CRC Press
Taylor & Francis Group

AIRCRAFT PROPULSION AND GAS TURBINE ENGINES

SECOND EDITION



AHMED F. EL-SAYED

Aircraft Propulsion and Gas Turbine Engines, Second Edition


Taylor & Francis
Taylor & Francis Group
http://taylorandfrancis.com

Aircraft Propulsion and Gas Turbine Engines, Second Edition

Ahmed F. El-Sayed



CRC Press
Taylor & Francis Group
Boca Raton London New York

CRC Press is an imprint of the
Taylor & Francis Group, an **informa** business

MATLAB® is a trademark of The MathWorks, Inc. and is used with permission. The MathWorks does not warrant the accuracy of the text or exercises in this book. This book's use or discussion of MATLAB® software or related products does not constitute endorsement or sponsorship by The MathWorks of a particular pedagogical approach or particular use of the MATLAB® software.

CRC Press
Taylor & Francis Group
6000 Broken Sound Parkway NW, Suite 300
Boca Raton, FL 33487-2742

© 2017 by Taylor & Francis Group, LLC
CRC Press is an imprint of Taylor & Francis Group, an Informa business

No claim to original U.S. Government works

Printed on acid-free paper

International Standard Book Number-13: 978-1-4665-9516-3 (Hardback)

This book contains information obtained from authentic and highly regarded sources. Reasonable efforts have been made to publish reliable data and information, but the author and publisher cannot assume responsibility for the validity of all materials or the consequences of their use. The authors and publishers have attempted to trace the copyright holders of all material reproduced in this publication and apologize to copyright holders if permission to publish in this form has not been obtained. If any copyright material has not been acknowledged, please write and let us know so we may rectify this in any future reprint.

Except as permitted under U.S. Copyright Law, no part of this book may be reprinted, reproduced, transmitted, or utilized in any form by any electronic, mechanical, or other means, now known or hereafter invented, including photocopying, microfilming, and recording, or in any information storage or retrieval system, without written permission from the publishers.

For permission to photocopy or use material electronically from this work, please access www.copyright.com (http://www.copyright.com/) or contact the Copyright Clearance Center, Inc. (CCC), 222 Rosewood Drive, Danvers, MA 01923, 978-750-8400. CCC is a not-for-profit organization that provides licenses and registration for a variety of users. For organizations that have been granted a photocopy license by the CCC, a separate system of payment has been arranged.

Trademark Notice: Product or corporate names may be trademarks or registered trademarks, and are used only for identification and explanation without intent to infringe.

Library of Congress Cataloging-in-Publication Data

Names: El-Sayed, Ahmed F., author.
Title: Aircraft propulsion and gas turbine engines / Ahmed F. El-Sayed.
Description: Second edition. | Boca Raton : Taylor & Francis, 2017. |
Includes bibliographical references and index.
Identifiers: LCCN 2016048776| ISBN 9781466595163 (hardback) | ISBN 9781466595170 (ebook) | ISBN 9781466595187 (ebook)
Subjects: LCSH: Airplanes--Turbojet engines. | Aircraft gas-turbines.
Classification: LCC TL709 .E42 2017 | DDC 629.134/353--dc23
LC record available at https://lccn.loc.gov/2016048776

Visit the Taylor & Francis website at
http://www.taylorandfrancis.com

and the CRC Press Web site at
http://www.crcpress.com

To

My wife Amany and sons Mohamed, Abdallah, and Khalid

for all their LOVE

AND UNDERSTANDING


Taylor & Francis
Taylor & Francis Group
http://taylorandfrancis.com

Contents

Preface xxiii
Author xxvii

Section I Aero Engines and Gas Turbines

1. History and Classifications of Aeroengines 3
1.1 Pre–Jet Engine History 4
1.1.1 Early Activities in Egypt and China 4
1.1.2 Leonardo da Vinci 6
1.1.3 Branca's Stamping Mill 6
1.1.4 Newton's Steam Wagon 6
1.1.5 Barber's Gas Turbine 7
1.1.6 Miscellaneous Aero-Vehicle's Activities in the Eighteenth and Nineteenth Centuries 7
1.1.7 Wright Brothers 10
1.1.8 Significant Events up to the 1940s 11
1.1.8.1 Aero-Vehicle Activities 11
1.1.8.2 Reciprocating Engines 14
1.2 Jet Engines 15
1.2.1 Jet Engines Inventors: Dr. Hans von Ohain and Sir Frank Whittle 15
1.2.1.1 Sir Frank Whittle (1907–1996) 15
1.2.1.2 Dr. Hans von Ohain (1911–1998) 16
1.2.2 Turbojet Engines 17
1.2.3 Turboprop and Turboshaft Engines 21
1.2.4 Turbofan Engines 25
1.2.5 Propfan Engine 28
1.2.6 Pulsejet, Ramjet, and Scramjet Engines 28
1.2.6.1 Pulsejet Engine 28
1.2.6.2 Ramjet and Scramjet Engines 30
1.2.7 Industrial Gas Turbine Engines 32
1.3 Classifications of Aerospace Engines 34
1.4 Classification of Jet Engines 35
1.4.1 Ramjet 35
1.4.2 Pulsejet 36
1.4.3 Scramjet 36
1.4.4 Turboramjet 37
1.4.5 Turborocket 38
1.5 Classification of Gas Turbine Engines 39
1.5.1 Turbojet Engines 39
1.5.2 Turboprop 42
1.5.3 Turboshaft 42
1.5.4 Turbofan Engines 43

1.5.5 Propfan Engines 48
1.5.6 Advanced Ducted Fan 49
1.6 Industrial Gas Turbines 50
1.7 Non-Airbreathing Engines 50
1.8 The Future of Aircraft and Powerplant Industries 51
1.8.1 Closure 59
Problems 63
References 72

2. Performance Parameters of Jet Engines 75
2.1 Introduction 75
2.2 Thrust Force 76
2.3 Factors Affecting Thrust 87
2.3.1 Jet Nozzle 87
2.3.2 Airspeed 87
2.3.3 Mass Airflow 87
2.3.4 Altitude 88
2.3.5 Ram Effect 89
2.4 Engine Performance Parameters 90
2.4.1 Propulsive Efficiency 91
2.4.2 Thermal Efficiency 96
2.4.2.1 Ramjet, Scramjet, Turbojet, and Turbofan Engines 97
2.4.2.2 Turboprop and Turboshaft Engines 98
2.4.3 Propeller Efficiency 98
2.4.4 Overall Efficiency 99
2.4.5 Takeoff Thrust 102
2.4.6 Specific Fuel Consumption 103
2.4.6.1 Ramjet, Turbojet, and Turbofan Engines 103
2.4.6.2 Turboprop Engines 104
2.4.7 Aircraft Range 104
2.4.8 Range Factor 108
2.4.9 Endurance Factor 108
2.4.10 Specific Impulse 110
2.4.11 Mission Segment Weight Fraction 114
2.4.12 Route Planning 117
2.4.12.1 Point of No Return 118
2.4.12.2 Critical Point 120
Problems 122
References 133

3. Pulsejet and Ramjet Engines 135
3.1 Introduction 135
3.2 Pulsejet Engines 135
3.2.1 Introduction 135
3.2.2 Valved Pulsejet 137
3.2.3 Valveless Pulsejet 143
3.2.4 Pulsating Nature of Flow Parameters in Pulsejet Engines 144
3.2.5 Pulse Detonation Engine 146

3.3 Ramjet Engines 151
3.3.1 Introduction 151
3.3.2 Classifications of Ramjet Engines 152
3.3.2.1 Subsonic–Supersonic Types 152
3.3.2.2 Fixed Geometry–Variable Geometry Types 153
3.3.2.3 Liquid-Fueled and Solid-Fueled Types 154
3.3.3 Ideal Ramjet 154
3.3.3.1 Real Cycle 158
3.4 Case Study 180
3.5 Nuclear Ramjet 191
3.6 Double-Throat Ramjet Engine 192
3.7 Solid-Fueled Ramjet Engine 193
3.8 Summary and Governing Equations for Shock Waves and Isentropic Flow 194
3.8.1 Summary 194
3.8.2 Normal Shock Wave Relations 195
3.8.3 Oblique Shock Wave Relations 195
3.8.4 Rayleigh Flow Equations 195
3.8.5 Isentropic Relation 196
Problems 196
References 200

4. Turbojet Engine 203
4.1 Introduction 203
4.2 Single Spool 206
4.2.1 Examples of Engines 206
4.2.2 Thermodynamic Analysis 207
4.2.3 Ideal Case 207
4.2.4 Actual Case 223
4.2.4.1 General Description 223
4.2.4.2 Governing Equations 225
4.2.5 Comparison between Operative and Inoperative Afterburner 234
4.3 Two-Spool Engine 239
4.3.1 Non-Afterburning Engine 239
4.3.1.1 Example of Engines 239
4.3.1.2 Thermodynamic Analysis 240
4.3.2 Afterburning Engine 244
4.3.2.1 Examples for Two-Spool Afterburning Turbojet Engines 244
4.3.2.2 Thermodynamic Analysis 245
4.4 Statistical Analysis 249
4.5 Thrust Augmentation 249
4.5.1 Water Injection 250
4.5.2 Afterburning 252
4.5.3 Pressure Loss in an Afterburning Engine 252
4.6 Supersonic Turbojet 257
4.7 Optimization of the Turbojet Cycle 260
4.8 Micro Turbojet 271
Problems 277
References 288

5. Turbofan Engines 289
5.1 Introduction 289
5.2 Forward Fan Unmixed Single-Spool Configuration 290
5.3 Forward Fan Unmixed Two-Spool Engines 296
5.3.1 The Fan and Low-Pressure Compressor (LPC) on One Shaft 296
5.3.2 Fan Driven by the LPT and the Compressor Driven by the HPT 307
5.3.3 A Geared Fan Driven by the LPT and the Compressor Driven by the HPT 308
5.3.3.1 Examples for This Configuration 308
5.4 Forward Fan Unmixed Three-Spool Engine 310
5.4.1 Examples for Three-Spool Engines 311
5.5 Forward Fan Mixed-Flow Engine 317
5.5.1 Mixed-Flow Two-Spool Engine 317
5.6 Mixed Turbofan with Afterburner 332
5.6.1 Introduction 332
5.6.2 Ideal Cycle 333
5.6.3 Real Cycle 335
5.7 Aft-Fan 335
5.8 VTOL and STOL (V/STOL) 338
5.8.1 Swiveling Nozzles 339
5.8.2 Switch-in Deflector System 343
5.8.2.1 Cruise 345
5.8.2.2 Takeoff or Lift Thrust 349
5.9 Performance Analysis 351
5.10 Geared Turbofan Engines 389
5.11 Summary 403
Problems 406
References 424

6. Shaft Engines: Internal Combustion, Turboprop, Turboshaft, and Propfan Engines 425
6.1 Introduction 425
6.2 Internal Combustion Engines 426
6.2.1 Introduction 426
6.2.2 Types of Aero Piston Engine 428
6.2.2.1 Rotary Engines 429
6.2.2.2 Reciprocating Engines 431
6.2.2.3 Supercharging and Turbocharging Engines 433
6.2.3 Aerodynamics and Thermodynamics of the Reciprocating Internal Combustion Engine 434
6.2.3.1 Terminology for the Four-Stroke Engine 434
6.2.3.2 Air-Standard Analysis 438
6.2.3.3 Engine Thermodynamics Cycles 438
6.2.3.4 Superchargers/Turbochargers 458
6.3 Aircraft Propellers 462
6.3.1 Introduction 462
6.3.2 Classifications 464
6.3.2.1 Source of Power 464
6.3.2.2 Material 464

6.3.2.3 Coupling to the Output Shaft 465
6.3.2.4 Control 465
6.3.2.5 Number of Propellers Coupled to Each Engine 466
6.3.2.6 Direction of Rotation 467
6.3.2.7 Propulsion Method 468
6.3.2.8 Number of Blades 470
6.3.3 Aerodynamic Design 470
6.3.3.1 Axial Momentum (or Actuator Disk) Theory 470
6.3.3.2 Modified Momentum or Simple Vortex Model 475
6.3.3.3 Blade Element Considerations 476
6.3.3.4 Dimensionless Parameters 482
6.3.3.5 Typical Propeller Performance 486
6.4 Turboprop Engines 495
6.4.1 Introduction to Turboprop Engines 496
6.4.2 Classification of Turboprop Engines 499
6.4.3 Thermodynamics Analysis of Turboprop Engines 501
6.4.3.1 Single-Spool Turboprop 501
6.4.3.2 Two-Spool Turboprop 507
6.4.4 Analogy with Turbofan Engines 510
6.4.5 Equivalent Engine Power 511
6.4.5.1 Static Condition 511
6.4.5.2 Flight Operation 511
6.4.6 Fuel Consumption 512
6.4.7 Turboprop Installation 513
6.4.8 Details of Some Engines 514
6.4.9 Performance Analysis 520
6.4.10 Comparison between Turbojet, Turbofan and Turboprop Engines 524
6.5 Turboshaft Engines 529
6.5.1 Power Generated by Turboshaft Engines 531
6.5.1.1 Single-Spool Turboshaft 531
6.5.1.2 Double-Spool Turboshaft 531
6.5.2 Examples for Turboshaft Engines 532
6.6 Propfan Engines 539
6.7 Conclusion 547
Problems 547
References 565

7. High-Speed Supersonic and Hypersonic Engines 567
7.1 Introduction 567
7.2 Supersonic Aircraft and Programs 567
7.2.1 Anglo-French Activities 568
7.2.1.1 Concorde 568
7.2.1.2 BAe-Aerospatiale AST 569
7.2.2 Russian Activities 570
7.2.2.1 Tupolev TU-144 570
7.2.3 The U.S. Activities 570
7.3 The Future of Commercial Supersonic Technology 572
7.4 Technology Challenges of Future Flight 573

7.5 High-Speed Supersonic and Hypersonic Propulsion 574
7.5.1 Introduction 574
7.5.2 Hybrid-Cycle Engine 575
7.6 Turboramjet Engine 575
7.7 Wraparound Turboramjet 576
7.7.1 Operation as a Turbojet Engine 577
7.7.2 Operation as a Ramjet Engine 579
7.8 Over/Under Turboramjet 580
7.8.1 Turbojet Mode 582
7.8.2 Dual Mode 582
7.8.3 Ramjet Mode 583
7.9 Turboramjet Performance 583
7.9.1 Turbojet Mode 583
7.9.2 Ramjet Mode 584
7.9.3 Dual Mode 584
7.10 Case Study 585
7.11 Examples for Turboramjet Engines 592
7.12 Hypersonic Flight 594
7.12.1 History of Hypersonic Vehicles 594
7.12.2 Hypersonic Commercial Transport 596
7.12.3 Military Applications 598
7.13 Scramjet Engines 598
7.13.1 Introduction 598
7.13.2 Thermodynamics 600
7.14 Intake of a Scramjet Engine 601
7.14.1 Case Study 601
7.15 Combustion Chamber 601
7.15.1 Fuel Mixing in Parallel Stream 603
7.15.1.1 Ramp Injectors 603
7.15.2 Fuel Mixing in Normal Stream 604
7.16 Nozzle 604
7.17 Case Study 605
7.18 Dual-Mode Combustion Engine (Dual Ram-Scramjet) 606
7.18.1 Aero-Thermodynamics of Dual-Mode Scramjet 607
Problems 613
References 617

8. Industrial Gas Turbines 619
8.1 Introduction 619
8.2 Categories of Gas Turbines 622
8.3 Types of Industrial Gas Turbines 624
8.4 Single-Shaft Engine 626
8.4.1 Single Compressor and Turbine 626
8.4.1.1 Ideal Cycle 626
8.4.1.2 Real Cycle 630
8.4.2 Regeneration 633
8.4.3 Reheat 635
8.4.4 Intercooling 638
8.4.5 Combined Intercooling, Regeneration, and Reheat 639

8.5 Double-Shaft Engine 645
8.5.1 Free-Power Turbine 645
8.5.2 Two-Discrete Shafts (Spools) 647
8.6 Three Spool 655
8.7 Combined Gas Turbine 662
8.8 Marine Applications 664
8.8.1 Additional Components for Marine Applications 665
8.8.2 Examples for Marine Gas Turbines 666
8.9 Offshore Gas Turbines 669
8.10 Micro-Gas Turbines (μ-Gas Turbines) 669
8.10.1 Micro- versus Typical-Gas Turbines 670
8.10.2 Design Challenges 670
8.10.2.1 Manufacturing 670
8.10.2.2 Selection and Design of Bearings 671
8.10.2.3 Compressor and Turbine 671
8.10.3 Applications 671
Problems 672
References 676

Section II Component Design

9. Powerplant Installation and Intakes 679
9.1 Introduction 679
9.2 Powerplant Installation 679
9.3 Subsonic Aircraft 680
9.3.1 Turbojet and Turbofan Engines 680
9.3.1.1 Wing Installation 680
9.3.1.2 Fuselage Installation 684
9.3.1.3 Combined Wing and Tail Installation (Three Engines) 687
9.3.1.4 Combined Fuselage and Tail Installation 688
9.3.2 Turboprop Installation 688
9.4 Supersonic Aircraft 691
9.4.1 Civil Transports 692
9.4.2 Military Aircraft 693
9.5 Air Intakes or Inlets 695
9.6 Subsonic Intakes 695
9.6.1 Inlet Performance 697
9.6.2 Performance Parameters 701
9.6.2.1 Isentropic Efficiency (η_d) 701
9.6.2.2 Stagnation-Pressure Ratio (r_d) 702
9.6.3 Turboprop Inlets 704
9.7 Supersonic Intakes 705
9.7.1 Review of Gas Dynamic Relations for Normal and Oblique Shocks 708
9.7.1.1 Normal Shock Waves 708
9.7.1.2 Oblique Shock Waves 709
9.7.2 External Compression Intake (Inlet) 710
9.7.3 Internal Compression Inlet (Intake) 716
9.7.4 Mixed Compression Intakes 717

9.8 Matching between Intake and Engine 719
9.9 Case Study 721
Problems 731
References 738

10. Combustion Systems 739
10.1 Introduction 739
10.2 Subsonic Combustion Chambers 740
10.2.1 Tubular (or Multiple) Combustion Chambers 740
10.2.2 Tubo-Annular Combustion Chambers 742
10.2.3 Annular Combustion Chambers 743
10.3 Supersonic Combustion Chamber 744
10.4 Combustion Process 744
10.5 Components of the Combustion Chamber 746
10.6 Aerodynamics of the Combustion Chamber 748
10.6.1 Aerodynamics of Diffusers 748
10.7 Chemistry of Combustion 753
10.8 The First Law Analysis of Combustion 757
10.9 Combustion Chamber Performance 759
10.9.1 Pressure Losses 760
10.9.2 Combustion Efficiency 760
10.9.3 Combustion Stability 762
10.9.4 Combustion Intensity 762
10.9.5 Cooling 763
10.9.5.1 Louver Cooling 763
10.9.5.2 Splash Cooling 763
10.9.5.3 Film Cooling 763
10.9.5.4 Convection-Film Cooling 764
10.9.5.5 Impingement-Film Cooling 764
10.9.5.6 Transpiration Cooling 765
10.9.5.7 Effective Cooling 765
10.10 Material 766
10.11 Aircraft Fuels 766
10.11.1 Safety Fuels 767
10.12 Emissions and Pollutants 768
10.12.1 Pollutant Formation 768
10.12.1.1 NO_x Emissions 768
10.12.1.2 Sulfur Dioxide (SO_2) Emissions 769
10.13 The Afterburner 770
10.14 Supersonic Combustion System 773
Problems 776
References 778

11. Exhaust System 781
11.1 Introduction 781
11.2 Nozzle 784
11.2.1 Governing Equations 785
11.2.1.1 Convergent-Divergent Nozzle 786
11.2.1.2 Convergent Nozzle 789

11.2.2 Variable Geometry Nozzles 790
11.2.3 Afterburning Nozzles 792
11.3 Calculation of the Two-Dimensional Supersonic Nozzle 795
11.3.1 Convergent Nozzle 796
11.3.2 Divergent Nozzle 802
11.3.2.1 Analytical Determination of the Contour of a Nozzle 805
11.3.2.2 Design Procedure for a Minimum Length Divergent Nozzle 807
11.3.2.3 Procedure of Drawing the Expansion Waves inside the Nozzle 808
11.4 Thrust Reversal 810
11.4.1 Classification of Thrust Reverser Systems 811
11.4.2 Calculation of Ground Roll Distance 817
11.5 Thrust Vectoring 819
11.5.1 Governing Equations 823
11.6 Noise 823
11.6.1 Introduction 823
11.6.2 Acoustics Model Theory 826
11.6.3 Methods Used to Decrease Jet Noise 828
11.7 High-Speed Vehicles 830
11.7.1 Conical Nozzles 830
11.7.2 Bell Nozzles 831
11.7.2.1 Advantages of Bell-Shaped Nozzle 832
11.7.2.2 Disadvantages of Bell-Shaped Nozzle 832
11.7.3 Annular Nozzles 832
11.7.3.1 Radial Out-Flow Nozzles 833
11.7.3.2 Radial Inflow Nozzles 834
Problems 834
References 836

12. Centrifugal Compressors 839
12.1 Introduction 839
12.2 Layout of Compressor 842
12.2.1 Impeller 843
12.2.2 Diffuser 844
12.2.3 Scroll or Manifold 845
12.3 Classification of Centrifugal Compressors 845
12.4 Governing Equations 849
12.4.1 The Continuity Equation 853
12.4.2 The Momentum Equation or Euler's Equation for Turbomachinery 853
12.4.3 The Energy Equation or the First Law of Thermodynamics 854
12.4.4 Slip Factor σ 858
12.4.5 Prewhirl 862
12.4.6 Types of Impeller 874
12.4.7 Radial Impeller 883
12.5 The Diffuser 885
12.5.1 Vaneless Diffuser 886
12.5.1.1 Incompressible Flow 886
12.5.1.2 Compressible Flow 887
12.5.2 Vaned Diffuser 888

12.6 Discharge Systems 896
12.7 Characteristic Performance of a Centrifugal Compressor 897
12.8 Erosion 899
12.8.1 Introduction 899
12.8.2 Theoretical Estimation of Erosion 905
Problems 909
References 925

13. Axial Flow Compressors and Fans 927
13.1 Introduction 927
13.2 Comparison between Axial and Centrifugal Compressors 930
13.2.1 Advantages of the Axial Flow Compressor over the Centrifugal Compressor 930
13.2.2 Advantages of Centrifugal-Flow Compressor over the Axial Flow Compressor 931
13.2.3 Main Points of Comparison between Centrifugal and Axial Compressors 932
13.3 Mean Flow (Two-Dimensional Approach) 933
13.3.1 Types of Velocity Triangles 935
13.3.2 Variation of Enthalpy Velocity and Pressure in an Axial Compressor 937
13.4 Basic Design Parameters 945
13.4.1 Centrifugal Stress 945
13.4.2 Tip Mach Number 948
13.4.3 Fluid Deflection 949
13.5 Design Parameters 950
13.6 Three-Dimensional Flow 954
13.6.1 Axisymmetric Flow 955
13.6.2 Simplified Radial Equilibrium Equation (SRE) 956
13.6.3 Free Vortex Method 958
13.6.4 General Design Procedure 963
13.7 Complete Design Process for Compressors 972
13.8 Rotational Speed (rpm) and Annulus Dimensions 973
13.9 Determine the Number of Stages (Assuming Stage Efficiency) 976
13.10 Calculation of Air Angles for Each Stage at the Mean Section 977
13.10.1 First Stage 977
13.10.2 Stages from (2) to $(n-1)$ 978
13.10.3 Last Stage 979
13.11 Variation of Air Angles from Root to Tip Based on Type of Blading (Either Free Vortex, Exponential, or First Power Methods) 980
13.12 Blade Design 982
13.12.1 Cascade Measurements 982
13.12.2 Choosing the Type of Airfoil 987
13.12.3 Stage Performance 988
13.13 Compressibility Effects 994
13.14 Performance 1003
13.14.1 Single Stage 1003
13.14.2 Multistage Compressor 1006
13.14.3 Compressor Map 1006

13.14.4 Stall and Surge 1008
13.14.5 Surge Control Methods 1011
13.14.5.1 Multi-Spool Compressor 1011
13.14.5.2 Variable Vanes 1012
13.14.5.3 Air Bleed 1013
13.15 Case Study 1019
13.15.1 Mean Section Data 1019
13.15.2 Variations from Hub to Tip 1019
13.15.3 Details of Flow in Stage Number 2 1021
13.15.4 Number of Blades and Stresses of the Seven Stages 1021
13.15.5 Compressor Layout 1023
13.16 Erosion 1023
Problems 1034
References 1056

14. Axial Turbines 1059
14.1 Introduction 1059
14.2 Comparison between Axial-Flow Compressors and Turbines 1062
14.3 Aerodynamics and Thermodynamics for a Two-Dimensional Flow 1062
14.3.1 Velocity Triangles 1062
14.3.2 Euler Equation 1065
14.3.3 Efficiency, Losses, and Pressure Ratio 1067
14.3.4 Nondimensional Quantities 1072
14.3.5 Several Remarks 1081
14.4 Three-Dimensional Analysis 1087
14.4.1 Free Vortex Design 1088
14.4.2 Constant Nozzle Angle Design (α_2) 1089
14.4.3 General Case 1091
14.4.4 Constant Specific Mass Flow Stage 1092
14.5 Preliminary Design 1108
14.5.1 Main Design Steps 1109
14.5.2 Aerodynamic Design 1109
14.5.3 Blade Profile Selection 1111
14.5.4 Mechanical and Structural Design 1112
14.5.4.1 Centrifugal Stresses 1113
14.5.4.2 Centrifugal Stresses on Blades 1113
14.5.4.3 Centrifugal Stresses on Disks 1115
14.5.4.4 Gas Bending Stress 1117
14.5.4.5 Centrifugal Bending Stress 1119
14.5.4.6 Thermal Stress 1120
14.5.5 Turbine Cooling 1120
14.5.5.1 Turbine Cooling Techniques 1120
14.5.5.2 Mathematical Modeling 1123
14.5.6 Losses and Efficiency 1129
14.5.6.1 Profile Loss (Y_p) 1129
14.5.6.2 Annulus Loss 1131
14.5.6.3 Secondary Flow Loss 1131
14.5.6.4 Tip Clearance Loss (Y_k) 1131
14.6 Turbine Map 1133

14.7 Case Study 1137
14.7.1 Design Point 1138
14.7.1.1 Mean Line Flow 1138
14.7.1.2 Three-Dimensional Variations 1138
14.7.1.3 Number of Blades for Nozzle and Rotor 1139
14.7.1.4 Chord Length at Any Section along Blade Height for Nozzle and Rotor 1140
14.7.1.5 Blade Material Selection 1144
14.7.1.6 Stresses on Rotor Blades 1144
14.7.1.7 Losses Calculations 1145
14.7.1.8 Turbine Efficiency 1145
14.8 Summary 1145
Problems 1146
References 1154

15. Radial Inflow Turbines 1157
15.1 Introduction 1157
15.2 Thermodynamic 1158
15.3 Dimensionless Parameters 1163
15.3.1 Stage Loading 1163
15.3.2 Flow Coefficient 1163
15.3.3 Rotor Meridional Velocity Ratio 1163
15.3.4 Specific Speed 1164
15.4 Preliminary Design 1164
15.5 Breakdown of Losses 1168
15.6 Design for Optimum Efficiency 1171
15.7 Cooling 1176
Problems 1177
References 1181

16. Module Matching 1183
16.1 Introduction 1183
16.2 Off-Design Operation of a Single-Shaft Gas Turbine Driving a Load 1183
16.2.1 Matching Procedure 1185
16.2.2 Different Loads 1190
16.3 Off-Design of a Free Turbine Engine 1190
16.3.1 Gas Generator 1191
16.3.2 Free Power Turbine 1192
16.4 Off-Design of Turbojet Engine 1197
Problems 1215
References 1220

17. Selected Topics 1221
17.1 Introduction 1221
17.2 New Trends in Aeroengines 1225
17.2.1 Intercooler 1226
17.2.2 Intercooler and Recuperator 1235
17.2.3 Inter-Turbine Burner 1243
17.2.4 Double-Bypass/Three-Stream Turbofan 1250

17.2.5 3D Printing as the Future of Manufacturing Aircraft and Aircraft Engines 1252
17.3 Aviation Environmental Issues 1252
17.3.1 Introduction 1252
17.3.2 Sustainable Alternative Fuels 1253
17.3.2.1 Introduction 1253
17.3.2.2 Potential Second-Generation Biofuel Feedstocks 1254
17.3.2.3 Key Advantages of Second-Generation Biofuels for Aviation 1254
17.3.2.4 Commercial and Demonstration Flights 1254
17.3.2.5 Biofuels for Aviation Economic Viability 1254
17.4 Unmanned Aircraft Vehicles 1255
17.4.1 Introduction 1255
17.4.2 Categorization of UAV 1256
17.4.2.1 Based on Function 1257
17.4.2.2 Based on Range/Altitude 1257
17.4.2.3 Based on Size 1259
17.4.2.4 European Classifications (EUROUVS) 1260
17.4.3 Power Plant of UAV 1260
17.4.3.1 Electric Engine 1260
17.4.3.2 Internal Combustion (IC) Engines 1262
17.4.3.3 Gas Turbine Engines 1263
17.4.3.4 Engine Characteristics 1263
Problems 1266
References 1269

Section III Rocket Propulsion

18. Introduction to Rocketry 1273
18.1 Introduction 1273
18.2 History 1274
18.2.1 Important Events 1274
18.2.2 Recent and Future Plans for Rocket and Space Flights (2014 and Beyond) 1276
18.3 Missile Configuration 1278
18.3.1 External Configuration 1278
18.3.2 Main Sections of a Missile Body 1279
18.3.2.1 Nose Section (Fore-Body) 1279
18.3.2.2 Mid-Section 1281
18.3.2.3 Tail Section 1281
18.3.3 The Auxiliary Components (Wings, Fins, and Canards) 1282
18.3.3.1 Wings 1282
18.3.3.2 Fins 1283
18.4 Classification 1285
18.4.1 Propulsion 1285
18.4.2 Energy Source 1285
18.4.3 Types of Missiles 1285
18.4.4 Launch Mode 1286

18.4.5 Range 1286
18.4.6 Warheads 1286
18.4.7 Guidance Systems 1286
18.4.8 Number of Stages 1287
18.4.9 Application 1287
18.4.10 Military Rockets 1287
18.4.10.1 According to Purpose and Use 1287
18.4.10.2 According to the Location of the Launching Site and Target 1288
18.4.10.3 According to the Main Characteristics 1288
18.5 Rocket Performance Parameters 1288
18.5.1 Thrust Force 1288
18.5.2 Effective Exhaust Velocity (V_{eff}) 1290
18.5.3 Exhaust Velocity (u_e) 1293
18.5.4 Important Nozzle Relations 1294
18.5.5 Characteristic Velocity (C^*) 1296
18.5.6 Thrust Coefficient (C_F) 1296
18.5.7 Total Impulse (I_t) 1298
18.5.8 Specific Impulse (I_{sp}) 1299
18.5.9 Specific Propellant Consumption 1303
18.5.10 Mass Ratio (MR) 1303
18.5.11 Propellant Mass Fraction (ζ) 1303
18.5.12 Impulse-to-Weight Ratio 1304
18.5.13 Efficiencies 1304
18.5.13.1 Thermal Efficiency 1304
18.5.13.2 Propulsive Efficiency 1305
18.5.13.3 Overall Efficiency (η_0) 1306
18.6 The Rocket Equation 1309
18.6.1 Single-Stage Rocket 1309
18.6.1.1 Negligible Drag 1311
18.6.1.2 Negligible Drag and Gravity Loss 1311
18.6.2 Multistage Rockets 1314
18.6.3 Rocket Equation for a Multistage Series Rocket 1316
18.6.4 Rocket Equation for a Parallel Multistage Rocket 1316
18.6.5 Advantages of Staging 1317
18.6.6 Disadvantages of Staging 1317
18.7 Space Flight 1324
18.7.1 Orbital Velocity 1324
18.7.2 Escape Velocity 1325
Problems 1326
References 1329

19. Rocket Engines 1331
19.1 Chemical Rocket Engines 1331
19.1.1 Introduction 1331
19.1.2 Performance Characteristics 1332
19.2 Solid Propellants 1333
19.2.1 Introduction 1333

19.2.2 Composition of a Solid Propellant 1335
19.2.3 Basic Definitions 1335
19.2.4 Burning Rate 1337
19.2.5 Characteristics of Some Solid Propellants 1346
19.2.6 Liquid-Propellant Rocket Engines (LRE) 1346
19.2.6.1 Introduction 1346
19.2.7 Applications 1348
19.2.7.1 Propellant Feed System of LREs 1348
19.3 Liquid Propellants 1350
19.3.1 Monopropellant 1350
19.3.2 Bipropellant 1351
19.3.3 Fundamental Relations 1353
19.4 Pump-Fed System 1355
19.5 Rocket Pumps 1359
19.5.1 Introduction 1359
19.5.2 Centrifugal Pumps 1359
19.5.3 Multistage Centrifugal Pumps 1362
19.5.4 Multistage Axial Pumps 1362
19.6 Performance of Centrifugal Pumps 1362
19.7 Pump Performance Parameters 1366
19.7.1 Pump Specific Speed (N_s) 1366
19.8 Features of Modules of the Space Shuttle Main Engine (SSME) 1372
19.9 Axial Pumps 1372
19.10 Parallel and Series Connections 1374
19.11 Pump Materials and Fabrication Processes 1377
19.12 Axial Turbines 1377
19.12.1 Single-Stage Impulse Turbine 1377
19.12.2 Multispool Impulse Turbines 1378
19.12.3 Reaction Turbines 1378
19.13 Hybrid Propulsion 1382
19.13.1 Introduction 1382
19.13.2 Mathematical Modeling 1384
19.13.3 Advantages and Disadvantages of Hybrid Engines 1386
19.14 Nuclear Rocket Propulsion 1387
19.14.1 Introduction 1387
19.14.2 Solid-Core Reactors 1387
19.14.3 Gas-Core Reactor 1390
19.15 Electric Rocket Propulsion 1390
19.15.1 Introduction 1390
19.15.2 Electrostatic Propulsion 1392
19.15.2.1 Introduction 1392
19.15.2.2 Mathematical Modeling 1393
19.15.2.3 Multiply Charged Ion Species 1395
19.15.2.4 Total Efficiency 1397
19.15.2.5 Electrical Efficiency 1397
19.15.3 Electrothermal 1400
19.15.3.1 Introduction 1400
19.15.3.2 Resistojets 1400

19.15.3.3 Arcjets 1401
19.15.3.4 Electromagnetic Engines 1402
Problems 1403
References 1406

Appendix A: Glossary 1409

Appendix B: Turbofan 1417

Appendix C: Samples of Gas Turbines (Representative Manufacturers) 1419

Index 1421

Preface

After accumulating a couple of thousand users (in academia and industry) from around the globe, this engine is due for an overhaul!

Since an overhaul is a heavy repair/maintenance process, then, in this second edition of my engine book, a number of significant changes have been made to the scope, organization, and focus. In this edition, I have strived to cope with the technological and environmental challenges associated with thrust/power production.

The scope of the book has been expanded to include rocket propulsion, unmanned aerial vehicles (UAVs), and biofuel. Therefore, three new chapters have been added. Two of them are on rocketry. The third is entitled "Selected Topics" and handles three hot topics: future trends in aeroengine design, UAV, and biofuel.

The book has 19 chapters organized in three parts. With this new material, it is now possible to teach two complete junior–senior-level courses—one on aircraft and rocket propulsion and one on aeroengine design.

Other major content changes include the addition of internal combustion engines and propeller design. Moreover, since a long-distance rocket incorporates an airbreathing engine side by side with a rocket engine for sustained flight, there is a thorough analysis and discussion in the relevant chapters of intermeshing a rocket engine with either a ramjet, turbojet, or turbofan engine. Also, unducted fan (UDF) or propfan engines have regained the interest they previously enjoyed in the 1970s after the oil embargo; this was sufficient motivation for adding a detailed case study. Many new solved examples and nearly 100 new end-of-chapter problems based on real airbreathing engines and rocket engines have been developed for this edition.

What's New in the Second Edition: Chapter-by-Chapter Content Changes

Chapter 1, History and Classifications of Aeroengines, includes all changes in airbreathing engines to cover the period between the two editions (2007–2016). There is particular emphasis on geared and three-spool turbofan engines, scramjet engines, and solar aircraft.

Chapter 2, Performance Parameters of Jet Engines, includes details for range and fuel consumption for each flight phase of military aircraft as well as the point of no return and critical point for airliners. Performance analyses of many flying aircraft are provided. Thrust of rockets is also introduced.

Chapter 3, Pulsejet and Ramjet Engines, includes major changes. The pulsating nature of pulsejet engines and the analysis of Flying Bomb V-1 and pulse detonation engine are discussed. Classifications of ramjets based on flight speed (subsonic/supersonic), geometry (fixed/variable), type of fuel (solid/liquid), and nuclear/nonnuclear engines are given. The thermodynamics of double-throat and solid-fuel ramjets is introduced. Finally, the Boeing IM-99/CIM-10 Bomarc rocket, using both a liquid-fuel rocket and a liquid-fuel ramjet for its sustained flight, is analyzed.

Chapter 4, Turbojet Engine, addresses small engines used in cruise missiles, target drones, and other small unmanned air vehicles (UAVs), since larger ones are no longer employed due to their high noise and fuel consumption. Data for several micro-turbojets are given. Turbojet engines integrated with rocket engines (e.g., in Harpoon and Storm shadow rockets) for sustained flight are analyzed.

Chapter 5, Turbofan Engines, adds new material on triple-spool mixed/afterburning turbofan engines. The effect of air bleed on the performance of large three-spool engines is enhanced. The subject of turbofan engines used in powering rockets during sustained flight has been added. Many examples are worked out, including the Williams International F107-WR-402 turbofan powering the AGM-86 ALCM cruise missile launched from the Boeing B-52H Stratofortress bomber. Since a geared turbofan engine represents the recommended choice for the coming decade—due to its low noise and fuel consumption—a detailed performance analysis for a typical geared turbofan is given.

Chapter 6 has undergone extensive changes including its title, which has been modified to Shaft Engines: Internal Combustion, Turboprop, Turboshaft, and Propfan Engines. Since aero-piston engines power both small aircraft and helicopters, FAA statistics in 2013 for flying vehicles powered by piston engines were fivefold those for aircraft powered by turbine engines, and the piston engine should continue its superiority but settling at a ratio of 3:1 by 2032. Thus, it was necessary to add new detailed material on aero-piston engines, including reciprocating, radial, and supercharged/turbocharged ones, with power, efficiency, and fuel consumption as the targets in each thermodynamic cycle analysis. However, a piston engine cannot propel an aircraft on its own, so a propeller must be installed on it. First, propeller classification is introduced, followed by detailed aerodynamic theories (momentum, modified momentum, and blade element). The generated thrust and the power from successive elements of the propeller are calculated using published experimental data. Next, the existing treatment of turboprop engines is augmented with the new section on propeller design. Analysis of a real engine powering the T116 aircraft is given. The third engine to be discussed is the turboshaft engine powering helicopters. Rotor aerodynamics is first added, and the thrust of the real engine powering the world's largest helicopter, the Mil Mi-26, is analyzed as an example. The fourth engine treated here is the propfan or UDF. Detailed analysis for a three-spool counter-rotating pusher-type propfan is given.

Chapter 7, High-Speed Supersonic and Hypersonic Engines, incorporates minor changes, wherein the thermodynamics and aerodynamics of the dual-mode combustion engine (dual ram-scramjet) are introduced.

Chapter 8, Industrial Gas Turbines, is modified to emphasize its relevance in various contemporary applications on land, sea, and air. A real engine (one of Siemens' gas turbines) is introduced as an example.

Chapter 9, Powerplant Installation and Intakes, addresses new features of subsonic divided intake as well as the quarter-circular intake of the F-111 fighter during its supersonic speeds.

Chapter 10, Combustion Systems, has new sections on the constituents of the combustion chamber, the aerodynamics of its diffuser section, and methods for calculating the lowest and highest heating value of fuel from the enthalpy of formation of the reactants and products.

Chapter 11, Exhaust System, includes a new part on nozzles for high-speed vehicles (mainly rockets). Formulae for geometries of different types of rocket nozzles (cone, bell, and annular types) are given.

Chapter 12, Centrifugal Compressors, includes tabulated formulae for governing equations of temperature rise, pressure ratio, torque, and consumed power appropriate for ideal and real conditions at impeller inlet and outlet. The subject of the radial impeller having inlet and outlet velocity triangles in radial–tangential plane is also added. The effect of fouling phenomena on its performance is discussed.

Chapter 13, Axial Flow Compressors and Fans, presents analyses of axial flow compressors and fans in real turbofan engines, including HF120 and V2500. Case studies for stall, surge control, and tip leakage are discussed. Combined axial–centrifugal layout is revisited.

In Chapter 14, Axial Turbines, a few materials regarding real turbines in commercial turbofans have been added.

Chapter 15, Radial Inflow Turbines, incorporates the performance of a turbine composed of a radial stage at inlet followed by multistage axial turbine.

Chapter 16, Module Matching, examines the matching of modules in a triple-spool turbofan engine as well as a turbojet engine.

New Chapters

Chapter 17, Selected Topics, examines three topics. The first is new trends in aeroengine design. Three options are discussed. The first examines a more complex thermodynamic cycle involving recuperation (for turboprop/turboshaft engines) and intercooling, together with recuperation for higher-pressure-ratio turbofan engines. The second proposes interturbine burners. The third suggests a three-stream turbofan. All are still under investigation. The second topic is biofuel, which has shared the currently used hydrocarbon fuel in several test flights. Since sources of jet fuel will diminish within some 50 years, biofuel is a potential candidate for future aviation fuel. The third topic deals with UAVs, which are now extensively used in both civil and military applications. The categories and benefits of UAVs are identified. Different power sources are defined.

Chapter 18, Introduction to Rocketry, presents the evolution of the rocket since its Chinese origin until now. Next, it classifies rockets based on type, launching mode, range, engine, warhead, and guidance system. A missile's main sections are then described: nose section, mid-section, tail section, nozzle, and auxiliary components. Rocket performance parameters are closely similar to those for airbreathing engines, which include thrust force, specific impulse, total impulse, thrust coefficient, effective exhaust velocity, characteristic velocity, and specific propellant consumption. The rocket equation is next derived for single- and multistage rockets. Both series and parallel staging are dealt with. The advantages and disadvantages of staging are described. Finally, space flight, orbital velocity, and escape velocity are derived.

Chapter 19, Rocket Engines: Rockets are propelled using one of the following energies: chemical, electrical, nuclear, and solar.

Chemical rockets are either of the solid, liquid, or hybrid types. The composition and characteristics of some solid propellants and their burning rate are given. Liquid-propellant rockets are either of the monopropellant or bipropellant type. The components of liquid-propellant rockets are defined. A pump-feed system is a vital component; thus, its type as well as series and parallel combinations are studied. The turbopump (normally seen in the Space Shuttle) includes both pumps and turbines and is studied here in detail.

Hybrid-propellant engines represent an intermediate group between solid- and liquid-propellant engines.

Nonchemical rockets, including nuclear and electrical rockets, are examined. Electrostatic, electrothermal, and electromagnetic types are thoroughly modeled and analyzed.

Insofar, the rapid infusion and implementation of information and computing facilities, I urge students to check the nearly daily developments in airbreathing and rocket engines through the various websites, of both industrial and academic nature. Also, many free or affordable programs are available on the Internet (e.g., MATLAB®, MATHCAD, and MATHEMATICA), which can be used in the design of both full engines and their modules, such as multistage axial compressors and turbines.

Supplements

As a further aid to instructors, a very detailed test manual is available, which includes some 80 full tests of 90 minutes each. An earlier version of this test manual, having some 60 full tests, accompanied the first edition. Many instructors liked it.

Also, a more complete solution manual is available.

Finally, I express my sincere appreciation and gratitude to Airbus Industries and Rolls-Royce plc for their permission to use illustrations and photographs within this text.

I thank the many kind instructors here and abroad who have communicated with me concerning various aspects of the first edition during its life of eight years. I am grateful to Darrel Pepper, Director of the Nevada Center for Advanced Computational Methods (NCACM), University of Nevada, Las Vegas, who invited me to teach an aircraft propulsion course (400/600 level). His continuous support and advice is most helpful. My gratitude extends also to Reda Mankabadi and Magdy S. Attia, College of Engineering, Embry–Riddle Aeronautical University, Daytona Beach, who used the first edition in teaching several propulsion and design courses and received many positive comments on the text. My gratitude extends to Louis Chow, Department of Mechanical and Aerospace Engineering, University of Central Florida, who carefully read and discussed the parts on heat transfer.

I am also so grateful to the continuous support and help of my students: Ahmed Z. Almeldein, Aerospace Department, Korea Advanced Institute of Science and Technology, South Korea; Amr Kamel, Egyptian Air Force; Mohamed Emera and Ibrahim Roufael, Mechanical Power Engineering Department, Zagazig University, Egypt; Ahmed Hamed, Senior Production Engineer, Engine Overhaul Directorate, EgyptAir Maintenance and Engineering Company; and Huessin Aziz and Eslam Abdel Ghany, Institute of Aviation Engineering and Technology, Cairo, Egypt.

And finally, my gratitude goes to my wife, Amany, for so patiently putting up with the turmoil surrounding a book in progress until we can breathe a joint sigh of relief at the end of the project. My sons, Mohamed, Abdallah, and Khalid, were the real inspiration and motivation behind this work.

Also, I am very grateful to Jonathan W. Plant, Executive Editor for Mechanical, Aerospace & Nuclear Engineering, Taylor & Francis Group/CRC Press, for his continuous support and encouragement that made this work possible.

Author

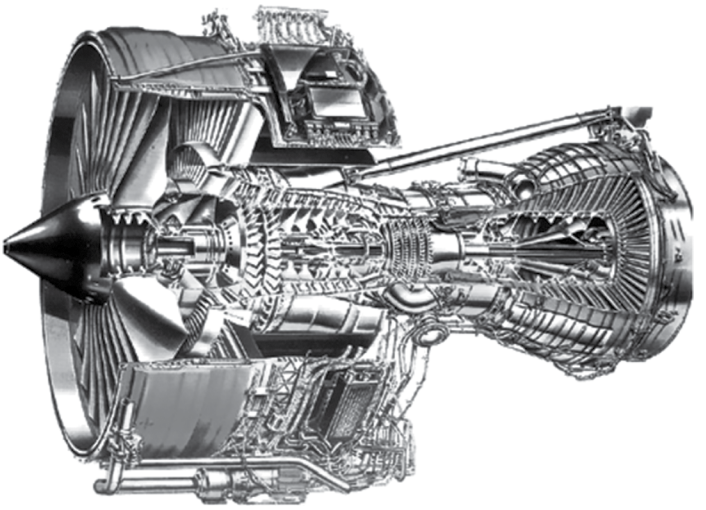
Professor Ahmed F. El-Sayed was a senior engineer for the Egyptian Airline EgyptAir for 10 years, working in the maintenance, technical inspection, and R&D departments, as well as the engine overhaul shop. He has worked as a researcher in corporate projects with Westinghouse (USA) and Rolls Royce (UK), and taught propulsion and turbomachinery courses in several universities in Egypt, the United States, and Libya.

Professor El-Sayed has lectured in the field of design and performance of aircraft engines in several universities in the United States, Russia, Belgium, United Kingdom, Austria, China, Syria, and Japan, as well as in the NASA Glenn Research Center, MIT, U.S. Air Force Academy, and the von Karman Institute. He is the author of eight books and more than 80 technical papers on aircraft propulsion, performance, and design aspects; FOD of intakes; fans and compressors; and cooling of axial turbines of aircraft engines.


Taylor & Francis
Taylor & Francis Group
http://taylorandfrancis.com

Section I

Aero Engines and Gas Turbines



Rolls-Royce Trent 800. (Reproduced from Rolls-Royce plc. with permission.)


Taylor & Francis
Taylor & Francis Group
http://taylorandfrancis.com

1

History and Classifications of Aeroengines

The idea of flying by imitating birds has been a dream since the dawn of human intelligence. Various ancient and medieval people who fashioned wings met with disastrous consequences when leaping from towers or roofs and flapping vigorously. The Greek myth of Daedalus and his son Icarus who were imprisoned on the island of Crete and tried to escape by fastening wings with wax and flying through the air is well known. This dream of flight was only achieved in the twentieth century, at approximately 10:35 AM on Tuesday, December 17, 1903, when Orville Wright managed to achieve the first successful flight in Kitty Hawk, North Carolina. That flying machine, the Wright Flyer I, was the first heavier-than-air flyer designed and flown by the Wright brothers: Wilbur (1867–1912) and Orville (1871–1948). The Wright brothers, who were the inventors of the first practical airplane, are certainly the premier aeronautical engineers in history. Comparing the Wright Flyer I with the twenty-first-century aircraft like the Boeing 787 and Airbus 350 underlines the unbelievable miracles that have taken place in the aviation industry. The Wright Flyer I did not even have a fuselage, and either brother had to lie prone on the bottom wing, facing into the cold wind. Nevertheless, such was the flight that marked the first stage in the magnificent evolution of human-controlled powered flight. Several years lapsed before the design of a conventional aircraft included a closed fuselage to which wings and a tail unit were attached and which had an undercarriage or landing gears. Tremendous development in the aviation industry eventually allowed passengers in civil aircraft to enjoy the hot/cold air-conditioned compartments of the fuselage, to have comfortable seats and delicious meals, and to enjoy video movies. However, it was a long time before people could be persuaded to use aircraft as transportation vehicles.

Some milestones in such a long journey might be briefly mentioned. For several decades, a piston engine coupled with propellers provided the necessary power for aircraft. The turbojet engine (the first jet engine), invented independently by Sir Frank Whittle in Britain and Dr. von Ohain in Germany, powered aircraft in the early 1940s and later. Such jet engines paved the way for the highly sophisticated military aircraft and the comfortable civil aircraft that we have now. In the middle of the last century, airliners relied upon low-speed subsonic aircraft. Flight speeds were less than 250 miles per hour (mph) and powered by turbojet and/or turboprop engines. In the late 1960s and the early 1970s, the wide-body aircraft (Boeing 747, DC-10, and Airbus A300) powered by turbofan engines flew at transonic speeds, less than 600 mph. Now even civilian transports fly at the same transonic speeds. Looking to the other side of military airplanes, you will find fighter airplanes fly at supersonic speeds; less than 1500 mph. Such fighters are fitted with turbofan engines with afterburners. Moreover, X-planes, which are hypersonic vehicles fitted with scramjet/rocket engines, fly at very high speeds of less than 6000 mph. Space shuttles, which have also rocket engines, fly at high hypersonic speeds less than 17,500 mph.

It is interesting to compare the flight time between popular destinations like Los Angeles and Tokyo in different airplanes; it is 9.6 h for Boeing 747, and only 2 h for hypersonic aircraft [1]. It should be stated here that the human race has endless

ambitions and one can hardly anticipate the shape, speed, and fuel of flying machines for even the next few decades.

It is a fact that the evolution of aero-vehicles and aero-propulsion is closely linked. Unlike the eternal question of the chicken and the egg, there is no doubt as to which came first. The lightweight and powerful engine enabled the human race to design the appropriate vehicle structure for both civil and military aircraft. Due to the tight interdependency of the performance characteristics of aero-vehicles (including aircraft, missiles, airships, and balloons) and their aero-propulsion systems, the evolution of both aero-propulsion and aero-vehicles will be concurrently reviewed in the following sections. This review of historical inventions will be divided into two phases. The first concerns pre–jet engine inventions, while the second describes the jet engine's invention and development.

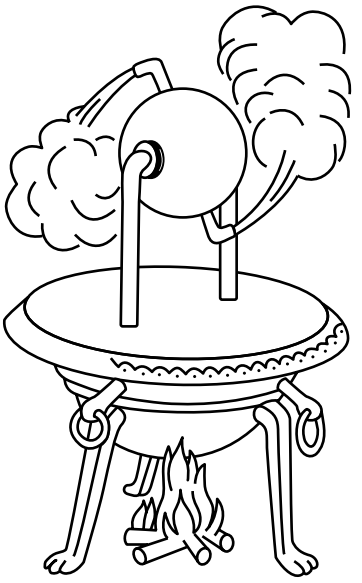
1.1 Pre–Jet Engine History

In this section, a brief summary is given of a long history of flight events. It starts with some activities in about 250 BC and ends just prior to the invention of the jet engine in the 1930s. First, there is a description of activities related to unpowered flight machines and some important patents, and next, a description of powered flights employing internal combustion gasoline.

1.1.1 Early Activities in Egypt and China

Jet propulsion is based on the reaction principle that governs the motion or flight of both aircraft and missiles. Though such a principle was one of the three famous laws of motion stated by Sir Isaac Newton in 1687, ancient Egyptians and Chinese were already utilizing this principle several hundred years before him. The first known reaction engine was built by the noted Egyptian mathematician and inventor Hero (sometimes called Heron) of Alexandria sometime around 250 BC [2] (some references refer to such an event in 150 BC [3]). Hero called his device an aeolipile (Figure 1.1). It consisted of a boiler or bowl that held a supply of water. Two hollow tubes extended up from the boiler and supported a hollow sphere, which was free to turn on these supports. When the steam escaped from two bent tubes mounted opposite one another on the surface of a sphere, these tubes became jet nozzles. A force was created at the nozzles, which caused the sphere to rotate about its axis. It is said that Hero attached a pulley, ropes, and linkages to the axle on which the sphere rotated to use his device to pull open a temple's doors without the aid of any visible power. Further details are found in numerous websites including [4].

The Chinese discovered gunpowder around about AD 1000. Some inventive person probably realized that a cylinder filled with gunpowder and open at one end could dart across a surface when it was ignited. This discovery was employed in battle by the Chinese tying tiny cylinders filled with gunpowder to their arrows. Thus, these arrows rocketed into the air when ignited (Figure 1.2). In records of a battle that took place in China in AD 1232, there is evidence that solid rockets were used as weapons. These early Chinese scientists were the first people to discover the principle of jet thrust. This same principle is the basis for today's jet engines. A Chinese scholar named Wan Hu planned to use these rockets for flight. A series of rockets were lashed to a chair under which a sled had been placed (Figure 1.3). When the rockets were ignited, both Hu and the chair were obliterated. Hu was thus the first flight martyr.

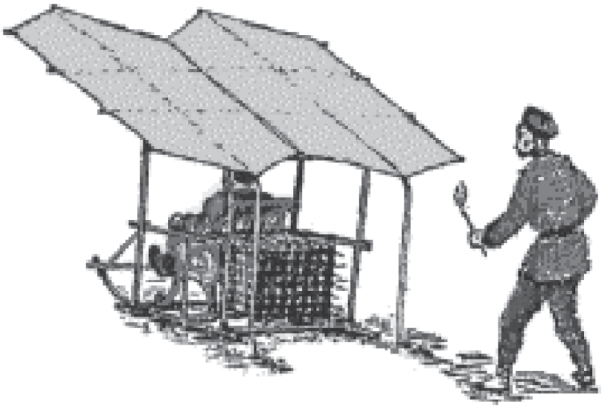


Hero's aeolipile

FIGURE 1.1
Aeolipile of Hero.



FIGURE 1.2
Chinese fire arrows.



Legendary Chinese official Wan Hu braces himself for "liftoff"

FIGURE 1.3
Wu and his chair.

1.1.2 Leonardo da Vinci

Leonardo da Vinci was possessed by the idea of human flight. He left surviving manuscripts, over 35,000 pages and 500 sketches, from AD 1486 to 1490 that deal with flight. One of his famous ornithopter designs illustrates human-powered flight achieved by flapping wings. Though this type of design was always doomed to failure, it is currently being studied again in some types of aircraft with hovering wings.

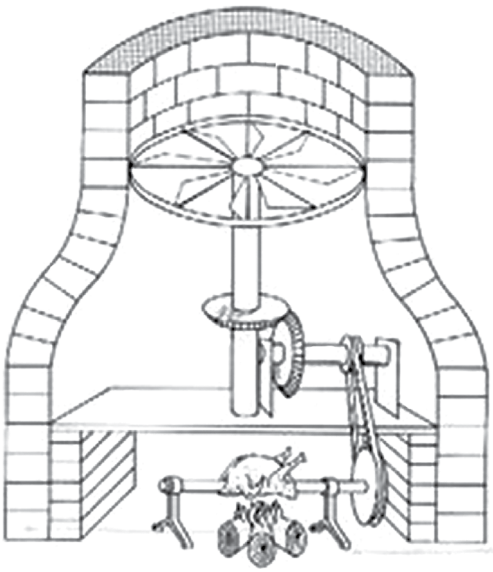
Around AD 1500, he introduced a sketch for a reaction machine, which was identified as the chimney jack [5]. It is a device for turning roasting spits (Figure 1.4). As the hot air rises, it causes several horizontal blades to rotate, which in turn rotate the roasting spit through bevel gears and a belt.

1.1.3 Branca's Stamping Mill

In 1629, Giovanni Branca, an Italian engineer, invented the first impulse turbine (Figure 1.5). Pressurized steam exited a boiler through a nozzle and impacted on the blades of a horizontally mounted turbine wheel. The turbine then turned the gear system that operated the stamping mill.

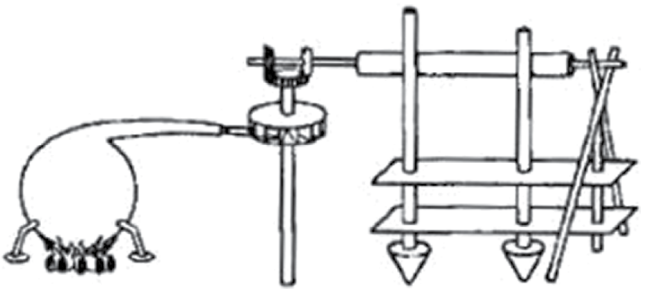
1.1.4 Newton's Steam Wagon

In 1687, Jacob Gravesand, a Dutchman, designed and built a carriage driven by steam power (Figure 1.6). Sir Isaac Newton may have only supplied the idea in an attempt to put his newly formulated laws of motion into test. The wagon consisted of a boiler fastened to four wheels. The fire beneath the boiler generated the pressurized steam exiting from a nozzle in the opposite direction of the desired movement. A steam cock in the nozzle



da Vinci's chimney jack

FIGURE 1.4
Chimney jack of Leonardo da Vinci.



Branca's jet turbine

FIGURE 1.5
Branca's stamping mill.

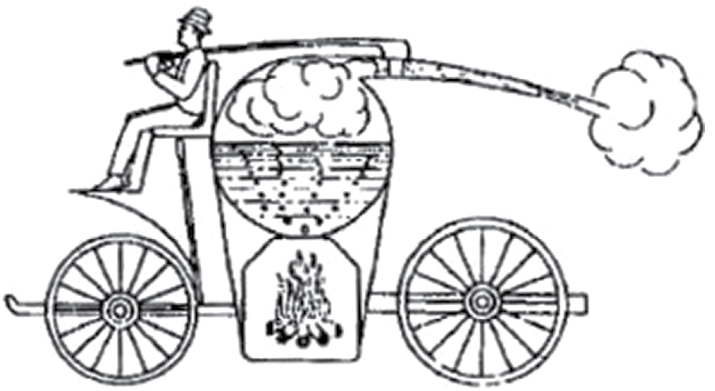


FIGURE 1.6
Newton's steam wagon.

controlled the speed of the carriage. The proposed motion of such a vehicle relied upon the reaction principle formulated in one of the three famous laws of Newton. However, the steam did not produce enough power to move the carriage.

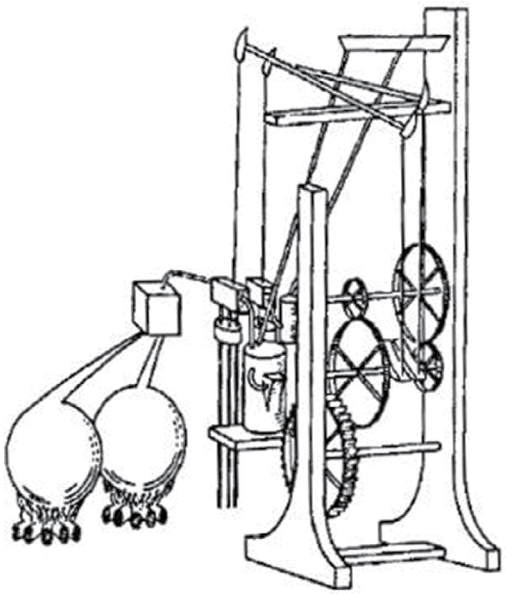
1.1.5 Barber's Gas Turbine

The first patent for an engine that used the thermodynamic cycle of a modern gas turbine (Figure 1.7) was given in 1791 by the Englishman John Barber. This engine included a compressor (of the reciprocating type), a turbine, and a combustion chamber.

1.1.6 Miscellaneous Aero-Vehicle's Activities in the Eighteenth and Nineteenth Centuries

Several red-letter dates may be listed here:

1. At 1:54 PM on November 21, 1783, the first flight of a hot-air balloon, designed by Joseph and Etienne Montgolfier and carrying Jean Pilatre de Rozier and Marquis d'Arlandes, ascended into the air and traveled in a sustained flight for a distance of



Barber's British patent (1791)

FIGURE 1.7
Barber's gas turbine.

5 miles across Paris. Next, the famous French physicist J.A.C. Charles built and flew a hydrogen-filled balloon (the first use of hydrogen in aeronautics) in its second flight on December 1, 1783. The trip lasted for 2 h and the balloon traveled 25 miles.

2. Sir George Cayley in 1799 engraved on a silver disk his concept of an aircraft composed of a fuselage, a fixed wing, and a horizontal and vertical tail, a very similar construction to that of the current aircraft [6]. In 1807, he also invented the reciprocating hot-air engine. This engine operated on the same principle as the modern closed-cycle gas turbine [5]. He also invented a triplane glider (known as the boy carrier) in 1853 and the human-carrier glider (1852). Sometime in 1852, he built and flew the world's first human-carrying glider. Consequently, he is considered the grandparent of the concept of the modern airplane.
3. The development of internal combustion engines took place largely in the nineteenth century [7]. These engines operated in a mixture of hydrogen and air. The first engine was described in 1820 by Reverend W. Cecil. In 1838, the English inventor William Barnett built a single-cylinder gas engine, which burnt gaseous fuel. The first practical gas engine was built in 1860 by the French inventor Jean Lenoir, which utilized illuminating gas as a fuel.

   The first four-stroke engine was built by August Otto and Eugen Langen in 1876. As a result, four-stroke engines are always called Otto cycle engines. George Brayton in the United States also built a gasoline engine that was exhibited in 1876 in Philadelphia. However, the most successful four-stroke engine was built in Germany in 1885 by Gottlieb Daimler. In the same year, a similar engine was also built in Germany by Karl Benz. The Daimler and Benz engines were used in early automobiles. Four-stroke engines were used extensively in the early aircraft.

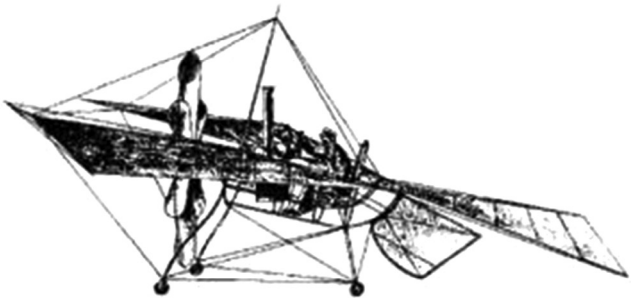


FIGURE 1.8
Du Temple's airplane.

4. The first airship designed and constructed by the Frenchman Henri Giffard was flown on September 24, 1852. This hydrogen-filled airship was powered by a steam engine (his personal design) that drove a propeller. In 1872, a German engineer, Paul Haenein, developed and flew an airship powered by an internal combustion engine also fueled by hydrogen gas. The first airship having adequate control was constructed and flown by Charles Renard and A.C. Kerbs on August 9, 1884.
5. The first powered airplanes, which only hopped off the ground, were built by the Frenchman Felix Du Temple in 1874 (Figure 1.8) and by the Russian Alexander F. Mozhaiski in 1884. They only managed hops, not a sustained controlled flight.
6. In 1872, Dr. F. Stoltz designed an engine very similar in concept to the modern gas turbine engine. However, the engine never ran under its own power due to the components' poor efficiencies.
7. The first fully successful gliders in the history were designed by Otto Lilienthal during the period 1891–1896 (Figure 1.9). Though he achieved over 2500 successful flights, he was killed in a glider crash in 1896.
8. Samuel Langley achieved the first sustained heavier-than-air unmanned powered flight in history with his small aerodrome in 1896. However, his attempt for manned flight was unsuccessful.



FIGURE 1.9
Glider of Otto Lilienthal.

1.1.7 Wright Brothers

The brothers Wilbur and Orville Wright achieved the first controlled, sustained, powered, heavier-than-air, manned flight in history. Several Internet sites deal with the subject, for example, the NASA website [8]. Also, many books describe the details of such achievements, for example, *The Bishop's Boys: A Life of Wilbur and Orville Wright* [9] best describes such invention. The time was ripe for such achievements since there had already been advancements in gliders, aerodynamics, and internal combustion engines. The Wright brothers designed and built three gliders (Gliders I, II, and III), a wind tunnel, propellers, and a light gasoline four-stroke, four-cylinder internal combustion engine.

At first, they designed and built their Glider I in 1900 (Figure 1.10) and Glider II in 1901. However, the obtained lift was only one-third of that obtained by Lilienthal according to his data. Thus, they had to build their own wind tunnel and test different wing models of their design. Through a balance system, they measured the lift and drag forces. They also used the wind tunnel to test light, long, twisted wooden propellers. Consequently, the Glider III in 1902 was much better from an aerodynamics point of view. Thus, powered flight was at their fingertips.

They designed and built their own engine because of the unsuitability of the available commercial engines for their mission. Their engine produced 12 hp and weighed 200 lb. It had 4.375 in. bore, 4 in. stroke, and 240 $in.^3$ displacement. The cylinders were made of cast iron with sheet aluminum water jackets. The crankcase was made of aluminum alloy. It also had in-head valves with an automatically operated intake valve and mechanically operated exhaust valve. A high-tension magneto was used for ignition.

Finally, they built their Flyer I (Figure 1.11). It had a wing span of 40 ft 4 in. and had a double rudder behind the wing and double elevator in front of the wing. The Wright

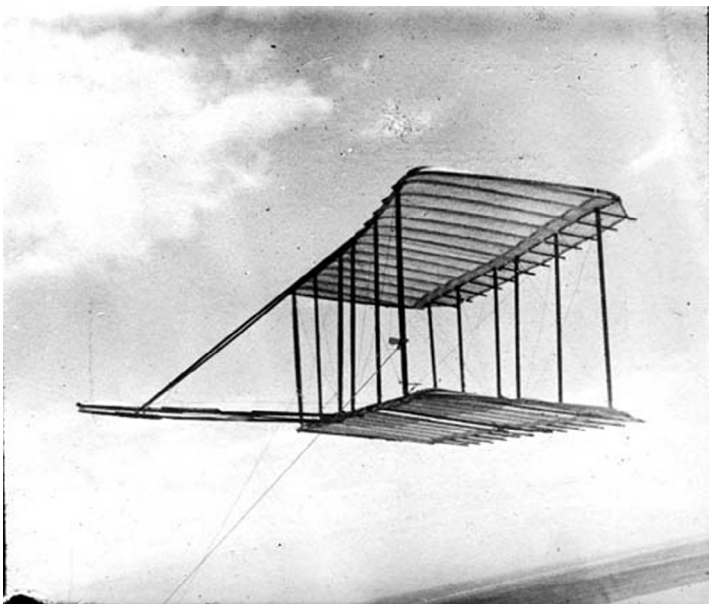


FIGURE 1.10
Glider I of the Wright brothers.

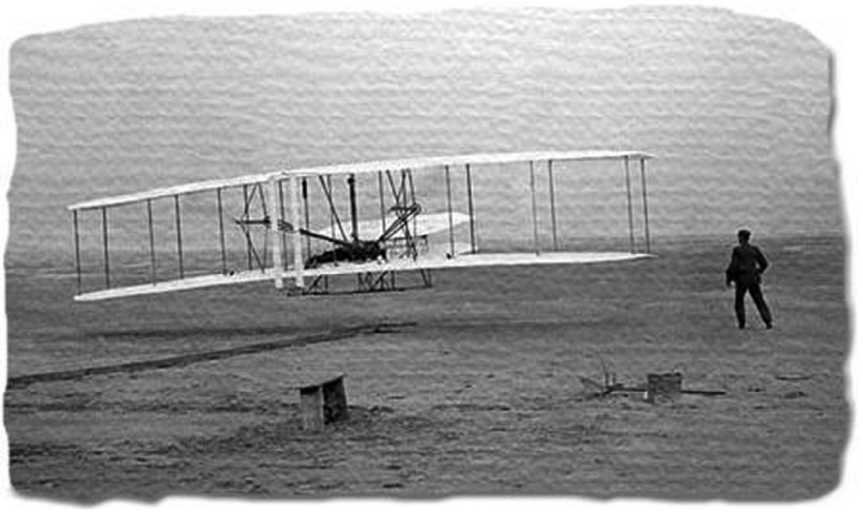


FIGURE 1.11
Flyer I of the Wright brothers.

gasoline engine drove two pusher propellers rotating in opposite directions by means of bicycle-type chains. The wing area was 505 ft^2. The total airplane weight with pilot was 750 lb. So, as mentioned earlier, it achieved the first powered flight under a pilot's control on December 17, 1903. On that day, four flights were made during the morning, with the last covering 852 ft and remaining in the air for 59 s.

After that epochal event, the Wright brothers did not stop. In 1904, they designed their Flyer II, which had a more powerful and efficient engine. They made 80 flights during 1904, including the first circular flight. The longest flight lasted 5 min and 4 s traversing 2.75 miles. Further developments led to the Wright Flyer III in June 1905. Both of the double rudder and biplane elevator were made larger. They also used a new improved rudder. This Flyer III is considered the first practical airplane in history. It made over 40 flights during 1905. The longest flight covered 24 miles and lasted for 38 min and 3 s.

Between 1905 and 1908, they designed a new flying machine, Wright type A, which allowed two persons to be seated upright between the wings. They also built at least six engines. Their Wright type A was powered by a 40 hp engine. The Wright brothers gave public displays by Orville in the United States in 1908 with impressive demonstrations for the army and by Wilbur at a show at Hunaudieres close to Le Mans in France.

1.1.8 Significant Events up to the 1940s

1.1.8.1 Aero-Vehicle Activities

1. In 1909, the Frenchman Louis Bleriot flew his XI monoplane across the English Channel (Figure 1.12). This was the first time an airplane crossed natural and political borders.
2. In 1910, the first seaplane was built and flown by Henri Fabri at Martigues, France. The plane, called a hydravion, powered by a 50 hp Gnome rotary engine, flew

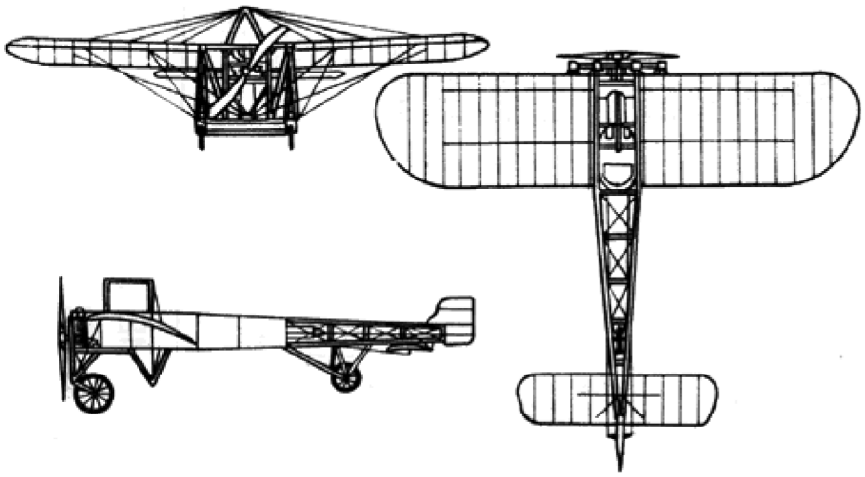


FIGURE 1.12
XI monoplane of Bleriot.

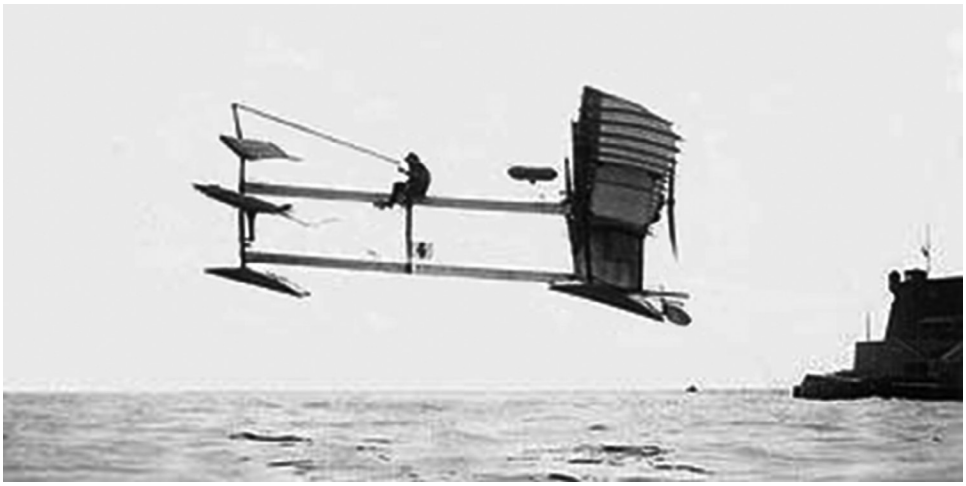


FIGURE 1.13
Henri Fabri hydravion.

1650 ft on water (Figure 1.13). However, the real and great pioneer of marine flying was Glenn Curtiss. In 1911, he fitted floats to one of his pusher biplanes and flew it off the water. His contribution to marine flying included flying boats and airplanes, which could take off and land on a ship.

3. In 1914, the war meant that airplanes had to be equipped with guns, bombs, and torpedoes. The Vickers Gunbus (Figure 1.14) in England was a biplane, which was considered the first aircraft specially designed as a fighter for the Royal Flying Crops. It was powered by one 100 hp Gnome radial-piston engine and had one or two Lewis machine guns.



FIGURE 1.14
Vickers Gunbus.

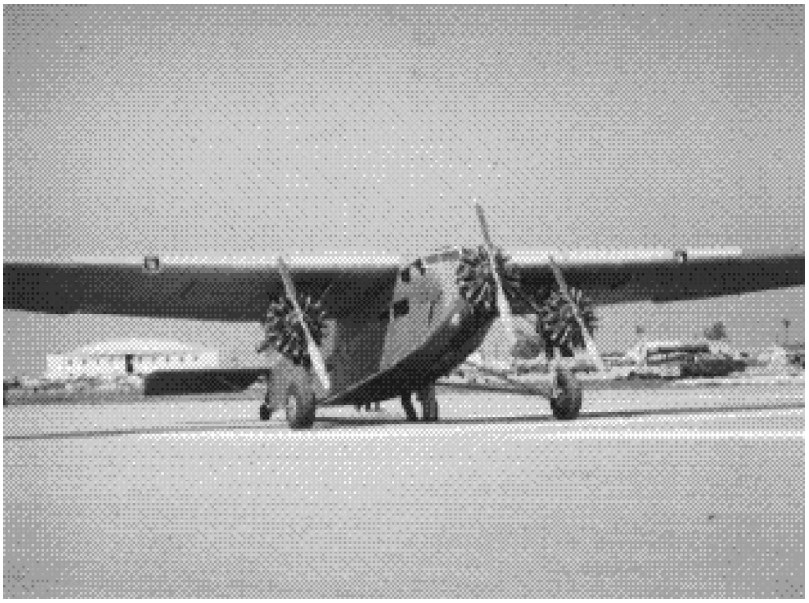


FIGURE 1.15
The Tin Goose.

4. The world's first airline services were in a dirigible in 1910. With the advances in aircraft design brought about by World War I, the enclosed cabin airplane became the standard for commercial airline travel by the early 1920s.
5. *Ford Trimotor*, nicknamed *The Tin Goose*, was a three-engine civil transport aircraft, first produced in 1926 by Henry Ford and which continued until about 1933 (Figure 1.15). This Trimotor was developed from several earlier designs and became the United States' first successful airliner.

   Throughout the Trimotor's lifespan, a total of 199 aircraft were produced. It was popular with the military and was sold all over the world. Ford did not make the



FIGURE 1.16
Zeppelin LZ-1 airship.

engines for these aircraft. The original (commercial production) 4-AT had three air-cooled Wright radial engines. The later 5-AT had more powerful Pratt & Whitney engines.

6. The first rigid airship filled with hydrogen was designed by Count Ferdinand von Zeppelin; the LZ-1 (Figure 1.16) made a successful flight in 1900. From 1911 to 1914, five Zeppelin airships were used in commercial air transportation in Germany. In the first decade of the twentieth century, there was significant ongoing development of airships in several countries, including Great Britain, France, the United States, Italy, Spain, Poland, Switzerland, and Japan. In 1936, there was the first commercial air service across the North Atlantic between Germany and the United Sates with the Hindenburg. At a cruising speed of 78 mph and carrying 50 passengers, it took 65 h for the eastbound crossing and 52 h for the westbound crossing.

1.1.8.2 Reciprocating Engines

Extensive development and use of airplanes during and after World War I led to a great improvement in engines. Some examples are given here:

1. Rotary-type engines, for example, the Gnome-Monosoupape (Figure 1.17) and the Bently.
2. In-line engines like the Hispano-Suiza; while an example of the inverted in-line engine is the Menasco Pirate, model C-4.
3. V-type engines like Rolls-Royce V-12 and the U.S.-made Liberty V-12. Both upright and inverted V-types were available.
4. Radial engines, which could be single-, double-, and multiple-row radial engines. The 28-cylinder Pratt & Whitney R-4360 engine was used extensively at the end of World War II and after that for both bombers and civil transports.
5. Opposed, Flat, or O-type engines.

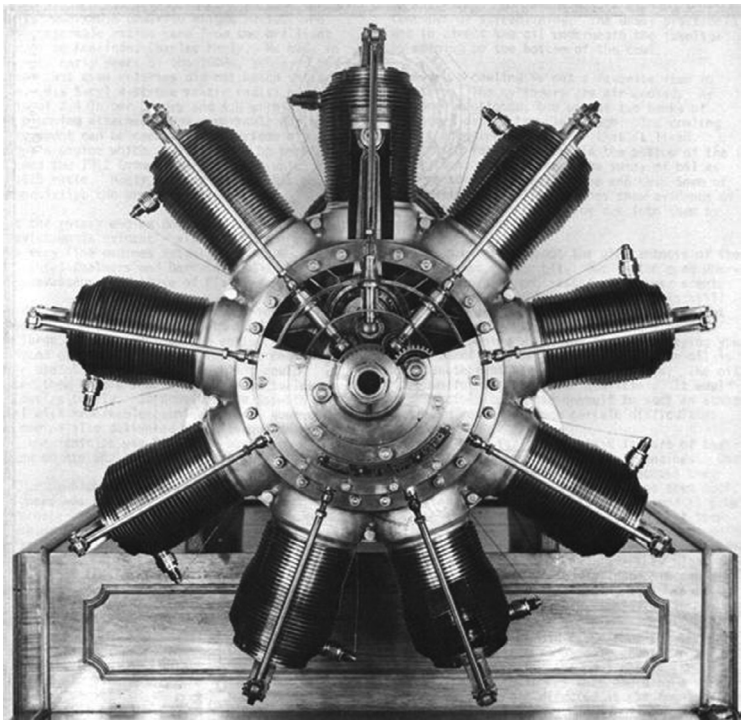


FIGURE 1.17
The radial piston Gnome.

1.2 Jet Engines

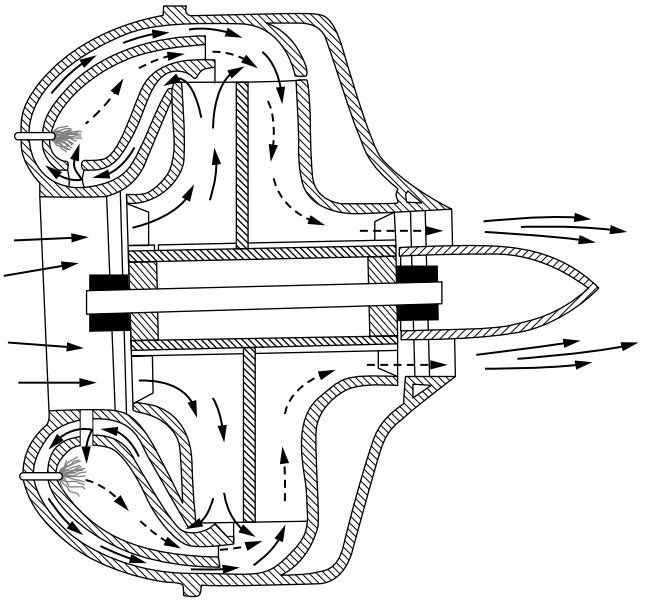
Before World War II, in 1939, jet engines existed only as laboratory items for testing. But at the end of the war, in 1945, it was clear that the future of aviation lay with jets. These jet engines, which had great power and thrust, were also compact in size and simple in their overall layout.

1.2.1 Jet Engines Inventors: Dr. Hans von Ohain and Sir Frank Whittle

Both Dr. Hans von Ohain and Sir Frank Whittle are recognized as the coinventors of the jet engine [10]. Each worked separately and knew nothing of the other's work. Hans von Ohain, a young German physicist, was at the forefront. He is considered the designer of the first operational turbojet engine. Frank Whittle was the first to register a patent for the turbojet engine in 1930. Hans von Ohain was granted a patent for his turbojet in 1936. However, von Ohain's jet engine was the first to fly in 1939. Frank Whittle's jet first flew in 1941. The detailed history of both inventors is given in several books, articles, and on numerous websites [11–14].

1.2.1.1 Sir Frank Whittle (1907–1996)

Whittle is considered by many to be the father of jet engine. In January 1930, Frank Whittle submitted his patent application for a jet aircraft engine (Figure 1.18). The patent was



Frank Whittle's patent drawing

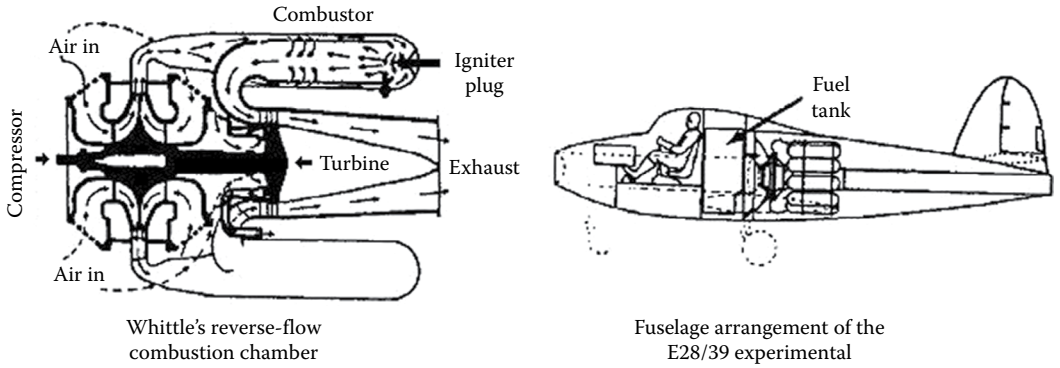
FIGURE 1.18
Patent of Frank Whittle.

granted in 1932. However, he received very little encouragement from the Air Ministry or industry. After receiving support from investment bankers, Power Jets were established in 1936 and Whittle was assigned to the company to work on the design and development of his first jet engine.

The first run of the experimental engine was in April 1937. This engine had a centrifugal compressor and axial-flow turbine. Many problems were encountered. Some were solved during the next year, and the experimental engine was reconstructed several times. The resulting engine with 10 combustion chambers performed well. In June 1939, the Air Ministry was finally convinced of the merits of Whittle's invention and decided to have a flight engine. Thus, the first Whittle flight engine was built and was called the Power Jet W.1. The W.1 turbojet engine was designed to produce 1240 lb at 17,750 rpm. The Air Ministry also decided to have the Gloster Aircraft Company build an experimental airplane called the E28/39. The aircraft was completed in March 1941 and the engine in May 1941. On May 15, 1941, the Gloster E28/39 powered with the W.1 Whittle engine (Figure 1.19) took off from Cranwell at 7.40 PM, flying for 17 min and reaching a maximum speed of around 545 km/h (340 mph). Within days, it was reaching 600 km/h (370 mph) at 7600 m.

1.2.1.2 Dr. Hans von Ohain (1911–1998)

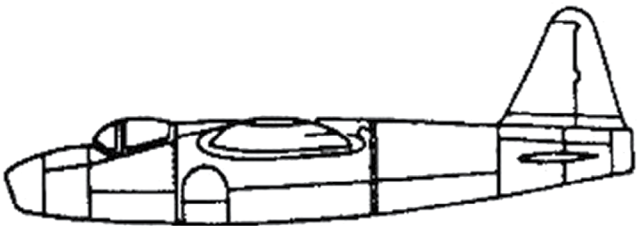
Hans von Ohain started the development of the turbojet engine in the early 1930s in the midst of his doctoral studies in Goettinger University in Germany. By 1935, he had developed a test engine to demonstrate his ideas. Ernst Heinkel, an aircraft manufacturer, supported him. At the end of February 1937, the He S-1 turbojet engine with hydrogen fuel was tested and produced a thrust of 250 lb at 10,000 rpm. Next, von Ohain started his development on the He S-3 engine, in particular the liquid-fuel combustor. Detailed design



Whittle's reverse-flow combustion chamber

Fuselage arrangement of the E28/39 experimental

FIGURE 1.19
Whittle's W.1 engine and the Gloster E28/39.



The German Heinkel He 178

FIGURE 1.20
Heinkel's He 178.

began in early 1938 on the test aircraft, the He 178 (Figure 1.20). In early 1939, both the engine and the airframe were completed. However, the thrust was below requirements. After several adjustments, the engine was ready. On August 27, 1939, Heinkel's test pilot, E. Warsitz, made the first successful flight of a jet-powered aircraft.

1.2.2 Turbojet Engines

1. The Messerschmitt Me 262 jet fighter, the first production jet aircraft, was powered by two Jumo 004B turbojet engines (Figure 1.21). The Me 262's first flight was on July 18, 1942. The Jumo 004 was designed by Dr. Anselm Franz of the Junkers Engine Company. The Jumo 004 was the most widely used turbojet engine during World War II. The flight speed of the Me 262 was 500 mph (805 km/h) and it was powered by two axial-flow jets, each of which provided 1980 lb of thrust. More than 1600 Me 262s were built. Germany allowed Japan to build its own version of the Me 262, known as the Kikka. The Junker Jumo 004 was also assembled in Czechoslovakia under the name Malsice M-04, and it was used to power the Avia S92/CS92.
2. The British shared Whittle's technology with the United States enabling General Electric Company—the first engine builder in the United States—to build its first

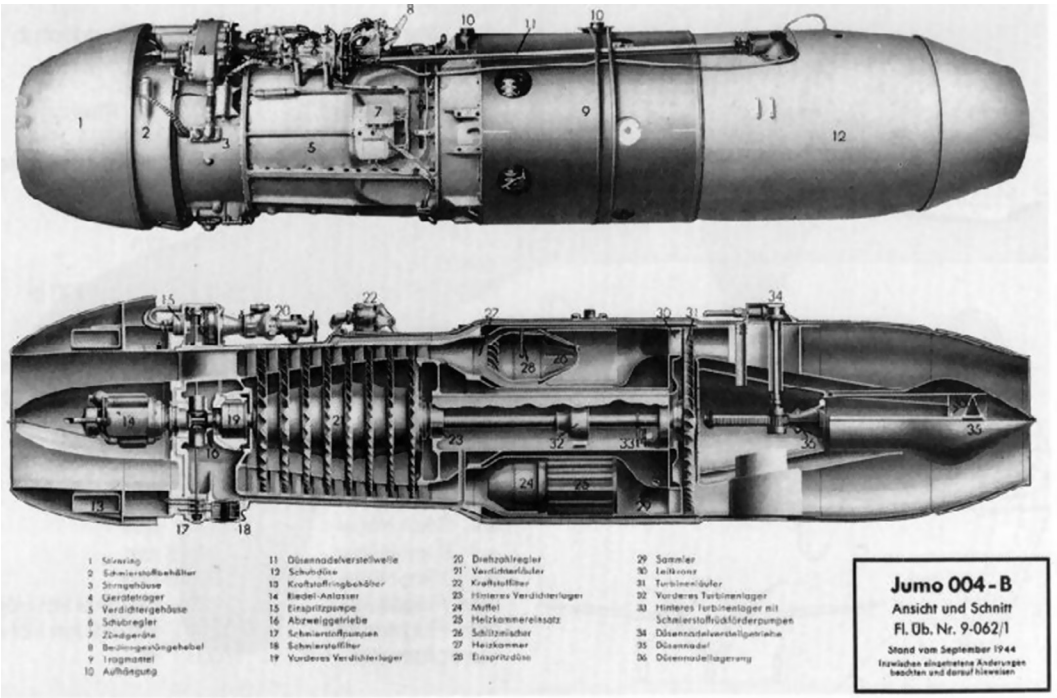


FIGURE 1.21
Jumo 004 jet engine.

jet engine, the I-A. On October 1, 1942, the U.S.'s first jet fighter, Bell XP-59, powered by the General Electric turbojet engine I-16, made its first flight. Thus, the jet engine age had come to the United States. GE shortly built its J-31 engine, which was the first turbojet engine produced in quantity in the United States.

3. The British continued developing jet engines based on Whittle's designs, with Rolls-Royce initiating work on the Nene engine in 1944 (Figure 1.22). The U.S. Navy selected the Nene for a carrier-based jet fighter, the Grumman Panther. Pratt & Whitney—another aircraft engine builder—built it under license. Rolls-Royce also sold the Nene to the Soviets. A Soviet-built version of the Nene engine subsequently powered the MiG-15 jet fighter that fought the United States in the Korean War.
4. Next, Rolls-Royce designed and built the Tay engine, which also powered later versions of the Panther fighter.
5. A.M. Lyu'ka is the father of the Soviet jet engine. In 1938, while he was working for the Kharkov Aviation Institute in a team developing the engine and compressor for the Tupolev Pe-8 heavy bomber, he designed a two-stage centrifugal compressor turbojet engine (RDT-1), which had 500 kg (1100 lb) of thrust. Further developments of this engine led to the Soviet Union's first turbojet engine, the RDT-1/VDR-2. The second Lyu'ka turbojet to run was the S-18/VDR-3, with 1250 kg of thrust, in August 1945. These two engines did not fly. His third engine, the TR-1, which is an eight-stage axial compressor developed from the S-18 and giving 1300 kg of thrust, was the first of his engines to fly. It was fitted to the Tu-22, the Su-11, and the Su-10 after clearance in December 1944.

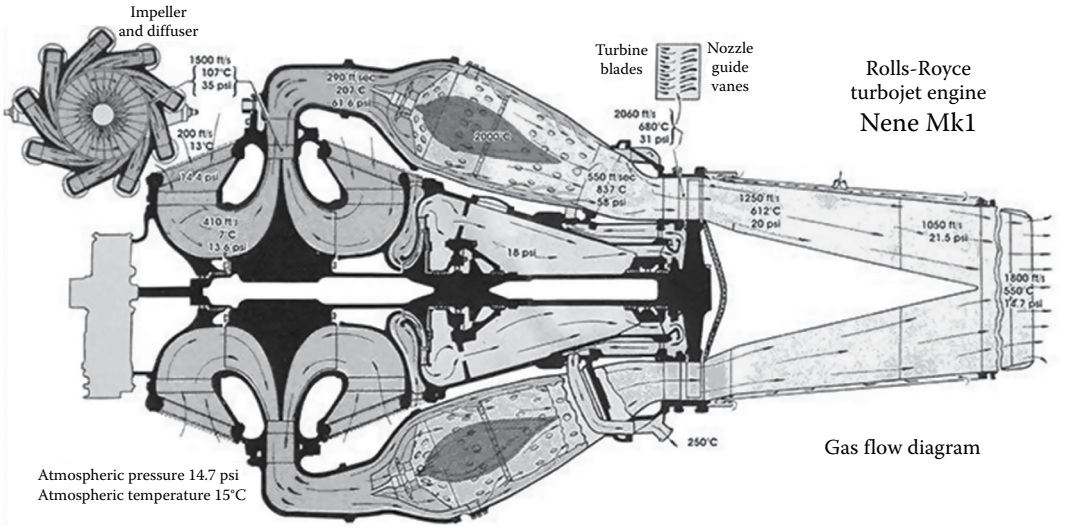


FIGURE 1.22
Nene turbojet engine.

6. The Lyulka AL-7 represents another famous Soviet engine. The prototype was tested in 1952 and the engine was planned to power the Ilyushin II-54 bomber. The afterburning version AL-7F was created in 1953. In 1957, the Sukhoi Su-9 equipped with this engine exceeded Mach 2 at 18,000 m. The engine was adopted for the Tupolev Tu-128P in 1960. The Lyulka AL-21 has close similarity to the GE J-79. It came into service in the early 1960s as it powered the interceptor Tu-28P. A later version Al-21-F3 used in Sukhoi Su-24 Fencer, Mikoyan Mig-23, and Sukhoi T-10.
7. Pratt & Whitney in the 1950s put together an innovative design for turbojet engines that overcome the drawback that earlier engines had of consuming large quantities of fuel. It was the "dual-spool" concept. The engine had two compressors. Each was rotated independently by a separate turbine, so that it looked as if two engines were combined in one. This approach led to the J-57 engine, which entered the U.S. Air Force in 1953. This engine powered several U.S. Air Force fighters, including the F-100, the first airplane to break the sound barrier without going into a dive. Also, eight J-57 engines powered the B-52 bomber. It also powered the commercial aircraft Boeing 707 and the Douglas DC-8. However, its military secrets were discovered when the Soviet Union brought down the U-2 spy plane powered by this engine on May 1, 1960.
8. Rolls-Royce also adopted the slender German engine design for its Avon series in 1953. The Avon powered the Hawker Hunter fighter of the 1950s. The Avon-powered Comet was the first turbojet engine to enter the transatlantic service. The Avon also powered the U.S. bomber B-57 and the French jet airliner Caravelle.
9. The other engine competitor was General Electric Company (GEC), which built its J-47 engine, which powered the F-86 fighter and the B-47 bomber. Successive developments of the J-47 led to the J-73 in the early 1950s. This more powerful engine was used instead of the J-47 in the F-86H aircraft.
10. After the dual-spool concept, another development for the turbojet engine was enhanced by GE. This was the "variable stator" concept, by which the turbojet

engines could avoid compressor stall. This phenomenon will be fully explained later in the compressor chapters, but it is worth mentioning here that stall leads to a loss in thrust and sometimes causes severe damage by breaking off compressor blades.

11. A third advancement was achieved by thrust augmentation or the afterburner. This is a second combustion chamber fitted between the last (low-pressure) turbine and the nozzle. This combustion chamber utilizes the remaining oxygen in the air to burn more fuel to a much higher temperature than that in the original combustion chamber. This provides some 50% or even greater increase in the thrust force generated by the original engine's configuration.
12. The variable stator design and the afterburner led to the GE engine J-79, which was the first true engine for supersonic flight. The Lockheed F-104 fighter powered by the J-79 flew at twice the speed of sound. In May 1958, the F-104 set a record of 1404 mph (2260 km/h) at the impressive altitude of 91,249 ft (27,813 m). Other fighters powered by the GE J-79 engines were the B-58 Hustler and the McDonnell Douglas Phantom F-4B.
13. It was interesting in 2001 to celebrate the fifties anniversary of the turbojet engine Viper produced by Rolls Royce (RR). It was used to power several military aircraft, including the two-seater Italian military trainer Aermacchi MB-326. Numerous versions of Viper were built during its history. The latest version was produced in Poland to power Poland's Irdya jet.
14. Allison, another builder of aircraft engines in the United States, built the J33 engine, which powered the Lockheed T-33 training version of the F-80 Shooting Star.
15. The Ishikawajima Ne-20, Japan's first turbojet engine, was developed during World War II. Only a small number of this engine was manufactured. Two of them were used to power the Kikka airplane on its only flight in August 7, 1945.
16. As an example of Chinese aircraft and its powerplants, we have the Shenyang J-8 fighter airplane powered by the turbojet engine PW13A (Figure 1.23).

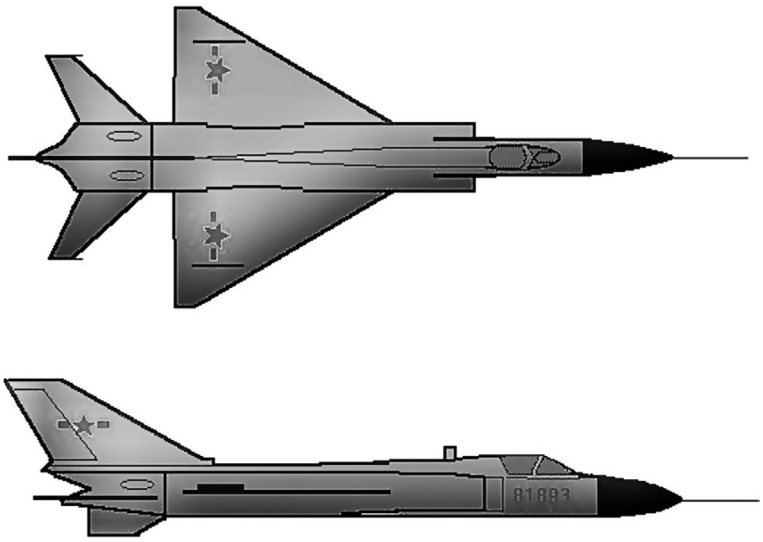


FIGURE 1.23
Shenyang J-8 Chinese fighter.

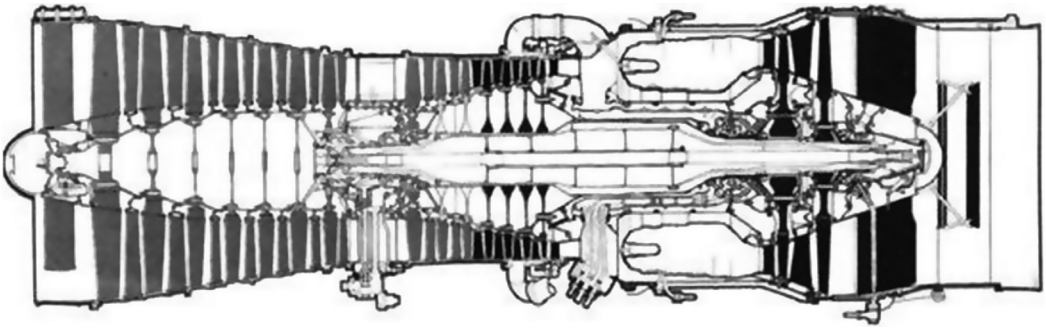


FIGURE 1.24
Rolls-Royce Olympus 593 turbojet engine powering Concorde airplane.

17. The Rolls-Royce/Snecma Olympus 593 turbojet (Figure 1.24) is unique in commercial aviation as the only afterburning turbojet to power a commercial aircraft, Concorde. The Olympus 593 project was started in 1964, using the Avro Vulcan's Olympus 320 as a basis for development. Bristol Siddeley of the United Kingdom and Snecma Moteurs of France were to share the project. Acquiring Bristol Siddeley in 1966, Rolls-Royce continued as the British partner. Rolls-Royce carried out the development of the original Bristol Siddeley Olympus and engine accessories, while Snecma had responsibility for the variable engine inlet system, the exhaust nozzle/thrust reverser, the afterburner, and the noise attenuation system. The United Kingdom was to have a larger share in the production of the Olympus 593 as France had a larger share in fuselage production. At 3:40 PM on March 2, 1969, Concorde prototype 001 started its first takeoff run, with afterburners lit. The four Olympus 593 engines briskly accelerated the aircraft, and after 4700 ft (1.4 km) of runway and at a speed of 205 knots (380 km/h), the aircraft lifted off for the first time.

1.2.3 Turboprop and Turboshaft Engines

1. Soon after turbojets were in the air, the turboprop engine was developed. This engine is a gas turbine driving a propeller (previously known as an airscrew). Its early name was the "airscrew turbine engine" and it was later given the neater title of turboprop [15]. Since it has mainly two parts, the core engine and the propeller, it produces two thrusts, one with the propeller and the other through the exhaust; a large gearbox makes it possible for the turbine to turn the propeller at a reduced speed to avoid any possible shock waves and flow separation at the propeller tip. There may be an additional turbine (called free or power turbine) that also drives the propeller through the gearbox. Turboprop engines are more efficient than other engines when they fly under 30,000 ft and at speeds below 400–450 mph.
2. Hungarian Gyorgy Jendrassik, who worked for the Ganz wagon works in Budapest, designed the very first working turboprop engine in 1938, called the "Cs-1." It was produced and used briefly in Czechoslovakia between 1939 and 1942. The engine was fitted to the Varga XG/XH twin-engine reconnaissance bomber but proved very unreliable. Jendrassik had also produced a small-scale 75 kW turboprop in 1937.

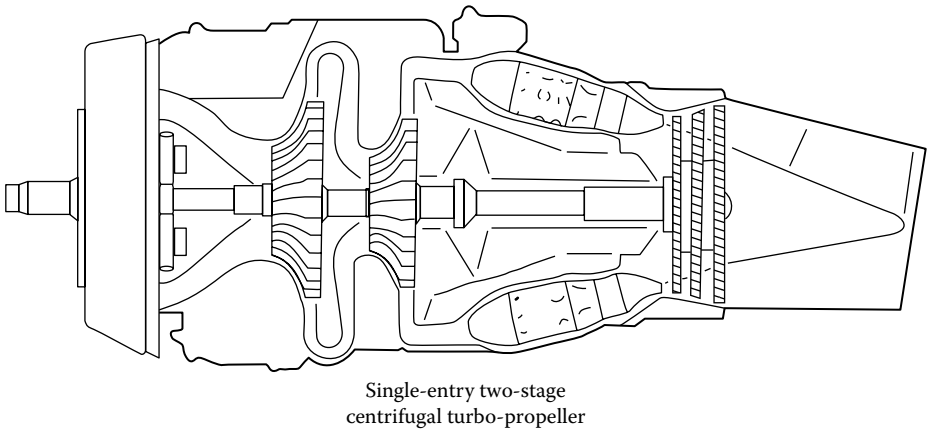


FIGURE 1.25
Rolls-Royce Dart turboprop engine.

3. In the 1940s, Rolls-Royce built several turboprop engines for flight speeds of around 400 mph. One of the first engines was the RB50 Trent, which, through a reduction gear, turned the five-blade Rotol propeller (7 ft 11 in. in diameter). On September 20, 1945, the Gloster Meteor fitted with two Trents became the world's first turboprop-powered aircraft to fly.
4. Later on, Rolls-Royce built the impressive Clyde; though it was one of its earliest turboprop engines, it reached 4200 hp plus 830 lb residual jet thrust, equivalent to 4543 equivalent horsepower. Also Dart (Figure 1.25) is one of the most famous turboprops of Rolls-Royce, and it powered Fairchild Industries' F-27, Grumman Gulfstream, and so on. More than 7100 Darts were sold, accumulating over 130 million hours of flight time. Another famous Rolls-Royce turboprop was the Tyne, which first ran in April 1955. It was a two-spool engine driving through a double-epicyclic gearbox a four-blade reverse propeller.
5. Another British manufacturer was Bristol, who built Theseus, which powered the Avro Lincoln aircraft. Next, Bristol built the Proteus that flew millions of hours and drove the biggest hovercraft across the British Channel from 1968 to 2000. A third British manufacturer is Armstrong Siddeley, which built the 4110 hp Python that powered the Wyvern carrier strike fighter. It also built Mamba and double Mamba, which powered the Fairey Gannet.
6. The first U.S. turboprop engine was the GE T-31 built by General Electric. The T-31's initial flight was in the Consolidated Vultee XP-81 on December 21, 1945. The T-31 was mounted in the nose, and the J-33 turbojet mounted in the rear fuselage provided added thrust. A similar turboprop/turbojet engine combination was also used in the Navy XF2R-1 aircraft. Another General Electric turboprop engine with increasing shaft horsepower was the T56 turboprop powering the Lockheed Martin C-130-H and C-2A Greyhound. Moreover, General Electric built the T64 powering de Havilland Canada DHC-5 and Buffalo aircraft.
7. Allison (another U.S. aeroengine manufacturer) produced several turboprop engines, such as the GMA 2100 powering the L100/C-130J and the T56-A-11 powering the AC-130A. It also built the T406 turboshaft engine that powers Bell Boeing's V-22 Osprey aircraft (Figure 1.26).



FIGURE 1.26
V-22 Osprey.

8. A third U.S. manufacturer of turboprop engines is AlliedSignal (previously Garrett AiResearch), which produced the famous TPF331 turboprop engine, which powered, for example, the Embraer/FAMA CBA-123. It is one of the few pusher turboprops in recent days.
9. The Soviet Union in the 1950s produced the Tu-95 Bear, which uses TV-12 engines having four contrarotating propellers with supersonic tip speeds to achieve maximum cruise speeds in excess of 575 mph, a ceiling of 11,300 m, and a range of about 15,000 km. The Bear represents one of the most successful long-range combat and surveillance aircraft and was a symbol of Soviet power projection throughout the end of the twentieth century.
10. Turboprops manufactured by the Ukrainian company Motor Sich PJSC are the AI-20D Series powering the AN-32 aircraft, which also successfully operates in a number of other countries like India, Bangladesh, Ethiopia, Peru, Nicaragua, etc., and the AI-24 installed in the AN-24 aircraft servicing short and medium-haul routes (both passenger and cargo).
11. Pratt & Whitney of Canada built a big family of the popular turboprop/turboshaft engines PT6 and PT6A (Figure 1.27). It is the most popular turboprop engine ever built, with 31,000 engines of the PT6A being sold to 5490 customers up to 1997. It powered numerous aircraft including Beechcraft 1900, Dornier DO 128-6, Bell 412, and Sikorsky S58T.
12. Turbomeca of France began producing small turboprop engines in 1947. Its first turboprops were the 400 hp Marcadau of 1953 and the 650 hp Bastan of 1957. Its 800–1100 shp Astazou was the only turboprop to sell in numbers. However, Turbomeca is recognized as the first company to build a true turboshaft engine.

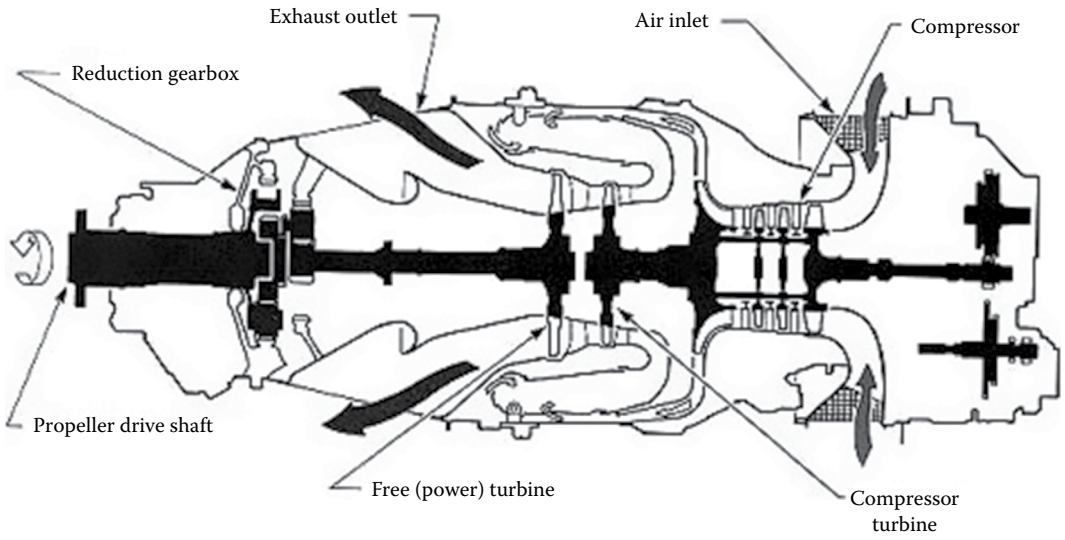


FIGURE 1.27
Pratt & Whitney Canada turboprop engine PT6.

In 1948, it built the first French-designed turbine engine, the 100 shp 782. In 1950, this work was used to develop the larger 280 shp Artouste, which was widely used on the Aerospatiale Alouette II and other helicopters [16].

13. Other worldwide companies include Fiat of Italy, which built the turboprop T64-P4D that powered the aircraft G222RM. The Japanese company IHI built the T56-IHI-14 and T58-IHI-110 turboprops, which powered the aircraft P-3C and KV-107, respectively.
14. The greatest power turboprop engine, the NK-12, built in 1946 to provide 12,000 hp by the Soviet company Kuznetsov and upgraded in 1957 to 15,000 hp, powers the huge aircraft An-22. Other famous Soviet turboprop engines are the TV3 VK-1500; Isotov company that power the aircraft An-140, medium helicopters and Canadair 540C.
15. The EPI Europrop International GmbH was created by the four leading European aeroengine companies (Industria de Turbo Propulsores, MTU Aero Engines, Rolls-Royce, and Snecma) to develop and produce three-shaft 11,000 shaft horsepower (shp). The TP400-D6 turboprop is used to power the Airbus A400M military transport. The A400M had short takeoffs and landings. It is a two-shaft engine with a free-power turbine and its first test will be in 2006.
16. Turboshaft engines are similar to turboprops. They differ primarily in the function of the turbine. Instead of driving a propeller, the turbine is connected to a transmission system that may drive a helicopter rotor. Other turboshaft engines that will be identified as industrial gas turbine engines (Section 1.2.5) are used for land and sea applications, such as in electrical generators, and compressors or pumps, and for marine propulsion for naval vessels, cargo ships, hydrofoils, and other vessels.
17. General Electric also built several turboshaft engines including the CT58, which powers the Sikorsky S-61, the Sikorsky S-62 and Boeing Vertol CH-47 helicopters.

The GE T700/CT7 is considered one of the company's most famous turboshaft engines; it powers the Bell AH-1W Super Cobra.

18. Rolls-Royce also built numerous turboshaft engines such as the Gem, which powers the AgustaWestland Lynx helicopter, and the AE1107C-Liberty turboshaft, which powers the Bell Boeing V-22 Osprey.
19. One of the earliest Soviet turboshaft engines was the D-25V manufactured in 1957, which had 4780 kW (5500 hp) and powered the Mi-6, Mi-10, and Mi-12 helicopters.
20. The Ukrainian three-spool turboshaft engine D-136 Series 1 powers the MI-26 transport helicopters, which are the largest in the world. Other famous Ukrainian turboshaft engines are the TB3-117 BMA used to power the KA helicopters and the TB3-117 BM powering the MI-17 and MI-8 AMT helicopters.

1.2.4 Turbofan Engines

1. During the period 1936–1946, Power Jet and Metropolitan pioneered several kinds of ducted fan jet engines, but they attracted no attention, as was the case with Whittle's patent for the jet engine. With its Conway engine, Rolls-Royce was the first company to introduce the "bypass" principle in the 1950s. It featured a large fan located in the front of the engine, which resembled a propeller but had many long blades set closely together. Bypass jet engines are frequently denoted as turbofan engines. Turbofan engines had three benefits, namely, a greater thrust, an improved fuel economy, and a quieter operation. The noise level was not a serious problem in those days, but now noise level is a strict condition for engine certification. The Conway powered the four-engine Vickers VC-10 jetliner as well as some Boeing 707s and DC-8s.
2. A smaller bypass engine, the Rolls-Royce Spey, was built under license in the United States, which powered the attack plane A-7, flown by both the U.S. Navy and Air Force. One Spey engine powers the Italian/Brazilian AMX airplane, while four Spey engines power the BAE Systems Nimrod aircraft.
3. Both General Electric and Pratt & Whitney built their own turbofan engines after 1965. The first aircraft to use turbofan engines in the United States was the Lockheed C-5A "Galaxy," using the GE TF-39 turbofan engines with a bypass ratio (BPR) of 8. Later on, all the U.S. Air Force cargo planes, including the C-17, as well as all the large airliners, including the Boeing 747, used turbofan engines.
4. With the emergence of wide-body airliners in the late 1960s, Rolls-Royce launched the three-spool turbofan engine RB211. This engine has three turbines, two compressors, and a fan. After some difficulties, this engine has now established itself at the heart of Rolls-Royce's world-class family of engines. One of the earliest aircraft powered by RB211 was the Lockheed L-1011 Tri-Star. Later on, this engine powered numerous aircraft, including Boeings 747, 757, and 767 and the Tupolev Tu 204-120.
5. In the 1960s, Pratt & Whitney built its high-BPR turbofan engine JT9D, which also powered the wide-body Boeing 747 (Figure 1.28). In the 1970s, Pratt & Whitney built its popular engine JT8D-200, which was the quieter, cleaner, and more efficient engine. In the 1990s, Pratt & Whitney built its PW4000 series that powered the Boeing 777.

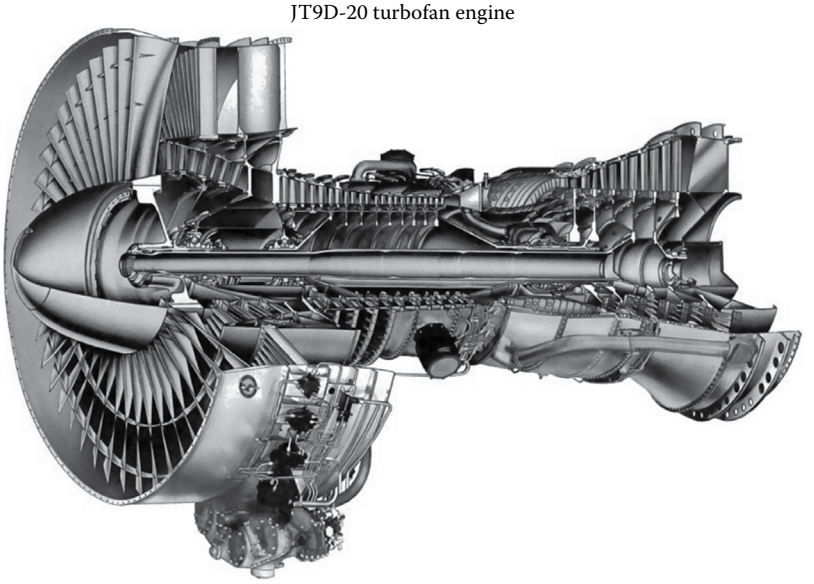


FIGURE 1.28
Pratt & Whitney JT9D.

6. The General Electric CF6 family of high-BPR turbofan engines have enjoyed great popularity since the early 1970s. They have powered numerous civil and military aircraft including Airbuses A300-600/600R, A310-22, A330, the Douglas DC-10, the McDonnell Douglas MD-11 Stretch, Boeings 747-200/300/400, and 767-200ER. By the late 1990s, more than 5500 CF6 engines were in service.
7. In 1974, collaboration between General Electric and SNECMA, the leading French aircraft engine manufacturer, resulted in establishing the CFM International, which received the first order for the CFM56-2 turbofan engine in 1979. CFM56-2 was chosen to re-engine the DC-8 Series Super 70s and its military version, designated F108, to re-engine the tanker aircraft KC-135. Since then, the General Electric and SNECMA CFM56 engines have powered the Boeing 737-300/400/500 series, Airbus Industries A318, A319, A320, and A321, and the long-range four-engine Airbus 380. The CFM56-7 powerplant was launched in 1993 to power the Boeing 737-600/700/800/900 series. In the second half of the 1990s, more than 3500 CFM engines were delivered worldwide.
8. In the 1980s, a unique five-nation consortium led to the establishment of the IAE International Aero Engines AG (the British Rolls-Royce, German MTU, Italian Fiat, American Pratt & Whitney, and the Japanese Aero Engine Corporation JAEC), which produced the turbofan engine V2500. Now the IAE is only a four-nation consortium without the Italian Fiat company. More than 2920 engines were delivered up to April 2006. V2500 powered numerous aircraft including the Boeing MD-90, the Airbus corporate jetliner, and Airbus A321, A320, A319.
9. Another alliance between General Electric and Pratt & Whitney was achieved in the 1990s to build the GP7000 series, which powered the superjumbo Airbus A380.



FIGURE 1.29
Rolls-Royce turbofan engine Trent 1000.

10. Rolls-Royce continued building high-technological aeroengines with its new family of Trent 500, 700, 800, 900, and 1000. These engines power a big family of Boeing and Airbus airplanes. The Trent 1000 powers the Dreamliner Boeing 787 aircraft.
11. GE90 is one of the largest turbofan engines with a BPR of nearly 9.
12. AlliedSignal Garrett is another aeroengine manufacturer in the United States. It built the famous engine TFE731 that powered the Lockheed Jetstar II, the Dassault Falcon 10, and the Hawker Siddeley125-700, as well as building the three-spool F109 (TFE76) engine.
13. The first turbofan engine built by former Soviet Union was the D-20P, which had advanced thrust, efficiency, and reliability performance. It is a two-spool engine and has been installed in the Tu-124 short-haul airplane for passenger transportation since October 1962. The two-spool D-30 series entered service in September 1967 and powered the Tu-134 aircraft. The D-30KP turbofan engine has a takeoff thrust of 12,000 kg_f. It powers IL-76T, IL-76TD, and IL-76MD versions of the popular long-haul IL-76 airplane for transportation of large-size equipment and cargo. It started commercial running for cargo transportation in July 1974.
14. Several three-spool engines manufactured by the famous Ukrainian company Motor Sich JSC are now in use. Examples are the D-18T Series 1 and Series 3, powering the AN-124 Ruslan and AN-225 Mriya transports. The same manufacturer and another Ukrainian manufacturer, also produce several three-spool turbofans including the D-436, which powers the short- and medium-haul airliners,

Tu-334-100 and Tu-334-120, while the turbofan engines D-36 series 1, 1E, 2A and 3A are installed to AN-72 and AN-74 aircrafts installed in AN-72 and AN-74 passenger aircraft. The same two manufacturers produce the low-BPR turbofan engine AI-25 TD, which powers the MIG UTS twin-engine trainer airplane.

1.2.5 Propfan Engine

1. The Metrovick F-2 turbojet engine was rebuilt in 1945 as a turbofan engine and was named the F.2/4. One of these F.2/4 turbofan engines was fitted with a two-stage open propfan to give an engine identical in layout to the GE UDF of over 40 years later, but nobody was interested [15].
2. Propfan engines emerged in the early 1970s as the price of fuel began to soar [15]. Propfan is a modified turbofan engine with the fan placed outside of the engine nacelle on the same axis of the compressor. They are also known as ultrahigh-bypass engines. It can be a single-rotation or a contrarotating engine. Propfan engines combine the best features of turboprop and turbofan engines. The main features of a propfan are more blades, reduced diameter; swept or scimitar-like profile and thinner blades in comparison with blades of turboprops; higher BPR than the turbofan; higher propulsive efficiency than both engines; higher flight speed than turboprop engines; and fuel-efficient engine like turboprop.
3. Hamilton Standard (HamStan) pioneered the idea of the propfan engine and NASA took it up. In 1974, HamStan tested a full-scale propfan having 8 blades, assuming a cruise altitude of 35,000 ft and a Mach number of 0.8 at NASA Ames and Lewis labs. The test resulted in a propfan having a tip sweep of 45° and a thickness/chord ratio of 2% outboard of 0.6 radius.
4. In 1981, NASA HamStan developed a single-rotation propfan driven by the 6000 shp Allison T701 mounted ahead of the swept wing of a Gulfstream II.
5. NASA contracts with General Electric led to the design of the GE UDF (unducted fan) (Figure 1.30). It is based on the aft-fan concept with contrarotating variable pitch propfan blades giving a BPR of about 34, which is 20%–30% more fuel efficient than subsonic turbofan engines.
6. The joint program of Pratt & Whitney/Allison led to the 578-DX engine, which was demonstrated in Indianapolis in pusher configuration. Similar to the General Electric (GE), it was flown on the same MD-80 from April 1989.
7. The Soviet Union and Ukraine designed their NK-93 propfan, which was tested in 1992 and flew in 1994. It powered the D Il-96M and the Tu-204 from1997.
8. The contrarotation D-27 (Figure 1.31) is the most famous propfan developed by Ukraine since 1991. A pusher version of D-27 powered the An-180, while a tractor version powered the An-70. Soviet and Ukrainian propfans are the only flying propfans to date.

1.2.6 Pulsejet, Ramjet, and Scramjet Engines

1.2.6.1 Pulsejet Engine

1. Pulsejet is a simple form of jet propulsion developed from the ramjet. It has spring-loaded inlet valves, which slam shut when the fuel ignites. The German Argus As



FIGURE 1.30
General electric unducted fan (GE UDF).

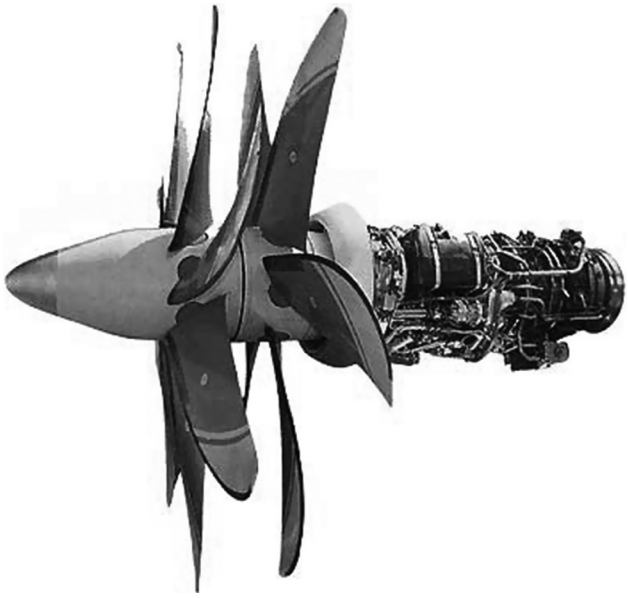


FIGURE 1.31
Ukrainian propfan (or turbopropfan) D-27.

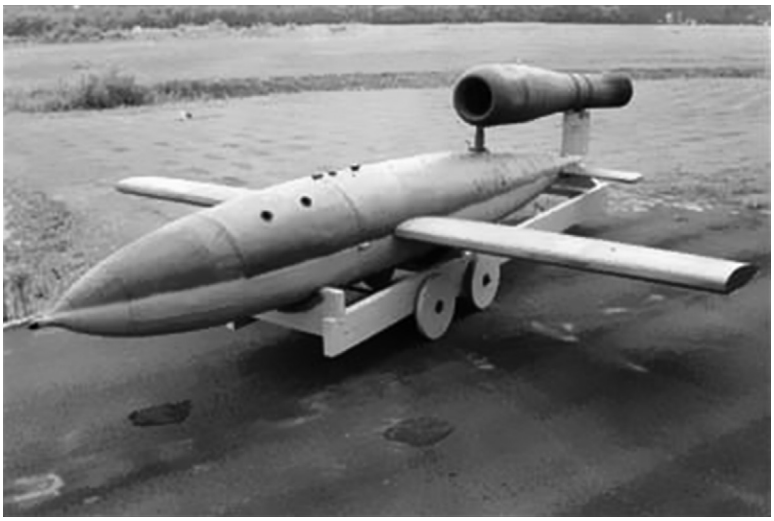


FIGURE 1.32
Pulsejet engine.

014 had its first flight at the end of 1942 when fitted to the Fieseler Fi 103 V-1 "Flying Bomb" producing about 750 lb of thrust (Figure 1.32). It was also used to power the Me 328 and versions of the He 280 and He 162A-10.

2. In the United States, Ford manufactured its pulsejet engine PJ-31-1, which was a copy of the Argus As 014. It was fitted to the Republic JB-2 "Thunderburg" and Northrop JB-10. A pair was fitted to the U.S. P 51 D Mustang for tests.
3. In Japan, a licensed copy of the Argus As 014 was manufactured and had the name Ka-10.
4. The Soviet RD-13/D-10 pulsejet with around 400 kg of thrust was developed from the Germany Argus As014/044 engines.
5. The pulsejet Jumo 226 with a thrust of 500 kg was developed in Dessau, Germany, at the end of World War II. Development continued after the Soviets occupied Dessau. Twelve engines were produced and tested in Germany by fitting it to the Junkers Ju 88G in the period from 1946 to 1947. Next, work was moved to Plant 30 near Moscow.

1.2.6.2 Ramjet and Scramjet Engines

1. The ramjet (sometimes known as "the flying stovepipe") was invented in 1908 by the French scientist René Lorin [17]. It consisted of just a tube, at one end of which air enters as a result of the forward motion of the plane. Air is compressed at the inlet and then fuel is added and burnt. The resulting hot gases are expelled at the other end. The ramjet does not contain any turbomachinery (compressor/turbine). A ramjet engine does not start to work until the speed of the flight vehicle is around 200 mph, but it gets more efficient the faster it goes. As an airplane increases its speed past Mach 1.0, the air pressure created from the speed of the airflow decreases the need for a compressor. As speeds approach Mach 3.5–4.0, a



FIGURE 1.33
Ramjet Leduc 010.

compressor is not even needed. The ramjet is the most efficient engine because it has few components.

2. Other ramjet pioneers (1913–1947) [18] are Albert Fono (General Electric, United States, patent in 1928), M. Stechkin (Soviet Union, ramjet theory, 1929), and René Leduc (France, patent, 1933).
3. In June 1936, René Leduc demonstrated the practical application of his ramjet engine, which he had been working on since the 1920s. The French government ordered the building of a plane using the new ramjet engine in 1937. However, work stopped due to the war.

   By November 1946, with the Leduc 010 fitted on top of a specially modified version of the aircraft Sud Est SE-161 Languedoc, four-engine transport plane "mother ship," the first test flights began on November 16, 1946. The first free-gliding flight of the Leduc 010 occurred on October 21, 1947 (Figure 1.33).
4. Other contributors in France were Marcel Warnner, Maurice Roy, and Georges Brun.
5. Soviet development of the ramjet ran from 1933 until 1939. The main contributors in the Soviet Union were MM. Bondaryuk (who patented the ramjet VRD-430 having 400 mm diameter, which was manufactured in 1940), Dudakov, Merkulov, Pobedonostsev, Tsander, and Zouyev.
6. In the United States, several contributions came from the General Electric people (Alexander Lippisch, O. Pabst, M. Trommsdorff, H. Walter), Roy Marquardt from APL/JHU, as well as staff from the NACA Lewis and Langley research centers. The subsonic ramjets developed by Roy Marquardt in 1945 were later adapted to the Bell Aircraft P-83 and the North American F-82 twin Mustang in 1947. In 1948, a pair of ramjets was fitted onto the wingtip of the Air Force's brand new F-80 "Shooting Star" made by Lockheed.
7. The supersonic ramjet developed by Marquardt powered the Rigel missile. The final Rigel flight (prior to August 1953, when the program was canceled) flew for 31 miles at an altitude of 42,000 ft while reaching a speed of Mach 2.5.



FIGURE 1.34
X-15.

Another supersonic ramjet (scramjet) engine powered the X-7 missile, which had its first flight on April 26, 1951. It achieved a new Mach record of 3.9 at 55,000 ft.

8. Other U.S. ramjets were used in operational missile programs such as the Bomarc missile (1949), Navaho, and Navy's Talos. Target missile drones were made such as XQ-5 "Kingfisher" (later the AQM-60A), "Red Roadrunner" MQM-42A, and the X-7A ramjet test vehicle by Lockheed Skunk Work, which later also developed the D-21 drone using a similar ramjet that was first mounted on top of the SR-71 and later used with the B-52. Other missiles powered by ramjets were the Vandal, Triton, super-Talos, and X-15 (Figure 1.34). A ramjet-powered version of a cruise missile for underwater launch was achieved and known as the IRR Torpedo Tube Vehicle [19].
9. In the United Kingdom, Bristol Aero Engines developed reliable and powerful ramjet engines for the Red-Duster Bloodhound II SAM missile. Hawker Siddeley Dynamics developed ramjet engines (Oden) for the Sea-Dart missiles, which were used in the Royal Navy on Type 21 and 22 destroyers in the 1970s.
10. Subsonic and supersonic ramjets were developed in other countries, for example, Sweden (RR2, RRX-1, RRX-5), USSR (SA4 Ganef—SA6 Gainful [SAN3 Goblet]), and France (ONERA Stataltex, Arsenal: SE4400, CT41 and VEGA as well as MARTA: Snecma ST 401, ST 402 and ST 407).
11. Then there was the development of other ramjets such as the "nuclear ramjet," that is, project "Pluto" when the world's first nuclear ramjet engine "Troy-II-A" was operated in 1961. There was also the "first NASP" program Hydrogen Research Engine (HRE) in 1964–1968, and the first "dual-mode" scramjet that burned both hydrogen and hydrocarbon fuel (1965–1968). There was also the ASALM flight test program in the 1970s that went to Mach 7.

    The Guinness World Records recognized NASA's X-43A scramjet's new world speed record for a jet-powered aircraft—Mach 9.6, or nearly 7000 mph. The X-43A set the new mark and broke its own world record on its third and final flight on November 16, 2004.

1.2.7 Industrial Gas Turbine Engines

1. As defined in Reference 20, the term industrial gas turbine is used for any gas turbine other than aircraft gas turbine. Industrial gas turbines have no limitations on their size and weight, nearly zero exhaust speeds, and a long time between

overhauls, which is of the order of 100,000 operating hours. The principal manufacturers for large industrial gas turbines are Alstom, General Electric, and Siemens-Westinghouse, all of whom designed single-shaft engines delivering more than 250 MW per unit. As the industrial gas turbine has proved itself as an extremely versatile prime mover, it has been used for a variety of applications, such as electric power generation, mechanical drive systems, pump drives for gas or liquid pipelines, chemical industries, and land and sea transport.

2. Since the 1970s, gas turbines for electric power generation have been primarily used for peaking and emergency applications. The main advantage of these turbines has been its ability to produce full power from cold in less than two minutes. Both Rolls-Royce Avon and Olympus engines were used in Great Britain, while the Pratt & Whitney FT-4 was used in North America. Countries with predominantly desert areas like Saudi Arabia extensively use gas turbines for generating electricity since they do not need cooling water.
3. Another application for the gas turbine is generating electricity for offshore platforms. Solar, Ruston turbines, and General Electric LM 500 are used for small power requirements (nearly 5 MW). Rolls-Royce RB211 as well as the Industrial Trent (50, 60) and the General Electric units LM 1600, LM 2500, LM 5000, and LM 6000 are used for larger power requirements (up to 60 MW).
4. Industrial gas turbines have been extensively used in pumping applications for gas and oil transmission pipelines.
5. Great engines in the sky equal great gas turbines aboard ships. Gas turbines have a long history of successful operation in navies. These engines have the advantages of compact size, high power density, and low noise. Several navies like those of the United Kingdom, the United States, Russia, Canada, Japan, and the Netherlands used gas turbines. Motor Gun Boat in 1947 was the first successful boat to use a gas turbine. In 1958, the Rolls-Royce Proteus gas turbine engines were first used in fast patrol boats. The General Electric LM Series was used in the U.S. Navy Bruke Destroyer, AEGIS Gruiser, Italian Lupo Frigate, as well as other large ferries, cargo and cruise ships, patrol boats, hydrofoils, and aircraft carriers. Rolls-Royce Trents were also used in container ships. In the late 1980s, the Canadian DDH-280 (which was the first warship to use gas turbines in 1970) used both of the Pratt & Whitney FT-4s for boost power and Allison 570s for cruise.
6. The AlliedSignal Lycoming AGT1500 gas turbine was used to power the U.S. tank M1A1 Abram. This tank was used in the Gulf War with great success.
7. Union Pacific used gas turbines for 15–20 years after 1955 to operate freight trains. PT6, the PWC turboshaft engine, was used to operate the CN TurboTrain. High-speed trains powered by turboshaft engines were built by the French and operated in the eastern United States. The Industrial Trent gas turbine allows the starting of large trains.
8. The PT6 turboshaft engine was used to operate the British Columbia Snow Plow. Moreover, the Pratt & Whitney Mobilepac engine, the gas-turbine-powered electric generating unit on wheels, was designed as a mobile power trailer.
9. The Rolls-Royce Industrial Trent family is designed to meet the higher power, variable speed demands required by other applications like natural gas liquefaction, gas transportation, and gas injection for oil recovery.

1.3 Classifications of Aerospace Engines

Aerospace engines [21] are classified into two broad categories, namely, airbreathing or non-airbreathing engines (Figure 1.35). Airbreathing engines (or airbreathers) are engines that use the *air* itself, through which the vehicle itself is flying, both as a source of *oxidizer* for the fuel in the combustion chamber and as a *working fluid* for generating thrust [22]. Non-airbreathing engines are the rocket engines wherein the propulsive gas originates onboard the vehicle. A rocket engine is defined as a jet propulsion device that produces thrust by ejecting *stored matter*, called the *propellant* [23].

Airbreathing engines are further divided into reciprocating engines and jet engines. It was the piston engine that powered the first successful flight of the Wright brothers. It remained the dominant source of power for aircraft propulsion for the next 40 years until jet engines took its place. From 1903 to 1908, piston engines employing water-cooled engines were used. The problem of excess drag and weight caused by the liquid-cooled engines affected the airplane performance at that time. By 1908, air-cooled engines replaced the liquid-cooled ones, which led to a substantial savings in weight (30%–40%). However, these air-cooled engines did not perform as well as expected. Thus, from about 1915 onward, better designs of liquid-cooled engines were able to develop more power than air-cooled ones. Many of the best fighters of World War II were powered by liquid-cooled engines. By the mid-1940s, the debate between water-cooled and air-cooled engines was over with air-cooled as the winner. NACA developed a cowling enclosing the engine to improve the efficiency of air-cooled aircraft. This enclosure for the engine limited the flow of air over the engine cylinders to the air actually in contact with the cooling fins of the cylinders.

However, piston engines were too heavy to compete with the jet engines for the same power generated. Jet engines have many advantages over reciprocating engines, the most

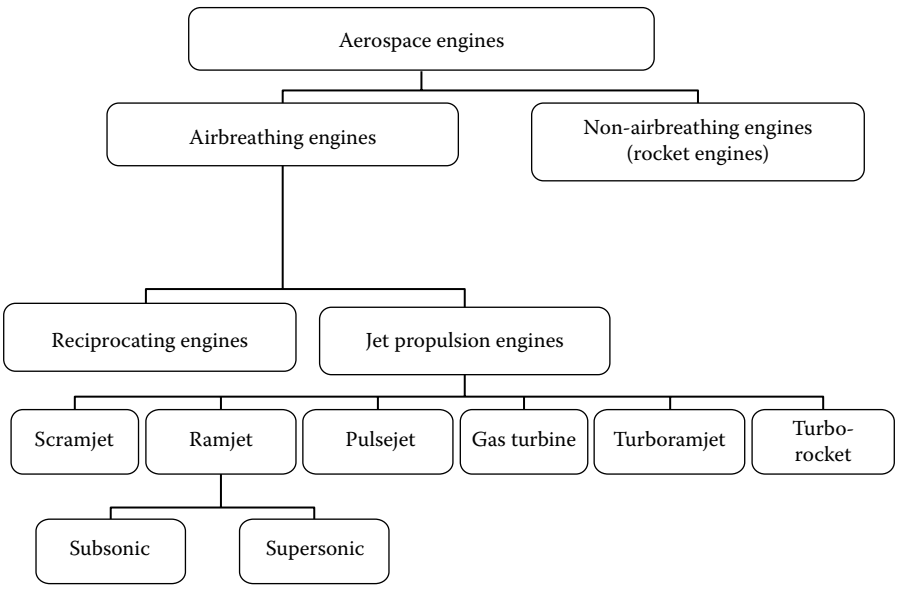


FIGURE 1.35
Classification of aerospace engines.

obvious being the capability of higher-altitude and higher-speed performance. Control is simpler because one lever controls both speed and power. With the large airflow, cooling is less complicated. Spark plugs are used only for starting, and the continuous ignition system of the reciprocating engines is not needed. A carburetor and mixture control are not needed.

The dawn of the jet engine was in the 1940s, and a tremendous development was achieved over the next 60 years and continues until now.

1.4 Classification of Jet Engines

Jet engines are further subdivided into numerous categories. Jet engines are subdivided into the following: ramjet, pulsejet, scramjet, gas turbines, turboram, and turborocket engines (Figure 1.35).

A brief description of each type follows, with further classification where appropriate.

1.4.1 Ramjet

The ramjet engine is an athodyd, or aero-thermodynamic-duct to give its full name [24]. It is composed of three elements, namely, an inlet, which is a divergent duct, a combustion zone, and a nozzle, either convergent or convergent–divergent. There are no rotating elements, neither a compressor nor a turbine. Layouts for subsonic and supersonic ramjets are illustrated in Figures 1.36 and 1.37, respectively.

When forward motion is imparted to the engine from an external source, air is forced into the inlet (or air intake). Air entering the inlet loses velocity or kinetic energy and increases its pressure energy since the inlet is a convergent duct. Next, it enters the combustion zone where it is mixed with the fuel and burned. The hot gases are then expelled in the nozzle where the thrust force is generated. The ramjet is inefficient at subsonic flight speeds. As described earlier, the ramjet has the virtue of maximum simplicity, as no turbomachinery is installed, and it has maximum tolerance to high-temperature operation and minimum mass-per-unit thrust at suitable flight Mach numbers [25].

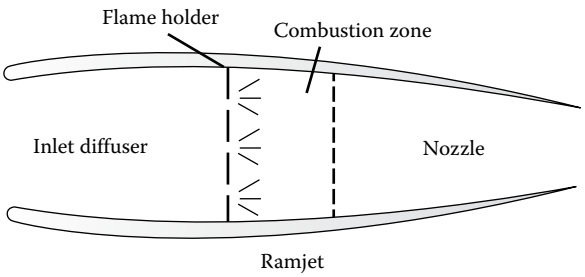


FIGURE 1.36
Subsonic ramjet engine.

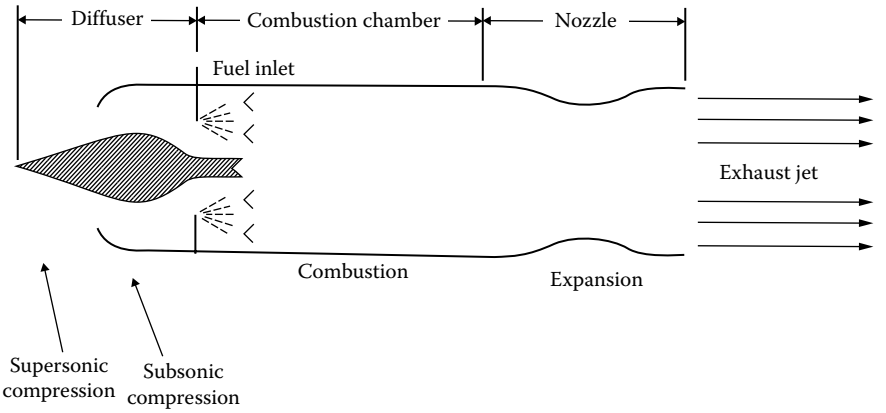


FIGURE 1.37
Supersonic ramjet engine.

1.4.2 Pulsejet

A pulsejet engine is a very simple form of internal combustion engine. A pulsejet is similar to a ramjet, except that a series of spring-loaded shutter-type valves (one-way valves) are located ahead of the combustion section. In a pulsejet, combustion is intermittent or pulsing rather than continuous. Air is admitted through the valves, and combustion is initiated, which increases the pressure, closing the valves to prevent backflow through the inlet. The hot gases are expelled through the rear nozzle, producing thrust and lowering the pressure to the point that the valves may open and admit fresh air. Then the cycle is repeated (Figure 1.38).

The most widely known pulsejet was the German V-1 missile, or buzz bomb, used near the end of World War II, which fired at a rate of about 40 cycles/s. The pulsing effect can also be achieved in a valveless engine, or wave engine, in which the cycling depends on pressure waves traveling back and forth through a properly scaled engine. A pulsejet engine delivers thrust at zero speed and can be started from rest, but the maximum possible flight speeds are below 960 km/h (600 mph). Poor efficiency, severe vibration, and high noise limited its use to low-cost, pilotless vehicles. Pulsejets use the forward speed of the engine and the inlet shape to compress the incoming air; then shutters at the inlet close while fuel is ignited in the combustion chamber and the pressure of the expanding gases force the jet forward. The shutters then open and the process starts again.

1.4.3 Scramjet

Scramjet is an acronym for supersonic combustion ramjet. The scramjet differs from the ramjet in that combustion takes place at supersonic air velocities through the engine. This allows the scramjet to achieve greater speeds than a conventional ramjet, which slows the incoming air to subsonic speeds before entering the combustion chamber. Projections for the top speed of a scramjet engine (without additional oxidizer input) vary between Mach 12 and Mach 24 (orbital velocity). It is mechanically simple but vastly more complex aerodynamically than a jet engine. Hydrogen is normally the fuel used. A typical scramjet engine is shown in Figure 1.39.

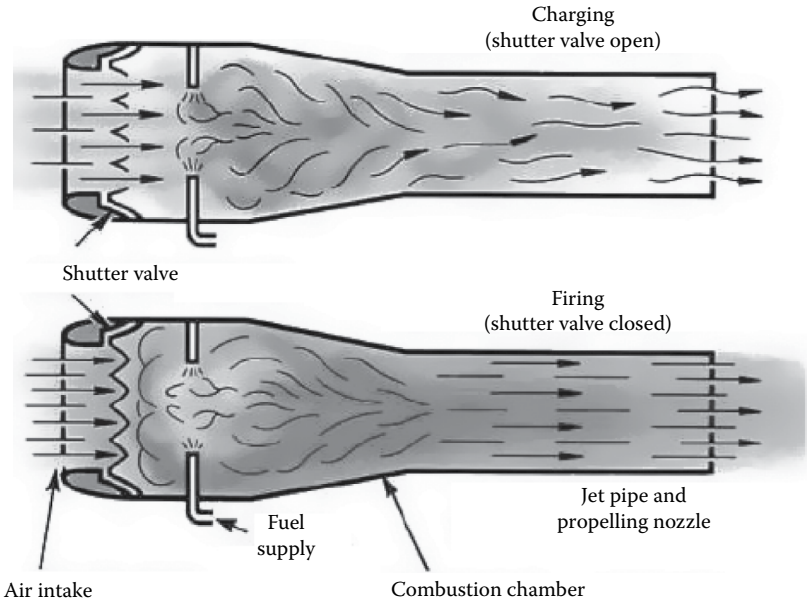


FIGURE 1.38
Pulsejet operation.

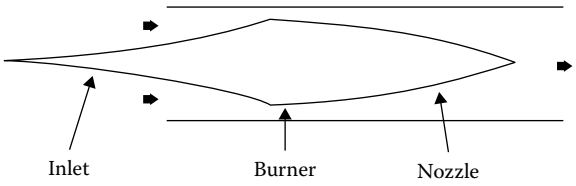


FIGURE 1.39
Scramjet engine.

1.4.4 Turboramjet

The turboramjet engine (Figure 1.40) combines the turbojet engine for speeds up to Mach 3 with the ramjet engine, which has good performance at high Mach numbers [24]. The engine is surrounded by a duct that has a variable intake at the front and an afterburning jet pipe with a variable nozzle at the rear. During takeoff and acceleration, the engine functions as a conventional turbojet with the afterburner lit, while at other flight conditions up to Mach 3, the afterburner is inoperative. As the aircraft accelerates through Mach 3, the turbojet is shut down and the intake air is diverted from the compressor, by guide vanes, and ducted straight into the afterburning jet pipe, which becomes a ramjet combustion chamber. This engine is suitable for an aircraft requiring high speed and sustained high Mach number cruise conditions where the engine operates in the ramjet mode.

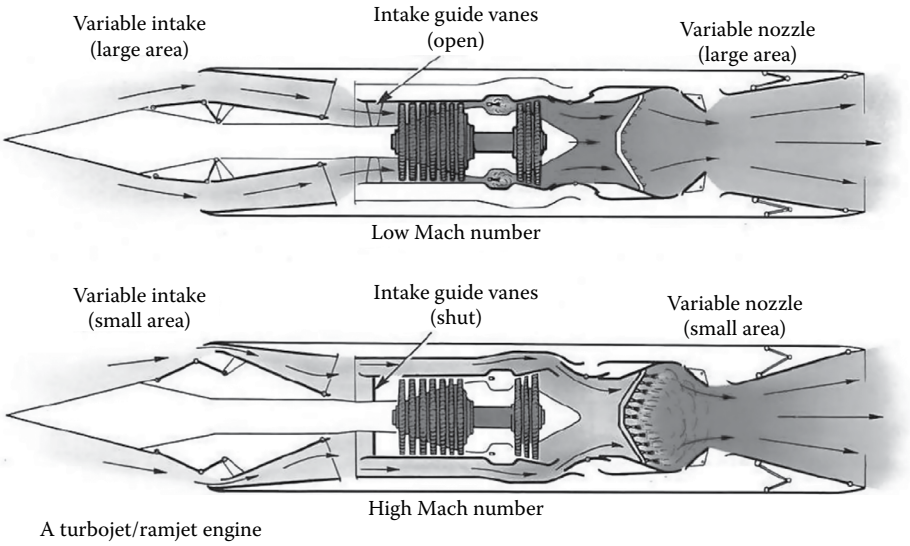


FIGURE 1.40
Turboram engine.

1.4.5 Turborocket

The turborocket engine figure (1-turborocket) could be considered as an alternative engine to the turboramjet. Its one major difference is that it carries its own oxygen to provide combustion [24]. The engine has a low-pressure compressor driven by a multistage turbine; the power to drive the turbine is derived from the combustion of kerosene and liquid oxygen in a rocket-type combustion chamber. Since the gas temperature will be in the order of 3500°C, additional fuel is sprayed into the combustion chamber for cooling purposes before the gas enters the turbine (Figure 1.41). This fuel-rich mixture (gas) is then diluted with air from the compressor and the surplus fuel burnt in a conventional afterburning system. Although the engine is smaller and lighter than the turboramjet, it has higher fuel consumption. This tends to make it more suitable for an interceptor or space-launcher type of aircraft that requires high-speed, high-altitude performance and normally has a flight plan that is entirely accelerative and of short duration.

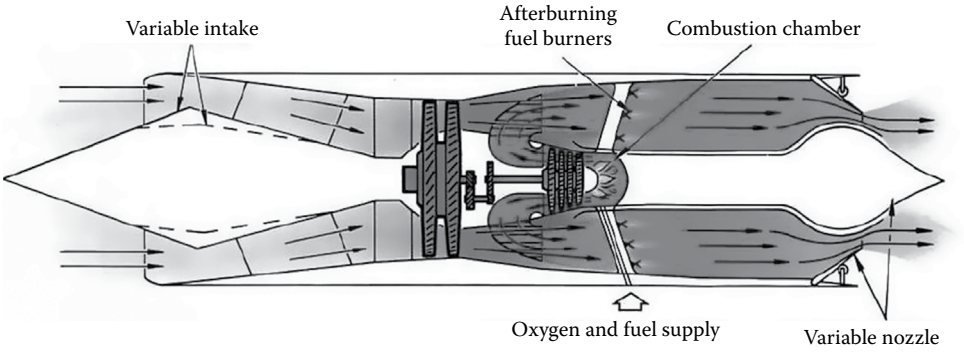


FIGURE 1.41
Turborocket engine.

1.5 Classification of Gas Turbine Engines

Gas turbine engines are the powerplants for all the flying aircraft/helicopters (and in this case may be denoted as *aeroengines* or aeroderivative gas turbines) and the source of power in miscellaneous industrial applications in automotives, tanks, marine vessels, and electric power generation. In addition to the advantages of the jet engines over the reciprocating engines mentioned in Section 1.3, vibration stresses are relieved as a result of rotating rather than the reciprocating parts. Gas turbines as classified are shown in Figure 1.42.

1.5.1 Turbojet Engines

Turbojet engines were the first type of jet engine used to power aircraft as early as the 1940s. This engine completely changed air transportation. It greatly reduced the expense of air travel and improved aircraft safety. The turbojet also allowed faster speeds, even supersonic speeds. It had a much higher thrust per unit weight ratio than the piston-driven engines, which led directly to longer ranges, higher payloads, and lower maintenance costs. Military fighters and fast business jets use turbojet engines:

1. Turbojet engines may be classified as single spool or double spool. Each may be further subdivided into centrifugal and axial compressor types. Figures 1.43 and 1.44 represent both types of compressors employed in the single-spool turbojet. The first turbojet engines of Frank Whittle (W.1) and Hans von Ohain (He S-1) incorporated centrifugal compressors.

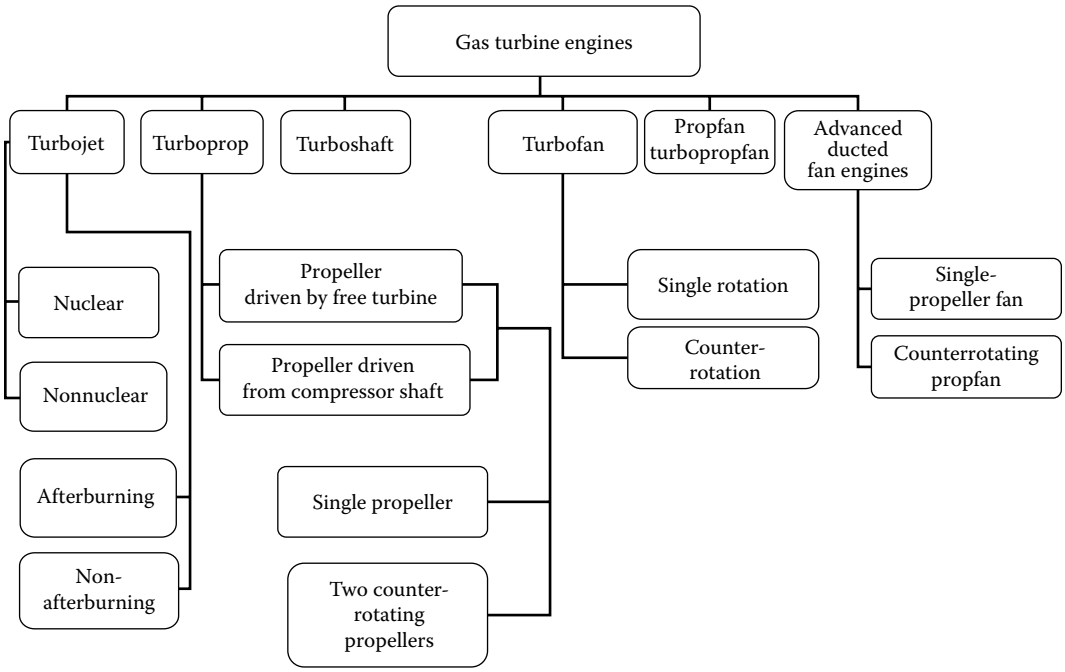
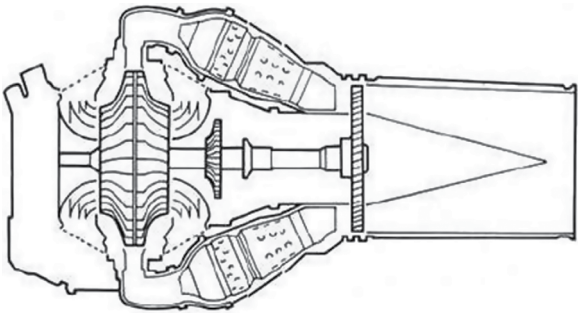
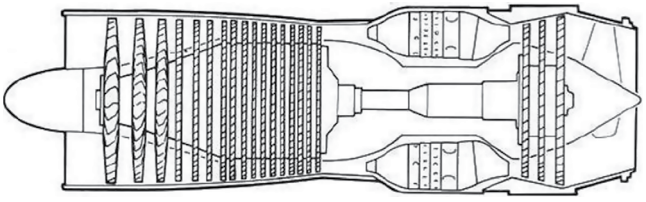


FIGURE 1.42
Classification of gas turbine engines.



Double-entry single-stage
centrifugal turbojet

FIGURE 1.43
Turbojet single-spool centrifugal compressor.



Single-spool axial-flow turbojet

FIGURE 1.44
Turbojet single-spool axial compressor.

2. Turbojets also may be classified as afterburning or non-afterburning. An afterburner is added to get an increased thrust (Figure 1.45). Fighter aircraft with afterburners only use them when absolutely necessary. If a pilot runs too long with the afterburner on, he or she risks running low on fuel before the mission is completed. The only civil transport aircraft that is fitted with afterburner was the Concorde. The turbojet engine was the most popular engine for most high-speed aircraft, in spite of the higher fuel consumption. When high speed and performance are important, the cost of fuel is less important.

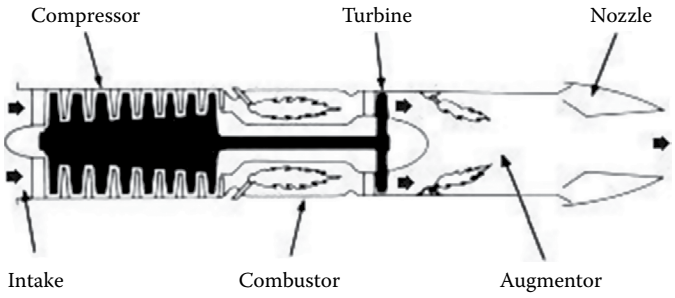


FIGURE 1.45
Turbojet engine with an afterburner.

3. Turbojet engines may be also classified as nuclear or nonnuclear engines. A typical nuclear turbojet engine is illustrated in Figure 1.46; the P-1 reactor/X39 engine complex (reactor P-1 combined to the GE X39 turbojet engine) where air duct scrolls for connection to the reactor (arrows) with a thrust output of 5000–7000 lb (Figure 1.47). It would have been flight tested aboard a highly modified B-36 bomber known as the X-6. The P-1 reactor would have been installed in the X-6's bomb bay for flight and removed shortly after landing.

Extensive studies were performed in the late 1940s and the early 1950s. However, all the nuclear engine projects were abandoned in favor of safety.

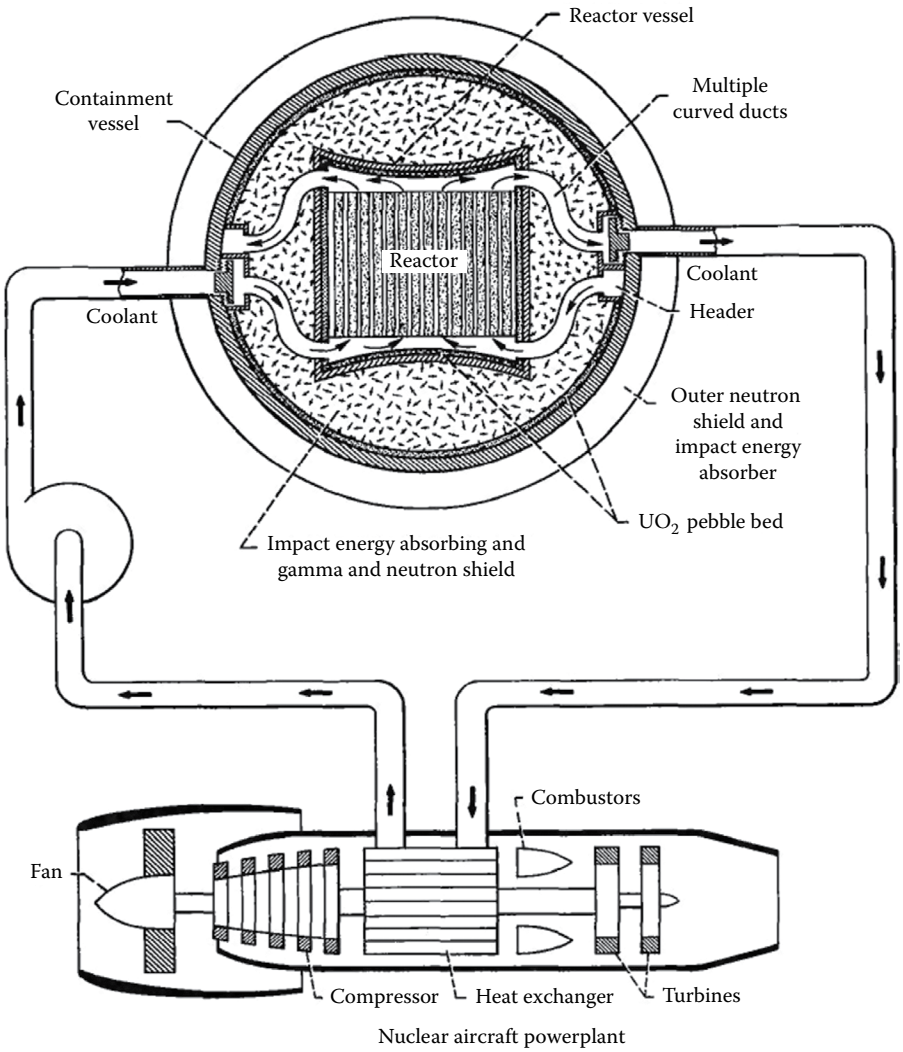


FIGURE 1.46
A typical nuclear turbojet engine.



FIGURE 1.47
Nuclear turbojet nuc x39.

1.5.2 Turboprop

Turboprop engines combine the best features of turbojet and piston engines. The former is more efficient at high speeds and high altitudes, while the latter is more efficient at speeds under 400–450 mph and below 30,000 ft. Consequently, commuter aircraft and military transports tend to feature turboprop engines. A turboprop engine differs from a turbojet engine in that the design is optimized to produce rotating shaft power to drive a propeller, instead of thrust from the exhaust gas. The turboprop uses a gas turbine to turn a large propeller. The shaft that connects the propeller to the turbine is also linked to a gearbox that controls the propeller's speed. The propeller is most efficient and quiet when the tips are spinning at just under supersonic speed. Moreover, no propeller is capable of withstanding the forces generated when it turns at the same speed as the turbine. Turboprop engines may be further classified into two groups, depending on the turbine driving the propeller. In the first group, the propeller is driven by the same gas turbine driving the compressor. In the second group, additional turbine (normally denoted as free-power turbine) turns the propeller. Figure 1.48 illustrates a turboprop engine with a single turbine driving the compressor and propeller. Figure 1.49 shows a turboprop engine with a free-power turbine.

Turboprop engines can be found on small commuter aircraft.

1.5.3 Turboshaft

Turboshaft engines are defined here as engines used in powering helicopters. The general layout of a turboshaft is similar to that of a turboprop, the main difference being the latter produces some residual propulsion thrust to supplement that produced by the shaft-driven propeller (Figure 1.49). Residual thrust on a turboshaft engine is avoided by further expansion in the turbine system and/or truncating and turning the exhaust through 90°. Another difference is that with a turboshaft the main gearbox is part of the vehicle (the helicopter here and identified as rotor reduction gearbox), not the engine. Virtually all turboshafts have a free power turbine, although this is also generally true for modern turboprop engines.

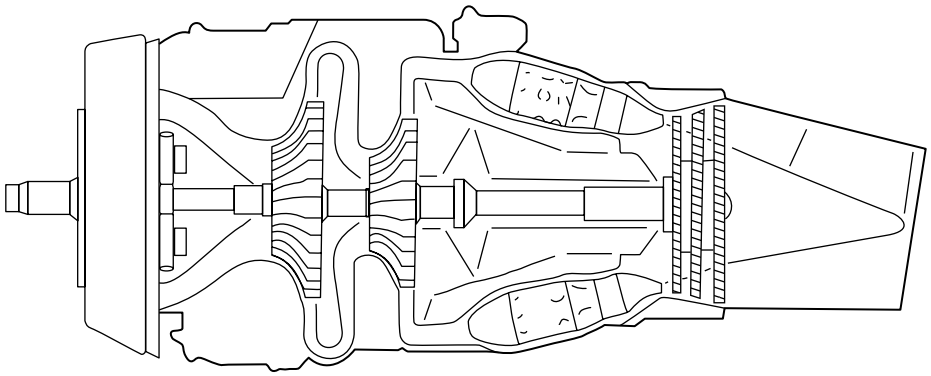


FIGURE 1.48
Turboprop engine with a turbine driving both compressor and propeller.

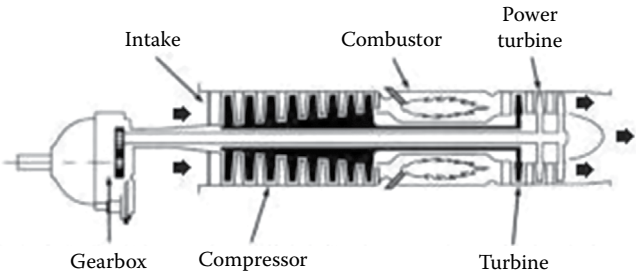


FIGURE 1.49
Turboprop–turboshaft engine with a free-power turbine.

1.5.4 Turbofan Engines

The turbofan engine was designed as a compromise between the turboprop and turbojet engines. It includes a large internal propeller (normally denoted a ducted fan) and two streams of air flowing through the engine. The primary stream travels through all the components like a turbojet engine, while the secondary air passes through the fan and is either ducted outside through a second nozzle identified as the cold nozzle or mixes with the hot gases leaving the turbine(s) and both are expelled from a single nozzle (Figure 1.50). Turbofan engines have a better performance and fuel economy than a turbojet at low power setting, low speed, and low altitude.

Figure 1.51 represents the numerous types of turbofan engines. Turbofan engines may be classified as

1. Forward-fan or aft-fan configuration (Figures 1.52 and 1.53)
2. Low bypass ratio or high bypass ratio (Figures 1.54 and 1.55)

   High-BPR turbofan jet engines like JT9, CF6, CFM56, PW4000, and GE90 are found in large commercial airliners. The BPR is now 5:1 or greater. At subsonic speed, high-bypass turbofans are more fuel efficient and quieter than other types of jet

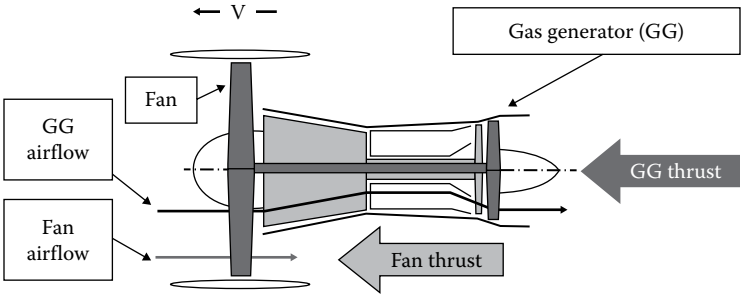


FIGURE 1.50
Turbofan layout.

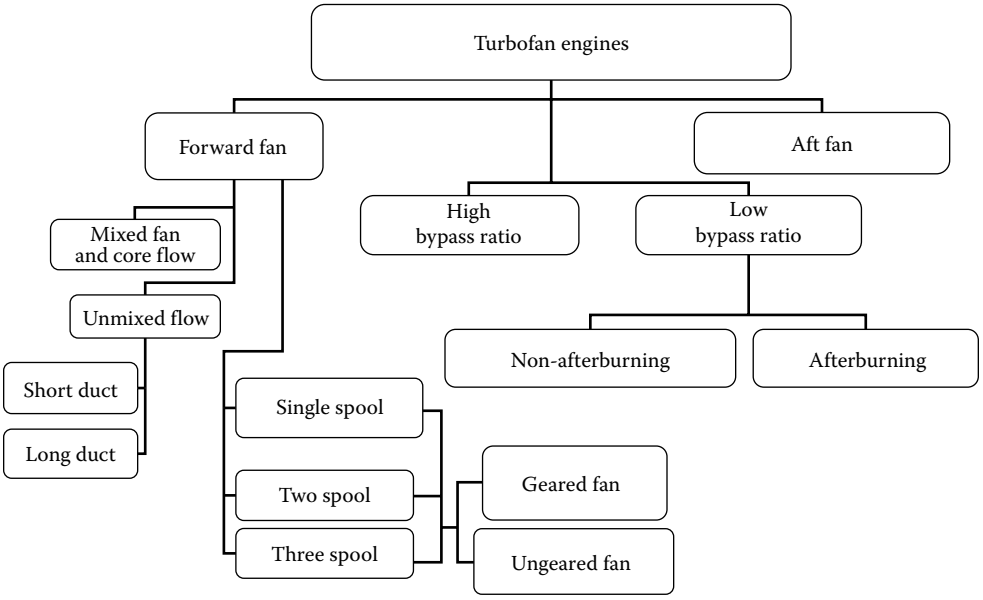


FIGURE 1.51
Classification of turbofan engines.

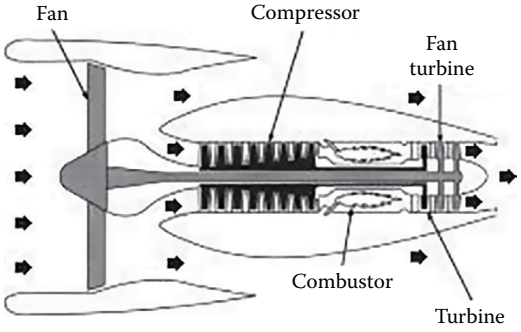


FIGURE 1.52
Forward fan.

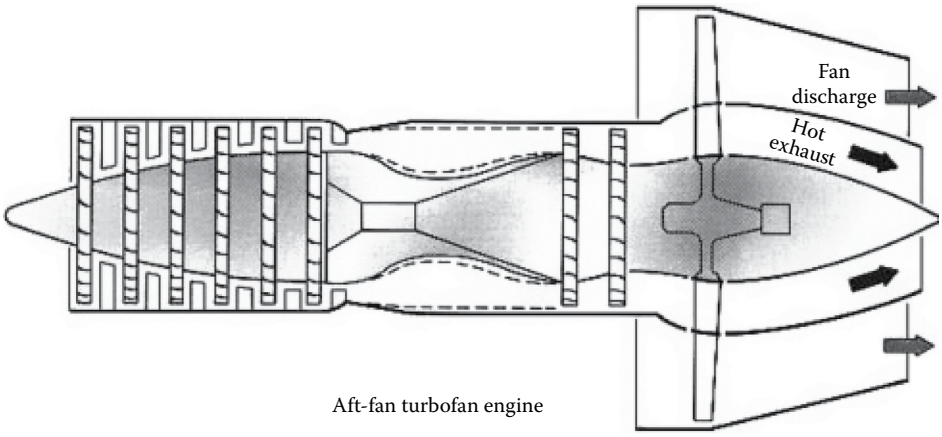


FIGURE 1.53
Aft fan.

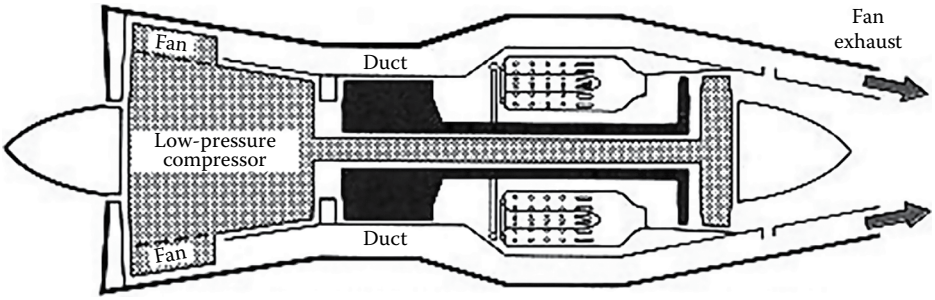


FIGURE 1.54
Low-bypass turbofan (short duct).

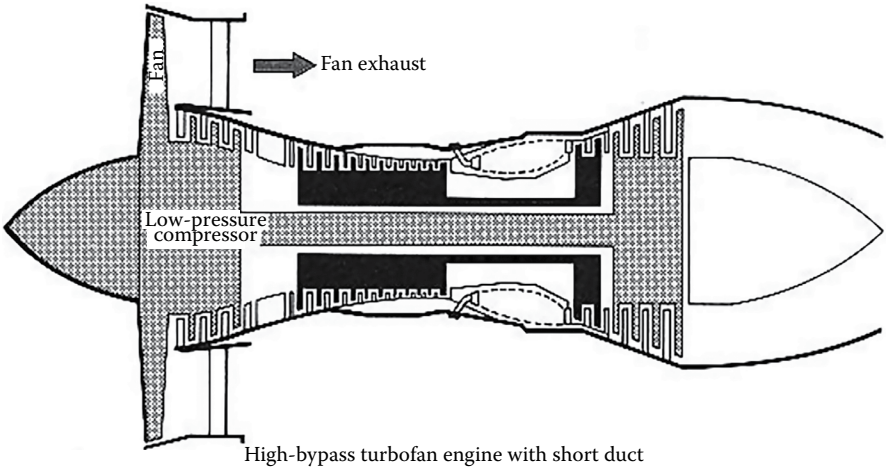


FIGURE 1.55
High-bypass turbofan.

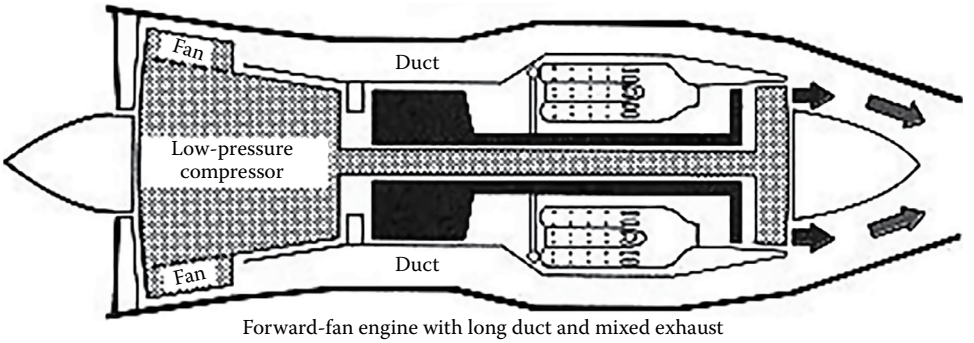


FIGURE 1.56
Mixed turbofan.

engines, making them ideally suited for commercial aircraft. Low-BPR turbofan engines are found mainly in military airplanes.

3. The forward fan may be of the mixed or unmixed types. In the former, the fan (cold) air stream passes through the fan where it is compressed and ejected from the cold nozzle, while the hot stream passes through the gas generator and is ejected through another hot nozzle. In the latter types, the cold stream leaving the fan mixes with the hot stream leaving the last turbine prior to leaving the engine from one nozzle. Figure 1.56 illustrates a mixed engine. A famous mixed engine is the Pratt & Whitney JT8 engine. The unmixed turbofan is already illustrated in Figure 1.54.
4. The unmixed turbofan may have short or long ducts. Figures 1.57 and 1.54 illustrate the general layout of both types. Mixed-flow engines are mostly military ones.
5. Forward fan also may be classified as single-, double- (two-), and triple- (three-) spool engines. Nowadays, single-spool turbofan engines are rare, while the majority of turbofan engines are of the two- or three-spool types. Figure 1.55 illustrates a two-spool unmixed turbofan engine having a high BPR and a short duct.

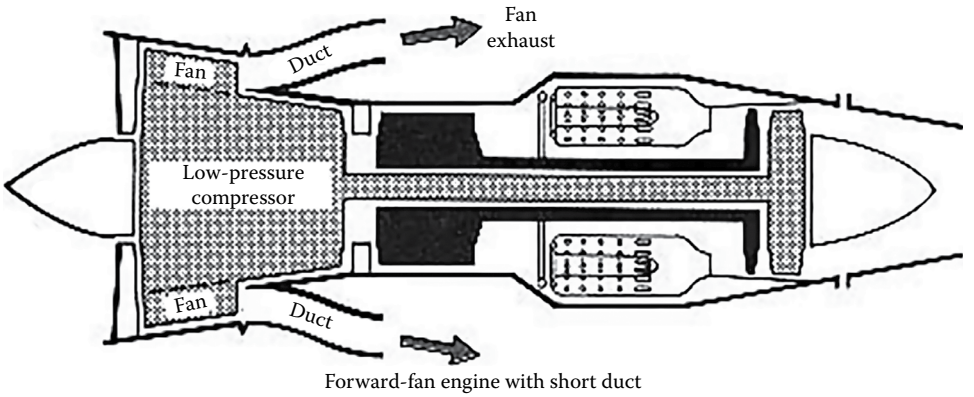


FIGURE 1.57
Unmixed turbofan (long duct).

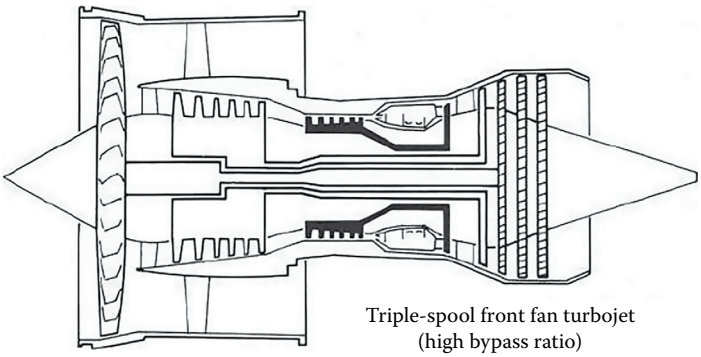


FIGURE 1.58
Typical three-spool turbofan forward fan.

Numerous high-BPR engines are two-spool engines, such as GE90, CF6, and PW4000. Figure 1.56 represents a typical turbofan engine employed in military applications. Three-spool engines are also prevailing these days. It includes many Rolls-Royce engines, including the RB211 and Trent series. Garrett AFT3 represents a medium BPR of 2.8 turbofan engine. A typical layout for a three-spool engine is depicted in Figure 1.58, an example for which is the Rolls-Royce Trent 800 engine.

6. Forward fan may be also classified either geared or ungeared fan. Lycoming ALF502R (Figure 1.59) and PW8000 are examples for such geared fans.
7. Low-BPR turbofan engines may also be classified as afterburning or non-afterburning engines. The former resembles all the recent military airplanes.

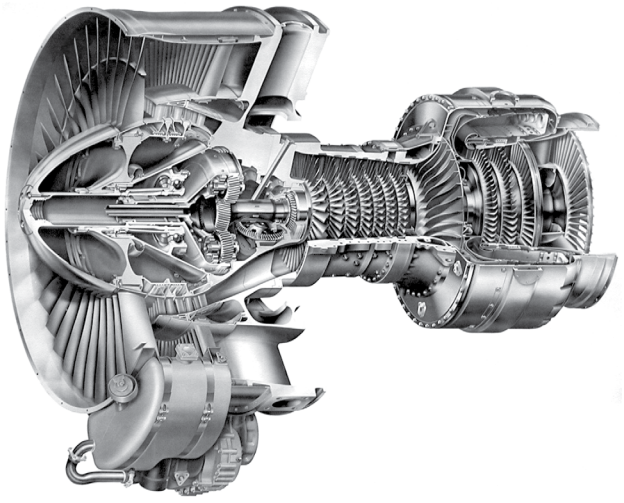


FIGURE 1.59
Lycoming ALF502R.

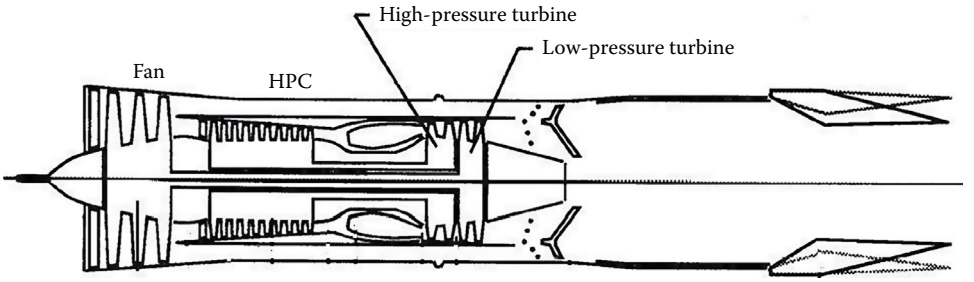


FIGURE 1.60
F-100 two-spool afterburning turbofan engine.

These engines are also of the mixed low BPR type. An example of these engines is the F100 (Figure 1.60). Due to their high fuel consumption, afterburners are not used for extended periods (a notable exception is the Pratt & Whitney J58 engine used in the SR-71 Blackbird). Thus, they are only used when it is important to have as much thrust as possible. This includes takeoffs from short runways (as in aircraft carriers) and combat situations.

8. Turbofan engines may also be classified as nuclear and nonnuclear engines. Though nuclear engines were abandoned in the early 1960s, extensive studies were performed after 1946 and up to 1961. The line of thought was that for aircraft with a gross weight of 0.45 million kg (1 million lb), such as the Boeing 747 and Lockheed C-5, it was practical to use nuclear fuel for their propulsion. Moreover, long operation (of the order of 10,000 h) between refueling and long range have an economic attraction. However, complete shielding of the flight and ground crew as well as the passengers was a dragging factor. Moreover, public safety in case of aircraft accidents furnishes another major concern. Though some studies made by NASA in the 1970s were in favor of using nuclear engines [26], these engines until now have not been adopted. Figure 1.46 nuclear engine represents a schematic drawing for a typical nuclear aircraft or air cushion powerplant that incorporates shielding and safety provision.
9. It is not common to find an airplane like Maritime patrol ASW (A-40) and SAR (Be-42) amphibian manufactured in the Soviet Union, which is powered by two 11 7.7 kN (26,455 lb) Aviadvigatel D-30KPV turbofan engines together with two 24.5 kN (5,510 lb) RKBM (formerly Klimov) RD-60K booster turbojet engines (Figure 1.61).

1.5.5 Propfan Engines

Propfan engines are sometimes identified in former Soviet Union countries as turboprop-fan (like D-27 engine), unducted fan, or ultrahigh BPR. There are two categories:

1. Single rotation
2. Counterrotating

Single rotation has a single forward unducted fan that combines the advantages of the propeller of a turboprop and the fan of a turbofan engine (Figure 1.62) [2]. The second type has two propellers, one behind the other that rotates in opposite directions (CR).



FIGURE 1.61
A-40 aircraft powered by two turbofans and two booster turbojets.

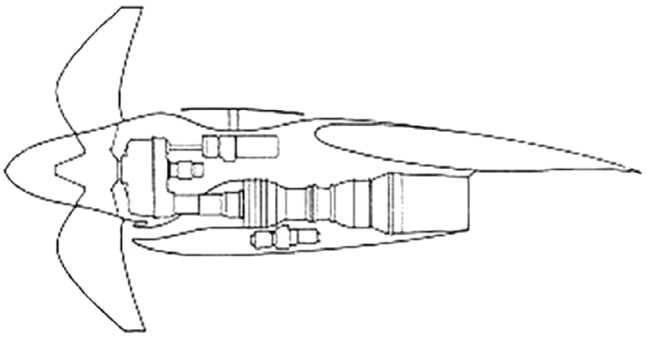


FIGURE 1.62
Single-rotation propfan. (From Pratt & Whitney, *The Aircraft Gas Turbine Engine and Its Operation*, Pratt & Whitney Operating Instructions 200, 1988, Section 1.)

Counterrotating designs offer the best performance [2]. It has some similarities with the aft fan type, but it is composed here of two counterrotating fans (Figure 1.63).

1.5.6 Advanced Ducted Fan

These designs are essentially turbofans with large, swept fan blades that have pitch control and reduction gearing similar to propfans, but the fans are enclosed in ducts like the turbofan. The BPR for an advanced ducted fan is from 15:1 to 25:1 [2]. There are two basic designs: one with geared, variable pitch, single-propeller fan and the other with counterrotating blades with pitch control (Figure 1.64). The need for such engines has been spurred by increasing airplane traffic, which raises noise, environmental, and fuel consumption issues. Extensive work in some aeroengine manufacturing companies like Pratt & Whitney, MTU, and Fiat Avio has been done for the design of this type of engines. A thin-lip, slim-line nacelle is required to make such a high BPR.

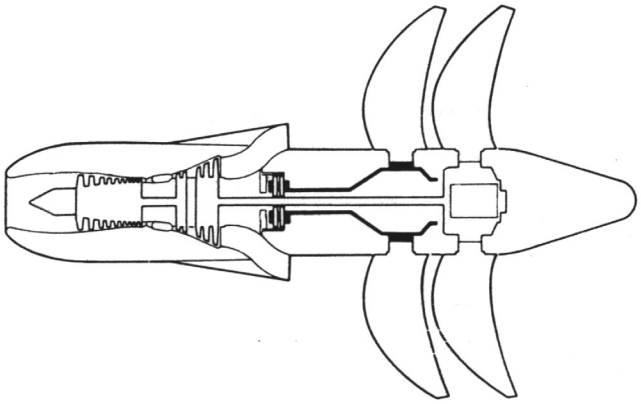


FIGURE 1.63
Counterrotating propfan.

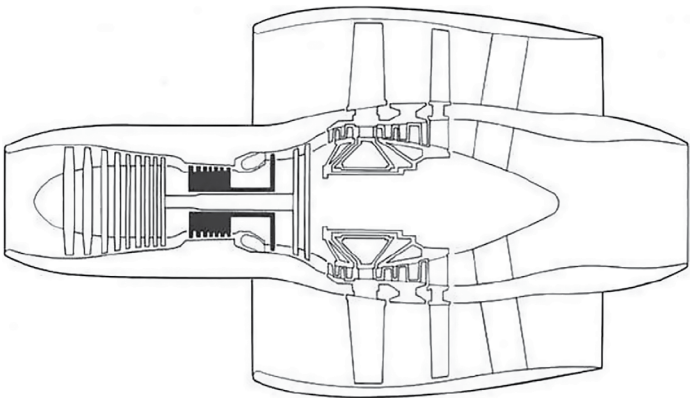


FIGURE 1.64
Counterrotating advanced ducted fan.

1.6 Industrial Gas Turbines

By "industrial gas turbine," it is meant here all turboshaft engines that are not installed in helicopters. Turboshaft engines are extremely versatile and are used in electric powerplants, offshore oil drilling, locomotives, tanks, trucks, hovercrafts, and marine vessels (Figure 1.65). In large powerplants used in generating electricity, it may be used in a combined cycle with steam powerplants (Figure 1.66).

1.7 Non-Airbreathing Engines

The different types of non-airbreathing engines (rocket engines) are illustrated in Figure 1.67. However, these types of engines are beyond the scope of this book.

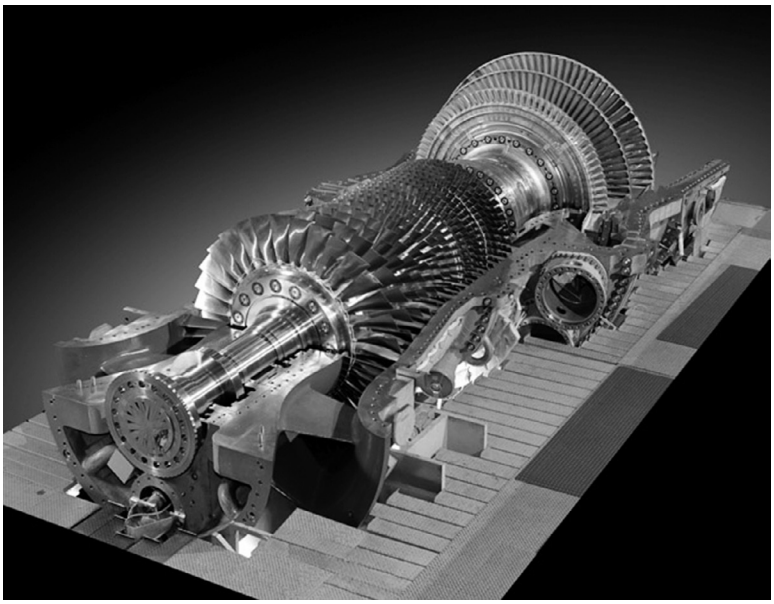


FIGURE 1.65
GE-7B gas turbine. (Courtesy of GE Power.)

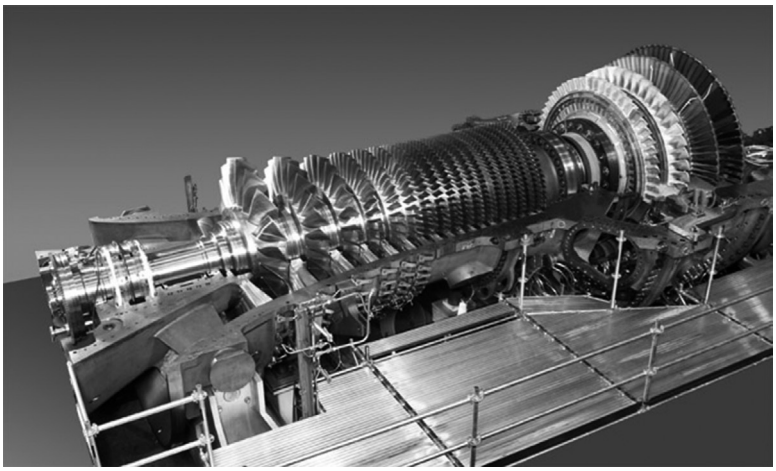


FIGURE 1.66
GE-7H combined-cycle gas turbine. (Courtesy of GE Power.)

1.8 The Future of Aircraft and Powerplant Industries

1. The twenty-first century is characterized by a revolutionary development in both aircraft and powerplant industry. On the *military side*, achieving air superiority is the main target of research and development (R&D) in giant companies. To that end, there are continuous developments in aircraft structure, materials, navigation and radar systems, exterior aerodynamic shape, other systems, computers,

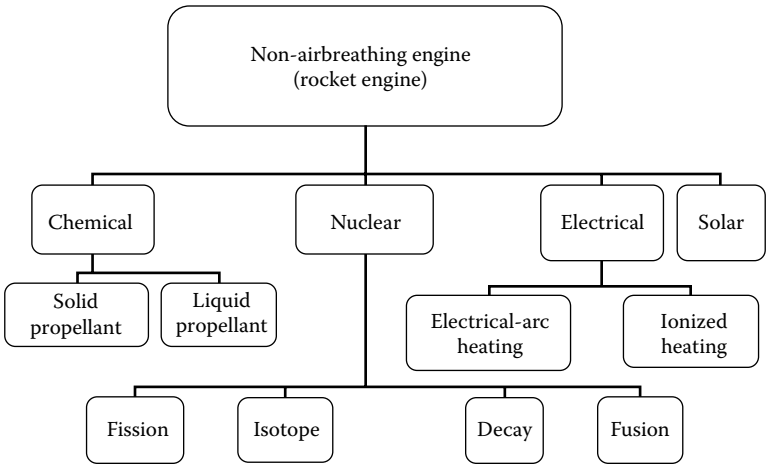


FIGURE 1.67
Classifications of non-airbreathing engines.

armaments, and jet engines. There are two distinct manufacturers in the United States developing the latest technological achievements in this regard: Boeing and Lockheed Martin.

The *Phantom Works* division is the main R&D arm of the Boeing company. Recent Phantom projects include some unmanned aerial vehicles (UAVs)—remotely piloted or self-piloted aircraft that can carry cameras, sensors, communications equipment, or other payloads—and a large-capacity transport aircraft. Examples of UAVs are

a. A160 Hummingbird UAV helicopter
b. X-45 series unmanned combat air vehicle (UCAV) powered by GE F404 engine, whose first flight was on May 22, 2002

The large-capacity transport craft Pelican ULTRA is intended for military or civilian use. It would have a wingspan of 500 ft, a cargo capacity of 1400 tons, and a range of 10,000 miles. Powered by four turboprop engines, its main mode would be to fly 20–50 ft over water, though it would also be capable of overland flight at a higher altitude but lesser range. The craft would be capable of carrying 17 M-1 battle tanks on a single sortie at speeds 10 times those of current container ships.

Lockheed Martin has several programs including the F-35 Lightning, X-35, F-22, and X-31.

The F-35 Lightning II—descended from the X-35 of the joint strike fighter (JSF) program—is a single-seat, single-engine military strike fighter. Demonstrator aircraft flew in 2000; first flight of production models first flew in 15 December 2006.

The X-35 [28] refers to a JSF having a short takeoff (400 ft runway at a speed of 80 mph) and a vertical landing by swiveling down the rear portion of the engine. It has a top speed of Mach 1.6 but can fly supersonically at a Mach 1.4 without afterburner, which gives the fighter a greater operating range and allows for stealthier flight operation. It is powered by two JSF119-611 afterburning turbofan engines (each of 35,000 lb thrust) manufactured by Pratt & Whitney and a shaft-driven lift fan manufactured by Rolls-Royce.

The F-22 Raptor [29] is an air superiority fighter having a top speed of Mach 1.7 and a ceiling of 50,000 ft. Its first flight was in 1997 and entered service in December 2005 as the F-22A. It flies at supersonic speeds without afterburner. It is a stealth aircraft so it carries its weapons in internal bays. It is powered by two Pratt & Whitney F119-PW-100 turbofan engines, each with 35,000 lb thrust. Thrust vectoring helps the pilot in both dog-fighting maneuverability and landing.

The X-31 is the first internationally experimental airplane [28]. It represents a joint project between the United States and Germany. It enhances super maneuvers with a top speed of Mach 1.3 and extremely short takeoff and landing. Thus, it can operate from a small airfield close to the enemy front line. It lifts the nose at final approach to reduce the speed at a steep angle with only 2 ft clearance from ground. It is powered by a single General Electric P404-GE-400 turbofan engine, producing 16,000 lb thrust.

The X-31 has three paddles mounted around the engine nozzles to redirect the flow of exhaust gases [27]. The moveable nozzles provide more control and maneuverability at high angles of attack when normal flight control surfaces are less effective. Information gained from the X-31 program could be used for future application to highly maneuverable aircraft.

Although the scheduled retirement of the F117 Nighthawk [30] is between 2017 and 2025, its retirement was surprisingly announced in January 2006. It is the world's number one stealth aircraft. It can penetrate deep in the enemy's aerospace and deliver its cargo of precision laser-guided bombs and head back for home. Its flat surface, designed in sharp angles, deflects incoming radar signals away from the aircraft. Moreover, its two GE F404-F1D2 turbofan engines are almost silent so it cannot be heard.

Another future field is employing solar- and fuel-cell systems for powering light airplanes like UAVs for extended flight time. Helios Prototype is a UAV solar- and fuel-cell system-powered UAV that NASA tested. On August 13, 2001, it sustained flight at above 96,000 ft (29,250 m) for 40 min, and at one time it flew as high as 96,863 ft (29,524 m). The solar-electric Helios Prototype flying wing is shown in Figure 1.68 over the Pacific Ocean during its first test flight on solar power from the U.S. Navy's Pacific Missile Range Facility at Kauai, Hawaii, on July 14, 2001. The 18-hour flight was a functional checkout of the aircraft's systems and performance in preparation for an attempt to reach sustained flight at 100,000 ft altitude.

Solar Impulse (Figure 1.69) is a Swiss long-range experimental solar-powered aircraft project, which has two operational aircraft. The aircraft are single-seater monoplanes powered by photovoltaic cells and capable of taking off under their own power. The prototype, often referred to as Solar Impulse 1, was designed to remain airborne for up to 36 h. It conducted its first test flight in December 2009. In July 2010, it flew an entire diurnal solar cycle, including nearly 9 hours of night flying in a 26-hour flight. Piccard and Borschberg completed successful solar-powered flights from Switzerland to Spain and then Morocco in 2012 and conducted a multistage flight across the United States in 2013.

A second aircraft, completed in 2014 and named Solar Impulse 2, carries more solar cells and more powerful motors, among other improvements.

2. Switching to civil transports, the two competitors Boeing and Airbus have their most recent airplanes, the Boeing 787 Dreamliner [31] and the Airbus A380 [32]. Comfort of passengers and fuel economy are the common features of both aircraft.



FIGURE 1.68
Solar-electric Helios.

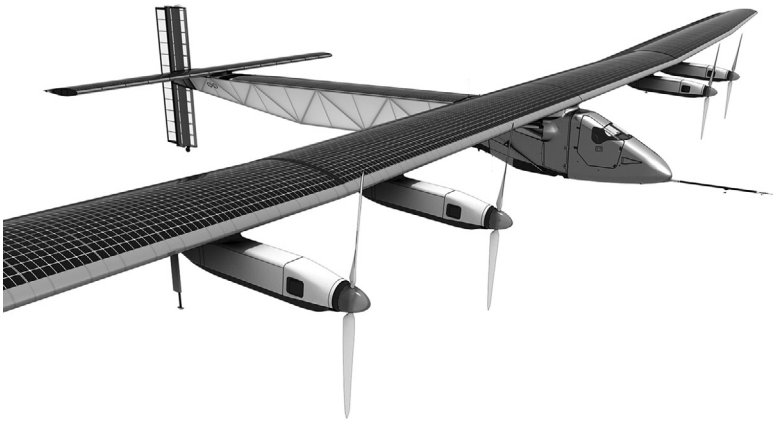


FIGURE 1.69
Solar Impulse aircraft.

The Boeing 787 Dreamliner, which was introduced on October 26, 2011, by All Nippon Airways, is a superefficient airplane with unmatched fuel efficiency and exceptional environmental performance. Passengers will have increased comfort and convenience. It has three different families, namely, 787-8, 787-9, and 787-10. The first family accomodates 290–330 passengers and be optimized for routes of 3000–3500 nautical miles. Boeing 787-8 dreamliner carries 210–250 passengers on routes of 8000–8500 nautical miles, while the 787-9 dreamliner will carries 260–290 passengers for routes of 8600–8800 nautical miles. Boeing 787 has as much as 50% of its structure made of composite materials. This reduces the risk of corrosion and lowers the overall maintenance costs and maximizes airline revenue by keeping airplanes flying as much as possible. Another innovative application is the

move from hydraulically actuated brakes to electric [38]. Moreover, its designers aim to incorporate health-monitoring systems that will allow the airplane to self-monitor and report maintenance requirements to ground-based computer systems. This will aid in troubleshooting the 787. Airplane systems information and fully integrated support will help maintenance and engineering organizations quickly isolate failed components and reduce return-to-service times. Boeing selected both General Electric and Rolls-Royce to develop engines for the 787. Advances in engine technology contributed as much as 8% of the increased efficiency of this airplane.

The airbus A380 [32] was introduced into service on October 25, 2007, by Singapore airlines. It has several configurations, namely, A380-800 and A380-800F. The first has different seating capacities, namely, 544, 644, and 853, while the second is the freight version having a payload of 150 tons. The powerplants are four turbofan engines, either the Rolls-Royce Trent 900 or the Engine Alliance GP7200, each having 68,000–84,000 lb thrust.

One of the most recent aircrafts is the Airbus A350 XWB, which is a family of long-range, twin-engine wide-body jet airliners powered by two Rolls-Royce Trent XWB, which had its first flight in 2013.

Various Internet sites that provide interesting information on aircraft are found in References 33–36.

Finally, the Bombardier CSeries is a family of narrow-body, twin-engine, medium-range jet airliners currently under development by Canadian manufacturer Bombardier Aerospace. The CSeries models are the 110-seat CS100 and the 135-seat CS300. These were initially named C110 and C130, respectively. In certification documentation, the CSeries family is designated Bombardier BD-500, with suffix -1A10 for the CS100 and -1A11 for the CS300. It is planned to be introduced by the second half of 2016 by SWISS and Airbaltic.

Work on hypersonic airplanes is being vigorously carried out in several countries. A hypersonic vehicle is an aerospace plane that would take off from a normal runway as a conventional airplane and then accelerate to near-orbital speeds within the atmosphere using scramjet engines (Figure 1.70). Hypersonic vehicles have long been touted as potential high-speed commercial transports to replace the current subsonic and supersonic airplanes.

The *Hyper-Soar* is planned to reach a flight Mach number of 10 (Figure 1.71). It is interesting to say that some aerospace companies, airlines, and government officials have proposed vehicles cruising at Mach 7 to 12 capable of carrying passengers from New York to Tokyo in less than 2 h.

Before 2020 an aurora scramjet-powered airplane will reach Mach 20 (Figure 1.72).

3. Now turning to the airbreathing engines, the technological developments assure that the ideal powerplant would be the most fuel efficient at its thrust, the most reliable, the lightest, the quietest, and the cleanest engine, all made at the lowest cost as thoroughly discussed by Rolls-Royce [37]. The fans in turbofan engines feature hollow swept blades with advanced aerodynamics, making them the lightest, strongest, quietest, and most efficient. Moreover, future engines use smarter ribbed steel and titanium casings. All recent Rolls-Royce engines employ three-shaft (spool) configurations. Future advancement in material and manufacturing technology will allow compressor weight savings of up to 70% with the introduction of blings. Blings are lightweight replacements of traditional compressor disks

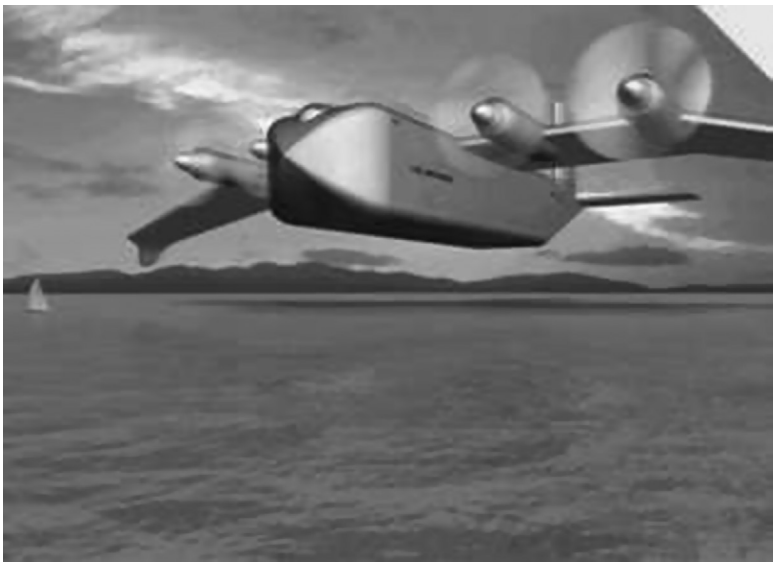


FIGURE 1.70
Hypersonic transport.



FIGURE 1.71
Hyper-soar aircraft.

featuring integral blades and using advanced silicon carbide–reinforced metal matrix to withstand high levels of stress.

The combustor is designed to have a stable flame over the different operating conditions. Advanced cooling methods are adopted to ensure integrity and long life as the flame temperature is nearly 1000°C above the melting temperature of

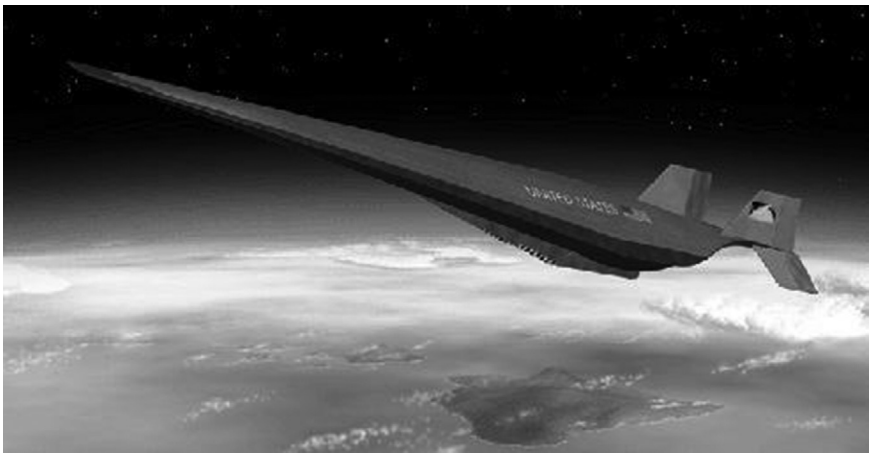


FIGURE 1.72
Hypersonic aurora aircraft.

the combustor material. The lean-burn combustion systems currently studied brought the NO_x level of the Rolls-Royce engines by 2010 to a level of half that required by legislation. By 2020, 80% NO_x reduction relative to those specified by CAEP 2 regulation is planned.

Advanced single-crystal material and thermal barrier coatings are used on static and rotating turbine components. Advanced cooling techniques allow the turbine temperature to be increased in order to improve the engine efficiency. Aerodynamic advancements, including counterrotating systems, 3-D design, and end-wall profiling, will lead to lighter blades with no efficiency penalty.

Engines are controlled by the Full Authority Digital Electronic Control (FADEC) system, which is becoming smaller, lighter, and more reliable.

The noise-reduction target is for noise by 2020 to be one-half its 2001 level. This is set as a strict goal.

A 10% reduction in fuel consumption of all newly designed engines by 2010 compared with the equivalent in 1998 engines is achieved.

Powerplant developments by Pratt & Whitney [26] cover the following aspects:

a. Integrally bladed rotors: In most stages, disks and blades are made of a single piece of metal for better performance and less air leakage.
b. Long-chord and shroudless fan blades: Wider and stronger fan blades with a ring of metal around most jet engines.
c. Low-aspect high-stage-loading compressor blades that have wider chord blades for greater strength.
d. Alloy C high-strength burn-resistant titanium compressor stator.
e. Alloy C in augmentor (if available) and nozzle: The same heat-resistant titanium alloy to protect the aft components.
f. Float wall combustor: Thermally isolated panels of oxidation-resistant high-cobalt material to make combustion chamber more durable.

g. Fourth-generation FADEC.
h. Improved supportability: Easy access for inspection, maintenance, and replacement of components/modules.

4. As regards supersonic transports (SST), two groups are performing studies in this area:
   a. Manufacturers of aircraft (Boeing) and aeroengines (Pratt & Whitney, General Electric, Rolls-Royce, and Snecma): Improvement of engine-specific fuel consumption (SFC) for high-speed civil transport (HSCT) at subsonic flight conditions has been one of the main concerns in the period 1990–2010. The original U.S. SST had very poor subsonic SFC. High subsonic SFC penalizes the mission performance by reducing the efficiency during subsonic mission legs and by requiring larger amounts of reserve fuel. The key to good subsonic and supersonic SFC is a variable-cycle engine (VCE). The major objective for a future HSCT application is to provide some degree of engine cycle variability that will not significantly increase the cost, the maintenance requirements, or the overall complexity of the engine. The VCE must have a good economic payoff for the airline while still providing more mission flexibility and reducing the reserve fuel requirements so that more payload can be carried. In the past, VCEs were designed with large variations in BPR to provide jet noise reduction. However, these types were complicated and did not perform well. Today, the trend is toward turbojets or low-bypass engines that have the ability to improve off-design performance by adjustment of compressor bleed or by a relatively small variation in BPR. The current engine offerings from Pratt & Whitney and General Electric fall into this category. Both of these engines will require an effective jet-noise suppressor. Rolls-Royce/SNECMA favors other approaches. One is a tandem fan that operates as a turbojet cycle for cruise but opens a bypass inlet and nozzle for higher flow at subsonic speeds. A second approach is to increase the BPR by incorporating an additional fan and turbine stream into the flow path at subsonic speeds.
   b. NASA Lewis

      The following are five of the most promising engine concepts studied:

      i. The turbine bypass engine (TBE) is a single-spool turbojet engine that has turbofan-like subsonic performance but produces the largest jet velocity of all the concepts. Hence, it needs a very advanced technology mixer–ejector exhaust nozzle with about 18 decibels (dB) suppression ability to attain FAR 36 Stage III noise requirements without oversizing the engine and reducing power during takeoff. This level of suppression could be reached if the ejector airflow equals 120% of the primary flow.
      ii. The VCE alters its BPR during flight to better match varying requirements. However, although its original version defined in the 1970s relied on an inverted velocity profile exhaust system to meet less stringent FAR 36 Stage II noise goals, the revised version needs a more powerful 15 dB suppression solution. A 60% mass flow–augmented mixer–ejector nozzle together with modest engine oversizing would satisfy this requirement. It should not be inferred from the discussion that the TBE needs a 120%

mass flow–augmented mixer–ejector nozzle while the VCE only needs one that is 60%. There is uncertainty concerning the best combination of mass flow augmentation, acoustic lining, and engine oversizing for both engines.

iii. A relative newcomer, the fan-on-blade ("Flade") engine is a variation of the VCE. It has an auxiliary third flow stream deployed during takeoff by opening a set of inlet guide vanes located in an external annular duct surrounding the VCE. The auxiliary annular duct is pressurized by extension to the fan blades and is scrolled into the lower half of the engine prior to exhausting in order to provide a fluid acoustic shield. It also requires a relatively modest mixer–ejector exhaust nozzle of approximately 30% flow augmentation.

iv. The fourth concept is the mixed-flow turbofan (MFTF) with a mixer–ejector nozzle.

v. The final engine concept is a TBE with an inlet flow valve (TBE/IFV). The IFV is activated during takeoff to permit auxiliary inlets to feed supplementary air to the rear compressor stages while the main inlet air is compressed by just the front compressor stages. While a single-spool TBE/IFV still needs a mixer–ejector exhaust nozzle, it seems possible to avoid that complexity with a two-spool version because of greater flow handling ability in the takeoff mode.

5. A list of the following points [38] in numbers for the period (2007–2017):
   a. More than 59,800 turbofan engines will be produced.
   b. Over 22,850 turboshaft engines will be produced.
   c. Sales of turboprop engines will be rebounded in the face of escalating airline fuel costs.
   d. Some 23,000 APU/GPUs will be produced.
   e. Nearly 27,700 engines for missiles, drones, and UAVs will be produced.
   f. Some 11,000 micro-turbines for electrical generation (30–500 kW) will be produced.
   g. Engines for marine power for surface vessels of all sizes, commercial and military, worth $4.7 billion will be manufactured.
   h. Concerning airplanes, 7900 large commercial jets and 3865 fighter/attack/jet trainer aircraft will be produced. Some 700 business jets will be produced annually. As regards military transport aircraft, Airbus will garner the lion's share (24%), Lockheed Martin will rank second (18% share), and the Boeing share will fall to 12.3%.

1.8.1 Closure

The evolution of flight vehicles since 1500 up to present (2016) is displayed in Figure 1.73.

A summary for the evolution of aeroengines is given in Figure 1.74. A concise table for the different propulsion system and the flight speeds for their powered vehicles is given in Figure 1.75.

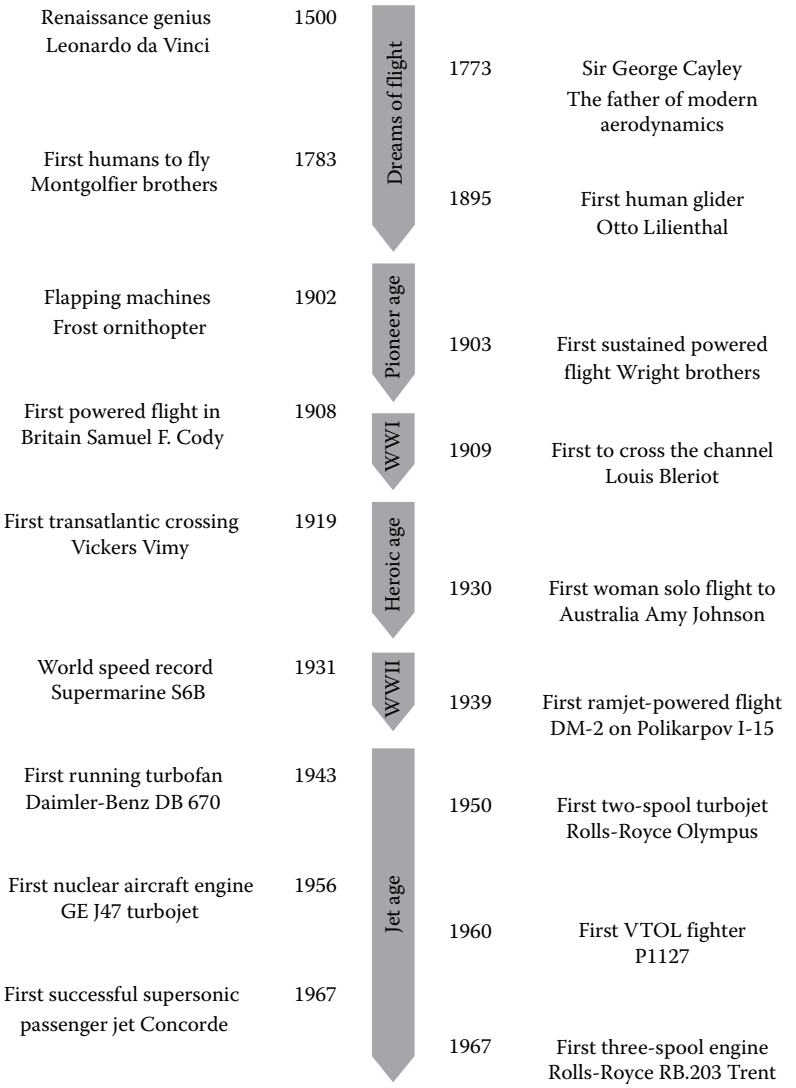


FIGURE 1.73
Historical events.

(*Continued*)

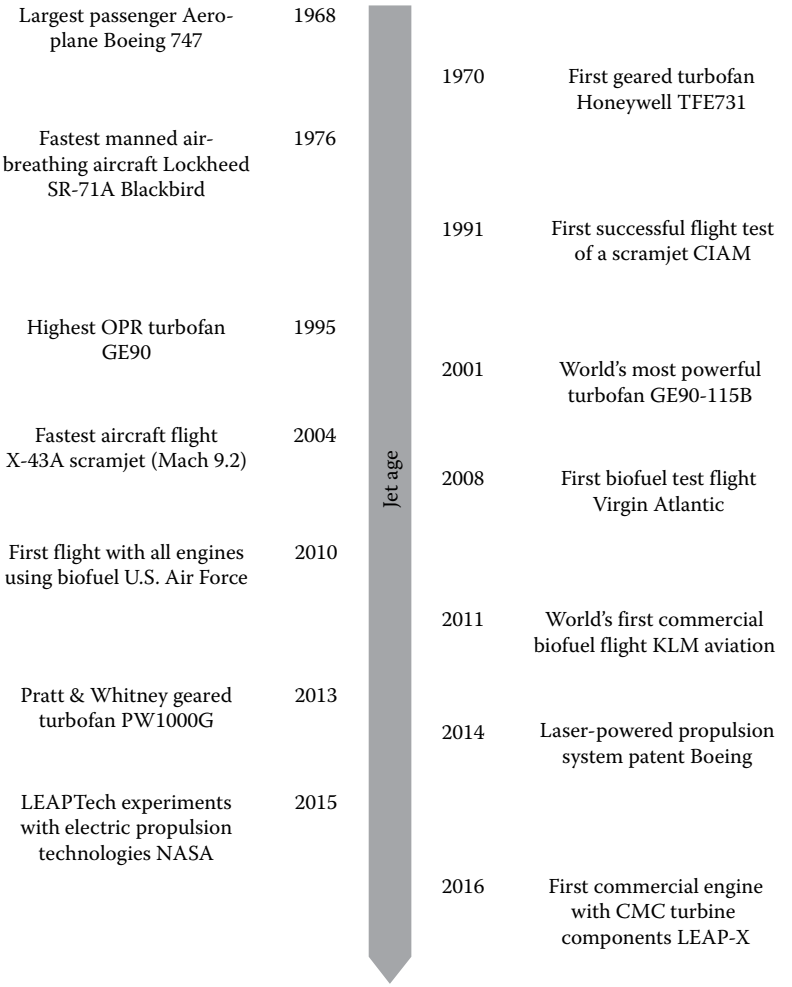


FIGURE 1.73 (*Continued*)
Historical events.

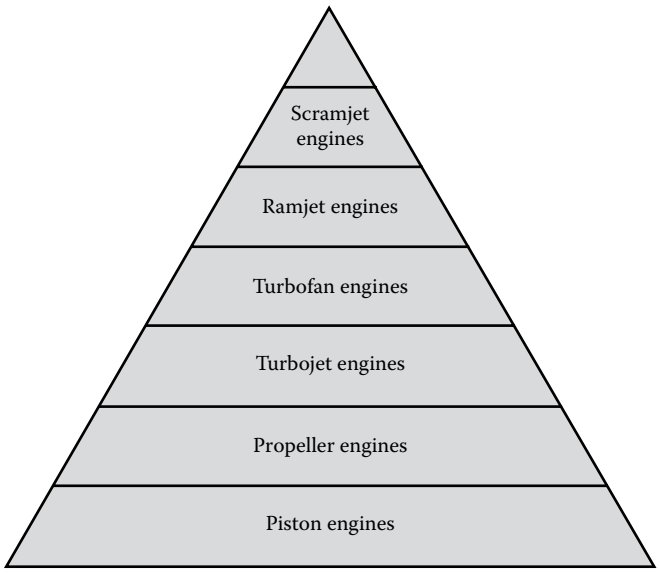


FIGURE 1.74
Evolution of aeroengines.

Propulsion System	**Jet Velocity (m/s)**
Helicopter lifting rotor	Up to 30
Propeller	30–200
Remote ducted fan, unducted fan or propfan	100–300
Turbofan	200–600
Turbojet (sea-level, static)	350–600
Turbojet (M = 2.0 at 36,000 ft, approx. 600 m/s)	900–1,200
Ramjet (M = 2.0 at 36,000 ft, approx. 600 m/s)	900–1,200
Ramjet (M = 4.0 at 36,000 ft, approx. 1200 m/s)	1,800–2,400
Solid-propellant rocket	1,500–2,600
Liquid-propellant rocket	2,000–3,500
↓impractical - - - - - - - practical↑	
Nuclear rocket (solid core reactor)	9,000–10,000
Nuclear rocket (fusion reactor)	25,000
Solar	20,000
Arc	6,000
Plasma and ion	$90–30 \times 10^6$
Photon	300×10^6

FIGURE 1.75
Classification of aeroengines based on their speeds.

Problems

1.1 Compare
1. Wrights Flyer I and Airbus 380.
2. Boeing 787 Dreamliner and Airbus 380.
3. Golden model found in Central and South America representing Maya and Inca empires and Grumman X-29 and F-102 aircraft.

1.2 Write short notes on the inventions of Leonardo da Vinci in the fields of aero-engines.

1.3
1. Describe the aeolipile device designed by the scientist Hero in Alexandria, Egypt, 100 BC.
2. Describe how aeolipile design preceded Newton and James Watt in applying action and reaction forces as well as steam power.

1.4 Describe how mankind tried to imitate birds in their flight. Refer to
1. Daedalus and Icarus in the eighteenth century BC.
2. Abbas Ibn Firnas (AD 810–887).

1.5 How is the tail of birds responsible for the stability of their flight?

1.6 Write short notes on
1. Inventions of Leonardo de Vinci in the fifteenth century in aviation fields.
2. Branca's stamp machine in 1629.
3. Balloons invented and designed by the Montgolfier brothers.
4. The first parachute-aided jump of André Jacques Garnerin in 1797.

1.7 Describe early attempts at designing flying vehicles prior to the Wright brothers.
Give short notes on the activities of
1. The Briton John Stringfellow in 1848.
2. The Briton Sir George Cayley in 1849.
3. French officer Félix du Temple in 1874.
4. French engineer Clément Ader in 1890.
5. German Otto Lilienthal in 1896.
6. Russian Alexander F. Mozhaiski in 1894.
7. Samuel Langley in 1896 and 1903.

1.8 Describe the attempts of the Wright brothers to design a glider between 1900 and 1902.

1.9 Draw figures to illustrate the developments of the Wright's airplanes (1900–1903), listing in a table the changes in: wing span—length—height-tail—engine.

1.10 Describe the first flying aircraft, Flyer I, designed and manufactured by the Wright brothers.

1.11 Describe the design aspects of the Wright brothers' manufacture of their Flyer I, including
1. Aircraft
2. Engine
3. Propeller
4. Wind tunnel

1.12 1. Define aerostats and aerodynes.
2. List the different types of powered aerostats and give example for each type.
3. List the different types of unpowered aerostats and give example for each type.

1.13 1. Classify the different types of aerodynes.
2. What are the different types of fixed-wing aircraft?
3. List the types of rotorcrafts and give examples for each type.
4. Give examples of hybrid fixed/rotary wing aircraft.
5. Give examples of flapping wing (ornithopter).

1.14 Give examples of aircraft and engines with
1. Tilt-wing.
2. Tilt-rotor engines.

1.15 Define, giving examples:
1. Aircraft powered by steam engines.
2. Aircraft powered by Stirling engines.
3. Aircraft powered by nuclear engines.

1.16 Since the first flight of Wright brothers in 1903, endless developments in aircraft and engine industries have been achieved. Identify some of the milestones in this long journey by listing the first engines of the following categories: turbojet engine, turbojet engine with afterburner, turbofan engine, supersonic turbofan engine, high-BPR turbofan engine, turboprop engine, and propfan engine.

1.17 Do you think the eternal chicken and egg question applies to the aircraft and engine?

1.18 Describe the British and German patents for the first jet engines.

1.19 Compare the first engines invented by Frank Whittle and Hans von Ohain.

1.20 Complete the following table:

Name	Contribution
Hero	
Wan Hu	
Leonardo da Vinci	
Giovanni Branca	
Isaac Newton	
Félix du Temple	
John Barber	
Samuel Langley	
Wright brothers	
Frank Whittle	

1.21 Which engines have no moving parts?

1.22 What is the type of engine that powers most of today's airliners?

1.23 What is the type of engine used in a helicopter?

1.24 How is a turboprop different from a turbojet?

1.25 List the names of some Chinese aircraft and engines.

1.26 Identify engines available for the following aircraft:

B787, B777, B767, B757, B747-200, B747-400, MD80, B737-800/500, A310, A320, A330, A340, B 787, A380, A350, the Sukhoi Su-9, Tupolev Tu-128P, DC-8, U-2 spy, Shenyang J-8, Rafale, Mirage 5, Swedish Ja-37 Viggen, Mig 23, Mig 29, Tornado ADV, Eurofighter V-22 Ospery, AN-225, Convair 580, Fairchild F-27, Lockheed L100 Hercules, Cessna Citation II, Gulfstream Aerospace (IAI) G100, Bombardier Canadair 415, Bell 412, Sikorsky S-58, Lockheed Martin F-117A Nighthawk, Lockheed Martin P-3 Orion, Mi-12, ATR 42-500, ATR 72, Panavia Tornado, AH-64 A Apache, SAAB 340B, Bombardier Dash 8, MiG-AT, Rutan Voyager

1.27 State the type of each of the following engines and mention the names of some aircraft they power:

F-100, F-101, F-110, RB-I99, RB 211, Nene, JT 8D, RR Pegasus T56, V2500, CFM56, GE90, Lyulka AL-7, JT9, CF6, TFE 731, TPE331, TV3 VK-1500, AL-31 F, Trent 700, Olympus 593, T700-GE, PW100, SM146, DR-1700, CF34-8, Ha 102

1.28 Why does the Rolls-Royce Pegasus have counterrotating shafts?

1.29 Write down the advantages of the following engines: RB-211 and the JT9D or CF6.

1.30 What are the key differences between the PT6 and the Garrett 331?

1.31 Compare turboprop, turbofan, and propfan engines (draw figures to illustrate their configurations).

1.32 Compare ramjet and scramjet engines.

1.33 Will the physical fitness of passengers influence the design of supersonic and hypersonic transports?

1.34 What engines are suitable for Airborne Warning and Control System (AWACS) aircraft?

1.35 Compare turboprop, turboshaft, and industrial gas turbines.

1.36 Write the names of two VTOL and V/STOL aircraft and discuss the requirements of their powerplants.

1.37 What is the possible engine type to be used in powering unmanned air vehicles (UAVs)?

1.38 What is the largest fan diameter, highest BPR, and largest overall pressure ratio of turbofan engines to date?

1.39 Which companies are associated with the following engines?

CFM 56, CF6, JT-3D, GP 7000, V 2500, RB 211

1.40 Compare

1. Piston engines powering aircraft and turboprop engines.
2. Turbojet/ramjet and turborocket engines.

1.41 Write short notes on the Curtiss flying boat illustrated here:



FIGURE P1.41

1.42 Classify the following engines:

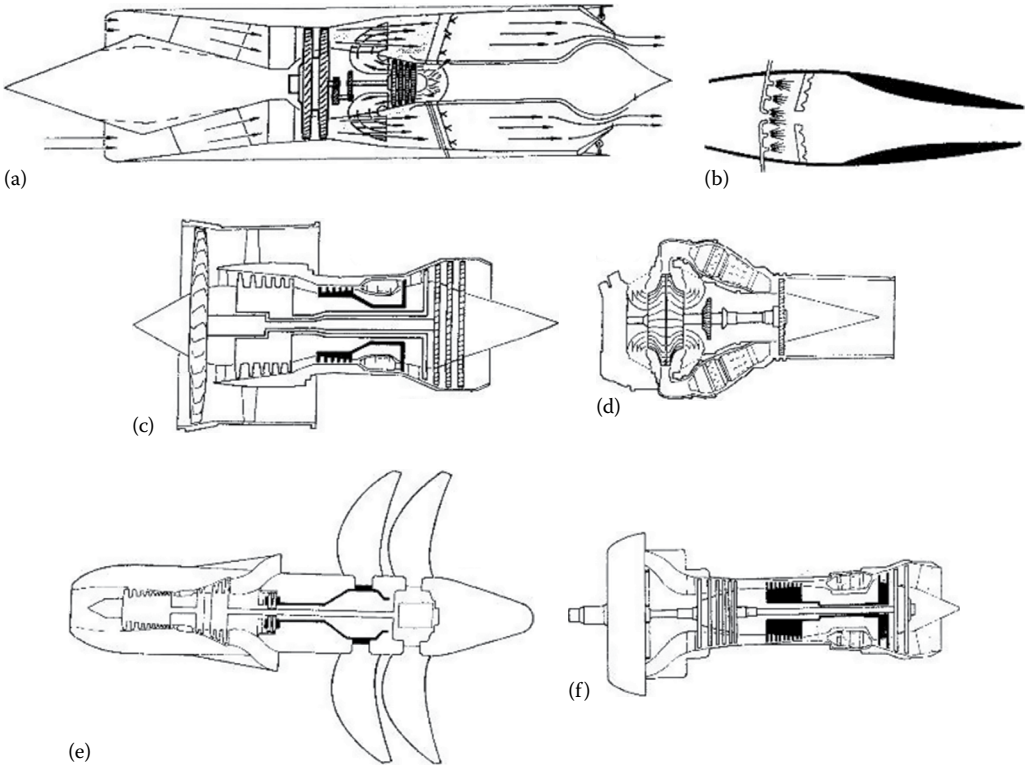
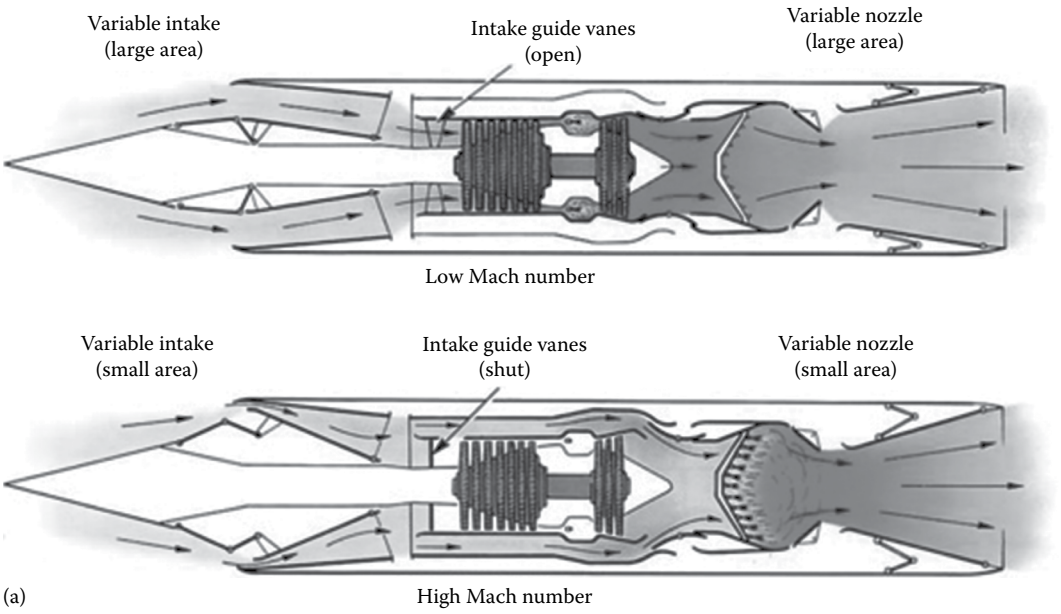


FIGURE P1.42

1.43 Classify and write short notes on the engines shown here:



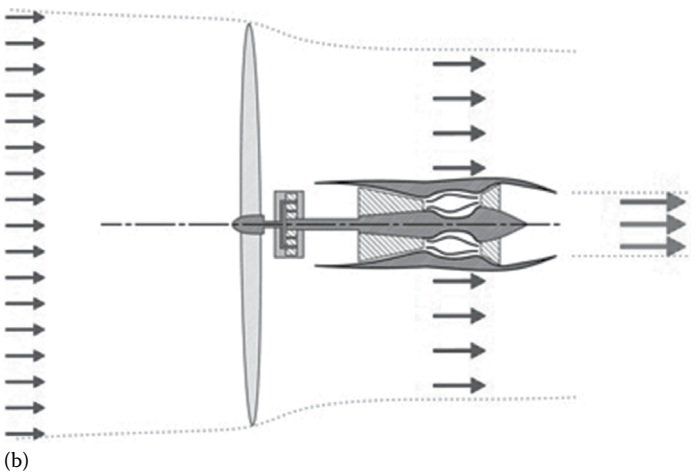
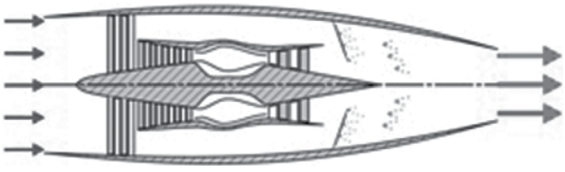
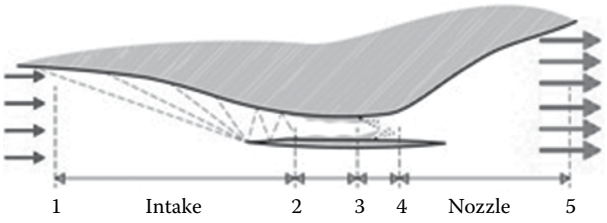


FIGURE P1.43

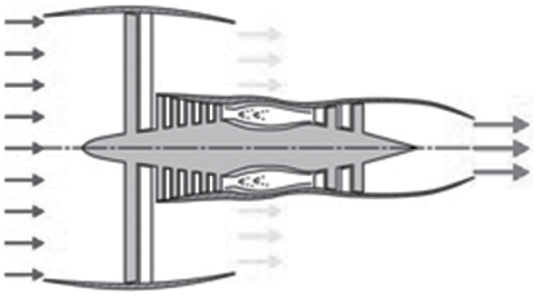
(*Continued*)



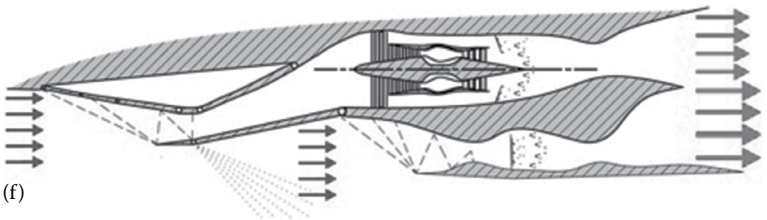
(c)



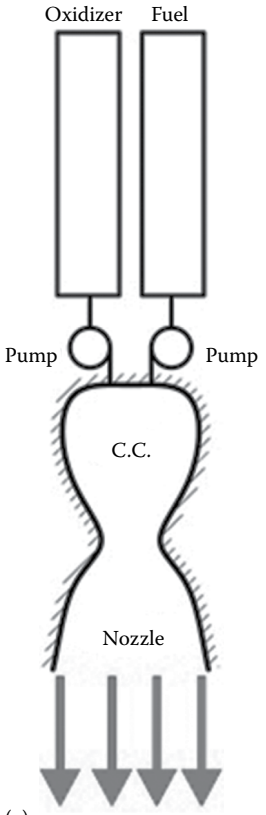
(d)



(e)



(f)



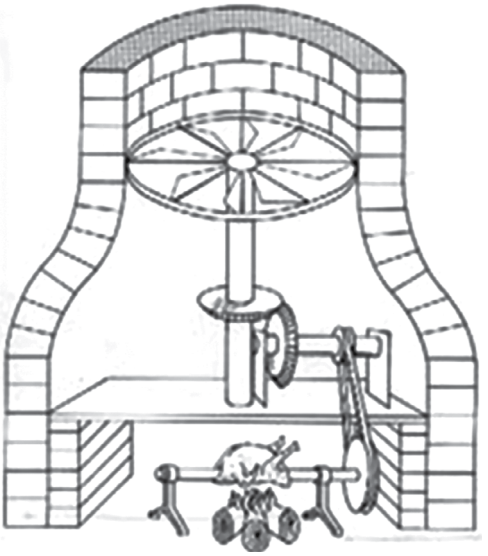
(g)

FIGURE P1.43 (*Continued*)

1.44 For the objects/vehicles shown in Figure P1.44, state the period in which it was made, who made it, and its contribution to the history of flight.



(a) The aeolipile



(b) Hot gases Chimney



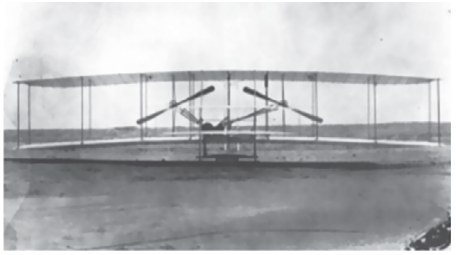
(c) Chinese rocket man



(d) Steam wagon

FIGURE P1.44

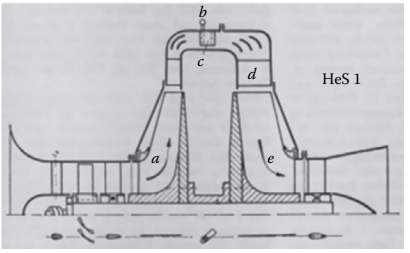
1.45 Describe the powerplant used for propelling the aircraft shown:



(a) Flyer III



(b) Vickers Gunbus



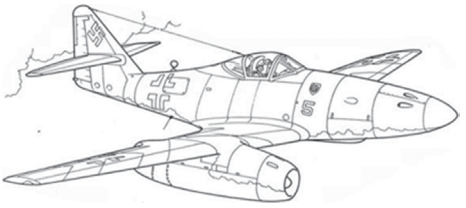
(c) HeS-1



(d) Heinkel He 178

FIGURE P1.45

1.46 What is the cruise Mach number for the aircraft shown? Describe its powerplant.



(a) Messerschmitt Me 262



(b) Bell X-1



(c) Concorde SST



(d) NASA X-43

FIGURE P1.46

1.47 Classify (giving examples for) turbojet engines according to
1. Compression system
2. Number of spools
3. Afterburning

1.48 Classify (with application) turbofan engines according to
1. BPR
2. Fan location
3. Number of spools
4. Afterburning

1.49 Classify (with application) turboprop and turboshaft engines.

1.50 Compare
1. Turboshaft and turboprop engines.
2. Turbojet and turbofan engines.
3. Turboprop and propfan engines.
4. Ramjet and scramjet engines.
5. Rockets powered by turbojet and rockets powered by turbofan.

1.51 Compare the two turbofans shown in Figure P1.51.

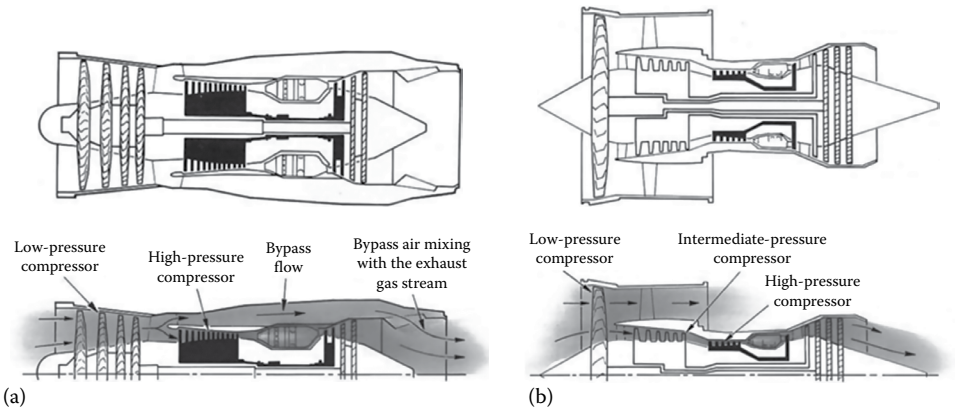


FIGURE P1.51

1.52 Identify the following engines and give one example for each type:

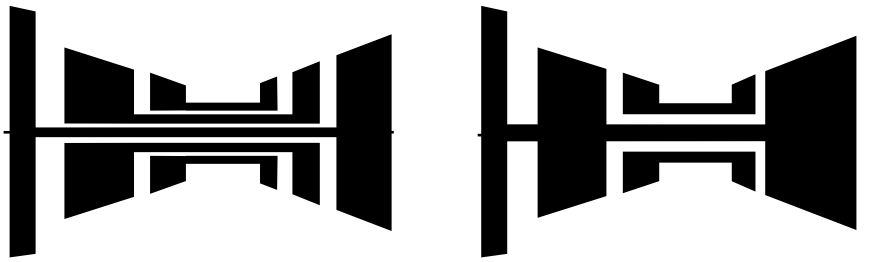


FIGURE P1.52

References

1. G. Daniel Brewer, *Hydrogen Aircraft Technology*, CRC Press Inc., 1991, p. 248.
2. Pratt & Whitney, *The Aircraft Gas Turbine Engine and Its Operation*, Pratt & Whitney Operating Instructions 200, 1988, Section 1.
3. J.V. Casamassa and R.D. Bent, *Jet Aircraft Power Systems*, 3rd edn., McGraw-Hill Book Co, 1965, Chapter 1.
4. http://www.smith.edu.hsc.museum/ancient_inventions/steamengine2.html.
5. I.E. Treager, *Aircraft Gas Turbine Engine Technology*, 3rd edn., McGraw-Hill, Inc., 1999.
6. J.D. Anderson, Jr., *Introduction to Flight*, 3rd edn., McGraw-Hill, Inc., 1989.
7. M.J. Kroes and T.W. Wild, Aircraft *Powerplants*, 7th edn., Glencoe/McGraw-Hill, 2002.
8. http://wright.nasa.gov/airplane/eng.html.
9. T.D. Crouch, *The Bishop's Boys : A Life of Wilbur and Orville Wright*, W. W. Norton & Company, April 17, 2003.
10. F.J. Malina, R.C. Truax, and A.D. Baxter, Historical development of jet propulsion. In: Lancaster, O.E. (ed.), *Part A of Jet Propulsion Engines*, Vol. XII of High Speed Aerodynamics and Jet Propulsion, C.D. Donaldson (ed.). Princeton, NJ: University Press.
11. H. von Ohain, 1979. The evolution and future of aeropropulsion systems. In: Boyne, W.J. and Lopez, D.S. (eds.), *The Jet Age*. Washington, DC: Smithsonian Institution Press, pp. 25–46.
12. H. von Ohain, *Face to Face*, AIAA Aerospace America, July 1990, pp. 8–9.
13. F.W. Whittle, *The Early History of the Whittle Jet Propulsion Gas Turbine*, IMechE Clayton Lecture, UK, October 5, 1945.
14. F.W. Whittle, 1979. The birth of jet engine in Britain. In: Boyne, W.J. and Lopez, D.S. (eds.), *The Jet Age*. Washington, DC: Smithsonian Institution Press, pp. 1–24.
15. B. Gunston, *The Development of Jet and Turbine Aero Engines*, Patrick Stephens Limited, imprint of Haynes Publishing, 1997.
16. C.D. Wilson and D.W. Riggins, Performance characterization of turboshaft engines: Work potential and second-law analysis, *58th Annual Forum of American Helicopter Society*, Montreal, Quebec, Canada, June 11–13, 2002.
17. M.J. Zucrow, *Aircraft and Missile Propulsion*, Vols. I and II, John Wiley & Son, Inc., 1958.
18. P.J. Mc Mahon, *Aircraft Propulsion*, Harper & Row, 1971.
19. P.J. Walterup, M.E. White, F. Zarlingo, and S. Garvlin, History of ramjet and scramjet propulsion development for U.S. Navy missiles, *John Hopkins APL Digest*, 18(2), 1997.
20. H.I.H. Saravanamuttoo, G.F.C. Rogers, and H. Cohen, *Gas Turbine Theory*, 5th edn., Prentice Hall, 2001.
21. http://www.geae.com/education/engines101.
22. R.D. Archer and M. Saarlas, *An Introduction to Aerospace Propulsion*, Prentice-Hall, Inc., 1996, p. 1.
23. G.P. Sutton, *Rocket Propulsion Elements—An Introduction to the Engineering of Rockets*, 5th edn., John Wiley & Sons, 1986, p. 1.
24. The Jet Engine, 5th edn., *Rolls Royce plc*, Reprinted 1996 with revisions, p. 3.
25. J.P. Hill and C. Peterson, *Mechanics and Thermodynamics of Propulsion*, 2nd edn., Addison Wesley Publication Company, Inc., 1992, p. 155.
26. F.E. Rom, Airbreathing nuclear propulsion—A new look, NASA TM X-2425, NASA, December 1971.
27. http://www.globalaircraft.org/planes/x-35_jsf.pl.
28. http://www.f22fighter.com/.
29. D. Logan, *Lockheed F-117 Nighthawks: A Stealth Fighter Roll Call*, Schiffer Publishing, Atglen, PA, 2009.
30. http://www.boeing.com/commercial/787family/.
31. http://www.airliners.net/info/stats.main?id=29.

32. http://www.globalsecurity.org/military/systems/aircraft/.
33. http://www.jetplanes.co.uk/.
34. http://www.pw.utc.com/prod_mil_f100.asp.
35. http://www.dfrc.nasa.gov/Gallery/Photo/index.html.
36. The future Now, Rolls Royce vcom 9362, April 2004.
37. Forecast International, *Aerospace, Defense, Electronics and Power Systems*, 2007.
38. J. Hale, Boeing 787 from the ground up, *Boeing Aero Magazine*, Issue 24 _Quarter 04, 2006.


Taylor & Francis
Taylor & Francis Group
http://taylorandfrancis.com

2

Performance Parameters of Jet Engines

2.1 Introduction

The designer of an aircraft engine must recognize the varying requirements for takeoff, climb, cruise, and maneuvering, the relative importance of these being different for civil and military applications and for long- and short-haul aircraft. In early aircraft, it was common practice to focus on the takeoff thrust. This is no longer adequate for later and present-day aircraft. For long-range civil transports like Boeing 747-8, 777-200 LR, and 777-300 ER, 787-8 and 787-9 Dreamliner, Airbus A340-500, A340-600, A380, A350-900 and A350-1000, the fuel consumption through some 10 or more flight hours is the dominant parameter. Military aircraft have numerous criteria: the rate of climb, maneuverability for fighters (some examples for the fifth generation: F-22 Raptor, Sukhoi Su-32, 34 and superjet 100, Chendu J-20 and Shenyang J-31), short takeoff distance for aircraft (F-35 series) operating from air carriers, and maximum ceilings for high-altitude reconnaissance aircraft like SR-71 Blackbird aircraft. For civil and military freighter airplanes (Airbus A400, Airbus Beluga, Boeing C-17, Lockheed Galaxy C-5, An 225, Il 76), the maximum payload is its main requirement.

In all types of aircraft, the engines are required to provide efficiently the thrust force necessary for their propelling during different flight phases and under different operating conditions, including the hottest/coldest ambient temperature, as well as rain, wind, and snow.

This chapter resembles a first window for performance of airbreathing engines. It starts by a derivation for the thrust force or the propelling force generated in the direction opposite to the flow of air entering the engine in accordance with Sir Isaac Newton's laws of motion. Consequently, all jet engines, including rocket motors, belong to the class of powerplants called *reaction engines*. It is the internal imbalance of forces within the gas turbine engines that gives the reaction engine its name. The propulsive force developed by a jet engine is the result of a complex series of actions and reactions that occur within the engine. These thrust constituents and the different factors affecting the thrust will be explained next. Some of these factors are related to the engine; others are related to the medium in which the engine operates.

The performance of jet engines is evaluated through the following efficiencies: propulsive, thermal, and overall. The propeller efficiency of turboprop engines is also evaluated. Fuel consumption is properly evaluated through a parameter identified as the thrust-specific fuel consumption (TSFC), which is the ratio of fuel flow rate into the engine to the generated thrust. Thus, different jet engines may be compared. The range of aircraft is a combined engine/aircraft parameter where the fuel consumption through the engine is coupled to the aircraft's lift and drag forces.

2.2 Thrust Force

Thrust force is the force responsible for propelling the aircraft in its different flight regimes.

Thrust, lift, drag, and weight represent the four forces that govern the aircraft motion. During the cruise phase of flight, when the aircraft is flying steadily at a constant speed and altitude, each pair of the four forces are in equilibrium—lift and weight as well as thrust and drag. During landing, thrust force is either fully or partially used in braking the aircraft by means of a thrust-reversing mechanism. The basic conservation laws of mass and momentum are used in their integral forms to derive an expression for thrust force.

Consider a schematic diagram (Figure 2.1) for an engine with a part of its pod installation (i.e., a structural support for hanging the engine to the wing). Next, define a control volume which control surface passes through the engine outlet (exhaust) plane (2) and extends far upstream at (1). The two side faces of the control volume are parallel to the flight velocity u. The upper surface side cuts the structural support while the lower one is far from the engine. The surface area at planes (1) and (2) are equal and denoted by A. The stream tube of air entering the engine has an area P_e at plane (1), while the exhaust area for gases leaving the engine is A_e. The velocity and pressure over plane (1) are u (which is the flight speed) and P_a (ambient pressure at this altitude). Over plane (2) the velocity and pressure are still u and P_a except over the exhaust area of the engine A_e which values will be u_e and P_e. The x and y directions employed here are chosen parallel and normal to the centerline of the engine.

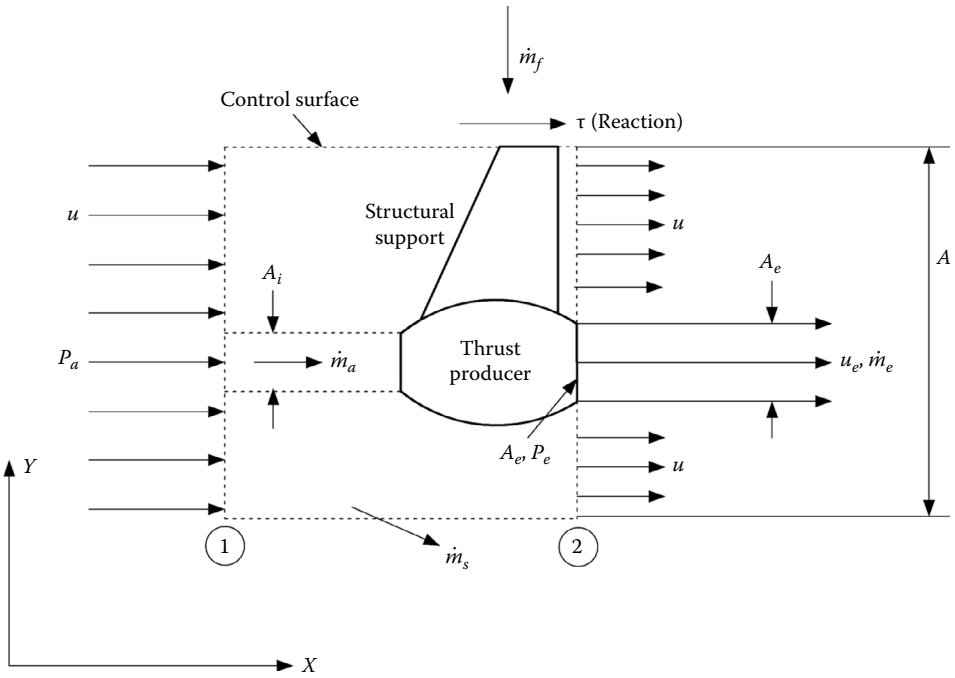


FIGURE 2.1
Thrust generated in an aeroengine.

The following assumptions are made:

1. The flow is steady within the control volume; thus, all the properties within the control do not change with time.
2. The external flow is reversible; thus, the pressures and velocities are constant over the control surface except over the exhaust area P_e of the engine.

Conservation of mass across the engine gives

$$\dot{m}_a + \dot{m}_f = \dot{m}_e$$

where $\dot{m}_a$ and $\dot{m}_e$ are the rate of mass flow of air entering the engine and exhaust gases leaving the engine, respectively, which are expressed as

$$\dot{m}_a = \rho u A_i, \quad \dot{m}_e = \rho_e u_e P_e$$

thus

$$\dot{m}_f = \rho_e u_e A_e - \rho u A_i \tag{2.1}$$

The fuel-to-air ratio is defined here as

$$f = \frac{\dot{m}_f}{\dot{m}_a}$$

Apply the continuity equation over the control volume

$$\frac{\partial}{\partial t}\iiint_{Cu} \rho \, d\upsilon + \oiint_{CS} \rho \bar{u} \cdot d\bar{A} = 0$$

For a steady flow, $\frac{\partial}{\partial t}\iiint_{Cu} \rho \, d\upsilon = 0$, then

$$\dot{m}_e + \dot{m}_s + \rho u\left(A - A_e\right) - \dot{m}_a - \dot{m}_f - \rho u\left(A - A_i\right) = 0$$

where $\dot{m}_s$ is the side air leaving the control volume.

Rearranging and applying Equation 2.1, we get the side mass flow rate as

$$\dot{m}_s = \rho u\left(A_e - A_i\right) \tag{2.2}$$

According to the momentum equation,

$$\sum \bar{F} = \frac{\partial}{\partial t}\iiint_{CS} \rho \bar{u} \, d\upsilon + \oiint_{CS} \bar{u}\left(\rho \bar{u} \cdot d\bar{A}\right)$$

where $\sum \bar{F}$ is the vector sum of all forces acting on the material within the control volume, which are surface forces (pressure force as well as the reaction to thrust force through the structural support denoted by τ) and the body force (which is the gravitational force here).

For steady flow,

$$\sum \bar{F} = \iint_{CS} \bar{u}\left(\rho \bar{u} \cdot d\bar{A}\right)$$

The x-component of the momentum equation

$$\sum F_x = \iint_{CS} u_x\left(\rho \bar{u} \cdot d\bar{A}\right) = \left(P_a - P_e\right)A_e + \tau \tag{a}$$

If the sides of the control volume are assumed sufficient distant from the engine, then the side mass flow rate leaves the control volume nearly in the x-direction.

$$\text{Now } \iint u_x\left(\rho \bar{u} \cdot d\bar{A}\right) = \dot{m}_e u_e + u\left[\rho u\left(A - P_e\right)\right] + \dot{m}_s u - \dot{m}_a u - u\left[\rho u\left(A - P_e\right)\right]$$
$$\therefore \iint u_x\left(\rho \bar{u} \cdot d\bar{A}\right) = \dot{m}_e u_e - \dot{m}_a u - \rho u^2\left(A_e - A_i\right) + \dot{m}_s u \tag{b}$$

with $\dot{m}_s = \rho u\left(A_e - A_i\right)$ (Equation 2.2)

$$\therefore \iint u_x(\rho \bar{u} \cdot d\bar{A}) = \dot{m}_e u_e - \dot{m}_a u$$

From Equations a and b, then

$$\dot{m}_e u_e - \dot{m}_a u = -\left(P_e - P_a\right)A_e + \tau$$
$$\therefore \tau = \dot{m}_a\left[\left(1+f\right)u_e - u\right] + \left(P_e - P_a\right)A_e \tag{2.3a}$$

where

τ is the net thrust
$\dot{m}_a\left[\left(1+f\right)u_e\right]$ is the momentum thrust
$(P_e - P_a)A_e$ is the pressure thrust
$\dot{m}_a\left[\left(1+f\right)u_e\right] + \left(P_e - P_a\right)A_e$ is the gross thrust
$\dot{m}_a u$ is the momentum drag

Equation 2.3a through c is then rewritten employing these definitions as

$$\text{Net thrust} = \text{Gross thrust} - \text{Momentum drag}$$

or

$$\text{Net thrust} = \text{Momentum thrust} + \text{Pressure thrust} - \text{Momentum drag}$$

If the nozzle is unchoked, then $P_e = P_a$, the pressure thrust cancels in Equation 2.3a. The thrust is then expressed as

$$\therefore \tau = \dot{m}_a \left[(1+f) u_e - u \right] \tag{2.3b}$$

In many cases, the fuel-to-air ratio is neglected in this equation and the thrust force equation is reduced to the simple form

$$\therefore \tau = \dot{m}_a (u_e - u) \tag{2.3c}$$

The thrust force in a turbojet engine attains high values as the exhaust speed is high and much greater than the air (flight) speed; $u_e/u \gg 1$. For turboprop engines, the high value of thrust is achieved by the very large quantity of the airflow rate, though the exhaust and flight speeds are very close.

In a similar way, the thrust force for two-stream engines like turbofan and propfan engines can be derived. It will be expressed as

$$\tau = \dot{m}_h \left[(1+f) u_{eh} - u \right] + \dot{m}_c (u_{ec} - u) + A_{eh} (P_{eh} - P_a) + A_{ec} (P_{ec} - P_a) \tag{2.4}$$

where

$f = \dot{m}_f / \dot{m}_h$ is the fuel-to-air ratio
$\dot{m}_h$ is the air mass flow passing through the hot section of engine (combustion chamber and turbine(s))
$\dot{m}_c$ is the air mass flow passing through the fan
u_{eh} is the velocity of hot gases leaving the turbine nozzle
u_{ec} is the velocity of cold air leaving the fan nozzle
P_{eh} is the exhaust pressure of the hot stream
P_{ec} is the exhaust pressure of the cold stream
A_{eh} is the exit area for the hot stream
A_{ec} is the exit area for the cold stream

The specific thrust is defined as the thrust per unit air mass flow rate ($T/\dot{m}_a$), which can be obtained from Equations 2.3a through c and 2.4. It has the dimensions of a velocity (say, m/s).

Example 2.1

Air flows through a jet engine at the rate of 30 kg/s and the fuel flow rate is 1 kg/s. The exhaust gases leave the jet nozzle with a relative velocity of 610 m/s. Pressure equilibrium exists over the exit plane. Compute the velocity of the airplane if the thrust power is 1.12×10^6 W.

Solution

The thrust force is expressed as

$$\tau = (\dot{m}_a + \dot{m}_f) u_e - \dot{m}_a u$$
$$\text{Thrust power} = t \times u$$

$$\text{Thrust power} = \left(\dot{m}_a + \dot{m}_f\right)u_e u - \dot{m}_a u^2$$
$$1.12\times10^6 = (31)(610)u - 30u^2$$
$$30u^2 - 18{,}910u + 1.12\times10^6 = 0$$

or

$$u = \frac{18{,}910 \pm 10^3\sqrt{357.588 - 134.4}}{60}$$

thus, either $u = 564.15$ m/s or $u = 66.17$ m/s.

Example 2.2

The idling turbojet engines of a landing airplane produce forward thrust when operating in a normal manner, but they can produce reverse thrust if the jet is properly deflected. Suppose that, while the aircraft rolls down the runway at 100 mph, the idling engine consumes air at 100 lb_m/s and produces an exhaust velocity of 450 ft/s.

1. What is the forward thrust of the engine?
2. What is the magnitude and direction (forward or reverse) if the exhaust is deflected 90° when the mass flow is kept constant?

Solution

Forward thrust has positive values and reverse thrust has negative values:

1. The flight speed is $U = 100\times1.4667 = 146.67$ ft/s.
   The thrust force represents the horizontal or the x-component of the momentum equation

$$T = \dot{m}_a\left(U_e - U\right)$$
$$T = \left(100\ \text{lb}_m/\text{s}\right)\times\left(450 - 146.67\right)\text{ft/s}\times\frac{1}{32.2}$$
$$T = 942\ \text{lb}_f$$

2. Since the exhaust velocity is now vertical due to thrust reverse application, then it has a zero horizontal component; thus, the thrust equation is

$$T = \dot{m}_a\left(U_e - U\right)$$
$$T = \frac{100}{32.2}\times\left(0 - 146.67\right)$$
$$T = -455.5\ \text{lb}_f\ \ (\text{reverse})$$

Example 2.3

It is required to calculate and plot the momentum drag as well as momentum, pressure, gross, and net thrusts versus the flight speed for a turbojet engine powering an aircraft flying at an altitude of 9 km (ambient temperature and pressure are 229.74 K and 30.8 kPa) and having the following characteristics: $A_i = 0.235$ m^2, $A_e = 0.25$ m^2, $f = 0.02$, $P_e = 200$ kPa, and $U_e = 600$ m/s.

The flight speed varies from 500 to 6000 km/h. Two cases are to be considered:

1. The air mass flow rate is constant and equal to 40 kg/s irrespective of the variation of flight speed.
2. The mass flow rate varies with the flight speed.

Solution

Case (*1*): The mass flow rate is constant and equal to 40 kg/s.

The momentum thrust ($T_{momentum}$) is constant and given by the relation

$$T_{momentum} = \dot{m}_a (1+f) U_e = 40 \times 1.02 \times 600 = 24,480 \text{ N}$$

The pressure thrust ($T_{pressure}$) is also constant and calculated as

$$T_{pressure} = A_e \times (P_e - P_a) = 0.25 \times (200 - 30.8) \times 10^3 = 42,300 \text{ N}$$

The gross thrust (T_{gross}) is constant and equal to the sum of momentum and pressure thrusts

$$T_{gross} = T_{momentum} + T_{pressure} = 66,780 \text{ N}$$

The momentum drag for flight speed varying from 500 to 6000 km/h is given by the relation

$$D_{momentum} = \dot{m}_a U = 40 \,(\text{kg/s}) \times \frac{U\,(\text{km/h})}{3.6} = 11.11 \times U \;(\text{N})$$

which is a linear relation in the flight speed U.

The net thrust is then

$$T_{net} = T_{gross} - D_{momentum} = 66,780 - 11.11 \times U \;(\text{N})$$

The net thrust varies linearly with the flight speed. The results are plotted in Figure 2.2. The net thrust must be greater than the total aircraft drag force during acceleration and equal to the drag at steady cruise flight. Zero net thrust results from the intersection of the gross thrust and ram drag.

Case (*2*): The mass flow rate varies linearly with the flight speed according to the relation

$$\dot{m}_a = \rho_a U A_i = \frac{P_a}{RT_a} U A_i = \frac{30.8 \times 10^3}{287 \times 229.74} \times \frac{U}{3.6} \times 0.235 \;(\text{kg/s})$$

$$\dot{m}_a = 0.03049 \times U \;(\text{kg/s})$$

The momentum thrust varies linearly with the flight speed as per the relation

$$T_{momentum} = \dot{m}_a (1+f) U_e = 0.03049 \times U \times 1.02 \times 600 = 18.66 \times U \;(\text{N})$$

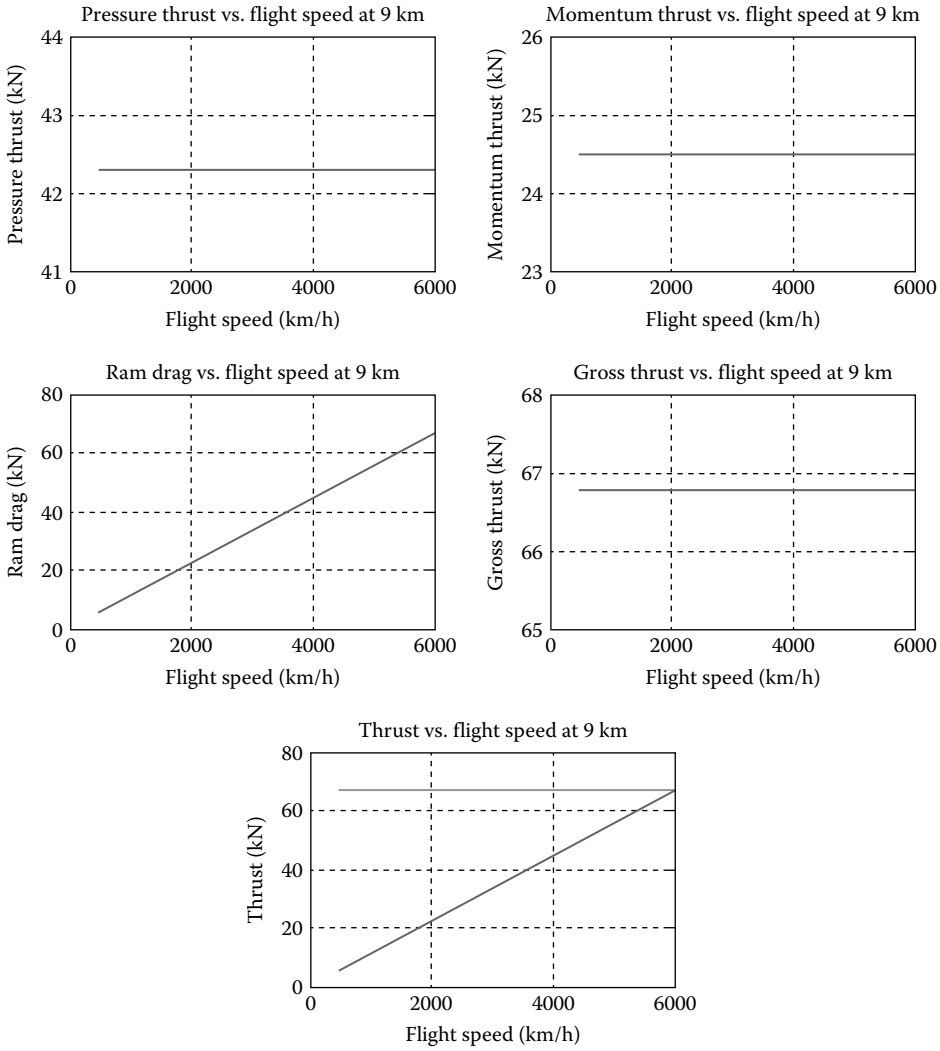


FIGURE 2.2
Thrust variations with constant mass flow rate.

The pressure thrust is constant and has the same value as in case (1)

$$T_{pressure} = A_e \times \left(P_e - P_a\right) = 0.25 \times \left(200 - 30.8\right) \times 10^3 = 42{,}300 \text{ N}$$

The gross thrust is varying linearly with the flight speed

$$T_{gross} = T_{momentum} + T_{pressure} = 18.66 \times U + 42{,}300 \ \left(\text{N}\right)$$

The momentum drag for flight speed varying from 500 to 6000 km/h is given by the relation

$$D_{momentum} = \dot{m}_a U = 0.03049 \times U\left(\text{kg/s}\right) \times \frac{U\left(\text{km/h}\right)}{3.6} = 8.47 \times 10^{-3} \times U^2 \ \left(\text{N}\right)$$

which is a quadratic relation in the flight speed U.

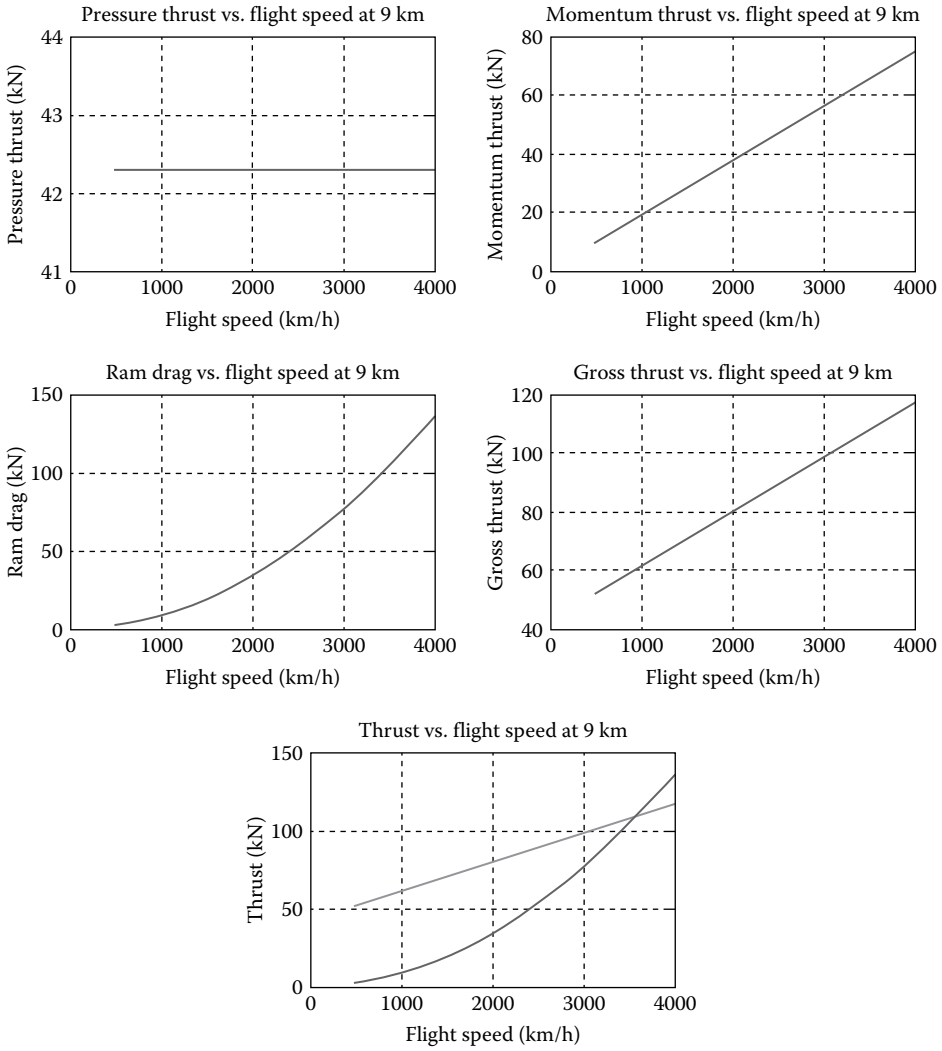


FIGURE 2.3
Thrust variations with variable mass flow rate.

The net thrust is then

$$T_{net} = T_{gross} - D_{momentum} = 42,300 + 18.66 \times U - 8.47 \times 10^{-3} \times U^2 \ \text{(N)}$$

These relations are plotted in Figure 2.2.

The same procedure is followed for case (2) for different altitudes starting from 3 to 15 km at 3 km intervals. The results are plotted in Figure 2.3.

Example 2.4

The shown diagram illustrates a typical single-spool axial-flow turbojet engine. It is required to calculate the distribution of the thrust force for each component (compressor, diffuser, combustion chamber, turbine, jet pipe, and nozzle).

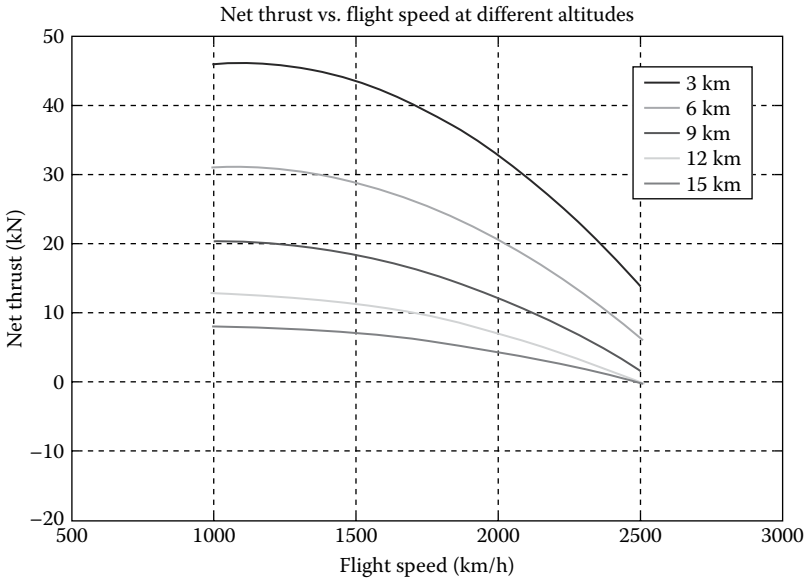


FIGURE 2.4
Thrust variations with variable mass flow rate at altitudes 3, 6, 9, 12, and 15 km.

Prove that the sum of these thrust forces is equal to the thrust force developed by the engine using the usual thrust force equation (Figure E2.1).

	Compressor	Diffuser	Combustion Chamber	Turbine	Jet Pipe	Nozzle
Outlet area (m^2)	0.117	0.132	0.374	0.310	0.420	0.214
Outlet velocity (m/s)	124	112	94	271	196	584
Outlet gage pressure (kPa)	648	655	641	145	145	41
Mass flow rate (kg/s)	69.4	69.4	69.4	69.4	69.4	69.4

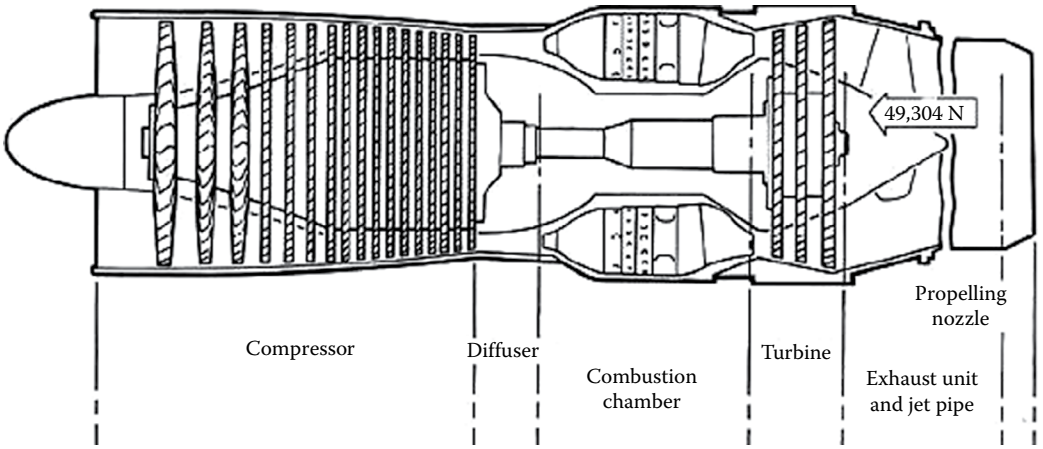


FIGURE E2.1
Modules of a typical single-spool turbojet engine.

Solution

This example illustrates how the thrust is generated from the unbalance forces and momentum created within the engine itself. For simple one-dimensional steady flow through an engine or any of its modules [1], the thrust force can be expressed as

$$\text{Thrust} = (PA)_e - (PA)_i + (\dot{m}U)_e - (\dot{m}U)_i$$

Neglecting the fuel mass flow rate, then this relation is reduced to the following formula:

$$\text{Thrust} = P_e A_e - P_i A_i + \dot{m}(U_e - U_i)$$

where U_e and P_e are the velocity and pressure at the exit of each component, while U_i and P_i are the velocity and pressure at the inlet to this component. Now this equation is applied to different components.

Compressor:

$$\begin{aligned} T_{comp} &= 648 \times 10^3 \times 0.117 + 69.4(124 - 0) \\ &= 75,816 + 8,605 \\ T_{comp} &= 84,421 \text{ N} \end{aligned}$$

Since the value is positive, then its direction is forward.

$$\begin{aligned} T_{diffueser} &= 655 \times 10^3 \times 0.132 - 648 \times 10^3 \times 0.117 + 69.4 \times 112 - 69.4 \times 124 \\ &= 86,460 + 7,773 - 84,421 \\ T_{diffueser} &= 9,812 \text{ N} \end{aligned}$$

Since the value is positive, then its direction is forward.

$$\begin{aligned} T_{CC} &= 641 \times 10^3 \times 0.374 + 69.4 \times 94 - 9,423^2 \\ &= 246,257 - 9,423^2 \\ T_{CC} &= 152,025 \text{ N} \end{aligned}$$

Since the value is positive, then its direction is forward.

Turbine assembly:

$$\begin{aligned} T_{Turbine} &= 145 \times 10^3 \times 0.31 - 69.4 \times 271 - 236,446 \\ &= 63,757 - 246,257 \\ T_{Turbine} &= -182,500 \text{ N} \end{aligned}$$

Since the value is negative, then its direction is rearward.

$$\begin{aligned} T_{Tailpipe} &= 145 \times 10^3 \times 0.42 + 69.4 \times 196 \\ &= 74,502 + 63,757 \\ T_{Tailpipe} &= 10,745 \text{ N} \end{aligned}$$

Since the value is positive, then its direction is forward.
Nozzle:

$$T_{Nozzle} = 4\times10^3\times0.214 + 69.4\times584 - 74,502$$
$$= 49,303 - 74,502$$
$$T_{Nozzle} = -25,118 \text{ N}$$

Since the value is negative, then its direction is rearward.

	Forward	Rearward
Force	84,421	−182,500
	9,811	−25,198
	152,025	
	10,745	
Total	257,002	−207,698

$$\text{Total thrust} = 49,304 \text{ N}$$

The magnitude and direction of the thrust forces generated at different components are plotted on the modules as shown in Figure E2.2.
Engine thrust equation:

$$T = \left(P_e - P_a\right)A_e + \dot{m}U_e$$
$$T = P_{e_{gage}}\times A_e + \dot{m}U_e$$
$$T = 41\times10^3\times0.214 + 69.4\times584$$
$$T = 49,304 \text{ N}$$

Equal values for the thrust force are obtained from the summation of the thrust forces generated at different elements and the general formula for the engine as a whole.

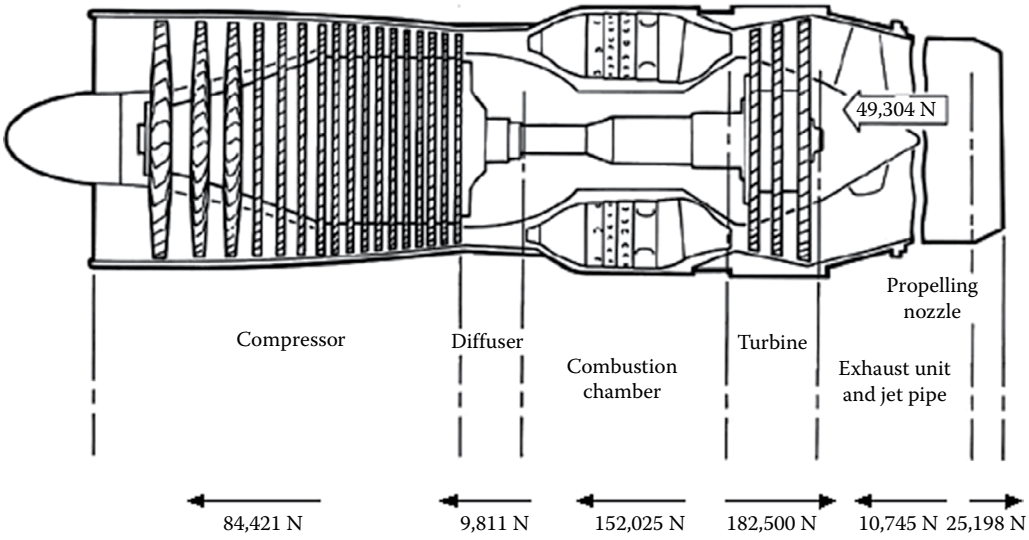


FIGURE E2.2
Thrust distribution across different modules of the engine. (Reproduced from Rolls-Royce plc, Copyright Rolls-Royce plc, 2016. With permission.)

2.3 Factors Affecting Thrust

As seen from Equation 2.3a through c, the thrust force of a single-stream aeroengine (ramjet or turbojet engine) depends on the inlet and outlet mass flow rates, fuel-to-air ratio, flight speed, exhaust speed, and exhaust pressure. Though it looked like a simple task to identify the factors listed earlier, each of them is dependent on several parameters. For example, the inlet air mass flow rate influencing both of the momentum thrust and momentum drag is dependent on several variables including the flight speed, ambient temperature and pressure, humidity, altitude, and rotational speed of the compressor. The outlet gas mass flow rate is dependent on the fuel added, air bleed, and water injection. The pressure thrust term depends on the turbine inlet temperature, flight altitude, and nozzle outlet area and pressure. The momentum thrust is also dependent on the jet nozzle velocity. These parameters [2] are further explained next.

2.3.1 Jet Nozzle

The outlet area and pressure of the exhaust nozzle affect the net thrust. The nozzle is either of the convergent or convergent–divergent type. Convergent nozzles may be choked or unchoked. For a choked convergent nozzle, the speed of the exhaust gases is equal to the sonic speed, which is mainly influenced by the exhaust gas temperature. The exhaust pressure for a choked nozzle is greater than the ambient pressure and thus the pressure thrust has a nonzero value. The pressure thrust depends on both the area of the exhaust nozzle and the difference between the exit and ambient pressures. If the nozzle is unchoked, then the jet velocity varies with the atmospheric pressure. The exhaust pressure is equal to the ambient pressure, and the pressure thrust is zero.

2.3.2 Airspeed

The airspeed, sometimes denoted as the approach speed, is equal to the flight speed in the thrust force (Equation 2.3a through c) derived from the control volume in Figure 2.1. Such a parameter has a direct effect on the net thrust. If the exhaust gas velocity is constant and the air velocity is increased, then the difference between both velocities $[(1+f)u_e - u]$ is decreased, leading to a decrease also in the net thrust. If the air mass flow and the fuel-to-air ratio are assumed constants, then a linear decrease in the net thrust is enhanced (Figure 2.5).

2.3.3 Mass Airflow

The mass airflow $\dot{m}_a$ is the most significant parameter in the thrust equation. It depends on the air temperature and pressure as both together determine the density of the air entering the engine. In free air, a rise in temperature will decrease the density. Thus, as the temperature increases, the thrust decreases. On the other hand, an increase in the pressure of free air increases its density and, consequently, its thrust increases. The effect of both of air temperature and pressure is illustrated in Figure 2.6. In brief, the density affects the inlet air mass flow and it directly affects thrust. A 10,000 lb thrust engine, for instance, might generate only about 8,000 lb of thrust on a hot day, while on a cold day this same engine might produce 12,000 lb of thrust.

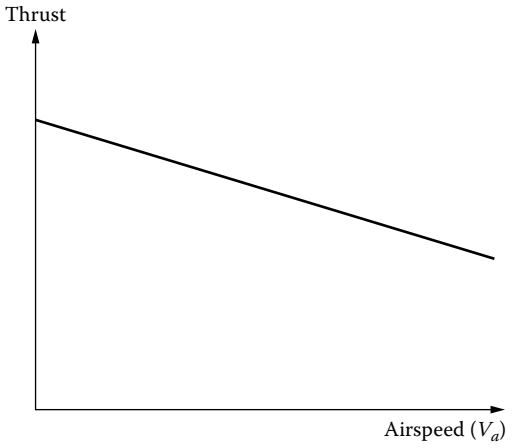


FIGURE 2.5
Variation of thrust force with airspeed.

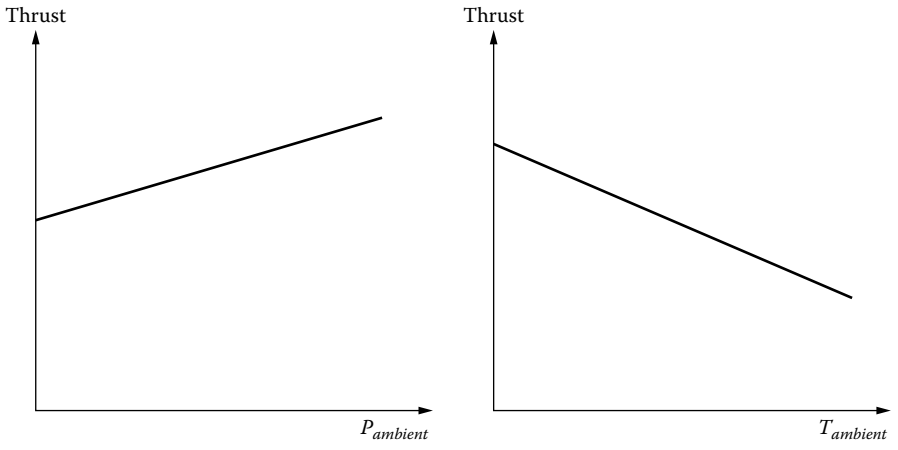


FIGURE 2.6
Variation of the thrust force with air temperature and pressure.

2.3.4 Altitude

As outlined earlier, the air temperature and pressure have significant effects on the thrust. Thus, we need to know how the ambient temperature and pressure vary with height above the sea level. The variation depends to some extent upon the season and latitude. However, it is usual to work with the "standard" atmosphere. The International Standard Atmosphere (ISA) corresponds to average values at middling latitudes and yields a temperature decreasing by about 3.2 K/500 m of altitude up to nearly 11,000 m (36,089 ft). The variations of ambient temperature and pressure are given by the following relations:

$$T(\mathrm{K}) = 288 - 0.0065 \times z$$
$$P(\mathrm{bar}) = 1.01325 - 0.000112 \times z + 3.8e^{-9} \times z$$

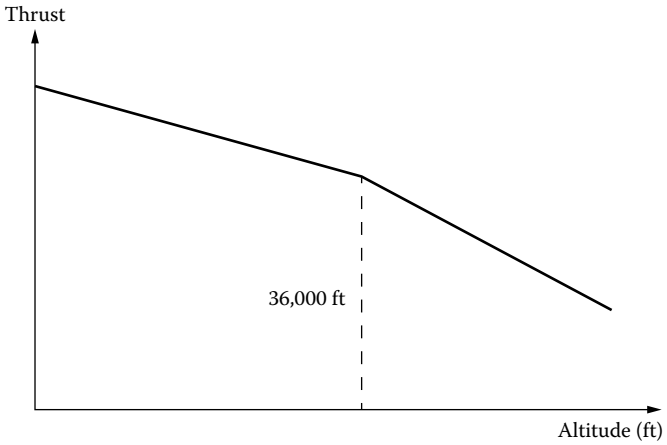


FIGURE 2.7
Variation of the thrust force with altitude.

After 11,000 m the temperature stops falling, but the pressure continues to drop steadily with increasing altitude. Consequently, above 11,000 m (36,089 ft) the thrust will drop off more rapidly (Figure 2.7). This makes 11,000 m the optimum altitude for long-range cruising at nominal speed, just prior to the rapidly increased effect of altitude on thrust. It may be concluded that the effect of altitude on thrust is really a function of density.

2.3.5 Ram Effect

The movement of the aircraft relative to the outside air causes air to be rammed into the engine inlet duct. Ram effect increases the airflow to the engine, which, in turn, means more gross thrust. However, it is not that simple; ram effects combine two factors, namely, the air speed increases and at the same time the pressure of the air and the airflow into the engine increases. As described earlier, the increase of airspeed reduces the thrust, which is sketched in Figure 2.8 as the "A" curve. The increase of the airflow will increase the thrust, which is sketched by the "B" curve in the same figure. The "C" curve is the result of combining curves "A" and "B." The increase of thrust due to ram becomes significant as the airspeed increases, which will compensate for the loss in thrust due to the reduced pressure at high altitude. Ram effect is thus important in high-speed fighter aircraft. Also, modern subsonic jet-powered aircraft fly at high subsonic speeds and higher altitudes to make use of the ram effect.

Finally, it is fruitful to classify the factors affecting thrust into two groups [3]:

1. Factors related to the engine
2. Factors related to the surrounding medium

The first group includes

1. The rotational speed (rpm), which influences both the compressor pressure ratio and the turbine work
2. Exhaust nozzle size, which influences the jet velocity

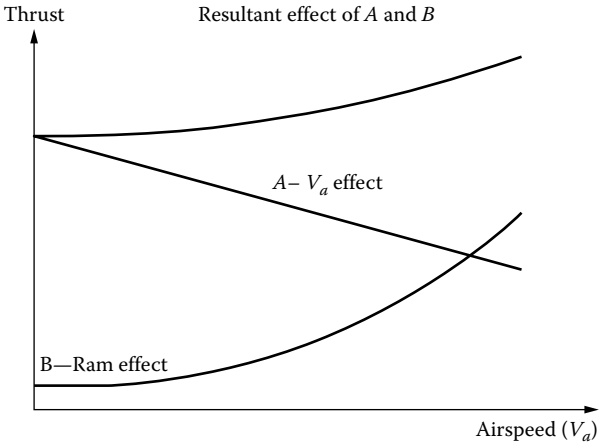


FIGURE 2.8
Effect of ram pressure on thrust.

3. Fuel flow rate and turbine inlet temperature, which affect the combustor heat generation
4. Compressor bleed flow, water injection, and components, performance, which lead to increase of the specific work

Thus, the first group contributes to both the air mass flow rate and jet velocity.
The second group includes

1. Forward (air) speed, which leads to thrust decrease and more fuel consumption
2. Air density (influenced by the flight altitude, humidity, hot/cold day), which influences the airflow leading to a thrust decreased if the airflow is increased and vice versa

2.4 Engine Performance Parameters

The performance of an aircraft engine may be criticized according to its ability to provide the necessary thrust force needed in propelling an aircraft efficiently in its different flight regimes.
The engine performance parameters are identified as

1. Propulsive efficiency
2. Thermal efficiency
3. Propeller efficiency
4. Overall efficiency
5. Takeoff thrust
6. Specific fuel consumption
7. Aircraft range

Military aircraft are powered by engines that fulfill their mission requirements. For this reason, the takeoff thrust and maneuverability are the critical issues, with some sacrifice of fuel consumption in some types such as fighters and interceptors. For civil transports, specific fuel consumption and the aircraft range are the critical design issues. In both types, several efficiencies related to the conversion of heat generated by fuel burning into thrust force are important.

2.4.1 Propulsive Efficiency

Propulsive efficiency is the conversion of the kinetic energy of air when it passes through the engine into a propulsive power. It is identified by manufacturers of aeroengines as an external efficiency. It is influenced by the amount of the energy wasted in the propelling nozzle(s) and denoted by (η_p).

It is defined as

$$\eta_p = \frac{\text{Thrust power}}{\text{Power imparted to engine airflow}} \tag{2.5a}$$

or simply

$$\eta_p = \frac{\text{Thrust power}}{\text{Thrust power} + \text{power wasted in the exhaust}} \tag{2.5b}$$

which will be denoted here as the *first* expression for the propulsive efficiency.

Another definition used in many texts is

$$\eta_p = \frac{\text{Thrust power}}{\text{Rate of kinetic energy added to engine airflow}} \tag{2.6}$$

This will be referred to as the *second* expression.

For *ramjet*, *scramjet*, and *turbojet* engines, the first expression has the form

$$\eta_p = \frac{uT}{uT + \frac{1}{2}\dot{m}_e\left(u_e - u\right)^2} \tag{2.7a}$$

$$\eta_p = \frac{u\left\{\dot{m}_a\left[\left(1+f\right)u_e - u\right] + A_e\left(P_e - P_a\right)\right\}}{u\left\{\dot{m}_a\left[\left(1+f\right)u_e - u\right] + A_e\left(P_e - P_a\right)\right\} + \frac{1}{2}\dot{m}_a\left(1+f\right)\left(u_e - u\right)^2} \tag{2.7b}$$

This expression is normally used by manufacturers of aeroengines [2–5], as well as some texts [6,7]. The second expression, adopted by other authors [8,9], is expressed as

$$\eta_p = \frac{2uT}{\dot{m}_a\left[\left(1+f\right)u_e^2 - u^2\right]} \tag{2.8a}$$

$$\eta_p = \frac{2u\left\{\dot{m}_a\left[\left(1+f\right)u_e - u\right] + A_e\left(P_e - P_a\right)\right\}}{\dot{m}_a\left[\left(1+f\right)u_e^2 - u^2\right]} \tag{2.8b}$$

The two expressions are identical if the nozzle is unchoked ($P_e = P_a$) and the fuel-to-air ratio (f) is negligible. Under such conditions, the following *third* expression is obtained:

$$\eta_p = \frac{2u}{u + u_e} = \frac{2}{1 + (u_e/u)} \tag{2.9}$$

Considering Equations 2.3c and 2.9, it is important to note that

1. If the exhaust speed is much greater than the air (flight) speed, $u_e \gg u$, then the thrust force $T \to$ maximum, $\eta_p \to 0$.

   This case represents the takeoff condition where $u = 0$.
2. If the exhaust speed is nearly equal to the flight speed, $u_e/u \approx 1$, then the thrust force $T \to 0$, $\eta_p \to$ maximum (100%).

For this reason, turboprop engines have higher propulsive efficiency compared to turbojet engines, as in the former the exhaust speed is close to the flight speed, while for turbojet engines, the exhaust speed is much higher than the flight speed.

For bypass engines (turbofan and propfan), the air coming into the engine is split into two streams: the first passes through the fan/propfan, and is known as the cold stream, while the other passes through the engine core—compressor, combustion chamber, and subsequent modules—and is known as the hot stream. Applying the same principle and employing the first expression, we get the following form:

$$\eta_p = \frac{u(T_h + T_c)}{u(T_h + T_c) + W_h + W_c} \tag{2.10a}$$

where

T_h and T_c are the thrust force generated by the hot and cold streams, respectively
W_h and W_c are the wake losses of the hot and cold streams, respectively

Their values are expressed as

$$T_h = \dot{m}_h\left[(1+f)u_{eh} - u\right] + A_{eh}(P_{eh} - P_a)$$
$$T_c = \dot{m}_c\left[u_{ec} - u\right] + A_{ec}(P_{ec} - P_a)$$
$$W_h = \frac{1}{2}\dot{m}_h(1+f)(u_{eh} - u)^2 = \frac{1}{2}\dot{m}_{eh}(u_{eh} - u)^2$$
$$W_c = \frac{1}{2}\dot{m}_c(u_{ec} - u)^2$$

where

$$\dot{m}_{eh} = (1+f)\dot{m}_h$$

This relation can also be written as

$$\eta_p = \frac{Tu}{Tu + 0.5\left\{\dot{m}_{eh}(u_{eh} - u)^2 + \dot{m}_c(u_{ec} - u)^2\right\}} \tag{2.10b}$$

this is the first expression for the propulsive efficiency in turbofan engine.

The *second* expression (Equation 2.6) can be also written using the two hot and cold streams:

$$\eta_p = \frac{2uT}{\dot{m}_h\left\{(1+f)u_{eh}^2 + \beta u_{ec}^2 - (1+\beta)u^2\right\}} \tag{2.11a}$$

When the two nozzles of the hot and cold streams are unchoked and the fuel-to-air ratio (f) is negligible, both expressions yield the following expression:

$$\eta_p = \frac{2u\left[u_{eh} + \beta u_{ec} - (1+\beta)u\right]}{u_{eh}^2 + \beta u_{ec}^2 - (1+\beta)u^2} \tag{2.11b}$$

where (β) is the bypass ratio (BPR), which is the ratio between the mass flow rates of the cold air and hot air, or $\beta = \dot{m}_c / \dot{m}_h$.

For turbofan engines, the simple relation expressed by Equation 2.9 cannot be applied.

The propulsive efficiency for turboprop, turbojet, and turbofan engines is illustrated in Figure 2.9. Figure 2.10 illustrates the propulsive efficiency for single and contrarotating propfan engines.

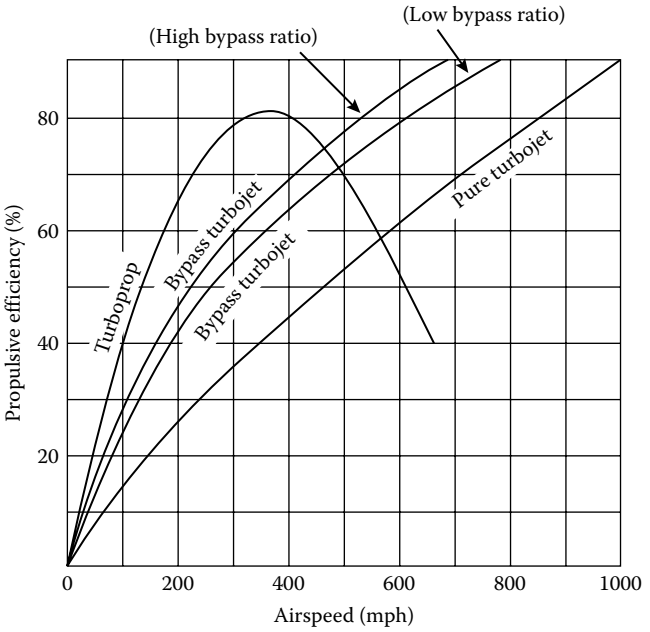


FIGURE 2.9
Propulsive efficiency for turboprop, turbojet, and turbofan engines. (Reproduced from Rolls-Royce plc, Copyright Rolls-Royce plc, 2016. With permission.)

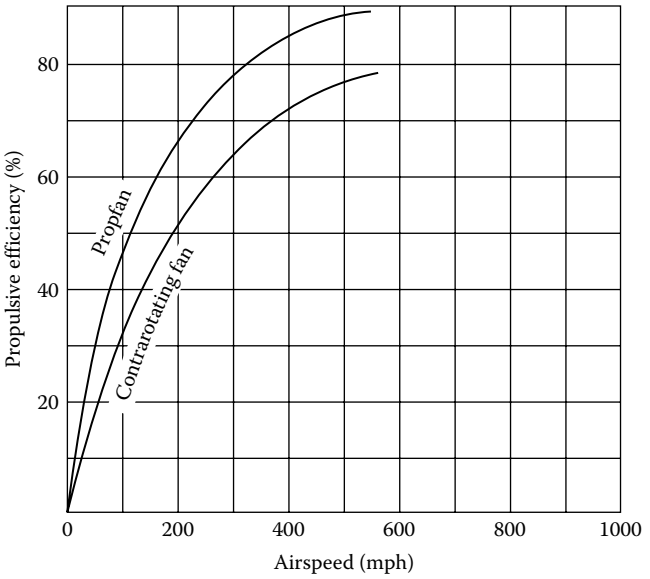


FIGURE 2.10
Propulsive efficiency for single and contrarotating propfan engines. (Reproduced from Rolls-Royce plc, Copyright Rolls-Royce plc, 2016. With permission.)

Example 2.5

A turbojet engine is powering a fighter airplane. Its cruise altitude and Mach number are 10 km and 0.8, respectively. The exhaust gases leave the nozzle at a speed of 570 m/s and a pressure of 0.67 bar. The exhaust nozzle is characterized by the ratio $A_e/\dot{m}_a = 0.006\ \text{m}^2 \cdot \text{s/kg}$. The fuel-to-air ratio is 0.02.

It is required to calculate

1. The specific thrust $(T/\dot{m}_a)$
2. The propulsive efficiency using the different expressions defined earlier

Solution

1. At altitude 10 km, the ambient temperature and pressure are

$$T_a = 223.3\ \text{K} \quad \text{and} \quad P_a = 0.265 \quad \text{bar}$$

The flight speed $u = M\sqrt{\gamma R T_a} = 239.6$ m/s.

From Equation 2.3a through c, the specific thrust is

$$\frac{T}{\dot{m}_a} = \left[\left(1+f\right)u_e - u\right] + \left(P_e - P_a\right)\frac{p_e}{\dot{m}_a}$$

$$\frac{T}{\dot{m}_a} = \left(1.02 \times 570 - 239.6\right) + 0.006 \times \left(0.67 - 0.265\right) \times 10^5$$

Then

$$\frac{T}{\dot{m}_a} = 584.77\ \text{N} \cdot \text{s/kg}$$

2. The propulsive efficiency is calculated using the different expressions. The first expression given by Equation 2.7a can be rewritten as

$$\eta_p = \frac{2\left(T/\dot{m}_a\right)u}{2\left(T/\dot{m}_a\right)u + \left(1+f\right)\left(u_e - u\right)^2}$$

Substitution will give

$$\eta_p = \frac{2\times 584.77\times 239.6}{2\times 584.77\times 239.6 + 1.02\times\left(570-239.6\right)^2} = 0.7156 = 71.56\%$$

Next, the second expression given by Equation 2.8a and b can be rewritten as

$$\eta_p = \frac{2\left(T/\dot{m}_a\right)u}{\left(1+f\right)u_e^2 - u^2}$$

which by substitution gives

$$\eta_p = \frac{2\times 584.77\times 239.6}{\left(1.02\right)\times\left(570\right)^2 - \left(239.6\right)^2} = 1.022 = 102.2\%$$

This value assures that this expression must *not* be used if the nozzle is choked. Finally, using the third expression given by Equation 2.9 gives

$$\eta_p = \frac{2u}{u_e + u} = 0.5918 = 59.18\%$$

Though this expression is simple, it gives a very rough estimate of the propulsive efficiency.

Example 2.6

A turbofan engine is powering an aircraft flying at Mach number 0.9, at an altitude of 33,000 ft, where the ambient temperature and pressure are –50.4° and 26.2 kPa. The engine BPR is 3, and the hot airflow passing through the engine core is 22.7 kg/s. Preliminary analysis provided the following results:

$$\text{Fuel-to-air ratio } f = 0.015$$

$$P_{ec} = 55.26 \text{ kPa}, \quad u_{ec} = 339.7 \text{ m/s}, \quad A_{ec} = 0.299 \text{ m}^2$$
$$P_{eh} = 32.56 \text{ kPa}, \quad u_{eh} = 452 \text{ m/s}, \quad A_{eh} = 0.229 \text{ m}^2$$

Calculate the thrust force and the propulsive efficiency using the first and second expressions.

Solution

From the given data, it is clear that both nozzles are choked since their exit pressures are higher than the ambient pressure of the flight altitude.

The flight speed is

$$u = M\sqrt{\gamma RT_a} = 269.2 \text{ m/s}$$

The cold airflow $\dot{m}_c = 3 \times 22.7 = 68.1$ m/s.

Fuel flow rate $\dot{m}_f = f \times \dot{m}_h = 0.015 \times 22.7 = 0.3405$ kg/s.

The hot exhaust flow rate $= \dot{m}_h + \dot{m}_f = 23.04$ kg/s.

The thrust force is calculated from the relation

$$\begin{aligned} T &= \dot{m}_h\left[(1+f)u_{eh} - u\right] + \dot{m}_c\left(u_{ec} - u\right) + A_{eh}\left(P_{eh} - P_a\right) + A_{ec}\left(P_{ec} - P_a\right) \\ &= (22.7)\left[(1.015)(452.1) - 269.2\right] + (68.1)\left[339.72 - 269.2\right] \\ &\quad + (0.229)\left[32.56 - 26.2\right]\times 10^3 + (0.299)\left[55.267 - 26.2\right]\times 10^3 \\ T &= 19.257 \text{ kN} \end{aligned}$$

The first expression for the propulsive efficiency (Equation 2.10b) is

$$\eta_p = \frac{Tu}{Tu + 0.5\left\{\dot{m}_{eh}\left(u_{eh} - u\right)^2 + \dot{m}_c\left(u_{ec} - u\right)^2\right\}} = 0.9032 = 90.32\%$$

The second expression for choked nozzle is given by Equation 2.11a:

$$\eta_p = \frac{2uT}{\dot{m}_h\left\{(1+f)u_{eh}^2 + \beta u_{ec}^2 - (1+\beta)u^2\right\}} = 1.7304 = 170.04\%$$

Comment: As demonstrated in Examples 2.5 and 2.6, the second expression for the propulsive efficiency provides efficiencies greater than unity. Such an astonishing value of a propulsive efficiency greater than unity can be overcome if the effective jet velocity proposed in [6,10] is employed. The proposed effective jet velocity is expressed as

$$u_e' = u_e + \left(P_e - P_a\right)\frac{P_e}{\dot{m}_e}$$

Such an effective jet velocity means that a full expansion of the gases to the ambient pressure is assumed. In such a case, the second expression for the propulsive efficiency will be exactly equal to the first expression. This effective velocity was also employed by Rolls-Royce [4]. The effective jet velocity is identified by aeroengine manufacturers as the fully expanded jet velocity (in the exhaust plume).

2.4.2 Thermal Efficiency

Thermal efficiency is the efficiency of energy conversion within the powerplant itself. So, it is considered as an internal efficiency while the propulsive efficiency resembles an external efficiency as stated earlier. Thermal efficiency is denoted by (η_{th}). Two forms for such efficiency are defined for the following two groups of engines identified in Sections 2.4.2.1 and 2.4.2.2.

2.4.2.1 Ramjet, Scramjet, Turbojet, and Turbofan Engines

$$\eta_{th} = \frac{\text{Power imparted to engine airflow}}{\text{Rate of energy supplied in the fuel}} \tag{2.12}$$

It is easy to note that the denominator in Equation 2.5a is equal to the numerator in Equation 2.12.

For a *ramjet* and *turbojet* engine: Using the first expression for the propulsive efficiency, the following expression for (η_{th}) is obtained:

$$\eta_{th} = \frac{Tu + \frac{1}{2}\dot{m}_a(1+f)(u_e - u)^2}{\dot{m}_f Q_R} \tag{2.13}$$

where (Q_R) is the heat of reaction of the fuel used. Other names for Q_R are the calorific value of fuel [8] or the lower heating value (LHV) [3]. It is also alternatively written as Q_{HV}.

Assuming an unchoked nozzle, then

$$\begin{aligned} \dot{W}_{out} &= \frac{1}{2}\left[(\dot{m}_a + \dot{m}_f)U_e^2 - \dot{m}_a U^2\right] \\ \eta_{th} &= \frac{\frac{1}{2}\left[(\dot{m}_a + \dot{m}_f)U_e^2 - \dot{m}_a U^2\right]}{\dot{m}_f Q_R} \\ \eta_{th} &= \frac{\left[(1+f)U_e^2 - U^2\right]}{2fQ_R} \end{aligned} \tag{2.14a}$$

For an unchoked nozzle and negligible (f), then

$$\eta_{th} = \frac{u_e^2 - u^2}{2fQ_R} \tag{2.14b}$$

For a two-stream engine (turbofan and propfan), the following expression is employed:

$$\eta_{th} = \frac{Tu + \frac{1}{2}\dot{m}_h(1+f)(u_{eh} - u)^2 + \frac{1}{2}\dot{m}_c(u_{ec} - u)^2}{\dot{m}_f Q_R} \tag{2.15}$$

Similarly, assuming unchoked nozzles and negligible (f), we get

$$\eta_{th} = \frac{u_{eh}^2 + \beta u_{ec}^2 - (1+\beta)u^2}{2fQ_R} \tag{2.16}$$

2.4.2.2 Turboprop and Turboshaft Engines

The output of a turboprop or turboshaft engine is largely a shaft power. In this case, thermal efficiency is defined as

$$\eta_{th} = \frac{SP}{\dot{m}_f Q_R} \tag{2.17}$$

where (SP) is the shaft power.

2.4.3 Propeller Efficiency

Propellers are used in two types of aeroengines: piston and turboprop. In both cases, shaft power is converted to thrust power. Propeller efficiency (η_{pr}) is defined as the ratio of the thrust power generated by the propeller ($TP \equiv uT_{pr}$) to the shaft power (SP):

$$\eta_{pr} = \frac{TP}{SP} = \frac{uT_{pr}}{SP} \tag{2.18}$$

when an appreciable amount of thrust is obtained from the exhaust gases T_e in a turboprop engine, an equivalent thrust power (ETP) is expressed in terms of the shaft power, propeller efficiency, and exhaust thrust power; thus,

$$ETP = (SP) \times \eta_{pr} + T_e u \tag{2.19a}$$

Alternatively, an equivalent shaft power is used instead of the equivalent thrust power. They are related to each other by the relation where

$$ESP = \frac{ETP}{\eta_{pr}} = SP + \frac{T_e u}{\eta_{pr}} \tag{2.19b}$$

Moreover, the exhaust thrust is expressed as

$$T_e = \dot{m}_h \left[(1+f) u_e - u \right] \tag{2.20a}$$

The total thrust force is given by the relation

$$T = T_{pr} + T_e \tag{2.20b}$$

The propeller efficiency is then expressed as

$$\eta_{pr} = \frac{uT}{ESP} \tag{2.21}$$

Such propeller efficiency replaces the propulsive efficiency of other types of aeroengines discussed earlier. More details will be given in Chapter 6.

2.4.4 Overall Efficiency

The product of the propulsive and thermal efficiencies ($\eta_p \times \eta_{th}$) or ($\eta_{pr} \times \eta_{th}$) as appropriate is called the overall efficiency.

In all cases,

$$\eta_o = \frac{Tu}{\dot{m}_f Q_R} \tag{2.22}$$

For a turbojet with unchoked nozzle and negligible fuel-to-air ratio (f), then from Equation 2.9

$$\eta_o = \eta_{th} \frac{2u}{u + u_e} \tag{2.23}$$

Example 2.7

The Boeing 747 aircraft is powered by four CF-6 turbofan engines manufactured by General Electric Company. Each engine has the following data:

Thrust force	24.0 kN
Air mass flow rate	125 kg/s
BPR	5.0
Fuel mass flow rate	0.75 kg/s
Operating Mach number	0.8
Altitude	10 km
Ambient temperature	223.2 k
Ambient pressure	26.4 kPa
Fuel heating value	42,800 kJ/kg

If the thrust generated from the fan is 75% of the total thrust, determine

1. The jet velocities of the cold air and hot gases
2. The specific thrust
3. The TSFC
4. The propulsive efficiency
5. The thermal efficiency
6. The overall efficiency

(Assume that the exit pressures of the cold and hot streams are equal to the ambient pressure.)

Solution

1. Since the total air mass flow rate through the engine is $\dot{m}_a = 125$ kg/s, then the flow rates are calculated from the BPR as follows:

$$\dot{m}_c \equiv \dot{m}_{Fan} = \frac{5}{6} \times 125 = 104.2 \text{ kg/s}$$

$$\dot{m}_h \equiv \dot{m}_{core} = (1/6) \times 125 = 20.8 \text{ kg/s}$$

Subscript *c*, which stands for both the cold section of the engine and fan, is used alternatively. Also, subscript *h*, which stands for both the hot section and core, is used alternatively.

$$\text{Fuel-to-air ratio } f = \dot{m}_{fuel}/\dot{m}_h = \frac{0.75}{20.8} = 0.036$$

$$T_{fan} = 0.75T = 18 \text{ kN}$$
$$T_{core} = 0.25T = 6 \text{ kN}$$

$$\text{Flight speed } U = M\sqrt{\gamma RT_a} = 0.8\sqrt{1.4 \times 287 \times 223.2}$$

$$U = 240 \text{ m/s}$$

Exit velocity from fan (cold air)

$$\text{Since } T_{Fan} = \dot{m}_{Fan}\left(U_{e_{Fan}} - U_{Flight}\right)$$

$$\therefore U_{e_{Fan}} = \frac{T_{Fan}}{\dot{m}_{Fan}} + U_{Flight} = \frac{18{,}000}{104.2} + 240 = 173 + 240$$
$$U_{e_{Fan}} = 413 \text{ m/s}$$

Exhaust velocity from engine core (hot gases)

$$\text{since } T_{Core} = \dot{m}_{Core}\left[(1+f)U_{e_C} - U\right]$$

$$\therefore U_{e_C} = \frac{\left[T_{Core}/\dot{m}_{Core} + U\right]}{1+f} = \frac{1}{1.036}\left[6000/20.8 + 240\right]$$
$$U_{e_{Core}} = 510 \text{ m/s}$$

2. Specific thrust $= \dfrac{T}{\dot{m}_a} = \dfrac{24}{125} = 0.192 \text{ kN} \cdot \text{s/kg} = 192 \text{ m/s}$.
3. $TSFC = \dfrac{\dot{m}_{Fuel}}{T} = \dfrac{0.75}{24} = 0.03125 \text{ kg} \cdot \text{Fuel/kN/s}$.
4. The propulsive efficiency
   Since both cold (fan) and hot (core) nozzles are unchoked, then the propulsive efficiency can be expressed as

$$\eta_P = \frac{T \times U}{\frac{1}{2}\dot{m}_h\left[(1+f)U_{e_h}^2 - U^2\right] + \frac{1}{2}\dot{m}_c\left[U_c^2 - U^2\right]}$$

$$\eta_P = \frac{2 \times 24{,}000 \times 240}{20.8\left[1.036 \times (510)^2 - (240)^2\right] + (104.2)\left[(413)^2 - (240)^2\right]}$$

$$\eta_P = \frac{11.52 \times 10^6}{4.409 \times 10^6 + 11.77 \times 10^6} = 0.712 = 71.2\%$$

Here also the propulsive efficiency can be written as

$$\eta_p = \frac{2U\left\{\left[(1+f)U_{e_{Core}} - U\right] + \beta\left(U_{e_{Fan}} - U\right)\right\}}{\left[(1+f)U_{e_{core}}^2 - U^2\right] + \beta\left(U_{fan}^2 - U^2\right)}$$

5. The thermal efficiency

$$\eta_{th} = \frac{\dot{m}_{Core}\left[(1+f)U_{e_{Core}}^2 - U^2\right] + \dot{m}_{Fan}\left(U_{e_{Fan}}^2 - U^2\right)}{2\dot{m}_{fuel}Q_{HV}}$$

$$\eta_{th} = \frac{16.179\times10^6}{2\times0.75\times42.8\times10^6} = 0.2546$$

$$\eta_{th} = 25.46\%$$

6. The overall efficiency

$$\eta_o = \eta_P\eta_{th} = 17.93\%$$

Example 2.8

For a turbofan engine with unchoked nozzles, prove that the value of the maximum overall efficiency is given by the relation

$$\eta_{o_{\max}} = \frac{(1+\beta)u^2}{fQ_R}$$

where the flight speed u is given by the relation

$$u = \frac{(1+f)u_h + \beta u_c}{2(1+\beta)}$$

Deduce the appropriate relations corresponding to a single-stream engine (ramjet, scramjet, and turbojet engines).

Solution

From Equation 2.4 with the cold mass flow rate equaling the BPR times the hot mass flow rate, the following relation is obtained:

$$T = \dot{m}_h(1+f)u_{eh} + \beta\dot{m}_h u_{ec} - \dot{m}_h(1+\beta)u$$

Substituting in the overall efficiency expression, we get

$$\eta_o = \frac{Tu}{\dot{m}_f Q_R} = \frac{u\left[(1+f)u_{eh} + \beta u_{ec} - (1+\beta)u\right]}{fQ_R} \qquad \text{(a)}$$

Differentiate with respect to the flight speed:

$$\frac{\partial \eta_o}{\partial u} = \frac{(1+f)u_{eh} + \beta u_{ec} - 2(1+\beta)u}{\text{constant}}$$

Setting $\partial \eta_o / \partial u = 0$ to obtain the maximum value of η_o

$$\therefore u = \frac{(1+f)u_h + \beta u_c}{2(1+\beta)} \tag{b}$$

Substitute to get the maximum value of the overall efficiency:

$$\eta_{o_{ma}} = \frac{1}{fQ_R}\left\{\frac{(1+f)u_h + \beta u_c}{2(1+\beta)}\right\}\left[(1+f)u_h + \beta u_c - (1+\beta)\left\{\frac{(1+f)u_h + \beta u_c}{2(1+\beta)}\right\}\right]$$

$$\eta_{o_{mx}} = \frac{(1+f)u_h + \beta u_c}{2(1+\beta)fQ_R}\left[(1+f)u_h + \beta u_c - \frac{(1+f)u_h + \beta u_c}{2}\right]$$

$$\eta_{o_{mx}} = \frac{\{(1+f)u_h + \beta u_c\}^2}{4(1+\beta)fQ_R}$$

This expression defines the maximum overall efficiency in terms of the exhaust speeds of both the hot and the cold stream.

To obtain an expression for the maximum overall efficiency in terms of the flight speed, substitute Equation b in a to get the requested relation

$$\eta_{o_{mx}} = \frac{(1+\beta)u^2}{fQ_R}$$

From this relation, the maximum overall efficiency for a single-stream engine (ramjet, scramjet, and turbojet engines) is obtained by setting the BPR equal to zero; thus, its value will be

$$\eta_{o_{mx}} = \frac{u^2}{fQ_R}$$

The corresponding value for the flight speed will be

$$u = \frac{(1+f)u_e}{2}$$

2.4.5 Takeoff Thrust

Takeoff thrust is an important parameter that defines the ability of an aeroengine to provide a static and low-speed thrust that enables the aircraft to take off under its own power. Both ramjet and scramjet engines are not self-accelerating propulsion systems

from static conditions: they require acceleration to an appreciable velocity by a boost system before they are capable of providing net positive thrust. Thus, they are excluded from this discussion.

From Equation 2.3a through c, the static thrust of a turbojet engine with an unchoked nozzle is expressed by the relation

$$T_{takeoff} = \dot{m}_a (1+f) u_e \tag{a}$$

From Equation 2.13 when $u = 0$, then

$$(\eta_{th})_{static} = \dot{m}_a (1+f) \frac{u_e^2}{2\dot{m}_f Q_R} \tag{b}$$

From Equations a and b, then the static or takeoff thrust is given by the relation

$$T_{takeoff} = \frac{2\eta_{th}\dot{m}_f Q_R}{u_e} \tag{2.24}$$

For a given flow rate and thermal efficiency, then

$$T_{takeoff} \propto \frac{1}{u_e}$$

This relation outlines one of the advantages of turboprop engines over turbojet and turbofan engines. Turboprop engines accelerate a large mass flow rate of air to a small exhaust velocity, which in turn increases the takeoff thrust. Consequently, aircraft powered by turboprop engines can take off from a very short runway.

2.4.6 Specific Fuel Consumption

This performance parameter of the engine has a direct influence on the costs of aircraft trip and flight economics. Fuel consumption is either defined per unit thrust force (for ramjet, turbojet, and turbofan engines) or per horsepower (e.g., for turboprop and piston-propeller engines).

2.4.6.1 Ramjet, Turbojet, and Turbofan Engines

The TSFC is defined as

$$TSFC = \frac{\dot{m}_f}{T} \tag{2.25a}$$

where the thrust force (T) is expressed by Equation 2.3a through c for a turbojet engine and Equation 2.4 for a turbofan engine; values of TSFC strongly depend on the flight speed.

So its typical values for both turbojet and turbofan are defined for static condition. Typical values [9] for turbojet engines are 0.075 – 0.11 kg/N·h (0.75 – 1.1 lb/lb$_f$·h), while turbofans are more economic and have the following range: 0.03 – 0.05 kg/N·h (0.3 – 0.5 lb/lb$_f$·h). However, for ramjets, reference values for TSFC are defined at a flight Mach number of 2. Typical values are 0.17 – 0.26 kg/N·h (1.7 – 2.6 lb/lb$_f$·h). Some empirical formulae are presented in [11] for TSFC. These formulae have the form

$$TSFC = \left(a + bM_0\right)\sqrt{\theta} \tag{2.25b}$$

where
- a and b are constants that vary from one engine to another
- M_0 is the flight Mach number
- θ is the dimensionless ratio (T_a/T_{ref}), which is the ratio between the ambient temperature at the flight altitude and the standard temperature at sea level (288.2 k)

For a high-BPR turbofan, the values of these constants are $a = 0.4$ and $b = 0.45$.

2.4.6.2 Turboprop Engines

For engines that produce shaft power, fuel consumption is identified by brake-specific fuel consumption (BSFC), or simply SFC, and defined as

$$\text{SFC} \equiv \text{BSFC} = \frac{\dot{m}_f}{SP} \tag{2.26}$$

When appreciable thrust is produced by the hot gases, the fuel consumption is identified by the equivalent brake-specific fuel consumption (EBSFC), or simply ESFC, and defined by

$$\text{ESFC} = \frac{\dot{m}_f}{\text{ESP}} \tag{2.27}$$

Typical values [9] for ESFC are 0.45–0.60 ((lb/h)/hp) or 0.27–0.36 (kg/kW·h). The values of the corresponding constants in the empirical relation (2.25b) are a = 0.2 and b = 0.9 [11].

2.4.7 Aircraft Range

Aircraft range is a design parameter of the aircraft, based on which the number, location, and capacity of fuel tanks in the aircraft are determined. The aircraft weight is composed of the structural weight, the payload (including the crew members, food, and service supply), and the fuel weight. During any trip, only the fuel weight is changeable.

Now consider the cruise phase in a flight trip where the aircraft flies at a constant speed. Ignoring the climb and descent phases, it may be assumed that the cruise distance is equal to the trip distance of the aircraft. During cruise, the aircraft is subjected to two vertical forces [lift (L) and weight (mg), which are equal in magnitude] and two horizontal forces [thrust (T) and drag (D), which are also equal in magnitude] (refer to Figure 2.11).

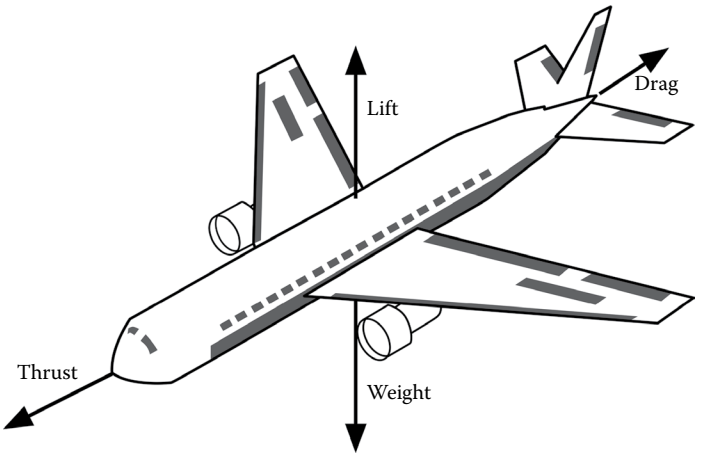


FIGURE 2.11
Forces on airplane during cruise.

Then

$$T = D = mg\left(\frac{D}{L}\right)$$

where
m is the instantaneous aircraft mass
g is the gravitational acceleration

Since the rate of fuel consumption is equal to the rate of decrease of the mass of aircraft, then

$$\dot{m}_f = -\frac{dm}{dt} = \left(-\frac{dm}{ds}\right) \times \left(\frac{ds}{dt}\right) = -u\frac{dm}{ds}$$

where s is the distance along the flight path:

$$\therefore \dot{m}_f = -u\left(\frac{T}{D}\right)\frac{dm}{ds}$$

$$= -\frac{uT}{D}\frac{L}{mg}\frac{dm}{ds}$$

$$\therefore ds = -\frac{u}{g}\frac{T}{\dot{m}_f}\frac{L}{D}\frac{dm}{m}$$

Integration of this equation yields the range of aircraft (S) as follows:

$$S = \frac{u}{g}\frac{T}{\dot{m}_f}\frac{L}{D}\ln\left(\frac{m_1}{m_2}\right) \tag{2.28}$$

where m_1 and m_2 are the initial and final mass of aircraft.

From Equation 2.25a and b, this equation is reformulated as

$$S = \frac{u}{g}\frac{1}{TSFC}\frac{L}{D}\ln\left(\frac{m_1}{m_2}\right) \tag{2.29}$$

This equation is known as Breguet's equation, which was derived in 1920. Another expression for the range is obtained from the propulsive efficiency (Equations 2.22 and 2.28) as follows:

$$S = \frac{\eta_o Q_R}{g}\frac{L}{D}\ln\left(\frac{m_1}{m_2}\right) \tag{2.30}$$

In Equations 2.29 and 2.30, the ratio between the lift and drag forces may be alternatively written as C_L/C_D, where the lift force coefficient is calculated as usual from the relation

$$C_L = \frac{W}{\frac{1}{2}\rho U^2 S_W}$$

where W and S_W are the aircraft weight and wing area.

The drag coefficient is calculated from the relation

$$C_D = K_1 C_L{}^2 + K_2 C_L + C_{D_o}$$

where the constants K_1, K_2, and C_{D_o} are typically functions of the flight Mach number and wing configuration (flap position, etc.). The C_{D_o} term is the zero-lift drag coefficient, which accounts for both frictional and pressure drag in the subsonic flight and wave drag in the supersonic flight [11]. The K_1 and K_2 terms account for the drag due to lift. Normally, K_2 is very small and approximately equal to zero in most fighter aircrafts.

It is clear from Equations 2.29 and 2.30 that to maximize the range of an aircraft flying at a specified speed [12], it must

1. Fly at the maximum lift-to-drag ratio
2. Have the highest possible overall efficiency
3. Have the lowest specific fuel consumption
4. Have the highest possible ratio between the aircraft weights at the start and end of cruise

Typical values for maximum lift-to-drag ratio are given in Table 2.1.

For a propeller/reciprocating or turboprop engine, a similar analysis may be followed.

TABLE 2.1

Typical Values for Maximum Lift-to-Drag Ratio

Type of Aircraft	$(L/D)_{max}$	Examples
Modern sailplanes	25–40	Voyager; (L/D) =40
Civil jet airliners	12–20	Boeing 747; (L/D) = 10
Supersonic fighter aircraft	4–10	F-45, F-5; (L/D) = 10

From Equations 2.21 and 2.27, then

$$\therefore \frac{uT}{\dot{m}_f} = \frac{\eta_{pr}}{ESFC}$$

Substituting this equation in Equation 2.28, the following equation for the range is obtained:

$$S = \frac{\eta_{pr}}{g}\frac{1}{ESFC}\frac{L}{D}\ln\left(\frac{m_1}{m_2}\right) \tag{2.31}$$

Similarly, in order to maximize the range, the lift-to-drag ratio, propeller efficiency, and the ratio of the aircraft weight at the start of cruise to that at the end of cruise have to be chosen as maximums while the fuel consumption (ESFC) has to be minimum.

Airlines and aircraft manufacturers normally use the following forms for *Breguet*'s equation:

For turbojet/turbofan engines

$$S = \frac{u}{c}\frac{L}{D}\ln\frac{m_1}{m_2} \tag{2.32}$$

For turboprop engines

$$S = \frac{\eta}{c}\frac{L}{D}\ln\frac{m_1}{m_2} \tag{2.33}$$

where c is the specific fuel consumption [13] expressed in (lb · fuel/lb · thrust/h) or (lb · fuel/ESHP/h).

Another definition is also employed, namely, the specific range [14], which is given in miles per pound of fuel (mi/lb).

a. For a turbojet/turbofan

$$\frac{\text{mi}}{\text{lb}} = \frac{u}{\left[c\left(\frac{D}{L}\right)W\right]} = \frac{u}{c}\frac{L}{D}\frac{1}{W} \tag{2.34a}$$

If u is in knots, mi/lb will be in nautical miles per pound of fuel.

b. For a turboprop engine

$$\frac{\text{mi}}{\text{lb}} = 325\left(\frac{\eta_{prop}}{c}\right)\left(\frac{L}{D}\right)\left(\frac{1}{W}\right) \tag{2.34b}$$

Example 2.9

A Boeing 747 aircraft has a lift-to-drag ratio of 17. The fuel-to-air ratio is 0.02 and the fuel heating value is 45, 000 kJ/kg. The ratio between the weight of the aircraft at the end and start of cruise is 0.673. The overall efficiency is 0.35.

1. Calculate the range of the aircraft.
2. What will be the fuel consumed in the cruise if the takeoff mass of aircraft is 385,560 kg?

3. If the fuel consumed during the engine start, warming, and climb is 4.4% of the initial aircraft weight and the fuel consumed during descent, landing, and engine stop is 3.8% of the aircraft weight at the end of cruise, calculate the fuel consumed in the whole trip.

Solution

From Equation 2.30 and the given data, the aircraft range (S) is

$$S = \frac{0.35 \times 45 \times 10^6}{9.8} \times 17 \times \ln\left(\frac{1}{0.673}\right) \text{ m}$$
$$= \frac{0.35 \times 45 \times 10^3}{9.8} \times 17 \times 0.396 \text{ km}$$
$$S = 10{,}819 \text{ km}$$

Fuel consumed in the trip = (1 − 0.673) × 385,650 = 126,078 kg

$$\text{Weight at landing} = \text{Weight at engine start} \times \frac{\text{Weight at the start of cruise}}{\text{Weight at engine start}} \times \frac{\text{Weight at the end of cruise}}{\text{Weight at the start of cruise}} \times \frac{\text{Weight after landing and engine stop}}{\text{Weight at the end of cruise}}$$
$$= 385{,}560 \times (1 - 0.044) \times 0.673 \times (1 - 0.038)$$
$$= 385{,}560 \times 0.956 \times 0.673 \times 0.962$$
$$\text{Weight at landing} = 238{,}638 \text{ kg}$$

Fuel consumed in the whole trip = 146,921 kg.

2.4.8 Range Factor

The range factor is defined as

$$RF = \frac{1}{g}\frac{u}{TSFC}\frac{L}{D} = \frac{1}{g}\frac{u}{TSFC}\frac{C_L}{C_D} \tag{2.35}$$

The minimum fuel consumption for a distance(s) occurs at the condition where the range factor is maximum.

2.4.9 Endurance Factor

The endurance factor is defined as

$$EF = \frac{1}{g}\frac{1}{TSFC}\frac{L}{D} = \frac{1}{g}\frac{1}{TSFC}\frac{C_L}{C_D} \tag{2.36}$$

The minimum fuel consumption as seen from Equation 2.36 for a time flight time (t) occurs when the endurance factor is maximum.

Example 2.10

Dassault Mirage G is a two-seat strike and reconnaissance fighter powered by one **Snecma TF-306C** turbofan engine. It has the following characteristics:

Flight Mach number	0.8
Altitude	65,000 ft
Ambient temperature	216.7 k
Ambient pressure	5.5 kPa
Fuel heating value	42,700 kJ/kg
Thrust force	53.4 kN
Air mass flow rate	45 kg/s
Fuel mass flow rate	2.5 kg/s
Aircraft gross weight (65,000 ft)	156 kN
Aircraft takeoff weight	173.3 kN
Wing area	26.4 m^2
Fuel weight	53 kN
Maximum lift coefficient	$C_{L\max=1.8}$
$C_{D0}=0.012 \quad K_1=0.2 \quad K_2=0.0$	
Air density at takeoff	1.225 kg/m^3
Air density at 650,000 ft	0.88 kg/m^3

Calculate

1. The specific thrust
2. The TSFC
3. The exit velocity
4. The thermal efficiency
5. The propulsive efficiency
6. The overall efficiency
7. The range factor (RF)

Solution

$$U = 0.8\sqrt{\gamma RT_o} = 0.8\sqrt{1.4\times 287\times 216.7} = 236 \text{ m/s}$$

1. The specific thrust $= \dfrac{T}{\dot{m}_a} = \dfrac{53.4\times 10^3}{45} = 1186.7$ m/s
2. $TSFC = \dfrac{\dot{m}_f}{T} = \dfrac{2.65}{53.4} = 0.046 \ \dfrac{\text{kg/s}}{\text{kN}} = 46 \ \dfrac{\text{mg}}{\text{N}\cdot\text{s}}$
3. The thrust force is $T = \left(\dot{m}_a + \dot{m}_f\right)U_e - \dot{m}_a U$

$$U_e = \frac{T + \dot{m}_a U}{\dot{m}_a + \dot{m}_f} = \frac{53{,}000 + 45\times 236}{45 + 2.5} = 1{,}339.4 \text{ m/s}$$

4. The thermal efficiency is given by the relation

$$\eta_{th} = \frac{\dot{W}_{out}}{\dot{Q}_{in}}$$

$$\dot{W}_{out} = \frac{1}{2}\left[\left(\dot{m}_a + \dot{m}_f\right)U_e^2 - \dot{m}_a U^2\right] = 0.5\left[(45+2.5)(1339.4)^2 - 45\times(236)^2\right]$$

$$\dot{W}_{out} = 41.35\times10^6 \text{ W}$$

$$\dot{Q}_{in} = \dot{m}_f Q_{HV} = 107\times10^6 \text{ W}$$

Substituting these values to get $\eta_{th} = 0.386 = 38.6\%$

5. The propulsive efficiency $\eta_p = \dfrac{TU}{\dot{W}_{out}} = \dfrac{53.4\times10^3\times236}{41.35\times10^6} = 0.3047 = 30.47\%$

$$\eta_o = \eta_p\eta_{th} = 0.1179 = 11.79\%$$

6. Overall efficiency

$$C_L = \frac{W}{\frac{1}{2}\rho U^2 S_W} = \frac{156{,}000}{0.5\times0.088\times(236)^2\times66.4} = 0.959$$

$$C_D = K_1 C_L^2 + K_2 C_L + C_{D_o}$$

$$C_D = 0.2\times0.919 + 0.012 = 0.195$$

7. The range factor

$$RF = \frac{C_L}{C_D}\frac{U}{TSFC}\frac{1}{g} = \frac{0.959}{0.195}\times\frac{236}{0.053*10^{-3}}\times\frac{1}{9.81} = 2232 \text{ km}$$

2.4.10 Specific Impulse

The specific impulse (I_{sp}) is defined as the thrust per unit fuel flow rate, or

$$I_{sp} = \frac{T}{\dot{m}_f g} \tag{2.37}$$

This quantity enters directly into the calculation of the fractional weight change of aircraft (or rocket) during flight. Thus, from Equation 2.28, the range can be expressed in terms of the specific impulse as follows:

$$S = uI_{sp}\frac{L}{D}\ln\left(\frac{m_1}{m_2}\right) \tag{2.38}$$

The specific impulse is equally applied for both rockets and aircrafts. The unit of specific impulse is time (seconds).

Example 2.11

The maximum range of an aircraft is given by the relation

$$S_{\max} = \left(\frac{V_g}{TSFC}\right)\left(\frac{1}{g}\right)\left(\frac{L}{D}\right)\ln\left(\frac{m_1}{m_2}\right)$$

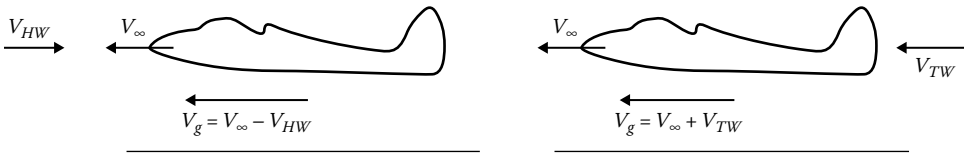


FIGURE 2.12
Head and tail wind conditions.

where V_g is the air relative speed including the effect of wind as shown in Figure 2.12 for either head wind or tail wind conditions.

1. Calculate the mass of the fuel consumed during a trip where its range is 4,000 km, flight speed is 250 m/s, $L/D = 10$, $TSFC = 0.08$ kg/N/h, and $m_1 = 50{,}000$ kg in the following two cases:
   a. Head wind = 50 m/s
   b. Tail wind = 50 m/s
2. Calculate the time for such a trip in these two cases.

Solution

This example illustrates the effect of wind on both fuel consumption and the time of a trip. Consider first the case:

1. Fuel consumption (*Tail wind*)
   The equation for the range is now rewritten in terms of the relative speed rather than the airplane speed:

$$S = \frac{V_g}{TSFC}\frac{1}{g}\frac{L}{D}\ln\frac{m_1}{m_2}$$

$$\therefore \ln\frac{m_1}{m_2} = \frac{(S)(g)(TSFC)}{V_g(L/D)}$$

When

$$V_g = V_\infty + V_{TW} = 250 + 50 = 300 \text{ m/s}$$

$$\ln\frac{m_1}{m_2} = \frac{4000 \times 10^3 \times 9.8 \times 0.08}{300 \times 10 \times 3600} = 0.2903$$

$$\frac{m_1}{m_2} = 1.3369$$

$$\text{Fuel consumed} = m_1 - m_2 = m_1\left(1 - \frac{1}{1.3369}\right) = 50{,}000 \times 0.252 = 12{,}600 \text{ kg}$$

Fuel consumed for the case of tail wind (i.e., supporting wind) = 12,600 kg

$$\therefore m_2 = 37400 \text{ kg}$$

a. *Head wind case:*

$$V_g = V_\infty - V_{HW} = 250 - 50 = 200 \text{ m/s}$$

$$\ln \frac{m_1}{m_2} = 0.43555$$

$$\frac{m_1}{m_2} = 1.54582$$

$$\text{Fuel consumed} = m_1\left(1 - \frac{1}{1.154582}\right)$$

Fuel consumed for the case of head wind = 17,654 kg

$$\therefore m_2 = 50{,}000 - 17{,}654 = 32{,}345 \text{ kg}$$

2. Trip time (t):

$$\text{Trip time } (t) = \frac{S}{V_g} = \frac{L/D}{(g)(TSFC)} \ln \frac{m_1}{m_2}$$

For tail wind case

$$\text{Time} = \frac{10}{(9.8)(0.08)} \ln \frac{50{,}000}{37{,}400}$$

$$\text{Time} = 3.70 \text{ h}$$

For the head wind case

$$\text{Time} = \frac{10}{(9.8)(0.08)} \ln \frac{50{,}000}{32{,}345}$$

$$\text{Time} = 5.556 \text{ h}$$

From this calculation, tail wind—as expected—helps in shortening the trip time and saves fuel. On the contrary, for head wind, the trip time and fuel consumed are increased. What are the corresponding values for zero wind speed?

Example 2.12

An airplane is powered by four engines and has the following data:

Drag coefficient	$C_d = 0.097$
Wing area	$A = 260$ m^2
Flight speed	$u = 300$ m/s
Air density	$\rho = 0.414$ kg/m^3
Inlet area of each engine	$A_i = 3.14$ m^2

It is required to calculate the jet speed assuming that the nozzles are unchoked and the fuel-to-air ratio is negligible.

Now, due to some troubles, one engine was shut down. Prove that the new flight speed u will be given by the relation

$$u = \frac{6A_i u_e}{C_d A + 6A_i}$$

where u_e is the speed of the exhaust gases, which is constant irrespective of other engine failures.

Calculate this flight speed based on the new available thrust forces.

Solution

For steady flight conditions, the drag force is equal to the sum of thrust forces generated by the four engines, or

$$\begin{aligned}
D &= \frac{1}{2}\rho u^2 A C_d \\
D &= \frac{1}{2} \times 0.414 \times (300)^2 \times 260 \times 0.097 \text{ N} \\
D &= 469.85 \text{ kN} \\
T &= \frac{D}{4} = 117.46 \text{ kN} \\
T &= \dot{m}(u_e - u) = \rho u A_i (u_e - u) \\
u_e &= u + \frac{T}{\rho u A_i} = 300 + \frac{117,460}{0.414 \times 300 \times 3.14} \\
u_e &= 601.2 \text{ m/s}
\end{aligned}$$

Since the air-mass flow rate into each engine is expressed as

$$\dot{m} = \rho u A_i$$

Thrust force for one engine is

$$\therefore T = \dot{m}(u_e - u) = \rho u A_i (u_e - u)$$

$$\text{Drag force} = D = \frac{1}{2}\rho u^2 A C_d$$

For n operative engines

$$\begin{aligned}
D &= nT \\
\frac{1}{2}\rho u^2 A C_d &= n\rho u A_i (u_e - u) \\
u A C_d &= 2nA_i (u_e - u) \\
u(C_d A + 2nA_i) &= 2nA_i u_e \\
\therefore \boldsymbol{u} &= \frac{2nA_i u_e}{C_d A + 2nA_i}
\end{aligned}$$

$\therefore$ For 3 operative engines, $n = 3$

$$\therefore u = \frac{6A_i u_e}{C_d A + 6A_i}$$

Keeping the exhaust speed the same as obtained earlier, then the new value for flight speed after one engine has been shut down is calculated from the relation

$$u = \frac{6A_f u_e}{C_d A + 6A_f}$$
$$= \frac{6 \times 3.14 \times 600}{0.0966 \times 260 + 6 \times 3.14}$$
$$u = \frac{11,304}{43.956} = 257.16 \text{ m/s}$$

Thus, the flight speed is reduced from 300 to 257.16 m/s.

Now, if a second engine was shut down; or, $n = 2$

$$u = \frac{4A_f u_e}{C_d A + 4A_f} = \frac{4 \times 3.14 \times 600}{0.0966 \times 260 + 4 \times 3.14}$$
$$u = \frac{7536}{34.536} = 218.2 \text{ m/s}$$

Again, the flight speed is reduced to only 218.2 m/s.

2.4.11 Mission Segment Weight Fraction

For analysis, the various mission segments, or "legs," are numbered, with (1) denoting the start of the mission. Mission leg 1 is usually engine warm-up and takeoff. The remaining legs are sequentially numbered [15]. For a simple passenger aircraft mission, the legs are (1) warm-up and takeoff, (2) climb, (3) cruise, (4) loiter, and (5) land. Table 2.2 gives typical weight fractions for mission legs [15].

From the endurance factor (Equation 2.36), then loiter-weight fractions are found as

$$\frac{W_2}{W_1} = e^{-\frac{E(TSFC)g}{(L/D)}}$$

It is important here to mention that the empty-weight fraction (W_e/W_0) is expressed by the relation

$$\frac{W_e}{W_0} = AW_0^C K_{vs} \tag{2.39}$$

The values of the constants (A and C) are given in Table 2.3 for different aircrafts.

TABLE 2.2

Mission Segments' Weight Fractions

	$\frac{m_{i+1}}{m_i}$
Warm-up and takeoff	0.97
Climb	0.985
Landing	0.995

Source: Raymer, D.P., *Aircraft Design: A Conceptual Approach* (*AIAA Education Series*), 1999.

TABLE 2.3

Empty Weight Fraction versus (W_0)

$\frac{W_e}{W_0} = AW_0^C K_{vs}$	A	C
Sailplane powered	0.91	−0.05
General aviation single engine	2.36	−0.18
General aviation twin engine	1.51	−0.10
Agricultural aircraft	0.74	−0.03
Twin turboprop	0.96	−0.05
Flying boat	1.09	−0.05
Jet trainer	1.59	−0.10
Jet fighter	2.34	−0.13
Military cargo/bomber	0.93	−0.07
Jet transport	1.02	−0.06

Source: Raymer, D.P., *Aircraft Design: A Conceptual Approach* (*AIAA Education Series*), 1999.
K_{vs} = variable sweep constant = 1.04 if variable sweep and equals unity for a fixed sweep.

Example 2.13

A bomber aircraft is in a mission whose profile is shown in Figure 2.13. A description of its phases is given in Table 2.4.

The crew members are two, totaling 200 kg, while the payload is 18,400 kg. The lift-to-drag ratio (L/D) is 21 for cruise and 22 for loiter. $TSFC$ = 0.04 kg/N/h. Using preliminary procedure for aircraft's sizing, calculate takeoff gross weight.

Solution

From Table 2.2:

1. Warm-up and takeoff (1-2)

$$W_2/W_1 = 0.97$$

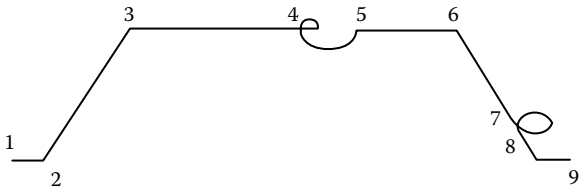


FIGURE 2.13
Flight segments of a bomber in a mission.

TABLE 2.4

Description of Different Segments of Bomber's Mission

Segment	**1-2**	**2-3**	**3-4**	**4-5**	**5-6**	**6-7**	**7-8**	**8-9**
Description	Warm-up and takeoff	Climb	Cruise 8000 km	Loiter 10 min	Cruise 3000 km	Descent	Loiter 15 min	Landing

2. Climb and acceleration

$$W_3/W_2 = 0.985$$

3. Cruise (3-4)

$$R = \frac{u}{g}\frac{1}{TSFC}\frac{L}{D}\ln\frac{W_3}{W_4}$$

$$\frac{W_4}{W_3} = e^{-\frac{R(TSFC)g}{u(L/D)}}$$

$$\frac{W_4}{W_3} = e^{-\frac{8,000,000(0.04/3600)9.81}{(870/3.6)(21)}} = e^{-0.17182}$$

$$\frac{W_4}{W_3} = 0.84213$$

4. Loiter (4-5)

$$W_5/W_4 = e^{-\frac{E(TSFC)g}{(L/D)}} = e^{-\frac{(10\times60)(0.04/3600)\times9.81}{(22)}} = e^{-0.00297}$$

$$W_5/W_4 = 0.997$$

5. Cruise (5-6)

$$W_6/W_5 = e^{-\frac{R(TSFC)g}{u(L/D)}}$$

$$W_6/W_5 = e^{-\frac{3,000,000(0.04/3600)9.81}{(870/3.6)(21)}} = e^{-0.0644}$$

$$W_4/W_3 = 0.93759$$

6. Descent (6-7)

$$W_7/W_6 = 0.995$$

7. Loiter (7-8)

$$W_8/W_7 = e^{-\frac{E(TSFC)g}{(L/D)}} = e^{-\frac{(15\times60)(0.04/3600)\times9.81}{(22)}} = e^{-0.004459}$$

$$W_5/W_4 = 0.99555$$

8. Descent and landing (8-9)

$$W_9/W_8 = 0.995$$

The weight ratio for the whole mission is then

$$\frac{W_9}{W_1} = \frac{W_9}{W_8}\frac{W_8}{W_7}\frac{W_7}{W_6}\frac{W_6}{W_5}\frac{W_5}{W_4}\frac{W_4}{W_3}\frac{W_3}{W_2}\frac{W_2}{W_1}$$

$$\frac{W_9}{W_1} = 0.995\times0.9955\times0.995\times0.9376\times0.997\times0.84213\times0.985\times0.97$$

$$\frac{W_9}{W_1} = 0.7417$$

TABLE 2.5

Guessed and Calculated Weight (W_0)

W_0 Guesses (kg)	$\frac{W_e}{W_0} = 0.93W_0^{-0.07}$	W_0 Calculated (kg)
100,000	0.446683	59,829
60,000	0.4305	62,888
61,000	0.43004	62,782
62,000	0.42955	62,679
62,500	0.42931	62,628
62,600	0.42926	62,618
62,610	0.429257	62,617
62,616	0.429255	62,616

The mission fuel fraction is

$$\frac{W_f}{W_0} = 1 - \frac{W_9}{W_1} = 1 - 0.7417 = 0.273798$$

Considering a 6% allowance for reserve and trapped fuel, the total fuel fraction may be estimated as

$$\frac{W_f}{W_0} = 1.06\left(1 - \frac{W_9}{W_1}\right) = 1.06 \times 0.273798 = 0.273798$$

The empty weight fraction for a fixed sweep is

$$\frac{W_e}{W_0} = AW_0^C K_{vs} = 0.93 \times W_0^{-0.07} \times 1 = 0.93W_0^{-0.07}$$

$$\frac{W_e}{W_0} = 0.93W_0^{-0.07}$$

Since $W_{crew} = 200$ kg and $W_{payload} = 18{,}400$ kg, then

$$W_0 = \frac{W_{crew} + W_{payload}}{1 - \frac{W_f}{W_0} - \frac{W_e}{W_0}} = \frac{18{,}600}{1 - 0.2737 - 0.93W_0^{-0.07}}$$

$$W_0 = \frac{18{,}600}{0.7263 - 0.93W_0^{-0.07}}$$

This equation is solved by trial and error. Guessed values for W_0 are assumed and the corresponding value is calculated, until both guessed and calculated values become identical (Table 2.5).

From Table 2.5, the gross weight of the bomber aircraft is $W_0 = 62{,}616$ kg.

2.4.12 Route Planning

A pilot planning a flight under VFR (visual flight rules) will usually use an aeronautical chart of the area published for the use of pilots. This map will depict controlled airspace,

radio navigation aids, and airfields prominently, as well as hazards to flying such as mountains, etc. It also includes sufficient ground detail—towns, roads, and wooded areas—to aid visual navigation.

The pilot will choose a route, taking care to avoid controlled airspace that is not permitted for the flight, restricted areas, danger areas, and so on. The chosen route is plotted on the map, and the lines drawn are called the *track*. During flight planning, two points must be taken into consideration:

1. Point of no return
2. Critical point

2.4.12.1 Point of No Return

The point of no return (*PNR*) is also known as the point of safe return (*PSR*). This is the furthest point along track that a pilot can fly toward the destination and have sufficient fuel to divert to an alternate destination, with safe reserves on arrival. In other words, it is the pilot's last chance to assess his/her prospect of a successful approach and landing at the destination and to decide whether to go on or to divert. If any doubt exists, he/she must *divert to the alternate*.

There are a number of methods that can be used to calculate a PNR/PSR, but the one most favored uses what are called specific fuel flows.

These are calculated by dividing the planned cruise fuel flow by the expected ground speeds toward the destination and toward the alternate field. Normally, two cases may be expected:

1. When the alternate is the departure field
2. When the alternate is on track between the departure point and the destination

Two examples to illustrate both cases follow.

Example 2.14

Consider a flight from airport A to airport B, with A as the alternate field (Figure 2.14). The distance from A to B is 2700 nms. Maximum range cruise power will be used, giving an FF of 800 L/h. The aircraft can carry 8000 L of useable fuel without exceeding the maximum AUW (all up weight (gross)). The fixed reserve is 1400 L. The used fuel for taxi and the climb are 100 and 500 L, respectively. A 15% of fuel is next maintained to provide a variable reserve. At this power setting, the planned TAS (true airspeed)

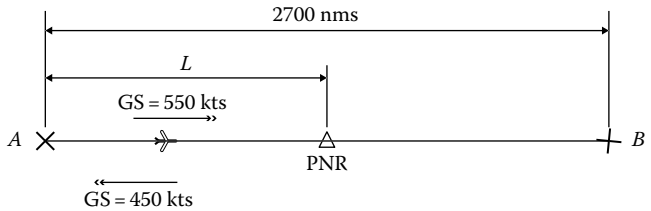


FIGURE 2.14
Flight track with departure airport as an alternate.

is 500 knots and a 50 knots tail wind is forecast A to B. Calculate the distance of PNR from the departure airport A.

Solution

The ground speed from A to B is

$$V_{AB} = V_0 + V_1 = 550 \text{ kts}$$

For a return to A, the ground speed is

$$V_{BA} = V_0 - V_1 = 450 \text{ kts}$$

Maximum range cruise power will be used, giving a fuel flow (FF) of 800 L/h, and this FF will also be used for a fixed reserve and any holding.

To establish the flight fuel available (FFA) for the PNR calculation, we must subtract from the useable fuel the fixed reserve (1400 L), the taxi fuel (100 L), and the climb allowance (500 L). The forecast for a possible return to A does not indicate the need for any holding fuel. Therefore, the FFA is

$$\text{FFA} = 8000 - (1400 + 100 + 500) = 6000 \text{ L}$$

This figure is now divided by 1.15 to provide a variable reserve, giving a final FFA of 5217 L.

Assume that L is the distance from airport A to PNR and fuel consumption as

Q_1 = Fuel quantity consumed in the root from A to PNR
Q_2 = Fuel quantity consumed in the root from PNR to A

Total fuel consumed $Q_1 + Q_2 = 5217$ L

$$Q_1 = FF \times T_1 = 800T_1 \quad Q_2 = FF \times T_2 = 800T_2$$

$$T_1 = \frac{L}{V_0 + V_1}, \quad T_2 = \frac{L}{V_0 - V_1}$$

$$Q = Q_1 + Q_2 = FF \times (T_1 + T_2) = FF \times \left(\frac{L}{V_0 - V_1} + \frac{L}{V_0 + V_1} \right)$$

$$Q = FF \times L \times \left(\frac{2V_0}{(V_0 - V_1)(V_0 + V_1)} \right)$$

$$L = Q \times \frac{(V_0 - V_1)(V_0 + V_1)}{2V_0 \times FF} = 5217 \times \frac{450 \times 550}{2 \times 500 \times 800} = 1614 \text{ nms}$$

The PNR is 1614 nautical miles (nms) apart from departure airport and 1086 nms apart from arrival airport.

Example 2.15

We will use the previous example of a flight from A to B over a distance of 2700 nms, but with the possible alternate (C) located at 700 nms along track toward A, that is, the

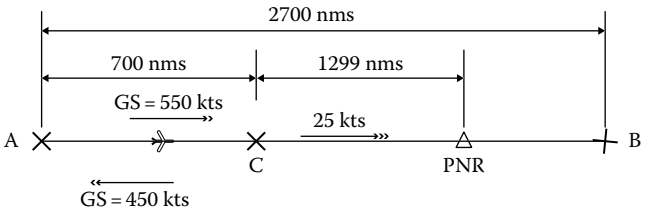


FIGURE 2.15
Flight track with alternate on track.

distance from C to B is 2000 nms. The other planning data remain the same as in the previous example, that is,

1. FFA at A = 5217 L (after allowing for a variable reserve)
2. Cruise fuel flow = 800 L/h
3. Ground speed away from home = 550 kts
4. Ground speed back to home = 450 kts

Calculate the distance between departure airport (A) and PNR.

Solution

We first determine how much fuel is required to fly from A to overhead C (Figure 2.15). This is equal to the distance from A to C (700 nms) divided by the speed (550 kts) and multiplied by the cruise fuel consumption (800 L/h).

Q = Fuel quantity consumed in the root from A to C

$$Q = FF \times T = 800T = 800\frac{700}{550} = 1018 \text{ L}$$

The fuel available to the trip from C to PNR and PNR to C is then

$$Q' = 5217 - 1018 = 4199 \text{ L}$$

The distance to PNR is L, given by the relation

$$L = Q' \times \frac{(V_0 - V_1)(V_0 + V_1)}{2V_0 \times FF} = 4199 \times \frac{450 \times 550}{2 \times 500 \times 800} = 1299 \text{ nms}$$

The distance of the PNR from C is therefore 1299 nms. This is 701 nms short of B and 1999 nms away from A. If the aircraft flies beyond this point, there will not be sufficient fuel to return to C with the fixed reserve intact.

2.4.12.2 Critical Point

Similarly, the equal time point, referred to as the ETP (also critical point (CP)), is the point in the flight where it would take the same time to continue flying straight, or track back to the departure aerodrome. The ETP is not dependent on fuel, but wind, giving a change in

ground speed out from and back to the departure aerodrome. In nil wind conditions, the ETP is located halfway between the two aerodromes, but in reality it is shifted depending on the wind speed and direction.

While the distance to a PNR is dependent on fuel availability and fuel flow, the distance to a critical point (*CP*) is independent of fuel considerations and is based on ground speeds only.

As an illustration, we will calculate a CP/ETP for the previous example flight.

Example 2.16

Consider a flight from airport A to airport B. The distance from A to B is 2700 nms. At this power setting, the planned TAS (true airspeed) is 500 kts and a 50 kts tail wind is forecast A to B. Calculate the critical point (CP) from the departure airport A.

Solution

As illustrated in Figure 2.16, the ground speed from CP to B is ($V_{AB} = V_0 + V_1 = 550$ kts), while the ground speed for a return to A is ($V_{BA} = V_0 - V_1 = 450$ kts).

T_1 = Flight time from critical point to departure airport A
T_2 = Flight time from critical point to arrival airport B

$$T_1 = \frac{L_1}{V_0 - V_1}, \quad T_2 = \frac{L_2}{V_0 + V_1}$$

Since $T_1 = T_2$ then $\frac{L_1}{450} = \frac{L_2}{550}$,

$$\frac{L_2}{L_1} = \frac{550}{450} = \frac{11}{9}$$
$$\because L_1 + L_2 = 2700$$
$$\therefore L_1 = 1215 \text{ kts}$$
$$L_2 = 1485 \text{ kts}$$

From this critical point, the time on to *B* is 2.7 h (1485/550), and the time back to A is also 2.7 h (1215/450).

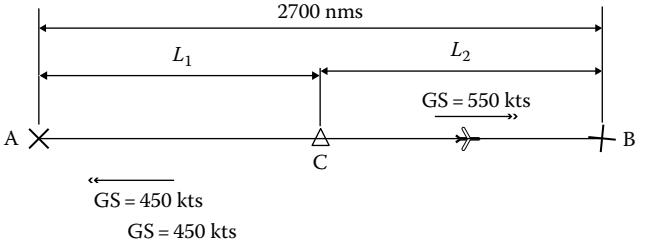


FIGURE 2.16
Flight track with critical point on track.

Problems

2.1 The following figure illustrates an airplane flying at an altitude of 10 km. Due to side and downward wind, the resultant speed is V_{p1} = 200 m/s. The angles (β_1 = 25°) and the angle (α = 15°) are encountered. The engine inlet area is 1.0 m². The exhaust speed is 400 m/s. Assuming

1. The angles ($\beta = \beta_1$)
2. The exhaust pressure is equal to the ambient pressure
3. The fuel-to-air ratio (f = 0.02)

It is required to calculate

a. What is the thrust force
b. What will be the value of thrust if only side gust is encountered (α =0)
c. What will be the thrust value if there is only upward gust (β_1 = 0)
d. What will be the value of thrust if no gust is encountered ($\alpha = \beta_1 = 0$)

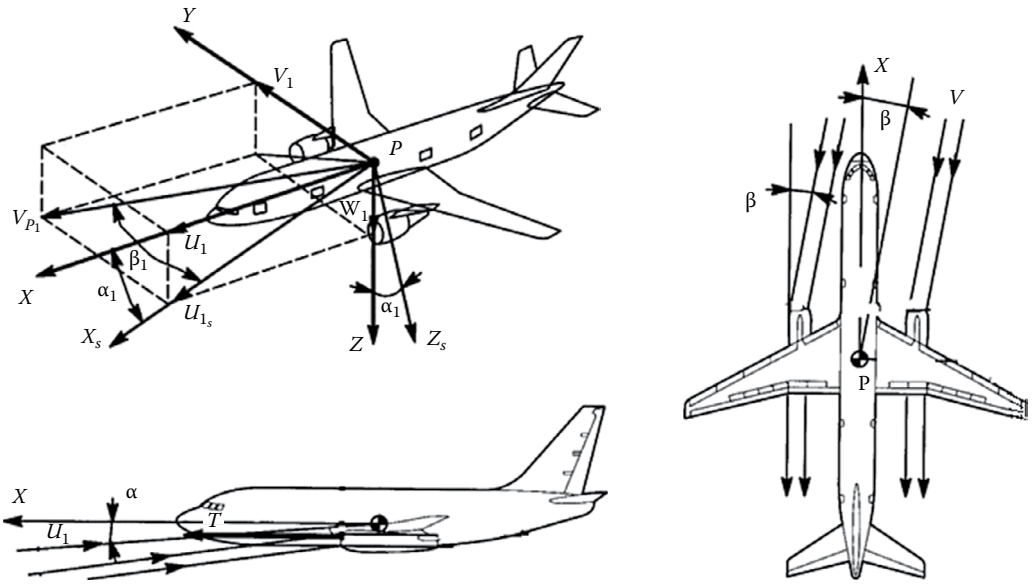


FIGURE P2.1

2.2 An aircraft flies with 280 m/s at an altitude of 20 km, where the ambient pressure and temperature are 26.5 kPa and 223.16 K, respectively. The jet speed, pressure, and temperature are 600 m/s, 750 K, and 30 kPa, respectively. The propulsion system of the aircraft consumes 200 kg/s of air and burns 6 kg/s of fuel having a heating value of Q_R = 42,600 kJ/kg.

Calculate

1. The specific thrust ($T/\dot{m}_a$)
2. The propulsive efficiency (η_{pr}), thermal efficiency (η_{th}), and overall efficiency (η_o)
3. The TSFC
4. The exhaust Mach number ($\gamma = \frac{4}{3}, R = 287\ \text{J/kg}\cdot\text{K}$)

2.3 A rocket has three nozzles canted at 30° with respect to the rocket's centerline. The gases exit at 2200 m/s through the exit area of 1.2 m^2. The density of the exhaust gases is 0.35 kg/m^3, and the pressure is 55 kPa. The atmospheric pressure is 12 kPa. Determine the thrust on the rocket.

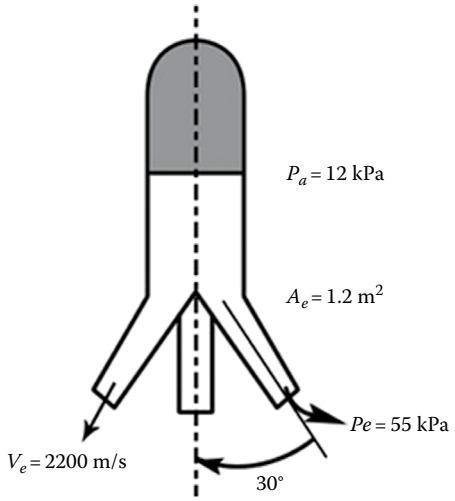


FIGURE P2.3

2.4 The pilot of a jet plane applied thrust reverse after the plane touched down. Air is sucked into the engine at the rate of 40 kg/s and the fuel-to-air ratio is 2.5%. The airplane speed is 80 m/s, while the exhaust gas speed is 500 m/s. The exhaust pressure is equal to the ambient pressure. What is the total reverse thrust of the airplane?

2.5 A turbojet engine powers an aircraft that is flying at a speed of 240 m/s, an exhaust speed of 560 m/s, and a specific thrust of 525 N·s/kg. Using the three different formulae, calculate the propulsive efficiency. What are your comments?

(Ignore the fuel-to-air ratio.)

Starting from the thrust force equation for an unchoked nozzle engine, prove that

$$\eta_{o\max} = \frac{(1+f)^2 u_e^2}{4fQ_R}$$

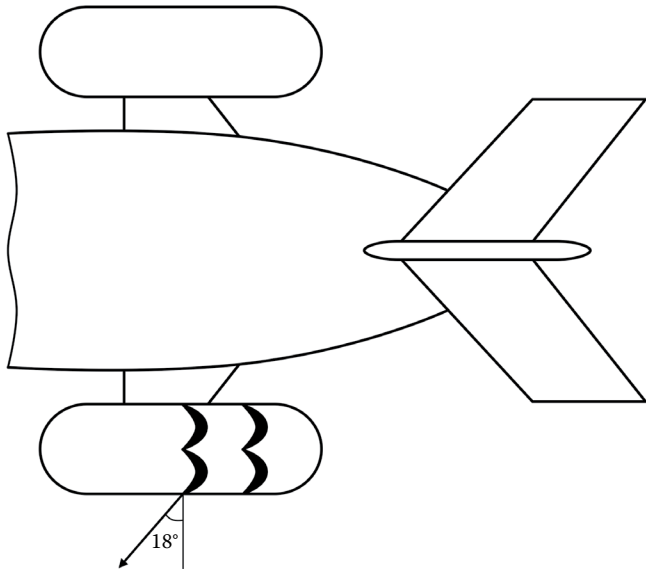


FIGURE P2.4

If λ is the ratio between the maximum overall efficiency and the overall efficiency ($\lambda = \eta_{o_{\max}}/\eta_o$), then prove that the flight speed u may be expressed by the relation $u = \dfrac{(1+f)u_e}{2}\left[1 \pm \sqrt{\dfrac{\lambda - 1}{\lambda}}\right]$.

Now, consider an aircraft fitted with a single engine that has the following data:

Air mass flow rate $\dot{m}_a = 100$ kg/s, exhaust speed $u_e = 770$ m/s,

Overall efficiency $\eta_o = 0.16$, maximum overall efficiency $\eta_{o_{\max}} = 0.18$,

Fuel-to-air ratio $f = 0.02$, lift/drag ratio $L/D = 10$, and

Aircraft mass ratio at takeoff and landing $m_1/m_2 = 1.2$

Calculate

1. The possible value(s) for flight speed
2. The heating value (Q_R)
3. The possible range(s) of aircraft
4. The trip time(s)
5. The aircraft masses m_1 and m_2
6. The thrust force(s)

2.6 For a turbojet engine, prove that the thrust force (T) and propulsive efficiency (η_p) are given by the following relations:

$$T = \dot{m}_a u(B + C) \quad \text{and} \quad \eta_p = \frac{B + C}{D + C - 1}$$

where

$$C = \frac{A_e P_a}{\dot{m}_a u}\left[\left(\frac{P_e}{P_a}\right) - 1\right]$$

$$D = \frac{1}{2}(1+f)\left[\left(u_e/u\right)^2 + 1\right]$$

Next, if the nozzle is unchoked, then

$$\eta_p = \frac{B}{D-1}$$

Moreover, if the nozzle is unchoked and (f) is negligible, then

$$\eta_p = \frac{2u}{u+u_e}$$

2.7 For a turbojet engine having the following data:

$$\dot{m}_a = 50 \text{ kg/s}, \quad f = 0.015, \quad u_e = 500 \text{ m/s}$$
$$P_a = 60 \text{ kPa}, \quad P_e = 120 \text{ kPa}, \quad A_e = 0.25 \text{ m}^2$$

Plot

1. The relation between the propulsive efficiency η_p and the speed ratio (u/u_e)
2. The relation between the thrust force and the speed ratio (u/u_e)

The flight speed u varies from 0 to 500 m/s.

2.8 To examine the effect of fuel-to-air ratio (f), plot the two relations for the following values of f: $f = 0.0$, 0.01, 0.015, and 0.02.

2.9 To examine the effect of exhaust pressure, plot the relations for the case in Problem 2.5, with variable P_e. Take $P_e = 60$, 90, 120, and 150 kPa.

2.10 Apply the Reynolds transport equation

$$\frac{DN}{Dt} = \oiint_{cs} \eta\rho\bar{u}\cdot d\bar{A} + \frac{\partial}{\partial t}\iiint_{cv} \eta\rho \, d\forall$$

to a turbofan engine to derive the thrust equation

$$T = \dot{m}_h(1+f)u_h + \dot{m}_c u_c - \dot{m}_a u + A_h(P_h - P_a) + A_c(P_c - P_a)$$

where $d\forall$ is the element of volume

$$\dot{m}_a = \dot{m}_c + \dot{m}_h$$

u_h, u_c are the exhaust speeds of the hot and cold streams, respectively
A_h, A_c are the exhaust areas of the hot and cold streams, respectively
P_a is the ambient pressure
u is the flight speed
f is the fuel-to-air ratio

2.11 Show that the specific thrust and the TSFC for a turbofan engine can be expressed as

$$\frac{T}{\dot{m}_a} = \frac{1+f}{1+\beta}u_{e_h} + \frac{\beta}{1+\beta}u_{e_c} - u$$

and

$$TSFC = \frac{f}{(1+\beta)(T/\dot{m}_a)}$$

2.12 The JT9D high-BPR turbofan engine at maximum static power ($V_0 = 0$) on a sea-level standard day ($P_0 = 14.696$ psia, $T_0 = 518.7°$ R) has the following data.

The air mass flow rate through the core is 247 lb_m/s, the air mass flow rate through the fan bypass duct is 1248 lb_m/s, the exit velocity from the core is 1190 ft/s, the exit velocity from the bypass duct is 885 ft/s, and the fuel flow rate into the combustor is 15,570 lb_m/h. For the case of exhaust pressures equal to ambient pressure ($P_0 = P_e$), estimate the following:

1. The thrust of the engine
2. The thermal efficiency of the engine (the heating value of jet fuel is about 18,400 Btu/lb_m)
3. The propulsive efficiency and TSFC of the engine

2.13 An aircraft is powered by two turbojet engines having the following characteristics:

Exhaust velocity $u_e = 2300$ km/h

Maximum overall efficiency $\eta_{o_{max}} = 0.15$

Fuel-to-air ratio $f = 0.0175$

Lift-to-drag ratio $L/D = 10$

Mass ratio at the beginning and end of the trip $m_1/m_2 = 1.2$

The maximum range is expressed by the relation

$$S_{max} = \frac{\eta_{o_{max}} Q_R}{g}\frac{L}{D}\ln\left(\frac{m_1}{m_2}\right)$$

where the maximum overall efficiency ($\eta_{o_{max}}$) is stated in Problem 2.2 and the corresponding flight speed is given by the relation $u = \frac{(1+f)}{2}u_e$.

Calculate

1. The flight speed (u)
2. The heating value (Q_R)
3. The maximum range of aircraft
4. The trip time
5. The value of m_1 and m_2

2.14 A fighter aircraft flies at a speed of 250 m/s. It is powered by a single turbojet engine having an inlet area of 0.35 m^2. Use the ISA standard tables for altitudes from 3 to 18 km to

1. Plot the air mass flow rate entering the engine versus altitude.
2. Plot the thrust force against the altitude, assuming the exhaust speed is constant and equal to 600 m/s, the fuel-to-air ratio $f = 0.025$, and the nozzle is unchoked.

2.15 The range factor of aircraft (*RF*) is defined as

$$RF = \frac{C_L}{C_D}\frac{u}{TSFC}$$

with

$$u = M\sqrt{\gamma R T_a}$$

and

$$TSFC = \left(1.7 + 0.26M\right)\sqrt{\theta}$$

Plot the range factor versus the Mach number for altitudes of 0, 5, 10, and 20 km, where $\theta = T/T_{S.L}$, T is the temperature at any altitude, and $T_{S.L}$ is the sea-level temperature (both are in Kelvin degrees). The aircraft weight is 150 kN, and the drag coefficient is given by the relation $C_D = K_1 C_L^2 + K_2 C_L + C_{D_0}$, where $C_{D_0} = 0.012$, $C_L = 0.3$, $K_1 = 0.2$, and $K_2 = 0.0$.

2.16

1. Prove that the wind has no effect on endurance factor (*EF*)
2. Prove that the range factor in the presence of wind is expressed by

$$RF = \left(RF\right)_{no\ wind} \mp V_w \times EF$$

where
$(RF)_{no\ wind}$ is the range factor for given flight schedule with no wind
EF is the endurance factor for the same flight schedule
V_w is the component of wind along the trajectory
+ is tail wind
– is head wind

2.17

1. Write the expressions for the effective jet velocity of both cold (fan) and hot (core) streams.
2. Use the expressions to find the global effective jet velocity based on the total air mass flow rate.
3. Find the expressions for the propulsive, thermal, and overall efficiencies employing the effective jet velocities obtained in (1).

2.18 Prove that the maximum range is expressed by

$$R = \frac{IU}{g}\left(\frac{L}{D}\right)_{\max} \ln\left(\frac{M_{initial}}{M_{final}}\right)$$

2.19 What is the ESFC of a turboprop engine that consumes 1500 lb of fuel per hour and produces 700 lb of exhaust thrust and 3300 shaft horsepower during flight at 250 mph? The propeller efficiency is 0.9.

2.20 An aircraft flies at 280 m/s at an altitude of 20 km, where the ambient pressure and temperature are 26.5 kPa and 223.16 K, respectively. If the propulsion system of the aircraft sucks 200 kg/s of air and burns 6 kg/s of fuel having a heating value of $Q_R = 42{,}600$ kJ/kg, calculate the specific thrust ($T/\dot{m}_a$), propulsive efficiency (η_{pr}), thermal efficiency (η_{th}), overall efficiency (η_o), and TSFC, if the jet speed, pressure, and temperature are 600 m/s, 750 K, and 30 kPa, respectively.

2.21 Prove that

$$\frac{\eta_0}{u_e^2} = \lambda\left(1 - \frac{u}{u_e}\right)\frac{u}{u_e}$$

where $\lambda = 1/fQ_R$

1. *Plot* $\left(\frac{\eta_0}{\lambda u_e^2}\right)$ versus $\left(\frac{u}{u_e}\right)$, with $\frac{u}{u_e}$ varying from (0 to 1.0)
2. *Deduce* when $\left(\frac{\eta_0}{\lambda u_e^2}\right)$ attains a maximum value. Comment!

2.22 An aircraft is powered by two turbofan engines, each generating 100 kN thrust force. The lift-to-drag ratio of the aircraft is 6.0. The aircraft has the following data:

1. Initial mass of the aircraft is 100,000 kg
2. $TSFC = 0.03$ kg/(N·h)
3. Overall efficiency $\eta_0 = 0.3$
4. Fuel heating value $Q_R = 43$ MJ/kg

For a trip of 3 h, calculate

a. The fuel consumed in the trip
b. The distance traveled by the aircraft

2.23 Oil price spikes and the need for increased energy security have generated extensive researches for a new energy source, namely, biofuels (fuels derived from plant or microalgae). On November 7, 2011, United Airlines flew the world's first commercial aviation flight on a microbially derived biofuel using Solazyme's algae-derived renewable jet fuel. The Eco-skies Boeing 737-800 plane was fueled with 40% biofuel, having a heating value of 37.27 MJ/kg, and 60% petroleum-derived jet fuel, having a heating value of 42 MJ/kg. If the aircraft mass is 70 tons at cruise with a speed of 530 mi/h (0.785 Mach number) at 35,000 ft, and the thrust/weight ratio of Boeing 737-800 is 0.2789, and if the aircraft uses 2187 kg/h fuel when using petroleum-derived jet fuel only, calculate

1. The propulsion system total thrust and overall efficiency (η_o)
2. The TSFC
3. Recalculate the TSFC in the following two cases:
   a. 100% biofuel
   b. 40% biofuel + 60% petroleum-derived fuel
4. Write your comments for biofuel usage.

2.24 An aircraft engine consumes 100 kg/s of air and 0.02 fuel-to-air ratio when it flies at 250 m/s at an altitude of 15 km (the ambient pressure and temperature are 12 kPa and 216.66 K, respectively).

1. Calculate the net thrust, propulsive efficiency (η_{pr}), thermal efficiency (η_{th}), overall efficiency (η_o), and TSFC in the following cases:

   Case 1. Jet speed of $u_e = 250$ m/s and pressure of $P_e = 12$ kPa

   Case 2. Jet speed of $u_e = 350$ m/s and pressure of $P_e = 12$ kPa

   Case 3. Jet speed of $u_e = 350$ m/s and pressure of $P_e = 16$ kPa

   Case 4. Jet speed of $u_e = 450$ m/s and pressure of $P_e = 12$ kPa

2. Plot the variation in net thrust, propulsive efficiency (η_{pr}), thermal efficiency (η_{th}), overall efficiency (η_o), and TSFC versus u/u_e for jet pressures of $P_e = 12$, 15, and 20 kPa.

   (Hint: Take $u/u_e = 0:1$.)

2.25 A turbofan engine is fixed on an open test rig (atmospheric pressure and temperature $P_a = 101$ kPa and $T_a = 288.16$ K). The test results are fuel mass flow rate 10 kg/s, net thrust of $T = 200$ kN, hot jet temperature $T_{eh} = 900$ K, hot jet pressure $P_{eh} = 150$ kPa, cold jet temperature $T_{ec} = 400$ K, and cold jet pressure $P_{eh} = 125$ kPa. For a BPR of $\beta = 4$ and a fuel heating value of $Q_R = 43{,}000$ kJ/kg, calculate

1. The total air mass flow rate
2. The specific thrust ($T/\dot{m}_a$)
3. The propulsive efficiency (η_{pr})
4. The thermal efficiency (η_{th})
5. The overall efficiency (η_o)
6. The TSFC

2.26 A turbofan-powered aircraft flies at an altitude of 13 km, where the ambient pressure and temperature are 16.52 kPa and 216.66 K, respectively. The turbofan engine consumes 500 kg/s of air and 2 kg/s of fuel having a heating value of $Q_R = 44{,}000$ kJ/kg. The exhaust speeds of hot and cold streams are 600 m/s and 320 m/s, respectively (full expansion in both nozzles).

Plot the variation in net thrust, propulsive efficiency (η_{pr}), thermal efficiency (η_{th}), overall efficiency (η_o), and TSFC versus aircraft speed for three BPRs of $\beta = 2$, 5, and 9.

(Hint: Assume that u varies from 0 to 300 m/s.)

2.27 For a turbofan engine with unchoked nozzles, prove that if the fuel-to-air ratio is negligible ($f \approx 0$), then the propulsive efficiency is expressed as

$$\eta_p = \frac{2u\left[u_{e_h} + \beta u_{e_c} - (1+\beta)u\right]}{u_{e_h}^2 + \beta u_{e_c}^2 - (1+\beta)u^2}$$

Next, plot the relation η_p versus u for the following cases:

β	u (m/s)				u_{e_c} (m/s)	u_{e_h} (m/s)
0.5	0	200	450	700	750	1000
2.0	0	200	400	400	700	950
5.0	0	100	200	300	500	800
8.0	0	100	200	302	450	750

2.28 Before the afterburners are turned on, an airplane is traveling at 475 mph. Twenty seconds after the afterburners are turned on, the plane is traveling at 560 mph.

1. What is the average acceleration of this airplane over those 20 s?
2. How far does the plane travel in those 20 s?

2.29 An airplane (m = 174,000 kg) is cruising at 241.40 m/s. The afterburners are ignited for 2.00 min providing an average thrust of 20 kN.

1. What is the velocity of the airplane after those 2.00 min?
2. How far did the airplane travel over those 2.00 min? (Assume that the mass of the airplane stays constant.)

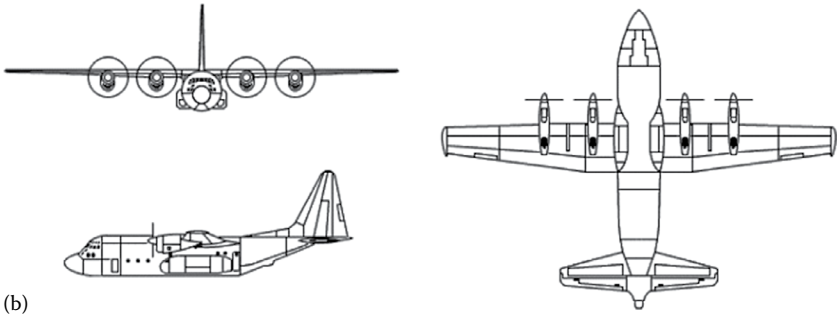
2.30 Compare the fuel consumed by the following four airplanes for a flight trip of 3600 km:

Aircraft	**Boeing 707**	**C-130**	**Airbus 320-200**	**Antonov AN-70**
Engines	4 Turbojet P&W JT3C	4 Turboprop T56-A-15	2 Turbofan IAV-V2500	4 Propfan Progress D-27
Thrust/power per engine	53.5 kN	4590 ehp	120 kN	14,000 ehp
Cruise speed (km/h)	885	592	828	750
TSFC/ESFC	22.24 g/(kN·s)	0.21 kg/(ehp·h)	14 g/(kN·s)	0.13 kg/(ehp·h)
Number of operative engines	4	4	2	2

ehp, equivalent horsepower.



(a)



(b)

FIGURE P2.30

(*Continued*)



(c)



(d)

FIGURE P2.30 (*Continued*)

2.31 The shown figure illustrates space shuttle Endeavor, sitting atop of carrier NASA Boeing 747-400, which is powered by 4 turbofan engines GE CF6-50E. If the thrust force is expressed by the relation

$$\tau = \dot{m}\left(u_e - u\right)$$

1. Prove that the thrust is a maximum when

$$u = 0.5\,u_e$$



FIGURE P2.31

2. Only the carrier Boeing 747-400 is considered here. It has the following data:

Gross mass	396,890 kg
Wing area	525 m^2
Drag coefficient	0.035
Exhaust jet speed	600 m/s
Engine thrust force	106 kN
Air density	0.414 kg/m^3
Engine inlet area	3.14 m^2

Calculate

a. The minimum flight speed
b. The maximum thrust that the engine can develop if ($u = 0.5u_e$)
c. The maximum acceleration

3. Consider the assembly case with space shuttle atop of Boeing 747 as shown in the figure. Space shuttle has the following data:

Gross mass	110,000 kg
Wing area	343 m^2
Drag coefficient	0.025

For the same minimum flight speed calculated earlier, calculate the maximum acceleration of the space shuttle Boeing assembly.

References

1. R. Crawford and R. Schulz, *Fundamentals of Air Breathing Propulsion*, University of Tennessee Space Institute, Knoxville, TN, Aero propulsion Short Course, PS-749, 2016.
2. United Technologies' Pratt Whitney, *The Aircraft Gas Turbine Engine and Its Operation*, P&W Operation Instruction 200, 1988, pp. 1–10.
3. H. Moustapha, *Turbomachinery & Propulsion*, Pratt & Whitney Canada Inc., Course Handbook p. 61.
4. *The Jet Engine*, 5th edn., Rolls Royce Plc, 2005, Reprinted 1996 with revisions.
5. J. Kurzke, *Aero-Engine Design: A State of the Art, Preliminary Design*, Von Karman Institute Lecture Series, 2002–2003, April 2003, p. 14.
6. M.J. Zucrow, *Aircraft and Missile Propulsion*, Belgium, Volume I: Thermodynamics and Fluid Flow and Application to Propulsion Engines, John Wiley & Sons, 1958, p. 21.
7. H. Ashly, *Engineering Analysis of Flight Vehicles*, Addison-Wesley Publication Co, 1974, p. 140.
8. H.I.H. Saravanamuttoo, G.F.C. Rogers, and H. Cohen, *Gas Turbine Theory*, 5th edn., Prentice Hall, 2001.
9. P. Hill and C. Peterson, *Mechanics and Thermodynamics of Propulsion*, 2nd edn., Addison Wesley Publication Company, Inc., 1992, p. 155.
10. D.G. Shepherd, *Aerospace Propulsion*, American Elsevier Publishing Company, Inc., 1972, p. 28.
11. J.D. Mattingly, *Elements of Gas Turbine Propulsion*, McGraw-Hill International Edition, 1996, p. 44.
12. J.D. Anderson, Jr., *Aircraft Performance and Design*, WCB/McGraw-Hill, 1999, p. 293.
13. G. Corning, *Supersonic and Subsonic CTOL and VTOL Airplane Design*, 4th edn., College Park, University of Maryland, 1979, Box No.14, p. 2.38.
14. R. Shevell, *Fundamentals of Flight*, Prentice-Hall, Inc., 1983, p. 265.
15. D.P. Raymer, *Aircraft Design: A Conceptual Approach,* AIAA Education Series, 1999.


Taylor & Francis
Taylor & Francis Group
http://taylorandfrancis.com

3

Pulsejet and Ramjet Engines

3.1 Introduction

This chapter introduces two types of airbreathing engines of the athodyd type. This abbreviation stands for Aero-THermODYnamic-Duct. Thus, these engines are pulsejet and ramjet engines. Both have no major rotating parts (fan/compressor or turbine) and include three stationary modules: an intake (or entry duct), a combustion chamber, and a nozzle [1].

The first engine, the pulsejet, operates intermittently and has limited applications [2]. The reasons are the difficulty of its integration into manned aircraft as well as its high fuel consumption, poor efficiency, severe vibration, and high noise. The second engine, the ramjet, is appropriate for supersonic flight speeds [3], where the ram compression of the air becomes sufficient to overcome the need for mechanical compression achieved normally by compressors or fans in other turbine-based or shaft-based jet engines. If the flight speed is so high that fuel combustion must occur supersonically, then this ramjet is called a scramjet [4]. The pulsejet, ramjet, and scramjet, then, are the three types of ram-based engines. As outlined earlier, this chapter will handle two types of the ram-based engine, while the third, the scramjet, will be discussed in Chapter 7, which deals with high-speed supersonic and hypersonic engines.

3.2 Pulsejet Engines

3.2.1 Introduction

The pulsejet engine is a very simple jet engine, which comprises an air intake, a combustion chamber, and an acoustically resonant exhaust pipe. It is a jet engine to which the intake of air is intermittent; thus, combustion occurs in pulses, resulting in a pulsating thrust rather than a continuous one.

Presently, there are two types of pulsejet: valved and valveless. The valved type is fitted with a one-way valve, while a valveless engine has no mechanical valves at its intake. A third future type, known as pulse detonation engine (PDE), is in the research and testing phase of production. The aim is to create a jet engine that operates on the supersonic detonation of fuel.

Martin Wiberg (1826–1905) developed the first pulsejet in Sweden. The first type, the valved or traditional pulsejet, was used to power a German cruise missile called the

Vergeltungswaffe 1 (Vengeance 1), or V1, and normally referred to as the V-1 flying bomb (see Figure 1.38). It was extensively used in bombing England and Belgium during World War II. The engines made a distinctive sound, leading the English to call them "buzz bombs."

In July 1944, captured V-1 components were shipped to the United States. Before long, the USAAF and U.S. industry had built their own V-1, which was designated the "Jet Bomb 2" (JB-2). The USAAF also experimented with air-launching the JB-2 from B-17 bombers, B-24s, and B-29s. The U.S. Navy experimented with their own V-1 variant, identified as the "KUW-1 (later LTV-N-2) Loon." Two submarines, the USS *Cusk* and the USS *Carbonero*, were modified and launched in 1949 and 1950.

The Soviets also built copies and derivatives of the V-1. In 1944, Japan also relied upon the Argus pulsejet Fieseler Fi-103 "Reichenberg" (Fi103R) manned version of the V-1 in designing their rocket-powered aircrafts for suicide missions, known as the "*Yokosuka MXY7 Ohka Japanese flying bomb*," against Allied naval forces. In the 1950s, the French operated a target drone, named the "Arsenal 5.501," based on the V-1. It was different from the original design in having twin tail fins and radio control. Pulsejet engines were attached to the extreme ends of the rotor blades in the 1950s and used to power experimental helicopters. In the twenty-first century, with the interest in unmanned aerial vehicles (UAVs), various agencies and contractors have started looking for ways to propel these tiny vehicles with an efficient, affordable, and robust power source. The pulsejet is one of these options. Finally, the flying bomb concept can be seen today in the modern cruise missile.

The pulsejet engine is extremely simple, cheap, and easy to construct. However, it has low reliability, poor fuel economy, and very high noise levels. The high noise levels make it impractical for other than military applications and similarly restricted applications. Pulsejets have been used to power experimental helicopters, the engines being attached to the extreme ends of the rotor blades. They have also been used in both tethered and radio-control model aircraft. The speed record for tethered model aircraft is 186 miles per hour (299 km/h), set in the early 1950s.

The valved type has a set of one-way valves (or check valves) through which the incoming air passes. The valving is accomplished through the use of reed valves, which consist of thin flexible metal or fiberglass strips fixed on one end that open and close upon changing pressures across opposite sides of the valve, much like heart valves do. Fuel in the form of a gas or liquid aerosol is either mixed with the air in the intake or injected into the combustion chamber. When the air/fuel is ignited, these valves slam shut, which means that the hot gases can only leave through the engine's tail pipe, thus creating forward thrust. The cycle frequency is primarily dependent on the length of the engine. For a small model-type engine, the frequency may be typically around 250 pulses per second, whereas for a larger engine such as the one used on the German V1 flying bomb, the frequency was closer to 45 pulses per second. Once the engine is running, it requires only an input of fuel, but it usually requires forced air and an ignition method for the fuel–air mix. Once running, the engine is self-sustaining. The main drawback of the valved type is that the valves require regular replacement and represent a weak link in the engine's reliability. The pulsejet-powered V1 flying bombs were only good for about 20–30 min of continuous operation. So, by eliminating the valves, it should be possible to make an engine that is as simple as a ramjet having absolutely no moving parts. Thus, a valveless type is employed.

The name valveless is really a misnomer. These engines have no mechanical valves, but they do have aerodynamic valves, which, for the most part, restrict the flow of gases to a single direction just as their mechanical counterparts do. Thus, this type of pulsejet has no mechanically moving parts at all and in that respect is similar to a ramjet.

3.2.2 Valved Pulsejet

Figure 3.1 illustrates the simple construction of valved type together with its cycle on the temperature entropy diagram.

The cycle can be described briefly as follows:

1. The air is sucked into the combustion chamber through a bank of spring-loaded check (reed) valves by the vacuum created by the exhaust of the previous cycle. These valves are normally closed, but if a predetermined pressure differential exists, they will open to permit high-pressure air from the diffusing section to pass into the combustion chamber. They never permit flow from the combustion chamber back into the diffuser.

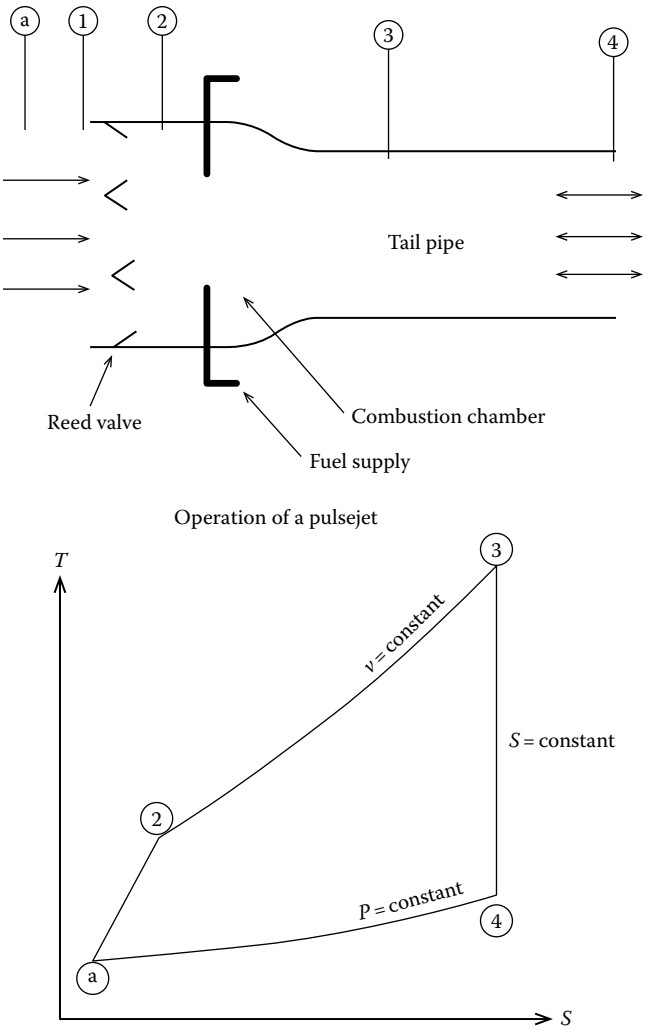


FIGURE 3.1
Valved pulsejet engine.

2. A spark plug initiates the combustion process, which occurs at something approaching a constant volume process [5]. Such combustion occurs in the form of an explosion, which raises the pressure in the combustion chamber to a high level and closes the spring valve at the intake.
3. The resultant high pressure and temperature force the gases to flow out of the tail pipe at high velocity.

   At the end of discharge, the inertia of the gas creates a vacuum in the combustion chamber, which, together with the ram pressure developed in the diffuser, causes sufficient pressure differential to open the check valves. A new charge of air enters the chamber and a new cycle starts. The frequency of the cycle depends on the size of the engine, and the dynamic characteristics of the valves must be matched carefully to this frequency. Small-size engines operate as high as 300–400 cycles/s, and large engines operate as low as 40 cycles/s.

To start the engine, a carefully adjusted amount of fuel is sprayed into the cold combustion chamber in order to create a mixture and the resultant strong explosion starts the cycle. The fuel flow, injected directly into the combustion chamber, is continuous throughout the cycle with some variation in fuel flow resulting from the pressure in the combustion chamber. This fuel flow fluctuation can be neglected.

1. Intake or diffuser

   This process occurs from state (a) to state (2) as shown in Figure 3.1. State (a) is far upstream, while state (1) is at the pulsejet inlet, and state (2) is just aft of the check valve upstream of the combustion chamber. Due to ram effect, both the pressure and temperature rise from the ambient conditions to the values to be calculated hereafter. The total conditions at state (1) are given by the relations

$$P_{01} = P_{0a} = P_a\left(1 + \frac{\gamma_c - 1}{2} M^2\right)^{\gamma_c/\gamma_c - 1} \tag{3.1}$$

   where

   M is the flight Mach number

   γ_c is the specific heat ratio for cold air

   The stagnation temperatures for states (a), (1), and (2) are also equal:

$$T_{01} = T_{0a} = T_a\left(1 + \frac{\gamma_c - 1}{2} M^2\right) \tag{3.2}$$

   If it is assumed that the diffuser is an ideal one, then the total pressure and temperature at state (2) are equal to those at state (1), or

$$P_{02} = P_{01} \tag{3.3}$$

   and

$$T_{02} = T_{01} \tag{3.4}$$

The total temperature at state (2) is always equal to its value at state (1). However, due to losses in the diffuser and check valves, the pressure at state (2) is less than that at (1). It may even reach half its value at state (1). In general, if the diffuser efficiency (η_d) is specified, then the total pressure will be calculated from the relation

$$P_{02} = P_a\left(1+\eta_d\frac{\gamma_c-1}{2}M_a^2\right)^{\gamma_c/\gamma_c-1} \tag{3.5}$$

2. Combustion chamber
Combustion takes place at a nearly constant volume process; thus,

$$P_{03} = P_{02}\left(T_{03}/T_{02}\right)$$

Fuel is added to the combustion chamber and burnt. The mass-flow rate of the burnt fuel is calculated from the energy balance of the combustion chamber:

$$\left(\dot{m}_a+\dot{m}_f\right)Cp_hT_{03} = \dot{m}_aCp_cT_{02}+\eta_b\dot{m}_fQ_R$$

where $f=\dot{m}_f/\dot{m}_a$, η_b being the burners (or combustion chamber) efficiency, and C_{pc}, C_{ph} are the specific heats for the cold air and hot gases.

The fuel-to-air ratio is determined from the relation

$$f = \frac{Cp_hT_{04}-Cp_cT_{03}}{\eta_bQ_R-Cp_hT_{04}} \tag{3.6}$$

Tail pipe: The gases expand isentropically in the tail pipe to the ambient pressure. Thus, $p_7=p_a$ and the temperature of the exhaust gases is determined from the relation

$$\left(\frac{T_{03}}{T_4}\right)=\left(\frac{P_{03}}{P_a}\right)^{\gamma_h-1/\gamma_h} \tag{3.7}$$

The exhaust velocity is now calculated from the relation

$$U_e = \sqrt{2Cp_hT_{03}\left[1-\left(P_a/P_{03}\right)^{\gamma_h-1/\gamma_h}\right]} \tag{3.8}$$

The thrust force is now calculated from the relation

$$T = m_a\left[\left(1+f\right)U_e-U\right] \tag{3.9}$$

The thrust-specific fuel consumption (TSFC) is given by the relation

$$\text{TSFC} = \frac{\dot{m}_f}{T} = \frac{f}{\left(T/\dot{m}_a\right)} \tag{3.10}$$

Example 3.1

A pulsejet engine is employed in powering a vehicle flying at a Mach number of 2 at an altitude of 40,000 ft. The engine has an inlet area of 0.084 m^2. The pressure ratio at combustion chamber is $P_{03}/P_{02}=9$, fuel heating value is 43,000 kJ/kg, and combustion efficiency is 0.96. Assuming ideal diffuser ($P_{02}=P_{0a}$), it is required to calculate

1. The air mass flow rate
2. The maximum temperature
3. The fuel-to-air ratio
4. The exhaust velocity
5. The thrust force
6. The TSFC

Solution

At an altitude of 40,000 ft, the ambient temperature and pressure are 216.65 K and 18.75 kPa, respectively.

The flight speed is

$$U = M\sqrt{\gamma RT_a} = 2\sqrt{1.4\times 287\times 216.65}$$

$$U = 590 \text{ m/s}$$

The air mass flow rate is

$$\dot{m}_a = \rho_a U A_i = \frac{P_a}{RT_a} U A_i = 14.99 \text{ kg/s}$$

Diffuser: The total temperature at the intake is equal to the total upstream temperature, or

$$T_{02} = T_{0a} = T_a\left(1+\frac{\gamma_c - 1}{2}M^2\right)$$

$$T_{02} = 216.65\left(1+\frac{1.4-1}{2}\times 2^2\right)$$

$$T_{02} = 390 \text{ K}$$

The total pressure at the diffuser outlet is also equal to the free-stream total pressure as the flow through the diffuser is assumed ideal:

$$P_{02} = P_{0a} = P_a\left(T_{0a}/T_a\right)^{\gamma/\gamma-1}$$

$$P_{02} = 146.7 \text{ kPa}$$

Combustion chamber: A constant volume process is assumed; then

$$T_{03} = T_{02}\left(P_{03}/P_{02}\right)$$

$$T_{03} = 9T_{02} = 3510 \text{ K}$$

The fuel-to-air ratio is calculated from Equation 3.6 as

$$f = \frac{1.148\times 3{,}510 - 1.005\times 390}{0.96\times 43{,}000 - 1.148\times 3{,}510}$$

$$f = 0.0976$$

Tail pipe: The exhaust speed is calculated from Equation 3.8 as

$$U_e = \sqrt{2 \times 1148 \times 3510\left[1 - \left(18.75_a/1320.3\right)^{0.25}\right]}$$
$$U_e = 2297 \text{ m/s}$$

The specific thrust is

$$\frac{T}{\dot{m}_a} = (1+f)U_e - U$$
$$\frac{T}{\dot{m}_a} = 1931.4 \text{ N} \cdot \text{s/kg}$$

The thrust force is then $T = \dot{m}_a\left(T/\dot{m}_a\right) = 28{,}955$ N.

The TSFC is calculated from Equation 3.10 as

$$\text{TSFC} = \frac{0.0976}{1931.4} = 5.06 \times 10^{-5} \text{ kg/N} \cdot \text{s}$$
$$\text{TSFC} = 0.182 \text{ kg/N} \cdot \text{h}$$

Example 3.2

Figure 3.2 illustrates three views of the flying bomb V-1 powered by a pulsejet engine. It has the following data:

- The static thrust is 2220 N with an air inlet speed of 180 m/s.
- The intake area is 0.1 m^2.
- The fuel is standard 80-octane gasoline having a heating value of $Q_R = 40$ MJ/kg.
- The burner efficiency is 0.92.
- The typical flight duration is 1800 s.
- The exhaust temperature is 740 K.

Assume that the specific heat of air is $Cp_a = 1.005$ kJ/kg · K and the specific heat of hot gases is $Cp_h = 1.1$ kJ/kg · K.

Calculate

1. The air-mass flow rate into engine
2. The exhaust velocity
3. The maximum temperature inside the engine
4. The maximum pressure
5. The TSFC
6. The average range
7. The fuel consumed during mission

Solution

The air properties at sea-level conditions are

$$\rho_a = 1.225 \text{ kg/m}^3, \quad T_a = 288.2 \text{ K}, \quad P_a = 101.325 \text{ kPa}$$

1. Air-mass flow rate into engine

$$\dot{m}_a = \rho_a U A_i = 1.225 \times 180 \times 0.1 = 22.05 \text{ kg/s}$$

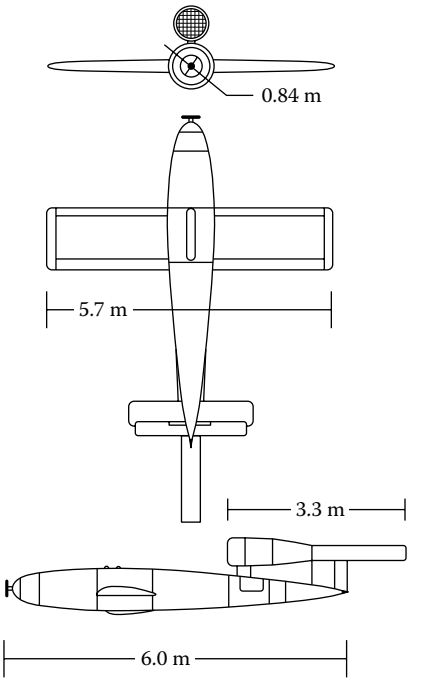


FIGURE 3.2
Flying bomb V-1.

2. Exhaust speed
   Since the thrust force is expressed by the relation

$$U_e = \frac{T + \dot{m}_a U}{\dot{m}_a (1 + f)}$$

   Assuming negligible fuel-to-air ratio, $f \cong 0$, then

$$U_e = \frac{T}{\dot{m}_a} + U = 280.7 \text{ m/s}$$

3. Maximum temperature at the engine (T_{03})

$$T_{03} = T_4 + \frac{U_e^2}{2Cp_h} = 740 + \frac{(280.7)^2}{2 \times 1100} = 775.8 \text{ K}$$

   The air temperature prior combustion is

$$T_{02} = T_{01} = T_{0a} = T_a + \frac{U^2}{2Cp_a} = 288.2 + \frac{(180)^2}{2 \times 1005} = 305.8 \text{ K}$$

   The fuel-to-air ratio is

$$f = \frac{Cp_h T_{03} - Cp_a T_{02}}{\eta_b Q_R - Cp_h T_{03}} = \frac{1.1 \times 775.8 - 1.005 \times 305.8}{0.92 \times 40,000 - 1.1 \times 775.8} = 0.01519$$

The fuel flow rate is

$$\dot{m}_f = f \times \dot{m}_a = 0.3349 \text{ kg/s}$$

Now, a better value for exhaust speed can be calculated from the original relation

$$U_e = \frac{T + \dot{m}_a U}{\dot{m}_a (1 + f)} = 276.5 \text{ K}$$

The maximum temperature can also be recalculated to be ($T_{03} = 778$ K).

4. Maximum pressure
   The air pressure prior combustion is

$$P_{02} = P_{01} = P_{0a} = P_a \times \left(\frac{T_{02}}{T_a} \right)^{\gamma/\gamma - 1} = 101.325 \times \left(\frac{305.8}{288.2} \right)^{3.5} = 124.69 \text{ kPa}$$

Since combustion takes place at a nearly constant volume process, then

$$P_{03} = P_{02} \times \frac{T_{03}}{T_{02}} = 124.69 \times \frac{778}{305.8} = 317.2 \text{ kPa}$$

Thus, the maximum pressure in engine is $P_{03} = 317.2$ kPa.

5. TSFC

$$\text{TSFC} = \frac{\dot{m}_f}{T} = \frac{0.3349}{2220} = 1.508 \times 10^{-4} \text{ kg/s} \cdot \text{N} = 0.543 \text{ kg/h} \cdot \text{N}$$

6. Average range

$$\text{Average range} = \text{Speed} \times \text{Time} = 180 \text{ m/s} \times 1800 \text{ s} = 324 \text{ km}$$

7. Fuel consumed

$$\text{Fuel consumed} = \dot{m}_f \times \text{Flight duration} = 602.9 \text{ kg}$$

3.2.3 Valveless Pulsejet

The valveless pulsejet engine is sometimes known as the acoustic jet engine [6]. This idea was the brainchild of the French propulsion research group SNECMA. They developed these valveless pulsejets in the late 1940s for use in drones. One application was the Dutch AT-21 target drone built by Aviolanda Aircraft from 1954 to 1958. The main design difficulties encountered for valved pulsejets result from difficult-to-resolve wear issues. So the valveless pulsejet was designed to replace the valved type. Valveless pulsejets are low in cost, lightweight, powerful, and easy to operate. They have all the advantages and most of the disadvantages of conventional valved pulsejets. Fuel consumption is excessively high and the noise level is unacceptable for recent standards. However, they do not have the troublesome reed valves that need frequent replacement. They can operate for their entire useful life with practically zero maintenance. They have been used to power model aircraft, experimental go-karts, and even some unmanned military aircraft such as cruise

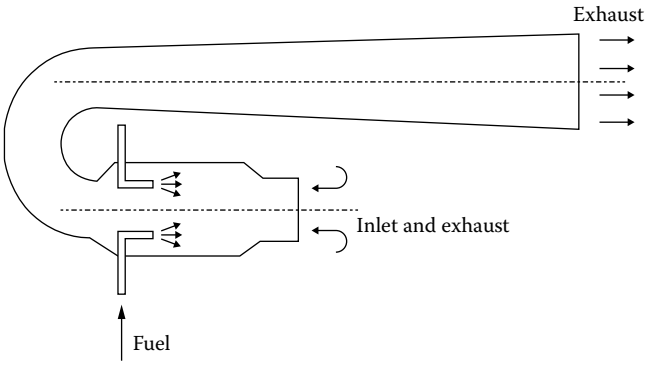


FIGURE 3.3
Valveless pulsejet engine.

missiles and target drones. These engines have no mechanical valves, but they do have aerodynamic valves, which, for the most part, restrict the flow of gases to a single direction just as their mechanical counterparts do. Thus, the intake and exhaust pipes usually face the same direction. This necessitates bending the engine into a "U" shape as shown in Figure 3.3 or placing a 180° bend in the intake tube. The Lockwood-Hiller is an example of the "U" shape design. When the air/fuel mixture inside the engine ignites, hot gases will rush out both the intake tube and the exhaust tube, since the aerodynamic valves "leak." If both tubes weren't facing in the same direction, less thrust would be generated because the reactions from the intake and exhaust gas flows would partially cancel each other.

In this type of pulsejet, the combustion process generates two shock-wave fronts, one traveling down each tube. By properly "tuning" the system, a stable, resonating combustion process can be achieved, which yields a considerable thrust.

Successful valveless pulsejets have been built from a few centimeters in length to huge sizes, though the largest and smallest have not been used for propulsion. The smallest ones are only successful when extremely fast-burning fuels are employed—acetylene or hydrogen, for example. Medium- and larger-sized engines can be made to burn almost any flammable material that can be delivered uniformly to the combustion zone, although of course volatile flammable liquids (gasoline, kerosene, various alcohols) and standard fuel gases (propane, butane, MAPP gas) are easiest to use. Because of the deflagration nature of pulsejet combustion, these engines are extremely efficient combustors, producing practically no hazardous pollutants, even when using hydrocarbon fuels. With modern high-temperature metals for the main structure, engine weight can be kept extremely low.

Up to the present, the physical size of successful valveless designs has always been somewhat larger than valved engines for the same thrust value, though this is theoretically not a requirement. An ignition system of some sort is required for engine start-up. In the smallest sizes, forced air at the intake is also typically needed for start-up. There is still much room for improvement in the development of really efficient, fully practical designs for propulsion uses.

3.2.4 Pulsating Nature of Flow Parameters in Pulsejet Engines

Several researches were performed to examine the fluctuating nature of flow properties within pulsejets since the 1940s [7]. Experimental investigations are still going on [8,9] as well as other numerical ones [6]. The fundamental operating frequency of the pulsejet

(f: cycles/s or Hz) is primarily related to the overall length of pulsejet (combustion and tail pipe) and can be expressed as

$$f \approx \frac{1}{L} \tag{3.11}$$

In acoustic terminology, a conventional pulsejet operates on a ($4L$) wave system. That is to say, four pressure waves (compression–rarefaction–rarefaction–compression; C_R_R_C) moving at or slightly above the local gas sound speed sequentially traverse the duct system (combustor + tail pipe = combustion tube of length $4L$) in one operational cycle. Thus, the operational period for one cycle in seconds is approximately

$$\Delta t_{cyc} \approx \frac{4L}{\mathrm{a}} \approx \frac{1}{f} \tag{3.12}$$

Various parameters in pulsejets like air mass flow rate, pressure, temperature, Mach number, and thrust force have a pulsating nature. Numerical simulation for various parameters in valved pulsejet was given in Reference 8.

As a trial for idealization of such pulsating behavior, a sinusoidal representation of the combustor pressure profile with time can be suggested [10]. Figure 3.4 illustrates the upper and lower absolute pressure limits about the idealized baseline pressure. Since they are nearly equal in magnitude, then $\Delta P = \mp 100\%$ for a symmetrical cycle (vacuum limit, $P \cong 0$, as the most negative trough point possible in the idealized sinusoidal cycle acting to enforce this limitation on performance).

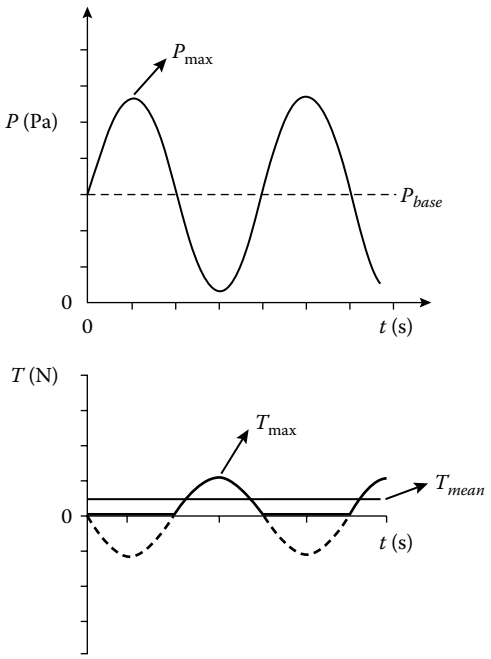


FIGURE 3.4
Idealized sinusoidal fluctuations in combustion pressure (P) and thrust force (T) versus time (t).

Analogous to the assumed idealized sinusoidal combustor pressure–time profile of Figure 3.4, one can assume a corresponding thrust–time profile would then have also a sinusoidal shape as shown in Figure 3.4. Assuming no appreciable negative thrust (resulting from backflow during the induction phase of the operational cycle), the remaining positive components of the cyclic thrust profile would produce a net mean thrust of

$$\bar{T} = \frac{T_{\max}}{\pi} \tag{3.13}$$

It is worth mentioning here that the results of numerical calculations in Reference 11 are far from Equation 3.13. In a case study, the maximum thrust was 110 N, while the average was 19.5 N.

3.2.5 Pulse Detonation Engine

The PDE marks a new approach toward noncontinuous combustion in jet engines and promises higher fuel efficiency compared even to turbofan jet engines. With the aid of the latest design techniques and high pulse frequencies, the drawbacks of the early designs can be overcome. To date, no practical PDE engine has been put into production, but several test bed engines have been built by Pratt & Whitney and General Electric that have proven the basic concept. Extensive research work is also carried out in different NASA centers. In theory, the design can produce an engine with an efficiency far surpassing gas turbine with almost no moving parts. These systems should be put to use in the near future.

All regular jet engines operate on the deflagration of fuel—that is, the rapid but subsonic combustion of fuel. The PDE is a concept currently in active development to create a jet engine that operates on the supersonic detonation of fuel.

PDEs are an extension of pulsejet engines. They share many similarities. However, there is one important difference between them: PDEs detonate, rather than deflagrate, their fuel. Detonation of fuel is a supersonic combustion of fuel that results in immense pressure, which in turn is used as thrust. These combustors have an advantage over traditional near-constant pressure combustors in being more thermodynamically efficient by approximating constant volume combustion. However, some analysis [12] suggests that detonation is neither a constant volume nor constant pressure combustion, but rather a distinctive change in the thermodynamic state properties specific to the detonation process [12].

The main objective of pulse detonation is to provide an efficient engine that is primarily used for high-speed (about Mach 5) civilian transport as well as many military applications, including supersonic vehicles, cruise missiles, afterburners, UAVs, single-stage to orbit (SSTO) launchers, and rockets.

PDEs use intermittent detonation waves to generate thrust. The cycle of a PDE is illustrated in Figure 3.5. Unlike the pulsejet, combustion in PDE is supersonic, effectively an explosion instead of burning, and the shock wave of the combustion front inside the fuel serves the purpose of the shutters in a valved pulsejet. A detonation propagating from the closed end of the tube is followed by an unsteady expansion wave (called Taylor wave) whose role is to bring the flow to rest near the closed end of the tube. When the shock wave reaches the rear of the engine and exits, the combustion products are ejected in "one go," the pressure inside the engine suddenly drops, and the air is pulled in from the front of the engine to start the next cycle.

The PDE operation is not determined by the acoustics of the system and can be directly controlled. PDEs typically operate at a frequency of 50–100 Hz, which means that a typical

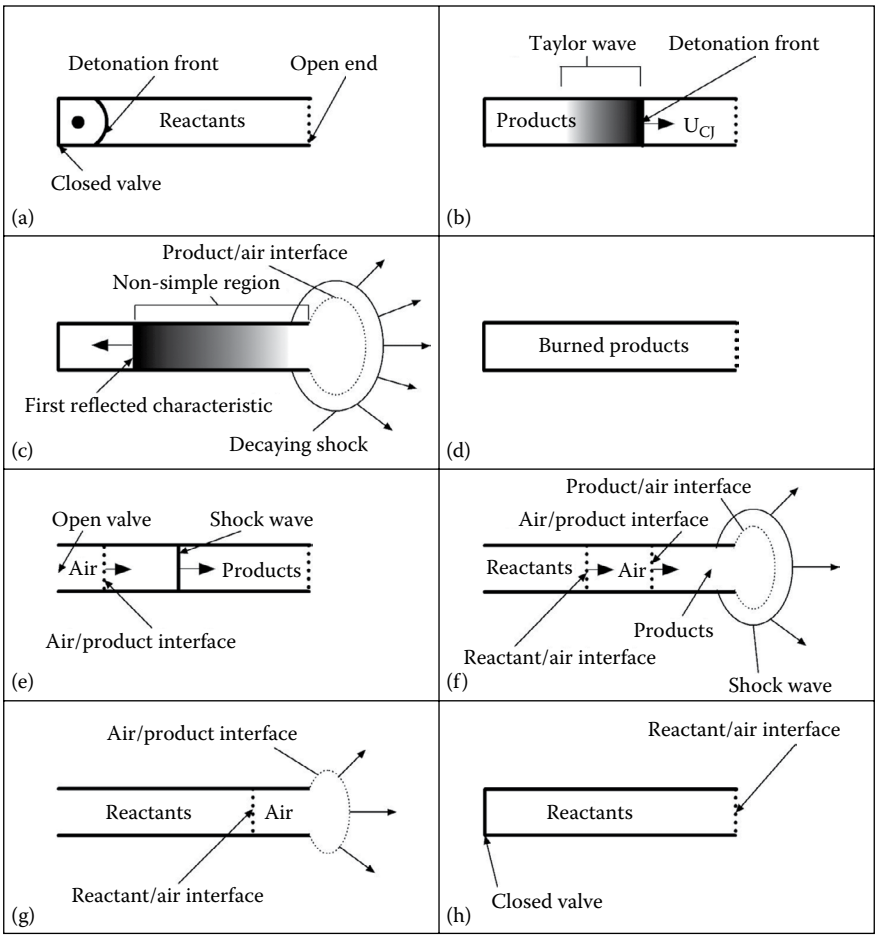


FIGURE 3.5
PDE thermodynamic cycle. (a) Initiation of detonation, (b) detonation, (c) wave reflection, (d) exhaust stage, (e) air/product interface, (f) purging start, (g) complete purging, and (h) filling.

cycle time is in the order of 10–20 ms. Since a PDE produces a higher specific thrust than a comparable ramjet engine at low supersonic speeds, it is suitable for use as part of a multistage propulsion system. The specific impulse for a PDE is plotted versus several other pulse and ramjet engines for comparison as shown in Figure 3.6. A single-tube supersonic impulse PDE with straight detonation has higher performance than ideal ramjet engines for flight Mach number up to 1.35. The PDE can provide static thrust for a ramjet or scramjet engine or operate in combination with turbofan systems.

A PDE can be classified as pure (stand-alone), combined cycle, or hybrid turbomachinery cycle [13]. Pure PDE, as the name implies, consists of an array of detonation tubes, an inlet, and a nozzle. The applications of pure PDEs are mainly military, as they are light and easy to manufacture and have higher performance around Mach 1 than current engine technologies. This makes them an ideal form of propulsion for missiles, unmanned vehicles, and other small-scale applications.

However, their noise and the drop in efficiency at higher Mach number imply that pure PDEs will likely not to be used often for large-scale applications.

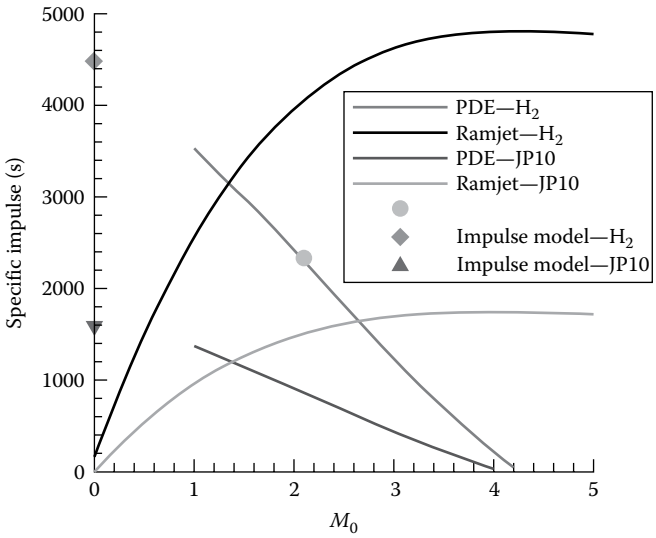


FIGURE 3.6
Specific impulse for PDE compared to other engines.

Combined-cycle PDEs may provide the most exciting possibilities for aviation. Adding a PDE to the flow path of a ramjet or scramjet would make an engine capable of operating efficiently as high as Mach 5.5. These engines would seem initially suitable for high-altitude, high-speed aircraft [14].

Hybrid PDEs make use of detonative combustion in place of constant pressure combustion, usually in combination with turbomachinery. For example, a hybrid turbofan PDE would combine both systems: the central core engine would still turn the large fan in front, but the bypass would flow into a ring of PDEs.

The bypass enters pulse detonation tubes that surround the standard combustion chamber (Figure 3.7). The tubes are then cyclically detonated; one detonates while the others fill with air or are primed with fuel. This combination promises to require simpler engine mechanisms and yield higher thrust with lower fuel consumption as examined by GE.

Hybrid PDEs will allow commercial aircraft powered by subsonic gas turbines to be faster, more efficient, and more environmentally friendly. NASA is projecting that intercontinental

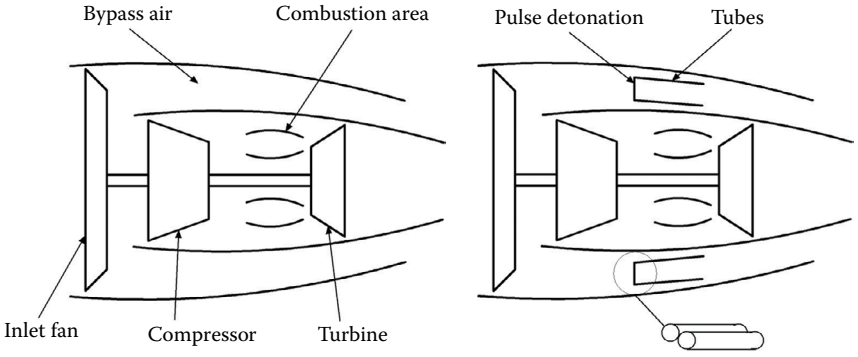


FIGURE 3.7
Hybrid turbofan PDE.

travel time will reduce by 2022. Similarly, hybrid supersonic gas turbines can also be used in military applications. Generally, hybrid PDEs will deliver the same thrust of a turbofan engine but with less fuel consumption. Moreover, they would produce significantly more thrust without requiring additional fuel.

Example 3.3

A PDE is employed in propelling a vehicle flying at a Mach number of 2 at an altitude of 40,000 ft. The engine has an inlet area of 0.084 m². The temperature ratio at combustion chamber is $T_{03}/T_{02} = 10.1$ and fuel heating value is 43,000 kJ/kg. Assuming that

- PDE operates on the simplified Humphrey thermodynamic cycle
- Ideal diffuser ($P_{02} = P_{0a}$)
- $\gamma_{air} = 1.4$, $\gamma_{gas} = 1.16$

It is required to calculate

1. The air mass flow rate
2. The maximum temperature
3. The fuel-to-air ratio
4. The exhaust velocity
5. The thrust force
6. The TSFC
7. The thermodynamic efficiency
8. The specific impulse

Solution

At an altitude of 40,000 ft, the ambient temperature and pressure are 216.65 K and 18.75 kPa, respectively.

The flight speed is

$$U = M\sqrt{\gamma RT_a} = 2\sqrt{1.4 \times 287 \times 216.65}$$

$$U = 590 \text{ m/s}$$

The *air mass flow rate* is

$$\dot{m}_a = \rho_a U A_i = \frac{P_a}{RT_a} U A_i = 14.99 \text{ kg/s}$$

$$Cp_{air} = \frac{\gamma_{air} R}{\gamma_{air} - 1} = \frac{1.4 \times 287}{1.4 - 1} = 1005 \text{ J/kg} \cdot \text{K}$$

$$Cp_{gas} = \frac{\gamma_{gas} R}{\gamma_{gas} - 1} = \frac{1.16 \times 287}{1.16 - 1} = 2081 \text{ J/kg} \cdot \text{K}$$

Diffuser: The total temperature at the intake is equal to the total upstream temperature, or

$$T_{02} = T_{0a} = T_a \left(1 + \frac{\gamma_c - 1}{2} M^2\right)$$

$$T_{02} = 216.65 \left(1 + \frac{1.4 - 1}{2} \times 2^2\right)$$

$$T_{02} = 390 \text{ K}$$

The total pressure at the diffuser outlet is also equal to the free-stream total pressure as the flow through the diffuser is assumed ideal:

$$P_{02} = P_{0a} = P_a\left(T_{0a}/T_a\right)^{\gamma/\gamma-1}$$

$$P_{02} = 146.7 \text{ kPa}$$

Combustion chamber: A constant volume process is assumed; therefore, the maximum temperature is

$$T_{03} = 10.1 T_{02} = 3939 \text{ K}$$

and the maximum pressure is

$$P_{03} = 10.1 P_{02} = 1482 \text{ kPa}$$

The fuel-to-air ratio is calculated from Equation 3.6 as

$$f = \frac{Cp_{gas}T_{03} - Cp_{air}T_{02}}{Q_R - Cp_{gas}T_{03}} = \frac{2.081 \times 3,939 - 1.005 \times 390}{43,000 - 2.081 \times 3,939} = 0.22427$$

$$f = 0.22427$$

The obtained fuel-to-air ratio is too large, which implies great fuel consumption.

Tail pipe: The exhaust speed is calculated from Equation 3.8 as

$$U_e = \sqrt{2Cp_h T_{03}\left[1 - \left(P_a/P_{03}\right)^{\gamma_h - 1/\gamma_h}\right]}$$

$$U_e = \sqrt{2 \times 2081 \times 3939 \times \left[1 - \left(18.75/1482\right)^{0.138}\right]}$$

$$U_e = 2725 \text{ m/s}$$

The specific thrust is

$$\frac{T}{\dot{m}_a} = \left(1 + f\right)U_e - U = 2746 \text{ N} \cdot \text{s/kg}$$

The thrust force is then

$$T = \dot{m}_a \times \frac{T}{\dot{m}_a} = 41{,}160 \text{ N} = 41.16 \text{ kN}$$

The TSFC is calculated from Equation 3.10 as

$$\text{TSFC} = \frac{0.22427}{2746} = 8.17 \times 10^{-5} \text{ kg/N} \cdot \text{s} = 0.294 \text{ kg/N} \cdot \text{h}$$

The thermal efficiency for different values of γ is calculated next.

For $\gamma = 1.16$,

$$\eta_{th} = 1 - \gamma \frac{T_a}{T_{02}} \left\{ \frac{\left(\frac{T_{03}}{T_{02}}\right)^{1/\gamma} - 1}{\frac{T_{03}}{T_{02}} - 1} \right\} = 1 - 1.16 \times \frac{216.65}{390} \times \left\{ \frac{\left(\frac{3939}{390}\right)^{0.862} - 1}{\frac{3939}{390} - 1} \right\} = 55.1\%$$

For $\gamma = 1.4$, then

$$\eta_{th} = 1 - \gamma \frac{T_a}{T_{02}} \left\{ \frac{\left(\frac{T_{03}}{T_{02}}\right)^{1/\gamma} - 1}{\frac{T_{03}}{T_{02}} - 1} \right\} = 1 - 1.4 \times \frac{216.65}{390} \times \left\{ \frac{\left(\frac{3939}{390}\right)^{0.714} - 1}{\frac{3939}{390} - 1} \right\} = 64\%$$

These two values for thermal efficiencies for the two values of specific heats are in complete compliance with the results in [15] for same temperature (pressure) ratio of 10.1.

Specific impulse:

$$I = \frac{T}{f\dot{m}_a g} = \frac{41160}{0.22427 \times 15 \times 9.81} = 1247.2 \text{ s}$$

3.3 Ramjet Engines

3.3.1 Introduction

A *ramjet* (*stato-réacteur*) is another type of athodyd airbreathing jet engine that was first proposed by Rene Lorin in 1913. It uses the forward motion of the engine to compress the incoming air, without a rotary compressor. Once the compressor is eliminated, the turbine is no longer required and it can also be omitted. Thus, a ramjet, which has no moving parts, is much like a valveless pulsejet, but it operates with continuous combustion rather than the series of explosions that give a pulsejet its characteristic noise.

Ramjet engines may be of the subsonic or supersonic type. Although a ramjet can operate at subsonic flight speed, the increasing pressure rise accompanying higher flight speeds renders the ramjet most suitable for supersonic flight [15]. For this reason, subsonic ramjets are seldom (if ever) used these days. The ramjet has been called a flying stovepipe, because it is open at both ends and has only fuel nozzles in the middle. A straight stovepipe would not work however; a ramjet must have a properly shaped inlet-diffusion section to produce low-velocity, high-pressure air at the combustion section and it must also have a properly shaped exhaust nozzle. High-speed air enters the inlet, is compressed as it is slowed down, is mixed with fuel and burned in the combustion chamber, and is finally expanded and ejected through the nozzle. The air rushing toward the inlet of an engine flying at high speed is partially compressed by the so-called ram effect. If the flight speed is supersonic, part of this compression actually occurs across a shock system that precedes the inlet. When the flight speed is high enough, this compression can be sufficient to operate an engine without a compressor. Once the compressor is eliminated, the turbine is no longer required and it can also be omitted. Ramjets can operate at speeds above 320 km/h (about 200 mph) or as low Mach number as 0.2. However, fuel consumption is horrendous at these low velocities. The operation of a ramjet does not become competitive with that of a turbojet until speeds of about $M_a = 2.5$ or even more are reached. Ramjets become practical for military applications only at very high or supersonic speeds. The combustion region is generally a large single combustor, similar to an afterburner [5]. For the combustion process to be efficient, the air must be compressed sufficiently. This is possible only when the free-stream Mach number exceeds

about 3, and so ramjets have been practical for only a few missile applications. A hybrid engine, and part turbojet, part ramjet (known as a turbo-ram engine), was also used on the SR-71 high-speed reconnaissance aircraft and is a topic of current research interest for several possible hypersonic applications. In brief, because the ramjet depends on the compression of the in-rushing air for its operation, or in other words depends on the flight speed, a vehicle powered by a ramjet cannot develop static thrust and therefore cannot accelerate a vehicle from a standing start. The vehicle must first be accelerated by other means to a sufficiently high speed prior to using a ramjet as a propulsive device. It may be dropped from a plane or launched by rocket assist.

In general, ramjet engines are used to power numerous guided missiles (ground and air launched). Since ramjet engines are one category of airbreathing engines that use atmospheric oxygen, it cannot be used in submarines (which cannot access atmospheric oxygen underwater) nor space vehicles, as they are surrounded by a vacuum. Moreover, they also appear to be the best choice for future hypersonic airplanes.

The main advantages and disadvantages of ramjet engines may be summarized as follows:

Advantages

- Able to attain high speeds (around Mach 5).
- No moving parts so less wear and tear as well as minimum losses.
- Reduced weight and smaller engine.
- Lighter and simpler than turbine-based engines.
- Higher temperatures can be employed.

Disadvantages

- Bad performance at lower speeds.
- Needs booster to accelerate it to a speed where ramjet begins to produce thrust.
- Higher fuel consumption.
- Maximum altitude is limited.
- High-temperature material is required.

3.3.2 Classifications of Ramjet Engines

Ramjets may be classified as follows.

3.3.2.1 Subsonic–Supersonic Types

A ramjet engine may be either of the subsonic or supersonic type. In either cases, the ramjet depends on the compression of the in-rushing air for its operation, or in other words depends on the flight speed. The air rushing toward the inlet of an engine flying at high speeds is partially compressed by the so-called ram effect. If the flight speed is supersonic, part of this compression actually occurs across a shock system that is either external or external–internal to the inlet.

Although a ramjet can operate at subsonic flight speed, the increasing pressure rise accompanying higher flight speeds renders the ramjet most suitable for supersonic flight

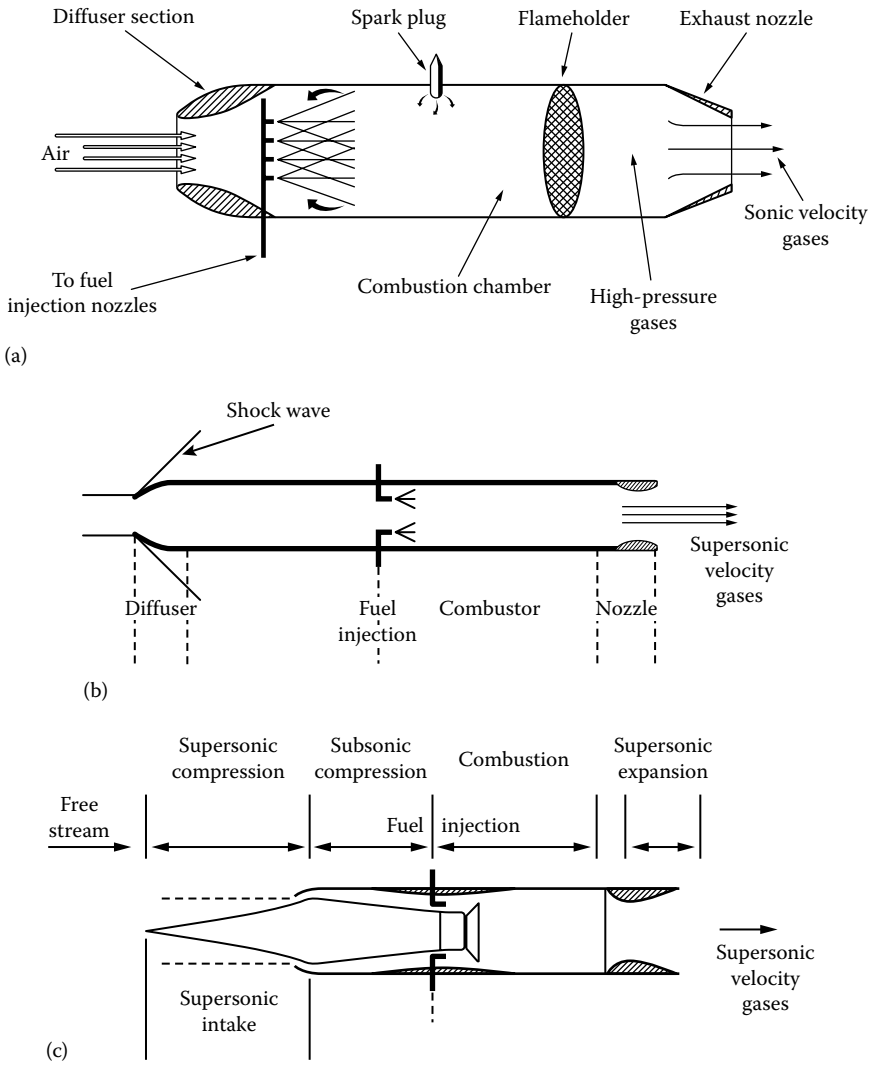


FIGURE 3.8
Types of ramjet engines: subsonic (a) and supersonic (b, c).

and most efficient at speeds around Mach 3. For this reason, subsonic ramjets are seldom (if ever) used these days.

Figure 3.8 illustrates a subsonic ramjet engine (a) and a supersonic engine (b and c).

Subsonic ramjets have very small overall efficiency and too high TSFC (TSFC $\approx 0.05-0.2$ kg/kN·s). However, the TSFC decreases to 0.05 kg/kN·s or less at supersonic speeds.

3.3.2.2 Fixed Geometry–Variable Geometry Types

Ramjets can be classified based on their geometry as

- Fixed geometry
- Variable geometry

Fixed geometry ramjets maintain the same geometric shape of the diffuser and the combustion chamber. Fixed geometry ramjets are much smaller and cheaper but only function at low speeds. *Variable geometry* ramjets are normally supersonic and can change the shape of their nose cones fitted to inlet according to velocity and use baffles in their combustion chamber to optimize the fuel burn. Variable geometry ramjets are much heavier and more expensive but can function at higher speeds.

3.3.2.3 Liquid-Fueled and Solid-Fueled Types

Finally, ramjet engines may be classified based on their fuel as

- Liquid fueled
- Solid fueled

The liquid-fuel ramjet (LFRJ) can use classical kerosene, high-density, or slurry fuels. An LFRJ can be fueled externally with a hydrazine-type fuel carried in fuel tanks (like a jet engine). The solid-fuel ramjet (SFRJ) has its fuel in solid form within the chamber, and the stoichiometry of combustion is controlled by the regression rate of the fuel. A wide range of fuels can be used from polymers such as poly(methyl methacrylate) (PMMA) or polyethylene (PE) to long-chain alkanes such as paraffin or cross-linked rubbers such as hydroxyl-terminated polybutadiene (HTPB).

An LFRJ is illustrated in Figure 3.9. It is characterized by high throttleability and excellent performance.

3.3.3 Ideal Ramjet

The ramjet engine as described earlier is composed of three modules (the same as the pulsejet engine), namely, an intake or diffuser, a combustion chamber, and a nozzle (Figure 3.10). To analyze ramjet performance, the different states of its three modules are defined here.

State (a), standing for ambient, is far upstream of the engine. The diffusion process takes place in part outside of the engine and in part inside the engine. The first part of diffusion

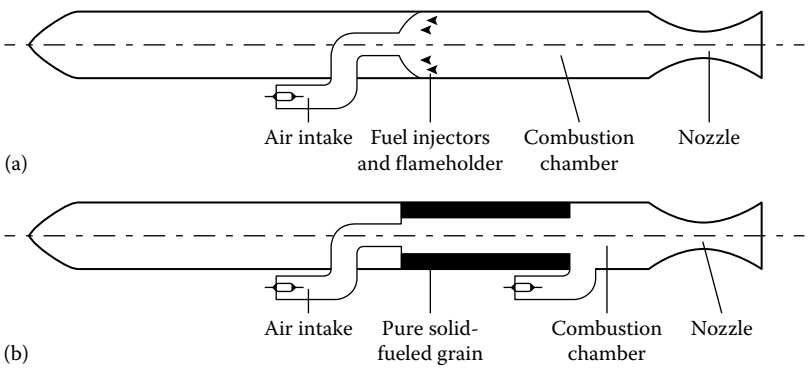


FIGURE 3.9
(a) LFRJs and (b) SFRJs in rockets.

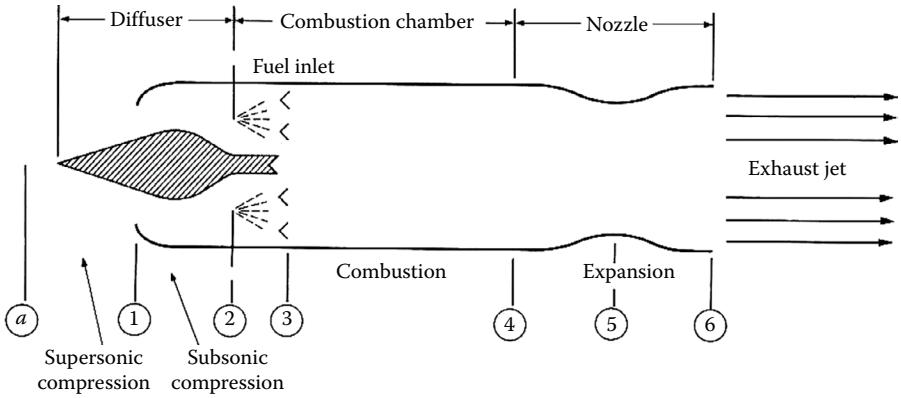


FIGURE 3.10
Ramjet engine and its different states.

takes place from the far upstream, state (a), to the engine entrance, state (1). The second part of diffusion takes place inside the engine, from state (1) to state (2), where state (2) is at the end of the diffusion section. Thus, the first module of the engine, the diffuser, is located between states (1) and (2). Air then enters the combustion chamber at subsonic speeds. This is achieved either as normal shock wave or as multiple oblique shock waves followed by a normal shock wave. Fuel is next injected as fine droplets, which mix rapidly with the mixture and are then ignited by a spark. The mixture then passes through a *flameholder* at state (3) to stabilize the flame and facilitate a good combustion process. The flameholder may be of the grill type, which provides a type of barrier to the burning mixture while allowing hot, expanding gases to escape through the exhaust nozzle. The high-pressure air coming into the combustion chamber keeps the burning mixture from effectively reacting toward the intake end of the engine.

The end of the combustion chamber is identified by state (4). Thus, the second module of the engine, combustion chamber, is located between states (2) and (4). Combustion in general raises the temperature of the mixture to some 3000 K before the products of combustion expand to produce high velocities in the nozzle. Though the walls of combustion chambers cannot tolerate temperature much above 1200 K, they can be kept much cooler than the main fluid stream by a fuel injection pattern that leaves a shielding layer of relatively cool air next to the walls [16]. The expansion process takes place at the third module of the engine, namely, the nozzle. Expansion starts at the convergent section between state (4) and the nozzle throat, state (5). The nozzle then has a diverging section that ends at state (6). Sometimes state (6) is denoted by (*e*) resembling the exhaust or exit condition. Thus, the nozzle is situated between states (4) and (6). The nozzle is shaped to accelerate the flow so that the exit velocity is greater than the free-stream velocity, and thus thrust is created.

The cycle of events within the engine (Figure 3.11) is described next. Here all the processes within the engine are assumed ideal with no losses.

For isentropic (reversible adiabatic) flow inside the engine, no pressure drop will be encountered in the three modules of the engine; thus,

$$P_{0a} = P_{02} = P_{04} = P_{06} \tag{3.14}$$

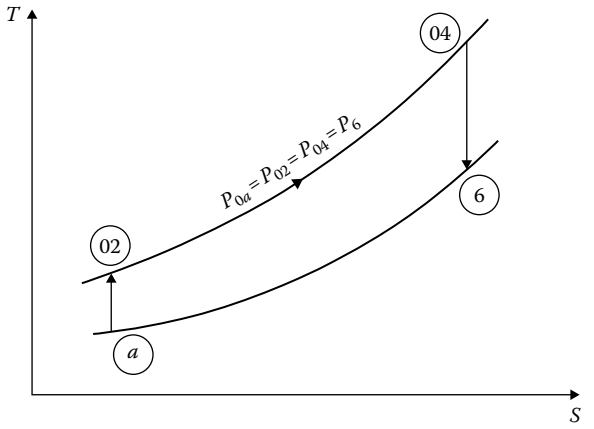


FIGURE 3.11
Ideal thermodynamic cycle for ramjet engine.

Moreover, since neither work nor heat addition nor rejection takes place in the intake and nozzle, then from the first law of thermodynamics, equal total enthalpy (and thus total temperature) is presumed. Thus,

$$\left.\begin{aligned} T_{0a} &= T_{02} \\ T_{04} &= T_{06} \end{aligned}\right\} \tag{3.15}$$

Full expansion of the hot gases within the nozzle is assumed; thus,

$$P_a = P_6 = P_e \tag{3.16}$$

The relations between total and static conditions (temperature and pressure) at the inlet and outlet of the engine, state (a) and (6 or e), are

$$\left.\begin{aligned} \frac{T_{0a}}{T_a} &= 1 + \frac{\gamma_a - 1}{2} M^2 = \frac{T_{02}}{T_a} \\ \frac{T_{0e}}{T_e} &= \frac{T_{06}}{T_6} = 1 + \frac{\gamma_6 - 1}{2} M_e^2 = \frac{T_{04}}{T_e} \end{aligned}\right\} \tag{3.17}$$

$$\left.\begin{aligned} \frac{P_{0a}}{P_a} &= \left(1 + \frac{\gamma_a - 1}{2} M^2\right)^{\gamma_a/\gamma_a - 1} \\ \frac{P_{06}}{P_e} &= \left(1 + \frac{\gamma_6 - 1}{2} M_e^2\right)^{\gamma_6/\gamma_6 - 1} \end{aligned}\right\} \tag{3.18}$$

In Equations 3.17 and 3.18, (γ_a, γ_6) are the specific heat ratios for air and exhaust gases, respectively. If we ignore the variations in fluid properties, (R, γ), then from Equations 3.14 and 3.16, we get

$$\frac{P_{06}}{P_e} = \frac{P_{0a}}{P_a} \tag{3.19}$$

Then from Equation 3.18, we have

$$M_e = M_a \tag{3.20}$$

or

$$u_e = \frac{a_e}{a}u = \sqrt{\frac{\gamma_6 R T_e}{\gamma_a R T_a}}u \tag{3.21a}$$

The flight and exhaust Mach numbers are equal, but the flight and exhaust speeds are not. This difference generates the thrust force.

Again, assuming constant (γ, R) within the engine, then

$$u_e = \sqrt{\frac{T_e}{T_a}}u$$

From Equation 3.17,

$$u_e = u\sqrt{\frac{T_{04}}{T_{0a}}} \equiv u\sqrt{\frac{T_{04}}{T_{02}}} \tag{3.21b}$$

Fuel-to-air ratio (f): To get the fuel-to-air ratio, apply the energy equation to the combustion process

$$\dot{m}_a h_{02} + \dot{m}_f Q_R = \left(\dot{m}_a + \dot{m}_f\right) h_{04}$$

$$Q_R = \text{Heating value of the fuel}$$

$$h_{02} + fQ_R = \left(1+f\right) h_{04}$$

$$C_{p_2} T_{02} + fQ_R = \left(1+f\right) C_{p_4} T_{04}$$

but

$$T_{02} = T_{0a}$$

$$\therefore f = \frac{\left(C_{p_4} T_{04}/C_{p_2} T_{0a}\right) - 1}{\left(Q_R/C_{p_2} T_{0a}\right) - \left(C_{p_4} T_{04}/C_{p_2} T_{0a}\right)} \tag{3.22}$$

Thrust force (T): Since full expansion in the nozzle is assumed, that is, $P_e = P_a$, then the thrust force is expressed as

$$T = \dot{m}_a\left(1+f\right)u_e - \dot{m}_a u$$

$$\frac{T}{\dot{m}_a} = \left(1+f\right)u_e - u = u\left[\left(1+f\right)\frac{u_e}{u} - 1\right]$$

Now, the flight speed and exhaust speed can be written as

$$u = Ma = M\sqrt{\gamma RT_a}$$

$$u_e = u\sqrt{\frac{T_{04}}{T_{0a}}} \equiv u\sqrt{\frac{T_{04}}{T_a}\times\frac{T_a}{T_{0a}}} = u\sqrt{\frac{T_{04}}{T_a}}\times\sqrt{\frac{1}{1+\frac{\gamma-1}{2}M^2}} \tag{3.23}$$

From Equation 3.22, a final expression for the thrust force will be expressed as

$$\frac{T}{\dot{m}_a} = M\sqrt{\gamma RT_a}\left[(1+f)\sqrt{\frac{T_{04}}{T_a}}\times\sqrt{\frac{1}{1+\frac{\gamma-1}{2}M^2}}-1\right] \tag{3.24}$$

The TSFC is

$$\text{TSFC} = \frac{\dot{m}_f}{T} = \frac{\text{f}}{T/\dot{m}_a} \tag{3.25}$$

3.3.3.1 Real Cycle

Now, consider the performance of a real ramjet engine. Aerodynamic losses in the intake, combustion chamber, and nozzle lead to a stagnation pressure drop in all of the three modules. Moreover, losses occur during combustion, which are accounted for by combustion or burner efficiency. Figure 3.12 illustrates the effect of irreversibility on the different processes in the cycle. Neither the compression process in the diffuser nor the expansion process in the nozzle is isentropic anymore. Moreover, combustion will not take place at a constant pressure.

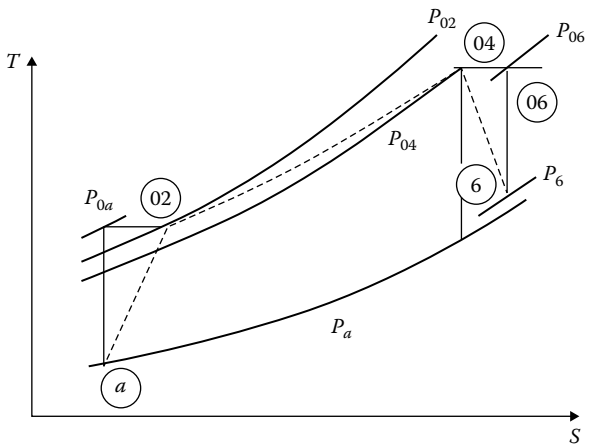


FIGURE 3.12
Real cycle of a ramjet engine.

The performance of the diffuser is characterized by a stagnation pressure ratio

$$r_d = \frac{P_{02}}{P_{0a}}$$

The stagnation pressure ratio in the combustion chamber is

$$r_c = \frac{P_{04}}{P_{02}}$$

The stagnation pressure ratio in the nozzle is

$$r_n = \frac{P_{06}}{P_{04}}$$

The overall stagnation pressure ratio is

$$\frac{P_{06}}{P_{0a}} = r_d r_c r_n \tag{3.26}$$

It will be shown that irreversibility will lead to the inequality of the flight and exhaust Mach numbers. The properties (γ, R) of the fluid through the different parts of the engine are assumed constant.

Now, since the stagnation pressure of the free stream is expressed as

$$\frac{P_{0a}}{P_a} = \left(1 + \frac{\gamma - 1}{2} M^2\right)^{\gamma/\gamma - 1}$$

$$\therefore \left(\frac{P_a}{P_{0a}}\right)^{\gamma/\gamma - 1} \left(1 + \frac{\gamma - 1}{2} M^2\right) = 1$$

and

$$\frac{P_{06}}{P_6} = \left(1 + \frac{\gamma - 1}{2} M_e^2\right)^{\gamma/\gamma - 1}$$

$$\therefore M_e^2 = \frac{2}{\gamma - 1}\left[\left(\frac{P_{06}}{P_6}\right)^{\gamma - 1/\gamma} - 1\right]$$

$$M_e^2 = \left(\frac{2}{\gamma - 1}\right)\left[\left(1 + \frac{\gamma - 1}{2} M^2\right)\left(\frac{P_a}{P_{0a}}\right)^{\gamma - 1/\gamma}\left(\frac{P_{06}}{P_6}\right)^{\gamma - 1/\gamma} - 1\right]$$

$$\therefore M_e^2 = \left(\frac{2}{\gamma_e - 1}\right)\left[\left(1 + \frac{\gamma - 1}{2} M^2\right)\left(\frac{P_{06}}{P_6}\frac{P_a}{P_{0a}}\right)^{\gamma - 1/\gamma} - 1\right]$$

Then from Equation 3.26, the exhaust Mach number is

$$M_e^2 = \left(\frac{2}{\gamma-1}\right)\left[\left(1+\frac{\gamma-1}{2}M^2\right)\left(r_d r_c r_n \frac{P_a}{P_e}\right)^{\gamma-1/\gamma} - 1\right] \tag{3.27a}$$

Now, define (m) as

$$m = \left(1+\frac{\gamma-1}{2}M^2\right)\left(r_d r_c r_n \frac{P_a}{P_e}\right)^{\gamma-1/\gamma} \tag{3.28a}$$

$$\therefore M_e^2 = \left(\frac{2}{\gamma-1}\right)(m-1) \tag{3.27b}$$

From Equation 3.27a and b, then another expression for (m) is

$$m = \left(1+\frac{\gamma-1}{2}M_e^2\right) \tag{3.28b}$$

If $r_d = r_c = r_n = 1$ and $P_e = P_a$, then $M_e = M$.

If heat transfer from the engine is assumed negligible (per unit mass of fluid), then the total exhaust temperature $T_{06} = T_{04}$

$$\frac{T_{06}}{T_6} = \frac{T_{04}}{T_e} = \left(1+\frac{\gamma-1}{2}M_e^2\right)$$

$$u_e = M_e\sqrt{\gamma R T_e} = M_e\sqrt{\gamma R T_{04}\frac{T_e}{T_{04}}}$$

$$u_e = M_e\sqrt{\gamma R T_{04}\Big/\left(1+\frac{\gamma-1}{2}M_e^2\right)}$$

$$u_e = M_e\sqrt{\gamma R T_{04}/m}$$

Substituting for M_e from Equation 3.27a, then

$$u_e = \sqrt{\frac{2\gamma R T_{04}(m-1)}{(\gamma-1)m}} \tag{3.29}$$

Since irreversibility has no effect on total temperatures throughout the engine, then the fuel-to-air ratio can be given by Equation 3.22 but modified for burner efficiency (η_b)

$$f = \frac{\left(C_{p4}T_{04}/C_{p2}T_{0a}\right)-1}{\eta_b Q_R/C_{p2}T_{0a} - \left(C_{p4}T_{04}/C_{p2}T_{0a}\right)} \tag{3.30}$$

The specific thrust is expressed as usual by the relation

$$\frac{T}{\dot{m}_a} = \left[(1+f)u_e - u_a\right] + \frac{1}{\dot{m}_a}(P_e - P_a)A_e \tag{3.31}$$

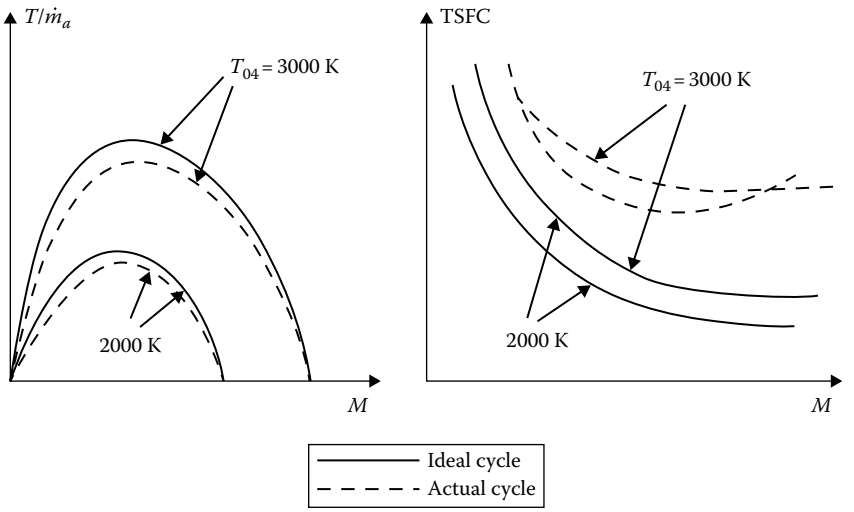


FIGURE 3.13
Specific thrust and TSFC for ideal and real ramjet engines.

Then since $u = M\sqrt{\gamma RT_a}$, specific thrust will be expressed as

$$\frac{T}{\dot{m}_a} = (1+f)\sqrt{\frac{2\gamma_e RT_{04}(m-1)}{(\gamma-1)m}} - M\sqrt{\gamma RT_a} + \frac{P_e A_e}{\dot{m}_a}\left(1-\frac{P_a}{P_e}\right) \tag{3.32}$$

The specific thrust and TSFC are plotted in Figure 3.13 for ideal and real engines. The ratio between specific heats is assumed constant, $\gamma = 1.4$. The maximum temperatures investigated are $T_{04} = 2000$ or 3000 K. The pressure ratios in the diffuser, combustion chamber, and nozzle are, respectively, $r_d = 0.7$, $r_c = 0.97$, and $r_n = 0.96$. The burner is assumed ideal ($\eta_b = 1$) and the fuel heating value is $Q_R = 43{,}000$ kJ/kg.

For any given peak temperature, the thrust per unit mass flow rate $\dot{m}_a$ for a real ramjet is less than the ideal. However, the TSFC for real is higher than the ideal. Also for a real ramjet, there is a reasonably well-defined minimum TSFC.

Example 3.4

A supersonic ramjet has a flight speed of $M_a = 2.0$ at an altitude of 16,200 m where the temperature is 216.6 K and the pressure is 10.01 kPa. An axisymmetric inlet is fitted with a spike having a deflection angle of 12°. Neglect frictional losses in the diffuser and combustion chamber. The inlet area is $A_1 = 0.2$ m^2. The maximum total temperature in the combustion chamber is 2500 K. The heating value of fuel is 45,000 kJ/kg. The burner efficiency is $\eta_b = 0.96$. The nozzle expands to atmospheric pressure for maximum thrust with $\eta_n = 0.96$. The velocity entering the combustion chamber is to be kept as large as possible but the Mach number is not greater than 0.25.

Assuming the fluid to be air ($\gamma = 1.4$), compute

1. The stagnation pressure ratio of the diffuser (r_d)
2. The inlet Mach number to the combustion chamber
3. The stagnation pressure ratio in the combustion chamber (r_c)

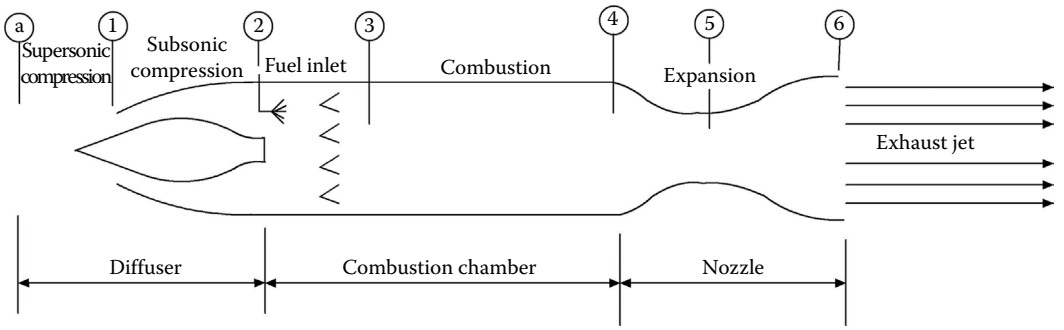


FIGURE E3.4

4. The stagnation pressure ratio in the nozzle (r_n)
5. The flight and exhaust speeds
6. The thrust force
7. The TSFC

Solution

The total conditions for air prior to entering the engine are

$$\frac{T_{0a}}{T_a} = 1 + \frac{\gamma - 1}{2} M_a^2 = 1.8$$

$$\frac{P_{0a}}{P_a} = \left(1 + \frac{\gamma - 1}{2} M_a^2\right)^{\gamma/\gamma - 1} = 7.824$$

Thus, $T_{0a} = 390$ K and $P_{0a} = 7.824 P_a$.

The total temperature is constant in the intake section and so

$$T_{0a} = T_{01} = T'_{01} = T_{02} = 390 \text{ K}$$

The flight speed is $U = M\sqrt{\gamma R T_a} = 590$ m/s.

Now, let us analyze the intake. Since the flight speed is supersonic, then two shock waves must be generated in the intake to deliver air at a subsonic speed to the combustion chamber as shown in Figure 3.14. The first shock is an oblique shock wave attached to the apex of the spike, which is to be followed by a normal shock wave.

1. Oblique shock wave
   The complete governing equations for oblique and normal shock waves are found in Section 3.8; some are rewritten here.

   With a free-stream Mach number $M_a = 2.0$ and a deflection angle $\delta = 12°$, the shock wave angle will be either determined from gas dynamics tables or iteratively from the following relation:

$$\tan\delta = \frac{2\cot\theta\left(M_1^2 \sin^2\theta - 1\right)}{(\gamma + 1)M_1^2 - 2\left(M_1^2 \sin^2\theta - 1\right)}$$

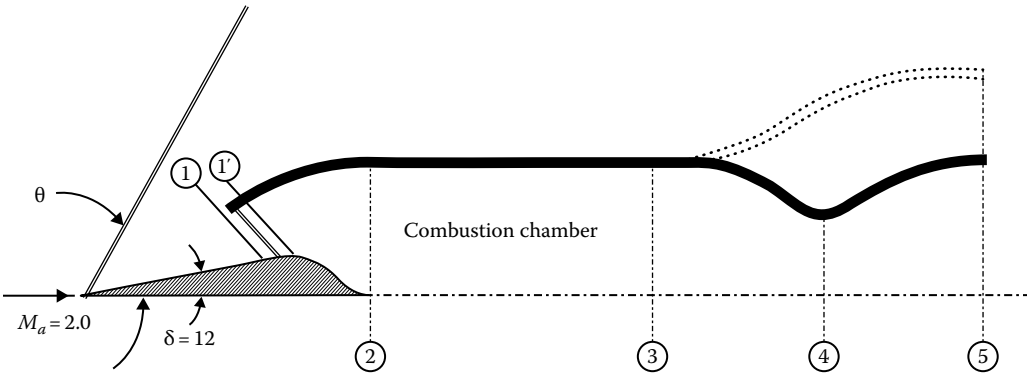


FIGURE 3.14
Shock wave pattern in ramjet engine.

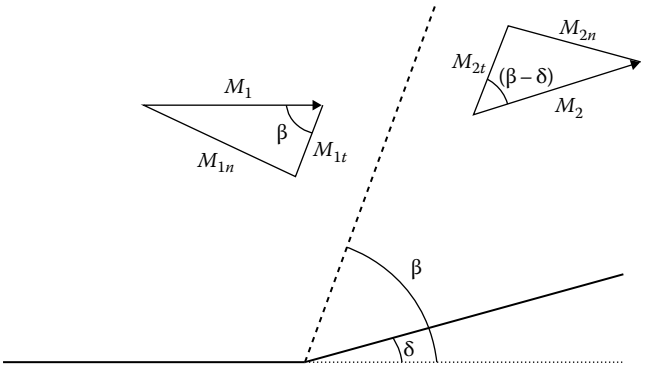


FIGURE 3.15
Oblique shock wave pattern.

Both result in the value θ = 41.56°. As shown in Figure 3.15, the Mach number upstream of the oblique shock wave can be decomposed into normal and tangential components. The normal component of the free-stream Mach number is

$$M_{an} = M_a \sin\theta = 2.0 \sin 41.56^\circ = 1.326$$

The normal component of the Mach number downstream of the normal shock wave will be determined also either from normal shock wave tables or from the relation

$$M_{1n}^2 = \frac{(\gamma - 1)M_{an}^2 + 2}{2\gamma M_{an}^2 - (\gamma - 1)} \tag{1}$$

The result is $M_{1n} = 0.773$.

The total pressure ratio also may be determined from normal shock wave tables or from the relation

$$\frac{P_{01}}{P_{0a}} = \left[\frac{(\gamma + 1)M_{an}^2}{2 + (\gamma - 1)M_{an}^2}\right]^{\gamma/\gamma - 1} \left[\left(\frac{2\gamma}{\gamma + 1}\right)M_{an}^2 - \left(\frac{\gamma - 1}{\gamma + 1}\right)\right]^{-(1/\gamma - 1)} \tag{2}$$

Thus, the pressure ratio is $P_{01}/P_{0a} = 0.9746$.

The Mach number for flow leaving the oblique shock wave is

$$M_1 = \frac{M_{1n}}{\sin(\theta - \delta)} = \frac{0.773}{\sin(41.56 - 12)} = 1.567$$

2. Normal shock wave
The second (normal) shock wave originates at the engine cowl (nose lips). With $M_1 = 1.567$, from normal shock wave tables, or Equation 1, then $M_1' = 0.678$, and the total pressure ratio also either from tables or Equation 2 is

$$\frac{P_{01}'}{P_{01}} = 0.90719$$

The pressure ratio is then

$$\frac{P_{01}'}{P_{0a}} = \frac{P_{01}'}{P_{01}}\frac{P_{01}}{P_{0a}} = 0.90719 \times 0.9746 = 0.884$$

Since there are no losses in the diffuser, then

$$P_{02} = P_{01}'$$

The stagnation pressure ratio in the intake is then

$$r_d = \frac{P_{02}}{P_{0a}} = 0.884$$

Combustion chamber: The flow in the combustion chamber is a flow with heat transfer or a Rayleigh flow. Now, if $M_2 = 0.25$, then Rayleigh flow tables or governing equations in Section 3.5

$$\frac{T_{02}}{T_0^*} = 0.2568$$

Then

$$T_0^* = T_{02}\frac{T_0^*}{T_{02}} = \frac{390}{0.2568} = 1518 \text{ K}$$

$$\frac{T_{03}}{T_0^*} = \frac{2500}{1518} = 1.64615 > 1.0$$

which is impossible.

Thus, adding fuel to make $T_{03} = 2500$ K means that the flow will be choked ($M_3 = 1.0$) and $M_2 < 0.25$. Thus, to find M_2,

$$\frac{T_{02}}{T_0^*} = \frac{T_{02}}{T_{03}}\frac{T_{03}}{T_0^*} = \frac{390}{2500}(1) = 0.156$$

From Rayleigh tables or equations, then $M_2 = 0.189$, and $P_{02}/P_0^* = 1.2378$.

The Mach number at state 3 is unity; thus, $P_{03} = P_0^* = \dfrac{P_0^*}{P_{02}} P_{02}$

$$P_{03} = \frac{1}{1.2378}\left(0.884 P_{0a}\right) = 0.714 P_{0a} = 5.586\, P_a$$

The stagnation pressure ratio in the combustion chamber is

$$r_c = \frac{P_{03}}{P_{02}} = \frac{1}{1.2378} = 0.808$$

The fuel-to-air ratio is

$$f = \frac{C_P\left(T_{03} - T_{0a}\right)}{\eta_b Q_R - C_P T_{0a}}$$

$$f = \frac{1.005\left(2{,}500 - 390\right)}{\left(0.98\right)\left(45{,}000\right) - \left(1.005\right)\left(2{,}500\right)} = 0.05099$$

Nozzle: Since $M_3 = 1.0$, the nozzle diverges immediately. The gases expand in the nozzle and leave at the same ambient pressure. The nozzle efficiency is

$$\eta_n = \frac{T_{03} - T_5}{T_{03} - T_{5s}}$$

$$T_5 = T_{03}\left[1 - \eta_n\left\{1 - \frac{T_{5s}}{T_{03}}\right\}\right]$$

$$T_5 = T_{03}\left[1 - \eta_n\left\{1 - \left(\frac{P_a}{P_{03}}\right)^{\gamma - 1/\gamma}\right\}\right]$$

with $P_{03}/P_a = 5.586$

$$T_5 = 2500\left[1 - 0.96\left\{1 - \left(5.586\right)^{-0.2857}\right\}\right] = 1567 \text{ K}$$

To calculate the stagnation pressure ratio in the nozzle, the isentropic total pressure at the nozzle outlet is then

$$\frac{P_{05}}{P_5} = \left(\frac{T_{05}}{T_5}\right)^{\gamma/\gamma - 1} = \left(\frac{2500}{1567}\right)^{3.5} = 5.129$$

$$\therefore P_{05} = 5.129 P_a$$

The nozzle total pressure ratio is then

$$r_n = \frac{P_{05}}{P_{03}} = 0.918$$

The engine overall pressure ratio is then

$$\frac{P_{05}}{P_{0a}} = r_d r_c r_n = 0.655$$

Since $T_5/T_{05} = 1567/2500 = 0.6268$, then from the isentropic flow tables:

The exhaust Mach number is $M_5 = 1.725$.
The exhaust speed is then $V_5 = M_5 a_5 = 1.725\sqrt{(1.4)(287)(1567)} = 1368$ m/s.

The mass flow rate is calculated from the known area at state (1); then with $M_1 = 1.567$, the static temperature and pressure at state (1) are given from normal shock tables as

$$T_1 = \frac{T_1}{T_a} T_a = 1.207 \times 216.66 = 261.5 \text{ K}$$

$$P_1 = \frac{P_1}{P_a} P_a = 1.8847 \times 10.01 = 18.8659 \text{ kPa}$$

The air density at state (1) is then $\rho_1 = \dfrac{P_1}{RT_1} = 0.2513$ kg/m^3
Moreover, the air speed is given by $V_1 = M_1\sqrt{\gamma RT_1} = 429.8$ m/s

$$\dot{m} = \rho_1 V_1 A_1$$
$$\dot{m} = \rho_1 V_1 A_1 = (0.2513)(0.2)(429.8) = 21.6 \text{ kg/s}$$

The thrust force is given by the relation

$$T = \dot{m}_a\left[(1+f)V_5 - V_a\right] = 21.6\left[1.05099 \times 1368 - 590\right]$$

$$T = 19{,}897 \text{ N}$$

$$\text{TSFC} = \frac{\dot{m}_f}{T} = \frac{f\dot{m}_a}{T}$$

$$\text{TSFC} = \frac{(0.05099)(21.6)}{19{,}897} = 0.00005535 \text{ kg/N} \cdot \text{s}$$

$$\text{TSFC} = 0.199 \text{ kg/N} \cdot \text{h}$$

Example 3.5

For an ideal ramjet, it is required to prove that the thermal efficiency is expressed by

$$\eta_{th} = 1 - (1/\tau_r)$$

where $\tau_r = T_{02}/T_a$.
(*Hint*: Use the following approximations—$f = Cp(T_{04} - T_{02})/Q_R$ and $\dot{m}_f \ll \dot{m}_a$.)

Solution

As derived in Chapter 2, the thermal efficiency is expressed by the relation

$$\eta_{th} = \frac{\left(\dot{m}_a + \dot{m}_f\right)V_6{}^2 - \dot{m}_a V^2}{2\dot{m}_f Q_R}$$

Now, with $\dot{m}_a \ll \dot{m}_f$, then

$$\eta_{th} = \frac{\dot{m}_a\left(V_6{}^2 - V^2\right)}{2\dot{m}_f Q_R}$$

with

$$f = \frac{\dot{m}_f}{\dot{m}_a} \quad \text{and} \quad f = \frac{Cp\left(T_{04} - T_{02}\right)}{Q_R}$$

$$\therefore \eta_{th} = \frac{\left(V_6{}^2 - V^2\right)}{2Cp\left(T_{04} - T_{02}\right)}$$

The flight speed is

$$V = M\sqrt{\gamma R T_a}$$

The exhaust velocity is

$$V_6 = M_e\sqrt{\gamma R T_6}$$

For an ideal ramjet,

$$M_e = M$$

$$\therefore \eta_{th} = \frac{M^2\left(\gamma R T_6 - \gamma R T_a\right)}{2Cp\left(T_{04} - T_{02}\right)}$$

$$\eta_{th} = \frac{\gamma R T_a M^2\left(\dfrac{T_6}{T_a} - 1\right)}{2Cp T_{02}\left(\dfrac{T_{04}}{T_{02}} - 1\right)} \tag{1}$$

Since

$$\frac{P_{04}}{P_6} = \frac{P_{02}}{P_a}$$

$$\left(\frac{T_{04}}{T_6}\right)^{(\gamma-1/\gamma)} = \left(\frac{T_{02}}{T_a}\right)^{(\gamma-1/\gamma)}$$

or

$$\frac{T_{04}}{T_6} = \frac{T_{02}}{T_a} \text{ as } \gamma = \text{constant}$$

$$\therefore \frac{T_{04}}{T_{02}} = \frac{T_6}{T_a} \tag{2}$$

From (1) and (2),

$$\therefore \eta_{th} = \frac{\gamma R T_a M^2}{2CpT_{02}} = \frac{\gamma R T_a M^2}{2\left(\frac{\gamma R}{\gamma - 1}\right) T_{02}}$$

But

$$\tau_r = \frac{T_{02}}{T_a} = \left(1 + \frac{\gamma - 1}{2} M^2\right)$$

Then

$$\eta_{th} = \frac{\left(\frac{\gamma - 1}{2}\right) M^2}{T_{02}/T_a} = \frac{\left(\frac{\gamma - 1}{2}\right) M^2}{\left(1 + \frac{\gamma - 1}{2} M^2\right)} = 1 - \frac{1}{\left(1 + \frac{\gamma - 1}{2} M^2\right)}$$

$$\therefore \eta_{th} = 1 - \frac{1}{\tau_r}$$

Example 3.6

For an ideal ramjet engine, prove that the thrust is expressed by the relation

$$T = \dot{m}_a u\left(\sqrt{\tau_b} - 1\right), \quad \tau_b = \frac{T_{04}}{T_{02}}$$

For a flow at stratosphere region of the standard atmosphere, where T_a = constant, and if the maximum temperature T_{04} = constant (full-throttle operation), prove that the thrust attains a maximum value when the flight Mach number M_0 is given by

$$M_0 = \sqrt{\frac{2}{\gamma - 1}\left(\tau_\lambda^{1/3} - 1\right)}, \quad \tau_\lambda = \frac{T_{04}}{T_a}$$

Plot the relation

$$\left(\frac{T}{\dot{m}_a a_0}\right) \text{ versus } M_0 \text{ for } \tau_\lambda = 9.0$$

where a_0 is the sonic speed at the flight altitude.

Solution

The specific thrust for an ideal ramjet engine with negligible fuel-to-air ratio f and unchoked nozzle is given by the relation

$$\frac{T}{\dot{m}} = \left(u_e - u\right) = u\left(\frac{u_e}{u} - 1\right)$$

From Equation 3.21b, the ratio between the exhaust and flight speeds is equal to the ratio between the maximum temperature and the total free-stream temperature:

$$\frac{u_e}{u} = \sqrt{\frac{T_{04}}{T_{0a}}}$$

Define this temperature ratio as

$$\tau_b = \frac{T_{04}}{T_{02}}$$

$$\therefore \frac{u_e}{u} = \sqrt{\tau_b}$$

$$\frac{T}{\dot{m}u} = \left(\frac{u_e}{u} - 1\right) = \left(\sqrt{\tau_b} - 1\right) \qquad \text{(a)}$$

Since $\tau_\lambda = \frac{T_{04}}{T_a}$ and $\tau_b = \frac{T_{04}}{T_{02}}$

$$\therefore \tau_\lambda = \frac{T_{04}}{T_{02}}\frac{T_{02}}{T_a} = \tau_b\left(1 + \frac{\gamma - 1}{2}M_0^2\right)$$

$$\tau_b = \frac{\tau_\lambda}{\left(1 + \frac{\gamma - 1}{2}M_0^2\right)} \qquad \text{(b)}$$

Since the flight speed (u) is equal to $M_0 a_0$, then from Equations a and b,

$$\therefore \frac{T}{\dot{m}} = M_0 a_0\left(\sqrt{\frac{\tau_\lambda}{\left(1 + \frac{\gamma - 1}{2}M_0^2\right)}} - 1\right)$$

$$\frac{\partial(T/\dot{m})}{\partial M_0} = a_0\left(\sqrt{\frac{\tau_\lambda}{\left(1 + \frac{\gamma - 1}{2}M_0^2\right)}} - 1\right) + + M_0 a_0\left((-0.5)\left(\frac{\gamma - 1}{2}\right)(2M_0)\frac{\sqrt{\tau_\lambda}}{\left(1 + \frac{\gamma - 1}{2}M_0^2\right)^{3/2}}\right)$$

The specific thrust is a maximum when

$$\frac{\partial(T/\dot{m})}{\partial M_0} = 0$$

$$\sqrt{\tau_\lambda}\left(1 + \cancel{\frac{\gamma - 1}{2}M_0^2}\right) - \left(1 + \frac{\gamma - 1}{2}M_0^2\right)^{3/2} - \cancel{\left(\frac{\gamma - 1}{2}M_0^2\right)}\sqrt{\tau_\lambda} = 0$$

$$\sqrt{\tau_\lambda} = \left(1 + \frac{\gamma - 1}{2}M_0^2\right)^{3/2}$$

$$\tau_\lambda^{1/3} = \left(1 + \frac{\gamma - 1}{2} M_0^2\right)$$

$$M_0^2 = \frac{2}{\gamma - 1}\left(\tau_\lambda^{1/3} - 1\right)$$

$$\left(M_0\right)_{\substack{\max. \\ thrust}} = \sqrt{\frac{2}{\gamma - 1}\left(\tau_\lambda^{1/3} - 1\right)}$$

Now to plot the relation $\left(T/\dot{m}a_0\right)$ against M_0, since

$$\frac{T}{\dot{m}a_0} = M_0\left(\sqrt{\tau_b} - 1\right)$$

From the earlier relation, the thrust or $T/\dot{m}a_0 = 0$, when (1) $M_0 = 0$ and (2) $\tau_b = 1$.

Since $\tau_\lambda = \tau_b\left(1 + \frac{\gamma - 1}{2} M_0^2\right)$, then at $\tau_b = 1$,

$$\tau_\lambda = \left(1 + \frac{\gamma - 1}{2} M_0^2\right)$$

and

$$M_0 = \sqrt{\frac{2}{\gamma - 1}\left(\tau_\lambda - 1\right)} = \sqrt{\frac{2}{0.4}\left(9 - 1\right)} = 6.32$$

Thus, the thrust is also equal to zero when the flight Mach number $M_0 = 6.32$. Since the thrust is equal to zero at $M_0 = 0$ and $M_0 = 6.32$, then it will attain a maximum value at an intermediate value calculated from the relation

$$M_0 = \sqrt{\frac{2}{\gamma - 1}\left(\tau_\lambda^{1/3} - 1\right)} = \sqrt{\frac{2}{0.4}\left(9^{1/3} - 1\right)} = 2.322$$

Thus, the thrust is maximum at $M_0 = 2.322$.

A plot for the relation $\left(\frac{T}{\dot{m}_a a_0}\right)$ versus M_0 for $\tau_\lambda = 9.0$ is illustrated in Figure 3.16.

Comments: This example illustrates the range of operation for an ideal ramjet engine. The engine can develop a thrust force when the flight Mach number is some value close to zero. However, this is normally not the case due to the different sources of irreversibility in the engine. Example 3.7 clarifies that a real ramjet engine can develop thrust force only at higher values of a Mach number that is close to or greater than 0.5 depending on the total pressure ratios within its three modules.

Example 3.7

A ramjet has low-speed stagnation pressure losses given by $r_d = 0.90$, $r_c = 0.95$, and $r_n = 0.96$. The ambient and maximum temperatures are 222 and 1950 K, respectively. The fuel-to-air ratio is assumed very small such that $f \ll 1$. What is the minimum flight Mach number at which the engine develops positive thrust? Assume that the nozzle is unchoked.

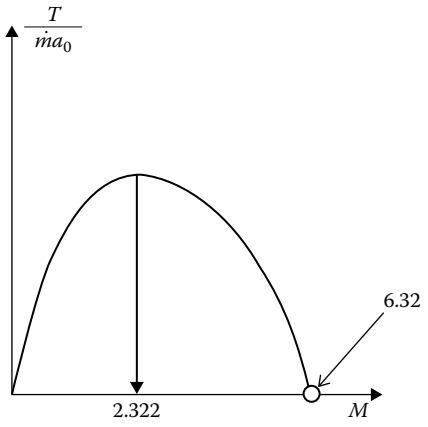


FIGURE 3.16
Plot for the relation $(T/\dot{m}_a a_o)$ versus M_0 for $\tau_\lambda = 9.0$.

Solution

The thrust equation is expressed by Equation 3.32 as follows:

$$\frac{T}{\dot{m}_a} = (1+f)\sqrt{\frac{2\gamma_e R_e T_{04}(m-1)}{(\gamma-1)m}} - M\sqrt{\gamma RT_a} + \frac{P_e A_e}{\dot{m}_a}\left(1-\frac{P_a}{P_e}\right)$$

where

$$m = \left(1+\frac{\gamma-1}{2}M^2\right)\left(r_d r_c r_n \frac{P_a}{P_e}\right)^{\gamma-1/\gamma}$$

for an unchoked nozzle $P_a = P_e$, also assuming small fuel-to-air ratio, $f \ll 1$, then

$$\frac{T}{\dot{m}_a} = \sqrt{\frac{2\gamma RT_{04}(m-1)}{(\gamma-1)m}} - M\sqrt{\gamma RT_a}$$

Rewrite m as

$$m = (1+\alpha_1 M^2)\alpha_2$$

where

$$\alpha_1 = \frac{\gamma-1}{2} \quad \text{and} \quad \alpha_2 = (r_d r_c r_n)^{\gamma-1/\gamma}$$

also define

$$\alpha_3 = \sqrt{\gamma RT_a} \quad \text{and} \quad \alpha_4 = \frac{2\gamma RT_{04}}{\gamma-1}$$

$$\therefore \frac{T}{\dot{m}_a} = \sqrt{\frac{\alpha_4\left[\alpha_2(1+\alpha_1 M^2)-1\right]}{\alpha_2(1+\alpha_1 M^2)}} - \alpha_3 M$$

When

$$\frac{T}{\dot{m}_a} = 0$$

$$\therefore \frac{\alpha_4\left[\alpha_2\left(1+\alpha_1 M^2\right)-1\right]}{\alpha_2\left(1+\alpha_1 M^2\right)} = \alpha_3^2 M^2$$

$$\therefore \alpha_2\alpha_4\left(1+\alpha_1 M^2\right)-\alpha_4 = \alpha_2\alpha_3^2 M^2\left(1+\alpha_1 M^2\right)$$

$$\alpha_1\alpha_2\alpha_3{}^2 M^4 + \alpha_2\alpha_3^2 M^2 - \alpha_1\alpha_2\alpha_4 M^2 - \alpha_2\alpha_4 + \alpha_4 = 0$$

Writing this equation in the general form

$$AM^4 + BM^2 + C = 0$$

where

$$A = \alpha_1\alpha_2\alpha_3^2$$

$$B = \alpha_2\alpha_3^2 - \alpha_1\alpha_2\alpha_4$$

$$C = \alpha_4\alpha_2\alpha_4 = \left(1-\alpha_2\right)\alpha_4$$

then

$$M^2 = \frac{-B \pm \sqrt{B^2 - 4AC}}{2A}$$

Now substitute the numerical values

$$\alpha_1 = 0.2, \quad \alpha_2 = 0.945, \quad \alpha_3 = 298.7, \quad \text{and} \quad \alpha_4 = 3917 \times 10^3$$

then

$$A = 16.86 \times 10^3, \quad B = -655.98 \times 10^3, \quad \text{and} \quad C = 215 \times 10^3$$

$$M^2 = \frac{656 \times 10^3 \pm 10^3\sqrt{430,336 - 14,499}}{2 \times 16.86 \times 10^3}$$

$$M^2 = 0.33, \quad \text{which gives } M = 0.574$$

or

$$M^2 = 38.55, \quad \text{which yields } M = 6.2088$$

Thrust starts to build up when the flight Mach number $M = 0.574$ and not zero as depicted in Example 3.6. A plot for the specific thrust versus the flight Mach number is given in Figure 3.17.

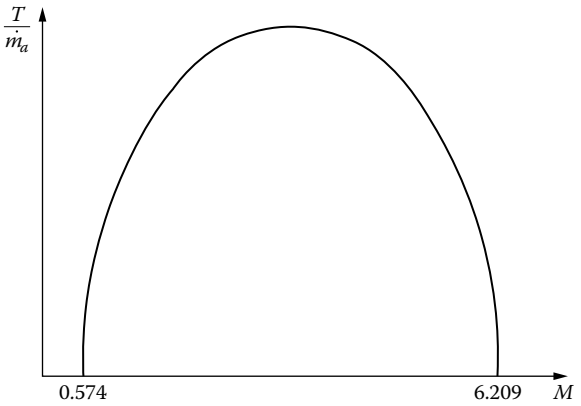


FIGURE 3.17
Specific thrust versus flight Mach number for a real ramjet engine.

Spike motion: A supersonic ramjet engine is fitted with a spike that moves axially in and out of the engine. This motion is necessary to adjust the oblique shock wave originating from the spike to the intake lips and avoid supersonic spillage and also penetrating shocks into the intake. This is the case for the turboram engine powering the SR-71 aircraft.

The motion of the spike is automatically adjusted by the engine control unit. The following example illustrates this motion.

Example 3.8

A ramjet engine is fitted with a variable geometry intake, where a center body moves forward or backward to adjust the oblique shock wave to the intake lips (Figure 3.18). The half angle of the spike is 10°. The flight Mach number M_1 in the supersonic regime varies from M_{min} to 3.5. The inlet radius of the intake is 250 mm.

1. Find the minimum Mach number $M_{min} > 1.0$ that corresponds to an attached shock wave to the apex.
2. Find the distance (S) wave to the apex of the center body.
3. Will the center body move forward or rearward when the flight Mach number increases?

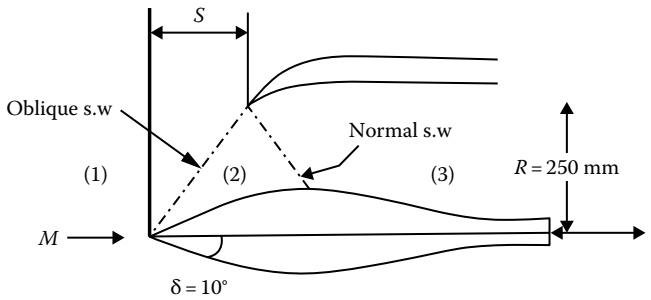


FIGURE 3.18
Variable geometry intake of a ramjet engine.

4. What would be the value of (*S*) if the Mach number $M_1 = 2.5$? Calculate the distance moved by the spike.
5. Calculate the total pressure ratio P_{03}/P_{01} in the case of $M_1 = 3.0$.

Solution

It is known that for a certain deflection angle, there is a minimum Mach number that provides an attached shock wave. If the Mach number is reduced, a detached shock wave exists.

1. From a shock wave graph (Figure 3.19), for a semi-vertex angle of the spike of 10°, then the minimum Mach number that corresponds to an attached shock wave is $M_{min} = 1.42$ and the corresponding wave angle $[\sigma]_{min} = 68°$.
2. The distance S corresponding to this minimum Mach number is

$$\tan 68 = \frac{R}{S}$$

$$S = \frac{R}{\tan 68} = \frac{250}{2.4751} = 101.0 \text{ mm}$$

3. Figure 3.19, illustrating the shock wave angle versus the deflection angle (σ vs. δ), defines two types of shock waves, namely, strong and weak shock waves. The strong shock wave is close to the normal one and has a large angle, where the flow downstream of the shock is subsonic. The weak shock wave occurs at small angles. The flow downstream of the weak shock wave is supersonic. The angle of the weak shock wave decreases as the Mach number increases. Thus, the spike (or the center body) moves forward to keep the shock wave attached to the intake lips.
4. At $M_1 = 2.5 \Rightarrow \sigma = 33°$

$$S = \frac{R}{\tan 33} = \frac{250}{0.6494} = 384.07 \text{ mm}$$

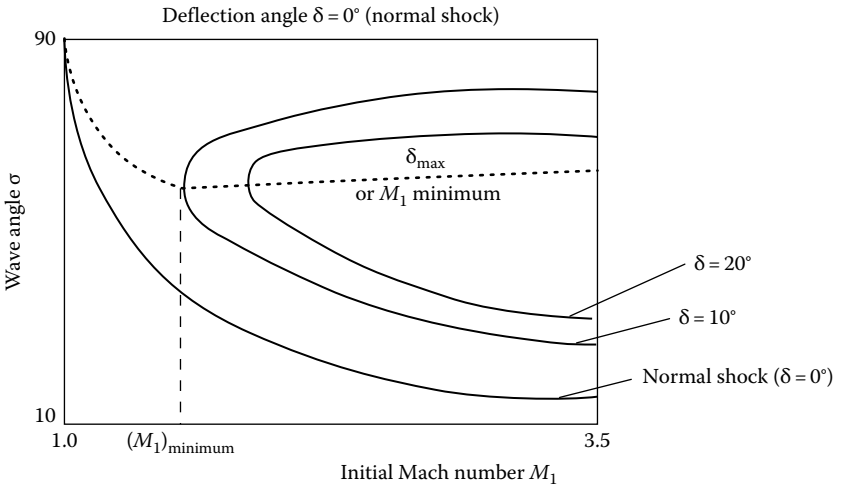


FIGURE 3.19
Shock angle for different Mach numbers. (From Hill, P. and Peterson, C., *Mechanics and Thermodynamics of Propulsion*, 2nd edn., Addison Wesley Publication Company, Inc., 1992, p. 155.)

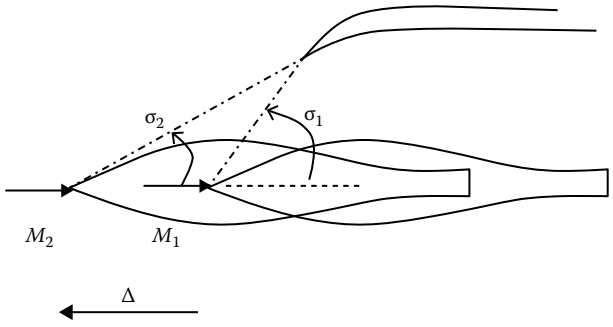


FIGURE 3.20
Spike motion due to the increase of the flight Mach number.

Thus, the spike moves forward by a distance (Δ) as shown in Figure 3.20:

$$\Delta = 384.07 - 101.0 = 283.07 \text{ mm}$$

5. Following the same procedure of Example 3.4, then for the flight Mach number $M_1 = 3.0$, the shock angle is $\sigma = 27°$.

The corresponding total pressure ratio is $P_{02}/P_{01} = 0.97$.

Now, to evaluate the pressure ratio between states (3) and (1), then the Mach number at state (2) is to be first determined. For the oblique shock wave, with $M_1 = 3.0$ and $\delta = 10°$, then $M_2 = 2.5$.

A normal shock wave is developed downstream of the oblique shock wave.

The corresponding pressure ratio (from the tables or equations in Section 3.8) is $P_{03}/P_{02} = 0.499$. The overall pressure ratio is

$$\frac{P_{03}}{P_{01}} = \frac{P_{03}}{P_{02}}\frac{P_{02}}{P_{01}} = 0.484$$

Example 3.9

Figure 3.21 illustrates a ramjet traveling in level flight at an altitude of 55,000 ft with a constant speed of 536 m/s. The intake conditions have been simplified to represent the formation of a normal shock wave immediately at the inlet. It may be assumed that the

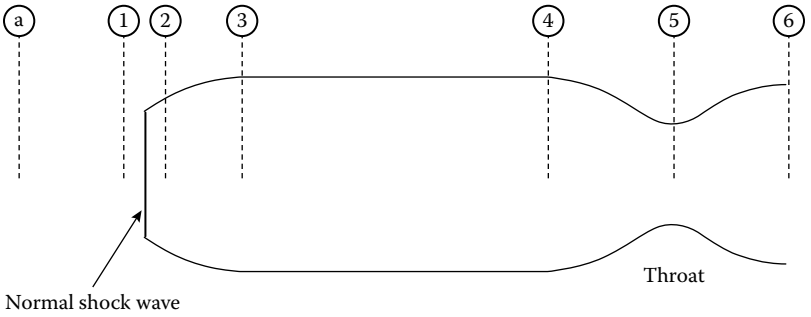


FIGURE 3.21
Ramjet engine with a normal shock wave at the inlet.

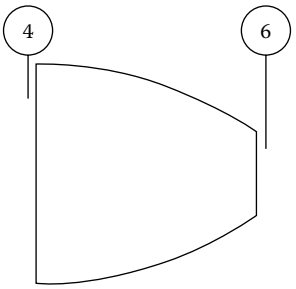


FIGURE E3.9

pressure external to the duct is everywhere that of the ambient atmosphere. The inlet process 2–3 is an isentropic diffusion, and the combustion process 3–4 occurs through the addition of fuel at constant area frictionless duct, the stagnation temperature at 4 being 1280 K. Process 4–5 is an isentropic expansion. Assume that the air/fuel ratio is 40:1. Take the working fluid as air with $\gamma = 1.4$ for all processes. The areas of the intake and combustion chamber are $A_2 = 0.0929$ m^2 and $A_3 = 0.1858$ m^2.

1. Calculate the mass flow rate.
2. Calculate the throat area at (5).
3. Calculate the pressure drop in the combustion chamber.
4. Calculate the thrust developed by the ramjet if the nozzle expands the gas down to the ambient pressure.
5. Repeat (3) for a convergent nozzle.
6. Calculate the propulsive efficiency for cases (3) and (4).
7. Calculate the TSFC in both cases.
8. Draw the cycle on *T*–*S* diagram for both cases of convergent–divergent and convergent nozzles.

Solution

At an altitude of 55,000 ft, the ambient conditions are

$$T_a = -56.5°\text{C} = 216.5 \text{ K}, \quad P_a = 9.122 \text{ kPa}$$

The sonic speed is

$$a = \sqrt{\gamma R T_a} = 295 \text{ m/s}$$

The flight Mach number is

$$M_1 = \frac{V_f}{a} = 1.818$$

$$\frac{T_{0a}}{T_a} = 1 + \frac{\gamma + 1}{2} M^2 = 1.82$$

$$\frac{P_{0a}}{P_a} = \left(1 + \frac{\gamma + 1}{2} M^2\right)^{\gamma/\gamma - 1} = 5.9$$

The ambient total conditions are $T_{0a} = 360$ K

$$P_{0a} = 53.86 \text{ kPa}$$

Just upstream of the engine, the static and total conditions are equal to the ambient conditions, or

$$P_{01} = P_{0a}, \quad P_1 = P_a, \quad T_1 = T_a, \quad T_{01} = T_{0a}$$

The density is

$$\rho_1 = \frac{P_1}{RT_1} = \frac{9122}{287 \times 216.5} = 0.147 \text{ kg/m}^3$$

Normal shock wave: Normal shock wave exists between states (1) and (2). From normal shock wave tables, or normal shock relations with $M_1 = 1.82$, then

$$\therefore M_2 = 0.6121, \quad \frac{T_{02}}{T_2} = 1.0773, \quad \frac{P_{02}}{P_{01}} = 0.803, \quad \frac{T_2}{T_1} = 1.5465$$

$$P_{02} = 43.25 \text{ kPa}, \quad T_2 = 334.8 \text{ K}, \quad T_{02} = 360 \text{ K} \equiv T_{01}$$

The mass flow rate is $\dot{m} = \rho_1 V_1 A_1$

$$\dot{m} = 0.147 \times 536 \times 0.0929 = 7.31 \text{ kg/s}$$

Intake: From state (2) to state (3), the flow is isentropic; thus,

$$P_{03} = P_{02} = 43.25 \text{ kPa} \quad \text{and} \quad T_{03} = T_{02} = 360 \text{ K}$$

From the isentropic flow tables or equations in Section 3.5, then with $M_2 = 0.6121$

$$\therefore \frac{A_2}{A^*} = 1.16565$$

since

$$\frac{A_3}{A^*} = \frac{A_3}{A^*}\frac{A^*}{A_2} = \frac{A_3}{A_2}\frac{A_2}{A^*} = 2 \times 1.16565$$

$$\frac{A_3}{A^*} = 2.3313$$

From the isentropic flow table or equation in Section 3.8, the Mach number at the inlet of combustion chamber is

$$M_3 = 0.26$$

This subsonic flow is appropriate for combustion.

Combustion chamber: From state (3) to state (4), a frictionless, heat addition constant area duct exists; thus, the process represents a Rayleigh flow. From the Rayleigh flow tables or equations, Section 3.8, with $M_3 = 0.26$

$$\therefore \frac{T_{03}}{T_0^*} = 0.27446, \quad \frac{P_{03}}{P_0^*} = 1.214$$

Next, with $T_{04} = 1278$ K

$$\therefore \frac{T_{04}}{T_0^*} = \frac{T_{04}}{T_{03}} \frac{T_{03}}{T_0^*} = \frac{1278}{360} \times 0.27446 = 0.9741$$

$\therefore$ From Rayleigh flow tables (or equations) $M_4 = 0.83$ and $P_{04}/P_0^* = 1.014$

$$\therefore \frac{P_{04}}{P_{03}} = \frac{P_{04}}{P_0^*} \frac{P_0^*}{P_{03}} = \frac{1.014}{1.214} = 0.8352$$

$$P_{04} = 36.12 \text{ kPa}$$

The pressure drop in the combustion chamber is $\Delta P_{CC} = P_{03} - P_{04} = (1 - \Delta P_{CC}) P_{03} = 7.125$ kPa.
This is a rather large pressure drop.
Nozzle: From state (4) to state (5), the flow in the nozzle is isentropic flow.
At $M_4 = 0.83$, then $A_4/A^* = 1.02696$.
The throat area is A^* and calculated as

$$A_5 \equiv A^* = \frac{A_4}{\left(A_4/A^*\right)} = \frac{0.1858}{1.02696} = 0.1809 \text{ m}^2$$

since

$$\frac{P_6}{P_{06}} = \frac{P_6}{P_{04}} = \frac{P_1}{P_{04}} = \frac{9.122}{36.12} = 0.2525$$

From the isentropic tables or the governing equations in Section 3.8, $M_6 = 1.555$.
Then $A_6/A^* = 1.211$ and $T_6/T_{06} = 0.67545$.
Thus, $A_6 = 1.211 \times 0.1809 = 0.21906$ m^2.
Since $T_{06} = T_{04} = 1277$ K, then $T_6 = 862.5$ K.
The jet speed is now calculated as $V_6 = M_6 \sqrt{\gamma R T_6} = 915.4$ m/s.
Thrust force $= \dot{m}\left[\left(1 + f\right)V_6 - V_f\right] + P_1\left(A_6 - A_1\right)$.
Since $f = \dfrac{1}{40} = 0.025$, then the thrust force is

$$T = (7.31)\left[(1.025)(915.4) - 536\right] + 9.122 \times 10^3 \left(0.219 - 0.929\right) = 4090 \text{ N}$$

If the nozzle is convergent (from state (4) to state (6)), check for choking

$$\frac{P_{04}}{P_a} = \frac{36.12}{9.122} = 3.959$$

$$\frac{P_{04}}{P_c} = \left(\frac{\gamma + 1}{\gamma}\right)^{\gamma/\gamma - 1} = 1.8929$$

$$T_6 = T_c = \frac{T_{04}}{\left(\dfrac{\gamma + 1}{2}\right)} = \frac{1278}{1.2} = 1065 \text{ K}$$

$$V_6 = \text{Sonic speed} = \sqrt{\gamma R T_6} = 654 \text{ m/s}$$

From the isentropic flow tables or equations, with $M_4 = 0.83$, then $\frac{A_4}{A^*} = 1.02708$

$$A_6 = A^* = \frac{0.1858}{1.02708} = 1809 \text{ m}^2$$

The thrust force equation is now expressed as $T = \dot{m}\left[\left(1+f\right)V_6\right] + P_6A_6 - P_1A_1$

$$T = 7.31\left[\left(1.025\right)\left(654\right) - 536\right] + 19.08\times10^3\times0.1809 - 9.122\times10^3\times0.0929$$

$$T = 3587 \text{ N}$$

Propulsive efficiency: The general expression for the propulsive efficiency is

$$\eta_p = \frac{TV_f}{TV_f + \frac{1}{2}\dot{m}_e\left(V_e - V_f\right)^2}$$

The exhaust mass flow rate is $\dot{m}_e = \dot{m}_a\left(1+f\right) = 7.31\times1.025 = 7.493$ kg/s.
Case (*1*): Convergent–divergent nozzle ($V_e = 915.4$ m/s)

$$\eta_p = \frac{4090\times536}{4090\times536 + \frac{1}{2}7.493\left(915.4-536\right)^2}$$

$$\eta_p = 80.25\%$$

Case (2): Convergent nozzle ($V_e = 654$ m/s)

$$\eta_p = \frac{4090\times536}{4090\times536 + \frac{1}{2}\times7.493\left(654-536\right)^2}$$

$$\eta_p = 97.6\%$$

The TSFC is expressed as $\text{TSFC} = \frac{\dot{m}_f}{T} = \frac{f}{T/\dot{m}_a}$
Case (*1*): With $T = 4090$ N, then $T/\dot{m}_a = 559.5$ N·s/kg

$$\text{TSFC} = \frac{0.025}{559.5} \text{ kg/N}\cdot\text{s} = 0.16 \text{ kg/N}\cdot\text{h}$$

Case (2): Now $T = 3587$ N

$$\text{TSFC} = \frac{0.025\times3600}{\left(3587/7.31\right)} = 0.1834 \text{ kg/N}\cdot\text{h}$$

Comments:

1. Convergent nozzle results in less thrust and consequently higher TSFC compared with a convergent–divergent nozzle.
2. The propulsive efficiency for the case of convergent nozzle is higher than that of a convergent–divergent nozzle as the exhaust speed is sonic in the former case and supersonic in the latter.

Figure 3.22 illustrates the cycle on the *T*–*S* diagram for both convergent and convergent–divergent nozzles.

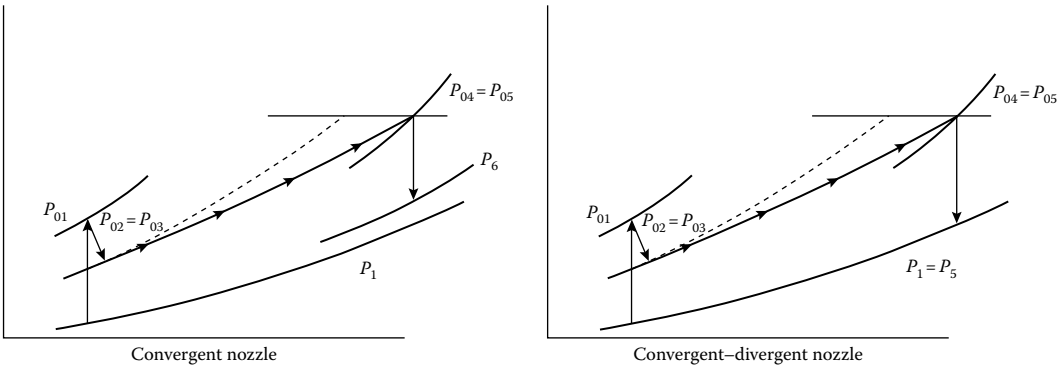


FIGURE 3.22
T–S diagram for convergent and convergent–divergent nozzles.

3.4 Case Study

The performance of a ramjet engine is examined here. The variables influencing the performance of ramjet engines are

1. Flight Mach number
2. Flight altitude
3. Maximum temperature of the engine
4. Fuel-heating value
5. Pressure ratio of three modules (intake, combustion chamber, and nozzle)

These parameters influence the engine performance. The measures for performance are

1. Specific thrust
2. Fuel-to-air ratio
3. Efficiencies: propulsive, thermal, and overall

The following ranges for variables are to be examined:

1. The flight Mach number is successively increased from 1.0 to 4.0.
2. Both sea level and 15 km altitudes.
3. Maximum temperature ranging from 2500 to 3000 K.
4. Two fuel types were considered:
   a. Hydrocarbon with a heating value ranging from 44,786 to 50,010 kJ/kg
   b. Hydrogen fuel having a heating value of 119,954 kJ/kg
5. Intake pressure ratio $r_d = 0.7$, combustion chamber pressure ratio $r_c = 0.97$, and nozzle pressure ratio $r_n = 0.96$.

Figure 3.23 illustrates the specific thrust versus Mach number for different maximum temperatures. As the maximum temperature increases, the specific thrust increases. At the

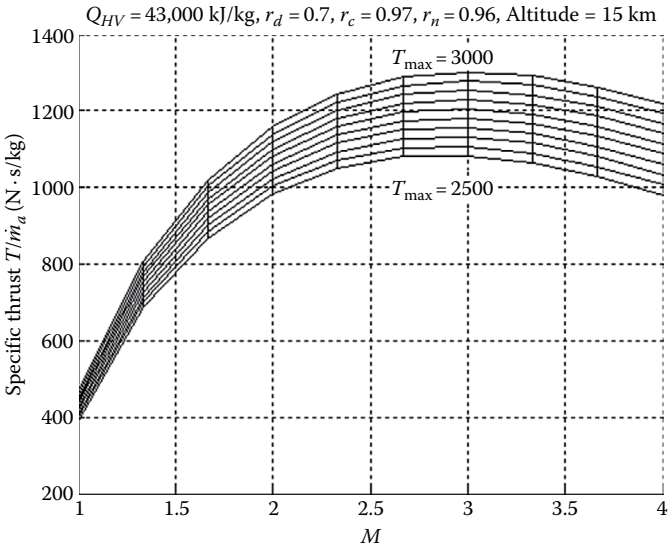


FIGURE 3.23
Variation of specific thrust with Mach number for different maximum temperatures.

same time, increasing the maximum temperature due to burning more fuel leads to an increase in the TSFC Figure 3.24 and increase of the fuel to air ratio, Figure 3.25.

Alternatively, the earlier variables can be drawn versus the maximum temperature for different Mach numbers. As an example, Figure 3.26 illustrates the variation of specific thrust versus maximum temperature for different Mach numbers. It is clarified from Figure 3.26 that a nearly linear relation persists between the specific thrust and the maximum temperature. The same conclusion is found for the fuel-to-air ratio variation with maximum temperature as shown in Figure 3.27.

The contribution of the fuel heating value on both TSFC and fuel-to-air ratio is plotted in Figures 3.28 and 3.29, respectively. As the fuel heating value increases, the fuel consumption decreases. Thus, the TSFC and fuel-to-air ratio decrease with the increase of the fuel heating value.

The variation of propulsive efficiency with Mach number for different maximum temperatures is plotted in Figure 3.30. This figure is distinct as the efficiency drops at first and then increases with Mach number. The increase of maximum cycle temperature leads to a drop in the propulsive efficiency for the same Mach number.

The variation of propulsive efficiency with maximum temperature for different Mach numbers is plotted in Figure 3.31. From Figures 3.30 and 3.31, the minimum propulsive efficiency is seen at Mach number close to 1.5.

The thermal efficiency increases with the Mach number. Figure 3.32 illustrates this relation for a maximum temperature of 2500 K.

The overall efficiency is plotted in Figure 3.33 versus Mach number for different maximum temperatures. It is interesting to notice that both the thermal and overall efficiencies increase continuously with the Mach number and the kink found in the propulsive efficiency is no longer seen.

It is interesting to have 3-D plots that illustrate the effect of two variables simultaneously on one of the performance parameters. Figures 3.34 through 3.39 illustrate these 3-D plots.

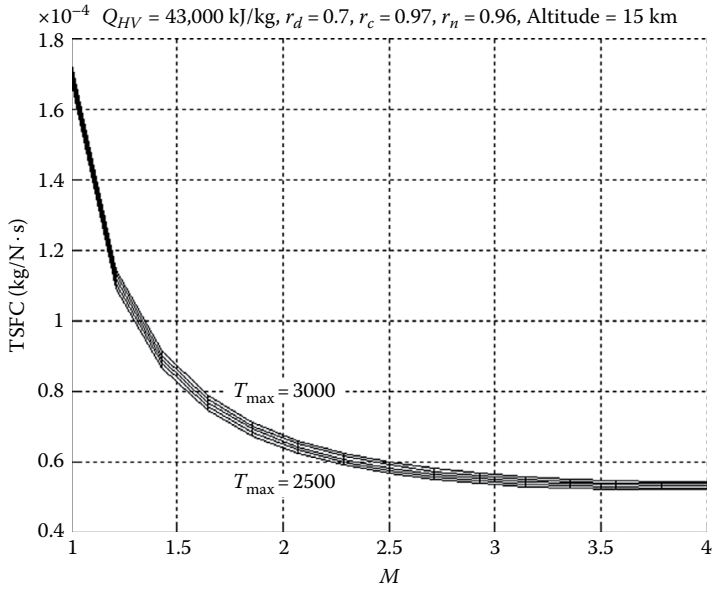


FIGURE 3.24
Variation of TSFC with Mach number for different maximum temperatures.

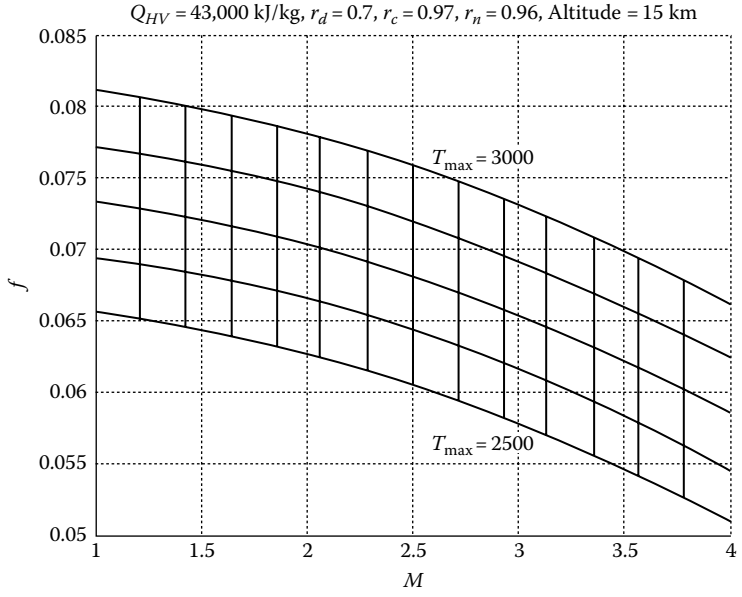


FIGURE 3.25
Variation of fuel-to-air ratio with Mach number for different maximum temperatures.

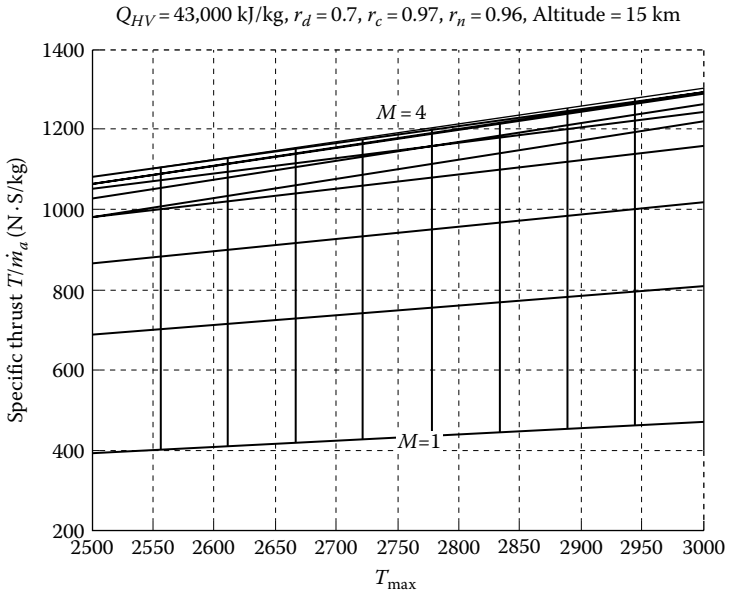


FIGURE 3.26
Variation of specific thrust versus maximum temperature for different Mach numbers.

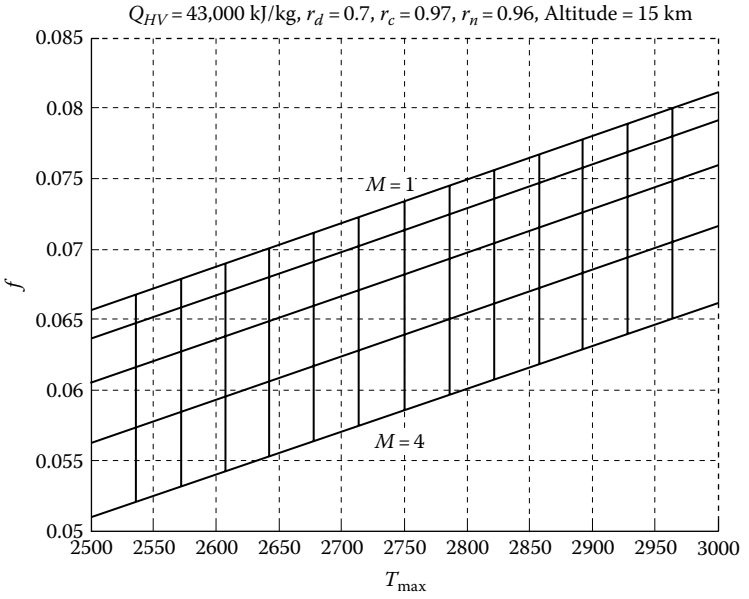


FIGURE 3.27
Variation of fuel-to-air ratio (*f*) versus maximum temperature for different Mach numbers.

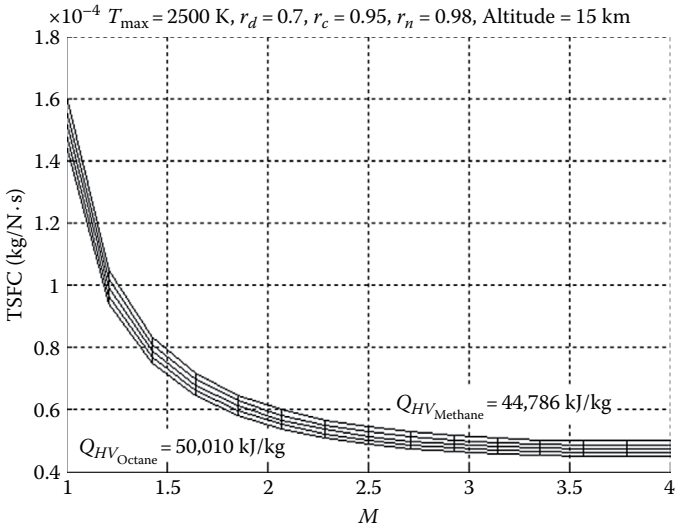


FIGURE 3.28
Variation of TSFC versus Mach number for different fuel heating values.

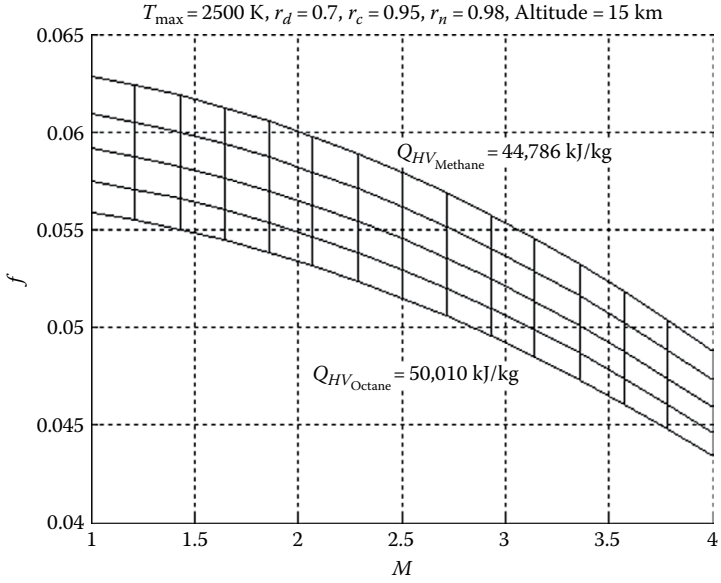


FIGURE 3.29
Variation of fuel-to-air ratio (*f*) versus Mach number for different fuel heating values.

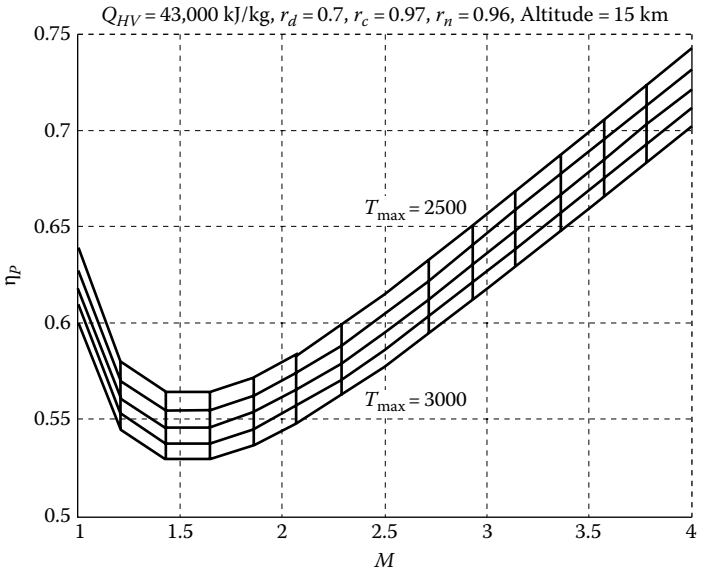


FIGURE 3.30
Variation of propulsive efficiency with Mach number for different maximum temperatures.

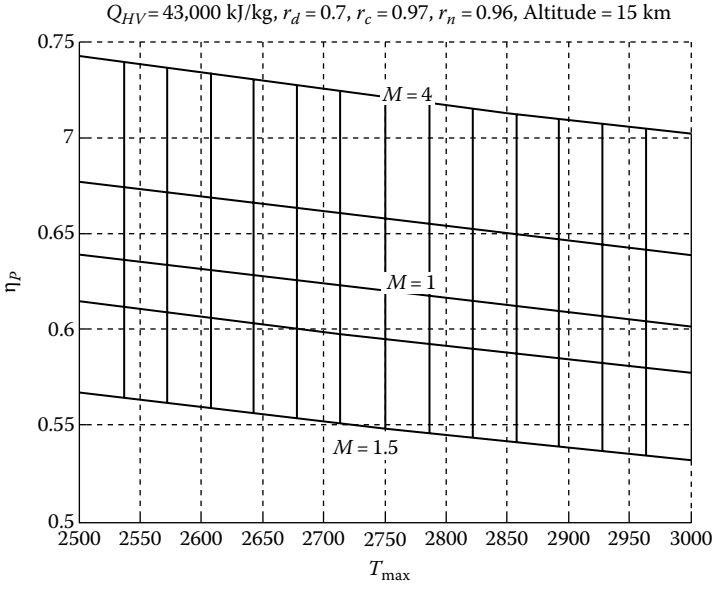


FIGURE 3.31
Variation of propulsive efficiency with maximum temperature for different Mach numbers.

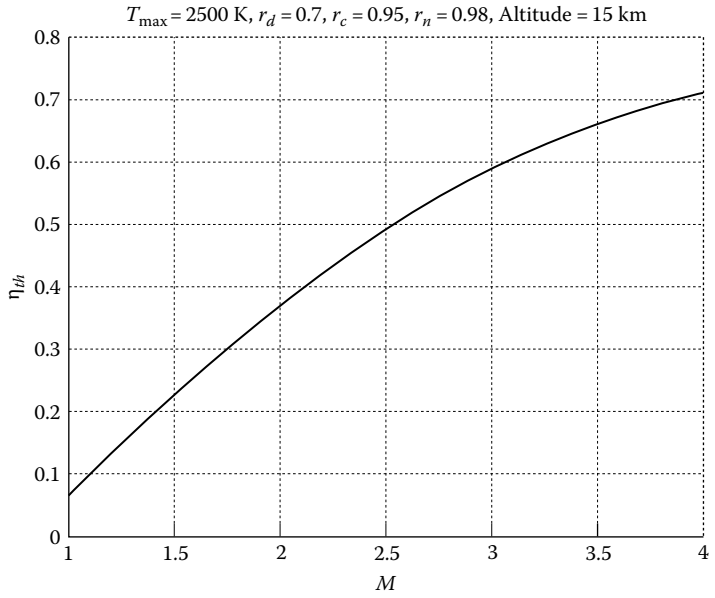


FIGURE 3.32
Variation of thermal efficiency with Mach number for a maximum temperature of 2500 K.

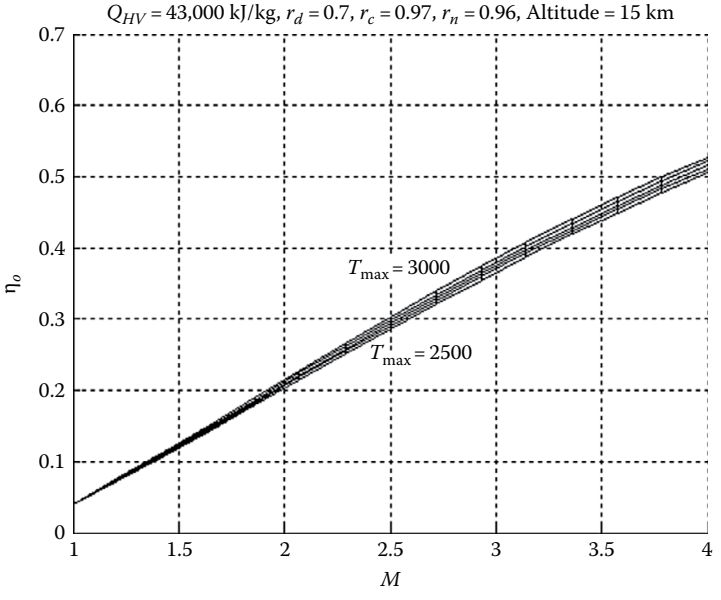


FIGURE 3.33
Variation of overall efficiency with Mach number for different maximum temperatures.

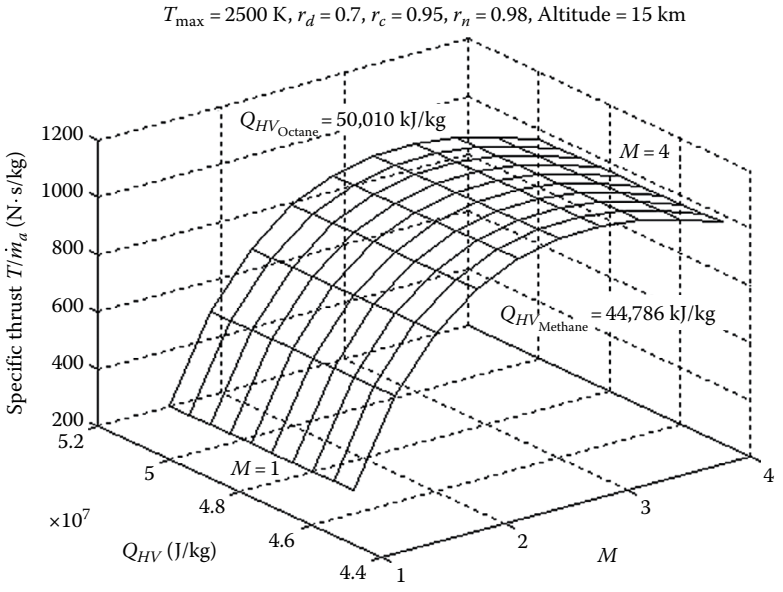


FIGURE 3.34
Variation of specific thrust with Mach number and heating value.

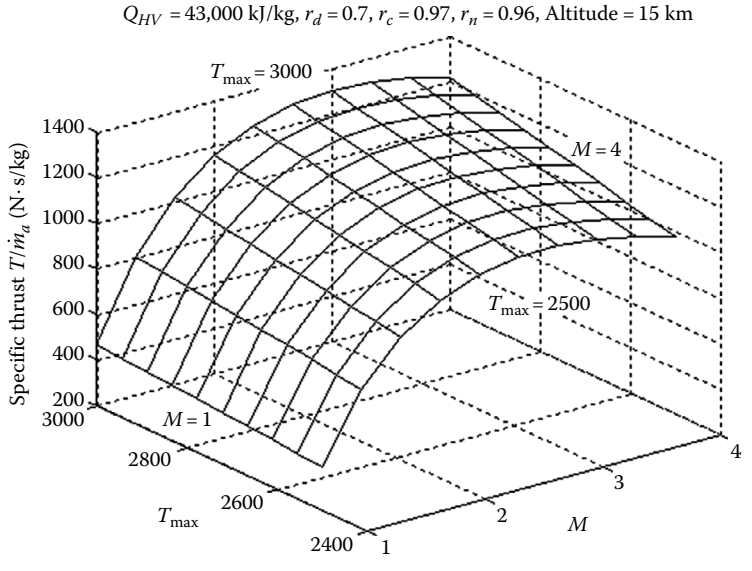


FIGURE 3.35
Variation of specific thrust with Mach number and maximum temperature.

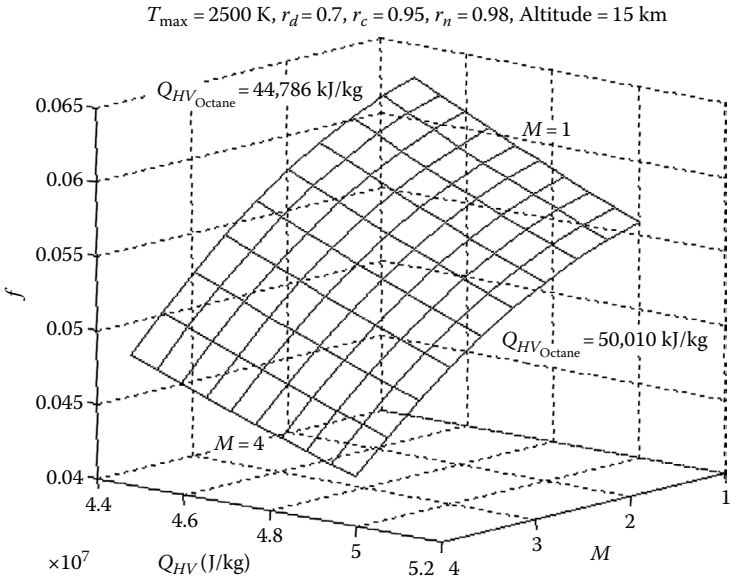


FIGURE 3.36
Variation of fuel-to- air ratio with Mach number and heating value.

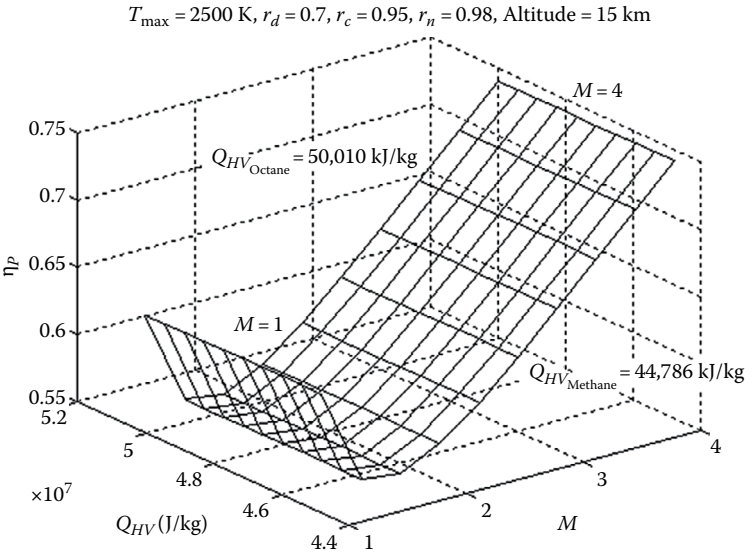


FIGURE 3.37
Variation of propulsive efficiency with Mach number and heating value.

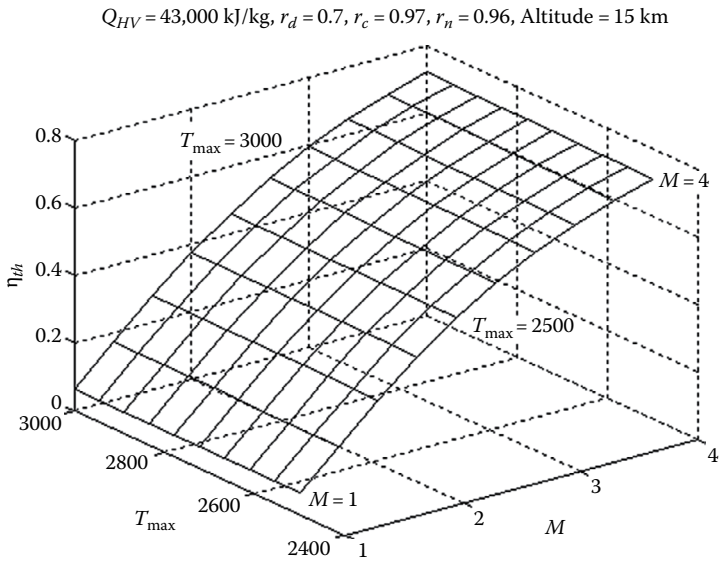


FIGURE 3.38
Variation of thermal efficiency with Mach number and maximum temperature.

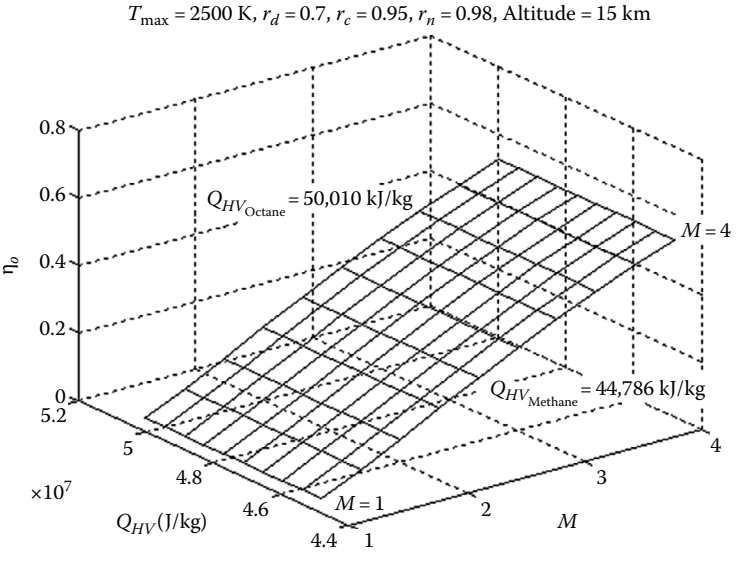


FIGURE 3.39
Variation of overall efficiency with Mach number and heating value.

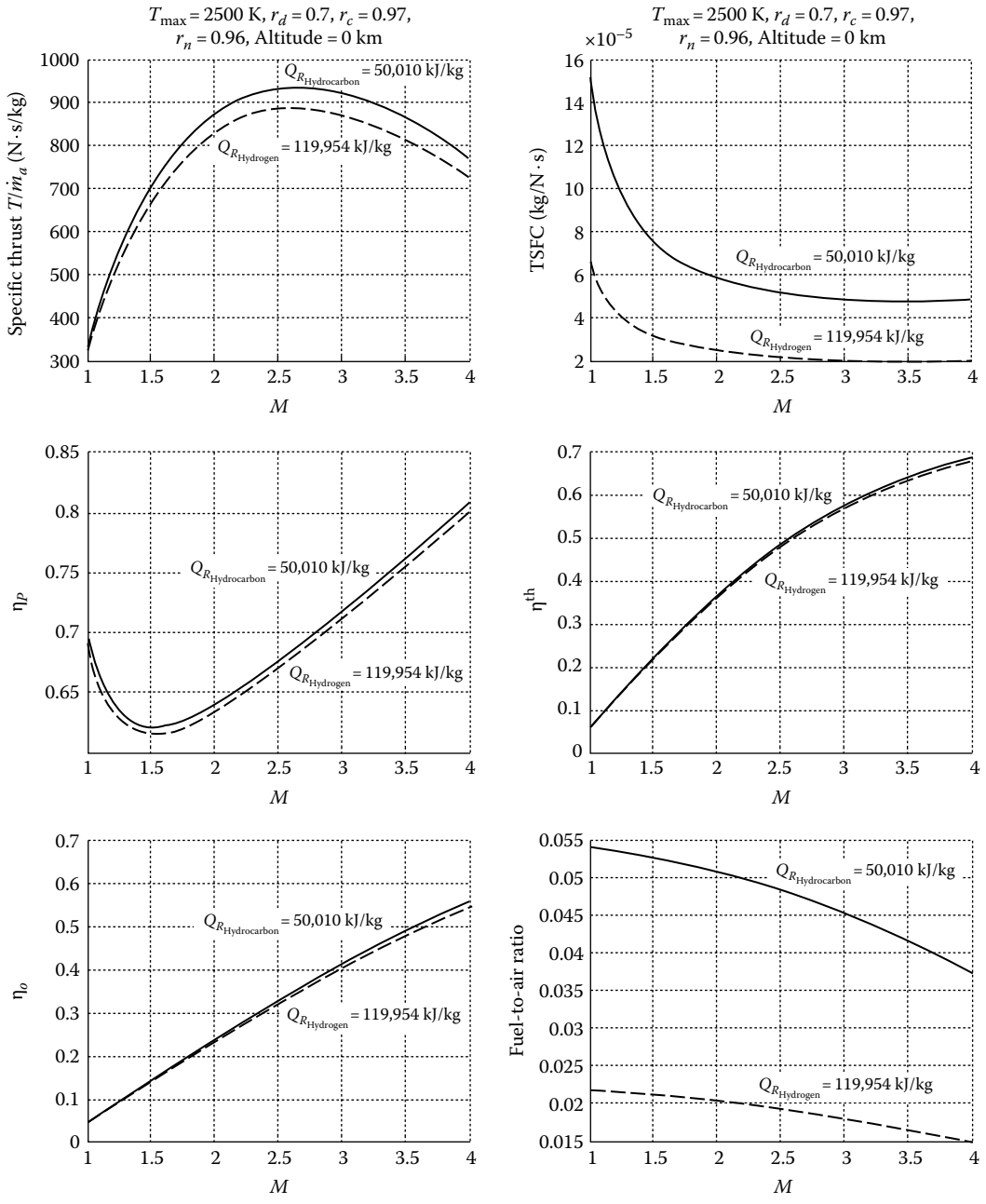


FIGURE 3.40
Performance parameters for hydrogen and hydrocarbon fuels at sea level.

Since hydrogen fuel is expected for future ramjet engines where its heating value is some 240% that of present hydrocarbon fuels, it was examined in this study also. The TSFC and the fuel-to-air ratio of hydrogen-fueled engines are very much less than those using hydrocarbon fuels. Their values for hydrogen fuel are nearly 40% those for hydrocarbon fuels. Figure 3.40 is an assembled figure for sea-level performance curves. It contains six figures representing the specific thrust, TSFC, fuel-to-air ratio, and propulsive, thermal, and overall efficiencies.

3.5 Nuclear Ramjet

The principle behind the nuclear ramjet was relatively simple: the three basic components of ramjet engines are the same, but a nuclear reactor is used to heat the air instead of burning fuel in a combustion chamber. Thus, additional components are used in nuclear ramjets: reactor core, radiation shield, and heat exchanger (Figure 3.41).

During the 1950s and 1960s, there was a government program in the United States to develop nuclear-powered ramjet engines for use in cruise missiles, namely, *Project Pluto*. Two experimental engines were tested at the United States Department of Energy Nevada Test Site in 1961 and 1964. Unlike commercial reactors, which are surrounded by concrete, the Pluto reactor had to be small and compact enough to fly but durable enough to survive a 7,000-mile (11,000 km) trip to a potential target. The nuclear engine could, in principle, operate for months, so a Pluto cruise missile could be left airborne for a prolonged time before being directed to carry out its attack. The project started on January 1, 1957 and, for many reasons, was canceled on July 1, 1964.

In the twenty-first century, interest rose in the possibility of a nuclear ramjet for planetary exploration. The long-term study of planetary atmospheres revealed a need for a probe that had the capabilities for several months' exploration and that had simplicity, reliability, and 3-D mobility. One proposed solution to this need is an autonomous supersonic aircraft powered by a nuclear ramjet engine. Since any gas could be used as a propellant in a nuclear reactor, then the nuclear ramjet can operate in any known planetary atmosphere. Venus's atmosphere is rich with N_2 and CO_2, while Jupiter's atmosphere includes H_2 and He. A nuclear ramjet called Jupiter Flyer [17] was designed to be part of the Galileo mission to Jupiter. Upon arrival at Jupiter, the companion orbiter and the entry

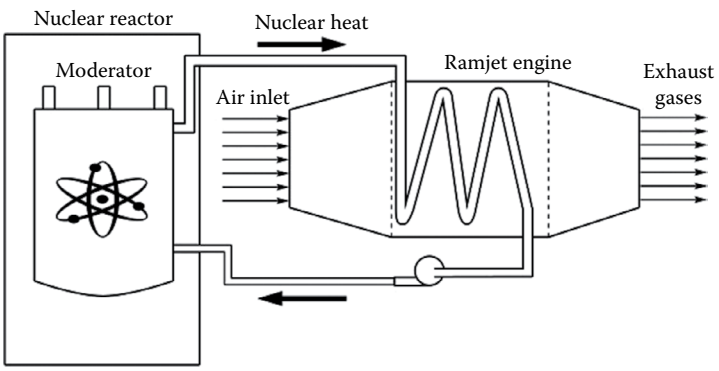


FIGURE 3.41
Nuclear energy ramjet.

capsule containing the Jupiter Flyer separate with the former entering an orbit around Jupiter and the latter entering Jupiter's atmosphere. When the entry capsule slowed to Mach 3, the Jupiter Flyer separated from thermal shield and the nuclear engine started using the ambient atmosphere.

3.6 Double-Throat Ramjet Engine

In the double-throat ramjet (DTR) engine (Figure 3.42), the flow stream needs to contain two throats: the first is to decelerate the flow to subsonic flow before the combustion chamber, and the second is to accelerate the flow to supersonic again in the nozzle.

Thus, the DTR is composed of a supersonic–subsonic intake followed by a subsonic combustion chamber and a subsonic–supersonic nozzle. The supersonic flow in the intake is decelerated to subsonic through either a normal shock or a number of oblique shock waves ended by a normal shock wave in the first throat. This subsonic flow will enter the combustion chamber where combustion process takes place in a nearly constant pressure. The subsonic flow leaving the combustion chamber is accelerated to supersonic speed in a convergent–divergent nozzle (incorporating the second throat). The main parameter affecting the engine performance is the amount of heat added per unit mass of air passing through the engine, which can be calculated from the fuel-to-air ratio in the engine.

Figure 3.42 shows the engine configuration, and Figure 3.43 shows the *T*–*S* diagram of a ramjet engine.

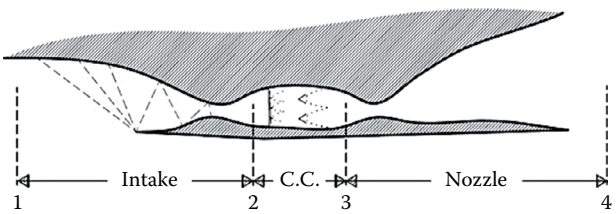


FIGURE 3.42
Configuration of a DTR engine.

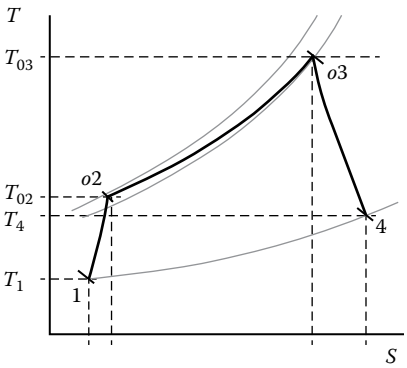


FIGURE 3.43
T–*S* diagram of a DTR engine.

3.7 Solid-Fueled Ramjet Engine

SFRJs are called ram rockets to differentiate them from the LFRJs or simply ramjets. A ram rocket must have all of the propellant in the motor casing (like a rocket). SFRJs are similar to LFRJs, being composed of three modules: diffuser, combustion chamber, and nozzle. Moreover, both can achieve the same high thermodynamic cycle and high performance [18]. An SFRJ has its fuel in solid form within the chamber, and the stoichiometry of combustion is controlled by the regression rate of the fuel.

Due to their inherent simplicity, SFRJs present a cost-effective option for a wide range of applications that demand a sustained thrust force during a substantial portion of their mission profile. UAVs and target drones are believed to be the primary candidates for SFRJ propulsion.

SFRJs offer some very significant advantages over LFRJs, such as

- Extreme *simplicity of construction*. Its simplest form is a tube with a fuel grain cast in it.
- Extreme *simplicity and ease of operation* (ease of ignition, stability, and availability).
- Low costs of fabrication and operation.
- Higher fuel density in the solid phase for pure hydrocarbons and even higher if metal additives are used.
- No need for pumps, external tankage, injectors, or plumbing for fuel delivery.
- Easy inclusion of metal fuels such as boron, magnesium, or beryllium, which raise the heat of combustion, compared with liquid ramjets.
- Solid fuel acts as an ablative insulator, allowing higher sustained combustion chamber exit temperature levels (and hence specific thrust) with less complexity.
- More efficient packaging and higher mass fractions since fuel is stored within the combustion chamber.

However, the main disadvantage of SFRJs is that it cannot be refueled without complex disassembly. LFRJs are much easier to refuel.

Two versions for SFRJ are seen in Figures 3.44 and 3.45 having two different intake constructions.

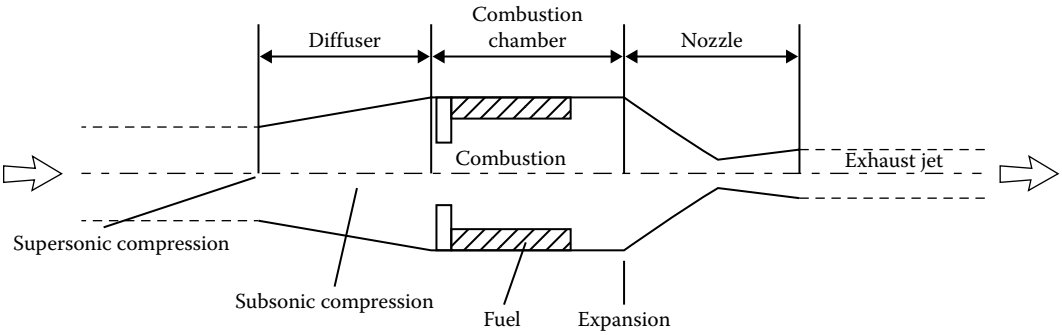


FIGURE 3.44
Schematic diagram of an SFRJ engine with normal shock.

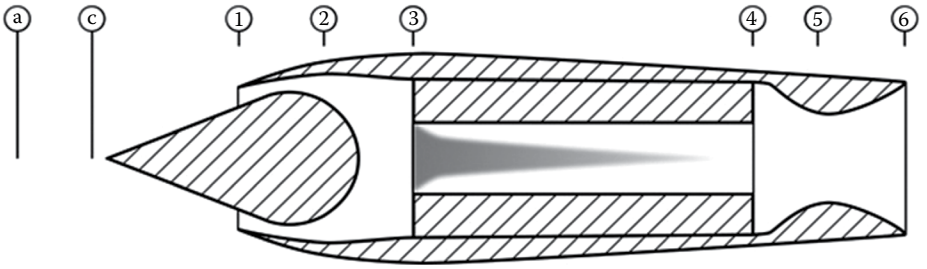


FIGURE 3.45
Schematic diagram of an SFRJ engine with oblique shock(s).

In Figure 3.44, a normal shock in the intake entrance is developed, while in Figure 3.45 one or more oblique shocks followed by a weak normal shock are encountered. Thus, for both cases, the internal flow in the combustion chamber is subsonic.

The combustion chamber entrance step is responsible for the formation of a recirculation region, increases the combustion reaction rates as well as playing the role of a flameholder. Thus it provides stability for the resulting flame.

3.8 Summary and Governing Equations for Shock Waves and Isentropic Flow

3.8.1 Summary (Figure 3.46)

$$T = \dot{m}_a\left[(1+f)u_e - u\right]$$

$$T/\dot{m}_a = \left[(1+f)u_e - u\right]$$

$$\eta_p = \frac{2u\left((1+f)u_e - u\right)}{(1+f)u_e^2 - u^2}$$

$$\eta_{th} = \frac{(1+f)u_e^2 - u^2}{2fQ_{HV}}$$

$$\eta_o = \frac{u\left((1+f)u_e - u\right)}{fQ_{HV}}$$

$$\text{TSFC} = \frac{f}{u\left((1+f)\dfrac{u_e}{u} - 1\right)}$$

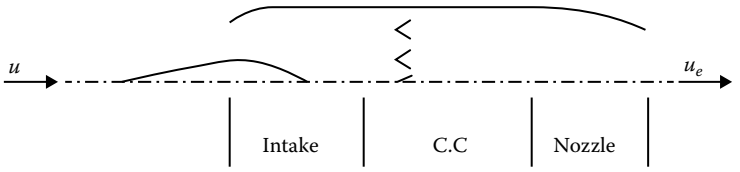


FIGURE 3.46
Schematic diagram of a ramjet engine.

3.8.2 Normal Shock Wave Relations

$$M_2^2 = \frac{(\gamma-1)M_1^2+2}{2\gamma M_1^2-(\gamma-1)}$$

$$\frac{T_2}{T_1} = \left[\frac{2}{(\gamma+1)M_1^2}+\left(\frac{\gamma-1}{\gamma+1}\right)\right]\left[\left(\frac{2\gamma}{\gamma+1}\right)M_1^2-\left(\frac{\gamma-1}{\gamma+1}\right)\right]$$

$$\frac{P_2}{P_1} = \left[1+\left(\frac{2\gamma}{\gamma+1}\right)\left(M_1^2-1\right)\right]$$

$$\frac{\rho_2}{\rho_1} = \left[\frac{(\gamma+1)M_1^2}{2+(\gamma-1)M_1^2}\right]$$

$$\frac{P_{02}}{P_{01}} = \left[\frac{(\gamma+1)M_1^2}{2+(\gamma-1)M_1^2}\right]^{\gamma/\gamma-1}\left[\left(\frac{2\gamma}{\gamma+1}\right)M_1^2-\left(\frac{\gamma-1}{\gamma+1}\right)\right]^{-(1/\gamma-1)}$$

3.8.3 Oblique Shock Wave Relations

$$\tan\delta = \frac{2\cot\beta\left(M_1^2\sin^2\beta-1\right)}{(\gamma+1)M_1^2-2\left(M_1^2\sin^2\beta-1\right)}$$

$$M_2^2\sin^2(\beta-\delta) = \frac{(\gamma-1)M_1^2\sin^2\beta+2}{2\gamma M_1^2\sin^2\beta-(\gamma-1)}$$

$$\frac{P_2}{P_1} = \left[1+\left(\frac{2\gamma}{\gamma+1}\right)\left(M_1^2\sin^2\beta-1\right)\right]$$

$$\frac{T_2}{T_1} = \left[\frac{2}{(\gamma+1)M_1^2\sin^2\beta}+\left(\frac{\gamma-1}{\gamma+1}\right)\right]\left[\left(\frac{2\gamma}{\gamma+1}\right)M_1^2\sin^2\beta-\left(\frac{\gamma-1}{\gamma+1}\right)\right]$$

$$\frac{\rho_2}{\rho_1} = \left[\frac{(\gamma+1)M_1^2\sin^2\beta}{2+(\gamma-1)M_1^2\sin^2\beta}\right]$$

$$\frac{P_{02}}{P_{01}} = \left[\frac{(\gamma+1)M_1^2\sin^2\beta}{2+(\gamma-1)M_1^2\sin^2\beta}\right]^{\gamma/\gamma-1}\left[\left(\frac{2\gamma}{\gamma+1}\right)M_1^2\sin^2\beta-\left(\frac{\gamma-1}{\gamma+1}\right)\right]^{-(1/\gamma-1)}$$

3.8.4 Rayleigh Flow Equations

$$\frac{P}{P^*} = \left[\frac{\gamma+1}{1+\gamma M^2}\right]$$

$$\frac{T}{T^*} = \frac{M^2(\gamma+1)^2}{(1+\gamma M^2)^2}$$

$$\frac{T_0}{T_0^*} = \frac{2(1+\gamma)M^2}{(1+\gamma M^2)^2}\left[1+\frac{\gamma-1}{2}M^2\right]$$

$$\frac{P_0}{P_0^*} = \frac{(1+\gamma)}{(1+\gamma M^2)}\left(\frac{1+\frac{\gamma-1}{2}M^2}{\frac{\gamma+1}{2}}\right)^{\gamma/\gamma-1}$$

3.8.5 Isentropic Relation

$$\frac{A}{A^*} = \frac{1}{M}\left(\frac{1+\frac{\gamma-1}{2}M^2}{\frac{\gamma+1}{2}}\right)^{\gamma+1/2(\gamma-1)}$$

Problems

3.1 A pulsejet similar to the German engine has the following data:

Net thrust	1,400 lb
Flight altitude	10,000 ft
Speed	400 mph
Inlet diameter	1.34 ft
Total pressure drop in the inlet	20%
Thrust-specific fuel consumption	10 $lb/lb_f \cdot h$
Fuel heating value	14,000 Btu/lb_m

Assume $\gamma = 1.4$ and $Cp = 0.24$ $Btu/lb_m{}^\circ R$.

Calculate

1. The fuel-to-air ratio
2. The maximum temperature in the combustion chamber
3. The exhaust velocity
4. The propulsive efficiency
5. The thermal efficiency

3.2 Why is mechanical efficiency not an issue with ramjets?

3.3 How is thrust created in ramjets?

3.4 A small vehicle is powered by a pulsejet. The available net thrust is 6000 N and the traveling speed is 200 km/h. The gases leave the engine with an average velocity of 360 m/s. Assume that the pressure equilibrium exists at the outlet plane and the fuel-to-air ratio is 0.06.

1. Compute the mass flow rate required.
2. Calculate the inlet area (assume 16°C and one atmosphere).

3. Calculate the thrust power.
4. Calculate the propulsive efficiency.

3.5 1. Prove that for an ideal ramjet having a choked nozzle, the specific thrust is expressed by the relation

$$\frac{T}{\dot{m}_a} = \sqrt{\gamma_c R T_a}\left[(1+f)\sqrt{\frac{2\gamma_h T_{o_4}}{\gamma_c(\gamma_h+1)T_a}} - M\right] + \frac{A_e P_a}{\dot{m}_a}\left[\frac{\left(1+\frac{\gamma_c-1}{2}M^2\right)^{\gamma_c/\gamma_c-1}}{\left(\frac{\gamma_h+1}{2}\right)^{\gamma_h/\gamma_h-1}} - 1\right]$$

2. Plot figures to illustrate TSFC and $T/\dot{m}_a$ versus the flight Mach number M for different values of the maximum cycle temperatures in both cases of ideal and real cycles.

3.6 A ramjet engine is powering an aircraft flying at a Mach number M. The thermodynamic cycle is considered ideal. Comparison is to be made between the two cases of choked and unchoked nozzles. Prove that

$$\frac{V_j}{V_c} = M\sqrt{\frac{\gamma+1}{2\left(1+\frac{\gamma-1}{2}M^2\right)}}$$

$$\frac{P_c}{P_a} = \left(\frac{2}{\gamma+1} + \frac{\gamma-1}{\gamma+1}M^2\right)^{\gamma/\gamma-1}$$

where V_j is the exhaust gas velocity when the nozzle is unchoked, while V_c and P_c are the exhaust velocity and pressure when the nozzle is choked.

Next, if $M = 1$,

1. Plot the thermodynamic cycle on the T–S diagram. Write also the thrust equation.
2. Prove that the thrust force is given by the relation

$$T = \rho_a A_i(\gamma R T_a)\left[\sqrt{\frac{2}{\gamma+1}\frac{T_{04}}{T_a}} - 1\right]$$

3.7 For the shown ramjet engine, if $T_{02} = T_6$, prove that

$$\frac{T_{04}}{T_a} = \left(1+\frac{\gamma-1}{2}M^2\right)^2$$

$$V_6 = V\left(1+\frac{\gamma-1}{2}M^2\right)^{1/2}$$

where

T_{04} is the maximum temperature

V_6 is the exhaust velocity

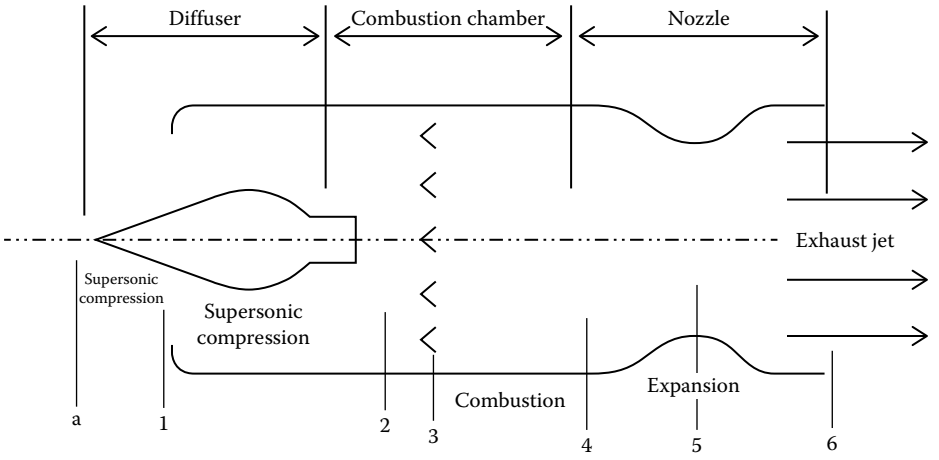


FIGURE P3.7

3.8 For an ideal ramjet engine, prove that if θ_b is constant, then the thrust parameter $\left(T/\dot{m}a_a\right)$ is maximum when $\theta_a = \theta_b^{1/3}$, where $\theta_a = T_{0a}/T_a$, $\theta_b = T_{0_{\max}}/T_a$, T = thrust, and $a_a = \sqrt{\gamma R T_a}$.

3.9 A ramjet engine is powering an airplane flying with Mach number $M = 4$, at an altitude of 50,000 ft, where the ambient temperature and pressure are 205 K and 11.6 kPa, respectively. The fuel heating value is 45,000 kJ/kg and the peak temperature is 3000 K. The air-mass flow rate is 50 kg/s. The ramjet diffuser losses are given by

$$\frac{P_{02}}{P_{0a}} = 1 - 0.1\left(M - 1\right)^{1.5}$$

where M is the flight Mach number. The stagnation pressure ratio across the flameholders (from states 2 to 3) is 0.97 and the stagnation pressure loss in the combustor (from states 3 to 4) is 5%. The nozzle and combustion efficiencies are 0.95 and 0.98, respectively. Assume that the propellant is a perfect gas having $R = 0.287$ kJ/(kg·K) throughout but having $\gamma = 1.4$ from state a (ambient) to state 3 and $\gamma = 1.3$ from states 3 to 6. Calculate

1. The fuel-to-air ratio
2. The nozzle exit area for the cases of choked (convergent nozzle) and unchoked (de Laval nozzle)
3. The thrust force in the two cases stated in item b
4. The TSFC

3.10 An ideal ramjet engine (Figure 5.21) operates at an altitude where the ambient temperature and pressure are 216.7 K and 10.287 kPa, respectively. The engine has the following data:

Thrust $T = 50.0$ kN

Inlet area $A_i = 0.5$ m^2

Propulsive efficiency $\eta_p = 80\%$

Fuel heating value $Q_R = 43$ MJ/kg

Mach number in the inlet of combustion chamber $M_2 = 0.15$

Assume that $M_2 = M_3 = M_4 = 0.15$ and the specific heat ratio is constant through the engine $Cp = 1005$ J/kg/K, $\gamma = 1.4$.

Neglecting the fuel-to-air ratio, calculate

1. The flight speed and Mach number (V, M)
2. The exhaust speed and Mach number (V_6, M_6)
3. The maximum total temperature (T_{04})
4. The air mass flow rate
5. The area at the inlet to the combustion chamber (A_2)
6. The area at throat of the nozzle (A_5)
7. Plot the static temperature, static pressure, and total temperature at different stations of the engine
8. Plot the internal areas at different stations within the engine

3.11 An ideal ramjet has the following characteristics:

$$T_a = 250 \text{ K}, \quad Q_R = 45 \text{ MJ/kg}, \quad C_p = 1005 \text{ J/kg} \cdot \text{K}, \quad \gamma = 1.4$$

The engine has the following constraints:

$$M_{\max} = 3.8$$

$$T_{0\max} = 2500 \text{ K}$$

$$f_{\max} = 0.04$$

Which of the following conditions may satisfy those conditions?

1. $M = 2.0$, $T_{0\max} = 2500$ K
2. $f = 0.035$, $T_{0\max} = 2400$ K
3. $M = 3.75$, $f = 0.04$

3.12 Figure P3.12 illustrates a Boeing IM-99/CIM-10 Bomarc rocket. It is designed to fly at a cruising altitude of 60,000 ft (18 km), where the ambient temperature and pressure are 216.5 K and 7.5 kPa, respectively. Its liquid-fueled rocket engine boosts the Bomarc to Mach 2.5, when its ramjet engines (Marquardt RJ43-MA-3) would take over for the remainder of the flight.

1. For ideal case and constant properties (γ, C_p), derive an expression for exhaust Mach number and prove that it will have a constant value $M_e = 2.5$.
2. Calculate the specific thrust if $T_{04} = 2000$ K (ignore fuel).
3. Calculate the propulsive efficiency.



FIGURE P3.12

References

1. *The Jet Engine*, 5th edn., Rolls-Royce plc, p. 3, Reprinted 1996 with revisions.
2. J.V. Foa, *Element of Flight Propulsion*, Wiley, New York, 1960.
3. R.D. Archer and M. Saarlas, *An Introduction to Aerospace Propulsion*, Prentice-Hall, Inc., 1996, p. 2.
4. F.S. Billing, Research on supersonic combustion, *AIAA Journal of Propulsion and Power*, 9(4), 499–514, July–August 1993.
5. R.D. Zucker and O. Biblarz, *Fundamental Gas Dynamics*, 2nd edn., John Wiley & Sons, Inc., 2002, p. 366.
6. J. Roskam and C.-T.E. Lan, *Airplane Aerodynamics and Design*, DAR Corporation, 1997, p. 258.
7. E.J. Manganiello, M.F. Valerino, and R.H. Essig, Sea-level performance tests of a 22-inch-diameter pulse-jet engine at various simulated Ram pressures, NACA MR No. E5J02, October 1945.
8. P.J. Litke, F.R. Schauer, D.E. Paxon, R.P. Bradley, and J.L. Hoke, Assessment of the performance of a pulsejet and comparison with a pulsed-detonation engine, *44th Aerospace Sciences Meeting and Exhibit, sponsored by the American Institute of Aeronautics and Astronautics*, Reno, Nevada, January 9–12, 2006, AIAA-2005-0228.
9. R.K.A. Kailasanathan, Experimental investigation on Pulsejet engines, MSc thesis, North Carolina State University, Mechanical engineering department, Raleigh, NC, 2007.
10. D.R. Greatrix, *Powered Flight—The Engineering of Aerospace Propulsion*, Springer, U.K., 2012.
11. T. Geng, D.E. Paxon, F. Zheng, A.V. Kuznetsov, and W.L. Roberts, Comparison between numerically simulated and experimentally measured flow field quantities behind a pulsejet, *44th Joint Propulsion Conference and Exhibit cosponsored by AIAA, ASME, SAE, and ASEE*, Hartford, Connecticut, July 21–23, 2008, NASA/TM-2008-215432.
12. M.L. Coleman, Overview of pulse detonation propulsion technology, Chemical propulsion Information Agency (CPIA), Report CPTR 70, April 2001.

13. D.E. Paxson, A performance map for ideal airbreathing pulse detonation engine, *37th Joint Propulsion Conference and Exhibit cosponsored by the AIAA, ASME, SAE, and ASEE*, Salt Lake City, Utah, July 8–11, 2001, AIAA- 2001-3465.
14. L.A. Povinelli, Pulse detonation engine for high speed flight, NASA/TM 2002-211908.
15. W. Heiser and D. Pratt, Thermodynamic cycle analysis of pulse detonation engines, *Journal of Propulsion and Power*, 18(1), 68–74, January–February 2002.
16. P. Hill and C. Peterson, *Mechanics and Thermodynamics of Propulsion*, 2nd edn., 1992, Addison Wesley Publication Company, Inc., p. 155.
17. G. Maise, J. Powell, J. Paniagua, E. Kush, P. Sforza, H. Ludewig, and T. Dowling, Application of the MITEE nuclear Ramjet for ultra long range flyer missions in the atmospheres of Jupiter and other giant planets, *54th International Astronautical Congress*, Bremen, Germany, September–October, 2003.
18. G.S. Moura and J.G. Ferreira, Performance of a Ramjet using polybutadiene as solid fuel, *Proceedings of 19th International Congress of Mechanical Engineering*, Brasilia, DF, November 5–9, 2007.


Taylor & Francis
Taylor & Francis Group
http://taylorandfrancis.com

4

Turbojet Engine

4.1 Introduction

The turbojet is the basic engine of the jet age. It is the simplest turbine-based jet engine. It is a reaction engine, which was invented by the two fathers of jet engines: Frank Whittle from Britain and von Ohain from Germany. The first flight of an airplane powered by a turbojet engine was the He178 German aircraft powered by the He S-3 engine on August 27, 1939. Based on von Ohain's work, the German engine designer Anslem Franz developed his turbojet engine that powered the jet fighter Me 262 built by the firm Messerschmitt. Frank Whittle in England, having no knowledge of Ohain's engine, built his W.1 turbojet engine, which powered the Gloster E28/39 aircraft. As described in Chapter 1, the future of aviation lay with jets.

The disadvantage of ramjet engine is that its pressure ratio depends on the flight Mach number. It cannot develop takeoff thrust and does not perform well unless the flight Mach number is much greater than one ([refer to the figure $\left(T/\dot{m}_a\right)$ vs. M]; Example 3.6, Ramjet). To overcome this disadvantage, a compressor is installed in the inlet duct so that even at zero flight speed, air cannot be drawn into the engine. This compressor is driven by the turbine installed downstream of the combustion chamber and connected to the compressor by a central shaft. Addition of the two rotating parts or modules (compressor and turbine) converts the ramjet into a turbojet. The compressor, combustion chamber, and turbine constitute what is called *gas generator*. The air is squeezed in the compressor to many times its normal atmospheric pressure and then forced into the combustion chamber. Fuel is sprayed into the compressed air, ignited, and burned continuously in the combustion chamber. This raises the temperature of the fluid mixture to about 1100°F – 1300°F. The resulting burning gases expand rapidly rearward and pass through the turbine, which drives the compressor. The turbine extracts energy from the expanding gases to drive the compressor, which intakes more air. If the turbine and compressor are efficient, the pressure at the turbine discharge will be nearly twice the atmospheric pressure, and this excess pressure is sent to the nozzle to produce a high-velocity stream of gases. These gases bounce back and shoot out of the rear of the exhaust, thus produce a thrust pushing the plane forward. Substantial increases in thrust can be obtained by employing an afterburner or augmenter. It is a second combustion chamber positioned after the turbine and before the nozzle. The afterburner increases the temperature of the gas ahead of the nozzle. The result of this increase in temperature is higher jet velocity and more push. Thus, an increase of about 40% in thrust at takeoff and a much larger percentage at high speeds once the plane is in the air.

Classification of turbojet engines is shown in Figure 4.1. Turbojet engines may be a *nuclear* or *non-nuclear* engine. In the late 1940s and through the 1950s [1,2], preliminary

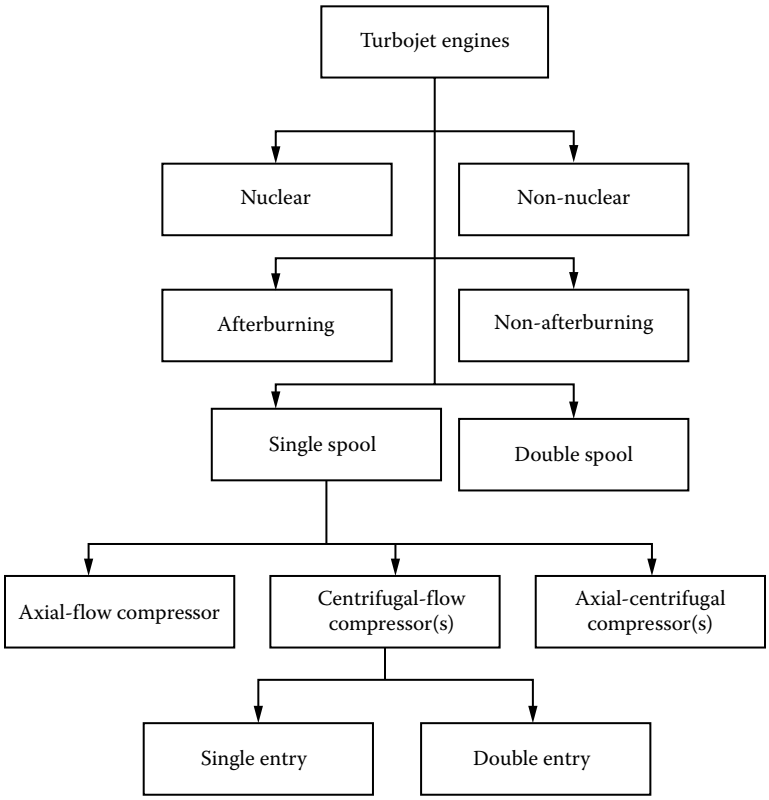


FIGURE 4.1
Classification of turbojet engines.

work was done on developing nuclear-powered rockets and jet engines. Both the United States and the Soviet Union conducted rigorous research and development (R&D) programs in this field, but ultimately canceled their respective programs, due to technical difficulties and growing safety concerns as catastrophic atomic radiation might be encountered in case of crashes/accidents of such nuclear airplanes. For the past 40 years, little research related to nuclear-powered jet engines has been done. However, recent discoveries in the field of controlled or triggered nuclear decay [3–5], together with the advancement of materials, airframe, and engine design, have reinvigorated the possibility of running aircraft on nuclear power.

Other classifications for turbojet engines may be emphasized as follows: Turbojet engines may be classified as *afterburning* or *non-afterburning*. As described earlier, the afterburner is a second chamber where afterburning (or reheat) is a method of augmenting the basic thrust of an engine to improve aircraft takeoff, climb, and (for military aircraft) combat performance. Afterburning consists of the introduction and burning of raw fuel between the engine turbine and the jet pipe propelling nozzle, utilizing the unburned oxygen in the exhaust gas to support combustion. The increase in the temperature of the exhaust gas increases the velocity of the jet leaving the propelling nozzle and therefore increases the engine thrust by 50% or more. This increased thrust could be obtained by the use of a larger engine, but this would increase the weight and overall fuel consumption.

A third classification of the turbojet engines is based on their *number of spools*. Turbojets may be single- or two-spool (sometimes identified as double or dual) engines. A single-spool turbojet has one shaft with a compressor and a turbine mounted at either shaft end, while a two-spool engine has two shafts, compressors, and turbines. The first compressor next to the intake is identified as the low-pressure compressor (LPC), which is driven by the low-pressure turbine (LPT). Both together with their shaft are denoted as the low-pressure spool. The high-pressure compressor (HPC) is situated downstream of the LPC. Also this compressor is driven by the high-pressure compressor (HPT). Both are coupled by the high-pressure shaft (which is concentric with the low-pressure shaft) and constitute the modules of the high-pressure spool. Figure 4.2 illustrates the layout and modules of the single- and double-spool turbojet engines.

The single-spool engine may be further classified based on the *type of compressor* employed. The compression section may be composed of either a single or double compressor. Moreover, the compressor may be of the axial or radial (centrifugal type). Thus numerous combinations may exist. A single-axial or centrifugal compressor is seen in

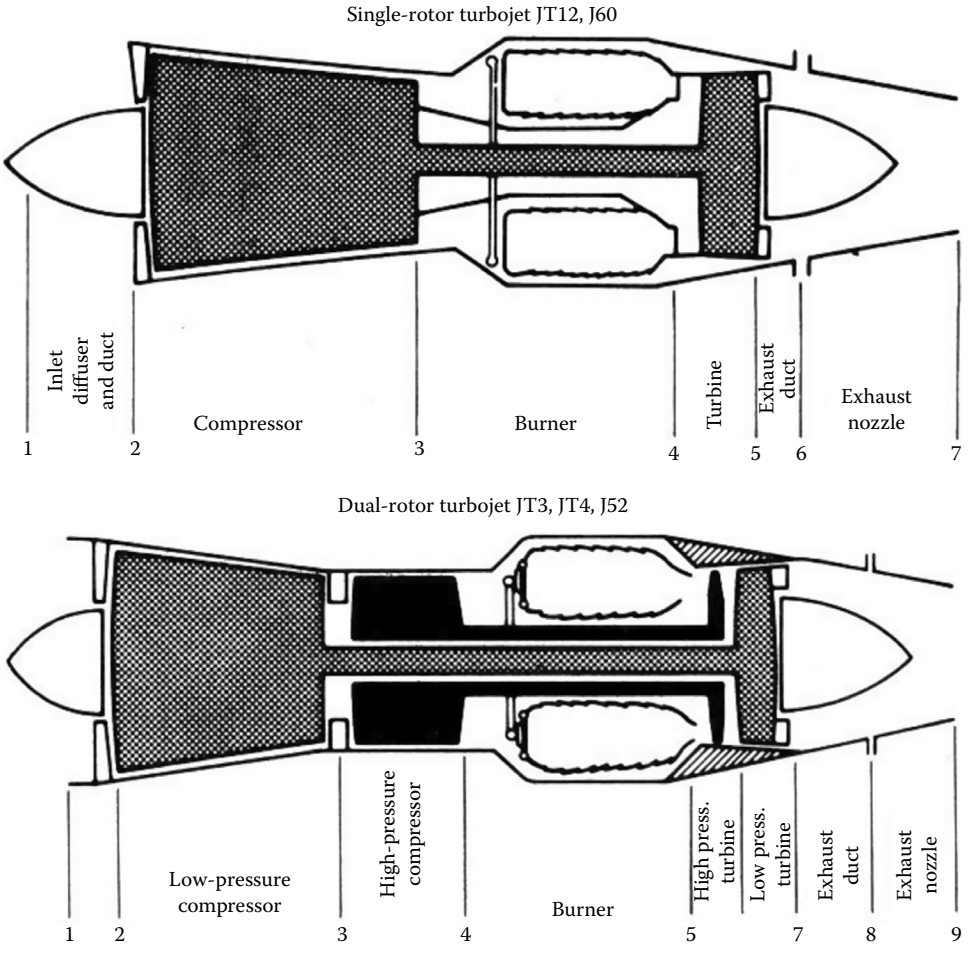


FIGURE 4.2
Layout of single- and dual-spool turbojet engines.

some turbojets. In other cases, two compressors assembled in series are found. These compressors may be either two centrifugal compressors or an axial compressor followed by a centrifugal compressor.

Lastly, turbojet engines with a centrifugal compressor may have either single entry or double entry. Double entry type is characterized by two inlets where two centrifugal compressors are manufactured back to back to increase the inlet mass flow rate.

4.2 Single Spool

4.2.1 Examples of Engines

1. *Rolls-Royce Nene* (powered Vickers_Viking_1a-G-Agrn aircraft)
   Non-afterburning engine
   Length: 97 in. (2464 mm)
   Diameter: 49.5 in. (1257 mm)
   Compressor: Dual-entry centrifugal compressor with two-sided impeller
   Combustors: 9 cans combustion chambers
   Turbine: Single-stage axial flow
   Fuel type: Aviation kerosene with 1% lubricating oil
   Thrust: 5,000 lbf (22.2 kN) at 12,400 rpm for takeoff
   Specific fuel consumption 1.04 lb/(h·lbf)
   Thrust-to-weight ratio 1:1
2. *Klimov_Vk-1* (powered MiG17 and Lim-R_B1 aircraft)
   Non-afterburning engine
   Length: 102 in. (2600 mm)
   Diameter: 51.0 in. (1300 mm)
   Compressor: Centrifugal
   Dry weight: 1395 lbf
   Thrust: 5955 lbf (26.5 kN)
   Specific fuel consumption 1.07 lb/(h·lbf) (109.1 kg/(kN·h))
   Thrust-to-weight ratio 4.27:1
   The *VK-1F*, an improved version with a simple afterburner and variable nozzle, was developed for the main production version, the MiG-17F
3. *General Electric J47*
   This engine was produced in at least 17 different series and was used to power various types of Air Force aircrafts including: F-86, XF-91, B-36, B-45, B-47, and XB-51.
   Compressor: 12-stage axial compressor
   Turbine: Single-stage axial turbine

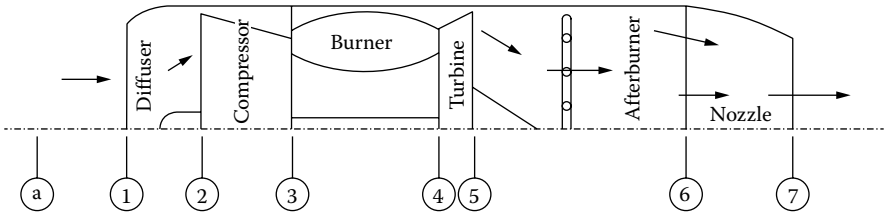


FIGURE 4.3
Single-spool afterburning turbojet.

Weight: 2707 lb
Thrust: 5670 lb
Maximum rpm: 7950
Maximum operating altitude: 50,000 ft

4.2.2 Thermodynamic Analysis

As described, single-spool turbojets may have either one or two compressors as well as a single driving turbine. It may or may not have an afterburner. Figure 4.3 illustrates a single-spool turbojet engine having a single compressor and an afterburner together with designations for each state. The different processes encountered within the engine are described here:

(a)–(1): Air flows from far upstream where the velocity of air relative to engine is the flight velocity up to the intake, usually with some deceleration during cruise and acceleration during takeoff.

(2)–(3): Air flows through the inlet diffuser and ducting system, where the air velocity is decreased as the air is carried to the compressor inlet.

(2)–(3): The air is compressed in a dynamic compressor.

(3)–(4): The air is "heated" by mixing and burring of fuel in the air.

(4)–(5): The air is expanded through a turbine to obtain power to drive the compressor.

(5)–(6): The air may or may not be further heated by the addition and burning of fuel in an afterburner.

(6)–(7): The air is accelerated and exhausted through the exhaust nozzle.

If the engine is not fitted with an afterburner, then states 5 and 6 are coincident. It would be simpler not to discard point 6 in the following analysis. Thus the flow in the nozzle remains from point 6 to point 7. The amount of mass flow is usually set by flow choking in the nozzle throat.

4.2.3 Ideal Case

The components except the burners are assumed to be reversible adiabatic or isentropic. Moreover, the burners are replaced by a frictionless heater, so the velocities at stations (2) through (6) are negligible.

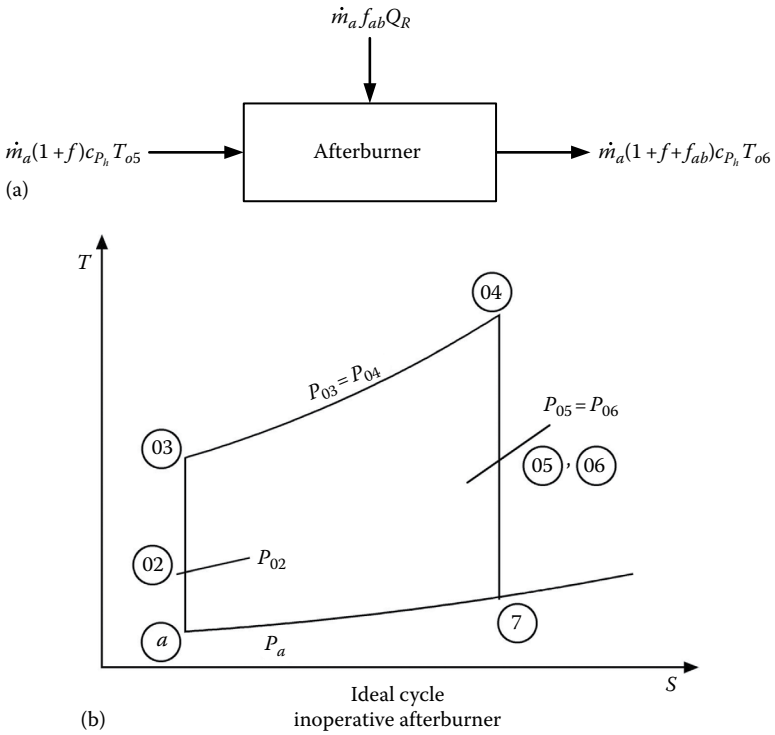


FIGURE 4.4
Temperature–entropy diagram for (a) ideal turbojet and (b) inoperative afterburner.

An analysis of the different components of the engine will be followed, refer to Figure 4.4.

1. Intake or Inlet
   During cruise, the static pressure rises from (a) to (1) outside the intake and from (1) to (2) inside the intake. The air is decelerated relative to the engine. Since the velocity at (2) is assumed to be zero and the deceleration is isentropic, then the total or stagnation pressure at states (a), (1), and (2) are constant and equal:

$$P_{02} = P_{01} = P_{0a} = P_a\left(1+\frac{\gamma-1}{2}M^2\right)^{\gamma/\gamma-1} \tag{4.1}$$

   The stagnation temperatures for states (a), (1), (2) are also equal:

$$T_{02} = T_{01} = T_{0a} = T_a\left(1+\frac{\gamma-1}{2}M^2\right) \tag{4.2}$$

2. Compressor
   The pressure ratio of the compressor π_C is assumed to be known, thus the pressure and temperature at the outlet of the compressor is evaluated from the

corresponding values at the inlet of the compressor (outlet of the intake) from the relations

$$P_{03} = \left(P_{02}\right)\left(\pi_c\right) \tag{4.3a}$$

$$T_{03} = T_{02}\left[\frac{P_{03}}{P_{02}}\right]^{\gamma-1/\gamma} \tag{4.3b}$$

3. Combustion Chamber
The turbojet here is assumed to be a single spool. Thus the outlet conditions of the compressor will be those at the inlet to the combustion chamber. Combustion process takes place from (3) to (4). In this process, fuel is injected in an atomized form, evaporated and mixed with air. Spark plugs initiate the combustion process. Since no pressure drop is assumed for the ideal case, then the pressures at the inlet and outlet of the combustion chamber are equal; or

$$P_{03} = P_{04} \tag{4.4}$$

The temperature at the outlet of the turbine is determined from metallurgical limits set by the turbine blade material and is known as the turbine-inlet temperature (TIT). Fuel is added to the combustion chamber and burnt. The mass flow rate of the burnt fuel is calculated from the energy balance of the combustion chamber.

$$\left(\dot{m}_a + \dot{m}_f\right) Cp_h T_{04} = \dot{m}_a Cp_c T_{03} + \dot{m}_f Q_R$$

with

$$f = \dot{m}_f / \dot{m}_a$$

then the fuel-to-air ratio is determined from the relation

$$f = \frac{Cp_h T_{04} - Cp_c T_{03}}{Q_R - Cp_h T_{04}} \tag{4.5}$$

4. Turbine
The power consumed in the compression from (2) to (3) must be supplied through the turbine in expansion from (4) to (5). If the ratio of the power needed to drive the compressor to the power available in the turbine is (λ) then, the energy balance for the compressor-turbine shaft is

$$W_c = \lambda W_t$$

Here (λ) is of the range 75%–85%. Thus in terms of the temperatures differences

$$Cp_c\left(T_{03} - T_{02}\right) = \lambda\left(1 + f\right) Cp_h\left(T_{04} - T_{05}\right)$$

$$\left(\frac{T_{05}}{T_{04}}\right)=1-\frac{\left(Cp_c/Cp_h\right)T_{02}}{\lambda\left(1+f\right)T_{04}}\left[\left(\frac{T_{03}}{T_{02}}\right)-1\right] \tag{4.6}$$

Then the turbine and compressor pressure ratios are related by

$$\left(\frac{P_{05}}{P_{04}}\right)=\left\{1-\frac{\left(Cp_c/Cp_h\right)T_{02}}{\lambda\left(1+f\right)T_{04}}\left[\left(\frac{P_{03}}{P_{02}}\right)^{\gamma_c-1/\gamma_c}-1\right]\right\}^{\gamma_h/\gamma_h-1} \tag{4.7a}$$

From Equation 4.2,

$$\left(\frac{P_{05}}{P_{04}}\right)=\left\{1-\frac{\left(Cp_c/Cp_h\right)T_a}{\lambda\left(1+f\right)T_{04}}\left(1+\frac{\gamma-1}{2}M^2\right)\left[\left(\frac{P_{03}}{P_{02}}\right)^{\gamma_c-1/\gamma_c}-1\right]\right\}^{\gamma_h/\gamma_h-1} \tag{4.7b}$$

If the pressure drop in the turbine is calculated prior to temperature drop calculation, then the temperature at the turbine outlet T_{05} may be calculated from the isentropic relation

$$\frac{T_{05}}{T_{04}}=\left(P_{05}/P_{04}\right)^{\gamma_h-1/\gamma_h} \tag{4.8}$$

5. Afterburner
If the jet engine is without an afterburner, then no work or heat transfer occurs downstream of station (5). The stagnation enthalpy remains constant throughout the rest of the engine. However, if there is an afterburner, we have two possibilities: either the afterburner is operative or inoperative. If the afterburner is inoperative, then states (5) and (6) are coincident. Both of the temperatures and pressures are equal:

$$T_{06}=T_{05}$$

$$P_{06}=P_{05}$$

For an operative afterburner, a subscript (A) is added to the symbols of the temperature and the pressure to denote an operative afterburner. In this case, an additional amount of fuel is burnt which raises the temperature to (T_{06A}), which is much higher than the TIT. The reason for such a higher temperature is that the downstream element is the nozzle, which is a non-rotating part. Thus the walls are subjected only to thermal stresses rather than the combined thermal and mechanical stresses as in the turbine(s). For an ideal cycle, then

$$P_{06A}=P_{05}$$

and

$$T_{06A}=T_{\max}$$

An additional fuel quantity ($\dot{m}_{fab}$) is added and burnt in the afterburner. The conservation of mass and energy within the afterburner yields the following equations:

$$\dot{m}_6 = \dot{m}_5 + \dot{m}_{fab}$$

$$\dot{m}_5 h_{05} + \dot{m}_{fab} Q_R = \dot{m}_6 h_{06A}$$

$$\therefore \dot{m}_5 Cp_5 T_{05} + \dot{m}_{fab} Q_R = \left(\dot{m}_5 + \dot{m}_{fab}\right) Cp_6 T_{06A}$$

with

$$f_{ab} = \dot{m}_{fab}/\dot{m}_a$$

$$\therefore \left(1+f\right) Cp_5 T_{05} + f_{ab} Q_R = \left(1+f+f_{ab}\right) Cp_6 T_{06A}$$

The corresponding fuel-to-air ratio within the afterburner (f_{ab}) is evaluated from the relation

$$f_{ab} = \frac{\left(1+f\right)\left(Cp_{6A} T_{06A} - Cp_5 T_{05}\right)}{Q_R - Cp_{6A} T_{06A}} \tag{4.9}$$

In Equation 4.9, the variation of the specific heat with temperature is taken into account

6. Nozzle
The exhaust velocity is obtained from the conservation of energy in the nozzle. The hot gases expand in the nozzle from (6) or (6A) to (7) depending on whether the afterburner is operative or inoperative. Hereafter, the two cases will be considered.
   a. Inoperative afterburner
   The nozzle is to be checked first to define whether it is choked or not. Thus the critical pressure is calculated from the relation

$$\left(\frac{P_{06}}{P_c}\right) = \left(\frac{\gamma_h + 1}{2}\right)^{\gamma_h/\gamma_h - 1} \tag{4.10a}$$

   The critical pressure is then compared with the ambient pressure. If it is greater or equal to the ambient pressure, then the nozzle is choked. This means that $P_7 = P_c$ and the nozzle outlet temperature (T_7) is then calculated from the relation

$$\left(\frac{T_{06}}{T_7}\right) = \left(\frac{\gamma_h + 1}{2}\right) \tag{4.11a}$$

   The exhaust velocity is then calculated as

$$V_7 = \sqrt{\gamma_h R T_7} \tag{4.12a}$$

On the other hand if the ambient pressure is greater than the critical pressure, then the exhaust pressure is equal to the ambient pressure, $P_7 = P_a$ and the temperature of the exhaust gases is determined from the relation

$$\left(\frac{T_{06}}{T_7}\right) = \left(\frac{P_{06}}{P_a}\right)^{\gamma_h - 1/\gamma_h} \tag{4.13a}$$

The exhaust velocity is now calculated from the relation

$$V_7 = \sqrt{2Cp_n\left(T_{06} - T_7\right)} = \sqrt{2Cp_n T_{06}\left[1 - \left(P_a / P_{06}\right)^{\gamma_h - 1/\gamma_h}\right]} \tag{4.14a}$$

b. Operative afterburner
In this case, the expansion process in the nozzle starts from the point (6A) to point (7) (refer to Figure 4.5). Again, a check for the state of the nozzle is performed by calculating the critical pressure from Equation 4.10a and b, or

$$\left(\frac{P_{06A}}{P_c}\right) = \left(\frac{\gamma_h + 1}{2}\right)^{\gamma_h/\gamma_h - 1} \tag{4.10b}$$

where $P_{06A} = P_{05}$. Again, the critical pressure is compared with the ambient pressure. If $P_{7A} = P_c$, then the nozzle is choked. The outlet temperature (T_{7A}) is much greater than that in the case of inoperative afterburner and calculated from the relation

$$\left(\frac{T_{06A}}{T_{7A}}\right) = \left(\frac{\gamma_h + 1}{2}\right) \tag{4.11b}$$

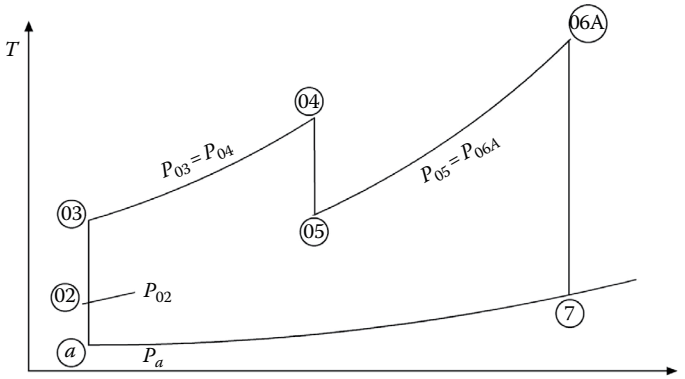


FIGURE 4.5
Temperature–entropy diagram for ideal turbojet, operative afterburner.

If the nozzle is choked, then the exhaust velocity may be calculated from the following equation:

$$V_{7ab} = \sqrt{\gamma_h R T_{7A}} \tag{4.12b}$$

If the nozzle is unchoked, then the exhaust pressure is again an ambient one. The velocity of the exhaust gases is calculated from the relation

$$V_{7ab} = \sqrt{2Cp_n T_{06A}\left[1-\left(P_a/P_{06A}\right)^{\gamma_h - 1/\gamma_h}\right]} \tag{4.14b}$$

The thrust force is expressed by Equation 2.3a as derived in Chapter 2:

$$T = \dot{m}_a\left[\left(1+f\right)V_e - V\right] + \left(P_e - P_a\right)A_e \tag{2.3a}$$

V_e is the exhaust jet speed which may be either V_7 or V_{7ab} depending on whether the afterburner is operative or inoperative.

Similarly, the propulsive, thermal, and overall efficiencies may be calculated from appropriate relations as described in Chapter 2.

Now, let us compare the velocity of the jet leaving the turbojet engine in the case of operative and inoperative afterburners. Since the shape of the constant pressure lines on the *T*–*S* diagram is divergent, the enthalpy drop in the nozzle for an operative afterburner is greater than in the case of an inoperative one. The jet velocity is proportional to the square of the enthalpy drop, as

$$h_{06} - h_7 = \frac{V_7^2}{2}$$

Hence, the exhaust velocity V_7 in the case of afterburning will be greater than that in the case of non-afterburning:

$$\left(V_7\right)_{afterburning} \approx 1.5\left(V_7\right)_{non\text{-}afterburning} \tag{4.15}$$

This is due to the absence of highly stressed material in the afterburner, which allows T_{06A} being much higher than turbine-inlet temperature T_{04}.

The big advantage of an afterburner is that the jet speed increases (Equation 4.15), which in turn significantly increases the thrust of the engine without adding much weight or complexity to the engine. Generally, an afterburner is nothing but a set of fuel injectors, a tube, and a flameholder that the fuel burns in, and an adjustable nozzle. A jet engine with an afterburner needs an adjustable nozzle so that it can work both with the afterburners on and off.

The disadvantage of an afterburner is that it uses a lot of fuel (Equation 4.9) for the power it generates. Therefore, most planes use afterburners sparingly. For example, a military jet would use its afterburners when taking off from the short runway on an aircraft carrier, or during a high-speed maneuver in a dogfight.

Example 4.1

A single-spool turbojet engine (without an afterburner) is running on ground ($M = 0$). Prove that for an ideal process and unchoked nozzle, then, the pressure ratio of the turbine (π_t) is related to the pressure ratio of the compressor (π_c) by the relation

$$\pi_t = \frac{1}{\left[1 - \frac{C_{P_c}}{C_{P_h}} \frac{T_a}{T_{04}} \left(\pi_c^{\gamma_c - 1/\gamma_c} - 1\right)\right]^{\gamma_t/\gamma_t - 1}}$$

and the jet speed is expressed as

$$V_j = \sqrt{2C_{P_h}\left[T_{04} - \frac{C_{P_c}}{C_{P_h}} T_a \left(\pi_c^{\gamma_c - 1/\gamma_c} - 1\right)\right]\left\{1 - \left(\frac{\pi_t}{\pi_c}\right)^{\gamma_h - 1/\gamma_h}\right\}}$$

where $\pi_t = \frac{P_{04}}{P_{05}}$, T_a and T_{04} are the ambient and maximum temperatures, respectively. Assume that the fuel-to-air ratio is negligible, and the work consumed by the compressor is equal to the work developed by the turbine.

Solution

The successive elements will be analyzed as follows:

1. Diffuser
   For a ground run of the engines ($M = 0$) and an ideal diffusion process, then from Equations 4.1 and 4.2,

$$T_a = T_{0a} = T_{02} = T_7$$

$$P_{02} = P_{0a} = P_a$$

2. Compressor
   For an ideal compression process, then

$$\frac{T_{03}}{T_{02}} = \pi_c^{\gamma_c - 1/\gamma_c} \qquad \text{(a)}$$

   where

$$\pi_c = \frac{P_{03}}{P_{02}}$$

3. Combustion chamber
   No pressure loss in the combustion chamber and negligible fuel-to-air ratio, then

$$P_{04} = P_{03}$$

$$f \ll 1$$

4. Turbine
   The pressure and temperature ratios at the turbine are expressed as

$$\frac{T_{04}}{T_{05}} = \pi_t^{\gamma_t - 1/\gamma_t}$$

   where

$$\pi_t = P_{04}/P_{05}$$

   Assuming that the work developed by the turbine is equal to the work consumed by the compressor, then

$$W_t = W_c$$

   for negligible fuel-to-air ratio

$$C_{P_t}\left(T_{04} - T_{05}\right) = C_{P_c}\left(T_{03} - T_{02}\right) \tag{b}$$

$$C_{P_t} T_{04}\left(1 - \frac{1}{\pi_t^{\gamma_t - 1/\gamma_t}}\right) = C_{P_c} T_{02}\left(\pi_c^{\gamma_c - 1/\gamma_c} - 1\right)$$

   With

$$T_{02} = T_a$$

$$\frac{1}{\pi_t^{\gamma_t - 1/\gamma_t}} = 1 - \frac{C_{P_c}}{C_{P_h}}\frac{T_a}{T_{04}}\left[\pi_c{}^{\gamma_c - 1/\gamma_c} - 1\right]$$

$$\pi_t = \frac{1}{\left[1 - \frac{C_{P_c}}{C_{P_h}}\frac{T_a}{T_{04}}\left(\pi_c^{\gamma_c - 1/\gamma_c} - 1\right)\right]^{\gamma_t/\gamma_t - 1}} \tag{c}$$

5. Nozzle
   For an unchoked nozzle and ideal expansion, the jet speed is

$$V_j = \sqrt{2C_{p_h} T_{06}\left[1 - \left(\frac{P_7}{P_{06}}\right)^{\gamma_h - 1/\gamma_h}\right]}$$

   From (a) and (b), then

$$T_{05} = T_{04} - \frac{C_{P_c}}{C_{P_h}} T_a\left[\pi_c^{\gamma_c - 1/\gamma_c} - 1\right] \equiv T_{06}$$

   Since

$$\frac{P_7}{P_{06}} = \frac{P_7}{P_{02}}\frac{P_{02}}{P_{03}}\frac{P_{03}}{P_{04}}\frac{P_{04}}{P_{05}}\frac{P_{05}}{P_{06}}$$

Then with $P_6 = p_a = P_{02}$, $P_{03} = P_{04}$, and $P_{05} = P_{06}$

$$\therefore \frac{P_7}{P_{06}} = \frac{\pi_t}{\pi_c}$$

$$V_j = \sqrt{2C_{P_h}\left[T_{04} - \frac{C_{P_c}}{C_{P_h}} T_a \left(\pi_c^{\gamma_c - 1/\gamma_c} - 1\right)\right]\left\{1 - \left(\frac{\pi_t}{\pi_c}\right)^{\gamma_h - 1/\gamma_h}\right\}} \tag{d}$$

Example 4.2

The airplane Fiat G91Y is a single-seat Strike and Reconnaissance fighter powered by two General Electric J85-GT-13A turbojets each rated at 12.12 kN at an altitude of 9150 m where the ambient conditions are 32 kPa and 240 K. The pressure ratio across the compressor is 12 and temperature at the turbine inlet is 1400 K. The aircraft speed is 310 m/s. Assume ideal operation for all components, assume unchoked nozzle and constant specific heat in all processes, $C_p = 1005\ \text{J/kg} \cdot \text{K}$. The heating value of the fuel is 42,700 kJ/kg.

Determine

1. Fuel-to-air ratio
2. The velocity of the exhaust gases
3. The air mass flow rate
4. The propulsive efficiency
5. The thermal efficiency
6. The overall efficiency

Solution

The given data are

Thrust $T = 12.12$ kN.
The flight altitude is 9150 m, at which the ambient pressure and temperature are

$$P_a = 32\ \text{kPa} \quad \text{and} \quad T_a = 240\ \text{K}$$

The compressor pressure ratio $\pi_c = 12$.
The turbine-inlet temperature and also the maximum temperature in the engine is

$$T_{\max} = 1400\ \text{K}$$

Fuel heating value $Q_R = 42,700\ \text{kJ/kg}$
Flight speed $V_f = 310\ \text{m/s}$
Specific heat $C_p = 1005\ \text{J/kg} \cdot \text{K}$

Diffuser: Since all the processes are ideal, then the total temperature is

$$T_{02} = T_{0a} = T_a + \frac{V_f^2}{2C_p} = 240 + \frac{(310)^2}{2 \times 1005} = 287.8\ \text{K}$$

The total pressure is calculated from the relation $\frac{P_{02}}{P_a} = \left(\frac{T_{02}}{T_a}\right)^{\gamma/\gamma - 1} = \left(\frac{287.8}{240}\right)^{3.5}$

$$P_{02} = 60.4\ \text{kPa}$$

Compressor: The compressor outlet pressure is obtained from the relation $P_{03} = \pi_c \times P_{02} = 725.1 \text{ kPa} \equiv P_{04}$.

The temperature at the outlet from the compressor is obtained from the relation

$$\frac{T_{03}}{T_{02}} = \pi_c^{\gamma-1/\gamma} = 12^{0.286} = 2.035$$

$$T_{03} = T_{02} \times 2.035 = 587.5 \text{ K}$$

Combustion chamber: From Equation 4.5, the fuel-to-air ratio is

$$f = \frac{C_P\left(T_{04} - T_{03}\right)}{Q_R - C_P T_{04}} = \frac{1.005(1{,}400 - 586)}{42{,}700 - 1.005 \times 1{,}400} = 0.0198$$

Assuming equal work in both the compressor and turbine, and equal specific heats, then from Equation 4.6,

$$T_{05} = T_{04} - \frac{T_{03} - T_{02}}{1+f} = 1106.1 \text{ K} = T_{06}.$$

The pressure at the outlet of the turbine is obtained as follows:

$$\frac{P_{04}}{P_{05}} = \left(\frac{T_{04}}{T_{05}}\right)^{\gamma/\gamma-1} = \left(\frac{1400}{1106.1}\right)^{3.5} = 2.281$$

$$P_{05} = 317.86 \text{ kPa} = P_{06}$$

Nozzle: For an isentropic flow in the nozzle, the temperature ratio within the nozzle is

$$\frac{T_{06}}{T_7} = \left(\frac{P_{06}}{P_7}\right)^{\gamma-1/\gamma} = \left(\frac{317.86}{32}\right)^{0.286} = 1.9283$$

$$T_7 = 563.6 \text{ K}$$

The exhaust speed is then $V_j = \sqrt{2C_P\left(T_{06} - T_7\right)} = 1044.34$ m/s.

Since the thrust force for an unchoked nozzle is expressed as $T = \dot{m}_a\left[\left(1+f\right)V_j - V_f\right]$ then the air mass flow rate is

$$\dot{m}_a = \frac{T}{\left(1+f\right)V_j - V_f} = \frac{12.12 \times 1{,}000}{1.0198 \times 1{,}044.2 - 310} = \frac{12{,}120}{754.9}$$

$$\dot{m}_a = 16.06 \text{ kg/s}$$

The fuel mass flow rate is $\dot{m}_f = f \times \dot{m}_a = 0.317$ kg/s.

The propulsive efficiency is calculated using two of the expressions discussed in Chapter 2 as follows:

a. Expression (1)

$$\eta_p = \frac{T \times V}{T \times V + 0.5\dot{m}_j\left(V_j - V\right)^2} = 45.97\%$$

b. Expression (2)

$$\eta_p = \frac{2V}{V + V_j} = 45.79\%$$

As shown, the results are very close as the nozzle is unchoked. The difference is due to the fuel addition in the jet mass flow in expression (1).

The thermal efficiency

$$\eta_{th} = \frac{T \times V + 0.5\dot{m}_j \left(V_j - V\right)^2}{\dot{m}_f Q_R} = 60.36\%$$

The overall efficiency

$$\eta_o = \eta_p \times \eta_{th} = 0.4597 \times 0.6036 = 0.2775 = 27.75\%$$

Example 4.3

A single-spool turbojet engine has the following data:

Flying Mach number	0.6
Ambient conditions	T_a = 222 K P_a = 25 kPa
Compressor pressure ratio	6
Maximum temperature	1,300 K
Fuel heating value	45,000 kJ/kg
Exhaust nozzle area	0.2 m^2

All the processes are assumed ideal and there is no pressure loss in either the combustion chamber or the inoperative afterburner:

1. Deduce that the nozzle is choked.
2. Calculate the thrust force.
3. Calculate the thrust force if the nozzle is unchoked.

Solution

1. The given data are rearranged as follows:

$$M = 0.6, \quad T_a = 222 \text{ K}, \quad P_a = 25 \text{ kPa}, \quad \pi_c = 6$$

$$T_{o\max} = 1300 \text{ K}, \quad Q_R = 45{,}000 \text{ kJ/kg}, \quad A_e = 0.2 \text{ m}^2$$

The flight speed

$$V = M\sqrt{\gamma R T_a} = 0.6\sqrt{1.4 \times 287 \times 222} = 179.2 \text{ m/s}$$

Diffuser:

$$T_{o2} = T_a\left(1 + \frac{\gamma - 1}{2} M^2\right) = 238 \text{ K}$$

$$P_{o2} = P_a\left(1 + \frac{\gamma - 1}{2} M^2\right)^{\gamma/\gamma - 1} = 31.88 \text{ kPa}$$

Compressor:

$$T_{o3} = T_{o2}\pi_c^{\gamma - 1/\gamma} = 397.3 \text{ K}$$

$$P_{o3} = \pi_c P_{o2} = 191.33 \text{ kPa}$$

Combustion chamber:

$$T_{o4} = 1300 \text{ K}$$

$$P_{o4} = P_{o3} = 191.33 \text{ kPa}$$

$$f = \frac{Cp\left(T_{o4} - T_{o3}\right)}{Q_R - CpT_{o4}} = \frac{1.01\left(1{,}300 - 397.3\right)}{45{,}000 - 1.01 \times 1{,}300} = 0.02087$$

Turbine: From Equation 4.6, with constant specific heats and $\lambda = 0.8$, then

$$T_{o5} = T_{o4} - \frac{\left(T_{o3} - T_{o2}\right)}{0.8\left(1 + f\right)} = 1105 \text{ K}$$

$$P_{o5} = P_{o4}\left(\frac{T_{o5}}{T_{o4}}\right)^{(\gamma/\gamma-1)} = 182.63 \text{ kPa}$$

Tail pipe: Ideal flow is assumed in the tail pipe. Thus no pressure or temperature drop, or

$$T_{06} = T_{05} \quad \text{and} \quad P_{06} = P_{05}$$

Nozzle: *Case* (1): Check if the nozzle is choked:

$$P_c = \frac{P_{06}}{\left(\frac{\gamma + 1}{2}\right)^{\gamma/\gamma-1}} = 96.48 \text{ kPa}$$

Since P_a = 25 kPa, then $P_c > P_a$; thus, the nozzle is choked:

$$\therefore P_7 = P_C = 96.48 \text{ kPa}$$

$$\therefore T_7 = T_c = \frac{T_{06}}{\left(\frac{\gamma + 1}{2}\right)} = 920.8 \text{ K}$$

$$V_7 = \text{sonic speed} = \sqrt{\gamma RT_7} = 608.26 \text{ K}$$

The mass flow rate is calculated as follows:

$$\dot{m} = \rho_7 V_7 A_7 = \frac{P_7}{RT_7} V_7 A_7 = \frac{96.48 \times 10^3}{287 \times 920.8} \times 608.26 \times 0.2 = 44.41 \text{ kg/s}$$

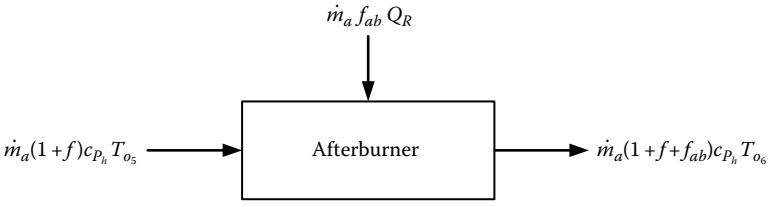


FIGURE E4.3

2. The thrust force T is expressed by the relation

$$T = \dot{m}_a\left[\left(1+f\right)V_7 - V\right] + A_e\left(P_e - P_a\right)$$

$$T = 44.41\times\left(1.02087\times 608.26 - 179.2\right) + 0.2\times 10^3\times\left(96.48 - 25\right)$$

$$T = 33,914 \text{ N} = 33.914 \text{ kN}$$

Case (2): The nozzle is unchoked, then

$$P_7 = P_a = 25 \text{ kPa}$$

$$\therefore T_7 = T_{o5}\left(\frac{P_7}{P_{o5}}\right)^{(\gamma-1/\gamma)} = 625.7 \text{ K}$$

The exhaust speed is calculated as follows: $V_7 = \sqrt{2Cp\left(T_{o5} - T_7\right)} = 983.96$ m/s.
This means that the exhaust Mach number, $M_7 = \dfrac{V_7}{\sqrt{\gamma R T_7}} = 1.962$.
The thrust force is calculated as follows:

$$T = \dot{m}_a\left[\left(1+f\right)V_7 - V\right] = 44.41\times\left(1.02087\times 983.96 - 179.2\right) = 36,651 \text{ N}$$
$$T = 36.65 \text{ kN}$$

Thus, the thrust force for a choked nozzle is less than its value for an unchoked nozzle.

Example 4.4

Compare the specific fuel consumption (TSFC) of a ramjet engine and an afterburning turbojet engine, when both have flight Mach number of 2 at 45,000 ft altitude, where ($T_a = -69.7$ °C, $P_a = 14.75$ kPa).

Both engines have the same maximum temperature of 2225 K and same exhaust speed. For the turbojet engine, the compressor pressure ratio is 8 and the turbine outlet temperature is 700 K.

Conventional hydrocarbon fuel is used with $Q_R = 43{,}000$ kJ/kg. For simplicity, assume constant specific heat ratio $\gamma = 1.4$, no aerodynamic loss in both engines, all the processes are ideal and no pressure losses in either the combustion chamber or afterburner. Assume also complete expansion of the gases in the nozzles to the ambient pressure.

Next, for the turbojet engine, what will be the ratio of the power consumed in the compressor to that available in the turbine?

Solution

1. Ramjet engine
   The gases in the nozzle expand to the ambient condition. With

$$T_a = -69.7 + 273.15 = 203.5 \text{ K}$$

$$P_a = 14.75 \text{ kPa} \quad \text{and} \quad M = 2$$

The flight speed is $u_a = M\sqrt{\gamma RT_a} = 2\sqrt{(1.4)(287)(203.5)}$

$$\therefore u_a = 571.8 \text{ m/s}$$

$$\frac{T_{0a}}{T_a} = 1 + \frac{\gamma - 1}{2} M^2 = 1 + 0.2 \times 4 = 1.8$$

$$\therefore T_{0a} = 366.3 \text{ K}$$

$$\frac{P_{0a}}{P_a} = \left(1 + \frac{\gamma - 1}{2} M^2\right)^{\gamma/\gamma - 1} = (1.8)^{3.5} = 7.824$$

$$P_{0a} = 115 \text{ kPa}$$

Diffuser: For ideal diffuser, then

$$T_{02} = T_{0a} = 366.3 \text{ K}$$

$$P_{0a} = P_{02} = P_{04} = 115 \text{ kPa}$$

Combustion chamber: The fuel-to-air ratio is $f = \dfrac{C_{P_h} T_{04} - C_{P_c} T_{0a}}{Q_R - C_{P_h} T_{04}}$

$$f = 0.0512$$

Nozzle: Since all the processes are ideal, then the velocity ratio is obtained from Equation 3.18b (Ra mjet sections in Chapter 3) as

$$\frac{u_e}{u_a} = \sqrt{\frac{T_{04}}{T_{0a}}} = \sqrt{\frac{2225}{366.3}} = 2.465$$

$$\therefore u_e = 1410 \text{ m/s}$$

The specific thrust is $\because \dfrac{T}{\dot{m}_a} = u_a \left[(1 + f) \dfrac{u_e}{u_a} - 1 \right] = 572 \left[1.0512 \times 2.465 - 1 \right]$

$$\frac{T}{\dot{m}_a} = 910 \text{ N/(kg/s)}$$

$$TSFC = \frac{f}{(T/\dot{m}_a)} = 0.2025 \text{ kg/N} \cdot \text{h}$$

2. Turbojet
   An ideal cycle is assumed and the nozzle is unchoked. The outlet conditions of the diffuser are the same as in the ramjet case,

$$\therefore T_{02} = 366.3 \text{ K} \quad \text{and} \quad P_{02} = 115 \text{ kPa}$$

Moreover, no pressure drop in the combustion chamber, thus $P_{04} = P_{03}$.
No pressure drop also in the afterburner, thus $P_{05} = P_{06A}$.

Nozzle: Since the nozzle is unchoked, and the exhaust speed is the same as in the case of ramjet,

$$T_{06A} = T_7 + \frac{V_7^2}{2C_P}$$

$$T_7 = T_{06A} - \frac{V_7^2}{2C_P} = 2225 - \frac{(1410)^2}{2 \times 1147}$$

$$T_7 = 1358 \text{ K}$$

$$\frac{P_{06A}}{P_7} \equiv \frac{P_{06A}}{P_a} = \left(\frac{T_{06A}}{T_7}\right)^{\gamma_h/\gamma_h - 1} = \left(\frac{2225}{1358}\right)^{1.33/0.33} = 7.206$$

$$P_{06A} = P_{05} = 106.3 \text{ kPa}$$

Compressor

$$\frac{P_{03}}{P_{02}} = \pi_c = 8$$

$$\therefore P_{03} = 923 \text{ kPa} \equiv P_{04}$$

$$\frac{T_{03}}{T_{02}} = (8)^{\gamma_c - 1/\gamma_c} = 8^{\frac{0.4}{1.4}} = 8^{0.286} = 1.811$$

$$T_{03} = 663 \text{ K}$$

Turbine

$$\frac{T_{04}}{T_{05}} = \left(\frac{P_{04}}{P_{05}}\right)^{\gamma_t - 1/\gamma_t} = \left(\frac{P_{03}}{P_{06A}}\right)^{0.33/1.33}$$

$$= \left(\frac{923}{106.3}\right)^{0.25} = 1.7166$$

$$\therefore T_{05} = 700 \text{ K}$$

$$\therefore T_{04} = 1201.6 \text{ K}$$

Combustion chamber

$$f = \frac{C_{P_h} T_{04} - C_{P_c} T_{03}}{Q_R - C_{P_h} T_{04}} = \frac{1.147 \times 1,201.6 - 1.005 \times 663}{43,000 - 1.147 \times 1,201.6}$$

$$f = 0.0171$$

To determine the fuel-to-air ratio of afterburner f_{ab}, consider the energy balance of afterburner.

From Equation 4.9, the afterburner fuel-to-air ratio is

$$f_{ab} = \frac{(1+f)c_{P_h}(T_{o_6} - T_{o_5})}{Q_R - c_{P_h}T_{o_6}} = \frac{(1.0171)(1.147)(2{,}225 - 700)}{43{,}000 - 1.147 \times 2{,}225}$$

$$f_{ab} = 0.04397$$

The total fuel-to-air ratio of the turbojet engine is $f_{total} = f + f_{ab}$:

$$f_{total} = 0.06107$$

$$\frac{T}{\dot{m}_a} = (1 + f_{tot})u_e - u = 1.06107 \times 1410 - 572$$

$$\frac{T}{\dot{m}_a} = 924.11 \text{ N/(kg/s)}$$

$$TSFC = 0.2379 \text{ kg/N} \cdot \text{h}$$

Summary

	Ramjet	**Turbojet**
$T/\dot{m}_a$ (N·s/kg)	910	924.11
TSFC (kg/N·h)	0.2025	0.2379

The afterburning turbojet engine produces more thrust at the expense of more fuel consumption compared to the ramjet.

The ratio between the power consumed in driving the compressor out of the total turbine power, i.e. (λ), is to be calculated from the relation

$$Cp(T_{03} - T_{02}) = \lambda Cp(T_{04} - T_{05})$$

$$\lambda = \frac{663 - 336}{1201.6 - 700} = 0.652$$

4.2.4 Actual Case

The temperature–entropy diagram for the real case is shown in Figure 4.6 for an inoperative afterburner and Figure 4.7 for an operative afterburner.

4.2.4.1 General Description

1. All components are irreversible but they are adiabatic (except burners), thus isentropic efficiencies for the intake, compressor, turbine, and nozzle are employed.
2. Friction in the air intake (or diffuser) reduces the total pressure from its free stream value and increases its entropy. The total temperature at the outlet of the intake is higher than the isentropic case, which depends on the intake or diffuser efficiency (η_d).

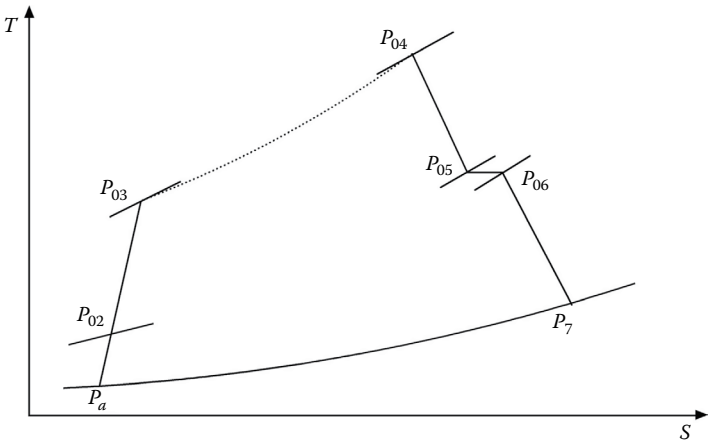


FIGURE 4.6
T–S diagram for real cycle of single-spool inoperative afterburner.

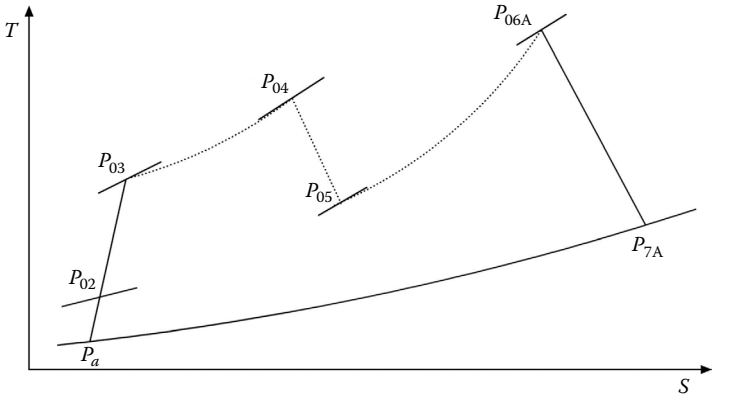


FIGURE 4.7
T–S diagram for real cycle of single-spool operative afterburner.

3. The compression of the air in the compressor is accompanied by losses due to friction, turbulence, separation, shocks, and so on. Consequently, the entropy of the air also increases during its flow through the compressor. Moreover, at the outlet of the compressor, the temperature is higher than the corresponding isentropic temperature. Such an increase in temperature depends on the compressor efficiency (η_c).
4. A portion of the compressed air is utilized in cooling the turbine disks, blades, and the supporting bearings through an air-bleed system. Thus, the air mass flow rate in the succeeding modules is somewhat smaller than that entering the compressor.
5. The burners are not simple heaters and the chemical composition of the working fluid changes during the combustion process. The larger the fuel-to-air ratio (*f*), the greater the deviation in the chemical composition of the products of combustion from that of the air. Losses in the combustion process are encountered due to many

factors including imperfect combustion, physical characteristics of the fuel as well as thermal losses due to conduction and radiation. Such losses are handled by introducing the burner efficiency (η_b). Pressure drop due to skin friction and pressure drag in the combustors (normally 3%–6% of the total pressure of the entering air) must be also taken into account.

6. The expansion process in the turbine is very nearly adiabatic. However, due to friction an increase in entropy is encountered. Moreover, the outlet temperature is higher than that of the isentropic case. Thus the available power from the turbine is less than that in the isentropic case. The expansion process is associated with the turbine efficiency (η_t).
7. Finally, the expansion process in the nozzle is similar to that in the turbine and influenced by skin friction. It is also governed by the adiabatic efficiency (η_n).
8. It is worth mentioning here that air/gas velocities within the gas generator are ignored. The velocities at the inlet to intake and outlet of nozzle are only calculated.

The engine performance is estimated by defining the adiabatic efficiencies as follows:

Diffuser efficiency: $0.7 < \eta_d < 0.9$ (depending strongly on flight Mach number)
Compressor efficiency: $0.85 < \eta_c < 0.90$
Burner efficiency: $0.97 < \eta_b \leq 0.99$ (same value applies for the efficiency of afterburner)
Turbine efficiency: $0.90 < \eta_t < 0.95$
Nozzle efficiency: $0.95 < \eta_n < 0.98$

4.2.4.2 Governing Equations

The different processes through the engine modules are described again here.

1. Intake
   The pressure ratio within the inlet may be given. The outlet pressure is obtained from the relation

$$r_d = \frac{P_{02}}{P_{0a}} \tag{4.16a}$$

   Alternatively, the efficiency (η_d) of the inlet (sometimes denoted as intake or diffuser) is given. The outlet pressure will be given by

$$P_{02} = P_a\left(1+\eta_d\frac{\gamma_c-1}{2}M_a^2\right)^{\gamma_c/\gamma_c-1} \tag{4.16b}$$

$$T_{02} = T_{0a} = T_a\left(1+\frac{\gamma_c-1}{2}M_a^2\right) \tag{4.2}$$

   Outside the engine, the total pressure remains constant; thus,

$$P_{01} = P_{0a} = P_a\left(1+\frac{\gamma-1}{2}M^2\right)^{\gamma/\gamma-1}$$

The outlet temperature of the diffuser is independent from the losses and so will be calculated from Equation 4.2 as in the ideal case.

2. Compressor
From state (2) to (3), an irreversible adiabatic compression process takes place, which is associated with the isentropic efficiency of the compressor, η_c. The outlet conditions are now

$$P_{03} = (P_{02})(\pi_c) \tag{4.17}$$

$$T_{03} = T_{02}\left[1 + \frac{\pi_c^{\gamma_c - 1/\gamma_c} - 1}{\eta_c}\right] \tag{4.18}$$

3. Combustion chamber
The stagnation pressure at the outlet of combustion chamber, state (4), is less than its value at inlet, state (3), because of fluid friction. The pressure drop is either given as a definite value or as a percentage. Thus the outlet pressure from the combustion chamber is expressed either as

$$P_{04} = P_{03} - \Delta P_{cc} \tag{4.19a}$$

or

$$P_{04} = P_{03}(1 - \Delta P_{cc}\%) \tag{4.19b}$$

The outlet temperature of the combustion chamber is defined as high as the turbine material limitations will allow. The fuel-to-air ratio is now calculated, taking into consideration the efficiency of burners η_b from the relation

$$f = \frac{Cp_h T_{04} - Cp_c T_{03}}{\eta_b Q_R - Cp_h T_{04}} \tag{4.20}$$

4. Turbine
From states (4) to (5), the fluid expands through the turbine, providing shaft power input to the compressor plus any mechanical losses or accessory power. Equation 4.6 is also valid here, and from it the outlet temperature to the turbine T_{05} is calculated. However, the outlet pressure is calculated considering the adiabatic efficiency of the turbine (η_t); thus,

$$\frac{P_{05}}{P_{04}} = \left[1 - \frac{1}{\eta_t}\left(1 - \frac{T_{05}}{T_{04}}\right)\right]^{\gamma_h/\gamma_h - 1} \tag{4.21a}$$

Other relations (similar to those of the ideal case) for evaluating the pressure ratio are

$$\left(\frac{P_{05}}{P_{04}}\right) = \left\{1 - \frac{(Cp_c / Cp_h)T_{02}}{\lambda(1+f)\eta_c \eta_t T_{04}}\left[\left(\frac{P_{03}}{P_{02}}\right)^{\gamma_c - 1/\gamma_c} - 1\right]\right\}^{\gamma_h/\gamma_h - 1} \tag{4.21b}$$

From Equation 4.2,

$$\left(\frac{P_{05}}{P_{04}}\right)=\left\{1-\frac{\left(Cp_c/Cp_h\right)T_a}{\lambda\left(1+f\right)\eta_c\eta_t T_{04}}\left(1+\frac{\gamma-1}{2}M^2\right)\left[\left(\frac{P_{03}}{P_{02}}\right)^{\gamma_c-1/\gamma_c}-1\right]\right\}^{\gamma_h/\gamma_h-1} \tag{4.21c}$$

5. Afterburner
State (6) depends on the geometry of the engine. The pressure at the outlet of the afterburner will be less than its value at the inlet whether the afterburner is operative or inoperative.
   a. Inoperative afterburner
   A treatment similar to the combustion chamber is considered. Thus, based on the value of the pressure drop within the afterburner due to the skin friction and the drag from the flameholders

$$P_{06}=P_{05}-\Delta P_{ab} \tag{4.22a}$$

   or

$$P_{06}=P_{05}\left(1-\Delta P_{ab}\%\right) \tag{4.22b}$$

   No further fuel is burnt as the afterburner is inoperative.
   The temperature is constant in the afterburner duct:

$$T_{06}=T_{05}$$

   b. Operative afterburner
   An additional amount of fuel is burnt in the afterburner, which leads to a steep rise in temperature to the maximum temperature in the cycle ($T_{06A}=T_{\max}$). The pressure drop is obtained using Equation 4.22a and b but P_{06A} replaces P_{06}. The afterburner fuel-to-air ratio is calculated from the relation

$$f_{ab}=\frac{\left(1+f\right)\left(Cp_{6A}T_{06A}-Cp_5T_{05}\right)}{\eta_{ab}Q_R-Cp_{6A}T_{06A}} \tag{4.23}$$

6. Nozzle
A check for nozzle choking is also performed first by calculating the critical pressure. The two cases of operative and inoperative are again considered.
   a. Inoperative afterburner
   The critical pressure is obtained from the relation

$$\frac{P_{06}}{P_c}=\frac{1}{\left[1-\frac{1}{\eta_n}\left(\frac{\gamma_h-1}{\gamma_h+1}\right)\right]^{\gamma_h/\gamma_h-1}} \tag{4.24}$$

Here η_n is the efficiency of the nozzle. If the nozzle is unchoked, then the outlet pressure is equal to the ambient pressure. The jet speed is now evaluated from the relation

$$V_7 = \sqrt{2Cp_h\left(T_{06} - T_7\right)} = \sqrt{2Cp_h\eta_n T_{06}\left[1-\left(P_a / P_{06}\right)^{\gamma_h - 1/\gamma_h}\right]} \tag{4.25a}$$

or

$$V_7 = \sqrt{\frac{2\gamma_h\eta_n RT_{06}}{\left(\gamma_h - 1\right)}\left[1-\left(P_a / P_{06}\right)^{\gamma_h - 1/\gamma_h}\right]} \tag{4.25b}$$

If the nozzle is choked, then the outlet temperature (T_7) is calculated from the following relation

$$\left(\frac{T_{06}}{T_7}\right) = \left(\frac{\gamma_h + 1}{2}\right) \tag{4.11a}$$

The jet speed is calculated from the following relation:

$$V_7 = \sqrt{\gamma_h RT_7} \tag{4.12a}$$

b. Operative afterburner

The expansion process in the nozzle starts from state (06A) to state (7).

The critical pressure is calculated from the relation

$$\frac{P_{06A}}{P_c} = \frac{1}{\left[1 - \frac{1}{\eta_n}\left(\frac{\gamma_h - 1}{\gamma_h + 1}\right)\right]^{\gamma_h/\gamma_h - 1}} \tag{4.26}$$

If the nozzle is unchoked, the jet speed will be

$$V_{7ab} = \sqrt{2Cp_h\eta_n T_{06A}\left[1-\left(P_a / P_{06}\right)^{\gamma_h - 1/\gamma_h}\right]} \tag{4.27a}$$

If the nozzle is choked, then

$$V_{7ab} = \sqrt{\gamma_h RT_{7A}} \tag{4.27b}$$

A general relation for the exhaust speed (whether choked or unchoked) may be obtained from Equation 4.25a and b by replacing P_a by P_7; thus,

$$V_{7ab} = \sqrt{2Cp_h\eta_n T_{06A}\left[1-\left(P_7 / P_{06A}\right)^{\gamma_h - 1/\gamma_h}\right]} \tag{4.28}$$

The two engine parameters defining the performance of the engine are the specific thrust and the specific fuel consumption.

The specific thrust is expressed by the relation

$$\frac{T}{\dot{m}_a} = \left[\left(1 + f + f_{ab}\right)V_7 - V\right] + \frac{A_7}{\dot{m}_a}\left(P_7 - P_a\right) \tag{4.29}$$

The thrust-specific fuel consumption (TSFC) is given by

$$TSFC = \frac{\dot{m}_f + \dot{m}_{fab}}{T} \tag{4.30a}$$

Substituting from Equation 4.26 to get

$$TSFC = \frac{f + f_{ab}}{\left(1 + f + f_{ab}\right)V_7 - V + \dfrac{A_7}{\dot{m}}\left(P_7 - P_a\right)} \tag{4.30b}$$

For an inoperative afterburner, the same Equations 4.29 and 4.30a and b are used but the afterburner fuel-to-air ratio f_{ab} is set equal to zero.

Example 4.5

A single-spool turbojet engine has the following data:

Compressor pressure ratio	8
Turbine-inlet temperature	1200 K
Air mass flow rate	15 kg/s
Aircraft's speed	260 m/s
Flight altitude	7000 m
Isentropic efficiency of intake	0.9
Isentropic efficiency of compressor and turbine	0.9
Combustion chamber pressure loss	= 6% of delivery pressure
Combustion chamber efficiency	0.95
Isentropic efficiency of propelling nozzle	0.9

Calculate the propelling nozzle area, the net thrust developed, and the TSFC.

If the gases in the jet pipe are reheated to 2000 K where a pressure loss of 3% is encountered, calculate

1. The percentage increase in net thrust
2. The percentage increase in nozzle area

$$\left(T_a = 242.7\ \text{K},\quad P_a = 41.06\ \text{kPa},\quad Q_R = 43{,}000\ \text{kJ/kg}\right)$$

Solution

Case (1) Inoperative afterburner

Diffuser:

$$T_{02} = T_a + \frac{V^2}{2Cp} = 242.7 + \frac{(260)^2}{2 \times 1005} = 276.3\ \text{K}$$

$$P_{02} = P_a\left[1+\eta_d\left(\frac{T_{02}-T_a}{T_a}\right)\right]^{\gamma/\gamma-1} = 1.5089\ P_a = 61.95\ \text{kPa}$$

Compressor

$$P_{03} = \pi_c P_{02} = 8\times 61.95 = 495.6\ \text{kPa}$$

$$T_{03} = T_{02}\left[1+\frac{\pi_C{}^{\gamma C-1/\gamma C}-1}{\eta_C}\right] = 525.7\ \text{K}$$

Combustion chamber

$$P_{04} = \left(1-\Delta P_{cc}\right)P_{03} = 0.94P_{03} = 475.8\ \text{kPa},$$

$$T_{04} = 1200\ \text{K}$$

$$f = \frac{Cp_t T_{04} - Cp_c T_{03}}{\eta_b Q_R - Cp_t T_{04}} = 0.023$$

Turbine: Energy balance for compressor and turbine

$$T_{05} = T_{04} - \frac{Cp_c\left(T_{03}-T_{02}\right)}{Cp_t\left(1+f\right)} = 1200 - \frac{1.005\times\left(525.7-276.3\right)}{1.157\times 1.023} = 988.2\ \text{K}$$

$$P_{05} = P_{04}\left[1-\frac{T_{04}-T_{05}}{\eta_t T_{04}}\right]^{\gamma_t/\gamma_t-1} = 476\left[1-\frac{1200-988.2}{0.9\times 1200}\right]^4 = 198.8\ \text{kPa}$$

Tail pipe: No losses is assumed if the afterburner is inoperative, then

$$T_{06} = T_{05}$$

$$P_{06} = P_{05}$$

Nozzle: Check whether the nozzle is choked or not:

$$\frac{P_{06}}{P_c} = \frac{1}{\left[1-\frac{1}{\eta_n}\frac{\gamma_n-1}{\gamma_n+1}\right]^{\gamma_n/\gamma_n-1}} = 1.907$$

$$P_c = 104.2\ \text{kPa}$$

Since $P_c > P_a$, the nozzle is choked:

$$\therefore P_7 = P_c = 104.2\ \text{kPa}$$

$$T_7 = \frac{T_{06}}{\left(\frac{\gamma_n + 1}{2}\right)} = 848.2 \text{ K}$$

$$V_7 = \sqrt{\gamma_n R T_7} = 569 \text{ m/s}$$

To get the nozzle area,

$$\dot{m} = \dot{m}_a\left(1 + f\right) = 15 \times 1.023 = 15.345 \text{ kg/s},$$

since $\dot{m} = \rho_7 V_7 A_7$.

And $\rho_7 = \frac{P_7}{RT_7} = 0.428 \text{ kg/m}^3$

$$\therefore A_7 = \frac{\dot{m}}{\rho_7 V_7} = 0.063 \text{ m}^2$$

$$T = \dot{m}_a\left[\left(1 + f\right)V_7 - V\right] + A_7\left(P_7 - P_a\right)$$

$$= 15\left[1.023 \times 569 - 260\right] + 0.063 \times 10^3\left(104.2 - 41.06\right)$$

$$T = 8809 \text{ N}$$

$$TSFC = \frac{\dot{m}_f}{T} = \frac{f\dot{m}_a}{T} = \frac{0.023 \times 15}{8809} = 3.916 \times 10^{-5} \text{ kg/N} \cdot \text{s}$$

Case (2) Operative afterburner

A pressure drop of 3% is encountered in the afterburner; thus,

$$P_{06A} = 0.97 \quad P_{05} = 192.836 \text{ kPa}$$

The maximum temperature is now $T_{06A} = 2000$ K:

$$f_{ab} = \frac{Cp_t\left(T_{06A} - T_{05}\right)}{\eta_{ab} Q_R - Cp_t T_{06A}} = \frac{1.157 \times \left(2{,}000 - 988.2\right)}{0.9 \times 43{,}000 - 1.157 \times 2{,}000} = 0.0322$$

Check also nozzle choking

$$\text{With } \frac{P_{06A}}{P_c} = \frac{1}{\left(1 - \frac{1}{\eta_n}\frac{\gamma_n - 1}{\gamma_n + 1}\right)^{\gamma_n/\gamma_n - 1}} = 1.907$$

$$\therefore P_c = 101.12 \text{ kPa}$$

$$\because P_c > P_a \quad \therefore \text{Nozzle is choked also.}$$

$$P_{7A} = P_c = 101.12 \text{ kPa},$$

$$T_{7A} = \frac{T_{06A}}{\left(\frac{\gamma_n + 1}{2}\right)} = 1716.7 \text{ K}$$

$$V_{7A} = a_{7A} = \sqrt{\gamma_n R T_{7A}} = 809.5 \text{ m/s}$$

The nozzle area is calculated from the relation

$$A_{7A} = \frac{\dot{m}_a\left(1 + f + f_{ab}\right)}{\rho_{7A} V_{7A}} = \frac{RT_{7A}\dot{m}_a\left(1 + f + f_{ab}\right)}{P_{7A} V_{7A}}$$

$$= \frac{287 \times (1716.7) \times (15) \times (1 + 0.023 + 0.0322)}{101.12 \times 10^3 \times (809.5)}$$

$$A_{7A} = 0.0952 \text{ m}^2$$

The thrust force for operative afterburner is

$$T_{ab} = \dot{m}_a\left[\left(1 + f + f_{ab}\right)V_{7A} - V\right] + A_{7A}\left(P_{7A} - P_a\right)$$

$$T_{ab} = 15\left[1.0552 \times 809.5 - 260\right] + 0.0952 \times 10^3\left(101.12 - 41.06\right) = 14,634.6 \text{ N}$$

$$T_{ab} = 14.635 \text{ kN}$$

1. The percentage increase in thrust when the after burner is operative:

$$\Delta T\% = \frac{T_{ab} - T}{T}\% = \frac{14.635 - 8.809}{8.809} = 66\%$$

2. The percentage increase in exhaust nozzle area is $\Delta A\%$:

$$\Delta A\% = \frac{A_{7A} - A_7}{A_7}\% = 51.1\%$$

Example 4.6

A single-spool turbojet engine is powering an aircraft flying at Mach number of 0.85 at an altitude where the ambient conditions are $T_a = 233$ K, $P_a = 26.4$ kPa. The nozzle is choked and the gases are leaving the nozzle with velocity of 600 m/s; the nozzle area is 0.2 m^2. The maximum temperature is 1,200 K and the fuel-heating value is 43,000 kJ/kg. It is required to calculate

1. Compressor pressure ratio
2. The fuel-to-air ratio
3. Thrust force
4. Overall efficiency

Solution

1. Compressor inlet temperature is

$$T_{02} = T_a\left(1+\frac{\gamma-1}{2}M^2\right) = 255 \text{ K}$$

Since no losses are assumed, then states (5) and (6) are coincident, or

$$T_{06} = T_{05}, \quad P_{06} = P_{05}$$

Since the nozzle is choked,

$$\frac{T_{05}}{T_C} = \frac{\gamma+1}{2}$$

$$V_j = \sqrt{\gamma R T_C} = \sqrt{\frac{2\gamma}{\gamma+1}RT_{05}}$$

$$T_{05} = \frac{\gamma+1}{2\gamma R}V_j^2 = 1075 \text{ K}$$

The temperature drop in the turbine is

$$\left(T_{04}-T_{05}\right) = 1200-1075 = 125 \text{ K}$$

The fuel-to-air ratio is

$$f = \frac{Cp_h T_{04} - Cp_c T_{03}}{Q_R - Cp_h T_{04}}$$

Since $W_c = W_t$

$$Cp_c\left(T_{03}-T_{02}\right) = \left(1+f\right)Cp_h\left(T_{04}-T_{05}\right)$$

$$\therefore \left(T_{03}-T_{02}\right) = \frac{Cp_h}{Cp_C}\left(1+\frac{Cp_h T_{04} - Cp_c T_{03}}{Q_R - Cp_h T_{04}}\right)\left(T_{04}-T_{05}\right)$$

$$T_{03} = \frac{T_{02} + \dfrac{Cp_h}{Cp_c}\left(1+\dfrac{Cp_h T_{04}}{Q_R - Cp_h T_{04}}\right)\left(T_{04}-T_{05}\right)}{\left(1+\dfrac{Cp_h\left(T_{04}-T_{05}\right)}{Q_R - Cp_h T_{04}}\right)} = 398 \text{ K}$$

$$\pi_c = \left(\frac{T_{03}}{T_{02}}\right)^{\gamma/\gamma-1} = \left(\frac{398}{255}\right)^{3.5} = 4.75$$

2. The fuel-to-air ratio is then

$$f = \frac{Cp_h T_{04} - Cp_c T_{03}}{Q_R - Cp_h T_{04}} = 0.02374$$

3. To calculate the thrust, the pressure at the exit of the engine must be first defined.
   It will be calculated from the ambient pressure as follows

$$P_{02} = P_a\left(1+\frac{\gamma-1}{2}M^2\right)^{\gamma_c/\gamma_c-1} = 42.34 \text{ kPa}$$

$$P_{03} = \pi_c P_{02} = 201.1 \text{ kPa}$$

$$P_{03} = P_{04}$$

$$P_{05} = P_{04}\left(\frac{T_{05}}{T_{04}}\right)^{\gamma_c/\gamma_c-1} = 129.5 \text{ kPa}$$

$$P_6 = P_C = \frac{P_{05}}{\left(\frac{\gamma_h+1}{2}\right)^{\gamma_h/\gamma_h-1}} = 70.31 \text{ kPa}$$

The mass flow rate is calculated from the outlet conditions

$$T_6 = T_C = \frac{T_{05}}{\frac{\gamma_h+1}{2}} = 922.7 \text{ K}$$

$$\rho_6 = \rho_c = \frac{P_c}{RT_c} = 0.266 \text{ kg/m}^3$$

$$\dot{m}_e = \rho_6 V_6 A_6 = 31.86 \text{ kg/s}$$

$$\dot{m}_a = \frac{\dot{m}_e}{1+f} = 31.12 \text{ kg/s}$$

$$\dot{m}_f = \dot{m}_e - \dot{m}_a = 0.74 \text{ kg/s}$$

$$T = \dot{m}_e V_j - \dot{m}_a V_f + A_e\left(P_e - P_a\right) = 19.98 \text{ kN}$$

4. The overall efficiency

$$\eta_o = \frac{TV_f}{\dot{m}_f Q_R} = 0.1597 = 15.97\%$$

4.2.5 Comparison between Operative and Inoperative Afterburner

For an inoperative afterburner, both the specific thrust $\left(T/\dot{m}_a\right)$ and the TSFC are dependent on

1. Compressor pressure ratio (π_c)
2. Flight Mach number
3. Maximum temperature or turbine-inlet temperature (T_{04})

For an operative afterburner or in the case of augmented thrust, an additional parameter is considered, namely, the maximum temperature in the engine T_{06A}.

Now consider the cases of an unchoked nozzle with and without thrust augmentation. If more precise analysis is assumed by considering the exact values for the specific

$$\frac{T_{ab}}{\dot{m}_a} = \left[\left(1+f+f_{ab}\right)V_{7ab} - V\right] + \frac{A_{7ab}}{\dot{m}_a}\left(P_{7ab} - P_a\right) \tag{4.31a}$$

$$\frac{T}{\dot{m}_a} = \left[\left(1+f\right)V_7 - V\right] + \frac{A_7}{\dot{m}_a}\left(P_7 - P_a\right) \tag{4.31b}$$

where

$$V_{7ab} = \sqrt{2Cp_{n_{ab}}T_{06A}\eta_{n_{ab}}\left\{1-\left(P_{7A}/P_{06A}\right)^{(\gamma-1/\gamma)_{n_{ab}}}\right\}} \tag{4.32a}$$

$$V_7 = \sqrt{2Cp_nT_{06}\eta_n\left\{1-\left(P_7/P_{06}\right)^{(\gamma-1/\gamma)_n}\right\}} \tag{4.32b}$$

$$\upsilon = V/V_7$$

Consider the case of unchoked nozzle

$$\frac{T_{ab}}{T} = \frac{\left(\dfrac{1+f+f_{ab}}{1+f}\right)\dfrac{V_{7ab}}{V_7} - \left(\dfrac{1}{1+f}\right)\upsilon}{1-\dfrac{\upsilon}{1+f}}$$

$$\frac{T_{ab}}{T} = \frac{\left\{\left(\dfrac{Cp_{n_{ab}}T_{06A}\eta_{n_{ab}}}{Cp_nT_{06}\eta_n}\dfrac{\left[1-\left(\dfrac{P_{7A}}{P_{06A}}\right)^{(\gamma-1/\gamma)_{n_{ab}}}\right]}{\left[1-\left(\dfrac{P_7}{P_{06}}\right)^{(\gamma-1/\gamma)_n}\right]}\right)^{1/2}\left(\dfrac{1+f+f_a}{1+f}\right)\right\} - \left(\dfrac{\upsilon}{1+f}\right)}{\left\{1-\left(\dfrac{\upsilon}{1+f}\right)\right\}} \tag{4.33}$$

Consider the following simplifying assumptions:

$$P_7 = P_{7A}, \quad P_{06} = P_{06A}, \quad \gamma_n = \gamma_{n_{ab}}$$

$$1+f+f_a \approx 1+f \approx 1$$

Then the ratio between the jet (exhaust) speeds for operative and inoperative afterburner is

$$\frac{V_{7_{ab}}}{V_7} = \sqrt{\frac{T_{06A}}{T_{06}}} \tag{4.34}$$

The ratio between the thrust force for operative and inoperative afterburner is given as

$$\frac{T_{ab}}{T} = \frac{\left(T_{06A}/T_{06}\right)^{1/2} - \upsilon}{1-\upsilon} \tag{4.35}$$

Since $T_{06} = T_{05}$ then the thrust ratio in fact is dependent on the temperature ratio between the temperature after and before the afterburner. When Equation 4.35 is plotted, Figure 4.8, the curves give an optimistic value of (T_{ab}/T) due to the assumptions made.

The curves show that

1. For any value of (T_{06A}/T_{06}), the increase in (υ), leads to an increase in (T_{ab}/T)
2. At any value of $\upsilon\left(\equiv \frac{V}{V_7}\right)$, the increase of (T_{06A}/T_{06}) will lead to an increase in the augmented thrust ratio
3. Since the afterburning engine can deliver large thrusts at larger values of $\upsilon\left(\equiv \frac{V}{V_7}\right)$ than are practical for a normal engine, the afterburning engine can operate with larger values of $\upsilon_{ab}\left(\equiv \frac{V}{V_{7ab}}\right)$ and still develop larger values of thrust per unit area
4. Since the propulsive efficiency for unchoked nozzle and negligible fuel burnt with respect to air mass flow rate is expressed as

$$\eta_p = \frac{2V}{V + V_{7ab}} = \frac{2}{1 + \frac{1}{\upsilon_{ab}}}$$

Then, as υ_{ab} increases, the propulsive efficiency increases

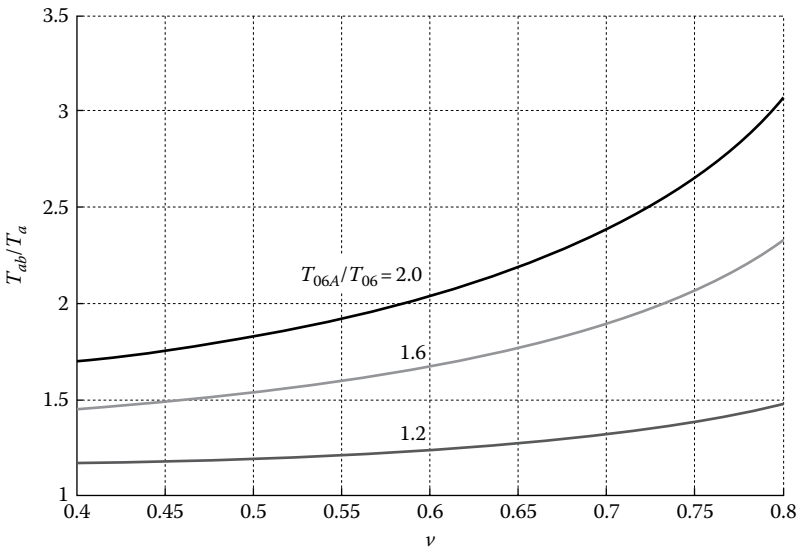


FIGURE 4.8
Ratio between thrust force for operative and inoperative afterburner.

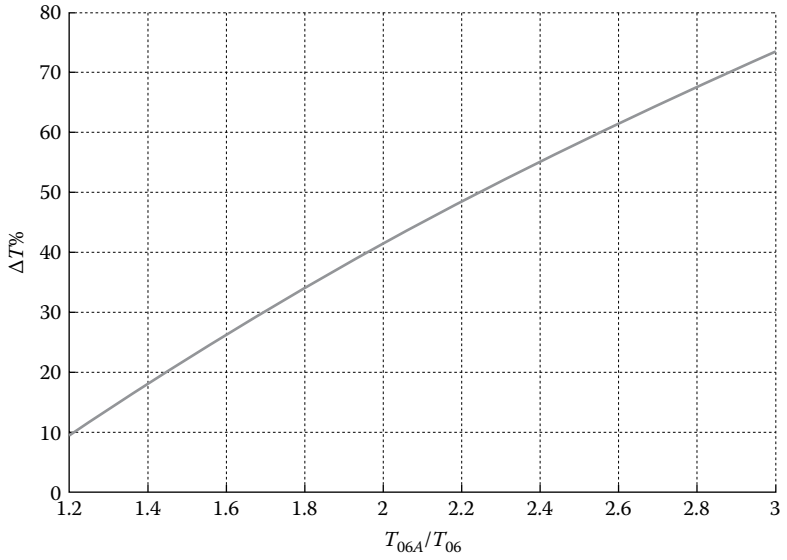


FIGURE 4.9
Percentage of thrust increase and temperature ratio.

During takeoff ($V=0$), from Equations 4.34 and 4.35, then:

$$\frac{T_{ab}}{T} = \left(T_{06A} / T_{06}\right)^{1/2} \equiv \frac{V_{7_{ab}}}{V_7} \tag{4.36}$$

Equation 4.36 is plotted in Figure 4.9 to illustrate the effect of temperature ratio.

Consider the following case for static operation with the following temperature values:

$$T_{06} = T_{05} = 959 \text{ K}$$

$$T_{06A} = 2000 \text{ K}$$

$$T_{04} = 1200 \text{ K}$$

$$T_{03} = 650 \text{ K}$$

From Equation 4.36, the increase in momentum thrust amounts to $\sqrt{2000/959} = 1.44$.

As an approximation, the increase in fuel-to-air ratio is obtained from the ratio of temperature differences for both cases of operative and inoperative afterburner, or

$$\frac{(2000-959)+(1200-650)}{(1200-650)} = 2.89$$

An increase in thrust of 44% is obtained at the expenses of 189% increase in fuel consumption, which represents the thrust augmentation during takeoff conditions. However, at high forward speed, the gain is much greater and is often more than 100%. This is due to the increase in momentum thrust for a fixed-ram drag (momentum drag).

It is interesting also to prove that for choked nozzles, the relation (4.34) is also correct. The exhaust temperature for an inoperative afterburner (or no afterburner at all) is

$$T_7 = \left(\frac{2}{\gamma+1}\right)T_{06} = \frac{\left(V_7^2\right)}{\gamma R}$$

For an operative afterburner, the exhaust temperature is

$$T_{7A} = \left(\frac{2}{\gamma+1}\right)T_{06A} = \frac{V_{7ab}^2}{\gamma R}$$

Again the ratio between the jet speeds for the operative and inoperative afterburner is expressed as

$$\therefore \frac{V_{7ab}}{V_7} = \sqrt{\frac{T_{06A}}{T_{06}}}$$

However, the thrust ratio is no longer expressed by Equation 4.36 as the pressure thrust must be included.

The increase in jet speed and thrust force when the afterburner is lit provides improved takeoff and climb characteristics as shown in Figure 4.10. Thus, for military applications the time saved in takeoff and reaching the necessary altitude is most important. Moreover, the short takeoff distance is needed if an airplane takes off from an air carrier. Operation of the afterburner is accompanied by an increase in fuel consumption as extra fuel is burnt, which is calculated from Equation 4.23. However, it was found that the amount of fuel required to reduce the time taken to reach the operation height in Figure 4.10 is not excessive [6].

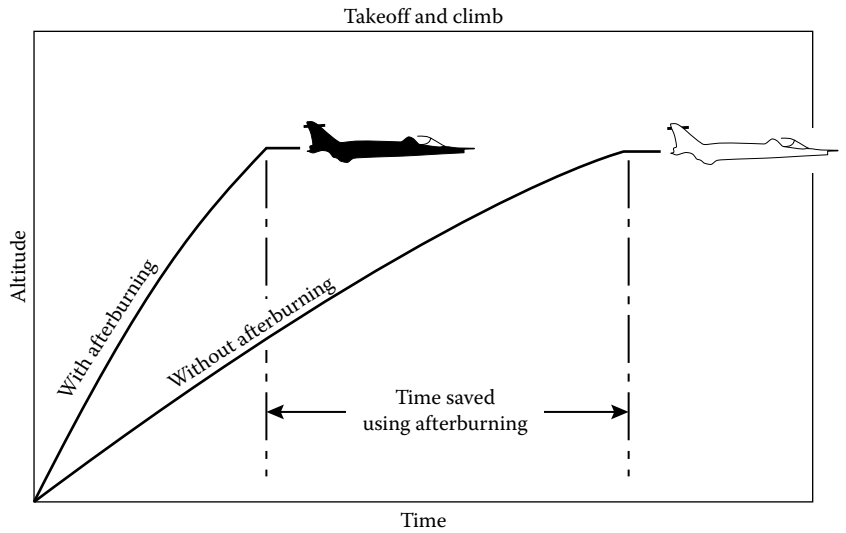


FIGURE 4.10
Effect of afterburning on takeoff and the rate of climb. (Reproduced from Rolls-Royce Plc. Copyright 2016. With permission.)

4.3 Two-Spool Engine

In this section the thermodynamic analysis of a two-spool turbojet engine is given. There are two types, namely, a turbojet engine with no afterburner and a turbojet engine with an afterburner (Figure 4.11). Mostly, the second type of turbojet engine is fitted to military airplanes. Rolls–Royce/SNECMA Olympus 593 Mrk 610 is the only engine that powered a supersonic commercial aircraft; namely, Concorde. The two-spool engines are composed of two compressors coupled to two turbines through two spools or shafts. As in the case of single spool with afterburner turbojet, the afterburning engines have two combustors, namely, the conventional combustion chamber and the afterburner installed downstream the LPT. Both variable area intake and nozzle are necessary here.

4.3.1 Non-Afterburning Engine

4.3.1.1 Example of Engines

GE J57-P-43 WB (Turbojet with water injection for thrust augmentation)

Length: 169 in. (4300 mm)
Diameter: 35 in. (900 mm)
Dry weight: 3875 lb (1757 kg)
Two axial compressors of total 16 stages
Overall pressure ratio 12:1
Turbine-inlet temperature: 1600°F (870°C)

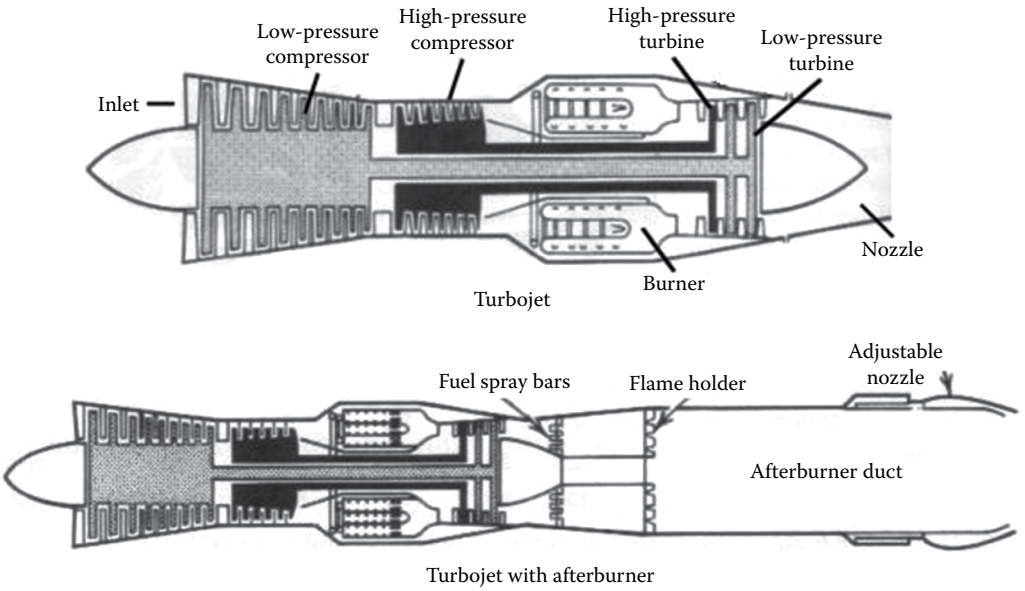


FIGURE 4.11
Layout of turbojet with and without afterburner.

Thrust: 11,200 lbf (49.9 kN) with water-methanol injection

Specific fuel consumption: 0.755 lb/(h·lbf) (77.0 kg/(h·kN)) at maximum military power

Thrust-to-weight ratio 2.9:1 (28.4 N/kg)

4.3.1.2 Thermodynamic Analysis

A simplified layout of a turbojet engine is shown in Figure 4.12. Moreover, the cycle or the successive processes are shown in Figure 4.13. Only a real case will be considered here,

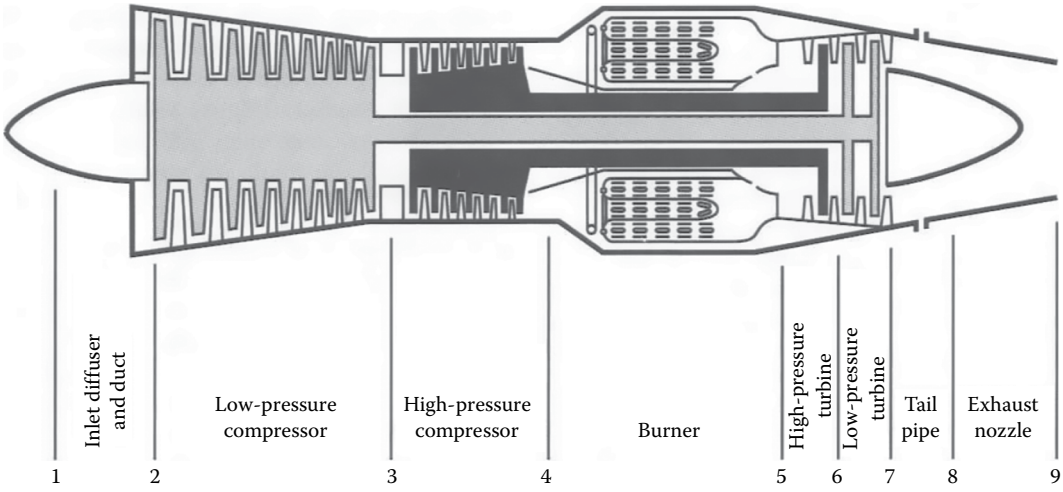


FIGURE 4.12
Stations of a turbojet engine.

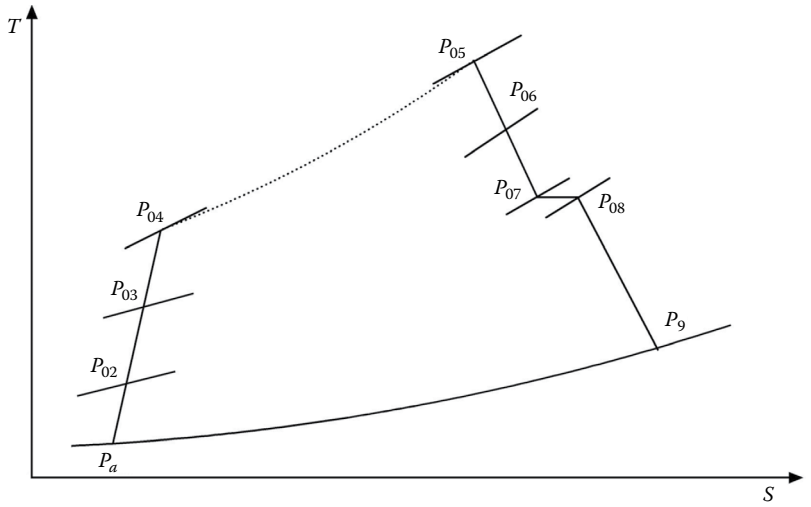


FIGURE 4.13
Cycle for inoperative two-spool turbojet.

as the ideal performance can be considered as a special case where the efficiencies are set equal to unity and no pressure losses.

Now the successive elements will be examined.

1. Intake
   The inlet conditions of the air entering the inlet are the ambient pressure and temperature (P_a and T_a, respectively). The intake has an isentropic efficiency (η_d). For a flight Mach number (M_a), the temperature and pressure at the outlet of the intake are T_{02} and P_{02} given by the same relations as the single spool, Equations 4.2 and 4.16b

$$P_{02} = P_a\left(1+\eta_d\frac{\gamma_c-1}{2}M_a^2\right)^{\gamma_c/\gamma_c-1} \tag{4.16b}$$

$$T_{02} = T_{0a} = T_a\left(1+\frac{\gamma_c-1}{2}M_a^2\right) \tag{4.2}$$

2. Low-pressure compressor
   For a known compressor pressure ratio (π_{c1}) and isentropic efficiency (η_{c1}), the temperature and pressure at the outlet of the LPC are given by the following relations:

$$P_{03} = \left(P_{02}\right)\left(\pi_{c1}\right) \tag{4.37}$$

$$T_{03} = T_{02}\left[1+\frac{{\pi_{c1}}^{\gamma_c-1/\gamma_c}-1}{\eta_{c1}}\right] \tag{4.38}$$

3. High-pressure compressor
   Similarly, both the pressure ratio (π_{c2}) and its isentropic efficiency (η_{c2}) are known. Thus the temperature and pressure at the outlet of the HPC are given by the following relations:

$$P_{04} = \left(P_{03}\right)\left(\pi_{c2}\right) \tag{4.39}$$

$$T_{04} = T_{03}\left[1+\frac{{\pi_{c2}}^{\gamma_c-1/\gamma_c}-1}{\eta_{c2}}\right] \tag{4.40}$$

4. Combustion chamber
   The temperature at the end of combustion process T_{05} is generally known. It is the maximum temperature in the cycle if the afterburner is inoperative. The pressure at the end of the combustion depends on the pressure drop in the combustion process itself. Thus, depending on the known expression for the pressure drop in the combustion chamber, it may be expressed as

$$P_{05} = P_{04} - \Delta P_{cc} \tag{4.41}$$

or

$$P_{05} = P_{04}\left(1 - \Delta P_{cc}\%\right) \tag{4.42}$$

The energy balance for the combustion chamber yields the following relation for the fuel-to-air ratio (f) defined as the ratio between the mass of fuel burnt to the air mass flow rate through the gas generator

$$\dot{m}_a\left(1+f\right)Cp_hT_{05} = \dot{m}_aCp_cT_{04} + \eta_b\dot{m}_fQ_R$$

with

$$f = \dot{m}_f/\dot{m}_a$$

$$f = \frac{\left(Cp_h/Cp_c\right)\left(T_{05}/T_{04}\right)-1}{\eta_b\left(Q_R/Cp_cT_{04}\right)-\left(Cp_h/Cp_c\right)\left(T_{05}/T_{04}\right)} \tag{4.43}$$

5. High-pressure turbine
The power generated in the HPT is used in driving the HPC in addition to some of the accessories. If the ratio of the power needed to drive the HPC to the power available from the HPT is (λ_1), then the energy balance for the compressor-turbine shaft is

$$W_{HPC} = \lambda_1 W_{HPT}$$

Here (λ_1) is of the range 75%–85%. Thus in terms of the temperatures differences

$$Cp_c\left(T_{04}-T_{03}\right) = \lambda_1\left(1+f\right)Cp_h\left(T_{05}-T_{06}\right)$$

$$\left(\frac{T_{06}}{T_{05}}\right) = 1 - \frac{\left(Cp_c/Cp_h\right)T_{03}}{\lambda_1\left(1+f\right)T_{05}}\left[\left(\frac{T_{04}}{T_{03}}\right)-1\right] \tag{4.44}$$

Then the pressure ratios of the HPT and HPC are related by

$$\left(\frac{P_{06}}{P_{05}}\right) = \left\{1 - \frac{\left(Cp_c/Cp_h\right)T_{03}}{\lambda_1\left(1+f\right)\eta_{c2}\eta_{t2}T_{05}}\left[\left(\frac{P_{04}}{P_{03}}\right)^{\gamma_c-1/\gamma_c}-1\right]\right\}^{\gamma_h/\gamma_h-1} \tag{4.45}$$

where η_{t2} is the isentropic efficiency of the HPT.

6. Low-pressure turbine (LPT)
The power consumed in the compression from (2) to (3) must be supplied through the LPT in expansion from (6) to (7). If the ratio of the power needed to drive the compressor to the power available in the turbine is (λ_2), then the energy balance for the low-pressure spool is

$$W_{LPC} = \lambda_2 W_{LPT}$$

Here (λ_2) is of the range 75%–85%. Thus, in terms of the temperature differences,

$$Cp_c\left(T_{03}-T_{02}\right)=\lambda_2\left(1+f\right)Cp_h\left(T_{06}-T_{07}\right)$$

$$\left(\frac{T_{07}}{T_{06}}\right)=1-\frac{\left(Cp_c/Cp_h\right)T_{02}}{\lambda_2\left(1+f\right)T_{06}}\left[\left(\frac{T_{03}}{T_{02}}\right)-1\right] \tag{4.46}$$

Then the turbine and compressor pressure ratios are related by

$$\left(\frac{P_{07}}{P_{06}}\right)=\left\{1-\frac{\left(Cp_c/Cp_h\right)T_{02}}{\lambda_2\left(1+f\right)\eta_{c1}\eta_{t1}T_{06}}\left[\left(\frac{P_{03}}{P_{02}}\right)^{\gamma_c-1/\gamma_c}-1\right]\right\}^{\gamma_h/\gamma_h-1} \tag{4.47}$$

From the diffuser part (Equation 4.2)

$$\left(\frac{P_{07}}{P_{06}}\right)=\left\{1-\frac{\left(Cp_c/Cp_h\right)T_a}{\lambda_2\left(1+f\right)\eta_{c1}\eta_{t1}T_{06}}\left(1+\frac{\gamma-1}{2}M^2\right)\left[\left(\frac{P_{03}}{P_{02}}\right)^{\gamma_c-1/\gamma_c}-1\right]\right\}^{\gamma_h/\gamma_h-1} \tag{4.48}$$

7. Jet pipe
   The jet pipe following the LPT and preceding the nozzle is associated with a slight pressure drop, while the total temperature remains unchanged:

$$P_{08}=P_{07}-\Delta P_{jet\ pipe} \tag{4.49a}$$

$$T_{08}=T_{07} \tag{4.49b}$$

8. Nozzle
   First of all a check for nozzle choking is performed. Thus for an isentropic efficiency of the nozzle η_n, the critical pressure is obtained from the relation

$$\frac{P_{08}}{P_c}=\frac{1}{\left[1-\frac{1}{\eta_n}\left(\frac{\gamma_h-1}{\gamma_h+1}\right)\right]^{\gamma_h/\gamma_h-1}} \tag{4.50}$$

   If the nozzle is unchoked, then the outlet pressure is equal to the ambient pressure. The jet speed is now evaluated from the relation

$$V_9=\sqrt{2Cp_h\eta_nT_{08}\left[1-\left(P_a/P_{08}\right)^{\gamma_h-1/\gamma_h}\right]} \tag{4.51a}$$

   If the nozzle is choked, then the outlet temperature (T_8) is calculated from the relation

$$\left(\frac{T_{08}}{T_9}\right)=\left(\frac{\gamma_h+1}{2}\right)$$

   The jet speed is expressed as

$$V_9=\sqrt{\gamma_hRT_9} \tag{4.51b}$$

4.3.2 Afterburning Engine

Most military engines together with the Rolls–Royce Snecma Olympus 593 Mrk 610 that powered the Concorde are fitted with an afterburner.

4.3.2.1 Examples for Two-Spool Afterburning Turbojet Engines

1. Pratt & Whitney J57-P-23

   This powered the following military aircraft: Boeing B-52, Boeing C-135, Convair F-102 Delta Dagger, Convair XB-60, Douglas A3D Skywarrior, Lockheed U-2, McDonnell F-101, and North America F-100.

   Length: 244 in. (6200 mm)

   Diameter: 39 in. (1000 mm)

   Dry weight: 5175 lb (2347 kg)

   Two-spool axial compressor of total 16 stages

   Overall pressure ratio: 11.5:1

   Turbine-inlet temperature: 1600°F (870°C)

   Thrust: 11,700 lbf (52.0 kN) dry

   17,200 lbf (76.5 kN) with afterburner

   Specific fuel consumption: 2.1 lb/(h·lbf) (214.2 kg/h·kN))

2. General Electric J79-GE-17

   This powered the following military aircraft: Lockheed F-104, B-58 Hustler, and the McDonnell Douglas Phantom F-4.

   Length: 17.4 ft (5.3 m)

   Diameter: 3.2 ft (1.0 m)

   Dry weight: 3850 lb (1750 kg)

   Two-spool axial compressor of total 17 stages with variable stator vanes

   Overall pressure ratio: 13.5:1

   Turbine-inlet temperature: 1210°F (655°C)

   Thrust: 11,905 lbf (52.9 kN) dry

   17,835 lbf (79.3 kN) with afterburner

   Specific fuel consumption: 1.965 lb/(h·lbf) or 200 kg/(h·kN) with afterburner

3. Rolls-Royce/SNECMA Olympus 593 Mrk 610:

   This powered the Concorde commercial airplane.

   Dry weight: 7000 lb

   Air mass flow rate: 410 lb/s

   Two-spool axial compressor of total 14 stages, 7 stages for each of the LPC and HPC

   Overall pressure ratio: 15.5:1

   Burner: Annular with 16 fuel nozzles

   Turbine: Single stage for each of the HPT and LPT

   Thrust: 32,000 lbf without afterburner at full power

   38,050 lbf with afterburner at full power

Exhaust: Constant diameter afterburning jet pipe, convergent primary nozzle, variable-area divergent secondary nozzle with thrust reverser

Specific fuel consumption: 0.59 lb/(h·lbf) dry

1.13 lb/(h·lbf) with afterburner

Thrust/weight: 5.4:1

4. Al-21

This powered the following Russian military aircraft: MiG-19S and MiG-19PF.

Two spools having axial compressors

Overall pressure ratio: 14.75:1

Turbine-inlet temperature: 2000°F (1100°C)

Thrust: 17,175 lbf (76.4 kN) dry

24,675 lbf (109.8 kN) with afterburner

Specific fuel consumption: 0.76 lb/(h·lbf) (77.5 kg/h·kN) at idle

0.86 lb/(h·lbf) (87.7 kg/h·kN) at maximum military power

1.86 lb/(h·lbf) (189.7 kg/h·kN) with afterburner

Thrust/weight: 6.6:1

4.3.2.2 Thermodynamic Analysis

A simplified diagrammatic sketch for the engine and cycle plotted on the *T*–*S* diagram is shown in Figures 4.14 and 4.15. The LPC is driven by the LPT while the HPC is driven by the HPT. Concerning the Olympus 593 engine, the high-pressure turbine also drives the accessory gearbox via a tower shaft and bevel gear in front of the HPC.

The same treatment for all the modules upstream to the afterburner is applied here. Now, consider the afterburner. Due to fuel addition in the afterburner, a steep rise in temperature to a value much greater than that obtained in the combustion chamber is visible. As expected due to the fuel lines, igniters, and flameholder, a pressure drop is

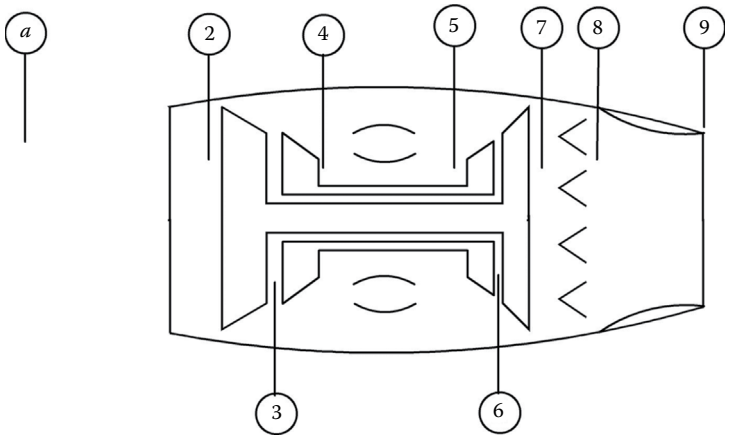


FIGURE 4.14
Stations for a two-spool turbojet engine with operative afterburner.

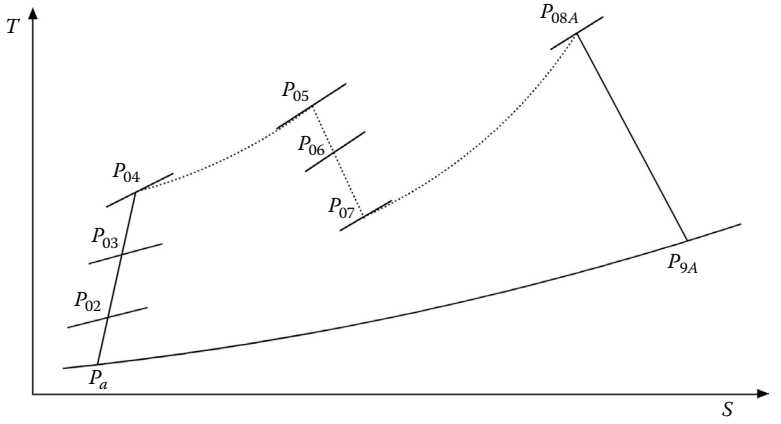


FIGURE 4.15
Cycle for a two-spool turbojet engine with operative afterburner.

encountered in the afterburner. Thus the pressure at the outlet to the afterburner is determined from one of the following relations:

$$P_{08A} = P_{07} - \Delta P_{ab} \tag{4.52a}$$

or

$$P_{08A} = P_{07}\left(1 - \Delta P_{ab}\%\right) \tag{4.52b}$$

The maximum temperature in the cycle is obtained at the end of the combustion process

$$T_{08A} = T_{\max}$$

The afterburner fuel-to-air ratio is calculated from the energy balance in the afterburner. The final relation is

$$f_{ab} = \frac{\left(1+f\right)\left(Cp_{8A}T_{08A} - Cp_7T_{07}\right)}{\eta_{ab}Q_R - Cp_{8A}T_{08A}} \tag{4.53}$$

Nozzle: The very hot gases leaving the afterburner expand in the nozzle from the state (08A) to state (9). As usual a check for nozzle choking is performed as follows:

$$\frac{P_{08A}}{P_c} = \frac{1}{\left[1 - \frac{1}{\eta_n}\left(\frac{\gamma_h - 1}{\gamma_h + 1}\right)\right]^{\gamma_h/\gamma_h - 1}} \tag{4.54}$$

If the nozzle is unchoked, the jet speed will be

$$V_{9ab} = \sqrt{2Cp_h\eta_nT_{08A}\left[1 - \left(P_a / P_{08}\right)^{\gamma_h - 1/\gamma_h}\right]} \tag{4.55a}$$

If the nozzle is choked, then the exhaust gases leave the nozzle with a temperature of T_{9A}, which is calculated from the relation

$$\left(\frac{T_{08}}{T_{9A}}\right)=\left(\frac{\gamma_h+1}{2}\right)$$

The exhaust speed is then calculated from the relation

$$V_{9ab}=\sqrt{\gamma_h R T_{9A}} \tag{4.55b}$$

The performance parameters are the specific thrust and the specific fuel consumption as well as the three efficiencies.

The specific thrust is expressed by the relation

$$\frac{T}{\dot{m}_a}=\left[\left(1+f+f_{ab}\right)V_9-V\right]+\frac{A_9}{\dot{m}_a}\left(P_9-P_a\right) \tag{4.56}$$

The thrust-specific fuel consumption (TSFC) is given by

$$TSFC=\frac{\dot{m}_f+\dot{m}_{fab}}{T}$$

Substituting from Equation 4.56, the TSFC is

$$TSFC=\frac{f+f_{ab}}{\left(1+f+f_{ab}\right)V_9-V+\dfrac{A_9}{\dot{m}_a}\left(P_9-P_a\right)} \tag{4.57}$$

For an inoperative afterburner, the same Equations 4.56 and 4.57 are used but the afterburner fuel-to-air ratio f_{ab} is set equal to zero.

Turbojet engines resemble a one-stream flow engine, and then from Equations 2.7a and 2.13, the efficiencies are calculated as follows. The propulsive efficiency is obtained from the relation

$$\eta_p=\frac{TV}{TV+\dfrac{1}{2}\dot{m}_e\left(V_e-V\right)^2}$$

where the mass and velocity of the gases leaving the nozzle are expressed in general as $\dot{m}_e$ and V_e.

The thermal efficiency is expressed as

$$\eta_{th}=\frac{TV+\dfrac{1}{2}\dot{m}_a\left(1+f\right)\left(V_e-V\right)^2}{\dot{m}_f Q_R}$$

The overall efficiency is then

$$\eta_0=\eta_p\times\eta_{th}$$

Example 4.7

A two-spool turbojet engine has the following data

η_d	$\eta c_1 \eta c_2$	η_{cc}	$\eta t_1 \eta t_2$	η_{ab}	η_n	πc_1	πc_2	ΔP_{cc}	ΔP_{ab}	TIT (K)	$T_{\max}$ (K)	A_i (m²)	$\dot{m}$ (kg/s)
0.9	0.88	0.95	0.94	0.95	0.96	3.35	4.65	0.03	0.05	1200	1500	0.9519	186

Fuel heating value is 45,000 kJ/kg

1. It is required to calculate
   a. The temperature and pressure at the inlet and outlet of each module of the engine
   b. Fuel-to-air ratio for both the combustion chamber and afterburner
   c. The exit area for both operative and inoperative afterburners
   d. The specific thrust and the TSFC
   e. The propulsive, thermal, and overall efficiency
2. Recalculate as for 1 but for when the airplane powered by the specified engine is flying at 8 km altitude with a Mach number 2.04. The maximum temperature at the afterburner is increased to 2000 K, and the air mass flow rate is increased to 314.64 kg/s.

In both cases the nozzle is unchoked.

Solution

Using the previous equations, the results are arranged in the following table:

Properties	Sea Level	Altitude 8 km (26,264 ft)
T_a (K)	288.16	236.23
P_a (Pa)	1.013125×10^5	3.5651×10^4
M	0	2.04
V (m/s)	0	628.5893
T_{02} (K)	288.16	432.9772
P_{02} (Pa)	1.013125×10^5	4.862×10^4
P_{03}	3.3944×10^5	1.6288×10^5
T_{03}	442.8617	635.3745
P_{04}	1.5784×10^6	7.5739×10^5
T_{04}	686.9657	1032.2
P_{05}	1.531×10^6	7.3467×10^5
T_{05} (TIT)	1200	1200
P_{06}	6.0126×10^5	1.6603×10^5
T_{06}	964.9536	849.7425
P_{07}	3.4105×10^5	6.0315×10^4
T_{07}	854.0723	671.0998
P_{08}	3.2399×10^5	6.0315×10^4
T_{08} ($T_{\max}$)	Operative A/B = 1500 Inoperative $A/B = T_{07}$ = 854.0723	Operative A/B = 2000 Inoperative $A/B = T_{07}$ =671.0998
$P_9 = P_a$	1.013125×10^5	3.5651×10^4
T_9	1136.9	1785.2
V_e (m/s)	913.1156	702.2306

(*Continued*)

Properties	Sea Level	Altitude 8 km (26,264 ft)
T (N)	Operative $A/B = 1.7582 \times 10^5$ Inoperative $A/B = 1.7266 \times 10^5$	Operative $A/B = 3.3388 \times 10^4$ Inoperative $A/B = 2.4987 \times 10^4$
η_p	0	0.9222
η_{th}	0.5977	0.1922
η_0	0	0.1802
f	0.0166	0.0082
f_{ab}	0.0186	0.038
Ae (m^2)	Operative $A/B = 0.4381$ Inoperative $A/B = 0.4032$	Operative $A/B = 1.0424$ Inoperative $A/B = 1.0045$

4.4 Statistical Analysis

A survey of many turbojet engines outlined that

1. The single-spool engine is nearly 85% of the turbojet engine and the rest (15%) is two-spool engines, Figure 4.16.
2. The turbojet engines fitted with afterburner is 48% of the total turbojet engines, Figure 4.17.

4.5 Thrust Augmentation

If the thrust of an engine has to be increased above the original design value, one of the following methods may be employed:

1. Increase of turbine-inlet temperature, which will increase the specific thrust and hence the thrust for a given engine size.
2. Increase of the mass flow rate through the engine without altering the cycle parameter.

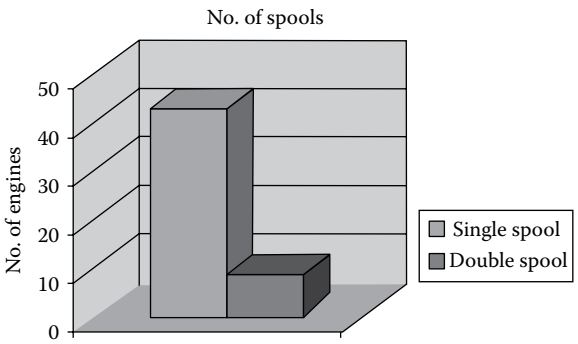


FIGURE 4.16
Survey for number of spools.

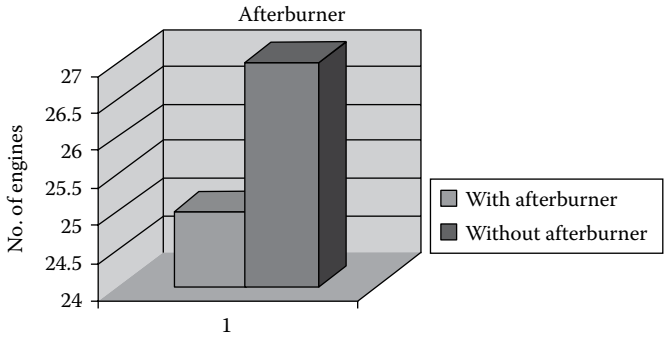


FIGURE 4.17
Survey for afterburning engines.

Both techniques imply some redesign of the engine and either/or both methods may be used to update the existing engine. For example, the inlet area may be increased, but this would be obtained at the expense of increased drag and weight. However, in some circumstances, there will be a requirement for temporary increase in thrust for a short time, for example, during takeoff, climb, and acceleration from subsonic to supersonic speed, or during combat maneuvers. In these circumstances, the thrust must be augmented for the fixed engine size. Numerous schemes have been proposed but the two methods most widely used are:

1. Water injection
2. Reheat or afterburning

4.5.1 Water Injection

Water injection is an old aviation technology that was previously used to enable an increase in engine thrust or power during takeoff. The thrust force depends to a large extent on the mass or the density of the air flow passing through the engine. There is, therefore, a reduction in thrust as the atmospheric pressure decreases with altitude, and/or the ambient air temperature increases (on very hot days).Thus it is frequently necessary to provide some means of thrust augmentation for non-afterburning turbojet or turbofan engines [7]. The thrust (or power for turboprop or turboshaft engines and stationary gas turbine) may be restored or even boosted as much as 10%–30% for takeoff by cooling the airflow with *water* or *water-methanol* (methyl alcohol) injection. The technique is to inject a finely atomized spray of water or W/M (a mixture of water and methanol) into either the inlet of compressor or into the combustion chamber inlet [7]. The compressor inlet water-injection system is either all water or a mixture of water and methanol, but the combustion-chamber water injection is always water/methanol. When methanol is added to water, it gives antifreezing properties and also provides an additional source of fuel. The maximum thrust of an engine using water or W/M injection is called the "wet rating." Figure 4.18 illustrates a typical turbojet engine thrust restoration. Water has to be very pure (so-called demineralized) since any impurities cause rapid buildup of hard deposits on vanes and rotor blades. It vaporizes rapidly causing intense cooling [8]. Turbojet engines usually employ water injection into the combustion chamber inlet, while in turboprop engines water or W/M is injected into the compressor inlet. Injected into the compressor inlet, the water both increases the air density

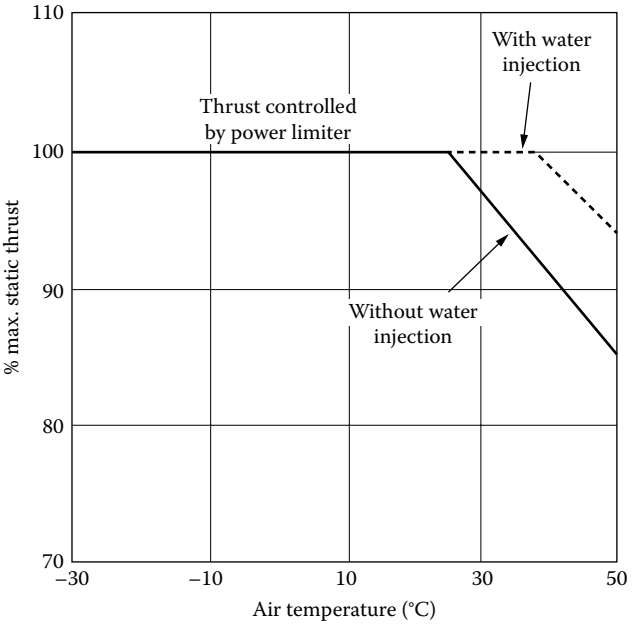


FIGURE 4.18
Thrust restoration of a turbojet engine using water injection. (Reproduced from Rolls-Royce Plc. Copyright 2016. With permission.)

and also cools the turbine gas temperature, enabling extra fuel to be burned, which further adds to the power. Injection into the combustion chamber gives better distribution and makes higher water flow rates possible. It increases the mass flow through the turbine, relative to that through the compressor. The pressure and temperature drop across the turbine is reduced as depicted from the following compressor—turbine energy balance:

$$\dot{m}_a C_{pc}\left(T_{03}-T_{02}\right)=\left(\dot{m}_a+\dot{m}_f+\dot{m}_{waterinjection}\right)C_{ph}\left(T_{04}-T_{05}\right)$$

This leads to an increased jet pipe pressure, which in turn results in additional thrust. Injection of water only reduces the turbine-inlet temperature, which enables an increase of fuel flow rate and an increase in the maximum rotational speed of the engine and thus provides additional thrust. When methanol is used with water, the turbine-inlet temperature is restored partially or fully by the burning of the methanol in the combustion chamber [6]. As aircraft engines have matured and became capable of generating ever more thrust, water injection for new engines has been abandoned, though there are still a few aircraft in service that continue to use water injection. This is due to the extra weight, cost, and extra maintenance arising from the additional system of tanks, pumps, and control system [8]. Moreover, for turbojets, "wet" takeoffs meant excruciating noise and usually a lot of black smoke [8].

Water injection was first used over 45 year ago on commercial transport aircraft Boeing's 707-120 with Pratt & Whitney JT3C-6 engines, and later on the Boeing 747-100 and -200 aircraft with Pratt & Whitney JT9D-3AW and -7AW engines for thrust augmentation. Its objective during these days had nothing to do with emission. Recently, water injection was revisited again to evaluate the feasibility of its use in commercial aircraft, but this time for emission reduction [9,10]. Moreover, newer high BPR engines experience higher

thrust-lapse rates with altitude, which results in higher core temperature. Again, water-injection systems are evaluated for possible use all the way to top of climb [11]. These recent studies are in favor of water injection in the combustion chamber inlet rather than injection into the inlet of compressor. Moreover, it ensured that water injection may reduce takeoff NO_x emission more than 50%. When using water injection throughout climb, turbine life would further improve but the water weight penalties would present unacceptable payload and airplane performance penalties.

4.5.2 Afterburning

Afterburning (or reheat) is a method of augmenting the basic thrust of an engine to improve the takeoff, climb, and (for military aircraft) combat performance. The increased thrust can be obtained by a larger engine, but this would increase the weight, frontal area, and overall fuel consumption [6]. Afterburning provides the best method for thrust augmentation for short periods. Afterburning requires another combustion chamber located between the low pressure turbine (or the turbine if only one turbine exists) and the jet pipe propelling nozzle. Fuel is burnt in this second combustion chamber utilizing the unburned oxygen in the exhaust gas. As described earlier, this increases the temperature and velocity of the exhaust gases leaving the propelling nozzle and therefore increases the engine thrust.

The burners of the afterburner are arranged so that the flame is concentrated around the axis of the jet pipe. Thus, a portion of the discharge gases flow along the walls of the jet pipe and protect these walls from the afterburner flame, the temperature of which is in excess of 1700°C. The area of the afterburning jet is larger than a normal jet pipe would be for the same engine in order to reduce the velocity of the gas stream. The afterburning jet pipe is fitted with either a two-position or a variable-area propelling nozzle.

The increase of thrust in an afterburning engine is also accompanied by an increase in specific fuel consumption. Therefore, afterburning is limited to periods of short duration. Fuel is not burnt in the afterburner as efficiently as in the engine combustion chamber since the pressure in the afterburner is not the peak pressure in the cycle. Figure 4.19 illustrates the thrust-specific fuel consumption for operative and inoperative afterburners at different flight Mach numbers.

4.5.3 Pressure Loss in an Afterburning Engine

In the afterburner diffuser, the velocity of the gases leaving the LPT in conventional turbojet engines ranges from 180 to 360 m/s, which is far too high for a stable flame to be maintained. Thus the flow is diffused before it enters the afterburner combustion zone, and the velocity is decreased and the static pressure is increased. A flame stabilizer is located downstream the fuel burner to provide a region in which turbulent eddies are formed to assist combustion. This reduction in speed also helps in reducing the total pressure losses due to momentum and friction. The conditions that must be satisfied to obtain an efficient diffusion make a compromise between a small diffusion angle to avoid separation losses and length to avoid excessive skin-friction losses. Since low velocities at the exit section, which tends to increase the frontal area of the engine, and efficient diffusion require a small diffusion angle, which tends to make the diffusion section too long, the design is usually dictated by the need to limit the afterburner diameter to the maximum diameter of the engine.

An additional state is defined now (5A) between the outlet of the turbine (5) and the outlet of the afterburner (6A) for a single-spool afterburning turbojet (Figure 4.20), while

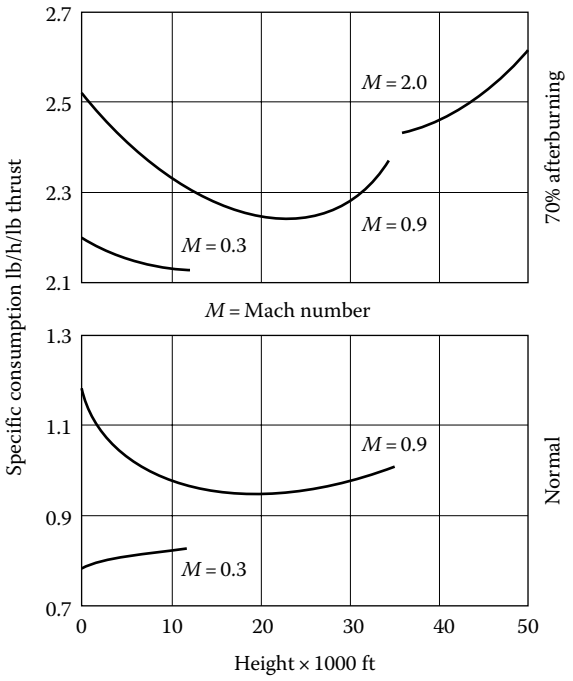


FIGURE 4.19
Thrust-specific fuel consumption. (Reproduced from Rolls-Royce Plc. Copyright 2016. With permission.)

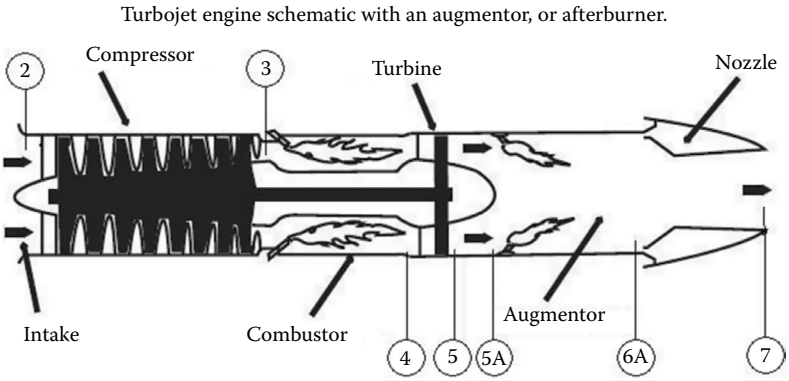


FIGURE 4.20
Stations for single-spool afterburning engine.

for a two-spool engine, the point (7A) is added between the points (8) and (8A) (Figure 4.21). The total pressure loss in the afterburner arises from three sources:

1. Loss in afterburning diffuser
2. Momentum pressure loss due to heat addition in the afterburner
3. Pressure loss due to drag of flameholders and wall friction known as afterburner friction pressure drop

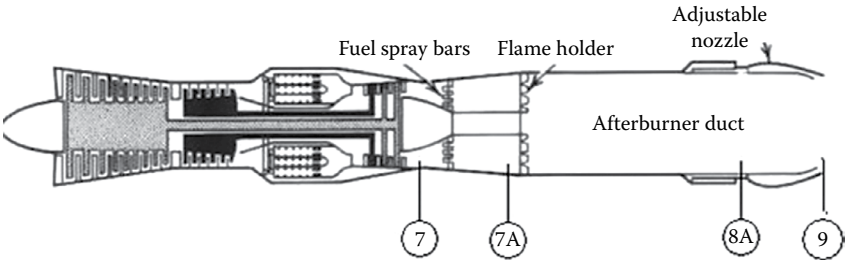


FIGURE 4.21
Stations in the afterburner for two-spool afterburning engine.

Hereafter, the case of a single spool will be considered. A comparison between the two engines would yield relevant relations.

1. Loss in the afterburning diffuser
   The isentropic efficiency of the diffuser will be expressed by the following total-to-static expression:

$$\eta_{d_{ab}} = \frac{\left(T_{05A}\right)_s - T_5}{T_{05A} - T_5} \quad \text{with } T_{05A} = T_{05},$$

   then

$$\eta_{d_{ab}} = \frac{\left[\left(T_{05A}\right)_s / T_{05}\right] - \left(T_5/T_{05}\right)}{1 - \left(T_5/T_{05}\right)}$$

   with

$$\frac{\left(T_{05A}\right)_s}{T_{05}} = \left(\frac{P_{05A}}{P_{05}}\right)^{\gamma-1/\gamma}$$

   and define A as

$$A = \frac{T_5}{T_{05}} = \left(1 + \frac{\gamma - 1}{2} M_5^2\right)^{-1} \tag{4.58a}$$

$$\therefore \eta_{d_{ab}} = \frac{\left(\dfrac{P_{05A}}{P_{05}}\right)^{\gamma-1/\gamma} - A}{1 - A}$$

   Thus,

$$\left(\frac{P_{05A}}{P_{05}}\right) = \left[A + \eta_{d_{ab}}\left(1 - A\right)\right]^{\gamma/\gamma-1} \tag{4.58b}$$

   The diffuser efficiency becomes increasingly important as V_5 is increased. The velocity of the gases discharged by the afterburner diffuser (V_{5A}) is determined

primarily by the cross-sectional area of the tailpipe, and it is desirable to keep it small without the frontal area of the afterburning engine exceeding that for the normal engine.

2. Momentum total pressure loss in afterburner
The pressure loss due to the rate of change in the momentum of gases flowing through the afterburner corresponds to the differential pressure required for accelerating the gases (due to heat addition) from V_{5A} to V_{6A}. The momentum total pressure loss ($P_{05A} - P_{06A}$) depends on the afterburner temperature rise ratio (T_{06A}/T_{05A}), the afterburner inlet Mach number M_{5A}, and the outlet Mach number M_{6A}.

Assuming the duct between stations 5A and 6A has a constant cross-sectional area and is frictionless, then, for such a simple adiabatic flow, the governing equations will be

Continuity $\rho_{5A} V_{5A} = \rho_{6A} V_{6A}$

State $P_{5A} = \rho_{5A} R_{5A} T_{5A}$ and $P_{6A} = \rho_{6A} R_{6A} T_{6A}$

Momentum $P_{5A} + \rho_{5A} V_{5A}^2 = P_{6A} + \rho_{6A} V_{6A}^2$

Energy $Cp_{5A} T_{05A} = Cp_{5A} T_{5A} + \dfrac{V_{5A}^2}{2}$

$$Cp_{6A} T_{06A} = Cp_{6A} T_{6A} + \frac{V_{6A}^2}{2}$$

From these equations, we get

$$\frac{T_{06A}}{T_{05A}} = \frac{Cp_{5A}\left(\gamma_{5A}-1\right)}{Cp_{6A}\left(\gamma_{6A}-1\right)} \frac{\gamma_{6A}^2 M_{6A}^2}{\gamma_{5A}^2 M_{5A}^2} \frac{\left[1+\gamma_{5A} M_{5A}^2\right]^2}{\left[1+\gamma_{6A} M_{6A}^2\right]^2} \frac{\left[1+\dfrac{\gamma_{6A}-1}{2} M_{6A}^2\right]}{\left[1+\dfrac{\gamma_{5A}-1}{2} M_{5A}^2\right]} \tag{4.59}$$

This equation gives the outlet Mach number M_{6A}. The total pressure ratio after some manipulation is thus

$$\frac{P_{06A}}{P_{05A}} = \frac{\left[1+\gamma_{5A} M_{5A}^2\right]}{\left[1+\gamma_{6A} M_{6A}^2\right]} \frac{\left[1+\dfrac{\gamma_{6A}-1}{2} M_{6A}^2\right]^{\gamma_{6A}/\gamma_{6A}-1}}{\left[1+\dfrac{\gamma_{5A}-1}{2} M_{5A}^2\right]^{\gamma_{5A}/\gamma_{5A}-1}} \tag{4.60}$$

From this equation, it is noticed that raising M_{5A} not only increases the loss in total pressure but also reduces the operating range of the afterburner.

3. Friction pressure loss
The friction pressure loss is determined experimentally with the afterburner inoperative. The friction pressure loss due to the drag of the flameholders and wall friction of the tailpipe is expressed in terms of drag coefficient C_D and inlet dynamic pressure of the gas

$$\Delta P_F = C_D \cdot \frac{1}{2} \rho_{5A} V_{5A}^2$$

$$C_D \leq 1.0$$

By careful design, the decrease in thrust of the normal engine due to friction pressure loss in the afterburner can be kept as small as 1% of the normal thrust.

Example 4.8

In an afterburning jet engine, the gases enter the afterburner at a temperature $T_0 = 900\,\text{K}$ whether the afterburner is operating or not. Then the gases' temperature rises to 2000 K when the burner is operating and the stagnation pressure is about 5% less than its value without burning. If the average specific heat in the nozzle rises from 1.1 to 1.315 kJ/kg·K, due to burning, how much relative change in exhaust nozzle area is required as the burner is ignited? It may be assumed that the nozzle is choked in both cases and that the mass flow is unchanged.

Solution

Since $R = 287\ \text{J/kg}\cdot\text{K}$, $Cp = \dfrac{\gamma R}{\gamma - 1}$, then

1. For $C_p)_{\substack{inoperative \\ ab}} = 1100\ \text{J/kg}\cdot\text{K}$, then $\gamma_1 = 1.353$
2. For $C_p)_{\substack{operative \\ ab}} = 1315\ \text{J/kg}\cdot\text{K}$, then $\gamma_2 = 1.279$

The process is plotted in Figure 4.22 for an operative and inoperative afterburner.

Since the mass flow rate $\dot{m} = P \times A \times M\sqrt{\dfrac{\gamma}{RT}}$, assuming no losses in the nozzle, then the mass flow for a choked nozzle is

$$\dot{m}_{choked} = P^* \times A^* \sqrt{\frac{\gamma}{RT^*}}$$

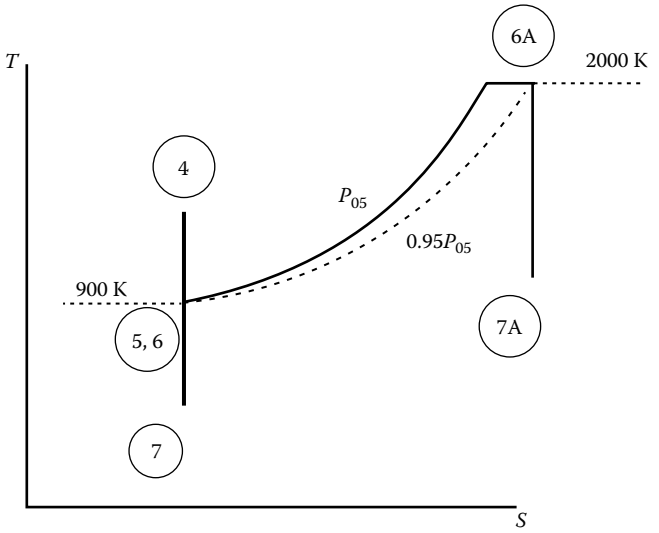


FIGURE 4.22
Temperature–entropy diagram for operative and inoperative afterburner.

This equation can be expressed in terms of the total conditions between states (6) and (7) as

$$\dot{m}_{choked} = \frac{A^* P_{06}}{\sqrt{RT_{06}}} \sqrt{\gamma} \left(\frac{2}{\gamma + 1} \right)^{\gamma + 1/2(\gamma - 1)}$$

where A^* is the outlet area of the convergent nozzle.

Since in both cases of operative and inoperative afterburner, the nozzle is choked and the mass flow is constant:

$$\therefore \frac{A_1^* P_0}{\sqrt{R \times 900}} \sqrt{\gamma_1} \left(\frac{2}{\gamma_1 + 1} \right)^{\gamma_1 + 1/2(\gamma_1 - 1)} = \frac{A_2^* \times 0.95 P_0}{\sqrt{R \times 2000}} \sqrt{\gamma_2} \left(\frac{2}{\gamma_2 + 1} \right)^{\gamma_2 + 1/2(\gamma_2 - 1)}$$

$$\therefore \frac{A_2^*}{A_1^*} = \sqrt{\frac{2000}{900}} \frac{1}{0.95} \sqrt{\frac{1.353}{1.279}} \frac{(0.85)^{3.3329}}{(0.8776)^{4.084}}$$

The area ratio is $\frac{A_2^*}{A_1^*} = 1.4907 \times 1.0526 \times 1.0285 \times \frac{0.5817}{0.5867} = 1.6.$

4.6 Supersonic Turbojet

Military airplanes fitted with turbojet engines are fitted with supersonic intakes. Figure 4.23 illustrates an example for such engines. When the afterburner is lit, the airplane will fly at a supersonic speed. Thus shock waves are generated in the intake as described in Chapter 3. A single normal shock wave is avoided due to the large losses encountered. Normally at least one oblique shock wave followed by a normal shock wave is seen in the diffuser or intake, upstream of the compressor. From the shock wave tables or graphs, the pressure ratio in the diffuser $\left(r_d \equiv \frac{P_{02}}{P_{0a}} \right)$ is determined. Then the intake efficiency (η_d), which is

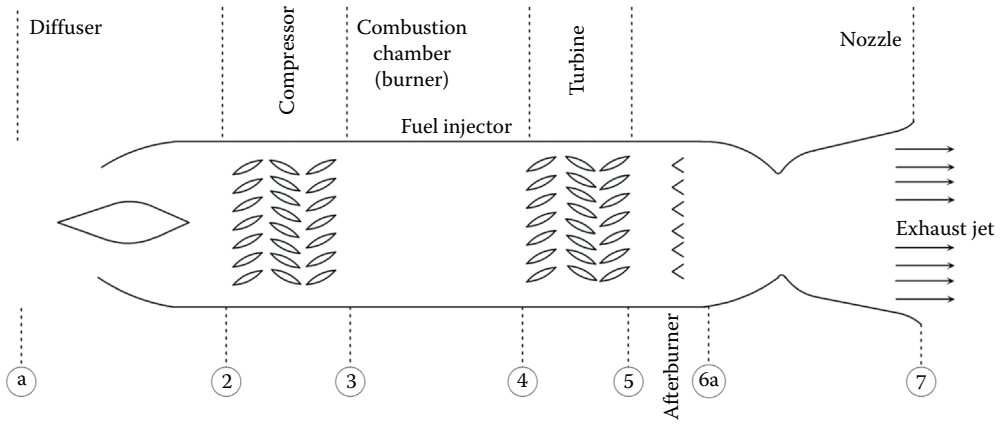


FIGURE 4.23
Layout for a supersonic afterburning turbojet.

dependent on both of the flight Mach number and the pressure ratio in the intake (r_d), is calculated from the relation

$$\eta_d = \frac{\left(1+\frac{\gamma-1}{2}M^2\right)\left(r_d\right)^{(\gamma-1)/\gamma}-1}{\frac{(\gamma-1)}{2}M^2} \tag{4.61}$$

Other modules are treated in the same procedure as described previously.

Example 4.9

A single-spool afterburning turbojet engine is powering a fighter airplane flying at Mach number $M_a = 2.0$ at an altitude of 16,200 m where the temperature is 216.6 K and the pressure is 10.01 kPa. The inlet is of the axisymmetric type, and fitted with a spike having a deflection angle of 12°. The air mass flow rate is 15 kg/s. The compressor has a pressure ratio of 5 and isentropic efficiency of 0.85. The pressure loss in the combustion chamber is 6% and the heating value of fuel is 45,000 kJ/kg. The burner efficiency is $\eta_b = 0.96$. The turbine-inlet temperature is 1200 K and its isentropic efficiency is 0.9. The maximum temperature in the afterburner is 2000 K. The pressure drop in the afterburner is 3% and the afterburner efficiency is 0.9. The nozzle efficiency is $\eta_n = 0.96$. Calculate

1. The stagnation pressure ratio of the diffuser (r_d) and its isentropic efficiency
2. The thrust force (total) pressure

Take $C_{pt} = 1.157$, $C_{pc} = 1.005$ kJ/kg·K

Solution

1. Intake
   The intake here is identical to that in Example 3.4. Two shock waves are developed in the intake; the first is an oblique one while the second is normal. The important results from this example are as follows.
   The total conditions for air upstream of the engine are $T_{0a} = 390$ K and $P_{0a} = 7.824P_a$.
   The flight speed is $V = M\sqrt{\gamma RT_a} = 590$ m/s.
   The stagnation pressure ratio in the intake is $r_d = \frac{P_{02}}{P_{0a}} = 0.884$.
   From Equation 4.61, the diffuser efficiency is

$$\eta_d = \frac{\left(1+0.2\times 4\right)\left(0.884\right)^{0.286}-1}{0.2\times 4} = 0.922$$

   The stagnation temperature of air leaving the diffuser is $T_{02} = T_{0a} = 390$ K.
   The stagnation pressure of air leaving the intake is

$$P_{02} = 0.884P_{0a} = 0.884\times 7.824P_a = 0.884\times 7.824\times 10.01 = 69.23 \text{ kPa}$$

2. Compressor

$$P_{03} = \pi_c P_{02} = 5\times 69.23 = 346.15 \text{ kPa}$$

$$T_{03} = T_{02}\left[1+\frac{\pi_C{}^{\gamma_C-1/\gamma_C}-1}{\eta_C}\right] = 658.2 \text{ K}$$

3. Combustion chamber

$$P_{04} = (1 - \Delta P_{cc}) P_{03} = 0.94 P_{03} = 325.38 \text{ kPa},$$

$$T_{04} = 1200 \text{ K, then}$$

$$f = \frac{Cp_t T_{04} - Cp_c T_{03}}{\eta_b Q_R - Cp_t T_{04}} = 0.0174$$

4. Turbine
   Energy balance for compressor and turbine

$$Cp_t (1 + f)(T_{04} - T_{05}) = Cp_c (T_{03} - T_{02})$$

$$T_{05} = T_{04} - \frac{Cp_c (T_{03} - T_{02})}{Cp_t (1 + f)} = 1200 - \frac{1.005 \times (658.2 - 390)}{1.157 \times 1.0174} = 970.9 \text{ K}$$

$$P_{05} = P_{04} \left[1 - \frac{T_{04} - T_{05}}{\eta_t T_{04}} \right]^{\gamma_t / \gamma_t - 1} = 325.38 \left[1 - \frac{1200 - 970.9}{0.9 \times 1200} \right]^4 = 125.37 \text{ kPa}$$

5. Tail pipe
   A pressure drop of 3% is encountered in the afterburner, thus

$$P_{06A} = 0.97 \quad P_{05} = 121.6 \text{ kPa}$$

The maximum temperature is now $T_{06A} = 2000$ K

$$f_{ab} = \frac{Cp_t (T_{06A} - T_{05})}{\eta_{ab} \ Q_R \ - \ Cp_t \ T_{06A}} = \frac{1.157 \times (2{,}000 - 970.9)}{0.9 \times 45{,}000 - 1.157 \times 2{,}000} = 0.0312$$

Check nozzle choking
With

$$\frac{P_{06A}}{P_c} = \frac{1}{\left(1 - \frac{1}{\eta_n} \frac{\gamma_n - 1}{\gamma_n + 1} \right)^{\frac{\gamma_n}{\gamma_n - 1}}} = 1.907$$

$$\therefore P_c = 63.77 \text{ kPa}$$

$$\therefore P_c > P_a$$

$\therefore$ Nozzle is chocked also

$$P_{7A} = P_c = 63.77 \text{ kPa}$$

$$T_{7A} = \frac{T_{06A}}{\left(\frac{\gamma_n + 1}{2} \right)} = 1716.9 \text{ K}$$

$$V_{7A} = a_{7A} = \sqrt{\gamma_n R T_{7A}} = 809.5 \text{ m/s}$$

The nozzle area is calculated from the relation

$$A_{7A} = \frac{\dot{m}_a\left(1+f+f_{ab}\right)}{\rho_{7A}V_{7A}} = \frac{RT_{7A}\dot{m}_a\left(1+f+f_{ab}\right)}{P_{7A}V_{7A}}$$

$$= \frac{287\times(1716.9)\times(15)\times(1+0.017+0.0312)}{63.77\times10^3\times(809.5)}$$

$$A_{7A} = 0.15 \text{ m}^2$$

The thrust force for operative afterburner is

$$T_{ab} = \dot{m}_a\left[\left(1+f+f_{ab}\right)V_{7A} - V\right] + A_{7A}\left(P_{7A}-P_a\right)$$

$$T_{ab} = 15\left[1.0486\times809.5-590\right] + 0.15\times10^3\left(63.77-10.01\right) = 11{,}946 \text{ N}$$

$$T_{ab} = 11.946 \text{ kN}$$

4.7 Optimization of the Turbojet Cycle

Performance parameters for a jet engine are the specific thrust, TSFC, fuel-to-air ratio, afterburner fuel-to-air ratio (for afterburning engines), as well as the propulsive, thermal, and overall efficiencies. The factors influencing these parameters are

1. Compressor(s) pressure ratio(s) (π_c for a single spool and π_{c1}, π_{c2} for dual spool).
2. Outlet temperature from the combustion chamber, which is the inlet temperature to the turbine (if single-spool engine) or the high-pressure turbine (if two-spool engine). It is normally denoted as TIT (turbine-inlet temperature) or TET (turbine-entry temperature).
3. Efficiencies (diffuser, compressor(s), combustion chamber, turbine(s), and nozzle).
4. Flight speed.
5. Flight altitude.
6. Maximum temperature in the afterburner if available.

Specific thrust

$$F_S = \frac{T}{\dot{m}_a} = \left(1+f\right)U_e - U_a + \frac{A_e}{\dot{m}}\left(P_e - P_a\right) \left(\text{N}\cdot\text{s}/\text{kg air}\right)$$

The TSFC

$$TSFC = \frac{\dot{m}_f}{T} = \frac{\dot{m}_f}{\dot{m}_a F_s}$$

$$TSFC = \frac{f}{F_s} \left(\text{kg fuel/N}\cdot\text{s}\right)$$

The following case study is considered for this parametric study:

1. Two altitudes are considered, sea level and 8 km
2. The compressor pressure ratio varies up to 50
3. The turbine-inlet temperature varies from 1200 to 1500 K
4. The flight Mach number varies from 0.1 to 1.5 for a non-afterburning engine and up to 2.7 for an afterburning engine
5. The maximum temperature in the afterburner varies from 2000 to 3000 K

The following values are considered for efficiencies: diffuser (0.9), compressor (0.88), combustion chamber (90.95), turbine (0.94), afterburner (0.95), nozzle (0.96). For a two-spool engine, the efficiencies of both compressors are equal and also both turbines have the same efficiency. Fuel heating value is 45,000 kJ/kg. The pressure drop in the combustion chamber and afterburner is 3% and 5%, respectively. The results of this analysis are discussed here.

Figures 4.24 and 4.25 illustrate the operation for a non-afterburning single-spool turbojet at sea level. Each figure combines four figures. Figure 4.24 represents the variations in specific thrust or the TSFC due to changes in Mach number, compressor pressure ratio, and turbine-inlet temperature.

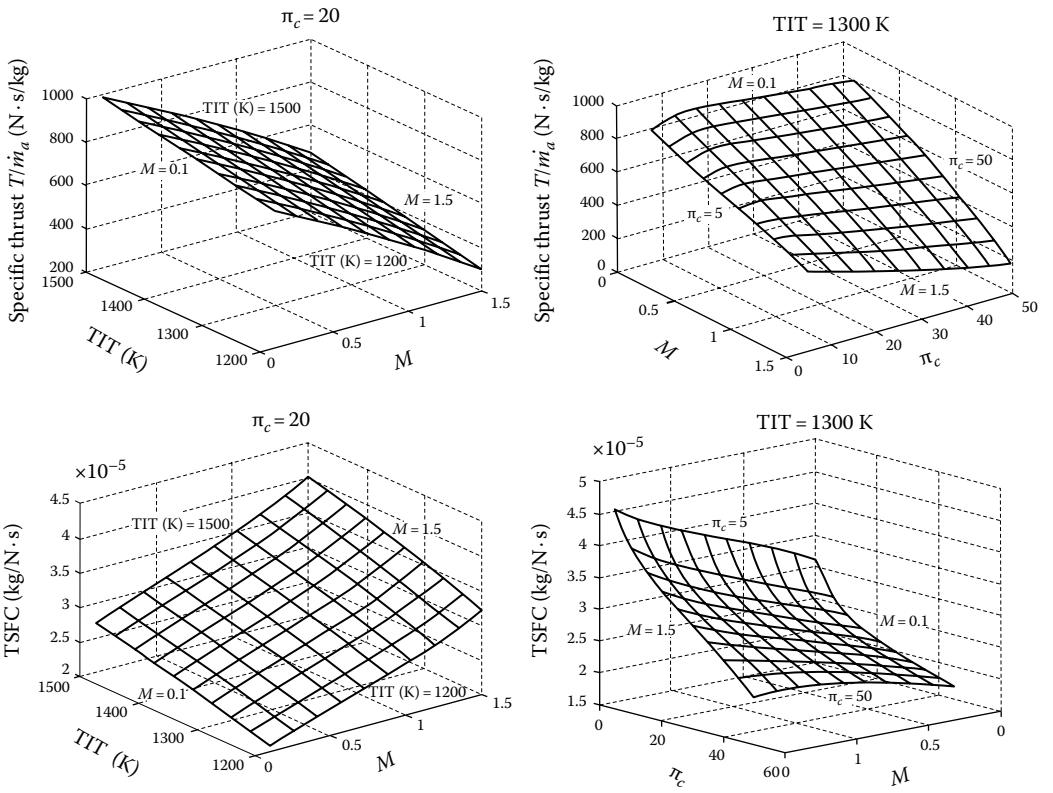


FIGURE 4.24
Variations of specific thrust and TSFC for a single-spool turbojet at sea level for inoperative afterburner.

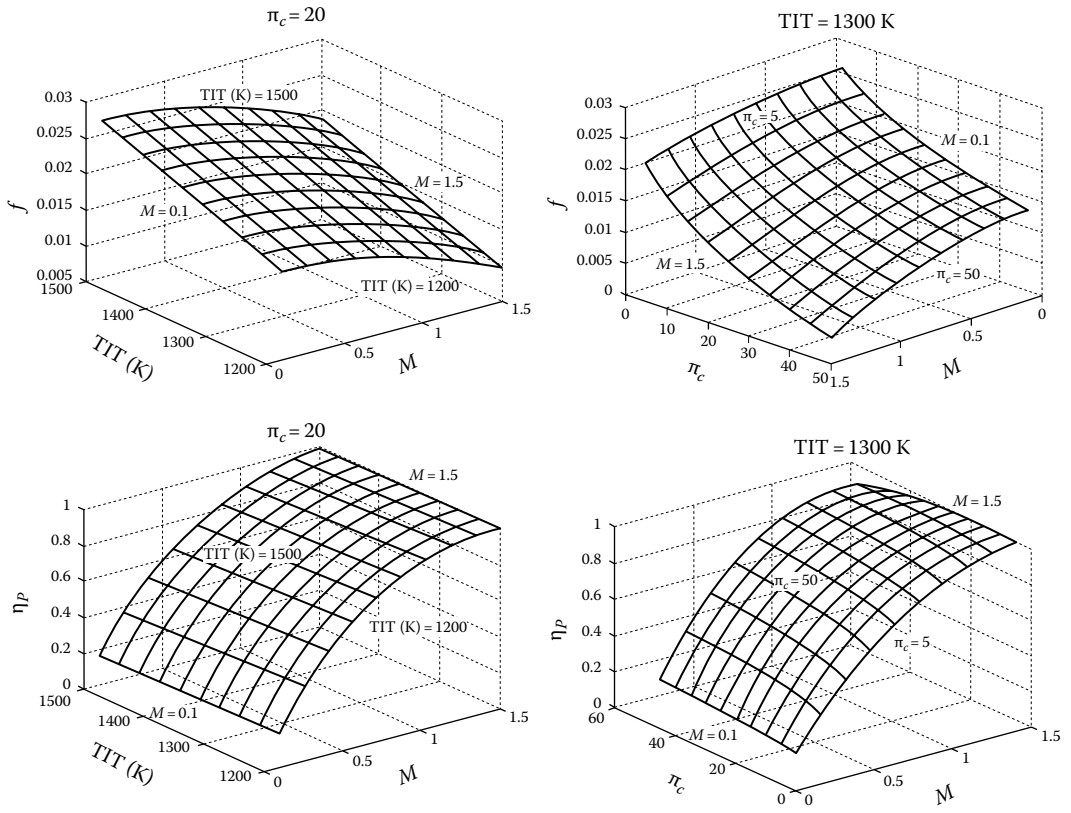


FIGURE 4.25
Variations of fuel-to-air ratio and propulsive efficiency for a single-spool turbojet at sea level for inoperative afterburner.

At a constant compressor pressure ratio π_c, an increase in TIT increases both specific thrust and thrust specific consumption TSFC which is an indication for fuel consumption. However the increase in specific thrust is more important than the penalty in increased TSFC as shown from the Figure 4.24.

1. For a fixed TIT, the increase of overall pressure ratio reduces the TSFC. The specific thrust increases at first then reduces. Thus for each TIT there is an optimum (π_c). The optimum (π_c) for maximum specific thrust increases as the turbine-inlet temperature increases.
2. For a constant pressure ratio and TIT, the increase in the flight Mach number leads to an increase in TSFC and a decrease in specific thrust. This is due to the increase in inlet momentum drag and the increase in compressor outlet temperature, and thus the decrease in fuel consumption.

Figure 4.25 illustrates the variations in the fuel-to-air ratio and propulsive efficiencies due to changes in flight Mach number, compressor pressure ratio, and turbine-inlet temperature.

- For a constant turbine-inlet temperature, the fuel-to-air ratio decreases with the increase of flight Mach number and the increase of the compressor pressure ratio.

- For a constant turbine-inlet temperature also, the propulsive efficiency increases with the increase of the flight Mach number and remains nearly unchanged with the increase in compressor pressure ratio.
- For a constant compressor pressure ratio, the fuel-to-air ratio increases with the increase of the turbine-inlet temperature. On the other hand, fuel-to-air ratio decreases as the flight Mach number increases.
- For a constant compressor pressure ratio, the propulsive efficiency increases with the increase of the flight Mach number and remains nearly unchanged with the increase in turbine-inlet temperature.

Figures 4.26 and 4.27 illustrate the operation of a single-spool turbojet with operative afterburner at sea level. Figure 4.26 represents the variations in specific thrust or the TSFC due to changes in the Mach number, compressor pressure ratio, and afterburner temperature, maintaining a constant TIT of 1300 K.

- At a constant compressor pressure ratio π_c, an increase in maximum temperature in the afterburner increases both the specific thrust and fuel consumption (TSFC). Moreover, the increase in the Mach number for a constant compressor pressure ratio decreases the specific thrust and increases TSFC.

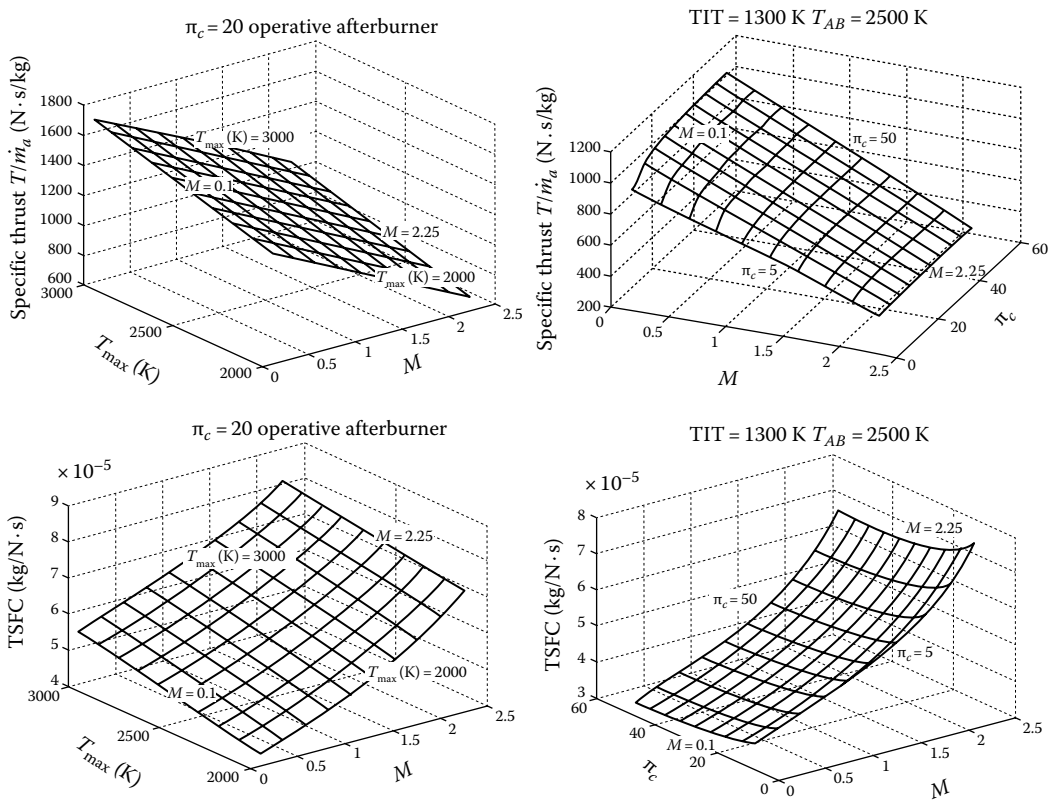


FIGURE 4.26
Variations of specific thrust and TSFC for a single-spool turbojet at sea level with operative afterburner.

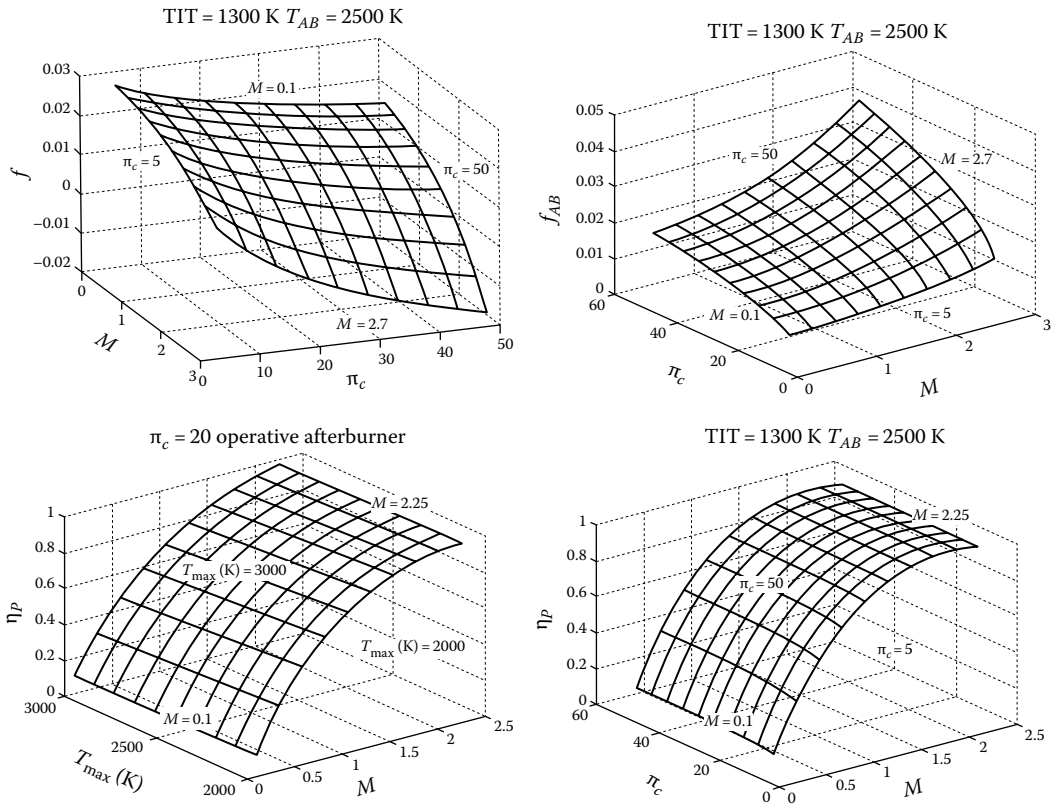


FIGURE 4.27
Variations of fuel-to-air ratio, afterburner fuel-to-air ratio, and propulsive efficiency for a single-spool turbojet at sea level.

- For a fixed maximum temperature in the afterburner, the increase of overall pressure ratio increases the specific thrust and slightly influences the TSFC. The increase in the Mach number for a constant maximum temperature decreases the specific thrust and increases TSFC.

Figure 4.27 illustrates the variation of fuel-to-air ratio (f), afterburner fuel-to-air ratio (f_{ab}), and propulsive efficiency at sea level for an operative afterburner.

- For a constant compressor pressure ratio, turbine-inlet temperature and maximum temperature, the fuel-to-air ratio decreases as the flight Mach number increases. It is important to notice that there is an upper limit for Mach number at takeoff. If the Mach number increases above a certain value, then the temperature rise in the intake and compressor yields greater temperature at the inlet to the combustion chamber than its design maximum temperature. This explains the negative values of fuel-to-air ratio at Mach numbers close or equal to 2.7.
- For a constant Mach number, turbine-inlet temperature, and maximum temperature, the fuel-to-air ratio decreases with the increase of the compressor pressure ratio.

- For a constant Mach number, turbine-inlet temperature, and maximum temperature, the afterburner fuel-to-air ratio increases with the increase of the compressor pressure ratio.
- For a constant compressor pressure ratio, turbine-inlet temperature, and maximum temperature, the afterburner fuel-to-air ratio increases as the flight Mach number increases.
- For a constant compressor pressure ratio, constant turbine-inlet temperature, and maximum temperature, the propulsive efficiency increases with the increase of the flight Mach number and remains nearly constant for different compressor pressure ratios.

Figures 4.28 and 4.29 illustrate the operation of a single-spool turbojet with inoperative afterburner at an altitude of 8 km. Comparing Figures 4.24 and 4.28 outlines that the performance is quite similar in both altitudes. TSFC is somewhat higher at 8 km than at sea level for the same compressor pressure ratio, Mach number and TIT. The reason is that the ambient temperature and pressure are less than the corresponding values at sea level particularly at low Mach numbers. This is quite clear from the fuel-to-air ratios (Figures 4.25 and 4.29). However, since the air mass flow rate at sea level is much higher than its value

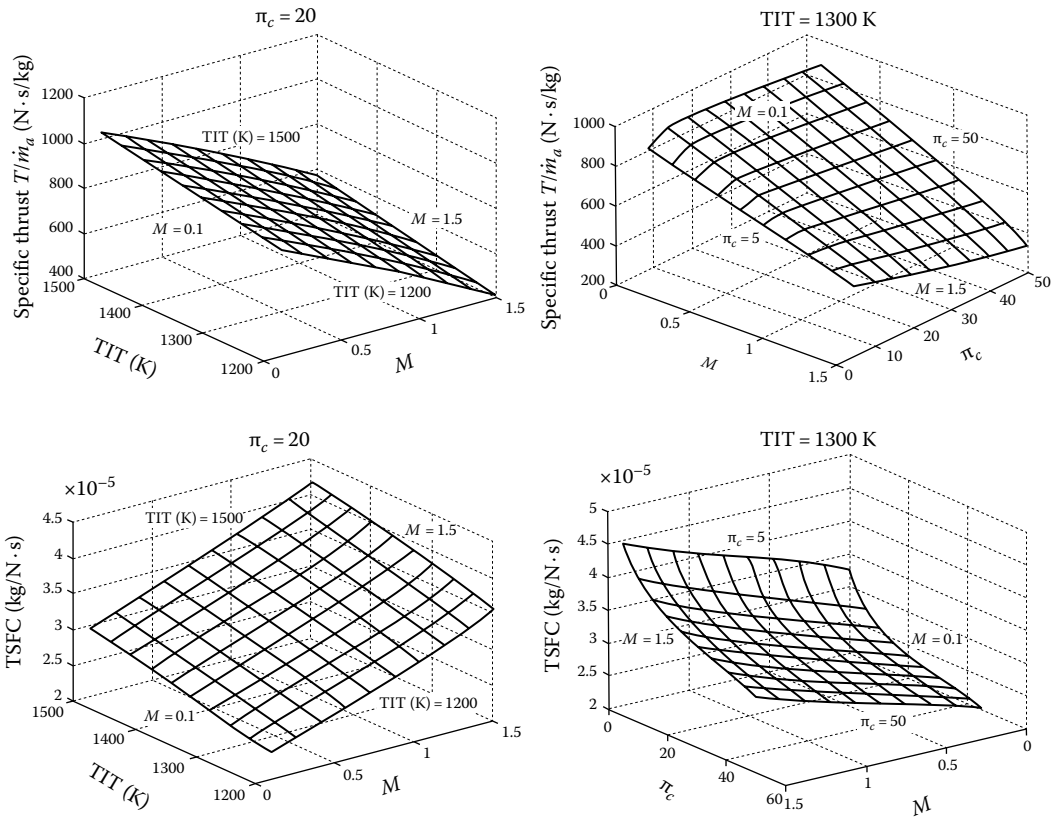


FIGURE 4.28
Variations of specific thrust and TSFC for a single-spool turbojet at altitude of 8 km for inoperative afterburner.

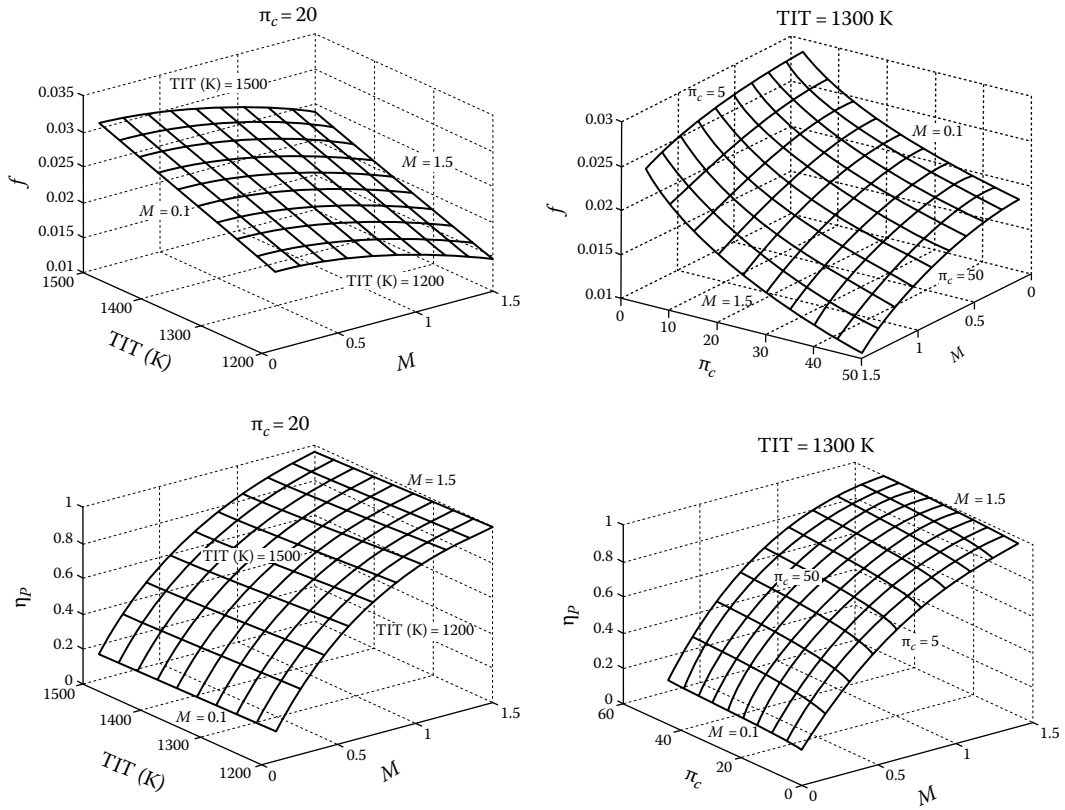


FIGURE 4.29
Variations of fuel-to-air ratio and propulsive efficiency for a single-spool turbojet at altitude of 8 km for inoperative afterburner.

at 8 km, then the thrust at sea level will be much greater than the altitude thrust. Also the fuel consumption is higher at sea level.

The propulsive efficiency at sea level is slightly higher at sea level than at 8 km for the same Mach number. This is due to the values of flight speed for the same Mach number at sea level is higher than at 8 km for the same reason of ambient conditions.

The effect of operating an afterburner on the engine performance at an altitude of 8 km is illustrated in Figures 4.30 through 4.32. Figure 4.30 illustrates the specific thrust and TSFC variations due to the Mach number, compressor pressure ratio, and maximum temperature variations. This figure has the same trends as at sea-level operation (Figure 4.26). Also TSFC is higher at 8 km compared with sea level.

The fuel-to-air ratio and afterburner fuel-to-air ratio is plotted in Figure 4.31 for 8 km altitude. Comparing Figures 4.27 and 4.31 yields a higher fuel-to-air ratio at 8 km compared to sea level, and lower afterburner fuel-to-air ratio at 8 km with respect to sea level values.

The propulsive efficiency for an afterburning engine at 8 km is plotted at Figure 4.32. It has the same trend as Figure 4.27.

The variations of TSFC are plotted versus specific thrust for different compressor pressure ratio and turbine-inlet temperature in Figure 4.33.

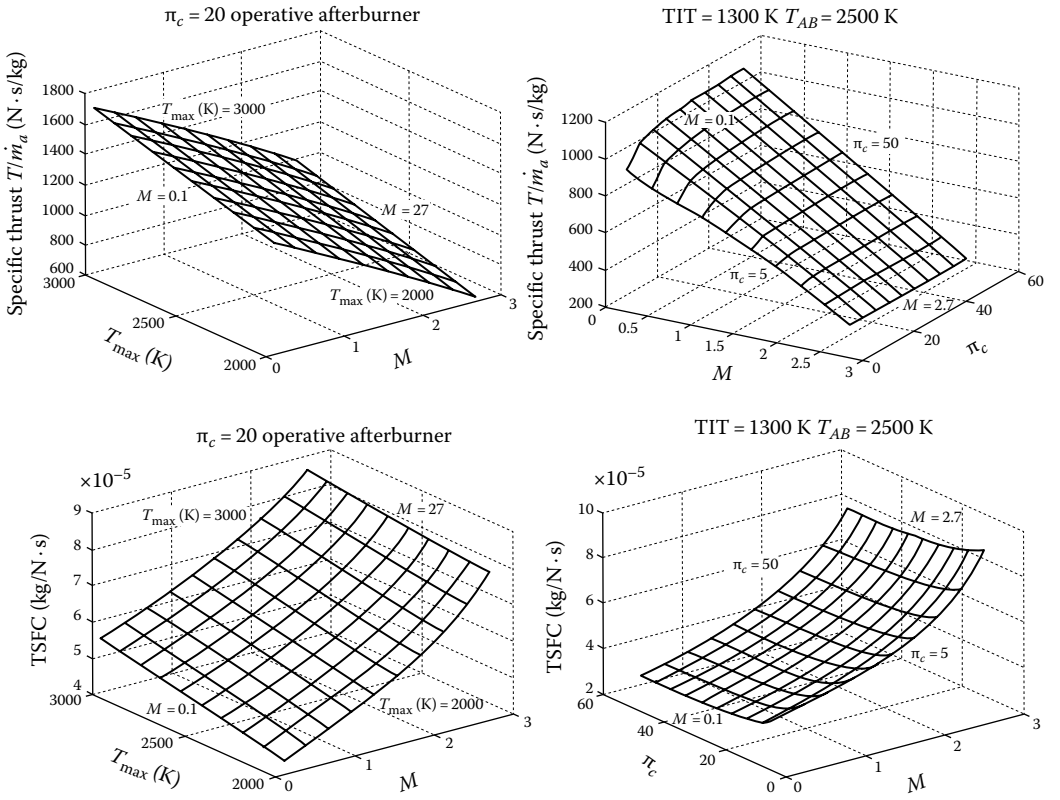


FIGURE 4.30
Variations of specific thrust and TSFC for a single-spool turbojet at altitude of 8 km for operative afterburner.

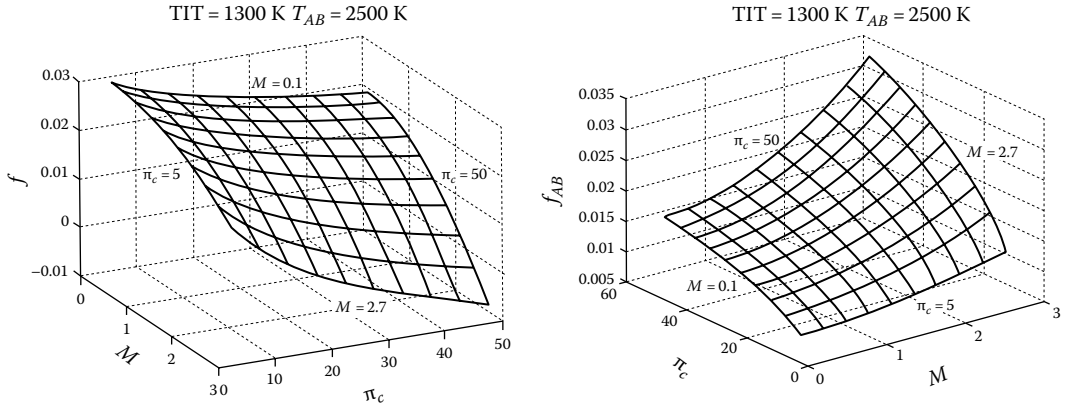


FIGURE 4.31
Variations of fuel-to-air ratio and afterburner fuel-to-air ratio for a single-spool turbojet at 8 km.

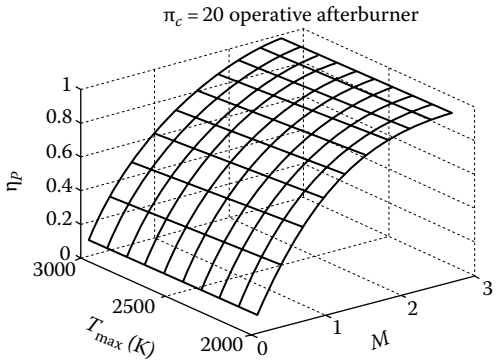


FIGURE 4.32
Variations of propulsive efficiency for a single-spool turbojet at 8 km.

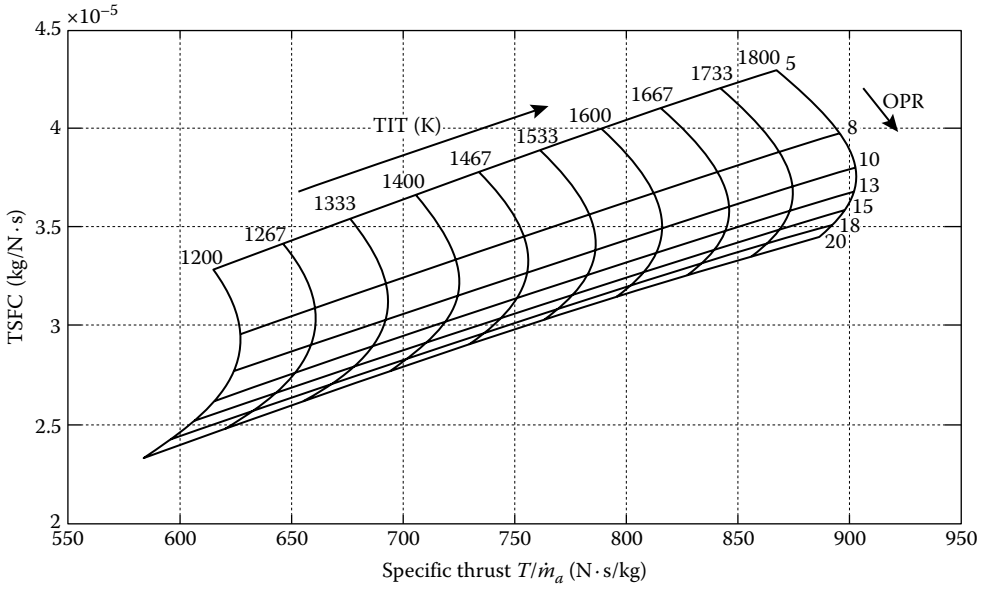


FIGURE 4.33
TSFC versus specific thrust.

Example 4.10

Figure 4.33 illustrates the performance map for a turbojet engine having the following operating conditions:

Ambient temperature	247.9 K	Ambient pressure	46.0 kPa
Compressor pressure ratio	10	Turbine-inlet temperature	1600 K
Diffuser efficiency	0.95	Compressor efficiency	0.8
Burner efficiency	0.98	Turbine efficiency	0.9
Nozzle efficiency	0.9	Pressure drop in combustion chamber	1%
Exhaust area	0.3 m²		
C_{ph} = 1.148 kJ/kg·K,	C_{pc} = 1.005 kJ/kg·K,		Q_R = 450,000 kJ/kg

It is required to calculate

1. The fuel-to-air ratio
2. The compressor outlet temperature
3. The flight Mach number
4. The turbine outlet temperature
5. The air mass flow rate
6. The inlet area.

Solution

From the performance map with known turbine-inlet temperature (1600 K) and compressor pressure ratio (10),

1. The specific thrust $\left(T/\dot{m}_a\right)$ is 815 $\mathrm{N\cdot s/kg}$
2. The specific fuel consumption is 3.5×10^{-5} $\mathrm{kg/N\cdot s}$

Since $\text{TSFC} = \dfrac{\dot{m}_f}{T}$

$$\therefore f = \frac{\dot{m}_f}{\dot{m}_a} = \frac{\dot{m}_f}{T}\frac{T}{\dot{m}_a} = \left(3.5\times10^{-5}\ \mathrm{kg/N\cdot s}\right)\left(815\ \mathrm{N\cdot s/kg}\right)$$

$$\therefore f = 0.02853$$

From the energy balance in the combustion chamber

$$f = \frac{Cp_{cc}T_{04} - Cp_cT_{03}}{\eta_bQ_R - Cp_{cc}T_{04}}$$

$$\therefore T_{03} = \frac{1}{Cp_c}\left[Cp_{cc}T_{04} - f\left(\eta_bQ_R - Cp_{cc}T_{04}\right)\right]$$

$$= \frac{1}{1.005}\left[1.148\times1{,}600 - 0.02853\left(0.98\times45{,}000 - 1.148\times1{,}600\right)\right]$$

$$\therefore T_{03} = 631\ \mathrm{K}$$

The compressor outlet temperature is given by the relation

$$T_{02} = \frac{T_{03}}{\left[1 + \dfrac{\pi_c^{\gamma_c-1/\gamma_c} - 1}{\eta_c}\right]} = 291.5\ \mathrm{K}$$

The temperature ratio within the diffuser is

$$\frac{T_{02}}{T_a} = \frac{T_{0a}}{T_a} = 1 + \frac{\gamma-1}{2}M^2$$

$$\therefore M = \sqrt{\frac{2}{\gamma-1}\left(\frac{T_{02}}{T_a} - 1\right)} = \sqrt{\frac{2}{0.4}\left(\frac{291.5}{247.9} - 1\right)}$$

$$M = 0.938$$

The flight speed is then

$$V_f = M\sqrt{\gamma RT_a} = 296 \text{ m/s}$$

The diffuser pressure ratio is

$$P_{02} = P_a\left(1+\eta_d\frac{\gamma_c-1}{2}M_a^2\right)^{\gamma_c/\gamma_c-1} = 79 \text{ kPa}$$

The compressor outlet pressure is

$$P_{03} = \left(P_{02}\right)\left(\pi_c\right) = 790 \text{ kPa}$$

Due to the pressure drop in the combustion chamber, the outlet pressure for the gases leaving the combustion chamber is

$$P_{04} = \left(1-\Delta P\right)P_{03} = 0.99\times 790 = 782.1 \text{ kPa}$$

From the energy balance between the compressor and turbine, the turbine-outlet temperature is

$$T_{05} = T_{04} - \frac{Cp_c\left(T_{03}-T_{02}\right)}{\left(1+f\right)Cp_h} = 1600 - \frac{1.005\left(631-291.5\right)}{1.02853\times 1.148}$$

$$T_{05} = 1311 \text{ K}$$

The pressure ratio in the turbine is

$$\frac{P_{05}}{P_{04}} = \left[1-\frac{1}{\eta_t}\left(1-\frac{T_{05}}{T_{04}}\right)\right]^{\gamma_h/\gamma_h-1} = \left[1-\frac{1}{0.9}\left(1-\frac{1311}{1600}\right)\right]^4 = 0.4082$$

Since $P_{03} = P_{04} = 782.1$ kPa, then

$$P_{05} = 319.2 \text{ kPa}$$

Now, the nozzle is to be checked out for choking:

$$\frac{P_{05}}{P_c} = \frac{1}{\left[1-\frac{1}{\eta_n}\left(\frac{\gamma_h-1}{\gamma_h+1}\right)\right]^{\gamma_h/\gamma_h-1}} = \frac{1}{\left(1-\frac{1}{0.95}\frac{0.33}{2.33}\right)^4} = 1.907$$

$$P_c = 167.4 \text{ kPa}$$

Since P_c is greater than P_a, then the nozzle is choked. The gases leave the nozzle at the temperature

$$T_7 = T_c = \frac{T_{05}}{\left(\frac{\gamma+1}{2}\right)} = 1123.7 \text{ K}$$

The jet speed is then

$$V_7 = V_c = \sqrt{\gamma RT}_7 = \sqrt{1.333\times 287\times 1123.7} = 655.75 \text{ m/s}$$

The specific thrust is given by the relation

$$\frac{T}{\dot{m}_a} = (1+f)V_7 - V_f + \frac{A_e}{\dot{m}_a}(P_7 - P_a)$$

$$815 = 1.02853 \times 655.75 - 296 + \frac{0.3}{\dot{m}_a}(167.4 - 46) \times 10^3$$

The mass flow rate is $\dot{m}_a = 83.43$ kg/s. Finally, since the mass flow rate is given by the relation

$$\dot{m}_a = \rho_i V_f A_i = \frac{P_i}{RT_i} V_f A_i$$

the inlet area is then $A_i = 0.436$ m^2.

Hint: From the performance map, it is seen that for a constant TIT, the specific thrust increases with the increase in compression pressure ratio at first then reduces. Thus for each TIT there is an optimum (π_c) that yields a maximum specific thrust. This optimum (π_c) increases as the turbine-inlet temperature increases.

4.8 Micro Turbojet

Small turbojet engines are developed for use in cruise missiles, target drones, and other small unmanned air vehicles (UAVs). Examples are the, whose different types (TRI 60-1, -2, -3, -20, and -30) produce a thrust force ranging from 3.5 to 5.3 kN. This engine is a single spool, having a length of 851 mm (33.5 in.), a diameter of 348 mm (13.7 in.), and dry weight of 61.2 kg (135 lb). March 20, 1983, represents the first-ever flight of a micro-turbojet-powered model aircraft, which had a three-minute flight. This engine measured 4¾ in. diameter, 13½ in. long, and weighed 3¾ lb. At 85,000 rpm, it produced over 9 lb of thrust and had a top speed of 97,000 rpm. Twenty years later, commercial engines of roughly similar dimensions and weight produced in average 30 lb thrust when running at 120,000 rpm.

The first commercial micro turbines were made available by JPX in the early 1990s [12]. Shortly after, Germany and the Netherlands sought to develop a powerful, lightweight, liquid-fueled micro turbine. AMT and Schreckling Designs were the first two companies to accomplish these goals. Figure 4.34 shows a cross-section of a micro turbojet engine (SR-30). Table 4.1 shows some data for micro turbojet engines.

Some cruise missiles are powered by both a rocket engine and an airbreathing engine (ramjet, turbojet, or turbofan) to increase their endurance and range [13]. Since the oxygen needed by an airbreathing engine is extracted from air, a cruise missile powered by a turbojet engine, for example, can generate more energy from the same weight of propellant than can a rocket-powered missile. Accordingly, the weight of fuel carried by a turbojet-powered cruise missile is only one third that needed by an identical rocket-propelled missile. An extra range as well as more war-head weight can be also

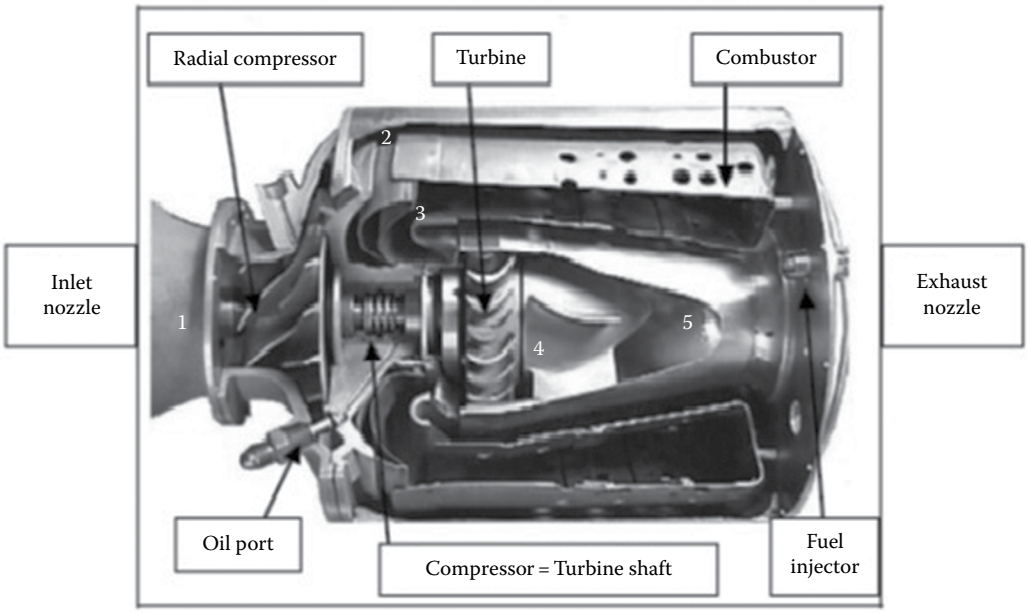


FIGURE 4.34
Cross-section of micro turbojet engine (SR-30).

TABLE 4.1

Some Micro Turbojet Engines

Manufacturer	Model	Diameter (in.)	Length (in.)	Weight (lb)	Max Thrust (lbf)
Wren	MW44	3.46	5.9	1.0	7.2
Schreckling	Piccolina	3.46	NA	1.3	4.95
BMT	BMT 80	4.25	9.7	2.5	17.98
Jetcat	P80	4.37	12.0	2.9	17
Ram	750F	4.37	9.4	2.4	16.9
Simjet	85N+	4.25	9.5	2.4	19.1
Artes/Espiell	JG100	4.33	9.4	2.3	22.5
Kamps		4.33	9.3	2.7	13.5
Phoenix	30/3	4.33	9.8	3.5	20.23
Schreckling	KJ66	4.37	9.5	2.1	16.9
AMT	Olympus	5.1	10.6	5.3	42.7

accomplished when a rocket is powered by a turbojet engine. The Chinese turbojet-powered C802 missile is based on the earlier rocket-powered C801 missile. It incorporates an air intake scoop for the Wopen turbojet engine. This turbojet engine increased the range of the C802 by 40% over that of the C801. The US Tomahawk missile has a range from 1300 to 2500 km [13].

Figure 4.35 illustrates the Harpoon missile which is an air-, surface-, or submarine-launched anti-surface (anti-ship) missile. It is powered by the Teledyne CAE J402 small turbojet engine (together with a solid-propellant booster). The Teledyne CAE J402 turbojet engine has the following specification: length 74 cm, diameter 32 cm, and dry weight 46 kg.

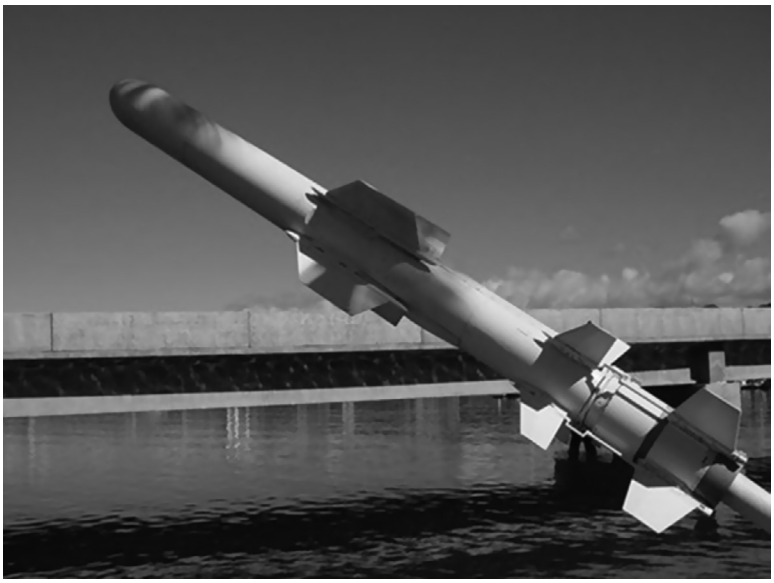


FIGURE 4.35
Harpoon missile.

Its modules are a single-stage axial compressor followed by a single-stage centrifugal compressor (overall pressure ratio: 5.6:1), annular combustor, and a single-stage high-pressure turbine. It generates a maximum thrust of 2.9 kN. Other performance data: fuel consumption 0.1224 g/(kN·h) and thrust-to-weight ratio 6.5:1.

Example 4.11

The Storm shadow missile; Figure 4.36 has been integrated into the RAF's Tornado GR4 and the Eurofighter Typhoon aircraft. It is a long-range air-to-surface missile that is powered by a single-spool turbojet for sustained flight. For a sea-level cruise operation (P_a = 101.325 kPa and T_a = 298 K) it has the following specification:

Flight Mach number = 0.8
Thrust = 5.4 kN
Compressor pressure ratio = 6.3
Fuel-to-air ratio f = 0.02
Fuel heating value Q_R = 43 MJ/kg
$P_e = P_a$
All processes are ideal
Constant values of (γ, C_p)

Calculate

1. Maximum temperature and pressure within the engine
2. Exhaust speed and Mach number
3. Air mass flow rate
4. Inlet area
5. TSFC



FIGURE 4.36
Storm shadow missile.

Solution

Figure 4.37 illustrates the Storm shadow missile with its inlet scoop:

$$V_f = M\sqrt{\gamma R T_a} = 276.82 \text{ m/s}$$

$$P_{02} = P_a\left(1+\frac{\gamma-1}{2}M^2\right)^{\gamma/\gamma-1} = 154.454 \text{ kPa}$$

$$T_{02} = T_a\left(1+\frac{\gamma-1}{2}M^2\right) = 336.144 \text{ K}$$

$$P_{03} = P_{02}\pi_c = 973.06 \text{ kPa}$$

$$T_{03} = T_{02}\left(\pi_c\right)^{\gamma-1/\gamma} = 569.0 \text{ K}$$

$$f = \frac{C_P T_{04} - C_P T_{03}}{\left(Q_R - T_{04}C_P\right)} \rightarrow T_{04} = \frac{fQ_R + C_P T_{03}}{C_P\left(1+f\right)} = 1396.78 \text{ K}$$

$$P_{04} = P_{03} = 973.06 \text{ kPa}$$

Balance between compressor and turbine (for constant C_p)

$$T_{05} = T_{04} - \frac{1}{\left(1+f\right)}\left(T_{03} - T_{02}\right) = 1168.49 \text{ K}$$

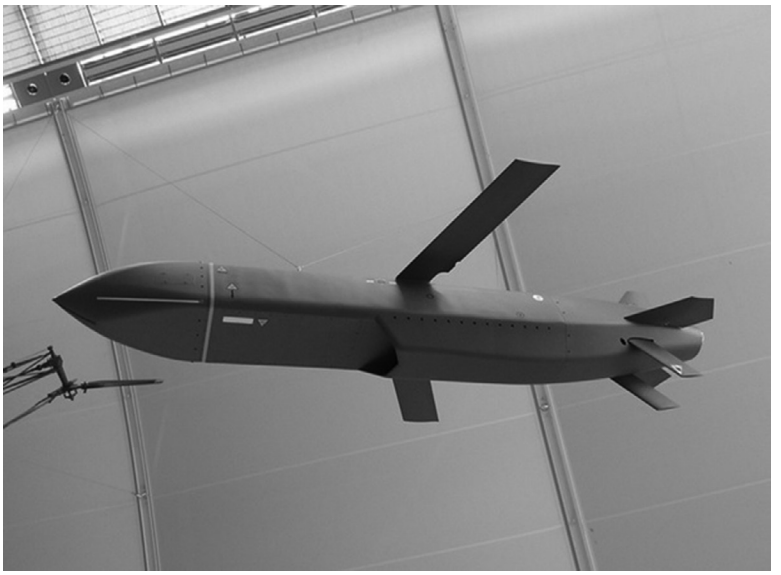


FIGURE 4.37
Storm shadow missile with its inlet scoop.

$$P_{05} = P_{04}\left(\frac{T_{05}}{T_{04}}\right)^{\gamma/\gamma-1} = 521.05 \text{ kPa}$$

$$P_e = P_a = 101.325 \text{ kPa}$$

$$T_e = T_{05}\left(\frac{P_e}{P_{05}}\right)^{\gamma-1/\gamma} = 731.53 \text{ K}$$

$$V_e = \sqrt{2C_P\left(T_{05} - T_e\right)} = 937.17 \text{ m/s}$$

$$M_e = \frac{V_e}{\sqrt{\gamma R T_e}} = 1.729$$

$$\frac{T}{\dot{m}_a} = \left(1+f\right)V_e - V_f = 679.09 \text{ m/s}$$

$$\dot{m}_a = \frac{T}{T/\dot{m}_a} = 7.95 \text{ kg/s}$$

$$\rho_a = \frac{P_a}{RT_a} = 1.185 \text{ kg/m}^3$$

$$A = \frac{\dot{m}_a}{\rho_a V_f} = 0.0242 \text{ m}^2$$

$$TSFC = \frac{\dot{m}_f}{T} = 2.944 \times 10^{-5} \text{ kg/N/s} = 29.44 \text{ mg/N/s}$$

Summary of Mathematical Relations

Ideal and Actual Cycles for a Turbojet Engine

Element	Ideal Cycle	Actual Cycle
Diffuser	$\eta_d = 1$	$T_{02} = T_a\left(1 + \frac{\gamma_c - 1}{2} M^2\right)$
		$P_{02} = P_a\left(1 + \eta_d \frac{\gamma_c - 1}{2} M^2\right)^{\gamma_c - 1/\gamma_c}$
Compressor	$\eta_c = 1$	$T_{03} = T_{02}\left(1 + \frac{\pi_c^{\gamma_c - 1/\gamma_c} - 1}{\eta_c}\right)$
		$P_{03} = \pi_c P_{02}$
Combustion chamber	$\eta_b = 1$	$T_{04} = TIT$
	$\Delta P_0\% = 0$	$P_{04} = (1 - \Delta P\%) P_{03}$
		$f = \frac{C_{p_h} T_{04} - C_{p_c} T_{03}}{\eta_b Q_R - C_{p_h} T_{04}}$
		$\dot{m}_f = f \dot{m}_a$
Turbine	$\eta_m = 1$	$T_{05} = T_{04} - \frac{C_{p_c}}{\eta_b \lambda (1 + f) C_{p_h}} (T_{03} - T_{02})$
	$\eta_f = 1$	$P_{05} = P_{04}\left(1 - \frac{T_{04} - T_{05}}{\eta_t T_{04}}\right)^{\gamma_h - 1/\gamma_h}$
Afterburner		$P_{06} = (1 - \Delta P_{ab}\%) P_{05}$
	$\Delta P_{ab} = 0$	For inoperative afterburner $T_{06} = T_{05}$ For operative afterburner $T_{06} = T_{0_{\max}}$
	$\eta_{ab} = 1$	$f_{ab} = \frac{(1 + f) C_{p_h} (T_{06} - T_{05})}{\eta_{ab} Q_R - C_{p_h} T_{06}}$
		$\dot{m}_{fab} = f_{ab} \dot{m}_a$
Nozzle	$\eta_n = 1$	$P_c = P_{06}\left(1 - \frac{1}{\eta_n} \frac{\gamma_h - 1}{\gamma_h + 1}\right)^{\gamma_h / \gamma_h - 1}$
		The nozzle is choked if $P_c \geq P_a$
		$P_7 = P_c$
		$T_7 = T_c = \frac{T_{06}}{\left(\frac{\gamma_h + 1}{2}\right)}$
		$V_7 = \sqrt{\gamma_h R T_7}$
		The nozzle is unchoked if $P_c < P_a$
		$P_7 = P_a$
		$T_7 = T_{06}\left[1 - \eta_n \left\{1 - \left(\frac{P_7}{P_{06}}\right)^{\gamma_h - 1/\gamma_h}\right\}\right]$
		$V_7 = \sqrt{2 C_{p_h} (T_{06} - T_7)}$

$$T = \dot{m}_a\left[(1 + f + f_{ab}) V_7 - V_f\right] + A_7 (P_7 - P_a)$$

$$TSFC = \frac{\dot{m}_f + \dot{m}_{ab}}{T} = \frac{f + f_{ab}}{T / \dot{m}_a}$$

$$\eta_p = \frac{TV}{TV + 0.5\dot{m}_a\left(1 + f + f_{ab}\right)\left(V_7 - V\right)^2}$$

$$\eta_{th} = \frac{TV + 0.5\dot{m}_a\left(1 + f + f_{ab}\right)\left(V_7 - V\right)^2}{\dot{m}_a\left(f + f_{ab}\right)Q_{HV}}$$

$$\eta_o = \frac{TV}{\dot{m}_a\left(f + f_{ab}\right)Q_{HV}}$$

C_{P_c}: Specific heat at constant pressure for cold air
C_{P_h}: Specific heat at constant pressure for hot gases
$\dot{m}_a$: Air mass flow rate
$\dot{m}_f$: Fuel mass flow rate
f: Fuel-to-air ratio
$\dot{m}_{f_{ab}}$: Fuel burnt in afterburner
f_{ab}: Afterburner fuel-to-air ratio
Q_R: Fuel heating value
γ_c: Ratio of specific heats for cold air
γ_h: Ratio of specific heats for hot gases

Problems

4.1 The following data refer to the operating conditions for an aircraft turbojet engine:

Barometric pressure	101 kPa
Aircraft speed	500 km/h
Compressor air flow	45 kg/s
Exhaust nozzle area	0.2 m^2
Exhaust nozzle pressure	200 kPa
Exhaust gas velocity	450 m/s
Fuel flow	0.8 kg/s

1. Calculate the ram drag, momentum thrust, pressure thrust, gross thrust, net thrust, and specific thrust.
2. If the aircraft speed is increased to 600, 700, 800, and 900 km/h, while all other data are maintained constant, plot the ram drag, gross thrust, and net thrust versus the aircraft speed.
3. If the mass flow rate is proportional to the aircraft speed, and the speed also changes to 600, 700, 800, and 900 km/h, calculate the new value of the air mass flow and plot again the ram drag, gross thrust, and net thrust versus the aircraft speed.

4.2 Calculate the specific thrust and the thrust-specific fuel consumption of a single-spool turbojet engine having the following specifications:

Cruise velocity of 280 m/s at altitude of 7000 m

Intake efficiency of 93%

Compressor pressure ratio of 8:1 and efficiency of 87%

Burner efficiency of 98%

Pressure drop in the combustion chamber of 4% of the delivery pressure of the compressor

Turbine-inlet temperature of 1200 K and efficiency of 90%

Mechanical efficiency of 99%

Nozzle efficiency of 95%

4.3 Derive an expression for the ratio between the thrust forces of a turbojet engine fitted with an afterburner when the afterburner is operative (T_{ab}) and inoperative (T) with choked nozzle similar to that in Equation 4.33.

4.4 A single-spool turbojet engine is used in powering an aircraft flying at Mach number of 0.5, at an altitude where T_a = 226.7 k and P_a = 28.7 kPa. It has the following data

Compressor pressure ratio	8
Maximum cycle temperature	1.200 K
Fuel heating value Q_R	43,000 kJ/kg

All the components of the engine are ideal.

Calculate the thrust force, fuel-to-air ratio, and TSFC.

4.5 Consider a simple turbojet engine with a compressor pressure ratio of 8, a turbine-inlet temperature 1200 K, and a mass flow of 15 kg/s, when the aircraft is flying at 260 m/s at an altitude of 7000 m. Assuming the following components efficiencies and I.S.A conditions, calculate the propelling nozzle area required, the net thrust developed, and the TSFC. If the gases in the jet pipe are reheated to 2000 K and the combustion chamber pressure loss is 3% of the pressure at outlet from turbine, calculate

Isentropic efficiency of intake	0.9
Isentropic efficiency of compressor	0.88
Isentropic efficiency of turbine	0.92
Isentropic efficiency of propelling nozzle	0.95
Combustion chamber pressure loss is 6% of compressor delivery pressure	
Combustion chamber efficiency	0.98

- The percentage increase in nozzle area required the mass flow is to be unchanged.
- The percentage increase in net thrust.

$$(T_a = 242.7\ \text{K},\quad P_a = 41.06\ \text{kPa},\quad Q_R = 43{,}000\ \text{kJ/kg})$$

4.6 A turbojet engine is installed in a fighter airplane flying at Mach number of 1.3. The ambient conditions are 236.21 K and 35.64 kPa. The exhaust conditions are 1800 K and 100 kPa. The compressor pressure ratio is 10. The engine's inlet and exhaust areas are 0.3 and 0.25 m^2, respectively. The afterburner is operating in this case. Assuming ideal processes, calculate

1. The maximum temperature and pressure at the afterburner
2. The outlet temperature and pressure of the compressor

3. The turbine inlet and outlet temperature (neglect fuel-to-air ratio *-f-* in power balance)

4.7 A turbojet engine is fitted with an afterburner. During a ground run, it has the following characteristics:

$$P_a = 101 \text{ kPa}, \quad T_a = 288 \text{ K}, \quad \pi_c = 6, \quad T_{04} = 1600 \text{ K}, \quad T_{06A} = 2600 \text{ K}, \quad Q_R = 45{,}000 \text{ kJ/kg}$$

Assuming that all the engine modules behave ideally and the afterburner is operative, calculate

1. The total fuel-to-air ratio of both the combustion chamber and afterburner
2. The exhaust speed
3. The specific thrust

Now, if another turbojet engine is theoretically investigated where no afterburner is available and the gases in the combustion chamber attain a maximum temperature of 2600 K, it is required to calculate the quantities calculated in items (1), (2), and (3). Next, compare both corresponding values. Write a brief note on the disadvantage of the second engine.

4.8 A fighter aircraft is powered by a single turbojet engine. The aircraft is flying at an altitude of 10 km where the ambient conditions are 223.23 K and 26.48 kPa with a Mach number of 1.2. The exhaust gases leave the nozzle at a speed of 900 m/s and the compressor has a pressure ratio of 8. Neglecting the fuel-to-air ratio, it is required to calculate the turbine-inlet temperature (TIT). Assume all efficiencies are equal to unity and the specific heat is constant.

4.9 A turbojet engine powers a fighter aircraft flying at an altitude of 13 km at a speed of 500 m/s. If the maximum temperature in the combustion chamber is 1600 K and the compressor pressure ratio 6, and the fuel heating value is 45,000 kJ/kg, assume the highest values of efficiency for each module, and calculate the exhaust speed.

If it is necessary to increase the turbine power by 30% for accessories' requirement and the exhaust speed is kept the same, what will be the increase necessary in the turbine-inlet temperature?

4.10 A turbojet engine is installed to a fighter airplane flying at Mach number of 1.3. The ambient conditions are 236.21 K and 35.64 kPa. The exhaust conditions are 1800 K and 100 kPa. The compressor pressure ratio is 10. The areas of the intake and exit are 0.3 and 0.25 m^2, respectively. The afterburner is operating in this case. Assuming ideal processes and variable properties (C_p and γ) within the engine, plot the cycle on the *T*–*S* diagram. Next, calculate

1. The maximum temperature and pressure at the afterburner
2. The outlet temperature and pressure of the compressor
3. The turbine-inlet and -outlet temperature (neglect f in power balance)
4. The thrust force (calculate *f* and the new turbine-outlet temperature assuming TIT is kept the same and $Q_R = 42{,}000$ kJ/kg)

Next, if a convergent-divergent nozzle is assumed to replace the convergent nozzle, what will be the new value of the thrust force? Write your comments.

4.11 A turbojet engine is operating under the following conditions:

Flight speed at sea level, standard day	0
Air flow entering compressor	1 lb/s (1 kg/s)
Compressor pressure ratio (total-to-total)	12
Efficiencies	
Diffuser	100%
Compressor	87%
Turbine	89%
Jet nozzle	100%
Turbine-inlet temperature (stagnation)	2530°R (1400 K)

Assuming mass of fuel added:

1. Calculate the thrust developed by and the heat added to this engine assuming a converging nozzle.
2. Calculate the thrust developed by, the heat added to, and the thread efficiency of this engine assuming a converging-diverging nozzle, that is, expansion in the nozzle back to ambient pressure.

4.12 Consider the turbojet in Example 4.1, Prove that if $\pi_t = \pi_c = \pi$, $\gamma_t = \gamma_c = \gamma$, and $C_{pc} = C_{pt}$ then the derived relations for the pressure ratio and the jet velocity are reduced to

$$\pi = \left(\frac{T_{04}}{T_a} \right)^{\gamma/\gamma - 1} \quad \text{and} \quad V_j = 0$$

Explain why the exhaust jet velocity attained a zero value.

4.13 The following data refer to a typical turbojet engine fitted with an afterburner; it is required to compare the afterburning and non-afterburning engine specific thrust, TSFC, and nozzle exit area.

The turbojet engine has the following characteristics and operating conditions:

Altitude	40,000 ft (12,200 m)
Ambient temperature	216.7 K
Ambient pressure	18.75 kPa
Flight Mach number	2.0
Mass flow rate	250 kg/s
Compressor stagnation pressure ratio	8.0

Pressure loss in burner and afterburner:

- Dry operation 1%
- Wet operation 3%

Turbine-inlet temperature 1400 K

Efficiencies:

- Diffuser 98%
- Compressor 85%
- Burner 98%

- Turbine 90%
- Nozzle 97%
- Mechanical 99%

Specific heat ratios:

- Cold stream 1.4
- Hot stream 1.33

Fuel heating value 45,000 kJ/kg

The maximum temperature with operative afterburner is 1900 K.

4.14 Prove that for an ideal turbojet engine,

$$\frac{T}{\dot{m}_a a_a} = \left\{ \sqrt{\left\{ 1 + \frac{2}{(\gamma - 1) M_a^2} \right\} (\tau_b - 1)(\tau_c - 1) + \tau_b} - 1 \right\}$$

where $a_a = \sqrt{\gamma R T_a}$, $\tau_c = T_{03}/T_{02}$, and $\tau_b = T_{04}/T_{03}$, and M_a is the flight Mach number

4.15 An airplane is weighing 182.24 kN and is powered by two turbojet engines. During flight at constant speed the following data was recorded:

Flight speed = 188 m/s, exhaust speed = 456 m/s

Ambient conditions T_a = 288 K, P_a = 101.3 kPa

Ratio of airplane drag to lift coefficients (C_D/C_L) = 0.135, fuel-to-air ratio f = 0.00913. Calculate the intake area of the engine. Next, when the airplane flew at altitude H = 9 km (where T_a = 229.5 K, P_a = 20.7 kPa), the drag decreased by 40% and fuel-to-air ratio (f) decreased by 20%, calculate

1. New air mass flow rate
2. Flight speed and Mach number
3. Exhaust speed

(Assume the nozzle is unchoked, C_D = constant)

4.16 Compare the specific fuel consumption of a turbojet and a ramjet that are being considered for flight at M = 1.5 and 50,000 ft altitude (ambient condition of pressure and temperature 11 kPa and 216 K, respectively). The turbojet pressure ratio is 8 and maximum temperature is 1130 K, for the ramjet the maximum temperature is 2240 K. For simplicity, ignore aerodynamics losses in both engines. Conventional hydrocarbon fuels having a heating value of 45,000 kJ/kg is used. Assume $\gamma = 1.4$ and $C_p = 1.005\ \text{kJ/kg} \cdot \text{K}$

4.17 The AGM-158A JASSM (joint air-to-surface standoff missile) is a low observable standoff air-launched cruise missile developed in the United States.

The missile has initial and final masses of 975 and 580 kg, respectively, and flight speed of 180 m/s for a range of 370 km. It is powered by a Teledyne CAE J402-CA-100 turbojet engine. The engine has the following data:

1. Thrust 2937 N
2. Overall pressure ratio: 5.6:1
3. Inlet area: A = 0.06 m^2

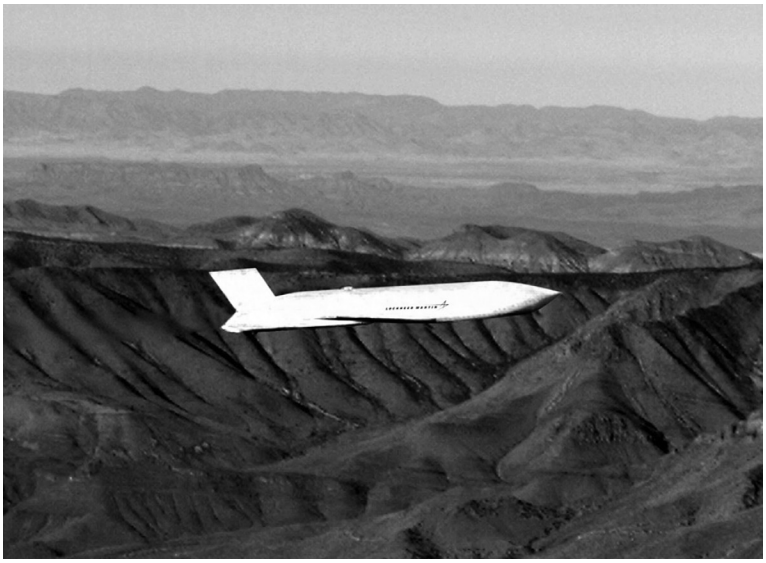


FIGURE P4.17
AGM-158A JASSM Missile.

4. Specific fuel consumption: 0.78 kg/kg·h
5. Fuel is JP10 having heating value = 39.5 MJ/kg

Consider the case when rocket is just impacting the target on ground ($T_a = 288$ K, $P_a = 100$ kPa)

Calculate

- Air mass flow rate
- Fuel-to-air ratio
- Exhaust gas speed
- Engine maximum temperature
- The lift-to-drag ratio using Breguet's equation for range

$$R = \left(\frac{u}{g}\right)\left(\frac{1}{TSFC}\right)\left(\frac{L}{D}\right)\ln\left(\frac{m_1}{m_2}\right)$$

4.18 A turbojet engine fitted with an afterburner is tested on ground (ambient temperature: T_a). The compressor pressure ratio is (π_c). The turbine-inlet temperature and maximum temperature when afterburner is on are, respectively, $T_{0t}, T_{0_{\max}}$.

Prove that the ratio between jet speeds when afterburner is on and off (V_{jab}, V_j) is given by the relation

$$\frac{V_{jab}}{V_j} = \sqrt{\frac{T_{0\max}}{T_{0t} - T_a\left(\pi_c^{\gamma-1/\gamma} - 1\right)}}$$

4.19 A single-spool turbojet engine is powering an airplane flying at a Mach number of 0.8 and an altitude of 11 km ($T_a = 216.7$ K and $P_a = 22.632$ kPa). The turbojet engine has the following data:

Thrust force	60 kN
Diffuser efficiency	$\eta_d = 0.85$
Inlet diameter of compressor	1.5 m
Mach number at compressor inlet	0.5
Compressor pressure ratio	$\pi_c = 10$
Isentropic efficiency of compressor	$\eta_c = 0.84$
Fuel-to-air ratio	$f = 0.025$
Fuel-heating value	43 MJ/kg
Burner efficiency	$\eta_b = 0.98$
Total temperature at turbine exit	960 K

Draw

1. A schematic diagram for the engine
2. A *T*–*S* diagram for cycle
3. Distribution of total temperature and total pressure within the engine

Calculate

1. Pressure ratio across the diffuser
2. Air mass flow rate
3. Exhaust Mach number
4. Maximum temperature in the engine
5. Percentage of energy extracted from turbine to drive the compressor

4.20 Figure P4.20 illustrates a turbojet engine powering aircraft flying at Mach number 2.0 and ambient conditions are 250 K and 48 kPa. Compressor pressure ratio is 6.0 and the turbine-inlet temperature is 1300 K. Fuel-heating value is 43 MJ/kg. The maximum temperature when the afterburner is operating is 1800 K.

The throats Mach numbers are $M_3 = M_9 = 1.0$. Gases expand in the nozzle to ambient pressure. If the compressor inlet diameter $D_4 = 0.6$ m, calculate

1. The thrust force
2. Propulsive efficiency

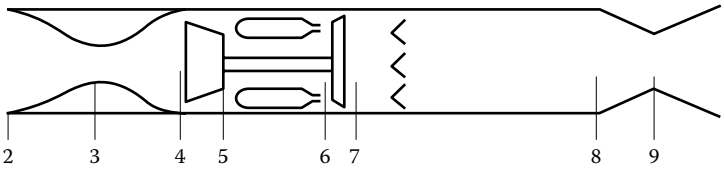


FIGURE P4.20

4.21 The Concorde airplane was the first SST worldwide. It was powered by four afterburning turbojet engines Rolls-Royce/Snecma Olympus 593. It is a two-spool engine having the following data:

Takeoff maximum thrust when afterburner is on 169.2 kN

Overall pressure ratio: 15.5

Exhaust gas temperature EGT = 806°C

Takeoff speed: 360 km/h

Air mass flow: 186 kg/s

Fuel-heating value: 43 MJ/kg

Assuming ideal processes, calculate

1. Exhaust jet speed (neglect fuel mass flow rate)
2. Maximum temperature in the engine when afterburner is operative
3. Maximum pressure in the engine
4. Total fuel burnt within the engine in both the combustion chamber and afterburner
5. TSFC

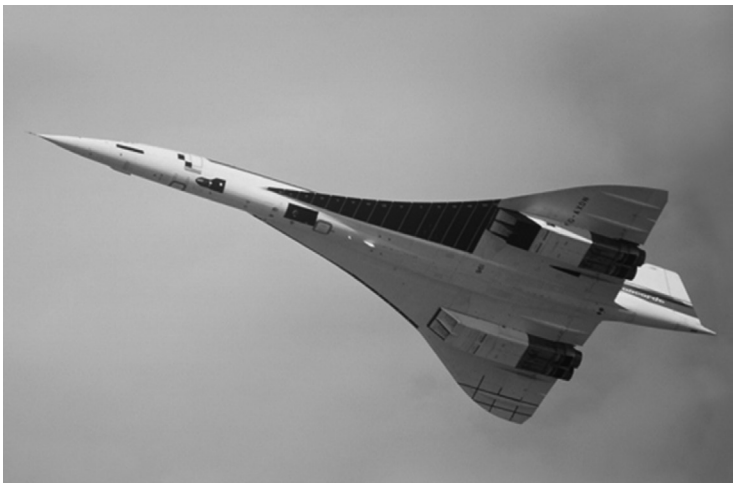


FIGURE P4.21

4.22 Figure P4.22 illustrates a turbojet engine with two pitot tubes for measuring total pressures at inlet to compressor (P_{02}) and outlet from turbine (P_{05}). These measurements are next displayed for the flight crew as exhaust pressure ratio (EPR defined as $EPR = P_{05}/P_{02}$).

Prove that for ideal conditions, exhaust Mach number is expressed by

$$M_e = \sqrt{\left(\frac{2}{\gamma_h - 1}\right)\left[(EPR)^{\gamma_h - 1/\gamma_h}\left(1 + \frac{\gamma_c - 1}{2}M^2\right)^{(\gamma_c/\gamma_c - 1)(\gamma_h - 1/\gamma_h)} - 1\right]}$$

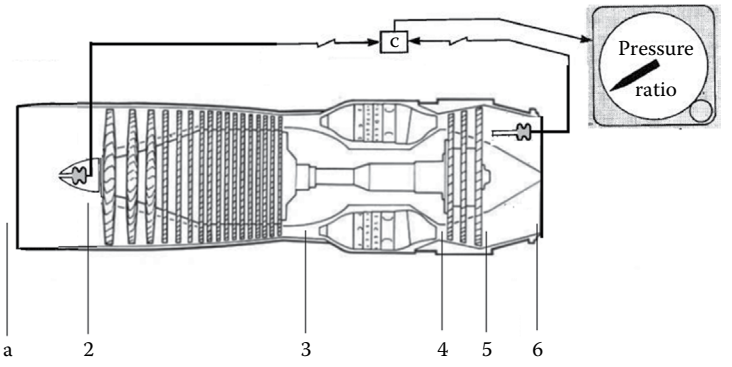


FIGURE P4.22

Calculate the exhaust Mach number from the equation for the case

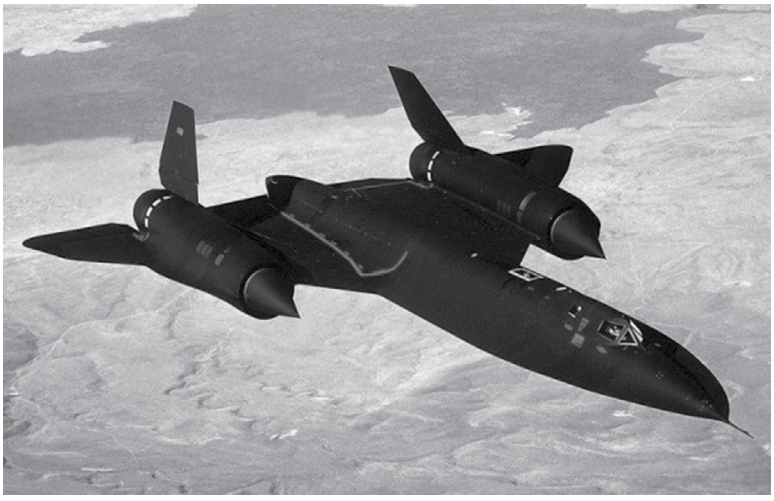
$$EPR = 1.6, \quad M = 2.0, \quad \gamma_c = 1.4, \quad \gamma_h = 4/3.$$

Now consider the case $M = 2, \pi_c = 6.0, T_a = 288\ \text{K}, T_{\max} = 1400\ \text{K}, \gamma = 1.4, Q_R = 43\ \text{MJ/kg}$.

Calculate

1. Exhaust Mach number
2. Turbine pressure ratio
3. The power delivered to accessories

4.23 Figure P4.23 illustrates the airplane SR-71 fitted with two Pratt & Whitney turbojet J58 engines that incorporates an afterburner. All processes are assumed ideal with constant values of both (C_p and γ).



(a)

FIGURE P4.23a

1. Draw a schematic diagram for the engine identifying each state by a number from (1–7)
2. Draw the corresponding cycle on *T*–*S* and *P*–*v* diagrams
3. Prove that
   a. The *thrust ratio* for an operative (τ_{AB}) and inoperative afterburner (τ) is expressed by the relation

$$\frac{\tau_{AB}}{\tau} = \frac{\sqrt{\left(\frac{2}{\gamma-1}\right)\left(\frac{T_{06A}}{T_a}\right)\left[1-\left(\frac{P_a}{P_{06A}}\right)^{\gamma-1/\gamma}\right]} - M}{\sqrt{\left(\frac{2}{\gamma-1}\right)\left(\frac{T_{05}}{T_a}\right)\left[1-\left(\frac{P_a}{P_{05}}\right)^{\gamma-1/\gamma}\right]} - M}$$

   where
   subscript (a) denotes ambient conditions
   ($6A$) denotes inlet conditions to nozzle when the afterburner is operative

   b. Next, when $M = 0$ and outlet temperatures of both compressor and turbine are equal, then

$$\frac{\tau_{AB}}{\tau} = \frac{\sqrt{\left(\frac{T_{06A}}{T_a}\right)}}{\pi^{(\gamma-1/2\gamma)}}$$



(b)

FIGURE P4.23b

The following table gives details of temperature and pressure at interior states of the turbojet engine:

	Diffuser Inlet	Compressor Inlet	Compressor Outlet	Turbine Inlet	Afterburner Inlet	Afterburner Outlet	Nozzle Outlet
T (K)	220	226	424.3	1300	1082	2200	1650
P (kPa)	23.1	25.1	188.25	182.5	82.5	79	23.1

4. Assuming variable values of both (C_p and γ), calculate
   a. Efficiency of diffuser, compressor and turbine
   b. Percentage of pressure drop in combustion chamber and afterburner
   c. Total rate of burnt fuel in engine if $Q_R = 44$ MJ/g, $\eta_{burner} = 0.96$ and air mass flow rate = 135 kg/s
   d. The thrust force if the inlet area is 0.25 m^2

4.24

1. Compare ramjet and afterburning turbojet engines.
2. Gripen multi-role fighter (Figure P4.24) is armed with an RBS15 MK3 anti-ship missile, which is powered by a French micro-turbo TRI-60 engine as shown in the figure. It is a single-spool turbojet engine with a sustained flight of 0.9 Mach number and nearly sea-level cruise altitude. The engine has the following data:

Thrust force = 4.4 kN	Compressor pressure ratio = 6.3
Air mass flow rate = 8.4 kg/s	TSFC = 0.11 kg/(N·h)
Fuel-heating value $Q_R = 43$ MJ/kg	

Gases expand in nozzle to ambient pressure.

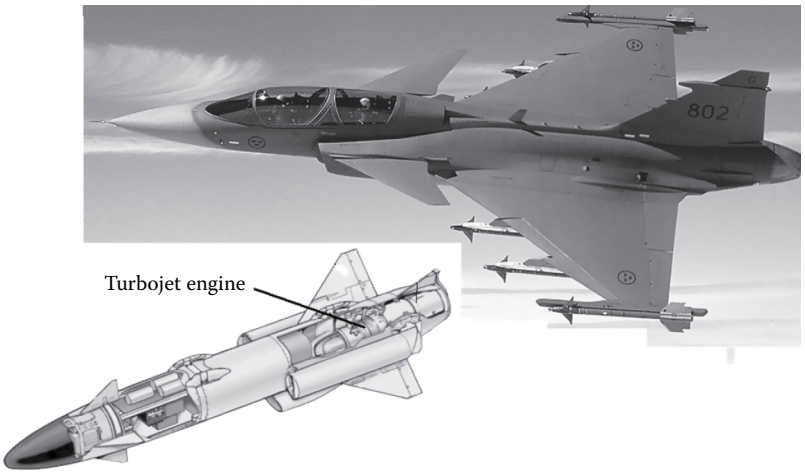


FIGURE P4.24

Assuming all processes are ideal and constant values of (γ, C_p), calculate

a. Fuel-to-air ratio
b. Maximum temperature and pressure within the engine
c. Exhaust speed and Mach number
d. Inlet area

References

1. R.G. Perel'Man, *Soviet Nuclear Propulsion (Yadernyye Dviagateli)*, Triumph Publishing Co., Washington, DC, 1959.
2. D.J. Keirn, The USAF nuclear propulsion programs, In K. F. Gantz (Ed.), *Nuclear Flight: The United States Air Force Programs for Atomic Jets, Missiles, and Rockets*, Duell, Sloan, and Pearce, New York, 1960.
3. C.B. Collins, M.C. Iosif, R. Dussart, J.M. Hicks, S.A. Karamian, C.A. Ur, I.I. Popsescu et al., Accelerated emission of gamma rays from the 31-years isomer of 178Hf induced by X-ray irradiation, *Physical Review Letters*, 82, 695–698, January 1999.
4. C.E. Hamilton, Design study of triggered isomer heat exchanger combustion hybrid jet engine for high altitude flight, Thesis, AFIT/GAE/ENY/02-6, Department of the Air Force, Air University, Air Force Institute of Technology, Wright-Patterson AFB, OH, 2002.
5. C.E. Hamilton, Design study of triggered isomer heat exchanger—Combustion hybrid jet engine for high altitude flight, MSc thesis, AFIT, WPAFB, OH.
6. *The Jet Engine*, 5th edn., Rolls-Royce Plc, 1996, p. 178, Reprinted 1996 with revisions.
7. W.W. Bathie, *Fundamentals of Gas Turbines*, 2nd edn., John Wiley & Sons, 1996, p. 227.
8. B. Gunston, *The Development of Jet and Turbine Aero Engines*, Patrick Stephens Limited, Imprint of Haynes Publishing, 1997, p. 79.
9. D.L. Daggett, S. Ortanderl, D. Eames, J.J. Berton, and C.A. Snyder, Revisiting water injection for commercial aircraft, World Aviation Congress and Exposition, Reno, NV, Volume: SAE Paper 2004-01-3108, 2004.
10. D.L. Daggett, Water misting & injection of commercial aircraft engines to reduce airport, NOx, NASA CR 2004-212957, 3/2004. World Aviation Congress & Exposition, November 2004, Reno, NV.
11. D.L. Daggett, L. Fucke, R.C. Hendricks, and D.J.H. Eames, Water injection on commercial aircraft to reduce airport nitrogen oxides, *40th Joint Propulsion Conference and Exhibit by the AIAA, ASME, SAE, and ASEE*, Fort Lauderdale, FL, July 11–14, 2004.
12. P.D. Lobik, Unmanned aerial vehicles: A study of gas turbine applications, MSc thesis, Naval Postgraduate School, September 1995.
13. W.C. Carus, *Cruise Missile Proliferation in the 1990s*, Praeger Publishers, Greenwood Publishing Group, 1992.

5

Turbofan Engines

5.1 Introduction

Turbofan engines were first named as bypass turbojets by Rolls-Royce. Boeing sometimes refers to them as fanjets [1]. Turbofan engines are the most reliable engines ever developed. Fundamentally, turbofan engines are fuel efficient and quiet, turbine-based engines. They feature continuous combustion and smooth rotation, unlike the internal combustion engine of automotives. The gas generator of a single-spool turbofan has three sections:

1. Fan unit and compressor section
2. Combustion chamber
3. Turbine section

The fan pressurizes air and feeds it aft. Most of this air goes around the engine core and is next ejected through a nozzle called a fan (or cold) nozzle. The rest goes through the engine core, where it is further compressed in a compressor and next then it mixes with the fuel and ignites. The hot expanding combustion efflux passes through the turbine section, spinning the turbine as it exits the engine.

The spinning turbine turns the engine shaft (also known as the spool). The rotating shaft spins the fan and compressor on the front of the engine. The fan sucks and compresses more air keeping this continuous cycle going.

Although during 1936–1946 the two companies, Power Jet and Metropolitan-Vickers, pioneered various kinds of ducted-fan jet engines, nobody had an interest in these engines and looked at them as some rather complicated turbojet engines. Ten years later, Rolls-Royce introduced bypass turbojet engines having a by pass ratio (BPR) of 3 or more [2]. General Electric led the way in 1965 with the TF39 (BPR 8) and still leads with the GE90 (BPR nearly 9).

There are several advantages to the turbofan engine over both turboprop and turbojet engines. The fan is not as large as the propeller, so the increase of speeds along the blade is less. Thus a turbofan engine can power civil transport flying at transonic speeds up to Mach 0.9. Also, by enclosing the fan inside a duct or cowling, the aerodynamics are better controlled. There is less flow separation at the higher speeds and less trouble with shock developing. The turbofan may suck in more air flow than a turbojet, and thus generate more thrust. Like the turboprop engine, the turbofan has low fuel consumption compared with the turbojet. The turbofan engine is the best choice for high-speed, subsonic commercial airplanes. The advantages of turbofan engines are as follows:

- The fan is not as large as the propeller; therefore, higher aircraft velocities can be reached before vibrations occur. The aircraft is able to reach transonic speeds of Mach 0.9.

- The fan is more stable than a single propeller; therefore, if the vibration velocity is reached, vibrations are less apparent and do not disrupt the airflow as significantly.
- The fan is encased in a duct or cowling; therefore, the aerodynamics of the airflow is controlled a lot better, providing greater efficiency.
- For geared turbofan engines, the gearbox required to translate the energy from the compressor/fan to the turbine is relatively small and less complex as the fan is smaller. This reduces the weight and aerodynamic drag loss that are present in the turboprop design.
- The smaller fan is more efficient and takes in air at a greater rate than the propeller, allowing the engine to produce greater thrust.
- The turbofan engine is a much more fuel-efficient design than the turbojet and is able to equal some of the high-performance velocities.

As illustrated in Figure 1.51, in the classification section of Chapter 1, numerous types of turbofan exist. Next, we present a detailed analysis of a few types of turbofans.

5.2 Forward Fan Unmixed Single-Spool Configuration

The main components here are the intake, fan, fan nozzle, compressor, combustion chamber, turbine, and turbine nozzle. The turbine drives both the fan and compressor. A schematic diagram of the fan as well as the cycle (successive processes) is illustrated in Figures 5.1 and 5.2. Here the BPR is defined as

$$\beta = \frac{\text{By-pass airflow}}{\text{Primary airflow}} = \frac{\dot{m}_{cold}}{\dot{m}_{hot}} \equiv \frac{\dot{m}_{fan}}{\dot{m}_{core}}$$

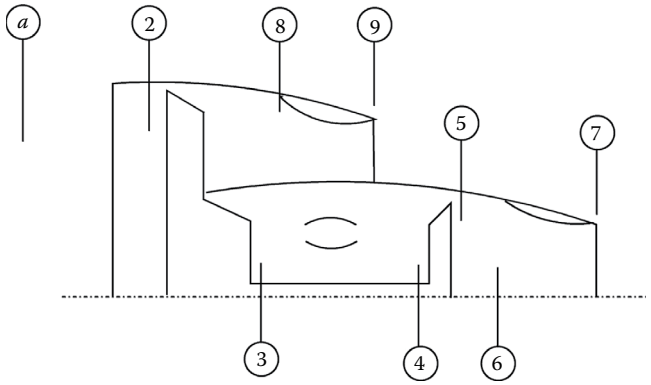


FIGURE 5.1
Schematic diagram of a single-spool turbofan engine.

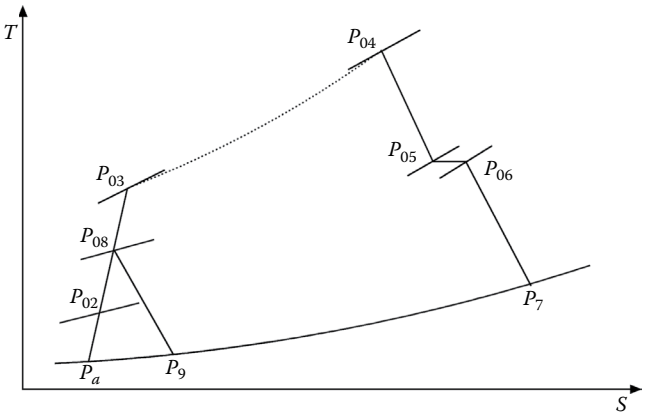


FIGURE 5.2
Temperature-entropy (*T*–*S*) diagram for the single-spool turbofan engine.

Thus if the air mass through the core (compressor) is ($\dot{m}_a$), then the bypass air mass flow rate is ($\beta\dot{m}_a$). Sometimes the core mass flow rate is identified as the gas generator mass flow rate $(\dot{m}_{GG})$. However, this designation will not be used in this text.

Now the successive elements will be examined.

1. Intake
   The inlet conditions of the air entering the inlet are the ambient temperature and pressure (P_a and T_a, respectively). The intake has an isentropic efficiency (η_d). For a flight Mach number of (M_a), the temperature and pressure at the outlet of the intake are T_{02} and P_{02}, given by the relations

$$P_{02} = P_a\left(1+\eta_d\frac{\gamma_c-1}{2}M_a^2\right)^{\gamma_c/\gamma_c-1} \tag{5.1}$$

$$T_{02} = T_{0a} = T_a\left(1+\frac{\gamma_c-1}{2}M_a^2\right) \tag{5.2}$$

   where
   η_d is the diffuser isentropic efficiency
   γ_c is the specific heat ratio for air (cold stream)

2. Forward fan
   For a known fan pressure ratio (π_f) and isentropic efficiency (η_f), the temperature and pressure at the outlet of the fan are given by the following relations

$$P_{08} = \left(P_{02}\right)\left(\pi_f\right) \tag{5.3}$$

$$T_{08} = T_{02}\left[1+\frac{1}{\eta_f}\left(\pi_f^{\gamma_c-1/\gamma_c}-1\right)\right] \tag{5.4}$$

3. Compressor
   Similarly, both of the compressor pressure ratio (π_c) and its isentropic efficiency (η_c) are known. Thus the temperature and pressure at the outlet of the compressor are given by the following relations

$$P_{03} = \left(P_{08}\right)\left(\pi_c\right) \tag{5.5}$$

$$T_{03} = T_{08}\left[1 + \frac{1}{\eta_c}\left(\pi_c^{\gamma_c - 1/\gamma_c} - 1\right)\right] \tag{5.6}$$

4. Combustion chamber
   The temperature at the end of combustion process T_{04} is generally known. It is here the maximum temperature in the cycle which is frequently identified as the turbine-inlet temperature (*TIT*). The pressure at the end of combustion depends on the pressure drop in the combustion process itself. Thus, depending on the known expression for the pressure drop in the combustion chamber, it may be expressed as

$$P_{04} = P_{03} - \Delta P_{cc} \tag{5.7}$$

   or

$$P_{04} = P_{03}\left(1 - \Delta P_{cc}\%\right) \tag{5.8}$$

   The energy balance for the combustion chamber yields the following relation for the fuel-to-air ratio (f), defined as the ratio between the mass of fuel burnt to the air mass flow rate through the core (hot)

$$f = \frac{\dot{m}_f}{\dot{m}_a}$$

$$\dot{m}_a\left(1 + f\right)Cp_h T_{04} = \dot{m}_a Cp_c T_{03} + \eta_b \dot{m}_f Q_R$$

$$f = \frac{\left(Cp_h/Cp_c\right)\left(T_{04}/T_{03}\right) - 1}{\eta_b\left(Q_R/Cp_c T_{03}\right) - \left(Cp_h/Cp_c\right)\left(T_{04}/T_{03}\right)} \tag{5.9}$$

5. Turbine
   Since the turbine drives both the compressor and turbine, the energy balance for this spool per unit air mass flow rate is given by the relation

$$W_t = W_c + W_f$$

   From this relation, the temperature ratio across the turbine is deduced as follows

$$\dot{m}_a\left(1 + f\right)Cp_h\left(T_{04} - T_{05}\right) = \dot{m}_a Cp_c\left(T_{03} - T_{08}\right) + \left(1 + \beta\right)\dot{m}_a Cp_c\left(T_{08} - T_{02}\right)$$

$$T_{04} - T_{05} = \frac{Cp_c\left\{\left[\left(T_{03} - T_{08}\right)\right] + \left(1 + \beta\right)\left[\left(T_{08} - T_{02}\right)\right]\right\}}{Cp_h\left(1 + f\right)}$$

$$\therefore \frac{T_{05}}{T_{04}} = 1 - \frac{\left[\left(T_{03} - T_{08}\right)\right] + \left(1+\beta\right)\left[\left(T_{08} - T_{02}\right)\right]}{\left(T_{04}\right)\left(Cp_h/Cp_c\right)\left(1+f\right)} \tag{5.10a}$$

This relation can be rewritten as

$$\frac{T_{05}}{T_{04}} = 1 - \frac{\left[\left(T_{03} - T_{02}\right)\right] + \beta\left[\left(T_{08} - T_{02}\right)\right]}{\left(T_{04}\right)\left(Cp_h/Cp_c\right)\left(1+f\right)} \tag{5.10b}$$

This temperature ratio can be further expressed as

$$\therefore \frac{T_{05}}{T_{04}} = \left\{1 - \frac{\left(1/\eta_c\right)\left[\left(P_{03}/P_{02}\right)^{\gamma_c - 1/\gamma_c} - 1\right] + \left(\beta/\eta_f\right)\left[\left(P_{08}/P_{02}\right)^{\gamma_c - 1/\gamma_c} - 1\right]}{\left(1+f\right)\left(Cp_h/Cp_c\right)\left(T_{04}/T_{02}\right)}\right\} \tag{5.10c}$$

The expansion ratio through the turbine can now be evaluated as long as its adiabatic efficiency (η_t) and the ratio of specific heats (γ_h) of the turbine working fluid are known

$$\frac{P_{05}}{P_{04}} = \left[1 - \frac{1}{\eta_t}\left(1 - \frac{T_{05}}{T_{04}}\right)\right]^{\gamma_h/\gamma_h - 1} \tag{5.11a}$$

$$\frac{P_{05}}{P_{04}} = \left[1 - \frac{1}{\eta_t}\left\{1 - \frac{\left(1/\eta_c\right)\left[\left(P_{03}/P_{02}\right)^{\gamma_c - 1/\gamma_c} - 1\right] + \left(\beta/\eta_f\right)\left[\left(P_{08}/P_{02}\right)^{\gamma_c - 1/\gamma_c} - 1\right]}{\left(1+f\right)\left(Cp_h/Cp_c\right)\left(T_{04}/T_{02}\right)}\right\}\right]^{\gamma_h/\gamma_h - 1} \tag{5.11b}$$

6. Turbine Nozzle
   Assume that there are no changes in the total pressure and total temperature in the jet pipe between the turbine and nozzle. Thus $P_{05} = P_{06}$ and $T_{05} = T_{06}$. Next, a check for nozzle choking is performed. Thus for a nozzle isentropic efficiency of η_{n_t}, the critical pressure is calculated from the relation

$$\frac{P_{06}}{P_c} = \frac{1}{\left[1 - \frac{1}{\eta_{n_t}}\left(\frac{\gamma_h - 1}{\gamma_h + 1}\right)\right]^{\gamma_h/\gamma_h - 1}}$$

   Now if the nozzle is an ideal one, then $\eta_{n_t} = 1$. This equation is reduced to

$$\left(\frac{P_{06}}{P_c}\right) = \left(\frac{\gamma_h + 1}{2}\right)^{\gamma_h/\gamma_h - 1}$$

   If $P_c \geq P_a$, then the nozzle is choked. The temperature of the gases leaving the nozzle is obtained from the relation

$$\left(\frac{T_{06}}{T_7}\right) = \left(\frac{\gamma_h + 1}{2}\right)$$

In this case, the gases leave the nozzle at a speed equal to the sonic speed or

$$V_7 = \sqrt{\gamma_h R T_7} \tag{5.12a}$$

If the nozzle is unchoked ($P_7 = P_a$), then the speed of the gases leaving the nozzle is given by

$$V_7 = \sqrt{2Cp_h T_{06}\eta_{n_t}\left[1-\left(\frac{P_a}{P_{06}}\right)^{\gamma_h - 1/\gamma_h}\right]} \tag{5.12b}$$

The pressure ratio in the nozzle is obtained from the relation

$$\frac{P_{06}}{P_a} = \frac{P_{06}}{P_{05}}\frac{P_{05}}{P_{04}}\frac{P_{04}}{P_{03}}\frac{P_{03}}{P_{02}}\frac{P_{02}}{P_{0a}}\frac{P_{0a}}{P_a}$$

7. Fan Nozzle
The fan nozzle is also checked to determine whether it is choked or unchoked. Thus the critical pressure is calculated from the relation

$$\frac{P_{08}}{P_c} = \frac{1}{\left[1-\frac{1}{\eta_{fn}}\left(\frac{\gamma_c - 1}{\gamma_c + 1}\right)\right]^{\gamma_c/\gamma_c - 1}}$$

Now if the flow in nozzle is an ideal one, then $\eta_{fn} = 1$ and this equation will be reduced to

$$\left(\frac{P_{08}}{P_c}\right) = \left(\frac{\gamma_c + 1}{2}\right)^{\gamma_c/\gamma_c - 1}$$

If $P_c \geq P_a$, then the fan nozzle is choked. The temperature of the gases leaving the nozzle is obtained from the relation

$$\left(\frac{T_{08}}{T_9}\right) = \left(\frac{\gamma_c + 1}{2}\right)$$

Then the gases leave the nozzle at a speed equal to the sonic speed or

$$V_9 = \sqrt{\gamma_c R T_9} \tag{5.13a}$$

If the nozzle is unchoked ($P_9 = P_a$), then the speed of the gases leaving the nozzle is given by

$$V_9 = \sqrt{\frac{2\gamma_c R T_{08}\eta_{fn}}{(\gamma_c - 1)}\left[1-\left(\frac{P_a}{P_{08}}\right)^{\gamma_c - 1/\gamma_c}\right]} \tag{5.13b}$$

$$\frac{P_{08}}{P_a} = \frac{P_{08}}{P_{02}}\frac{P_{02}}{P_a}$$

The thrust force is now obtained from the general relation

$$\frac{T}{\dot{m}_a} = (1+f)V_7 + \beta V_9 - U(1+\beta) + \frac{1}{\dot{m}_a}\left[A_7(P_7 - P_a) + A_9(P_9 - P_a)\right]$$
$$= (1+f)V_7 + \beta(V_9 - U) - U + \frac{1}{\dot{m}_a}\left[A_7(P_7 - P_a) + A_9(P_9 - P_a)\right] \quad (5.14a)$$

The specific thrust, the thrust force per total air mass flow rate ($\dot{m}_{at}$), is further evaluated from the relation

$$\frac{T}{\dot{m}_{at}} = \frac{T}{\dot{m}_h + \dot{m}_c} = \frac{T}{\dot{m}_a(1+\beta)} = \frac{(1+f)}{(1+\beta)}V_7 + \frac{\beta}{(1+\beta)}V_9 - U$$
$$+ \frac{1}{\dot{m}_a(1+\beta)}\left[A_7(P_7 - P_a) + A_9(P_9 - P_a)\right] \quad (5.14b)$$

The TSFC is

$$\text{TSFC} = \frac{\dot{m}_f}{T} = \frac{\dot{m}_f}{\dot{m}_a}\frac{\dot{m}_a}{T} = \frac{f}{T/\dot{m}_a} \quad (5.15)$$

There are two important questions related to the design of turbofan engines:

1. What is the best value for the BPR (β)?
2. What is the best pressure ratio of the secondary (bypass) stream (π_f)?

The answer to these questions depends on a number of factors including

1. Components efficiencies
2. Structural weights
3. Nature of application

The increase in thrust ΔT gained by adding a fan to a turbojet engine will be of the form shown in Figure 5.3. Associated with the increase in mass flow, an increase in drag ΔD is achieved due to the larger engine installation. Thus, for the desired flight conditions the best BPR would be that which corresponds to the maximum difference between the increased thrust and the increased drag, $(\Delta T - \Delta D)$, the maximum net thrust.

If, on the other hand, takeoff thrust is a very important consideration, then it might be worthwhile to increase the BPR beyond this value, since at takeoff the drag would be small.

Moreover, both of the jet velocities of the cold air from the fan nozzle and the hot gases from the turbine nozzle are less than the jet velocity of turbojet engines. This represents an additional advantage of a turbofan engine over simple turbojet engines, as the jet noise is correlated to the jet velocity. The intensity of jet noise has been shown to be proportional to the eighth power of the velocity of the jet relative to the ambient air, thus small reductions

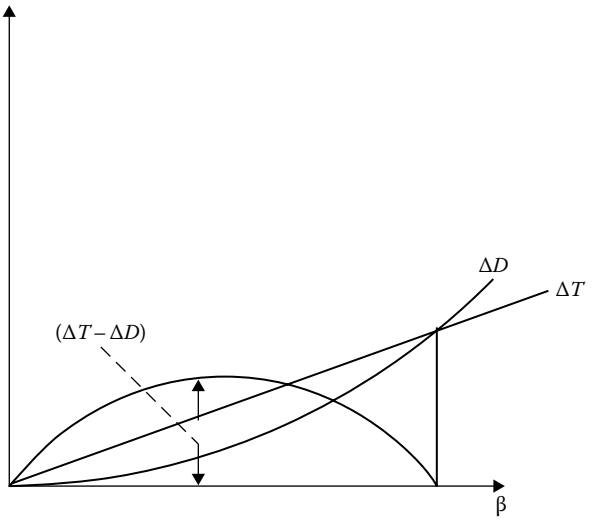


FIGURE 5.3
Thrust and drag variation of a turbofan engine with BPR β.

in velocity means significant reductions in noise. It is well-known that the noise of the jet engine, especially those noise components with frequencies disagreeable to humans, appear to come from the compressor.

Another possible advantage of turbofan engines over the turbojet ones is associated with the lower temperature of the hot exhausts before the nozzle. Thus the exhaust is then much less susceptible to infra-red detection.

5.3 Forward Fan Unmixed Two-Spool Engines

5.3.1 The Fan and Low-Pressure Compressor (LPC) on One Shaft

The famous engine of this configuration is the General Electric CF6 engine series. This engine is composed of a low-pressure spool with a single-stage fan and a three-stage low-pressure compressor (LPC, sometimes denoted as a booster by aeroengine manufacturers). Both are driven by a five-stage low-pressure turbine (LPT). The high-pressure spool is composed of a 14-stage high-pressure compressor (HPC) driven by a two-stage high-pressure turbine (HPT).

Another famous example is the Pratt and Whitney PW4000 series.

A typical turbofan of this configuration together with the corresponding *T*–*S* diagram is shown in Figures 5.4 and 5.5.

The different modules will now be analyzed.

1. Intake
   The same governing equations for the intake in the single-spool configuration, Equations 5.1 and 5.2, are applied here.

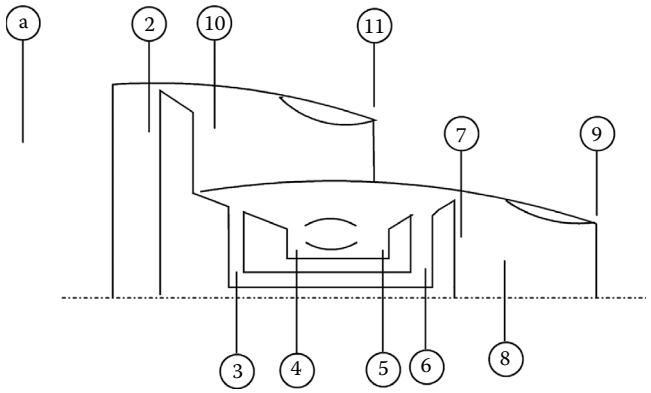


FIGURE 5.4
Layout of a two-spool turbofan engine (fan and compressor driven by an LPT).

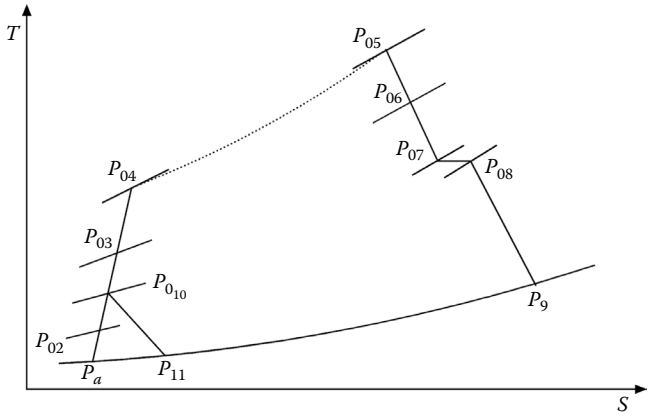


FIGURE 5.5
Temperature-entropy diagram of a two-spool turbofan engine.

2. Fan

   The following equations are applied:

$$P_{0_{10}} = \left(P_{02}\right)\left(\pi_f\right) \tag{5.16}$$

$$T_{0_{10}} = T_{02}\left[1 + \frac{1}{\eta_f}\left(\pi_f^{\gamma-1/\gamma} - 1\right)\right] \tag{5.17}$$

3. LPC

   The pressure ratio achieved in this compressor is less than two:

$$P_{03} = \left(P_{0_{10}}\right)\left(\pi_{lpc}\right) \tag{5.18}$$

$$T_{03} = T_{0_{10}}\left[1 + \frac{1}{\eta_{lpc}}\left(\pi_{lpc}^{\gamma-1/\gamma} - 1\right)\right] \tag{5.19}$$

4. HPC

$$P_{04} = \left(P_{03}\right)\left(\pi_{hpc}\right) \tag{5.20}$$

$$T_{04} = T_{03}\left[1 + \frac{1}{\eta_{hpc}}\left(\pi_{hpc}^{\gamma-1/\gamma} - 1\right)\right] \tag{5.21}$$

5. Combustion Chamber
   The pressure at the outlet of the combustion chamber is obtained from the pressure drop in the combustion chamber

$$P_{05} = P_{04} - \Delta P_{cc} \tag{5.22a}$$

   or

$$P_{05} = P_{04}\left(1 - \Delta P_{cc}\%\right) \tag{5.22b}$$

   The temperature at the outlet of the combustion chamber is also the maximum temperature in the engine and known in advance. Thus the fuel-to-air ratio is calculated from the relation

$$f = \frac{\left(Cp_h/Cp_c\right)\left(T_{05}/T_{04}\right) - 1}{\eta_b\left(Q_R/Cp_cT_{04}\right) - \left(Cp_h/Cp_c\right)\left(T_{05}/T_{04}\right)} \tag{5.23}$$

6. High-pressure turbine (HPT)
   To calculate the temperature and pressure at the outlet of the HPT, an energy balance between the HPC and HPT is performed as follows:

$$\dot{m}_aCp_c\left(T_{04} - T_{03}\right) = \dot{m}_a\left(1 + f\right)Cp_h\left(T_{05} - T_{06}\right) \tag{5.24}$$

   From this relation, the temperature at the outlet of the turbine T_{06} is defined. Moreover, from the known isentropic efficiency of the HPT η_{hpt}, then the outlet pressure from the HPT P_{06} is calculated as explained previously in the single-spool turbofan.

7. LTP
   An energy balance between the fan and LPC from one side and the LPT on the other side is expressed by the relation

$$\beta\dot{m}_aCp_c\left(T_{0_{10}} - T_{02}\right) + \dot{m}_aCp_c\left(T_{03} - T_{02}\right) = \dot{m}_a\left(1 + f\right)Cp_h\left(T_{06} - T_{07}\right) \tag{5.25a}$$

   or

$$\left(1 + \beta\right)\dot{m}_aCp_c\left(T_{0_{10}} - T_{02}\right) + \dot{m}_aCp_c\left(T_{03} - T_{0_{10}}\right) = \dot{m}_a\left(1 + f\right)Cp_h\left(T_{06} - T_{07}\right) \tag{5.25b}$$

$$\therefore T_{07} = T_{06} - \left(\frac{1+\beta}{1+f}\right)\left(\frac{C_{pc}}{C_{ph}}\right)\left(T_{0_{10}} - T_{o2}\right) - \left(\frac{C_{pc}}{C_{ph}}\right)\left(\frac{T_{03} - T_{0_{10}}}{1+f}\right)$$

The pressure at the outlet is obtained from the relation

$$P_{o7} = P_{o6}\left(1 - \frac{T_{o6} - T_{o7}}{\eta_{t2} \times T_{o6}}\right)^{\gamma_h/\gamma_h - 1}$$

Now, if there is an air bleed from the HPC at a station where the pressure is P_{03b}, then the energy balance with the HPT gives

$$\dot{m}_a Cp_c \left(T_{03b} - T_{03}\right) + \dot{m}_a \left(1 - b\right)\left(T_{04} - T_{03b}\right) = \dot{m}_a \left(1 + f - b\right) Cp_h \left(T_{05} - T_{06}\right) \tag{5.26}$$

where $b = \dot{m}_b/\dot{m}_a$ is the air-bleed ratio defining the ratio between the air bled from the HPC to the core air flow rate.

Moreover, such a bleed has its impact on the energy balance of the low-pressure spool as the air passing through the LPT is now reduced.

$$\left(1 + \beta\right)\dot{m}_a Cp_c \left(T_{0_{10}} - T_{02}\right) + \dot{m}_a Cp_c \left(T_{03} - T_{0_{10}}\right) = \dot{m}_a \left(1 + f - b\right) Cp_h \left(T_{06} - T_{07}\right) \tag{5.27}$$

The flow in the jet pipe is frequently associated with a pressure drop, mainly due to skin friction.

Thus, the pressure upstream of the turbine nozzle is slightly less than the outlet pressure from the turbine. The temperature, however, is the same. Thus,

$$P_{08} = P_{07}\left(1 - \Delta P_{jetpipe}\right)$$
$$T_{08} = T_{07}$$

Concerning the other modules or components, a similar procedure is followed. The exhaust velocities of both the cold air from the fan nozzle and the hot gases from the turbine nozzles are obtained after checks for choking. The thrust force, specific thrust, and TSFC are calculated.

Example 5.1

A two-spool turbofan engine is to be examined here. The low-pressure spool is composed of a turbine driving the fan and the LPC. The high-pressure spool is composed of an HPC and an HPT. Air is bled from an intermediate state in the HPC.

The total pressure (in psia) and total temperature (in °C) during a ground test ($M = 0.0$) is recorded and shown in the following table.

Station	Fan Inlet	Fan Outlet	LPC Outlet	Air Bleed Location	HPC Outlet	CC Outlet	HPT Outlet	LPT Outlet
P_0 (psia)	14.7	23.2	35.6	110	347	332	86.4	21.4
T_0 (°C)	15	62.7	109.3	275	501	1286	906	512

The fan and turbine nozzles have an isentropic efficiency of 0.9.

We need to calculate

1. The fan isentropic efficiency (station 2–station 10)
2. The high-pressure ratio isentropic efficiency (station 3–station 4)
3. The fuel-to-air ratio (f)

4. The air-bleed ratio (b)
5. The BPR (β)
6. The thrust force if the total air mass flow rate is 280 kg/s

Assume the following values for the different variables

$$\eta_b = 0.96$$
$$Q_{HV} = 45{,}000 \text{ kJ/kg}$$
$$\gamma_{air} = 1.4$$
$$\gamma_{gases} = 1.33$$

Solution

The modules of the engine and its different processes are plotted on the T–S diagram as shown in Figures 5.4 and 5.5.

Fan module (from station 2 to 3)

$$T_{02} = 15 + 273 = 288 \text{ K}$$

$$T_{03} - T_{02} = 62.7 - 15 = 47.7 \text{ K}$$

The fan isentropic efficiency may be expressed as in Figure 5.6.

$$\eta_f = \frac{T_{03S} - T_{02}}{T_{03} - T_{02}} = \frac{T_{02}\left[\left(\frac{P_{03}}{P_{02}}\right)^{\gamma-1/\gamma} - 1\right]}{T_{03} - T_{02}} = \frac{288\left[\left(\frac{23.2}{14.7}\right)^{0.286} - 1\right]}{47.7} = \frac{288 \times 0.1394}{47.7}$$

$$\eta_f = 0.8416$$

HPC

With $T_{04} = 382.3$ K, the isentropic efficiency of the HPC is given from the relation

$$\eta_{HPC} = \frac{T_{05S} - T_{04}}{T_{05} - T_{04}} = \frac{T_{04}\left[\left(\frac{P_{05}}{P_{04}}\right)^{\gamma-1/\gamma} - 1\right]}{T_{05} - T_{04}} = \frac{382.3[0.9178]}{391.7}$$

$$\eta_{HPC} = 0.895$$

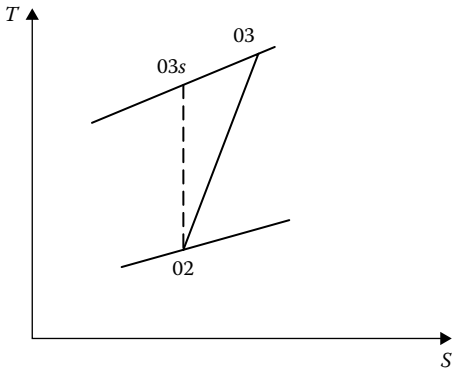
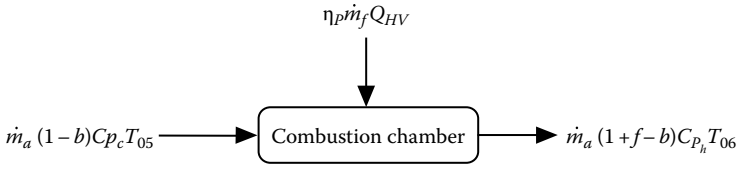


FIGURE 5.6
Isentropic efficiency.



Fuel-to-air ratio

$$f = \frac{\dot{m}_f}{\dot{m}_a} = \frac{(1-b)(Cp_h T_{06} - Cp_c T_{05})}{\eta_b Q_{HV} - Cp_h T_{05}} = (1-b)\frac{1.147 \times 1559 - 1.005 \times 774}{0.96 \times 45000 - 1.147 \times 1559} \quad (1)$$

$$f = 0.0244(1-b)$$

Energy balance for high-pressure spool

$$Cp_h(1+f-b)(T_{06} - T_{07}) = Cp_c(T_{04b} - T_{04}) + Cp_c(1-b)(T_{05} - T_{04b})$$

Substitute from (1)

$$1.147\left[1 + 0.0244(1-b) - b\right](380) = 1.005\left[165.7 + 226 - 226b\right]$$

$$1.147\left[1.0244 - 1.0244b\right](380) = 393.65 - 227.13b$$

$$b = 0.2406$$

$$\text{Bleed} = 24.06\%$$

Comment: This bleed ratio looks like a great percentage; however, as will be described in the turbine cooling sections, each blade row may need some 2% for cooling and the two turbines here have a total of five stages and therefore 10 blade rows. In addition, bleeding has its applications for cabin-air conditioning as well as other anti-icing functions.

Fuel-to-air ratio $f = 0.0185$. This ratio is a reasonable figure, which assures the value previously obtained for the bleed ratio.

Energy balance for low-pressure spool

$$(1+f-b)Cp_h(T_{07} - T_{08}) = \beta Cp_c(T_{03} - T_{02}) + Cp_c(T_{04} - T_{02})$$

$$0.7779 \times 1.147 \times 394 = \beta \times 1.005 \times 47 + 1.005 \times 94$$

$$\beta = 5.4425$$

Thus the BPR of this engine is 5.4425.

Fan nozzle: The first step in nozzle analysis is to check whether it is choked or not by calculating the pressure ratio:

$$\frac{P_{03}}{P_c} = \frac{1}{\left(1 - \frac{1}{\eta_{fn}}\frac{\gamma_c - 1}{\gamma_c + 1}\right)^{\gamma_c/\gamma_c - 1}} = \frac{1}{\left(1 - \frac{1}{0.9}\frac{1.4-1}{1.4+1}\right)^{1.4/1.4-1}} = 2.0478$$

$$P_c = 11.32 \text{ psi}$$

Since $P_c < P_a$, the fan nozzle is unchoked:

$$V_{e_{fan}} = \sqrt{2C_{p_c}\eta_n T_{03}\left\{1-\left(\frac{P_a}{P_{03}}\right)^{\gamma_c-1/\gamma_c}\right\}} = \sqrt{2\times 1005\times 0.9\times 335.7\times 0.1223} = 272.7 \text{ m/s}$$

Turbine Nozzle: Here a check for the choking of the turbine nozzle also followed:

$$\frac{P_{08}}{P_c} = \frac{1}{\left(1-\frac{1}{\eta_{tn}}\frac{\gamma_h-1}{\gamma_h+1}\right)^{\gamma_h/\gamma_h-1}} = \frac{1}{\left(1-\frac{1}{0.9}\frac{1.33-1}{1.33+1}\right)^{1.33/1.33-1}} = 1.9835$$

$$P_c = 10.78 \text{ psi}$$

Since $P_c < P_a$, the turbine nozzle is also unchoked:

$$V_{e_h} = \sqrt{2Cp_h\eta_n T_{08}\left\{1-\left(\frac{P_a}{P_{08}}\right)^{\gamma_h-1/\gamma_h}\right\}} = \sqrt{2\times 1147\times 0.9\times 785\left\{1-\left(\frac{14.7}{21.4}\right)^{0.25}\right\}}$$

$$V_{eh} = 381 \text{ m/s}$$

Since the total air mass flow rate is
$\dot{m}_a = 280$ kg/s, the fan (cold) air mass flow rate is

$$\dot{m}_{fan} = \frac{\beta}{1+\beta} \quad \dot{m}_a = \frac{5.4425}{6.4425}\times 280 = 236.5 \text{ kg/s}$$

and the core (hot) mass flow rate is

$$\dot{m}_{core} = 43.5 \text{ kg/s}$$

Thrust Force (T)

$$T = \dot{m}_{fan}V_{eFan} + (1+f-b)\dot{m}_{core}V_{eCore}$$

$$T = 236.5\times 272.7 + 0.7779\times 43.5\times 381 = 77,375 \text{ N}$$

$$\therefore T = 77.4 \text{ kN}$$

Example 5.2

One of the techniques used in short takeoff and landing (STOL) fighters is the flap blowing turbofan engine. Air is bled from the LPC and ducted to the flap system in the wing trailing edge (see Figure 5.7). Such accelerated air flow creates greater lift than would be possible by the wings themselves. Here is the data for one of these engines. During takeoff at sea level ($T_a = 288$ K and $P_a = 101$ kPa), the engine has a BPR of 3.0 and the core engine air flow is 22.7 kg/s; 15% of this air is bled at the exit of the LPC. The components' efficiencies are

$$\eta_f = 0.9, \quad \eta_c = 0.88, \quad \eta_b = 0.96, \quad \eta_t = 0.94, \quad \eta_n = 0.95$$

The total pressure recovery factor for the intake is $r_d = P_{02}/P_{0a} = 0.98$. The pressure ratio of the fan and both the LPC and HPC are 2.5, 3.0, and 5.0, respectively. The maximum

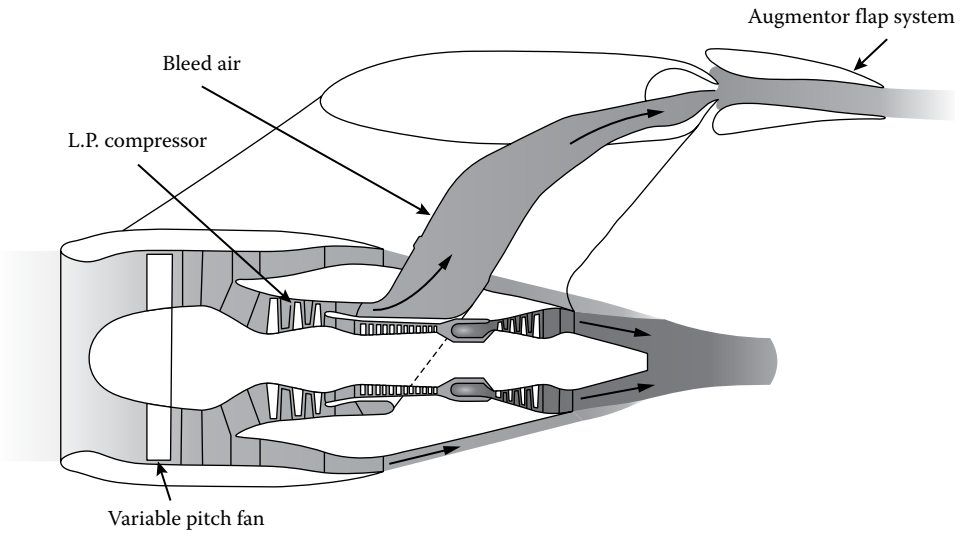


FIGURE 5.7
Flap blowing engine. (From Rolls-Royce, *The Jet Engine*, 1986, p. 189.)

allowable turbine total inlet temperature is 1400 K. The total pressure loss in the combustion chamber is 3%. The fuel heating value is 43,000 kJ/kg. We need to calculate

1. The properties of the working fluid in all the states
2. The thrust force
3. The TSFC
4. The overall efficiency

Solution
The given data are
$T_a = 288$ K, $P_a = 101$ kPa,

$$\beta = 3.0, \quad \dot{m}_{core} = 22.7 \text{ kg/s}, \quad \text{bleed } b = 15\%$$

$$\eta_c = 0.88, \quad \eta_f = 0.9, \quad \eta_b = 0.94, \quad \eta_n = 0.95$$

$$r_d = \frac{P_{o2}}{P_{oa}} = 0.98$$

$$\pi_c)_{total} = 15, \quad \pi_{LPC} = 3.0, \quad \pi_{HPC} = 5.0, \quad \pi_f = 2.5, \quad T_{0\max} = 1400 \text{ K}, \quad \Delta P_{cc} = 3\%,$$
$$\text{and} \quad Q_{HV} = 43{,}000 \text{ kJ}$$

Figure 5.8a illustrates the core and bleed mass flow rates, (b) illustrates the core and fan mass flow rates, and (c) and (d) illustrate the modules and stations of the engine and the *T*–*S* diagram.

For takeoff operation:

$$P_{02} = P_a = 101 \text{ kPa}$$
$$T_{02} = T_a = 288 \text{ K}$$
$$P_{03} = P_{02} \times \pi_{fan} = 101 \times 2.5 = 252.5 \text{ kPa}$$

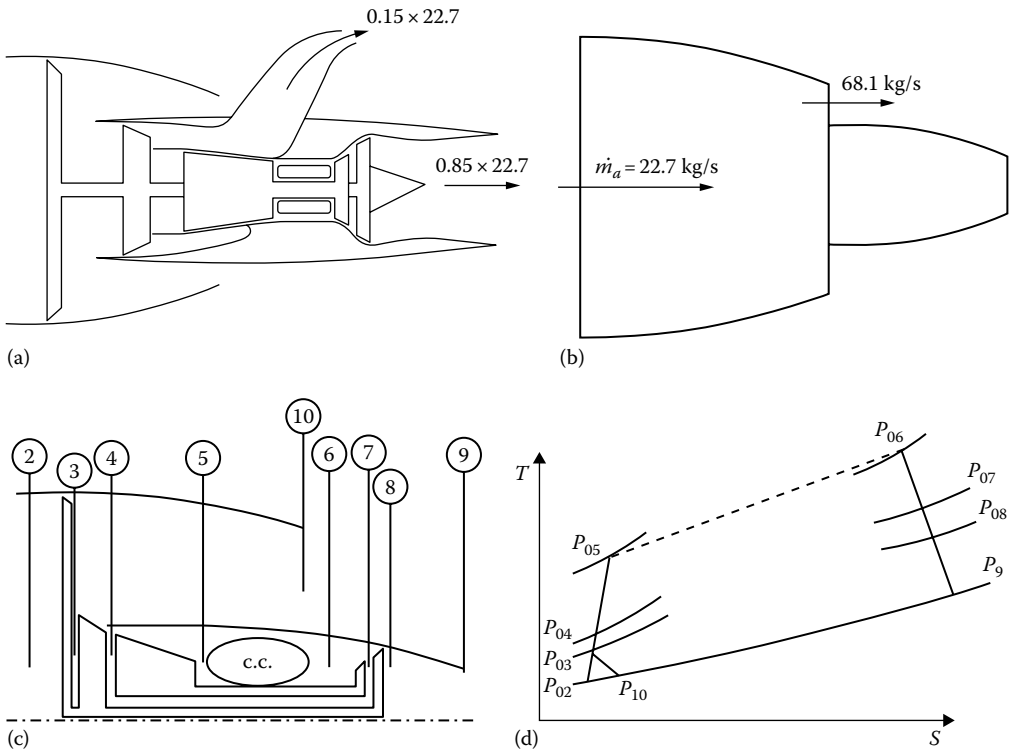


FIGURE 5.8
Example 5.2.

The isentropic efficiency of the fan will be calculated as seen from Figure 5.6.

$$\eta_f = \frac{T_{03s} - T_{02}}{T_{03} - T_{02}} = \frac{T_{02}\left[\left(\pi_{fan}\right)^{\gamma-1/\gamma} - 1\right]}{T_{03} - T_{02}}$$

$$T_{03} = 383.9 \text{ K}$$

$$P_{04} = P_{03} \times \pi_{LPC} = 757.5 \text{ kPa}$$

$$T_{04} = T_{03}\left[1 + \frac{1}{\eta_c}\left(\pi_{LPC}^{\gamma-1/\gamma} - 1\right)\right] = 383.9\left[1 + \frac{1}{0.88}(1.369 - 1)\right] = 544.9 \text{ K}$$

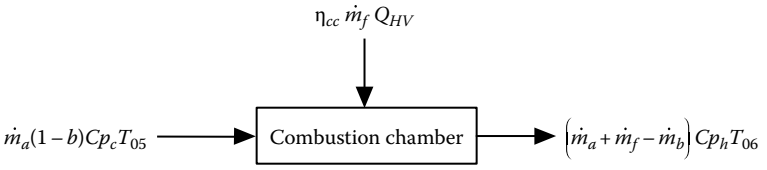
$$P_{05} = P_{04} \times \pi_{HPC} = 3787.5 \text{ kPa}$$

$$T_{o5} = T_{o4}\left[1 + \frac{1}{\eta_c}\left(\pi_{HPC}^{\gamma-1/\gamma} - 1\right)\right] = 544.9[1.4193] = 773.4 \text{ K}$$

$$P_{06} = P_{05} \times \left[1 - \Delta P_{56}\%\right] = P_{o5} \times 0.97 = 3673.9 \text{ kPa}$$

$$\dot{m}_a)_{LPC} = 22.7 \text{ kg/s}$$

$$\dot{m}_a)_{HPC} = \dot{m}_a)_{LPC} \times (1 - b) = 19.3 \text{ kg/s}$$



$$\dot{m}_f=\frac{\left(\dot{m}_a-\dot{m}_b\right)\left[Cp_hT_{06}-Cp_cT_{05}\right]}{\eta_{cc}Q_{HV}-Cp_hT_{06}}$$

$$\dot{m}_a-\dot{m}_b=0.85\dot{m}_{Core}=19.3\ \text{kg/s}$$

$$f=\frac{\dot{m}_f}{\dot{m}_a-\dot{m}_b}=\frac{\left[1.147\times1{,}400-1.005\times773.4\right]}{0.96\times43{,}000-1.147\times1{,}400}=\frac{828.5}{39{,}674.2}=0.02088$$

Energy Balance for High-Pressure Spool

From the layout shown above the energy balance assuming no mechanical losses in power transmission from the turbine to the compressor, will be expressed as:

$$\dot{m}_a\left(1-b\right)Cp_c\left(T_{05}-T_{04}\right)=\dot{m}_a\left(1+f-b\right)Cp_h\left(T_{o6}-T_{o7}\right)$$

$$T_{07}=T_{06}-\left(\frac{1-b}{1+f-b}\right)\frac{Cp_c}{Cp_h}\left(T_{05}-T_{04}\right)=1400-\frac{0.85}{0.87088}\frac{1.005}{1.147}\left(773.4-544.9\right)$$

$$T_{07}=1204.6\ \text{K}$$

$$\eta_t=\frac{T_{06}-T_{07}}{T_{06}-T_{07s}}=\frac{T_{06}-T_{07}}{T_{06}\left[1-\left(\frac{P_{07}}{P_{06}}\right)^{\gamma-1/\gamma}\right]}$$

$$\frac{P_{07}}{P_{06}}=\left[1-\frac{T_{06}-T_{07}}{\eta_tT_{06}}\right]^{\gamma/\gamma-1}=\left(1-\frac{195.4}{0.94\times1400}\right)^4=0.5257$$

$$P_{07}=1931.55\ \text{kPa}$$

Energy Balance for Low-Pressure Spool (Figure 5.9)

$$\beta\dot{m}_aCp_c\left(T_{03}-T_{02}\right)+\dot{m}_aCp_c\left(T_{04}-T_{02}\right)=\dot{m}_a\left(1+f-b\right)Cp_h\left(T_{07}-T_{08}\right)$$

$$T_{o8}=1204.6-\frac{1.005}{0.87008\times1.147}\left\{3\times\left(383.9-288\right)+\left(544.9-288\right)\right\}$$

$$T_{08}=656.6\ \text{K}$$

$$\frac{P_{08}}{P_{07}}=\left[1-\frac{T_{07}-T_{08}}{\eta_tT_{07}}\right]^{\gamma/\gamma-1}=0.0709$$

$$P_{08}=137.04\ \text{kPa}$$

Check hot nozzle choking

$$\frac{P_{o8}}{P_C}=\frac{1}{\left(1-\frac{1}{\eta_{tn}}\frac{\gamma-1}{\gamma+1}\right)^{\gamma/\gamma-1}}=\frac{1}{\left(1-\frac{1}{0.9}\frac{1.33-1}{1.33+1}\right)^4}=1.907$$

$$P_C=71.86\ \text{kPa}$$

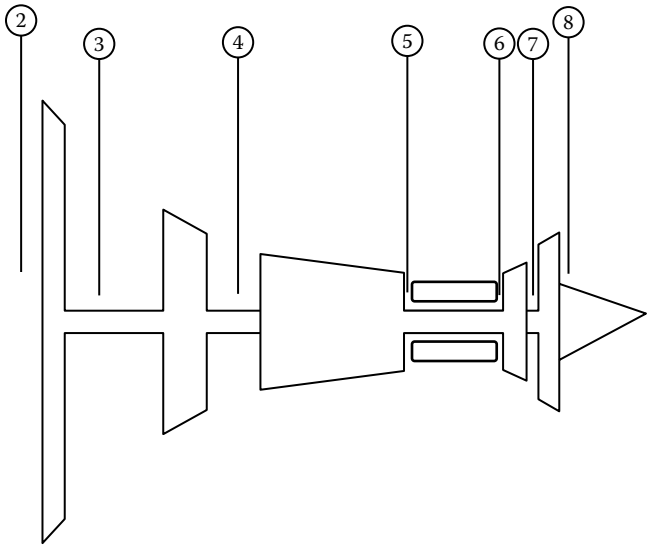


FIGURE 5.9
The engine two spools.

Since $P_C < P_a$, the hot nozzle is unchoked

$$P_9 = P_a = 101 \text{ kPa}$$

$$\eta_{tn} = \frac{T_{08} - T_9}{T_{08} - T_{9s}} = \frac{T_{08} - T_9}{T_{08}\left[1 - \left(\frac{P_a}{P_{08}}\right)^{\gamma-1/\gamma}\right]}$$

$$T_9 = 610.78 \text{ K}$$

$$V_9 = \sqrt{2C_P\left(T_{08} - T_9\right)} = \sqrt{1.147 \times 287 \times \left(656.6 - 610.78\right)} = 324.2 \text{ m/s}$$

Check cold (fan) nozzle

$$\frac{P_{o3}}{P_C} = \frac{1}{\left(1 - \frac{1}{\eta_n}\frac{\gamma - 1}{\gamma + 1}\right)^{\gamma/\gamma-1}} = \frac{1}{\left(1 - \frac{1}{0.95}\frac{1.4 - 1}{1.4 + 1}\right)^{3.5}} = 1.9643$$

$$P_C = 128.54 \text{ kPa}$$

Since $P_C > P_a$, the fan nozzle is choked.

$$P_{10} = P_C = 128.54 \text{ kPa}$$

$$T_{10} = T_{03}\left[1 - \eta_{fn}\left\{1 - \left(\frac{P_C}{P_{03}}\right)^{\gamma-1/\gamma}\right\}\right] = 383.9\left[1 - 0.95\left\{1 - \left(\frac{1}{1.964}\right)^{0.286}\right\}\right] = 319.8 \text{ m/s}$$

$$V_{10} = \sqrt{\gamma R T_{10}} = \sqrt{1.4 \times 287 \times 319.8}$$

$$V_{10} = 358.5 \text{ m/s}$$

The thrust force

$$T = \beta \dot{m}_a \left(V_{10} - V_{Flight}\right) + \dot{m}_a \left[\left(1 + f - b\right)V_9 - V_{Flight}\right] + A_{10}\left(P_{10} - P_a\right)$$
$$V_{Flight} = 0$$

The exhaust area of the fan nozzle must be first calculated

$$A_{10} = \frac{\beta \dot{m}_a R T_{10}}{P_{10} V_{10}} = \frac{3 \times 22.7 \times 287 \times 319.8}{128,540 \times 358.5} = 0.136$$

$$T = 3 \times 22.7 \times 358.5 + 22.7 \times 0.87088 \times 324.2 + 0.136 \times 128.54 \times 1,000$$
$$T = 24,414 + 6,409 + 17,481 = 48,304$$
$$T = 48.304 \text{ kN}$$

$$\text{TSFC} = \frac{\dot{m}_f}{T} = \frac{f \times \dot{m}_{cc}}{T} = \frac{0.02088 \times 19.3}{48.304} = 0.00834 \text{ kg} \cdot \text{s/kN}$$

The overall efficiency is

$$\eta_o = \frac{TV}{\dot{m}_f Q_{HV}} = 0$$

Since the flight speed is zero as the aircraft is still on the ground, then both the propulsive and overall efficiencies are zero.

5.3.2 Fan Driven by the LPT and the Compressor Driven by the HPT

The most famous example of such an engine is the GE Rolls-Royce F136 engine, which is manufactured by General Electric and Rolls Royce companies. It delivers 40,000 lb of thrust. Three-stage fan (manufactured by RR), five-stage compressor (manufactured by GE), advanced annular combustor (RR), one-stage HPT (GE), and three-stage LPT which first stage is manufactured by GE while its second and third stages re manufactured by RR.

Here each spool is composed of a single compressing element, either a fan or a compressor. A schematic drawing for such a configuration together with its *T*–*S* diagram is shown in Figures 5.10 and 5.11.

Only the changes in the analysis between this case and that in Section 5.3.1 will be discussed here.

1. Energy balance between the fan and the LPT taking a possible bleed from the HPC.

$$\left(1 + \beta\right)\dot{m}_a Cp_c \left(T_{03} - T_{02}\right) = \dot{m}_a \left(1 + f - b\right) Cp_h \left(T_{06} - T_{07}\right) \tag{5.28}$$

2. Energy balance between the HPC and the high-pressure turbine (HPT).
   Assuming that there is an air bleed from station 3b, then

$$\dot{m}_a Cp_c \left(T_{03b} - T_{03}\right) + \dot{m}_a \left(1 - b\right) Cp_c \left(T_{04} - T_{03b}\right) = \dot{m}_a \left(1 + f - b\right) Cp_h \left(T_{05} - T_{06}\right) \tag{5.29}$$

If there is no bleed from the compressor, then put $b = 0$ in Equations 5.28 and 5.29.

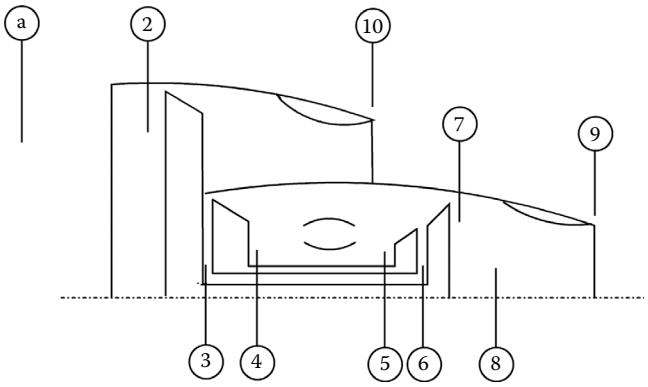


FIGURE 5.10
Layout for a three-spool turbofan (fan driven by LPT and compressor driven by HPT).

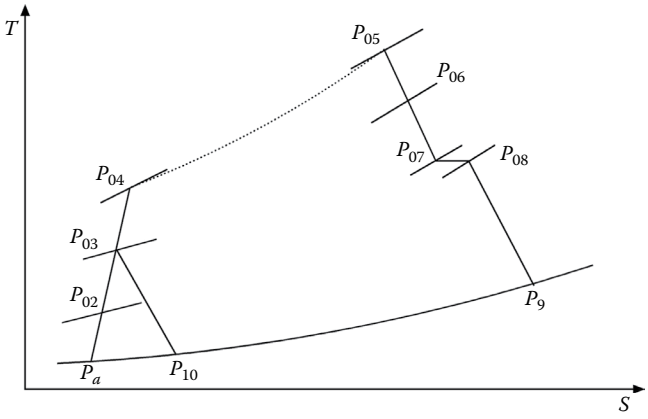


FIGURE 5.11
Temperature-entropy diagram for the two-spool engine in Figure 5.10.

5.3.3 A Geared Fan Driven by the LPT and the Compressor Driven by the HPT

Geared turbofans are the next big step in engine performance, efficiency, and economy. Conventional turbofans consist of a high-pressure spool and a low-pressure spool. Since the fan is normally part of the low spool, both are turning at the same speed. This speed, however, is often a compromise. The fan really operates more efficiently at low rotational speeds (rpm) while the rest of the low spool is more efficient at higher speeds. Putting a reduction gear in between these components makes it possible for the fan and the low spool to run at their optimum speed. This in turn will minimize the possibility of the formation of shock waves in the fan, leading to a higher efficiency. The other advantages are more fuel efficiency, reduced noise levels, and fewer engine parts (compressors and turbine stages).

5.3.3.1 Examples for This Configuration

An example for this new design is the aeroengine PW8000 [3]. Pratt & Whitney launched its program Advanced Technology Fan Integrator (AFTI) and combined Hartford-based

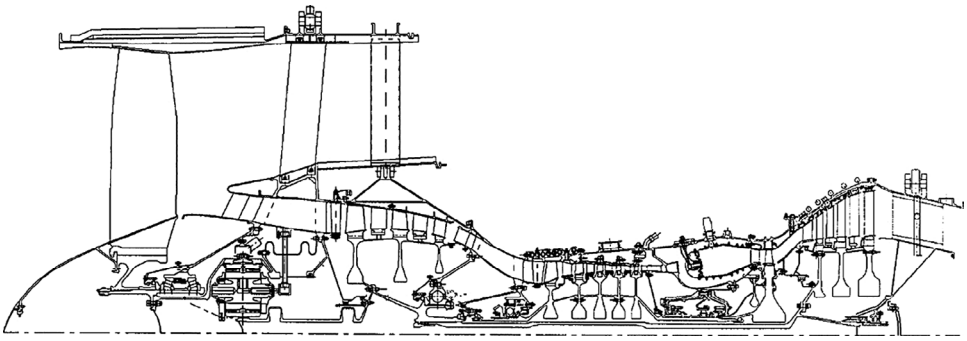


FIGURE 5.12
Geared fan. (From SAE International Aerospace Engineering online.)

engineering resources with those of Pratt & Whitney Canada, and made use of the ADP project (Advanced Ducted Propulsion) of the German manufacturer MTU together with its partner Fiat, for several key components, particularly their gearbox.

The fan rotates at nearly one-third of the speed of the low-pressure spool (3200/9000 rpm). Moreover, the fan BPR is either 10 or 11 for a fan diameter of 1.93 or 1.83 m.

The fan is a single-stage axial configuration; Figure 5.12 driven by a planetary gearbox. The LPC is a three-stage axial type. The HPC is also a five-stage axial type. The HPC is a single-stage axial type. The LPC is a three-stage axial type. Thus the total number of stages is 13, while similar turbofan engines have 20 or more stages. The fuel saving is 9%. The reduction in noise is 30 dB (cumulated) below current stage-three limitations.

The PW8000 shared its core with the PW6000, which is Pratt's other new engine but is designed as a conventional turbofan. While the PW6000 is designed for the thrust class of 70–101 kN (15,750–22,950 lb), the more powerful PW8000 geared fan is aimed at the 110–155 kN (24,750–34,875 lb) category. Its first run was in 2008.

Another geared fan is the P&W Canada PW800 [4].

The PW800 was shown for the first time in its stand at the 2001 Paris Air Show, Le Bourget. Its thrust is in the 10,000–20,000 lb range. It represents a new family of environmentally friendly "green" engines that will burn 10% less fuel, and be quieter and cleaner. The German partner MTU will provide both the HPC and the LPT. Moreover, their partner Fiat Avio will provide the fan-drive gearbox assembly and the accessory gearbox.

A third example is the Lycoming ALF502R (Figure 5.13).

Now, to examine this engine, no changes in the thermodynamic analysis from the preceding case except in the energy balance for the low spool.

If the mechanical efficiency of the gearbox is η_{gb} and the ratio of the bled air in the compressor is (b), then the energy balance of the low-pressure spool is expressed by the relation

$$(1+\beta)\dot{m}_a Cp_c (T_{03} - T_{02}) = \eta_{gb}\dot{m}_a (1 + f - b) Cp_h (T_{06} - T_{07}) \tag{5.30}$$

The energy balance relation for the high-pressure spool is given by the relation (5.29).

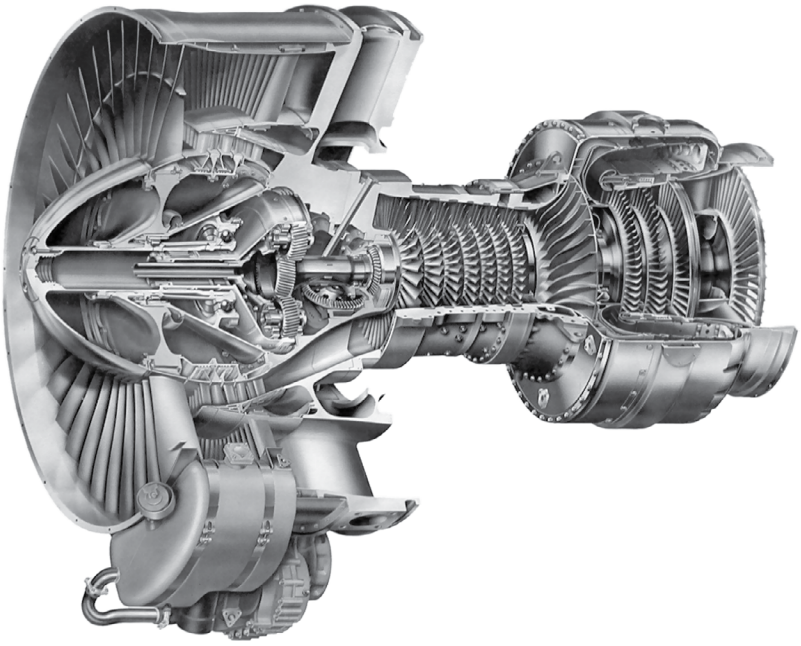


FIGURE 5.13
Lycoming ALF502R Geared Turbofan.

5.4 Forward Fan Unmixed Three-Spool Engine

The three-spool engine is composed of a low-pressure, an intermediate-pressure, and a high-pressure spool running at different speeds. The fan and the LPT make up the low-pressure spool. The intermediate spool is composed of an intermediate-pressure compressor and an intermediate-pressure turbine. The high-pressure spool is also composed of an HPC and an HPT. Rolls-Royce was the first aeroengine manufacturer to design, develop, and produce the three-spool turbofan engine. The Rolls-Royce RB211 was the first three-spool engine to enter service. Later on, several manufacturers developed and manufactured this type of engine.

The main advantages of the three-spool arrangement are

1. Shorter modules and shafts, which result in a shorter engine
   a. Single-stage fan with no booster stages
   b. Fewer overall compressor stages and fewer variable stages
   c. Shorter HPC
2. Higher efficiencies as each spool is running at its "right speed"
3. Greater engine rigidity
4. Lighter weight
5. Fan and core compressors can run at their individual optimum speeds

The main drawbacks of this three-spool category are that they are more complex to build and maintain [5].

5.4.1 Examples for Three-Spool Engines

1. Rolls-Royce RB211
   RB211-22 series [5]: This is the first of the whole series that first saw service in 1972. Its thrust rating is 42,000 lbf (169 kN). Being the pioneer three-shaft engine, it underwent a difficult gestation. However, it improved during service and matured into a reliable engine.
   RB211-524 series: A development of the -22, it featured a very mature design. Its thrust rating is 50,000–60,600 lbf (222–270 kN). It was first fitted into the Boeing 747 in 1977. Its excellent service record led it to be fitted to the improved Lockheed L-1011 in 1981.
   Improved versions—the -524G rated at 58,000 lbf (258 kN) and the -524H rated at 60,600 lbf (270 kN), featuring FADEC—were offered with the Boeing 747-400 and Boeing 767. The -524G and -524H are the first to feature the wide-chord fan, which increases efficiency, reduces noise, and gives added protection against foreign object damage. This was later adopted by GE and Pratt & Whitney for their engines.
   RB211-535 series: This is essentially a scaled-down version of the -524. Its thrust range spans from 37,000 to 43,100 lbf (165 to 192 kN). It powers the Boeing 757 and the Russian Tupolev Tu-204 airliner. The later series shares common features with the later series -524, such as a wide-chord fan and FADEC.
2. Rolls-Royce Trent
   This is a family of high-bypass ratio turbofan engines developed from the RB211 with thrust ratings spanning between 53,000 and 95,000 lbf (236 to 423 kN). The Trent's advanced layout provides lighter weight and better performance compared to the original RB211 and other similar competing engines. It features the wide-chord fan and single crystal HPT blades inherited from later generations of the RB211, but with improved performance and durability.
   The core turbomachinery is brand new, giving better performance, noise, and pollution levels.
   Here also the main points different from two-spool engine, Section 5.3, is introduced. The layout of this engine and the *T*–*S* diagram are shown in Figures 5.14 and 5.15. Air bleed is extracted from the intermediate-pressure compressor at station (3b).

1. Energy balance for the first spool (fan and LPT)

$$(1+\beta)\dot{m}_a Cp_c (T_{03} - T_{02}) = \dot{m}_a (1 + f - b) Cp_h (T_{08} - T_{09}) \tag{5.31}$$

2. Energy balance for the intermediate spool (Intermediate-pressure compressor [IPC] and [IPT])

$$\dot{m}_a Cp_c (T_{03b} - T_{03}) + (1-b)\dot{m}_a Cp_c (T_{04} - T_{03b}) = \dot{m}_a (1 + f - b) Cp_h (T_{07} - T_{08}) \tag{5.32}$$

3. Energy balance for the high-pressure spool (HPC and HPT)

$$\dot{m}_a (1-b) Cp_c (T_{05} - T_{04}) = \dot{m}_a (1 + f - b) Cp_h (T_{06} - T_{07}) \tag{5.33}$$

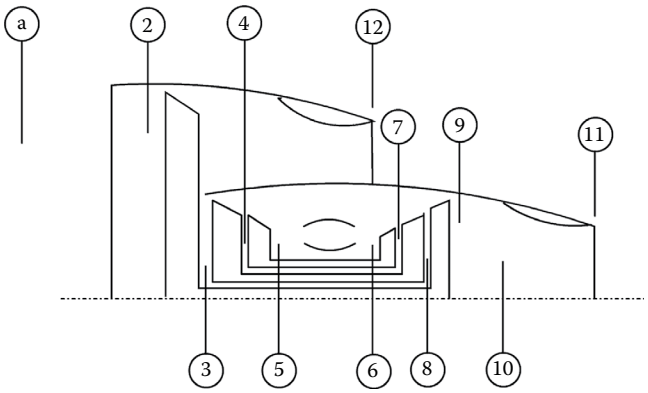


FIGURE 5.14
Layout of a three-spool engine.

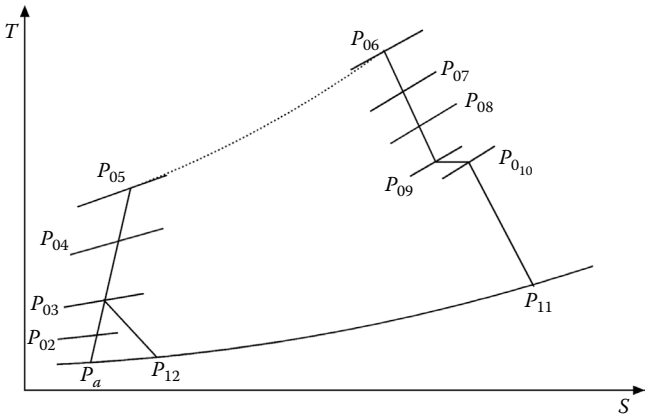


FIGURE 5.15
T–S diagram for a three-spool turbofan.

The procedure discussed earlier for evaluating the fuel-to-air ratio, jet velocities of the cold air, and hot gases from the fan and turbine nozzles may also be followed here. The propulsive, thermal, and overall efficiencies are obtained following the appropriate equations from Chapter 2.

Example 5.3

A three-spool turbofan (forward fan) is shown in Figure 5.14. It has the following data

Fan pressure ratio	1.42:1
Overall compressor pressure ratio	25
HPC pressure ratio	5
BPR ($\dot{m}_{cold}/\dot{m}_{hot}$)	5:1
Fan air mass flow rate	500 kg/s
Fuel-to-air ratio (at takeoff thrust)	0.0177
Ambient pressure	1.0 bar

(*Continued*)

Ambient temperature	288 K
Total pressure recovery at inlet	98%
Efficiencies:	
Fan	99%
Intermediate compressor	89%
HPC	90%
HPT	90%
Intermediate-pressure turbine	90%
LPT	90%
Combustion chamber	98%
Mechanical efficiency	99%
Percentage bleeding air of core mass flow	2%
Fuel heating value	45,000 kJ/kg
Specific heat at constant pressure	$Cp_{air} = 1.005$ kJ/kg/K
	$Cp_{gases} = 1.147$ kJ/kg/K
Hot gases nozzle and fan nozzle efficiency	87%
Percentage total pressure drop in combustion chamber relative HPC	2%
Percentage pressure losses in the jet pipe relative to LPT	2%
$\gamma_{air} = 1.4$, $\gamma_{gases} = 1.33$	
Engine weight	28.8 kN
Maximum diameter	2172 mm
Maximum frontal area	2.79 m^2

Calculate the takeoff thrust at $M = 0.2$.

For all elements up to the combustion chamber $\gamma = 1.4$, $C_p = 1.005$ kJ/kg·k.

Solution

The states numbering of Figure 5.14 is used here. The T–S will be as shown in Figure 5.15.

1. Air inlet

$$U_a = M\sqrt{\gamma RT}_a = 68 \text{ m/s}$$

$$T_{02} = T_{oa} = T_a\left(1 + \frac{\gamma - 1}{2}M_a^2\right) = 290.3 \text{ K}$$

$$P_{oa} = P_a\left(1 + \frac{\gamma - 1}{2}M_a^2\right)^{\gamma/\gamma - 1} = 1.0283 \text{ bar}$$

$$P_{02} = 0.98 \quad P_{oa} = 1.008 \text{ bar}$$

2. Fan

$$P_{03} = \pi_f \times P_{02} = 1.42 \times 1.008 = 1.431 \text{ bar}$$

$$T_{03} = T_{02}\left(1 + \frac{\pi_f^{\gamma-1/2} - 1}{\eta_f}\right) = 290.3\left(1 + \frac{1.42^{0.286} - 1}{0.99}\right) = 321 \text{ K}$$

3. Intermediate-pressure compressor

$$P_{04} = \pi_{LPC} \times P_{03} = 5 \times 1.431 = 7.155 \text{ bar}$$

$$T_{04} = T_{o3}\left(1 + \frac{\pi_{IPC}^{\gamma-1/2} - 1}{\eta_{IPC}}\right) = 321 \times 1.656 \text{ K} = 532 \text{ K}$$

4. HPC

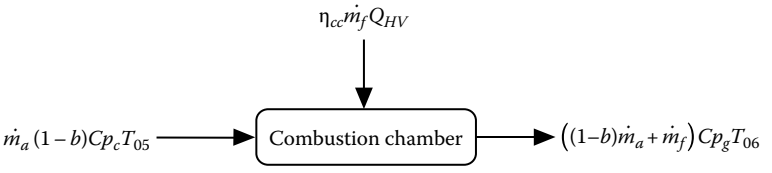
$$P_{05} = \pi_{HPC} \times P_{04} = 5 \times 7.155 = 35.775 \text{ bar}$$

$$T_{05} = T_{04}\left\{1 + \left[\frac{\pi_{HPC}{}^{\gamma-1/\gamma} - 1}{\eta_{HPC}}\right]\right\} = 532\left\{1 + \left[\frac{(5)^{0.286} - 1}{0.90}\right]\right\} = 532 \times 1.6489 = 877.2 \text{ K}$$

5. Combustion chamber: For all the hot elements including combustion chamber, turbines, and nozzles

$$\gamma = 1.33, \quad {}^{\circ}C_p = 1.147 \text{ kJ/kg} \cdot \text{k}$$

Energy balance of combustion chamber: A bleed from the outlet of the HPC is considered here



$$b = \dot{m}_b/\dot{m}_a \quad \text{and} \quad f = \dot{m}_f/\dot{m}_a$$

$$\left[(1-b)\ Cp_a\, T_{05}\right] + \eta_{cc}\dot{m}_f Q = \left[(1-b)\dot{m}_a + \dot{m}_f\right]C_{pg}\, T_{06}$$

$$(1-b)Cp_a\, T_{05} + \eta_{cc} fQ = (1 + f - b)Cp_g T_{06}$$

$$T_{06} = \left[(1-b)Cp_a\, T_{05} + \eta_{cc} fQ\right] \Big/ \left[(1 + f - b)Cp_g\right] = 1437 \text{ K}$$

$$P_{06} = 0.98 \quad P_{05} = 0.98 \times 35.775 = 35.06 \text{ bar}$$

6. HPT

$$\eta_m W_{HPT} = W_{HPT}$$

$$\eta_m \dot{m}_{hot} Cp_g\left(T_{06} - T_{07}\right) = \dot{m}_{a_{core}} Cp_a\left(T_{05} - T_{04}\right)$$

$$\dot{m}_{hot} = (1 + f - b)\dot{m}_{a_{core}} = 0.9977\ \dot{m}_{a_{core}}$$

$$\Delta T_{0_{67}} = T_{06} - T_{07} = \frac{Cp_a\left(T_{05} - T_{04}\right)}{0.9977 \times \eta_m \times C_{pg}} = \frac{1.005(877.2 - 532)}{0.9977 \times 0.99 \times 1.147} = 306.22 \text{ K}$$

$$T_{07} = T_{06} - \Delta T_{0_{67}} = 1130 \text{ K}$$

$$P_{07} = P_{06}\left[1 - \frac{\left[1 - \left(T_{07}/T_{06}\right)\right]}{\eta_{HPT}}\right]^{\gamma_g/\gamma_g - 1} = 35.06\left[1 - \frac{\left[1 - \left(1130/1437\right)\right]}{0.9}\right]^{1.33/0.33} = 11.859 \text{ bar}$$

7. Intermediate-pressure turbine
   From energy balance

$$\eta_m W_{IPT} = W_{IPC}$$

$$\eta_m \dot{m}_{hot} Cp_g \left(T_{07} - T_{08}\right) = \dot{m}_{a-core} Cp_a \left(T_{04} - T_{03}\right)$$

$$\Delta T_{o78} = \frac{Cp_a \left(T_{04} - T_{03}\right)}{0.9977 \times \eta_m \times C_{pg}} = \frac{1.005\left(532 - 321\right)}{0.9977 \times 0.99 \times 1.147} = 187.2 \text{ K}$$

$$T_{08} = T_{07} - \Delta T_{078} = 1130 - 187.2 = 942.8 \text{ K}$$

$$P_{08} = P_{07}\left[1 - \frac{\left[1 - \left(T_{08} \diagup T_{07}\right)\right]}{\eta_{IPT}}\right]^{\gamma_g/\gamma_g - 1} = 0.44 \quad P_{07} = 5.24 \text{ bar}$$

8. Low-pressure turbine
   From energy balance

$$\eta_m W_{LPT} = W_{Fan}$$

$$\eta_m Cp_g \dot{m}_{hot} \left(T_{08} - T_{09}\right) = Cp_a \left(\dot{m}_{a_{core}} + \dot{m}_{fan}\right)\left(T_{03} - T_{02}\right)$$

$$\eta_m Cp_g \times 0.9977 \dot{m}_{a_{core}} \left(T_{08} - T_{09}\right) = Cp_a \left(\dot{m}_{a_{core}} + \beta \dot{m}_{a_{core}}\right)\left(T_{03} - T_{02}\right)$$

$$\Delta T_{089} = \frac{Cp_a \left(1 + \beta\right)}{\eta_m Cp_g \times 0.9977}\left(T_{03} - T_{02}\right) = 165 \text{ K}$$

$$T_{09} = T_{08} - \Delta T_{089} = 943 - 165 = 778 \text{ K}$$

$$P_{09} = P_{08}\left[1 - \frac{\left(1 - \dfrac{T_{o9}}{T_{o8}}\right)}{\eta_{LPT}}\right]^{\gamma_g/\gamma_g - 1} = 5.24\left[1 - \frac{\left(1 - \dfrac{778}{943}\right)}{0.9}\right]^{1.33/0.33} = 5.24 \times 0421 = 2.207 \text{ bar}$$

9. Hot nozzle
   The inlet temperature and pressure to the hot nozzle are

$$T_{0_{10}} = T_{0_9} = 778 \text{ K}$$

$$P_{0_{10}} = P_{0_9} \times \left(1 - \Delta P_{jet\ pipe}\right) = 0.98 \quad P_{0_9} = 2.163 \text{ bar}$$

   To check whether the hot nozzle is choked or not

$$\frac{P_{0_{10}}}{P_C} = \frac{1}{\left(1 - \dfrac{1}{\eta_n}\dfrac{\gamma - 1}{\gamma + 1}\right)^{\gamma/\gamma - 1}} = 1.8892$$

But

$$\frac{P_{0_{10}}}{P_a} = 2.163$$

since $\frac{P_{0_{10}}}{P_a} \succ \frac{P_{0_9}}{P_C}$, then the nozzle is choked

$$\therefore P_{11} = P_C = \frac{P_{0_{10}}}{P_{0_{10}}/P_C} = \frac{2.163}{1.8892} = 1.1449 \text{ bar}$$

$$\frac{T_{11}}{T_{0_{10}}} = \frac{2}{\gamma+1} = \frac{2}{1.33+1} = 0.858$$
$$T_{11} = 667.5 \text{ K}$$

$$U_{11} = a_{11} = \sqrt{\gamma R T_{11}} = \sqrt{1.33 \times 287 \times 667.5} = 505 \text{ m/s}$$

$$\rho_{11} = \frac{P_{11}}{RT_{11}} = \frac{1.1449 \times 10^5}{287 \times 667.5} = 0.597 \text{ kg/m}^3$$

$$\dot{m}_{core} = 0.9977\ \dot{m}_{hot}$$

but

$$\dot{m}_{hot} = \frac{\dot{m}_{Fan}}{\beta} = \frac{500}{5} = 100 \text{ kg/s}$$

$$\therefore \dot{m}_{a_{core}} = 99.77 \text{ kg/s}$$
$$\dot{m}_{a_{core}} = \rho_{11} U_{11} A_{11}$$

$$A_{11} = \frac{\dot{m}_{a_{core}}}{\rho_{11} U_{11}} = \frac{99.77}{0.59 \times 505} = \frac{99.77}{301.7} = 0.3307 \text{ m}^2$$

Thrust due to hot gases

$$\begin{aligned} T_{hot} &= \dot{m}_{core} U_{11} - \dot{m}_{hot} U_a + A_{11}\left(P_{11} - P_a\right) \\ &= 99.77 \times 505 - 100 \times 68 + 0.3307\left(1.145 - 1.0\right) \times 10^5 \\ T_{hot} &= 48.39 \text{ kN} \end{aligned}$$

10. Fan nozzle
Next the fan nozzle is also checked for choking

$$\frac{P_{03}}{P_a} = 1.431$$
$$\frac{P_{03}}{P_C} = \frac{1}{\left(1 - \frac{1}{\eta_{fn}} \frac{\gamma-1}{\gamma+1}\right)^{\gamma/\gamma-1}} = \frac{1}{\left(1 - \frac{1}{0.97} \frac{1.4-1}{1.4+1}\right)^{1.4/1.4-1}}$$
$$\frac{P_{03}}{P_c} = 1.899$$
$$\frac{P_{03}}{P_a} < \frac{P_{03}}{P_c}$$

∴ The fan nozzle is unchoked

$$P_{12} = P_a$$

$$\frac{T_{12}}{T_{03}} = \left[1 - \eta_n \left\{1 - \left(\frac{P_{12}}{P_{03}}\right)^{\gamma-1/\gamma}\right\}\right]$$

$$\frac{T_{12}}{T_{03}} = \left[1 - 0.97\left[1 - \left(\frac{1}{1.431}\right)^{0.4/1.4}\right]\right] = 0.9054$$

$$T_{12} = 290.65 \text{ K}$$

$$U_{12} = \sqrt{2Cp_a\left(T_{03} - T_{12}\right)} = \sqrt{2 \times 1005 \times \left(321 - 290.65\right)} = 247 \text{ m/s}$$

Thrust generated by the fan is T_{fan}

$$T_{fan} = \dot{m}_{fan}\left(u_{12} - u_a\right) = 500\left(247 - 68\right)$$
$$T_{fan} = 89.49 \text{ kN}$$

$$\text{Total thrust} = T_{hot\ gases} + T_{Fan} = 137.88 \text{ kN}$$

$$\dot{m}_f = f\dot{m}_a = 0.017 \times 100 \times 3600 = 6120 \text{ kg/h}$$

$$\text{TSFC} = \frac{\dot{m}_f}{T} = \frac{6120}{137.88 * 10^3} = 0.04438 \text{ kg/N} \cdot \text{h}$$

5.5 Forward Fan Mixed-Flow Engine

Mixed turbofan engines are always found in either single or two-spool engines. It was used in the past for military applications only. Nowadays it is used in both civil and military aircraft. An example of a two-spool engine is the CFM56 series. The cold compressed air leaving the fan is not directly exhausted as previously described but flows in a long duct surrounding the engine core and then mixes with the hot gases leaving the LPT. Thus the cold air is heated while the hot gases are cooled. Only one mixed exhaust is found.

A layout of a single-spool mixed turbofan and its *T*–*S* diagram are shown in Figure 5.16.

5.5.1 Mixed-Flow Two-Spool Engine

Most of the mixed turbofan engines now are two-spool ones. If mixed turbofan engines are analyzed versus unmixed turbofan engines, the following points are found [6]

1. The optimum fan pressure ratio for a mixed-flow engine is generally lower than that for a separate flow for a given BPR
2. At a given fan pressure ratio, the mixed-flow engine has a lower BPR and therefore a higher specific thrust
3. The amount of power, which the LPT supplies to drive the fan, will be smaller

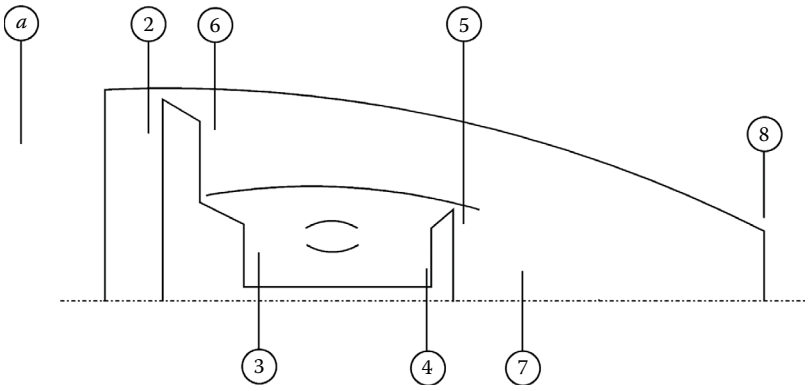


FIGURE 5.16
Single-spool mixed-flow turbofan.

4. Possibly one LPT stage less is sufficient
5. Other features to be considered are
   a. Thrust gain due to mixing
   b. Noise
   c. Weight
   d. Reverse thrust

Hereafter, a detailed analysis of this category will be given. Figures 5.17 through 5.19 present the engine layout and its temperature-entropy diagram.

The requirements for the mixing process are equal static pressures and also equal velocities. Thus from the layout designation these two conditions are specified as $P_3' = P_7$ and $V_3' = V_7$ which means that if there are no pressure losses in the bypass duct connecting the cold and hot streams, and there is no pressure loss in the mixing process, then

$$P_{03} = P_{03}' = P_{07} = P_{08} \tag{5.34}$$

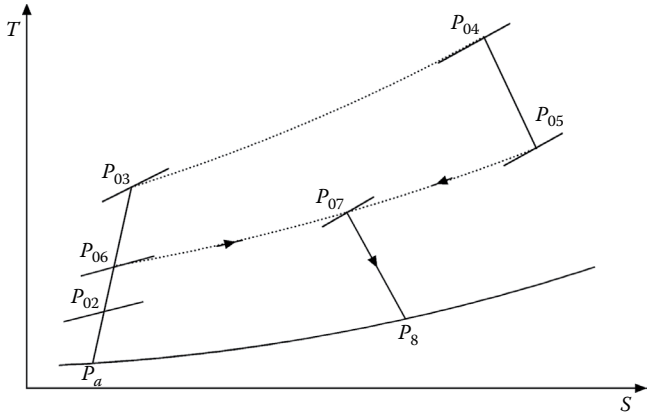


FIGURE 5.17
T–S diagram of single-spool mixed flow turbofan.

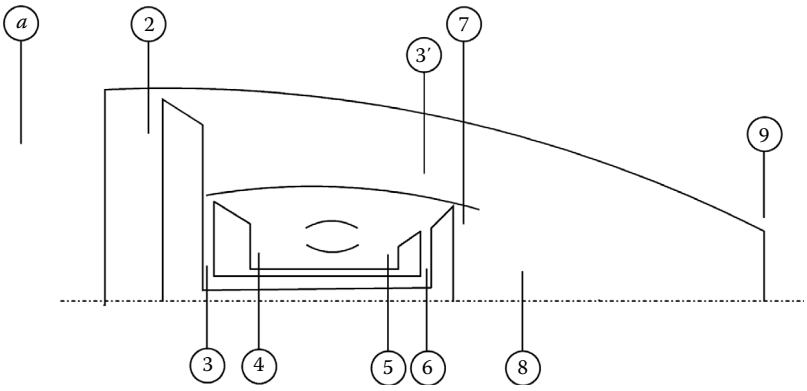


FIGURE 5.18
Layout of a mixed two-spool turbofan.

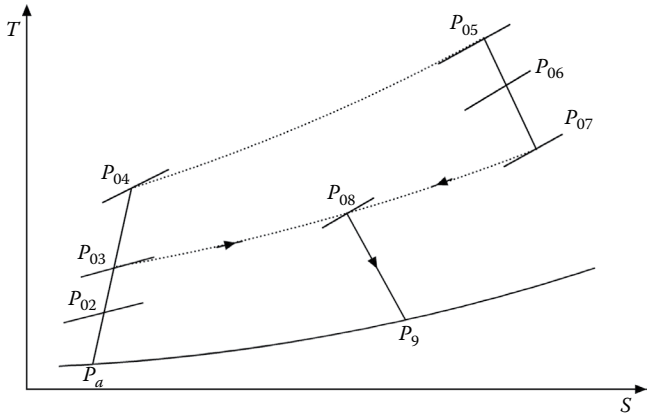


FIGURE 5.19
Temperature-entropy diagram for two-spool mixed turbofan.

If there are losses in the fan bypass duct, then

$$P'_{03} = P_{03} - \Delta P_{fan/duct}$$
$$P_{07} = P_{08} = P_{03} - \Delta P_{fan/duct}$$

In the above equation, no pressure drop is considered during the mixing process.

In some engines like the CFM56 series, the mixing process takes place in a mixer preceding the nozzle. It results in a quieter engine than if the mixer was not present. Figure 5.20 illustrates a typical mixed two-spool engine with a mixer.

1. Energy balance for the low-pressure spool:
   Considering a mechanical efficiency for the low-pressure spool of (η_{m1}), then

$$W_{fan} = \eta_{m1} W_{LPT}$$

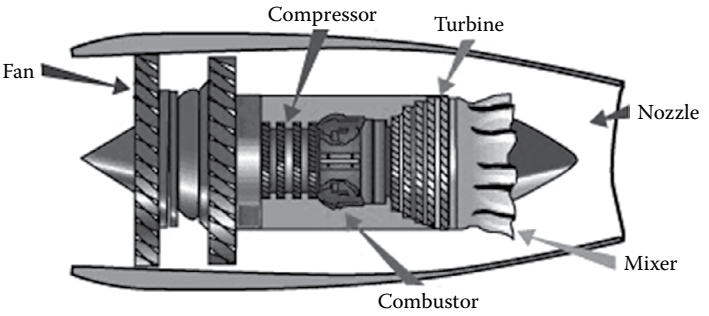


FIGURE 5.20
Two-spool mixed turbofan engine with a mixer.

or

$$\dot{m}_a(1+\beta)Cp_c(T_{03}-T_{02}) = \eta_{m1}\dot{m}_a(1+f)Cp_h(T_{06}-T_{07}) \tag{5.35}$$

2. Energy balance for the high-pressure spool:
A second mechanical efficiency for the high-pressure spool is (η_{m2}) assumed.

$$W_{HPC} = \eta_{m2}(1+f)\dot{m}_a Cp_h(T_{05}-T_{06})$$

thus

$$\dot{m}_a Cp_c(T_{04}-T_{03}) = \eta_{m2}\dot{m}_a(1+f)Cp_h(T_{05}-T_{06}) \tag{5.36}$$

3. Mixing process:
The hot gases leaving the LPT and the cold air leaving the fan bypass duct are mixed and getting new properties at state (8). Thus such a process is governed by the first law of thermodynamics as follows:

$$H_{03}+H_{07}=H_{08}$$
$$\dot{m}_c Cp_c T_{03}+(1+f)\dot{m}_h Cp_h T_{07} = \left[\dot{m}_c+(1+f)\dot{m}_h\right]Cp_c T_{08}$$

which is reduced to

$$\beta Cp_c T_{03}+(1+f)Cp_h T_{07} = (1+\beta+f)Cp_h T_{08} \tag{5.37}$$

Now for a better evaluation of the gas properties after mixing we can use the mass weighted average properties of the gases at state (8) as follows:

$$Cp_8 = \frac{Cp_7+\beta Cp_3}{1+\beta}$$
$$R_8 = \frac{R_7+\beta R_3}{1+\beta}$$
$$\gamma_8 = \frac{Cp_8}{Cp_8-R_8}$$

Consider the real case of mixing where normally losses are encountered and where pressure drop is associated with the mixing process. Such pressure losses are either given as the value ΔP_{mixing} or as a ratio r_m in the mixing process

$$P_{08} = P_{07} - \Delta P_{mixing} \quad \text{or}$$
$$P_{08} = r_m P_{07} \quad \text{where } r_m < 1 \approx 0.98$$

The thrust force is then given by the relation

$$T = \dot{m}_a \left[(1 + f + \beta) U_e - (1 + \beta) U \right] \tag{5.38}$$

Example 5.4

Figure 5.21 illustrates the mixed high-BPR turbofan engine CFM56-5C. It has the following data

Bypass ratio	6.6
Typical TSFC	0.04 kg/(N·h)
Cruise thrust	29,360 N
Total mass flow rate at cruise	100 kg/s

During takeoff operation:

Takeoff thrust	140,000 N
Total air mass flow rate	474.0 kg/s
Overall pressure ratio	37.5
Total temperature at inlet to the LTP	1,251 K
Exhaust gas temperature	349 K
Ambient temperature	288.0 K
Ambient pressure	101 kPa

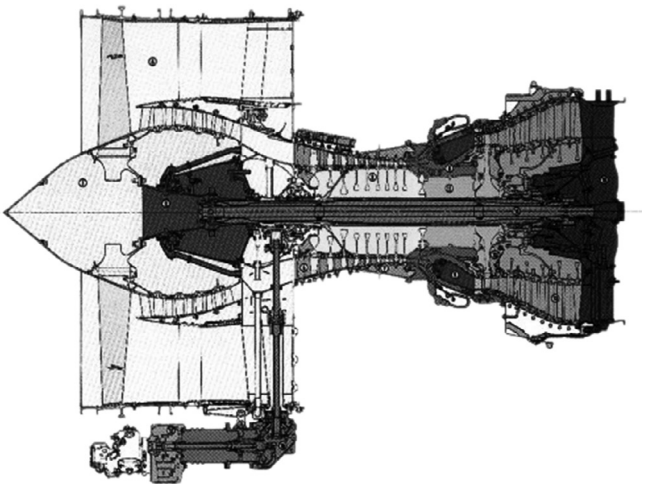


FIGURE 5.21
CFM56-5C mixed high-BPR turbofan engine.

Assuming that all the processes are ideal and there are no losses in either the combustion chamber or the mixing process,

1. Prove that the thrust force is given by the relation

$$T = \frac{\dot{m}_a(1+\beta)(u_e - u)}{1 - u_e(TSFC)}$$

2. Calculate
   a. The exhaust velocity at both takeoff and cruise (use the above relation)
   b. The fuel-to-air ratios at both takeoff and cruise conditions.
3. Under takeoff conditions, calculate
   a. The total temperature at the outlet of the HPC
   b. The total temperature at the inlet to the HPT
   c. The pressure ratio of the HPC
   d. The fan pressure ratio
   e. The temperature of the hot gases prior to mixing
   f. The pressure ratio of the LPC (booster)

Assume that the nozzle is unchoked.

Solution

1. For a mixed-flow turbofan engine, with an unchoked nozzle, the thrust force is expressed as

$$T = \dot{m}_a\left[(1 + f + \beta)u_e - (1+\beta)u\right] \tag{a}$$

$$TSFC = \frac{\dot{m}_f}{T} = \frac{f\dot{m}_a}{T} \tag{b}$$

From (a) and (b)

$$\therefore T = \dot{m}_a(1+\beta)u_e + TSFC \times Tu_e - \dot{m}_a(1+\beta)u$$
$$T(1 - TSFC \times u_e) = \dot{m}_a(1+\beta)(u_e - u)$$

or

$$T = \frac{\dot{m}_a(1+\beta)(u_e - u)}{1 - TSFC \times u_e}$$

2. Rearrange the above relation to get

$$u_e = \frac{T + \dot{m}_a(1+\beta)u}{T(TSFC) + \dot{m}_a(1+\beta)} \tag{c}$$

At cruise, the flight speed is

$$u = M\sqrt{\gamma RT_a} = 0.8\sqrt{1.4 \times 287 \times 218.7} = 237.3 \text{ m/s}$$
$$\therefore u_e = \frac{29{,}360 + 100 \times 237.3}{29{,}360 \times \dfrac{0.04}{3{,}600} + 100} = 529.17 \text{ m/s}$$

From Equation c, at takeoff $u = 0$

$$u_e)_{Takeoff} = \frac{T}{T(TSFC) + \dot{m}_a(1+\beta)}$$

$$u_e)_{Takeoff} = \frac{140{,}000}{140{,}000 \times \dfrac{0.04}{3{,}600} + 474} = 294.4 \text{ m/s}$$

3. Since $f = \dot{m}_f/\dot{m}_h$ and $\dot{m}_h = \dot{m}_t/1+\beta$ where $\dot{m}_h$ is the air passing through the hot section of the engine (sometimes called the core air) and $\dot{m}_t$ is the total mass flow rate through the engine.

$$\therefore f = \frac{\dot{m}_f(1+\beta)}{\dot{m}_t}$$

Moreover

$$TSFC = \frac{\dot{m}_f}{T}$$

$$\therefore f = \frac{T(TSFC)(1+\beta)}{\dot{m}_t}$$

$$f)_{cruise} = \frac{29{,}360 \times 0.04 \times 7.6}{100} = 0.02479$$

$$\dot{m}_f)_{cruise} = \frac{0.02479 \times 100}{7.6} = 0.326 \text{ kg/s}$$

Moreover

$$f)_{T/O} = \frac{140{,}000 \times 0.04 \times 7.6}{474} = 0.02494$$

$$\dot{m}_f)_{T/O} = \frac{0.02494 \times 474}{7.6} = 1.555 \text{ kg/s}$$

4. At the end of the compression process, that is, the delivery total temperature of the HPC (state 5) is

$$T_{o_5} = T_a(OPR)^{\gamma_c - 1/\gamma_c} = 288(37.5)^{0.286} = 812 \text{ K}$$

5. The energy balance at the combustor (from state 5 to 6)

$$\dot{m}_f h_{o_5} + \dot{m}_f Q_R = (\dot{m}_a + \dot{m}_f) h_{o_6}$$

Then

$$\dot{m}_f C_{P_c} T_{o_5} + \dot{m}_f Q_R = (\dot{m}_a + \dot{m}_f) C_{P_h} T_{o_6}$$

$$T_{o_6} = \frac{fQ_R + C_{P_c} T_{o_5}}{(1+f) C_{P_h}}$$

Then substituting the value of (f) at takeoff

$$T_{o_6} = \frac{0.02494 \times 45{,}000 + 1.005 \times 812}{1.02494 \times 1.148} = 1{,}647.4 \text{ K}$$

6. The energy balance of the high-pressure spool yields

$$C_{P_c}\left(T_{o_5} - T_{o_4}\right) = \left(1+f\right)C_{P_h}\left(T_{o_6} - T_{o_7}\right)$$

$$C_{P_c}T_{o_5}\left[1 - \left(\frac{P_{o_4}}{P_{o_5}}\right)^{\gamma_c - 1/\gamma_c}\right] = \left(1+f\right)C_{P_h}\left(T_{o_6} - T_{o_7}\right)$$

The pressure ratio P_{o4}/P_{o5} may be calculated as follows:

$$\frac{P_{o_4}}{P_{o_5}} = \left[1 - \frac{\left(1+f\right)C_{P_h}\left(T_{o_6} - T_{o_7}\right)}{C_{Pc}T_{o_5}}\right]^{\gamma_c/\gamma_c - 1}$$

$$\frac{P_{o_4}}{P_{o_5}} = \left[1 - \frac{1.02494 \times 1.148 \times \left(1647.4 - 1251\right)}{1.005 \times 812}\right]^{3.5} = 0.05148$$

The pressure ratio of the HPC

$$\pi_{HPC} = \frac{P_{o5}}{P_{o4}} = 19.423$$

7. The exhaust velocity is obtained from the relation

$$u_e^2 = 2C_P\left(T_{09} - T_{10}\right) = 2C_PT_{10}\left[\left(\frac{P_{09}}{P_{10}}\right)^{\gamma_c - 1/\gamma_c} - 1\right]$$

$$\frac{P_{09}}{P_{10}} = \left[1 + \frac{u_e^2}{2C_PT_{10}}\right]^{\gamma_c/\gamma_c - 1} = \left[1 + \frac{\left(294.4\right)^2}{2 \times 1005 \times 349}\right]^{3.5}$$

$$\frac{P_{09}}{P_{10}} = 1.503$$

The conditions to be satisfied for proper mixing yield equal total pressure at the fan outlet, LPT, and the end of the mixing process, that is,

$$P_{03} = P_{08} = P_{09}$$

Also, since a complete expansion is assumed at the nozzle, $P_{10} = P_a$

$$\therefore \frac{P_{09}}{P_{10}} = \frac{P_{03}}{P_a} = \pi_f$$

$\therefore$ Fan pressure ratio

$$\pi_f = 1.503$$

8. Since the fan pressure ratio is now calculated, then

$$T_{03} = T_{02}\pi_f^{\gamma_c - 1/\gamma_c} = (288)(1.503)^{0.286} = 323.6 \text{ K}$$

Also

$$\frac{T_{09}}{T_{10}} = \pi_f^{\gamma_c - 1/\gamma_c}$$

$$T_{09} = (349)(1.503)^{0.286} = 398.6 \text{ K}$$

Now, from the energy balance within the mixing process

$$\beta \dot{m}_a C_{pc} T_{03} + (1+f)\dot{m}_a C_{ph} T_{08} = (1+f+\beta)\dot{m}_a C_{pc} T_{09}$$

$$T_{08} = \left(\frac{1+f+\beta}{1+f}\right)\frac{C_{P_c}}{C_{P_h}} T_{09} - \left(\frac{\beta}{1+f}\right)\frac{C_{P_c}}{C_{P_h}} T_{03}$$

$$T_{08} = \left(\frac{1+0.02494+6.6}{1.024949}\right)\frac{1.005}{1.148} \times 398.6 - \frac{6.6}{1.02494}\frac{1.005}{1.148} \times 323.6 = 775.15 \text{ K}$$

9. The booster pressure ratio (π_{LPC})

$$\pi_{LPC} = \frac{OPR}{\pi_f \times \pi_{HPC}} = \frac{37.5}{19.423 \times 1.503}$$

$$\pi_{LPC} = 1.2846$$

Example 5.5

A two-spool turbofan engine is in its preliminary design stages. Two configurations for the engine are to be compared: namely the mixed and the unmixed types (Figures 5.22 and 5.23a respectively). The following characteristics are to be considered

M = 0.9, altitude = 33,000 ft (where T_a = 222 K and P_a = 26.2 kPa), fan pressure ratio ($\pi_f = 2$), compressor pressure ratio ($\pi_c = 8$), maximum temperature = 1,400 K, pressure drop in combustion chamber $\Delta P_{cc} = 3\%$, fuel-to-air ratio $f = 0.017$, fuel heating value Q_R = 43,000 kJ/kg, efficiencies for diffuser, compressor, fan, combustion chamber, turbines, and nozzles are, respectively, $\eta_d = 0.98$, $\eta_c = 0.88$, $\eta_f = 0.9$, $\eta_{cc} = 0.96$, $\eta_t = 0.94$, $\eta_n = 0.95$. variations in the specific heats are considered within the engine for cold and hot streams as follows:

$$c_{P_d} = c_{p_c} = c_{P_f} = 1.005 \text{ kJ/kg} \cdot \text{K}, \quad \gamma_c = 1.4, \quad c_{P_t} = c_{P_n} = 1.2 \text{ kJ/kg/K}, \quad \gamma_h = 1.33$$

Both cases have the same BPR. For the mixing type, the outlet streams of the fan and the LPT have the same total pressure just prior to mixing. Calculate

1. The BPR (β). Comment on this value.
2. TSFC.

$M = 0.9$

$H = 33{,}000 \text{ ft}, \quad P_a = 26.2 \text{ kPa}, \quad T_a = 222 \text{ K}, \quad f = 0.017, \quad Q_R = 43{,}000 \text{ kJ/kg}$

$\pi_f = 2, \quad \pi_c = 8, \quad T_{\max} = 1400 \text{ K}, \quad \Delta P_{cc} = 3\%$

$\eta_d = 0.98, \quad \eta_c = 0.88, \quad \eta_f = 0.9, \quad \eta_{cc} = 0.96, \quad \eta_t = 0.94, \quad \eta_n = 0.95, \quad \eta_{nf} = 0.95$

$c_{P_d} = c_{P_c} = c_{P_f} = 1.005 \text{ kJ/kg} \cdot \text{K}, \quad \gamma_c = 1.4$

$c_{P_t} = c_{P_n} = 1.2 \text{ kJ/kg} \cdot \text{K}, \quad \gamma_h = 1.33$

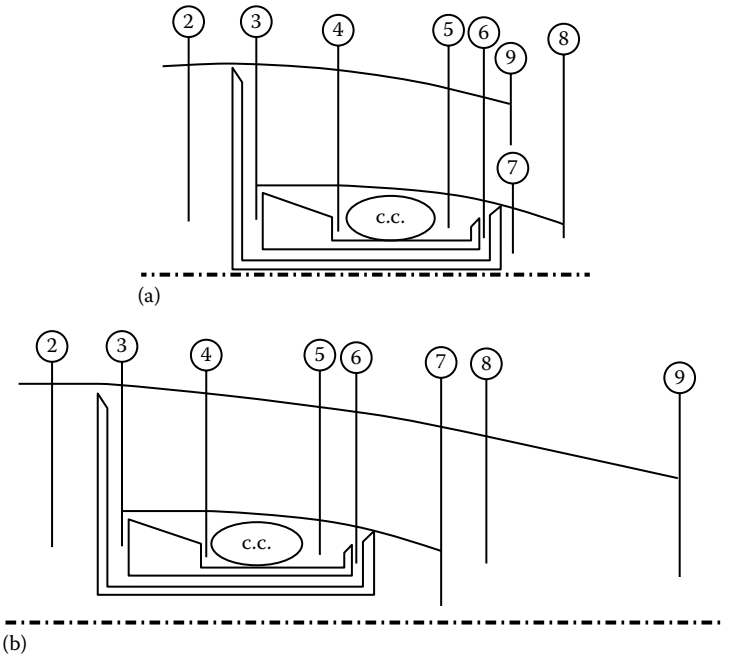


FIGURE 5.22
(a) Mixed and (b) unmixed turbofan engines.

1. Mixed turbofan

$$u = 0.9\sqrt{\gamma RT_a} = 0.9\sqrt{(1.4)(287)(222)} = 268.2 \text{ m/s}$$

$$T_{o_2} = T_a\left[1 + \frac{\gamma - 1}{2}M^2\right] = 222\left[1 + 0.2(0.9)^2\right] = 258.8 \text{ K}$$

$$T_{o_2} = 258.8 \text{ K}$$

$$\frac{P_{o_2}}{P_a} = \left(1 + \eta_d \frac{\gamma - 1}{2}M^2\right)^{\gamma/\gamma - 1} = \left[1 + (0.98)(0.2)(0.9)^2\right]^{3.5} = (1.15876)^{3.5} = 1.676$$

$$\therefore P_{o_2} = 43.9 \text{ kPa}$$

$$P_{o_3} = P_{o_2}(2) = 87.8 \text{ kPa}$$

$$T_{o_3} = T_{o_2}\left[1 + \frac{1}{\eta_f}\left(\pi_f^{\gamma - 1/\gamma} - 1\right)\right] = T_{o_2}\left[1 + \frac{1.219 - 1}{0.9}\right]$$

$$T_{o_3} = 322 \text{ K}$$

$$\frac{P_{o_4}}{P_{o_3}} = r_c = 8$$

$$P_{o_4} = 702.4 \text{ kPa}$$

$$T_{o_4} = T_{o_3}\left[1 + \frac{1}{\eta_c}\left\{\pi_c^{\gamma - 1/\gamma} - 1\right\}\right]$$

$$T_{o_4} = 344\left[1 + \frac{1}{0.88}\left(8^{0.286} - 1\right)\right] = 612 \text{ K}$$

$$P_{o_5} = 0.97 \quad P_{o_4} = 681.3 \text{ kPa}$$

$$T_{o_5} = 1400 \text{ K}$$

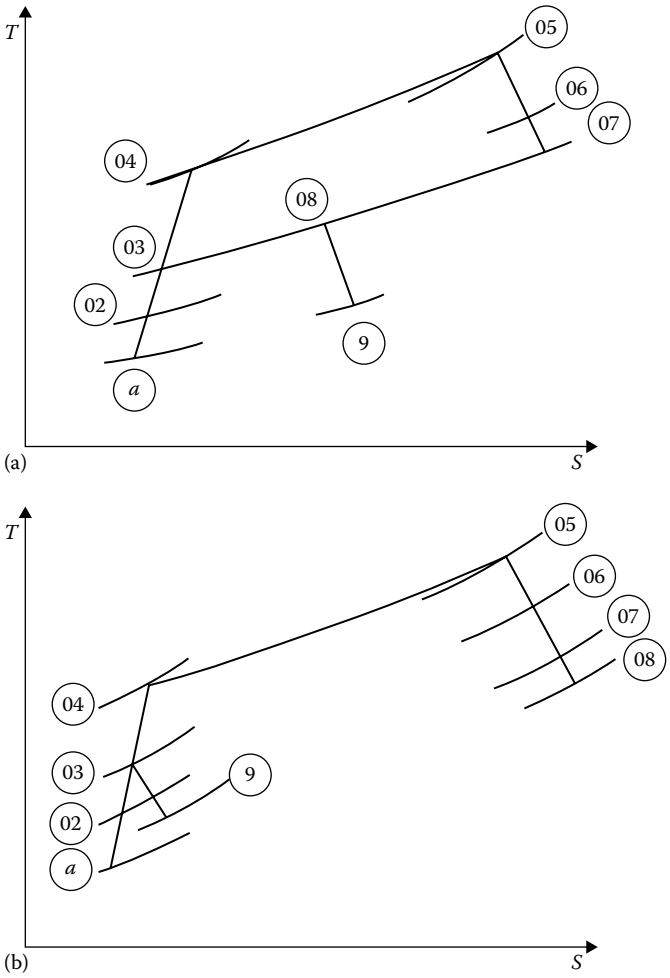


FIGURE 5.23
Temperature-entropy diagram of mixed and unmixed turbofan engines. (a) *T–S* diagram of mixed turbofan engines (b) *T–S* diagram of unmixed turbofan engines.

With $\eta_m = 1.0$, then $W_{HPT} = W_{HPC}$

$$\therefore \dot{m}_a (1+f) c_{P_t} (T_{o_5} - T_{o_6}) = \dot{m}_a c_{P_c} (T_{o_4} - T_{o_3})$$

With $f = 0.017$

$$1.017 \times 1200 (1400 - T_{o_6}) = 1005 (612 - 322)$$

$$T_{o_6} = 1161 \text{ K}$$

$$\frac{P_{o_6}}{P_{o_5}} = \left[1 - \frac{1}{\eta_t} \left(1 - \frac{T_{o_6}}{T_{o_5}} \right) \right]^{\gamma/\gamma - 1}$$

$$\frac{P_{o_6}}{P_{o_5}} = \left[1 - \frac{1}{0.94} \left(1 - \frac{1161}{1400} \right) \right]^4 = 0.4485$$

$$P_{o_6} = 305.6 \text{ kPa}$$

Mixing condition

$$P_{o_7} = P_{o_3} = P_{o_8}$$
$$\therefore P_{o_7} = 87.8 \text{ kPa}$$
$$\frac{T_{o_7}}{T_{o_6}} = 1 - \eta_t \left\{ 1 - \left(\frac{P_{o_7}}{P_{o_6}} \right)^{\gamma - 1/\gamma} \right\}$$
$$T_{o_7} = 1 - 0.94 \left\{ 1 - \left(\frac{87.8}{305.6} \right)^{0.25} \right\} = 869 \text{ K}$$

Power balance between LPT and Fan

$$W_F = W_{LPT}$$

$$\therefore \left(\dot{m}_h + \dot{m}_c \right) c_{P_f} \left(T_{o_3} - T_{o_2} \right) = \left(1 + f \right) \dot{m}_h c_{P_t} \left(T_{o_6} - T_{o_7} \right)$$

with $\beta = \dot{m}_c / \dot{m}_h$, then

$$\therefore (1 + \beta)(1005)(322 - 259) = (1.017)(1200)(1161 - 869)$$
$$1 + \beta = 5.635$$
$$\beta = 4.635$$

The process from 7 to 8 is a mixing process:

$$\therefore H_{o_3} + H_{o_7} = H_{o_8}$$

$$\dot{m}_c c_{P_c} T_{o_3} + \left(1 + f \right) \dot{m}_h c_{P_h} T_{o_7} = \left[\dot{m}_c + \dot{m}_h \left(1 + f \right) \right] c_{P_h} T_{o_8}$$
$$\beta c_{P_c} T_{o_3} + \left(1 + f \right) c_{P_h} T_{o_7} = \left[\left(1 + f \right) + \beta \right] c_{P_h} T_{o_8}$$
$$T_{o_8} = \frac{4.635 \times 1005 \times 322 + 1200 \times 869 \times 1.017}{\left(1 + 0.017 + 4.635 \right) \times 1200} = 377.5 \text{ K}$$

Propelling nozzle (process 8–9)

$$\frac{P_{o_8}}{P_a} = \frac{87.8}{26.2} = 3.35$$

But the critical pressure is calculated from the relation

$$\frac{P_{o_8}}{P_c} = \left(\frac{1}{1 - \frac{1}{\eta_n} \frac{\gamma - 1}{\gamma + 1}} \right)^{\gamma / \gamma - 1}$$
$$\frac{P_{o_8}}{P_c} = \left(\frac{1}{1 - \frac{1}{0.95} \frac{0.33}{2.33}} \right)^4 = \left(1.1752 \right)^4 = 1.9076$$
$$\frac{P_{o_8}}{P_a} > \frac{P_{o_8}}{P_c}$$

$\therefore$ Nozzle is choked

$$P_9 = P_c = \frac{P_{o_8}}{1.9076} = 46.026 \text{ kPa}$$
$$T_9 = T_c = \frac{T_{o_8}}{\frac{\gamma+1}{2}} = \frac{T_{o_8}}{1.1752} = 321.22 \text{ K}$$
$$\rho_9 = \frac{P_9}{RT_9} = \frac{46.026 \times 10^3}{287 \times 321.22}$$
$$\rho_9 = 0.499 \text{ kg/m}^3$$
$$u_9 = C_9 = \sqrt{\gamma RT_9} = \sqrt{1.33 \times 287 \times 321.22}$$
$$u_9 = 350.16 \text{ m/s}$$
$$\dot{m}_9 = \dot{m}_a + \dot{m}_f = \dot{m}_a(1+f) = \rho_9 u_9 A_9$$
$$\therefore \frac{A_9}{\dot{m}_a} = \frac{1+f}{\rho_9 u_9} = \frac{1.017}{0.499 \times 350.16}$$
$$\frac{A_9}{\dot{m}_a} = 5.81 \times 10^{-3} \left(\text{m}^2/\text{kg/s}\right)$$

Specific thrust $\frac{T}{\dot{m}_a} = \left[(1+f)u_9 - u\right] + \frac{A_9}{\dot{m}_a}(P_9 - P_a)$

$$\frac{T}{\dot{m}_a} = \left[(1.017)(350.16) - 268.8\right] + 5.81 \times 10^{-3} \times (46.026 - 26.2) \times 10^3$$
$$\frac{T}{\dot{m}_a} = 87.31 + 115.19 = 202.5 \left(\text{N} \cdot \text{s/kg}\right)$$
$$\text{TSFC} = \frac{f}{\left(T/\dot{m}_a\right)} = 0.30204 \text{ kg fuel/N} \cdot \text{h}$$

2. Unmixed turbofan

$$\frac{P_{o_3}}{P_a} = \frac{87.8}{26.2} = 3.35$$
$$\frac{P_{o_3}}{P_c} = \left(\frac{1}{1 - \frac{1}{\eta_{nf}}\frac{\gamma-1}{\gamma+1}}\right)^{\gamma/\gamma-1} = \left(\frac{1}{1 - \frac{1}{0.95}\frac{0.4}{2.4}}\right)^{3.5} = (1.2127)^{3.5} = 1.964$$
$$\frac{P_{o_3}}{P_a} > \frac{P_{o_3}}{P_c}$$

$\therefore$ Fan nozzle is choked

$$P_9 = P_c$$
$$P_9 = \frac{P_{o_3}}{1.964} = \frac{87.8}{1.964} = 44.7 \text{ kPa}$$
$$T_9 = T_c = \frac{T_{o_3}}{1.2127} = \frac{322}{1.2127} = 265.5 \text{ K}$$
$$\rho_9 = \frac{P_9}{RT_9} = \frac{44.7 \times 10^3}{287 \times 265.5} = 0.587 \text{ kg/m}^3$$
$$u_9 = \sqrt{\gamma RT_9} = \sqrt{1.4 \times 287 \times 265.5} = 326.6 \text{ m/s}$$
$$T = \beta\dot{m}_a(u_9 - u) + A_9(P_9 - P_a) + \dot{m}_a\left[u_8(1+f) - u\right] + A_8(P_8 - P_9)$$

As previously defined

$$T_{o_3} = 322\ \text{K}$$
$$T_{o_4} = 612\ \text{K}$$

Since $T_{o_5} = 1400$ K, then the energy balance between the HPC and HPT yields

$$W_{HPC} = W_{HPT}$$
$$c_{P_c}\left(T_{o_4} - T_{o_3}\right) = \left(1+f\right)c_{P_h}\left(T_{o_5} - T_{o_6}\right)$$
$$1005 \times \left(612 - 322\right) = \left(1.017\right) \times 1200\left(1400 - T_{o_6}\right)$$
$$T_{o_6} = 1161\ \text{K}$$

Since

$$\frac{P_{o_6}}{P_{o_5}} = \left\{1 - \frac{1}{\eta_t}\left(1 - \frac{T_{o_6}}{T_{o_5}}\right)\right\}^{\gamma/\gamma-1} = \left\{1 - \frac{1}{0.94}\left(1 - \frac{1161}{1400}\right)\right\}^4 = 0.4486$$

with $P_{o_5} = 681.3$ kPa, then $P_{o_6} = 305.6$ kPa.

Now, from the energy balance between the fan and LPT, since

$$W_f = W_{LPT}$$
$$\therefore \left(1+\beta\right)c_{P_c}\left(T_{o_3} - T_{o_2}\right) = \left(1+f\right)c_{P_h}\left(T_{o_6} - T_{o_7}\right)$$

With the same β

$$5.635 \times 1005 \times \left(322 - 259\right) = 1.017 \times 1200 \times \left(1161 - T_{o_7}\right)$$
$$T_{o_7} = 869\ \text{K}$$
$$\frac{P_{o_7}}{P_{o_6}} = \left\{1 - \frac{1}{\eta_t}\left(1 - \frac{T_{o_7}}{T_{o_6}}\right)\right\}^{\gamma/\gamma-1} = \left\{1 - \frac{1}{0.94}\left(1 - \frac{869}{1161}\right)\right\}^4 = 0.288$$
$$P_{o_7} = 88.02\ \text{kPa}$$
$$\frac{P_{o_7}}{P_a} = \frac{88.02}{26.2} = 3.359$$
$$\frac{P_{o_7}}{P_c} = \left(\frac{1}{1 - \frac{1}{\eta_n}\frac{\gamma-1}{\gamma+1}}\right)^{\gamma/\gamma-1} = \left(\frac{1}{1 - \frac{1}{0.95}\frac{0.33}{2.33}}\right)^4 = \left(1.1752\right)^4$$
$$\frac{P_{o_7}}{P_c} = 1.9076$$
$$\because \frac{P_{o_7}}{P_{o_6}} > \frac{P_{o_7}}{P_c}$$
$$\therefore P_c > P_a$$

The hot nozzle is choked

$$P_8 = P_c = \frac{P_{o7}}{1.9076} = 46.14 \text{ kPa}$$
$$T_8 = T_c = \frac{T_{o7}}{1.1752} = 739.4 \text{ K}$$
$$\rho_8 = \frac{P_8}{RT_8} = \frac{46.14 \times 10^3}{287 \times 739.4}$$
$$\rho_8 = 0.217 \text{ kg/m}^3$$
$$u_8 = \sqrt{\gamma RT_8} = \sqrt{1.33 \times 287 \times 739.4}$$
$$u_8 = 531 \text{ m/s}$$
$$\rho_8 u_8 A_8 = (1+f)\dot{m}_h$$
$$\frac{A_8}{\dot{m}_h} = \frac{1+f}{\rho_8 u_8} = \frac{1.017}{0.217 \times 531}$$
$$\frac{A_8}{\dot{m}_h} = 8.33 \times 10^{-3} \text{ m}^2/(\text{kg/s})$$

Define the total mass flow rate

$$\dot{M} = \dot{m}_h + \dot{m}_c = (1+\beta)\dot{m}_h$$

Since the thrust force is defined as

$$T = \beta\dot{m}_h(u_9 - u) + A_9(P_9 - P_a) + \dot{m}_h\left[(1+f)u_8 - u\right] + A_8(P_8 - P_a)$$
$$\frac{T}{\dot{M}} \equiv \frac{T}{(1+\beta)\dot{m}_h} = \frac{\beta}{1+\beta}(u_9 - u) + \frac{A_9}{(1+\beta)\dot{m}}(P_9 - P_a) + \left(\frac{1}{1+\beta}\right)\left\{(1+f)u_8 - u\right\}$$
$$+ \frac{A_8}{(1+\beta)\dot{m}_h}(P_8 - P_a)$$

Now, since $\rho_9 u_9 A_9 = \beta\dot{m}_h$

$$\therefore \frac{A_9}{\beta\dot{m}_h} = \frac{1}{\rho_9 u_9} = \frac{1}{0.587 \times 326.6} = 5.216 \times 10^{-3} \text{ m}^2/(\text{kg/s})$$
$$\therefore \frac{A_9}{(1+\beta)\dot{m}_h} = \frac{A_9}{\beta\dot{m}_h}\frac{\beta}{1+\beta} = 5.216 \times 10^{-3} \times \frac{4.635}{5.635}$$
$$\frac{A_9}{(1+\beta)\dot{m}_h} = 4.29 \times 10^{-3} \text{ m}^2/(\text{kg/s})$$

$$\frac{T}{\dot{M}} = \frac{4.635}{5.635}(326.6 - 268.8) + 4.29 \times 10^{-3}(44.7 - 26.2) \times 10^3$$
$$+ \frac{1}{5.635}\left\{(1.017)(531) - 268.8\right\} + \frac{8.83 \times 10^{-3}}{5.635}(46.14 - 26.2) \times 10^3$$
$$= 47.5 + 79.3 + 48.13 + 31.245$$
$$\frac{T}{\dot{M}} = 206.17 \text{ N/(kg/s)}$$
$$TSFC = \frac{f}{(T/\dot{M})} = \frac{0.017}{206.17} \times 3600 = 0.29664 \text{ (kg fuel/N} \cdot \text{h)}$$

From the above results, it may be deduced that, for the same BPR, fan, and compressor pressure ratios, the unmixed flow ensures higher specific thrust and better fuel economy.

5.6 Mixed Turbofan with Afterburner

5.6.1 Introduction

Since 1970, most military aircraft have been powered by a low-BPR turbofan fitted with an afterburner [7]. The first afterburning turbofan engine was the Pratt & Whitney TF30. Afterburning gives a significant thrust boost for takeoff particularly from short runways such as those on aircraft carriers, for transonic acceleration, and for combat maneuvers, though it is very fuel intensive. This engine has a mixed low-BPR forward fan. The mixed flow still has a sufficient quantity of oxygen for another combustion process. Thus, an afterburner is installed downstream of the LPT and upstream of the nozzle. Prodigious amounts of fuel are burnt in the afterburner when it is lit. This raises the temperature of exhaust gases by a significant amount which results in a higher exhaust velocity/engine specific thrust. For a turbofan engine, afterburning (or reheat) offers greater gains because of the relatively low temperature after the mixing of the hot and cold streams and the large quantity of the excess air available for combustion.

This nozzle is normally of the variable area type to furnish a suitable medium for different operating conditions. The variable-geometry nozzle must open to a larger throat area to accommodate the extra volume flow when the afterburner is lit. Unlike the main combustor, where the integrity of the downstream turbine blades must be preserved, an afterburner can operate at the ideal maximum (stoichiometric) temperature (about 2100 K [3780 R]). Now, at a fixed total applied fuel-to-air ratio, the total fuel flow for a given fan airflow will be the same, regardless of the dry specific thrust of the engine. A high specific thrust turbofan will, by definition, have a higher nozzle pressure ratio, resulting in a higher afterburning net thrust and, therefore, lower afterburning specific fuel consumption. High specific thrust engines have a high dry specific fuel consumption. A typical photo for such an engine is shown in Figure 5.24.

Examples of this type of engine and its maximum thrust are Pratt & Whitney series F100-220 (40K), F100-229 (48K), F100-232 (28K), F101 (51K), F119 (65K), Pratt & Whitney F119, Eurojet EJ200, and General Electric F110.

Some details on the afterburning engine *Adour Mk.104* will now be presented.

This engine is installed in Sepecat Jaguar aircraft. It has the following characteristics:

- Length 117 in. (with afterburner removed 77 in.) and inlet diameter 22 in.
- Two-stage axial fan, five-stage axial compressor
- Annular straight-through flow combustion chamber
- One-stage for the HPT, One-stage for the LPT
- Fully modulated afterburner
- Takeoff thrust (dry) 5260 lb and with afterburner 8000 lb

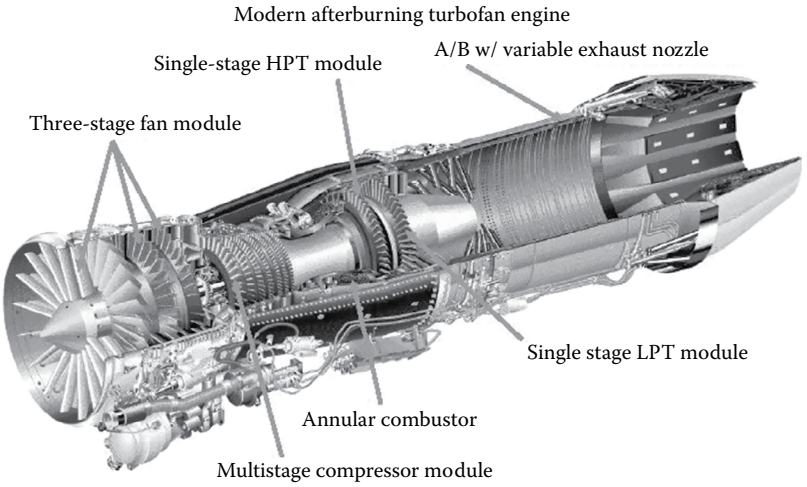


FIGURE 5.24
Afterburning two-spool turbofan engine (GE).

A Russian engine is the RD-133 afterburning turbofan TVC engine

- Length 4230 mm, maximum diameter 1040 mm
- Weight 1055 kg
- Full reheat power setting ($H = 0$, $V = 0$, ISA), 89 kN
- Maximum dry power setting ($H = 0$, $V = 0$, ISA), 55 kN
- Bypass ratio 0.437
- Maximum turbine-inlet temperature 1720 K

5.6.2 Ideal Cycle

A typical layout of such an engine together with its T–S diagram for an ideal cycle is shown in Figures 5.25 and 5.26.

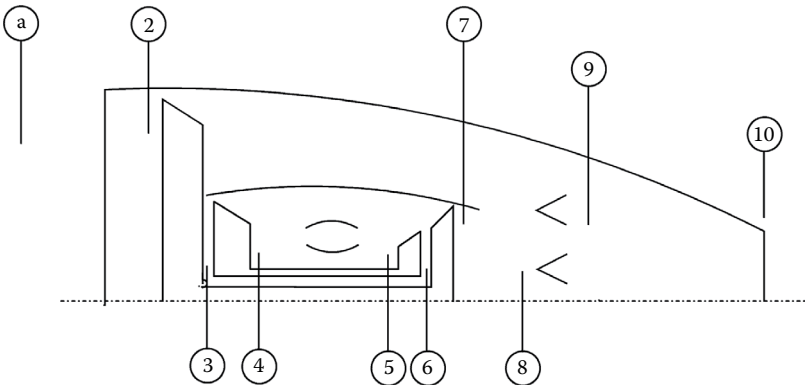


FIGURE 5.25
Layout of a typical two-spool mixed afterburning engine.

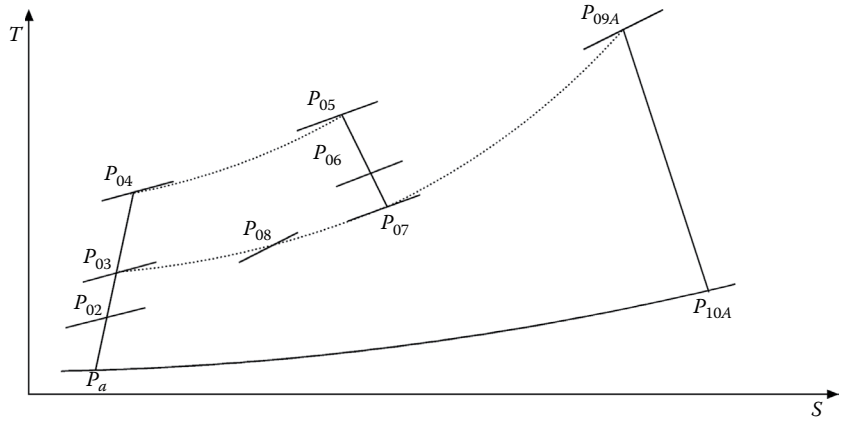


FIGURE 5.26
T–S diagram for two-spool mixed afterburning engine.

The conditions described earlier for mixing still hold. Thus, the following relation for the total pressure may be stated:

$$P_{0_3} = P_{0_7} = P_{0_8} = P_{0_9A}$$

where P_{0_9A} is the total pressure at the outlet of the afterburner, when it is operative. Moreover, the outlet temperature of the afterburner T_{0_9A} is the maximum temperature within the engine, which is known in advance. It is limited by the maximum temperature that the material of the afterburner can withstand. However, it is much higher than the total turbine-inlet temperature (TIT) due to the absence of centrifugal stresses created by the rotation of the turbine blades.

Now the energy balance in the afterburner gives the following afterburner fuel-to-air ratio (f_{ab}).

With (f_{ab}) defined as

$$f_{ab} = \frac{\dot{m}_{fab}}{\dot{m}_c + \dot{m}_h} \tag{5.39a}$$

then the balance of the afterburner yields the relation

$$f_{ab} = \frac{Cp_{9A}T_{0_9A} - Cp_8T_{0_8}}{Q_{HV} - Cp_{9A}T_{0_9A}} \tag{5.39b}$$

Now a convergent–divergent nozzle, a full expansion to the ambient pressure occurs. Thus the jet speed will be given by the relation

$$\therefore V_{10A} = \sqrt{2Cp_{10A}T_{0_9A}}\left[1 - \left(\frac{P_a}{P_{0_9A}}\right)^{\gamma_{10}-1/\gamma_{10}}\right] \tag{5.40}$$

The thrust force is now

$$T = \dot{m}_e V_{10A} - \dot{m}_a V_\infty$$

With the exhaust mass flow rate defined as

$$\dot{m}_e = m_c + \dot{m}_h\left(1+f\right)+\dot{m}_{f_{ab}}$$
$$\dot{m}_e = \left\{\dot{m}_c + \dot{m}_h\left(1+f\right)\right\}\left(1+f_{ab}\right)$$

then the thrust is now expressed as

$$T = \left\{\dot{m}_c + \dot{m}_h\left(1+f\right)\right\}\left(1+f_{ab}\right)V_{10A} - \left(\dot{m}_c + \dot{m}_h\right)V_\infty \tag{5.41}$$

5.6.3 Real Cycle

The same procedure described in the real mixed turbofans previously mentioned will be followed.

The losses in the mixing process are also governed by either one of the following equations for losses

$$P_{08} = P_{07} - \Delta P_{mixing}$$

or

$$P_{08} = r_m P_{07} \quad \text{where } r_m < 1 \approx 0.98$$

The losses in the afterburner are also governed by the relation

$$P_{09A} = P_{08} - \Delta P_{ab}$$

The afterburning combustion is no longer ideal but controlled by the efficiency of the burners. Thus the afterburning fuel-to-air ratio is now

$$f_{ab} = \frac{Cp_{9A}T_{09A} - Cp_8T_{08}}{\eta_{ab}Q_{HV} - Cp_{9A}T_{09A}} \tag{5.39c}$$

5.7 Aft-Fan

There are few turbofan engines of the aft-fan types. The most famous is the GE CF700 engine.

CF700: The CF700 turbofan engine was developed as an aft-fan engine to power the Rockwell Sabre 75 version of the Sabreliner aircraft as well as the Dassault Falcon. The CF700 was the first small turbofan to be certified by the FAA. Moreover, it was also used to train moon-mounted astronauts in the Apollo program as the powerplant for the lunar landing training vehicle.

Specifications

- Fan/compressor stages: 1/8, core/power turbine stages: 2/1
- Maximum diameter: 33 in., length: 75.5 in.
- Dry weight (lb): 725–737.

Application examples: Falcon 20 and Sabreliner 75A/80A.

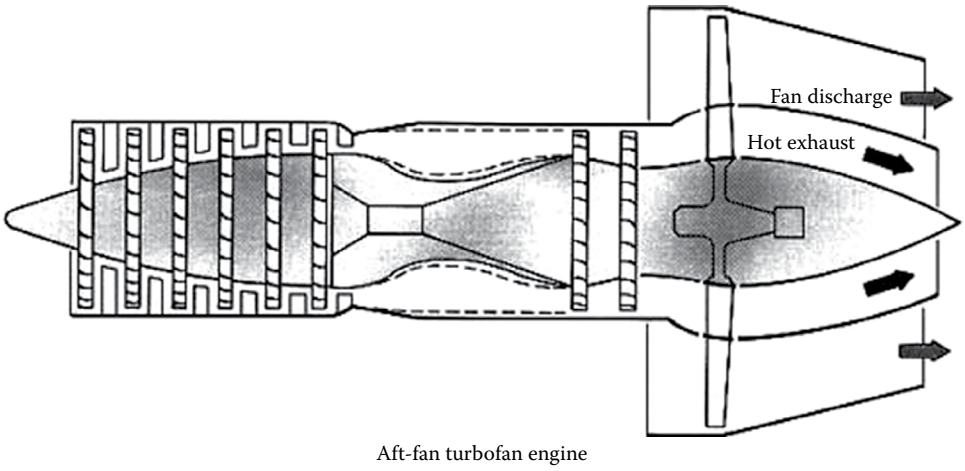


FIGURE 5.27
Layout of aft-fan configuration.

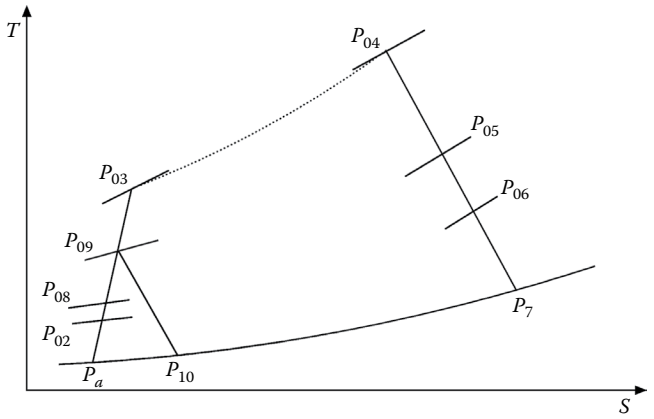


FIGURE 5.28
T–S diagram for aft-fan.

Figures 5.27 and 5.28 show the layout of a typical aft-fan together with its *T–S* diagram.

The engine is composed of a single spool (compressor driven by turbine as normal) and another turbine/fan configuration. This LPT has blades extending outside the engine core to form the fan section. The blading of the turbine fan must be designed to give turbine blade sections for the hot stream and a compressor blade section for the cold stream. Thus a blading of high cost arises, because the entire blade must be made from the turbine material of high weight.

Moreover, manufacturing of these blades is so complicated when the inner part is a turbine blade and the outer part is a fan blade. The convex shape of the inner part of the blade becomes a concave in the outer part of the blade and vice versa. This is a necessity as the direction of rotation of the compressor blades must be from the pressure side to the suction side of the opposite blade, while the turbine is from the suction side to the pressure side.

In addition, if the turbine blades have to be cooled, then a highly sophisticated manufacturing process is needed. Finally, sealing between the hot and cold streams is needed.

1. Core or gas generator intake
   The intake for the core or the gas generator has the same governing equations: Equations 5.1 and 5.2.
2. Fan intake
   Similar governing equations are used with the efficiency of fan diffuser rather than the efficiency of the core diffuser

$$P_{08} = P_a\left(1+\eta_{fd}\frac{\gamma_c-1}{2}M_a^2\right)^{\gamma_c/\gamma_c-1} \tag{5.42}$$

$$T_{08} = T_{0a} = T_a\left(1+\frac{\gamma_c-1}{2}M_a^2\right) \tag{5.43}$$

   Note that

$$T_{02} = T_{08} \quad \text{while} \quad P_{02} \neq P_{08} \text{ as } \eta_{fd} \neq \eta_d$$

3. Compressor
   For known values of the pressure ratio and efficiency of the compressor, the outlet pressure and temperature of the compressor are obtained as

$$P_{03} = \pi_c P_{02}$$
$$T_{03} = T_{02}\left[1+\frac{1}{\eta_c}\left(\pi_c^{\gamma_c-1/\gamma_c}-1\right)\right]$$

4. Fan
   The outlet pressure and temperature of the fan section are determined as follows;

$$P_{09} = \pi_f P_{08}$$
$$T_{09} = T_{08}\left[1+\frac{1}{\eta_f}\left(\pi_f^{\gamma_c-1/\gamma_c}-1\right)\right]$$

5. Combustion chamber
   The pressure at the outlet of the combustion chamber is defined as

$$P_{o4} = P_{03} - \Delta P_{cc}$$
$$P_{o4} = P_{03}\left(1-\Delta P_{cc}\%\right)$$

   While the maximum cycle temperature T_{04} is known, the fuel-to-air ratio is defined as usual from the typical relation

$$f = \frac{Cp_h T_{04} - Cp_c T_{03}}{\eta_b Q_{HV} - Cp_h T_{04}}$$

6. Compressor turbine or the HPT
   The temperature at the outlet from the turbine driving the compressor is determined from the energy balance between the compressor and turbine incorporating a mechanical efficiency η_{m1}

$$\begin{gathered} W_c = \eta_{m1} W_{HPT} \\ Cp_c\left(T_{03} - T_{02}\right) = \eta_{m1}\left(1+f\right) Cp_h\left(T_{04} - T_{05}\right) \end{gathered} \tag{5.44}$$

   Thus the temperature at the outlet of the HPT T_{05} is now known. From this temperature and the isentropic efficiency of the HPT, P_{05} can be calculated as follows

$$P_{05} = P_{04}\left(1 - \frac{T_{04} - T_{05}}{\eta_{t1} \times T_{04}}\right)^{\left(\gamma_h/\gamma_h - 1\right)} \tag{5.44a}$$

7. Fan turbine
   Also, from the energy balance between the fan and the LPT incorporating a second mechanical efficiency η_{m2},

$$\begin{gathered} W_f = W_{LPT} \\ \beta \dot{m}_a Cp_c\left(T_{09} - T_{08}\right) = \eta_{m2} \dot{m}_a\left(1+f\right) Cp_h\left(T_{05} - T_{06}\right) \end{gathered} \tag{5.45}$$

8. Nozzles
   The aft-fan is also of the unmixed type. Thus it has also two outlet streams: one exits from the cold (fan) section through the fan nozzle, the other is the hot stream and exits from the turbine nozzle. For both nozzles, a check for their choking is needed. Thus the outlet pressures of the hot and cold streams (P_7, P_{10}) are calculated if different from the ambient pressure. The outlet velocities (V_7, V_{10}) are also calculated.
   The general thrust equation is now

$$T = \dot{m}_a\left[\left(1+f\right)V_7 - V\right] + \beta \dot{m}_a\left(V_{10} - V\right) + A_7\left(P_7 - P_a\right) + A_{10}\left(P_{10} - P_a\right) \tag{5.46}$$

5.8 VTOL and STOL (V/STOL)

Vertical takeoff and landing (VTOL) or short takeoff and landing (STOL) are desirable characteristics for any type of aircraft, provided that its normal performance characteristics are fulfilled [8]. This type of engine requires a takeoff thrust of about 120% of the takeoff weight, because the lift has to be produced by the propulsion system [9]. Many approaches were tried after the 1950s for both civil and military applications. However, it became clear that VTOL was not economical for civil applications and there were major problems with engine noise in urban areas. Development then focused on military applications, primarily for fighters; the VTOL capability offered the chance to operate from unprepared areas, aircraft carriers, or from battle-damaged airfields. This is achieved by what is known as the

lift/propulsion engine. This type of engine is capable of providing thrust for both normal wing prone flight and for lift. It is achieved by changing the direction of thrust either by a deflector system consisting of one, two, or four swiveling nozzles or by a device known as a switch-in deflector, which redirects the exhaust gases from a rearward-facing propulsion nozzle to one or two downward-facing lift nozzles.

5.8.1 Swiveling Nozzles

The only really successful system to date is the single-engined vectored thrust installation of the Rolls-Royce Pegasus in the Harrier; see Figure 5.29. The Pegasus is basically a conventional unmixed turbofan engine having separate exhausts, with vectoring nozzles for both hot and cold streams. The bypass cold air is exhausted into a pair of swiveling nozzles, one on each side of the aircraft. In addition, the hot gases are also exhausted via two swiveling nozzles, one on each side of the airplane. In this way, the Pegasus, the first ducted-fan lift/propulsion engine (Figure 5.30) evolved. The Pegasus engine develops a vertical takeoff thrust up to 98 kN (17,000 lb_f). The exhaust nozzles may be rotated to provide any combination of horizontal and vertical thrust.

The Pegasus engine is of the two-spool unmixed type and has a three-stage fan, while the compressor has eight stages. Each is driven by a two-stage turbine. A schematic diagram for the Pegasus engine and its *T*–*S* diagram are shown in Figures 5.31 and 5.32.



FIGURE 5.29
Harrier aircraft.

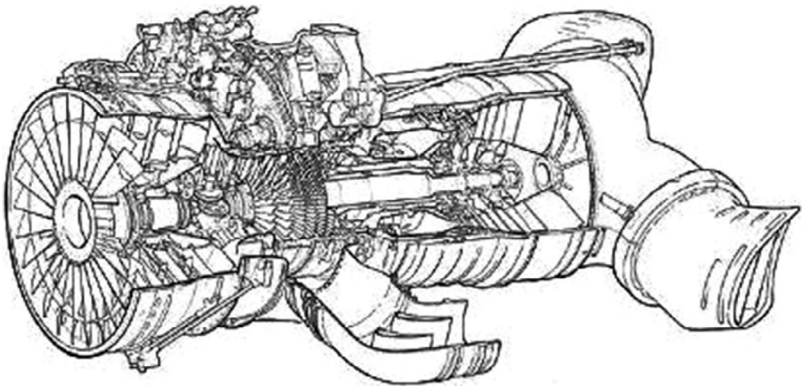


FIGURE 5.30
The Harrier engine: Pegasus.

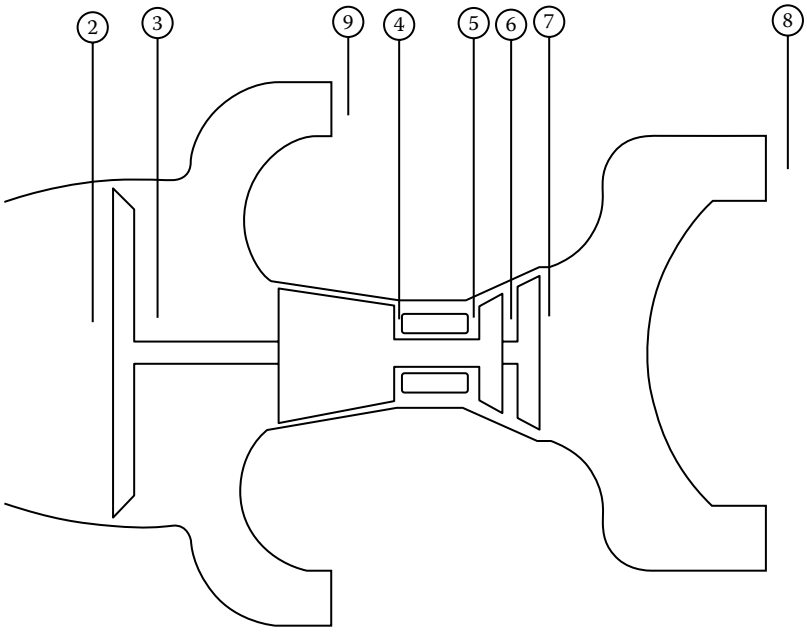


FIGURE 5.31
Schematic diagram of the Harrier engine: Pegasus.

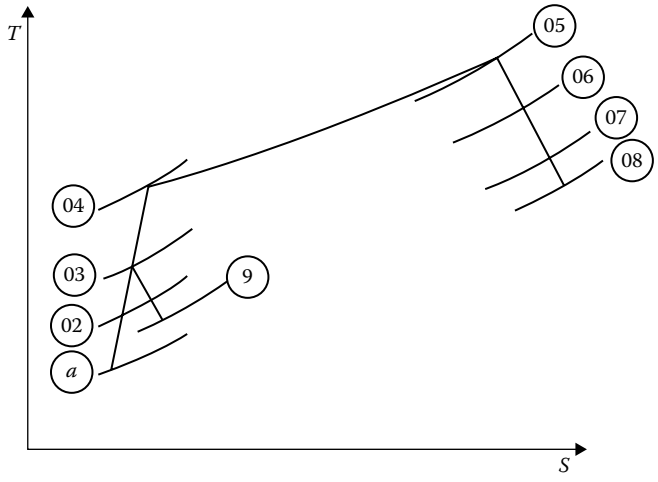


FIGURE 5.32
T–S diagram of the Harrier engine.

Example 5.6

Hawker Siddeley Harrier G.R.MK.1 illustrated in Figure 5.29 is a single seat V/STOL ground attack fighter. It is powered by a single turbofan engine. The fan and turbine exhausts pass through two pairs of swiveling nozzles as shown. During takeoff the plane moves vertically. The nozzles are rotated at 90° such that the thrust force is now a lift force. The turbofan engine has the following characteristics (Figure 5.33).

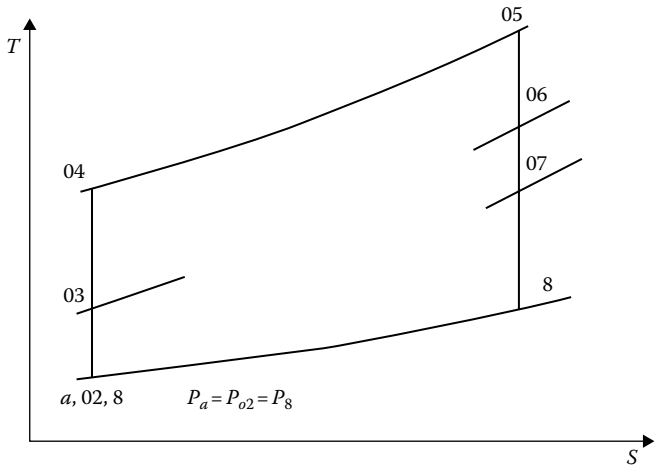


FIGURE 5.33
Temperature-entropy diagram for ideal processes of the Pegasus at takeoff.

Static takeoff thrust	98.0 kN
Fan pressure ratio	1.7
Compressor pressure ratio	6.0
Maximum temperature	1,200 K
Fuel heating value	43,000 kJ/kg
Bypass ratio	1.0

The fan is driven by the HPT. For sea-level conditions ($T_a = 288\,\text{K}, P_a = 101$ kPa), assume that

1. All the processes are ideal
2. Both fan nozzle and turbine nozzle are unchoked
3. Constant properties equivalent to the cold air ($Cp = 1.005$ kJ/kg/K and $\gamma = 1.4$)

Calculate

a. The total mass flow rate
b. The thermal efficiency.

Solution

Since the BPR $\beta = 1$

$$\therefore \dot{m}_C = \dot{m}_h = \frac{1}{2}\dot{m}_a$$

Diffuser: For static operation

$$P_{O_2} = P_a = 101\,\text{kPa}$$

and

$$T_{02} = T_a = 288\,\text{K}$$

Fan

$$P_{O3} = \pi_f \quad P_{O2} = 1.7 \times 101$$
$$P_{O3} = 171.7 \text{ kPa}$$

$$T_{O2} = T_a = 288 \text{ K}$$

$$T_{O3} = T_{O2}\pi_f^{\gamma_c - 1/\gamma_c} = 335.2 \text{ K}$$

Compressor

$$P_{O4} = \pi_C P_{O3} = 1030.2 \text{ kPa}$$
$$T_{O4} = \left(T_{O3}\right)\pi^{\gamma_c - 1/\gamma_c} = 559.6 \text{ K}$$

Combustion chamber

$$f = \frac{Cp\left(T_{O5} - T_{O4}\right)}{Q_R - CpT_{O4}} = \frac{1.005 \times \left(1{,}200 - 559.6\right)}{43{,}000 - 1.005 \times 1{,}200} = \frac{643.6}{41{,}794} = 0.0154$$

$$P_{O5} = P_{O4} = 1030.2 \text{ kPa}$$

Energy balance for the high-pressure spool

$$W_C = W_t$$

$$\dot{m}_h Cp\left(T_{O4} - T_{O3}\right) = \dot{m}_h\left(1 + f\right)Cp\left(T_{O5} - T_{O6}\right)$$

$$T_{O4} - T_{O3} = \left(1 + f\right)\left(T_{O5} - T_{O6}\right)$$

$$T_{O6} = T_{O5} - \frac{\left(T_{O4} - T_{O6}\right)}{\left(1 + f\right)} = 1200 - \frac{\left(559.6 - 335.2\right)}{\left(1 + 0.0154\right)} = 979 \text{ K}$$
$$P_{O6} = P_{O5}\left(\frac{T_{O6}}{T_{O5}}\right)^{\gamma/\gamma - 1} = 1030.2\left(\frac{979}{1200}\right)^{3.5} = 505 \text{ kPa}$$

Energy balance for the low-pressure spool (*fan and free power turbine*)

$$W_f = W_{ft}$$

$$\dot{m}_a Cp\left(T_{O3} - T_a\right) = \dot{m}_h\left(1 + f\right)Cp\left(T_{O6} - T_{O7}\right) = \left(\frac{\dot{m}_a}{1 + \beta}\right)\left(1 + f\right)Cp\left(T_{O6} - T_{O7}\right)$$

$$T_{O7} = T_{O6} - \left(\frac{1 + \beta}{1 + f}\right)\left(T_{O3} - T_a\right) = 979 - \frac{2}{1.0154}\left(335.2 - 288\right) = 886 \text{ K}$$
$$P_{O7} = P_{O6}\left(\frac{T_{O7}}{T_{O6}}\right)^{\gamma/\gamma - 1} = 505\left(\frac{886}{979}\right)^{3.5} = 356.2 \text{ kPa}$$

$$T_8 = T_{O7}\left(\frac{P_8}{P_{O7}}\right)^{\gamma - 1/\gamma} = 886\left(\frac{101}{356.2}\right)^{0.286} = 617.9 \text{ K}$$

$$V_8 = \sqrt{2Cp\left(T_{O7} - T_8\right)} = \sqrt{2 \times 1005 \times \left(886 - 617.9\right)} = 734 \text{ m/s}$$

$$V_9 = \sqrt{2Cp\left(T_{O3} - T_a\right)} = \sqrt{2 \times 1005 \times \left(335.2 - 288\right)} = 308 \text{ m/s}$$

The thrust force will be

$$\frac{T}{\dot{m}_a} = \frac{\beta}{1+\beta} V_9 + \frac{\left(1+f\right)}{\left(1+\beta\right)} V_8 = \left[\frac{308}{2} + \frac{1.0154}{2} \times 734\right] = 525.65 \text{ N} \cdot \text{s/kg}$$

Since the thrust force is 98 kN, then

$$98 \times 10^3 = 526.65 \dot{m}_a$$
$$\therefore \dot{m}_a = 186.07 \text{ kg/s}$$

Thermal Efficiency: The general equation for η_{th} of a turbofan engine (unchoked case) is

$$\eta_{th} = \frac{\frac{\beta}{1+\beta} V_{cc}^2 + \frac{1+f}{1+\beta} V_{eh}^2 - V_f^2}{\frac{2f}{1+\beta} Q_R}$$

For takeoff conditions

$$\eta_{th} = \frac{\dot{m}_a \left[\frac{\beta}{1+\beta} V_9^2 + \frac{1+f}{1+\beta} V_8^2\right] - 0}{2\dot{m}_f Q_R}$$

with $\beta = 1$,

$$f = \frac{\dot{m}_f}{\dot{m}_h} = \frac{2\dot{m}_f}{\dot{m}_a}$$
$$\therefore 2\dot{m}_f = f\dot{m}_a$$

$$\eta_{th} = \frac{V_9^2 + \left(1+f\right)V_8^2}{2fQ_R} = \frac{\left(308\right)^2 + \left(1.0154\right)\left(734\right)^2}{2 \times 0.0154 \times 43 \times 10^6} = 0.484 = 48.4\%$$

5.8.2 Switch-in Deflector System

Another suggested technique for thrust vectoring is the switch-in deflector. It is not been available in reality until now. However, it is visible. One of the switch-in-deflector systems is used in the tandem fan or hybrid fan vectored thrust engine [8]; see Figure 5.34.

The illustrated turbofan is of the mixed-flow afterburning turbofan type. A deflector is positioned inbetween the tandem fan. During cruise, the engine operates as a mixed-flow turbofan engine with the valve switched in the off position. During takeoff or lift thrust, the valve is switch so that the exhaust flow from the front part of the fan exhausts through a downward-facing lift nozzle and a secondary inlet is opened to provide the required

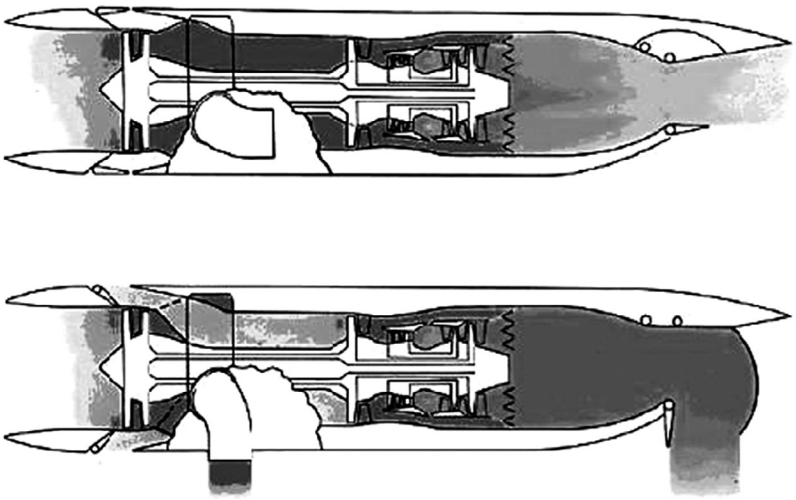


FIGURE 5.34
Vectored thrust engine.

airflow to the rear part of the fan and the main engine. In fact, it cannot truly be called a typical unmixed turbofan engine. The only difference is that the air passing through the fan is not split into two streams, cold and hot. However, two exhaust streams exist as in the unmixed turbofan engines (Figures 5.34 and 5.35b).

A detailed thermodynamic analysis of the engine illustrated is given here.

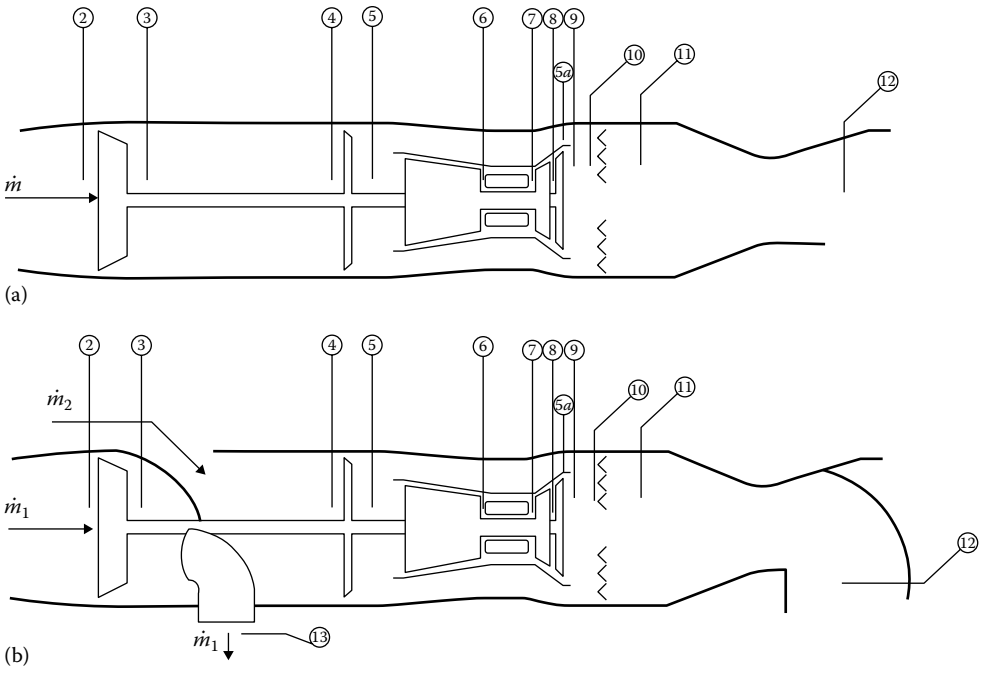


FIGURE 5.35
Illustration of schematic diagram for the engine during (a) cruise and (b) takeoff conditions.

5.8.2.1 Cruise

The different processes are presented by Figure 5.36.

Intake: Air is sucked into the engine core through the intake. The ambient conditions depend on the cruise altitude. The process from state (a) to state (2) is governed by the flight speed (V) or the free stream Mach number (M) and the isentropic efficiency of the diffuser (η_d). The outlet pressure and temperature are

$$P_{02} = P_a\left(1+\eta_d\frac{\gamma_c-1}{2}M_a^2\right)^{\gamma_c/\gamma_c-1} \tag{5.47}$$

$$T_{02} = T_{0a} = T_a\left(1+\frac{\gamma_c-1}{2}M_a^2\right) \tag{5.48}$$

Fan: First part: The first part (stage) of the fan has a pressure ratio and isentropic efficiency of (π_{f1}, η_{f1}).

The inlet conditions are (T_{02}, P_{02}). The outlet pressure and temperature are calculated as follows

$$P_{03} = \left(P_{02}\right)\left(\pi_{f1}\right) \tag{5.49}$$

$$T_{03} = T_{02}\left[1+\frac{1}{\eta_{f1}}\left(\pi_{f1}^{\gamma_c-1/\gamma_c}-1\right)\right] \tag{5.50}$$

Second part: A pressure drop in the long duct separating the two parts of the fan is ΔP_f, then

$$P_{04} = P_{03} - \Delta P_f$$

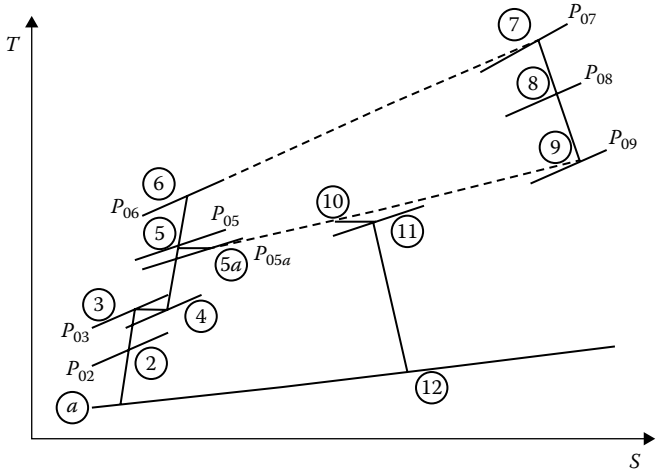


FIGURE 5.36
Temperature-entropy diagram for cruise conditions. Cruise operation inoperative afterburner.

The total temperature remains the same

$$T_{04} = T_{03}$$

Concerning the second part (stage) of the fan with a pressure ratio and isentropic efficiency of (π_{f2}, η_{f2}), the pressure and temperature at the fan outlet are

$$P_{05} = \left(P_{04}\right)\left(\pi_{f2}\right) \tag{5.51}$$

$$T_{05} = T_{04}\left[1 + \frac{1}{\eta_{f2}}\left(\pi_{f2}^{\gamma_c - 1/\gamma_c} - 1\right)\right] \tag{5.52}$$

Compressor: The compressed air leaving the fan is divided into two streams. The cold stream passes in an annulus duct surrounding the engine (from state 5 to state 5*a*), while the hot stream proceeds forward toward the compressor and the subsequent hot section. This division occurs in a proportion of the BPR (β), where

$$\beta = \frac{\dot{m}_c}{\dot{m}_h}$$

Only one compressor exists here and the compression process within the compressor depends on its pressure ratio and isentropic efficiency (π_c, η_c). The outlet conditions are

$$P_{06} = \left(P_{05}\right)\left(\pi_c\right) \tag{5.53}$$

$$T_{06} = T_{05}\left[1 + \frac{1}{\eta_c}\left(\pi_c^{\gamma_c - 1/\gamma_c} - 1\right)\right] \tag{5.54}$$

A quantity of air is bled from a position downstream of the compressor for several reasons including turbine cooling.

This bled air is $\dot{m}_b$, where the bleed ratio is expressed as

$$b = \frac{\dot{m}_b}{\dot{m}_h}$$

Combustion chamber: The maximum temperature in the outlet of the combustion chamber is known (T_{07}) and the pressure within the combustion chamber enhances a pressure drop, thus

$$P_{07} = P_{06}\left(1 - \Delta P_{cc}\right) \tag{5.55}$$

The fuel burnt in the combustion chamber is determined from the energy balance

$$f = \frac{\left(1-b\right)\left(Cp_h T_{07} - Cp_c T_{06}\right)}{\eta_b Q_R - Cp_h T_{07}} \tag{5.56}$$

HPT: The HPT drives the high-pressure compressor. The mechanical efficiency of the high-pressure spool is (η_{m1}). The outlet pressure and temperature are obtained from the energy balance between the compressor and turbine

$$\eta_{m1} W_{HPT} = W_c$$
$$\eta_{m1} \dot{m}_h (1 + f - b) Cp_h (T_{07} - T_{08}) = \dot{m}_c Cp_c (T_{06} - T_{05})$$

The outlet temperature is then obtained from the preceding relation as

$$T_{08} = T_{07} - \frac{Cp_c (T_{06} - T_{05})}{\eta_{m1} Cp_h (1 + f - b)} \tag{5.57}$$

The outlet pressure depends on the isentropic efficiency of the HTP (η_{t1}) and is given by the relation

$$\frac{P_{08}}{P_{07}} = \left[1 - \frac{1 - (T_{08}/T_{07})}{\eta_{t1}} \right]^{\gamma_h/\gamma_h - 1} \tag{5.58}$$

LPT: The LPT drives the tandem fan. If the mechanical efficiency for the low pressure spool is (η_{m2}), then the energy balance for the turbine and fan is

$$\eta_{m2} W_{LPT} = W_{f1} + W_{f2}$$
$$\eta_{m2} \dot{m}_h (1 + f - b) Cp_h (T_{08} - T_{09}) = \dot{m}_a Cp_c (T_{05} - T_{02})$$

Since

$$\dot{m}_h = \frac{\dot{m}_a}{1 + \beta}$$

the outlet temperature from the low-pressure turbine will be

$$T_{09} = T_{08} - \frac{(1 + \beta)}{\eta_{m2} (1 + f - b)} (T_{05} - T_{02}) \tag{5.59}$$

Mixing process: The cold air passes through the fan duct which surrounds the hot section, will experience a pressure drop (ΔP_{fd}), where

$$P_{05a} = P_{05} - \Delta P_{fd} \tag{5.60a}$$

The air leaves the fan duct at the same temperature as it enters; thus

$$T_{05a} = T_{05} \tag{5.61}$$

This cold air mixes with the hot gases leaving the LPT. An energy balance is necessary to determine its state prior to entering the subsequent elements. The conditions for this mixing process are equal static pressure and equal speeds, which assures equal total pressures, for air and gases at states (5*a*) and (9) respectively, or

$$P_{05a} = P_{09} \tag{5.60b}$$

The energy balance for the mixing process is

$$\dot{m}_c Cp_c T_{05a} + \left(1 + f - b\right)\dot{m}_h Cp_h T_{09} = \left[\dot{m}_c + \left(1 + f - b\right)\dot{m}_h\right] Cp_h T_{010}$$

Thus the total temperature after mixing process will be

$$T_{010} = \frac{\beta Cp_c T_{05a} + \left(1 + f - b\right) Cp_h T_{09}}{\left(1 + \beta + f - b\right) Cp_h} \tag{5.62}$$

This mixing process experience also a slight pressure drop of (ΔP_m) where

$$P_{010} = \left(1 - \Delta P_m\right) P_{09}$$

Afterburner: During cruise, the afterburner is inoperative. Thus the hot gases pass through it. Again the presence of flameholders, igniters, and other elements in the afterburner results in a pressure drop (ΔP_{ab}), thus

$$P_{11} = \left(1 - \Delta P_{ab}\right) P_{010} \tag{5.63}$$

The total temperature remains the same as in the inlet to afterburner; thus

$$T_{011} = T_{010} \tag{5.64}$$

Nozzle: The gases expend through the nozzle to the ambient pressure, so the outlet temperature is

$$T_{12} = T_{011}\left[1 - \eta_n\left\{1 - \left(\frac{P_{12}}{P_{011}}\right)^{\gamma_h - 1/\gamma_h}\right\}\right] \tag{5.65}$$

The jet or exhaust speed is

$$V_j = \sqrt{2Cp_h\left(T_{011} - T_{12}\right)} \tag{5.66}$$

Thrust force: The thrust force for such an unchoked nozzle is given by the relation

$$T = \dot{m}_a\left[\left(1 + \frac{f - b}{1 + \beta}\right)V_j - V\right] \tag{5.67}$$

5.8.2.2 Takeoff or Lift Thrust

During takeoff or lift thrust, the valve is switched so that the air mass flow rate ($\dot{m}_1$) passing through the front part of the fan exhausts through a downward-facing lift nozzles at the cold exhaust speed (V_{ef}). A secondary inlet is opened to provide the required airflow rate ($\dot{m}_2$) to the rear part of the fan and the main engine. The resulting hot gases also leave the engine vertically downward to generate a second lift thrust. Figure 5.37 illustrates the *T*–*S* diagram for takeoff conditions.

Now, the different processes are discussed.

Intake: The outlet conditions are same as the ambient ones

$$T_{02} = T_a, \quad P_{02} = P_a$$

Fan: The first part of the fan compresses the air to the same outlet conditions as expressed in the earlier cruise case. However, this compresses air flows through the downward nozzles to the ambient pressure. The exhaust speed is then

$$V_{ef} = V_{13} = \sqrt{2Cp_c\eta_{fn}T_{o3}\left\{1-\left(\frac{P_a}{P_{o3}}\right)^{\gamma_c-1/\gamma_c}\right\}} \tag{5.68}$$

The second part of the fan receives the secondary airflow rate ($\dot{m}_2$), which enters the engine through the secondary port. This air enters at the ambient conditions, thus

$$T_{04} = T_a, \quad P_{04} = P_a \tag{5.69}$$

The outlet conditions will be calculated by the same Equations 5.51 and 5.52.

Compressor: The compressed air leaving the fan ($\dot{m}_2$) is divided into two streams. The cold stream passes in an annulus duct surrounding the engine, while the hot stream proceeds toward the compressor and the subsequent hot section. This division occurs in a proportionality of the BPR (β).

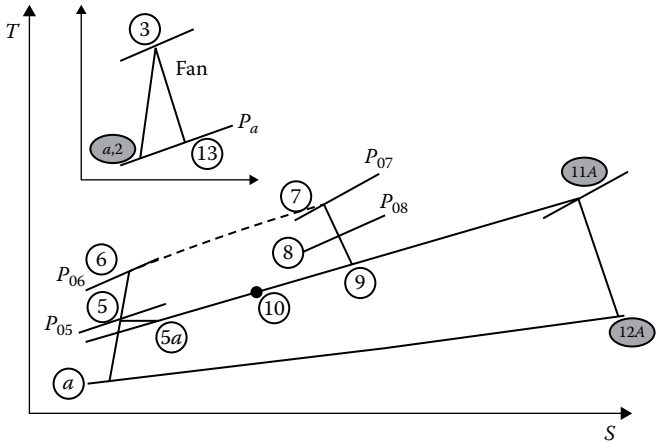


FIGURE 5.37
Temperature-entropy diagram for takeoff condition. Takeoff operative afterburner.

The outlet conditions are determined from the same Equations 5.53 and 5.54.

A quantity of air is bled from a position downstream the compressor for several reasons including turbine cooling.

Also an amount of air $\dot{m}_b$ is bled just downstream of the compressor.

Combustion chamber: The combustion process raises the temperature to (T_{07}), which is known in advance. The pressure within the combustion chamber enhances a pressure drop, thus Equation 5.55 is used to determine the outlet pressure. The fuel burnt in the combustion chamber is determined from Equation 5.56.

HPT: The HPT drives the HPC. The mechanical efficiency of the high-pressure spool is (η_{m1}). The outlet pressure and temperature are obtained from Equations 5.57 and 5.58.

LPT: The LPT drives the tandem fan. Considering a mechanical efficiency for this low-pressure spool of (η_{m2}), the energy balance for the turbine and fan is

$$\eta_{m2} W_{LPT} = W_{f1} + W_{f2}$$
$$\eta_{m2} \dot{m}_h (1 + f - b) Cp_h (T_{08} - T_{09}) = \dot{m}_1 Cp_c (T_{03} - T_{02}) + \dot{m}_2 Cp_c (T_{05} - T_{04})$$

The outlet temperature from the LPT will be

$$T_{09} = T_{08} - \frac{Cp_c}{\eta_{m2}(1 + f - b)} \left[\dot{m}_1 (T_{03} - T_{02}) + \dot{m}_2 (T_{05} - T_{04}) \right] \tag{5.70}$$

The outlet temperature is determined from the relation

$$\frac{P_{09}}{P_{08}} = \left[1 - \frac{1 - (T_{09}/T_{08})}{\eta_{t2}} \right]^{\gamma_h/\gamma_h - 1}$$

Mixing process: The cold air passes through the cold duct (denoted here as a fan duct) surrounding the hot section. Equations 5.60 and 5.61 are again used to determine the properties of the cold air just prior to mixing.

This cold air mixes with the hot gases leaving the LPT. Thus the total temperature after the mixing process will be also calculated from Equation 5.62. The total pressure after the mixing process is determined from Equation 5.63.

Afterburner: During takeoff the afterburner is operative, so another combustion process takes place. The temperature of these hot gases is raised to the maximum temperature in the engine, which is (T_{011A}). This combustion process is associated with a pressure loss ($\overline{\Delta P_{ab}}$). A bar is added to this pressure drop to discriminate between the dry and wet operation of the afterburner, thus

$$P_{11} = \left(1 - \overline{\Delta P_{ab}}\right) P_{010} \tag{5.71}$$

The total temperature remains the same as in the inlet to afterburner; thus

$$T_{011A} = T_{\max} \tag{5.72}$$

A large quantity of additional fuel is burnt during the operation of the afterburner. The energy balance for the afterburner yields the following afterburner fuel–to-air ratio

$$f_{ab} = \frac{(1+\beta+f-b)Cp_h(T_{\max}-T_{010})}{\eta_{ab}Q_R - Cp_h T_{\max}} \tag{5.73}$$

where $f_{ab} = \dot{m}_{fab}/\dot{m}_h$.

Nozzle: The gases expand through the nozzle to the ambient pressure, thus the outlet temperature is

$$T_{12A} = T_{011A}\left[1-\eta_n\left\{1-\left(\frac{P_a}{P_{011A}}\right)^{\gamma_h-1/\gamma_h}\right\}\right] \tag{5.74}$$

The jet or exhaust speed is

$$V_{12A} = \sqrt{2Cp_h(T_{011A}-T_{12A})} \tag{5.75}$$

Thrust force: The thrust force for such an unchoked nozzle is given by the relation

$$T = \dot{m}_1 V_{13} + \frac{\dot{m}_2}{(1+\beta)}(1+\beta+f+f_{ab}-b)V_{12A} \tag{5.76}$$

5.9 Performance Analysis

The turbofan engine GE90 represents the investment of General Electric in the future of wide-body aircraft. Over the period 1980–2000, GE's CF6 and CFM56 engines have been chosen to power more than 50% of all new aircraft ordered with a capacity of 100 passengers or more.

Example 5.7

The data of a highBPR (similar to GE90) during cruise operation is listed below. We need to calculate thrust, fuel mass flow rate, fuel consumption, TSFC, specific thrust, propulsive efficiency, thermal efficiency, and overall efficiency. Sketch the *T*–*S* diagram and plot the engine map for TIT from 1380 to 1600 and OPR form 15 to 43 (Figure 5.38).

GE90 ENGINE DATA

Area of hot nozzle = 1.0111 m^2

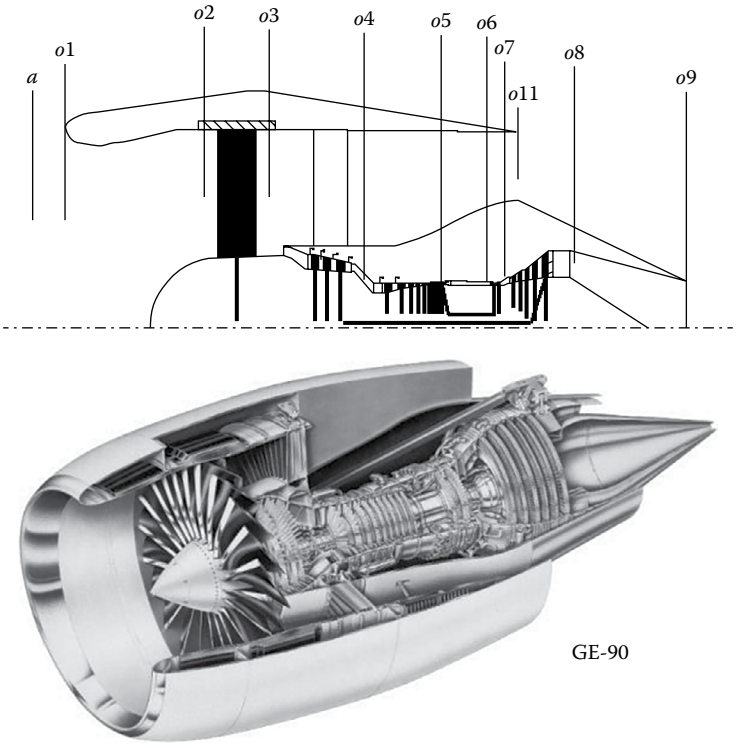


FIGURE 5.38
High-BPR (similar to GE90 turbofan engine).

Area of cold nozzle = 3.5935 m^2
Main engine parameters

Component	Real Case
η_d (Intake efficiency)	0.98
η_{fn} (Isentropic fan nozzle efficiency)	0.95
η_f (Fan polytropic efficiency)	0.93
$\eta_{C_{LPC}}$ (LPC efficiency)	0.91
$\eta_{C_{HPC}}$ (HPC efficiency)	0.91
η_{CC} (Combustion chamber's efficiency)	0.99
ΔP_{cc} Combustion pressure loss (ratio)	0.02
Q_{hv} (J/kg)	4.80E+07
η_m (Mechanical efficiency)	0.99
$\eta_{t_{HPT}}$ (HPT efficiency)	0.93
$\eta_{t_{LPT}}$ (LPT efficiency)	0.93
η_n (Isentropic nozzle efficiency)	0.95
β (BPR)	8.1
π_f (Fan pressure ratio)	1.7
$\pi_{C_{LPC}}$ (LPC pressure ratio)	1.14
$\pi_{C_{HPC}}$ (HPC pressure ratio)	21.0

The engine operation conditions

M (Mach number)	0.85
Altitude (m)	10,668
T_a (K)	218.934
P_a (kPa)	23.9
TIT (K)	1,380

Solution

Diffuser

$$P_{o2} = P_a\left[1+\eta_d\left(\frac{\gamma_c-1}{2}\right)M^2\right]^{\gamma_c/\gamma_c-1} = 34.994 \text{ kPa}$$

$$T_{o2} = T_a\left[1+\left(\frac{\gamma_c-1}{2}\right)M^2\right] = 250.44 \text{ K}$$

Fan

$$P_{o3} = \pi_f \times P_{o2} = 62.689 \text{ kPa}$$

$$T_{o3} = T_{o2}\left[1+\frac{\left(\pi_f{}^{(\gamma_c-1)/\gamma_c}-1\right)}{\eta_{fn}}\right] = 291.86 \text{ K}$$

LPC

$$P_{o4} = \pi_{C_{LPC}} \times P_{o3} = 71.466 \text{ kPa}$$

$$T_{o4} = T_{o3}\left(1+\frac{\left(\pi_{C_{LPC}}{}^{(\gamma_c-1)/\gamma_c}-1\right)}{\eta_{C_{LPC}}}\right) = 304.10 \text{ K}$$

HPC

$$P_{o5} = \pi_{C_{HPC}} \times P_{o4} = 1500.0 \text{ kPa}$$

$$T_{o5} = T_{o4}\left(1+\frac{\left(\pi_{C_{HPC}}{}^{(\gamma_c-1)/\gamma_c}-1\right)}{\eta_{C_{HPC}}}\right) = 788.46 \text{ K}$$

Combustion chamber

$$T_{06} = 1380 \text{ K}$$

$$P_{o6} = 0.98 \times P_{o5} = 1471.0 \text{ kPa}$$

$$f = \frac{\left(C_{ph} \times T_{o6} - C_{pc} \times T_{o5}\right)}{\left(\eta_b \times Q_{hv} - C_{ph} \times T_{o6}\right)} = 0.018$$

HPT: From energy balance

$$W_{HPT} = W_c$$

$$T_{o7} = T_{o6} - \left(\frac{C_{pc} \times \left(T_{o5} - T_{o4}\right)}{C_{ph}\left(1+f\right)}\right) = 984.7 \text{ K}$$

$$P_{o7} = P_{o6}\left(1-\frac{T_{o6}-T_{o7}}{\eta_{t_{HPT}} \times T_{o6}}\right)^{(\gamma_h/\gamma_h-1)} = 333.5 \text{ kPa}$$

LPT: From the energy balance

$$W_{LPT} = W_{fan} + W_{LPC}$$

$$(1+\beta)\dot{m}_a Cp_c (T_{03} - T_{02}) + \dot{m}_a Cp_c (T_{04} - T_{03}) = \dot{m}_a (1+f) Cp_h (T_{07} - T_{08})$$

$$T_{o8} = T_{o7} - \left(\frac{1+\beta}{1+f}\right)\left(\frac{C_{pc}}{C_{ph}}\right)(T_{o3} - T_{o2}) - \left(\frac{C_{pc}}{C_{ph}(1+f)}\right)(T_{o4} - T_{o3}) = 652.7 \text{ K}$$

$$P_{o8} = P_{o7}\left(1 - \left(\frac{T_{o6} - T_{o7}}{\eta_{t_{LPT}} \times T_{o6}}\right)\right)^{(\gamma_h/\gamma_h - 1)} = 54.33 \text{ kPa}$$

Hot nozzle

$$P_{c1} = P_{o8}\left(1 - \frac{1}{\eta_n}\left(\frac{\gamma_h - 1}{\gamma_h + 1}\right)\right)^{\gamma_h/\gamma_h - 1} = 28.34 \text{ kPa}$$

$$\because P_{c1} \rangle P_a$$

$\therefore$ Chocked nozzel $M_e = 1$ and $P_9 = P_{c1}$

$$P_9 = P_{c1} = 28.34 \text{ kPa}$$

$$T_{c1} = \frac{T_{o8}}{\left(\frac{\gamma_h + 1}{2}\right)} = 560.27 \text{ K}$$

$$T_9 = T_{c1} = 560.27 \text{ K}$$

$$V_9 = \sqrt{\gamma_h R T_9} = 462.45 \text{ m/s}$$

For cold nozzle

$$P_{c2} = P_{o3}\left(1 - \frac{1}{\eta_{fn}}\left(\frac{\gamma_c - 1}{\gamma_c + 1}\right)\right)^{\gamma_c/\gamma_c - 1} = 31.91 \text{ kPa}$$

$$\because P_{c2} \rangle P_a$$

$\therefore$ The nozzle is choked $M_e = 1$ and $P_{11} = P_{c2}$

$$P_{11} = P_{c2} = 3.1914 \times 10^4 \text{ Pa}$$

$$T_{c2} = \frac{T_{o3}}{\left(\frac{\gamma_h + 1}{2}\right)} = 243.22 \text{ K}$$

$$T_{11} = T_{c2} = 243.22 \text{ K}$$

$$V_{11} = \sqrt{\gamma_c R T_{11}} = 312.61 \text{ m/s}$$

Specific thrust

$$\frac{T}{\dot{m}_a} = \frac{\beta}{1+\beta} V_{11} + \frac{1}{1+\beta}(1+f) V_9 - V_f + \left(\frac{1+f}{1+\beta}\right)\left(\frac{RT_9}{P_9 V_9}\right)(P_9 - P_a)$$

$$+ \frac{\beta}{1+\beta}\frac{RT_{11}}{P_{11} V_{11}}(P_{11} - P_a) = 133.96 \text{ N} \cdot \text{s/kg}$$

Thrust

$$\begin{aligned}\dot{m}_a &= \rho_a \times A_{inlet} \times V_{inlet} \\ &= \frac{P_a}{R \times T_a} \times 6.006 \times M \times \sqrt{\gamma_c \times R \times T_a} = 576.1 \text{ kg/s} \\ T &= \left(T/\dot{m}_a\right) \times \dot{m}_a = 77.2 \text{ kN}\end{aligned}$$

TSFC

$$TSFC = \frac{f}{T/\dot{m}_a} = 1.47 \times 10^{-5} \text{ kg/N/s}$$

Mass flow rate

$$\dot{m}_f = f \times \dot{m}_{hot} = 1.1086 \text{ kg/s}$$

Fuel consumption

$$\text{Fuel consumpation} = \dot{m}_f \times \frac{3600}{1000} = 3.99 \text{ tons/h}$$

Propulsive efficiency

$$\eta_p = \frac{\left(T/\dot{m}_a\right)V_f}{\left(T/\dot{m}_a\right)V_f + \left(0.5 \times \frac{(1+f)}{(1+\beta)}\right)\left(V_9 - V_f\right)^2 + 0.5 \times \left(\frac{\beta}{1+\beta}\right)\left(V_{11} - V_f\right)^2} = 0.89$$

Thermal efficiency: Since the nozzles are choked, the expression for thermal efficiency will be given by the following relation (Figures 5.39 and 5.40)

$$\eta_{th} = \frac{\left(T/\dot{m}_a\right)V_f + \left(0.5 \times \frac{(1+f)}{(1+\beta)}\right)\left(V_9 - V_f\right)^2 + 0.5 \times \left(\frac{\beta}{1+\beta}\right)\left(V_{11} - V_f\right)^2}{\left(\frac{f}{1+\beta}\right) \times Q_{HV}}$$

Substituting in the above equation gives the following result

$$\eta_{th} = 0.61$$

If the nozzles are unchoked, then the above relation is reduced to the well-known form

$$\eta_{th} = \frac{0.5\left[\left(\frac{\beta}{1+\beta}\right)\left(V_{11}\right)^2 + \left(\frac{1+f}{1+\beta}\right)\left(V_9\right)^2 - \left(V_f\right)^2\right]}{\left(\frac{f}{1+\beta}\right) \times Q_{HV}}$$

Overall efficiency

$$\eta_o = \eta_{th} \times \eta_p = 0.54$$

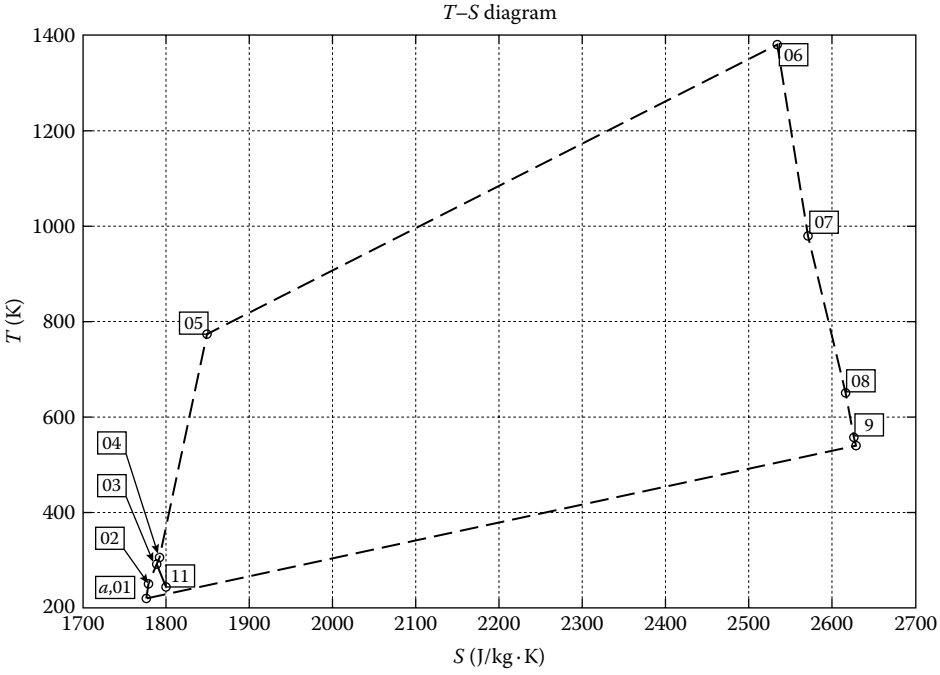


FIGURE 5.39
Temperature-entropy diagram for high-bypass turbofan (similar to GE-90).

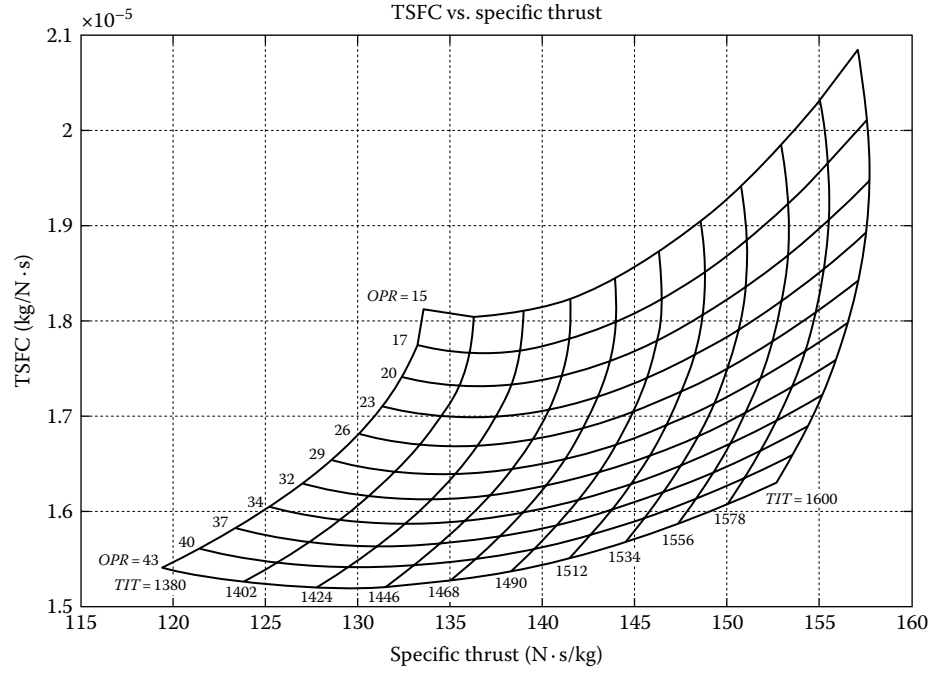


FIGURE 5.40
Engine map for high-bypass turbofan (similar the GE-90).

Example 5.8

A gas generator (Figure 5.41a) is composed of a single spool [compressor (C_1) and turbine (T_1)]. It is employed in two versions of turbofan engines, namely, forward fan (Figure 5.41b) and aft-fan (Figure 5.41c) to increase the thrust force.

Forward fan: A second turbine (T_2) is added together with the forward fan (F_1) to form a second low-pressure spool.

Aft-fan: A free power turbine is installed after the turbine T_1 which has an outer blade part forming the aft-fan (F_2). The operation parameters and the engine's characteristics are as follows: flight Mach Number M_o = 0.8, altitude 33,000 ft with ambient conditions P_a = 26.2 kPa and T_a = 222 K, fan pressure ratio (both cases) π_f=1.8, compressor pressure ratio π_c=8, maximum temperature 1500 K, BPR (both cases) β = 5, mass flow rate to the compressor 50 kg/s, efficiencies of the compressor, combustion chamber, fans, turbine, free power turbine, hot and cold nozzles are equal to 0.9, fuel heating value 42,000 kJ/kg, combustion chamber pressure loss 5%.

$$C_{Pc} = 1020\,\text{J/kg}\cdot\text{K}, \quad C_{Ph} = 1160\,\text{J/kg}\cdot\text{K}, \quad R = 287\,\text{J/kg}\cdot\text{K}$$

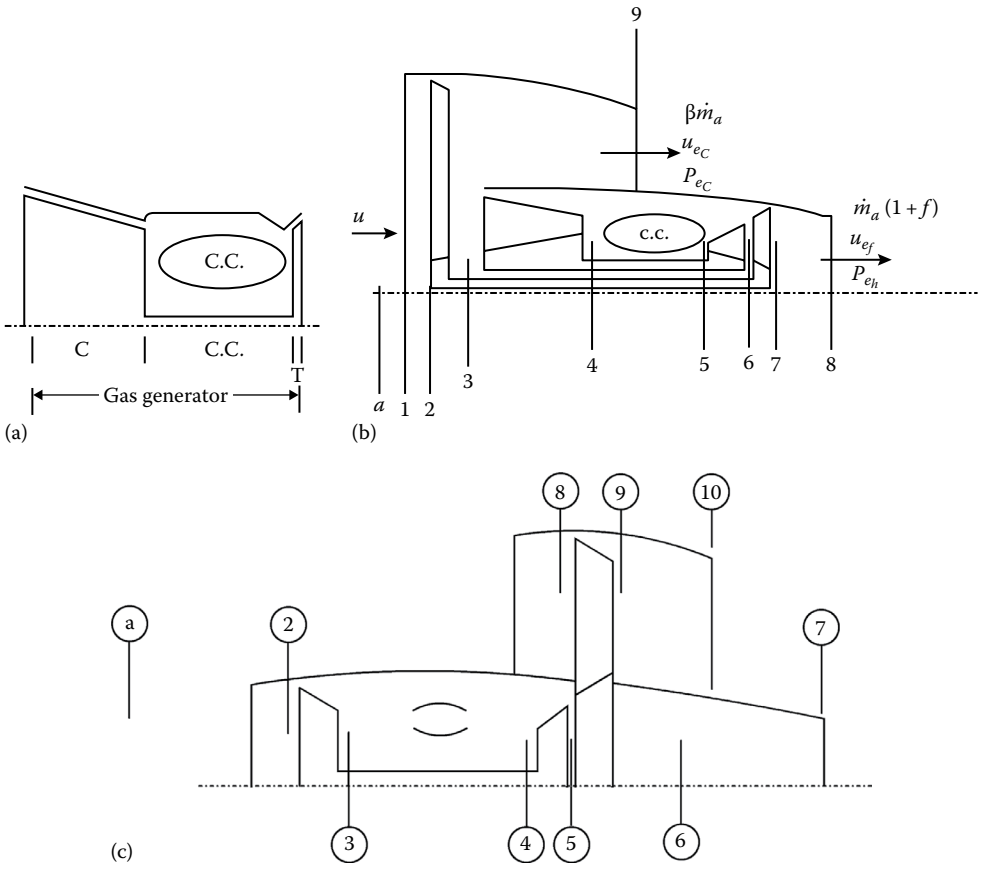


FIGURE 5.41
Layout of aft-fan turbofan engine.

We need to

1. Calculate the TSFC in both cases
2. Compare both cases, clarifying which is to be preferred

$$P_a = 26.2 \text{ kPa}, \quad T_a = 222 \text{ K}$$

$$C_{Vc} = C_{Pc} - R = 1020 - 287 = 733 \text{ J/kg/K}$$

$$\gamma_C = \frac{C_{Pc}}{C_{Vc}} = \frac{1020}{733} = 1.391$$

$$\gamma_h = \frac{C_{Ph}}{C_{Vh}} = \frac{1160}{873} = 1.328$$

$$T_{o2} = T_a\left(1 + \frac{\gamma_c - 1}{2}M^2\right) = 222 \times 1.125$$

$$T_{o2} = 249.82 \text{ K}$$

$$P_{o2} = P_a\left(1 + \frac{\gamma_c - 1}{2}M^2\right)^{\gamma_c/\gamma_c - 1} = 26.2 \times 1.5221 = 39.878 \text{ kPa}$$

$$P_{o3} = P_{o2} \times \pi_f = 71.78 \text{ kPa}$$

$$T_{o3} = T_{o2}\left[1 + \frac{\left\{\left(\pi_f\right)^{\gamma-1/\gamma} - 1\right\}}{\eta_f}\right] = 249.82\left[1 + 0.1995\right] = 299.67 \text{ K}$$

$$P_{o4} = 574.24 \text{ kPa}$$

$$T_{o4} = T_{o3}\left[1 + \frac{\pi_c^{\lambda-1/\gamma} - 1}{\eta_c}\right] = 564 \text{ K}$$

$$f = \frac{C_{Ph}T_{o5} - C_{Pc}T_{o4}}{\eta_{cc}Q_R - C_{Ph}T_{o5}} = \frac{1.16 \times 1{,}500 - 1.02 \times 564}{0.9 \times 42{,}000 - 1.16 \times 1{,}500}$$

$$f = 0.0322$$

$$P_{o5} = P_{o4}\left(1 - 0.05\right) = 545.3 \text{ kPa}$$

Energy balance (high-pressure spool)

$$C_{Pc}\left(T_{o4} - T_{o3}\right) = C_{Ph}\left(1 + f\right)\left(T_{o6} - T_{o5}\right)1.02\left[564 - 299.7\right] = 1.16\left(1 + 0.0322\right)\left[T_{o6} - 1500\right]$$

$$T_{o6} = 1274.8 \text{ K}$$

$$\eta_{T1} = \frac{T_{o5} - T_{o6}}{T_{o5} - T_{o6S}} = \frac{T_{o5} - T_{o6}}{T_{o5}\left[1 - \left(\frac{P_{o6}}{P_{o5}}\right)^{\gamma_h - 1/\gamma_h}\right]}$$

$$0.9 = \frac{1500 - 1274.8}{1500\left[1 - \left(\frac{P_{o6}}{P_{o5}}\right)^{\gamma_h - 1/\gamma_h}\right]}$$

$$\left(\frac{P_{o6}}{P_{o5}}\right)^{\gamma_h - 1/\gamma_h} = 1 - 0.1675 = 0.8324$$

$$\frac{P_{o6}}{P_{o5}} = 0.4757$$

$$P_{o6} = 259.4 \text{ kPa}$$

Energy balance (low-pressure spool)

$$\beta C_{Pc}\left(T_{o3}-T_{o2}\right)=C_{Ph}\left(1+f\right)\left(T_{o6}-T_{o7}\right)$$
$$5\times 1.02\left(299.7-249.8\right)=1.16\left(1.0322\right)\left(1274.8-T_{o7}\right)$$
$$T_{o7}=1062.2\ \text{K}$$
$$\frac{P_{o7}}{P_{o6}}=\left[1-\frac{T_{o6}-T_{o7}}{\eta_{T2}T_{o6}}\right]^{\gamma_h/\gamma_h-1}=\left[1-\frac{1274.8-1062.2}{0.9\times 1274.8}\right]^{4.05}=0.436$$
$$P_{o7}=113.11\ \text{kPa}$$
$$\frac{P_{o7}}{P_a}=4.31$$
$$\frac{P_{o7}}{P_C}=\frac{1}{\left[1-\dfrac{\gamma_h-1}{\eta_n\left(\gamma_h-1\right)}\right]^{\gamma_h-1/\gamma_h}}=1.993$$

Since $\frac{P_{o7}}{P_a}>\frac{P_{o7}}{P_C}$, then the nozzle is choked

$$P_8=P_C=\frac{113.11}{1.993}=56.75\ \text{kPa}$$
$$T_8=\left(\frac{2}{\gamma_h+1}\right)T_{o7}=912.3\ \text{K}$$
$$V_F=M\sqrt{\gamma RT_a}=238.25\ \text{m/s}$$
$$V_8=\sqrt{\gamma RT_8}=589.7\ \text{K}$$
$$\dot{m}_8=\rho_8 A_8 V_8$$
$$\dot{m}_a\left(1+f\right)=\frac{P_8}{RT_8}A_8V_8$$
$$A_8=\frac{\dot{m}_a\left(1+f\right)RT_8}{P_8V_8}=\frac{50\left(1.0332\right)\left(287\right)\left(912.13\right)}{56.75\times 10^3\times 589.7}=0.4038\ \text{m}^2$$

For the hot section

$$\text{Thrust}=T_h=\dot{m}\left[\left(1+f\right)V_8-V_F\right]+A_8\left(P_8-P_a\right)$$
$$\frac{T_h}{\dot{m}}=\left\{\left(1.0322\right)\left(589.7\right)-238.25\right\}+\frac{0.4038}{50}\left(56.75-26.2\right)\times 10^3=370.43+246.7$$
$$\frac{T_h}{\dot{m}}=617.138\ \text{N}\cdot\text{s/kg}$$
$$\text{Thrust})_{\textit{hot section}}=30{,}856\ \text{N}$$

For the cold section

$$\frac{P_{o3}}{P_C}=\frac{1}{\left[1-\dfrac{\gamma_c-1}{\eta_n\left(\gamma_c+1\right)}\right]^{\gamma_c/\gamma_c-1}}=\frac{1}{0.4899}=2.04$$
$$\frac{P_{o3}}{P_a}=\frac{71.78}{26.2}=2.739$$

Choked cold nozzle

$$P_9 = P_c = 35.18 \text{ kPa}$$
$$T_9 = \left(\frac{2}{\gamma_c + 1}\right) T_{o3} = 299.67 \times 0.836 = 250.66 \text{ K}$$
$$\rho_9 = \frac{P_9}{RT_9} = 0.489 \text{ kg/m}^3$$
$$V_9 = \sqrt{\gamma R T_9} = 316.33 \text{ m/s}$$
$$A_9 = \frac{\beta \dot{m}}{\rho_9 V_9} = \frac{5 \times 50}{0.489 \times 316.33} = 1.616 \text{ m}^2$$

Thrust of cold section

$$T_c = \beta \dot{m}_a (V_9 - V_F) + A_9 (P_9 - P_a)$$
$$T_c = 5 \times 50(316.33 - 283.25) + 1.616(35.18 - 26.2) \times 10^3 = 34{,}031 \text{ N}$$
$$\text{Total thrust} = 30{,}856.9 + 34{,}031 = 64{,}887.9 \text{ N}$$
$$TSFC = \frac{\dot{m}_F}{T} = \frac{f \times \dot{m}_a}{T} = \frac{0.0322 \times 50}{64{,}887} = 2.4812 \times 10^{-5} \text{ kg fuel/N} \cdot \text{s}$$

Aft-fan
Cold section

$$P_{o3} = 71.75 \text{ kPa}, \quad T_{o3} = 299.67 \text{ K}$$
$$\frac{P_{o3}}{P_a} = \frac{71.75}{26.2} = 2.738$$
$$\frac{P_{o3}}{P_c} = \frac{1}{\left[1 - \dfrac{\gamma_c - 1}{\eta_n (\gamma_c + 1)}\right]^{\gamma/\gamma_c - 1}} = 2.04$$

Choked nozzle

$$T_4 = 250.66 \text{ K}$$
$$V_4 = 316.33 \text{ m/s}$$
$$A_4 = 1.616 \text{ m}^2$$
$$T_{Fan} = T_{cold} = 34{,}031 \text{ N}$$

Hot section

$$T_{o2'} = T_{o2} = 249.82 \text{ K}$$
$$P_{o2'} = P_{o2} = 39.878 \text{ kPa}$$
$$P_{o5} = r_c P_{o2'} = 8 \times 39.878 = 319.024 \text{ kPa}$$
$$T_{o5} = T_{o2}\left[1 + \frac{r_c^{\gamma - 1/\gamma} - 1}{\eta_c}\right] = 470 \text{ K}$$
$$P_{o6} = 0.95 \times 319 = 303 \text{ kPa}$$

Energy balance
(between compressor and turbine)

$$\dot{m}_a C_{Pc}\left(T_{o5}-T_{o2'}\right)=\dot{m}_a\left(1+f\right)C_{\ Ph}\left(T_{o6}-T_{o7}\right)$$

$$T_{o6}-T_{o7}=\left(T_{o5}-T_{o22'}\right)\frac{C_{Pc}}{C_{Ph}\left(1+f\right)}=\frac{\left(470-300\right)\times 1.02}{1.03495\times 1.16}=144.4\ \text{K}$$

$$T_{o7}=1355.6\ \text{K}$$

$$f=\frac{C_{Ph}T_{o6}-C_{Pc}T_{o3}}{\eta_b Q_R-C_{Ph}T_{o6}}=\frac{1.16\times 1{,}500-1.02\times 470}{0.9\times 42{,}000-1.16\times 1{,}500}=0.03495$$

$$\frac{P_{o7}}{P_{o6}}=\left[1-\frac{T_{o6}-T_{o7}}{\eta_t T_{o6}}\right]^{\gamma/\gamma-1}=\left[1-\frac{1500-1355}{0.9\times 1500}\right]^{4.05}=\left(0.893\right)^{4.05}$$

$$\frac{P_{o7}}{P_{o6}}=0.6323$$

$$P_{o7}=191.6\ \text{kPa}$$

Energy balance (fan and LPT)

$$\dot{m}_a\left(1+f\right)C_{Ph}\left(T_{o7}-T_{o8}\right)=\beta\dot{m}_a C_{Pc}\left(T_{o3}-T_{o2}\right)$$

$$f=0.03495$$

$$\left(1.03495\right)\left(1.16\right)\left(1355-T_{o8}\right)=5\times 1.102\left(299.67-222\right)$$

$$T_{o8}=1355-\frac{429.78}{1.2}=997.4\ \text{K}$$

$$\eta_t=\frac{T_{o7}-T_{o8}}{T_{o7}-T_{o8S}}=\frac{T_{o7}-T_{o8}}{T_{o7}\left[1-\left(\frac{P_{o8}}{P_{o7}}\right)^{\gamma_h-1/\gamma_h}\right]}$$

$$\frac{P_{o8}}{P_{o7}}=\left[1-\frac{T_{o7}-T_{o8}}{\eta_t T_{o7}}\right]^{\gamma_h/\gamma_h-1}=\left[1-\frac{1355-997}{0.9\times 1355}\right]^{4.05}=\left(0.6229\right)^{4.05}$$

$$P_{o8}=46.9\ \text{kPa}$$

$$\frac{P_{o8}}{P_a}=1.79$$

Since $P_{o8}/P_c=1.993$, then the nozzle is unchoked

$$\text{Hot thrust}\equiv T_{hot}=\dot{m}_h\left[\left(1+f\right)V_9-V_F\right]=15{,}386\ \text{N}$$

$$\eta_n=\frac{T_{o8}-T_9}{T_{o8}-T_{9S}}=\frac{T_{o8}-T_9}{T_{o8}\left[1-\left(\frac{P_9}{P_{o8}}\right)^{\gamma_h-1/\gamma_h}\right]}$$

$$T_9=T_{o8}\left[1-\eta_n\left\{1-\left(\frac{P_a}{P_{o8}}\right)^{\gamma_h-1/\gamma_h}\right\}\right]=997.4\left[1-0.9\left\{1-\left(\frac{26.2}{46.9}\right)^{0.247}\right\}\right]$$

$$T_9=877.2\ \text{K}$$

$$V_9=\sqrt{2C_P\left(T_{o8}-T_9\right)}=527.3\ \text{m/s}$$

$$\text{Total thrust})_{aft\ fan}=15{,}386+34{,}031=49{,}417\ \text{N}$$

$$TSFC=\frac{\dot{m}_F}{T}=\frac{f\times\dot{m}_a}{T}=\frac{0.03495\times 50}{19{,}417}$$

$$TSFC)_{aft\ fan}=3.536\times 10^{-5}\ \text{kg fuel/N}\cdot\text{s}$$

$$TSFC)_{Forward\ fan}<TSFC)_{Aft\ fan}$$

Example 5.9

The performance of a brand-new and a deteriorated engine is dependent on the efficiency of different components. Here the efficiencies of new and deteriorated high-BPR turbofan engines are listed. Calculate and plot the variation of the propulsive, thermal, and overall efficiencies as well as the thrust, specific thrust, and TSFC with the BPR if the same operating conditions listed in Example 5.7 are applied.

Component	New	Deteriorated
η_d (Intake efficiency)	0.98	0.95
η_{fn} (Isentropic fan nozzle efficiency)	0.95	0.95
η_f (Fan polytrophic efficiency)	0.93	0.925
$\eta_{C_{LPC}}$ (LPC efficiency)	0.91	0.88
$\eta_{C_{HPC}}$ (HPC efficiency)	0.91	0.87
η_{CC} (Combustion chambers' efficiency)	0.99	0.99
ΔP_{cc} Combustion pressure loss (ratio)	0.02	0.05
Q_{hv}(J/kg)	4.80E+07	4.80E+07
η_m (Mechanical efficiency)	0.99	0.99
$\eta_{t_{HPT}}$ (HPT efficiency)	0.93	0.91
$\eta_{t_{LPT}}$ (LPT efficiency)	0.93	0.91
η_n (Isentropic nozzle efficiency)	0.95	0.95

Solution

Deterioration of the components of the turbofan engine leads to a decrease in all the efficiencies (propulsive, thermal, and overall). It will also reduce both the thrust and specific thrust. Moreover, higher fuel consumption is expected, which increases the TSFC. These results are depicted in Figures 5.42 through 5.47.

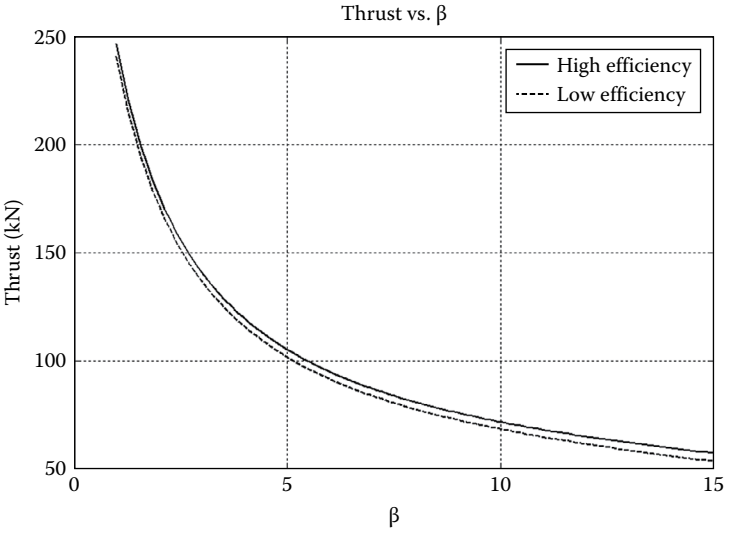


FIGURE 5.42
Variation of the thrust with the BPR.

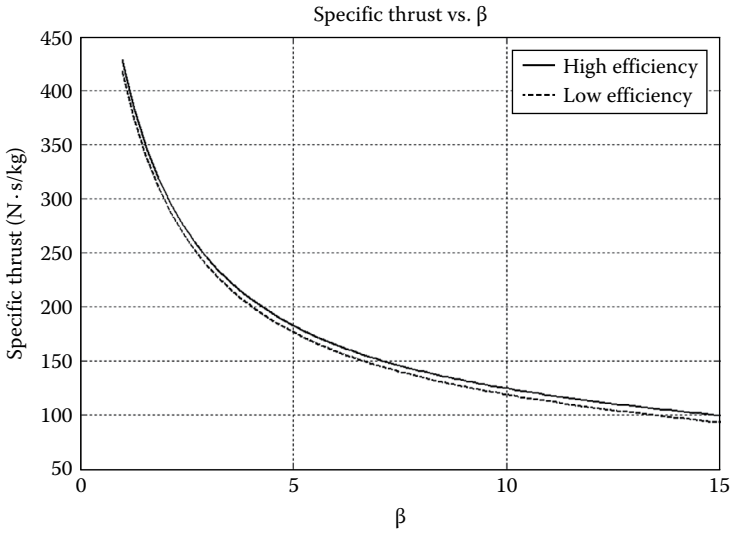


FIGURE 5.43
Variation of the specific thrust with the BPR.

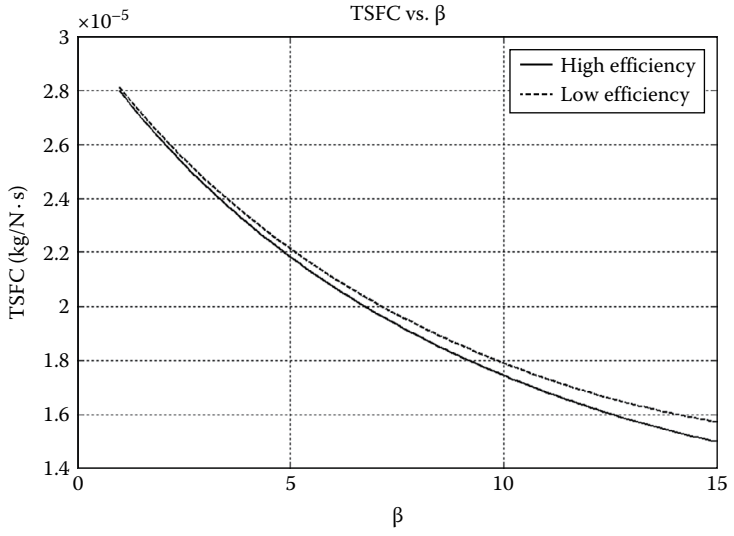


FIGURE 5.44
Variation of the specific fuel consumption with the BPR.

Example 5.10

The most important performance specifications of an aircraft engine are the propulsive efficiency of the engine and the TSFC. They are important for the airlines that install the engine in its aircraft. Both the propulsive efficiency and the TSFC may be used as an indication of the required working cost. Two engine parameters have a direct influence on its performance, namely

- Turbine-inlet temperature
- The ratio of the bleed air drawn from the cold section to the air mass flow rate.

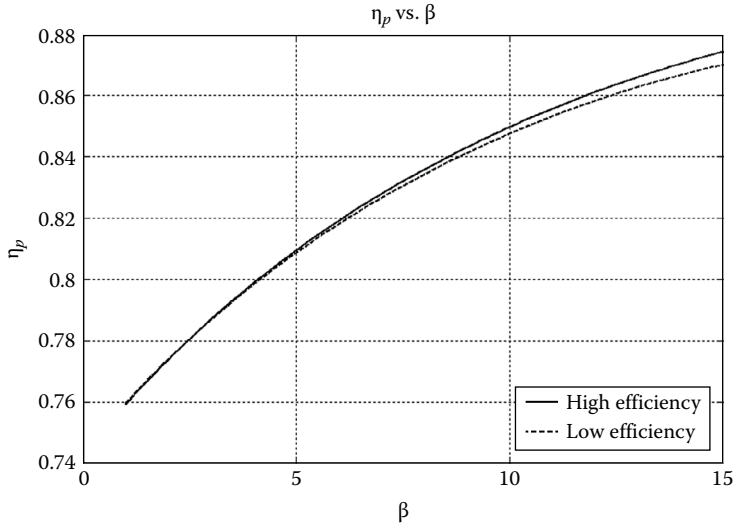


FIGURE 5.45
Variation of the propulsive efficiency with the BPR.

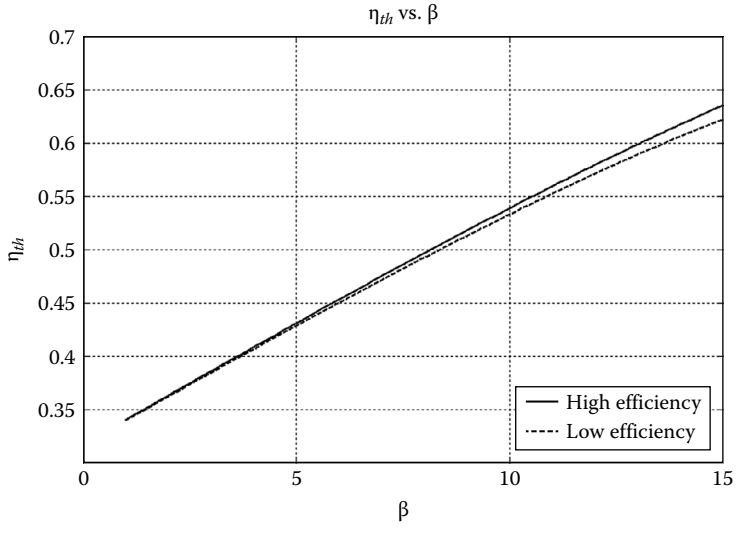


FIGURE 5.46
Variation of the thermal efficiency with the BPR.

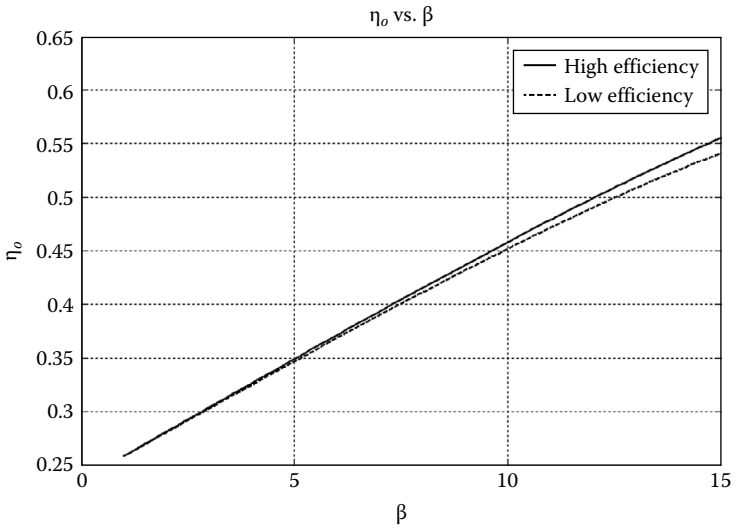


FIGURE 5.47
Variation of the overall efficiency with the BPR.

Use the following data to calculate and plot the variation of the propulsive efficiency and the TSFC for the engine for successive variations of TIT from 1850 to 2000 K and bleed ratio ranging from 0.05 to 0.15.

η_d (Intake efficiency)	0.98
η_{fn} (Isentropic fan nozzle efficiency)	0.95
η_f (Fan polytrophic efficiency)	0.93
η_C (LPC and HPC efficiencies)	0.91
η_{CC} (Combustion chambers' efficiency)	0.99
ΔP_{cc} Combustion pressure loss (ratio)	0.02
Q_{hv} (J/kg)	4.80E+07
η_m (Mechanical efficiency)	0.99
η_t (HPT and LPT efficiencies)	0.93
η_n (Isentropic nozzle efficiency)	0.95
π_f (Fan pressure ratio)	0.98
π_{LPC} (LPC pressure ratio)	0.95
π_{HPC} (HPC pressure ratio)	0.93
Ambient	Altitude sea level
β (BPR)	2
TIT (For the study of bleed ratio)	1850–2000
$b = \frac{\dot{m}_{bleed}}{\dot{m}_a}$ (For the study of TIT)	0.05–0.15

Solution

The effect of the turbine-inlet temperature on the propulsive efficiency is plotted in Figure 5.48 and its effect on the TSFC is plotted in Figure 5.49.

The effect of the bleed air to air mass flow ratio on the propulsive efficiency is plotted in Figure 5.50 and its effect on the TSFC is plotted in Figure 5.51.

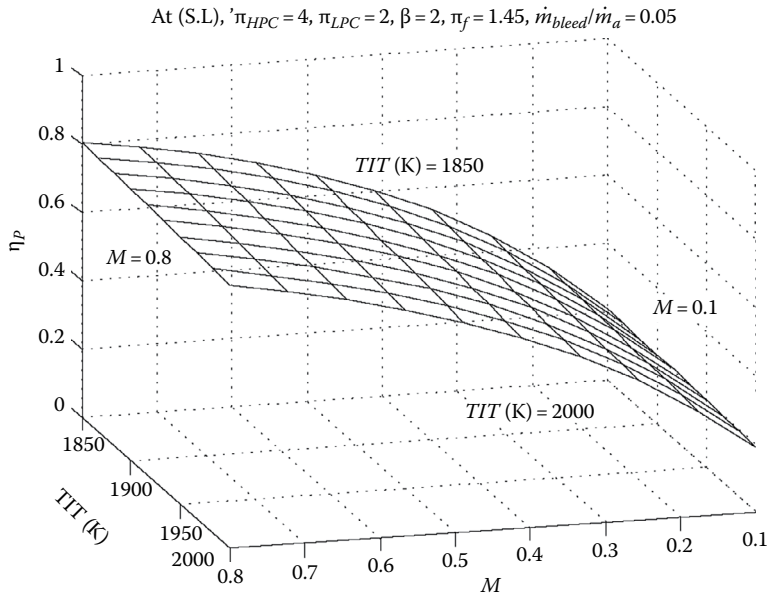


FIGURE 5.48
Variation of the propulsive efficiency with the TIT.

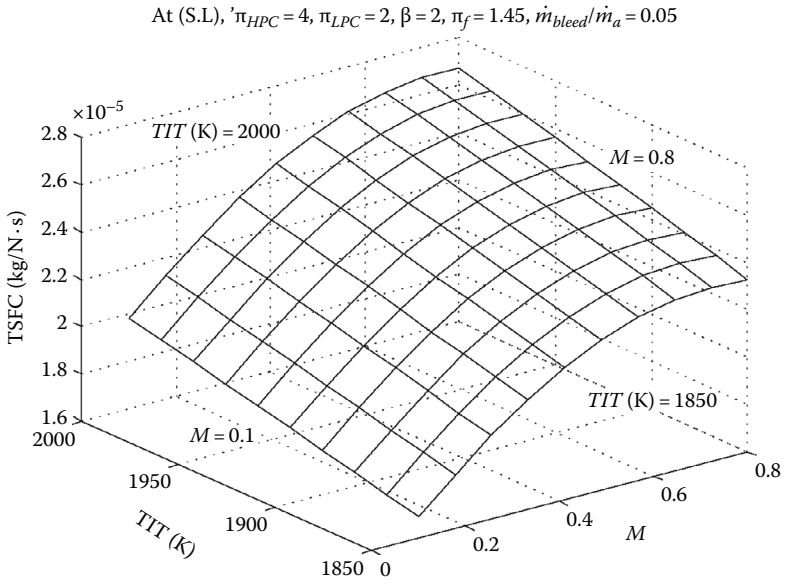


FIGURE 5.49
Variation of the specific fuel consumption with the TIT.

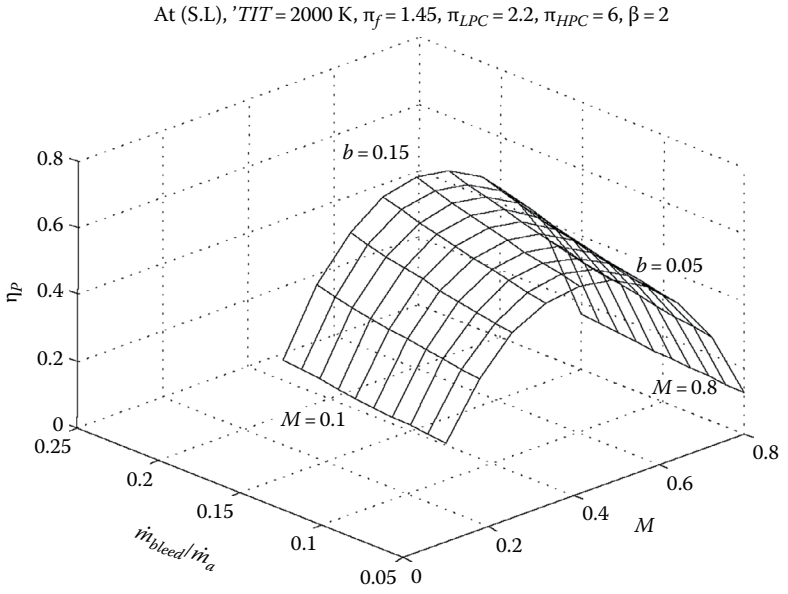


FIGURE 5.50
Variation of the propulsive efficiency with the *b*.

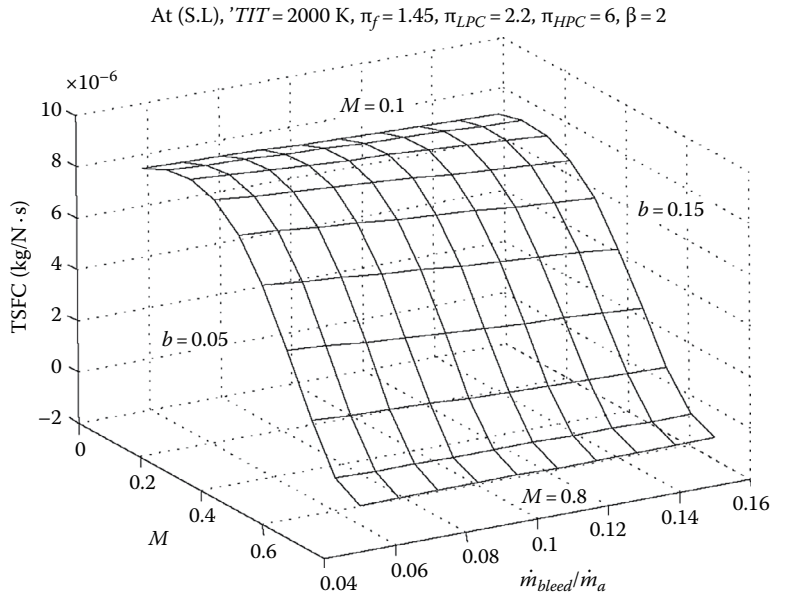


FIGURE 5.51
Variation of the specific fuel consumption with the bleed ratio.

Example 5.11

For the engine in Example 5.7 (a high-bypass engine similar to GE-90) and at the same operating conditions, plot the effect of TIT and OPR together on (Figures 5.52 through 5.58)

1. Thrust
2. Specific thrust
3. TSFC
4. Fuel-consumption rate
5. Propulsive efficiency
6. Thermal efficiency
7. Overall efficiency

Solution

As discussed earlier, there are four thermodynamic parameters that control the performance of turbofan engines. These are

1. The BPR
2. The fan pressure ratio
3. The overall pressure ratio
4. The turbine-inlet temperature

Consider the case of an engine with both

- Overall pressure ratio fixed
- BPR fixed

Then, change the turbine-inlet temperature and fan pressure ratio.

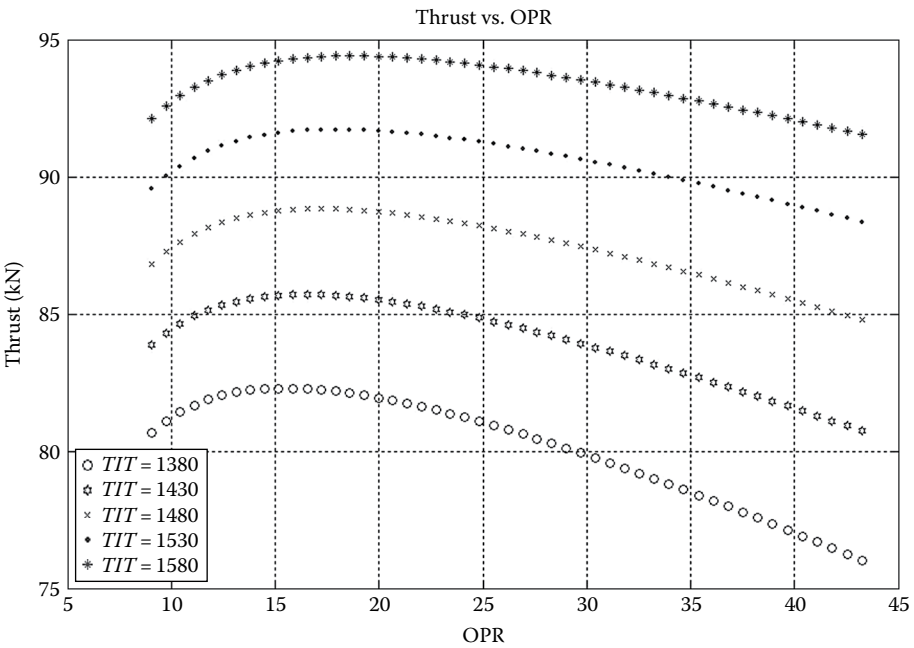


FIGURE 5.52
Variation of the thrust with the overall pressure ratio.

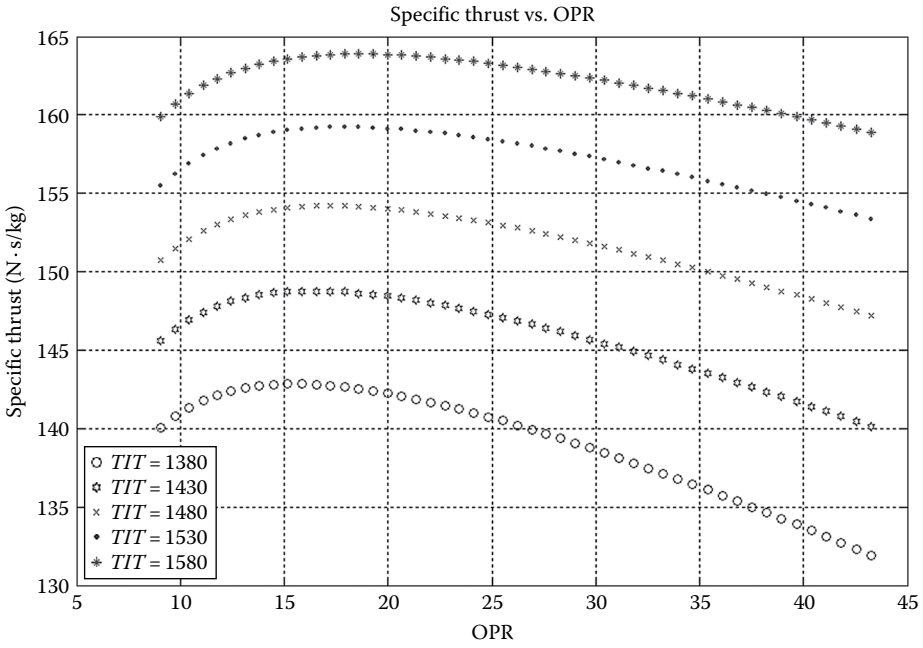


FIGURE 5.53
Variation of the specific thrust with the overall pressure ratio.

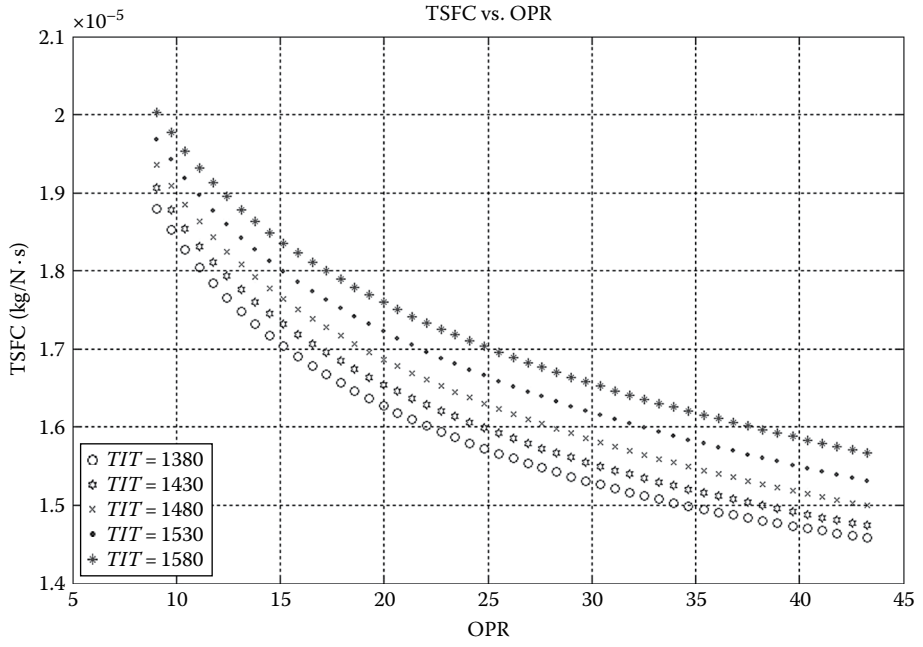


FIGURE 5.54
Variation of the specific fuel consumption with the overall pressure ratio.

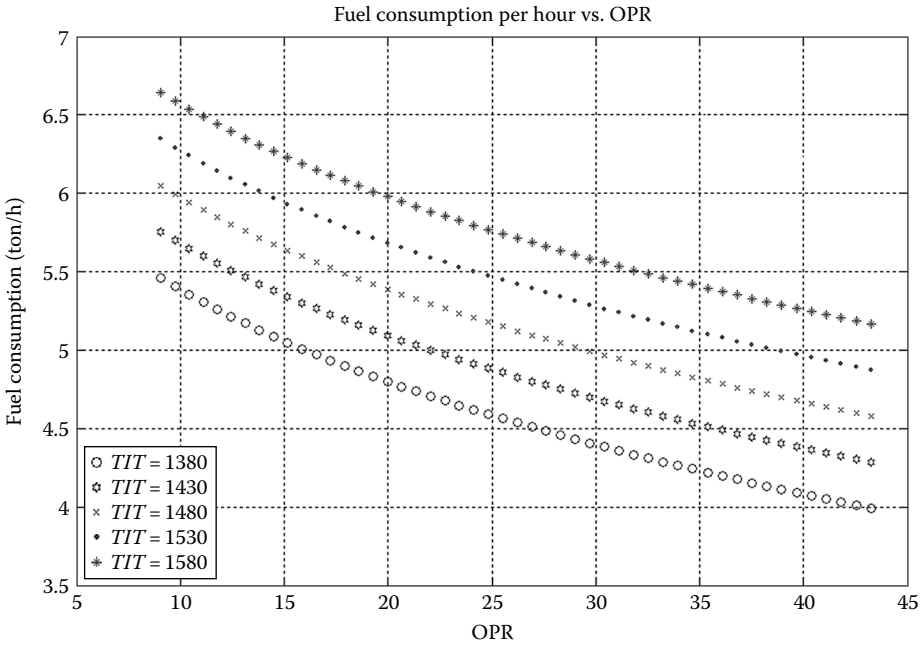


FIGURE 5.55
Variation of the rate of fuel consumption with the overall pressure ratio.

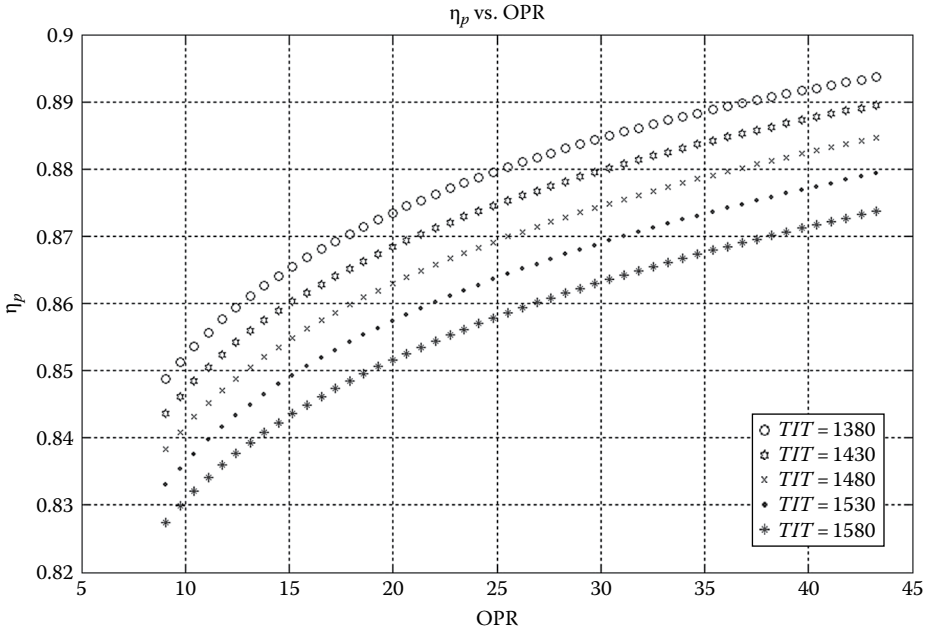


FIGURE 5.56
Variation of the propulsive efficiency with the overall pressure ratio.

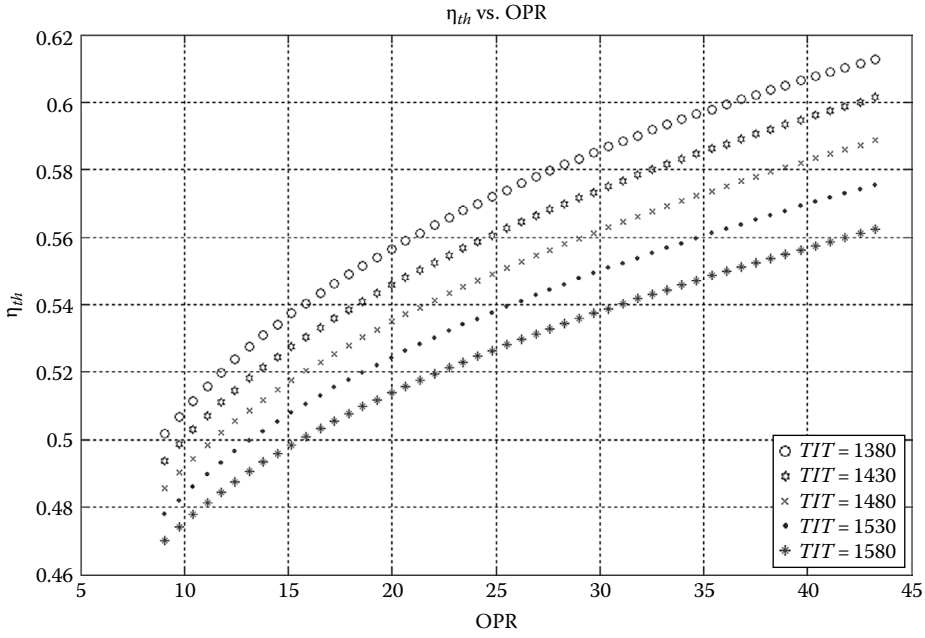


FIGURE 5.57
Variation of the thermal efficiency with the overall pressure ratio.

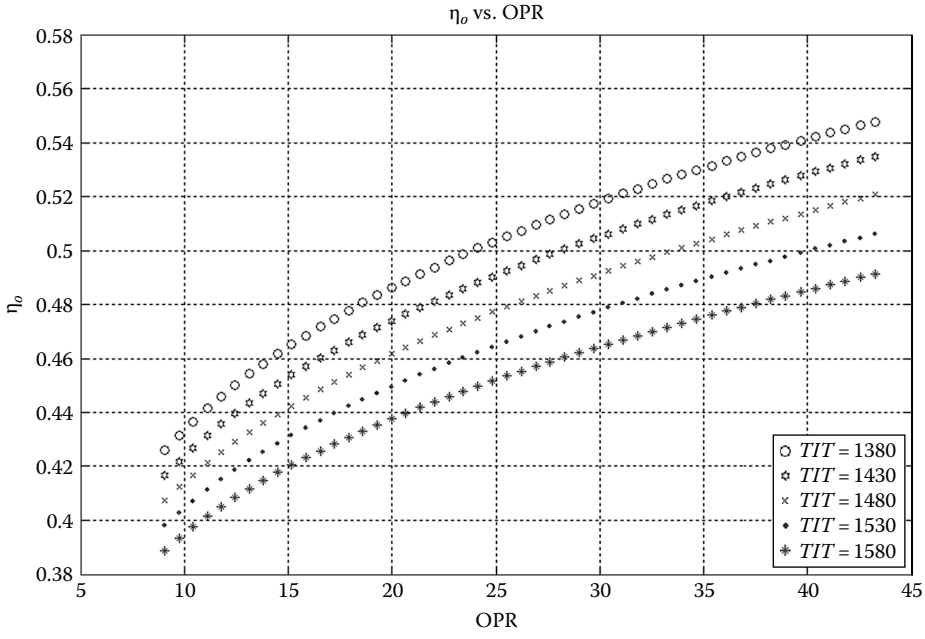


FIGURE 5.58
Variation of the overall efficiency with the overall pressure ratio.

Remarks

1. Increasing the BPR improves TSFC at the expense of a significant reduction in specific thrust.
2. The optimum fan pressure ratio increases with the increase of turbine-inlet temperature.
3. Optimum fan pressure ratio decreases with the increase of BPR.

When $\beta = 5$, r_f may be small enough to permit the use of a single-stage fan.

Aircraft application

1. Long range subsonic transport
   The TSFC is of major importance. This is achieved through BPR in the range (4–6), high overall pressure ratio, and a low turbine-inlet temperature.
2. Military aircraft
   Maneuverability and supersonic capabilities as well as good subsonic fuel consumption are the major objectives. This is achieved through low BPR ranging from 0.5 to 1.0, which results in a small frontal area as well as adding an afterburner.
3. Short-haul commercial aircraft
   The BPR is similar to that of the long-range subsonic transport, which also minimizes noise.

Example 5.12

The "White Swan" is the nickname among Russian airmen for the Tupolev TU-160 aircraft (see Figure 5.59). The aircraft also has the NATO reporting name "Blackjack." The aircraft is powered by four Kuznetsov NK-32 triple-spool mixed and afterburning turbofan engines as shown in Figure 5.60.

During aircraft flight at an altitude of 12.2 km (T_a = 220.5 K and P_a = 20.744 kPa) and a Mach number of 2.05, the engine characteristics at maximum speed (operative afterburner) are



FIGURE 5.59
Tu-160.



FIGURE 5.60
Kuznetsov NK-32 triple-spool afterburning mixed turbofan engine.

Total mass flow rate = 365 kg/s.
Thrust = 245 kN.
Specific fuel consumption = 4.8136 * 10^{-5} kg/N · S (1.70 kg_f/h).
Overall pressure ratio = 28.4.
Bypass ratio = 1.4 (mixed).
Turbine-inlet temprature = 1630 K.
Fuel heating value = 43 MJ/kg.

Component	Data	γ	*Cp* (J/kg/K)
Air intake	$r_d = 0.95$	1.4	1005
Fan	$\eta_f = 0.85$, $\pi_f = 1.5$	1.4	1005
LPC	$\eta_{LPC} = 0.87$, $\pi_{LPC} = 3$	1.4	1005
HPC	$\eta_{HPC} = 0.9$	1.4	1005
Burner	$\eta_b = 0.99$, $r_b = 0.98$	1.33	1147
LPT	$\eta_{LPT} = 0.88$	1.33	1147
IPT	$\eta_{IPT} = 0.88$	1.33	1147
HPT	$\eta_{HPT} = 0.9$	1.33	1147
Shaft	$\eta_m = 0.98$	—	—
Afterburner	$r_{ab} = 0.98$	1.33	1147
Jet pipe	$r_{jet\ pipe} = 0.99$	1.33	1147
Nozzle	$\eta_n = 0.95$	1.33	1140

Assuming *full expansion* in the nozzle calculate

1. Combustor fuel mass flow
2. Afterburner fuel mass flow
3. Nozzle exit static pressure
4. Nozzle exit velocity

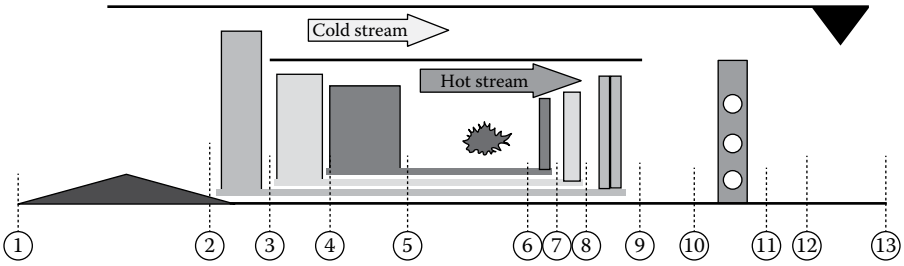


FIGURE 5.61
Layout for three-spool afterburning turbofan engine.

5. Thrust force
6. Propulsive efficiency
7. Thermal efficiency
8. Overall efficiency

Solution

Figure 5.61 illustrates the engine modules and its states.

Flight speed

$$U = M\sqrt{\gamma RT_a} = 2.05 \times \sqrt{1.4 \times 287 \times 220.5} = 610.2 \text{ m/s}$$

Upstream conditions of engine

$$T_{o1} = T_a\left(1 + \frac{\gamma_c - 1}{2} M_a^2\right) = 405.83 \text{ K}$$

$$P_{o1} = P_a\left(1 + \frac{\gamma_c - 1}{2} M_a^2\right)^{\gamma_c/\gamma_c - 1} = 175.46 \text{ kPa}$$

Intake

$$T_{o2} = T_{o1} = 405.83 \text{ K}$$

$$P_{o2} = r_d P_{o1} = 166.68 \text{ kPa}$$

Fan

$$T_{o3} = T_{o2}\left(1 + \frac{\pi_f^{\gamma_c - 1/\gamma_c} - 1}{\eta_f}\right) = 464.4724 \text{ K}$$

$$P_{o3} = P_{o2}\pi_f = 250.02 \text{ kPa}$$

$$\dot{m}_c = \frac{\beta}{1+\beta}\dot{m} = 212.9167 \text{ kg/s}$$

$$\dot{m}_h = \frac{1}{1+\beta}\dot{m} = 152.0833 \text{ kg/s}$$

LPC

$$T_{o4} = T_{o3}\left(1 + \frac{\pi_{LPC}^{\gamma_c - 1/\gamma_c} - 1}{\eta_{LPC}}\right) = 661.33 \text{ K}$$

$$P_{o4} = P_{o3}\pi_{LPC} = 750.06 \text{ kPa}$$

HPC

$$\pi_{HPC} = \frac{\pi_{overall}}{\pi_f \times \pi_{LPC}} = 6.311$$

$$T_{o5} = T_{o4}\left(1 + \frac{\pi_{HPC}^{\gamma_c - 1/\gamma_c} - 1}{\eta_{HPC}}\right) = 1170 \text{ K}$$
$$P_{o5} = P_{o4}\pi_{HPC} = 4.73 \text{ MPa}$$

Burner

$$T_{o6} = TIT = 1630 \text{ K}$$
$$P_{o6} = P_{o5}r_b = 4.6391 \text{ MPa}$$
$$f = \frac{TIT \times Cp_h - T_{o5} \times Cp_c}{\eta_b Q_{HV} - TIT \times Cp_h} = 0.0170$$

$$\left(\dot{m}_f\right)_{burner} = f \times \dot{m}_f = 2.5908 \text{ kg/s}$$

HPT: Compressor consumed power

$$W_{HPC} = \dot{m}_h \times Cp_c \times \left(T_{o5} - T_{o4}\right) = 77.808 \text{ MJ}$$

Turbine delivered power

$$W_{HPT} = W_{HPC}/\eta_m = 79.396 \text{ MJ}$$
$$T_{o7} = T_{o6} - \frac{W_{HPT}}{Cp_h\left(\dot{m}_h + \dot{m}_f\right)} = 1182.5 \text{ K}$$
$$P_{o7} = P_{o6}\left(1 - \left(1 - \frac{T_{o7}}{T_{o6}}\right)\frac{1}{\eta_{HPT}}\right)^{\gamma_h/\gamma_h - 1} = 1.071 \text{ MPa}$$

Intermediate-pressure turbine: Consumed power by LPC

$$W_{LPC} = \dot{m}_h \times Cp_c\left(T_{o4} - T_{o3}\right) = 30.089 \text{ MJ}$$

Delivered power by intermediate-pressure turbine

$$W_{IPT} = W_{LPC}/\eta_m = 30.703 \text{ MJ}$$
$$T_{o8} = T_{o7} - \frac{W_{IPT}}{Cp_h\left(\dot{m}_h + \dot{m}_f\right)} = 1009.4 \text{ K}$$
$$P_{o8} = P_{o7}\left(1 - \left(1 - \frac{T_{o8}}{T_{o7}}\right)\frac{1}{\eta_{IPT}}\right)^{\gamma_h/\gamma_h - 1} = 514.115 \text{ kPa}$$

LPT: Power consumed by fan

$$W_{fan} = \dot{m} \times Cp_c \times \left(T_{o3} - T_{o2}\right) = 21.511 \text{ MJ}$$

Delivered power by LPT

$$W_{LPT} = \frac{W_{fan}}{\eta_m} = 21.95 \text{ MJ}$$

$$T_{o9} = T_{o8} - \frac{W_{LPT}}{Cp_h\left(\dot{m}_h + \dot{m}_f\right)} = 885.6892 \text{ K}$$

$$P_{o9} = P_{o8}\left(1 - \left(1 - \frac{T_{o9}}{T_{o8}}\right)\frac{1}{\eta_{LPT}}\right)^{\gamma_h/\gamma_h - 1} = 280.88 \text{ kPa}$$

Mixer: Since specific fuel consumption = 1.70 kg/kg$_f$/h
Then, specific fuel consumption = $1.7/(9.81 \times 3600) = 4.8136 \times 10^{-5}$ kg/N · s
Total fuel mass flow = $\left(\dot{m}_f\right)_{total} = \text{TSFC} \times \text{Thrust} = 11.7933$ kg/s

$$\left(\dot{m}_f\right)_{after\ burner} = \left(\dot{m}_f\right)_{total} - \left(\dot{m}_f\right)_{burner} = 9.2025 \text{ kg/s}$$

$$\dot{m}_3 = \dot{m}_c = 212.9167 \text{ kg/s}$$

$$\dot{m}_9 = \dot{m}_h + \left(\dot{m}_f\right)_{burner} = 154.6742 \text{ kg/s}$$

$$T_{010} = \frac{\dot{m}_9 \times C_{ph} \times T_{09} + \dot{m}_3 \times C_{pc} \times T_{03}}{\left(\dot{m}_3 + \dot{m}_9\right) \times C_{ph}} = 562.2665 \text{ K}$$

The mixer is a constant pressure duct, thus

$$P_{o10} = P_{o9} = 280.88 \text{ kPa}$$

Afterburner

$$\dot{m}_{11} = \dot{m}_3 + \dot{m}_9 + \left(\dot{m}_f\right)_{Afterburner} = 376.7933 \text{ kg/s}$$

$$T_{011} = \frac{\left(\dot{m}_3 + \dot{m}_9\right) \times C_{ph} \times T_{010} + \left(\dot{m}_f\right)_{Afterburner} \times Q_{HV} \times \eta_b}{\dot{m}_{11} \times C_{ph}} = 1500 \text{ K}$$

$$P_{o11} = P_{o9} \times r_{ab} = 275.26 \text{ kPa}$$

Jet pipe

$$T_{013} = T_{012} = T_{011} = 1500 \text{ K}$$

$$P_{o12} = r_{jet_pipe} P_{o11} = 275.26 \text{ kPa}$$

C-D Nozzle: This nozzle is unchocked

$$P_{13} = P_a = 20.744 \text{ kPa}$$

$$T_{13} = T_{012}\left[1 - \eta_n\left\{1 - \left(\frac{P_a}{P_{012}}\right)^{\gamma - 1/\gamma}\right\}\right]$$

$$T_{13} = 1500\left[1 - 0.95\left\{1 - \left(\frac{20.744}{275.27}\right)^{0.25}\right\}\right] = 821.62\ \text{K}$$

$$U_{13} = \sqrt{2 \times C_P \times \left(T_{013} - T_{13}\right)} = 1243.66\ \text{m/s}$$

$$\rho_{13} = \frac{P_{13}}{RT_{13}} = \frac{20.744}{0.287 \times 821.62} = 0.08797\ \text{kg/m}^3$$

$$\dot{m}_{13} = \dot{m}_{11}$$

$$A_{13} = \frac{\dot{m}_{13}}{\rho_{13} U_{13}} = 3.444\,\text{m}^2$$

$$T = \dot{m}_{13} U_{13} - \dot{m} U = 235.88\ \text{kN}$$

$$\text{Losses} = 0.5 \times \dot{m}_{13} \times \left(U_{13} - U\right)^2 = 75.598\ \left(\text{MN} \cdot \text{m/s}\right)$$

$$\eta_P = \frac{TU}{TU + \text{Losses}} = 0.6556$$

$$\eta_{th} = \frac{TU + \text{Losses}}{\left[\left(\dot{m}_f\right)_{burner} \eta_{burner} + \left(\dot{m}_f\right)_{after\ burner} \eta_{after\ burner}\right] \times Q_{HV}}$$

$$\text{If } \eta_{after\ burner} = \eta_{burner} \equiv \eta_b$$

$$\eta_{th} = \frac{TU + \text{Losses}}{\eta_b \times \left(\dot{m}_f\right)_{total} \times Q_{HV}} = 0.43728$$

$$\eta_{th} = \frac{TU + \text{Losses}}{\dot{m}_f \eta_b Q_{HV}} = 0.43723$$

$$\eta_o = \eta_{th} \times \eta_P = 0.2867$$

Example 5.13

Figure 5.62 illustrates the *AGM-86 ALCM*, which is an American subsonic air-launched cruise missile (ALCM) built by Boeing and operated by the United States Air Force. The Boeing B-52H Stratofortress bomber carries six AGM-86B or AGM-86C missiles on each of two externally mounted pylons, and eight internally on a rotary launcher, giving the B-52H a maximum capacity of 20 missiles per aircraft. The missile after launch deploys its folded wings, tail surfaces, and inlet to its turbofan engine; namely, Williams International for F107-WR-400; see Figure 5.63.

The rocket weight is 1430 kg, its speed is 890 km/h, and it has a range of 2400 km. It is launched at an altitude of 15,000 m, where the ambient conditions are

$$T_a = 216.5\ \text{K}, \quad P_a = 12.11\ \text{kPa}, \quad \rho_a = 0.1948\ \text{kg/m}^3.$$



FIGURE 5.62
AGM-86 ALCM subsonic air-launched cruise missile (ALCM).

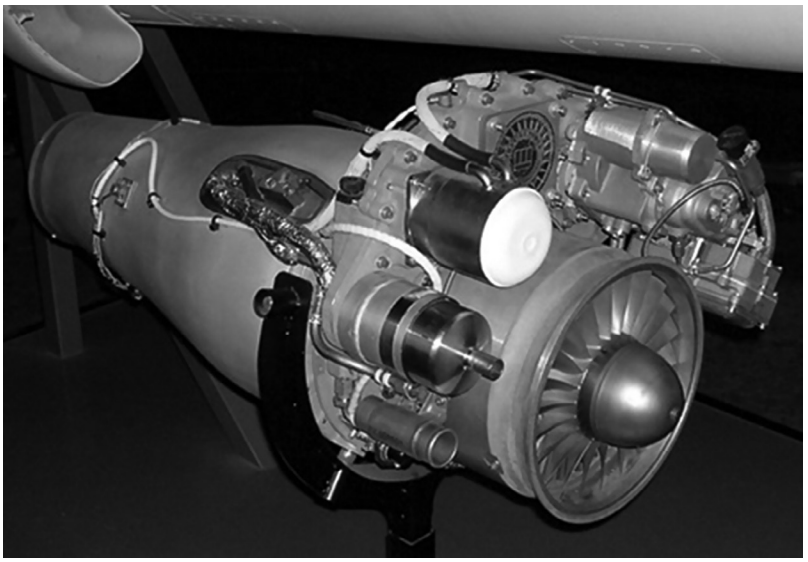


FIGURE 5.63
Williams F107-WR-402 turbofan engine.

The turbofan engine develops thrust for a sustained flight the rocket. Assume the engine cycle is ideal and has the following characteristics:

Thrust = 1.8 kN
Specific fuel consumption = 0.682 kg/kg · h
BPR = 1
Overall pressure ratio = 13.8
Fan pressure ratio = 2.1
Inlet area A = 0.07306 m^2
Fuel heating value = 43,000 kJ/kg

1. Calculate
   a. Air mass flow rate
   b. Fuel-to-air ratio

c. Exhaust gas speed
d. Engine maximum temperature

2. Using Breguet's equation for the range

$$R = \left(\frac{u}{g}\right)\left(\frac{1}{\text{TSFC}}\right)\left(\frac{L}{D}\right)\ln\left(\frac{m_1}{m_2}\right)$$

calculate the lift-to-drag ratio $\left(\frac{L}{D}\right)$ for the rocket

3. Calculate the overall efficiency (η_0) of the engine

Solution

The flight speed $V_f = 870/3.6 = 247.22$ m/s
Since the inlet area is $A = 0.07306$ m^2
Then, the *air mass flow* rate is $\dot{m}_a = \rho_a V_f A = 3.518$ kg/s
Moreover, with BPR $\beta = 1.0$, then $\dot{m}_c = \dot{m}_h = 1.75922$ kg/s

$$\frac{T}{\dot{m}_a} = 511.6 \text{ m/s}$$

$$TSFC = 0.682\ \frac{\text{kg}}{\text{kgf}\cdot\text{h}} = \frac{0.682}{9.81\times 3600} = 0.0000193 \text{ kg/N}\cdot\text{s} = 19.3 \text{ g/kN}\cdot\text{s}$$

Fuel-to-air ratio

$$TSFC = \frac{\dot{m}_f}{T} = \frac{\dot{m}_f/\dot{m}_h}{T/\dot{m}_h} = \frac{\left(\dot{m}_f/\dot{m}_h\right)}{\left(T/\dot{m}_a\right)\times\left(1+\beta\right)} = \frac{f}{\left(T/\dot{m}_a\right)\times\left(1+\beta\right)}$$

$$f = TSFC\times\left(\frac{T}{\dot{m}_a}\right)\left(1+\beta\right) = 0.0000193\times 511.6\times 2 = 0.01976$$

Exhaust gas speed

$$T = \left[\dot{m}_c + \dot{m}_h\left(1+f\right)\right]V_e - \dot{m}_a V_f$$

$$\frac{T}{\dot{m}_a} = \left[\frac{\beta}{1+\beta} + \frac{\left(1+f\right)}{1+\beta}\right]V_e - V_f = \left(\frac{\beta+1+f}{1+\beta}\right)V_e - V_f$$

$$V_e = \frac{\left(T/\dot{m}_a\right)+V_f}{\left(\frac{\beta+1+f}{1+\beta}\right)} = \frac{511.6+247.22}{\left(\frac{2.01976}{2}\right)} = 751.4 \text{ m/s}$$

Engine cycle analysis
Intake

$$M = \frac{V_f}{\sqrt{\gamma R T_a}} = 0.8505$$

$$P_{02} = P_a\left(1+\frac{\gamma-1}{2}M^2\right)^{\gamma/\gamma-1} = 19.43 \text{ kPa}$$

$$T_{02} = T_a\left(1+\frac{\gamma-1}{2}M^2\right) = 247.82 \text{ K}$$

Fan

$$P_{03} = P_{02}\pi_f = 40.8 \text{ kPa}$$

$$T_{03} = T_{02}\left(\pi_f\right)^{\gamma-1/\gamma} = 306.4 \text{ K}$$

Compressor pressure ratio of compressor = 6.57

$$P_{04} = P_{03}\pi_c = 268.1 \text{ kPa}$$

$$T_{04} = T_{03}\left(\pi_c\right)^{\gamma-1/\gamma} = 524.9 \text{ K}$$

Combustion chamber

$$\dot{m}_f Q_R + \dot{m}_h C_{pc} T_{04} = \left(\dot{m}_h + \dot{m}_f\right) C_{ph} T_{05}$$

$$T_{05} = \frac{fQ_R + C_{pc}T_{04}}{\left(1+f\right)C_{ph}} = \frac{0.01976\times 43{,}000 + 1.005\times 524.9}{1.01976\times 1.148} = 1{,}176\,\text{K}$$

Maximum temperature is then $T_{0\max} = 1176$ K.
Since the range of AGM-86B version is 2400 km, then

Average flight time $t = \dfrac{2400}{890} = 2.6966\,\text{h}$
Fuel consumed $m_f = f \times \dot{m}_a \times t = 0.01976 \times 3.518 \times 2.6966 \times 3600 = 674.85$ kg
Initial rocket mass $m_1 = 1430$ kg
Final mass of rocket $m_2 = m_1 - m_f = 1430 - 674.854 = 755.15$ kg

Range equation

$$S = \left(\frac{u}{g}\right)\left(\frac{1}{TSFC}\right)\left(\frac{L}{D}\right)\ln\left(\frac{m_1}{m_2}\right)$$

$$\frac{L}{D} = \frac{g\times S\times \text{TSFC}}{u\times\ln\left(\dfrac{m_1}{m_2}\right)} = \frac{9.81\times 2400\times 10^3\times 0.0000193}{247.22\times\ln\left(\dfrac{1430}{755.15}\right)} = 2.878$$

The overall efficiency is related to the range by Equation 2.30

$$S = \left(\frac{\eta_0 Q_R}{g}\right)\left(\frac{L}{D}\right)\ln\left(\frac{m_1}{m_2}\right)$$

Then

$$\eta_0 = \frac{S\times g}{Q_{R\times}\left(\dfrac{L}{D}\right)\times\ln\left(\dfrac{m_1}{m_2}\right)} = 0.2979 \equiv 29.79\%$$

Example 5.14

A triple-spool unmixed turbofan engine (Trent 700) is shown in Figure 5.64. Of the 8% of air bled from the HPC, 5% is employed in cooling high and intermediate-pressure turbines while the remaining 3% is used in anti-icing systems.

Data for the engine is listed in Table 5.1.

For takeoff condition ($M = 0.2$), at sea level

1. Consider air bleed from HPC ($b = 8\%$)

Calculate

a. The total temperature at the outlet of the fan, intermediate- and high-pressure compressors
b. The total temperature at the outlet to the high-, intermediate- and low-pressure turbines

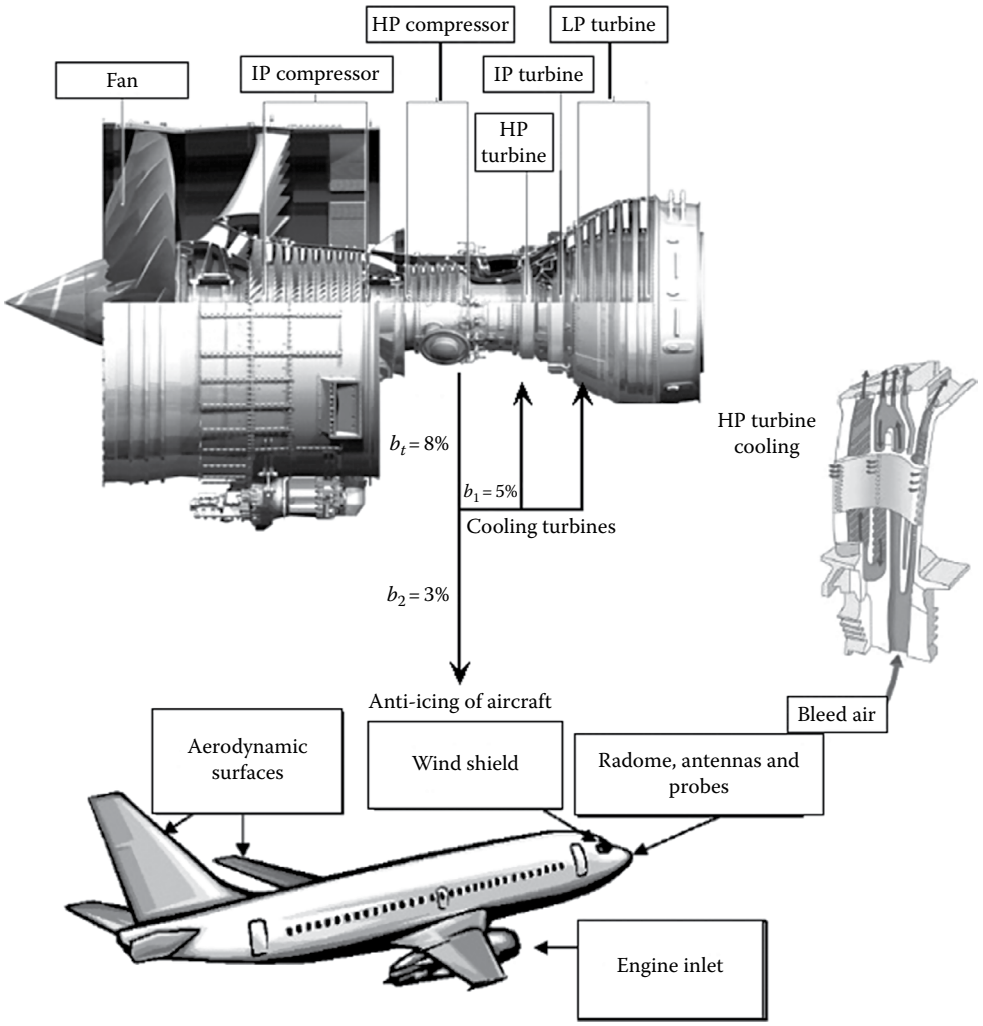


FIGURE 5.64
Layout of unmixed three-spool engine (Trent 700) and bleed air utilities.

TABLE 5.1

Operating Conditions for a Triple-Spool Unmixed Turbofan Engine

Properties	Value	Properties	Value
η_d	0.88	$\Delta p_{c.c}$	0.03
η_f	0.9	$\Delta p_{fan\,duct}$	0
η_c	0.89	cp_c (J/kg·K)	1005
η_b	0.98	cp_h (J/kg·K)	1148
η_t	0.93	R (J/kg·K)	287
η_n	0.98	γ_c	1.4
η_m	0.99	γ_h	1.33
λ_1	0.84	b	0.08
λ_2	1	β	5.05
λ_3	1	TIT (K)	1543
M	0.82	π_{IPC}	5.8
π_F	1.45	π_{HPC}	4.2

   c. The pressure and temperature at the outlet of the cold and hot nozzles
   d. Specific thrust and TSFC
   e. Propulsive, thermal, and overall efficiencies
2. Ignoring bleed (b = 0%)
   Recalculate as above in (1)
3. Compare both cases

Solution

Figures 5.65 and 5.66 illustrate the layout and T–S diagram for a three-spool unmixed turbofan engine with a bleed from HPC.

1. At takeoff (M = 0.2) at sea level with 8% bleed air
   Flight speed

$$V = M\sqrt{\gamma RT_a} = 68.035 \text{ m/s}$$

Diffuser (a–2)

$$P_{o2} = P_a\left(1+\eta_d\frac{\gamma_c-1}{2}M_a^2\right)^{\gamma_c/\gamma_c-1} = 1.0384\times10^5 \text{ Pa}$$

$$T_{o2} = T_a\left(1+\frac{\gamma_c-1}{2}M_a^2\right) = 290.4653 \text{ K}$$

Fan (2–3)

$$P_{o3} = P_{o2}\pi_f = 1.5057\times10^5 \text{ Pa}, \quad T_{o3} = T_{o2}\left(1+\frac{\pi_f^{\gamma_c-1/\gamma_c}-1}{\eta_f}\right) = 326.6124 \text{ K}$$

Intermediate pressure compressor (IPC) (3–4)

$$P_{o4} = P_{o3}\times\pi_{IPC} = 8.7333\times10^5 \text{ Pa} \quad T_{o4} = T_{o3}\left(1+\frac{\pi_{IPC}^{\gamma_c-1/\gamma_c}-1}{\eta_{IPC}}\right) = 566.0401 \text{ K}$$

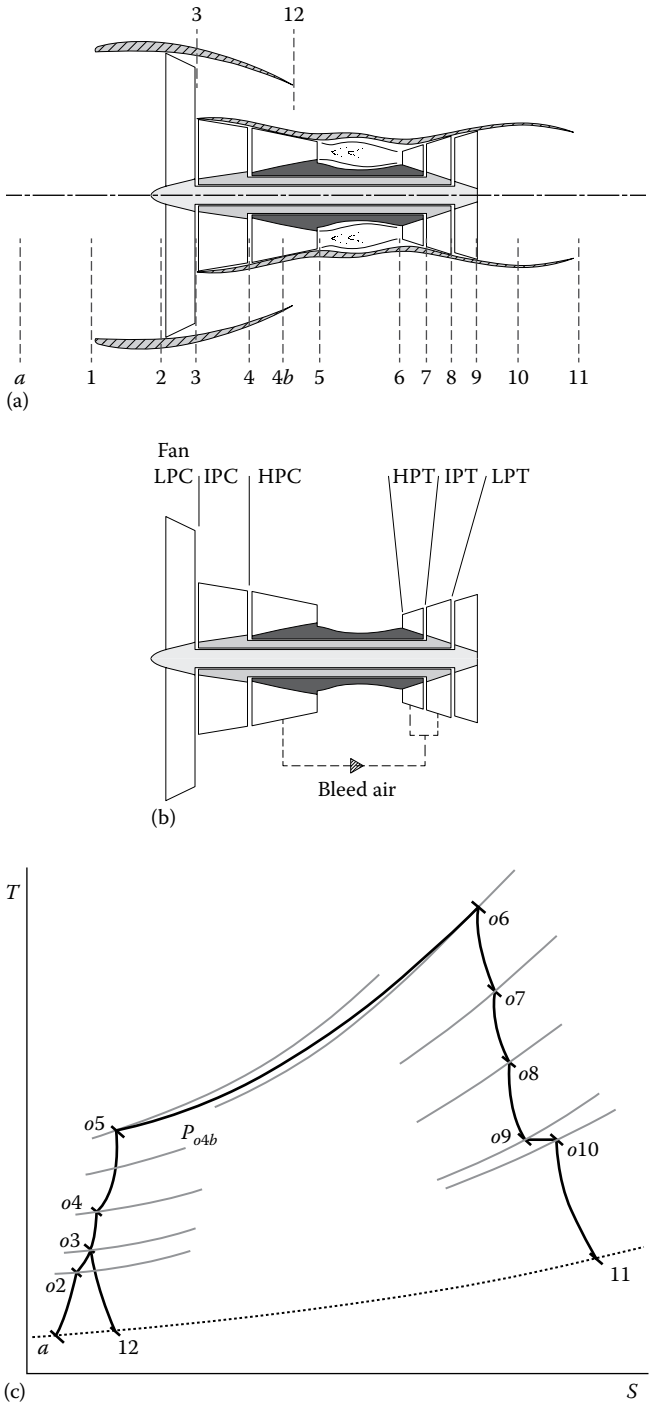


FIGURE 5.65
(a) Layout of unmixed three-spool engine with states and bleed air station. (b) Bleed air system. (c) *T*–*S* diagram.

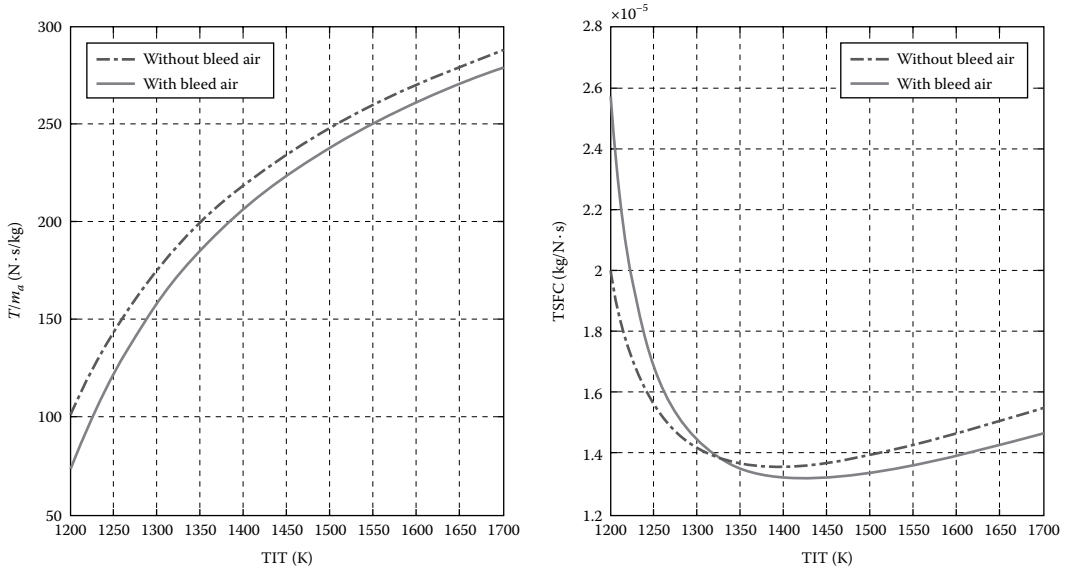


FIGURE 5.66
Variation of specific thrust and TSFC with TIT for cases of bleed and no bleed air.

HPC (4–5)

$$P_{o4b} = P_{o4} \times \sqrt{\pi_{HPC}} = 1.7898 \times 10^6 \text{ pa}$$
$$T_{o4b} = T_{o4}\left(1 + \frac{\pi_{HPC}^{\gamma_c - 1/2\gamma_c} - 1}{\eta_{HPC}}\right) = 710.7556 \text{ K}$$

$$P_{o5} = P_{o4b} \times \sqrt{\pi_{HPC}} = 3.6680 \times 10^6$$
$$T_{o5} = T_{o4b}\left(1 + \frac{\pi_{HPC}^{\gamma_c - 1/2\gamma_c} - 1}{\eta_{HPC}}\right) = 892.4693 \text{ K}$$

Combustion chamber (5–6)

$$T_{o6} = TIT, \quad P_{o6} = P_{o5} \times \left(1 - \Delta p_{c.c}\right) = 3.5579 \times 10^6$$

$$f = \left(1 - b_t\right)\left(\frac{C_{ph} \times T_{o6} - C_{pc} \times T_{o5}}{\eta_b \times Q_R - C_{ph} \times T_{o6}}\right) = 0.0204$$

HPT (6–7)

$$T_{o7} = T_{o6} - \left[\left(\frac{C_{pc}}{\eta_{m1} \times \lambda_1 \times \left(1 + f - b_t\right) \times C_{ph}}\right) \times \left(\left[T_{o4b} - T_{o4}\right] + \left(1 - b_t\right) \times \left[T_{o5} - T_{o4b}\right]\right)\right] = 1207.1 \text{ K}$$

$$P_{o7} = P_{o6}\left(1 - \frac{\left(T_{o6} - T_{o7}\right)}{\eta_{HPT} \times T_{o6}}\right)^{\gamma/\gamma_h - 1} = 1.2145 \times 10^6 \text{ Pa}$$

Intermediate-pressure turbine (IPT) (7–8)

$$T_{o8} = T_{o7} - \left(\frac{C_{pc} \times \left[T_{o4} - T_{o3} \right]}{\lambda_2 \times \eta_{m2} \times \left(1 + f - \frac{b_1}{2} - b_2 \right) \times C_{ph}} \right) = 987.7755 \text{ K}$$

$$P_{o8} = P_{o7} \left(1 - \frac{\left[T_{o7} - T_{o8} \right]}{\eta_{IPT} \times T_{o7}} \right)^{\gamma_h / \gamma_h - 1} = 5.0576 \times 10^5 \text{ Pa}$$

Low-pressure turbine (LPT) (8–9)

$$T_{o9} = T_{o8} - \left(\frac{\left(1 + \beta \right) \times C_{pc} \times \left[T_{o3} - T_{o2} \right]}{\lambda_3 \times \eta_{m3} \times \left(1 + f - b_2 \right) \times C_{ph}} \right) = 792.5231 \text{ K}$$

$$P_{o9} = P_{o8} \left(1 - \frac{\left[T_{o8} - T_{o9} \right]}{\eta_{LPT} \times T_{o8}} \right)^{\gamma_h / \gamma_h - 1} = 1.9306 \times 10^5 \text{ Pa}$$

Hot nozzle (10–11)

$$P_{o10} = P_{o9} \left(1 - \Delta p_{duct} \right) = 1.8727 \times 10^5 \text{ Pa}$$

The critical pressure

$$P_c = P_{o10} \left(1 - \frac{1}{\eta_n} \left[\frac{\gamma_h - 1}{\gamma_h + 1} \right] \right)^{\gamma_h / \gamma_h - 1} = 9.9828 \times 10^4 \text{ Pa}$$

With ambient pressure

$$P_a = 1.01325 \times 10^5 \text{ Pa}$$

Since $P_c > P_a$, the hot nozzle is choked.

$$\therefore P_{11} = P_a, \quad T_{11} = T_{o10} \left[1 - \eta_n \left(1 - \left(\frac{P_a}{P_{o10}} \right)^{\gamma_h - 1 / \gamma_h} \right) \right] = 682.7351 \text{ K},$$

$$V_{12} = \sqrt{2 C_{ph} \left(T_{o10} - T_{11} \right)} = 502.0690 \text{ m/s}$$

Cold nozzle (3–12): The critical pressure

$$P_c = P_{o3} \left(1 - \frac{1}{\eta_n} \left[\frac{\gamma_h - 1}{\gamma_h + 1} \right] \right)^{\gamma_h / \gamma_h - 1} = 7.8415 \times 10^4 \text{ Pa}$$

with $P_a = 101{,}325$ Pa since $P_c > P_a$, then the cold nozzle is also choked.

$$P_{12} = P_a, \quad T_{12} = T_{o3} \left[1 - \eta_n \left(1 - \left(\frac{P_a}{P_{o3}} \right)^{\gamma_h - 1 / \gamma_h} \right) \right] = 292.3616 \text{ K}, \quad V_{12} = \sqrt{2 C_{ph} \left(T_{o3} - T_{12} \right)} = 280.4278 \text{ m/s}$$

Specific thrust

$$\frac{T}{\dot{m}_a}=\left[\left(\frac{1}{1+\beta}\right)\left[\left(1+f-b_2\right)\times V_{11}+\beta\times V_{12}+\left(1+f-b_2\right)\left(\frac{RT_{11}}{P_{11}V_{11}}\right)\left(P_{11}-P_a\right)+\beta\left(\frac{RT_{12}}{P_{12}V_{12}}\right)\left(P_{12}-P_a\right)\right]-V\right]$$
$$=248.2143\ \text{N}\cdot\text{s/kg}$$

where
T is the thrust force
$\dot{m}_a$ is the air mass flow rate
V is the flight speed
V_{11} is the hot gases exhaust speed
V_{12} is the cold gases exhaust speed

TSFC

$$TSFC=\frac{f/(1+\beta)}{T/\dot{m}_a}=1.3601\times10^{-5}$$

Propulsive efficiency

$$\eta_p=\frac{T/\dot{m}_a\times V}{T/\dot{m}_a\times V+\left[0.5\left(\frac{1+f-b_2}{1+\beta}\right)\left(V_{11}-V\right)^2\right]+\left[0.5\left(\frac{\beta}{1+\beta}\right)\left(V_{12}-V\right)^2\right]}=0.3303$$

Thermal efficiency

$$\eta_{th}=\frac{T/\dot{m}_a\times V+\left[0.5\left(\frac{1+f-b_2}{1+\beta}\right)\left(V_{11}-V\right)^2\right]+\left[0.5\left(\frac{\beta}{1+\beta}\right)\left(V_{12}-V\right)^2\right]}{\left(\frac{f}{1+\beta}\right)Q_R}=0.3606$$

Overall efficiency

$$\eta_o=\eta_p\times\eta_{th}=\frac{T/\dot{m}_a\times V}{\left(\frac{f}{1+\beta}\right)Q_R}=0.1191$$

2. At takeoff (M = 0.2) at sea level with 0% bleed air
Cycle analysis
Results for case (A) are applied here up to the combustion chamber
Combustion chamber (5–6)

$$T_{o6}=TIT,\quad P_{o6}=P_{o5}\times\left(1-\Delta p_{c.c}\right)=3.5579\times10^6$$

$$f=\left(\frac{C_{ph}\times T_{o6}-C_{pc}\times T_{o5}}{\eta_b\times Q_R-C_{ph}\times T_{o6}}\right)=0.0222$$

HPT (6–7)

$$T_{o7} = T_{o6} - \left[\left(\frac{C_{pc}}{\eta_{m1} \times \lambda_1 \times (1+f) \times C_{ph}} \right) \times \left(\left[T_{o4b} - T_{o4} \right] + \left[T_{o5} - T_{o4b} \right] \right) \right] = 1206 \text{ K}$$

$$P_{o7} = P_{o6} \left(1 - \frac{(T_{o6} - T_{o7})}{\eta_{HPT} \times T_{o6}} \right)^{\gamma_h/\gamma_h - 1} = 1.2099 \times 10^6 \text{ Pa}$$

Intermediate-pressure turbine (HPT) (7–8)

$$T_{o8} = T_{o7} - \left(\frac{C_{pc} \times \left[T_{o4} - T_{o3} \right]}{\lambda_2 \times \eta_{m2} \times (1+f) \times C_{ph}} \right) = 998.9187 \text{ K}$$

$$P_{o8} = P_{o7} \left(1 - \frac{\left[T_{o7} - T_{o8} \right]}{\eta_{IPT} \times T_{o7}} \right)^{\gamma_h/\gamma_h - 1} = 5.3137 \times 10^5 \text{ Pa}$$

Low-pressure turbine (HPT) (8–9)

$$T_{o9} = T_{o8} - \left(\frac{(1+\beta) \times C_{pc} \times \left[T_{o3} - T_{o2} \right]}{\lambda_3 \times \eta_{m3} \times (1+f) \times C_{ph}} \right) = 809.7359 \text{ K}$$

$$P_{o9} = P_{o8} \left(1 - \frac{\left[T_{o8} - T_{o9} \right]}{\eta_{LPT} \times T_{o8}} \right)^{\gamma_h/\gamma_h - 1} = 2.1224 \times 10^5 \text{ Pa}$$

Hot nozzle (10–11)

$$P_{o10} = P_{o9} \left(1 - \Delta p_{duct} \right) = 2.0588 \times 10^5 \text{ Pa}$$

The critical pressure

$$P_c = P_{o10} \left(1 - \frac{1}{\eta_n} \left[\frac{\gamma_h - 1}{\gamma_h + 1} \right] \right)^{\gamma_h/\gamma_h - 1} = 1.0975 \times 10^5 \text{ Pa}$$

with

$$P_a = 1.01325 \times 10^5 \text{ Pa}$$

since $P_c > P_a$, then the hot nozzle is choked

$$\therefore P_{11} = P_c, \quad T_{11} = T_{o10} \left(\frac{2}{\gamma_h + 1} \right) = 695.0523 \text{ K}, \quad V_{11} = \sqrt{\gamma_h R T_{11}} = 515.0810 \text{ m/s}$$

Cold nozzle (3–12): The critical pressure

$$P_c = P_{o3} \left(1 - \frac{1}{\eta_n} \left[\frac{\gamma_h - 1}{\gamma_h + 1} \right] \right)^{\gamma_h/\gamma_h - 1} = 7.8415 \times 10^4 \text{ Pa}$$

with $P_a = 101{,}325$ Pa where η_n: is the nozzle's total-to-static isentropic efficiency.

Since $P_c < P_a$, then the cold nozzle is unchoked.

$$P_{12} = P_a, \quad T_{12} = T_{o3}\left[1 - \eta_n\left(1 - \left(\frac{P_a}{P_{o3}}\right)^{\gamma_h - 1/\gamma_h}\right)\right] = 292.3616 \text{ K},$$
$$V_{12} = \sqrt{2C_{ph}\left(T_{o3} - T_{12}\right)} = 280.4278 \text{ m/s}$$

Specific thrust

$$\frac{T}{\dot{m}_a} = \left[\left(\frac{1}{1+\beta}\right)\left[(1+f)\times V_{11} + \beta \times V_{12} + (1+f)\left(\frac{RT_{11}}{P_{11}V_{11}}\right)(P_{11} - P_a) + \beta\left(\frac{RT_{12}}{P_{12}V_{12}}\right)(P_{12} - P_a)\right] - V\right]$$
$$= 258.0705 \text{ N} \cdot \text{s/kg}$$

TSFC

$$TSFC = \frac{f/(1+\beta)}{T/\dot{m}_a} = 1.4219 \times 10^{-5}$$

Propulsive efficiency

$$\eta_p = \frac{T/\dot{m}_a \times V}{T/\dot{m}_a \times V + \left[0.5\left(\frac{1+f}{1+\beta}\right)(V_{11} - V)^2\right] + \left[0.5\left(\frac{\beta}{1+\beta}\right)(V_{12} - V)^2\right]} = 0.3297$$

Thermal efficiency

$$\eta_{th} = \frac{T/\dot{m}_a \times V + \left[0.5\left(\frac{1+f}{1+\beta}\right)(V_{11} - V)^2\right] + \left[0.5\left(\frac{\beta}{1+\beta}\right)(V_{12} - V)^2\right]}{\left(\frac{f}{1+\beta}\right)Q_R} = 0.3456$$

Overall efficiency

$$\eta_o = \eta_p \times \eta_{th} = \frac{T/\dot{m}_a \times V}{\left(\frac{f}{1+\beta}\right)Q_R} = 0.1140$$

3. Comparison between the cases with bleed and without bleed

Case	$T/\dot{m}_a$ (N · s/kg)	$TSFC \times 10^5$ kg/(N · s)	η_p(%)	η_{th} (%)	η_o (%)
8% bleed	248.21	1.36	33.03	36.06	11.91
0% bleed	258.07	1.42	32.97	34.56	11.4

A parametric study for the cases of zero bleed and 8% bleed air is performed for different turbine-inlet temperatures (from 1200 to 1700 K). The final results are plotted in Figure 5.66.

5.10 Geared Turbofan Engines

The concept of a geared turbofan is not new, and the first designs for this engine type date back to the 1980s. The gear system decouples the engine's turbine from the large air intake fan at its front, making it possible to run both at optimum speeds.

However, old gearboxes were heavy. Using lighter alloys, the problem is then overcome, and the rewards in terms of *efficiency gains* are significant.

Since most of the thrust generated by a turbofan engine comes from the bypassed air, a smaller jet engine leads to less burnt fuel. The space around the engine also helps reduce noise.

Currently, the average BPR is around 8:1. However, for geared turbofans the ratio is increased to be 12:1.

The new engine lets the inlet fan rotate at a third of the speed of the turbine, improving the propulsive efficiency. This allows both the turbine and the inlet fan to run at their optimal speeds.

A geared turbofan has the following advantages:

1. Lower emissions (CO_2 and NO_x)
2. Lower cost
3. Less weight and size through
   a. Fewer number of stages of LPC
   b. Fewer number of stages of HPC
   c. Fewer number of stages of LPT
4. Higher propulsive efficiency
5. Higher thermal efficiency since maximum cycle temperature is reduced
6. Lower fuel consumption (up to 15%)
7. Lower noise pollution
8. Lower nitrous oxide emissions (fuel saving implies that each aircraft will emit 3600 fewer tons of carbon dioxide annually)

Example 5.15 will present a comprehensive analysis of a geared turbofan engine.

Example 5.15

The Bombardier C Series is a narrow-body, twin-engine airliner powered by two geared turbofans, the Pratt & Whitney PW1000G. The cruise altitude is 12,000 m at which pressure is equal to 19,300 Pa and the temperature is 216.7 K with a Mach number of 0.78. The PW1000G is a twin-spool, high-BPR turbofan having a BPR of 11.4 and an OPR of 42 during cruise. The fan, LPC, and HPC have pressure ratios of 1.6, 2.2, and 11.93, respectively. The turbine-inlet temperature is 1520 K. Fuel used has a heating value of 43 MJ/kg.

1. We need to calculate the following
   a. Total temperature and total pressure at each station.
   b. Specific thrust, thrust, TSFC, and fuel-to-air ratio knowing that the air mass flow rate is 173 kg/s.
   c. The thermal, propulsive, and total efficiencies.

2. Next, investigate the effect of changing BPR, TIT, flight Mach number, and altitude on the calculated results.
   Take the following constants

η_{intake}	$\eta_{mechanical}$	η_{fan}	$\eta_{compressor}$	η_{CC}	$\eta_{turbine}$	$\eta_{nozzles}$
0.98	0.993	0.91	0.90	0.95	0.95	0.95

Cp_c	Cp_h	γ_h	γ_c	R	$\%\Delta P_{cc}$
1005 J/kg · K	1148 J/kg · K	1.333	1.4	287 J/kg · K	2%

Solution

1. *Diffuser*

$$P_{02} = P_a\left[1+\eta_{intake}\left(\frac{\gamma_c-1}{2}\right)M^2\right]^{\gamma_c/\gamma_c-1}$$

$$P_{02} = 19.3*\left[1+0.98\left(\frac{1.4-1}{2}\right)0.78^2\right]^{3.5}$$

$$P_{02} = 28.628 \text{ kPa}$$

$$T_{02} = T_a\left[1+\left(\frac{\gamma_c-1}{2}\right)M^2\right]$$

$$T_{02} = 216.7*\left[1+\left(\frac{1.4-1}{2}\right)0.78^2\right]$$

$$T_{02} = 243.068 \text{ K}$$

Fan

$$P_{03} = \pi_f * P_{02} = 1.6*28.628$$

$$P_{03} = 45.805 \text{ kPa}$$

$$T_{03} = T_{02}\left[1+\frac{\left(\pi_f{}^{\gamma_c-1/\gamma_c}-1\right)}{\eta_{fan}}\right] = 243.068*\left[1+\frac{\left(1.6^{0.4/1.4}-1\right)}{0.91}\right]$$

$$T_{03} = 281.457 \text{ K}$$

LPC

$$P_{04} = \pi_{LPC} * P_{03} = 2.2*45.805$$

$$P_{04} = 100.772 \text{ kPa}$$

$$T_{04} = T_{03}\left[1+\frac{\left(\pi_{LPC}{}^{\gamma_c/\gamma_c-1}-1\right)}{\eta_{LPC}}\right] = 281.457\left[1+\frac{\left(2.2^{0.4/1.4}-1\right)}{0.9}\right]$$

$$T_{04} = 360.473 \text{ K}$$

HPC

$$P_{05} = \pi_{HPC} * P_{04} = 11.93 * 100.772$$

$$P_{05} = 1202.393 \text{ kPa}$$

$$T_{05} = T_{04}\left[1 + \frac{\left(\pi_{HPC}{}^{\gamma_c/\gamma_c - 1} - 1\right)}{\eta_{HPC}}\right] = 360.473\left[1 + \frac{\left(11.93^{0.4/1.4} - 1\right)}{0.9}\right]$$

$$T_{05} = 773.266 \text{ K}$$

Combustion chamber

$$T_{06} = 1520 \text{ K}$$

$$P_{06} = \left(1 - \%\Delta Pcc\right) * P_{05} = \left(1 - 0.02\right) * 1202.393$$

$$P_{06} = 1178.345 \text{ kPa}$$

$$f = \frac{Cp_h * T_{06} - Cp_c * T_{05}}{\eta_{cc} QHV - Cp_h * T_{06}} = \frac{1148 * 1520 - 1005 * 773.266}{0.95 * 43 * 10^6 - 1148 * 1520}$$

$$f = 0.024749$$

HPT

$$T_{07} = T_{06} - \left(\frac{Cp_c * \left(T_{05} - T_{04}\right)}{\eta_m Cp_h \left(1 + f\right)}\right) = 1520 - \left(\frac{1005 * \left(773.266 - 360.473\right)}{0.993 * 1148 * \left(1 + 0.024749\right)}\right)$$

$$T_{07} = 1163.792 \text{ K}$$

$$P_{07} = P_{06} * \left(1 - \frac{T_{06} - T_{07}}{\eta_{HPT} * T_{06}}\right)^{\gamma_h/(\gamma_h - 1)} = 1178.345 * \left(1 - \frac{1520 - 1163.792}{0.95 * 1520}\right)^4$$

$$P_{07} = 379.478 \text{ kPa}$$

LPT

$$T_{08} = T_{07} - \left(\frac{1 + \beta}{1 + f}\right)\left(\frac{Cp_c}{\eta_m Cp_h}\right)\left(T_{03} - T_{02}\right) - \left(\frac{Cp_c}{\eta_m Cp_h \left(1 + f\right)}\right)\left(T_{04} - T_{03}\right)$$

$$T_{08} = 1163.792 + -\left(\frac{12.4}{1.024749}\right)\left(\frac{1005}{0.993 * 1148}\right)\left(281.457 - 243.068\right) - \left(\frac{1005}{0.993 * 1148 * 1.024749}\right)\left(360.473 - 281.457\right)$$

$$T_{08} = 684.837 \text{ K}$$

$$P_{08} = P_{07} * \left(1 - \frac{T_{07} - T_{08}}{\eta_{HPT} * T_{07}}\right)^{\gamma_h/\gamma_{h-1}} = 379.48 * \left(1 - \frac{1163.79 - 684.837}{0.9 * 1163.792}\right)^4$$

$$P_{08} = 39.163 \text{ kPa}$$

Hot nozzle: Find critical pressure

$$P_{c1} = P_{08}\left(1 - \frac{1}{\eta_n}\left(\frac{\gamma_h - 1}{\gamma_h + 1}\right)\right)^{\gamma_h/(\gamma_h - 1)} = 39.163\left(1 - \frac{1}{0.95}\left(\frac{0.333}{2.333}\right)\right)^4$$

$$P_{c1} = 20.571 \text{ kPa}$$

$$P_{c1} > P_a$$

$\therefore$ The nozzle is choked

$$\therefore P_9 = P_{c1}$$

$$T_9 = \frac{To8}{\frac{\gamma_h + 1}{2}} = 587.087 \text{ K}$$

$$V_9 = \sqrt{\gamma_h R T_9} = 473.923 \text{ m/s}$$

Cold nozzle: Find critical pressure

$$P_{c2} = P_{03}\left(1 - \frac{1}{\eta_n}\left(\frac{\gamma_c - 1}{\gamma_c + 1}\right)\right)^{\gamma_c/(\gamma_c - 1)}$$

$$P_{c2} = 23.499 \text{ kPa}$$

$$P_{c2} > P_a$$

$\therefore$ The nozzle is choked

$$\therefore P_{11} = P_{c1}$$

$$T_{11} = \frac{T_{o3}}{\frac{\gamma_c + 1}{2}} = 234.547 \text{ K}$$

$$V_{11} = \sqrt{\gamma_c R T_{11}} = 306.987 \text{ m/s}$$

Specific thrust

$$\frac{T}{\dot{m}a} = \frac{\beta}{1+\beta}V_{11} + \frac{(1+f)}{1+\beta}V_9 - V_f + \left(\frac{1+f}{1+\beta}\right)\left(\frac{RT_9}{P_9V_9}\right)(P_9 - P_a) + \left(\frac{\beta}{1+\beta}\right)\left(\frac{RT_{11}}{P_{11}V_{11}}\right)(P_{11} - P_a)$$

$$\frac{T}{\dot{m}a} = 129.079\ \mathrm{N \cdot s/kg}$$

TSFC

$$TSFC = \frac{f}{T/\dot{m}_a}$$

$$TSFC = 0.00019174\ \mathrm{kg/N \cdot s}$$

Thrust

$$T = \frac{T}{\dot{m}a} * \dot{m}a = 129.079 * 173 = 22339.2\ \mathrm{N}$$

Propulsive efficiency

$$\eta_p = \frac{\frac{T}{\dot{m}a} * Vf}{\frac{T}{\dot{m}a} * V_f + 0.5 * \left(\left(\frac{1+f}{1+\beta}\right) * (V_9 - V_f)^2 + \left(\frac{\beta}{1+\beta}\right) * (V_{11} - V_f)^2\right)}$$

$$V_f = M * \sqrt{\gamma RT_a} = 0.78 * \sqrt{1.4 * 287 * 216.7} = 230.16\ \mathrm{m/s}$$

$$\eta_p = \frac{129.079 * 230.16}{129.079 * 230.16 + 0.5 * \left(\left(\frac{1.024749}{12.4}\right) * (473.923 - 230.16)^2 + \left(\frac{11.4}{12.4}\right) * (306.987 - 230.16)^2\right)}$$

$$\eta_p = 0.852$$

Thermal efficiency

$$\eta_{th} = \frac{\frac{T}{\dot{m}a} * Vf + 0.5 * \left(\left(\frac{1+f}{1+\beta}\right) * (V_9 - V_f)^2 + \left(\frac{\beta}{1+\beta}\right) * (V_{11} - V_f)^2\right)}{(f/(1+\beta)) * QHV}$$

$$\eta_{th} = \frac{129.079 * 230.16 + 0.5 * \left(\left(\frac{1.024749}{12.4}\right) * (473.923 - 230.16)^2 + \left(\frac{11.4}{12.4}\right) * (306.987 - 230.16)^2\right)}{(0.024749 / (12.4)) * 43 * 10^6}$$

$$\eta_{th} = 0.406$$

Overall efficiency

$$\eta_o = 0.852 * 0.406 = 0.346$$

2. To study the effects of these variations, a computer program is developed.
   - I. TIT effect
     Vary TIT from 1370 to 1900 K to get the curves shown in Figures 5.67 through 5.73.
   - II. BPR
     Vary BPR from 4 to 12.8 to get the curves shown in Figures 5.74 through 5.77.
   - III. Mach number
     Varying flight Mach number from 0.1 to 0.9 to get the curves shown in Figures 5.78 through 5.81.
   - IV. Altitude analysis
     Vary altitude from 1,500 to 12,000 m to get the curves shown in Figures 5.82 and 5.83.
   - V. Mach number: BPR analysis (Figures 5.84 and 5.85)
   - VI. Mach number: TIT analysis (Figures 5.86 and 5.87)
   - VII. BPR: TIT analysis (Figures 5.88 and 5.89)

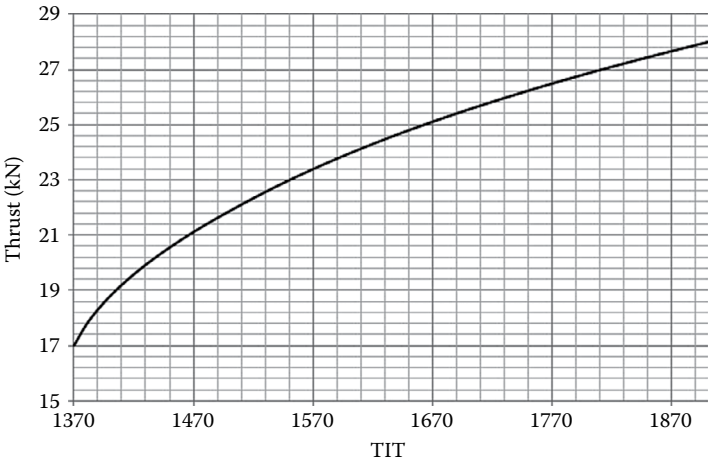


FIGURE 5.67
Variation of thrust with turbine inlet temperature TIT.

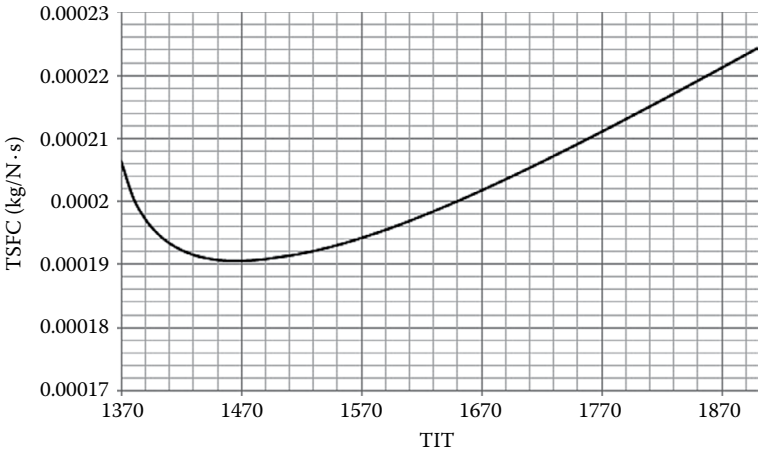


FIGURE 5.68
Variation of thrust specific fuel consumption TSFC with turbine inlet temperature TIT.

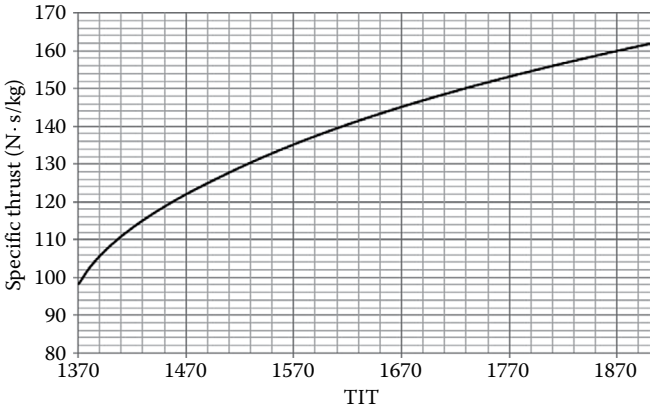


FIGURE 5.69
Variation of specific thrust with turbine inlet temperature TIT.

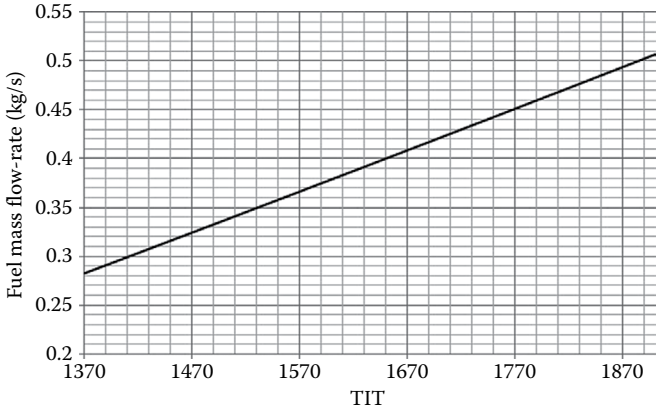


FIGURE 5.70
Variation of fuel mass flow-rate with turbine inlet temperature TIT.

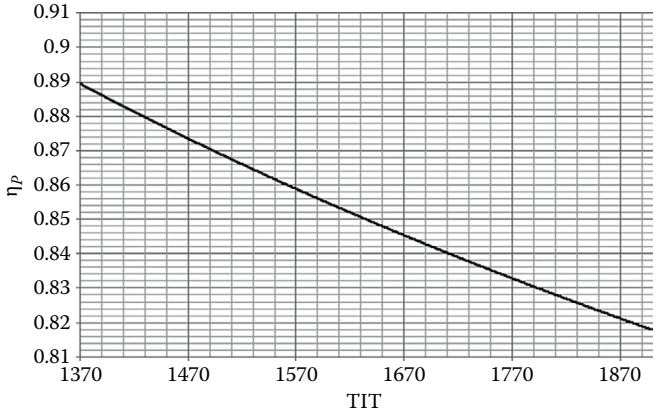


FIGURE 5.71
Variation of propulsive efficiency with turbine inlet temperature TIT.

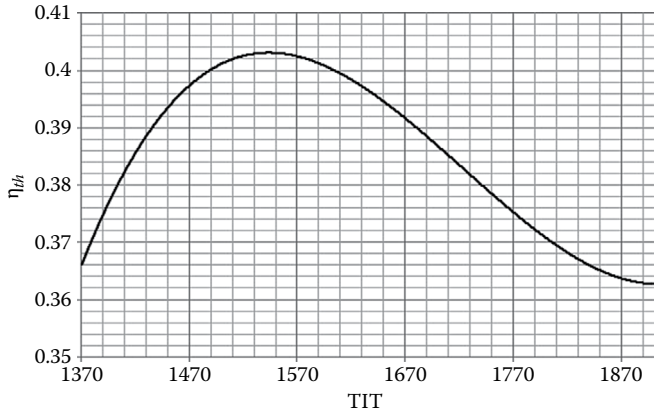


FIGURE 5.72
Variation of thermal efficiency with turbine inlet temperature TIT.

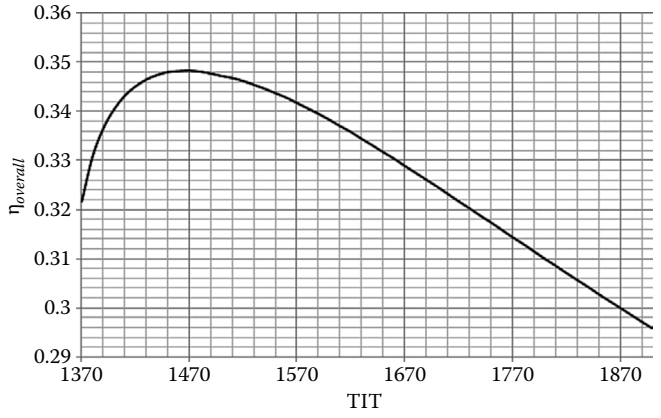


FIGURE 5.73
Variation of overall efficiency with turbine inlet temperature TIT.

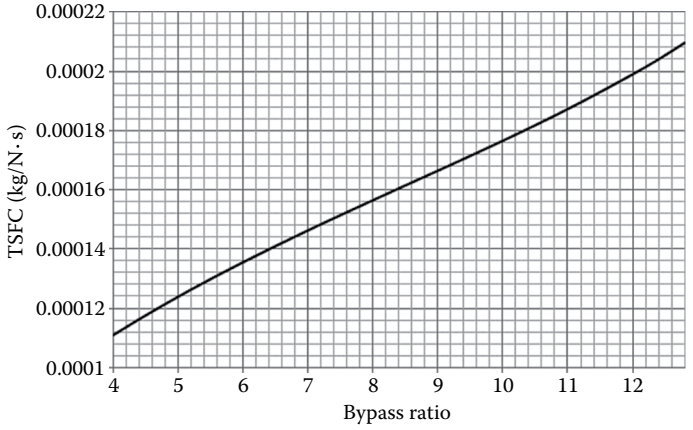


FIGURE 5.74
Variation of thrust specific fuel consumption TSFC with bypass ratio.

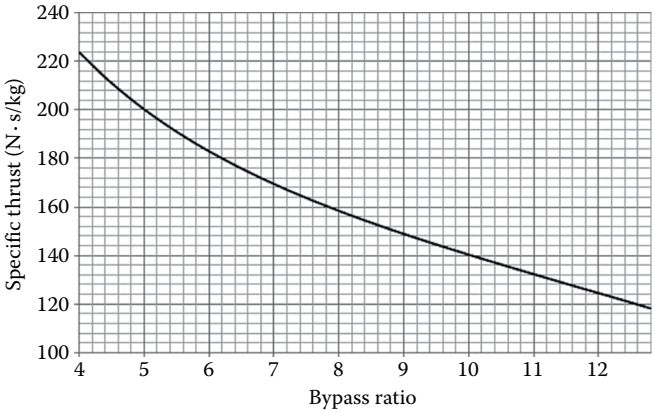


FIGURE 5.75
Variation of specific thrust with bypass ratio.

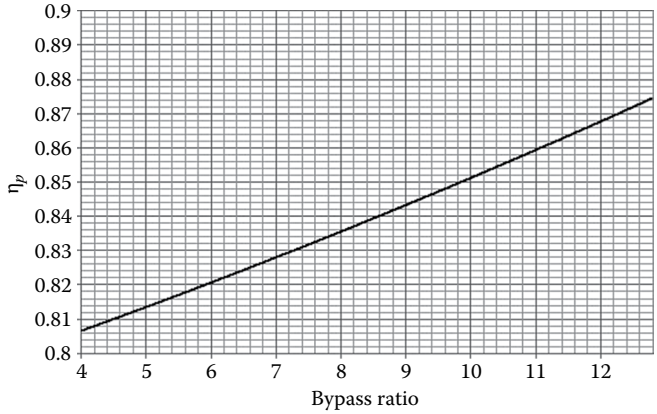


FIGURE 5.76
Variation of propulsive efficiency with bypass ratio.

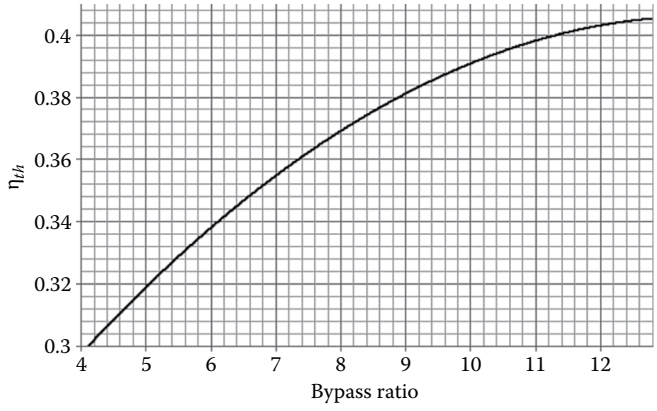


FIGURE 5.77
Variation of thermal efficiency with bypass ratio.

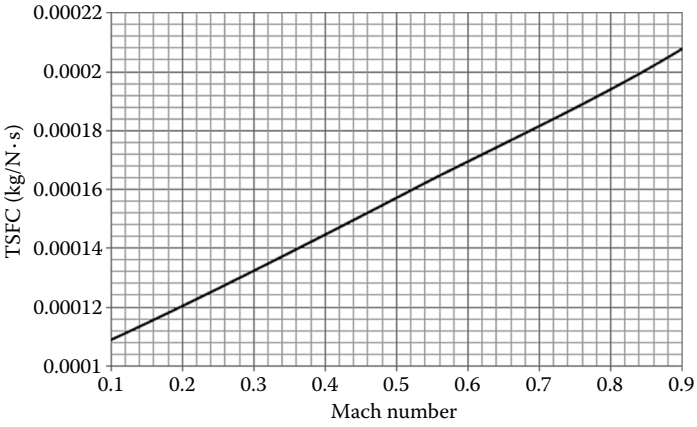


FIGURE 5.78
Variation of thrust specific fuel consumption TSFC with flight Mach number.

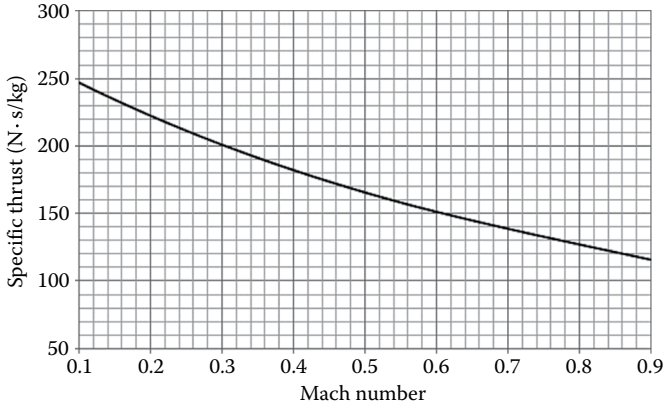


FIGURE 5.79
Variation of specific thrust with flight Mach number.

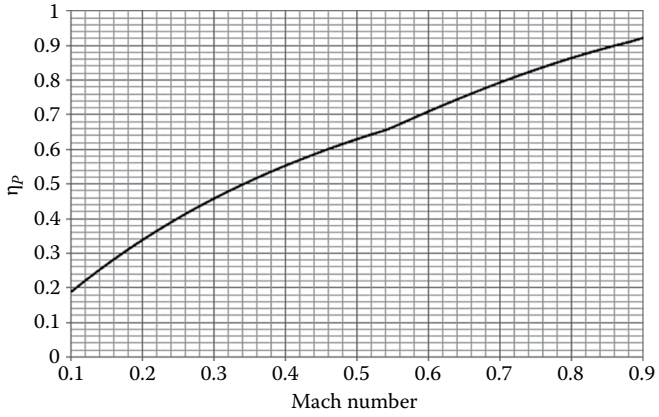


FIGURE 5.80
Variation of propulsive efficiency with flight Mach number.

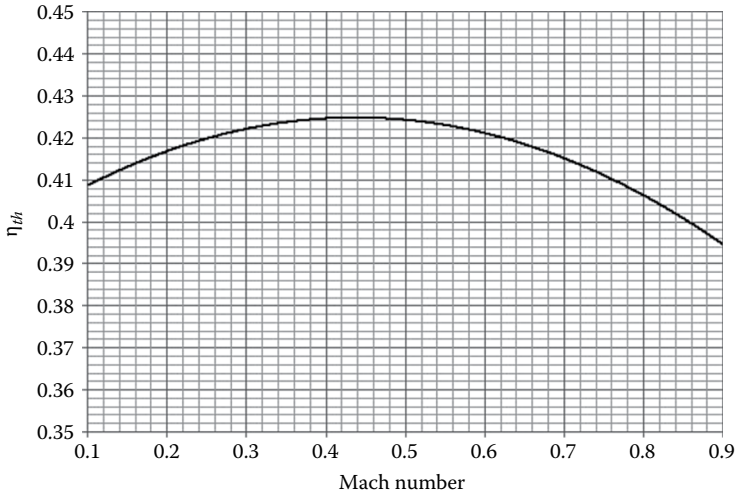


FIGURE 5.81
Variation of thermal efficiency with flight Mach number.

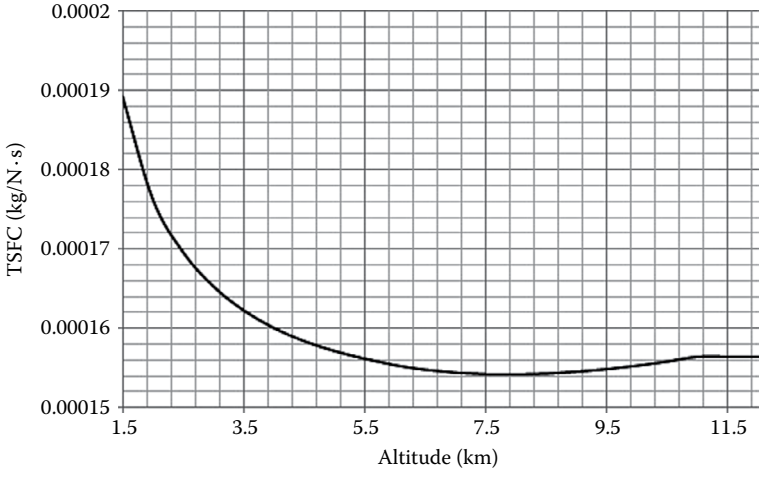


FIGURE 5.82

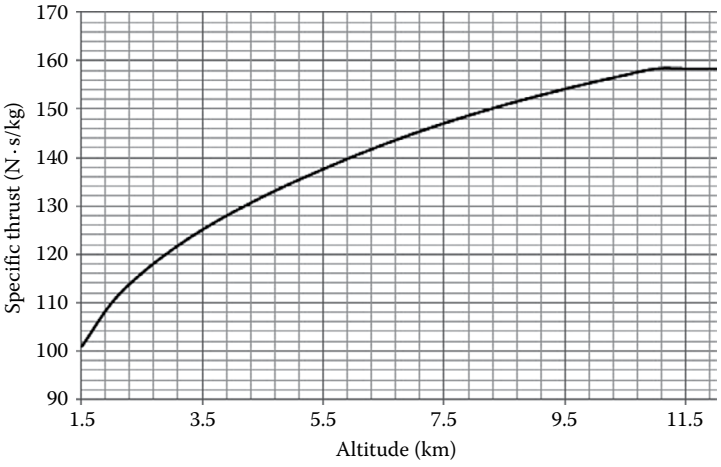


FIGURE 5.83
Variation of thrust specific fuel consumption TSFC with flight altitude.

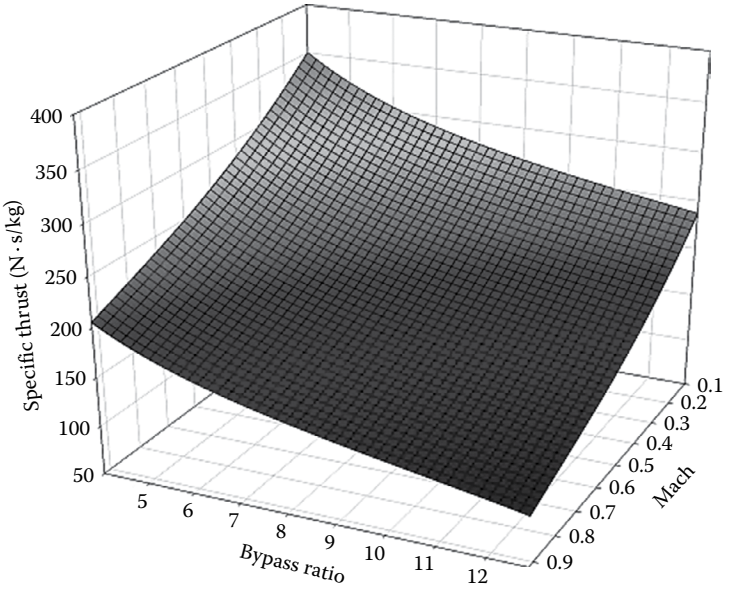


FIGURE 5.84
Variations of specific thrust with bypass ratio and flight Mach number.

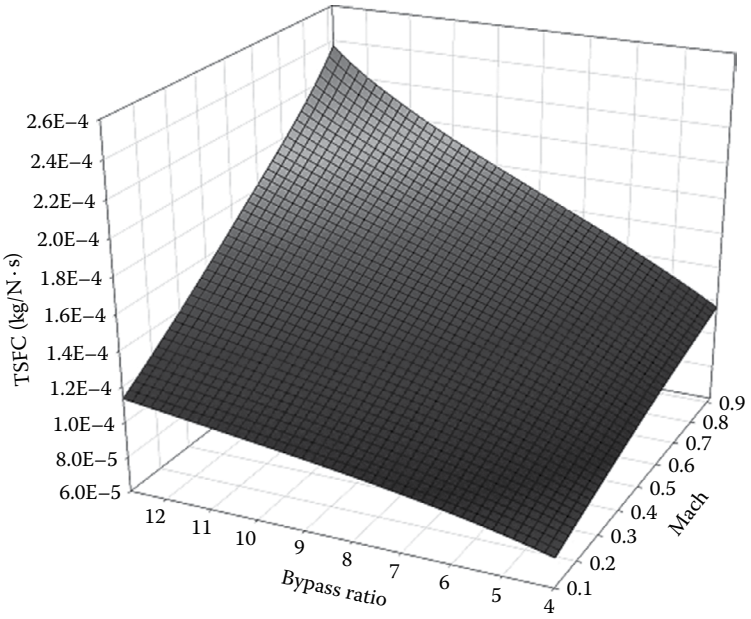


FIGURE 5.85
Variations of thrust specific fuel consumption with bypass ratio and flight Mach number.

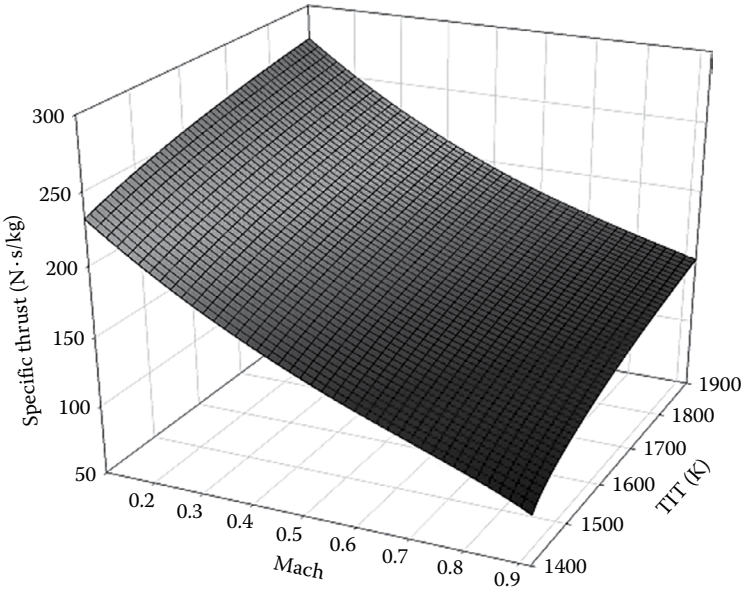


FIGURE 5.86
Variations of specific thrust with flight Mach number and turbine inlet temperature TIT.

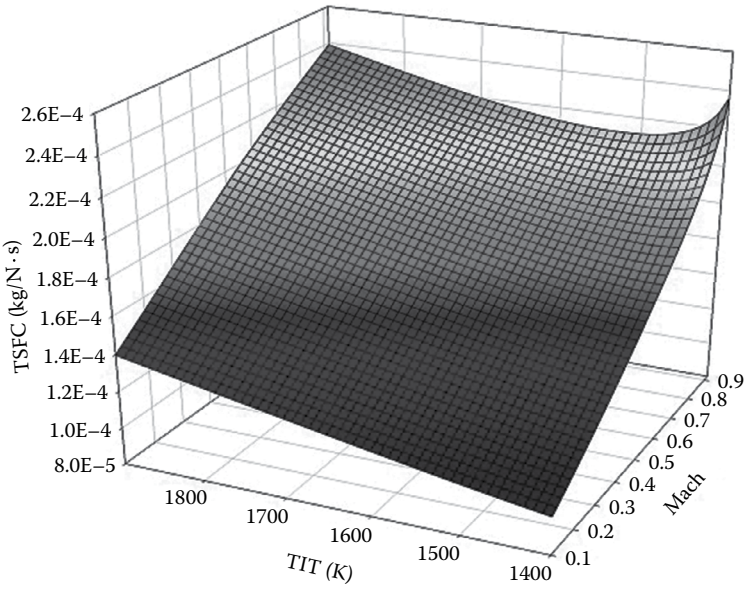


FIGURE 5.87
Variations of thrust specific fuel consumption TSFC with flight Mach number and turbine inlet temperature TIT.

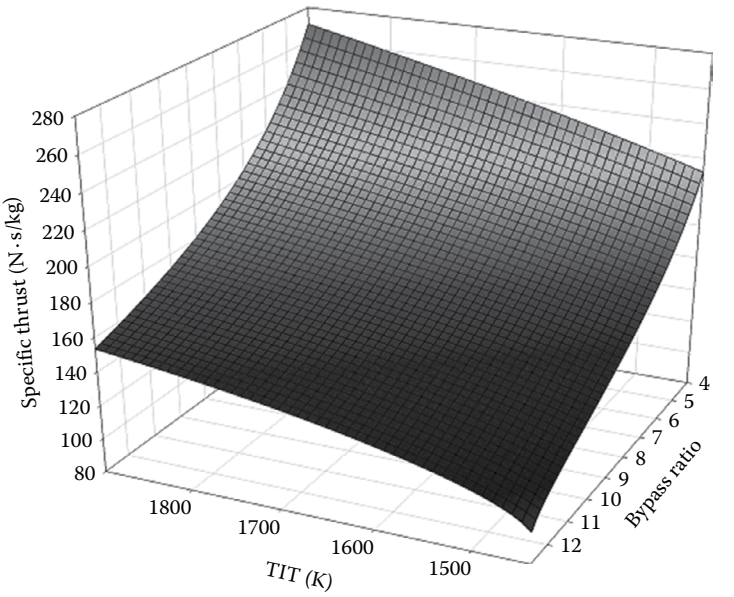


FIGURE 5.88
Variations of specific thrust with bypass ratio and turbine inlet temperature TIT.

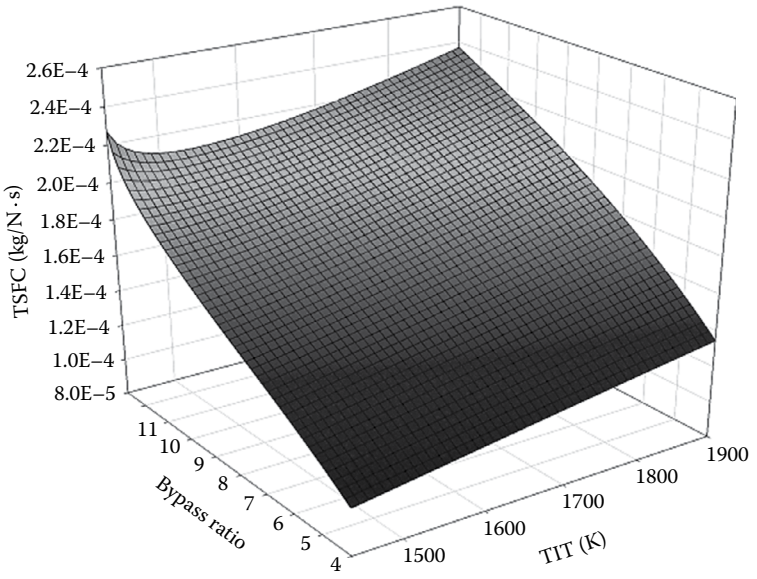


FIGURE 5.89
Variations of thrust specific fuel consumption TSFC with bypass ratio and turbine inlet temperature TIT.

5.11 Summary

1. Ideal and actual cycles for a single-spool turbofan engine

Element	Ideal Cycle	Actual Cycle
Diffuser	$\eta_d = 1$	$T_{o2} = T_a\left(1 + \frac{\gamma_c - 1}{2}M^2\right)$ $P_{o2} = P_a\left(1 + \eta_d \frac{\gamma_c - 1}{2}M^2\right)^{\gamma_c/\gamma_c - 1}$
Fan	$\eta_f = 1$	$T_{o3} = T_{o2}\left(1 + \frac{\pi_f^{\gamma_c - 1/\gamma_c} - 1}{\eta_f}\right)$ $P_{o3} = \pi_f P_{o2}$
Compressor	$\eta_c = 1$	$T_{o4} = T_{o3}\left(1 + \frac{\pi_c^{\gamma_c - 1/\gamma_c} - 1}{\eta_c}\right)$ $P_{o4} = \pi_c P_{o3}$
Combustion chamber	$\eta_b = 1$ $\Delta P\% = 0$	$T_{o5} = TIT$ $f = \frac{Cp_h T_{o5} - Cp_c T_{o4}}{\eta_b Q_R - Cp_h T_{o5}}$ $\dot{m}_f = f\dot{m}_a$ $P_{o5} = (1 - \Delta P\%)P_{o4}$

(*Continued*)

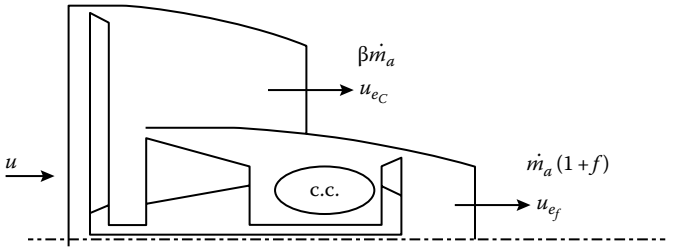
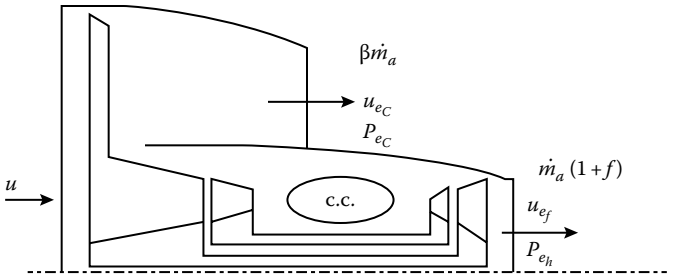
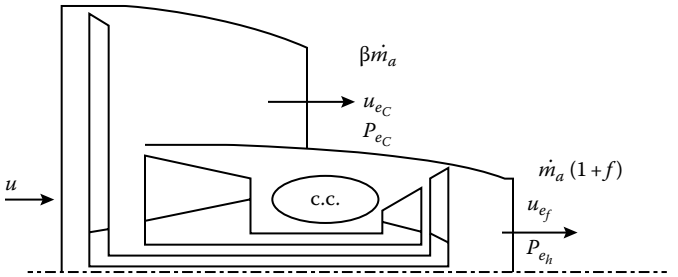
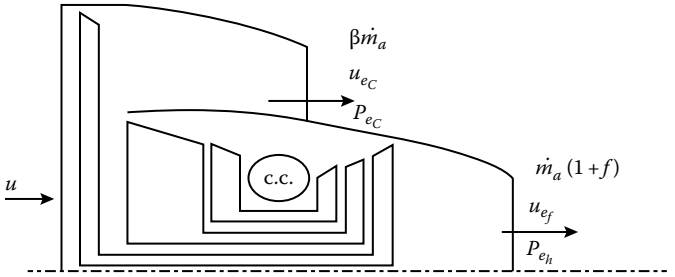
Element	Ideal Cycle	Actual Cycle
Turbine	$\eta_m = 1$ $\eta_t = 1$	$T_{o6} = T_{o5} - \dfrac{Cp_c}{\eta_m \lambda (1+f) Cp_c}\left(T_{o4} + \beta T_{o3} - (1+\beta) T_{o2}\right)$ $P_{o6} = P_{o5}\left(1 - \dfrac{T_{o5} - T_{o6}}{\eta_t T_{o5}}\right)^{\gamma_h/\gamma_h - 1}$
Nozzle	$\eta_n = 1$	$P_c = P_{o6}\left(1 - \dfrac{1}{\eta_n}\dfrac{\gamma_h - 1}{\gamma_h + 1}\right)^{\gamma_h/\gamma_h - 1}$ If $P_c \geq P_a$ the nozzle is choked $P_7 = P_c$ $T_7 = T_c = \dfrac{T_{o6}}{\left(\dfrac{\gamma_h + 1}{2}\right)}$ $V = \sqrt{\gamma_h R T_7}$ If $P_c < P_a$ the nozzle is unchoked $P_7 = P_a$ $T_7 = T_{o6}\left(1 - \eta_n\left(1 - \left(\dfrac{P_7}{P_{o6}}\right)^{\gamma_h - 1/\gamma_h}\right)\right)$ $V_7 = \sqrt{2Cp_h\left(T_{o6} - T_7\right)}$
Fan nozzle	$\eta_{fn} = 1$	$P_c = P_{o3}\left(1 - \dfrac{1}{\eta_{fn}}\dfrac{\gamma_c - 1}{\gamma_c + 1}\right)^{\gamma_h - 1/\gamma_c}$ If $P_c \geq P_a$ the nozzle is choked $P_8 = P_c$ $T_8 = T_c = \dfrac{T_{o3}}{\dfrac{\gamma_c + 1}{2}}$ If $P_c < P_a$ the nozzle is unchoked $P_8 = P_a$ $T_8 = T_{o3}\left(1 - \eta_n\left\{1 - \left(\dfrac{P_8}{P_{03}}\right)^{\gamma_c - 1/\gamma_c}\right\}\right)$ $V_8 = \sqrt{2Cp_C\left(T_{o3} - T_8\right)}$

$$T = \dot{m}_a(1+f)V_7 + \beta\dot{m}_a V_8 - (1+\beta)\dot{m}_a V_f + A_7(P_7 - P_a) + A_8(P_8 - P_a)$$

$$\text{Specific thrust} = \frac{T}{\dot{m}_a(1+\beta)} \quad TSFC = \frac{\dot{m}_f}{T}$$

C_{p_c} is the specific heat at constant pressure for cold air
C_{p_h} is the specific heat at constant pressure for hot gases
$\dot{m}_a$ is the air mass flow rate
$\dot{m}_f$ is the fuel mass flow rate
f is the fuel-to-air ratio
Q_R is the fuel heating value
γ_c is the ratio of specific heats for cold air
γ_h is the ratio of specific heats for hot gas
β BPR

2. Layout and governing equations of some types of engines

Engine Type	**Governing Equations**
Forward fan, single spool, unmixed, no afterburner 	$P_T = P_C + P_F$ $T = \dot{m}_a\left[(1+f)u_{e_h} + \beta u_{e_C} - (1+\beta)u\right] + A_{e_c}(P_{e_c} - P_a) + A_{e_h}(P_{e_h} - P_a)$
Forward fan, double spool, unmixed, no afterburner 	$P_{HPT} = P_{HPC}$ $P_{LPT} = P_F + P_{LPC}$ $T = \dot{m}_a\left[(1+f)u_{e_h} + \beta u_{e_C} - (1+\beta)u\right] + A_{e_c}(P_{e_c} - P_a) + A_{e_h}(P_{e_h} - P_a)$
Forward fan, double spool, unmixed, no afterburner 	$P_{HPT} = P_{HPC}$ $P_{LPT} = P_F$ $T = \dot{m}_a\left[(1+f)u_{e_h} + \beta u_{e_C} - (1+\beta)u\right] + A_{e_c}(P_{e_c} - P_a) + A_{e_h}(P_{e_h} - P_a)$
Forward fan, three-spool, unmixed, no afterburner 	$P_{LPT} = P_F$ $P_{IPT} = P_{IPC}$ $P_{HPT} = P_{HPC}$ $T = \dot{m}_a\left[(1+f)u_{e_h} + \beta u_{e_C} - (1+\beta)u\right] + A_{e_c}(P_{e_c} - P_a) + A_{e_h}(P_{e_h} - P_a)$

Governing equations

Specific thrust

$$\frac{T}{\dot{m}_a} = \frac{\beta}{1+\beta}u_{e_C} + \frac{1}{1+\beta}(1+f)u_{e_h} - u + \left(\frac{1+f}{1+B}\right)\left(\frac{RT_{e_h}}{P_{e_h}u_{e_h}}\right)(P_{e_h} - P_a) + \frac{\beta}{1+\beta}\frac{RT_a}{P_a u_{e_h}}(P_{e_C} - P_a)$$

TSFC

$$TSFC = \frac{f}{T/\dot{m}_a}$$

Propulsive efficiency

$$\eta_p = \frac{(T/\dot{m}_a)u}{(T/\dot{m}_a)u + \left(0.5\times\frac{(1+f)}{(1+B)}\right)(u_{e_h} - u)^2 + 0.5\times\left(\frac{\beta}{1+\beta}\right)(u_{e_C} - u)^2}$$

Thermal efficiency

For choked nozzle

$$\eta_{th} = \frac{(T/\dot{m}_a)u + \left(0.5\times\frac{(1+f)}{(1+B)}\right)(u_{e_h} - u)^2 + 0.5\times\left(\frac{\beta}{1+\beta}\right)(u_{e_C} - u)^2}{\left(\frac{f}{1+B}\right)\times Q_{hv}}$$

For unchoked nozzles, it is reduced to

$$\eta_{th} = \frac{0.5\left[\left(\frac{\beta}{1+\beta}\right)(u_{e_C})^2 + \left(\frac{1+f}{1+\beta}\right)(u_{e_h})^2 - (u)^2\right]}{\left(\frac{f}{1+B}\right)\times Q_{hv}}$$

Overall efficiency

$$\eta_o = \eta_{th}\times\eta_p$$

Problems

5.1 A single-spool turbofan engine has the following data

Ambient temperature	288 K
Ambient pressure	101.3 kN/m^2
BPR β	0.7
Overall pressure ratio	25
Fan pressure ratio	3.375
Fuel heating value Q_R	44,000 kJ/kg
Turbine-inlet temperature	2,000 K
Diffuser pressure recovery factor r_d	0.9
Compressor efficiency η_c	0.89
Fan efficiency η_f	0.91
Combustion efficiency η_b	0.98
Burner pressure recovery factor r_b	0.95
Turbine efficiency η_t	0.98
Nozzle efficiency η_n	1.0

Calculate the thrust per unit mass flow rate and the TSFC.

5.2 A V/STOL aircraft is powered by the tandem fan vectored thrust with a switch-in deflector engine described in Section 5.8.2. The following data applies for the case of takeoff (lift thrust)

$$T_a = 288\ \text{K}, \quad P_a = 1.01\ \text{bar}, \quad \dot{m}_1 = 80\ \text{kg/s}, \quad Q_R = 45{,}000\ \text{kJ/k},$$

$$\pi_{f1} = 1.6, \quad \pi_{f2} = 1.2, \quad \pi_c = 10, \quad TIT = 1400\ \text{K}, \quad T_{\max} = 2200\ \text{K},$$

$$P_{04}/P_{03} = 97\%, \quad P_{07}/P_{06} = 94\%, \quad P_{010}/P_{05} = 97\%, \quad \Delta P_{ab} = 5\%$$

Bleed from compressor (b) = 2%, by-pass ratio (β) = 0.9
Efficiencies:

$$\eta_d = 0.97, \quad \eta_{f1} = \eta_{f2} = \eta_c = 0.85, \quad \eta_b = 0.99, \quad \eta_{t1} = \eta_{t2} = 0.9,$$

$$\eta_{fn} = \eta_n = 0.98, \quad \eta_m = 0.99$$

Calculate

1. The mass flow rate $\dot{m}_2$ that gives equal lift forces from both nozzles
2. The total lift force

5.3 For the V/STOL engine described in Problem 5.2 consider the cruise operation of the aircraft. The flight Mach number is 0.8 at an altitude of 32,000 ft. The afterburner is inoperative as described in Section 5.8.2 and the engine is considered as a mixed two-spool configuration. The values of the pressure ratios, fuel heating value, turbine-inlet temperature, pressure losses in the different ducts given as pressure ratios, bleed, and efficiencies are the same as in Problem 5.2. The total mass flow rate is $\dot{m}_1 = 80$ kg/s and $\Delta P_{ab} = 5\%$. The nozzle is also unchoked.
Calculate

1. The BPR
2. The thrust force
3. The propulsive, thermal, and overall efficiencies

5.4 1. Write expressions for the thrust, fan, and core effective jet velocities (V_{jf},V_{jc}).
2. Using these two parameters, find the expression for the global effective jet velocity ($\bar{V}_e$), based on the total mass flow rate ($\dot{m}_{fan} + \dot{m}_{core}$).
3. Find the expressions for the thermal, propulsive, and overall efficiencies, employing the fan and core effective jet velocities.

5.5 1. Prove that for a two-stream turbofan engine, with a constant sum of "relative" kinetic power, the thrust and propulsive efficiency are maximum when $V_{ef} = V_{eC}$.
2. A turbofan engine cruises at $M_o = 0.85$ and at an altitude of 34,000 ft. The fan and core effective jet velocities are 350 and 470 m/s respectively. The total air mass flow rate is 270 kg/s and the BPR (β) is 4.2. The engine has an overall pressure ratio of 31.3 and a maximum turbine-inlet temperature (TIT) equal to 1405 K. Assuming ideal intake compressors and combustion chamber, determine
   a. Combustion chamber "ideal" fuel–air ratio
   b. Thrust, various efficiencies (η_{th}, η_p, η_o), and specific fuel consumption (TSFC)

5.6 Compare the performance of a twin-spool turbofan engine with separate fan and compressor, Section 5.3.2 to that of a turbojet engine, both with an overall pressure ratio of 30 and a turbine inlet temperature of 1300 K, and designed for an altitude of 12 km and a flight speed of 275 m/s. The BPR is 6 and the fan pressure ratio is 1.6. Assume that the efficiency of fan, compressor, and turbine is 90% and a combustor loss of 3% of the compressor exit total pressure. Compare specific thrusts for engines built from the same core engine. Compare also the specific fuel consumption and jet velocities.

5.7 Consider the V/STOL ground attack fighter Hawker Siddeley Harrier G.R.MK.1, discussed in Example 5.6. It has the same static takeoff thrust of 98 kN and the other data cited in the example. However, the real case is considered with the following efficiencies

1. Isentropic efficiencies of the intake, fan, and compressor are, respectively, 93%, 88%, and 85%
2. Isentropic efficiencies of both turbines is 91%
3. Isentropic efficiency of the fan nozzle and turbine nozzles is 93%
4. The pressure drop in the combustion chamber is 2%

Recalculate

a. The air mass flow rate

b. The thermal efficiency.

Take $Cp_c = 1.005$ J/kg/K, $Cp_h = 1.148$ J/kg/K, $\gamma_c = 1.4$, $\gamma_h = 4/3$.

What are your comments?

5.8 A turbofan engine of the mixing type, where the fan is driven by the LPT and the compressor is driven by the HPT. During a ground run of the engine, the following readings were recorded: P_a = 100 kPa, T_a = 300 K, fan pressure ratio = 2, compressor pressure ratio = 8.0, turbine inlet temperature = 1600 K, $\eta_c = \eta_f = \eta_t = 0.9$, f = 0.065, $\gamma_{air} = 1.4$, $\gamma_{gass} = 1.33$

Calculate

1. The BPR on the assumption that the outlet streams of the fan and LPT have the same total pressure just prior to mixing
2. The specific thrust
3. The TSFC

5.9 A turbofan engine has a fan and LPC driven by the LPT. It operates at a flight velocity of 200 m/s at 12,000 m altitude, where the ambient temperature and pressure are 216.65 K and 0.1933 bar, respectively. The overall pressure ratio of the engine is 19, the fan and LPC pressure ratios are 1.65 and 2.5 respectively. The fan, compressors, and turbines have a 90% polytrophic efficiency. Assume an isentropic inlet and separate isentropic convergent nozzles, a fuel heating value of 43,000 kJ/kg, and a combustor total pressure loss of 6.5%.

Determine the core engine and bypass duct exit velocities, the engine TSFC, thrust and specific thrust for an engine inlet air flow of 100 kg/s and BPR of 3.0. Determine whether the nozzles are choked.

5.10 A low-BPR turbofan engine is powering an aircraft flying at a Mach number M. Assuming all the processes are isentropic except for the combustion process, in which no pressure drop is encountered

1. Draw the cycle on the T–S diagram.

2. Plot the new cycle on the same *T*–*S* diagram in (1) if the compressor pressure ratio is increased while the maximum cycle temperature is maintained constant.
3. If a zero flight Mach number is assumed, plot a third graph for the cycle on the same *T*–*S* diagram in (1).
4. Calculate the specific thrust and the fuel-to-air ratio in the following cases.
   a. Flight Mach number is 0.8
   b. Flying altitude is 34,000 ft, where the ambient pressure and temperature are 0.2472 bar and 220 K, respectively
   c. The fan pressure ratio is 1.5 and the compressor pressure ratio is 6.0
   d. The BPR is 1.0
   e. Lowest fuel heating value is 45,000 kJ/kg
   f. Specific heats for air and gases are, respectively, 1.005 and 1.148 kJ/(kg·K)
   g. Maximum cycle temperature is 1500 K
   Assume full expansion in the nozzles to ambient pressure.
5. If the fan and the LPT are removed and the turbofan engine is replaced with a turbojet engine with an afterburner
   a. Plot on the same *T*–*S* diagram in (1) the cycle if the maximum temperature of the afterburner is also 1500 K.
   b. Calculate the new specific thrust and the fuel-to-air ratio assuming also an unchoked nozzle and no pressure drop in the afterburner.
   c. What are your comments?

5.11 Figure P5.11 illustrates several turbofan engines together with their BPR and flight-specific fuel consumptions. Construct a similar figure and plot these engines: CF6, GE90, Trent 700, 900, 1000, F-100, F-101, F-110, RB-I99, RB 211, Nene, RR Pegasus T56, V2500, CFM56, Lyulka AL-7, CF6, TFE 731, TPE331, TV3 VK-1500, and AL-31 F.

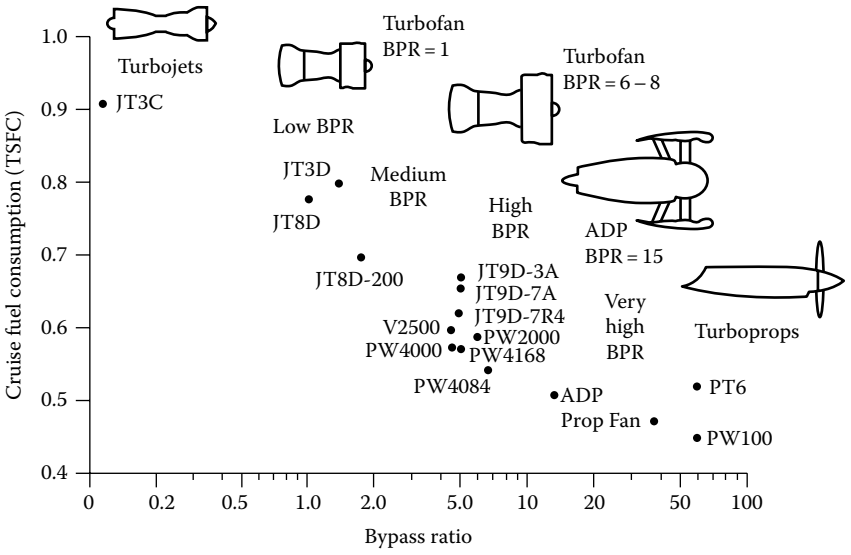


FIGURE P5.11

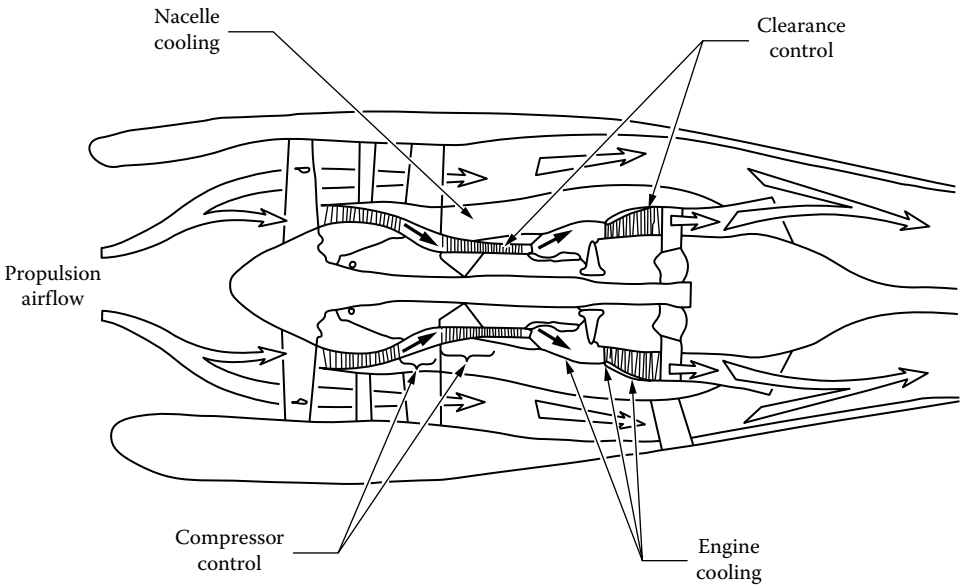


FIGURE P5.12

5.12 Figure P5.12 illustrates the mixed high-BPR turbofan engine (similar to CFM56-SC). It has the following data:

- BPR 6.6
- Typical TSFC 0.04 kg/(N · h)
- Cruise thrust 29,360 N
- Total mass flow rate at cruise 100 kg/s

During takeoff operation

Takeoff thrust	140,000 N
Total air mass flow rate at takeoff	474.0 kg
Overall pressure ratio	37.5
Total temperature at inlet to the LPT	1251 K
Exhaust gas temperature	349 K
Ambient temperature	288.0 K
Ambient pressure	101 kPa

Assuming that all the processes are ideal and there are no losses in either the combustion chamber or mixing process,

1. Prove that the thrust force is given by the relation

$$T = \frac{\dot{m}_a(1+\beta)(u_e - u)}{1 - u_e(\text{TSFC})}$$

2. Calculate
   a. The exhaust velocity at both takeoff and cruise (use the preceding relation)
   b. The fuel-to-air ratios at both takeoff and cruise conditions

3. At takeoff condition, calculate
   a. The total temperature at the outlet of the HPC
   b. The total temperature at the inlet to the HPT
   c. The pressure ratio of the HPC
   d. The fan pressure ratio
   e. The temperature of the hot gases prior to mixing
   f. The pressure ratio of the LPC (booster)

Assume that the nozzle is unchoked.

5.13 Figure P5.13 illustrates a supersonic turbofan engine that has the following characteristics during flight at high-altitude ambient conditions 216.7 K and 9.28 kPa. The semi-vertex angle of the fan nose is 16°, the Mach number at the fan is $M_2 = 1.5$, the Mach number at the fan exhaust $M_3 = 2.6$, the maximum cycle temperature is 1800 K.

Fan pressure ratio	2
Overall pressure ratio	6
BPR	1.0
Isentropic efficiency for fan and compressor	0.83
Isentropic efficiency for cold and hot nozzle	0.95
Burner efficiency	0.99
Isentropic efficiency for HPT and LPT	0.9
Fuel heating value	43,000 kJ/kg
No pressure drop in the combustion chamber	
Total air mass flow rate	330 kg/s

1. Plot the cycle on the *T*–*S* diagram
2. Calculate the flight speed and pressure recovery in the intake
3. Calculate the fuel-to-air ratio
4. Calculate the supersonic Mach number of the hot gases
5. Calculate the thrust force
6. Calculate the TSFC

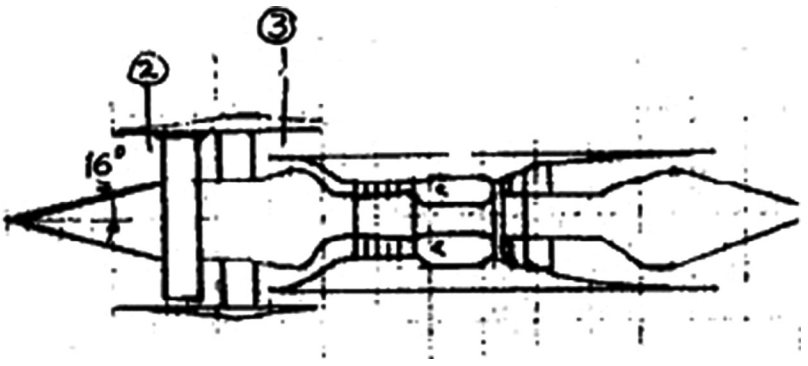


FIGURE P5.13

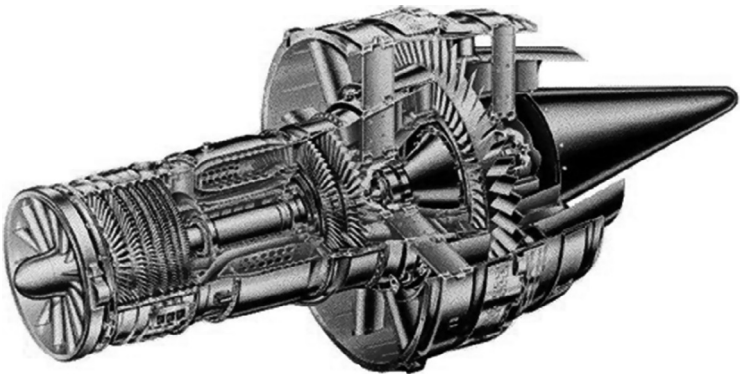


FIGURE P5.14

5.14 The fan illustrated in Figure P5.14, the General Electric CF 700 aft-fan turbofan engine. During a ground test ($M = 0$) assume that

- Ideal compression and expansion processes in the fan, compressor, turbines, and nozzles
- Negligible fuel-to-air ratio

Required

1. Prove that the exhaust speeds of the cold air and hot gases are equal if the BPR (β) is expressed by the relation

$$\beta = \frac{(A-B)(B-1)}{B(C-1)} - 1$$

where

$$A = T_{o4} / T_a \quad \text{and} \quad B = \pi_c^{\gamma-1/\gamma} \quad \text{and} \quad C = \pi_f^{\gamma-1/\gamma}$$

2. Now consider the following case study

$$T_a = 300 \text{ K}, \quad \pi_c = 4.0, \quad \pi_f = 1.5, \quad T_{o4} = 1200 \text{ K}$$

Evaluate the BPR β that satisfies equal exhaust speeds for the hot and cold streams.

5.15 A Boeing 747 civil transport airplane is fitted with four high-BPR turbofan engines similar to CF6-50C turbofan engines. Each engine has the following data:

Thrust force	24.0 kN
Air flow rate $\dot{m}_a$	125 kg/s
BPR	5.0
Fuel mass flaw rate $\dot{m}_r$	0.75 kg/s
Operating Mach number	0.8
Altitude	10 km
Ambient temperature T_a	223.2 K
Ambient pressure P_a	26.4 kPa
Fuel heating value $Q_{H \cdot V}$	42,800 kJ/kg

If the thrust generated from the fan is 75% of the total thrust, determine

1. The specific thrust
2. The TSFC
3. The jet velocity of the hot gases
4. Thermal efficiency
5. Propulsive efficiency
6. The overall efficiency

Assume that the exit pressure is equal to the ambient pressure.

5.16 One of the techniques used in STOL fighters is the flap-blowing turbofan engines. Air is bled from the LPC and ducted to the flap system in the wing trailing edge. Such accelerated air flow creates greater lift than would be possible by the wings themselves. Here is the data for one of these engines. During takeoff at sea level ($T_a = 288$ K, $P_a = 101$ kPa), the engine has a BPR of 3.0 and the core engine air flow is 22.7 kg/s. Fifteen percent of this air is bled at the exit of the LPC. The component efficiencies are given as

$$\eta_c = 0.88, \quad \eta_f = 0.90, \quad \eta_b = 0.96, \eta_t = 0.94, \quad \eta_n = 0.95.$$

The total pressure recovery factor of the diffuser (related to the free stream) is $r_d = 0.98$, compressor total pressure ratio is 15, fan total pressure ratio is 2.5 maximum allowable turbine-inlet temperature is 1,400 K, total pressure loss in the combustor is 3% , and heating value of the fuel is 43,000 kJ/kg. Assume the working medium to be air and treat it as a perfect gas with constant specific heats.

Compute

1. The properties at each section
2. The thrust force
3. The TSFC
4. The overall efficiency

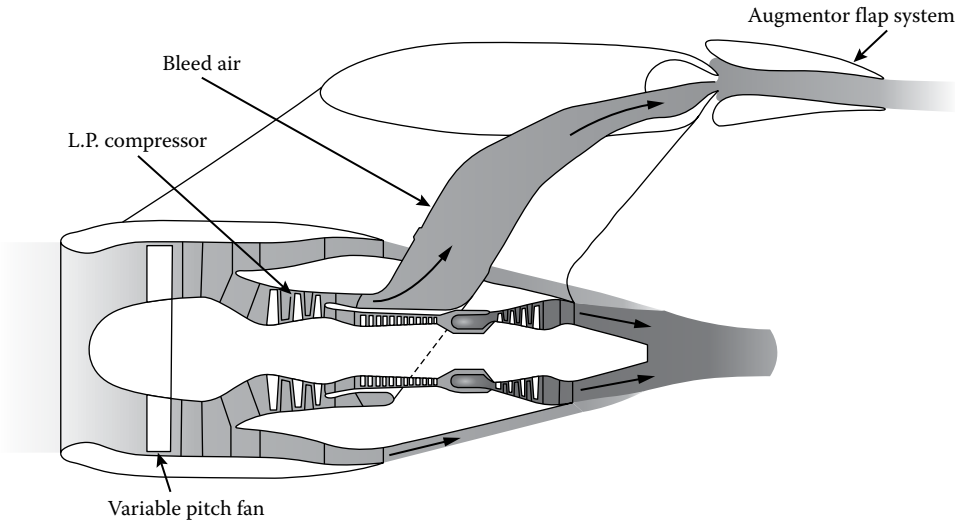


FIGURE P5.16
(Courtesy of Rolls-Royce.)

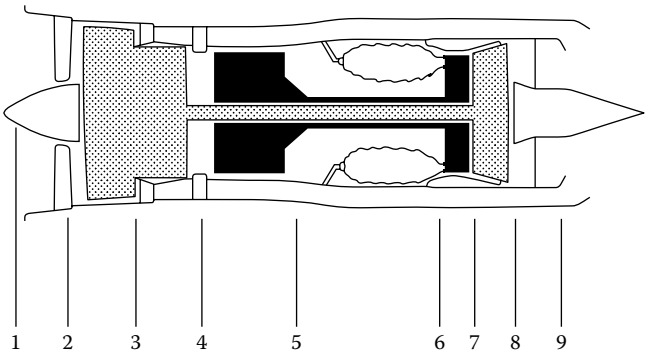


FIGURE P5.17
Dual-rotor turbofan full duct JT8D.

5.17 Figure P5.17 illustrates the Pratt & Whitney dual-rotor turbofan full duct mixed-type JT8D Engine. It has the following characteristics:

Compressor pressure ratio	10
Fan pressure ratio	1.8
Inlet temperature to HPT	1628 K
Mechanical efficiency	0.85
Fuel-to-air ratio	0.06
Efficiencies of fan/compressors	0.9
Efficiencies of turbines/nozzle	0.95
Ambient temperature	300 K
Ambient pressure	100 kPa

Assume that the outlet streams from the fan and LPT have the same total pressure before mixing.

1. Determine
   a. The BPR
   b. The specific thrust
   c. The TSFC
2. Plot the temperature and pressure distributions along the different components of the engine.

   For the fan and compressor C_p =1.0 kJ/kg/K and $\gamma = 1.4$

   For the turbines and nozzle C_p =1.2 kJ/kg/K and $\gamma = 1.33$

5.18 For a turbofan engine write down the mathematical expressions for

1. The thrust force
2. The overall efficiency

Prove that the maximum overall efficiency is given by

$$\eta_{0\max} = \frac{(1+\beta)u^2}{fQ_R}$$

5.19 Figure P5.19 illustrates a turbofan engine during testing in a test cell. It has the following characteristics:

1. $\beta = 3, f = 2\%, V_2 = 3V_1$

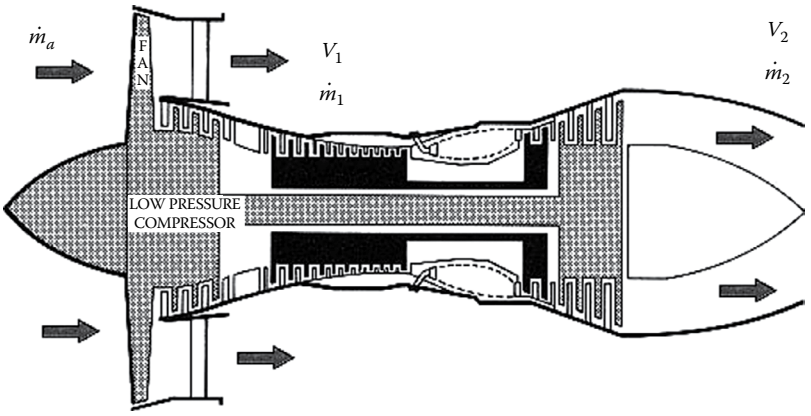


FIGURE P5.19

2. $\dot{m}_a = 200$ kg, thrust = 60 kN
   a. Calculate: $\dot{m}_1$, $\dot{m}_2$ and $\dot{m}_f$.
   b. Evaluate V_1, V_2 if f is neglected.
   c. Calculate the propulsive efficiency.
   What are your comments?

5.20 Reconsider the engine Kuznetsov NK-32 triple-spool afterburning turbofan engine examined in Example 5.12. Assuming the nozzle is choked, calculate

1. Nozzle exit static pressure
2. Nozzle exit velocity
3. The thrust force
4. Propulsive efficiency
5. Thermal efficiency
6. Overall efficiency

5.21 Kh-55 (Russian: X-55) is a Russian subsonic air-launched cruise missile as illustrated in Figure P5.21a and b. The missile is launched from the Tu-160; Figure P5.22. The missile after launch deploys its folded wings, tail surfaces, and engine inlet of its turbofan engine TVD-50.

The rocket speed is 960 km/h. It is launched at an altitude of 15,000 m, where the ambient conditions are $T_a = 216.5$ K, $P_a = 12.11$ kPa, $\rho_a = 0.1948$ kg/m^3). The turbofan engine during a sustained flight of the rocket has the following characteristics:

Thrust force = 4.0 kN

Specific fuel consumption = 0.65 kg/kg · h

Fuel-to-air ratio = 0.018

BPR = 1.2

Overall pressure ratio = 14

Fan pressure ratio = 2.1

Maximum temperature = 1100 K

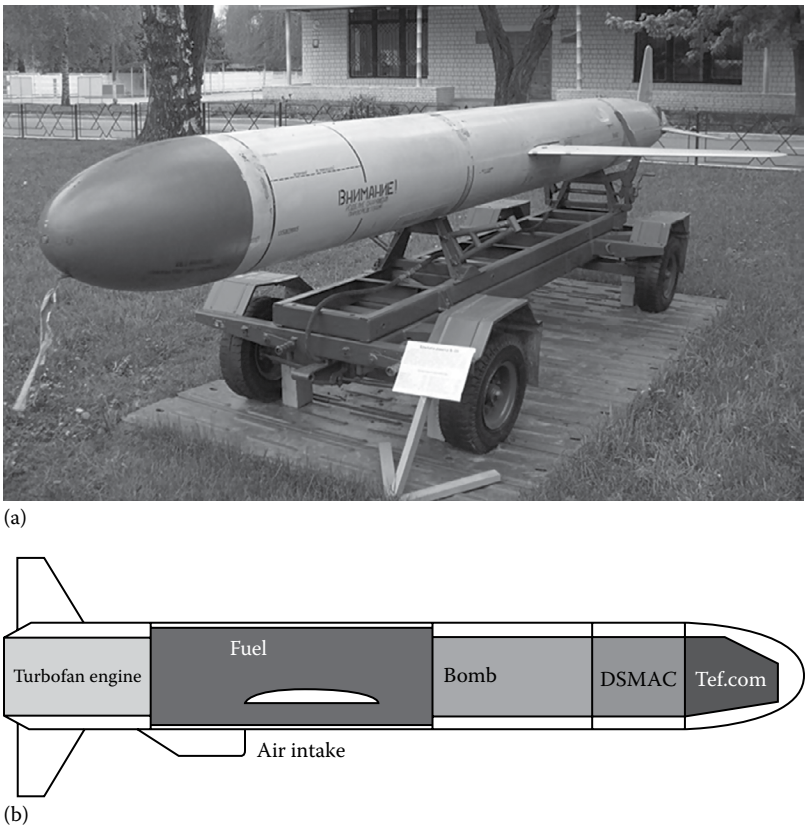


FIGURE P5.21
Kh-55 Russian subsonic *air-launched cruise missile.* (a) Display of missile and (b) modules of missile.

Calculate

1. Air mass flow rate
2. Specific thrust
3. Exhaust gas speed
4. Inlet area
5. Fuel heating value

5.22 In Problem 5.21, the Kh-55 rocket has a weight of 1210 kg and a range of 2500 km. Calculate

1. The lift-to-drag ratio $\left(\frac{L}{D}\right)$ using Breguet's equation for range

$$R = \left(\frac{u}{g}\right)\left(\frac{1}{TSFC}\right)\left(\frac{L}{D}\right)\ln\left(\frac{m_1}{m_2}\right)$$

2. The overall efficiency (η_0)



FIGURE P5.22
Kh-55 launched from Tu-160.

5.23 The Tomahawk is a long-range subsonic cruise missile powered by a solid-fuel rocket booster and the small two-spool turbofan engine Williams International F107-WR-402; see Figure P5.23. It has the following data

Flight speed $V_f = 247.22$ m/s

Ambient temperature $T_a = 275$ K

Ambient pressure $P_a = 0.79$ bar

Thrust force $T = 3.1$ kN

Specific fuel consumption = 0.682 kg/kg · h



FIGURE P5.23
Tomahawk missile and Williams F107-WR-402 turbofan engine.

BPR = 1

Overall pressure ratio = 13.8

Fan pressure ratio = 2.1

Fan diameter = 0.305 m

Fuel heating value = 42,500 kJ/kg

Calculate

Air mass flow rate

Fuel-to-air ratio

Exhaust gas speed

Engine maximum temperature

5.24 Consider a triple-spool, afterburning, mixed turbofan engine. The engine characteristics at maximum speed (operative afterburner) are given as

Altitude: 12.2 km (T_a = 220.5 K and P_a = 20.744 kPa)

Mach number: 2.05

Total mass flow rate: 365 kg/s

Thrust: 245 kN

Overall pressure ratio: 28.4

BPR: 1.4 (mixed)

Turbine-inlet temperature: 1630 K

Afterburning temperature: 1630 K

Fuel heating value: 43 MJ/kg

Component		**γ**	***Cp* (J/kg · K)**
Air intake	$r_d = 0.95$	1.4	1005
Fan	$\eta_f = 0.85$, $\pi_f = 1.5$	1.4	1005
LPC	$\eta_{LPC} = 0.87$, $\pi_{LPC} = 3.0$	1.4	1005
HPC	$\eta_{HPC} = 0.90$	1.4	1005
Burner	$\eta_b = 0.99$, $r_b = 0.98$	1.33	1147
LPT	$\eta_{LPT} = 0.88$	1.33	1147
IPT	$\eta_{IPT} = 0.88$, $\lambda_{IPT} = 1.0$	1.33	1147
HPT	$\eta_{HPT} = 0.90$, $\lambda_{HPT} = 1.0$	1.33	1147
Shaft	$\eta_m = 0.90$		
Afterburner	$r_{ab} = 0.98$		
Jet pipe	$r_{jet\ pipe} = 0.99$	1.33	1147
Nozzle	$\eta_n = 0.95$	1.33	1147

Assuming full expansion in the nozzle (supersonic nozzle), calculate

1. λ_{LPT}
2. Combustor fuel mass flow
3. Afterburner fuel mass flow
4. Nozzle exit static pressure

5. Nozzle exit velocity
6. Propulsive efficiency
7. Thermal efficiency
8. Overall efficiency

5.25 For the triple-spool afterburning engine described in Problem 5.24, consider its operation with an inoperative afterburner.

A. Check whether the nozzle is choked or unchoked

B. Recalculate

1. λ_{LPT}
2. Combustor fuel mass flow
3. Nozzle exit static pressure
4. Nozzle exit velocity
5. Propulsive efficiency
6. Thermal efficiency
7. Overall efficiency

5.26 Consider the triple-spool unmixed turbofan engine examined in Example 5.14. Recalculate as in the example for the cruise condition at Mach number ($M = 0.82$) and altitude 12,000 m. Analyze the engine also for 8% and 0% air bleed.

Compare

1. Cruise conditions with no bleed and 8% air bleed
2. Takeoff and cruise conditions with 8% bleed
3. Takeoff and cruise conditions for 0% bleed

5.27 A double spool high-BPR turbofan (Figure P5.27) has the following flight and design conditions

$M_0 = 0.9$, $P_0 = 20$ kPa and $T_0 = 216$ K

$\dot{m}_o = 500$ kg/s and BPR, $\beta = 500$

$T_{t4} = 1700$ K and heating value $Q = 42.8$ MJ/kg

Component		**γ**
Diffuser	$r_d = 0.95$	1.4
Fan	$\eta_f = 0.85$, $\pi_f = 2$	1.4
LPC	$\eta_{LPC} = 0.87$, $\pi_{LPC} = 4$	1.4
HPC	$\eta_{HPC} = 0.9$, $\pi_{HPC} = 6$	1.4
Burner	$\eta_b = 0.99$, $r_b = 0.98$	1.33
HPT	$\eta_{HPT} = 0.9$	1.33
LPT	$\eta_{LPT} = 0.88$	1.33
Shaft	$\eta_m = 0.99$	
Hot gases nozzle	$\eta_{nozzle} = 0.95$, $r_n = 0.98$	1.33
Fan nozzle	$\eta_{Fan-nozzle} = 0.97$	1.4

Calculate

1. The specific thrust
2. The TSFC
3. Thermal efficiency, propulsive efficicency, and overall efficiency

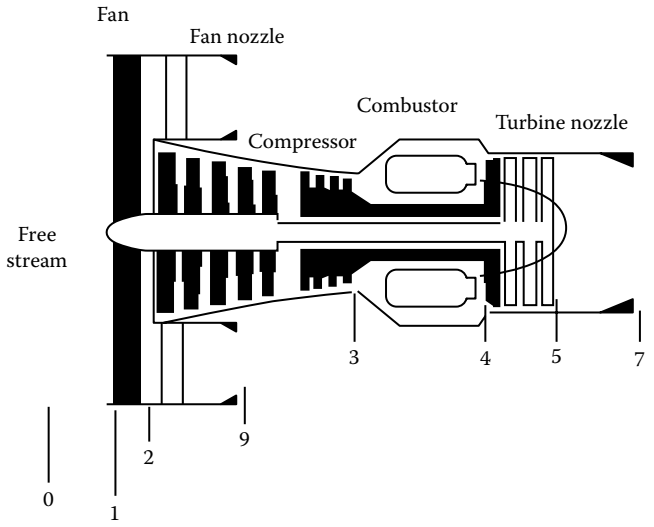


FIGURE P5.27
Double spool turbofan.

5.28 The supersonic business aircraft is powered with twin-engine, low-bypass turbofans Pratt &Whitney F119; (see Figure P5.28), with takeoff weight of 444 kN. The aircraft is assumed to have lift-to-drag ratios $L = D$ of 5 at takeoff. The engine characteristics at full takeoff thrust ($h = 0$ ft, $M_1 = 0$) are given as

$T_a = 288$ K and $P_a = 100$ kPa

Total mass flow rate = 139 kg/s

Overall pressure ratio = 30

Fan pressure ratio = 5

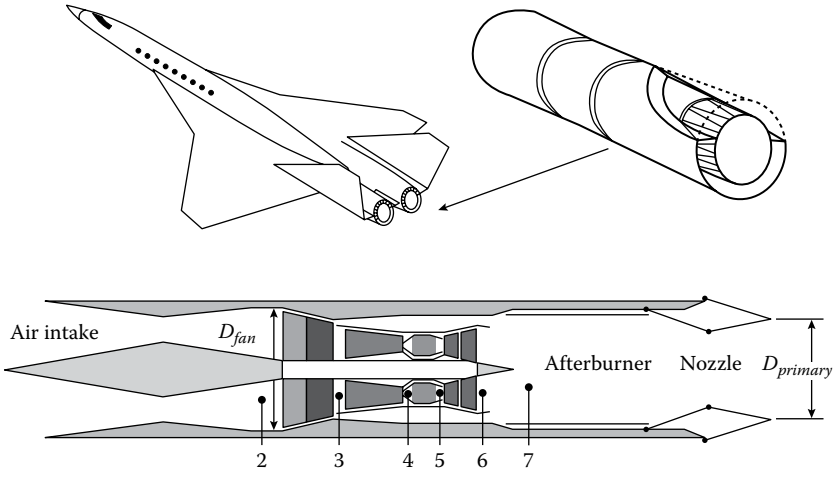


FIGURE P5.28
Supersonic business aircraft and low-bypass afterburning turbofan.

BPR = 0.45 (mixed)
Turbine-inlet temprature = 1800 K
Fuel heating value (43.4 MJ/kg)
Exit Mach number = 1.4
Exit diameter = 0.65 m

Component		γ
Air intake	$r_d = 0.95$	1.4
Fan	$\eta_f = 0.85$	1.4
Compressor	$\eta_c = 0.85$	1.37
Burner	$\eta_b = 0.98$, $r_b = 0.98$	1.35
LPT	0.92	1.33
HPT	0.9	1.33
Shaft	$\eta_m = 0.99$	
Jet nozzle	$\eta_n = 0.98$, $r_{jet\ pipe} = 0.98$	1.4

If the afterburner is turned off, calculate

1. Nozzle exit velocity
2. Nozzle exit static pressure
3. Engine thrust
4. Engine fuel consumption
5. Whether the engine thrust is sufficent to overcome the aircraft drag

5.29 Consider the engine described in Problem 5.28, while the aircraft is at cruise condition (h = 50,000 ft, M = 2.0), where T_a = 216.5 K, P_a = 12.11 kPa. The aircraft is assumed to have lift-to-drag ratios $L = D$ of 10. Engines will run at a turbine temperature about 100 K lower than takeoff conditions in order to improve the turbine life. Moreover, the engine characteristics will be

Overall pressure ratio = 25
Fan pressure ratio = 4.5
BPR = 0.45 (mixed)
Turbine-inlet temprature = 1700 K
Total mass flow rate = 103 kg/s
Fuel heating value (43.4 MJ/kg)
Exit Mach number = 2.15
Exit diameter = 1.3 m

Component	Efficiency	Specific Heat Ratio
Air intake	0.97	1.4
Fan	0.85	1.4
Compressor	0.85	1.37
Burner	0.98	1.35
Turbine	0.9	1.33
Jet nozzle	0.98	1.4

For the case of the operative afterburner, calculate

1. The engine thrust
2. The TSFC
3. Propulsive efficiency
4. Thermal efficiency
5. Overall efficiency

5.30 If the variation of the entropy for any process in the cycle is computed approximately from the thermodynamic relation

$$s_f - s_i = c_p \left(\frac{T_{0_f}}{T_{0_i}} \right) - R \ln \left(\frac{P_{0_f}}{P_{0_i}} \right)$$

where the initial and final states are denoted as (i) and (f), plot the *T*–*S* diagram for Problems 5.29 and 5.30.

5.31 At Mach number 1.5, compare four engines (ramjet, turbojet, high-BPR, and low-BPR turbofan) assuming the ideal cycles. The flight conditions are P_a = 20 kPa, T_a = 216 K. Inlet area is constant (0.5 m^2) for the four engines. The fuel has a heating value of 43.4 MJ/kg. Calculate the mass flow rate, the jet speed, engine thrust, TSFC, and propulsive efficiency. Use the following engine data:

Engine	Fan, Compressor	$T_{0\max}$ (K)
Ramjet	—	1100
Turbojet	$\pi_c = 25$	1100
Turbofan ($\beta = 5$)	$\pi_f = 2$, $\pi_c = 12.5$	1100
Turbofan ($\beta = 0.5$)	$\pi_f = 5$, $\pi_c = 5$	1100

5.32 Figure P5.32 shows a fighter airplane propelled by a low-BPR *mixed* afterburning turbofan engine during takeoff from an aircraft carrier. The temperature and pressure of the ambient air are 290 K and 101 kPa. Air is ingested into the engine intake at a



FIGURE P5.32

Mach number of 0.2. The turbofan engine has the following data: $\pi_f = 1.8$, $\pi_c = 5$, $f = 0.02$, $f_{ab} = 0.04$, $Q_R = 45$ MJ/kg, percentages of power extracted by fan and compressor from the driving turbines are, respectively, $\lambda_1 = \lambda_2 = 0.8$. Assume ideal processes and variable properties (γ, C_p).

Calculate

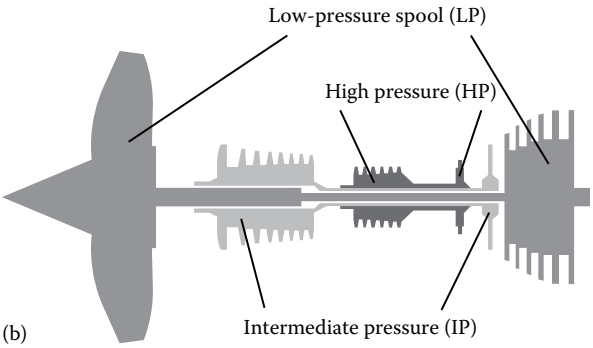
1. BPR
2. Jet speed
3. TSFC

5.33 1. Classify turbofan engines.

2. Compare turbojet and turbofan engines (maximum Mach number, ceiling, noise, fuel consumption).
3. Figure P5.33a illustrates the Antonov An-225 aircraft powered by six engines (Progress D-18T): the triple-spool unmixed high-BPR turbofan engine, Figure P5.33b.



(a)



(b)

FIGURE P5.33
(a) Russian space shuttle (b) Three-spool turbofan engine.

Bleed air is 8% extracted from HPC to cool HPT (5%) and IP turbine (3%). It has the following data:

Parameter	Value	Parameter	Value	Parameter	Value	Parameter	Value
η_d	0.88	$\Delta p_{c.c}$	0.03	π_F	1.35	λ_1	0.84
η_f	0.9	$\Delta p_{fan\,duct}$	0.0	π_{IPC}	5.0	$\lambda_2 = \lambda_3$	1.0
η_c	0.88	cp_c (J/kg·K)	1005	π_{HPC}	4.1	η_n	0.96
η_b	0.98	cp_h (J/kg·K)	1148	β	5.7	η_m	0.99
η_t	0.92	R (J/kg·K)	287	TIT (K)	1600	b	8%
γ_c	1.4	γ_h	4/3				

For *takeoff* conditions (M = 0.2), *at* sea level, *calculate*

a. The pressure and temperature at the outlets of the cold and hot nozzles
b. Specific thrust, TSFC

References

1. F. Zimmer, Engines, *BOEING, AERO Magazine*, QTR_03, 2008, pp. 21–28.
2. B. Gunston, *The Development of Jet And Turbine Aero Engines*, Haynes Publishing Group, PATRICK Stephens Limited, U.K., 1997, p. 67.
3. C. Hess, *Pratt & Whitney Geared Turbofan*, Flug Revue 10/98, p. 54.
4. G. Norris, PW800 For Gulfstream G600 Progresses. *Aviation Week*, May 26, 2016.
5. http://en.wikipedia.org/wiki/Rolls-Royce_RB211.
6. P. Jeschke, J. Kurzke, R. Schaber and C. Riegler, Preliminary gas turbine design using the multidisciplinary design system MOPEDS. ASME Paper No. GT2002-30496, pp. 75–84, 2002.
7. http://en.wikipedia.org/wiki/Turbofan.
8. *The Jet Engine*, 5th edn., Rolls-Royce Plc, Derby, U.K., 1996, p. 189.
9. H.I.H. Saravanamuttoo, G.F.C. Rogers, and H. Cohen, *Gas Turbine Theory*, 5th edn., Prentice Hall, 2001, p. 146.

6

Shaft Engines: Internal Combustion, Turboprop, Turboshaft, and Propfan Engines

6.1 Introduction

This chapter is devoted to the aerodynamics and thermodynamics of four shaft engines: internal combustion (IC), turboprop, turboshaft, and propfan engines (Figure 6.1). The tree presented in Figure 6.1 illustrates air-breathing engines, which are so named as they need only air for combustion while carrying appropriate fuels [1]. Consequently, these propulsion systems stop working outside the atmosphere of Earth. The aim when designing shaft-based engines is to achieve higher power (or thrust) and less weight (using advanced composite materials), thus achieving a high thrust-to-weight ratio. Other goals are to achieve a smaller frontal area, reduced chemical emissions (CO_2, SO_x, and NO_x), low-level exterior noise, better cooling characteristics, and lower fuel consumption. Moreover, during production, it can be built using green processes and materials.

Power, rather than thrust, is the key factor in these four types of engine. Internal combustion engines work on an intermittent combustion pattern, while the other three engines operate by continuous combustion. Internal combustion engines power small aircrafts and helicopters that fly at low-to-moderate subsonic speeds; aero piston engines are either of the rotary engine or reciprocating engine families. Rotary engines are categorized as being either conventional or Wankel engines, while reciprocating engines have different configurations, including in-line, horizontally opposed, V-type, X-type, H-type, and radial type engines. Superchargers or turbochargers are added to reciprocating engines to boost either pressure or power. By itself, an internal combustion engine cannot propulsion, so the engine is coupled to a propeller to generate the required thrust force.

The exhaust gases of turboprop and turboshaft engines leave the engine at a very low speed, nearly zero in some designs. Turboprop engines power many heavy transport aircraft flying at moderate subsonic speeds. The turboshaft engines discussed here are limited to helicopters only. Turboshaft engines employed in other applications will be treated in Chapter 8 and identified as gas turbines, which are employed in numerous industrial applications both on land and at sea. Propfan engines combine many of the advantages of both turbofan and turboprop engines. There is no separate chapter allocated to propfan engines as this design still has limited applications in the aviation industry.

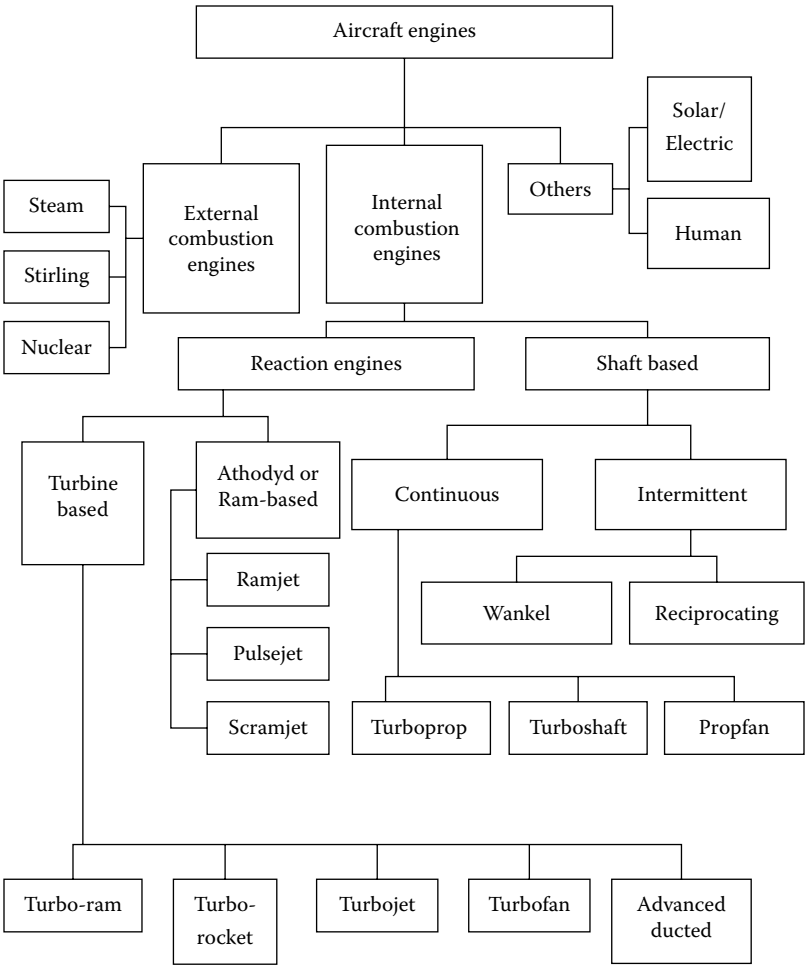


FIGURE 6.1
Classification of propulsion systems.

6.2 Internal Combustion Engines

6.2.1 Introduction

The Wright Flyer I was the first plane to be propelled by a simple four-cylinder piston engine and propeller. Piston engines employed in this way are identified as *aero piston engines* to differentiate them from automotive piston engines. Aero piston engines were the primary powerplant used during the first 50 years of manned flight. However, they continue to power small aircrafts and helicopters. Nearly 80% of current small flying machines (aircraft/helicopters or home-made planes) are powered by internal combustion engines.

Piston-powered aircraft and helicopters most commonly use 100 octane low-leaded fuel. Aero piston engines are able to power small aircraft and helicopters. Small airplanes have one or more piston-powered engines connected to the propeller(s). Table 6.1 provides

TABLE 6.1

Aviation Statistics (2000–2032)[a]

	Fixed Wing				Rotorcraft		Total	
	Piston		Turbine					
Year	Single Engine	Multi-Engine	Turbo Prop	Turbo Jet	Piston	Turbine	Piston	Turbine
2000	149,422	21,091	5,762	7,001	2,680	4,470	173,193	17,233
2005	148,101	19,412	7,942	9,823	3,039	5,689	170,552	23,454
2010	139,519	15,900	9,369	11,484	3,588	6,514	159,007	27,367
2013	136,650	15,660	9,570	12,410	3,875	7,165	156,185	29,145
2020	132,335	15,175	10,120	16,265	4,505	8,940	152,015	35,325
2026	132,370	14,745	10,740	20,865	5,075	10,650	152,190	42,255
2032	135,340	14,350	11,445	26,935	5,705	12,550	155,395	50,930

[a] FAA Aerospace Forecast, Fiscal Years 2012–2032, FAA Report.

statistics for current and forecast piston and jet engines for the period 2000–2032. In 2000, the number of aircraft powered by jet engines equaled 10% of those powered by piston engines. However, this ratio is expected to increase to 27.8% by 2032. The number of aircraft powered by piston engines dropped by 10% in the period 2000–2032, while the number of aircraft powered by jet engines increased by 195% in the same period. Many of the piston aircraft used for business typically fly relatively short missions of 300–400 miles, at altitudes below 15,000 ft, using very small general aviation airports that often do not have air traffic control towers. Helicopters are often attractive to business people because of their ability to land at a variety of heliports and outlying airports. Among the companies manufacturing piston-driven airplanes are the Cirrus Aircraft Corporation, Cessna Aircraft Company, Beechcraft Corporation (formerly the Hawker Beechcraft Corporation), Diamond Aircraft Industries, and the Mooney International Corporation. Manufacturers of helicopters include AgustaWestland (whose activities merged with Leonardo-Finmeccanica's Helicopter Division on January 1, 2016), Bell Aircraft, Enstrom Helicopter Corporation, Airbus Helicopters (formerly Eurocopter Group), Robinson Helicopter Company, and the Sikorsky Aircraft Corporation.

Piston engines are sources of power for land, sea, and air applications. They are the only source of power for almost all automotive vehicles, as very few current vehicle designs use electrical or solar power. Most locomotives and maritime applications use piston engines. In the field of aviation, also, most small or short-range aircraft are powered by piston engines. Piston engines alone cannot propel these craft and must be coupled to propellers. Marine craft are also coupled to marine screws, which were invented and employed long before air propellers or air screws. The Wright brothers designed and manufactured the first air propeller for use in their Flyer I (or 1903 Flyer), having tested it in a wind tunnel. Their light-weight four-stroke piston engine powered the twin propellers via a sprocket chain drive.

Section 6.2.2 discusses aero piston engines and Section 6.2.3 deals with propellers. Propellers installed in combination with piston engines are very similar to those fitted to turboprop engines. Propellers are classified based on their source of power, material, coupling to the output shaft, control, number of propellers coupled to each engine, direction of rotation, propulsion method, and the number of blades. Detailed aerodynamic theories are discussed regarding propeller design, covering axial momentum (or actuator disk), modified momentum, and the blade element. Nondimensional

parameters are derived defining propeller performance; namely, thrust and power coefficients, as well as the advance ratio. Detailed analysis of the thrust generated by each blade segment and the total thrust are described through worked examples. Charts are given for the thrust, power, and propulsive efficiency of two- and three-bladed propellers.

Propeller aerodynamics and design are also introduced.

6.2.2 Types of Aero Piston Engine

Aero piston engines are further classified into the following three types:

1. Rotary engines
2. Reciprocating engines
3. Supercharged/turbocharged reciprocating engines

Piston engines are further classified based on

- Number of cylinders
- Arrangement of cylinders
- Fuel used
- Cooling methods

Regarding cooling, most aircraft engines are air-cooled. However, a few liquid-cooled engine designs are in operation. In both cases, excess air is transferred to the surrounding air. In an air-cooled system, heat is transferred directly to the surrounding air. A liquid-cooled engine transfers heat from the cylinders to a liquid coolant, which, in turn, transfers the heat to the surrounding air through a radiator.

Two principal types of piston engine are the

1. Spark-ignition engine (SI), which is also identified as a petrol engine or gasoline engine
2. Compression-ignition engine (CI), which is also identified as a diesel engine

Moreover, piston engines may be specified as

- Two-stroke engines
- Four-stroke engines

In a spark-ignition engine, a mixture of fuel and air is ignited by a spark plug. In most petrol engines, the fuel and air are usually pre-mixed before compression. The pre-mixing was formerly done in a carburetor, but now it is achieved by electronically controlled fuel injection, except in small engines. Spark-ignition engines are advantageous for applications requiring low power (up to about 225 kW; 300 hp). In a compression-ignition engine, air is compressed to a sufficiently high pressure and temperature for combustion to occur spontaneously when fuel is injected. Petrol engines run at higher speeds than diesel engines, partially due to their lighter pistons, connecting rods and crankshaft and due to petrol burning faster than diesel. However, the lower compression ratios of a petrol engine

give a lower efficiency than that of a diesel engine. Compression-ignition engines are more reliable and are usually preferred for applications when fuel economy and relatively large amounts of power are required. New diesel engines may bring fuel efficiency and lead-free emissions to small aircraft, representing the biggest change in light aircraft engines in decades. The diesel engine has the highest thermal efficiency of any regular internal or external combustion engine due to its very high compression ratio. In the mid-range, spark-ignition and compression-ignition engines are used.

6.2.2.1 Rotary Engines

6.2.2.1.1 Conventional Types

The *rotary engine* was an early type of internal combustion engine, usually designed with an odd number of cylinders per row in a radial configuration. In rotary engines, the crankshaft remained stationary and the entire cylinder block rotated around it. This type of engine was widely used during World War I and the years immediately preceding that conflict. They have been described as very efficient in terms of power output, weight, cost, manufacture, and reliability.

The rotary engine met these goals, the Gnome Omega No. 1 Rotary Engine being an example (Figure 6.2). The entire engine rotates with the propeller, providing plenty of airflow for cooling regardless of the aircraft's forward speed. Some of these engines were a two-stroke design, giving them a high specific power and power-to-weight ratio. Unfortunately, the severe gyroscopic effects from the heavy rotating engine made the aircraft very difficult to fly. The engines also consumed large amounts of castor oil, spreading it all over the airframe and creating fumes, which caused pilots to feel nauseated.

6.2.2.1.2 Wankel Engines

The *Wankel engine* is a type of internal combustion engine using an eccentric rotary design to convert pressure into a rotating motion, instead of using reciprocating pistons**.** Its four-stroke cycle (shown in Figure 6.3) takes place in a space between the

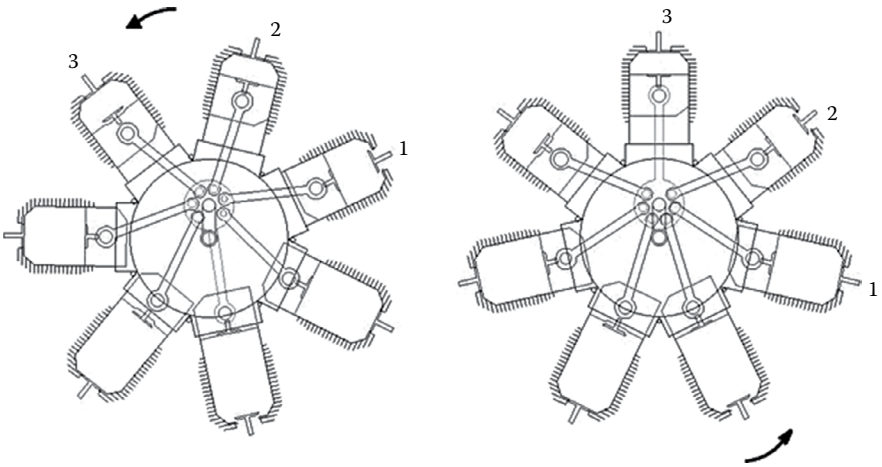


FIGURE 6.2
Rotary engine (Gnome engine).

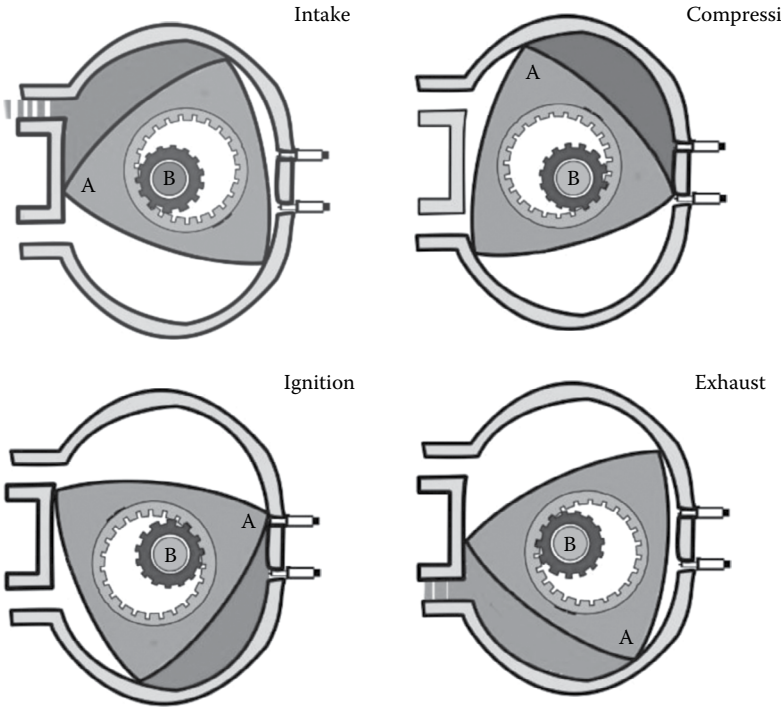


FIGURE 6.3
The four strokes of the Wankel engine.

inside of an oval-like epitrochoid-shaped housing and a rotor that is similar in shape to a Reuleaux triangle but having somewhat flatter sides. The very compact Wankel engine delivers smooth power at high rpm. It also has high horsepower per displacement compared with other internal combustion engines. The lubrication system is similar to that of the two-stroke engine and thus it does not need a separate system, unlike the four-stroke engine.

A Wankel engine is considered to be the optimum powerplant for a light aircraft, as it is light, compact, almost vibrationless, and has a high power-to-weight ratio. Further aviation benefits of a Wankel engine include that

1. The rotors cannot seize, since rotor casings expand more than rotors
2. It is not susceptible to "shock-cooling" during descent
3. It does not require an enriched mixture for cooling at high power

The first Wankel rotary engine aircraft was the experimental Lockheed Q-Star civilian version of the United States Army's reconnaissance QT-2 in 1967. It was subsequently installed in a variety of aircrafts including the Diamond DA20, a general aviation aircraft designed for flight training. Moreover, Wankel engines, due to their compact size and quiet operation, are used in drones or UAVs; an example of this, the AAI RQ-7 Shadow is shown in Figure 6.4.

Wankel engines are also becoming increasingly popular in home-built experimental aircraft.



FIGURE 6.4
AAI RQ-7 Shadow AUV.

6.2.2.2 Reciprocating Engines

Based on the cylinder arrangement, there are the following types:

1. In-line engine (or straight)
2. Horizontally opposed engine
3. V-type engine (twin-five-six-eight cylinders)
4. X-type engine
5. H-type engine
6. Radial type engine

6.2.2.2.1 In-Line Engines

An in-line engine has cylinders aligned in a single row. Mostly, it has an even number of cylinders (Figure 6.5). Many in-line engines were developed during World War I, including the Wright Flyer as well as the Hispano-Suiza engine and the Benz BZ-4. The cylinders are either upright above the crankshaft or inverted; that is, below the crankshaft. Most in-line engines are liquid-cooled since it is difficult to achieve sufficient air flow to cool the rear cylinders directly in air-cooled engines. The biggest advantage of an in-line engine is that it allows the aircraft to be designed with a narrow frontal area for low drag. The disadvantages of an in-line engine include a poor power-to-weight ratio, as the crankcase and crankshaft are long and thus heavy. Consequently, the in-line design was abandoned and is a rarity in modern aviation.

6.2.2.2.2 Horizontally Opposed Engines

A horizontally opposed engine, also called a "flat" or "boxer" engine, has two banks of cylinders on opposite sides of a centrally located crankcase. The engine is either air-cooled or liquid-cooled, but air-cooled versions predominate. Opposed engines are mounted in airplanes with the crankshaft horizontal, but may be mounted in helicopters with the crankshaft vertical. This type of engine is streamlined, resulting in less drag and good visibility for pilots. Due to the cylinder layout, reciprocating forces tend to cancel each other

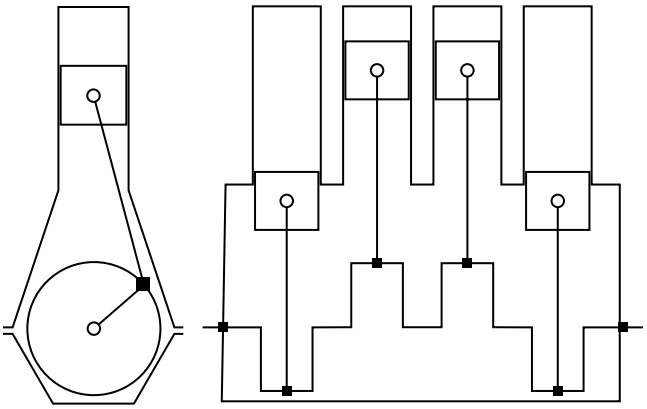


FIGURE 6.5
Four-cylinder straight engine scheme.

out, resulting in a smooth running engine. Opposed, air-cooled four- and six-cylinder piston engines are by far the most common engines used in small, general aviation aircraft requiring up to 400 hp (300 kW) per engine. The Continental O-360 is an example of a horizontally-opposed engine.

6.2.2.2.3 V-Type Engines

Cylinders in this type of engine are arranged in two in-line banks, tilted between 30° and 90° apart from each other. The vast majority of V engines are water-cooled. The V design provides a higher power-to-weight ratio than an in-line engine, while still providing a small frontal area. Perhaps the most famous example of this design is the legendary Rolls-Royce Merlin engine, a 27 L 60° V12 engine used in, among others, Spitfires. Similarly, two types of V-engines, the upright V-type and the inverted V-type, are frequently seen in World War I engines.

6.2.2.2.4 X-Type Engines

An *X engine* comprises twinned V-block engines horizontally opposed to each other. Thus, the cylinders are arranged in four banks, driving a common crankshaft. The Rolls-Royce Vulture, is an example of this type of engine, which powered the Avro Manchester bomber and the Hawker Tornado fighter.

6.2.2.2.5 H-Type Engine

An *H engine* (or "H-block") is an engine configuration in which the cylinders are aligned so that, if viewed from the front, they appear to be in a vertical or horizontal letter H. An H engine can be viewed as two flat engines, one either above or beside the other. The "two engines" each have their own crankshaft, which are then geared together at one end for power takeoff. The Napier Sabre was a British H-24-cylinder, liquid-cooled, piston aeroengine, used to power the Hawker Typhoon aircraft in mid-1941.

6.2.2.2.6 Radial Type Engine

This type of engine has one or two rows of cylinders arranged in a circle around a centrally located crankcase (Figure 6.6). Each row must have an odd number of cylinders in order to produce smooth operation. Rotary and radial engines look strikingly similar when they

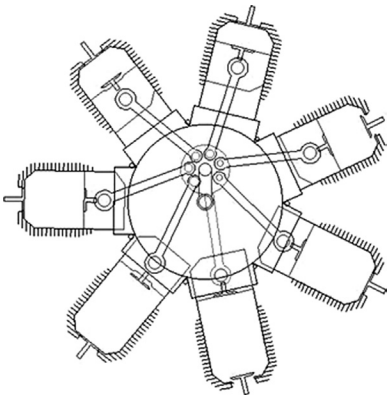


FIGURE 6.6
Single-row radial type engine.

are not running and can easily be confused, since both have cylinders arranged radially around a central crankshaft. Unlike the rotary engine, however, radial engines use a conventional rotating crankshaft in a fixed engine block. A radial engine has only one crank throw per row and a relatively small crankcase, resulting in a favorable power-to-weight ratio. Because the cylinder arrangement exposes a large proportion of the engine's heat-radiating surfaces to the air and tends to cancel reciprocating forces, radials tend to cool evenly and run smoothly. The lower cylinders, which are under the crankcase, may collect oil when the engine has been stopped for an extended period, which can cause hydrostatic lock. In military aircraft designs, the large frontal area of the engine acted as an extra layer of armor for the pilot. However, the large frontal area also resulted in an aircraft with a blunt and aerodynamically inefficient profile.

6.2.2.3 Supercharging and Turbocharging Engines

Superchargers and turbochargers are two types of forced induction employed in piston engines to add large amounts of power to their motor. In the field of aviation, *supercharging* and *turbocharging* allow piston engines to develop maximum power when operating at high altitudes or boost a craft's power during takeoff. At high altitudes, an engine without a supercharger will lose power because of the reduced density of the air entering the induction system of the engine. Both superchargers (Figure 6.7) and turbochargers (Figure 6.8) have compressors mounted in the intake system; these are used to raise the pressure and density of the incoming air. The advantage of compressing the air is that it allows more air to enter a cylinder, which increases the amount of fuel that can be taken into the cylinder, so more power is obtained from each combustion in each cylinder. The typical boost provided by either a turbocharger or a supercharger is 20–50 kPa. Two types of compressor are used in superchargers and turbochargers: positive displacement or dynamic. Three types of positive displacement compressors are used extensively: the roots, vane, and screw types. Two types of dynamic compressors are used: centrifugal or axial. This power can be supplied by a separate drive for the supercharger, or by connecting the supercharger directly to the engine shaft or to a gas turbine driven by the engine exhaust gases. As shown in Figure 6.8, turbochargers consist of a centrifugal compressor coupled to a radial inflow turbine through a vaneless or vaned diffuser housing.

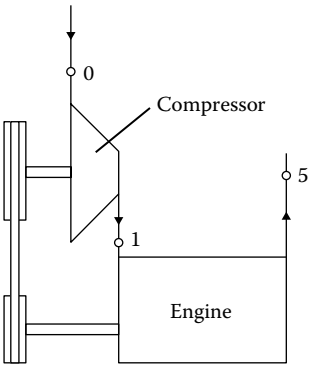


FIGURE 6.7
Supercharger.

The key difference between a turbocharger and a supercharger is the power supply. Superchargers are mechanically driven directly off the engine through belts, gears, shafts, or chains connected to the engine's crankshaft. The supercharger is normally located between the carburetor and inlet manifold. A turbocharger, on the other hand, is powered by a turbine mounted in the exhaust stream, which, in turn, spins the compressor element situated between the air intake and the carburetor or injector [2].

In theory, a turbocharger is more efficient as it uses the "wasted" energy in the exhaust stream for its power source. On the other hand, a turbocharger causes a certain amount of back pressure in the exhaust system and tends to provide less boost until the engine is running at higher RPMs. Generally, turbocharging is commonly found on high-power four-stroke engines, but it can also be used on two-stroke engines. Superchargers are easier to install but tend to be more expensive. A supercharger is considerably safer because of the simplicity of its design. More details are given in Table 6.2.

Superchargers and turbochargers are used in the following aircraft: Spitfire Mark I, Hurricane Mark I, Defiant fighter, Wellington bomber, Halifax bomber, Lancaster bomber, and Mosquito fighter.

6.2.3 Aerodynamics and Thermodynamics of the Reciprocating Internal Combustion Engine

6.2.3.1 Terminology for the Four-Stroke Engine

Figure 6.9 is a sketch of a reciprocating internal combustion engine consisting of a piston that moves within a cylinder fitted with two valves. The sketch is labeled with some special terms. The *bore* of the cylinder is its diameter. The *stroke* is the distance the piston moves in one direction. The piston is said to be at top dead center (TDC) when it has moved to a position where the cylinder volume is at the minimum [3]. This minimum volume is known as the *clearance volume*. When the piston has moved to the position of maximum cylinder volume, the piston is at bottom dead center (BDC). The distance between the TDC and the BDC is the largest distance that the piston can travel in one direction, and it is called the *stroke* of the engine. The volume swept out by the piston as it

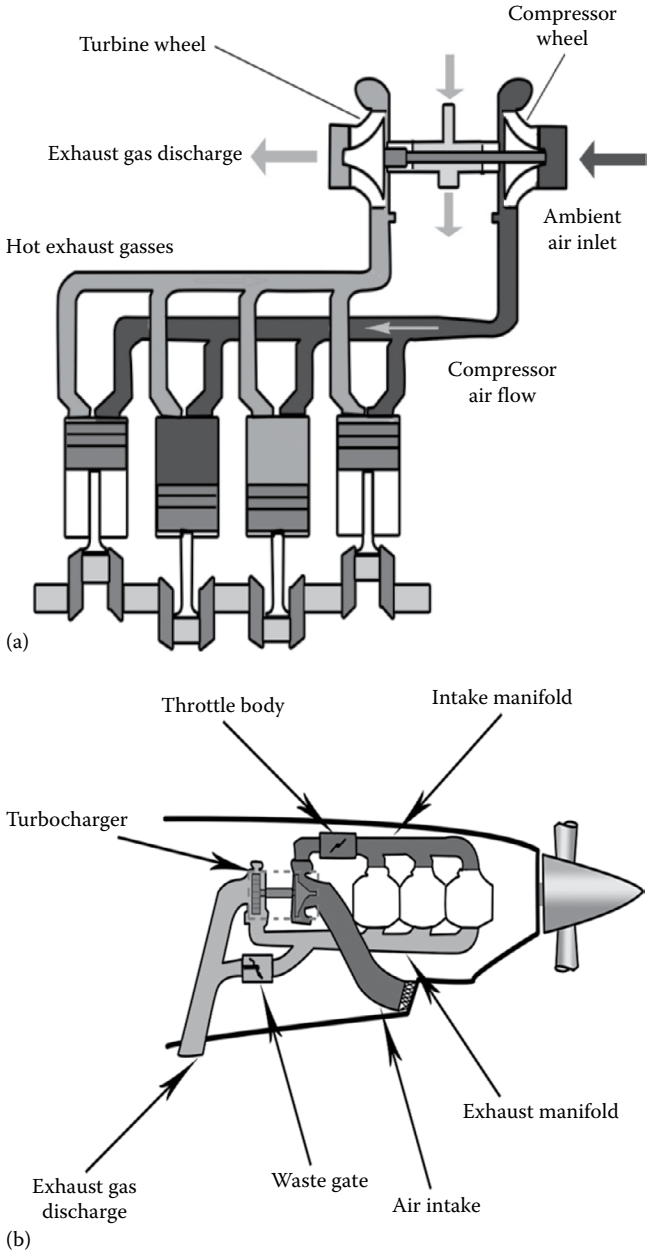


FIGURE 6.8
Turbo-charger (a) typical layout and (b) turbocharger. (From Rolls Royce Merlin III engine.)

TABLE 6.2

Supercharger versus Turbocharger

Parameter	Supercharger	Turbocharger
Driving method	Compressor is driven by the power taken directly from the engine via belts, gears, or chains	Compressor is driven by a turbine that is driven by the exhaust gases
Advantages	Drives vehicles to faster speeds	High fuel economy
Disadvantages	1. Losses due to mechanical friction 2. More expensive	1. Increased engine back pressure 2. Less expensive

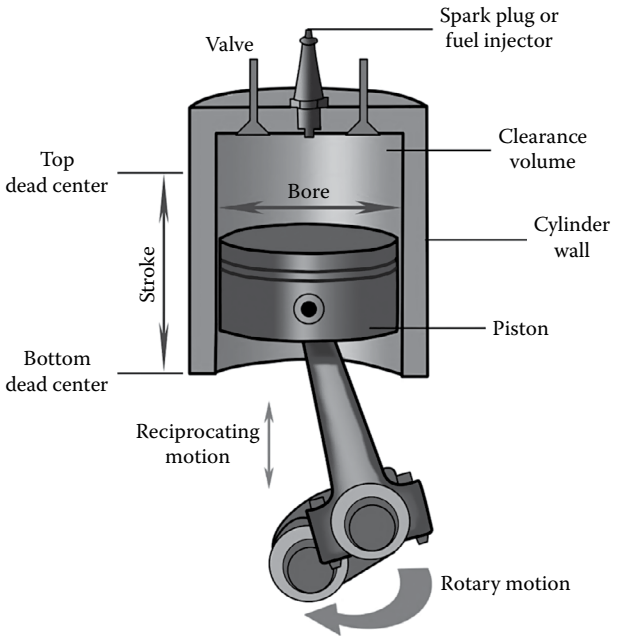


FIGURE 6.9
Nomenclature for reciprocating piston-cylinder engines.

moves from the top dead center to the bottom dead center position is called the *displacement volume*. The reciprocating motion of the piston is converted to rotary motion by a crank mechanism.

The *compression ratio* (r_c) is defined as the volume at bottom dead center (maximum volume) divided by the volume at top dead center (minimum volume or clearance).

$$r_c = \frac{V_{\max}}{V_{\min}} = \frac{V_{BDC}}{V_{TDC}} \tag{6.1}$$

Note that the compression ratio is a volume ratio and should not be confused with the pressure ratio [4].

In a four-stroke internal combustion engine, the piston executes four distinct strokes within the cylinder for every two revolutions of the crankshaft. Figure 6.10 gives a pressure–volume diagram such as might be displayed electronically.

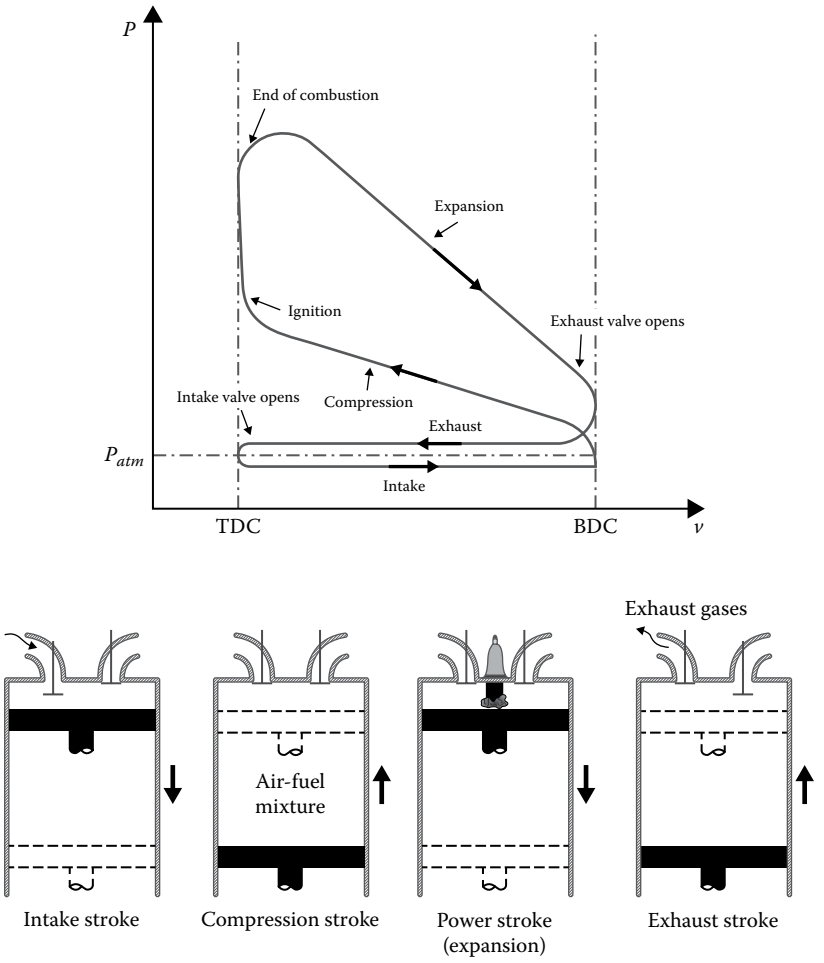


FIGURE 6.10
Pressure–volume diagram for a reciprocating internal combustion engine.

1. With the intake valve open, the piston makes an intake stroke to draw a fresh charge into the cylinder. For spark-ignition engines, the charge is a combustible mixture of fuel and air. Air alone is the charge in compression-ignition engines.
2. With both valves closed, the piston undergoes a compression stroke, raising the temperature and pressure of the charge. This requires work input from the piston to the cylinder contents. Combustion is induced by the spark plug near the end of the compression stroke in spark-ignition engines. In compression ignition engines, combustion is initiated by injecting fuel into the hot compressed air, beginning near the end of the compression stroke and continuing through the first part of the expansion. This combustion process results in a high-pressure, high-temperature gas mixture.
3. A power stroke follows the compression stroke, during which the gas mixture expands and applies direct force to the piston so that it returns to bottom dead center.
4. The piston then executes an exhaust stroke in which the burned gases are purged from the cylinder through the open exhaust valve.

6.2.3.2 Air-Standard Analysis

The analysis of real flow within an internal combustion engine is very complex due to the mechanical and thermal losses associated with friction and the combustion process. Other complexities are associated with heat transfer between the gases and the cylinder walls, as well as the work required to charge the cylinder and exhaust the products of combustion. Accurate modeling of reciprocating internal combustion engines normally involves computer simulation. To conduct elementary thermodynamic analyses of internal combustion engines, considerable simplification is required. One procedure is to employ an *air-standard analysis*; this deals with the following elements:

1. The almost-constant pressure intake and exhaust strokes are assumed to be at constant pressure. At wide-open throttle (WOT) (or fully open throttle valve), the intake stroke is assumed to be at the ambient pressure. At partially closed throttle or when supercharged, the inlet pressure will assume a constant value other than the ambient pressure [5]. The exhaust stroke pressure is assumed constant at the ambient pressure.
2. All processes are internally reversible.
3. Compression and expansion strokes are approximated by isentropic processes (reversible and adiabatic). Heat transfer for any stroke is negligible due to its very short duration.
4. The combustion process is replaced by a heat addition process from an external source in a constant-volume process (spark-ignition: SI cycle), a constant-pressure process (compression-ignition: CI cycle), or a combination of both (dual cycle).
5. Exhaust blow-down is approximated by a constant-volume process.

In air-standard cycles, air is considered an ideal gas such that the following ideal gas relations are used

$$Pv = RT, \quad P = \rho RT, \quad PV = mRT \tag{6.2a}$$

$$dh = C_p dT, \quad du = C_v dT \tag{6.2b}$$

$$a = \sqrt{\gamma RT} \tag{6.3}$$

For an isentropic process

$$Pv^{\gamma} = \text{constant}, \quad Tv^{\gamma-1} = \text{constant}, \quad TP^{(1-\gamma/\gamma)} = \text{constant} \tag{6.4}$$

Work-done for an isentropic process from state (1) to state (2)

$$w_{1-2} = \frac{P_2 v_2 - P_1 v_1}{1-\gamma} = \frac{R\left(T_2 - T_1\right)}{1-\gamma} \tag{6.5}$$

6.2.3.3 Engine Thermodynamics Cycles

Two cycles will be discussed here: the Otto and diesel cycles. The Otto cycle is an ideal cycle for spark-ignition engines, while the diesel cycle is ideal for compression-ignition cycles.

Specific air heats are functions of temperature. The temperature within piston engines may vary from room temperature up to several thousand degrees. At the low-temperature

end of the cycle (during intake and start of compression), the specific heat ratio has a value of $\gamma = 1.4$, while at the end of combustion, due to a rise in temperature, the specific heat ratio will be $\gamma = 1.3$. To simplify cycle analysis, *specific heat will be assumed constant*, having the average value of $\gamma = 1.35$.

In the next sections, the following values will be used:

$$C_p = 1.108 \text{ kJ/(kg·K)} \quad C_v = 0.821 \text{ kJ/(kg·K)} \tag{6.6a}$$

$$R = C_p - C_v = 0.287 \text{ kJ/(kg·K)}, \tag{6.6b}$$

$$\frac{C_p}{C_v} = 1.35 \tag{6.6c}$$

6.2.3.3.1 Four-Stroke Spark Ignition Otto Cycle Engines at WOT

The Otto cycle is the ideal cycle for spark-ignition reciprocating engines. It is named after Nikolaus A. Otto who, in 1876, built a successful four-stroke engine in Germany. In most spark-ignition engines, the piston executes four complete strokes (two mechanical cycles) within the cylinder, and the crankshaft completes two revolutions for each thermodynamic cycle. These engines are called four-stroke internal combustion engines. Schematic drawings for the ideal cycle on both *P–v* and *T–S* diagrams are shown in Figure 6.11.

Detailed thermodynamic analysis of Otto cycle

1. *Process 0–1*: Constant pressure suction (intake) stroke of air at ambient pressure P_0 With the intake valve open and exhaust valve closed, the piston makes an intake stroke to draw a fresh charge (a combustible mixture of fuel and air) into the cylinder

$$P_1 = P_5 = P_0 \tag{6.7a}$$

$$w_{0-1} = P_0(v_1 - v_0) \tag{6.7b}$$

Here, specific and total volumes are identified as v, V, respectively.

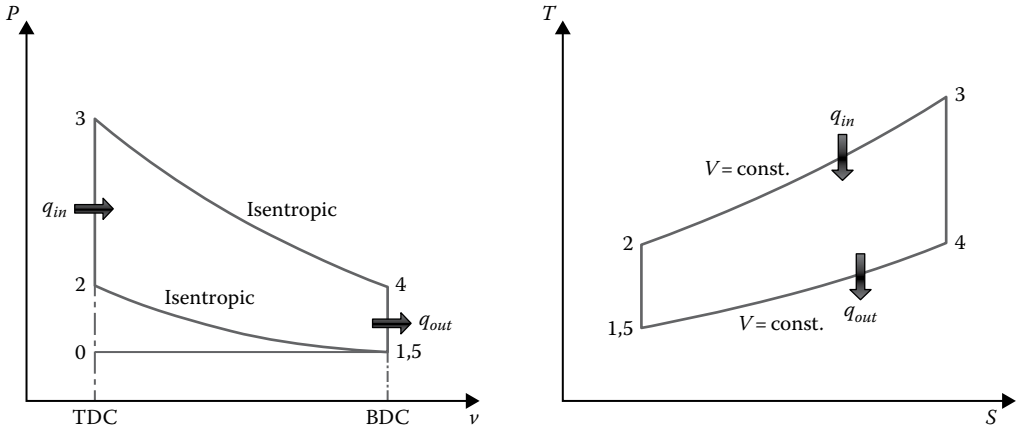


FIGURE 6.11
P–v and *T–S* diagram of ideal Otto cycle.

2. *Process 1–2*: Isentropic compression stroke
With both valves closed, the piston undergoes a compression stroke, raising the temperature and pressure of the charge. This requires work input from the piston to the contents of the cylinder.

$$T_2 = T_1\left(\frac{v_1}{v_2}\right)^{\gamma-1} = T_1\left(\frac{V_1}{V_2}\right)^{\gamma-1} = T_1\left(r_c\right)^{\gamma-1} \tag{6.8a}$$

$$P_2 = P_1\left(\frac{v_1}{v_2}\right)^{\gamma} = P_1\left(\frac{V_1}{V_2}\right)^{\gamma} = P_1\left(r_c\right)^{\gamma} \tag{6.8b}$$

$$q_{1-2} = 0 \tag{6.8c}$$

$$w_{1-2} = \frac{P_2v_2 - P_1v_1}{1-\gamma} = \frac{R\left(T_2 - T_1\right)}{1-\gamma} = \left(u_1 - u_2\right) = C_v\left(T_1 - T_2\right) \tag{6.8d}$$

3. *Process 2–3*: Constant-volume heat addition (combustion)

$$T_3 = T_{\max}, \quad P_3 = P_{\max}, \quad v_3 = v_2 = v_{TDC}, \quad w_{2-3} = 0 \tag{6.9a}$$

The specific heat added is (q_{in}), given by the relation

$$q_{2-3} = q_{in} = C_v\left(T_3 - T_2\right) = \left(u_3 - u_2\right) \tag{6.9b}$$

$$Q_{2-3} = Q_{in} = m_f Q_{HV}\eta_c = m_m C_v\left(T_3 - T_2\right) = \left(m_a + m_f\right)C_v\left(T_3 - T_2\right) \tag{6.9c}$$

$$Q_{HV}\eta_c = \left(AF + 1\right)C_v\left(T_3 - T_2\right) \tag{6.9d}$$

where

Q_{HV} is the heating value of fuel, while AF is the air-to-fuel ratio (m_a/m_f)

η_c is the combustion efficiency

The combustion process results in a gas mixture having the maximum pressure and maximum temperature.

Combustion is induced by the spark plug near the end of the compression stroke.

4. *Process 3–4*: Isentropic power or expansion stroke
During this stroke, which follows the compression stroke, the gas mixture expands and force is applied to the piston, returning it to bottom dead center. All valves are closed.

$$T_4 = T_3\left(\frac{v_3}{v_4}\right)^{\gamma-1} = T_3\left(\frac{V_3}{V_4}\right)^{\gamma-1} = T_3\left(r_c\right)^{\gamma-1} \tag{6.10a}$$

$$P_4 = P_3\left(\frac{v_3}{v_4}\right)^{\gamma} = P_3\left(\frac{V_3}{V_4}\right)^{\gamma} = P_3\left(r_c\right)^{\gamma} \tag{6.10b}$$

$$q_{3-4} = 0 \tag{6.10c}$$

$$w_{3-4} = \frac{P_4 v_4 - P_3 v_3}{1-\gamma} = \frac{R\left(T_4 - T_3\right)}{1-\gamma} = \left(u_3 - u_4\right) = C_v\left(T_3 - T_4\right) \tag{6.10d}$$

5. *Process 4–5*: Constant volume heat rejection (exhaust blow-down)
   The exhaust valve is open and the intake valve is closed

$$v_5 = v_4 = v_{BDC}, \quad w_{4-5} = 0 \tag{6.11a}$$

$$q_{4-5} = q_{out} = C_v\left(T_5 - T_4\right) = C_v\left(T_1 - T_4\right) = \left(u_5 - u_4\right) \tag{6.11b}$$

$$Q_{4-5} = Q_{out} = m_m C_v\left(T_5 - T_4\right) = m_m C_v\left(T_1 - T_4\right) \tag{6.11c}$$

6. *Process 5–0*: Constant pressure exhaust stroke at P_0
   The piston then executes an exhaust stroke in which the burned gases are purged from the cylinder through the open exhaust valve.

$$P_5 = P_1 = P_0 \tag{6.12a}$$

$$w_{5-0} = P_0\left(v_0 - v_5\right) = P_0\left(v_0 - v_1\right) \tag{6.12b}$$

Thermal efficiency of Otto cycle: Since the Otto cycle is executed in a closed system, and disregarding the changes in kinetic and potential energies, the energy balance for any process is expressed, on a unit-mass basis, as

$$w_{net} = \left(q_{in} - q_{out}\right) \text{kJ/kg} \tag{6.13}$$

with

$$w_{net} = q_{in} - q_{out} = \left(u_3 - u_2\right) - \left(u_4 - u_1\right)$$

The thermal efficiency is defined as

$$\eta_{th,Otto} = \frac{w_{net}}{q_{in}} = 1 - \frac{q_{out}}{q_{in}} = 1 - \frac{\left(u_4 - u_1\right)}{\left(u_3 - u_2\right)} = 1 - \frac{c_v\left(T_4 - T_1\right)}{c_v\left(T_3 - T_2\right)} = 1 - \frac{\left(T_4 - T_1\right)}{\left(T_3 - T_2\right)} = 1 - \frac{T_1\left(\frac{T_4}{T_1} - 1\right)}{T_2\left(\frac{T_3}{T_2} - 1\right)} \tag{6.14a}$$

Since processes 1–2 and 3–4 are isentropic, $v_2 = v_3$ and $v_4 = v_1$.

Thus

$$\frac{T_1}{T_2} = \left(\frac{v_2}{v_1}\right)^{\gamma-1} = \left(\frac{v_3}{v_4}\right)^{\gamma-1} = \frac{T_4}{T_3} \tag{6.14b}$$

Rearranging

$$\frac{T_4}{T_1} = \frac{T_3}{T_2} \tag{6.14c}$$

From Equation 6.14a through c, then

$$\eta_{th,Otto} = 1 - \frac{1}{r_c^{\gamma-1}} \tag{6.15}$$

where

$$r_c = \frac{v_{\max}}{v_{\min}} = \frac{v_1}{v_2} \tag{6.16}$$

From Equation 6.15, thermal efficiency is seen to be dependent on both of the compression ratio (r_c) and specific heat ratio (γ). A plot of Otto thermal efficiency versus the compression ratio for different values of (γ) is given in Figure 6.12.

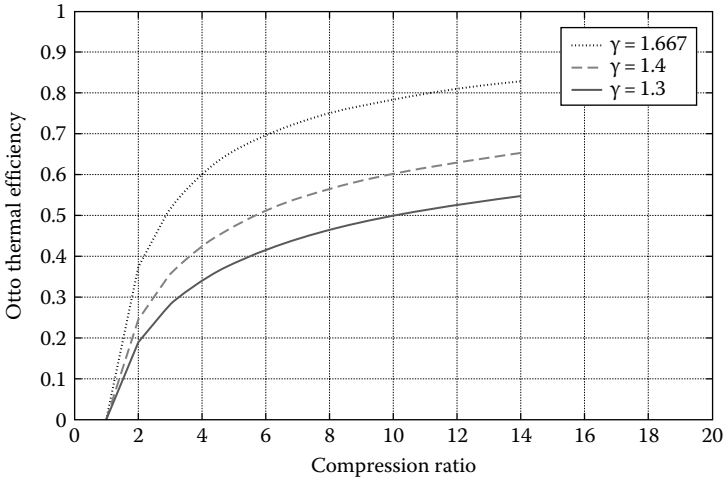


FIGURE 6.12
Thermal efficiency of the Otto cycle versus the compression ratio for different values of specific heat ratio (γ) of the working fluid.

From Figure 6.12, it is noticed that

1. The thermal efficiency curve is rather steep at low compression ratios but starts to flatten out at a compression ratio value of about 8. Therefore, the increase in thermal efficiency with the compression ratio is not as pronounced at high compression ratios.
2. For a given compression ratio, thermal efficiency increases with the specific heat ratio. Thus, it is maximum for a monatomic gas (such as argon or helium, $\gamma = 1.667$) and minimum for the least specific heat ratio ($\gamma = 1.3$).

General remarks

1. The working fluid in actual engines contains larger molecules, such as carbon dioxide, and the specific heat ratio decreases with temperature; thus, the actual cycles have lower thermal efficiencies than the ideal Otto cycle.
2. A spark-ignition engine has less efficiency than an ideal Otto cycle for a given compression ratio because of irreversible elements, such as friction and incomplete combustion.
3. The thermal efficiencies of spark-ignition engines range from about 25% to 30%.

Power generation and fuel consumption: The torque generated in piston engines is normally measured with a dynamometer. The torque exerted by the engine T is

$$T = Fb \tag{6.17}$$

The power P delivered by the engine and absorbed by the dynamometer is given by

$$P = T \times \omega = 2\pi NT \tag{6.18}$$

This value of engine power is called BRAKE POWER (P_b), where

$$P_b(\text{kW}) = 2\pi N\,(\text{rev/s}) \times T\,(\text{N}\cdot\text{m}) \times 10^{-3}$$

The indicated power is correlated to the indicated work, as illustrated in Figure 6.13.

The indicated work per cycle per cylinder

$$W_{C,i} = \oint p\,dv \tag{6.19a}$$

The *Net indicated work per cycle per cylinder* $W_{C,i}$ is the work delivered to the piston over the entire four-stroke cycle

$$W_{c,i} = \text{Area}(A) - \text{Area}(B) \tag{6.19b}$$

The power per cylinder is related to the indicated work per cylinder by

$$P_i = \frac{W_{C,i}N}{n_R} \tag{6.19c}$$

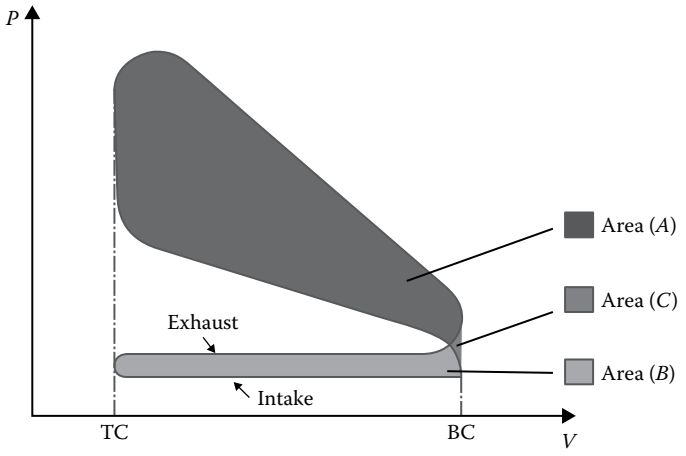


FIGURE 6.13
P–v diagram for a four-stroke SI engine.

where n_R is the number of crank revolutions for each power stroke per cylinder. For a four-stroke cycle engine $n_R = 2$, for two-stroke engine $n_R = 1$. This power is the indicated power defined as the rate of work transfer from the gas within the cylinder to the piston. From Equation 6.19c, then

$$W_{C,i} = \frac{P_i n_R}{N} \tag{6.19d}$$

For a four-stroke engine

$$W_{C,i} = \frac{2P_i}{N} \tag{6.19e}$$

For a two-stroke engine

$$W_{C,i} = \frac{P_i}{N} \tag{6.19f}$$

The brake power P_b is related to the indicated power P_i by the relation

$$P_i = P_b + P_f \tag{6.20}$$

where P_f is the power consumed in

- Overcoming the friction of the bearings, pistons, and other mechanical components of engine
- Driving accessories
- Induction and exhaust strokes

The ratio of brake (or useful) power delivered by the engine to the indicated power is called the mechanical efficiency (η_m), defined as

$$\eta_m = \frac{P_b}{P_i} \tag{6.21}$$

$\eta_m = 90\%$ for modern automotive engines at speeds below 30–40 rev/s (1800–2400 rev/min) and $\eta_m = 75\%$ at maximum rated speed

A parameter used to describe the performance of reciprocating piston engines is the mean effective pressure (*MEP*) (see Equation 6.22). The mean effective pressure is a fictitious pressure that, if it acted on the piston during the entire power stroke, would produce the same amount of network as that produced during the actual cycle (see Figure 6.14). That is

$$W_{net} = \text{MEP} \times \text{Piston area} \times \text{Stroke} = \text{MEP} \times \text{Displacement volume}$$

or

$$\text{Mean effective pressure} = \frac{\text{Net work for one cycle}}{\text{Displacement volume}} = \frac{W_{net}}{V_{\max} - V_{\min}} = \frac{w_{net}}{v_{\max} - v_{\min}} \tag{6.22}$$

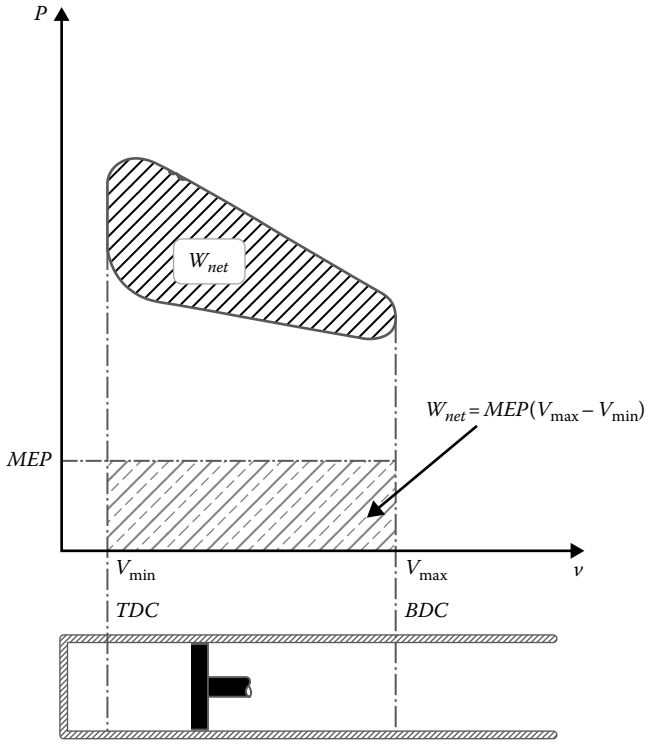


FIGURE 6.14
Mean effective pressure.

Various mean effective pressures can be defined by using different work terms in Equation 6.22. If *indicated work* is used, then the indicated mean effective pressure is obtained.

$$imep = \frac{W_{C,i}}{V_d} = \frac{P_i n_R}{N V_d} \tag{6.23}$$

If brake work is used, then the *brake mean effective pressure* (BMEP) is obtained

$$bmep = \frac{P_b\, n_R}{N V_d} \tag{6.24a}$$

Both mean effective pressures are related by

$$bmep = \eta_m \times imep \tag{6.24b}$$

Also *friction mean effective pressure* is given by

$$fmep = imep - bmep \tag{6.25}$$

Moreover, with

$$P_b = 2\pi NT$$

then

$$bmep = \frac{2\pi T n_R}{V_d} \tag{6.24c}$$

Other expressions for thermal efficiency: Thermal efficiency is also identified as *fuel-conversion efficiency* ($\eta_f \equiv \eta_{th}$). From Equation 6.14a, thermal efficiency may be expressed as

$$\eta_{th} = \frac{\text{Indicated power}}{\text{Fuel mass flow rate} \times \text{Heating value}}$$

$$\eta_{th} = \frac{P_i}{\dot{m}_f \times Q_{HV}} \tag{6.26a}$$

In British units, the indicated thermal efficiency is expressed as

$$\eta_{th} = \frac{ihp \times 33{,}000}{(\text{Mass of fuel burned/min}) \times (\text{heat value}) \times 778} \tag{6.26b}$$

Air/fuel and fuel/air ratios

$$\text{Air/Fuel ratio}\,(A/F) = \frac{\dot{m}_a}{\dot{m}_f} \tag{6.27a}$$

$$\text{Fuel/Air ratio}\left(F/A\right)=\frac{\dot{m}_f}{\dot{m}_a} \tag{6.27b}$$

Normal operating range for

SI engine using gasoline fuel

$$12 \ll A/F \ll 18^\circ \quad \left(0.056 \ll F/A \ll 0.083\right)$$

CI engine using diesel fuel

$$18 \ll A/F \ll 70^\circ \quad \left(0.014 \ll F/A \ll 0.056\right)$$

Specific fuel consumption: Specific fuel consumption is defined as the fuel flow rate per unit power output, or

$$SFC=\frac{\dot{m}_f}{P} \tag{6.28a}$$

Indicated specific fuel consumption

$$ISFC=\frac{\dot{m}_f}{P_i} \tag{6.28b}$$

Brake specific fuel consumption

$$BSFC=\frac{\dot{m}_f}{P_b} \tag{6.28c}$$

Friction specific fuel consumption

$$FSFC=\frac{\dot{m}_f}{P_f} \tag{6.28d}$$

Then, from Equation 6.26a, we get

$$\eta_{th}=\frac{1}{SFC\,Q_{HV}} \tag{6.29}$$

Thus, specific fuel consumption (SFC) is inversely proportional to the thermal (or fuel conversion) efficiency for normal hydrocarbon fuels. Introducing several units, then

$$\eta_{th}=\eta_f=\frac{1}{SFC\left(\text{mg/J}\right)Q_{HV}\left(\text{MJ/kg}\right)} \tag{6.30a}$$

or

$$\eta_{th}=\eta_f=\frac{3600}{SFC\left(\text{g/kW}\cdot\text{h}\right)Q_{HV}\left(\text{MJ/kg}\right)} \tag{6.30b}$$

or

$$\eta_{th} = \eta_f = \frac{2545}{SFC\left(\text{ib}_m/\text{hp}\cdot\text{h}\right)Q_{HV}\left(\text{Btu}/\text{ib}_m\right)} \tag{6.30c}$$

The typical heating value for the commercial hydrocarbon fuels used in engines

$$Q_{HV} = 42 - 44\ \text{MJ/kg} \tag{6.31a}$$

or

$$Q_{HV} = 18{,}000 - 19{,}000\ \text{Btu/ib}_m \tag{6.31b}$$

Note that low values of SFC are desirable. The typical best values of brake specific fuel consumption are equal or less than the following values.

For SI engines

$$75\ \mu\text{g/J} = 270\ \text{g/kW}\cdot\text{h} = 0.47\ \text{ib}_m/\text{hp}\cdot\text{h} \tag{6.32a}$$

For CI engines

$$55\ \mu\text{g/J} = 200\ \text{g/kW}\cdot\text{h} = 0.32\ \text{ib}_m/\text{hp}\cdot\text{h} \tag{6.32b}$$

Volumetric efficiency (η_V): Volumetric efficiency is only used with four-stroke cycle engines, which have a distinct induction process. It is a measure for the effectiveness of an engine's induction process, as the intake system (air filter, carburetor, intake manifold, and intake valve) restricts the amount of air induced to the engine [6]. It is defined as the volume flow rate of air into the intake system divided by the rate at which volume is displaced by the piston

$$\eta_V = \frac{\dot{V}_a}{V_s} = \frac{2\dot{m}_a}{\rho_{a,i}V_d N} \tag{6.33a}$$

where
$\rho_{a,i}$ is the air density at the inlet
$\dot{V}_a$ is the rate of naturally aspirated induced air volume
V_s is the rate at which volume is displaced by the piston

Since piston speed is defined as

$$\bar{S}_P = 2LN$$

where L is the stroke
then

$$\eta_V = \frac{4\dot{m}_a L}{\rho_{a,i}V_d\bar{S}_P} \tag{6.33b}$$

or

$$\eta_V = \frac{m_a}{\rho_{a,i} V_d} \tag{6.33c}$$

where m is the mass of air inducted into the cylinder per cycle. The maximum value for volumetric efficiency has the following range

$$(\eta_V)_{\max} = 80\% - 90\%$$

Propulsive efficiency: A piston engine is coupled to one or more propellers to furnish the forward thrust force. The propulsive efficiency here is a propeller efficiency, which is the ratio of the thrust horsepower to the brake horsepower. On average

$$\eta_P \equiv \eta_{Pr} = 80\%$$

Thus, thrust horsepower constitutes approximately 80% of the brake horsepower; the other 20% is lost in friction and slippage controlling the blade angle of the propeller.

Engine specific weight and specific volume:

$$\text{Specific weight} = \frac{\text{Engine weight}}{\text{Rated power}} \tag{6.34}$$

$$\text{Specific volume} = \frac{\text{Engine volume}}{\text{Rated power}} \tag{6.35}$$

Relationships between performance parameters: From the previous relations, the following performance parameters can be developed as

Power

$$P = \frac{\eta_f m_a N Q_{HV} (F/A)}{n_R}$$

$$P = \frac{\eta_f \eta_V N V_d Q_{HV} \rho_{a,i} (F/A)}{n_R}$$

Torque

$$T = \frac{\eta_f \eta_V V_d Q_{HV} \rho_{a,i} (F/A)}{2\pi n_R}$$

Mean-effective pressure

$$MEP = \eta_f \eta_V Q_{HV} \rho_{a,i} (F/A)$$

The power per piston area, often called *SPECIFIC POWER* is

$$\frac{P}{A_P} = \frac{\eta_f \eta_V N L Q_{HV} \rho_{a,i} (F/A)}{n_R} \tag{6.36a}$$

Introducing mean piston speed, $\overline{S}_p = 2LN$, then

$$\frac{P}{A_P} = \frac{\eta_f \eta_V \overline{S}_P Q_{HV} \rho_{a,i} (F/A)}{2n_R} \tag{6.36b}$$

For a four-stroke engine

$$P/A_P = (mep)\overline{S}_P/4 \tag{6.37a}$$

For a two-stroke engine

$$P/A_P = (mep)\overline{S}_P/2 \tag{6.37b}$$

Example 6.1

A four-cylinder 2.0 L, SI engine operates at WOT on a four stroke air standard Otto cycle. The engine has a compression ratio of 8:1, a stroke-to-bore ratio S/B = 1.025 at 3000 rpm and mechanical efficiency of 86%. Air to fuel ratio AF = 15, fuel heating value is 44,000 kJ/kg. At the start of compression stroke, condition at the cylinder are 100 kPa and 30°C. It is assumed that a 4% exhaust residual is left over from previous cycle.

1. Perform a complete thermodynamic analysis of the engine
2. Calculate thermal efficiency
3. Mean piston speed
4. Brake power
5. Brake specific fuel consumption

Solution

1. Displacement volume for one cylinder

$$V_d = \frac{2.0\ \text{L}}{4} = 0.5\ \text{L} = 0.0005\ \text{m}^3$$

Compression ratio:

$$r_c = \frac{V_1}{V_2} = \frac{V_d + V_c}{V_c} = \frac{0.5 + V_c}{V_c} = 8.0$$

$$V_c = 0.714\ \text{L} = 0.0000714\ \text{m}^3$$

Since the displacement volume is expressed as

$$V_d = \frac{\pi}{4} B^2 S = \frac{\pi}{4} \times B^2 \times 1.025B$$

Then the bore $B = 0.0853$ m $= 8.53$ cm

The stroke $S = 0.0874$ m $= 8.74$ cm

Now, let us calculate the air/gas properties at different states.

State (*1*)

$$T_1 = 30°\text{C} = 303 \text{ K}, \quad P_1 = 100 \text{ kPa}$$

$$V_1 = V_d + V_c = 0.0005714 \text{ m}^3$$

Mass of mixture at state (1) is $m_m = \dfrac{P_1 V_1}{RT_1} = \dfrac{100 \times 10^3 \times 0.0005714}{287 \times 303} = 0.000657 \text{ kg}$

State (*2*)

Since process 1–2 is an isentropic compression, then

$$P_2 = P_1 (r_c)^{\gamma} = 100 \times (8)^{1.35} = 1656 \text{ kPa}$$

$$T_2 = T_1 (r_c)^{\gamma - 1} = 303 \times (8)^{0.35} = 627.4 \text{ K}$$

$$V_2 = \frac{mRT_2}{P_2} = \frac{0.000657 \times 0.287 \times 627.4}{1656} = 0.0000714 \text{ m}^3$$

Or simply

$$V_2 = \frac{V_1}{r_c} = \frac{0.0005714}{8} = 0.0000714 \text{ m}^3$$

The mass of mixture (m_m) within the cylinder can be decomposed as follows:

$$m_m = m_a + m_f + m_{ex} = 0.000657 \text{ kg}$$

where

(m_a) is the mass of fresh air sucked into the cylinder

(m_f) is the mass of fuel mixed with fresh air

(m_{ex}) is the exhaust residual left in the cylinder

$$(m_{ex}) = 0.04\, m_m = 0.00002628 \text{ kg}$$

Since, $AF = \dfrac{m_a}{m_f} = 15$, then $0.96 m_m = 16 m_f$

$$m_f = 0.00003942 \text{ kg}, \quad m_a = 0.0005913 \text{ kg}$$

State (*3*)

Heat added $Q_{in} = m_f Q_{HV} = 0.00003942 \times 44{,}000 = 1.73448$ kJ

Heat added can be also expressed as

$$Q_{in} = m_m C_v (T_3 - T_2) = 0.000657 \times 0.821 \times (T_3 - 627.4)$$

Then $T_3 = 3842 \text{ K} \equiv T_{\max}$

$$V_3 = V_1 = 0.0005714 \text{ m}^3$$

For a constant volume process; $P_3 = P_2 \left(\dfrac{T_3}{T_2} \right) = 10{,}143$ kPa

State (*4*)
Power stroke; isentropic expansion

$$P_4 = P_3\left(\frac{1}{r_c}\right)^{\gamma} = \frac{10{,}143}{(8)^{1.35}} = 612.3 \text{ kPa}$$

$$T_4 = T_3\left(\frac{1}{r_c}\right)^{\gamma-1} = \frac{3843}{(8)^{0.35}} = 1856 \text{ K}$$

$$v_4 = \frac{mRT_4}{P_4} = 0.000571 \equiv V_1$$

Work produced in power expansion:

$$W_{3-4} = \frac{mR(T_4 - T_3)}{1-\gamma} = \frac{0.000657 \times 0.287 \times (1856 - 3843)}{1 - 1.35} = 1.07047 \text{ kJ}$$

Work absorbed in isentropic compression stroke:

$$W_{1-2} = \frac{mR(T_2 - T_1)}{1-\gamma} = \frac{0.000657 \times 0.287 \times (627.4 - 303)}{1 - 1.35} = -0.17476 \text{ kJ}$$

$$W_{net} = W_{3-4} + W_{1-2} = 0.8957 \text{ kJ}$$

2. Thermal efficiency $\eta_{th} = W_{net}/Q_{in} = 0.5166 = 51.7\%$
Thermal efficiency can be also evaluated from the relation

$$\eta_{th} = 1 - \frac{1}{r_c^{\gamma-1}} = 0.517$$

3. Mean piston speed

$$\bar{S}_P = 2LN = 2 \times 0.0874 \times \left(\frac{3000}{60}\right) = 8.74 \text{ m/s}$$

4. Brake power
Net brake work per cylinder for one cycle:

$$W_b = \eta_m W_i = 0.86 \times 0.8957 = 0.77 \text{ kJ}$$

Brake power at 3000 rpm

$$P_b = (W_b N/n_R) \times (\text{number of cylinders})$$

$$P_b = \left(0.77 \times \frac{3000}{60} \times \frac{1}{2}\right) \times (4) = 77 \text{ kW} = 103.4 \text{ hp}$$

5. Brake specific fuel consumption

$$\text{Fuel mass flow rate } \dot{m}_f = \left(\frac{m_f N}{n_R}\right) \times (\text{number of cylinders})$$

$$\dot{m}_f = \left(0.00003942 \times \frac{3000}{60} \times \frac{1}{2}\right) \times (4) = 0.003942 \text{ kg/s}$$

$$bsfc = 0.003942 \times 1000 \times \frac{3600}{77} = 184.3 \text{ g/(kW} \cdot \text{h)}$$

6.2.3.3.2 Two-Stroke Spark Ignition (Otto Cycle) Engines

Two-stroke engines are small engines that may be used in ultra-light aircrafts. Similar to four-stroke engines, two-stroke engine is constructed with a cylinder, piston, crankshaft, connecting rod, and crankcase.

Petrol engine includes a spark plug, while diesel engine replaces the spark plug with fuel injector (Figure 6.15). The cycle is illustrated in Figure 6.16 and described as follows: A fresh charge of fuel-air mixture enters when the piston uncovers the intake port while moving upwards (Figure 6.16a). There is already a fuel-air mixture being compressed in the cylinder head above the piston. At the top of the compression stroke, the compressed fuel-air mixture is ignited by the spark plug (Figure 6.16b). The resulting explosion of gases is what drives the piston downwards and more fuel-air mixture has been drawn into the cylinder. As the piston moves downwards, it uncovers the exhaust port. The exhaust gases flow out of that port (Figure 6.16c). As the piston moves down even further, Figure 6.16d, the transfer port becomes uncovered and the compressed fuel-air mixture in the crankcase rushes into the cylinder head above the piston, helping to displace any remaining exhaust gases. The piston now starts back on its upward stroke.

Table 6.3 presents a quick comparison between two-stroke and four-stroke engines.

6.2.3.3.3 Four Stroke Diesel Engines

The diesel cycle is the ideal cycle for CI reciprocating engines. The CI engine, first proposed by Rudolph Diesel in the 1890s, is very similar to the SI engine discussed in the last

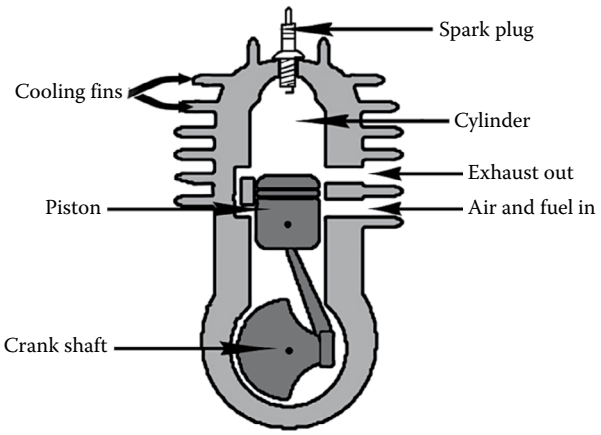


FIGURE 6.15
Two-stroke spark ignition engine.

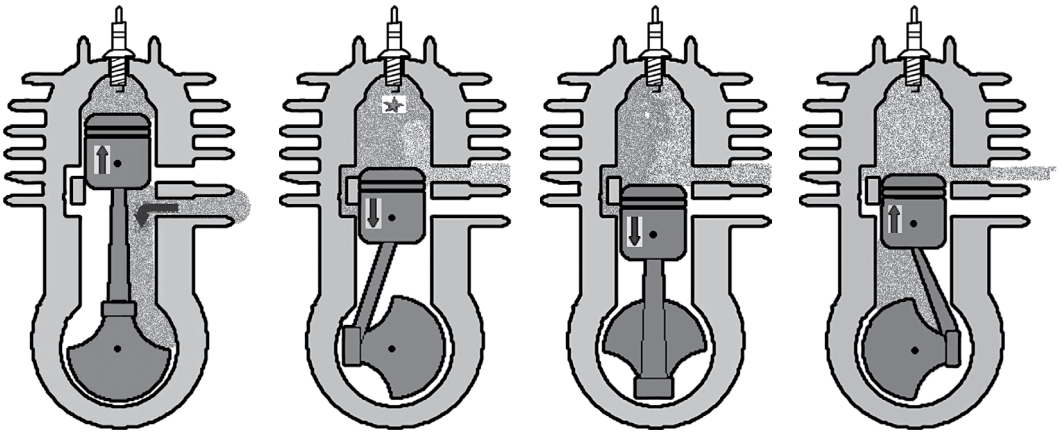


FIGURE 6.16
Two-stroke Otto Cycle. (a) Charging, (b) combustion, (c) exhaust, and (d) compression.

TABLE 6.3
Two-Stroke versus Four-Stroke Engines

		Two Stroke	Four Stroke
1	Compression ratio	18:1–100:1	10:1–20:1
2	Speed	2000–6000	400–3500
3	Power stroke	One working stroke per one revolution of crankshaft	One working stroke per two revolutions of crankshaft
4	Weight and size	Lighter and compact for same power	Heavier and larger
5	Flywheel size	Smaller	Larger
6	Construction	Simpler and easy to manufacture	More complicated due to valve mechanisms
7	Mechanical efficiency	Higher due to few moving parts	smaller
8	Thermal efficiency	Small	Higher
9	Noise	High	smaller
10	Fuel consumption	High	Low
11	Maintenance	Less	High

section, differing mainly in the method of initiating combustion. In CI engines (also known as diesel engines), the air is compressed to a temperature that is above the auto-ignition temperature of the fuel, and combustion starts as the fuel is injected into this hot air. Therefore, the spark plug and carburetor are replaced by a fuel injector in diesel engines. The four strokes of diesel engines are plotted on both P–v and T–S diagrams in Figure 6.17.

In diesel engines, only air is compressed during the compression stroke, eliminating the possibility of auto-ignition. Therefore, diesel engines can be designed to operate at much higher compression ratios, typically between 12 and 24. Fuels that are less refined (thus less expensive) can be used in diesel engines. The fuel injection process in diesel engines starts when the piston approaches TDC and continues during the first part of the power stroke. Therefore, the combustion process in these engines takes place over a longer interval. Because of this longer duration, the combustion process in the ideal diesel cycle is

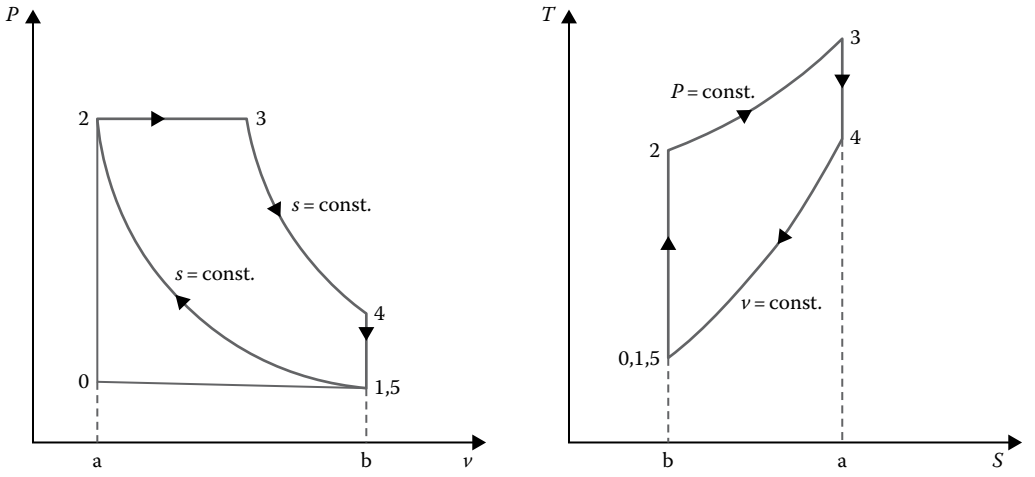


FIGURE 6.17
Air-standard diesel cycle.

approximated as a constant-pressure heat-addition process. In fact, this is the only process where the Otto and the diesel cycles differ. The remaining three processes are the same for both ideal cycles. That is, process 1–2 is isentropic compression, process 2–3 constant-pressure heat addition, process 3–4 is isentropic expansion, and process 4–1 is constant-volume heat rejection. The similarity between the two cycles is also apparent by comparing the *P–v* and *T–S* diagrams of both cycles illustrated in Figures 6.11 and 6.17.

Thermodynamic analysis of air-standard diesel cycle

1. *Process 0–1*: Constant pressure induction of air at ambient pressure P_0
   Intake valve open and exhaust valve closed, Equation 6.7a and b are also used here.
2. *Process 1–2*: Isentropic compression stroke
   Both valves closed, Equation 6.8a through d are applied here.
3. *Process 2–3*: Constant-pressure heat addition (combustion)

$$T_3 = T_{\max}, \quad P_3 = P_2, \quad v_2 = v_{TDC} \tag{6.38a}$$

$$q_{2-3} = q_{in} = C_p\left(T_3 - T_2\right) = \left(h_3 - h_2\right) \tag{6.38b}$$

$$Q_{2-3} = Q_{in} = m_f Q_{HV}\eta_c = m_m C_p\left(T_3 - T_2\right) = \left(m_a + m_f\right)C_p\left(T_3 - T_2\right) \tag{6.38c}$$

$$Q_{HV}\eta_c = \left(AF + 1\right)C_p\left(T_3 - T_2\right) \tag{6.38d}$$

$$w_{2-3} = q_{2-3} - \left(u_3 - u_2\right) = P_2\left(v_3 - v_2\right) \tag{6.38e}$$

Cutoff ratio β is defined as the change in volume that occurs during combustion, given by

$$\beta = V_3/V_2 = v_3/v_2 = T_3/T_2 \tag{6.38f}$$

4. *Process 3–4*: Isentropic power or expansion stroke
   All valves are closed; Equation 6.10a through d are used also here.
5. *Process 4–5*: Constant volume heat rejection (exhaust blow-down)
   Exhaust valve open and intake valve closed; Equation 6.11a and c are also applicable.
6. *Process 5–0*: Constant pressure exhaust stroke at P_0
   The piston then executes an exhaust stroke in which the burned gases are purged from the cylinder through the open exhaust valve. Equation 6.12a and b are used here.

Thermal efficiency of diesel cycle:

$$\eta_{th,Diesel} = \frac{w_{net}}{q_{in}} = 1 - \frac{q_{out}}{q_{in}} = 1 - \frac{C_v(T_4 - T_1)}{C_P(T_3 - T_2)} = 1 - \frac{(T_4 - T_1)}{\gamma(T_3 - T_2)} \tag{6.39a}$$

With rearrangement,

$$\eta_{th,Diesel} = 1 - \frac{1}{r_c^{\gamma-1}}\left[\left(\beta^{\gamma} - 1\right)/\gamma(\beta - 1)\right] \tag{6.39b}$$

where r_c as previously defined

$$r_c \frac{v_{\max}}{v_{\min}} = \frac{v_1}{v_2}, = C_P/C_v$$

and

$$\beta = v_3/v_2$$

Example 6.2

A large CI engine operates on air-standard diesel cycle using diesel fuel having latent heating value of 41,000 kJ/kg and a combustion efficiency of 98%. The engine has a compression ratio of 16:1, cutoff ratio of 3.0. Inlet temperature and pressure are 35°C and 101 kPa. Calculate

1. Pressure, temperature, and specific volume at each point of the cycle
2. Air-fuel ratio
3. Thermal efficiency

Solution

State 1:

$$T_1 = 35°\text{C} = 308\ \text{K}, \quad P_1 = 101\ \text{kPa}$$

$$v_1 = \frac{RT_1}{P_1} = \frac{0.287 \times 308}{101} = 0.8752\ \text{m}^3/\text{kg}$$

State 2: Isentropic compression

$$P_2 = P_1\left(r_c\right)^{\gamma} = 101 \times \left(16\right)^{1.35} = 4264.6 \text{ kPa}$$

$$T_2 = T_1\left(r_c\right)^{\gamma-1} = 308 \times \left(16\right)^{0.35} = 627.4 \text{ K}$$

$$v_2 = \frac{RT_2}{P_2} = \frac{0.287 \times 812.8}{4264.6} = 0.0547 \text{ m}^3/\text{kg}$$

or simply

$$v_2 = \frac{V_1}{r_c} = 0.0547 \text{ m}^3/\text{kg}$$

Work

$$W_{1-2} = \frac{R\left(T_2 - T_1\right)}{1-\gamma} = \frac{0.287 \times \left(812.8 - 308\right)}{1-1.35} = -413.94 \text{ kJ/kg}$$

State 3: $v_3 = v_2 \times \beta = 0.1641 \text{ m}^3/\text{kg}$

$$P_3 = P_2 = 4264.6 \text{ kPa}$$

$$T_3 = \frac{P_3 v_3}{R} = \frac{4264.6 \times 0.1641}{0.287} = 2438.4 \text{ K}$$

$$w_{2-3} = P_2\left(v_3 - v_2\right) = 4264.6 \times \left(0.1641 - 0.0547\right) = 466.5 \text{ kJ/kg}$$

$$q_{in} = q_{2-3} = C_p\left(T_3 - T_2\right) = 1.108 \times \left(2438.4 - 812.8\right) = 1801.2 \text{ kJ/kg}$$

State 4: $v_4 = v_1 = 0.8752 \text{ m}^3/\text{kg}$

$$T_4 = T_3 \times \left(\frac{v_3}{v_4}\right)^{\gamma-1} = 2438.4 \times \left(\frac{0.1641}{0.8753}\right)^{0.35} = 1357.2 \text{ K}$$

$$P_4 = P_3 \times \left(\frac{v_3}{v_4}\right)^{\gamma} = 4264.6 \times \left(\frac{0.1641}{0.8753}\right)^{1.35} = 445.1 \text{ kPa}$$

Air-to-fuel ratio is obtained from Equation 6.38d as follows:

$$Q_{HV}\eta_c = \left(AF + 1\right)C_p\left(T_3 - T_2\right)$$

$$AF = \frac{Q_{HV}\eta_c}{C_p\left(T_3 - T_2\right)} - 1 = \frac{41{,}000 \times 0.98}{1.108 \times \left(2{,}438.4 - 812.8\right)} - 1 = 21.3$$

$$W_{3-4} = \frac{R\left(T_4 - T_3\right)}{1-\gamma} = \frac{0.287 \times \left(1357.2 - 2438.4\right)}{1-1.35} = 886.6 \text{ kJ/kg}$$

$$W_{net} = W_{1-2} + W_{2-3} + W_{3-4} = -413.9 + 466.5 + 886.6 = 939.2 \text{ kJ/kg}$$

Thermal efficiency

$$\eta_{th,Diesel} = 1 - \frac{W_{net}}{q_{in}} = 1 - \frac{939.2}{1801.2} = 0.5214 = 52.14\%$$

Or it can be evaluated from the relation:

$$\eta_{th,Diesel} = 1 - \frac{1}{r_c^{\gamma-1}}\left[\left(\beta^{\gamma} - 1\right)/\gamma(\beta - 1)\right]$$

$$\eta_{th,Diesel} = 1 - \frac{1}{(16)^{0.35}}\left[\left(3^{1.35} - 1\right)/(1.35)(3 - 1)\right] = 0.5214 = 52.14\%$$

6.2.3.3.4 Two-Stroke Diesel Engines

In a two-stroke cycle C.I. engine all the operations are exactly the same as those in two-stroke S.I. engine except that in this case only air is taken in instead of air-fuel mixture and the fuel is injected at the end of compression stroke, a fuel injector being fitted instead of a spark plug.

6.2.3.3.5 Summary for Piston Engines Used in Land, Sea, and Air applications

Table 6.4 provides a comparison of piston engines used in land, sea, and air applications.

6.2.3.4 Superchargers/Turbochargers

Superchargers or turbochargers will increase the power and efficiency of an internal combustion engine through increasing the pressure and density of the inlet air using compressors. Two types of compressors are used; namely, positive displacement and dynamic. Positive displacement compressors are either of the roots, vane, or screw types. Two types of dynamic compressors used are either centrifugal or axial.

Figure 6.18 illustrates the P–v and T–S diagrams for a supercharger coupled to an aero piston engine performing an Otto cycle. Since the boost pressure (P_1) is greater than the ambient pressure (P_0), then the pumping loop represents a positive work.

TABLE 6.4

Data for Piston Engines Used in Different Land, Sea, and Air Applications

			Predominant Type		
Class	**Services**	**Power Range (kW)**	**D or SI**	**Cycle**	**Cooling**
Road vehicles	Passengers	15–200	D	4	W
	Heavy commercial	120–400	D	4	W
Rail road	Locomotive	400–3,000	D	2/4	W
Marine	Ships	3,500–22,000	D	2/4	W
Stationary	Electric power	35–22,000	D	2/4	W
Airborne	Airplanes	45–2,700	SI	4	A
	Helicopters	45–1,500	SI	4	A

Source: Heywood, J., *Internal Combustion Engine Fundamentals*, 1st edn., McGraw-Hill, 1988.
Note: SI, spark ignition; D, diesel; A, air-cooled; W, water-cooled.

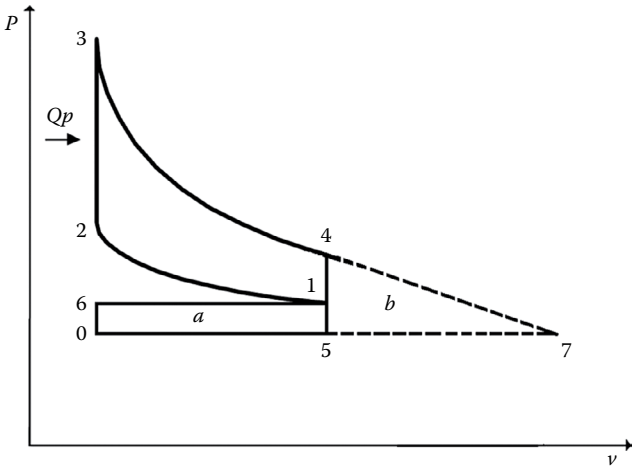


FIGURE 6.18
P–v diagram for Super/Turbo-charger.

Hence to get the net indicated power (P_i), the power represented by pumping loop is to be added:

$$P_i = \text{Area}(1-2-3-4) + \text{Area}(0-6-1-5) \tag{6.40}$$

The power required for driving the supercharger can be calculated by considering flow in as an adiabatic steady flow. The air enters the compressor at a pressure, temperature, and enthalpy (P_0, T_0, h_0). The work supplied to the supercharger is (w). The air leaves the supercharger at a pressure, temperature, and enthalpy (P_1, T_1, h_1). From Figure 6.19, the work is calculated as

$$w = h_1 - h_0 = C_p(T_1 - T_0) = \frac{C_p T_0}{\eta_s}\left[\left(\frac{P_1}{P_0}\right)^{\gamma-1/\gamma} - 1\right] \tag{6.41a}$$

where η_s is the efficiency of supercharger. The power required to drive the supercharger is then equal to;

$$P_{supercharger} = \dot{m}_a C_p(T_1 - T_0) = \frac{\dot{m}_a C_p T_0}{\eta_s}\left[\left(\frac{P_1}{P_0}\right)^{\gamma-1/\gamma} - 1\right] \tag{6.41b}$$

Assuming a mechanical efficiency for coupling between supercharger and piston engine (η_m), then the power extracted from engine to drive the supercharger is

$$P_{supercharger} = \frac{\dot{m}_a C_p T_0}{\eta_s \times \eta_m}\left[\left(\frac{P_1}{P_0}\right)^{\gamma-1/\gamma} - 1\right] \tag{6.41c}$$

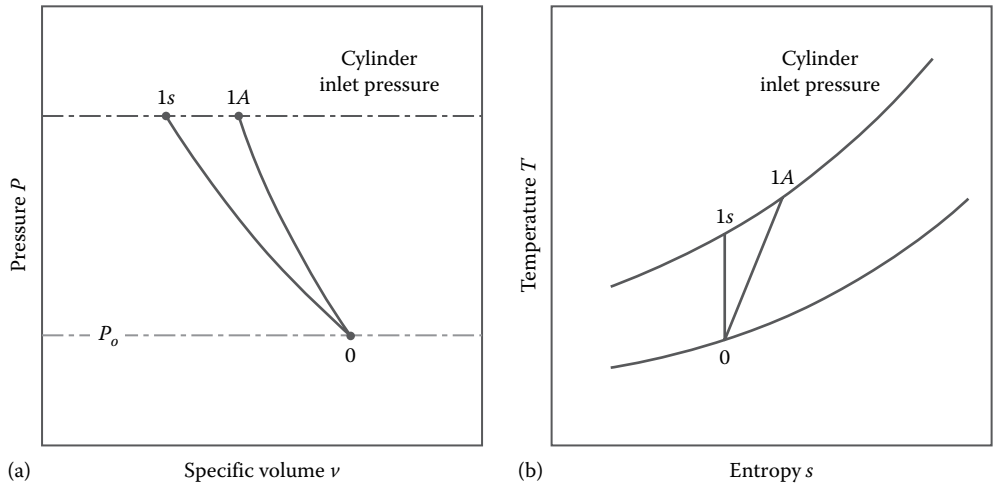


FIGURE 6.19
Compression process in compressor of super/turbo-charger. (a) *P–v* diagram and (b) *T–S* diagram.

Example 6.3

A four-stroke diesel engine of 3000 cc develops 15.0 kW/m³ of free air induced per minute. When running at 3600 rev/min, it has a volumetric efficiency of 90% when referred to free air conditions of 1.01 bar and 25°C. A supercharger is added to boost the engine power. It has a pressure ratio of 1.75 and an isentropic efficiency of 80%, and the overall mechanical efficiency is at 80%.

Assuming that, at the end of induction, the cylinders contain a volume of charge equal to the swept volume, at the pressure and temperature of the delivery from the blower, calculate

1. The increase in indicated and brake powers
2. Recalculate for altitudes of 3, 6, and 9 km
3. Plot the increase in indicated and brake powers versus altitude

Solution

1. *Sea-level conditions*

Swept volume $V_s \equiv V_1 = 3000 \times \dfrac{3600}{2} = 5.4 \times 10^6 \text{ cm}^3/\text{min} = 5.4 \text{ m}^3/\text{min}$

From Equation 6.33a, the rate of naturally aspirated induced air volume ($\dot{V}_a$) is

$$\dot{V}_a = V_s \times \eta_V = 5.4 \times 0.9 = 4.86 \text{ m}^3/\text{min}$$

Supercharger

Inlet conditions of 1.01 bar and 25°C = 25 + 273 = 298 K

Exit pressure $P_1 = 1.75 \times 1.01 = 1.7675$ bar

Exit temperature $T_1 = T_0\left(1 + \dfrac{\pi_s^{\gamma-1/\gamma} - 1}{\eta_s}\right) = 298\left(1 + \dfrac{1.75^{0.286} - 1}{0.8}\right) = 362.7 \text{ K}$

The process in the compressor is governed by the relation

$$\frac{P_1 V_1}{T_1} = \frac{P_0 V_0}{T_0}$$

Using the rate of volume flow instead, the above relation can be expressed as

$$\frac{P_1V_1}{T_1} = \frac{P_0V_0}{T_0}$$

Thus, $V_0 = \dfrac{\pi_s \times T_0 \times V_1}{T_1} = \dfrac{1.75 \times 298 \times 5.4}{362.7} = 7.76\ \text{m}^3/\text{min}.$

The inlet air flow rate into the supercharger is 7.76 m^3/min at pressure = 1.01 bar and temperature 25°C.

The increase in indicated power $(\Delta P)_i$ due to increased induction pressure is

$$(\Delta P)_i = \frac{(P_1 - P_0) \times V_s}{60} = \frac{(1.7675 - 1.01) \times 100 \times 5.4}{60} = 6.8175\ \text{kW}$$

The increase in brake power $(\Delta P)_b$ due to increased induction pressure is

$$(\Delta P)_b = (\Delta P)_i \times \eta_m = 6.8175 \times 0.8 = 5.454\ \text{kW}$$

Increase in induced air volume = 7.76 – 4.86 = 2.9 m^3/min

Increase in power due to induced air = 15 × 2.9 = 43.5 kW

The mass of air delivered by the supercharger is

$$\dot{m}_a = \frac{P_1V_1}{RT_1} = \frac{1.7675 \times 10^5 \times 5.4}{287 \times 362.7} = 9.17\ \text{kg/min}$$

The power extracted to drive the supercharger is, then, as shown in Equation 6.41c:

$$(\Delta P)_{supercharger} = \dot{m}_a \frac{C_p(T_1 - T_0)}{\eta_m} = \frac{9.17 \times 1.005 \times (362.7 - 298)}{0.8 \times 60} = 12.422\ \text{kW}$$

Net increase in indicated power = 43.5 + 6.8175 – 12.422 = 37.8955 kW

Net increase in brake power = 43.5 + 5.454 – 12.422 = 36.532 kW

Net power for original engine (without supercharger) = 15 × 4.86 = 72.9 kW

2. *Altitudes*

The above procedure is followed and the results of calculations are listed in Table 6.5. Moreover, the power gained (both indicated and brake) is plotted in Figure 6.20. A plot for the increase in indicated and brake powers versus altitude is given in Figure 6.20.

TABLE 6.5

Variation of Power versus Altitude

Altitude (km)	$V_s \equiv V_1$ (m^3/min)	P_1 (bar)	T_1 (K)	$\dot{m}_a$ (kg/min)	Net Increase in Indicated Power (kW)	Net Increase in Brake Power (kW)
0	5.4	1.768	362.7	9.17	37.90	36.53
3	5.4	1.225	326.7	7.06	39.63	38.68
6	5.4	0.823	303.0	5.11	40.90	40.27
9	5.4	0.543	279.2	3.66	41.79	41.37

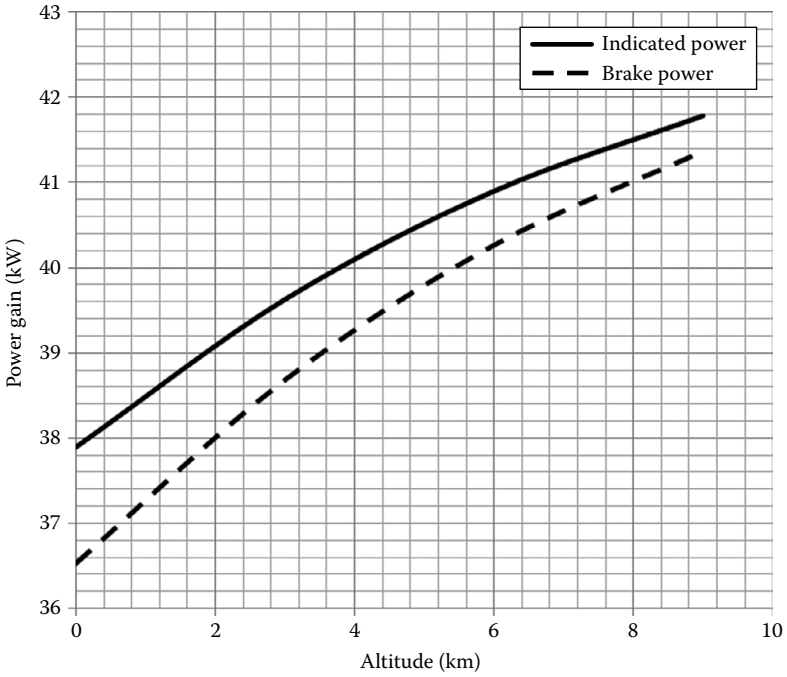


FIGURE 6.20
Power gain by supercharger at different altitudes.

6.3 Aircraft Propellers

6.3.1 Introduction

Aircraft propellers or *airscrews* convert rotary motion from piston engines or turboprops to provide propulsive force (Figure 6.21). Figure 6.21a illustrates a propeller installed in conjunction with a piston engine, while Figure 6.21b illustrates a propeller fitted with a turboprop engine.

Propellers may be of fixed or variable pitch. In both cases, the propeller accelerates a large quantity of air through a small velocity change. In turboprop engines, 80%–90% of the thrust is produced by a turbine-driven propeller and 10%–20% by the jet. In piston engines, propellers produce 100% of the thrust force.

There are several definitions for propellers:

- A device having a central revolving hub with radiating blades, for *propelling* an airplane, ship, etc. [7]
- A device consisting of a set of two or more twisted, airfoil-shaped blades mounted around a shaft and spun to provide propulsion of a vehicle through air or water
- A type of fan that transmits power by converting rotational motion from a piston engine or turboprops into thrust to pull or push the airplane through the air
- A series of rotating wings (or airfoils) of equal length meeting at a central hub attached to the crankshaft of an aircraft engine

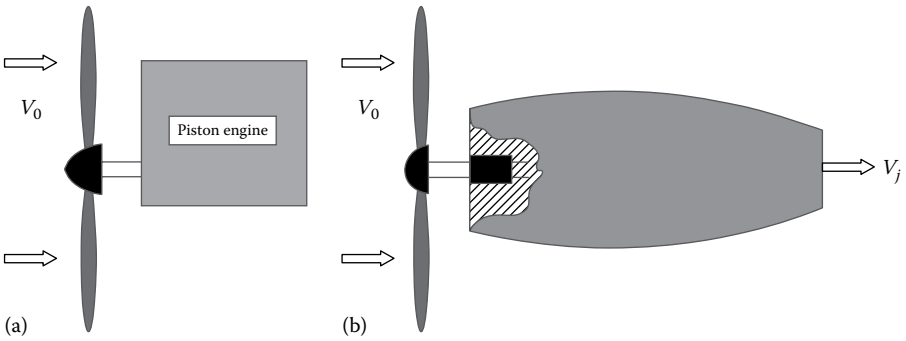


FIGURE 6.21
Propeller installed in conjunction with (a) a piston engine (b) a turboprop engine.

In brief, the history of propellers has the following important milestones:

1. In the third century BC, the Greek scientist Archimedes figured out how to enclose a long spiral screw inside a cylinder to lift water.
2. In the sixteenth century, Leonardo da Vinci sketched an upward-facing screw propeller on his design for a helicopter, which he never built.
3. John Fitch, in 1796, made the first basic propeller, shaped like a screw, for a steamboat.
4. In 1836, Francis Petit-Smith and John Ericsson independently developed modern-style propellers with blades for ships.
5. In 1903, the Wright brothers designed and manufactured twisted propellers to make possible the first powered flight.
6. In 1919, fixed pitch propellers entered service.
7. In 1924, the constant speed propeller was patented by H. S. Hele-Shaw and T. E. Beacham.
8. In 1932, variable pitch propellers were introduced into air force service.
9. In 1935, constant speed propellers became available.
10. In 1945, five-blade propellers were installed to Rolls-Royce RB50 Trent turboprop engines to power the Gloster Meteor, the first British jet fighter.
11. In 1980, high speed propellers were tested by NASA for propfans to power transport aircraft.

The cross-section of a propeller blade is a typical airfoil section; Figure 6.22 shows two views and various cross-sections of a propeller blade. The blade shank is that the portion of the blade that is near the butt of the blade. It is usually thick to give it strength, and it is cylindrica1 where it fits the hub barrel, but the cylindrical portion of the shank contributes little or nothing to thrust. In an attempt to obtain more thrust, some propeller blades are designed so that the airfoil section (shape) is carried all the way along the blade from the tip to the hub.

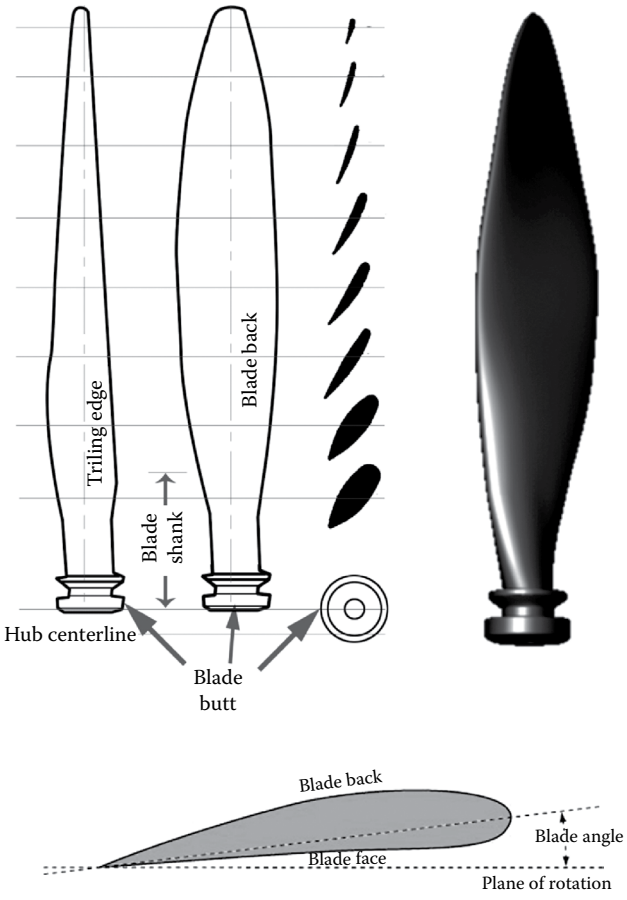


FIGURE 6.22
Cross-sections of a propeller.

6.3.2 Classifications

This section identifies classifications for propellers based on a variety of points. It is important to state here that the classifications listed here are applied to both piston engines and turboprop engines. Classifications will be followed hereafter based on various considerations.

6.3.2.1 Source of Power

As seen in Figure 6.21, a propeller may be either driven by

- Piston engines (crankshaft of a piston engine)
- Turboprops (turbine shaft of a turboprop engine)

6.3.2.2 Material

- *Wood* (solid or laminated)
  Very early types were used exclusively on personal and business aircraft prior to World War II

- *Metal* (later types)
  After 1940, propellers were made of steel but recent propellers have been fabricated from high-strength, heat-treated, aluminum alloy. Metal propellers have thinner.
- *Composite materials* (most modern designs)
  In the 1960s, glass and fiber polymer composite propeller materials were used for manufacturing propellers. Today, nearly all the large propellers for aircrafts have carbon fiber blades (Lockheed Hercules C-130J). These are light-weight, have high specific strength, rigidity, and excellent fatigue resistance. Also, carbon fiber is three times more resistant to erosion than aluminum alloys [8].

6.3.2.3 Coupling to the Output Shaft

Two methods are available by which to couple a propeller to the output shaft (see Figure 6.23):

- Direct coupling
- Through a reduction unit

6.3.2.4 Control

Two principal designs of propeller are used: fixed and variable pitch.

1. *Fixed pitch*: Blades are fixed at a specific fixed angle to the hub; this usually never changes (it can be altered on the ground only and not during flight). The Wright

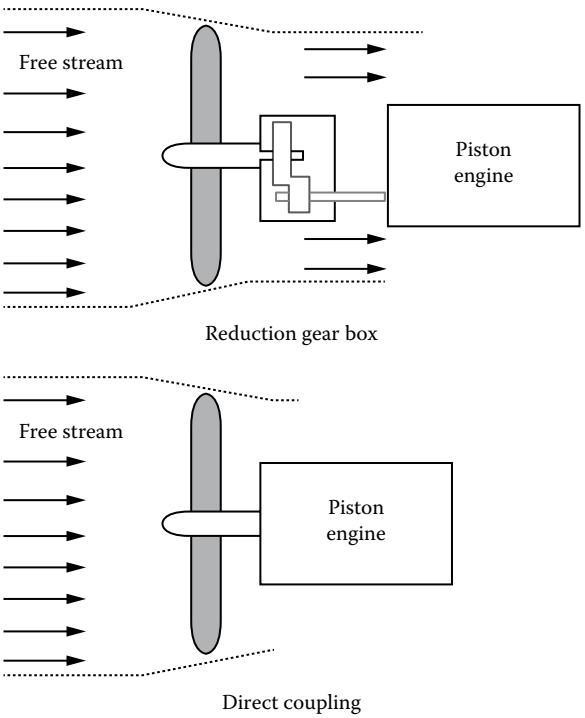


FIGURE 6.23
Coupling between propeller and engine.

brothers developed the first successful fixed pitch propellers, and this design is still employed in small aircraft.

2. *Variable pitch*: Variable pitch propellers are used in larger and more sophisticated planes. Blades may be rotated about a long axis. This classification may be further categorized into two-position propellers and adjustable pitch propellers.
   a. *Two-position propeller*
   Blades are limited to two angles, one for takeoff and climb (low-speed operation) and the other for cruising (high-speed operation)
   b. *Adjustable pitch* (blades whose pitch can be altered by the pilot)
   Controllable pitch has an automatic mechanism to adjust the pitch to match the plane's flying speed. Such adjustable pitch propellers are seen in the following types:
      i. *Constant-speed* (designed to change pitch automatically, allowing the engine always to turn over at a constant speed)
      ii. *Feathered* (turning the propeller blades so they are edgeways on, making a very shallow angle to the oncoming air, minimizing air resistance). On single-engine aircraft, the effect is to increase the gliding distance. On a multi-engine aircraft, feathering the propeller on a failed engine allows the aircraft to maintain altitude with the reduced power from the remaining engines.
      iii. *Thrust reversal* (the pitch of the blades can be reversed so a propeller makes a forward draft of air instead of one moving backwards—handy for extra braking (especially, if the main brakes on the wheels suddenly fail).

6.3.2.5 Number of Propellers Coupled to Each Engine

- Single (Figure 6.21)
- Double (contra-rotating) (Figure 6.24)



FIGURE 6.24
Contra-rotating propellers on a Rolls-Royce–Griffon–powered P-51 unlimited racer.

Contra-rotating propellers, also referred to as *coaxial contra-rotating propellers* or *high-speed propellers*, apply the maximum power of an engine (or engines) to drive two propellers one behind the other about the same axis in opposite directions.

6.3.2.6 Direction of Rotation

1. Nose installation (single engine)
   a. Left-handed propeller, which, when viewed from the cockpit, rotates in an anti-clockwise direction
   b. Right-handed propeller, which rotates clockwise when viewed from the cockpit
2. Wing installation (even number of engines; two, four, six, and so on)
   a. All propellers may have same direction of rotation (for both wings)
   b. Counter-rotating (the right wing has clockwise propeller rotation and the left wing has counter-clockwise propeller rotation, or vice versa). The advantage of such designs is that counter-rotating propellers balance the effects of torque and p-factor.
   c. Counter-rotating pairs on each wing (Airbus A400M Atlas)

The two propellers on each wing of the A400M, shown in Figure 6.25, rotate in opposite directions, with the tips of the propellers advancing from above toward the midpoint between the two engines. The Wright Flyer had a single engine and a chain to drive its two propellers in counter-rotational directions.

The following twin-engine aircrafts (one engine per wing) have counter-rotating propellers: the de Havilland Hornet, Lockheed P-38 Lightning, Henschel Hs 129, Piper PA-31 Navajo, Piper PA-34 Seneca, Piper PA-39 Twin Comanche C/R, Piper PA-40 Arapaho, and Piper PA-44 Seminole.

The Messerschmitt Me 323 was powered by six engines, three on each wing. All engines in each wing rotated in the same direction and opposite to those on the other wing.

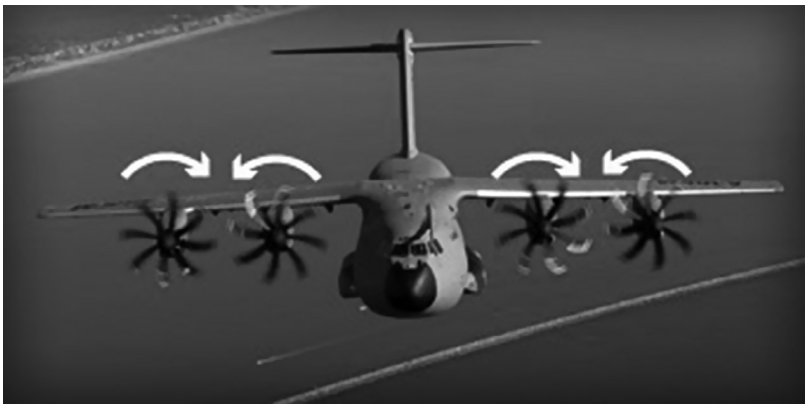


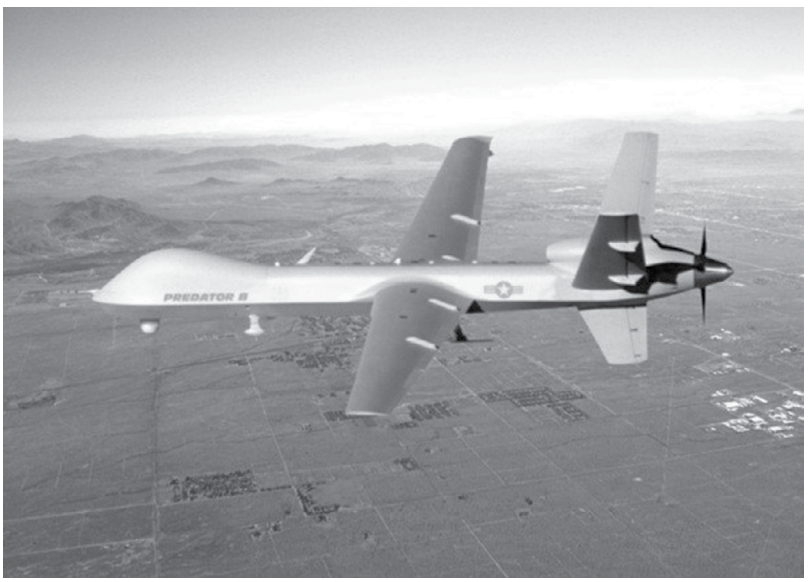
FIGURE 6.25
Airbus A400 M aircraft (pair of propellers on each wing turn in opposite directions).

6.3.2.7 Propulsion Method

- Pusher (Figure 6.26)
- Puller (tractor) (Figure 6.27)
- Combination of the pusher and puller types mounted in-line on a small aircraft (refer to Burton [10]), as shown in Figure 6.28



(a)



(b)

FIGURE 6.26
Pusher propeller (a) Piaggio P-180 Avanti Rennes and (b) An AUV.



FIGURE 6.27
Puller propeller installed to Antonov An-140-100 aircraft.

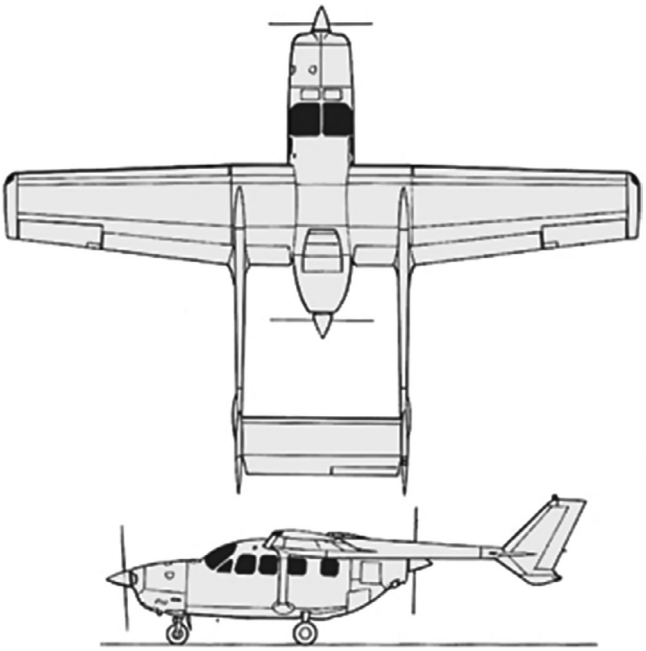


FIGURE 6.28
Combination of puller-pusher layout (Cessna 337 Skymaster).

6.3.2.8 Number of Blades

One has the option of setting the number of blades (B) for a given application. While there are only two blades to choose from, one can presently go as high as around eight blades at the high-performance end for an unducted propeller.

- Two
- Three
- Four
- Six
- Eight

Multiple (greater than four, as an example: Eight-bladed Hamilton Sundstrand NP2000).

6.3.3 Aerodynamic Design

Aerodynamic developments in propellers started with the simple Rankine-Froude momentum theory. Next, blade element theories provided more realistic results and lead to practical propeller design calculations. Initially, lumped inflow factors (see Glauert [9]) are used to evaluate flow velocities around a blade element.

This section will only deal with actuator disk and blade element theories. For more advanced work, the reader can review the work of Bocci [11]. Detailed descriptions for advanced methods are highlighted by Archer and Saarlas [12]. There is also interest in transonic and supersonic propellers, but shock-wave losses and noise present severe problems.

6.3.3.1 Axial Momentum (or Actuator Disk) Theory

Actuator disk theory is also sometimes known as *Rankine-Froude* or *slip stream* theory (1865). The actuator disk theory replaces the propeller with an infinitely thin plane "actuator" disk, which imparts a certain momentum to the fluid passing through it, thus produces an increase in axial velocity and axial momentum (Figure 6.29). This theory provides an initial idea regarding the performance of a propeller (say, efficiency) but fails to furnish the required design data for the propeller blades.

The following assumptions and definitions are stated:

- Fluid is one dimensional, perfect, incompressible, and isentropic.
- Flow has uniform properties (velocity and pressure) across any plane normal to the flow except for the discontinuous jump in pressure across the disk itself.
- Rotation imparted to the flow is ignored.
- The streamlines at the edge of the disk define the outer limit of the contracting streamtube, which passes through the disk and separates it from the surrounding flow. The streamtube has cylindrical sections both far upstream and far downstream.
- The flow outside the propeller streamtube has constant stagnation pressure (no work is imparted to it).

Figure 6.29 illustrates fluid streamlines, velocities, and pressures around the plane of the propeller with the following designations for points: (1) far upstream of the propeller,

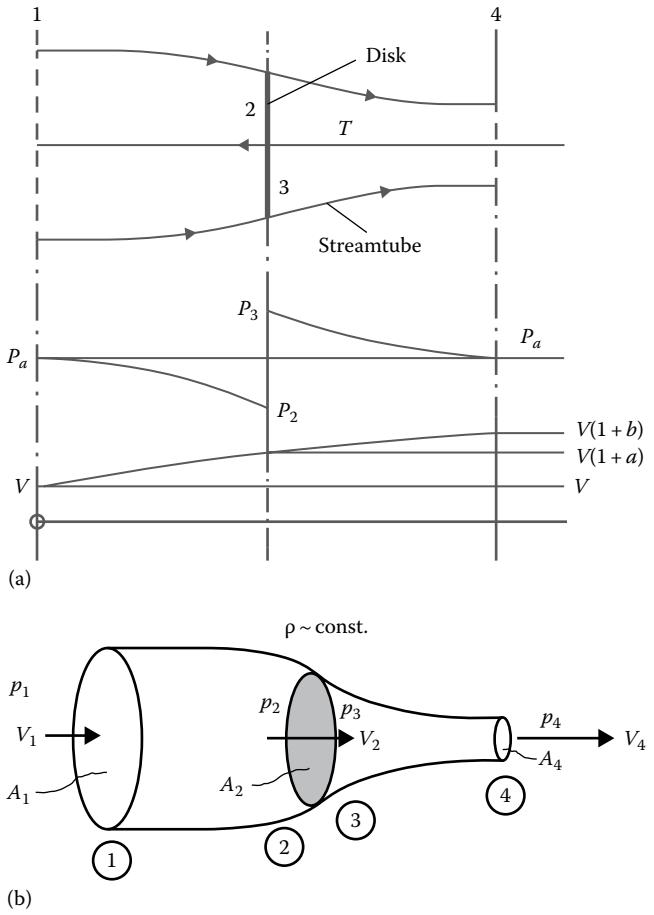


FIGURE 6.29
(a) Actuator disk—pressure and velocity distribution, (b) Actuator disk in physical plan and its pressure and velocity distribution.

(2) just in front of the propeller, (3) just after the propeller, and (4) far downstream of the propeller. The distance between (2) and (3) is assumed to be infinitesimal.

Along the streamtube between stations 1 and 4, the velocity increases from the free upstream value V_1, at cross-sectional area A_1, to the value V_4 in the cross-sectional area A_4. The static pressure at stations 1 and 4 is the ambient atmospheric value P_a ($P_1 = P_4 = P_a$), while pressure difference builds up across the disc.

The velocity at the disk, $V_2 = V_3$, is written as $V_2 = V_1(1+a)$, where $aV_1 = V_2 - V_1$ is the increase in velocity through the disk and a is called the *axial inflow factor*.

In the fully developed slipstream, the velocity $V_4 = V_1(1+b)$, where $bV_1 = V_4 - V_1$ is the increase in velocity there and b is called the *slipstream factor*. So

$$a = \frac{V_2 - V_1}{V_1} \tag{6.42}$$

and

$$b = \frac{V_4 - V_1}{V_1} \tag{6.43}$$

1. Thrust
   Apply Newton's second law of motion (the principle of the conservation of momentum) in the axial flow direction to the control region between stations 1 and 4 (Figure 6.29). The thrust (T) is simply the rate of increase of momentum of the airflow in the downstream direction

$$T = \dot{m}\left(V_4 - V_1\right) \tag{6.44}$$

Dropping the subscript (1) on the free-stream velocity, put $V = V_1$

$$T = \dot{m}\left[V\left(1+b\right) - V\right] = \dot{m}bV \tag{6.45}$$

where $\dot{m}$ is the mass flow through the actuator disk, and

$$\dot{m} = \rho A V_2 = \rho A V\left(1+a\right) \tag{6.46}$$

Equations 6.44 through 6.46 give

$$T = \rho A V_2\left(V_4 - V_1\right) = \rho A V^2\left(1+a\right)b \tag{6.47}$$

Force balance across the disk requires that

$$T = A\Delta p \tag{6.48}$$

where, from Figure 6.35

$$\Delta p = p_3 - p_2 \tag{6.49}$$

Eliminating (T) from Equations 6.47 and 6.48 gives

$$\Delta p = \rho V^2\left(1+a\right)b \tag{6.50}$$

Since the flow is assumed incompressible, then Bernoulli's equation applied between stations (1) and (2) yields

$$p_a + \frac{1}{2}\rho V^2 = p_2 + \frac{1}{2}\rho V^2\left(1+a\right)^2$$

Applying Bernoulli's equation also between stations (3) and (4) yields

$$p_3 + \frac{1}{2}\rho V^2 (1+a)^2 = p_a + \frac{1}{2}\rho V^2 (1+b)^2$$

So

$$p_3 - p_2 = \Delta p = \frac{1}{2}\rho V^2 (1+b)^2 - \frac{1}{2}\rho V^2$$

or

$$\Delta p = \rho V^2 b\left(1 + \frac{b}{2}\right) \tag{6.51}$$

Eliminating (Δp) from Equations 6.50 and 6.51 gives

$$1 + a = 1 + \frac{b}{2}$$

thus

$$a = \frac{b}{2} \quad \text{or} \quad b = 2a \tag{6.52}$$

From Equations 6.42 and 6.43, it is easy to prove that

$$V_2 = \frac{V_1 + V_4}{2} \tag{6.53a}$$

Moreover, at zero forward speed ($V = V_1 = 0$), then $(V_4 = 2V_2)_{V=0}$

This simple but important result means that at any speed, including zero, one half of the final increase in velocity in the slipstream has already occurred at the rotor disk itself. Using Equations 6.47 and 6.52, the following relations between thrust and the inflow factor (a), or the slipstream factor (b), can be derived:

$$T = \rho A V^2 (1+a) 2a = \rho A V^2 \left(1 + \frac{b}{2}\right) b \tag{6.54}$$

Equation 6.54 is quadratic in the parameters (a) or (b), which have the solutions

$$a = -\frac{1}{2} \pm \sqrt{\left(\frac{1}{2}\right)^2 + \frac{T}{2\rho A V^2}} \tag{6.55a}$$

Denoting, $v = aV$, where (v) is the induced velocity at the propeller (disk), then

$$v = aV = -\frac{V}{2} \pm \sqrt{\left(\frac{V}{2}\right)^2 + \frac{T}{2\rho A}} \tag{6.55b}$$

Moreover

$$b = -1 \pm \sqrt{1 + \frac{2T}{\rho A V^2}} \tag{6.55c}$$

Denoting $w = bV$, where (w) is the induced velocity far downstream the propeller (disk), then

$$w = bV = -V \pm \sqrt{(V)^2 + \frac{2T}{\rho A}} \tag{6.55d}$$

2. Propulsive efficiency
The propulsive efficiency (η_p) of a propeller is the ratio of the available power; this is also sometimes identified as useful thrust power ($P_A = TV$) to the power delivered to the propeller. For piston engines, this is the shaft brake power (P)

$$\eta_p = \frac{P_A}{P} = \frac{TV}{P} \tag{6.56}$$

For the actuator disk model, this efficiency is an ideal propulsive efficiency because it ignores all losses except that associated with the streamwise kinetic energy. Using Equations 6.52 and 6.54 gives

$$\text{Useful thrust power} = TV = \rho A V^3 (1+a)(2a) \tag{6.57}$$

Power expended on the air = P = rate of change of kinetic energy

$$\begin{aligned} P &= \frac{1}{2}\dot{m}\left[V^2(1+b)^2 - V^2\right] \\ P &= \rho A V^3 (1+a)^2 (2a) \end{aligned} \tag{6.58}$$

The ratio of these two powers, seen in Equations 6.57 and 6.58, for the ideal actuator disk model is called the ideal *Froude* efficiency (η_F) and is therefore the upper limit to propeller performance

$$\eta_F = \frac{1}{1+a} = \frac{V_1}{V_2} = \frac{V}{V+v} \tag{6.59}$$

Equation 6.59 proves that a higher efficiency of propulsion can be achieved by large rotors with a very small increase in fluid velocity (achieving thrust by means of large surfaces rather than velocity) [13]. The ideal Froude efficiency (η_F) is always greater than the actual propulsive efficiency (η_P).

Example 6.4

An internal combustion engine drives a propeller. The propeller has a diameter of 2.0 m and discharges air at a rate of 360 kg/s. The aircraft flight speed is 80.0 m/s. Determine the thrust, ideal, and actual power of the propeller, the Froude efficiency, and the pressure rise across the propeller. Assume air density to be 1.225 kg/m^3.

Solution

Given data: $V_1 = 80$ m/s, $\rho = 1.225$ kg/m^3

Velocity at propeller plane $V_2 = \dfrac{\dot{m}}{\rho A} = \dfrac{4\dot{m}}{\rho \pi D^2} = \dfrac{4 \times 360}{1.225 \times \pi \times (2)^2} = 93.54$ m/s

Since $V_2 = \dfrac{V_1 + V_4}{2}$, then

$$V_4 = 2V_2 - V_1 = 107.08 \text{ m/s}$$

Thrust force $T = \rho A V_2 (V_4 - V_1) = 9{,}748$ N $= 9.75$ kN
Ideal power $P_{ideal} = T \times V_2 = 9.748 \times 93.54 = 911.83$ kW
Actual power $P_{actual} = T \times V_1 = 9.748 \times 80.0 = 779.84$ kW
Froude efficiency

$$\eta_F = \frac{P_{actual}}{P_{ideal}} = \frac{V_1}{V_2} = \frac{80}{93.54} = 0.855 \equiv 85.5\%$$

Since thrust $T = A\Delta p$, then the pressure rise across propeller is

$$\Delta p = \frac{T}{A} = \frac{T}{\pi R^2} = \frac{9.75}{\pi \times 1} = 3.104 \text{ kPa}$$

6.3.3.2 Modified Momentum or Simple Vortex Model

A practical assessment of propeller performance and the design of realistic propellers requires inclusion of at least some of the foregoing effects and allowance for blading details. In this simple vortex model, the effect of rotational flow will be discussed.

Consider a streamtube that passes through the propeller section at radius (r) (Figure 6.30). The corresponding angular speed at this blade section is Ωr where Ω is the angular speed of the propeller and r is the local radius of the propeller. When fluid passes through the propeller section, it acquires an angular speed due to the swirling nature of the flow induced by the propeller. Thus, the rotational speeds at propeller sections are

$$u = a_\Omega \Omega r \tag{6.60}$$

where a_Ω is the angular induced factor.

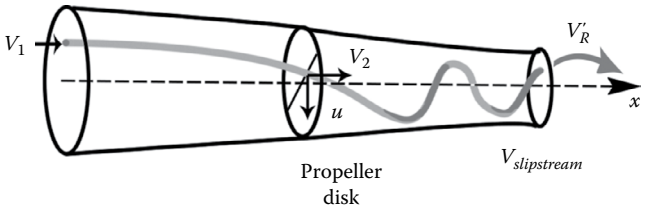


FIGURE 6.30
Modified actuator disk.

The local flow velocity just downstream of the propeller blade is expressed as

$$V_R = \sqrt{V_2^2 + u^2} = \sqrt{V_1^2(1+a)^2 + (a_\Omega \Omega r)^2}$$

The local flow velocity far downstream of the propeller is expressed as

$$V_R' = \sqrt{V_4^2 + u^2} = \sqrt{V_1^2(1+b)^2 + (a_\Omega \Omega r)^2}$$

The local propulsive efficiency at any radius, r, based on modified momentum theory η_{mm}, is defined as

$$\eta_{mm} = \frac{T \times V_1}{T \times V_1 + (KE)_{Losses}} = \frac{\dot{m}(V_4 - V_1) \times V_1}{\dot{m}(V_4 - V_1) \times V_1 + \frac{1}{2}\dot{m}(b^2 V_1^2 + u^2)} = \frac{bV_1^2}{bV_1^2 + \frac{b^2 V_1^2 + u^2}{2}}$$

$$\eta_{mm} = \frac{1}{1 + \frac{b}{2} + \frac{u^2}{2bV_1^2}} = \frac{1}{1 + a + \frac{u^2}{4aV_1^2}} \tag{6.61}$$

$$\eta_{mm} = \frac{1}{1 + a + \frac{a_\Omega^2 \Omega^2 r^2}{4aV_1^2}}$$

6.3.3.3 Blade Element Considerations

Blade element theory is similar to wing theory. In this theory, the blade is divided into small sections, which are handled independently of each other. Each segment has a chord, a blade angle, and associated airfoil characteristics. This isolated airfoil assumption is found to be substantially correct for two- or three-bladed propellers, except near the hub.

At any given radius, r, the circumferential distance between two successive blades is called spacing, s, while the length of blade section between the leading and trailing edges is called chord, c (see Figure 6.31). Since the s/c for two- and three-bladed propellers is much greater than unity, this justifies the use of isolated airfoil characteristics in this theory. Multi-blade propellers for which the s/c ratio has fallen to a value of the order of 1, or less, will have to be treated as cascades.

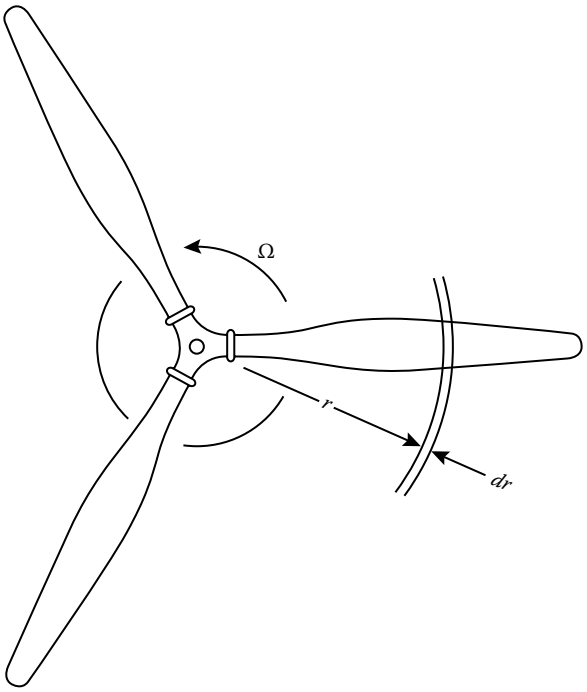


FIGURE 6.31
Blade segment in a three-bladed propeller.

The forces acting on a small section of the blade (lift and drag) are determined and then integrated over the propeller radius in order to predict the thrust, torque, and power characteristics of the propeller.

The forces acting on a small section of the blade (lift and drag) are first determined (Figure 6.32). These are then resolved into two perpendicular components in the axial and tangential directions, and are finally integrated over the propeller radius in order to predict the thrust, torque, and power characteristics of the propeller.

A differential blade element of chord, c, and width, dr, located at a radius, r, from the propeller axis, is shown in Figure 6.32a. The element is shown acting under the influence of rotational velocity $\bar{V}_t$, forward velocity $\overline{V'}$, and induced velocity, $\bar{w}$. The resultant or relative velocity, $\bar{V}_R$, is then expressed by the relation

$$\bar{V}_R = \overline{V'} + \bar{V}_t + \bar{w} \tag{6.62}$$

where the axial velocity and rotational velocities are given by

$$V' = V\left(1 + a\right) \tag{6.63}$$

and

$$V_t = \Omega r\left(1 - a_\Omega\right) \tag{6.64}$$

The relative fluid velocity varies from hub to tip, primarily under the influence of the rotational velocity component, Ωr, and the inflow factor, a. Figure 6.32 shows the velocities and

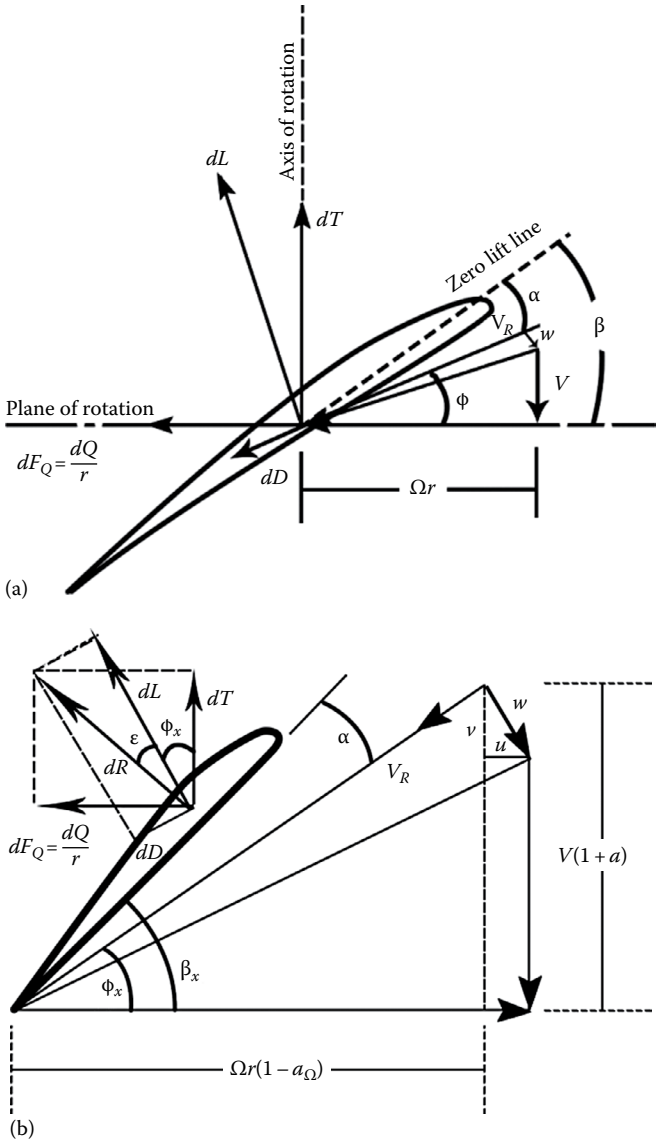


FIGURE 6.32
Blade element theory (a) Velocity components and (b) force components.

forces on a blade element that lies between radial stations r and $r+\delta r$, and whose local chord length is c. The section has a geometric pitch angle, or blade angle, β, where

$$\beta = \alpha + \phi \tag{6.65}$$

with α as the local two dimensional incidence angle (or angle of attack) and ϕ as the advance angle, given by

$$\tan\phi = \frac{V_1(1+a)}{\Omega r(1-a_\Omega)} \tag{6.66}$$

Defining the dimensionless radius, $x = r/R$, then

$$\tan\phi = \frac{V_1(1+a)}{\Omega r(1-a_\Omega)} = \frac{J(1+a)}{\pi x(1-a_\Omega)} \tag{6.67}$$

The blade angle, β, is calculated from the advance of the propeller during one revolution, known as the geometric pitch, p, as follows:

$$\tan\beta = \frac{p}{\pi D} \tag{6.68}$$

Radial pitch distribution will be specified for a given blade, but a representative *pitch* is quoted at a *reference radius* conventionally taken at either *70%* or *75% radius*. Overall solid body pitch may be varied by rotation of the blade about its radial axis.

1. Thrust and torque
   The axial and tangential forces on a blade element generate the thrust, δT, and torque, $\delta F_Q = \delta Q/r$, contributions of the blade elements and can now be written as

$$\delta T = \delta L\cos\phi - \delta D\sin\phi = (l\cos\phi - d\sin\phi)\delta r \tag{6.69}$$

$$\frac{\delta Q}{r} = \delta L\sin\phi + \delta D\cos\phi = (l\sin\phi + d\cos\phi)\delta r \tag{6.70}$$

   δL and δD are the lift and drag forces on the blade element. Introducing the definitions for lift and drag coefficients, C_l and C_d, as well as dynamic pressure, q, then the lift and drag forces per unit span length, l and d, are expressed as

$$C_l = \frac{l}{\frac{1}{2}\rho V_R^2 c}, \quad C_d = \frac{d}{\frac{1}{2}\rho V_R^2 c}, \quad \text{and} \quad q = \frac{1}{2}\rho V^2 \tag{6.71}$$

   Moreover, from Figure 6.32b the relative velocity is given by

$$V_R = \frac{V(1+a)}{\sin\phi} \tag{6.72}$$

   Introducing the relations in Equations 6.71 and 6.72 into Equations 6.69 and 6.70, and assuming the number of blades is (B), we obtain the following relations for thrust and torque gradients

$$\frac{\delta T}{\delta r} = Bcq(1+a)^2\frac{c_l\cos\phi - c_d\sin\phi}{\sin^2\phi} \tag{6.73}$$

$$\frac{\delta Q}{\delta r} = Brcq(1+a)^2\frac{c_l\sin\phi + c_d\cos\phi}{\sin^2\phi} \tag{6.74}$$

with $x = r/R$, the local solidity (σ_r), at station (r) is defined as

$$\sigma_r = \frac{Bc}{\pi r} \tag{6.75a}$$

The solidity at the propeller tip is then

$$\sigma_R = \frac{Bc}{\pi R} = x\sigma_r \tag{6.75b}$$

In the succeeding equations, the thrust force is nondimensionalized by ($\rho n^2 D^4$) to obtain the thrust coefficient, Equation 6.81, and the torque will be nondimensionalized by ($\rho n^2 D^5$) to obtain the torque coefficient (C_Q) (see Equation 6.82).

Introducing them into Equations 6.73 and 6.74 yields the following relations

$$\frac{dC_T}{dx} = \frac{\pi}{8}\sigma_R J^2 (1+a)^2 \frac{c_l \cos\phi - c_d \sin\phi}{\sin^2\phi} \tag{6.76a}$$

$$\frac{dC_Q}{dx} = \frac{\pi}{16}\sigma_R J^2 (1+a)^2 x \frac{c_l \sin\phi + c_d \cos\phi}{\sin^2\phi} \tag{6.76b}$$

The relation between the drag and lift forces on the blade element is given by

$$\tan\varepsilon = \frac{l}{d} = \frac{c_l}{c_d} \tag{6.77}$$

Introducing Equation 6.77 into Equation 6.76a and b obtains

$$\frac{dC_T}{dx} = \frac{\pi}{8}\sigma_R J^2 (1+a)^2 c_l \frac{\cot\phi - \tan\varepsilon}{\sin\phi} \tag{6.78}$$

and

$$\frac{dC_Q}{dx} = \frac{\pi}{16}\sigma_R J^2 (1+a)^2 x c_l \cot\phi \frac{\tan\phi + \tan\varepsilon}{\sin\phi} \tag{6.79}$$

Integrating Equations 6.78 and 6.79 obtains the thrust, T and torque, Q.

2. Propulsive efficiency

Propulsive efficiency for a *blade element* is defined as the ratio between useful work, $V\delta T$, to the supplied torque power, $\Omega\delta Q$, or

$$\eta_{be} = \frac{V\delta T}{\Omega\delta Q}$$

From Equations 6.67 and 6.72 , as well as Figure 6.32b, we get

$$\eta_{be} = \frac{V\delta T}{\Omega \delta Q} = \frac{1-a_\Omega}{1-a} r \quad \tan\phi \frac{\delta T}{\delta Q} = \frac{1-a_\Omega}{1-a} \quad \tan\phi \frac{\delta T}{(\delta Q/r)}$$

$$\eta_{be} = \frac{(1-a_\Omega)}{(1-a)} \quad \tan\phi \frac{c_l \cos\phi - c_d \sin\phi}{c_l \sin\phi + c_d \cos\phi} = \frac{(1-a_\Omega)}{(1-a)} \quad \tan\phi \frac{1-\tan\varepsilon \ \sin\phi}{\tan\varepsilon + \tan\phi}$$

$$\therefore \eta_{be} = \frac{(1-a_\Omega)}{(1-a)} \frac{\tan\phi}{\tan(\phi+\varepsilon)} \tag{6.80}$$

As noticed from Equation 6.80, the local propeller efficiency is dependent on the angle $\varepsilon = \tan^{-1}(c_d/c_l)$ and the interference factors, a, $a\Omega$. Figure 6.33 illustrates the variation of blade element efficiency as a function of the advance angle, ϕ, and the angle ε.

The following two cases are identified

$$\eta_{be} = 100\%$$

This is the straight line case when

$$\varepsilon = a = a_\Omega = 0$$

$$\eta_{be} = \text{variable}$$

$$\varepsilon \neq 0, \quad a \neq 0, \quad a_\Omega \neq 0$$

In this case, the blade element efficiency has the value zero when $\phi = 0$ and $\phi = 90° - \varepsilon$.

At an in-between value, the blade element efficiency acquires a maximum value, which can be obtained by differentiating Equation 6.80 with respect to ϕ and equating the differential to zero, then

$$\phi = 45° - (\varepsilon/2)$$

Several curves are obtained for different ratios of drag to lift coefficients.

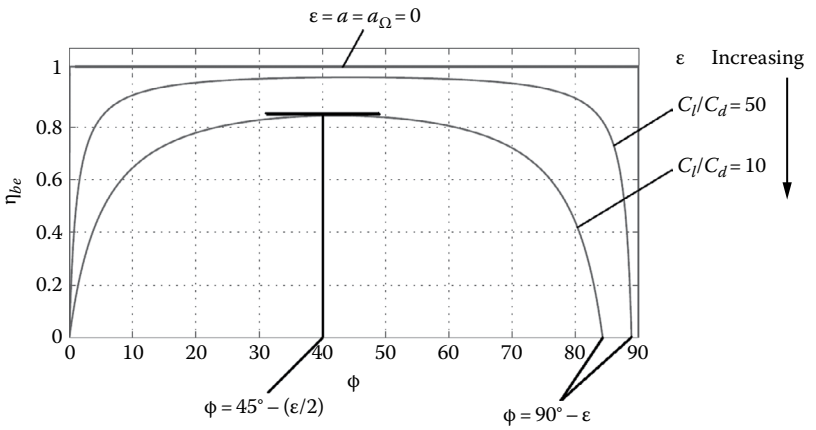


FIGURE 6.33
Variation of blade element efficiency versus the angle ϕ.

6.3.3.4 Dimensionless Parameters

There are nine independent variables needed to define the performance of a fixed-pitch propeller in subsonic flight: thrust force, torque, power, air density, compressibility, air viscosity, propeller diameter, approach speed, and rotational speed, expressed by the variables $T, Q, P, \rho, \beta, \mu, D, V, n$, respectively. From these nine variables, and with the three fundamental units of mass, M, length, L, and time, T, using dimensional analysis we get six (6 = 9–3) dimensionless groups or parameters. These are

$$1.\ \text{Thrust coefficient: } C_T = \frac{T}{\rho n^2 D^4} \quad \text{or} \quad T_c = \frac{T}{\rho V^2 D^2} \tag{6.81}$$

$$2.\ \text{Torque coefficient: } C_Q = \frac{Q}{\rho n^2 D^5} \quad \text{or} \quad Q_c = \frac{Q}{\rho V^2 D^5} \tag{6.82}$$

$$3.\ \text{Power coefficient: } C_P = \frac{P}{\rho n^3 D^5} \tag{6.83a}$$

A relation between power and torque coefficients can be derived as follows:

$$C_P = \frac{P}{\rho n^3 D^5} = \frac{2\pi n Q}{\rho n^3 D^5} = 2\pi C_Q \tag{6.83b}$$

$$4.\ \text{Advance ratio (or speed coefficient): } J = \frac{V}{nD}$$

$$5.\ \text{Reynolds number: } R_e = \frac{VD\rho}{\mu}$$

$$6.\ \text{Mach number: } M = \frac{V}{a} \equiv \frac{V}{\sqrt{\gamma RT}} \tag{6.84}$$

The first four dimensionless quantities are correlated by the following relations

$$C_T = T_c J^2 \tag{6.85a}$$

and

$$C_Q = Q_c J^2 \tag{6.85b}$$

Another important dimensionless quantity is the *speed power coefficient*, denoted sometimes as C_S and sometimes as C_{P_S}, which is defined as

$$C_S = \left(\frac{\rho V^5}{P n^2} \right)^{1/5} \tag{6.86a}$$

or

$$C_S^5 = \frac{\rho V^5}{Pn^2} = \frac{\rho n^3 D^5}{P}\frac{V^5}{n^5 D^5} = \frac{J^5}{C_P}$$

$$C_S = \frac{J}{(C_P)^{1/5}} \tag{6.86b}$$

As noted from Equation 6.86a and b, the speed power coefficient eliminates the propeller diameter, D. Now, back to Equation 6.55a and c: using Equation 6.81, we can express the factors a and b by the relation

$$b = 2a = -1 \pm \sqrt{1 + \frac{8}{\pi} T_c} \tag{6.87}$$

The actual propulsive efficiency can be expressed in terms of the thrust and power coefficients, Equations 6.81 and 6.83b

$$\eta_p = \frac{TV}{P} = \frac{TV}{\Omega Q} = \frac{JC_T}{2\pi C_Q} = \frac{JC_T}{C_P} \tag{6.88}$$

As discussed earlier, the maximum value of ideal Froude efficiencies, η_F, is 100%, while the peak for the actual propulsive efficiency of propellers, Equation 6.88, is much less than this value. This is due to the ignored losses in the ideal actuator disk model arising from:

- Rotational flow (whirl) about the rotor axis in the wake
- Profile drag (viscous friction and form drag) of the flow over the propeller blades—near the high-speed zero-thrust condition, profile drag is dominant (Glauert [9])
- Interference effects in the hub region between multiple blades and the nacelle
- Compressibility effects (shock waves and shock/boundary layer interaction)—lateral components of incoming flow that occur when a propeller is yawed

Two other important parameters relevant to propeller power are power loading and the activity factor, defined as

Power loading (*PL*)

$$PL = \frac{P}{D^2} = \frac{C_P \rho n^3 D^5}{D^2} = \frac{C_P}{J^3}\rho V^3 \tag{6.89}$$

Activity factor (*AF*)

$$AF = 10^5 \int_{root}^{tip} \left[\frac{c}{D}\left(\frac{r}{D}\right)^3\right] d\left(\frac{r}{D}\right) \tag{6.90}$$

Both of these are a measure of power absorption by the propeller and are used to compare the performance of different propeller designs. *PL* is a simple disk loading, whereas the *AF* is designed to express the capacity of a blade to absorb power. *AF* is dimensionless, with a value of about 80% per blade.

Example 6.5

A four-bladed propeller has the following data:

- Generated power = 3000 hp
- Sea-level conditions
- Relative tip speed = 320 m/s
- Flight speed = 75 m/s
- The blade section has a lift and drag coefficients equal, respectively, to 0.85 and 0.0425

Calculate

1. Rotational speed of tip
2. Thrust and torque coefficients
3. Propeller efficiency
4. Rotational speed
5. Propeller diameter
6. Reference blade chord

For a preliminary analysis assume that

- The blade has a constant chord equal to the reference chord (c_{ref}) where $c_{ref} = 0.06D$ and D is the propeller diameter
- $a = a_\Omega = 0$
- Ignore the drag coefficient

Solution

From the velocity triangle at tip section, the relative speed at the tip is related to the flight speed and rotational speed by the following relation (Figure 6.34).

$$V_R^2 = U_t^2 + V^2, \text{thus } U_t = \sqrt{V_R^2 - V^2}$$

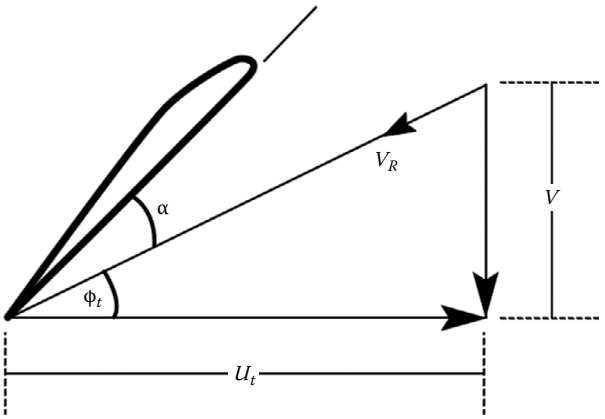


FIGURE 6.34
Velocity triangle.

With $V_R = 320$ m/s and a flight speed of 75 m/s, then the rotational speed of the tip is

$$U_t = 311 \text{ m/s},$$
$$nD = U_t/\pi = 99 \text{ m/s}$$

$$J = V/nD = 0.76, \quad \text{since } a = a_\Omega = 0$$

Then

$$\phi_t = \tan^{-1}\left(V/U_t\right) = 14°$$

Ignoring the drag coefficient, then, for ($a = 0$), the thrust coefficient (Equation 6.78) and the torque coefficient (Equation 6.79) are reduced to

$$\frac{dC_T}{dx} = \frac{\pi}{8}\sigma_R J^2 \frac{c_l}{\sin\phi\tan\phi}$$
$$\frac{dC_Q}{dx} = \frac{\pi}{16}\sigma_R J^2 x \frac{c_l}{\sin\phi}$$

Now, since

$$\sigma_R = \frac{Bc}{\pi R} = \frac{2Bc_{ref}}{\pi\times(2R)} = \frac{2B\left(c_{ref}/D\right)}{\pi} = \frac{2\times 4\times 0.06}{\pi} = \frac{0.48}{\pi}$$

$$\therefore \frac{dC_T}{dx} = \frac{\pi}{8}\sigma_R J^2 \frac{c_l}{\sin\phi\tan\phi} = \frac{0.051J^2}{\sin\phi\tan\phi}$$

Thus, at any radius along the blade, with $c_l = 0.85$ and $J = 0.76$, then

$$\frac{dC_T(x)}{dx} = \frac{0.0295}{\sin\phi(x)\tan\phi(x)} \tag{a}$$

$$\frac{dC_Q(x)}{dx} = \frac{0.0147x}{\sin\phi(x)} \tag{b}$$

For the present case, the following values of $\phi(x)$, $dC_t(x)/dx$, and $dC_Q(x)/dx$ can be calculated and tabulated in Table 6.6:

$$V = 75 \text{ m/s}, \quad U_t = 311 \text{ m/s}, \quad J = 0.76, \quad \text{and} \quad \phi_t = 14°$$

$$C_t = \Sigma\left(dC_t/dx\right)\times\Delta x = 0.204$$
$$C_Q = \Sigma\left(dC_Q/dx\right)\times\Delta x = 0.024983$$

Propeller efficiency may be calculated next from Equation 6.56

$$\eta_p = \frac{TV}{P} = \frac{TV}{\Omega Q} = \frac{JC_T}{2\pi C_Q} = 0.9876$$

TABLE 6.6

Variation of Flow Parameters along Blade Span

$x(\equiv r/R)$	U (m/s)	ϕ(°)	$dC_t(x)/dx$	$dC_Q(x)/dx$
0.1	31.1	67	0.0136	0.001597
0.2	62.2	50	0.0323	0.00384
0.3	93.3	39	0.0579	0.00701
0.4	124.4	31	0.0953	0.01142
0.5	155.5	26	0.1380	0.01677
0.6	186.6	22	0.1949	0.02544
0.7	217.7	19	0.2632	0.03161
0.8	248.8	17	0.3300	0.04022
0.9	279.9	15	0.4254	0.05117
1.0	311	14	0.4891	0.06076

TABLE 6.7

V (m/s)	nD	J	C_t	C_Q	$\eta_p = \frac{JC_T}{2\pi C_Q}$	$T = \frac{\eta_p P}{V}$ (N)	n (rps)	D (m)
75	99	0.76	0.204	0.024983	98.76%	29.458	28.36	3.48

The thrust force can be calculated from the relation

$$T = \frac{\eta_p P}{V} = 29{,}458 \text{ N}$$

The diameter and rotational speed can then be calculated.

From Equations 6.81 and 6.84, we get

$$n = \left(\frac{V}{J}\right)^2 \sqrt{\frac{\rho C_t}{T}} = 28.36 \text{ rps} \tag{c}$$

and

$$D = \frac{J}{V}\sqrt{\frac{T}{\rho C_t}} = 3.48 \text{ m} \tag{d}$$

A summary of the calculated results for the preliminary design of a propeller are listed in Table 6.7.

6.3.3.5 Typical Propeller Performance

Experimental testing of propellers was started long ago by the Wright Brothers during the design process of their first airborne flight machine. Extensive experimental work continued and full-scale propeller testing was performed in a National Advisory Committee for Aeronautics (NACA) 20 ft wind tunnel at NASA, Langley. Detailed analyses of two-, three- and four-bladed propellers with the CLARK Y and RAF series airfoil section was published in Hartman and Biermann [14]. During the late 1930s, some NACA four-digit airfoils were used extensively in propellers. The blade thickness decreases from root to tip along

the blade length, as shown in Figure 6.26. The following NACA series are used for sections from hub to tip [19]:

NACA 4424/NACA 4418/NACA 2415/NACA 2412/NACA 2410/NACA 2408/
NACA 1412/NACA 1410/NACA 1408/NACA 0012/NACA 0009

To remind readers of airfoil designations, consider the section NACA 4428:

- The first integer (4) means that the airfoil has a maximum camber (maximum value of mean line ordinate) as a percentage of the chord (4%)
- Second integer (4) means the position of maximum camber in tenths of the chord from leading edge (40%)
- Last two integers (15) denote the maximum thickness as a percentage of the chord (15%)

After World War II, NACA series 16-airfoils were derived for use at high speeds, particularly for propeller applications [15]. This series has thin-profile airfoils and thus has low drag at high speeds. Consequently, it is appropriate for transonic propeller sections near the tip [16]. Continuous efforts have continued, performing computational analyses side by side with experimental ones. A detailed computational analysis of propeller performance using the commercial code FLUENT 6.2 is presented in Farghaly [17].

In general, the performance of a propeller is indicated by the thrust coefficient, C_T, the power coefficient, C_P, and efficiency, η_p. These values depend on the advance ratio, J.

Figure 6.39 presents the propeller efficiency for a two-bladed propeller. As clarified, it depends on the advance ratio, J, and the pitch angle, β.

As expected, efficiency values are less than unity, since the available power is less than that delivered due to losses. These losses are attributed to translational and rotational kinetic energy in the wake of propeller, as discussed earlier in the Froude and modified momentum theories. Skin friction and the profile drag of the propeller blades add to these losses. For high-speed propellers where the relative tip speed approaches sonic values, shock waves as well as boundary layer interaction on the suction sides of the blade section result in additional losses.

For any pitch angles, propeller efficiency starts with a zero value at $J=0$, increases to a maximum value and drops again to zero at a high finite value of J. When $J=0$, then $V=0$, and consequently the available or thrust power $P_A \equiv TV=0$, therefore $\eta_P \equiv P_A/P=0$.

The other case of zero efficiency corresponds to a higher value of advance ratio, $J>0$; this corresponds to a high flight speed. The corresponding relative speed coincides with zero lift (which, in turn, leads to zero thrust and zero efficiency). For higher flight (forward) speed, a negative lift is produced, leading to reverse thrust as shown in Figure 6.35.

The maximum value of η_p is seen to be around 80%–85%. However, the value of J at which the maximum of η_p occurs depends on the pitch angle, β. This indicates that, for a single pitch or fixed pitch propeller, the efficiency is high (80%–85%) but only over a narrow range of flight speeds (Figure 6.36).

At other flight velocities, a fixed pitch propeller will operate at smaller efficiencies, which severely influences aircraft performance. For this reason, commercial airplanes use a variable pitch propeller. In such a propeller, the entire blade is rotated through a chosen angle during the flight and the pitch of all the blade elements changes. Such propellers have high efficiency over a wide range of speeds. However, propellers with variable pitch arrangements are expensive and heavy. Hence, small (personal) airplanes, where the cost of the

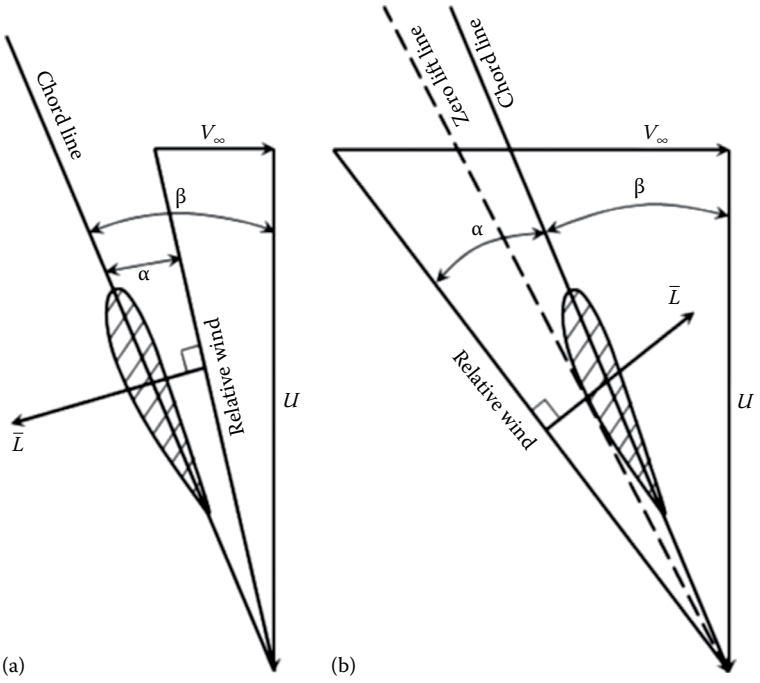


FIGURE 6.35
Variation of propeller efficiency with advance ratio: (a) small positive angle of attack and (b) large negative angle of attack.

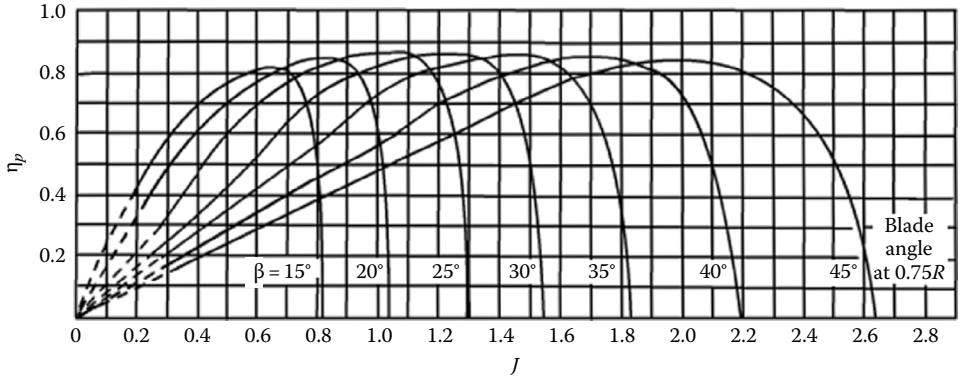


FIGURE 6.36
Propeller efficiency, η_p, versus advance ratio, J, for a two-bladed propeller at various pitch angles, β.

airplane is an important consideration, employ a fixed pitch propeller. As a compromise, in some designs propellers with two or three pitch settings are employed.

Figure 6.37 presents the variation of thrust coefficient C_T versus J for a two-bladed propeller with different values of β.

Figure 6.38 presents the variation of power coefficient C_P versus J for a two-bladed propeller with β and C_T as parameters.

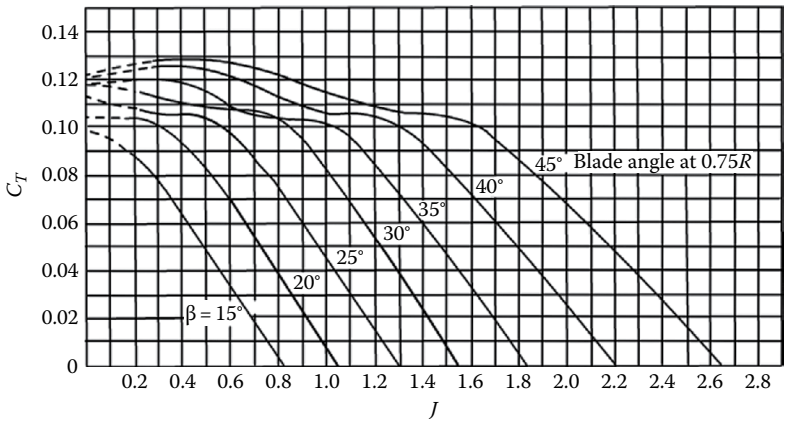


FIGURE 6.37
Thrust coefficient C_T versus advance ratio J for a two-bladed propeller with pitch angle parameter (β).

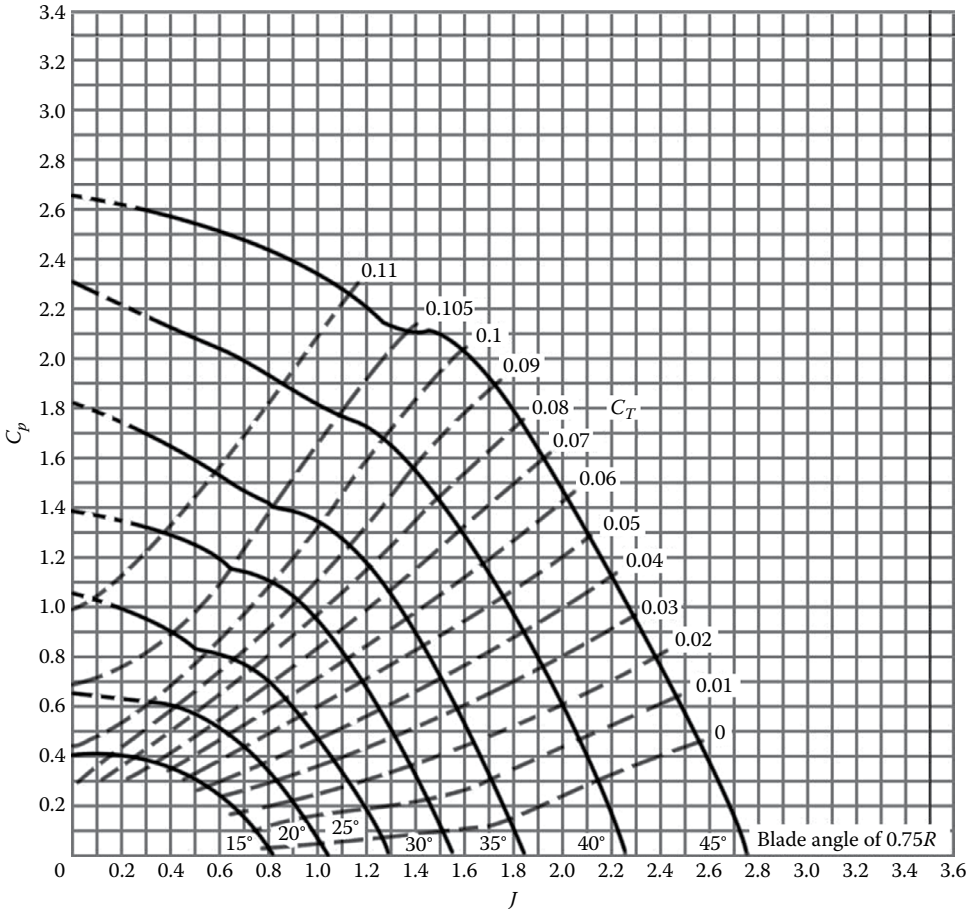


FIGURE 6.38
Power coefficient C_P versus advance ratio J for a two-bladed propeller with pitch angle parameter β and thrust coefficient C_T as parameters.

Figures 6.36 through 6.38 demonstrate that

1. For each pitch angle (β), efficiency has a value of zero at both $J=0$ and thrust coefficient $C_T=0$.
2. The condition $C_T=0$ corresponds to the axial interference factor $a=0$ and Froude efficiency $\eta_F=100\%$.
3. At small values of pitch angle, the thrust coefficient is greater than the power coefficient for any value of advance ratio. On the contrary, at high value of pitch angle, the power coefficient is greater than the thrust coefficient at any advance ratio.

Other figures for three- and four-bladed propellers (similar to Figures 6.36 through 6.38) are found in Hartman and Biermann [14]. However, recent propellers may have different numbers of blades (between 5 and 8). Performance parameters such as thrust coefficient can be obtained from the following equation [18]. The thrust coefficient for an eight-bladed propeller is then

$$C_T)_{B=8} = C_T)_{B=4} + \{C_T)_{B=4} - C_T)_{B=3}\} \times (B-4) \tag{6.91}$$

At the preliminary design stages, when the propeller diameter has not yet been determined, the speed-power coefficient (Equation 6.86a and b) may be used. Thus, new plots for the speed-power coefficient and for efficiency are plotted versus the advance ratio. Two method for plotting these relations are found in Figures 6.39 and 6.40.

Figure 6.39 provides the locus of maximum efficiency for different speed power coefficients.

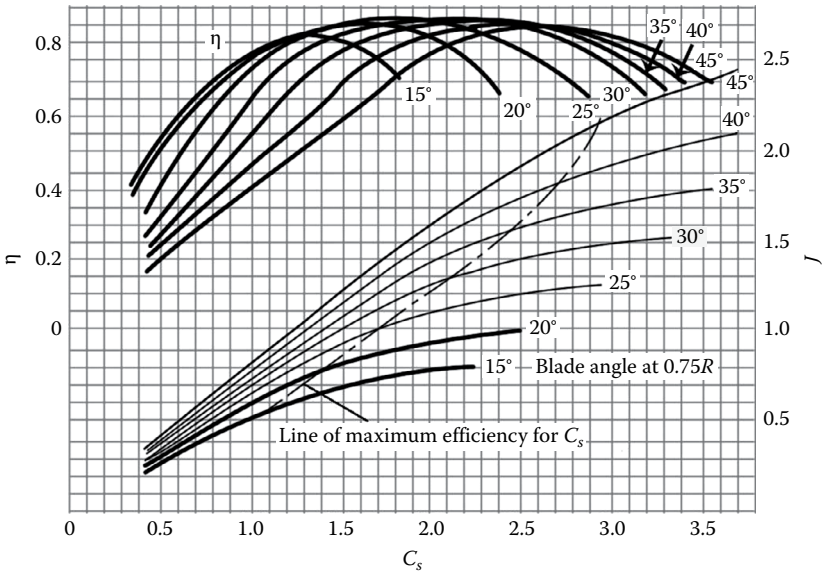


FIGURE 6.39
Combined speed-power coefficient and propeller efficiency for different advance ratio and pitch angle parameters.

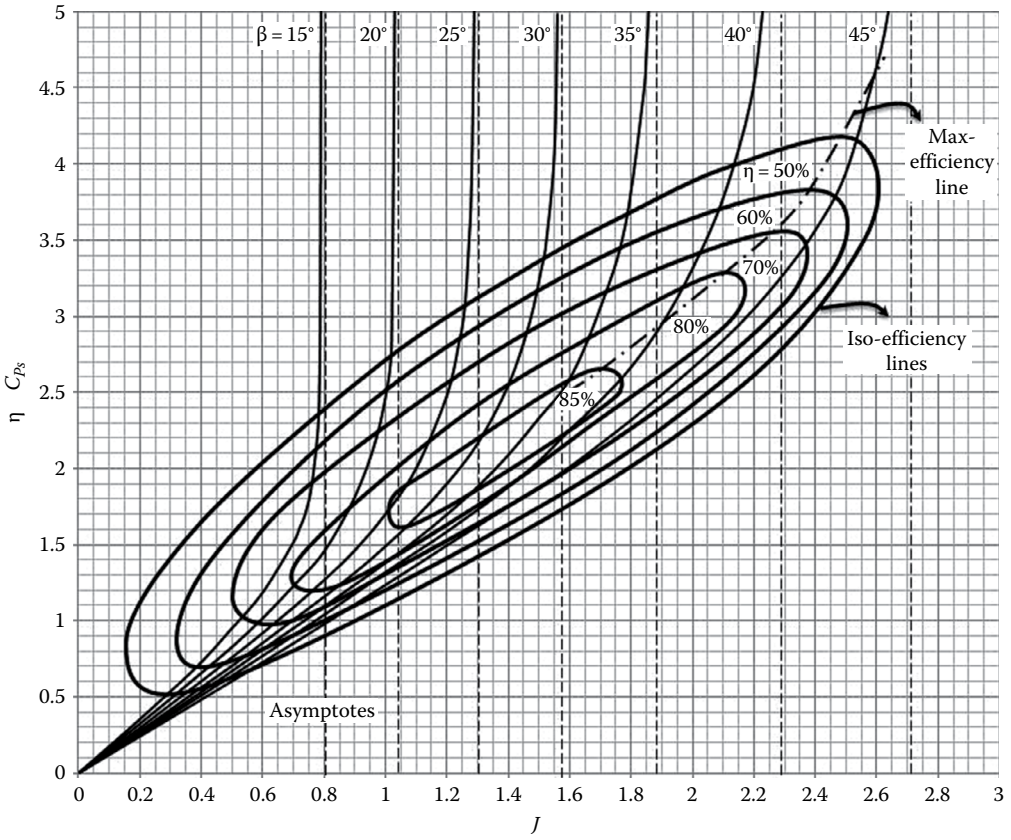


FIGURE 6.40
Other versions of speed-power coefficient and propeller efficiency curves for different advance ratio and pitch angle parameters.

Figure 6.40 provides iso-efficiency lines plotted over a constant speed-power coefficient and advance ratio parameter. It is quite similar to the compressor map, as will be explained later on in the turbomachinery sections.

Figure 6.41 provides values of efficiency at different pitch angles corresponding to a constant speed-power coefficient. As can be noted from Figure 6.41, efficiency increases in line with the increase of pitch angle for the same speed-power coefficient value.

Example 6.6

A preliminary design is required for a four-bladed propeller having the following data:

- Power = 1965 kW
- Sea-level conditions
- Relative speed at tip is 330 m/s
- Flight speed is 125 m/s

$$\phi_{root} = 70°$$
$$a_{\Omega} = 0.00787$$

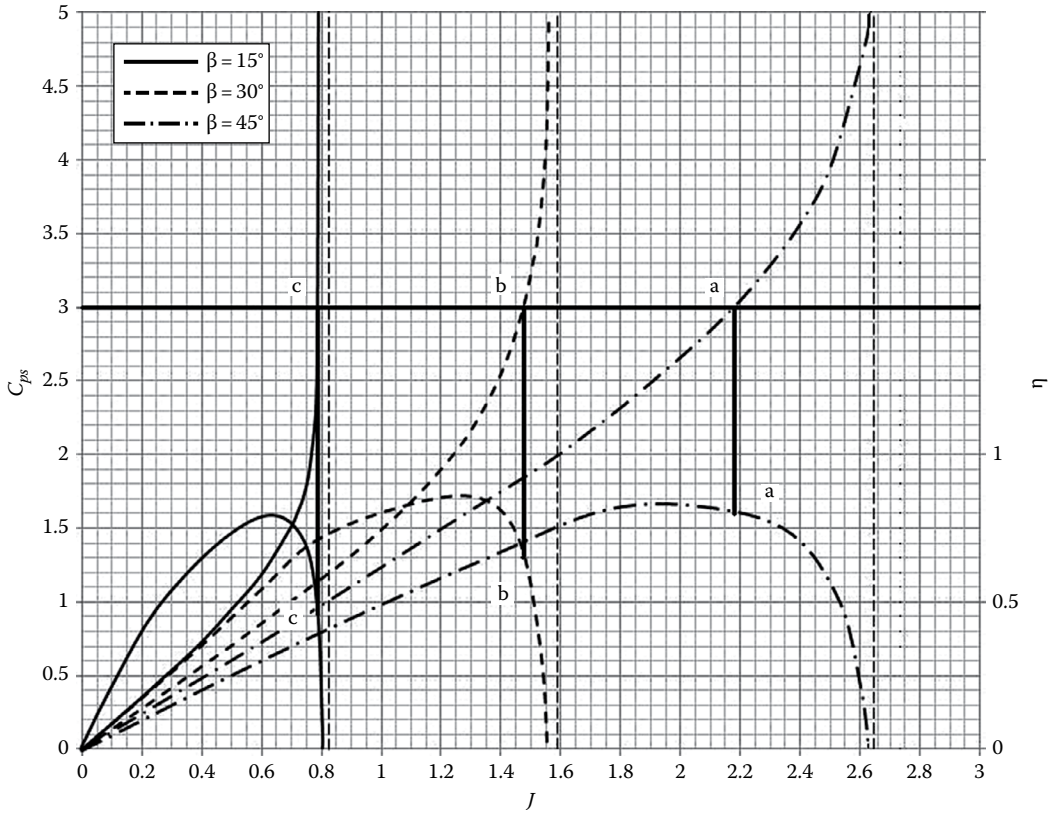


FIGURE 6.41
Constant speed-power coefficient and corresponding efficiency values.

Assume that the chord distribution is linear, with the following defined sections: $c_{0.3h} = c_{0.75h} = 0.054D$ and $c_{0.5h} = 0.074D$, where D is the propeller diameter and h is the blade height. The blade section has lift and drag coefficients equal to 0.85 and 0.035, respectively.

At 0.75R, it has a pitch angle $\beta = 40°$ and the following data:

- Thrust coefficient $c_T = 0.1764$
- Propeller efficiency is $\eta_b = 0.85$

The angle of attack is constant along the blade height: $\alpha = 3°$.

Calculate

1. Thrust force
2. Propeller diameter and rotational speed
3. Blade height
4. Chord and the advance angle (ϕ) along the blade length
5. The thrust distribution along the blade height

Solution

1. The thrust force can be obtained from the relation

$$T = \frac{\eta_p P}{V} = \frac{0.85 \times 1765 \times 10^3}{125} = 12{,}000 \text{ N}$$

2. Rotational speed limit

$$U_t = \sqrt{W_t^2 - V^2} = \sqrt{330^2 - 125^2} = 305.4 \text{ m/s}$$

$$nD = \frac{U_t}{\pi} = 97.2 \text{ m/s} \tag{a}$$

The advance ratio is $J = \dfrac{V}{nD} = \dfrac{125}{97.2} = 1.285$

3. Power limit
From Equations 6.81 and 6.84, we obtain

$$n = \left(\frac{V}{J}\right)^2 \sqrt{\frac{\rho C_t}{T}} = \left(\frac{125}{1.285}\right)^2 \sqrt{\frac{1.225 \times 0.1764}{12{,}000}} = 40.155 \text{ rps}$$

and

$$D = \frac{J}{V}\sqrt{\frac{T}{\rho C_t}} = \frac{1.285}{125}\sqrt{\frac{12{,}000}{1.225 \times 0.1764}} = 2.423 \text{ m}$$

$$T_c = \frac{c_T}{J^2} = 0.1068$$

$$b = 2a = -1 + \sqrt{1 + \frac{8}{\pi} T_c} = 0.1278$$

$$a = 0.0639$$

Forward speed is $V(1+a) = 125 \times 1.0639 = 132.99$ m/s.
Rotational speed is $U_t = \Omega r(1 - a_\Omega) = \pi D n(1 - a_\Omega) = \pi \times 97.2 \times (1 - 0.007876) =$ 302.95 m/s.

$$\tan\phi_t = \frac{V(1+a)}{\pi D n(1 - a_\Omega)} = \frac{132.99}{302.95} = 0.4387$$

$$\phi_t = 23.7^\circ$$

At the hub section, assuming the interference factors a, a_Ω are constant

$$\tan\phi_{root} = \tan 70 = \frac{V(1+a)}{U_{root}(1 - a_\Omega)} = \frac{132.99}{0.99213 U_r} = 2.747$$

$$U_r = 48.79 \text{ m}$$

$$D_{root}/D_{tip} = U_{root}/U_{tip} = 0.161$$

$$D_{root} = 0.39 \text{ m}$$

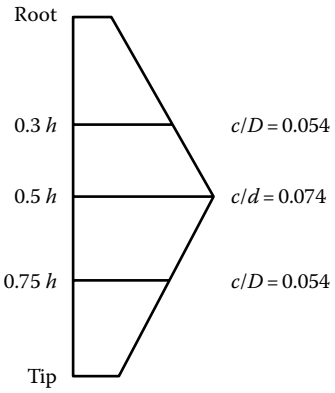


FIGURE 6.42
Chord distribution.

The blade height is

$$h = \frac{D_{tip} - D_{root}}{2} = U_{root} / U_{tip} = 1.016 \text{ m}$$

4A. Chord length

$$c_{0.3h} = c_{0.75h} = 0.054D = 0.131 \text{ m}$$

and

$$c_{0.5h} = 0.074D = 0.179 \text{ m}$$

The linear variation of the chord is displayed in Figure 6.42. The variation of the chord is calculated from the known values at the mean blade section, 0.3 and 0.75 heights above and tabulated in Table 6.8.

TABLE 6.8

Station x/R	C (m)	U (m/s)	ϕ	$c \times \frac{c_l \cos\phi - c_d \sin\phi}{\sin^2\phi}$	ΔT (N)
0.1	0.083	74.46	60.9	0.0416	180.25
0.2	0.107	100.12	53.23	0.0801	347.1
0.3	0.131	125.78	46.81	0.1371	594.1
0.4	0.155	151.44	41.5	0.2165	938.1
0.5	0.179	177.1	37.11	0.3229	1399.12
0.6	0.1598	202.76	33.46	0.3626	1571.14
0.7	0.1406	228.42	30.4	0.3928	1702
0.8	0.1214	254.08	27.8	0.4105	1778.7
0.9	0.1022	279.74	25.6	0.4114	1782.6
1.0	0.083	305.4	23.7	0.3926	1701.13

4B. Advance angle (ϕ)

At *root*	$\phi_{R=0}=70°$
At 0.75*R*:	$\beta=40°$
thus	$\phi_{0.75R}=\beta-\alpha=40°-3°=37°$
Also at *tip*	$\phi_t=23.7°$

At *any location* along the blade:

$$\tan\phi(x)=\frac{(1+a)}{(1-a_\Omega)}\frac{V}{U(x)}=\frac{132.99}{0.99213U(x)}=\frac{134}{U(x)}$$

The distribution of angle ϕ will be given in Table 6.8.

5. Thrust force distribution

Dividing the blade into 10 increments, then $\Delta r=\frac{h}{10}=0.10$ m

From Equation 6.73, the thrust increment for each blade element is expressed by

$$\Delta T=Bcq(1+a)^2\frac{c_l\cos\phi-c_d\sin\phi}{\sin^2\phi}\Delta r$$

We have

$$Bq(1+a)^2\Delta r=4\times\left(0.5\times1.225\times125^2\right)\times(1.0639)^2\times0.1=4333\ \text{N/m}$$

thus

$$\Delta T(r)=4333c\frac{c_l\cos\phi-c_d\sin\phi}{\sin^2\phi}$$

The torque distribution is given in Table 6.8.

$$T=\sum\Delta T=11,994.24\ N$$

Since the thrust force was obtained before, =12,000 N, the summation of the thrust increment obtained in Table 6.8 yields nearly the same design value (12,000 N), the assumptions set earlier are satisfactory. If this is not the case, then an iteration procedure should be employed by altering one or more of the following variables:

- Flight speed
- Chord length of blade
- Airfoil section, which contributes different lift and drag coefficients

6.4 Turboprop Engines

A turboprop engine is a hybrid engine that provides jet thrust and also drives a propeller. It is basically similar to a turbojet except that the turbine works through a shaft and speed-reducing gears to turn a propeller at the front of the engine (Figure 6.43).

Many low-speed and small commuter aircraft (King Air A100, Mitsubishi MU-2, Saab 340, and De Havilland Canada Dash 8), military transport aircraft (Hercules C-130,

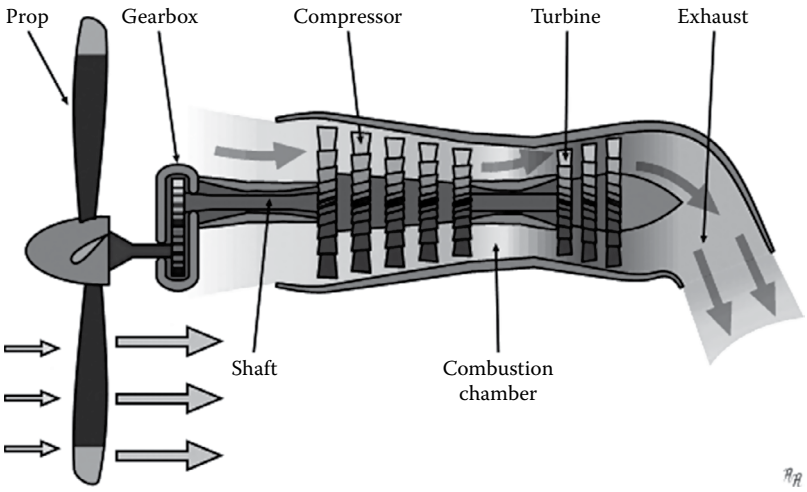


FIGURE 6.43
Turboprop engine.



FIGURE 6.44
Russian Tu-95.

Lockheed P-3A, and Antonov An -38,-140) as well as long range aircraft (the Russian Tu-95; Figure 6.44 and the CP-140 Aurora) use turboprop propulsion. Turboprop engines are basically propellers driven by a turbine.

6.4.1 Introduction to Turboprop Engines

Soon after the first turbojets were in the air, the turboprop engine was developed. A turboprop engine has a concept similar to that of the turbofan, though having a higher bypass ratio.

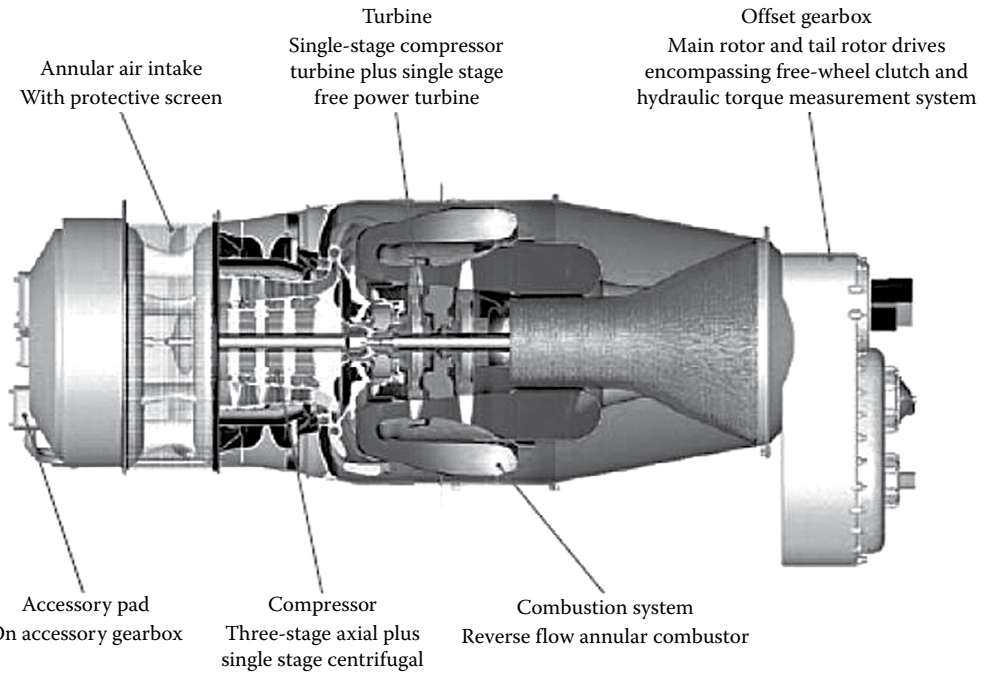


FIGURE 6.45
PT 6B. (Courtesy of Pratt & Whitney, Longueuil, Quebec, Canada.)

Moreover, instead of the turbine driving a ducted fan, it drives a completely external propeller. The turboprop uses a gas turbine core to turn a propeller. The propeller is driven either by the gas generator turbine (Figure 6.45), or by another turbine classified as a free or power turbine (Figure 6.46). In this case, the free turbine is independent of the compressor-drive turbine and is free to rotate by itself in the engine exhaust gas stream. Another configuration of the free turbine turboprop has a rather unconventional rear-to-front air and gas direction. This configuration provides great flexibility in the design of nacelle installations: the space behind the engine that is not used for an exhaust duct end can be used for wheel wells or fuel tanks. The compressor is a combination of the axial/centrifugal flow designs. An example of such an engine is the PT6, manufactured by Pratt & Whitney of Canada.

In either case, a heavy gear box is installed between the turbine and the propeller and provides a speed reduction of nearly 1:15. A turboprop engine produces two thrusts, one with the propeller and the other through the exhaust. The thrust developed by the propeller is nearly 85% of the total thrust, while the remaining 15% is produced by the jet core exhaust due to the low-speed exhaust.

As stated previously, the propeller rotates at a very low speed compared with its driving turbine. The speed reduction may be 1:15. This speed reduction is necessary for two reasons:

1. A large centrifugal force arises from the rotation of the large diameter propeller blades (2–4 m, or even more). These blades are fixed to the propeller hub in a cantilever fixed-end configuration. Consequently, such centrifugal force generates a large tensile stress

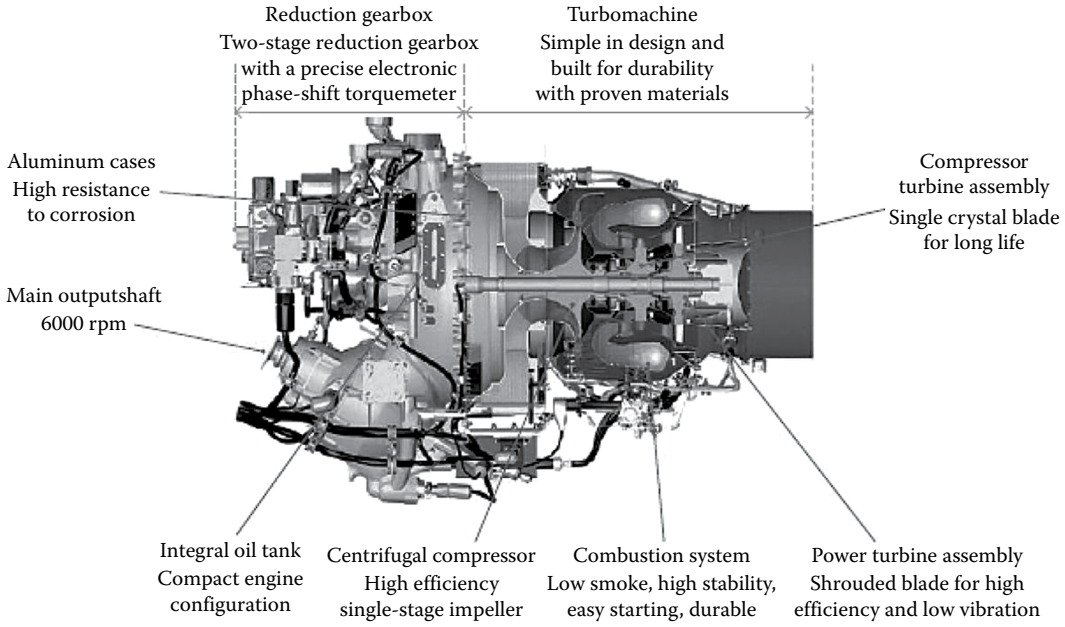


FIGURE 6.46
PW200. (Courtesy of Pratt & Whitney, Longueuil, Quebec, Canada.)

at the blade root. Stress limitations require that a large diameter propeller rotates at a much slower speed. It is a fact that no propeller can withstand the tensile force (and stress) that is generated when it is turned at the same speed as the turbine.

2. Due to the rotation of the propeller, the relative velocity at the propeller tip will approach the speed of sound before the aircraft approaches the speed of sound. This compressibility effect when approaching the speed of sound limits the design of propellers. At high subsonic flight speeds ($M > 0.7$), the tips of the blades may approach supersonic speeds. If this happens, the flow may separate and shock waves may form. As a consequence, the performance of a turboprop engine deteriorates due to both the poor propeller efficiency and the decrease in air flow rate into the engine.

The propeller is pitch controlled to be suitable for a wider range of satisfactory applications.

If the shaft of a free turbine is used to drive something other than an aircraft propeller, the engine is called a "turboshaft" engine. This is one of the turboshaft engines that will be discussed later in this chapter. Turboshaft engines are similar to turboprop engines, except that the hot gases are expanded to a lower pressure in the turbine, thus providing greater shaft power and little exhaust velocity. Turboshaft engines are those used in helicopters.

Now, let us discuss the *advantages* of turboprop engines:

1. Turboprops have high fuel efficiency, even greater than turbofan engines. This is due to the small amount of air flow burned inside the engine. Turboprop engines can then generate considerable thrust at low fuel consumption.
2. Turboprop engines may find application in vertical takeoff and landing (VTOL). The Osprey V-22 aircraft shown in Figure 6.47 is one of the famous VTOL aircraft that is powered by a turboprop engine.



FIGURE 6.47
V-22 Osprey.

3. Turboprop engines have a high takeoff thrust that enables aircraft to have a short airfield takeoff.
4. They have the highest propulsive efficiency for flight speeds of 400 mph compared with turbofan and turbojet engines.

However, turboprop engines have several *disadvantages*:

1. The noise and vibration produced by the propeller is a significant drawback.
2. Turboprop engines are limited to subsonic flights (less than 400 mph) and low altitudes (below 30,000 ft).
3. The propeller and its reduction gear, pitch control mechanism and the power turbine contribute additional weight, so the turboprop engine may be 1.5 times as heavy as a conventional turbojet of the same gas-generator size.
4. The large size gearbox connected to the propeller is situated upstream of the air path to the engine inlet. Thus, the intake shapes are different from those of turbojet and turbofan engines. Moreover, the gearbox (normally a single or double planetary version) has many moving parts that could break and could foul the air stream going into the engine.

6.4.2 Classification of Turboprop Engines

There is a great similarity between aero piston and turboprop engines, as will now be described.

1. Based on engine-aircraft configuration
   Turboprop engines may be either a *tractor* type (sometimes identified as *puller*) or a pusher type. The word puller (tractor) denotes a turboprop engine with a propeller that precedes the intake and compressor. The thrust force (mostly generated by



FIGURE 6.48
Pusher configuration of Jetcruzer 500, AASI airplane.

the propeller) is thus a pulling force. Most aircrafts are powered by a puller (tractor) configuration (see Figure 6.44 for an example). If the propeller is downstream of the inlet and compressor, then this type turboprop is identified as pusher, as shown in Figure 6.48.

Advantages of pusher turboprop engines

a. A higher-quality (clean) airflow prevails over the wing.
b. Engine noise in the cabin area is reduced.
c. The pilot's front field of view is improved.

Disadvantages of pusher turboprop engines

a. The heavy gearbox is at the back, which shifts the center of gravity rearward thus reducing the longitudinal stability.
b. The propeller is more likely to be damaged by flying debris on landing.
c. Engine cooling problems are more severe.

The "pusher" configuration is not very common.

Example

Jetcruzer 500 powered by Pratt & Whitney Canada (PT6A-66) driving five blades at constant speed.

2. Hartzell propeller

Advantages of puller (tractor) turboprop engines:

a. The heavy gearbox is at the front, which helps to move the center of gravity forward and therefore allows a smaller tail for stability.
b. The propeller works in an undisturbed free stream. There is a more effective flow of cooling air for the engine.

Disadvantages of puller (tractor) turboprop engines:

a. The propeller slipstream disturbs the quality of the airflow over the wing.
b. The increased velocity and flow turbulence over the fuselage due to the propeller slipstream increase the local skin friction on the fuselage.

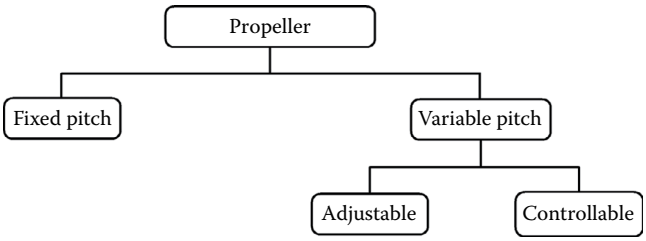


FIGURE 6.49
Classification of propellers.

Example

Most, if not all, aircraft powered by turboprops have the puller configuration. The Pratt & Whitney Canada (PW 120A), which powers the Dash 8 aircraft, is a model for this type.

3. Propeller-engine coupling
   This classification has already been mentioned and is dependent on the way the propeller and the turbine are coupled. The propeller may be driven by the gas generator or by a separate turbine (identified as a "free power" turbine).
4. Number of spools
   Turboprop engines may be single-, double-, or triple-spooled. Propellers driven by the gas generator are found either in a single- or double-spool turboprop engine. Conversely, a propeller driven by a free (power) turbine may be a part of either a double- or triple-spooled turboprop engine. The number of spools is the same as the number of turbines in the engine.
5. Propeller type
   Propeller types may also be classified, as shown in Figure 6.49, as either fixed pitch or variable pitch. Variable pitch propellers may be further sub-divided into adjustable or controllable ones.
6. Type of intake
   Intakes may have different shapes, as shown in Figure 6.50. These shapes depend on the size and location of the reduction gear box coupled to the propeller. The shapes of the intake may be axial, axisymmetric, axisymmetric through a plenum or a scoop, which, in turn, may have an elliptical, rectangular, annular, or a u-shape.

6.4.3 Thermodynamics Analysis of Turboprop Engines

The different modules for a turboprop engine are the intake or inlet, one or two compressors, a combustion chamber and one or more (up to three) turbines, and the exhaust nozzle. Only one compressor is found in single- or double-spooled engines. Triple-spooled engines have two compressors. There is one turbine for each spool.

6.4.3.1 Single-Spool Turboprop

A simplified layout of a single-spool turboprop engine in its different states and the corresponding temperature-entropy diagram is shown in Figures 6.51 and 6.52. The same procedure used in previous chapters will be followed.

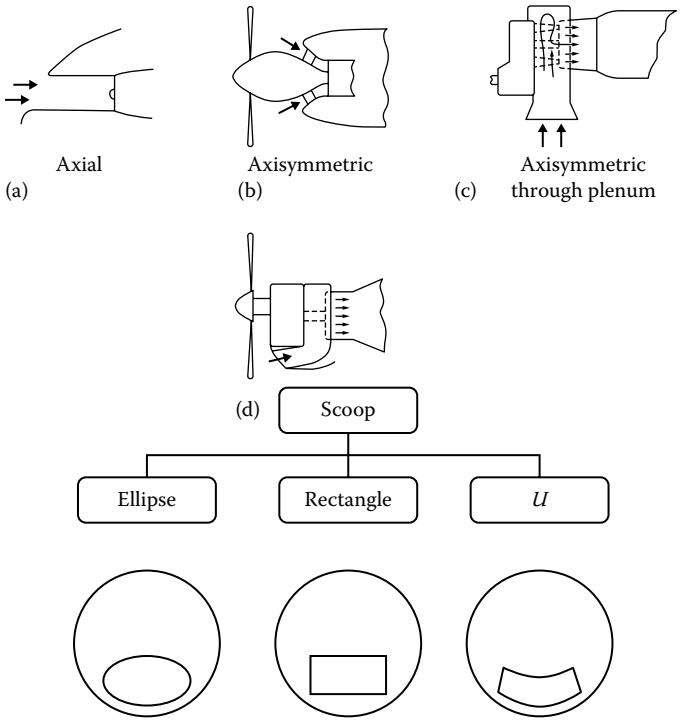


FIGURE 6.50
Types of inlets.

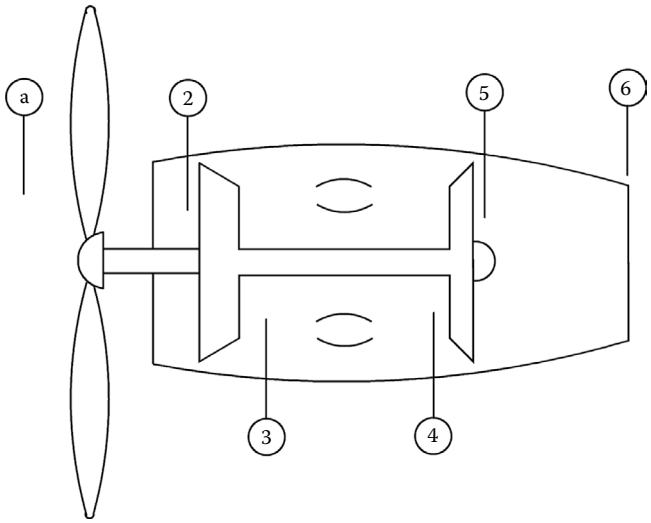


FIGURE 6.51
Layout of a single spool (direct drive turboprop engines).

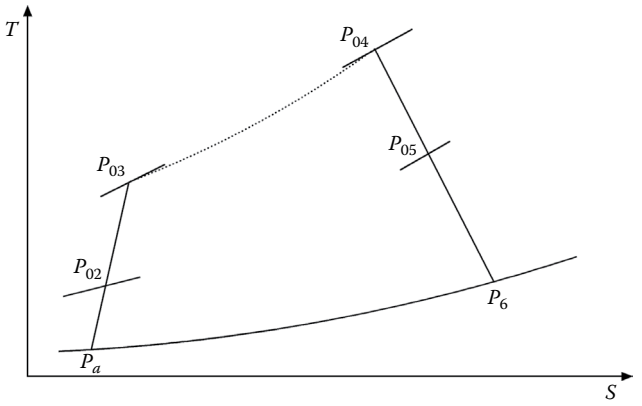


FIGURE 6.52
Temperature–entropy diagram of single-spool turboprop.

The flight speed is expressed as $U = M_a\sqrt{\gamma RT_a}$.

The thermodynamic properties at different locations within the engine are obtained as follows

$$\gamma_c = Cp_c/\left(Cp_c - R\right), \quad \gamma_{cc} = Cp_{cc}/\left(Cp_{cc} - R\right), \quad \gamma_t = Cp_t/\left(Cp_t - R\right), \quad \gamma_n = Cp_n/\left(Cp_n - R\right)$$

The different modules of the engine are treated as described in Chapters 3 through 5.

1. Intake
   The intake has an isentropic efficiency, η_d, the ambient temperature and pressure are P_a and T_a, respectively, and the flight Mach number is M_a. The temperature and pressure at the intake outlet is T_{02} and P_{02}, given by the relations

$$P_{02} = P_a\left(1 + \eta_d \frac{\gamma_c - 1}{2} M_a^2\right)^{\gamma_c/\gamma_{c-1}} \tag{6.92}$$

$$T_{02} = T_a\left(1 + \frac{\gamma_c - 1}{2} M_a^2\right) \tag{6.93}$$

2. Compressor
   For a known compressor pressure ratio, π_c, its isentropic efficiency is η_c, thus the temperature and pressure at the outlet of the compressor, as well as the specific power of the compressor, are given by the following relations

$$P_{03} = \left(P_{02}\right)\left(\pi_c\right) \tag{6.94}$$

$$T_{03} = T_{02}\left(1 + \frac{\pi_c^{\gamma_c - 1/\gamma_c} - 1}{\eta_c}\right) \tag{6.95}$$

$$\Delta h_c = Cp_c\left(T_{03} - T_{02}\right)$$

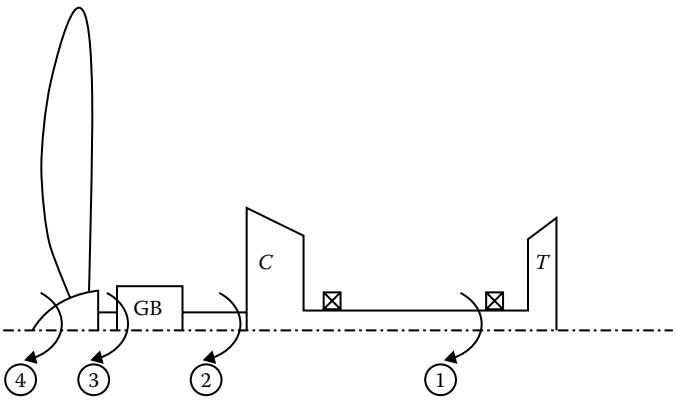
3. Combustion chamber
   The combustion process takes place in the combustor with an efficiency of η_b, while the products of combustion experience a pressure drop equal to $-\Delta P$. The pressure at the outlet of the combustion chamber and the fuel to air ratio are given by

$$P_{04} = (1 - \Delta P) P_{03}$$

$$f = \frac{Cp_{cc} T_{04} - Cp_c T_{03}}{\eta_b Q_R - Cp_{cc} T_{04}} \tag{6.96}$$

4. Turbine
   In this case, it is not easy to determine the outlet pressure and temperature of the turbine. The reason is that the turbine drives both the compressor and propeller. The proportion of each is not known in advance. Let us first examine the power transmission from the turbine to the propeller, as illustrated in Figure 6.53.

The output power from the turbine is slightly less than the extracted power due to friction of the bearings supporting the turbine [23,24]. This loss is accounted for by the turbine's mechanical efficiency, η_{mt}. Moreover, the mechanical losses encountered in the bearings supporting the compressor are accounted for by the compressor mechanical efficiency, η_{mc}. The difference between the turbine and the compressor powers is the shaft power delivered to the reduction gear box, where additional friction losses are encountered and accounted for by the gearbox's mechanical efficiency, η_g. Finally, the output power available from the propeller is controlled by the propeller efficiency, η_{pr}.



Power transmission

at (1) $\eta_{mt} W_t$

at (2) $\left(\eta_{mt} W_t - \frac{W_c}{\eta_{mc}}\right)$

at (3) $\eta_{gb}\left(\eta_{mt} W_t - \frac{W_c}{\eta_{mc}}\right)$

at (4) $\eta_{pr}\eta_g\left(\eta_{mt} W_t - \frac{W_c}{\eta_{mc}}\right)$

FIGURE 6.53
Power transmission through a single-spool turboprop engine.

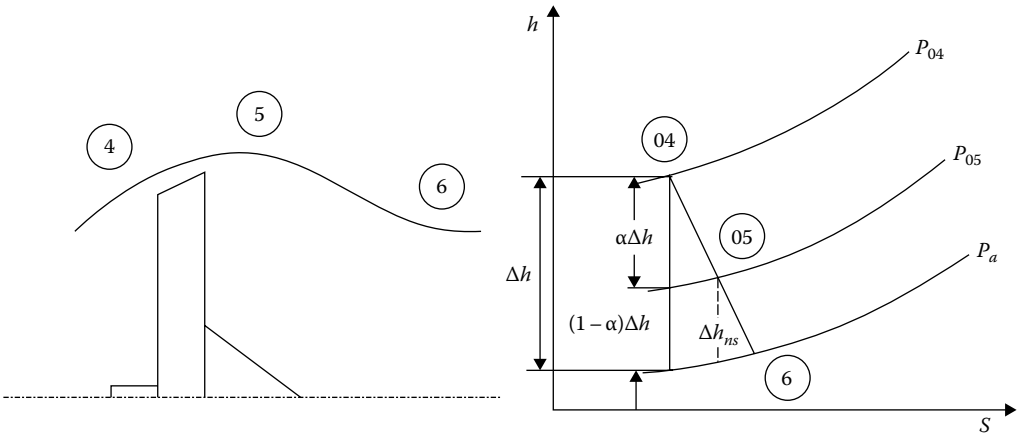


FIGURE 6.54
Expansion in the turbine and nozzle of a single-spool turboprop engine.

Now, Figure 6.54 illustrates the enthalpy-entropy diagram for the expansion processes through both the turbine and the exhaust nozzle. It has been shown by Lancaster [20] that there is an optimum exhaust velocity that yields the maximum thrust for a given flight speed, turbine inlet temperature, and given efficiencies. Now define the following symbols as shown in Figure 6.54.

Δh = enthalpy drop available in an ideal (isentropic) turbine and exhaust nozzle.

$\alpha\Delta h = \Delta h_{ts}$, which is the fraction of Δh that would be available from an isentropic turbine having the actual pressure ratio.

$$\Delta h_{ns} = (1-\alpha)\Delta h$$

which is also the fraction of Δh that may be available from an isentropic nozzle.

η_t = isentropic efficiency of turbine.

η_n = isentropic efficiency of the exhaust nozzle.

Now, to evaluate these values from the following thermodynamic relations

$$\Delta h = Cp_t T_{04}\left[1-\left(\frac{P_a}{P_{04}}\right)^{\gamma_h-1/\gamma_h}\right] \tag{6.97}$$

It was assumed in Equation 6.97 that the ratios between specific heats within the turbine and nozzle are constant, or

$$\gamma_t = \gamma_n = \gamma_h$$

The exhaust gas speed, U_e, is given by the relation

$$\frac{U_e^2}{2} = \eta_n(1-\alpha)\Delta h$$

$$U_e = \sqrt{2(1-\alpha)\Delta h\eta_n} \tag{6.98}$$

The procedure to be followed here is to deduce a mathematical expression for the thrust force generated by the propeller, T_{pr}. from the power generated by the propeller. Adding this thrust to the thrust generated by the exhaust gases, the total thrust is obtained as a function of α. Differentiate with respect to α to obtain the optimum value of α giving the maximum thrust.

The propeller thrust, T_{pr}, is correlated to the propeller power by the relation

$$T_{pr} = \frac{\dot{m}_a \eta_{pr} \eta_g W_{shaft}}{U}$$

The shaft power is

$$W_{shaft} = \eta_{mt}\left(1 + f - b\right)\Delta h_t - \frac{\Delta h_c}{\eta_{mc}}$$

where the turbine specific power is

$$\Delta h_t = \eta_t \alpha \Delta h$$

$\dot{m}_a$ is the air induction rate per second, and the fuel-to-air ratio and the bleed ratio are defined as

$$f = \frac{\dot{m}_f}{\dot{m}_a} \quad \text{and} \quad b = \frac{\dot{m}_b}{\dot{m}_a}$$

$$T_{pr} = \frac{\dot{m}_a \eta_{pr} \eta_g}{U}\left[\left(1 + f - b\right)\eta_{mt}\eta_t \alpha \Delta h - \frac{\Delta h_c}{\eta_{mc}}\right] \tag{6.99}$$

The thrust force obtained from the exhaust gases leaving the nozzle is abbreviated as T_n. If the fuel mass flow rate and the air bled from the compressor are considered, then it will be given by the relation

$$T_n = \dot{m}_a\left[\left(1 + f - b\right)U_e - U\right]$$

Total thrust

$$T = T_{pr} + T_n$$

$$\frac{T}{\dot{m}} = \frac{\eta_{pr}\eta_g}{U}\left[\left(1 + f - b\right)\eta_{mt}\eta_t \alpha \Delta h - \frac{\Delta h_c}{\eta_{mc}}\right] + \left[\left(1 + f - b\right)\sqrt{2\left(1 - \alpha\right)\eta_n \Delta h} - U\right] \tag{6.100}$$

Maximizing the thrust, T, for fixed component efficiencies, flight speed, U, compressor specific power, Δh_c, and expansion power, Δh, yields the following optimum value of α_{opt}

$$\alpha_{opt} = 1 - \frac{U^2}{2\Delta h}\left(\frac{\eta_n}{\eta_{pr}^2 \eta_g^2 \eta_{mt}^2 \eta_t^2}\right) \tag{6.101}$$

Substituting this value of α in Equation 6.100 gives the maximum value of the thrust force. The corresponding value of the exhaust speed is given by the following equation

$$U_e = U\frac{\eta_n}{\eta_{pr}\eta_g\eta_{mt}\eta_t} \tag{6.102}$$

6.4.3.2 Two-Spool Turboprop

A schematic diagram of a two-spool engine with a free power turbine together with its temperature-entropy diagram is shown in Figures 6.55 and 6.56. The low-pressure spool is composed of the propeller and the free power turbine, while the high-pressure spool is composed of the compressor and the high-pressure or gas generator turbine.

The different components are examined here.

1. Intake
   The same relations for the outlet pressure and temperature in the single spool, Equations 6.92 and 6.93, are applied here.
2. Compressor
   The same relations in Equations 6.94 and 6.95 are applied here. The specific work of the compressor (the work per kg of air inducted into the engine) is

$$\Delta h_c = Cp_c\left(T_{03} - T_{02}\right)$$

3. Combustion chamber
   The fuel-to-air ratio is obtained from the same relation, Equation 6.96.

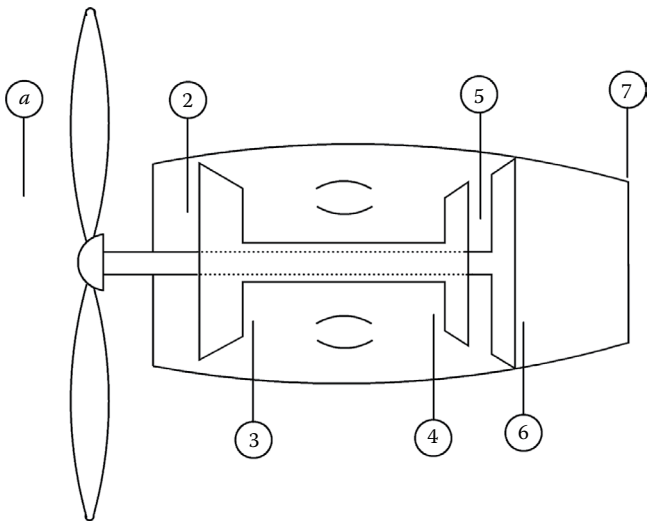


FIGURE 6.55
Layout of a free power turbine turboprop engine.

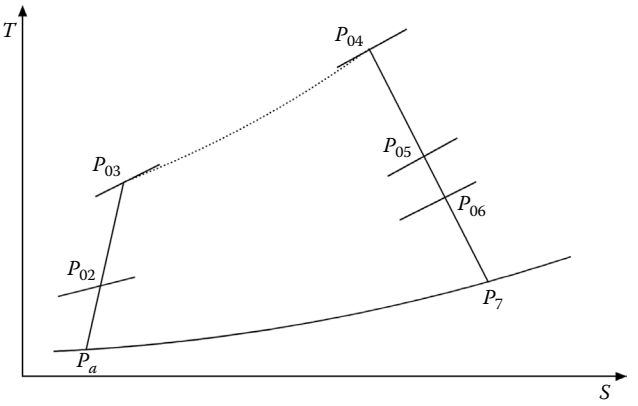


FIGURE 6.56
Temperature–entropy diagram for a free power turbine.

4. Gas generator turbine
An energy balance between the compressor and this high-pressure turbine gives

$$\frac{\Delta h_c}{\eta_{mc}} = \eta_{mt}\Delta h_t \tag{6.103a}$$

The specific work generated in the turbine of the gas generator is

$$\Delta h_t = Cp_t\left(T_{04} - T_{05}\right)\left(1 + f - b\right) \tag{6.103b}$$

From Equation 6.103a and b with a known turbine inlet temperature, the outlet temperature (T_{05}) is calculated from the relation

$$T_{05} = T_{04} - \frac{Cp_c\left(T_{03} - T_{02}\right)}{Cp_t\eta_{mc}\eta_{mt}\left(1 + f - b\right)}$$

Moreover, from the isentropic efficiency of the gas generator turbine, the outlet pressure, P_{05}, is calculated from the relation

$$P_{05} = P_{04}\left[1 - \left(\frac{T_{04} - T_{05}}{\eta_t T_{04}}\right)\right]^{\gamma_t/\gamma_t - 1}$$

5. Free power turbine
Figure 6.57 illustrates the power flow from the free turbine to the propeller. The work developed by the free power turbine per unit mass inducted into the engine is

$$\Delta h_{ft} = Cp_{ft}\left(1 + f - b\right)\left(T_{05} - T_{06}\right)$$

As observed from the above equation and previously explained in Section 6.4.3.1, the temperature T_{06} is unknown and cannot be calculated. Therefore a similar

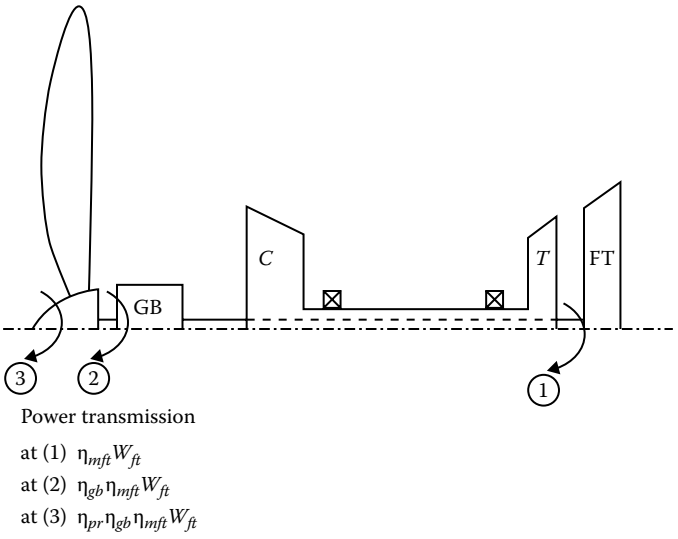


FIGURE 6.57
Power transmission through a double-spool turboprop engine.

procedure to that described in Section 6.4.3.1 will be followed. Referring to Figure 6.58, which defines the successive expansion processes in the free power turbine and the nozzle, we have Δh = enthalpy drop available in an ideal (isentropic) turbine and exhaust nozzle, assuming a full expansion to the ambient pressure is assumed in the nozzle $P_7 = P_a$, is calculated as

$$\Delta h = Cp_t T_{05}\left[1 - \left(\frac{P_7}{P_{05}}\right)^{\gamma_t - 1/\gamma_t}\right]$$

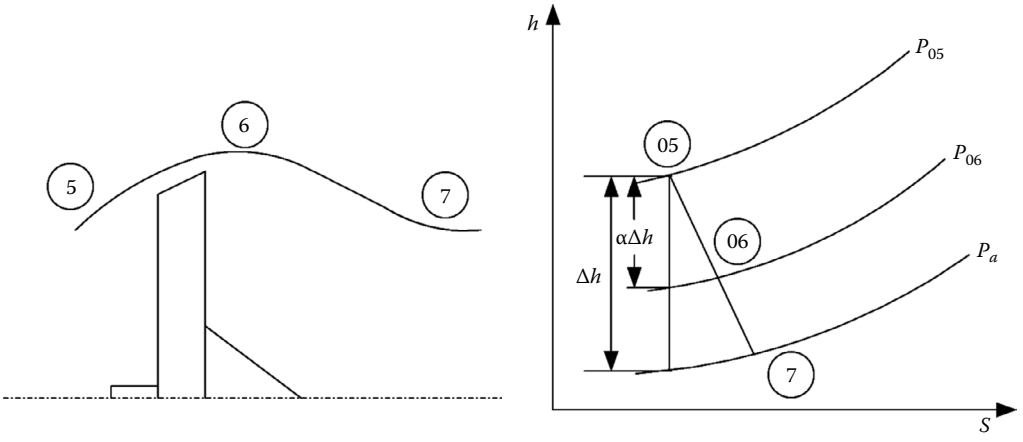


FIGURE 6.58
Expansion in the turbine and nozzle of a double-spool turboprop engine.

$\alpha\Delta h = \Delta h_{fts}$, which is the proportion of Δh that would be available from an isentropic free power turbine having the actual pressure ratio

$$\Delta h_{ft} = \eta_{ft}\Delta h_{ft}$$

η_{ft} = isentropic efficiency of the free power turbine.

Following the same procedure described above to determine the optimum α, the propeller thrust and the exhaust thrust are determined from the relations

$$T_{pr} = \frac{\dot{m}_a \eta_{pr}\eta_g}{U}\left[\left(1+f-b\right)\eta_{mft}\eta_{ft}\alpha\Delta h\right] \tag{6.104}$$

$$T_n = \dot{m}_a\left[\left(1+f-b\right)U_e - U\right]$$

The total thrust is then $T = T_{pr} + T_n$

$$\frac{T}{\dot{m}} = \frac{\eta_{pr}\eta_g}{U}\left[\left(1+f-b\right)\eta_{mft}\eta_{ft}\alpha\Delta h\right] + \left[\left(1+f-b\right)\sqrt{2\left(1-\alpha\right)\eta_n\Delta h} - U\right] \tag{6.105}$$

where η_{mft} is the mechanical efficiency of the free power turbine.

Maximizing the thrust, T, for fixed component efficiencies, flight speed, U, and Δh, yields the following optimum value of α_{opt}

$$\alpha_{opt} = 1 - \frac{U^2}{2\Delta h}\left(\frac{\eta_n}{\eta_{pr}^2\eta_g^2\eta_{mt}^2\eta_t^2}\right) \tag{6.106}$$

Substituting this value of α in Equation 6.105 gives the maximum value of the thrust force. The corresponding value of the exhaust speed is given by the following equation:

$$U_e = U\frac{\eta_n}{\eta_{pr}\eta_g\eta_{mft}\eta_{ft}} \tag{6.107}$$

The outlet conditions at the free turbine outlet are easily calculated from the known values of Δh and α_{opt}.

6.4.4 Analogy with Turbofan Engines

Turboprop engines are analogous to high-bypass turbofan engines. The propeller itself is an un-ducted fan with a bypass ratio equal to or greater than 25. The air flow through the propeller is slightly accelerated and thus acquires speeds slightly higher than the aircraft flight speed. The momentum difference between the inlet flow and outlet flow through the propeller produces the propeller thrust. Next, this accelerated air passes through the engine core and is accelerated to higher speeds. The momentum difference between the outlet and inlet core flow results in the core thrust. The thrust force is given by the relation

$$T = \dot{m}_0\left[\left(u_1 - u_0\right)\right] + \dot{m}_a\left[\left(1+f-b\right)u_e - u_1\right] \tag{6.108a}$$

Introducing the bypass ratio into Equation 6.17a obtains

$$T = \dot{m}_a\left[\beta u_1 + (1+f-b)u_e - (1+\beta)u_0\right] \tag{6.108b}$$

The specific thrust related to the engine core mass flow rate obtains

$$\frac{T}{\dot{m}_a} = \left[\beta u_1 + (1+f-b)u_e\right] + (1+\beta)u_0) \tag{6.108c}$$

6.4.5 Equivalent Engine Power

6.4.5.1 Static Condition

During testing (on a test bench) or takeoff conditions, the total equivalent horsepower (TEHP) is equal to the shaft horsepower (SHP) plus the SHP equivalent to the net jet thrust. For estimation purposes, it is assumed that, under sea-level static conditions, one SHP is equivalent to approximately 2.6 lb of jet thrust [21]. Thus

$$(\text{TEHP})_{Take-off} = \text{SHP} + \frac{\text{Jet thrust}(\text{ib})}{2.6} \tag{6.109a}$$

Switching to SI units, experiments [22] have also shown that the total equivalent power (TEP) in kW is related to the shaft power (SP), also in kW, by the relation

$$\{\text{TEP}(\text{kW})\}_{Take-off} = \text{SP}(\text{kW}) + \frac{\text{jet thrust}(\text{Newton})}{8.5} \tag{6.109b}$$

The thrust on a test bench (ground testing) or during takeoff is given by

$$T = \dot{m}(1+f-b)U_e$$

6.4.5.2 Flight Operation

For a turboprop engine during flight, the equivalent shaft horsepower (ESHP) is equal to the SHP plus the jet thrust power, as per the following relation

$$\text{ESHP} = \text{SHP} + \frac{T \times U}{\text{Constant} \times \eta_{pr}} \tag{6.110a}$$

where the thrust is

$$T = \dot{m}\left[(1+f-b)U_e - U\right]$$

The constant in Equation 6.19a depends on the units employed, thus

$$\text{ESHP} = \text{SHP} + \frac{T(\text{lb}) \times U(\text{ft/s})}{550 \times \eta_{pr}} \tag{6.110b}$$

$$\text{ESHP} = \text{SHP} + \frac{T(\text{lb}) \times U(\text{mph})}{375 \times \eta_{pr}} \tag{6.110c}$$

$$\text{ESHP} = \text{SHP} + \frac{T(\text{lb}) \times U(\text{knots})}{325 \times \eta_{pr}} \tag{6.110d}$$

$$\text{ESHP} = \text{SHP} + \frac{T(\text{lb}) \times U(\text{in. ft/s})}{550 \times \eta_{pr}} \tag{6.110e}$$

Usually, a value of $\eta_{pr} \approx 80\%$ is employed as an industrial standard.

6.4.6 Fuel Consumption

As previously explained for turbojet and turbofan engines, fuel consumption is identified by the thrust specific fuel consumption (TSFC), defined as TSFC = $\dot{m}f/T$ and expressed in terms of kg fuel/N · h.

For turboprop engines, fuel consumption is identified by the equivalent specific fuel consumption (ESFC), defined as

$$ESFC = \frac{\dot{m}f}{ESHP}$$

and expressed in the following units lb fuel/hp · h or kg fuel/kW · h.

Typical values for this are $ESFC = 0.45 - 0.60$ lb fuel/hp · h, or $0.27 - 0.36$ kg fuel/kW · h

Example 6.7

A two-spool turboprop engine with the propeller driven by a free power turbine. It is required to calculate the ESHP and ESFC in the following two cases:

1. Static conditions

$$\dot{m}_f = 1500 \text{ lb/h}, \quad T = 600 \text{ lb}_f, \quad \text{and} \quad SHP = 2800$$

2. Flight conditions

$$V = 330 \text{ ft/s}, \quad \dot{m}_f = 1000 \text{ lb/h}, \quad T = 300 \text{ lb}_f, \quad \text{and} \quad SHP = 2000$$

Solution

1. For static or ground-run conditions, the equivalent shaft horsepower and equivalent specific fuel consumption are calculated from the relations

$$ESHP = SHP + \frac{T}{2.5} = 2800 + \frac{600}{2.5} = 3040 \text{ hp}$$

$$ESFC = \frac{\dot{m}_f}{ESHP} = \frac{1500}{3040} = 0.4934 \text{ lb/ESHP} \cdot \text{h}$$

2. During flight

$$ESHP = SHP + \frac{TV}{550} = 2000 + \frac{300 \times 330}{550} = 2180 \text{ hp}$$

$$ESFC = \frac{\dot{m}_f}{ESHP} = \frac{1000}{2180} = 0.4587 \text{ lb/ESHP} \cdot \text{h}$$

6.4.7 Turboprop Installation

Turboprop (or turbo-propeller) engines are installed in one of the following positions:

1. Wing
2. Fuselage, either at the nose or empennage of the aircraft for a single-engined aircraft
3. Horizontal tail installation

Details of the powerplant installation will be given in Chapter 9. A brief overview is given here. Most present day turboprops are *wing*-mounted engines on either passenger or cargo transports (Figure 6.59). Either puller or pusher turboprops may be installed to the wing. A typical wing installation of the puller type is seen in the Fokker F-27, which is powered by two RR Dart puller engines. In some aircraft, a pair of counter-rotating propellers is installed to each engine; the Antonov An-70 is an example of these aircraft.

Small aircrafts may be powered by turboprop engines mounted to the fuselage. With regard to nose installation, a single turboprop engine fitted to the nose of an aircraft having either a single propeller or contra-rotating propellers can be found (Figure 6.60). As an

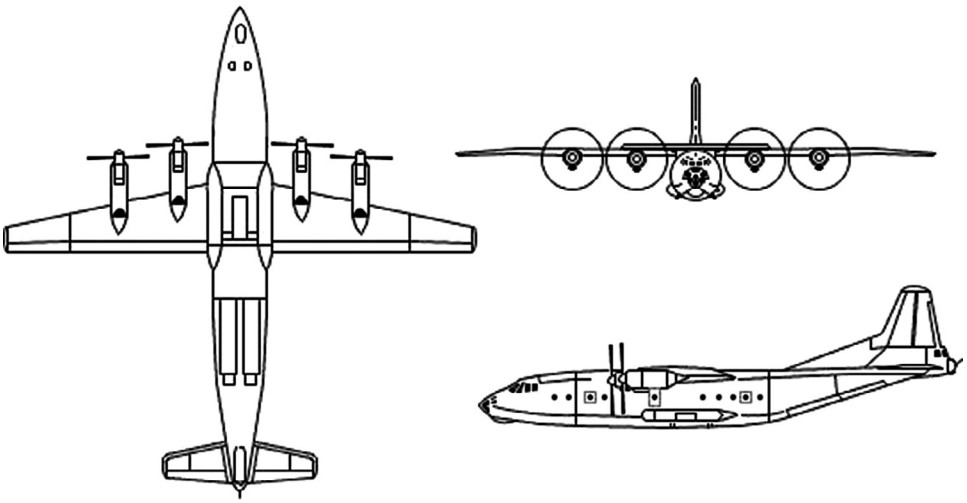


FIGURE 6.59
Wing installation of turboprop engine.



FIGURE 6.60
Counter-rotating nose turboprop engines.

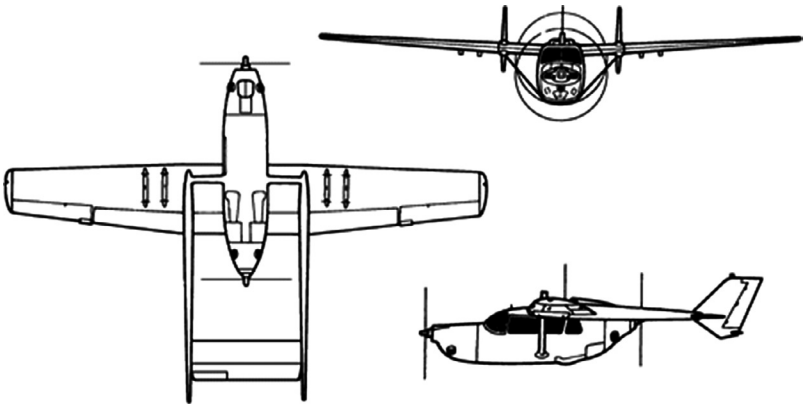


FIGURE 6.61
Nose and tail turboprop engines; Cessna O-2 Skymaster.

alternative, a turboprop engine with contra-rotating propellers can be installed in the tail, as seen in the Jetcruzer 500, AASI airplane (Figure 6.48). A combination of nose and tail installations is seen in the Cessna O-2 Skymaster (Figure 6.61).

The Antonov AN-180, a medium-sized turboprop airliner (around 175 passengers), is under development. It is powered by two turboprop engines attached to the tips of the horizontal tail and each has contra-rotating propellers.

6.4.8 Details of Some Engines

Some of the data for two turboprop engines is given in Table 6.9.

TABLE 6.9

Engine	A-T53-L13B	LTS101-600A
Power (SHP)	1570	640
No. of shafts	1	1
Compressor type	Axial + Centrifugal	Axial + Centrifugal
Compressor stages	5 Axial + 1 Centrifugal	1 Axial + 1 Centrifugal
Turbine stages	2	1
Compression ratio	7	14
Mass flow rate (lb/s)	11.5	5
Propeller RPM	2200	2000
T/O SFC (lb/ESHP/h)	0.6	0.551
Cruising SFC (lb/ESHP/h)	0.6	0.551
Max PWR pressure ratio	9.4	8.5
Length (in.)	47.6	37.4
Diameter (in.)	23	21
Weight (lb)	545	290

Example 6.8

A single-spool turboprop engine when running at maximum rpm at sea-level conditions, $P_a = 1$ bar and $T_a = 288$ K, has the following particulars:

$m_a = 14.6\,\text{kg/s}$	$\pi_c = \dfrac{P_{03}}{P_{02}} = 8.5$	$P_{04} = 0.96\,P_{03}$
$T_{04} = 1220\,\text{K}$	$V_J = 250\ \text{m/s}$	
$\eta_c = 0.87$	$\eta_{C.C} = 0.98$	$\eta_t = 0.9$
$\eta_n = 0.95$	$\eta_m = 0.98$	$\eta_{pr} \times \eta_g = 0.78$
$C_{P_c} = 1.01\ \text{kJ/kg}\cdot\text{K}$	$C_{P_{C\text{-}C}} = 1.13\ \text{kJ/kg}\cdot\text{K}$	$C_{P_t} = C_{P_t} = 1.14\ \text{kJ/kg}\cdot\text{K}$
$Q_R = 43{,}000\,\text{kJ/kg}\cdot\text{K}$		

It is required to calculate the equivalent brake horsepower (EBHP)

Solution

A sketch for the turboprop engine and the cycle on the temperature-entropy diagram is given in Figure 6.62. Successive analysis of the elements will be given here.

Intake: During a ground test (zero flight speed and Mach number), the total engine conditions are equal to the static conditions.

Moreover, the flow in the diffuser is isentropic, thus

$$T_{02} = T_{0a} = T_a = 288\ \text{K}$$
$$P_{02} = P_{0a} = P_a = 1\ \text{bar}$$

Compressor: The outlet conditions are

$$P_{03} = \pi_c \quad P_{02} = 8.5\ \text{bar}$$
$$T_{03} = T_{02}\left[1 + \frac{\pi^{\gamma_c - 1/\gamma_c} - 1}{\eta_C}\right]$$
$$W = C_{P_c}\left(T_{03} - T_{02}\right) = 281.88\ \text{kJ/kg}$$

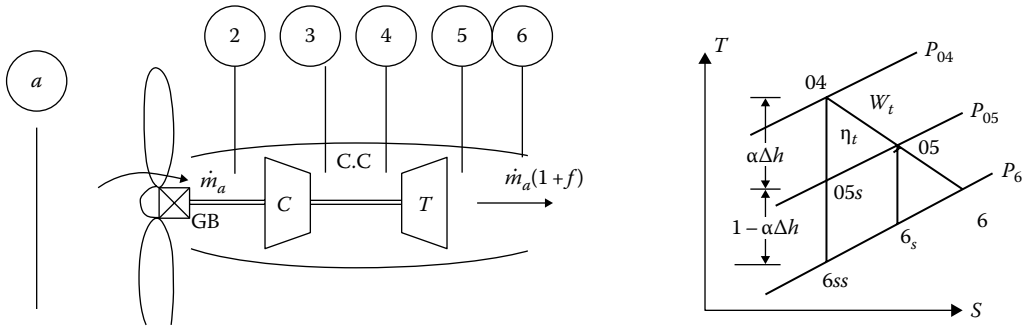


FIGURE 6.62
Sketch for the engine and cycle.

Combustion chamber: The pressure for gases leaving the combustion chamber is

$$P_{04} = 0.96 \quad P_{03} = 8.16 \text{ bar}$$

The fuel-to-air ratio and fuel mass flow rate are

$$f = \frac{C_{P_{C.C}} T_{04} - C_{P_C} T_{03}}{\eta_{C.C} Q_R - C_{O_{C.C}} T_{04}} = 0.017$$
$$\dot{m}_f = 0.017 \dot{m}_a = 0.248 \text{ kg/s}$$

Turbine: The enthalpy drop in the turbine and nozzle is

$$\Delta h = C_{P_t}\left(T_{04} - T_{6s}\right) = C_{P_t} T_{04}\left(1 - \frac{T_{6s}}{T_{04}}\right) = C_{P_t} T_{04}\left[1 - \left(\frac{P_6}{P_{04}}\right)^{\gamma_t - 1/\gamma_t}\right]$$

with $P_6 = P_a$, $\gamma_t = 1.336$, then

$$\Delta h = 527.25 \text{ kJ/kg}$$

From Figure 6.62 since $\eta_n = \dfrac{V_j^2/2}{(1-\alpha)\Delta h}$, then $\alpha = 1 - \dfrac{V_j^2}{2\eta_n \Delta h} = 0.938$.

The turbine output specific power is

$$W_t = \eta_t \alpha \Delta h = 445.104 \text{ kJ/kg}$$

The specific power delivered to the propeller shaft is

$$W_{Shaft} = \eta_m W_t - W_C = 154.322 \text{ kJ/kg}$$

The corresponding shaft power is

$$P_{Shaft} = \dot{m}_a W_{Shaft} = 2253.107 \text{ kW}$$

The jet thrust for zero flight speed is

$$T_J = \dot{m}_a\left[\left(1+f\right)V_J\right] = 3712.05 \text{ N}$$

The total power is the sum of propeller and jet thrust contributions

$$P_{Total} = \eta_{pr} \times \eta_g \times P_{Shaft}\left(\text{kW}\right) + \frac{T_J\left(\text{N}\right)}{8.5} = 2194.1 \text{ kW}$$

The horsepower is then

$$EBHP = \frac{P_{Total}\left(\text{kW}\right)}{0.7457} = 2942.3 \text{ hp}$$

Example 6.9

The turboprop considered in Example 6.8 is re-examined here. The engine is fitted to an aircraft flying at a Mach number of 0.6. The maximum temperature is 1120 K and fuel having a heating value of 438,778 kJ/kg is used. All other data are unchanged. It is required to calculate the specific equivalent shaft horsepower (S.E.S.H.P.) if the aircraft is flying at sea level and altitudes of 3, 6, and 9 km.

Solution

The ambient temperature and pressure at the requested altitudes are

At sea level	$T_a = 288$ K	$P_a = 1$ bar
3 km	$T_a = 268.5$ K	$P_a = 0.701$ bar
6 km	$T_a = 249$ K	$P_a = 0.472$ bar
9 km	$T_a = 229.5$ K	$P_a = 0.308$ bar

A general formulation for the problem will be followed to account for the variations in the inlet conditions due to altitude change

Intake:

$$T_{02} = T_{0a} = T_a\left[1+\frac{\gamma-1}{\gamma}M^2\right] = 1.072T_a \text{ K}$$

$$P_{02} = P_{0a} = P_a\left[1+\frac{\gamma-1}{\gamma}M^2\right]^{\gamma_c/\gamma_c-1} = 1.276T_a^{\gamma_c/\gamma_c-1} \text{ bar}$$

Compressor:

$$P_{03} = \pi_C P_{02} = 8.5 \times P_{02} \text{ bar}$$

With $\gamma_c = 1.397$, then the outlet temperature and the compressor specific work are

$$T_{03} = T_{02}\left[1+\frac{\pi^{\gamma_c-1/\gamma_c}-1}{\eta_C}\right] = T_{02}\left[1+\frac{\pi^{0.286}-1}{0.87}\right] = 1.97T_{02}$$

$$W_c = \frac{C_{P_c}\left(T_{03}-T_{02}\right)}{\eta_{mc}} = \frac{1.01\times 0.97}{0.98} = T_{02} \text{ kW/kg}$$

Combustion chamber:

$$P_{04} = 0.96P_{03}$$

$$f = \frac{C_{p_{cc}}T_{04} - C_{P_C}T_{03}}{\eta_c Q_R - C_{P_{>CC}}T_{04}} = \frac{1{,}265 - 1.01T_{03}}{43{,}000 - 1{,}265} = \frac{1{,}265 - 1.01T_{03}}{41{,}735}$$

Turbine: From Figure 6.62

$$T_{05} - T_{6ss} = T_{05} - T_{6s} = \frac{V_j^2}{2Cp_n\eta_n} = \frac{(250)^2}{2\times 1140\times 0.95} = 28.8\ \text{K}$$

with $\frac{\gamma_n - 1}{\gamma_n} = \frac{R}{Cp_n} = \frac{287}{1140} = 0.252$, thus $\gamma_n = \gamma_t = 1.336$.

Since $C_{P_t} = C_{P_n} = 1.14$, and $\frac{\gamma_n - 1}{\gamma_n} = \frac{R}{Cp_n} = \frac{287}{1140} = 0.252$, then $\gamma_n = \gamma_t = 1.336$

$$\frac{T_{04}}{T_{6ss}} = \left(\frac{P_{04}}{P_a}\right)^{\gamma_n - 1/\gamma_n} = \left(\frac{P_{04}}{P_{03}}\frac{P_{03}}{P_{02}}\frac{P_{02}}{P_a}\right)^{\gamma_n - 1/\gamma_n} = \left[(0.96)(8.5)(1.275)\right]^{0.252} = 1.8$$

$$T_{6ss} = \frac{1120}{1.8} = 621\ \text{K}$$

$$T_{05s} \approx T_{6ss} + (T_{05} - T_{6s}) = 621 + 28.8 = 648.8\ \text{K}$$

$$\frac{P_{04}}{P_{05}} = \left(\frac{T_{04}}{T_{05s}}\right)^{\gamma_t/\gamma_t - 1} = \left(\frac{1120}{648.8}\right)^{3.97} = 8.6$$

$$W_t = \eta_{mt}\Delta h_t = \eta_{mt}\eta_t Cp_t (T_{04} - T_{05s}) = 0.98\times 0.9\times 1.14\times (1120 - 648.8)$$

$$W_t = 470\ \text{kJ/kg}$$

$$W_{Shaft} = (1+f)W_t - W$$

$$\frac{P_{propeller}}{\dot{m}_a} = \eta_{pr}\eta_8 W_{shaft} = 0.78W_{shaft}$$

$$\frac{T}{\dot{m}_a} = (1+f)V_j - V_f = (1+f)V_j - 0.6\sqrt{\gamma_c RT_a}$$

$$\frac{P_{jet}}{\dot{m}_a} = \frac{T}{\dot{m}_a}\times V_f = \frac{T}{\dot{m}_a}\times\left(0.6\sqrt{\gamma_c RT_a}\right)$$

$$\frac{P_{total}}{\dot{m}_a} = \frac{P_{propeller}}{\dot{m}_a} + \frac{P_{jet}}{\dot{m}_a}$$

$$\text{S.E.S.H.P} = \frac{P_{total}}{0.7456\dot{m}_a}$$

The results can be arranged as given in Table 6.10.

TABLE 6.10

Altitude (km)	W_C (kJ/kg)	f	W_{SHAFT} (kJ/kg)	$\frac{P_{propeller}}{\dot{m}_a}$	V_f (m/s)	$\frac{T}{\dot{m}_a}$	$\frac{P_{jet}}{\dot{m}_a}$	$\frac{P_{total}}{\dot{m}_a}$ (kJ/kg)	S.E.S.H.P hp/(kg/s)
0	308	0.0152	169	132	204	49.8	10.16	142.16	190.35
3	288	0.0164	190	148	196	57	11.17	159.17	213.13
6	267	0.0176	211	165	190	63	12	177	237.26
9	246	0.0183	232	181	182	71	12.92	193.92	260

Example 6.10

The Bell/Boeing V-22 Tilt-rotor multi-mission aircraft is shown in Figure 6.47. It is powered by an Allison T406 engine. The T406 engine has the following characteristics:

Rotor is connected to a free power turbine

Air mass flow rate	14 kg/s
Compressor pressure ratio	14
Turbine inlet temperature	1,400 K
Fuel heating value	43,000 kJ/kg

During landing, it may be assumed that the air entering and the gases leaving the engine have nearly zero velocity. The ambient conditions are 288 K and 101 kPa. The propeller efficiency and gear box efficiencies are 0.75 and 0.95. Assuming all the processes are ideal, calculate the propeller power during landing $\gamma_c = 1.4$ and $\gamma_h = 1.3299$.

Solution

The ambient conditions are

$$T_a = 288\ \text{K}, \quad P_a = 101\ \text{kPa}$$

The flight and jet speeds are $V_f = V_j = 0$

with $\gamma_c = 1.4$, then $Cp_c = \dfrac{\gamma_c R}{\gamma_c - 1} = 1004.5\ \text{J/kg/k}$

Since $\gamma_h = 1.3299$, then $Cp_h = \dfrac{\gamma_h R}{\gamma_h - 1} = 1156.7\ \text{J/kg/K}.$

Intake: Since the flight Mach number is zero, then

$$T_{o2} = T_{oa} = T_a\left(1 + \frac{\gamma_c - 1}{2}M^2\right) = 288\ \text{K}$$

$$P_{o2} = P_{oa} = P_a\left(1 + \frac{\gamma_c - 1}{2}M^2\right)^{\gamma_c/\gamma_c - 1} = 101\ \text{kPa}$$

Compressor: For an ideal compressor

$$T_{o3} = T_{o2}\left(\frac{P_{o3}}{P_{o2}}\right)^{\gamma_c - 1/\gamma_c} = T_{o2}\left(\pi_c\right)^{\gamma_c - 1/\gamma_c} = 612.15\ \text{K}$$

$$P_{o3} = \pi_c \times P_{o2} = 1414\ \text{kPa}$$

Combustion chamber:

$$T_{o4} = 1400\ \text{K} \quad \text{and} \quad P_{o4} = P_{o3} = 1414\ \text{kPa}$$

Fuel-to-air ratio

$$f = \frac{Cp_h T_{o4} - Cp_c T_{o3}}{Q_{HV} - Cp_h T_{o4}} = 0.02$$

Turbine: Energy balance between the compressor and turbine of the gas generator

$$W_c = W_t$$
$$\dot{m}_a Cp_c\left(T_{o3} - T_{o2}\right) = \dot{m}_a\left(1+f\right)Cp_h\left(T_{o4} - T_{o5}\right)$$
$$T_{o5} = T_{o4} - \frac{Cp_c}{Cp_h\left(1+f\right)}\left(T_{o3} - T_{o2}\right) = 1125.37 \text{ K}$$
$$P_{o5} = P_{o4}\left(\frac{T_{o5}}{T_{o4}}\right)^{\left(\gamma_h/\gamma_h - 1\right)} = 586.47 \text{ kPa}$$

Free power turbine:

$$\Delta h = h_{o5} - h_{7S} = Cp_h\left(T_{o5} - T_{7S}\right)$$
$$\Delta h = Cp_h T_{o5}\left(1 - \left(\frac{P_7}{P_{o5}}\right)^{\left(\gamma_h - 1/\gamma_h\right)}\right) = 460376.7 \text{ J/kg}$$
$$\alpha_{opt} = 1 - \frac{\cancel{V_J^2}\,\eta_n}{2\eta_{pr}^2\eta_g^2\eta_m^2\eta_{fpt}^2\Delta h} = 1$$

The free power turbine absorbs all the power in the gases leaving the gas generator turbine. Points (6) and (7) in Figure 6.16 are coincident. Thus

$$\Delta h = Cp_h\left(T_{o5} - T_{6S}\right) = Cp_h\left(T_{o5} - T_{o6}\right)$$

From which $T_{o6} = 727.36$ K.

Nozzle: There is no thrust generated as

$$Tj = \dot{m}_a\left(\left(1+f\right)V_J - V_f\right) = 0$$
$$P_j = 0$$

The specific power absorbed in the propeller is

$$W_{pr} = \eta_{pr}\eta_g\eta_m\eta_{fpt}\alpha\Delta h = 0.75 \times 0.95 \times 1 \times 1 \times 1 \times 460.3767 = 328.02 \text{ kJ/kg}$$

The power consumed in the propeller is then

$$P_{pr} = \dot{m}_a W_{pr} = 4592.26 \text{ kW}$$
$$P_t = P_{pr} + P_j = 4592.26 \text{ kW}$$

The corresponding shaft horsepower is then

$$\text{SHP} = \frac{P_t}{0.7457} = \frac{4592.26}{0.7457} = 6158.32 \text{ hp}$$

6.4.9 Performance Analysis

A case study for a turboprop fitted with a free power turbine is examined. The flight altitude considered is 6 km. The effect of the flight Mach number on the thrust and power of both the propeller and jet is examined. The Mach number is increased from 0.1 to 0.8. The fuel is of the hydrocarbon type, having a heating value of 43,000 kJ/kg, a compressor

pressure ratio of 6, and a turbine inlet temperature of 1,200 K. The efficiencies of the diffuser, compressor, and combustion chamber are 0.95, 0.87, and 0.98, respectively. The efficiency of the two turbines and nozzle is 0.9. The mechanical efficiency for the compressor and turbine is 0.98. The efficiencies of the gearbox and propeller are 0.95 and 0.8. The air mass flow rate is 25 kg/s. The specific heat ratios for the cold section, combustion chamber, and hot section are, respectively, $\gamma_c = 1.3798$, $\gamma_{cc} = 1.3405$, and $\gamma_h = 1.3365$.

Figure 6.63 illustrates the variation of four parameters: fuel-to-air ratio, enthalpy drop across the free turbine and nozzle, optimum α_{opt}, and inlet diameter with the flight Mach number.

Figure 6.64 examines the contribution of both the jet and propeller to the engine thrust and power. It also evaluates the percentage of the jet thrust to the propeller thrust. As can be seen, this percentage ranges from 1% to 12% as the Mach number increases from 0.1 to 0.8.

The total power expressed in ESHP and the fuel consumption expressed as ESFC is illustrated in Figure 6.65.

To examine the effect of the compressor pressure ratio and turbine inlet temperature, the above case is re-examined but for a larger engine with a compressor pressure ratio of 23 and a turbine inlet temperature of 1600 K. All other data are unchanged. The variations of fuel-to-air ratio, enthalpy drop across the free turbine and nozzle, optimum α_{opt}, and inlet diameter with the flight Mach number are given in Figure 6.66.

Figure 6.67 examines the contribution of both the jet and propeller to the engine thrust and power. It also evaluates the percentage of the jet thrust to the propeller thrust. As can be seen, this percentage ranges from 1% to 7% as the Mach number increases from 0.1 to 0.8.

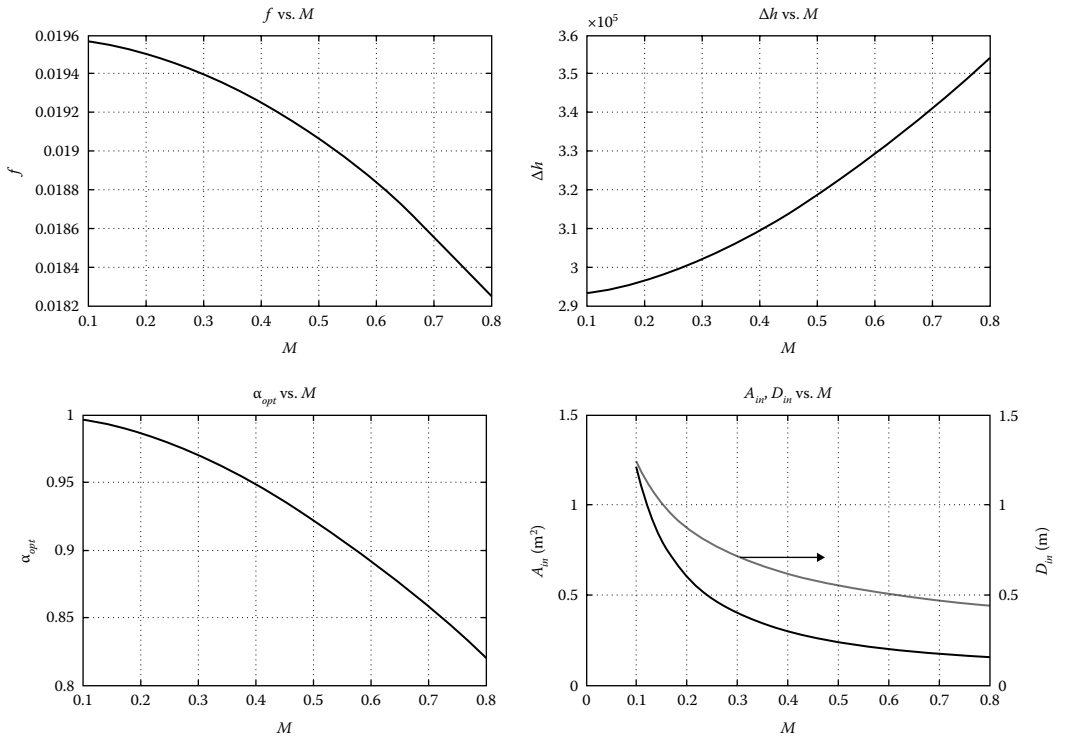


FIGURE 6.63
Variation of f, Δh, α_{opt}, and inlet area with the flight Mach number.

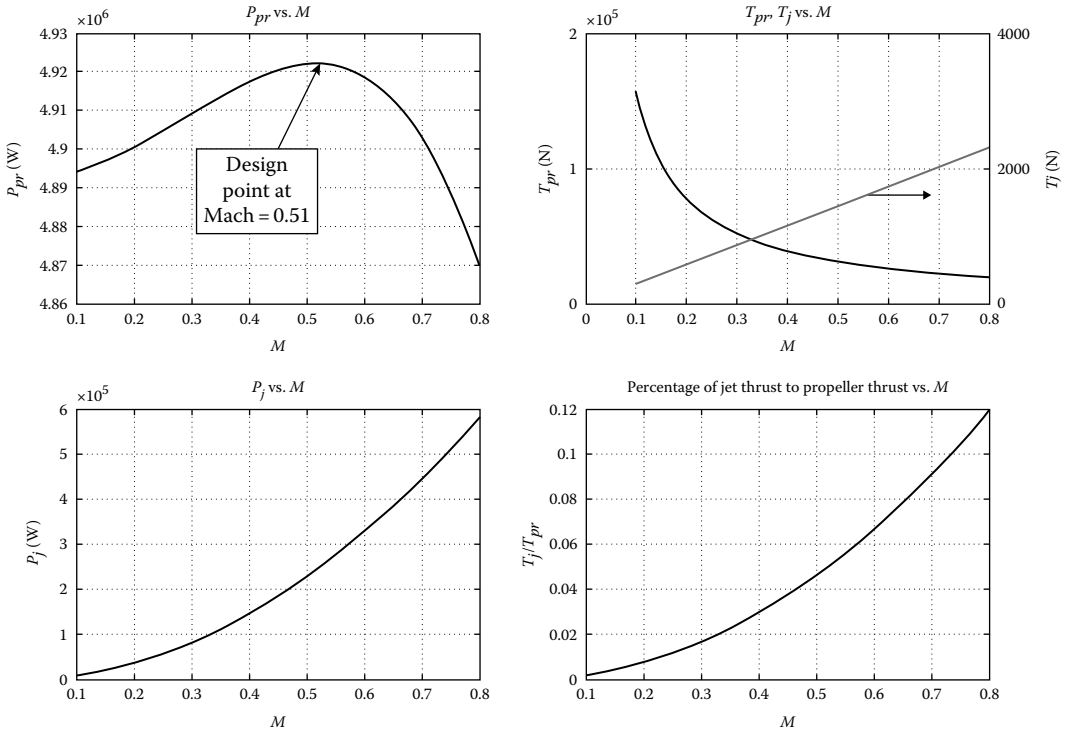


FIGURE 6.64
Thrust and power contribution of both propeller and jet.

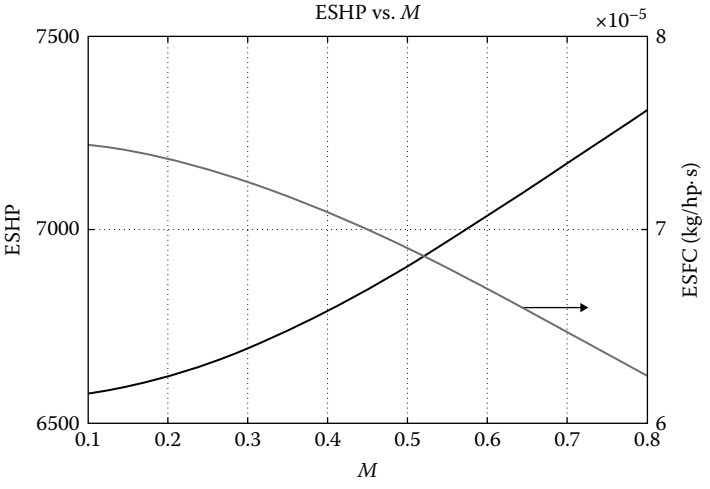


FIGURE 6.65
Variation of ESHP and ESFC with Mach number.

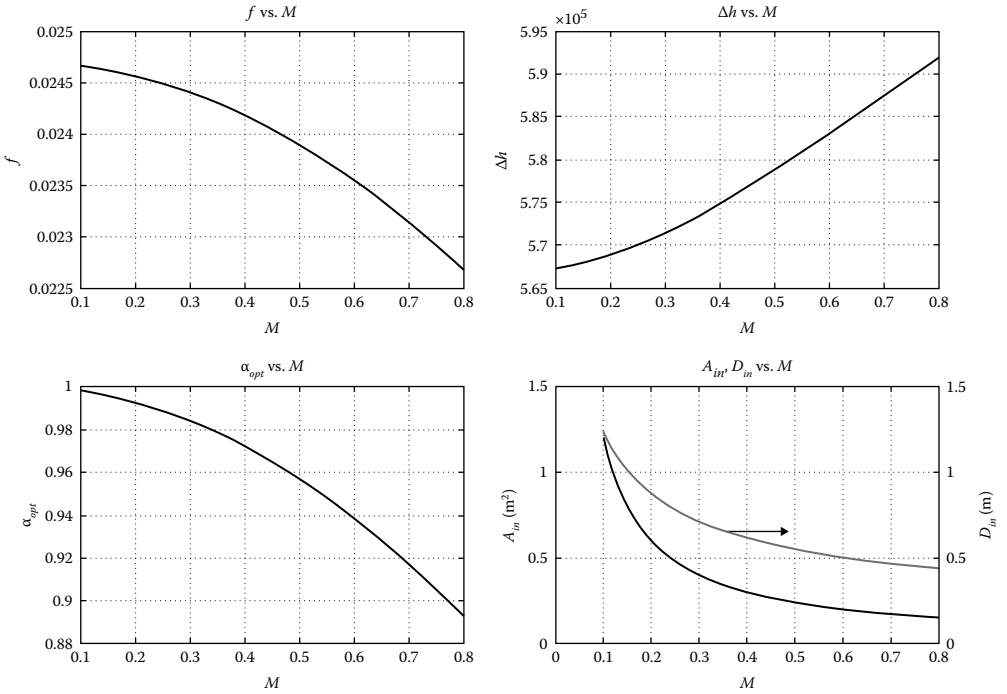


FIGURE 6.66
Variation of f, Δh, α_{opt}, and inlet area with flight Mach number for the larger engine.

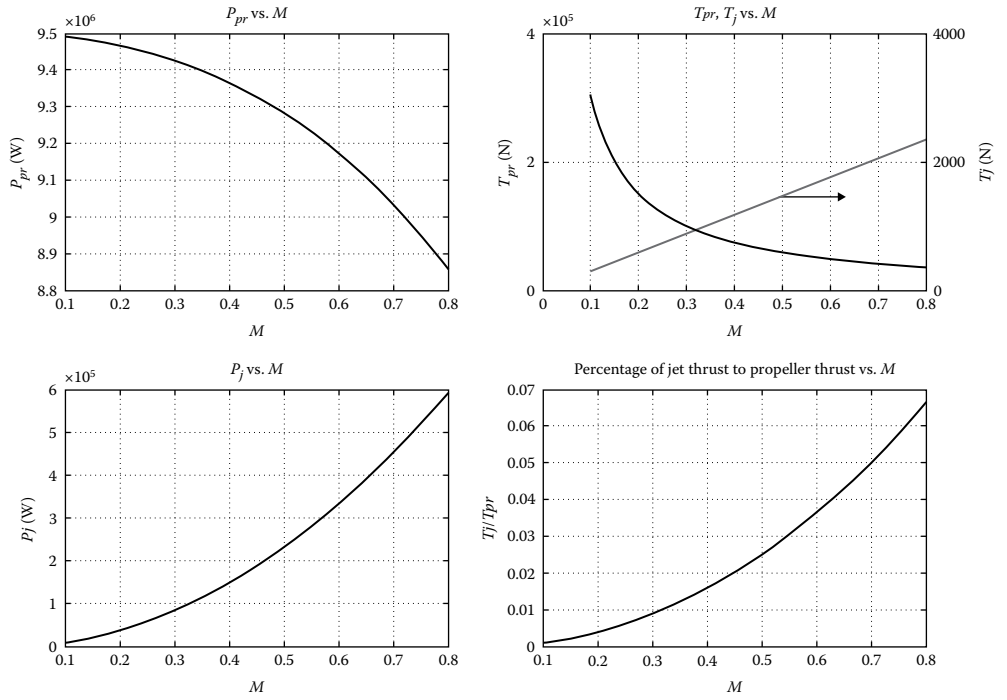


FIGURE 6.67
The thrust and power contributions of both the propeller and jet for the larger engine.

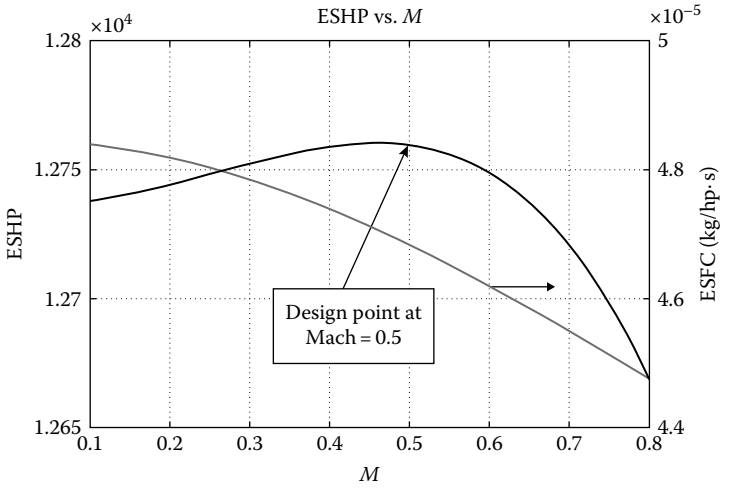


FIGURE 6.68
Variation of ESHP and ESFC with the Mach number.

The total power expressed in ESHP and the fuel consumption expressed as ESFC is illustrated in Figure 6.68. A peak value at a Mach number of 0.5 is seen for the ESHP. This point may be selected for the continuous cruise of aircraft.

6.4.10 Comparison between Turbojet, Turbofan and Turboprop Engines

Certain important characters of the three engine types are

1. Turbojet engine
   a. Low thrust at low forward speed
   b. High-thrust specific fuel consumption
   c. Low specific weight (W/T)
   d. Small frontal area
   e. Good ground clearance
2. Turbofan engine
   a. High thrust even at low speed
   b. Thrust-specific fuel consumption is better than that in a turbojet engine
   c. Less noise compared with turbojet engine
   d. Low propulsive efficiency at very high speed, though higher than turbojet; generally better performance in the range of subsonic and transonic speeds
   e. Fair ground clearance
3. Turboprop engine
   a. High propulsive efficiency at low speed
   b. More complicated and heavier than turbojet and turbofan engines

c. Low SFC
d. Large ground clearance as high wing design is employed in turboprop powered aircraft
e. Highest noise level

Example 6.11

A Tupolev Tu-114 turboprop-powered aircraft (Figure 6.69) is cruising at velocity of 770 km/h at an altitude of 10,000 m. The aircraft is powered by four Kuznetsov NK-12 MV engines. At this altitude, the engines have a compression ratio of 11 and a turbine inlet temperature of 1250 K; the propeller and gear box efficiencies are 0.80 and 0.95, respectively. Let each engine have the following properties

η_{intake}	$\eta_{compressor}$	$\eta_{turbine}$	$\eta_{combustion}$	η_{nozzle}
0.95	0.91	0.91	0.98	0.95

Assume the engines are operating in conditions of α_{opt} and each engine has an equivalent power of 5940 kW.

Calculate

1. α_{opt}
2. V_e
3. $\dot{m}_a$
4. Jet thrust
5. Propeller thrust
6. ESFC

Solution

The cycle on the *T*–*S* diagram is plotted in Figure 6.70.

$$\text{At } 10{,}000 \text{ m}; \quad T_a = 223.1 \text{ K}, \quad P_a = 26.5 \text{ kPa}$$



FIGURE 6.69
Tu116.

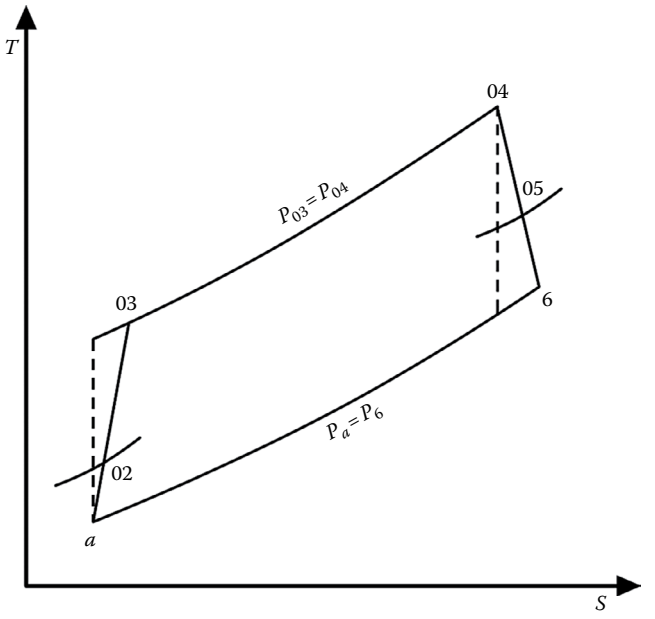


FIGURE 6.70
T–S diagram.

$$V = 770 \text{ km/h} = 213.9 \text{ m/s}$$

$$M = \frac{V}{\sqrt{\gamma R T_a}} = 0.7144$$

Diffuser

$$P_{02} = P_a\left[1 + \eta_{intake}\left(\frac{\gamma_c - 1}{2}\right)M^2\right]^{\gamma_c/\gamma_c - 1}$$

$$\therefore P_{02} = 26.5 * \left[1 + 0.95 * \left(\frac{1.4 - 1}{2}\right)0.7144^2\right]^{3.5}$$

$$P_{02} = 36.64 \text{ kPa}$$

$$T_{02} = T_a\left[1 + \left(\frac{\gamma_c - 1}{2}\right)M^2\right]$$

$$\therefore T_{02} = 223.1 * \left[1 + \left(\frac{1.4 - 1}{2}\right)0.7144^2\right]$$

$$T_{02} = 245.9 \text{ K}$$

Compressor

$$P_{03} = \pi_c * P_{02}$$

$$\therefore P_{03} = 11 * 36.64$$

$$P_{03} = 403 \text{ kPa}$$

$$T_{03} = T_{02}\left[1 + \frac{\left(\pi_c{}^{\gamma_c - 1/\gamma_c}\right)}{\eta_c}\right]$$

$$\therefore T_{03} = 245.9 * \left[1 + \frac{\left(11^{0.4/1.4} - 1\right)}{0.91}\right]$$

$$T_{03} = 511.8 \text{ K}$$

Combustion chamber

$$T_{04} = 1250 \text{ K}$$

$$P_{04} = P_{03}$$

$$P_{04} = 403 \text{ kPa}$$

$$f = \frac{Cp_h * T_{04} - Cp_c * T_{03}}{\eta_b QHV - Cp_h * T_{04}}$$

$$\therefore f = \frac{1.148 * 1,250 - 1.005 * 511.8}{0.98 * 43,000 - 1.148 * 1,250}$$

$$f = 0.0226174$$

Turbine and nozzle

$$\Delta h = Cp_h T_{04}\left(1 - \left(\frac{P_a}{P_{04}}\right)^{\gamma_h - 1/\gamma_h}\right) = 1.148 * 1250 * \left(1 - \left(\frac{26.5}{403}\right)^{0.25}\right) = 708.33 \text{ kJ/kg}$$

For α_{opt} condition

$$\alpha_{opt} = 1 - \frac{V^2}{2\Delta h}\left(\frac{\eta_n}{\eta_{pr}^2 \eta_g^2 \eta_m^2 \eta_t^2}\right)$$

$$\therefore \alpha_{opt} = 1 - \frac{213.9^2}{2 * 708330}\left(\frac{0.95}{0.80^2 * 0.95^2 * 1^2 * 0.91^2}\right)$$

$$\alpha_{opt} = 0.9359$$

$$V_e = V\left(\frac{\eta_n}{\eta_{pr}\eta_g\eta_m\eta_t}\right)$$

$$\therefore V_e = 213.9 * \left(\frac{0.95}{0.80 * 0.95 * 1 * 0.91}\right)$$

$$V_e = 293.82 \text{ m/s}$$

Equivalent power

$$\text{Equivalent power} = P_{propeller} + T_{jet} * V$$

$$\therefore \text{Equivalent power} = \dot{m}_a * \eta_p * \eta_{gb} * W_{shaft} + \dot{m}_a\left[\left(1+f\right)V_e - V)\right] * V$$

$$\therefore \text{Equivalent power} = \dot{m}_a * \eta_p * \eta_{gb} * \left[\left(1+f\right)\eta_t\alpha\Delta h - \Delta h_c\right] + \dot{m}_a\left[\left(1+f\right)\sqrt{2\eta_n\left(1-\alpha\right)\Delta h} - V)\right] * V$$

$$\therefore \text{Equivalent power} = \dot{m}_a\left[\eta_p * \eta_{gb} * \left[\left(1+f\right)\eta_t\alpha\Delta h - \Delta h_c\right] + \left[\left(1+f\right)\sqrt{2\eta_n\left(1-\alpha\right)\Delta h} - V)\right] * V\right]$$

$$\Delta h = Cp_h T_{04}\left(1 - \left(\frac{P_a}{P_{04}}\right)^{\gamma_h - 1/\gamma_h}\right) = 1.148 * 1250 * \left(1 - \left(\frac{26.5}{403}\right)^{0.25}\right) = 708.33 \text{ kJ/kg}$$

$$\Delta h_c = Cp_h\left(T_{03} - T_{02}\right) = 1.005 * \left(511.8 - 245.9\right) = 267.23 \text{ kJ/kg}$$

$$\therefore 5{,}940 * 10^3 = \dot{m}_a[0.8 * 0.95 * \left[1.0226174 * 0.91 * 0.9359 * 708{,}330 - 267{,}230\right]$$

$$+\left[1.0226174\sqrt{2 * 0.95 * \left(1 - 0.9359\right) * 708{,}330} - 213.9)\right] * 213.9]$$

$$\therefore \dot{m}_a = 20.88 \text{ kg/s}$$

Jet and propeller thrust

$$T_{Pr} = \frac{\dot{m}_a * \eta_p * \eta_{gb} * W_{shaft}}{V}$$

$$W_{shaft} = \left(1+f\right)\eta_t\alpha\Delta h - \Delta h_c = 1.0226174 * 0.91 * 0.9359 * 708.33 - 267.23 = 349.677 \text{ kJ/kg}$$

$$\therefore T_{Pr} = \frac{20.88 * 0.80 * 0.95 * 349.677}{213.9}$$

$$\therefore T_{Pr} = 25.94 \text{ kN}$$

$$T_{jet} = \dot{m}_a\left[\left(1+f\right)V_e - V)\right] = 20.88 * \left[1.0226174 * 293.82 - 213.9\right]$$

$$T_{jet} = 1.8075 \text{ kN}$$

ESFC

$$ESFC = \frac{\dot{m}_f}{\text{Equiv. power}} = \frac{f * \dot{m}_a}{\text{Equiv. power}}$$

$$\therefore ESFC = \frac{0.0226174 * 20.88}{5940}$$

$$\therefore ESFC = 0.795036 * 10^{-4}\ \text{kg/kW} \cdot \text{s} = 0.286213\ \text{kg/kW} \cdot \text{h}$$

6.5 Turboshaft Engines

A turboshaft engine is defined as a gas turbine engine designed to produce only shaft power. Turboshaft engines are similar to turboprop engines, except that the hot gases are expanded to a lower pressure in the turbine, thus providing greater shaft power and little exhaust velocity.

Turboshaft engines are used in helicopters, boats, ships, trains and automobiles, tanks, pumping units for natural gas in cross-country pipelines, and various types of industrial equipment.

In this chapter, analysis and discussions will be limited to the turboshaft engines used in helicopters.

All the other applications will be thoroughly analyzed in Chapter 8. Many aeroengine manufacturers produce two versions of an engine, one as a turboprop and the other as a turboshaft engine. Examples are the PT6B and PW206 produced by Pratt & Whitney of Canada, the Allied Signal LTS101-600A-3, and the Allison 250-C30M.

A turboshaft engine also has two configurations; either the load is driven by the same gas generator shaft (Figure 6.71) or it is driven by the free power turbine (Figure 6.72). The first configuration resembles a single-spool engine, while the second is a two-spool configuration.

The corresponding cycles plotted on the temperature-entropy axes are shown in Figure 6.73 for the single-spool configuration and Figure 6.74 for double-spool engines.

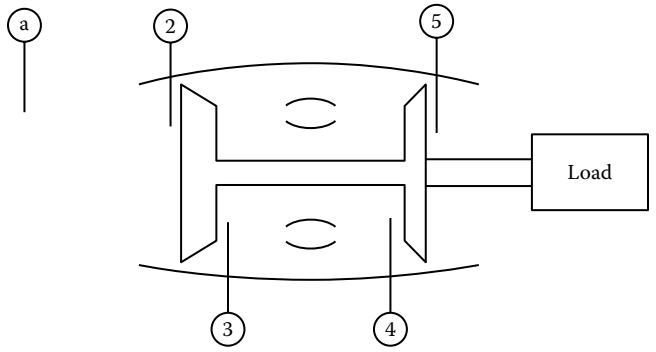


FIGURE 6.71
Single-spool turboshaft engine.

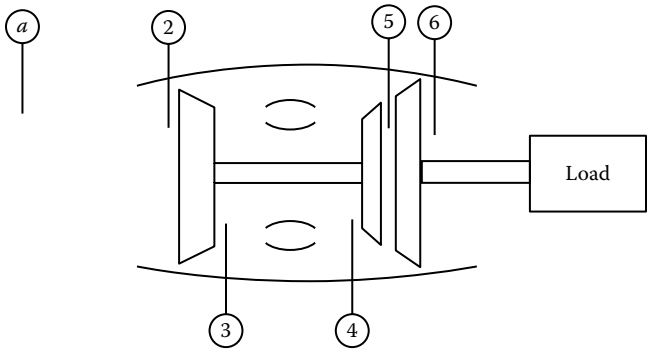


FIGURE 6.72
Two-spool turboshaft engine.

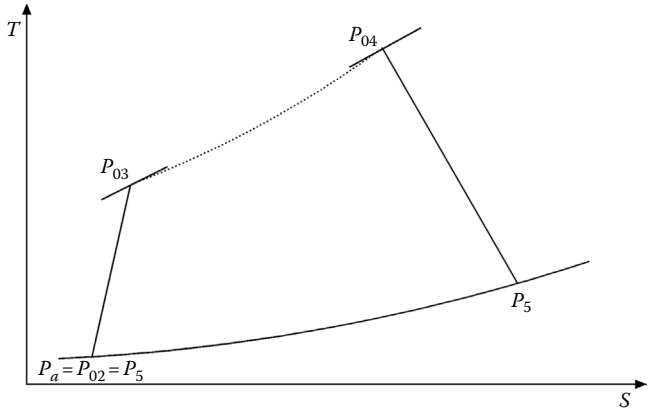


FIGURE 6.73
T–S diagram for a single-spool turboshaft.

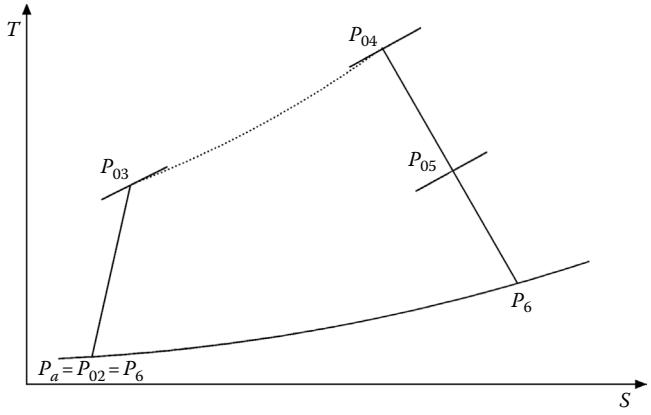


FIGURE 6.74
T–S diagram for a double-spool turboshaft.

The hot gases do not expand in the turbine (single-spool) or free turbine (double-spool) to nearly the ambient pressure, thus providing greater shaft power and low exhaust velocity.

6.5.1 Power Generated by Turboshaft Engines

6.5.1.1 Single-Spool Turboshaft

From Figure 6.69, the following point may be drawn.

Diffuser: Due to the nearly zero or low flight speed

$$P_{02} = P_{0a} = P_a \tag{6.111}$$

and

$$T_{02} = T_{0a} = T_a \tag{6.112}$$

Compressor: The outlet temperature and pressure are determined from Equations 6.94 and 6.95.

Combustion chamber: The fuel-to-air ratio is evaluated from Equation 6.96.

Turbine: The turbine drives both the compressor and load. The specific power delivered to the output shaft, W_{shaft}, is expressed as

$$W_{shaft} = (1 + f - b)\eta_{mt} W_t - \frac{W_c}{\eta_{mc}} \tag{6.113}$$

where f, b is the fuel-to-air ratio and bleed ratio. The mechanical efficiencies for the turbine and compressor are, respectively, η_{mt}, η_{mc}.

This shaft will drive the load (here, the rotor of a helicopter) and will experience some mechanical losses due to friction in the gearbox and bearings, thus

$$W_{load} = \eta_m W_{shaft} \tag{6.114}$$

The load power is, then,

$$P_{load} = \dot{m}_a W_{load} \tag{6.115}$$

6.5.1.2 Double-Spool Turboshaft

Various points will be given here. The diffuser, compressor, and combustion chamber are treated as in Section 6.5.1.1.

Gas generator turbine: The turbine provides sufficient energy to drive the compressor, thus the outlet temperature is obtained from the energy balance between the compressor and turbine, or

$$T_{05} = T_{04} - \frac{Cp_c (T_{03} - T_{02})}{Cp_t \eta_{mc} \eta_{mt} (1 + f - b)} \tag{6.116}$$

and

$$P_{05} = P_{04}\left[1-\left(\frac{T_{04}-T_{05}}{\eta_t T_{04}}\right)\right]^{\gamma_t/\gamma_t-1} \tag{6.117}$$

Free power turbine: The gases are assumed to have complete expansion to the ambient pressure, thus the power delivered to the load is

$$P_{load} = \dot{m}_a\left(1+f-b\right)\eta_m Cp_{ft} T_{05}\left[1-\left(\frac{P_a}{P_{05}}\right)^{\gamma_t-1/\gamma_t}\right] \tag{6.118}$$

6.5.2 Examples for Turboshaft Engines

Examples for turboshaft engines used in helicopters are the Lycoming T-55-L-7C, powering the Boeing Vertol Chinook CH-47 helicopter [25], or the Turbomeca Arrius 2K1, powering the Eurocopter EC120 Colibri used in tourism over New York City [26]. Both are two-spool engines where the helicopter rotor is driven by a free power turbine.

Example 6.12

Figure 6.75 illustrates the world's largest helicopter, the Mi-26, a Russian multipurpose transport helicopter, lifting and transporting a retired Tupolev Tu-134 airliner. It is powered by two Lotarev D-136 turboshaft engines. Moreover, Figure 6.76 illustrates the hovering operation of the Mi-26 close to the ground, together with a control volume surrounding it and its inlet and outlet diameters. The total mass of the helicopter is 56,000 kg. The exit static pressure is atmospheric. Assuming the flow is one-dimensional, steady, and incompressible, calculate

1. The inlet and exit velocities of air V_1, V_2
2. The power of the turboshaft engine

Solution

Figure 6.76 shows a control volume enclosing the helicopter with states (1) and (2) identifying upstream and downstream of the rotor. Both ends have a diameter of 32.0 m, while the helicopter downwash diameter, state (2), is circular, having a diameter of 29.0 m. Now, conservation equations will be applied as follows

Continuity equation:

$$\dot{m}_1 = \dot{m}_2 = \dot{m}$$

$$\dot{m} = \rho_1 V_1 A_1 = \rho_2 V_2 A_2$$

For an incompressible flow, then

$$V_1 = V_2\left(\frac{A_2}{A_1}\right) \tag{A}$$



FIGURE 6.75
Mil Mi-26 transporting a Tu-95 airliner.

Momentum equation:

$$\bar{F}_S + \bar{F}_B = \frac{\partial}{\partial t}\int_{C.V.} \bar{V}\,\rho\, dV + \int_{C.S.} \bar{V}\left(\rho \bar{V}\cdot d\bar{A}\right)$$

For a steady flow

$$mg + P_{1g}A_1 - P_{2g}A_2 = \dot{m}\left(V_2 - V_1\right) \tag{B}$$

where, P_{1g} and P_{2g} are gauge pressures.
Moreover, from Bernoulli's Equation

$$P_{atm} + \frac{1}{2}\rho V_\infty^2 = P_1 + \frac{1}{2}\rho V_1^2$$

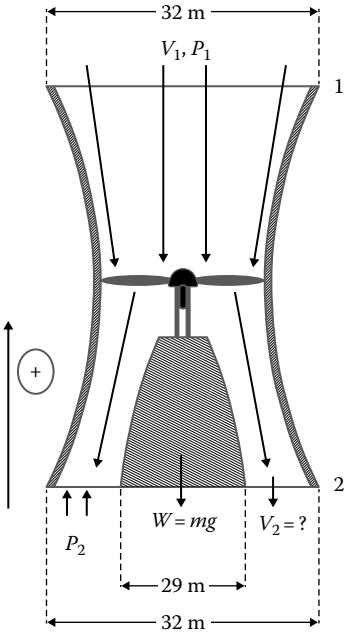


FIGURE 6.76
Control volume.

with $V_\infty = 0$

$$P_{1g} \equiv P_1 - P_{atm} = -\frac{1}{2}\rho V_1^2$$

$$P_{1g} A_1 = -\frac{1}{2}\rho V_1^2 A_1 = -\frac{1}{2}\rho V_2^2 A_2 \frac{A_2}{A_1}$$

With $P_{2g} = 0$, then, from Equations A and B

$$mg + P_{1g} A_1 = \rho V_2 A_2 \left[V_2 - V_2 \left(\frac{A_2}{A_1} \right) \right]$$

$$mg - \frac{1}{2}\rho V_2^2 A_2 \frac{A_2}{A_1} = \rho V_2 A_2 \left[V_2 - V_2 \frac{A_2}{A_1} \right]$$

$$mg = \rho V_2^2 A_2 \left[1 - \frac{A_2}{2A_1} \right] \Rightarrow \boldsymbol{V_2} = \sqrt{\frac{\boldsymbol{mg}}{\rho \boldsymbol{A_2} \left[1 - \dfrac{\boldsymbol{A_2}}{2\boldsymbol{A_1}} \right]}}$$

Since $A_1 = \frac{\pi}{4}(32)^2 = 804\ \text{m}^2$, $A_2 = \frac{\pi}{4}\left(32^2 - 29^2\right) = 143.5\ \text{m}^2$

$$\rho = \frac{P}{RT} = \frac{101 \times 10^3}{287 \times 288} = 1.22\ \text{kg/m}^3$$

$$\therefore V_2 = \sqrt{\frac{56{,}000 \times 9.81}{1.22 \times 143.5 \times \left[1 - \frac{143.5}{2 \times 804}\right]}} = 58.7 \text{ m/s}$$

From Equation A

$$V_1 = V_2\left(\frac{A_2}{A_1}\right) = 10.5 \text{ m/s}$$

Finally, applying the energy equation for the same control volume

$$\dot{Q} + \dot{W} = \int_{CS}\left(\frac{V^2}{2}\right)\left(\rho \overline{V} \cdot dA\right) + \frac{\partial}{\partial t}\int_{CV} V^2 \rho \, dV$$

For adiabatic flow $\dot{Q} = 0$ and steady conditions

$$\frac{\partial}{\partial t}\int_{CV} V^2 \rho \, dV = 0$$

$$\therefore \dot{W} = \dot{m}\left(\frac{V_2^2 - V_1^2}{2}\right) = \frac{1}{2} \times 1.22 \times 58.7 \times 143.5 \times \left[58.7^2 - 10.5^2\right]$$

The power of the propulsion system is

$$\dot{W} = 17{,}138 \text{ kW}$$

Since two turboshaft engines are installed, then the power of each engine is

$$P = 8569 \text{ kW}$$

Example 6.13

A single-spool turboshaft engine has an exhaust speed of approximately zero, and equal compressor and turbine pressure ratios. Prove that, if the fuel-to-air ratio, *f*, is negligible and constant thermal properties C_p and γ are assumed through the engine, then the power available for driving the load attains a maximum value if the compressor pressure ratio has the value

$$\pi_c = \left(T_{04}/T_a\right)^{\gamma/2(\gamma-1)}$$

where
π_c is the compressor pressure ratio
T_{04} is the turbine inlet temperature (TIT)
T_a is the ambient temperature

The maximum available specific power is then equal to

$$CpT_a\left[\sqrt{\frac{T_{04}}{T_a}} - 1\right]^2$$

Ignore all mechanical losses and pressure drop, and assume that the processes in the compressor and turbine are isentropic.

Solution

From Figure 6.73, the following peculiarities may be listed

$$P_5 = P_a \quad \text{and} \quad \pi_c = \pi_t$$

The specific power consumed in the compressor is

$$\Delta h_c = Cp\left(T_{03} - T_{02}\right) = CpT_{02}\left(\pi_c^{\gamma-1/\gamma} - 1\right) = CpT_a\left(\pi_c^{\gamma-1/\gamma} - 1\right)$$

The available specific power from the turbine is

$$\Delta h_t = Cp\left(T_{o4} - T_5\right) = CpT_{04}\left(1 - \frac{T_5}{T_{04}}\right) = CpT_{04}\left(1 - \frac{1}{\pi_c^{\gamma-1/\gamma}}\right)$$

The specific power available to the load with negligible mechanical efficiencies is, then

$$P_{load} = \Delta h_t - \Delta h_c$$

$$P_{load} = CpT_{04}\left(1 - \frac{1}{\pi_c^{\gamma-1/\gamma}}\right) - CpT_a\left(\pi_c^{\gamma-1/\gamma} - 1\right)$$

$$P_{load} = CpT_a\left[\frac{T_{04}}{T_a}\left(1 - \frac{1}{\pi_c^{\gamma-1/\gamma}}\right) - \left(\pi_c^{\gamma-1/\gamma} - 1\right)\right]$$

Define the following variables

$$\lambda = CpT_a, \quad x^b = \pi_c^{\gamma-1/\gamma}, \quad A = \frac{T_{04}}{T_a}$$

$$P_{load} = \lambda\left[A\left(1 - \frac{1}{x^b}\right) - \left(x^b - 1\right)\right]$$

$$\frac{\partial P_{load}}{\partial x} = \lambda\left[A\left(\frac{b}{x^{1+b}}\right) - bx^{b-1}\right]$$

At maximum power supplied to the load $\frac{\partial P_{load}}{\partial x} = 0$, thus

$$\frac{A}{x^{1+b}} = x^{b-1} \quad \text{or} \quad A = x^{2b}$$

$$x = A^{\frac{1}{2b}} = \left(\frac{T_{o4}}{T_a}\right)^{\gamma/2(\gamma-1)}$$

The maximum available power is, then

$$\left(P_{load}\right)_{\max} = \lambda\left[A\left(1 - \frac{1}{\sqrt{A}}\right) - \left(\sqrt{A} - 1\right)\right] = \lambda\left[A - \sqrt{A} - \sqrt{A} + 1\right]$$

$$\left(P_{load}\right)_{\max} = \lambda\left[\sqrt{A} - 1\right]^2$$

or, finally

$$\left(P_{load}\right)_{\max} = CpT_a\left[\sqrt{\frac{T_{04}}{T_a}} - 1\right]^2$$

Example 6.14

The Boeing CH-47 Chinook is a twin-engine, tandem rotor, heavy-lift helicopter. Its primary roles are troop movement, artillery placement, and battlefield resupply. It is powered by two Lycoming T55 turboshaft engines (Figure 6.77).

The T-55 turboshaft engine has the following characteristics:

- Maximum power output: 3631 kW
- Power turbine inlet temperature: 815°C
- Cruise speed: 240 km/h
- Service ceiling: 5640 m
- Compressor pressure ratio: 9.32
- Fuel heating value: 44 MJ/kg
- Pressure drop in combustion: 2%
- Modules efficiencies: $\eta_d = 092$, $\eta_c = 0.84$, $\eta_b = 0.98$, $\eta_{gt} = \eta_{pt} = 0.88$, $\eta_m = 0.99$

Calculate

1. Fuel-to-air ratio
2. Air mass flow rate



FIGURE 6.77
Boeing CH-47 Chinook.

Solution

At service ceiling 5640 m, $T_a = 252.1$ K, $P_a = 50.5$ kPa

Flight speed

$$V = \frac{240}{3.6} = 66.7\,\text{m/s}$$

Sonic speed

$$a = \sqrt{\gamma R T_a} = \sqrt{1.4 \times 287 \times 252.1} = 318.3\,\text{m/s}$$

Flight Mach number

$$M = \frac{V}{a} = 0.21$$

Intake (*a*–2): Outlet conditions

$$T_{02} = T_a\left(1 + \frac{\gamma - 1}{2}M^2\right) = 254.3\ \text{K}$$

$$P_{02} = P_a\left(1 + \eta_d \frac{\gamma - 1}{2}M^2\right)^{\gamma/\gamma - 1} = 51.95\ \text{kPa}$$

Compressor (states 2–3): Outlet conditions:

$$P_{03} = \pi_c P_{02} = 484.2\ \text{kPa}$$

$$T_{03} = T_{02}\left(1 + \frac{\pi_c^{\gamma_c - 1/\gamma_c} - 1}{\eta c}\right) = 524.8\ \text{K}$$

Combustion chamber (states 3–4):

$$P_{04} = \left(1 - \Delta P_{cc}\right) \times P_{03} = 474.5\ \text{kPa}$$

Gas turbine (states 4–5): First iteration for evaluating fuel-to-air ratio

$$Cp_c\left(T_{03} - T_{02}\right) = \left(1 + f\right)Cp_h\left(T_{04} - T_{05}\right)$$

Assuming negligible fuel to air ratio

$$T_{04} \approx T_{05} + \frac{Cp_c}{Cp_h}\left(T_{03} - T_{02}\right) = 1088 + \frac{1.005}{1.148}\left(524.8 - 254.3\right) = 1324.8\ \text{K}$$

$$f = \frac{Cp_{cc}T_{05} - Cp_c T_{04}}{\eta_b Q_R - Cp_{cc}T_{05}} = \frac{1.148 \times 1,324.8 - 1.005 \times 524.8}{0.98 \times 44,000 - 1.148 \times 1,324.8} = 0.02388$$

$$T_{04} = T_{05} + \frac{Cp_c}{Cp_h(1+f)}(T_{03} - T_{02}) = 1088 + \frac{1.005}{1.02388 \times 1.148}(524.8 - 254.3) = 1319.3 \text{ K}$$

Second iteration: Thus, a more accurate value is obtained as follows

$$f = \frac{Cp_{cc}T_{05} - Cp_cT_{04}}{\eta_b Q_R - Cp_{cc}T_{05}} = \frac{1.148 \times 1,319.3 - 1.005 \times 524.8}{0.98 \times 44,000 - 1.148 \times 1319.3} = 0.0237$$

1. Fuel-to-air ratio: $f = 0.0237$

$$P_{06} = 235.126 \text{ kPa}$$

$$P_{05} = P_{04}\left(1 - \frac{T_{04} - T_{05}}{\eta_t T_{04}}\right)^{\gamma/\gamma-1} = 474.5 \times \left(1 - \frac{1319.3 - 1088}{0.88 \times 1319.3}\right)^4 = 195.1 \text{ kPa}$$

Power Turbine (states 5–6)

$$P_6 = P_a = 50.5 \text{ kPa}$$

$$T_6 = T_{05}\left[1 - \eta_{ft}\left\{1 - \left(\frac{P_a}{P_{05}}\right)^{\gamma-1/\gamma}\right\}\right]$$

$$T_6 = 1088 \times \left[1 - 0.88\left\{1 - \left(\frac{50.5}{195.1}\right)^{0.25}\right\}\right] = 813.5 \text{ K}$$

2. Air mass flow rate:
   The specific power delivered to the rotor is

$$\frac{P_{rotor}}{\dot{m}_a} = (1+f)C_{ph}(T_{05} - T_6) = 1.0237 \times 1.148 \times (1088 - 813.5) = 322.63 \text{ kJ/kg}$$

Since the power of rotor is 3631 kW, then the *air mass flow rate* is obtained as follows

$$\dot{m}_a = \frac{P}{P/\dot{m}_a} = \frac{3631}{322.63} = 11.254 \text{ kg/s}$$

6.6 Propfan Engines

The propfan engine emerged in the early 1970s when the price of fuel began to soar. A *propfan* is a modified turbofan engine, with the fan placed outside the engine nacelle on the same axis as the compressor. Propfans are also known as *ultra-high bypass* (UHB) engines.

The design is intended to offer the speed and performance of a turbofan with the fuel economy of a turboprop. There are two main types of propfan:

1. Propfans similar to a forward fan with the fan placed outside the engine nacelle. This type is subsequently divided into either the single- or contra-rotating category; as an example, the contra-rotating propfan installed to the AN-70 aircraft (Figure 6.78).
2. Propfans similar to an aft fan where the fan is coupled to the turbine. It is always of the contra-rotating type (Figure 6.79).

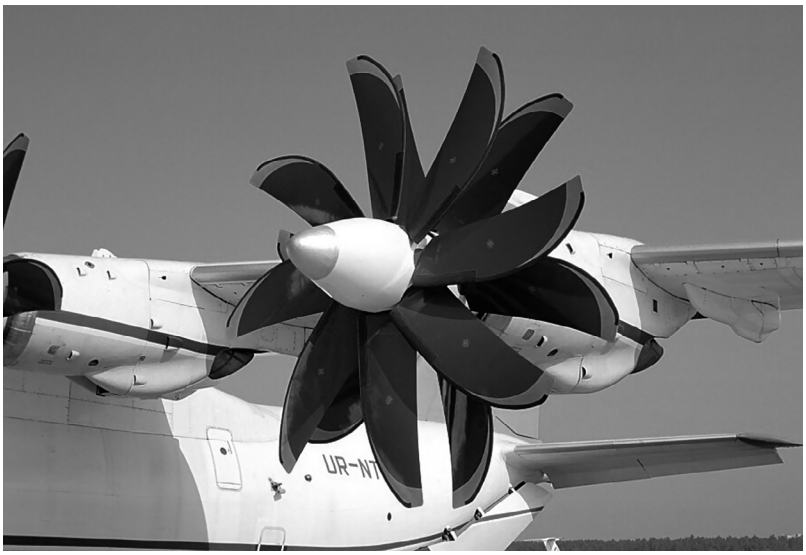


FIGURE 6.78
Contra-rotating forward propfan installed to AN-70 aircraft.

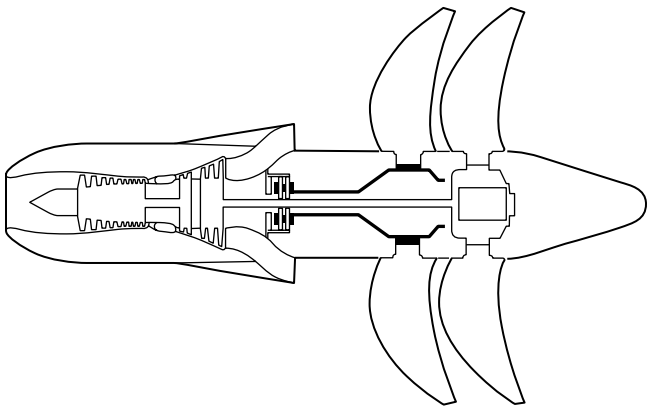


FIGURE 6.79
Contra-rotating aft propfan. (Reproduced from Rolls-Royce Plc. Copyright 2016. With permission.)

TABLE 6.11

Engine	Turboprop	Propfan
Number of blades	3–6	8–12
Diameter	Large	Smaller
Power/Square of diameter	Small	Larger
Blade shape	Nearly straight	Swept or scimitar-like profile
Maximum thickness	Thick	Thinner
Tip speed	Subsonic	Supersonic
BPR	Nearly 50	25 or more
Propulsive efficiency	High	Higher
ESFC(kg/hp·h)	0.19–0.23	0.17
Mach number	0.5–0.6	0.68
Cruise altitude	6000 m	11,000 m

Propfan engines have the best propulsive efficiency. Single-rotation engines have propulsive efficiency of around 80%, while contra-rotating engines have greater efficiency, close to 90%.

The main features of propfan engines versus turboprop engines are given in Table 6.11.

The only flying aircraft powered by a propfan engine is AN-70. During the 1970s, due to the escalating prices of oil, several projects for developing propfans or unducted fans (UDF) were introduced. The propfan concept was intended to deliver 35% better fuel efficiency in comparison with contemporary turbofans. In static and air tests on a modified DC-9, propfans achieved a 30% improvement. This efficiency comes at a price, as one of the major problems with the propfan is noise, particularly in an era where aircraft are required to comply with increasingly strict Stage III and Stage IV noise limitations.

GE introduced its unducted fan (UDF), which appears similar to a turboprop of the pusher configuration. GE's UDF has a novel direct drive arrangement, where the reduction gearbox is replaced by a low-speed 7-stage turbine. The turbine rotors drive one propeller, while the other prop is connected to the "unearthed" turbine stators and rotates in the opposite direction. So, in effect, the power turbine has 14 stages. Boeing intended to offer GE's pusher UDF engine on the 7J7 platform, and McDonnel Douglas were going to do likewise on their MD-94X airliner. Both airliners were to use rear-fuselage mounted General Electric GE-36 engines.

McDonnell Douglas developed a proof-of-concept aircraft by modifying their MD-80. They removed the JT8D turbofan engine from the left-hand side of the fuselage and replaced it with the GE36 (Figure 6.80). A number of test flights were conducted, which proved the airworthiness, aerodynamic characteristics, and noise signature of the design. The test and marketing flights of the GE-outfitted "Demo Aircraft" concluded in 1988, demonstrating a 30% reduction in fuel burn over the turbofan powered MD-80, full Stage III noise compliance, and low levels of interior noise/vibration. Due to a fall in the price of jet fuel and shifting marketing priorities, Douglas shelved the program the following year.

In the 1980s, Allison collaborated with Pratt & Whitney on demonstrating the 578-DX propfan. Unlike the competing General Electric GE-36 UDF, the 578-DX was fairly conventional, having a reduction gearbox between the LP turbine and the propfan blades. The 578-DX was successfully flight tested on a McDonnell Douglas MD-80. Figures 6.81 and 6.82 illustrate details of the contra-rotating fan blades, as well as ground testing of the GE36 UDF.

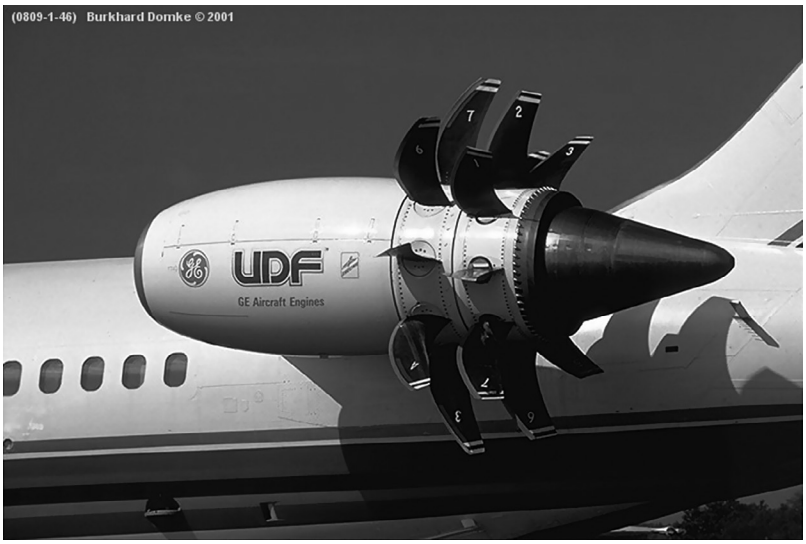


FIGURE 6.80
Unducted fan installed in the MD-80.

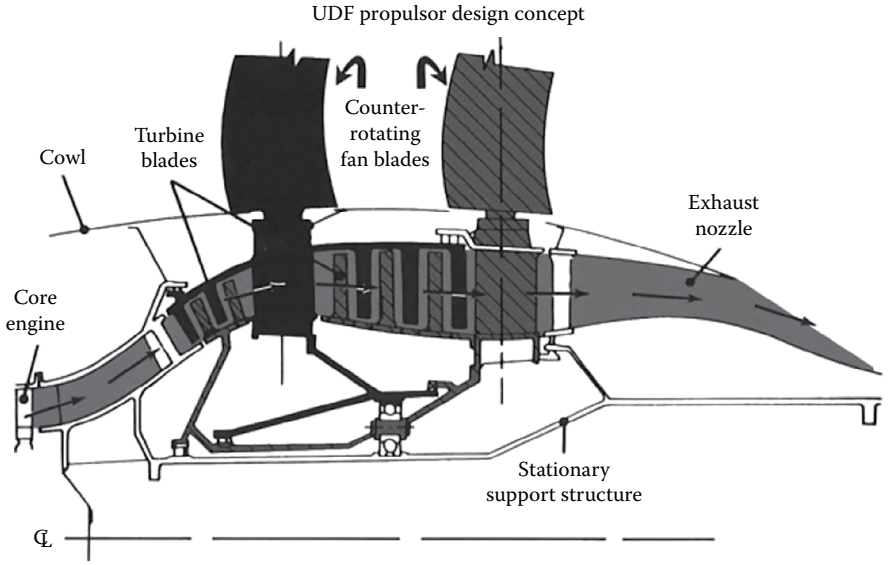


FIGURE 6.81
General Electric propulsor design concept.

The Progress D-27 propfan, developed in the U.S.S.R., is even more conventional in layout, with the propfan blades at the front of the engine in a tractor configuration. Two rear-mounted D-27 propfans propelled the Antonov An-180, which was scheduled for entry into service in 1995. Another Russian propfan application was the Yakovlev Yak-46.

However, none of the above projects came to fruition, mainly because of excessive cabin noise and low fuel prices.



FIGURE 6.82
GE36 UDF during ground testing in a test cell.

During the 1990s, Antonov also developed the An-70, powered by four Progress D-27 engines in a tractor configuration; this still remains available for further investment and production.

Example 6.15

A three-spool pusher type propfan, or UDF, is fitted to an aircraft flying at a speed of 220 m/s and altitude of 6 km, $T_a = 249$ K and $P_a = 47.182$ kPa (Figure 6.83). The engine is composed of three spools: an intermediate pressure spool composed of an intermediate pressure compressor driven by an intermediate pressure turbine, a high-pressure compressor driven by a high-pressure turbine, and the UDF (resembling a low-pressure compressor) driven by a low-pressure turbine. The maximum temperature is 1400 K and fuel with a heating value of 43,000 kJ/kg is used. It has the following particulars: $\dot{m}_a = 40.0$ kg/s, $\pi_{IPC} = 3.1$, $\pi_{HPC} = 5.6$, $\pi_{UDF} = 1.2$, $\Delta P_{CC} = 6\%$, $\eta_d = 0.92$, $\eta_{IPC} = 0.84$, $\eta_{HPC} = 0.85$, $\eta_b = 0.965/0.98$, $\eta_{IPT} = 0.91$, $\eta_{HPT} = 0.93$, $\eta_{FT} = 0.92$, $\eta_n = 0.96$, $\eta_{UDF} = 0.825$, $(\eta_m)_{UDF} = 0.98$, $\alpha = 0.85$, bleed ratio; $b = 0.06$, $C_{P_c} = 1.005$ kJ/kg·K, $C_{P_t} = C_{P_n} = 1.148$ kJ/kg·K.

It is required to calculate

1. Bypass ratio β
2. Ratio between thrust force generated by the unducted fan and nozzle
3. Total equivalent horsepower

Solution

Figure 6.84 illustrates the *T*–*S* diagram for the different states identified above.

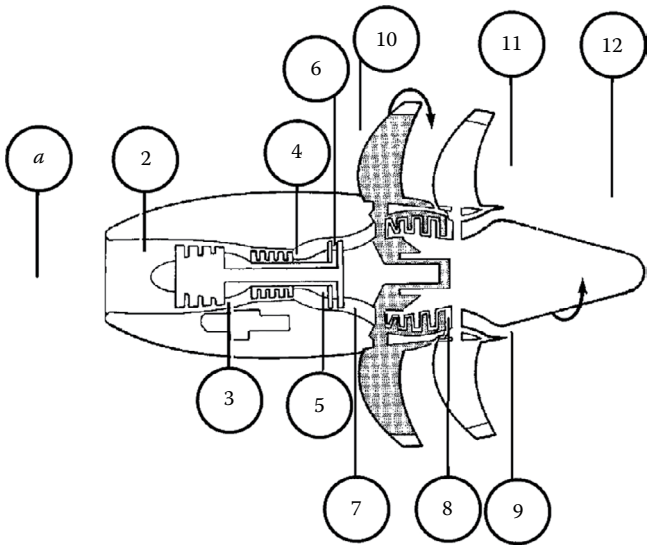


FIGURE 6.83
Layout of a propfan engine.

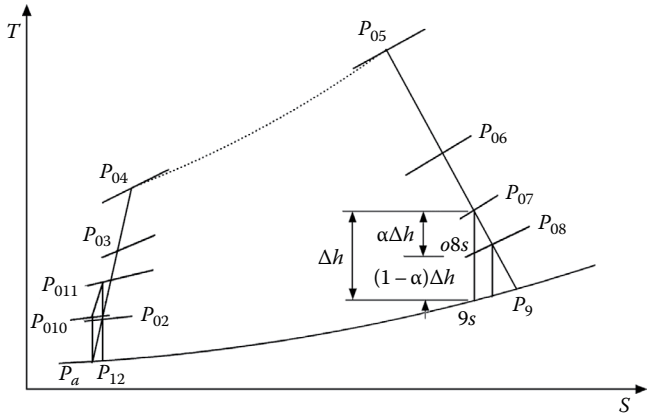


FIGURE 6.84
T–S diagram for a propfan (UDF) engine.

Intake (state *a*–2): The engine is examined during flight at a speed of 220 m/s and altitude where the ambient conditions are $T_a = 216.7$ K and $P_a = 22.632$ kPa, then the total conditions at the diffuser outlet are calculated as follows.

Sonic speed and flight mach number are

$$a = \sqrt{\gamma_c R T_a} = \sqrt{1.4 \times 287 \times 216.7} = 295 \text{ m/s}$$

$$M = U/a = 0.745$$

$$T_{02} = T_a\left(1 + \frac{\gamma_c - 1}{2} M^2\right) = 240.8 \text{ K}$$

$$P_{02} = P_a\left(1 + \eta_d \frac{\gamma_c - 1}{2} M^2\right)^{\gamma_c/\gamma_c - 1} = 31.8 \text{ kPa}$$

Intermediate-pressure compressor (states 2–3):

$$P_{03} = P_{02} \times \pi_{IPC} = 3.1 \times 60.52 = 98.6 \text{ kPa}$$

$$T_{03} = T_{02}\left(1 + \frac{\pi_{IPC}^{\gamma_c - 1/\gamma_c} - 1}{\eta_{IPC}}\right) = 240.8 \times \left(1 + \frac{3.1^{0.286} - 1}{0.84}\right) = 350.3 \text{ K}$$

High-pressure compressor (states 3–4):

$$P_{04} = P_{03} \times \pi_{HPC} = 552.2 \text{ kPa}$$

$$T_{04} = T_{03}\left(1 + \frac{\pi_{HPC}^{\gamma_c - 1/\gamma_c} - 1}{\eta_{HPC}}\right) = 350.3 \times \left(1 + \frac{5.6^{0.286} - 1}{0.85}\right) = 612.7 \text{ K}$$

Combustion chamber (states 4–5):

$$P_{05} = \left(1 - \Delta P_{cc}\right) \times P_{04} = 0.94 \times 552.2 = 519 \text{ kPa}$$

$$f = \left(1 - b\right)\frac{Cp_{cc}T_{05} - Cp_cT_{04}}{\eta_b Q_R - Cp_{cc}T_{05}} = \left(0.92\right)\frac{1.148 \times 1,400 - 1.005 \times 612.7}{0.98 \times 43,000 - 1.148 \times 1,400} = 0.0225$$

High Pressure Turbine (HPT) (states 5–6): Energy balance for the high-pressure spool

$$Cp_c\left(T_{04} - T_{03}\right) = \left(1 + f - b\right)Cp_h\left(T_{05} - T_{06}\right)$$

$$T_{06} = T_{05} - \frac{Cp_c}{\left(1 + f - b\right)Cp_h}\left(T_{04} - T_{03}\right) = 1400 - \frac{1.005}{1.148 \times 0.962}\left(612.7 - 350.3\right) = 1161.3 \text{ K}$$

$$\frac{P_{06}}{P_{05}} = \left[1 - \frac{1}{\eta_{HPT}}\left(1 - \frac{T_{06}}{T_{05}}\right)\right]^{\gamma_h/\gamma_{h-1}} = \left[1 - \frac{1}{0.93}\left(1 - \frac{1161.3}{1400}\right)\right]^4 = 0.4448$$

$$P_{06} = 230.85 \text{ kPa}$$

Intermediate-pressure turbine (IPT) (states (6–7): *Energy balance*

$$T_{07} = T_{06} - \frac{Cp_c}{\left(1 + f - b\right)Cp_h}\left(T_{03} - T_{02}\right) = 1161.3 - \frac{1.005}{1.148 \times 0.962}\left(109.5\right) = 1061.7 \text{ K}$$

$$\frac{P_{07}}{P_{06}} = \left[1 - \frac{1}{\eta_{IPT}}\left(1 - \frac{T_{07}}{T_{06}}\right)\right]^{\gamma_h/\gamma_{h-1}} = \left[1 - \frac{1}{0.91}\left(1 - \frac{1061.7}{1161.3}\right)\right]^4 = 0.673$$

$$P_{07} = 155.4 \text{ kPa}$$

Unducted Fan (UDF) (states 10–11):

$$T_{010} = T_{02} = 240.8 \text{ K}$$

$$P_{010} = P_a\left(1 + \frac{\gamma_c - 1}{2}M^2\right)^{\gamma_c/\gamma_c - 1} = 32.71 \text{ kPa}$$

$$P_{011} = P_{010} \times \pi_{UDF} = 39.25 \text{ kPa}$$

$$T_{011} = T_{010}\left(1 + \frac{\pi_{UDF}^{\gamma_c - 1/\gamma_c} - 1}{\eta_{UDF}}\right) = 240.8 \times \left(1 + \frac{1.2^{0.286} - 1}{0.84}\right) = 256.1 \text{ K}$$

$$\frac{T_{12}}{T_{011}} = \left(\frac{P_a}{P_{011}}\right)^{\gamma_{c-1}/\gamma_c} = \left(\frac{22.632}{39.25}\right)^{0.286} = 0.8543$$

$$T_{12} = 218.8 \text{ K}$$

$$\left(U_e\right)_{UDF} = \sqrt{2Cp_c\left(T_{011} - T_{12}\right)} = 273.86 \text{ m/s}$$

Free turbine and hot gases nozzle (states 7–9):

$$\frac{T_{07}}{T_{9s}} = \left(\frac{P_{07}}{P_a}\right)^{\gamma_h - 1/\gamma_h} = \left(\frac{155.4}{22.632}\right)^{0.25} = 1.618$$

$$T_{9s} = 655.9 \text{ K}$$

Temperature drop in free turbine:

$$T_{07} - T_{08} = \eta_{FT} \times \left(T_{07} - T_{08s}\right) = \eta_{FT} \times \alpha \times \left(T_{07} - T_{9s}\right) = 0.92 \times 0.85 \times \left(1061.7 - 655.9\right) = 317.4 \text{ K}$$

$$T_{08} = 744.3 \text{ K}$$

$$T_{08s} = 716.7 \text{ K}$$

$$\frac{P_{07}}{P_{08}} = \left(\frac{T_{07}}{T_{08s}}\right)^{\gamma_h/\gamma_h - 1} = \left(\frac{1061.7}{716.7}\right)^4 = 3.21/4.82$$

$$P_{08} = 32.27 \text{ kPa}$$

$$\left(U_e\right)_n = \sqrt{2Cp_h \times \eta_n \left(T_{08} - T_{9s}\right)} = 450.5 \text{ m/s}$$

The thrust force obtained from the exhaust gases leaving the nozzle is denoted as T_n, given by the relation

$$T_n = \dot{m} \times \left[\left(1 + f - b\right)\left(U_e\right)_n - U\right] = 7887 \text{ N}$$

Energy balance

$$\beta Cp_c \left(T_{011} - T_{010}\right) = \left(1 + f - b\right) Cp_h \left(T_{07} - T_{08}\right)$$

$$\beta = \left(1 + f - b\right) \frac{Cp_h \left(T_{07} - T_{08}\right)}{Cp_c \left(T_{011} - T_{010}\right)} = 0.926 \times \frac{1.148 \times \left(1061.7 - 744.3\right)}{1.005 \times \left(256.1 - 240.8\right)} = 21.94$$

The thrust force obtained from an unducted fan denoted as (T_{UDF}) is given by the relation

$$T_{UDF} = \beta \dot{m} \times \left[\left(U_e\right)_{UDF} - U\right] = 47,268 \text{ N}$$

Total thrust

$$T_{tot} = T_{UDF} + T_n = 55,155 \text{ N}$$

The ratio between unducted fan and nozzle thrusts is

$$\frac{T_{UDF}}{T_n} = \left(\frac{41,804}{4,459}\right) = 6$$

The unducted fan power is

$$P_{UDF} = U \times T_{UDF} = 10,399 \text{ kW} = 13,945 \text{ hp}$$

The jet nozzle power is

$$P_n = U \times T_n = 1735 \text{ kW} = 2326 \text{ hp}$$

Total equivalent power is

$$P = T_{tot} \times U = 12,134 \text{ kW} = 15,271 \text{ hp}$$

6.7 Conclusion

The chapter focuses on the aerodynamics and thermodynamics of shaft engines, which comprise four types: aero-piston, turboprop, turboshaft, and propfan (or unducted fan/UDF) engines.

Aero piston engines were the first prime-mover used in propelling aircraft since the early Flyer of the Wright brothers in 1903 and they have been extensively used until now. Both petrol and diesel engines were analyzed. Superchargers used for boosting power at high altitudes were also discussed. Since piston engines alone cannot support an aircraft's flight, a propeller is installed either directly or via a reduction gearbox. Basic theories for propeller aerodynamics were reviewed: momentum, modified momentum, and blade-element theories.

Turboprop engines were discussed next. Single-, double, and triple spool designs were analyzed.

Propellers are also necessary here to transform shaft power into thrust force. Propellers employed in turboprop engines are high-speed propellers.

The third engine discussed was the turboshaft, which is the main source of power in helicopters. Shaft power is used for propelling helicopters via one or more rotors in different arrangements.

The last type of engine discussed was the propfan or unducted fan engine (UDF). A propfan engine develops the highest propulsive efficiency, as discussed in Chapter 2, as well as having the lowest fuel burn requirement.

Numerous examples for all four engine groups were thoroughly solved and discussed.

Summary of turboprop relations

$$T = \dot{m}_a\left(\left(1+f\right)\sqrt{2\eta_n\left(1-\alpha\right)\Delta h} - u\right) + \eta_t\eta_m\eta_g\eta_{pr}\frac{\alpha\Delta h}{u}\dot{m}_a\left(1+f\right)$$

$$T/\dot{m}_a = \left[\left(1+f\right)u_e - u\right] + \eta_t\eta_m\eta_g\eta_{pr}\frac{\alpha\Delta h}{u}\left(1+f\right)$$

$$\eta_p = \frac{2uT/\dot{m}_a}{\left(1+f\right)u_e^2 - u^2}$$

$$\eta_{th} = \frac{\left(1+f\right)u_e^2 - u^2}{2fQ_{HV}}$$

$$\eta_o = \frac{u\,T/\dot{m}_a}{fQ_{HV}}$$

Problems

Choose the correct answer:

6.1 The benefit of liquid (as opposed to air) to cool aircraft piston engine is that

1. A steady operating temperature will be more easily maintained
2. The engine will be lighter

3. The engine will be simpler
4. The cost of engine production will be lower

6.2 The purpose of the "fins" which are arranged about the cylinder and cylinder head of an air-cooled engine is

1. To allow heat to dissipate rapidly
2. To reduce the engine weight
3. To direct air through the engine compartment
4. To support the engine cooling

6.3 Which of these statements applies to a propeller that has been "feathered":

1. Its leading edges are facing forward in the direction of flight
2. It is operating at its maximum rotational speed
3. It is producing maximum power
4. Its leading edges are facing 90° to the direction of flight

6.4 On a variable pitch propeller, the largest obtainable pitch angle is known as

1. Fine pitch
2. Optimum pitch
3. Coarse pitch
4. Takeoff pitch

6.5 When the airflow over the propeller blades of a failed engine keeps the propeller turning, this is known as

1. Reverse thrust
2. Windmilling
3. Contra-rotating
4. Reverse thrust

6.6 "Blade twist" in a propeller helps to

1. Reduce noise levels
2. Make feathering possible
3. Make the blade stronger and lighter
4. Even out the thrust along the blade

6.7 Define the following terms related to aero-piston engines:

stroke—bore—top dead center—bottom dead center—clearance volume

6.8 The Dornier is a light freighter and feeder liner aircraft powered by two Lycoming IGSO-540-A1A six-cylinder horizontally opposed engines, each rated at 260 kW. Assume that *Otto cycle* represent the cycle for such a spark-ignition engine. Data for the engine is as follows:

1. Compression ratio: 8
2. Temperature and pressure at the beginning of the compression stroke: 300 K and 96 kPa
3. Rate of heat transfer during the constant volume stroke: 760 kJ/kg
4. Specific heat at constant volume: 0.72 kJ/(kg · K)

Calculate

a. The pressure and temperature at the end of the heat addition process
b. Network output
c. Air mass flow rate
d. Mean effective pressure

6.9 A large CI engine operates on air-standard *diesel cycle*, using diesel fuel with a latent heating value of 41,500 kJ/kg and a combustion efficiency of 98%. The inlet temperature and pressure are 298 K and 1 atmosphere, respectively. For a parametric study, it is required to calculate and plot the thermal efficiency versus the pressure ratio in the two cases of a cutoff ratio of 3.0 and 4.0. Consider the following values for the compression ratio: 7.5, 9, 12.5, 15, and 17.5 and maximum temperatures of 1500, 1700, and 1900 K.

6.10 The pressure and temperature at the start of compression in air—standard *Otto cycle*—are 101 kPa and 300 K. The compression ratio is 8. The amount of heat addition is 2100 kJ/kg of air. Determine

1. The cycle thermal efficiency
2. The maximum cycle temperature
3. The maximum cycle pressure
4. The mean effective pressure

Figure P6.10 illustrates the Beech S35 Bonanza light aircraft powered by a single Continental IO-550 six-cylinder, horizontally opposed, air-cooled aircraft engine.

It has the following data:

- Bore: 133.4 mm
- Stroke: 108.0 mm
- Displacement: 9.05 L



FIGURE P6.10

- Power output: 224 kW at 2700 rpm
- Specific power: 24.6 kW/L
- Compression ratio: 8.5:1
- Power-to-weight ratio: 1.15 kW/kg

Calculate

1. Specific speed
2. Brake mean effective pressure
3. Engine weight
4. Fuel conversion efficiency

6.11 Figure P6.11 illustrates the *Robinson R44*, a four-seat, light helicopter produced by the Robinson Helicopter Company, the first delivery having been in February 1993. It is powered by one Lycoming IO-540-AE1A5 six-cylinder air-cooled, horizontally opposed engine of 183 kW. The engine has the following characteristics:

- Engine operates on the ideal Otto cycle
- Displacement: 8.9 L
- Compression ratio: 8.7:1
- The temperature and pressure at the beginning of the compression process of an air-standard Otto cycle are 290 K and 1 atm, respectively

Calculate

1. Heat supplied per cylinder
2. Thermal efficiency
3. Mean effective pressure
4. Rotational speed



FIGURE P6.11

6.12 Consider a cold air-standard diesel cycle. The following table illustrates various properties at different cycle states.

State	T (K)	P (kPa)	$v(\mathrm{m_3/kg})$
1	300	101	0.85
2	910	4916	0.05
3	1820	4916	0.10
4	790	267	0.85

For $\gamma = 1.4, C_p = 1.005\ \mathrm{kJ/(kg \cdot K)}$, determine

1. Heat transfer and work per unit mass for each process
2. Thermal efficiency

6.13 The thermal efficiency of a diesel cycle is expressed by the relation

$$\eta_{th,Diesel} = 1 - \frac{1}{r_c^{\gamma-1}}\left[\frac{\left(\beta^{\gamma} - 1\right)}{\gamma(\beta - 1)}\right]$$

While the thermal efficiency for an Otto cycle is expressed by the relation

$$\eta_{th,Otto} = 1 - \frac{1}{r_c^{\gamma-1}}$$

Plot both relations on the same figure for a compression ratio ranging from 4 to 12.

6.14 A four-cylinder internal combustion engine has the following design values:

- Maximum brake torque of 200 $\mathrm{N \cdot m}$
- Mid-speed range of 3000 rpm
- Maximum bmep = 950 kPa

Estimate the engine displacement, bore and stroke (assume the bore and stroke to be equal).

Consider a six-cylinder ICE having a stroke of 9.5 cm, a bore of 8.0 cm, and a compression ratio of 10. The pressure and temperature in the intake manifold are 0.8 atm and 250 K, respectively. The fuel-to-air ratio is 0.06. The mechanical efficiency of the engine is 75%. If the crankshaft is connected to a propeller with an efficiency of 83%, calculate the *available power from the propeller* for an engine speed of 3000 rpm. The fuel heating value is 42.9 MJ/kg and the Otto cycle is assumed.

6.15 A diesel engine has the following data:

- Fuel used: Diesel
- Type: Vertical cylinder, DI diesel engine
- Number of cylinders: 1
- Bore Stroke (mm): 88 × 110
- Compression ratio: 17.5:1

- Cutoff ratio: 3.0
- Cooling system: Water cooling
- Speed (rpm): 1500
- Rated brake power (kW): 5.4 at 1500 rpm
- Ignition system: Compression ignition
- Chemical formula of fuel: $C_{12}H_{26}$
- Stoichiometric air/fuel ratio (wt/wt): 14.6
- Lower heating value (kJ/kg): 42,800
- Inlet total temperature and pressure: 280 K and 0.95 bar, respectively

6.16 The displacement volume of an internal combustion engine is 5.8 liters. The processes within each cylinder of the engine are modeled as an air-standard diesel cycle with a cutoff ratio of 2.4. The state of the air at the beginning of compression is: $P_1 = 9$ 6 kPa , $T_1 = 300$ K, and $V_1 = 6.0$ L. Draw the cycle on the P–v diagram and determine the work per cycle in kJ, the power developed in kW, and the thermal efficiency, if the engine speed is 1600 rpm.

6.17 A four-stroke petrol engine operates on a standard air cycle and has a volume of 0.46 m^3). Operating conditions at the beginning of a compression stroke are 1 bar and 27°C, respectively. At the end of the compression stroke, the pressure is 11 bar and 220 kJ of heat is added at constant volume. The engine runs at 215 rpm. Determine

1. $P, T,$ *and* v at all cycle points
2. Clearance percentages
3. Thermal efficiency
4. Network per cycle
5. Mean effective pressure

6.18 Starting from the following definition for propeller efficiency

$$\eta_P = \frac{\text{Thrust power}}{\text{Thrust power} + \text{Wasted power in jet}} = \frac{TV_1}{TV_1 + \frac{1}{2}\dot{m}(V_4 - V_1)^2}$$

prove that

$$\eta_F = \frac{2}{1 + V_4/V_1}$$

6.19 Prove that the thrust force generated by a propeller is related to the supplied power by the relation

$$T = \frac{PC_T}{nDC_P}$$

6.20 Prove that the available power of a propeller is expressed by the relation

$$P = \frac{TV_1}{2}\left(\sqrt{\frac{8T}{\rho V_1^2 \pi D^2} + 1} + 1\right)$$

6.21 Compute the diameter of the flow field in the far wake of a 3.0 m diameter propeller, which produces a thrust of 9.0 kN at sea-level conditions while flying at a speed of 330 km/h.

6.22 An aircraft is propelled by a 4.6 m diameter propeller, which produces 36.0 kN of thrust. The aircraft is flying at an altitude where the air density is 0.9 kg/m^3. Using momentum theory, calculate

1. The induced velocity through the disk
2. The final velocity of the flow in the far wake
3. Propeller efficiency, using actuator disk theory
4. The pressure jump across the propeller

6.23 A three-bladed propeller has the following data:

Generated power = 2250 hp

Sea-level conditions

Relative tip speed = 320 m/s

Flight speed = 75 m/s

Blade section has a lift and drag coefficients equal to 0.85 and 0.0425, respectively

Calculate

1. Tip rotational speed
2. Thrust and torque coefficients
3. Propeller efficiency
4. Rotational speed
5. Propeller diameter
6. Reference blade chord

6.24 For a preliminary analysis, assume that

- The blade has a constant chord equal to the reference chord, c_{ref}, where $c_{ref} = 0.06D$ and D is the propeller diameter

$$a = 0.1, \quad a_\Omega = 0$$

Figure P6.24 illustrates a Cessna R172K Hawk XP single-engine aircraft. The airplane has a maximum cruise speed of 243 km/h. It is powered by a single, fuel-injected, Continental IO-360K 195 hp (145 kW). The propeller has the following characteristics:

Number of blades (B) = 2

Diameter (D) = 2.80 m

Blade chord at 0.75R = 0.16 m



FIGURE P6.24
Cessna 172 Hawk XP on floats.

Rotational speed = 2880 rpm
Inflow factor (a) = 0.05
Lift coefficient = 0.7

It is required to calculate C_T, C_Q, C_P, η

Hints

1. Divide the propeller blade into five stations: x = 0.12, 0.34, 0.56, 0.78, and 1.0
2. Ignore the drag coefficient

6.25 A four-bladed propeller has the following data:

- Generated power = 3000 hp
- Sea-level conditions
- Relative tip speed = 320 m/s
- Flight speed = 75 m/s
- The blade section has lift and drag coefficients equal to 0.85 and 0.0425, respectively

Calculate

1. Tip rotational speed
2. Thrust and torque coefficients
3. Propeller efficiency
4. Rotational speed
5. Propeller diameter
6. Reference blade chord

Hints

For a preliminary analysis, assume that

- The blade has a constant chord equal to the reference chord, c_{ref}, where $c_{ref} = 0.06D$ and D is the propeller diameter

$$a = a_\Omega = 0$$

- Ignore drag coefficient

6.26 The following data is for a four-stroke spark-ignition engine:

Displacement volume V_d	2.2 L
Bore	87.5 mm
Stroke	92.0 mm
Compression ratio	8.9
Maximum power	65 kW
Speed	5000 rpm
Number of cylinders	4
Mean piston speed	10 m/s
Air flow rate	60 g/s

Calculate

1. Volumetric efficiency based on atmospheric conditions
2. Brake mean effective pressure
3. Specific power

Assume mixture density = 1.184 (g/L)

6.27 Figure P6.27 illustrates a Cessna 335/340 aircraft that is powered by two piston engines, each producing 2900 N thrust force. Each propeller is three-bladed with a diameter of 1.92 m. If the service ceiling of airplane is 30,000 ft and the cruise speed is 450 km/h.



FIGURE P6.27
Cessna 335/340 aircraft.

Calculate

1. Propeller efficiency, using actuator disk theory
2. The pressure jump across the propeller

6.28 An aircraft is flying at a speed of 540 km/h speed at sea level. It is powered by a three-bladed propeller developing 1600 kW. The propeller is connected to a piston engine rotating at 2600 rpm, through a 1:2 gear box. The propeller is designed with NACA 5869-9 blade sections. At 0.75 R, it has a pitch angle of $\beta = 35°$. Use the chart provided for the speed-power coefficient to compute the propeller diameter and the efficiency of the propeller in these operating conditions; Figure 6.39.

6.29 The V-22 Osprey aircraft takes off and lands as a helicopter. Once airborne, its engine nacelles can be rotated to convert the aircraft to a turboprop aircraft capable of a high speed and high-altitude flight. It can transport internal and external cargo. The V-22 Osprey is powered by two *turboprop* engines. Each has the following data:

Shaft horsepower	6150
Specific fuel consumption	0.42 ib/shp/h
Compressor pressure ratio	14.1
Compressor isentropic efficiency	0.85
Burner efficiency	0.94
Pressure drop in combustion chamber	2%
Fuel heating value	45,000 kJ/kg
Turbine inlet temperature	1,300 K
Turbines isentropic efficiency	0.92
Gearbox mechanical efficiency	0.94
Propeller efficiency	0.823
Ambient conditions	288 K and 101 kPa

It is required to

1. Calculate the air mass flow rate into the engine
2. Check that the power is 6150 hp

6.30 The total work coefficient (W) in turboprop engines is defined as the ratio of propulsive power to the thermal energy of the airflow inducted into the engine; or

$$W = \frac{\eta_{pr} P_s + U_0 T}{m_a C p T_a}$$

It is required to

1. Prove that the total work coefficient, W, in the case of an ideal turboprop engine is given by the relation

$$W_{ideal} = (\gamma - 1) M_a^2 \left\{ \sqrt{\left(\frac{\theta_t}{\theta_a \tau_c} \right) \left(\frac{\theta_a \tau_c \tau_t - 1}{\theta_a - 1} \right)} - 1 \right\} + \theta_t (1 - \tau_t) - \theta_a (\tau_c - 1)$$

$$\theta_a = \frac{T_{02}}{T_a}, \quad \tau_c = \frac{T_{03}}{T_{02}}, \quad \tau_t = \frac{T_{05}}{T_{04}}, \quad \theta_t = \frac{T_{04}}{T_a}$$

2. Prove that the work coefficient is at maximum value in takeoff conditions (the flight speed is zero)

6.31 It is required to design a three-bladed propeller with the following data:

- Power = 260 kW
- Rotational speed = 2500 rpm
- Flight speed = 300 km/h
- Tip Mach number = 0.8 and sonic speed = 340 m/s
- The rotational induction factor is assumed constant and given by $a_\Omega = 0.001$

Other data are

(r/R)	0.2	0.4	0.6	0.75	0.9
$\frac{c}{R}$	0.1	0.15	0.16	0.18	0.09
C_d	0.05	0.04	0.025	0.015	0.01
$\left(\frac{dT}{dr}\right)_{3-blades}$ (N/m)	500	2500	4400	5900	3150

It is required to calculate

1. The radius of the propeller
2. Propeller efficiency
3. *At each blade section*, calculate
   a. The axial interference factor (a)
   b. Lift coefficient C_L
   c. Angle of attack (α)
   d. Blade angle (β)
   e. Local propeller efficiency

Hint

To calculate the angle of attack, use one of the following relations:

$$\alpha = \frac{C_l}{2\pi} \quad \text{for } M_W \cong 0.3 - 0.6$$

$$\alpha = \frac{C_l\sqrt{1 - M_W^2}}{2\pi} \quad \text{for } M_W \cong 0.7 - 0.9$$

6.32 For a particular section of a propeller ($r/R = 0.4$), the following data was recorded:

$$V_1 = 83.3 \text{ m/s}, \quad \Omega r = 104.7 \text{ m/s}, \quad a = 0.05544, \quad a_\Omega = 0.001$$

The blade element theory developed a propeller efficiency of $\eta_P = 83.89$ %. Compare between the propulsive efficiencies using Froude and modified momentum theory to that obtained using blade element theory.

6.33 As an extension to Example 6.3, for the same turboprop engine it is required to calculate the specific equivalent specific fuel consumption defined as

$$\text{S.E.S.F.C} = \frac{f}{\text{S.E.S.H.P}}$$

at sea level and the same three altitudes. Next, to calculate the equivalent shaft horsepower and the fuel flow rate at different altitudes, the mass flow rate at different altitudes must first be determined. Prove that the air mass flow rate at any altitude is related to the air mass flow rate at sea level by the relation

$$\dot{m}_{alt} = \dot{m}_{s.l}\frac{\delta}{\sqrt{\theta}} \equiv \dot{m}_{s.l}\frac{P_{alt}}{P_{s.l}}\sqrt{\frac{T_{s.l}}{T_{alt}}}$$

If the mass flow rate at sea level is 14.6 kg/s, calculate the air mass flow rate, fuel mass flow rate, equivalent shaft horsepower (ESHP) and (ESFC) at the four levels.

6.34 A turboprop engine with a free power turbine has the following data:

$\dot{m}_a = 15$ kg/s	$H = 6$ km
$T_a = 249$ K	$P_a = 47.2$ kPa
$M_0 = 0.6$	$\pi_C = \frac{P_{03}}{P_{02}} = 6$
$P_{04} = 0.96P_{03}$	$T_{04} = 1120$ K
$\eta_{id} = 0.95$	$\eta_C = 0.87$
$\eta_{C.C} = 0.98$	$\eta_t = \eta_{FPT} = \eta_n = 0.9$
$\eta_g = 0.95$	$\eta_{Pr} = 0.8$
$C_{P_C} = 1.01$ kJ/kg·K	$C_{P_t} = C_{P_{FPT}} = C_{P_n} = 1.14$ kJ/kg·K
$Q_R = 43{,}000$ kJ/kg	

The power in the gases leaving the gas generator turbine is divided between the free power turbine and the nozzle, based on the optimum condition $\alpha = \alpha_{opt}$, calculate the ESHP and the ESFC.

6.35 A medium-range military and civil freighter (a typical example is the U.S.S.R ANTONOV AN-12 CUB) is powered by four turboprop engines. The mass of the airplane (m) is expressed in terms of the flight distance(s) as

$$m = a(10)^6 - 10^5(s)^{-0.3} \text{ kg}$$

where s is expressed in (km). The takeoff mass is 65,000 kg. The maximum range is 3500 km. The heating value of the fuel used is Q_R = 45,000 kJ/kg, the lift-to-drag ratio (L/D) is 16, the airplane speed is 100 m/s, the propeller efficiency is 0.8.

It is required to

1. Calculate the value of the constant (a) in the above mass-distance equation
2. Calculate the final mass of airplane if the distance traveled were 3500 km
3. Calculate the overall efficiency η_0
4. Calculate the thrust force T
5. Calculate the SHP if the ESHP is 4015

6.36 An aircraft is fitted with four turboprop engines and is flying at Mach number 0.7 at an altitude of 9 km where the ambient conditions are 30.8 kPa and 229.7 K. When the engines are running at maximum rpm, each engine has an ESHP of 1280. The engine components have the following isentropic efficiencies: Intake (0.9), compressor (0.87), burner (0.98), turbine (0.89), nozzle (0.95). Other data are

Compressor pressure ratio	7.5
Combustion chamber pressure drop	3%
Exhaust velocity	250 m/s
Turbine inlet temperature	1,180 K
Fuel heating value	43,000 kJ/kg

Calculate the air mass flow rate into the engine.

6.37 A commuter airplane is powered by two turboprop engines. The propeller is driven by a compressor-turbine shaft; the expansion process in the turbine and nozzle is governed by the optimum ratio

$$\alpha_{opt} = 1 - \frac{u^2}{2\Delta h} \frac{\eta_n}{\eta_{pr}^2 \eta_g^2 \eta_{mt}^2 \eta_t^2}$$

Prove that, in this case, the optimum exhaust speed is given by

$$u_e = \frac{u\eta_t}{\eta_{pr}\eta_g\eta_{mt}\eta_t}$$

Find the corresponding maximum thrust. Explain how to handle a problem such as this during takeoff; $u = 0$ while u_e is greater than zero.

6.38 A short-haul commercial transport (an example of which is the FOKKER F-27 manufactured in the Netherlands) is powered by two turboprop engines. At sea-level conditions, each engine delivers 2250 ESHP and 260 lb thrust. The maximum flight speed is 330 mph at 20,000 ft. Find

1. The SHP at sea level
2. Corrected thrust at 20,000 ft
3. Corrected SHP at 20,000 ft
4. ESHP at 20,000 ft

(Ambient conditions at sea level are T = 288 K and P = 14.69 psia, and at altitude 20,000 ft are T = 248.4 K, P = 6.754 psia.)

6.39 A turboprop engine has the following specifications:

Air mass flow rate	15 kg/s
Flight Mach no.	$M = 0.6$
Flight altitude	6 km
Ambient temperature and pressure	249 K and 47.2 kPa
Compressor pressure ratio	6
Pressure loss in the combustion chamber	4%
Maximum total temperature	1,120 K
Fuel heating value	43,000 kJ/kg

Efficiencies: Diffuser = 0.95, compressor = 0.87, combustion chamber = 0.98, turbines and nozzle = 0.9, gearbox = 0.95, propeller = 0.8.

Specific heats at constant pressure: Compressor = 1.01, combustion chamber = 1.13, turbines = nozzle = 1.14 kJ/kg K.

Assuming $\alpha_{opt} = 0.87$, calculate

1. The ESHP
2. The ESFC

6.40 Compare the thrust forces of the following three engines, which have the same maximum temperature (1600 K) and a compressor pressure ratio of (8), the same core mass flow rate $\dot{m}_a$ of 30 kg/s and use the same fuel with a heating value Q_R of 44,000 kJ/kg. Assume no losses in the fan, compressor, combustion chamber, turbine(s), or nozzle(s). Moreover, all nozzles are unchoked. These engines power aircraft flying at an altitude of 8 km, where the ambient conditions are 236.21 K and 35.64 kPa, and at Mach 0.7.

1. Turboprop engine

   The propeller is driven by a power turbine. The propeller efficiency is $\eta_{pr} = 0.8$, the gearbox and power shaft mechanical efficiencies are both 0.98.
2. Forward fan turbofan engine

   The bypass ratio is $\beta = 3$ and the fan pressure ratio is $\pi_f = 1.5$
3. Aft fan turbofan engine

   The bypass ratio is $\beta = 3$ and the fan pressure ratio is $\pi_f = 1.5$

6.41 The Kuznetsov NK-12 is a Soviet turboprop engine from the 1950s. It is known to be the most powerful turboprop engine ever built. One of its variants, the NK-12MA, has an equivalent power of 11,185 kW. The engine has a single-spool configuration with a 5-stage axial turbine driving the 14-stage axial compressor and two contra-rotating propellers. Consider the engine operation on takeoff (M = 0.25) with a compression ratio of 9.5 and a turbine inlet temperature of 1250 K. The air mass flow is 55.8 kg/s. The propeller and gear box efficiencies are 0.75 and 0.95, respectively. Assume the engine components are not ideal and have the following efficiencies

η_{intake}	$\eta_{compressor}$	$\eta_{turbine}$	$\eta_{combustion}$	η_{nozzle}
0.95	0.91	0.91	0.98	0.95

It is required to calculate

1. α
2. Jet thrust
3. Propeller thrust
4. The ESFC



FIGURE P6.41

6.42 The Tupolev Tu-114 is a Russian turboprop-powered long-range aircraft built in 1955. It has the distinction of being the fastest propeller-driven aircraft in the world, a record it has held since 1960. The aircraft is powered by four Kuznetsov NK-12MV engines. During its record-breaking flight, it reached a speed of 876.5 km/h at an altitude of 8000 m. At this altitude, the engines have a compression ratio of 11, a turbine inlet temperature of 1250 K, and the propeller and gear box efficiencies are 0.75 and 0.95, respectively. Let each engine have the following properties

α	η_{intake}	$\eta_{compressor}$	$\eta_{turbine}$	$\eta_{combustion}$	η_{nozzle}
0.94	0.95	0.91	0.91	0.98	0.95

Assume the aircraft has a drag coefficient of 0.05 and a 100 m^2 frontal area, and cruises at a constant speed of 876.5 km/h.

It is required to calculate

1. Thrust per engine
2. $\dot{m}_a$
3. Jet thrust
4. Propeller thrust
5. Equivalent power
6. ESFC



FIGURE P6.42

6.43 For a two-stream engine (turboprop or turbofan), prove that the ratio between the exhaust speed of the hot stream and the inlet speed, u_{eh}/u, is expressed by the relation

$$\frac{u_{eh}}{u} = \frac{1 \pm \sqrt{1 - \eta_p C}}{\eta_p}$$

where

$$C = \eta_p \beta \left(\frac{u_{ec}}{u} \right)^2 - 2\beta \left(\frac{u_{ec}}{u} \right) + (1 + \beta)(2 - \eta_p)$$

η_p is the propulsive efficiency

β is the bypass ratio

$\frac{u_{ec}}{u}$ is the ratio between the exhaust speed of the cold stream and the inlet speed

Four engine types are considered in the following table.

	Turboprop	High-Bypass Ratio Turbofan	Low-Bypass Ratio Turbofan	Turbojet
β	30.0	10.0	1.0	0
η_p	0.9	0.75	0.62	0.5
$\frac{u_{ec}}{u}$	1.05	1.2	1.4	0

1. Calculate $\left(\frac{u_{eh}}{u} \right)$ for each case
2. Comment



FIGURE P6.44

6.44 Figure P6.44 illustrates the Bell Boeing V-22 Osprey aircraft, which takes off and lands as a helicopter. It is powered by two Rolls Royce Allsion T406 two-spool turboprop engines. Each engine has the following data during takeoff

Propeller power	4586 kW
Compressor pressure ratio	16.7
Fuel heating value	43.0 MJ/kg
Gas turbine inlet temperature	1400 K
Gearbox mechanical efficiency	0.95
Propeller efficiency	0.72
Ambient conditions	288 K and 101 kPa
Exhaust speed	200 m/s
Propulsive efficiency	60% $\left(\text{defined as; } \eta_{propulsive} = \dfrac{2V}{V+V_e}\right)$

Assuming ideal conditions and variable properties γ, C_p, calculate

1. The speed of air flowing into the intake (V)
2. The inlet temperature and pressure for the power turbine driving the propeller
3. The air mass flow rate
4. The ESFC

6.45 1. What are the advantages and disadvantages of turboprop engines
2. Compare piston engines, turboprop engines, and propfan engines
3. Figure P6.45 illustrates a de Havilland Canada DHC-5 Buffalo aircraft, which it is powered by a T64-GE-100 turboprop engine. It is a two-spool engine where the low-pressure turbine drives the propeller and the high-pressure turbine drives the compressor.



FIGURE P6.45

The turboprop engine has the following specifications:

a. Maximum power output: 3228.88 kW
b. Compressor pressure ratio: 14.9:1
c. Turbine inlet temperature: 770°C
d. Fuel heating value 42.8 MJ/kg
e. Propeller efficiency 0.85
f. Gearbox efficiency 0.99

The maximum thrust is obtained when

$$\alpha_{optimum} = 1 - \frac{1}{2\Delta h}\left(\frac{U}{\eta_{pr}\eta_g\eta_{pt}}\right)^2$$

If the engine is tested in an engine shop and all processes are assumed ideal:

1. What will be the value of $\alpha_{optimum}$? Plot the cycle on the *T*–*S* diagram.
2. Calculate the air mass flow rate.
3. Calculate the power specific fuel consumption.
4. Calculate the thermal efficiency.
5. If $\alpha = 0.85$, plot the cycle on the *T*–*S* diagram and calculate the equivalent power.

References

1. A.F. El-Sayed, *Aircraft Propulsion and Gas Turbine Engines*, Taylor & Francis, 2008.
2. U.S. Department of Energy, *DOE Fundamentals Handbook Mechanical Science*, Vol. 1 of 2, 1993, DOE-HDBK-1018/1-93.
3. J.M. Michael, H.N. Shapiro, D.D. Boettner, and M.B. Bailey, *Fundamentals of Engineering Thermodynamics*, 7th edn., John Wiley & Sons, 2011.
4. Y.A. Cengel and M.A. Boles, *Thermodynamics: An Engineering Approach*, 7th edn., McGraw-Hill, 2010.
5. W.W. Pulkrabek, *Engineering Fundamentals of the Internal Combustion Engine*, 2nd edn., Pearson Prentice Hall, 2004.
6. J. Heywood, *Internal Combustion Engine Fundamentals*, 1st edn., McGraw-Hill, 1988.
7. *Collins English Dictionary: Complete & Unabridged*, 10th edn., HarperCollins Publishers, 2009.
8. M. Burden, R. McCarthy and B. Wiggins, Chapter 6: Advanced polymer composite propeller blades, In H. Assender and P. Grant (Eds.), *Aerospace Materials*, Institute of Physics, 2012.
9. H. Glauert, On the vortex theory of screw propellers, *Proceedings of the Royal Society of London, A*, 123(792), 440–465, April 6, 1947.
10. M. Burton, The professional pilot study guide series, PROPELLERS, Airlife Publishing Ltd., U.K., pp. 6–7, 1992.
11. A.J. Bocci, A new series of aerofoil sections suitable for aircraft propellers, *RAeS Aeronautical Quarterly*, 29–73, 1977.
12. R. Douglas Archer and M. Saarlas, *An Introduction to Aerospace Propulsion*, Prentice Hall, 1996.
13. H.S. Ribner and S.P. Foster, Ideal efficiency of propellers: Theodorsen revisited, *AIAA Journal of Aircraft*, 37(9), 810–819, 1990.
14. E.P. Hartman and D. Biermann, The aerodynamic characteristics of full-scale propellers having 2, 3 and 4 blades of CLARK Y and R.A.F. 6 airfoil sections, N.A.C.A. Report No. 640, 1938.
15. W.F. Lindsey, D.B. Stevenson, and B.N. Daley, Aerodynamic characteristics of 24 NACA 16-series airfoils at Mach numbers between 0.3 and 0.8, NACA TN-1546, 1948.
16. J.D. Anderson, Jr, *Introduction to Flight*, 7th edn., McGraw-Hill, Publishing Company, 2011.
17. M.B. Farghaly, Erosion of propeller blades for turboprop engine, MSc thesis, Cairo University, Cairo, Egypt, 2012.
18. J. Roskam, *Airplane Aerodynamics and Performance*, DAR Corporation, 1997.
19. I.H. Abbott and A.E.V. Doenhoff, *Theory of Wing Sections*, Pan American and International Copyright Conventions, 1959.
20. O.M. Lancaster (Ed.), *Jet Propulsion Engines*, Vol. 12, High Speed Aerodynamics and Jet Propulsion, Princeton University Press, Princeton, NJ, pp. 199–267, 1959.
21. *The Jet Engine*, 5th edn., Rolls-Royce plc, 1986, p. 217. Reprinted 1996 with revisions.
22. H.I.H. Saravanamuttoo, G.F.C. Rogers, and H. Cohen, *Gas Turbine Theory*, 5th edn., Prentice Hall, p. 137, 2001.
23. P. Hill and C. Peterson, *Mechanics and Thermodynamics of Propulsion*, 2nd edn., Addison Wesley Publication Company, Inc, p. 155, 1992.
24. B. Gunston, *The Development of Jet and Turbine Aero Engines*, 2nd edn., Patrick Stephens Limited, an imprint of Haynes Publishing, p. 107, 1997.
25. http://www.minihelicopter.net/CH47Chinook/index.htm.
26. http://www.turbokart.com/about_arrius.htm.


Taylor & Francis
Taylor & Francis Group
http://taylorandfrancis.com

7

High-Speed Supersonic and Hypersonic Engines

7.1 Introduction

In the previous four chapters four broad categories of aeroengines were discussed. The powered vehicles have flight speeds ranging from low subsonic speeds, as in the case of helicopters, up to moderate supersonic speeds. Supersonic vehicles are mainly military airplanes and the limited number of supersonic transports (SSTs), such as the Concorde (retired on November 26, 2003) and Tu-144 airplanes. Passengers become bored by the long time of trips, say across the Atlantic, or in general during flights having more than 5–7 flight hours. Extensive efforts are given these days to satisfy passengers' needs. It is expected in the forthcoming decades that airplanes will satisfy the increasing demand for more comfortable and faster flights. This chapter will concentrate on engines that power such airplanes or airspace planes that will fly at high supersonic and hypersonic flight speeds (Mach 5 and above). The corresponding flight altitudes in such circumstances will be much higher than today's subsonic/transonic civil airliners, for some technical reasons which will be discussed later.

In this chapter two engines will be analyzed: the turboramjet and the scramjet. Both were highlighted in Chapter 1. The turboramjet either combines a turbojet/turbofan and a ramjet engine in one conduit or assembles them in an over/under configuration. In Chapters 3 through 5, the ramjet, turbojet, and turbofan engines were analyzed. Here, a brief discussion will be given with a special analysis of their combined layout and combined operation in the dual mode.

Next, the scramjet will be analyzed, and its similarity with the ramjet will be emphasized. Scramjets are employed in hypersonic vehicles, which must be boosted at first by other engines to reach the starting Mach number for their operation.

7.2 Supersonic Aircraft and Programs

On October 14, 1947, the Bell X-1 [1] became the first airplane to fly faster than the speed of sound. Piloted by U.S. Air Force Capt. Charles E. Yeager, the X-1 reached a speed of 1127 km (700 miles) per hour, Mach 1.06, at an altitude of 13,000 m (43,000 ft).

It was the first Aircraft to have the designation X. The X-1 was air-launched at an altitude of approximately 20,000 ft from the Boeing B-29 (Figure 7.1).

By that flight the supersonic age was started. The second generation of Bell X-1 reached a Mach number of 2.44 at an altitude of 90,000 ft. Later on, many aircraft shared the supersonic race. Until now, the fastest manned aircraft is the Blackbird SR-71 (Figure 7.2),

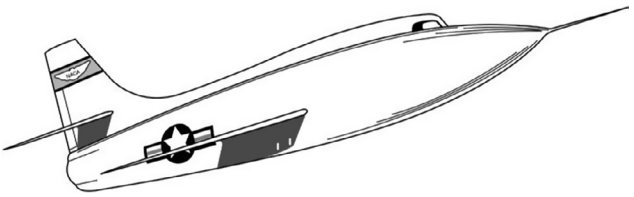


FIGURE 7.1
The first supersonic aircraft X-1E.

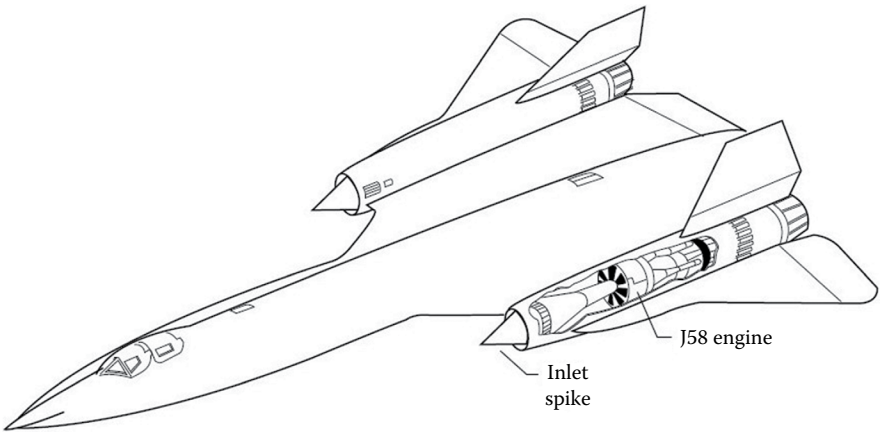


FIGURE 7.2
The fastest manned aircraft SR-71.

a long-range, strategic reconnaissance aircraft, which can fly at Mach number of 3+ having a maximum speed (2200+ mph/3530+ km/h) at 80,000 ft (24,000 m). It is powered by 2 P&W J58-1s, with continuous-bleed afterburning turbojet 32,500 lb force (145 kN) each [2,18]. It was in service from 1964 to 1998.

Continuous R&D programs and testing are performed in the United States, France, Russia, the United Kingdom, and Japan. However, the first supersonic programs started by National Advisory Committee for Aeronautics (NACA) first conceptual design of a supersonic commercial transport designed to carry 10 passengers for a range of about 1500 miles at a cruise speed of Mach number 1.5.

After that design, there were a lot of other conceptual designs of supersonic commercial aircraft. Very few designs reached completion, like Concorde and Tu-144 did. Many others, such as the Boeing 2707-100, 200, 300 and the Lockheed L-2000, were only tested in wind tunnels. Research on supersonic commercial air transport started in the United States in 1958 and somewhat earlier in France and United Kingdom. The date for the start of the Russian projects is unknown. Hereafter, a brief description of several programs will be given.

7.2.1 Anglo-French Activities

7.2.1.1 Concorde

The "Supersonic Transport Aircraft Committee (STAC)" was established in 1956. STAC conducted a series of design studies, leading to the Bristol Company's "Bristol 198," which



FIGURE 7.3
Concorde supersonic airplane.

was a slim, delta-winged machine with eight turbojet engines designed to cross the Atlantic at Mach 2. This evolved into the somewhat less ambitious "Bristol 223," which had four engines and 110 seats.

In the meantime, Sud-Aviation of France designed the "Super Caravelle," which, surprisingly, was very similar to the Bristol 223. On November 29, 1962, the British and French governments signed a collaborative agreement to develop an Anglo-French SST, which became the "Concorde." It was to be built by the *British Aircraft Corporation (BAC)*, into which Bristol had been absorbed in the meantime, and *Rolls-Royce*, in the United Kingdom, and by *Sud-Aviation* and the *Snecma* engine firm in France. In total, 20 Concordes (Figure 7.3), were built between 1966 and 1979 [3]. The first two Concordes were prototype models, one built in France and the other in United Kingdom. Another two preproduction prototypes were built to refine design further and test out ground-breaking systems before the production runs. Thus only 16 aircraft in total were started between the two countries. Concorde is powered by four turbojet engines (Olympus 593) fixed in the wing. The maximum thrust produced during supersonic cruise per engine is 10,000 lb. The maximum weight without fuel (Zero fuel weight) is 203,000 lb (92,080 kg). The maximum operating altitude is 60,000 ft.

7.2.1.2 BAe-Aerospatiale AST

The European advanced supersonic transport (AST) was based on the Concorde design, although it was much larger and more efficient. It had canard fore-planes for extra stability. The new AST design featured the curved Concorde wing, unlike all other delta supersonic transport designs up to that time. It was designed as two aircraft, the first to carry 275 passengers, and the second to carry 400 passengers, and this second version would weigh the same on takeoff as two Concordes. Moreover, the second version had a slimmer delta shape and a double-delta leading-edge wing shape similar to AST designs coming out of the United States.

7.2.2 Russian Activities

7.2.2.1 Tupolev TU-144

In the former Soviet Union, plans were underway for a trans-Soviet continental SST. The Tupolev Tu-144 "Concordski" looked superficially similar to the Anglo-French aircraft (Figure 7.4). It was quite different however. It began life with all four NK144 turbofan engines in a main block underneath the fuselage [4]. This arrangement was changed to a design similar to the Concorde, with the four engines in boxes of two each side. The wing design had two delta angles in it. The last passenger flight for the Tu-144 was in June 1978, and it was last flown in 1999 by NASA.

7.2.3 The U.S. Activities

In the United States, there were fears about being left behind in the supersonic airliner race as the Soviet and European SSTs started to take form on paper. Boeing and Lockheed competed in the design of an SST paper plane. The Boeing model was the 2707-100, 200, and 300. Lockheed had also proposed an SST of its own, the Lockheed L-2000.

Boeing 2707-100/200: This was a large aircraft, 318 ft long from nose to tail, and it had a complex swing-wing design with a tail plane behind the main swing-wing. This tail place formed the back section of the delta wing when the wings were swung back during supersonic flight, and it held four large General-Electric GE-4 turbojet engines. The Boeing 2707-100/200 would fly at a high Mach of 2.7 over 3900 miles, with a passenger load of at least 300. This was a truly large aircraft—bigger than a Boeing 747 (Figure 7.5).

Lockheed L-2000: This jet had a similar range and size to the Boeing jets but was designed as a simpler delta; Figure 7.6. The Lockheed L-2000 was powered by Four General Electric GE4/J5P or P&W JTF17A-21L turbojets with augmentation which are fixed in the wing. Empty weight was 238,000 lb (107,955 kg) and maximum takeoff weight was 590,000 lb (276,620 kg).



FIGURE 7.4
Tupolev TU-144.

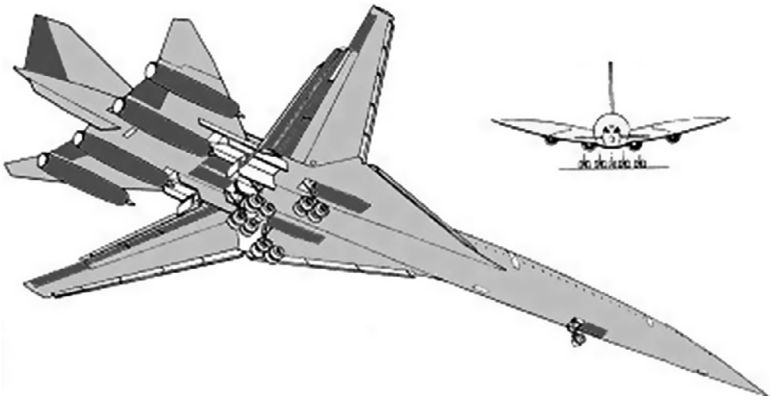


FIGURE 7.5
Boeing 2707-200. (From Boeing 2707 SST specifications, http://www.globalsecurity.org/military/systems/aircraft/b2707-specs.htm.)

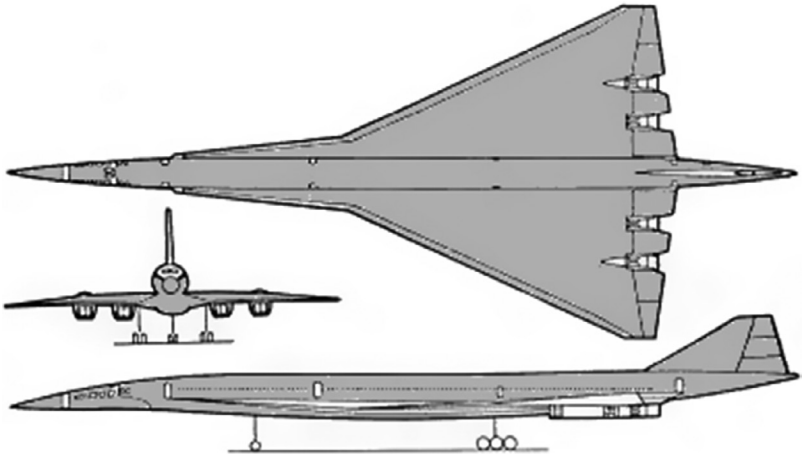


FIGURE 7.6
Lockheed L-2000.

Boeing 2707-300: Boeing looked again at the 2707-200 and replaced it with the Boeing 2707-300 design. This was a more conventional design, although it still had a tail plane, but with a conventional SST delta wing and the four GE-3 engines mounted separately underneath the wing.

Convair BJ-58: The Convair BJ-58 was designed to fly at Mach 2.5 and cruise at more than 70,000 ft (Figure 7.7). It was powered by four J-58 engines (each of 23,000 lb) and had payload capacity of 52 passengers.

NASA AD-1: was both an aircraft and an associated flight test program conducted between 1979 and 1982 at the NASA Dryden Flight Research Center, Edwards California. It successfully demonstrated an aircraft wing that could be pivoted obliquely from zero to 60° during flight. Powered by two small turbojet engines, each producing 220 lb of static thrust at sea level, the aircraft was limited for reasons of safety to a speed of about 170 mph. If flying at speeds up to Mach 1.4,

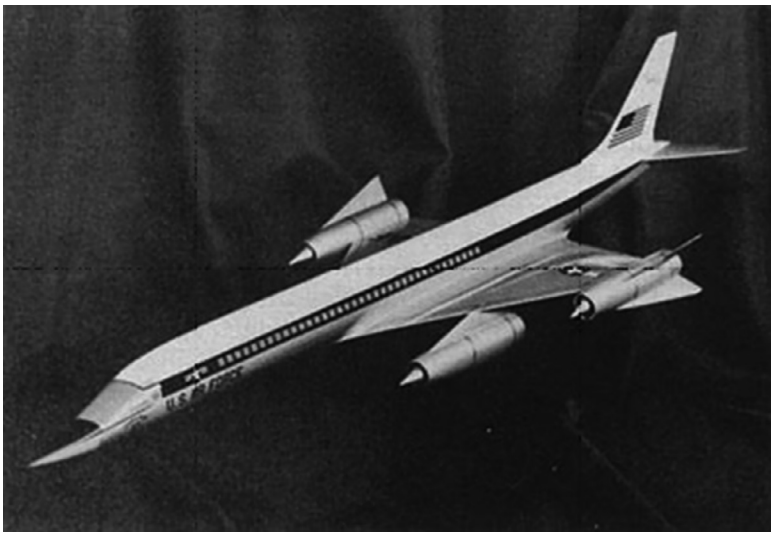


FIGURE 7.7
Convair BJ-58.



FIGURE 7.8
The HSCT.

it would have substantially better aerodynamic performance than aircraft with more conventional wings.

The high speed civil transport (HSCT): was a project for a supersonic airliner, contracted between NASA subdivision HSR (high-speed research), Boeing, General Electric, and Pratt & Whitney (Figure 7.8). This contract was able to solve a lot of the SST problems, such as the emissions problem and the sonic boom problem. But the problems of landing noise, takeoff noise, and materials still remain.

7.3 The Future of Commercial Supersonic Technology

Both Lockheed Martin (*LMT*) and Boeing (*BA*) are working with NASA to develop the Commercial Supersonic Technology (CST) project. Its objectives are developing the tools, technologies, and knowledge to help eliminate today's technical barriers to practical commercial supersonic flight: sonic boom, fuel inefficiency, airport community noise,

high-altitude emissions, and problems of aeroelasticity. The aim is to develop the ability to design future vehicles in an integrated, multidisciplinary manner. It is planned to have the first in a series of "X-planes" in NASA's New Aviation Horizons initiative by the fiscal year 2017 budget. Moreover, NASA believes it is making good progress (largely through aircraft design), and sometime after 2022, it may be acceptable to exceed the speed of sound over land. That would put many more routes in play, and open the door to potential commercial supersonic service.

The governments of France, Japan, Russia, and the United Kingdom are also sponsoring the development of supersonic technology with commercial applications, although none has embarked on a formal program to produce a new commercial supersonic aircraft.

However, supersonic planes will likely first appear in the private and business jet market. Thus, a small supersonic jet could be developed by a single aircraft manufacturer and might lead to important technological innovation.

At least two companies are currently working on such planes. Aerion company (based in Reno, Nevada) is developing a $110-million, 12-passenger business jet capable of hitting Mach 1.6—or over 1200 mph. That is roughly twice as fast as the $65-million Gulfstream G650, and would cut the travel time between New York and London from 7 to just over 4.

The company hopes to deliver the first plane in 2022.

Spike Aerospace (Boston-based) is working on a similar plane that would also carry business passengers at a speed of Mach 1.6.

7.4 Technology Challenges of Future Flight

The key technology challenges coming from customer requirements for vehicle characteristics are related to the environment, economics, and certification [5].

- Environment
  - Benign effect on climate and atmospheric ozone
  - Low landing and takeoff noise
  - Low sonic boom
- Economics (range, payload, fuel burn, and so on)
  - Low weight and low empty weight fraction
  - Improved aerodynamic performance
  - Highly integrated airframe/propulsion systems
  - Low thrust-specific fuel consumption (TSFC)
  - Long life
- Certification for commercial operations
  - Acceptable handling and ride qualities
  - Passenger and crew safety at high altitudes
  - Reliability of advanced technologies, including synthetic vision
  - Technical justification for revising regulations to allow supersonic operations over land

7.5 High-Speed Supersonic and Hypersonic Propulsion

7.5.1 Introduction

For an aircraft cruising at Mach 6, the aircraft must be fitted with an engine that can give sufficient thrust for takeoff, climb, and cruise, and again deceleration, descent, and landing. There are two suggestions for such a vehicle and its prolusion:

1. *Multi-stage vehicle*: In this method the aircraft is to be composed of two stages (Figure 7.9). The first stage has turbine engines (either a turbojet or turbofan) to power the aircraft during takeoff, climb, and acceleration to supersonic speed. At such speed the first stage separates and the engines of the second stage start working, which are either ramjet or scramjet engines.
2. *Hybrid-cycle engine*: The hybrid or combined engine is an engine that works on two or more cycles (Figure 7.10). The first cycle is a cycle of a normal turbojet or turbofan engine. The engine stays working with that cycle until the aircraft reaches a specified speed, at which the engine changes its cycle and works on a ramjet, scramjet, or even a rocket cycle, depending on the aircraft mission and concept.

Most certainly, the second concept will be used because in the first concept there will be a lot of problems, such as those concerning connecting/disconnecting the stages, and working out how the first stage will be brought back to the airport.

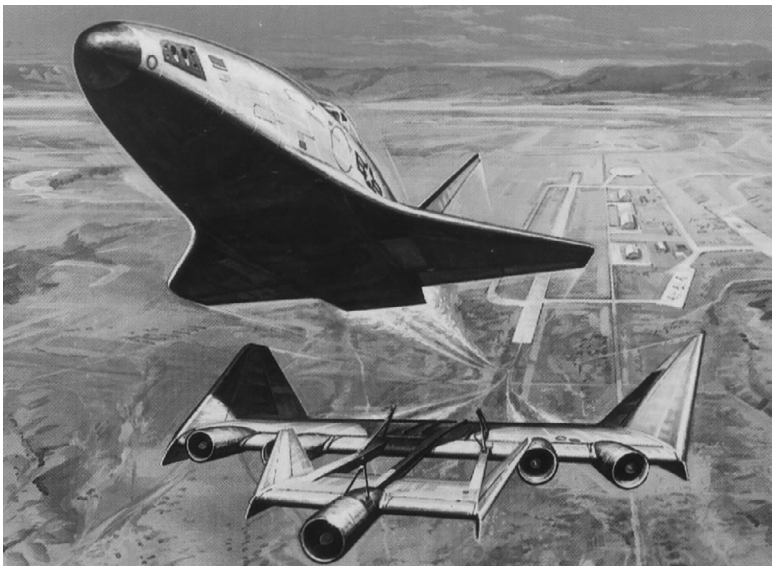


FIGURE 7.9
Multistage aircraft concept.

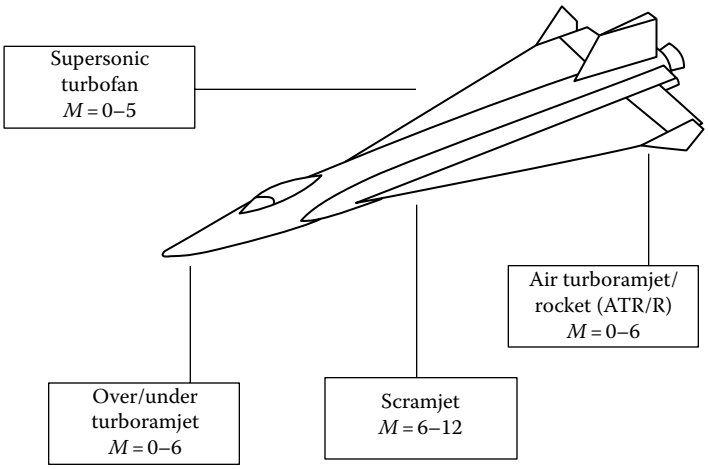


FIGURE 7.10
Hybrid (combined) cycle engine.

7.5.2 Hybrid-Cycle Engine

The question arising here is why a hybrid- (combined) cycle is needed.

The main engine for the aircraft is to be a turbine engine (turbojet or turbofan), but from the performance analysis of those engines—Chapters 4 and 5—it was found that the engine thrust would start decreasing after a certain Mach number (about 2–3) depending on the overall pressure ratio of the engine and the BPR for turbofans. By contrast, a ramjet would still have a reasonable thrust for Mach numbers up to 5 or 6, and a scramjet engine can provide thrust theoretically up to a Mach number of 20. Ramjet and scramjet engines, however, cannot generate thrust at static conditions or at low Mach numbers. A ramjet can start generating thrust at Mach numbers close to unity, while a scramjet develops thrust at Mach numbers greater than 2.5. So the hypersonic aircraft needs both the turbine engine and the ram/scram engine. The above argument is displayed in Figure 7.11, illustrating the specific impulse versus Mach number.

The hybrid engine works on the combined cycle, where in the first flight segment the engine works as a turbojet or a turbofan and is then switched to a ramjet or a scramjet. It may also have a poster rocket to help the engine in the transition region or to drive the vehicle alone if it is to fly in space (the aerospace plane).

In the following sections both turboramjet and scramjet engines will be treated in detail.

7.6 Turboramjet Engine

As defined earlier, the turboramjet engine is a hybrid engine composed of a ramjet engine in conjunction with either a turbojet or turbofan engine. The turboramjet can be run in

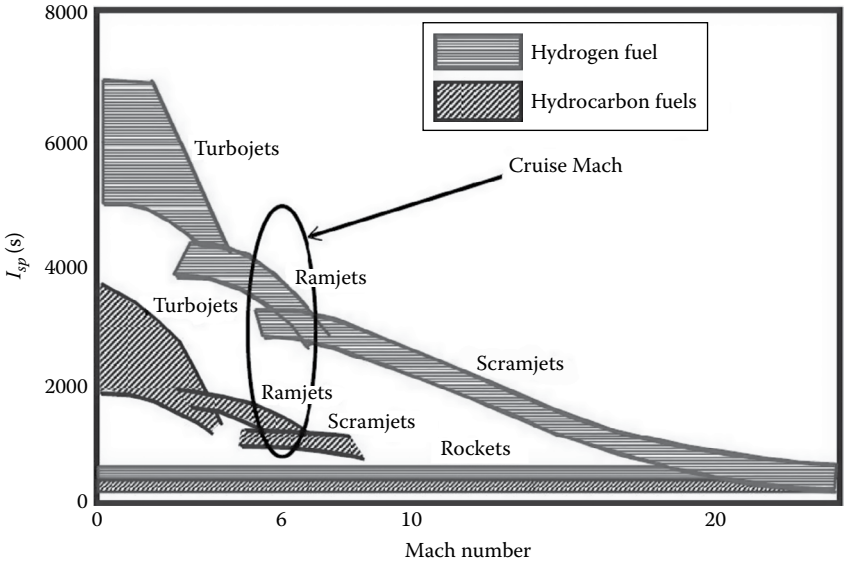


FIGURE 7.11
Specific impulse versus Mach number.

turbojet mode at takeoff and during low-speed flight but will then switch to ramjet mode to accelerate to high Mach numbers. It is constructed in either of the following forms:

1. Wraparound turboramjet
2. Over/under turboramjet

The differences between them are

- The position of the ram with respect to the turbojet
- The position of the afterburner of the turbojet with respect to the ram

7.7 Wraparound Turboramjet

In this configuration, the turbojet is mounted inside a ramjet (Figure 7.12). The turbojet core is mounted inside a duct that contains a combustion chamber downstream of the turbojet nozzle. The operation of the engine is controlled using bypass flaps located just downstream of the diffuser. During low-speed flight, these controllable flaps close the bypass duct and force air directly into the compressor section of the turbojet. During high-speed flight, the flaps block the flow into the turbojet, and the engine operates like a ramjet using the aft combustion chamber to produce thrust.

The wraparound turboramjet layout is found in Convair BJ-58 and SR-71 aircraft.

The engine cycle is plotted on the *T*–*S* diagram in Figure 7.13. It has two modes of operation: either working as a simple turbojet or as a ramjet. A plot for the cycle on the temperature–entropy plane is illustrated in Figure 7.13.

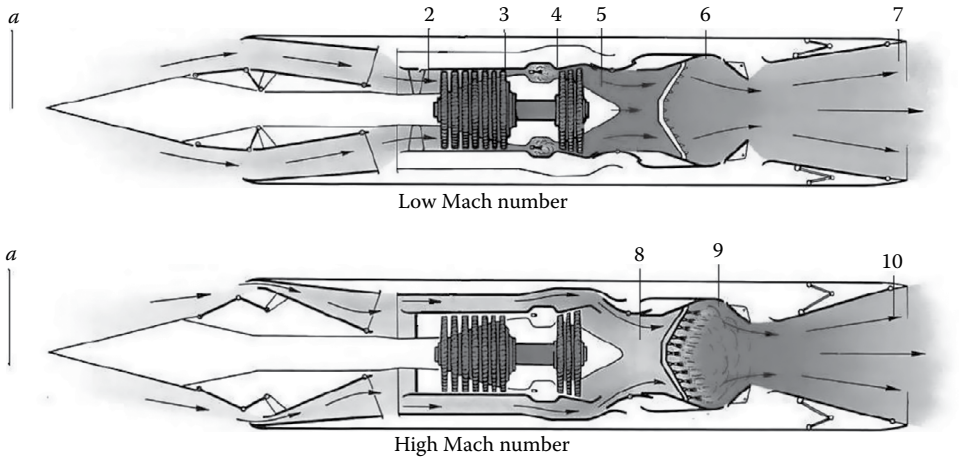


FIGURE 7.12
Wraparound turboramjet.

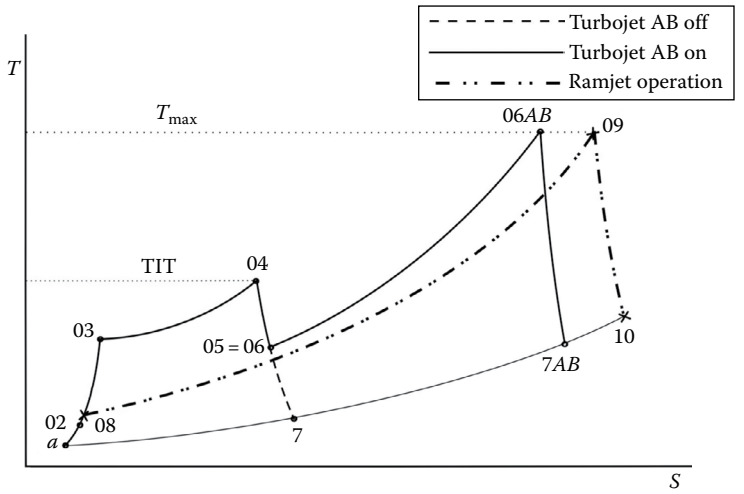


FIGURE 7.13
T–S diagram of the wraparound turboramjet engine.

7.7.1 Operation as a Turbojet Engine

In the turbojet mode, a chain description of the different processes through the different modules is described in Table 7.1.

A brief description of the different processes is given hereafter.

Intake: As previously described, the inlet conditions are the ambient ones. For a flight Mach number of (M), the outlet conditions will be

$$T_{o2} = T_a \left(1 + \frac{\gamma_c - 1}{2} M^2\right)^{\gamma_c/\gamma_c - 1} \tag{7.1}$$

TABLE 7.1

Thermodynamic Processes in Modules of Wraparound Turboramjet Engine

Part	States	Processes
Intake	*a* to 2	Compression process with isentropic efficiency η_d
Compressor	2 to 3	Compression process with isentropic efficiency η_C
Combustion chamber	3 to 4	Heat addition at constant pressure process, with pressure drop $\Delta P_{c.c.}$
Turbine	4 to 5	Expansion process with isentropic efficiency η_t
Afterburner	5 to 6	Heat addition at constant pressure process with pressure drop ΔP_{AB}
Nozzle	6 to 7	Expansion process with isentropic efficiency η_N

$$P_{o2} = P_a\left(1+\eta_d\frac{\gamma_c-1}{2}M^2\right)^{\gamma_c/\gamma_c-1} \tag{7.2}$$

Compressor: With a pressure ratio of π_C the outlet conditions will be

$$P_{o3} = \pi_C \times P_{o2} \tag{7.3}$$

$$T_{o3} = T_{o2}\left(1+\frac{\pi_C{}^{\gamma_{c-1}/\gamma_c}-1}{\eta_c}\right) \tag{7.4}$$

Combustion chamber: Due to friction, a pressure loss $\Delta P_{C.C}$ will be encountered. The output of the combustion chamber is to be controlled by the turbine inlet temperature (TIT), which depends on the turbine material. The outlet pressure and fuel-to-air ratio are then

$$P_{o4} = P_{o3}\left(1-\Delta P_{C.C}\right) \tag{7.5}$$

$$f = \frac{C_{Ph}T_{o4}-C_{Pc}T_{o3}}{\eta_{c.c}Q_{HV}-C_{Ph}T_{o4}} \tag{7.6}$$

Turbine: As usual, the turbine is the main source of power in the aircraft, so its power must be equal to the power needed to drive the compressor plus the power needed by all systems in the aircraft. For a preliminary design, it is assumed that the power of both turbine and compressor are equal. Thus power balance results in the following:

$$T_{o5} = T_{o4}-\frac{C_{Pc}\left(T_{o3}-T_{o2}\right)}{\eta_{mech}C_{Ph}\left(1+f\right)} \tag{7.7}$$

$$P_{o5} = P_{o4}\left(1-\frac{T_{o4}-T_{o5}}{\eta_t T_{o4}}\right)^{\gamma_h/\gamma_h-1} \tag{7.8}$$

Afterburner: The afterburner will be lit if more thrust is needed from the engine. When no extra thrust is needed the afterburner is to be turned off and treated as a pipe. Combustion in

the afterburner is associated with pressure loss ΔP_{AB}. The fuel burned in the afterburner and the outlet pressure are calculated

$$f_{AB} = C_{Ph}\left(1+f\right)\frac{T_{o5}-T_{o4}}{\eta_{AB}Q_{HV}-C_{Ph}T_{o6}} \tag{7.9}$$

$$P_{o6} = P_{o5}\left(1-\Delta P_{AB}\right) \tag{7.10}$$

Nozzle: The gases expand in the nozzle to high velocities to generate the required thrust. The outlet conditions of the gases and nozzle exit area are

$$T_7 = T_{o6} - \eta_N T_{o6}\left[1-\left(\frac{P_a}{P_{o6}}\right)^{\gamma_h-1/\gamma_h}\right] \tag{7.11}$$

$$V_7 = \sqrt{2C_{Ph}\left(T_{o6}-T_7\right)} \tag{7.12}$$

$$\rho_7 = \frac{P_a}{RT_7} \tag{7.13}$$

$$\frac{A_{ex}}{m_a} = \frac{1+f+f_{AB}}{\rho_7 V_7} \tag{7.14}$$

7.7.2 Operation as a Ramjet Engine

In the ramjet mode, the flow is passing through the processes and states described in Table 7.2.

Analysis of the processes is briefly described as follows.

Intake: The delivery pressure and temperature will be evaluated in term of the total pressure ratio of (r_d) which is to be calculated from Equation 7.15:

$$r_d = \begin{cases} 1 & M \le 1 \\ 1-0.75\left(M-1\right)^{1.35} & 1 \le M \le 5 \\ \dfrac{800}{M^4+938} & M \ge 5 \end{cases} \tag{7.15}$$

TABLE 7.2

Thermodynamic Processes in Modules of Ramjet Engine

Part	States	Processes
Intake	*a* to 8	Compression process with total pressure ratio r_d
Combustion chamber	8 to 9	Heat addition at constant pressure with pressure drop $\Delta P_{c.c}$
Nozzle	9 to 10	Expansion with isentropic efficiency (η_N)

The outlet temperature and pressure are

$$T_{o8} = T_a\left(1+\frac{\gamma_c-1}{2}M^2\right)^{\gamma_c/\gamma_c-1} \tag{7.16}$$

$$P_{o8} = P_a\, r_d\left(1+\frac{\gamma_c-1}{2}M^2\right)^{\gamma_c/\gamma_c-1} \tag{7.17}$$

The combustion chamber is treated in the same way as the afterburner of the turbojet:

$$P_{o9} = P_{o8}\left(1-\Delta P_{C.C.R}\right) \tag{7.18}$$

$$f_R = \frac{C_{Ph}T_{o9}-C_{Pc}T_{o8}}{\eta_{C.C.R}Q_{HV}-C_{Ph}T_{o9}} \tag{7.19}$$

Nozzle: This will also be handled in the same way as in the turbojet engine:

$$T_{10} = T_{o9}-\eta_N T_{o9}\left[1-\left(\frac{P_a}{P_{o9}}\right)^{\gamma_h-1/\gamma_h}\right] \tag{7.20}$$

$$V_{10} = \sqrt{2C_{Ph}\left(T_{o9}-T_{10}\right)} \tag{7.21}$$

$$\rho_{10} = \frac{P_a}{RT_{10}} \tag{7.22}$$

$$\frac{A_{ex}}{m_a} = \frac{1+f_R}{\rho_{10}V_{10}} \tag{7.23}$$

7.8 Over/Under Turboramjet

As is clear from the name "over/under," this configuration has separated turbojet and ramjet engines, but may have the same intake (inlet) and nozzle (outlet) as in the wrap-around configuration. However, in some cases each engine has a separate intake and nozzle. In such configurations, the turbojet engine operates at takeoff and low subsonic flight and the movable inlet ramp is deployed to allow for the maximum air-flow rate into its intake. At higher Mach numbers the engine operates at a dual mode, where both turbojet and ramjet engines are operative for few seconds until the Mach number reaches 2.5 or 3.0. Next, the turbojet engine is shut down and the ramjet alone becomes operative. An example for such a layout is found in the four over/under airbreathing turboramjet engines powering the Mach 5 Waverider [7]. The complexity of both the aerodynamic and mechanical design of two variable throat nozzles and necessary flaps led to another design including only one nozzle [8]. The suggested nozzle uses a single-expansion ramp nozzle (SERN) instead of a conventional, two-dimensional, convergent-divergent nozzle.

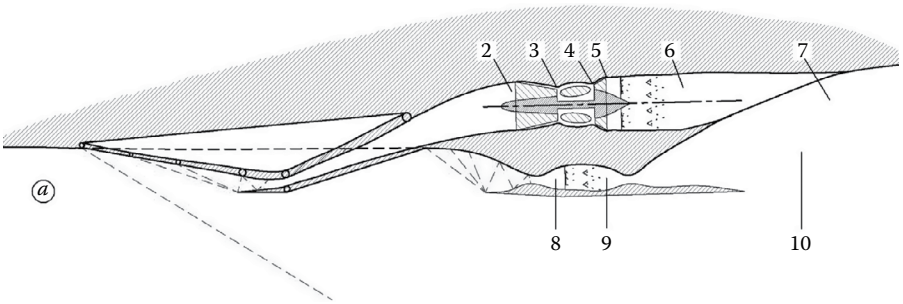


FIGURE 7.14
Over/under layout of turboramjet engine.

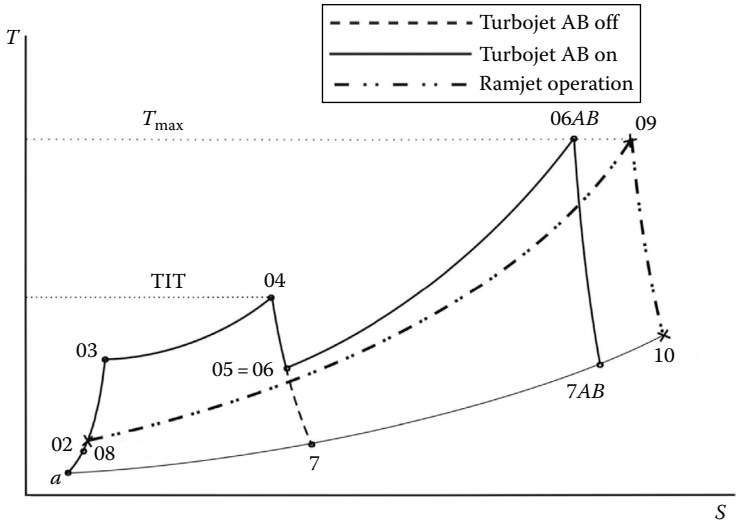


FIGURE 7.15
T–S diagram of the over/under layout of turboramjet engine.

Figures 7.14 and 7.15 illustrate a layout and *T–S* diagram of the over/under configuration of the turboramjet engine.

For the over/under configuration of a turboramjet engine, the engine height is large compared to the wraparound configuration. The reason is clear as the height in this case is the sum of the heights of the turbojet and ramjet engines. Usually, a part of the engine is to be buried inside the fuselage or inside the wing. Since the engine will operate at a high Mach number, it needs a long intake. Thus, a part of the aircraft forebody is used as part of the intake. Concerning installation, the engine is either installed under the fuselage or in the wing. For fuselage installation, the turbojet is buried inside the fuselage and the ramjet is located under the fuselage as in Figures 7.16 and 7.17. For wing installation, the turbojet is situated above the wing and the ramjet is under the wing.

Concerning the thermodynamic cycle of an over/under configuration, there are three modes of operation: a turbojet, a ramjet, or a dual mode. Dual mode represents the combined or transition mode in which both the turbojet and ramjet are operating simultaneously.

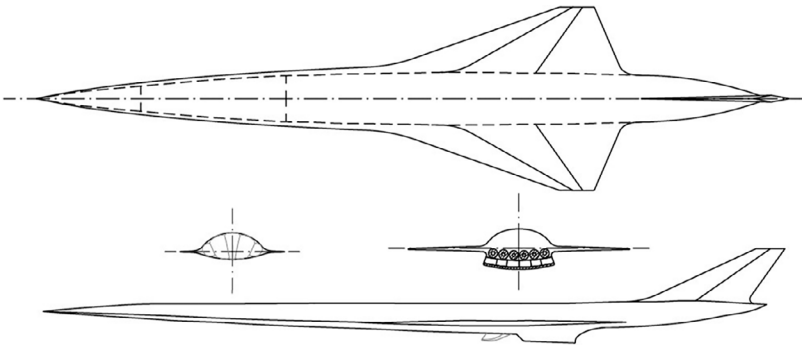


FIGURE 7.16
Hypersonic aircraft (HYCAT-1). (From Gregory, D.R., Aerodynamic characteristics including effect of body shape of a Mach 6 aircraft concept, NASA-TP-2235, December 1983.)

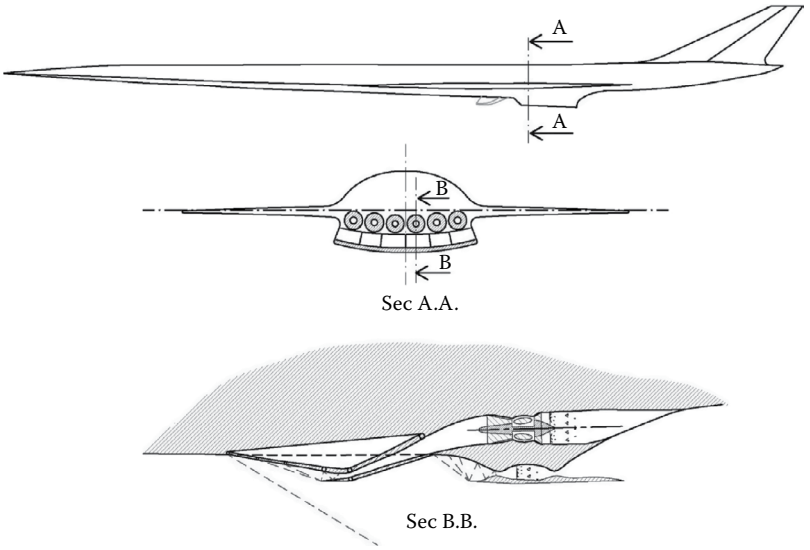


FIGURE 7.17
Turboramjet engine installed under the fuselage.

7.8.1 Turbojet Mode

In that operation mode the engine is working as a simple turbojet engine and develops all the thrust needed by the aircraft. The states and governing equations are the same as for the turbojet in the wraparound configuration.

7.8.2 Dual Mode

In dual mode, both the turbojet and the ramjet are operating simultaneously. The turbojet starts declining and the thrust it has developed will be intentionally decreased by reducing the inlet air-mass flow rate via its variable-geometrical inlet. The ramjet starts working by adding fuel and starting the ignition in its combustion chamber. The thrust generated in the ramjet is increased by also increasing the air-mass flow rate through its

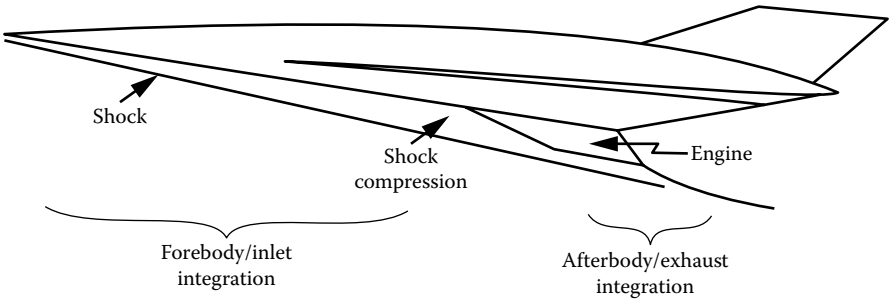


FIGURE 7.18
Intake of the ramjet of the turboramjet engine.

variable area inlet. The generated thrust force will be then the sum of the thrusts of both the turbojet and ramjet engines.

7.8.3 Ramjet Mode

In this mode, the turbojet stops working and its intake is completely closed. All the air-mass flow passes through the ramjet intake. As the Mach number increases, the forebody acts as part of the intake with the foremost oblique shock wave located close to the aircraft nose, as shown in Figure 7.18.

7.9 Turboramjet Performance

The performance parameters—specific thrust, TSFC, total thrust, and propulsive, thermal and overall efficiencies—are defined here. The following equations are valid for both types of turboramjet engines.

7.9.1 Turbojet Mode

The specific thrust is

$$\left.\frac{T}{\dot{m}_a}\right)_{T.J} = \left(1 + f + f_{AB}\right)V_7 - V \tag{7.24}$$

The TSFC

$$TSFC)_{T.J} = \frac{\left(f + f_{AB}\right)}{T/\dot{m}_a} \tag{7.25}$$

The engine propulsive, thermal, and overall efficiencies are

$$\eta_p = \frac{\dfrac{T}{\dot{m}_a}V}{\dfrac{T}{\dot{m}_a}V + \dfrac{\left(V_7 - V\right)^2}{2}\left(1 + f + f_{AB}\right)} \tag{7.26}$$

$$\eta_{th} = \frac{\frac{T}{\dot{m}_a}V + \frac{(V_7 - V)^2}{2}(1 + f + f_{AB})}{Q_{HV}(f + f_{AB})} \tag{7.27}$$

$$\eta_o = \eta_p \times \eta_{th} \tag{7.28}$$

7.9.2 Ramjet Mode

For the ramjet engine, the performance parameters will be calculated in the same way.
The thrust per unit air mass flow $T/\dot{m}_a$

$$\left.\frac{T}{\dot{m}_a}\right)_{R.J} = (1 + f_R)V_{10} - V \tag{7.29}$$

The TSFC

$$TSFC)_{R.J} = \frac{f_R}{\left.\frac{T}{\dot{m}_a}\right)_{R.J}} \tag{7.30}$$

The engine propulsive, thermal, and overall efficiencies

$$\eta_p = \frac{\left.\frac{T}{\dot{m}_a}\right)_{R.J} V}{\left.\frac{T}{\dot{m}_a}\right)_{R.J} V + \frac{(V_{10} - V)^2}{2}(1 + f_R)} \tag{7.31}$$

$$\eta_{th} = \frac{\left.\frac{T}{\dot{m}_a}\right)_{R.J} V + \frac{(V_{10} - V)^2}{2}(1 + f_R)}{Q_{HV} f_R} \tag{7.32}$$

$$\eta_o = \eta_p \times \eta_{th} \tag{7.33}$$

7.9.3 Dual Mode

Both turbojet and ramjet are operating simultaneously. The total thrust will be

$$T = T)_{T.J} + T)_{R.J} \tag{7.34}$$

$$T = (\dot{m}_a)_{T.J}\left[(1 + f + f_{AB})V_7 - V\right] + (\dot{m}_a)_{R.J}\left[(1 + f_R)V_{10} - V\right] \tag{7.35a}$$

$$T = (\dot{m}_a)_{T.J}(1 + f + f_{AB})V_7 + (\dot{m}_a)_{R.J}(1 + f_R)V_{10} - (\dot{m}_a)_{Total}V \tag{7.35b}$$

The specific thrust is

$$\frac{T}{\dot{m}_a} = \frac{T_{total}}{(\dot{m}_a)_{total}} = \frac{(T)_{T.J} + (T)_{R.J}}{(\dot{m}_a)_{T.J} + (\dot{m}_a)_{R.J}} \tag{7.36}$$

The total fuel mass flow rate is

$$\dot{m}_f = (\dot{m}_a)_{T.J}(f + f_{AB}) + (\dot{m}_a)_{R.J} \times f_R \tag{7.37}$$

The TSFC is

$$\frac{(\dot{m}_f)_{Total}}{(T)_{Total}} = \frac{(\dot{m}_f)_{T.J} + (\dot{m}_f)_{R.J}}{(T)_{T.J} + (T)_{R.J}} \tag{7.38}$$

7.10 Case Study

A simplified design procedure for a turboramjet engine will be given here. The procedure is the same followed in any airliner design. It starts by a selecting a proper engine for a certain aircraft. This is not an easy task like selecting a tie for a suit, but a very complicated process. The following steps among many others are to be followed. The function of the air vehicle is first defined and then its mission is to be specified. The drag and lift forces are calculated for each point on the flight envelop. Based on this lift force, the lifting surfaces are designed and a variation of the lift coefficient against Mach number is determined. The corresponding drag force is also calculated and a graph for drag coefficient versus Mach number is also plotted. Now, from this last curve, the appropriate powerplant is selected. The case of one engine type, as described in the previous four chapters, is a straightforward process. But a hybrid engine is a rather complicated design procedure. The difficulty arises from the proper selection of switching points—in other words, when one engine is stopped and another one takes over. If more than two engines are available, the process gets more and more complicated. In addition, even for only two engines, there are also the combined or dual modes. Such a transition process must be carefully analyzed to keep safe margins of lift and thrust forces above the weight and drag forces. A sophisticated system is needed here to control the air and fuel mass-flow rates into different engines. Variable intakes or inlet doors, nozzles, and possibly stator vanes in compressors are activated during such a transition mode.

The following steps summarize the procedure for high supersonic/hypersonic cruise aircraft propulsion integration:

1. The mission or flight envelop has to be selected. The cruise altitude is important from a fuel economy point of view, while takeoff, climb, and acceleration are critical from the surplus thrust that must be available over the aircraft drag force.
2. Calculate the drag force based on drag coefficient variations with the Mach number.
3. The necessary thrust force must be greater than the drag value all over its Mach number operation. A margin of 10% is selected here.

4. The determination of the number of engines is based on the maximum thrust suggested for the hybrid engine at its different modes.
5. The performance of each constituent of the hybrid engine is separately determined. For example, if the hybrid engine includes a ramjet, turbojet, and scramjet, each module is examined separately. Thus, the performance of the turbojet engine running alone is considered first. The specific thrust and TSFC are determined for the cases of operative and inoperative afterburner. Next, the performance of the ramjet operating alone is also considered. Since the ramjet operates up to a Mach number of 6, liquid hydrogen is considered for its fuel. If a scramjet is available, then its performance is determined separately also.
6. Optimization of the hybrid engine represents the next difficult step. The switching points are defined from the specific thrust and TSFC. So, in this step, the designer selects at which Mach number the turbojet operates or stops the afterburner, and also at which Mach number the turbojet must be completely stopped and replaced by the ramjet. If a scramjet is also available, another decision has to be made concerning the Mach number for switching from ramjet to scramjet. The switching process duration and the accompanying procedures regarding the air and fuel flow rates and inlet doors actuation have to be defined.

Since the aim of the twenty-first century is to have hypersonic/high supersonic civil transports, a modified version of the HYCAT-1 aircraft [9] is selected for this analysis as its aerodynamic characteristics up to Mach 6 are available. This aircraft, identified as HYCAT-1-A, includes a completely buried turbojet engine in the fuselage. Other studies for supersonic aircraft having test results up to Mach 6 are also available [10]. Test results for supersonic aircraft of Mach 2.96, 3.96, and 4.63 are found in Reference 11, while results for a supersonic aircraft flying at Mach number of 4 are discussed in Reference 12. Some data of the aircraft is given in Table 7.3.

TABLE 7.3

Mission of HYCAT-1-A

Passengers	200
Range	9,260 km
Cruise Mach number	6
Field length	3,200 m
Fuel	JA-7 For Turbojet LH2 for Ramjet
Aircraft life	Commensurate with current aircraft
Fuel reserves	5% of block fuel
Subsonic flight to alternate airport	482 km
Descent Mach at which turbojet turns on	0.8 Mach
Cruise altitude	90,000 ft
Fuselage length	118.26 m
Wing reference area	816.8 m^2
Horizontal tail total area	177.8 m^2
Vertical tail area	90.2 m^2
Gross weight	350,953 kg
Payload	19,051 kg
Empty weight	198,729 kg

Now, after selecting the aircraft, illustrated in Figures 7.16 and 7.17, the drag force is calculated for different Mach numbers. Concerning the turbojet engine, here is some important data: compressor pressure ratio of 10, turbine inlet temperature of 1750 K, maximum temperature in the afterburner of 3,000 K, and heating value of hydrocarbon fuel of 45,000 kJ/kg. The efficiencies of the diffuser, compressor, turbine, and nozzle are 0.9, 0.91, 0.92, and 0.98, respectively. The efficiency of the combustion chamber and afterburner are 0.99. The pressure drop in the combustion chamber and afterburner is 2% for both. The mechanical efficiency of the compressor turbine shaft is 0.99. Concerning the ramjet, the maximum temperature is 3,000 K, and the heating value of liquid hydrogen is 119,000 kJ/kg. The efficiencies of the diffuser, combustion chamber, and nozzle are respectively 0.9, 0.99, and 0.98. The pressure drop in the combustion chamber is 2%.

The specific thrust and specific fuel consumption for the individual turbojet engine and ramjet engine are calculated and plotted in Figures 7.19 and 7.20.

From Figures 7.19 and 7.20, the following points may be selected as the switching points (refer to Figure 7.21):

1. The ramjet starts burning fuel. (R1)
2. The turbojet starts its gradual shut down. (T1)
3. The ramjet works with its maximum burner temperature. (R2)
4. The turbojet completely shuts down. (T2)

Details of selections and identification of these points is given in Table 7.4.

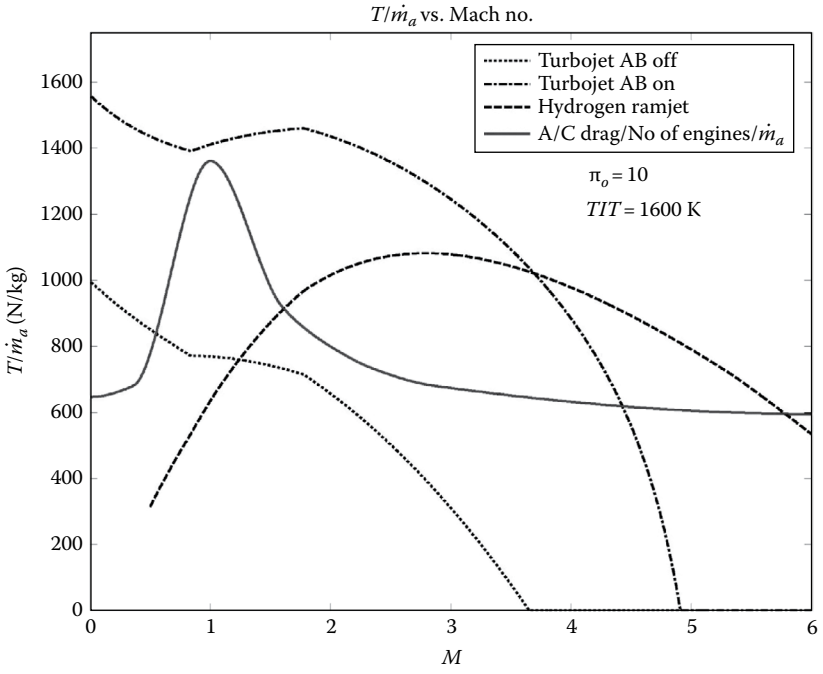


FIGURE 7.19
Specific thrust for individual turbojet and ramjet engines.

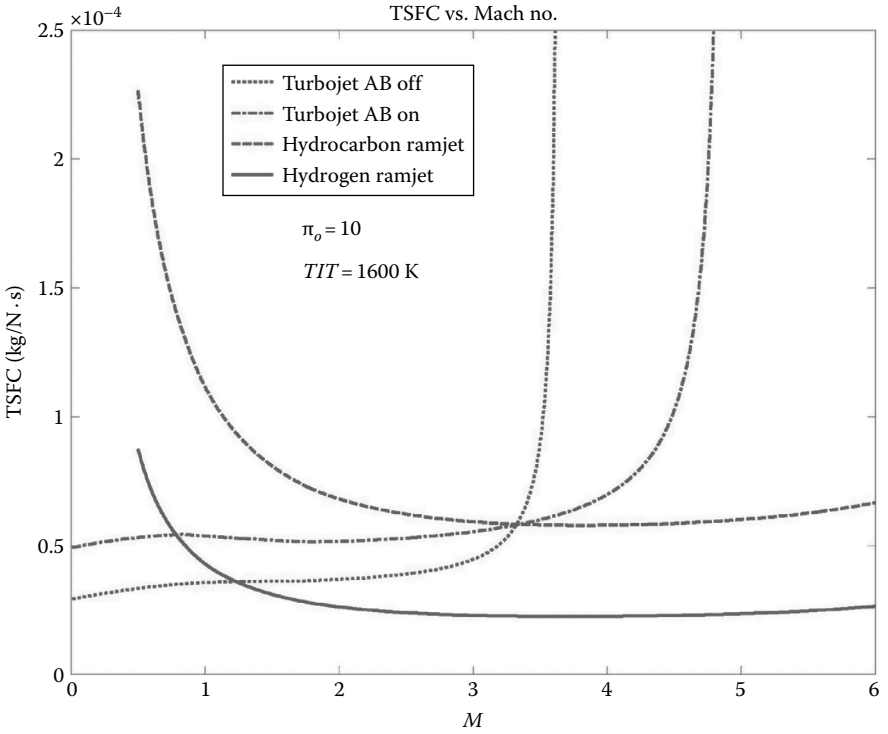


FIGURE 7.20
TSFC for individual turbojet and ramjet engines.

The following two assumptions are identified here concerning both engines:

1. *Concerning the turbojet engine*: The turbojet has three regions of operation, namely:
   a. Constant mass-flow rate with afterburner off (from $M = 0$ to $M = 0.5$)
   b. Constant mass-flow rate with afterburner on (from $M = 0.5$ to $M = 1.5$)
   c. Decreasing mass-flow rate with afterburner off (from $M = 1.5$ to $M = 2.5$)

   The air flow in this last region decreases gradually and linearly from point T1 to Point T2.
2. *Concerning the ramjet engine*: The ramjet has three regions of operation, namely:
   a. The cold flow region (burner is off) in which the ramjet does not generate any thrust but generates drag (from $M = 0$ to point R1).
   b. The starting region, in which the burner temperature increases gradually and linearly. At the end of this region, the temperature reaches its maximum value (from point R1 to point R2).
   c. The working region, in which the burner temperature reaches its maximum value and keeps working (from point R2 to the maximum Mach number).

Based on the above explanation, the operation of the hybrid engine is divided into four regions, which are identified in Table 7.4 and in Figures 7.21 through 7.25.

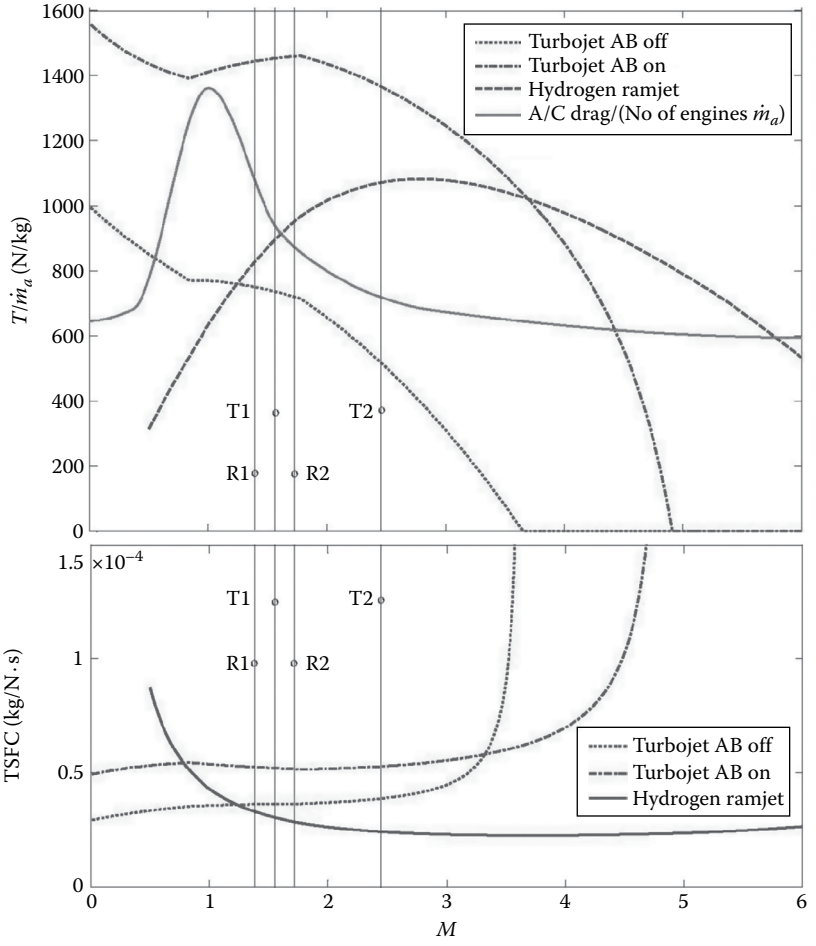


FIGURE 7.21
Regions boundaries.

TABLE 7.4

Regions of Turboramjet Operation

Region		**I**	**II**	**III**	**IV**
Mach number		0–0.5	0.5–1.5	1.5–2.5	2.5–6
Ramjet		Off (cold flow)	Off (cold flow)	Starting (combustion starts and $(\dot{m}_a)_{R.J}$ increases to required value)	On (working alone and stable)
Turbojet	Gas generator	On $(\dot{m}_a)_{T.J} = 160$ kg/s (alone and stable)	On $(\dot{m}_a)_{T.J} = 160$ kg/s (alone and stable)	On $((\dot{m}_a)_{T.J}$ starts to decrease to reach zero at $M = 2.5)$	Off $(\dot{m}_a)_{T.J} = 0$
	After burner	Off	On $T_{max} = 3000$ K	Off	Off

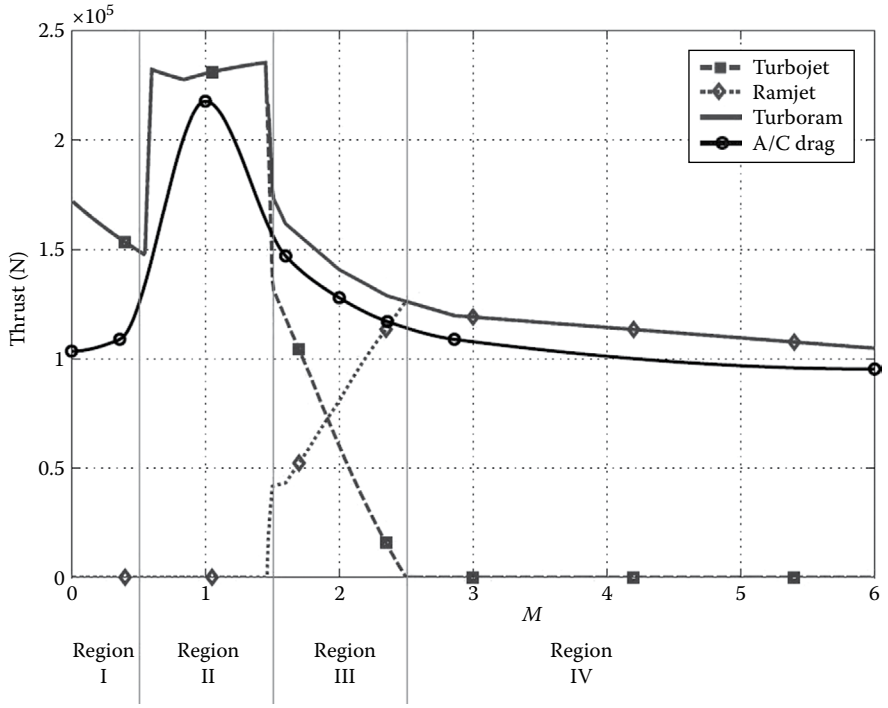


FIGURE 7.22
Thrust versus drag of hybrid engine.

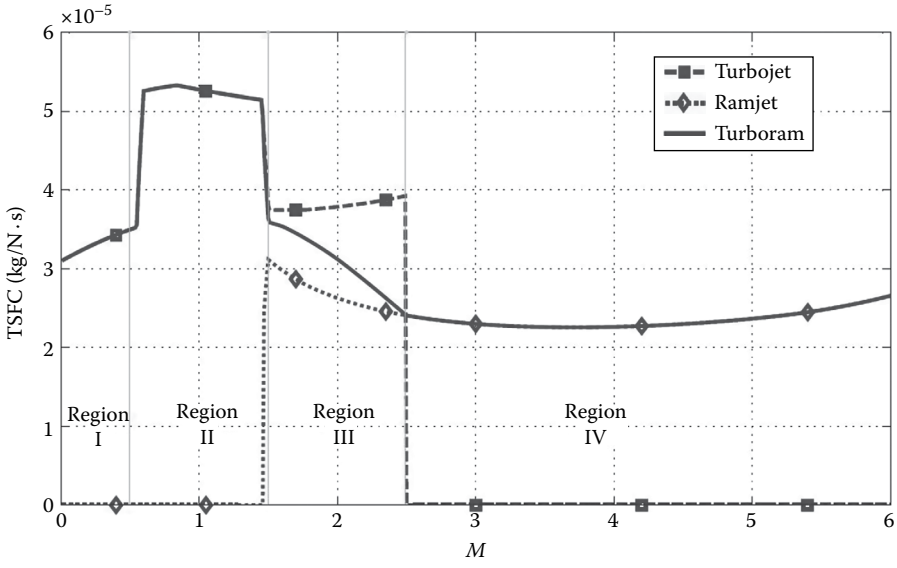


FIGURE 7.23
TSFC of hybrid engine.

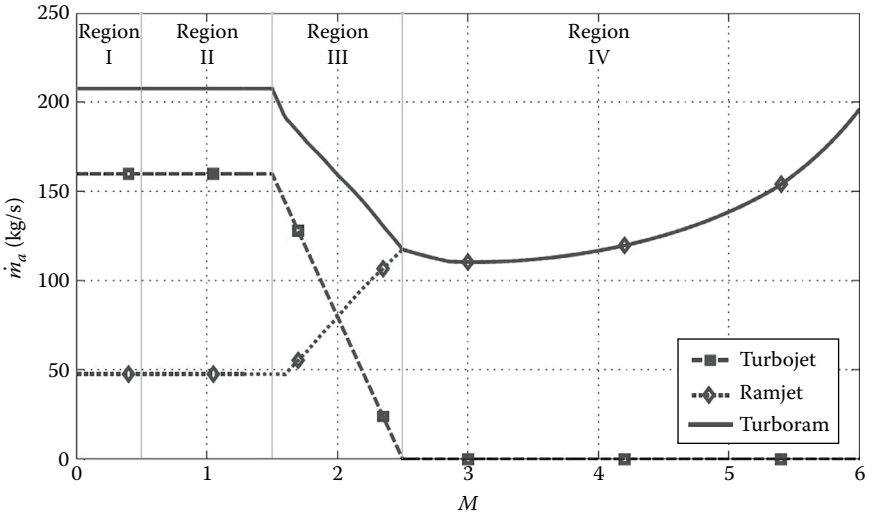


FIGURE 7.24
Air mass flow rate of hybrid engine.

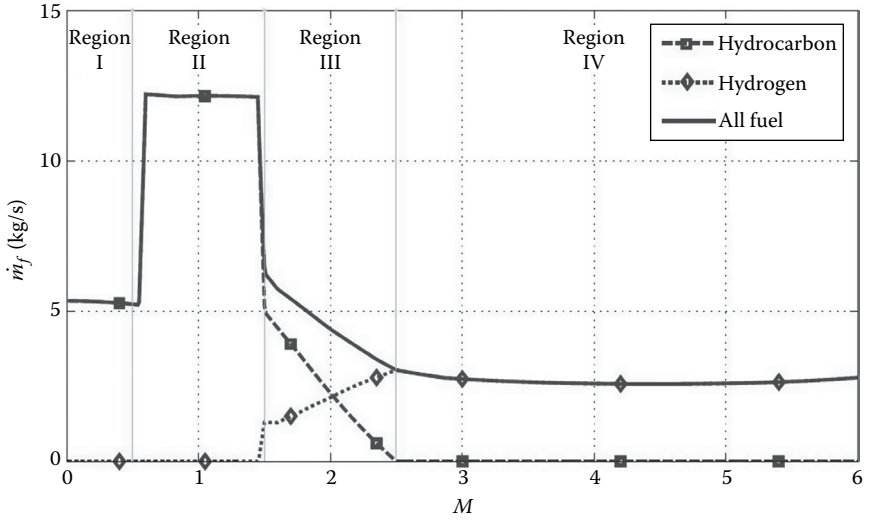


FIGURE 7.25
Fuel mass flow rate of hybrid engine.

Region III (dual region) is important as in this transition region the ramjet engine is starting to build up thrust while the turbojet engine is declining. A linear variation of the air mass-flow rate in the turbojet is assumed during its shutdown (region III); thus, at any Mach number, the thrust generated by the turbojet engine is known. The thrust needed from the ramjet is the difference between the aircraft's required thrust and the turbojet thrust. Since the specific thrust of the ramjet is known at this Mach number, then the air mass-flow rate through the ramjet can be calculated from the following relations:

$$T)_{R.j} = T_R)_{A/C} - T)_{T.j} \tag{7.39}$$

where $(T_R)_{A/C}$ is the thrust required by airplane, say 110% of aircraft drag

$$\dot{m}_a)_{R.J} = \frac{T)_{R.j}}{\left(\frac{T}{\dot{m}_a}\right)_{R.j}} \tag{7.40}$$

In region IV, the ramjet is working alone so the desired thrust from ramjet is equal to the aircraft's required thrust. In the same way, the ramjet air mass-flow rate can be calculated from Equations 7.41 and 7.42.

$$T)_{R.j} = T_R)_{A/C} \tag{7.41}$$

$$\dot{m}_a)_{R.J} = \frac{T)_{R.j}}{\left(\frac{T}{\dot{m}_a}\right)_{R.j}} \tag{7.42}$$

The mass-flow rate of the ramjet engine is known all over the engine working interval. Thus the different performance parameters of the turboramjet engine can be calculated and plotted as illustrated in Figures 7.22 through 7.26.

7.11 Examples for Turboramjet Engines

Turboramjet engines are not as common as the pure ramjet engine. Two famous such engines may be identified. (Most of the others are either secret or only in experimental phases.)

1. P&W J58-1, continuous-bleed afterburning turbo (145 kN), two of which powered the SR-71 strategic reconnaissance aircraft (1964–1998). This enabled it to take off under turbojet power and switch to ramjets at higher super-sonic speeds. Cruise speed was between $M = 3$ and $M = 3.5$.
2. The ATREX turboramjet engine [13].

The ATREX was developed in Japan. As shown in Figure 7.27, the airflow is pressurized inside the engine by an air fan, while the liquid hydrogen (fuel used) is pressurized by a turbopump. Highlights for both flows are given here.

- *Air flow*: The air intake that reduces the velocity of incoming air at a high flight Mach number. Next, this air is cooled down by the pre-cooler. The cooled air is pressurized by a fan and injected into the combustion chamber through the mixer together with the hydrogen discharged out of the tip turbine. The plug nozzle provides the effective nozzle expansion over the wide range of the flight environment.
- *Hydrogen* (H_2) *flow*: The hydrogen supplied from the storage tank is pressurized by a turbopump and heated regeneratively in the pre-cooler.

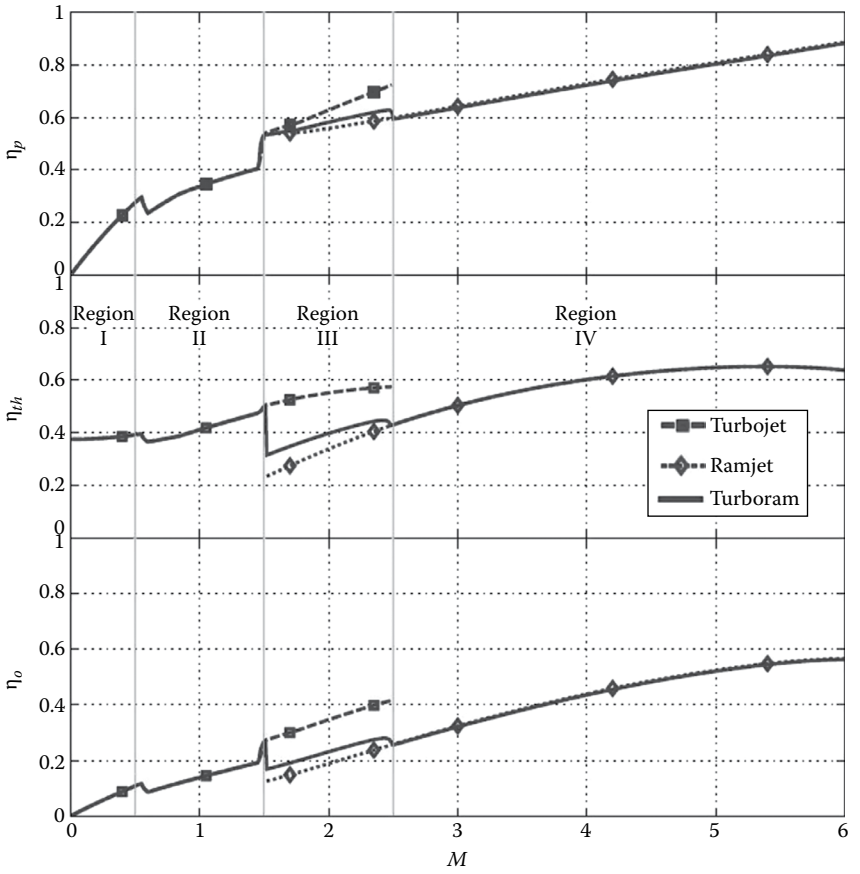


FIGURE 7.26
Propulsive, thermal, and overall efficiencies.

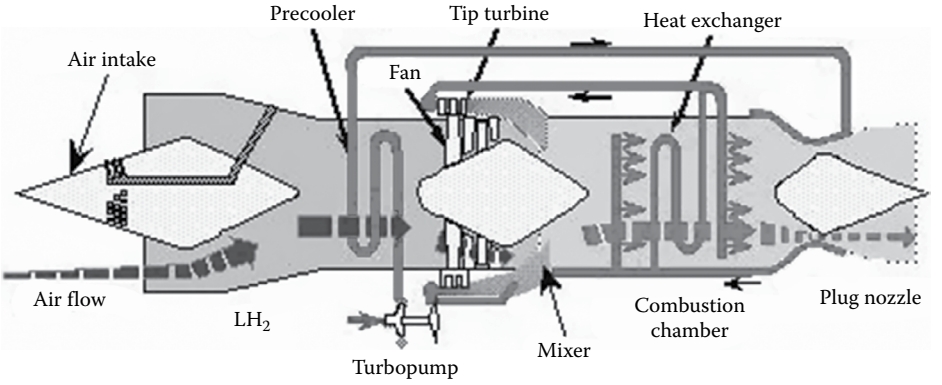


FIGURE 7.27
ATREX turboramjet engine.

7.12 Hypersonic Flight

Hypersonic flight is identified as flight with a Mach number exceeding 5 [14]. The main problem of that speed range is the very large wave drag. To minimize this, both the aircraft and engine must be completely reconfigured. Until now, apart from in research work, no civil aircraft can fly at hypersonic speeds. Only rockets can.

7.12.1 History of Hypersonic Vehicles

Some important events will be highlighted here.

WAC Corporal: The first vehicle ever to achieve hypersonic speeds was the WAC Corporal, a U.S. Army second-stage rocket mounted atop a captured German V-2 rocket. On February 24, 1949, the WAC Corporal separated from the V-2 at 3500 mph before its own engine powered it to an altitude of 244 miles and a top speed of 5150 mph upon atmospheric re-entry.

Bell Aircraft Corporation X-2: First flight was on June 27, 1952. The fastest flight recorded a Mach of 3.169. The last flight was on September 27, 1956.

Lockheed missiles & Space Co. X-7: First flight was on April 24, 1951. The fastest flight was at a Mach number of 4.31. The last flight was on July 20, 1960 [21].

North American Aviation X-10: First flight on October 14, 1953. The fastest flight speed was at Mach 2.05. The last flight was on January 29, 1959.

North American Aviation X-15: American Robert White flew the X-15 rocket-powered research aircraft at Mach 5.3, thereby becoming the first pilot to reach hypersonic velocities (Figure 7.28). White's mark was later topped by fellow X-15 pilot Pete Knight who flew the craft (denoted X15A-2) to a maximum speed of Mach 6.72 in 1967. The record still stands as the highest velocity ever reached by an aircraft.

National Aerospace Plane (*NASP*) *X-30*: During the 1980s, NASA began considering a hypersonic single-stage-to-orbit (SSTO) vehicle to replace the Space Shuttle. The proposed National Aerospace Plane (NASP) would takeoff from a standard runway using some kind of low-speed jet engine. Once the aircraft had reached

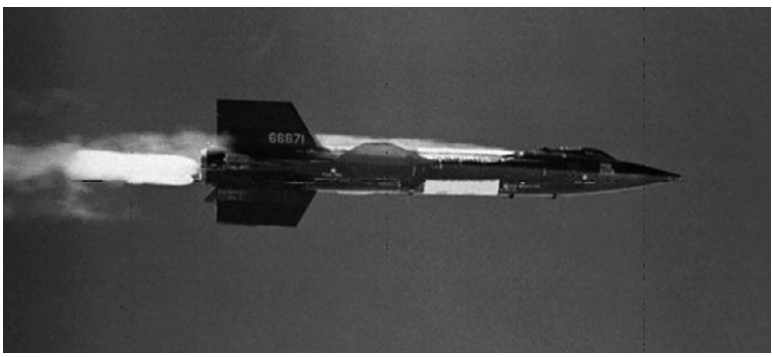


FIGURE 7.28
X-15.

sufficient speed, air-breathing ramjet or scramjet engines would power the aircraft to hypersonic velocities (Mach 20 or more) and to the edge of the atmosphere. A small rocket system would provide the final push into orbit, but the attractiveness of the concept was using the atmosphere to provide most of the fuel needed to get into space. NASP eventually matured into the X-30 research vehicle, which used an integrated scramjet propulsion system.

X-43 Hyper-X: X-43 is a part of the NASA's Hyper-X project (Figure 7.29). A winged booster rocket with the X-43 itself at the tip, called a "stack," is launched from a carrier plane (B-52). After the booster rocket (a modified first stage of the Pegasus rocket) brings the stack to the target speed and altitude. It is discarded, and the X-43 flies free using its own scramjet engine (Figure 7.30). The first X-43 test flight,

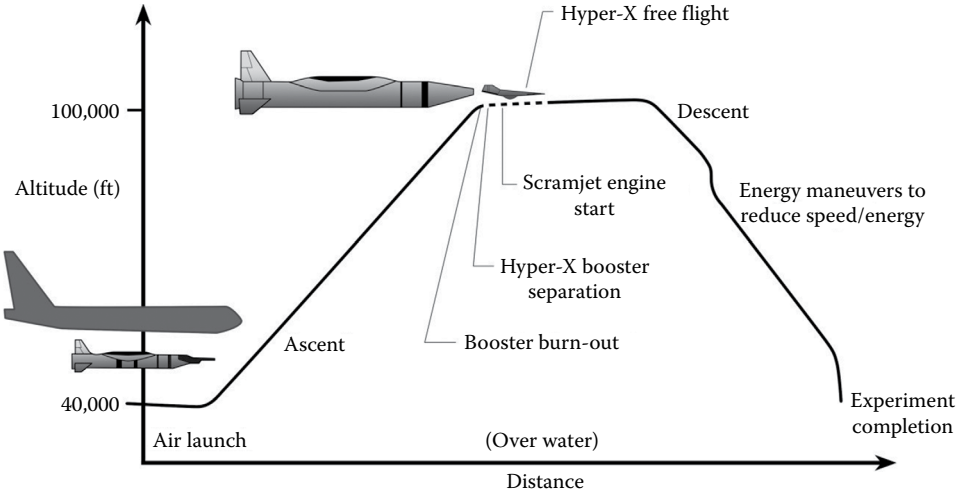


FIGURE 7.29
X-43.



FIGURE 7.30
Booster rocket and X-43.



FIGURE 7.31
The German sänger space transportation systems.

conducted in June 2001, ended in failure after the Pegasus booster rocket became unstable and went out of control. The X-43A's successful second flight made it the fastest free-flying air-breathing aircraft in the world, although it was preceded by an Australian Hyshot as the first operating scramjet engine flight. The third flight of a Boeing X-43A set a new speed record of 7,546 mph (12,144 km/h), or Mach 9.8, on November 16, 2004. It was boosted by a modified Pegasus rocket which was launched from a Boeing B-52 at 13,157 m (43,166 ft). After a free flight in which the scramjet operated for about 10 s, the craft made a planned crash into the Pacific Ocean off the coast of southern California.

LoFlyte: To further research in this area, the U.S. Air Force and NASA sponsored the LoFlyte test vehicle to study the flight characteristics of a Waverider at low-speed conditions, like takeoff and landing. LoFlyte is another small, unmanned vehicle that can be reconfigured with different types of control surfaces and flight control algorithms to determine the most effective combination. Though designed using a Mach 5.5 conical flow field, the LoFlyte vehicle is not actually capable of flying at hypersonic speeds. It has instead been tested for basic handling characteristics at low-speeds.

The German Sänger space transportation systems: The German hypersonic technology program was initiated in 1988. The reference configuration is known as sänger space transportation systems and it is reusable in two stages (Figure 7.31). The piloted first stage is also known as the European hypersonic transport vehicle (EHTV); the EHTV is propelled up to the stage separation Mach number of 6.8 by a hydrogen-fueled turboramjet propulsion system. There are two identical second stages similar to the Space Shuttle orbiter and powered by a hydrogen oxygen rocket.

7.12.2 Hypersonic Commercial Transport

Hypersonic vehicles in general, and Waveriders in particular, have long been touted as potential high-speed commercial transports to replace the Concorde. Some aerospace companies, airlines, and government officials have proposed vehicles cruising at Mach 7 to 12 capable of carrying passengers from New York to Tokyo in under 2 h. Perhaps one of the best-known concepts along these lines was the Orient Express, envisioned as a commercial derivative of the NASP project. Figures 1.70 and 7.32 illustrate a recent artist's concept of hypersonic transports.

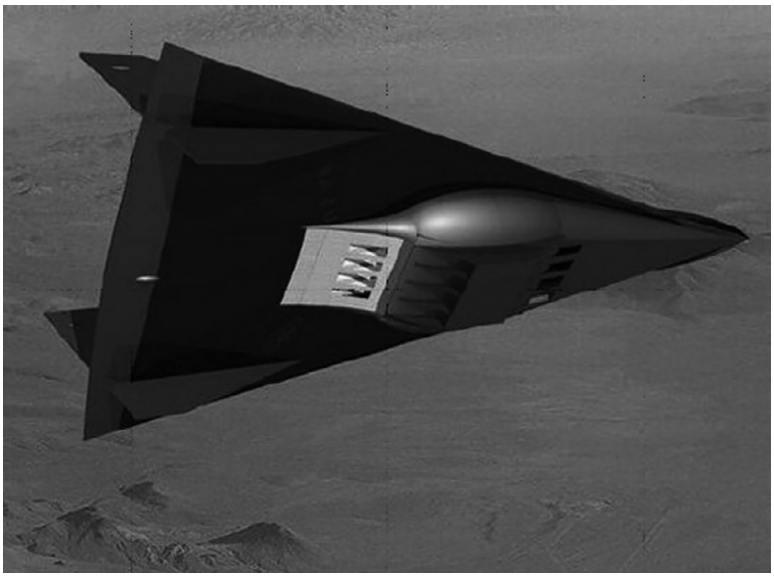


FIGURE 7.32
Artist's concept of a hypersonic aircraft (Aurora).

The expected flight path for the commercial flight is something unbelievable. Hypersonic vehicles escapes heat build-up on the airframe by skipping along the edge of the Earth's atmosphere, much like a rock skipped across water. A hypersonic vehicle would ascend via its power outside the Earth's atmosphere, and then turn off its engines and coast back to the surface of the atmosphere. There, it would again fire its air-breathing engines and skip back into space. The craft would repeat this process until it reached its destination. A flight from United States to Japan would take 25 such skips (Figure 7.33). The skips would be angled at only 5°. The passengers would feel a force of 1.5 Gs, which is what you would experience on a child's swing. The plane would power up to 39 km, from where it would coast to double that altitude, before it started to descend. Each skip would be 450 km long.

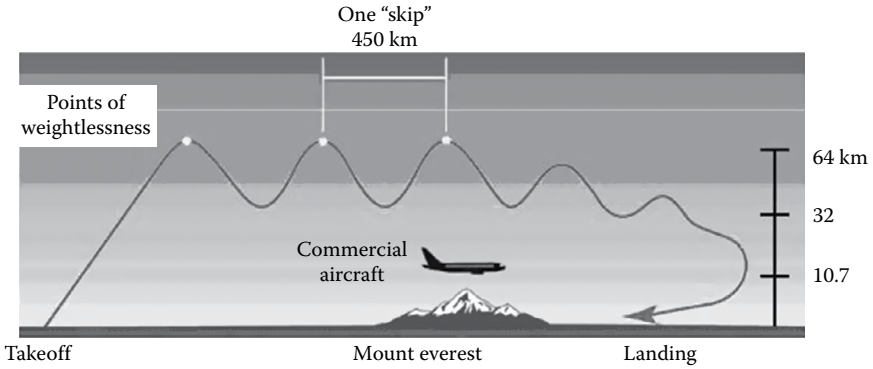


FIGURE 7.33
The expected flight path for hypersonic civil transports.

7.12.3 Military Applications

Trends of the 1950s and 1960s indicated that military aircraft had to fly faster and higher to survive, so concepts for high-altitude fighters and bombers cruising at Mach 4 or more were not uncommon. Although the trends soon fizzled out and military planners looked to maneuverability and stealth for survival, the military has recently shown renewed interest in hypersonic flight. For example, many have conjectured about the possible existence of a Mach 5 spy plane, the Aurora; Figure 1.72, which may be either under development or perhaps already flying. If so, the Aurora may be scramjet-powered.

7.13 Scramjet Engines

7.13.1 Introduction

The scramjet engine find its applications in many recent hypersonic speed vehicles such as rockets, commercial transports in the twenty-first century, as well as single-stage-to-orbit (SSTO) launchers. Scramjet is an acronym for Supersonic Combustion Ramjet.

From a thermodynamic point of view, a scramjet engine is similar to a ramjet (Figure 7.34) engine as both consist of an intake, a combustion chamber, and a nozzle. A dominant characteristic of airbreathing engines for hypersonic flight is that the engine is mostly inlet and nozzle (Figure 7.35), and the engine occupies the entire lower surface of the vehicle body.

In both engines, the cycle pressure rise is achieved purely by ram compression [15]. The main difference between ramjet and scramjet is to be found in the speed of combustion, which is subsonic in a ramjet engine and supersonic in a scramjet engine. A conventional

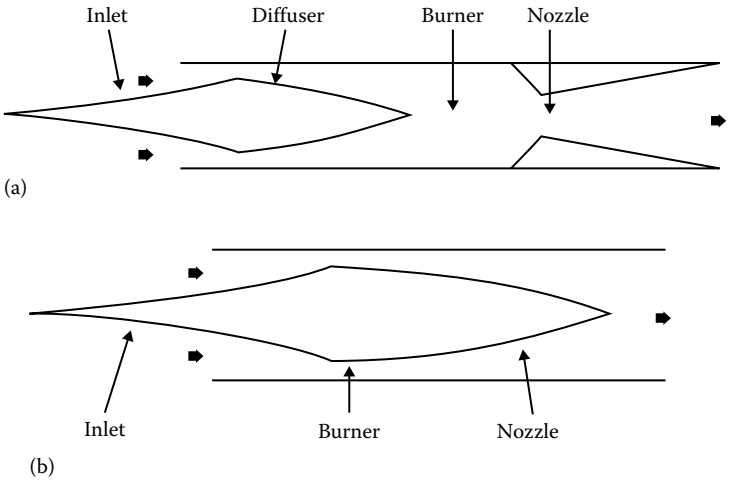


FIGURE 7.34
(a) Ramjet and (b) scramjet engines.

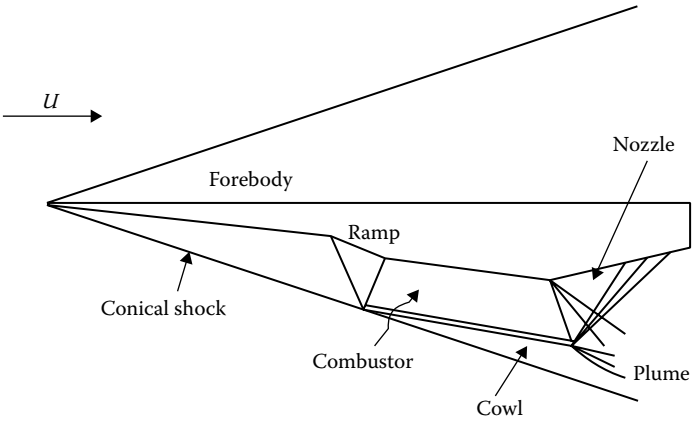


FIGURE 7.35
Schematic representation of a hypersonic scramjet engine powering a hypersonic aircraft.

hydrogen-fuelled ramjet with a subsonic combustor is capable of operating up to around Mach 5–6, at which speed the limiting effect of dissociation reduces the effective heat addition to the airflow, resulting in a rapid loss in net thrust.

The idea behind the scramjet engine is to avoid dissociation limit by partially slowing the air stream through the intake system (thus reducing the static temperature rise) and hence permitting greater useful heat addition in the now supersonic combustor. Consequently, scramjet engines offer a tantalizing prospect of achieving a high specific impulse up to a very high Mach number (Figure 7.11). Scramjet engines have a relatively low specific thrust due to the moderate combustor temperature rise and pressure ratio, and therefore a very large air mass-flow rate is required to give adequate vehicle thrust/weight ratio. As outlined in Reference 15, the captured air mass flow reduces for a given intake area as speed rises above Mach 1. Consequently, the entire vehicle frontal area is needed to serve as an intake at scramjet speeds and similarly the exhaust flow has to be re-expanded back into the original streamtube in order to achieve a reasonable exhaust speed. Employing the vehicle forebody and aftbody as part of the propulsion system has the following disadvantages:

1. The forebody boundary layer reaches nearly 40% of the intake flow which upsets the intake flow stability. The conventional solution of bleeding the boundary layer off would be unacceptable due to the prohibitive momentum drag penalty.
2. The vehicle surface must be flat in order to provide the intake with a uniform flow field. This flattened vehicle cross-section is not really suitable for pressurized tankage and has a higher surface area/volume than a circular cross-section.
3. Since the engine and airframe are physically inseparable, little freedom is available to the designer to control the vehicle pitch balance. The single-sided intake and nozzle generate both lift and pitching moments and this adds difficulties when trying to achieve both vehicle pitch balance over the entire Mach number range and center of gravity (CG) movement to trim the vehicle.

4. Normally, scramjet engines are clustered into a compact package underneath the vehicle. This results in interdependent flowfield and thus the failure in one engine with a consequent loss of internal flow is likely to unstart the entire engine installation precipitating a violent change in vehicle pitching moment.
5. In order to focus the intake shock system and to generate the correct duct flow areas over the whole Mach number, variable-geometry intake/combustor and nozzle surfaces are required. The large variation in flow passage shape forces the adoption of a rectangular engine cross-section with flat moving ramps, thereby incurring a severe penalty in the pressure vessel mass.
6. To maximize the installed engine performance a high dynamic pressure trajectory with the high Mach number is required, which imposes severe heating rates on the airframe. Active cooling of significant portions of the airframe will be necessary with further penalties in mass and complexity.
7. The net thrust of a scramjet is very sensitive to the intake, combustion, and nozzle efficiencies due to the exceptionally poor work ratio of the cycle. Since the exhaust velocity is only slightly greater than the incoming free-stream velocity, a small reduction in pressure recovery is likely to convert a small net thrust into a small net drag.

7.13.2 Thermodynamics

A typical layout of a scramjet engine is shown in Figure 7.36. Three processes only are found: compression, combustion, and expansion. Both compression and expansion take place internally and externally. The first part of compression takes place external to the engine while the last part of expansion occurs outside the engine. The same governing equations described in Section 7.7.2 are applied here. Thus, Equations 7.15 through 7.23 are also applicable here. The five performance parameters (specific thrust, TSFC, and the propulsive, thermal, and overall efficiencies) are also calculated from equations similar to Equations 7.29 through 7.33.

The previously described pressure-recovery factors in Chapter 3 for the ramjet engine may also be employed here. Thus Equations 3.23 through 3.29 may also be applied.

Hereafter, the different modules will be briefly described.

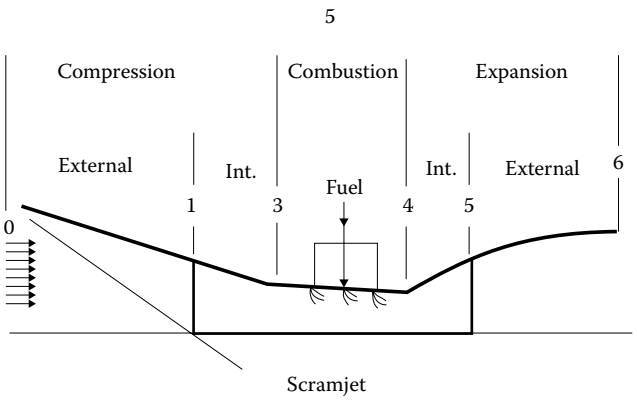


FIGURE 7.36
Layout of a scramjet engine.

7.14 Intake of a Scramjet Engine

The design of an air intake (inlet) of any airbreathing engine is crucial in achieving optimal engine performance. The flow pattern for supersonic flow is more complicated due to shock waves/turbulent boundary layer interaction in an adverse pressure gradient. It is necessary to design such intake for a maximum pressure recovery; $r_d = P_{02}/P_{0a}$.

Supersonic intakes are classified into three basic types, characterized by the location of the supersonic compression wave system: internal compression, external compression, and mixed compression. The first type (*internal compression*) achieves compression through a series of internal oblique shock waves. The second (*external compression*) achieves compression through either one or a series of external oblique shock waves. The last type (*mixed compression*) makes oblique shock waves in various external and internal blends in order to achieve compression and flow turn. Apart from the scramjet engine, in all other types of airbreathing engines the oblique shock waves previously described are followed by a normal shock to convert the flow into a subsonic one. The intake of a scramjet engine is unique by itself. It is of the supersonic-supersonic type. Both inlet and outlet flow are supersonic. The flow is decelerated through several shock waves in the intake, but all of them are of the oblique type. The flow is to be decelerated to the supersonic speed suitable for the succeeding supersonic combustion chamber. The outlet Mach number could be 3 or higher [16].

The pressure recovery of the intake may be calculated from Equation 7.15 based on the flight Mach number or calculated from the product of the pressure ratio across different shock waves.

The details of intake design are given in Chapter 9 together with the governing equations. The pressure recovery for scramjet engines attains very small values. It depends both on the flight Mach number and the number of shocks in the intake. It reaches small values for large Mach numbers. It is in the range of 0.1–0.2 for Mach numbers close to 10 and 0.01–0.02 for Mach numbers close to 20 [16].

7.14.1 Case Study

The intake of a scramjet engine is designed in two cases, 4 and 12 external shock waves. The free-stream Mach number is 8. The outlet pressure for the 4 shocks 2.66 and for the 12 shocks is 2.43. The intake shape together with the shock train is shown in Figure 7.37. The intake aspect ratios (height/length) are 1:5.5 and 1:12.5, respectively. The efficiency is 0.87 and 0.42 for the 4- and 12-shock intakes, respectively. Such low efficiency outlines how external shock is not appropriate. Moreover, its length is too large and increases continuously with the increase of the number of shocks.

7.15 Combustion Chamber

The combustion process here represents a heat-addition process at high-speed flow (supersonic flow). Generally, the Mach number at the inlet to the combustion chamber is nearly one-third of the flight Mach number. The cross-sectional area of the combustion chamber

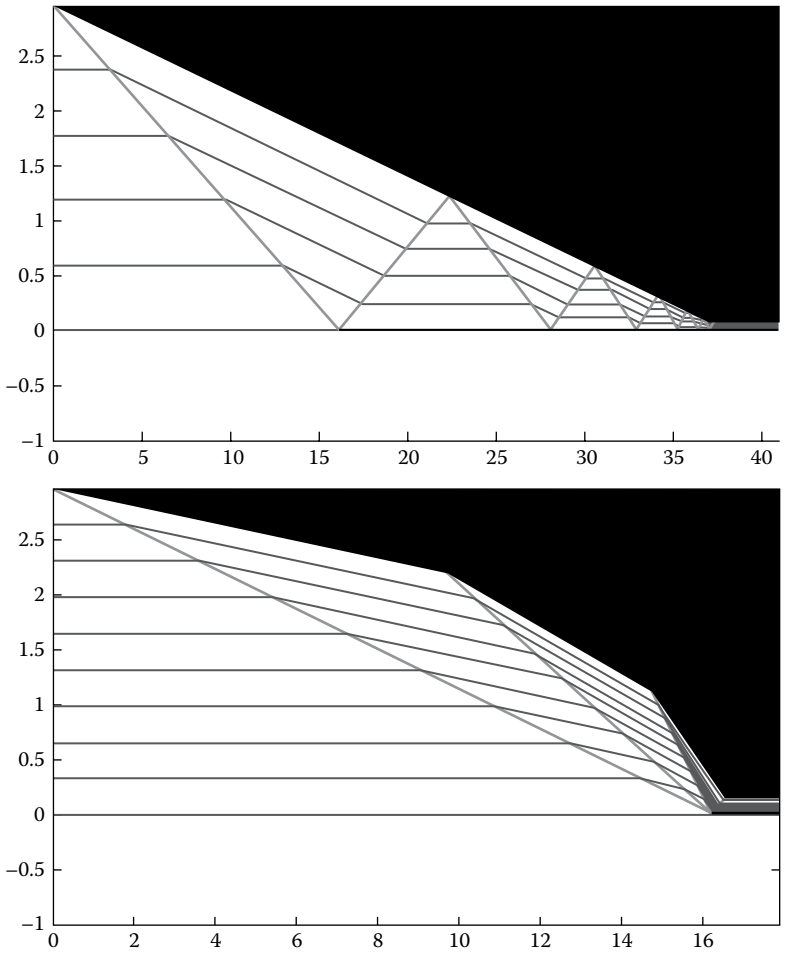


FIGURE 7.37
Eight versus four external shock wave intakes.

is assumed constant for simplicity. The flow may be treated as a Rayleigh flow as a first approximation. In such a simplified model, both the specific heat at constant pressure and the specific heat ratio are assumed constant. Supersonic combustion will be treated in detail in Chapter 11. Here some highlights will be given. First, the practical problems of employing supersonic combustion may be stated as follows:

1. Capture a stream tube of supersonic air.
2. Inject fuel into the air stream.
3. Achieve a fairly uniform mixture of fuel and air.
4. Carry out the combustion process within a reasonable length without causing a normal shock within the engine.

For a hydrocarbon fuel C_xH_y, the maximum combustion temperature occurs when hydrocarbon fuel molecules are mixed with just enough air so that all of the hydrogen atoms

form water vapor and all of the carbon atoms form carbon dioxide. The stoichiometric fuel-to-air ratio is

$$f_{st} = \frac{36x + 3y}{103(4x + y)} \text{ kg fuel/kg air}$$

Fuel mixtures could be rich or lean depending on the equivalence ratio; the ratio of the actual fuel/air ratio to the stoichiometric fuel/air ratio, or

$$\phi = \frac{f}{f_{st}}$$

Combustion includes successive processes including fuel injection, mixing, and ignition.

The fuel injector for supersonic combustion should be capable of generating vertical motions which cause the fuel-air interface area to increase rapidly and enhance the micromixing at molecular level, leading to efficient combustion. Injection and mixing are correlated. There are two types of injection which exist either in parallel or normal streams.

7.15.1 Fuel Mixing in Parallel Stream

7.15.1.1 Ramp Injectors

Ramp injectors are passive mixing devices that produce counterrotating stream-wise vortices to enhance the mixing of fuel and air (Figure 7.38).

Compression ramps (configuration (a)) are associated with an oblique shock standing at the base of the ramp, while the compressed air above the ramp spills over the sides into the lower pressure, forming a counterrotating pair of axial vortices. In expansion ramps (configuration (b)), the wall is turned away from the flow while the top surface of the ramp remains in the plane of the upstream wall, leading to a Prandtl-Meyer expansion so a pressure difference between the flow on the upper ramp surface and the expanded flow is produced. The location of the shock was found to affect the mixing performance, and the expansion design produces higher combustion efficiencies despite having lower overall mixing performance. This was attributed to the improved local, small-scale mixing near the fuel injection port.

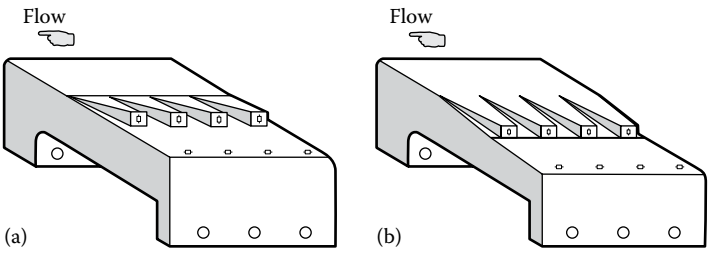


FIGURE 7.38
(a) Compression ramps. (b) Expansion ramps. (From Heiser, W.H. and Pratt, D.T., *Hypersonic Airbreathing Propulsion*, AIAA Education Series, 1994, p. 278. With permission.)

7.15.2 Fuel Mixing in Normal Stream

The performance of very high-speed combustor systems requires fuel and air mixing at the molecular level in the near-field of the fuel injection. One of the simplest approaches is the transverse (normal) injection of fuel from a wall orifice. As the fuel jet, sonic at the exit, interacts with the supersonic cross flow, an interesting but rather complicated flow-field is generated.

Fuel air mixing is very important and numerous studies for this process are available. Two types of mixing are examined: laminar and turbulent. Upon ignition and flame generation, it is necessary to have a flameholder to reduce the ignition delay time and to provide a continuous source of radicals for the chemical reaction to be established in the shortest distance possible.

Analysis of the combustion chamber may be simplified and treated as a one-dimensional flow. If the flow is supersonic, adding heat lowers the Mach number. A case study examined in Reference 16 demonstrated that if the inlet Mach number to the combustion chamber is 3.0 and the heat added due to fuel burning increases the total temperature by 30%, then the outlet Mach number will be 1.7, and the total pressure ratio between the outlet and inlet states will be 0.37 [16]. Finally, two points may be added here:

1. Hydrogen fuel is mostly used in scramjet engines, which generally has a heating value per unit mass some 2.3 times the conventional hydrocarbon or jet fuel.
2. Computational fluid dynamics (CFD) are extensively used in the analysis of combustion chambers to verify and overcome any difficulties in performing a complete experimental analysis.

7.16 Nozzle

The nozzle is very similar to the intake. It has an internal part and an external part formed by the vehicle body. The internal part is a typical two-dimensional nozzle, while the aft-body is the external part, which is a critical part of the nozzle component.

A two-dimensional (or planar rather than axisymmetric or circular) nozzle is used in scramjet engines planned for powering hypersonic aircraft. The Mach number is greater than 5 for the following reasons:

First: Circular nozzles are comparatively heavy and do not lend themselves easily to variable geometry, and the need for tight integration.

Second: The flow at the exhaust nozzle entry is supersonic, rather than the sonic or choked-throat condition of convergent-divergent nozzles.

Third: The design produces a uniform, parallel flow at the desired exit Mach number which maximizes the resulting thrust.

Fourth: The design is a minimum-length exhaust nozzle. This is achieved by placing sharp corners that generate centered simple or Prandtl-Meyer expansion fans at the nozzle entry.

7.17 Case Study

An axisymmetric nozzle of a scramjet has the following data:

Inlet Mach number = 1.56
Outlet Mach number = 3.65
Inlet radius = 0.366 m

An analytical procedure is followed for drawing the nozzle contour and the Mach number within the nozzle. The procedure is described in full detail in Section 11.3.2.1 of the Chapter 11. Here, only the final results are given in Table 7.5. The nozzle contours are plotted in Figure 7.39 and the Mach number within the nozzle is also given in Figure 7.40.

TABLE 7.5
Nozzle Characteristics

	1	2	3	4	5	6	7	8	9	10
M	1.56	1.79	2.02	2.25	2.49	2.72	2.95	3.18	3.42	3.65
μ	39.94	33.96	29.64	26.33	23.71	21.58	19.81	18.34	17.02	15.91
θ_o	47.21	47.21	47.21	47.21	47.21	47.21	47.21	47.21	47.21	47.21
θ	47.21	40.38	33.83	27.69	22.01	16.79	12.01	7.65	3.65	0
r_c					0.366					
r	0.366	0.429	0.517	0.632	0.782	0.974	1.215	1.515	1.886	2.340
x	0	0.146	0.394	0.789	1.391	2.272	3.527	5.270	7.638	10.798
y	0.404	0.542	0.728	0.961	1.237	1.544	1.863	2.16	2.389	2.484

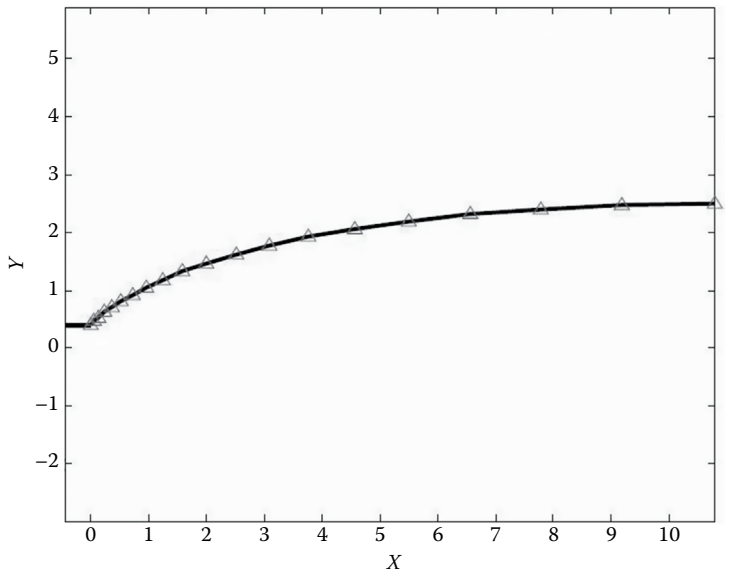


FIGURE 7.39
Nozzle geometry for a scramjet engine.

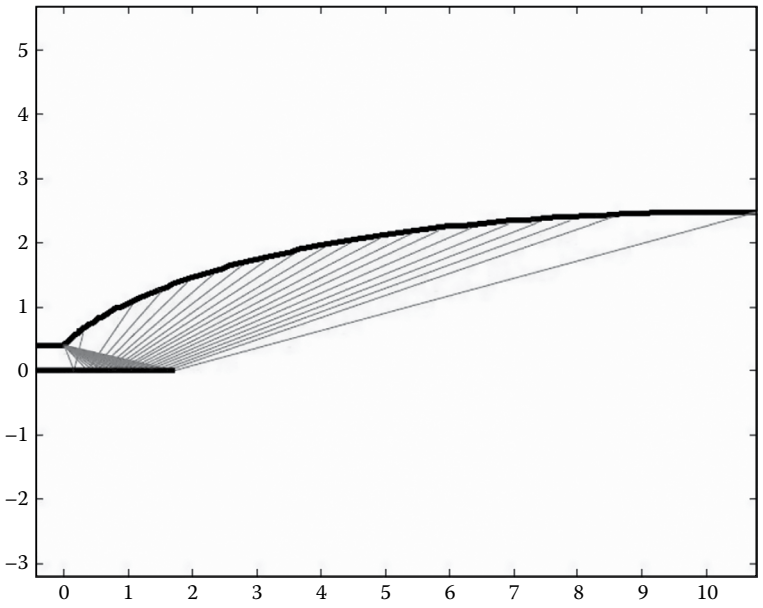


FIGURE 7.40
Mach number distribution within the nozzle.

7.18 Dual-Mode Combustion Engine (Dual Ram-Scramjet)

The dual-mode ramjet (DRM), also known as the dual-mode scramjet, is a ramjet that operates as a ramjet at low supersonic speeds and transforms into a scramjet at high Mach numbers (Dual Ram-Scramjet). It normally operates in the lower hypersonic regime between Mach 4 and 8. In ramjet operations, the air-flow needs to contain two throats: the first is to decelerate the flow to subsonic before the combustion chamber, and the second is to accelerate the flow to supersonic again in the nozzle. For a scramjet, these two throats are no longer needed. Thus, a complicated control system is needed to modify scramjet geometry to match flight-speed requirements. Aerodynamists suggested a simpler solution—adding a short duct between the inlet and the combustor known as an *isolator* [19] and keeping the other engine geometry unchanged. The isolator is a constant area duct that can maintain normal or oblique shock trains (Figures 7.41 and 7.42). Figure 7.41a illustrates the configuration of a dual ram-scramjet engine, while Figure 7.41b defines station numbering for a dual ram-scramjet engine.

The main concern in the isolator is that the shock pattern that occurs during subsonic combustion operation might not reach the inlet, since this condition can cause the engine to unstart. For high supersonic flight Mach numbers (and correspondingly high combustor Mach numbers), the boundary layers in the isolator will be very thin and no waves of any importance will form in the isolator [20]. The shock train formed in the isolator and its performance depend on the back pressure acting on it and the isolator height-to-length ratio, which is a new parameter affecting the system. Other components are treated the same as in the scramjet. The *T*–*S* diagram of a dual ram-scramjet engine are shown in

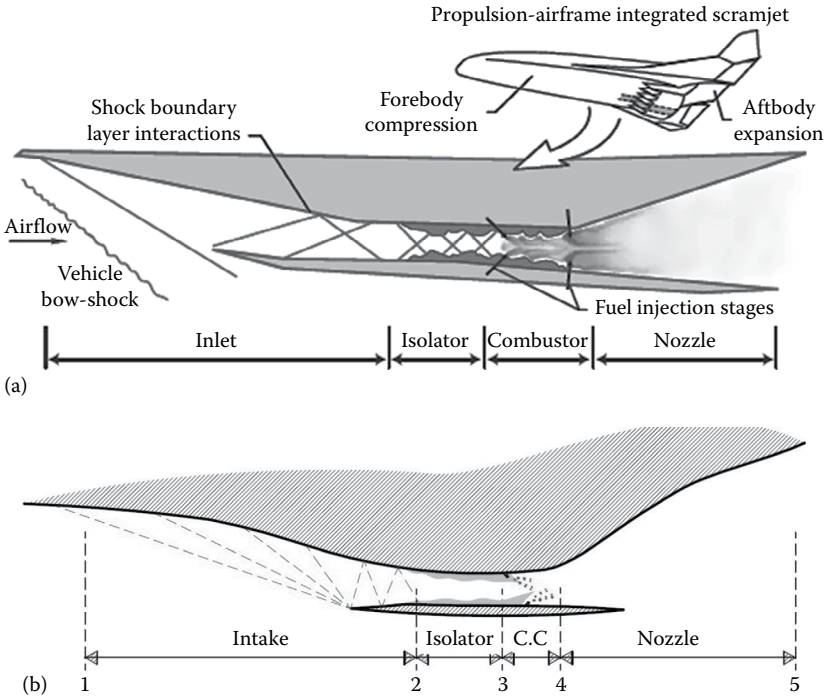


FIGURE 7.41
(a) Configuration of dual ram-scramjet engine. (b) Stations for dual ram-scramjet engine.

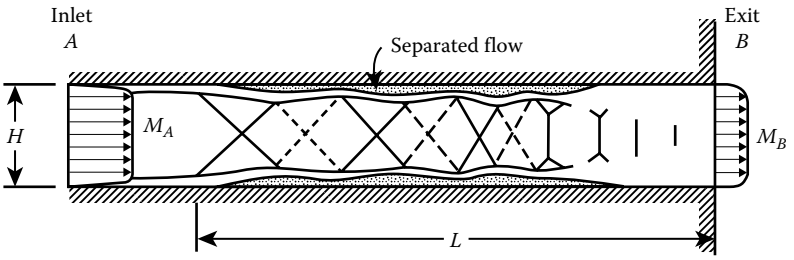


FIGURE 7.42
Configuration of isolator. (From Conners, T.R., Predicted performance of a thrust-enhanced SR-71b aircraft with an external payload, NASA TM 104330, 1997.)

Figures 7.43 and 7.44. Static states are displayed in Figure 7.43, while total and static states are shown in Figure 7.44 for both ideal and real processes.

7.18.1 Aero-Thermodynamics of Dual-Mode Scramjet

The same designations for the states of a scramjet as described previously are used here, thus

Station 1 is downstream of the vehicle forebody shock and represents the properties of the flow that enters the inlet.

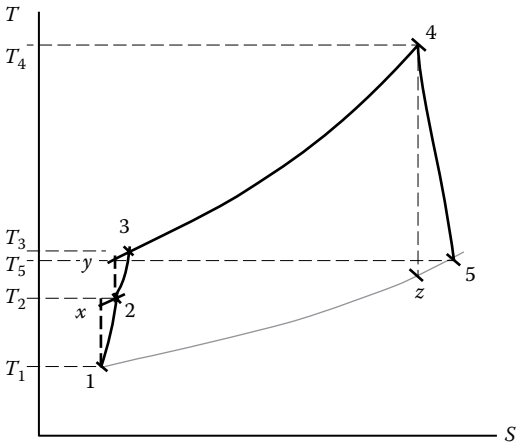


FIGURE 7.43
T–S diagram for dual ram-scramjet engine (static states only).

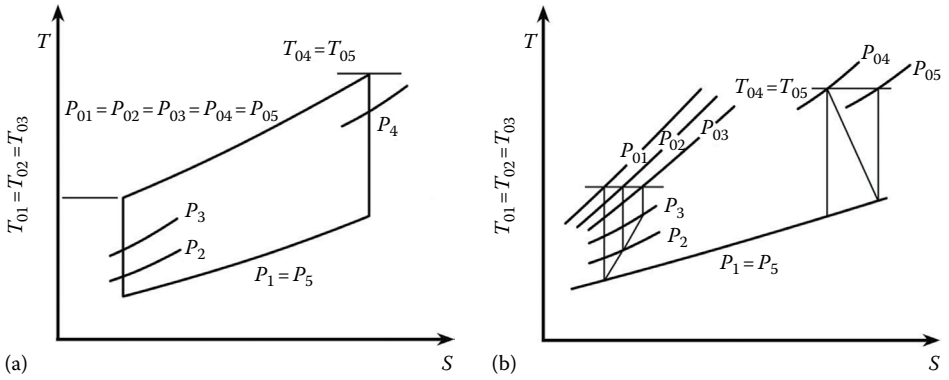


FIGURE 7.44
Ideal and real cycle on *T–S* diagram: (a) ideal cycle and (b) real cycle.

Station 2 is at the inlet throat, which is usually the minimum area of the flowpath, and the isolator extends between stations 2 and 3.
Station 3 represents the start of the combustor, where fuel and air are mixed and burned.
Station 4 represents the end of the combustor.
Station 5 represents the end of the expansion process, which includes an internal expansion within the nozzle and an external expansion to the end of the vehicle.

A. Intake
The intake is modeled as adiabatic supersonic flow with adiabatic compression efficiency. The governing equations are same as listed in scramjet (Equations 7.1 through 7.4).

B. Isolator
The isolator behavior will be governed by Equation 7.43, which relates isolator outlet pressure ratio to its dimensions, inlet Mach number, and boundary layer

parameters at inlet [19]. In Equation 7.43, L/H are isolator dimensions according to Figure 5.38, while θ is the momentum thickness at isolator inlet, and R_θ is the Reynolds number related to momentum thickness. The maximum pressure ratio that can take place in the duct module with no energy addition or subtraction will be equal to the pressure ratio through a normal shock wave. So the pressure ratio in the isolator will be limited to Equation 7.44. The flow in the isolator will be treated also as adiabatic supersonic flow with adiabatic compression efficiency defined by Equation 7.45 and Figure 5.39a. The combustion inlet temperature and Mach number can be calculated through Equations 7.46 and 7.47.

$$\frac{L}{H}=\frac{\sqrt{\frac{\theta}{H}}}{\sqrt[4]{\mathrm{Re}_\theta}}\cdot\frac{50\left(\frac{P_3}{P_2}-1\right)+170\left(\frac{P_3}{P_2}-1\right)^2}{M_2^2-1} \tag{7.43}$$

$$\frac{P_3}{P_2}=\frac{2\gamma_c}{\gamma_c+1}\times M_2^2-\frac{\gamma_c-1}{\gamma_c+1} \tag{7.44}$$

$$\eta_{Iso}=\frac{T_y-T_2}{T_3-T_2} \tag{7.45}$$

$$T_3=T_2\left[1+\frac{1}{\eta_{Iso}}\left(\left(\frac{P_3}{P_2}\right)^{\gamma_c-1/\gamma_c}-1\right)\right] \tag{7.46}$$

$$M_3=\sqrt{\frac{T_1}{T_3}\left(\frac{2}{\gamma-1}+M_1^2\right)-\frac{2}{\gamma-1}} \tag{7.47}$$

C. Combustion Chamber

The burnering process is modeled as a Rayleigh flow. When the Mach number at the combustion chamber is supersonic, the combustion chamber will be similar to the scramjet combustion. Combustion chamber outlet data is obtained using Rayleigh flow and energy Equations 7.48 through 7.50.

$$T_{o4}=\frac{\dot{m}_f\eta_b QV}{C_{ph}\left(\dot{m}_a+\dot{m}_f\right)}+\frac{\dot{m}_a C_{pc}T_3}{C_{ph}\left(\dot{m}_a+\dot{m}_f\right)}\left(1+0.5\times\left(\gamma_c-1\right)M_3^2\right) \tag{7.48}$$

$$\frac{T_{o4}}{T_{o3}}=\left(\frac{M_4}{M_3}\right)^2\left(\frac{1+\gamma_c M_3^2}{1+\gamma_h M_4^2}\right)^2\left(\frac{1+0.5\times\left(\gamma_h-1\right)M_4^2}{1+0.5\times\left(\gamma_c-1\right)M_3^2}\right) \tag{7.49a}$$

$$\frac{T_4}{T_3}=\left(\frac{M_4}{M_3}\right)^2\left(\frac{1+\gamma_c M_3^2}{1+\gamma_h M_4^2}\right)^2 \tag{7.49b}$$

$$\frac{P_4}{P_3}=\frac{1+\gamma_c M_3^2}{1+\gamma_h M_4^2} \tag{7.50}$$

For subsonic combustion the amount of heat added will be equal to the critical value to reach a choking condition at combustion chamber exit $M_4 = 1.0$, to convert the flow to supersonic. The combustion chamber outlet data is obtained using Rayleigh flow and energy equation: Equations 7.51 and 7.52

$$T_{o4} = \frac{T_{o3}}{M_3^2}\left(\frac{1+\gamma_c M_3^2}{1+\gamma_h}\right)^2\left(\frac{1+0.5\times(\gamma_h-1)}{1+0.5\times(\gamma_c-1)M_3^2}\right) \tag{7.51}$$

$$P_4 = P_3\frac{1+\gamma_c M_3^2}{1+\gamma_h} \tag{7.52}$$

The definition of adiabatic expansion (nozzle) efficiency is Equation 7.53 and Figure 5.37a. Assuming complete expansion in the nozzle output flow can be calculated using Equations 7.54 and 7.55:

$$\eta_N = \frac{T_4 - T_5}{T_4 - T_z} \tag{7.53}$$

$$T_5 = T_4 - T_4\eta_N\left(1-\left(\frac{P_1}{P_4}\right)^{\gamma_h - 1/\gamma_h}\right) \tag{7.54}$$

$$V_5 = \sqrt{2C_{Ph}\left(T_{o4} - T_5\right)} \tag{7.55}$$

Example 7.1

Figure 7.45 illustrates a scram jet engine powering an airplane flying at Mach number equal to 5.0 at an altitude of 55,000 ft where $T_a = 216.67$ K and $P_a = 9.122$ kPa. Two oblique shock waves are formed in the intake prior to entering the combustion chamber at supersonic speed. Hydrogen fuel is burned that develops a maximum temperature of 2000 K. The fuel-to-air ratio is 0.025. The nozzle has an expansion ratio $A_5/A_4 = 5$. The inlet and exit areas of the engine are equal, $A_1 = A_5 = 0.2$ m^2. Hydrogen fuel heating value is 120,900 kJ/kg. It is required to:

1. Calculate the inlet Mach number to the combustion chamber.
2. Calculate exhaust jet velocity.
3. Calculate the overall efficiency.

$(C_p)_{cc} = 1.51$ kJ/kg K, $\gamma_n = 1.238$, and burner efficiency is 0.8.

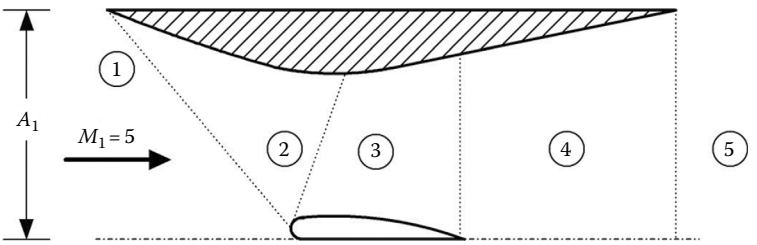


FIGURE 7.45
Scramjet layout.

Solution

Diffuser Section: Flight speed $V_f = M_1\sqrt{\gamma RT_a} = 5\sqrt{1.4\times 287\times 216.7} = 1475.4$ m/s

$$T_{01} = T_a\left(1+\frac{\gamma-1}{2}M^2\right) = 1300 \text{ K}$$

An oblique shack wave separates region (1) and (2) with $M_1 = 5$ and $\delta = 10°$, then either from the governing equations listed in Chapter 3 or from oblique shock-wave table/figure, then the shock wave inclination angle is $\sigma_1 = 19.38°$. The normal component of the Mach number ahead of the shock is

$$M_{1n} = M_1 \sin(\sigma-\delta) = 1.659$$

The normal component of the Mach number behind (downstream) the shock wave is $M_{2n} = 0.65119$.

The corresponding Mach number is then

$$M_2 = \frac{M_{2n}}{\sin(\sigma-\delta)} = 4.0$$

The static temperature ratio across the shock is $T_2/T_1 = 1.429$.

A second oblique shock wave is developed between regions (2) and (3). With the inlet Mach number and wedge angle having the values $M_2 = 4.0$ and $\delta = 10°$, the shock angle is $\sigma_2 = 22.23°$ and the normal component of the inlet Mach number is $M_{2n} = M_2 \sin\sigma = 1.513$.

From oblique shock tables, the normal component of the outlet Mach number is obtained from tables or normal shock relations as

$$M_{3n} = 0.698$$

$$M_3 = \frac{M_{3n}}{\sin(\sigma-\delta)} = \frac{0.698}{\sin 12.23} = 3.295$$

$$\frac{T_3}{T_2} = 1.328$$

The inlet Mach number to combustion chamber is $M_3 = 3.295$.

Combustion chamber (*Rayleigh flow*): Within the combustion chamber (from 3–4), heat is added. The flow is a Rayleigh flow.

With $M_3 = 3.316$, from Rayleigh Flow tables:

$$\frac{T_{03}}{T_0^*} = 0.6282, \quad \frac{P_{03}}{P_0^*} = 4.53$$

Since $T_{01} = T_{02} = T_{03} = 1300$ K and $T_{04} = 2000$ K, then

$$\frac{T_{04}}{T_0^*} = \frac{T_{04}}{T_{03}}\frac{T_{03}}{T_0^*} = \frac{2000}{1300}\times 0.6282 = 0.966$$

From Rayleigh flow tables

$$M_4 = 1.26 \quad \text{and} \quad \frac{P_{04}}{P_0^*} = 1.0328$$

The outlet Mach number from the combustion chamber is $M_4 = 1.26$. This confirms the fact that adding heat to a supersonic flow reduces its speed.

The pressure ratio in the combustion chamber (P_{04}/P_{03}) is calculated as

$$\frac{P_{04}}{P_{03}} = \frac{P_{04}}{P_0^*}\frac{P_0^*}{P_{03}} = \frac{1.0328}{4.53} = 0.2279$$

Note that this value is rather a small value, as normally ($P_{04}/P_{03} \approx 0.3-0.4$).

The fuel-to-air ratio

$$f = \frac{C_p T_{04} - C_p T_{03}}{\eta_b Q_R - C_p T_{04}} = \frac{1.51(2{,}000 - 1{,}300)}{0.8 \times 120{,}900 - 1.51 \times 2{,}000} = 0.01128$$

sometimes the following simple formula is used for (f)

$$f = \frac{C_p (T_{04} - T_{03})}{\eta_b Q_R} = \frac{1.51(2{,}000 - 1{,}300)}{0.8 \times 120{,}900} = 0.011$$

Nozzle: The flow in the nozzle is isentropic. From isentropic flow tables with the inlet Mach number $M_4 = 1.26$, then $A_4/A^* = 1.05$ and $T_{04}/T_4 = 1.317$.

$$\frac{A_5}{A^*} = \frac{A_5}{A_4}\frac{A_4}{A^*} = 5 \times 1.05 = 5.25$$

The outlet Mach number and temperature ratio are

$$M_5 = 3.23 \quad \text{and} \quad \frac{T_{05}}{T_5} = 3.11$$

$$T_5 = \frac{T_5}{T_{05}}\frac{T_{05}}{T_{04}}\frac{T_{04}}{T_4}\frac{T_4}{T_3}\frac{T_3}{T_2}\frac{T_2}{T_1}T_1$$

With $T_{05} = T_{04}$, then

$$T_5 = \frac{1}{3.11} \times 1.317 \times 3.744 \times 1.333 \times 1.429 \times 216.7 = 654.5 \text{ K}$$

The exhaust speed is

$$V_5 = M_5\sqrt{\gamma_h R T_5} = 1558 \text{ m/s}$$

Note also that the difference between flight and exhaust speeds are very small as previously identified, which is one of the drawbacks of scramjet engines.

The air mass flow rate is

$$\dot{m} = \rho_1 V_1 A_1 = \frac{P_1}{RT_1} V_1 A_1 = \frac{9122}{287 \times 216.67} \times 1475.4 \times 0.2 = 43.3 \text{ kg/s}$$

Thrust force: For unchoked nozzle as usual in scramjet engines, the thrust force is

$$T = \dot{m}\left[(1+f)V_5 - V\right]$$

$$T = (43.3)\left[1.012 \times 1558 - 1475.4\right] = 4386 \text{ N}$$

This value is small and it is appropriate for the high-altitude flights as the drag force on air vehicles is also small.

Overall efficiency:

$$\eta_0 = \frac{TV_F}{\dot{m}_f Q_{HV}} = \frac{TV_F}{f\dot{m}_a Q_{AV}} = \frac{4386 \times 1475}{0.012 \times 43.3 \times 120.9 \times 10^6} = 10.29\%$$

A summary for Mach numbers at different stations in the engine is given as

$$M_1 = 5, \quad M_2 = 4, \quad M_3 = 3.295, \quad M_4 = 1.26, \quad M_5 = 3.23$$

Problems

7.1 The drag of a hypersonic future businesses jet is to be simplified by the following equations (Figure P7.1):

Flight Mach Number	Drag (N)
M = 0–0.75	$D = 10^5 \cdot (4.1M^2 - 1.1M + 2.1)$
M = 0.75–1.25	$D = 10^5 \cdot (-9.7M^2 + 20M - 5.9)$
M = 1.25–6	$D = 10^5 \cdot \left(\frac{21}{M^4} - \frac{37}{M^3} + \frac{26}{M^2} - \frac{5.9}{M} + 2.3\right)$

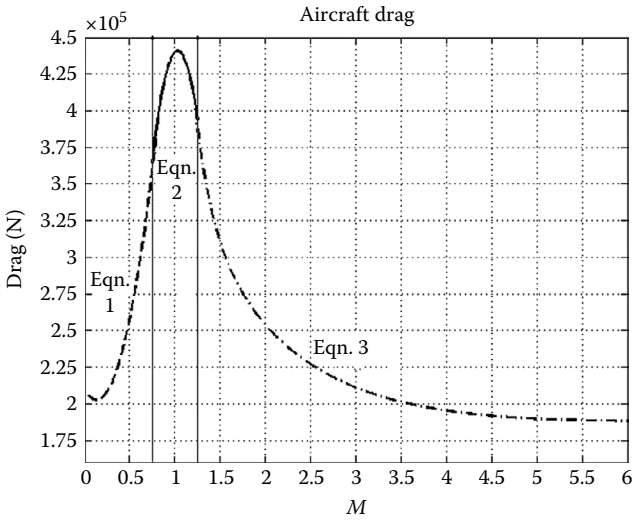


FIGURE P7.1
Drag versus Mach no.

If that aircraft is to be driven by two turbojet engines with afterburner, each having the following parameters:

$$\text{Turbine inlet temperature}(TIT) = 1750\ \text{K}$$

$$\text{Maximum temperature } T_{\max} = 2500\ \text{K}$$

$$\text{Pressure ratio } \pi_o = 10$$

Efficiencies of different components:

$$\eta_d = 0.9 \quad \eta_N = 0.98 \quad \eta_C = 0.91$$

$$\eta_T = 0.91 \quad \eta_m = 0.99 \quad \eta_b = 0.99$$

Pressure losses:

$$\Delta P_{C.C.} = 0.02 \quad \Delta P_{AB} = 0.02$$

The fuel used is a hydrocarbon fuel having a heating value of 45,000 kJ/kg. It is required to consider the following two cases:

1. Afterburner is off.
2. Afterburner is on.

In each case calculate and plot for a Mach number varying from 0 to 4

- The air mass flow rate ($\dot{m}_a$)
- The fuel flow rate ($\dot{m}_f$)
- The TSFC

7.2 The aircraft of Problem 7.1 is to be driven by two ramjet engine having the following parameters:

$$T_{\max} = 2500\ \text{K}$$
$$\eta_d = 0.9 \quad \eta_N = 0.98$$
$$\eta_b = 0.99 \quad \Delta P_{C.C.} = 0.02$$

Calculate and plot

1. The air mass flow rate ($\dot{m}_a$)
2. The fuel flow rate ($\dot{m}_f$)
3. The TSFC

If the engine is using the same fuel as in Problem 7.1 and if it is using a hydrogen fuel having a heating value of 119,000 kJ/kg for a Mach range: $M = 0.75$ to $M = 6$.

7.3 Compare the four cases of the previous Problems 7.1 and 7.2 at the following values of Mach number $M = 0.9$, $M = 1.5$, and $M = 3.5$ and write your comments.

7.4 If the mass flow through the turbojet engine is limited to $\dot{m}_a = 200$ kg/s find the point at which the afterburner will start burning fuel. Then plot

1. The air mass flow rate ($\dot{m}_a$)
2. The fuel flow rate ($\dot{m}_f$)
3. The TSFC

For a Mach number ranging from $M = 0$ to $M = 4$

7.5 The aircraft of Problem 7.1 is to be fitted with an over/under turboramjet, which is constructed from both of the turbojets described in Problem 7.1 and the ramjet described in Problem 7.2. The air mass flow in the turbojet engine is to be limited to $\dot{m}_a = 200$ kg/s as in Problem 7.4. During the flight instants where the turbojet needs to develop more thrust and needs extra air flow rate ($\dot{m}_a > 200$ kg/s), the following switching mode is selected: the afterburner is put off and the ramjet starts to operate with an appropriate mass flow that increases the total thrust to overcome the drag of the aircraft (110% drag). For that transition case calculate and plot

1. The air mass flow rate ($\dot{m}_a$)
2. The fuel flow rate ($\dot{m}_f$)
3. The TSFC

7.6 Compare the TSFC in Problems 7.1, 7.2, and 7.5 write your comments.

7.7 If the aircraft is to be driven with the over/under turboramjet of Problem 7.5 and to work on the following regimes:

Regime	Engine Condition
$M = 0$ to $M = 0.5$	Turbojet with AB off
$M = 0.5$ to $M = 1.5$	Turbojet with AB on
$M = 1.5$ to $M = 3$	Turbojet with AB off Mass flow in turbojet is decreasing from 100% $\dot{m}_a$ at $M = 1.5$ to 0% $\dot{m}_a$ at $M = 2.5$ Ramjet is operating as a support for the turbojet engine
$M = 3$ to $M = 6$	The turbojet is off. The ramjet is driving the A/C alone

For that case calculate and plot

1. The air mass flow rate ($\dot{m}_a$)
2. The fuel flow rate ($\dot{m}_f$)
3. The TSFC

Write your comments.

7.8 For the wraparound turboramjet engine, the following data was recorded when the turbojet engine was operating with operative afterburner at an altitude of 60,000 ft:

Flight Mach number	2.5
Turbine inlet temperature	1300 K
Maximum temperature	2000 K
Air mass flow rate	60 kg/s

If the pilot is planning to switch operations to ramjet and stop the turbojet, what is the procedure he has to follow for this transition time?

If the maximum temperature of the ramjet is 2500 K, what will be the necessary air mass flow rate to keep the same thrust as the turbojet mode?

Do you expect a dual mode is possible? Explain why or why not.

7.9 A military airplane is powered by a scramjet engine. The airplane is flying at an altitude of 60,000 ft where the ambient temperature and pressure are 216.5 K and 7.17 kPa. The flight Mach number is 7.0. The fuel used is hydrogen, where its gas constant $R = 4.124$ kJ/kg·K, its heating value is 130,000 kJ/kg, and an average specific heat of

1.4 may be assumed all over the engine components. The maximum temperature in the engine is 3000 K. The exhaust gases leave the combustion chamber at a Mach number equal to unity. The efficiency of combustion is 0.98. The exit pressure is equal to the ambient pressure. Assume that in the nozzle the outlet total pressure to the inlet total pressure is 0.1.

It is required to calculate

1. The flight speed
2. The fuel-to-air ratio (f)
3. The Mach number at the inlet to the combustion chamber
4. The total pressure ratio at the diffuser ($P_{o_{outlet}}/P_{o_{inlet}}$)
5. The total pressure ratio at the combustion chamber
6. The exhaust jet speed
7. The specific thrust
8. The TSFC

7.10 Compare turboramjet and scramjet engines with respect to the following points:

1. Flight altitude
2. Maximum Mach number
3. Fuel consumption

7.11 When do you expect to fly via a hypersonic vehicle?

7.12 A scramjet engine is used to power a hypersonic vehicle that flies at an altitude of 25,000 m, Mach number $M=8$, using hydrocarbon fuel (heating value: $Q_{HV}=43.4$ MJ/kg).

The momentum thickness is $\theta=3$ mm, height of isolator $H=0.08$ m, and the Reynolds number based on momentum thickness boundary layer is $Re_\theta=3.5\times10^5$. Detailed data of its four elements are given in table below:

Air and Gas Properties

Element	γ	R (J/kg·K)	C_P (J/kg·K)	M_{inlet} Mach Number at Inlet	η (%)
Intake (states 1–2)	1.4	287	1005	8.0	92
Isolator (states 2–3)	1.37	287	1063	4.0	86
Burner (states 3–4)	1.30	297	1275	2.5	97
Nozzle (states 4–5)	1.33	290	1170	2.0	98

Calculate:

1. Specific thrust and TSFC
2. Thermal efficiency, propulsive efficiency, and overall efficiency
3. Mach number of gases leaving scramjet
4. Isolator length (L)

7.13 Figure P7.13 illustrates a scramjet engine powering an aerospace vehicle flying at a Mach number of 4.0 at an altitude where the ambient conditions are: $T_a=216$ K, $P_a=20$ kPa. Air is decelerated to a Mach number of 2.0 at the inlet of combustion chamber. Heat is added at the combustion chamber to bring the Mach number at the exit of combustion chamber to 1.0. The flow expands to the ambient pressure at exit of nozzle ($P_e=P_a$).

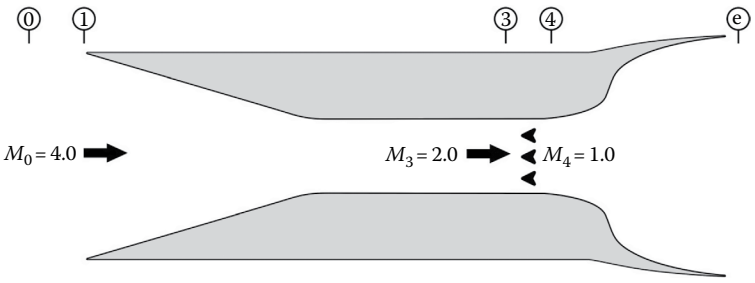


FIGURE P7.13

Assume that all processes in the engine are *ideal* and the flow has constant properties ($\gamma = 1.4$, $R = 287 \dfrac{\text{J}}{\text{kg} \cdot \text{K}}$, $C_p = 1005\ \text{J/kg} \cdot \text{K}$),

1. With $M_e = M_a$ and assuming negligible fuel-to-air ratio ($f \ll 1$), prove that

$$\frac{T}{P_a A_a} = \gamma M_a^2 \left(\frac{U_e}{U_a} - 1 \right) + \frac{A_e}{A_a} \left(\frac{P_e}{P_a} - 1 \right)$$

2. Assuming Rayleigh flow in the combustion chamber, calculate the maximum temperature in the engine.
3. Calculate $\dfrac{T}{P_0 A_0}$.

References

1. J. Miller, *The X-Planes: X-1 to X-45*, Midland, Hinckley, U.K., 2001.
2. B. Calvert, *Flying Concorde: The Full Story*, Crowood Press, London, U.K., 2002.
3. Y. Gordon, *Tupolev Tu-144*, Midland, Leicestershire, U.K., 2006.
4. S.J. Morris, Jr., K.A. Geiselhart, and P.G. Coen, Performance potential of an advanced technology Mach 3 turbojet engine installed on a conceptual high-speed civil transport, NASA-TM-4144, November 1989.
5. J.C. Ellison, Investigation of the aerodynamic characteristics of a hypersonic transport model at Mach numbers to 6, NASA TN-6191, April 1971.
6. R.J. Pegg et al., Design of hypersonic waverider-derived airplane, AIAA Paper 93-0401, January 1993.
7. D.W. Lam, Use of the PARC code to estimate the off-design transopnic performance of an over/under turboramjet noise, NASA TM-106924, AIAA-95-2616.
8. R.E. Morris and G.D. Brewer, Hypersonic Cruise Aircraft Propulsion Integration Study, Vols. I and II, NASA-CR-158926-1 and NASA-CR-158926-2, September 1979.
9. D. Robert, J.M.A. Longo, C. Gerald, D. Philippe, I. Salah El Din, and Remi, Multi-disciplinary analysis and optimization of hypersonic transport aircrafts, Thepot2elib.dlr.de/68247/1/ESA_paper_final.pdf.
10. G.D. Riebe, Aerodynamic characteristics including effect of body shape of a Mach 6 aircraft concept, NASA-TP-2235, December 1983.

11. J.L. Pittman and G.D. Riebe, Experimental and theoretical aerodynamic characteristics of two hypersonic cruise aircraft concepts at Mach numbers of 2.96, 3.96, and 4.63, NASA-TP-1767, December 1980.
12. C.S. Domack, S.M. Dollyhigh, F.L. Beissner, Jr., K.A. Geiselhart, M.E. McGraw, Jr., E.W. Shields, and E.E. Swanson, Concept development of a Mach 4 high-speed civil transport, NASA-TM-4223, December 1990.
13. https://web.archive.org/web/20061108134907/; http://atrex.isas.ac.jp/index.html.
14. R. Varvill and A. Bond, A comparison of propulsion concepts for SSTO reusable launchers, *JBIS*, 56, 108–117, 2003.
15. J.L. Kerrebrock, *Aircraft Engines and Gas Turbines*, MIT Press, 1992, p. 405.
16. W.H. Heiser and D.T. Pratt, *Hypersonic Airbreathing Propulsion*, AIAA Education Series, Reston, VA, 1994, p. 278.
17. T.R. Conners, Predicted performance of a thrust enhanced SR-71b aircraft with an external payload, NASA TM 104330, 1997.
18. M.K. Smart, Scramjet isolators, RTO-EN-AVT-185.
19. S.M. Torrez, D.J. Dalle, and J.F. Driscoll, Dual mode scramjet design to achieve improved operational stability, AIAA 2010-6957.
20. Boeing 2707 SST specifications, http://www.globalsecurity.org/military/systems/aircraft/b2707-specs.htm.
21. D.R. Jenkins, T. Landis, and J. Miller, American X-vehicles, SP-2003-4531, Monographs in aerospace history No. 31, June 2003.

8

Industrial Gas Turbines

8.1 Introduction

Industrial gas turbines are defined as all gas turbines other than aircraft gas turbines, or aeroengines [1]. An industrial gas turbine is basically a turboshaft engine. Historically, the industrial gas turbine had its roots planted much further back in time than its aeroengine sister, and again these routes sprouted in European soil [2].

The industrial gas turbine proves itself as an extremely versatile and cost-effective prime mover as it has been used for a variety of applications on land and sea.

It may be used as load topping because of its rapid start-up ability. It is used in conjunction with a steam turbine in a "combined cycle plant," which is at present the most efficient form of large-scale power generation. Moreover, it has many applications in the chemical industry. In the oil industry, gas turbines drive the compressor/pump for natural-gas or liquid-oil transmission pipelines. Land transport also employs gas turbines in freight trains and as starters for large trains. Some military tanks, such as the M1A1, are powered by gas turbines. Gas turbines are also used in numerous naval vessels, cargo ships, hydrofoils, patrol boats, frigates, and others.

Industrial gas turbines differ from aeroengines in that they have no limitations on their size and weight. They have nearly zero exhaust speeds. Moreover, they have something in the order of 100,000 operating hours between overhauls.

Today there are gas turbines that run on natural gas, diesel fuel, naphtha, crude, low-Btu gas, vaporized fuel oils, and biomass.

The principal manufacturers of large industrial gas turbines are as follows: Allied Signal, Alstom, Aviadvigatel, Bharat Heavy Electricals, Centrax Gas Turbine, Dresser Rand, Ebara, Fiat Avio, General Electric, Hitachi, Japan Gas Turbine, Kawasaki Heavy Industries, Mitsubishi Heavy Industries, MTU, Motoren, Nuovo Pignone-Turbotecnicaall, Pratt & Whitney, Pratt & Whitney Canada, Rolls-Royce, Ruston Turbines, Siemens, Simens-Westinghouse, Solar Turbines, Sulzer Turbines, Toshiba, Turbomeca, and Volvo Aero.

There are now many single-shaft engines delivering more than 250 MW per unit on the market.

The most important advantages for industrial gas turbines may be described as

1. Compactness (small mass and volume) for a given power output, that is, high W/m^3 or W/kg. This is an advantage for its use in naval applications.
2. Low vibration as its parts are rotating and not reciprocating like internal combustion engines.

3. Reliable: low dynamic stresses from near constant rotational speed operation.
4. Low cost per kg at larger sizes.
5. Low emissions, low installation costs, and low-cost power generation [3].
6. Changeover from primary to secondary fuel with constant load is automatically achieved.
7. Transportation is easily done by air, land, or sea.
8. An on-site maintenance is performed with inspection intervals from 25,000 to 30,000 h.

Advantages in special applications:

1. Units used in generating electricity have the ability to produce full power from cold in less than 2 min. Moreover, they can be erected in deserts (or in general away from water sources) since they do not need cooling water.
2. Gas turbines may be installed on trailers as a mobile source for generating electricity.
3. Engines used in naval applications are of compact size and have high power density and low noise in comparison with diesel engines.
4. Electrical power units have a very compact size in comparison with any other power sources; for example, the ABB ALSTOM power unit GT 26, which generates 265 MW, has the dimensions of 12.3 × 5.0 × 5.5 m [4].

Disadvantages:

1. Lower thermal efficiency compared with diesel engines.
2. Relatively poor dynamic performance—less suitable for cars and other "stop-start" applications.

A brief history of gas turbines and pioneering work in that field:

1. John Barber (1734–1801)—gas turbine patent, including several inventions in 1791.
2. John Dumbell—patented a device in 1808, having "a series of vanes, or fliers, within a cylinder, like the sails of a windmill, causing them to rotate together with the shaft to which they were fixed."
3. Bresson—in 1837, suggested heating and compressing air, delivering it to a combustion chamber and mixing this with fuel gas, and then burning it. The combustion products would then drive "a wheel like a water wheel."
4. Franz Stolze (1836–1910)—a patent for a gas turbine engine in 1872. This engine used a multi-stage reaction turbine and a multi-stage axial flow compressor. He called this a "Fire Turbine."
5. Sir Charles Algernon Parsons—invented the steam turbine in 1884, patented a gas turbine, which he called a Multiple Motor. In addition, designed and manufactured industrial compressors.

6. René Armengaud and Charles Lemale—in 1903, they built and successfully tested the first of several experimental gas turbines with internally water-cooled disks and blades.
7. Dr. Holzwarth—in 1905, proposed an explosion (constant-volume) turbine. A prototype was built and experiments were carried out between 1909 and 1913. This worked without a compressor. Several of these turbines were built but not put into commercial use.
8. Matthew Henry Phineas Riall Sankey (1853–1925)—recognized the future role of the gas turbine as early as 1917.
9. Charles Gordon Curtis (1860–1953)—designed the Curtis steam turbine in 1896. He sold the rights of the turbine to General Electric in 1901.
10. Prof. Aurel Boleslav Stodola (1859–1942)—published a book in 1903, which had an appendix on gas turbines. He tested the world's first industrial gas turbine at Neuchâtel in 1940.
11. Charles Brown (1863–1924)—co-founder of the Brown Boveri Company in 1891, in Baden, Switzerland, and founded the Swiss Locomotive and Machine Works (SLM).
12. Walter Boveri (1865–1924)—co-founder of the Brown Boveri Company in 1891, in Baden, Switzerland.
13. Aegidius Elling (1861–1949)—considered to be the father of the gas turbine. In 1903, he designed and constructed the first constant-pressure gas turbine. His first machine had an output of 11 hp and the second 44 hp.
14. Auguste Camille Rateau (1863–1930)—designed the compressor for the gas turbine. His work was largely on compressors; he founded Rateau Industries.
15. Sanford Alexander Moss (1872–1946)—carried out research into compressor design in General Electric.
16. Jakob Ackeret (1898–1981)—considered an expert on gas turbines; known for his research on axial-flow compressors, airfoil theory, aerodynamics, and high-speed propulsion problems. He is recognized as a pioneer of modern aerodynamics.
17. Sir Harold Roxbee Cox (1902–1997)—chairman and managing director of the nationalized Power Jets, which was restyled in 1946 as the National Gas Turbine Establishment.
18. Alan Howard (1905–1966)—considered the key figure in General Electric's efforts to develop the gas turbines for military aircraft propulsion.
19. Basil Wood (1905–1992)—an expert in all matters relating to gas turbines. For many years he edited the gas turbine section of Kemps Yearbook.
20. Air Commodore Sir Frank Whittle (1907–1996)—inventor of the jet engine, he was a British Royal Air Force (RAF) engineer officer, who shared credit with Germany's Dr. Hans Von Ohain for independently inventing the jet engine. Whittle is hailed as the father of jet propulsion and the contribution he made to the development of the industrial gas turbine was significant.
21. Geoffrey Bertram Robert Feilden (1917–2004)—produced the first Ruston-type TA gas turbine. Later in life he was the author of a widely acclaimed work on engineering design.

22. Dr. Waheeb Rizk (1921–2009)—born and educated in Cairo and then in Cambridge University. He joined the English Electric Company in 1954, to become a founder member of the mechanical engineering laboratory at Whetstone, Leicester, and in 1957 he became chief engineer of the gas turbine division.
23. Prof. Dr. Rudolf Friedrich (1909–1998)—Chief Technical Officer for gas turbines at Siemens and full professor for turbine technology at Karlsruhe Technical University. He was given the nickname "Mr. Siemens-Gas Turbine" by his colleagues.
24. Andrew T. Bowden (1968)—joined C A Parsons as Chief Research Engineer, setting up the Gas Turbine Department and recruiting a team of engineers.
25. Dr. Claude Seippel (1900–1986)—employed by Brown Boveri and in 1939, the person in charge of conceptual design for the Neuchatel gas turbine plant.
26. John Lamb (1890–1958)—arranged for one of the diesel-electric engines on the tanker Auris to be replaced by a gas turbine.

8.2 Categories of Gas Turbines

Based on their application, industrial gas turbines may be classified as pertaining to land, sea, or air, as illustrated in Figure 8.1a.

Next, based on the generated power, the simple cycle gas turbine is classified into five broad groups [5] (Figure 8.1b):

1. *Heavy-duty gas turbines*: These are large power-generation units ranging from 3 to 480 MW in a simple cycle configuration, with efficiencies ranging from 30% to 46%.
2. *Aircraft-derivative gas turbines* (*aero-derivatives*): As the name indicates, these power-generation units were originally aircraft engines, which were later on adapted for the electricity-generation industry by adding a power turbine to absorb the kinetic energy of the exhaust. An engine of this class is the General Electric LM2500. For example, the aero RR RB211 turbofan engine is modified by removing the fan and replacing the bypass fans and adding a power turbine at their exhaust. Other examples for the aero-derivatives are Avco Lycoming TF25, rated at 2000 hp and weighing approximately 1020 lb. The power ranges from 3 MW to about 50 MW. The efficiencies of these units range from 35% to 45%. The outstanding characteristic of the aircraft-derived engines is their lightness. For example, the LM2500 weighs 34,000 lb, including typical mounts, base, and enclosure, for approximate 1.5 lb per horsepower [X]. For marine applications, the material of these jet engines was either changed or coated to resist sea-salt corrosion.
3. *Industrial-type gas turbines*: These vary in range from 2.5 to 15 MW. They are used extensively in petro-chemical plants for compressor drive trains. The efficiencies of these units is less than 30%.

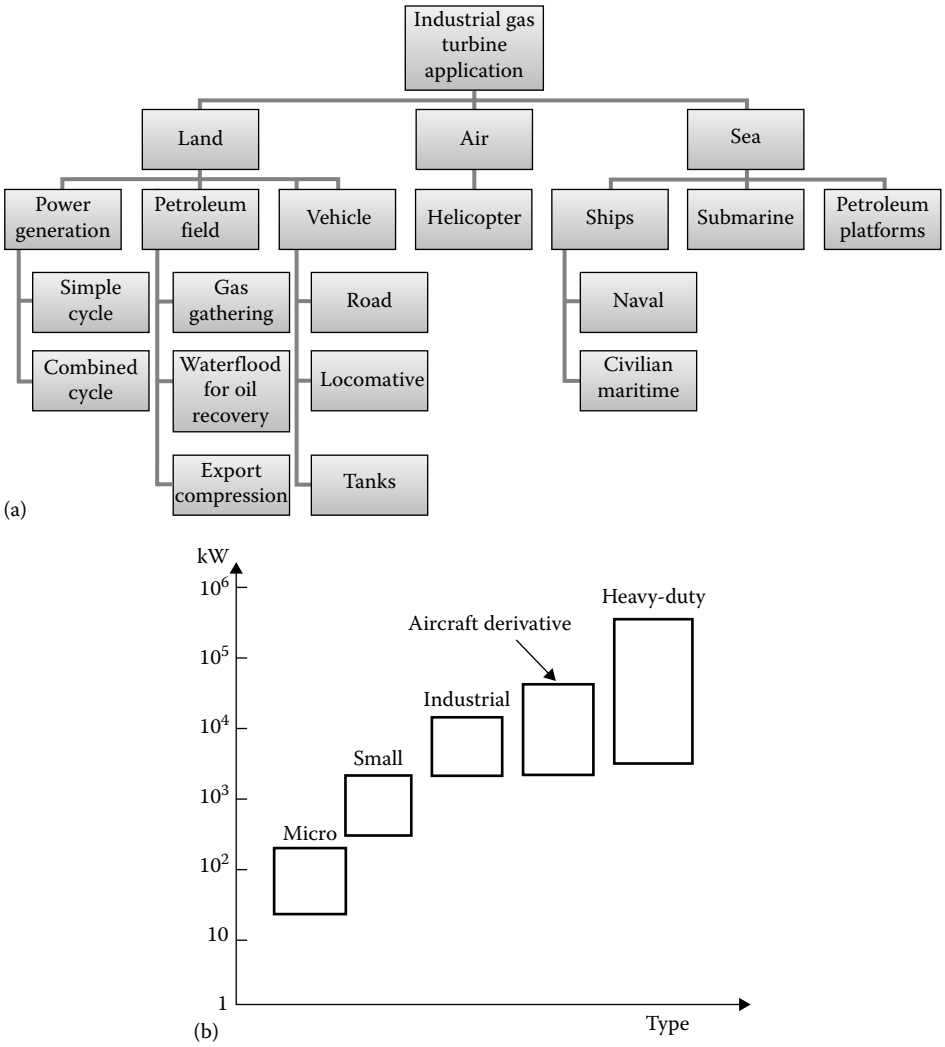


FIGURE 8.1
(a) Classifications of industrial gas turbines. (b) Categories of gas turbine engines.

4. *Small gas turbines*: These gas turbines range from 0.5 to 2.5 MW. They usually have centrifugal compressors and radial inflow turbines. Efficiencies in the simple cycle applications are in the range of 15%–25%.
5. *Micro-turbines*: These turbines are in the range of 20–350 kW. They have had a dramatic growth since the late 1990s.

Successive developments in gas turbines through 50 years are summarized in Table 8.1. Power has doubled 50 times, turbine inlet-temperature increased by 250%, and the pressure ratio has increased by a factor of seven. Such developments have led to an increase in thermal efficiency by some 200% and a decrease of emission by less than 25%.

TABLE 8.1

Development of Gas Turbines in the Period 1940–2000

Year	1940	1950	1960	1970	1980	1990	2000
Unit output (MW)	5	12	20	50	120	185	250
Turbine inlet temperature (industrial gas turbine) (°C)	550	760	816	899	1068	1124	1316
Temperature of turbine blade material (°C)	550	730	800	825	840	870	900
Turbine inlet temperature (aeroengines) (°C)	—	820	900	1050	1200	1350	1460
Compressor pressure ratio	4.2	5	6.5	9.4	14	15.7	30
Overall thermal efficiency (%)	17.4	24	25.8	27.3	31.5	34.4	38.6
Maximum exhaust emission NOx PPMV (15% O_2)	—	110	110	200	200	55	25

Source: Hunt, R.J., The history of the industrial gas turbine (Part 1 The first fifty years 1940–1990), IDGTE 582, PPMV: parts per million volume 2011, http://www.idgte.org/.

8.3 Types of Industrial Gas Turbines

Open-cycle engines take a number of different forms. They may be

1. Single-shaft engine
2. Multiple-shaft engines

These different layouts are illustrated in Figures 8.2 through 8.4. The single shaft (Figure 8.2) has also two forms as is shown in Figure 8.2a and b. In both figures, the gas

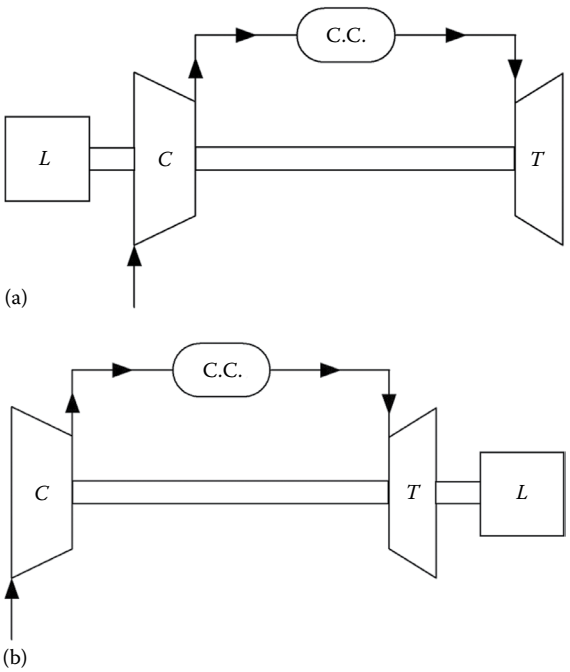


FIGURE 8.2
(a) Single spool with load coupled to the cold side. (b) Single spool with load coupled to the hot side.

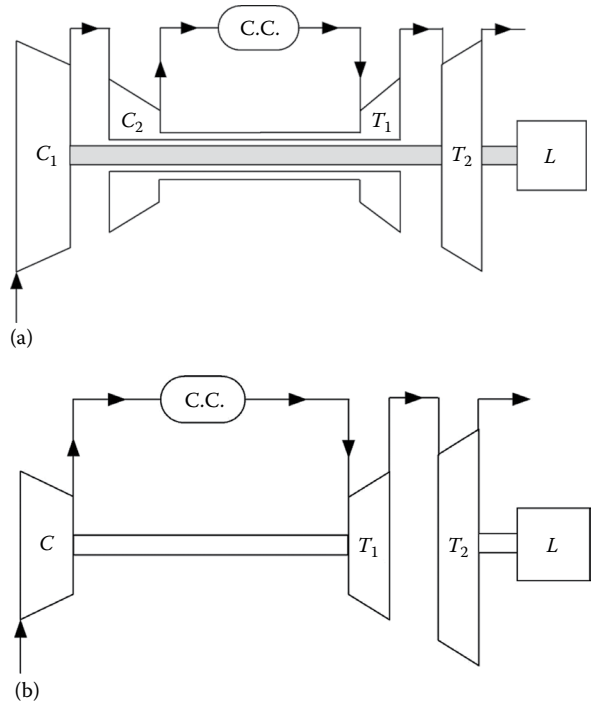


FIGURE 8.3
(a) Two spool with load coupled to low-pressure spool. (b) Two spool with free-power turbine.

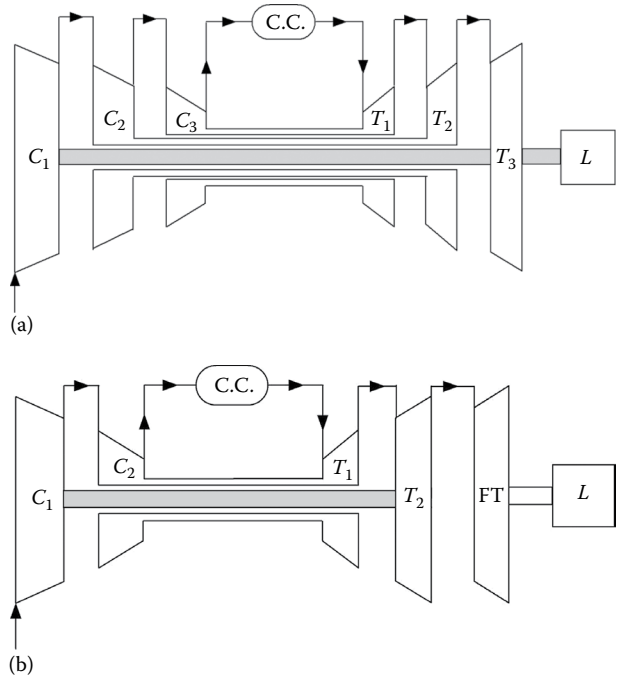


FIGURE 8.4
(a) Three spool with load coupled to low-pressure spool. (b) Three spool with free-power turbine.

generator (compressor, combustion chamber, and turbine) is coupled to an industrial load. This industrial load may be coupled to the cold end (compressor side) (Figure 8.1a) or coupled to the hot end (turbine side) (Figure 8.1b). The second type is the multiple shaft, which is either a two-shaft or three-shaft engine. The two-shaft configuration may be found in one of these two layouts. The two shafts may be concentric (sometimes identified as split-shaft or compound form) (Figure 8.3a) and the load may be coupled to either shaft. The other two-shaft configuration (Figure 8.3b) includes a power turbine driving the load through a separate shaft downstream the main shaft comprising the gas-generator. The three-shaft engines are either similar to the three-spool turbofan, but here the load is driven by one of the three shafts (Figure 8.4a), mostly the low-pressure spool or a two-spool (low-pressure and high-pressure shafts) or a free-power turbine driving the load (Figure 8.4b).

The single shaft promotes simplicity in design, compactness and has high inertia to handle large load step-up and step-down (which is favorable in electrical generation units). However, the two-shaft configuration is normally quicker to start and needs less starting power.

8.4 Single-Shaft Engine

The basic gas turbine cycle is named for the Boston engineer, George Brayton, who first proposed the Brayton cycle around 1870. The gas turbine first successfully ran in 1939 at the Swiss National Exhibition at Zurich. The early gas turbines built in the 1940s and even the 1950s had simple-cycle efficiencies of about 17% because of the low compressor and turbine efficiencies and low turbine-inlet temperatures due to the metallurgical limitations of those times. The gas turbine has experienced phenomenal progress and growth since its first successful development in the 1930s. The efforts to improve the cycle efficiency concentrated on three areas:

1. Increasing the turbine-inlet (or firing) temperatures
2. Increasing the efficiencies of turbo-machinery components
3. Adding modifications to the basic cycles

These added modules include regeneration (or reproduction), inter-cooling, and reheating. This will be discussed in the succeeding sections.

An example for this single spool is Siemens (SGT-800) gas turbine (45 MW).

8.4.1 Single Compressor and Turbine

8.4.1.1 Ideal Cycle

Gas turbines usually operate on an open Brayton cycle, as shown in Figure 8.5**.** The T – S and $P-v$ diagrams of an ideal Brayton cycle are shown in Figure 8.6.

Frequently, gas turbines are designated symbolically by several letters that identify their constituents. The letter "C" refers to the compressor, the letter "B" refers to the burner or combustion chamber, and the letter "T" refers to the turbine, thus the simple Brayton cycle is denoted as "**CBT**."

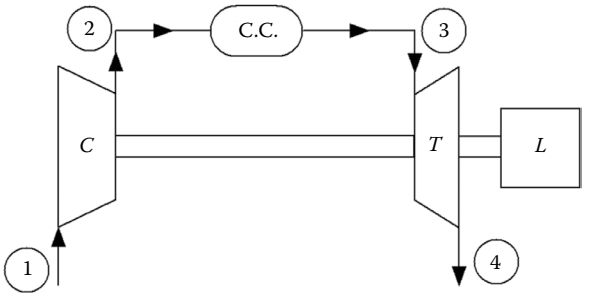


FIGURE 8.5
A typical single-spool gas turbine.

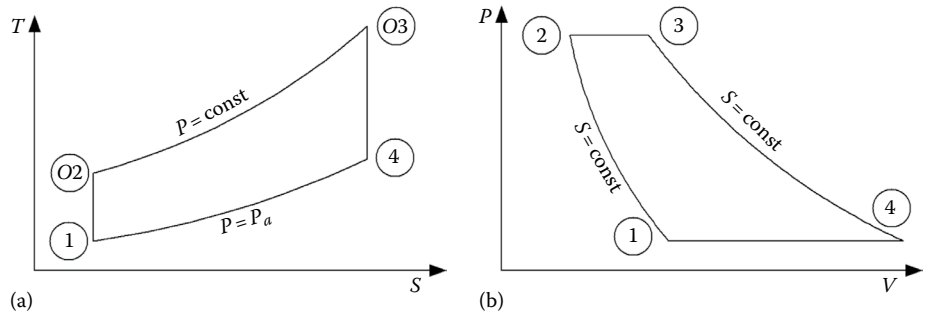


FIGURE 8.6
(a) Temperature–entropy and (b) pressure–specific volume diagrams.

The following are assumed:

1. All processes are steady.
2. The compression and expansion processes are isentropic.
3. No pressure drop in the combustion chamber.
4. Constant properties (specific heat and specific heat ratio Cp, γ).
5. The working fluid is assumed air.
6. The amount of fuel added is also neglected in the energy balance relations.

The different modules are described as follows:

Air inlet assembly: The engine inlet sucks air from the nearby area and delivers it to the compressor. It is assumed that there are no changes in either the total temperature or pressure from its ambient values $T_{01} = T_a$ and $P_{01} = P_a$.

Compressor: Fresh air at ambient conditions is drawn into the compressor. The compressor is either axial or centrifugal. The axial compressor has higher efficiency, higher air-flow rate, and more stages than the centrifugal compressor. The centrifugal compressor is used in small and medium-size industrial engines. It has fewer stages. Moreover, it is simple and rugged. The most recent axial compressor is the Electron Beam (EB)-welded rotor, which gives low vibration, straightforward torque transfer, good control of blade tip clearance, and still

offers the possibility of replacing individual blades in situ, provided that the casings in the compressor section have a longitudinal split.

Next, the air temperature and pressure are raised in an isentropic compression process. Since the compression process is isentropic, then

$$\frac{T_{02}}{T_{01}} = \left(\frac{P_{02}}{P_{01}}\right)^{(\gamma-1)/\gamma} = \pi_c^{(\gamma-1)/\gamma}$$

The specific work in the compressor is

$$W_c = Cp\left(T_{02} - T_{01}\right) = Cp\left(T_{02} - T_a\right) = CpT_a\left(\pi_c^{\gamma-1/\gamma} - 1\right) \tag{8.1}$$

Combustion chamber: The combustion chamber, also known as the "burner" must be compact and must provide even temperature distribution of the hot gases as delivered next to the turbines. The three basic configurations of the combustion chamber are annular, can, and can-annular. The annular is a donut-shaped, single continuous chamber that encircles the turbine. It requires less cooling air due to less hot surface area and gives a better flow inlet into the turbine. It also has simple cross-ignition during start-up. However, acoustic control can be difficult owing to flame instability at ultra-low emission levels. The can-annular is made of multiple, single burners ("cans") evenly spaced around the rotor shaft. It requires more cooling air and cross-over tubes for start-up, alternatively one igniter per can. Single cans can be removed without the removal of the turbine module. Cans are either one or more combustion chambers mounted external to the gas turbine body. Generally, the high-pressure air proceeds into the combustion chamber, where the fuel is burned at constant pressure. The heat added per unit air mass flow rate is

$$Q_{in} = h_{03} - h_{02} = Cp\left(T_{03} - T_{02}\right) \tag{8.2}$$

Turbine: The resulting high-temperature gases then enter the turbine, where they expand in an isentropic process to atmospheric pressure, thus producing power. The exhaust gases leaving the turbine are thrown out (not recirculated), causing the cycle to be classified as an open cycle. The expansion process in the turbine is also isentropic. Moreover, since $P_{02} = P_{03}$ and $P_{04} = P_{01}$, then

$$\frac{T_{03}}{T_{04}} = \left(\frac{P_{03}}{P_{04}}\right)^{(\gamma-1)/\gamma} = \left(\frac{P_{02}}{P_{01}}\right)^{(\gamma-1)/\gamma} = \pi_c{}^{\gamma-1/\gamma}$$

The specific work generated in the turbine is

$$W_t = Cp\left(T_{03} - T_{04}\right) = CpT_{03}\left[1 - \frac{1}{\pi_c{}^{\gamma-1/\gamma}}\right] \tag{8.3}$$

The net specific work of the cycle that is delivered to the load is

$$W_{net} = W_t - W_c = Cp\left(T_{03} - T_{04}\right) - Cp\left(T_{02} - T_{01}\right) \tag{8.4}$$

The thermal efficiency of the ideal Brayton cycle under the cold air standard assumptions becomes

$$\eta_{th,\,Brayton} = \frac{W_{net}}{Q_{in}} = 1 - \frac{Cp\left(T_{04} - T_{01}\right)}{Cp\left(T_{03} - T_{02}\right)} = 1 - \frac{T_{01}\left(T_{04}/T_{01} - 1\right)}{T_{02}\left(T_{03}/T_{02} - 1\right)}$$

Since the processes 1–2 and 3–4 are isentropic, and $P_{02} = P_{03}$ and $P_{04} = P_{01}$. Thus

$$\frac{T_{02}}{T_{01}} = \left(\frac{P_{02}}{P_{01}}\right)^{(\gamma-1)/\gamma} = \left(\frac{P_{03}}{P_{04}}\right)^{(\gamma-1)/\gamma} = \frac{T_{03}}{T_{04}} \quad \text{or} \quad \frac{T_{04}}{T_{01}} = \frac{T_{03}}{T_{02}}$$

Substituting these equations into the thermal efficiency relation and simplifying gives

$$\eta_{th,\,Brayton} = 1 - \frac{1}{\pi_c^{(\gamma-1)/\gamma}} \tag{8.5}$$

where $\pi_c = P_{02}/P_{01}$.

Thus the thermal efficiency depends only on the compressor pressure ratio and the specific heat ratio. As will be described next, the thermal efficiency of the real cycle depends on other parameters as well.

The specific power ($\mathscr{P}$) is the net power per unit mass flow rate (W·s/kg), which can be rearranged from Equation 8.4 as follows

$$\mathscr{P} = W_t - W_c = Cp\left(T_{03} - T_{04}\right) - Cp\left(T_{02} - T_{01}\right)$$

$$\mathscr{P} = W_t - W_c = CpT_{03}\left(1 - \frac{T_{04}}{T_{03}}\right) - CpT_{01}\left(\frac{T_{02}}{T_{01}} - 1\right)$$

$$\mathscr{P} = CpT_{03}\left(1 - x^{-1}\right) - CpT_{01}\left(x - 1\right)$$

where $x = \pi_c^{\gamma-1/\gamma}$.

From the above equation, the specific power depends on the ambient temperature, compressor pressure ratio and maximum temperature of the turbine. The specific work attains a maximum value when its derivative w.r.t. the compressor pressure ratio is equal to zero

$$\frac{d\mathscr{P}}{dx} = 0$$

$$\frac{CpT_{03}}{x^2} - CpT_{01} = o$$

$$\frac{T_{03}}{T_{01}} = x^2 = \pi_c^{2(\gamma-1)/\gamma} \tag{8.6a}$$

or

$$\pi_c = \left(T_{03}/T_{01}\right)^{\gamma/2(\gamma-1)} \tag{8.6b}$$

A plot for the above relation is given in Figure 8.7.

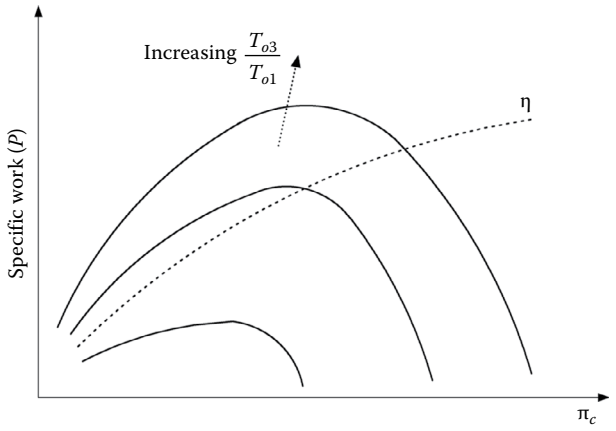


FIGURE 8.7
Variation of specific power and thermal efficiency with the compressor pressure ratio.

8.4.1.2 Real Cycle

The real case is associated with losses due to friction. The changes in specific heat at constant pressure are considered. A schematic diagram for the engine and its processes on the temperature-entropy diagram is shown in Figure 8.8. The different modules will be again analyzed as follows:

Compressor: The inlet conditions are also the ambient conditions, thus the outlet pressure and temperature are given by the relations

$$P_{02} = (P_{01})(\pi_c) = P_a \times \pi_c \tag{8.7}$$

$$T_{02} = T_a\left[1 + \frac{\pi_c^{\gamma_c - 1/\gamma_c} - 1}{\eta_c}\right] \tag{8.8}$$

where
η_c is the isentropic efficiency of the compressor
γ_c is the specific heat ratio of ambient air

The specific work of the compressor is

$$W_c = Cp_c\,(T_{02} - T_a)$$

where Cp_c is the air specific heat.

Combustion chamber: The combustion process is associated with a pressure drop, thus the outlet pressure is given by the relation

$$P_{03} = P_{02} - \Delta P_{cc} \tag{8.9a}$$

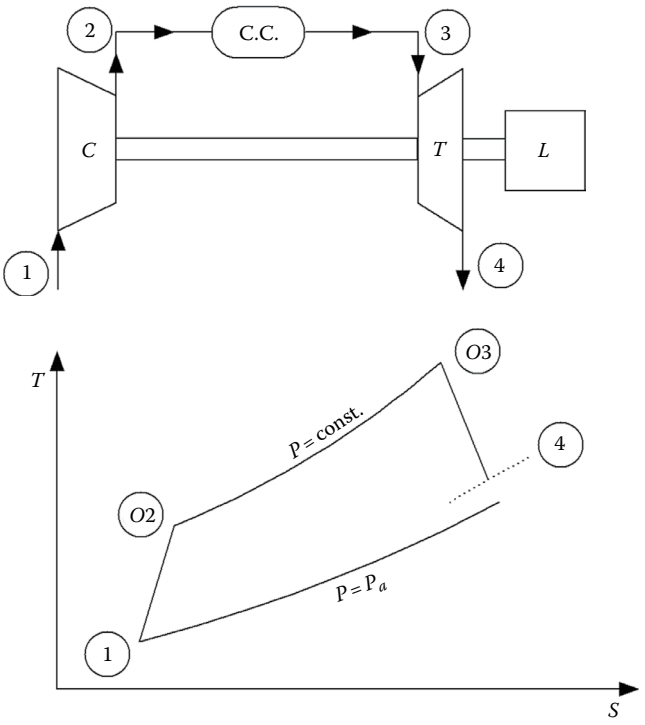


FIGURE 8.8
Real Brayton cycle.

Some gas turbine manufacturers employ a fraction pressure loss, *fpl* (about 0.05 or 5%) to account for combustor or burner losses, thus $fpl = \dfrac{P_{02} - P_{03}}{P_{02}}$.

Thus

$$P_{03} = P_{02}\left(1 - fpl\right) \tag{8.9b}$$

The maximum temperature is known (T_{03}), thus the mass of burnt fuel is calculated from the energy balance in the combustion chamber. The resulting fuel-to-air ratio is given by the relation

$$f = \frac{Cp_h T_{03} - Cp_c T_{02}}{\eta_b Q_R - Cp_h T_{03}} \tag{8.10}$$

where

η_b is the burner efficiency
Q_R is the fuel heating value
Cp_h is the hot gases specific heat

Turbine: The hot gases expand in the turbine to a pressure very near to the ambient pressure. The exhaust gases must leave with some velocity so that it can get clear

of the engine before its kinetic energy is dissipated in the atmosphere. Therefore, a typical pressure ratio [6] would be

$$\frac{P_{04}}{P_a} = 1.1 - 1.2 \tag{8.11a}$$

It was suggested in Reference 1 that the outlet pressure will be very close to the ambient pressure, or

$$P_{04} - P_a = 0.01 - 0.04 \text{ bar} \tag{8.11b}$$

Thus the turbine outlet pressure is known. The temperature drop in the turbine is

$$T_{03} - T_{04} = \eta_t T_{03}\left[1 - \frac{1}{\left(P_{03}/P_{04}\right)^{\gamma-1/\gamma}}\right] \tag{8.12}$$

where η_t is the isentropic efficiency of the turbine.

The specific turbine work is given by the relation

$$W_t = Cp_h\left(T_{03} - T_{04}\right) \tag{8.13}$$

The specific power to the load is given by the relation

$$P = \left[\left(1+f\right)\eta_{mt}W_t - \frac{1}{\eta_{mc}}W_c\right] \tag{8.14}$$

where (η_{mc}, η_{mt}) are the mechanical efficiencies of the compressor and turbine, respectively. The units of the specific power in Equation 7.13 are kJ/kg or kW·s/kg.

The specific fuel consumption (SFC) is defined as

$$\text{SFC} = \frac{f}{P} \tag{8.15}$$

The units of the specific fuel consumption in the above equation is as usual kg/(kW·s).

The thermal efficiency is expressed as

$$\eta_{th} = \frac{P}{fQ_R} = \frac{1}{\text{SFC} \times Q_R} \tag{8.16}$$

If the following are assumed

1. All processes are steady
2. The mechanical efficiencies of the compressor and turbine are assumed unity
3. No pressure drop in the combustion chamber
4. Constant properties (specific heat and specific heat ratio Cp, γ)
5. The working fluid is assumed air
6. The amount of fuel added is also neglected in the energy balance relations

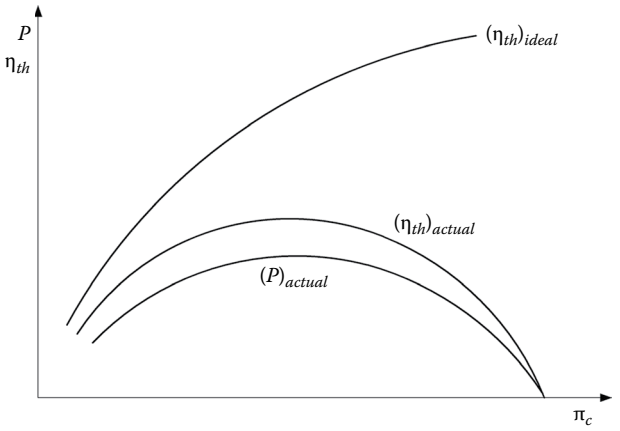


FIGURE 8.9
Real versus actual specific power and thermal efficiency.

then the thermal efficiency will be expressed by the relation

$$\eta_{th} = \left(\frac{\alpha \eta_c \eta_t - \beta}{\alpha \eta_c - \beta + (1 - \eta_c)} \right) \left(1 - \frac{1}{\beta} \right) \tag{8.17}$$

where $\alpha = (T_{03}/T_{01})$ and $\beta = \pi_c^{\gamma - 1/\gamma}$.

The specific power is expressed as

$$P = CpT_{01}(\beta - 1) \left(\frac{\eta_t \alpha}{\beta} - \frac{1}{\eta_c} \right) \tag{8.18}$$

Equation 8.17 will be reduced to the form in Equation 8.5 if the compressor and turbine efficiency are set equal to unity. A plot of Equations 8.17 and 8.18 versus the compressor pressure ratio is shown in Figure 8.9. A comparison between Figures 8.7 and 8.9 yields that

1. The thermal efficiency is dependent on the turbine inlet temperature and thus the turbine material limits the maximum thermal efficiency.
2. The loss due to compressor efficiency is partially compensated for by the reduction in heat added due to fuel burning in the combustion chamber, thus the compressor efficiency appears both in the numerator and denominator.
3. The loss in turbine is lost from the system, thus the turbine efficiency appears only in the numerator.

8.4.2 Regeneration

In a gas-turbine engine, the temperature of the exhaust gas leaving the last turbine (if there is more than one turbine) is often considerably higher than the temperature of the air leaving the last compressor (also, if there is more than one compressor).

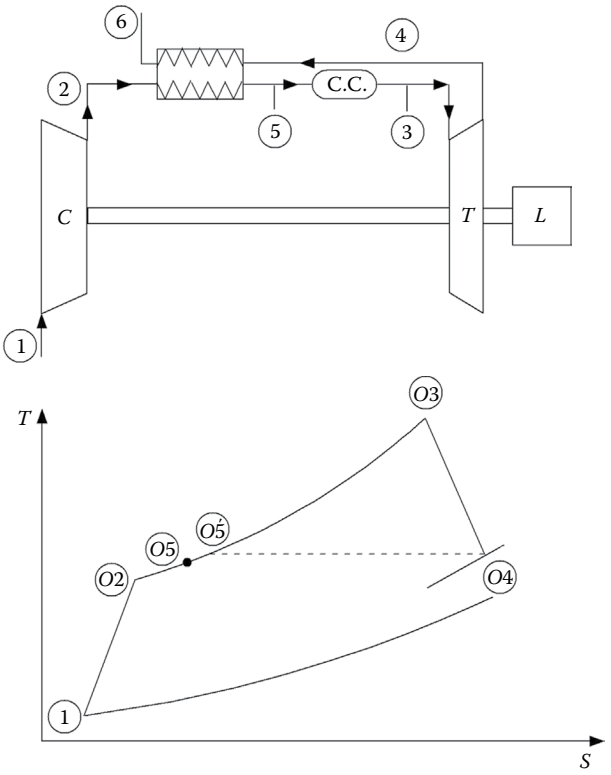


FIGURE 8.10
Single spool with regeneration.

Therefore, the high-pressure air leaving the compressor can be heated by transferring heat to it from the hot exhaust gases in a counter-flow heat exchanger, which is also known as a regenerator or a recuperator. A sketch of the single-shaft gas-turbine engine utilizing a regenerator together with its T-S diagram of the new cycle is shown in Figure 8.10. The regenerator is normally referred to by the letter "**X**," thus the engine is referred to "**CXBT**."

The highest temperature occurring within the regenerator is (T_{04}), the temperature of the exhaust gases leaving the turbine and entering the regenerator. Under no conditions can the air be preheated in the regenerator to a temperature above this value [7]. Air normally leaves the regenerator at a lower temperature (T_{05}). In the limiting (ideal) case, the air will exit the generator at the inlet temperature of the exhaust gases (T_{04}). The actual heat transfers from the exhaust gases to the air can be expressed as

$$q_{regen,\,act} = h_{05} - h_{02}$$

Assuming the regenerator to be well insulated and any changes in kinetic and potential energies to be negligible, the maximum heat transfers from the exhaust gases to the air can be expressed as

$$q_{regen,\,\max} = h_{05'} - h_{02} = h_{04} - h_{02}$$

The extent to which a regenerator approaches an ideal regenerator is called the effectiveness ε and is defined as

$$\varepsilon = \frac{q_{regen,\,act}}{q_{regen,\,\max}} = \frac{h_{05} - h_{02}}{h_{04} - h_{02}}$$

When the cold-air-standard assumptions are utilized, it reduces to

$$\varepsilon = \frac{T_{05} - T_{02}}{T_{04} - T_{02}} \tag{8.19}$$

A regenerator with a higher effectiveness will obviously save a greater amount of fuel since it will preheat the air to a higher temperature prior to combustion. However, achieving a higher effectiveness requires the use of a larger regenerator of higher price and causes a larger pressure drop. The effectiveness of most regenerators used in practice is below 0.85.

Thus, the new value for the fuel-to-air ratio is now

$$f = \frac{Cp_h T_{03} - Cp_c T_{05}}{\eta_b Q_R - Cp_h T_{03}} \tag{8.20}$$

Concerning the thermal efficiency of an ideal Brayton cycle with regeneration under the cold-air-standard assumptions, its value is

$$\eta_{th,\,regen} = 1 - \left(\frac{T_{01}}{T_{03}}\right)(\pi_c)^{(\gamma-1)/\gamma} \tag{8.21}$$

Therefore, the thermal efficiency of an ideal Brayton cycle with regeneration depends on the ratio of the minimum to maximum temperatures as well as the compressor-pressure ratio.

Concerning the actual cycle, the specific work in both the compressor and the turbine are the same as in Section 8.4.1.2. The real cycle efficiency will then be obtained from Equation 8.16 by substituting the new value of the fuel-to-air ratio from Equation 8.15. The main advantage of regeneration is its reduction in fuel consumption and, consequently, the reduction in the fuel-to-air ratio. This leads to an increase in the thermal efficiency as shown by Equation 8.16.

8.4.3 Reheat

In this case, reheat is proposed at some point in the expansion process for a single-shaft configuration. Thus, a second combustion chamber is installed between the two turbines. The engine layout, together with its temperature-entropy diagram is shown in Figure 8.11. Reheat is referred to by the letter "**R**," thus the engine is identified by "**CBTRT**." Again, an analysis of the cycle is considered here.

The compressor and the first combustion chamber (downstream of the compressor) are treated in the same way as shown in Figure 8.11. But, since there are two combustion

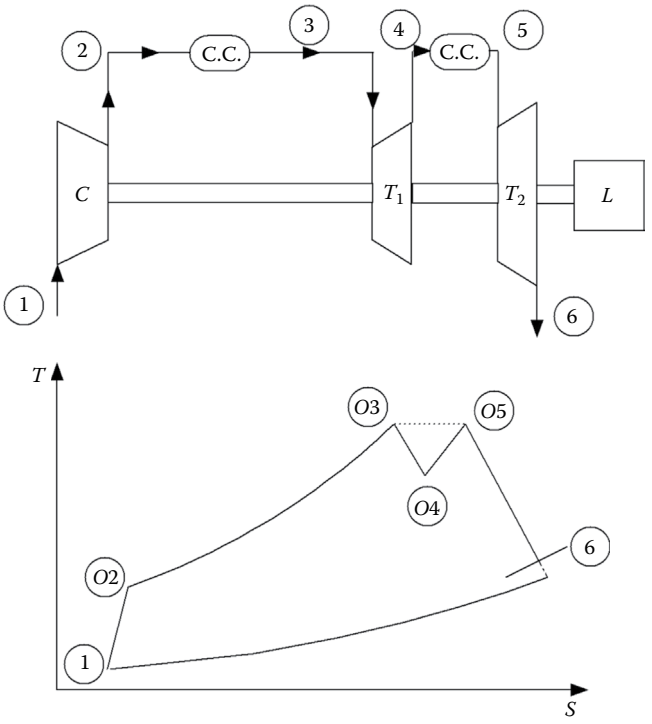


FIGURE 8.11
Single spool with reheat.

chambers, then the fuel burnt in this combustion chamber is denoted by $\dot{m}_{f1}$ and the corresponding fuel-to-air ratio are also denoted by f_1 where

$$f_1 = \frac{Cp_h T_{03} - Cp_c T_{02}}{\eta_{b1} Q_R - Cp_h T_{03}} \tag{8.22}$$

The subsequent elements are analyzed hereafter.

High-pressure turbine (*HPT*) *or turbine* (*1*): The inlet total temperature of the turbine is defined from metallurgical capabilities of the turbine material. Moreover, its total pressure is known from the pressure drop in the first combustion chamber. However, a problem arises; namely, how to determine the outlet conditions of this first turbine. Theoretically, the optimum pressure ratio for each turbine is equal, and its value would be equal to the square root of the overall pressure ratio of both turbines. Now, since the outlet pressure of the second turbine is slightly higher than the ambient pressure (say 0.01–0.04 bar greater than the ambient pressure), then the outlet pressure of the second turbine (P_{06}) is known. It can be shown also that to maximize the total turbine work output, the pressure ratio of both turbines must be equal. Thus, for optimum operation we have

$$\frac{P_{03}}{P_{04}} = \frac{P_{05}}{P_{06}} = \sqrt{\frac{P_{03}}{P_{06}}} \tag{8.23}$$

The temperature drop in the first (high-pressure) turbine is

$$T_{03} - T_{04} = \eta_{t1} T_{03} \left[1 - \frac{1}{\left(P_{03}/P_{04} \right)^{\gamma - 1/\gamma}} \right] \tag{8.24}$$

The specific work of the first turbine is

$$W_{t1} = Cp_h \left(T_{03} - T_{04} \right) \tag{8.25}$$

Second combustion chamber (*reheat*): Here for simplicity, the pressure drop in this combustion chamber is neglected. The corresponding fuel-to-air ratio is

$$f_2 = \frac{Cp_h \left(T_{05} - T_{04} \right)}{\eta_{b2} Q_R - Cp_h T_{05}} \tag{8.26}$$

This equation is written in a general form where the second burner has a new efficiency (η_{b2}). The maximum temperature in both combustion chambers is assumed equal

$$T_{05} = T_{03} \tag{8.27}$$

Low-pressure turbine (LPT) or turbine (2): The temperature drop in the turbine is

$$T_{05} - T_{06} = \eta_{t2} T_{05} \left[1 - \frac{1}{\left(P_{05}/P_{06} \right)^{\gamma - 1/\gamma}} \right] \tag{8.28}$$

where η_{t2} is the isentropic efficiency of the second turbine. The specific work of the second turbine is

$$W_{t2} = Cp_h \left(T_{05} - T_{06} \right) \tag{8.29}$$

The specific power to the load is given by the relation

$$P = \left[\left(1 + f_1 \right) \eta_{mt1} W_{t1} + \left(1 + f_1 + f_2 \right) \eta_{mt2} W_{t2} - \frac{1}{\eta_{mc}} W_c \right] \tag{8.30}$$

The specific fuel consumption is defined as

$$\text{SFC} = \frac{f_1 + f_2}{P} \ \text{kg/(kW} \cdot \text{s)} \tag{8.31}$$

The thermal efficiency is expressed as

$$\eta_{th} = \frac{P}{\left(f_1 + f_2 \right) Q_R} = \frac{1}{\text{SFC} \times Q_R} \tag{8.32}$$

The main advantage here is that reheat increases in the power output. This is very similar to reheat in aircraft engines, which also increase the thrust force. However, there is an increase in turn in the fuel consumption and the fuel-to-air ratio. The outcome of both points is a slight reduction in the thermal efficiency of the engine.

8.4.4 Intercooling

The third module that may be added is the intercooler. The single-shaft gas turbine is now composed of two compressors (low pressure and high pressure) with an intercooler in between; the second compressor is followed by a combustion chamber, with a turbine driving the two compressors and the load (Figure 8.12). The cycle is also illustrated on the T-S diagram in the same figure. The intercooler is referred to by the letter "I" and this engine is then referred to as "**CICBT.**" Air is cooled in station (2) prior to proceeding to the high-pressure compressor (HPC). The minimum possible temperature is again the ambient temperature. The effectiveness of the intercooler can be defined as

$$\varepsilon_{IC} = \frac{T_{02} - T_{03}}{T_{02} - T_{01}}$$

This lower temperature means that the HPC will be compact or, in other words, will be smaller than its normal size in a non-intercooled engine. Another advantage for the intercooled gas turbine is that the HPC power requirement is reduced. Thus higher power will be available for driving the load. However, the reduced HPC delivery temperature leads to

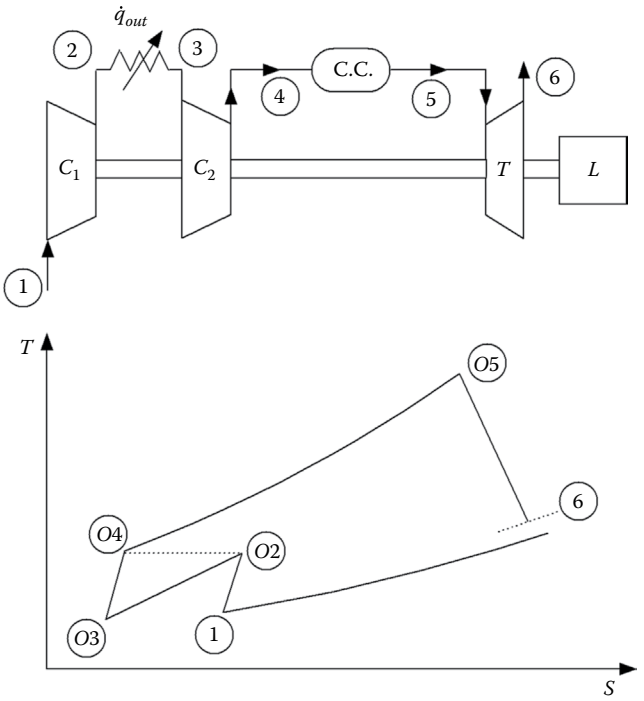


FIGURE 8.12
Single spool with intercooler.

substantially more fuel attaining the same maximum temperature of a normal gas turbine engine. The analysis of the cycle will be briefly discussed.

The low-pressure compressor (LPC) is typical of the basic case described in Section 8.4.1.2 with appropriate pressure ratio and isentropic efficiency (π_{c1}, η_{c1}).

HPC: The HPC has a pressure ratio and isentropic efficiency (π_{c2}, η_{c2}).

The output conditions are

$$P_{04} = (P_{03})(\pi_{c2}) \tag{8.33}$$

$$T_{04} = T_{03}\left[1 + \frac{\pi_{c2}^{\gamma_c - 1/\gamma_c} - 1}{\eta_{c2}}\right] \tag{8.34}$$

Combustion chamber: More fuel will be needed to reach the maximum temperature of the basic cycle engine. The fuel-to-air ratio is then

$$f = \frac{Cp_h T_{05} - Cp_c T_{04}}{\eta_b Q_R - Cp_h T_{05}}$$

Turbine: The outlet pressure (P_{06}) is known through either a ratio to the ambient pressure or a specified difference between its value and the ambient pressure. Then the outlet temperature is obtained from the relation

$$T_{06} = T_{05}\left[1 - \eta_t\left\{1 - \left(\frac{P_{06}}{P_{05}}\right)^{\gamma_h - 1/\gamma_h}\right\}\right]$$

Load: The specific power available for driving the load is

$$P = \eta_{mt1}(1+f)Cp_h(T_{05} - T_{06}) - Cp_c\left(\frac{T_{02} - T_a}{\eta_{mc1}} + \frac{T_{04} - T_{03}}{\eta_{mc2}}\right) \tag{8.35}$$

where $\eta_{mc1}, \eta_{mc2}, \eta_{mt}$ are the mechanical efficiencies of the LPCs, HPCs, and the turbine, respectively.

8.4.5 Combined Intercooling, Regeneration, and Reheat

Figure 8.13 illustrates this combined case together with its temperature entropy diagram. The engine is then symbolically designated by "**CICXBTRT**."

Example 8.1

A preliminary design analysis is to be made for a stationary gas turbine powerplant. The proposed powerplant is to incorporate one stage of intercooling and a regenerator "**CICXBT**" having an effectiveness of $\varepsilon_R = 0.75$ as shown in Figure 8.14. The inlet

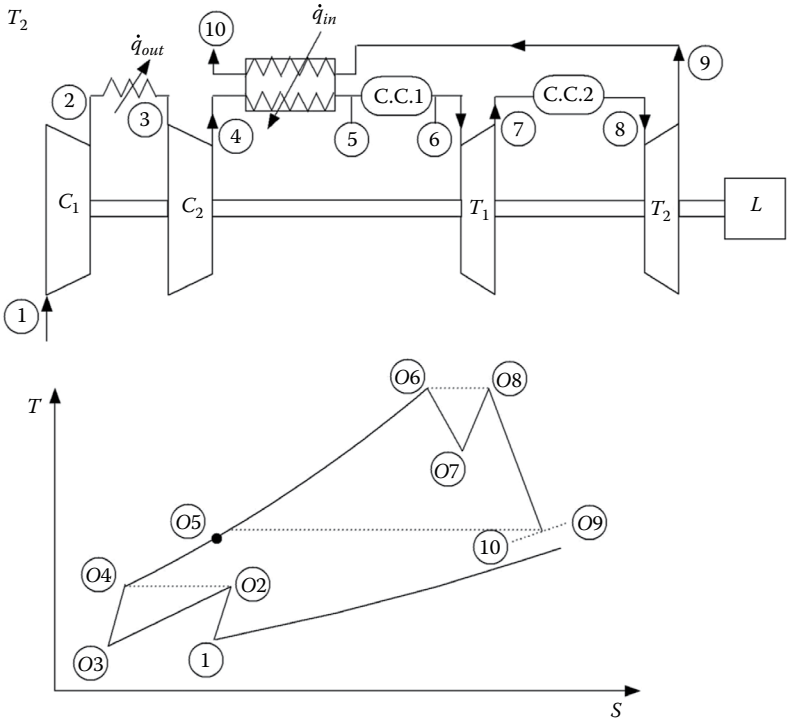


FIGURE 8.13
Single spool with intercooler, reheat, and regenerator.

temperature to the turbine at the maximum load condition is limited to 650°C. Derive a general relation for the intermediate pressure (P_{02}) as a function of the inlet and outlet pressures of the compression process; $P_{02}=f(P_{01},P_{04})$ that gives the maximum thermal efficiency. *Prove* that the specific work of the two compressors of the intercooler is minimum if the intermediate pressure of the intercooler is related to the inlet and outlet pressure of the intercooler set by the relation

$$P_{02}^2 = \left(\frac{\eta_{c1}+\varepsilon-1}{\eta_{c2}+\varepsilon-1}\right)^{\gamma/\gamma-1} P_{01}P_{04}$$

Next, if the isentropic efficiency of both compressors is equal, then the minimum specific work attains a maximum value when the pressure ratio of both compressors is equal; thus

$$\frac{P_{02}}{P_{01}} = \frac{P_{04}}{P_{02}} = \sqrt{\frac{P_{04}}{P_{01}}}$$

Determine this pressure ratio and also the corresponding thermal efficiency if the component efficiencies are as follows:

$$\eta_{c1}=0.83,\quad \eta_{c2}=0.83,\quad \eta_t=0.85,\quad \eta_b=0.98,\quad \eta_{mc1}=\eta_{mc2}=\eta_{mt}=0.98,\quad \varepsilon_{IC}=0.9$$

Air inlet temperature to the first compressor is 20°C, and the maximum temperature in the cycle is 650°C. For overall pressure ratios of 2, 3, 4, 6, and 8, calculate and plot the

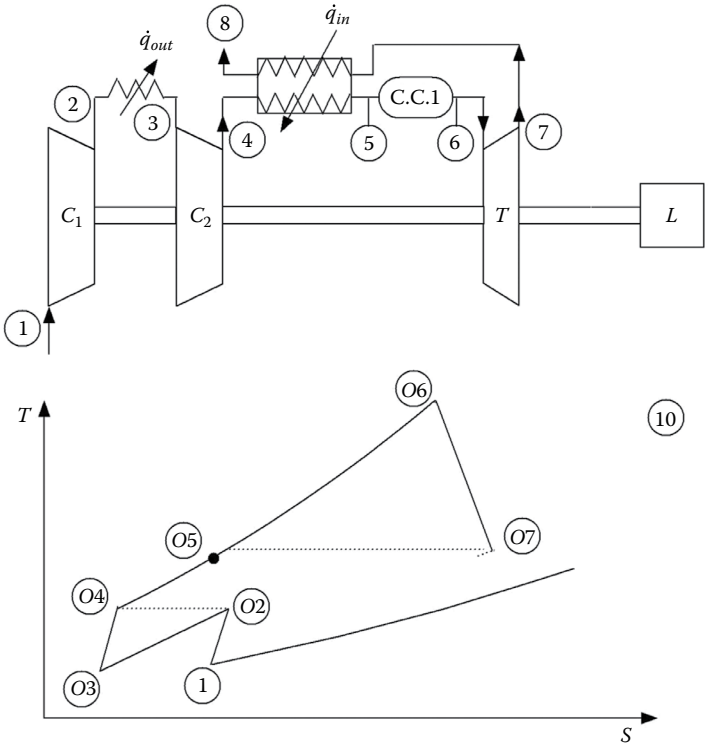


FIGURE 8.14
Single spool with intercooler and regenerator.

specific power and thermal efficiency for optimum pressure ratios in the compression system $\left(\frac{P_{02}}{P_{01}} = \frac{P_{04}}{P_{02}} = \sqrt{\frac{P_{04}}{P_{01}}}\right)$ and determine the value of the overall pressure ratio corresponding to the maximum specific power and maximum thermal efficiency.

Solution

Figure 8.14 illustrates a layout of the gas turbine together with its temperature entropy diagram.

The efficiencies of different modules are

$$\eta_{c_1} = \eta_{c_2} = 0.83, \quad \eta_t = 0.85, \quad \eta_{mc_1} = \eta_{mc_2} = \eta_t = 0.98, \quad \eta_B = 0.98$$

The effectiveness of the intercooler and regenerators are $\varepsilon_{IC} = 0.9$, $\varepsilon_R = 0.75$.

The operating conditions are

$$T_{06} = 650 + 273 = 823 \text{ K}, \quad T_{01} = 20 + 273 = 293 \text{ K}, \quad P_{01} = 1.0 \text{ bar}$$

For general procedure we first assume that η_{c1} and η_{c2} have unequal values

$$\varepsilon_{IC} = \frac{T_{02} - T_{03}}{T_{02} - T_{01}}$$
$$\therefore T_{03} = T_{02} - \varepsilon_{IC}\left(T_{02} - T_{01}\right) = T_{02}\left(1 - \varepsilon\right) + \varepsilon T_{01}$$

But the outlet temperature of the first compressor (C_1) is

$$T_{02} = T_{01}\left[1+\frac{1}{\eta_{c_1}}\left\{\left(\frac{P_{02}}{P_{01}}\right)^{\gamma-1/\gamma}-1\right\}\right]$$

$$T_{03} = T_{01}\left[\varepsilon+(1-\varepsilon)\left\{1+\frac{1}{\eta_{c_1}}\left(\frac{P_{02}}{P_{01}}\right)^{\gamma-1/\gamma}-\frac{1}{\eta_{c_1}}\right\}\right]$$

$$T_{03} = T_{01}\left[1-\left(\frac{1-\varepsilon}{\eta_{c_1}}\right)+\left(\frac{1-\varepsilon}{\eta_{c_1}}\right)\left(\frac{P_{02}}{P_{01}}\right)^{\gamma-1/\gamma}\right]$$

Define $B=\dfrac{1-\varepsilon}{\eta_{c_1}}$ and $\lambda=1-B$.

$$\therefore T_{03} = T_{01}\left[\lambda+B\left(P_{02}/P_{01}\right)^{\gamma-1/\gamma}\right]$$

The specific work of compressors (C_1) and (C_2) are

$$W_{c1} = \frac{C_P}{\eta_{m_1}\eta_{c_1}}T_{01}\left\{\left(\frac{P_{02}}{P_{01}}\right)^{\gamma-1/\gamma}-1\right\}$$

$$W_{c2} = \frac{C_P}{\eta_{m2}\eta_{c2}}T_{03}\left\{\left(\frac{P_{04}}{P_{02}}\right)^{\gamma-1/\gamma}-1\right\}$$

For $\eta_{m2}=\eta_{m1}=\eta_m$ and the total specific work of the compressor W_{CT} defined as $W_{CT}=W_{C1}=W_{C2}$, then

$$W_{CT} = \frac{C_PT_{01}}{\eta_m\eta_{c1}}\left[\left(\frac{P_{02}}{P_{01}}\right)^{\gamma-1/\gamma}-1\right]+\frac{C_PT_{01}}{\eta_m\eta_{c2}}\left[\left\{\lambda+B\left(\frac{P_{02}}{P_{01}}\right)^{\gamma-1/\gamma}\right\}\left\{\left(\frac{P_{04}}{P_{02}}\right)^{\gamma-1/\gamma}-1\right\}\right]$$

$$W_{CT} = \frac{C_PT_{01}}{\eta_m}\left[\frac{1}{\eta_{c1}}\left(\frac{P_{02}}{P_{01}}\right)^{\gamma-1/\gamma}-\frac{1}{\eta_{c1}}+\frac{\lambda}{\eta_{c2}}\left(\frac{P_{04}}{P_{02}}\right)^{\gamma-1/\gamma}-\frac{\lambda}{\eta_{c2}}+\frac{B}{\eta_{c2}}\left(\frac{P_{04}}{P_{01}}\right)^{\gamma-1/\gamma}-\frac{B}{\eta_{c2}}\left(\frac{P_{02}}{P_{01}}\right)^{\gamma-1/\gamma}\right]$$

$$W_{CT} = A\left[\left(\frac{1}{\eta_{c1}}-\frac{B}{\eta_{c2}}\right)\left(\frac{P_{02}}{P_{01}}\right)^{\gamma-1/\gamma}+\frac{\lambda}{\eta_{c2}}\left(\frac{P_{04}}{P_{02}}\right)^{\gamma-1/\gamma}+\frac{B}{\eta_{c2}}\left(\frac{P_{04}}{P_{01}}\right)^{\gamma-1/\gamma}-\frac{\lambda}{\eta_{c2}}-\frac{1}{\eta_{c1}}\right]$$

To obtain the value of minimum work, differentiate with respect to the intermediate pressure (P_{02}) and equate the differential to zero, or $\partial W_{CT}/\partial P_{02}=0$.

$$\frac{\partial W_{CT}}{\partial P_{02}} = A\left[\left(\frac{1}{\eta_{c1}}-\frac{1-\varepsilon}{\eta_{c1}\eta_{c2}}\right)\left(\frac{\gamma-1}{\gamma}\right)\frac{(P_{02})^{-1/\gamma}}{(P_{01})^{\gamma-1/\gamma}}-\frac{\lambda}{\eta_{c2}}\left(\frac{\gamma-1}{\gamma}\right)(P_{04})^{\gamma-1/\gamma}(P_{02})^{-2+\frac{1}{\gamma}}\right]$$

$$\therefore\left(\frac{1}{\eta_{c1}}-\frac{1-\varepsilon}{\eta_{c1}\eta_{c2}}\right)\frac{P_{02}^{-1/\gamma}}{(P_{01})^{\gamma-1/\gamma}} = \frac{1}{\eta_{c2}}\left(1-\frac{1-\varepsilon}{\eta_{c1}}\right)(P_{04})^{\gamma-1/\gamma}(P_{02})^{-2+\frac{1}{\gamma}}=0$$

$$\left(\frac{\eta_{c2}-1+\varepsilon}{\eta_{c1}\eta_{c2}}\right)(P_{02})^{2(\gamma-1/\gamma)} = \left(\frac{\eta_{c1}-1+\varepsilon}{\eta_{c1}\eta_{c2}}\right)(P_{01}P_{04})^{\gamma-1/\gamma}$$

Then the general relation requested is

$$P_{02}^2 = \left(\frac{\eta_{c1} + \varepsilon - 1}{\eta_{c2} + \varepsilon - 1}\right)^{\gamma/\gamma-1} P_{01}P_{04}$$

If the efficiency of both compressors is equal, then $\eta_{c1} = \eta_{c2} = \eta_c$.

The above equation is reduced to the well-known formula

$$P_{02}^2 = P_{01}P_{04}$$

Thus, the requested relation is proved as

$$\frac{P_{02}}{P_{01}} = \frac{P_{04}}{P_{02}} = \sqrt{\frac{P_{04}}{P_{01}}}$$

Now, returning to the numerical values in this example

$$T_{02} = T_{01}\left[1 - \frac{1}{\eta_c} + \frac{1}{\eta_c}\left(\frac{P_{02}}{P_{01}}\right)^{\gamma-1/\gamma}\right]$$

Then for $\gamma = 1.4$, $T_{01} = 293\,^\circ\text{K}$, and $\eta_c = 0.83$

$$T_{02} = 293\left[1 - \left(P_{02}/P_{01}\right)^{0.286} - 0.202\right] \tag{1}$$

$$T_{03} = T_{01}\left[1 - \left(\frac{1-\varepsilon}{\eta_c}\right) + \left(\frac{1-\varepsilon}{\eta_c}\right)\left(\frac{P_{02}}{P_{01}}\right)^{\gamma-1/\gamma}\right]$$

$$T_{03} = 293\left[0.88 + 0.12\left(P_{02}/P_{01}\right)^{0.286}\right] \tag{2}$$

$$T_{04} = T_{03}\left[1 - \frac{1}{\eta_c} + \frac{1}{\eta_c}\left(\frac{P_{04}}{P_{02}}\right)^{\gamma-1/\gamma}\right]$$

$$T_{04} = T_{03}\left[1.202\left(P_{04}/P_{02}\right)^{0.286} - 0.202\right] \tag{3}$$

The total compression work of the two compressors (W_{CT}) is reformulated as

$$W_{CT} = \frac{C_p T_{01}}{\eta_m \eta_c}\left[(1-B)\left\{\left(\frac{P_{02}}{P_{01}}\right)^{\gamma-1/\gamma} + \left(\frac{P_{04}}{P_{02}}\right)^{\gamma-1/\gamma}\right\} + B\left(\frac{P_{04}}{P_{01}}\right)^{\gamma-1/\gamma} - (1+\lambda)\right]$$

Since

$$P_{02}^2 = P_{01}P_{04}$$

Then

$$\frac{P_{02}}{P_{01}} = \frac{P_{04}}{P_{02}} = \sqrt{\frac{P_{04}}{P_{01}}}$$

Then

$$W_{CT} = \frac{293}{(0.83)(0.98)}\left[(0.88)(2)\left(\frac{P_{02}}{P_{01}}\right)^{0.286} + 0.12\left(\frac{P_{04}}{P_{01}}\right)^{0.286} - 1.88\right] \text{ kJ/kg}$$

$$W_{CT} = 360\left[1.76\left(\frac{P_{02}}{P_{01}}\right)^{0.286} + 0.12\left(\frac{P_{04}}{P_{01}}\right)^{0.286} - 1.88\right] \tag{4}$$

The specific power generated in the turbine is (W_t) which is expressed as

$$W_T = \eta_m \eta_t T_{06}\left[1 - \left(\frac{P_{01}}{P_{04}}\right)^{0.286}\right] = 770\left[1 - \left(\frac{P_{04}}{P_{01}}\right)^{-0.286}\right] \text{ kJ/kg} \tag{5}$$

The heat added in the combustion chamber per unit air mass flow rate is

$$q = \frac{1}{\eta_B}(h_{06} - h_{05}) = \frac{Cp}{\eta_B}(T_{06} - T_{05})$$

$$q = 1.02\left[(T_{06} - T_{04}) - \varepsilon_R (T_7 - T_{04})\right] \text{ kJ/kg} \tag{6}$$

$$T_7 = 923\left[0.15 + 0.85\left(\frac{P_{04}}{P_{01}}\right)^{-0.286}\right]$$

The thermal efficiency of the powerplant is

$$\eta_{th} = \frac{W_T - W_{CT}}{q}$$

P_{04}/P_{01}	$P_{02}/P_{01} = P_{04}/P_{02} = \sqrt{P_{04}/P_{01}}$	T_{03} (K)	T_{04} (K)	W_{CT} (kJ/kg)	T_7 (K)
2	1.414	296	330	75.2	785
3	1.732	299	360	124.1	714
4	2	300	376	158	668
6	2.45	304	410	212	608
8	2.729	306	444	254	572

P_{04}/P_{01}	$T_7 - T_{04}$ (K)	$T_{06} - T_{04}$ (K)	q (kJ/kg)	W_T (kJ/kg)	$W_{net} = W_T - W_{CT}$ (kJ/kg)	η_{th}
2	455	593	257	138.2	63	24.8%
3	356	565	300	207	83	27.7%
4	292	547	326	251.8	93	28.6%
6	199	514	371	308	96	25.9%
8	127	478	390	344	90	23.3%

From the above table, we can plot the thermal efficiency and specific power versus the compressor overall efficiency (Figure 8.15).

The maximum thermal efficiency is obtained when $P_{04}/P_{01} = 4.0$ and the maximum thermal efficiency is $\eta_{th} = 0.286$. The maximum power is 96 kJ/kg at a compression ratio of 6.0.

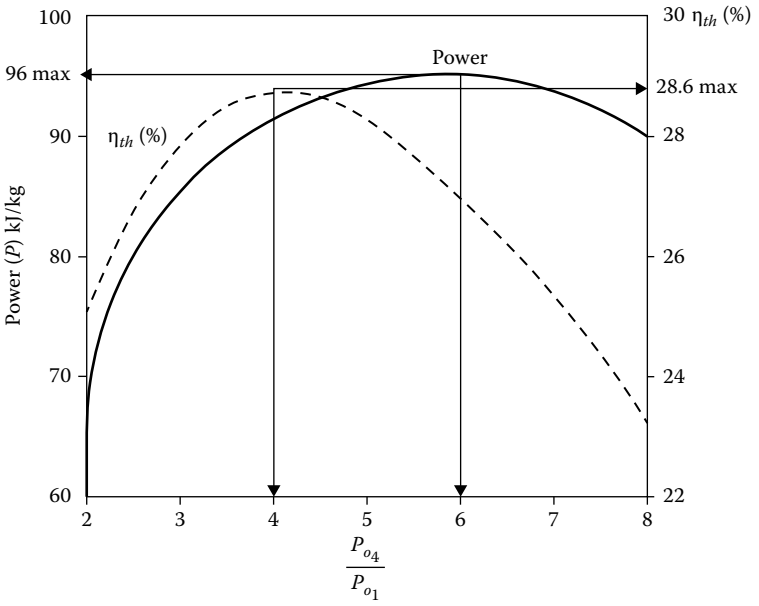


FIGURE 8.15
Plot of specific work and thermal efficiency versus pressure ratio.

8.5 Double-Shaft Engine

The double-shaft engines—as described in Section 8.1—have two main configurations: the split-shafts and the free-power turbine.

8.5.1 Free-Power Turbine

Figure 8.16 illustrates the case of a two spool having a free turbine. The compressor is directly connected and driven by the turbine (HPT), while the load is coupled and driven by the free-power turbine, thus denoted by "**CBTT**." Only a single combustion chamber is found, which is located as part of the gas generator.

The different processes are described as follows:

Compressor: The same treatment described in Section 8.4.1 is followed here for a real case. Thus the outlet pressure and temperature are given by Equations 8.1 and 8.2.

Combustion chamber: Also, the same methodology is followed to obtain the outlet pressure and the fuel-to-air ratio. The maximum temperature is known in advance. The fuel-to-air ratio is also calculated as above.

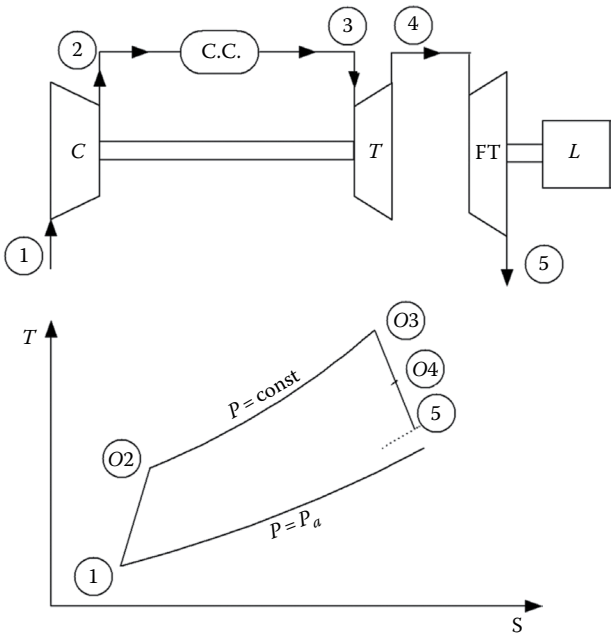


FIGURE 8.16
Layout and temperature-entropy diagram for a double spool with a free-power turbine.

HPT (*the compressor-turbine*): The power generated in the turbine is just sufficient to drive the compressor. Thus the energy balance for the compressor-turbine coupling is

$$(1+f)\eta_{mt}W_t = \frac{1}{\eta_{mc}}W_c$$

$$T_{04} = T_{03} - \frac{1}{\eta_{mc}\eta_{mt}(1+f)}\frac{Cp_c}{Cp_h}(T_{02} - T_a)$$

The turbine pressure ratio is calculated from the relation

$$\frac{P_{04}}{P_{03}} = \left(1 - \frac{T_{03} - T_{04}}{\eta_t T_{03}}\right)^{\gamma_h/\gamma_h - 1}$$

Free-power turbine: Assuming that there are no pressure losses in the ducts between the compressor-turbine and the free-power turbine, then the inlet pressure to the free-power turbine is also (P_{04}). The outlet pressure (P_{05}) is also very close to the ambient pressure. It is either defined as a ratio to the ambient pressure ($P_{05}/P_a \approx 1.1$) or $P_{05} = P_a + 0.04$ bar.

The exhaust gas temperature (T_{05}) at the outlet to the free-power turbine is given by the relation

$$T_{05} = T_{04}\left[1 - \eta_{pt}\left\{1 - \left(\frac{P_{05}}{P_{04}}\right)^{\gamma_h - 1/\gamma_h}\right\}\right] \tag{8.36}$$

The specific power, in kJ/kg (or kW·s/kg), delivered to the load is

$$P = (1+f)Cp_h(T_{04} - T_{05}) \tag{8.37}$$

The specific fuel consumption is defined as

$$\text{SFC} = \frac{f}{P} \text{ kg/kW·s}$$

The thermal efficiency is expressed as

$$\eta_{th} = \frac{P}{fQ_R} = \frac{1}{(\text{SFC})Q_R}$$

8.5.2 Two-Discrete Shafts (Spools)

The two-shaft arrangement here is composed of two compressors, two turbines, and a single combustion chamber, thus denoted by "**CCBTT**." It is similar to the two-spool turbofan engine. The low-pressure spool, as demonstrated in Figure 8.17, is composed of a compressor (C_1) and a turbine (T_1). The high-pressure spool is composed of a compressor (C_2) and a turbine (T_2). The load is driven by the low-pressure spool.

Low-pressure spool: The inlet conditions are the ambient pressure and temperature. The outlet conditions are obtained from the relations (8.7) and (8.8).

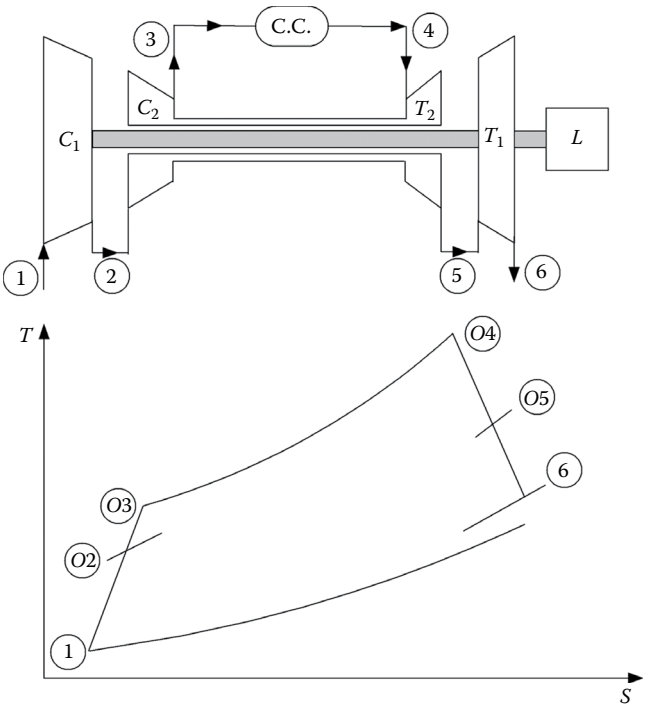


FIGURE 8.17
Layout of a two-spool engine (load coupled to the low-pressure spool with temperature-entropy diagram).

The specific work of the low-pressure compressor (C_1) is

$$W_{c1} = Cp_c\left(T_{02} - T_a\right)$$

High-pressure spool: The outlet conditions are obtained from the relations

$$P_{03} = \left(P_{02}\right)\left(\pi_{c2}\right) \tag{8.38}$$

$$T_{03} = T_{02}\left[1 + \frac{\pi_{c2}^{\gamma_c - 1/\gamma_c} - 1}{\eta_{c2}}\right] \tag{8.39}$$

The specific work of the high-pressure compressor (C_2) is

$$W_{c2} = Cp_c\left(T_{03} - T_{02}\right) \tag{8.40}$$

Combustion chamber: The combustion process is associated with a pressure drop, thus the outlet pressure is given by the relation

$$P_{04} = P_{03} - \Delta P_{cc}$$

The maximum temperature is known (T_{04}), thus the mass of burnt fuel is calculated from the energy balance in the combustion chamber. The resulting fuel-to-air ratio is given by the relation

$$f = \frac{Cp_h T_{04} - Cp_c T_{03}}{\eta_b Q_R - Cp_h T_{04}} \tag{8.41}$$

HPT: The HPT (T_2) drives the HPC (C_2). The energy balance gives the outlet temperature of the turbine (T_2) as

$$T_{05} = T_{04} - \frac{1}{\eta_{mc2}\eta_{mt2}\left(1+f\right)}\frac{Cp_c}{Cp_h}\left(T_{03} - T_{02}\right) \tag{8.42}$$

The turbine pressure ratio is calculated from the relation

$$\frac{P_{05}}{P_{04}} = \left(1 - \frac{T_{04} - T_{05}}{\eta_{t2} T_{04}}\right)^{\gamma_h/\gamma_h - 1} \tag{8.43}$$

LPT (T_1): The outlet pressure (P_{06}) is known to be slightly higher than the ambient pressure. The outlet temperature (T_{06}) is determined from the relation

$$T_{06} = T_{05}\left[1 - \eta_{t2}\left\{1 - \left(\frac{P_{06}}{P_{05}}\right)^{\gamma_h - 1/\gamma_h}\right\}\right] \tag{8.44}$$

The specific power consumed in the load is

$$P = \eta_{mt1}(1+f)Cp_h(T_{05}-T_{06}) - \frac{1}{\eta_{mc1}}Cp_c(T_{02}-T_a) \tag{8.45}$$

The specific fuel consumption is also given by the

$$\text{SFC} = \frac{f}{P} \text{ kg/kW}\cdot\text{s}$$

The thermal efficiency is expressed as

$$\eta_{th} = \frac{P}{fQ_R} = \frac{1}{(\text{SFC})Q_R}$$

Example 8.2

A two-spool industrial gas turbine, in which the load is coupled to a free-power turbine, "**CBTT**," operates at the following conditions:

Ambient temperature	288 K
Ambient pressure	101.3 kPa
Compressor pressure ratio	9
Turbine-inlet temperature	1380 K

The efficiencies of the different elements are

$$\eta_c = 0.87, \quad \eta_b = 0.99, \quad \eta_t = \eta_{ft} = 0.89$$

The fuel heating value = 43,000 kJ/kg.
The delivery pressure of the free turbine = 120 kPa.
Calculate

1. The fuel-to-air ratio
2. The net specific power
3. The thermal efficiency

Solution

The engine examined is illustrated in Figure 8.16. The successive processes are described as follows:

Compressor: The outlet conditions from the compressor are determined from Equations 8.7 and 8.8 as $P_{o2} = \pi \times P_a = 9 \times 101.3 = 911.7$ kPa.

$$T_{02} = 288\left[1 + \frac{9^{0.286}-1}{0.87}\right] = 577.53 \text{ K}$$

Combustion chamber: The fuel-to-air ratio

$$f = \frac{C_{P_h}T_{o3} - C_{P_c}T_{o2}}{\eta_b Q_R - C_{P_h}T_{o3}} = \frac{1.148\times 1{,}380 - 1.005\times 577.53}{0.99\times 43{,}000 - 1.148\times 1{,}380} = 0.0245$$

Since no pressure drop is assumed in the combustion chamber, then

$$P_{03} = P_{02} = 911.7 \text{ kPa}$$

Gas generator turbine: From the energy balance between the compressor and the turbine ($W_t = W_c$), the turbine outlet temperature and pressure are

$$T_{o4} = T_{o3} - \frac{C_{Pc}\left(T_{o2} - T_{o1}\right)}{\left(1+f\right)C_{Ph}} = 1380 - \frac{1.005}{1.0245 \times 1.148}\left(577.53 - 288\right) = 1132.6 \text{ K}$$

$$P_{o4} = P_{o3}\left(1 - \frac{T_{o3} - T_{o4}}{\eta_t T_{o3}}\right)^{\gamma/\gamma-1} = 911.7 \times \left(1 - \frac{247.4}{0.89 \times 1380}\right)^4 = 370.8 \text{ kPa}$$

Free-power turbine: The outlet pressure is 120 kPa, thus

$$T_{o5} = T_{o4}\left[1 - \eta_{ft}\left\{1 - \left(\frac{P_{o5}}{P_{o4}}\right)^{\gamma-1/\gamma}\right\}\right] = 1128.77\left[1 - 0.89\left\{1 - \left(\frac{120}{370.8}\right)^{0.25}\right\}\right]$$

$$T_{o5} = 884.9 \text{ K}$$

The specific power is equal to the specific power available in the free-power turbine as no mechanical looses are considered, thus

$$W_{ft} = \left(1+f\right)C_{Ph}\left(T_{o4} - T_{o5}\right) = 291.35 \text{ kJ/kg}$$

The corresponding thermal efficiency is calculated as follows

$$\eta_{th} = \frac{W_{ft}}{fQ_R} = \frac{291.35}{0.0245 \times 43{,}000} = 0.2765 = 27.65\%$$

Example 8.3

It is required to improve the thermal efficiency of the gas described in Example 8.2 by splitting the compressor into two compressors and adding an *intercooler* in between: a "**CICBTT**" configuration. The delivery pressure of the second compressor is kept at 911.7 kPa , or the same as in Example 8.2. The intercooler pressure is assumed to be the optimum one. Both compressors have the same efficiency (87%). The inlet total temperature of the second compressor is the same as the first compressor (288 K).

Calculate

1. The new value of the fuel-to-air ratio
2. The net specific power
3. The thermal efficiency

Solution

A layout of the engine is shown in Figure 8.18. Since the intercooler operates at the optimum pressure, then

$$P_{02} = \sqrt{P_{01}P_{04}} = 303.9 \text{ kPa} \quad \text{and} \quad \frac{P_{02}}{P_{01}} = \frac{P_{04}}{P_{03}} = \sqrt{\frac{P_{04}}{P_{01}}} = 3$$

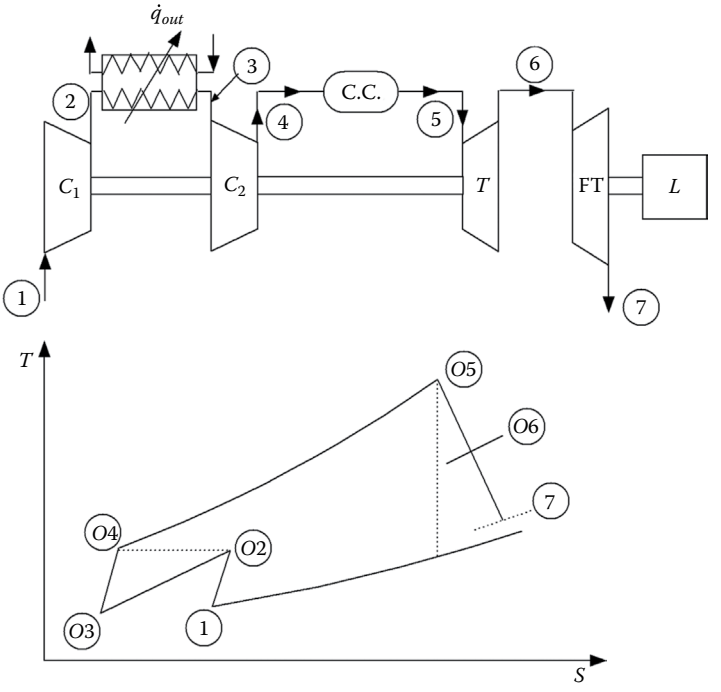


FIGURE 8.18
Layout of a two-spool engine having a free-power turbine and an intercooler.

Compressor (1)

$$T_{02} = T_a\left[1 + \frac{\eta_{c_1}^{\gamma_c - 1/\gamma_c} - 1}{\eta_{c_1}}\right] = 288\left[1 + \frac{3^{0.286} - 1}{0.87}\right] = 410.2 \text{ K}$$

Compressor (2)

$$P_{03} = P_{02} = 303.9 \text{ kPa}$$

Since $T_{03} = T_a$, and $\eta_{c1} = \eta_{c2}$, then

$$T_{04} = T_{02} = 410.2 \text{ K}$$

Combustion chamber: The fuel-to-air ratio is

$$f = \frac{C_{P_h} T_{05} - C_{P_c} T_{04}}{\eta_b Q_R - C_{P_h} T_{05}} = \frac{1.148 \times 1{,}380 - 1.005 \times 410.2}{0.99 \times 43{,}000 - 1.148 \times 1380} = \frac{1{,}172}{40{,}985.8} = 0.0286$$

Gas generator turbine: The turbine here drives both compressors, thus

$$W_t = W_{c_1} + W_{c_2}$$

$$T_{06} = T_{05} - \frac{C_{P_c}\left[T_{04} - T_{03} + T_{02} - T_{01}\right]}{(1+f)C_{P_h}} = T_{05} - \frac{2C_{P_c}(T_{02} - T_a)}{(1+f)C_{P_h}}$$

$$T_{06} = 1380 - \frac{2 \times 1.005 \times (410.2 - 288)}{1.0286 \times 1.148} = 1380 - 208 = 1172 \text{ K}$$

$$\frac{P_{06}}{P_{05}} = \left(1 - \frac{T_{05} - T_{06}}{\eta_t T_{05}}\right)^{\gamma/\gamma-1} = \left(1 - \frac{1380 - 1172}{0.98 \times 1380}\right)^4 = 0.476$$

$$P_{06} = 911.7 \times 0.476 = 434 \text{ kPa}$$

Free-power turbine

$$T_{07} = T_{06}\left[1 - \eta_{ft}\left\{1 - \left(\frac{P_{07}}{P_{06}}\right)^{\gamma-1/\gamma}\right\}\right] = 1276\left[1 - 0.89\left\{1 - \left(\frac{120}{434}\right)^{0.25}\right\}\right] = 963.9 \text{ K}$$

$$W_{ft} = (1+f)C_{P_h}(T_{06} - T_{07}) = 1.0286 \times 1.148 \times (1276 - 963.9) = 368.6 \text{ kJ/kg}$$

$$\eta_{th} = \frac{W_{ft}}{fQ_R} = \frac{368.6}{0.0286 \times 43{,}000} = 0.2996 = 29.96\% \approx 30\%$$

The increase in fuel consumption is $\frac{0.0286 - 0.0245}{0.0245} = 14.3\%$.

While the increase in thermal efficiency is $\frac{30 - 26.76}{26.76} = 12.1\%$.

Example 8.4

A two-shaft industrial gas turbine operates on the *regenerative* cycle. The efficiency of the regenerator is 0.85. The data in Example 8.2 is applied here. Determine

1. The thermal efficiency
2. Fuel-to-air ratio
3. The improvement in thermal efficiency and fuel-to-air ratio

Solution

A layout for the regenerative cycle and its temperature-entropy diagram are shown in Figure 8.19: "**CXBTT**" configuration. From Example 8.2, the following information is known:

State	1	2	3	4	5	6
P_o (kPa)	101.3	911.7	911.7	911.7	364.7	120
T_o (K)	288	577.5	?	1380	1128.8	885

The regenerator efficiency is

$$\varepsilon = \frac{T_{03} - T_{02}}{T_{06} - T_{02}}$$

$$\therefore T_{03} = T_{02} + \varepsilon(T_{06} - T_{02}) = 795.5 \text{ K}$$

$$W_{ft} = 291.35 \text{ kJ/kg}$$

$$f = \frac{C_{P_h}T_{o4} - C_{P_c}T_{o3}}{\eta_b Q_R - C_{P_h}T_{o4}} = \frac{1.148 \times 1{,}380 - 1.005 \times 795.5}{0.99 \times 43{,}000 - 1.148 \times 1{,}380} = 0.091$$

$$\eta_{th} = \frac{W_{ft}}{fQ_R} = \frac{291.35}{0.0191 \times 43{,}000} = 35.47\%$$

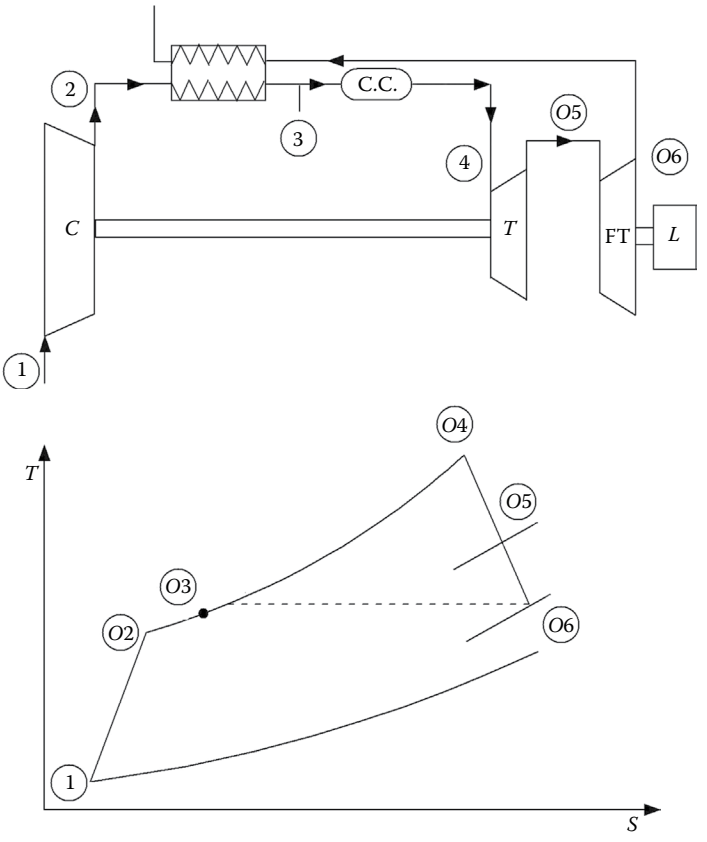


FIGURE 8.19
Two-spool engine with a free-power turbine and regenerator.

The improvement in fuel consumption is $\frac{0.0191 - 0.0245}{0.0245} = -22\%$.
This represents a substantial improvement in fuel consumption.
The improvement in thermal efficiency is $\frac{0.3547 - 0.2676}{0.2676} = 32.6\%$.

Example 8.5

A two-shaft gas turbine engine operates with reheat between the gas turbine and the free-power turbine: "**CBTRT**" configuration. Assuming that the data of the engine is same as in Example 8.2, calculate

1. The net specific power.
2. The fuel-to-air ratio.
3. The thermal efficiency.
4. Compare these values with the basic gas-turbine results in Example 8.2.
5. If the power of the engine is 20 MW, what will be the air mass flow rate?

Solution

A layout and temperature entropy diagram is shown in Figure 8.20.

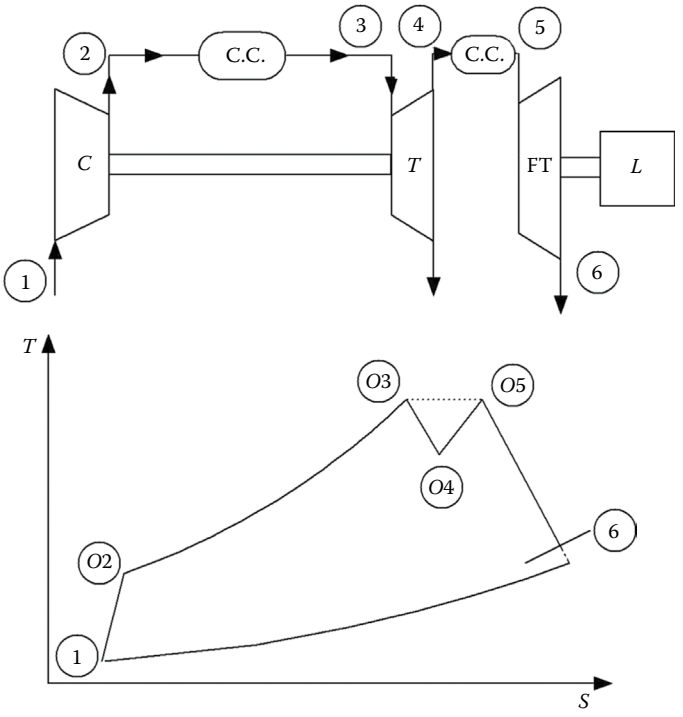


FIGURE 8.20
Two-spool with a free-power turbine and reheat.

Since reheat means adding a new combustor, this means an additional fuel is burnt. The temperature is raised from the outlet temperature of the gas generator 1129 K to turbine inlet temperature, namely, 1380 K. Thus, the additional fuel-to-air ratio is

$$f_1 = \frac{Cp_h\left(T_{05} - T_{04}\right)}{\eta_b Q_R - Cp_h T_{05}} = \frac{1.148\left(1380 - 1129\right)}{0.99 \times 43{,}000 - 1.148 \times 1380} = 0.007$$

$$\therefore \text{Total fuel-to-air ratio} = f + f_1 = 0.0245 + 0.007 = 0.0315.$$

Free-power turbine: Since $P_{05} = P_{04} = 364.68$ kPa

$$T_{06} = T_{05}\left[1 - \eta_{ft}\left\{1 - \left(\frac{P_{06}}{P_{05}}\right)^{\gamma-1/\gamma}\right\}\right]$$

$$T_{06} = 1380\left[1 - 0.89\left\{1 - \left(\frac{120}{364.68}\right)^{0.25}\right\}\right] = 947.6 \text{ K}$$

$$W_{ft} = (1 + f + f_1) C_{P_h} (T_{05} - T_{06}) = 1.0315 \times 1.148 \times (1380 - 947.6) = 512 \text{ kJ/kg}$$

$$\eta_{th} = \frac{W_{ft}}{f_{total} \times Q_R} = \frac{512}{0.0315 \times 43{,}000} = 37.8\%$$

Thus an improvement in thermal efficiency equal to $\frac{37.8 - 26.76}{26.76} = 41.3\%$.

The increase in fuel consumption is $\frac{0.0315 - 0.0245}{0.0245} = 28.6\%$.

For a power of 20 MW, then the air mass flow rate $= \frac{\text{Power}}{W_{ft}} = \frac{20. \times 10^3}{512} = 39$ kg/s.

Summary of the results of the basic and new added modules:

Description	Basic Engine	Regeneration	Intercooling	Reheat
Thermal efficiency (%)	27.65	35.47	30	37.8
Fuel-to-air ratio	0.0245	0.0191	0.0286	0.0315
Net specific power (kJ/kg)	291.35	291.35	368.6	512

8.6 Three Spool

The basic layout of a three-spool gas turbine was previously illustrated in Figure 8.4a and b. In Figure 8.4a three compressors and three turbines are seen. The load is derived by the low-pressure spool. This engine is denoted by "**CCCBTTT**." In Figure 8.4b, two gas turbines drive the corresponding two compressors. The load is driven by the free-power turbine. The engine is denoted by "**CCBTTT**." As described in the single- and double-spool configurations, an intercooler may be added between the compressors: so one intercooler may be added in the layout of Figure 8.4b or two in the configuration of Figure 8.4a. In addition, one or two reheat stages may be added between turbines.

If more than one intercooler is added between the compressors, then, for equal inlet temperature of all compressors, the optimum pressure ratio for each compressor [8] that yields a minimum overall compression work will be given by the relation

$$\pi_{c,stage} = \sqrt[Nc]{\pi_{c,overall}} \tag{8.46}$$

where (Nc) is the number of compressors. Thus for an overall pressure ratio of 27 with three compressors employed, the pressure ratio for each compressor is $\sqrt[3]{27} = 3$ (not 27/3 = 9).

Moreover, if more than reheat stages are used in between turbines, then, for equal inlet temperature for all turbines, the optimum turbine pressure ratio that yields maximum power is given by the relation

$$\pi_{t,stage} = \sqrt[Nt]{\pi_{t,overall}} \tag{8.47}$$

where (Nt) is the number of turbines.

The corresponding maximum specific power for layout of Figure 8.4a, if the compressors have equal efficiencies and the turbines also have equal efficiencies, will be

$$\frac{P}{\dot{m}Cp} = T_{0\max}\eta_t\left(n_{RH}+1\right)\left(1-\frac{1}{\pi_t^{\gamma-1/\gamma}}\right)-T_a\frac{\left(n_{IC}+1\right)}{\eta_C}\left(\pi_c^{\gamma-1/\gamma}-1\right) \tag{8.48}$$

where

n_{RH} is the number of reheat stages
n_{IC} is the number of intercoolers

In Equations 8.47 and 8.48 the working fluid is assumed air with constant properties throughout the thermodynamic cycle.

The rate of heat added is given by the relation

$$\frac{Q}{\dot{m}Cp} = T_{0\max}\left\{\left(n_{RH}+1\right)-\left(n_{RH}+\varepsilon_R\right)\left[1-\eta_t\left(1-\frac{1}{\pi_t^{\gamma-1/\gamma}}\right)\right]\right\} - T_a\left(1-\varepsilon_R\right)\left[1+\frac{\left(\pi_c^{\gamma-1/\gamma}-1\right)}{\eta_C}\right] \tag{8.49}$$

where (ε_R) is the effectiveness of the regenerator installed between the HPC and HPT.

Example 8.6

A three-shaft industrial gas turbine with a free-power turbine is modified by incorporating an intercooler between the two compressors, a regenerator, and a reheater. The intercooler pressure is assumed to be the optimum one. The inlet temperature to the two compressors is 288 K. The inlet pressure to the first compressor is 101.3 kPa. The overall pressure ratio of both compressors is 25. The inlet temperature to both gas turbines is 1500 K. The exhaust pressure is 110 kPa. The pressure drop in the regenerator and first combustor is 2% and 3% of the delivery pressure of the second compressor. The pressure drop in the second combustor is 4% of the delivery pressure of the second gas turbine. Assume equal pressure ratios of both gas turbines. The efficiencies of the different modules are

$$\eta_{c_1}=\eta_{c_2}=88\%,\quad \varepsilon_R=80\%,\quad \eta_{b_1}=\eta_{b_2}=99\%,\quad \eta_{t_1}=\eta_{t_2}=\eta_{ft}=90\%,\quad Q_R=43{,}000\ \text{kJ/kg}$$

Calculate

1. The net power
2. The thermal efficiency

If the power required is 300 MW, what will be the air and fuel mass flow rate?

Consider variable specific heat based on the relation $C_P=950+0.21T_{o1}$, where T_{o1} is the total temperature at the start of the process.

Solution

The three-spool layout with the three elements (intercooler, regenerator, and reheater) together with the temperature-entropy diagram is shown in Figure 8.21, which is denoted by "**CICXBTRTT**."

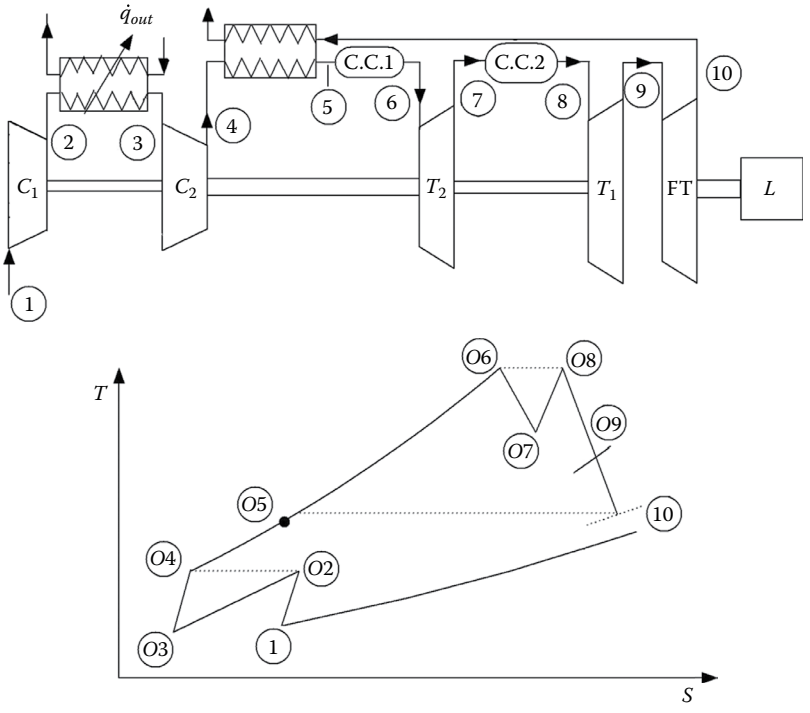


FIGURE 8.21
Three-spool engine with a free-power turbine, intercooler, regenerator, and reheater.

Since the intercooler operates at the optimum pressure, then

$$\frac{P_{02}}{P_{01}} = \frac{P_{04}}{P_{03}} = \sqrt{\frac{P_{04}}{P_{01}}} = \sqrt{25} = 5$$

Compressor (1)

$$C_{P_1} = 950 + 0.21T_{o_1} = 950 + 0.21 \times 288 = 1010.5 \text{ J/kg/K}$$

$$\therefore \frac{\gamma}{\gamma - 1} = \frac{C_{P_1}}{R} = 3.521 \quad \text{and} \quad \frac{\gamma - 1}{\gamma} = 0.284$$

$$\therefore T_{02} = T_a\left[1 + \frac{5^{0.286} - 1}{0.88}\right] = 477.6 \text{ K}$$

$$P_{02} = 5P_{01} = 506.5 \text{ kPa}$$

Compressor (2): Since $T_{03} = T_{01}$, then the same values for C_P and γ as compressor (1) are obtained.

Also $T_{04} = T_{02} = 477.6$ K

$$P_{03} = P_{02} = 506.5 \text{ kPa} \quad \text{and} \quad P_{04} = 5P_{03} = 2532.5 \text{ kPa}$$

Gas turbine (2): Turbine (2) is driving the compressor (2) and together they form the high-pressure spool.

$$P_{06} = P_{04}\left(1 - \Delta P_R - \Delta P_{CC_1}\right) = 2532.5\left(1 - 0.02 - 0.03\right) = 2405.9 \text{ kPa}$$

Moreover

$$Cp_6 = Cp_8 = 950 + 0.21 \times 1200 = 1265 \text{ J/kg/K},$$

$$\left(\frac{\gamma}{\gamma - 1}\right)_6 = \left(\frac{\gamma}{\gamma - 1}\right)_8 = 4.4$$

Energy balance for both compressors and turbines forming the low- and high-pressure spools gives

$$W_{C_1} + W_{C_2} = W_{t_1} + W_{t_2}$$

$$\begin{aligned} 2Cp_1\left(T_{02} - T_{01}\right) &= Cp_6\left(T_{06} - T_{07}\right) + Cp_8\left(T_{08} - T_{09}\right) \\ &= \eta_t Cp_6 T_{06}\left[\left(1 - \frac{1}{\pi_{t_1}^{(\gamma-1/\gamma)_6}}\right) + \left(1 - \frac{1}{\pi_{t_2}^{(\gamma-1/\gamma)_8}}\right)\right] \end{aligned}$$

For a maximum power available from the turbines, both turbines must have equal pressure ratios

$$\pi_{t_1} = \pi_{t_2} = \pi_t$$

Solving to get

$$\pi_t = 1.688$$

The outlet turbine from the high-pressure turbine is then

$$P_{07} = \frac{P_{06}}{\pi_t} = 1425.3 \text{ kPa}$$

$$T_{07} = T_{06}\left[1 - \eta_{t_1}\left\{1 - \left(\frac{1}{\pi_t}\right)^{(\gamma-1/\gamma)_6}\right\}\right] = 1500\left[1 - 0.9\left\{1 - \left(\frac{1}{1.688}\right)^{0.227}\right\}\right] = 1348 \text{ K}$$

Gas turbine (1): The inlet pressure is

$$P_{08} = P_{07}\left(1 - \Delta P_{cc_2}\right) = 1423.6 \times 0.96 = 1294.5 \text{ kPa}$$

The outlet pressure is

$$P_{09} = \frac{P_{08}}{\pi_t} = 766 \text{ kPa}$$

The outlet temperature is then

$$T_{09} = T_{08}\left[1 - \eta_{t_2}\left\{1 - \left(\frac{1}{\pi_t}\right)^{(\gamma-1/\gamma)_8}\right\}\right] = 1348 \text{ K}$$

Free-power turbine

$$Cp_9 = 950 + 0.21 \times 1348 = 1233 \text{ J/kg/K}, \quad \left(\frac{\gamma}{\gamma - 1}\right)_9 = 4.296$$

$$T_{010} = T_{09}\left[1 - \eta_{ft}\left\{1 - \left(\frac{T_{010}}{T_{09}}\right)^{(\gamma-1/\gamma)_9}\right\}\right] = 1348\left[1 - 0.9\left\{1 - \left(\frac{110}{766}\right)^{0.233}\right\}\right] = 906.7 \text{ K}$$

$$W_{net} = Cp_9\left(T_{09} - T_{010}\right) = 1233\left(1348 - 906.7\right) = 544 \text{ kJ/kg}$$

Regenerator

$$\varepsilon_R = \frac{T_{05} - T_{04}}{T_{010} - T_{04}}$$

$$T_{05} = T_{04} + \varepsilon_R\left(T_{010} - T_{04}\right) = 477.6 + 0.8\left(906.7 - 477.6\right) = 820.9 \text{ K}$$

$$Cp_5 = 950 + 0.21 \times 820.9 = 1122.4 \text{ J/kg/K}$$

First combustor: The fuel-to-air ratio in the first combustor

$$f_1 = \frac{Cp_6 T_{06} - Cp_5 T_{05}}{\eta_b Q_R - Cp_6 T_{06}} = \frac{1.265 \times 1,500 - 1.1224 \times 820.9}{0.99 \times 43,000 - 1.265 \times 1,500} = 0.02399$$

$$Cp_7 = 950 + 0.21 \times 1348 = 1233 \text{ J/kg/K}$$

Second combustor: The fuel-to-air ratio in the second combustor

$$f_2 = \frac{Cp_8 T_{08} - Cp_7 T_{07}}{\eta_b Q_R - Cp_8 T_{08}} = \frac{1.265 \times 1,500 - 1.233 \times 1,348}{0.99 \times 43,000 - 1.265 \times 1,500} = 0.0058$$

The total fuel-to-air ratio $f_{total} = f_1 + f_2 = 0.02977$.

For a power of 300 MW, the needed air mass flow rate is

$$\dot{m} = \frac{Power}{\left(1 + f_{total}\right)W_{net}} = \frac{300 \times 10^3}{544 \times 1.0298}$$

$$\dot{m} = 535.5 \text{ kg/s}$$

Example 8.7

Consider an aeroderivative gas turbine that is developed from the turbofan engine described in Example 5.3. The fan is removed and the by-pass duct of the engine is cancelled. The gases leaving the intermediate-pressure turbine (IPT) are used to drive a power turbine, which in turn drives the load as shown in Figure 8.22. The efficiency of

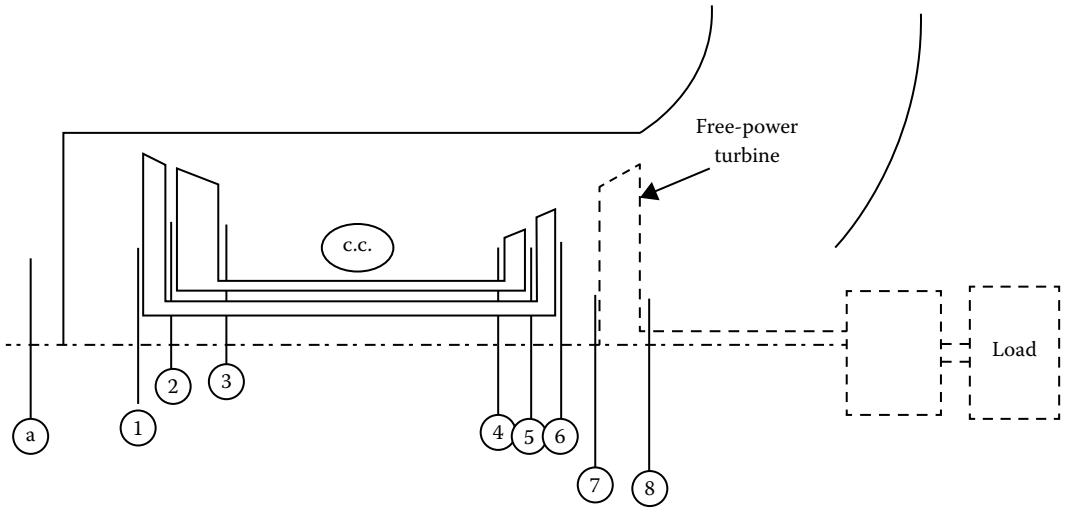


FIGURE 8.22
Aeroderivative engine.

the free-power turbine is $\eta_{Ft} = 0.9$. Calculate the power delivered to the load. All other data are kept the same as in the previous example.

Solution

Inlet mass flow to the whole engine

$$\dot{m}_a = 100 \text{ kg/s}, \quad P_{o1} = P_a = 1.0 \text{ bar}, \quad T_{o1} = T_a = 288 \text{ K}$$

1. Air inlet

$$T_{01} = T_a = 288 \text{ K}, \quad P_{o1} = P_a = 1.0 \text{ bar},$$

2. Intermediate pressure compressor

$$P_{02} = \pi_{LPC} \times P_{01} = 5 \times 1.0 = 5.0 \text{ bar}$$

$$T_{02} = T_{01}\left(1 + \frac{\pi_{IPC}^{\gamma-1/\gamma} - 1}{\eta_{IPC}}\right) = 288 \times 1.656 = 477.2 \text{ K}$$

3. HPC

$$P_{03} = \pi_{\text{HPC}} \times P_{04} = 5 \times 5 = 25 \text{ bar}$$

$$T_{03} = T_{02}\left\{1 + \left[\frac{\pi_{HPC}{}^{\gamma-1/\gamma} - 1}{\eta_{HPC}}\right]\right\} = 477.2\left\{1 + \left[\frac{(5)^{0.286} - 1}{0.90}\right]\right\} = 477.2 \times 1.6489 = 787 \text{ K}$$

4. Combustion chamber
   For all the hot elements including the combustion chamber, turbines, and nozzles

$$\gamma = 1.33, Cp = 1.147 \text{ kJ/kg k}$$

Energy balance of combustion chamber: A bleed from the outlet of the high pressure compressor is considered here

$$\text{with } b = \dot{m}_b/\dot{m}_a \quad \text{and} \quad f = \dot{m}_f/\dot{m}_a$$

$$\dot{m}_a\left[(1-b)Cp_a T_{03}\right] + \eta_{cc}\dot{m}_f Q = \left[(1-b)\dot{m}_a + \dot{m}_f\right]C_{pg}T_{04}$$
$$(1-b)Cp_a T_{05} + \eta_{cc} fQ = (1+f-b)Cp_g T_{06}$$

$$T_{04} = \left[(1-b)Cp_a T_{03} + \eta_{cc} fQ\right]/\left[(1+f-b)Cp_g\right] = 1359.4 \text{ K}$$
$$P_{04} = 0.98\,P_{03} = 0.98 \times 25 = 24.5 \text{ bar}$$

5. HPT

$$\eta_m W_{HPT} = W_{HPT}$$

$$\eta_m \dot{m}_{hot} Cp_g\left(T_{04} - T_{05}\right) = \dot{m}_a Cp_a\left(T_{03} - T_{02}\right)$$

$$\dot{m}_{hot} = (1+f-b)\dot{m}_a = 0.9977\,\dot{m}_a$$
$$\Delta T_{0_{45}} = T_{04} - T_{05} = \frac{Cp_a\left(T_{03} - T_{02}\right)}{0.9977 \times \eta_m \times C_{pg}} = \frac{1.005(787 - 477.2)}{0.9977 \times 0.99 \times 1.147} = 274.82 \text{ K}$$
$$T_{05} = T_{04} - \Delta T_{0_{45}} = 1084.6 \text{ K}$$
$$P_{05} = P_{04}\left[1 - \frac{\left[1 - \left(T_{05}/T_{04}\right)\right]}{\eta_{HPT}}\right]^{\gamma_g/\gamma_g - 1} = 24.5\left[1 - \frac{\left[1 - \left(1084.6/1359.4\right)\right]}{0.9}\right]^{1.33/0.33} = 8.855 \text{ bar}$$

6. Intermediate-pressure turbine: From energy balance

$$\eta_m W_{IPT} = W_{IPC}$$

$$\eta_m \dot{m}_{hot} Cp_g\left(T_{05} - T_{06}\right) = \dot{m}_a Cp_a\left(T_{02} - T_{01}\right)$$

$$\Delta T_{o_{56}} = \frac{Cp_a\left(T_{02} - T_{01}\right)}{0.9977 \times \eta_m \times C_{pg}} = \frac{1.005(477.2 - 288)}{0.9977 \times 0.99 \times 1.147} = 167.84 \text{ K}$$
$$T_{06} = T_{05} - \Delta T_{0_{56}} = 1084.6 - 167.84 = 916.76 \text{ K}$$
$$P_{06} = P_{05}\left[1 - \frac{\left[1 - \left(T_{06}/T_{05}\right)\right]}{\eta_{IPT}}\right]^{\gamma_g/\gamma_g - 1} = 0.47 \quad P_{05} = 4.1632 \text{ bar}$$

Expansion in the power turbine to ambient pressure

$$T_7 = T_{06}\left\{1 - \eta_{ft}\left[\left(\frac{P_{07}}{P_8}\right)^{\gamma_h - 1/\gamma_h} - 1\right]\right\} = 916.7\left\{1 - 0.9\left[(4.1632)^{0.25} - 1\right]\right\} = 563.2 \text{ K}$$

The power delivered to the load = $\mathscr{P}$

$$\mathrm{P} = \dot{m}_a(1+f-b)Cp_g\left(T_{07} - T_8\right) = 100 \times 0.997 \times 1.147(916.76 - 563.2) = \mathscr{P} = 40{,}340 \text{ kW} = 40.34 \text{ MW}$$

8.7 Combined Gas Turbine

Though gas-turbine cycles have a greater potential for higher thermal efficiencies because of the higher average temperature at which gas is supplied, they have an inherent disadvantage; namely, the gas leaves the gas turbine at very high temperatures (usually above 500 °C), which wipes out any potential gains from the thermal efficiency. The continued quest for higher thermal efficiencies has resulted in rather innovative modifications to conventional powerplants. A popular modification is to use the high-temperature exhaust gases of the gas turbine as the energy source for bottoming such steam power cycle. Thus, the suggested powerplant here is a gas-powered cycle topping a vapor-powered cycle, which is called the *combined gas-vapor cycle*, or just the combined cycle. The combined cycle of greatest interest is the gas-turbine (Brayton) cycle topping a steam-turbine (Rankine) cycle, which has a higher thermal efficiency than either of the cycles executed individually.

Gas-turbine cycles typically operate at considerably higher temperatures than steam cycles. The maximum fluid temperature at the turbine inlet is about 620 °C (1150 °F) for modern steam powerplants, but over 1150 °C (2100 °F) for gas-turbine powerplants. The use of higher temperatures in gas turbines is made possible by recent developments in cooling the turbine blades and coating them with high-temperature-resistant materials such as ceramics. A combined gas-turbine-Rankine cycle may be implemented in several ways. The open-cycle gas turbine may be linked to a steam cycle through what may be considered a gas-turbine heat exchange containing an economizer and a boiler. This combined gas-steam plant is called a heat-recovery steam generator (HRSG), which is shown in Figure 8.23. The T-S diagram for the steam-bottoming cycle is shown in Figure 8.24. In this cycle, the energy is recovered from the exhaust gases by transferring it to the steam in the heat exchanger that serves as the boiler.

Assuming constant specific heat for the gases leaving the turbine, then the energy balance gives

$$\dot{m}_s\left(h_{12}-h_{11}\right)=\dot{m}_g Cp_g\left(T_{06}-T_{07}\right)=\dot{m}_s A_1 \tag{8.50}$$

$$\dot{m}_s\left(h_{13}-h_{12}\right)=\dot{m}_g Cp_g\left(T_{05}-T_{06}\right)=\dot{m}_s A_2 \tag{8.51}$$

$$\dot{m}_s\left(h_{8}-h_{13}\right)=\dot{m}_g Cp_g\left(T_{04}-T_{05}\right)=\dot{m}_s A_3 \tag{8.52}$$

where $\dot{m}_s$ and $\dot{m}_g$ are the steam and gas mass flow rates. Combining Equations 8.50 through 8.52 gives

$$\dot{m}_s\left(h_{8}-h_{11}\right)=\dot{m}_g Cp_g\left(T_{04}-T_{07}\right)=\dot{m}_s\left(A_1+A_2+A_3\right) \tag{8.53}$$

The total power from the combined cycle is $W_{gt}+W_{st}$ while the heat input is only from the gas turbine (Q) which is unchanged. The overall efficiency is then given by

$$\eta=\frac{W_{gt}+W_{st}}{Q}$$

The combined cycle increases the efficiency without appreciably increasing the initial cost. Consequently, many new powerplants operate on combined cycles, and many more existing steam- or gas-turbine plants are being converted to combined-cycle powerplants. Thermal efficiencies well over 40% are reported as a result of conversion.

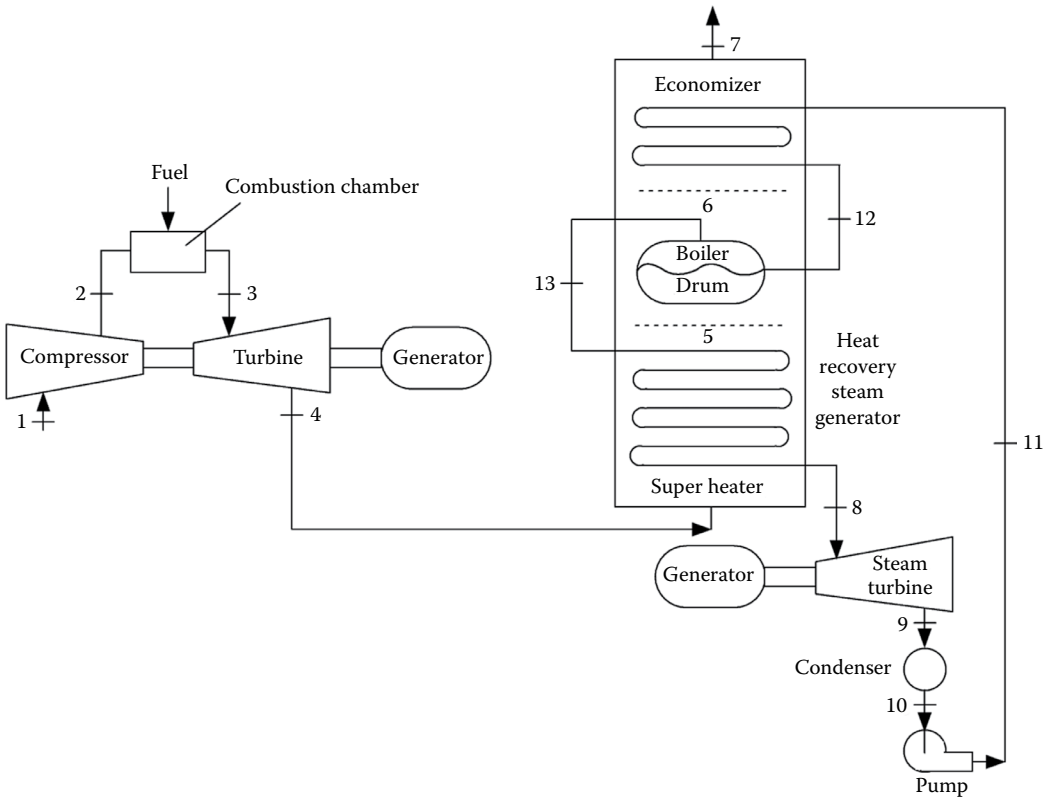


FIGURE 8.23
Combined cycle gas and steam turbines.

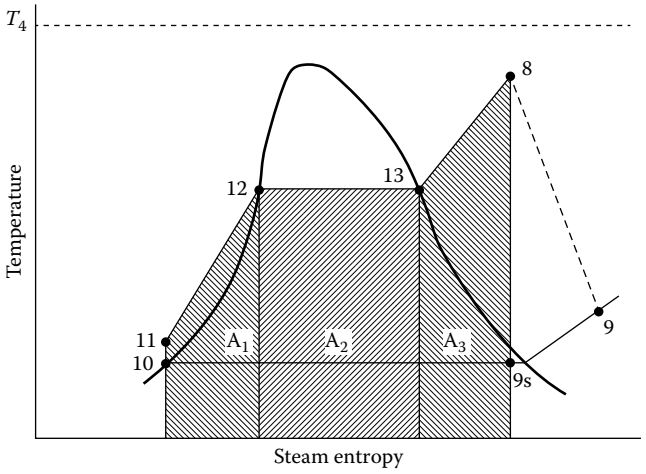


FIGURE 8.24
Temperature-entropy diagram for steam-bottoming cycle.

8.8 Marine Applications

The marine gas turbine like most of the engines used for marine propulsion is usually an adaptation of a machine that was originally developed for some other purpose. The aeroderivative gas turbine is a prominent example, whereby aircraft-derivative gas-turbine engines are used for both main propulsion and the ship's service electrical power. A high degree of plant automation is achieved with an integrated system of control and monitoring consoles.

A wide range of vessels are powered by marine gas-turbine engines ranging from modest-sized pleasure craft requiring several hundred horsepower, to major naval vessels and the largest merchant ships, which may require 20,000–50,000 horsepower by shaft [9]. These vessels belong to the following categories: merchant ships, coastguard vessels, naval vessels, and small craft.

The advantages of a gas-turbine plant as compared to a steam plant of comparable horsepower include

1. Weight reduction of 70%
2. Simplicity (fewer propulsion auxiliaries)
3. Reduced manning due to automated propulsion plant control
4. Quicker response time
5. Faster acceleration/deceleration

The load to be driven by a marine propulsion engine is usually a screw propeller, a jet pump, and an electrical generator or a hydraulic pump. The load changes rapidly in maneuvering situations, especially when an emergency stop is required. The gas turbine is the optimum choice that satisfies these requirements due to its small inertia of the moving part compared to diesel engines. Moreover, for a rearward motion of the vessel, the propulsion load must be reversed. Gas turbines use some auxiliary methods to satisfy this requirement such as reversing the propeller pitch or using a reverse train in the reduction gear.

Marine gas turbines operate in a wet and salty environment. Vessel motions have widely ranging magnitudes and frequencies. Air sucked into the compressor is wet with salty sprays that may leave deposits on the engine with consequent corrosive effects and obstruction of air passages. Moreover, the products of combustion have a polluting effect on the surrounding environment.

There are two types of gas turbines used in marine applications; namely, the single-shaft engine (as an example Allison 501-K17 engine) and the two-spool engine. This two-spool type is sometimes known as a split-shaft engine. An example of the latter type is the General Electric LM2500. The power turbine is aerodynamically coupled to the gas generator but the two shafts are not mechanically connected. The power turbine converts the thermal energy from the gas generator to mechanical energy to drive the load. The output speed is varied by controlling the speed of the gas generator, which determines the amount of exhaust gases sent to the power turbine. Split-shaft gas-turbine engines are suitable for main propulsion applications. The advantages in this application are

1. The gas generator is more responsive to load demands because the compressor is not restricted in operation by the load on the power turbine.
2. The gas-generator section and the power-turbine section operate near their most efficient speeds throughout a range of load demands.

To cope with environmental protection, extensive research is also performed to design super-marine gas turbines in a variety of ship classes that develop a low NO_x (below 1 g/kWh) and high efficiency (at least 38%) and for the application of marine diesel oil [10] gas turbines. The engine is a two-split-shaft gas turbine consisting of a gas generator and the power system, and incorporating a regenerative (recuperator) unit.

8.8.1 Additional Components for Marine Applications

For naval applications, gas turbines have the same components as described previously. However, three important components (modules) are added, namely, the *intake* and *exhaust systems*, and the *propeller*. Gas turbines use a high rate of air, nearly 5 $ft^3/hp \cdot min$, which is roughly twice that of diesels. This large mass flow rate means high velocity and high pressure drop, and an increase of salt-laden droplets of sea spray. Other requirements for inlet and exhaust systems are silencing, avoidance of reingestion or injection into the intake, and finally keeping the hot exhaust gases away from the wooden structure of the vessel if applicable.

As shown in Figure 8.25, the *intake system* is composed of the following elements: high-hat assembly, intake duct, anti-icing manifold, silencers, and expansion unit. The *high-hat assembly* supports the moisture separators that remove water droplets and dirt from the intake air to prevent erosion of compressor components. Electric-strip heaters prevent ice formation on the louvers. In addition, it houses the blow-in door that prevents engine air starvation when the moisture separators become dirty [11].

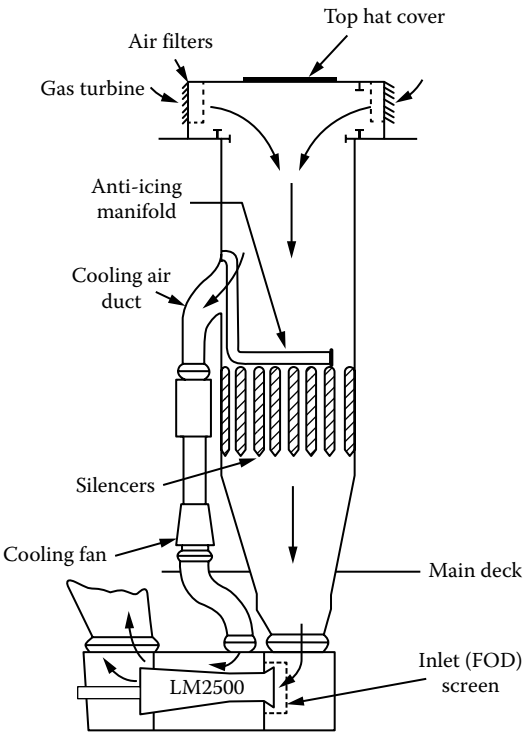


FIGURE 8.25
A typical intake system for a marine gas turbine.

The *intake duct* provides combustion air for the engine and cooling air for the module. The module-cooling system routes a portion of the intake air to the engine enclosure for module ventilation and external engine cooling. The module cooling air swirls about the engine removing heat and ventilating the module before exiting via a small air gap around the aft end of the power turbine. The *anti-icing manifold* injects hot bleed air into the intake trunk, below the module cooling air duct, to prevent ice formation that may occur when the outside air temperature drops to 38°F. Icing at the compressor inlet can restrict airflow causing a stall and also presents a serious foreign-object damage hazard to the engine. *Intake silencers* are located halfway down the intake duct to reduce airborne noise. The silencers consist of vertical vanes of sound-deadening material encased in perforated stainless-steel sheets. The module-cooling air duct contains a single bullet-shaped silencer to silence the noise created by the cooling air. The *expansion joint* is a rubber boot connecting the intake duct to the module inlet plenum. This prevents the noise of the module from being transmitted to the hull of the ship.

The *exhaust-duct system* routes engine exhaust gases to the atmosphere while reducing both the heat and noise of the exhaust (Figure 8.26). It is composed of an exhaust collector, uptake ducting, silencing, exhaust eductors, and a boundary-layer infrared suppression system (BLISS). The *exhaust elbow* directs exhaust gases into the exhaust-uptake duct. A gap between the exhaust elbow and ship's uptake causes an *eductor* effect, drawing module-cooling air into the exhaust uptake. Exhaust-uptake ducting is insulated to control heat and noise as the exhaust is passed to the atmosphere. A vane-type *silencer* is located in the center of the duct. These silencers are the same as those in the intake ducting but are permanently mounted. Exhaust eductors are located at the uppermost end of the exhaust ducting. It cools the exhaust gases by mixing them with cool ambient air to reduce the infrared signature of the ship. *Bliss* caps are installed on the top of each mixing tube to further cool the exhaust air by mixing it with layers of ambient air. This is accomplished by the use of several louvers that are angled to create an eductor effect. This allows cool ambient air to mix with the hot exhaust gases.

The *propeller* in a marine gas turbine is similar to the propeller in turboprop engines. It is the propulsor element that converts the mechanical energy into thrust power. First, the gas turbine converts the thermal energy into mechanical energy. Next, the transmission system transmits the mechanical energy to its point of use. It often includes a speed-reducing gear set and may include clutches, brakes, and couplings of various types. The propulsor is most often the familiar screw propeller. The propeller is either of the fixed or variable-pitch type. The rotational speed of the propeller is proportional to the vessel speed. The propeller torque and power are proportional to the square and cube of its rotational speed, respectively.

8.8.2 Examples for Marine Gas Turbines

1. General Electric LM2500: It has various series of somewhat different power;—LM2500PE (22,346 kW), LM2500PH (26,463 kW), LM2500RC (32,916 kW), LM2500RC (35,842 kW), and LM2500RD (32,689 kW).
   Figure 8.27 illustrates the details of the LM2500. A brief description of the LM2500 is given here.
   a. Gas generator components
      Compressor section: The LM2500 has a 16-stage axial-flow compressor (17 for the advanced LM2500+). The compressor casing contains one stage of inlet guide vanes (IGV), followed by six stages of variable stator vanes (VSV) to prevent compressor stall, and finally 10 stages of stationary stator vanes. Bleed air is extracted from the compressor for use in the ship's bleed-air system and for internal use in the engine.

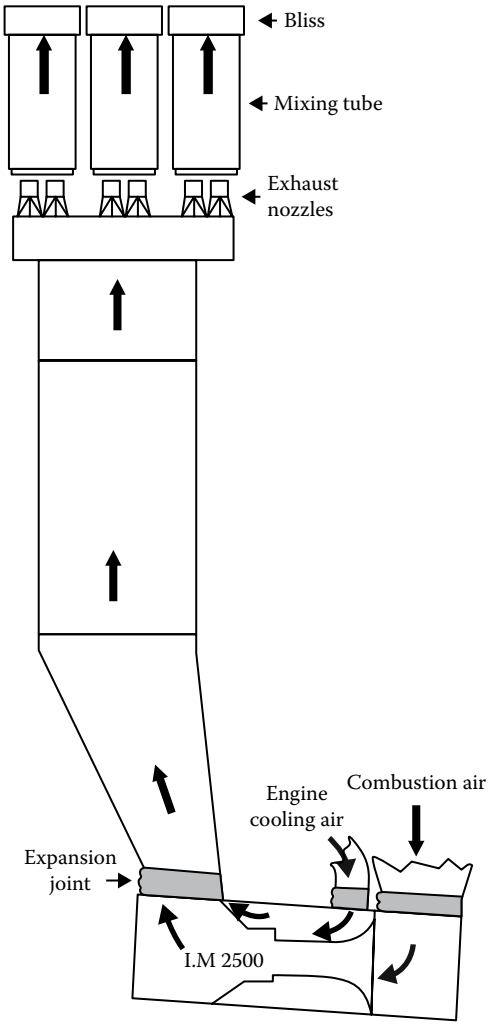


FIGURE 8.26
A typical exhaust system for a marine engine.

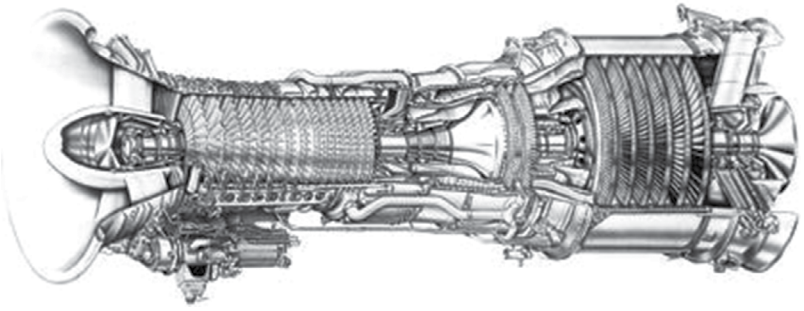


FIGURE 8.27
LM2500. (Courtesy of General Electric Energy. http://www.fi-powerweb.com/Engine/Industrial/GE-LM2500.html.)

Combustor: The combustor is an annular type with 30 fuel nozzles and 2 spark ignitors. Of the air from the compressor, approximately 30% is mixed with fuel to support combustion. The other 70% is used to cool and center the flame within the combustion liner.

HPT section: The HPT is a two-stage axial-flow type. It uses approximately 65% of the thermal energy from the combustor to drive the compressor and engine-mounted accessories.

b. Power turbine
The power turbine is a six-stage axial-flow type turbine. It extracts the remaining 35% of useable energy and uses this to drive the main reduction gear through a high-speed flexible-coupling shaft and clutch assembly. Depending on the series, the power-to-weight ratio ranges from 5.86 to 5.95 kW/kg, the power-to-footprint ranges from 2019 to 2310 kW/m^2, and the specific fuel consumption is from 200 to 215 (g/(kW·h)).

2. Rolls Royce MT30 [12]
This turbine delivers a broad range of available power for commercial marine and naval applications in an exceptionally lightweight package. It is derived from the Trent 800, which efficiently powers the Boeing 777 aircraft. Its power is 36 MW at 26°C. The MT30 is also designed to burn commercially available distillate fuels, giving a high degree of flexibility and associated through-life cost benefits. It is a twin-spool high-pressure ratio gas generator with an eight-stage variable geometry intermediate pressure compressor and a six-stage HPC. Both intermediate-pressure and high-pressure turbines have only one stage. The four-stage free-power turbine is derived from the Trent 800, incorporating the latest cooling technique. The key parts are protectively coated for service in the marine environment to reduce maintenance and ensure a long service life. The annular combustor, similar to its parent aeroengine, is employed to meet all current and anticipated legislation on emission and smoke. The gas-turbine change unit includes the power turbine and weighs 6200 kg (dry).

Table 8.2 outlines a comparison between gas turbine and diesel engines. The values given represent average values. The comparison is in favor of gas turbines if the power per weight and power per footprint are examined. Diesel engines have better specific fuel consumption. The difference in fuel consumption decreases as the power rating increases.

TABLE 8.2

Comparison between Gas Turbine and Diesel Engines Used in Marine Applications

Power Rating (MW)		**5–10**	**10–20**	**20–30**	**30–40**
Power/weight (kW/kg)	GT	4.0	3.5	3.0	2.9
	Diesel	0.3	0.2	0.15	0.15
Power/footprint (kW/m^2)	GT	1000	1100	1500	1750
	Diesel	250	250	250	250
SFC (g/(kW·h))	GT	240	210	200	195
	Diesel	190	175	170	168

Source: Gee, N., Fast Ferry powering and propulsors: The options, http://www.ngal.co.uk/downloads/techpapers/paper7.pdf.

8.9 Offshore Gas Turbines

Gas turbines are widely used offshore for a variety of purposes, including power generation, gas and water injection, pumping, gas lift, and export compression. Gas turbines have been adapted in place of diesel-generation systems on a significant number of platforms because they can be locally powered (self-fueled); and since 70% of the operational costs are in fuel, they can be very cost effective on a platform where the gas supply comes at well-head prices. Moreover, since they are lightweight (and thus have a high power-to-weight ratio) and compact in size, gas turbines are well suited to such tasks. In addition, availability, reliability, and ruggedness are additional key factors for selecting gas turbines as offshore powerplants. The only operational constraints are on efficiency, as there is no combined-cycle efficiency gain [14].

Aeroderivative gas turbines are increasingly favored offshore because of the requirements for low weight, simple change-out, and ease of maintenance. For example the GE LM series is now favored over General Electric's older industrial frame series. Industrial gas turbines of a compact modular system utilizing aerospace rotor technology are very different from the earlier bulkier technology commonly used in onshore power generation.

Factors that need to be considered in designing turbines offshore include weight and dimensions, minimizing vibration, resistance to saltwater, and resistance to pitch and roll—particularly in floating installations. They are prone to material degradation: corrosion, environmental attack, erosion, oxidation, and foreign object damage. For these reasons, turbines are made of Nimonic alloys, while Co-Ni-based alloys are used in compressors. Ceramics have been used in some Rolls-Royce designs [15]. Offshore engines are either single-shaft or two-shaft gas turbines.

Offshore main gas-turbine suppliers are Rolls-Royce (RB211, Avon, Coberra), Solar Turbines (Saturn, Mars, Titan), General Electric (GE Industrial Gas Turbine, Nuovo Pigneone, Partners like John Brown), Siemens-Westinghouse, Pratt & Whitney, ABB, Allison, Dresser, and MAN.

8.10 Micro-Gas Turbines (μ-Gas Turbines)

Though micro-gas turbines are defined as those generating less than 350 kW power [16], the same name has been extensively used recently for gas turbines whose dimensions are of the order of centimeters. The current trend toward miniaturization, portability, and ubiquitous intelligence has led to the development of a wide range of new tiny products. The power units appropriate for such products may be fuel cells, thermo-electric devices, combustion engines, and gas turbines. While fuel cells are expected to offer the highest efficiency, micro-gas turbines are expected to offer the highest power density. The gas turbine was invented in the twentieth century and micro-gas turbines are considered the key to powering twenty-first-century technology. Though no bigger than a regular shirt button, a micro-gas-turbine engine uses the same process for power generation as its big brother powerplant. Numerous research work was performed in the last decade for micro-gas turbines. Extensive work for design, development, and production of micro-gas turbines is carried out in many institutions worldwide. Epstein [17] and his coworkers in MIT (USA) finished making micro-gas-turbine engines, in which each of the individual parts

functions; inside a tiny combustion chamber, fuel and air quickly mix and burn at the melting point of steel. Turbine blades (spanning an area less than a dime) made of low-defect, high-strength, micro-fabricated materials spin at 20,000 revolutions per second—100 times faster than those in jet engines. A mini-generator produces 10 W of power. A little compressor raises the pressure of air in preparation for combustion. And cooling (always a challenge in hot micro devices) appears manageable by sending the compression air around the outside of the combustor. The resulting device is sealed all around, with holes on the top and bottom for air intake, fuel intake, and exhaust.

8.10.1 Micro- versus Typical-Gas Turbines

The main difference between a small and a large gas turbine is the amount of gas submitted to an almost unchanged thermodynamic cycle. Velocity and pressure levels remain the same when scaling down a gas turbine. Only the dimensions are smaller. The work exchange between the compressor or turbine and the fluid is proportional to the peripheral speed, such that the rotational speed should scale inversely proportional to the diameter, resulting in speeds of more than 500,000 rpm for rotor diameters below 20 mm.

A major problem with miniaturization of micro-turbines is a large decrease in Reynolds number, resulting in higher viscous losses and a lower overall cycle efficiency.

Also the required temperature is a problem. As a pressure ratio of 3 is envisaged, the turbine inlet temperature should be at least 1200 K to obtain positive cycle efficiency, and higher temperatures would considerably boost the overall efficiency. In large turbines, the blades are cooled by internal cooling channels and protected by thermal barrier coatings. In the case of micro-turbines, internal cooling of blades a few millimeters in size is unrealistic. Therefore, temperatures of 1200 K and higher can only be reached with ceramic materials.

Another major consequence of the small dimensions is the extreme temperature gradient between the hot turbine and colder compressor. The resulting massive heat flux provokes a non-negligible decrease of both compressor and turbine efficiency.

A gas turbine net power output is the small difference between the large turbine power output and the large compressor energy requirements. The deterioration of aero-performance of the components with decreasing dimensions and increased heat transfer results in a larger decrease of power output and cycle efficiency. Therefore, careful optimization is needed to also guarantee positive output at the smallest dimensions. However, little knowledge is available on aero-thermodynamics at these small scales. There is also no guarantee that the existing flow-solvers and turbulence models are still accurate for these extremely low Reynolds numbers [18].

8.10.2 Design Challenges

8.10.2.1 Manufacturing

Gas turbines are amongst the most advanced systems as they combine extreme conditions in terms of rotational speed with elevated gas temperatures (up to 2100 K for military engines). Miniaturization of such a system poses tremendous technical problems as it leads to extremely high rotational speeds (e.g., 10^6 rpm). Moreover, scaling down the system unfavorably influences the flow and combustion process. Fabricating such devices requires new materials to be explored (such as Si_3N_4 and SiC) and also requires three-dimensional micro manufacturing processes. Combining "best-of-both-worlds," that is, photolithographic micromanufacturing techniques with more traditional micromechanical manufacturing will be essential for reaching the envisaged objectives.

8.10.2.2 Selection and Design of Bearings

The bearings must operate throughout the whole range of possible temperature conditions during startup and in steady state operation. Maximum temperatures between 100°C and 1000°C can be expected depending on the exact location of the bearings. Rotor imbalance can result in dangerously high dynamic radial loading, and, therefore, the eccentricity of the mass center should be balanced within a few micrometers.

It is clear that conventional ball bearings are not feasible for these sorts of speed and temperature. Magnetic bearings could offer a solution regarding speed, but the high temperature dissuades the use of permanent magnets as these could demagnetize. Consequently, such bearings should be constructed with electromagnets, which consume a considerable amount of electrical energy.

Air bearings seem most suited for this application. Aerostatic as well as aerodynamic ones can be used. Aerostatic bearings can be fed by tapping a small amount of compressed air from the compressor. This results in problems at startup and moreover decreases the overall efficiency.

Aerodynamic bearings are self-pressurizing and therefore need no external supply. However, the phase of dry friction during startup is a major drawback. Additionally, self-excited instabilities (half-speed whirl) limit the maximum attainable speed. Nevertheless, aerodynamic bearings are the most promising choice on condition that the issue of instability is tackled.

Several stabilizing techniques exist, but most promising for this application are bearings with conformable surfaces—more specifically, aerodynamic foil bearings. These bearings are virtually immune to half-speed whirl and suffer less from centrifugal and thermal rotor growth. Several research work focuses on designing new foil bearing concepts, suitable for small dimensions [18].

8.10.2.3 Compressor and Turbine

As stated before, the efficiency of all components is critical. This is especially true for the compressor and turbine, requiring efficiencies of at least 60%–70%. Thus, it is clearly a challenge to obtain the required efficiency despite the low Reynolds numbers, increased heat transfer, and lower relative geometric accuracy of the components. Manufacturers of 3D micro-impellors with sufficiently high accuracy and low roughness [18] face various technical problems.

8.10.3 Applications

1. Electric generation

   The micro-gas turbine developed [18] will be in the cm range (2 cm diameter and 5 cm long) and will produce a power output of about 100 W. The system basically consists of a compressor, regenerator, combustion chamber, turbine, and electrical generator, as illustrated in Figure 8.28.

   Generally micro-gas turbines can produce enough electricity to power handheld electronics. In the foreseeable future, these tiny turbines will serve as a battery replacement. They could run for ten or more hours on a container of diesel fuel slightly larger than a D battery; when the fuel cartridge runs out, a new one can easily replace it. Each disposable cartridge would pack as much energy as a few heavy handfuls of lithium-ion batteries. As a result, a small pack of the cheap and

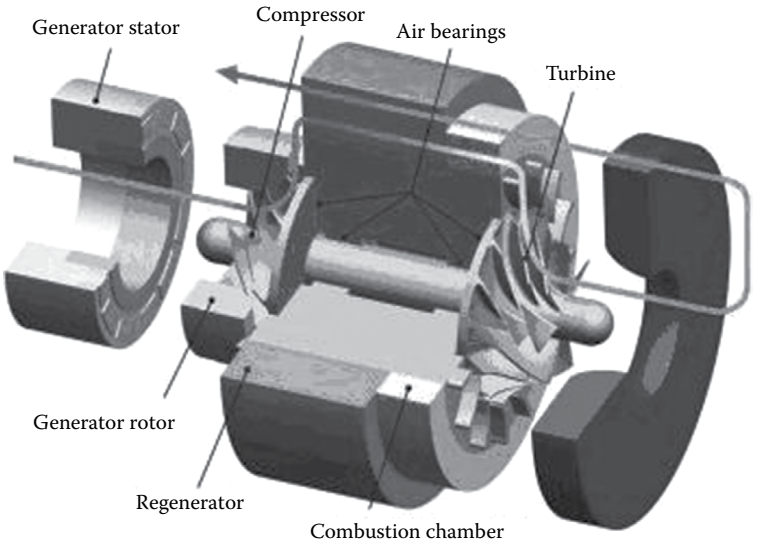


FIGURE 8.28
Micro-gas turbine layout. (From Ultra micro gas turbine generator, http://www.powermems.be/gasturbine.html.)

light cartridges could power a PDA or cell phone through several days of heavy usage, no wall-outlet recharging required; this would be a highly attractive feature for soldiers in remote locations or for travelers. Moreover, a cluster of tiny engines, each capable of producing up to a hundred Watts, could supply a home with an efficient and reliable source of electricity.

2. Turbopumps for liquid-rocket propellant
   A micro turbopump has the following components and systems:
   a. Micro axial/centrifugal compressor
   b. Micro burners
   c. Micro radial inflow/axial turbines
   d. Gearboxes and reduction drives, and associated shaft dynamics analysis [19]

   Figure 8.29 illustrates the microcentrifugal compressor for the turbopump.
3. UAV and scaled aircrafts/helicopters
   A miniature aircraft engine may be used for as small as 15-cm-long planes that could carry small cameras for surveillance. Moreover, micro-turboshaft engines may be used for scaled helicopters [19].

Problems

In the following problems unless otherwise stated, use the following data: Ambient conditions are 288 K and 101 kPa, fuel heating value is 42,000 kJ/kg.

8.1 A single-spool gas turbine is composed of a compressor, combustion chamber, and turbine. The isentropic efficiencies of the compressor and turbine are respectively

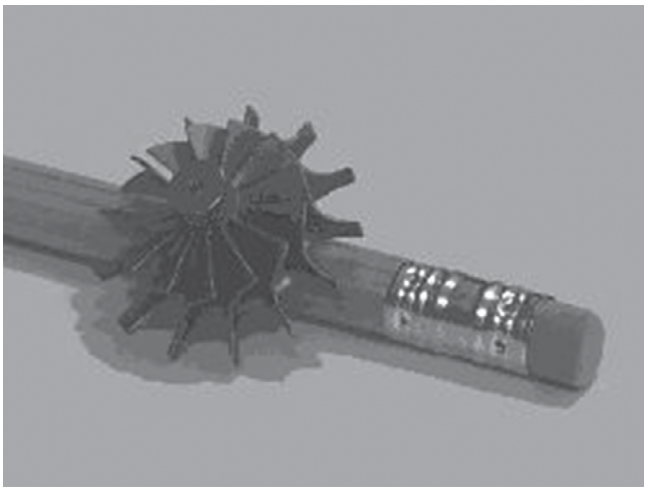


FIGURE 8.29
Microcentrifugal compressor for a turbopump.

η_c and η_t. Assume that there is no pressure drop in the combustion chamber, the working fluid has constant properties in all the components, fuel flow rate is negligible, and expansion in the turbine to the ambient pressure. Prove that the power attains a maximum value if the compressor-pressure ratio satisfies the following relation:

$$\pi_c^* = \left(\eta_c \eta_t T_{03}/T_{01}\right)^{\gamma/2(\gamma-1)}$$

Plot the relation of the specific power and thermal efficiency versus the compressor-pressure ratio for compression ratios in the range 4–10. The compressor and turbine efficiencies are 86% and 89%, respectively, while the turbine inlet temperature is 1100 K.

What will be the value of (π_c^*) if real conditions are assumed instead of the above assumption?

8.2 A regenerator is added to the gas turbine in Problem 8.1. The compressor-pressure ratio is 6, while the pressure drops in the regenerator and in the combustion chamber are 2% and 4%, respectively. Other data remains the same as above. It is required to

1. Plot the processes in the four modules on the temperature-entropy diagram
2. Calculate and plot the specific power versus the regenerator effectiveness ranging from 20% to 85%
3. Determine what the effect is of regenerator effectiveness on the fuel consumption

8.3 The compressor in a single-spool gas turbine has a pressure ratio of 15 and isentropic efficiency of 85%. The pressure drop is 2% of the compressor delivery pressure. The turbine-inlet temperature and isentropic efficiency are 1100 K and 90%. Gases leave the turbine at a pressure of 110 kPa.

1. Calculate
   a. Fuel-to-air ratio
   b. Specific power
   c. SFC
   d. Thermal efficiency

2. If all the gas turbine components are assumed ideal, there is no pressure drop in the combustion chamber, and the gases leave the turbine at the ambient conditions, what will be the ideal efficiency?

8.4 For the same gas turbine in Problem 8.3 calculate and plot the thermal efficiency and specific power if the compressor-pressure ratio attains the values of 6, 8, 10, 12, and 14.

8.5 For the same data of Problem 8.4 repeat the above procedure for turbine-inlet temperatures of 1000, 1200, and 1400 K. Plot the thermal efficiency and specific power versus the compressor-pressure ratio.

8.6 Consider a single-spool gas turbine incorporating an intercooler, regenerator and a reheat stage. The compression and expansion processes in the compressors and turbines are isentropic. The pressure ratio in both compressors is equal and the expansion ratio at both turbines is equal. Full expansion is assumed for the gases leaving the second turbine to ambient pressure.

1. Sketch a layout for the industrial gas turbine and draw the T-S diagram.
2. Calculate
   a. Fuel-to-air ratio
   b. Specific power
   c. SFC
   d. Thermal efficiency

8.7 During testing of the gas turbine illustrated in Figure 8.13 the following values for temperature are recorded:

$$T_{03} = 288, \quad T_{04} = 750, \quad T_{06} = 1400, \quad T_{07} = 1270 \text{ K}.$$

The regenerator effectiveness is 75%.
Calculate

1. The compression ratio in both compressors
2. The expansion ratio in both turbines
3. The temperature of air leaving the regenerator
4. The specific power
5. The thermal efficiency

8.8 The Ruston TA2500 gas turbine is two-shaft engine rated at 2500 bhp at ISO conditions. The compressor is a fourteen-stage axial type. The combustion system employs one large diameter chamber. It is possible for fuels other than natural gas and distillate oil to be burned. The gas turbine (compressor turbine) is a two-stage axial turbine. The free-power turbine is also a two-stage one. The conditions to the elements are as follows:

Module	Compressor Inlet	Compressor Outlet	Turbine Inlet	Free Power Inlet	Exhaust Duct Inlet
Temperature	59°F, 15°C	415°F, 213°C	1564°F, 851°C	1203°F, 651°C	944°F, 507°C
Pressure	14.7 psia 1.03 ata	72.0 psia 5.06 ata	70.1 psia 4.93 ata	29.2(psia) 2.05 ata	14.7(psia) 1.03 ata

It is required to calculate

1. The isentropic efficiency of the compressor, compressor-turbine, and free-power turbine
2. The pressure drop in the combustion chamber

3. The fuel to air ratio
4. The thermal efficiency of the engine
5. The air mass flow rate

8.9 A single-spool industrial gas turbine has the following data:

$$\dot{m}_a = 715\,\text{kg/s}, \quad P_{01} = 1\,\text{bar}, \quad T_{01} = 300\,\text{K}, \quad \pi_c = 18, \quad TIT = 1620°\text{C}, \quad Q_R = 48\text{MJ/kg}$$

$$\eta_c = 0.9, \quad \eta_{cc} = 0.98, \quad \eta_t = 0.95, \quad \eta_m = 0.98, \quad \gamma_c = 1.4, \quad \gamma_h = \frac{4}{3},$$

$$C_{pc} = 1.005\,\text{kJ/kg}\cdot\text{K}, \quad C_{ph} = 1.148\,\text{kJ/kg}\cdot\text{K}$$

Calculate

1. The generated power
2. SFC
3. Thermal efficiency

8.10 The Siemens gas turbine SGT5-8000H is a single-spool gas turbine Figure 8.30 with the following data:

Pressure ratio	19.2
Exhaust temperature (°C)	625
Exhaust mass flow (kg/s)	820
Lower heating value	45 MJ/kg

Reasonable assumptions for efficiencies and air/gas properties are

$$\eta_c = 0.9, \quad \eta_{cc} = 0.98, \quad \eta_t = 0.95, \quad \eta_m = 0.98, \quad \gamma_c = 1.4, \quad \gamma_h = \frac{4}{3},$$
$$C_{pc} = 1.005\ \text{kJ/kg}\cdot\text{K}, \quad C_{ph} = 1.148\ \text{kJ/kg}\cdot\text{K}$$



FIGURE 8.30
Siemens gas turbine SGT5-8000H.

Calculate

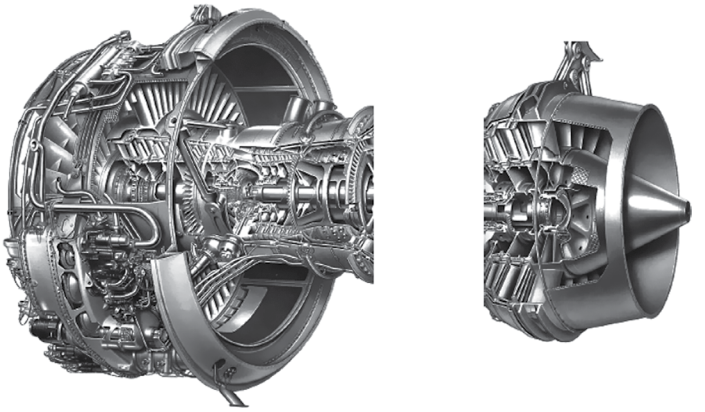
1. Turbine-inlet temperature
2. Fuel-to-air ratio
3. The generated power
4. SFC
5. Thermal efficiency

References

1. H.I.H. Saravanamuttoo, G.F.C. Rogers, and H. Cohen, *Gas Turbine Theory*, 5th edn., Prentice Hall, Upper Saddle River, NJ, 2001.
2. Ruston, *A Range of Industrial Gas Turbines below 10,000 B.H.P*, Publication 028, England, U.K., Revised July 1981.
3. A. Secareanu, D. Stankovic, L. Fuchs, V. Mllosavljevic, and J. Holmborn, Experimental investigation of airflow and spray stability in an air blast injector of an industrial gas turbine, GT2004-53961, ASME TURBO EXPO, Vienna, Austria, June 14–17, 2004.
4. Gas Turbine World 1999–2000 Performance Specs, *Performance Rating of Gas Turbine Power Plants for Project Planning, Engineering, Design & Procurement*, Vol. 19, 1999, pp. 10–48.
5. M.P. Boyce, *Gas Turbine Engineering Handbook*, 2nd edn., Gulf-Professional Publishing, Houtson, TX, 2002, p. 16.
6. R.T.C. Harman, *Gas Turbine Engineering Applications, Cycles and Characteristics*, Halsted Press Book/John Wiley & Sons, New York, 1981, p. 31.
7. Y.A. Cengel and M.A. Boles, *Thermodynamics: An Engineering Approach*, McGraw-Hill, New York, Inc., 3rd edn., 1998, p. 517.
8. M.M. El-Wakil, *Powerplant Technology*, McGraw-Hill International Edition, New York, 1984, p. 325.
9. J.B. Woodward, *Marine Gas Turbines*, John Wiley & Sons, New York, 1975, p. 7.
10. M. Arai, T. Sugimoto, K. Imai, H. Miyaji, K. Nakanishi, and Y. Hamachi, Research and development of gas turbine for next-generation marine propulsion system (Super marine Gas Turbine), *Proceeding of the International Gas Turbine Congress*, IGTC 2003 Tokyo OS-202, Tokyo, Japan, November 2–7, 2003.
11. wrc.navair-rdte.navy.mil/warfighter_enc/SHIPS/shipeng/Thermo/thermo.htm.
12. www.rolls-royce.com (MP/46/Issue 8, May 03).
13. N. Gee, Fast Ferry powering and propulsors: The options, http://www.ngal.co.uk/downloads/techpapers/paper7.pdf.
14. http://www.iso.ch/iso/en/commcentre/pdf/Oilgas0002.pdf.
15. M. Wall, R. Lee and S. Frost, *Offshore Gas Turbines (and Major Driven Equipment) Integrity and Inspection Guidance Notes*, ESR Technology Ltd., Cheshire, U.K., 2006.
16. A.S. Rangwala, *Turbomachinery Dynamics*, McGraw-Hill, New York, 2005, p. 62.
17. http://web.mit.edu/newsoffice/2006/microengines.html.
18. http://www.powermems.be/gasturbine.html.
19. http://www.m-dot.com.
20. R.J. Hunt, The history of the industrial gas turbine (Part 1 The first fifty years 1940–1990), IDGTE 582, 2011, http://www.idgte.org/.
21. http://www.fi-powerweb.com/Engine/Industrial/GE-LM2500.html.
22. Ultra micro gas turbine generator. http://www.powermems.be/gasturbine.html.

Section II

Component Design



Rolls-Royce RB211-22B. (Reproduced from Rolls-Royce plc. With permission.)


Taylor & Francis
Taylor & Francis Group
http://taylorandfrancis.com

9

Powerplant Installation and Intakes

9.1 Introduction

All airbreathing engines installed in an aircraft must be provided with an air intake and a ducting system (which is also known as an inlet or diffuser) to diffuse the air from free-stream velocity to a lower velocity acceptable for further processing by other engine components [1]. The inlet component is designed to capture the exact amount of air required to accomplish the diffusion with maximum static pressure rise and minimum total pressure loss, to deliver the air with tolerable flow distortion (as uniform as possible), and to contribute the least possible external drag to the system. For a gas turbine engine (turbojet, turbofan, and turboprop), the airflow entering subsonic compressors or fans must be of low Mach number, of the order 0.4–0.5 or less, even if the aircraft speed is supersonic. For a ramjet also, the inlet reduces the speed to a subsonic value to have a subsonic combustion. Thus the entrance duct usually acts as a diffuser.

Inlets may be classified as

1. Subsonic or supersonic
2. Fixed or variable geometry

The intake geometry and performance are closely related to the method of powerplant installation. The position of the powerplant must not affect the efficiency of the air intake. In the following sections, the different methods of powerplant installation will be first discussed for both civil and military aircraft; next subsonic and supersonic intakes will be analyzed.

9.2 Powerplant Installation

Powerplant installation is sometimes referred to as propulsion-airframe integration. It is the process of locating the powerplants and designating their installation to meet many operating requirements while minimizing drag and weight penalties [2]. The installation of the engines influences aircraft safety, structural weight, flutter, drag, control, maximum lift, performance and reliability of engine, maintainability, and aircraft growth potential. Powerplant installation influences the design of the air-inlet system, the exhaust system (which will be discussed in Chapter 11), the cooling arrangement, and the mounting structure.

These elements are largely the responsibility of the airframe manufacturer. However, the engine manufacturer is also involved as the engine data must be available to the airframe manufacturer to design a suitable installation.

Hereafter, powerplant installation will be discussed for both subsonic and supersonic aircraft.

9.3 Subsonic Aircraft

Powerplant installations for both civil and military aircraft are similar as long as their flight speeds are subsonic or transonic. However, for supersonic aircraft there are great differences in the installation methods of civil and military aircraft, as will be described later on. Turbojet and turbofan engines have the same methods for installation, while turboprops employ other methods.

9.3.1 Turbojet and Turbofan Engines

Although most present-day transport aircraft (passenger or cargo) are powered by turbofan engines, turbojet engines still have small avenues. The following forms are frequently seen for turbojet and turbofan engines:

1. Wing installation (even number of engines: 2, 4, 6, or 8)
2. Fuselage (2 or 4 engines)
3. Wing and tail combination (3 engines)
4. Fuselage and tail combination (3 engines)

9.3.1.1 Wing Installation

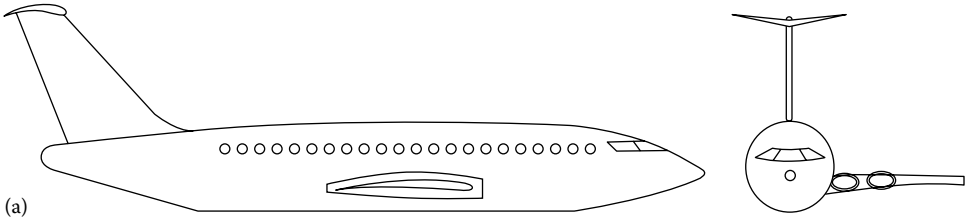
Three forms for powerplants installed in the wings, namely,

1. Buried in the wing (2 or 4 engines)
2. Pod installation (2, 4, 6, or 8 engines)
3. Above the wing (2 or 4 engines)

The first type of wing installation, "buried in the wing," is found in early aircraft such as the DeHaviland Comet 4 and the Hawker Siddeley Nimrod. In both aircraft, four engines are buried in the wing root (Figure 9.1a and b). The B-2's four General Electric F118-GE-110 non-afterburning turbofans are buried in the wings, with two engines clustered together inboard on each wing (Figure 9.1c). The intakes of the B-2 aircraft have a zigzag lip to scatter radar reflections, and there is a zigzag slot just before each intake to act as a "boundary layer splitter," breaking up the stagnant turbulent airflow that tends to collect on the surface of an aircraft.

This method of installation has the following advantages:

1. Minimum parasite drag and probably the minimum weight
2. Minimum yawing moment in case of engine failure, which counteracts the asymmetric thrust, allowing the pilot to maintain a straight level flight easily



(a)



(b)



(c)

FIGURE 9.1
(a) Buried wing installation, (b) Nimrod aircraft as a typical buried wing installation, and (c) B-2 aircraft. (Courtesy of Nortrop Grumman.)

However, it has the following disadvantages:

1. It poses a threat to the wing structure in the case of the failure of a turbine blade or disk.
2. Very difficult to maximize the inlet efficiency.
3. If a larger diameter engine is desired in a later version of the airplane, the entire wing may have to be redesigned.
4. Difficult accessibility for maintenance and repair.
5. It eliminates the flap in the region of the engine exhaust, therefore reducing the maximum lift coefficient $C_{L_{MAX}}$ [2].

The second type of wing installation is the "pod installation," whereby engines are attached to the wings via pylons (Figure 9.2a and b). Most engines nowadays have a pod installation; either two or four engines are found in the following aircraft: Boeing 707, 737, 747, 757, 767, 777, MD-11, 787; Airbus A 300, 320, 330, 340, 350, and 380; and Antonov An-148. Six engines power the Antonov An-225, while eight P&W TF33 turbofan engines power the B-52.

This type of engine installation has the following advantages:

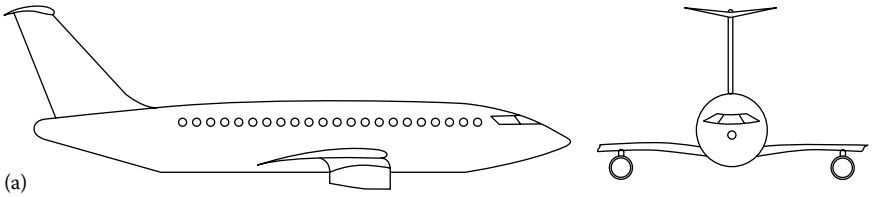
1. It minimizes the risk of wing structural damage in case of blade/disk failure.
2. It is simple to obtain high ram recovery in the inlet since the angle of attack at the inlet is minimized and no wakes are ingested.
3. Engine maintenance and replacement is easy.

However, it has the following disadvantages:

1. For low-wing aircraft like the Boeing 737, the engines are mounted close to ground and so tend to suck dirt, pebbles, rocks, snow, and so on, into the inlet. This is known as foreign object damage (FOD) which may cause serious damage to the engine blades.
2. The high temperature and high dynamic pressure of the exhaust impinging on the flap increases flap loads and weight, and may require titanium structure, which is more expensive.
3. Pylon-wing interference affects the local velocities near the wing's leading edge, thus increasing the drag and reducing the maximum lift coefficient. (However, this drawback can be remedied by choosing the nacelle locations sufficiently forward and low with respect to the wing as shown in Figure 9.3.)

Engines installed "*above the wing*" represent the third type of wing installation. This can be found on sea planes like the A-40 Albatros, which is powered by two Soloviev D-30KPV engines of 117.7 kN thrust each plus two Klimov RD-60K booster engines of 24.5 kN thrust (Figure 9.4) and on conventional aircraft like the Antonov An-74TK-200 aircraft, powered by two turbofan engines D-36, series 3-A, mounted over the wing. This type of installation has the following advantages:

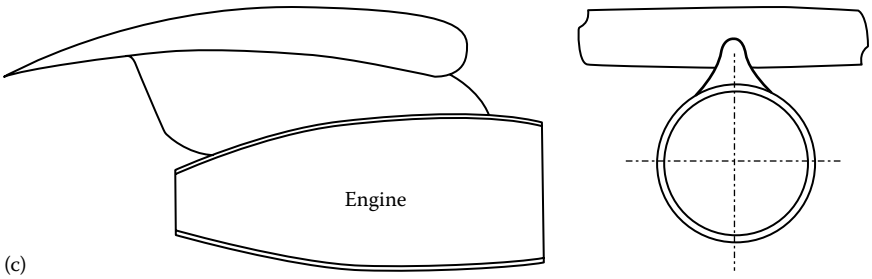
1. It prevents (or greatly reduces) foreign object ingestion into the engines from the surface of a runway during takeoff and landing.
2. It prevents water ingestion into the engine for seaplanes during takeoff and landing.



(a)



(b)



(c)



(d)

FIGURE 9.2
Pod installation to wing. (a) General aircraft/engine layout. (b) Airbus A340-600 EgyptAir airliner. (c) Close view of pod. (d) Antonov An-225. (Courtesy of Airbus Industries and EgyptAir Company.)

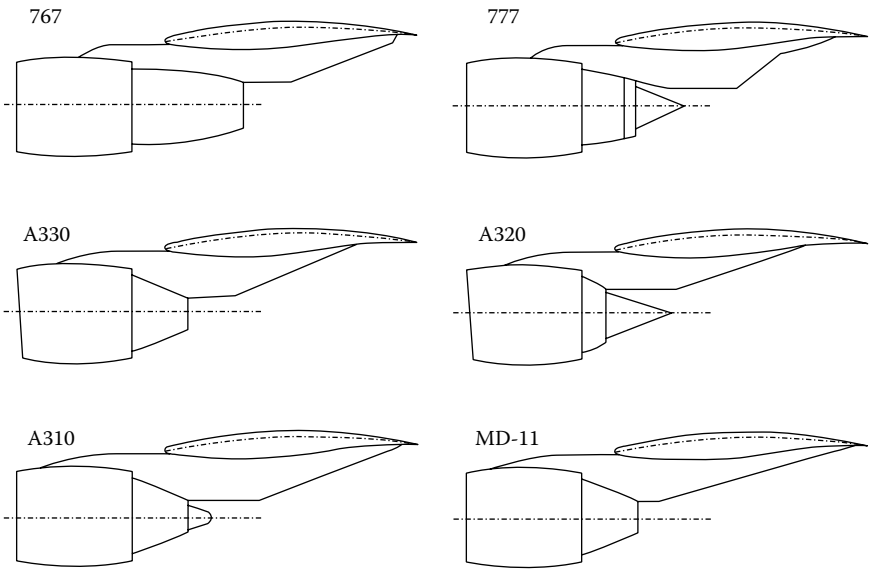


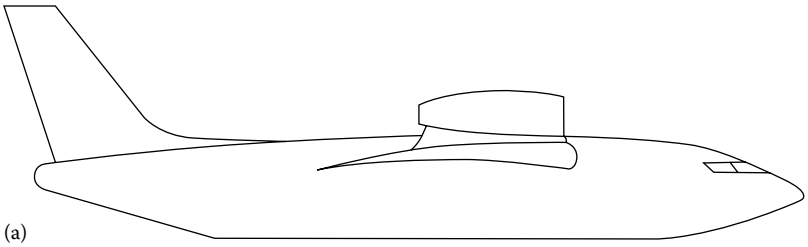
FIGURE 9.3
Different nacelle configuration for several aircraft.

3. It improves wing lift due to the blowing over of the wing upper surface and inboard flaps by engine streams.
4. It reduces noise level at the terrain due to screening engine streams by the wing, which complies with the increasingly stringent civilian aviation noise regulations.

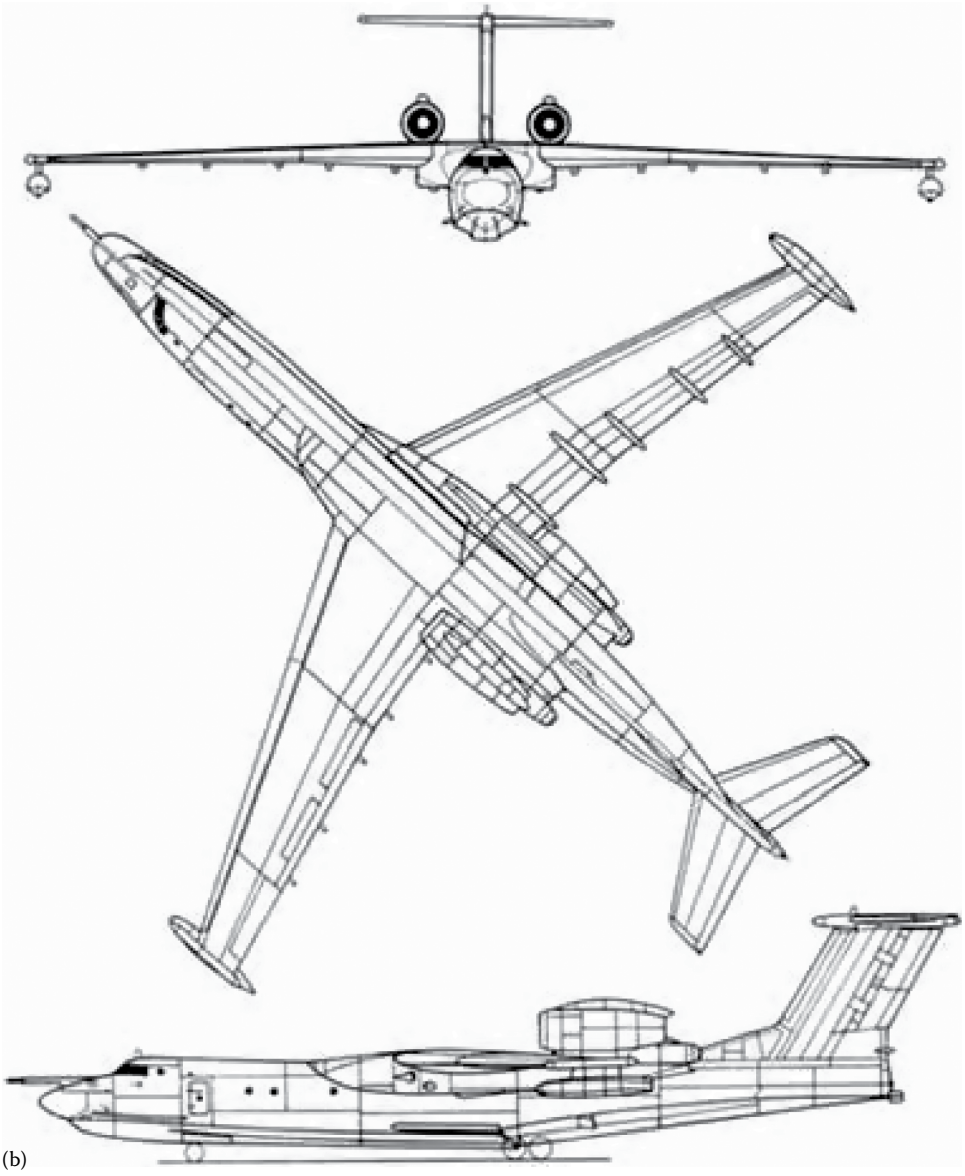
As at present and in the future, increasingly stringent civilian aviation noise regulations will require the design and manufacture of extremely quiet commercial aircraft. Also, the large fan diameters of modern engines with increasingly higher BPRs pose significant packaging and aircraft installation challenges. The design approach that addresses both of these challenges is to mount the engines above the wing. In addition to allowing the performance trend toward large diameters and high BPR-turbofan engines to continue, this approach allows the wing to shield much of the engine noise from people on the ground.

9.3.1.2 Fuselage Installation

As described in [2], fuselage installation (which is sometimes identified as *aft-engine* arrangements) is most suitable for small aircraft, in which it is difficult to install engines under the wing and maintain adequate wing-nacelle and nacelle ground clearances. Same as wing, pod installation to engine mounting is used. Engine pods are mounted on struts to allow an air gap between the pod and the fuselage (and also in wing installation). Thus, there is a minimum of aerodynamic interference with the smooth flow of air over the structure adjacent to the engine pod. The engines are attached to the sides of the rear fuselage with short stub wings. Aircraft are either powered by two engines (Figure 9.5a) or four engines. Examples of two-engine aircraft are the DC-9, MD-80, Gates Learjet Model 25, Fokker F-28, Cessna 550 Citation II, Tu-324 and 334, and Sud aviation Caravelle 12. Examples of four-engine aircraft are the Jetstar and BAC Super VC-10 (Figure 9.5b).

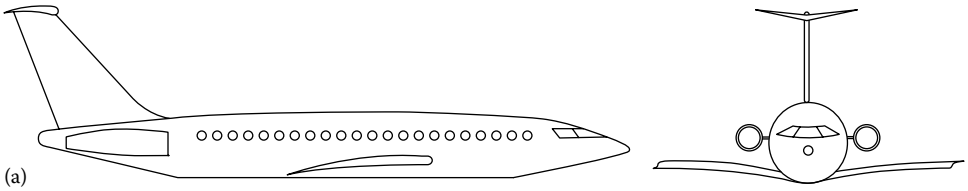


(a)



(b)

FIGURE 9.4
Above the wing installation. (a) Typical layout. (b) Three views for A-40 Albatros aircraft.



(a)



(b)

FIGURE 9.5
(a) Two-engine fuselage installation and (b) four-engine fuselage installation; Super VC-10.

Fuselage installation has the following advantages [2]:

1. Greater maximum lift coefficient and less drag due to elimination of wing-pylon and exhaust-flap interference
2. Less asymmetric yaw after engine failure as the engines are close to the fuselage
3. Lower fuselage height above the ground, which permits shorter landing gear and air stair length

However, this installation has the following disadvantages [3]:

1. The center of gravity of the empty airplane is moved aft, well behind the center of gravity of the payload. Thus a greater center of gravity range is required, which leads to difficult balance problems and larger tail.
2. On wet runway, the wheels kick water and special deflectors on the landing gear may be needed to avoid water ingestion into the engine.
3. At very high angles of attack, the nacelle wake blankets the T-tail and may cause stall, necessitating a larger tail span.
4. Vibration and noise isolation are difficult problems.

It appears that for DC-9 size aircraft, the fuselage installation is to be slightly preferred. In general, smaller aircraft employ the fuselage arrangement.

9.3.1.3 Combined Wing and Tail Installation (Three Engines)

Tail installation represents a *center-engine* installation. Only one turbofan engine is installed in all available tail combinations with either wing or fuselage arrangement. Examples are found in Lockheed Tristar and DC-10 aircraft. There are four arrangements of this type of installation as seen in Figure 9.6 for center- (or tail-)engine installation, where layout (a) represents bifurcated inlet, (b) represents a long inlet, (c) represents a long tail pipe, and (d) represents an "S" bend inlet. Each possibility entails compromises of weight, inlet-total pressure loss, inlet-flow distortion drag, thrust reverser effectiveness, and maintenance accessibilities.

The two usually used are the S-bend and the long-inlet configurations. Both installation methods have the following advantages:

1. Mounted very far aft so a ruptured turbine blade or disc will not impact on the basic tail structure.
2. High thrust reverser without interfering with control surface effectiveness. This is achieved by shaping and tilting the cascades used to reverse the flow.

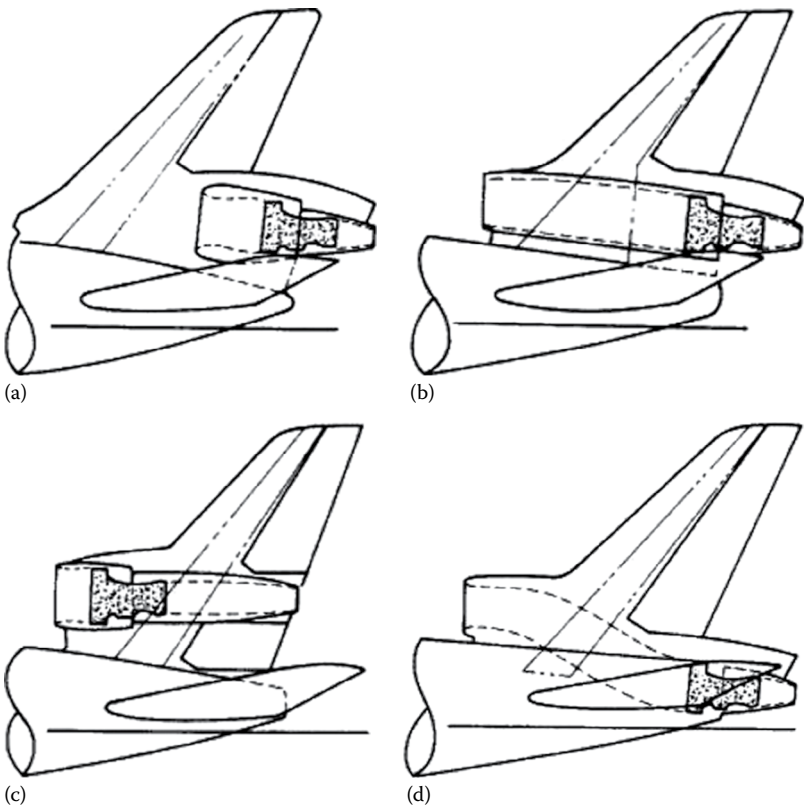


FIGURE 9.6
Tail engine installation (DC-10) transport aircraft. (a) Bifurcated inlet, (b) long inlet, (c) long tail pipe, and (d) "S" bend inlet. (Copyright Boeing, Chicago, IL. All rights reserved.)

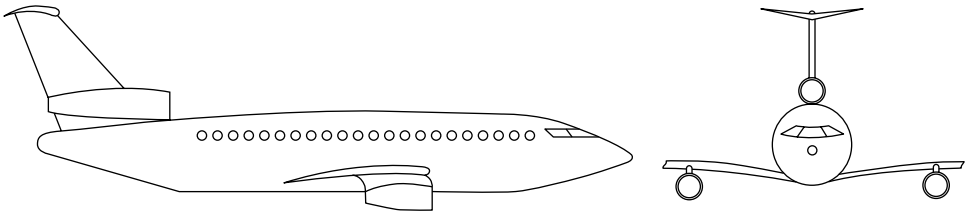


FIGURE 9.7
Wing and tail installation.

But both arrangements also have the following disadvantages:

1. Large inlet losses due to the long length of intake
2. Difficult accessibility for maintenance and repair

The *S-bend* has lower engine location and uses the engine exhaust to replace part of the fuselage boat-tail (saving drag) but has several disadvantages; namely, a distortion risk, a drag from fairing out the inlet, and the serious drawback of cutting a huge hole in the upper fuselage structure.

The long (or straight-through) inlet has the engine mounted on the fin, which has an ideal aerodynamic inlet free of distortion, but does have an increase in fin structural weight to support the engine. Figure 9.7 illustrates a typical wing and tail installation.

9.3.1.4 Combined Fuselage and Tail Installation

Examples of this type of installation are the Boeing 727 aircraft, Tu-154 and Yak-42D. A typical layout for this configuration is shown in Figure 9.8.

9.3.2 Turboprop Installation

Turboprop (or turbo-propeller) engines, however, have limited options. The propeller requirements always place the engine in one of the following positions:

1. Installation in the wing
2. Installation in the fuselage, either at the nose or empennage of the aircraft for a single-engine aircraft
3. Horizontal tail installation

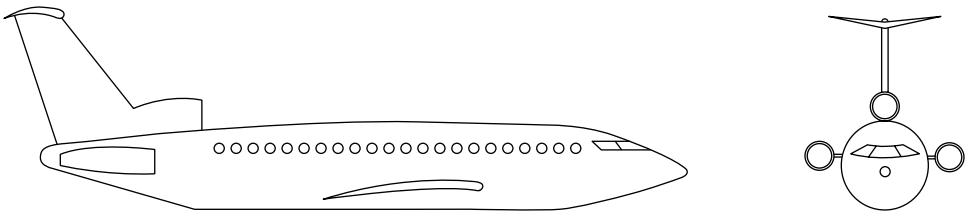


FIGURE 9.8
Fuselage and tail installation.

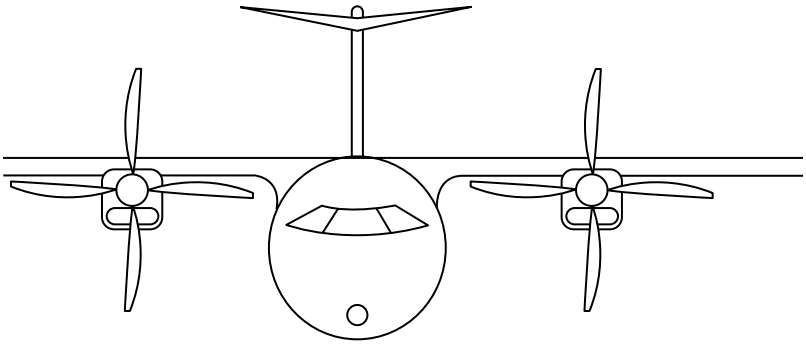


FIGURE 9.9
Puller turboprop engines installed to wing.

Most present day turboprops are wing-mounted engines on either passenger or cargo transports. Either puller or pusher turboprops may be installed in the wing. Typical wing installation of the puller type is shown in Figure 9.9. Examples of wing installation are the DeHavilland DHC-8 Commuter airplane powered by two PW120 puller engines, the Fokker F-27 powered by two RR Dart puller engines, and the Beech Starship powered by two PT6A-67A pusher engines (Figure 9.10). In some aircraft, a pair of



FIGURE 9.10
Starship aircraft powered by two PT6A-67A pusher engines.

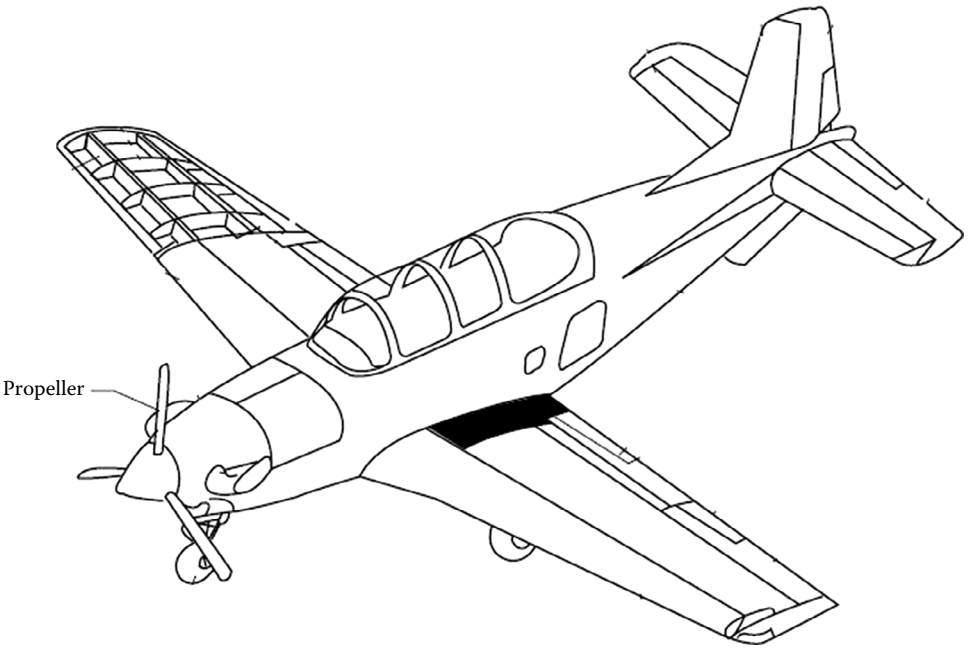


FIGURE 9.11
Nose-mounted turboprop engine.

counterrotating propellers is installed to each engine. Antonov An-70 is an example of an aircraft powered by four engines.

A small aircraft may be powered by a single turboprop engine fitted to its nose (Figure 9.11).

Nose-mounted turboprop engines may have two "counterrotating" propellers. An example of this type of aircraft is the Westland Wyvern TF MK2 long-distance ship airplane, developed for the Royal navy in 1944. This was the last fixed-wing aircraft at the Westland Company, and it was the first ship airplane in the world equipped with the turboprop engines having contra rotating propellers (Figure 9.12).

Another engine fitted with a turboprop engine having contra rotating propellers in the tail was the XB-42, which allowed the wing to have a clean unfettered design (Figure 9.13).

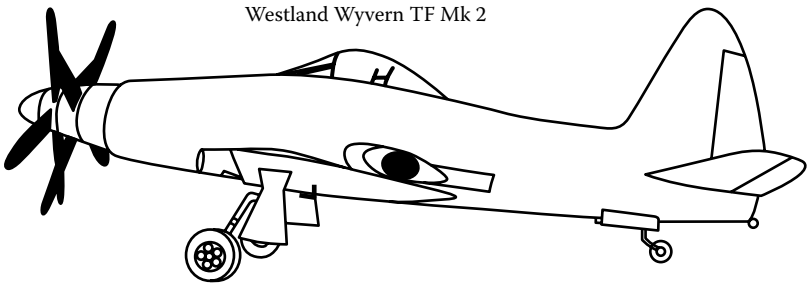


FIGURE 9.12
Contrarotating propeller of a turboprop (nose installation).

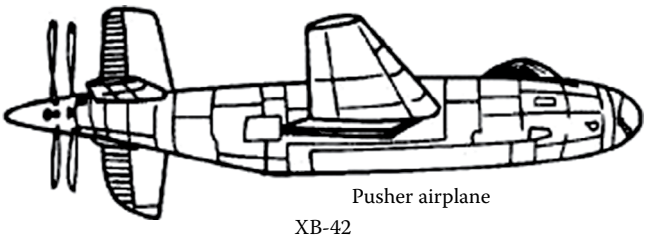


FIGURE 9.13
Contrarotating propeller of a turboprop (empennage installation).



FIGURE 9.14
Turboprop engines mounted in the horizontal tail.

The Antonov AN-180 medium turboprop airliner (around 175 passengers) is powered by two turboprop engines attached to the tips of the horizontal tail and each has contra rotating propellers (Figure 9.14).

9.4 Supersonic Aircraft

Supersonic aircraft are mostly military ones. There were a few supersonic civil aircraft, including the Anglo-French Concorde (powered by turbojet engines) and the Russian Tu-144 (powered by turbofan engines). Concorde was retired on April 10, 2003, while the Tu144 was retired on July 1, 1983. All the remaining supersonic aircraft are military ones.

9.4.1 Civil Transports

The engines of the two civil supersonic transports (SST) are installed in the wing. Concorde is powered by four Rolls Royce/SNECMA Olympus 593 turbojets (Figure 9.15), while the Tu-144 is powered by four turbofan engines. All engines are installed onto the lower surface and aft part of the wing. The engine nacelle is flush to wing surface and has a rectangular inlet (Figure 9.16).

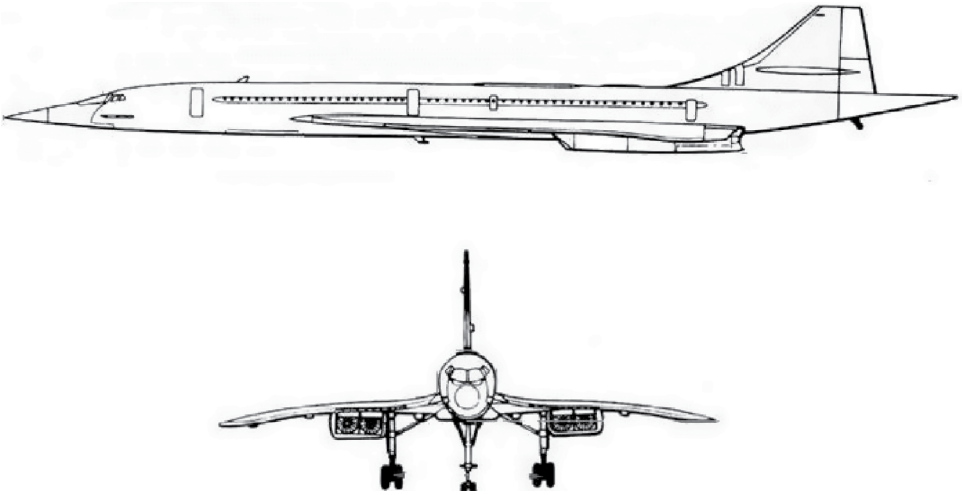


FIGURE 9.15
Concorde aircraft.



FIGURE 9.16
Inlet of Olympus 593 engine of the Concorde.

9.4.2 Military Aircraft

Most, if not all, military aircraft are powered by fuselage installation engines. Turbojet or turbofan engines are installed at the aft end of the fuselage. Fighters powered by a single engine may have a single intake (Figure 9.17) or divided intakes (Figure 9.18). Nose intake involves the use of either a short duct as in the case of the F-86 or a long duct as in the case of the F-8 and F-16. Nose intake enjoys good characteristics through a wide range of angle of attack and sideslip. It is free from aerodynamic interference effects—such as flow separation—from other parts of the aircraft. Perhaps the largest

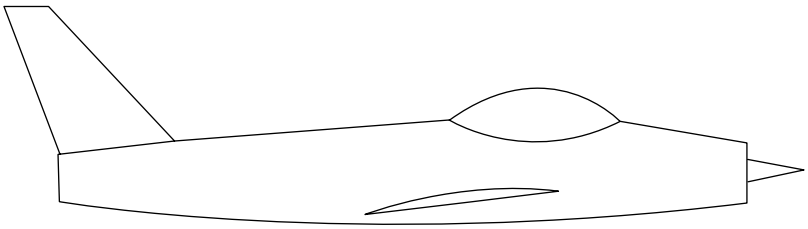


FIGURE 9.17
Nose intake for a single engine fuselage-mounted engine.

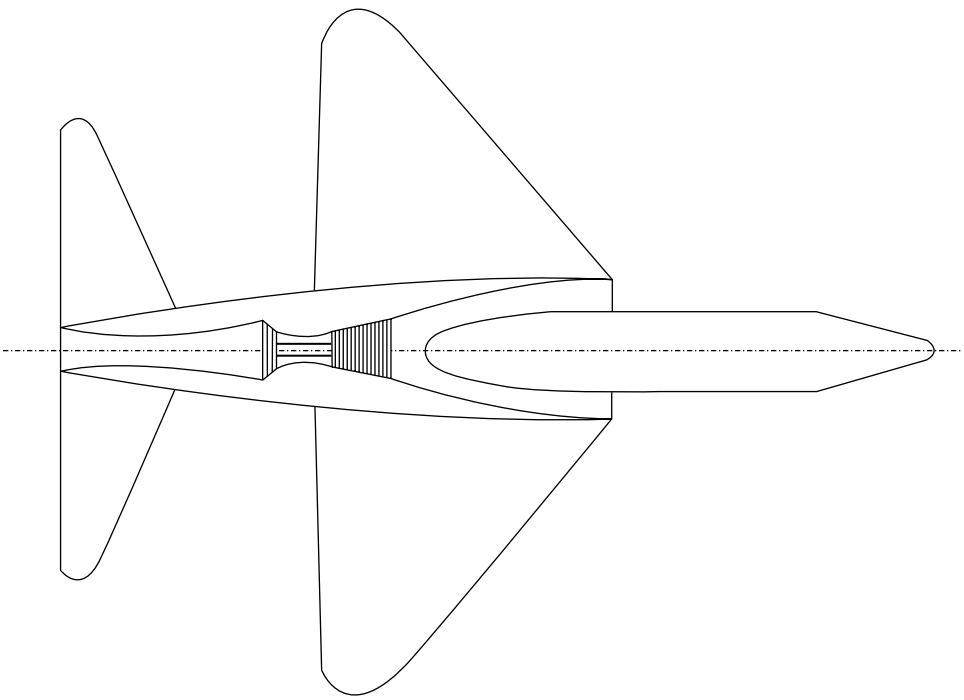


FIGURE 9.18
Divided intake for a single engine fuselage-mounted engine.

drawback of the nose inlet, however, is that neither guns nor radar can be mounted in the front of the fuselage. Moreover, the long internal duct leading from the inlet to the engine generates excessive friction and thus has relatively high pressure losses. In addition, interference between the duct and the pilot's cockpit may be encountered. For this reason, divided intake is often used where the inlets are located at the roots of aircraft wings.

Another type of nose inlet is the chin inlet employed on the F-8 airplane, which has many of the advantages of the simple nose inlet but leaves space in the front of the fuselage for radar or guns, and has a somewhat shorter internal duct. Care should be taken in such a design to avoid a separated or unsteady flow entering the inlet from the nose of the aircraft. The proximity of the inlet to the ground introduces a possible risk of foreign-object ingestion, and, obviously, the nose wheel must be located behind the inlet. The chin inlet, however, is employed on the General Dynamics F-16.

Twin-engine fighters mostly have wing-root inlet installation, examples being the F-15; Figure 9.19, and F-101. Inlets located in this manner offer several advantages. Among these are short, light, internal flow ducts, avoidance of fuselage boundary-layer air ingestion, and freedom to mount guns and radar in the nose of the aircraft. Further, no interference between the cockpit and internal ducting is encountered in this arrangement.

Different types of inlet will be discussed later on. A unique wing installation is found in the SR-71 aircraft (Figure 9.20).

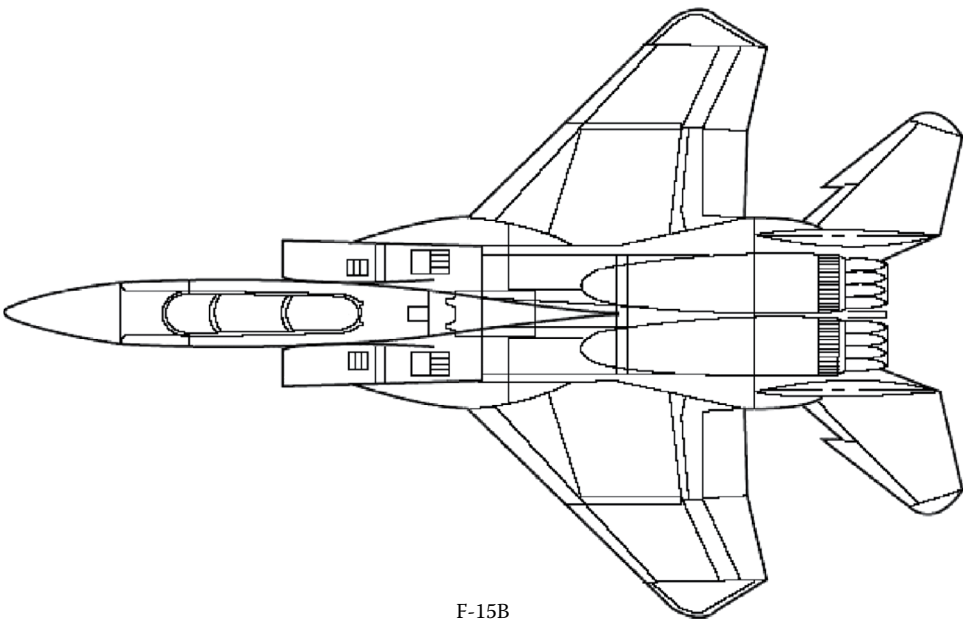


FIGURE 9.19
F-15.

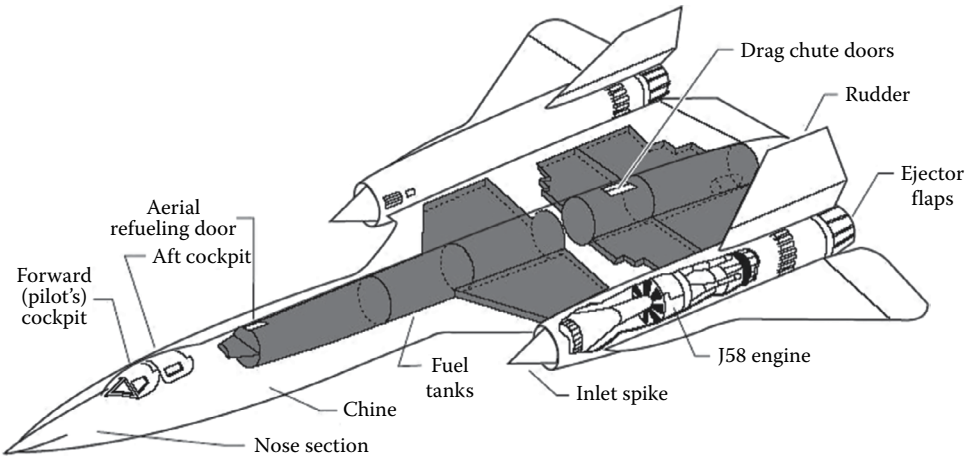


FIGURE 9.20
General arrangement of the SR-71 aircraft (NASA TM 104330).

9.5 Air Intakes or Inlets

The intake is the first part of all airbreathing propulsion systems. Both of the words "intake" and "inlet" are used alternatively. Intake is used in Britain while inlet is used in the United States. The air-intake duct is designed and manufactured by the airframe manufacturer and not by the engine manufacturer. Both manufacturers cooperate in testing air intakes. An aircraft will require one or more intakes to capture (collect) the atmospheric air (working fluid) at free-stream Mach number, sometimes changing its direction of flow, and supplying this flow to the engine with as little distortion as possible, to ensure smooth running and efficient propulsion. Moreover, the intake has to achieve all this with minimum disturbance to the external flow around the aircraft and thus minimum external drag. So, for a successful operation of the engine within the desired flight envelope, engine-intake compatibility is essential. Subsonic inlets in modern-day aircraft contain noise-absorbing materials to cope with international acoustics limitations [4].

9.6 Subsonic Intakes

Subsonic intakes are found in the turbojet or turbofan engines powering most of the current civil transports (commercial and cargo aircraft). Examples of these engines are the JT8, JT9, PW 4000 series, RB211, Trent series, and the V2500. All these engines power many of the Boeing and Airbus aircraft transports. The surface of the inlet is a continuous smooth curve, whose very front (most upstream portion) is called the inlet lip. A subsonic aircraft has an intake with a relatively thick lip. Concerning turboprop engines, the intakes are much complicated by the propeller and gear box at the inlet to the engine.

Subsonic inlets have fixed geometry, although inlets for some high-BPR turbofan engines are designed with blow-in-doors. These doors are spring-loaded parts installed in the perimeter of the inlet duct designed to deliver additional air to the aeroengine during takeoff and climb conditions, as this is when the highest thrust is needed and the aircraft speed is low [5]. The most common type of subsonic intake is the pitot intake. This type of intake makes the fullest use of ram due to forward speed, and suffers the minimum loss of ram pressure with changes of aircraft altitude [4]. However, as sonic speed is approached, the efficiency of this type of air intake begins to fall because of the formation of a shock wave at the intake lip. Pitot intake consists of a simple forward entry hole with a cowl lip. The three major types of pitot intakes as shown in Figure 9.21 are

1. Podded intakes
2. Integrated intakes
3. Flush intakes

Podded intake is common in transport aircraft (civil or military). Examples of commercial aircraft with this intake are Boeing 707, 767, 777, 787 and Airbus A330, 340, 350, and 380. The B-52 is an example of a military aircraft with this intake. The integrated intake is used in combat (military) aircraft, an example being the British Aerospace Harrier. For integrated intakes, the internal flow problems are of dominant concern, due to (1) the duct being longer, usually containing bends and shape changes, and (2) the presence of aircraft surface ahead of the intake, wetted by the internal flow [6]. The flush intake is usually used in missiles since it can be more readily accommodated into those airframes.

For typical podded intakes, the friction losses are insignificant while the flow separation is of prime importance. The internal flow has the shortest and most direct route possible to

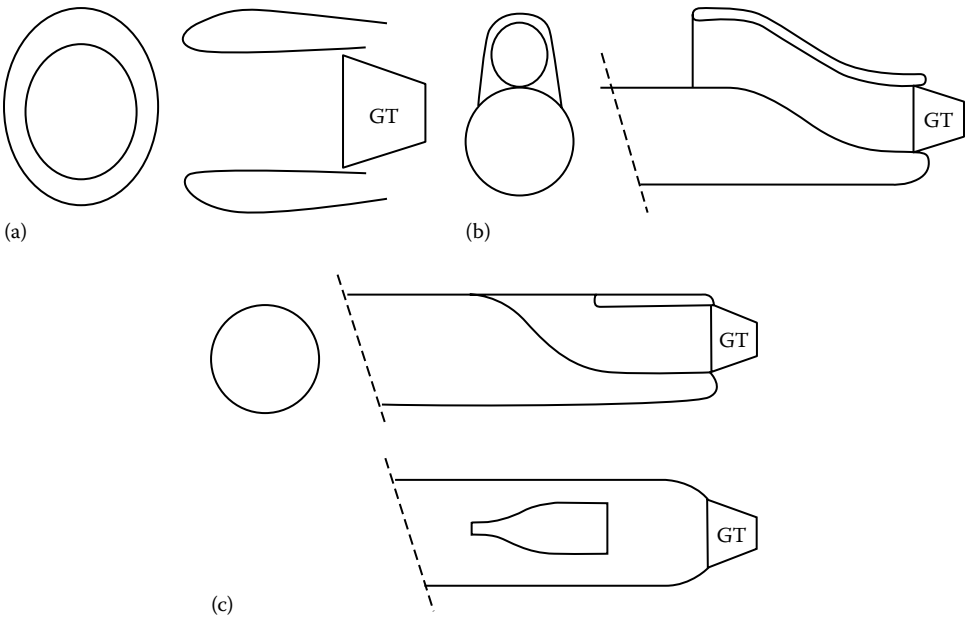


FIGURE 9.21
Types of pitot subsonic intakes: (a) podded pitot, (b) integrated pitot, and (c) flush pitot.

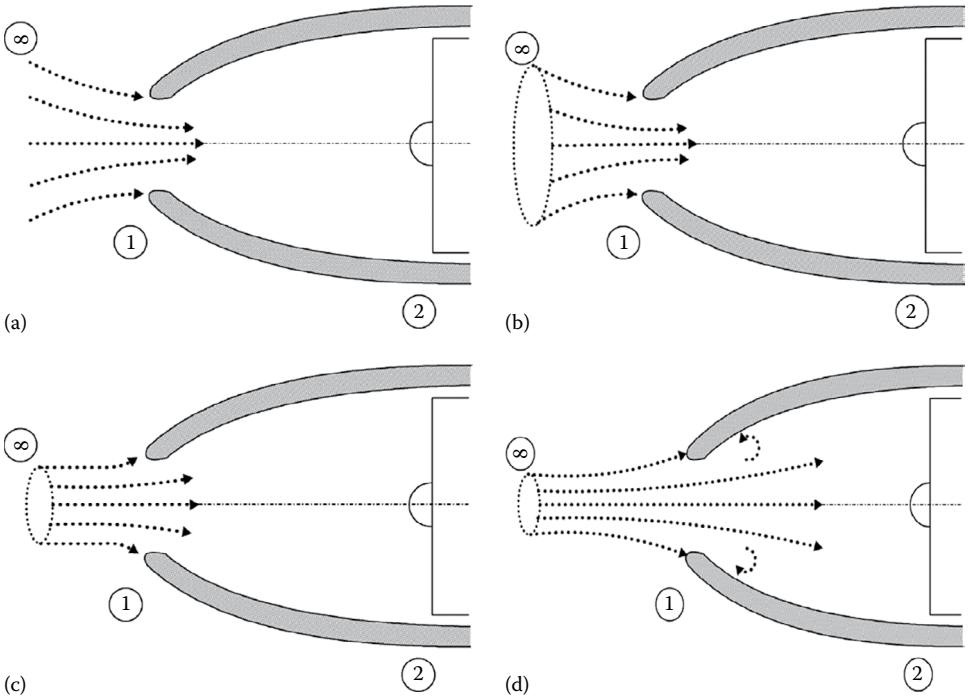


FIGURE 9.22
Flow characteristics of podded intakes: (a) ground run, (b) climb, (c) high-speed cruise, and (d) top speed.

the engine and its pressure recovery is almost 100% [6]. From an aerodynamic point of view, the flow in the intake resembles the flow in a duct. The duct "captures" a certain stream tube of air, thus dividing the air stream into an internal flow and an external flow. The external flow preserves the good aerodynamics of the airframe, while the internal flow feeds the engine. The flow characteristics in podded intakes are illustrated in Figure 9.22 for four flow conditions. In ground run, case (a), there will be no effective free-stream velocity, which will result in a large induced flow capture area causing the streamlines to converge into the intake area. The ratio between the upstream capture area to the inlet area approaches infinite. The stream tube has a bell-shape pattern. During climb, case (b), the free stream velocity will be lower than the intake velocity due to the high mass-flow rates required. This will also result in a larger entry stream tube area than the intake area (a convergent stream-tube pattern). At high-speed cruise, case (c), (M = 0.85) the entry-stream tube will be smaller than the intake area and diffusion will take place partially outside the intake and partially inside the intake, and hence the air velocity will attain lower values in the intake with a small resultant rise in pressure (15%). At top speed, case (d), (higher than cruise [M = 0.95]), the high-pressure gradient on the intake lip can cause separation and an unstable flow into the intake.

9.6.1 Inlet Performance

Depending on the flight speed and the mass flow demanded by the engine, the inlet may have to operate with a wide range of incident stream conditions. Figure 9.23 shows the

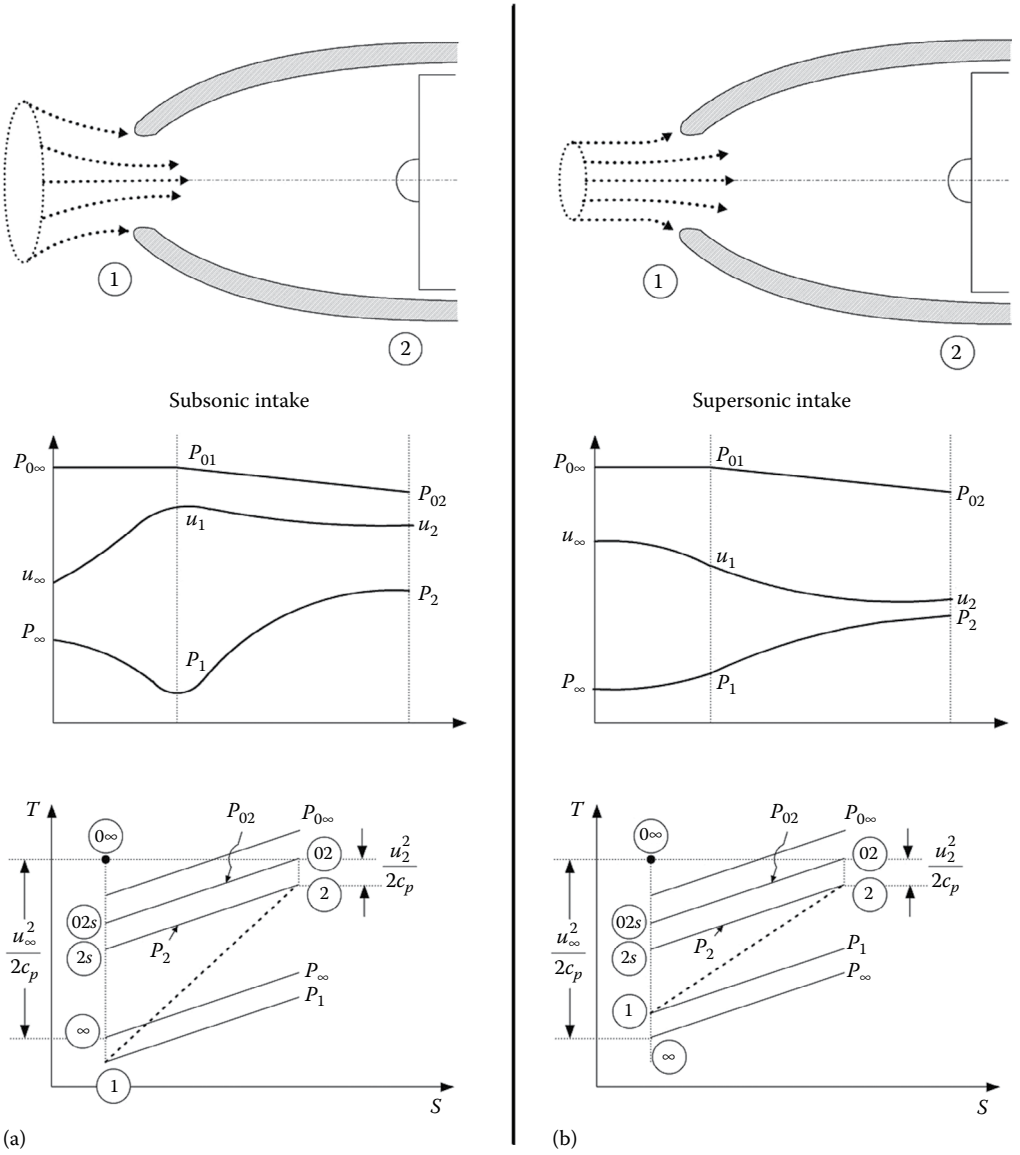


FIGURE 9.23
Subsonic inlet during (a) takeoff and (b) cruise.

performance of subsonic intake during two typical subsonic conditions, namely takeoff (Figure 9.23a) and cruise (Figure 9.23b).

For each operating condition, three plots are given in Figure 9.23. The first illustrates the stream tube, while the second depicts the pressure and speed variation, and the third is a temperature entropy diagram. The flow-in intake is identified by three states: far upstream, which is denoted as (∞), at the duct entry, denoted as (1), and at the engine face, denoted as (2). The flow outside the engine (from state ∞ to 1) is an isentropic one, where no losses

are associated with the total temperature and pressure. For high speed, or cruise condition (Figure 9.23a), the stream tube will have a divergent shape and following conditions can be stated:

$$u_1 < u_\infty, \quad P_1 > P_\infty, \quad P_{01} = P_{0\infty}, \quad T_{01} = T_{0\infty}$$

During low-speed high-thrust operation (e.g., during takeoff and climb), Figure 9.23b, the same engine will demand more mass flow and the air stream upstream the intake will be accelerated. The stream tube will have a converging shape and the following conditions will be satisfied:

$$u_1 > u_\infty, \quad P_1 < P_\infty, \quad P_{01} = P_{0\infty}, \quad T_{01} = T_{0\infty}$$

For both cases of takeoff and cruise, there will be internal diffusion within the intake up to the engine face. The static pressure will rise and the air speed will be reduced. The total pressure will also decrease due to skin friction while the total temperature will remain unchanged as the flow through the diffuser is adiabatic. Thus, for both takeoff and cruise conditions

$$P_2 > P_1, \quad P_{02} < P_{0\infty}, \quad u_2 < u_1$$

Since the inlet speed to the engine (compressor/fan) should be nearly constant for different operating conditions, then

$$\left(\frac{P_2}{P_1}\right)_{takeoff} > \left(\frac{P_2}{P_1}\right)_{cruise}$$

If this pressure increase is too large, the diffuser may stall due to boundary layer separation. Stalling usually reduces the stagnation pressure of the stream as a whole [7]. Conversely, for cruise conditions, Figure 9.23b, to avoid separation, or to have a less severe loading on the boundary layer, it is recommended to have a low velocity ratio (u_1/u_∞) and consequently less internal pressure rise [8]. Therefore, the inlet area is often chosen so as to minimize external acceleration during takeoff, with the result that external deceleration occurs during level-cruise operation. Under these conditions the "upstream capture area" A_∞ is less than the inlet area A_1, and some flow is spilled over the inlet.

The serious problem is the change in M_∞ from zero at takeoff to about 0.8 at cruise.

If optimized for the $M_\infty = 0.8$ cruise, the inlet would have the dashed contour in the lower half of figure with a thin lip to minimize the increase in Mach number as the flow is divided.

But this inlet would separate badly on the inside at takeoff and low subsonic conditions because the turn around the sharp lip would impose severe pressure gradients. To compromise, the lip is rounded, making it less sensitive to flow angle, but incurring some loss due to separation in the exterior flow.

When fully developed a good inlet will produce a pressure recovery $P_{o2}/P_{oa} = 0.95 - 0.97$ at its optimum condition.

Example 9.1

Prove that the capture area (A_∞) for a subsonic diffuser is related to the free-stream Mach number (M_∞) by the relation

$$A_\infty = \lambda/M_\infty \quad \text{where } \lambda = \frac{\dot{m}_\infty}{P_\infty}\sqrt{\frac{RT_\infty}{\gamma}}$$

A turbofan engine during ground run ingests airflow at the rate of $\dot{m}_\infty = 500$ kg/s through an inlet area (A_1) of 3.0 m^2. If the ambient conditions (T_∞, P_∞) are 288 K and 100 kPa, respectively, calculate the area ratio (A_∞/A_1) for different free-stream Mach numbers. What is the value of the Mach number where the capture area is equal to the inlet area? Draw the air-stream tube for different Mach numbers.

Solution

The mass flow rate is

$$\dot{m}_\infty = \rho_\infty V_\infty A_\infty = \frac{P_\infty}{RT_\infty}\left(M_\infty\sqrt{\gamma RT_\infty}\right)A_\infty$$

Then

$$A_\infty = \frac{\dot{m}_\infty}{P_\infty M_\infty}\sqrt{\frac{RT_\infty}{\gamma}}$$

or

$$A_\infty = \frac{\lambda}{M_\infty}$$

where

$$\lambda = \frac{\dot{m}_\infty}{P_\infty}\sqrt{\frac{RT_\infty}{\gamma}}$$

From the given data, then

$$\lambda = \frac{\dot{m}_\infty}{P_\infty}\sqrt{\frac{RT_\infty}{\gamma}} = \frac{500}{100\times10^3}\sqrt{\frac{287\times288}{1.4}} = 1.215$$

or

$$\frac{A_\infty}{A_1} = \frac{0.405}{M_\infty} \qquad \text{(a)}$$

From (a), the capture area is equal to the engine inlet area ($A_\infty/A_1 = 1$) when $M_\infty = 0.405$.

From relation (a), the following table is constructed:

M_∞	0.05	0.1	0.2	0.3	0.4	0.5
$\frac{A_\infty}{A_1}$	8.1	4.05	2.025	1.35	1.0125	0.81
$\frac{D_\infty}{D_1}$	2.84	2.0125	1.42	1.162	1.006	0.9

Figure 9.24 illustrates the stream tube for different free-stream Mach numbers.

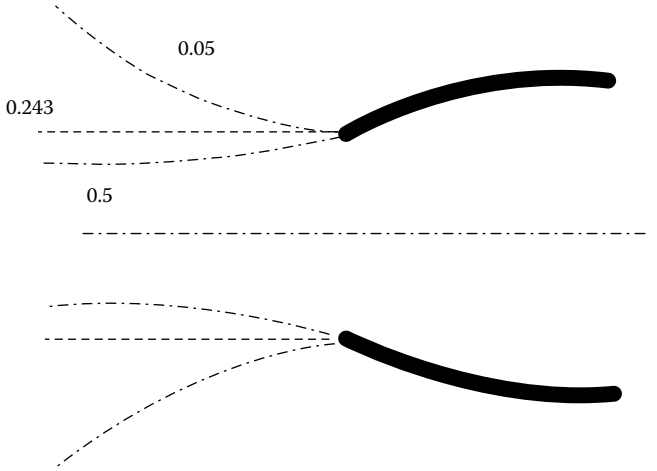


FIGURE 9.24
Stream tubes for different free-stream Mach numbers.

9.6.2 Performance Parameters

Two parameters will be discussed here:

1. Isentropic efficiency (η_d)
2. Stagnation-pressure ratio (r_d)

9.6.2.1 Isentropic Efficiency (η_d)

The isentropic efficiency of the intake η_d is a static-to-total efficiency and as previously defined in Chapters 3 through 7, it is a measure for the losses from the far upstream conditions to the engine face. The efficiency is then expressed by the following relation (refer to Figure 9.23a):

$$\eta_d = \frac{h_{02s} - h_\infty}{h_{02} - h_\infty} = \frac{T_{02s} - T_\infty}{T_{02} - T_\infty} = \frac{\left(T_{02s} / T_\infty\right) - 1}{\left(T_{02} / T_\infty\right) - 1}$$

Since

$$\frac{T_{o2}}{T_\infty} = \frac{T_{o\infty}}{T_\infty} = 1 + \frac{\gamma - 1}{2} M_\infty^2$$

$$\therefore \eta_d = \frac{\left(P_{02} / P_\infty\right)^{\gamma - 1/\gamma} - 1}{\left[\left(\gamma - 1\right)/2\right] M_\infty^2} \tag{9.1}$$

$$\frac{P_{02}}{P_\infty} = \left(1 + \eta_d \frac{\gamma - 1}{\gamma} M_\infty^2\right)^{\gamma/\gamma - 1} \tag{9.2}$$

9.6.2.2 Stagnation-Pressure Ratio (r_d)

Modern jet transports may cruise with values of the pressure recovery of 97%–98%. Supersonic aircraft with well-designed, practical inlet and internal flow systems may have pressure recoveries of 85% or more for Mach numbers in the 2.0–2.5 range.

Stagnation-pressure ratio is defined as the ratio between the average total pressure of the air entering the engine to that of the free-stream air, or

$$r_d = \frac{P_{02}}{P_{0\infty}}$$

$$\frac{P_{02}}{P_a} = \frac{P_{02}}{P_{0\infty}}\frac{P_{0\infty}}{P_\infty} = r_d\left[1+\frac{\gamma-1}{2}M_\infty^2\right]^{\gamma/\gamma-1} \tag{9.3}$$

From Equations 9.2 and 9.3 and

$$\therefore \eta_d = \frac{\left(r_d\right)^{\gamma-1/\gamma}\left[1+\frac{\gamma-1}{2}M_\infty^2\right]-1}{\left(\frac{\gamma-1}{2}\right)M_\infty^2} \tag{9.4}$$

Moreover, the pressure recovery can be expressed as

$$r_d = \frac{P_{02}}{P_{0\infty}} = \left[\frac{1+\eta_d\frac{\gamma-1}{\gamma}M_\infty^2}{1+\frac{\gamma-1}{\gamma}M_\infty^2}\right]^{\gamma/\gamma-1} \tag{9.5}$$

Thus, if the isentropic efficiency is known, the pressure recovery can be obtained from Equation 9.5, while if the pressure recovery is known, the diffuser efficiency can be determined from Equation 9.4.

However, since the flow upstream of the intake is isentropic, then all the losses are encountered inside the intake, or from state (1) to state (2). In some cases, the efficiency is defined for the *internal part* of diffuser (η_d'). In this case, the diffuser efficiency is defined as

$$\eta_d' = \frac{h_{02s}-h_1}{h_{02}-h_1} = \frac{T_{02s}-T_1}{T_{02}-T_1} = \frac{\left(T_{02s}/T_1\right)-1}{\left(T_{01}/T_1\right)-1}$$

$$\eta_d' = \frac{\left(P_{02}/P_1\right)^{\gamma-1/\gamma}-1}{\left(P_{01}/P_1\right)^{\gamma-1/\gamma}-1} = \frac{\left(P_{02}/P_1\right)^{\gamma-1/\gamma}-1}{\frac{\gamma-1}{2}M_1^2}$$

$$\left(\frac{P_{02}}{P_1}\right) = \left(1+\eta_d'\,\frac{\gamma-1}{2}M_1^2\right)^{\gamma/\gamma-1} \tag{9.5}$$

Example 9.2

Consider the turbofan engine described in Example 9.1 during flight at a Mach number of 0.9 and altitude of 11 km where the ambient temperature and pressure are, respectively, −56.5°C and 22.632 kPa. The mass ingested into the engine is now 235 kg/s. If the diffuser efficiency is 0.9 and the Mach number at the fan face is 0.45, calculate

1. The capture area
2. The static pressures at the inlet and fan face
3. The air speed at the same stations as above
4. The diffuser pressure recovery factor

Solution

1. The ambient static temperature is $T_\infty = -56.5 + 273$ K.
   The free stream speed is $u_\infty = M_\infty\sqrt{\gamma RT_\infty} = 271.6$ m/s.
   The free stream density $\rho_\infty = \dfrac{P_\infty}{RT_\infty} = 0.3479$ kg/m^3.
   The capture area is $A_\infty = \dfrac{\dot{m}}{\rho_\infty u_\infty} = 2.486$ m^2, which is smaller than the inlet area.
2. To calculate the static pressures at states (1) and (2), two methods may be used:
   a. Gas dynamics tables
   b. Isentropic relations
   The first method
3. From gas dynamics tables, at Mach number equal to 0.9, the area ratio A/A^*=1.00886.
   Then $A^* = 2.486/1.0086 = 2.465$ m^2

$$A_1/A^* = 3/2.465 = 1.217 \text{ m}^2$$

   from tables, $M_1 = 0.577$
   The corresponding temperature and pressure ratios are $P_1/P_{01} = 0.798$, $T_1/T_{01} = 0.93757$.
   Since $T_{01} = T_{0\infty}$, $P_{01} = P_{0\infty}$, then $P_1 = 30.547$ kPa, $T_1 = 246.9$ K.
4. Moreover, $u_1 = M_1\sqrt{\gamma RT_1} = 181.7$ m/s.
   Since $M_2 = 0.45$, then $P_2/P_{02} = 0.87027$.
   Now from the diffuser efficiency, then from Equation 9.2, the pressure ratio

$$\frac{P_{02}}{P_\infty} = \left(1 + 0.9 \times 0.2 \times 0.9^2\right)^{3.5} = 1.6102$$

$$P_{02} = 36.442 \text{ kPa}$$

   But $P_2 = \dfrac{P_{02}}{\left(1 + \dfrac{\gamma - 1}{\gamma} M_2^2\right)^{\gamma/\gamma - 1}} = 31.714$ kPa

   and $T_2 = \dfrac{T_{02}}{\left(1 + \dfrac{\gamma - 1}{\gamma} M_2^2\right)} = 253.1$ K

   Then $u_2 = M_2\sqrt{\gamma RT_2} = 143.5$ m/s.

   The pressure recovery factor $r_d = P_{02}/P_{0\infty} = 36.442/38.278 = 0.952$.

These results can be summarized in the following table:

State	∞	1	2
T (K)	226.65	246.9	253.1
T_0 (K)	263.36		
P (kPa)	22.632	30.547	31.71
P_0 (kPa)	38.278		36.442
u (m/s)	271.6	181.7	143.5
M	0.9	0.577	0.45

The second method: The continuity equation

$$\frac{\dot{m}}{A} = \rho u = \frac{P}{RT} M\sqrt{\gamma RT} = PM\sqrt{\frac{\gamma}{RT}}$$

$$\frac{\dot{m}}{A} = \frac{MP_0}{\left(1+\frac{\gamma-1}{2}M^2\right)^{\gamma/\gamma-1}}\sqrt{\frac{\gamma}{R}}\frac{\left(1+\frac{\gamma-1}{2}M^2\right)}{T_0}$$

$$\frac{\dot{m}}{A} = \frac{MP_0}{\left(1+\frac{\gamma-1}{2}M^2\right)^{\gamma+1/2(\gamma-1)}}\sqrt{\frac{\gamma}{RT_0}}$$

Applying this equation at station (1), then

$$\frac{\dot{m}}{A_1 P_{01}}\sqrt{\frac{RT_{01}}{\gamma}} = \frac{M_1}{\left(1+\frac{\gamma-1}{2}M_1^2\right)^{\gamma+1/2(\gamma-1)}}$$

The left-hand side is known, and the Mach number M_1 is unknown, which can be determined iteratively. From M_1, determine T_1:

$$T_1 = T_{0\infty}\Big/\left(1+\frac{\gamma-1}{2}M_1^2\right)$$

Determine $P_1 = P_{0\infty}\Big/\left(1+\frac{\gamma-1}{2}M_1^2\right)^{\gamma/\gamma-1}$ and u_1 as above.

Determine P_{02} from Equation 9.2, thus determine the recovery pressure ratio.

Determine $P_2 = P_{02}\Big/\left(1+\frac{\gamma-1}{\gamma}M_2^2\right)^{\gamma/\gamma-1}$ and $T_2 = T_{0\infty}\Big/\left(1+\frac{\gamma-1}{2}M_2^2\right)$.

Next, determine the air speed at the fan face from the relation $u_2 = M_2\sqrt{\gamma RT_2}$.

9.6.3 Turboprop Inlets

The intake for turboprop engines is very complicated due to the bulk gearbox. However, an aerodynamically efficient turboprop intake can be achieved by use of a ducted spinner [9] as shown in Figure 9.25. Improvement of intake performance is achieved by choosing a large entry area. In addition, minimum cylindrical roots are encased in fairings of low thickness/chord, which form the structural members supporting the spinner cowl [6].

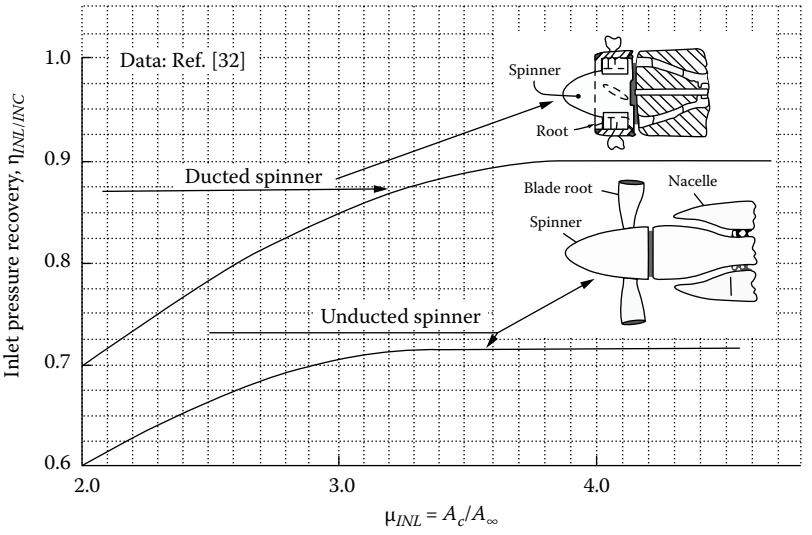


FIGURE 9.25
Efficiency of inlets of turboprop engine. (From Seddon, J. and Goldsmith, E.L., *Intake Aerodynamics*, AIAA Education Series, 1989, p. 19.)

The efficiency of the intake, defined as the ratio between the difference between the static pressure at the engine face and the free stream value to the dynamic pressure, is plotted versus the ratio between the capture area and the duct entry.

9.7 Supersonic Intakes

The design of inlet systems for supersonic aircraft is a highly complex matter involving engineering trade-offs between efficiency, complexity, weight, and cost. A typical supersonic intake is made up of a supersonic diffuser, in which the flow is decelerated by a combination of shocks, diffuse compression, and a subsonic diffuser, which reduces the Mach number from high subsonic value after the last shock to the value acceptable to the engine [10]. Subsonic intakes that have thick lips are quite unsuitable for supersonic speeds. The reason is that a normal shock wave ahead of the intake is generated, which will yield a very sharp static pressure rise without change of flow direction and a correspondingly big velocity reduction. The adiabatic efficiency of compression through a normal shock wave is very low as compared with oblique shocks. At Mach 2.0 in the stratosphere adiabatic efficiency would be about 80% or less for normal shock waves, whereas its value will be about 95% or even more for an intake designed for oblique shocks.

Flight at supersonic speeds complicates the diffuser design for the following reasons [10]:

1. The existence of shock waves, which lead to large decrease in stagnation pressure even in the absence of viscous effects.
2. The large variation in capture stream tube area between subsonic and supersonic flight for a given engine, as much as a factor of four between $M_\infty = 1$ and $M_\infty = 3$.

3. As M_∞ increases, the inlet compression ratio becomes a larger fraction of the overall cycle compression ratios and as a result the specific thrust becomes more sensitive to diffuser pressure ratio.
4. It must operate efficiently both during the subsonic flight phases (takeoff, climb and subsonic cruise) and at supersonic design speed.

Generally supersonic intake may be classified as

1. Axisymmetric or two-dimensional (Figure 9.26)
   Axisymmetric intakes use an axisymmetric central cone to shock the flow down to subsonic speeds. The two-dimensional inlets have rectangular cross-sections as found in the F-14 and F-15 fighter aircraft.
2. Variable- or fixed-geometry (Figure 9.27)
   For variable-geometry axisymmetric intakes, the central cone may move fore and aft to adjust the intake area. Alternatively, the inlet area is adjusted in the case of the rectangular section through hinged flaps (or ramps) that may change its angles.

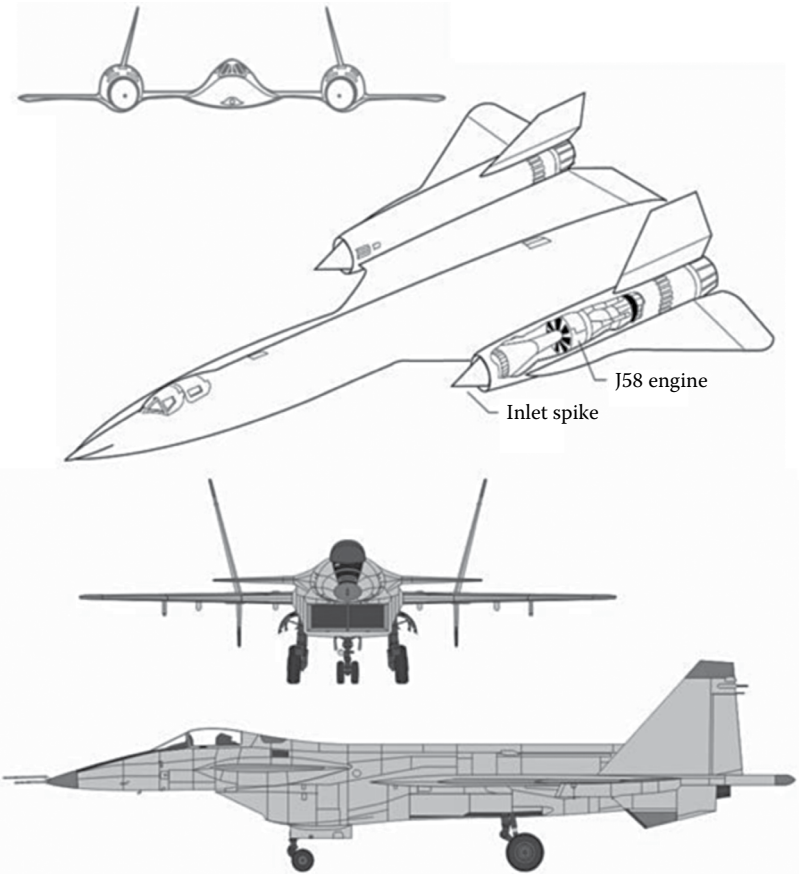


FIGURE 9.26
Axisymmetric and two-dimensional supersonic intakes.

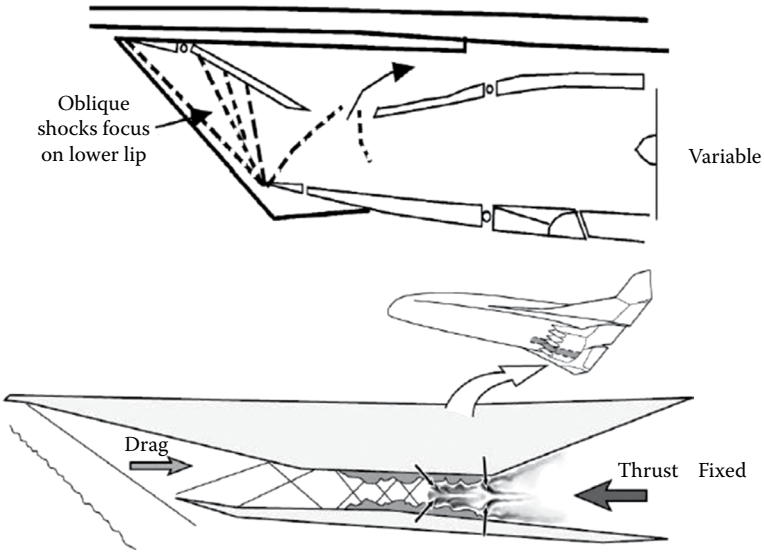


FIGURE 9.27
Variable- and fixed-geometry supersonic intakes.

For flight at Mach numbers much beyond 1.6, variable-geometry features must be incorporated in the inlet to achieve high inlet pressure recoveries together with low external drag. The General Dynamics F-111 airplane has a quarter-round inlet equipped with a translating center body or spike. The inlet is bounded on the top by the wing and on one side by the fuselage. An installation of this type is often referred to as an "armpit" inlet. The spike automatically translates fore and aft as the Mach number changes. The throat area of the inlet also varies with the Mach number. This is accomplished by the expansion and contraction of the rear part of the spike.

3. Internal, external, or mixed-compression (Figure 9.28)
   As shown in Figure 9.28, the set of shocks situated between the forebody and intake lip are identified as external shocks, while those found between the nose lip

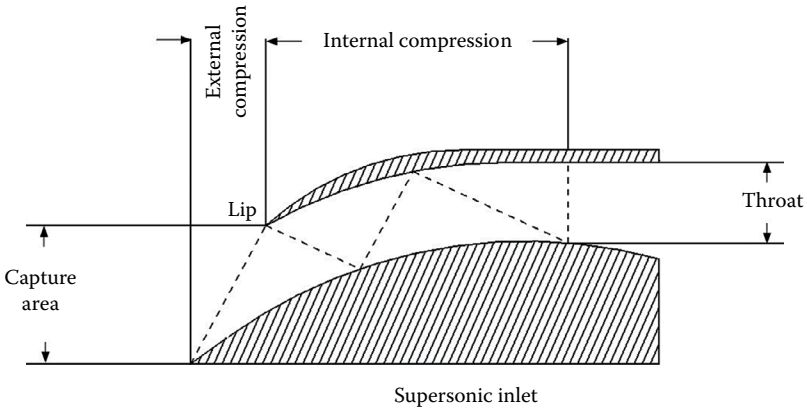


FIGURE 9.28
External and internal compression supersonic intake.

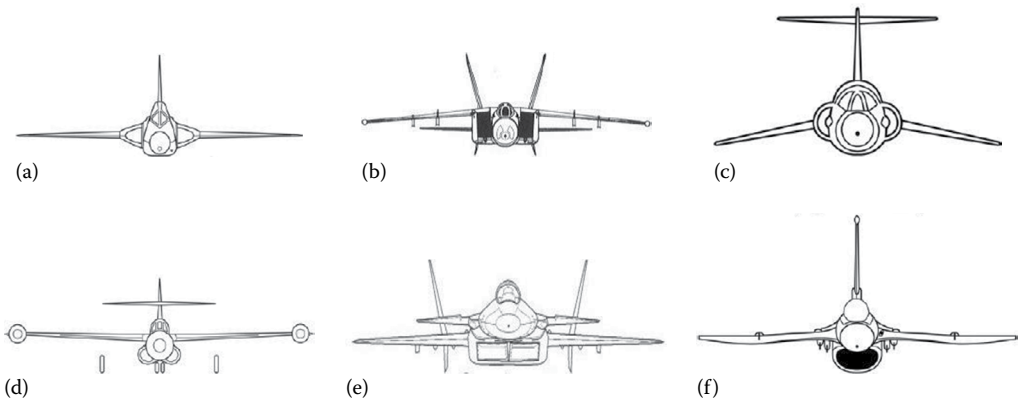


FIGURE 9.29
Intakes for military aircraft: (a) F5D-1 Skylancer, (b) MIG-25, (c) F-104, (d) F-89, (e) MIG-FMI, and (f) F-16-A.

and the intake throat are called internal shocks. Some intakes have one type of shock, either external or internal, and are given that name, while others have both types and are denoted as mixed compression intakes.

A constant-area (or fixed-geometry) intake may be either axisymmetric or two dimensional. The supersonic pitot intake is a constant cross-sectional area intake similar to the subsonic pitot intake, but it requires a sharp lip for the shock wave attachment. This will substantially reduce intake drag compared with that of the subsonic rounded-edged lip operating at the same Mach number. Sharp edges unfortunately result in poor pressure recovery at low Mach numbers. However, this design presents a very simple solution for supersonic intakes. Variable-geometry intakes may involve the use of a translating center body, a variable-geometry center body, and a cowl with a variable lip angle, variable ramp angles and/or a variable throat area. Using variable-geometry inlets requires the use of sensors, which add complexity and weight to the inlet.

The use of axisymmetric or 2-D inlets is dependent on the method of engine installation on the aircraft, the cruise Mach number, and the type of the aircraft (i.e., military or civil), as clearly illustrated in Figures 9.15 and 9.29.

9.7.1 Review of Gas Dynamic Relations for Normal and Oblique Shocks

9.7.1.1 Normal Shock Waves

For a normal shock wave, denoting the conditions upstream and downstream the shock by subscripts (1) and (2), respectively, the following relations give the downstream Mach number, static temperature and pressure ratios, density ratio, and total pressure ratio across the shock:

$$M_2^2 = \frac{(\gamma-1)M_1^2+2}{2\gamma M_1^2-(\gamma-1)} \tag{9.6}$$

$$\frac{T_2}{T_1} = \left[\frac{2}{(\gamma+1)M_1^2}+\left(\frac{\gamma-1}{\gamma+1}\right)\right]\left[\left(\frac{2\gamma}{\gamma+1}\right)M_1^2-\left(\frac{\gamma-1}{\gamma+1}\right)\right] \tag{9.7}$$

$$\frac{P_2}{P_1} = \left[1 + \left(\frac{2\gamma}{\gamma+1}\right)\left(M_1^2 - 1\right)\right] \tag{9.8}$$

$$\frac{\rho_2}{\rho_1} = \left[\frac{(\gamma+1)M_1^2}{2+(\gamma-1)M_1^2}\right] \tag{9.9}$$

$$\frac{P_{02}}{P_{01}} = \left[\frac{(\gamma+1)M_1^2}{2+(\gamma-1)M_1^2}\right]^{\gamma/\gamma-1}\left[\left(\frac{2\gamma}{\gamma+1}\right)M_1^2 - \left(\frac{\gamma-1}{\gamma+1}\right)\right]^{(1/\gamma-1)} \tag{9.10}$$

9.7.1.2 Oblique Shock Waves

The shown oblique shock, Figure 9.30 has a shock angle β and a deflection angle δ. Oblique shock can be treated as a normal shock having an upstream Mach number $M_{1n} = M_1 \sin\beta$ and a tangential component $M_{1t} = M_1 \cos\beta$. The tangential velocity components upstream and downstream the shocks are equal. From References 11 and 12, the following relations are given:

$$\tan\delta = \frac{2\cot\beta\left(M_1^2\sin^2\beta - 1\right)}{(\gamma+1)M_1^2 - 2\left(M_1^2\sin^2\beta - 1\right)} \tag{9.11a}$$

For $\gamma = 7/4$, then

$$\tan\delta = 5\frac{M_1^2\sin 2\beta - 2\cot\beta}{10 + M_1^2(7 + 5\cos 2\beta)} \tag{9.11b}$$

$$M_2^2\sin^2(\beta-\delta) = \frac{(\gamma-1)M_1^2\sin^2\beta + 2}{2\gamma M_1^2\sin^2\beta - (\gamma-1)} \tag{9.12a}$$

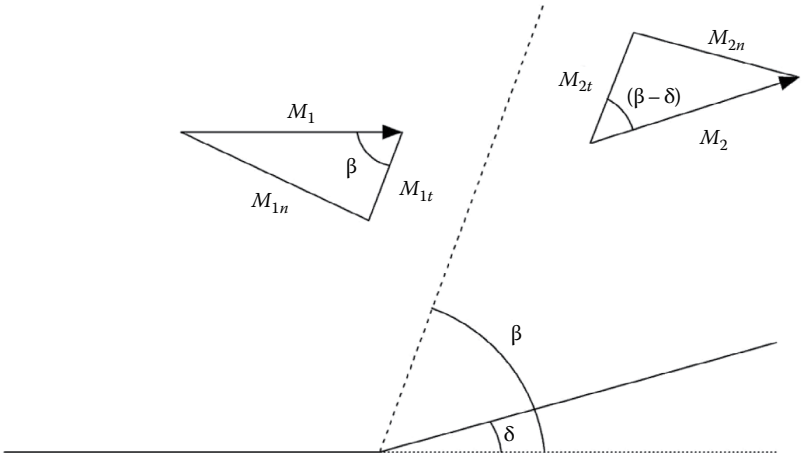


FIGURE 9.30
Nomenclature of oblique shock wave.

For $\gamma = 7/4$, then

$$M_2^2 = \frac{36M_1^4 \sin^2\beta - 5\left(M_1^2 \sin^2\beta - 1\right)\left(7M_1^2 \sin^2\beta + 5\right)}{\left(7M_1^2 \sin^2\beta - 1\right)\left(M_1^2 \sin^2\beta + 5\right)} \tag{9.12b}$$

$$\frac{P_2}{P_1} = \left[1 + \left(\frac{2\gamma}{\gamma+1}\right)\left(M_1^2 \sin^2\beta - 1\right)\right] \tag{9.13a}$$

For $\gamma = 7/4$, then

$$\frac{P_2}{P_1} = \left(\frac{7M_1^2 \sin^2\beta - 1}{6}\right) \tag{9.13b}$$

$$\frac{T_2}{T_1} = \left[\frac{2}{(\gamma+1)M_1^2 \sin^2\beta} + \left(\frac{\gamma-1}{\gamma+1}\right)\right]\left[\left(\frac{2\gamma}{\gamma+1}\right)M_1^2 \sin^2\beta - \left(\frac{\gamma-1}{\gamma+1}\right)\right] \tag{9.14a}$$

For $\gamma = 7/4$, then

$$\frac{T_2}{T_1} = \frac{\left(7M_1^2 \sin^2\beta - 1\right)\left(M_1^2 \sin^2\beta + 5\right)}{36M_1^2 \sin^2\beta} \tag{9.14b}$$

$$\frac{\rho_2}{\rho_1} = \left[\frac{(\gamma+1)M_1^2 \sin^2\beta}{2 + (\gamma-1)M_1^2 \sin^2\beta}\right] \tag{9.15a}$$

For $\gamma = 7/4$, then

$$\frac{\rho_2}{\rho_1} = \left[\frac{6M_1^2 \sin^2\beta}{M_1^2 \sin^2\beta + 5}\right] \tag{9.15b}$$

$$\frac{P_{02}}{P_{01}} = \left[\frac{(\gamma+1)M_1^2 \sin^2\beta}{2 + (\gamma-1)M_1^2 \sin^2\beta}\right]^{\gamma/\gamma-1}\left[\left(\frac{2\gamma}{\gamma+1}\right)M_1^2 \sin^2\beta - \left(\frac{\gamma-1}{\gamma+1}\right)\right]^{-(1/\gamma-1)} \tag{9.16a}$$

For $\gamma = 7/4$, then the relation for total pressure ratio will be

$$\frac{P_{02}}{P_{01}} = \left[\frac{6M_1^2 \sin^2\beta}{M_1^2 \sin^2\beta + 5}\right]^{7/2}\left[\frac{6}{7M_1^2 \sin^2\beta - 1}\right]^{(5/2)} \tag{9.16b}$$

9.7.2 External Compression Intake (Inlet)

External compression intakes complete the supersonic diffusion process outside the covered portion of the inlet where the flow is decelerated through a combination of oblique shocks (single, double, triple, or multiple). These oblique shocks are followed by a normal shock

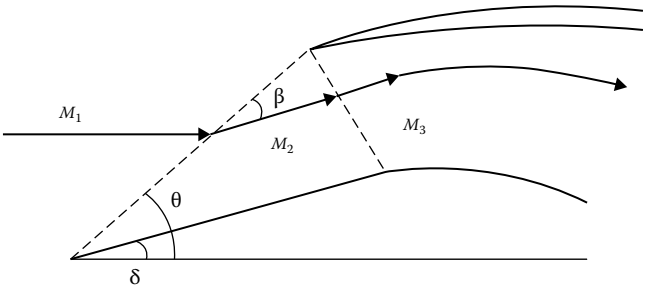


FIGURE 9.31
Single oblique shock external compression intake.

wave that changes the flow from supersonic to subsonic. Both the normal shock wave and the throat are ideally located at the cowl lip. The supersonic diffuser is followed by a subsonic diffuser, which reduces the Mach number from high subsonic value after the last shock to the value acceptable to the engine. The simplest form of staged compression is the single oblique shock, produced by a single-angled wedge or cone projecting forward of the duct, followed by a normal shock as illustrated in Figure 9.31. The intake in this case is referred to as a *two-shock* intake. With a wedge, the flow after the oblique shock wave is at a constant Mach number and is parallel to the wedge surface. With a cone, the flow behind the conical shock is itself conical, the Mach number is constant along rays from the apex and varies along streamline. Forebody intake is frequently used for "external compression intake of wedge or cone form" [6].

The capture area (A_c) for supersonic intakes is defined as the area enclosed by the leading edge, or "highlight," of the intake cowl, including the cross-sectional area of the forebody in that plane. The maximum flow ratio is achieved when the boundary of the free stream tube (A_∞) arrives undisturbed at the lip. This means

$$\frac{A_\infty}{A_c} = 1.0$$

This condition is identified as the *full flow* [6] or the critical flow [5]. This condition depends on the Mach number, angle of the forebody, and the position of the tip. In this case, the shock angle θ is equal to the angle subtended by lip at the apex of the body and corresponds to the maximum possible flow through the intake (Figure 9.32). This is the design point for constant area intake and the goal of the variable area intake as to stay at that condition over the flight operating range. At Mach numbers (or speeds) below the value of the critical (design) value described earlier, the mass flow is less than that at the critical condition, and the normal shock wave occurs in front of the cowl lip, and this case is identified as *subcritical*. It is to be noticed here that

$$\frac{A_\infty}{A_c} < 1.0$$

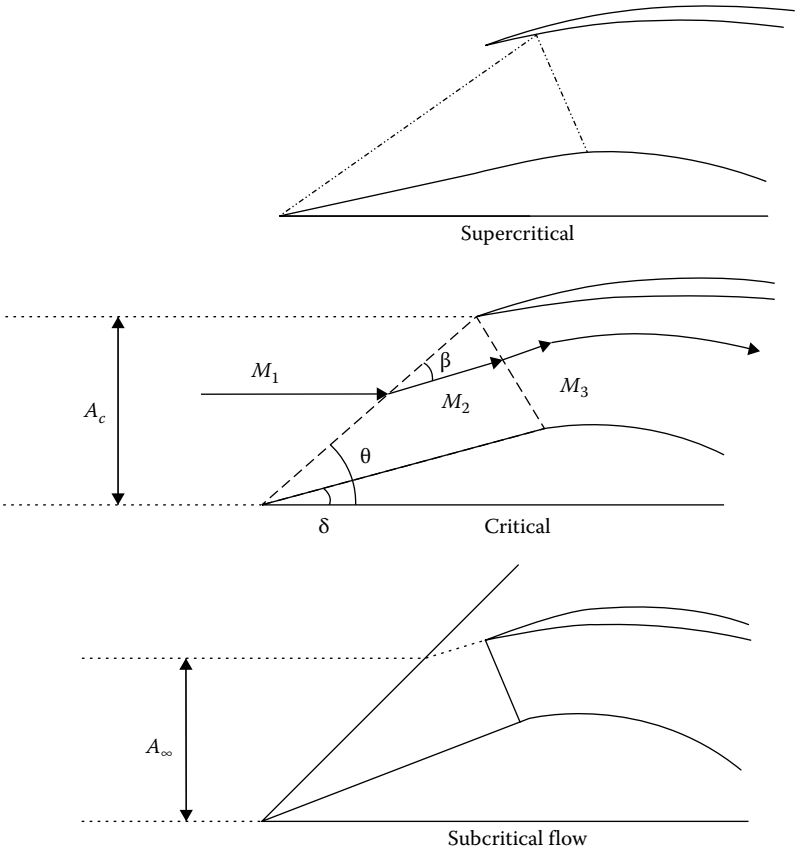


FIGURE 9.32
Types of flow in an external compression intake.

Moreover, the outer drag of the intake becomes very large and smaller pressure recovery is obtained. If the air speed is greater than the design value, then the oblique shock will impinge inside the cowl lip and the normal shock will move to the diverging section. This type of operation is referred to as the *supercritical* operation.

The two-shock intake is only moderately good at Mach 2.0 and unlikely to be adequate at higher Mach numbers [4]. The principle of breaking down an external shock system can be extended to any desired number of stages. The next step is the three-shock intake, whereby two oblique shocks are followed by a normal shock, where the double-wedge and double-cone are the archetypal forms (Figure 9.33).

Continuing the process of breaking down the external shock system, three or more oblique shocks may be used ahead of the normal shock. For a system of $(n-1)$ oblique shocks, the pressure recovery factor will be

$$\frac{P_{02}}{P_{0\infty}} = \frac{P_{02}}{P_{01}}\frac{P_{03}}{P_{02}}\frac{P_{04}}{P_{03}}\cdots\frac{P_{0n}}{P_{0n-1}}\left(\frac{P_{0n}}{P_{0n-1}}\right)_{normal\ shock} \tag{9.17}$$

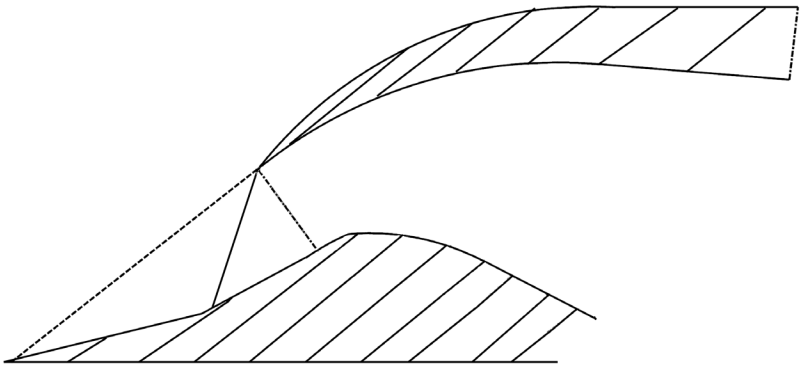


FIGURE 9.33
Three shocks for double-cone (or double-wedge) geometry.

Two remarks are to be made here:

1. As the number of oblique shocks increases, the pressure recovery factor increases.
2. Up to Mach 2, equal deflections of the successive wedge angles give the best results, while for higher Mach numbers, the first deflection angle needs to be the smallest and the last the largest [4].

Extending the principle of multi-shock compression to its limit leads to the concept of *isentropic compression*, in which a smoothly contoured forebody produces an infinitely large number of infinitely weak oblique shocks (Figure 9.34). In this case the supersonic stream is compressed with no losses in the total pressure.

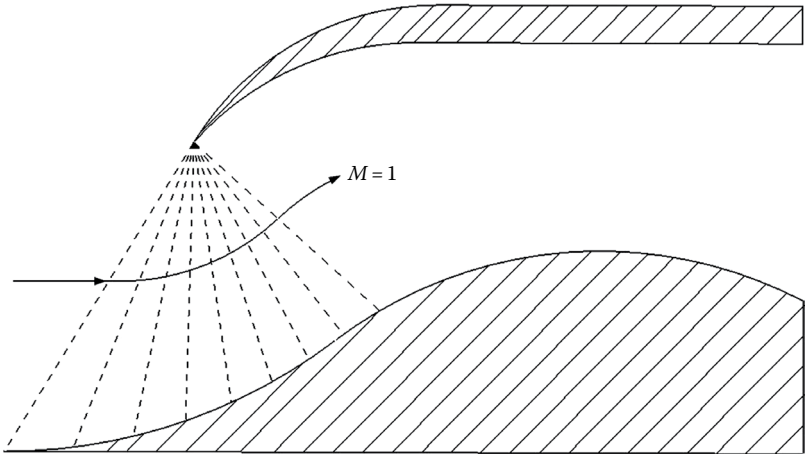


FIGURE 9.34
Isotropic compression supersonic inlet.

Example 9.3

A fighter aircraft is flying at an altitude of 50,000 ft where the ambient pressure and temperature are, respectively, 1.682 psia and 390°R. The aircraft has the two-dimensional inlet (illustrated in Figure 9.35) through which air enters with a Mach number of 2.5. Within the intake diffuser a single oblique shock wave is developed followed by a normal shock. The two-dimensional oblique shock has an oblique shock angle of 30°. Assuming constant specific heats ($C_P = 0.24$ Btu/Ib$_m$ °R), determine

1. The total temperature and pressure of the air entering the oblique shock
2. The static and total conditions after the oblique shock
3. The Mach number after the oblique shock
4. The flow deflection angle (δ)
5. The Mach number after the normal shock
6. The static and total conditions after the normal shock (Figure 9.35)

Solution

1. With γ = 1.4

$$V_1 = 2.5\sqrt{\gamma g_C R T_1}$$

$$V_1 = 2.5\sqrt{(1.4)(32.174)(53.35)(390)}$$

$$V_1 = 2420 \text{ ft/s}$$

$$T_{01} = T_1 + \frac{V^2}{2g_C C_P J} = 390 + \frac{(2420)^2}{(2)(32.174)(0.24)(778)} = 390 + 487$$

$$T_{01} = 877°\text{R}$$

$$P_{01} = P_1\left(\frac{T_{01}}{T_1}\right)^{\gamma/\gamma-1} = 1.682\left(\frac{877}{390}\right)^{1.4/0.4}$$

$$P_{01} = 28.68 \text{ psia}$$

2. Since an oblique shock wave can be treated as a normal shock wave with the normal component of the Mach number as the Mach number upstream the normal shock wave, then for a shock angle of 30°, the normal and tangential components of the Mach number are

$$M_{1n} = 2.5(\sin 30) = 1.25$$
$$M_{1t} = 2.5(\cos 30) = 2.165$$

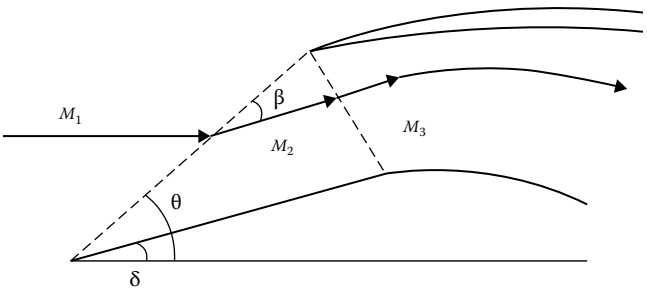


FIGURE 9.35
Two-shock intake.

The conditions downstream the oblique shock waves are either determined from tables of normal shock waves or from the mathematical expressions of normal shock waves, noting that in both methods the normal component of the Mach number are used.

From normal shock-wave tables with $M_{1n} = 1.25$, then

$$\mathrm{M}_{2n} = 0.814, \quad \frac{P_2}{P_1} = 1.659, \quad \frac{P_{02}}{P_{01}} = 0.986, \quad \frac{T_2}{T_1} = 1.159$$

As an alternative, the relations (9.6) through (9.10) are used.

From Equation 9.6 with $M_{1n} = 0.814$, then

$$M_{2n} = 0.813$$

$$\frac{P_2}{P_1} = 1.656, \quad \frac{P_{02}}{P_{01}} = 0.987, \quad \text{and} \quad \frac{T_2}{T_1} = 1.159$$

Both procedures give nearly the same results.

The total pressure after the oblique shock wave is

$$P_{02} = \frac{P_{02}}{P_{01}} P_{01} = (0.986)(26.68)$$

$$P_{02} = 26.31 \text{ psia}$$

The static pressure after the oblique shock wave is

$$P_2 = (P_2/P_1)P_1 = (1.695)(1.682)$$

$$P_2 = 2.7904 \text{ psia}$$

The static temperature after the oblique shock wave is

$$T_2 = (T_2 / T_1)T_1 = (1.159)(390)$$
$$T_2 = 452.2^\circ\mathrm{R}$$

3. The tangential velocity across an oblique shock does not change, but since the static temperature changes, the tangential Mach numbers before and after the shock are unequal. Now since

$$V_{1t} = V_{2t}$$
$$\therefore \frac{V_{1t}}{\sqrt{\gamma R T_1}}\sqrt{T_1} = \frac{V_{2t}}{\sqrt{\gamma R T_2}}\sqrt{T_2}$$
$$M_{1t}\sqrt{T_1} = M_{2t}\sqrt{T_2}$$
$$M_{2t} = M_{1t}\sqrt{\frac{T_1}{T_2}}$$
$$\therefore M_{2t} = 2.165\sqrt{\frac{1}{1.159}} = 2.0106$$
$$\therefore M_2 = \sqrt{M_{2n}^2 + M_{2t}^2} = \sqrt{(0.814)^2 + (2.0106)^2}$$
$$M_2 = 2.169$$

4. The angle of the streamline leaving the oblique shock is β where

$$\tan\beta = \frac{M_{2n}}{M_{2t}} = \frac{0.814}{2.0106} = 0.4048$$

$$\therefore \beta = 22.04^{\circ}$$

$\therefore$ The deflection angle $\delta = \theta - \beta = 30 - 22.04 = 7.96°$.

5. The Mach number after the normal shock wave is to be calculated from Equation 9.5

$$M_3^2 = \frac{(0.4)(2.0106)^2 + 2}{(2)(1.4)(2.0106)^2 - 0.4}$$

$$M_3 = 0.5755$$

6. The total pressure ratio across the normal shock wave may be obtained from Equation 9.10

$$\frac{P_{03}}{P_{02}} = \left[\frac{(2.4)(2.0106)^2}{2 + (0.4)(2.0106)^2}\right]^{3.5} \left[\left(\frac{2.8}{2.4}\right)(2.0106)^2 - \frac{0.4}{2.4}\right]^{-2.5}$$

$$\frac{P_{03}}{P_{02}} = 0.7159$$

$$P_{03} = 0.7159 \times 26.31 = 18.835 \text{ psia}$$

7. The static temperature is calculated from Equation 9.7

$$\frac{T_3}{T_2} = \left[\frac{2}{(2.4)(2.0106)^2} + \frac{0.4}{2.4}\right]\left[\left(\frac{2.8}{2.4}\right)(2.0106)^2 - \frac{0.4}{2.4}\right]$$

$$\frac{T_3}{T_2} = 1.696$$

$$T_3 = (1.696)(452.2) = 767°\text{R}$$

The static pressure is obtained from Equation 9.8

$$\frac{P_3}{P_2} = 1 + \frac{2.8}{2.4}\left[(2.0106)^2 - 1\right] = 4.55$$

$$P_3 = (4.55)(2.7904) = 12.695 \text{ psia}$$

9.7.3 Internal Compression Inlet (Intake)

The internal compression inlet locates all the shocks within the covered passage way (Figure 9.36). The terminal shock wave is also a normal one, which is located near or at the throat.

A principal difference between internal and external compression intakes is that with internal compression, since the system is enclosed, oblique shocks are reflected from an opposite wall, which have to be considered. The simplest form is a three-shock system. The single-wedge turns the flow toward the opposite wall. The oblique shock is reflected from the opposite wall and the flow passing the reflected shock is restored to an axial direction.

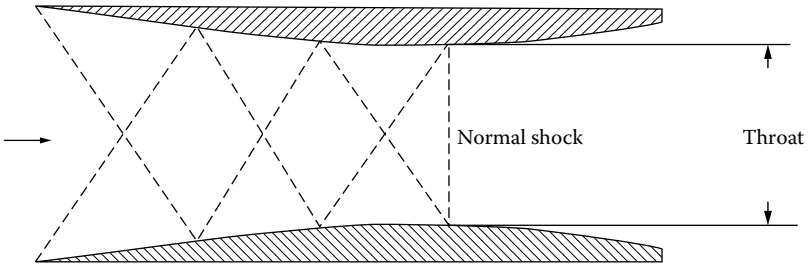


FIGURE 9.36
Internal compression supersonic intake.

A normal shock terminates the supersonic as usual. For a symmetrical intake, as shown in Figure 9.34, there are four oblique shocks. The reflected shocks are part of the symmetrical four-shock intersection system.

Again here, there are three flow patterns resembling critical (design), subcritical, and supercritical cases. The inlet is said to be operating in the critical mode when the normal shock wave is located at the throat resulting in the highest pressure recovery factor. In subcritical operation, the terminal (normal) shock wave is located upstream of the throat, or in the converging part of the diffuser. The supercritical mode occurs when the terminal shock is located downstream of the throat, or in the diverging part of the diffuser.

A subcritical flow operation is an unstable mode [5]. The terminal shock may move upstream, or ahead of the cowl lip, producing a condition called unstart. During an unstart condition, the pressure recovery factor will drop and flow will spill over the cowl, which will produce high drag.

For the above reason, internal supersonic compression intakes operate in the supercritical mode rather than the critical one. This represents a margin of stability if the inlet flow is suddenly changed.

9.7.4 Mixed Compression Intakes

These inlets use a combined external and internal compression system (Figure 9.28). Currently, all the supersonic intakes are of the mixed compression type.

Example 9.4

For the shown mixed-compression two-dimensional supersonic inlet, the free-stream Mach number is 3.0. A three-shock system (two oblique and shocks ended by a normal shock) reduces the speed from supersonic to subsonic speeds. Calculate

1. The overall total pressure ratio
2. The overall static pressure ratio (Figure 9.37)

Solution

1. The first oblique shock wave has an upstream Mach number $M_1 = 3$ and δ_1=15°, then from tables $\beta_1 = 32.25°$.
   Alternatively, from the Equation 9.11a and b, the angle (β_1) is determined iteratively. The same value of $\beta_1 = 32.25°$ is obtained.

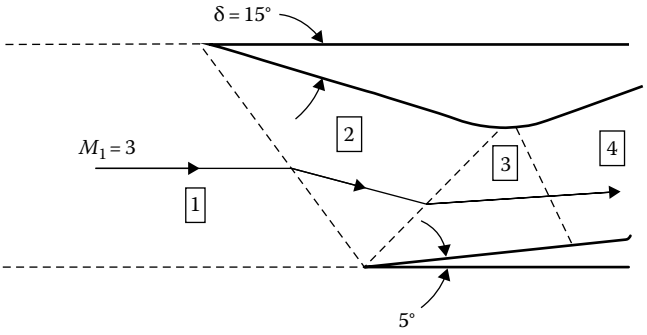


FIGURE 9.37
Three-shock system.

The Mach number after the shock wave is determined from the relation

$$M_2^2 = \frac{(\gamma-1)M_1^2\sin^2\beta + 2}{2\gamma M_1^2\sin^2\beta - (\gamma-1)}\frac{1}{\sin^2(\beta-\delta)}$$

With $\beta_1 = 32.25°$ and $\delta_1 = 15°$, then

$$M_2 = 2.25$$

From Equation 9.16a and b, the total pressure ratio is

$$\frac{P_{02}}{P_{01}} = 0.8935$$

The flow in the region 2 is deflected by an angle

$$\delta_2 = 15 + 5 = 20°$$

Then with $M_2 = 2.25$, from either tables or equations, $\beta_2 = 46.95°$

$$M_2^2 = \frac{36M_1^4\sin^2\beta - 5\left(M_1^2\sin^2\beta - 1\right)\left(7M_1^2\sin^2\beta + 5\right)}{\left(7M_1^2\sin^2\beta - 1\right)\left(M_1^2\sin^2\beta + 5\right)}$$

$$M_3 = 1.444$$

The total pressure ratio is then

$$\frac{P_{03}}{P_{02}} = 0.878$$

The flow in region 4 is downstream a normal shock wave

$$M_4 = 0.7219$$

$$\frac{P_{04}}{P_{03}} = 0.9465$$

$$\therefore \frac{P_{04}}{P_{01}} = \frac{P_{04}}{P_{03}} \times \frac{P_{03}}{P_{02}} \times \frac{P_{02}}{P_{01}}$$

$$= 0.9465 \times 0.878 \times 0.8935$$

The intake pressure recovery factor is

$$\frac{P_{04}}{P_{01}} = 0.7865$$

2. To evaluate the static pressure ratio, tables of the normal shock waves will be used (or Equations 9.6 through 9.10).
   For the first oblique shock, with $M_1 = 3$ and $\beta_1 = 32.25$

$$\therefore M_{1n} = M_1 \sin\beta_1$$

$$= 3 \times \sin 32.25 = 3 \times 0.5446$$

$$M_{1n} = 1.6008$$

The static pressure ratio $\frac{P_2}{P_1} = 2.82$.

For $M_2 = 2.25$ and $\beta_2 = 47$

$$\therefore M_{2n} = M_2 \sin\beta_2 = 2.25 \times 0.682$$

$$M_{2n} = 1.6455$$

The static pressure ratio $\frac{P_3}{P_2} = 2.992$.

For the last normal shock

$M_3 = 1.444$, then $\frac{P_4}{P_3} = 2.333$

The overall static pressure ratio is

$$\frac{P_4}{P_1} = \frac{P_4}{P_3} \times \frac{P_3}{P_2} \times \frac{P_2}{P_1} = 2.333 \times 2.992 \times 2.82$$

The overall static pressure ratio is

$$\frac{P_4}{P_1} = 19.691$$

9.8 Matching between Intake and Engine

As other engine modules, the intake is designed for certain operating conditions. However, the aircraft operates through a flight envelope containing an enormous variety of operating conditions. Therefore the intake has to cope with these different situations. This is accomplished by different capabilities for ingesting extra air quantity in some cases

(takeoff) and dumping unneeded air through bleeding in other cases. Some engines, particularly supersonic ones, are fitted with variable-geometry intakes. The engine control unit (ECU) controls both air and fuel flow into the engine that fulfill the requirements of different operating conditions.

Example 9.5

A ramjet engine is powering an aircraft flying at an altitude of 15 km where the ambient temperature and pressure are 216.5 K and 12.11 kPa, respectively. The maximum temperature is 2500 K and the fuel heating value is 43,000 kJ/kg. To examine the effect of intake design on the performance of the engine, it is assumed that only one normal shock converts the supersonic flow into subsonic flow. Moreover, all the other components are ideal. Plot the specific thrust and TSFC versus the Mach number.

Solution

Since only one normal shock exists in the intake, then the pressure recovery is the ratio between the total pressures upstream and downstream the shock wave, or

$$r_d = \frac{P_{02}}{P_{01}}$$

This ratio is obtained either from the normal shock tables or from the relation (9.11). The procedure for obtaining the specific thrust is described in Chapter 3 and only here the obtained results will be plotted. Figure 9.38 illustrates the relation between the free-stream Mach number and the pressure recovery factor. At a Mach number of nearly 2.0, the pressure recovery is nearly 0.72, while for a Mach number of 3.5 the pressure recovery is 0.212. This ensures that the efficient intake cannot use only one normal shock wave to reduce the air speed from supersonic speed to low subsonic speed suitable for subsonic combustors.

Figure 9.39 illustrates the drastic drop in thrust with the Mach number increase if the intake employs one normal shock wave. For the same case at Mach number 2.0, and pressure recovery of 0.72, the thrust drops by nearly 20%. Moreover, at Mach number 3.5, the shock losses would become so severe that all the engine thrust would be lost.

Comment: A similar case was discussed for a turbojet engine in Reference 13; the examined intake also had only one normal shock wave. The thrust was completely lost at Mach number 3.5.

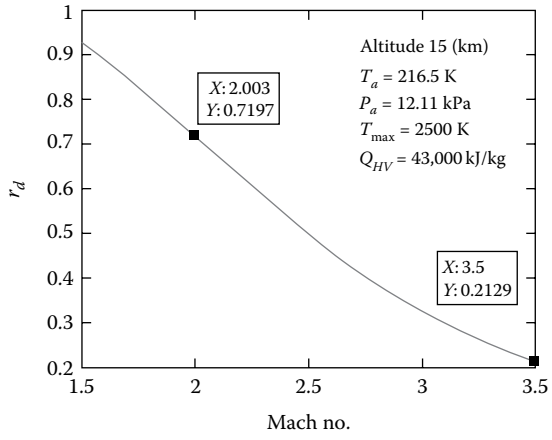


FIGURE 9.38
Pressure recovery due to a normal shock versus the Mach number for ramjet engine.

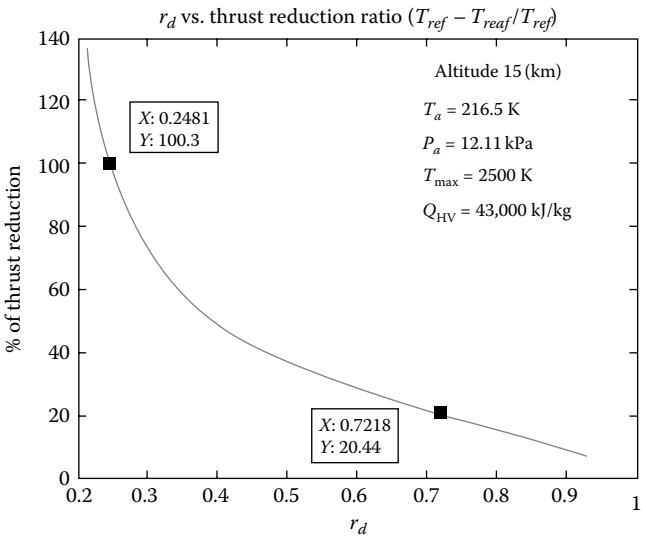


FIGURE 9.39
Percentage of thrust loss versus pressure recovery for a ramjet engine.

9.9 Case Study

The turbo ramjet engine previously described in Chapter 7 is analyzed here. The geometry of the intake for the turbojet engine operating at low supersonic speeds (up to Mach number 2.0) is shown in Figure 9.40. Two designs are examined: four oblique shocks and eight oblique shocks. In both cases, a normal shock wave exists downstream the oblique shocks.

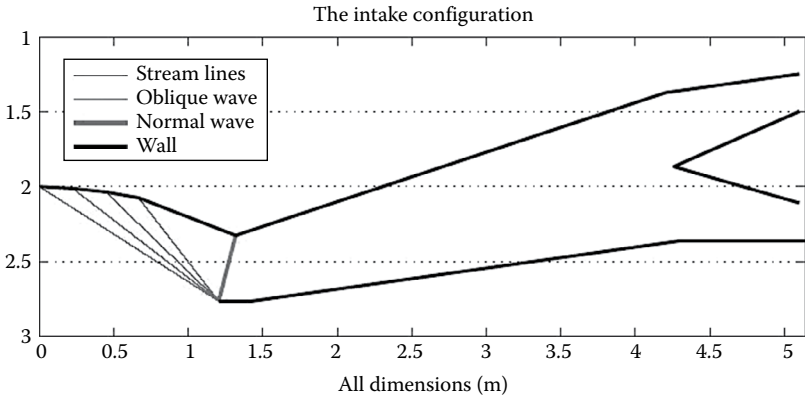


FIGURE 9.40
Intake geometry.

The design point of the turbojet intake is given in the following table:

	Intake Design Point
Mach number M	2
Altitude	12.507 km
Ambient temperature T_a	216.66 K
Ambient pressure P_a	17.857 kPa
Ambient density ρ_a	0.2872 kg/m^3
Flight speed V_∞	590.0983 m/s
Mass flow rate	130 kg/s

The following table presents the shock characteristics as well as the Mach number and speed downstream four successive shocks.

Position	**δ (deg)**	**β (deg)**	M_e	V_e **(m/s)**	P_{0e}/P_{0i}
After 1st wave	3	32.5055	1.8924	571.8126	0.9995
After 2nd wave	3.1026	34.6033	1.7839	552.0081	0.9995
After 3rd wave	4.0353	37.8574	1.6454	524.6129	0.9991
After 4th wave	4.4098	41.9685	1.4953	492.0425	0.9989
After normal wave	—	—	0.7027	265.3856	0.93127
After diffuser	—	—	0.3386	132.5240	0.98620

The pressure recovery factor for the four oblique shocks is 91.57% and the intake efficiency is 94.41%. The static pressure, temperature, and density variation along the diffuser is plotted in Figure 9.41. The Mach number, speed, and overall total pressure ratio are plotted along the diffuser in Figure 9.42.

The following table presents the shock wave characteristics for the 10 oblique shock case.

Position	**δ (deg)**	**β (deg)**	M_e	V_e **(m/s)**	P_{0e}/P_{0i}
After 1st wave	1.5	31.2259	1.9459	581.0759	0.9999
After 2nd wave	2.0263	33.1751	1.8518	564.5681	0.9998
After 3rd wave	2.6578	34.4534	1.7814	551.5333	0.9997
After 4th wave	2.74903	37.1048	1.6713	529.9305	0.9996
After 5th wave	3.2082	39.4409	1.5781	510.3819	0.9995
After 6th wave	3.5027	43.5466	1.4449	480.4076	0.9994
After 7th wave	3.9039	48.2073	1.3219	450.4606	0.9993
After 8th wave	4.0155	55.8417	1.1659	409.2317	0.9991
After normal wave	—	—	0.8642	319.0882	0.9956
Subsonic diffuser	—	—	0.3704	144.6517	0.9813

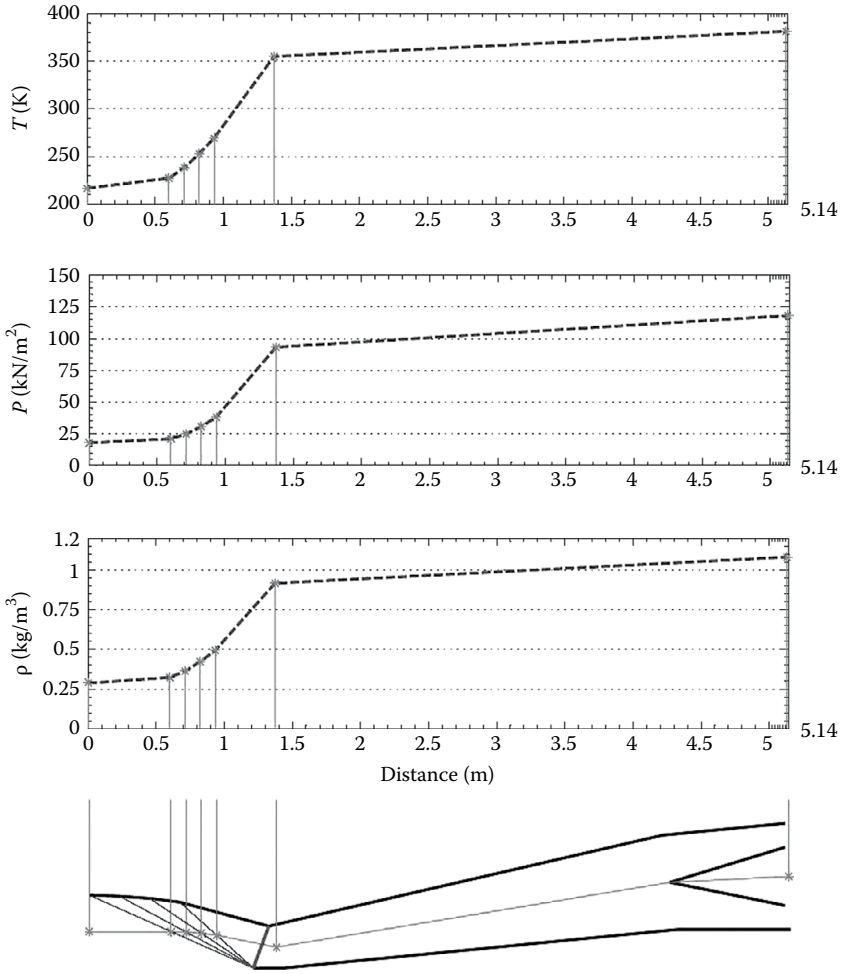


FIGURE 9.41
Static pressure and temperature as well as density distribution for a four-oblique-shock case.

Pressure recovery for the eight oblique shocks case is 97.37% while the intake efficiency is 98.29%. The static pressure, temperature, and density variation along the diffuser is plotted in Figure 9.43. The Mach number, speed, and overall total pressure ratio are plotted along the diffuser in Figure 9.44.

From both cases, it can be seen that increasing the number of shocks increases the effectiveness of the intake, and consequently the pressure recovery and adiabatic efficiency of the intake. Ultimately, by a continuous increase of the number of oblique shocks, there will be no need for the normal shock and the case of isentropic diffuser will be reached.

The intake is of the variable-geometry type. A simplified layout for the actuation system is shown in Figure 9.45.

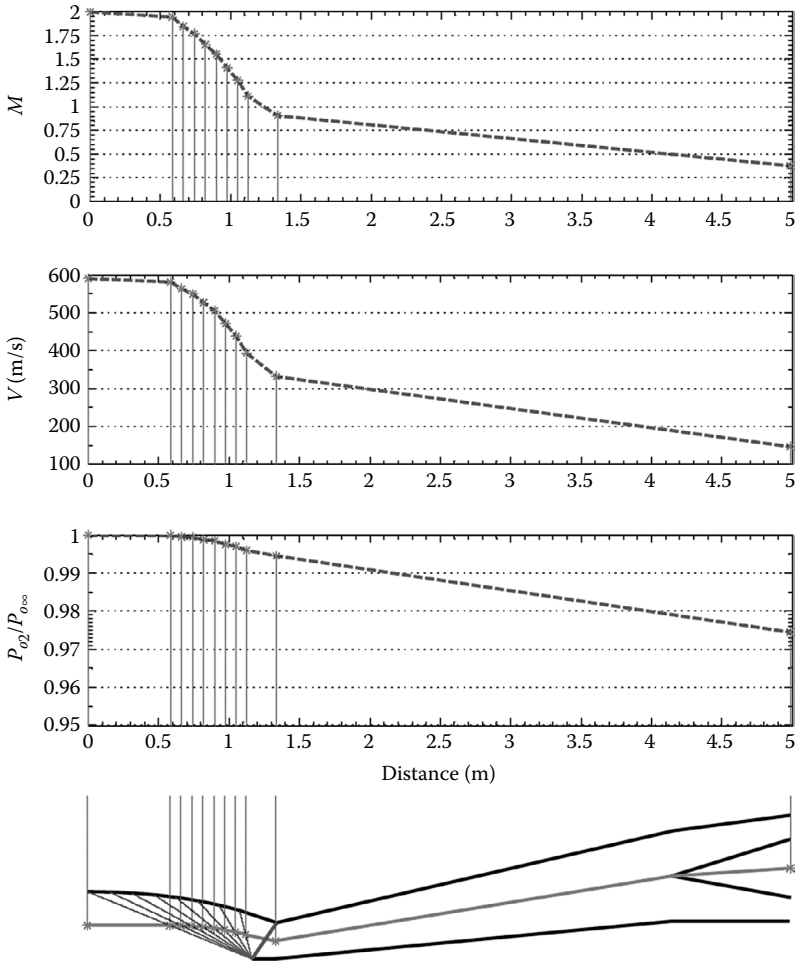


FIGURE 9.42
Mach number, speed, and total pressure ratio distribution for a four-oblique-shock case.

Example 9.6

A fighter aircraft (F-111A) is flying at an altitude of 13,700 m where the ambient pressure and temperature are, respectively, 14,794 Pa and 216.66 K, Figure 9.46. The F-111A is powered by two Pratt & Whitney TF30 afterburning turbofan engines. The engine has the one-quarter-circle (r = 0.846 m) axisymmetric external compression inlets under the wing (Figure 9.47). Air enters the intake with a Mach number of 2.2. The intake diffuser has *single oblique shock wave followed by a normal shock wave*, Figures 9.48 and 9.49. The deflection angle of spike is 12.5°.

Find

1. The total pressure and temperature of air entering the oblique shock wave
2. The oblique shock-wave angle (θ)
3. The static and total conditions after the oblique shock
4. The Mach number after the oblique shock wave
5. The Mach number after the normal shock wave
6. The static and total conditions after the normal shock wave

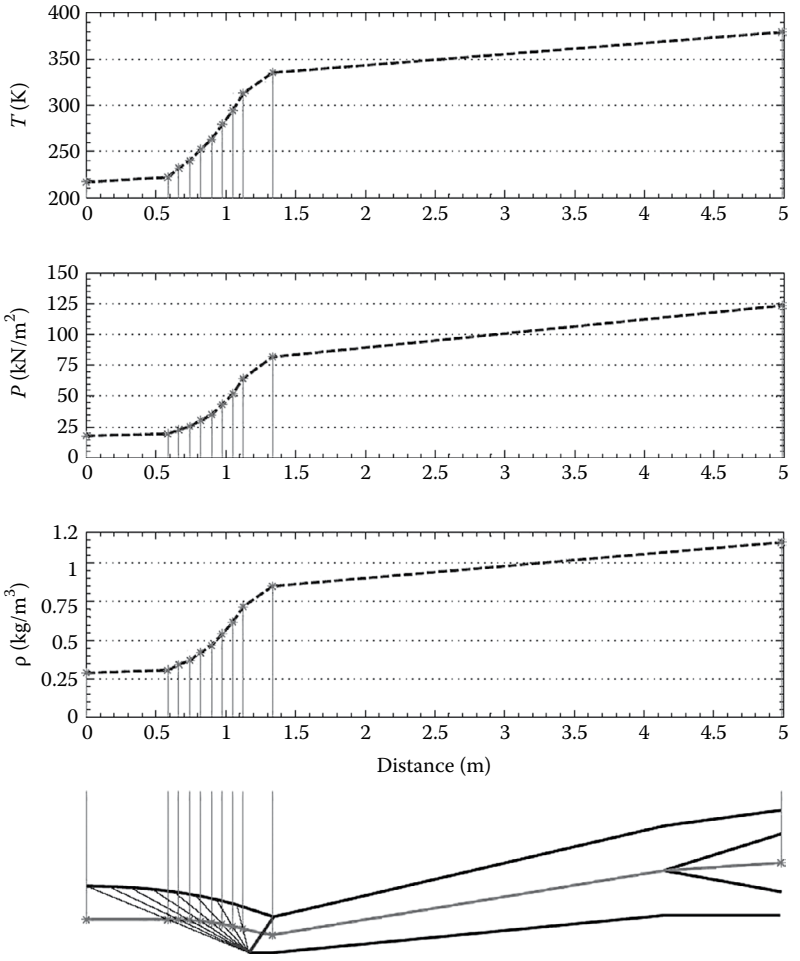


FIGURE 9.43
Static temperature and pressure as well as density distribution for an eight-oblique-shock case.

7. The total pressure recovery (assume that the pressure recovery for subsonic section of intake = 0.98)
8. The mass flow rate inlet engine
($\gamma = 1.4$ and $R = 287$ J/kg·K)

Solution

1. The total pressure and temperature of air entering the oblique shock wave are

$$T_{0\infty} = T_a \times \left(1 + \frac{\gamma - 1}{2} M_a^2\right) = 426.66\,\text{K}$$

$$P_{0\infty} = P_a \times \left(1 + \frac{\gamma - 1}{2} M_a^2\right)^{\gamma/\gamma - 1} = 1.58187 \times 10^5\ \text{Pa}$$

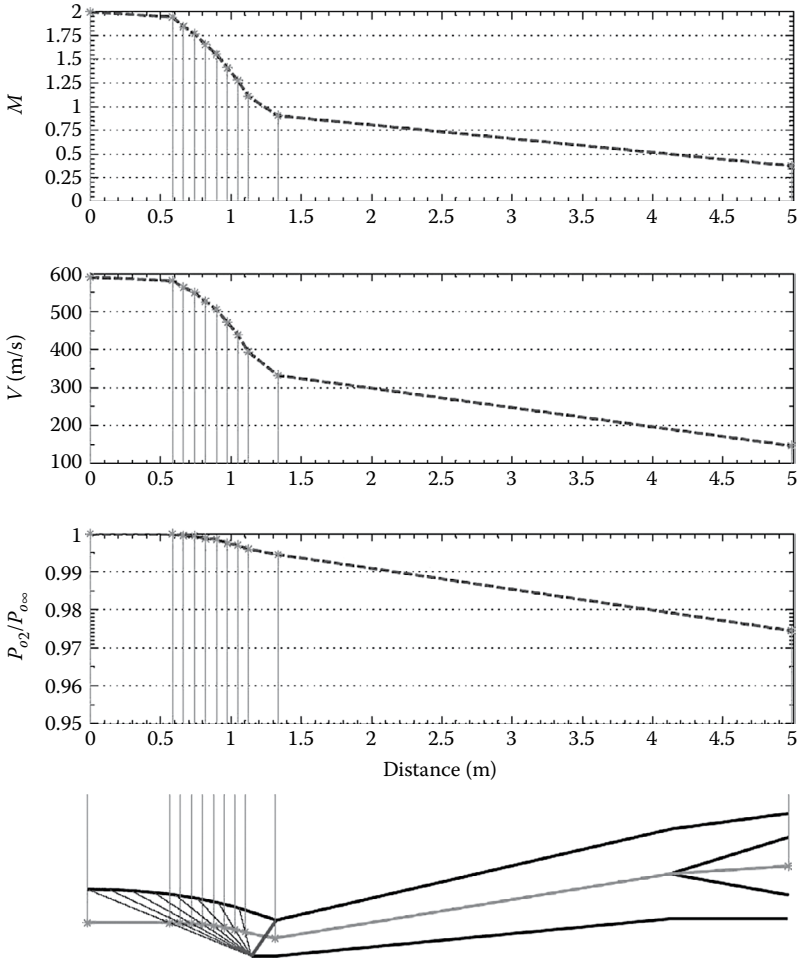


FIGURE 9.44
Mach number, speed, and total pressure ratio distribution for an eight-oblique-shock case.

2. The oblique shock-wave angle is (θ)
   With a free-stream Mach number $M_a = 2.2$ and a deflection angle $\delta = 12.5°$, then the shock-wave angle will be either determined from gas dynamics tables or iteratively from the following relation:

$$\tan\delta = \frac{2\cot\theta\left(M_a^2\sin^2\theta - 1\right)}{(\gamma+1)M_a^2 - 2\left(M_a^2\sin^2\theta - 1\right)} \tag{A}$$

   Both methods give the value $\theta = 38.411°$.
3. The static and total condition after oblique shock
   The Mach number upstream the oblique shock wave can be decomposed into normal and tangential components. The normal component of the free stream Mach number is

$$M_{an} = M_a\sin\theta = 2.2\sin 38.411° = 1.36685$$

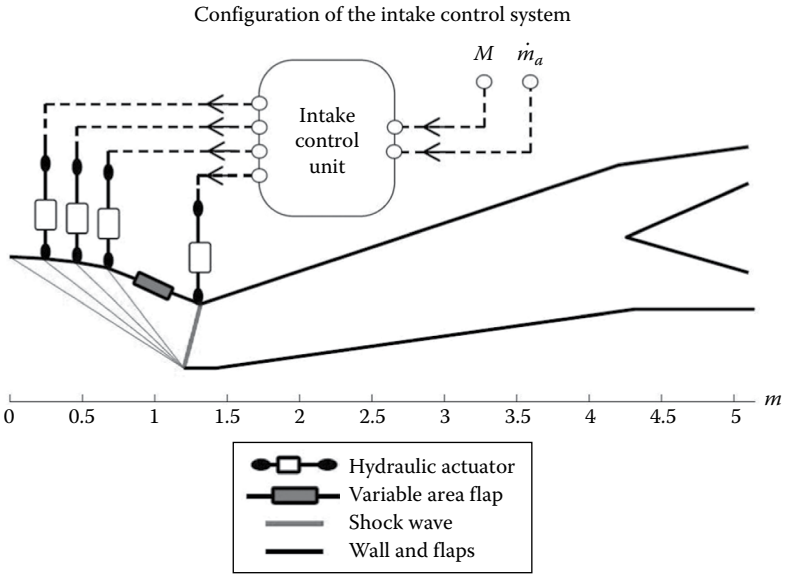


FIGURE 9.45
Actuation system for the variable geometry four-oblique-shock intake.

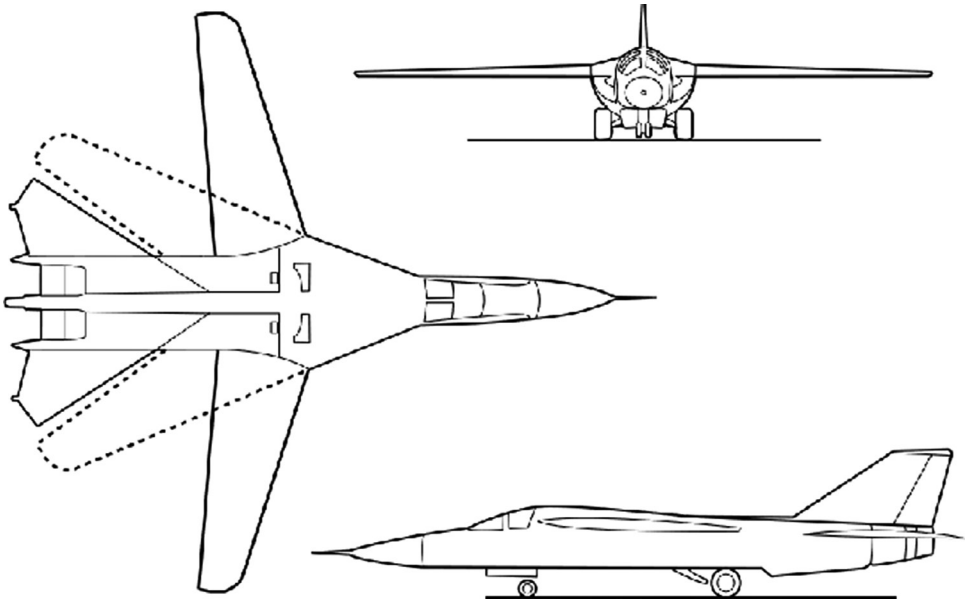


FIGURE 9.46
A fighter aircraft (F-111A).



FIGURE 9.47
A fighter aircraft (F-111A) supersonic intake.

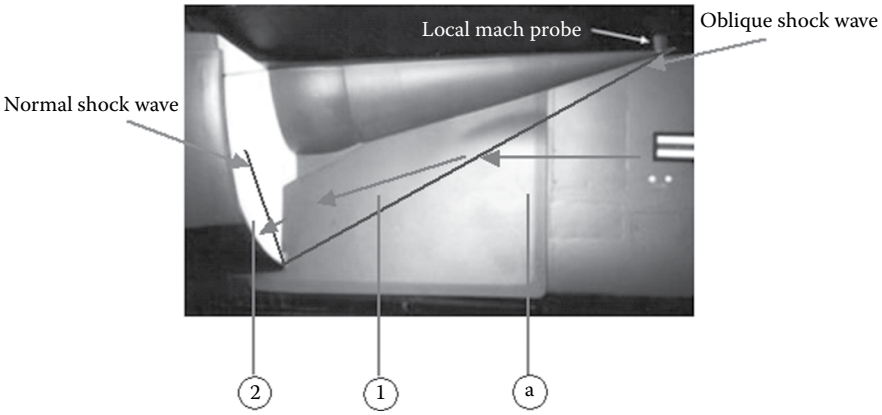


FIGURE 9.48
A fighter aircraft (F-111A) supersonic intake with single-oblique shock wave followed by a normal shock wave.

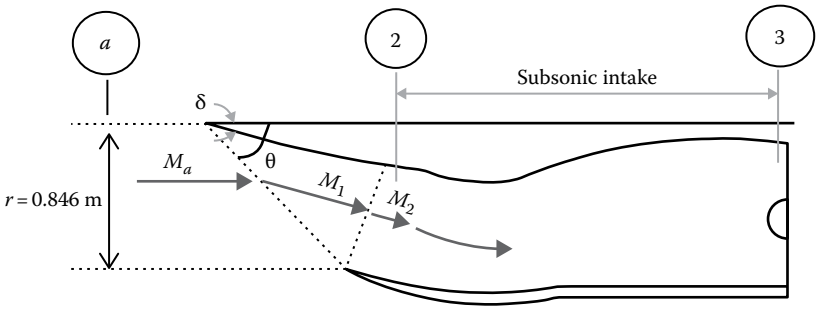


FIGURE 9.49
A fighter aircraft (F-111A) supersonic intake with states for a single-oblique shock wave followed by a normal shock wave.

The normal component of the Mach number downstream the normal shock wave will be determined also either from normal shock-wave tables or from the relation

$$M_{1n}^2 = \frac{(\gamma-1)M_{an}^2 + 2}{2\gamma M_{an}^2 - (\gamma-1)}, \quad M_{1n} = 0.7541$$

The static and total conditions after the oblique shock wave can be determined from normal shock-wave tables or from the relations

$$\frac{P_{01}}{P_{0a}} = \left[\frac{(\gamma+1)M_{an}^2}{2+(\gamma-1)M_{an}^2}\right]^{\gamma/\gamma-1}\left[\left(\frac{2\gamma}{\gamma+1}\right)M_{an}^2 - \left(\frac{\gamma-1}{\gamma+1}\right)\right]^{-(1/\gamma-1)} = 0.966$$

$$\frac{P_1}{P_a} = \left[1+\left[\frac{2\gamma}{\gamma+1}\right]\left(M_{an}^2-1\right)\right] = 2.013$$

$$\frac{T_1}{T_a} = \left[\frac{2}{(\gamma+1)M_{an}^2} + \frac{(\gamma-1)}{(\gamma+1)}\right]\left[\left(\frac{2\gamma}{\gamma+1}\right)M_{an}^2 - \left(\frac{\gamma-1}{\gamma+1}\right)\right] = 1.233$$

We get

$$P_{01} = 1.528086\times10^5 \text{ Pa}, \quad P_1 = 2.97803\times10^4 \text{ Pa}, \quad T_1 = 267.149 \text{ K}, \quad T_{o1} = T_{oa}$$

4. The Mach number after oblique shock wave

$$M_1 = \frac{M_{1n}}{\sin(\theta-\delta)} = \frac{0.7541}{\sin(38.411-12.5)} = 1.726$$

5. The Mach number after normal shock wave

$$M_2^2 = \frac{(\gamma-1)M_1^2 + 2}{2\gamma M_1^2 - (\gamma-1)}, \quad M_2 = 0.634$$

6. The static and total condition, after normal shock wave, may be determined from normal shock-wave tables or from the relation

$$\frac{P_{02}}{P_{01}} = \left[\frac{(\gamma+1)M_1^2}{2+(\gamma-1)M_1^2}\right]^{\gamma/\gamma-1}\left[\left(\frac{2\gamma}{\gamma+1}\right)M_1^2 - \left(\frac{\gamma-1}{\gamma+1}\right)\right]^{-(1/\gamma-1)} = 0.8448$$

$$\frac{P_2}{P_1} = \left[1+\left[\frac{2\gamma}{\gamma+1}\right]\left(M_1^2-1\right)\right] = 3.308$$

$$\frac{T_2}{T_1} = \left[\frac{2}{(\gamma+1)M_1^2} + \frac{(\gamma-1)}{(\gamma+1)}\right]\left[\left(\frac{2\gamma}{\gamma+1}\right)M_1^2 - \left(\frac{\gamma-1}{\gamma+1}\right)\right] = 1.477$$

We get

$$P_{02} = 1.290958\times10^5 \text{ Pa}, \quad P_2 = 9.854068\times10^4 \text{ Pa}, \quad T_2 = 394.6025 \text{ K}, \quad T_{o1} = T_{o2}$$

7. From Figure 9.49, the total pressure recovery

$$\frac{P_{03}}{P_{0a}} = \frac{P_{03}}{P_{02}} \times \frac{P_{02}}{P_{01}} \times \frac{P_{01}}{P_{0a}} = 0.98 \times 0.8448 \times 0.966 = 0.79975$$

8. The mass flow rate inlet engine

$$\dot{m}_{inlet} = \rho_a \times V_a \times A = \frac{P_a}{RT_a} \times M_a \times \sqrt{\gamma RT_a} \times \frac{\pi r^2}{4} = 86.8105 \text{ kg/s}$$

Example 9.7

F-111A is fitted with an automatic inlet control system. This system senses the local Mach number and then changes the spike angle, (δ). Calculate the spike angle appropriate for flight Mach numbers of M = 1.9 and M = 2.5.

Solution

From Example 9.6 with a free-stream Mach number M_a=2.2 and a deflection angle δ=12.5°, the shock-wave angle was calculated as θ = 38.411°, which will be assumed constant for different Mach numbers.

Now for a free-stream Mach number M_a=1.9 and a shock-wave angle θ=38.411°, the deflection angle of spike will be determined either from gas dynamics tables or iteratively from Equation A in Example 9.6. The final result is δ=7.181°.

Next, for a free stream Mach number M_a=2.5 and a shock-wave angle θ=38.411°, the deflection angle of spike will be δ=16.312°.

Since when the flight Mach number was M = 2.2, the deflection angle was δ = 12.5°, then if the flight Mach number is increased to 2.5 the spike angle will be increased by Δδ=3.8°. While, if the Mach number is 1.9, the spike angle will be decreased by Δδ=5.319°, as shown in Figure 9.50.

A plot for the deflection angle of spike and the corresponding Mach number is plotted in Figure 9.51.

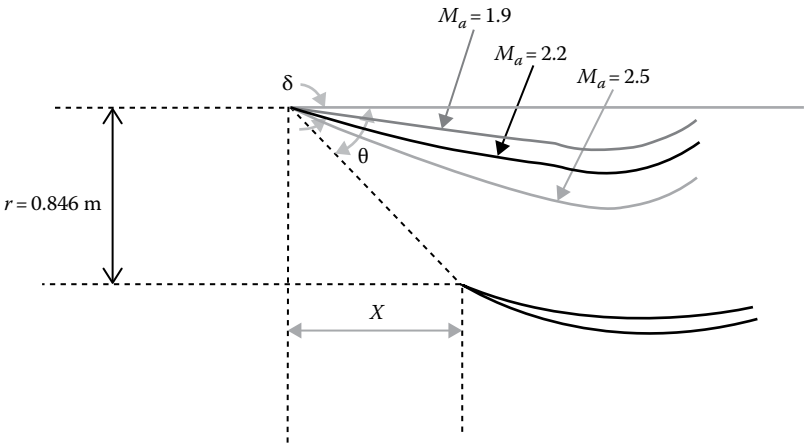


FIGURE 9.50
Variation of intake spike angle with different Mach number.

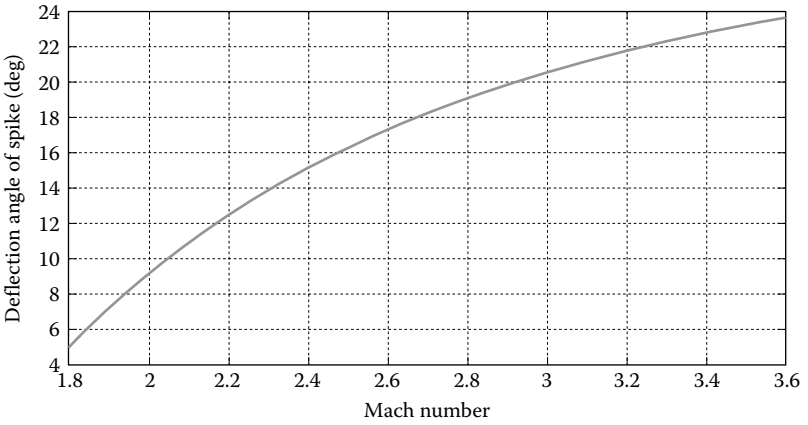


FIGURE 9.51
Variation of deflection angle with Mach number at constant wave angle of θ = 38.411°.

Problems

9.1 A fighter airplane is flying at an altitude where the ambient pressure and temperature are 11.6 kPa and 216.7 K. The intake is composed of a supersonic part followed by a subsonic part. Within the supersonic part, two shock waves are generated: an oblique shock followed by a normal shock wave. After the normal shock wave, the Mach number is 0.504. Within the subsonic part, pressure recovery is 98.7% and the total temperature remains constant. The static pressure and temperature after the normal shock wave are 111.5 kPa and 600 K. It is required to

1. Calculate the turning angle of the supersonic diffuser δ
2. Calculate the Mach number at the inlet of the supersonic diffuser

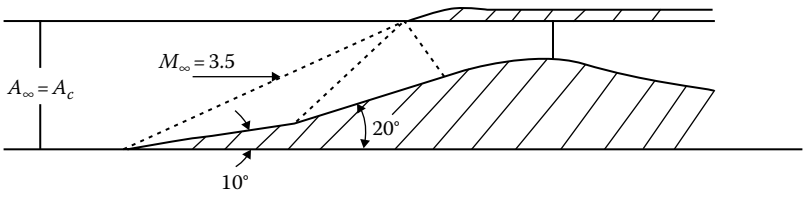


FIGURE P9.1

9.2 The following Figure P9.2 illustrates a four-shock type intake where three oblique shocks are followed by a normal shock. The Mach number after the normal shock is 0.6. Find

1. The free-stream Mach number
2. The static pressure ratio after the four shocks

3. The pressure recovery factor for the intake if the total pressure ratio within the subsonic diffuser is 0.99

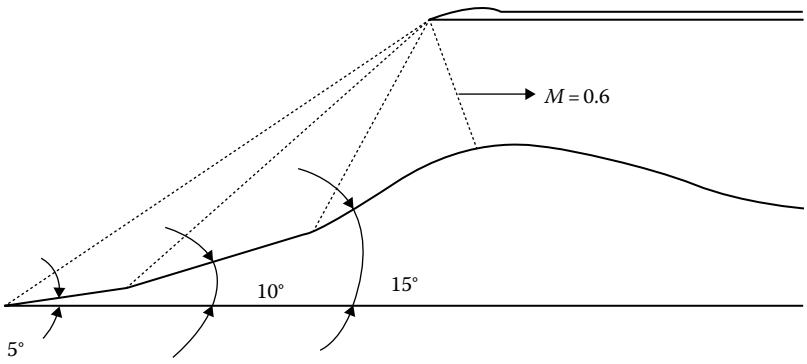


FIGURE P9.2

9.3 A supersonic fighter has the shown intake that is fitted with a movable spike. The circular intake has an inlet radius $R = 1$ m. During ground run, the following data was recorded:

Air mass flow rate	350 kg/s
Ambient temperature	288 K
Ambient pressure	101 kPa
Free stream velocity	100 m/s

What will be the distance x of the outer portion of the spike?

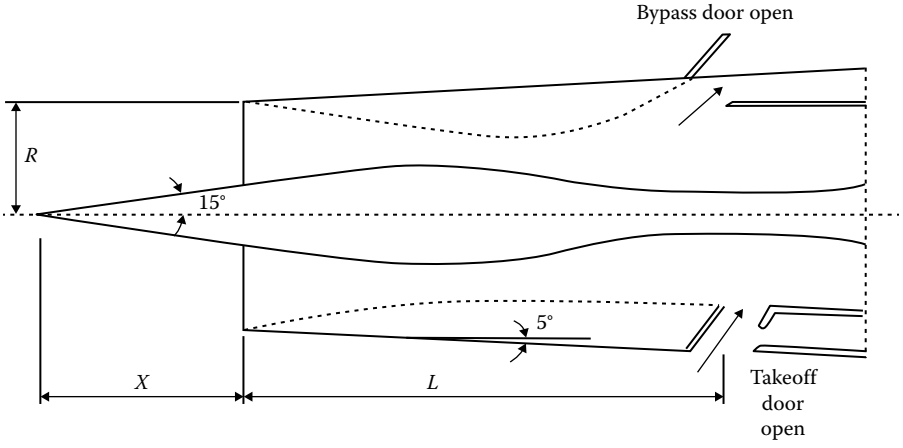


FIGURE P9.3

If the needed mass flow rate becomes 380 m/s, two options are suggested: either retracting the spike to increase the inlet area or opening the 8 blow-up doors. Calculate the new position of the spike (x'). If the blow-up doors are opened, calculate the length of the doors, if the subtended angle to each door is 30° and the length L is equal to 1.6 m.

9.4 The two-dimensional or wedge-type diffuser consists of two external oblique shocks: a normal shock and a subsonic diffuser, as shown in the following figure. Assuming that the external losses are due to the shock losses and the pressure drop in the subsonic part is 4.5%,

1. Determine the total pressure ratio for the shown Mach number of 3.5.
2. What will be the external length of the wedge if the height of intake is 0.5 m?

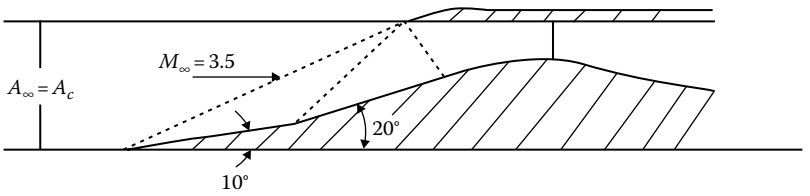


FIGURE P9.4

9.5 A two-dimensional wedge-type diffuser of a military aircraft is flying at a Mach number of 2.5 and at an altitude where the ambient conditions are −56.5°C and 12 kPa is shown in Figure P9.5. The Mach number of the flow leaving the throat is 0.7; what is the value of the wedge angle δ_1? For the shown two-dimensional supersonic inlet calculate the static and total temperatures and pressures at different states of the inlet.

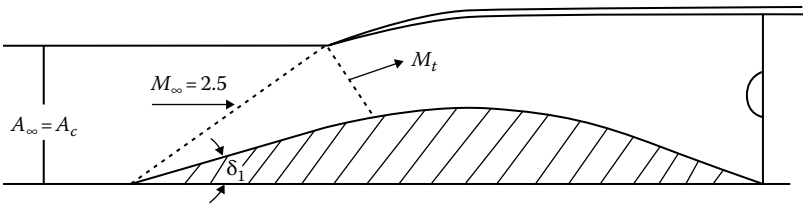


FIGURE P9.5

9.6 It is required to examine the case of a subsonic inlet if installed to a fighter airplane flying at a Mach number of 1.8 as shown in Figure P9.6. Calculate the Mach number downstream of the normal shock wave. If the Mach number at the lips of the subsonic intake is 0.5, what will be the ratio between the mass flow rate entering the engine and the approaching mass upstream the normal shock and having the same area ($A_\infty = A_c$)?

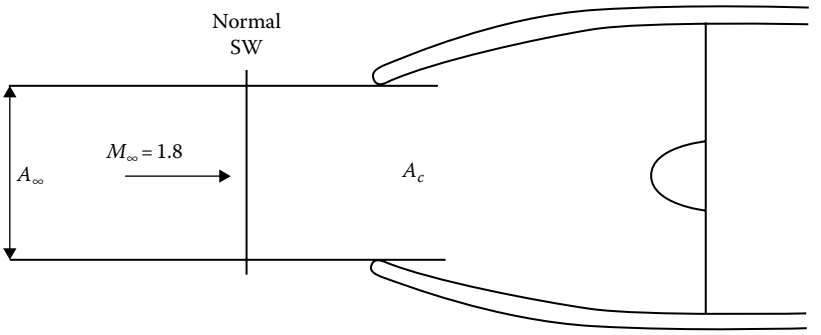


FIGURE P9.6

9.7 The supersonic axisymmetric intake shown is fitted to an aircraft flying at Mach number of 2.1 at an altitude of 12 km. If the supersonic turbofan engine powering this fighter consumes 35 kg/s and the spike length outside the intake is 0.8 m and intake radius is 0.6 m, determine whether the intake side doors are injecting or ejecting airflow from the intake. What will be the spike length that allows exact airflow rate into the engine if the side doors are closed?

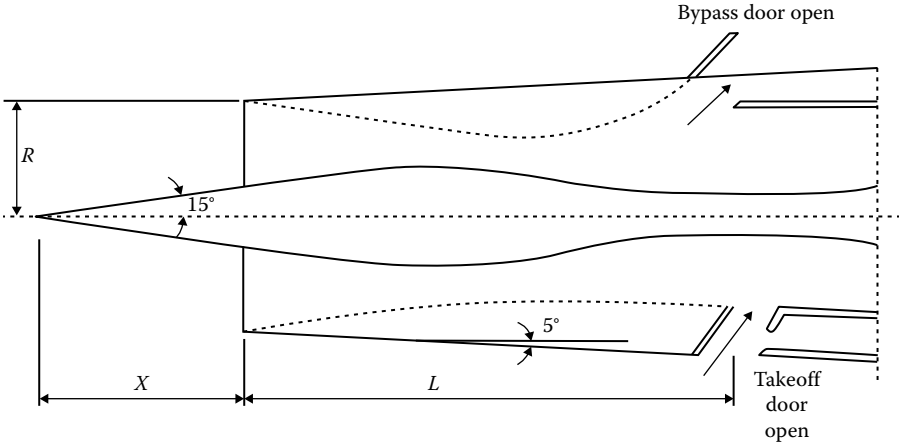


FIGURE P9.7

9.8 The figure shown illustrates a supersonic intake of an engine installed on the lower surface of the wing of a fighter airplane. The airplane has a maximum Mach number of 2.3. Two shocks are generated (oblique and normal) and the long duct upstream of the engine is a subsonic part having a pressure drop of 10%. The Mach number at the engine inlet is 0.5, which is 15% less than the Mach number downstream of the normal shock wave. Calculate the wedge angle of the oblique shock wave. What will be the overall pressure ratio of this intake? Have you any suggestions?

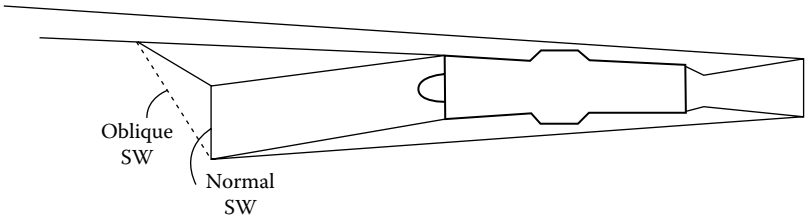


FIGURE P9.8

9.9 Is the intake shown in its design or off-design conditions? The flight Mach number is 2.5 and the flight altitude is 18 km (Figure P9.9). The wedge angle is 10°. Calculate the ratio A_∞/A_c if the spike length outside the engine is 1.0 m and the intake width is 1.0 m. What is the total pressure ratio of the intake if the subsonic part develops 15% losses?

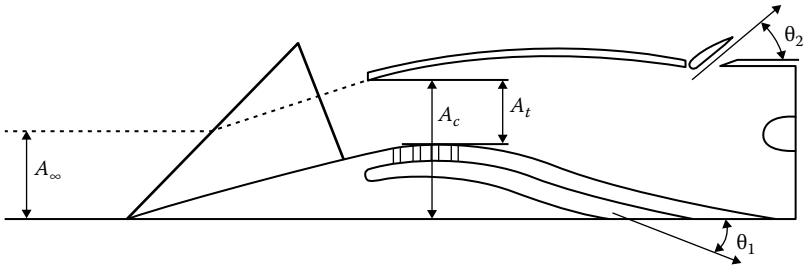


FIGURE P9.9

9.10 The supersonic two-dimensional intake shown in Figure P9.10 has three oblique shocks and a final normal shock. The first wedge angle is δ = 5°. Each subsequent wedge has an additional 1°. The flight Mach number is 2.2. What will be the efficiency of the intake? For a flight altitude of 9 km, calculate the static and total pressures downstream each shock.

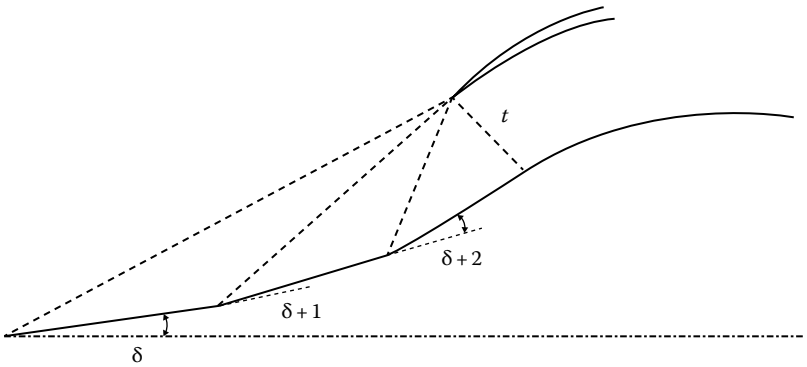


FIGURE P9.10

9.11 During cruise flight, the ambient conditions and the intake conditions in a turbofan engine are P_∞= 23.824 kPa, T_∞ = 218.665 K, total air mass flow rate of engine $\dot{m}$= 118 kg/s.

Mach numbers are as follows: Far upstream: M_∞ = 0.85, at diffuser inlet (capture section) M_c = 0.8 and fan inlet M_f = 0.50.

Assuming the diffuser pressure recovery: π_d = 0.95.

1. Determine the diameters at far upstream (d_∞), intake inlet section (d_c), and intake outlet section (or fan inlet section: d_f). Assume the hub-tip ratio of fan is 0.3.
2. Diffuser length L (assume that the diffuser angle 2θ is 12°).

9.12 The fighter aircraft (F-111A) described in Example 9.6 has an automatic inlet control system. This system senses the local Mach number and then moves the spike longitudinally. If the spike deflection angle is constant (δ = 12.5°), calculate the distance (x) for spike at flight Mach number M = 1.9, M = 2.2, and M = 2.5.

9.13 A fighter aircraft (F-111A) is flying at an altitude of 13,700 m where the ambient pressure and temperature are respectively 14,794 Pa and 216.66 K, as shown in Figure P9.13. The F-111 is powered by two Pratt & Whitney TF30 afterburning turbofan engines. The engine has a one-quarter-circle (r = 0.846 m) axisymmetric external compression inlet under the wing, as shown in Figure P9.13. The aircraft flies at a Mach number of 2.2. An oblique shock wave is attached to the aircraft nose having a shock wave angle θ_1 = 35°. At intake diffuser a second oblique shock wave having a wave angle θ_2 = 38.411°, followed by a normal shock wave are generated as shown in Figure P9.13.

Calculate

1. The total pressure and temperature of air entering the first oblique shock wave
2. The deflection angle of aircraft nose (δ_1)

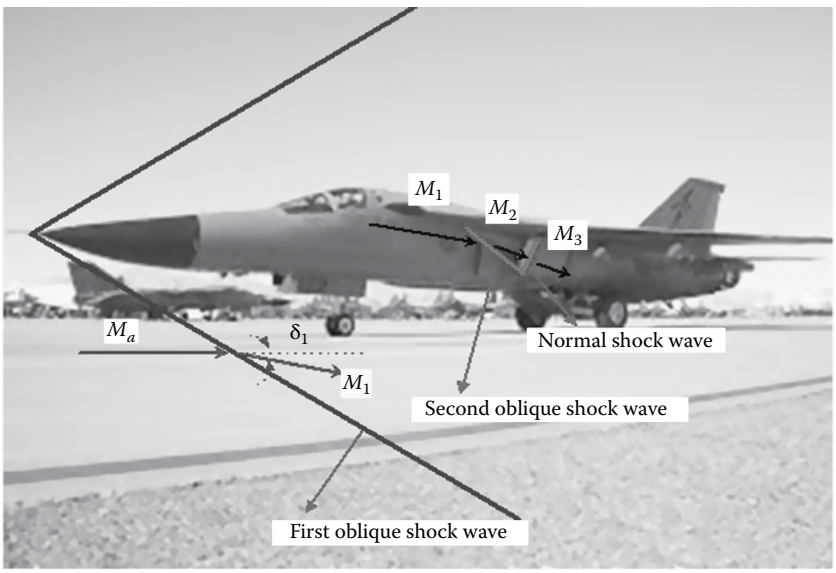


FIGURE P9.13

3. The pressure recovery across the first oblique shock
4. The Mach number after the first oblique shock wave
5. The deflection angle of a spike (δ_2)
6. The Mach number after the second oblique shock wave
7. The pressure recovery across the second oblique shock
8. The Mach number after the normal shock wave
9. The pressure recovery across the normal shock wave
10. The total pressure recovery (where pressure recovery for the subsonic intake = 0.98)
11. The external distance of spike (X)

($\gamma = 1.4$ and $R = 287\ \mathrm{J/kg \cdot K}$)

9.14 The following Figure P9.14 illustrates a divided intake having two circular inlets, each has a diameter of 0.3 m (section A–A). The branched part of intake ends with an elliptical section (B–B) having major and minor diameters of 0.6 and 0.5 m. Air then

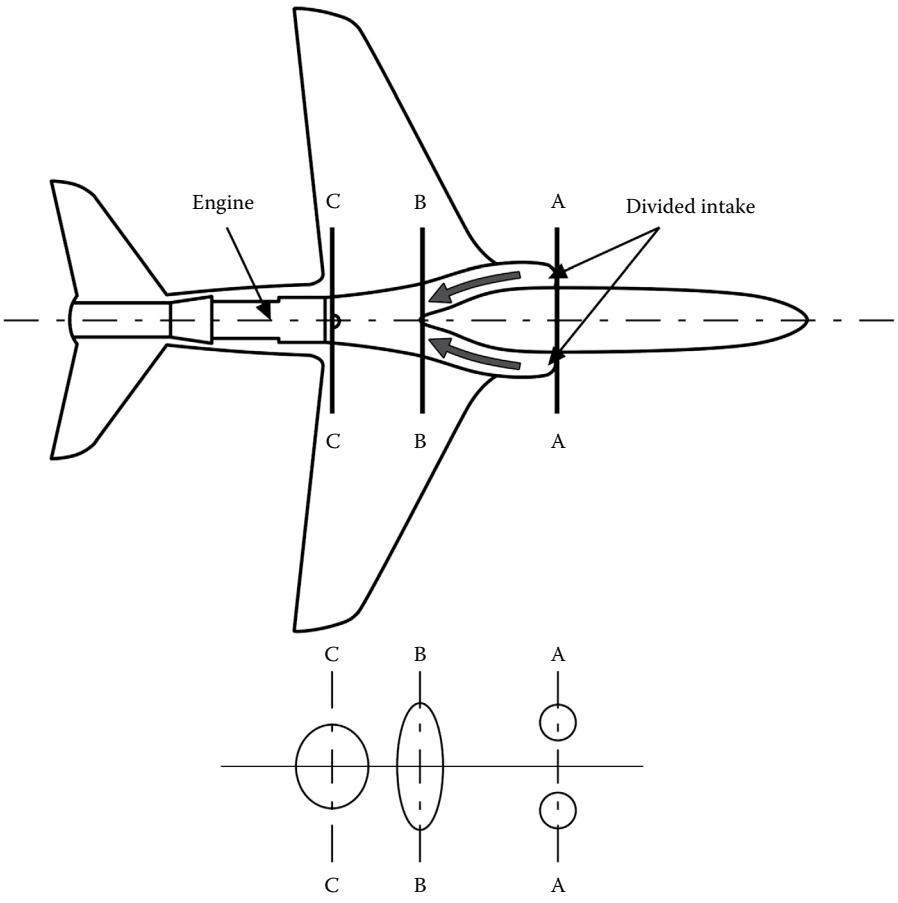


FIGURE P9.14

continues to diffuse to the engine inlet (Section C–C) that has a circular shape with a diameter of 0.6 m.

1. If the air velocity at engine inlet (Section C–C) is 60 m/s, calculate the air inlet velocity at the inlet and outlet of the divided section (Sections A–A and B–B, respectively).
2. If the ambient conditions are $T_a = 288$ K, $P_a = 101$ kPa, calculate the inlet total temperature and pressure at Section A-A.
3. Assume the total pressure drops in the branching, and the succeeding diffuser parts up to the engine inlet are respectively 2% and 1%. Calculate the total pressure and temperature at section C–C.

References

1. J.J. Mahoney, *Inlet for Supersonic Missiles*, AIAA Education Series, New York, 1990, p. 1.
2. R.S. Shevel, *Fundamentals of Flight*, Prentice-Hall, Inc., Englewood Cliffs, NJ, 1983, p. 348.
3. I. Kroo and R. Shevel, *Aircraft Design: Synthesis and Analysis, Digital Textbook*, version 0.99, Stanford University, Stanford, CA, January 2001, p. 374.
4. *The Jet Engine*, 5th edn., Rolls-Royce plc, Derby, U.K., p. 245, Reprinted 1996 with revisions.
5. W.W. Bathie, *Fundamentals of Gas Turbines*, 2nd edn., John Wiley& Sons, Inc., New York, 1996, p. 330.
6. J. Seddon and E.L. Goldsmith, *Intake Aerodynamics*, AIAA Education Series, New York, 1989, p. 19.
7. P. Hill and C. Peterson, *Mechanics and Thermodynamics of Propulsion*, 2nd edn., Addison Wesley Publication Company, Inc., Boston, MA, 1992, p. 219.
8. *Power Plant*, Volume II, Boeing Publication, D6-1420, pp. 2–36.
9. J. Roskam, *Airplane Design*, Volume VI: Preliminary Calculation of Aerodynamic, Thrust and Power Characteristics, Roskam Aviation and Engineering Corporation, Lawrence, KS, 1990, p. 152.
10. J.L. Kerrebrock, *Aircraft Engines and Gas Turbines*, 2nd edn., MIT Press, Cambridge, MA, 1992, p. 121.
11. *Compressible Flow Data Book for Data Book for Engineering Tripos*, Cambridge University Engineering Department, Cambridge, U.K., 2004.
12. Equations, tables and charts for compressible flow, NACA Report 1153, Ames Research Staff, 1953.
13. D.D. Wyatt. A review of supersonic air intake problems, In: Fabri, J. (eds.), *Air Intake Problems in Supersonic Propulsion*, Pergamon Press, London, U.K., 1958, p. 21.

10

Combustion Systems

10.1 Introduction

The combustion process in aircraft engines and gas turbines is one in which heat is added to the compressed air in the combustor or burner. Thus, the combustion is a direct-fired air heater in which fuel is burned. The combustor is situated between the compressor and turbine, where it accepts air from the compressor and delivers it at an elevated temperature to the turbine. Some engines have a second combustion system that either reheats the flow for the later turbine stages (as described in Chapter 8) or burns more fuel in an afterburner behind the turbines to provide the high exhaust velocity required for the propulsion of supersonic aircraft (as described in Chapters 4 and 5). A part of the supplied energy provides useful work absorbed by the turbine(s) and the remainder goes to waste as heat in the exhaust gas [1]. Combustion in gas turbines is a continuous process that takes place at high pressure in a smaller space and usually at a very high temperature. Fuel is burned in the air supplied by the compressor; an electric spark is required for initiating the combustion process, and thereafter the flame must be self-sustaining.

The design of combustors is a very complicated process where aerodynamics, chemical reactions, and mechanical design are linked together [2]. The interweaving of the various processes and the hardware geometry is reflected in the empirical nature of much of the design process. Though the individual processes are well known, their combination into a working combustion system owes much to experimentation and experience rather than to mathematical modeling. Recent developments in computational fluid mechanics (CFD) have helped reduce this experimentation. To understand how complex the design of a combustion chamber is, it is necessary to identify the main requirements from gas turbine combustors. These requirements may be summarized as follows [3]:

1. Its length and frontal area remain within the limits set by other engine components, that is, size and shape must be compatible with the engine envelope.
2. Its diffuser minimizes the pressure loss.
3. The presence of a liner to provide stable operation (that is, the flame should stay alight over a wide range of air to fuel ratios [AFRs]).
4. It meets the pollutant emissions regulations (low emissions of smoke, unburned fuel, and gaseous pollutant species).
5. Ability to utilize a much broader range of fuels.
6. Durability and relighting capability.

7. High combustion efficiency at different operating conditions: (a) altitude ranging from sea level to 11 km for civil transport, and higher for some military aircraft; and (b) Mach numbers ranging from zero during ground run to supersonic for military aircraft.
8. Design for minimum cost and ease of maintenance.
9. An outlet temperature distribution (pattern form) that is tailored to maximize the life of the turbine blades and nozzle guide vanes.
10. Freedom from pressure pulsations and other manifestations of combustion-induced instabilities.
11. Reliable and smooth ignition both on the ground (especially at very low ambient temperature) and, in the case of aircraft engine flameout, at high altitude.
12. The formation of carbon deposits (coking) must be avoided, particularly the hard brittle variety. Small particles carried into the turbine in the high-velocity gas stream can erode the blades. Furthermore, aerodynamically excited vibration in the combustion chamber might cause sizeable pieces of carbon to break free, resulting in even worse damage to the turbine.

According to the present aircraft, combustors may be classified as either *subsonic* or *supersonic*, depending on the velocity of combustion. Moreover, subsonic combustors may be subdivided into *axial* flow, *reverse* flow, and *cyclone* types. The last type is little used with present gas turbines. Axial flow combustors may be subdivided into *tubular*, *tubo-annular*, and *annular* types. Subsonic combustion chambers have three zones: (1) a recirculation zone, (2) a burning zone, and (3) a dilution zone [4].

10.2 Subsonic Combustion Chambers

The combustion process occurs at subsonic speeds; air normally leaves the compressor at 150 m/s or at Mach numbers less than unity (0.3–0.5). Apart from scramjet engines, all the available aeroengines and gas turbines have subsonic combustors. There are three main types of subsonic combustion chambers in use in gas-turbine engines, namely, multiple chamber (tubular or can type), tubo-annular chamber, and the annular chamber.

10.2.1 Tubular (or Multiple) Combustion Chambers

The first turbojet engines invented by Frank Whittle and Dr. von Ohain had subsonic tubular combustors. The tubular type is sometimes identified as multiple- or can-type combustion chamber.

As shown in Figure 10.1, this type of combustor is composed of cylindrical chambers disposed around the shaft connecting the compressor and turbine. Compressor delivery air is split into a number of separate streams, each supplying a separate chamber [5]. These chambers are interconnected to allow stabilization of any pressure fluctuations. Ignition starts sequentially with the use of two igniters. The Rolls-Royce Dart uses a tubular type combustor.

The number of combustion chambers varies from 7 to 16 per engine. The present trend is to have fewer (8 or 10) and even a single tubular chamber may be preferred. On U.S.-built

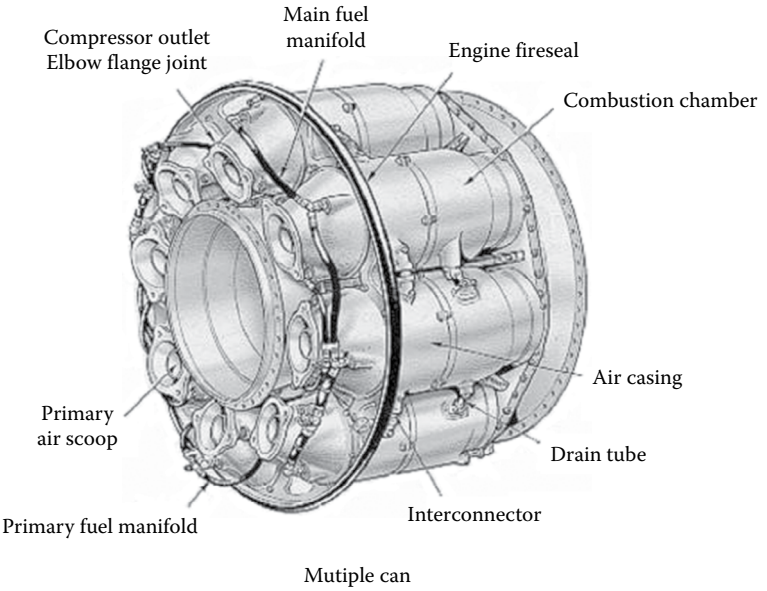


FIGURE 10.1
Multiple combustion chambers. (From Rolls-Royce plc, *The Jet Engine*, 5th edn., Derby, U.K., 1996.)

engines these chambers are numbered in a clockwise direction facing the rear of the engine with the number (1) chamber at the top. The can-type combustion chamber is typical of the type used on both centrifugal and axial-flow engines. It is particularly well suited for the centrifugal compressor engine since the air leaving the compressor is already divided into equal portions as it leaves the diffuser vanes. It is then a simple matter to duct the air from the diffuser into the respective combustion chambers arranged radially around the axis of the engine. The advantages of tubular type are as follows:

- Mechanically robust
- Fuel-flow and airflow patterns are easily matched
- Rig testing necessitates only a small fraction of total engine air mass flow
- Easy replacement for maintenance

The disadvantages are as follows:

- Bulky and heavy
- High pressure loss
- Requires interconnectors
- Incurs problem of light-round
- Large frontal area and high drag

For these reasons, the tubular type is no longer used in current designs. Small gas turbines used in auxiliary power units (APUs) and automotives are designed with a single can.

10.2.2 Tubo-Annular Combustion Chambers

This type may also be identified as can-annular or cannular. It consists of a series of cylindrical burners arranged within a common single annulus as is shown in Figure 10.2. Thus, it bridges the evolutionary gap between the tubular (multiple) and annular types. It combines the compactness of the annular chamber with the best features of the tubular type.

The combustion chambers are enclosed in a removable shroud that covers the entire burner section. This feature makes the burners readily available for any required maintenance. Can-annular combustion chambers must have fuel-drain valves in two or more of the bottom chambers. This ensures drainage of residual fuel to prevent its being burned at the next start. The flow of air through the holes and louvers of the can-annular system is almost identical to the flow through other types of burners. Reverse-flow combustors are mostly of the can-annular type. Reverse-flow combustors make the engine more compact. Pratt & Whitney use a can-annular-type combustion chamber in their JT3 axial-flow turbojet engine. Moreover, General Electric and Westinghouse use this type in their industrial gas turbines. Advantages of can-annular types are as follows:

- Mechanically robust
- Fuel flow and airflow patterns are easily matched
- Rig testing necessitates only a small fraction of total engine air mass flow
- Shorter and lighter than tubular chambers
- Low pressure loss

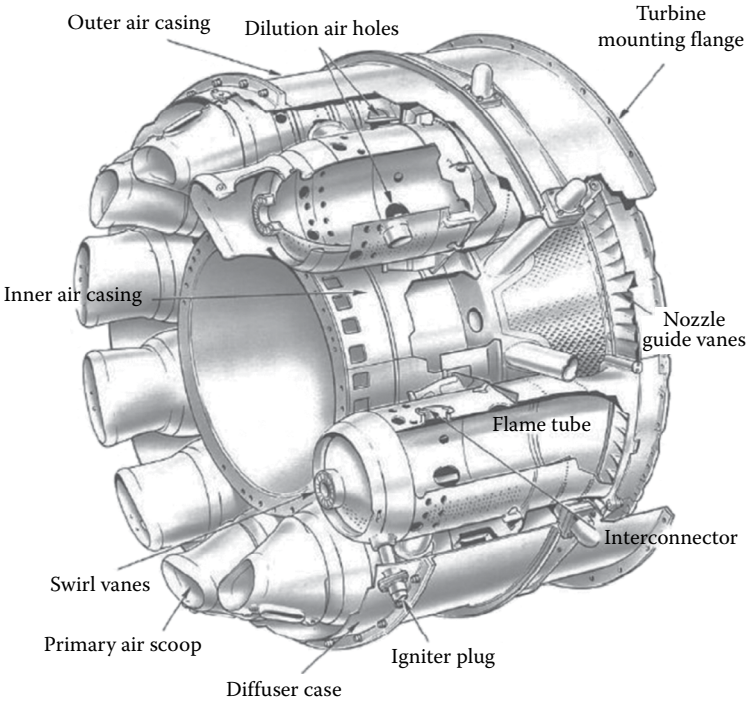


FIGURE 10.2
Tubo-annular combustion chamber. (From Rolls-Royce plc, *The Jet Engine*, 5th edn., Derby, U.K., 1996.)

Their disadvantages are as follows:

- Less compact than annular
- Requires connectors
- Incurs a problem of light around

10.2.3 Annular Combustion Chambers

In this type, an annular liner is mounted concentrically inside an annular casing. This combustor represents the ideal configuration for combustors since its "clean" aerodynamic layout results in compact dimensions (and consequently an engine of small diameter) (see Figure 10.3) and lower pressure loss than other designs. Usually, enough space is left between the outer liner wall and the combustion chamber housing to permit the flow of cooling air from the compressor. Normally, this type is used in many engines using an axial-flow compressor and also others incorporating dual-type compressors (combinations of axial flow and centrifugal flow). Currently, most aeroengines use annular type combustors, examples of which are the V2500 engine, Rolls-Royce Trent series, General Electric's GE-90, and Pratt & Whitney's PW4000 series. Moreover, several industrial gas turbines such as ABB and Siemens plants of over 150 MW fall into this category.

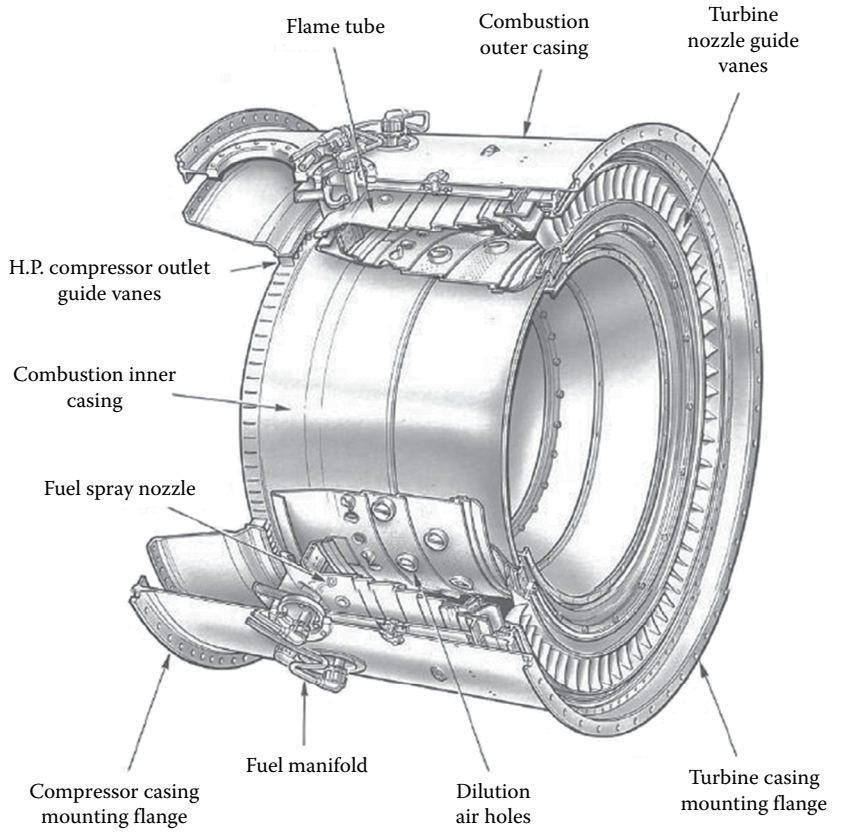


FIGURE 10.3
Annular type combustor. (From Rolls-Royce plc, *The Jet Engine*, 5th edn., Derby, U.K., 1996.)

The advantages of annular type may be summarized as follows:

- Minimum length and weight (its length is nearly 0.75 of can-annular combustor length)
- Minimum pressure loss
- Minimum engine frontal area
- Less wall area than can-annular and thus less cooling air is required—so the combustion efficiency rises as the unburnt fuel is reduced
- Easy light-round
- Design simplicity
- Combustion zone uniformity
- Permits better mixing of the fuel and air
- Simple structure compared to can burners
- Increased durability

However, it has the following disadvantages:

- Serious buckling problem on outer liner
- Rig testing necessitates full engine air mass flow
- Difficult to match fuel flow and airflow patterns
- Difficult to maintain stable outlet temperature transverse
- Must remove the engine from aircraft to disassemble for maintenance and overhaul

10.3 Supersonic Combustion Chamber

Supersonic combustion exists only in scramjet engines. The supersonic combustor is mechanically simple but aerodynamically vastly more complex than a subsonic one. Hydrogen is normally the fuel used. The scramjet engine has a 2D combustor as found in the combustor of X-43 aircraft. Details of supersonic combustion will be discussed later in this chapter.

10.4 Combustion Process

The objectives of the combustion process are to introduce and burn a fuel in the compressed air flowing through the combustor with the minimum pressure loss and with as complete a utilization of fuel as possible. From a thermodynamic viewpoint the process occurring in the combustor takes place in two major steps:

1. The introduction of the liquid fuel in the form of a fine spray of droplets, mixing it with the primary air and vaporizing it.
2. The combustion (chemical reaction) of vaporized fuel and the thorough mixing of the resulting combustion products with the secondary air.

Step 1 results in a decrease in the temperature of the working fluid before combustion since both the enthalpy used in raising the temperature of the liquid fuel to its boiling point and the latent heat of evaporation of the fuel are absorbed from the enthalpy of the warm compressed air.

In Step 2, the combustion process raises the temperature of the mixture of combustion products and secondary air to the desired temperature for the gases entering the turbine nozzle ring. That temperature is limited by the permissible operating temperature for the turbine blades. For a complete combustion process, the rate of reaction must be defined as the process efficiency depends on it.

These steps will be explained in detail here as regards the simple combustion chamber illustrated in Figure 10.4.

Air from the engine compressor enters the combustion chamber at a velocity in the range of 150 m/s. This air speed is far too high for combustion. The first step is to decelerate

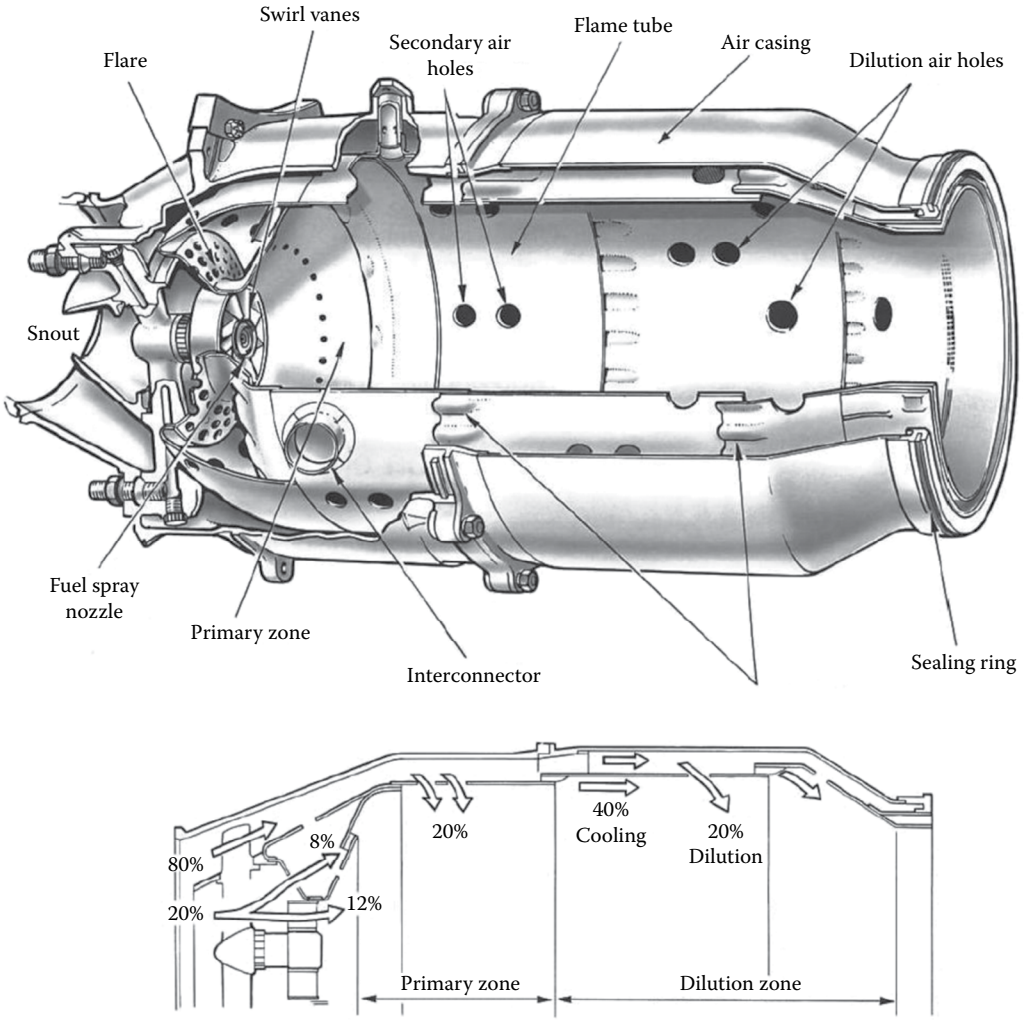


FIGURE 10.4
Combustion chamber and the corresponding air-flow rates. (From Rolls-Royce plc, *The Jet Engine*, 5th edn., Derby, U.K., 1996.)

(diffuse) this airflow to say 20–30 m/s and raise its static pressure. Since the speed of burning kerosene at normal mixture ratios is only a few meters per second, any fuel lit even in the diffused air steam would be blown away [5]. A region of low axial velocity has therefore to be created in the chamber. In normal operation, the overall AFR of a combustion chamber can vary between 45:1 and 130:1. However, kerosene will only burn efficiently at, or close to, a ratio of 15:1, so the fuel must be burned with only part of the air entering the chamber in what is called the *primary combustion zone*. Approximately 20% of the air-mass flow is taken in by the snout or entry section Figure 10.4. Immediately downstream of the snout are swirl vanes and a perforated flare, through which air passes into the primary combustion zone. The swirling air induces a flow upstream of the center of the flame tube and promotes the desired recirculation. The air not picked up by the snout flows into the annular space between the flame tube and the air casing. Through the wall of the flame tube body, adjacent to the combustion zone, are a selected number of secondary holes through which a further 20% of the main flow of air passes into the primary zone. The air from the swirl vanes and that from the secondary air holes interact and create a region of low velocity recirculation. This takes the form of a toroidal vortex, similar to a smoke ring, which has the effect of stabilizing and anchoring the flame. The recirculating gases hasten the burning of freshly injected fuel droplets by rapidly bringing them to ignition temperature. It is arranged such that the conical fuel spray from the nozzle intersects the recirculation vortex at its center, which assists in breaking up the fuel and mixing it with the incoming air. The temperature of the gases released by combustion is about 1800°C–2000°C, which is far too hot for entry into the nozzle guide vanes of the turbine. The air not used for combustion, which amounts to about 60% of the total airflow, is therefore introduced progressively into the flame tube. Approximately a third of this is used to lower the gas temperature in the dilution zone before it enters the turbine, and the remainder is used in film cooling of the walls of the flame tube. An electric spark from an igniter plug initiates combustion and the flame is then self-sustained.

10.5 Components of the Combustion Chamber

As illustrated in Figure 10.5, the combustion chamber of the multiple can or tubo-annular type has the following components:

Casing (*or case*): The case is the outer shell of the combustor, which has a fairly simple structure needing little maintenance. The case is protected from thermal loads by the air flowing in it, so thermal performance is of limited concern.

Diffuser: The purpose of the diffuser is to slow the high-speed, highly compressed air from the compressor to a velocity optimal for the combustor. Reducing the velocity results in an unavoidable loss in total pressure and flow distortion. So one of the design challenges is to limit the loss of pressure and reduce the flow separation. Like most other gas-turbine engine components, the diffuser is designed to be as short and light as possible.

Liner: The liner contains the combustion process and introduces the various airflows (intermediate, dilution, and cooling) into the combustion zone. The liner must be designed and built to withstand extended high-temperature cycles. For that reason, liners tend to be made from super alloys like Hastelloy X or thermal barrier coatings.

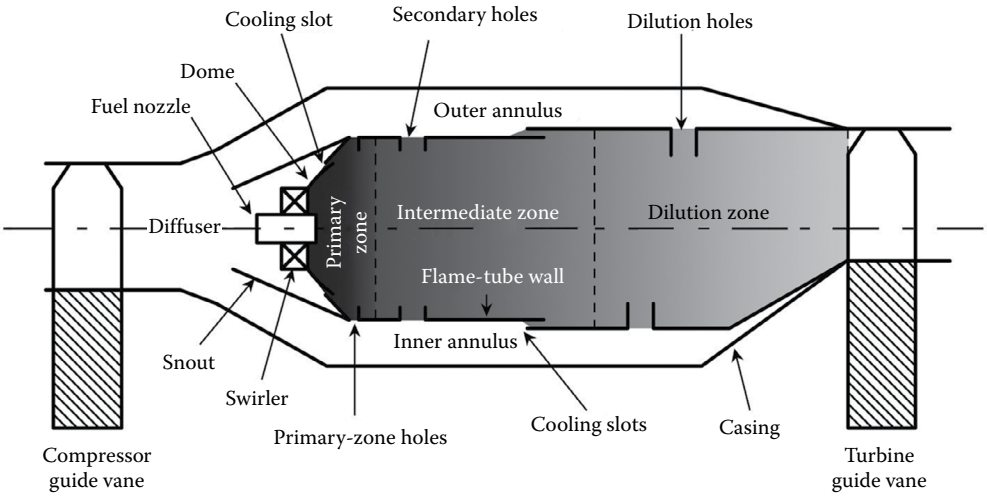


FIGURE 10.5
Components of the combustion chamber.

However, air cooling is still needed in either case. In general, there are two main types of liner cooling; namely, film and transpiration methods. In film cooling, cool air is injected from outside of the liner to just inside of the liner. This creates a thin film of cool air that protects the liner, reducing the temperature at the liner from around 1800 K to around 830 K. Transpiration cooling is a more modern approach that uses a porous material for the liner, thus allowing a small amount of cooling air to pass through it, providing better performance than film cooling. Transpiration cooling results in a much more even temperature profile since the cooling air is uniformly introduced. Film cooling air is generally introduced through slats or louvers, resulting in an uneven profile where it is cooler at the slat and warmer between the slats.

More importantly, transpiration cooling uses much less cooling air (in the order of 10% of total airflow, rather than 20%–50% for film cooling). Since less air is used for cooling, more air is available for combustion, which is more and more important for high-performance, high-thrust engines.

Snout: The snout is an extension of the dome; Figures 10.4 and 10.5 that acts as an air splitter, separating the primary air from the secondary air flows (intermediate, dilution, and cooling air).

Dome/swirler: The dome and swirler are the part of the combustor that the primary air flows through as it enters the combustion zone. Their role is to generate turbulence in the flow to rapidly mix the air with fuel. The swirler establishes a local low-pressure zone that forces some of the combustion products to recirculate, creating the high turbulence. However, the higher the turbulence, the higher the pressure loss will be for the combustor. Thus the dome and swirler must be carefully designed so as not to generate more turbulence than is needed to mix the fuel and air sufficiently.

Fuel injector: The fuel injector is responsible for introducing fuel to the combustion zone and, along with the swirler, is responsible for mixing the fuel and air. There are four primary types of fuel injectors: pressure-atomizing, air blast, vaporizing, and premix/pre-vaporizing injectors.

Igniter: Most igniters in gas-turbine applications are electrical-spark igniters, similar to automotive spark plugs. The igniter needs to be in the combustion zone where the fuel and air are already mixed, but it needs to be far enough upstream so that it is not damaged by the combustion itself.

Once the combustion is started by the igniter, it is self-sustaining and the igniter is no longer used. In can-annular and annular combustors, the flame can propagate from one combustion zone to another, so igniters are not needed at each one.

10.6 Aerodynamics of the Combustion Chamber

Aerodynamic processes play a vital role in the design and performance of gas-turbine combustion systems. Aerodynamic design of combustor provides its size and performance analysis. In the next sections, flow through diffuser and liner holes will be thoroughly analyzed.

10.6.1 Aerodynamics of Diffusers

In its simplest form, a diffuser is merely a divergent passage in which the flow is decelerated and the reduction in velocity head is converted into a rise in static pressure. The ideal diffuser achieves the required velocity reduction in the shortest possible length with minimum loss in total pressure as well as uniform and stable flow conditions at its outlet.

The different types of diffusers are illustrated in Figure 10.6, where Figure 10.6a represents a two-dimensional model, Figure 10.6b shows a conical type, Figure 10.6c illustrates a straight core annular, and finally Figure 10.6d resembles an equiangular type.

These straight-walled diffusers may be defined in terms of three geometric parameters; namely, area ratio (AR), geometrical length (either the wall length L or axial

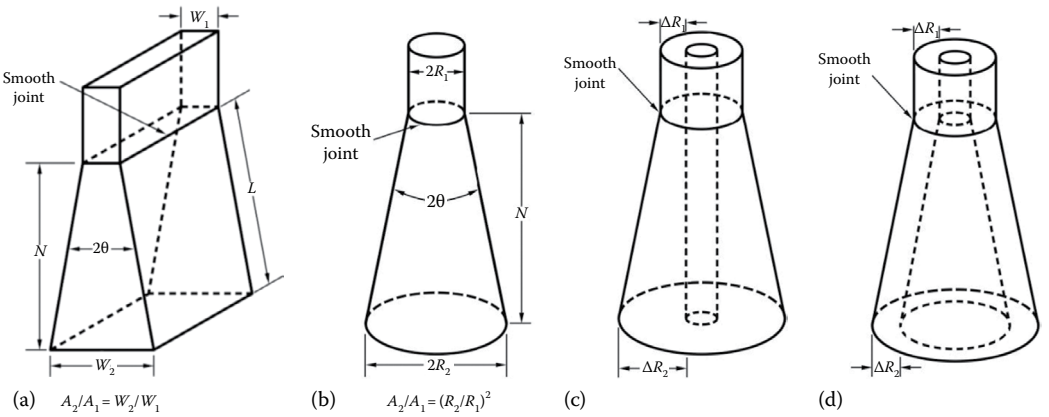


FIGURE 10.6
Different shapes of diffuser: (a) two-dimensional, (b) conical, (c) straight core annular, and (d) equiangular annular.

length N), and the divergence angle (2θ). The area ratio is expressed by the following relations.

For two-dimensional

$$AR = 1 + 2\frac{L}{W_1}\sin\theta \tag{10.1}$$

For conical

$$AR = 1 + 2\frac{L}{R_1}\sin\theta + \left(\frac{L}{R_1}\sin\theta\right)^2 \tag{10.2}$$

For annular

$$AR = \frac{\Delta R_2}{\Delta R_1}$$

where ΔR_1 is the annulus height at diffuser inlet.

For straight-core annular the area ratio is then

$$AR = 1 + 2\frac{L}{\Delta R_1}\sin\theta + \left(\frac{L}{\Delta R_1}\sin\theta\right)^2 \tag{10.3a}$$

For can-angular annular diffuser

$$AR = 1 + 2\frac{L}{\Delta R_1}\left(\sin\theta_i + \sin\theta_0\right) + \left(\frac{L}{\Delta R_1}\left(\sin\theta_i + \sin\theta_0\right)\right)^2 \tag{10.3b}$$

The first systematic study of flow pattern in 2-D straight-walled diffusers was carried out by Kline et al. [6]. As the divergence angle increased, different flow patterns were seen, including no appreciable stall, transitory stall, fully developed stall, and jet flow in which the main flow is separated from the wall. The first appreciable stall for different types of diffusers is plotted in Figure 10.7. It was measured by Howard et al. [7] and agreed with the data obtained by McDonald and Fox [8] and Reneau et al. [9].

For one-dimensional incompressible flow

$$\dot{m} = \rho_1 A_1 U_1 = \rho_2 A_2 U_2$$

Hence

$$\frac{A_2}{A_1} = \frac{U_1}{U_2} = AR \tag{10.4}$$

The pressure-recovery coefficient is calculated as

$$C_p = \frac{\left(P_2 - P_1\right)}{q_1}$$

where $q_1 = \rho U_1^2$.

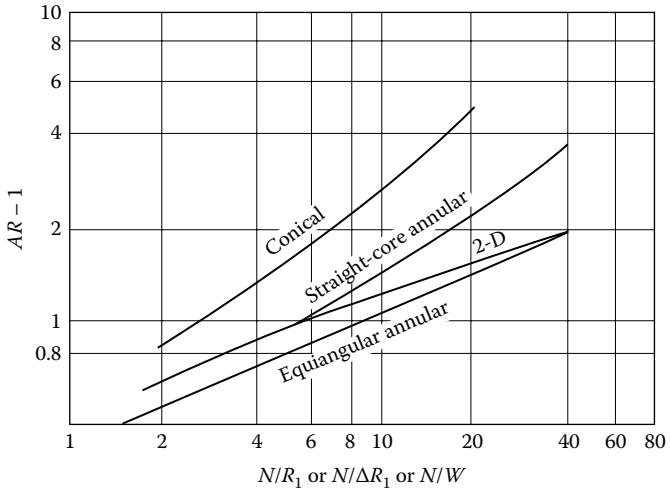


FIGURE 10.7
First stall lines for different types of diffusers. (From Howard, J.H.G. et al., *Performance and Flow Regimes for Annular Diffusers*, ASME Paper 67-WA/FE-21, New York, 1967.)

The static-pressure rise in the diffuser is given by

$$P_1 + q_1 = P_2 + q_2 + \Delta P_{diff}$$

$$P_2 - P_1 = q_1\left(1 - \frac{1}{AR^2}\right) - \Delta P_{diff}$$

In ideal diffuser, there are no losses, then

$$\left(P_2 - P_1\right)_{ideal} = q_1\left(1 - \frac{1}{AR^2}\right)$$

$$C_{p_{ideal}} = \frac{\left(P_2 - P_1\right)_{ideal}}{q_1} = \left(1 - \frac{1}{AR^2}\right) \tag{10.5}$$

Overall effectiveness of diffuser is expressed by

$$\eta = \frac{C_{p_{measured}}}{C_{p_{ideal}}} = \frac{C_p}{\left(1 - \frac{1}{AR^2}\right)} \tag{10.6}$$

Figure 10.8 illustrates the performance of conical diffusers. The $\left(C_p^*\right)$ is the locus of points that define the diffuser divergence angle (2θ) producing the maximum pressure recovery in a prescribed non-dimensional length.

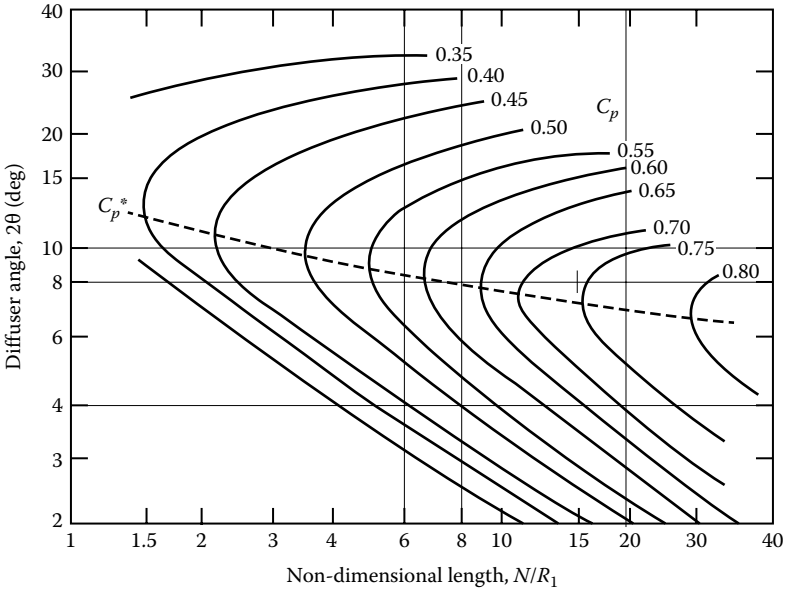


FIGURE 10.8
Performance chart for conical diffusers.

Example 10.1

The combustion chamber in a General Electric GEnx turbofan engine is a straight core annular one having the following data:

Inlet total pressure: $P_{01} = 1639.2$ kPa
Inlet total temperature: $T_{01} = 792.2$ K
Inlet Mach number: $M_1 = 0.3$
Air mass flow rate: $\dot{m} = 57.242$ kg/s
Inner radius of annular diffuser at inlet is: $r_1 = 0.3047$ m
Area ratio: $AR = 2.02$

Calculate

1. Dimensions of diffuser
2. Exit Mach number M_2

Solution

The static inlet pressure is determined from the isentropic relationship

$$P_1 = \frac{P_{01}}{\left(1 + \frac{\gamma - 1}{2} M_1^2\right)^{\gamma/\gamma - 1}} = \frac{1639.2}{\left(1 + 0.2 \times 0.3^2\right)^{0.286}} = 1540 \text{ kPa}$$

The static inlet pressure is determined from the isentropic relationship

$$T_1 = \frac{T_{01}}{1 + \frac{\gamma - 1}{2} M_1^2} = \frac{792.2}{1 + 0.2 \times 0.3^2} = 778.2 \text{ K}$$

Air density at inlet is

$$\rho_i = \frac{P_i}{RT_i} = 6.895 \text{ kg/m}^3$$

Inlet air velocity is

$$U_1 = M_1\sqrt{\gamma RT_1} = 167.75 \text{ m/s}$$

The mass-flow rate is expressed by

$$\dot{m} = \rho_1 U_1 A_1$$

Then the inlet area is

$$A_1 = \frac{\dot{m}}{\rho_1 U_1} = \frac{57.242}{6.895 \times 167.75} = 0.04949 \text{ m}^2$$

$$A_1 = 2\pi \times r_1 \times h_1$$

$$h_i = 0.02585 \text{ m}$$

Since

$$h_1 = 2\Delta R_1$$

Then

$$\Delta R_1 = 0.01292 \text{ m}$$

From Figure 10.7 for straight core annular diffuser

$$\frac{N}{\Delta R_1} = 6$$

The axial length of diffuser $N = 0.0775$ m.
Since

$$L = \frac{N}{\cos\theta}$$

and the area ratio is

$$AR = 1 + \frac{2L\sin\theta}{R_1} + \left(\frac{L\sin\theta}{R_1}\right)^2$$

Then by trial and error, the angle $\theta = 4$, gives an acceptable area ratio:

$$AR = 1 + 0.8388 + 0.1758 = 2.0147$$

Then outlet speed and area are

$$U_2 = \frac{U_1}{AR} = 83.0 \text{ m/s}$$

$$A_2 = 0.0999 \text{ m}^2$$

Performance criteria: At $M_1 = 0.3$, from isentropic flow tables, $\frac{A_1}{A^*} = 2.035$

$$A^* = \frac{0.04949}{2.035} = 0.02432 \text{ m}^2$$

And for the exit

$$\frac{A_2}{A^*} = \frac{0.0999}{0.02432} = 4.1106 \text{ m}^2$$

Again from isentropic flow tables, $M_2 = 0.1425$.
Alternatively, since

$$T_2 = T_{02} - \frac{U_2^2}{2 \times Cp} \equiv T_{01} - \frac{U_2^2}{2 \times Cp}$$

$$T_2 = 788.8 \text{ K}$$

Thus

$$\frac{T_{02}}{T_2} = 1.0043$$

Then from isentropic flow tables, $M_2 = 0.1425$.

10.7 Chemistry of Combustion

Under most operating conditions, the rate of combustion is limited by the rate at which the fuel is vaporized and mixed with air. In most combustors, the fuel is injected as an atomized liquid droplet spray into the hot reaction zone where it mixes with air and hot combustion gases.

The rate of reaction depends on both static pressures P and temperature T in a very complex way. For many situations, the reaction rate can be approximated by a form of the Arrhenius equation written for the mass rate of reaction as

$$\text{Reaction rate} \propto P^n f(T) e^{-E/RT} \tag{10.7}$$

where

- n is an exponent that depends on the number of molecules involved in a reactive collision (e.g., $n = 2$ for two molecules, for hydrocarbon–air combustion, $n = 1.8$)
- $f(T)$ is a function that relates the reaction rate to the forms of energy (translation, rotation, and vibration)

The term $e^{-E/RT}$ accounts for the number of molecular collisions in which the energy of one molecule relative to another exceeds the active energy (E) and R is the universal gas constant [10].

At low pressure, the reaction rate becomes slow and can become limiting for aircraft engines at very high altitudes. However, under most operating conditions, the rate of combustion is limited by the rate at which the fuel is vaporized and mixed with air.

If the temperature and pressure in the reaction zone are sufficiently high, the reaction rate will be fast and the fuel vapor will react as it comes in contact with sufficient oxygen. Thus, for fast or more acceptable reaction, the combustion should occur with sufficient oxygen and this is called by *stoichiometric ratio*.

The stoichiometric ratio is the required ratio for complete combustion of a hydrocarbon fuel to convert the fuel completely to carbon dioxide (CO_2) and the hydrogen to water vapor (H_2O).

Since 23% by mass of oxygen in the air participates in combustion, the stoichiometric AFR can be calculated from the reaction equation as follows. Consider the complete combustion of a general hydrocarbon fuel of average molecular composition C_aH_b with air. The overall complete combustion equation is

$$C_aH_b + \left(a + \frac{b}{4}\right)\left(O_2 + 3.773N_2\right) = aCO_2 + \frac{b}{2}H_2O + 3.773\left(a + \frac{b}{4}\right)N_2 \tag{10.8}$$

where the molecular weights of oxygen, atmospheric nitrogen, atomic carbon, and atomic hydrogen are, respectively, 32, 28.16, 12.011, and 1.008. The fuel composition could have been written CH_y, where $y = b/a$.

The combustion equation defines the stoichiometric (or chemically correct or theoretical) proportions of fuel and air (just enough oxygen for conversion of all the fuel into completely oxidized products). The stoichiometric AFR or fuel–air ratio (FAR) depends on fuel composition and can be defined as

$$\left(\frac{A}{F}\right)_S = \left(\frac{F}{A}\right)_S^{-1} = \frac{\left(1 + y/4\right)\left(32 + 3.773 \times 28.16\right)}{12.011 + 1.008y} = \frac{34.56\left(4 + y\right)}{12.011 + 1.008y} \tag{10.9}$$

Note that if the fuel is burned at a numerically large AFR, the mixture is referred to as lean or weak, and if the combustion at an AFR lower than the stoichiometric value implies a deficiency of oxygen and hence combustion is incomplete, then the fuel is partially burned, resulting in carbon monoxide (CO) and unburned hydrocarbons.

Example 10.2

A hydrocarbon fuel of composition 84.1% by mass **C** and 15.9% by mass **H** has a molecular weight of 114.15. Determine the number of moles of air required for stoichiometric combustion and the number of moles of products produced per mole of fuel. Calculate air-to-fuel ratio (A/F).

Solution

Assume a general form for fuel composition, namely, C_aH_b. The molecular weight relation gives

$$114.15 = 12.011a + 1.008b$$

The gravimetric analysis of the fuel gives

$$\frac{b}{a} = \frac{15.9/1.008}{84.1/12.011} = 2.25$$

Thus, $a = 8$ and $b = 18$; therefore, the fuel is octane C_8H_{18}. The burning equation then becomes

$$\underset{\text{Fuel}}{C_8H_{18}} + \overbrace{12.5\left(O_2 + 3.773N_2\right)}^{\text{Air}} = \overbrace{8CO_2 + 9H_2O + 47.16N_2}^{\text{Products}}$$

Relative mass:

$$114.15 + 59.66 \times 28.96 = 8 \times 44.01 + 9 \times 18.02 + 47.16 \times 28.16$$
$$114.15 + 1727.8 = 1842.3$$

Per unit mass fuel:

$$1 + 15.14 = 16.14$$

The stoichiometric air-to-fuel ratio is then $(A/F) = 15.14$ and fuel-to-air ratio $(F/A) = 0.0661$.

Fuel–air mixtures with more than or less than the stoichiometric air requirement can be burned. With excess air or fuel-lean combustion, the extra air appears in the products in uncharged form. With less than the stoichiometric air requirement, that is, with fuel-rich combustion, there is insufficient oxygen to oxidize fully the fuel constituents (C) and (H) to CO_2 and H_2O. The products are a mixture of CO_2 and H_2O with carbon monoxide CO and hydrogen H_2 (as well as N_2). The product composition cannot be determined from an element balance alone and an additional assumption about the chemical composition of the product species must be made.

Because the composition of the combustion products is significantly different for fuel-lean and fuel-rich mixtures and because the stoichiometric FAR depends on fuel composition, the ratio of the actual FAR to the stoichiometric ratio (or its inverse) is a more informative parameter for defining mixture composition. The fuel-air equivalence ratio Φ

$$\Phi = \frac{(F/A)_{actual}}{(F/A)_{stoich}} \tag{10.10a}$$

For fuel-lean mixtures	$\Phi < 1$
For stoichiometric mixtures	$\Phi = 1$
For fuel-rich mixtures	$\Phi > 1$

Equation 10.4 can be rewritten in terms of the F/A (f) as

$$\Phi = \frac{f}{f_{stoich}} \tag{10.10b}$$

To prevent excessive temperatures at the exit of the main burner or the afterburner and to protect its walls, the overall F/A ratio must be much less than stoichiometric ratio where $\Phi < 1$.

Example 10.3

An aeroengine is using octane $C_{12}H_{24}$ as a fuel. The temperature of the working fluid at the inlet and outlet of combustion chamber are T_{01} = 650 K and T_{02} = 1600 K. The fuel heating value is Q_{HV} = 42,800 kJ/kg. The specific heats of cold and hot streams are Cp_c = 1.005 kJ (kg · K) and Cp_h = 1.23 kJ/(kg·K). Calculate the equivalence ratio.

Solution

The chemical reaction of fuel is

$$C_{12}H_{24} + 18\left(O_2 + \frac{79}{21}N_2\right) \rightarrow 12CO_2 + 12H_2O + 18\left(\frac{79}{21}N_2\right)$$

Thus, the stoichiometric FAR is found to be

$$f_{stoich} = \frac{12 \times 12.011 + 24 \times 1.008}{18 \times 32 + 18 \times (79/21) \times 28.16} = 0.067795$$

The F/A is given by the relation

$$f = \frac{Cp_h T_{02} - Cp_c T_{01}}{Q_{Hv} - Cp_h T_{02}} = \frac{1.23 \times 1,600 - 1.005 \times 650}{42,800 - 1.23 \times 1,600} = 0.032199$$

The equivalence ratio is

$$\Phi = \frac{f}{f_{stoich}} = 0.4749$$

This case then represents lean fuel mixture.

Example 10.4

Consider a stoichiometric mixture of *propane* (C_3H_8) and air, Calculate the air to fuel ratio in the cases:

1. Stoichiometric flow
2. Less air (70% of stoichiometric)

Solution

1. The general chemical relation for stoichiometric mixture will be

$$C_3H_8 + 5\left(O_2 + \frac{79}{21}N_2\right) \rightarrow 3CO_2 + 4H_2O + 5\left(\frac{79}{21}N_2\right)$$

$$\left(\frac{A}{F}\right)_{stioch} = \frac{m_{air}}{m_{fuel}} = \frac{5 \times \left(32 + \frac{79}{21} \times 28.16\right)}{3 \times 12.011 + 8 \times 1.005} = 15.648$$

$$\left(\frac{A}{F}\right)_{stioch} = 15.648 \text{ kg-air/kg-fuel}$$

Thus

$$\left(\frac{F}{A}\right)_{stoich} = 0.0639$$

2. Less air
Less air means a Rich Mixture. Thus

$$\lambda C_3H_8 + 0.7\times 5\left(O_2 + 3.76N_2\right) \rightarrow aCO + bH_2O + 0.7\times 18.8N_2$$

Then

$$a = 3\lambda, \quad b = 4\lambda, \quad a + b = 7$$

Thus

$$\lambda = 1, \quad a = 3, \quad b = 4$$

$$C_3H_8 + 0.7\times 5\left(O_2 + 3.76N_2\right) \rightarrow 3CO + 4H_2O + 0.7\times 18.8N_2$$

$$\left(\frac{A}{F}\right)_{stioch} = \frac{m_{air}}{m_{fuel}} = \frac{3.5\times\left(32 + \frac{79}{21}\times 28.16\right)}{3\times 12.011 + 8\times 1.005} = 10.954$$

$$\left(\frac{A}{F}\right)_{rich} = 10.954 \text{ kg-air/kg-fuel}$$

$$\left(\frac{F}{A}\right)_{rich} = 0.0913$$

Figure 10.9 illustrates the flammability limits for air mixture. Fuel–air mixtures will react over only a rather narrow range of F/A ratio (corresponding also to a narrow range of equivalence ratio). The equivalence ratio for hydrocarbon is in the range from 0.5 to 3, while hydrogen fuel has a wider range from 0.25 to nearly 6 [10].

10.8 The First Law Analysis of Combustion

The main purpose of combustion is to produce heat through a change of enthalpy from the reactants to the products. From the First Law equation in a control volume bounding the combustion chamber, ignoring kinetic and potential energy changes and assuming no work is done [11], we have the combustion heat expressed as

$$Q_{cv} = \sum_p N_p h_p - \sum_r N_r h_r \tag{10.11}$$

where the summations are taken over all the products (p) and the reactants (r). Also (N) refers to the number of moles of each component and (h) in [kJ/kmol] refers to the molar enthalpy of each component.

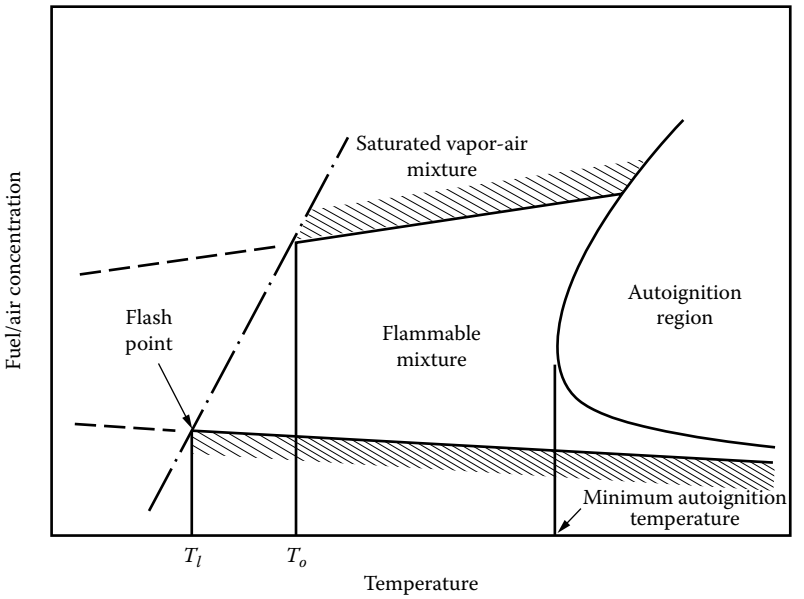


FIGURE 10.9
Effect of temperature on flammability limits. (Adapted from Lefebvre, A.H., *Gas Turbine Combustion*, 2nd edn., Taylor & Francis, Philadelphia, PA, 1999. With permission.)

Since there are a number of different substances involved, we need to establish a common reference state to evaluate the enthalpy, the common choice being 25°C and 1 atm, which is normally denoted with a superscript (°).

Example 10.5

Consider the complete combustion of methane (CH_4) with theoretical air. If the enthalpy of formation of the reactants and products are as follows:

Substance	Chemical Expression	h_{fo} (kJ/kmol)
Carbon dioxide	$CO_2(g)$	−393,520
Water vapor	$H_2O(g)$	−241,820
Water	$H_2O(l)$	−285,820
Methane	$CH_4(g)$	−74,850

where (g) refers to gas and (l) refers to liquid. Calculate the lower and higher heating values of CH_4.

Solution

The chemical relation for complete combustion of CH_4 is

$$CH_4 + 2(O_2 + 3.76N_2) \rightarrow CO_2 + 2H_2O + 7.25N_2$$

It is noted that [12]

1. The enthalpy of formation of basic elements O_2 and N_2 is zero.
2. The enthalpy of formation, (h_{fo}) has negative sign which indicates that the process is exothermic, i.e., heat is given off when the compound is formed.

Assume here that there is sufficient heat transfer such that both the reactants and the products are at 25°C and 1 atm pressure, and that the lower heating value is obtained when the water product is vapor, while the higher heating value is obtained when the water product is liquid.

Since there is no sensible enthalpy change, the energy equation; (10.11), the higher heating value becomes

$$Q_{cv} = \sum_p N_p h_{fo_p} - \sum_r N_r h_{fo_r} = 1(-393{,}520) + 2(-285{,}820) - 1(-74{,}850)$$

$$Q_{cv} = -890{,}310 \text{ kJ/kmol fuel}$$

Now, on a unit mass basis

$$q_{cv} = \frac{Q_{cv}}{M_{CH_4}} = \frac{-890{,}310}{(12+4)} = -55{,}644 \text{ kJ/kg fuel}$$

The lower heating value is then

$$Q_{cv} = \sum_p N_p h_{fo_p} - \sum_r N_r h_{fo_r} = 1(-393{,}520) + 2(-241{,}820) - 1(-74{,}850)$$

$$Q_{cv} = -802{,}310 \text{ kJ/kmol fuel}$$

Now, on a unit mass basis,

$$q_{cv} = \frac{Q_{cv}}{M_{CH_4}} = \frac{-890{,}310}{(12+4)} = -50{,}144 \text{ kJ/kg fuel}$$

This heat (q_{cv}) is called the *enthalpy of combustion* or the *heating value* of the fuel. If the products contain liquid water, then it is the *higher heating value* (as in the preceding example), however if the product contains water vapor then it is the *lower heating value* of the fuel. The enthalpy of combustion is the largest amount of heat that can be released by a given fuel.

10.9 Combustion Chamber Performance

A combustion chamber must be capable of allowing fuel to burn efficiently over a wide range of operating conditions without incurring a large pressure loss. So, the combustion chamber performance can be evaluated by some conditions or performance as follows:

1. Pressure loss
2. Combustion efficiency
3. Combustion stability
4. Combustion intensity

10.9.1 Pressure Losses

The sources of pressure drop or loss are either cold or hot losses. Cold losses arise from sudden expansion, wall friction, turbulent dissipation, and mixing. Cold losses can be measured by flowing air without fuel through all the slots, holes, orifices, and so on. The hot losses (fundamental losses) are due to temperature increase. Generally, the fundamental loss due to heat addition in an aeroengine will be low compared with the losses due to friction and mixing. Experiments have shown that the overall pressure loss can be expressed by the relation

$$\text{Pressure loss factor (PLF)} = \underbrace{\frac{\Delta P_0}{m^2/\left(2\rho_1 A_m^2\right)}}_{\text{Cold}} = \overline{K_1} + \overline{K_2\left(\frac{T_{02}}{T_{01}} - 1\right)} \quad \text{(Hot)} \tag{10.12}$$

where

m is the air mass flow rate
A_m is the maximum cross-sectional area of chamber
ρ_1 is the inlet density
K_1 and K_2 are determined by measurement of the performance of the system

Equation 10.5 is plotted in Figure 10.10.

Typical values of pressure loss factor (PLF) at design operating conditions for can, can-annular, and annular combustion chambers are 35, 25, and 18, respectively.

10.9.2 Combustion Efficiency

The main objective of the combustor is to transfer all the energy of the fuel to the gas stream. In practice, this will not occur for many reasons; for example, some of the fuel may

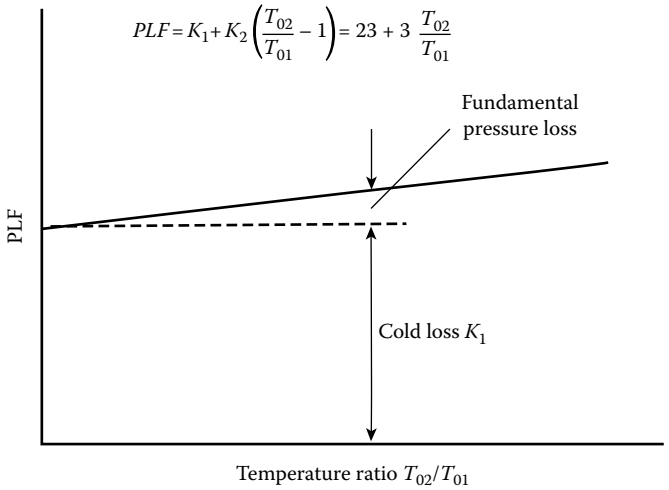


FIGURE 10.10
Variation of pressure loss factor.

not find oxygen for combustion in the very short time available. Therefore, it is necessary to define the efficiency of the combustion.

To obtain high efficiency from the combustor, the following conditions must be achieved:

- Fuel and air have adequate time and adequate space to mix and react
- Fuel should be completely vaporized and mixed with air before burning

The combustion efficiency may be expressed as [3]

$$\eta_b = f\left(\text{airflow rate}\right)^{-1}\left(\frac{1}{\text{evaporation rate}}+\frac{1}{\text{mixing rate}}+\frac{1}{\text{reaction rate}}\right)^{-1} \tag{10.13}$$

As stated in Reference 5 and illustrated in Figure 10.11 the combustion efficiency of most gas turbine engines at sea level takeoff conditions is almost 100%. It is reduced to 98% at altitude cruise.

Another definition for efficiency is discussed in Reference 1 and introduces it in terms of the heat release during combustion. Thus,

$$\eta_b = \frac{\left(h_{02}-h_{01}\right)_{actual}}{\left(h_{02}-h_{01}\right)_{ideal}} = \frac{\left(T_{02}-T_{01}\right)_{actual}}{\left(T_{02}-T_{01}\right)_{ideal}} = \frac{\dot{m}_{f\ ideal}}{\dot{m}_{f\ actual}} \tag{10.14}$$

Since heat release from combustion arises from the formation of (CO_2, H_2O), the combustion efficiency is determined by the quantity of these two constituents in the exhaust gas relative to the maximum possible quantity. Before combustion is completed, the gas contains various molecules and radicals of hydrocarbon as well as carbon monoxide. These represent unused chemical energy and, if allowed to remain in the exhaust gas, constitute two of the major pollutants.

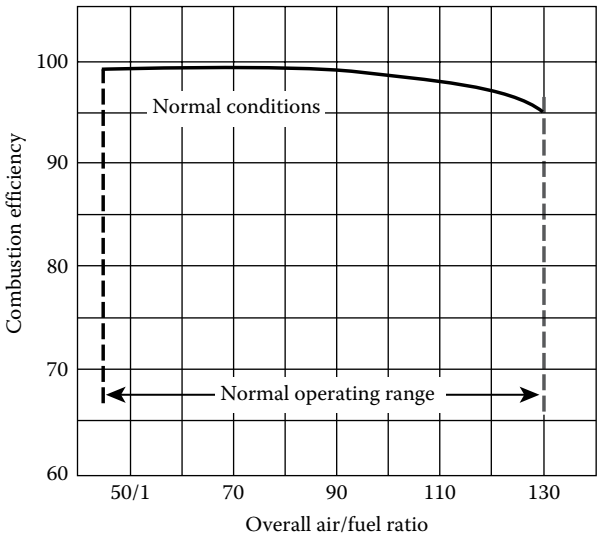


FIGURE 10.11
Combustion efficiency. (From Rolls-Royce plc, *The Jet Engine*, 5th edn., Derby, U.K., 1996.)

10.9.3 Combustion Stability

Combustion stability means smooth burning and the ability of the flame to remain alight over a wide operating range. For any particular type of combustion chamber, there is both a rich and a weak limit to the AFR beyond which the flame is extinguished.

Actually when a new system is tested, the stability limits, which represent the highest and lowest FARs at which combustion will take place, will be investigated. Normally, the limits will be well away from the normal operating point. The range of stable operation will reduce with the increase of air velocity, and if the air mass flow rate is increased beyond a certain value, the flame will be extinguished. A typical stability loop is illustrated in Figure 10.12.

There are two causes of instability of combustion. The first is, if the fuel–air mixture becomes too lean or too rich, the temperatures and reaction rates drop below the level necessary to effectively heat and vaporize the incoming fuel and air. The second reason is, if the velocity of gas stream U becomes higher than the flame speed S, it causes a blow out of the flame. Stability loops provide two basic kinds of information.

10.9.4 Combustion Intensity

The heat released by a combustion chamber is dependent on the volume of the combustion area. So, the combustion area must be increased. Therefore, the average velocities increasing in the combustor will make efficient burning more and more difficult. However, it is found that if the intensity of combustion is kept within certain limiting values and the fuel is atomized adequately, it is possible to obtain combustion efficiencies of 98%–100% at design conditions with conventionally designed combustion chamber.

The larger volume will achieve a low-pressure drop, high efficiency, good outlet temperature distribution, and satisfactory stability characteristics.

The design problem is also eased by an increase in the pressure and temperature of the air entering the chamber.

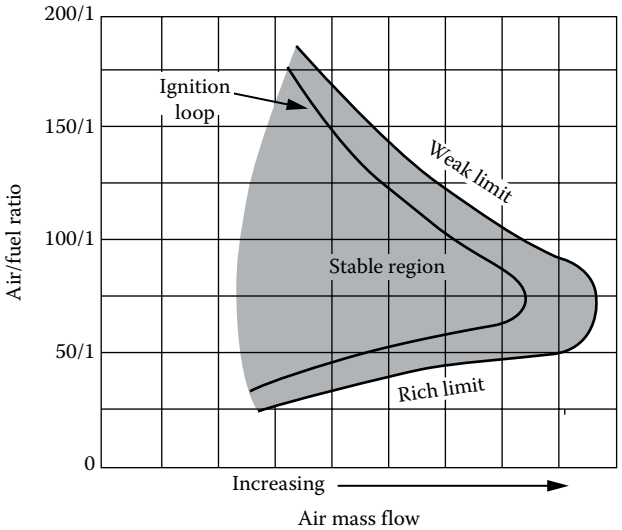


FIGURE 10.12
Combustion stability limits. (From Rolls-Royce plc, *The Jet Engine*, 5th edn., Derby, U.K., 1996.)

The combustion intensity (CI) can be defined as

$$\text{CI} = \frac{\text{Heat release rate}}{\text{Combustion volume} \times \text{pressure}} \quad \text{kW}/\left(\text{m}^3\ \text{atm}\right) \tag{10.15}$$

Certainly the lower the value of the CI the easier it is to design a combustion system that will meet all the design requirements.

For aircraft system the CI is in the region of $(2 - 5) \times 10^4$ kW/m^3 atm.

10.9.5 Cooling

Cooling air must be used to protect the burner liner and dome from the high radiative and connective heat loads produced within the burner. The heat release from burning the fuel in the combustor introduces products with a high temperature that can reach 2000°C. Thus, as shown in Figure 10.4 about 60% of the total airflow is introduced progressively into the flame tube for cooling. Approximately, one-third of this is used to lower the gas temperature in the dilution zone before it enters the turbine, while the remainder is used for cooling the flame tube.

More than one cooling technique is used in cooling as illustrated in the following.

10.9.5.1 Louver Cooling

Many early gas turbine combustors used the louver cooling technique whereby the liner was fabricated in the form of cylindrical shells that, when assembled, formed annular passages at the shell intersection points as shown in Figure 10.13.

These passages permitted a film of cooling air to be injected along the hot side of the liner wall to provide a protective thermal barrier.

10.9.5.2 Splash Cooling

Through splash cooling, air enters the liner through a row of holes of small diameter as is shown in Figure 10.14. The air jets impinge on a cooling skirt, which then directs the flow so as to form a film along the inside of the liner wall.

10.9.5.3 Film Cooling

The air is normally introduced through liner in a film of air that is formed between the combustion gases and liner hardware as is shown in Figure 10.15.

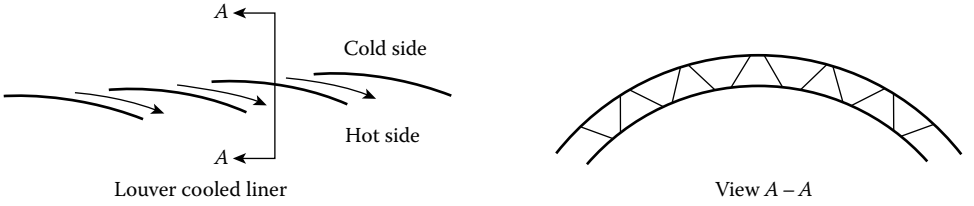


FIGURE 10.13
Louver cooling. (Reprinted from Mattingly, J.D., *Elements of Gas Turbine Propulsion*, AIAA Educations Series, American Institute of Aeronautics and Astronautics, Inc., Reston, VA, 2005, p. 817. With permission.)

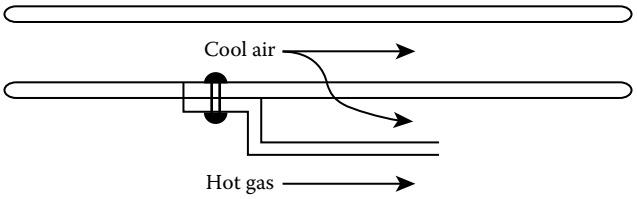


FIGURE 10.14
Splash cooling. (Reprinted from Mattingly, J.D., *Elements of Gas Turbine Propulsion*, AIAA Educations Series, American Institute of Aeronautics and Astronautics, Inc., Reston, VA, 2005, p. 817. With permission.)

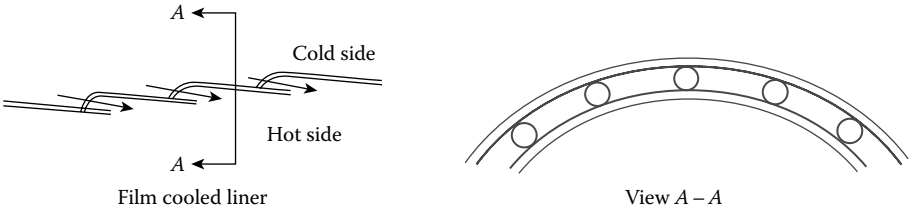


FIGURE 10.15
Film cooling. (Reprinted from Mattingly, J.D., *Elements of Gas Turbine Propulsion*, AIAA Educations Series, American Institute of Aeronautics and Astronautics, Inc., Reston, VA, 2005, p. 817. With permission.)

10.9.5.4 Convection-Film Cooling

Convection-film cooling utilizes simple but controlled convection cooling enhanced by roughened walls while providing a protective layer of cool air along the hot side of the wall at each cooling panel (Figure 10.16).

10.9.5.5 Impingement-Film Cooling

This method is well suited to high temperature combustion as shown in Figure 10.17. However, its complex construction poses difficulties in manufacture and repair.

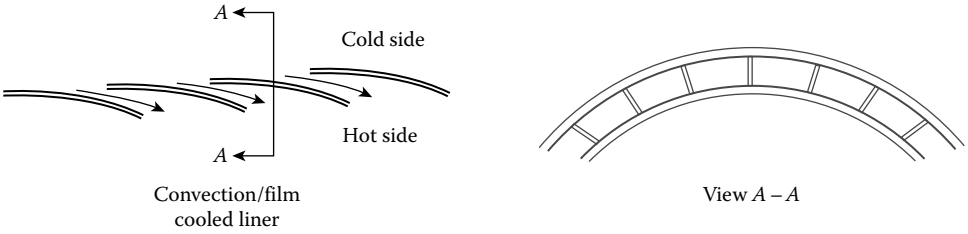


FIGURE 10.16
Convection-film cooling. (Reprinted from Mattingly, J.D., *Elements of Gas Turbine Propulsion*, AIAA Educations Series, American Institute of Aeronautics and Astronautics, Inc., Reston, VA, 2005, p. 817. With permission.)

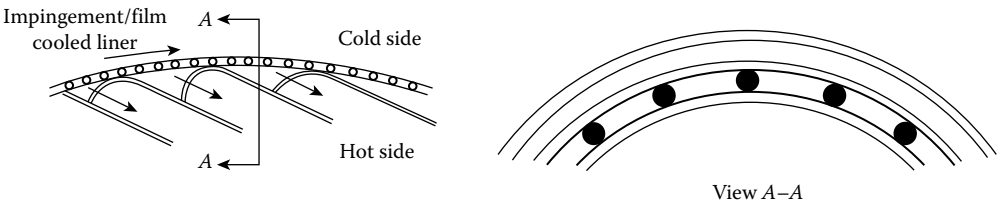


FIGURE 10.17
Impingement-film cooling. (Reprinted from Mattingly, J.D., *Elements of Gas Turbine Propulsion*, AIAA Educations Series, American Institute of Aeronautics and Astronautics, Inc., Reston, VA, 2005, p. 817. With permission.)

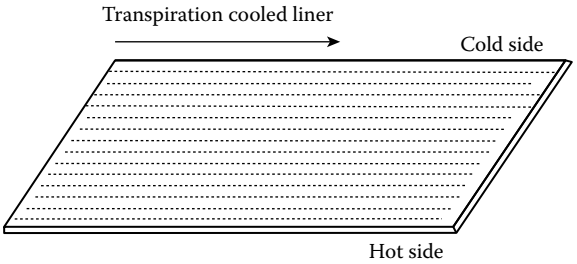


FIGURE 10.18
Transpiration cooling. (Reprinted from Mattingly, J.D., *Elements of Gas Turbine Propulsion*, AIAA Educations Series, American Institute of Aeronautics and Astronautics, Inc., Reston, VA, 2005, p. 817. With permission.)

10.9.5.6 Transpiration Cooling

Transpiration is the most advanced form of wall cooling developed now (Figure 10.18). It has the potential of reducing the required amount of cooling air by as much as 50%. With this scheme, the cooling air flows through a porous liner wall, first removing heat from the wall itself and then providing a barrier between the wall and the hot combustion gases.

10.9.5.7 Effective Cooling

The following parameter is introduced to evaluate the effectiveness of different cooling techniques. It is the cooling effectiveness and is defined by

$$\Phi = \frac{T_g - T_m}{T_g - T_c} \tag{10.16}$$

where
T_g is the main stream gas temperature
T_m is the average metal temperature
T_c is the cooling air temperature

Figure 10.19 illustrates a comparison between the quantities of air needed for cooling with respect to that employed in a simple film cooling. The total pressure and temperature of the inlet to the combustion chamber are 2.425 MPa and 850 K, respectively, while the outlet temperature of the hot products is 2000 K.

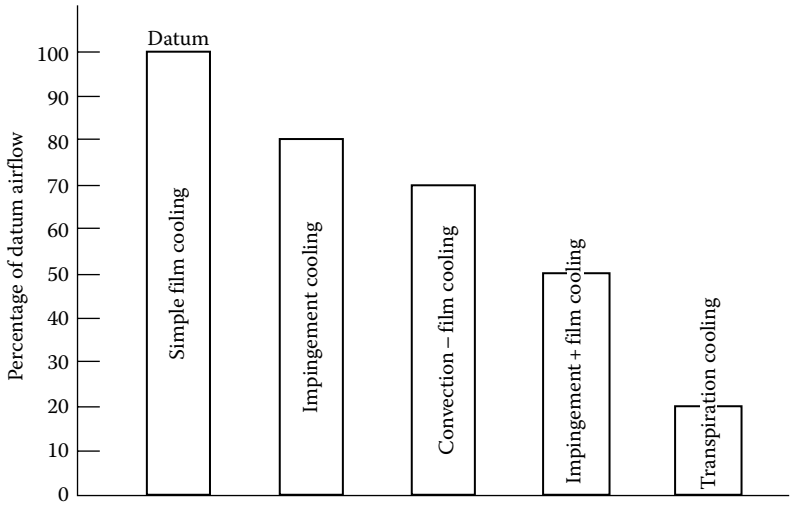


FIGURE 10.19
Comparison between different cooling techniques.

10.10 Material

The walls and internal parts of the combustion chamber must be capable of resisting the very high gas temperature in the primary zone. In practice, this is achieved by using the best heat-resisting materials available. Normally the selected material must withstand severe operating conditions. For example, the combustor is designed for a lifetime of some 9000 hot hours at an average temperature around 2800°F. Moreover, the combustor liners are subjected to high thermal stresses due to temperature gradient and transient stresses during takeoff. Thus, they must withstand these critical conditions together with the possible corrosion. The most commonly used material at present is a nickel-based alloy, with a ceramic composite planned for the future.

10.11 Aircraft Fuels

The fuel specification for aircraft engines is more severe than for all other types of gas turbine. Several requirements by different sources have to be fulfilled.

Operation requirements set by aircraft and engine

1. Low cost and high availability
2. Low fire risk (which implies low vapor pressure, low volatility, high flash point, and high conductivity to minimize the buildup of static electricity during fueling)

3. High heat content for maximum range and/or payload
4. High thermal stability to avoid filter plugging, sticking of control valves, and so on
5. Low vapor pressure to minimize vaporization losses at high altitude
6. High specific heat to provide effective heat absorption on high-speed aircraft

Fuel system requirements

1. Pumping ability (fuel must remain in the liquid phase and flow freely to the atomizer)
2. Freedom from filter clogging by ice or wax crystals
3. Freedom from vapor locking
4. High lubricity for minimum pump wear

Combustion chamber requirements

1. Freedom from contaminants that cause blockage of small passage in fuel nozzle
2. Good atomization
3. Rapid vaporization
4. Minimum carbon formation for low flame radiation and freedom from coke deposition and exhaust smoke
5. Less carbon content to avoid excessive carbon deposits in the combustion chamber
6. Relatively small amount of ash
7. Freedom from alkali metals (such as sodium, which combines with sulfur in the fuel to form corrosive sulfates)
8. Freedom from vanadium

Nowadays, provided an aircraft combustion chamber has been properly designed, its performance and operating characteristics are fairly insensitive to the type of fuel employed.

Probably the only flight condition during which fuel properties become significant is the relight and pull away phase after a flameout at high altitude.

10.11.1 Safety Fuels

One of the greatest hazards in aviation is the possibility of fire after a crash landing. Fuel released from ruptured tanks may be ignited by friction sparks, hot surfaces, or flames. Once a fire has started, it will spread rapidly to all regions where the vapor–air ratio is within the limits of flammability. One method of reducing this fire hazard is by the use of thickened fuels, which have a reduced tendency to flow and a lower rate of evaporation than liquid fuels; if a tank containing thickened fuel is ruptured, then both the spread of fuel and the rate of formation of flammable mists are drastically reduced, and more time is available for passenger evacuation (45–50 min). Thickened fuels may be produced by gelling or emulsification.

10.12 Emissions and Pollutants

Recently, control of emissions has become one of the most important factors in the design of aeroengines and industrial gas turbines. Solutions for emissions from aeroengines are quite different from those for land-based gas turbines.

The pollutants appearing in the exhaust will include oxides of nitrogen (NO_x), CO, and unburned hydrocarbons (UHC); any sulfur in the fuel will result in oxides of sulfur (SO_x), the most common of which is SO_2. Although all these represent a very small proportion of the exhaust, the large flow of exhaust gases produces significant quantities of pollutants that can become concentrated in the area close to the plant. The oxides of nitrogen, in particular, can react in the presence of sunlight to produce "smog," which can be seen as a brownish cloud. This has led to major efforts to clean up the emissions from vehicle exhausts and stringent restrictions on emissions from all types of powerplant. NO_x also cause acid rain, in combination with moisture in the atmosphere, and ozone depletion at high altitudes, which may result in a reduction in the protection from ultraviolet rays provided by the ozone layer, leading to increases in the incidence of skin cancer. UHC may also contain carcinogens, and CO is fatal if inhaled in significant amounts. With an ever-increasing worldwide demand for power and transportation, control of emissions is becoming essential.

10.12.1 Pollutant Formation

For many years the attention of combustion engineers was focused on the design and development of high-efficiency combustors that were rugged and durable, followed by a relatively simple solution to the problem of smoke. When the requirements for emission control emerged, much basic research was necessary to establish the fundamentals of pollutant formation. The single most important factor affecting the formation of NO_x is the flame temperature; this is theoretically a maximum at stoichiometric conditions and will fall off at both rich and lean mixtures. Unfortunately, while NO_x could be reduced by operating well away from stoichiometric conditions, these result in increasing formation of both CO and UHC, as shown in Figure 10.20.

10.12.1.1 NO_x Emissions

NO_x emissions are a considerable environmental problem. They also react with hydrocarbons to form ground-level ozone. They are the main contributors to acid rain together with sulfur dioxide (SO_2). NO_x comes from many natural resources; the majority of the NO_x emissions come from the combustion of biomass and fossil fuels. The combustion of fossil fuels accounts for approximately 42% of the world's total NO_x emissions. These NO_x emissions have steadily increased since the 1970s, but controlling them can be simply accomplished by changing the combustion process.

There are several methods used to reduce atmospheric NO_x pollution. There are two primary solutions: the first method involves combustion modification techniques, while the second utilizes new technologies. Selective catalytic reduction (SCR) is currently the most prominent technology. SCR uses a process that mixes the exhaust air with gaseous reagents such as ammonia or urea and carries that mixture over a catalyst bed at air stream temperature. Another technology currently being used is called selective noncatalytic reduction (SNCR). This technology uses the same basic plan as SCR, only it utilizes

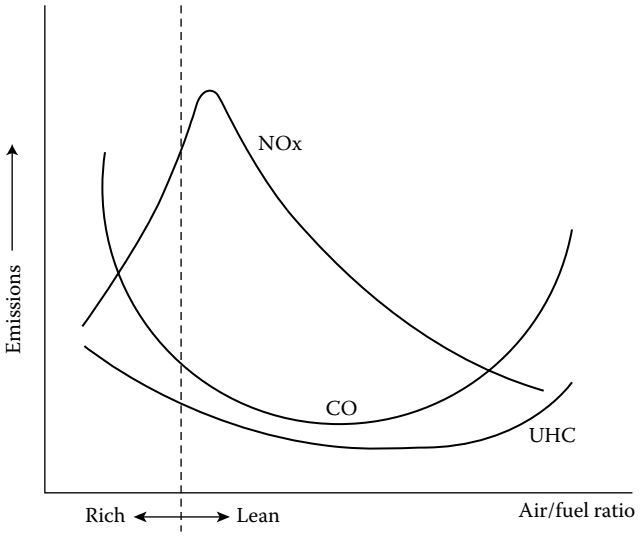


FIGURE 10.20
Effect of fuel–air ratio on emission. (From Saravanamuttoo, H.I.H. et al., *Gas Turbine Theory*, 5th edn., Pearson Prentice Hall, Essex, U.K., 2001, p. 109. With permission.)

gas-phase free-radical reactions instead of a catalyst. In order to reduce NO_x in the SNCR method, the gas must be kept within the range of 1600°F–2100°F.

New technologies have combined the SCR and SNCR processes in order to create even greater reductions. This technology reduces NO_x emissions by using the low-temperature injections as well as the ammonia reagent from the SCR system.

General Electric approaches the NO_x issue by trying to avoid NO_x-producing temperature spikes. Its first attack on NO_x was its low emissions combustor (LEC) on the CF6-80C, which used the existing case and fuel nozzles, optimized mixing for reduced NO_x and smoke, and controlled fuel spray and cooling to cut unburned hydrocarbons. This LEC combustor is used in the GE90, CF34, and GP7000 engine families.

For a larger NO_x cut, General Electric introduced the dual annular combustor (DAC) as an option for CFM56-5B and CFM56-7B engines. The DAC has two combustion zones or stages, a rich pilot stage optimized for emissions during ignition and low power conditions, and then a lean main stage optimized for low NO_x production for high-power conditions.

10.12.1.2 Sulfur Dioxide (SO_2) Emissions

The amount of SO_2 emissions are rising considerably every year, causing damage to the environment and the human population as sulfuric acid, formed when sulfur dioxide combines with water, is the primary component in acid rain. Many respiratory problems can be a result of SO_2 inhalation. Bronchial constriction can be caused by any amount of SO_2 in the range of 1-10 ppm can cause eye, throat, and nose irritation, which can lead to chronic bronchitis. Much larger amounts of sulfur dioxide can be lethal. SO_2 emissions are a result of the combustion of sulfur and oxygen, when one sulfur atom and two oxygen atoms combine.

In conclusion, gas turbine emissions are regulated to increasingly stringent levels in both aircraft and industrial applications. As regards limitations for industrial gas turbines, NO_x was limited to 15/9 ppm by 2010 and will be to 9/5 ppm by 2020. The approaches suggested are as follows:

1. Advanced fuel mixers
2. Novel configurations (that is, variable geometry, fuel staging)
3. Advanced cooling
4. Instability and noise control methods

10.13 The Afterburner

The afterburner, as described previously, is a second combustion chamber located downstream of the turbine and is fitted to supersonic aircraft (mostly military) to develop a greater thrust force. An afterburner consists of only two fundamental parts:

1. The spray bars or the fuel nozzle
2. The flameholder

The afterburner is quite similar to the combustion chamber in ramjet engines as both have a maximum temperature much greater than conventional combustion chambers. For the case of afterburners (in turbojet and turbofan engines), the gases leave the turbine at very high speeds (250–400 m/s), which is far too high for a stable flame to be maintained. Though the flow is diffused before entering the afterburner combustion zone, the gas speed is still high and the diffused air stream would be blown away. For this reason, the afterburner is provided with flameholders downstream of the spray bars. The flameholders have different forms, as shown in Figure 10.21. The vee-gutter flameholder type has been widely used as it has the advantages of low flow blockage, low total pressure loss (dry loss), being simple and lightweight, and having a good development history.

The specific design requirements for an afterburner are larger temperature rise and easy ignition.

First, the afterburner is not subjected to the physical and temperature limits of combustion chamber as the outlet of the afterburner passes through a fixed element (nozzle) rather than a rotating element (turbine) as in the case of combustion chamber. The temperature rise is limited by the amount of oxygen that is available for combustion and limited by the liner and nozzle cooling air. Moreover, combustion takes place easily because 75% of the air (oxygen) entering the afterburner, while no longer need for cooling, is still available for burning with fuel. Ignition in an afterburner is either by a special spark igniter, or by a flash of flame through the turbines of the basic engine or arc igniter or a pilot burner.

Example 10.6

A turbofan engine fitted with an afterburner has the following data:
Fuel is octane: $C_{12}H_{24}$ having lowest heating value LHV = 42,800 kJ/kg
Inlet Mach number to afterburner $M = 0.14$
Inlet temperature of combustion chamber 650 K

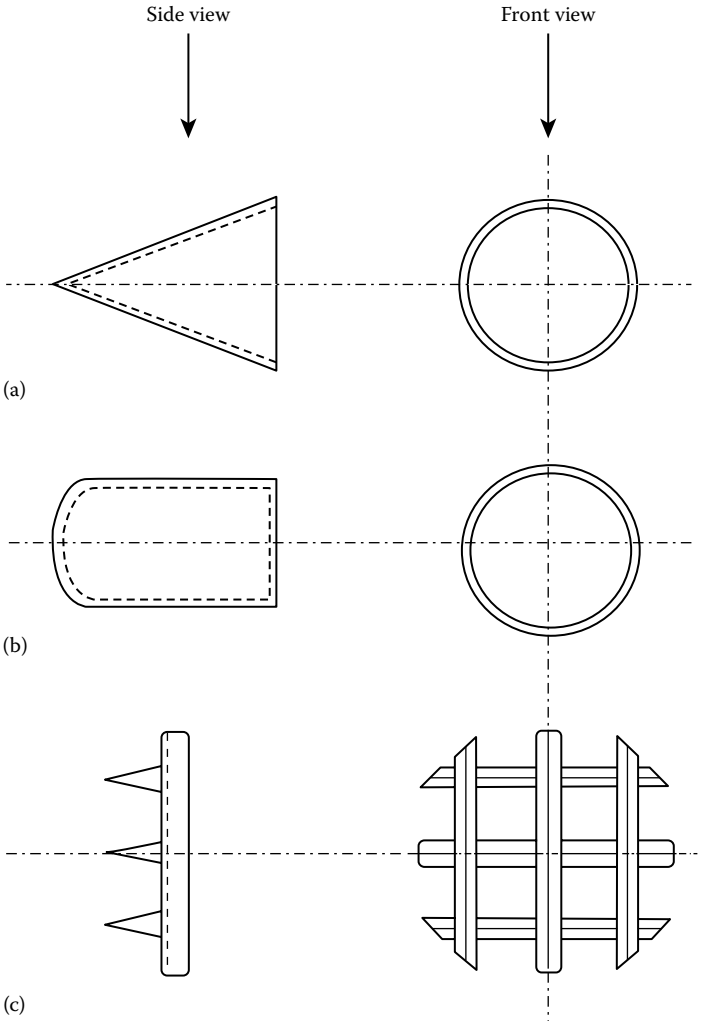


FIGURE 10.21
Different shapes for flameholder: (a) conical baffle, (b) cylindrical baffle, and (c) vee-gutter.

Outlet temperature of combustion chamber 1600 K
Inlet Mach number to afterburner $M = 0.2$
Inlet temperature to afterburner 800 K
Outlet temperature to afterburner 2000
Using these values for specific heat for cold and hot streams: $Cp_c = 1.005$ kJ/kg/K,

$$Cp_h = 1.23 \text{ kJ/kg/K}$$

Calculate

1. Exit Mach number in the combustion chamber
2. Exit Mach number in the afterburner
3. Equivalence ratio in the combustion chamber
4. Equivalence ratio in the afterburner

Solution

1. Temperature ratio in the combustion chamber

$$\frac{T_{02}}{T_{01}} = \frac{1600}{650} = 2.4615$$

At $M = 0.14$

$$\frac{T_0^*}{T_{01}} = 1 / 0.08947$$

Since

$$\frac{T_0^*}{T_{02}} = \frac{T_0^*}{T_{01}} \frac{T_{01}}{T_{02}} = \frac{1}{0.08947 \times 2.4615} = 4.54$$

$$\frac{T_{02}}{T_0^*} = 0.22$$

Mach number at outlet of combustion ratio is $M_2 = 0.22845$.

2. Temperature ratio in the afterburner

$$\frac{T_{0e}}{T_{0i}} = \frac{2000}{800} = 2.5$$

At $M = 0.2$

$$\frac{T_0^*}{T_{0i}} = 1/0.17355$$

Since

$$\frac{T_0^*}{T_{0e}} = \frac{T_0^*}{T_{0i}} \frac{T_{0i}}{T_{0e}} = \frac{1}{0.17355 \times 2.5} = 2.3048$$

$$\frac{T_{0e}}{T_0^*} = 0.4339$$

The corresponding exit Mach number is then $M_e = 0.32726$.

3. The chemical reaction of fuel is

$$2C_{12}H_{24} + 18\left(O_2 + 3.76N_2\right) \rightarrow 12CO_2 + 12H_2O + 18 \times 3.76N_2$$

Thus the stoichiometric FAR is calculated as

$$f_{stoich} = \frac{12 \times 12.011 + 24 \times 1.008}{18 \times 32 + 18 \times 3.76 \times 28.16} = 0.067795$$

F/A for combustion chamber

$$f = \frac{Cp_h T_{02} - Cp_c T_{01}}{LHV - Cp_h T_{02}} = \frac{1.23 \times 1,600 - 1.005 \times 650}{42,800 - 1.23 \times 1,600} = 0.032199$$

Equivalence ratio

$$\phi = \frac{f}{f_{stoich}} = 0.4749$$

4. Equivalence ratio for afterburner
   F/A for afterburner

$$f = \frac{Cp_h T_{0e} - Cp_c T_{0i}}{LHV - Cp_h T_{0e}} = \frac{1.23 \times 2,000 - 1.005 \times 800}{42,800 - 1.23 \times 2,000} = 0.04105$$

Equivalence ratio

$$\phi = \frac{f}{f_{stoich}} = 0.6055$$

10.14 Supersonic Combustion System

As described in Chapter 7, the scramjet engine has a supersonic combustor to avoid the possible large total pressure loss and high static temperature rise that would be caused by the deceleration of hypersonic flow to subsonic. Incomplete combustion occurs in a scramjet engine because of short flowtime available for combustion. Similar to subsonic combustion, there are two scales of mixing: macro and micro. In macromixing, fluids are mixed to a very fine scale but there is no molecular mixing, while in micromixing, molecular mixing occurs.

As a typical value, the ratio of burner length L to entry duct height H, which we might call the burner aspect ratio, is $L/H \sim 10$. The fuel injector for supersonic combustion should be capable of generating vertical motions that cause the fuel–air interface area to increase rapidly and enhance the micromixing at molecular level, hence leading to efficient combustion. Different injection strategies have been proposed with particular concern for rapid, near-field mixing; these injection strategies typically rely on the generation of strong streamwise counter-rotating vortices. Fuel is both injected and mixed in parallel or normal streams [13]. In parallel mixing, ramp injectors are used. These injectors are passive mixing devices that produce counter-rotating streamwise vortices to enhance the mixing of fuel and air (Figure 10.22). Figure 10.22a and b represents the compression and expansion ramps, respectively. Figure 10.22c and d represents the swept and unswept ramp types, respectively.

Finally, swept expansion ramp has the highest performance in parallel of all the designs investigated.

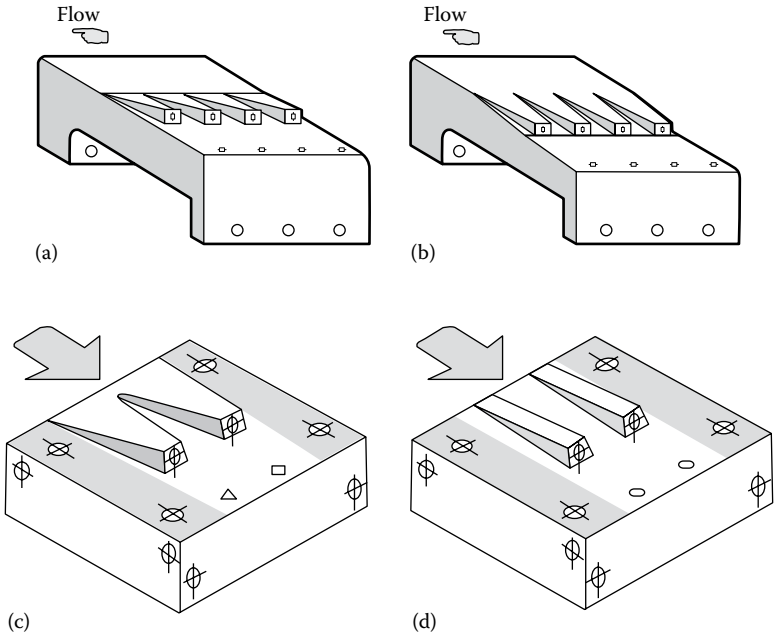


FIGURE 10.22
Supersonic injectors: (a) compression, (b) expansion, (c) swept ramp injectors, and (d) unswept ramp injectors. (Reprinted from Heiser, W.H., *Hypersonic Airbreathing Propulsion*, American Institute of Aeronautics and Astronautics, Inc., Washington, DC, 1994. With permission.)

Now, the other type of mixing, that is, normal mixing, is discussed. One of the simplest approaches is the transverse (normal) injection of fuel from a wall orifice. As the fuel jet interacts with the supersonic cross flow, an interesting but rather complicated flow field is generated. Figure 10.23 illustrates the general flow features of an under-expanded transverse jet injected into a cross flow. As the supersonic cross flow is displaced by the fuel jet, a 3-D bow shock is produced due to the blockage produced by the flow. The bow shock causes the upstream wall boundary layer to separate, providing a region where the boundary layer and jet fluids mix subsonically upstream of the jet exit. This region, confined by the separation shock wave formed in front of it, is important in transverse injection flow fields owing to its flameholding capability in combusting situations.

The stabilization of flames in supersonic flow is a difficult task for two primary reasons: the first is that the flow time is merely a short second. The second is that the strain rates tend to be high in compressible flows, which can suppress combustion.

The primary objective of a flameholder in supersonic combustion, therefore, is to reduce the ignition delay time and to provide a continuous source of radicals for the chemical reaction to be established in the shortest distance possible. In general, flameholding is achieved by three techniques:

1. Organization of a recirculation area where the fuel and air can be mixed partially at low velocities
2. Interaction of a shock wave with partially or fully mixed fuel and oxidizer
3. Formation of coherent structures containing unmixed fuel and air, wherein a diffusion flame occurs as the gases are convected downstream

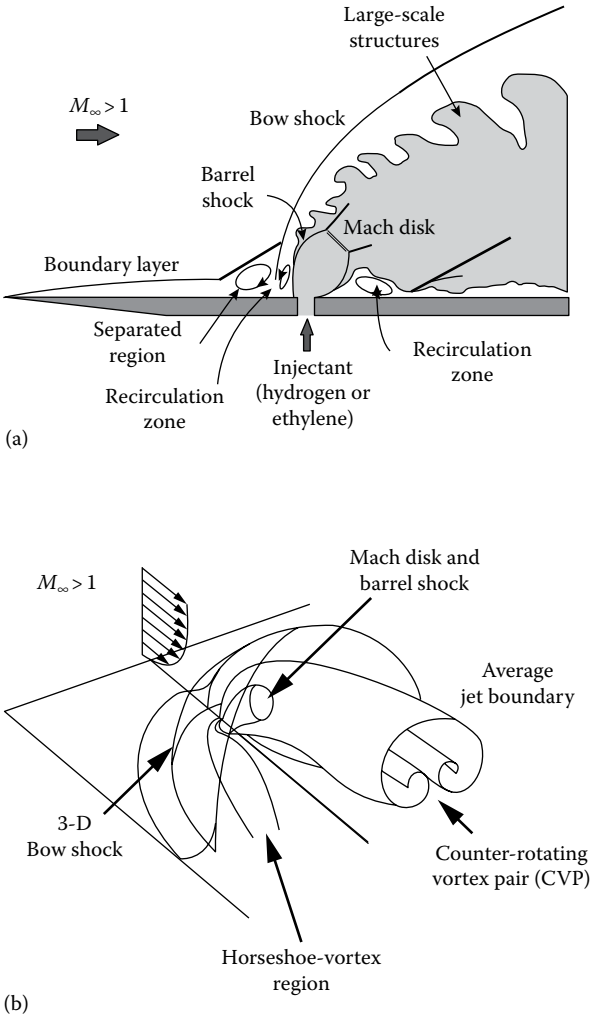


FIGURE 10.23
Normal mixing. (a) Boundary layer separation and recirculation zone. (b) 3-D Bow shock. (Reprinted from Heiser, W.H., *Hypersonic Airbreathing Propulsion*, American Institute of Aeronautics and Astronautics, Inc., Washington, DC, 1994. With permission.)

Cavity-based fuel injection is one of the simplest approaches in flameholding. It uses the backward facing step. While generating a recirculation zone behind the step, that contains the hot gases in it, it serves as a continuous ignition source. This approach can provide sustained combustion, but it has a disadvantage of relatively high stagnation pressure loss. In recent years, a cavity flameholder, which is an integrated fuel injection flameholding approach, has been proposed as a new concept for flameholding and stabilization in a supersonic combustor.

Burners are of two types: either a constant area type or a constant pressure type.

Problems

10.1 Describe the three basic designs for a combustion chamber.

10.2 Explain afterburning (or reheat) operation.

10.3 Describe the gas flow through a typical combustion chamber.

10.4 How it is possible to burn additional fuel in the exhaust system?

10.5 With the aid of tree illustration, identify the different types of combustion chamber.

10.6 Describe briefly the possible configuration for short annular combustors.

10.7 Describe the combustion chamber of the following engines:
1. Turbojet engine P&W JT3
2. Turboprop P&W C PT6
3. Turbofan engines GE CF6, RR Trent 700, PW 4000

10.8 Describe afterburners of the following engines:
1. Turbojet GE J47
2. Turbofan PW F135

10.9 Compare the different types of subsonic combustion chambers, giving the advantages and disadvantages of each type.

10.10 Compare subsonic and supersonic combustion chambers.

10.11 What are the design requirements for a good combustion chamber?

10.12 The temperature rise in combustion chamber (ΔT) depends on the fuel to air ratio (f) and air temperature upstream of the combustion chamber. For an upstream temperature of 650 K, this relation may be expressed as

$$\Delta T\ \left(\mathrm{K}\right) = af + b = 3393 \times 10^4 f + 21.08$$

For C_8H_{18} fuel described in Example 10.2
1. Calculate the fuel-to-air ratio if the temperature rise in combustion chamber is 950 K.
2. Calculate the equivalence ratio ϕ.
3. Write down the chemical reaction equation.

10.13 As an extension to Example 10.3, consider a lean mixture ($\phi < 1.0$). The chemical reaction is expressed by the relation

$$\phi C_{12}H_{24} + 18\left(O_2 + \frac{79}{21}N_2\right) \rightarrow 12\phi\left(CO_2 + H_2O\right) + 18\left(1-\phi\right)O_2 + 18\left(\frac{79}{21}\right)N_2$$

Calculate the percentage of unburnt oxygen.

10.14 If the combustion efficiency (η_c) is also considered in the preceding case of lean mixture, then the chemical reaction equation becomes

$$\phi C_{12}H_{24} + 18\left(O_2 + \frac{79}{21}N_2\right) \rightarrow 12\eta_c\phi\left(CO_2 + H_2O\right) + \left(1-\eta_c\right)\phi C_{12}H_{24}$$
$$+ 18\left(1-\eta_c\phi\right)O_2 + 18\left(\frac{79}{21}\right)N_2$$

For a combustion efficiency of 0.98 and the same equivalence ratio, calculate the percentage of

1. Unburnt fuel
2. Unused oxygen

10.15 Consider the case of a rich mixture ($\phi > 1.0$) for the same fuel discussed in Example 10.3. The chemical reaction for a combustion efficiency of (η_c) is given by

$$\phi C_{12}H_{24} + 18\left(O_2 + \frac{79}{21}N_2\right) \rightarrow 12\eta_c\phi\left(CO_2 + H_2\right) + \left(1-\eta_c\right)\phi C_{12}H_{24} + 18\left(1-\eta_c\phi\right)O_2 + 18\left(\frac{79}{21}\right)N_2$$

For combustion efficiency $\eta_c = 98\%$ and equivalence ratio $\phi = 1.02$, calculate

1. The percentage increase of fuel injected into the combustion chamber
2. The percentage of unburnt fuel
3. The percentage of unused oxygen

10.16 In a 2-year study for low emission combustor technology (LOWNOX I) by numerous aeroengine manufacturers, including RR, MTU, and Volvo as well as other institutions and agencies [14], the following data were deduced for a turbofan engine:

Condition	Idle	Takeoff	Cruise
Inlet temperature to combustion chamber	550 (K)	917 (K)	846 (K)
A/F ratio	114.8	36.9	39.9

The fuel used is C_8H_{18}; it is required for the three operating conditions to

1. Write down the chemical reaction equation.
2. Calculate the equivalence ratio.
3. Calculate the temperature rise in combustion chamber assuming that

$$Q_{HV} = 42{,}800\,\text{kJ/kg}, \quad CP_c = 1.005\,\text{kJ/(kg·K)}, \quad Cp_h = 1.23\,\text{kJ/(kg·K)}.$$

4. Calculate the combustion efficiency.

10.17 What are the operation requirements in aircraft fuels set by aircraft and engines?

10.18 If the combustion gases have a temperature of 1400 K and the coolant temperature is 500 K, calculate the average metal temperature if the effective cooling parameter (ϕ) has the values of 0.2, 0.4, and 0.6.

10.19 A turbofan engine powering a military aircraft is fitted with an afterburner. The inlet condition to the afterburner are $T_{01} = 600$ K, $M_1 = 0.2$ and the outlet temperature is $T_{02} = 3000$ K. Using Rayleigh flow equations (or tables)

1. Calculate the Mach number at the outlet of the afterburner M_2.
2. If the afterburner is designed to have an outlet Mach number $M_2 = 1.0$, what will be the value of the outlet temperature T_{02}?
3. If the Mach number at the outlet of afterburner is $M_2 = 1.0$ and the inlet and outlet total temperatures are $T_{01} = 600$ K and $T_{02} = 3000$ K, respectively, what will be the value of the inlet Mach number M_1?

10.20 A conical diffuser of a combustion chamber has the following data:

1. Area ratio (AR) = 1.6
2. Divergence angle = 12°
3. Air density = 5.42 kg/m^3
4. Inlet velocity of air V_i = 133.304 m/s
5. Mass flow rate of air (Diffuser) = 4 kg/s

Calculate

1. Diffuser geometry
2. Overall effectiveness

10.21 Consider the complete combustion of Octane (C_8H_{18}) with theoretical air. If the enthalpy of formation of the reactants and products are as follows:

Substance	Chemical Expression	h_{fo} (kJ/kmol)
Carbon dioxide	$CO_2(g)$	−393,520
Water vapor	$H_2O(g)$	−241,820
Water	$H_2O(l)$	−285,820
Methane	$C_8H_{18}(g)$	−208,447

where (g) refers to gas and (l) refers to liquid. Calculate the lower and higher heating values of C_8H_{18}.

Develop the combustion equation and determine the air-fuel ratio for the complete combustion of *n-Butane* (C_4H_{10}) with

1. Theoretical air
2. 50% excess air

References

1. R.T.C. Harman, *Gas Turbine Engineering: Applications, Cycles and Characteristics*, Halsted Press Book, John Wiley & Sons, New York, 1981, p. 88.
2. H.I.H. Saravanamuttoo, G.F.C. Rogers and H. Cohen, *Gas Turbine Theory*, 5th edn., Pearson Prentice Hall, Essex, U.K., 2001.
3. A.H. Lefebvre, *Gas Turbine Combustion*, 2nd edn., Taylor & Francis, Philadelphia, PA, 1999, p. 39.
4. M.P. Boyce, *Gas Turbine Engineering Handbook*, 2nd edn., Butterworth-Heinemann, Houston, TX, 2002, p. 370.
5. *The Jet Engine*, 5th edn., Rolls-Royce plc, Derby, U.K., 1996.
6. S.J. Kline, D.E. Abbott, and R.W. Fox, Optimum design of straight-walled diffusers, *Journal of Basic Engineering*, 81, 321–331, 1959.
7. J.H.G. Howard, A.B. Thornton-Trump, and H.J. Henseler, *Performance and Flow Regimes for Annular Diffusers*, ASME Paper 67-WA/FE-21, ASME, New York, 1967.
8. A.T. McDonald and R.W. Fox, An experimental investigation of incompressible flow in conical diffusers, *International Journal of Mechanical Sciences*, 8, 125–139, 1966.
9. L.R. Reneau, J.P. Johnson, and S.J. Kline, Performance and design of straight, two-dimensional diffusers, *Journal of Basic Engineering*, 95, 141–150, 1967.

10. J.D. Mattingly, *Elements of Gas Turbine Propulsion*, AIAA Education Series, American Institute of Aeronautics and Astronautics, Inc., Reston, VA, 2005, p. 817.
11. I. Urieli, *Engineering Thermodynamics—A Graphical Approach*, Ohio State University, Ohio, 2010, http://www.ohio.edu/mechanical/thermo/Applied/Chapt.7_11/Chapter11.html.
12. A.F. El-Sayed, *Fundamentals of Aircraft and Rocket Propulsion*, Springer, London, U.K., 2016.
13. W.H. Heiser and D.T. Pratt, *Hypersonic Airbreathing Propulsion*, AIAA Education Series, American Institute of Aeronautics and Astronautics, Inc., Washington, DC, 1994.
14. R. Dunker, *Advances in Engine Technology, European Commission Directorate—General XII, Science, Research and Development*, John Wiley & Sons, Chichester, U.K., 1993, pp. 105–152.


Taylor & Francis
Taylor & Francis Group
http://taylorandfrancis.com

11

Exhaust System

11.1 Introduction

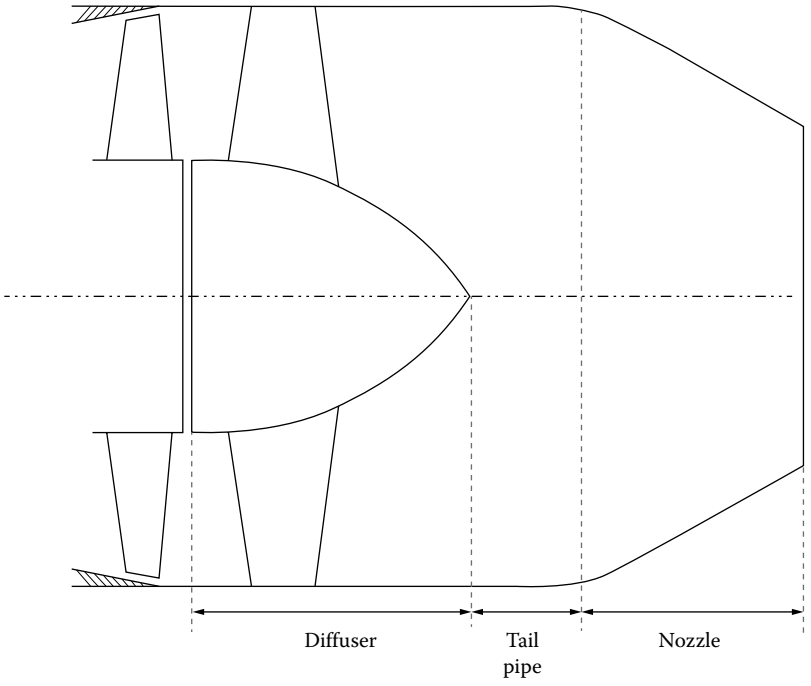
Aero gas turbines have an exhaust system that passes the turbine discharge gases into the atmosphere at a velocity and direction appropriate to the flight condition. A second nozzle exists in (high bypass) for discharging the air that has bypassed the fan. Thus it provides the thrust force required for all flight conditions except landing where the thrust reverse system may provide the dragging force needed for the aircraft to stop within an appropriate distance. For turbo-propeller engines, the major part of thrust is developed by the propeller, and the exhaust gases make little contribution.

The main components of the exhaust system for non-afterburning engines are the tail cone, the exhaust duct (which is often referred to as the tail pipe), and the exhaust nozzle, Figure 11.1.

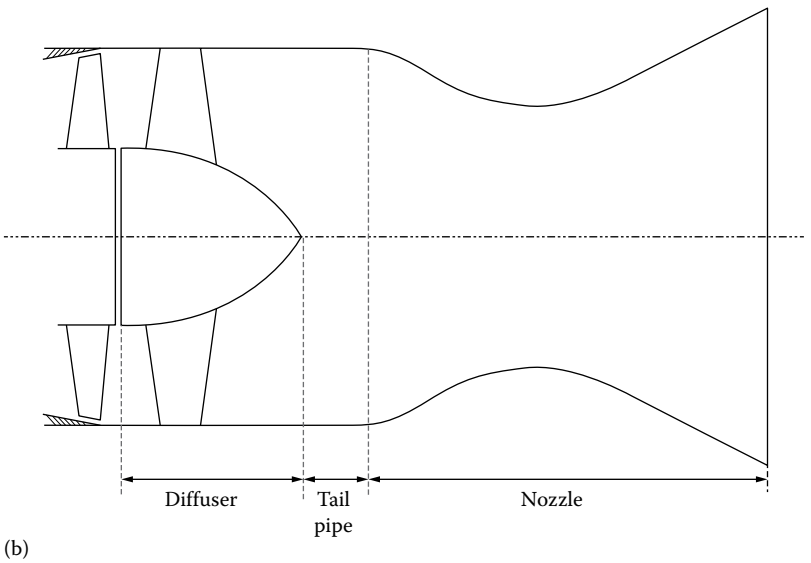
Gas from the engine turbine enters the exhaust system at velocities from 750 to 1200 ft/s [1]. This high velocity produces high friction losses; thus these high speeds have to be reduced by diffusion. Diffusion is accomplished by increasing the passage area between the exhaust cone and the outer wall as shown in Figure 11.1. The tail cone is fastened to the casing by turbine rear support struts. These struts straighten out the flow before the gases pass into the jet pipe. The exhaust gases pass into atmosphere through the propelling nozzle. In a non-afterburning turbojet engine, the exit velocity of the exhaust gases is subsonic at low-thrust conditions and reaches the speed of sound in most operating conditions. As shown in Figure 11.1a, the nozzle is of the convergent type. For supersonic flow, the nozzle is always of the convergent-divergent (C-D) type (Figure 11.1b). Both figures apply for simple ramjet and turbojet engines. In the case of afterburning engines, the afterburner fuel nozzle and flameholder are located in the tail pipe, which is also identified as jet pipe (Figure 11.1c). Figure 11.1d illustrates the case of a low-BPR turbofan engine of the mixed type with an afterburner. Both hot and cold streams are mixed before entering the propelling nozzle or the afterburner.

Many of these engines use separate nozzles for exhausting core and fan streams.

Unmixed turbofan engines have two separate nozzles for exhausting core and fan streams as described in Chapter 5. The hot nozzle is located downstream of the turbine, or the low-pressure turbine for multi-spool engines, which is similar to that in Figure 11.1. The cold nozzle is downstream of the fan section and identified as the fan nozzle. The vast majority of jet-powered aircraft use what are known as axisymmetric nozzles. These nozzles, like those illustrated in Figure 11.1, direct thrust purely along the axis of the engine, hence the term axisymmetric. However, in some aircraft, two-dimensional nozzles are used (Figure 11.2). These nozzles are not only capable for directing the thrust along the axis of the engine, but also of deflecting to vector the thrust and produce a force that points the

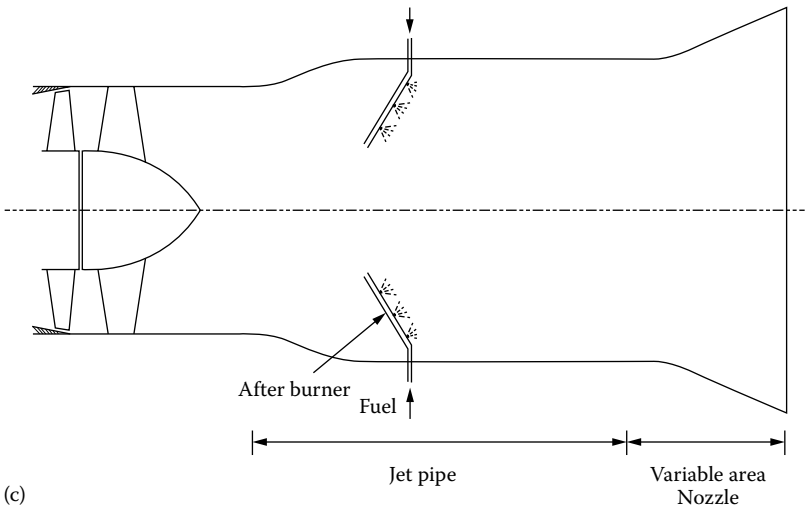


(a)

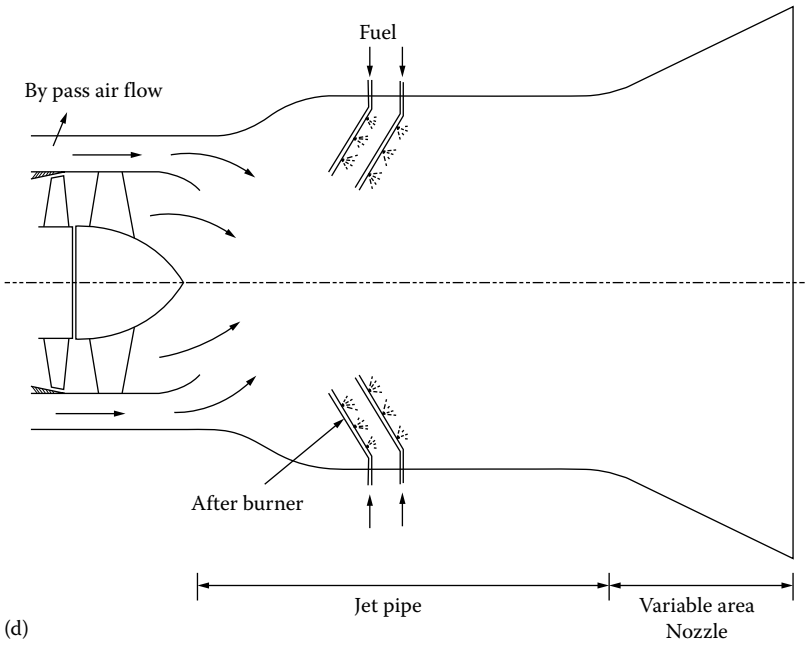


(b)

FIGURE 11.1
Arrangements of exhaust system. (a) Simple exhaust system. (b) Supersonic aircraft exhaust. (*Continued*)



(c)



(d)

FIGURE 11.1 (*Continued*)
Arrangements of exhaust system. (c) Exhaust system for afterburning engines. (d) Exhaust system for low BPR afterburning turbofans.

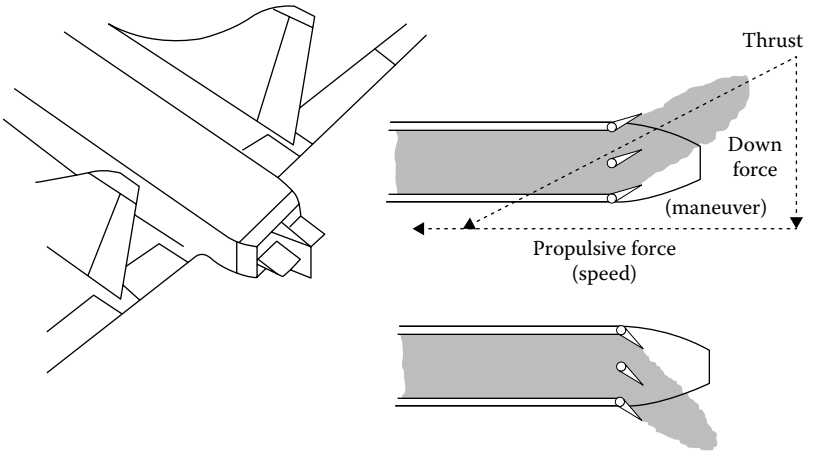


FIGURE 11.2
Two-dimensional nozzles for thrust vectoring.

nose of the plane in a different direction. This type of nozzle is at the heart of what is known as *thrust vectoring*. The nozzles depicted in Figure 11.2 are capable of vectoring the thrust up or down to produce an up force or down force. Down force will force the aircraft nose to pitch upward while up force has the opposite effect. The two nozzles can also be deflected differentially (one producing up force, the other down force) to provide roll control.

Two important topics are incorporated with the exhaust system, namely thrust reverse and noise suppressor. Thrust reversing is an engine system used for bringing to a stop all the civil and some of the military airplanes in service nowadays. When deployed by the pilot, these devices reverse the engine's thrust by closing in and pushing the air out the front of the engine rather than the back. This motion decreases the speed of the aircraft and is the loud noise always heard when landing.

Presently regulations specify certain noise levels that must not be exceeded by new aircraft. The noise sources are the fan or compressor, the turbine, and the exhaust jet or jets. The noise of these sources increases to varying degrees with greater relative airflow velocity. Exhaust-jet noise varies by a larger factor than the compressor- or turbine-noise, therefore a reduction in exhaust-jet velocity has a stronger influence than an equivalent reduction in compressor or turbine blade speeds. The amount of energy in the exhaust that is transformed into noise varies as approximately tile eighth power of the exhaust velocity. Details of noise suppression will be discussed later in this chapter.

11.2 Nozzle

The exhaust nozzles may be classified as

1. Convergent or convergent-divergent (C-D) types
2. Axisymmetric or two-dimensional types
3. Fixed-geometry or variable-geometry types

The simplest form is the fixed-geometry convergent type as no moving parts or control mechanisms are needed. It is found in subsonic commercial aircrafts. Sophisticated nozzle mechanisms are normally found in thrust-vectoring types like that in F-22 Raptor and F-15 S, X-36, and Sukhoi Su-35.

Nozzles should fulfill the following requirements [2]:

1. Be matched to other engine components for all engine operating conditions
2. Provide the optimum expansion ratio
3. Have minimum losses at design and off-design conditions
4. Permit afterburner operation (if available) without affecting main engine operation
5. Allow for cooling of walls if necessary
6. Provide reversed thrust when necessary
7. Suppress jet noise and infrared radiation (IR) if desired
8. Provide appropriate force for takeoff/landing for vertical takeoff and landing (VTOL) or vertical/short takeoff and landing (V/STOL) aircraft
9. Provide necessary maneuvering for military aircrafts fitted with thrust-vectoring systems
10. Do 1–9 with minimal cost, weight, and boat-tail-drag while meeting life and reliability goals

Convergent nozzles are used in almost all the present subsonic transports. Moreover, in most cases these convergent nozzles are also choked, and incomplete expansion of the flowing gases to the ambient pressure is encountered. At nozzle outlet, the gases exit at sonic speed while the pressure is greater than the ambient pressure. Thus a pressure-thrust force is developed. On the contrary, a convergent-divergent nozzle (C-D) satisfies a full expansion to the ambient pressure.

Thus the exit and ambient pressures are equal and the exit velocity is higher than the sonic speed. The C-D nozzle develops higher momentum thrust, which is greater than the pressure thrust of a convergent nozzle operating at the same inlet conditions. Thus if both types are examined in the case of subsonic civil transports, a C-D nozzle provides higher thrust. However, it has the penalties of increased weight, length, diameter leading to an increase of aircraft weight and possibly drag [3].

11.2.1 Governing Equations

The flow of a calorically perfect gas in a nozzle is considered here. The mass flow rate $\dot{m}$ may be determined in terms of the local area from the relation

$$\dot{m} = \rho u A = \left(\frac{P}{RT}\right)\left(M\sqrt{\gamma RT}\right)A = (MA)\left(\frac{P}{P_0}\right)P_0\frac{\sqrt{\gamma T_0}}{\sqrt{R}}\sqrt{\frac{T_0}{T}}$$

$$\dot{m} = \frac{\sqrt{\gamma}P_0}{\sqrt{T_0 R}}MA\frac{\left\{1+\frac{\gamma-1}{2}M^2\right\}^{1/2}}{\left\{1+\frac{\gamma-1}{2}M^2\right\}^{\gamma/\gamma-1}}$$

Finally, the mass flow is

$$\dot{m} = \frac{AP_0}{\sqrt{T_0}}\sqrt{\frac{\gamma}{R}}\frac{M}{\left\{1+\frac{\gamma-1}{2}M^2\right\}^{\gamma+1/2(\gamma-1)}} \tag{11.1a}$$

11.2.1.1 Convergent-Divergent Nozzle

The flow in nozzles can be assumed adiabatic as the heat transfer per unit mass of fluid is much smaller than the difference in enthalpy between inlet and exit. Figure 11.3 illustrates a C-D nozzle together with its T–S diagram. Three states are identified, namely, inlet (i), throat (t) and exit (e). Flow is assumed to be isentropic from the inlet section up to the throat, thus $P_{oi}=P_{ot}$, $T_{oi}=T_{ot}$. Flow from the throat and up to the exit is assumed to be adiabatic but irreversible due to possible boundary layer separation; thus, $P_{ot}>P_{oe}$ but $T_{ot}=T_{oe}$. Gases expand to the static pressure P_e with an adiabatic efficiency η_n in the range from 0.95 to 0.98.

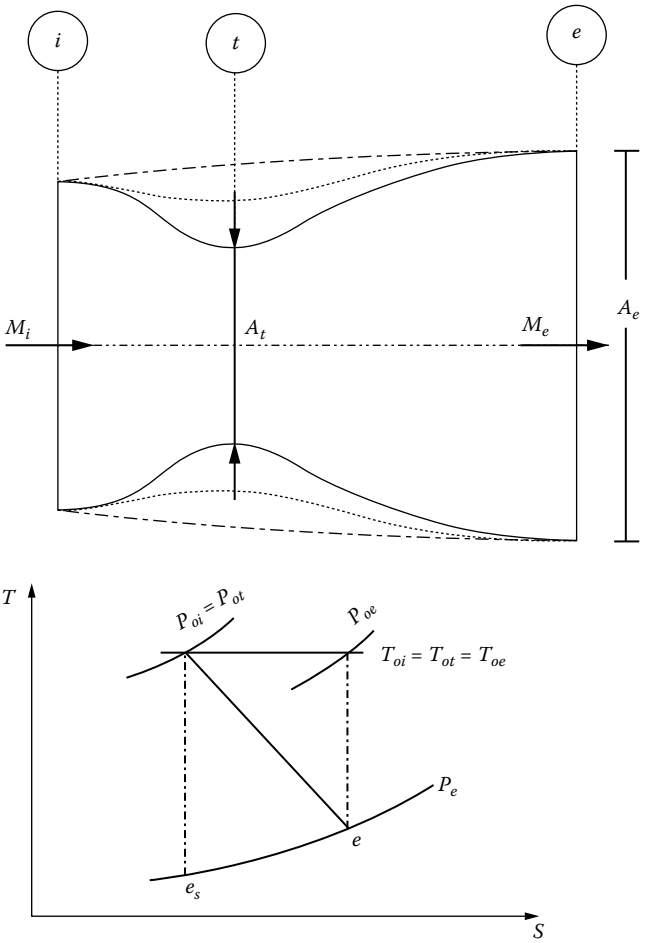


FIGURE 11.3
Convergent-divergent nozzle.

This efficiency is used to evaluate the pressure ratio in the nozzle (P_{0i}/P_{0e}) as follows. The efficiency is defined as

$$\eta_n = \frac{h_{oi} - h_e}{h_{oi} - h_{es}} = \frac{T_{0i} - T_e}{T_{0i} - T_{es}} = \frac{1 - T_e/T_{0e}}{1 - T_{es}/T_{0i}}$$

Since $T_{oi} = T_{oe}$, $\eta_n = \dfrac{1 - \left(P_e/P_{0e}\right)^{\gamma-1/\gamma}}{1 - \left(P_e/P_{0i}\right)^{\gamma-1/\gamma}}$

Thus

$$\frac{P_e}{P_{0e}} = \left[1 - \eta_n \left\{1 - \left(\frac{P_e}{P_{0i}}\right)^{\gamma-1/\gamma}\right\}\right]^{\gamma/\gamma-1}$$

Rewriting $P_{0i}/P_{0e} = (P_e/P_{0e})(P_{0i}/P_e)$, then the nozzle pressure ratio is

$$\frac{P_{0i}}{P_{0e}} = \frac{P_{0i}}{P_e}\left[1 - \eta_n \left\{1 - \left(\frac{P_e}{P_{0i}}\right)^{\gamma-1/\gamma}\right\}\right] \tag{11.2}$$

The exit velocity is evaluated from the relation $u_e = \sqrt{2\left(h_{0i} - h_e\right)} = \sqrt{2\eta_n\left(h_{0i} - h_{es}\right)}$

$$u_e = \sqrt{2C_p\eta_n\left(T_{0i} - T_{es}\right)} = \sqrt{2C_p\eta_n T_{0i}\left\{1 - \left(\frac{P_e}{P_{oi}}\right)^{\gamma-1/\gamma}\right\}}$$

$$u_e = \sqrt{\frac{2\gamma R}{(\gamma - 1)}\eta_n T_{0i}\left\{1 - \left(\frac{P_e}{P_{oi}}\right)^{\gamma-1/\gamma}\right\}}$$

The exit Mach number is then $M_e^2 = u_e^2/a_e^2 = u_e^2/\gamma R T_e$

Since

$$\frac{T_{0e}}{T_e} = 1 + (\gamma - 1/2)M_e^2 \equiv \frac{T_{0e}}{T_e}$$

$$M_e^2 = \frac{2\eta_n}{\gamma - 1}\left\{1 + \frac{\gamma - 1}{2}M_e^2\right\}\left\{1 - \left(\frac{P_i}{P_{0i}}\right)^{\gamma-1/\gamma}\right\}$$

$$M_e^2 = \frac{2}{\gamma - 1}\left[\frac{\eta_n\left\{1 - \left(P_e/P_{0i}\right)^{\gamma-1/\gamma}\right\}}{1 - \eta_n\left\{1 - \left(P_e/P_{0i}\right)^{\gamma-1/\gamma}\right\}}\right] \tag{11.3}$$

From Equation 11.1a, and noting that isentropic flow is assumed from nozzle inlet until the throat ($P_{oi} = P_{ot}$), the ratio between the throat area and exit area variation with Mach number can be expressed as

$$\frac{A_t}{A_e} = \frac{P_{0e}}{P_{ot}}\frac{M_e}{M_t}\left[\frac{1 + \dfrac{\gamma - 1}{2}M_t^2}{1 + \dfrac{\gamma - 1}{2}M_e^2}\right]^{\gamma+1/2(\gamma-1)} = \frac{P_{0e}}{P_{oi}}\frac{M_e}{M_t}\left[\frac{1 + \dfrac{\gamma - 1}{2}M_t^2}{1 + \dfrac{\gamma - 1}{2}M_e^2}\right]^{\gamma+1/2(\gamma-1)} \tag{11.4a}$$

Since in most cases the throat will be choked, or $M_t = 1$, then the equation will be

$$\frac{A^*}{A_e} = \frac{P_{0e}M_e}{P_{0i}^*}\left[\frac{\frac{\gamma+1}{2}}{1+\frac{\gamma-1}{2}M_e^{\,2}}\right]^{\gamma+1/2(\gamma-1)} \tag{11.4b}$$

The mass flow rate in this case will be expressed as

$$\dot{m} = \frac{A^* P_{0i}^*}{\sqrt{T_{0i}^*}}\sqrt{\frac{\gamma}{R}}\frac{1}{\left\{\frac{\gamma+1}{2}\right\}^{\frac{\gamma+1}{2(\gamma-1)}}} \tag{11.1b}$$

The velocity and static pressure is plotted along the longitudinal axis of nozzle as shown in Figure 11.4. The C-D nozzle is designed to have the exit pressure equal to the ambient pressure. If the nozzle operates at higher or lower altitudes, then the nozzle will have different behaviors as shown in Figure 11.5. Figure 11.5a illustrates the design conditions. This may be the case of a nozzle fitted to a turbojet and have an area ratio of 4 and flight Mach number $M \approx 2$.

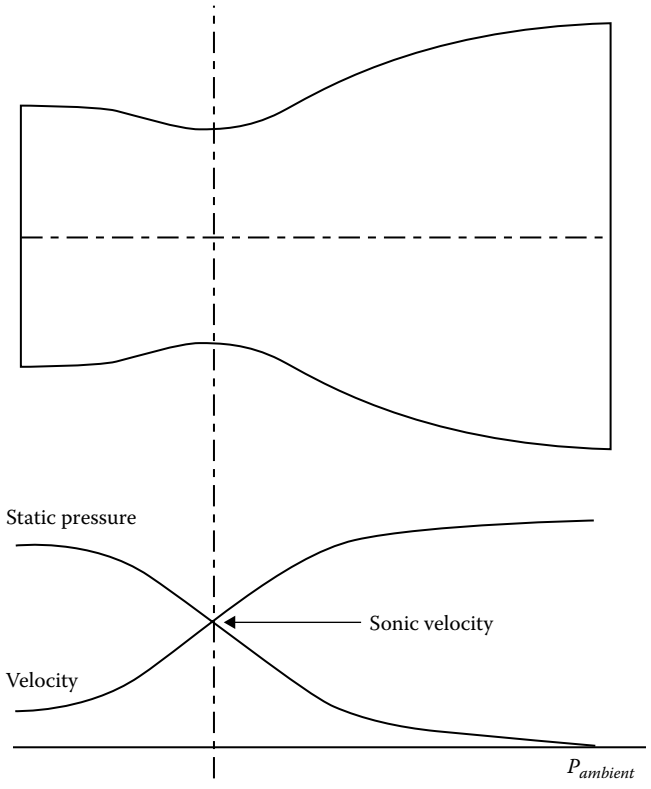


FIGURE 11.4
Velocity and static pressure distribution in convergent-divergent nozzle.

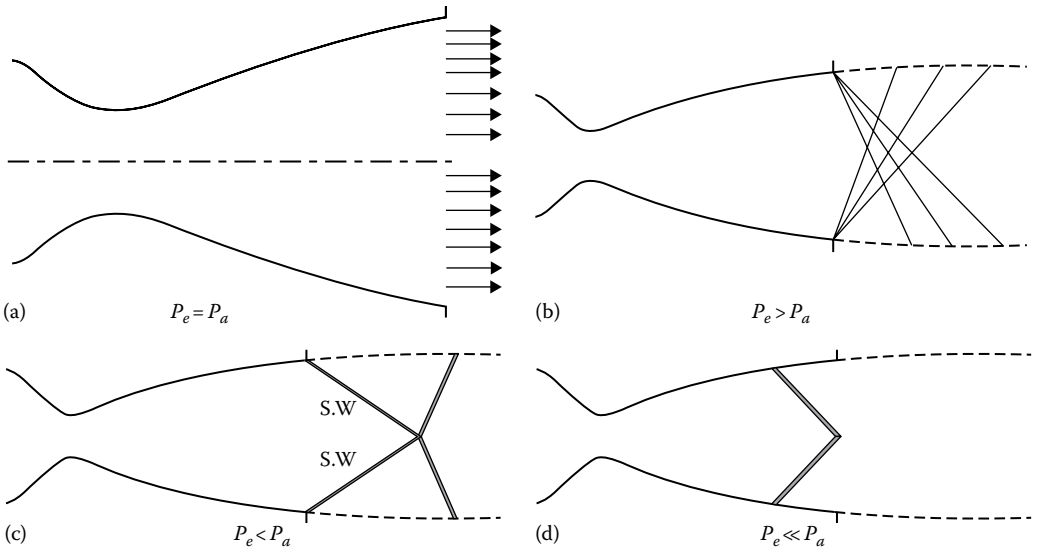


FIGURE 11.5
Behavior of convergent-divergent nozzle. (a) Design condition. (b) Exit pressure exceeds ambient pressure. (c) Ambient pressure exceeds exit pressure. (d) Ambient pressure greatly exceeds exit pressure.

When the exit pressure exceeds ambient pressure (under expansion case, $M > 2$), expansion waves exist on nozzle lip (Figure 11.5b). The opposite case: when the ambient pressure exceeds the exit pressure (over expansion, $M < 2$, $P_e > P_a/2$), oblique shock waves are generated at the exit plane (Figure 11.5c). If the ambient pressure is much greater than the exit pressure ($M < 2$, $P_e \ll P_a$), the oblique shock waves exist within the nozzle (Figure 11.5d).

11.2.1.2 Convergent Nozzle

The convergent nozzle has close similarity to the convergent part of the previously discussed C-D nozzle. However, the main difference is that the flow in the C-D nozzle is assumed isentropic while the flow in the convergent nozzle is assumed to be only adiabatic.

If the nozzle is choked, then the exit Mach number is unity and all conditions are denoted by subscript (c). The temperature ratio is then

$$\frac{T_{0e}}{T_e} = \frac{T_{0e}}{T_c} = \frac{\gamma + 1}{2} \tag{11.5}$$

The efficiency of the nozzle is also defined as

$$\eta_n = \frac{h_{oi} - h_e}{h_{oi} - h_{es}} = \frac{T_{0i} - T_e}{T_{0i} - T_{es}} = \frac{1 - T_e / T_{0e}}{1 - T_{es} / T_{0i}} = \frac{1 - \dfrac{\gamma + 1}{2}}{1 - \left(\dfrac{P_c}{P_{0i}}\right)^{\gamma - 1/\gamma}}$$

Thus the pressure ratio is expressed as

$$\frac{P_{0i}}{P_c} = \frac{1}{\left(1 - \frac{1}{\eta_n}\frac{\gamma-1}{\gamma+1}\right)^{\gamma/\gamma-1}} \tag{11.6}$$

In general an estimate for the critical value is obtained by assuming that the nozzle is isentropic, thus Equation 11.6 is reduced to $\frac{P_{0i}}{P_c} = \left(\frac{\gamma+1}{2}\right)^{\gamma/\gamma-1}$ and for $\gamma = 4/3$, and this ratio will be $\frac{P_{0i}}{P_c} = 1.853$. If $\frac{P_{0i}}{P_a} > \frac{P_{0i}}{P_c}$, then the nozzle is choked.

11.2.2 Variable Geometry Nozzles

Variable area nozzle, which is sometimes identified as an adjustable nozzle, is necessary for engines fitted with afterburners. Generally, as the nozzle is reduced in area, the turbine inlet temperature increases, and the exhaust velocity and thrust increase. Three methods are available, namely,

1. Central plug at nozzle outlet
2. Ejector type nozzle
3. IRIS nozzle

Central plug, Figure 11.6, is the exact analogue of spike at the inlet as described in Chapter 9. The plug employs an external expansion fan as the spike employs external oblique shocks [4].

The second type is the *ejector nozzle*, which creates an effective nozzle through a secondary airflow and spring-loaded petals. At subsonic speeds, the airflow constricts the exhaust to a convergent shape. As the aircraft speeds up, the two nozzles dilate, which allows the exhaust to form a convergent-divergent shape, speeding the exhaust gases past Mach 1, Figure 11.7. More complex engines can actually use a tertiary airflow to reduce exit area at very low speeds. Advantages of the ejector nozzle are relative simplicity and reliability. Disadvantages are average performance (compared to the other nozzle type) and

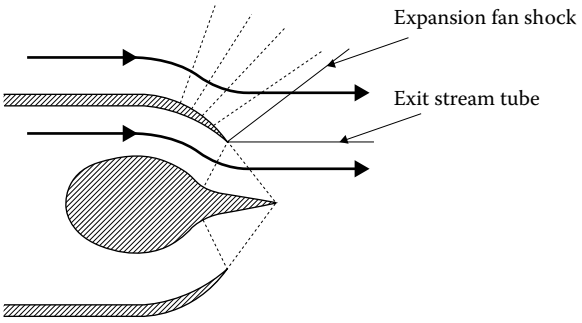


FIGURE 11.6
Plug nozzle at design point. (From Kerrebrock, J.L., *Aircraft Engines and Gas Turbines*, 2nd edn., The MIT Press, Cambridge, MA, 1992, 142pp.)

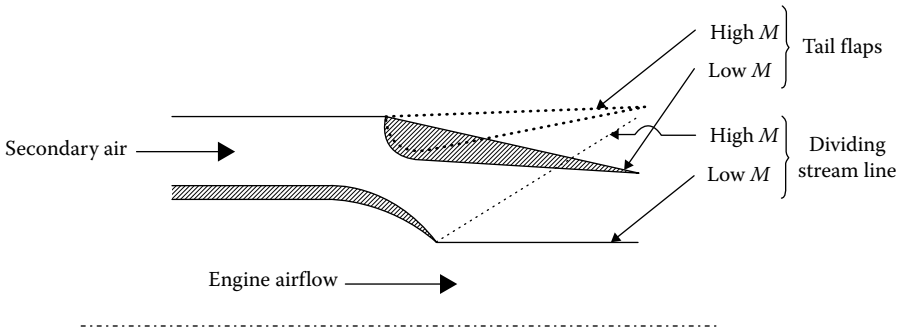


FIGURE 11.7
Variable geometry ejector nozzle. (From Kerrebrock, J.L., *Aircraft Engines and Gas Turbines*, 2nd edn., The MIT Press, Cambridge, MA, 1992, 142pp.)

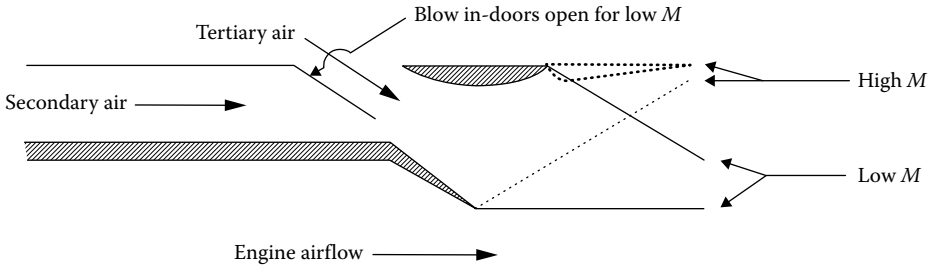


FIGURE 11.8
Ejector nozzle with blow-in doors for tertiary air. (From Kerrebrock, J.L., *Aircraft Engines and Gas Turbines*, 2nd edn., The MIT Press, Cambridge, MA, 1992, 142pp.)

relatively high drag due to the secondary airflow (Figure 11.8). Some of the aircraft that have utilized this type of nozzle are the SR-71, Concorde, F-111, and Saab Viggen.

The third type is an iris nozzle, which is used for higher performance nozzles (Figure 11.9). This type uses overlapping, hydraulically adjustable "petals." Although more complex than the ejector nozzle, it has significantly higher performance and smoother airflow. It is employed primarily on high-performance fighters such as the F-14, F-15, F-16, and the high-speed bomber B-1B. Some modern iris nozzles have the ability to change the angle of the thrust.

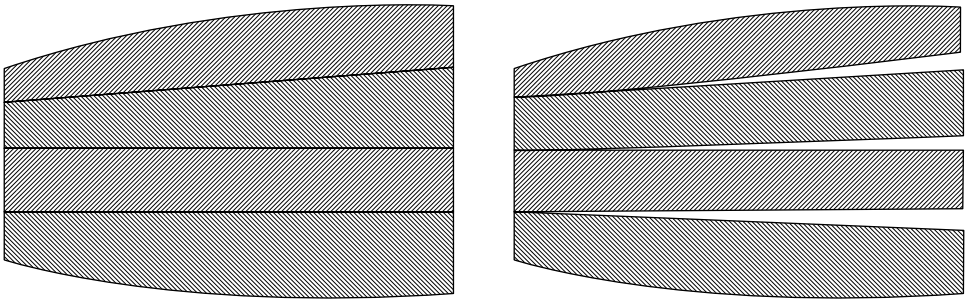


FIGURE 11.9
Iris variable nozzle.

11.2.3 Afterburning Nozzles

Afterburning is a method for augmenting the basic thrust of an engine to improve the takeoff, rate of climb, and combat performance of military aircrafts. Supersonic civil transports are also fitted with afterburners. The thrust of an afterburning engine, with inoperative afterburner, is slightly less than that of a similar engine not fitted with afterburning equipment due to the added restrictions in the jet pipe (Figure 11.1). The temperature of the afterburner flame may exceed 1700°C. The area of the afterburning jet pipe is larger than a normal jet pipe to obtain a reduced velocity gas stream. The rear fan duct and turbine exhaust cone form a diffuser section to reduce the velocity of fan discharge air and engine exhaust gases [5]. Fuel is introduced through a series of perforated spray bars located inside the forward section. A flameholder is mounted behind the manifolds and reduces the velocity of gases to ensure flame stability.

The afterburning jet pipe is made of a heat-resistant nickel alloy and requires more insulation than the normal jet pipe. The jet pipe may be of a double-skin construction with a part of the fan bypass air is induced between both inner and outer skins for its cooling [1]. A circular heatshield of similar material to the jet pipe is often fitted to the inner wall of the jet pipe to improve cooling at the rear of the burner section. The propelling nozzle is of similar material and construction as the jet pipe. A variable geometry nozzle is achieved by either a two-position nozzle or a nozzle whose area varies automatically in proportion to the total thrust produced by the basic engine and the afterburner together. A two-position propelling nozzle has two movable eyelids that are operated by actuators (Figure 11.10), or pneumatic rams, to give an open or closed position.

The most common type of variable area propelling nozzle for axial-flow compressor engines has a ring of interlocking flaps spaced around the perimeter of the nozzle and actuated either by powered rams [1] or pneumatic actuators [5]. The iris-type camera shutter (Figure 11.9) is not often used today. Balanced-beam nozzle is the most sophisticated recent exhaust nozzle, which automatically varies the size of nozzle opening. The F100 engine is fitted with this type of nozzle.

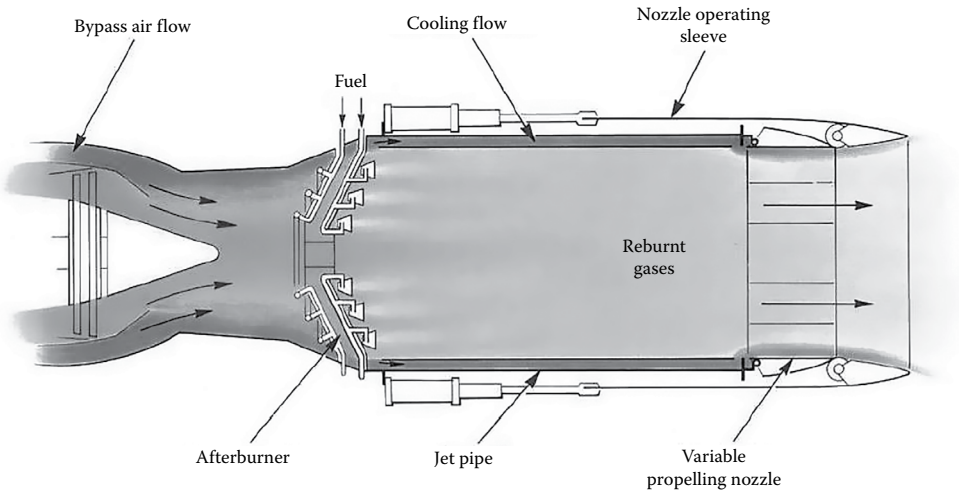


FIGURE 11.10
Variable geometry nozzle for afterburning engine. (Courtesy of Rolls-Royce plc. Copyright 2016.)

Example 11.1

A turbojet engine is powering an aircraft flying at an altitude of 11,000 m where $T_a = 216.7$ K and $P_a = 24.475$ kPa. The flight Mach number is 0.9. The inlet conditions to the nozzle are 1000 and 60 kPa. The specific heat ratio of air and gases at nozzle are 1.4 and 4/3.

1. Determine the thrust per inlet frontal area in the following two cases:
   a. C-D nozzle
   b. Convergent nozzle
2. Calculate the ratio between the thrust forces in both cases.
3. Calculate the exit total pressure in both cases.

Neglect the mass of added fuel.

Solution

Case 1: C-D Nozzle

From Equation 11.3, with $P_a/P_{oi} = 24.475/60 = 0.4074$

Then

$$M_e^2 = \frac{2}{\gamma - 1}\left[\frac{\eta_n\left\{1-\left(\frac{P_a}{P_{oi}}\right)^{\gamma-1/\gamma}\right\}}{1-\eta_n\left\{1-\left(\frac{P_a}{P_{oi}}\right)^{\gamma-1/\gamma}\right\}}\right] = \frac{2}{(1/3)}\left[\frac{0.98\left\{1-(0.4074)^{0.25}\right\}}{1-0.98\left\{1-(0.4074)^{0.25}\right\}}\right]$$

$$M_e = 1.27276$$

Since

$$\dot{m} = \rho u A = \frac{P}{RT} u A$$

Then

$$\frac{\dot{m}}{A} = \rho u = \frac{P}{RT} u = \frac{P\sqrt{\gamma}}{\sqrt{RT}} \frac{u}{\sqrt{\gamma RT}} = M\sqrt{\frac{\gamma}{R}} \frac{P}{\sqrt{T}}$$

The mass flow per unit area of the inlet of intake is

$$\left(\frac{\dot{m}}{A}\right)_a = M_a\sqrt{\frac{\gamma_a}{R}} \frac{P_a}{\sqrt{T_a}} \tag{a}$$

Similarly, the mass flow rate per unit area of the exit of nozzle is

$$\left(\frac{\dot{m}}{A}\right)_e = M_e\sqrt{\frac{\gamma_e}{R}} \frac{P_e}{T_e} \tag{b}$$

From Equations a and b the ratio between the areas of the nozzle exit and inlet of intake, assuming negligible fuel mass

$$\frac{A_e}{A} = \frac{M_a}{M_e}\sqrt{\frac{\gamma_a}{\gamma_e}}\sqrt{\frac{T_e}{T_a}} \frac{P_a}{P_e} \tag{c}$$

With $T_e = \dfrac{T_{oe}}{1+\dfrac{\gamma-1}{2}M_e^2} = \dfrac{1000}{1+\dfrac{0.333}{2}(1.27276)^2} = 787.4 \text{ K}$

From Equations a through c

$$\frac{A_e}{A} = \frac{0.9}{1.273}\sqrt{\frac{1.4}{1.333}}\sqrt{\frac{787.4}{216.7}} \times 1 = 1.381$$

The thrust force is

$$T = \dot{m}_a\left[(1+f)u_e - u\right] + A_e\left(P_e - P_a\right)$$

With $f \approx 0$ and $P_e = P_a$, then the thrust equation becomes

$$T = \dot{m}_e u_e - \dot{m}_a u_e = \rho_e u_e^2 A_e^2 - \rho u^2 A \tag{d}$$

where A is the area of the inlet of intake section.

With $\rho u^2 = \dfrac{P}{RT}u^2 = \dfrac{\gamma P}{\gamma RT}u^2 = \gamma P M^2$, then from Equation d

$$T = \gamma_e P_e M_e^2 A_e - \gamma P M^2 A$$

$$\frac{T}{A} = \gamma_e P_e M_e^2 \frac{A_e}{A} - \gamma P M^2 = \frac{4}{3} \times 24.475 \times (1.273)^2 - 1.4 \times 24.475 \times (0.9)^2$$

$$\left(\frac{T}{A}\right)_1 = 45.27 \text{ kN/m}^2 \tag{e}$$

From Equation 11.2,

$$\frac{P_{oi}}{P_{oe}} = \frac{P_{oi}}{P_e}\left[1 - \eta_n\left\{1 - \left(\frac{P_e}{P_{oi}}\right)^{\gamma-1/\gamma}\right\}\right]^{\gamma/\gamma-1} = \frac{60}{24.475}\left[1 - 0.98\left\{1 - \left(\frac{24.475}{60}\right)^{0.25}\right\}\right]^4$$

$$\frac{P_{oi}}{P_{oe}} = 1.02$$

The total pressure at the nozzle exit is $P_{oe} = 58.8$ kPa.

Case 2: Convergent nozzle

The nozzle is first checked for choking. From Equation 11.6,

$$\frac{P_{oi}}{P_c} = \frac{1}{\left(1 - \dfrac{1}{\eta_n}\dfrac{\gamma-1}{\gamma+1}\right)^{\gamma/\gamma-1}} = \frac{1}{\left(1 - \dfrac{1}{0.98}\dfrac{1}{7}\right)^4} = 1.878$$

Since

$$\frac{P_{oi}}{P_c} = \frac{60}{24.475} = 2.45$$

Then

$$\frac{P_{o\max}}{P_a} > \frac{P_{o\max}}{P_c}$$

Consequently

$$P_c > P_a \Rightarrow \text{Choked nozzle}$$

$$P_e = P_c = \frac{60}{1.878} = 31.95 \text{ kPa}$$

The pressure thrust term is no longer zero; thus,

$$T = \dot{m}_e u_e - \dot{m}_a u_e + (P_e - P_a) A_e$$

From Equation c and noting that $M_e = 1$, then the nozzle to inlet area ratio is

$$\frac{A_e}{A} = \frac{M_a}{M_e}\sqrt{\frac{\gamma_a}{\gamma_e}}\sqrt{\frac{T_e}{T_a}}\frac{P_a}{P_e} = \frac{0.9}{1.0}\sqrt{\frac{1.4}{1.333}}\sqrt{\frac{787.4}{216.7}}\frac{24.475}{31.95}$$

$$\frac{A_e}{A} = 1.3466$$

(Note that this ratio is less than in the case of C-D nozzle)

The thrust per unit area of the inlet of intake is

$$\left(\frac{T}{A}\right)_2 = \gamma_e P_e M_e^2 \frac{A_e}{A} - \gamma_a P_a M^2 + (P_e - P_a)\frac{A_e}{A}$$

$$\left(\frac{T}{A}\right)_2 = \frac{4}{3} \times 31.95 \times 1.3466 - 1.4 \times 24.475 \times (0.9)^2 + 10.07$$

$$= 39.68 \text{ kN/m}^2$$

$$\frac{(T/A)_1}{(T/A)_2} = \frac{45.27}{39.68} = 1.141$$

Total pressure ratio in nozzle is determined also from Equation 11.2 but for a choked nozzle becomes

$$\frac{P_{oi}}{P_{oe}} = \frac{P_{oi}}{P_c}\left[1 - \eta_n\left\{1 - \left(\frac{P_c}{P_{oi}}\right)^{\gamma-1/\gamma}\right\}\right]^{\gamma/\gamma-1} = 1.0137$$

$$P_{0e} = 59.19 \text{ kPa.}$$

11.3 Calculation of the Two-Dimensional Supersonic Nozzle

The profile of a subsonic nozzle is totally convergent while a supersonic nozzle has a convergent part followed by a divergent part. In this section, a preliminary design for the subsonic convergent nozzle and the supersonic divergent nozzle will be given.

11.3.1 Convergent Nozzle

A convergent nozzle is used in all the present subsonic/transonic civil transports. The convergent part is assumed to have a linear shape in the present preliminary design. Curved nozzle profiles need rather a complicated fluid dynamics modeling using computer programs. The linear nozzle shape and the relation between the exit pressure and back pressure are plotted in Figure 11.11.

Design steps:

1. Calculate the nozzle radius at inlet (r_i) or exit (r_e) from the relation

$$r = \sqrt{\frac{\dot{m}}{\pi \rho V}} \tag{11.7a}$$

2. Calculate the length of nozzle (L) from the relation

$$L = \frac{r_i - r_e}{\tan \theta} \tag{11.7b}$$

where $\theta = 11° - 15°$.

3. The area at any section along the nozzle length is obtained as follows
   Assume that the nozzle radius decreases linearly along its length; thus

$$r_x = ax + b$$

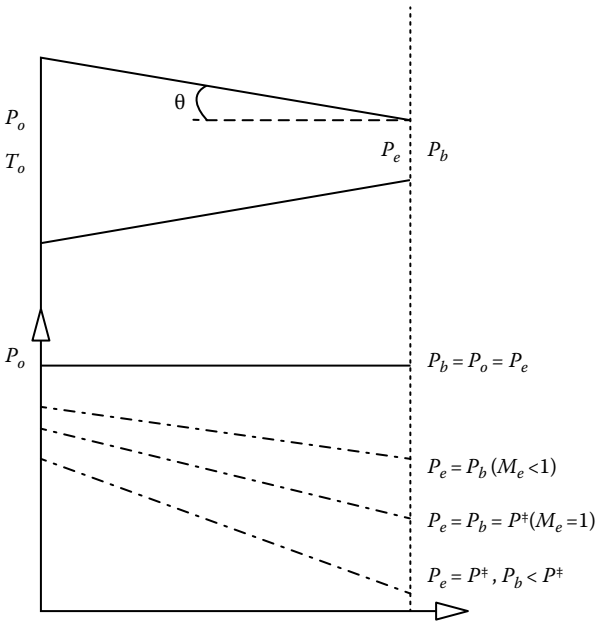


FIGURE 11.11
Convergent nozzle.

where $a = \dfrac{r_e - r_i}{L}$ and $b = r_i$. Thus the corresponding area

$$A_x = \pi r_x^2$$

4. The area ratio at any station; (A_x/A^*) is related to the corresponding Mach number at this location by the isentropic relation

$$\frac{A_x}{A^*} = \frac{1}{M_x}\left[\frac{2}{\gamma+1}\left(1+\frac{\gamma-1}{2}M_x^2\right)\right]^{(\gamma+1)/[2(\gamma-1)]}$$

The local Mach number M_x is obtained iteratively from the relation

$$M_x = \frac{A^*}{A_x}\left[\frac{2}{\gamma+1}\left(1+\frac{\gamma-1}{2}M_x^2\right)\right]^{(\gamma+1)/[2(\gamma-1)]} \tag{11.8}$$

5. Next, the corresponding static to total pressure, density and temperature ratios are obtained as follows:

$$\frac{P}{P_0} = \left[1+\frac{\gamma-1}{2}M_x^2\right]^{-\gamma/\gamma-1} \tag{11.9a}$$

$$\frac{\rho}{\rho_0} = \left[1+\frac{\gamma-1}{2}M_x^2\right]^{-1/\gamma-1} \tag{11.9b}$$

$$\frac{T}{T_0} = \left[1+\frac{\gamma-1}{2}M_x^2\right]^{-1} \tag{11.9c}$$

6. Since the total temperature (T_o) is constant through the nozzle, the static temperature (T) is obtained at any location (x)
7. The velocity is calculated from the Mach number and static temperature as

$$V = M\sqrt{\gamma RT}$$

8. The static density is then calculated from the continuity equation

$$\rho = \frac{\dot{m}}{VA}$$

9. The static pressure is calculated from equation of state

$$P = \rho RT$$

10. The total pressure and density are calculated from Equation 11.9a and b

Example 11.2

A convergent nozzle is to be designed based on the procedure described in Section 11.3.1. A linear shape is assumed. The following data is given at the inlet and exit sections:

$$\dot{m} = 64.36 \text{ kg/s}, \quad \theta = 14°, \quad \gamma = 4/3$$
$$P_i = 63.23 \text{ kPa}, \quad T_i = 747.5 \text{ K}, \quad V_i = 131.56 \text{ m/s}$$
$$P_e = 36.13 \text{ kPa}, \quad T_e = 647.1 \text{ K}, \quad V_e = 497.617 \text{ m/s}$$

Solution

The density at inlet and outlet sections are calculated from the given static pressures and temperatures as

$$\rho_i = 0.2994 \text{ kg/m}^3 \quad \text{and} \quad \rho_e = 0.1945 \text{ kg/m}^3$$

The inlet and outlet areas are calculated as

$$A_i = \frac{\dot{m}}{\rho V_i} = 1.66 \text{ m}^2 \quad \text{and} \quad A_e = \frac{\dot{m}}{\rho V_e} = 0.665 \text{ m}^2$$

Then the inlet and exit radii are $r_i = 0.7269$ m, $r_e = 0.4601$ m.

The nozzle length is then $L = 1.0703$ m.

The inlet and exit Mach numbers are calculated as

$$M_i = \frac{V_i}{\sqrt{\gamma R T_i}} = 0.2463 \quad M_e = \frac{V_e}{\sqrt{\gamma R T_e}} = 1.00$$

The nozzle is choked as the exit Mach number equals unity.

Assuming a linear relation for the radius, or $r_x = ax + b$.

Then $a = \dfrac{r_e - r_i}{L} = -0.2493 \text{ m}^{-1}$ and $b = r_i = 0.7269$ m.

The corresponding area along any axial position is $A_x = \pi r_x^2$.

The results of calculations are listed in Table 11.1.

Figure 11.12 illustrates the variations of the different parameters inside the nozzle.

TABLE 11.1

Variation of Aerodynamic and Thermodynamic Properties of Flow within the Convergent Nozzle

Station	x/L (%)	M	T (K)	V (m/s)	ρ (kg/m³)	P (kPa)	P_0 (kPa)	T_0 (K)	ρ_0 (kg/m³)
1	0	0.246	747.46	131.55	0.294	63.22	64.50	755	0.299
2	10	0.27	746.17	142.35	0.293	62.78	64.28	755	0.299
3	20	0.29	744.58	154.66	0.291	62.25	64.00	755	0.298
4	30	0.32	742.59	168.82	0.289	61.58	63.66	755	0.297
5	40	0.35	740.05	185.29	0.286	60.74	63.22	755	0.296
6	50	0.39	736.74	204.75	0.282	59.67	62.66	755	0.294
7	60	0.43	732.32	228.19	0.277	58.25	61.91	755	0.292
8	70	0.49	726.18	257.25	0.270	56.32	60.88	755	0.289
9	80	0.56	717.08	295.06	0.260	53.55	59.36	755	0.285
10	90	0.67	701.84	349.37	0.244	49.14	56.86	755	0.277
11	100	1	647.13	497.63	0.194	36.13	48.60	755	0.251

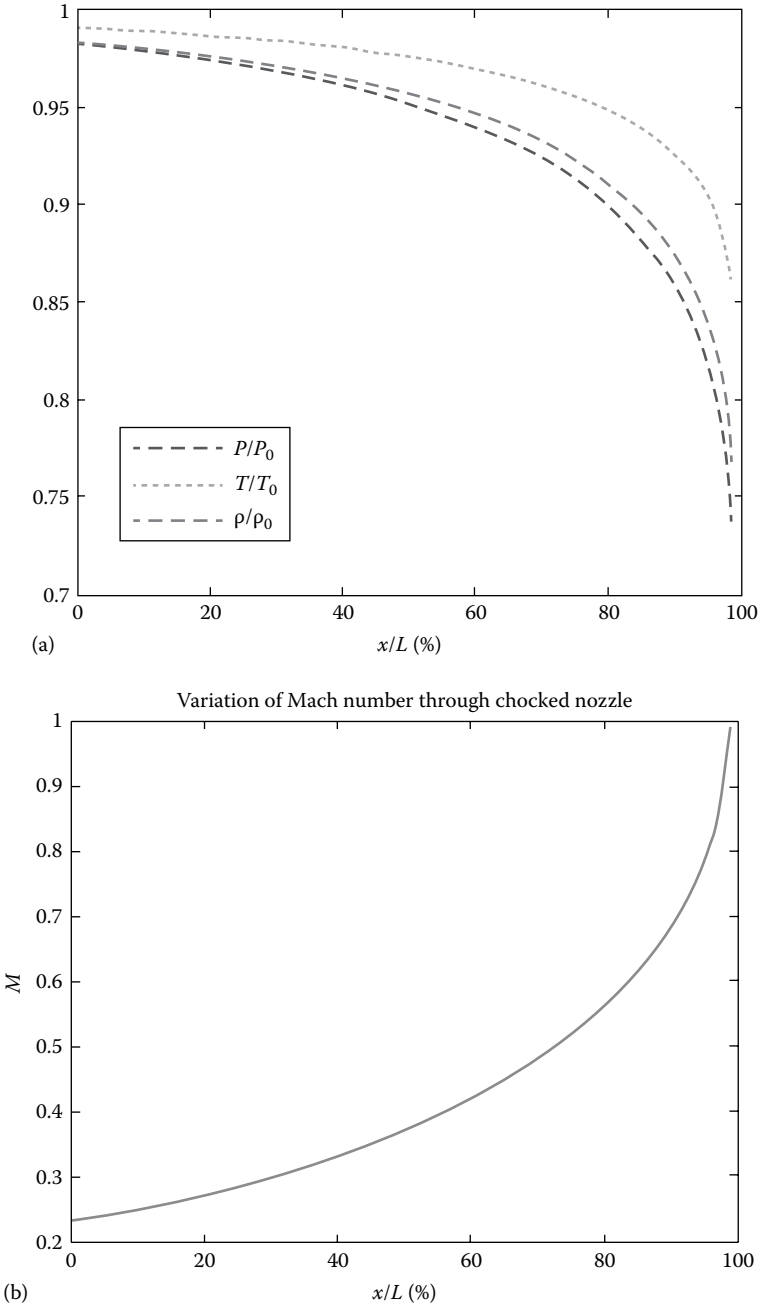
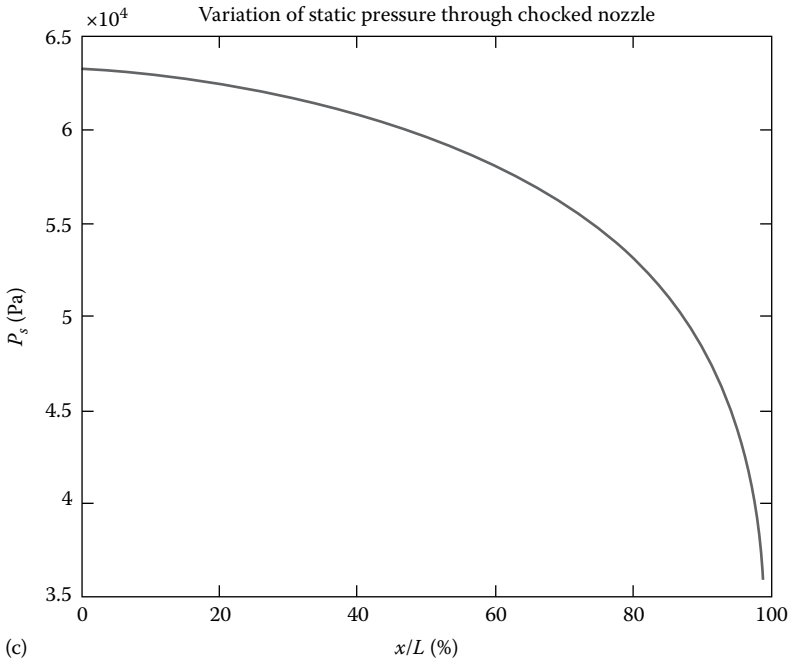


FIGURE 11.12
(a) Variation of ratios of static to total conditions through chocked nozzle. (b) Variation of Mach number through chocked nozzle. (*Continued*)



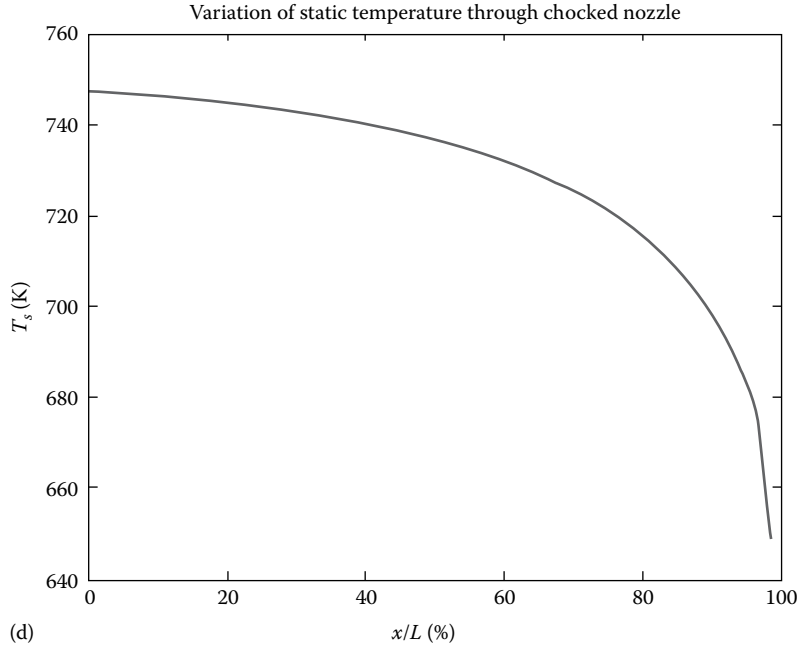
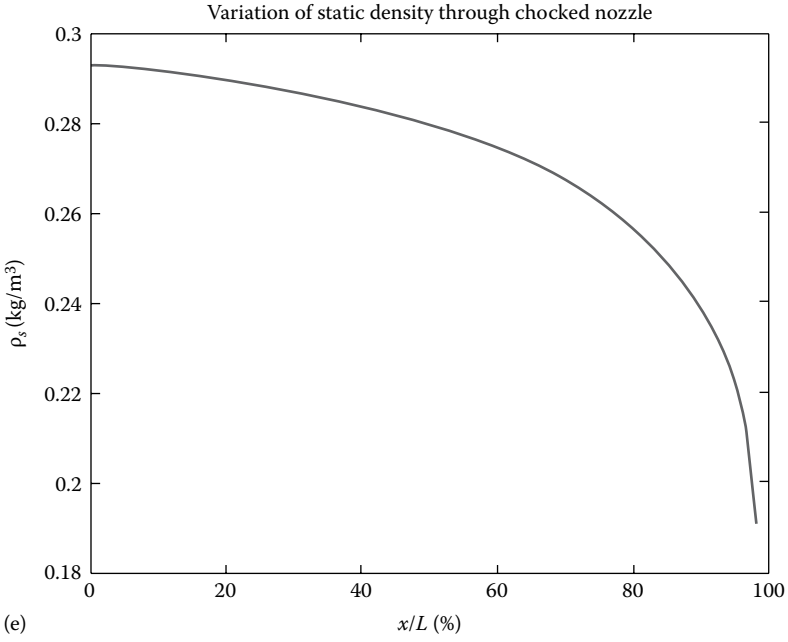
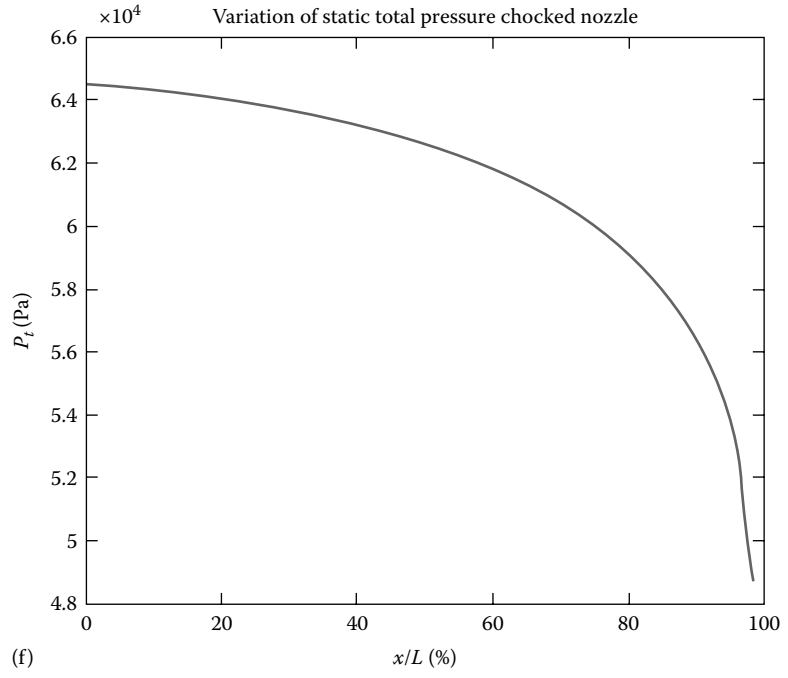


FIGURE 11.12 (*Continued*)
(c) Variation of static pressure through chocked nozzle. (d) Variation of static temperature through chocked nozzle. (*Continued*)



(e)



(f)

FIGURE 11.12 (*Continued*)
(e) Variation of static density through chocked nozzle. (f) Variation of total pressure through chocked nozzle.
(*Continued*)

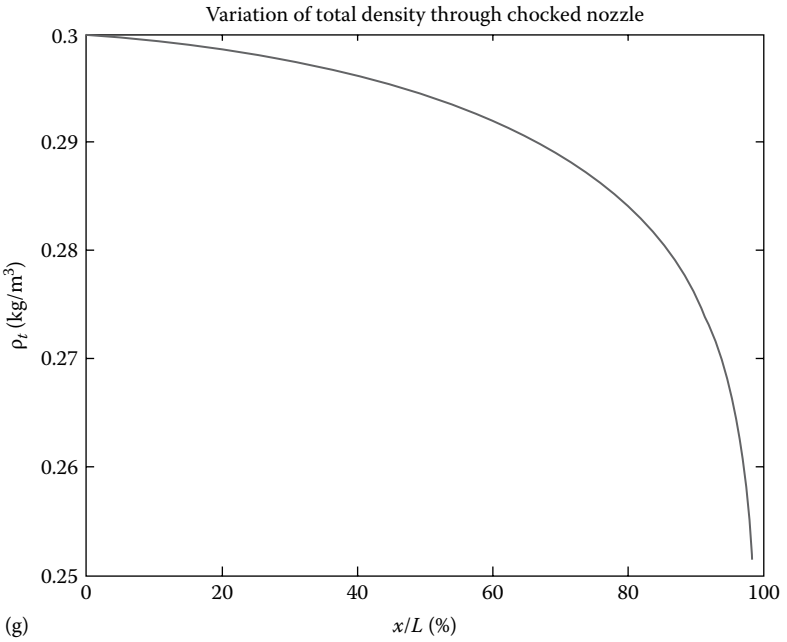


FIGURE 11.12 (*Continued*)
(g) Variation of total density through chocked nozzle.

11.3.2 Divergent Nozzle

A supersonic nozzle that produces uniform, parallel flow is shown in Figure 11.13. Since it is required that the flow be parallel and supersonic, the wall must first curve outward (AD) and then curve in again (DE), so that the wall is again parallel to the initial flow [6]. Point D is the point where the wall has its maximum slope. It is usually assumed that the flow at throat is uniform, parallel, and sonic $M = 1$. Because of the nozzle symmetry, the nozzle axis is a streamline and may for design processes be replaced by a solid boundary. Therefore, only one half of the longitudinal section of the nozzle is designed.

The flow region ABCDA is called the expansion zone. The curved wall AD generates expansion waves that reflect off the centerline. The region DCED is called the straightening

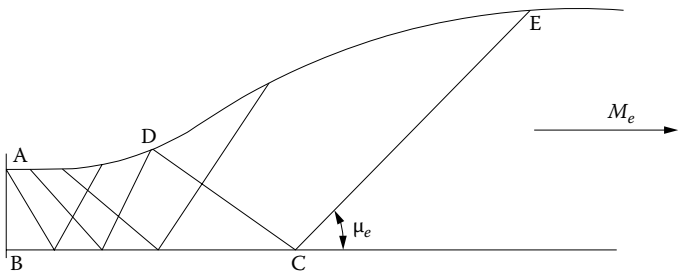


FIGURE 11.13
Divergent nozzle producing parallel flow.

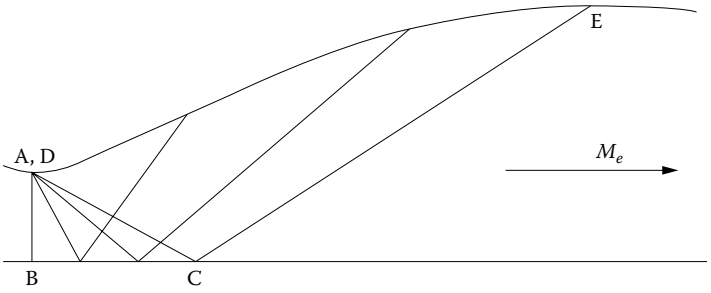


FIGURE 11.14
Sharp corner nozzle.

section, and the wall in this section is curved so that the incoming expansion waves are cancelled. The flow past CE is uniform, parallel and supersonic. Point D is the inflection point and is the point where the wall has the maximum slope.

The most important parameter is the Mach number in the exit section (M_e). It depends on how much expansion occurs between A and D. For a large exit Mach number, a nozzle of this type may be too long for jet engine applications. In these cases, a limiting form of this nozzle is used. A nozzle with sharp-edged throat, as shown in Figure 11.14, produces uniform, parallel flow in the shortest possible length. It is a limiting form of the nozzle shown in Figure 11.13, where points A and D coincide. The flow expands around a sharp edge producing waves that are reflected by the centerline. Cancellation of the reflected waves is again used to obtain uniform parallel flow at the exit. Thus the straightening contour extends from the corner to the exit.

Now, from symmetry if the flow expansion is accomplished by the means of the two walls enclosing an angle (θ), then expansion corresponding to a single wall is ($\theta/2$).

The waves are reflected on the axis, producing a total expansion of the same intensity as that of the incident wave, thus the expansion referring to one wall is ($\theta/2$), the remaining expansion to (θ) being completed by the waves reflected by the axis of symmetry.

It must be further noted that all the reflected waves complete the restoring of the stream to its initial direction, since they are of opposite sense.

Consider any expansion corresponding to a deflection (θ) (Figure 11.15). The incoming Mach number is M and the leaving Mach number is M_e. The wave angles corresponding to M and M_e are μ and μ' forming what is called a Mach fan at the corner.

The angle ω is given by the relation

$$\omega = \mu - \mu' + \theta = -\Delta\mu + \theta \tag{11.10}$$

Since

$$\tan\mu = \frac{1}{\sqrt{M^2 - 1}} \tag{11.11}$$

Then

$$\frac{d\mu}{\cos^2\mu} = -\frac{M^2}{M^2 - 1}\frac{dM}{M} = -\frac{1}{\cos^2\mu}\frac{dM}{M}$$

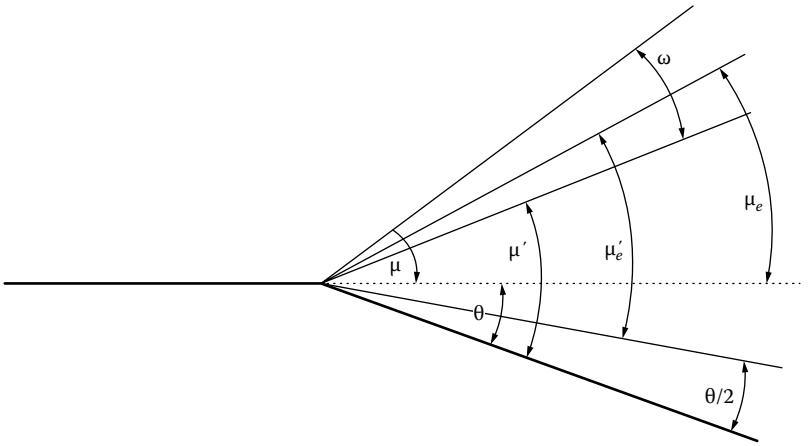


FIGURE 11.15
Mach angles distribution.

or

$$d\mu = -\frac{dM}{M} \tag{11.12}$$

If the deflection angle θ is divided into several incremental $d\theta$, the incremental increase in Mach number due to this small expansion is expressed by the relation

$$d\theta = \frac{\sqrt{M^2-1}}{1+\dfrac{n-1}{2}M^2}\frac{dM}{M} \tag{11.13}$$

It follows from Equations 11.11 through 11.13 that

$$-d\mu = \left(1+\frac{n-1}{2}M^2\right)\tan\mu \; d\theta \tag{11.14}$$

From Equations 11.10 and 11.14 by considering small finite increments, replacing $d\mu$ by $\Delta\mu$ and $d\theta$ by θ, then

$$\begin{aligned} \omega &= \theta + \theta\left(1+\frac{n-1}{2}M^2\right)\tan\mu \\ \omega &= \theta\left[1+\left(1+\frac{n-1}{2}M^2\right)\tan\mu\right] \end{aligned} \tag{11.15}$$

For small angle (θ) the Mach fan in figure (N.3/11.13) can be replaced by a single line, a mean line is taken. In that case the average Mach angle will be

$$\mu_e = \mu - \frac{\omega}{2} \tag{11.16}$$

This angle corresponds approximately to a stream deflected by $\theta/2$, since the limits of approximation

$$\omega_e = \frac{\theta}{2}\left[1+\left(1+\frac{n-1}{2}M^2\right)\tan\mu\right] = \frac{\omega}{2} \tag{11.17}$$

The mean angle μ_e will correspond to a stream deflected by μ'_e and

$$\mu'_e = \mu_e + \frac{\theta}{2} \tag{11.18}$$

If the deflection is so great that the approximation entails a great error, the deflection is divided into several parts, applying to each separate part the preceding procedure.

The determination of the inclination of the waves after intersection is of primary importance for the graphical calculation of the nozzle, since small errors in the orientation of the waves after intersection could lead to major errors in the contour of the walls.

Two methods are used in nozzle design, namely, the graphical and analytical solutions. The graphical solution is best illustrated in [7]. Although the graphical design of a nozzle is simple, it entails laborious calculations and yields approximate results. For this reason, only the analytical solution is considered here [8].

11.3.2.1 Analytical Determination of the Contour of a Nozzle

Although the graphical design of a nozzle is simple, it entails laborious calculations and yields approximate results. Atkin [8] had indicated a method through which the contour can be determined as an analytical curve with parameter representation. The basic idea in this method is the transformation of radial supersonic system due to a source into a uniform parallel stream. If the single expansion slope is prolonged, the point of intersection with the axis is the center of the source and also the origin of the polar system of coordinates (r,θ). Such a flow can only exist from a radius r_c onwards, for which the Mach number is unity, hence close to the sonic throat; Figure 11.16.

The Mach number varies along a radius vector (supersonic source flow) according to the formula

$$\frac{r}{r_c} = \frac{1}{M}\left(\frac{\gamma-1}{\gamma+1}M^2+\frac{2}{\gamma+1}\right)^{\gamma+1/2(\gamma-1)} \tag{11.19}$$

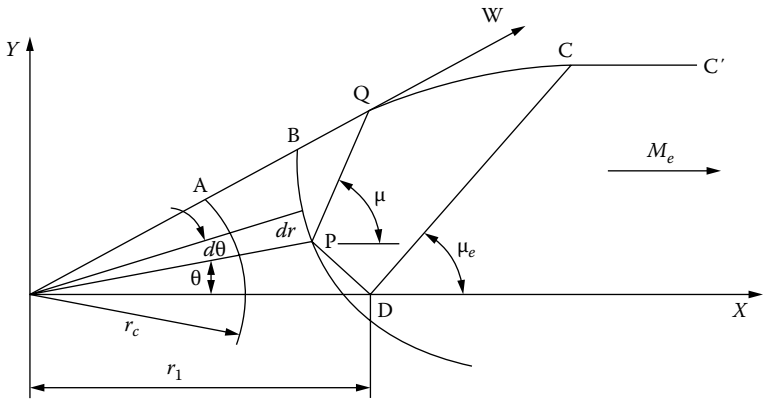


FIGURE 11.16
Notations for analytical treatment.

For a Mach number M_e in the nozzle outlet (the corresponding radius r_1 where $r_1 = OD$) can be derived from the preceding formula by setting $M = M_e$. The wave DC is inclined an angle μ_e where $\mu_e = \sin^{-1}\left(\frac{1}{M_e}\right)$. Beyond DC the streamlines are uniform and the wall CC′ is parallel to the axis of nozzle. The slope begins to decrease at point B and the curve BQC must ensure the transition from the radial flow AB to the parallel flow CC′. At each point Q on this curve, a wave Q arises along which the velocity is parallel to the tangent at the wall and to the radial velocity at point P. Two characteristics pass through P, the first is the wave PQ at an angle μ with direction of the velocity, the second is PD at an angle (−μ). The locus of P is a characteristics curve, defined by the equation

$$\frac{dy}{dx} = \tan(\theta \pm \mu)$$

In polar coordinates this equation has the form

$$\frac{rd\theta}{dr} = \pm \tan\mu = \pm \frac{1}{\sqrt{M^2 - 1}}$$

which can be integrated. From Equation 11.13 setting (r) and (dr) in terms of M, then

$$\frac{dr}{r} = \frac{M^2 - 1}{1 + \frac{\gamma - 1}{2} M^2} \frac{dM}{M}$$

and

$$\pm d\theta = \frac{M^2 - 1}{1 + \frac{\gamma - 1}{2} M^2} \frac{dM}{M\sqrt{M^2 - 1}}$$

Setting $\sqrt{M^2 - 1} = y$, then $\frac{MdM}{\sqrt{M^2 - 1}} = dy$.

The equation is readily integrated with the result

$$\pm d\theta = \frac{dy}{1 + \frac{\gamma - 1}{\gamma + 1} y^2} - \frac{dy}{1 + y^2}$$

and

$$\pm\theta = \sqrt{\frac{\gamma + 1}{\gamma - 1}} \tan^{-1}\left[\sqrt{\frac{\gamma - 1}{\gamma + 1}}\sqrt{M^2 - 1}\right] - \tan^{-1}\sqrt{M^2 - 1} + C \tag{11.20a}$$

as obtained in continuous expansion around a corner. The constant C is determined by setting $\theta = 0$ for $M = M_e$:

$$C = \tan^{-1}\sqrt{M_e^2 - 1} - \sqrt{\frac{\gamma + 1}{\gamma - 1}} \tan^{-1}\left[\sqrt{\frac{\gamma - 1}{\gamma + 1}}\sqrt{M_e^2 - 1}\right] \tag{11.20b}$$

The curve required is BQC whose coordinates are

$$X = r\cos\theta + PQ\cos(\mu + \theta)$$

$$Y = r\sin\theta + PQ\sin(\mu + \theta)$$

For the length PQ we can put

$$PQ = \frac{r(\theta_o - \theta)}{\sin\mu}$$

So that

$$X = r\cos\theta + r(\theta_o - \theta)\frac{\cos(u + \theta)}{\sin\mu} \tag{11.21a}$$

$$Y = r\sin\theta + r(\theta_o - \theta)\frac{\sin(u + \theta)}{\sin\mu} \tag{11.21b}$$

For the practical construction of this curve, the angles μ will be first taken from the equation or from tables of characteristics as a function of M, decreasing from M_e. The parameter of variation is thus M and the plot of the curve will be more accurate, the more numerous the values of M are taken. This method being easy to apply and yielding fairly exact results, which is recommended compared with the graphical methods, especially in view of the errors generally associated with geometrical constructions.

11.3.2.2 Design Procedure for a Minimum Length Divergent Nozzle

1. Decide number of characteristics used for calculations.
2. Divide Mach number from M^* (nozzle entry) to M_e (nozzle exit) into the number of characteristics.
3. Calculate the Mach wave angle μ from the relation

$$\mu = \sin^{-1}\left(\frac{1}{M}\right)$$

4. Calculate the maximum turning angle θ_o and deflection angle θ for each characteristic, where

$$2\theta_o = \sqrt{\frac{\gamma+1}{\gamma-1}}\tan^{-1}\left[\sqrt{\frac{\gamma-1}{\gamma+1}}\sqrt{M_e^2-1}\right] - \tan^{-1}\sqrt{M_e^2-1}$$

5. From Equation 11.20a and b then

$$\theta = \sqrt{\frac{\gamma+1}{\gamma-1}}\tan^{-1}\left[\sqrt{\frac{\gamma-1}{\gamma+1}}\sqrt{M^2-1}\right] - \tan^{-1}\sqrt{M^2-1} + \tan^{-1}\sqrt{M_e^2-1} - \sqrt{\frac{\gamma+1}{\gamma-1}}\tan^{-1}\left[\sqrt{\frac{\gamma-1}{\gamma+1}}\sqrt{M_e^2-1}\right]$$

6. Calculate r_c where, $r_c = \dfrac{h_o}{\tan\theta_o}$, and

$$h_o = \frac{D_{throat}}{2} = \text{the height of the throat section.}$$

7. Calculate the radius (r):

$$r = \frac{r_c}{M}\left(\frac{\gamma-1}{\gamma+1}M^2 + \frac{2}{\gamma+1}\right)^{\gamma+1/2(\gamma-1)}$$

8. Calculate X and Y from Equation 11.21a and b.

11.3.2.3 Procedure of Drawing the Expansion Waves inside the Nozzle

1. Decide number of characteristics used for calculations.
2. Assign (θ) for each characteristic, normally uniformly distributed starting with a small value up to θ_{max} with constant incremental step $\Delta\theta$.
3. Calculate the Mach number and Mach angle μ at every (θ) from Prandtl-Meyer tables.

   Note: We assume that there is a small expansion fan and the angle of this fan starts with μ_1 and ends with μ_2. Then get the equivalent μ of the expansion fan (Figure 11.17), where

$$\mu = \frac{1}{2}\left[\mu_1 + \mu_2 - \Delta\theta\right]$$

4. Draw the characteristics lines.

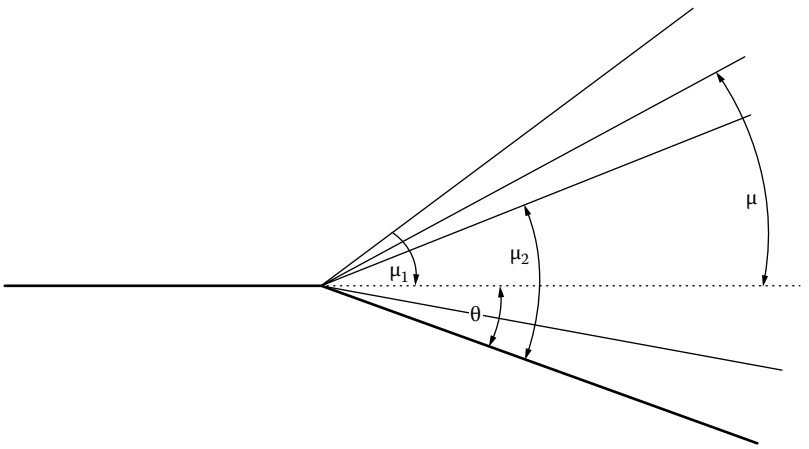


FIGURE 11.17
Expansion fan notation.

Example 11.3

An axisymmetric nozzle has a throat of 1.0 m diameter and an outlet Mach number of 2.4.

Calculate and draw the profile of the divergent part of the nozzle. Draw also the expansion Mach numbers.

Solution

The procedure is followed here. Ten characteristics are selected between the inlet and exit Mach numbers and the corresponding nozzle profile is considered. All the results are tabulated in Table 11.2.

Figure 11.18 illustrates the nozzle contour together with the expansion Mach number.

TABLE 11.2

Geometry of the Divergent Nozzle and the Expanding Mach Waves

	1	**2**	**3**	**4**	**5**	**6**	**7**	**8**	**9**	**10**
M	1	1.156	1.311	1.467	1.622	1.778	1.933	2.089	2.244	2.4
μ	90	59.93	49.70	42.90	38.06	34.23	31.15	28.60	26.46	24.62
θ_0	36.75	36.75	36.75	36.75	36.75	36.75	36.75	36.75	36.75	36.75
θ	36.75	34.24	30.27	25.82	21.23	16.67	12.22	7.947	3.87	0
r_c	0.738	0.738	0.738	0.738	0.738	0.738	0.738	0.738	0.738	0.738
r	0.738	0.752	0.790	0.852	0.936	1.044	1.179	1.343	1.539	1.773
x	0	0.027	0.112	0.262	0.491	0.820	1.27	1.871	2.656	3.663
y	0.441	0.461	0.514	0.593	0.692	0.804	0.919	1.025	1.105	1.137

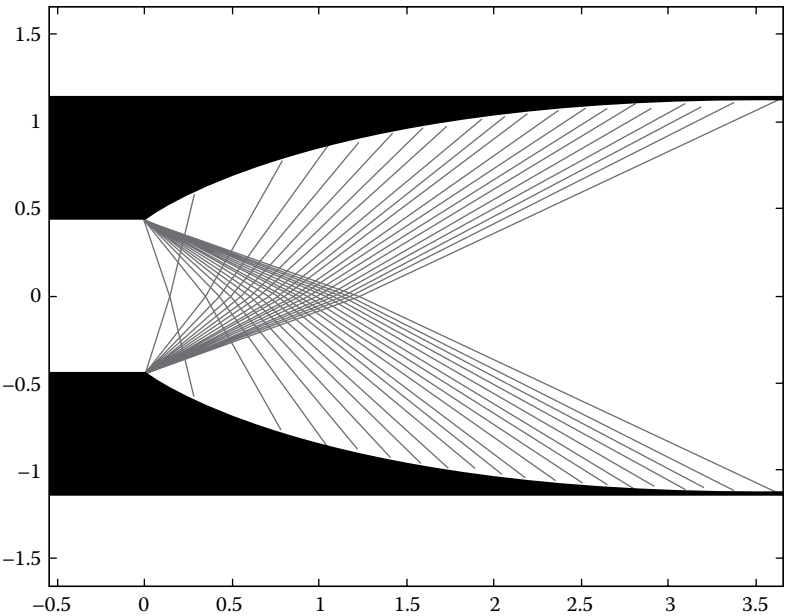


FIGURE 11.18
Nozzle contours and expansion waves.

11.4 Thrust Reversal

Stopping an aircraft after landing is not an easy problem to solve due to the increases in its gross weight, wing loadings, and landing speeds [5]. The amount of force required to stop an aircraft in a given distance after touchdown increases with the gross weight of the aircraft and the square of the landing speed. The size of modern transport aircraft, which results in higher wing loadings and increased landing speeds, makes the use of wheel brakes alone unsatisfactory for routine operations [5]. Moreover, in the case of wet, icy or snow-covered runways, the efficiency of aircraft brakes may be reduced by the loss of adhesion between aircraft tire and the runway [1]. Thus for current large aircraft and under such runway conditions, there is a need for additional methods for augmenting the stopping power provided by the brakes to bring the aircraft to rest within the required distance. The reversible pitch propeller has solved the problem for reciprocating-engine and turboprop-powered aircrafts. Turbojet and turbofan aircraft, however, must rely upon either some device such as a parabrake or runway arrester gear or some means for reversing the thrust produced by their engines. For military aircraft, parabrake or drag parachutes are in use. Arrester gears are primarily for aircraft-carrier-decks, although they are sometimes used at military bases. One or multiple parachutes may be deployed in some military aircraft as well as space shuttle after touchdown. Figure 11.19 illustrates the three parachutes used in braking the XB-70 aircraft. Following each landing, the parachutes must be detached from the aircraft and repacked. The use of these devices for deceleration is not an attractive alternative for any type of routine operation and is completely unacceptable for commercial airline operations.

However, a number of Soviet transport aircraft, including early versions of the Tupelov Tu-134 twinjet transport, were equipped with braking parachutes. For civilian transport, reversing the engine thrust is the simplest and effective way to reduce the aircraft landing run on both dry and slippery runways. Thus turbojet- and turbofan-powered transport aircraft are equipped with some form of diverter that, when activated, reverses the thrust

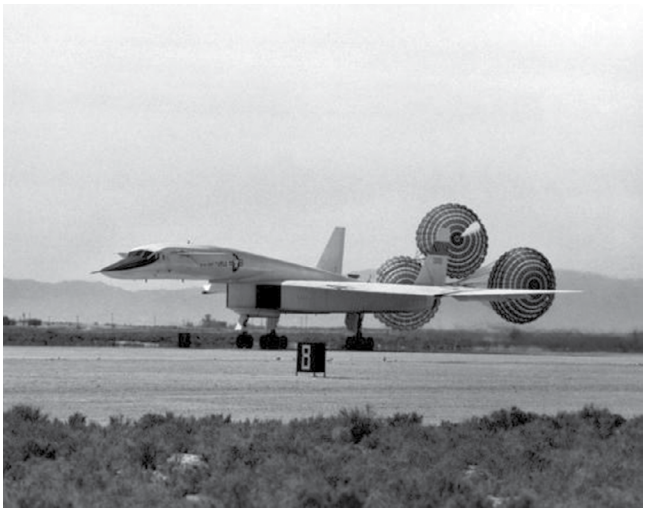


FIGURE 11.19
XB-70 during landing.

and thus provides a powerful stopping force. The direction of the exhaust (gas or air) is reversed so the engine power is used as a deceleration force. The landing runs could be reduced by some 500 ft by applying thrust reversal [2]. An engine thrust reverser provides an effective braking force on the ground. Some reversers are suitable for use in flight to reduce airspeed during descent to slow the aircraft's rate of descent, allowing it to land at steeper angles. However, they are not commonly used in modern aircraft. Ideally, the gas should be directed in a completely forward direction, which is not possible due to aerodynamic reasons. Actually, a discharge angle of approximately 45° is appropriate.

On turbojet engines, low bypass turbofan engines—whether fitted with afterburner or not—and mixed turbofan engines, the thrust reverser is achieved by reversing the exhaust gas flow (hot stream). On high BPR turbofan engines, reverse thrust is achieved by reversing the fan (cold stream) airflow. Mostly, in this case it is not necessary to reverse the hot stream as the majority of the engine thrust is derived from the fan, though some engines use both systems.

A good thrust reverser must fulfill the following conditions [5]:

1. Must not affect the engine operation whether the thrust reverser is applied or stowed
2. Must withstand high temperature if it is used in the turbine exhaust
3. Must be mechanically strong
4. Must be relatively light in weight
5. When stowed should be streamlined into the engine nacelle and should not add appreciably to the frontal area of the engine
6. Must be reliable and fail-safe
7. Should cause few increased maintenance problems
8. Provide at least 50% of the full forward thrust

11.4.1 Classification of Thrust Reverser Systems

The most commonly used reversers are clamshell-type, external bucket-type doors, and blocker doors, as shown in Figure 11.20.

The clamshell door system is a pneumatically operated. When reverse thrust is applied, the doors rotate to uncover the ducts and close the normal gas stream. Sometimes clamshell doors are employed together with cascade vanes (Figure 11.20) or buckets [9] that direct the gas stream in a forward direction to generate a thrust force that opposes the aircraft motion. Clamshell type is normally used for non-afterburning engines. When the thrust reverser is applied, the reverser automatically opens to form a "clamshell" approximately three-quarters to one nozzle diameter to the rear of the engine exhaust nozzle.

The bucket target system is hydraulically actuated and uses bucket-type doors to reverse the hot gas stream. In the forward (stowed) thrust mode, the thrust reverser doors form the C-D final nozzle for the engine. The thrust reverser in Boeing 737-200 aircrafts is an example for this type of thrust reverser.

High bypass turbofan engines normally use blocker doors to reverse the cold stream airflow type (C) in Figure 11.20. A cascade-type reverser uses numerous turning vanes in the gas path to direct the gas flow outward and forward during operation. Some types utilize a sleeve to cover the fan cascade during forward thrust. Aft movement of the reverse sleeves causes blocker doors to blank off the cold stream final nozzle, and deflect fan

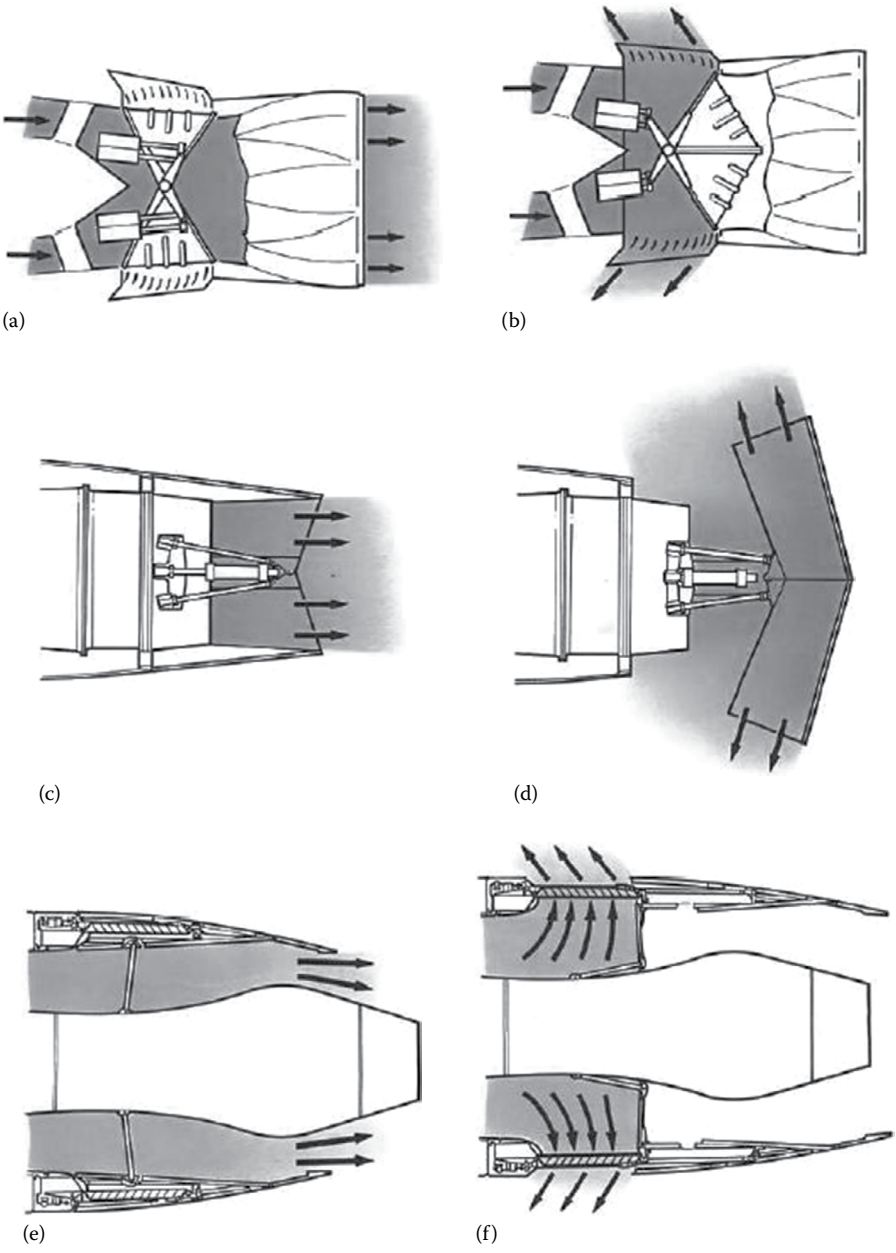


FIGURE 11.20
Methods of thrust reversal. (a) Clamshell doors in forward thrust position, (b) Clamshell doors in reverse thrust position, (c) actuator extended and bucket doors in forward thrust position, (d) actuator and bucket doors in reverse thrust position, (e) cold streams reverser in forward thrust position, and (f) cold streams reverser in reverse thrust position. (Courtesy of Rolls-Royce plc. Copyright 2016.)

discharge air forward through fixed cascade vanes, producing reverse thrust. In some installations, cascade turning vanes are used in conjunction with clamshell to reverse the turbine exhaust gases. Both the cascade and the clamshell are located forward of the turbine exhaust nozzle. For reverse thrust, the clamshell blocks the flow of exhaust gases and exposes the cascade vanes, which act as an exhaust nozzle. Some installations in low-bypass turbofan unmixed engines use two sets of cascade, forward and rearward. For the forward cascade, the impinging exhaust is turned by the blades in the cascade into the forward direction. Concerning the rearward cascade, the exhaust from the hot-gas generator strikes the closed clamshell doors and is diverted forward and outward through the cascade installed in these circumferential openings in the engine nacelle.

Thrust reverser of all types are not used if the forward speed is approximately 60 knots, otherwise recirculating exhaust air or gases together with any foreign objects will be ingested into the engine.

Example 11.4

Prove that the force developed by thrust reverser during landing is given by the relation

$$F = \dot{m}_a\left[\left(1+f\right)V_j\cos\beta + V_f\right]$$

where

V_f is the flight speed
V_j is the exhaust speed
f is the fuel-to-air ratio
β is the inclination of the exhaust gases leaving the buckets measured from the engine longitudinal axis

Next, calculate the dragging force developed by thrust reversers of the *two* engine aircraft in the following case $\dot{m}_a = 50\ \text{kg/s}$, $f = 0.02$ and $\beta = 60°$.

Solution

For the shown control volume in Figure 11.21a, the gases leave the engine at (j) with a jet velocity (V_j) and rate $\left(\dot{m}_j\right)$. These gases impact the buckets and leave the control volume at (1) and (2).

From the continuity equation assuming constant density, then

$$\rho V_j A_j = \rho V_1 A_1 + \rho V_2 A_2$$

or

$$V_j A_j = V_1 A_1 + V_2 A_2 \tag{a}$$

Applying Bernoulli's equation twice between states (j) and (1) and between states (j) and (2) gives

$$\frac{P_j}{\rho} + \frac{V_j^2}{2} = \frac{P_1}{\rho} + \frac{V_1^2}{2}$$

and

$$\frac{P_j}{\rho} + \frac{V_j^2}{2} = \frac{P_2}{\rho} + \frac{V_2^2}{2}$$

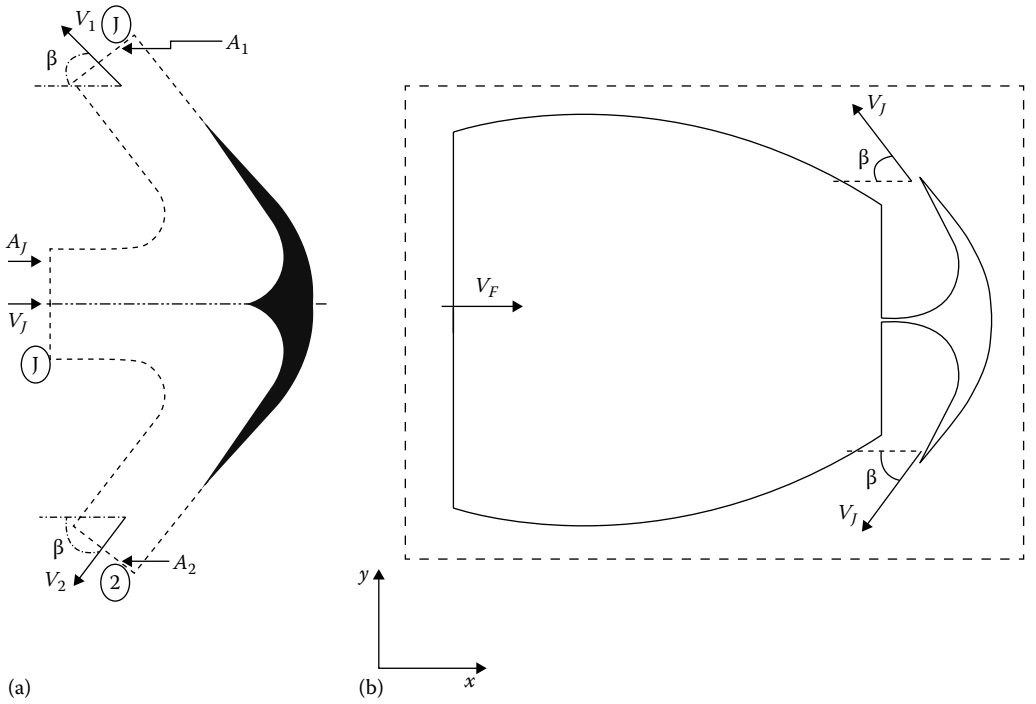


FIGURE 11.21
(a) Control volume for the exhaust jet. (b) Control volume for aircraft engine.

Assuming $P_j = P_1 = P_2$ yields $V_j = V_1 = V_2$, then from Equation a

$$A_j = A_1 + A_2 \tag{b}$$

Writing the y-momentum equation

$$F_y = 0 = \rho A_1 V_1^2 \sin\beta - \rho A_2 V_2^2 \sin\beta$$

Then $A_1 = A_2$.
From Equation b

$$A_1 = A_2 = \frac{A_j}{2}$$

Next, for the control volume shown in Figure 11.21b and assuming $P_j = P_a$

$$F_x = -\dot{m}_e V_j \cos\beta - \dot{m}_a V_f$$
$$F_x = -\dot{m}_a \left[(1+f) V_j \cos\beta + V_f \right]$$

This force is the force on the control volume. Then the force on the engine is in its opposite direction and so is a positive value. This means that it is in the positive x-direction or a dragging force:

$$F_x = \dot{m}_a \left[(1+f) V_j \cos\beta + V_f \right]$$

For (n) engines, the force applied on the aircraft due to thrust reverses is

$$F_x = n\dot{m}_a\left[(1+f)V_j\cos\beta + V_f\right]$$

Substituting the given data,

$$F_x = (2)(50)\left[(1+0.02)\times 600\times\cos 60 + 80\right]$$
$$F_x = 38{,}600\ \text{N} = 38.6\ \text{kN directed rearward}$$

Example 11.5

During landing, the pilot is applying thrust reverse to shorten the landing distance (Figure 11.22). The thrust reverse exhaust is inclined an angle (β) to the normal of flight speed. If the aircraft is powered by (***n***) engines, and assuming the average drag force on the airplane during landing is D_{av}, it is required to prove that the time necessary to decelerate the airplane from the touch down speed (V_0) to any value (V) during landing is given by

$$t = -\frac{m}{n\dot{m}_a}\ln\frac{V + V_j\sin\beta + \left(D_{av}/n\dot{m}_a\right)}{V_0 + V_j\sin\beta + \left(D_{av}/n\dot{m}_a\right)}$$

where

m is the airplane total mass

$\dot{m}_a$ is the mass-flow rate of air entering or leaving one engine (i.e., negligible fuel mass flow rate)

Next, for a particular aircraft having the following data:

$$n = 2,\quad m = 50{,}000\ \text{kg},\quad D_{av} = 5000\ \text{N},\quad \dot{m}_a = 50\ \text{kg/s},$$
$$V_0 = 40\ \text{m/s},\quad V_j = 600\ \text{m/s},\quad \beta = 30^\circ$$

Calculate the time needed for complete stop and the distance needed.

From the control surface shown in Figure 11.22, the force generated by each engine when the thrust reverser is applied is

$$F = m_e V_j\sin\beta + \dot{m}_a V$$

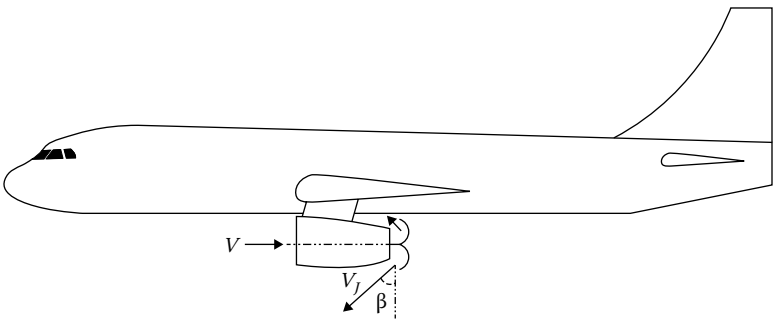


FIGURE 11.22
Thrust reversal.

Neglecting the fuel mass flow rate, then

$$\dot{m}_a \approx \dot{m}_e$$

Then the force is

$$F = \dot{m}_a \left(V + V_j \sin\beta \right)$$

The thrust force in this case is a resistance force that adds to the drag force.

For an aircraft powered by (n) engines, since acceleration during landing is negative (i.e., deceleration) then the equation of motion is:

$$\therefore -m\frac{dV}{dt} = n\dot{m}_a \left(V + V_j \sin\beta \right) + D_{av}$$

$$\frac{dV}{dt} + \frac{n\dot{m}_a}{m} V = -\left(\frac{n\dot{m}_a}{m} V_j \sin\beta + \frac{D_{av}}{m} \right)$$

The equation may be written in the form

$$\dot{x} + Ax = B$$

where

$$A = \frac{n\dot{m}_a}{m}$$

$$B = -\left(\frac{n\dot{m}_a}{m} V_j \sin\beta + \frac{D_{av}}{m} \right)$$

The general solution for the preceding differential equation is

$$x = \lambda e^{-At} + \frac{B}{A}$$

where

λ is a constant

t is the time

Thus

$$V = \lambda e^{-\frac{n\dot{m}_a}{m}t} - \left(V_j \sin\beta + \frac{D_{av}}{n\dot{m}_a} \right)$$

To determine the value of the constant (λ), assuming that at touch down ($t = 0$) the aircraft speed is V_0, then

$$V_0 = \lambda - \left(V_j \sin\beta + \frac{D_{av}}{n\dot{m}_a} \right)$$

$$\lambda = V_0 + V_j \sin\beta + \frac{D_{av}}{n\dot{m}_a}$$

Thus,

$$V = \left(V_0 + V_j \sin\beta + \frac{D_{av}}{n\dot{m}_a}\right) e^{-\frac{n\dot{m}_a}{m}t} - \left(V_j \sin\beta + \frac{D_{av}}{n\dot{m}_a}\right)$$

or

$$e^{\frac{-n\dot{m}_a}{m}t} = \frac{V + V_j \sin\beta + \frac{D_{av}}{n\dot{m}_a}}{V_0 + V_j \sin\beta + \frac{D_{av}}{n\dot{m}_a}}$$

The time is then expressed as

$$t = -\frac{m}{n\dot{m}_a} \ln \frac{V + V_j \sin\beta + \frac{D_{av}}{n\dot{m}_a}}{V_0 + V_j \sin\beta + \frac{D_{av}}{n\dot{m}_a}}$$

To determine the time and distance between touch down and aircraft stop, the given data are substituted in the preceding equation. For two engines, then

$$t = -\frac{50{,}000}{2 \times 50} \ln \frac{0 + 600 \times \sin 30 + \frac{5{,}000}{2 \times 50}}{40 + 600 \sin 30 + \frac{5{,}000}{2 \times 50}} = 54.1 \text{ s} = 0.9 \text{ min}$$

The deceleration is determined from the relation

$$a = -\frac{V_0}{t} = -\frac{40}{54.1} = -0.739 \text{ m/s}^2$$

The distance is then $s = -V_0^2 / 2a = 1082$ m.

11.4.2 Calculation of Ground Roll Distance

As the aircraft approaches the ground, the aircraft goes in what is known as ground roll just prior to its touchdown. The normal landing procedure after touchdown may be described as follows. Immediately after touch down at the speed of V_{TD} the aircraft goes in what is identified as free roll for few seconds. It is next followed by applying the thrust-reversal system for some 600–800 m. Finally, the thrust lever is returned to the idle detent giving a small amount of forward thrust, and the pilot applies the brake intermittently until there is a final stop. Thus the three landing distances will be analyzed here at first and next it will be applied to a large civil transport like Boeing 777 or Airbus A330.

The landing distance may be then written as

$$S = S_1 + S_2 + S_3 \tag{11.22}$$

Where the free roll distance is

$$S_1 = S_{fr} = tV_{TD} \tag{11.23}$$

And the time (t) is 1 s for small airplanes and 3 s for large airplane [10]. The touchdown speed is related to the stall speed of aircraft given by the relation

$$V_{TD} = iV_{stall} = i\sqrt{\frac{2W}{\rho S C_{L\max}}}$$

where (i) is equal to (1.15) for civil airplanes and (1.1) for military airplanes. The wing area is (S).

The second landing distance (S_2) is governed by the aircraft equation of motion:

$$F = T_{rev} + D + \mu_r (W - L) = -m\frac{dV}{dt}$$

The forces here are the thrust reverse force (T_{rev}), aerodynamic drag (D) and frictional force with the runway coefficient of friction ($\mu_r = 0.01 - 0.04$) depending on the runway condition.

The resultant force is correlated to the aircraft speed and landing distance as follows:

$$F = -m\frac{dV}{dt} = -m\frac{dV}{dS}\frac{dS}{dt} = -mV\frac{dV}{dS} = -\frac{m}{2}\frac{dV^2}{dS}$$

The preceding equation is integrated keeping in mind the landing procedure described earlier. Thus the integration is from the instant of application the thrust reversal until stowing the thrust reversal barrel in turbofan engines, for example, or in general ending thrust reversal application:

$$S_2 = -\frac{m}{2F}\left[\int_{V_{TD}}^{V_{brake}} dV^2\right]$$

$$S_2 = \frac{m}{2}\frac{V_{TD}^2 - V_{brake}^2}{\left[T_{rev} + D + \mu_r (W - L)\right]_{0.7V_{TD}}} \tag{11.24}$$

The total reverse thrust force for (n) engines is given by the relation

$$T_{rev} = n\dot{m}_{ac}\left[(V_e \cos\beta) + V_{TD}\right]$$

Here the lift and drag forces are calculated at an average speed equal to 7/10th of the touchdown speed ($V_{av} = 0.7V_{TD}$).

The third segment is when the brakes are applied and the thrust again in the normal direction but at idle condition:

$$S_3 = \frac{m}{2}\frac{V_{brake}^2}{\left[-T + D + \mu_r (W - L)\right]_{0.35V_{TD}}} \tag{11.25}$$

where $V_{brake} \approx 0.3 - 0.5V_{TD}$.

11.5 Thrust Vectoring

Thrust vectoring is the ability of an aircraft or other vehicle to direct the thrust from its main engine(s) in a direction other than parallel to the vehicle's longitudinal axis. Thrust vectoring is a key technology for current and future air vehicles. The primary challenge is to develop a multi-axis thrust-vectored exhaust nozzle, which can operate efficiently at all flight conditions while satisfying the design constraint of low cost, low weight, and minimum impact on radar cross-section signature. The technique was originally envisaged to provide upward vertical thrust as a means to give aircraft vertical takeoff and landing (VTOL) or short takeoff and landing (STOL) capability. Subsequently, it was realized that the use of vectored thrust in combat situations enabled an aircraft to perform various maneuvers and have better rates of climb not available to conventional-engined planes. Additionally, which is most important, thrust vectoring can control the aircraft by engine forces, even beyond its stall limit, i.e., during "impossible" post-stall (PS) maneuvers at extremely high-nose turn rates [11]. An interesting "definition" for thrust vectoring is introduced in Reference 12 as a *maneuver effector that can be used to augment aerodynamic control moments throughout and beyond the conventional flight envelop*. Rockets or rocket-powered aircraft can also use thrust vectoring. Examples of rockets and missiles that use thrust vectoring are the space shuttle SRB, S-300P, UGM-27 Polaris nuclear ballistic missile, and Swingfire small battlefield.

Aircraft that do not use thrust vectoring have to rely on ailerons or flaps to facilitate turns, while aircrafts that do still have to use ailerons, but to a lesser extent. For pure-vectored propulsion, the flight-control forces generated by conventional aerodynamic control surfaces of the aircraft have been replaced by the stronger internal thrust forces of the jet engines [11]. These forces may be simultaneously or separately oriented in all directions, i.e., in the yaw, pitch, roll, thrust reversal, and forward-thrust directions of the aircraft. Thrust vectoring is also used as a control mechanism for airships, particularly modern non-rigid airships. In this application, the majority of the load is typically supported by buoyancy, and vectored thrust is used to control the motion of the aircraft.

There are two methods for achieving thrust vectoring—either mechanically or by fluidic control. Mechanical-thrust vectoring includes deflecting the engine nozzle and thus physically changing the direction of the primary jet. Fluidic-thrust vectoring involves injecting fluid into or removing it from the boundary layer of a primary jet to enable vectoring. A mechanical-thrust vectoring system is heavy and complex, while fluidic-thrust vectoring is simple, lightweight, inexpensive, and free from moving parts (fixed geometry).

Mechanical thrust vectoring can be further subdivided into engine/nozzle internal-thrust vectoring (ITV) and engine/nozzle external-thrust vectoring (ETV). An ITV system is illustrated by Figure 11.23, where only pitch-control is available. Figure 11.23a illustrates unvectored engine operation, while Figure 11.23b illustrates a down-pitch thrust-vectoring operation. ETV is based on post-nozzle exit; (three or four) jet-deflecting vanes that deflect exhaust jet(s) in the yaw and pitch coordinates, and in a few designs, also in roll coordinates [13]. Figure 11.24 illustrates three and four vanes (pedals) ETV [14].

The two-dimensional nozzle depicted in Figure 11.25 is capable of vectoring the thrust up or down to produce an up force or down force. Down force will force the aircraft nose to pitch upward while up force has the opposite effect.

If the two nozzles of a twin-engined plane can also be deflected differentially (one producing up force, the other down force) it will provide roll control. This type of nozzle may

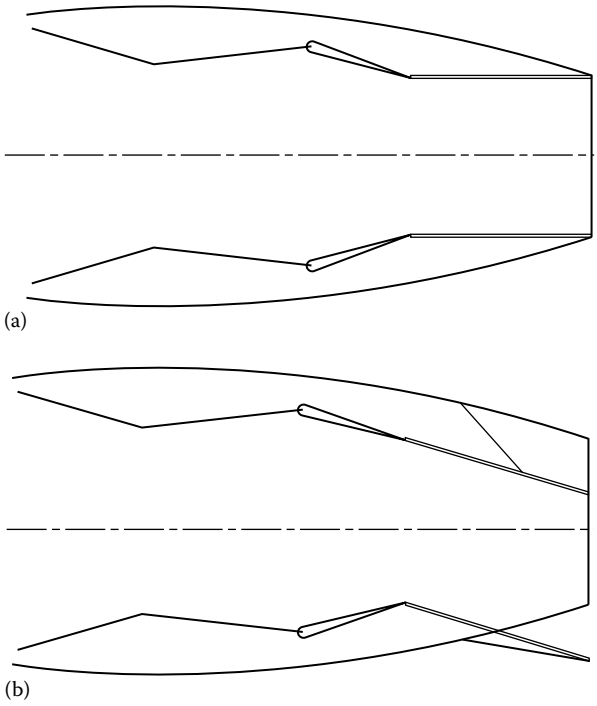


FIGURE 11.23
Example for pitch-control internal thrust-vectoring nozzle (ITV). (a) Normal operation. (b) Down-pitch operation.

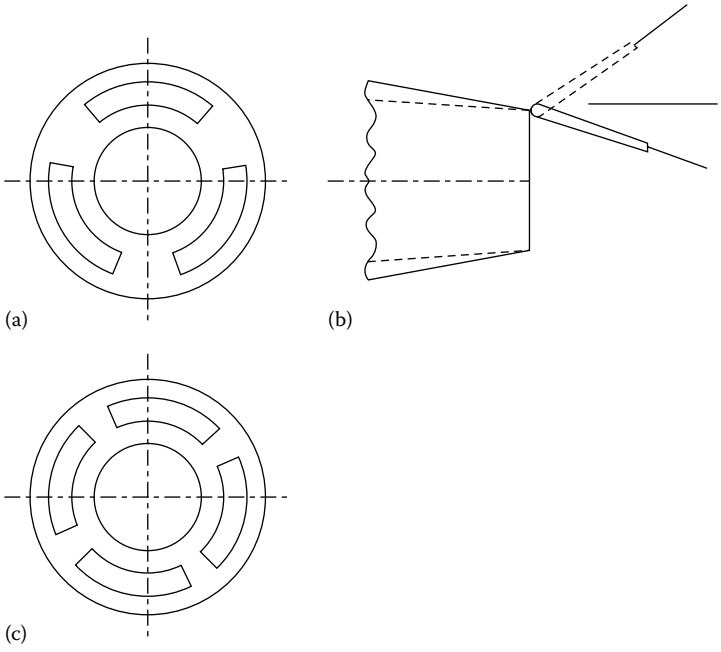


FIGURE 11.24
External thrust vectoring. (a) Three pedals. (b) Side view. (c) Four pedals.

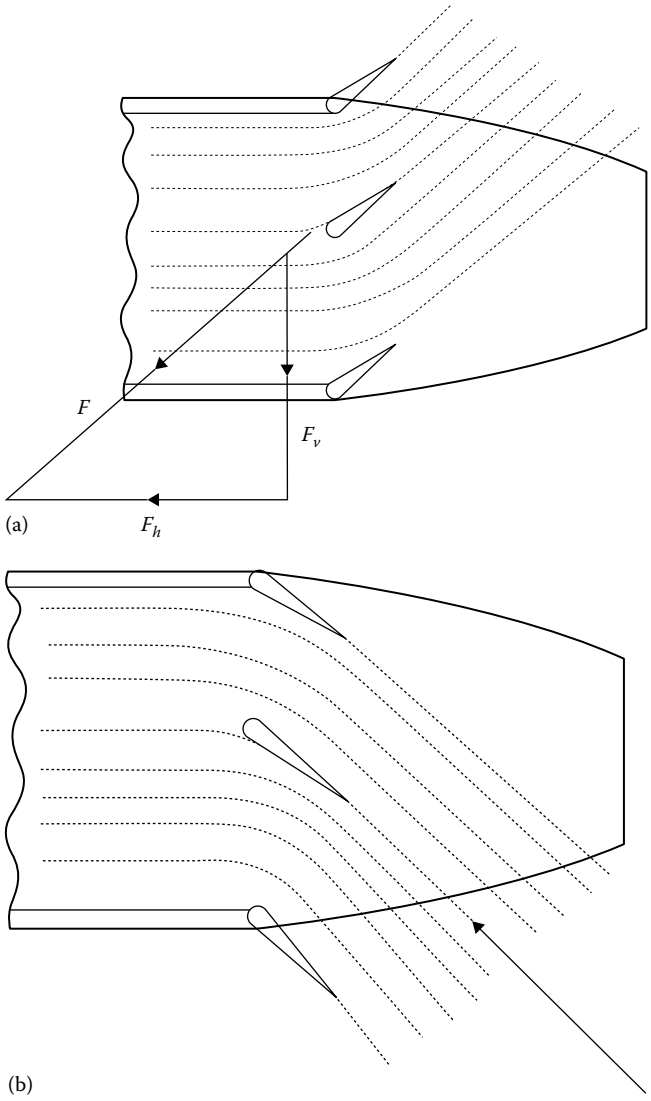


FIGURE 11.25
Thrust vectoring nozzle: (a) up-pitch and (b) down-pitch.

be identified as 3-D thrust vectoring. Examples for aircrafts using a 2-D nozzle are Harrier, Boeing X-32, F-35, Yak-38, and Yak-141.

Examples for aircrafts employing 3-D thrust vectoring (pitch and yaw moments) are F-15, F-16, F-18, MiG-29, MiG-35, Sukhoi Su-30, Su-37, and Su-47.

For example, the F-22 carries two Pratt & Whitney F119-PW-100, reheated engines. The exhaust nozzles move 20° in all directions, providing it with 3-D thrust vectoring capabilities. Heat-resistant components give the nozzles the durability needed to vector thrust, even in afterburner conditions. With precision digital controls, the nozzles work like another aircraft flight control surface. Thrust vectoring is an integrated part of the F-22's

flight control system, which allows for seamless integration of all components working in response to pilot commands.

Concerning MiG-29M OVT, the nozzle vectoring mechanism employs three hydraulic actuators mounted 120° apart around the engine; the nozzle can deflect the engine's full thrust by up to 18° in any direction [15].

Most currently, operational vectored thrust aircraft use turbofans with rotating nozzles or vanes to deflect the exhaust stream. This method can successfully deflect thrust through as much as 90°, relative to the aircraft centerline.

Now turning attention to fluidic nozzles, they divert thrust via fluid effects. Tests have shown that air forced into the exhaust stream can affect deflected thrust of up to 15°. Extensive experimental studies for utilizing a fluidic injection system instead of the heavy and mechanically complex door system is now performed by scientists in academia, research centers, and military aircraft manufacturers. In addition to its light weight and simplicity, it has minimal aircraft observability penalty (or lower radar cross section). For this reason, some studies were performed to utilize it in low observable unmanned air vehicles operating in the subsonic flight regime [12]. However, the main challenges with fluidic vectoring are in obtaining an effective, efficient system with reasonably linear control response.

Fluidic thrust vectoring must be implemented at the outset of the design process unlike a mechanical system that can be retrofitted to existing aircraft currently in use today [13]. The basic idea of fluidic thrust-vectoring systems is to use a secondary air jet to control the direction of the primary jet. It has several types; namely, shock vector control, coflow, counter flow, synthetic jet actuators, and sonic throat skewing. Figure 11.26 illustrates the first three cases.

Shock thrust-vector control involves injecting a secondary jet into the primary jet from one of the divergent flaps. An oblique shock wave is formed, which deflects the primary jet in the pitch plane. Both coflow and counterflow concepts involve the use of a secondary jet together with the coanda effect. Curved reaction surfaces are positioned downstream of the nozzle exit to which the jet may attach according to the coanda effect. The side onto which the jet attaches is controlled by tangential injection of a secondary jet of air upstream of the surfaces. The resulting thrust vector force generated on the reaction surface can then be used to provide useful moments for aircraft control.

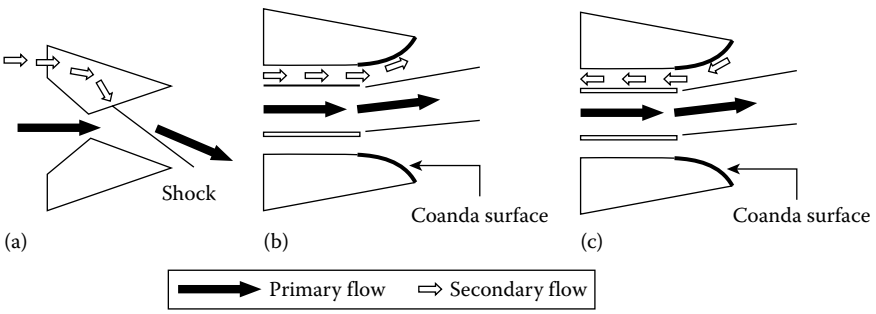


FIGURE 11.26
(a) Shock vector, (b) coflow, and (c) counter flow fluidic thrust-vectoring concepts.

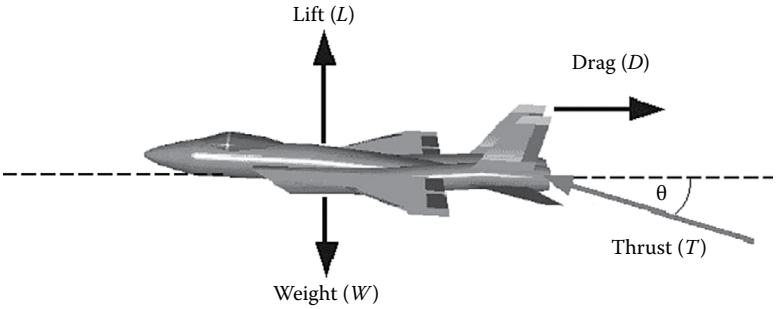


FIGURE 11.27
Forces on aircraft for thrust vectoring.

11.5.1 Governing Equations

Here only 2-D thrust vectoring will be discussed. As shown in Figure 11.27, four forces influencing the aircraft motion are the lift (L), weight (W), drag (D), and thrust (T). For thrust vectoring, the thrust force is inclined an angle (θ) to the horizontal. Thus the governing equations in the horizontal and vertical directions, respectively, are

$$T\cos\theta - D = ma_x \tag{11.26a}$$

$$L - W + T\sin\theta = ma_y \tag{11.26b}$$

where a_x and a_y are the acceleration in the horizontal and vertical directions, respectively. The first acceleration controls the forward motion while the second acceleration controls the rate of climb or descent. The angle (θ) is the inclination of the exhaust jet stream from the axis of aircraft. For a vertical flight this angle is 90°. This angle also develops a pitching moment necessary for nose up or down depending on whether the jet nozzle is deflecting upward or downward.

11.6 Noise

11.6.1 Introduction

Since airline travel has become much more common and widely available, resulting in an increased amount of air traffic, an increasing number of people are affected by aircraft noise, both as passengers and as members of communities located near airports. Aeroengine manufacturers have to stick to the international legislation norms concerning noise by measuring noise around an engine on a bench in an open environment. Noise may be defined as *unwanted and usually irritating sound* [16]. The unit used to express noise annoyance is the Effective Perceived Noise deciBel (ENPdB), where Bel is the basic unit and Db is 1/10th of Bel.

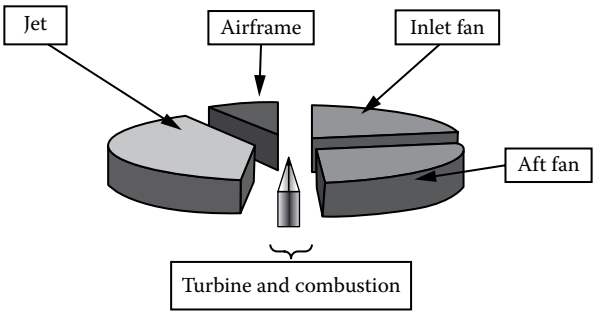


FIGURE 11.28
Different sources of noise in aircraft.

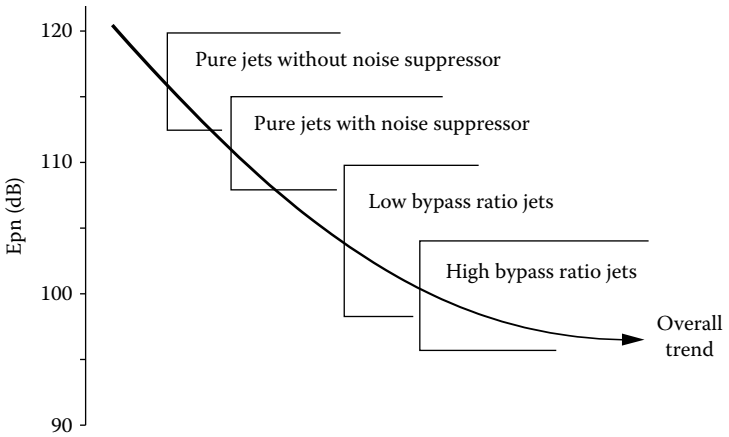


FIGURE 11.29
Comparative noise level of various jet engines. (Courtesy of Rolls-Royce plc. Copyright 2016.)

Aircraft noise derives primarily from engines (or the propulsion systems) and from airframe structure. Figure 11.28 illustrates the contribution of several noise sources for an aircraft, where the inlet fan stands for fan in turbofan engines and compressor in turbojet engines. The biggest source of aircraft noise is the engines (although the air rushing over the airframe also creates noise). Concerning the engine modules, the significant noise originates in the fan or compressor, the turbine, and the exhaust jet or jets. Exhaust jet noise varies by a larger factor than the compressor or turbine noise, therefore a reduction in the exhaust jet velocity has a stronger influence than an equivalent reduction in compressor and turbine blade speed [1]. The intensity of the sound produced by a jet engine at takeoff may attain a value of 155 dB (15.5B) while the threshold of feeling for a human being is 130. The different noise levels of jet engines with and without noise suppressors are plotted in Figure 11.29.

Jet exhaust noise is caused by turbulent mixing of the exhaust gases "efflux" with the lower velocity surrounding air. The small eddies near the exhaust duct cause high-frequency noise, while the larger eddies downstream the exhaust jet create low-frequency noise. Accelerating the mixing rate or reducing the velocity of the exhaust jet reduces the noise level. Additionally, when the exhaust jet velocity exceeds the local speed of sound, a regular shock pattern is formed within the exhaust core. This produces a discrete (single frequency) tone and selective amplification of the mixing noise as depicted in Figure 11.30.

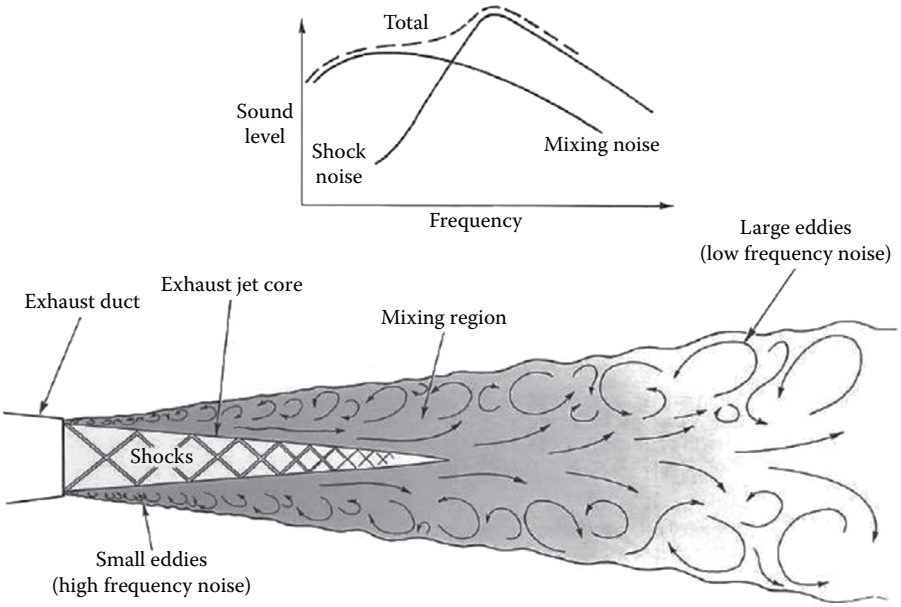


FIGURE 11.30
Exhaust mixing and shock structure. (Courtesy of Rolls-Royce plc. Copyright 2016.)

In turbojet engine, there are three types of noise: noise radiated from the air intake, noise radiated from vibrations of the engine shell, and exhaust noise. For a turbofan engine fan exhaust has lower velocity, resulting in quieter operation for a given total thrust [17].

The second type of noise, namely, the airframe noise, includes the noise that is produced by the passing of air around the aircraft. Under normal cruising conditions, this type of noise predominates, especially among higher frequencies. However, propulsion noise tends to predominate at the lower takeoff and landing speeds [17].

In subsonic flight, which is typical for the vast majority of passenger flights, aircraft noise peaks when the aircraft is approximately overhead and then gradually diminishes to the ambient noise level. Additionally, noise that is heard as the aircraft approaches tends to be dominated by higher frequency sound, whereas noise that is heard after the aircraft has passed tends to include lower-frequency sound [17].

As illustrated in Figure 11.31, for turbojet engines (which dominated in 1960s), lower-frequency exhaust noise predominates over the rearward-propagating while higher-frequency noise is produced by the compressor and turbine. In turbofan engines (which have dominated since the 1990s), on the other hand, higher-frequency sound radiating from the fan, compressor, and turbine predominates over exhaust noise and propagates both forward and rearward from the aircraft.

This may be a moot point, however, since the vast majority of commercial aircraft now use turbofan engines. Thus, contemporary aircraft noise pollution generally includes higher-frequency noise than aircraft noise pollution of yesteryear.

Supersonic airplanes produce a unique noise phenomenon: the sonic boom. In most cases, a sonic boom is experienced as a shock wave sweeping across the ground below the aircraft. However, sonic booms can also occur during acceleration periods such as diving, and in such cases are more transient. Though sonic booms are obviously much more damaging than noise produced during subsonic flight, they are generally restricted to military

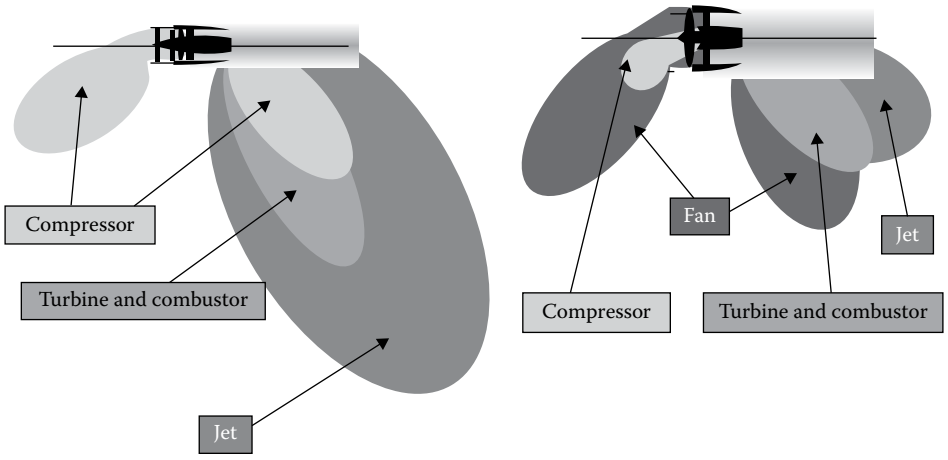


FIGURE 11.31
Noise of the 1960s and 1990s aeroengines. (Courtesy of Airbus Industries.)

aircraft and are banned above most urban areas, and thus contribute less to the noise pollution experienced by most people.

Historically, the first complaints about "noise pollution" arose from the Boeing 707, first delivered in 1958, which was powered by turbojet engines. The establishment of the Federal Aviation Administration (FAA) noise regulations in the early 1970s called for a 25%–50% reduction in maximum noise generated by the existing long-range Boeing 707, Douglas DC-8, and Vickers VC-10 aircraft. Larger aircraft then entering service such as the Lockheed L-1011, Douglas DC-10, and Airbus A300 were designed with the more stringent noise requirements in mind, while the Boeing 747 needed some modification to cope with the new regulations. In 1971, the U.S. FAA implemented its own rules in Federal Aviation Regulations (FAR) Part 36. FAR Part 36 set the maximum noise that could be produced at an airport at three points—two on either end of the runway beneath takeoff and landing paths and one at the middle and sides of the runway. The FAA regulations on aircraft noise were tightened several times after the initial rules were set. Naturally, this has prompted aircraft/engine manufacturers to try to develop quieter aircrafts/engines. The development of high-bypass turbofans resulted in a beneficial reduction in noise. Since 1966–2000 more than 20 dB improvement in lateral noise level corrected to aircraft thrust have been achieved (Figure 11.32). The main challenge for the aircraft industry is to reduce the noise level by a factor of (20 EPNdB) by 2022.

The maximum perceived noise level of different turbofan modules at approach and takeoff are illustrated in Figure 11.33. The jet has a larger noise level during takeoff than approach, while the fan exhaust is nearly equal.

11.6.2 Acoustics Model Theory

The main model used in the study of the jet noise is the Ffowcs Williams and Hawkings (FW-H) model. The FW-H equation is essentially an inhomogeneous wave equation that

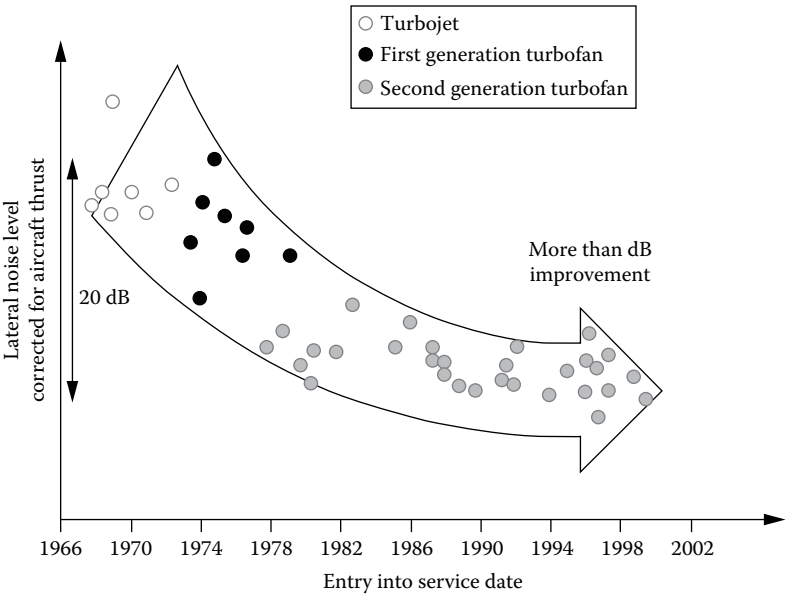


FIGURE 11.32
Improvement of engine noise level.

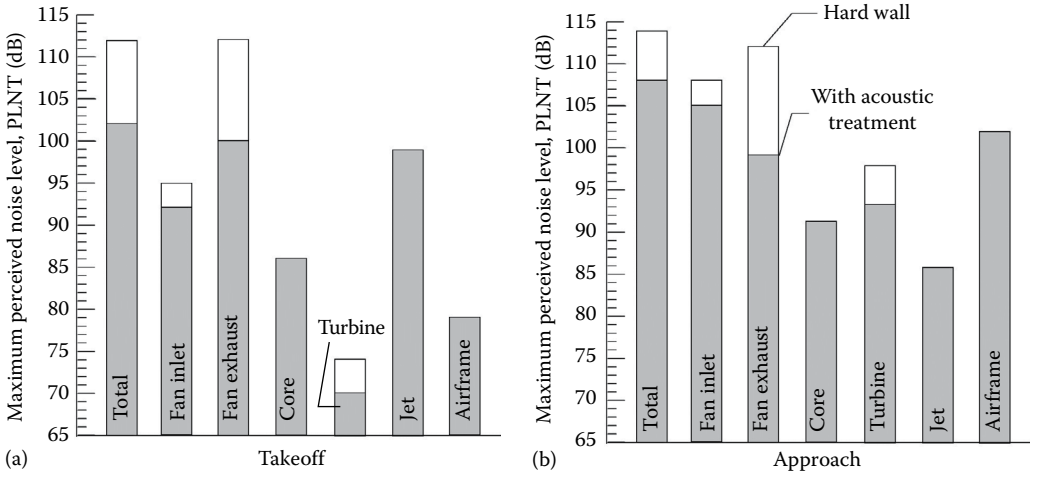


FIGURE 11.33
(a) Maximum perceived noise of turbofan modules during takeoff. (b) Maximum perceived noise of turbofan modules during approach. (From Leylekian, L. et al., *J. AerospaceLab*, AL07-01, Issue 7, 1, 2014.)

can be derived by manipulating the continuity equation and the Navier–Stokes equations [18]. This equation is capable of addressing three-dimensional, nonlinear, and unsteady flow problems of compressible and viscous fluids. An alternative equation is the Kirchhoff (K) equation [19]. Using generalized function theory, both the FW-H and the K equations can be written with inhomogeneous source terms involving the Dirac delta function.

11.6.3 Methods Used to Decrease Jet Noise

Noise suppression of internal sources is approached in two ways; by basic design to minimize noise originating within or from engine, and by the use of acoustically absorbent lining [20–22]. The noise suppressor is usually combined with the engine thrust reverser and is called a suppressor-reverser [5].

As described earlier, exhaust jet is the major source of noise in turbojet and low-BPR turbofan engines, and this can be reduced by inducing a shorter mixing region. This is achieved by increasing the contact area of atmosphere with the exhaust gas stream by using a propelling nozzle incorporating either a *corrugated* or *lobe-type* (multiple-tube) noise suppressor. Corrugated perimeter type is warped or angled, often looking like a flower (Figure 11.34). It breaks up the single main jet exhaust into a number of smaller jet streams. The shape of the suppressor increases the total perimeter of the nozzle area, and reduces the size of eddies created as the gases are discharged to the open air, which promote rapid mixing. The size of eddies scales down linearly with the size of the exhaust stream. This has two effects. First, the change in frequency may put some noise above the audibility range of human ear. Second, high frequencies within the audible range are more highly attenuated by atmospheric absorption than are low frequencies.

In the lobe-tube nozzle, the exhaust gases are divided to flow through the lobes and a small central nozzle. These form a number of separate exhaust jets that rapidly mix with the air entrained by the suppressor lobes (Figure 11.35). This principle can be extended by the use of a series of tubes to give the same overall area as the basic circular nozzle. This type of noise suppressor was used by military aircraft and early commercial aircrafts. But both of these methods increased drag and reduced engine performance, and the multi-tube approach also increased weight, sometimes substantially.

Another solution that emerged in the 1960s was the *ejector-suppressor*. This was essentially a large tube fitted aft of the engine around the exhaust nozzle that allowed air from outside the engine to mix with the exhaust, reducing the final efflux velocity.



FIGURE 11.34
Corrugated perimeter noise suppressor (rear view). (Courtesy of Rolls-Royce plc. Copyright 2016.)

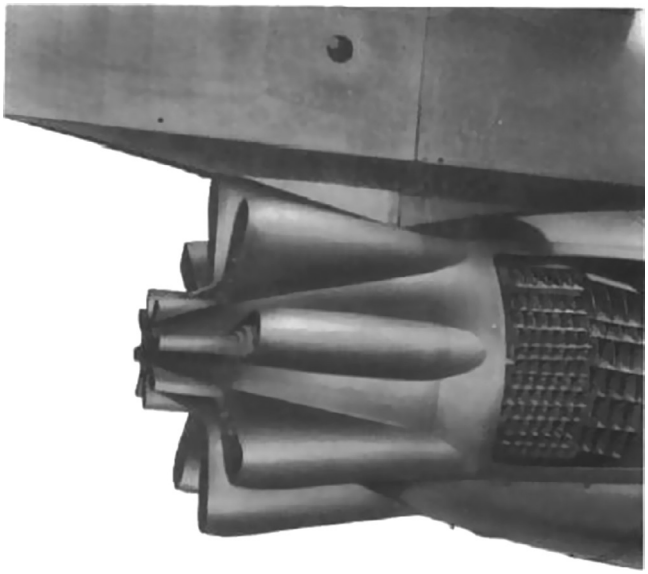


FIGURE 11.35
Lobe type nozzle. (Courtesy of Rolls-Royce plc, 2016. Copyright 2016.)

Turbofan engines are quieter than turbojet engines as the exhaust velocities of both streams of turbofans are less than those for turbojets. Mixing of the flows in turbofan engines for the purpose of noise reduction was examined as early as the 1970s [23]. Extensive research was carried out by air forces in the 1980s as they started looking for ways to reduce fighters' infrared signature. It was noticed that those same nozzles had an effect on noise emissions as well. Several nozzle designs were tested to reduce the fully expanded jet velocity by mixing (1) core flow with fan flow only, (2) fan flow with ambient flow only, or (3) both flows simultaneously. Depending on the type of mixing attempted, these designs fell into two broad categories: tabs and chevrons. Tabs are severe protrusions into the flow at the nozzle exit plane. Chevrons are also protrusions, but of much less severity than tabs. The aggressive mixing produced by the tabs greatly reduced low-frequency noise, but with the penalty of tab-induced high-frequency noise. Chevrons, which provided a more balanced approach to mixing, reduced low-frequency noise without significant chevron-induced high-frequency noise. Other nozzle designs attempted to shield the core flow by using a scarf-fan nozzle and an offset-fan nozzle for mixed-flow turbofan engines; mixing of both hot and cold streams greatly reduces the noise.

Generally, the most successful method employed by numerous aeroengine manufacturers is to mix the hot and cold exhaust streams within the confines of the engine and to expel the lower velocity exhaust gas flow through a single nozzle. This single nozzle may also have the corrugated or lobe-type shape [1]. Numerous numerical research works are carried out to examine the mixing process for turbofan engines—for example refer to Reference 24.

Another technique for noise suppression that may be applied to both turbojet and turbofan engines, which has been recently investigated, is the eccentric coannular nozzle [25]. The eccentric nozzle has some 10% improvement for low-frequency noise and some 5% for high-frequency noise.

11.7 High-Speed Vehicles

By high-speed vehicles is meant missiles or rockets, which will be treated in Chapters 18 and 19. They employ convergent–divergent nozzles, which have three main types [26]:

1. Cone
2. Bell
3. Annular

Hereafter, the main characteristics of these types will be briefly described [27].

11.7.1 Conical Nozzles

The conical nozzle was used in early rockets due to its simplicity and ease of construction. The main geometrical parameters for a conical nozzle are half-angle α, length L, and throat diameter D^*. The ratio of exit to throat area is

$$\frac{A_e}{A^*} = \left(\frac{D^* + 2L\tan\alpha}{D^*} \right)^2 \tag{11.27}$$

The length of nozzle is also expressed as

$$L = \frac{D^* \left(\sqrt{\frac{A_e}{A^*}} - 1 \right)}{2\tan\alpha} \tag{11.28}$$

The length of the nozzle is then calculated knowing the area ratio, throat diameter, and desired nozzle half angle. Throat diameter D^* is fixed by combustion chamber conditions and desired thrust. Moreover, the nozzle length and mass are strongly dependent on α.

Figure 11.36 illustrates three conical nozzles having constant (A_e/A^*) and different (L/D^*). The longest nozzle (case a) has nearly uniform axial outlet speed. Case (b) has

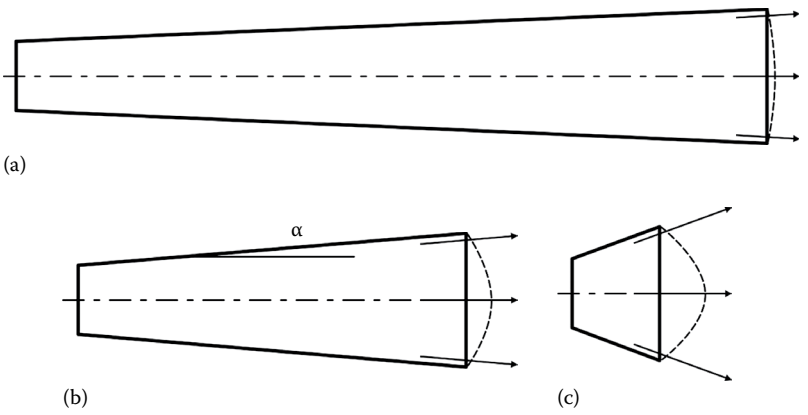


FIGURE 11.36
(a–c) Three conical nozzles having constant (A_e/A^*) and different (L/D^*).

almost axial flow at nozzle outlet. Case (c) is the shortest nozzle, where the flow has a reasonable radial velocity component with possible separation. Soviet nozzles look more conical.

Example 11.6

Calculate the length of a nozzle for area ratio of 50 and half angle α of 20° and 10°.

Solution

From Equation 11.28,

$$\frac{L}{D^*} = \frac{\left(\sqrt{\frac{A_e}{A^*}} - 1\right)}{2\tan\alpha}$$

If α = 20°,

$$\frac{L}{D^*} = 8.34$$

If α = 10°,

$$\frac{L}{D^*} = 17.2$$

Reducing α from 20° to 10° would more than double the length and consequently mass of the divergent portion of the nozzle. However, a small angle produces a great thrust as it maximizes the axial component of exit velocity and produce higher specific impulse. On the contrary, large angle reduces performance as it causes flow separation.

11.7.2 Bell Nozzles

The bell is the most commonly used nozzle shape. It offers significant advantages over the conical nozzle. Concerning length, it is nearly 10%–25% shorter than the conical as illustrated in Figure 11.37. Thus it has less weight. It has also better performance as its contour avoids oblique shocks. However, its shape is only optimum at one altitude.

The bell consists of two sections: near throat section and divergent section. It diverges at a relatively large angle. The degree of divergence tapers off further downstream. Near the nozzle exit, the divergence angle is very small ~2°–8° [28].

The performance of the bell nozzles depends on flight altitude (refer to Figure 11.38). At optimum (intermediate) altitude the exhaust gases are ideally expanded ($P_e = P_a$), exhaust plume is column shaped, producing the maximum efficiency. At lower altitudes and sea level, the nozzle is over-expanded ($P_e < P_a$), but gases do not expand beyond $P_e = 0.4P_a$. The exhaust plume is pinched by high ambient air pressure. At high altitudes, the nozzle is underexpanded where $P_e > P_a$. The exhaust plume continues to expand past the nozzle exit. Efficiency is reduced for low and high altitudes.

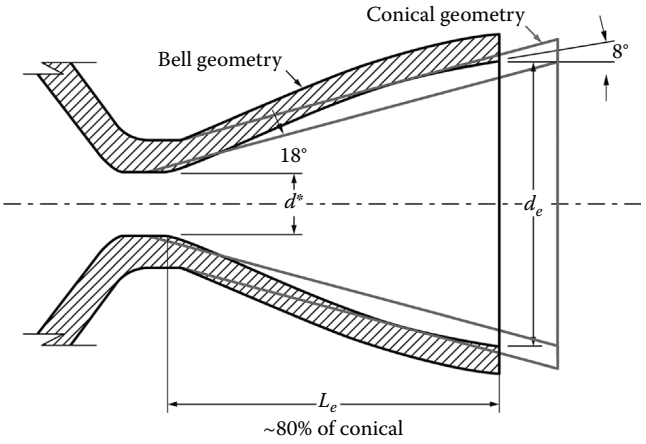


FIGURE 11.37
Bell versus conical nozzle.

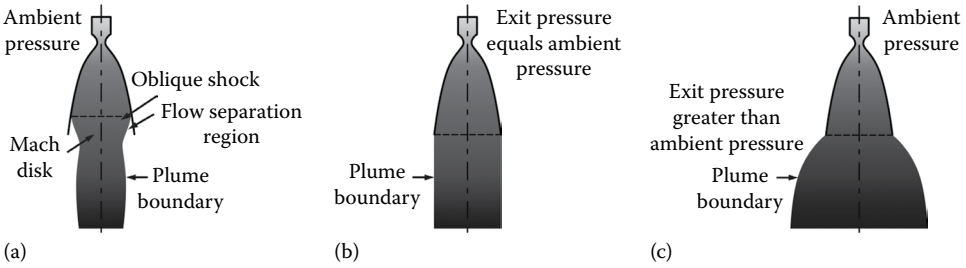


FIGURE 11.38
Plume shapes for different altitudes. (a) Sea level, (b) optimum altitude, and (c) high altitude.

11.7.2.1 Advantages of Bell-Shaped Nozzle

1. Mechanical design is simple as tangential stresses are dominant, which is easiest to design for
2. Cooling is easy as it is fabricated with walls of simple tubular construction that enables cooling in a straightforward way
3. Matching to combustion chamber is simple as it is most naturally a simple cylinder

11.7.2.2 Disadvantages of Bell-Shaped Nozzle

Over-expansion case leads to both thrust loss and flow instability as well as uncertainty or unsteadiness of the thrust direction. Generally, U.S. nozzle designs tend to have bell shapes and are usually designed by method-of-characteristics methods.

11.7.3 Annular Nozzles

Annular nozzles are sometimes known as the plug or "altitude-compensating" nozzles. They have recently received significant research attention. However, they are least

employed due to their greater complexity. "Plug" refers to the center-body that blocks flow from what would be the center portion of a traditional nozzle.

Annular nozzles are classified into two major types depending on the method in which they expand exhaust, namely, outward or inward.

1. *Radial out-flow nozzles*: Examples of this type are the expansion-deflection (E-D), reverse-flow (R-F), and horizontal-flow (H-F) nozzles.
2. *Radial in-flow nozzles*: Examples of this type are spike nozzles and linear-aerospike nozzles for X-33.

Brief discussion will be given hereafter for some of the annular nozzles.

11.7.3.1 Radial Out-Flow Nozzles

Figure 11.39 shows an example of an E-D nozzle, which works much like a bell nozzle. Exhaust gases are forced into a converging throat before expanding in a bell-shaped nozzle. Flow is deflected by a plug, or center-body, that forces the gases away from the center of the nozzle, which thus stays attached to nozzle walls. Center-body position may move to optimize performance. As altitude or back-pressure varies, flow is free to expand into "void" which allows the nozzle to compensate for altitude.

Expansion ratio

$$\varepsilon = \frac{A_{exit} - A_{plug}}{A_{throat}}$$

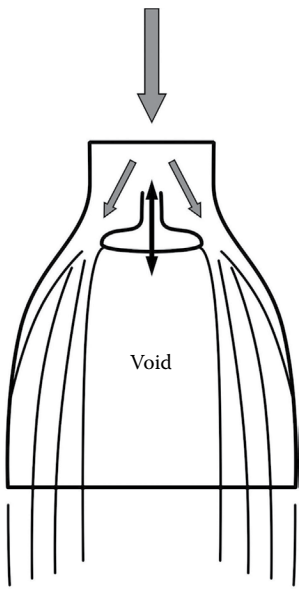


FIGURE 11.39
An expansion-deflection (E-D) radial outflow nozzle.

Another parameter

$$\text{Annular diameter ratio} = D_{plug}/D_{throat}$$

This ratio is used as a measure of nozzle geometry for comparison with other plug nozzle shapes.

11.7.3.2 Radial Inflow Nozzles

Radial inflow nozzles [29] are often referred to as

- Spike nozzles
- Aerospike or truncated aerospike

The spike nozzle is named for its prominent spike center-body. It may be thought of as a bell turned inside out. Each type of spike nozzles features a curved, pointed spike. The spike shape allows exhaust gases to expand through an isentropic process. An isentropic spike may be the most efficient but it tends to be prohibitively long and heavy.

The aerospike or truncated aerospike is generated by removing the pointed spike altogether and replacing it with a flat base. The main disadvantage of a "flat" plug is turbulent wake forms aft of base at high altitudes resulting in high base drag and reduced efficiency. However, it may be alleviated by introducing a "base bleed," or secondary subsonic flow. Circulation of this secondary flow and its interaction with the engine exhaust creates an "aerodynamic spike" that behaves much like the ideal, isentropic spike.

Problems

11.1 A turbojet engine is powering an aircraft flying at altitude of 8000 m where the temperature and pressure are 236.2 K and 35.6 kPa, respectively. At a flight Mach number of 0.8, the inlet conditions to the nozzle were 600 K and 16 kPa. For a convergent nozzle, check whether the nozzle is choked or not. Calculate the thrust per unit frontal area. Next, the pilot lit the afterburner to increase the Mach number to 1.6. The nozzle's geometry was changed to a convergent-divergent shape. The inlet temperature and pressure to the nozzle were 1200 K and 16 kPa, respectively. Recalculate the thrust per unit frontal area. Compare the nozzle outlet areas in both cases. Calculate the throat area of the C-D nozzle.

11.2 Figure P11.2 illustrates a turbofan engine during the application of thrust reverse. The exhaust from the fan is leaving through reverse cascade at a speed of $V_1 = 300$ m/s and an inclination angle with respect to the longitudinal axis of engine of $\theta_1 = 50°$. The hot gases are also leaving the engine through reverse cascades at a speed of $V_2 = 600$ m/s and an inclination angle of $\theta_2 = 60°$ to the engine axis. The touchdown speed is $V_f = 80$ m/s. Prove that the force developed by thrust reversers is

$$F = \beta \dot{m}_a V_1 \cos\theta_1 + \dot{m}_a (1+f) V_2 \cos\theta_2 + (1+\beta)\dot{m}_a V_f$$

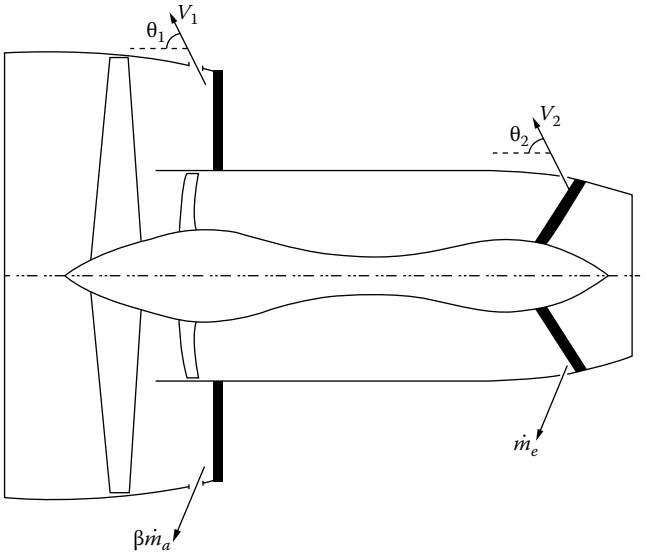


FIGURE P11.2

Calculate the resulting drag force due to the application of thrust reverser in the following case: fuel to air ratio $f = 0.02$ and $\dot{m}_a = 50$ kg/s, BPR $\beta = 5$.

11.3 The time needed for landing when the thrust reverse is applied up to a complete stop and assuming a mean value for drag force was derived in Example 11.5 given by

$$t = -\frac{m}{n\dot{m}_a}\ln\frac{V + V_j\sin\beta + \left(D_{av}/n\dot{m}_a\right)}{V_0 + V_j\sin\beta + \left(D_{av}/n\dot{m}_a\right)}$$

where

V_0 is the touchdown velocity
V is the velocity at any time during landing and is equal to zero at aircraft stop
V_j is the exhaust jet velocity
m is the mass of the airplane during landing
$\dot{m}_a$ is the mass-flow rate of air sucked and exhausted by the engine (assume $\dot{m}_f \gg 0$)
n is the number of engines

For a twin-engine airplane, with $m = 50{,}000$ kg, $m_a = 50$ kg/s, $V_j = 600$ m/s, $V_0 = 80$ m/s, examine

1. The effect of the angle β on the time and distance for landing. Assume β changes from 0° to 60° in intervals of 10°.
2. For the airplane in question with the angle $\beta = 60°$, examine the effect of exhaust speed V_j, assuming it varies from 200 to 600 in 100 intervals.

11.4 A wide body civil transport aircraft powered with two turbofan engine is examined during landing. The pilot is applying the thrust reverse to shorten the ground landing distance, the thrust reverse is inclined angle $\beta = 60°$ to the axial direction.

The runway is dry concrete/asphalt where the coefficient of friction with brakes on and off is 0.4 and 0.04, respectively. The aircraft has the following data: Maximum weight = 187 tons, wingspan = 60.3 m, wing area = 361.6 m^2, fan air mass flow rate $\dot{m}_{ac} = 500$ kg/s, engine maximum thrust = 320 kN, idle thrust = 50 kN, lift and drag coefficient factors are $C_{Do} = 0.02$ and $C_{L\,\max} = 3.2$, span efficiency factor (e) = 0.9.

Calculate

1. The ground landing distance with applied thrust reverse
2. The ground landing distance without thrust reversal

11.5 The convergent nozzle discussed in Example 11.2 is to be re-examined to determine the effect of the angle θ on the length of the nozzle. What will be the length of the nozzle if θ changes in one-degree increment from 11 to 14?

Follow the same procedure and recalculate the variation of the gas properties through the nozzle for an angle $\theta = 11°$.

11.6 Follow the same procedure in Example 11.3 and calculate and plot the nozzle contour for an outlet Mach number of 4.0 and the same throat diameter. How does the length of the nozzle changes with the outlet Mach number?

11.7 Air flows through a convergent divergent nozzle having a circular cross-section area $A(x)$ expressed by the relation $A(x) = 0.15 + x^2$, where $A(x)$ is in square meters and (x) is in meters. The duct extends from $x = -0.6$ m to $x = +1.8$ m.

1. Draw a layout for the nozzle
2. If the inlet air speed is subsonic, plot the variation of the following variables along the nozzle:
   a. Mach number
   b. Static to total temperature ratio: $\frac{T}{T_o}$
   c. Static to total pressure: $\frac{P}{P_o}$
3. Replot the three variables if the inlet speed is supersonic

11.8 Discuss why fluidic-thrust reverse is not used in large aircrafts.

11.9 Discuss how the runway length will be drastically longer if aircrafts land without the application of thrust reverse. Consider the wide body civil transport in Problem 11.4 and recalculate the landing distance without thrust-reversal force.

11.10 Why is thrust reversal not applied at low speeds? Consider again the civil transport in Problem 11.4 and calculate the needed distance for an aircraft to reach zero speed if the pilot depends totally on the thrust reverse and does not use the brakes at all.

References

1. Rolls-Royce plc, *The Jet Engine*, 5th edn., Rolls-Royce plc, Derby, U.K., 1996, 159pp. Reprinted 1996 with revisions.
2. W.W. Bathie, *Fundamentals of Gas Turbines*, 2nd edn., John Wiley & Sons, Inc., New York, 1996, 343pp.
3. H.I.H. Saravanamuttoo, G.F.C. Rogers, and H. Cohen, *Gas Turbine Theory*, 5th edn., Prentice Hall, Harlow, U.K., 2001, 109pp.

4. J.L. Kerreebrock, *Aircraft Engines and Gas Turbines*, 2nd edn., The MIT Press, Cambridge, MA, 1992, 142pp.
5. United Technologies Pratt Whitney, *The Aircraft Gas Turbine Engine and Its Operation*, Vol. 200, P&W Operation Instruction, East Hartford, CT, 1988, pp. 3–33.
6. A. Glassman, *Turbine Design and Application*, Vol. III, NASA, Washington, DC, SP-290, 14pp.
7. A.H. Shapiro, *The Dynamics and Thermodynamics of Compressible Flow Field*, 1st edn.,Vol. I, 1954.
8. M.A. Khan, S.K. Sardiwal, M.V. Sai Sharath and D.H. Chowdary, Design of a supersonic nozzle using method of characteristics, *International Journal of Engineering Research and Technology*, 2(11), 19–24, 2013.
9. I.E. Treager, *Aircraft Gas Turbine Engine Technology*, 3rd edn., McGraw-Hill, Inc., New York, 1999, 220pp.
10. J.D. Anderson, Jr., *Aircraft Performance and Design*, McGraw-Hill Book Co., Boston, MA, 1999, 370pp.
11. B. Gal-Or, Fundamental concepts of vectored propulsion, *Journal of Propulsion and Power*, 6(6), 747–757, November–December 1990.
12. M.S. Mason and W.J. Crowther, Fluidic thrust vectoring of low observable aircraft, *CEAS, Aerospace Aerodynamic Research Conference*, Cambridge, U.K., June 10–12, 2002.
13. B.L. Berrier and M.L. Mason, *Static Performance of an Axisymmetric Nozzle with Post-Exit Vanes for Multiaxis Thrust-Vectoring*, NASA TP-2800, Washington, DC, May 1988.
14. E.A. Bare and D.E. Reubush, *Static Internal Performance of a Two-Dimensional Convergent-Divergent Nozzle with Thrust Vectoring*, NASA TP-2721, Washington, DC, July 1987.
15. Farnborough: MiG-29 thrust vectoring rekindles spirit, FLIGHT 25/07/2006.
16. M.J. Kroes and T.W. Wild, *Aircraft Powerplants*, 7th edn., McGraw-Hill, Glencoe, Scotland, 2002, 303pp.
17. J.P. Raney and J.M. Cawthorn, Aircraft noise, In C.M. Harris (Ed.), *Handbook of Noise Control*, 2nd edn., McGraw-Hill Book Company, New York, 1979, Chapter 34.
18. J.E.W. Ffowcs and D.L. Hawings, Sound generation by turbulence and surfaces in arbitrary motion, *Philosophical Transactions of the Royal Society*, A264(1151), 321–542, 1969.
19. F. Farassat and K.S. Brentner, *A Study of Supersonic Surface Sources—The Ffowcs Williams-Hawkings Equation and the Kirchhoff Formula*, NASA-AIAA-98-2375, 1998.
20. M.J.T. Smith, *Aircraft Noise*, Cambridge University Press, Cambridge, U.K., 1989, p. 4.
21. D. Papamoschou and M. Debiasi, Directional suppression of noise from a high-speed jet, *AIAA Journal*, 39(3), 380–387, 2001.
22. M. Harper-Bourne, Physics of jet noise suppression, *Proceedings of Jet Noise Workshop*, NASA/CP–2001-211152, 2001, pp. 701–719.
23. G.C. Paynter and S.C. Birch, An experimental and numerical study of the 3-D mixing flows of a turbofan engine exhaust system, *15th Aerospace Science Meeting, AIAA-77-204*, Los Angeles, CA, 1977.
24. N.J. Cooper and P. Merati, Numerical simulation of the vortical structures in a lobed jet mixing flow, *43rd AIAA Aerospace Sciences Meeting and Exhibit*, January 10–13, 2005, AIAA-2005-0635, Reno, NV.
25. K. Zaman, Noise- and flow-field of jets from an eccentric coannular nozzle, AIAA-2004-0005, 2004.
26. Aerospace web, Aircraft design, http://www.aerospaceweb.org/design/aerospike/shapes.shtml.
27. A.F. El-Sayed, *Fundamentals of Aircraft and Rocket Propulsion*, Springer, London, U.K., 2016.
28. D.R. Kirk, Rocket nozzles, MAE 4262: Rocket and mission analysis, nozzles, PPT.
29. D.R. Kirk, *Rocket Nozzles*, Mechanical and Aerospace Engineering Department, Florida Institute of Technology, Melbourne, FL, 2016, http://docshare01.docshare.tips/files/26389/263891559.pdf.
30. L. Leylekian, M. Lebrun and P. Lempereur, An overview of aircraft noise reduction technologies, ONERA, *Journal of AerospaceLab*, AL07-01(7), 1–15, 2014.


Taylor & Francis
Taylor & Francis Group
http://taylorandfrancis.com

12

Centrifugal Compressors

12.1 Introduction

This chapter and the following three chapters deal with the rotating modules of both aeroengines and gas turbines. These four chapters discuss compressors, fans, and turbines. Since all of these are identified as *turbomachines*, it is necessary here to introduce a definition for turbomachines. The word *turbo* (or *turbines*) is of Latin origin meaning "that which spins or whirls around." Turbomachines are often referred to as rotor dynamic devices that transfer energy to or from a working fluid through the forces generated by a rotor. For compressors or fans, energy is transferred from the rotor to the fluid. The reverse occurs in turbines, which deliver shaft power in exchange of thermal energy taken from the working fluid.

This chapter and the next deal with dynamic compressors. Compressors are classified as either intermittent flow or continuous flow (Figure 12.1), Brown [1]. Intermittent-flow compressors are positive-displacement ones. They are classified as either reciprocating or rotary types. Such positive-displacement compressors achieve their pressure rise by trapping fluid in a confined space and transporting it to the region of higher pressure. Continuous-flow compressors are classified as either ejectors or dynamic compressors. Dynamic compressors are further classified as radial flow, mixed flow, or axial flow. In radial-flow compressors outlet air flows in a plane perpendicular to the rotation axis, while in axial compressors outlet flow is mainly parallel to the axis of rotation. Finally, in the case of mixed-flow compressors, outlet flow is partly radial and partly axial.

Dynamic compressors are also very similar to propellers and propfans. In both, energy is transferred from the blades to the working fluid. However, they differ in the influenced fluid quantity. Dynamic compressors accommodate a finite quantity of working fluid that flows steadily in an annular duct comprising a hub and casing. Consequently, it is defined as an *enclosed* machine. In contrast, propellers and propfans influence an unbounded quantity of air—in other words, they are turbomachines without shrouds or annulus walls (or casing) near the tip. Thus these machines are defined as extended turbomachines.

Dynamic compressors work by conversion of the velocity to pressure in a continuous flow. They are efficient, compact, and handle vast quantities of working fluid. Considering air as the working fluid at 1.013 bar and 288 K, the inlet flow is typically 150 kg/s (122 m^3/s or 259,000 ft^3/min) per square meter of inlet area at Mach 0.4 [2]. The intake diameters of the various types range from 0.1 m (4 in.) to 2.44 m (8 ft). The range of mass flow varies from about 1.2 to 700 kg/s. The isentropic efficiency ranges typically from 0.7 to 0.9.

In this chapter, the aerodynamic and mechanical design of centrifugal compressors are presented. Axial compressors will be treated in Chapter 13. Mixed-flow compressors are rarely used in aeroengines or gas turbines.

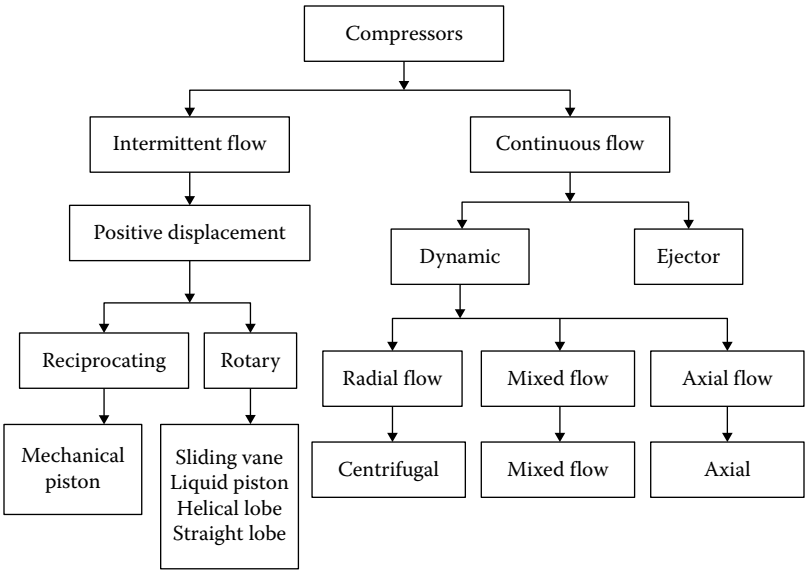


FIGURE 12.1
Classification of compressors.

Centrifugal compressors and radial-inflow turbines are identified as radial turbomachines. Radial turbomachines have a surprisingly long history, and predate axial-flow turbomachines, both compressors and turbines [3]. In 1705, Papin published descriptions of the centrifugal pumps and blowers that he had developed. In the closing years of the nineteenth century, relatively crude centrifugal pumps and blowers were in use for ventilation. In the twentieth century, the gas turbine engine came to prominence, and pushed turbomachine design to the limits of technology and materials. The most efficient turbomachines available to the early gas-turbine engineers were the centrifugal compressors and axial turbines [3]. For this reason, centrifugal compressors were employed in the first jet engines developed by Frank Whittle and von Ohain, thanks to the previous experience gained in the design of superchargers. Through the development of aeroengines, axial compressors have nearly replaced the centrifugal compressors. Thus centrifugal compressors are found in small turbofan engines like the Allied Signal 731 turbofan engines and small turboprop/turboshaft engines like the Rolls Royce DART, Allied Signal 331, and the famous engine manufactured by Pratt and Whitney of Canada, the PT6 (Figure 12.2). It is found also in auxiliary power units (APUs) found in many civil transport like Garrett GTCP-85 for DC8 and 9, the MD-80, the Boeings 707,737, Sunstrand Turbomach APS 200 for the B737-500 and A321, as well as Hamilton Sunstrand's APS 5000 for the B787. Other applications for the centrifugal compressors are aircraft-cabin air conditioning like the Hamilton Standard 777(ACTCS) and the Multi Purpose Small Power Units (MPSPU), represented by the SunStrand Turbomach T-100. In few gas-turbine engines, a centrifugal compressor is used for the final stage of compression downstream of multistage of axial compressor. This arrangement, called an *axial-centrifugal* compressor, is to be found, for example, in the General Electric T700 engine, the very popular PT6 Pratt & Whitney Canada engine, and the T53 Lycoming engine.

Centrifugal compressors in aeroengines provide small-to-moderate air flows (up to nearly 50 kg/s). They have either single or double stages (sometimes identified as

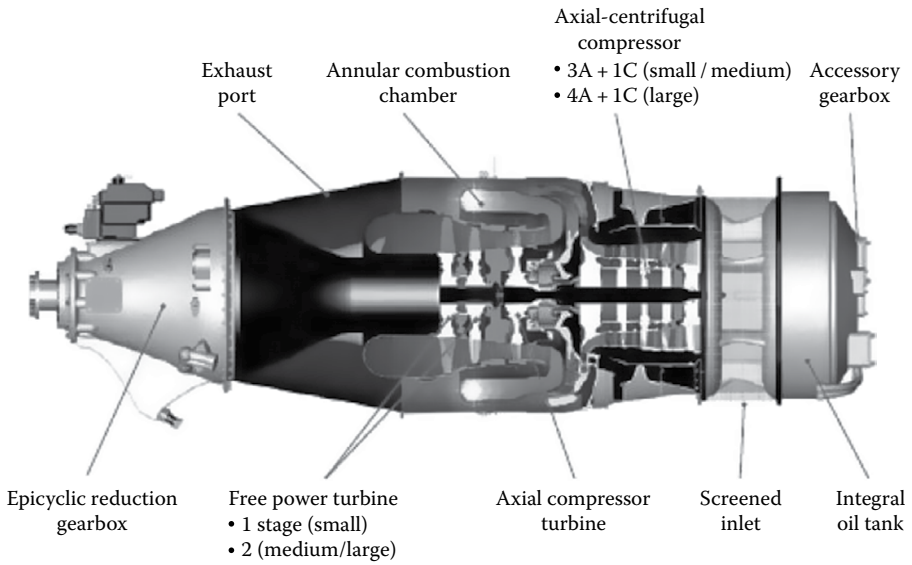


FIGURE 12.2
Centrifugal compressor in the turboprop engine PT6. (Courtesy of Pratt & Whitney of Canada.)

impellers in tandem). The pressure ratio per stage ranges from 4:1 to 8:1, while for double (two) stages in series, a pressure ratio of 15:1 is found in Pratt & Whitney PW100. The evolution of centrifugal compressors since Frank Whittle engines up to the mid 1980s was reviewed by Kenny [4]. An ambitious program by Pratt & Whitney, Canada, as well as other manufacturers, to reach a higher value of pressure ratios (16:1 or more) in the near future.

Centrifugal compressors are used in many industrial applications, such as refineries, chemical and petrochemical plants, natural gas processing and transmission plants, very large-scale refrigeration, and iron and steel mills. These centrifugal compressors may have single or multiple stages (up to five) and can operate at very high inlet pressures. Rolls Royce RFA36 and RFA24 giant compressors may have pressures up to 155 bar, flow rate of 200 at design speed from 3,600 to 12,800 rpm. The General Electric Power Systems, Oil and Gas, and Nuovo Pignone centrifugal compressors for re-injection services have discharge pressure up to 500 bar. Hitachi had manufactured 800 sets of centrifugal compressors since first unit delivered in 1911 to be employed in different applications. Earlier types manufactured by Hitachi in 1978 had an approximate pressure ratio of 260 for four groups CO_2 applications [5]. On the other hand, centrifugal compressors are employed by PCA in its micro-gas turbine generator.

Centrifugal compressors have the following advantages: lightweight, low cost, rigidity, high-pressure ratio per stage, easily made in relatively small sizes thus suitable for handling small volume flows, simplicity, better resistance to foreign object damage (FOD), less susceptibility to loss of performance by build up of deposits on the blade surfaces, and the ability to operate over a wider range of mass flow at a particular speed. The disadvantages of the centrifugal compressor are that it is generally less efficient than an axial compressor (by perhaps 4%–5%), and it has a large cross-section compared to the cross-section of the inlet flow. A detailed comparison between centrifugal and axial compressors will be given in the Chapter 13.

12.2 Layout of Compressor

Figure 12.3 illustrates a typical centrifugal compressor [2]. Nomenclature for a single-sided compressor with channel-types diffuser is given here.

F:	Impeller	G:	Inducer (rotating guide vane)
H:	Diffuser	J:	Impeller vane
K:	Half vane	L:	Impeller tip
M:	Impeller hub	N:	Shroud (casing)
O:	Impeller eye	P:	Vane less gap

Generally, a centrifugal compressor is so called because the flow through the compressor is turned perpendicular to the axis of rotation. This type of compressors is composed of three main elements: the rotating part or impeller, the stationary part or stator, and a manifold or a collector (denoted by scroll or volute). The impeller has several blades referred to as vanes.

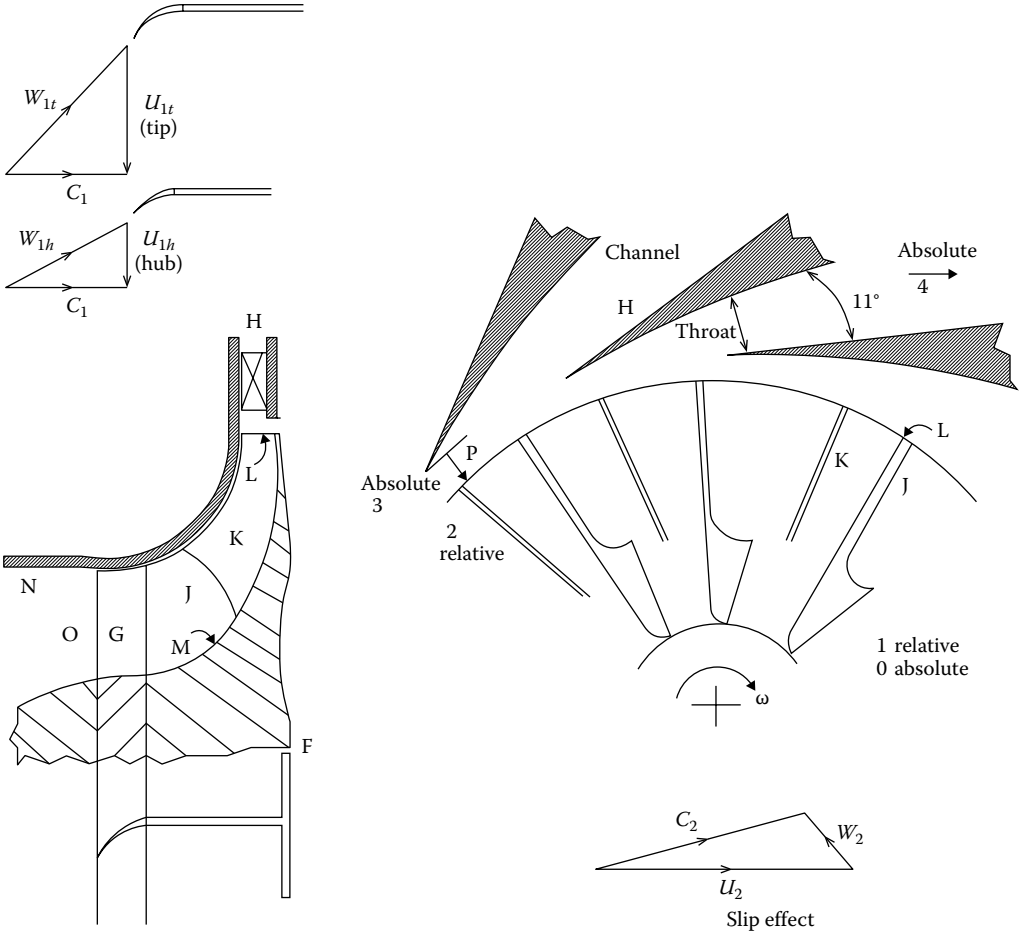


FIGURE 12.3
Layout of a typical centrifugal compressor.

The diffuser may have vanes or may be vaneless. Other arrangements for the diffuser will be discussed later on in the diffuser section.

An important part upstream of the impeller is the *inducer duct.* The nature of flow through the impeller is strongly dependent upon the duct arrangement upstream. This could be a simple straight duct, a curved inlet duct, a curved return passage of a multi-stage compressor, or the final stage of an axial compressor. These alternative configurations can lead to distorted flow conditions at the impeller inlet, which in turn will lead to an overall deterioration of the compressor's performance.

12.2.1 Impeller

The impeller scoops in the working fluid (air/gas). Air is drawn at the center or eye of the impeller, then accelerated through the fast spinning speed of the impeller and finally thrown out at the tip. The forces exerted on the air are centripetal. At the eye (inlet), the vanes are curved to induce the flow: this axial portion is called the inducer or known as the rotating guide vanes and may be integral with or made separately from the main impeller. The divergence (increasing cross-sectional area) of these passages diffuses (slows) the flow to a lower relative velocity and higher static pressure. The impeller is a complicated diffuser compared with the conventional straight conical diffuser as the passage is doubly curved first in the axial plane and then in the radial plane (Figure 12.4). The impeller vanes are aligned radially, but may be curved near the tip, having forward or backward configurations. The impeller may have double sides (sometimes denoted double entry) as shown in Figure 12.5, to pass the maximum flow rate relative to its diameter and to balance the stresses of single-sided impeller. The vanes are cast, forged, or machined integrally with the impeller hub. The hub is the curved surface of revolution extending from the eye root to the outlet. The number of vanes is usually a prime number, typically from 19 to 37, to avoid vibration problems [2]. Half vanes (splitter blades) are sometimes used toward the tip to improve the flow pattern where the full vanes are widely spaced (denoted K in Figure 12.3). The outer curve of the vanes is sealed by the shroud, which may be part of the stationary structure or may rotate with the rotor. Typical impeller proportions are that the eye root diameter is about half the eye tip diameter and the tip (outlet) diameter is nearly twice the eye tip diameter.

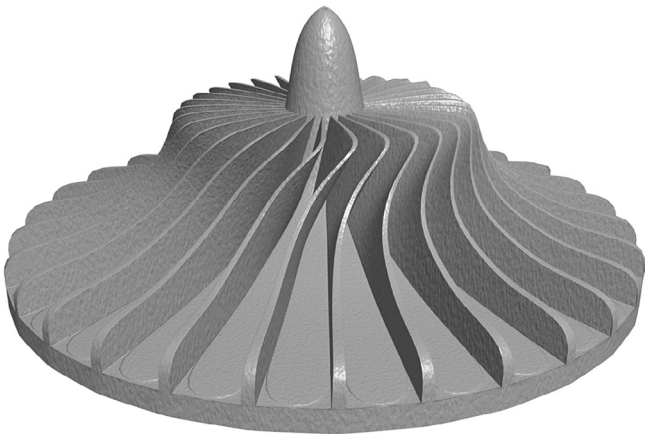


FIGURE 12.4
Impeller shape.

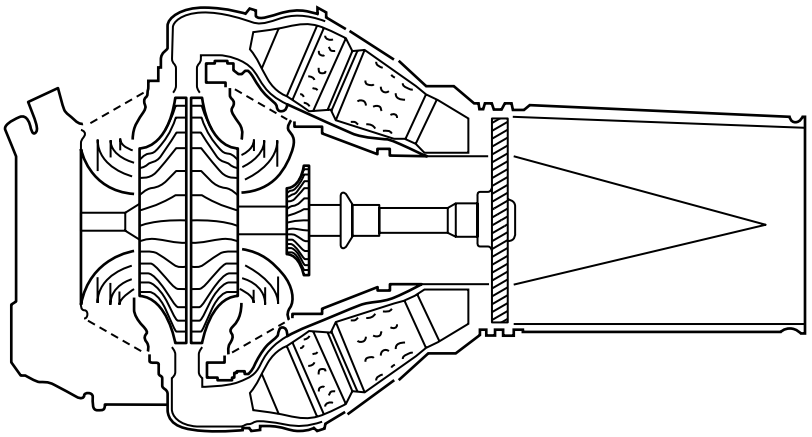


FIGURE 12.5
Double-sided centrifugal compressor. (Courtesy of Rolls-Royce plc, Copyright 2007. With permission.)

The impeller material is often aluminum, with titanium or steel for smaller, high-duty machines. To conclude this part, it is worthy mentioning that the part of the compression process achieved in the impeller is caused by moving the fluid outward in a centrifugal force field produced by the rotation of the impeller. This part of pressure rise differs from the pressure rise in axial flow compressor rotors and stators; instead of arising from the exchange of kinetic energy for thermal energy in a diffusion process, it arises from the change in potential energy of the fluid in the centrifugal force field of the rotor. It is therefore less limited by the problems of boundary layer growth and separation in adverse pressure gradients. Probably for this reason, the centrifugal compressor first attained a range of pressure ratio and efficiency useful for turbojet engines and was used in the von Ohain engine (1939) and the Whittle engine (1941).

12.2.2 Diffuser

The impeller blades sling the air radially outward where it is once again collected (at higher pressure) before it enters the diffuser. The diffuser represents a part of the fixed structure of the compressor. It discharges air from the compressor impeller with a high absolute velocity and the role of diffusion is to reduce the kinetic energy, thereby increasing the static pressure. The diffuser is either a vaneless passage or a vaneless passage followed by a vaned section. The vaned diffuser represents a large group including the vanes together with the cascade, channel, and pipe types (Figure 12.6) [2].

All diffusers have an initial vaneless gap outboard of the impeller in which the flow settles. The vaneless diffuser is bulky and can be inefficient relative to the other types. The cascade may involve one, two, or three rows of vanes, with performance similar to that of axial cascades. Vaned diffusers may use curved or straight vanes, having a longer path length than the cascade diffuser. Vaned diffusers may be made variable, the vanes pivoting about an axis, as shown in figure, to accommodate different incident flow angles through the speed range.

Vaneless, cascade, and vaned diffusers collect the flow in a one-volute-type collector, which is suitable for industrial applications. Channel and pipe diffusers are suitable for aeroengines and gas turbines.

The channel and pipe diffusers collect the flow in separate passages, sometimes with corner vanes at their outlet. The passage diverges slowly, the pipe consisting of a conical

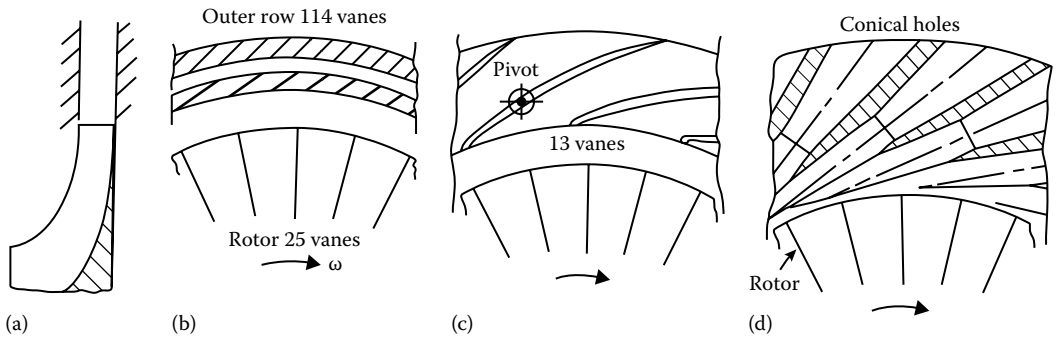


FIGURE 12.6
Different types of diffuser. (a) Vaneless, (b) cascade (2) rows, (c) vaned diffuser, and (d) pipe diffuser.

hole and the channel type being rectangular in section with one pair of opposed walls diverging at 10°–11°, the others being parallel.

The pipe and channel diffusers may feed separate combustors or may merge downstream. Recently, it had been shown that the pipe-type diffuser (a diffuser comprising channel of circular cross section) is more efficient than the conventional type with rectangular channels. The passages are formed by drilling holes tangentially through a ring surrounding the impeller, and after the throat the passages are conical. Overall isentropic efficiencies of over 85% are claimed for compressors using this new pipe diffuser.

12.2.3 Scroll or Manifold

The final element of centrifugal compressors is either a manifold or a scroll. Centrifugal compressors with manifolds are used when the compressor is a part of a gas generator—in either a gas turbine or an aeroengine—and thus the compressor is followed by a combustion chamber. In this case, the diffuser is bolted to the manifold, and often the entire assembly is referred to as the diffuser. In case of industrial applications for the oil and gas industry (up-, mid-, and downstream), chemical industries and petrochemicals, iron and steel mining, and the paper industry, the working fluid is collected in a scroll or volute. The working fluid leaving the stators is collected in a spiral casing surrounding the diffuser called a *volute* or *scroll*. The area of the cross-section of the volute increases along the flow path in such a way that the velocity remains constant. Finally, the total fluid leaving all the stator passages is ejected from a pipe/duct normal to the inlet duct. The possible shapes of volute are shown in Figure 12.7.

12.3 Classification of Centrifugal Compressors

Centrifugal compressors may be classified as

1. *Single or multiple stages*: For aeroengines, centrifugal compressors have either single stage (Figure 12.8) or double (two or tandem) stages (Figure 12.9). In some cases, two (or double) stages are mounted on the same shaft, handling the fluid in

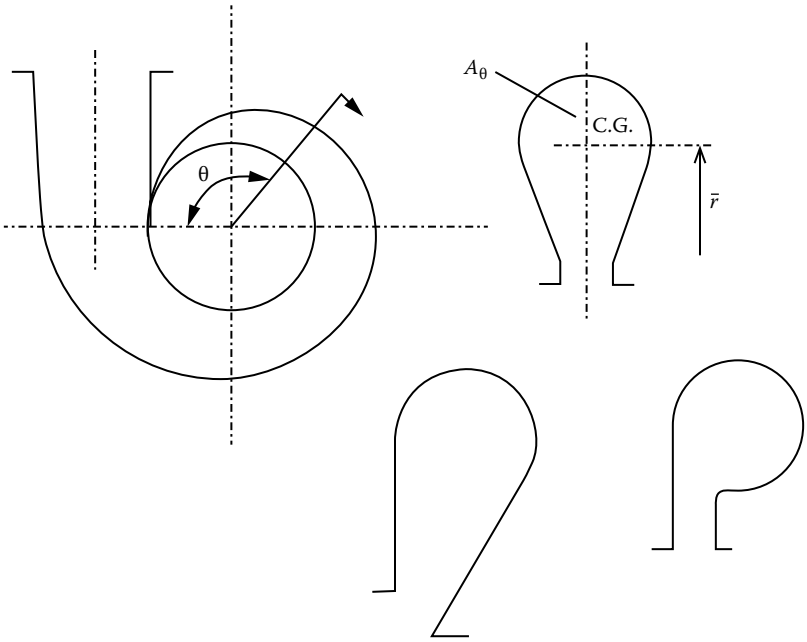


FIGURE 12.7
Different shapes of volute. (From Saravanamuttoo, H.I.H. et al., *Gas Turbine Theory*, 5th edn., Prentice Hall, Harlow, U.K., 2001, p. 167.)

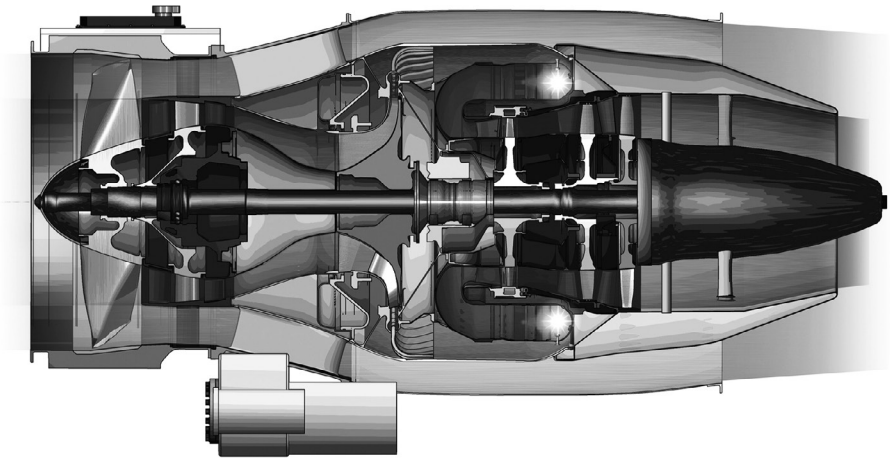


FIGURE 12.8
Single-stage centrifugal compressor. (Courtesy of Pratt & Whitney of Canada.)

series to boost its final pressure. In industrial gas turbines like pipeline compressors, there are up to five stages.

2. *Single-entry* (*or single-face*) *or double* (*dual*) *entry* (*or double-face*): The principal differences between the single-entry and dual-entry are the size of the impeller and the ducting arrangement. The single-entry impeller permits ducting directly to

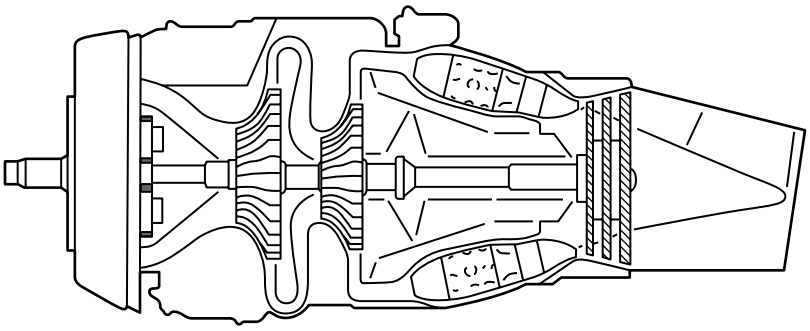


FIGURE 12.9
Two-stage centrifugal compressor. (Courtesy of Rolls-Royce plc, Copyright 2007. With permission.)

the inducer vanes, as opposed to the more complicated ducting needed to reach the rear side of the dual-entry type. Although slightly more efficient in receiving air, single-entry impellers must be of greater diameter to provide sufficient air. Dual-entry impellers are smaller in diameter and rotate at higher speeds to ensure sufficient airflow. Most gas turbines of modern design use the dual-entry compressor to reduce engine diameter.

3. *Shrouded or unshrouded impeller*: Unshrouded impeller means that there is a clearance between the ends of the impeller vanes and a stationary shroud, while shrouded means that there is a rotating shroud fixed to the impeller vanes. Shrouding reduces the losses due to leakage of air from the pressure side to the suction side of the blade. However, it increases the friction and weight of the impeller. For gas turbine and turbocharger applications the impeller is usually unshrouded and the stationary cover is referred to as the shroud. For large process compressors the impeller is often constructed with an integral shroud.
4. The impeller may have a non-, semi-, or full-inducer section as shown in Figure 12.10. For a full inducer impeller, the impeller vanes are continued around into the axial direction and the compressor resembles an axial compressor at inlet.

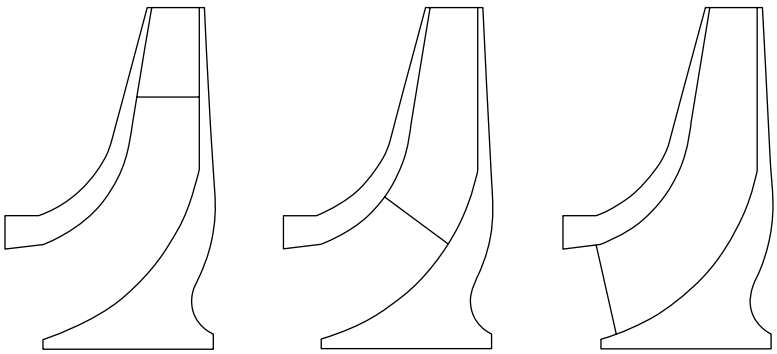


FIGURE 12.10
Types of inducers.

5. The impeller vanes may be radial at outlet or they may be inclined backward or forward, thus identified as a backward-leaning (commonly now described as backswept) or forward-leaning compressor (Figure 12.11).
6. The impeller layout may be either open, semi-closed, or closed. The open type is built with blades in a radial direction without enclosing covers on either front or back sides, and is normally found in turbochargers. Semi-closed types are built with blades in a radial direction with an enclosed cover on the back side which extends to the periphery of the blades, and is normally found in air compressors. The closed type is built with backward- or forward-leaning blades and has enclosing covers on both the front and back sides, and is normally found in multi-stage compressors.
7. The intake or inlet passage to the compressor may be fitted with inlet guide vanes (IGV) or may not. The IGVs are designed to give either positive or negative prewhirl, Figure 12.12. The IGVs giving a positive prewhirl are frequently found in high-speed compressors, say in aeroengines, to minimize the possibility of air reaching or exceeding the sonic speed. In this case shock waves may be formed, which will lead to great losses in the intake. Negative prewhirl is employed to increase the inlet relative speed at some applications. These IGVs may also be set at a fixed angle or they can be rotated to vary the inlet flow angle.
8. Outlet through a collector (denoted as scroll or volute) or a manifold: In the aviation field, the air leaving the compressor must be directed toward the combustion

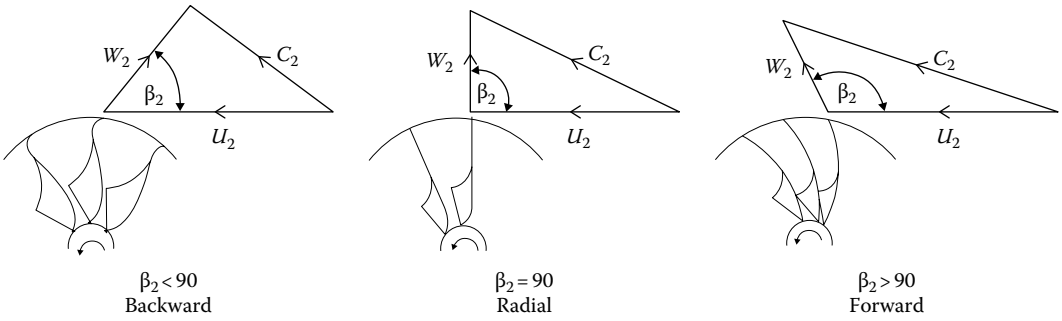


FIGURE 12.11
Different types of impeller.

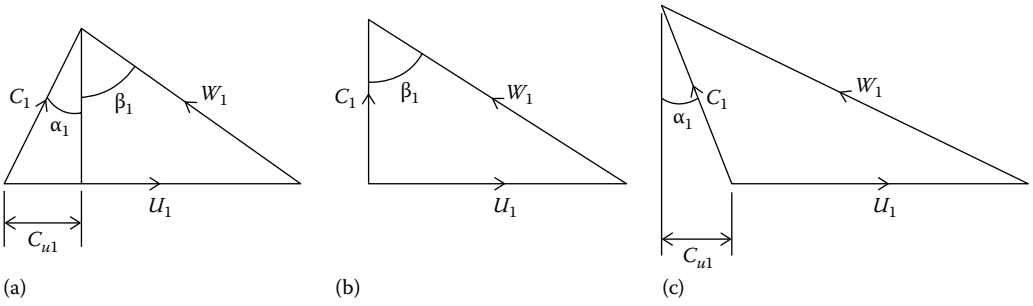


FIGURE 12.12
(a) Positive, (b) negative, and (c) no prewhirl.

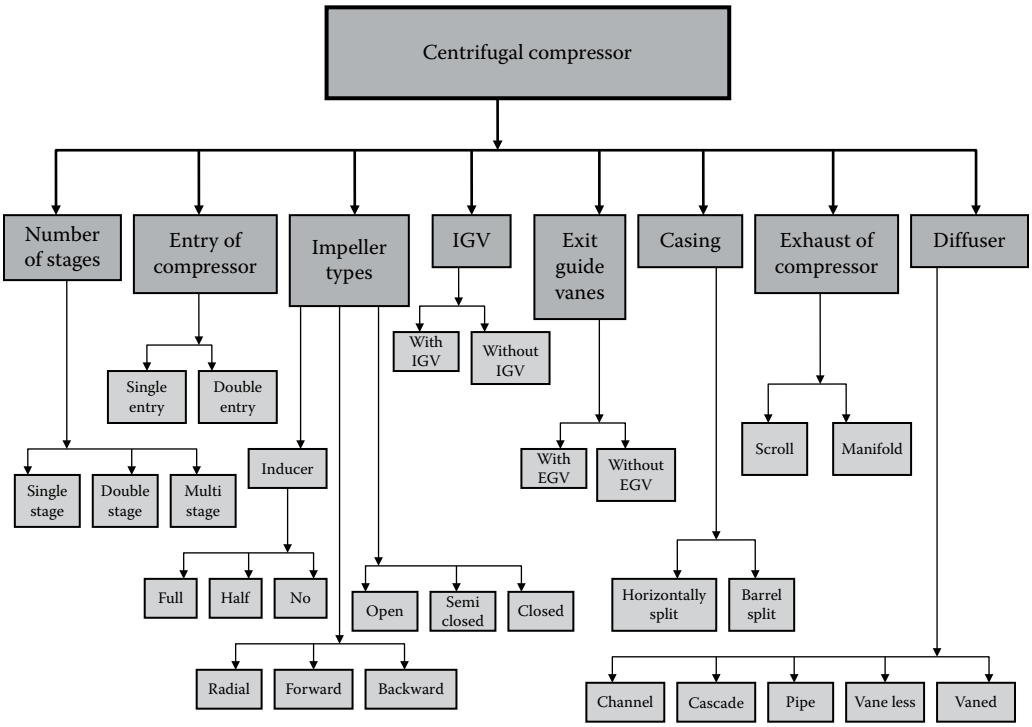


FIGURE 12.13
Classification of centrifugal compressors.

chamber with the minimum ducting losses. The diffuser is either constructed or ended by a 90° bend to satisfy this requirement. If the compressor is used in other industrial applications, then the air leaving the successive passages of the stators is collected in a scroll or volute and ducted from a single pipe.

9. The exit may be fitted with exit-guide vanes or without.
10. The casing of the compressor may be horizontally or vertically split casing or a bell casing.

To conclude this section of classification, a break-down of different classifications is illustrated in Figure 12.13.

12.4 Governing Equations

The thermodynamic state of an ideal fluid is described by two properties, which may be the pressure and the temperature. For fluid in motion, its velocity (magnitude and direction) must also be specified. The centrifugal compressor illustrated in Figure 12.14 defines three states: the impeller inlet (state 1), impeller outlet (state 2), and diffuser outlet (state 3). These states are also plotted on the T–S diagram in Figure 12.15. Each state is defined by two points: the static and total (stagnation) conditions. Thus two pressure lines

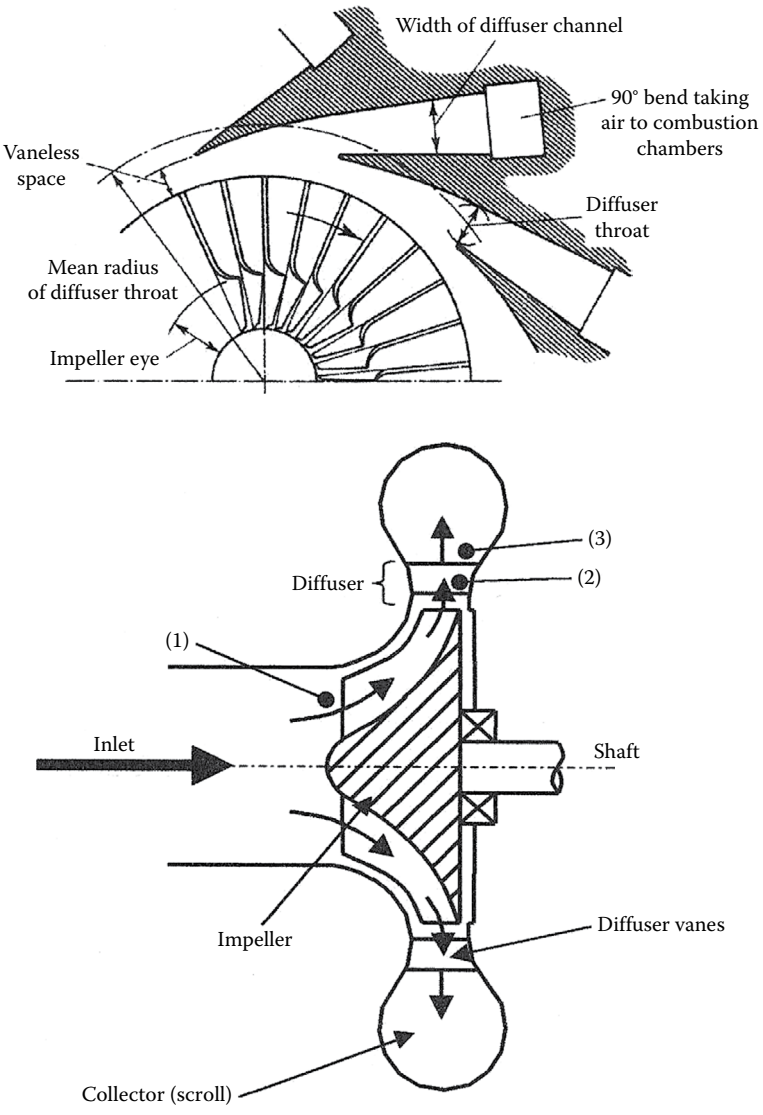


FIGURE 12.14
Layout of centrifugal compressor.

(static and total) are seen for each state. The compression processes are assumed adiabatic irreversible, thus entropy increase is found in each process.

The velocity triangles at the inlet and outlet of the impeller are shown in Figure 12.16. The velocity triangles in any turbomachine are governed by the relation:

$$\vec{C} = \vec{U} + \vec{W} \tag{12.1}$$

where $\vec{C}, \vec{U}$, and $\vec{W}$ are the absolute, rotational, and relative velocities, respectively. As shown in Figure 12.14, the flow at approach to the eye may be axial (C_1) with a typical velocity of 150 m/s for air, or may have a swirl angle (in case of prewhirl as will be discussed later).

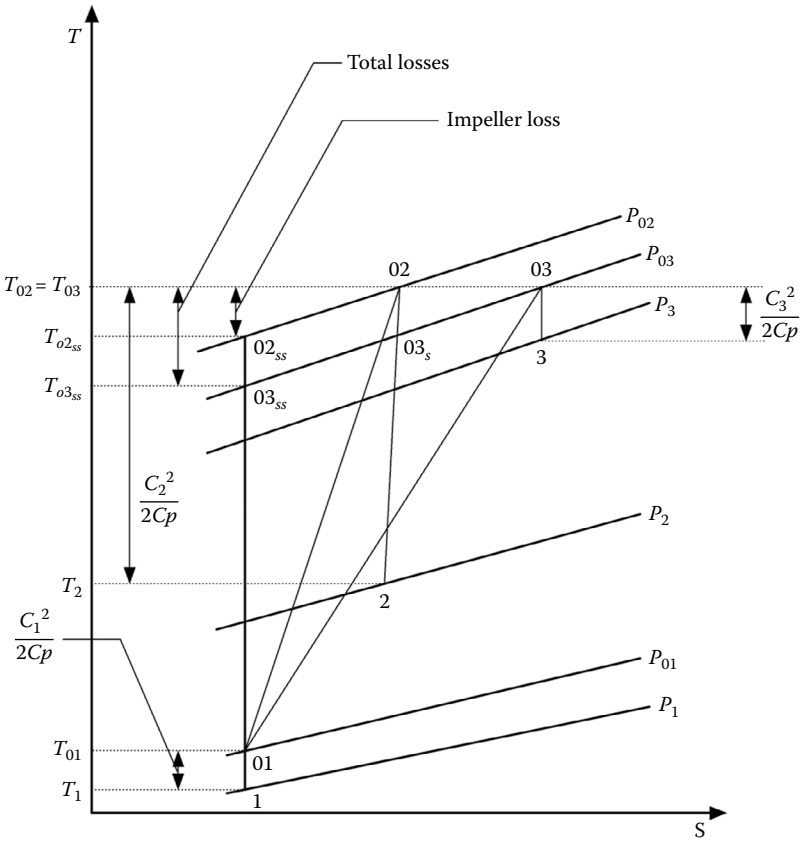


FIGURE 12.15
T–S diagram for a centrifugal compressor.

The flow velocity when added to the impeller tangential (rotational) velocity (U_1) will give the relative velocity (W_1), which varies in magnitude and direction from eye hub to tip since U_1 varies with radii. This requires the inducer vane to be twisted to align with the flow at all radii. It is normal for the relative Mach number at the eye tip to be below 0.9 and falls to below 0.5 for most of the subsequent passage length to minimize frictional losses. This inlet velocity is drawn in the axial- tangential plane. At the impeller outlet, the air leaves the passage with a relative velocity (W_2), which, when added vectorially to the tangential speed (U_2), will give the absolute velocity (C_2) which is greater than (C_1) and represents the effect of work input to the rotor shaft. The tip tangential velocity (U_2) at outlet is slightly greater than the whirl velocity (Cu_2), the difference is called the *slip*. It is interesting to note here that the outlet velocity triangle is at the radial-tangential plane. Thus the inlet and outlet velocity triangle at the inlet and outlet of impeller are in two different planes as shown in Figure 12.16.

Returning to the thermodynamics and velocities at the three states of the compressor

1. State (1)—Impeller inlet:
   a. The static and total temperatures are T_1 and T_{01}. The static and total pressures are P_1 and P_{01}.
   b. The absolute, relative and rotational velocities are: C_1, W_1, and U_1.

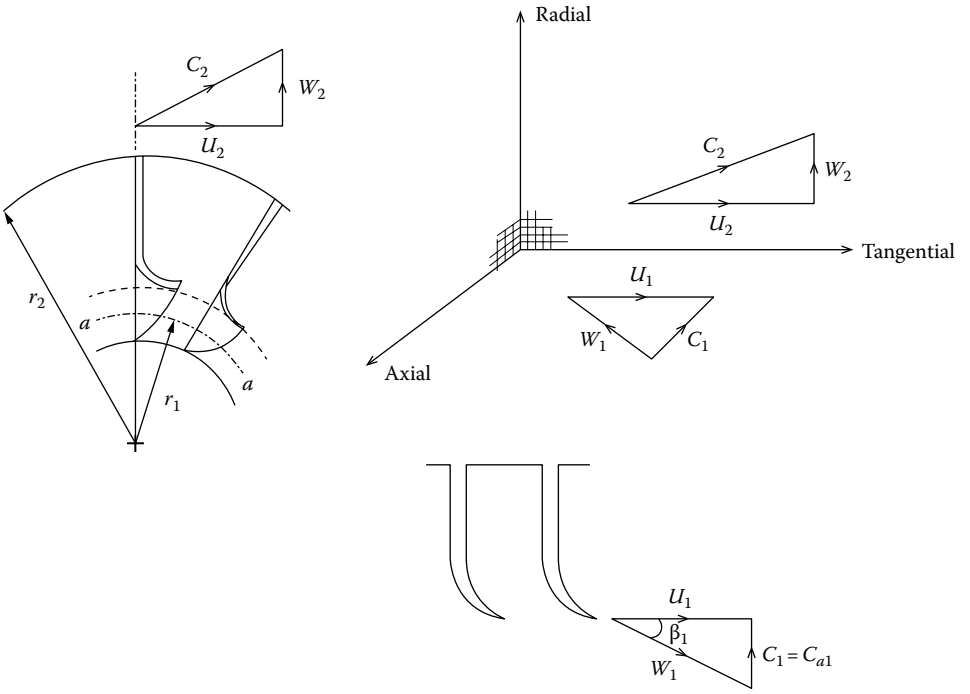


FIGURE 12.16
Inlet and outlet velocity triangles at space.

2. State (2)—Tip (outlet) of impeller:
   a. The static and total temperatures are T_2 and T_{02}. The static and total pressures are P_2 and P_{02}.
   b. The absolute, relative and rotational velocities are $C_2, W_2,$ and U_2, respectively. The relations between inlet and outlet conditions are:

$$P_2 > P_1, \quad T_2 > T_1, \quad C_2 \gg C_1, \quad P_{02} \gg P_{01}, \quad T_{02} \gg T_{01}.$$

   c. Both of the total temperature and total pressure increase as all the energy is added to the air or in general the fluid) in the impeller. Moreover, since the impeller is a rotating diffuser then the static pressure rises while the relative speed decreases ($W_2 < W_1$).
3. State (3)—Stator outlet:
   a. The outlet pressures, temperatures, and absolute velocity are

$$P_3, P_{03}, T_3, T_{03}, \text{and} C_3.$$

   b. The relations between the inlet and outlet conditions in the stator are

$$T_3 > T_3, \quad T_{03} = T_{o2}, \quad P_3 > P_2, \quad P_{o3} < P_{o2}, \quad C_3 < C_2, \quad \left(C_3 \approx C_1\right).$$

In the diffuser, there is merely a conversion of the kinetic energy into pressure energy. Thus, the total temperature at the inlet and outlet of the stator are equal from the first law. The outlet total pressure is less than the inlet total pressure due to friction. The static pressure rises in the diffuser while the absolute velocity decreases as found in any diffusing passage.

The governing equations for a moving fluid are

1. Conservation of mass or continuity equation
2. Momentum equation or Newton's second law
3. Conservation of energy or the first law of thermodynamics

12.4.1 The Continuity Equation

This equation is simply a statement that in steady flow the mass rates of fluid entering and leaving a control volume are identical. Thus, considering a control volume between the impeller inlet (state 1) and outlet (state 2), then the continuity equation is written as follows:

$$\dot{m}_1 = \dot{m}_2$$

Air mass flow rate ($\dot{m}$) at the inlet is

$$\dot{m} = \rho_1 C_{a1} \times \text{inlet area} = \rho_1 C_{a1}\left[\left(\frac{\pi}{4}\right)\left(D_{1t}^2 - D_{1r}^2\right)\right] \tag{12.2}$$

where

ρ_1 and C_{a1} are the density and axial velocity at the inlet section
D_{1r} and D_{1t} are the eye root and tip diameters at inlet

and at the exit it is

$$\dot{m} = \rho_2 C_{r2} A_2 = \rho_2 C_{r2}\left[b\left(\pi D_2 - nt\right)\right] \tag{12.3}$$

where

ρ_2 and C_{r2} are the density and radial velocity at the impeller tip
n is the number of blades
t is the thickness of blade at impeller outlet

12.4.2 The Momentum Equation or Euler's Equation for Turbomachinery

Newton's second law of motion applied to the fluid passing through a control volume states that the rate of change of momentum of the fluid is equal to the net applied force on the fluid in the control volume, or

$$\vec{F} = \frac{d}{dt}\left(m\vec{C}\right)$$

For a steady flow between states 1 and 2, this can be written as

$$\vec{F} = \dot{m}\left(\vec{C}_2 - \vec{C}_1\right)$$

This equation is used to obtain the torque arising from the net force, which is related to the angular momentum of the fluid within the control volume by multiplying the equation by the appropriate radii, thus

$$\vec{T} = \vec{r} \otimes \vec{F} = \dot{m}\left(\vec{r_2} \otimes \vec{C}_2 - \vec{r_1} \otimes \vec{C}_1\right)$$

This vectorial equation is reduced to the following scalar relation for the torque about the axis of rotation

$$T = \dot{m}\left[r_2 C_{u2} - r_1 C_{u1}\right]$$

Or the final form known as Euler's equation is given by the relation

$$T = \dot{m}\left[\left(rC_u\right)_2 - \left(rC_u\right)_1\right] \tag{12.4}$$

where C_{u1} and C_{u2} are the swirl velocities at the inlet and outlet to the impeller. The mean inlet radius and the impeller tip radius are r_1 and r_2, respectively. For the case when the flow enters the impeller axially, there is no swirl velocity at the inlet ($C_{u1} = 0$), then Euler equation is reduced to

$$T = \dot{m} r_2 C_{u2} \tag{12.4a}$$

Since the power is equal to the torque times the rotational speed, then the power P is expressed as

$$P = T \times \omega = \dot{m}\left(\omega r_2\right) C_{u_2} = \dot{m} U_2 C_{u2} \tag{12.5}$$

The power needed to drive the compressor is greater than the power derived that is shown. A part of this power is consumed in overcoming the friction between the casing and the air carried round by the vanes, the disk friction or the windage, and the bearing friction. Thus the power input to the compressor (P_i) is equal to the power derived but multiplied by a power input factor ψ:

$$P_i = \psi P = \psi \dot{m} C_{u2} U_2 \tag{12.6}$$

where $\psi = 1.035 - 1.04$.

12.4.3 The Energy Equation or the First Law of Thermodynamics

The first law of thermodynamics states that the net change of energy of a fluid undergoing any process is equal to the net transfer of work and heat between the fluid and its surroundings.

Thus

$$\frac{\dot{Q}-\dot{W}}{\dot{m}}=\left(h_2-h_1\right)+\frac{1}{2}\left(C_2^2-C_1^2\right)+g\left(z_2-z_1\right)$$

In most turbomachines, the potential energy is negligible. Moreover, turbomachines are adiabatic. Thus the heat term is negligible, by adjusting the sign of the rate of work, then

$$\frac{\dot{W}}{\dot{m}}=\left(h_2+\frac{1}{2}C_2^2\right)-\left(h_1+\frac{1}{2}C_1^2\right)=H_{02}-H_{01}=H_{03}-H_{01}$$

Since the rate of work is the power ($P_i=\dot{W}$), then the left-hand side (LHS), which is the mechanical input power per unit mass flow rate is equal to the enthalpy rise through the compressor. Thus from Equation 12.6

$$Cp\left(T_{03}-T_{01}\right)=\psi C_{u2}U_2$$

The temperature rise in the compressor is then

$$\Delta T_0=T_{03}-T_{01}=\frac{\psi C_{u2}U_2}{Cp} \tag{12.7}$$

The pressure ratio of compressor (π_c) is defined as

$$\pi_c\equiv\frac{P_{03}}{P_{01}}=\left(\frac{T_{03s}}{T_{01}}\right)^{\gamma/\gamma-1}$$

The isentropic efficiency of the compressor is defined as

$$\eta_c=\frac{T_{03s}-T_{01}}{T_{03}-T_{01}}=\frac{T_{01}\left[\left(T_{03s}/T_{01}\right)-1\right]}{T_{03}-T_{01}}$$

The pressure ratio of the compressor is

$$\pi_c\equiv\frac{P_{03}}{P_{01}}=\left[1+\eta_c\frac{T_{03}-T_{01}}{T_{01}}\right]^{\gamma/\gamma-1}$$

Then from Equation 12.4a,

$$\therefore\ \pi_c\equiv\frac{P_{03}}{P_{01}}=\left[1+\eta_c\frac{\psi C_{u2}U_2}{CpT_{01}}\right]^{\gamma/\gamma-1} \tag{12.8}$$

Since in the ideal case

$$U_2=C_{u2}$$

then, the torque-Equation 12.4a will be expressed as

$$T = \dot{m} r_2 U_2$$

The power, from Equation 12.5, is

$$P = \dot{m} U_2^2 \tag{12.5a}$$

The input power, from Equation 12.6, is

$$P_i = \psi P = \psi \dot{m} U_2^2 \tag{12.6a}$$

The temperature rise, from Equation 12.7, is

$$\Delta T_0 = \frac{\psi U_2^2}{Cp} \tag{12.7a}$$

and the pressure ratio, from Equation 12.8a, is

$$\pi_c = \left[1 + \eta_c \frac{\psi U_2^2}{Cp T_{01}} \right]^{\gamma/\gamma - 1} \tag{12.8a}$$

From that relation, it is justified to say that centrifugal compressor has the following performance characteristics, often called "*the three fan laws*":

1. Flow is proportional to impeller speed.
2. Differential pressure across an impeller is proportional to the square of the impeller speed.
3. Power absorbed by the impeller varies with the cube of the impeller speed.

Example 12.1

A two-stage centrifugal compressor as shown in the Figure 12.17 has an overall pressure ratio of π_c. The isentropic efficiencies of both stages are η_1, η_2, respectively. If no losses are assumed in the passage between the two stages, derive a mathematical expression for T_{o3} in terms of π_c, T_{o1}, T_{o6}, η_1, and η_2.

Next, if $\pi_c = 11$, $T_{o1} = 290$ K, $T_{o6} = 660$ K, $\eta_1 = \eta_2 = 0.8$, then calculate T_{o3}.

Solution

The two-stage centrifugal compressor has an overall pressure ratio Π_c, is defined as

$$\Pi_c = \frac{P_{o6}}{P_{o1}} \quad \text{and} \quad \frac{P_{o4}}{P_{o3}} = 1$$

$$\frac{P_{o6}}{P_{o1}} = \frac{P_{o3}}{P_{o1}} \times \frac{P_{o6}}{P_{o4}}$$

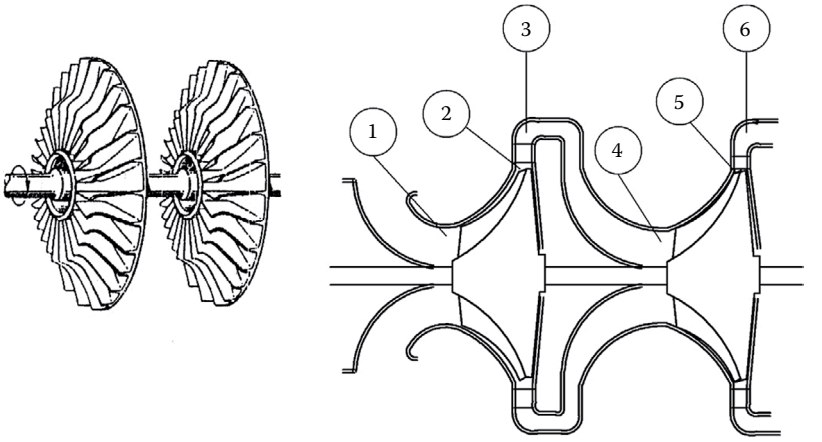


FIGURE 12.17
Two-spool centrifugal compressor.

$$\frac{P_{o3}}{P_{o1}} = \left(1 + \eta_1 \frac{\Delta T_{os1}}{T_{o1}}\right)^{\gamma/\gamma-1}$$

$$\Delta T_{os1} = T_{o3} - T_{o1}$$

$$\frac{P_{o3}}{P_{o1}} = \left(1 + \left[\eta_1 \frac{T_{o3}}{T_{o1}} - 1\right]\right)^{\gamma/\gamma-1}$$

$$\frac{P_{o6}}{p_{o4}} = \left(1 + \eta_2 \frac{\Delta T_{os2}}{T_{o4}}\right)^{\gamma/\gamma-1}$$

$$T_{o4} \equiv T_{o3}$$

$$\Delta T_{os2} = T_{o6} - T_{o4} \equiv T_{o6} - T_{o3}$$

$$\frac{P_{o6}}{P_{o4}} = \left(1 + \eta_2 \left[\frac{T_{o6}}{T_{o3}} - 1\right]\right)^{\gamma/\gamma-1}$$

$$\Pi_c = \frac{P_{o6}}{P_{o1}} = \left(1 + \eta_1 \left[\frac{T_{o3}}{T_{o1}} - 1\right]\right)^{\gamma/\gamma-1} \times \left(1 + \eta_2 \left[\frac{T_{o6}}{T_{o3}} - 1\right]\right)^{\gamma/\gamma-1}$$

$$\Pi_c^{\gamma-1/\gamma} = \left(1 + \frac{T_{o3}}{T_{o1}}\eta_1 - \eta_1\right)\left(1 + \frac{T_{o6}}{T_{o3}}\eta_2 - \eta_2\right)$$

$$\Pi_c^{\gamma-1/\gamma} = 1 + \frac{T_{o6}}{T_{o3}}\eta_2 - \eta_2 + \frac{T_{o3}}{T_{o1}}\eta_1 + \frac{T_{o6}}{T_{o1}}\eta_1\eta_2 - \frac{T_{o3}}{T_{o1}}\eta_1\eta_2 - \eta_1 - \frac{T_{o6}}{T_{o3}}\eta_1\eta_2 + \eta_1\eta_2$$

$$\Pi_c^{\gamma-1/\gamma} = T_{o3}\left(\frac{\eta_1}{T_{o1}} - \frac{\eta_1\eta_2}{T_{o1}}\right) + \frac{1}{T_{o3}}\left(T_{o6}\eta_2 - T_{o6}\eta_1\eta_2\right) + 1 - \eta_1 - \eta_2 + \eta_1\eta_2\left(\frac{T_{o6}}{T_{o1}} + 1\right)$$

$$\Pi_c^{\gamma-1/\gamma} = A_1 T_{o3} + \frac{A_2}{T_{03}} + A_3$$

where

$$A_1 = \frac{\eta_1}{T_{o_1}} - \frac{\eta_1\eta_2}{T_{o_1}}, \quad A_2 = T_{o_6}\eta_2 - T_{o_6}\eta_1\eta_2$$

$$A_3 = 1 - \eta_1 - \eta_2 + \eta_1\eta_2\left(\frac{T_{o_6}}{T_{o_1}} + 1\right)$$

$$\Pi_c^{\gamma-1/\gamma} = \frac{A_1 T_{o_3}^2 + A_2 + A_3 T_{o_3}}{T_{o_3}}$$

$$A_1 T_{o_3}^2 + A_2 + A_3 T_{o_3} = \Pi_c^{\gamma-1/\gamma} T_{o_3}$$

$$T_{o_3}^2 + \left(\frac{A_3 - \Pi_c^{\gamma-1/\gamma}}{A_1}\right) T_{o_3} + \frac{A_2}{A_1} = 0$$

Define:

$$\lambda_1 = \frac{A_3 - \Pi_c^{\gamma-1/\gamma}}{A_1} \quad \text{and} \quad \lambda_2 = \frac{A_2}{A_1}$$

$$T_{o_3} = \frac{-\lambda_1 \pm \sqrt{\lambda_1^2 - 4\lambda_2}}{2} \tag{a}$$

Now substitute the given data in Equation a to get the value of T_{o3}:

$$\Pi_c = 11, \quad T_{o_1} = 290 \text{ K}, \quad T_{o_6} = 660 \text{ K}, \quad \eta_1 = \eta_2 = 0.8$$

The values of the constants are then

$$A_1 = 5.517 \times 10^{-4}, \quad A_2 = 105.6, \quad A_3 = 1.497 \quad \text{and} \quad \Pi_c^{\gamma-1/\gamma} = 1.984$$

$$\frac{\left(A_3 - \Pi_c^{\gamma-1/\gamma}\right)}{A_1} = -882.726 \quad \text{and} \quad \frac{A_2}{A_1} = 19.141 \times 10^4$$

From Equation a, then

$$T_{o_3} = \frac{+882.726 \pm \sqrt{882.726^2 - 4 \times 19.141 \times 10^4}}{2}$$

$$T_{o_3} = 441.363 \pm 58.235$$

$$T_{o_3} = 499.598 \text{ K} \quad \text{or} \quad T_{o_3} = 383.128 \text{ K}.$$

12.4.4 Slip Factor σ

If the flow at impeller discharge is perfectly guided by the impeller blades, then the tangential component of the absolute velocity (swirl velocity) is equal to the rotational velocity ($C_{u2} = U_2$). In practice the flow cannot be perfectly guided by a finite number of blades and it is said to slip. Thus, at the impeller outlet, the swirl velocity is less than the

impeller rotational speed ($C_{u2} < U_2$). The classical explanation for the slip phenomenon [3] uses the concept of the relative eddy. As the flow into the impeller is normally irrotational, that is, it has no initial rotation, then at the impeller discharge the flow relative to the impeller must rotate with an angular velocity equal and opposite to the impeller (Figure 12.18).

By combining this relative eddy and the radial through flow, the resultant relative velocity vector has a component in the opposite direction to the impeller rotation.

The slip factor is denoted by σ and defined as

$$\sigma = \frac{C_{u_2}}{U_2} \tag{12.9}$$

Though Stodola and Busemann derived formulae for this slip factor, the correlation proposed by Staintz [7] has a wide range of application. The Stanitz formula is expressed as

$$\sigma = 1 - \frac{0.63\pi}{n} \tag{12.10}$$

where n is the number of blades. It was considered satisfactory for both radial blades, forward- and backward-leaning blades having blade angles ranging from −45° to +45°. As the number of vanes of impeller is increased, then the slip factor is also increased; slip lag at the tip of the impeller reduces as shown in Figure 12.19.

The effect of slip is to reduce the magnitude of the swirl velocity from the ideal case. This in turn will reduce the pressure ratio. In this way, slip will also reduce the compressor power consumption. The detrimental effect of slip is that the impeller must be larger or the rotational speed must be higher to deliver the same pressure ratio. This leads to an increased stress level; it will also lead to increased relative velocity, which will lead to increased friction loss and a reduced efficiency.

Then from Equation 12.7, the temperature rise will be

$$\Delta T_0 = \frac{\sigma \psi U_2^2}{Cp} \tag{12.7b}$$

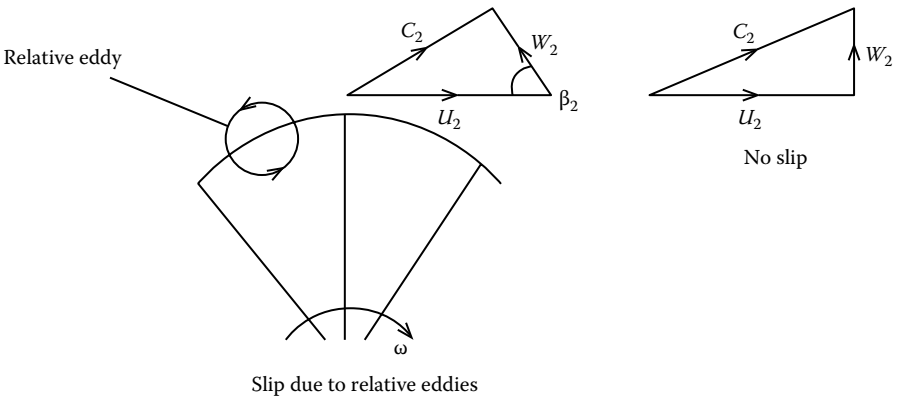


FIGURE 12.18
Velocity triangles with slip.

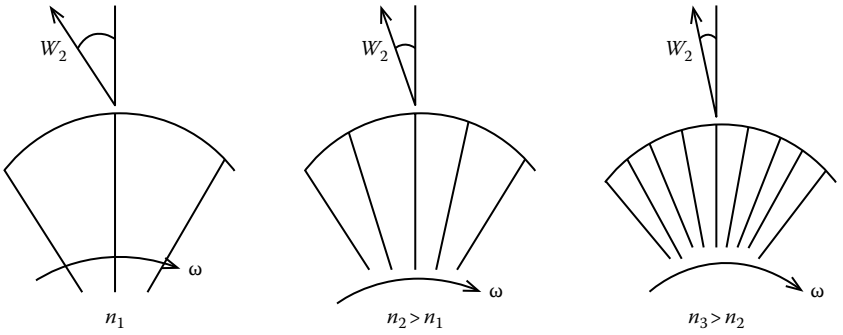


FIGURE 12.19
Effect of the number of blades on the outlet relative velocity.

The pressure ratio will be reduced and has the value

$$\pi_c = \left(1 + \frac{\eta_c \psi \sigma U_2^2}{Cp T_{01}}\right)^{\gamma/\gamma-1} \tag{12.8b}$$

From Equation 12.8b, with $Cp = \dfrac{\gamma R}{\gamma - 1}$ and $a_{01}^2 = \gamma R T_{01}$, then, the pressure ratio can be expressed as

$$\pi_c = \left(1 + \frac{(\gamma - 1)\eta_c \psi \sigma U_2^2}{a_{01}^2}\right)^{\gamma/\gamma-1} \tag{12.8c}$$

where a_{01} is the total sonic speed or the sonic speed referred to the total temperature at the compressor inlet.

Note that when there is no slip, then the slip factor σ is equal to unity and this yields the maximum temperature rise and pressure ratio that may be achieved by this compressor. These values are expressed by the relations

$$(\Delta T_o)_{\max} = \frac{\psi U_2^2}{Cp}$$

$$(\Pi_c)_{\max} = \left(1 + \frac{\eta_c \psi U_2^2}{Cp T_{o_1}}\right)^{\gamma/\gamma-1}$$

Example 12.2

At inlet of a centrifugal compressor eye, the relative Mach number is to be less than 0.97 to eliminate the formation of shock waves and its attendant losses. The hub-to-tip radius ratio of the inducer is 0.4. There is no inlet guide vane and the inlet velocity is axial and uniform over the impeller eye. The eye tip diameter is 20 cm.

Determine

1. The maximum mass flow rate throughout for a given rotational speed of 486 rps.

2. The blade angle at the inducer tip corresponding to this mass flow rate. (Take air inlet conditions to be 101.3 kPa, 288 K.)

Solution

The given data are

$$M_{1_{relt}} = 0.97 \quad \zeta = \frac{r_h}{r_t} = 0.4 \quad D_{e_t} = 20 \text{ cm}$$

$$N = 486 \text{ rps} \quad P_{o_1} = 101.3 \text{ kPa} \quad T_{o_1} = 288 \text{ K}$$

The rotational speed at the inducer tip is

$$U_{1_t} = \pi D_{e_t} N = \pi \times 0.2 \times 486 = 305.363 \text{ m/s}$$

The maximum relative Mach number is at the eye tip; thus,

$$M_{1_{rel}} = \frac{W_{1_t}}{\sqrt{\gamma R T_1}} = \frac{\sqrt{C_1^2 + U_{1_t}^2}}{\sqrt{\gamma R\left(T_{o_1} - \dfrac{C_1^2}{2C_P}\right)}} = \frac{\sqrt{C_1^2 + U_{1_t}^2}}{\sqrt{\gamma R T_{o_1} - \dfrac{(\gamma - 1)C_1^2}{2}}}$$

$$0.97^2 = \frac{C_1^2 + 305.363^2}{115{,}718.4 - 0.2C_1^2}$$

$$C_1^2 + 93{,}246.443 = 108{,}879.44 - 0.19C_1^2$$

$$1.19C_1^2 = 15{,}633$$

The absolute velocity at inlet is

$$C_1 = 114.62 \text{ m/s}$$

$$T_1 = T_{o_1} - \frac{C_1^2}{2C_P} = 281.464 \text{ K}$$

$$\frac{P_{o_1}}{P_1} = \left(\frac{T_{o_1}}{T_1}\right)^{\gamma/\gamma - 1}$$

$$P_1 = 93.48 \text{ kPa}$$

$$\rho_1 = \frac{P_1}{RT_1} = 1.157 \text{ kg/m}^3$$

$$A_1 = \frac{\pi}{4}\left(D_{e_t}^2 - D_{e_r}^2\right) = \frac{\pi}{4} D_{e_t}^2 \left(1 - \zeta^2\right)$$

$$A_1 = 0.0264 \text{ m}^2$$

Since the flow is axial, then $C_{a1} = C_1$. The mass flow rate is calculated from the inlet conditions as

$$\dot{m} = \rho_1 C_{a_1} A_1 = 1.157 \times 114.62 \times 0.0264 = 3.5 \text{ kg/s}$$

The blade inlet angle at the tip β_{1t} is given from the relation

$$\tan\beta_{1_t} = \frac{C_1}{U_{1_t}}$$

$$\beta_{1_t} = 20.57°.$$

12.4.5 Prewhirl

The tangential component of velocity at the inlet to the impeller is usually zero as the flow enters the impeller axially. If prewhirl (or inlet guide) vanes are installed to the inlet duct prior to the impeller, then the incoming air has a tangential component of velocity. This velocity component depends on the vane outlet angle. Prewhirl may be positive or negative as shown in Figure 12.12. Positive prewhirl reduces the inlet relative velocity, while negative prewhirl increases the inlet relative velocity. In aeroengines, positive prewhirl is frequently used to reduce the inlet relative speed. The objective here is to avoid the formation of shock waves on the blade suction side. The designer of a compressor aims for a small inlet area of the engine to reduce the drag force. At the same time the air mass flow rate is chosen as high as possible to maximize the thrust force. Both factors lead to the increase of the axial absolute velocity at inlet, which in turn increases the relative velocity. Since the relative velocity is a maximum at the tip radius of the inlet then when accelerated there is always a tendency for the air to break away from the convex face of the curved part of the impeller vane. Here a shock wave might occur, which upon interaction with the boundary layer over the convex surface of blades causes a large increase in boundary layer thickness. Thus excessive pressure loss occurs.

The value of the inlet relative Mach number must be in the range from 0.8 to 0.85 to avoid the shock wave losses previously described, or

$$M_1 = \frac{W_1}{\sqrt{\gamma R T_1}} \approx 0.8 - 0.85$$

where T_1 is the static inlet temperature. Though this Mach number may be satisfactory on ground operation, it may be too high at altitude as the ambient temperature decreases with altitude. For this reason, inlet guide vanes (IGV) are added to decrease the Mach number. These IGV are attached to the compressor casing to provide a positive prewhirl that decreases the magnitude of the maximum relative velocity (W_1) at the eye tip.

The inlet guide vanes, sometimes denoted as swirl vanes, may swivel about radial axes to vary the swirl angle with speed. Keeping W_1 aligned with the inducer leading edge results in a minimum incidence or shock losses. Thus they widen the operating speed range, increase efficiency and reduce the relative Mach number at the eye tip, but they also reduce the mass flow by reducing the inlet area (Figure 12.20).

Assuming that the axial velocity is uniform from the root to the tip of the eye then the maximum relative Mach number at the eye tip is given by the relation

$$M_{1\max} = \frac{W_{1\max}}{a_1} = \sqrt{\frac{C_{a_1}^2 + \left(U_{1t} - C_{a1}\sin\zeta\right)^2}{\gamma R T_1}} \tag{12.11}$$

where

U_{1t} is the rotational speed at the eye tip

ζ is the prewhirl angle which is the angle between the absolute velocity leaving the IGV and the axial direction

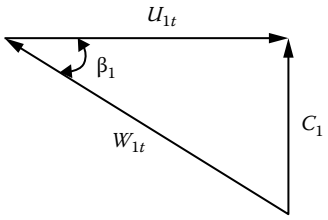


FIGURE 12.20
Inlet velocity triangle at tip.

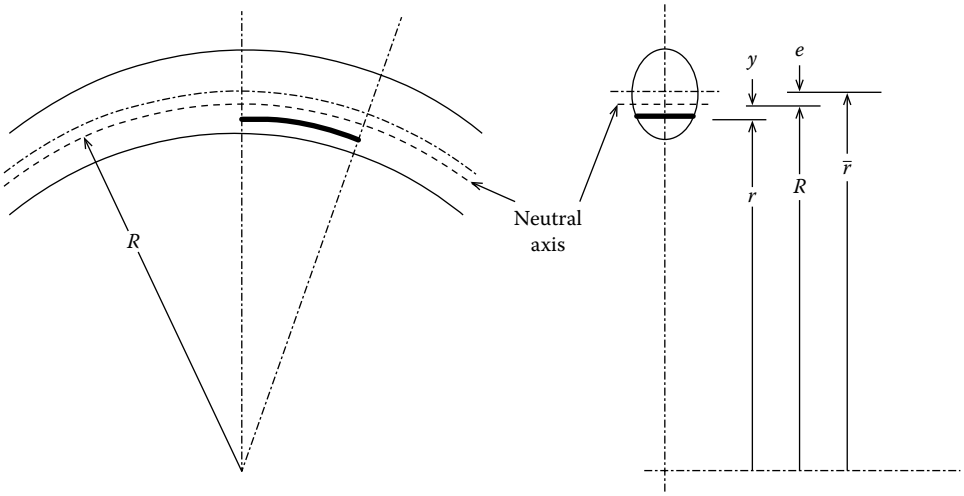


FIGURE 12.21
Curved-beam nomenclature.

Another advantage of the prewhirl is that the curvature of the impeller vanes at the inlet will be reduced and so the radius of curvature will increase. Thus the bending stress is decreased. The reason is that the inducer of the impeller resembles a curved beam (Figure 12.21). The bending stress for curved beams is inversely proportional to the radius of curvature [8]. The bending stress is obtained from the relation

$$\sigma = \frac{My}{Ae(R-y)} \tag{12.12}$$

where

$$e = \bar{r} - R \quad \text{and} \quad R = \frac{A}{\int dA/r}$$

with

M is the bending moment
A is the cross-sectional area
e is the distance from centroidal axis to the neutral axis
R is the radius of the neutral axis
$\bar{r}$ is the radius of centroidal axis
r is the radius of a general point at a distance (y) from the neutral axis at which the stress is to be calculated

The critical stresses occur at the inner and outer surfaces of the curved beam. Since the pressure side here is the concave side of the inducer, then the bending stresses on this side is greater than that on the convex (suction) side. Moreover, prewhirl increases the radius of curvature of the inducer at its inlet ($\bar{r}$), thus the stress decreases (Equation 12.12).

Prewhirl also increases the relative angle (β_1) measured between the relative velocity (W_1) and the tangent. Thus

$$\beta_{1 prewhirl} > \beta_{1 without\ prewhirl}$$

However, prewhirl leads to a decrease in the work-capacity compressor as the angular momentum is reduced leading to a decrease of the pressure ratio of the compressor. Since prewhirl creates a swirl component of the absolute inlet velocity then it reduces the temperature rise in the compressor and also the compressor pressure ratio:

$$\Delta T_0 = \frac{\psi\left(C_{u2}U_2 - C_{u1}U_{1m}\right)}{Cp} \tag{12.13}$$

where $C_{u1} = C_1 \sin\zeta$. Also, U_{1m} is the rotational speed at the mean radius of the eye. The pressure ratio is then

$$\pi_c = \left\{1 + \eta_c \frac{\psi\left[\sigma U_2^2 - U_{1m}C_1 \sin\zeta\right]}{CpT_{01}}\right\}^{\gamma/\gamma-1} \tag{12.14}$$

The previous relations governing the flow in radial compressors can be summarized in Table 12.1.

Further discussions for power input factor, slip factor, and efficiency will be given here:

- Power input factor and slip factor are neither independent of one another, nor of efficiency.
- The *power input factor* represents an increase in the work input shown that is needed for deriving the impeller (rotating element) of the compressor.

TABLE 12.1

Summary of Governing Relations for Radial Impeller

	Ideal No Slip No Inlet Swirl	**Real With Slip No Inlet Swirl**	**Real With Slip With Inlet Swirl**
Temperature rise ΔT_0	$\frac{\psi U_2^2}{Cp}$ Maximum value	$\frac{\psi\sigma U_2^2}{Cp}$	$\frac{\psi\left\{\sigma U_2^2 - (UC_u)_1\right\}}{Cp}$ Minimum value
Pressure ratio π_c	$\left(1 + \eta_c \frac{\psi U_2^2}{CpT_{01}}\right)^{\gamma/\gamma-1}$ Maximum value	$\left(1 + \eta_c \frac{\psi\left\{(UC_u)_2\right\}}{CpT_{01}}\right)^{\gamma/\gamma-1}$	$\left(1 + \eta_c \frac{\psi\left\{(UC_u)_2 - (UC_u)_1\right\}}{CpT_{01}}\right)^{\gamma/\gamma-1}$ Minimum value
Torque T	$\dot{m}r_2U_2$ Maximum value	$\dot{m}r_2C_{u2}$	$\dot{m}\left(r_2C_{u2} - r_1C_{u1}\right)$ Minimum value
Consumed power $\mathscr{P}$	$\dot{m}U_2^2$ Maximum value	$\dot{m}U_2C_{u2}$	$\dot{m}\left(U_2C_{u2} - U_1C_{u1}\right)$ Minimum value
Input power $\mathscr{P}_i$	$\dot{m}\psi U_2^2$ Maximum value	$\dot{m}\psi U_2C_{u2}$	$\dot{m}\psi\left(U_2C_{u2} - U_1C_{u1}\right)$ Minimum value

- This increase is absorbed in overcoming frictional loss and therefore degraded into thermal energy.
- Power input factor should be as close as possible to unity.
- Low values of power input factor imply that the impeller is very efficient.
- However, the value of compressor efficiency also depends on friction losses in the diffuser, which do not affect power input factor.
- The *slip factor* limits the capacity of the compressor and this should be as high as possible.
- A high value of slip factor requires a higher number of vanes.
- A higher number of vanes will increase frictional losses and hence increase the value of power input factor and decrease the value of *efficiency*.
- A suitable compromise must be found, and present day practice is 19–34 vanes to get a slip factor value of 0.9.

Finally, it is worth mentioning that an efficient compressor may be better than a compact compressor. Moreover, historically, trends showed that its value was 70% in 1950, raised to 75% in 1960, then to 82% in 1980, that it reached 85% in 2000, and finally scored 87% by 2010. Its projected value is 90% in 2040.

Example 12.3

An aircraft engine is fitted with a single-sided centrifugal compressor. The aircraft flies at a Mach number 0.85 and altitude of 35,000 ft. The inlet duct of the impeller is fitted with inlet guide vanes. The hub and shroud diameters of the eye are 14 cm and 28 cm, respectively, and the rotational speed is 270 rev/s. Estimate the prewhirl angle if the mass flow is 3.6 kg/s and the maximum relative inlet Mach number is 0.8.

Solution

The given data are

$$d_{eh} = 14 \text{ cm} \quad d_{et} = 28 \text{ cm} \quad N = 270 \text{ rps} \quad \dot{m} = 3.6 \text{ kg/s}$$

At altitude 35,000 ft, the ambient conditions are

$$P_a = 23.844 \text{ kPa} \quad T_a = 218.67 \text{ K}$$

$$T_{o1} = T_a\left[1 + \frac{\gamma - 1}{2} M_{flight}^2\right]$$

$$T_{o1} = 218.67\left[1 + \frac{0.4}{2}(0.85)^2\right] = 250.67 \text{ K}$$

$$P_{o1} = P_a\left(\frac{T_{o1}}{T_a}\right)^{\gamma/\gamma-1} = 23,844.24\left(\frac{250.27}{218.67}\right)^{\frac{1.4}{0.4}} = 38,243 \text{ Pa}$$

$$U_{1t} = \pi D_t \frac{N}{60}$$

$$U_{1t} = \pi \times 0.28 \times 270 = 237.5 \text{ m/s}$$

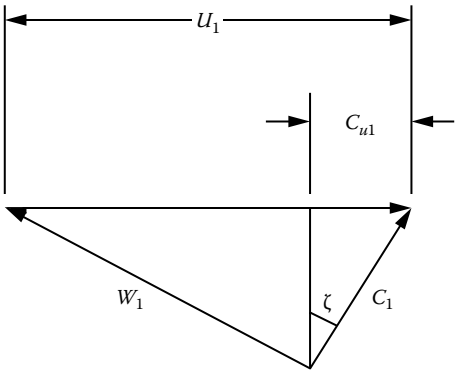


FIGURE 12.22
Velocity triangle at inlet with slip.

$$M_{1_t} = \frac{W_{1_T}}{\sqrt{\gamma R T_1}}$$

$$W_{1_t}^2 = M_{1_t}^2 \gamma R T_1$$

From Figure 12.22, the velocity triangle at inlet with slip

$$C_{a1}^2 + \left(U_{1_t} - C_{a1}\tan\zeta\right)^2 = M_{1_t}^2 \gamma R T_1$$
$$\left(U_{1_t} - C_{a1}\tan\zeta\right)^2 = M_{1_t}^2 \gamma R T_1 - C_{a1}^2$$
$$U_{1_t} - C_{a1}\tan\zeta = \sqrt{M_{1_t}^2 \gamma R T_1 - C_{a1}^2}$$
$$C_{a1}\tan\zeta = U_{1_t} = -\sqrt{M_{1_t}^2 \gamma R T_1 - C_{a1}^2}$$

$$\tan\zeta = \frac{U_{1_t}}{C_{a1}} - \sqrt{\frac{M_{1_t}^2 \gamma R T_1}{C_{a1}^2} - 1}$$
$$\zeta = \tan^{-1}\left(\frac{U_{1_t}}{C_{a1}} - \sqrt{\frac{M_{1_t}^2 \gamma R T_1}{C_{a1}^2} - 1}\right)$$
$$\zeta = \tan^{-1}\left(\frac{237.5}{C_{a1}} - \sqrt{\frac{(0.8)^2 \times 1.4 \times 287 T_1}{C_{a1}^2} - 1}\right)$$
$$\zeta = \tan^{-1}\left(\frac{237.5}{C_{a1}} - \sqrt{\frac{257.15 T_1}{C_{a1}^2} - 1}\right)$$

$$A_1 = \frac{\pi}{4}\left(D_t^2 - D_h^2\right) = \frac{\pi}{4}\left[(0.28)^2 - (0.14)^2\right] = 0.0461814 \text{ m}^2$$

As a first assumption, calculate the inlet density from the total temperature and pressure; thus,

$$\rho_1 = \frac{P_{o1}}{RT_{o1}} = \frac{38,243}{287 \times 250.27} = 0.532428461 \text{ kg/m}^3 \qquad \text{(a)}$$

Calculate now the axial inlet velocity:

$$C_{a1} = \frac{\dot{m}}{\rho_1 A_1} = \frac{3.5}{0.53242861 \times 0.0461814} = 142.344 \text{ m/s}$$

The prewhirl angle is now calculated from the relation

$$\zeta = \tan^{-1}\left(\frac{237.5}{C_{a1}} - \sqrt{\frac{257.15 T_{01}}{C_{a1}^2} - 1} \right)$$

$$\zeta = \tan^{-1}\left(\frac{237.5}{142.344} - \sqrt{\frac{257.15 \times 250.27}{(142.344)^2} - 1} \right) = 10.94^\circ$$

The inlet absolute velocity is now calculated as

$$C_1 = \frac{C_{a1}}{\cos\zeta} = \frac{142.244}{\cos 10.94} = 144.98 \text{ m/s}$$

The static inlet temperature is

$$T_1 = T_{01} - \frac{C_1^2}{2C_p} = 250.27 - \frac{(144.98)^2}{2 \times 1005} = 239.81 \text{ K}$$

The static inlet pressure is calculated as

$$P_1 = P_{01}\left(\frac{T_1}{T_{01}} \right)^{\gamma/\gamma - 1} = 32{,}840.86 \text{ Pa}$$

The density is recalculated from the static temperature and pressure just obtained as

$$\rho_1 = \frac{P_1}{RT_1} = 0.47755 \text{ kg/m}^3 \tag{b}$$

A large difference is noticed between this value and the value obtained in Equation a, thus iteration is performed until equal values for the density is obtained in two successive iterations as shown in Table 12.2.

Eleven iterations were needed for convergence. Only some were displayed in the figure shown. The final results are

$$C_{a1} = 167.04 \text{ m/s}, \quad \zeta = 18.94^\circ, \quad C_1 = 176.6 \text{ m/s}$$

$$P_1 = 30{,}567 \text{ Pa}, \quad T_1 = 234.75 \text{ K}, \quad \rho_1 = 0.4537 \text{ kg/m}^3$$

Example 12.4

To examine how prewhirl reduces the bending stress for the blades of centrifugal compressors, consider the following case where the blade shape at tip of the eye is shown in Figure 12.23 for the two cases with prewhirl and without prewhirl.

$$r_i)_{Prewhirl} = 15 \text{ cm}, \quad r_i)_{no\,Prewhirl} = 5 \text{ cm}, \quad t = 0.4 \text{ cm}, \quad A = 0.4 \text{ cm}^2$$

If the bending moment $M = 10.0 \text{ N} \cdot \text{m}$, calculate the maximum stresses in both cases and the percentage of stress reduction when prewhirl is employed.

TABLE 12.2

Iteration Procedure

Iteration No.	**1**	**2**	**10**	**11**
$C_{a1} = \dfrac{\dot{m}}{\rho_1 A_1}$	142.344	158.702	167.04	167.04
$\zeta = \tan^{-1}\left(\dfrac{237.5}{C_{a1}} - \sqrt{\dfrac{257.15T_1}{C_{a1}^2} - 1}\right)$	13.44	16.375	18.9395	18.94
$C_1 = \dfrac{C_{a1}}{\cos\zeta}$	146.35	165.411	176.6	176.6
$T_1 = T_{01} - \dfrac{C_1^2}{2C_p}$	239.614	236.66	234.754	234.75
$P_1 = P_{01}\left(\dfrac{T_1}{T_{01}}\right)^{\gamma/\gamma-1}$	32,840.86	31,444.4	30,567.98	30,567.8
$\rho_1 = \dfrac{P_1}{RT_1}$	0.47755	0.46295	0.453703	0.4537

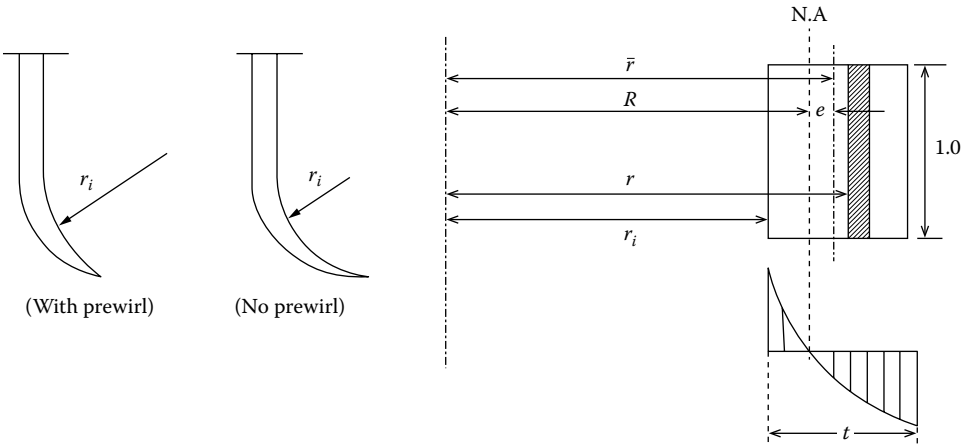


FIGURE 12.23
Stresses over the section of a curved beam of the impeller with prewhirl.

Solution

The stress in such curved beams is given by

$$\sigma = \frac{My}{Ae(R-y)}$$

where $R = A/(\int dA/r)$ is the radius of the neutral axis, which is here for a rectangular cross-section is expressed by

$$R = \frac{t}{\ln\left(1+\dfrac{t}{r_i}\right)} \quad \text{and} \quad e = \bar{r} - R$$

TABLE 12.3

Results for Cases of Prewhirl and No Prewhirl

	No Prewhirl	**With Prewhirl**
$R = t/\ln\left(1+\frac{t}{r_i}\right)$	5.1974 cm	15.199 cm
$e = \bar{r} - R$	2.565×10^{-3} cm	0.001 cm
$y_{inner} = R - r_i$	0.1974 cm	0.199 cm
$r_{inner} = R - y$	5.0 cm	15.0 cm
$\sigma = \frac{My}{Ae(R-y)}$	384.8 MPa	331.6 MPa

$\bar{r}$ is the radius of the center of gravity of the section,

$$\bar{r} = r_i + \frac{t}{2}$$

$$r = R - y$$

r is any radius defining any point within the rectangular cross section.

Since the maximum stress occurs at the point having minimum radius, then the critical point is at the concave side of the blades ($r = r_i$).

Calculation for the two cases will be summarized in Table 12.3.

These results show that prewhirl reduced the maximum stresses by a percentage of 13%.

Example 12.5

A centrifugal compressor has the following data:

$$D_{eh} = 0.12 \text{ m}, \quad D_{et} = 0.24 \text{ m}, \quad D_t = 0.5 \text{ m}$$

$$C_1 = 100 \text{ m/s}, \quad N = 300 \text{ rev/s}, \quad T_{01} = 300 \text{ K}$$

$$\psi = 1.04, \quad \sigma = 0.92, \quad \eta_c = 0.85$$

Now inlet guide vanes are added upstream to the compressor. Two designs are suggested:

1. Inlet guide vanes having constant prewhirl angle ($\zeta = 25°$)
2. Inlet guide vanes having constant inlet relative angle (β_1) as its value at the hub if no prewhirl is employed

Assuming that the axial velocity is kept constant and equal to 100 m/s, it is required in the following three cases:

1. No prewhirl
2. Design (A)
3. Design (B)
   a. Calculate the inlet relative Mach number (M_{1rel}) at the hub, mean, and tip sections of the eye.
   b. Calculate the compressor pressure ratio.
   c. Write down your comments and suggestions.

Solution

$$U_{1h} = \pi D_{eh} \frac{N}{60} = \pi \times 0.12 \times 300 = 113.1 \text{ m/s}$$

$$U_{1m} = \pi D_{em} \frac{N}{60} = \pi \times 0.18 \times 300 = 169.65 \text{ m/s}$$

$$U_{1t} = \pi \times D_{et} \frac{N}{60} = \pi \times 0.24 \times 300 = 226.2 \text{ m/s}$$

$$U_2 = \pi \times D_{et} \frac{N}{60} = \pi \times 0.5 \times 300 = 471.24 \text{ m/s}$$

Case (*A*) *No prewhirl* (Figure 12.24)

$$T_1 = T_{o1} - \frac{C_1^2}{2C_P} = 300 - \frac{(100)^2}{2 \times 1005} = 295 \text{ K}$$

1. At the hub

$$W_{1h} = \sqrt{U_{1h}^2 + C_a^2}$$
$$W_{1h} = \sqrt{(113.1)^2 + (100)^2} = 150.97 \text{ m/s}$$

$$(M_{1_{rel}})_h = \frac{W_{1h}}{\sqrt{\gamma R T_1}} = \frac{150.97}{\sqrt{1.4 \times 287 \times 295}} = 0.4385$$

$$\tan \beta_{1h} = \frac{C_a}{U_{1h}} = \frac{100}{113.1} \quad \beta_{1h} = 41.48$$

2. At the mean

$$W_{1m} = \sqrt{U_{1m}^2 + C_a^2}$$
$$W_{1m} = \sqrt{(169.65)^2 + (100)^2} = 196.93 \text{ m/s}$$

$$M_{1_{rel}})_m = \frac{W_{1m}}{\sqrt{\gamma R T_1}} = \frac{196.93}{\sqrt{1.4 \times 287 \times 295}} = 0.572$$

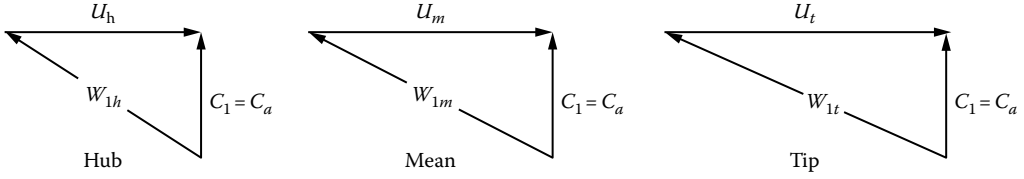


FIGURE 12.24
Velocity triangles with no prewhirl.

3. At the tip

$$W_{1t} = \sqrt{U_{1t}^2 + C_a^2}$$
$$W_{1t} = \sqrt{(226.2)^2 + (100)^2} = 247.32 \text{ m/s}$$

$$M_{1_{rel}})_t = \frac{W_{1t}}{\sqrt{\gamma R T_1}} = \frac{247.32}{\sqrt{1.4 \times 287 \times 295}} = 0.7184$$

$$\pi_c = \frac{P_{o3}}{P_{o3}} = \left(1 + \eta_c \frac{\sigma U_2^2 - U_1 C_{u1}}{C_P T_{o1}}\right)^{\gamma/\gamma - 1}$$

$$\pi_c = \left(1 + 0.85 \frac{0.92 \times (471.24)^2 - 0}{1005 \times 300}\right)^{1.4/0.4} = 4.914$$

Case (*B*) *Constant prewhirl angle* ($\zeta = 25$) (Figure 12.25)

Since the same axial velocity is kept constant in all cases then

$$C_1 = \frac{C_a}{\cos\zeta} = \frac{100}{\cos 25} = 110.34 \text{ m/s}$$

$$T_1 = T_{01} - \frac{C_1^2}{2C_P} = 300 - \frac{(110.34)^2}{2 \times 1005} = 293.94 \text{ K}$$

1. At the hub

$$C_{u1h} = C_a \tan\zeta = 100 \tan 25 = 46.63 \text{ m/s} = C_{u1m} = C_{u1h}$$

Note that $C_{u1h} = C_{u1m} = C_{u1t}$

$$W_{1h} = \sqrt{(U_{1h} - C_{u1h})^2 + C_a^2}$$
$$W_{1h} = \sqrt{(113.1 - 46.63)^2 + (100)^2} = 120.07 \text{ m/s}$$

$$M_{1_{rel}})_h = \frac{W_{1h}}{\sqrt{\gamma R T_1}} = \frac{120.07}{\sqrt{1.4 \times 287 \times 293.94}} = 0.3494$$

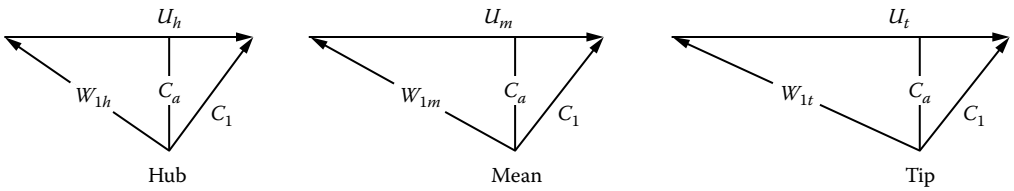


FIGURE 12.25
Velocity triangles with constant prewhirl angle.

2. At the mean

$$W_{1m} = \sqrt{\left(U_{1m} - C_{u1m}\right)^2 + C_a^2}$$
$$W_{1m} = \sqrt{\left(169.65 - 46.63\right)^2 + \left(100\right)^2} = 158.54 \text{ m/s}$$

$$M_{1_{rel}})_m = \frac{W_{1m}}{\sqrt{\gamma R T_1}} = \frac{158.54}{\sqrt{1.4 \times 287 \times 293.94}} = 0.4613$$

3. At the tip

$$W_{1t} = \sqrt{\left(U_{1t} - C_{u1t}\right)^2 + C_a^2}$$
$$W_{1t} = \sqrt{\left(226.2 - 46.63\right)^2 + \left(100\right)^2 = 205.54 \text{ m/s}}$$

$$M_{1_{rel}})_t = \frac{W_{1t}}{\sqrt{\gamma R T_1}} = \frac{205.54}{\sqrt{1.4 \times 287 \times 293.94}} = 0.598$$

$$\pi_c = \frac{P_{o3}}{P_{o3}} = \left(1 + \eta_c \frac{\sigma U_2^2 - U_1 C_{u1}}{C_P T_{o1}}\right)^{\gamma/\gamma - 1}$$
$$\pi_c = \left(1 + 0.85 \frac{0.92 * \left(471.24\right)^2 - 169.65 * 46.63}{1005 * 300}\right)^{1.4/0.4} = 4.6747$$

Case (C) *Constant inlet relative angle* ($\beta_1 = 41.48$) Figure 12.26

1. At the hub

$$T_1 = T_{01} - \frac{C_1^2}{2C_P} = 300 - \frac{\left(100\right)^2}{2 * 1005} = 295 \text{ K}$$

$$W_{1h} = \sqrt{U_{1h}^2 + C_a^2}$$
$$W_{1h} = \sqrt{\left(113.1\right)^2 + \left(100\right)^2} = 150.97 \text{ m/s} = W_{1m} = W_{1t}$$

$$M_{1_{rel}})_h = \frac{W_{1h}}{\sqrt{\gamma R T_1}} = \frac{150.97}{\sqrt{1.4 \times 287 \times 295}} = 0.4385$$

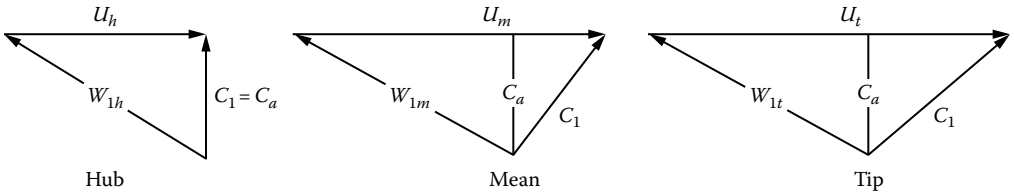


FIGURE 12.26
Velocity triangles with constant inlet relative angle.

2. At the mean

$$C_{u1})_m = U_m - U_h = 169.65 - 113.1 = 56.55$$

$$C_{1m} = \sqrt{C_{u1m}^2 + C_a^2} = \sqrt{(56.55)^2 + (100)^2} = 114.88 \text{ m/s}$$

$$T_1 = T_{01} - \frac{C_1^2}{2C_P} = 300 - \frac{(114.88)^2}{2 * 1005} = 293.43 \text{ K}$$

$$M_{1_{rel}})_m = \frac{W_{1m}}{\sqrt{\gamma R T_1}} = \frac{150.97}{\sqrt{1.4 \times 287 \times 293.43}} = 0.4397$$

3. At the tip

$$C_{u1})_t = U_t - U_h = 226.2 - 113.1 = 113.1 \text{ m/s}$$

$$C_{1t} = \sqrt{C_{u1t}^2 + C_a^2} = \sqrt{(113.1)^2 + (100)^2} = 150.96 \text{ m/s}$$

$$T_1 = T_{01} - \frac{C_1^2}{2C_P} = 300 - \frac{(150.96)^2}{2 \times 1005} = 288.66 \text{ K}$$

$$M_{1_{rel}})_t = \frac{W_{1t}}{\sqrt{\gamma R T_1}} = \frac{150.97}{\sqrt{1.4 \times 287 \times 288.66}} = 0.4433$$

$$\pi_c = \frac{P_{03}}{P_{01}} = \left(1 + \eta_c \frac{\sigma U_2^2 - \overline{U_1 C_{u1}}}{C_P T_{01}}\right)^{\gamma/\gamma - 1}$$

$$\overline{U_1 C_{u1}} = \frac{\int_{r_h}^{r_t} U C_u \, dr}{r_t - r_h} = \frac{\int_{r_h}^{r_t} \omega r C_u \, dr}{r_t - r_h}$$

but $C_u = U - C_a \tan\beta$ or $C_u = U - A$

$$\overline{U_1 C_{u1}} = \frac{\omega \int_{r_h}^{r_t} r(U - A) \, dr}{r_t - r_h} = \frac{\omega \int_{r_h}^{r_t} r(\omega r - A) \, dr}{r_t - r_h}$$

$$\overline{U_1 C_{u1}} = \frac{\omega \int_{r_h}^{r_t} (\omega r^2 - Ar) \, dr}{r_t - r_h}$$

$$\overline{U_1 C_{u1}} = \frac{\omega}{r_t - r_h} \left[\omega \frac{r^3}{3} - A \frac{r^2}{2}\right]_{r_h}^{r_t}$$

$$\overline{U_1 C_{u1}} = \frac{\omega}{r_t - r_h} \left[\frac{\omega}{3}(r_t^3 - r_h^3) - \frac{A}{2}(r_t^2 - r_h^2)\right]$$

$$\overline{U_1 C_{u1}} = \omega \left[\frac{\omega}{3}(r_t^2 + r_t r_h + r_h^2) - \frac{A}{2}(r_t + r_h)\right]$$

$$\overline{U_1 C_{u1}} = \frac{1}{6}\left[2U_t^2 + 2U_t U_h + 2U_h^2 - 3AU_t - 3AU_h\right]$$

$$\overline{U_1 C_{u1}} = \frac{1}{6}\left[2U_t(U_t - A) + 2U_h(U_h - A) + U_t(U_h - A) + U_h(U_t - A)\right]$$

$$\overline{U_1 C_{u1}} = \frac{1}{6}\left[2U_t C_{ut} + 2U_h C_{uh} + U_t C_{uh} + U_h C_{ut}\right]$$

TABLE 12.4

Variation of Mach Number and Pressure Ratio for Different Design Methods

	$M_{1_{rel}})_h$	$M_{1_{rel}})_m$	$M_{1_{rel}})_t$	π_c
No prewhirl	0.4385	0.572	0.7184	4.914
Constant prewhirl angle ($\zeta = 25$)	0.3494	0.4613	0.598	4.6747
Constant inlet relative angle ($\beta_1 = 41.48$)	0.4385	0.4397	0.4433	4.5936

But $C_{uh} = 0$

$$\therefore \overline{U_1 C_{u1}} = \frac{1}{6}\left[2U_t C_{ut} + U_h C_{ut}\right]$$

$$= \frac{1}{6}\left[2 \times 226.2 \times 113.1 + 113.1 \times 113.1\right] = 10{,}659.675 \ \left(\text{m/s}\right)^2$$

$$\pi_c = \left(1 + \eta_c \frac{\sigma U_2^2 - \overline{U_1 C_{u1}}}{C_P T_{01}}\right)^{\gamma/\gamma - 1}$$

$$\pi_c = \left(1 + 0.85 \frac{0.92\left(471.24\right)^2 - 10{,}659.675}{1{,}005 \times 300}\right)^{1.4/0.4} = 4.5936$$

Table 12.4 shows that the selection will be in favor of the constant relative angle (β) as it achieves the lowest relative Mach number at tip. Moreover, the pressure ratio is close to the constant prewhirl angle (ζ).

12.4.6 Types of Impeller

As described previously, the impeller may be shrouded or unshrouded. In general, shrouded impellers are common with multi-stage configuration. A shroud fixed to the impeller reduces the axial load on the thrust bearing and may be very important in high-pressure applications. However, the shroud complicates the design of the impeller and increases its mass, which means that lower peripheral speeds are required for stress reasons. For steel impellers in industrial applications, the maximum tip speed for shrouded impellers is 300–360 m/s while for unshrouded it is 380–430 m/s [9].

The impeller may have full-, half-, or no-inducer at inlet as classified previously. The inducer improves the aerodynamic performance [9]. For the impeller of Eckardt, the inducer is capable of increasing the maximum mass flow rate. For a compressor without inducer running at 16,000 rev/min, the flow appears choked at 6 kg/s, whereas the same-sized machine with an inducer is able to pass 7 kg/s with no sign of choking [9].

The impeller may also be classified based on blading into three types: straight radial, forward leaning, or backward leaning. Figure 12.11 shows the three types schematically, together with typical velocity triangles in the radial plane for the outlet of each type. The three velocity triangles have the same rotational speed U_2 and same radial velocity component $C_r = W_r$. As a first approximation assume that the relative fluid velocity leaving the impeller W_2 is assumed parallel to the blade. The angle of the blade at exit with respect to the radial direction is denoted by β_2', and is positive for a backward-leaning blade (Figure 12.27). On the same figure, the velocity triangles for radial impeller with and without slip are shown.

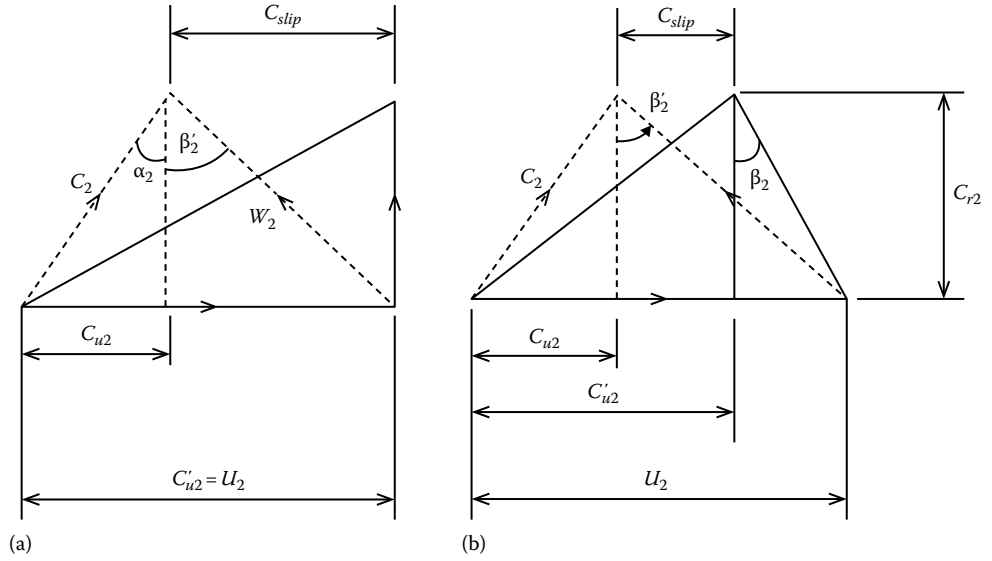


FIGURE 12.27
Slip for (a) radial and (b) backward impellers.

The swirl (or tangential) component of the absolute velocity is

$$C_{u2} = U_2 - W_{u2} \tan \beta_2' \tag{12.15}$$

From Equation 12.13,

$$\frac{T_{03} - T_{01}}{T_{01}} = \frac{\Delta T_0}{T_{01}} = \frac{(C_{u2}U_2 - C_{u1}U_{1m})}{CpT_{01}}$$

$$\frac{T_{03} - T_{01}}{T_{01}} = \frac{(\gamma - 1)(C_{u2}U_2 - C_{u1}U_{1m})}{\gamma RT_{01}} = \frac{(\gamma - 1)U_2^2}{a_{01}^2}\left[\frac{C_{u2}}{U_2} - \left(\frac{U_1}{U_2}\right)^2 \frac{C_{u1}}{U_1}\right]$$

$$\frac{T_{03} - T_{01}}{T_{01}} = (\gamma - 1)\left(\frac{U_2}{a_{01}}\right)^2 \left[\frac{C_{u2}}{U_2} - \left(\frac{r_1}{r_2}\right)^2 \frac{C_{u1}}{U_1}\right]$$

If the flow enters the impeller axially then $C_{u1} = 0$, and the temperature relation shown is expressed as

$$\frac{T_{03} - T_{01}}{T_{01}} = (\gamma - 1)\left(\frac{U_2}{a_{01}}\right)^2 \frac{C_{u2}}{U_2} = (\gamma - 1)\left(\frac{U_2}{a_{01}}\right)^2 \left(1 - \frac{W_{r2}}{U_2} \tan \beta_2'\right) \tag{12.16}$$

$$\frac{T_{03} - T_{01}}{(\gamma - 1)\left(\frac{U_2}{a_{01}}\right)^2 T_{01}} = \left(1 - \frac{W_{r2}}{U_2} \tan \beta_2'\right) \tag{12.16a}$$

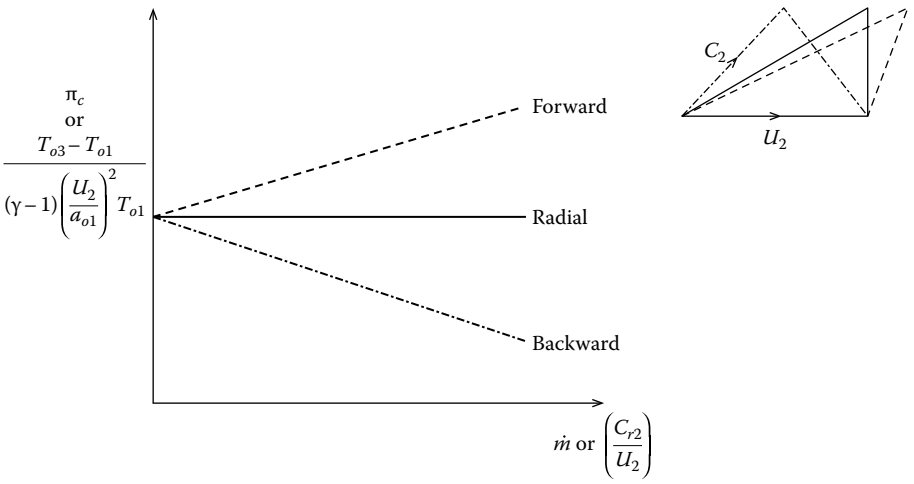
From Equation 12.3, neglecting the blade thickness (t), thus

$$W_{r2} = \frac{\dot{m}}{\pi \rho_2 b D_2} \tag{12.17}$$

The variable $(T_{03} - T_{01})/(\gamma - 1)(U_2/a_{01})^2 T_{01}$ represents the relative stage temperature rise and consequently an index for pressure ratio, while the variable W_{r2}/U_2 (which is equivalent to C_{r2}/U_2) represents the mass-flow parameter for a certain rotational speed. Plotting relation (12.15) yields a straight line provided that the blade angle β_2' is constant (Figure 12.28). At the same mass flow rate and tip speed, U_2, the rotor with *forward-leaning* blades will do more work on the fluid. At first sight, it might be expected to produce the highest pressure ratio compared to the radial or backward-leaning blades. However, as will be explained in the Chapter 13, for an axial compressor, positive slope is not advantageous as the higher pressure ratio and temperature rise will lead to dynamic instability [10]. Moreover, the resulting absolute velocity at exit C_2 is the maximum (for the same Wr_2 and U_2) that increases the pressure rise necessary in the diffuser. For these reasons forward-leaning blades are not suitable for high-speed compressors and never used for aircraft engines.

For radial blades ($\beta_2' = 0$), a horizontal line is obtained which means that the pressure ratio is independent from the mass flow rate.

For backward-leaning (backswept) blades, the relation yields a straight line having a negative slope. Backward-leaning blades often have higher efficiency than straight radial blades since the absolute velocity (C_2) for backward is less than that for straight radial. This means less stringent diffusion requirements in both the impeller and diffuser, tending to increase the efficiency of both components [6]. The backswept angle may be in the range 30°–40°. The use of backswept vanes gives the compressor a wider



Pressure ratio for different impeller blading

FIGURE 12.28
Temperature rise versus the mass flow rate for different types of impellers.

operating range of the airflow at a given rotational speed, which is important for matching the compressor to its driving turbine.

Since the pressure ratio is given by the relation

$$\frac{P_{03}}{P_{01}} = \left[1 + \eta_c \frac{T_{03} - T_{01}}{T_{01}}\right]^{\gamma/\gamma-1}$$

with

$$\frac{T_{03} - T_{01}}{T_{01}} = (\gamma - 1)\left(\frac{U_2}{a_{01}}\right)^2 \frac{C_{u2}}{U_2}$$

The slip factor as defined by Dixon [11] is

$$\sigma_s = \frac{C_{u2}}{C'_{u2}} = 1 - \frac{0.63\pi/N_b}{1 - \phi_2 \tan\beta'_2} \tag{12.18}$$

where N_b is the number of blades, thus

$$\frac{C_{u2}}{U_2} = \sigma \frac{C'_{u2}}{U_2}$$

and

$$C'_{u2} = U_2 - C_{r_2} \tan\beta'_2 = U_2\left(1 - \frac{C_{r_2}}{U_2} \tan\beta'_2\right)$$

The swirl velocity ratio is then $C_{u2}/U_2 = \left(1 - \phi_2 \tan\beta'_2\right)$ where $\phi = C_{r_2}/U_2$ or

$$\frac{C_{u2}}{U_2} = \sigma_s\left(1 - \phi_2 \tan\beta'_2\right)$$

Since the pressure ratio is expressed as

$$\frac{P_{03}}{P_{01}} = \left[1 + \eta_c(\gamma - 1)\frac{U_2 C_{u2}}{a_{01}^2}\right]^{\gamma/\gamma-1}$$

Thus

$$\frac{P_{03}}{P_{01}} = \left[1 + (\gamma - 1)\eta_c \sigma_s \left(\frac{U_2}{a_{01}}\right)^2 \left(1 - \phi_2 \tan\beta'_2\right)\right]^{\gamma/\gamma-1} \tag{12.19}$$

Other correlations for the slip factor are found in References 3 and 9.

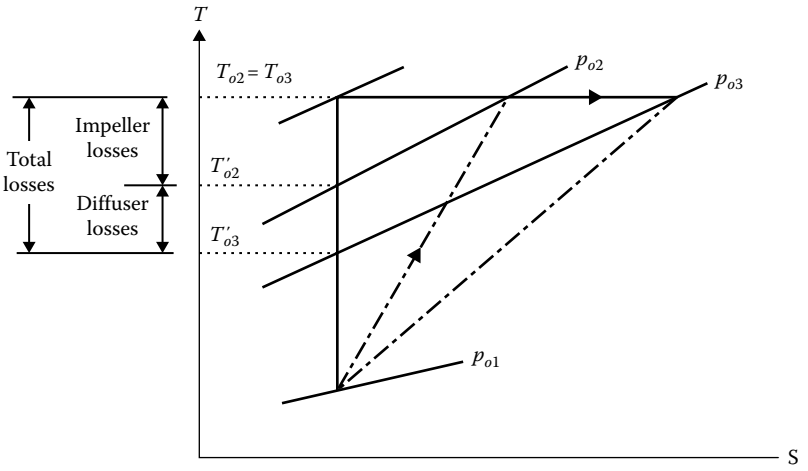


FIGURE 12.29
Impeller and diffuser losses.

The pressure ratio of the *impeller* only is defined in a similar way to the whole compressor and expressed as

$$\frac{P_{02}}{P_{01}} = \left[1 + \eta_{imp}\frac{\psi C_{u2} U_2}{CpT_{01}}\right]^{\gamma/\gamma-1} \tag{12.20}$$

This value is greater than the pressure ratio of the compressor due to the losses in the diffuser.

The impeller isentropic efficiency is related to the compressor efficiency. Now, if the losses in the impeller are equal to a certain fraction of the total losses, say λ, then from the T–S diagram (Figure 12.29), the impeller loss and the compressor loss are, respectively, $(T_{02} - T_{02SS})$ and $(T_{02} - T_{03SS})$.

The impeller efficiency is defined as $\eta_{imp} = (T_{02ss} - T_{01})/(T_{03} - T_{01})$; from this definition and compressor efficiencies,

$$\frac{T_{02} - T_{02SS}}{T_{02} - T_{03SS}} = \frac{1 - \eta_{imp}}{1 - \eta_c} = \lambda$$

$$\eta_{imp} = 1 - \lambda + \lambda\eta_c \tag{12.21}$$

for the case of equal losses in impeller and diffuser then

$$\eta_{imp} = 0.5\left(1 + \eta_c\right) \tag{12.21a}$$

Example 12.6

A single-sided centrifugal compressor is to deliver 14 kg/s of air when operating at a pressure ratio of 4:1 and a speed of 200 rev/s. The inlet stagnations conditions are 288 K and 0.1 MPa. The number of blades is 20, power input factor is 1.04, and the compressor isentropic efficiency is 0.8. If the Mach number is not to exceed unity at the impeller tip, and 60% of the losses are assumed to occur in the impeller (Figures 12.30 and 12.31).

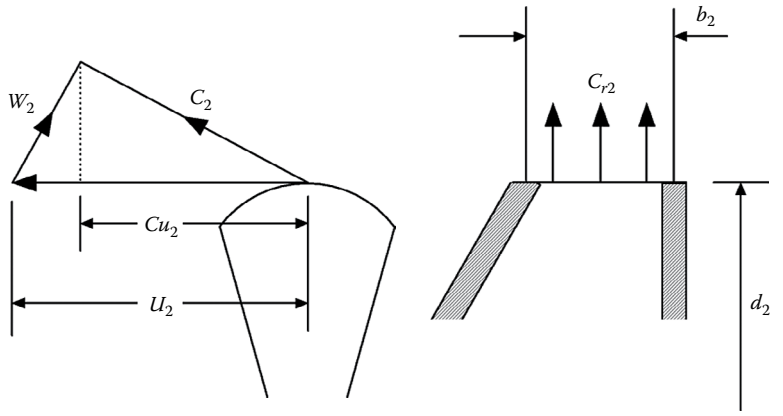


FIGURE 12.30
Outlet flow from impeller.

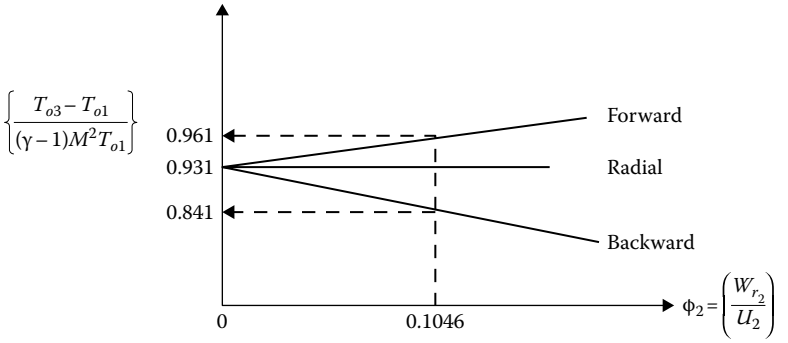


FIGURE 12.31
Temperature rise for different impellers having a constant diameter.

Find

1. The overall diameter of the impeller if its blades are radial
2. The minimum possible axial depth of the diffuser for the impeller described in (1)
3. The corresponding pressure ratio and temperature rise if the radial impeller in (1) is to be replaced by a backward-leaning impeller having the same diameter, same flow coefficient at impeller outlet $\phi_2 = C_{r2}/U_2$ and the backswept angle $\beta_2' = 30°$
4. The same as in (3) but a forward-leaning impeller is employed with $\beta_2' = -30°$
5. The corresponding impeller diameter d_2 and tip speed U_2 if the three impellers (radial, forward, and backward-leaning) are to have the same pressure ratio, same flow coefficient ϕ_2 and same rotational speed; $N = 200$ rev/s and same isentropic efficiency

Solution

1. For a radial impeller blades having 20 blades, then the slip factor is

$$\therefore \sigma = 1 - \left(\frac{0.63\pi}{N_b}\right) = 0.901$$

The compressor pressure ratio is related to the impeller tip speed U_2 by the relation

$$\pi_c^{\gamma-1/\gamma} = \left(1 + \frac{\eta_c \sigma \psi U_2^2}{C_P T_{o_1}}\right)$$

$$\therefore 4^{1.4-1/1.4} = 1 + \frac{0.8 \times 1.04 \times 0.901 \times U_2^2}{1005 \times 288}$$

$$\therefore U_2 = 435.16 \text{ m/s}$$

The impeller tip diameter is then

$$d_2 = \frac{U_2}{\pi \times N} = \frac{435.16}{\pi \times 200} = 0.69 \text{ m}$$

The temperature rise across the impeller is then

$$\Delta T_o = T_{o_2} - T_{o_1} = \frac{\sigma \psi U_2^2}{C_P} = \frac{0.901 \times 1.04 \times 18.94 \times 10^4}{1005} = 175.6 \text{ K}$$

The total temperature at the impeller outlet is thus $T_{02} = T_{03} = 463.6$ K.

From Equation 12.21, the impeller efficiency

$$\eta_{imp} = 1 - \lambda + \lambda \eta_c$$

$$\eta_{imp} = 1 - 0.6 + 0.6 \times 0.8 = 0.88$$

The pressure ratio across the impeller is

$$\frac{P_{o_2}}{P_{o_1}} = \left[1 + \eta_{imp}\left(\frac{T_{o_2} - T_{o_1}}{T_{o_1}}\right)\right]^{\gamma/\gamma-1}$$

$$\frac{P_{o_2}}{P_{o_1}} = \left[1 + 0.88\left(\frac{175.6}{288}\right)\right]^{1.4/0.4} = (1.5366)^{3.5} = 4.498$$

The total pressure at the impeller outlet $P_{o2} = 4.498$ bar.

2. Since the Mach number at impeller outlet must not exceed unity, then the absolute velocity at outlet is taken as equal to the sonic speed, then C_2 = sonic speed = $\sqrt{\gamma R T_2}$.

   The total to static temperature in this case is expressed as

$$\frac{T_{0_2}}{T_2} = \frac{\gamma + 1}{2} = \frac{1.4 + 1}{2} = 1.2$$

The static temperature is then $T_2 = 386.8$ K, and the absolute velocity is

$$C_2 = \sqrt{1.4 \times 287 \times 386.8} = 394 \text{ m/s}$$

The total and static pressure ratio is also

$$\frac{P_{0_2}}{P_2} = \left(\frac{\gamma+1}{2}\right)^{\gamma/\gamma-1} = (1.2)^{3.5} = 1.8929$$

Thus

$$P_2 = \frac{4.498}{1.8929} = 2.376 \text{ bar}$$

The air density at the impeller outlet is

$$\rho_2 = \frac{P_2}{RT_2} = \frac{2.376\times10^5}{287\times386.8} = 2.14 \text{ kg/m}^3$$

The mass flow rate is $\dot{m} = \rho_2 C_{r_2} A_2$

$$\dot{m} = \rho_2 C_{r_2}(\pi \times d_2 \times b_2) \qquad \text{(a)}$$

$$\dot{m} = \rho_2\sqrt{C_2^2 - (\sigma U_2)^2}\,(\pi d_2 b_2) = \rho_2\sqrt{C_2^2 - (\sigma U_2)^2}\,(\pi d_2 b_2)$$

With a constant $\dot{m}$ and rotational speed, then at maximum (C_2) the impeller width b_2 will be a minimum;

$$C_{r_2}^2 = C_2^2 - (\sigma U_2)^2 = (394)^2 - (0.9\times435)^2$$

$$C_r = 45.5 \text{ m/s}$$

from Equation a

$$\therefore b_2 = \frac{\dot{m}}{\rho_2 C_{r_2}\pi d_2} = \frac{14}{(2.14)(45.5)(\pi\times0.69)} = \frac{14}{211.0} = 0.066 \text{ m}$$

3. Backward-leaning impeller $(\beta_2') = 30°$

$$\phi_2 = \frac{C_{r_2}}{U_2} = \frac{W_{r_2}}{U_2} = \frac{45.5}{435} = 0.1046$$

Slip factor is given by the relation

$$\sigma_S = 1 - \frac{0.63(\pi/N_b)}{1-\phi_2\tan\beta_2'} = 1 - \frac{(0.63\pi/20)}{1-(0.1046)\times\tan30°} = 0.8951$$

The total sonic speed is $a_{0_1} = \sqrt{\gamma RT_{o_1}} = \sqrt{1.4\times287\times288} = 340$ m/s.

The pressure ratio is determined from Equation 12.19 as follows

$$\frac{P_{0_3}}{P_{0_1}} = \left\{1 + 0.4\times0.8\times0.8951\times\left(\frac{435}{340}\right)^2(1-0.1046\times0.5774)\right\}^{3.5} = 3.5876$$

The temperature ratio is then

$$\frac{T_{0_2}}{T_{0_1}} = \frac{T_{0_3}}{T_{0_1}} = 1 + \frac{\pi_c^{\gamma-1/\gamma} - 1}{\eta_c} = 1 + \frac{1.4405 - 1}{0.8}$$

The impeller and compressor outlet temperature is then $T_{02} = 446.6$ K.

4. Forward-leaning impeller $\left(\beta_2'\right) = -30°$
The slip factor is

$$\sigma_S = 1 - \frac{0.63\pi/N_b}{1 - \phi_2 \tan\beta_2'} = 1 - \frac{0.63\pi/20}{1 - 0.1046 \times \left(-0.5774\right)} = 0.9067$$

The pressure ratio calculated also from Equation 12.19

$$\frac{P_{0_3}}{P_{0_1}} = \left\{1 + 0.4 \times 0.8 \times 0.9067 \times \left(\frac{435}{340}\right)^2 \left(1 + 0.1046 \times 0.5774\right)\right\}^{\gamma/\gamma-1} = 4.1687$$

The corresponding temperature ratio is

$$\frac{T_{0_3}}{T_{0_1}} = 1 + \frac{\pi_c^{\gamma/\gamma-1} - 1}{\eta_c} = 1 + \frac{1.50365 - 1}{0.8} = 1.6296$$

The outlet temperature is then $T_{03} = 469.3$ K.

5. If the pressure rise in backward-leaning impeller = pressure rise in radial impeller

$$\left(\frac{P_{0_3}}{P_{0_1}}\right)^{\gamma-1/\gamma} = \left[1 + \left(\gamma - 1\right)\eta_c \sigma_{S_b} \left(\frac{U_2}{a_{o_1}}\right)_b^2 \left(1 - \phi_2 \tan\beta_2'\right)_b\right] = \left[1 + \left(\gamma - 1\right)\eta_c \sigma_{S_r} \left(\frac{U_2}{a_{o_1}}\right)_r\right]$$

Subscripts (b) and (r) stand for backward leaning and radial impellers

$$\therefore \sigma_{S_b} U_{2_b}^2 \left(1 - \phi_2 \tan\beta_2'\right)_b = \sigma_{S_r} U_{2_r}^2$$

$$\left(\frac{U_{2_b}}{U_{2_r}}\right)^2 = \frac{\sigma_{S_r}}{\sigma_{S_b}\left(1 - \phi_2 \tan\beta_2'\right)_b} = \frac{0.901}{0.8951\left(1 - 0.1046 \times 0.5774\right)} = 1.0713$$

$$U_{2_b} = 1.035 U_{2_r} = 450 \text{ m/s}$$

The diameter ratio between the backward and radial impellers is then

$$\frac{d_{2_b}}{d_{2_r}} = \frac{U_{2_b}}{U_{2_r}} = 1.035$$

The diameter of the backward impeller is then $d_{2_b} = 0.714$ m.

Moreover, since

$$\phi_2 = 0.1046 = \frac{C_{r_2}}{U_2}$$

The radial velocity at the impeller outlet is $C_{r2} = 47.07$ m/s.

For a forward-leaning impeller, by equating the pressure rise in forward-leaning and radial impellers, then

$$\sigma_{S_f}\left(\frac{U_2}{a_{o_1}}\right)_f^2\left(1-\phi_2\tan\beta_2'\right)_f=\sigma_{S_r}\left(\frac{U_2}{a_{o_1}}\right)_r^2$$

Where subscript (f) stands for forward-leaning impeller, the rotational speed is

$$U_{2_f}=U_{2_r}\left\{\frac{\sigma_{S_r}}{\sigma_{S_f}\left(1-\phi_2\tan\beta_2'\right)_f}\right\}^{1/2}=435\left\{\frac{0.901}{0.9067\left(1+0.1046\times0.5774\right)}\right\}^{1/2}=421.09\ \text{m/s}$$

The tip diameter is then

$$d_{2_f}=d_{2_r}\frac{U_{2_f}}{U_{2_r}}=0.69\times0.968=0.6679\ \text{m}$$

$$C_{r_2}=\phi_2\times U_2=0.1046\times421.09=44.05\ \text{m/s}$$

12.4.7 Radial Impeller

Impeller has no inducer section. The blade starts and ends in the radial plane. Thus both velocity triangles are drawn in the $(r-\theta)$ plane. Figure 12.32 illustrates both blade shape and velocity triangles at inlet and outlet [11].

Example 12.7

Air is compressed in a centrifugal compressor having the following properties:

Rotational speed is 5400 rpm
Mass flow rate is 20 kg/s
Air density at impeller inlet is 1.115 kg/m^3
Air density at impeller outlet is 1.45 kg/m^3

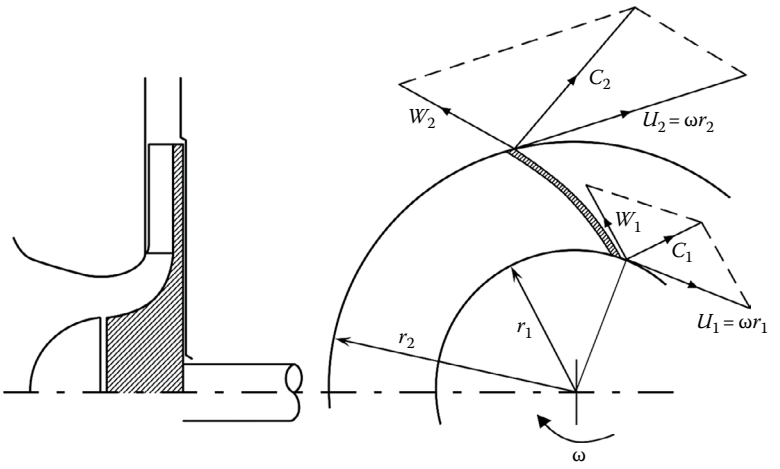


FIGURE 12.32
Radial impeller.

Impeller inlet radius is 0.3 m
Impeller outlet radius is 0.56 m

Power consumed in driving the impeller is 750 kW, and entry is radial with a component of 60 m/s which is constant throughout.

Calculate

1. The width at inlet and outlet
2. Temperature rise in compressor
3. Angles: α_1, α_2, β_1, β_2

Solution

1. *Continuity equation*:

$$\dot{m} \equiv 20\,\text{kg/s} = \rho_1 C_1 A_1 = 1.115 \times 60 \times A_1$$

$$A_1 = \frac{20}{66.9} = 0.2989\,\text{m}^2$$

$$A_1 = 2\pi r_1 b_1$$

Width of impeller at inlet is $b_1 = \dfrac{0.2989}{2\pi \times 0.3} = 0.1586$ m.

Similarly, impeller blade width at outlet is $b_2 = \dfrac{\dot{m}}{\rho_2 C_{r2} \times 2\pi r_2} = \dfrac{20}{1.45 \times 60 \times 2 \times \pi \times 0.56} =$ 0.065 m.

Rotational speeds:

$$U_1 = 2\pi r_1 N = 2\pi \times 0.3 \times \frac{5400}{60} = 169.6\ \text{m/s}$$

$$U_2 = 2\pi r_2 N = 2\pi \times 0.56 \times \frac{5400}{60} = 316.7\ \text{m/s}$$

Power:

$$\mathscr{P} = \dot{m} U_2 C_{u2} \tag{A}$$

$$C_{u2} = \frac{750 \times 10^3}{20 \times 316.7} = 118.4\ \text{m/s}$$

$$\mathscr{P} = \dot{m} C_p \Delta T_0 \tag{B}$$

2. Temperature rise: From Equations A and B

$$\Delta T_0 = \frac{U_2 C_{u2}}{C_p} = 37.3\,\text{K}$$

$$W_{u2} = U_2 - C_{u2} = 316.7 - 118.4 = 198.3\ \text{m/s}$$

3. Flow angles

$$\tan\beta_1 = \frac{U_1}{C_1} = \frac{169.6}{60} = 2.8267$$

$$\beta_1 = 70.52°$$

$$\alpha_1 = 0.0$$

$$\tan\beta_2 = \frac{W_{u2}}{C_{r2}} = \frac{198.3}{60} = 3.305$$

$$\beta_2 = 73.17°$$

$$\tan\alpha_2 = \frac{C_{u2}}{C_{r2}} = \frac{118.4}{60} = 1.973$$

$$\alpha_2 = 63.12°$$

12.5 The Diffuser

The function of the diffuser is to decelerate the flow leaving the impeller, thus reducing the absolute velocity of the gas at impeller exit from (C_2) to a lower velocity (C_3) as shown in the T–S diagram. The static pressure of the gas at the impeller exit is further raised by passing through the diffuser. The amount of deceleration and the static pressure rise ($P_3 - P_2$) in the diffuser depend on the degree of reaction and the efficiency of the diffusion process. An efficient diffuser must have minimum losses ($P_{02} - P_{03}$) for maximum efficiency.

There are broadly two types of diffuser, vaneless and vaned. The vaned diffuser has many types, including not only with fixed or pivoting vanes but also the cascade, channel, and pipe types. All diffusers have an initial vaneless gap outboard of the impeller in which the flow settles. The vaneless diffuser is bulky and can be inefficient relative to the other types. The cascade may involve one, two, or three rows of vanes, with performance similar to that of axial cascades. Vaned diffusers may use curved or straight vanes, having a longer path length than the cascade diffuser. Vaneless, cascade, and vaned diffusers collect the flow in a volute-type collector. The channel and pipe diffusers collect the flow in separate passages, sometimes with corner vanes at their outlet. The passage diverges slowly, the pipe consisting of a conical hole and the channel type being rectangular in section with one pair of opposed walls diverging at 10°–11°, the others being parallel.

The pipe and channel diffusers may feed separate combustors or may merge downstream. The channel type is sometimes known as the vane-island or wedge-type diffuser. The blunt end causes as much loss as 5% of the overall efficiency. The pipe-type diffuser was originally proposed and patented by Pratt & Whitney of Canada [9]. It had been shown that the pipe-type diffuser is more efficient than the conventional type with rectangular channels. The passages are formed by drilling holes tangentially through a ring surrounding the impeller, and after the throat the passages are conical. Overall isentropic efficiencies of over 85% are obtained for compressors using this pipe diffuser. Of all the types of diffuser, the vaned diffuser may be made variable, the vanes pivoting about an axial axis.

In general the performance of a diffuser is examined by considering the pressure coefficient

$$Cp = \frac{P_3 - P_2}{P_{02} - P_2}$$

where stations 2 and 3 are the inlet and outlet of diffuser, respectively. The pressure coefficient is sometimes identified as the pressure rise coefficient and given by the symbol C_{pr}.

12.5.1 Vaneless Diffuser

12.5.1.1 Incompressible Flow

As the name implies, the gas in a vaneless diffuser is diffused in the vaneless space around the impeller before it leaves the stage of compressor through a volute casing. The gas in the vaneless diffuser gains static pressure rise simply due to the diffusion process from a smaller diameter (d_2) to a larger diameter (d_3). The corresponding areas of cross-sections in the radial direction are

$$\begin{aligned} A_2 &= \pi d_2 b_2 = 2\pi r_2 b_2 \\ A_3 &= \pi d_3 b_3 = 2\pi r_3 b_3 \end{aligned} \tag{12.22}$$

Such a flow in the vaneless space is axisymmetric inviscid. Since no external torque is applied, the angular momentum is constant, or

$$r_2 C_{u2} = r_3 C_{u3} \tag{12.23}$$

From the continuity equation, at the entry and exit section of the vaneless diffuser

$$\rho_2 C_{r2} A_2 = \rho_3 C_{r_3} A_3$$

$$\rho_2 C_{r_2} \left(2\pi r_2 b_2\right) = \rho_3 C_{r_3} \left(2\pi r_3 b_3\right)$$

$$\rho_2 C_{r2} r_2 b_2 = \rho_3 C_{r3} r_3 b_3 \tag{12.24}$$

For a small pressure rise across the diffuser, then $\rho_2 \approx \rho_3$ therefore

$$C_{r_2} r_2 b_2 = C_{r_3} r_3 b_3$$

For a constant width (parallel wall) diffuser $b_2 = b_3$,

$$C_{r_2} r_2 = C_{r_3} r_3 \tag{12.24a}$$

From Equations 12.23 and 12.24a,

$$\therefore \frac{C_{u3}}{C_{u2}} = \frac{C_{r_3}}{C_{r_2}} = \frac{C_3}{C_2} = \frac{r_2}{r_3} \tag{12.25}$$

Equation 12.25 gives

$$\alpha_2 = \alpha_3 = \tan^{-1} \frac{C_{u_2}}{C_{r2}} = \tan^{-1} \frac{C_{u_3}}{C_{r3}} = \alpha \tag{12.26}$$

This equation is valid for incompressible flow through a constant width diffuser. Equation 12.20 clearly shows that the diffusion is directly proportion to the diameter ration (d_3/d_2).

This leads to a relatively large-sized diffuser, which is a serious disadvantage of the vaneless type. This leads to an impractically large compressor, which prohibits the use of vaneless diffuser in aeronautical applications.

The streamlines for incompressible flow in a vaneless diffuser of constant axial width make a constant angle with the radial direction α. Thus its shape is sometimes called logarithmic spiral.

$$\theta_3 - \theta_2 = \tan\alpha_2 \ell n \frac{r_3}{r_2} \tag{12.27}$$

12.5.1.2 Compressible Flow

Assuming that the flow is reversible, then the fluid properties at any point is related to their values at a point where the Mach number is unity (denoted here after by *).

From Equation 12.19, the continuity equation gives

$$\rho_2 C_{r_2} r_2 = \rho^* C_r^* r^*$$

Conservation of angular momentum requires

$$r_2 C_{u_2} = r^* C_u{}^*$$

Combining these two equations, with $\alpha = \tan^{-1}(C_u/C_r)$ then

$$\frac{\tan\alpha^*}{\tan\alpha} = \frac{\rho^*}{\rho}$$

$$\frac{\rho^*}{\rho} = \frac{\rho_0}{\rho}\frac{\rho^*}{\rho_0} = \frac{\left(1+\frac{\gamma-1}{2}M^2\right)^{1/\gamma-1}}{\left(\frac{\gamma+1}{2}\right)^{1/\gamma-1}}$$

$$\frac{\tan\alpha^*}{\tan\alpha} = \frac{\rho^*}{\rho} = \left[\frac{2}{\gamma+1}\left(1+\frac{\gamma-1}{2}M^2\right)\right]^{1/\gamma-1} \tag{12.28}$$

From the conservation of angular momentum

$$\frac{r^*\sin\alpha^*}{r\sin\alpha} = \frac{C}{C^*} = M\sqrt{T/T^*}$$

with

$$\frac{T}{T^*} = \frac{T_0}{T^*}\frac{T}{T_0}\left[\frac{(\gamma+1)/2}{1+\frac{\gamma-1}{2}M^2}\right]$$

Then

$$\frac{r^* \sin\alpha^*}{r \sin\alpha} = M\left\{\frac{(\gamma+1)/2}{1+\frac{\gamma-1}{2}M^2}\right\}^{1/2} \tag{12.29}$$

From Equations 12.28 and 12.29 since α* is constant, then for a desired Mach number at the diffuser outlet, the corresponding angle and radius can be obtained from the relations

$$\tan\alpha_3 = \tan\alpha_2\left[\frac{1+\frac{\gamma-1}{2}M_2^2}{1+\frac{\gamma-1}{2}M_3^2}\right]^{1/\gamma-1} \tag{12.30}$$

and

$$r_3 = r_2\frac{\sin\alpha_2}{\sin\alpha_3}\frac{M_2}{M_3}\left[\frac{1+\frac{\gamma-1}{2}M_3^2}{1+\frac{\gamma-1}{2}M_2^2}\right]^{1/2} \tag{12.31}$$

The vaneless diffuser is a very efficient device with an essentially limitless operating range, since the angle of attack sensitivity is absent. Unfortunately, however, the desired diffusion usually requires an excessively large radius ratio across the vaneless diffuser. This is especially critical in aircraft applications where large engine diameters are to be avoided.

12.5.2 Vaned Diffuser

To save space, vanes are employed to reduce the fluid angular momentum and thereby reduce C_u more rapidly. The layout of a channel diffuser is shown in Figure 12.33. It is composed of three domains: vaneless, semi-vaneless, and channel. The channel section represents a low-aspect ratio diffuser. It is extensively studied and summarized by Runstadler [12] and Japikse [13]. The crucial parameters are the inlet (throat) Mach number, inlet Reynolds number, stagnation pressure level, and inlet boundary layer blockage in addition to some geometrical parameters. The dimensional parameters for a typical channel diffuser (Figure 12.33) may be defined as follows [3]:

1. Aspect ratio $AS = b_{th}/W_{th}$
2. Area ratio $AR = A_{exit}/A_{throat}$
3. Nondimensional length $LWR = L/W_{th}$
4. Divergence angle 2θ, where $\tan\theta = (AR-1)/(2LWR)$
5. Inlet boundary layer blockage BK where:

$$BK = 1 - \frac{\text{Effective flow area}}{\text{Geometric flow area}}$$

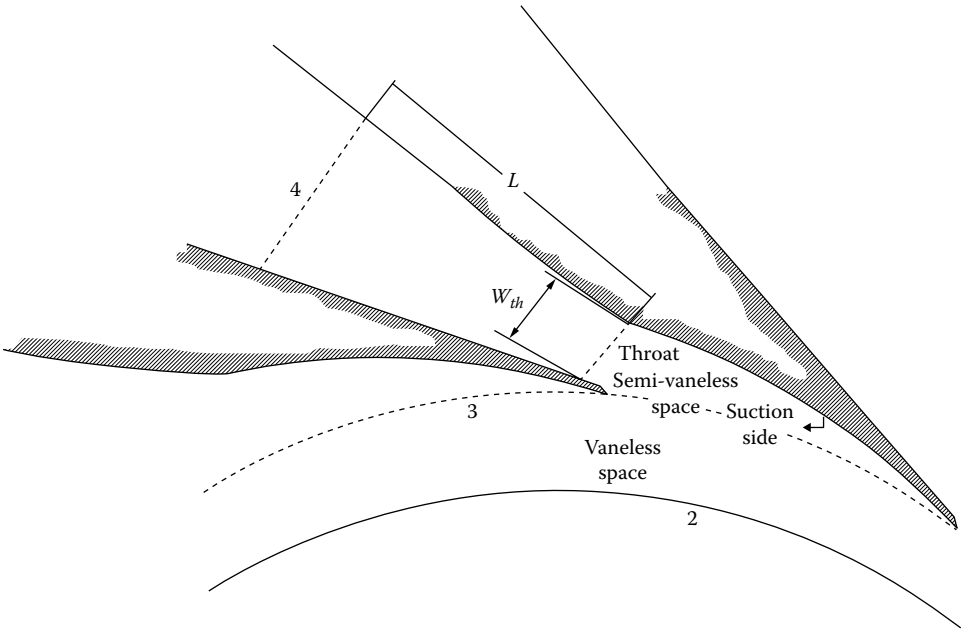


FIGURE 12.33
Channel diffuser.

6. Inlet Reynolds number, $R_e = C_{in} d_{th} \rho / \mu$, where d_h is the hydraulic diameter which is defined as:

$$d_h = 4 \times \text{cross sectional area/passage perimeter}$$

A series of performance maps was presented in Reference 12 to show the effect of inlet blockage, Mach number, and Reynolds number on the diffusers with different aspect ratios. A typical map is shown in Figure 12.34. As outlined in Reference 14, the static pressure rise can be approximated by the values of total pressures and absolute velocities at inlet and outlet.

At any state, the isentropic relation between the static and total pressures is given as

$$\frac{P_S}{P_0} = \left(\frac{T_S}{T_0}\right)^{\gamma/\gamma-1} = \left(\frac{T_S}{T_0}\right)^{C_p/R} = \left(\frac{T_0 - \dfrac{C^2}{2C_p}}{T_0}\right)^{C_p/R} = \left(1 - \frac{C^2}{2C_p T_0}\right)^{C_p/R}$$

Using only two terms only for the binomial expansion gives

$$\frac{P_S}{P_0} \approx 1 - \left(\frac{C_p}{R}\right)\left(\frac{C^2}{2C_p T_0}\right) \approx 1 - \frac{C^2}{2RT_0}$$

With

$$\frac{P_0}{\rho_0} = RT_0$$

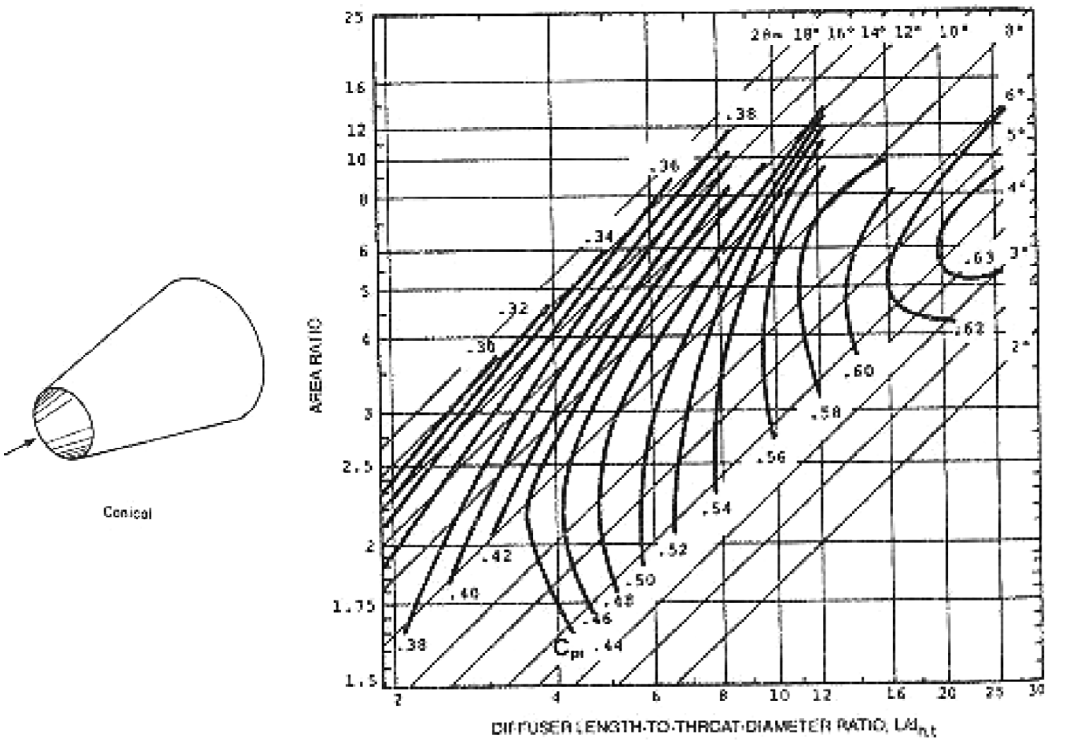


FIGURE 12.34
A typical diffuser performance map.

Then

$$\frac{P_S}{P_0} \approx 1 - \frac{C^2}{2}\frac{\rho_0}{P_0}$$

or

$$P_S \approx P_0 - \frac{\rho_0 C^2}{2}$$

Then the static pressure rise coefficient for a conical diffuser $\left(C_{P_r} \equiv (P_3 - P_2)/(P_{02} - P_2)\right)$ may be approximated by

$$C_{P_r} \approx \frac{\left(P_{03} - \frac{\rho_{03}C_3^2}{2}\right) - \left(P_{02} - \frac{\rho_{02}C_2^2}{2}\right)}{P_{02} - \left(P_{02} - \frac{\rho_{02}C_2^2}{2}\right)} = \frac{P_{03} - P_{02}}{\rho_{02}C_2^2/2} + \left[1 - \frac{\rho_{03}}{\rho_{02}}\left(\frac{C_3}{C_2}\right)^2\right]$$

or

$$C_{P_r} \approx \frac{P_{03} - P_{02}}{\rho_{02}C_2^2/2} + \left[1 - \frac{\rho_{03}}{\rho_{02}}\left(\frac{C_3}{C_2}\right)^2\right]$$

Since for an adiabatic diffuser $T_{02}=T_{03}$, then $P_{02}/\rho_{02}=P_{03}/\rho_{03}$

$$C_{P_r} \approx 2\frac{(P_{03}-P_{02})}{\rho_{02}C_2^2}+\left[1-\frac{P_{03}}{P_{02}}\left(\frac{C_3}{C_2}\right)^2\right] \tag{12.32}$$

Example 12.8

The performance of a conical-diffuser is illustrated in Figure 12.34. The diffuser to be examined has a length-to-throat diameter ratio of 8 and a conical angle (2θ) equals to 8°. The absolute velocity at impeller outlet, $C_2=356$ m/s, and the impeller outlet diameter is 0.5 m. The rotational speed of impeller N = 290 rev/s. The number of diffuser conical passages is 12 and the inlet diffuser area per passage is 7.8×10^{-4} m^2. The total temperature and pressure at diffuser inlet are 488 K and 5.48 bar. Using the approximate static pressure rise coefficient relation given by the relation

$$C_{P_r} \approx \frac{2(P_{03}-P_{02})}{\rho_{02}C_2^2}+\left[1-\frac{P_{03}}{P_{02}}\left(\frac{C_3}{C_2}\right)^2\right]$$

It is required to calculate

1. Mass flow rate
2. Outlet velocity C_3.

Solution

From Figure 12.34, the pressure coefficient and area ratio are

$$C_{P_r} \approx 0.52 \quad \text{Area ratio} = 4.5$$

The static temperature and pressure are

$$T_2 = T_{02}-\frac{C_2^2}{2C_P} = 488-\frac{(356)^2}{2\times1005} = 424.95 \text{ K}$$

$$P_2 = P_{02}\left(\frac{T_2}{T_{02}}\right)^{\gamma/\gamma-1} = 3.376 \text{ bar}$$

The density

$$\rho_2 = \frac{P_2}{RT_2} = 2.768 \text{ kg/m}^3$$

The mass flow rate $\dot{m}$ is given by $\dot{m}=\rho_2 C_2 (A_d\times12)$, with $A_d=7.8\times10^{-4}$ m^2, then

$$\dot{m} = 2.768\times356\times7.8\times10^{-4}\times12 = 9.223 \text{ kg/s}$$

An approximate value for C_3 can be evaluated based on the following arguments

The continuity equation is $\dot{m} = \rho_2 C_2 A_2 = \rho_3 C_3 A_3$
For incompressible flow

$$A_2 C_2 = A_3 C_3, \quad \text{or} \quad C_3 = C_2 \frac{A_2}{A_3} = \frac{C_2}{\text{Area ratio}}$$

However, since the flow is compressible, then the static pressure and consequently the density increase in the diffuser i.e., $\rho_3 > \rho_2$, thus $C_3 < C_2/\text{Area ratio}$
Now for our case, the area ratio is 4.5, then $C_3 < 356/4.5$, or $C_3 < 79.1$ m/s
Try $C_3 = 70$ m/s

$$C_{P_r} \approx \frac{2(P_{03} - P_{02})}{\rho_{02} C_2^2} + \left[1 - \frac{P_{03}}{P_{02}} \left(\frac{C_3}{C_2}\right)^2\right]$$

$$C_{P_r} = \frac{2P_{02}}{\rho_{02} C_2^2}\left[\frac{P_{03}}{P_{02}} - 1\right] + \left[1 - \frac{P_{03}}{P_{02}} \left(\frac{C_3}{C_2}\right)^2\right] = \frac{2RT_{02}}{C_2^2}\left[\frac{P_{03}}{P_{02}} - 1\right] + \left[1 - \frac{P_{03}}{P_{02}} \left(\frac{C_3}{C_2}\right)^2\right]$$

Define $\lambda = P_{03}/P_{02}$, then

$$C_{P_r} = \frac{2 \times 287 \times 488}{(356)^2}[\lambda - 1] + \left[1 - \lambda \left(\frac{70}{356}\right)^2\right]$$

Or

$$0.52 = 2.21(\lambda - 1) + (1 - 0.039\lambda) = 2.171\lambda - 1.21$$

Thus $\lambda = 0.796$ and thus $P_{03} = 4.366$ bar.
The static properties at the diffuser outlet are then

$$T_3 = T_{03} - \frac{{C_3}^2}{2C_P} = 488 - \frac{(70)^2}{2 \times 1005} = 485.6 \text{ K}$$

$$P_3 = P_{03}\left(\frac{T_3}{T_{03}}\right)^{\gamma/\gamma - 1} = 4.366 \times \left(\frac{485.6}{488}\right)^{3.5} = 4.291 \text{ bar}$$

$$\rho_3 = \frac{P_3}{RT_3} = \frac{4.291 \times 10^5}{287 \times 485.6} = 3.079 \text{ kg/m}^3$$

The outlet speed is then

$$C_3 = \frac{\dot{m}}{\rho_3 A_3} = \frac{9.223}{\left(4.079 \times 4.5 \times 7.8 \times 10^{-4} \times 12\right)} = 71.1 \text{ m/s}\cdot$$

Example 12.9

In the early phase of design, two possibilities for the diffuser of a centrifugal compressor, namely, vaned and vaneless diffuser, are considered. The diffuser has an inlet radius of 0.42 and the flow has inlet Mach number of 0.9, and at angle of 68° with respect to the radial direction.

1. First, if a vaned diffuser is selected, it is required to calculate the Mach number at diffuser outlet if the outlet radius of the vanes is 0.525 m, their axial width is constant. Consider an isentropic flow with a pressure coefficient, $c_{pd}=(p_3-p_2)/(p_{o2}-p_2)=0.65$, what would be the outlet blade angle?
2. If a vaneless diffuser replaced the vaned diffuser what would be the outlet radius and flow outlet angle if the outlet Mach number is maintained the same as for a vaned diffuser?
3. If the flow in the vaned diffuser is no longer isentropic but a drop in stagnation pressure of 10 % is encountered, but the same value of $c_{pd}=0.65$ is maintained, determine the required exit blade angle. (Assume as a first approximation that the vane and flow angles are the same.)

Solution

1. Isentropic vaned diffuser (Figure 12.35)
   Since

$$c_{pd}=\frac{P_3-P_2}{P_{o2}-P_2}=\frac{\dfrac{P_3}{P_2}-1}{\dfrac{P_{02}}{P_2}-1}=0.65,$$

   then

$$\frac{P_3}{P_2}=1+0.65\left[\left(\frac{P_{o2}}{P_2}\right)-1\right]=1+0.65\left[\left(1+\frac{\gamma-1}{2}M^2\right)^{\gamma/\gamma-1}-1\right]=1.449$$

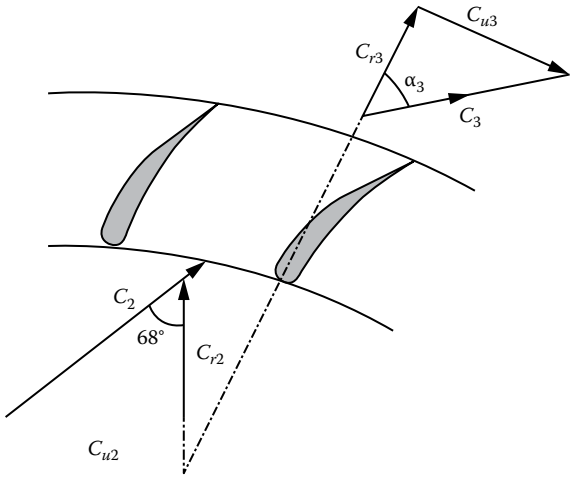


FIGURE 12.35
Vaned diffuser.

Since $P_{03} = P_{02}$, then

$$\frac{P_3}{P_2} = \frac{P_3}{P_{o3}} \frac{P_{o2}}{P_2} = \frac{\left(1 + \frac{\gamma - 1}{2} M_2^2\right)^{\gamma/\gamma - 1}}{\left(1 + \frac{\gamma - 1}{2} M_3^2\right)^{\gamma/\gamma - 1}} = \left(\frac{1.162}{1 + 0.2 M_3^2}\right)^{3.5}$$

Or

$$(1.449)^{1/3.5} = \frac{1.162}{1 + 0.2 M_3^2} \quad \text{or} \quad 1 + 0.2 M_3^2 = \frac{1.162}{1.112} = 1.044964$$

The outlet Mach number is $M_3 = 0.474$.
Since the flow is isentropic in the vaned diffuser, i.e., $T_{03} = T_{02}$ and $P_{03} = P_{02}$

$$\frac{P_3}{P_2} = \frac{\rho_3}{\rho_2} \frac{T_3}{T_2} = \frac{\rho_3}{\rho_2} \frac{(T_3/T_{o3})}{(T_2/T_{o2})} = \frac{\rho_3}{\rho_2} \frac{1 + \frac{\gamma - 1}{2} M_2^2}{1 + \frac{\gamma - 1}{2} M_3^2}$$

$$\therefore 1.449 = \frac{\rho_3}{\rho_2} \frac{1.162}{1.04496}$$

$$\frac{\rho_3}{\rho_2} = 1.303$$

From the continuity equation

$$\rho_2 c_{r2} (\pi d_2 b_2) = \rho_3 c_{r3} (\pi d_3 b_3)$$

with $b_2 = b_3$, then

$$\frac{C_3}{C_2} = \frac{\rho_2 d_2}{\rho_3 d_3} \tag{1}$$

From the conservation of angular momentum in the vaned diffuser

$$r_2 C_{u2} = r_3 C_{u3}, \quad \text{thus} \frac{C_{u3}}{C_{u2}} = \frac{r_2}{r_3} = \frac{d_2}{d_3} \tag{2}$$

From Equations 1 and 2

$$\frac{C_{u3}/C_{r3}}{C_{u2}/C_{r2}} = \frac{\rho_3}{\rho_2}$$

or

$$\frac{\tan \alpha_3}{\tan \alpha_2} = \frac{\rho_3}{\rho_2} = 1.303$$

$$\tan \alpha_3 = 1.303 \tan \alpha_2 = 1.303 \times 2.4751$$

$$\alpha_3 = 72.766°$$

2. Vaneless diffuser
   The following data are assumed also for the vaneless diffuser

$$M_2 = 0.9, \quad r_2 = 0.42 \text{ m}, \quad M_3 = 0.474, \quad \text{and} \quad \alpha_2 = 68°$$

The flow is compressible and isentropic, then from Equation 12.30

$$\alpha_3 = 72.7833$$

Also from Equation 12.31

$$r_3 = 0.744 \text{ m}$$

It is clear from cases (1) and (2) that the outlet diameter of the vaneless diffuser (0.744 m) is much greater than the outlet diameter of the vaned diffuser (0.525 m), thus a vaneless diffuser enlarges the outer diameter of the compressor, which in turn increases the frontal area of aeroengines and increases the drag force.

3. If $P_{o3} = 0.9P_{o2}$ and $T_{o3} = T_{o2}$ and $P_3/P_2 = 1.449$

$$\therefore \frac{P_{o2}/P_2}{P_{o3}/P_3} = \left(\frac{1 + \frac{\gamma - 1}{2} M_2^2}{1 + \frac{\gamma - 1}{2} M_3^2} \right)^{\gamma/\gamma - 1} = \left(\frac{1.162}{1 + 0.2M_3^2} \right)^{3.5}$$

but

$$\frac{P_{o2} / P_2}{P_{o3} / P_3} = \frac{P_{o2}}{P_{o3}} \frac{P_3}{P_2} = \frac{1.449}{0.9} = 1.61$$

then

$$M_3 = 0.2805$$

$$\frac{P_3}{P_2} = \frac{\rho_3}{\rho_2} \frac{T_3}{T_2} = \frac{\rho_3}{\rho_2} \frac{(T_3/T_{o3})}{(T_2/T_{o2})} = \frac{\rho_3}{\rho_2} \frac{1 + \frac{\gamma - 1}{2} M_2^2}{1 + \frac{\gamma - 1}{2} M_3^2} = \frac{\rho_3}{\rho_2} \frac{1.0157}{1.162} = \frac{\rho_3}{\rho_2} (0.87413)$$

$$\frac{\rho_3}{\rho_2} = \frac{1.449}{0.87413} = 1.6576$$

Since $\tan\alpha_3 / \tan\alpha_2 = \rho_3 / \rho_2$, then $\tan\alpha_3 = 1.6576 \times 2.4751 = 4.1028$ or $\alpha_3 = 76.3°$.

Note that the outlet diameter of the vaneless diffuser is much greater than the vaned diffuser. Also the outlet angle from the radial direction is greater in the case of a vaneless diffuser than vaned one (Figure 12.36).

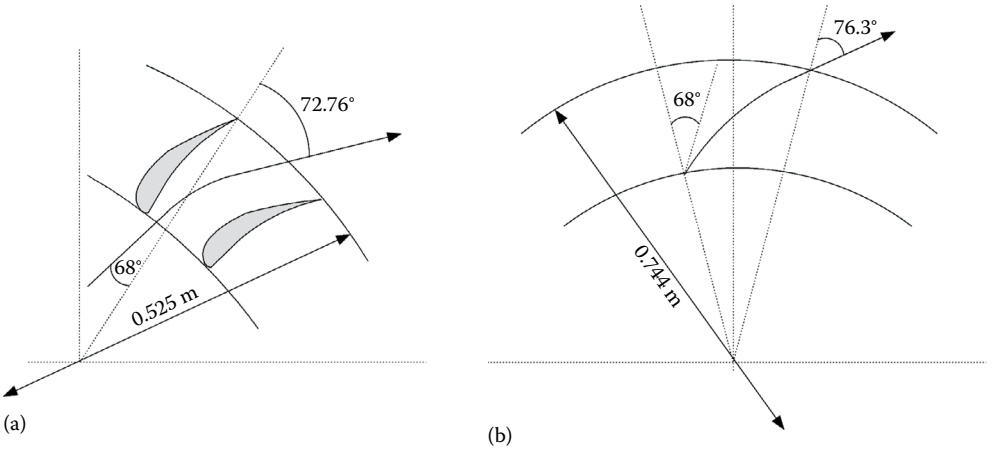


FIGURE 12.36
(a) Vaned versus (b) vaneless diffuser.

12.6 Discharge Systems

The discharge system as described earlier is either a manifold, a crossover duct (an inverted U-shaped passage), or a collector (scroll or volute). Aeroengines and many gas turbines require the discharged air to be turned into axial direction for transmission to the combustion chamber. Multi-stage compressors have an inverted U-shaped passage to turn the flow from radially outward to radially inward, and then to axial direction for transmission to the inlet of the next stage. In many industrial gas turbines and turbochargers, the fluid is collected in one pipe for delivery to the subsequent modules of the system.

Very little research work treated the volute design. Figure 12.37 illustrates the volute shape. In general the cross-sectional area of the volute must increase with the azimuth

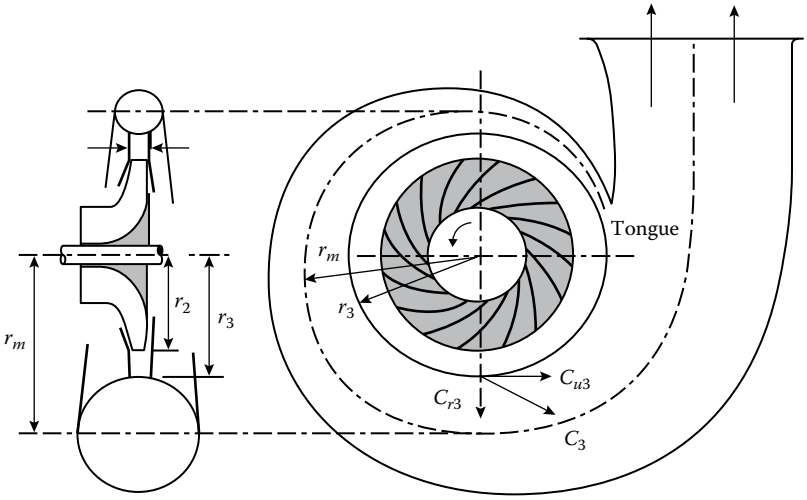


FIGURE 12.37
Volute geometry.

angle to accommodate the increasing flow. The cross sectional area of the volute may be very close to the circular shape. The simplest method of volute design assumes that the angular momentum of the flow remains constant ($rC_u = K$). The area at any azimuth angle A_θ at any angle θ is expressed as

$$\frac{A_\theta}{\bar{r}} = Q\frac{\theta}{2\pi K} \tag{12.33}$$

where $\bar{r}$ and Q are the radius of the centroid of the cross-section of the volute and volume flow.

12.7 Characteristic Performance of a Centrifugal Compressor

Here, the characteristic behavior of a centrifugal compressor operating between inlet station denoted by 1 and outlet station denoted by 2 will be described. Changing nomenclature a little, the overall stagnation pressure ratio to be P_{02}/P_{01}. For any compressor, the stagnation pressure at outlet and the overall compressor efficiency are dependent on other physical properties as follows

$$P_{02}, \eta_c = f\left(\dot{m}, P_{01}, T_{01}, \gamma, R, D, N, \text{ and } \upsilon\right)$$

In the above relation, subscripts 01 and 02 denote the compressor inlet and outlet total conditions, the mass flow rate is denoted by $\dot{m}$, specific heat ratio and gas constant are γ and R and the kinematic viscosity υ. Based on the Buckingham's theory, there are nine physical quantities and four basic dimensions, and then the number of dimensionless quantities is 9 − 4 = 5. The dimensionless analysis will give the following relationship

$$\frac{P_{02}}{P_{01}}, \quad \eta_C = f\left(\frac{\dot{m}\sqrt{\gamma RT_{01}}}{P_{01}D^2}, \frac{ND}{\sqrt{RT_{01}}}, \frac{ND^2}{\upsilon}, \gamma\right) \tag{12.34}$$

The specific heat ratio γ does not vary much with compressing the air. The viscous effects are insensitive to the variation of Reynolds number, ND^2/υ, if the Reynolds number itself is high. Since the Reynolds number range is sufficiently high then the compressor performance can be adequately described by

$$\frac{P_{02}}{P_{01}}, \quad \eta_C = f\left(\frac{\dot{m}\sqrt{\gamma RT_{01}}}{P_{01}D^2}, \frac{ND}{\sqrt{RT_{01}}}\right) \tag{12.35}$$

Moreover, if for a given air compressor both of the diameter and gas constant are fixed, then the performance can be described by the following pseudo dimensionless variables:

$$\frac{P_{02}}{P_{01}}, \quad \eta_C = f\left(\frac{\dot{m}\sqrt{T_{01}}}{P_{01}}, \frac{N}{\sqrt{T_{01}}}\right) \tag{12.36}$$

To account for the air properties at different altitudes (when this compressor is a part of an aeroengine), the right-hand-side variables are referred to the standard day conditions. Thus again the performance relation shown is described by

$$\frac{P_{02}}{P_{01}}, \quad \eta_C = f\left(\frac{\dot{m}\sqrt{\theta}}{\delta}, \frac{N}{\sqrt{\theta}}\right) \tag{12.37}$$

$$\theta = \frac{T_{01}}{(T_{01})_{std\ day}} \quad \text{and} \quad \delta = \frac{P_{01}}{(P_{01})_{std\ day}} \tag{12.38}$$

where $(T_{01})_{std\ day} = 288.15$ K and $(P_{01})_{std\ day} = 101.325$ kPa.

The compressor performance is defined (either experimentally or numerically) and plotted in what is called a *compressor map*. This map has the vertical axis as the pressure ratio—or the compressor efficiency—and the mass flow parameter as the vertical axis for varying rotational speed parameter. If the performance of compressor is to be defined experimentally, the test rig provides capabilities for both speed and air mass flow rate. For each rotational speed, the air mass flow is varied and the corresponding pressure ratio and efficiency are determined. Next, the rotational speed is changed and another set of experiments is followed the mass flow rate, pressure ratio and efficiency are changing. A schematic of the compressor map is shown in Figure 12.38.

In general, three forms for this map are found:

1. The actual values for the mass and speed parameters are used $\left(\dot{m}\sqrt{T_{01}}/P_{01}, N/\sqrt{T_{01}}\right)$.
2. The values of the mass and speed parameters will be here non-dimensionalized by the design values, or, $\left(\dot{m}\sqrt{T_{01}}/P_{01}\right)/\left(\dot{m}\sqrt{T_{01}}/P_{01}\right)_d$ and $\left(N/\sqrt{T_{01}}\right)/\left(N/\sqrt{T_{01}}\right)_d$ in such a case at the design point the values of both parameters are unity and other range say from 0.4 to 1.1 (Figure 12.39).
3. The values of these parameters referred to the standard day temperature and pressure, or $\left(\dot{m}\sqrt{\theta}/\delta, N/\sqrt{\theta}\right)$. This form of map is usually used by manufacturers of aeroengines [15] (Figure 12.40).

Each speed line (or corrected speed) has two limiting points, namely, surging and choking points. The choking point is the point at the farthest right on the curve. Choking point represents the maximum obtained mass flow rate, beyond which no further mass flow rate can be obtained and choking is said to occur. The farthest left point on the constant speed curve represents *surging*. Surging is associated with a drop in delivery pressure with violent aerodynamic pulsation, which is propagated into the whole machine [6]. Surging may be described as follows: if the operating point is on the part of the speed line having a positive slope, then a decrease in the mass flow will be accompanied by a drop in the delivery pressure. If the pressure downstream the compressor does not fall quickly enough, the air will tend to reverse and flow back in the direction of the resulting pressure gradient. This leads to a rapid drop in the pressure ratio. Meanwhile, the pressure downstream the compressor has fallen also, so that the compressor will be able to pick up again and repeat the cycle of events that occurs at high frequency.

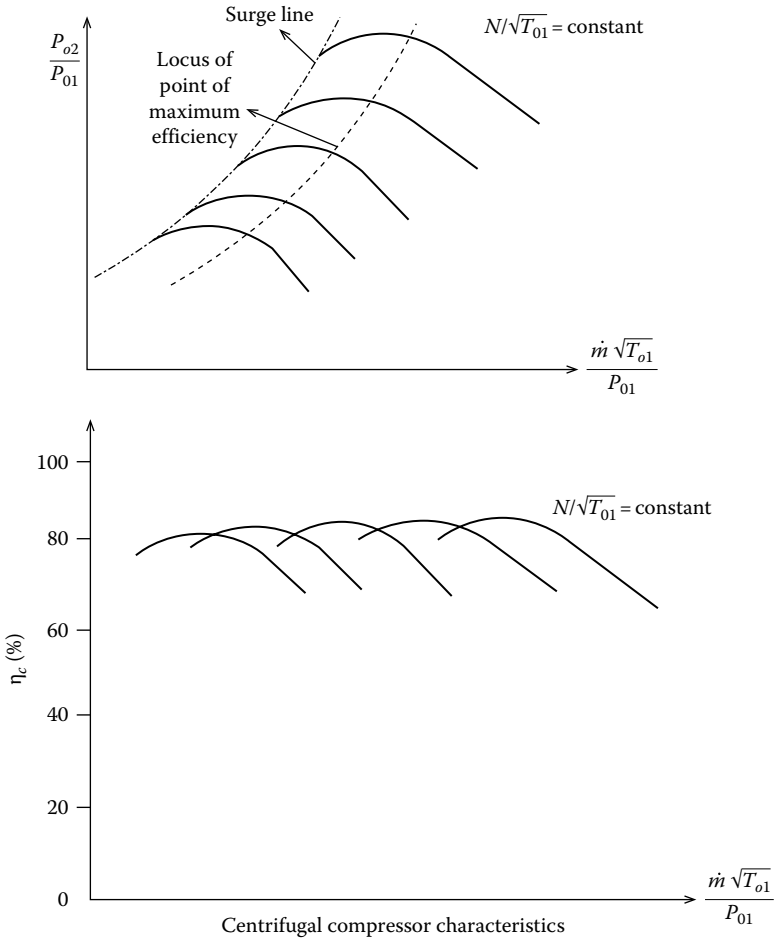


FIGURE 12.38
Compressor map.

12.8 Erosion

12.8.1 Introduction

Erosion studies have been of great importance due to the increased usage of gas turbines in polluted or dusty environments. This is primarily a result of the stepped-up employment of helicopters, which have the inherent ability to land on dusty terrains.

Extensive studies for particulate flows in the aviation field and the resulting erosion/fouling of turbomachines started in the 1970s. These studies examined gas turbines as well as aircraft propulsion components in helicopters, hovercrafts, V/STOL and some conventional airplanes like 737–200 which have the ability to operate from 5000 ft unpaved runways in small cities and villages [16]. In such circumstances billions of high-velocity, abrasive dust particles are ingested into the core of turbomachines eroding away the thin metal areas of engine hardware such as blade tips. For this reason,

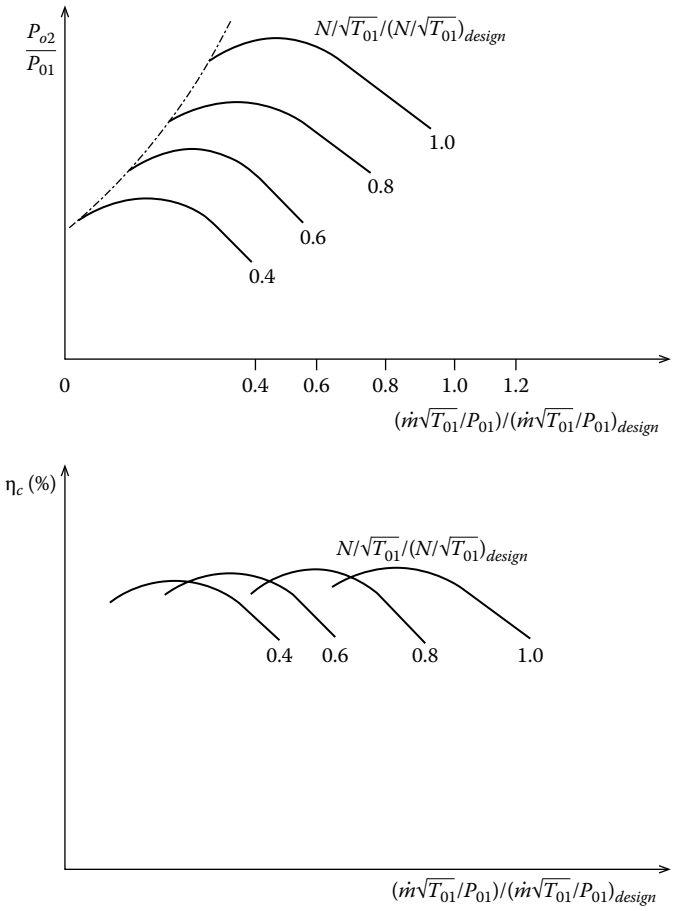


FIGURE 12.39
Compressor map with reference to design point.

theoretical studies were initiated for analyzing particulate flows in axial turbomachines [17], radial turbines [18] and centrifugal compressors [19], respectively. However very few experimental results have been available until now. The missing experimental results may be compensated for by the consensus between the field and theoretical erosion results.

Operating a small gas-turbine-powered helicopter over dusty unimproved land areas routinely results in the ingestion of up to 25 lb of sand and dust for every hour of low-altitude operation. Consequently, many billions of high-velocity, abrasive dust particles impact the surfaces of compressor blades eroding away the thin metal areas. The inevitable result is progressive and rapid degradation of engine performance often to the extent of premature engine failure within 10%–20% of the normal overhaul time [20]. This is in addition to the numerous in-flight stall/power losses and unscheduled maintenance.

Centrifugal compressors are found in many turboshaft engines powering helicopters and turboprop engines. Particles ingestion into these compressors results in erosion

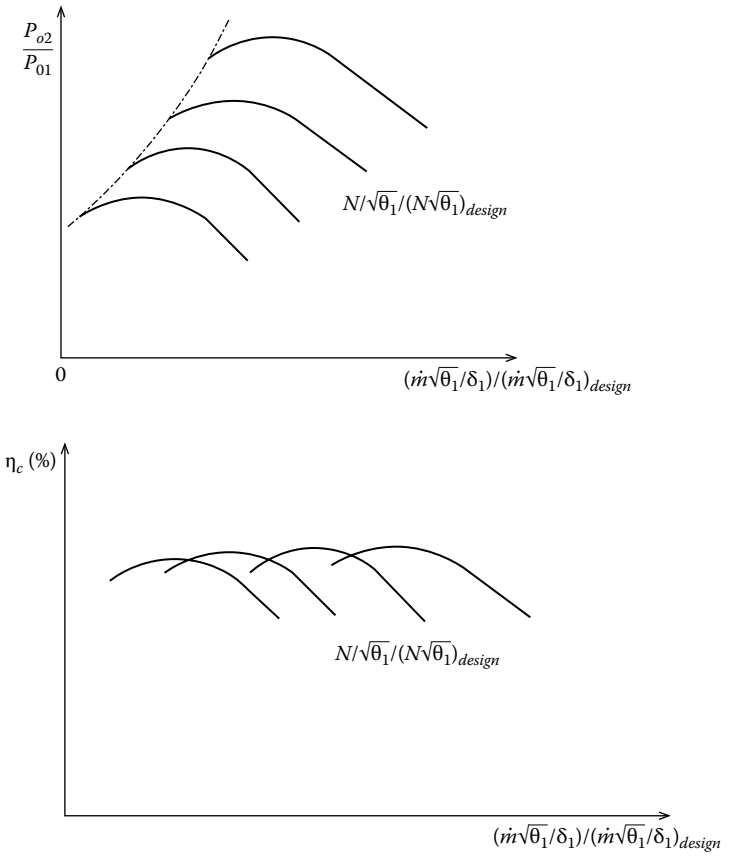


FIGURE 12.40
Compressor map based on ISA standard conditions.

damage of many critical parts of the blades of both rotating and stationary elements. This structural wear results in aerodynamic performance losses and possible boundary-layer separation. Consequently, both the compressor–pressure ratio and efficiency are reduced.

As compressor efficiency is reduced, excessive heating occurs to produce a constant power level. Moreover, the compressor operating line becomes closer to the surge line, resulting in a smaller surge margin and stable range of operation.

Sand/dust particles are ingested into the core of aeroengines in three different circumstances. First, during takeoff, climb, cruise, and descent of aircraft, particles of variable size, different materials, and different concentrations are sucked in by the intakes. Second, during the landing ground roll, the trust reverser operation leads to reingestion of hot gases and debris into the intakes of the engines as described in Reference 21 for military aircraft. The videotape [22] prepared by Pratt & Whitney illustrated the same problem for civil transports. The third circumstances—rarely encountered—is when volcanic ash is ingested into the engines of commercial airplanes. The first recorded volcanic eruption which had its impact on aviation occurred on March 22, 1944, when Mount Vesuvius erupted. Eighty-eight North American B-25 Mitchells had enough damage to be scrapped [23]. Later on,

several incidents were encountered by a Lockheed C-130 Hercules on May 25, 1980, and by two Boeing 727 airplanes in the same year. Several incidents for Boeing 747 airplanes were next recorded where they encountered volcanic debris. Some of these airplanes were powered by Rolls-Royce RB-211 -524 engines while others were powered by P&W JT 9D-7As and GE CF6-80C2. In all of these cases, volcanic dust caused rapid erosion and damage to the internal components of the engines.

The science and technology of multiphase flows has advanced in the past few years because of enhanced computational and experimental capabilities. Three steps are followed in theoretical treatment of erosion problems:

1. Gas-flow analysis
2. Particle trajectories
3. Erosion calculations

Generally particulate flows are two-phase flow problems. They are treated as either a continuum or a discrete flow. In the continuum approach, each phase is considered homogeneous. The particle phase is treated as a continuum phase that interacts with the fluid phase. The mechanisms of the two phases are solved simultaneously through an Eulerian solution technique. The main disadvantage of this approach is its limited ability to provide information for individual particle trajectories. Moreover, it does not account for particle-to-particle or particle-to-surface interactions. These disadvantages made this approach unsuitable for the prediction of erosion due to particulate flow. In the discrete approach, the particles are treated in discrete manner and are solved based on a Lagrangian approach. The particle collisions and particle-wall interactions can be considered as well. Coupling between the two phases is considered through mass, momentum, and energy exchange. This coupling may be considered as one-way or two-way coupling. In one-way coupling (dilute flow), the particles have no influence on the gas flow, and the fluid properties can be evaluated as if no particles are carried. In the two-way coupling (dense flow), each phase is mutually affected by the other.

The particle trajectories can be obtained by solving the equations of the motion of solid particles in the pre-defined flow field. These trajectories depend on many factors such as the air-flow field, domain geometry, wall and particle material combination, particle size and shape, particle density, and particle initial injection velocity, and location [19]. Particles are assumed to have a spherical shape in most of the published papers. The trajectories of nonspherical particles (ellipsoid, cylinder, disc, and so on) are also investigated [24]. After defining the particle trajectories, the internal surfaces of turbomachines subjected to excessive impacts are determined and the erosion rates are defined.

The *erosion rate* is defined as the mass removed from a surface per unit mass of particles impinging on the surface. According to most of the experimental results that have been conducted, the erosion depends on

1. Impact velocity and impact angle
2. Gas temperature
3. Material properties of erodent and target
4. Particle concentration
5. Mass of the particle

6. Particle composition
7. Erodent size
8. Other factors such as the time duration, the shape, and orientation of the particles during impacts

The erosion phenomenon can be classified into two categories, namely ductile and brittle erosion, depending on the target materials [25]. For the ductile mode, maximum erosion occurs at some angle between 20° and 30°. In brittle mode erosion increases with impingement angle and reaches its maximum at 90 degrees. Brittle mode in this case, the erosion leads to surface and subsurface cracking, and spalling of the target.

In one of the earliest analyses of ductile erosion [26] the particles were liken to the cutting edge of a tool which moves into the surface causing plastic deformation of the material and removal of the debris so formed (Figure 12.41). The erosion parameter was inter-related as a function of impact velocity, and impact angle.

Another model that accounts for erosion at all attack angles considered erosion to consist of two simultaneous processes, indentation deformation wear for high angle of attack and cutting wear for low angles [27]. A two-stage mechanism of erosion model [28] proposed that particles impacting at near-normal incidence may fragment, and the fragments may subsequently erode exposed surface features. Moreover, a decrease of erosion with decreasing particle size was noticed and the concept of a minimum particle size for effective erosion was introduced.

The model proposed in Reference 29 assumes that erosion occurs as the result of Hertzian contact stresses during impact. These stresses cause cracks to grow from pre-existing flaws in the target surface. The volume removed per impact is set proportionally to both the penetration depth and the area of the crack.

Both the impact angle and the impact velocity have the dominant effect on the erosion pattern. Figure 12.42 shows the effect of the impact angle on the erosion for different target materials:

$$\varepsilon = k_1 f(\beta) V^2 \cos^2\beta\left(1 - R_T^2\right) + k_3 \left(V \sin\beta\right)^4 \tag{12.39}$$

where

ε is the erosion parameter (g/g)
V is the impact velocity (m/s)
β is the impact angle (°)

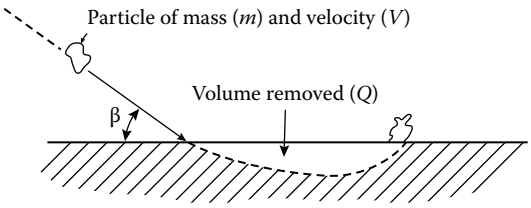


FIGURE 12.41
Ductile erosion simulation.

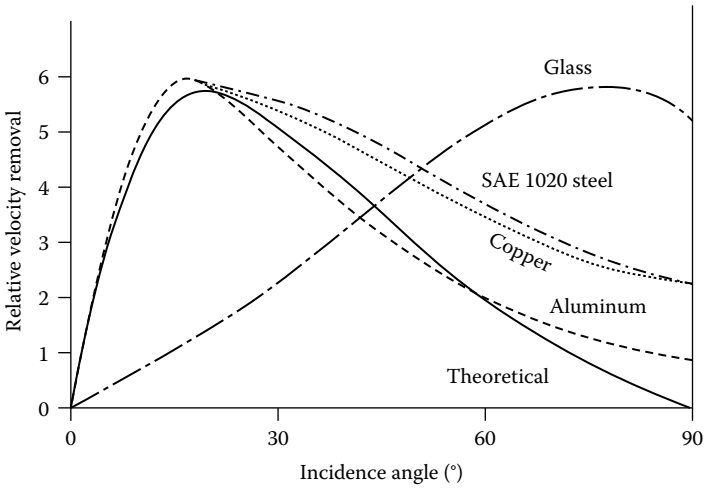


FIGURE 12.42
Effect of impingement angle on the erosion for different target material.

$$R_T = 1.0 - 0.00525V \sin\beta$$

$$f(\beta) = 1.0 + CK\left(k_{12} \sin\frac{\pi}{2}\frac{\beta}{\beta_0}\right)^2 \tag{12.40}$$

where

$$CK = \begin{cases} 1 & \beta \le \beta_0 \\ 0 & \beta > \beta_0 \end{cases} \quad \beta_0 \approx 20°$$

The values for the constants k_1, k_2, k_{12} are given in Table 12.5 for different particles and target material combinations.

In Equation 4.20, β_o is the impact angle at which the maximum erosion occurs. It has a value near 20° in case of the ductile erosion.

TABLE 12.5

Constants Used in Erosion Prediction by Equation 12.39

Material Particle	Surface	k_1 (g/g/(m/s)²)	k_{12}	k_3 (g/g/(m/s)⁴)
SiO_2	2024 Al	3.95×10^{-8}	0.585	6.95×10^{-13}
Al_2O_3	2024 Al	5.73×10^{-8}	0.585	10.43×10^{-13}
SiO_2	410 SS	6.53×10^{-8}	0.293	8.94×10^{-13}
Al_2O_3	410 SS	12.46×10^{-8}	0.293	25.3×10^{-13}
SiO_2	Ti–6Al–4v	5.32×10^{-8}	0.192	8.94×10^{-13}
Al_2O_3	Ti–6Al–4v	11.13×10^{-8}	0.192	24.9×10^{-13}

Source: Clevenger, W.B. and Tabakoff, W., *Erosion in Radial Inflow Turbines, Volume III: Trajectories of Erosive Particles in Radial Inflow Turbines*, NASA-CR 134700, Washington, DC, 1974.

12.8.2 Theoretical Estimation of Erosion

A theoretical estimation of the erosion rates of the internal surfaces of a centrifugal compressor is presented [30]. This estimation is based on an analytical study of the trajectories of particles through the impeller [31]. The analytical treatment of this problem may be described as follows: The particles are assumed to have no influence on the gas flow field. Thus the gas flow properties are obtained as if no particles were suspended. Next, the particle motion is obtained through the integration of the equations of motion of a particle superimposed on the fluid flow field. Both silicon dioxide and aluminum oxide particles were considered.

Figures 12.43 and 12.44 illustrate the trajectories of silicon dioxide particles having radii of 3 and 60 μm. Reviewing the different particle trajectories allowed the definition of the

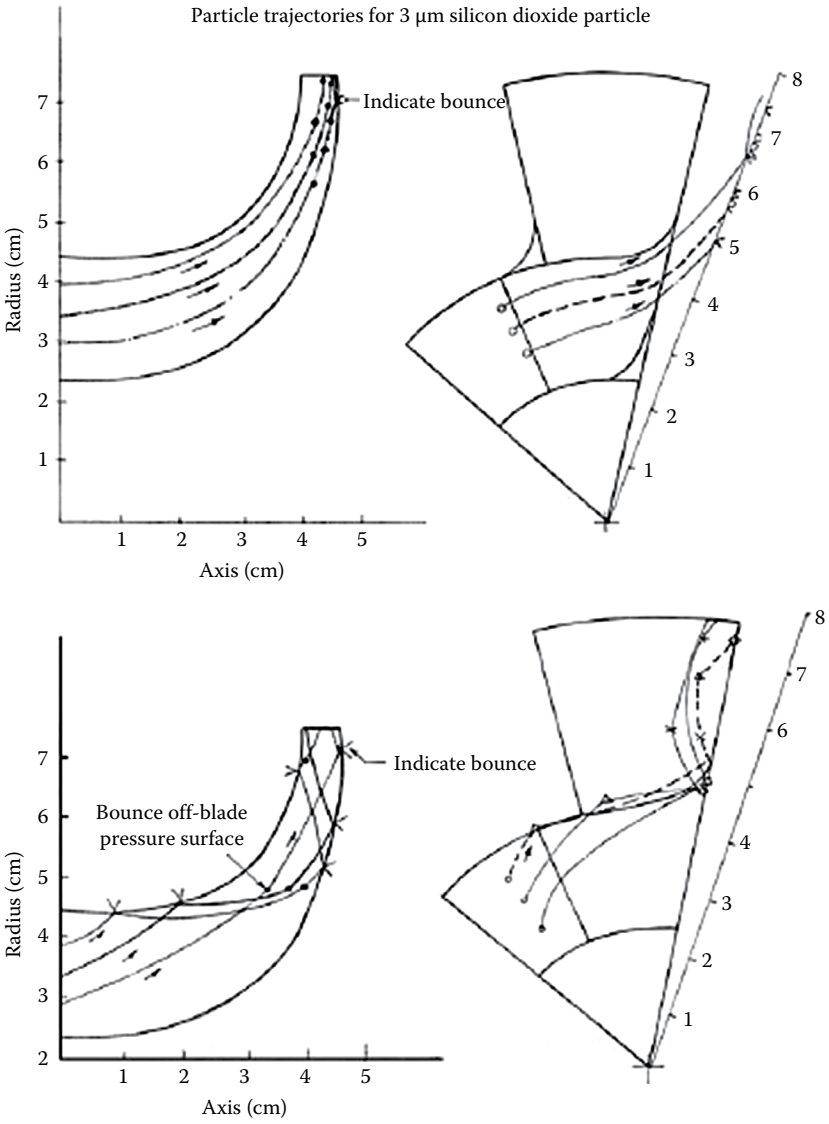


FIGURE 12.43
Particle trajectories of 3 and 15 μm silicon dioxide particles.

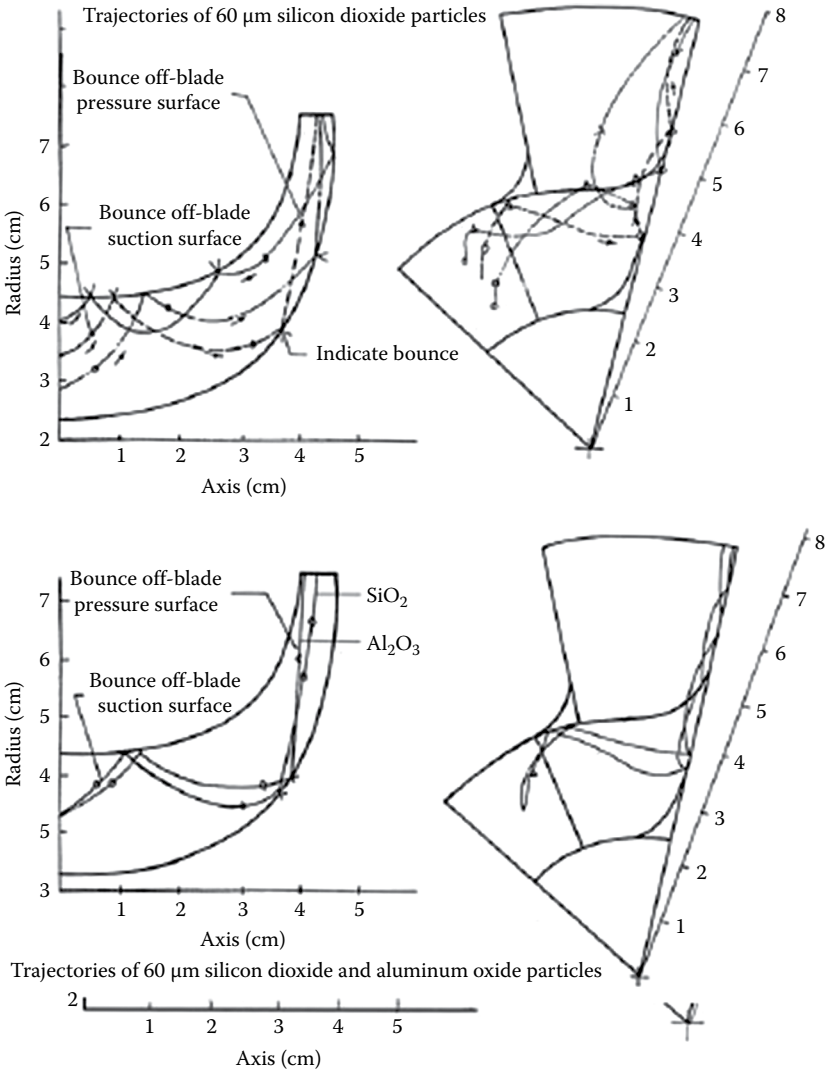


FIGURE 12.44
Particle trajectories of 60 μm silicon dioxide and aluminum oxide particles.

areas that are subjected to severe erosion rates. These will be the areas that are subjected to a higher number of collisions. Figure 12.45 or Figure 12.46 summarizes the data on the number and location of particle impacts with the impeller surfaces. Four critical areas were identified: namely, casing surface close to the inlet, two areas on the blade pressure surface and hub surface near the outlet of impeller. The blade suction surface was occasionally impacted by only massive particles. Even these few impacts occurred at relatively low-to-moderate incidence velocities and at relatively small incidence angles. On the contrary, the blade pressure surface was subjected to a great number of collisions. It is worth noting that the leading edge of the inducer and the curved section connecting to the straight blade of the impeller was subjected to a low number of impacts. The straight blade of the impeller was repeatedly impacted by small-and large-sized particles. The shroud surface was

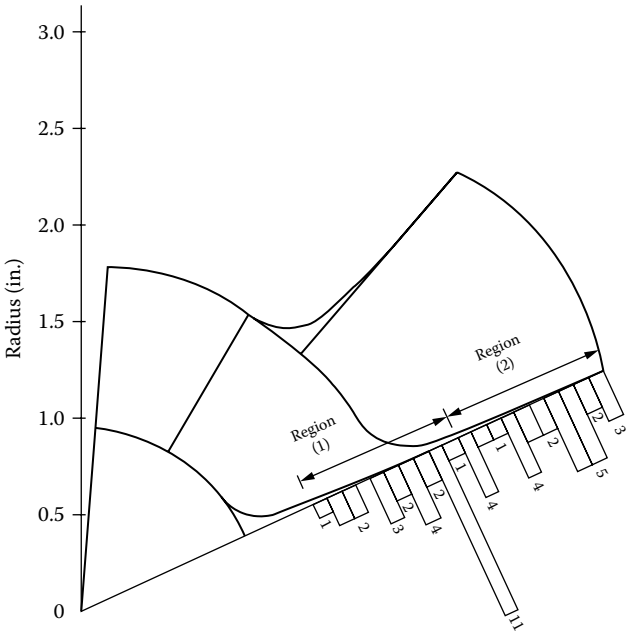


FIGURE 12.45
Summary of particle bounces and selected erosion test area (front view).

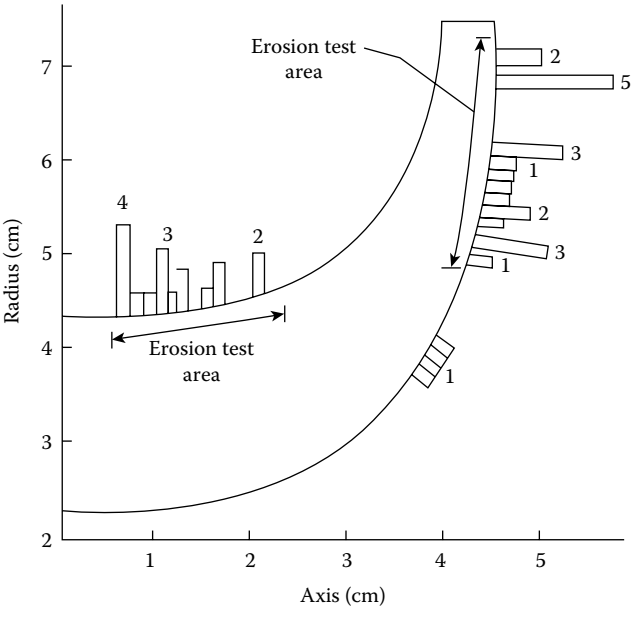


FIGURE 12.46
Summary of particle bounces and selected erosion test area (side view).

subjected to a moderate number of collisions. Two materials for the impeller were considered: 410 stainless steel and 2024 aluminum alloy.

The rates of erosion penetration of these different surfaces were calculated from a specified concentration of particulate flow. Particles diameters ranged from 3 to 60 μm. From the rates of erosion over the four selected areas, the depth of penetration after certain operating hours was defined. For the shroud surface, the depth of erosion of an aluminum alloy after 1000 operating hours was 0.688 mm, while this depth will be 0.4 mm for the 410ss. Concerning the blade pressure surface (region 1), the depth of penetration of a 2024 Al material was 1.3025 mm, while this depth was 1.166 mm for a 410ss material after 100 operating hours as

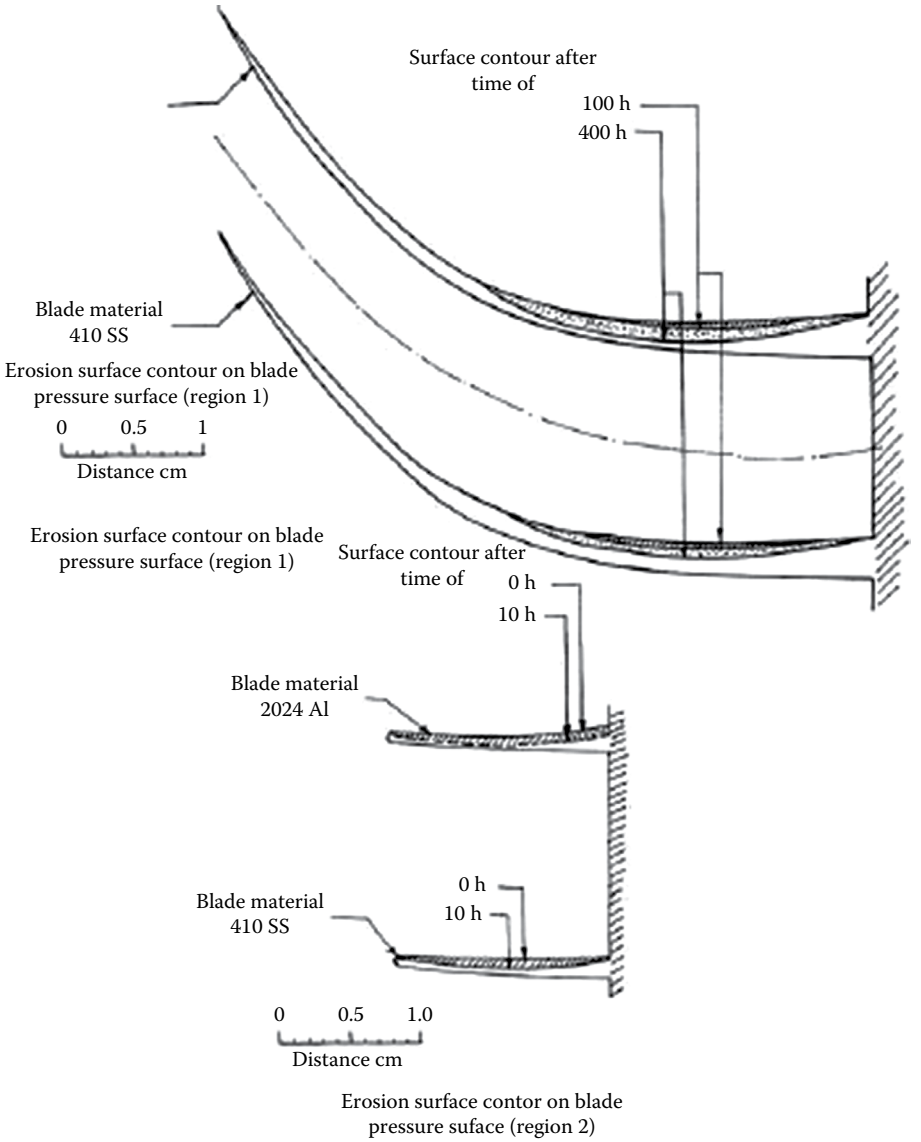


FIGURE 12.47
Erosion results for aluminum Al 2024 and 410 stainless steel impellers.

shown in Figure 12.34. Concerning region 2 of the blade pressure surface, after 100 operating hours, the depths of erosion of 2024 Al and 410ss materials were, respectively, 1.81 and 1.228 mm. The hub surface was subjected to the most severe erosion rates where after only one operating hour the depth of erosion will be 5.6 mm for 2024 Al material and 3.87 mm for 410ss material. These results are summarized in Figure 12.47 for both 410ss and 2024 aluminum alloy. The experimental work of Montgomery [20] outlined that after 25 operating hours there was visual evidence of severe erosion of the impeller. Tip wear at the top of the blades in addition to the undercutting of the blade near its root were reported. The hub surface was subjected to severe erosion damage as it was reported that particles with 0–5 μm diameter polished the leading side of the compressor blades and the area between the blades to an excellent micro finish. Further, the area near the blade root suffered from the worst erosion damage. This fact complies with the particle trajectory patterns, as most particles tended to strike the hub surface near the blade pressure surface. Similar results were reported in Reference 32 for a centrifugal compressor with splitter blades [33].

The severe erosion rates described emphasize that the material of the impeller must be changed to a more erosion-resistant one. Moreover, coatings may be added to increase the life time as well as time between overhaul (TBO) of the centrifugal compressor.

The titanium impeller of the engine powering the V-22 tilt-rotor aircraft (Osprey) had three different coatings. High-velocity sand-erosion tests were conducted with sand particles impacting these coatings and tested [34]. Erosion rates were reduced to 10%–30% of those of its original uncoated base material.

Problems

12.1 Choose the appropriate answer or answers:

1. Types of diffuser in centrifugal compressors (reaction-cascade-impulse- vaneless)
2. Types of prewhirl (positive-negative-zero-pipe)
3. The number of stages in centrifugal compressors in aircraft engines are (1–2–5–9)

12.2

1. Prove that the torque applied to the shown shaft of a centrifugal compressor is given by

$$\text{Torque } \tau = \dot{m}\left[\left(rC_u\right)_2 - \left(rC_u\right)_1\right]$$

   where C_u is the tangential component of the absolute velocity C.
2. For the centrifugal compressor diffuser, if the free vortex flow is assumed (rC_u = constant) and the static pressure and temperature (P and T) are constant, then prove that the absolute Mach number is inversely proportional to the radius r ($M \propto 1/r$). Also prove that $\alpha = \tan^{-1}(C_r/C_u) = \text{constant}$ which implies that the streamlines in the diffuser have a logarithmic spiral shape.

12.3 A turbojet engine incorporates a centrifugal compressor having the following data

$$T_1 = 283 \text{ K}, \quad P_{o_1} = 1 \text{ bar}, \quad M_1 = 0.3,$$

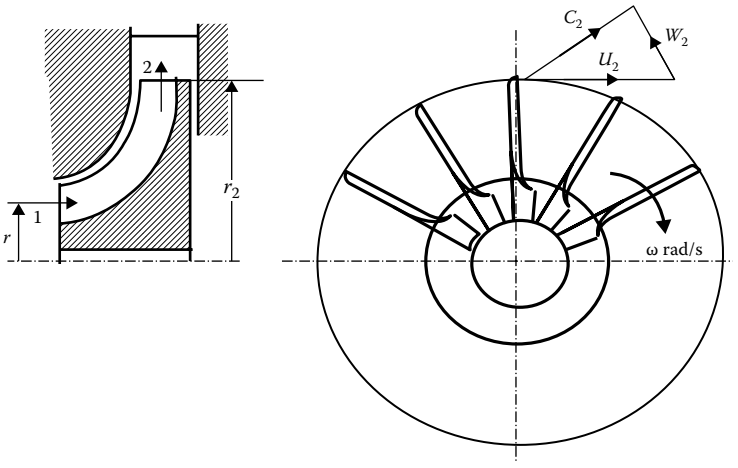


FIGURE 12.48
Problem_3.

$$\Psi = 1.04, \quad \sigma = 0.9, \quad \frac{P_{o_3}}{P_{o_1}} = 4.0 \text{ bar},$$

$$D_{e_r} = 0.15 \text{ m}, \quad D_{e_t} = 0.3 \text{ m}, \quad D_2 = 0.5 \text{ m}, \quad C_p = 1.005 \text{ kJ/kg} \cdot \text{K}$$

1. Calculate
   a. Temperature rise ΔT_o
   b. The velocities U_2, W_2, C_1 (assume flow enters axially and $C_{a_1} = C_{r_2}$)
   c. Relative Mach number at impeller tip
   d. Mass flow rate $\dot{m}$
2. Draw the velocity triangles at impeller inlet and outlet
3. Plot this operating point on the compressor map (Figure 12.48)

12.4 The figure is a cut-away view of the SR-30 gas-turbine engine that represents a small turbojet engine. It contains an inlet nozzle (intake), centrifugal compressor, combustion chamber, and an axial turbine and exhaust nozzle (Figure 12.49).

The centrifugal compressor has the following data:

$T_{01} = 300$ K	$P_{01} = 100$ kPa	$P_{03}/P_{01} = 3.0$
$P_2/P_1 = 1.94$	$P_3/P_2 = 1.48$	$C_1 = 106$ m/s
Maximum inlet relative Mach number $W_{1\max}/a_1 = 0.84$		
Maximum absolute Mach number at outlet $C_2/a_2 = 0.9$		
$D_h = 20.6$ mm	$D_s = 60.3$ mm	$D_2 = 102$ mm
$\psi = 1.04$	Number of blades = 18	

Assuming no prewhirl, it is required to

1. Calculate the air mass flow rate
2. Calculate the rotational speed
3. Calculate the temperature rise in the compressor

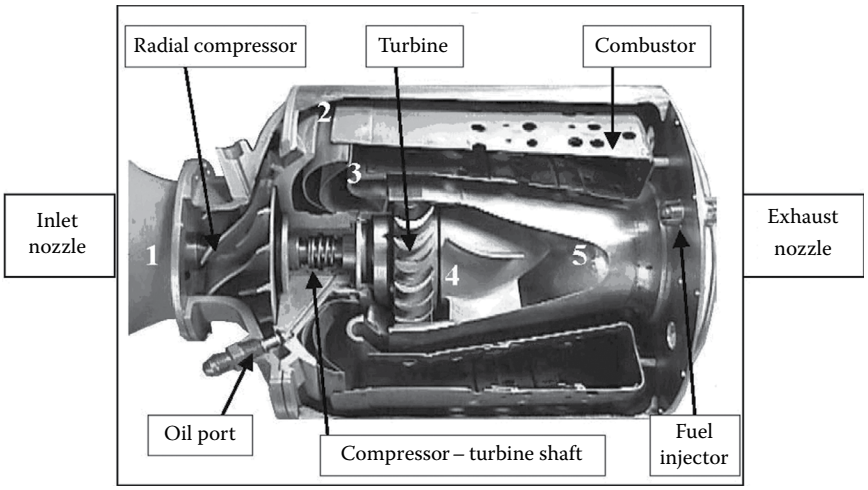


FIGURE 12.49
Problem_4. (From Witkowski, T. et al., Characterizing the performance of the SR-30 turbojet engine, ASE 2003-1133, *Proceedings of the 2003 American Society for Engineering Education Annual Conference & Exposition*, 2003.)

4. Prove that: $C_2 = \sqrt{2\gamma R M_2^2 T_{02}/2 + (\gamma - 1) M_2^2}$
5. Calculate the compressor efficiency
6. Calculate the losses in the impeller as a percentage of the total losses in the compressor
7. Calculate the impeller efficiency

12.5 A centrifugal compressor has a noninducer impeller (refer to Figure 12.10). It has 30 straight radial blades extending from an inlet radius of 0.12 m to an outer radius of 0.2 m and has a thickness of 0.5 cm. The velocity triangles have $C_{u1} = U_1$ and $C_{u2} = U_2$. The air mass flow rate is 30 kg/s. The impeller rotates at 300 rps. The impeller is made of an aluminum alloy with yield-shear strength—based on the distortion energy theorem—of 60 MPa. The blade roots are considered as 30 rectangles of dimensions 8 × 0.5 cm and its center has a radius of 16 cm.

Calculate the maximum shear stress at the roots of the blades and the corresponding factor of safety using the relation $\tau_{max} = Tr_{max}/J_o$.

12.6 A centrifugal compressor used in a small turbojet engine fitted with a can type combustion chamber is shown in Figure 12.50.

Measurement of the pressure, temperature, and velocity components at different locations in the compressor is listed in Table 12.6.

Other data are

Power input factor ψ = 1.04
Rotational speed N = 200 rps
Eye tip diameter = 0.3 m
Eye hub diameter = 0.14 m

If the flow in the stator is assumed to be a free vortex flow, it is required to

1. Draw the velocity triangles at impeller inlet and outlet
2. Calculate the percentage of the impeller losses out of the total losses in the compressor

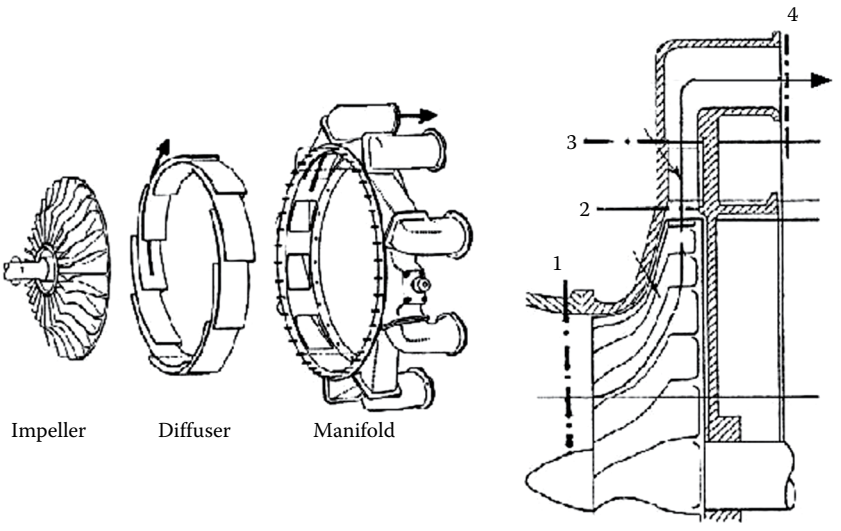


FIGURE 12.50
Problem_6.

TABLE 12.6

Measured Parameters at Different Locations Inside Compressor

Location	1	2	3	4
T_o (K)	290	374.7	374.7	374.7
P_o (kPa)	85	188.5	172	170
T (K)	288.4	339.8	351.1	374.5
P (kPa)	83.36	133.9	150.1	169.8
C_u (m/s)	—	263.4	216.8	—
C_r (m/s)	—	27.1	21.86	—
C_a (m/s)	57.0	—	—	16.8

3. Calculate the air mass flow rate into the compressor
4. Calculate the diffuser outlet diameter and width
5. Calculate the power needed to drive the compressor
6. Calculate the diameter of each manifold if air leaving the compressor is assembled in eight circular manifolds to direct the air to the eight cans of the combustion chamber

12.7 Three cases for a centrifugal compressor, namely radial, forward, and backward impellers are considered. The design conditions are as follows:

Inlet total temperature	$T_{o1} = 288$ K	Impeller outlet diameter	$D_2 = 0.50$ m
Inlet total pressure	$P_{o1} = 101$ kPa	Eye hub diameter	$d_{1h} = 0.15$ m
Mass flow rate	$\dot{m} = 9.0$ kg/s	Eye tip diameter	$d_{1t} = 0.30$ m
Rotational speed	$N = 270$ rev/s	Impeller isentropic efficiency	$\eta = 0.90$
Power input factor	$\psi = 1.04$		

Outlet angle for radial, backward, and forward impellers are 90°, 70°, and 110°, respectively. The impeller losses equal to 50% of the total compressor losses. Assume the inlet axial velocity is equal to the radial velocity ($C_a = C_r$).

1. Calculate the pressure ratio for the three types of compressors.
2. If the mass flow rate is decreased such that the new axial velocity at the inlet is reduced by 30% ($C'_a = 0.7C_a$) and, due to losses at the inducer, the impeller adiabatic efficiency is decreased to 0.87, calculate the new pressure ratio and power for the three cases.

Comment on the results (Figure 12.51).

12.8 The velocity triangles at inlet and outlet of the impeller of a centrifugal compressor are illustrated in Figure 12.52 drawn to a common apex.

1. Identify the velocities C and W at the inlet and outlet
2. What is the physical meaning of ζ_1 and ζ_2?
3. Prove that the power necessary for driving the compressor if the power input factor ψ is unity is given by

$$P = \frac{\omega \dot{m}^2}{\rho_1 \pi \left(r_{et}^2 - r_{eh}^2\right)} \left(r_2 \tan\zeta_2 - r_{em} \tan\zeta_1\right)$$

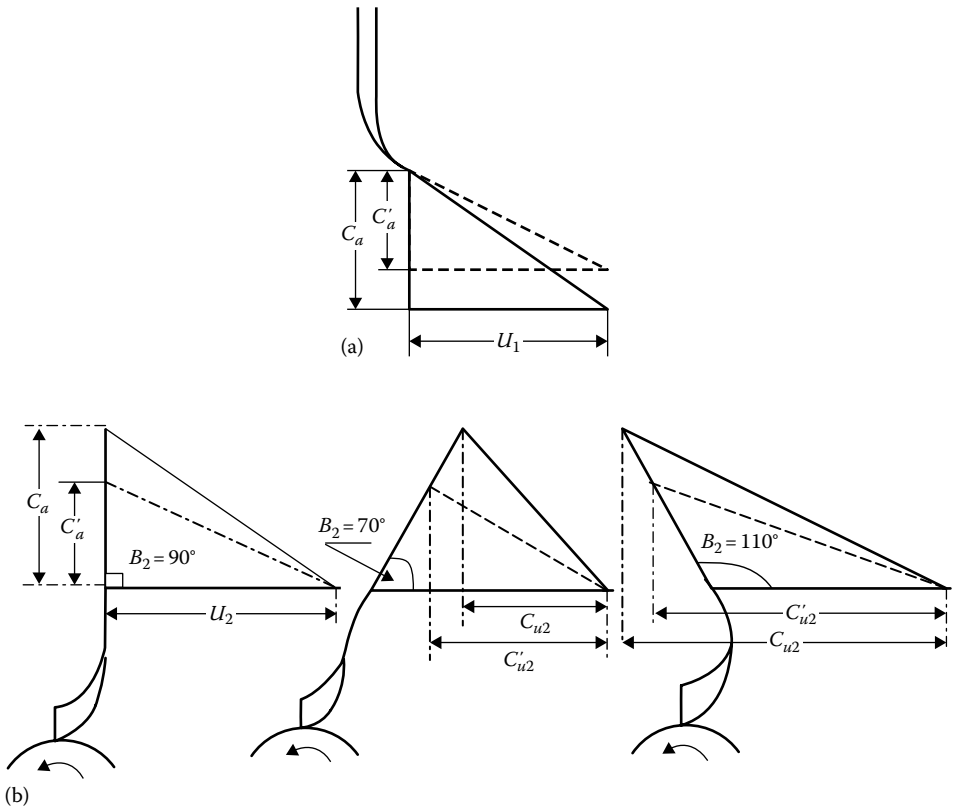


FIGURE 12.51
(a) Velocity triangle at inlet. (b) Velocity triangles at outlet.

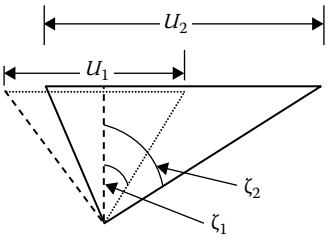


FIGURE 12.52
Inlet and outlet velocity triangles.

where subscripts (*et*, *eh*, and *em*) refer to the eye tip, eye hub, and eye mean respectively, and subscripts 1 and 2 refer to the compressor inlet and outlet.

4. What are the conditions of maximum power? Draw the velocity triangles in this case.
5. Prove that the compressor pressure ratio π_C is expressed as

$$\pi_C = \left[1 + \frac{\eta_C \omega \dot{m}}{\rho_1 \pi \left(r_{et}^2 - r_{eh}^2\right) C_P T_{o1}} \left(r_2 \tan\zeta_2 - r_{em} \tan\zeta_1\right)\right]^{\gamma/\gamma-1}$$

6. Write three disadvantages for each of the centrifugal and axial compressors.

12.9

1. For a centrifugal compressor, plot the process from the impeller inlet (state) to the volute outlet (state 4) on the T–S diagram.
2. Compare between the geometry of centrifugal compressors used in aircraft engines and those used in wind tunnels.
3. Explain why total-to-total isentropic efficiency cannot be employed for the diffuser of a centrifugal compressor.
4. Compare the compressor maps for axial and centrifugal compressors.
5. If the isentropic efficiency of the diffuser in a centrifugal compressor is defined as $\eta_d = (T_{3s} - T_2)/(T_3 - T_2)$, prove that $\eta_d = (AC - BD)/BE$, where

$$A = 1 + \eta_c \frac{\Delta T_0}{T_{01}}$$

$$B = 1 + \eta_{imp} \frac{\Delta T_0}{T_{01}}$$

$$C = T_{03} - \frac{C_3^2}{2C_P}$$

$$D = T_{03} - \frac{C_2^2}{2C_P}$$

$$E = \frac{C_2^2 - C_3^2}{2C_P}$$

12.10 A two stage centrifugal compressor has the following data:

	First Stage	**Second Stage**
Power input factor	1.04	1.04
Slip factor	0.90	0.90
Overall diameter of the impeller (m)	0.60	0.60
Eye root diameter (m)	0.16	0.16
Eye tip diameter (m)	0.32	0.28
Isentropic efficiency	0.78	0.80

The rotational speed is 240 rev/s, the air mass flow rate is 10 kg/s, and inlet stagnation conditions are $T_{o1} = 290$ K and $P_{o1} = 1.1$ bar. The total pressure drop in the inverted U-shape duct between the two stages is 5%. The first stage is identified by states from 1 to 3, while the second stage is identified by states from 4 to 6.

Calculate

1. The overall pressure ratio of the compressor.
2. If $\rho_1 = 1.234$ kg/m^3, $C_{a_1} = C_{r_2}$, $C_{a_4} = C_{r_5}$, calculate the diffuser depth for each stage.
3. The power needed to drive the compressor.

12.11 The following results were obtained from a test on a small single-sided centrifugal compressor:

Compressor delivery stagnation pressure	2.97 bar
Compressor delivery stagnation temperature	429 K
Static pressure at impeller tip	1.92 bar
Mass flow rate	0.6 kg/s
Rotational speed	766 rps
Ambient pressure	0.99 bar
Ambient temperature	288 K

Calculate the overall isentropic efficiency of the compressor. The diameter of the impeller is 16.5 cm, the axial depth of the vaneless diffuser is 1.0 cm and the number of the impeller vanes is 17. Making use of Stanitz equation for the slip factor, calculate the stagnation pressure at the impeller tip and hence find the fraction of the overall losses that occur in the impeller.

12.12 A single-stage, centrifugal compressor receives air at a stagnation pressure of 1.013 bar and a stagnation temperature of 288 K. The rotor tip speed is 450 m/s and the velocity at the impeller eye is 100 m/s. The inlet (eye) hub and shroud diameters are 6 and 12 cm, respectively. There are 12 blades on the impeller. Determine the vane angle, β_2' required to obtain a stagnation pressure ratio across the compressor of 2.0. The rotational speed is 36,000 rpm. Assume that the slip factor is 0.95.

12.13 A double-sided centrifugal compressor has the following characteristics:

1. Mass flow rate 50 kg/s, which is divided equally between the front and back faces of impeller
2. Power input factor $\psi = 1.04$
3. Number of impeller blades $n = 20$
4. Rotational speed $N = 300$
5. Isentropic efficiency $\eta_c = 0.78$
6. Inlet stagnation temperature $T_{01} = 295$ K
7. Inlet stagnation pressure $P_{01} = 1.05$ bar
8. Power required to drive the compressor 9.8 = MW
9. Absolute Mach number at impeller outlet $M_2 = 1.1$
10. Eye tip diameter is double the eye root diameter
11. Assuming that $C_{r2} = C_{a1}$, it is required to calculate:
    1. Temperature rise in the compressor $(T_{03} - T_{01})$
    2. Overall diameter of impeller D_2
    3. The absolute velocity at impeller outlet C_2
    4. Axial velocity at impeller inlet C_{a1}
    5. Eye root and tip diameters
    6. Pressure drop in the stator $(P_{02} - P_{03})$

12.14 In what case, is the specific work of a centrifugal compressor expressed by the relation

$$w = U_2^2 - U_1^2$$

Next, it is required to

1. Draw the impeller shape
2. Draw the corresponding velocity triangles
3. Prove that if $C_{a1} = C_{r2}$, then $W_1 = W_2$
4. if $W_1/U_1 = 0.6$ and $U_1/U_2 = 0.4$, prove that

$$\frac{C_2}{C_1} = 2.2$$

12.15 A light business executive transport is powered by two turboprop engines. Each engine is fitted with two centrifugal compressors. The engines are running in polluted weather; hence they are subjected to sand-particle ingestion that erodes the blades of the low-pressure compressor. Such erosion of the impeller blades at inlet causes separation of flow from the suction side of impeller blades at inlet and increases eddies and vortices in the flow leaving the impeller. Thus, the circumferential component of the absolute velocity leaving the impeller is reduced by 10% $\left(C'_{u2} = 0.9C_{u2}\right)$. It is required to Problem 12.16

1. Calculate the ratio between the temperature rise before and after erosion:

$$\frac{\Delta T_0'}{\Delta T_0}$$

2. Prove that the drop in the pressure ratio due to erosion is given by

$$\pi_c - \pi_c' \approx 0.1 \frac{\gamma}{\gamma - 1} \eta_c \frac{\Delta T_0}{T_{01}}$$

3. Now to restore the same pressure ratio of the eroded compressor, the rotational speed of the compressor has to be increased. What will be the ratio between this rotational speed and the original one?
4. Next, if the angle of the relative velocity (W_1) at impeller inlet is maintained constant with axial direction before and after increasing the rotational speed, what will be the increase in the mass flow rate in this case?
5. Plot the original and final state on the compressor map.

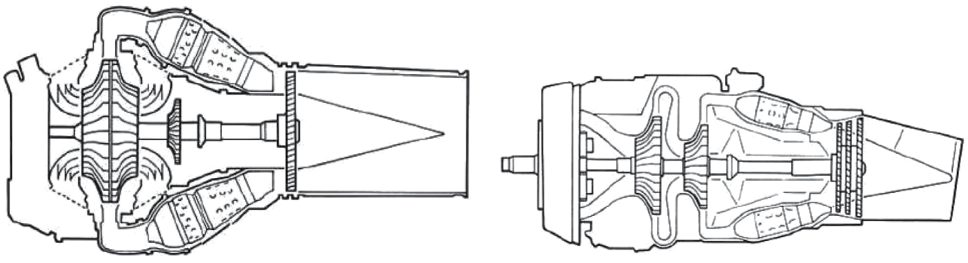
12.16 Figure 12.53 illustrates two centrifugal compressors in two arrangements (I) double entry and (II) single entry. If the overall pressure ratio of the two arrangements is equal, compare between the pressure ratios of each compressor.

Why the second compressor in arrangement (II) is smaller than the first?

12.17 A centrifugal compressor has the following characteristics:

Power coefficient	$\Psi = 1.042$
Tip rotational speed	$U_2 = 450$ m/s
Rotational speed	$N = 18{,}000$ rpm
Inlet total pressure	$P_{01} = 1.0$ bar
Inlet total temperature	$T_{01} = 288$ K
Inlet absolute velocity	$C_1 = 140$ m/s
Mean eye diameter	0.2 m
Isentropic efficiency	0.8

Figure 12.54 represents combined inlet and outlet velocity triangles at three cases of operation.



(a) (b)

FIGURE 12.53
(a) Double entry versus (b) single entry two-stage compressor.

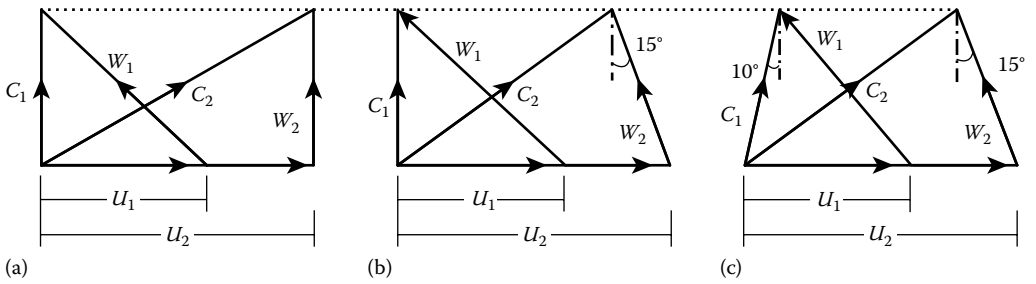


FIGURE 12.54
Three cases of compressor with and without prewhirl. (a) Zero pre-whirl and zero outlet slip, (b) zero pre-prewhirl and finite slip at outlet, and (c) finite Inlet prewhirl and finite slip at outlet.

1. It is required in *each case* to define:
   a. Slip factor (σ) and prewhirl angle (ξ)
   b. Temperature rise (ΔT_0) and compressor pressure ratio (π_c)
2. Compare between the three cases and explain the advantages and disadvantages of prewhirl

12.18 The centrifugal compressor stage of the compressor has backward-swept blades as shown in Figure 12.55. It has also the following data:

$$U_{1m} = 300 \text{ m/s}, \quad \dot{m} = 10 \text{ kg/s}, \quad T_{01} = 450 \text{ K}$$
$$P_{01} = 4 \text{ bar}, \quad U_2 = 500 \text{ m/s}, \quad W_2 = 200 \text{ m/s}$$
$$\beta_2 = 30°, \quad \eta = 0.85$$

Zero swirl and zero slip are assumed at inlet and outlet stages respectively.

1. Calculate stage pressure ratio and the impeller outlet area (A_2).
2. If the relative velocity (W_2) is doubled while the rotational speed is kept constant as shown in Figure 12.56, recalculate the stage pressure ratio and mass flow rate.
3. Plot the relation between the specific total enthalpy (Δh) and the mass flow rate ($\dot{m}$)
4. If the mass air flow is $\dot{m} = 12$ kg/s, what will be the pressure ratio and the relative velocity W_2?

12.19 A centrifugal compressor has radial blades as well as the following data:

$$M_1 = 0.4, \quad M_{1rel} = 0.7, \quad T_{01} = 290 \text{ K}, \quad P_{01} = 110 \text{ kPa},$$
$$r_{1m} = 0.2 \text{ m}, \quad r_2 = 0.5 \text{ m}, \quad W_2 = C_1, \quad \rho_2 = 2.5 \text{ kg/m}^3,$$
$$\Delta P_{0diffuser} = 101 \text{ kPa}, \quad C_1 = C_{a1}, \quad W_{r2} = W_2, \quad b_2 = 0.04 \text{ m}$$

Losses in the impeller are 55% of the compressor total losses. Diffuser outlet radius $r_3 = 0.65$ m.

Calculate

1. Rotational speed (N)
2. Absolute Mach number at impeller exit M_2

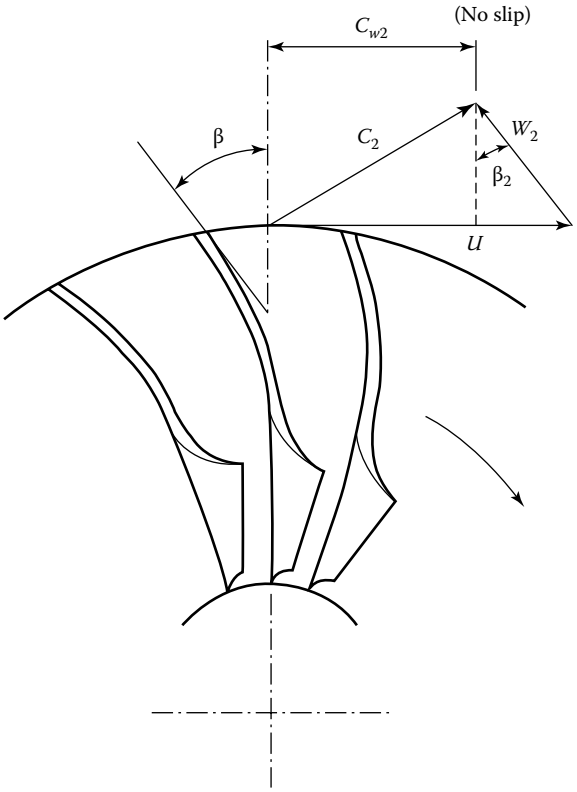


FIGURE 12.55
Backward swept centrifugal compressor.

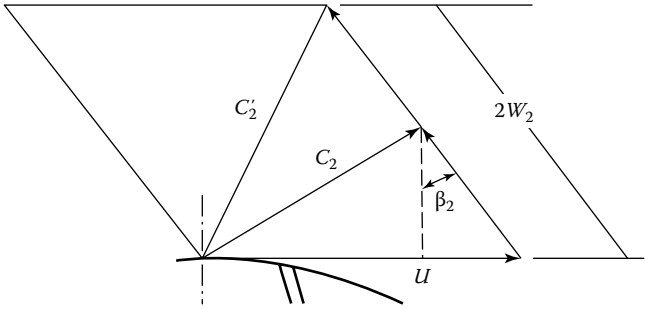


FIGURE 12.56
Velocity triangles for two cases of outlet relative speed.

3. Total pressures P_{02} and P_{03}
4. Impeller and compressor efficiencies η_{imp}, η_c
5. Radius inside the diffuser ($r*$) where the absolute speed is sonic ($C = a$)
6. Mach number at diffuser outlet M_3
7. Mass flow rate
8. Inlet hub to tip ratio $\zeta_i = r_{1h}/r_{1t}$

Assume that

$$\frac{C_2}{C_3}=\frac{C_{r2}}{C_{r3}}=\frac{C_{u2}}{C_{u3}}=\frac{r_3}{r_2}$$

12.20 The performance of a centrifugal compressor is illustrated by the shown map. Prove that the pressure ratio is given by the relation

$$\pi_c=\left[1+\eta_c\frac{\Delta T_0}{T_{01}}\right]^{\gamma/\gamma-1}\approx 1+\frac{\gamma}{\gamma-1}\eta_c\frac{\Delta T_0}{T_{01}}$$

During acceleration from state (1) to state (2), the operating conditions were changed from

$$N_1,\pi_1,\dot{m}_1,\eta_{c1}\ \text{ to }\ N_2,\pi_2,\dot{m}_2,\eta_{c2}$$

Prove that the increase in pressure ratio is expressed by the relation

$$\Delta\pi_c=B\left(\eta_{c2}N_2^2-\eta_{c1}N_1^2\right)$$

where

$$B=\left(\frac{\sigma\psi}{RT_{01}}\right)\left(\pi D_2\right)^2$$

The compressor has the following data:

$$\sigma=0.9,\quad \psi=1.04,\quad A_1=0.1\ \text{m}^2,\quad D_2=0.5\ \text{m},\quad \eta_{c1}=0.8,\quad \eta_{c2}=0.82,$$

$$N_1=280\ \text{rps},\quad N_2=300\ \text{rps},\quad C_1=150\ \text{m/s},\quad T_{01}=295\ \text{K},\quad P_{01}=110\ \text{kPa}$$

Calculate

1. The mass flow rate $\dot{m}_1$
2. The increase in compressor pressure ratio $\Delta\pi_c$.
3. If the mass flow rates are related by the equation: $\dot{m}_2=1.1\dot{m}_1$, the density at compressor inlet ρ_1 is assumed constant in both cases of N_1 and N_2, calculate the new mass flow rate ($\dot{m}_2$).
4. If a variable angle stator is employed in the diffuser, draw the two velocity triangles at impeller outlet and calculate the necessary angle of rotation of stator from cases (1) and (2). Assume the relation between the axial velocity at impeller inlet and radial velocity at impeller outlet are given by the relation: $C_{a1}=W_{r2}$ (Figure 12.57).

12.21 Figure 12.58 illustrates a single-stage centrifugal compressor where states are identified as follows:

1. Compressor inlet
2. Impeller outlet

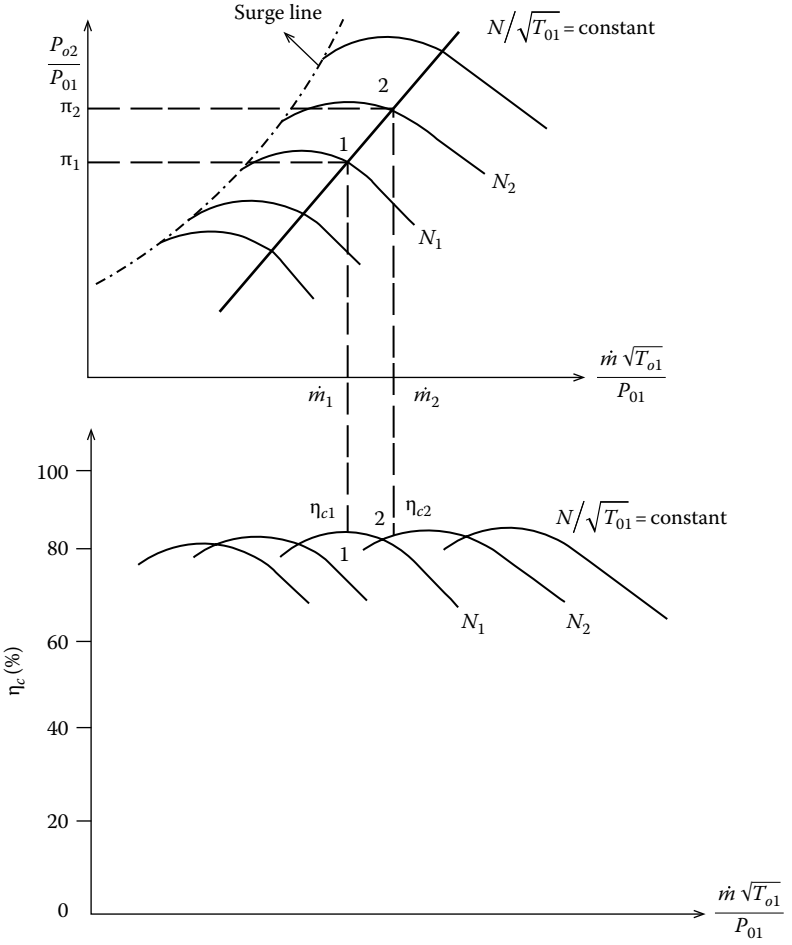


FIGURE 12.57
Compressor map.

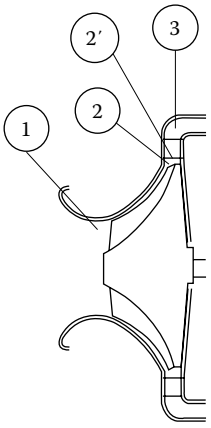


FIGURE 12.58
Single stage centrifugal compressor map.

2′: Stator inlet

3: Stator outlet

Rotational speed N = 200 rps

$$\eta_{imp} = 0.87, \quad \eta_{comp} = 0.85, \quad b_2 = b_{2'} = b_3 = 0.05 \text{ m}$$
$$P_{02'} = 0.998 P_{02}, \quad r_2 C_{u2} = r_{2'} C_{u2'} = r_3 C_{u3}$$

Other data are listed in the following table:

State	1	2	2′	3
T_0 (K)	290.3	374.5	?	?
P_0 (kPa)	?	?	?	?
T (K)	?	?	?	?
P (kPa)	101	?	?	?
C_u (m/s)	15	263.4	?	?
C_r (m/s)	—	30	?	?
C_a (m/s)	60	—	—	—
C (m/s)	?	?	258.4	215
r (m)	0.12	?	0.2692	0.3235

1. Calculate

$$\text{Rotational speed}(U_2), \text{ Mass flow rate}(\dot{m}), \text{ Slip factor}(\sigma)$$

2. Complete the table
3. Draw velocity triangles at inlet and outlet of impeller
4. Draw on T-s (Mollier) diagram static and total conditions of states (1, 2, 2′ and 3)

12.22 The blades shown in Figure 12.59 illustrates a radial impeller of a centrifugal compressor. Blades are made of stainless steel AISI 1010 having a density of 7832 kg/m^3 and welded to the hub as shown. The pressure values at the blade inlet and outlet have the following values:

$$P_1 = 80 \text{ kPa}, \quad P_1' = 65 \text{ kPa}, \quad P_2 = 180 \text{ kPa}, \quad P_2' = 150 \text{ kPa}$$

The blade dimensions are: $L = 150$ mm, $b = 40$ mm and $t = 5$ mm. The blade is welded using AWS Electrode number E60xx which yield strength is 900 MPa, calculate the weld thickness (t_1) if each blade is welded from both sides and the factor of safety is assumed 5.0. $r_1 = 200$ mm, $N = 100$ rev/s

12.23 The shown centrifugal compressor in Figure 12.60 is of the backward-leaning type. The impeller is fouled due to operating in a polluted environment. Fouling is defined as an accumulation of debris in the impeller or blade passage that reduces the flow area and roughens the surface finish. This leads to an increase of radial velocity of air at the impeller outlet as well as a reduction of compressor efficiency. A brand-new compressor has the following data:

$$\dot{m} = 20 \text{ kg/s}, \; C_{a1} = C_{r2} = 100 \text{ m/s}, \; U_2 = 400 \text{ m/s}, \; P_{01} = 1.0 \text{ bar}, \; T_{01} = 300 \text{ K}, \; \eta_c = 82\%, \; \beta_2 = 30°$$

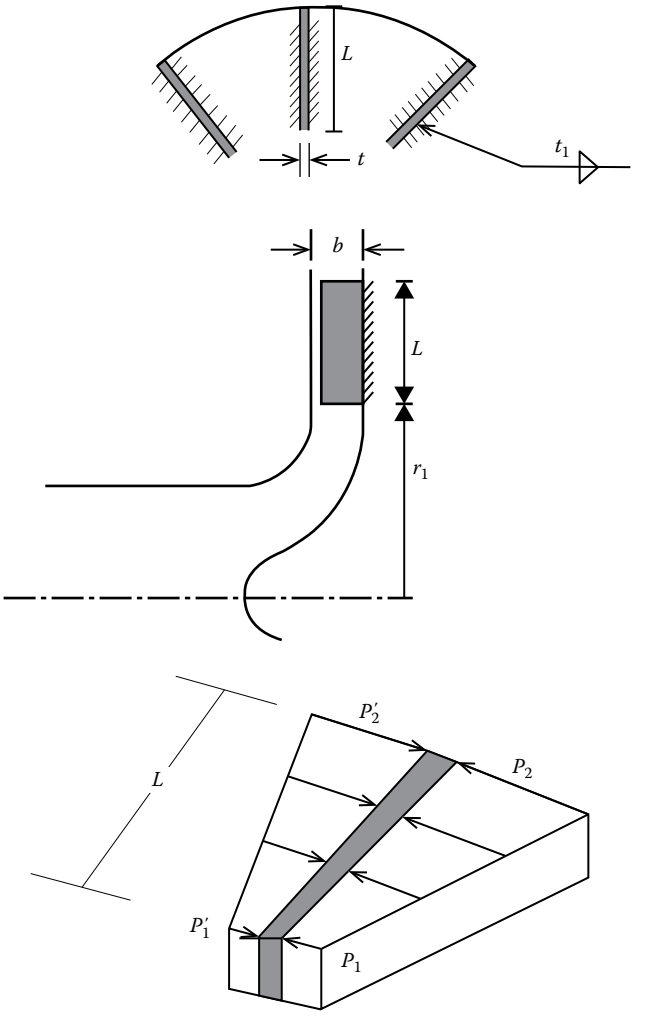


FIGURE 12.59
Radial blade impeller.

Due to fouling; radial velocity increased by 10%, while compressor efficiency decreases; thus,

$$\left(C_{r2}\right)_{fouled} = 110\%\left(C_{r2}\right)_{new} \quad \text{and} \quad \left(\eta_c\right)_{fouled} = 80\%$$

If $r_2 = 2r_{1mean}$, calculate for both new and fouled cases:

1. Total temperature rise (ΔT_0)
2. Compressor pressure ratio (π_c)
3. Absolute outlet velocity (C_2)
4. Angle (α_2) between (U_2) and (C_2)
5. Percentage of decrease in outlet area (A_2)

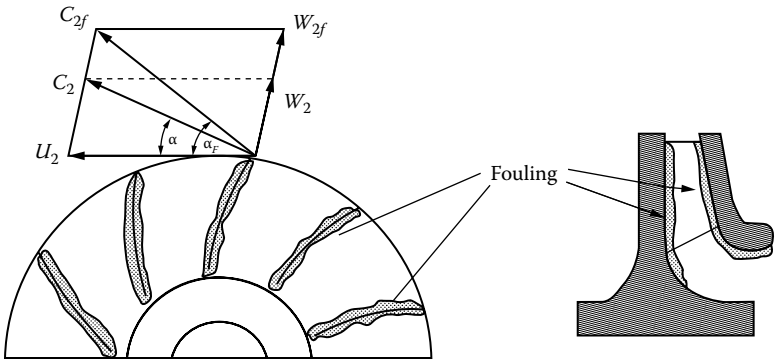


FIGURE 12.60
Velocity triangles for new and fouled centrifugal compressor.

12.24 A two-stage centrifugal compressor (Figure 12.17) has the following data:

	First Stage	Second Stage
Power input factor	1.04	1.04
Slip factor	0.9	0.9
Overall diameter of the impeller (m)	0.6	0.6
Eye root diameter (m)	0.16	0.16
Eye tip diameter (m)	0.32	0.32
Isentropic efficiency	0.78	0.8
Mechanical efficiency	0.95	0.8

The rotational speed is 240 rps, air mass flow rate is 10 kg/s, inlet stagnation conditions are T_{01} = 330 K and P_{01} = 1.15 bar. The total pressure drop in the duct between the two stages is ΔP_{03-4} = 5%. Calculate

1. The overall pressure ratio of the compressor
2. If $\rho_1 = 1.234$ kg/m^3, $C_{a1} = C_{r2}$, $C_{a4} = C_{r5}$, calculate the diffuser depth for each stage
3. The power needed to drive the compressor

12.25

1. Compare the stator in a centrifugal compressor with a radial turbine
2. Compare the impeller of a centrifugal compressor with the rotor of an axial compressor
3. A centrifugal compressor has the following data:

Mass flow rate is 80 kg/s
Inlet conditions: $T_{01} = 300$ K, $P_{01} = 1.1$ bar, $C_1 = 100$ m/s
Impeller: $\dfrac{P_{02}}{P_{01}} = 4.0$, $\eta_{imp} = 0.84$, $U_2 = C_2 = 400$ m/s, $N = 6000$ rpm
Diffuser: $\dfrac{P_3}{P_2} = 1.2$, $\dfrac{r_3}{r_2} = 1.2$, $b_2 = b_3 = 0.1$ m, $\rho_2 = \rho_3$
Calculate

a. Impeller outlet conditions (T_{02}) and (P_{02})
b. Slip factor (σ)

c. Total pressure drop in stator ($P_{02} - P_{03}$)
d. Compressor efficiency (η_c)
e. Ratio between losses in impeller and stator

References

1. R.N. Brown, *Compressors-Selection and Sizing*, Gulf Publication Co., Houston, TX, 1981, Chapter 1.
2. R.T.C. Harman, *Gas Turbine Engineering, Applications, Cycles and Characteristics*, John Wiley & Sons, New York, 1981, 7pp.
3. A. Whitfield and N.C. Baines, *Design of Turbomachines*, Longman and Scientific & Technical, Harlow, U.K., 1990, 3pp.
4. D.P. Kenny, The history and future of the centrifugal compressor in aviation gas turbines, First Cliff Garrett Turbomachinery Award Lecture, SAE paper SAE/SP-802/602.
5. Hitachi Compressor. Centrifugal Compressor: Hitachi Centrifugal Compressor. www.hitachi.com/businesses/infrastructure/.../compressor/pdf/E35_04(H)_English.pdf.
6. H.I.H. Saravanamuttoo, G.F.C. Rogers and H. Cohen, *Gas Turbine Theory*, 5th edn., Prentice Hall, Harlow, U.K., 2001, 167pp.
7. J.D. Staintz, Some theoretical aerodynamic investigations of impellers in radial and mixed flow centrifugal compressors, *Transactions of ASME*, 74, 473, 1952.
8. J.E. Shigley and C.R. Mischke, *Mechanical Engineering Design*, 5th edn., McGraw-Hill Book Company, New York, 1989, 65pp.
9. N.A. Cumpsty, *Compressor Aerodynamics*, Longman Scientific & Technical, Harlow, U.K., 1989, 71pp.
10. P. Hill and C. Peterson, *Mechanics and Thermodynamics of Propulsion*, 2nd edn., Addison Wesley Publication Company, Inc., Reading, MA, 1992, 431pp.
11. S.L. Dixon and C.A. Hall, *Fluid Mechanics and Thermodynamics of Turbomachinery*, 6th edn., Butterworth/Heinemann, Boston, MA, 2010, 155pp.
12. S.L. Dixon, *Fluid Mechanics and Thermodynamics of Turbomachinery*, 4th edn., Butterworth-Heinemann, Boston, MA, 1998, 213pp.
13. P.W. Runstadler, F.X. Dolan, and R.C. Dean, *Diffuser Data Book*, Vol. 186, Creare TN, Hanover, Germany, 1975.
14. D. Japikse, *Turbomachinery Diffuser Design Technology*, DTS-1, Concepts ETI, Norwich, VT, 1984.
15. D.G. Wilson and T. Korakianiti, *The Design of High-Efficiency Turbomachinery and Gas Turbines*, 2nd edn., Prentice-Hall, 1998, 180pp.
16. *The Aircraft Gas Turbine Engine and Its Operation*, P&W Oper. Instr. 200, Part No. Pratt & Whitney P&W 182408, 1988, pp. 3–81.
17. Unpaved runways operation-737, Boeing Airliner, *Boeing Magazine*, April 1975.
18. M.F. Hussein, Dynamic characteristics of solid particulate flow in rotating turbomachinery, PhD dissertation, University of Cincinnati, Cincinnati, OH, 1972.
19. W.B. Clevenger and W. Tabakoff, *Erosion in Radial Inflow Turbines, Volume III: Trajectories of Erosive Particles in Radial Inflow Turbines*, NASA-CR 134700, Washington, DC, 1974.
20. A.F. El-Sayed, Aerodynamics of air carrying sand- particulate flow in centrifugal compressors, PhD dissertation, Cairo University, Cairo, Egypt, 1978.
21. J.E. Newhart, Evaluating and controlling erosion in aircraft turbine engines, Paper No. 21, *Proceedings of the National Conference on Environmental Effects on Aircraft and Propulsion Systems*, 1974.
22. W. Kurz, Comparison of model and flight testing with respect to hot gas reingestion and debris ingestion during thrust reversal, Paper No. 13, *Proceedings of the Fifth International Symposium on Airbreathing Engines (5th ISABE)*, Bangalore, India, February 1981.

23. United Technologies Pratt & Whitney, Reingestion caused by thrust reverser operation, Videotape P/N 807833, December 1988.
24. A.T. Lloyd, Vulcan's blast, *BOEING Airliner*, April–June 1990, pp. 15–21.
25. A.F. El-Sayed and W.T. Rouleau, The effect of different parameters on the trajectories of particulate in a stationary turbine cascade, *Proceedings of the Third Multi-Phase Flow and Heat Transfer Symposium Workshop*, Miami Beach, FL, 1983.
26. C.E. Smeltzer, M.G. Gulden, and W.A. Compton, Mechanisms of metal removal by impacting dust particles, *Journal of Basic Engineering*, 92, 639, 1970.
27. I. Finnie, The mechanism of erosion of ductile materials, *Proceeding of Third National Congress of Applied Mechanics*, pp. 527–532, 1958.
28. J.G.A. Bitter, A study of erosion phenomena, Part I and II, *Wear*, 6, 5–21, 169–190, 1963.
29. G.P. Tilly, A two stage mechanism of ductile erosion, *Wear*, 23, 87–96, 1973.
30. G.L. Sheldon and I. Finnie, The mechanism of material removal in the erosive cutting of brittle materials, *Journal of Engineering for Industry*, 88, 393–400, 1966.
31. M.I.I. Rashed and A.F. Abd-el-Azim El-Sayed, Erosion in centrifugal compressor, *Proceedings of the Fifth International Conference on Erosion by Solid and Liquid Impact, ELSI V*, Cambridge, U.K., September 1979.
32. A.F.A.A. El-Sayed and M.I.I. Rashed, Particulate trajectories in centrifugal compressors, *Proceedings of Gas Borne Particles Conference, Institute of Mechanical Engineers, Paper C61/81, I. Mech. E*, Oxford, U.K., 1981.
33. S. Elfekki and W. Tabakoff, Erosion study of radial flow compressor with splitter, *ASME Journal of Turbo-Machinery*, 109, 62–69, 1987.
34. G.Y. Richardson, C.S. Lei, and W. Tabakoff, Erosion testing of coatings for V-22 aircraft applications, *International Journal of Rotating Machinery*, 9(1), 35–40, 2003.
35. T. Witkowski, S. White, C. Ortiz Dueñas, P. Strykowski, and T. Simon, Characterizing the performance of the SR-30 turbojet engine, ASE 2003-1133, *Proceedings of the 2003 American Society for Engineering Education Annual Conference and Exposition*, 2003.

13

Axial Flow Compressors and Fans

13.1 Introduction

Since day one of the gas turbine engine, the compressor was the key component for success and always required high development efforts and costs. The importance of the compressor for modern high bypass ratio engines is demonstrated by the fact that 50%–60% of the engine length, up to 40%–50% of the weight, 35%–40% of the manufacturing costs, and 30% of the maintenance costs are taken up by the compression system. The advances in compressors allow aeroengines to operate with core engine thermal efficiency in the range of 50% while the propulsive efficiency approaches 80% [1].

Axial compressors are those in which the air flows mainly parallel to the rotational axis. Axial flow compressors have a large mass flow capacity, high reliability, and high efficiency, but have a smaller pressure rise per stage (1.1:1–1.4:1) than centrifugal compressors (4:1–5:1). However, it is easy to link together several stages and produce a multistage axial compressor having pressure ratios up to 40:1, as in recent compressors. Integrally bladed rotors permit blade speeds significantly above conventional rotors and hence stage pressure ratios greater than 1.8 [1]. Axial compressors are widely used in gas turbines, notably jet engines, wind tunnels, air blowers, and blast furnaces. Engines using an axial compressor are known as axial flow engines. Almost all present-day jet engines use axial flow compressors, the notable exception being those used in helicopters, where the smaller size of the centrifugal compressor is useful. The fan in turbofan engines is also an axial compression module, which is treated as an axial compressor having less blades of very large height, wide chord, and large twist. These fans may be single stage, or up to three stages, in low bypass turbofan engines. Jet engines nowadays use two or three axial compressors for higher pressure ratios. Nearly all the turbojet engines are of the two-spool type, which have two compressors identified as low and high pressure. Two-spool turbofan engines have the fan as the low-pressure spool. Sometimes, this fan represents the first stage of the low-pressure compressor. The fan in this case is followed by a few stages of an axial compressor, which represents the first module of the engine core. In other turbofans the fan on its own represents the low-pressure compressor, which is followed by the high-pressure compressor. Three-spool turbofan engines have a fan, an intermediate pressure, and a high-pressure compressor. The low-pressure compressor turns at the lowest rpm while the high-pressure compressor turns at the highest speed.

A typical axial compressor depicted in Figure 13.1 has a series of rotating "rotor" blades followed by a stationary "stator" set of blades that are concentric with the axis of rotation. The compressor blades/vanes are relatively flat in section. Each pair of rotors and stators

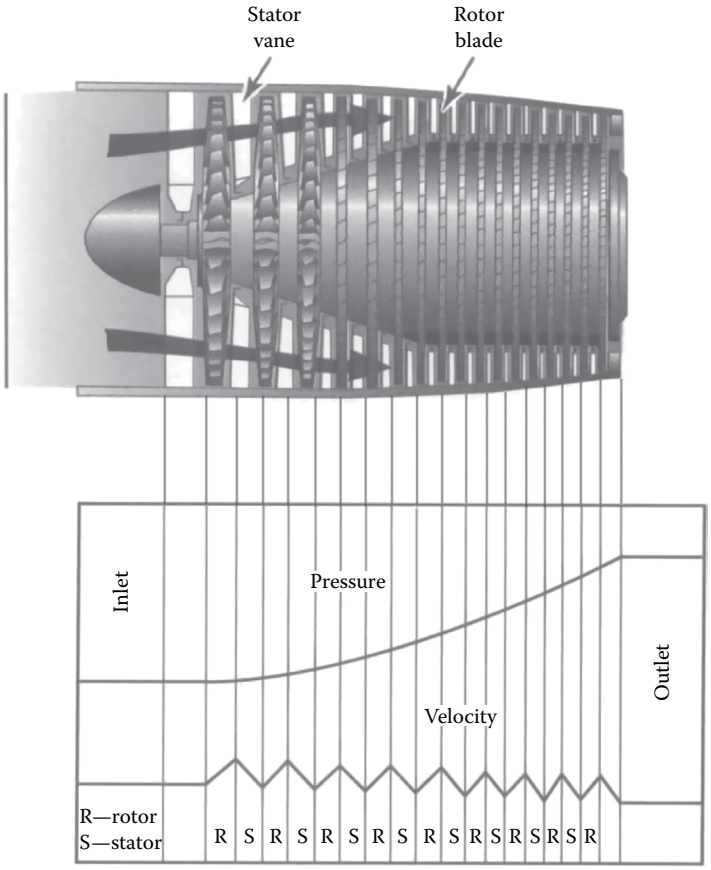


FIGURE 13.1
Layout of an axial compressor.

is referred to as a "stage," and most axial compressors have a number of such stages placed in a row along a common power shaft in the center. The stator blades are required in order to ensure reasonable efficiency; without them the gas would rotate with the rotor blades resulting in a large drop in efficiency. The axial compressor compresses the working fluid (here only air will be treated) by first accelerating the air and then diffusing it to obtain a pressure increase. The air is accelerated in the rotor and then diffused in the stator. This is illustrated in Figure 13.1 where the absolute velocity (C) increases in the rotor and decreases in the diffuser. For successive stages, a saw-teeth pattern for the velocity is obtained, while the static pressure continuously increases in both of the rotor and stator rows of all stages.

The axial compressor is built of a series of stagers, each consisting of a disk of rotor blades followed by a ring of stator vanes. The axial compressor is generally composed of four main elements: front frame, casing with inlet (stator) vanes, rotor with rotor blades, and rear frame [2].

The *front frame* in turbojet engines is a ring-shaped single-piece lightweight structure made of aluminum alloy or steel, usually cast and then machined. It is composed of an outer ring, an inner hub, and 6–8 streamlined supporting struts. If the compressor is a part

of a turbofan engine, then this front frame is replaced by a row of inlet guide vanes. The compressor *casing* is a tube-like construction split length-wise to facilitate engine assembly and maintenance. The inner surfaces of the casing are machined with circumferential T-section grooves to retain the stator blades and variable inlet guide vanes in modern engines. The final ring of stator blades (vanes) are called the outlet guide vanes, as they guide the flow to the axial direction to suit the compressor outlet. After installing the rotor, both casing halves are bolted together through longitudinal flanges. The compressor casing is made of light weight titanium. In recent engines, like the Pratt & Whitney 4084 that powers the Boeing 777 for example, the casing is made of the "Thermax" alloy of Inconel to allow for the expansion of the casing and for maintaining an acceptable tip-clearance margin. The third constituent of the compressor is the *rotor assembly*. The rotor blades (like the stator ones) have an aerofoil section like the aircraft wing, but they are highly twisted from root to tip to obtain the optimum angle-of-attack to the flow everywhere along the blade length. The reason for that twist is that the root section travels much slower than the tip section. Thus, for a constant axial velocity, the relative velocity and angle change from root to tip.

The length of the blades decreases progressively downstream in the same proportion as the pressure increases. The rotor blades are attached by a dovetail root, pin fixing, fir tree, and straddle *T* root [3]. These sets of rotors are mounted on the rotor shaft through drums, individual disks, and bolted disks, or are clamped. The disks are assembled with a number of tie-bolts, with the bolt-circle diameter selected to produce a dynamically stiff rotor and good torque transmission. The last constituent is the compressor *rear frame*, which guides and delivers the pressurized air stream to the combustion chamber. The center of the rear frame accommodates the rearward bearing of the rotor that absorbs the longitudinal thrust of the rotor. Moreover, the struts of the rear frame provide structural strength, lubrication, and venting of the bearing as well as a supply of bleed air. As the flow usually has a constant axial velocity through the compressor, the cross-sectional area of the annular passage reduces toward the outlet (or from the front to the rear). This is due to the decrease of the volume of air (thus increasing the density) as compression progresses from stage to stage. Three different layouts are possible; see Figure 13.2. The first maintains a constant casing diameter through successive stages, while increasing the hub diameter. This design provides the maximum Mach number and pressure ratio. In the second pattern, the hub radius is kept constant while the casing diameter is increased, which provides the best geometry for a compressor. The final pattern has a constant mean diameter, which is associated with a decrease in casing diameter along with an increase in the hub diameter. This typical layout is generally employed in deriving the basic theory of axial compressors.

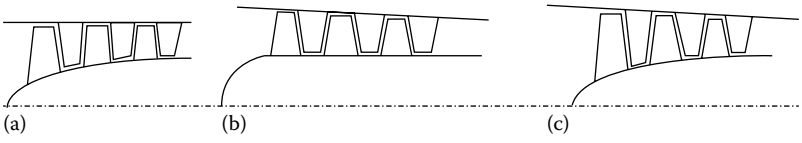


FIGURE 13.2
Variations of the annulus section. (a) Constant casing diameter, (b) constant hub diameter, and (c) constant mean diameter.

13.2 Comparison between Axial and Centrifugal Compressors

The centrifugal compressor achieves part of the compression process by causing the fluid to move outward in the centrifugal force field produced by the rotation of the impeller. Thus, the pressure rises due to the change in potential energy of the fluid in the centrifugal force field of the rotor. Conversely, the pressure rise in the axial flow compressor rotors and stators is achieved by the exchange of kinetic energy with thermal energy in a diffusion process. The pressure rise in a centrifugal compressor is therefore less limited by the problems of boundary layer growth and separation in adverse pressure gradients. Probably, for this reason, the centrifugal compressor was the first to attain a range of pressure ratio and efficiency that was useful for turbojet engines and so was used in the von Ohain engine (1939) and Whittle engine (1941).

The essential feature of air flow in the impeller of a centrifugal compressor is that all the fluid leaves the rotor at the tip radius rather than over a range of radii as in the axial compressor.

13.2.1 Advantages of the Axial Flow Compressor over the Centrifugal Compressor

1. Smaller frontal area for a given mass rate of flow (perhaps 1/2 or 1/3), thus the aerodynamic drag or nacelle housing the engine is smaller, as shown in Figure 13.3.
2. Much greater mass flow rates; for example, present-day axial compressors have mass flow rates up to 200 kg/s (up to 900 kg/s for high bypass ratio turbofan engines [2]), while centrifugal compressors have mass flow rates less than 100 kg/s.

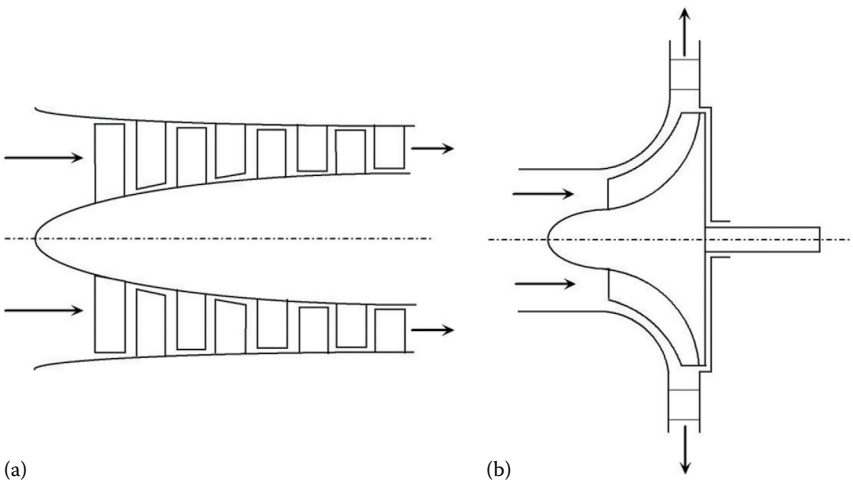


FIGURE 13.3
Layouts of (a) axial and (b) centrifugal-flow compressors.

3. Flow direction discharge is more suitable for mitigating viscous effects, hence is suitable for large engines.
4. May use cascade experiment research in developing compressors.
5. Somewhat higher efficiency at high-pressure ratio (perhaps 4%–5% higher than centrifugal compressors).
6. Higher maximum pressure ratio, which was about 17 in the 1960s and achieved up to 45 for the present transonic compressors [1].

13.2.2 Advantages of Centrifugal-Flow Compressor over the Axial Flow Compressor

1. Higher stage pressure ratio (5:1 or even 10:1)
2. Simplicity and ruggedness of construction
3. Shorter length for the same overall pressure ratio
4. Generally less severe stall characteristics
5. Less drop in performance with the adherence of dust to blades
6. Cheaper to manufacture for equal pressure ratio
7. Flow direction of discharged air is convenient for the installation of an intercooler and/or heat exchanger in gas turbines
8. Wider range (margin) of stable operation between surging and choking limits at a given rotational speed, as shown in Figure 13.4

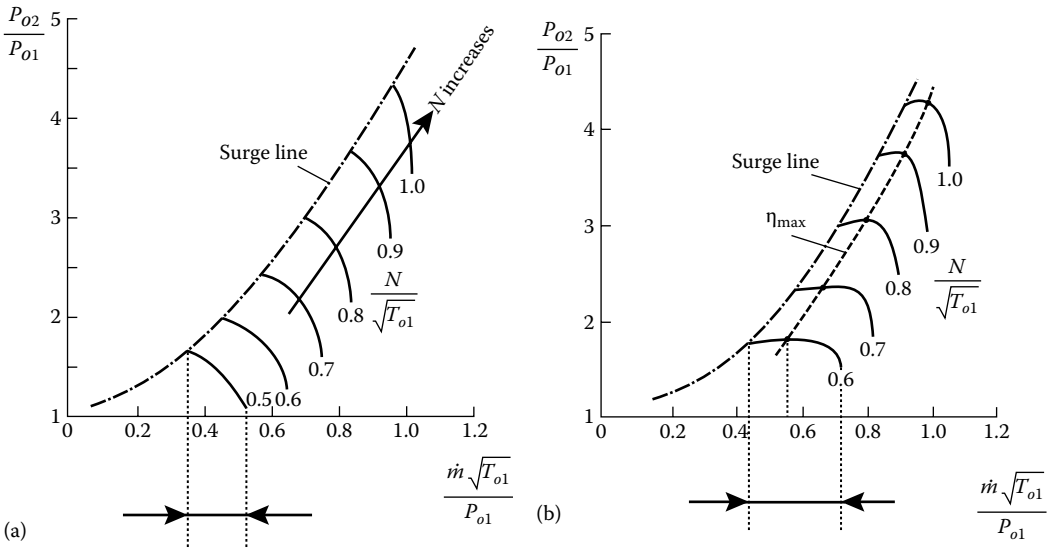


FIGURE 13.4
Compressor maps for axial (a) and centrifugal (b) compressors.

13.2.3 Main Points of Comparison between Centrifugal and Axial Compressors (Table 13.1)

TABLE 13.1

Main Points of Comparison between Axial and Centrifugal Compressors

	Axial Compressor	Centrifugal Compressor
Dimensions (frontal area)	Smaller	Larger
Dimensions (length)	Longer	Shorter
Number of blades per stage	More	Less
Weight	Heavier	Lighter
Rpm	Low	High
Efficiency	High (85% or greater)	Moderate (75%–80%)
Pressure ratio per stage	Small	High
Overall pressure ratio	Higher (30:1)	Much smaller (<10)
Mass flow rate	Higher	Smaller
Flow direction at outlet	Axial	Radial
Manufacturing and its cost	Difficult and expensive	Simple and cheaper
Balance	Difficult	Easier
Construction	Complex	Simple
Rapid change of inlet mass flow	Cannot accept	Can accept
Maintenance and its cost	Difficult and expensive	Simple and cheap
Balancing	More difficult due to blade scatter effect	Easier owing to support bearings
Foreign object damage (FOD)	Less resistant	More resistant
Fouling	Greatly influenced	Less influenced
Reliability	Lower	Higher
Operating range (between choking and surge points)	Narrow	Wide
Ruggedness	Fragile	Strong
Material	Impeller (aluminum alloy) inlet section (steel)	Rotor: • Front stages (steel alloy) • Mid-stages (aluminum alloy) • Rear stages (titanium alloys) Drum or disks: steel Casing: Magnesium alloy at the front Steel at the rear
Engine operation	1. Trouble usually experienced when starting due to lack of initial axial flow (blade stall) 2. Reluctant to respond to rapid acceleration	1. Works satisfactorily at all speeds provided turbine is properly matched 2. Can accept rapid changes of mass air flow (acceleration)
Starting power requirement	Higher	Lower
Engine thrust	Higher	Lower
Engine specific fuel consumption	Lower	Higher
Aircraft altitude	Higher	Lower
Application	All aeroengines	Small aeroengines and auxiliary power units (APU)

13.3 Mean Flow (Two-Dimensional Approach)

The flow is considered to be occurring in the tangential plane at the mean blade height where the peripheral rotation velocity is U; see Figure 13.5. This two-dimensional approach means that the flow velocity will have two velocity components, one axial denoted by subscript (a) and one peripheral denoted by subscript (u). The radial velocity component is neglected here. The mean section for both of the axial compressor and axial turbine is shown side by side in Figure 13.5, which illustrates how the hub-to-tip ratio of the axial compressor is much smaller than its value in the axial turbine. For an axial compressor having a constant casing diameter, the radius of the mean section increases in a rearward direction as shown in Figure 13.6. The velocity triangles at the inlet and outlet of a single stage are shown in Figure 13.7.

The air approaches the rotor with an absolute velocity (C_1), at an angle (α_1) to the axial direction; when combined with the rotational speed (U), the relative velocity will be (W_1), at an angle (β_1) to the axial; refer to Figure 13.8. After passing through the diverging passages formed between the rotor blades the absolute velocity (C_2) of the air will increase ($C_2 > C_1$) while its relative velocity W_2 decreases ($W_2 < W_1$) and the flow exit angle β_2 will be

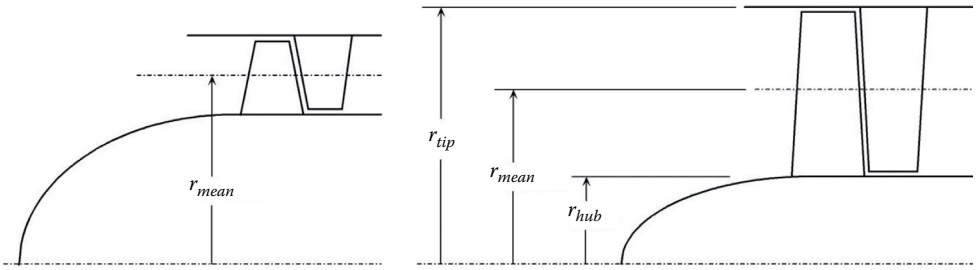


FIGURE 13.5
Mean tangential plane for both axial turbine (a) and axial compressor (b).

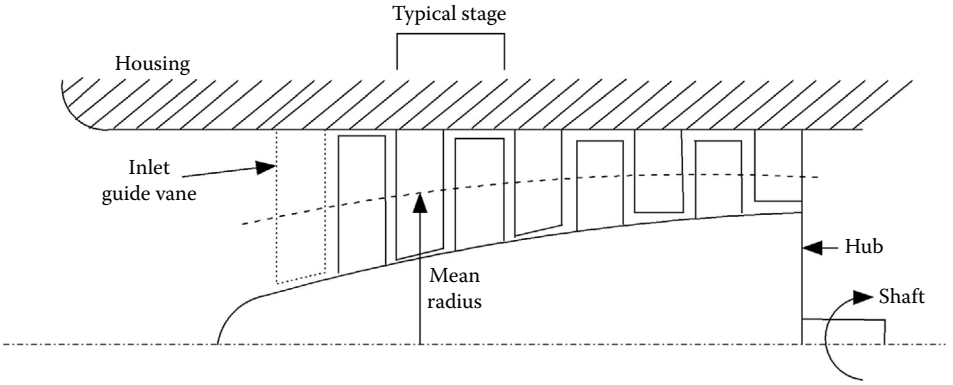


FIGURE 13.6
Variation of mean radius for a constant casing multistage axial compressor.

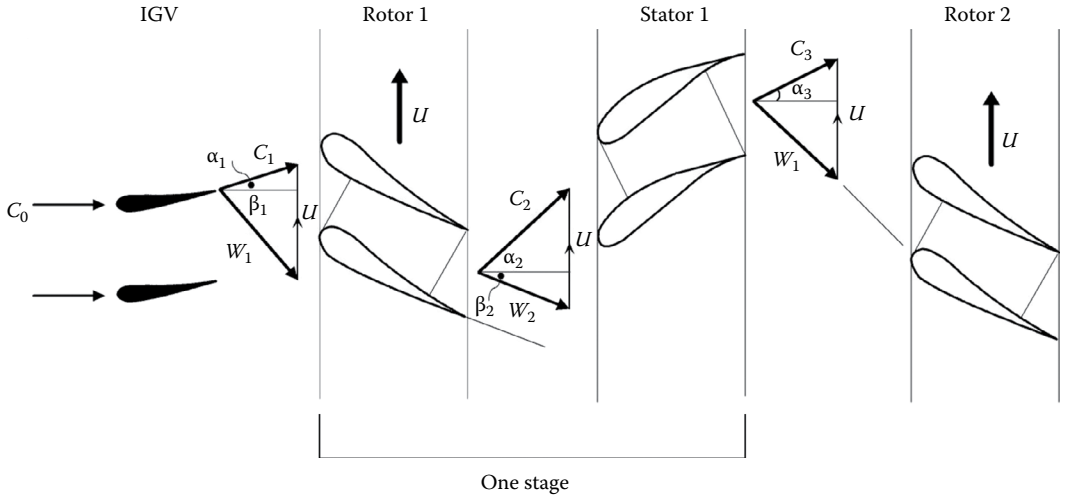


FIGURE 13.7
Velocity triangles at the inlet and outlet of a constant mean radius.

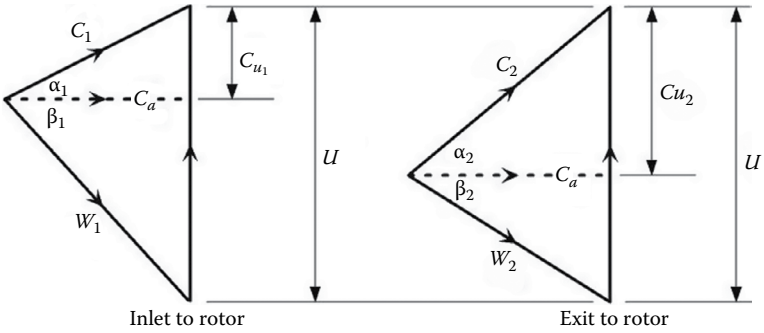


FIGURE 13.8
Airflow in an IGV as well as one and a half stages of an axial compressor.

less than the flow inlet angle β_1, ($\beta_2 < \beta_1$). This turning of flow toward the axial direction is necessary to increase the effective flow area.

Since the relative velocity is decreased due to diffusion ($W_2 < W_1$), then the static pressure increases ($P_2 > P_1$), that is, a pressure rise will be developed in the rotor.

The absolute velocity of the flow leaving the rotor is C_2. The flow then passes through the stator passages, which are also diverging, thus the absolute velocity is decreased, due to diffusion, and the static pressure is increased, that is, $C_3 < C_2$ and $P_3 > P_2$. The flow angle at the outlet of the stator will be equal to the inlet angle to the rotor in most designs, that is, $\alpha_3 = \alpha_1$.

From Figure 13.8, the following kinematical relations are derived

$$\frac{U}{C_{a_1}} = \tan\alpha_1 + \tan\beta_1 \tag{13.1a}$$

$$\frac{U}{C_{a_2}} = \tan\alpha_2 + \tan\beta_2 \tag{13.1b}$$

If the axial velocity is constant at the inlet and outlet of the stage, then $C_{a1} = C_{a_2} = C_a$.

The kinematical relations in Equation 13.1a and b will be

$$\frac{U}{C_a} = \tan\alpha_1 + \tan\beta_1 = \tan\alpha_2 + \tan\beta_2 \tag{13.1c}$$

13.3.1 Types of Velocity Triangles

These velocity diagrams assume equal axial velocities at inlet and outlet, implying that the density is varying inversely with area.

The separate velocity triangles are superimposed either on the common base, namely, the blade rotational speed (U) (see Figure 13.9a) or are superimposed with a common apex (see Figure 13.9b).

$$\left(C_{u_2} - C_{u_1}\right) \equiv \Delta C_u$$

which is the essential element in the energy transfer.

Another useful concept is that of the mean fluid angle and mean velocities shown by the mean velocity triangle; see Figure 13.9c. The velocities of this mean triangle are C_m, W_m, and U.

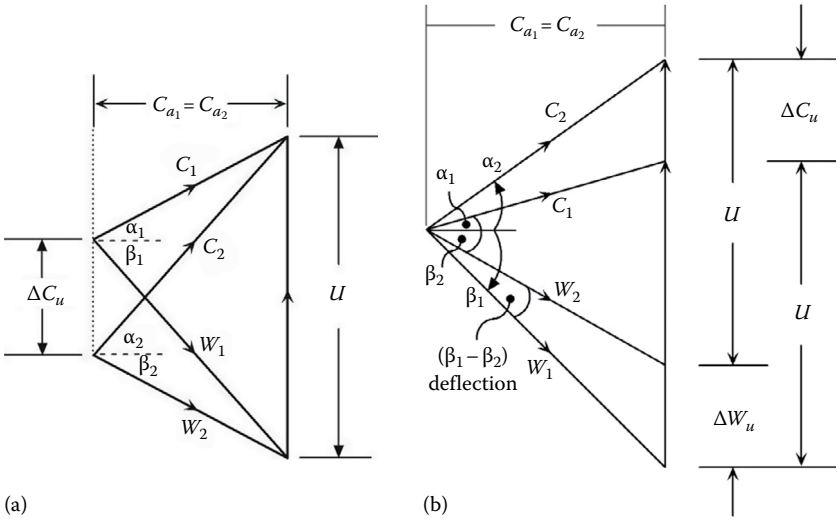


FIGURE 13.9
Different layouts for mean velocity triangle. (a) Common apex velocity triangles. (b) Common base velocity triangles. (*Continued*)

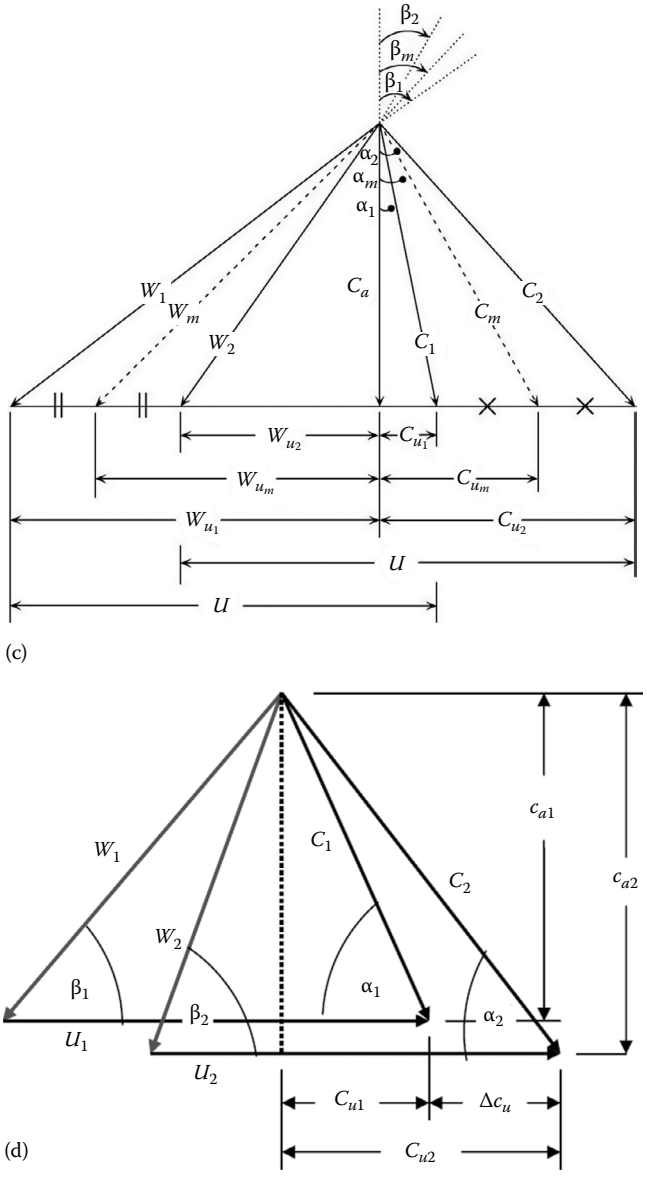


FIGURE 13.9 (*Continued*)
Different layouts for mean velocity triangle. (c) Mean velocity triangle. (d) Common apex for different axial speeds at inlet and outlet.

The angles are α_m and β_m. With constant axial and rotational velocities, the absolute and relative swirl velocities are calculated from the following relations.

$$\left.\begin{aligned} C_{um} &= \frac{(C_{u1} + C_{u2})}{2} \\ W_{um} &= \frac{(W_{u1} + W_{u2})}{2} \end{aligned}\right\} \tag{13.2}$$

$$\left.\begin{aligned}\tan\alpha_m &= \frac{C_{um}}{C_a}\\ \tan\beta_m &= \frac{W_{um}}{C_a}\end{aligned}\right\} \tag{13.3a}$$

Thus the mean absolute and relative angles are obtained from the relations

$$\left.\begin{aligned}\tan\alpha_m &= \frac{(\tan\alpha_1 + \tan\alpha_2)}{2}\\ \tan\beta_m &= \frac{(\tan\beta_1 + \tan\beta_2)}{2}\end{aligned}\right\} \tag{13.3b}$$

13.3.2 Variation of Enthalpy Velocity and Pressure in an Axial Compressor

The gain in energy of the gas is shown by the enthalpy achieved in the rotor blade row only. The total enthalpy increases in the rotor and remains constant in the stator as shown in Figure 13.10. In the same figure, the variations of the absolute velocity and static pressure

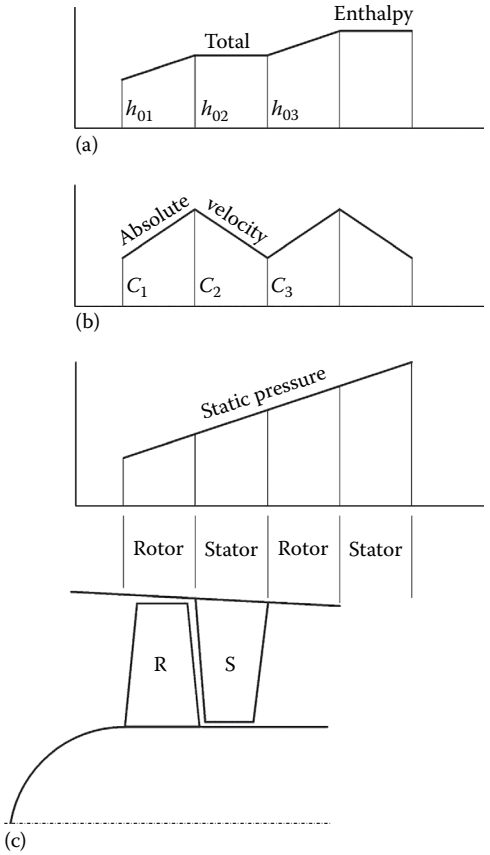


FIGURE 13.10
Variations of the (a) enthalpy, (b) absolute velocity, and (c) static pressure across two successive stages.

are plotted for any two successive stages. While energy can only be added at the rotor blades, as shown by the horizontal line at the stator, the gain in *static* pressure can be divided between the rotor and stator, as indicated by the continuous increase in pressure as the gas moves from the rotor through the stator.

The energy equation (or the first law of thermodynamics) is expressed in terms of the inlet and outlet conditions of a stage, states (1) and (3), respectively, as

$$Q_{13} + h_{01} = W_{13} + h_{03}$$

Since an adiabatic process is assumed, then the change in total enthalpy will be equal to the work done on the rotor, or

$$\Delta h_0 = U_2 C_{u2} - U_1 C_{u1} \tag{13.4}$$

For an axial compressor, with constant mean radius at inlet and outlet of the rotor, or $U_1 = U_2 = U$, then Euler's equation for turbomachinery is again expressed for axial compressors as

$$\Delta h_0 = U\left(C_{u2} - C_{u1}\right) = W_{13} \tag{13.5}$$

All the energy transfer between the fluid and rotor is accounted for by the difference between the two UC_u terms. Now from the velocity triangles shown in Figure 13.11, Euler's equation can be mathematically expressed in a different form.

$$C_a^2 = C^2 - C_u^2$$

$$W_a^2 = W^2 - W_u^2 = W^2 - \left(U - C_u\right)^2$$

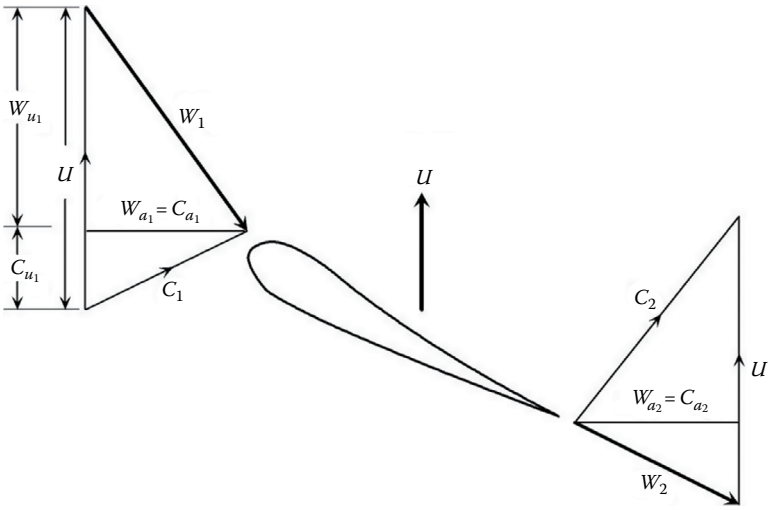


FIGURE 13.11
Detailed velocity triangles.

$$\text{Since} \quad C_a = W_a$$

$$\therefore C^2 - C_u^2 = W^2 - U^2 + 2UC_u - C_u^2$$

$$\therefore UC_u = \frac{1}{2}\left(C^2 + U^2 - W^2\right)$$

$$\therefore U_1 C_{u_1} = \frac{1}{2}\left(C_1^2 + U_1^2 - W_1^2\right)$$

$$U_2 C_{u_2} = \frac{1}{2}\left(C_2^2 + U_2^2 - W_2^2\right)$$

$$\because \Delta h_0 = \left(UC_u\right)_2 - \left(UC_u\right)_1$$

$$\therefore \Delta h_o = \frac{1}{2}\left(C_2^2 - C_1^2 + U_2^2 - U_1^2 + W_1^2 - W_2^2\right) \tag{13.6}$$

This equation is an alternative form of the basic energy one, by definition

$$\Delta h_0 = h_{02} - h_{01} = h_2 + \frac{C_2^2}{2} - h_1 - \frac{C_1^2}{2}$$

$$\therefore \Delta h = h_2 - h_1 = \frac{1}{2}\left(U_2^2 - U_1^2 + W_1^2 - W_2^2\right) \tag{13.7}$$

Thus, the terms U^2 and W^2 represent the change in static across the rotor, while the C^2 terms represent the absolute kinetic energy across the rotor.

From Equation 13.5, the specific work input is equal to the change in the total enthalpy across the stage, or

$$W_s \equiv h_{03} - h_{01} = h_{02} - h_{01} = U\left(C_{u_2} - C_{u_1}\right)$$

where h_0 is the total enthalpy, or

$$W_s \equiv Cp\left(T_{02} - T_{01}\right) = U\Delta C_u \equiv Cp\Delta T_0$$
$$\therefore \Delta T_0 = \frac{U\Delta Cu}{Cp}$$

or

$$\frac{\Delta T_0}{T_{01}} = \frac{U\Delta C_u}{CpT_{01}} \tag{13.8}$$

From Figure 13.12, Equation 13.8 can be expressed in terms of the axial and rotational velocities and the absolute and relative angles as follows:

$$\Delta C_u = C_{a1}\tan\beta_1 - C_{a2}\tan\beta_2$$

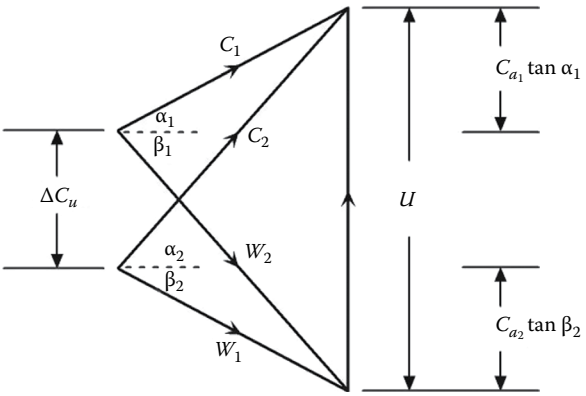


FIGURE 13.12
Velocity triangles over a stage.

or

$$\Delta C_u = C_{a2} \tan \alpha_2 - C_{a1} \tan \alpha_1$$

or

$$\Delta C_u = U - C_{a1} \tan \alpha_1 - C_{a2} \tan \beta_2$$

If $C_{a1} = C_{a2} = C_a$

$$\therefore \Delta C_u = U\left[1 - \frac{C_a}{U}\left(\tan \alpha_1 + \tan \beta_2\right)\right]$$

or

$$\Delta C_u = C_a\left(\tan\ \beta_1 - \tan\ \beta_2\right) \equiv C_a\left(\tan \alpha_2 - \tan \alpha_1\right)$$

The stage temperature rise is now expressed as

$$\Delta T_0 = \frac{UC_a}{Cp}\left(\tan \alpha_2 - \tan \alpha_1\right) = \frac{UC_a}{Cp}\left(\tan \beta_1 - \tan \beta_2\right) \tag{13.9a}$$

and

$$\frac{\Delta T_0}{T_{01}} = \frac{U^2}{CpT_{01}}\left[1 - \frac{C_a}{U}\left(\tan \alpha_1 + \tan \beta_2\right)\right] \tag{13.10a}$$

or

$$\frac{\Delta T_0}{T_{01}} = \frac{UC_a}{CpT_{01}}\left(\tan \beta_1 - \tan \beta_2\right) = \frac{UC_a}{CpT_{01}}\left(\tan \alpha_2 - \tan \alpha_1\right) \tag{13.10b}$$

The specific work is also given by the relation

$$W_s = UC_a\left(\tan\alpha_2 - \tan\alpha_1\right) = UC_a\left(\tan\beta_1 - \tan\beta_2\right) \tag{13.11}$$

Figure 13.13 illustrates the temperature–entropy variation for the compression process through the stage. If the whole processes were isentropic, the final stagnation pressure for the same work input would be $P_{0\max}$. However, due to losses in the rotor and stator, the pressure at the outlet of the rotor is less than that maximum value and so the pressure for air leaving the stator is also less than the pressure at the outlet of the rotor, or $P_{03} < P_{02} < P_{0\max}$.

If the stage total-to-total efficiency (η_{st}) is defined as

$$\eta_{st} = \frac{h_{03ss} - h_{01}}{h_{03} - h_{01}}$$

$$\therefore \eta_{st} = \frac{T_{03ss} - T_{01}}{T_{03} - T_{01}} = \frac{T_{03ss} - T_{01}}{\Delta T_0} = \frac{\dfrac{T_{03ss}}{T_{01}} - 1}{\dfrac{\Delta T_0}{T_{01}}}$$

$$\therefore \frac{T_{03ss}}{T_{01}} - 1 = \eta_{st}\frac{\Delta T_0}{T_{01}}$$

Since

$$\frac{P_{03}}{P_{01}} = \frac{T_{03ss}}{T_{01}}$$

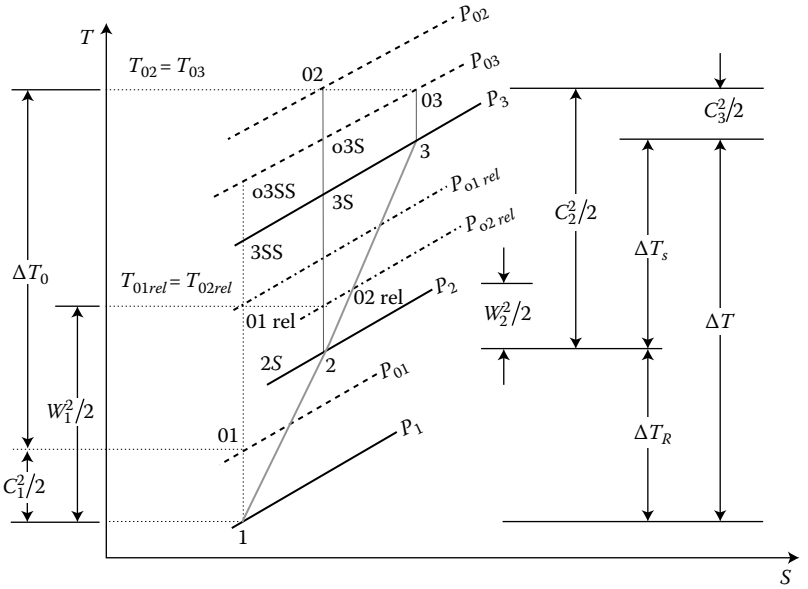


FIGURE 13.13
Temperature–entropy diagram for a compressor stage.

Then

$$\pi_{stage} \equiv \frac{P_{03}}{P_{01}} = \left(1 + \eta_{st} \frac{\Delta T_0}{T_{01}}\right)^{\gamma/\gamma-1}$$

But

$$\left(\frac{\Delta T_0}{T_{01}}\right)_{stage} = \frac{UCa}{CpT_{01}}\left(\tan\alpha_2 - \tan\alpha_1\right)$$

Then

$$\pi_{stage} = \left[1 + \eta_{st} \frac{UCa\left(\tan\alpha_2 - \tan\alpha_1\right)}{CpT_{01}}\right]^{\gamma/\gamma-1} \tag{13.12a}$$

An actual stage temperature rise will be less than the above value due to the three-dimensional effects in the compressor annulus. Analysis of experimental results shows that it is necessary to multiply the results by a factor less than unity, identified as the work done factor (λ), due to the radial variation of the axial velocity. The latter is not constant across the annulus but is peaky as the flow proceeds, settling down to a fixed profile at about the fourth stage, as shown in Figure 13.14. The stage temperature rise, Equation 13.12a and b, should be modified to

$$\therefore \Delta T_0 = \frac{\lambda}{Cp} UC_a\left(\tan\alpha_2 - \tan\alpha_1\right) = \frac{\lambda}{Cp} UC_a\left(\tan\beta_1 - \tan\beta_2\right) \tag{13.9b}$$

$$\pi_S = \left[1 + \frac{\lambda\eta_{st}}{CpT_{01}} UC_a\left(\tan\alpha_2 - \tan\alpha_1\right)\right]^{\gamma/\gamma-1} \tag{13.12b}$$

Thus, the pressure ratio across the stage could be determined. It is entirely possible to achieve a very high work input per stage, but it is not possible to achieve a high $\Delta T_0/T_{01}$ while maintaining high efficiency. For a single-stage axial compressor, the temperature rise for efficient operation is always limited such that $(\Delta T_0/T_{01}) \ll 1$. Then Equation 13.12b may be approximated to

$$\frac{P_{03}}{P_{01}} = \pi_{stage} \approx 1 + \frac{\gamma}{\gamma - 1} \eta_{st} \frac{\Delta T_0}{T_{01}} \tag{13.12c}$$

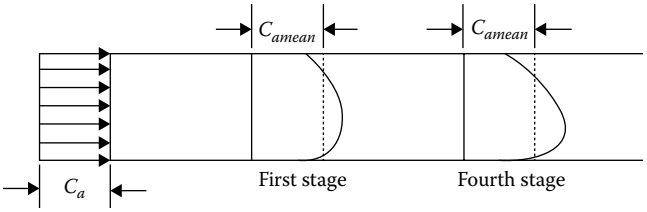


FIGURE 13.14
Variations of the axial velocity through successive stages.

It is highly desirable to achieve high work input per compressor stage in order to minimize the total number of stages necessary to provide the desired overall compression ratio.

Example 13.1

Air at 1 bar and 15°C enters a three-stage axial compressor with a velocity of 120 m/s. There are no inlet guide vanes, and constant axial velocity is assumed throughout. In each stage the rotor turning angle is 25°. The annular flow passages are shaped so that the mean blade radius is everywhere 20 cm. The rotor speed is 9000 rpm. The polytropic efficiency is constant at 0.9. The blade height at the inlet is 5 cm.

Draw the velocities diagram and calculate

1. Specific work for each stage
2. The mass flow rate
3. The power necessary to run the compressor
4. The stage temperature ratios
5. The overall compressor pressure ratio
6. The blade height at the exit from the third stage
7. The degree of reaction of the first stage

Solution

The given data are

$$P_{01} = 1 \text{ bar},\ r_m = 0.2 \text{ m},\ N = 9000 \text{ rpm},\ \eta_S = 0.9,\ \beta_1 - \beta_2 = 25°,\ h = 0.05 \text{ m},$$
$$\text{Number of stages} = 3,\ C_1 \equiv C_{a1} = 120 \text{ m/s}$$

Since the flow is axial, then $\alpha_1 = zero$, $C_{u1} = zero$, $\Delta C_u \equiv C_{u2}$.
The inlet total temperature is $T_{01} = 15 + 273 = 288$ K.
With $U_m = 2\pi r_m N = 188.496$ m/s.
then $\tan \beta_1 = U/C_{a1}$

$$\beta_1 = 57.52° = \text{constant for all stages}$$
$$\beta_2 = \beta_1 - 25 = 32.52° = \text{constant also for all stages}$$

since

$$\tan \beta_2 = \frac{U - C_{u2}}{C_{a2}}$$

then $C_{u2} = 111.989$ m/s $\equiv \Delta C_u$
The axial compressor is composed of three identical stages, where (Figure 13.15)

1. The flow enters axially.
2. The rotor turning angle is the same, $\beta_1 - \beta_2 = \text{constant}$, thus $\Delta C_u = \text{constant}$.
3. The polytropic efficiency is constant.
4. The compressor has a constant mean radius layout $U_m = \text{constant}$.

Thus, the temperature rise per stage as well as the specific work are constants.
The specific work per stage is $w_S = U\Delta C_u = 21.11$ kJ/kg $\equiv$ constant for all stages [or $w_S = U\Delta C_u = UC_a(\tan\beta_1 - \tan\beta_2) = 21.11$ kJ/kg].
The specific work for the three-stage compressor is $W_s = 3w_s = 3 \times 21.11 = 63.33$ kJ/kg.
The mass flow rate $\dot{m} = \rho_1 C_{a1} A_1$
at the compressor inlet, the static temperature $T_1 = T_{01} - \left(C_1^2/2Cp\right) = 280.836$ K,
and the static pressure $P_1 = P_{01}/(T_{01}/T_1)^{\gamma/\gamma-1} = 0.916$ bar.
The density $\rho_1 = P_1/RT_1 = 1.136$ kg/m^3.
The annulus area $A = 2\pi r_m h = 0.0628$ m^2

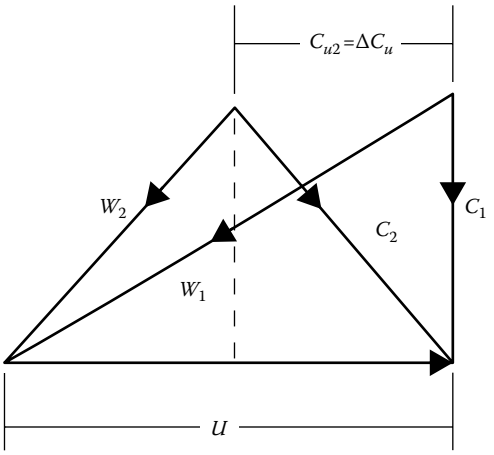


FIGURE 13.15
Velocity triangles of the first stage.

$$\therefore \dot{m} = \rho_1 C_{a1} A = 8.565 \text{ kg/s}.$$

$$\text{Power} = \dot{m} w_S = 180.81 \text{ kW}$$

The temperature rise per stage is $\Delta T_{0S} = w_S / Cp = 21$ K ≡ constant for all stages.
Pressure ratio of stage # 1

$$\pi_1 = \left(1 + \eta_S \frac{\Delta T_{0S}}{T_{01}}\right)^{\gamma/\gamma-1} = 1.249$$

Pressure ratio of stage # 2

$$\pi_2 = \left(1 + \eta_S \frac{\Delta T_{0S}}{T_{01} + \Delta T_{0S}}\right)^{\gamma/\gamma-1} = 1.231$$

Pressure ratio of stage # 3

$$\pi_3 = \left(1 + \eta_S \frac{\Delta T_{0S}}{T_{01} + 2\Delta T_{0S}}\right)^{\gamma/\gamma-1} = 1.215$$

Overall pressure ratio $\pi_{comp} = \pi_1 \times \pi_2 \times \pi_3 = 1.87$
The pressure at the outlet of the compressor is $P_{03})_{S3} = \pi_C \times P_{01})_{S1} = 1.87$ bar
The temperature at the exit of the compressor is $T_{03})_{S3} = T_{01})_{S1} + 3\Delta T_{0S} = 351$ K
With $C_3 = C_1$

$$T_3)_{S3} = T_{03})_{S3} - \frac{C_3^2}{2Cp} = 343.836 \text{ K}$$

$$P_3)_{S3} = \frac{P_{03})_{S3}}{\left[\left(T_3/T_{03}\right)^{\gamma/\gamma-1}\right]_{S3}} = 1.74 \text{ bar}$$

$$\rho_3 = \frac{P_3}{RT_3}\Big)_{S3} = 1.763 \text{ kg/m}^3$$

Since

$$\dot{m} = (\rho_3 C_3 A_3)_{S3} = \left[\rho_3 C_3 (2\pi r_m h_3)\right]_{S3}$$

then

$$(h_3)_{S3} = 3.2 \text{ cm}$$

The degree of reaction is expressed as

$$\Lambda = 1 - \frac{C_{u1} + C_{u2}}{2U}$$

$$\Lambda = 1 - \frac{C_{u2}}{2U} = 1 - \frac{112}{2 \times 188.5} = 0.7$$

13.4 Basic Design Parameters

The pressure ratio per stage is expressed by the relation

$$\pi_s = \left[1 + \eta_s \frac{\lambda U C_a}{C p T_{01}} (\tan\beta_1 - \tan\beta_2)\right]^{\gamma/\gamma - 1}$$

To obtain high-pressure ratio per stage, we need to have

1. High blade speed (U)
2. High axial velocity (C_a)
3. High fluid deflection ($\beta_1 - \beta_2$) in the rotor blade

However, the increase in the rotational speed is limited by the maximum acceptable tensile stress at the rotor hub. Furthermore, the increase in the rotational and axial velocities (U and C_a) is limited by the tip Mach number. Compressors of the 1960s had a maximum tip Mach number of less than 0.8. This limit was increased for the present transonic compressors to reach the value of 1.4 [4]. The fluid deflection has upper limits determined by the diffusion or de Haller parameters.

13.4.1 Centrifugal Stress

Centrifugal stress depends on the rotational speed (ω), blade material density (ρ_b), and height of the blade. The maximum centrifugal stress occurs in the root. As shown in Figure 13.16, the centrifugal force arising from any element of the blade is evaluated as

$$dF_c = \omega^2 r \delta m$$

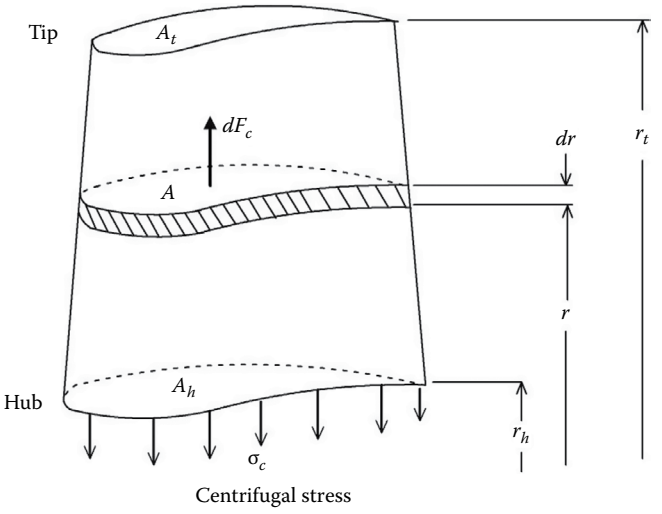


FIGURE 13.16
Nomenclature for centrifugal stress on a rotor blade.

where (ω) and (*r*) are the rotational speed and the radius of any blade element having a mass of (δ*m*) and length of (*dr*)

$$\delta m = \rho_b A dr$$

Then the maximum centrifugal stress at the root is the summation of the centrifugal forces of all the elements of the blade from the hub to the tip divided by the blade's cross-sectional area at the root, or

$$\left(\sigma_c\right)_{\max} = \frac{\omega^2}{A_{root}} \int_{rh}^{rt} r\delta m$$

$$\left(\sigma_c\right)_{\max} = \frac{\rho_b \omega^2}{A_{root}} \int_{rh}^{rt} rAdr \tag{13.13}$$

Special cases:

1. If the blade has a constant area (*A*) along the blade height, then the maximum stress will be

$$\left(\sigma_c\right)_{\max} = \frac{\rho_b}{2}\left(2\pi N\right)^2\left(r_t^2 - r_r^2\right)$$
$$\sigma_{\max} = 2\pi N^2 \rho_b A$$

where

$$A = \pi\left(r_t^2 - r_r^2\right) = \text{annulus area}$$

$$U_t = \omega r_t = 2\pi N r_t$$

$$(\sigma_c)_{\max} = \frac{\rho_b U_t^2}{2}\left[1 - \left(\frac{r_r}{r_t}\right)^2\right]$$

$$(\sigma_c)_{\max} = \frac{\rho_b U_t^2}{2}\left[1 - \zeta^2\right] \tag{13.14}$$

where

$$\zeta = \frac{r_r}{r_t}$$

2. For linear variation of the cross-sectional area with radius

$$(\sigma_{ct})_{\max} = \frac{\rho_b U_t^2}{2}\left(1 - \zeta^2\right) \text{ K} \tag{13.15}$$

$$K = 1 - \frac{(1-d)\left(2 - \zeta - \zeta^2\right)}{3\left(1 - \zeta^2\right)}$$

where $d = A_{tip}/A_{root}$ and K = 0.55–0.65 for tapered blades.

3. If the area is inversely proportional to the radius, (or $A = \text{constant}/r$), since $r_r A_r = r_t A_t = rA = K$

$$\frac{A_t}{A_r} = \frac{r_r}{r_t} = \zeta$$

$$\therefore \sigma_{c\max} = \frac{\rho_b \omega^2}{A_r}\int_{r_r}^{r_t} rA\,dr = \frac{\rho_b \omega^2 K}{A_r}\int_{r_r}^{r_t} dr$$

$$\sigma_{c\max} = \frac{\left(\rho_b \omega^2\right)K}{A_r}\left[r_t - r_r\right]$$

$$\sigma_{c\max} = \frac{\rho_b \omega^2}{A_r}\left[r_t^2 A_t - r_r^2 A_r\right] = \rho_b U_t^2\left[\frac{A_t}{A_r} - \zeta^2\right]$$

$$\sigma_{c\max} = \rho_b U_t^2\left(\zeta - \zeta^2\right) = \rho_b U_t^2 \zeta\left(1 - \zeta\right) \tag{13.16}$$

The same equations are applied for both fans and compressors. If the tip speed of a fan at a high bypass ratio turbofan is 450 m/s and the blades are long (low hub-to-tip ratios), then the design of the disk becomes critical.

13.4.2 Tip Mach Number

The maximum Mach number is found at the rotor tip of the first stage as it has the maximum radius for any layout of axial compressor (constant, tip, mean, or hub radius). Thus the rotational speed (U) attains a maximum value. For the first stage, the axial velocity is equal to the inlet absolute velocity and has a constant value along the annulus. The corresponding maximum Mach number is

$$M_{tip} = M_{1_{\max}} = \frac{W_{1\max}}{a} = \frac{\sqrt{C_1^2 + U_{tip}^2}}{\sqrt{\gamma R T_1}} = \sqrt{\frac{C_1^2 + U_{tip}^2}{\gamma R\left(T_{01} - \dfrac{C_1^2}{2Cp}\right)}}$$

$$M_{1_{\max}} = U_{tip}\sqrt{\frac{\left(C_1/U_{tip}\right)^2 + 1}{\gamma R\left(T_{01} - \dfrac{C_1^2}{2Cp}\right)}} \tag{13.17}$$

The relation between the maximum relative Mach number (at rotor tip) is plotted versus the tip rotational speed (U_t) for different axial velocities (C_1); see Figure 13.17. Thus for a specified tip Mach number and rotational speed, the axial velocity at the inlet is determined.

For a transonic compressor, an acceptable value for the maximum Mach number at the tip is about 1.1 ($M_{1tip} \cong 1.1$), while for the fan in turbofan engines a much higher Mach number is expected and allowed, thus M_{1tip} = 1.5–1.7. A challenging design is to increase the

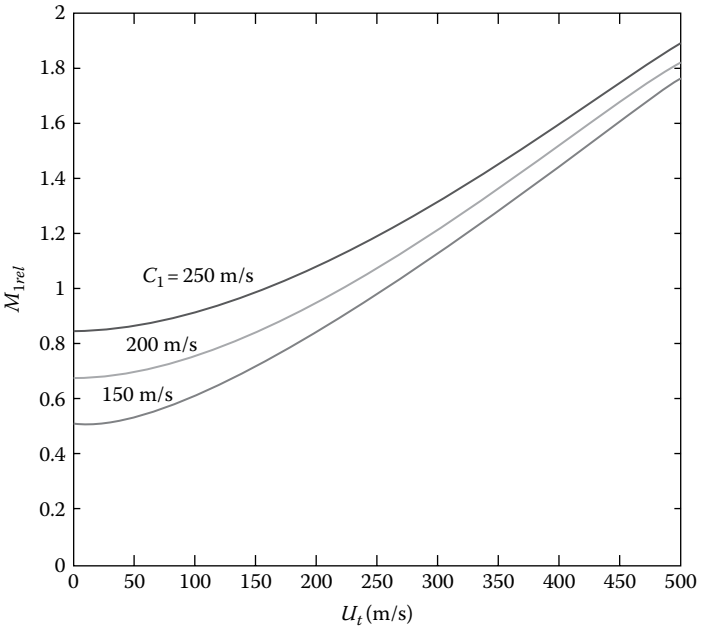


FIGURE 13.17
Relation between tip Mach number and tip rotational speed.

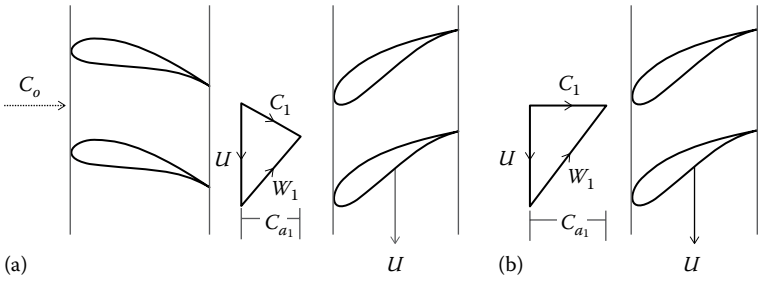


FIGURE 13.18
Inlet velocity triangle with (a) and without IGV (b).

rotational speed U and keep the Mach number within acceptable limits. Since increasing the rotational speed automatically increases the maximum relative speed ($W_{1\max}$), inlet guide vanes (an additional ring of stator vanes) are installed upstream of the first stage of the compressor as shown in Figure 13.18 to add a swirl component to the inlet speed (C_1) and thus reduce the relative speed (W_1). Note that the passages of the inlet guide vanes are nozzles to increase the absolute speed ($C_1 > C_0$) and thus keep a constant axial velocity C_a.

The maximum relative Mach number at the rotor tip is

$$\left(M_{1rel}\right)_{\max} = \frac{W_{1\max}}{\sqrt{\gamma R T_1}} = \sqrt{\frac{\left(U - C_1 \sin\alpha_1\right)^2 + \left(C_1 \cos\alpha_1\right)^2}{\gamma R\left(T_{01} - \dfrac{C_1^2}{2Cp}\right)}}$$

where α_1 is the angle between the absolute velocity and axial direction. Thus the maximum relative Mach number can be rewritten as

$$\left(M_{1rel}\right)_{\max} = \sqrt{\frac{U^2 + C_1^2 - 2UC_1 \sin\alpha_1}{\gamma R\left(T_{01} - \dfrac{C_1^2}{2Cp}\right)}} \tag{13.18}$$

13.4.3 Fluid Deflection

By "fluid deflection," is meant the difference between the outlet and inlet angles; $(\beta_2 - \beta_1)$ at the rotor and $(\alpha_3 - \alpha_2)$ for a stator. Excessive deflection, which means a high rate of diffusion, will lead to blade stall. To maximize the specific work, the difference between the flow angles in the rotor must attain its maximum allowable value. If the inlet relative velocity maintains a constant angle, β_1, then the outlet relative angle, β_2, will control either a good design or a stall condition. Since a constant axial velocity is assumed, then the relative angle is a measure of the magnitude of the relative velocities (W_1, W_2). An earlier method for assessing the diffusion was the "de Haller number," defined as V_2/V_1, where a limit of $(V_2/V_1 / < 0.72)$ was set. Because of its simplicity it is still used today at the preliminary design stage. However, for final design calculations the criterion known as the "diffusion factor" (DF) developed by National Advisory Committee for Aeronautics (NACA) is preferred [5]. The velocity distribution over the suction and pressure sides of a typical

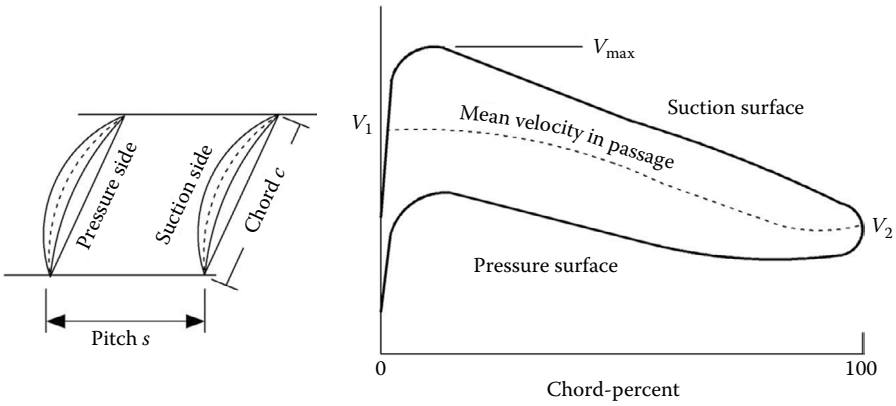


FIGURE 13.19
Velocity distribution in the passage of a cascade.

passage of cascade is shown in Figure 13.19. The velocities V_1, V_2, and V_{max} are, respectively, the velocities at the inlet and outlet of the cascade and the maximum velocity over the suction surface. The diffusion factor (DF) is defined as

$$DF \approx \frac{V_{max} - V_2}{V_1} \approx 1 - \frac{V_2}{V_1} + \frac{\Delta C_u}{2\sigma V_1} \tag{13.19a}$$

where $\sigma = c/s$ is the solidity.

A more precise expression, if the mean radii at the inlet and outlet of the blade are not equal, is expressed as [6]

$$DF = 1 - \frac{V_2}{V_1} + \frac{\Delta r C_u}{2\sigma r V_1} \tag{13.19b}$$

Values of DF in excess of 0.6 are thought to indicate blade stall, and a value of 0.45 might be taken as a typical design choice [5].

13.5 Design Parameters

The following three design parameters are frequently used in the parametric study of a repeating axial stage

1. Flow coefficient ϕ
2. Stage loading ψ
3. Degree of reaction Λ

The flow coefficient is defined as the ratio between the axial and the rotational speeds, or

$$\phi = \frac{C_a}{U} \tag{13.20}$$

The stage loading is defined as the ratio between the total enthalpy rise per stage to the square of the rotational speed, or

$$\psi = \frac{\Delta h_0}{U^2} = \frac{W_s}{U^2} = \frac{\Delta C_u}{U} \tag{13.21}$$

The degree of reaction of a compressor stage has several definitions. For an incompressible flow, the degree of reaction is defined as the ratio of the static pressure rise in the rotor to the static pressure rise in the stage [7], or

$$\Lambda = \frac{p_2 - p_1}{p_3 - p_1}$$

For a compressible flow, the degree of reaction is defined as the ratio of the static enthalpy (or temperature) rise in the rotor to the enthalpy (or temperature) rise in the whole stage, or

$$\Lambda = \frac{h_2 - h_1}{h_3 - h_1} = \frac{\Delta T_R}{\Delta T_R + \Delta T_S} \tag{13.22}$$

A third definition [8] states that the degree of reaction is equal to the change of the static enthalpy rise across the rotor as a fraction of the change in the absolute enthalpy rise in a stage,

$$\Lambda = \frac{h_2 - h_1}{h_{03} - h_{01}} = \frac{h_2 - h_1}{h_{02} - h_{01}}$$

The expression given in Equation 13.22 will be employed in this text.

The following general relation will be derived for the degree of reaction, assuming that the axial velocities are not equal ($C_{a2} \neq C_{a1}$). Since the absolute velocities at the inlet and outlet of the stage are assumed to be equal, that is, $C_1 = C_3$, then the static and total temperature rise in a stage are also equal, or $\Delta T = \Delta T_0$. The temperature rise in the stage is

$$\Delta T \equiv \Delta T_0 = \frac{U\left(C_{u2} - C_{u1}\right)}{C_p}$$

Since the rothalpy (I) is equal at the rotor inlet and outlet, then

$$I_2 = I_1$$

where $I = h_{0rel} - \frac{1}{2}U^2$, $\quad h_{0rel} = h + \frac{1}{2}W^2$.

Since equal mean radii at the rotor inlet and inlet is assumed, that is, $U_2 = U_1$ and $h_{01rel} = h_{02rel}$, or

$$h_1 + \frac{1}{2}W_1^2 = h_2 + W_2^2$$

The temperature rise within the rotor is

$$\Delta T_R = T_2 - T_1 = \frac{W_1^2 - W_2^2}{2C_p}$$

with $W^2 = C_a^2 + (U - C_u)^2$

$$\therefore \Delta T_R = \frac{C_{a1}^2 + (U - C_{u1})^2 - C_{a2}^2 + (U - C_{u2})^2}{2C_p}$$

$$\Delta T_R = \frac{C_{a1}^2 - C_{a2}^2 + 2U(C_{u2} - C_{u1}) - C_{u2}^2 + C_{u1}^2}{2C_p}$$

The degree of reaction is then

$$\Lambda = 1 + \frac{C_{a2}^2 - C_{a1}^2}{2U(C_{u2} - C_{u1})} - \frac{C_{u1} + C_{u2}}{2U} \tag{13.23a}$$

When the axial velocities at the rotor inlet and outlet are assumed to be equal, then $C_{a2} = C_{a1}$, and Equation 13.23a is reduced to the following relation

$$\Lambda = 1 - \frac{C_{u1} + C_{u2}}{2U} \tag{13.23b}$$

In terms of the flow angles, Equation 13.23b may be rewritten as

$$\Lambda = 1 - \frac{C_a}{2U}(\tan\alpha_1 + \tan\alpha_2) \tag{13.23c}$$

From Equation 13.1c, with some manipulation, we arrive at the following expressions for the degree of reaction

$$\Lambda = \frac{1}{2} - \frac{C_a}{2U}(\tan\alpha_1 - \tan\beta_2) \tag{13.23d}$$

$$\Lambda = \frac{C_a}{2U}(\tan\beta_1 + \tan\beta_2) \tag{13.23e}$$

From Equation 13.23e, another expression for the degree of reaction is obtained

$$\Lambda = \frac{1}{U}\left(\frac{C_a \tan\beta_1 + C_a \tan\beta_2}{2}\right)$$

$$\Lambda = \frac{1}{U}\left(\frac{W_{u_1} + W_{u_2}}{2}\right)$$

$$\Lambda = \frac{W_{umean}}{U} = \frac{C_a \tan\beta_m}{U} \tag{13.23f}$$

Three special cases are found here

1. $\Lambda = 0\%$
2. $\Lambda = 50\%$
3. $\Lambda = 100\%$

The 50% reaction stage provides the best efficiency. If the degree of reaction is much different from 50% one of the blade rows must tolerate a greater pressure rise than the other. This means that its boundary layer will be more highly loaded and more likely to stall or at least create higher losses. The velocity triangles of this case will now be examined. From Equation 13.23d

$$\therefore \tan\alpha_1 = \tan\beta_2$$
$$\therefore \alpha_1 = \beta_2$$

From Equation 13.1c

$$\frac{U}{C_a} = \tan\alpha_1 + \tan\beta_1 = \tan\alpha_2 + \tan\beta_2$$
$$\therefore \alpha_2 = \beta_1$$

This means that these velocity triangles are symmetrical. It is interesting to notice that if the degree of reaction is greater than 50% then $\beta_2 > \alpha_1$ and the velocity triangles will be skewed in the direction of the rotational speed [9]. The static enthalpy rise across the rotor exceeds that of the stator (this is also true for the static pressure). If the degree of reaction is less than 50%, then $\beta_2 < \alpha_1$ and the velocity triangles will be skewed in the opposite direction of the rotational speed. The stator enthalpy rise (and pressure) exceed that in the rotor.

The case of a zero degree of reaction is known as impulse blading. From Equation 13.23e, the magnitude of the relative angles at the inlet and outlet of the rotor are equal but have opposite signs, $\beta_2 = -\beta_1$. There is no contribution for the rotor row here. All the enthalpy (or pressure) rises occur in the stator blade row. The rotor just redirects the incoming flow, such that the outlet angle is equal in magnitude to the inlet angle with opposite sign.

The case of a 100% degree of reaction necessitates that $\alpha_2 = -\alpha_1$. All the enthalpy (and static pressure) rises occur in the rotor, while the stator makes no contribution.

The three cases described above are illustrated in Figure 13.20.

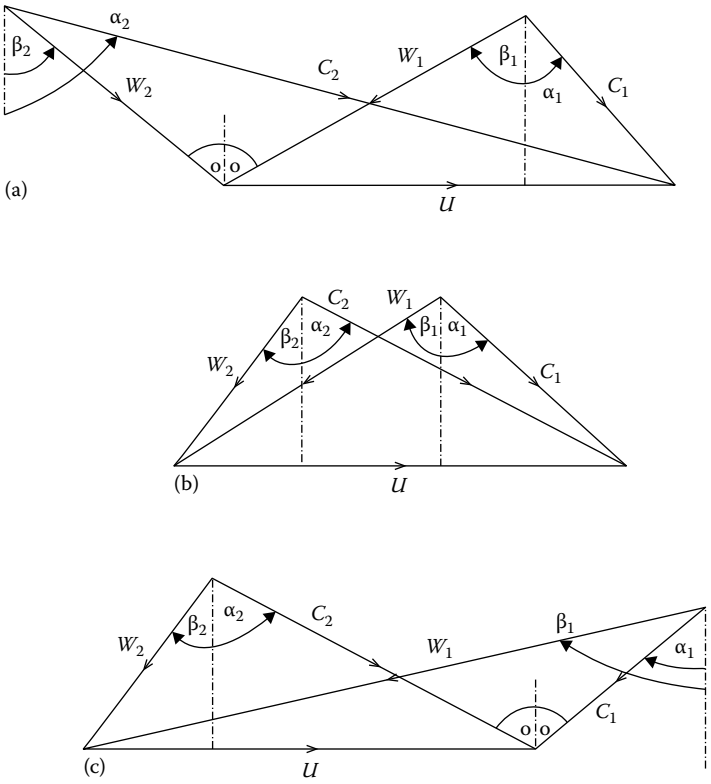


FIGURE 13.20
Velocity triangles for different degrees of reaction. (a) $\Lambda = 0\%$ ($\beta_2 = -\beta_1$), (b) $\Lambda = 50\%$ ($\alpha_1 = \beta_2$, $\alpha_2 = \beta_1$), and (c) $\Lambda = 100\%$ ($\alpha_1 = \alpha_2$).

13.6 Three-Dimensional Flow

In present-day turbomachinery, the three-dimensional effects are hardly negligible and their incorporation into the design or analysis is essential for the accurate prediction of the performance or improved design of either compressors or turbines [10]. Some of the three-dimensional effects are due to

1. Compressibility, radial density, and pressure gradients
2. Radial variation in blade thickness and geometry
3. Presence of finite hub and annulus walls, annulus area changes, flaring, curvature, and rotation
4. Radially varying work input or output
5. Presence of a two-phase flow (water injection, rain, sand, ice) and coolant injection
6. Radial component of blade force and effects of blade skew, sweep, lean, and twist
7. Leakage flow due to tip clearance and axial gaps
8. Non-uniform inlet flow and presence of upstream and downstream blade rows

9. Mixed-flow (subsonic, supersonic, and transonic flow) regions along the blade with shock-boundary-layer interaction
10. Secondary flow caused by inlet velocity/stagnation pressure gradient and flow turning
11. Air bleed in some intermediate stages of a multistage compressor for surge control
12. Injection of bulky foreign objects like stones, birds, and humans

Most of these are caused by inviscid effects, which can be treated by the use of inviscid equations of motion. The secondary flow is caused primarily by the presence of viscous layers on the wall.

In the previous sections, a two-dimensional flow was assumed in the sense that radial (i.e., spanwise) velocities did not exist. It was assumed that the radial variations in the flow parameters through the compressor's annulus are negligible. For a compressor in which the blade height is small relative to the mean diameter, that is, those with high hub/tip ratios (of the order of 0.8 or more), this assumption is reasonable. But for blades with low hub-to-tip ratios (say 0.4, as in the case of the fan of a turbofan engine), radial variations are important.

13.6.1 Axisymmetric Flow

The equations of motion governing the turbulent flow through turbomachinery are highly nonlinear, and hence most of the analytical solutions available are for simple flows. These solutions involve several assumptions depending on the type of machinery and the geometry of the blade row and flow parameters. Numerical solutions for the governing equations started in the late 1960s [11]. The three-dimensional flow in turbomachines is solved by techniques classified as either axisymmetric or non-axisymmetric. The axisymmetric solutions [10] include

1. Simplified radial equilibrium analysis (SRE)
2. Actuator disk theories
3. Passage averaged equations and their solutions

The non-axisymmetric solutions can generally be classified as [10]

1. Lifting line and lifting surface approach
2. Quasi-three-dimensional methods
3. Numerical solutions of exact equations (potential, Euler, and Navier–Stokes)

The axisymmetric solution is used to predict radial or spanwise variation of properties of flow far upstream and downstream of blade rows. Once the local values of flow parameters are known, the cascade theories can be used to predict the blade-to-blade variation of flow properties.

The equations governing the axisymmetric inviscid and steady flow motion of a fluid particle subjected to a body force having radial, tangential, and axial components (F_r, F_u, F_a) in the cylindrical coordinate system (Figure 13.21) are expressed as

$$\text{Continuity equation} \quad \frac{\partial}{\partial r}(\rho r C_r) + \frac{\partial}{\partial z}(\rho r C_z) = 0 \tag{13.24}$$

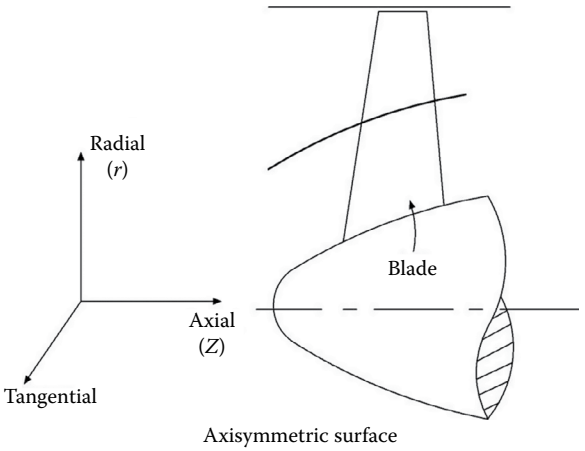


FIGURE 13.21
Axisymmetric flow notations.

$$\text{Radial momentum} \quad \frac{\partial C_r}{\partial t} + C_r \frac{\partial C_r}{\partial r} + C_z \frac{\partial C_r}{\partial z} - \frac{C_u^2}{r} = -\frac{1}{\rho}\frac{\partial p}{\partial r} + F_r \tag{13.25}$$

$$\text{Tangential momentum} \quad \frac{\partial C_u}{\partial t} + C_r \frac{\partial C_u}{\partial r} + C_z \frac{\partial C_u}{\partial z} + \frac{C_u C_r}{r} = F_u \tag{13.26}$$

$$\text{Axial momentum} \quad \frac{\partial C_z}{\partial t} + C_r \frac{\partial C_z}{\partial r} + C_z \frac{\partial C_z}{\partial z} = -\frac{1}{\rho}\frac{\partial p}{\partial z} + F_z \tag{13.27}$$

13.6.2 Simplified Radial Equilibrium Equation (SRE)

It is assumed that all the radial motion of the particle takes place within the blade row passages, while in the axial spacing between the successive blade rows (rotor/stator combination) radial equilibrium is assumed. Thus the axisymmetrical stream surface in the spacing between the blade rows has now a cylindrical stream surface shape; see Figure 13.22. The radial component of velocity is neglected in the spaces between blade rows as

$$C_r \ll C_a, \quad C_r \ll C_u, \quad \text{thus} \quad C_r \approx 0$$

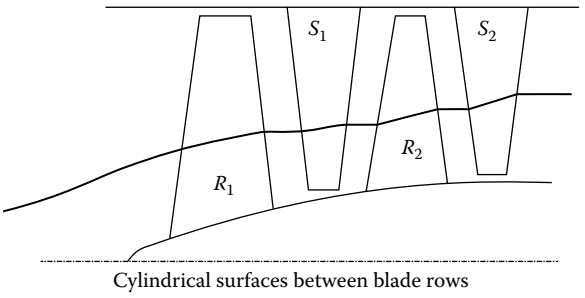


FIGURE 13.22
Axisymmetric and cylindrical surfaces in a one-stage compressor.

For a steady flow, when Equations 13.24 through 13.27 are solved over these cylindrical surfaces, they are simplified considerably, and the resulting radial momentum equation is called the "simplified radial equilibrium equation" (SRE). These equations are strictly valid away from the blade row. Only the radial equilibrium equation is relevant because the flow does not vary in either the tangential or axial direction. This is because, for a steady inviscid flow in the cylindrical surface without any body force, the variables, C_u, C_a, h, and h_0, are functions of the radius (r). Therefore, the radial component of the angular momentum equation is given by

$$\frac{1}{\rho}\frac{dp}{dr} = \frac{c_u^2}{r} \tag{13.28}$$

Equation 13.28 is the radial equilibrium equation.

The stagnation enthalpy is written now as

$$h_0 = h + \frac{C^2}{2} = h + \frac{C_a^2}{2} + \frac{C_u^2}{2} \quad (C_r \approx 0)$$

$$\frac{dh_0}{dr} = \frac{dh}{dr} + C_a\frac{dC_a}{dr} + C_u\frac{dC_u}{dr}$$

The thermodynamic relation $Tds = dh - \dfrac{dp}{\rho}$

$$dh = Tds + \frac{dp}{\rho}$$

$$\frac{dh}{dr} = T\frac{ds}{dr} + \frac{dT}{dr}ds + \frac{1}{\rho}\frac{dp}{dr}$$

Neglecting second-order terms and substituting from Equation 13.28

$$\frac{dh}{dr} = T\frac{ds}{dr} + \frac{1}{\rho}\frac{dp}{dr} = T\frac{ds}{dr} + \frac{C_u^2}{r}$$

$$\frac{dh_0}{dr} = T\frac{ds}{dr} + \frac{C_u^2}{r} + C_a\frac{dC_a}{dr} + C_u\frac{dC_u}{dr}$$

The term Tds/dr represents radial variations across the annulus, and may be significant only in detailed design and when the flow is supersonic and shock losses occur. Neglect entropy gradient

$$\frac{dh_0}{dr} = C_a\frac{dc_a}{dr} + C_u\frac{dC_u}{dr} + \frac{C_u^2}{r} \tag{13.29}$$

Equation 13.29 is denoted as the vortex energy equation, which is also applicable (as the radial equilibrium equation) only in the axial space between a pair of blade rows. Equation 13.29 is an ordinary differential equation and can be easily solved when all the variables, with the exception of one, are known. For example, for isentropic flow, if C_u and h_0 are known or prescribed, then Equation 13.29 can be solved for C_a.

13.6.3 Free Vortex Method

The free vortex method is one of the simplest design methods in axial compressors. It is based on the general equation (13.29) with the following simplifications:

1. Assuming constant specific work at all radii, $\frac{dh_0}{dr} = 0$

$$\therefore C_a \frac{dC_a}{dr} + C_u \frac{dC_u}{dr} + \frac{C_u^2}{r} = 0$$

2. Assuming constant axial velocity at all radii, $\frac{dC_a}{dr} = 0$

$$\therefore C_u \frac{dC_u}{dr} + \frac{C_u^2}{r} = 0$$

$$\frac{dC_u}{C_u} = -\frac{dr}{r}$$

Integrating, we obtain

$$rC_u = \text{constant} \tag{13.30}$$

Thus, the whirl velocity component of the flow varies inversely with the radius, which is known as a free vortex.

It is clear that if the three variables (h_0, C_a, rC_u) are not varying in the radial direction, then the radial equilibrium equation, $dp/\rho dr = c_u^2/r$, is satisfied. The resulting blading is denoted free vortex blading. Though it represents a simple mathematical treatment for blade twist, it has two main disadvantages; namely, the large variation of the degree of reaction and the large blade twist along the blade span (or height).

The degree of reaction from Equation 13.23c is expressed as

$$\Lambda = 1 - \frac{C_a}{2U}\left(\tan\alpha_1 + \tan\alpha_2\right) = 1 - \frac{C_{u1} + C_{u2}}{2U}$$

$$\Lambda = 1 - \frac{rC_{u1} + rC_{u2}}{2rU}$$

but

$$\frac{U}{U_m} = \frac{r}{r_m}$$

$$\Lambda = 1 - \frac{\text{constant}}{2U_m r/r_m}$$

$$\Lambda = 1 - \frac{\text{constant}}{r^2} \tag{13.31}$$

A great variation in the degree of reaction from the blade hub-to-tip is represented by Equation 13.31. Moreover, some suspect that at the blade root, where its radius is a

minimum, a negative reaction is possible. One final note to mention here is that the free vortex relation (Equation 13.30) is applied twice at stations 1 and 2. The following example illustrates the above points.

Example 13.2

Consider a free vortex design for a compressor stage having a degree of reaction at the mean section equals to 0.5, a hub-to-tip ratio of 0.6, and flow angles $\alpha_{1m}=30°$, $\beta_{1m}=60°$. Calculate the absolute and relative angles at the hub (α_h, β_h) and tip (α_t, β_t) for both stations 1 (upstream of the rotor) and 2 (downstream of the rotor). Calculate also the degree of reaction at both hub and tip.

Solution

Since the degree of reaction is 50% at the mean section, then

$$\alpha_{1m}=\beta_{2m} \quad \text{and} \quad \alpha_{2m}=\beta_{1m}$$

Since the hub-to-tip ratio is equal to 0.6, then at both stations (1) and (2)

$$r_t=\frac{5}{4}r_m \quad \text{and} \quad r_h=\frac{3}{4}r_m$$

$$U_t=U_m\frac{r_t}{r_m} \quad U_t=\frac{5}{4}U_m$$
$$U_h=U_m\frac{r_h}{r_m} \quad U_h=\frac{3}{4}U_m$$

For a free vortex design, rC_u = Constant at stations 1 and 2

$$r_hC_{uh}=r_mC_{um} \quad C_{uh}=\frac{r_m}{r_h}C_{um}$$
$$r_tC_{ut}=r_mC_{um} \quad C_{ut}=\frac{r_m}{r_t}C_{um}$$

The swirl velocity components are

$$C_{uh}=\frac{4}{3}C_{um} \quad C_{ut}=\frac{4}{5}C_{um}$$

Then, for both stations 1 and 2

$$C_{u1h}=\frac{4}{3}C_{u1m} \quad C_{u2h}=\frac{4}{3}C_{u2m} \quad U_h=\frac{3}{4}U_m$$
$$C_{u1t}=\frac{4}{5}C_{u1m} \quad C_{u2t}=\frac{4}{5}C_{u2m} \quad U_t=\frac{5}{4}U_m$$

$$\tan\alpha_h=\frac{C_{uh}}{C_a}=\frac{4}{3}\frac{C_{um}}{C_a}=\frac{4}{3}\tan\alpha_m$$
$$\tan\alpha_t=\frac{C_{ut}}{C_a}=\frac{4}{5}\frac{C_{um}}{C_a}=\frac{4}{5}\tan\alpha_m$$
$$\tan\beta_h=\frac{U_h-C_{uh}}{C_a}=\frac{(3/4)U_m-(4/3)C_{um}}{C_a}$$

TABLE 13.2

Characteristics of a Single-Stage Axial Compressor Based on the Free Vortex Design Method

	α_1	β_1	α_2	β_2	Λ	$\beta_1 - \beta_2$
Hub	37.6	43.9	66.6	−30	0.11	73.9
Mean	30	60	60	30	0.5	30
Tip	24.8	67.5	54.2	56.3	0.68	11.3

Note: All angles in degrees.

but

$$\frac{U_m}{C_a} = \tan\alpha_m + \tan\beta_m \quad \text{and} \quad \frac{C_{um}}{C_a} = \tan\alpha_m$$

$$\therefore \tan\beta_h = \frac{3}{4}\tan\beta_m - \frac{7}{12}\tan\alpha_m$$

Similarly

$$\frac{U_m}{C_a} = \tan\alpha_m + \tan\beta_m \quad \text{and} \quad \frac{C_{um}}{C_a} = \tan\alpha_m$$

$$\tan\beta_t = \frac{U_t - C_{ut}}{C_a} = \frac{(5/4)U_m - (4/5)C_{um}}{C_a}$$

$$\therefore \tan\beta_t = \frac{9}{20}\tan\alpha_m + \frac{5}{4}\tan\beta_m$$

From Equations 13.1a and 13.23e, the degree of reaction at any radius may be expressed as

$$\Lambda = \frac{\tan\beta_1 + \tan\beta_2}{2(\tan\alpha_1 + \tan\beta_1)}$$

The difference in the angles $\beta_1 - \beta_2$ at different stations along the blade span represents the blade twist. Thus adopting the free vortex design yields a highly twisted blade and much variation in the degree of reaction from hub to tip. The degree of reaction is only 0.11 at the hub. As explained in [5], because of the lower blade speed at the root section, more fluid deflection is required for a given work input, that is, a great rate of diffusion is required at the root section. It is therefore undesirable to have a low degree of reaction in this region, and the problem is aggravated as the hub–tip ratio is reduced.

The velocity triangles and the blade twist are shown in Figure 13.23.

Example 13.3

For an axial compressor stage, using the vortex energy equation

$$\frac{1}{r^2}\frac{d}{dr}\left(r^2C_u^2\right) + \frac{d}{dr}\left(C_a^2\right) = 0$$

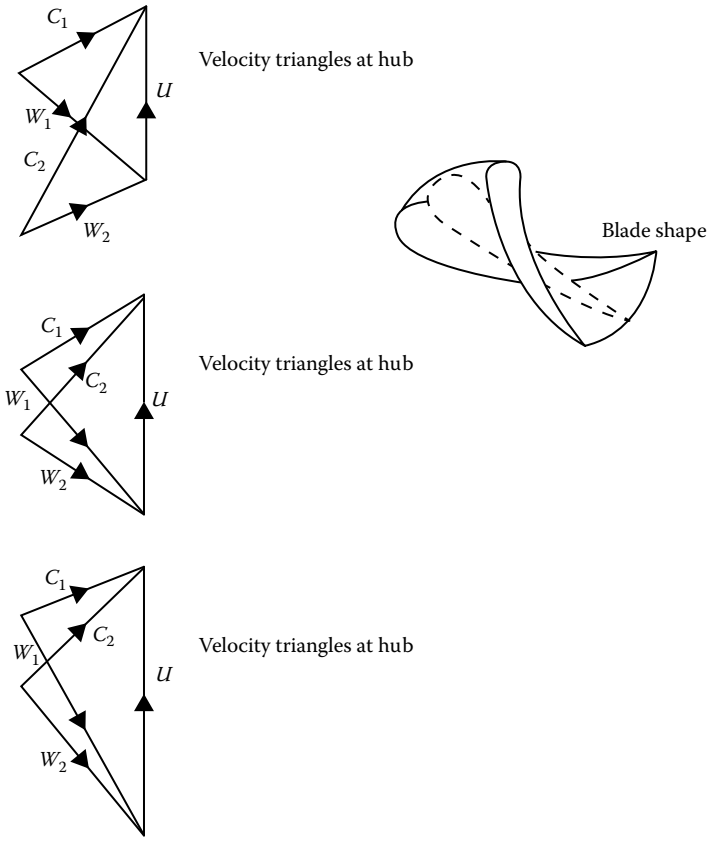


FIGURE 13.23
Free vortex velocity triangle and blade shape.

prove that, if the flow is represented by a free vortex and $rC_u = \text{constant}$,

1. $C_a = \text{constant}$
2. $\tan\alpha_{1h} = \left(\dfrac{1+\zeta}{2\zeta}\right)\tan\alpha_{1m}$
3. $\tan\beta_{1h}\left(\dfrac{2\zeta}{1+\zeta}\right)\tan\beta_{1h} + \dfrac{(3\zeta+1)(\zeta-1)}{2\zeta(1+\zeta)}\tan\alpha_{1m}$

where
ζ is the hub–tip ratio
α_1 is the angle between the inlet absolute velocity and the axial direction
β_1 is the angle between the inlet relative velocity and the axial direction

Subscripts (h) and (m) refer to the hub and mean sections, respectively (Figure 13.24).

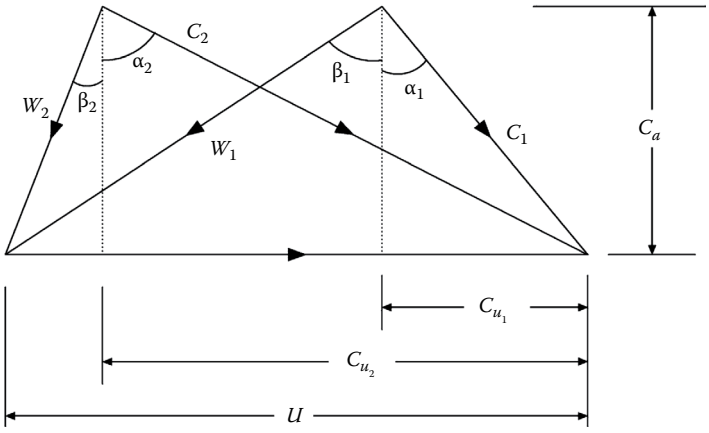


FIGURE 13.24
Velocity triangle.

Solution

1. For $rC_u = \text{Constant}$

$$\therefore \frac{d}{dr}\left(rC_u\right) = 0$$

Then, from the vortex energy equation,

$$\frac{1}{r^2}\frac{d}{dr}\left(r^2C_u^2\right) + \frac{d}{dr}\left(C_a^2\right) = \frac{d}{dr}\left(C_a^2\right) = 0$$

Thus

$$C_a^2 = \text{Constant}$$
$$\therefore C_a = \text{Constant}$$

2. Since $\tan\alpha_{1h} = \dfrac{C_{u1h}}{C_a}$, $\tan\alpha_{1m} = \dfrac{C_{u1m}}{C_a}$, and $C_a = \text{constant}$

Then $\dfrac{\tan\alpha_{1h}}{\tan\alpha_{1m}} = \dfrac{C_{u1h}}{C_{u1m}}$

$$\tan\alpha_{1h} = \frac{C_{u1h}}{C_{u1m}}\tan\alpha_{1m} \tag{1}$$

but

$$rC_u = \text{Constant}, \quad \text{or} \quad r_hC_{uh} = r_mC_{um}$$

Then at state (1)

$$r_hC_{u1h} = r_mC_{u1m}$$

$$\frac{C_{u1h}}{C_{u1m}} = \frac{r_m}{r_h}$$

then from Equation 1

$$\therefore \tan\alpha_{1h} = \frac{r_m}{r_h}\tan\alpha_{1m}$$

$$\frac{r_m}{r_h} = \frac{r_h + r_t}{2r_h} = \frac{\frac{r_h}{r_t}+1}{2\frac{r_h}{r_t}} = \frac{1+\zeta}{2\zeta}$$

$$\tan\alpha_{1h} = \frac{1+\zeta}{2\zeta}\tan\alpha_{1m}$$

3. From the kinematical relations

$$\tan\alpha_{1h} + \tan\beta_{1h} = \frac{U_h}{C_a}$$

$$\tan\alpha_{1m} + \tan\beta_{1m} = \frac{U_m}{C_a}$$

$$\therefore \frac{\tan\alpha_{1h} + \tan\beta_{1h}}{\tan\alpha_{1m} + \tan\beta_{1m}} = \frac{U_h}{U_m}$$

$$\tan\alpha_{1h} + \tan\beta_{1h} = \frac{U_h}{U_m}\left(\tan\alpha_{1m} + \tan\beta_{1m}\right)$$

$$\tan\beta_{1h} = \frac{U_h}{U_m}\left(\tan\alpha_{1m} + \tan\beta_{1m}\right) - \tan\alpha_{1h}$$

Since

$$\frac{U_h}{U_m} = \frac{r_h}{r_m} = \frac{2\zeta}{\zeta+1}$$

and

$$\tan\alpha_{1h} = \frac{1+\zeta}{2\zeta}\tan\alpha_{1m}$$

$$\therefore \tan\beta_{1h} = \frac{2\zeta}{\zeta+1}\left(\tan\alpha_{1m} + \tan\beta_{1m}\right) - \frac{1+\zeta}{2\zeta}\tan\alpha_{1m}$$

$$\tan\beta_{1h} = \frac{2\zeta}{1+\zeta}\tan\beta_{1m} + \left[\frac{2\zeta}{\zeta+1} - \frac{1+\zeta}{2\zeta}\right]\tan\alpha_{1m}$$

$$\tan\beta_{1h} = \frac{2\zeta}{\zeta+1}\tan\beta_{1m} + \frac{4\zeta^2 - (1+\zeta)^2}{2\zeta(1+\zeta)}\tan\alpha_{1m}$$

$$\tan\beta_{1h} = \frac{2\zeta}{\zeta+1}\tan\beta_{1m} + \frac{(3\zeta+1)(\zeta-1)}{2\zeta(1+\zeta)}\tan\alpha_{1m}$$

13.6.4 General Design Procedure

The disadvantages of the free vortex method mentioned above motivate searching for other design methods. Thus, if the design is based on the arbitrarily chosen radial distribution of any two variables of the three (h_0, C_a, C_u), then the variation of the other is

determined from Equation 13.29. However, it is always preferable to employ a constant specific work at all radii along the blade together with an arbitrary whirl velocity distribution for C_{u1}, C_{u2} that is compatible with the constant specific work condition. Next, the variation of the axial velocity C_a and the degree of reaction Λ with the radius r are calculated. Equation 13.29 is to be solved twice, at both stations (1) and (2), to obtain the radial variation of the axial velocities C_{a1}, C_{a2}.

The designer usually prescribes the whirl velocity somewhere between a *forced-vortex* and a *free vortex* design according to the relation

$$C_{u1} = aR^n - \frac{b}{R} \quad C_{u2} = aR^n + \frac{b}{R} \tag{13.32}$$

where

$$R = \frac{r}{r_m} = \frac{U}{U_m}$$

The value a is determined from the degree of reaction

$$\Lambda = 1 - \frac{C_{u1} + C_{u2}}{2U}$$

At the mean section, the degree of reaction will be

$$\Lambda_m = 1 - \frac{C_{u1m} + C_{u2m}}{2U_m}$$

Substitute the values of the whirl velocities at the mean section from Equation 13.32, then

$$\Lambda_m = 1 - \frac{\left(aR_m^n + \frac{b}{R_m}\right) + \left(aR_m^n - \frac{b}{R_m}\right)}{2U_m}, \quad R_m = 1$$

$$\therefore \Lambda_m = 1 - \frac{a}{U_m}$$

$$a = U_m\left(1 - \Lambda_m\right) \tag{13.33}$$

The constant b is calculated from the condition of constant specific work

$$\Delta h_0 = \text{constant} \equiv h_{02} - h_{01}$$

$$W_s \equiv \Delta h_0 = U\left(C_{u2} - C_{u1}\right)$$

$$\Delta h_0 = U_m R\left(aR^n + \frac{b}{R} - aR^n + \frac{b}{R}\right)$$

$$\Delta h_0 = 2bU_m$$

$$b = \frac{\Delta h_0}{2U_m} \tag{13.34}$$

The values of (a) and (b) are constants and independent of the radius (r) as verified by Equations 13.33 and 13.34.

The above relation cannot be applied for either $n = 0$ or $n = 1$. Thus Equation 13.29.

Consider the following three special cases for n; namely $n = -1$, 1, and 0.

$$\begin{aligned} n = -1 \quad &\text{Free vortex} \quad rC_u = A \\ n = 0 \quad &\text{Exponential} \quad rC_u = Ar + B \\ n = 1 \quad &\text{Free power} \quad rC_u = Ar^2 + B \end{aligned}$$

Rewriting Equation 13.33

$$\frac{dh_0}{dr} = C_a \frac{dC_a}{dr} + C_u \frac{dC_u}{dr} + \frac{C_u^2}{r}$$

The total enthalpy upstream of the stage h_{01} is assumed constant and independent of the radius (r). Since the specific work, $W_s \equiv h_{02} - h_{01}$, is assumed to be constant, then the downstream enthalpy (h_{02}) is also constant. Now Equation 13.33 is to be solved both at state (1) and (2). In both cases the LHS of Equation 13.33 is zero. The equation to be solved is now reduced to

$$C_a \frac{dC_a}{dr} + C_u \frac{dC_u}{dr} + \frac{C_u^2}{r} = 0$$

This equation is to be integrated at station (1), for example, from the mean radius to any station (r). At the mean radius

$$R_m = 1, \quad C_{u1m} = a - b \quad \text{and} \quad C_{u2m} = a + b$$

Thus the following equation is obtained

$$\begin{aligned} \frac{1}{2}\left(C_{a1}^2 - C_{am}^2\right) &= -\frac{1}{2}\left(C_{u1}^2 - C_{u1m}^2\right) - \int_1^R \left(aR^n - \frac{b}{R}\right)^2 \frac{dR}{R} \\ &= -\frac{1}{2}\left[\left(aR^n - \frac{b}{R}\right)^2 - (a-b)^2\right] - \int_1^R \left(a^2R^{2n-1} - 2abR^{n-2} + \frac{b^2}{R^3}\right) dR \\ \frac{1}{2}\left(C_{a1}^2 - C_{a1m}^2\right) &= \frac{1}{2}\left[\left(a^2R^{2n} - 2abR^{n-1} + \frac{b^2}{R^2}\right) - \left(a^2 - 2ab + b^2\right)\right] + Integral \end{aligned}$$

$$Integral \equiv \int_1^R \left(a^2 R^{2n-1} - 2abR^{n-2} + \frac{b^2}{R^3} \right) dR$$

$$Integral = \left[\left(\frac{a^2 R^{2n}}{2n} - \frac{2abR^{n-1}}{n-1} - \frac{b^2}{2R^2} \right) - \left(\frac{a^2}{2n} - \frac{2ab}{n-1} - \frac{b^2}{2} \right) \right]$$

This integral represents a general solution for any value of (n). However, the general solution cannot be applied for the cases of n equals (0) or (1). A similar relation is also obtained for state (2) at the outlet of the rotor stage. Thus, the value of n must be substituted first and the integral is next evaluated. A similar procedure is followed for state (2) downstream of the rotor.

The resulting values for the axial velocities at any radius in stations (1) and (2) are calculated. These results are assembled in Table 13.3 together with the values of the whirl speeds and the degree of reaction.

As stated in [10], for the exponential method, the loading as well as the blade twists are moderate. The new blade design tends toward low-aspect ratio blading. The velocity triangles for any type of blading except $n = -1$ is plotted in Figure 13.25. The variation of axial velocities at states (1) and (2), C_{a1}, C_{a2}, are plotted along the blade height, as illustrated in Figure 13.26.

TABLE 13.3

Governing Equations for Different Design Methods

	$C_{u1} = aR^n - \frac{b}{R}\ C_{u2} = aR^n + \frac{b}{R}$		$a = U_m(1-\Lambda_m)$ $b = Cp\Delta T_{0s}/2U_m$
Blading	Ca	Λ	Cu
Free vortex $n = -1$	$C_{a1} = C_{a1m}$ $C_{a2} = C_{a2m}$ $C_{a1m} = C_{a2m}$	$\Lambda = 1 - \frac{a}{U_m R^2}$ $\Lambda = 1 - \frac{(1-\Lambda_m)}{R^2}$	$C_{u1} = \frac{a-b}{R}$ $C_{u2} = \frac{a+b}{R}$
Exponential $n = 0$	$C_{a1}^2 - C_{a1m}^2 = -2\left[a^2 \ln R + \frac{ab}{R} - ab \right]$ $C_{a2}^2 - C_{a2m}^2 = -2\left[a^2 \ln R - \frac{ab}{R} + ab \right]$ $C_{a1m} = C_{a2m}$ $C_{a2}^2 - C_{a1}^2 = 4ab\left(\frac{1}{R} - 1 \right)$	$\Lambda = 1 + \frac{a}{U_m} - \frac{2a}{U_m R}$ $\Lambda = 1 + \left(1 - \frac{2}{R} \right)(1-\Lambda_m)$	$C_{u1} = a - \frac{b}{R}$ $C_{u2} = a + \frac{b}{R}$
First power $n = 1$	$C_{a1}^2 - C_{a1m}^2 = -2\left[a^2 \left(R^2 - 1 \right) - 2ab \ln R \right]$ $C_{a2}^2 - C_{a2m}^2 = -2\left[a^2 \left(R^2 - 1 \right) + 2ab \ln R \right]$ $C_{a2}^2 - C_{a1}^2 = -8ab \ln R$ $C_{a1m} = C_{a2m}$	$\Lambda = 1 + \frac{2a \ln R}{U_m} - \frac{a}{U_m}$ $\Lambda = 1 + (2 \ln R - 1)(1 - \Lambda_m)$	$C_{u1} = aR - \frac{b}{R}$ $C_{u2} = aR + \frac{b}{R}$

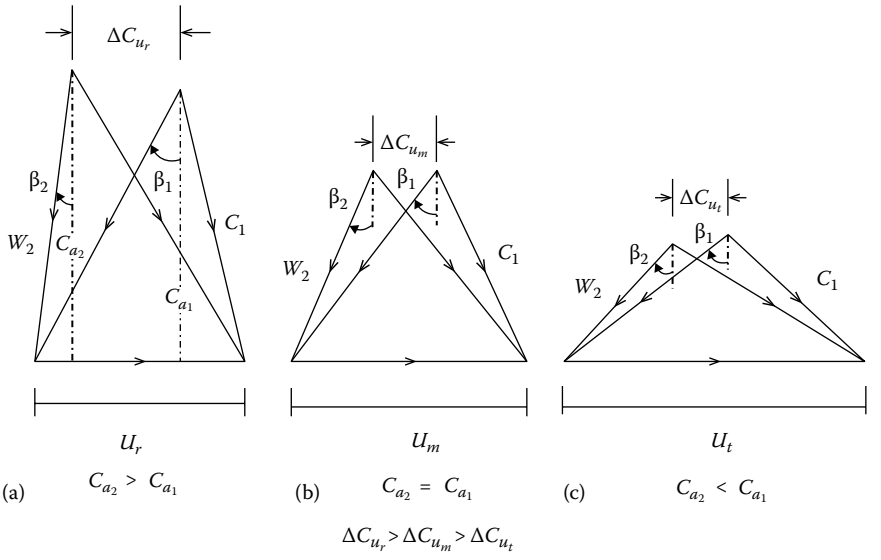


FIGURE 13.25
Velocity triangles at (a) hub, (b) mean, and (c) tip stations for $n \neq -1$.

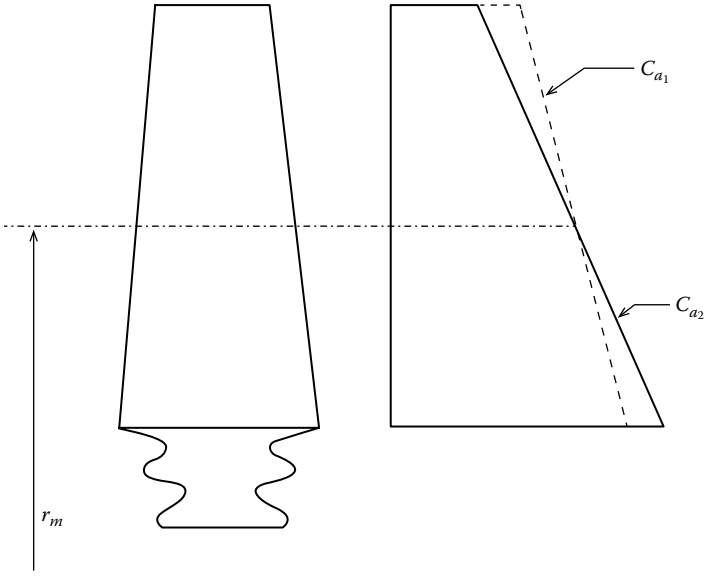


FIGURE 13.26
Variation of axial velocities C_{a1}, C_{a2} along the blade height for $n \neq -1$.

Example 13.4

If the whirl velocities in an axial stage are expressed as

$$C_{u1} = aR^n - \frac{b}{R} \qquad C_{u2} = aR^n + \frac{b}{R}$$

prove that, if a constant specific work is assumed and the exponent $n = 2$,

$$C_{a1}^2 - C_{a2}^2 = 12ab(R-1)$$

Solution

Since the vortex energy equation is expressed by

$$\frac{dh_o}{dr} = C_a \frac{dC_a}{dr} + C_u \frac{dC_u}{dr} + \frac{C_u^2}{r}$$

assume the specific work = constant in the radial direction

$$-C_a \frac{dC_a}{dr} = C_u \frac{dC_u}{dr} + \frac{C_u^2}{r}$$

$$-C_a dC_a = C_u dC_u + \frac{C_u^2}{r} dr$$

$$R = \frac{r}{r_m}$$

$$-\int_{C_{am}}^{C_a} C_a dC_a = \int_{C_{um}}^{C_u} C_u dC_u + \int_1^R C_u^2 \frac{dR}{R}$$

$$-\frac{1}{2}\left[C_a^2 - C_{a_m}^2\right] = \frac{1}{2}\left[C_u^2 - C_{u_m}^2\right] + I$$

$n = 2$

$$C_{u1} = aR^2 - \frac{b}{R}$$

$$C_{u2} = aR^2 + \frac{b}{R}$$

$$-\frac{1}{2}\left[C_{a1}^2 - C_{a1_m}^2\right] = \frac{1}{2}\left[C_{u1}^2 - C_{u1_m}^2\right] + \int_1^R \left(aR^2 - \frac{b}{R}\right)^2 \frac{dR}{R}$$

$$-\frac{1}{2}\left[C_{a1}^2 - C_{a1_m}^2\right] = \frac{1}{2}\left[\left(aR^2 - \frac{b}{R}\right)^2 - (a-b)^2\right] + \int_1^R \left(a^2R^3 - 2ab + \frac{b^2}{R^3}\right) dR$$

$$-\frac{1}{2}\left[C_{a1}^2 - C_{a1_m}^2\right] = \frac{1}{2}\left[\left(aR^2 - \frac{b}{R}\right)^2 - (a-b)^2\right] + \left[\frac{a^2R^4}{4} - 2abR - \frac{b^2}{2R^2}\right]_1^R$$

$$-\frac{1}{2}\left[C_{a1}^2 - C_{a1_m}^2\right] = \frac{1}{2}\left[\left(a^2R^4 - 2abR + \frac{b^2}{R^2}\right) - \left(a^2 - 2ab + b^2\right)\right]$$

$$+\left[\left(\frac{a^2R^4}{4} - 2abR - \frac{b^2}{2R^2}\right) - \left(\frac{a^2}{4} - 2ab - \frac{b^2}{2}\right)\right]$$

$$C_{a1}^2 - C_{a1_m}^2 = \left(\frac{3}{2}a^2 - 6ab\right) - \left(\frac{3}{2}a^2R^4 - 6abR\right)$$

Similarly

$$C_{a2}^2 - C_{a2_m}^2 = \left(\frac{3}{2}a^2 + 6ab\right) - \left(\frac{3}{2}a^2R^4 + 6abR\right)$$

Since $C_{a1m} = C_{a2m}$

$$C_{a1}^2 - C_{a2}^2 = 12ab(R-1)$$

From the above equation, the following conclusions are deduced:

$R<1$	$R=1$	$R>1$
$Ca_1 < Ca_2$	$Ca_{1m} = Ca_{2m}$	$Ca_1 > Ca_2$

Example 13.5

1. Consider a free vortex design for a compressor stage having a degree of reaction at the mean section equal to 0.6, a hub-to-tip ratio of 0.6, and the flow angles $\alpha_{1m} = 30°$, $\beta_{1m} = 60°$. *Calculate* the absolute and relative angles at the hub (α_h, β_h) and tip (α_t, β_t) for both stations 1 (upstream of the rotor) and 2 (downstream of the rotor). *Calculate* also the degree of reaction at both hub and tip.
2. If the above compressor stage is to be designed by the *exponential method* instead of the free vortex, *recalculate* the absolute and relative angles at the hub (α_h, β_h) and tip (α_t, β_t) for both stations 1 (upstream of the rotor) and 2 (downstream of the rotor) and also the degree of reaction at both hub and tip (Figure 13.27). Additional data are

$$a = 100 \text{ m/s}, \quad b = 40 \text{ m/s}$$

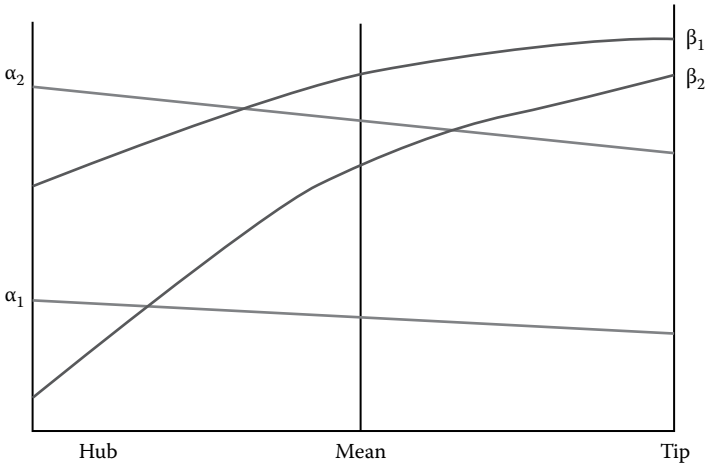


FIGURE 13.27
Variation of angles from hub to tip.

Solution

Given data

$$\alpha_{1m} = 30°, \quad \beta_{1m} = 60°, \quad \text{and} \quad \zeta = 0.6$$

1. Free vortex design
   The data here are the same as in Example 13.2, except for the degree of reaction. Thus the following same results are obtained for the inlet flow along the blade.

$$\alpha_{1h} = 37.6°, \quad \alpha_{1t} = 24.8°, \quad \beta_{1h} = 43.9°, \quad \beta_{1t} = 67.5°$$

   It was proved in Example 13.2 that the degree of reaction may be expressed by the relation

$$\Lambda = \frac{\tan\beta_1 + \tan\beta_2}{2(\tan\alpha_1 + \tan\beta_1)}$$

   Applying this equation at the mean section, then

$$\tan\beta_{2m} = 2\Lambda_m(\tan\alpha_{1m} + \tan\beta_{1m}) - \tan\beta_{1m}$$
$$\tan\beta_{2m} = 2 \times 0.6 \times 2.3094 - 1.732 = 1.0392$$
$$\beta_{2m} = 46.1°$$
$$\tan\alpha_{2m} = \frac{U_m}{C_a} - \tan\beta_{2m} = 1.2702$$
$$\alpha_{2m} = 51.78°$$

$$\Lambda = \frac{\tan\beta_1 + \tan\beta_2}{2(\tan\alpha_1 + \tan\beta_1)}$$
$$\Lambda_h = \frac{\tan\beta_{1h} + \tan\beta_{2h}}{2(\tan\alpha_{1h} + \tan\beta_{1h})} = 0.2905$$
$$\Lambda_t = \frac{\tan\beta_{1t} + \tan\beta_{2t}}{2(\tan\alpha_{1t} + \tan\beta_{1t})} = 0.7438$$

2. Exponential design method
   Since $a = U_m(1 - \Lambda_m) = 100$, $\Lambda_m = 0.6$, then

$$U_m = \frac{100}{0.4} = 250 \text{ m/s}$$

   Moreover, with $b = 40$ m/s

$$\Delta T_0 = \frac{2bU_m}{Cp} = \frac{2 \times 40 \times 250}{1005} = 19.9 \text{ K}$$

$$Cu_1 = a - \frac{b}{R}$$

$$Cu_{1h} = 46.7 \text{ m/s}, \quad Cu_{1t} = 68 \text{ m/s}$$

Since

$$\frac{U_m}{C_{am}} = \tan\alpha_{1m} + \tan\beta_{1m}$$

$$C_{am} = \frac{250}{\tan 30 + \tan 60} = 108.25 \text{ m/s}$$

$$Ca_{1h}{}^2 = Ca_m{}^2 - 2\left[a^2 \ln R + \frac{ab}{R} - ab\right]$$

$$Ca_{1h}{}^2 = (108.25)^2 - 2\left((100)^2 \ln\frac{3}{4} + \frac{100\times 40}{(3/40)} - 100\times 40\right)$$

$Ca_{1h} = 121.7$ m/s, similarly $Ca_{1t} = 94.1$ m/s

$$C_{a2}^2 = C_{a2m}^2 - 2\left[a^2 \ell nR - \frac{ab}{R} + ab\right]$$

$$Ca_{2h} = 141.9 \text{ m/s} \quad \text{and} \quad Cu_{2h} = a + \frac{b}{R_h} = 153.3 \text{ m/s}$$

$$Cu_{2t} = 132 \text{ m/s}$$

$$\tan\alpha_{1h} = \left(\frac{C_{u1}}{C_{a1}}\right)_h = 0.384, \quad \alpha_{1h} = 21°$$

$$\tan\alpha_{2h} = \left(\frac{Cu_2}{Ca_2}\right)_h = 0.93, \quad \alpha_{2h} = 42.9°$$

$$\tan\alpha_{1t} = \left(\frac{C_{u1°}}{C_{a1}}\right)_t = 0.722, \quad \alpha_{1t} = 35.85°$$

$$\tan\alpha_{2t} = \left(\frac{C_{u2}}{C_{a2}}\right)_t = 1.755, \quad \alpha_{2t} = 60.32°$$

$$U_h = \frac{3}{4}U_m = 187.5 \text{ m/s} \quad U_t = 312 \text{ m/s}$$

$$\left(\frac{U}{C_{a1}}\right)_h = \tan\alpha_{1h} + \tan\beta_{1h}$$

$$\tan\beta_{1h} = \frac{187.5}{121.7} - \tan 21 = 1.1568$$

$\beta_{1h} = 49.15°$ similarly $\beta_{1t} = 68.95°$

$$\tan\beta_{2h} = \left(\frac{U}{C_{a2}}\right)_h - \tan\alpha_{2h} = 0.392$$

$\beta_{2h} = 21.4°$, similarly $\beta_{2t} = 67.388°$

TABLE 13.4

Summary of Results for Free Vortex Design

	$\frac{U}{Ca}$	α_1	β_1	α_2	β_2	Λ	$(\beta_1-\beta_2)$
Hub	1.725	37.6	43.9	59.25	2.53	0.2905	41.37
Mean	2.3	30	60	51.78	46.1	0.6	13.9
Tip	2.875	24.8	67.5	45.25	61.8	0.7438	5.7

TABLE 13.5

Summary of Results for Exponential Method

	U (m/s)	Ca_1	Ca_2	α_1	β_1	α_2	β_2	Λ	$(\beta_1-\beta_2)$
Hub	187.5	121.7	141.9	21	49.2	42.9	21.4	0.59	27.8
Mean	250	108.25	108.25	30	60	51.78	46.1	0.6	13.9
Tip	312.5	94.1	75.2	38.9	69	60.32	67.4	0.734	1.6

From both tables the following conclusions may be deduced (Tables 13.4 and 13.5):

1. The degree of reaction for the exponential design is much higher than the case of the free vortex design.
2. The rotor twist $(\beta_1-\beta_2)$ for the exponential design is less than the free vortex design.

13.7 Complete Design Process for Compressors

Compressors are designed by the *indirect method* [6]. That is, first one defines the flow path (casing and hub) radii and then one decides on the thermodynamic and aerodynamic properties as well as the work input that air must have at each axial location (station) along the flow path. An iterative analysis is conducted in which the continuity, momentum, energy, and state equations are satisfied at each station. Although there are no blades or blade shape in the analysis, their presence is recognized by work input, turning ability, and loss. Then one designs the blade and vanes to achieve the desired thermodynamic and aerodynamic properties. The designer is constrained to achieve the overall pressure ratio and mass flow rate. The full design details are given in Reference 12.

A concise design procedure is presented in Reference 6. The steps for this design are

1. Choice of the compressor rotational speed (rpm) and annulus dimensions
2. Determine number of stages (assuming efficiency)
3. Calculate air angles for each stage at the mean section
4. Determine the variation of air angles from root to tip based on type of blading (either free vortex, exponential, or first power)
5. Selection of compressor blading using experimentally cascade data

6. Check efficiency (previously assumed) using cascade data
7. Investigation of compressibility effects
8. Estimate off-design performance
9. Rig testing

The details of these steps will be described here.

13.8 Rotational Speed (rpm) and Annulus Dimensions

From past experience of subsonic compressor design [6], the maximum tip speed, axial velocity, as well as the hub–tip ratio of the first stage may have the following typical values

$$U_t \approx 350 \text{ m/s}$$

$$C_a \approx 150 - 200 \text{ m/s}$$

$$\zeta \equiv \frac{r_h}{r_t} \approx 0.4 - 0.6$$

Another design procedure also for subsonic compressors is to rely on the Mach number rather than specific values of speeds. Thus the following values are suggested:

Axial Mach number $M_a \approx 0.5 (<0.7)$

Hub–tip ratio at inlet $\zeta > 0.3$ and at outlet $\zeta < 0.9$

Relative Mach number: at tip $M_{1tip} < 1.2$ for the high-pressure compressor (HPC), for fan $M_{1tip} < 1.8$

Relative Mach number at hub $M_{1hub} < 0.9$

However, if this compressor is a part of an aeroengine powering a supersonic or future hypersonic aircraft, the total temperature at the inlet to compressor approaches or exceeds 1000 K. In this case, the static temperature is very close to the total values, which leads to very high values for sonic speeds. Thus, the Mach number values suggested above develop unaffordable stresses in the blades. Consequently, these values are drastically reduced to as much as half the suggested values. Alternatively, specific values for the mean blade and axial speeds are to be employed.

If this compressor is connected to a turbine, then the rotational speed of the compressor must be the same as the rotational speed of the turbine. This will be a design constraint. Moreover, for the same compressor/turbine spool, the outer dimensions (tip diameter) must be equal or comparable. This will be another constraint.

For the first stage, the flow is axial or $C_1 = C_{a1}$. The axial Mach number is calculated as

$$C_1 = M_1 \sqrt{\gamma R T_1}$$

$$C_1 = M_1 \sqrt{\frac{\gamma R T_{01}}{1 + \frac{\gamma - 1}{2} M^2}} \tag{13.35}$$

Similarly, the relative speed at the blade tip is

$$W_1 = M_{1rel} \sqrt{\frac{\gamma R T_{01}}{1 + \frac{\gamma - 1}{2} M^2}} \tag{13.36}$$

The rotational speed is then

$$U_t^2 = W_{1tip}^2 - C_1^2$$

$$U_t^2 = \left(M_{1tip}^2 - M_1^2\right)\left(\frac{\gamma R T_{01}}{1 + \frac{\gamma - 1}{2} M^2}\right) \tag{13.37}$$

The outer diameter and the rotational speed are related by the equation

$$r_t = \frac{U_t}{2\pi N}$$

If either the tip speed or the rotational speed is specified (or have some constraint), then the hub–tip ratio is calculated from the continuity equation as follows:

$$\dot{m} = \rho_1 C_{a1} A = \rho_1 C_{a1} \pi \left(r_t^2 - r_h^2\right)$$

$$\zeta^2 = \left\{\frac{\dot{m}}{\rho_1 C_{a1} \pi \left(1 - r_t^2\right)}\right\}$$

The density is calculated as

$$C_1 = C_{a1}, \quad T_1 = T_{01} - \frac{C_1^2}{2Cp} \quad \text{and} \quad P_1 = P_{01}\left(\frac{T_1}{T_{01}}\right)^{\gamma/\gamma - 1}$$

$$\therefore \rho_1 = \frac{P_1}{R T_1}$$

A check is required here for the hub–tip ratio to be within the specified range.

Example 13.6

A preliminary design for the low-pressure axial compressor that is connected to an axial turbine of a small turbojet engine is required. The compressor has an inlet total temperature and pressure of 322.2 K and 141 kPa. The mass flow rate is 50 kg/s. The turbine rotational speed is 180 rev/s, with a tip diameter of 0.285 m. Assume the flow to be axial at the compressor inlet.

Solution

Based on the suggested inlet Mach numbers, assume that the relative tip Mach number $M_{1tip}=1.1$ and the axial Mach number $M_a=0.5$. The procedure is to calculate the static temperature and pressure and then the density. Next, the axial, relative, and rotational speeds are calculated. Finally, the tip radius is calculated, and from this the hub–tip ratio. If the tip diameter is far from the turbine outer diameter, the axial Mach number is to be changed within its design range. The results for the example are arranged in the following table where the axial Mach number varies from 0.5 to 0.6 (Table 13.6). Since, from turbine calculations,

$$N = 180 \text{ rps} \quad \text{and} \quad (r_t)_{turbine} = 0.285 \text{ m}$$

choose $M_1=0.6$, where $\zeta = 0.5$ and $r_t=0.283$ m, which is close to the tip radius of the turbine. The corresponding blade rotational speed at the tip is $U_t=320$ m/s.

The mean radius is $r_m = \dfrac{1+\zeta}{2} r_t = 0.213$ m. The hub radius is 0.143 m. The mean rotational speed U_m or simply U is 241 m/s. Here, a decision has to be made concerning the type of variation of the compressor passage at its successive stages. One has to decide whether the compressor will have a constant mean, tip, or hub radius through all stages.

Now, to determine the outlet dimensions of the compressor, assume the stage efficiency (or the polytropic efficiency) of the compressor is η_s. The outlet temperature of the compressor is then calculated as

$$\frac{T_{02}}{T_{01}} = \left(\frac{P_{02}}{P_{01}}\right)^{n-1/n}$$

where

$$\frac{n-1}{n} = \frac{1}{\eta_s}\frac{\gamma-1}{\gamma}$$

Assume that air leaves the stator of the last stage of the compressor axially. Thus

$$C_2 = C_a = C_1$$

TABLE 13.6

Results for a Preliminary Design of an Axial Compressor

M_1	0.5	0.55	0.6
T_1 (K)	307	304	301
P_1 (kPa)	119	115	111
ρ_1 (kg/m^3)	1.349	1.317	1.28
C_1 (m/s)	175.6	192.2	209
W_1 (m/s)	386.3	386	382
Ut (m/s)	344.1	335	320
rt	0.304	0.296	0.283
ζ	0.522	0.531	0.506

which was previously calculated based on the assumed axial Mach number. The static pressure and temperature will be

$$T_2 = T_{02} - \frac{C_2^2}{2C_p}, \quad P_2 = P_{02}\left(\frac{T_2}{T_{02}}\right)^{\gamma/\gamma-1}$$

The density and the annulus area are $\rho_2 = P_2/RT_2$, $A_2 = \dot{m}/\rho_2 C_{a2}$.

If the constant mean radius option is selected, then the mean radius is already known and the blade height at outlet is calculated as follows, $h = A_2/2\pi r_m$, the tip, and root radii at the outlet are calculated from the relations

$$r_t = r_m + \frac{h}{2} \quad r_r = r_m - \frac{h}{2}$$

The polytropic efficiency is related to the compressor efficiency by the relation

$$\eta_c = \frac{\pi_c^{(\gamma-1)/\gamma} - 1}{\pi_c^{(\gamma-1)/\gamma\eta_s} - 1}$$

13.9 Determine the Number of Stages (Assuming Stage Efficiency)

To determine the number of stages, the overall temperature rise within the compressor is firstly determined as $\Delta T_{comp} = T_{02} - T_{01}$. Secondly, the stage temperature rise is determined. Then divide both values to obtain the number of stages. This figure will be rounded to the nearest integer.

The stage temperature rise will be obtained from Equation 13.9a and b as follows:

$$\Delta T_0 = \frac{UC_a}{Cp}\left(\tan\beta_1 - \tan\beta_2\right)$$

Since the rotor de Haller number $DH_r = W_2/W_1$, then, for constant axial velocity,

$$DH_r = \frac{\cos\beta_1}{\cos\beta_2} = \frac{\sec\beta_2}{\sec\beta_1} = \sqrt{\frac{1+\tan\beta_2^2}{1+\tan\beta_1^2}}$$

$$\therefore \tan\beta_2 = \sqrt{\left(DH_r\right)^2\left(1+\tan\beta_1^2\right)-1} \tag{13.38}$$

$$\Delta T_0 = \frac{UC_a}{Cp}\left(\tan\beta_1 - \sqrt{\left(DH_r\right)^2\left(1+\tan\beta_1^2\right)-1}\right) \tag{13.39}$$

As a guide, from past experience [5], the temperature rise per stage for the available compressor has the following range

$$\Delta T_{0s} = 10 - 30 \text{ K} \quad \text{subsonic stages}$$
$$\Delta T_{0s} = 45 - 55 \text{ K} \quad \text{transonic stage}$$

Then the number of stages is determined as

$$n = \frac{(\Delta T_0)_{compressor}}{(\Delta T_0)_{stage}}$$

Again, the above values for temperature rise per stage are only a guide for present-day compressors. Aeroengine manufacturers are working hard to increase these values to reach 70°C or 80°C for transonic compressors.

13.10 Calculation of Air Angles for Each Stage at the Mean Section

For a constant mean diameter and known axial and mean blade speeds (C_a, U_m), the angles $\alpha_1, \beta_1, \alpha_2,$ and β_2 will be calculated for each stage. The degree of reaction at the mean section will also be calculated and checked for reasonable values.

13.10.1 First Stage

The first stage is characterized by an axial inlet flow ($\alpha_1 = 0$), thus the relative inlet velocity and angle are calculated from the relations

$$W_1 = \sqrt{U_m^2 + C_a^2}$$

$$\tan\beta_1 = \frac{U_m}{C_a}$$

For simplicity U_m will be written here as U. The outlet relative angle is to be calculated from Equation 13.38, where the rotor de Haller number selected is equal to or greater than 0.72.

The absolute angle at the rotor outlet is calculated from Equation 13.1b as follows:

$$\tan\alpha_2 = \frac{U}{C_a} - \tan\beta_2$$

which is the inlet angle to the stator. The outlet angle to the stator (α_3) may be calculated from the de Haller number of the stator defined as

$$DH_s = \frac{C_3}{C_2} = \frac{\cos\alpha_2}{\cos\alpha_3}$$

The value of the de Haller number of the stator has to be carefully selected otherwise it may yield an imaginary value for α_3 (if $\cos\alpha_3 > 1.0$). Thus, it must satisfy the condition

$$DH_s > \cos\alpha_2 \tag{13.40}$$

Thus

$$\cos\alpha_3 = \frac{\cos\alpha_2}{DH_s} \tag{13.41}$$

A better value for the stage temperature rise can now be calculated by incorporating the work done factor (λ), Equation 13.9b.

The value of the work done factor for different stages is given by the following table:

Stage Number	First	Second	Third	Fourth–Last
λ	0.98	0.93	0.88	0.83

The pressure ratio is calculated from the relation

$$\pi_s = \left(\frac{P_{03}}{P_{01}}\right)_s = \left(1 + \frac{\eta_s \Delta T_{01}}{T_{01}}\right)^{\gamma/\gamma-1} \tag{13.42}$$

The degree of reaction is calculated from Equation 13.23e.

13.10.2 Stages from (2) to (*n* – 1)

The procedure is straightforward and as follows:

1. The inlet total conditions to any stage (i) are

$$(P_{01})_{stage(i)} = (P_{01})_{stage(i-1)} \left(\frac{P_{03}}{P_{01}}\right)_{stage(i-1)}$$

$$(T_{01})_{stage(i)} = (T_{01})_{stage(i-1)} + (\Delta T_0)_{stage(i-1)}$$

2. The flow is no longer axial, but the outlet angle α_3 for any stage will be equal to the inlet absolute angle α_1 of the next angle. In general

$$(\alpha_1)_{stage(i)} = (\alpha_3)_{stage(i-1)}$$

3. The inlet relative angle β_1 is obtained as

$$\tan\beta_1 = \frac{U}{C_a} - \tan\alpha_1$$

4. The outlet relative angle β_2 is obtained from Equation 13.38 with a de Haller number equal to 0.72.
5. The absolute outlet angle α_2 is calculated from the relation

$$\tan\alpha_2 = \frac{U}{C_a} - \tan\beta_2$$

6. The stage temperature rise ΔT_{0s} is calculated from Equation 13.9b using the appropriate work done factor.
7. The stage pressure ratio π_s is calculated from the relation (13.42).
8. The degree of reaction Λ is calculated from Equation 13.23e.
9. The appropriate de Haller number DH_s for the stator is calculated from Equation 13.40.
10. The stator outlet angle α_3 is calculated from Equation 13.41.

The above procedure is repeated for all stages up to the last.

13.10.3 Last Stage

1. The pressure ratio of the stage is evaluated from the overall pressure ratio of the compressor and the product of the stage pressure ratios of all the previous $(n-1)$ stages as

$$\pi_{last} = \frac{\pi_c}{\Pi\pi_i}$$

2. The corresponding temperature rise is obtained from the relation

$$(\Delta T_0)_{last} = \frac{(T_{01})_{last}}{\eta_s}\left(\pi_{last}^{\gamma-1/\gamma} - 1\right)$$

3. The inlet relative angle β_1 is calculated as in section (b)—steps 2 and 3 above.
4. The relative outlet blade angle is obtained from the relation

$$\tan\beta_2 = \tan\beta_1 - \frac{Cp\Delta T_0}{\lambda U C_a}$$

   Check for the rotor de Haller number.
5. The outlet absolute angle α_2 is calculated as step 5 above.
6. The degree of reaction Λ is calculated from (13.23e) as above.
7. The outlet absolute angle α_3 is assumed to be zero; check the stator de Haller number.

TABLE 13.7

Calculated Parameters for the 7 Stages of Compressor

Stage	1	2	3	4	5	6	7
T_{01} (K)	288	315.4	340.4	364.1	386.6	409.2	431.8
ΔT_{0s} (K)	27.4	25	23.7	22.5	22.6	22.6	21.5
π_s	1.333	1.273	1.238	1.208	1.196	1.185	1.165
α_1	0	11.86	11.73	9.48	9.05	9.05	9.05
β_1	60.6	57.4	57.5	58.05	58.05	58.05	58.05
α_2	35.16	41.59	41.51	40.5	40.5	40.5	39.56
β_2	47	41.65	42.69	42.7	42.7	42.7	43.57
α_3	11.86	11.73	9.84	9.05	9.05	9.05	0
Λ	0.804	0.69	0.692	0.71	0.71	0.71	0.72
DH_r	0.72	0.72	0.72	0.72	0.72	0.72	0.73
DH_s	0.72	0.764	0.76	0.77	0.77	0.77	0.77

Example 13.7

A seven-stage axial compressor has the following data. Calculate the following variables for each stage π_s, ΔT_{0s}, α_1, β_1, α_2, β_2, α_3, Λ, DH_s, DH_r.

Overall pressure ratio	4.15
Mean rotational speed	266 m/s
Axial velocity	150 m/s
Stage efficiency	0.9
Inlet temperature and pressure	288 K, 101 kPa

Solution

The total temperature rise for the compressor is 164.5 K.

The above procedure is followed and the results are arranged in Table 13.7. The summation of the total temperature rise for the seven stages is 165.3, which is in good agreement with the value calculated above (164.5).

13.11 Variation of Air Angles from Root to Tip Based on Type of Blading (Either Free Vortex, Exponential, or First Power Methods)

The three methods that estimate the variations of air properties in the radial direction from blade hub to tip are applied here. The procedure is as follows:

1. Calculate the dimensions at the rotor inlet and outlet for each stage
2. Calculate the values of the constants (*a*) and (*b*) from Equations 13.33 and 13.34
3. Use Table 13.1 to calculate the variations in axial and whirl velocities as well as the degree of reaction.

Now, to calculate the dimensions upstream and downstream of the rotor, states (1) and (2), the dimensions at state (3) are first calculated from the continuity equation. The air density

is calculated from the perfect gas law, and then the annulus area is calculated as the axial speed (at the mean section it is already known).

$$\rho_3 = \frac{P_3}{RT_3}, \quad A_3 = \frac{\dot{m}}{\rho_3 C_a}$$

This annulus area is used to calculate the blade height (h), $h_3 = A/2\pi r_m$, from which and assuming constant mean radius the root and tip radii are then calculated as

$$r_{r3} = r_{m3} - \frac{h_3}{2} \quad r_{t3} = r_{m3} + \frac{h_3}{2}$$

The corresponding hub and tip radii at the rotor outlet are the mean value of those at states (1) and (3), as shown in Figure 13.28.

$$r_{r2} = \frac{r_{r1} + r_{r3}}{2} \quad r_{t2} = \frac{r_{t1} + r_{t3}}{2}$$

It only remains for us to calculate the corresponding nondimensional radii ($R = r/r_m$) at the root and tip at states (1) and (2). After calculating the constants (a) and (b), the whirl velocities (C_{u1} and C_{u2}) are calculated for any design methods from the known values at the mean radius. Moreover, the axial velocities C_{a1} and C_{a2} are calculated for any design method other than the free vortex. The degree of reaction is also calculated. It is important to have as high degree of reaction at the hub as possible.

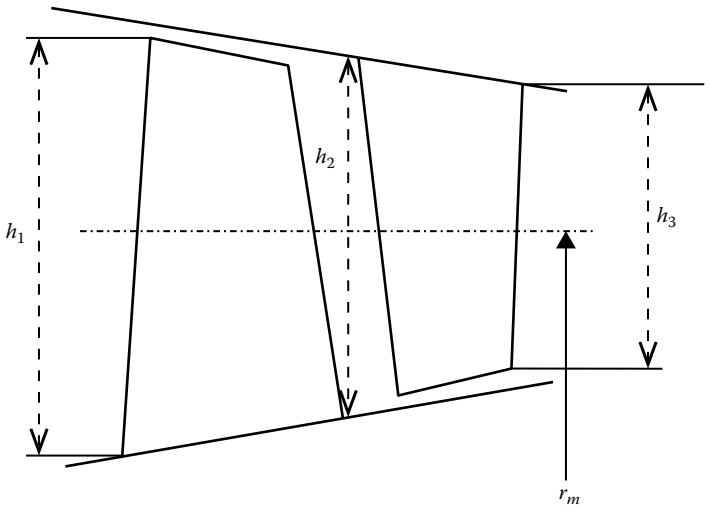


FIGURE 13.28
A single-stage geometry.

13.12 Blade Design

13.12.1 Cascade Measurements

In order to obtain information on the effect of different blade designs on air flow angles, pressure losses, and energy transfer across blade rows, one must resort to cascade wind tunnels and cascade theory. Experimentation here is performed to ensure that the blade row satisfies its objectives. The first objective is to turn air through the required angles $\beta_1 - \beta_2$ for the rotor and $\alpha_2 - \alpha_3$ for the stator, with the angle $\beta_1 - \beta_2$ as great as possible to maximize the stage pressure ratio. The second objective is to achieve the diffusing process with optimum efficiency, that is, with minimum loss of stagnation pressure. Experiments are generally performed in a straight wind tunnel (Figure 13.29), rather than an annular form of tunnel. By the word "cascade," it is meant a row of identical (geometrically similar) blades equally spaced and parallel to each other and aligned with the flow direction as shown in Figure 13.30a. The height and length of cascade in a cascade wind tunnel are made as large as the available air supply will allow, eliminating the interference effects due to the tunnel walls. Boundary layer suction on the walls is frequently applied to prevent contraction of the air stream. The cascade is mounted on a turntable so that its angular direction with respect to the inflow duct (α_1) can be set at any desired value and thus the incidence angle (i) may be varied. The vertical traverses over

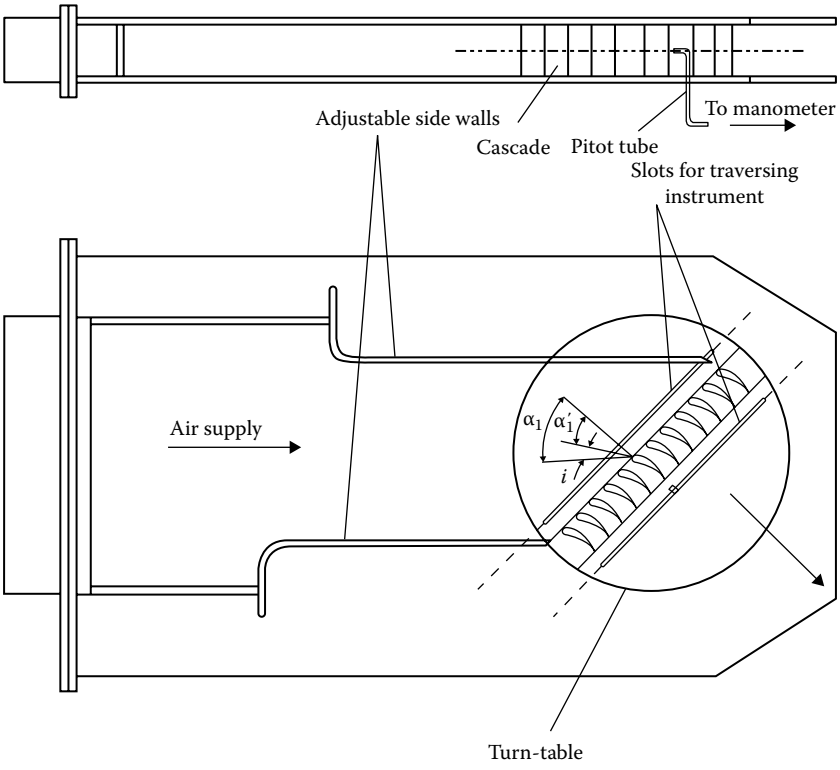


FIGURE 13.29
Cascade wind tunnel.

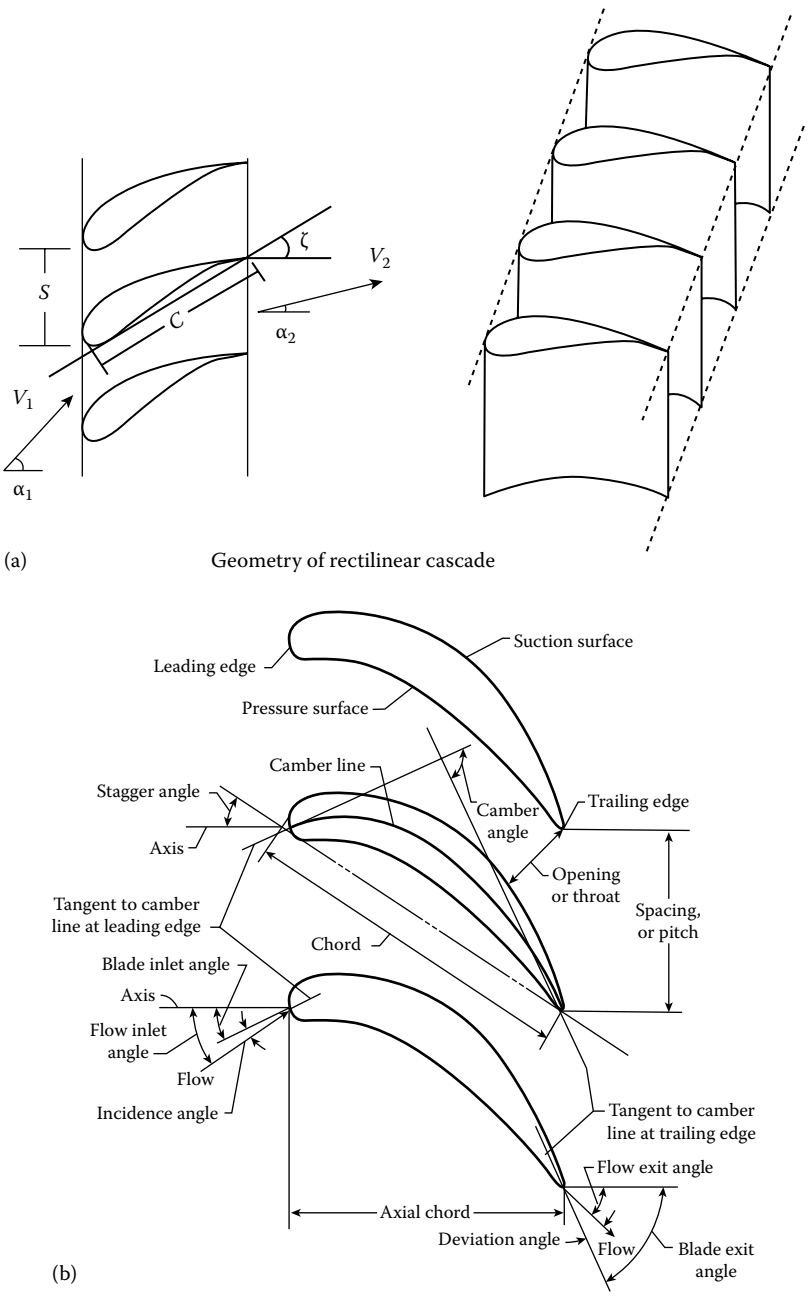


FIGURE 13.30
(a) Three-dimensional illustration for cascade and (b) cascade nomenclature.

the two planes, usually at a distance of one blade chord upstream and downstream of the cascade, are provided with pitot tubes and yaw meters to measure the pressure and air flow angles.

Pressure and velocity measurements are made by the usual L-shaped pitot-static tubes. The air direction is found by either claw or cylindrical yaw meters.

TABLE 13.8

Cascade Nomenclature

α_1'	Blade (metal) inlet angle	α_1	Air inlet angle
α_2'	Blade (metal) outlet angle	α_2	Air outlet angle
θ	Blade camber angle = $\alpha_1' - \alpha_2'$	i	Incidence angle = $\alpha_1 - \alpha_1'$
ζ	Setting or stagger angle	δ	Deviation angle = $\alpha_2 - \alpha_2'$
s	Pitch (or space)	C	Chord
ε	Air deflection = $\alpha_1 - \alpha_2$	a	Location of maximum camber
V_1	Air inlet velocity	V_2	Air outlet velocity

Before proceeding further into cascade testing and blade design, it is necessary to define various important geometrical issues and angles relevant to the design. Figure 13.30a and b represents a cascade that has the nomenclature listed in Table 13.8. The measured velocities and angles above have different meanings for rotor and stator rows, as defined in Table 13.9.

Other definitions here are

$$\text{Solidity} \quad \sigma = \text{chord}/\text{spacing}\,(c/s)$$

$$\text{Aspect ratio} = \text{height}/\text{chord}\,(h/c)$$

$$\text{Stagnation pressure loss} \quad \frac{P_{01} - P_{02}}{\frac{1}{2}\rho V_1^2} = \frac{w}{\frac{1}{2}\rho V_1^2}$$

When the pressure and flow direction measuring instruments are traversed along the blade row in the upstream and downstream positions, the results are as plotted in Figure 13.31. An averaging for this stagnation pressure loss (expressed hereafter as $\bar{w}/\frac{1}{2}\rho V_1^2$) and also an average for the deflection angle ($\bar{\varepsilon}$) is evaluated at this particular incidence angle. The same measurements and averaging process are repeated for different incidence angles. The results are plotted in Figure 13.32. The deflection increases with the angle of incidence up to a maximum angle ε_s. This is the stall point where separation occurs on the suction surface of the blade. Since this angle may not be well defined, it is taken as the angle of incidence where the mean pressure loss is twice the minimum. The practice has been to select

TABLE 13.9

Rotor and Stator Equivalent Parameters for the Measured Velocities and Angles

Cascade	Rotor	Stator
V_1	W_1	C_2
V_2	W_2	C_3
α_1	β_1	α_2
α_2	β_2	α_3

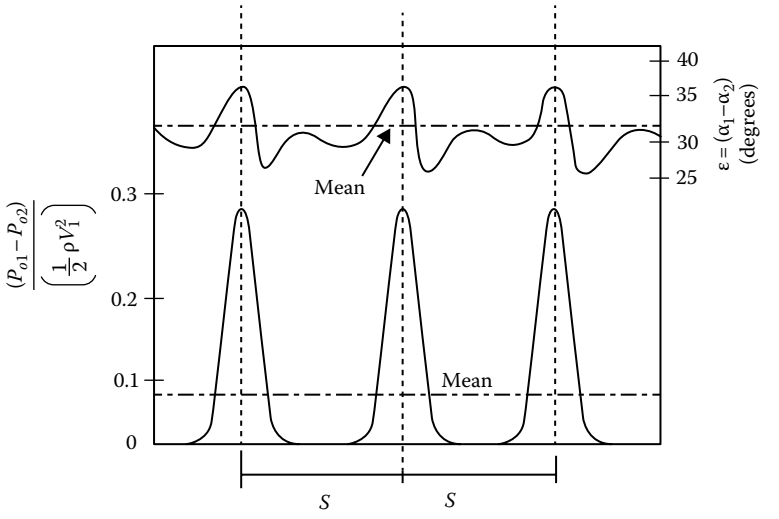


FIGURE 13.31
Variation of stagnation pressure loss and deflection for cascade at a certain incidence angle. (From Saravanamuttoo, H.I.H. et al., *Gas Turbine Theory*, 5th edn., Prentice Hall, Harlow, U.K., 2001, p. 191. With permission.)

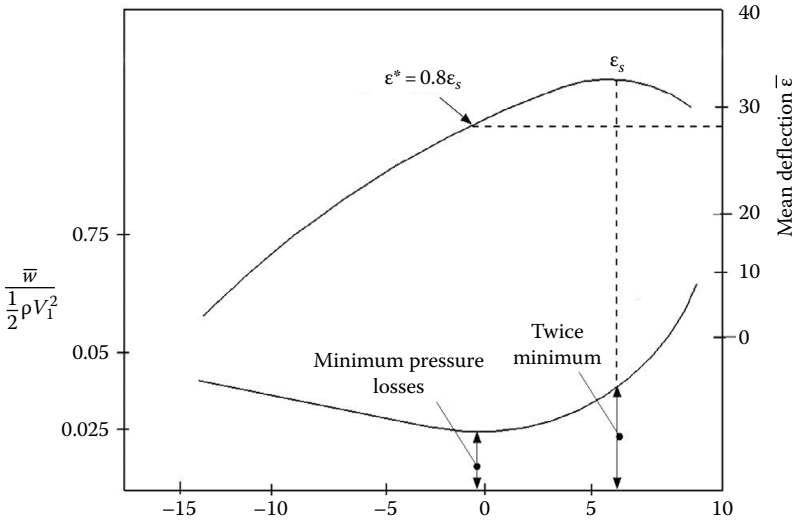


FIGURE 13.32
Mean deflection and mean stagnation pressure loss curves.

a deflection that corresponds to a definite proportion of the stalling deflection. The proportion found to be most suitable is 80%, thus the selected or nominal deflection $\varepsilon^* = 0.8\varepsilon_s$.

It was found that the nominal deflection angle is mainly dependent on the pitch/chord (s/c) ratio and the air outlet angle (α_2),

$$\varepsilon^* = f\left(\frac{s}{c}, \alpha_2\right)$$

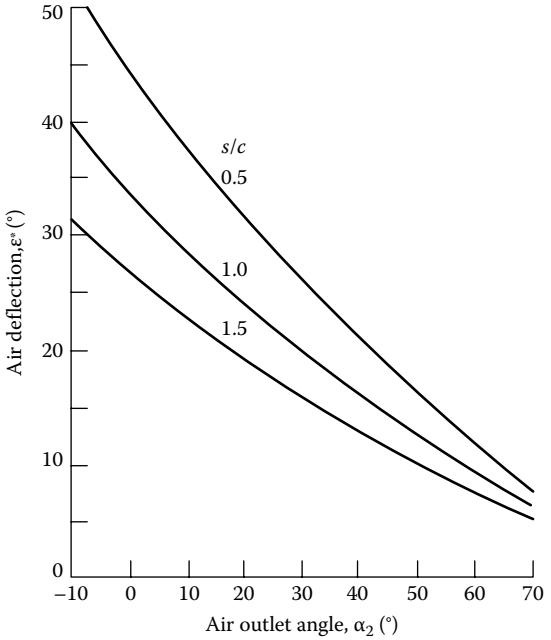


FIGURE 13.33
Cascade nominal deflection versus outlet angle. (From Saravanamuttoo, H.I.H. et al., *Gas Turbine Theory*, 5th edn., Prentice Hall, Harlow, U.K., 2001, p. 191. With permission.)

Thus a large number of tests covering different forms of cascade were performed. The results are shown in Figure 13.33. For known flow angles, the deflection angle is calculated. Next, from this deviation angle and the flow outlet angle, the ratio of (s/c) can be obtained. Since the blade height is known from previous sections, and the blade height/chord is a known ratio ($h/c = 3$ for typical subsonic compressors), then, from this known chord, the spacing (s) is calculated. The number of blades is then calculated as

$$n = \frac{2\pi r_m}{s}$$

It is recommended to avoid numbers with common multiples for blades in successive rows (rotor/stator or stator/rotor) to prevent introducing resonant forcing frequencies.

The blade inlet angle (α_1') could be determined from the air inlet angle, assuming a zero incidence angle $\alpha_1' = \alpha_1(i = 0)$. However, the blade outlet angle (α_2') cannot be determined from the flow outlet angle α_2 until the deviation angle $\delta(\alpha_2 - \alpha_2')$ has been determined. The deflection angle is determined from the empirical relation

$$\delta = m\theta\sqrt{\frac{s}{c}} \tag{13.42a}$$

where

$$m = 0.23\left(\frac{2a}{c}\right)^2 + 0.1\left(\frac{\alpha_2^\circ}{50}\right) \tag{13.42b}$$

$$\theta = \alpha_1' - \alpha_2'$$

a is the distance of the point of maximum camber from the leading edge of the blade and the angle α_2 is in degrees. For a circular arc, $2a/c = 1$, then

$$m = 0.23 + 0.1\left(\frac{\alpha_2^\circ}{50}\right) \tag{13.42c}$$

For inlet guide vanes (IGVs)

$$\delta = 0.19\theta\left(s/c\right) \tag{13.42d}$$

For a circular arc blade camber, the blade setting angle ζ (Figure 13.27b) is given by the relation

$$\zeta = \alpha_1' - \frac{\theta}{2} \tag{13.42e}$$

The axial chord of any blade row is then $c_a = c\cos\zeta$. The chord of the blade in a subsonic compressor is one-third of the blade height $c = h/3$. The gap between two successive blade rows is $w = c_a/4$. Thus the axial length of one stage (including a rotor-gap and stator-gap) will be equal to $l = \frac{5}{4}\left\{\left(c_a\right)_r + \left(c_a\right)_s\right\}$.

The same procedure can be followed for any other blade ratios. The length of the compressor is then the sum of the axial lengths of all compressor stages.

13.12.2 Choosing the Type of Airfoil

After the radial distribution of air angles and velocities have been determined, the blading can be designed. First, incidence and deviation angles are selected so that the slope of the airfoil's mean line (camber line) at the leading and trailing edges can be established [6]. Incidence angles are selected in the low loss region of its performance envelope. Generally, the incidence angle (i) is in the range $-5° \le i \le 5°$. The deviation angle is calculated from Equation 13.42 which is also in the range $5° \le \delta \le 20°$. The mean line shape and thickness are selected to achieve the desired airfoil loadings. The pressure increase is achieved by the diffusion process. The amount of diffusion is monitored by computing the diffusion factor, Equation 13.19a. Values of the diffusion factor greater than 0.65 mean that flow separation is imminent.

The nature and type of blading depends on the application and Mach number. Subsonic blading usually consists of circular arcs, parabolic arcs, or combinations thereof. Many countries developed their own profiles (e.g., the United States, Britain, Japan, West Germany) for subsonic flows. One of the famous American profiles is the NACA 65 series blade. The famous British profile is the C-series. The NACA 65 series designation is NACA 65(x)y, or 65 – x – y, where x is 10 times the design lift coefficient for an isolated airfoil and y is the maximum thickness in percent of the chord. An example for the C-series is 10C4/20P40, where the blade is a 10% thick C4 profile with a 20° camber angle, using a parabolic camber line with maximum camber at 40% of the camber. A 10C4/20C40 blade would be similar, but with a circular arc. Another British series is the RAF 27 profiles. The NACA 65 series and similar British profiles are used in low subsonic flows [12].

13.12.3 Stage Performance

The performance, particularly the efficiency, for a given work input will govern the final pressure ratio. The efficiency is dependent on the total drag coefficient for each of the blade rows comprising the stage. Consider a control volume around a single blade of a cascade; see Figure 13.34. Two forces are generated, namely, the axial and tangential forces (F_a, F_t). These two forces are decomposed into the lift and drag forces (L, D), from which the lift and profile drag coefficients can be obtained. The static pressure rise across the blade can be written as

$$\Delta P = P_2 - P_1 = \left(P_{02} - \frac{1}{2}\rho_2 V_2^2\right) - \left(P_{01} - \frac{1}{2}\rho_1 V_1^2\right) \tag{13.43}$$

If the changes in density are negligible then

$$\Delta P = \frac{1}{2}\rho\left(V_1^2 - V_2^2\right) - \bar{w} = \frac{1}{2}\rho V_a^2\left(\sec^2\alpha_1 - \sec^2\alpha_2\right) - \bar{w}$$
$$\Delta P = \frac{1}{2}\rho V_a^2\left(\tan^2\alpha_1 - \tan^2\alpha_2\right) - \bar{w}$$

The axial force per unit length is then $F_a = s\Delta P$

$$F_a = \frac{1}{2}\rho V_a^2 s\left(\tan^2\alpha_1 - \tan^2\alpha_2\right) - s\bar{w} \tag{13.44}$$

The tangential force per unit length is $F_t = \dot{m}\Delta V_u$

$$F_t = \dot{m} \times \left(\text{change in velocity component along cascade}\right)$$

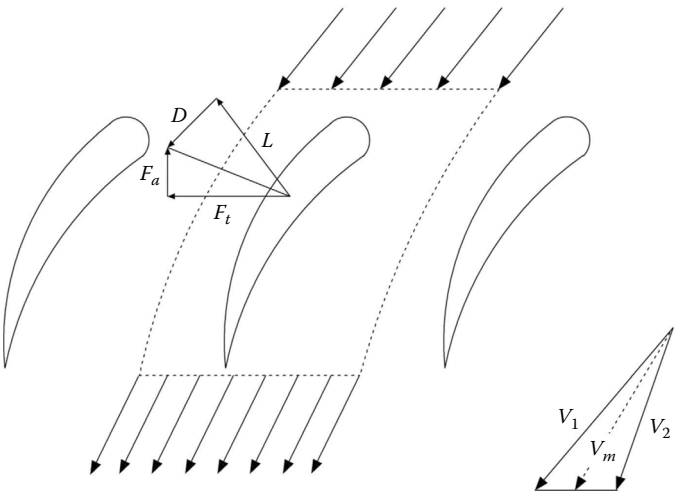


FIGURE 13.34
Forces on cascade.

$$F_t = s\rho V_a \times \left(V_a \tan\alpha_1 - V_a \tan\alpha_2\right)$$

$$F_t = s\rho V_a^2 \left(\tan\alpha_1 - \tan\alpha_2\right) \tag{13.45}$$

The lift and profile drag coefficient C_L, C_{Dp} depend on the mean angle (α_m). The drag and lift force can be obtained from the axial and tangential forces as follows:

$$D = F_t \sin\alpha_m - F_a \cos\alpha_m$$

$$L = F_t \cos\alpha_m + F_a \sin\alpha_m$$

The lift and drag forces are also expressed as

$$D = \frac{1}{2}\rho V_m^2 c C_{Dp}$$

$$L = \frac{1}{2}\rho V_m^2 C C_L$$

Now with

$$D = F_t \sin\alpha_m - s\Delta P \cos\alpha_m$$

$$D = s\rho V_a^2 \left(\tan\alpha_1 - \tan\alpha_2\right)\sin\alpha_m - \frac{1}{2}\rho V_a^2 s\left(\tan^2\alpha_1 - \tan^2\alpha_2\right)\cos\alpha_m + s\bar{w}\cos\alpha_m$$

$$\tan^2\alpha_1 - \tan^2\alpha_2 = \left(\tan\alpha_1 - \tan\alpha_2\right)\left(\tan\alpha_1 + \tan\alpha_2\right)$$

and

$$\tan\alpha_m = \frac{1}{2}\left(\tan\alpha_1 + \tan\alpha_2\right)$$

$$\tan^2\alpha_1 - \tan^2\alpha_2 = 2\left(\tan\alpha_1 - \tan\alpha_2\right)\tan\alpha_m$$

$$\therefore D = s\bar{w}\cos\alpha_m$$

but

$$D = \frac{1}{2}\rho V_m^2 c C_{Dp}$$

$$\therefore C_{Dp} = \left(\frac{s}{c}\right)\left(\frac{\bar{w}}{\frac{1}{2}\rho V_1^2}\right)\left(\frac{\cos^3\alpha_m}{\cos^2\alpha_1}\right) \tag{13.47}$$

$$\therefore C_L = 2\left(\frac{s}{c}\right)\left(\tan\alpha_1 - \tan\alpha_2\right)\cos\alpha_m - C_{Dp}\tan\alpha_m \tag{13.48a}$$

The lift and drag coefficients depend on the angles α_1, α_2, and α_m, which can be determined as

$$\alpha_1 = \alpha_1' + i, \quad \alpha_2 = \alpha_1 - \varepsilon * \quad \text{and} \quad \alpha_m = \tan^{-1}\left[\frac{1}{2}\left(\tan\alpha_1 + \tan\alpha_2\right)\right]$$

Using the values of $\bar{w}/\left((1/2)\rho V_1^2\right)$ and the known value of (s/c), calculate the lift and drag coefficients, C_L and C_{Dp}. Since $C_{Dp}\tan\alpha_m$ is small then we can write the conventional theoretical values of C_L as

$$C_L = 2\left(\frac{s}{c}\right)\left(\tan\alpha_1 - \tan\alpha_2\right)\cos\alpha_m \tag{13.48b}$$

Figure 13.35 illustrates the coefficients of lift and profile drag versus the incidence angle for certain values of (s/c). Figure 13.36 illustrates the lift coefficient versus the air outlet angle for different (s/c) values.

There are two additional factors affecting the drag:

1. Drag due to the walls of the compressor (annulus drag)
2. Drag due to secondary flow

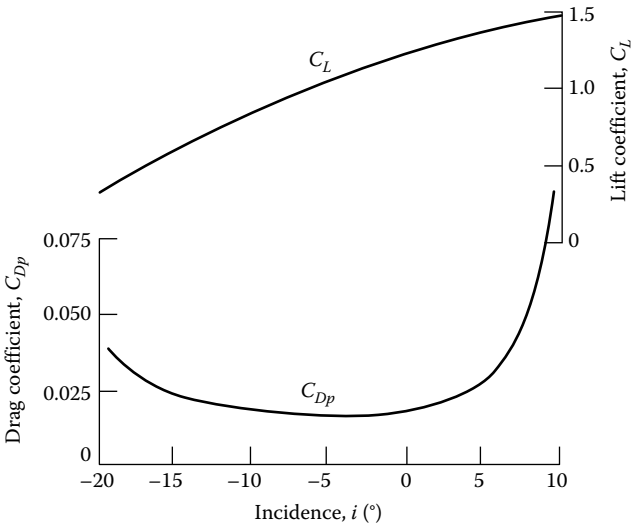


FIGURE 13.35
Variation of the lift and profile drag coefficients with incidence angle. (From Saravanamuttoo, H.I.H. et al., *Gas Turbine Theory*, 5th edn., Prentice Hall, Harlow, U.K., 2001, p. 191. With permission.)

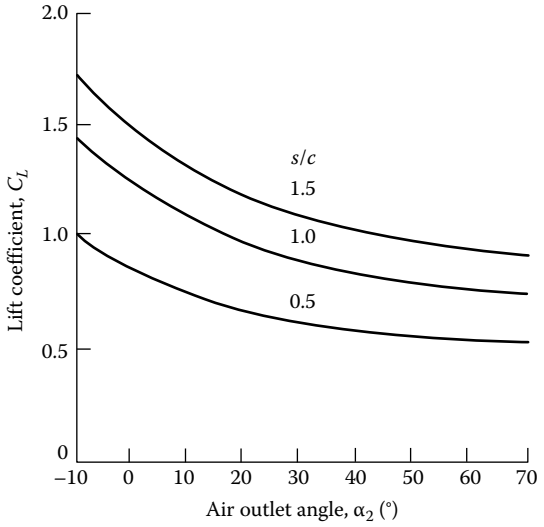


FIGURE 13.36
Variation of the lift coefficient with air outlet angle. (From Saravanamuttoo, H.I.H. et al., *Gas Turbine Theory*, 5th edn., Prentice Hall, Harlow, U.K., 2001, p. 191. With permission.)

Annulus drag is developed due to the boundary layer over the hub and casing. These boundary layers together with the developed boundary layers over the suction and pressure sides of the blades are illustrated in Figure 13.37.

The annulus drag is expressed by the relation

$$C_{DA} = 0.020(s/h) \tag{13.49}$$

Secondary flow is generated due to the curved blade shape leading to the generation of two opposite circulations as shown in Figure 13.38. Tip clearance will influence the

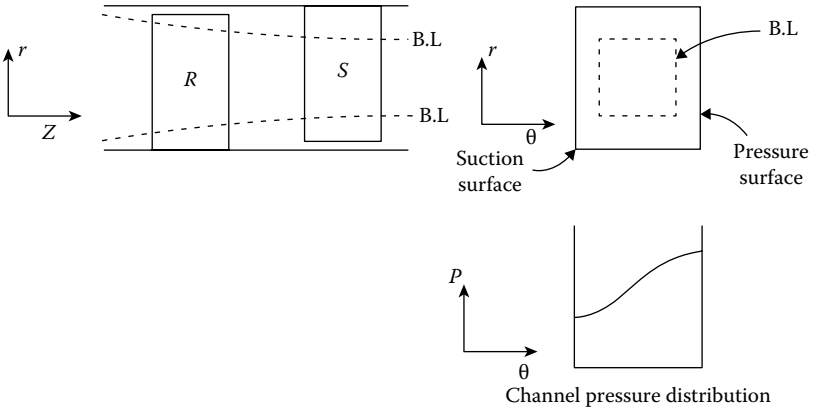


FIGURE 13.37
Annulus drag.

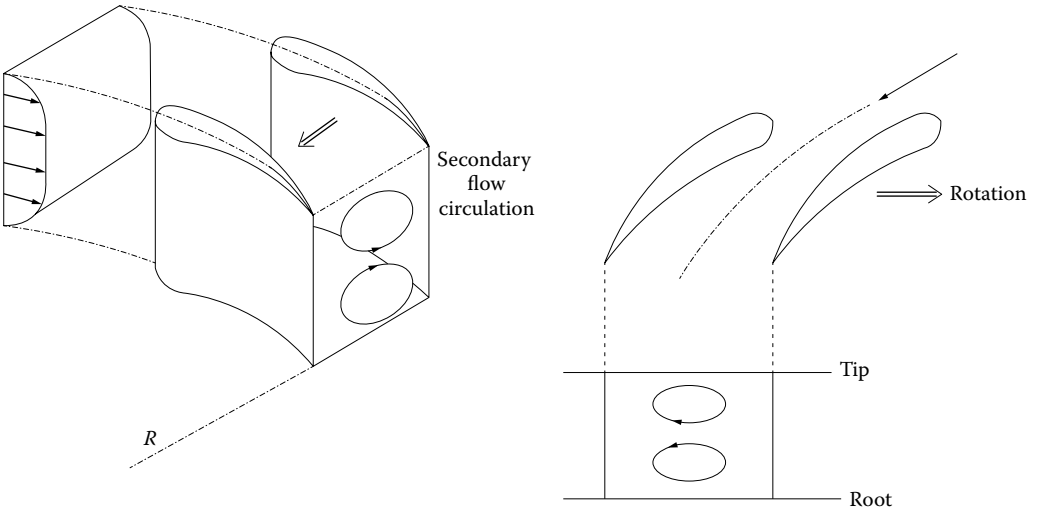


FIGURE 13.38
Secondary flow in a cascade.

secondary flow. The secondary loss is of the same order of magnitude as the profile drag and may be represented by the relation

$$C_{DS} = 0.018C_L^2 \tag{13.50}$$

The total drag is then equal to the sum of the three types of drag described above, or

$$\text{Total drag} = \text{Profile drag} + \text{Secondary flow drag} + \text{Annulus drag}$$

$$C_D = C_{DP} + C_{DS} + C_{DA}$$

Thus the loss coefficient can be determined from the relation

$$\frac{\bar{w}}{\frac{1}{2}\rho V_1^2} = \frac{C_D}{\left(\frac{s}{c}\right)\left(\frac{\cos^3 \alpha_m}{\cos^2 \alpha_1}\right)} \tag{13.51}$$

Now to determine the stage efficiency from the cascade measurements, with cascade data, efficiency is evaluated from the pressure rise.

Blade efficiency and stage efficiency: Since the static pressure rise ΔP is given by the relation

$$\Delta P = \frac{1}{2}\rho V_a^2\left(\tan^2 \alpha_1 - \tan^2 \alpha_2\right) - \bar{w}$$

then the ideal or theoretical pressure rise will be

$$\Delta P_{th} = \frac{1}{2}\rho V_a^2\left(\tan^2 \alpha_1 - \tan^2 \alpha_2\right)$$

The blade row efficiency is defined as

$$\eta_b = \frac{\text{Actual pressure rise in compressor blade row}}{\text{Theoretical pressure rise in blade row}}$$

$$\eta_b = \frac{\Delta P}{\Delta P_{th}} = \frac{\Delta P_{th} - \bar{w}}{\Delta P_{th}} = 1 - \frac{\bar{w}}{\Delta P_{th}} = 1 - \frac{\bar{w}/\left(\rho V_1^2/2\right)}{\Delta P_{th}/\left(\rho V_1^2/2\right)}$$

$$\eta_b = 1 - \frac{\bar{w}/\left(\rho V_1^2/2\right)}{\Delta P_{th}/\left(\rho V_1^2/2\right)} \tag{13.52}$$

$$\frac{\Delta P_{th}}{\left(\rho V_1^2/2\right)} = \frac{\left(\rho V_a^2/2\right)\left(\tan^2\alpha_1 - \tan^2\alpha_2\right)}{\left(\rho V_a^2/2\right)\sec^2\alpha_1} = \frac{\sec^2\alpha_1 - \sec^2\alpha_2}{\sec^2\alpha_1}$$

$$\frac{\Delta P_{th}}{\left(\rho V_1^2/2\right)} = 1 - \frac{\sec^2\alpha_2}{\sec^2\alpha_1} \tag{13.53}$$

From Equations 13.51 through 13.53 the blade row efficiency can be obtained. For the normal stage, $C_1 = C_3$, the stage isentropic efficiency can be approximated to

$$\eta_s = \frac{T_{3ss} - T_3}{T_3 - T_1}$$

For Λ = 0.5, half the temperature rise occurs in the rotor and half at the stator, or $T_3 - T_2 = T_2 - T_1$

$$\eta_b \approx \eta_s \tag{13.54a}$$

If the degree of reaction is far from 50%

$$\eta_s = \Lambda\eta_{rotor} + \left(1 - \Lambda\right)\eta_{stator} \tag{13.54b}$$

Example 13.8

Boeing 737 airplanes have the ability to take off and land from unpaved runways. Moreover, their engines are close to the ground, thus they are more susceptible to ingestion of solid particles into their core, which erode the compressor blades. An examination of one of the compressor blades revealed that erosion led to

1. Shortening of the chord by 10%
2. An increase in the incidence angle (i) from 4° to 8°

Other data for the compressor stage are

1. Stage temperature rise at entry to the stage is $T_{01} = 320$ K
2. Stage total temperature rise = $\Delta T_{0s} = 25$ K



FIGURE 13.39
Boeing 737 aircraft.

For the new blade

$$s/c_{new} = 1.0 \quad \text{and} \quad \alpha_{1_{new}} = 50°$$

For both new and eroded blade $\alpha_2 = 30°$ and $s/h = 0.25$

1. Calculate the stage efficiency for both the new and eroded blade.
2. Calculate the stage pressure ratio for the new and eroded blade.
3. Comment.

Solution

Calculations are arranged in Table 13.10.
Comments

1. The stage efficiency has been decreased by 6%.
2. The stage pressure ratio has been decreased by 1.4%.

13.13 Compressibility Effects

High performance gas turbines and aeroengines use large air flow rates per unit frontal area in which the blade tip speed is large, leading to high velocity and Mach numbers in compressors. Early compressors were designed with subsonic velocity throughout. In present-day compressors, the axial and absolute Mach numbers at the inlet are always subsonic. However, since the blade speed (Ωr) is higher at higher radii, the relative Mach numbers may reach supersonic

Near the outer sections of the rotor, the relative flow near the inner radii remains subsonic. A *transonic* compressor is one where the relative flow remains subsonic at the inner

TABLE 13.10

Performance of a Compressor Stage In Cases of New and Eroded Blades

	New Blade	Eroded Blade
i	4°	8°
α_1	50°	54°
α_2	30°	30°
$\tan\alpha_m = \frac{1}{2}(\tan\alpha_1 + \tan\alpha_2)$		
α_m	41.5°	44.33°
s/c	1.0	$\frac{1}{0.9} = 1.11$
s/h	0.25	0.25
C_{Dp} (from Figure 13.35)	0.025	0.075
C_L (from Figure 13.35)	0.9	0.94
$C_{Ds} = 0.018C_L^2$	0.01458	0.0159
$C_{DA} = 0.02s/h$	0.005	0.005
$C_D = C_{Dp} + C_{DA} + C_{Ds}$	0.04458	0.0959
$\frac{\Delta P_{th}}{\frac{1}{2}\rho v_1^2} = 1 - \frac{\cos^2\alpha_1}{\cos^2\alpha_2}$	0.449	0.5393
$\frac{\bar{w}}{\frac{1}{2}\rho V_1^2} = \frac{C_D}{\frac{s}{c}\frac{\cos^3\alpha_m}{\cos^2\alpha_1}}$	0.04384	0.08154
$\eta_b = 1 - \frac{\bar{w}/\frac{1}{2}\rho V_1^2}{\Delta P_{th}/\frac{1}{2}\rho V_1^2}$	0.90236	0.84878
$\eta_b = \eta_s$	0.9024	0.8488
$\pi_s = \left(1 + \eta_s \frac{\Delta T_{0s}}{T_1}\right)^{\gamma/\gamma-1}$	1.2693	1.2519

radii and supersonic at the outer radii, with a transonic region in the middle. This is especially true for high aspect ratio or low hub–tip ratio compressors [10]. In some low-aspect ratio and compact compressors, there may be cases where the entire flow, from hub to tip, has supersonic relative flow. Such a compressor is known as a *supersonic compressor* and has sharp leading edges and thin blades. The flow pattern in such a compressor is shown in Figure 13.36. The oblique shock wave is followed by a normal shock wave initiated at the leading edge and propagated toward the suction side of the opposite blade in the blade passage; see Figure 13.40. This normal shock wave leads to a jump in both static and total pressures. Nowadays, the most successful designs have custom-tailored airfoils whose design is based on the controlled diffusion airfoil and shock-free airfoil concepts [6]. Thus the efficiency of a supersonic compressor (a single stage) which was as low as 40% during the 1940s now has an efficiency of nearly 90%. The highest relative Mach number has increased to 2.4 in the experimental compressor stage [10]. A historical account of transonic and supersonic compressor development can be found in References 13 and 14.

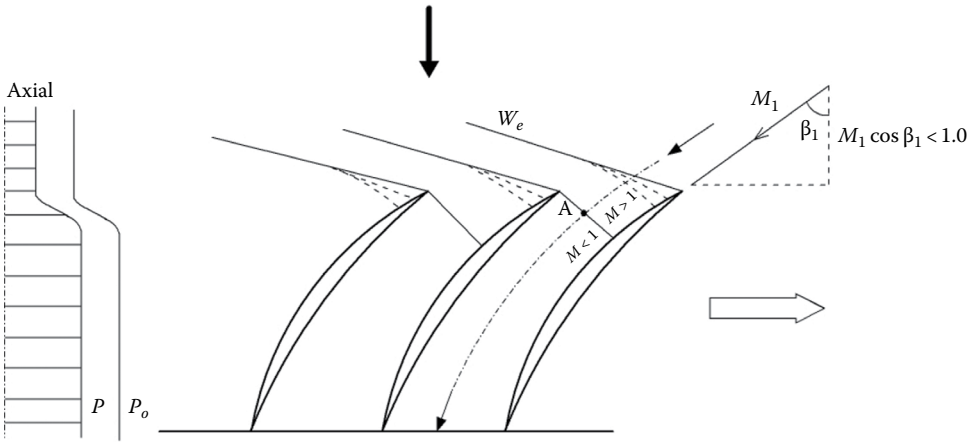


FIGURE 13.40
Flow pattern in a supersonic rotor.

The velocity triangles for a high turning supersonic impulse cascade are shown in Figure 13.41, and the velocity triangles for a low turning supersonic compressor cascade are shown in Figure 13.42.

The different flow patterns for a single stage in a supersonic compressor may be classified as

1. Shock-in-stator
2. Shock-in-rotor
3. Shock-in-rotor/shock-in-stator

In the first impulse type (Figure 13.37), the flow in both rotor and stator are supersonic, thus shocks are found in both blade rows see Figure 13.43. In general [15], if the rotor has a reaction type of blading rather than an impulse one, and has a large turning angle, the flow in the rotor may be subsonic, though the inlet absolute velocity to the stator is supersonic.

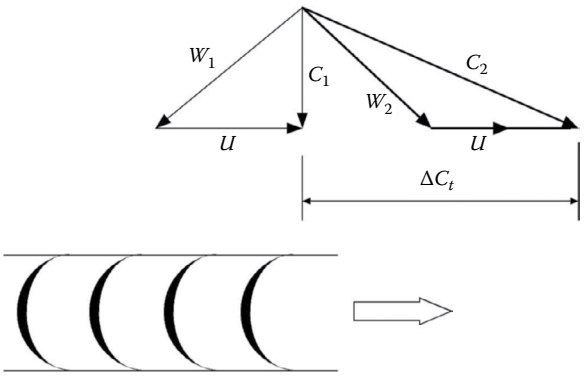


FIGURE 13.41
Velocity triangles of high turning supersonic impulse cascade.

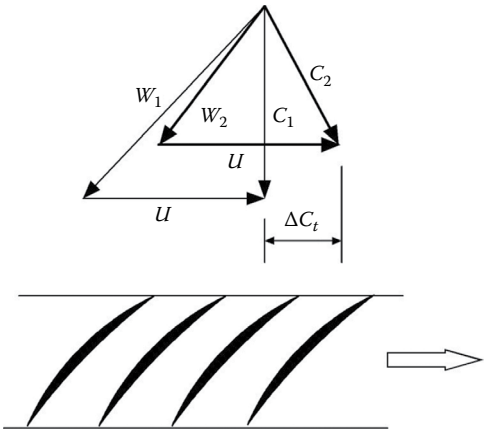


FIGURE 13.42
Velocity triangles low turning supersonic compressor cascade.

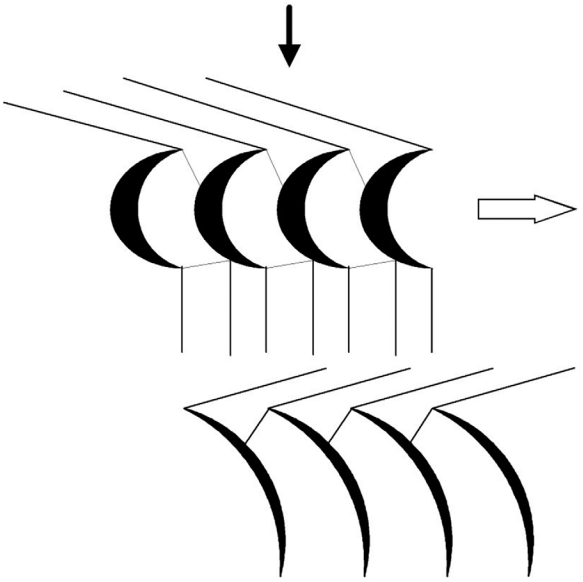


FIGURE 13.43
Shock-in-stator.

Thus, the rotor is a subsonic one while the stator is supersonic and a normal shock is generated in the stator. Concerning the second case of reaction blading (Figure 13.38), there are two cases: either (1) the flow in the rotor is supersonic while the flow in the stator is purely subsonic ($M_{1rel} > 1, M_2 < 1$) (Figure 13.44), which is identified as a "shock-in-rotor" configuration; or (2) the flow in both cases is supersonic ($M_{1rel} > 1, M_2 > 1$) (Figure 13.45) and the flow is identified as shock-in-rotor/shock-in-stator. More details are found in Reference 10.

For subsonic flow, the flow is completely specified if the upstream Mach number and the incidence angle are set. For supersonic flow, it is also necessary to specify the

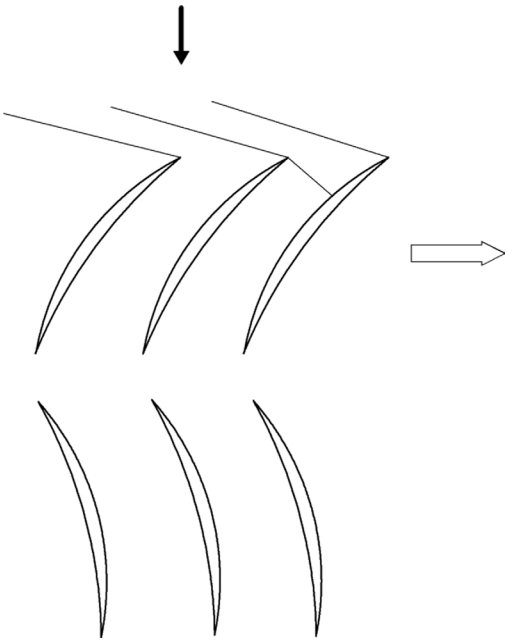


FIGURE 13.44
Shock-in-rotor.

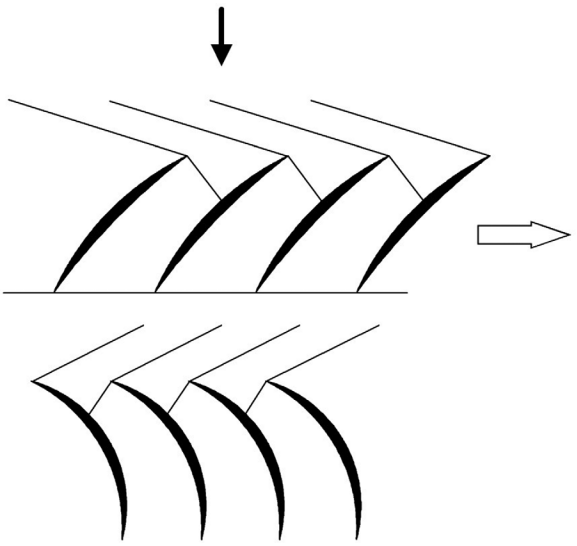


FIGURE 13.45
Shock-in-rotor/shock-in-stator.

downstream pressure, in ratio to that upstream, in order to locate the shock position. The loss coefficient is now defined as

$$\bar{\omega} = \frac{P_{01} - \overline{P_{02}}}{P_{01} - P_1} \tag{13.46}$$

where $\overline{P_{02}}$ is the mass average total pressure over the flow downstream cascade. The effect of the inlet Mach number on losses is experimentally measured for different blading [16]. Figure 13.42 illustrates the losses for two types of compressor blading; namely, the C4 and double circular arc (DCA). Compressibility effect will be most important at the front compressor where the temperature and sonic speed are the lowest. The Mach number corresponding to the velocity relative to the tip of the rotor is the highest. The stator Mach number is highest at the hub. A simplified model for estimating the shock losses [5] is explained with reference to Figure 13.46. In the figure, a pair of DCA are shown, with a supersonic velocity (M_1) entering in a direction aligned with the leading edge. The supersonic expansion along the uncovered portion of the suction side can be analyzed by Prandtl–Meyer expansion relations or tables. The Mach number will increase as the flow proceeds along the suction surface. A normal shock wave stands near the entrance to the passage, striking the suction surface at B. The procedure to be followed here is mainly particular to the author and is different from that described in Reference 5. The Mach number at point B, M_2, prior to the normal shock, is evaluated from Prandtl–Meyer tables once the deflection angle $\Delta\theta$ is known. This angle may be roughly assumed to be a portion of the deflection angle $(\beta_1 - \beta_2)$ depending on the (s/c) ratio, say half or less. The static to total pressure ratio is also evaluated from the Prandtl–Meyer tables (P_1/P_{01}). Then a normal shock wave is assumed with inlet Mach number equal to that just obtained. From normal shock tables, the outlet Mach number and the pressure ratio (P_{02}/P_1) are determined. Assuming that the downstream pressure is nearly equal to the averaged total pressure, $P_{02} \approx \overline{P_{02}}$, then the supersonic loss can be calculated from Equation 13.46.

As an example, if the Mach number at the tip of a rotor is $M_1 = 1.2$, the air inlet and outlet angles are $\beta_1 = 67°$ and $\beta_2 = 62°$. The total turning angle is 5°. The turning angle from the inlet to the normal shock wave location, $\Delta\theta$, depends on the ratio of the spacing to the

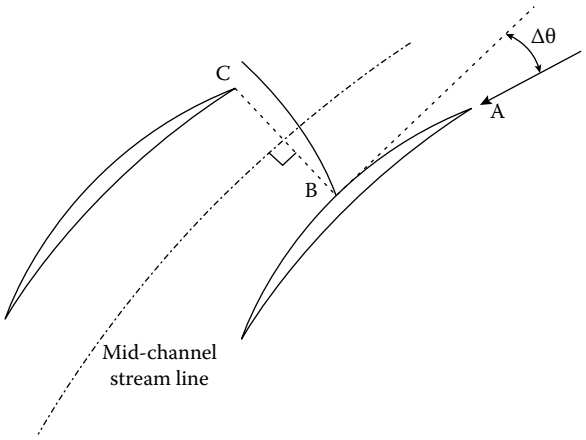


FIGURE 13.46
Shock loss model.

chord (s/c). A reasonable assumption for this angle is 2°. From the Prandtl–Meyer tables, the Mach number just before the normal shock wave is 1.2774. The pressure ratio is $P_1/P_{01} = 0.3721$. From normal shock wave tables with Mach number of 1.2774, the pressure ratio is $P_{02}/P_1 = 2.642$. Substituting in Equation 13.46 will give the losses $\bar{\omega} = 0.0269$.

Example 13.9

Figure 13.47 illustrates the flow pattern and balding at the tip of a transonic fan rotor. The inlet and outlet angles of the flow relative to the blades are $\beta_1 = 68.8°$ and $\beta_2 = 65°$, respectively. The flow approaches the rotor in the axial direction with an absolute velocity $C_1 = 200$ m/s. The inlet stagnation temperature and pressure are 300 K and 1.15 bar, respectively (radially uniform). The hub–tip ratio is 0.4 and the rotor tip diameter is 2.0 m. Inside the rotor blade passage, two oblique shocks are generated. Experimental measurements of the static pressure over the blade-to-blade surface indicated that the turning angles of both oblique shocks are $\delta_1 = 10°$ and $\delta_2 = 10°$.

At the outlet to the rotor, the relative Mach number equals that in region 3. The absolute inlet speed (C_1) and the specific work (W_s) are assumed to be constant at all radii.

1. Calculate the static and total pressure ratios across the rotor.
2. Calculate the absolute and relative velocities at the outlet to the rotor, then draw the velocity triangles.
3. Define which portion of the blade is subjected to supersonic relative inlet speed; draw the velocity triangles at its minimum radius.

Solution

The given data are $T_{01} = 300$ K, $P_{01} = 1.15$ bar, and $C_1 = 200$ m/s.

The sonic speed is then $a_1 = \sqrt{\gamma R T_1} = 335$ m/s.

The static conditions are then $T_1 = T_{01} - \left(C_1^2 / 2C_p\right) = 300 - \left(200^2/2\times 1005\right) = 280$ K.

$$P_1 = P_{01}\left(\frac{T_1}{T_{01}}\right)^{3.5} = 1.15\left(0.933\right)^{3.5} = 0.90319 \text{ bar}$$

$$\rho_1 = \frac{P_1}{RT_1} = 1.1239 \text{ kg/m}^3$$

The first shock wave

$$W_1 = \frac{C_1}{\cos\beta_1} = \frac{200}{\cos 68.8} = 553 \text{ m/s}$$

$$M_{w1} = \frac{W_1}{a} = 1.65 \text{ m/s}$$

since $M_{W1} = 1.65$ and $\delta = 10°$, then $\theta = 50°$. The normal component of the inlet relative Mach number is then

$$M_{W1n} = M_{W1}\sin\theta = 1.65\sin 50 = 1.2639$$

From normal shock wave tables, $M_{W2n} = 0.8052$

$$M_{W2} = \frac{M_{W2n}}{\sin\left(\theta - \delta\right)} = \frac{0.8052}{\sin 40°} = 1.2526$$

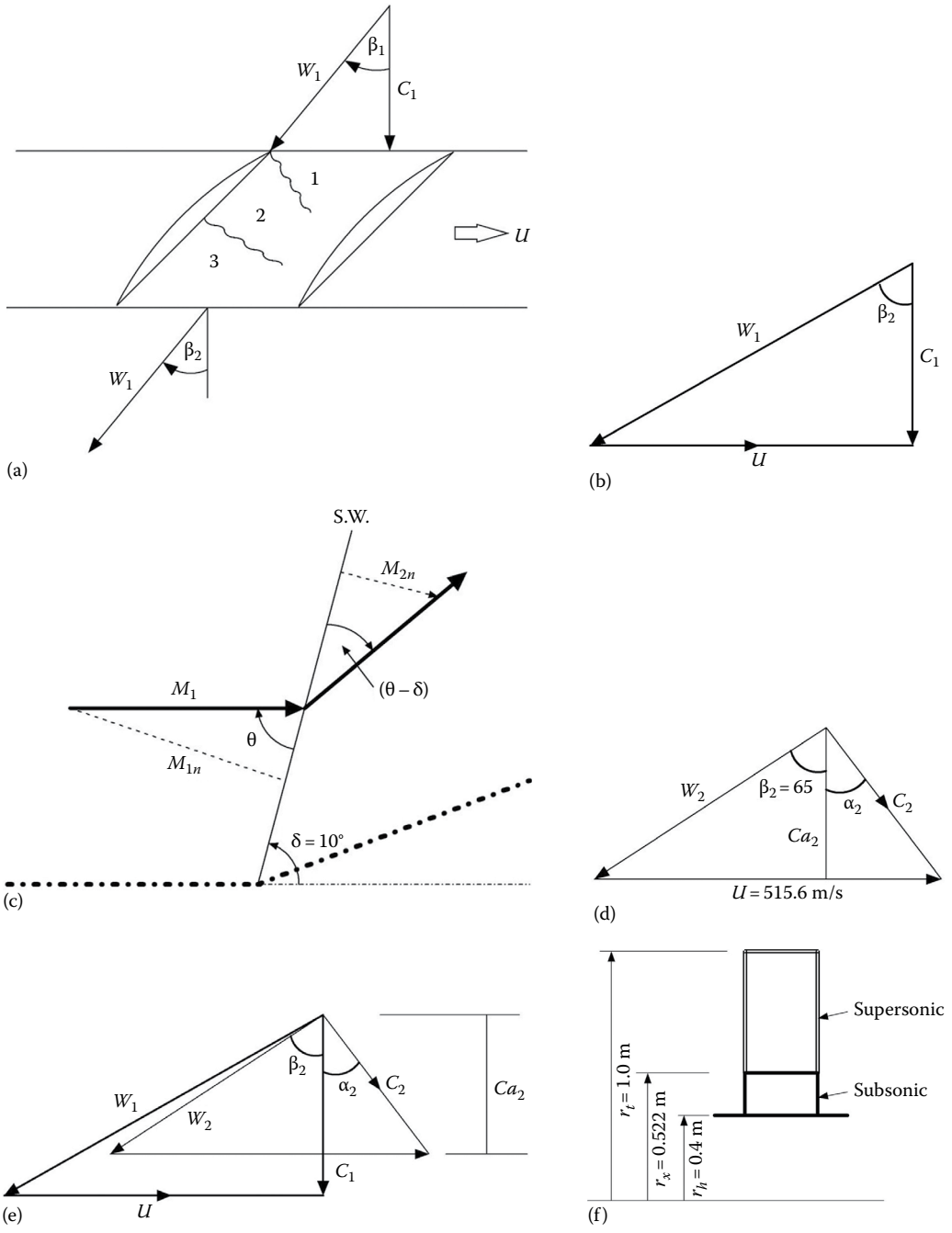


FIGURE 13.47
Transonic axial fan. (a) Layout and shock pattern at tip. (b) Inlet velocity triangle. (c) Oblique shock wave pattern. (d) Outlet velocity triangle. (e) Inlet and outlet velocity triangles in a common apex pattern. (f) Subsonic and supersonic domains on the blade.

Also from tables

$$\frac{P_2}{P_1} = 1.6976, \quad \frac{\rho_2}{\rho_1} = 1.4528, \quad \frac{T_2}{T_1} = 1.1682, \quad \frac{P_{02}}{P_{01}} = 0.9849$$

The second shock wave

Since $M_{W2} = 1.2526$ and $\delta = 10°$,

then from shock table $\theta = 57°$

The normal component of the Mach number. $M_{W2n} = 1.2526 \sin 57 = 1.0513$.

From normal shock wave tables $M_{W3n} = 0.952$

The Mach number is then $M_{W3} = \dfrac{M_{W3n}}{\sin(\theta - \delta)} = \dfrac{0.952}{\sin(57 - 2)} = 1.1621.$

From tables

$$\frac{P_3}{P_2} = 1.1229, \quad \frac{\rho_3}{\rho_2} = 1.08619$$

$$\frac{T_3}{T_2} = 1.03365, \quad \frac{P_{03}}{P_{02}} = 0.9985$$

$$P_{03} = \frac{P_{03}}{P_{02}} \frac{P_{02}}{P_{01}} P_{01} = (0.9985)(0.984918)(1.15) = 1.1325 \text{ bar}$$

The static conditions at state 3 are $\dfrac{P_3}{P_1} = \dfrac{P_3}{P_2} \dfrac{P_2}{P_1} = 1.906$

$$P_3 = 1.7217 \text{ bar}$$

$$T_3 = \frac{T_3}{T_2} \frac{T_2}{T_1} T_1 = 338 \text{ K}$$

$$\rho_3 = \frac{\rho_3}{\rho_2} \frac{\rho_2}{\rho_1} \rho_1 = 1.7738 \text{ kg/m}^3$$

The sonic speed is $a_3 = 368.5$ m/s.

Since at the outlet to the rotor the Mach number is $M_{W3} = 1.1621$, then the rotor outlet relative speed is

$$W_2 = 1.1621 \times 368.5 = 428 \text{ m/s}$$

$$C_{a2} = W_2 \cos 65 = 428 \times 0.4226 = 180.8 \text{ m/s}$$

$$\frac{U}{C_{a2}} = \tan \beta_2 + \tan \alpha_2$$

$$\tan \alpha_2 = \frac{515.6}{180.8} - \tan 65 = 0.7073$$

$$\alpha_2 = 35.27°$$

$$C_2 = \frac{C_{a2}}{\cos \alpha_2} = 221.4 \text{ m/s}$$

$$M_{C2} = \frac{221.4}{368.5} = 0.6$$

Next determine which part of the blade is subjected to supersonic flow and the location at which the inlet relative speed equals the sonic speed ($W_1 = a_1 = \sqrt{\gamma RT_1} = 335$ m/s) is first determined. Denoting the relative speed in this case with $W_{1s} = 335$ m/s, then

$$\cos\beta_{1s} = \frac{C_1}{W_{1s}} = \frac{200}{335} \quad \text{or} \quad \beta_{1s} = 53.3°$$

From the velocity triangle, then the rotational speed

$$U_s = C_1 \tan\beta_{1s} = 200 \times 1.3416 = 268.32 \text{ m/s}$$

Since the ratio between rotational speeds at two positions is related to their radii ratio, then

$$\frac{U_s}{U_t} = \frac{r_s}{r_{tip}}$$

$$r_s = r_{tip}\frac{U_s}{U_{tip}} = (1.0)\left(\frac{268.3}{515.6}\right) = 0.52 \text{ m}$$

The hub radius is

$$r_h = \left(\frac{r_h}{r_t}\right) r_t = (0.4)(1.0) = 0.4 \text{ m}$$

As shown, the part of the blades extending from the hub (radius equals 0.4 m) to a radius of 0.544 m represents the subsonic part of the blade. The outer portion is then a supersonic part. The fan is thus a transonic fan.

13.14 Performance

13.14.1 Single Stage

Compressor balding has a limited range for incidence before losses become excessive and low efficiency is encountered. At incidence angles away from the design point, blade stalling may occur and lead to a surging of the whole compressor, which may lead to engine damage and aircraft hazard. Equation 13.10a may be rewritten again as

$$\frac{Cp\Delta T_{0s}}{U^2} = 1 - \frac{C_a}{U}(\tan\alpha_1 + \tan\beta_2) \tag{13.10a}$$

where

α_1 is the absolute inlet angle to the rotor or the outlet angle from the previous stator for a multistage compressor

β_2 is the air outlet angle from the rotor

Generally α_1 and β_2 remain unchanged for a fixed geometry compressor. Now defining the *loading coefficient* ψ as

$$\psi = \frac{Cp\Delta T_{0s}}{U^2} = \frac{\Delta C_u}{U}$$

and the *flow coefficient* ϕ as

$$\phi = \frac{C_a}{U}$$

then

$$\psi = 1 - K\phi \tag{13.47a}$$

where

$$K = \tan\alpha_1 + \tan\beta_2 \tag{13.47b}$$

Plotting relation (13.37a), it is shown that the loading coefficient ψ is a linear function of the flow coefficient (or mass flow parameter) ϕ if α_1 and β_2 are constants; see Figure 13.48. The actual performance drops rapidly at flow coefficients above and below the design operating condition. A plot of the efficiency for the actual performance is also plotted in Figure 13.48. The critical points in this figure are the stall and choking points. The velocity triangles corresponding to both points are also drawn.

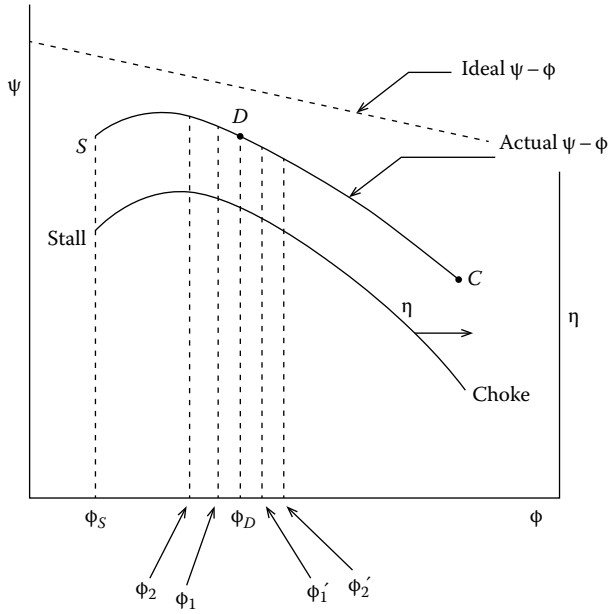


FIGURE 13.48
Actual and ideal performance of a compressor stage.

As shown in Figure 13.48, for the ideal case the temperature coefficient decreases as the flow coefficient increases. Moreover, if $\phi = 0$, then $\psi = 1$, or $\Delta C_u = U$, which provides a very large diffusion factor (D) and a drastic drop in efficiency. For satisfactory operation, the temperature coefficient must be in the range $\psi = 0.3$–0.4. The real performance indicates that, for a flow coefficient ϕ smaller than its design value, that is, $C_a < (C_a)_d$, then the relative inlet angle (β_1) and an incidence angle will increase, which will possibly lead to a positive stall. On the other hand an increase in the flow coefficient ϕ, that is, $C_a > (C_a)_d$, a decrease in the relative inlet angle (β_1), and a negative incidence result may lead to a negative stall (see Figure 13.49).

It was emphasized previously that the stage performance is a function of the temperature coefficient, flow coefficient, and efficiency, or

$$\text{Stage performance} = f(\phi, \psi, \eta_s)$$

Designers sometimes employ a pressure coefficient instead of the temperature coefficient in estimating stage performance. The pressure coefficient is defined as $\psi_p = \Delta P_{0s} / \rho_{01} U^2$

$$\frac{P_{02}}{P_{01}} = 1 + \frac{\Delta P_{0s}}{P_{01}} = \left(1 + \frac{\eta_s \Delta T_{0s}}{T_{01}}\right)^{\gamma/\gamma - 1}$$

since

$$\frac{\Delta T_{0s}}{T_{01}} \ll 1$$

$$\therefore \frac{\Delta P_{0s}}{P_{01}} \cong \frac{\gamma}{\gamma - 1} \frac{\eta_s \Delta T_{0s}}{T_{01}} = \frac{\eta_s Cp \Delta T_{0s}}{R T_{01}}$$

$$\frac{\Delta P_{0s}}{\rho_{01}} = \eta_s Cp \Delta T_{0s}$$

$$\therefore \psi_p \equiv \frac{\Delta P_{0s}}{\rho_{01} U^2} = \frac{\eta_s Cp \Delta T_{0s}}{U^2} = \eta_s \psi$$

$$\psi_p = f(\eta_s, \psi)$$

Thus the stage performance can be expressed as

$$\text{Stage performance} = G(\phi, \psi_p, Cp)$$

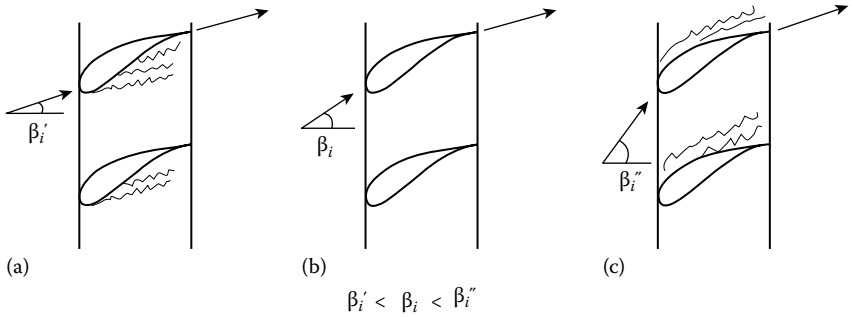


FIGURE 13.49
(a) Negative, (b) normal, and (c) positive stall.

13.14.2 Multistage Compressor

So far, we have considered an isolated single-stage performance over a range of off-design conditions. For a multistage compressor, the simplest method for examining its performance is to assume that the compressor consists of stages having identical characteristics, which is known as "stage stacking." It is assumed that all stages operate at the design point ϕ_d. A small departure from the design point at the first stage will lead to a progressively increasing departure from design conditions from the first stage onward. Consider the following two cases:

1. If, at constant speed, the compressor is subjected to a slight decease in the mass flow rate, this slightly decreases the flow coefficient of the first stage to $\phi_1 < \phi_d$ and slightly increases the specific work or the pressure ratio, $\psi_1 > \psi_d$. Thus, the density of air entering the second stage will increase and the flow coefficient will decrease due to two reasons; the first is the decrease in mass flow rate while the second is the increase in the density of the air leaving the first stage. Then the axial velocity of air entering the second stage will decrease ($\phi_2 < \phi_1$). This effect is propagated through the compressor and eventually some of the latter stages will stall at decreased ϕ_n (positive stall).
2. Increasing the mass flow in the first stage from the design point, $\phi_1' > \phi_d$, decreases the temperature rise and pressure ratio at the inlet to the second stage, $\psi_1' < \psi_d$, which similarly will lead to another increase in the axial velocity and flow coefficient of air entering the second stage $\phi_2' > \phi_1'$. Thus the pressure and temperature coefficients will decrease, or $\psi_2' < \psi_1'$, due to the increase in the air flow rate and the decrease in the air density. This continuous increase in axial flow velocity is propagated through the compressor, which at some stage will become choked.

13.14.3 Compressor Map

Compressor performance is usually presented in the form of a compressor map, as described in the previous chapter. The dimensionless parameters influencing compressor performance are derived as

$$\frac{P_{02}}{P_{01}}, \quad \eta_C = f\left(\frac{\dot{m}\sqrt{\gamma RT_{01}}}{P_{01}D^2}, \frac{ND}{\sqrt{RT_{01}}}\right)$$

which for a certain working fluid and a specific compressor are reduced to either

$$\frac{P_{02}}{P_{01}}, \quad \eta_C = f\left(\frac{\dot{m}\sqrt{T_{01}}}{P_{01}}, \frac{N}{\sqrt{T_{01}}}\right) \quad \text{or} \quad \frac{P_{02}}{P_{01}}, \quad \eta_C = f\left(\frac{\dot{m}\sqrt{\theta}}{\delta}, \frac{N}{\sqrt{\theta}}\right)$$

One point in this map represents the design point. However, the compressor has to perform efficiently in other operating conditions, frequently identified as "off-design conditions," namely during engine starting, idling, reduced power, maximum power, acceleration, and deceleration.

Consequently, the compressor has to operate satisfactorily over a wide range of rotational speeds (rpm) and inlet conditions. But since the annulus area and compressor blading are chosen to satisfy the design point condition then at other conditions they will not function correctly [5].

The compressor map of an axial compressor is shown in Figure 13.50. It may be noticed that, for a fixed value of $N/\sqrt{T_{01}}$, the range of the mass flow rate is narrower than that in a centrifugal compressor. At high rotational speed, the lines become very steep and ultimately may be vertical.

The surge point occurs before the curves reach a maximum value. Stage characteristics are similar to overall characteristics but with a much lower pressure ratio. Mass flow is limited by choking in various stages. Before examining the compressor map, it is worthy mentioning that the annulus area of the compressor decreases from the front to the rear stages, the reason being that the density increases in the rearward direction (due to pressure increase) and the axial velocity is maintained.

The following are remarks concerning the compressor map:

1. At rotational speeds lower than the design speed, $N/\sqrt{T_{01}} < \left(N/\sqrt{T_{01}}\right)_{design}$, choking will occur at the latter stages. This low speed will provide a smaller temperature and pressure rise compared to the design values. Thus, the air density will decrease, which will lead to an increase in the axial velocity in the rear stages. Thus, choking will occur in the last stages and limit the mass flow, which, when coupled with the original density at the inlet, will lead to smaller axial velocities at the first stage and a positive stall will follow. Hence, lower speeds result in the choking of the rear stages and the stalling of the first stage.

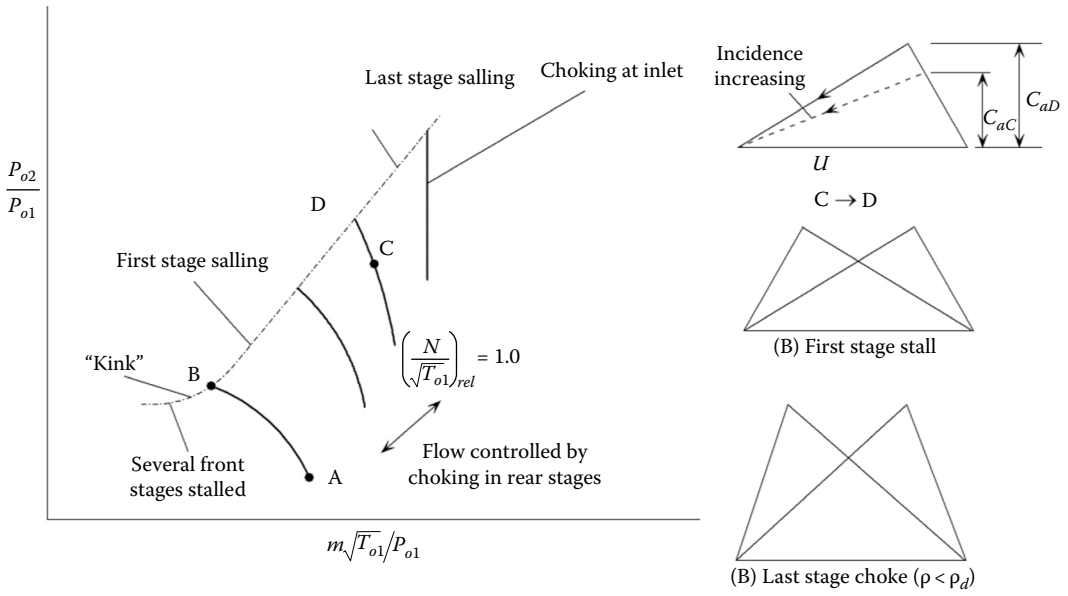


FIGURE 13.50
Compressor map with different operating conditions.

2. When the rotational speed increases, the air density is increased to the design value and the rear stages will pass all the flow provided by the first stages. Then choking will occur at the inlet of the compressor. Thus, the vertical line is due to inlet choking.
3. At the design speed, the speed line is very steep, thus any decrease in the mass flow rate will bring a reasonable increase in pressure. This will also increase the density and decrease the axial velocity. This effect will propagate in the rearward direction and be magnified to the limit where it causes a stall of the rear stages.

13.14.4 Stall and Surge

A stall is a situation of abnormal airflow through single or multiple stages of the compressor, while a whole compressor stall, known as a "compressor surge," results in a loss of engine power. This power failure may only be momentary, or it may shut the engine down completely and cause a flameout. The appropriate response to compressor stalls varies according to the engine type and situation, but it usually involves an immediate and steady decrease of the thrust in the affected engine. The most likely cause of a compressor stall is a sudden change in the pressure differential between the intake and combustion chamber. The following factors can induce compressor stall:

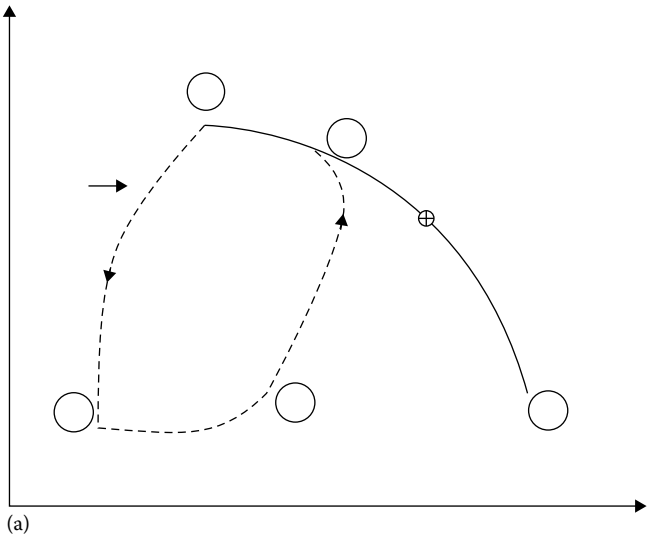
- Engine over-speed
- Engine operation outside specified engineering parameters
- Turbulent or disrupted airflow to the engine intake
- Contaminated or damaged engine components

Jet aircraft pilots must be careful when dropping the airspeed or increasing the throttle.

Physically, rotating stall and surge phenomena in axial flow compressors are the most serious problems in compressors. Severe performance and reliability problems arise if the compressor is unable to recover from a stall. Surge and rotating stalls can be described as follows [6]. Consider the performance map in Figure 13.51, which plots the pressure coefficient and flow coefficient variables ($\psi_p - \phi$). As the mass flow is decreased (throttle closed), then the pressure increases and the compressor will be stable and operate along the unstalled characteristics from points *A* to *B*. A further reduction in mass flow below point *B* will generate a rotating stall and the operating point will suddenly drop to a new stable condition in the rotating stall, point *C*. If the mass flow is increased (throttle opened), then the compressor will not jump back to point *B*, but operate by the stalled characteristics to point *D*. A further increase of mass flow beyond *D* causes the operating point to jump to point *E* of the unstalled characteristics. Regions *B*, *C*, *D*, *E*, *B* is the stall *hysteresis* region. Now the *rotating stall* [6] is defined as a breakdown at one or more compressor blades. A rotating stall is a stagnated region of air which moves in the opposite circumferential direction of rotor rotation, but at 50%–70% of the blade speed [10], which will now be described.

If the throttle is closed or the back pressure is increased, the blade loading or the incidence is increased. Then the adverse pressure gradient on the suction surfaces increases the boundary layer growth, which leads to separation and stall. Not all the blade passages will stall at the same time. The stalling of a blade passage will lead to an increase of the incidence angle of the next passage in the opposite direction of rotation.

Thus it will stall (Figure 13.52). There may be several stall cells in a blade row rotating in the same time; see Figure 13.53. As described in Reference 17, a part span is usually



(a)



(b)

FIGURE 13.51
Performance characteristics for (a) unstalled and (b) stalled operation. (From Wisler, D.C., *Advanced Compressor and Fan Systems*, GE Aircraft Engines, Cincinnati, OH, 1988. With permission.)

encountered in the front stages of the compressor with large aspect ratio blades and low speeds. This is usually encountered during takeoff or start-up. A full span stall occurs in the medium speed range and its effect is much more damaging. In brief, a rotating stall does not move axially in either direction, although it may cause pressure waves to move upstream (compression wave) or downstream (rarefaction waves). Moreover, such standing rotating pockets prevent fresh air from the intake passing over the stalled rotor blades, leading to blades overheating and consequently engine wear and possible damage. Compressor surge occurs when there is a complete breakdown of the flow field in the entire engine (not just blading). Upon surge, a compression component will unload by permitting the compressed fluid in the downstream stages to expand in the upstream direction, forming waves strong enough to lead to flow reversal. The compressor can then recover and begin again to pump flow. However, if the cause of the surge is not removed,

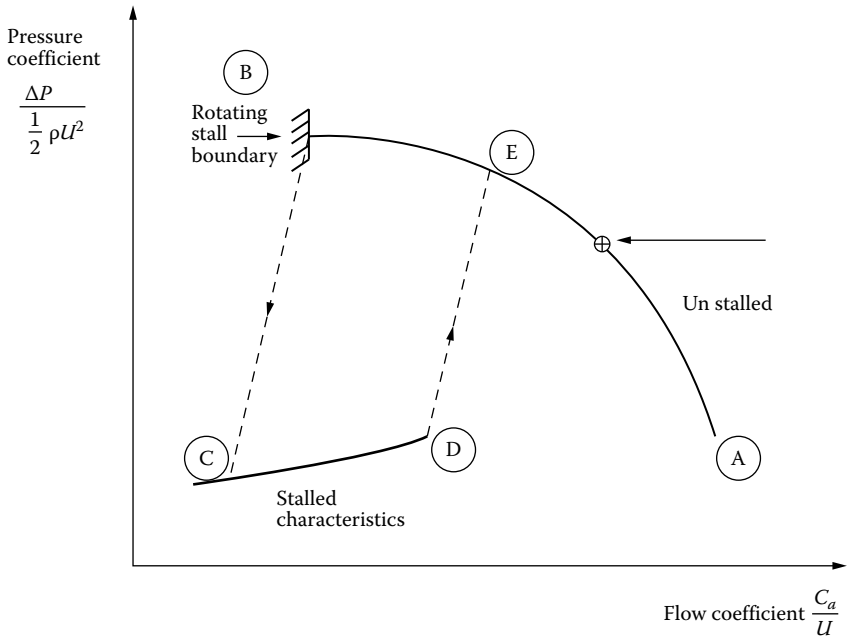


FIGURE 13.52
The propagation of a rotating stall.

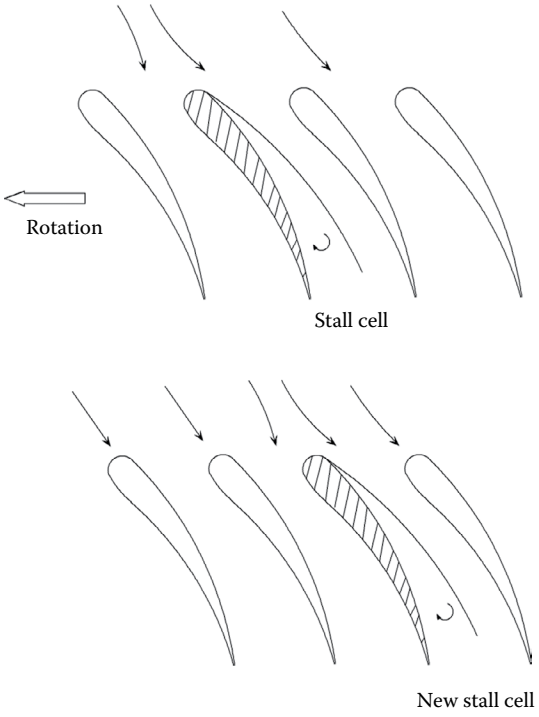


FIGURE 13.53
Rotating stall and surge.

the compressor will surge again and continue the surge/recovery cycle until some relief is provided. Otherwise, the surge will result in violent oscillations in pressure, propagation of pressure waves, and the failure of the entire compression system.

Precautions to avoid surge have led to defining what is called a "surge margin" (very similar to the factor of safety in mechanical system design). It is defined as

$$\text{Stall margin} = \left\{ \frac{\left(P_{02}/P_{01}\right)_{stall}}{\left(P_{02}/P_{01}\right)_{design\ point}} \times \frac{\left(\dot{m}\sqrt{T_{01}/P_{01}}\right)_{design\ point}}{\left(\dot{m}\sqrt{T_{01}/P_{01}}\right)_{stall}} - 1 \right\} \%$$

When a surge occurs in an operating engine, it causes at the least a stoppage of the airflow through the compressor [18], which leads to a straightforward expulsion of air back out of the intake. In civil transport, this is evidenced by a loud bang emanating from the engine as the combustion process "backfires," which is unsettling to passengers. This may be accompanied by an increase in exhaust gas temperature and a yawing of the aircraft in the direction of the affected engine. If repeated enough times, it can do structural damage to the engine inlet or perhaps to the fan (in turbofan engines) or the fan frame. Violent compressor surge might completely destroy the engine and set it on fire. But absent of such structural damage, the engine will usually recover and continue to run. In supersonic aircraft, the consequences can be more serious, because the blockage due to a surge can generate a shock wave in the inlet, which may produce overpressures large enough to damage the structure.

13.14.5 Surge Control Methods

As described above, a surge causes serious problems to compressor, engine, and aircraft. Though it is in many circumstances unavoidable, its recovery is possible. Since a rotating stall represents the onset of a surge, by avoiding a stall a surge will not occur. However, this is rather a difficult task due to the different operating conditions for the compressors installed in aeroengines powering airplanes during any trip or mission. For compressors in industrial power plants different conditions are also found during say starting, idling, acceleration, and deceleration. FOD is another serious circumstance that influences the fluid mass flow rate. Compressor designers have been proposed for surge control. In the design phase, the single-spool engine is replaced by a two-spool engine. Each spool (and consequently compressor) rotates at a different speed. During operation, two alternatives are found, namely, the variable geometry compressor and air bleed. Later techniques are activated by the engine control unit, which represents a computerized control system that has its inputs from sensors within the engine.

13.14.5.1 Multi-Spool Compressor

A reduction in compressor speed from the design value will cause an increase of incidence angle in the first stage and a decrease of incidence angle in the last stage. The incidence could be maintained at the design value by decreasing the speed of the first stages and increasing the speed of the last stage. These conflicting requirements can be met by splitting the compressor into two (or more) sections, each driven by separate turbines (the low-pressure turbine drives the low-pressure compressor and the high-pressure turbine

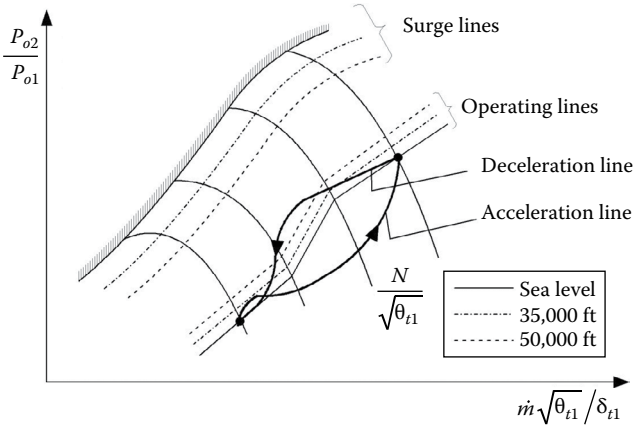


FIGURE 13.54
Map for a low-pressure compressor. (From United Technologies Pratt Whitney, *The Aircraft Gas Turbine Engine and Its Operation*, P&W Operation Instruction 200, East Hartford, CT, pp. 3–81, 1988.)

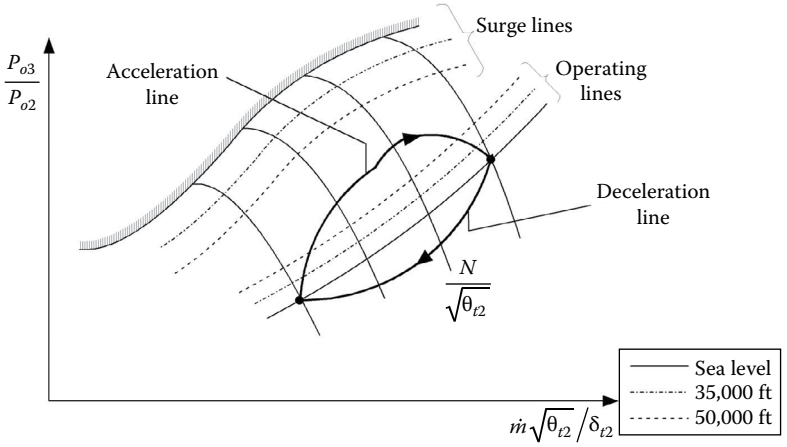


FIGURE 13.55
Map for a high-pressure compressor. (From United Technologies Pratt Whitney, *The Aircraft Gas Turbine Engine and Its Operation*, P&W Operation Instruction 200, East Hartford, CT, pp. 3–81, 1988.)

drives the high-pressure compressor). Examples for the two-spool engines are the CF6, CFM56, GE90, V2500, and JT9 turbofan engines. Examples for three spools are the RB211 and Trent family. Typical compressor maps for the low-pressure and high-pressure spools are illustrated in Figures 13.54 and 13.55.

13.14.5.2 Variable Vanes

Variable stators may be used to unstall those stages precipitating general compressor stall. Since it is the front end and/or the back end stages of a compressor that are most likely to encounter a stall, the use of variable geometry is normally confined to these stages. Furthermore, with the tendency of the back end stages to be more lightly loaded (due to

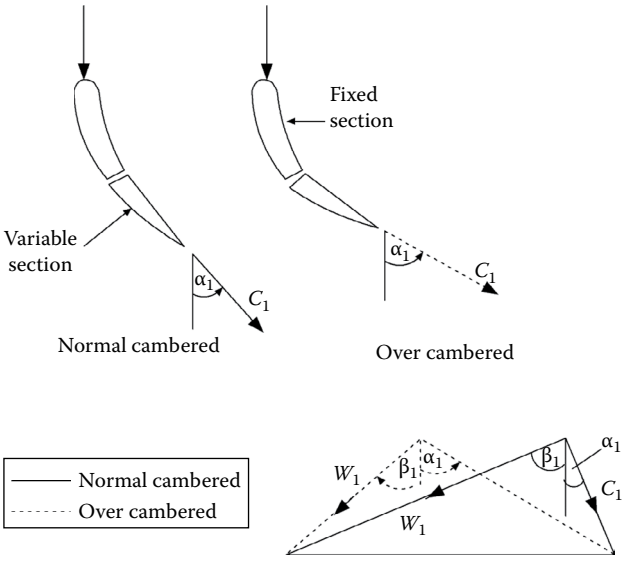


FIGURE 13.56
Variable stator blades.

lower Mach numbers), the stall problem is not as severe in those stages. As a result, variable stators are normally confined to the front stages and their principal use is to provide acceptable starting and/or low speed acceleration of the engine. Positive stall is encountered when the inlet relative angle, β_1, and consequently the incidence angle are increased. To reduce this value two methods are employed. In the first, the inlet guide vanes or the stators of the first stages are rotated away from the axial direction to increase the absolute angle at inlet α_1 and thus reduce the relative inlet angle β_1. As an alternative, the rear part of the blade is rotated, which becomes over cambered; hence, it achieves the same job as the completely rotated stators (see Figure 13.56).

13.14.5.3 Air Bleed

The bleeding of air downstream of a stalled stage or stages will allow the flow to increase ahead of the bleed location. This increase in airflow will in turn result in a reduction of the rotor incidence and unstall the blade (Figure 13.57). The amount of the bled air will exceed by a small amount the increase in front flow. The flow to the back stages will thereby be reduced. This reduction of flow reduces the axial velocity component to the rear stages and will increase their work output, compensating to a certain degree the loss of output in the front stages (refer to Equation 13.47a).

Example 13.10

The compressor in a single-spool turbojet engine is composed of a four-stage axial compressor and a single-stage centrifugal compressor. The rotational speed is 290 rev/s. The detailed data of both compressors is given as

The inlet total conditions to the compressor section are

$$T_{01} = 298 \text{ K}, \quad P_{01} = 1.0 \text{ bar}$$

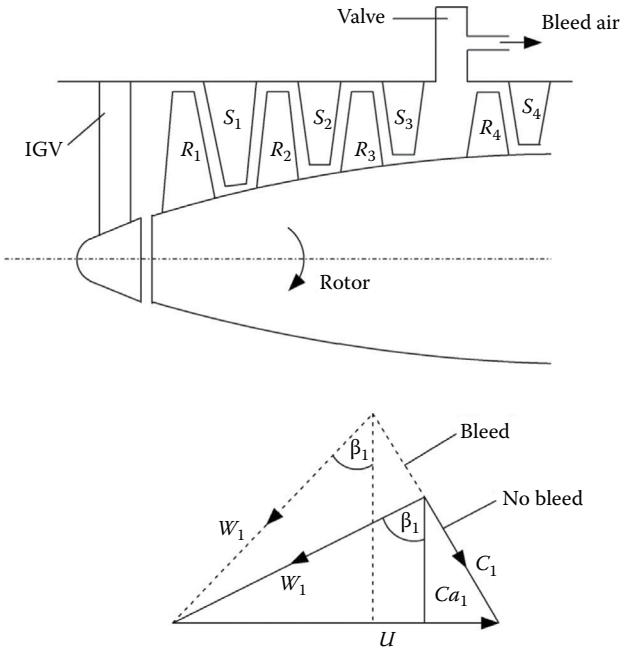


FIGURE 13.57
Bleed as a surge controller.

Two arrangements are investigated; namely, the axial compressor (*A*) installed upstream of the centrifugal compressor (*C*) (Figure 13.58a), and the reverse (Figure 13.58b).

1. Compare the overall stagnation pressure ratio and temperature rise in both cases.
2. Plot these operating conditions on the maps of both compressors ($\dot{m} = 20$ kg/s)
3. Calculate the overall efficiency for both arrangements.
4. Do as in (1) and (3) above but with a reduced value for the efficiency of the centrifugal compressor ($\eta_c = 0.8$).
5. Compare between both layouts from an aerodynamic, performance, and mechanical point of view.

Axial compressor (*A*)	
Temperature rise per stage	25 K
Polytropic efficiency η_{pc}	0.9
Centrifugal compressor (*B*)	
Impeller tip diameter	0.5 m
Power input factor ψ	1.04
Slip factor σ	0.9
Efficiency η_c	0.9

Solution

1. The temperature difference across these compressors is given by

$$\left(T_{0_e} - T_{0_i}\right)_{axial} = N\Delta T_{0_s}$$

$$\left(T_{0_e} - T_{0_i}\right)_{centrifugal} = \frac{\Psi \sigma U_{tip}^2}{C_p}$$

Both are constants for the two arrangements
Arrangement (1): For the axial compressor (Table 13.11)

$$\Delta T_{0_{axial}} = N\Delta T_{0_s} = 4 \times 25 = 100 \text{ K}$$

$$T_{01} = 298 \text{ K}, \quad T_{02} = 398 \text{ K}$$

$$\frac{n}{n-1} = \eta_{PC} \frac{\gamma}{\gamma - 1} = 0.9 \frac{1.4}{0.4} = 3.15$$

$$\pi_{axial} = \left(1 + \frac{\Delta T_0}{T_{01}}\right)^{n/n-1}$$

$$\pi_{axial} = \left(1 + \frac{100}{298}\right)^{n/n-1} = \left(1.3356\right)^{3.15} = 2.488$$

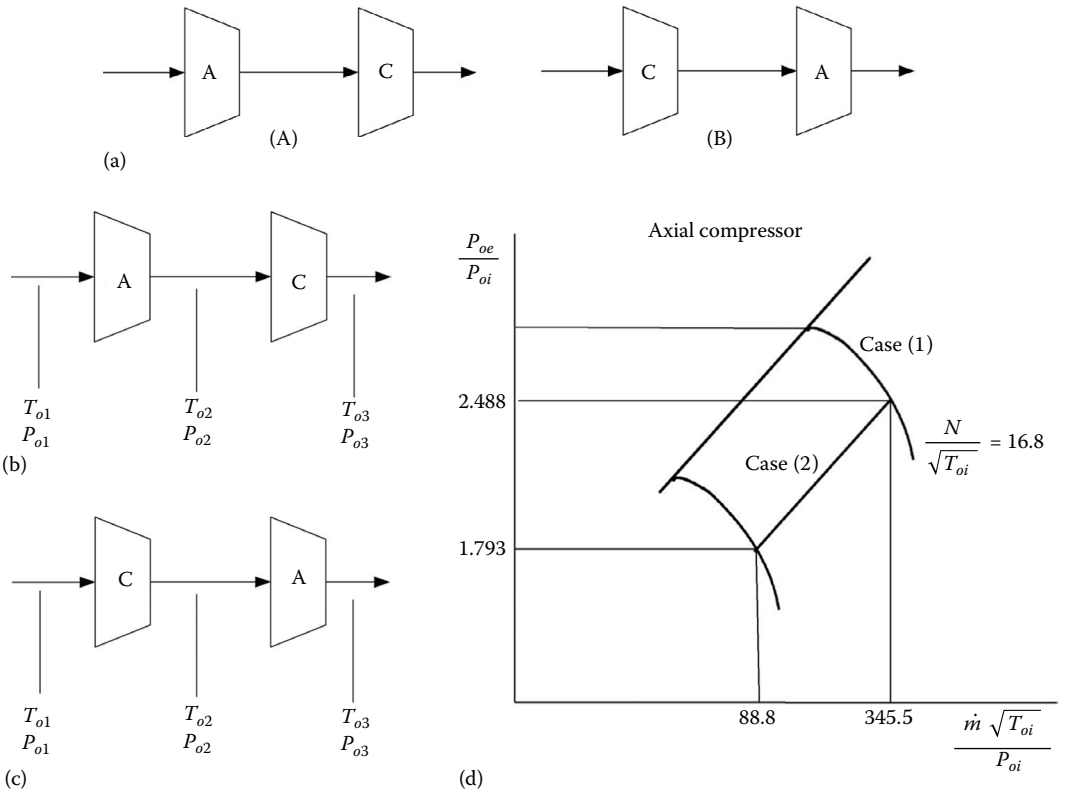


FIGURE 13.58
(a) Two arrangements for axial and centrifugal compressors. (b) Axial-centrifugal compressor (arrangement 1). (c) Centrifugal-axial layout (arrangement 2). (d) Compressor map for axial compressor. (*Continued*)

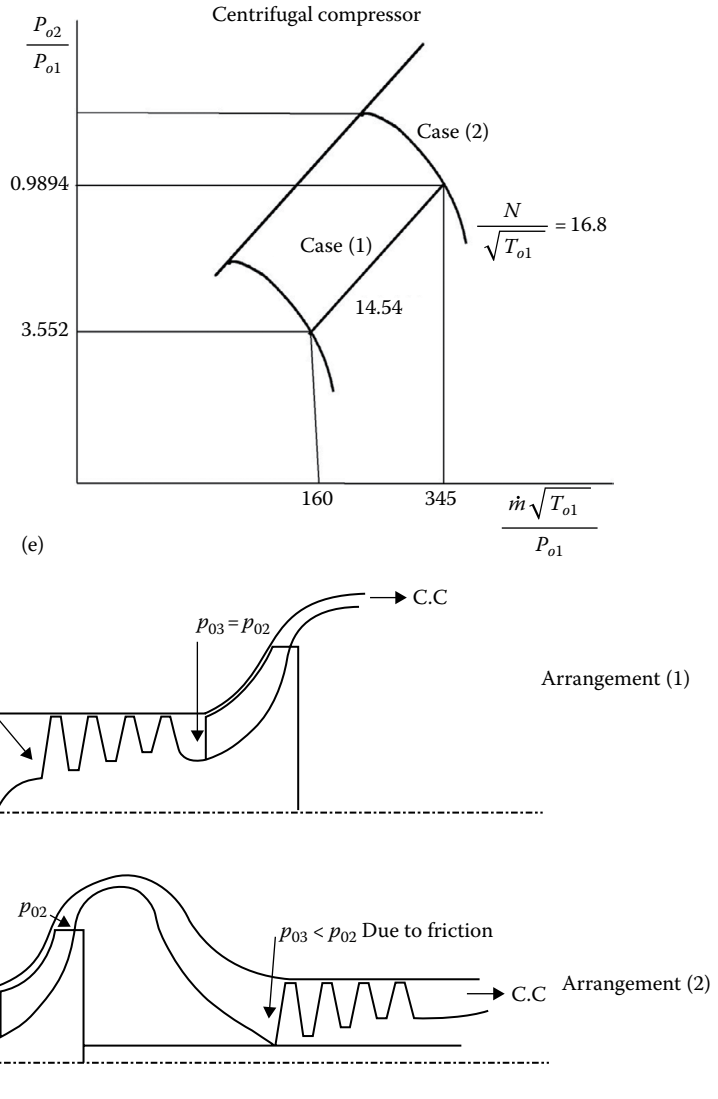


FIGURE 13.58 (*Continued*)
(e) Compressor map for centrifugal compressor. (f) Length and diameter pattern for the combined compressor in the two arrangements.

TABLE 13.11

Output Results for Axial Compressor

	Axial Compressor						
Arrangement	T_{oinlet} **(K)**	$T_{0_{exit}}$ **(K)**	P_{0i} **(bar)**	P_{0e} **(bar)**	π	$\dot{m}\sqrt{T_{0_i}}/P_{0_i}$	$N/\sqrt{T_{0_{inlet}}}$
(1)	298	398	1.0	2.488	2.488	345.5	16.8
(2)	491	591	4.989	8.9465	1.793	88.83	13.09

TABLE 13.12

Output Results for Centrifugal Compressor

Centrifugal Compressor							
Arrangement	T_{oinlet} **(K)**	T_{0exit} **(K)**	P_{0i} **(bar)**	P_{0e} **(bar)**	π	$\dot{m}\sqrt{T_{0i}}/P_{0i}$	$N/\sqrt{T_{0inlet}}$
(1)	398	591	2.488	8.838	3.5522	160.4	14.91
(2)	298	491	1.0	4.9897	4.9897	345.2	13.09

For the centrifugal compressor (Table 13.12)

$$U_{tip} = \pi d_t N = \pi \times 0.5 \times 290 = 455.5 \text{ m/s}$$

$$\left(\Delta T_0\right)_{centrifugal} = \frac{\Psi \sigma U_{tip}^2}{C_p}$$

$$\left(\Delta T_0\right)_{centrifugal} = \frac{1.04 \times 0.9 \times \left(455.5\right)^2}{1005} = 193 \text{ K}$$

$$T_{03} = T_{02} + \left(\Delta T_0\right)_{centrifugal} = 591 \text{ K}$$

$$\pi_{centrifugal} = \left(1 + \eta_c \frac{\Delta T_0}{T_{02}}\right)^{\gamma/\gamma-1} = \left(1 + 0.9\frac{193}{398}\right)^{3.5} = 3.5522$$

$$\pi_{total} = \pi_{axial} \times \pi_{centrifugal} = 8.838$$

The overall temperature rise across the two compressors is constant in both arrangements and equal to 293 K.

Arrangement (2):

$$\pi_{centrifugal} = \left(1 + 0.9\frac{193}{298}\right)^{3.5} = \left(1.5828859\right)^{3.5} = 4.98969$$

$$\pi_{axial} = \left(1 + \frac{100}{491}\right)^{3.15} = 1.793$$

$$\pi_{total} = 8.9465$$

2. The overall efficiency ($\eta_a = \eta_c = 0.9$)

$$\eta = \frac{T_{02'} - T_{01}}{T_{02} - T_{01}} = \frac{T_{01}\left\{\left(\frac{p_{02}}{p_{01}}\right)^{\gamma-1/\gamma} - 1\right\}}{T_{02} - T_{01}}$$

$$\eta_{arrangement(1)} = \frac{298\left\{\left(8.839\right)^{0.4/1.4} - 1\right\}}{293} = \frac{298\left(1.8638 - 1\right)}{293} = 0.8785$$

$$\eta_{arrangement(2)} = \frac{298\left\{\left(8.9465\right)^{0.4/1.4} - 1\right\}}{293} = \frac{298\left(1.8702 - 1\right)}{293} = 0.8851$$

3. The efficiency of the axial compressor is unchanged while the efficiency of the centrifugal compressor drops, or $\eta_a = 0.9$, $\eta_c = 0.8$.
   The compression ratio for the axial compressor will not change

$$\therefore \pi_{axial} = 2.488, \quad T_{02} = 398 \text{ K}$$

$$\pi_{centrifugal} = \left(1 + 0.8\frac{193}{398}\right)^{3.5} = (1.3879396)^{3.5} = 3.1496$$

$$T_{03} = 591 \text{ K}$$

$$\pi_{Total} = 7.836$$

Arrangement (2) $T_{01} = 298$ K

$$\pi_{centrifugal} = \left(1 + 0.8\frac{193}{298}\right)^{3.5} = 4.3099$$

$$T_{02} = 491 \text{ K}$$

$$\pi_{axial} = \left(1 + \frac{100}{491}\right)^{3.15} = 1.793$$

$$\pi_{Total} = 7.7276$$

The overall efficiency (Table 13.13)

$$\eta_{arrangement(1)} = \frac{298\left\{(7.836)^{0.4/1.4} - 1\right\}}{293} = \frac{298(1.8007 - 1)}{293} = 0.81436$$

$$\eta_{arrangement(2)} = \frac{298\left[(7.7276)^{0.4/1.4} - 1\right]}{293} = \frac{298(1.7936 - 1)}{293} = 0.8071$$

4. From the above calculations it can be deduced that
   a. The overall pressure ratio is slightly higher for arrangement (2) if both compressors have the same efficiency, but if the efficiency of the centrifugal compressor is dropped then arrangement (1) gives a higher pressure ratio.
   b. When the efficiency of centrifugal compressor is less than that of the axial one, then the overall efficiency of the compressor in arrangement (1) is larger than the overall efficiency in arrangement (2).

TABLE 13.13

Summary for Both Arrangements

	1		2	
Arrangement	$\eta_a = \eta_c = 0.9$	$\eta_a = 0.9, \eta_c = 0.8$	$\eta_a = \eta_c = 0.9$	$\eta_a = 0.9, \eta_c = 0.8$
Overall pressure ratio	8.838	7.836	8.9465	7.7276
Overall efficiency	0.8785	0.81436	0.8851	0.8071

c. Arrangement (1) is much more appropriate for the installation of a combustion chamber, while arrangement (2) needs some piping system between both compressors, which adds some mechanical complications to the compressor section. This piping increases the skin friction and thus reduces the total pressure upstream of the axial compressor. The external drag force in arrangement (2) is larger than in arrangement (1), as shown in Figure 13.58f.

13.15 Case Study

A complete design for a seven-stage axial compressor is presented here. The compressor pressure ratio is 4.15 and the air mass flow rate is 20 kg/s. The ambient temperature and pressure are 288 K and 101 kPa. The rotational speed is 15,000 rpm. The mean flow calculations are given in Table 13.14. The air flow properties along the mean radius of all stages will be given hereafter. Only the fourth stage will be examined in detail where the variations of different aerodynamic and thermodynamic properties from hub to tip will be given using the three-design method. The reader can follow similar steps for the other stages. Finally, the seven-stage compressor will be constructed.

13.15.1 Mean Section Data

The temperature rise, pressure ratio, flow angles, hub and tip radii, hub–tip ratio, and degree of reaction at the mean section of the seven stages are given in Table 13.14.

13.15.2 Variations from Hub to Tip

The free vortex, exponential, and first power methods are employed for calculating the variations in the flow angles.

Tables 13.15 and 13.16 give the variation of the flow angles and degree of reaction at hub and tip using the free vortex method.

Tables 13.17 and 13.18 give the variation of the flow angles and degree of reaction at hub and tip using the exponential method.

TABLE 13.14

Mean Radius Characteristics

Stage	1	2	3	4	5	6	7
ΔT_o (K)	27.35	25.24	23.86	22.50	22.50	22.50	19.85
π	1.3325	1.2756	1.2386	1.2084	1.1955	1.1841	1.1524
α_1	0	8.91	9.21	9.22	9.22	9.22	9.22
α_2	35.06	40.0	40.16	40.17	40.17	40.17	37.37
β_1	60.62	58.30	58.22	58.21	58.21	58.21	58.21
β_2	47.04	43.13	43.0	43.0	43.0	43.0	45.35
α_3	8.91	9.21	9.22	9.22	9.22	9.22	0
Λ	0.8024	0.7196	0.7168	0.7167	0.7166	0.7166	0.7393
ζ	0.5000	0.5722	0.6275	0.6714	0.7066	0.7368	0.7629
r_h (m)	0.1131	0.1234	0.1308	0.1363	0.1404	0.1439	0.1468
r_t (m)	0.2261	0.2158	0.2084	0.2029	0.1988	0.1953	0.1924

TABLE 13.15

Results at Hub Section Using Free Vortex Method

Stage	1	2	3	4	5	6	7
α_1	0.6033	13.9411	14.7497	15.3312	14.8955	14.5530	13.8522
α_2	46.1905	40.0043	46.1618	44.3795	43.5140	42.8187	39.4638
β_1	49.5638	58.3016	47.8898	49.0587	50.3051	51.2802	52.2299
β_2	8.0584	43.1313	18.1698	24.1482	27.5327	30.1270	35.5230
α_3	9.6806	9.2082	9.6782	9.5291	9.4608	9.4077	0
Λ	0.5553	0.7196	0.5237	0.5610	0.5868	0.6064	0.6520

TABLE 13.16

Results at Tip Section Using Free Vortex Method

Stage	1	2	3	4	5	6	7
α_1	0.3017	8.0837	9.3814	10.4300	10.6450	10.8290	10.6542
α_2	27.5295	32.6567	33.1656	33.3068	33.8570	34.3237	32.1321
β_1	67.0605	64.7190	63.6313	62.7436	62.1591	61.6569	61.3031
β_2	61.5658	58.2889	56.8135	55.7395	54.6639	53.7210	54.2055
α_3	8.5645	8.7875	8.8125	8.8196	8.8475	8.8716	0
Λ	0.8888	0.8267	0.8124	0.8021	0.7937	0.7863	0.7975

TABLE 13.17

Results at Hub Section Using Exponential Method

Stage	1	2	3	4	5	6	7
α_1	−9.4648	3.4821	6.3719	8.4192	9.0155	9.4839	9.7826
α_2	38.1211	39.5878	38.9146	38.2140	38.1791	38.1577	35.6433
β_1	53.7386	50.3613	50.8903	51.3491	52.1309	52.7709	53.3723
β_2	16.0130	17.6198	23.3691	27.7422	30.2142	32.1828	36.8703
α_3	9.0875	9.1807	9.1372	9.0932	9.0911	9.0897	0
Λ	0.6047	0.5099	0.5486	0.5780	0.5990	0.6154	0.6583

TABLE 13.18

Results at Tip Section Using Exponential Method

Stage	1	2	3	4	5	6	7
α_1	5.3419	14.3196	14.8613	15.2608	14.9480	14.6812	13.8377
α_2	33.1587	39.6580	39.1979	38.5404	38.4783	38.4300	35.4744
β_1	66.3833	64.1605	63.1053	62.2515	61.6808	61.1976	60.8916
β_2	62.0826	59.1892	57.4469	56.1676	54.9707	53.9351	54.2632
α_3	8.8122	9.1853	9.1553	9.1135	9.1096	9.1066	0
Λ	0.9012	0.8396	0.8223	0.8098	0.7998	0.7912	0.8011

TABLE 13.19

Results at Hub Section Using First Power Method

Stage	1	2	3	4	5	6	7
α_1	−16.2068	−4.1368	−0.0633	2.9039	4.1835	5.2170	6.2860
α_2	33.0091	33.6940	33.6545	33.5219	33.9764	34.3799	32.4509
β_1	56.5061	53.3604	53.2427	53.2377	53.6923	54.0817	54.3961
β_2	20.6067	22.4275	26.9203	30.4135	32.3290	33.8832	38.0480
α_3	8.8048	8.8391	8.8371	8.8304	8.8536	8.8746	0
Λ	0.6421	0.5415	0.5695	0.5926	0.6098	0.6235	0.6640

TABLE 13.20

Results at Tip Section Using First Power Method

Stage	1	2	3	4	5	6	7
α_1	12.1762	22.6717	21.8930	21.2576	20.1468	19.2322	*17.5194*
α_2	41.5821	50.2022	47.6596	45.5026	44.3990	43.5324	*39.4774*
β_1	65.7243	63.8804	62.7671	61.8879	61.2868	60.7944	*60.5044*
β_2	63.5145	61.8772	59.2382	57.3591	55.8235	54.5476	*54.5261*
α_3	9.3171	10.0627	9.8127	9.6217	9.5307	9.4622	*0*
Λ	0.9161	0.8546	0.8335	0.8184	0.8065	0.7966	*0.8051*

Tables 13.19 and 13.20 give the variation of the flow angles and degree of reaction at hub and tip using the first power method.

13.15.3 Details of Flow in Stage Number 2

The variations of the aerodynamic and thermodynamic properties from hub to tip of the flowing air through the fourth stage are calculated and plotted here:

1. Degree of reaction is illustrated by Figure 13.59.
2. Radial variation of air angles using free vortex for 6th stage.
3. Blade deflection angle ($\beta_1 - \beta_2$) is shown in Figure 13.61.
4. The absolute and relative velocities at inlet and outlet C_1, C_2, W_1, W_2 are shown in Figure 13.62.
5. The tangential and axial components of the absolute velocities are C_{u1}, C_{u2}, C_{a1}, C_{a2}, as shown in Figure 13.63.
6. Flow angles β_1, β_2, α_1, α_2 are shown in Figure 13.64.
7. Variation of inlet condition from hub to tip T_1, P_1, ρ_1 are given in Figure 13.65.

13.15.4 Number of Blades and Stresses of the Seven Stages

Table 13.21 gives the number of blades for the stator and rotor blade rows for all stages. Moreover, the maximum stress and the factor of safety for the rotors in each stage are given. It is assumed that the first three stages are made of titanium alloy while the remaining four are made of steel.

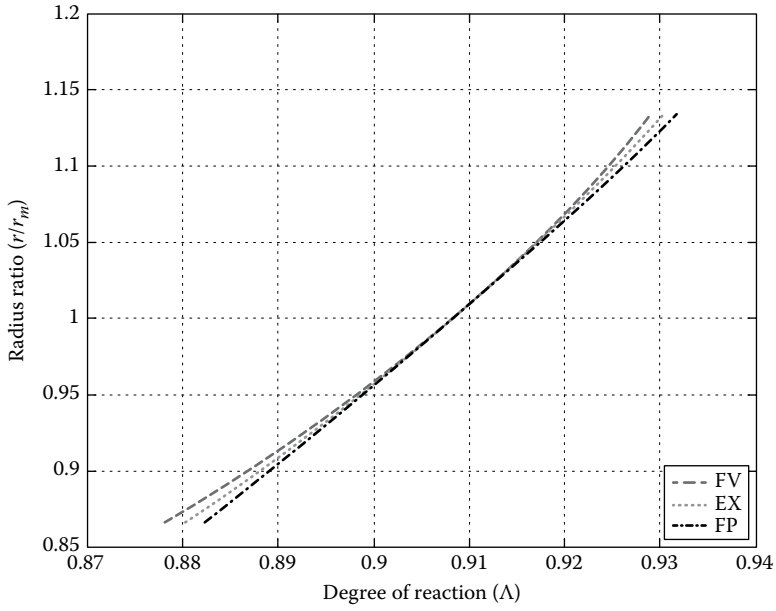


FIGURE 13.59
Variation of degree for reaction from hub to tip.

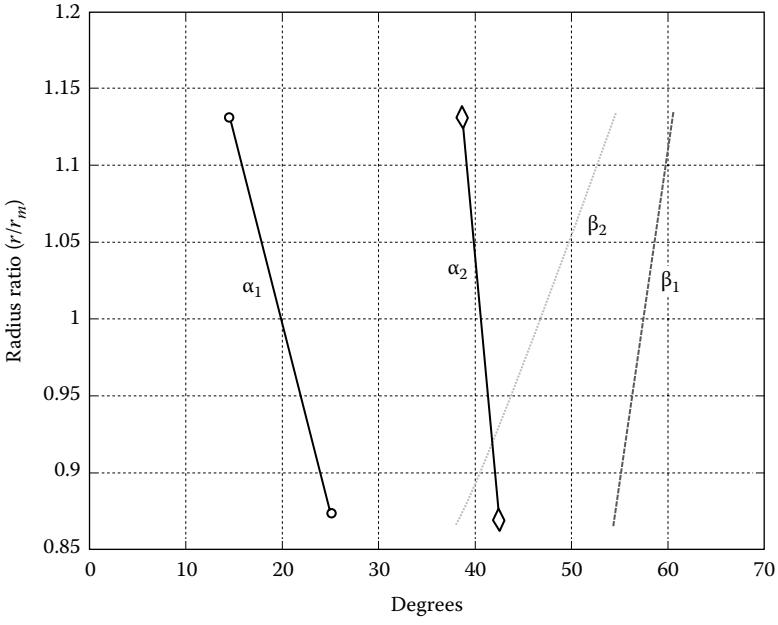


FIGURE 13.60
Variation of stage angles from hub to tip.

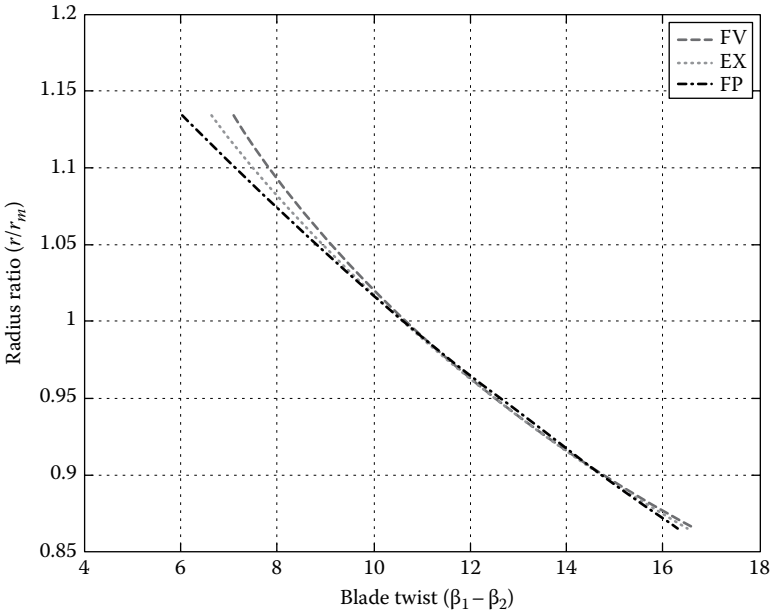


FIGURE 13.61
Variation of blade twist from hub to tip ($\beta_1 - \beta_2$).

13.15.5 Compressor Layout

A complete layout for the seven stages is drawn in Figure 13.66. The number of blades increases in the rearward direction while the blade height as well as their chord at root increases in the forward direction.

13.16 Erosion

As described in Chapter 12, the flowing air into gas turbine/aeroengines is frequently laden with solid particles such as sand, dust, fly ashes, ice, and volcanic ashes. These particles are ingested into the engine from outside. Due to their high inertia, they do not follow the carrier phase streamlines and tend to impact on the internal surfaces. In the case of aeroengines, sand particles are ingested into the core during all flight phases. However, the critical flight phases are takeoff and landing, when particles of different (but large diameter) sizes are sucked into the intakes. Moreover, the operation of thrust reversal leads to re-ingestion of the hot gases and debris during landing (Figure 13.67).

Particle–surface interactions lead to pitting and cutting of the blade's leading and trailing edges, increasing the tip clearance due to changes in the blade geometry, and increasing

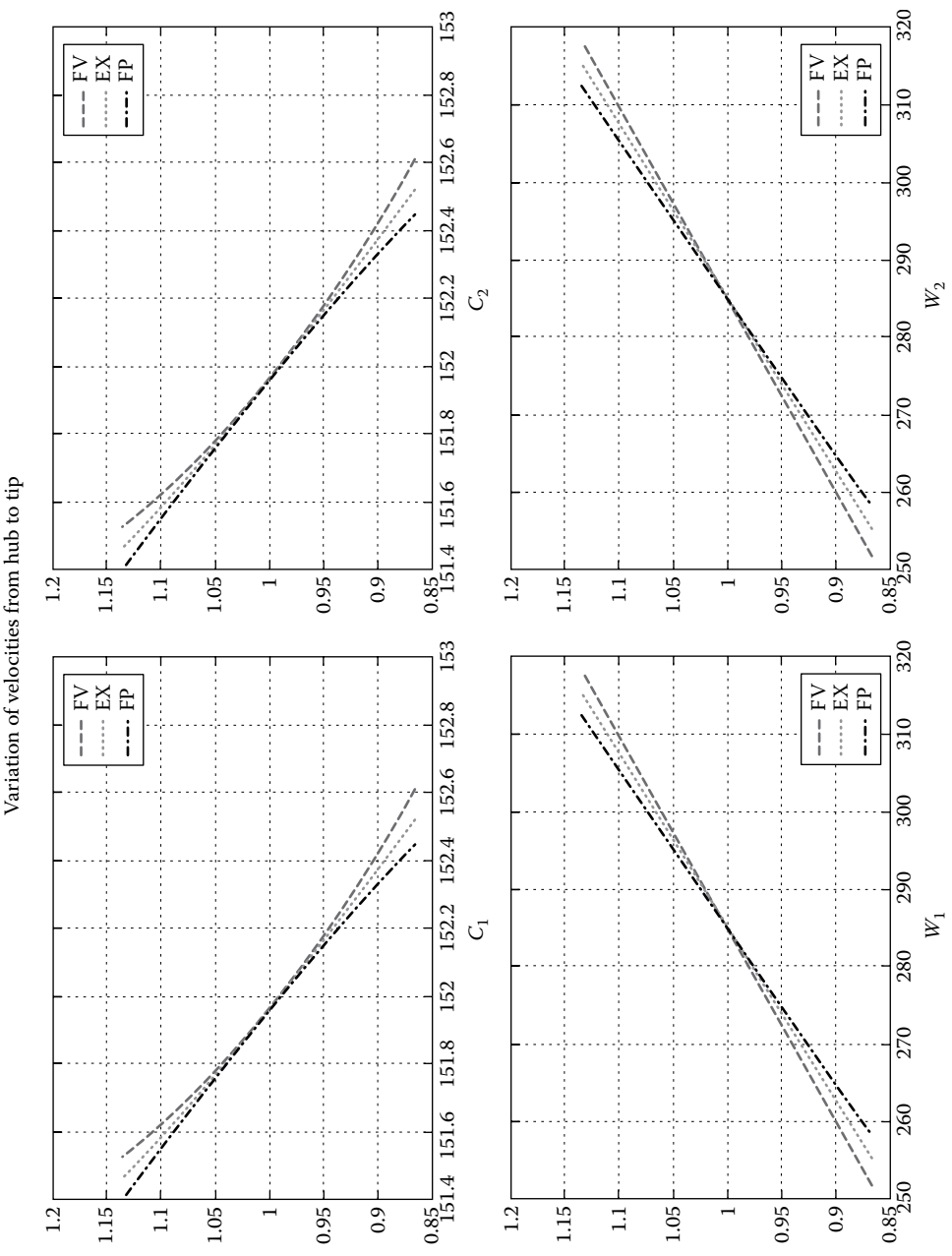


FIGURE 13.62
Variation of velocities from hub to tip C_1, C_2, W_1, W_2.

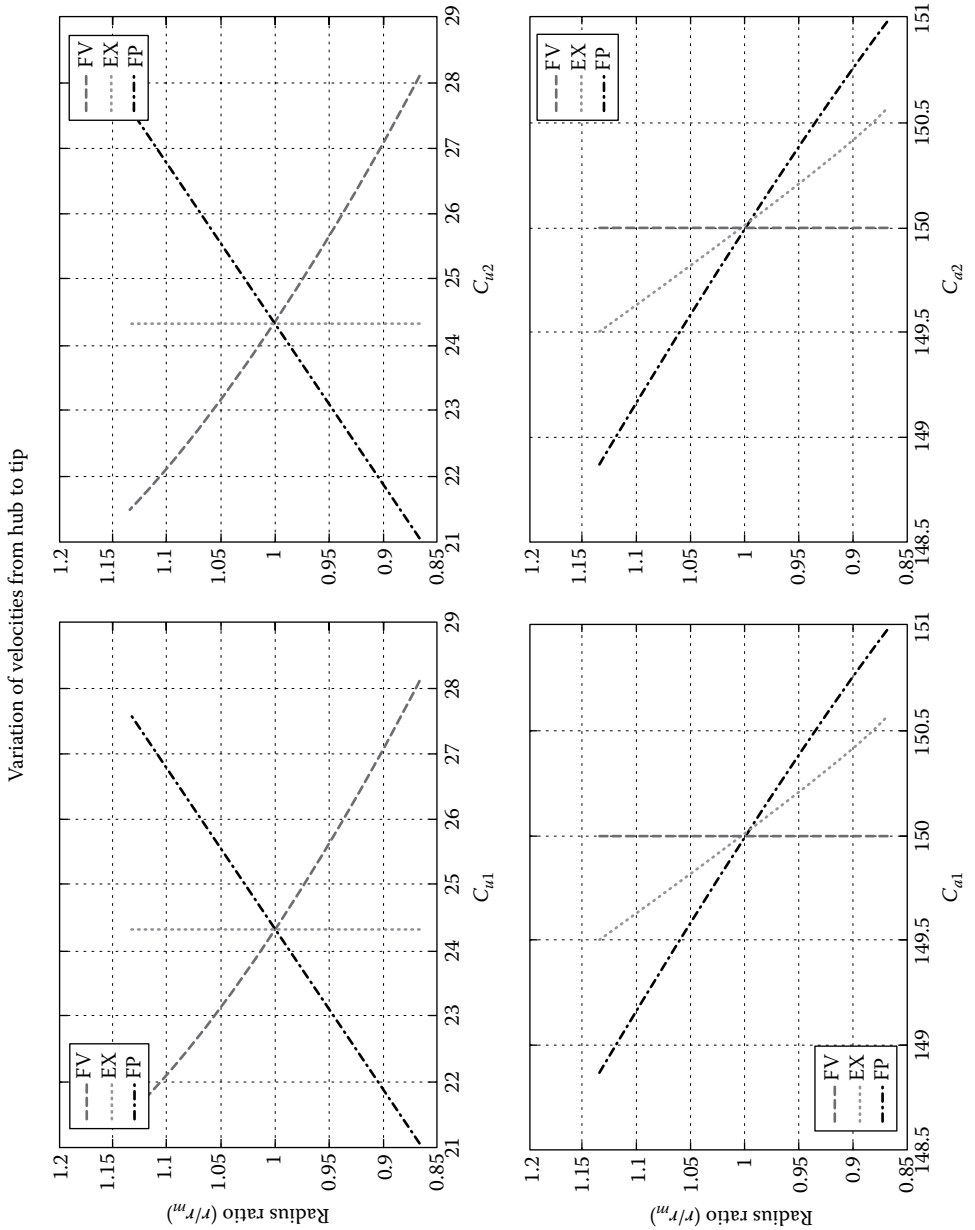


FIGURE 13.63
Variation of velocities from hub to tip (C_{u1}, C_{u2}, C_{a1}, C_{a2}).

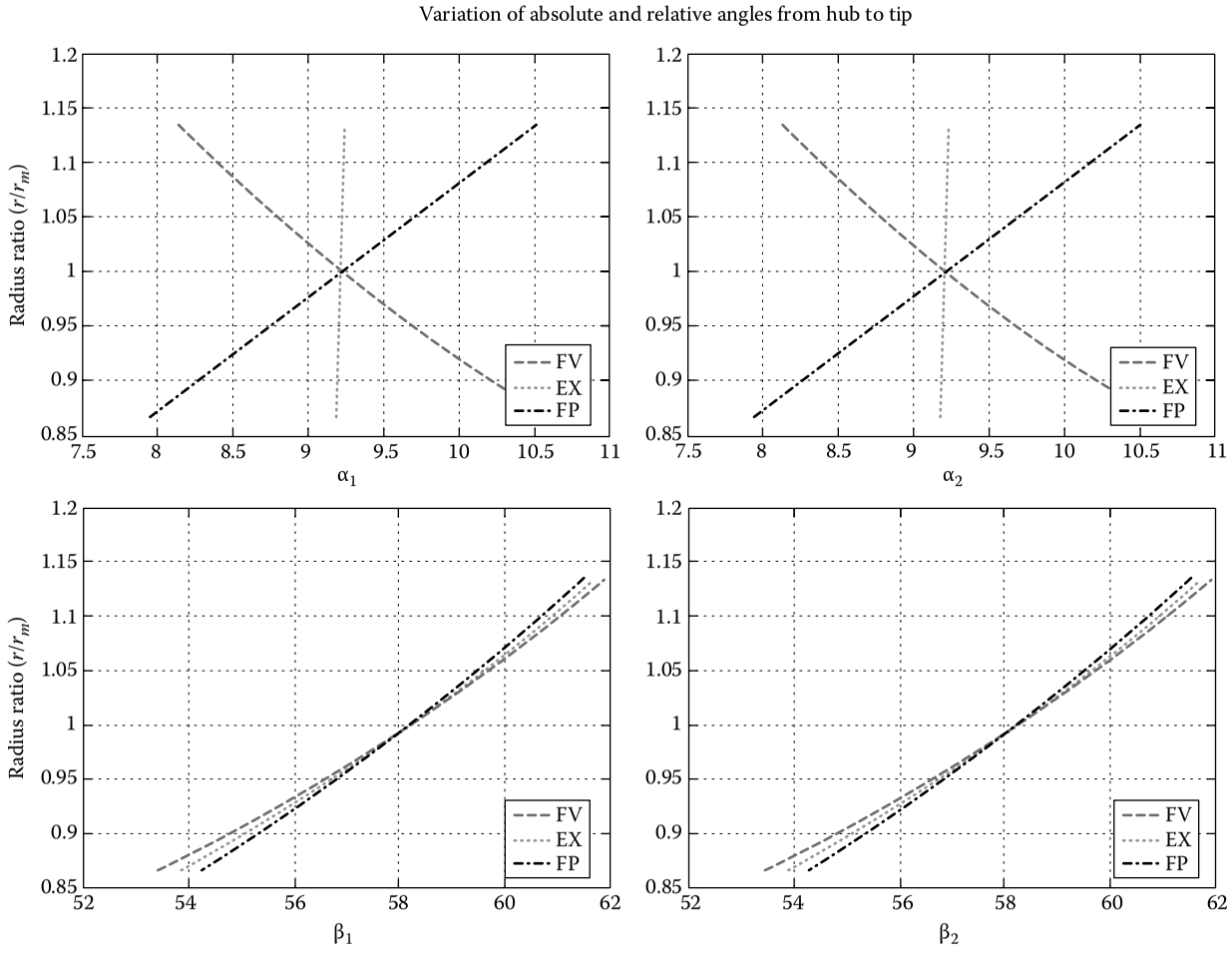


FIGURE 13.64
Variation of absolute and relative angles from hub to tip β_1, β_2, α_1, α_2.

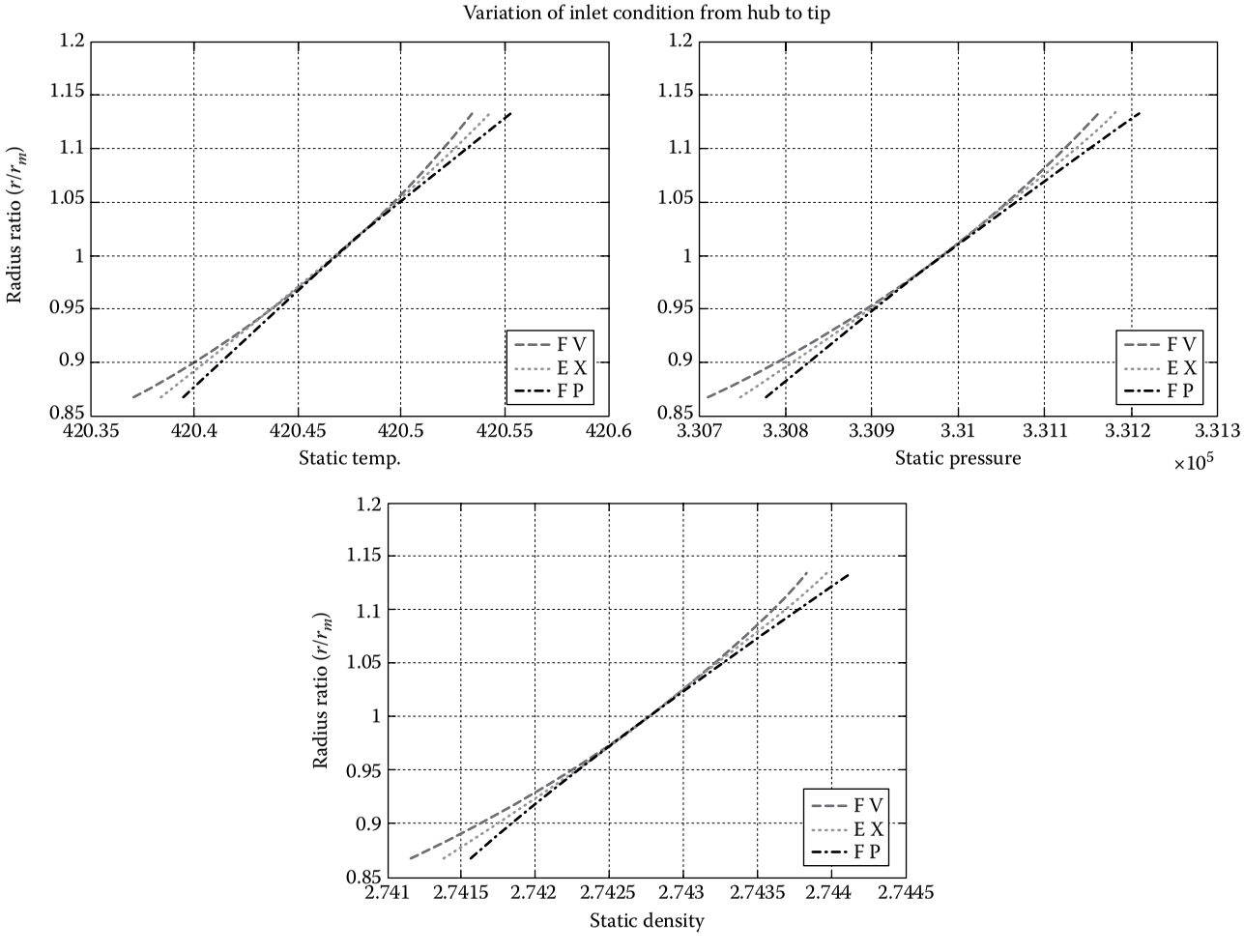


FIGURE 13.65
Variation of inlet condition from hub to tip T_1, P_1, ρ_1.

TABLE 13.21

Number of Blades and Maximum Stresses for the Rotors of the Seven Stages

Stage	1	2	3	4	5	6	7
No. of blade (rotor)	28	34	42	48	56	62	56
No. of blade (stator)	32	39	47	55	63	71	67
σ_{max} (MPa)	158.0	137.0	121.0	190.7	172.3	156.3	142.3
Material	Titanium	Titanium	Titanium	Steel	Steel	Steel	Steel
Factor of safety	4.8	5.5	6.29	2.62	2.90	3.2	3.52

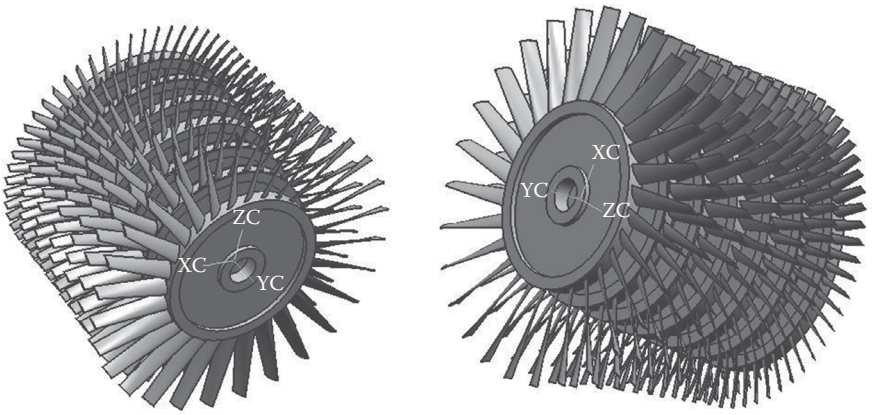


FIGURE 13.66
Three-dimensional illustration for seven-stage axial compressor.

the blade's surface roughness; see Figure 13.68. This will cause changes in the aerodynamic performance of the fan/compressor modules, which influences their stability, efficiency, and operating range and results in a progressive and rapid degradation of engine performance. The damage of the blades is caused mainly by direct material impingement of large particles, and even by recirculation of fine particles due to secondary flow through the blade passage [20]. Particles as small as 1–5 μm lead to severe erosion in axial flow turbomachinery [21] and [22].

Extensive studies by the Pratt and Whitney Aircraft Group proved that erosion was one of the four sources of JT9D engine performance deterioration [23]. This study was based on historical records and data obtained from five airlines covering the period from early 1973 through to December 31, 1976. Erosion of airfoils and outer air seals of compressors resulted in increased roughness and bluntness, loss of camber, loss of blade length, and increased operating clearances. Figure 13.69 shows the effect of flight cycles on the JT9D ninth stage HPC rotor erosion. The estimated performance losses due to erosion after 3500 flights were about 40% of the total losses.

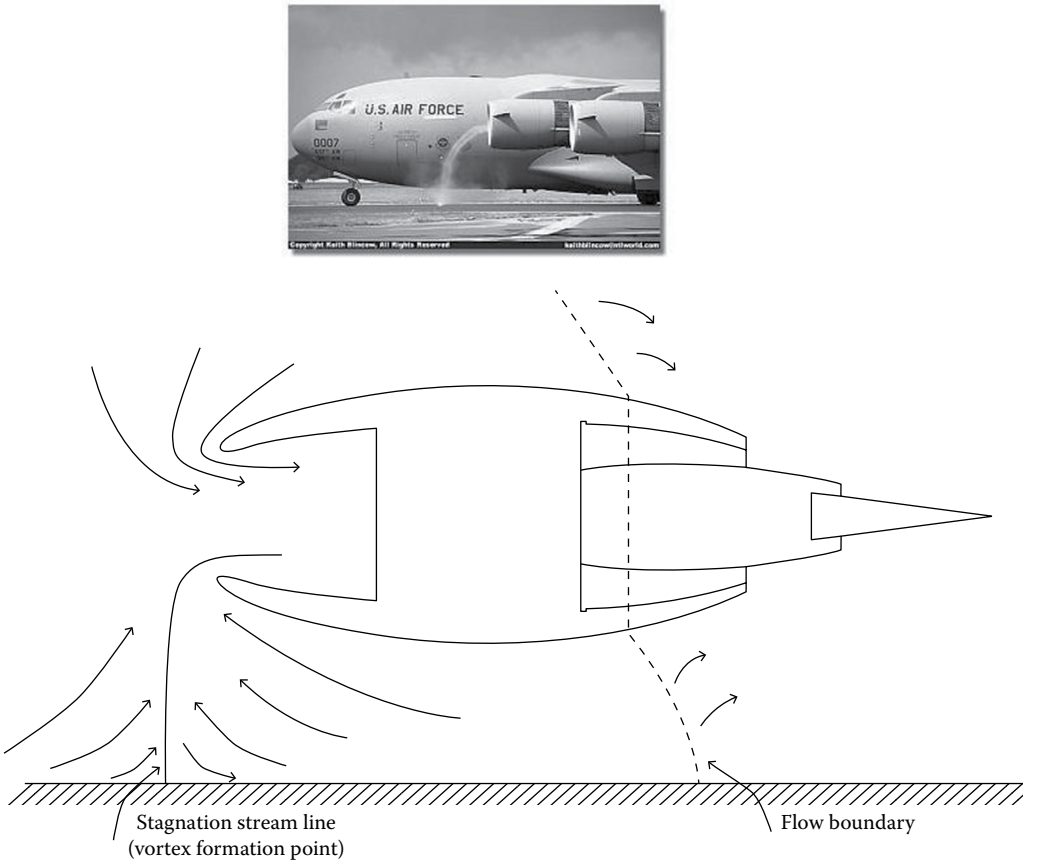


FIGURE 13.67
Particle ingestion during aircraft landing.

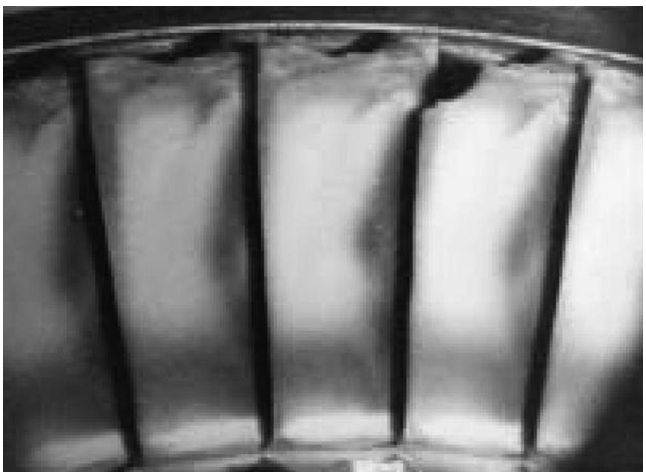


FIGURE 13.68
Erosion of axial compressor.

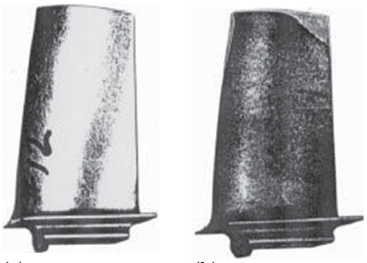


FIGURE 13.69
Erosion of ninth stage HPC of JT9D. (a) 800 h, 2000 cycles and (b) 8700 h, 5500 cycles.

The strong pressure gradient within the flow passages due to the turning of fluid within the rotor/stator blades affects the trajectories of particles and their impact locations [24]. As reported [25], within 6000–8000 h of jet engine operation, compressor blades had blunt leading edges with an increased surface roughness [25]. The inspection of a new CFM56 turbofan after particle ingestion on its high-pressure compressor showed similar effects [26].

Erosion of compressor blades reduces their efficiency. Moreover, the operating line becomes closer to the surge line.

The three-dimensional particle trajectory calculations through axial flow turbomachines were first reported in Reference 27. Later on, numerous studies were performed for predicting such trajectories through rotating and stationary turbomachinery blade rows, for example refer to [28]. These studies showed many particles impacting on the blade's leading edges, pressure sides, and trailing edges.

Experimental work was also performed by ingestion of 2.5 kg of sand to examine the effect of erosion on axial compressor performance. These measurements [29] showed that the blade's leading edge and the pressure side were severely eroded with an increase in surface roughness. As a result, the pressure distribution around the blade profile changed. This caused an early boundary layer transition. The blade suction surface remained unaffected for most of the experiments. These tests showed also that the loss in efficiency was related to erosion of the blade's leading edge and increased tip leakage. Stage performance deterioration is linearly related to the erosion rate, and there is an overall shift of the pressure coefficient and efficiency versus flow coefficient. The notable conclusions were a 3.5% deterioration of the in-stage loading coefficient and a 4% deterioration in efficiency.

Erosion of axial fans and compressors in aeroengines results in the blunting of their leading edges and a reduction of their chords. The aerodynamic performance of a transonic compressor rotor operating with variable chord length blades was examined in Reference 30. The test results indicated that both the surge margin and compressor efficiency were decreased by decreasing the blade chord.

A better analysis of erosion may be developed if the successive changes in blade geometry are continuously employed in the three steps of erosion previously described in Chapter 12. The study may be examined in stepwise time intervals. Thus, after a

certain time period, say 1000 h, the new shape of the blades is calculated and the gas flow, particle trajectories, and the resulting erosion rates may be calculated again and used as initial data for the next 1000 h time interval. This procedure was used to examine the erosion of turbomachines by dividing the 12,000 flight hours into four segments, each of 3000 h [31] and [32].

The erosion of an axial fan exposed to particulate flow [33] caused a loss in the fan performance due to tip clearance increase and a change in stalling incidence caused by alterations to the blade profile, particularly near the leading edge tip region.

The effect of erosion (due to particulate flow) on the performance of the axial transonic fan of a high bypass ratio turbofan engine (similar to GE-CF6) has been investigated [34]. The dynamic behavior of the ingested particles through the intake and fan have been investigated in both takeoff and cruise conditions. The effect of the particle size on its trajectory, impact location, and predicted erosion rate have also been examined. Moreover, a Rosin Rambler particle diameter distribution was assumed at takeoff and cruise conditions in order to simulate the problem in a more realistic manner. The mean particle radius during takeoff is 150 μm and during cruise is 15 μm. Table 13.22 shows the different parameters of the particles at both takeoff and cruise conditions.

In general, it is found that the deviation of the particle trajectories from the streamlines increases with increasing particle size. Consequently, large particle trajectories are greatly influenced by the centrifugal force and successively impact on the walls at high speeds and centrifuge faster after impacts. Small size particles are accelerated to high velocities and their trajectories are as close as possible to the gas streamlines. These particle trajectories define the impact locations on the intake casing, fan nose, blade pressure and suction sides, and the fan hub and casing.

The erosion rate of the fan blade during takeoff is shown in Figure 13.70. Along the blade span, the erosion rate is concentrated near both the trailing and leading edges of the pressure side and near the leading edge of the suction side. On the suction side, the upper half of the blade is exposed to an erosion rate ranging from 6.6×10^{-6} to 1.3×10^{-5} mg/g. Other regions on the suction side are less affected by erosion. On the pressure side, the region of maximum erosion rate appears at the corner of the blade between the tip and trailing edge. The value of the erosion rate reaches its maximum in this region, at about 3.34×10^{-5} mg/g. This is because it is exposed to a high frequency, high erosion parameter. Moreover, the

TABLE 13.22

Parameters of the Particles at Both Takeoff and Cruise Conditions

Particle Parameter	Takeoff	Cruise
Material	Sand	Fly ashes
Density (kg/m^3)	2650	600
Concentration (mass of particles per unit volume of the air, kg/m^3)	0.176×10^{-3}	0.176×10^{-4}
Particle mass flow rate (g/s)	97.5	8.83
Particle initial velocity (m/s)	128.6	133.5
Initial injection location	Intake inlet	Intake inlet

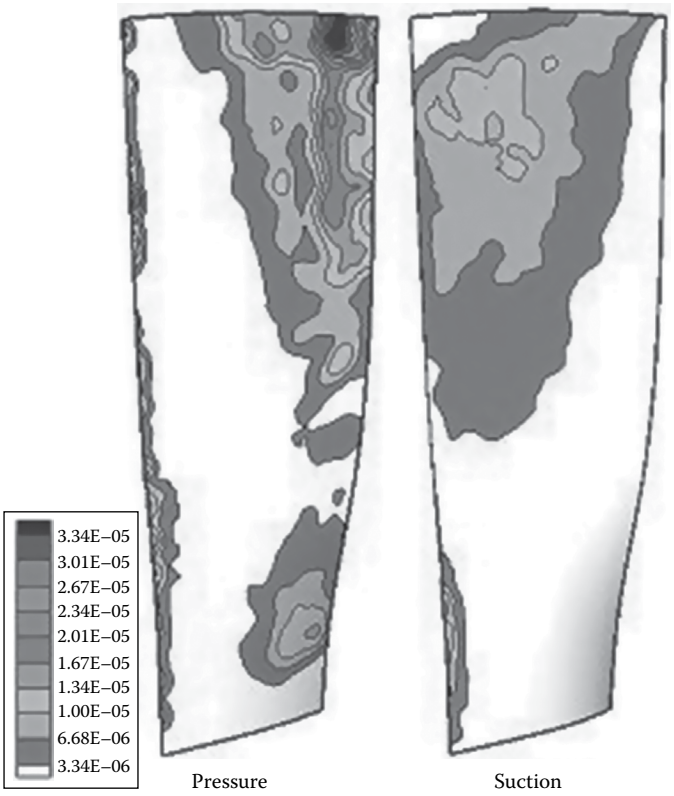


FIGURE 13.70
Erosion of axial fan during takeoff (mg/g).

region on the blade pressure side at about the upper third of the blade height and at about a 20% chord from the trailing edge shows increased erosion rates as well. Also, we can see that, near the leading edge of the pressure side, the erosion rate contours are condensed, indicating moderate values (about 10^{-5}) along the span.

The results of erosion during cruise conditions is shown in Figure 13.71. One can observe high erosion and penetration rate values at the pressure side's leading edge. The pressure side's trailing edge is exposed to moderate values of erosion and penetration rates. On the blade's suction side, the erosion and penetration rates are limited to the blade's leading edge at the upper half-span.

Figure 13.72 illustrates the real shape of eroded fan blades due to solid particle ingestion. A close similarity between the calculated and real erosion patterns. Figures 13.73 and 13.74 illustrate the damage in fan blades after exposure to different foreign objects. This is what is known as FOD. This abbreviation equally stands for foreign object damage or foreign object debris. These causes of FOD could be wildlife, soft objects, ice/hard objects as well as several unknown sources [35].

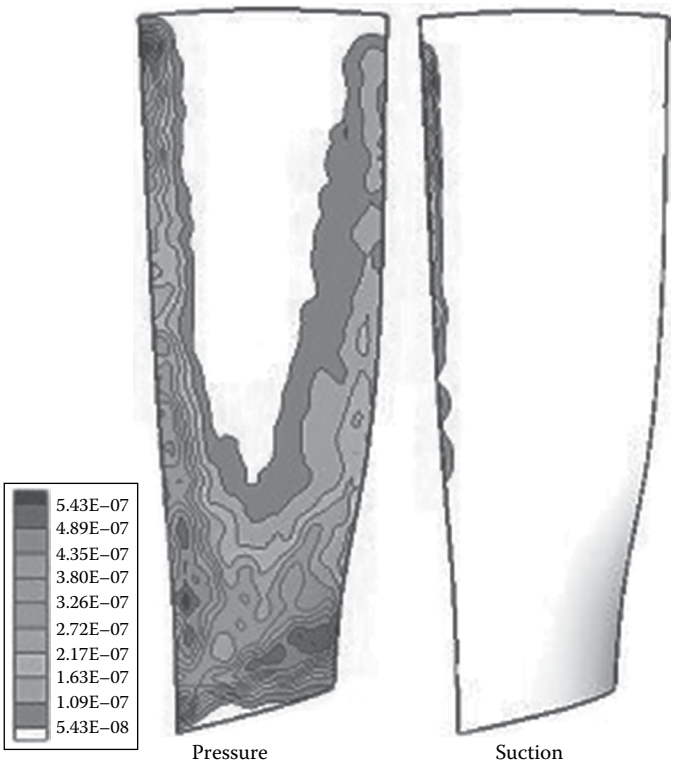


FIGURE 13.71
Erosion of axial fan during cruise (mg/g).



FIGURE 13.72
Erosion of the fan of a high bypass ratio turbofan engine.

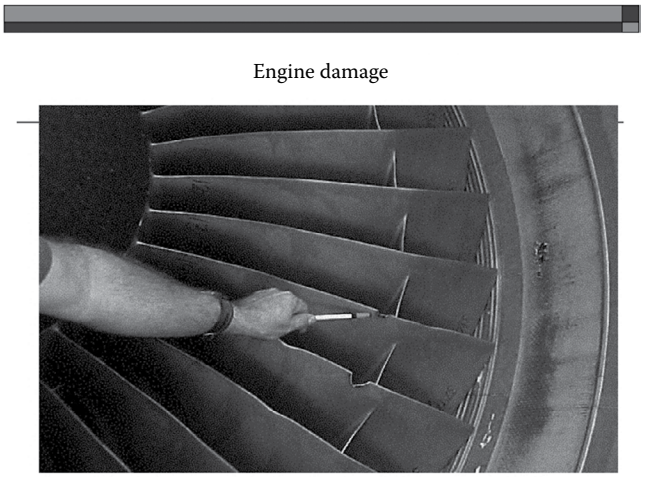


FIGURE 13.73
Foreign object damage of an axial fan of a turbofan engine.

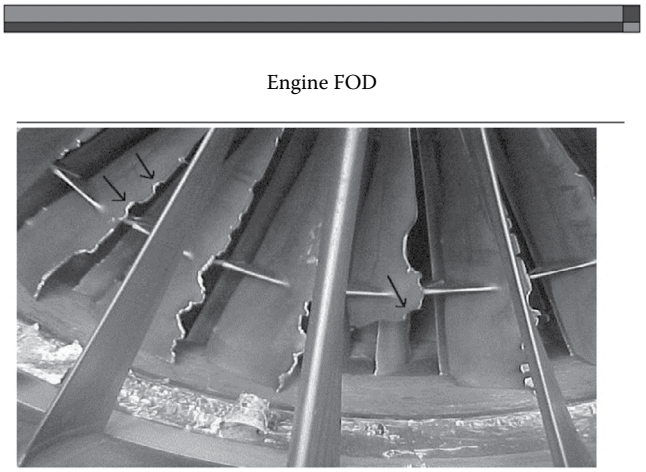


FIGURE 13.74
Excessive damage of an axial fan of a turbofan.

Problems

13.1 The power plant of a helicopter is a twin-spool turboshaft engine. The compression section is composed of an axial compressor followed by a centrifugal compressor. The expansion section is composed of the two axial turbines followed by a free power turbine. Compare between axial and centrifugal compressors.

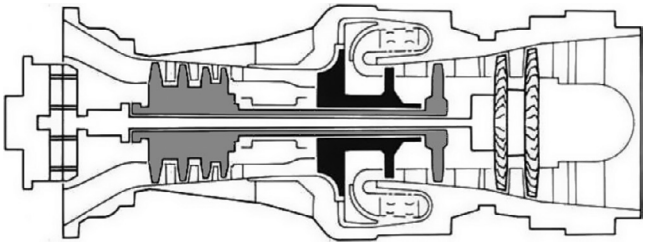


FIGURE P13.1
Turboshaft engine. (From Rolls-Royce plc, *The Jet Engine*, 5th edn., Derby, U.K., 1996.)

13.2

1. For a multistage axial flow compressor, if the pressure ratio in two successive stages $i-1$, i are equal (i.e., $\pi_{i-1}=\pi_i$), prove that the ratio between the total temperature rise in the two stages ΔT_i, ΔT_{i-1} is given by

$$\frac{\Delta T_i}{\Delta T_{i-1}}=\frac{\eta_{i-1}T_i}{\eta_i T_{i-1}}$$

   where η_i, η_{i-1} are the stages' efficiencies, respectively.
2. The following data refers to the rotor inlet of the first stage axial compressor

Axial velocity C_a	150 m/s
Mass flow rate	20 kg/s
Mean rotational speed U_m	267 rev/s
Mean radius	0.1697 m
Tip radius	0.2262 m
Outlet total temperature T_{03}	310 K
Outlet total pressure P_{03}	1.25 bar

$$C_{u2m}=77 \text{ m/s}, \quad a_{3m}=11^\circ$$

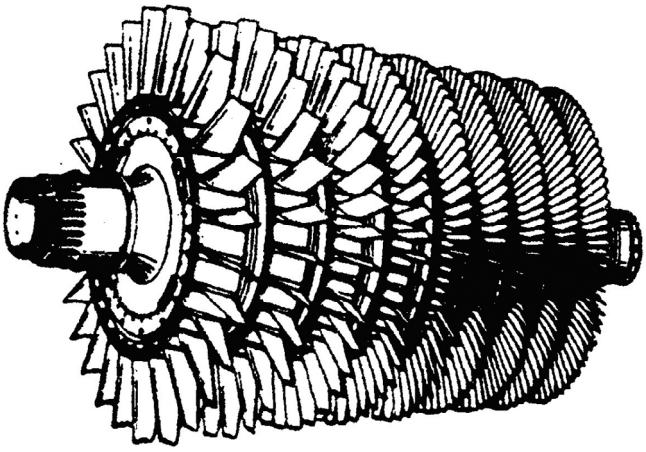


FIGURE P13.2B

Using the free vortex condition rc_u = constant, calculate

1. The angles β_1, α_2, β_2 and the degree of reaction Δ at the root, mean, and tip sections.
2. Draw the velocity triangles for the root, mean, and tip sections.
3. Draw the blade shape.

13.3 One of the intermediate stages of an axial compressor has the following characteristics:

Flow coefficient φ	0.5
Mean rotational speed U	250 m/s
Inlet flow angle α_1	30°
Rotor outlet angle β_1	35°

If these parameters are kept constant, plot the ideal relation $\psi - \varphi$.

Next, if the blade inlet angle is constant and equal to 50°, calculate the incidence angle.

Now, if negative and positive stalls occur when the incidence angles are (15°) and (−6°), respectively, calculate the corresponding values of C_a, ψ, and ΔT_{os}.

Draw the velocity triangles in the original and the two stall cases as well as the flow pattern around the airfoil.

Note that in all cases C_a and U are constants.

13.4

1. An axial flow compressor is made of AISI 1043 heat treated steel with yield strength S_y = 1520 MPa. Prove that for a constant blade cross-section from root to tip the maximum centrifugal tensile stress at the blade root is given by

$$\sigma_{\max} = \frac{\rho_b}{2} U_t^2 \left(1 - \zeta^2\right)$$

where
ρ_b is the blade material density (8160 kg/m^3)
U_t is the tip speed (350 m/s)
ζ is the hub-to-tip ratio (0.4)

Evaluate the factor of safety ($S_y/\sigma_{\max}$). If the blade is tapered with a linear variation of cross-sectional area, then

$$\sigma_{\max} = \frac{\rho_b}{2} U_t^2 \left(1 - \zeta^2\right) \text{ K}$$

where

$$k = 1 - \frac{(1-d)\left(2 - \zeta - \zeta^2\right)}{3\left(1 - \zeta^2\right)}$$

and where d is the ratio of the cross-sectional area at the tip to that at the root (d = 0.4). Calculate the new value for the factor of safety.

2. For supersonic compressors, draw figures to illustrate
   a. Velocity triangles for a high turning impulse cascade
   b. Velocity triangles for a low turning compressor cascade
   c. A wave pattern of shock–in-stator configuration

13.5 A multistage axial flow compressor has the following characteristics:

Inlet total temperature	T_{01}	288 K
Inlet total pressure	P_{01}	1 bar
Hub-to-tip ratio at inlet	ζ_{in}	0.5
Axial velocity	C_a	150 m/s
Overall pressure ratio	r_p	4.0
Compressor isentropic efficiency	η_c	0.9
Mass flow rate	m_o	20 kg/s
Tip speed	U_t	300 m/s

Assuming that the flow enters and leaves axially, calculate

a. The root and tip radii at the inlet
b. The geometry of the compressor at the outlet in the following three cases:
   i. Constant mean diameter for all stages
   ii. Constant tip diameter for all stages
   iii. Constant root diameter for all stages
c. The compressor rotational speed
d. The number of stages

13.6 The following table gives some data for the design parameters of the rotor in an axial flow compressor stage using free vortex blading.

Variable	**Root Section**	**Mean Section**	**Tip Section**
C_{u1} (m/s)	32	24	?
Cu_2 (m/s)	?	150	?
$R(r/r_m)$	?	?	?
U_1 (m/s)	?	?	?
U_2 (m/s)	?	?	?
Λ	?	?	?
C_{a1} (m/s)	109	?	?
C_{a2} (m/s)	?	?	?
ΔT_0 (K)	?	?	?
$U\Delta C_u$ (J/kg)	?	?	?
α_1 (°)	?	?	?
α_2 (°)	?	?	?
β_1 (°)	?	?	?
β_2 (°)	?	?	?
Cord (cm)	6.0	5.5	5.0

1. Complete the above table.
2. Draw the angles α_1, β_1, α_2, β_2 against the nondimensional radius (R).
3. Plot the degree of reaction (Λ) versus R.
4. Draw a plan view of the blade.

13.7 Centrifugal stresses on the rotor of an axial compressor depend on the rotational speed (ω). Prove that the maximum centrifugal stress that occurs in the root (for constant rotor cross-sectional area along the blade height) is given by

$$\sigma_{C_{\max}} = \rho_b U_1^2 \left(1 - \zeta^2\right)/2$$

Next, if the rotor cross-sectional area is inversely proportional to the radius (i.e., $A = \dfrac{\text{Constant}}{r}$), then

$$\sigma_{C_{\max}} = \rho_b U_1^2 \left(\frac{A_t}{A_r} - \zeta^2 \right)$$

where A_t, A_r are the root and tip blade cross-sectional areas.

13.8 For a three-dimensional design of an axial flow compressor stage, the first power method may be used where

$$C_{u_1} = aR - b/R$$

and

$$C_{u_2} = aR + b/R$$

Also

$$\zeta = 0.6$$

$$C_{a1m} = C_{a2m} = 150 \text{ m/s}$$

$$C_{u1m} = 60 \text{ m/s}, \quad C_{u2m} = 150 \text{ m/s}, \quad \text{Specific work} = 21.6 \text{ kJ/kg}$$

Calculate

1. ΔT, Λ_m, a, b
2. Λ_r, Λ_t
3. C_{a1}, C_{a2} at the root and tip
4. The angles α_1, α_2, β_1, and β_2 at the root, mean, and tip sections

13.9

1. For a supersonic axial flow compressor, draw the shock patterns and velocity triangles for both impulse and reaction stages.
2. Describe three methods for avoiding surge in axial compressors.
3. What are the types of drag in an axial compressor?
4. Define the design and off-design conditions of an axial compressor.
5. Explain three different methods for drawing the compressor map.

13.10 Prove that for an axial compressor stage the pressure ratio is

$$\frac{P_{03}}{P_{01}} = \left[1 + \eta_c \frac{M_u^2(\gamma - 1)}{1 + \frac{\gamma - 1}{2} M_1^2} \left\{1 - \frac{M_{a1}}{M_u}\left(\tan\alpha_1 + \frac{C_{a2}}{C_{a1}}\tan\beta_2\right)\right\}\right]^{\gamma/\gamma-1}$$

where

η_c is the compressor efficiency

$M_u = U/\sqrt{\gamma R T_1}$

$M_{a1} = C_{a1}/\sqrt{\gamma R T_1}$ and $C_{a1} \neq C_{a2}$

13.11 In a cascade testing of an axial compressor, the nearby figure illustrates the relation between the angle (ε^*) and the air outlet angle (α_2) for different (s/c) ratios. The rotor of an intermediate stage was designed using a *free vortex design*. The results for the root, mean, and tip sections are given in the following table.

	Root	Mean	Tip
β_1	400°	50.9°	60.6°
β_2	−10.0°	28°	55°

The number of rotor blades is 49.

Mean radius is 0.17 m.

Blade height is 0.08 m.

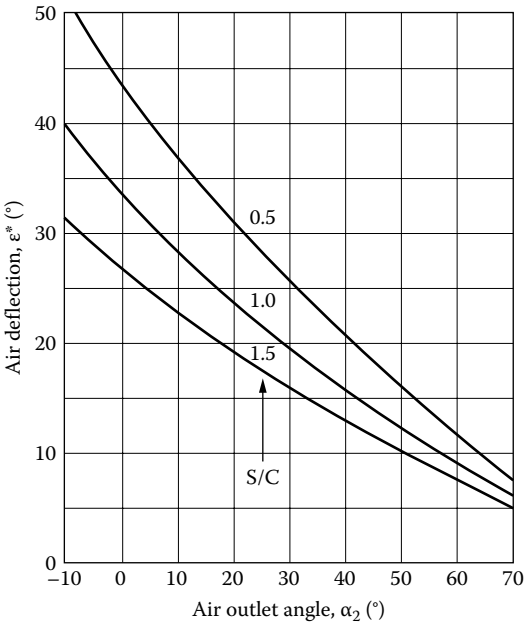


FIGURE P13.11

1. Draw the blade shape at the tip, mean, and root sections using an airfoil with

$$\left(\frac{t}{c}\right)_{\max} = 0.1$$

2. Draw a plan view of the blade by assembling the above sections, employing a stacking axis at the quarter of chord.

13.12 For the illustrated velocity triangles at the mean section of an axial flow compressor calculate Λ and ψ.

Draw the velocity triangles on a common base and with common apex configurations.

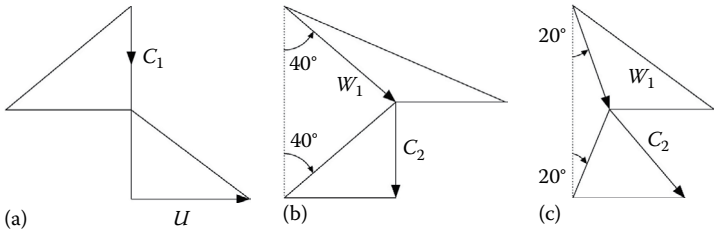


FIGURE P13.12

13.13 The degree of reaction at the mean section of an axial compressor stage is 0.5. The radial variation of the air flow from hub to tip is considered using the three methods of free vortex, exponential, and first power. The minimum degree of reaction is to be chosen as zero. The hub radius is 0.3 m. For the three design methods

1. Calculate
   a. Hub-to-tip ratio
   b. The tip radius
   c. Blade height
   d. Degree of reaction
   e. Nondimensional radius at tip (R_t)
2. Plot the relation between Λ and R

13.14

1. The maximum centrifugal stress occurs at the root of the blades of axial flow compressors. If the blade cross-sectional area is inversely proportional to the radius (r), prove that

$$\sigma_{c\max} = \rho_b U_t^2 \zeta (1-\zeta)$$

where
ρ_b is the blade's material density
U_t is the rotational speed at the blade tip
ζ is the hub-to-tip ratio

2. Define the degree of reaction of an axial compressor stage. Prove that
   a. If $C_1 \neq C_3$ and $Ca_1 \neq Ca_2$, then

$$\Delta = \frac{2U\left(C_{u2} - C_{u1}\right) - \left(C_2^2 - C_1^2\right)}{2U\left(C_{u2} - C_{u1}\right) - \left(C_3^2 - C_1^2\right)}$$

   b. If $C_{a1} = C_{a2}$ and $C_1 \neq C_3$, then

$$\Delta = \frac{\left(C_{u2} - C_{u1}\right)\left\{2U - \left(C_{u1} - C_{u2}\right)\right\}}{2U\left(C_{u2} - C_{u1}\right) - \left(C_3^2 - C_1^2\right)}$$

   What will be the value of the degree of reaction if $C_1 = C_3$ and $Ca_1 = Ca_2$?

13.15

1. Draw figures to illustrate shock-in-stator and shock-in-rotor for a supersonic axial compressor.
2. At a particular operating condition, an axial flow compressor has a degree of reaction of 60%, a flow coefficient of 0.5, and a stage loading of 0.35. If the flow exit angles of both the stator and rotor blade rows are assumed to remain unchanged when the mass flow is throttled, determine the degree of reaction and stage loading when the mass of air flow is reduced by 10%. Sketch the velocity triangles for the two cases and write your comments. If at a positive stall the angle $\beta_1 = 65°$ and at choking conditions $\beta_1 = 45°$, calculate the ratios of the mass flow in these two cases to the original mass flow rate (assume α_1 and β_2 are constants).

13.16

1. For the illustrated high-pressure compressor of the turbofan engine CFM56-5C
   a. How many stages are at the compressor?
   b. Compare between the rotor of the first and last stages.
   c. Plot the variation of the static temperature and pressure, the total temperature and pressure, and the absolute and relative velocities along the compressor stages.
2. Figure P13.16 shows one of the rotor blades of the high-pressure compressor of the CFM56-5C turbofan engine. It is manufactured from a titanium alloy. The concave side of the upper portion of the blade (extending from radius r_1 to r_1) is coated with tungsten carbide, which is an erosion resistant alloy. The average density of this blade portion is p while the inner portion of the blade (extending from hub to r_1) is ρ_2. The yield strength of the blade root is S_y. If the requested factor of safety is (FS),

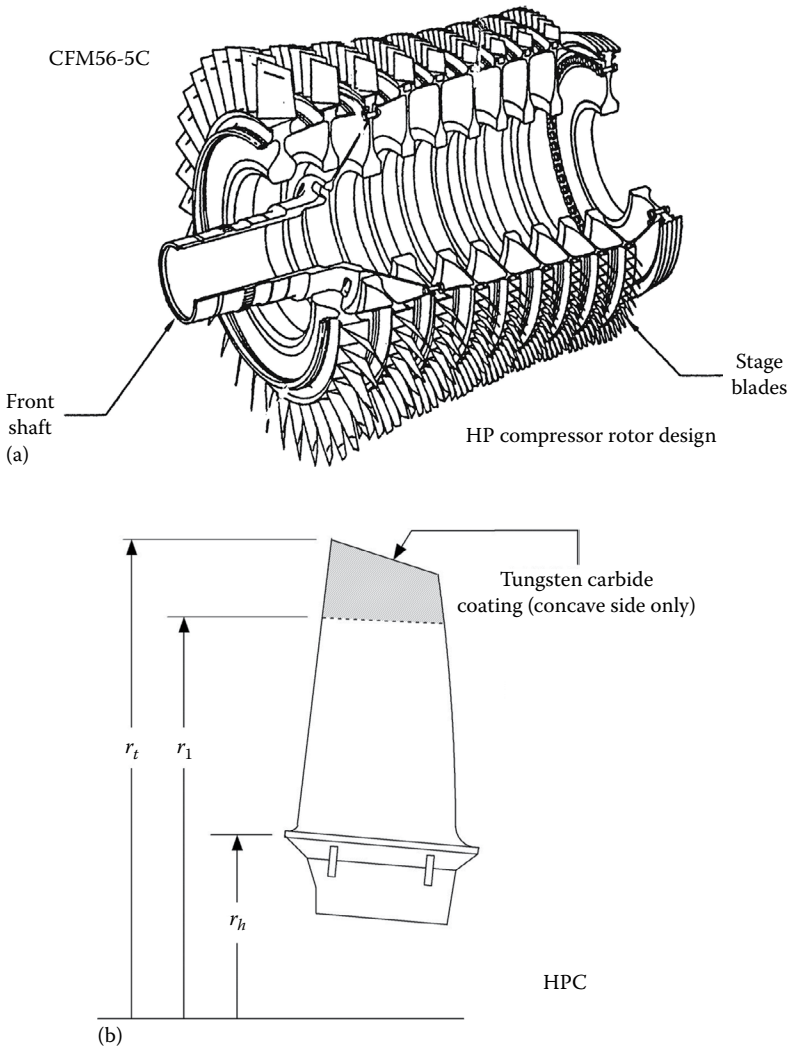


FIGURE P13.16

prove that for a constant blade cross-sectional area from hub to tip, the factor of safety, *FS*, is given by

$$FS = \frac{2S_y}{U_1^2\left[\left(\rho_2 - \rho_1\right)\zeta_1^2 + \rho_1 - \rho_2\zeta^2\right]}$$

where

U_1 is the tip rotational speed

$\zeta_1 = r_1/r_1$

$\zeta = r_h/r_1$

13.17

1. For a free vortex design, prove that

$$\Delta = 1 - \left(1 - \Delta_m\right) / R^2$$

2. The illustrated figures show C_{u1} versus R, where $R = r/r_m$
   If $C_{u1} = aR^n - b/R$ then identify the value of (n) for each case.
   Next, with $C_{u2} = aR^n + b/R$, plot the curves of C_{u2} on the same figures for different (n).
3. The velocity triangles at the inlet of an axial compressor stage at the hub, mean, and tip sections are shown. Other data for this stage are

$$U_h = 200\,\text{m/s}, \quad \zeta = 0.5, \quad \dot{m} = 20\ \text{kg/s}, \quad T_{01} = 290\,\text{K}, \quad P_{01} = 1.05\,\text{bar}$$

   a. Draw the velocity triangles at the outlet.
   b. Do these velocity triangles represent a free vortex design?

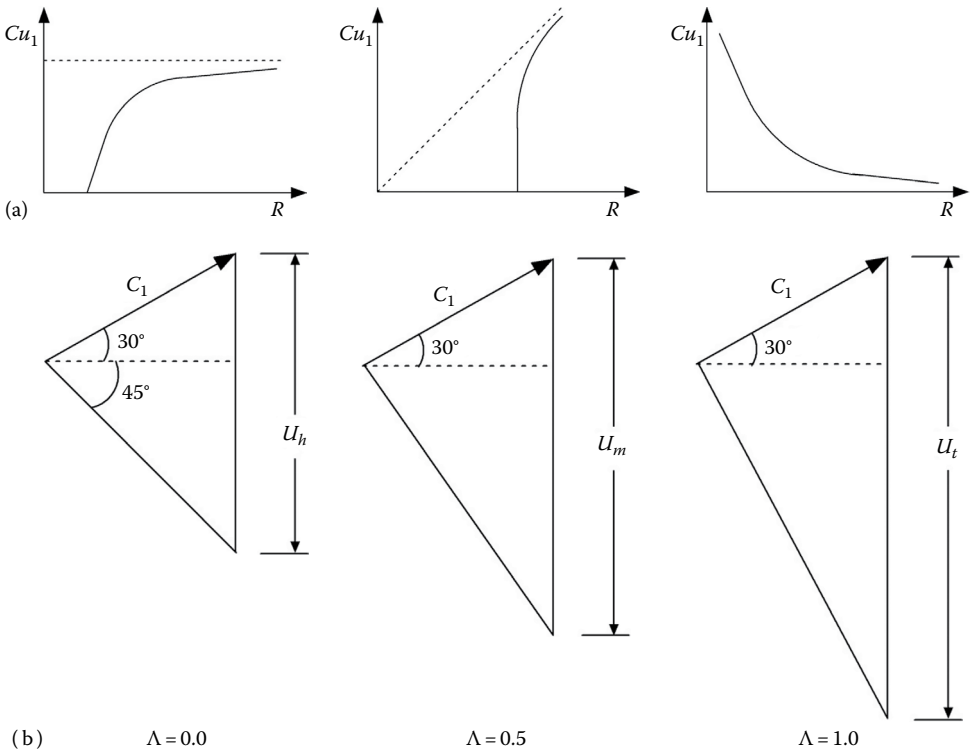


FIGURE P13.17

13.18 The three-dimensional behavior of an axial compressor stage is to be designed based on the exponential method.

The stage has the following data

$$Ca_{1_h} = 170 \text{ m/s}, \quad Ca_{2_h} = 170 \text{ m/s}, \quad R_h = 0.5, \quad \alpha_{1_h} = 6°, \quad U_h = 150 \text{ m/s}$$

1. Calculate the constants (a) and (b).
2. Do these constants vary from one design method to another?
3. Calculate the temperature rise in the stage.
4. Calculate the degree of reaction at the mean section.
5. Complete the following table using both the first power and exponential design methods.

	Exponential Method	First Power Method
Ca_{1h} (m/s)		
Ca_{2h} (m/s)		
Ca_{11} (m/s)		
Ca_{21} (m/s)		
Δ_h		
Δ_1		

13.19

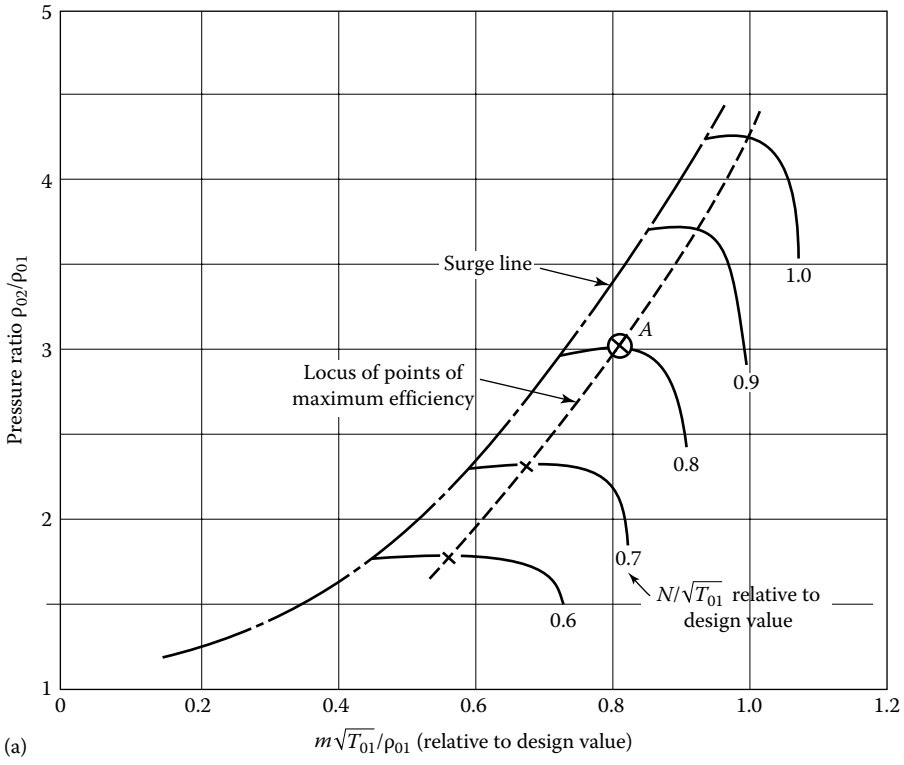
1. The illustrated figure shows a compressor map. The design point has the following values

$$\dot{m} = 50 \text{ kg/s}, \quad T_{01} = 288 \text{ K}, \quad P_{01} = 101.3 \text{ kPa}, \quad N = 6000 \text{ rpm}$$

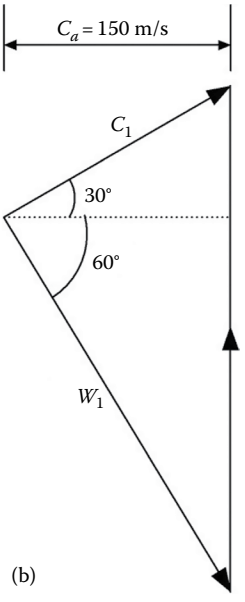
   a. Calculate the values of m, N at point (A), when
      i. The inlet total pressure and temperature are maintained at a constant
      ii. When the aircraft is flying at an altitude where T_{01} = 225 K and P_{01} = 15 kPa

   b. Calculate the inlet total pressure and temperature (T_{01}, P_{01} (if, relative to the design point, the parameter
   $N/\sqrt{To} = 0.9$ and $\dot{m}\sqrt{To}/P_{01} = 0.9$, and both N and m are equal to the design values.

2. The triangle (Figure P13.19b) shows the flow conditions at the inlet rotor of a stage of a multistage axial compressor. Calculate the following parameters α_2, β_2, W_2, C_2, the temperature rise per stage (ΔTo_s), and the pressure rise per stage (R_s) if the degree of reaction is zero, 0.5, and 1.0. Take the work done factor λ = 0.95 and the stage efficiency $\eta_s = 0.9$. Give a clear explanation for your answers.



(a)



(b)

FIGURE P13.19

13.20 The following data describes the characteristics of an axial compressor stage

$$W_s = 2.1\times10^4 \text{ m}^2/\text{s}^2 \quad C_a = 150 \text{ m/s}$$

$$U_m = 300 \text{ m/s} \quad \tau = 0.5$$

$$\Lambda_m = 0.5 \quad r_m = 0.1697 \text{ m}$$

1. Calculate the mean flow angles.
2. If $R_h = 2/3$, using the exponential method for blade design, calculate the parameters Ca_1, Ca_2, C_{u1}, C_{u2} and draw the velocity triangles at the root section.

13.21 The illustrated figure shows the civil transport Boeing 747 airplane powered by the turbofan engine CF6.

1. For an axial compressor define the symbols Φ and ψ.

   Prove that for the first stage (where $C_1 = C_{a1}$)

$$\tan\beta_1 = 1/\varphi,\ \tan\alpha_2 = \frac{\psi}{\varphi} \text{ and } \tan\beta_2 = (1-\psi)/\varphi$$

2. The engine CF6 is a two-spool engine. The low-pressure spool is composed of a fan and low-pressure compressor driven by the low-pressure turbine at speed N_1.

The fan has the following characteristics at takeoff

Rotational Speed	N_1	**3445 rpm**
Mass flow rate	$\dot{m}$	593 kg/s
Fan tip diameter		2.18 m
Fan hub-to-tip	(τ)	0.4
Ambient air temperature		15°
Ambient air density		1.225 kg/m^3
De Haller number at tip radius		0.95
De Haller number at mean radius		0.95

a. Define the portion of the fan blade subjected to supersonic flow.
b. Calculate the angles $\alpha_1, \beta_1, \alpha_2 \ldots$ and β_2 at the mean section. Use Figure P13.21c where $\Delta\theta°$ is the difference between the flow inlet and outlet angles and ω is the shock losses coefficient.

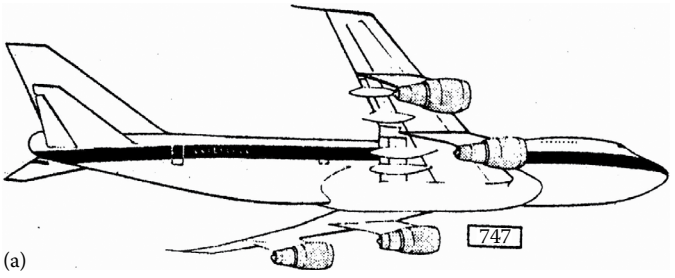


FIGURE P13.21a
Two-spool turbofan engine. (Courtesy of General Electric.)

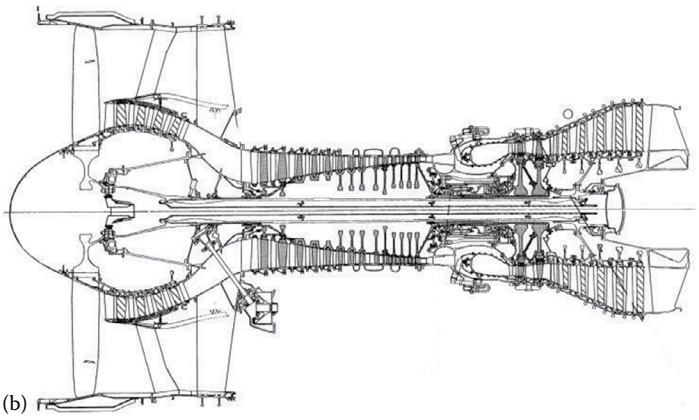


FIGURE P13.21b
High bypass ratio turbofan engine. (Courtesy of General Electric.)

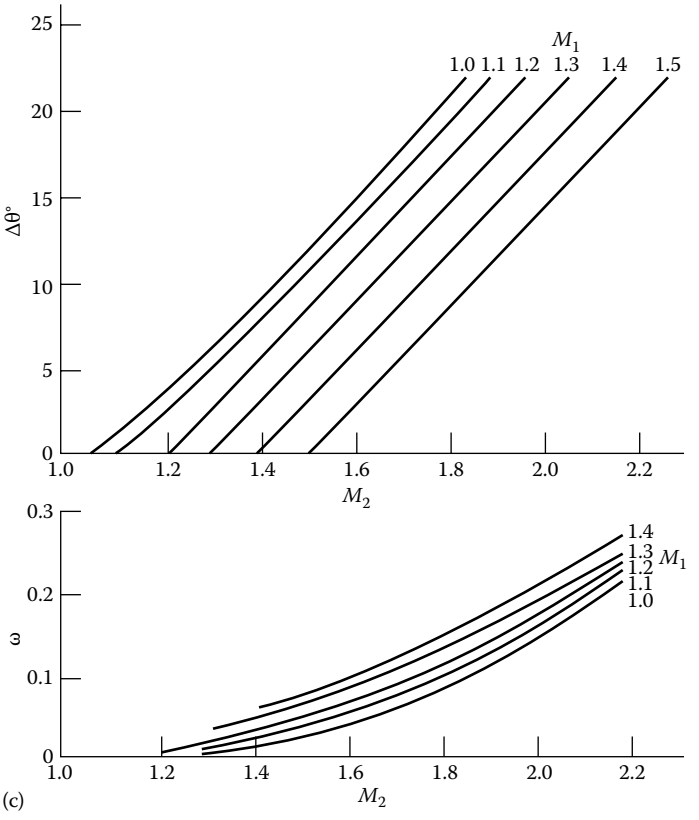


FIGURE P13.21c
Shock wave losses. (From Saravanumuttoo, H.I.H. et al., *Gas Turbine Theory*, 5th edn., Prentice Hall, Harlow, U.K., 2001, p. 191. With permission.)

13.22 The high-pressure axial compressor is composed of 14 stages. The first six stator stages have variable-angle vanes (see Figure P13.21c), where $\Delta\theta°$ is the difference between the flow inlet and outlet angles and ω is the shock losses coefficient. The last stage has the following data:

Axial velocity = 160 m/s		
Tip diameter	0.64 m	$\alpha_1 = 24°$
Speed N_2	8000 rpm	$\Omega_m = 0.50$
De Haller number at tip = 0.85		

1. Calculate the degree of reaction at the tip radius.
2. Calculate the hub-to-tip ratio (τ).
3. For a free vortex design, calculate and plot the values of α_1, α_2, β_1, β_2, and Ω at the hub, mean, and tip sections of the blade.
4. Describe two methods for improving the surge margin of axial compressors.

13.23 An axial compressor is composed of four stages and to be designed using the exponential blading method where

$$Cu_1 = a - \left(b/R\right) \quad \text{and} \quad Cu_2 = a + \left(b/R\right)$$

One of these stages has the following data:

	Ca_1 (m/s)	Ca_2 (m/s)	R_{Inlet}	R_{exit}
Root	168	186	0.754	0.79
Mean	150	150	1.0	1.0
Tip	132	116	1.246	1.21

$$r_{mean} = 0.4 \text{ m}, \quad \alpha_{1_{mean}} = \beta_{2_{mean}}, \quad \lambda = 0.88, \quad \eta_c = 0.92,$$
$$\text{inlet temperature to compressor} = 300 \text{ K}$$

ΔT_{0stage} = constant for the four stages.

1. Draw the velocity triangles for the hub, mean, and tip sections.
2. Prove that h_{02} = constant along the blade height.
3. Calculate the pressure ratio across the compressor.

13.24 Figure P13.24 illustrates a GE Honda (HF120 Turbofan engine) powering a very light jet.

The engine is a two-spool engine where the low-pressure spool is composed of an axial fan and a low-pressure compressor composed of two axial stages both driven by a single-stage low-pressure turbine. The high-pressure spool is composed of a single-stage high-pressure centrifugal compressor driven by a single-stage axial flow turbine. A reverse flow combustor is used to shorten the engine length. For flight at cruise altitude, the inlet total conditions to the fan are 238 K and 30 kPa.

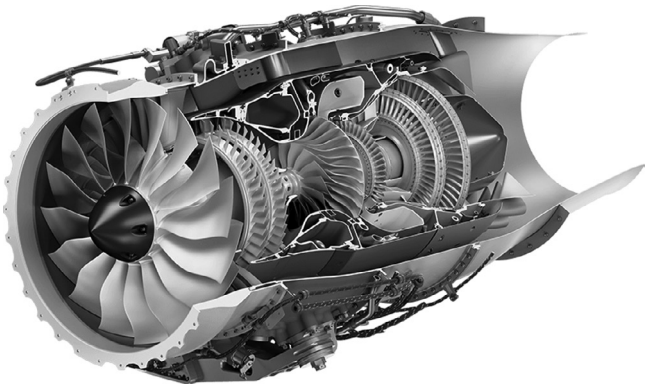


FIGURE P13.24
HF 120 Turbofan engine.

Pressure ratios and efficiencies for the different elements are as follows:

	Fan	First Stage of LPC	Second Stage of LPC	Centrifugal Compressor
Pressure ratio	2.5	1.4	1.37	5.0
Efficiency	0.86	0.87	0.87	0.85

Calculate the temperature rise in each of the above four elements.

13.25 Consider the axial fan in engine HF120 described in Problem 12.24.

It has the following peculiarities:

The axial fan has a hub-to-tip ratio $\zeta = 0.3$.

Axial speed $C_{a1} = 150$ m/s = constant in the radial direction.

Hub degree of reaction $\Lambda_h = 0.2$.

The flow is assumed to be axial along the blade height; thus $C_{u1} = 0$.

Assuming constant specific work along the blade height (Δh = constant), calculate $U_h, U_t, \beta_{1t}, \beta_{2t}, \alpha_{2t}, \Lambda_t$.

13.26 Consider the first stage of the low-pressure axial compressor in engine HF120 described in Problem 12.24. The following vortex energy equation is used for its aerodynamic design:

$$\frac{dh_0}{d_r} = C_a \frac{dC_a}{dr} + C_u \frac{dC_u}{dr} + \frac{C_u^2}{r}$$

1. If the inlet axial velocity is assumed to be constant, C_{a1} = constant, then using the above equation, prove that the swirl velocity is a free vortex, or

$$C_{u1} = \frac{A}{r}$$

2. Assuming the outlet swirl speed is expressed by the relation

$$C_{u2} = ar^2$$

prove (also using the above vortex energy equation) that the axial speed is expressed by the relation

$$C_{a2m}^2 - C_{a2}^2 = \frac{3a^2}{2}\left(r^4 - r_m^4\right)$$

The degree of reaction $\Lambda = 1 - \dfrac{A + ar^3}{2\omega r^2}$.

3. Draw figures to illustrate the variation from hub to tip of the following velocities:

$$C_{a1}, C_{a2}, C_{u1}, C_{u2}.$$

13.27 If the degree of reaction of an axial compressor is expressed by the relation

$$\Lambda = A + B\tan\alpha_1 + C\tan\alpha_2 + D\tan\beta_1 + E\tan\beta_2$$

find the values of the constants *A*, *B*, *C*, *D*, and *E*.

Next, if

$$C_a = 150 \text{ m/s}, \quad U = 300 \text{ m/s}, \quad \alpha_1 = -\alpha_2 = 45°,$$

find Λ, β_1, β_2.

13.28 The figure illustrates a V2500 Turbofan engine. The high-pressure compressor is a 10-stage axial compressor. Flow is axial at the inlet and has the following data:

$$T_{01} = 337 \text{ K}, \quad P_{01} = 179 \text{ kPa}, \quad r_m = 0.265 \text{ m}, \quad \eta_s = 0.92$$

The compressor has a constant mean radius. Other data for the first stage is

$$U_m = 280 \text{ m/s}, \quad C_{u2} = 160 \text{ m/s}, \quad C_a = 100 \text{ m/s}$$

If the stage pressure is expressed by the relation

$$\pi_s = \frac{k}{n} + 1.22$$

where
k is constant
n is the stage number

1. Calculate the pressure ratio of the first stage.
2. Calculate the value of the constant (*k*).
3. Calculate the pressure ratio of the second and third stages.
4. Draw velocity triangles for the mean section of the first stage.

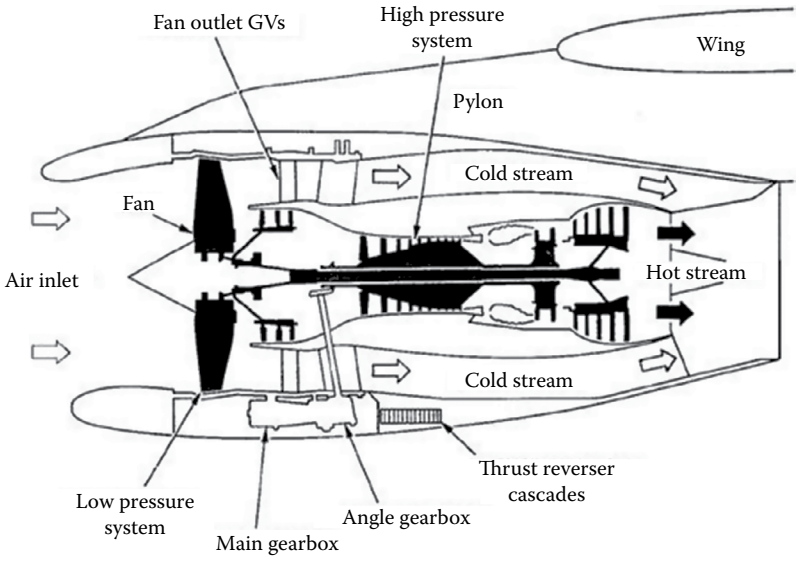


FIGURE P13.28
V2500 Turbofan engine.

13.29 Consider the axial compressor in Problem 13.28. If the hub-to-tip ratio of the first stage is $\zeta = 0.6$, and the variation of velocities from hub to tip is expressed by the free vortex equation $rC_u = \text{constant}$

1. Draw the velocity triangles at the hub and tip.
2. Sketch the blade shape of the first stage.
3. What are the disadvantages of free vortex blading?

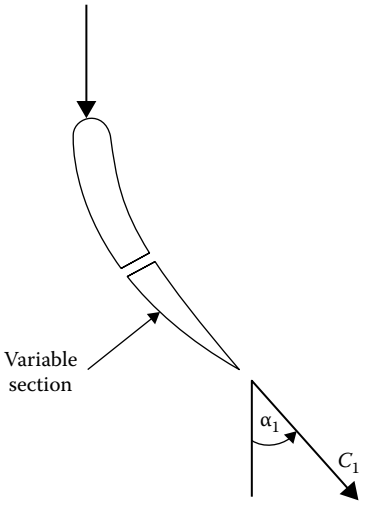


FIGURE P13.29
Variable inlet guide vanes.

4. For a surge control, variable inlet guide vanes are added upstream of the first stage to reduce the inlet relative angle, such that $\beta_1 \leq 60°$. Calculate the angle (α_1). (Use the results obtained in item 4 of Problem 2.28.)

13.30 Figure P13.30 illustrates a 10-stage axial compressor. The pressure ratio of each stage is given by the empirical relation

$$\pi_i = Ae^{-Bi}$$

where $A = 1.577$ and $B = 0.025$.

Stage efficiency is constant; $\eta_s = 90\%$. Inlet conditions are $P_{01} = 1.0$ bar, $T_{01} = 300$ K. Flow enters the compressor axially; $C_1 = C_{a1} = 200$ m/s. Axial velocity is constant for all stages. Other data are $\dot{m} = 80$ kg/s, hub-to-tip ratio of first stage (ζ) *first stage* = 0.5. The compressor has a constant tip diameter for all stages and $U_{tip} = 330$ m/s. The last stage has an inlet relative angle, $\beta_1 = 68°$.

1. Calculate the pressure ratio for each stage π_I, where $i = 1 \rightarrow 10$.
2. Calculate the total temperature rise for each stage $(\Delta T_0)_i$, where $i = 1 \rightarrow 10$.
3. Plot π_i versus stage number (i).
4. Plot $(\Delta T_0)i$ versus stage number (i).
5. Calculate the hub-to-tip ratio at the compressor outlet (note that $C_3 = 200$ m/s).
6. For the last stage, calculate the de Haller number and degree of reaction.
7. Using *free vortex blading*, calculate and draw velocity triangles at the tip and hub for the last stage rotor.

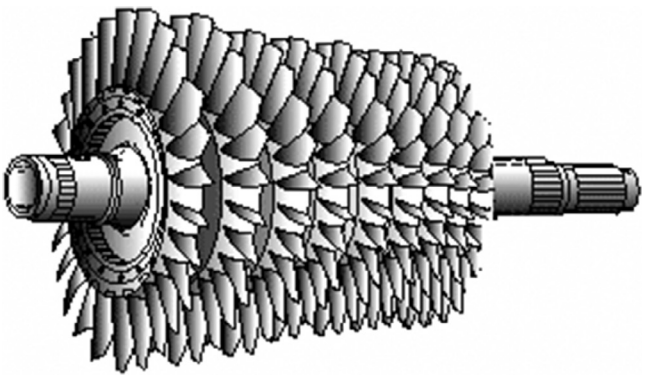


FIGURE P13.30
Multistage axial compressor.

13.31 Figure P13.31 illustrates the onset (starting) of stall in one blade-to-blade passage. Explain how surge is propagating from one passage to the other. Define the direction of rotation and the direction of stall progress.

13.32 For an axial compressor stage, the *ideal* relation between the stage loading (Ψ) and flow coefficient ($\phi = C_a/U$) is expressed by the relation

$$\Psi = 1 - \frac{C_a}{U}\left(\tan\alpha_1 + \tan\beta_2\right)$$

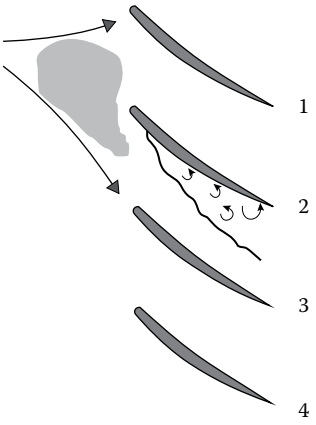


FIGURE P13.31
Stall of compressor.

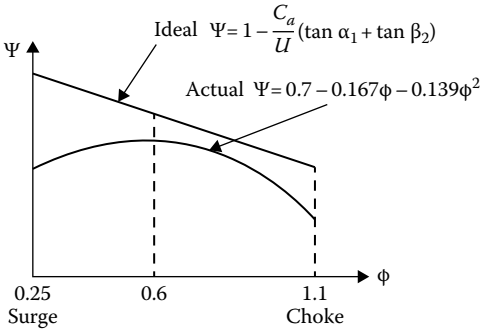


FIGURE P13.32
Ideal and real relation for stage loading vs flow coefficient.

while the *actual* relation is expressed as

$$\Psi = 0.7 - 0.167\phi - 0.139\phi^2$$

Both ideal and real cases are plotted in Figure P13.32. The design point is given by the following characteristics:

$$\phi = 0.6, \quad \Delta T_0 = 30 \text{ K}, \quad \Lambda = 0.5, \quad U = 220 \text{ m/s}, \quad P_{01} = 1.0 \text{ bar}$$

$$T_{01} = 288 \text{ K}, \quad \eta_{st} = 0.85, \quad \dot{m} = 15 \text{ kg/s}, \quad N = 10000 \text{ rpm}$$

Assume $C_1 = C_3$.

1. *For the actual case* ($\Psi = 0.7 - 0.167\phi - 0.139\phi^2$), calculate the blade loading Ψ and the temperature rise of the stage ΔT_0 at the design point ($\phi = 0.6$).
2. *For the ideal case* [$\Psi = 1 - C_a/U(\tan\alpha_1 + \tan\beta_2)$]

a. Calculate the flow angles α_1, β_1 and the blade loading Ψ at the design point ($\phi = 0.6$ and $\Delta T_0 = 30$ K).
b. At the surge point ($\phi = 0.25$) and for the same angles (α_1, β_1) calculated above, calculate the blade loading and the relative flow angle β_1. If the incidence angle in the design point $i = 1.52°$, calculate the incidence angle leading to stall.
c. Calculate the blade heights at the inlet and outlet of stage h_1, h_3.
d. At choking point ($\phi = 1.1$) and for the same angles (α_1, β_1) calculated in (a), calculate the maximum mass flow rate.

13.33 An axial compressor stage has the following data:

$$C_a = 150 \text{ m/s}, \quad U = 250 \text{ m/s}, \quad \eta_s = 0.89,$$

$$\alpha_1 = 20°, \quad \beta_2 = 30°, \quad T_{01} = 290 \text{ K}$$

Calculate the total temperature rise and pressure ratio of the stage.

Due to tip clearance between the rotor blades and casing, a tip leakage flow occurs as shown in Figure P13.33.

The axial velocity is decreased by 3%, while the angles α_1 and β_2 are kept constant.

1. Draw the velocity triangles in both cases.
2. Calculate the new total temperature rise of the stage.
3. If the pressure ratio of the stage is decreased by 3%, what is the new value of stage efficiency?
4. How can the effects of tip leakage flow be minimized?

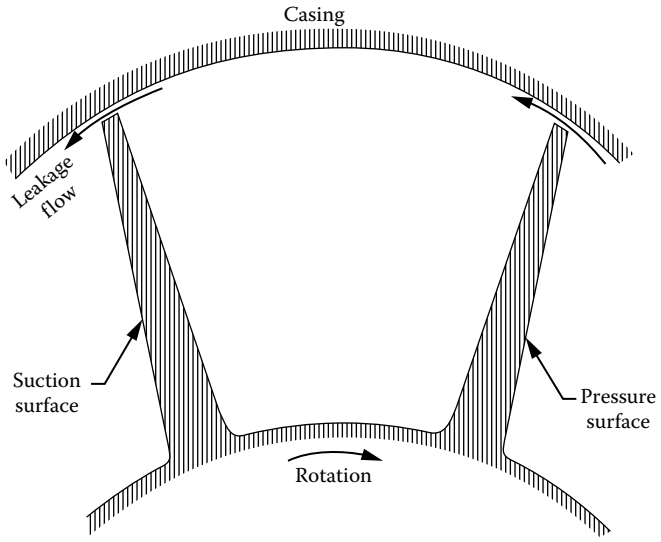


FIGURE P13.33
Fouled axial compressor.

13.34 Figure P13.34 illustrates a small turboshaft engine that may be used for air, land, and sea applications. It is composed of a compressor-turbine gas generator that is aerodynamically coupled to a free power turbine. The compressor is composed of a three-stage axial flow and a centrifugal single stage. The combustor is of the reversed type, which is followed by a single-stage axial turbine. The power turbine is a two-stage axial flow one.

The axial compressor has the following data:

$$T_{01} = 300 \text{ K}, \quad P_{01} = 1.1 \text{ bar}, \quad C_1 \equiv C_a = 150 \text{ m/s}$$

$$N = 18000 \text{ rpm}, \quad r_m = 0.15 \text{ m}, \quad \dot{m} = 10.0 \text{ kg/s}$$

All three stages have the following characteristics:

$$P_{02rel} = 0.95P_{01rel}, \quad P_{03} = 0.98P_{02}, \quad \alpha_1 = \alpha_3 = 0$$

$$\beta_2 = 35°, \quad \Delta T_{0stage} = \text{constant}, \quad \eta_{stage} = \text{constant}$$

1. Draw the compression process for a single stage on the T–S diagram.
2. Draw the velocity triangles for each stage.
3. Calculate the pressure ratio for each stage.
4. Using the exponential design method, calculate and draw the velocity triangles for the first stage using the below equations.

$$(C_{a1})^2 - (C_{a1m})^2 = 2\left[a^2 \ln R + \frac{ab}{R} - ab\right]$$

$$(C_{a2})^2 - (C_{a2m})^2 = 2\left[a^2 \ln R - \frac{ab}{R} + ab\right]$$

$$\Omega = 1 + \frac{a}{U_m} - \frac{2a}{U_m R}$$

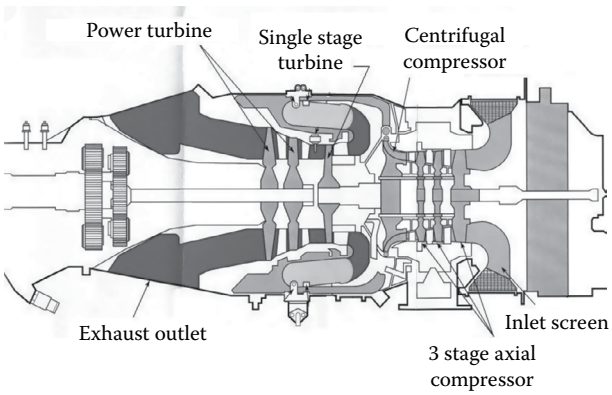


FIGURE P13.34
Turboshaft engine.

References

1. K. Steffens, Advanced compressor technology—Key success factor for competitiveness in modern aero engines, MTU Aero Engines Internal Report.
2. K. Hunecke, *Jet Engines, Fundamentals of Theory, Design and Operation*, 1st edn., Motor Books International Publishers & Wholesalers, Osceola, WI, 6th impression, 2003.
3. R.T.C. Harman, *Gas Turbine Engineering, Applications, Cycles and Characteristics*, John Wiley & Sons, New York, 1981, 78pp.
4. N.A. Cumpsty, *Compressor Aerodynamics*, Longman Scientific & Technical, Malabar, FL, 1989, 48pp.
5. H.I.H. Saravanamuttoo, G.F.C. Rogers, and H. Cohen, *Gas Turbine Theory*, 5th edn., Prentice Hall, Harlow, U.K., 2001, 191pp.
6. D.C. Wisler, *Advanced Compressor and Fan Systems*, GE Aircraft Engines, Cincinnati, OH, 1988, General Electric Co. USA, All Rights Reserved.
7. R.N. Brown, *Compressors-Selection and Sizing*, Gulf Publication Co., Oxford, U.K., 1981, 219pp.
8. A. Glassman (Ed.), *Turbine Design*, Vol. I, NASA SP-290, Washington, DC, 32pp, 1975.
9. S.L. Dixon, *Fluid Mechanics and Thermodynamics of Turbomachinery*, 4th edn., SI/Metric Units, Butterworth/Heinemann, Boston, MA, 1998, 144pp.
10. B. Lakshminarayana, *Fluid Dynamics and Heat transfer of Turbomachinery*, John Wiley & Sons, Inc., New York, 1996, 261pp.
11. H. Mars, *A Computer Program for the Through Flow Fluid Mechanics in an Arbitrary Turbomachine Using a Matrix Method*, H.M.S.O., London, U.K., British ARC R&M 3509.
12. I.A. Johnsen and R.O. Bullock (Eds.), *Aerodynamic Design of Axial Flow Compressors*, NASA SP-36, Washington, DC, 1965.
13. G.K. Serovy, Axial flow compressor aerodynamics, In G.C. Oates, Ed., *Aerothermodynamics of Aircraft Engine Components*, 1985.
14. A. Wennerstrom, *Low Aspect Ratio Axial Flow Compressors, Why and What It Means*, SAE SP 683, Warrendale, PA, 1986.
15. J.H. Horlock, *Axial Flow Compressors, Fluid Mechanics and Thermodynamics*, Krieger Publishing Co., Melbourne, FL, 1973, 164pp.
16. D.E. Hobbs and H.D. Weingold, Development of controlled diffusion airfoils for multistage compressor applications, *ASME Journal of Engineering for Gas Turbines and Power*, 106, 271, 1984.
17. I.J. Day, Stall and surge in axial flow compressors, VKI Lecture Series 1992-02, January 1992.
18. J.L. Kerreebrock, *Aircraft Engines and Gas Turbines*, 2nd edn., The MIT Press, Cambridge, MA, 1992, p. 264.
19. United Technologies Pratt Whitney, *The Aircraft Gas Turbine Engine and Its Operation*, P&W Operation Instruction 200, East Hartford, CT, 1988, pp. 3–81.
20. J.H. Neilson and A. Gilchrist, Erosion by a stream of solid particles, *Wear*, 11, 112–122, 1968.
21. A.F. El-Sayed, R. Lasser, and W.T. Rouleau, Three dimensional viscous particulate flow in a typical turboexpander, *International Journal of Energy Systems*, 5(2), 146–154, 1985.
22. A.F. El-Sayed, R. Lasser, and W.T. Rouleau, Effect of secondary flow on particle motion and erosion in a stationary cascade, *International Journal of Heat and Fluid Flow*, 7(2), 146–154, June 1986.
23. G.P. Sallee, *Performance Deterioration Based On Existing (Historical) Data: JT9D Jet Engine Diagnostics Program*, United Technologies Corporation, Pratt & Whitney Aircraft Group Commercial Products Division, NASA CR-135448, PWA-5512-21, Washington, DC, 1978.
24. D. Japikse, Review—Progress in numerical turbo-machinery analysis, *ASME Journal of Fluids Engineering*, 98, 592–606, 1976.
25. R.H. Wulf, W.H. Kramer, and J.E. Paas, *CF6-6D Jet Engine Performance Deterioration*, NASA/CR-159786, Washington, DC, 1980.

26. R.C. Peterson, Design features for performance retention in the CFM56 engine, Turbo-machinery Performance Deterioration FED: Vol. 37 the AIAA/ASME 4th Joint Fluid Mechanics Plasma Dynamics and Lasers Conference, Atlanta, GA.
27. M.F. Hussein and W. Tabakoff, Dynamic behavior of solid particles suspended by polluted flow in a turbine stage, *Journal of Aircraft*, 10(7), 334–340, 1973.
28. M.F. Hussein and W. Tabakoff, Computation and plotting of solid particle flow in rotating cascades, *Computers and Fluids*, 2, 1974.
29. W. Tabakoff and C. Balan, *Effect of Sand Erosion on the Performance Deterioration of a Single Stage Axial Flow Compressor*, AIAA, 1983, pp. 83–7053.
30. W.B. Roberts, A. Armin, G. Kassaseya, K.L. Suder, S.A. Thorp, and A.J. Strazisar, The effect of variable chord length on transonic axial rotor performance, *Journal of Turbomachinery*, 124, July 2002.
31. A.F. El-Sayed and A. Brown, Computer prediction of erosion damage in gas turbine, ASME Paper 87-GT-127, *32nd ASME International Gas Turbine Conference*, Anaheim, CA, 1987.
32. A.F.A.A. El-Sayed and A. Hegazy, An iterative procedure for estimating the effect of erosion on turbine blades life, Paper 95-YOKOHAMA-IGTC-58, 1995 Yokohama International Gas Turbine Congress, October 22–27, 1995.
33. A. Ghenaiet, R.L. Elder, and S.C. Tan, *Particles Trajectories through an Axial Fan and Performance Degradation due to Sand Ingestion*, ASME TURBO EXPO, June 2001.
34. H.H. Zoheir, Solid particulate flow in an axial transonic fan in a high bypass ratio turbofan engine, MSc thesis, Mechanical Power Engineering Department, Zagazig University, Zagazig, Egypt, 2006.
35. G. Chaplin et al., *Make it FOD Free- the Ultimate FOD Prevention Program Manual*, FOD, The FOD Corporation, 2004.
36. Rolls-Royce plc, *The Jet Engine*, 5th edn., Derby, U.K., 1996.


Taylor & Francis
Taylor & Francis Group
http://taylorandfrancis.com

14

Axial Turbines

14.1 Introduction

Turbines may be defined as turbomachines that extract energy from the fluid and convert it into mechanical/electrical energy. A classification of turbines is shown in Figure 14.1. Turbines may be classified based on whether the surrounding fluid is extended or enclosed. An example of an extended fluid turbine is a *wind turbine*, which may be a horizontal axis wind turbine or a vertical axis wind turbine. Enclosed turbines may be classified based on whether the working fluid is either incompressible or compressible. Hydraulic turbines (mostly *water turbines*) deal with incompressible fluids. Compressible turbines may deal with either steam or gas. Gas turbines may operate as subsonic or supersonic turbines. Turbines may also be classified based on whether the gas flow direction within its passage is axial, radial, or mixed. In axial turbines, the flow moves parallel to the axis of rotation. In radial turbines, the gas moves perpendicular to the axis of rotation. In mixed-flow turbines, the gases have a combined radial and axial motion. Another classification is related to the role of the turbine rotor in extracting power from the gas flowing through its passages; thus, there may be either impulse or reaction turbines. In reaction turbines, both stator and rotor share power extraction from the gas, while in impulse types, stator only do the job.

Historically, water turbines were built first, followed by *steam turbines* and finally *gas turbines*. A water, or hydraulic, turbine is used to drive electric generators in hydroelectric power stations. The first such station was built in Wisconsin in 1882. The three most common types of hydraulic turbine are the Pelton wheel, the Francis turbine, and the Kaplan turbine.

Toward the end of the nineteenth century, two engineers—Charles A. Parsons of Great Britain and Carl G. P. de Laval of Sweden—were pioneers in the building of steam turbines. Continual improvements of their basic machines have caused steam turbines to become the principal power sources used to drive most large electric generators and the propellers of most large ships. Most steam turbines are multistage engines. At the inlet of the turbine, high-pressure steam enters from a boiler and moves through the turbine parallel to the shaft, first striking a row of stationary vanes that directs the steam against the first bladed disk at an optimum speed and angle. The steam then passes through the remaining stages, forcing the disks and the shaft to rotate. At the last end of the turbine, the shaft sticks out and can be attached to machinery.

The gas turbine is a relative newcomer. The term "gas turbine" refers to a turbine in which the hot gases released from the combustion system are the working fluid. Axial turbines are handled in this chapter, while radial turbines will be analyzed in the next chapter. Virtually all turbines in aircraft engines are of the axial type, regardless of the type of compressor used. An axial turbine is similar to an axial compressor operating in reverse.

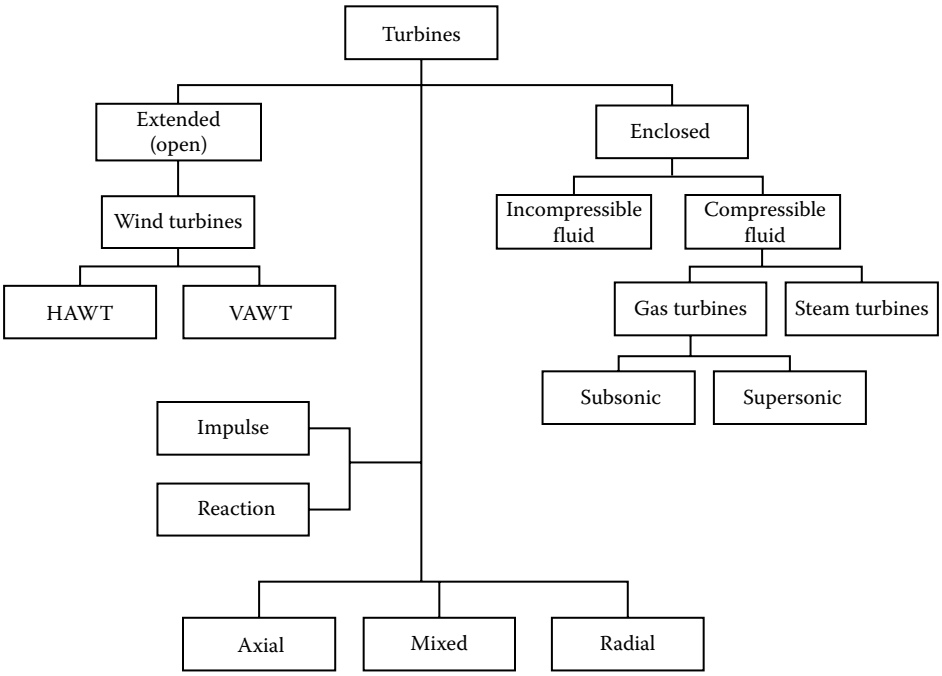


FIGURE 14.1
Classification of turbines.

The turbine is composed of a few stages; each has two successive stators (called nozzles or nozzle guide vanes) and rotor blade rows of small airfoil-shaped blades (Figure 14.2). The stators keep the flow from spiraling around the axis by bringing the flow back parallel to the axis. Depending on the engine type, there may be multiple turbine stages present in the engine. *Turbofan* and *turboprop* engines usually employ a separate turbine and shaft to power the fan and gearbox, respectively, and are termed *two-spool* engines. *Three-spool* configurations exist for some high-performance engines where an additional turbine and shaft power separate parts of the compressor. Nearly three fourths of the energy extracted by the turbine is used to drive the connected module (fan/compressor). When energy is extracted from the flow, pressure drops across the turbine. The pressure gradient helps keep the flow attached to the turbine blades; therefore, turbines, unlike compressors, are easier to design. The pressure drop across a single turbine stage can be much greater than the pressure increase across a corresponding compressor stage, without the danger of separating the flow. A single turbine stage can be used to drive multiple compressor stages. Therefore, higher efficiencies can be achieved in a turbine stage. To keep flow from leaking around the edges of the turbine blades because of the higher pressure gradient, the blade is shrouded at the tip. The shrouded blades form a band around the perimeter of the turbine that serves to cut down gas leakage around the tips of the turbine blades, and thus improve the airflow characteristics and increase the efficiency of the turbine (Figure 14.3). The shrouds also serve to reduce blade vibrations.

The turbine blades exist in a much more hostile environment than compressor blades. Sitting just downstream of the burner, the blades are exposed to an entry temperature of 850°C–1700°C [1]. Turbine blades therefore make use of advancements in metallurgy and

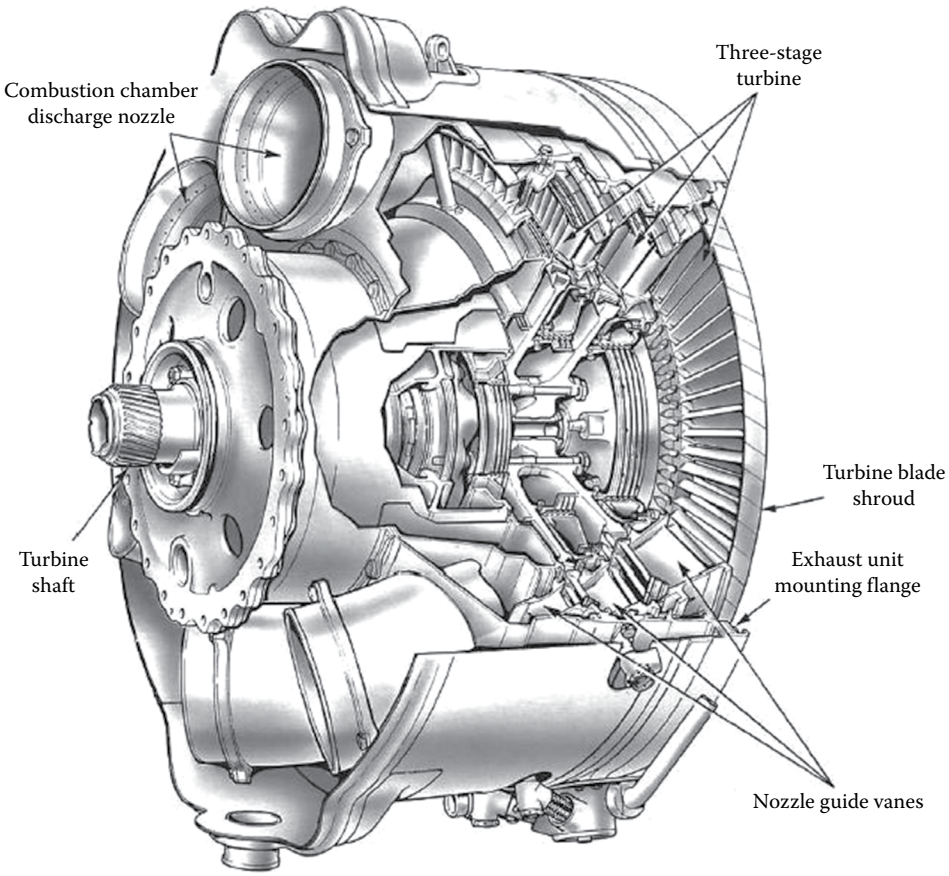


FIGURE 14.2
A triple-stage turbine with a single shaft. (Reproduced from Rolls-Royce plc, Copyright Rolls-Royce plc 2007. With permission.)

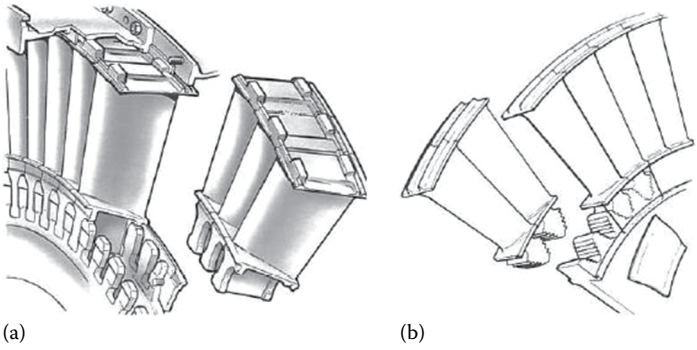


FIGURE 14.3
Shrouded blades of both (a) the nozzle and (b) rotor. (Reproduced from Rolls-Royce plc, Copyright Rolls-Royce plc 2007. With permission.)

manufacturing processes and are either made of special metals that can withstand the heat, or actively cooled. The blade is hollow, and cool air that is bled off the compressor is pumped through the blade and out through the small holes on the surface to keep the surface cool. Moreover, for efficient operation, the turbine rotates at very high speed—over 40,000 rpm for small engines to 8,000 rpm for larger engines—which makes the turbine wheel one of the most highly stressed parts in the engine.

14.2 Comparison between Axial-Flow Compressors and Turbines

A single stage of an axial turbine drawn side by side with an axial compressor stage is shown in Figure 14.4. The relative speeds in both cases are drawn. Through the turbine the flow is accelerated, while it is decelerated for the compressor. From this figure, it is shown that the blade-to-blade passage is convergent for a turbine and divergent for a compressor. The meridional plane (axial-radial directions) is convergent for a compressor and divergent for a turbine. Other comparisons are listed in Table 14.1.

14.3 Aerodynamics and Thermodynamics for a Two-Dimensional Flow

14.3.1 Velocity Triangles

One stage of an axial turbine is shown in Figure 14.5. The gases leaving the combustion chamber approach the stator (or nozzle) with an absolute velocity (C_1), normally in an axial direction, thus the absolute angle to the axial direction ($\alpha_1 = 0$). Since the passage represents a nozzle with either a convergent or convergent-divergent passage, the flow is accelerated, leading to an increase in the absolute velocity. The flow leaves the stator passage at a speed (C_2), where ($C_2 > C_1$). The static pressure decreases as usual as gases pass through the nozzle. Moreover, total pressures decrease due to skin friction and other sources of losses, as will be described later on. Thus $P_1 > P_2$, $P_{01} > P_{02}$. The static enthalpy and total enthalpy also drop at the end of the nozzle. The flow leaves the stator with an absolute speed of (C_2) and angle (α_2); when combined with the rotational speed (U) the relative velocity will be (W_2), inclined at an angle (β_2) to the axial. The velocity triangles at the exit of the nozzle and the

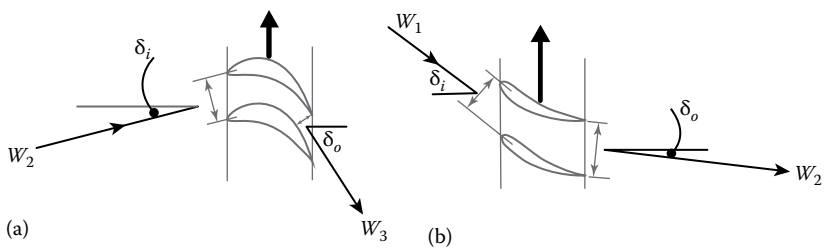


FIGURE 14.4
The rotor passage for an (a) axial turbine and (b) axial compressor.

TABLE 14.1

Comparison between Axial-Flow Compressor and Axial-Flow Turbine

	Compressor	**Turbine**
Flow	Decelerating	Accelerating
Meridional passage	Divergent	Convergent
Blade-to-blade passage	Diffuser	Nozzle
Maximum blade thickness	Small	Large
Direction of rotation	From suction to pressure surfaces	From pressure to suction surfaces
Number of stages	3–20	1–4
Hub-to-tip ratio (first stage)	0.4–0.6	≥0.7
Blade height	Large	Small
Annulus area in a multistage	Decreasing	Increasing
Number of blades	Small	Large
$(\Delta T_0)_{stage}$	• Positive • Small	• Negative • Large
P_0, h_0, and T_0	Increase	Decrease
Operating temperature (°R) [2]	500–1000	1000–3500
Specific work	$U(C_{u2} - C_{u1})$	$U(C_{u2} - C_{u3})$
Stage arrangement	Rotor-stator	Stator-rotor
$\psi - \phi$ relation	ψ is proportional to $(-\phi)$	ψ is proportional to (ϕ)
Maximum stage efficiency	0.8–0.9	>0.9
Erosion	Due to foreign objects like sand, polluted air, ice, etc.	Due to particles in combustion products
Flow deflection (°)$(\delta_i - \delta_o)$	20–35	50–180

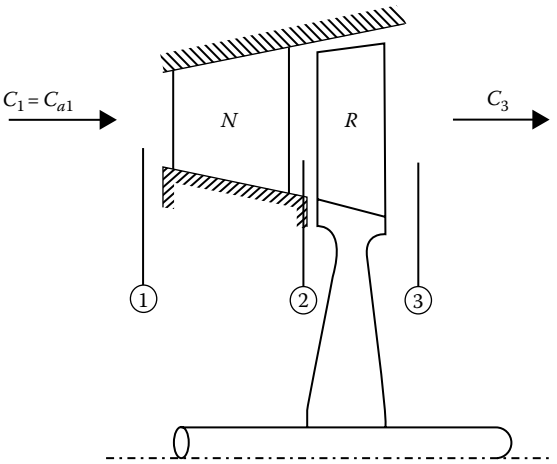


FIGURE 14.5
Layout of an axial turbine stage.

exit of the rotor are shown in Figure 14.6. The rotor blades extract work from the gases. Since the rotor blade-to-blade passages also resemble the nozzle shape, the gases' relative velocity (W_3) will increase, ($W_3 > W_2$), while their absolute velocity (C_3) decreases; ($C_3 < C_2$) and the flow exit angle (β_3) will be greater than the flow inlet angle, ($\beta_3 > \beta_2$). The static and total pressures also drop in the rotor passage, ($P_3 < P_2$, $P_{02} < P_{03}$). The static enthalpy and

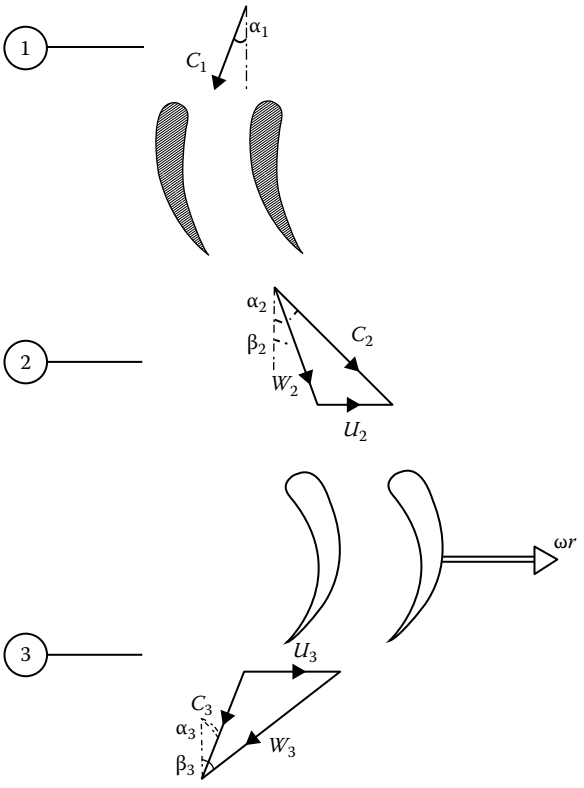


FIGURE 14.6
Velocity triangles.

total enthalpy also drop at the end of the rotor. If there is no static pressure and static enthalpy drop in the rotor, the turbine is called an *impulse turbine*. Since the static pressure and temperature decrease in the turbine, the density decreases. The annulus area is increased to avoid excessively high velocities.

The analysis of a turbine stage is very similar to that of a compressor stage, as will be emphasized here. The same kinematical relation described in centrifugal and axial compressors is valid:

$$\vec{C} = \vec{W} + \vec{U}$$

The three-dimensional velocity field can be further expressed in terms of the axial, radial, and tangential components as

$$\begin{pmatrix} C_a \\ C_r \\ C_u \end{pmatrix} = \begin{pmatrix} W_a \\ W_r \\ W_u \end{pmatrix} + \begin{pmatrix} 0 \\ 0 \\ \pm U \end{pmatrix}$$

In a similar way to the axial compressor, the following kinematical relations are derived from Figure 14.6:

$$\frac{U}{C_{a2}} = \tan\alpha_2 - \tan\beta_2 \tag{14.1a}$$

$$\frac{U}{Ca_3} = \tan\beta_3 - \tan\alpha_3 \tag{14.1b}$$

If the axial velocity is constant at the inlet and outlet of the stage, $C_{a2} = C_{a3} = C_a$.

The kinematical relations in Equation 14.1a and b will be

$$\frac{U}{C_a} = \tan\alpha_2 - \tan\beta_2 = \tan\beta_3 - \tan\alpha_3 \tag{14.1c}$$

Thus the following relation is reached:

$$\tan\alpha_2 - \tan\alpha_3 = \tan\beta_2 - \tan\beta_3 \tag{14.2}$$

Moreover, assuming a constant rotational speed ($U_2 = U_3 = U$), then the following kinematical relation between the absolute and relative velocities at the rotor inlet and outlet is simply arrived at

$$C_{u2} + C_{u3} = W_{u2} + W_{u3} \tag{14.3}$$

The velocity triangles shown in Figure 14.6 may be combined in three different ways. For equal axial velocities, the common bases (Figure 14.7a) and the common apex velocity triangles (Figure 14.7b) may be drawn. Alternatively, the velocity triangles having parallel rotational speed vectors [3] are shown in Figure 14.7c. Unequal axial velocities may also be drawn on common base form, as shown in Figure 14.7d.

14.3.2 Euler Equation

Euler's equation in turbomachinery represents the conservation of angular momentum, from which the specific work is expressed by the relation

$$W_s = \left(\vec{U} \times \vec{C}_u\right)_3 - \left(\vec{U} \times \vec{C}_u\right)_2 \tag{14.4a}$$

Since the swirl velocities $\vec{C}_{u3}$ and $\vec{C}_{u2}$ are in opposite directions, then

$$W_s = \left(UC_u\right)_3 - \left(UC_u\right)_2 \tag{14.4b}$$

In some cases the turbine has a continuously varying mean radius, as shown in Figure 14.8.

The corresponding velocity triangles shown in Figure 14.9 represent the most general case in which neither the rotational speed nor the axial speed is equal at the inlet and outlet of the rotor.

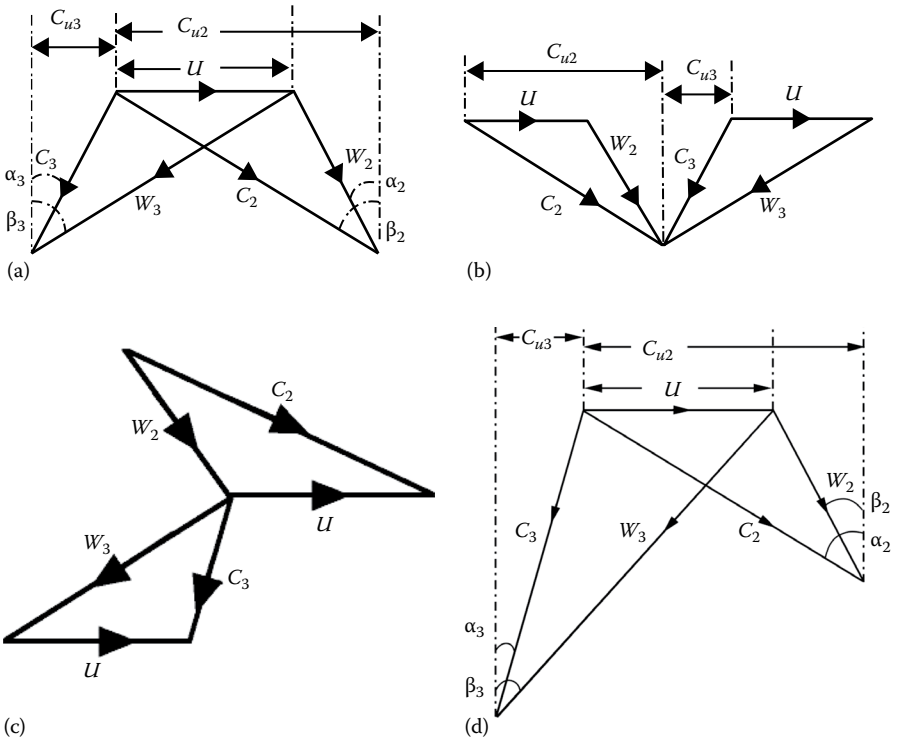


FIGURE 14.7
(a) Common base velocity triangles. (b) Common apex velocity triangles. (c) Parallel rotational speed velocity triangles. (d) Unequal axial velocity.

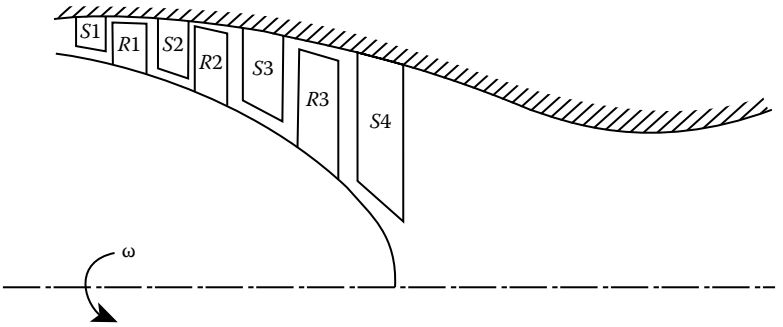


FIGURE 14.8
Layout of an axial turbine having variable mean radius.

The specific work will be expressed in the general form

$$W_s = U_2 C_{a2} \tan\alpha_2 + U_3 C_{a3} \tan\alpha_3 = U_2 C_{a2} \tan\beta_2 + U_3 C_{a3} \tan\beta_3 \tag{14.5a}$$

If the axial velocities are unequal but the mean radius and consequently the rotational speed are equal, $U_2 = U_3 = U$, then

$$W_s = U\left(C_{a2} \tan\alpha_2 + C_{a3} \tan\alpha_3\right) = U\left(C_{a2} \tan\beta_2 + C_{a3} \tan\beta_3\right) \tag{14.5b}$$

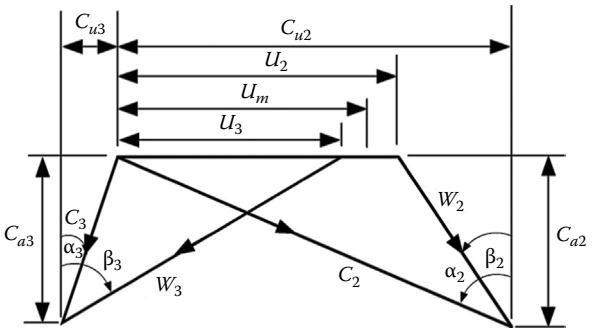


FIGURE 14.9
Velocity triangles for the general case.

If in addition, the axial speeds are equal, $C_{a2} = C_{a3} = C_a$, then Equation 14.5b is reduced to

$$W_s = UC_a\left(\tan\alpha_2 + \tan\alpha_3\right) \tag{14.5c}$$

Then from Equation 14.2, the specific work is

$$W_s = UC_a\left(\tan\beta_2 + \tan\beta_3\right) \tag{14.5d}$$

The working fluid in a turbine are hot gases, which have the following properties:

$$\gamma = 1.33 \quad Cp = 1.148\ \left(\approx 1.15\ \text{kJ/kg}\cdot\text{K}\right) \quad R = 287\ \text{J/kg}\cdot\text{K}$$

14.3.3 Efficiency, Losses, and Pressure Ratio

The expansion processes in the stator and rotor of an axial turbine are drawn on the T–S diagram shown in Figure 14.10. State (1) represents the inlet to the stator, while states (2) and (3) are the inlet and outlet to the rotor. Across the *nozzle* (stator), no work or heat is added to or rejected from the flow, thus

$$Q_{1-2} = W_{1-2} = 0$$

Accordingly, the inlet and outlet stagnation enthalpy and temperature are equal, or

$$h_{01} = h_{02} \quad \text{and} \quad T_{01} = T_{02} \tag{14.6}$$

Thus

$$h_1 - h_2 = \frac{\left(C_2^2 - C_1^2\right)}{2}$$

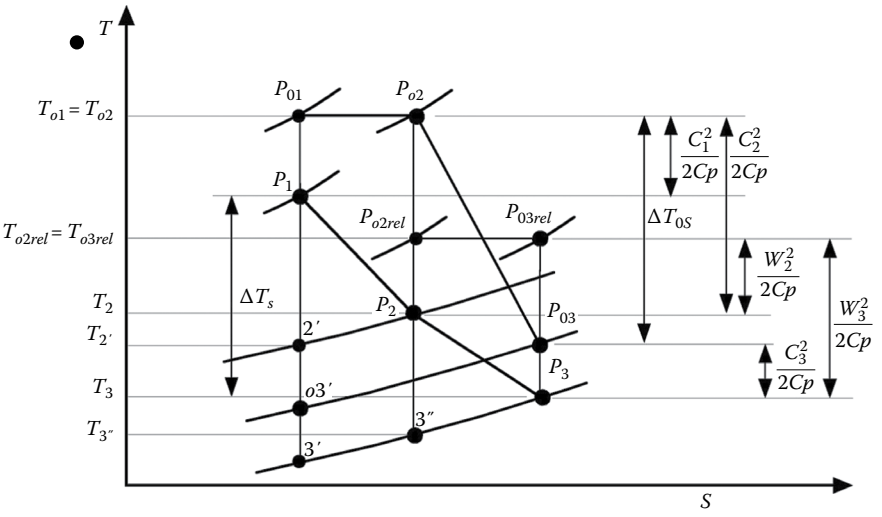


FIGURE 14.10
T–S diagram for a reaction turbine stage having equal mean radii at the inlet and outlet of the rotor.

Across the *rotor*, no heat is exchanged with the surroundings (outside a typical control volume surrounding the stage), thus

$$Q_{2-3} = 0$$

The rotor, however, extracts energy from the hot gases, thus the enthalpy drops. The corresponding specific work is

$$W_{2-3} = h_{02} - h_{03} = Cp\left(T_{02} - T_{03}\right)$$

Now, across the *stage*, no heat is transferred, thus

$$Q_s = 0 \tag{14.7}$$

The specific work is then

$$\begin{aligned} W_{1-3} &= h_{01} - h_{03} = \left(h_{01} - h_{02}\right) + \left(h_{02} - h_{03}\right) = \left(h_{02} - h_{03}\right) = Cp\left(T_{02} - T_{03}\right) \\ W_s &= \left(h_{02} - h_{03}\right) = Cp\left(T_{02} - T_{03}\right) \equiv Cp\left(T_{01} - T_{03}\right) = Cp\Delta T_{0s} \end{aligned} \tag{14.8}$$

The temperature drop in the stage from Equations 14.5a and 14.8 will be expressed as

$$\Delta T_{0s} = \frac{\left(U_2 C_{a2} \tan\alpha_2 + U_3 C_{a3} \tan\alpha_3\right)}{C_p} \tag{14.9a}$$

For a constant mean diameter, the rotational speeds are equal, then the temperature drop will be

$$\Delta T_{0s} = \frac{U\left(C_{a2} \tan\alpha_2 + C_{a3} \tan\alpha_3\right)}{Cp} \tag{14.9b}$$

For constant axial speed in addition, it will be

$$\Delta T_{0s} = \frac{UC_a\left(\tan\alpha_2 + \tan\alpha_3\right)}{Cp} = \frac{UC_a\left(\tan\beta_2 + \tan\beta_3\right)}{Cp} \tag{14.9c}$$

Across the rotor, the *rothalpy* (*I*)—rotational enthalpy—is frequently employed. It is defined as

$$I = h_{0r} - U^2/2 \tag{14.10}$$

Across the rotor, the rothalpy is constant, or

$$I_2 = I_3$$

$$h_{02r} - U_2^2/2 = h_{03r} - U_3^2/2 \tag{14.11}$$

When the rotor has equal mean diameter at inlet and outlet, then the relative total enthalpy

$$h_{02r} = h_{03r}$$

$$T_{02r} = T_{03r} \tag{14.11b}$$

which is shown on the T–S diagram, Figure 14.10.

Since the relative total enthalpy is expressed by

$$h_{0r} = h + W^2/2$$

then for equal relative total enthalpy

$$h_2 - h_3 = \frac{\left(W_3^2 - W_2^2\right)}{2}$$

and so

$$T_2 - T_3 = \frac{\left(W_3^2 - W_2^2\right)}{2Cp} \tag{14.12}$$

The *stage efficiency* (total-to-total) is defined as

$$\eta_{stage} = \frac{T_{01} - T_{03}}{T_{01} - T_{03}'} = \frac{\Delta T_{0stage}}{T_{01}\left[1 - \left(\frac{P_{03}}{P_{01}}\right)^{\gamma-1/\gamma}\right]}$$

$$\Delta T_{0stage} = \eta_{stage} T_{01}\left[1 - \left(\frac{P_{03}}{P_{01}}\right)^{\gamma-1/\gamma}\right]$$

$$\Delta T_{0s} = \eta_s T_{01}\left[1-\left(\frac{1}{\pi_s}\right)^{\gamma-1/\gamma}\right] \tag{14.13}$$

The pressure ratio of a stage, π_s, is given by the relation

$$\pi_s = \frac{P_{01}}{P_{03}} = \frac{1}{\left(1-\dfrac{\Delta T_{0s}}{\eta_s T_{01}}\right)^{\gamma/\gamma-1}} \tag{14.14}$$

The axial velocity ratio (AVR) is expressed as

$$AVR = \frac{C_{a3}}{C_{a2}} \tag{14.15}$$

$$\frac{\Delta T_{0s}}{T_{01}} = \frac{(\gamma-1)U^2 C_{a2}}{\gamma R T_{01} U}\left(\tan\alpha_2 + AVR\tan\alpha_3\right)$$

Moreover, $T_{01} = T_1\left(1+\dfrac{\gamma-1}{2}M_1^2\right)$ and defines the rotational and axial Mach numbers as

$$M_u = \frac{U}{\sqrt{\gamma R T_1}} \quad \text{and} \quad M_{a2} = \frac{C_{a2}}{\sqrt{\gamma R T_1}}$$

Thus the temperature drop in the stage as a ratio of the inlet total temperature becomes

$$\frac{\Delta T_{0s}}{T_{01}} = \frac{(\gamma-1)M_u^2}{\left(1+\dfrac{\gamma-1}{2}M_1^2\right)}\frac{M_{a2}}{M_u}\left(\tan\alpha_2 + AVR\tan\alpha_3\right) \tag{14.16a}$$

The pressure ratio of the stage [2] is now in terms of Mach numbers and may be expressed as

$$\frac{P_{03}}{P_{01}} = \left[1-\frac{(\gamma-1)M_u^2}{\eta_S\left(1+\dfrac{\gamma-1}{2}M_1^2\right)}\frac{M_{a2}}{M_u}\left(\tan\alpha_2 + AVR\tan\alpha_3\right)\right]^{\gamma/\gamma-1} \tag{14.16b}$$

The turbine efficiency η_t is related to the stage efficiency η_s by the relation

$$\eta_t = \frac{1-\pi_t^{(\gamma-1/\gamma)}}{1-\pi_t^{\eta_s(\gamma-1/\gamma)}} \tag{14.17}$$

where the turbine pressure ratio is $\pi_t = \dfrac{(P_0)_{turbine\ inlet}}{(P_0)_{turbine\ outlet}}$

Loss coefficient in the nozzle: This is expressed either as an enthalpy loss coefficient (λ_N) or pressure loss coefficient (Y_N) [4], where

$$\lambda_N = \frac{T_2 - T_2'}{C_2^2/2Cp} \tag{14.18}$$

and

$$Y_N = \frac{P_{01} - P_{02}}{P_{02} - P_{02}} \tag{14.19}$$

A third loss coefficient, namely, the velocity loss coefficient [5], is defined as

$$\varphi_N = \frac{C_2}{C_{2S}} \tag{14.20}$$

Loss coefficient in the rotor: The enthalpy loss in the rotor is

$$\lambda_R = \frac{T_3 - T_3''}{W_3^2/2Cp} \tag{14.21}$$

The pressure loss in the rotor is

$$Y_R = \frac{P_{02rel} - P_{03rel}}{P_{03rel} - P_3} \tag{14.22}$$

The velocity loss in the rotor is

$$\varphi_R = \frac{W_3}{W_{3S}} \tag{14.23}$$

The pressure loss may be measured in a cascade tunnel, while the enthalpy loss is used in the blade row design. Both are nearly equal, or

$$Y \approx \lambda \quad \text{or} \quad Y_R \approx \lambda_R, \quad Y_N \approx \lambda_N$$

The total-to-total isentropic efficiency, after a lengthy mathematical manipulation [4], can be written as

$$\eta_s \cong \frac{1}{1 + \dfrac{C_a}{2U}\left[\dfrac{\lambda_R \sec^2\beta_3 + (T_3/T_2)\lambda_N \sec^2\alpha_2}{\tan\beta_3 + \tan\alpha_2 - (U/c_a)}\right]} \tag{14.24}$$

Another expression correlating the stage efficiency and the nozzle and rotor loss coefficients [5] is given by

$$\eta_s = \frac{1}{1+\left[\dfrac{\lambda_N C_2^2 + \lambda_R W_3^2}{2\left(h_{01} - h_{03}\right)}\right]} \tag{14.25}$$

14.3.4 Nondimensional Quantities

1. Blade loading or temperature drop coefficient
2. Flow coefficient
3. Degree of reaction

The temperature drop or blade loading is expressed as

$$\psi = \frac{Cp\Delta T_{0s}}{U^2} \tag{14.26a}$$

Most text and reference books adopt the expression expressed by Equation 14.26a for blade loading [2,3,5]. However, the National Gas Turbine Establishment in the United Kingdom defines this parameter as

$$\psi_{NGTE} = \frac{Cp\Delta T_{0s}}{1/2U^2} = \frac{2Cp\Delta T_{0s}}{U^2} \tag{14.26b}$$

This form is adopted in some texts [4]. Thus

$$\psi = \frac{\psi_{NGTE}}{2}$$

The flow coefficient has the same definition as in the axial compressor, namely

$$\phi = \frac{C_{a2}}{U} \tag{14.27a}$$

The temperature drop can be expressed as

$$\psi = \phi\left(\tan\alpha_2 + AVR\tan\alpha_3\right) \tag{14.28a}$$

If $C_{a2} = C_{a3} = C_a$ then

$$\phi = \frac{C_a}{U} \tag{14.27b}$$

The corresponding temperature drop is now

$$\psi = \phi\left(\tan\alpha_2 + \tan\alpha_3\right) = \phi\left(\tan\beta_2 + \tan\beta_3\right) \tag{14.28b}$$

The degree of reaction is defined in terms of static enthalpy change as

$$\Lambda = \frac{T_2 - T_3}{T_1 - T_3} \equiv \left.\begin{matrix}\text{Static enthalpy drop in rotor} \\ \text{Static enthalpy drop in stage}\end{matrix}\right\} \tag{14.29}$$

If equal absolute speeds are assumed in the inlet and outlet of the stage, $C_1 = C_3$, then from Figure 14.10 and Equation 14.9c

$$\Delta T \equiv T_1 - T_3 = \Delta T_0 = \frac{UC_a\left(\tan\beta_2 + \tan\beta_3\right)}{Cp} \tag{14.30}$$

Moreover, since the relative total enthalpy (and temperature) at the inlet and outlet of the rotor are equal, then

$$h_{02rel} = h_{03rel}$$

$$h_2 + \frac{W_2^2}{2} = h_3 + \frac{W_3^2}{2}$$

$$T_2 - T_3 = \frac{1}{2Cp}\left(W_3^2 - W_2^2\right) = \frac{C_a^2}{2Cp}\left(\sec^2\beta_3 - \sec^2\beta_2\right) = \frac{C_a^2}{2Cp}\left(\tan^2\beta_2 - \tan^2\beta_3\right) \tag{14.31}$$

From Equations 14.30 and 14.31, the degree of reaction is

$$\Lambda \equiv \frac{T_2 - T_3}{T_1 - T_3} = \left(\frac{C_a^2}{2Cp}\right)\left(\frac{\left(\tan^2\beta_2 - \tan^2\beta_3\right)}{\left(\tan\beta_2 + \tan\beta_3\right)}\right)$$

$$\Lambda = \frac{C_a}{2U}\left(\tan\beta_3 - \tan\beta_2\right) \tag{14.32a}$$

or in terms of the flow coefficient

$$\Lambda = \frac{\phi}{2}\left(\tan\beta_3 - \tan\beta_2\right)$$

From Equation 14.27a, for an impulse turbine, $\Lambda = 0$, the rotor's relative angles at the inlet and outlet are equal, or $\beta_2 = \beta_3$.

From Equation 14.1c, the following other expressions for the degree of reaction are obtained:

$$\Lambda = \frac{1}{2} - \frac{C_a}{2U}\left(\tan\alpha_2 - \tan\beta_3\right) \tag{14.32b}$$

or

$$\Lambda = \frac{1}{2} - \frac{\phi}{2}\left(\tan\alpha_2 - \tan\beta_3\right)$$

$$\Lambda = 1 - \frac{C_a}{2U}\left(\tan\alpha_2 - \tan\alpha_3\right) \tag{14.32c}$$

or

$$\Lambda = 1 - \frac{\phi}{2}\left(\tan\alpha_2 - \tan\alpha_3\right)$$

Equation 14.32a through c may be used to construct Table 14.2.

The three non-dimensional variables may be coupled to give the following relations: if $C_{a2} = C_{a3}$, then

$$\psi = \phi\left(\tan\alpha_2 + \tan\alpha_3\right) = \phi\left(\tan\beta_2 + \tan\beta_3\right)$$

$$\Lambda = \frac{\phi}{2}\left(\tan\beta_3 - \tan\beta_2\right)$$

$$\tan\beta_2 = \frac{1}{2\phi}\left(\psi - 2\Lambda\right) \tag{14.33}$$

$$\tan\beta_3 = \frac{1}{2\phi}\left(\psi + 2\Lambda\right) \tag{14.34}$$

Since

$$\frac{1}{\phi} = \tan\beta_3 - \tan\alpha_3 = \tan\alpha_2 - \tan\beta_2$$

then

$$\tan\alpha_2 = \tan\beta_2 + \frac{1}{\phi} = \frac{1}{2\phi}\left(\psi - 2\Lambda + 2\right) \tag{14.35}$$

and

$$\tan\alpha_3 = \tan\beta_3 - \frac{1}{\phi} = \frac{1}{2\phi}\left(\psi + 2\Lambda - 2\right) \tag{14.36}$$

TABLE 14.2

Variation of Rotor Blade Characteristics for Different Degrees of Reaction

Λ	Blading	Characteristics	Velocity Triangle	Thermodynamics
0	Impulse	$\beta_2 = \beta_3$	Skewed	$T_2 = T_3$
0.5	Reaction	$\alpha_2 = \beta_3$, $\alpha_3 = \beta_2$	Symmetrical	$T_2 = (T_1 + T_3)/2$
1.0	Reaction	$\alpha_2 = \alpha_3$	Skewed	$T_1 = T_2$

Thus, the temperature loading will be expressed by the relations

$$\psi = 2\phi \tan\alpha_2 + 2\Lambda - 2 \tag{14.37a}$$

$$\psi = 2\phi \tan\alpha_3 - 2\Lambda + 2 \tag{14.37b}$$

$$\psi = 2\phi \tan\beta_2 + 2\Lambda \tag{14.37c}$$

$$\psi = 2\phi \tan\beta_3 - 2\Lambda \tag{14.37d}$$

Figure 14.11 illustrates relations (14.37a) and (14.37b) for a degree of reaction of 0.4 for different absolute angles, $\alpha_2 = 50°$, 60°, 70°, and 80° and $\alpha_3 = -10°$, 0°, 10°, 20°. A plot for relations (14.37c) and (14.37b) for different values of the degree of reaction (0.4, 0.5, and 0.6) and relative angles ($\beta_2 = 10°$ and $\beta_3 = 70°$) is illustrated in Figure 14.12.

For the special case of

$$\tan\beta_3 = \frac{1}{2\phi}(\psi + 1)$$

thus

$$\psi = 2\phi \tan\beta_3 - 1 = 2\phi \tan\alpha_2 - 1 \tag{14.38a}$$

$$\psi = 2\phi \tan\beta_2 + 1 = 2\phi \tan\alpha_3 + 1 \tag{14.38b}$$

Figure 14.13 illustrates the relation between temperature loading and flow coefficient as expressed by the relations (14.38a) and (14.38b) for $\beta_2 = 0°$, 15° and 30° and $\beta_3 = 50°$, 65° and 80° and a 50% reaction.

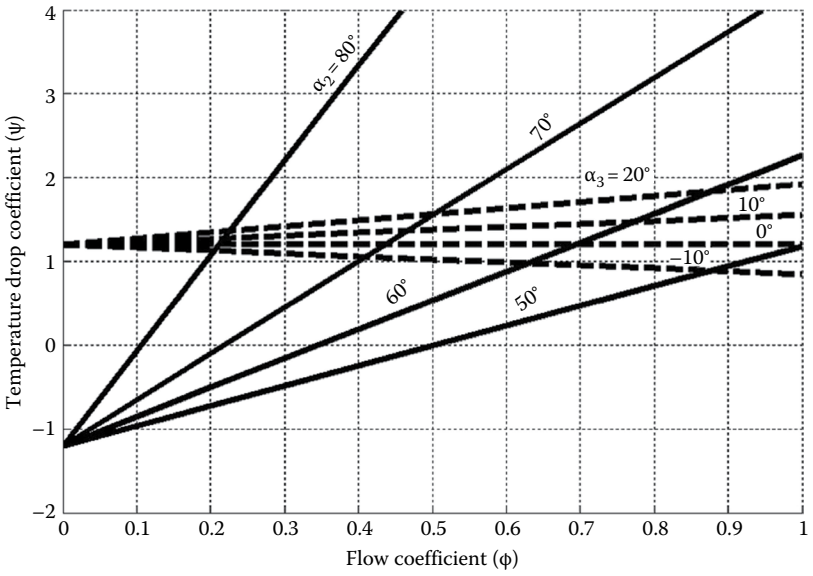


FIGURE 14.11
Temperature loading versus flow coefficient for 0.4° of reaction.

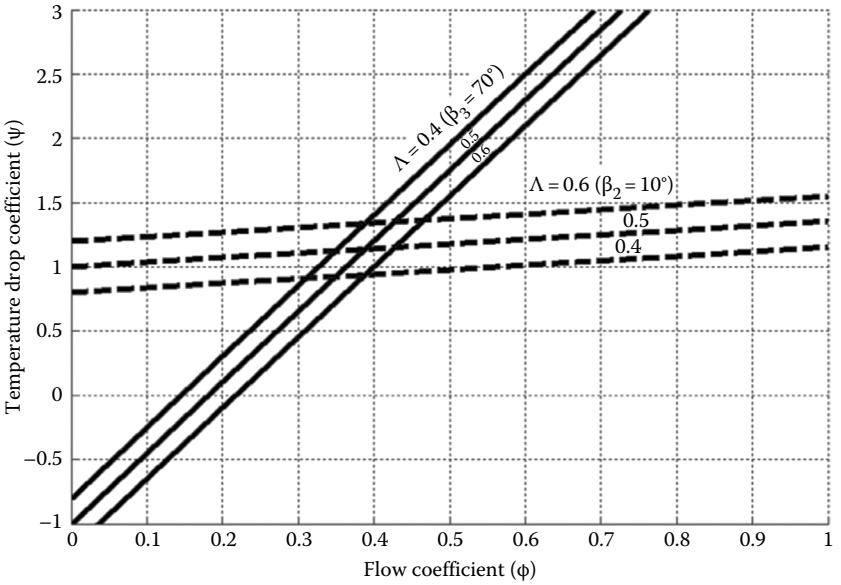


FIGURE 14.12
Temperature loading versus flow coefficient for different degrees of reaction.

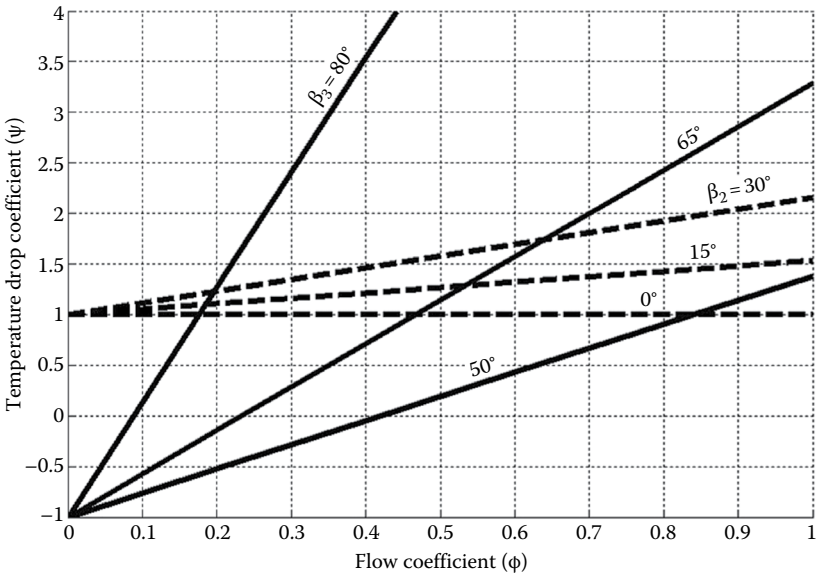


FIGURE 14.13
Temperature loading versus flow coefficient for Λ = 0.5.

For an impulse turbine ($\Lambda = 0$), then

$$\psi = 2\phi \tan \beta_2 \tag{14.39}$$

$$\psi = 2\phi \tan \alpha_3 + 2 \tag{14.40}$$

Example 14.1

Consider a three-stage axial-flow turbine where the inlet total temperature is 1100 K, the flow coefficient is 0.8, and the mean rotational speed is constant for all stages and equal to 340 m/s. Other data is given in the following table:

Stage	Angles	Degree of Reaction Λ_m	Efficiency η_s	Inlet Temperature (K)	Temperature Drop ΔT_o (K)
1	$\alpha_1 = 0$	0.5	0.938	1100	145
2	$\alpha_1 = \beta_2$	0.5	0.938	?	145
3	$\alpha_3 = 0$	?	0.94	?	120

It is required to

1. Sketch the turbine shape.
2. Draw the velocity triangles at the mean sections for each stage (assume constant mean radius for all stages).
3. Calculate the degree of reaction at the mean section for the third stage.
4. Calculate the pressure ratio of each stage.
5. Prove that, for equal pressure ratios of the three stages, the efficiencies must have the following relations:

$$\frac{\eta_{s2}}{\eta_{s1}} = \frac{T_{01} \times \Delta T_{02}}{\Delta T_{01} \times \left(T_{01} - \Delta T_{01}\right)}$$

$$\frac{\eta_{s3}}{\eta_{s1}} = \frac{T_{01} \Delta T_{03}}{\Delta T_{01} \times \left(T_{01} - \Delta T_{01} - \Delta T_{02}\right)}$$

Solution

1. The sketch in Figure 14.14 illustrates the three-stage axial turbine having a constant mean radius.
2. To draw the velocity triangles, the angles (α_2, α_3, β_2, β_3) must be calculated first. The appropriate governing equations are the temperature drop and the degree of reaction. From Equations 14.9c and 14.32a, then

$$\tan \beta_3 + \tan \beta_2 = \frac{C_p \Delta T_0}{U C_a} \tag{1}$$

$$\tan \beta_3 - \tan \beta_2 = \frac{2\Lambda}{\phi} \tag{2}$$

Now, solving these two equations simultaneously we obtain the angles β_2 and β_3.

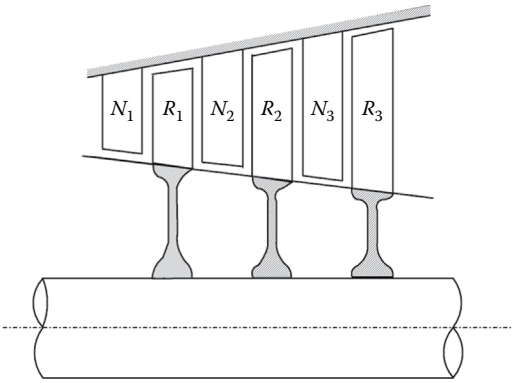


FIGURE 14.14
Layout of the three-stage axial turbine.

Stage 1: Since $T_{01} = 1100$ K and $T_{0S} = 145$ K, then $T_{03} = 955$ K
Also, as $\Lambda_m = 1/2$, then $\alpha_2 = \beta_3$, $\alpha_3 = \beta_2$

$$\tan\beta_3 + \tan\beta_2 = \frac{1148 \times 145}{340 \times 272} = 1.8 \tag{a}$$

$$\tan\beta_3 - \tan\beta_2 = \frac{2 \times 0.5}{0.8} = 1.25 \tag{b}$$

Then $\beta_2 = \alpha_3 = 15.376°$ and $\beta_3 = \alpha_2 = 56.746°$
Stage 2: The same results are obtained for stage 2 as both have the same temperature drop per stage, axial-flow coefficient, and axial and rotational speeds.

$$\beta_2 = \alpha_3 = 15.376°$$

$$\beta_3 = \alpha_2 = 56.746°$$

Stage 3: From Equation 14.9c,

$$\tan\alpha_3 + \tan\alpha_2 = \frac{C_p \Delta T_{0s}}{UC_a}$$

With $\alpha_3 = 0°$ and $\Delta T_{0s} = 120$ K

$$\therefore \tan\alpha_2 = \frac{C_p \Delta T_{0s}}{UC_a}$$

$$\therefore \alpha_2 = 56.125°$$

To calculate the angles β_2 and β_3, we again use Equations 1 and 2:

$$\tan\beta_3 + \tan\beta_2 = \frac{1148 \times 120}{340 \times 272} = 1.4896$$

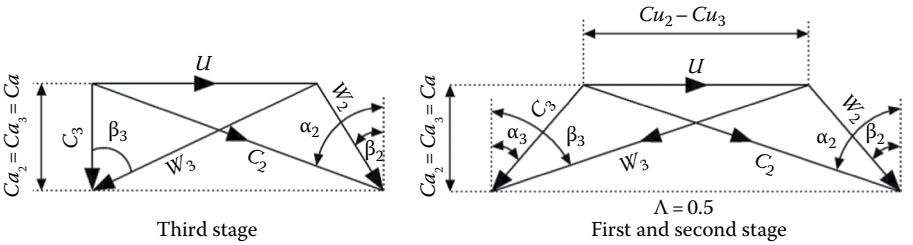


FIGURE 14.15
Velocity triangles for the three stages.

$$\text{Also} \quad \tan\beta_3 - \tan\beta_2 = \frac{2 \times 0.4042}{0.8} = 1.0105$$

Solving both equations, we get $\beta_2 = 13.471°$ and $\beta_3 = 51.341°$.

Now the velocity triangles can be drawn. Stages 1 and 2 have the same velocity triangle, while the third stage has zero exit swirl, as shown in Figure 14.15.

3. The degree of reaction for the third stage can be calculated from Equation 14.32c, namely

$$\Lambda = 1 - \frac{\phi}{2}\left(\tan\alpha_3 - \tan\alpha_2\right)$$

With $\alpha_3 = 0°$ and $\alpha_2 = 56.125°$

$$\Lambda = 0.4042$$

4. The pressure ratio of any stage is calculated from Equation 14.14:

$$\left(\frac{P_{03}}{P_{01}}\right)_{stage} = \left[1 - \frac{\Delta T_{0s}}{\eta_s T_{01}}\right]^{\gamma/\gamma - 1}$$

Stage 1:

$$T_{01} = 1100\ \text{K} \quad \text{and} \quad \Delta T_{os} = 145\ \text{K} \quad \text{then } T_{03} = 955\ \text{K}$$

$$\left(\frac{P_{03}}{P_{01}}\right) = \left[1 - \frac{145}{(0.938) \times (1100)}\right]^{1.33/0.33} = 0.5432$$

Stage 2:

$$T_{01} = 955\ \text{K} \quad \text{and} \quad \Delta T_0 = 145\ \text{K} \quad \text{then } T_{03} = 810\ \text{K}$$

$$\frac{P_{03}}{P_{01}} = 0.4908$$

Stage 3:

$$T_{01} = 810\,\text{K} \quad \text{and} \quad \Delta T_o = 120\,\text{K} \quad \text{then} \frac{P_{03}}{P_{01}} = 0.50097$$

5. Now to correlate the efficiencies of the first two stages to the temperature drop per stage, since

$$\left(\frac{P_{03}}{P_{01}}\right)_1 = \left(\frac{P_{03}}{P_{01}}\right)_2$$

$$\left(1 - \frac{\Delta T_{01}}{\eta_{s1} T_{01}}\right)^{\gamma/\gamma-1} = \left(1 - \frac{\Delta T_{02}}{\eta_{s2}\left(T_{01} - \Delta T_{01}\right)}\right)^{\gamma/\gamma-1}$$

$$\frac{\Delta T_{01}}{\eta_{s1} T_{01}} = \frac{\Delta T_{02}}{\eta_{s2}\left(T_{01} - \Delta T_{01}\right)}$$

$$\frac{\eta_{s2}}{\eta_{s1}} = \frac{T_{01}\Delta T_{02}}{\Delta T_{01}\left(T_{01} - \Delta T_{01}\right)}$$

Similarly, assuming equal pressure ratios for all stages

$$\therefore \left(\frac{P_{03}}{P_{01}}\right)_1 = \left(\frac{P_{03}}{P_{01}}\right)_3$$

$$\left(1 - \frac{\Delta T_{01}}{\eta_{s1} T_{01}}\right)^{\gamma/\gamma-1} = \left[1 - \frac{\Delta T_{03}}{\eta_{s3}\left(T_{01} - \Delta T_{01} - \Delta T_{02}\right)}\right]^{\gamma/\gamma-1}$$

$$\therefore \frac{\Delta T_{01}}{\eta_{s1} T_{01}} = \frac{\Delta T_{03}}{\eta_{s3}\left(T_{01} - \Delta T_{01} - \Delta T_{02}\right)}$$

$$\frac{\eta_{s3}}{\eta_{s1}} = \frac{T_{01}\Delta T_{03}}{\Delta T_{01}\left(T_{01} - \Delta T_{01} - \Delta T_{02}\right)}$$

Summary of Results

	Stage		
Parameters	**Stage 1**	**Stage 2**	**Stage 3**
T_{01}	1100	955	810
α_2 (degrees)	56.746	56.746	56.126
β_3 (degrees)	56.746	56.746	51.341
α_3 (degrees)	15.376	15.376	0
β_2 (degrees)	15.376	15.376	13.471
Λ_m	0.5	0.5	0.4042
P_{03}/P_{01}	0.5432	0.4908	0.50097

14.3.5 Several Remarks

1. The mass flow parameter can be calculated at any of the three states of the stage. Conservation of mass gives the following relation:

$$\dot{m} = \rho_1 C_{a1} A_1 = \rho_2 C_{a2} A_2 = \rho_3 C_{a3} A_3 \tag{14.41}$$

The thrust force on the turbine is a combination of pressure thrust and axial thrust.

$$\text{Thrust} = \text{Pressure thrust} \pm \text{Axial thrust}$$

$$\text{Pressure thrust} = \left(A_2 P_2 - P_3 A_3\right)$$

$$\text{Axial thrust} = \dot{m}\left(Ca_2 - Ca_3\right)$$

The thrust force (T) is then expressed as

$$T = \left(A_2 P_2 - P_3 A_3\right) + \dot{m}\left(C_{a2} - C_{a3}\right) \tag{14.42}$$

A pure impulse stage, with no pressure drop and a constant axial velocity component across the rotor, will have zero net axial loads. The thrust force generated by the compressor either partially or fully balances the thrust force generated on the turbine, as shown in Figure 14.16. If the axial velocity is constant through the rotor, then the thrust forces arise only from the pressure difference.

2. Aeroengines need an axial turbine to have a high blade loading or temperature drop coefficient (ψ), and a high flow coefficient (ϕ). High blade loading means high-temperature drop per stage and consequently fewer stages for a certain power output, thus the weight and size of the aeroengine is at a minimum to satisfy flight needs. Moreover, high flow coefficient implies high axial velocity and consequently a small annulus area. This leads to a small frontal area and low drag.

   On the contrary, the axial turbines in industrial gas turbines are characterized by low blade loading and low axial velocity. These conditions are associated with the best stage efficiency [4]. High efficiency provides the best fuel economy or the lowest specific fuel consumption. Though low blade loading will lead to a large

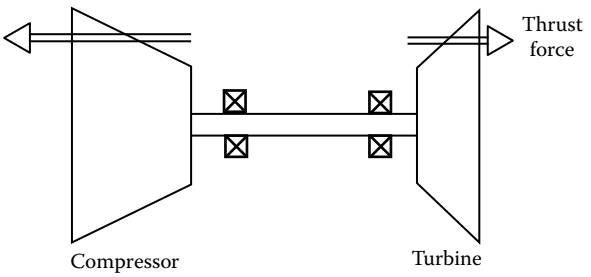


FIGURE 14.16
Thrust force on a spool.

number of stages, and a low flow coefficient also leads to a large frontal area, both are of minor importance for ground engines.

Smith [6] examined the data of some 70 turbine tests with a degree of reaction between 0.2 and 0.6, and an aspect ratio (blade height/chord) in the region 3–4. He plotted these data as $\psi - \phi$ curves for constant efficiencies. This data was published in 1965 for specific data, and modern-day turbine stages, even though they have different geometry and data, have the same trends. For this reason, Smith's work is still used for the preliminary design of turbines. From the earlier discussion and Smith's work, the following conclusions may be deduced. For aeroengines, the optimum value for ψ is from 1.5 to 2.5 and for ϕ is from 0.8 to 1.2. The efficiency ranges from 86% to 91%. For industrial gas turbines, the optimum value for ψ ranges from 1.0 to 1.5, while ϕ ranges from 0.4 to 0.8. The corresponding efficiency ranges from 93% to 95%.

3. Stator blade rows have nozzle shapes and for this reason are frequently identified as nozzle vanes. The stator passage may be of a convergent or convergent-divergent shape. The latter type is not recommended for two reasons: first, convergent-divergent nozzles are inefficient at part loads or generally at any pressure ratios other than the design value; second, the outlet speed from the nozzle, C_2, will be high and consequently the rotor inlet relative speed, W_2, will be also high enough to form shockwaves within the rotor passage.

   The convergent nozzle must be checked for choking. Thus, if $(P_{01}/P_2 < P_{01}/P_c)$, then the nozzle is unchoked. Each ratio can be calculated as follows:

$$\frac{P_{01}}{P_2} = \left(\frac{T_{01}}{T_2'}\right)^{\gamma/\gamma-1}$$

   where $T_2' = T_2 - \lambda_N C_2^2/2Cp$ and

$$\frac{P_{01}}{P_c} = \left(\frac{\gamma+1}{2}\right)^{\gamma/\gamma-1} = \left(\frac{2.33}{2}\right)^{1.33/0.33} = 1.853$$

   For a choked nozzle, the absolute velocity is equal to the sonic speed.

   The annulus of turbine stages is generally flared (Figure 14.17). The flare angle is calculated when the blade heights and widths are first calculated. The blade heights are calculated as follows: the axial velocities at states (1), (2), and (3) are determined first. Next, the absolute velocities at the three states are determined. The static temperature and pressure are calculated as follows: $T = T_0 - C^2/2C_p$ and $P = P_0(T/T_0)^{\gamma/\gamma-1}$, thus the density is $\rho = P/RT$. The blade height is then obtained for a constant mean radius from the relation $h = \dot{m}/\pi\rho C_a D_m$. The blade mean height is then calculated as follows: $h_{nozzle} = (h_1 + h_2)/2$ and $h_{rotor} = (h_2 + h_3)/2$. The blade chord ranges from $(h/4)$ to $(h/2)$. The spacing between the blade rows must be greater than 20% of the chord. The flare can then be calculated.

   If the included angle of divergence of the walls is large, flow separation from the inner wall may be encountered. A safe value for the included angle is to be less than or equal to 25° [7]. The flare angles, height-to-width ratio of the stator/rotor blades, and the spacing between the stator and rotor blade rows are design parameters. They depend on aerodynamics and the mechanical stresses of the stator and rotor blades. Rotor blades are subjected to *vibration stresses* as well as *mechanical stresses*.

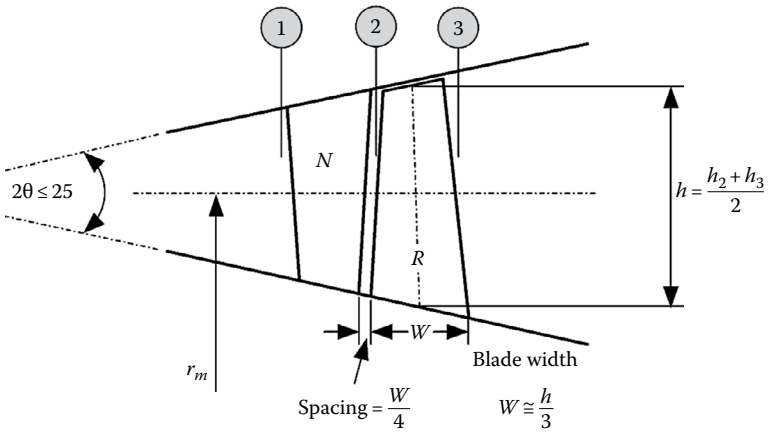


FIGURE 14.17
Suggested geometry for an axial turbine stage.

Vibration stresses arise as the rotor blades pass through the wake of the nozzle blades. Excessive vibration stresses arise when the space between the blade rows is less than 0.2 of the blade width. A value of nearly 0.5 is often used, which will reduce both the vibration stresses and the annulus flare [4].

Example 14.2

A single-stage axial-flow gas turbine has the following data:

• Turbine inlet total temperature	=1100 K
• Turbine inlet total pressure	=3.4 bar
• Stage temperature drop	$\Delta T_0 = 144\,\text{K}$
• Isentropic efficiency	$\eta = 0.9$
• Mean blade speed	$U = 298$ m/s
• Mass flow rate	$\dot{m} = 18.75$ kg/s
• Flow coefficient	$\phi = 0.95$
• Loss coefficient for nozzle blade	$\lambda_N = 0.05$
• Rotational speed	=200 rps
• The convergent nozzle is choked	

Calculate

1. The blade loading coefficient (Ψ)
2. The pressure ratio of the stage
3. The flow angles α_2, α_3, β_2, and β_3

Solution

The gas properties are

$$C_P = 1148\ \text{J/kg}\cdot\text{K}, \quad R = 287\ \text{J/kg}\cdot\text{K}, \quad \gamma = \frac{4}{3}$$

1. The blade loading is $\psi = \dfrac{C_P \Delta T_0}{U^2} = \dfrac{1148 \times 144}{298^2}$

$$\psi = 1.8615$$

2. $T_{02}/T_{01} = 1100$ K

$$T_{03} = T_{01} - \Delta T_0 = 1100 - 144 = 956 \text{ K}$$

$$\frac{P_{03}}{P_{01}} = \left[1 - \frac{\Delta T_0}{\eta_t T_{01}}\right]^{\gamma/\gamma-1} = \left[1 - \frac{144}{0.9 \times 1100}\right]^4 = 0.533$$

The pressure ratio in the turbine is $P_{01}/P_{03} = 1.875$, or $P_{03} = 1.813$ bar.

3. Since the nozzle is choked, then

a. $C_2 = \sqrt{\gamma R T_2}$

b. $\dfrac{T_{02}}{T_2} = \dfrac{\gamma + 1}{2} = 1.165$

The static temperature at the nozzle outlet is then $T_2 = 944.2$ K.

The absolute speed of the gases leaving the choked nozzle is $C_2 = \sqrt{\gamma R T_2} =$ 600.3 m/s.

Since the nozzle losses are expressed by the relation

$$T_2 - T_2' = \lambda_N \frac{C_2^2}{2C_P} = \frac{0.05 \times 600^2}{2 \times 1148} = 7.839 \text{ K}$$

$$T_2' = 936.4 \text{ K}$$

The pressure ratio $\dfrac{P_{01}}{P_2} = \left(\dfrac{T_{01}}{T_2'}\right)^{\gamma/\gamma-1} = \left(\dfrac{1100}{936.4}\right)^4 = 1.904.$

$$P_2 = 1.785 \text{ bar}$$

$$C_{a2} = U\phi = 298 \times 0.95 = 283 \text{ m/s}$$

$$\cos\alpha_2 = \frac{C_{a2}}{C_2} = \frac{283}{600} = 0.4716$$

$$\alpha_2 = 62°$$

Since

$$\frac{U}{C_a} = \tan\alpha_2 - \tan\beta_2 = \frac{1}{\phi}$$

then

$$\tan\beta_2 = \tan\alpha_2 - \frac{1}{\phi} = 0.828$$

$$\beta_2 = 39.6°$$

The specified work, W_s, is expressed as

$$W_s = C_P \Delta T_0 = U\left(C_{U2} + C_{U3}\right) = UC_a\left(\tan\alpha_2 + \tan\alpha_3\right)$$

$$\tan\alpha_2 = \frac{C_P \Delta T_0}{UC_a} - \tan\alpha_3 = \frac{1148 \times 144}{298 \times 283} - 1.8807 = 0.0793$$

$$\alpha_3 = 4.54°$$

$$\frac{U}{C_a} = \tan\alpha_3 - \tan\beta_3$$

$$\tan\beta_3 = \frac{1}{\phi} + \tan\alpha_3 = 1.0526 + 0.0794 = 1.132$$

$$\beta_3 = 48.54°$$

Example 14.3

A single-stage axial-flow turbine has a mean radius of 30 cm and a blade height at the stator inlet of 6 cm. The hot gases enter the turbine stage at 1900 kPa and 1200 K, and the absolute velocity leaving the stator (C_2) is 600 m/s and inclined at an angle of 65° to the axial direction. The relative angles at the inlet and outlet of the rotor blade are 25° and 60°, respectively. The stage efficiency is 0.88.

Calculate

1. The absolute angle α_3
2. The rotor rotational speed in rpm
3. The stage pressure ratio
4. The flow coefficient, blade loading coefficient and degree of reaction
5. The mass flow rate
6. The power delivered by the turbine

Take $\gamma = 1.33$, $R = 290$ J/kg·K, and Ca/U as constant through the stage.

Solution

1. The given angles are $\alpha_2 = 65°$, $\beta_2 = 25°$, $\beta_3 = 60°$.
   From Equation 14.1c,

$$\tan\alpha_3 = \tan\beta_3 - \tan\alpha_2 + \tan\beta_2 = 0.0539$$

   Then

$$\alpha_3 = 3.08°$$

2. Since $C_a = C_2 \cos\alpha_2 = 600\cos 65 = 253.57$ m/s.
   From Equation 14.1c,

$$U = C_a\left(\tan\alpha_2 - \tan\beta_2\right) = 253.57 \times \left(\tan 65 - \tan 25\right) = 425.5 \text{ m/s}$$

But $U = \pi ND/60$, so then

$$N = 60 \times 425.5/\pi \times 0.6 = 13{,}545 \text{ rpm}$$

3. From Equation 14.9c, with $\beta_2 = 25°$, $\beta = 60°$ and

$$Cp = \gamma R/(\gamma - 1) = 1168.8 \text{ J/kg} \cdot \text{K}$$

$$\Delta T_{0stage} = \frac{425.5 \times 253.37}{1168.8}(\tan 25 + \tan 60) = 202.77 \text{ K}$$

From Equation 14.14, the stage pressure ratio is

$$\pi_{stage} = \frac{P_{01}}{P_{03}} = \frac{1}{\left(1 - \frac{\Delta T_{0s}}{\eta_s T_{01}}\right)^{\gamma/\gamma - 1}} = \frac{1}{\left(1 - \frac{202.77}{0.88 \times 1200}\right)^4} = 2.346$$

4. The flow coefficient $\phi = C_a/U = 0.6$.
   The blade loading coefficient, ψ, is given by the relation

$$\psi = \frac{C_p \Delta T_{0stage}}{U^2} = \frac{1168.8 \times 202.77}{(425.5)^2} = 1.309$$

From the degree of reaction Equation 14.32a,

$$\Lambda = \phi(\tan\beta_3 - \tan\beta_2)/2 = 0.41$$

5. From Equation 14.1c,

$$\tan\beta_3 - \tan\alpha_3 = \frac{U}{C_a}$$

$$\tan\alpha_3 = \tan 60 - \frac{425.5}{253.57} = 3.1°$$

$$C_3 = \frac{C_a}{\cos\alpha_3} = \frac{253.57}{\cos 3.1} = 253.94 \text{ m/s}$$

Assuming that $C_1 = C_3$, then the static conditions at the stage inlet are calculated as follows:

$$T_1 = T_{01} - \frac{C_1^2}{2C_p} = 1200 - \frac{(253.94)^2}{2 \times 1168.8} = 1172.4 \text{ K}$$

$$P_1 = P_{01}\left(\frac{T_1}{T_{01}}\right)^{\gamma/\gamma - 1} = 1900 \times 10^3 \left(\frac{1172.4}{1200}\right)^4 = 1731 \times 10^3 \text{ Pa}$$

$$\rho_1 = \frac{P_1}{RT_1} = \frac{1731 \times 10^3}{290 \times 1172.4} = 5.09 \text{ kg/m}^3$$

The annulus area at the inlet is $A_1 = \pi D_m h = \pi \times 0.6 \times 0.06 = 0.1131$ m^2.
The mass flow rate is $\dot{m} = \rho_1 C_a A_1 = 5.09 \times 253.57 \times 0.1131 = 145.97$ kg/m^3.

6. Power $= \dot{m} C_p \Delta T_{0stage} = 145.97 \times 1.1688 \times 202.77 = 34{,}600$ kW

Power = 34.6 MW

14.4 Three-Dimensional Analysis

A similar procedure to that followed in Chapter 13 will be followed here. It is assumed that all the radial motion of the particle takes place within the blade row passages, while radial equilibrium is assumed in the axial spacing between the successive blade rows. Thus the stream surface in the spacing between the blade rows has a cylindrical stream surface shape.

$$C_r \ll C_a, \quad C_r \ll C_u, \quad \text{thus} \quad C_r \approx 0$$

For steady flow, the *simplified radial equilibrium equation*, Equation 13.28, is valid.

$$\frac{1}{\rho}\frac{dp}{dr} = \frac{C_u^2}{r} \tag{14.43}$$

Substituting the radial equilibrium equation into the stagnation enthalpy, neglecting second-order terms and also neglecting entropy changes in the radial direction, the vortex energy equation, Equation 13.29, is also derived.

$$\frac{dh_0}{dr} = C_a \frac{dc_a}{dr} + C_u \frac{dC_u}{dr} + \frac{C_u^2}{r} \tag{14.44}$$

Solution of Equation 13.29 provides a simplified three-dimensional analysis of the flow. The three-dimensional nature of the flow affects the variation of the gas angles with the radius (from root to tip) as U increases with the radius. Also, the whirl component in the flow outlet from the nozzles causes the static pressure and temperature to vary across the annulus. Twisted blading designed to account for the changing gas angles is called *vortex blading*.

The following three methods will be examined:

1. Free vortex
2. Constant nozzle angle, which is subdivided into three cases:
   a. General case
   b. Zero exit swirl
   c. Free vortex at rotor outlet
3. General N-case, where the swirl velocity is proportional to the radius raised to the power N

14.4.1 Free Vortex Design

As pointed out Reference 3, for design purposes, it is usually assumed that the total enthalpy (h_{01}) and entropy are constant at entry to the stage, or $dh_{01}/dr = 0$. A *free vortex stage* will be obtained if $dh_{01}/dr = 0$, and the whirl velocity components at the rotor inlet and outlet satisfy the conditions

$$rC_{u2} = \text{constant} \quad \text{and} \quad rC_{u3} = \text{constant}$$

This can be justified as follows. Since no work is done by the gases in the nozzle then the total enthalpy at the nozzle outlet (h_{02}) must also be constant over the annulus at the outlet. At the nozzle outlet, if the whirl velocity component of the flow (C_u) is inversely proportional to the radius, rC_{u2} = constant, then it follows from the radial equilibrium equation (13.28) that $dC_{a2}/dr = 0$, and the axial velocity (C_{a2}) is constant across the annulus. Assuming also that the whirl velocity at the rotor inlet is inversely proportional to the radius, or rC_{u3} = constant, then the specific work is

$$h_{o2} - h_{03} = U\left(C_{u2} + C_{u3}\right) = \omega\left(rC_{u2} + rC_{u3}\right) = \text{constant}$$

Thus, the total enthalpy at the rotor outlet (h_{03}) is constant over the annulus. With rC_{u3} = constant, the axial velocity (C_{a3}) is also constant.

To evaluate the angles at any radius, since axial velocity is constant, then $rC_{u2} = rC_{a2}\tan\alpha_2 = \text{constant}$ or $r\tan\alpha_2 = \text{constant}$.

From Equation 14.1a, the relative angle β_2 may be obtained. The same procedure may be followed for the rotor outlet.

As a summary of the free vortex design:

State (*1*): All the properties are constant along the annulus.

State (*2*): $rC_{u2} = \text{constant}$, $C_{a2} = \text{constant}$,

$$\tan\alpha_2 = \left(\frac{r_m}{r}\right)_2 \tan\alpha_{2m} \tag{14.45a}$$

$$\tan\beta_2 = \left(r_m/r\right)_2 \tan\alpha_{2_m} - \left(r/r_m\right)_2 \frac{U_m}{C_{a2}} \tag{14.46a}$$

State (*3*): $rC_{u3} = \text{constant}\ C_{a3} = C_{a2} = \text{constant}$,

$$\tan\alpha_3 = \left(\frac{r_m}{r}\right)_3 \tan\alpha_{3m} \tag{14.45b}$$

$$\tan\beta_3 = \left(r_m/r\right)_3 \tan\alpha_{3m} + \left(r/r_m\right)_3 \frac{U_m}{C_{a3}} \tag{14.46b}$$

14.4.2 Constant Nozzle Angle Design (α_2)

An alternative design procedure to free vortex flow is the constant nozzle angle. The appropriate conditions that also provide radial equilibrium are

1. Uniform flow in the annulus space between the nozzles and rotor blades, which is satisfied when the outlet flow to the nozzle is uniform; $dh_{o2}/dr = 0$
2. Constant nozzle outlet angle (α_2), which avoids having to manufacture nozzles with varying outlet angles

Since

$$\cot\alpha_2 = \frac{C_{a2}}{C_{u2}} = \text{constant} \tag{14.47}$$

then

$$C_{a2} = C_{u2}\cot\alpha_2 \quad \text{and} \quad \frac{dC_{a2}}{dr} = \frac{dC_{u2}}{dr}\cot\alpha_2$$

From the vortex energy equation (Equation 13.29) and Equation 14.47,

$$C_{u2}\cot^2\alpha_2\frac{dC_{u2}}{dr} + C_{u2}\frac{dC_{u2}}{dr} + \frac{C_{u2}^2}{r} = 0$$

$$C_{u2}\left(1+\cot^2\alpha_2\right)\frac{dC_{u2}}{dr} + \frac{C_{u2}^2}{r} = 0$$

$$\frac{dC_{u2}}{C_{u2}} = -\sin^2\alpha_2\frac{dr}{r}$$

Integrate to get

$$C_{u2}r^{\left(\sin^2\alpha_2\right)} = \text{constant} \tag{14.48a}$$

or

$$C_{u2} = C_{u2m}\left(\frac{r_m}{r}\right)^{\sin^2\alpha_2} \tag{14.48b}$$

Similarly

$$C_{a2}r^{\left(\sin^2\alpha_2\right)} = \text{constant} \tag{14.49a}$$

or

$$C_{a2} = C_{a2m}\left(\frac{r_m}{r}\right)^{\sin^2\alpha_2} \tag{14.49b}$$

Also, the absolute velocity will have the expression

$$C_2 = C_{2m}\left(\frac{r_m}{r}\right)^{\sin^2\alpha_2} \tag{14.50}$$

Normally, nozzle angles are greater than 60°, and thus quite a good *approximate* solution is obtained by designing with a constant nozzle angle and constant angular momentum, or

$$\alpha_2 = \text{constant} \quad \text{and} \quad rC_{u2} = \text{constant}$$

Or in other words,

$$\alpha_2 = \text{constant} \quad \text{and} \quad \frac{C_{u2}}{C_{u2m}} = \frac{C_{a2}}{C_{a2m}} = \frac{C_2}{C_{2m}} = \frac{r_m}{r} \tag{14.51}$$

So far the conditions at the rotor inlet are properly defined. It remains to define the conditions at the rotor exit, or at state (3). Three cases are available for the rotor outlet, namely

1. Constant total enthalpy at outlet
2. Zero whirl at outlet
3. Free vortex at outlet

Case (*1*): *Constant total enthalpy at outlet*

The total enthalpy is constant at all the states of the turbine stages, which means that the specific work is also constant.

Since

$$U\left(C_{u2} + C_{u3}\right) = \Delta h_0$$

then

$$C_{u3} = \frac{\Delta h_0}{U} - C_{u2} = \frac{K}{r} - C_{u2} = \frac{K}{r} - C_{a2}\tan\alpha_2$$

where $K = \Delta h_0/\omega$

Or

$$C_{u3} = \frac{K}{r} - C_{a2m}\left(\frac{r_m}{r}\right)^{\sin^2\alpha_2}\tan\alpha_2 \tag{14.52}$$

The axial velocity at station 3 (Figure 14.17) obtained from the vortex energy equation and has the following expression [8]:

$$C_{a3}^2 = C_{a2m}^2\left(\frac{r_m}{r}\right)^{2\sin^2\alpha_2} - \frac{\sin\left(2\alpha_2\right)}{1+\sin^2\alpha_2}\frac{c_{a2m}K}{r_m}\left[\left(\frac{r_m}{r}\right)^{1+\sin^2\alpha_2} - 1\right] + C_{a3m}^2 - C_{a2m}^2 \tag{14.53}$$

Case (2): *Zero whirl angle* ($\alpha_3 = zero$)

Since the flow leaves the rotor axially, then $C_{u3} = 0$, and so the vortex energy equation (Equation 13.29) becomes

$$\frac{dh_{03}}{dr} = C_{a3}\frac{dC_{a3}}{dr} \tag{14.54}$$

Also

$$h_{03} = h_{01} - UC_{u2} = h_{01} - UC_{u2m}\left(\frac{r_m}{r}\right)^{\sin^2\alpha_2}$$

$$\frac{dh_{03}}{dr} = -\frac{d}{dr}\left[UC_{u2m}\left(\frac{r_m}{r}\right)^{\sin^2\alpha_2}\right] \tag{14.55}$$

From Equations 14.54 and 14.55,

$$C_{a3}^2 = C_{a3m}^2 + 2U_mC_{u2m}\left[1-\left(\frac{r}{r_m}\right)^{\cos^2\alpha_2}\right] \tag{14.56}$$

Case (3): *Free vortex at rotor outlet* ($rC_{u3} = constant$)

The whirl component at different radii is expressed as $C_{u3} = \frac{r_m}{r}C_{u3m}$.

Following the same procedure as before, the axial velocity will have the same expression in Equation 14.56.

14.4.3 General Case

According to the vortex energy equation (Equation 13.29), if the total enthalpy is radially constant it is expressed by

$$C_a\frac{dC_a}{dr} + C_u\frac{dC_u}{dr} + \frac{C_u^2}{r} = 0 \tag{14.57}$$

Consider a general variation for swirl velocity (C_u) with the radius [9] as

$$C_u = Kr^N \tag{14.58a}$$

or in terms of mean-section conditions

$$\frac{C_u}{C_{um}} = \left(\frac{r}{r_m}\right)^N \tag{14.58b}$$

Substituting Equation 14.58a into the vortex energy equation and then integrating between the limit of r_m and r,

$$\frac{C_a}{C_{am}} = \left\{1 - \tan^2\alpha_m\left(\frac{N+1}{N}\right)\left[\left(\frac{r}{r_m}\right)^{2N} - 1\right]\right\}^{1/2} \qquad N \neq 0 \tag{14.59}$$

Equation 14.59 is not valid for the special case of $N = 0$ (constant C_u). For this special case, Equation 14.57 will be reduced to

$$\frac{C_u^2}{r} + \frac{1}{2}\frac{d}{dr}\left(C_a^2\right) = 0$$

Integrate to get

$$\frac{C_a}{C_{am}} = \left[1 - 2\tan^2\alpha_m \ln\frac{r}{r_m}\right]^{1/2} \qquad N = 0 \tag{14.60}$$

In the general case, Equation 14.58a and b is valid for any value of $N \neq 0$. The case of free vortex, $N = -1$, provides constant axial velocity in the radial direction (or $C_a = C_{am} = 1$), as was proved earlier. The radial variation in the axial velocity is largely dependent on the specified swirl velocity variation (value of N). Two important notes have to be stated here [9]:

1. Axial velocities and flow angles (α_2) associated with certain values of N cannot be obtained with all blade lengths.
2. The range of N that can be used for design purposes becomes larger as the blades become shorter (values of r_h/r_m and r_t/r_m become closer to 1).

As described in Reference 9, free vortex is so commonly used that all other designs are often classified under the common heading of *non-free vortex*. The non-free vortex designs are used to alleviate some of the potential disadvantages associated with the free vortex design, namely, large variations in the degree of reaction across the blade, and large blade twist. Thus a turbine blade has the potential to have low degree of reaction at root, thus nearly an impulse blading may be the case at blade root and large degree of reaction at tip. The latter can also be troublesome because it increases the leakage across the blade tip clearance space. The following cases are distanced:

1. $N = -2$, the super vortex
2. $N = -1$, the free vortex
3. $N = 0$, the constant swirl velocity
4. $N = 1$, the wheel flow or solid rotation

14.4.4 Constant Specific Mass Flow Stage

Another design procedure that satisfies the radial equilibrium equation is the constant specific mass flow or the constant mass flow per unit area at all radii. Consider an infinitesimal annulus area between the hub and the casing of an axial turbine (Figure 14.18).

$$d\dot{m} = \rho C_a dA$$

$$\frac{d\dot{m}}{dA} = \rho C_a = \text{constant} \equiv K_1$$

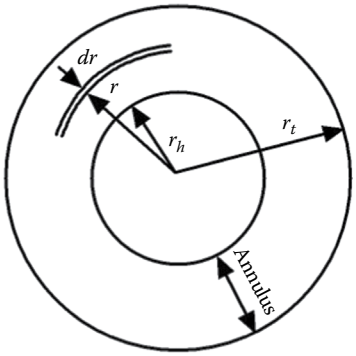


FIGURE 14.18
Flow through infinitesimal annulus in axial turbine.

$$\rho^2 = \frac{K_1^2}{C^2 \cos^2 \alpha} \tag{14.61a}$$

$$\cos \alpha = \frac{\rho_m C_m}{\rho C} \cos \alpha_m \tag{14.61b}$$

But in the radial equilibrium equation (Equation 14.43)

$$\frac{1}{\rho}\frac{dp}{dr} = \frac{1}{\rho}\left(\frac{dp}{d\rho}\right)_s \frac{d\rho}{dr} = \frac{a^2}{\rho}\frac{d\rho}{dr} = \frac{C_u^2}{r} = \frac{C^2 \sin^2 \alpha}{r} \tag{14.62}$$

where $a = \sqrt{\gamma RT}$ is the speed of sound.

The density temperature relation

$$\frac{T}{\rho^{\gamma-1}} = K_2 = \text{constant} \tag{14.63}$$

From Equations 14.62 and 14.63

$$\frac{1}{\rho}\left(K_2 \gamma R \rho^{\gamma-1}\right)\frac{d\rho}{dr} = \frac{C^2 \sin^2 \alpha}{r}$$

$$\gamma R K_2 \frac{\rho^\gamma}{\rho^2}\frac{d\rho}{dr} = \frac{C^2 \sin^2 \alpha}{r}$$

Substituting ρ^2 from Equation 14.62

$$\therefore \frac{\gamma R K_2 \rho^\gamma}{\left(K_1^2 / C^2 \cos^2 \alpha\right)}\frac{d\rho}{dr} = \frac{C^2 \sin^2 \alpha}{r}$$

$$\frac{K_2}{K_1^2}\gamma R \int_{\rho_m}^{\rho} \rho^\gamma d\rho = \int_{r_m}^{r} \tan^2 \alpha \frac{dr}{r}$$

$$\left(\frac{K_2}{K_1^2}\right)\left(\frac{\gamma R}{\gamma+1}\right)\left(\rho^{\gamma+1}-\rho_m^{\gamma+1}\right)=\int_{r_m}^{r}\tan^2\alpha\frac{dr}{r}$$

$$\rho=\left[\rho_m^{\gamma+1}+\left(\frac{K_1^2}{K_2}\right)\left(\frac{\gamma+1}{\gamma R}\right)\int_{r_m}^{r}\tan^2\alpha\frac{dr}{r}\right]^{1/\gamma+1} \tag{14.64}$$

To derive a relation for the absolute velocity variation across the annulus from the total enthalpy relation ($h=h_0-C^2/2$) and entropy enthalpy relation ($Tds=dh-dp/\rho$), and assuming that the total enthalpy and entropy are constants along the radial direction, then

$$\frac{dh}{dr}=\frac{dh_0}{dr}-\frac{1}{2}\frac{d}{dr}\left(C^2\right)$$

$$T\frac{ds}{dr}=\frac{dh}{dr}-\frac{1}{\rho}\frac{dp}{dr}=\frac{dh_0}{dr}-\frac{1}{2}\frac{d}{dr}\left(C^2\right)-\frac{1}{\rho}\frac{dp}{dr}$$

$$\frac{1}{\rho}\frac{dp}{dr}=-C\frac{dC}{dr} \tag{14.65a}$$

From the radial equilibrium equation

$$\frac{1}{\rho}\frac{dp}{dr}=\frac{C_u^2}{r}=\frac{C^2\sin^2\alpha}{r} \tag{14.65b}$$

From Equation 14.65a and b

$$\frac{C^2\sin^2\alpha}{r}=-C\frac{dC}{dr}$$

$$\int_{C_m}^{C}\frac{dC}{C}=-\int_{r_m}^{r}\sin^2\alpha\frac{dr}{r}=\int_{r}^{r_m}\sin^2\alpha\frac{dr}{r}$$

$$\ln\frac{C}{C_m}=\int_{r}^{r_m}\sin^2\alpha\frac{dr}{r}$$

$$C=C_m\exp\left(\int_{r}^{r_m}\sin^2\alpha\frac{dr}{r}\right) \tag{14.66}$$

Then, Equations 14.61a, b, 14.64, 14.65a, and b are used to determine the variations in density (ρ), velocity (C), and angle (α), respectively, along the radial direction. The calculations

can be done by adopting a step-by-step method for infinitesimal lengths Δr along the blade height. The value of (α) may be assumed to be constant over the small span Δr [10].

Example 14.4

An axial turbine has the following data:

$$\zeta = 0.8, \quad \alpha_{2m} = 60, \quad \alpha_3 = 0, \quad \Lambda_m = 0.5, \quad \text{and} \quad C_{am} = 200 \text{ m/s}$$

Three design methods are to be examined. The governing equations for each are given as follows:

Method (*1*)

$$C_{u2m} = C_{u2h}$$

Method (*2*)

$$\frac{C_{a2t}}{C_{a2h}} = \zeta^{\sin^2 \alpha_2}$$

Method (*3*)

$$\frac{C_{u2t}}{C_{u2h}} = \zeta$$

It is required to

1. Identify the design method.
2. Calculate the values of the angles α_2, α_3, β_2, β_3 at the hub, mean, and tip sections.
3. Draw the velocity triangles at the hub and tip.

Solution

Given data

$$\zeta = 0.8 \quad \alpha_3 = 0 \quad \alpha_{2m} = 60$$

$$\Lambda_m = 0.5 \quad Ca_m = 200 \text{ m/s}$$

At any radius along the blade

$$\alpha_2 = \tan^{-1}\left(\frac{C_{u2}}{C_{a2}}\right), \quad \beta_2 = \tan^{-1}\left(\frac{C_{u2} - U}{C_{a2}}\right)$$

$$\frac{r_h}{r_m} = \frac{2\zeta}{1+\zeta} = \frac{1.6}{1.8} = 0.889$$

$$\frac{r_t}{r_m} = \frac{2}{1+\zeta} = \frac{2}{1.8} = 1.111$$

At the mean section

$$C_{a2} = 200 \text{ m/s}$$

$$C_{u2} = C_{a2} \times \tan\alpha_2 = 346.41 \text{ m/s}$$

$$C_{u3} = 0$$

$$U = C_{u2} = 346.41 \text{ m/s}$$

Moreover, since $\Lambda = 0.5$, then

$$\alpha_2 = \beta_3 = 60^\circ, \quad \alpha_3 = \beta_2 = 0$$

The rotational speed at any radius is $U_i = (r_i/r_m) \times U_m$, thus

$$U_h = 307.92 \text{ m/s} \quad \text{and} \quad U_t = 384.9 \text{ m/s}$$

Method (*1*): Since C_{u2} = constant along the blade height, then from Equation 14.57 this design method is the *general power case* with $N = 0$.

The axial speed (C_{a2}) is calculated from Equation 14.59, which is expressed in state (2) as

$$C_{a2} = C_{am}\left[1 - 2\tan^2\alpha_m \ln\frac{r}{r_m}\right]^{1/2}$$

Since $\alpha_3 = 0$, then from the same Equation 14.59 but applied at state (2), C_{a3} = constant from blade hub to tip. Moreover, since $\alpha_3 = 0$, then $C_{u3} = 0$ along the blade height. The angles β_2 and β_3 are calculated from Equation 14.1c. The results are summarized in Table 14.3.

A plot for the results is shown in Figure 14.19.

The velocity triangles are shown in Figure 14.20.

Method (*2*): Since $C_{a2t} = C_{a2h} = \varsigma^{\sin^2\alpha_2}$, then

$$\frac{Ca_{2t}}{Ca_{2h}} = \left(\frac{r_h}{r_t}\right)^{\sin^2\alpha_2} = \left(\frac{r_m}{r_t}\right)^{\sin^2\alpha_2}\left(\frac{r_h}{r_m}\right)^{\sin^2\alpha_2}$$

TABLE 14.3

Hub-to-Tip Variations of Flow Characteristics in the Rotor Blade

	C_{a2} (m/s)	C_{a3} (m/s)	C_{u2} (m/s)	C_{u3} (m/s)	α_2	α_3	β_2	β_3
Hub	261.3	200	346.4	0	52.97	0	8.4	56.99
Mean	200	200	346.4	0	60	0	0	60
Tip	121.3	200	346.4	0	70.7	0	−17	62.54

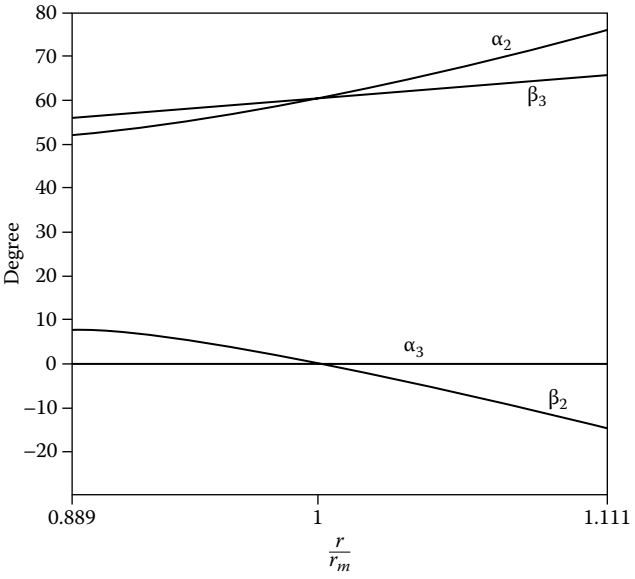


FIGURE 14.19
Variation of flow angles for case (1).

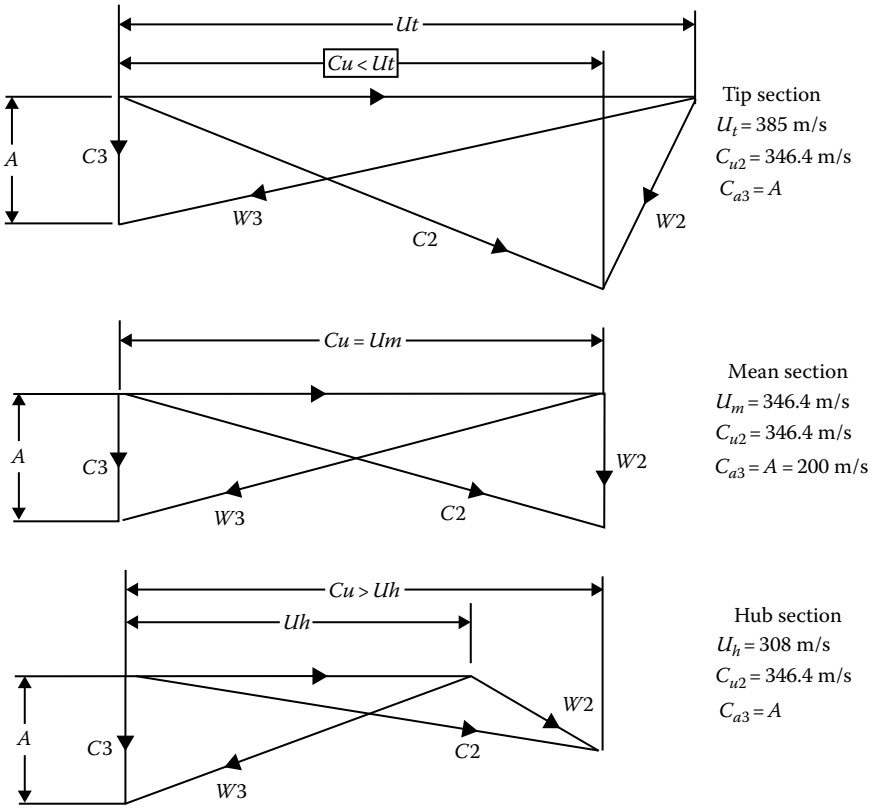


FIGURE 14.20
Velocity triangles for case (1).

This design method is the *constant nozzle angle* at state (2), or

$$Ca_2 = Ca_{2m}\left(\frac{r_m}{r}\right)^{\sin^2\alpha_2}, \quad Cu_2 = Cu_{2m}\left(\frac{r_m}{r}\right)^{\sin^2\alpha_2}, \quad C_2 = C_{2m}\left(\frac{r_m}{r}\right)^{\sin^2\alpha_2}$$

At state (3), $\alpha_3 = 0$, $C_{u3} = 0$

$$C_{a3}^2 = C_{a3m}^2 + 2U_m C_{u2m}\left[1 - \left(\frac{r}{r_m}\right)^{\cos^2\alpha_2}\right]$$

It is deduced here that all the velocity components C_{u2}, C_{a2}, and C_{a3} are variables.

	C_{a2}	C_{a3}	C_{u2}	C_{u2}	α_2	α_3	β_2	β_3
Hub	218.47	216.71	378.4	0	60	0	17.885	54.86
Mean	200	200	346.41	0	60	0	0	60
Tip	184.8	183.29	320.09	0	60	0	−19.35	64.53

A plot for the results is shown in Figure 14.21.
The velocity triangles are shown in Figure 14.22.

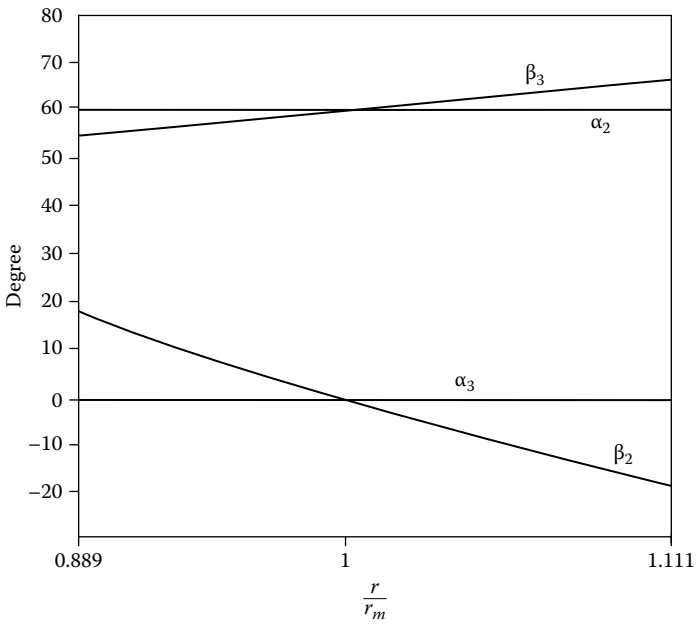


FIGURE 14.21
Variation of flow angles for case (2).

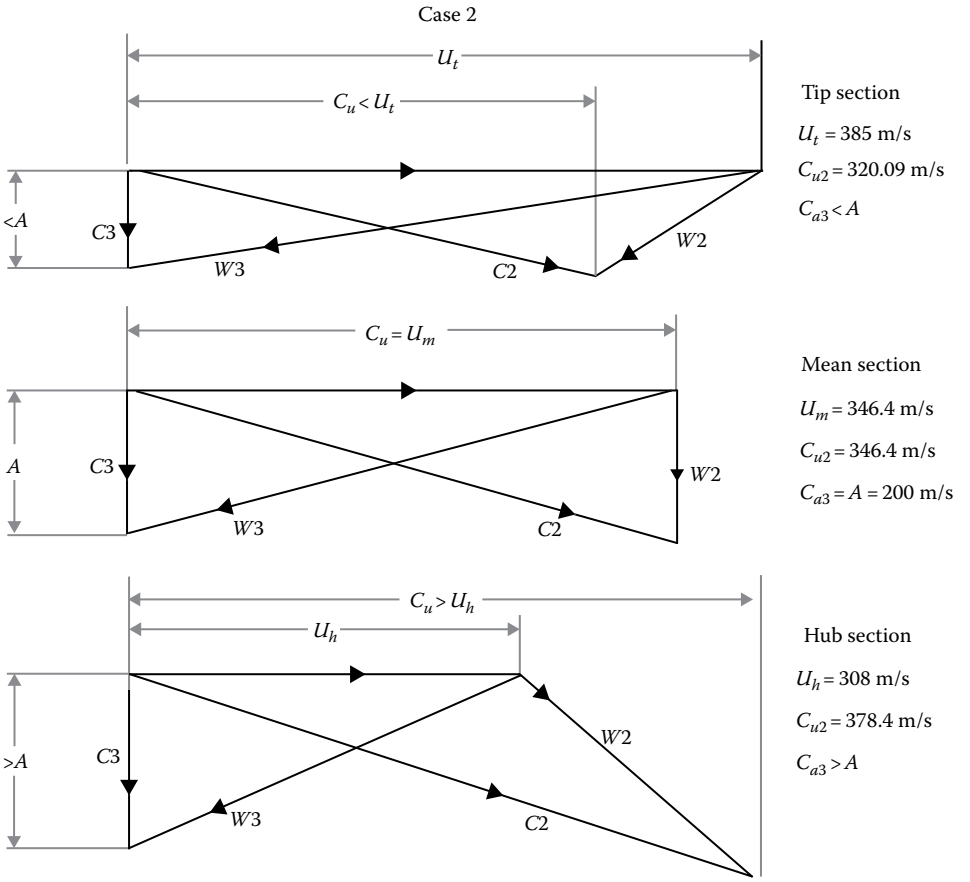


FIGURE 14.22
Velocity triangles for case (2).

Method (3): Since

$$\frac{Cu_{2t}}{Cu_{2h}} = \zeta = \frac{r_h}{r_t}$$

or rCu_2 = constant, then this design method is *free vortex*.

At the rotor outlet, the flow is also a free vortex, or rCu_3 = constant.

The axial velocity is then constant at both states (2) and (3), or

$$Ca_2 = Ca_{2m} = Ca_3 = Ca_{3m} = \text{constant}$$

	Ca_2	Ca_3	Cu_2	Cu_3	α_2	α_3	β_2	β_3
Hub	200	200	389.7	0	62.833	0	22.247	56.994
Mean	200	200	346.41	0	60	0	0	60
Tip	200	200	311.77	0	57.32	0	−20.85	62.549

A plot for the results is shown in Figure 14.23.

The velocity triangles are shown in Figure 14.24.

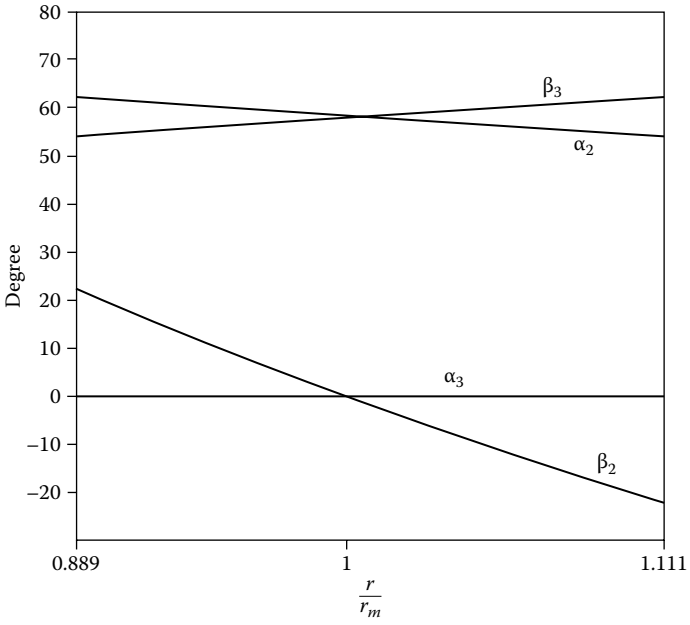


FIGURE 14.23
Variation of flow angles for case (3).

Example 14.5

1. Two design methods are used in an axial turbine design. In the first method, the swirl velocity at radius (r) is (C_u), and the swirl velocity at the same radius (r) in the second method is (C'_u). If the ratio between the two swirl velocities is given by the ratio

$$\frac{C_u}{C'_u} = \lambda r^2$$

   a. What will be the value of the constant (λ) and what may be those design methods?
   b. Deduce a relation for the ratio between the axial velocities (C_a/C'_a) at radius (r) for both design methods.
2. A constant nozzle design method is used for the design of an axial turbine stage with a free vortex design at state (3). Use the following data to obtain the variations in the angles and speeds from hub to tip:

$$\alpha_{2m} = 58.5, \quad \beta_{2m} = 20.5, \quad \alpha_{3m} = 10, \quad \beta_{3m} = 55$$

$$\left(\frac{r_m}{r_r}\right)_2 = 1.16, \quad \left(\frac{r_m}{r_t}\right)_2 = 0.88, \quad \left(\frac{r_m}{r_r}\right)_3 = 1.22, \quad \left(\frac{r_m}{r_t}\right)_3 = 0.85$$

$$\frac{U_m}{C_{a2}} = \frac{U_m}{C_{a3}} = 1.25, \quad U_m = 340 \text{ m/s}$$

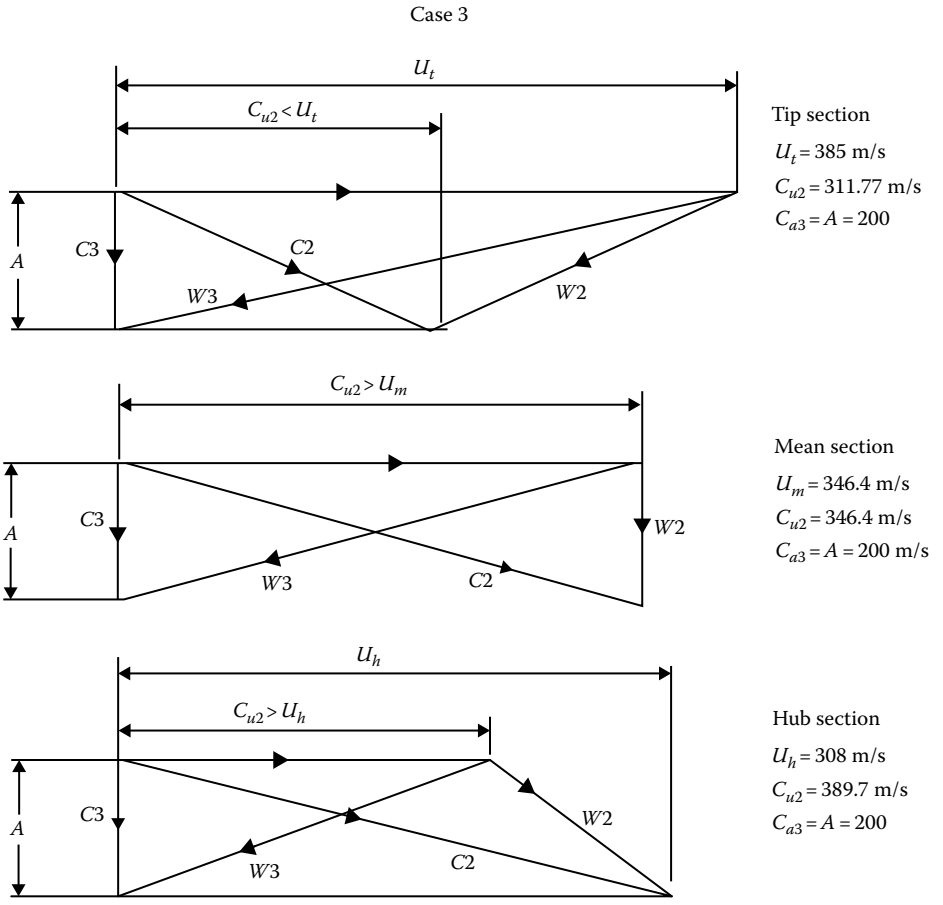


FIGURE 14.24
Velocity triangles for case (3).

Solution

1. a. For general power with $N = 1$ at radius (r), the whirl velocity is C_u.

$$C_u = C_{um}\left(\frac{r}{r_m}\right)^N$$

For $N = 1$, then $C_u = C_{um}(r/r_m)$

Next, for free vortex design at radius (r), the whirl velocity is C'_u.

$$rC'_u = \text{constant} \quad \text{or} \quad rC'_u = r_m C_{um}$$

$$C'_u = \frac{r_m}{r} C_{um}$$

Then

$$\frac{C_u}{C'_u} = \frac{r}{r_m} \times \frac{r}{r_m} = \frac{r^2}{r_m^2}$$

The value of the constant in both cases is $\lambda = 1/r_m^2$.

The relation between the axial velocities

b. For general power with $N = 1$ at radius (r), the axial velocity is C_a.

$$\frac{C_a}{C_{am}} = \left\{1 - \tan^2 \alpha_m \left(\frac{N+1}{N}\right)\left[\left(\frac{r}{r_m}\right)^{2N} - 1\right]\right\}^{1/2}$$

For $N = 1$

$$\frac{C_a}{C_{am}} = \left\{1 - 2\tan^2 \alpha_m \left[\left(\frac{r}{r_m}\right)^{2} - 1\right]\right\}^{1/2}$$

Next, for free vortex design at radius (r), the whirl velocity is C'_a.

$$C'_a = C_{am} \quad \text{or} \quad \frac{C'_a}{C_{am}} = 1$$

2. i. At the mean (Figure 14.25)

$$U_m = 340 \text{ m/s}, \quad \frac{U_m}{C_{a2}} = 1.25, \quad \frac{340}{C_{a2}} = 1.25, \quad C_{a2m} = C_{a3m} = 272 \text{ m/s}$$

$$C_{u2} = C_{a2} \tan \alpha_2$$

$$C_{u2} = 272 \tan(58.5) \quad C_{u2m} = 443.86 \text{ m/s}$$

$$C_{u3} = C_{a3} \tan \alpha_3$$

$$C_{u3} = 272 \tan(10) \quad C_{u3m} = 47.96 \text{ m/s}$$

ii. At the hub section (Figure 14.26)

$$\alpha_{2r} = \alpha_{2m} = 58.5$$

$$\frac{U_m}{U_{r2}} = \left(\frac{r_m}{r_r}\right)_2$$

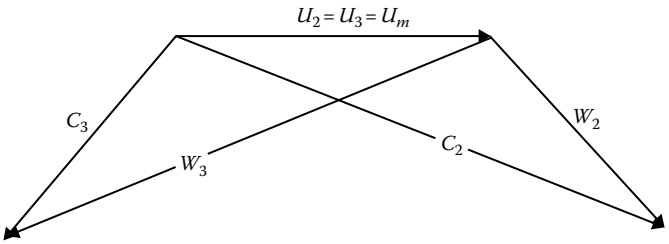


FIGURE 14.25
Mean section velocity triangles.

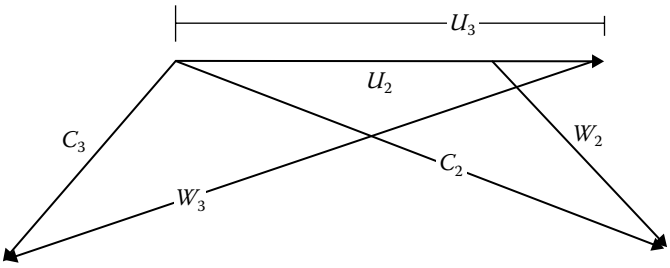


FIGURE 14.26
Velocity triangles at hub section.

$$\frac{340}{U_{r2}} = 1.16 \quad U_{r2} = 293.1 \text{ m/s}$$

$$\frac{U_m}{U_{r3}} = \left(\frac{r_m}{r_r}\right)_3$$

$$\frac{340}{U_{r3}} = 1.22 \quad U_{r3} = 278.69 \text{ m/s}$$

$$C_{a2r} = C_{a2m}\left(\frac{r_m}{r_r}\right)_2^{\sin^2\alpha_2}$$

$$C_{a2r} = 272\left(1.16\right)^{\sin^2(58.5)} = 302.99 \text{ m/s}$$

$$C_{u2r} = C_{u2m}\left(\frac{r_m}{r_r}\right)_2^{\sin^2\alpha_2}$$

$$C_{u2r} = 443.86\left(1.16\right)^{\sin^2(58.5)} = 494.43 \text{ m/s}$$

$$\tan\alpha_2 - \tan\beta_2 = \frac{U_2}{C_{a2}}$$

$$\tan\left(58.5\right) - \tan\beta_2 = \frac{293.1}{302.99} \quad \beta_{2r} = 33.6$$

$$C_{a3r}^2 = C_{a3m}^2 + 2U_m C_{u2m}\left[1 - \left(\frac{r_r}{r_m}\right)_3^{\cos^2\alpha_2}\right]$$

$$C_{a3r}^2 = \left(272\right)^2 + 2\times 340\times 443.86\left[1 - \left(\frac{1}{1.22}\right)^{\cos^2(58.5)}\right] \quad C_{a3r} = 299.89 \text{ m/s}$$

$$\left(rC_u\right)_3 = \text{constant}$$

$$(r_r C_{ur})_3 = (r_m C_{um})_3$$

$$C_{u3r} = C_{u3m}\left(\frac{r_m}{r_r}\right)_3$$

$$C_{u3r} = 47.96 \times 1.22 = 58.511 \text{ m/s}$$

$$\tan\alpha_3 = \frac{C_{u3}}{C_{a3}} = \frac{58.11}{299.89} \quad \alpha_3 = 11.04$$

$$\tan\beta_3 - \tan\alpha_3 = \frac{U_3}{C_{a3}}$$

$$\tan\beta_3 - \tan(11.04) = \frac{278.69}{299.89} \quad \beta_3 = 48.35$$

iii. At the tip (Figure 14.27)

$$\alpha_{2t} = \alpha_{2m} = 58.5$$

$$\frac{U_m}{U_{t2}} = \left(\frac{r_m}{r_t}\right)_2$$

$$\frac{340}{U_{t2}} = 0.88 \quad U_{t2} = 386.36 \text{ m/s}$$

$$\frac{U_m}{U_{t3}} = \left(\frac{r_m}{r_t}\right)_3$$

$$\frac{340}{U_{t3}} = 0.85 \quad U_{t3} = 400 \text{ m/s}$$

$$C_{a2t} = C_{a2m}\left(\frac{r_m}{r_t}\right)_2^{\sin^2\alpha_2}$$

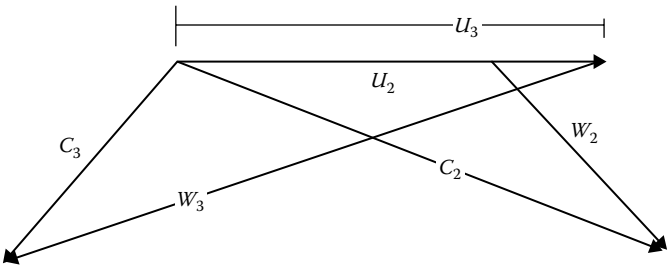


FIGURE 14.27
Velocity triangles at tip section.

$$C_{a2r} = 272\left(0.88\right)^{\sin^2(58.5)} = 247.86 \text{ m/s}$$

$$C_{u2t} = C_{u2m}\left(\frac{r_m}{r_t}\right)_2^{\sin^2\alpha_2}$$

$$C_{u2r} = 443.86\left(0.88\right)^{\sin^2(58.5)} = 404.46 \text{ m/s}$$

$$\tan\alpha_2 - \tan\beta_2 = \frac{U_2}{C_{a2}}$$

$$\tan\left(58.5\right) - \tan\beta_2 = \frac{386.36}{247.86} \quad \beta_{2t} = 3.87$$

$$C_{a3t}^2 = C_{a3m}^2 + 2U_m C_{u2m}\left[1 - \left(\frac{r_t}{r_m}\right)_3^{\cos^2\alpha_2}\right]$$

$$C_{a3t}^2 = \left(272\right)^2 + 2\times 340\times 443.86\left[1 - \left(\frac{1}{0.85}\right)^{\cos^2(58.5)}\right]$$

$$C_{a3t} = 245.54 \text{ m/s}$$

$$\left(rC_u\right)_3 = \text{constant}$$

$$\left(r_t C_{ut}\right)_3 = \left(r_m C_{um}\right)_3$$

$$C_{u3t} = C_{u3m}\left(\frac{r_m}{r_t}\right)_3$$

$$C_{u3r} = 47.96\times 0.85 = 40.766 \text{ m/s}$$

$$\tan\alpha_3 = \frac{C_{u3}}{C_{a3}} = \frac{40.766}{245.54} \quad \alpha_3 = 9.43$$

$$\tan\beta_3 - \tan\alpha_3 = \frac{U_3}{C_{a3}}$$

$$\tan\beta_3 - \tan\left(9.43\right) = \frac{400}{245.54} \quad \beta_3 = 60.88$$

Example 14.6

An axial turbine stage is to be designed with a constant nozzle design. It has the following data:

$\Delta T_o = 150$ K, $U_{2h} = 300$ m/s, $U_{2t} = 400$ m/s, $\alpha_2 = 60$, $\alpha_3 = 0$, and $\zeta_3 = 0.75$

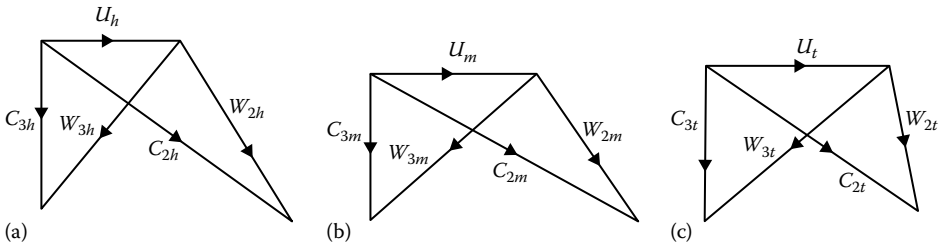


FIGURE 14.28
Velocity triangles at (a) hub, (b) mean, and (c) tip sections.

1. Draw the velocity triangles at the hub, mean, and tip sections using the following relations (Figure 14.28):

$$\frac{C_2}{C_{2m}} = \frac{C_{a_2}}{C_{a2m}} = \frac{C_{u2}}{C_{u2m}} = \left(\frac{r_m}{r}\right)^{(\sin\alpha_2)^2}$$

$$\left(C_{a3}\right)^2 = \left(C_{a3m}\right)^2 + 2U_m \times C_{u2m}\left(1 - \left(\frac{r}{r_m}\right)^{(\cos\alpha_2)^2}\right)$$

2. Use the approximate solution for the constant nozzle blading, namely $\alpha_2 = \text{constant}$ and $rC_{u2} = \text{constant}$, to calculate the axial and tangential velocities at the hub, mean, and tip sections at stations 2 and 3.
3. Using free vortex design, calculate the axial and tangential velocity, as earlier.

Solution

1. Constant nozzle angle design: The axial turbine stage has a constant nozzle outlet angle and zero exit swirl. Since $\zeta = 0.75$, then

$$\frac{r_m}{r_t} = \frac{U_m}{U_t} = \frac{1+\zeta}{2} = 0.875$$

and

$$\frac{r_m}{r_h} = \frac{U_m}{U_h} = \frac{1+\zeta}{2\zeta} = 1.166$$

The specific work is given by the relation

$$Cp\Delta T_o = U_m \Delta C_{um} = U_m C_{u2m}$$

$$C_{u2m} = \frac{Cp\Delta T_o}{U_m} = 492 \text{ m/s}$$

$$C_{a2m} = C_{u2m} \cot\alpha_2$$

$$C_{a2m} = C_{a3m} = 284 \text{ m/s}$$

$$\frac{C_{a2}}{C_{a2m}} = \frac{C_{u2}}{C_{u2m}} = \left(\frac{r_m}{r}\right)^{(\sin\alpha_2)^2}$$

At the hub

$$C_{a2h} = C_{a2m}\left(\frac{r_m}{r_h}\right)^{(\sin\alpha_2)^2} = 318.8 \text{ m/s}$$

$$C_{u2h} = C_{u2m}\left(\frac{r_m}{r_h}\right)^{(\sin\alpha_2)^2} = 552.2 \text{ m/s}$$

At the tip

$$C_{a2t} = C_{a2m}\left(\frac{r_m}{r_t}\right)^{(\sin\alpha_2)^2} = 256.93 \text{ m/s}$$

$$C_{u2t} = C_{u2m}\left(\frac{r_m}{r_t}\right)^{(\sin\alpha_2)^2} = 446.6 \text{ m/s}$$

$$\frac{C_{a2}}{C_{a2m}} = \frac{C_{u2}}{C_{u2m}} = \left(\frac{r_m}{r}\right)^{(\sin\alpha_2)^2}$$

At the rotor outlet

$$\left(C_{a3}\right)^2 - \left(C_{a3m}\right)^2 = 2U_m \times C_{u2m}\left(1 - \left(\frac{r}{r_m}\right)^{(\cos\alpha_2)^2}\right)$$

$$\left(C_{a3t}\right) = \sqrt{\left(C_{a3m}\right)^2 + 2U_m \times C_{u2m}\left(1 - \left(\frac{r_t}{r_m}\right)^{(\cos\alpha_2)^2}\right)} = 262.1 \text{ m/s}$$

$$\left(C_{a3h}\right) = \sqrt{\left(C_{a3m}\right)^2 + 2U_m \times C_{u2m}\left(1 - \left(\frac{r_h}{r_h}\right)^{(\cos\alpha_2)^2}\right)} = 306 \text{ m/s}$$

2. *Approximate constant nozzle* ($\alpha_2 = \text{costant}$, $r\,C_{u2} = \text{constant}$):

$$r_m C_{u2m} = r_h C_{u2h} = r_t C_{u2t}$$

$$C_{u2h} = \frac{r_m C_{u2m}}{r_h}$$

$$C_{a2h} = C_{u2h} \cot\alpha_2$$

$$C_{u2t} = \frac{r_m C_{u2m}}{r_t}$$

$$C_{a2t} = C_{u2t} \cot \alpha_2$$

$$C_{u3h} = C_{u3h} = Zero$$

$$C_{a3}^2 = C_{a3m}^2 + 2U_m C_{u2m} \left[1 - \left(\frac{r}{r_m} \right)^{\cos^2 \alpha_2} \right]$$

$$\left(C_{a3t} \right) = \sqrt{\left(C_{a3m} \right)^2 + 2U_m \times C_{u2m} \left(1 - \left(\frac{r_t}{r_m} \right)^{(\cos \alpha_2)^2} \right)}$$

$$\left(C_{a3h} \right) = \sqrt{\left(C_{a3m} \right)^2 + 2U_m \times C_{u2m} \left(1 - \left(\frac{r_h}{r_h} \right)^{(\cos \alpha_2)^2} \right)}$$

3. *Free vortex design*:

$$\left(rC_u \right)_2 = \text{constant}$$

C_a = constant at inlet and outlet to rotor

Summary of the Velocity Variations Using Different Design Methods

	Constant Nozzle (m/s)	Approximate Constant Nozzle (m/s)	Free Vortex (m/s)
C_{a2h}	318.8	331.2	284
C_{a2m}	284	284	284
C_{a2t}	256.9	248.5	284
C_{u2h}	552.2	573.7	573.7
C_{u2m}	492	492	492
C_{u2t}	446.6	430.5	430
C_{a3h}	306	331.2	284
C_{a3m}	284	284	284
C_{a3t}	262.6	248.5	284

14.5 Preliminary Design

As usual, design procedure is started by *need recognition*. Here, market research defines specific customer requirements. The design itself begins with preliminary studies such as cycle selection and analysis, as described in Chapters 4 through 8; the type of turbomachinery that is used (axial/mixed/radial); as well as the suggested layout. This preliminary procedure defines that the inlet total conditions, expansion ratio, power required, mass flow rate, and shaft speed are known.

If an axial turbine is selected, then the design process starts by preliminary design, including aerodynamic, mechanical, and thermal steps, which are next followed by sophisticated analyses using computational fluid dynamics for simulating the real flow to the best available accuracy. This last step is followed by numerous experimental tests for scaled and prototype models. This design procedure is known as an *iterative procedure*. Thus several checks are carried out during the previous steps, and modifications are adopted when there is a necessity.

14.5.1 Main Design Steps

The following steps are used in preliminary analysis:

1. The number of stages (n) is first determined by assuming the temperature drop per stage. For an aeroengine it is between 140 and 200 K, thus

$$n = \frac{\left(\Delta T_0\right)_{turbine}}{\left(\Delta T_0\right)_{stage}}$$

2. Aerodynamic design. This may be subdivided into mean line design and variations along the blade span.
3. Blade profile selection. The blade profile and the number of blades for both stator and rotor are determined.
4. Structural analysis. This includes mechanical design for blades and disks, rotor dynamic analysis, and modal analysis. Normally both aerodynamic and mechanical designs are closely connected and there is considerable iteration between them.
5. Cooling. The different methods of cooling are examined. In most cases, combinations of these methods are adopted to satisfy an adequate lifetime. Structural and cooling analyses determine the material of both stator and rotor blades.
6. Checking stage efficiency.
7. Off-design.
8. Rig testing.

14.5.2 Aerodynamic Design

This may be subdivided into mean blade design and variations along the blade span.

1. Mean blade design analysis starts by making preliminary choices for the stage loading, flow coefficient, and degree of reaction. For aeroengines, the following design parameters may be used as a guide:
   a. Stage loading ranges from 1.5 to 2.5.
   b. Flow coefficient ranges from 0.8 to 1.0.
   c. Stage efficiency ranges from 0.89 to 0.94.

d. Absolute outlet angle ranges from 0° to 20°.
e. Stator and rotor blade loss coefficients $\lambda_N \approx \lambda_R \approx 0.05$.

The following procedure can be followed next:

i. The stage expansion ratio is determined from Equation 14.14.
ii. The rotational speed is determined from Equation 14.26a, $U_m = \sqrt{Cp\Delta T_{0s}/\psi}$.
iii. If the turbine drives a compressor, the compressor design may require a certain speed or speed range to hold a stable operation at high efficiency. Since the stable range of operation of a compressor and the region of high efficiency of a compressor is much limited in comparison with the turbine, usually the compressor determines the turbine speed, rather than vice versa [11].
The mean radius is next obtained from the relation $r_m = U_m/2\pi N$.
iv. The angles β_2, β_3, α_2, α_3 are determined from Equations 14.33 through 14.36.
v. The axial speed is determined from Equation 14.27b, $C_{a1} = \phi U$.
Assuming the flow is axial at the stage inlet, then

$$C_1 = C_{a1} = C_3$$

vi. Thus, the velocity triangles for the stage can be drawn and the speeds (C_2, W_2, W_3) calculated.
vii. The thermodynamic properties at the inlet and outlet of both stator and rotor blade rows are calculated (T_1, T_2, T_3), (P_1, P_2, P_3) and (ρ_1, ρ_2, ρ_3).
viii. The blade heights (h_1, h_2, h_3), blade widths (W_1, W_2), and spacing between the nozzle and rotor blade rows are calculated.

Some checks are performed here:

I. Flare angle, which is recommended to be less than 25°.
II. Low swirl angle at the stage exit ($\alpha_3 < 20°$), otherwise exit guide vanes may be needed to minimize the losses in the jet pipe and propelling nozzle.
III. The pressure ratio in the nozzle must be less than the critical pressure ratio, or $P_{01}/P_2 < P_{01}/P_c$, if a convergent nozzle is chosen.

2. Three-dimensional flow
The variation of properties in the radial direction is considered using different methods; namely, free vortex, constant nozzle angle, and general power N and constant specific mass flow methods are employed. Early turbine designs relied on the free vortex method, and this is still used in a large number of applications for which it has proved its suitability [11]. In several applications, there is a need to vary the blade angle in an arbitrary function of radius; thus, non-free vortex methods may be employed. The radial equilibrium equation must still apply and implies a certain, not necessarily constant, distribution of work across the span.

Proper selection of the design method may be based on which method satisfies the minimum losses and the highest degree of reaction at root.

14.5.3 Blade Profile Selection

Originally, airfoil sections were laid out manually using a set of circular arcs and straight lines according to various empirical rules based on experience of successful designs. Turbine airfoil sections are thicker than those of compressors to withstand the very high temperatures and allow for cooling holes. Special series are used for turbine airfoils like NACA 4412 and 4415, as well as the British series T6, C7, and RAF 27. Gas turbine airfoil sections were originally derived from steam turbine airfoils with some modifications [4]. These include increasing the maximum thickness and radiusing the trailing edge. As defined in [12], the airfoil is described by a set of eleven parameters including the airfoil radius, axial and tangential chords, inlet and exit blade angles, and leading and trailing edge radii, together with the number of blades and throats. A modern airfoil section generator will typically define the blade pressure and suction surfaces using Bezier polynomials, which provide the designer with great flexibility while maintaining a high degree of continuity in the curve and the derivatives.

Usually, a minimum of three sections at the hub, mean, and tip radii are used. This suffices only for the simplest blade geometries. For complex or three-dimensional shapes, 10 or more sections may be used. Once the blade sections have been generated, cascade testing or a simple computational two-dimensional blade-to-blade analysis may be used. Thus, the velocity or Mach number distribution over the suction and pressure surfaces is determined. The next step is to stack the airfoil section in order to create the three-dimensional blade shape. A stacking line is defined, which determines the relative position of each of the sections with one another. The stacking line does not have to be straight or radial, but it can be curved or leaned to produce complex blade shapes [11]. Sections may be stacked on the center area of each section, or the leading edge, the trailing edge, or some other arbitrary line.

The blade profile and the number of blades for both stator and rotor are determined from Figure 14.29. From known inlet and efflux angles for stator (α_1, α_2) and rotor (β_2, β_3)

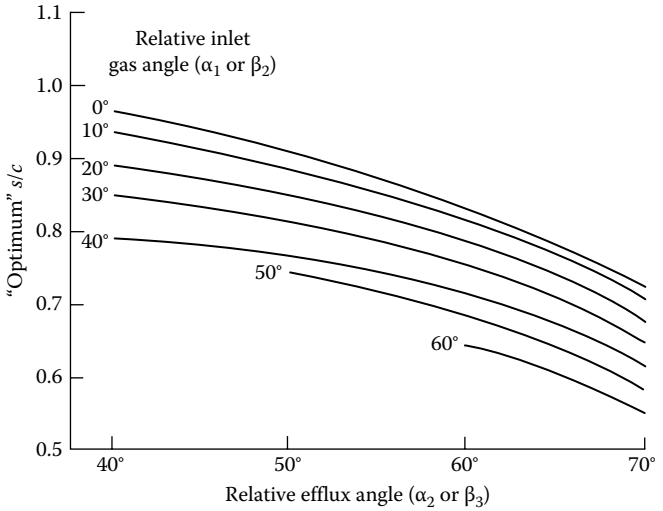


FIGURE 14.29
Optimum pitch/chord ratio. (From Saravanamuttoo, H.I.H. et al., *Gas Turbine Theory*, 5th edn., Prentice Hall, Harlow, U.K., 2001, p. 313. With permission.)

of the mean line flow, the optimum pitch/chord ratio (s/c) is determined. The blade aspect ratio (h/c) ranges from 3 to 4. Since the mean blade height for the nozzle and rotor are determined as

$$h_N = (h_1 + h_2)/2 \quad \text{and} \quad h_R = (h_2 + h_3)/2$$

the corresponding chords for the nozzle and rotor (c_N, c_R) are determined, and thus the spacing for the nozzle and rotor blade rows (s_N, s_R) is determined. Now the number of blades is determined from the relation

$$n_N = 2\pi r_m / s_N \quad \text{and} \quad n_R = 2\pi r_m / s_R$$

It is usual to avoid numbers with common multiples to reduce the possibilities of resonant frequencies. It is common practice to use an even number for the nozzle, and a prime number for the rotor blades.

14.5.4 Mechanical and Structural Design

Mechanical and structural design has a direct impact on aerodynamic design. Both designs are interrelated to achieve high aerodynamic performance, adequate life, and structural integrity. Vibration analysis is so important for rotor blades to avoid resonance and the possibility of blade breakage. An assessment of stress level is considered here.

There are two types of stresses that must be considered, namely, *steady* and *unsteady* stresses.

Steady state stresses arise from the centrifugal, pressure-loading, and thermal sources. Unsteady state stresses arise from the interaction of the rotating blade with stationary features of stators, thermal cycling for turbines downstream combustion chambers as the products of combustion are not completely uniform in the tangential direction [11]. There will be also some mechanical effects caused by residual imbalance and rub-out of bearings. Failure in both cases has different features. Failure due to steady stresses causes the ductile blade material to creep or elongate and ultimately fail in plastic deformation. Failure due to unsteady stresses causes the blade to fail through fatigue due to crack initiation and growth.

Turbine blades in aero engines are designed to avoid creep. The allowable stress in turbines depends strongly on the operating temperature and is specified as that stress that will not exceed a creep extension of, say, 1% for 100,000 h at the specified temperature, since 100,000 h (11.4 years) is a long period of testing [13]. It is common to compare materials to see the stress that causes rupture after 100 h. The rupture stress divided by the blade material density is plotted versus the working temperature. Increasing the working temperature is associated with a reduction of the 100 h rupture stress/density (σ/ρ) ratio. Ceramics have superior strength-temperature characteristics. However, they tend to be brittle and unreliable. Adopting ceramic composites—for example by including very high-strength tin whiskers—may provide a solution to the problem, where high strength and reliability may be achieved. For example, Si_3N_4 ceramic may have a 100 rupture stress/density ratio of 35 (kPa/kg/m^3) at as high a working temperature as 1200°C.

There are three types of mechanical stresses for turbomachines in general. For turbines, there is an additional *thermal stress* due to a high temperature gradient within the blades. The mechanical stresses are

1. Centrifugal stress
2. Gas bending stress
3. Centrifugal bending stress

Centrifugal stress (which is a tensile stress) is important for both the blades and the disks that support them. It is the largest but not necessarily the most important, since it is a steady stress [4]. Bending stress arises in the blades from the aerodynamic forces acting on them due to steady or unsteady conditions. Thermal stress arises due to the temperature gradient within the blade that may be caused by surrounding high-temperature gases and cold air flowing in the cooling passages.

14.5.4.1 Centrifugal Stresses

For a given hub/tip ratio, centrifugal stress at blade root depends on

1. Blade density (ρ_b)
2. Hub-tip radius ratio (ζ)
3. Blade tip speed (U_t)

This increases with blade twist due to centrifugal loading. It can be reduced by tapering the blade's cross-section.

14.5.4.2 Centrifugal Stresses on Blades

Consider the layout of a rotor blade row shown in Figure 14.30. Consider an element on the blade at a radius of (r) having a cross-sectional area A_b and thickness (dr). The element is subjected to a radial stress (σ_r) and a centrifugal force due to its rotation with an angular speed Ω. Force balance of this element yields the following relation:

$$\frac{d}{dr}\left(\sigma_r A_b\right) = -\left(\rho_b A_b\right)\Omega^2 r$$

where ρ_b is the blade material density. If the cross-sectional area is assumed constant, then the previous relation is reduced to

$$\frac{d\sigma_r}{dr} = -\rho_b \Omega^2 r$$

Integrating from any radius to the tip radius and noting that the centrifugal stress is zero at blade tip, the stress at any radius will be

$$\sigma_r = \rho_b \frac{\Omega^2}{2}\left[r_t^2 - r^2\right] = \rho_b \frac{\Omega^2 r_t^2}{2}\left[1 - \left(\frac{r}{r_t}\right)^2\right] = \rho_b \frac{U_t^2}{2}\left[1 - \left(\frac{r}{r_t}\right)^2\right]$$

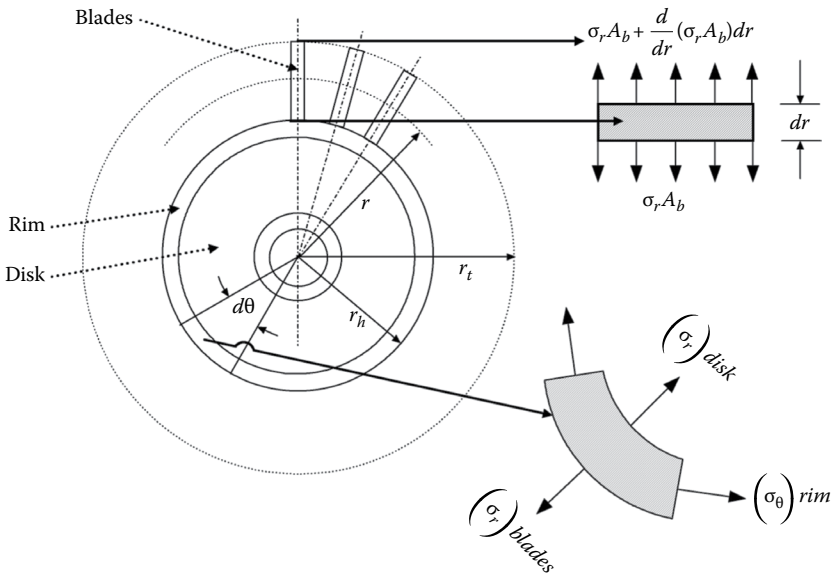


FIGURE 14.30
Stresses in blades.

The maximum centrifugal stress occurs at the blade hub radius ($r = r_h$), or

$$\sigma_b = \rho_b \frac{U_t^2}{2}\left[1-\zeta^2\right] = 2\rho_b \pi N^2 A \tag{14.67}$$

where
$\zeta = r_h/r_t$ is the hub-tip ratio
N is the rotational speed in rev/s
A is the annulus area

From Equation 14.67, the maximum blade stress factor $\sigma_b/\rho_b U_t^2$ has a maximum value of 0.5 (at a fictitious hub-tip ratio of 0) and decreases rapidly as the hub-tip ratio increases.

Since turbine blades are tapered both in chord and thickness, the ratio between the tip and root areas (a_t/a_h) is between 1/4 and 1/3; thus it is accurate enough to assume that tapering of the blade reduces the stress to 2/3 of its value [4] given in Equation 14.67, or

$$(\sigma_b)_{tapered} \approx \rho_b \frac{U_t^2}{3}\left[1-\zeta^2\right] \approx \frac{4}{3}\rho_b \pi N^2 A \tag{14.68}$$

For linear tapering, the exact expression is

$$(\sigma_b)_{tapered} = \frac{\rho_b \omega^2 A}{4\pi}\left[2-\frac{2}{3}\left(1-\frac{a_t}{a_h}\right)\left(1+\frac{1}{1+\zeta}\right)\right] \tag{14.69}$$

14.5.4.3 Centrifugal Stresses on Disks

The centrifugal stress is checked in three locations, namely, the outer and inner rims and in the disk material between both rims (Figure 14.31). The following assumptions are considered:

1. Centrifugal force applied by the blades to the rims can be considered equivalent to a radial, uniformly distributed load.
2. The disk is tapered such that its circumferential and radial stresses are constant everywhere and equal to (σ).
3. The rims are thin enough to have uniform tangential stress equal to (σ).

14.5.4.3.1 Outer Rim

Applying Newton's second law of motion to a small element on the outer rim (Figure 14.32), the sum of force (on the left-hand side) will be equal to the mass multiplied by acceleration (right-hand side).

$$2\sigma A_o \frac{d\theta}{2} - N_b \sigma_b A_b \left(\frac{d\theta}{2\pi}\right) + \sigma\left(r_h d\theta\right) t_o = \rho_b \left(A_o r_h d\theta\right) r_h \Omega^2$$

Dividing by $A_o d\theta \rho_b U_t^2$ gives

$$\frac{\sigma}{\rho_b U_t^2} = \frac{\dfrac{N_b}{2\pi}\dfrac{A_b}{A_o}\dfrac{\sigma_b}{\rho_b U_t^2} + \zeta^2}{1 + \dfrac{r_h t_o}{A_o}} \tag{14.70}$$

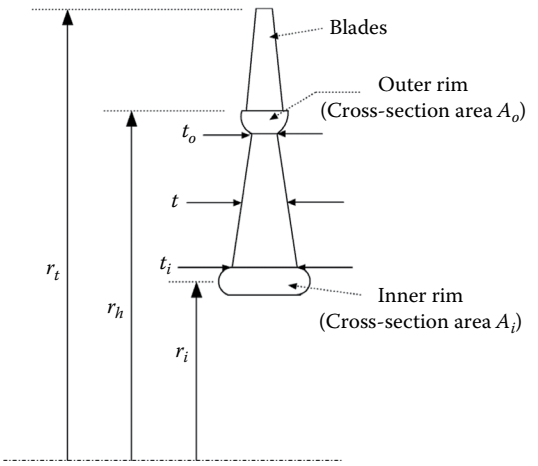


FIGURE 14.31
Nomenclature of disk.

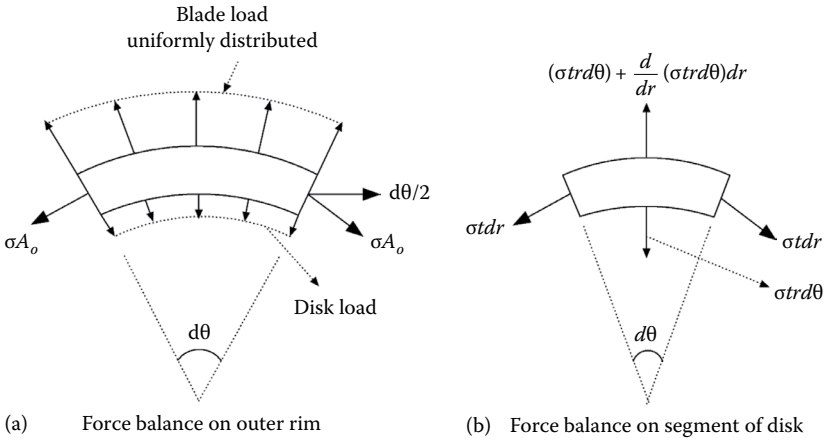


FIGURE 14.32
Stresses on (a) outer and (b) inner rims of disk.

14.5.4.3.2 Disk Segment

Also apply Newton's second law to a segment on the disk. Referring to Figure 14.31, the segment of the disk has a width of (dr), arc length of ($rd\theta$), and thickness of (t). Force balance will give the relation

$$\left(2\sigma t dr\right)\frac{d\theta}{2} - \frac{d}{dr}\left(\sigma t r d\theta\right)dr = \rho_b\left(t r d\theta dr\right)\Omega^2 r$$

Since σ is assumed constant, then simplify to get

$$t - \frac{d}{dr}\left(tr\right) = -r\frac{dt}{dr} = \frac{\rho_b \Omega^2 r^2 t}{\sigma}$$

$$\frac{dt}{t} = -\frac{\rho\Omega^2}{\sigma} r dr$$

Integrate between the radii of the inner and outer rims to get

$$\ln\frac{t_o}{t_i} = -\frac{\rho\Omega^2}{2\sigma}\left(r_h^2 - r_i^2\right)$$

The stress in the disk can also be rewritten as a stress factor in the following form:

$$\frac{\sigma}{\rho_b U_t^2} = \frac{\zeta^2\left[1 - \left(\frac{r_i}{r_h}\right)^2\right]}{2\ln\left(\frac{t_i}{t_o}\right)} \tag{14.71}$$

14.5.4.3.3 Inner Rim

Force balance also gives

$$2\sigma A_i \frac{d\theta}{2} - \sigma\left(r_i d\theta\right) t_i = \Omega^2 r_i \left(\rho_b A_i r_i d\theta\right)$$

which gives

$$\frac{\sigma}{\rho_b U_i^2} = \frac{\zeta^2 \left(\frac{r_i}{r_h}\right)^2}{1 - \frac{t_i r_i}{A_i}} \tag{14.72}$$

From Equations 14.70 through 14.72, the stresses at any point in the disk can be calculated and compared with the blade root stress using Equation 14.68. Disk stresses can exceed the blade root stress at high hub-tip ratios.

14.5.4.4 Gas Bending Stress

The gas flow through the rotor passages generates two forces, namely, tangential and axial forces (F_t, F_a). For a stator blade row, only axial force is generated. The tangential force also develops a gas bending moment (M_t) about the axial direction, while the axial force develops another gas bending moment (M_a) about the tangential direction (Figure 14.33). The neutral axes are inclined at an angle ϕ to the original axial and tangential axes.

Resolve M_a and M_t in the new X and Y directions to get

$$M_x = M_t \cos\phi + M_a \sin\phi, \quad M_Y = M_a \cos\phi - M_t \sin\phi$$

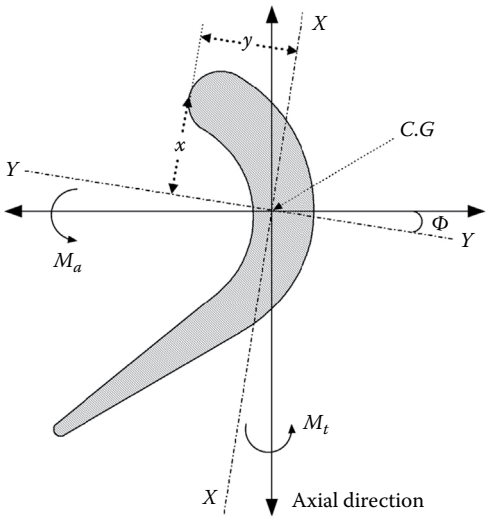


FIGURE 14.33
Gas bending stress.

The corresponding gas bending stress is

$$\sigma_{gb} = \frac{-M_x Y}{I_{xx}} + \frac{M_Y X}{I_{YY}}$$

which is tensile at the blade leading edge and compressed at the blade trailing edge. Now, to evaluate the order of magnitude of each term, the axial force is evaluated first. The axial force is developed from two sources:

1. Momentum change, which is the case when there is a change in axial velocity ($C_{a2} \neq C_{a3}$). The axial force per blade is then

$$|F_a| = \frac{\dot{m}|C_{a2} - C_{a3}|}{n}$$

   where n is the number of blades.
2. Pressure difference, thus the *force per unit blade height* is

$$F_a = (P_2 - P_3)(2\pi r/n)$$

   The tangential force is determined from the power, which is correlated to the specific work w_s by the relation

$$P = \dot{m} w_s = \dot{m} U (Cu_{2m} + Cu_{3m})$$

   But the power is also expressed as $P = F_t \times U$.

Then the tangential force is $F_t = \dot{m}(Cu_{2m} + Cu_{3m})$.

The tangential force per blade is then

$$F_{t1} = \frac{\dot{m}(Cu_2 + Cu_3)}{n}$$

The tangential moment per blade is

$$M_t \cong F_{t1} \frac{h}{2} = \frac{\dot{m}(Cu_{2m} + Cu_{3m})}{n} \frac{h}{2},$$

The tangential momentum is far greater than the axial momentum and the angle ϕ is small, so the gas bending moment is approximated as

$$(\sigma_{gb})_{\max} \approx -\frac{M_t y}{I_{xx}}$$

$$\left|(\sigma_{gb})_{\max}\right| = \frac{\dot{m}(Cu_{2m} + Cu_{3m})}{n} \times \frac{h}{2} \times \frac{y}{I_{xx}} \tag{14.73}$$

where $I_{XX}/y = S = zc^3$ is the smallest value of section modulus.

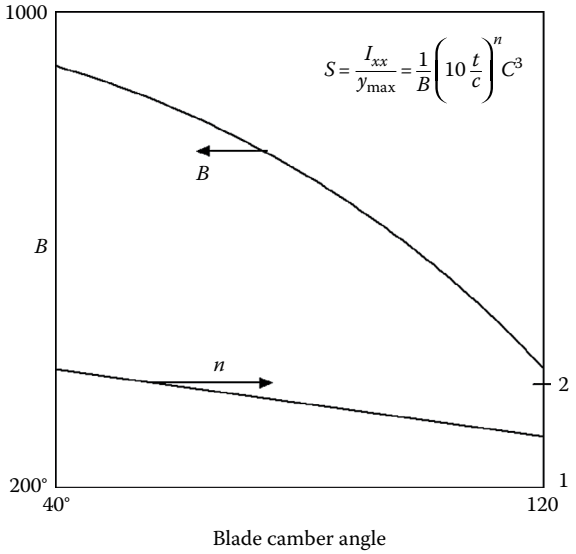


FIGURE 14.34
Approximate rule for section module. (From Saravanamuttoo, H.I.H. et al., *Gas Turbine Theory*, 5th edn., Prentice Hall, Harlow, U.K., 2001, p. 313.)

As reported in Reference 4, the section modulus is expressed as

$$S = \frac{I_{xx}}{y_{max}} = \frac{1}{B}\left(10\frac{t}{c}\right)^n c^3 \tag{14.74}$$

The variables (B, n) are plotted as a function of the blade camber angle in Figure 14.34. As depicted in Equations 14.73 and 14.74, the gas bending stress is inversely proportional to the cube of the blade chord. By doubling the chord, the stress will be reduced by nearly one order of magnitude. Thus, it is possible always to keep the gas bending stress smaller than the centrifugal one.

Equations 14.73 and 14.74 represent the gas bending stress for the case of steady aerodynamics. However, as each blade row passes through the wake shed by the blades of the preceding blade row, it experiences a small aerodynamic force fluctuation that could be serious if one of the critical vibration frequencies of the blade were to coincide with the wake passing frequency. During such resonance, destructive strain amplitudes can develop even if the force amplitude is small. These stresses are not serious in turbines compared with compressors. They are much less than centrifugal stresses.

14.5.4.5 Centrifugal Bending Stress

Centrifugal bending stresses arise if the centroids of the blade cross-sections at different radii do not lie on a radial line. However, the torsion stress arising from this source is small enough to be neglected [4].

14.5.4.6 Thermal Stress

The blade temperature is not uniform either along the blade height or across its cross-section. The blade is surrounded by hot gases, and cold air flows through the internal passages used for cooling. At each cross-section there is an average temperature depending on its position along the blade height. For any point in this section there is a temperature difference ΔT above or below the average temperature. Thus, local thermal stress is developed, which is proportional to the product ($E\ \alpha\ \Delta T$), where E is the modulus of elasticity of the blade material and α is the coefficient of thermal expansion. For average values of $E \approx 2 \times 10^5$ MPa, $\alpha \approx 7 \times 10^{-7}/^\circ$C, $\Delta T \approx 50$, the thermal stress will be 70 MPa, which will have a serious effect on turbine blades, particularly if the cooling passages are small.

14.5.5 Turbine Cooling

Designers of gas turbines and aircraft engines aim to increase specific power output (or specific thrust for an aero engine), increasing the thermal efficiency, reducing the specific fuel consumption, and reducing the engine weight. One way to achieve these objectives is to increase the turbine inlet temperature. Turbine inlet temperature has increased considerably over the past years and will continue to do so. This trend has been made possible by advancements in materials and technology, and the use of advanced turbine blade cooling techniques. Improvement in materials has allowed a slow increase in turbine inlet temperature, while cooling has allowed for a faster rate of increase of turbine inlet temperatures. Since 1950, advancements in material and cooling technology have led to an annual increase of about 10°C [14]. Cooling allows the turbine's operational temperature to exceed the material's melting point without affecting the blade and vane integrity. Coolant is either air that is bled from a compressor, or liquid, which is impractical in aeroengines. When air is used as a coolant, 1.5%–2% of air mass flow rate (bled from the compressor) is used for cooling each turbine blade row. Then the blade temperature can be reduced by 200°C–300°C. On practically all large aeroengines, the first-stage nozzle and rotor are cooled. Cooling is accomplished by directing compressor bleed air through passages inside the engine to the turbine area, where the air is led to longitudinal holes, tubes, or cavities in the vanes and the blades [15]. After entering the passages in the vanes and blades, the air (coolant) in all present gas turbines is distributed through holes at the leading and trailing edges of the vanes and blades. The air impinges on the vane and blade surfaces and then passes out of the engine through the engine exhaust.

The use of current alloys permits the turbine inlet temperature to reach 1650 K. Generally, ceramics and carbon-based materials promise substantial further increase in blade temperature. However, some problems have to be solved to overcome these materials' inherent brittleness [11].

14.5.5.1 Turbine Cooling Techniques

As shown in Figure 14.35, the following methods are used in turbine cooling:

1. Convection
2. Impingement
3. Film cooling
4. Full coverage film cooling
5. Transpiration

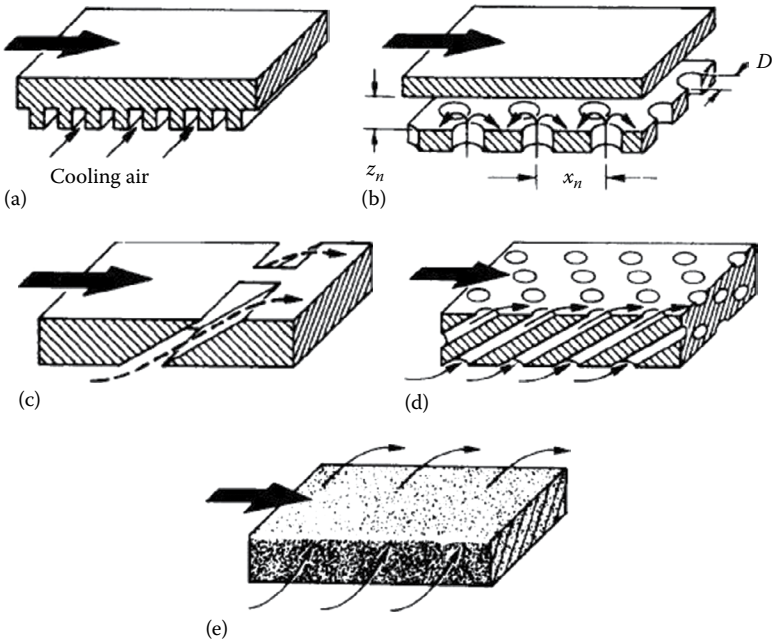


FIGURE 14.35
Cooling methods: (a) convection, (b) impingement, (c) film, (d) full-coverage film, and (e) transpiration. (From Glassman, A.J. (ed.), *Turbine Design and Applications*, NASA SP-290, Washington, DC, 1973, p. 88.)

14.5.5.1.1 Convection

Convection cooling with a single internal passage was the only available cooling technique in the 1960s (Figure 14.36). Cooling air was injected through the airfoil attachment and to the inside of airfoil; the cold air was discharged at the blade tip. Development has led to multipass internal cooling. The blades are either casted using cores to from the cooling passages, or forged with holes of any size and shape, which are produced by electrochemical drilling. The effectiveness of convection cooling is limited by

- Size of the internal passages
- Quantity of cooling air available

The main disadvantage of early convection technique is its failure to cool the trailing edges of blades, which is serious as the trailing edge is very thin. Moreover, convection fails to cool the leading edge, which is subjected to the highest temperature. However, in the 1970s the evolution in convection cooling led to the cooling of the trailing edge by discharging the cold air through the trailing edges (Figure 14.35).

14.5.5.1.2 Impingement Cooling

This is a form of convection; the main difference between this method and the conventional cooling method is that air flows radially in convection cooling, but in the impingement method air is brought radially to one or more center section, then turned normal to the radial direction and passed through a series of holes so that it impinges on the inside of blade, usually just opposite the stagnation point of the blade. It is mostly used

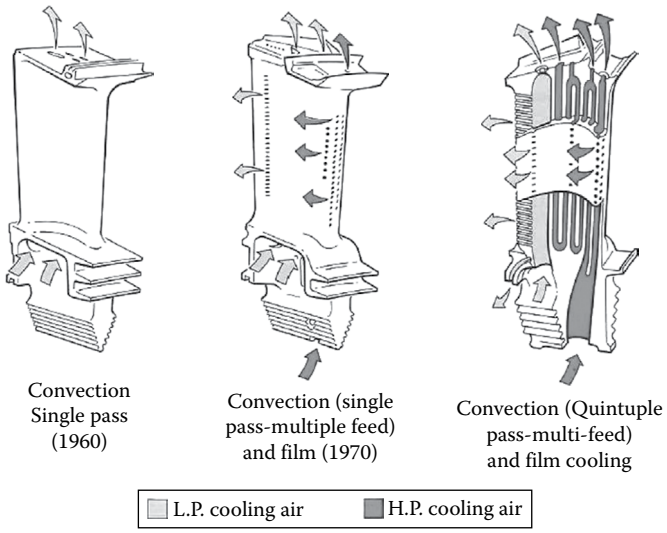


FIGURE 14.36
Development of high-pressure turbine cooling. (Reproduced from Rolls-Royce plc, Copyright Rolls-Royce plc 2007. With permission.)

in stators and may be used in a rotor if sufficient space is available to include the required hardware inside the blade.

14.5.5.1.3 Film Cooling

This involves the injection of a secondary fluid (cold air) into the boundary layer of the primary fluid (hot gases). This is an effective method to protect the surface from the hot gases as the cooling air acts as an insulating layer to maintain a lower blade material temperature.

Disadvantages include

1. Turbine losses due to injection into the boundary layer
2. Penetration of the boundary layer if too much air is used or if it is ejected at high speeds
3. Stress concentration if close holes are used

However, film cooling is more effective than normal convection or impingement methods. The cooling air absorbs energy as it passes inside the blade and through the holes, and then it further reduces the blade temperature by reducing the amount of energy transferred from the hot gases to the blade. It must be noted that the cold air used must be at a high pressure; this is not always satisfied, especially for the leading edge of the first stator (nozzle).

Current cooled airfoils use a combination of sophisticated internal convection and film cooling.

14.5.5.1.4 Transpiration Cooling

This is the most efficient technique. It is sometimes referred to as *full-blade film cooling* (full coverage) or *porous blade cooling*. It involves the use of a porous material through which the cooling air is forced into the boundary layer to form a relatively cooling, insulating film or layer.

Generally, transpiration cooling has the following detrimental effects [16]:

1. Added cost of producing turbine blades
2. Drop in turbine blade reliability
3. Loss of turbine work due to the cooling air bypassing one or two of the turbine stages
4. Drop in total temperature due to the cooling air being mixed with hot gas steam

14.5.5.2 Mathematical Modeling

In this section, the temperature of the turbine blade material will be calculated in three different cases, namely, no cooling at all, film cooling, and convection cooling.

14.5.5.2.1 No Cooling

The rotor blade of the first stage represents the critical section from a mechanical point of view because it is subjected to the maximum mechanical stress. If for some reason there is no cooling for this part, this section be subject to the highest thermal stress [13]. Now, let us assume that there is

- No blade cooling
- No conduction of heat away from the blade root into the turbine disk

We assume that, in this case, the blade temperature is nearly equal to the relative stagnation temperature of the hot gases, ($T_s = T_{02rel}$).

At the hub section

$$T_{2h} = T_{02} - \frac{C_{2h}^2}{2Cp} = T_{02} - \frac{\gamma - 1}{2\gamma R}\left(Cu_{2h}^2 + Ca_{2h}^2\right)$$

where subscripts (u) and (a) refer to tangential and axial, respectively.

Dividing by the rotational speed at the tip (U_t) and noting that $\zeta = r_h/r_t = U_h/U_t$, then

$$\frac{T_{2h}}{T_{02}} = 1 - \frac{\gamma - 1}{2}\left(\frac{U_t}{a_o}\right)^2 \zeta^2 \left[\left(\frac{Cu_2}{U}\right)_h^2 + \left(\frac{Ca_2}{U}\right)_h^2\right] \tag{14.75}$$

Subscripts (h) and (t) in Equation 14.75 refer to the hub and tip sections. The relative stagnation temperature is

$$T_{02rel} = T_{2h} + \frac{W_{2h}^2}{2Cp}$$

With no blade cooling or conduction into the disk, the blade would take a temperature somewhat less than T_{02rel}, or

$$T_s = T_{2h} + r_f \frac{W_{2h}^2}{2Cp} \tag{14.76}$$

where r_f is the recovery factor, which reflects the fact that the deceleration process in the surrounding boundary layer is not adiabatic. Some heat transfer takes place between the streamlines and the surrounding moving boundaries. The recovery factor has the following range: $r_f = 0.9 - 0.95$. Since

$$\frac{W_{2h}^2}{2CpT_o} = \frac{\gamma - 1}{2\gamma RT_o}\left[W_{u2h}^2 + W_{a2h}^2\right] = \frac{\gamma - 1}{2}\left(\frac{U_t}{a_o}\right)^2 \zeta^2 \left[\left(\frac{C_{u2}}{U} - 1\right)_h^2 + \left(\frac{C_{a2}}{U}\right)_h^2\right] \tag{14.77}$$

then, from the previous equation and Equation 14.75, the surface temperature at the hub is

$$\left(\frac{T_{shub}}{T_{o_1}}\right) = 1 - \frac{\gamma - 1}{2}\left(\frac{U_t}{a_o}\right)^2 \zeta^2 \left[\left(\frac{C_{u2}}{U}\right)_h^2 + \left(\frac{C_{a2}}{U}\right)_h^2 - r_f\left\{\left(\frac{C_{u2}}{U} - 1\right)_h^2 + \left(\frac{C_{a2}}{U}\right)_h^2\right\}\right] \tag{14.78}$$

It will be found in the succeeding examples that, even without cooling, the blade temperature is less than the stagnation (absolute total temperature) at the inlet to the turbine. With blade cooling, the blade root temperature is 300–400 K below the absolute stagnation temperature of gas entering the turbine [13]. This necessitates extracting cold air from both of the low- and high-pressure compressors to cool the turbine blades, as shown in Figure 14.37. Both the disk, stator and rotor blades need less than 10% of the compressor exit airflow for their cooling.

Hereafter, the cases of blade cooling using either film or convection methods will be analyzed.

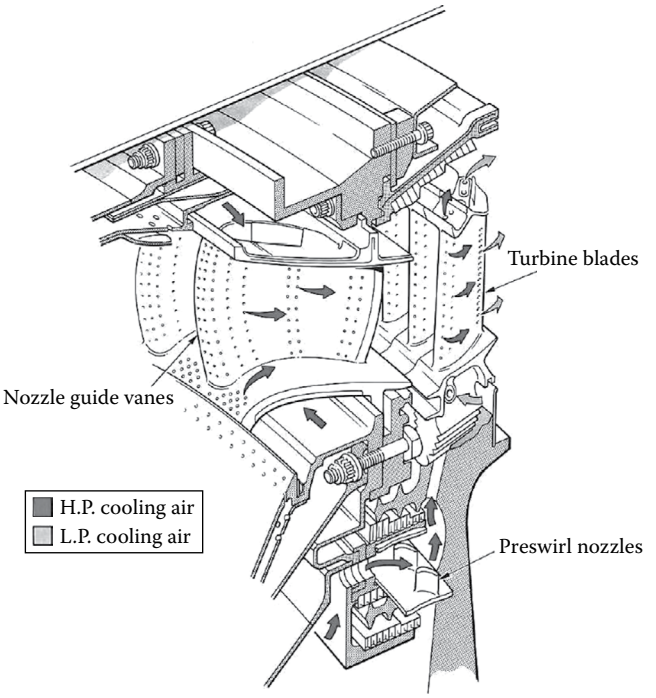


FIGURE 14.37
Cooled high-pressure turbine stage. (Reproduced from Rolls-Royce plc, Copyright Rolls-Royce plc 2007. With permission.)

14.5.5.2.2 Film Cooling

From the Eckert relation, the heat flux from the hot gas to the wall q is given by

$$q = h_o\left(T_{aw} - T_w\right) \tag{14.79}$$

where
h_o is the film coefficient for convective heat transfer to the wall
T_w is the wall temperature
T_{aw} is the adiabatic wall temperature

Air is bled from the compressor at a certain location, where its temperature is T_i, and ejected into the turbine disk, where its temperature becomes T_c. Thus, the heat added to the bled air up to the point of injection will be expressed as:

$$\dot{Q}_a = \dot{m}_a Cp_a\left(T_c - T_i\right) \tag{14.80}$$

If heat conduction from blade to disk is small, then this heat $\dot{Q}_a$ will be balanced by the heat transfer from the hot gases to the blade surface $\dot{Q}_g$. Using the Eckert law, $\dot{Q}_g$ will be expressed as

$$\dot{Q}_g = h_o\left(T_{aw} - T_b\right)A_s \tag{14.81}$$

where
A_s is the surface area of the blade
T_b is the blade temperature

From Equations 14.80 and 14.81, the air mass flow rate is

$$\dot{m}_a = \frac{h_o\left(T_{aw} - T_b\right)A_s}{Cp_a\left(T_c - T_i\right)}$$

The Stanton number is defined as

$$st_o = \frac{h_o}{\rho_g Cp_g W_g}$$

where (ρ_g, Cp_g, W_g) are the gas density, specific heat at constant pressure, and inlet speed. With the gas mass flow rate defined as $\dot{m}_g = \rho_g W_g A_g$, where A_g is the hot gas flow area, or the area perpendicular to the gas speed, then the Stanton number will be expressed as $st_o = h_o A_g / Cp_g \dot{m}_g$. The ratio between the mass flow rates of the bled air and hot gases is then

$$\frac{\dot{m}_a}{\dot{m}_g} = st_o \frac{A_s}{A_g}\frac{Cp_g}{Cp_a}\left(\frac{T_{aw} - T_b}{T_c - T_i}\right)$$

Now, if the cooling effectiveness η_f is defined as

$$\eta_f = \frac{T_g - T_{aw}}{T_g - T_c}$$

then the adiabatic wall temperature will be $T_{aw} = T_g - \eta_f (T_g - T_c)$.

The ratio between the bled air and gas flow rates is then

$$\frac{\dot{m}_a}{\dot{m}_g} = st_o \frac{A_s}{A_g} \frac{Cp_g}{Cp_a} \left(\frac{T_g - T_b}{T_c - T_i} - \eta_f \frac{T_g - T_c}{T_c - T_i} \right) \tag{14.82}$$

In Equation 14.82, four temperatures are listed, which are again summarized as follows:

T_g is the gas temperature.
T_b is the blade temperature.
T_i is the cold air temperature as it is bled from the compressor.
T_c is the coolant ejection temperature.

The Stanton number is dependent on the gas Reynolds number and ranges from 0.002 to 0.003 for the prevailing values of Reynolds numbers. The typical value for the average film cooling effectiveness is 0.2.

14.5.5.2.3 Convection Cooling

Figure 14.38 illustrates a turbine blade cooled by a forced convection method [4]. Cold air bled from the compressor is pumped inside the internal cooling holes of the turbine blade. This cold air is heated as it passes within the blade and becomes less effective in cooling. For this reason, together with the low thermal conductivity of the blade, it may be assumed that the spanwise conduction is negligible.

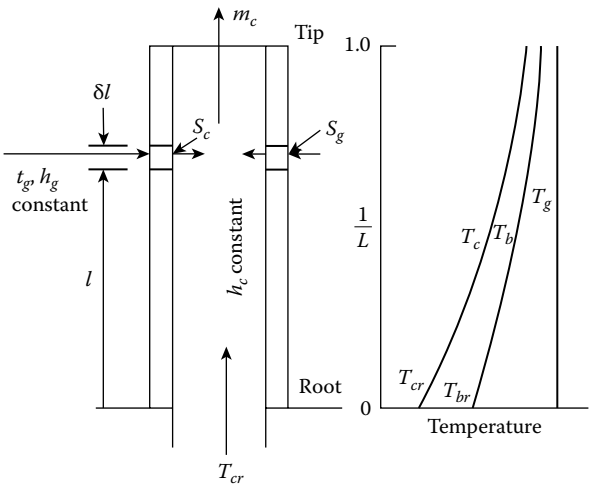


FIGURE 14.38
Forced convection of a turbine blade.

Consider a blade element of length (dl) at a distance (l) from the root. The heat balance between the outer gases and the blade outer surface from one side, and the through cold air and the inner surface of blade from the other side results in

$$h_g S_g \left(T_g - T_b\right) = h_c S_c \left(T_b - T_c\right) \tag{14.83a}$$

or

$$T_c = T_b - \frac{h_g S_g}{h_c S_c}\left(T_g - T_b\right) \tag{14.83b}$$

Since the gas temperature is constant, then

$$\frac{dT_c}{dl} = \left[1 + \frac{h_g S_g}{h_c S_c}\right]\frac{dT_b}{dl} \tag{14.83c}$$

where h_g, h_c are the convection heat transfer coefficients for the hot gases/blade and cold air/blade, respectively. Moreover, S_g, S_c are the wetted perimeters of the outer blade surface and the combined coolant passages, respectively. The coolant temperature gradient in the radial direction will be given by the relation

$$\dot{m}_c C_{pc} \frac{dT_c}{dl} = h_c S_c \left(T_b - T_c\right) \tag{14.84}$$

From Equations 14.83a and 14.84, then

$$\frac{dT_c}{dl} = \frac{h_c S_c}{\dot{m}_c C_{pc}}\left(T_b - T_c\right) = \frac{h_g S_g}{\dot{m}_c C_{pc}}\left(T_g - T_b\right)$$

From Equation 14.83c, then

$$\frac{dT_c}{dl} = \left[1 + \frac{h_g S_g}{h_c S_c}\right]\frac{dT_b}{dl} = \frac{h_g S_g}{\dot{m}_c C_{pc}}\left(T_g - T_b\right)$$

With $\dfrac{dT_b}{dl} = -\dfrac{d\left(T_g - T_b\right)}{dl}$, then

$$-\frac{d\left(T_g - T_b\right)}{dl}\left[1 + \frac{h_g S_g}{h_c S_c}\right] = \frac{h_g S_g}{\dot{m}_c C_{pc}}\left(T_g - T_b\right)$$

Integrating from the root to any distance along the blade gives

$$\int_{T_{br}}^{l} \frac{d\left(T_g - T_b\right)}{\left(T_g - T_b\right)} = K\int_0^l dl$$

$$T_g - T_b = \left(T_g - T_{br}\right)e^{-Kl/L} \tag{14.85a}$$

where

$$\frac{K}{L} = \frac{h_g S_g}{\dot{m}_c C_{p_c}\left[1 + \frac{h_g S_g}{h_c S_c}\right]} \tag{14.85b}$$

From Equation 14.83b, by adding T_g to both sides, then

$$T_g - T_c = \left(T_g - T_b\right)\left[1 + \frac{h_g S_g}{h_c h_c}\right]$$

From Equation 14.85a,

$$T_g - T_c = \left(T_g - T_{br}\right)\left[1 + \frac{h_g S_g}{h_c S_c}\right] \times e^{-Kl/L} \tag{14.86}$$

At root $l = 0$, the coolant temperature is $T_c = T_{cr}$.

$$T_g - T_{cr} = \left(T_g - T_{br}\right)\left[1 + \frac{h_g S_g}{h_c S_c}\right] \tag{14.87}$$

Combine Equations 14.86 and 14.87 to get

$$T_g - T_c = \left(T_g - T_{cr}\right)e^{-Kl/L} \tag{14.88}$$

From Equations 14.86 and 14.87 one gets

$$T_b - T_{cr} = \left(T_g - T_{br}\right)\left[1 + \frac{h_g S_g}{h_c S_c} - e^{-Kl/L}\right] \tag{14.89}$$

The blade relative temperature at any radius is determined from the relation

$$\frac{T_b - T_{cr}}{T_g - T_{cr}} = 1 - \frac{e^{-Kl/L}}{\left[1 + \left(\frac{h_g S_g}{h_c S_c}\right)\right]} \tag{14.90}$$

Equation 14.90 allows calculation of the blade temperature at any radius. This temperature depends on the ratio between the mass flow rates of both coolant and gas $\left(\dot{m}_c/\dot{m}_g\right)$. An increase of this ratio decreases the blade temperature. Moreover, the heat transfer coefficients (h_c, h_g) depend on the Nusselt numbers for the coolant and gas main stream: N_{uc}, N_{ug}.

Finally, it is important to assess the cooling performance of a blade using the effectiveness parameter (ϕ), defined as

$$\phi = \frac{T_G - T_M}{T_G - T_C} \tag{14.91}$$

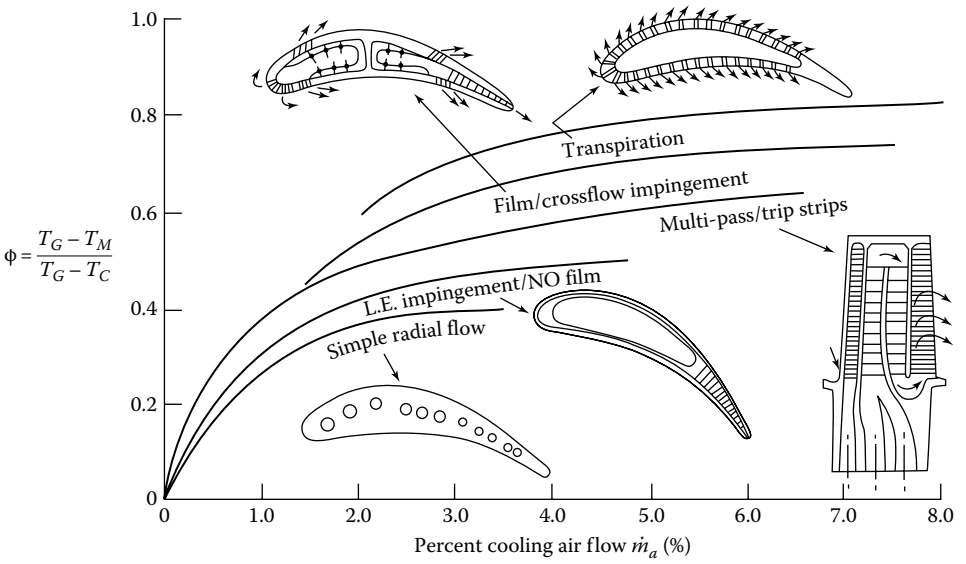


FIGURE 14.39
Effectiveness of different cooling methods as a function of coolant airflow ratio. (From Moustapha, H. et al., *Axial and Radial Turbines*, Concepts NREC, White River Junction, VT, 2003, 31pp.)

where subscripts *C*, *G*, and *M* refer to the coolant, gas, and metal, respectively. The value of $\phi = 0$ represents no cooling, while the value $\phi = 1$ is the ideal case of perfect cooling where the blade metal and coolant temperatures are equal. Figure 14.39 illustrates the effectiveness of typical cooling methods for different cooling airflow ratios.

The cooling effectiveness is a function of many variables such as the blade design, the arrangement of cooling air passages, the way in which the coolant air is ejected, and the percentage of the coolant air as a ratio of the hot gas main stream.

14.5.6 Losses and Efficiency

Losses are dependent on several parameters, including the blade geometry, incidence angle, Reynolds number, ratios s/c, $h/c \cdot t_{max}/c$, Mach number, and turbulence level. There are three major components of loss, namely, profile loss, annulus and secondary flow losses, and tip clearance loss. The overall blade loss coefficient is either identified as Y or λ, which is equal to the sum of these three types.

14.5.6.1 Profile Loss (Y_p)

Profile loss is the loss due to skin friction on the area of the blade's surface. It depends on several factors including the area of blade in contact with fluid, the surface finish, and the Reynolds and Mach numbers of the flow through the passage. These factors directly influence the boundary layer over the blade surface and any possible boundary layer separation. The surface finish itself is in turn influenced by both erosion and fouling. Profile loss is measured directly in cascade wind tunnels, similar to the compressors.

One of the most commonly used approaches in defining the profile loss coefficient from a set of cascade test results is extracted from [7]. The profile loss coefficient (Figure 14.40)

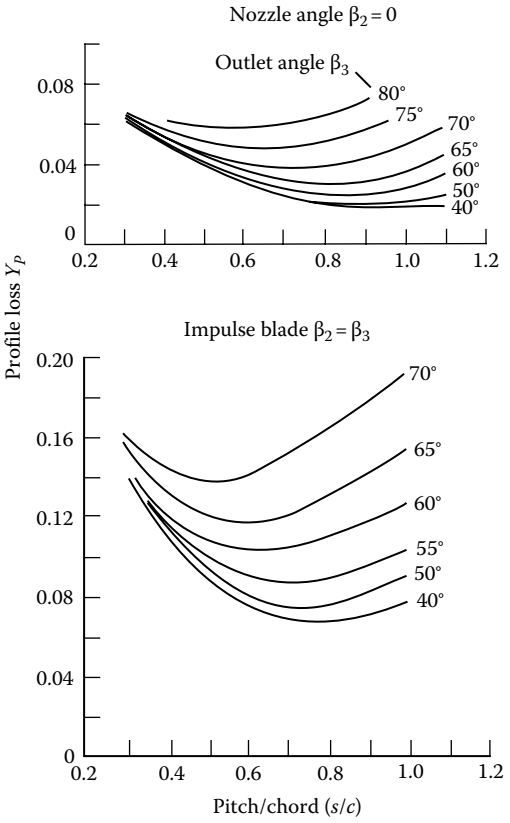


FIGURE 14.40
Profile loss coefficient for conventional blading with t/c = 0.2. (From Saravanamuttoo, H.I.H. et al., *Gas Turbine Theory*, 5th edn., Prentice Hall, Harlow, U.K., 2001, p. 313. With permission.)

is expressed in terms of pitch/chord ratio and cascade exit angle (β_3) for two special cases of (β_2), namely, axial approach of flow ($\beta_2 = 0$) and impulse blading ($\beta_2 = \beta_3$).

For any other combination of angles, these graphs are interpolated by means of the following relation:

$$Y_p = \left\{ Y_{p(\beta_2=0)} + \left(\frac{\beta_2}{\beta_3}\right)^2 \left[Y_{p(\beta_2=\beta_3)} - Y_{p(\beta_2=0)} \right] \left(\frac{t/c}{0.2}\right)^{\beta_2/\beta_3} \right\} \tag{14.92a}$$

When Equation 14.92a is used for a stator blade row, then the angle α_1 is used instead of β_2, and α_2 is used instead of β_3.

The main assumptions for the validity of Equation 14.92a are

- Subsonic flow turbine stage
- The trailing edge thickness to pitch ratio; $t_e/s \approx 0.02$
- Zero incidence angle; $i = 0$
- Reynolds number; $R_e = 2 \times 10^5$

Since cascade data and other loss correlation are limited to subsonic conditions, a correction to Equation 14.92a was suggested in [16] to account for supersonic Mach numbers at either of the outlets of the rotor or stator blade row, as follows:

$$Y_p = \left(Y_p\right)_{\text{Equation 14.92a}} \times \left[1 + 60\left(M - 1\right)^2\right] \tag{14.92b}$$

where M is the absolute Mach number at the nozzle outlet and the relative Mach number at the rotor outlet.

14.5.6.2 Annulus Loss

The profile loss is caused by friction and also associated with the boundary layer growth over the inner and outer walls of the annulus. Annulus losses are similar to profile losses as both are caused by friction. However, a fresh boundary layer grows from the leading edge of the blade, whereas the annulus boundary layer may have its origin some way upstream of the leading edge depending on the details of the annulus itself.

14.5.6.3 Secondary Flow Loss

Secondary flows are contrarotating vortices that occur due to curvature of the passage and boundary layers. Secondary flows tend to scrub both the endwall and blade boundary layers and redistribute low momentum fluid through the passage [11]. Secondary flow losses represent the major source of losses.

Both annulus loss and secondary flow loss cannot be separated, and they are accounted for by a secondary loss coefficient (Y_s).

14.5.6.4 Tip Clearance Loss (Y_k)

Tip clearance loss occurs in the rotors. Some fluid leaks through the gap between the blade tip and the shroud, and therefore contributes little or no expansion work.

The combined secondary loss and tip leakage are expressed by the relation

$$Y_s + Y_k = \left[\lambda + B\left(\frac{k}{h}\right)\right]\left(\frac{C_L}{s/c}\right)^2\left[\frac{\cos^2\beta_3}{\cos^3\beta_m}\right] \tag{14.93}$$

where

$$\frac{C_L}{\left(s/c\right)} = 2\left(\tan\beta_2 + \tan\beta_3\right)\cos\beta_m$$

and

$$\beta_m = \tan^{-1}\left[\frac{\left(\tan\beta_3 - \tan\beta_2\right)}{2}\right]$$

The parameter B depends on whether or not the blade is shrouded. For unshrouded, $B = 0.5$, while for shrouded, $B = 0.25$. Moreover, the parameter λ is a function of the parameter

$$\lambda = f\left[\frac{\left(A_3 \cos\beta_3 / A_2 \cos\beta_2\right)^2}{\left(1 + \left(r_r / r_t\right)\right)}\right]$$

and is evaluated from Figure 14.41 [4].

The total losses for the nozzle are then

$$Y_N = \left(Y_p\right)_N + \left(Y_s + Y_k\right)_N$$

and, similarly, the total losses for the rotor are then

$$Y_R = \left(Y_p\right)_R + \left(Y_s + Y_k\right)_R$$

The equivalent loss coefficients defined in temperature are given hereafter for the nozzle and rotor as

$$\lambda_N = \frac{Y_N}{T_{02} / T_2'} \quad \text{and} \quad \lambda_R = \frac{Y_R}{T_{03rel} / T_3''}$$

The stage efficiency is then calculated as

$$\eta_s = \frac{1}{1 + \lambda_R \left(W_3^2 / 2C_p\right) + \left(T_3 / T_2\right)\lambda_N \left(C_2^2 / 2C_p\right) / \left(T_{01} - T_{03}\right)} \tag{14.94}$$

The value calculated from Equation 14.94 is checked with the assumed value. If not satisfactory, some changes to the previously assumed degree of reaction, the stage loading coefficient and flow coefficient must be carried out.

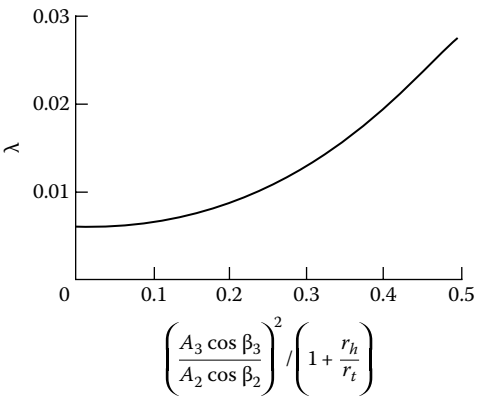


FIGURE 14.41
Secondary loss parameter. (From Saravanamuttoo, H.I.H. et al., *Gas Turbine Theory*, 5th edn., Prentice Hall, Harlow, U.K., 2001, p. 313. With permission.)

14.6 Turbine Map

The overall turbine performance is defined in the same way as that of the compressor, in terms of similar nondimensional parameters, namely, the mass flow parameter ($\dot{m}\sqrt{T_{0i}}/P_{0i}$), speed parameter ($N/\sqrt{T_{0i}}$), pressure ratio, and thermal efficiency. If the turbine is composed of more than one stage, then the efficiency previously calculated by Equation 14.94 is considered as a polytrophic efficiency and the turbine efficiency is calculated from the relation

$$\eta_t = \frac{1-\left(P_{0e}/P_{0i}\right)^A}{1-\left(P_{0e}/P_{0i}\right)^B}$$

where

$$A = \frac{\eta_s\left(\gamma-1\right)}{\gamma}$$
$$B = \frac{\left(\gamma-1\right)}{\gamma}$$

The maximum mass flow rate is called the choking condition, which is constant for a certain range of the turbine pressure ratio, as shown in Figure 14.42a. The efficiency is also plotted versus the turbine pressure ratio (Figure 14.42b). It is noticeable here that the variations in the mass flow parameter and efficiency are not sensitive to the speed parameter, as in the case of the compressor.

Example 14.7

An axial-flow turbine is to be cooled by forced convection. The hot gases' temperature is 1200 K and the temperature of the coolant air extracted from the compressor is 350 K. The gas mass flow rate is 50 kg/s and the coolant air is 2% of the hot gases. The heat transfer coefficients of the hot gases and coolant are, respectively, 1200 and 1000 W/m²·K.

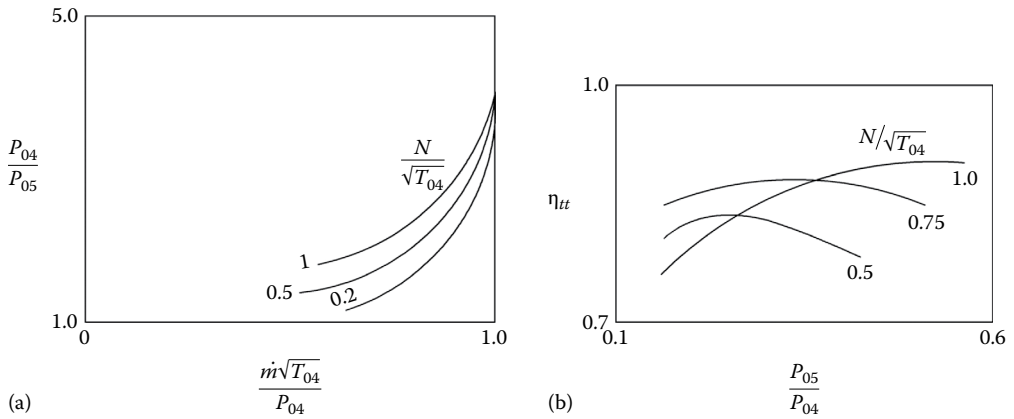


FIGURE 14.42
Turbine characteristics: (a) mass flow versus pressure ratio and (b) efficiency versus pressure ratio.

The perimeters of the turbine blade section and the cooling passages are, respectively, 0.12 and 0.06 m. The blade height is 0.1 m.

It is required to

Calculate the temperatures of the coolant and blade height along the blade.

Solution

The previous data can be rewritten as

$$T_g = 1200 \text{ K}, \quad T_{cr} = 350 \text{ K}, \quad \dot{m}_g = 50 \text{ kg/s}, \quad \dot{m}_c = 1 \text{ kg/s}$$

$$h_g = 1200 \text{ W/m}^2\text{/K}, \quad h_C = 1000 \text{ W/m}^2\text{/K}, \quad S_g = 0.12 \text{ m}, \quad S_c = 0.06 \text{ m}$$

$$L = 0.1 \text{ m}$$

From Equation 14.85a,

$$\frac{K}{L} = \frac{h_g S_g}{\dot{m}_c C_{PC}\left[1 + \dfrac{h_g S_g}{h_c S_c}\right]} = \frac{1200 \times 0.12}{1 \times 1005\left[1 + \dfrac{1200 \times 0.12}{1000 \times 0.06}\right]} = 0.04214$$

1. The *temperature of the coolant* (T_c) is obtained from Equation 14.88, namely

$$\frac{T_g - T_c}{T_g - T_{cr}} = e^{-Kl/L}$$

$$\frac{1200 - T_c}{1200 - 350} = e^{-0.042141L}$$

Thus, an expression for the coolant temperature along the blade height is expressed as

$$T_C = 1200 - 850\, e^{-0.04214l}$$

2. The *temperature of the blade* (T_b) is obtained from Equation 14.90, or

$$\frac{T_b - T_{cr}}{T_g - T_{cr}} = 1 - \frac{e^{-Kl/L}}{\left[1 + \dfrac{h_g S_g}{h_c S_c}\right]}$$

$$\frac{T_b - 350}{1200 - 350} = 1 - \frac{e^{-0.04214l}}{\left[1 + \dfrac{1200 \times 0.12}{1000 \times 0.06}\right]}$$

Thus, the blade temperature at any point along its height is shown in Table 14.4.

Example 14.8

For forced convection cooling of an axial-flow turbine blade, the following data are given:

Gas temperature T_g = 1500 K
Coolant temperature at inlet T_{cr} = 320 K

TABLE 14.4

Variation of Blade and Coolant Temperatures along Blade Height

l	l/L	T_C	T_b	T_g
0.0	0.0	350	950	1200
0.01	0.1	350.36	950.1	1200
0.02	0.2	350.716	950.21	1200
0.03	0.3	351.074	950.316	1200
0.04	0.4	351.432	950.421	1200
0.05	0.5	351.789	950.526	1200
0.06	0.6	352.146	950.631	1200
0.07	0.7	352.504	950.736	1200
0.08	0.8	352.86	950.841	1200
0.09	0.9	353.218	950.946	1200
0.1	1	353.574	951.05	1200

Coolant mass flow rate $\dot{m}_c = 1$ kg/s
Gas flow rate $\dot{m}_g = 33$ kg/s
Blade height $L = 0.1$ m
Gas heat transfer coefficient $h_g = 1500$ W/m$^2 \cdot$K
Wetted perimeter of blade profile $S_g = 0.15$ m
Parameter $(h_g S_g / h_c S_c) = 2$

It is required to

1. Calculate and plot the temperature of the blade material and coolant along the blade height.
2. Calculate the parameter $\phi = (T_G - T_M)/(T_G - T_C)$ from Figure 14.39, where T_M is the maximum blade temperature at tip as calculated earlier, and T_C is the coolant temperature at the compressor outlet, here at 695 K.
3. Calculate the value of the parameter ϕ for forced convection.
4. Use the same bleed mass flow rate ratio $\dot{m}_c/\dot{m}_g$ to calculate the maximum blade temperature T_m at the blade tip for other cooling techniques shown in Figure 14.39.

Solution

1. The blade temperature is expressed by the relation (14.90), from which

$$T_b = T_{cr} + \left(T_g - T_{cr}\right)\left[1 - \frac{e^{-Kl/L}}{1 + \dfrac{h_g S_g}{h_c S_c}}\right] = 320 + 1180\left[1 - \frac{e^{-Kl/L}}{3}\right]$$

$$\frac{K}{L} = \frac{h_g S_g}{\dot{m}_c Cp_c\left[1 + \dfrac{h_g S_g}{h_c S_c}\right]} = \frac{1500 \times 0.15}{1.0 \times 1005(1+2)} = 0.0746$$

$$\therefore T_b = 320 + 1180\left[1 - \frac{e^{-0.0746l}}{3}\right] \qquad (1)$$

TABLE 14.5

Blade and Coolant Temperatures along the Blade Height

l (m)	T_b (K)	T_C (K)	
	1106.6	319.8	Root
0.025	1107.4	322.2	
0.05	1108.1	324.3	Mean
0.075	1108.8	326.4	
0. 1	1109.9	329.7	Tip

The coolant temperature is to be calculated from the relation

$$\therefore T_C = T_g - \left(T_g - T_b\right)\left[1 + \frac{h_g S_g}{h_c S_c}\right]$$

$$\therefore T_C = 1500 - 3\left(1500 - T_b\right) \tag{2}$$

From Equations 1 and 2, T_b and T_g are calculated at different blade heights as shown in Table 14.5.

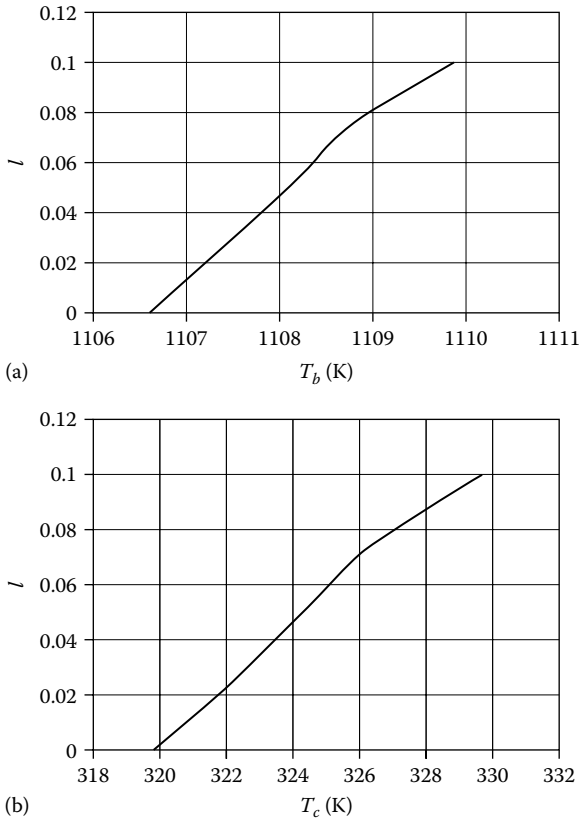


FIGURE 14.43
(a) Blade and (b) coolant temperature distribution along the blade height.

TABLE 14.6

Cooling Parameter for Different Cooling Techniques

	Cooling Technique	ϕ	T_m (K)
1	Simple radial flow	0.395	1182
2	Leading edge impingement/no film	0.466	1124.9
3	Multipass/trip strips	0.536	1068.5
4	Film/cross-flow impingement	0.611	1008
5	Transpiration	0.69	944.6

The blade and coolant temperature distribution along the blade height is plotted in Figure 14.43.

Variation of blade and coolant temperatures along the blade height

2. Calculate the parameter (ϕ) and (T_M)
Since

$$\phi = \frac{T_G - T_M}{T_G - T_C}$$

$$T_M = T_G - \phi\left(T_G - T_C\right)$$

Since $\dot{m}_c/\dot{m}_g = 3\%$, then from Figure 14.39 the value of ϕ is determined, and the maximum blade temperature for different cooling techniques is calculated and plotted in Table 14.6.

As seen from Table 14.6, the transpiration method gives the minimum value of the maximum temperature, which assures that this is the best cooling technique.

14.7 Case Study

The following section represents a complete preliminary design of an axial turbine. The steps followed in the design are given hereafter.

Design steps:

1. Calculation of flow properties at mean sections: flow angles, absolute and relative velocities, as well as total and static pressures and temperatures
2. Calculation of annulus dimensions
3. Calculation of the values of flow properties at different sections along the blade height from hub to tip, including airflow angles, absolute and relative velocities, together with the static pressures and temperatures
4. Estimation of the number of blades from data at the mean section for nozzles and rotors
5. Calculation of the chord length at any section along the blade height for nozzles and rotors
6. Selection of blade material that resists thermal and mechanical stresses
7. Calculation of stresses on rotor blades
8. Estimation of design point performance
9. Calculation of turbine efficiency
10. Turbine cooling

14.7.1 Design Point

The turbine to be designed is a part or module of either an aeroengine or gas turbine. The following data represent the values of the design variables determined from the performance analysis of the complete aeroengine or gas turbine.

Parameter	Value
$\dot{m}$ (kg/s)	110
Inlet pressure (bar)	10.803
Outlet pressure (bar)	6.584
Inlet temperature (K)	1600
Outlet temperature (K)	1430.5
Temperature drop (ΔT_{0S}) (K)	169.5
Isentropic efficiency (ηt)	0.91
Suggested number of stages	1

Only one stage is needed for this temperature drop. The rotational speed of the turbine is determined from the compressor coupled to the turbine as 150 rev/s. Moreover, the mean radius is assumed to be 0.4 m. The following values of some parameters are suggested:

Λ_m	ϕ_m	α_{1m} (°)	λ_N
0.45	0.8	0.0	0.05

The specific heat ratio and specific heat are assumed to be $\gamma = 1.333$ and $C_p = 1148\ \mathrm{J/kg \cdot K}$. From the temperature drop $\Delta T_{0S} = 169.5$ K, the stage loading coefficient is $\psi_m = 1.5717$. The design assumes a constant mean radius along the nozzle (stator) and rotor blade rows.

14.7.1.1 Mean Line Flow

The governing equations for mean flow calculations have previously been described. The results of the mean flow analysis are given in Table 14.7 for the three stations upstream of the stator and rotor and downstream of the rotor.

The annulus areas, blade heights, tip, and hub radii at the three stations are given in Table 14.8.

14.7.1.2 Three-Dimensional Variations

Variation of the flow parameters from hub to tip is calculated at three sections only (hub, mean, and tip) using the different design methods. The results of the free vortex method are given in Table 14.9. The flow is assumed to enter the stage axially, $\alpha_1 = 0$.

The following points may be concluded from Table 14.9:

1. The flow leaves the rotor at a non-zero absolute angle.
2. The static temperature and pressure increase from hub to tip at stations 2 and 3.
3. The maximum relative Mach number occurs at the hub for the rotor inlet and the tip for the rotor outlet.

TABLE 14.7

Flow and Geometrical Parameters at Different Turbine Stations

	Station 1	Station 2	Station 3
α_m (°)	0	59.0841	16.4269
β_m (°)	—	22.7740	57.0841
U_m (m/s)	—	351.8584	351.8584
Ca_m (m/s)	293.4656	281.4867	281.4867
Cu_m (m/s)	—	470.0339	82.9897
W_m (m/s)	—	305.2871	518.0035
T_0 (K)	1600	1600	1430.5
T_m (K)	1562.5	1469.3	1393
P_0 (bar)	10.803	10.612	6.5847
P_m (bar)	9.8250	7.5460	5.9208
ρ_m (kg/m^3)	2.1910	1.7895	1.4810
A (m^2)	0.1711	0.2184	0.2639
h (m)	0.0681	0.0869	0.1050
r_t (m)	0.4340	0.4434	0.4525
r_m (m)	0.4	0.4	0.4
r_h (m)	0.3660	0.3566	0.3475

TABLE 14.8

Geometrical Parameters at Different Stations

	Station 1	Station 2	Station 3
A_m (m^2)	0.1711	0.2184	0.2639
h (m)	0.0681	0.0869	0.1050
r_t (m)	0.4340	0.4434	0.4525
r_m (m)	0.4	0.4	0.4
r_h (m)	0.3660	0.3566	0.3475

It is worth mentioning here that the ordinate of any line in Figures 14.44 through 14.50 is proportional to the annulus height at stations 1, 2, and 3.

14.7.1.3 Number of Blades for Nozzle and Rotor

From calculations at the mean section, the blade heights at stations 1, 2, and 3 are determined. Next, assuming that the aspect ratio (h/c) is in the range (2–4), the blade chord at the mean section (c) is calculated.

From Figure 14.29, we can get the optimum pitch/chord ratio (s/c), since the flow angles at the mean section are known. Then the number of blades is estimated from the relation

$$\text{Number of blades} = \frac{2\pi r_m}{s}$$

The results for the calculations about the number of blades for the nozzle and rotor, after rounding, are given in Table 14.10.

TABLE 14.9

Flow Parameters at Different Turbine Stations

	Hub	Mean	Tip
α_1 (°)	0	0	0
α_2 (°)	61.9057	59.0841	56.4195
α_3 (°)	18.7453	16.4269	14.6076
β_2 (°)	37.2001	22.7740	6.8695
β_3 (°)	54.9466	57.0841	59.1572
U_2 (m/s)	313.6432	351.8584	390.0735
U_3 (m/s)	305.6816	351.8584	398.0352
Ca_1 (m/s)	293.4656	293.4656	293.4656
Ca_2 (m/s)	281.4867	281.4867	281.4867
Ca_3 (m/s)	281.4867	281.4867	281.4867
C_{u2} (m/s)	527.3041	470.0339	423.9851
C_{u3} (m/s)	95.5263	82.9897	73.3619
C_1 (m/s)	293.4656	293.4656	293.4656
C_2 (m/s)	597.7327	547.8747	508.9186
C_3 (m/s)	297.2542	293.4656	290.8896
W_2 (m/s)	353.3918	305.2871	283.5221
W_3 (m/s)	490.1046	518.0035	549.0446
T_{o1} (K)	1600	1600	1600
T_{o2} (K)	1600	1600	1600
T_{o3} (K)	1430.5	1430.5	1430.5
T_1 (K)	1562.5	1562.5	1562.5
T_2 (K)	1444.4	1469.3	1487.2
T_3 (K)	1392	1393	1393.6
P_{01} (bar)	10.803	10.803	10.803
P_{o2} (bar)	10.612	10.612	10.612
P_{03} (bar)	6.5847	6.5847	6.5847
P_1 (bar)	9.8250	9.8250	9.8250
P_2 (bar)	7.1746	7.6818	8.0638
P_3 (bar)	5.9042	5.9208	5.9319
M_{w2}	0.4753	0.4071	0.3758
M_{w3}	0.6715	0.7095	0.7518

14.7.1.4 Chord Length at Any Section along Blade Height for Nozzle and Rotor

After calculating the number of blades and pitch/chord at any station, the chord at any station will be recalculated as follows. The spacing or pitch is

$$s = \frac{2\pi r_m}{\text{Number of blades}}$$

$$c = \frac{s}{(s/c)}$$

	Hub	Mean	Tip
Chord of nozzle (c_N) (m)	0.0357	0.0380	0.0403
Chord of rotor (c_R) (m)	0.0443	0.0468	0.0498

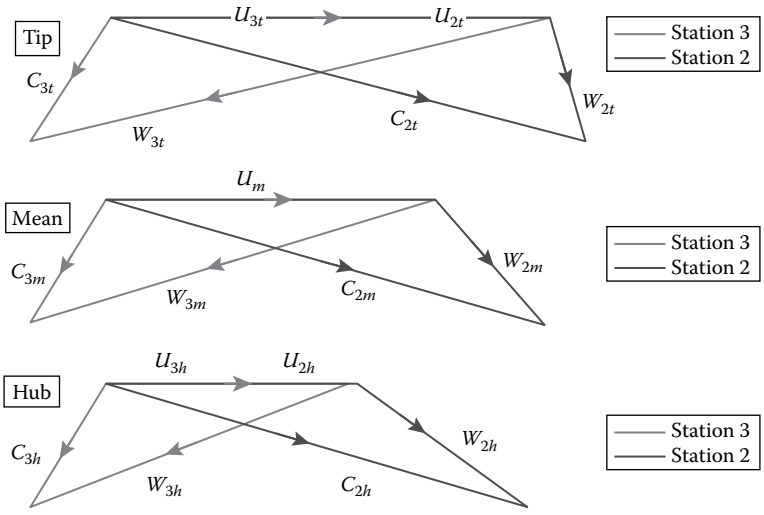


FIGURE 14.44
Variation of velocity triangles at HPT.

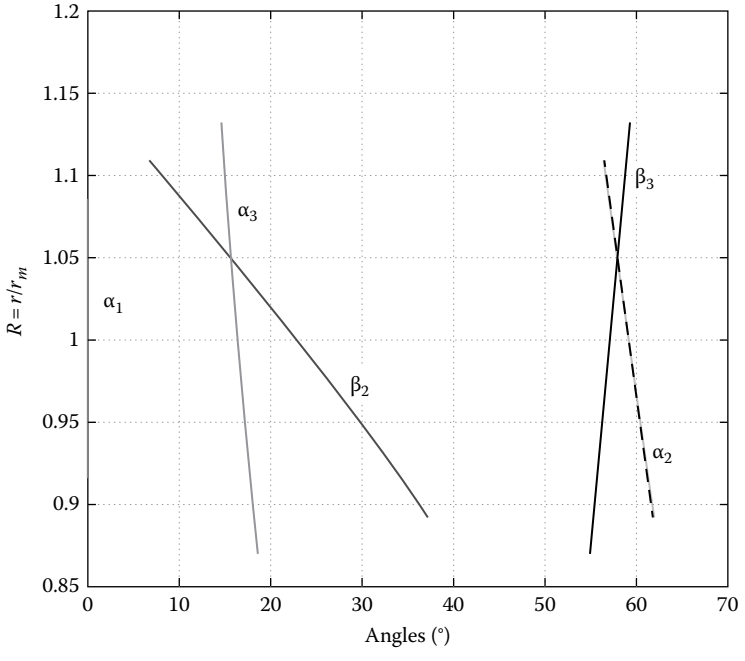


FIGURE 14.45
Variation of angles.

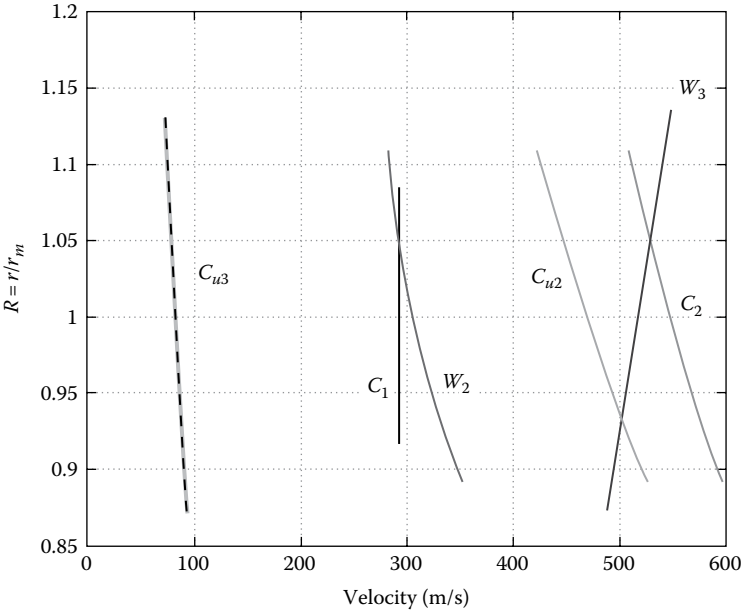


FIGURE 14.46
Variation of velocities.

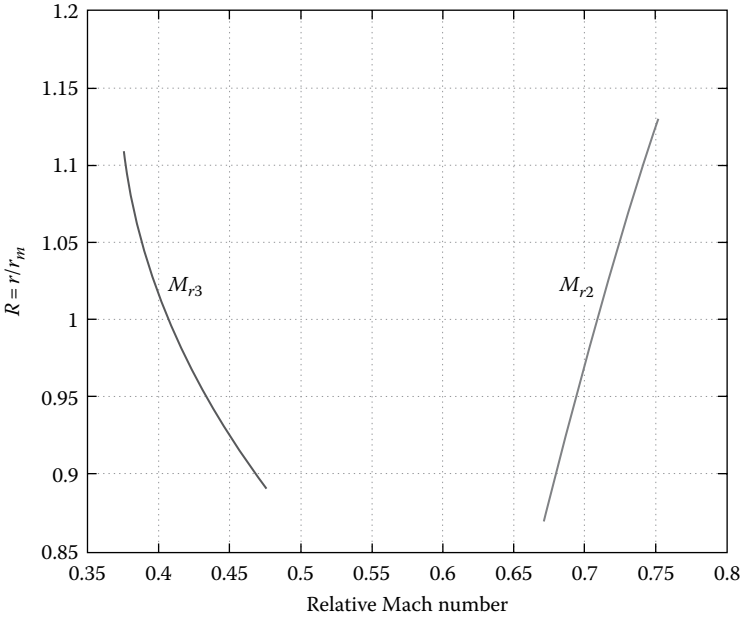


FIGURE 14.47
Variation of relative Mach number.

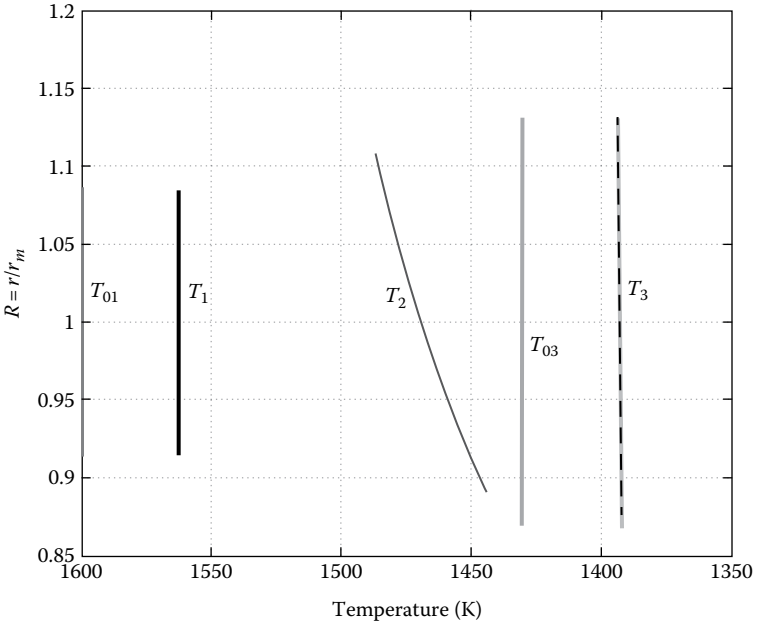


FIGURE 14.48
Variation of temperatures.

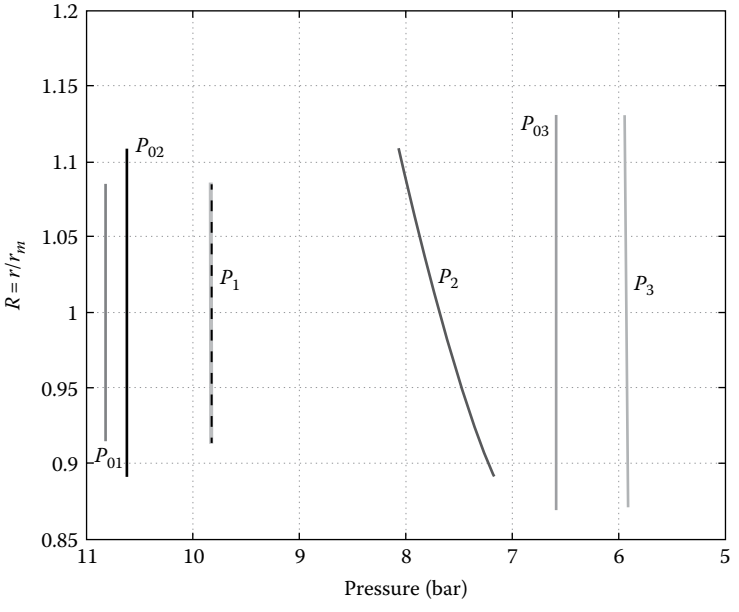


FIGURE 14.49
Variation of pressures.

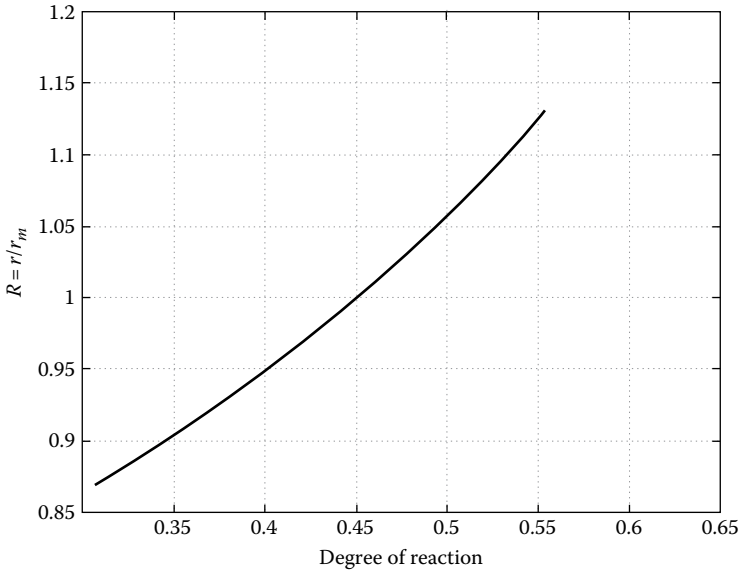


FIGURE 14.50
Variation of degree of reaction.

TABLE 14.10

Geometry and Number of Blades for Nozzle and Rotor

	Nozzle	Rotor
h/c	2	2
s/c	0.8490	0.8015
No. of blades	78	67

14.7.1.5 Blade Material Selection

The nozzle and rotor blade materials are selected to resist very high thermal and mechanical stresses. A suggested material for the present turbine blades is (SiC/SiC Ceramic Matrix Composites) as it can resist very high temperatures (up to 1900 K), and it is lightweight ($\rho_b = 3200$ kg/m^3) to reduce stresses on the blades.

14.7.1.6 Stresses on Rotor Blades

Based on the rotational speed of the rotor, as well as its dimensions and material, the centrifugal stress is calculated from Equation 14.68, while the gas bending stress is calculated from Equations 14.73 and 14.74. The following values of stresses are obtained:

$(\sigma_{ct})_{max}$ (MPa)	$(\sigma_{gb})_{max}$ (MPa)
95	118.69

14.7.1.7 Losses Calculations

The procedure described in Section 14.5.6 is followed here. Equations 14.92a, b, and 14.93 are used to evaluate the loss coefficients for nozzle and rotor. The following results are obtained:

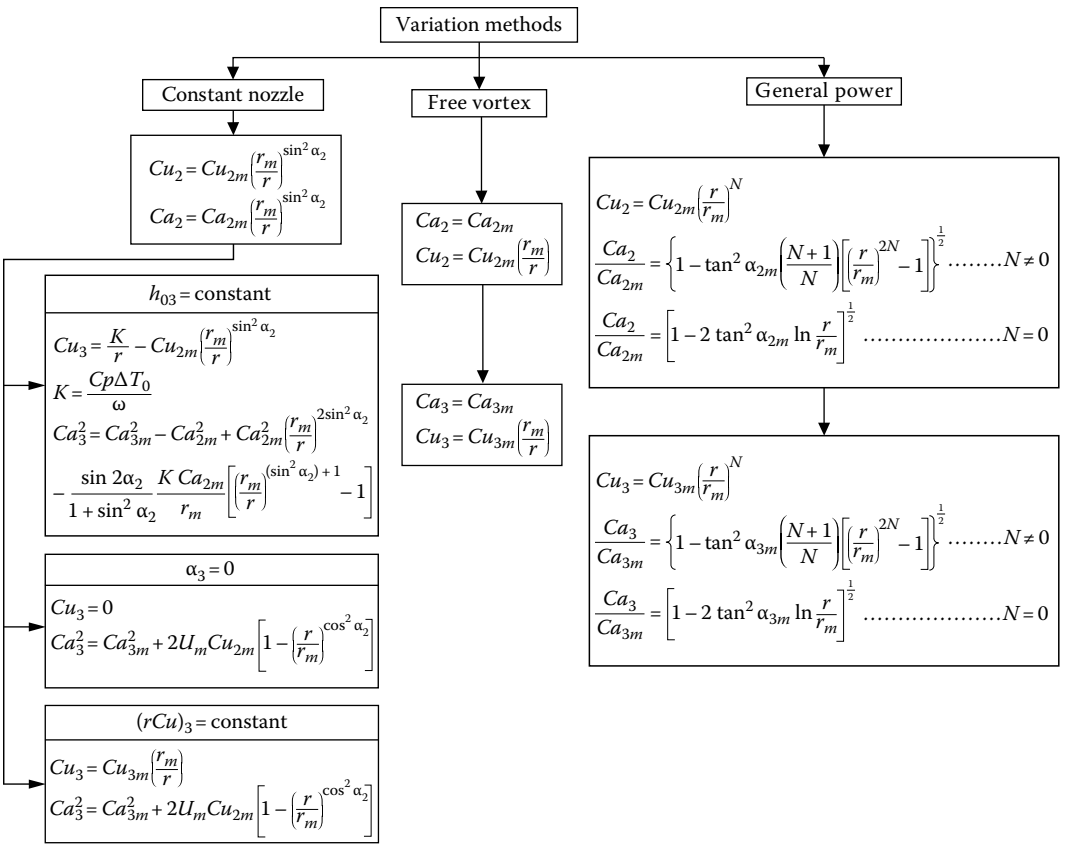
	Nozzle	Rotor
Total loss coefficient (Y)	0.1002	0.1508
Equivalent loss coefficient (λ)	0.0916	0.1381

14.7.1.8 Turbine Efficiency

From the previous values of loss coefficients and Equation 14.94, the value of the efficiency of the turbine is $\eta_t = 0.8904$. The assumed value was 0.91. The deviation between the assumed and calculated values is nearly 2%.

14.8 Summary

The following table summarizes the different methods that handle the variations of air properties from the root to tip sections:



Problems

14.1 A single-stage axial-flow gas turbine has the following data:

Inlet Stagnation Temperature T_{01}	**1200 K**
Stator outlet angle, α_2	60°
Rotor blade inlet angle, β_2	20°
Rotor blade outlet angle, β_3	60°

Calculate

1. The flow coefficient
2. The stage loading coefficient
3. The degree of reaction
4. If the blade speed $U = 360$ m/s
   a. The stage total temperature drop
   b. The stage pressure ratio if its efficiency is 0.9

14.2 An axial-flow gas turbine stage has a flow coefficient of 0.65, a constant axial velocity, and the gas leaves the stator blades at an angle of 65° to axial direction.

Calculate

i. The blade loading coefficient
ii. The rotor blade relative flow angle
iii. The degree of reaction

14.3 A single-stage axial-flow gas turbine has a mean radius of 30 cm. The hot gases enter the turbine stage at 1900 kPa and 1200 K, and the absolute velocity leaving the stator (C_2) is 600 m/s, making 65° with the axial direction (α_2). The rotor inlet and outlet blade angles (β_2 and β_3) are 25° and 60°, respectively.

Draw the velocity triangles and calculate

1. The rotor rotational speed (rpm)
2. The stage pressure ratio if its efficiency is 0.88
3. The flow coefficient, loading coefficient, and degree of reaction
4. The power delivered by the turbine if the mass flow rate is 50 kg/s

14.4 An axial-flow turbine stage is designed for zero exit swirl ($\alpha_3 = 0$). Sketch the velocity triangles for the speed-to-work ratios of ($\lambda = U/\Delta C_u$) 0.33, 0.5, and 1. Compare the three designs with respect to the work obtained and the degree of reaction.

14.5 A single-stage axial-flow turbine with axial leaving velocity has the following data:

Static temperature at stator inlet	= 750 K
Gas velocity at stator inlet	= 165 m/s
Blade mean velocity	= 300 m/s
Degree of reaction at mean radius	= 0.5

Plot the velocity triangles and determine

1. The fluid angle (α_2)
2. The stage loading coefficient
3. The flow coefficient
4. The stage total pressure ratio if $\eta_s = 0.9$

14.6 In a *zero-reaction* gas turbine, the blade speed at the mean diameter is 290 m/s. Gas leaves the nozzle ring at an angle 65° to the axial direction, while the inlet stage temperature is 1100 K. The following pressures were measured at various locations:

At nozzle entry, stagnation pressure	400 kPa
At nozzle exit, stagnation pressure	390 kPa
At nozzle exit, static pressure	200 kPa
At rotor exit, static pressure	188 kPa

Assuming the magnitude and direction of the velocities at the entry and exit of the stage are the same, determine the total-to-total efficiency of the stage.

14.7 Figure 14.51 shows velocity diagrams for *impulse* (zero-reaction) and *50%-reaction* turbine stages at different rotor speeds. In both cases, the rotor's absolute inlet velocity C_2 is 400 m/s at an angle $\alpha_2 = 70°$, and the absolute exit angle C_3 is axial. Complete the following table:

Quantity	Impulse	50% Reaction
U		
Φ		
Ψ		
β_1		
β_2		
$\Delta T_{0\,stage}$		
Work		

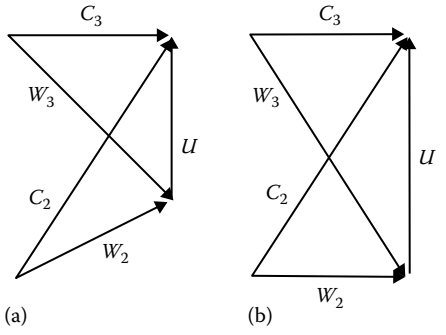


FIGURE 14.51
Velocity triangles for (a) impulse turbine and (b) 50%-reaction turbine.

14.8 A small axial-flow gas turbine with equal stage inlet and outlet velocities has the following design data based on the mean diameter:

Inlet temperature, T_{01}	1100 K	Inlet pressure, P_{01}	350 kPa
Axial velocity, C_a	260 m/s	Blade speed, U	350 m/s
Nozzle efflux angle, α_2	60°	Stage exit angle, α_3	12°
Mass flow rate	18 kg/s		

Calculate

1. The rotor blade angles
2. The blade loading coefficient and degree of reaction
3. The power output
4. The nozzle throat area required if the throat is situated at the nozzle outlet and the nozzle losses coefficient is 0.05

14.9 A single-stage axial-flow gas turbine with convergent nozzles has the following data:

Inlet stagnation temperature, T_{01}	1150 K	Mass flow rate	25 kg/s
Inlet stagnation pressure, P_{01}	420 kPa	Mean blade speed, U	340 m/s
Stage stagnation temperature drop	150 K	Rotational speed, N	15,000 rpm
Pressure ratio, P_{01}/P_{03}	1.9	Flow coefficient, Φ	0.75
Angle of gas leaving stage, α_3	12^0	Nozzle coefficient, λ_N	0.05

If the axial velocity remains constant and the gas velocities at the inlet and outlet are the same, determine at the mean radius:

1. The blade angles
2. The stage efficiency
3. The blade loading coefficient and degree of reaction
4. The required nozzle inlet area
5. The annulus area at rotor inlet and outlet
6. The blade height at the above locations

14.10 The following data apply to a single-stage axial-flow gas turbine:

Inlet stagnation temperature, T_{01}	1200 K	Mass flow rate	36 kg/s
Inlet stagnation pressure, P_{01}	8.0 bar	Mean blade speed, U	320 m/s
Stage stagnation temperature drop	150 K	Rotational speed, N	250 rev/s
Isentropic stage efficiency	0.9	Outlet velocity, C_3	400 m/s

Assuming that the outlet velocity is axial, calculate

1. The stage specific work and the stage power
2. The velocity triangle, and determine the blade and flow angles
3. The stage pressure ratio
4. The inlet rotor and exit Mach numbers
5. The blade height at rotor inlet and exit if $\lambda_N = 0.05$

14.11 A single-stage axial-flow gas turbine with convergent nozzles has the following data:

Inlet stagnation temperature, T_{01}	1100 K	Mass flow rate	18.75 kg/s
Inlet stagnation pressure, P_{01}	3.4 bar	Mean blade speed, U	298 m/s
Stage stagnation temperature drop	144 K	Rotational speed, N	200 rps
Nozzle losses coefficient, λ_N	0.05	Flow coefficient, Φ	0.95
Isentropic stage efficiency	0.9		

The convergent nozzle is choked.

Calculate

1. The pressure ratio in the turbine
2. The flow angles α_2, β_2, α_3, and β_3
3. The blade loading coefficient
4. The degree of reaction
5. The blade height and annulus radius ratio at stations 1, 2, and 3

14.12 The following particulars relate to a single-stage turbine of a free vortex design:

Inlet stagnation temperature, T_{01}	1050 K	Outlet velocity, C_3	275 m/s
Inlet stagnation pressure, P_{01}	3.8 bar	Root blade speed, U	300 m/s
Pressure ratio, P_{01}/P_{03}	2.0	Isentropic efficiency	0.88

The turbine is designed for zero reaction ($\Lambda = 0$) at the root radius, and the velocities at the inlet and outlet (C_1, C_3) are both equal and axial.

Calculate

1. The nozzle efflux angle α_2 and the blade inlet angle β_2 at the root radius
2. The nozzle efflux angle and degree of reaction at the tip radius if the tip-to-root radius ratio of the annulus at the exit from the nozzle blades is 1.4
3. The static pressure at the inlet and outlet of the rotor blades at root radius, assuming a nozzle blade losses coefficient of 0.05

14.13 A single-stage axial-flow gas turbine has a degree of reaction at the mean radius $\Lambda_m = 0.5$. If the free vortex design is considered, what is the minimum hub-to-tip ratio (ζ) such that the degree of reaction remains positive along the blade height?

14.14 The following data apply to a single-stage axial-flow gas turbine designed on free vortex theory. The outlet velocity is axial, and the turbine is designed with a constant annulus area through the stage.

Inlet stagnation temperature, T_{01}	1225 K	Mass flow rate	30 kg/s
Inlet stagnation pressure, P_{01}	800 kPa	Mean blade speed, U	330 m/s
Stage stagnation temperature drop	160 K	Rotational speed, N	15,000 rpm
Isentropic stage efficiency	0.9	Outlet velocity, C_3	390 m/s
Angle of gas leaving stage, α_3	12°	Nozzle coefficient, λ_N	0.05

Calculate

1. The stage pressure ratio
2. The flow and blade angles at the mean radius
3. The flow coefficient, loading stage coefficient, and degree of reaction
4. The blade height at inlet and exit from the rotor
5. The flow and blade angles at the root and tip radius using free vortex design

14.15 A single-stage turbine receives a supply of gases at a temperature of 1400 K and a pressure of 3.2 bar. The inlet and exit flows for the stage are both axial. The rotational speed of the turbine is 10,000 rpm, and it provides a power output of 4 MW. The mean radius of the blades is 0.25 m. The stage loading coefficient is 1.4, and the turbine operates with a flow coefficient of 0.5. It is required to perform a preliminary mean radius design for this stage, specifically

1. Calculate the axial velocity and mass flow rate.
2. Calculate the blade height at the inlet and outlet of stator, as well as at the rotor outlet.
3. Calculate the number of stator and rotor blades.
4. Calculate the relative flow angles at the rotor entry and exit.
5. Sketch the velocity triangles.
6. Estimate the stage efficiency.

The gas may be taken as $C_P = 1148\ \text{J/kg}\cdot\text{K}$, $\gamma = 4/3$.

14.16 1. Compare the degree of reaction in an axial turbine and axial compressor.

2. For an axial turbine, compare the values of ψ and ϕ in the case of
   a. Aircraft engines
   b. Industrial gas turbines

14.17 A single-spool turbojet engine has a seven-stage axial-flow compressor driven by a single axial turbine. The engine's components have the following data:

1. Compressor

Inlet total conditions	$T_{01} = 288$ K, $P_{01} = 1.01$ bar
Mean blade speed	$U = 250$ m/s
Flow coefficient	$\phi = 0.6$
Bleed from compressor outlet	$b = 8\%$
Mass flow rate	$m^{o} = 20$ kg/s

Stage	Flow Angles (°)	Rotor's de Haller No.	Work-Done Factor (λ)	Degree of Reaction (Λ)
1		0.8	0.98	0.5
2		0.75	0.93	0.5
3	$\beta_2 = 42°$	0.74	0.88	0.5
4	$\alpha_1' = 28.5°$	0.73	0.83	0.5
5		0.73	0.83	0.5
6		0.73	0.83	0.5
7		0.73	0.83	0.5

2. Combustion chamber

Pressure drop	$\Delta P_{occ} = 2.25\%$
Fuel-to-air ratio	$f = 1.7\%$

3. Turbine

Turbine inlet temperature	1100 K
Isentropic efficiency	$\eta_t = 0.9$
Mechanical efficiency	$\eta_m = 0.95$
Mean blade speed	$U = 298$ m/s
Flow coefficient	$\phi = 0.95$
Loss coefficient for the nozzle blades	$\lambda_N = 0.05$
Rotational speed	200 rps

The convergent nozzle is choked.
Calculate

a. The temperature rise in the compressor
b. The pressure ratio of the compressor
c. The blade loading coefficient in the turbine (Ψ)
d. The pressure ratio in the turbine
e. The flow angles in the turbine (β_3, β_2, α_2, α_3)
f. The degree of reaction of the turbine
g. The blade height and the annulus radius ratio at stations 1, 2, and 3 of the turbine

14.18 At midradius, an axial turbine stage is designed with 50% reaction, zero outlet swirl, and an axial velocity component of 200 m/s (constant through the stage). The absolute flow angle at outlet from the stator is 65° from the axial direction.

1. At the design point, what is the work done by the fluid at midradius on the rotor (kJ/kg)?
2. With no change to the turbine design flow conditions, but with a 20% drop in the design rotor rpm, estimate the work done (kJ/kg) by the rotor at midradius.
3. Calculate the flow coefficient for the design point.
4. Calculate the work coefficient for the design point.
5. If the air enters the stator at 1200 K, calculate the stagnation temperature and pressure ratios, ($\eta_s = 0.94$), for the design point.
6. If the tip diameter is 0.8 m, the hub-to-tip ratio is 0.9, and the blade material density is 8000 kg/m^3, calculate the maximum centrifugal stress and specify where it occurs (for the design point).
7. If the blade's maximum, average, and minimum temperatures are 1300, 1000, and 900 K, respectively, calculate the maximum and minimum thermal stresses for the design point ($E = 2 \times 10^5$ MPa, $\alpha = 7 \times 10^{-6}$ K^{-1}).

14.19 For a single stage, prove that

$$\frac{P_{02}}{P_{01}} = \left(1 - \frac{\lambda_N C_2^2}{2C_p T_2}\right)^{\gamma/\gamma-1}$$

$$\frac{P_{03r}}{P_{02r}} = \left(1 - \frac{\lambda_R W_3^2}{2C_p T_3}\right)^{\gamma/\gamma-1}$$

14.20 A single stage has the following characteristics:

Power generated	1200 kW
Inlet total temperature	1200 K
Inlet total pressure	3 bar
Outlet absolute velocity	$C_3 = C_{a3} = C_1 = 150$ m/s
Mean rotational speed	$U_2 = U_3 = 300$ m/s
Degree of reaction	$\Lambda = 0.5$
Nozzle and rotor loss coefficients	$\lambda_N = \lambda_R = 0.05$

Calculate

1. The parameters T_1, P_1, T_2, P_2, T_{02}, T_{02r}, P_{02r}, P_{02}, T_3, T_{03}, T_{03r}, P_{03}, P_{03r}
2. The gas mass flow rate
3. The flow and loading coefficients ϕ, ψ
4. The maximum mass flow rate that the turbine can pass at the same T_2

14.21 A high-pressure turbine is a single-stage axial turbine with the following properties:

$$T_{01} = 1200 \text{ K}, \quad P_{01} = 710 \text{ kPa}, \quad U_m = 450 \text{ m/s}, \quad \eta = 0.89, \quad \phi = 0.7, \quad \alpha_3 = 0, \quad \lambda_N = 0.05$$

Fuel-to-air ratio = 0.02

1. Calculate ψ, $\beta_3, \beta_2, \Lambda, \alpha_2, T_2'$.
2. Check whether or not the nozzle is choked.

14.22 The high-pressure turbine of a high-bypass turbofan engine is a two stage, axial turbine which drives the high-pressure compressor. It has the following data:

$$U_m = 380 \text{ m/s}, \quad \phi \equiv C_a/U_m = 0.8, \quad \eta_s = 0.94$$

Complete the following table. Comment on the degree of reaction of the second stage.

Stage	α_1	α_3	β_2	β_3	Λ	T_{01} **(K)**	ΔT_{os} **(K)**	(P_{01}/P_{03})
1	0	?	?	?	0.5	1400	235	?
2	?	0	?	?	?	?	235	?

14.23 A single-stage high-pressure axial-flow turbine has a mean radius of 0.3 m and blade height of 6 cm. The hot gases enter the turbine stage at 1900 kPa and 1200 K;

the absolute velocity leaving the stator (C_2) is 600 m/s and $\alpha_2 = 65°$. The rotor inlet and outlet blade angles (β_2 and β_3) are 25° and 60°, respectively.

1. Draw the velocity triangles.
2. Calculate
   a. The rotational speed of the rotor (rpm)
   b. The stage pressure ratio if its efficiency is 0.88
   c. The flow coefficient, loading coefficient, and degree of reaction
   d. The mass flow rate
   e. The power delivered by the turbine

   [$\gamma = 1.33$, $R = 290$ J/kg·K, and C_a/U is constant through the stage]

14.24 A single-stage axial turbine has the following characteristics: $\dot{m} = 110$ kg/s, $\eta_t = 0.91$, $T_{01} = 1140$ K, $P_{01} = 1280$ kPa, $\Delta T_0 = 150$ K, $U_m = 340$ m/s, nozzle losses coefficient $\lambda_N = 0.05$, flow coefficient $\phi = 1.0$, $\alpha_1 = 0$, $\alpha_3 = 10°$.

Calculate

1. The angles α_2, β_2, and β_3
2. The variables Ψ, Λ
3. The density at the nozzle outlet (ρ_2)

14.25 An axial turbine has the following data:

$$T_{01} = 1300 \text{ K}, \quad P_{01} = 11.5 \text{ bar}, \quad Y_N = 0.05, \quad \Delta T_0 = 300 \text{ K}$$

$$\phi = 0.7, \quad \psi = 2.0, \quad \Lambda = 0.5, \quad \eta_t = 0.9$$

Calculate

1. C_2 and hence identify the type of nozzle used
2. The rotor pressure loss factor (Y_R)

14.26 The high-pressure turbine of a turbofan engine is a single stage. It has the following data:

Inlet total temperature 1563 K	Stage efficiency 0.92
Inlet total pressure 43.6 bar	Rotational speed at mean radius 490 m/s
Stage temperature drop 352 K	Absolute outflow angle $\alpha_3 = 25°$
Flow coefficient $\phi = 0.8$	

Calculate

1. The stage pressure ratio
2. The absolute Mach numbers M_1, M_2, M_3
3. The parameters ψ and Λ
4. The angles α_2, β_2, β_3

14.27 An axial turbine stage has the following characteristics:
Mass flow rate 18 kg/s
Inlet total conditions $T_{01} = 1000$ K, $P_{01} = 400$ kPa
Temperature drop $\Delta T_0 = 151$ K
The nozzle is choked ($P_2 = P_c$).
At rotor inlet, annulus area $A_2 = 0.08$ m^2, $\alpha_2 = 60°$ and $U_2 = 350$ m/s
Stage efficiency $\eta_s = 0.92$
The axial speed is assumed constant through the rotor.
Specific heat ratio $\gamma = 4/3$

1. Draw the stage velocity triangles and plot the expansion process on a T–S diagram.
2. Calculate
   a. The velocities (C_2) and (C_{a2})
   b. The flow angles (β_2, α_3 and β_3)
   c. The degree of reaction (Λ)
   d. The stage pressure ratio (P_{01}/P_{03})
   e. The *maximum tensile stress* for a constant cross-sectional area rotor blade is given by the relation

$$\sigma_{\max} = 2\pi\rho_b N^2 A$$

If the blade is manufactured from Inconel 718, with the material density $\rho_b = 8220$ kg/m^3, rotational speed $N = 300$ rps, and $A = 0.08$ m^2, calculate the corresponding maximum stress.

References

1. Rolls-Royce plc, *The Jet Engine*, 5th edn., Rolls-Royce plc, Reprinted 1996, 45pp.
2. B. Lakshminarayana, *Fluid Dynamics and Heat Transfer of Turbomachinery*, John Wiley & Sons, Inc., New York, 1996, 145pp.
3. J.H. Horlock, *Axial Flow Turbine—Fluid Mechanics and Thermodynamics*, Robert E. Krieger Publishing Co. Inc., Malabar, FL, 1982, 51pp.
4. H.I.H. Saravanamuttoo, G.F.C. Rogers, and H. Cohen, *Gas Turbine Theory*, 5th edn., Prentice Hall, Harlow, U.K., 2001, 313pp.
5. H. Moustapha, *Gas Turbine Design*, Pratt & Whitney Canada Inc., Lecture Notes, 81pp.
6. S.F. Smith, A simple correlation of turbine efficiency, *Journal of Royal Aeronautical Society*, 69, 467–470, 1965.
7. D.G. Ainley and G.C.R. Mathieson, An examination of the flow and pressure losses in blade row of axial flow turbines, Aeronautical Research Council R&M 2891 (HMSO), 1955.
8. M.H. Vavra, *Aero-Thermodynamics and Flow in Turbomachines*, Robert E. Krieger Publishing Co. Inc., 1974, 456pp.
9. A.J. Glassman (ed.), *Turbine Design and Applications*, NASA SP-290, Washington, DC, 1973, 88pp.
10. S.M. Yahya, *Turbines Compressors and Fans*, TATA McGraw-Hill, New York, 1983, 334pp.

11. H. Moustapha, M.F. Zelessky, N.C. Baines, and D. Japikse, *Axial and Radial Turbines*, Concepts NREC, White River Junction, VT, 2003, 31pp.
12. L.J. Pritchar, An eleven parameter axial turbine airfoil geometry model, ASME P85-GT-219, 1985.
13. P. Hill and C. Peterson, *Mechanics and Thermodynamics of Propulsion*, 2nd edn., Addison Wesley Publication Company, Inc., Reading, MA, 1992, 387pp.
14. P.B. Meherwan, *Gas Turbine Engineering Handbook*, 2nd edn., Butterworth-Heinemann, Waltham, MA, 2002, 351pp.
15. W.W. Bathie, *Fundamentals of Gas Turbines*, 2nd edn., John Wiley & Sons, Inc., New York, 1996, 325pp.
16. J. Dunham and P.M. Came, Improvements to the Ainley-Mathieson method of turbine performance prediction, Paper 70-GT-2, ASME, New York, 1970.


Taylor & Francis
Taylor & Francis Group
http://taylorandfrancis.com

15

Radial Inflow Turbines

15.1 Introduction

Radial inflow turbines have a long history and predate axial machines by many years. The oldest turbine was that Hero's turbine that dates back to 150 BC. The other old one is the Ljungstrom outward flow type which dates back to 1894. This chapter deals solely with radial inflow turbines working with compressible fluids. Radial inflow turbines are not as common as radial flow (centrifugal) compressors. Like the latter, most radial inflow turbines are machines with relatively low specific speed suitable for applications with low flow rates and large pressure drops. They are also simpler and cheaper than axial turbines and so are used when weight and cost are more important than efficiency. The inward-flow radial (IFR) turbine covers tremendous ranges of power, rates of mass flow, and rotational speeds, and their uses range from very large Francis turbines used in hydroelectric power generation and developing hundreds of megawatts down to tiny closed cycle gas turbines employed in aerospace applications requiring power generation of a few kilowatts [1].

Most applications are relatively small scale in situations where compact power sources are required. Examples are turbochargers for cars, buses and trucks, railway locomotives and diesel power generators, cryogenic and process expanders, small gas turbines as the auxiliary power unit (APU) in most current airliners, helicopter engines, aerospace power systems, and rocket engine turbopumps.

Radial inflow turbines (similar to centrifugal compressors) are found in one of two layouts: either as part of a small gas generator or as part of a module where the first element is an inlet scroll or volute. In the first layout, the radial inflow turbine is coupled to a compressor and situated downstream of a combustion chamber. In this case, the turbine is coupled to a centrifugal compressor, usually in a back-to-back configuration. Moreover, the combustion chamber in between the two units is frequently of the reverse-flow type. This small gas turbine will therefore be of a minimal length, which is advantageous in many situations, particularly aerospace applications.

In the second layout, the turbine is a part of a module, for example, a cryogenic expander. The flow enters from a pipe and is dispersed around the annulus of the turbine in the volute, which is very similar to a centrifugal compressor and its outward scroll.

The characteristics that make radial turbines desirable are

- High efficiency
- Ease of manufacture
- Sturdy construction
- High reliability

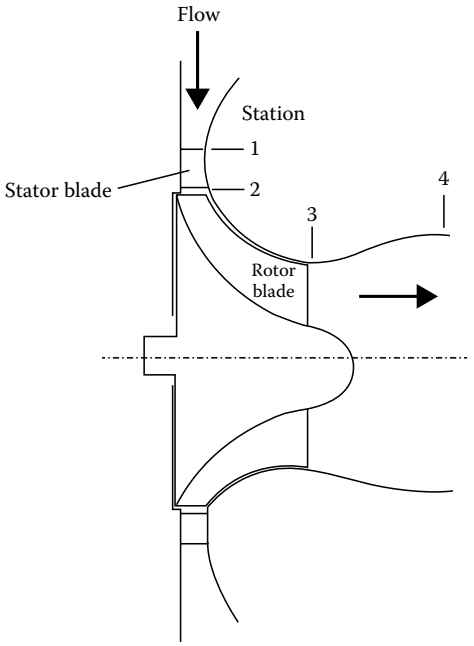


FIGURE 15.1
Layout of a radial inflow turbine.

Radial turbines are similar to centrifugal compressors as in both fluid enters and leave in two perpendicular directions. For radial turbines, the flow enters radially and leaves axially close to the axis of rotation. This turning of the flow takes place in the rotor passage, which is relatively long and narrow. Figure 15.1 illustrates a radial inflow turbine.

A radial inflow turbine is composed of four elements; namely, a volute (or scroll), nozzle vanes, a rotor, and a discharge diffuser. The flow enters the turbine via a scroll, which provides some swirl velocity before distributing the flow in the stator blades. Small turbines used in turbochargers do not have stator blades and rely on the scroll to provide all the angular momentum entering the rotor. The ring of nozzle vanes upstream of the rotor accelerates the flow. Flow enters the diffuser at a large radius and leaves it at a smaller radius. At the rotor inlet, where the flow velocity relative to the rotor has little or no tangential component, the rotor blades are usually straight and radial. Generally, this straight section of the rotor blade is rather highly loaded, due to the momentum being angular $(r \times C_u)$ (where (r) is the radius and (C_u) is the tangential component of absolute velocity). Usually, there is a diffuser downstream of the rotor to reduce the exhaust velocity to a negligible value.

15.2 Thermodynamic

The expansion process in a radial turbine differs appreciably from that in an axial turbine because of the change of radius in the rotor. The relative total temperature and pressure decrease with the decreasing radius, which is a distinct advantage for the radial

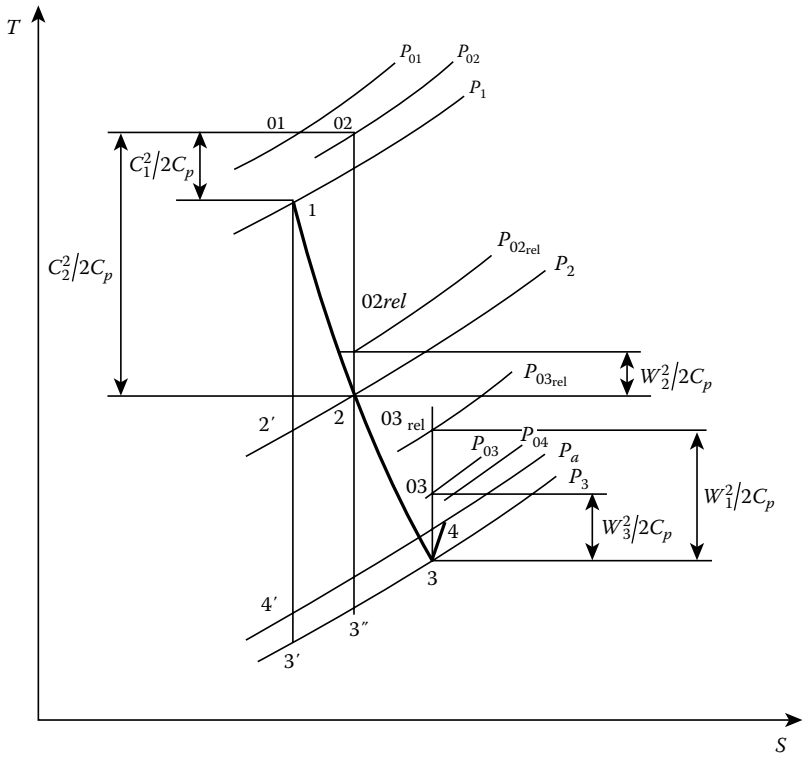


FIGURE 15.2
Temperature–entropy diagram.

turbine because it permits the use of a lower velocity for a given overall expansion. This can be seen from the temperature–entropy diagram in Figure 15.2.

For the radial turbine, as shown in Figure 15.1, the turbine is situated downstream from either a volute or a combustion chamber. The first element considered in this analysis is the nozzle. The flow may experience a slight drop in total pressure, but the total temperature remains unchanged.

$$T_{02} = T_{01}, \quad P_{02} = P_{01} - \Delta P_{0\ nozzle} \tag{15.1}$$

For preliminary design, it is sufficient to assume that $\Delta P_{0\ nozzle} = 0$. For the rotor, the outlet total pressure (P_{03}) is much less than the (P_{02}). This difference is mainly due to the energy extraction from the working fluid to produce shaft power together with the loss.

Figure 15.3 shows a radial turbine velocity diagram for a turbine with prewhirl in the inlet volute and a mean diameter ratio (exit mean to inlet) of about 0.5.

The absolute inlet velocity to the rotor C_2 has two components in the radial and tangential directions: (C_{r2}, C_{u2}). The radial component is compatible with the mass flow rate

$$\dot{m} = \rho_2 A_2 (1 - B_2) C_{r2} \tag{15.2}$$

where

A_2 is the annulus area at the rotor tip

B_2 is the allowance for boundary layer blockage [2]

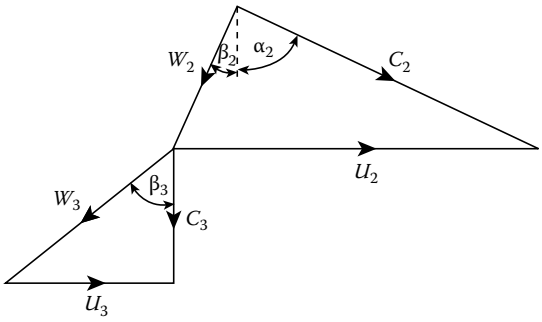


FIGURE 15.3
Velocity triangles in a radial inflow turbine.

The specific work output is given by Euler's equation for turbomachinery

$$W = U_2 C_{u2} - U_3 C_{u3} \tag{15.3}$$

which is expressed in terms of enthalpy drop as

$$W = C_P \left(T_{01} - T_{03} \right) = h_{01} - h_{03}$$

If the flow at the rotor inlet is radial, then the relative angle β_2 is zero (thus $U_2 = C_{u2}$). The flow leaves the rotor axially, thus C_{u3} is zero.

$$W = C_p \left(T_{01} - T_{03} \right) = U_2 C_{u2} = U_2^2 \tag{15.4}$$

If the flow is assumed to be ideal isentropic through the turbine with a perfect diffuser, then define the specific work output as

$$W' = Cp \left(T_{01} - T_4 \right) = \frac{C_0^2}{2} \tag{15.5a}$$

$$C_0^2 = 2CpT_{01} \left[1 - \left(\frac{P_4}{P_{01}} \right)^{\gamma - 1/\gamma} \right] \tag{15.5b}$$

where C_0 is the spouting velocity defined as the velocity equivalent of the isentropic enthalpy drop. From Equations 15.4 and 15.5a,

$$U_2^2 = \frac{C_0^2}{2} \tag{15.6}$$

This velocity ratio is identified as

$$v = \frac{U_2}{C_0}$$

For an ideal case, $\nu \equiv U_2 / C_0 = 0.707$. For non-isentropic flow [3], this speed ratio becomes $U_2 / C_0 \approx 0.68 - 0.71$.

Three efficiencies are defined here: the isentropic efficiency of the turbine alone and the isentropic efficiency for the turbine and for the diffuser. The isentropic efficiency of the turbine is expressed either as total-to-total or as total-to-static efficiency. The turbine total-to-static efficiency is defined as

$$\eta_{ts} = \frac{T_{01} - T_{03}}{T_{01} - T_3'} \tag{15.7}$$

The total-to-total efficiency is defined as

$$\eta_{tt} = \frac{T_{01} - T_{03}}{T_{01} - T_{03s}} = \frac{\Delta T_0}{T_{01} - T_{03s}} \tag{15.8}$$

The combined turbine and diffuser efficiency is

$$\eta_o = \frac{T_{01} - T_{03}}{T_{01} - T_4'} \tag{15.9}$$

The nozzle loss coefficient is also defined as

$$\lambda_N = \frac{T_2 - T_2'}{\left(C_2^2/2C_p\right)} \tag{15.10}$$

The rotor loss coefficient is

$$\lambda_R = \frac{T_3 - T_3''}{\left(W_3^2/2C_p\right)} \tag{15.11}$$

For the constant pressure process $C_p \delta T = T \delta s$, the nozzle loss coefficient can be expressed as

$$\lambda_N = \frac{T_3'' - T_3'}{\left(C_2^2/2C_p\right)} \frac{T_2'}{T_3'}$$

The turbine isentropic efficiency can be expressed in terms of the nozzle and rotor loss coefficients

$$\eta_{ts} = \left[1 + \frac{1}{2C_p\left(T_{01} - T_{03}\right)} \left\{ C_3^2 + \lambda_R W_3^2 + \lambda_N \frac{T_3'}{T_2'} C_2^2 \right\}\right]^{-1} \tag{15.12}$$

The term T_3'/T_2' can be calculated from the relation

$$\frac{T_3'}{T_2'} = 1 - \frac{U_2^2}{2CpT_2}\left[1 + \left(\frac{r_3}{r_2}\right)^2 \left\{\left(1 + \lambda_R\right)\text{cosec}^2\,\beta_3 - 1\right\} - \cot^2\alpha_2\right] \tag{15.13}$$

where

$$T_2 = T_{01} - \frac{U_2^2}{2Cp}\text{cosec}^2\alpha_2 \tag{15.14}$$

Example 15.1

A small radial inflow turbine develops 60 kW of power when its rotor is running at 60,000 rpm. The pressure ratio P_{o1}/P_3 is 2.0. The inlet total temperature is 1200 K. The rotor has an inlet tip diameter of 12 cm and a rotor exit tip diameter of 7.5 cm. The hub/tip ratio at exit is 0.3. The mass flow rate of gases is 0.35 kg/s. The gases enter the rotor radially and leave axially and have the following inlet and outlet angles $\alpha_2 = 70$ and $\beta_3 = 40°$, respectively. The nozzle loss coefficient $(\lambda_N) = 0.07$. It is required to calculate

1. The isentropic efficiency (η_{ts})
2. The rotor loss coefficient (λ_R)

Solution

The rotor tip rotational speed is $U_2 = \pi \times D_2 \times N = 377$ m/s.

From the inlet velocity triangle, Figure 15.3, with $\beta_2 = 0$, then

$$\sin\alpha_2 = \frac{U_2}{C_2}$$

The absolute velocity at the inlet is $C_2 = U_2 \times \text{cosec}\ \alpha_2 = 401.185$ m/s.

The static temperature at the inlet is $T_2 = T_{o2} - \dfrac{C_2^2}{2Cp} = 1130$ K.

$$T_{o1} - T_3' = T_{o1}\left[1 - \frac{T_3'}{T_{o1}}\right] = T_{o1}\left[1 - \left(\frac{P_3}{P_{o1}}\right)^{\gamma-1/\gamma}\right] = 190.92 \text{ K}$$

The turbine power is

$$\mathscr{P} = \dot{m} \times Cp \times \left(T_{o1} - T_{o3}\right)$$

$$T_{o1} - T_{o3} = \frac{60{,}000}{0.35 \times 1148} = 149.328 \text{ K}$$

Since

$$\eta_{ts} = \frac{T_{o1} - T_{o3}}{T_{o1} - T_3'} = 0.782$$

$$\frac{r_3}{r_2} = \frac{D_{3h} + D_{3s}}{D_2} = \frac{\xi \times D_{3s} + D_{3s}}{2 \times D_2} = 0.40625$$

From Equation 15.13,

$$\frac{T_3'}{T_2'} = 1 - \frac{U_2^2}{2 \times Cp \times T_2}\left[1 + \left(\frac{r_3}{r_2}\right)^2 \left\{\left(1 + \lambda_R\right)\text{cosec}^2\beta_3 - 1\right\} - \cot^2\alpha_2\right]$$

$$\frac{T_3'}{T_2'} = 0.9396 - 0.02187 \times \lambda_R$$

Substituting the value of T_3'/T_2' in Equation 15.12,

$$\eta_{ts} = \left[1 + 0.5\left\{\left(\frac{r_3}{r_2}\right)^2 \left(\cot^2\beta_3 + \lambda_R \operatorname{cosec}^2\beta_3\right) + \lambda_N \frac{T_3'}{T_2'} \operatorname{cosec}^2\alpha_2\right\}\right]^{-1}$$

$$(0.782) - 1 = 1.1544 + 0.191 \times \lambda_R$$

$$\lambda_R = 0.65.$$

15.3 Dimensionless Parameters

The following dimensionless parameters are frequently used in the preliminary design of radial inflow turbines: stage loading, flow coefficient, rotor meridional velocity ration, and specific speed.

15.3.1 Stage Loading

The stage loading coefficient can be expressed using the Euler turbomachinery equation as

$$\psi = \frac{C_{u2}U_2 - C_{u3}U_3}{U_2^2} \tag{15.15a}$$

$$\psi = \frac{C_{u2}}{U_2} - \frac{r_3}{r_2}\frac{C_{u3}}{U_3}$$

where r_3/r_2 is the rotor radius ratio. The exit is normally fairly small so that the second term on the right-hand side is small in comparison with the first, and the loading coefficient can be approximated as

$$\psi \approx \frac{C_{u2}}{U_2} \tag{15.15b}$$

15.3.2 Flow Coefficient

The flow coefficient is defined in terms of the exit meridional velocity, also non-dimensionalized by the inlet blade speeds

$$\phi = \frac{C_{a3}}{U_2} \tag{15.16}$$

15.3.3 Rotor Meridional Velocity Ratio

The rotor meridional velocity ratio ξ

$$\xi = \frac{C_{r2}}{C_{a3}} \approx 1.0 \tag{15.17}$$

15.3.4 Specific Speed

Specific speed is defined as

$$N_s = \frac{N\sqrt{Q}}{\left(\Delta h_{0s}\right)^{3/4}} \tag{15.18}$$

where
N is the rotational speed
Q is the volume rate

Substituting for Δh_{0s} and considering the volume flow rate at station 3, the specific speed has the form

$$N_s = 0.18\sqrt{\frac{Q_3}{ND_2^3}}$$

or

$$\Omega_s = 1.131\sqrt{\frac{Q_3}{ND_2^3}} \text{ rad}$$

Specific speed is a function only of the operating conditions and contains no parameters relating directly to the turbine geometry [2]. Performance measurements of a large number of radial inflow turbines indicate that the best efficiencies occur at specific speeds in the range of about 0.4–0.8.

15.4 Preliminary Design

Appropriate values for the following variables are to be selected such that optimum efficiency is attained:

- Stage loading (ψ), in the range 0.8–1.0
- Flow coefficient (ϕ), in the range 0.3–0.4
- Total-to-total or total-to-static efficiency, equal to or greater than 0.7
- Meridional velocity ratio (ξ), in most cases selected as unity
- The ratio between the exit hub and the inlet radii (r_{3h}/r_2), in the range of 0.25–0.35

Generally, some data will be available for the turbine to be designed. These include

- Power
- Rotational speed
- Working fluid
- Mass flow rate
- Inlet total conditions

The design steps are presented in points 1–23.

1. Calculate the total enthalpy (or temperature) drop from the relation

$$\mathscr{P} = \dot{m} \times Cp \times \left(T_{o1} - T_{o3}\right)$$

$$\Delta T_0 \equiv \left(T_{o1} - T_{o3}\right) = \mathscr{P} / \left(\dot{m} \times Cp\right)$$

2. Calculate the rotor tip speed from

$$U_2 = \sqrt{\Delta h} = \sqrt{C_p \left(T_{01} - T_{03}\right)}$$

3. Calculate the axial speed at exit from the relation

$$C_{a3} = \phi U_2$$

The axial velocity at the rotor outlet is nearly equal to the absolute velocity at the rotor outlet, or

$$C_3 \cong C_{a3}$$

4. Calculate the rotor inlet radial velocity component from the relation

$$C_{r2} = \xi \phi U_2 = \xi C_{a3}$$

5. Calculate the rotor inlet swirl speed from the relation

$$C_{u2} = \psi U_2$$

6. Calculate the rotor inlet absolute flow angle from the relation

$$\alpha_2 = \tan^{-1} \frac{C_{u2}}{C_{r2}}$$

7. Calculate the rotor inlet relative angle

$$\beta_2 = \tan^{-1} \frac{C_{u2} - U_2}{C_{r2}}$$

8. Calculate the inlet absolute velocity

$$C_2 = \left(C_{r2} + C_{u2}\right)^{1/2}$$

9. Calculate the rotor inlet static temperature

$$T_2 = T_{02} - \frac{C_2^2}{2C_p}$$

10. Calculate the rotor inlet static pressure

$$P_2 = P_{02}\left(T_2/T_{02}\right)^{\gamma/\gamma-1}$$

For preliminary calculations, it may be first assumed that $P_{02} = P_{01}$

11. Calculate the rotor inlet area

$$A_2 = \frac{\dot{m}RT_2}{P_2 C_{r2}}$$

12. Calculate the rotor inlet radius

$$r_2 = \frac{U_2}{2\pi N}$$

13. Calculate the rotor inlet width

$$b_2 = \frac{A_2}{2\pi r_2}$$

14. Calculate the rotor outlet total temperature

$$T_{03} = T_{01} - \Delta T_0$$

15. Calculate the static temperature at the rotor outlet

$$T_3 = T_{03} - \frac{C_3^2}{2C_p}$$

16. Calculate the rotor total outlet pressure

$$P_{03} = P_{01}\left(1 - \frac{\Delta T_0}{T_{01}\eta_{tt}}\right)^{\gamma/\gamma-1}$$

17. Calculate the static pressure at the rotor outlet

$$P_3 = P_{03}\left(T_3/T_{03}\right)^{\gamma/\gamma-1}$$

Alternatively, if the total-to-static efficiency is given, then the static pressure is obtained from the relation

$$\frac{P_3}{P_{01}} = \left[1 - \frac{1}{\eta_{ts}}\left(1 - \frac{T_{03}}{T_{01}}\right)\right]^{\gamma/\gamma-1}$$

The total pressure at the rotor outlet is calculated as

$$P_{03} = P_3\left(T_{03}/T_3\right)^{\gamma/\gamma-1}$$

18. The rotor outlet area is calculated as

$$A_3 = \frac{\dot{m} R T_3}{C_3 P_3}$$

19. The hub radius at the rotor outlet is calculated from the known ratio (r_{3h}/r_2) as

$$r_{3h} = \left(r_{3h}/r_2\right) \times r_2$$

20. The tip radius is calculated as

$$r_{3t} = \sqrt{\frac{A}{\pi} - r_{3h}^2}$$

21. The mean rotational speed at the rotor outlet is calculated as

$$U_3\left(RMS\right) = \pi\left(r_{3h} + r_{3t}\right)N$$

22. For the design followed here, zero swirl is assumed at the outlet, thus the flow leaves the rotor axially or $C_{u3} = 0$. The outlet relative angle is then

$$\beta_3 = \tan^{-1}\frac{U_3}{C_3}$$

23. The outlet relative speed is

$$W_3 = U_3\left(RMS\right)\text{cosec}\ \beta_3$$

Some notes may be added here:

- In this procedure, no exit swirl is assumed. The effect of exit swirl is discussed in detail in Chen and Baines [4]. However, for most practical purposes, it suffices to say that designers usually add exit swirl only when it is necessary to increase or decrease the power output without changing the speed of rotation. This is clear from Equation 15.3. It must be noted that if the exit swirl angle exceeds about 15°–20°, diffuser performance falls in conventional diffuser cases. This constraint is similar to that in nozzles following axial turbines.
- Rotor blade inlet and exit angles are determined from the flow inlet and outlet angles with known incidence and deviation angles

$$\beta_{b2} = \beta_2 - i$$

$$\beta_{b3} = \beta_3 + \delta_3$$

- Concerning the angle of incidence, it must be consistent with general experience, from which it is noticed that the best efficiency occurs at a value in the range of 20°–30° in magnitude.

15.5 Breakdown of Losses

Figure 15.4 illustrates a division of the losses in a radial turbine stage and emphasizes the large contribution made to the stage by the rotor and by rotor-related losses [5]; namely,

1. Nozzle blade row boundary layer
2. Rotor passage boundary layer
3. Rotor blade tip clearance
4. Disk windage (or the back surface of the rotor)
5. Kinetic energy loss at exit

From Figure 15.4, it may be concluded that, for low values of specific speed, the stator and rotor viscous losses are very large due to the high ratio of wall area to flow area. Also, the clearance loss is considerable as the blade-to-shroud clearance is a relatively large proportion of the passage height. The windage loss, which depends primarily on the diameter and rotational speed, is also large at a low specific speed due to the low flow rate. As specific speed increases, the stator and rotor losses, clearance loss, and windage loss all decrease due to the increased flow and area. The exit kinetic energy loss becomes predominant at high values of specific speed.

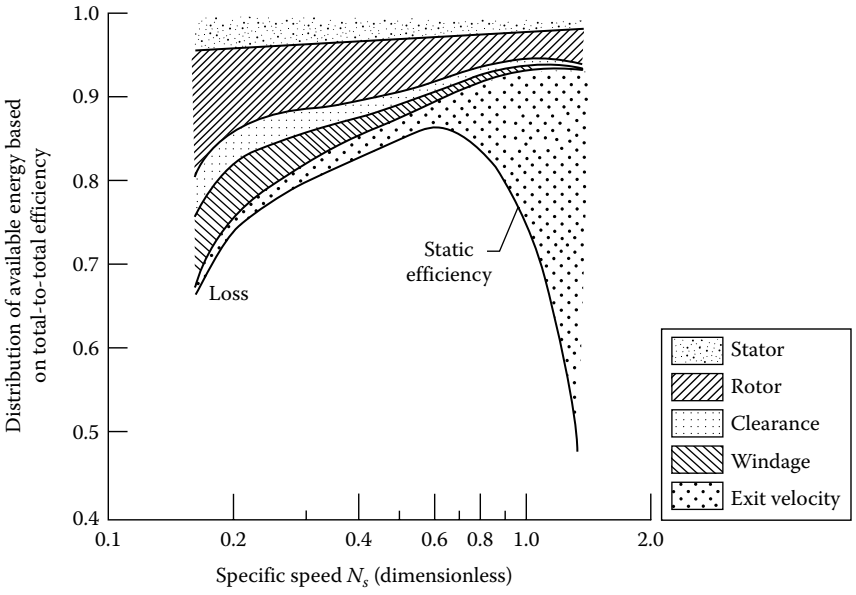


FIGURE 15.4
Breakdown of losses of radial turbine. (From Rohlik, H.E., *Analytical Determination of Radial Inflow Turbine Design Geometry for Maximum Efficiency*, NASA TN D-4384, Washington, DC. With permission.)

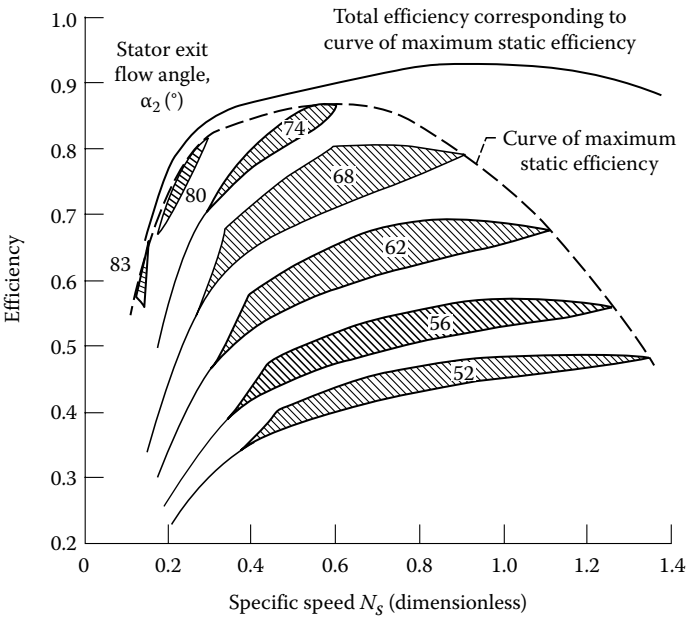


FIGURE 15.5
Effect of design speed on total-to-static efficiency. (From Glassman, A.J., *Turbine Design and Application*, NASA SP-290, Washington, DC, p. 279. With permission.)

The effects of geometry and velocity diagram characteristics were examined by calculating the previously mentioned losses for a large number of combinations of the following parameters:

- Nozzle exit angle α_2
- Rotor diameter ratio D_{3av}/D_2
- Rotor blade entry height to exit diameter ratio b_2/D_{3av}

The static efficiency is plotted against specific speed; see Figure 15.5. For the range of values used in the study, all of the calculated points fell in the shaded areas in Figure 15.5. The stator-exit angle is seen to be a prime determinant of efficiency, which falls into a small region for each stator exit flow angle. The dashed curve is the envelope of all the computed static efficiencies and the solid curve above it represents the corresponding total efficiencies.

Example 15.2

A radial inflow turbine has the following characteristics and operating conditions:

Inlet total temperature	1400 K
Inlet total pressure	3.0 bar
Rotor tip rotational speed	500 m/s
Rotational speed	40,000 rpm
Specific speed	$\Omega_S \equiv 1.131\sqrt{\dfrac{Q_3}{ND_2^3}} = 0.58$

$$\beta_{3_{av}} = 63°, \quad \frac{D_{3_s}}{D_2} = 0.7, \quad \alpha_2 = 74°$$

$$\frac{D_{3_h}}{D_{3_s}} = 0.4, \quad \frac{U_2}{C_0} = 0.7, \quad \text{and} \quad \frac{b}{D_2} = 0.0873$$

Using Figure 15.5, it is required to find

a. The turbine total-to-static efficiency
b. The geometrical dimensions of the turbine $D_2, b_2, D_3, D_{3h}, D_{3av}$
c. The outlet total and static temperatures and the outlet static pressure (T_{03}, T_3, P_3)
d. Rate of mass flow $(\dot{m})$

Solution

1. Total-to-static efficiency: From Figure 15.5, with a specific speed of $\Omega_S = 0.58$ rad and $\alpha_2 = 74°$, then $\eta_{ts} = 0.85$
2. Geometrical dimensions

$$D_2 = \frac{60U_2}{\pi N} == \frac{60 \times 500}{\pi \times 40{,}000} = 0.2387 \text{ m}$$

$$\frac{b_2}{D_2} = 0.0873$$

$$b_2 = 0.0873 \times 0.2387 \text{ m}$$

$$\frac{D_{3s}}{D_2} = 0.7$$

$$D_{3s} = 0.1671 \text{ m}$$

$$\frac{D_{3h}}{D_{3s}} = 0.4$$

$$D_{3h} = 0.06684 \text{ m}$$

$$D_{3av} = \frac{D_{3h} + D_{3s}}{2} = \frac{0.06684 + 0.1671}{2}$$

$$D_{3av} = 0.11697 \text{ m}$$

3. The outlet conditions: From Equation 15.4, the specific work is

$$W = C_P(T_{01} - T_{03}) = U_2 C_{u_2} = U_2^2$$

Then

$$1148 \times (1400 - T_{03}) = (500)^2$$

$$T_{03} = 1182.23 \text{ K}$$

The specific speed $\Omega_S = 1.131\sqrt{\dfrac{Q_3}{ND_2^3}}$

$$0.58 = 1.131\sqrt{\frac{Q_3}{\dfrac{40{,}000}{60}(0.2387)^3}}$$

Then

$$Q_3 = 2.3845 \text{ m}^3/\text{s}$$

Since

$$Q_3 = C_{a3}\frac{\pi}{4}\left(D_{S3}^2 - D_{h3}^2\right)$$

Then

$$2.3845 = C_{a3}\frac{\pi}{4}\left((0.1671)^2 - (0.06684)^2\right)$$

$$C_{a3} = 129.44 \text{ m/s} = C_3$$

$$T_3 = T_{03} - \frac{C_3^2}{2C_P} = 1182.23 - \frac{(129.44)^2}{2\times 1148}$$

$$T_3 = 1174.93 \text{ K}$$

The static pressure is correlated to the total-to-static efficiency by the relation

$$\frac{P_3}{P_{01}} = \left[1 - \frac{1}{\eta_{ts}}\left(1 - \frac{T_{03}}{T_{01}}\right)\right]^{\gamma/\gamma-1} = \left[1 - \frac{1}{0.85}\left(1 - \frac{1182.23}{1400}\right)\right]^{\gamma/\gamma-1} = 0.4455$$

$$P_3 = 1.337 \text{ bar}$$

4. Mass flow rate

$$\dot{m} = \rho_3 Q_3 = \frac{P_3}{RT_3}\times Q_3$$

$$\dot{m} = \frac{1.337\times 10^5}{287\times 1174.93}\times 2.3845 = 0.9454 \text{ kg/s.}$$

15.6 Design for Optimum Efficiency

A general one-dimensional design procedure for the radial inflow turbines was presented in Whitefield [7]. Starting from the kinematical relation for velocities at the rotor inlet

$$U_2 - C_{u2} = C_{r2}\tan\beta_2 = C_{u2}\tan\beta_2/\tan\alpha_2$$

the following relation is reached:

$$U_2 C_{u2}/C_{r2}^2 - C_{u2}^2/C_{r2}^2 - \tan\alpha_2 \tan\beta_2 = 0$$

Solving this relation gives, for positive values of (α_2), the following relation:

$$\tan\alpha_2 = \frac{\sin\alpha_2}{1-\cos\alpha_2} \tag{15.19a}$$

The relation given in Equation 15.19a yields the following simple numerical relation between the absolute and relative angles at the inlet [7]:

$$\alpha_2 = 90 - \beta_2/2 \tag{15.19b}$$

From Equation 15.19a and b, the following relation can be obtained

$$\frac{C_{u2}}{U_2} = \cos\beta_2 \tag{15.20}$$

The number of blades is obtained from the following relation, which is known as the Whitefield equation:

$$n = \frac{1}{\cos^2\alpha_2} \tag{15.21}$$

Thus, for a given number of rotor blades, the absolute flow angle at the rotor inlet is calculated from Equation 5.21. The relative flow angle at the rotor inlet is next determined from Equation 15.19b.

The ratio between the swirl velocity and the rotational speed at the rotor inlet is determined from Equation 15.20. From Equation 15.4 and for a known specific power, both the rotational speed and swirl velocity are determined. The next step is to determine the rotor inlet diameter from the rotational speed and the blade speed (rev/s). Other dimensions at the rotor outlet are determined from known ratios between the outlet mean radius and the rotor inlet radius and the hub-to-shroud ratio at the outlet. The rotor inlet width may be calculated from the conservation of mass.

Here are certain other expressions that define the number of blades. Jamieson [8] developed the following relation:

$$n_{\min} = 2\pi\tan\alpha_2 \tag{15.22}$$

Glassman [9] developed the relation

$$n = \frac{\pi}{30}(110^\circ - \alpha_2)\tan\alpha_2 \tag{15.23}$$

Example 15.3

An IFR turbine with 12 vanes is required to develop 229.6 kW from a supply of hot gases available at a stagnation temperature of 1000 K and a flow rate of 1 kg/s. The following data refer $C_{a3}/U_2 = 0.25$, $\zeta = 0.4$, $r_{3s}/r_2 = 0.7$, and $W_{3m}/W_2 = 2.0$.

Total-to-static efficiency 0.85.
Static pressure at the rotor is 100 kPa.
The nozzle enthalpy loss coefficient is $\lambda_N = 0.06$.
Use the optimum efficiency design method.

Determine

1. Absolute and relative flow angles at the rotor inlet (α_1, α_2)
2. Overall pressure ratio P_{01}/P_3
3. Rotor tip speed (U_2) and inlet absolute Mach number M_2
4. Ratio of relative velocity W_{3s}/W_2 at shroud
5. Diameter and width of rotor and its speed of rotation

Solution

Whitefield equation

$$\cos^2 \alpha_2 = \frac{1}{n} = \frac{1}{12} = 0.08333$$

$$\alpha_2 = 73.22°$$

Also

$$\beta_2 = 2(90 - \alpha_2) = 2(90 - 73.22) = 33.56°$$

$$\Delta T_0 = \frac{W}{Cp} = \frac{229.6}{1.148} = 200 \text{ K}$$

$$\frac{P_{01}}{P_3} = \frac{1}{\left(1 - \dfrac{\Delta T_0}{\eta_{ts} T_{01}}\right)^{\gamma/\gamma - 1}} = \left(1 - \frac{0.2}{0.81}\right)^{-4} = 2.924$$

From the specific power relation, with

$$\frac{C_{u2}}{U_2} = \cos\beta_2$$

$$W = U_2 C_{u2} = U_2^2 \cos\beta_2$$

$$U_2 = 524.9 \text{ m/s}$$

$$\frac{r_{3m}}{r_{3s}} = \frac{r_{3s} + r_{3h}}{2} \frac{1}{r_{3s}} = \frac{1 + \zeta}{2} = 0.7$$

$$\frac{r_{3m}}{r_2} = \frac{r_{3av}}{r_{3s}} \frac{r_{3s}}{r_2} = 0.7 \times 0.7 = 0.49$$

$$\cos\beta_{3m} = \frac{C_{a3}}{U_2} \frac{r_2}{r_{3m}} = \frac{0.25}{0.49} = 0.5102$$

$$\beta_{3m} = 62.97°$$

$$\cos\beta_{3s} = \frac{C_{a3}}{U_2} \frac{r_2}{r_{3s}} = \frac{0.25}{0.7} = 0.3571$$

$$\beta_{3s} = 70.35°$$

$$\frac{W_{3s}}{W_2} = \frac{W_{3s}}{W_{3m}}\frac{W_{3m}}{W_2} = \frac{\sec\beta_{3s}}{\sec\beta_{3m}} \times 2.0 = 2.702$$

The relative velocity ratio increases from the hub to the shroud

$$\frac{W_{3h}}{W_2} = \frac{W_{3h}}{W_{3m}}\frac{W_{3m}}{W_2}$$

$$T_{03} = T_{01} - \Delta T_0 = 1000 - 200 = 800 \text{ K}$$

$$T_3 = T_{03} - \frac{C_3^2}{2 \times Cp} = T_{03} - \left(\frac{C_{a3}}{U_2}\right)^2 \frac{{U_2}^2}{2 \times Cp} = 800 - (0.25)^2 \frac{(524.9)^2}{2 \times 1148} = 792.5 \text{ K}$$

$$\dot{m} = \rho_3 C_{a3} A_3 = \left(\frac{P_3}{RT_3}\right)\left(\frac{C_{a3}}{U_2}\right) U_2 \pi \left(\frac{r_{3s}}{r_2}\right)^2 \left(1 - \zeta^2\right) {r_2}^2$$

$$1.0 = \left(\frac{10^5}{287 \times 792.5}\right)(0.25) \times 524.9 \times \pi \times 0.7^2 \times \left(1 - 0.4^2\right) r_2^2$$

$$r_2^2 = 0.0134$$

$$r_2 = 0.1158 \text{ m}$$

$$D_2 = 0.2316 \text{ m}$$

$$\omega = \frac{U_2}{r_2} = 4{,}532.8 \text{ rad/s } (N = 43{,}285.2 \text{ rpm})$$

Also, since

$$\dot{m} = \rho_2 C_{r2} A_2$$

$$\frac{b_2}{D_2} = \frac{\dot{m}}{4\pi \times \rho_2 \times C_{r2} \times r_2^2}$$

Now

$$C_{u2} = U_2 \cos\beta_2 = 437.4 \text{ m/s}$$

$$C_{r2} = \frac{C_{u2}}{\tan\alpha_2} = \frac{437.4}{3.3163} = 131.89 \text{ m/s}$$

$$C_2 = \frac{C_{u2}}{\sin\alpha_2} = \frac{437.4}{0.9574} = 456.8 \text{ m/s}$$

$$T_2 = T_{02} - \frac{C_2^2}{2Cp} = 1000 - \frac{456.8^2}{2 \times 1148} = 909.1 \text{ K}$$

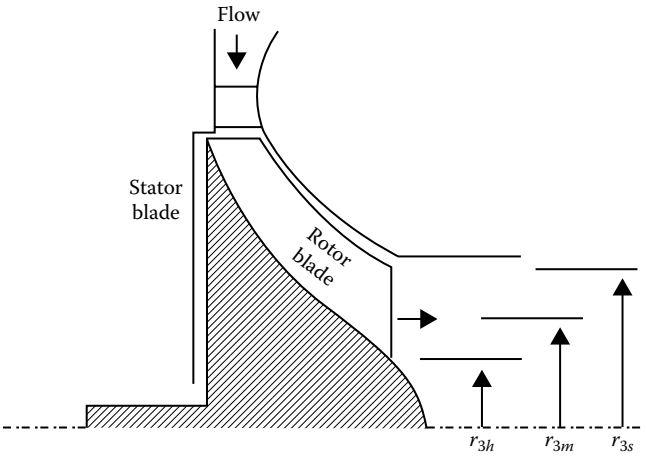


FIGURE 15.6
Geometry of radial turbine.

$$T_2' = T_2 - \frac{\lambda_N C_2^2}{2Cp} = 909.1 - \frac{0.06 \times 456.8^2}{2 \times 1148} = 903.64 \text{ K}$$

$$P_2 = P_{01}\left(\frac{T_2'}{T_{01}}\right)^{\gamma/\gamma-1} = 2.924 \times 10^5 \times \left(\frac{903.64}{1000}\right)^4 = 1.9497 \times 10^5 \text{ Pa}$$

$$\frac{b_2}{D_2} = \frac{\dot{m}}{4\pi \times \left(\frac{P_2}{RT_2}\right) \times C_{r2} \times r_2^2} = \frac{1.0}{4\pi \times \left(\frac{1.9496 \times 10^5}{287 \times 954.5}\right) \times 131.89 \times 0.0134} = 0.06322$$

$$b_2 = 0.0146 \text{ m}$$

The geometry of a radial turbine is shown in Figure 15.6.

Example 15.4

Make comparison between the specific power of the axial and radial turbines in the following case (Figure 15.7):

Axial flow turbine having the following angles: $\alpha_2 = \beta_3 = 60$ and $\alpha_3 = \beta_2 = 0$.
Radial inflow turbine with $\alpha_2 = 60$, $\alpha_3 = \beta_2 = 0$, and $\beta_3 = 0$.

The rotational speed U_2 is equal in both turbines.

Solution

1. *Axial flow turbine*: Since $\alpha_2 = \beta_3 = 60$ and $\alpha_3 = \beta_2 = 0$, the specific work is

$$W_{axial} = U_2 C_{u2} + U_3 C_{u3}$$

$$W_{axial} = U_2^2$$

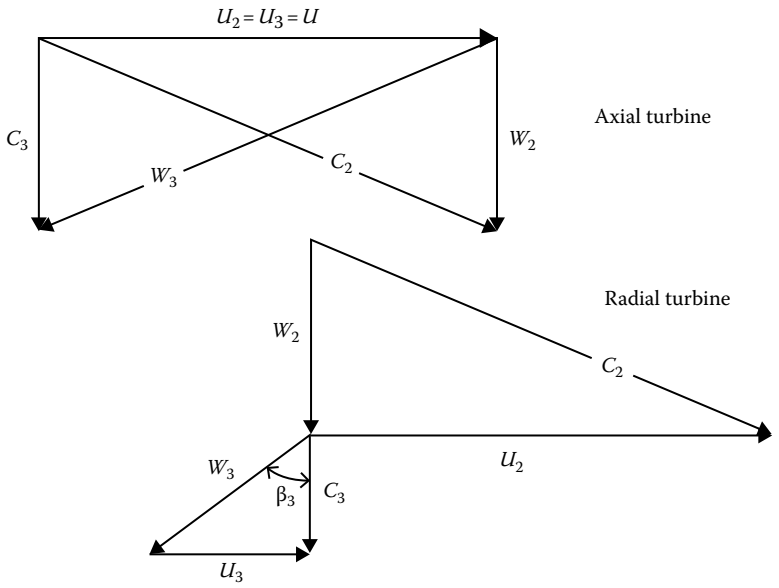


FIGURE 15.7
Velocity triangles at inlet and outlet for both axial and radial turbines.

2. *Radial flow turbine*: Since $\alpha_2 = 60°$, $\alpha_3 = \beta_2 = 0$, and $\beta_3 = 45°$, the specific work is

$$W_{radial} = U_2 C_{u2} - U_3 C_{u3}$$

$$W_{radial} = U_2 U_2 - U_3 \times 0$$

$$W_{radial} = U_2^2$$

$$\frac{W_{axial}}{W_{radial}} = \frac{U_2^2}{U_2^2} = 1$$

Thus, in this particular case, the specific power of both turbines is equal.

15.7 Cooling

Increasing the turbine entry temperature has preoccupied gas turbine designers for many years. As described in Whitefield and Baines [10], cooling of the rotor nozzle and rotor is achieved using a variety of techniques. Convection, impingement, and film cooling are used for the rotor. Figure 15.8 illustrates different cooling methods for the rotor. In Figure 15.8a, convection cooling with leading edge ejection is employed, which provides good cooling in the hottest part of the blade. Figure 15.8b illustrates impingement cooling of the leading edge together with tip surface ejection. Figure 15.8c illustrates trailing edge ejection together with leading edge impingement. Figure 15.8d illustrates film cooling through different holes in the blade surface together with leading edge impingement.

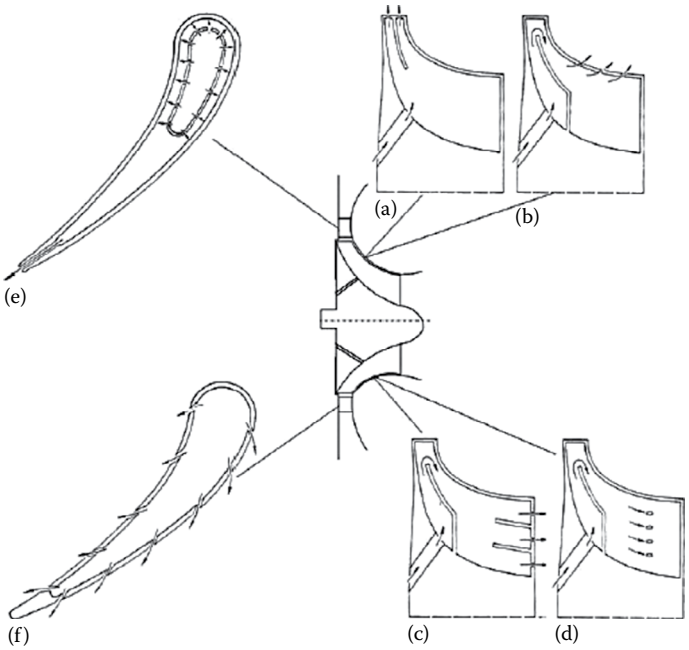


FIGURE 15.8
Cooling techniques for both the rotor and stator of a radial inflow turbine. (a) Convection cooling and leading edge ejection. (b) Impingement cooling of the leading edge and tip surface ejection. (c) Trailing edge ejection and leading edge impingement. (d) Film cooling through different holes in the blade surface and leading edge impingement. (e) Impingement plus trailing edge ejection. (f) surface film ejection.

Concerning nozzle cooling, this may be achieved either by impingement plus trailing edge ejection (Figure 15.8e) or by surface film ejection (Figure 15.8f).

Problems

15.1 A radial inflow turbine for a small application, such as an auxiliary power unit (APU) in an aircraft, is shown in Figure 15.1 and has the following data:

Pressure ratio	P_{01}/P_3	2.1
Inlet temperature	T_{01}	1100 K
Output work		43 kW
Rotational speed		800 rps
Gas mass flow rate $\dot{m}$		0.35 kg/s
Rotor inlet tip diameter		12.0 cm
Rotor exit tip diameter		7.5 cm
Hub/tip ratio at exit		0.3
Nozzle efflux angle	α_2	70°
Rotor vane outlet angle	β_3	40°
Nozzle loss coefficient	λ_N	0.07

Calculate that

1. The isentropic efficiency is η_{ts}
2. The rotor loss coefficient is λ_R

15.2 1. Prove that the specific work for any turbomachinery is expressed by Euler's equation

$$W = \frac{1}{2}\left[\left(U_2^2 - U_3^2\right) - \left(W_2^2 - W_3^2\right) + \left(C_2^2 - C_3^2\right)\right]$$

2. Make comparison between axial and radial inflow turbines.
3. Plot on a *T*–*S* diagram the expansion process in a radial inflow turbine and an axial flow turbine.
4. Describe the different methods of cooling in a radial inflow turbine.

15.3 A radial inflow turbine has the following characteristics and operating conditions:

Inlet total temperature	1,000 K
Inlet total pressure	2.0 bar
Rotor tip rotational speed	500 m/s
Rotational speed	140,000 rpm
$\beta_{3_{su}}$, $D_{3s}/D_2 = 0.7$, $\alpha_2 = 62°$	and $b_2/D_2 = 0.0873$

The turbine operates at the maximum total-to-static efficiency.

Using Figure 15.6, find

1. The specific speed
2. The geometrical dimensions of turbine $D_2, b_2, D_{3s}, D_{3h}, D_{3av}$
3. The outlet total and static temperatures and the outlet static pressure (T_{03}, T_3, P_3)
4. Rate of mass flow $(\dot{m})$
5. Rotor inlet static temperature and pressure (T_2, P_2)

15.4 A small inward flow radial gas turbine, comprising a radial vaned impeller, a ring of nozzle blades, and an axial diffuser, operates at its design point with a total-to-total efficiency of 0.91. At turbine entry, the stagnation pressure and temperature of the gas are 410 kPa and 1100 K. The flow leaving the turbine is diffused to a pressure of 101 kPa and has negligible final velocity. Given that the flow is simply choked at the nozzle exit, determine the peripheral speed of the impeller and the flow outlet angle from the nozzle. The working fluid is hot gases having $\gamma = 1.333$ and $R = 287$ J/kg °C.

15.5 A radial turbine is proposed as the gas expansion element in a chemical plant. The pressure and temperature conditions through the stage at the design point are as follows:

Upstream of the nozzle, $P_{01} = 700$ kPa, $T_{01} = 1150$ K

Nozzle exit, $P_2 = 530$ kPa, $T_2 = 1030$ K

Rotor exit, $P_3 = 385$ kPa, $T_3 = 915$ K, $T_{03} = 925$ K

The ratio of the rotor exit mean diameter to the rotor inlet tip diameter is chosen to be 0.45 and the rotational speed is 25,000 rpm. Assume that the relative flow at the rotor inlet is radial and the absolute flow at the rotor exit is axial. The gases have a molecular weight of 40 and a specific heat ratio of 1.6. Determine

1. The total-to-static efficiency of the turbine
2. The rotor diameter

15.6 A small inward flow radial gas turbine fitted with an axial diffuser operates at its design point with a total-to-total efficiency of 0.9. At entry into the turbine, the stagnation pressure and the temperature of the gas are 410 kPa and 1100 K, respectively. The flow leaving the turbine is diffused to a pressure of 101 kPa and has negligible final velocity. Given that the flow is simply choked at the nozzle exit, determine the peripheral speed of the impeller and the flow outlet angle from the nozzle. The working fluid is hot gases having $\gamma = 1.333$ and $R = 287$ J/kg °C.

15.7 Following the design procedure described in Section 15.4, it is required to design a radial inflow turbine having the following specifications:

Mass flow rate	0.145 kg/s
Speed	130,000 rpm
Power	20.0 kW
Inlet total temperature	1,080 K
Inlet total pressure	2.1 bar
Stage loading ψ	0.9
Flow coefficient ϕ	0.3
Meridional velocity ratio C_{r2}/C_{a3}	1.0
Total-to-total efficiency	0.8
r_{3h}/r_2	0.3

Calculate

1. The velocities $U_2, C_2, W_2, U_3, C_3, W_3$
2. The dimensions at inlet r_2, b_2
3. The dimensions at outlet r_{3h}, r_{3t}

15.8 A gas turbine is composed of a radial turbine followed by a two-stage axial turbine; see Figure 15.9. It has the following characteristics:

$$N = 12{,}000 \text{ rpm}, \quad P_{01} = 14.0 \text{ bar}, \quad T_{01} = 1400 \text{ K},$$
$$(\Delta T_0)_{radial} = (\Delta T_0)_{axial} = 300 \text{ K}, \quad \text{thus}, T_{08} = 800 \text{ K}$$

$$C_1 = W_2 = C_3 = 200 \text{ m/s}$$

$$\beta_2 = \alpha_3 = \alpha_5 = \alpha_7 = 0$$

For the two-stage axial turbine:

$$\Lambda_{1st\ stage} = \Lambda_{2nd\ stage}$$

Axial velocity is constant and the mean radius at stations 3, 4, 5, 6, and 7 is constant.

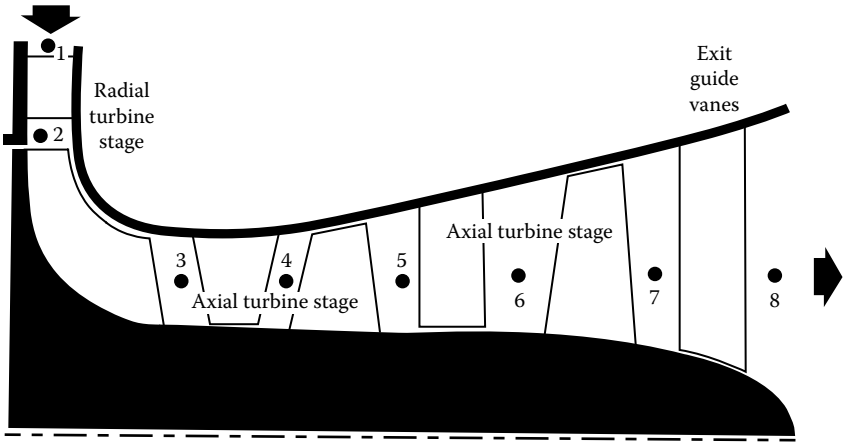


FIGURE 15.9
Radial–axial gas turbine.

For the whole turbine:

$$\eta_{radial} = \eta_{1st\ stage} = \eta_{2nd\ stage} = 0.92$$

1. Draw velocity triangles for radial turbine.
2. Draw velocity triangles for stages 1 and 2 of axial turbine.
3. *Prove* that $r_2 = \sqrt{2} r_3$.
4. Plot a *T*–*S* diagram for the whole (radial–axial) turbine.
5. Calculate the pressure ratio for both radial and axial turbines.
6. Calculate the overall efficiency of the turbine.
7. Calculate the degree of reaction of radial turbine.

15.9 A radial inflow turbine has the following data:

$$T_{01} = 1400\ \text{K}, \quad P_{02} = 1000\ \text{kPa}, \quad U_2 = 600\ \text{m/s}, \quad r_2 = 0.25\ \text{m}, \quad b_2 = 0.05\ \text{m},$$
$$C_{r2} = C_{a3}, \quad \left(C_{a3}/U_2\right) = 0.25, \quad \left(r_{3m}/r_2\right) = 0.4, \quad \beta_2 = \alpha_3 = 0$$

1. Calculate
   a. Temperature drop through the turbine
   b. $C_2, \rho_2, \alpha_2, \beta_3$
   c. Mass flow rate
2. Draw inlet and outlet velocity triangles
3. Describe two methods for radial turbine cooling
4. Compare between radial and axial turbines

15.10 A *radial turbine* has the following data: Output power of 3000 kW and gas mass flow rate of 10 kg/s,

$$T_{01} = 1000\ \text{K}, \quad P_{01} = 3.52\ \text{bar}, \quad P_a = 0.76\ \text{bar}, \quad \Delta P_{0nozzle} = 3\%$$
$$C_3 = W_2, \quad \eta_{tt} = 0.85, \quad b_2 = 0.05\ \text{m}, \quad r_{3m}/r_2 = 0.6, \quad r_2 = 0.218\ \text{m}$$

1. Draw the velocity triangles at the inlet and the outlet of the rotor.
2. Calculate the rotational speed (N).
3. Calculate $T_2, P_2, T_3, P_3, P_{02r}, P_{03r}$.
4. Calculate the rothalpy I_2, I_3.

15.11 A radial inflow turbine runs at 60,000 rpm. The inlet conditions are $T_{01} = 1000$ K, $P_{01} = 400$ kPa. The turbine pressure ratio is $P_{01}/P_3 = 2.3$, and the mass flow rate is 0.3 kg/s. The rotor tip diameter is $D_2 = 0.12$ m, and the specific heat ratio $\gamma = 1.35$. Other data are $\beta_2 = C_{u3} = 0$, $W_2 = C_3$, $\alpha_2 = 75°$, and $P_{02}/P_{01} = 0.98$.

Calculate

1. The ratio of tip speed to spouting velocity (U_2/C_0)
2. The power produced by the turbine
3. The total-to-total efficiency

References

1. S.L. Dixon, *Fluid Mechanics and Thermodynamics of Turbomachinery*, 4th edn., 1998, Butterworth-Heinemann, Boston, MA, 236pp.
2. H. Moustapha, M.F. Zelessky, N.C. Baines, and D. Japikse, *Axial and Radial Turbines*, Concepts NREC, White River Junction, VT, 2003, 209pp.
3. H.I.H. Saravanamuttoo, G.F.C. Rogers, and H. Cohen, *Gas Turbine Theory*, 5th edn., Prentice Hall, Harlow, U.K., 2001, 367pp.
4. H. Chen and N.C. Baines, Analytical optimization design of radial and mixed flow turbines, *Proceedings of the Institution of Mechanical Engineers*, Vol. 206, 1992, pp. 177–187.
5. H.E. Rohlik, *Analytical Determination of Radial Inflow Turbine Design Geometry for Maximum Efficiency*, NASA TN D-4384, Washington, DC, 1968.
6. A.J. Glassman, *Turbine Design and Application*, NASA NASA-SP 290, Washington, DC, 1994, 279pp.
7. A. Whitefield, The preliminary design of radial inflow turbines, *Journal of Turbomachinery*, 112, 50–57, 1990.
8. A.W. Jamieson, Chapter 9: The radial turbine, In: Sir H. Roxbee-Cox (Ed.), *Gas Turbine Principles and Practice*, Newnes, London, U.K., 1955.
9. A.J. Glassman, *Computer Program for Design and Analysis of Radial Inflow Turbines*, NASA TN 8164, Washington, DC, 1976.
10. A. Whitefield and N.C. baines, *Design of Radial Turbomachines*, Longmans Scientific & Technical, Harlow, U.K., 1990, 357pp.


Taylor & Francis
Taylor & Francis Group
http://taylorandfrancis.com

16

Module Matching

16.1 Introduction

"Module matching" means the successful interplay of engine geometry and engine parameters. This relates not only to matching between a turbine and the driven compressor, but also to the global synchronization of the different modules, including the diffuser, combustion chamber, nozzle and fan (for turbofan engines), afterburner (for afterburning engines), propeller (for turboprop engines), and load (for gas turbines and turboshaft engines). A turbine is coupled to either a compressor or a fan, thus forming an engine spool, as described in Chapters 4 through 8. However, the performance matching between these two modules is influenced by their front and back modules. A choked nozzle influences the performance of its preceding elements. The diffuser on the contrary controls the mass flow and total pressure/temperature of all the succeeding modules. If the diffuser incorporates a water injection system, the mass flow in the succeeding elements is affected. Fuel addition and pressure drop in the combustion chamber influence the performance of the succeeding turbine and nozzle. The afterburner influences the mass flow rate and inlet pressure to the succeeding nozzle.

As described in the preceding four chapters, each compressor/turbine has a certain design point where the rotational speed (N), pressure ratio (π_c), and mass flow ($\dot{m}$) are specified. However, it is required that these modules operate efficiently over the complete range of speed and power output for aeroengines and powerplants. These conditions are identified as the "off-design conditions" and include starting, idling, reduced flow, maximum power, part load, acceleration, and deceleration. For aeroengines, performance is more complex as the inlet conditions are further changed due to flying at different speeds and altitudes.

No matter what type of engine is being considered, the steady-state performance of an engine at each speed (N) is determined by two conditions: conservation of mass (or continuity of flow) and conservation of energy (or power balance), which leads to the "match point." However, for aeroengines a third condition is added, namely, conservation of momentum, which develops the necessary thrust at different flight conditions.

16.2 Off-Design Operation of a Single-Shaft Gas Turbine Driving a Load

A single spool composed of a turbine driving both the compressor and load is shown in Figure 16.1. The load could be a generator, marine screw, or propeller of a turboprop engine. It is assumed that the losses in the inlet and exhaust modules are ignored. Thus, the

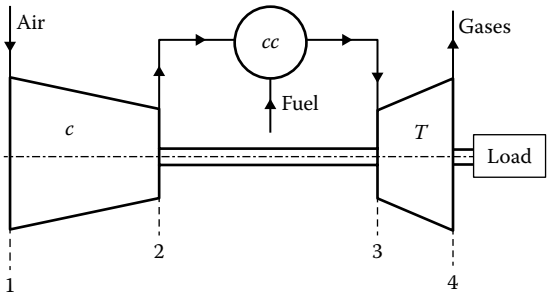


FIGURE 16.1
Single-shaft gas turbine.

inlet total pressure and temperature of the compressor (T_{01}, P_{01}) are equal to the ambient conditions (T_a, P_a). Moreover, the gases expand in the turbine toward the ambient pressure.

The cycle of this layout is illustrated in Figure 16.2. Due to the conservation of mass through the spool, the mass flow rate through the turbine ($\dot{m}_3$) is equal to the mass flow rate through the compressor ($\dot{m}_1$) less any bleeds ($\dot{m}_b$), but supplemented by the fuel flow ($\dot{m}_f$) and any water injection ($\dot{m}_{w.i}$) that is added. The mass of fuel added is approximately equal to the bled air. The fuel-to-air ratio (f) and the bleed ratio (b) may be given instead.

The compressor and turbine maps are known, together with other data like the ambient conditions (T_a, P_a) together with the fuel flow rate (f) and bleed ratio (b), the pressure drop in the combustion chamber (ΔP_{cc}), as well as the load power. The turbine pressure is then related to the compressor outlet pressure by the relation

$$P_{03} = P_{02}\left(1 - \Delta P_{cc}\right) \tag{16.1}$$

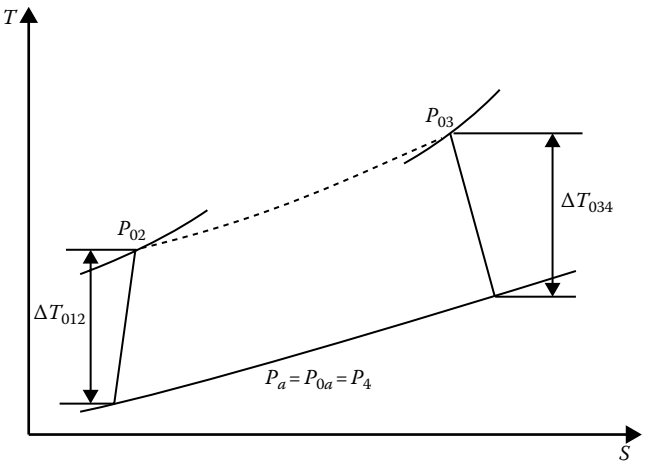


FIGURE 16.2
T–S diagram for single-shaft gas turbine.

16.2.1 Matching Procedure

The following steps summarize the matching procedure.

1. Select a rotational speed (N).
   Thus from the known ambient conditions determine ($N/\sqrt{T_{01}}$) that defines the operating line on the compressor map.
2. Assume a turbine inlet temperature (T_{03}).
   Thus calculate ($N/\sqrt{T_{03}}$) that also determines the turbine operating line.
3. Assume the compressor pressure ratio (P_{02}/P_{01}).
   Thus from the compressor map the operating point is completely defined (i.e., the mass flow parameter $\dot{m}_1\sqrt{T_{01}}/P_{01}$ and compressor efficiency η_c); see Figure 16.3.
4. The compressor mass flow rate is calculated from the relation

$$\dot{m}_1 = \frac{\dot{m}_1\sqrt{T_{01}}}{P_{01}}\frac{P_{01}}{\sqrt{T_{01}}} \tag{16.2}$$

   and the turbine mass flow rate is then obtained from the relation

$$\dot{m}_3 = \dot{m}_1\left(1+f-b\right) \tag{16.3}$$

5. Calculate the compressor specific work from the relation

$$w_c = \frac{Cp_cT_{01}}{\eta_c}\left[\left(\frac{P_{02}}{P_{01}}\right)^{\gamma_c-1/\gamma_c} - 1\right] \tag{16.4}$$

   As seen earlier, the variations in specific heat and specific heat ratio are taken into account in the different gas turbine modules.

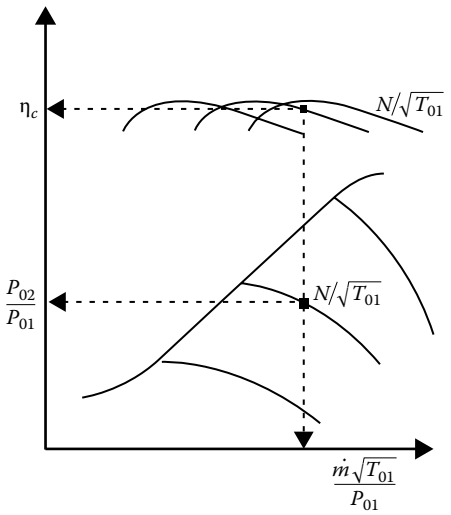


FIGURE 16.3
Operating point on compressor map.

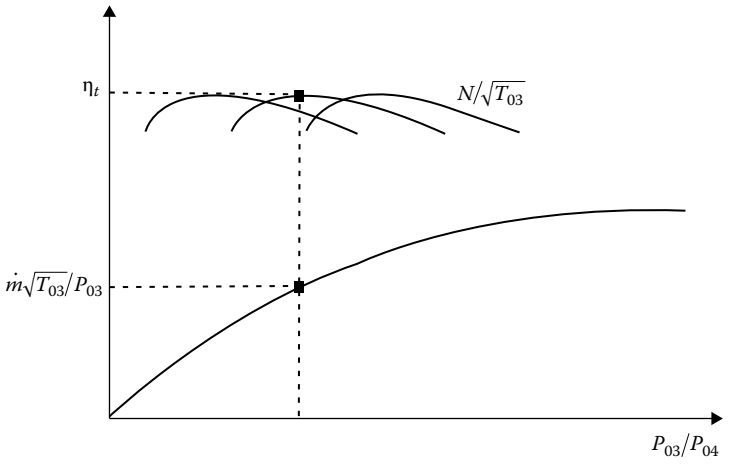


FIGURE 16.4
Operating point of turbine map.

6. The turbine mass flow parameter is determined as follows:

$$\frac{\dot{m}_3\sqrt{T_{03}}}{P_{03}} = \frac{\dot{m}_1\sqrt{T_{01}}}{P_{01}}\frac{P_{01}}{P_{02}}\frac{P_{02}}{P_{03}}\sqrt{\frac{T_{01}}{T_{03}}}\frac{\dot{m}_3}{\dot{m}_1} \tag{16.5}$$

   From this mass parameter and the operating speed line, the turbine efficiency can be determined; see Figure 16.4. It is worth saying again here that the turbine pressure ratio (P_{03}/P_{04}) is equal to the compressor pressure ratio (P_{02}/P_{01}).
7. The turbine work can then be determined from the relation

$$w_t = \eta_t C p_t T_{03}\left[1 - \frac{1}{\left(\frac{P_{03}}{P_{04}}\right)^{\gamma_t - 1/\gamma_t}}\right] \tag{16.6}$$

8. The net power ($\mathscr{P}$) is then evaluated from the relation

$$\mathscr{P} = \dot{m}_3 w_t - \frac{\dot{m}_1 w_c}{\eta_m} \tag{16.7}$$

   where η_m is the mechanical efficiency for the spool. This net power is then checked with the load power. If they are unequal, then a new value for the compressor pressure ratio is selected and the earlier procedure is repeated until convergence occurs.

Now if the nozzle is choked, then the left-hand side of Equation 16.5 will be constant, or

$$\frac{\dot{m}_3\sqrt{T_{03}}}{P_{03}} = \frac{\dot{m}_1\sqrt{T_{01}}}{P_{01}}\frac{P_{01}}{P_{02}}\frac{P_{02}}{P_{03}}\sqrt{\frac{T_{01}}{T_{03}}}\frac{\dot{m}_3}{\dot{m}_1} = \text{constant}.$$

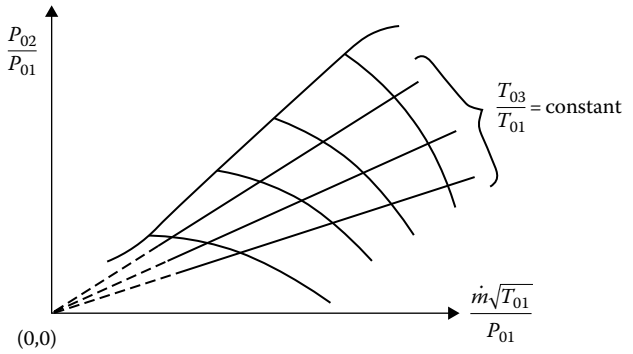


FIGURE 16.5
Constant turbine inlet temperature on the compressor map.

For a constant pressure ratio within the combustion chamber (P_{03}/P_{02} = constant) and a constant mass flow rate in both the compressor and turbine ($\dot{m}_3 = \dot{m}_1$), then

$$\frac{P_{02}}{P_{01}} = K_1 \frac{\dot{m}_1\sqrt{T_{01}}}{P_{01}} \sqrt{\frac{T_{03}}{T_{01}}}$$

If (T_{03}/T_{01}) = constant, then the compressor pressure ratio will be expressed as

$$\frac{P_{02}}{P_{01}} = K \frac{\dot{m}_1\sqrt{T_{01}}}{P_{01}} \tag{16.8}$$

This linear relation when plotted on the compressor map will have the shape illustrated in Figure 16.5. However, this relation shows that the pressure ratio is zero when the mass flow rate is zero, which is impossible. Since Equation 16.8 assumes that the turbine is choked, which never occurs at a low mass flow rate, it is then logical to assume that these lines are used for mass flow rates away from the origin [1–3].

Example 16.1

The following data refer to a single shaft of a turboprop engine during a ground run. The gas turbine is running at its design point.

Compressor Characteristics			Turbine Characteristics		
P_{02}/P_{01}	$\dot{m}_1\sqrt{T_{01}}/P_{01}$	η_C	$\dot{m}_3\sqrt{T_{03}}/P_{03}$	P_{03}/P_{04}	η_t
4.0	350	0.76	130	4.2	0.88
4.5	330	0.80	144	4.6	0.90
5.0	310	0.84	144	5.0	0.91

The compressor delivery pressure and the ambient conditions are 1.01 bar and 288 K. The non-dimensional flows are based on $\dot{m}$ in kg/s and P in bar and T in K. Neglecting mechanical losses, the pressure losses in the combustion chamber are 3%. Assume also that the mass flow rate in both compressor and turbine is equal. Calculate the power consumed in the propeller when the turbine inlet temperature is 1200 K.

Solution

Flow compatibility is expressed by the relation (16.5)

$$\frac{\dot{m}_3\sqrt{T_{03}}}{P_{03}} = \frac{\dot{m}_1\sqrt{T_{01}}}{P_{01}}\frac{P_{01}}{P_{02}}\frac{P_{02}}{P_{03}}\sqrt{\frac{T_{01}}{T_{03}}}\frac{\dot{m}_3}{\dot{m}_1}$$

For equal mass flow rate through the compressor and turbine, 3% pressure loss in the combustion chamber, and equality of compressor inlet pressure and turbine outlet pressure ($P_{01} = P_{04}$),

$$\frac{\dot{m}\sqrt{T_{03}}}{P_{03}} = \frac{\dot{m}\sqrt{T_{01}}}{P_{01}}\frac{P_{01}}{P_{03}}\sqrt{\frac{288}{1200}} = 2.041\frac{\dot{m}\sqrt{T_{01}}}{P_{01}}\frac{P_{04}}{P_{03}} \tag{1}$$

The mass flow parameter is calculated from Equation 1 for different turbine pressure ratios and tabulated side by side with the values given in the data earlier in the following table:

P_{03}/P_{04}	$\dot{m}_3\sqrt{T_{03}}/P_{03}$ From Turbine Map	$\dot{m}_3\sqrt{T_{03}}/P_{03}$ From Equation 1
4.2	130	170.10
4.6	144	146.42
5.0	144	126.54

The two sets of turbine mass flow parameters are plotted in Figure 16.6.

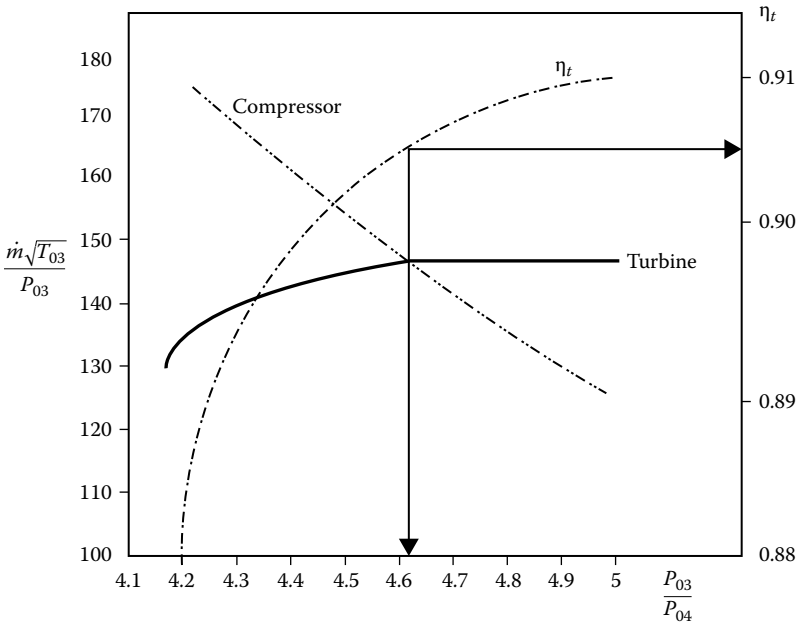


FIGURE 16.6
Equilibrium point for compressor and turbine.

From Figure 16.6, it can be seen that equilibrium between compressor and turbine occurs at $P_{03}/P_{04}=4.64$, $\dot{m}_3\sqrt{T_{03}}/P_{03}=144$. Plotting the turbine efficiency on the same figure gives the corresponding turbine efficiency as $\eta_t=0.9012$.

The corresponding compressor pressure ratio is

$$P_{02}/P_{01}=\frac{P_{03}/P_{04}}{0.97}=\frac{4.64}{0.97}=4.7835$$

The corresponding value of the compressor mass flow rate and efficiency is determined from Figure 16.7, which is $\dot{m}_1\sqrt{T_{01}}/P_{01}=319$ and $\eta_C=0.82$.

From Equation 16.2, the mass flow rate is

$$\dot{m}_1=\frac{\dot{m}_1\sqrt{T_{01}}}{P_{01}}\frac{P_{01}}{\sqrt{T_{01}}}=\frac{319\times1.01}{\sqrt{288}}=18.98\ \text{kg/s}$$

The available power is evaluated from Equation 16.7

$$\mathscr{P}=\dot{m}_3w_t-\dot{m}_1w_c=w_t=\dot{m}\left\{\eta_tCp_tT_{03}\left[1-\frac{1}{\left(\frac{P_{03}}{P_{04}}\right)^{\gamma_t-1/\gamma_t}}\right]-\frac{Cp_cT_{01}}{\eta_c}\left[\left(\frac{P_{02}}{P_{01}}\right)^{\gamma_c-1/\gamma_c}-1\right]\right\}$$

$$\mathscr{P}=19.98\left\{0.9012\times1.148\times1200\left[1-\left(\frac{1}{4.64}\right)^{0.25}\right]-\frac{1.005}{0.82}\left[(4.7835)^{0.286}-1\right]\right\}$$

$$\mathscr{P}=3922.3\ \text{kW}$$

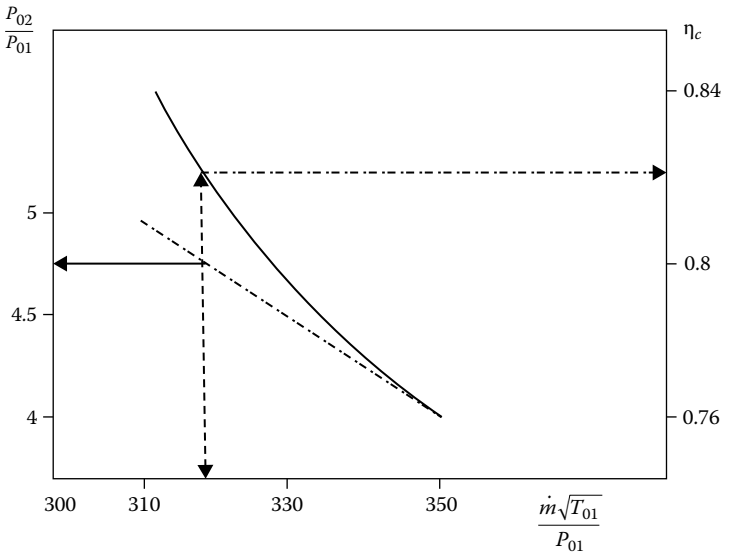


FIGURE 16.7
Matching point on compressor map.

16.2.2 Different Loads

The load could be either a propeller or an electrical generator. The propeller could be of the constant or variable speed type. For a fixed pitch propeller, the propeller power is proportional to the cube of its rotational speed. This speed is equal to the turbine speed multiplied by the gear reduction ratio. Thus, if this ratio and the mechanical efficiency of the gearbox are known, then the propeller power can be plotted against the turbine speed. Thus for each speed line on the compressor map, only a single point will provide the required power [2], which is determined by trial and error after taking several points on the compressor map and finding the available power. Repeating this procedure for different speed lines a series of points are obtained, which when joined together form the equilibrium running line. Variable pitch propellers are commonly used in aircraft, which run at constant rotational speed. The load in this case varies by changing the pitch. Thus, the equilibrium lines for these loads would correspond to a particular line of constant non-dimensional speed. Each point on this line corresponds to a different value of fuel flow, turbine inlet temperature, and power outpour.

The case of an electrical generator is similar to the variable pitch propeller.

16.3 Off-Design of a Free Turbine Engine

Figure 16.8 illustrates the gas turbine incorporating a free (power) turbine. The corresponding temperature entropy diagram is shown in Figure 16.9.

The gas generator is in equilibrium, or in other words the power of the gas generator turbine is exactly equal to the compressor power. The remaining power in the gases leaving the first (generator) turbine is absorbed by the free turbine and used to drive the load. The analysis to be followed here is divided into two steps:

1. Matching between the compressor and turbine of the gas generator
2. Off-design analysis of the free turbine.

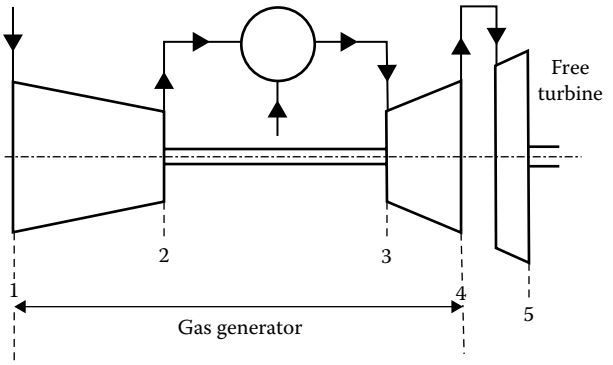


FIGURE 16.8
Gas turbine with a free turbine.

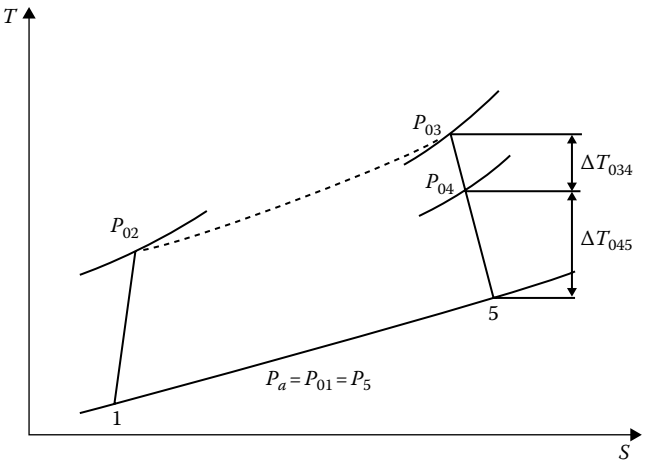


FIGURE 16.9
Temperature–entropy diagram for a gas turbine with a free turbine.

16.3.1 Gas Generator

The procedure is an alternative to that described in Section 16.2. The following parameters are known in advance: inlet conditions (T_a, P_a), fuel-to-air ratio (f), bleed ratio (b), and pressure drop in the combustion chamber (ΔP_{cc}).

1. Select a constant speed line on the compressor map and choose any point on this line, thus the parameters $N/\sqrt{T_{01}}$, P_{02}/P_{01} and $\dfrac{\dot{m}\sqrt{T_{01}}}{P_{01}}$ are determined.
2. The compressor specific work is determined from Equation 16.4.
3. Estimate a value of the turbine pressure ratio (P_{03}/P_{04}), thus the value of the turbine mass flow parameter is determined. It is assumed here that the turbine non-dimensional flow is independent of the non-dimensional speed and is a function in the turbine pressure ratio. The turbine mass flow rate is determined from Equation 16.3.
4. Calculate the turbine temperature ratio (T_{03}/T_{01}) from Equation 16.5:

$$\left(\frac{T_{03}}{T_{01}}\right)_A = \left(\frac{\left(\dot{m}_1\sqrt{T_{01}}/P_{01}\right)}{\left(\dot{m}_3\sqrt{T_{03}}/P_{03}\right)}\frac{P_{01}}{P_{02}}\frac{P_{02}}{P_{03}}\frac{\dot{m}_3}{\dot{m}_1}\right)^2 \tag{16.9}$$

   Thus, the turbine inlet temperature is defined, from which $N/\sqrt{T_{03}}$ and the turbine efficiency η_t are determined.
5. Calculate another value for the turbine inlet temperature ratio from the energy balance of the gas generator ($w_t = w_c$). The following relation is obtained:

$$\left(\frac{T_{03}}{T_{01}}\right)_B = \frac{\dot{m}_1}{\dot{m}_3}\frac{Cp_c}{\eta_c\eta_t Cp_t}\frac{\left[\left(P_{02}/P_{01}\right)^{\gamma_c-1/\gamma_c}-1\right]}{\left[1-\dfrac{1}{\left(P_{03}/P_{04}\right)^{\gamma_t-1/\gamma_t}}\right]} \tag{16.10}$$

In general, the values of $(T_{03}/T_{01})_A$ and $(T_{03}/T_{01})_B$ obtained from Equations 16.9 and 16.10 are not equal, thus the estimated value of the turbine pressure ratio (P_{03}/P_{04}) is not valid for an operating point on the equilibrium running line. Thus, another value for the turbine pressure ratio is assumed and the procedure is repeated until convergence is satisfied.

Note that in the matching procedure it was assumed that the turbine non-dimensional mass flow parameter is independent from the speed parameter. Thus, only one line exists for the unchoked part of the mass flow parameter. If the mass flow parameter is dependent on the non-dimensional speed parameter then another matching procedure is to be followed where steps 3 and 4 are to be modified:

3. Assume a turbine temperature ratio (T_{03}/T_{01}), thus the turbine speed parameter $N/\sqrt{T_{03}}$ and the turbine mass flow parameter $\dot{m}_3\sqrt{T_{03}}/P_{03}$ are obtained from Equation 16.5. From both parameters, the turbine pressure ratio and efficiency η_t are determined.
4. From work compatibility, the value of turbine temperature ratio (T_{03}/T_{01}) is obtained from Equation 16.10. This value is compared with the assumed value. If unequal, another turbine temperature ratio is assumed and the procedure is repeated until convergence occurs.

The steps described are arranged in the flowchart given in Figure 16.10.

16.3.2 Free Power Turbine

The parameters of the power turbine are the mass flow parameter $\dot{m}\sqrt{T_4}/P_4$, the pressure ratio P_{04}/P_a, the speed parameter $N/\sqrt{T_{04}}$, and efficiency η_{ft}. The free turbine map is illustrated in Figure 16.11.

Here are the additional compatibility conditions after the proper matching of the gas generator modules. The outlet conditions of the gas generator turbine (T_{04}, P_{04}) are known and from which the mass flow parameter and speed parameter can be determined.

The mass flow parameter is

$$\frac{\dot{m}\sqrt{T_{04}}}{P_{04}} = \frac{\dot{m}\sqrt{T_{03}}}{P_{03}} \times \frac{P_{03}}{P_{04}} \times \sqrt{\frac{T_{04}}{T_{03}}} \tag{16.11}$$

The pressure ratio across the free power turbine is determined from the relation

$$\frac{P_{04}}{P_a} = \frac{P_{04}}{P_{03}}\frac{P_{03}}{P_{02}}\frac{P_{02}}{P_{01}}\frac{P_{01}}{P_a} \tag{16.12}$$

It may be noted that the outlet pressure of the free turbine is assumed to be equal to the compressor inlet pressure by neglecting the losses in the inlet diffuser and outlet duct of industrial gas turbines; or

$$P_a = P_5 = P_{01}$$

The matching procedure for a free power turbine is straightforward.

1. Select a constant speed line on the compressor map.
2. Select a point on this speed line.

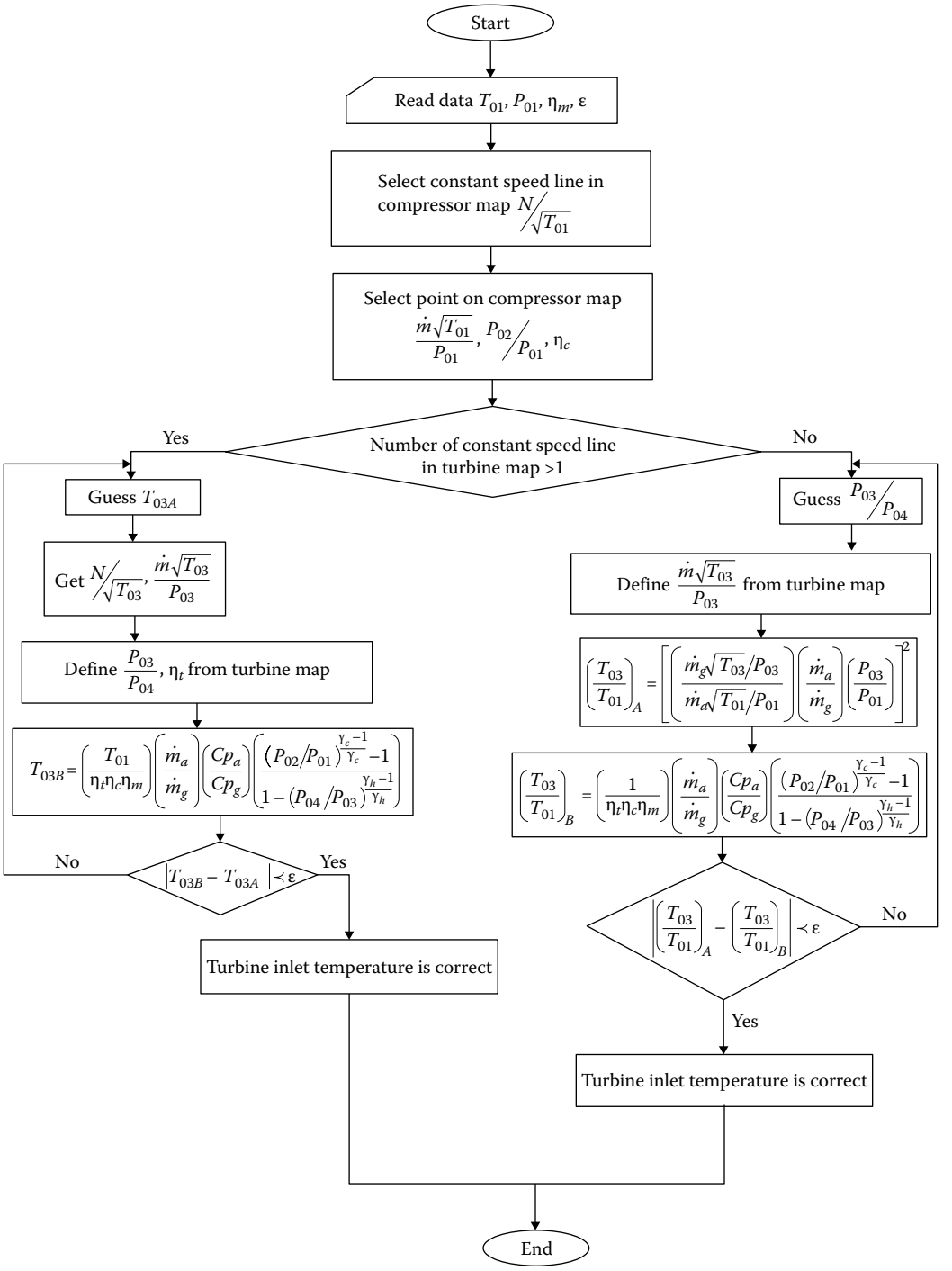


FIGURE 16.10
Flowchart for gas generator matching.

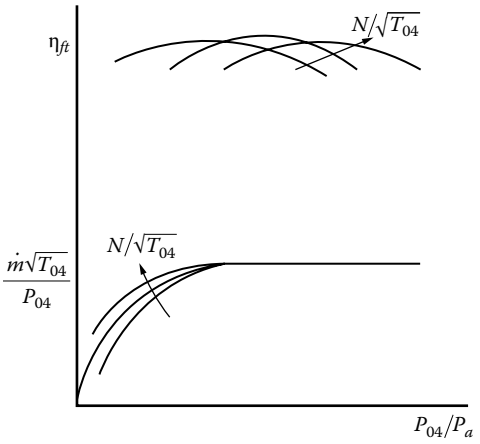


FIGURE 16.11
Map of free turbine.

3. Follow the same procedure described for matching between this point and a corresponding point on the gas generator turbine.
4. Calculate the pressure ratio of the free power turbine from Equation 16.12.
5. Determine the mass flow parameter from the free turbine map.
6. Compare this value with the value calculated from Equation 16.11.
7. If agreement is not reached, the procedure is repeated by selecting another point on the same constant speed line of the compressor and repeating the procedure until convergence is achieved.
8. Repeat this procedure for other constant speed lines.
9. The successful points on the compressor map are joined together to provide an operating line for such an application as shown in Figure 16.12.

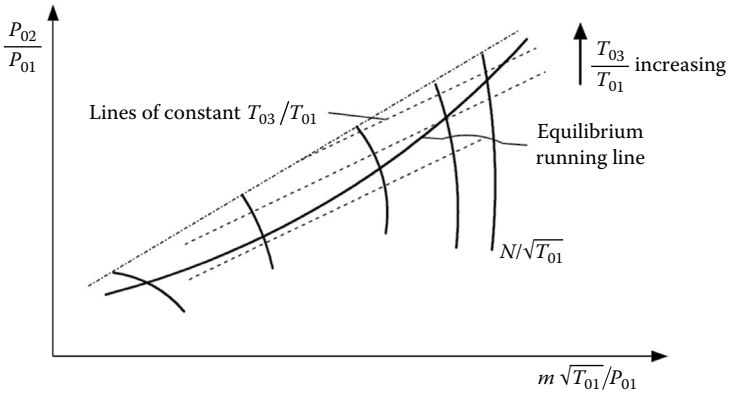


FIGURE 16.12
Operating line for a free power turbine.

As concluded in Reference 2, the equilibrium running line for the free power turbine is independent of the load and is determined by the swallowing capacity of the free power turbine.

The power generated from the free power turbine is

$$\text{Power output} = \dot{m}_4 C p_4 \Delta T_{045} \tag{16.13a}$$

$$\text{Power output} = \dot{m}_4 C p_4 \eta_{ft} T_{04} \left[1 - \left(\frac{1}{P_{04}/P_a} \right)^{\gamma_t - 1/\gamma_t} \right] \tag{16.13b}$$

The mass flow rate can be obtained from the known output conditions of the gas generator turbine

$$\dot{m}_4 = \frac{\dot{m}\sqrt{T_{04}}}{P_{04}} \frac{P_{04}}{\sqrt{T_{04}}}$$

The efficiency can also be obtained from the known speed and mass flow parameters.

The gas generator turbine and free power turbines represent two turbines in series. An important rule for them is that if the free turbine is choked, the gas generator turbine will be constrained to operate at a fixed non-dimensional point, thus $(\Delta T_{034}/T_{03})$ has a constant value equal to the design value.

Example 16.2

The following data refer to a gas turbine with a free power turbine, operating at design speed.

Compressor Characteristic			Gas Generator Turbine Characteristic		
P_{02}/P_{01}	$\dot{m}\sqrt{T_{01}}/P_{01}$	η_C	P_{03}/P_{04}	$\dot{m}\sqrt{T_{03}}/P_{03}$	η_t
6.0	250	0.83	2.8	100	0.85
5.6	270	0.84	2.5	100	0.85
5.2	290	0.83	2.2	95	0.85

Assuming that the power turbine is choked, the value of $\dot{m}\sqrt{T_{04}}/P_{04}$ being 220 determines the design values of the compressor pressure ratio and turbine inlet temperature. Assume pressure losses in the combustion chamber of 3% and assume the mechanical efficiency of the gas generator rotor to be 0.98 and take the ambient temperature as 288 K. The non-dimensional flows quoted are based on $\dot{m}$ in kg/s and P in bar and T in K, all pressures and temperatures being stagnation values.

Solution

For a choked free turbine $\dot{m}\sqrt{T_{04}}/P_{04} = \text{constant}$, or $\dot{m}\sqrt{T_{04}}/P_{04} = 220$.

The compatibility of mass flow rates between two turbines

$$\frac{\dot{m}\sqrt{T_{04}}}{P_{04}} = \frac{\dot{m}\sqrt{T_{03}}}{P_{03}} \times \sqrt{\frac{T_{04}}{T_{03}}} \times \frac{P_{03}}{P_{04}}$$

where

$$\frac{T_{04}}{T_{03}} = 1 - \eta_t \left(1 - \frac{1}{\pi_t^{\frac{G_t}{}}}\right)$$

π_t is the pressure ratio of the gas generator turbine

$$G_t = \gamma_t - 1/\gamma_t.$$

Define the calculated mass flow parameter of the free power turbine as $\left(\dot{m}\sqrt{T_{04}}/P_{04}\right)_A$, which is calculated from

$$\left(\frac{\dot{m}\sqrt{T_{04}}}{P_{04}}\right)_A = \frac{\dot{m}\sqrt{T_{03}}}{P_{03}} \times \left[1 - \eta_t \left(1 - \frac{1}{\pi_t^{\frac{G_t}{}}}\right)\right]^{0.5} \times \pi_t \tag{1}$$

P_{03}/P_{04}	η_t	$\dot{m}\sqrt{T_{03}}/P_{03}$	$\left(1-\left(1/\pi_t^{Gt}\right)\right)$	$\left[1-\eta_t\left(1-\left(1/\pi_t^{Gt}\right)\right)\right]^{0.5}\times\pi_t$	$\left(\dot{m}\sqrt{T_{04}}/P_{04}\right)_A$
2.8	0.85	100	0.2269	2.5155	251.54
2.5	0.85	100	0.2047	2.2721	227.2
2.2	0.84	95	0.1789	2.0279	192.7

The calculated mass flow parameter of the free turbine $\left(\dot{m}\sqrt{T_{04}}/P_{04}\right)_A$ is plotted together with the given choked value $\dot{m}\sqrt{T_{04}}/P_{04} = 220$ as shown in Figure 16.13.

The intersection point gives the matching point data

$$\pi_t = \frac{P_{03}}{P_{04}} = 2.438 \quad \text{and} \quad \frac{\dot{m}\sqrt{T_{03}}}{P_{03}} = 98.9667$$

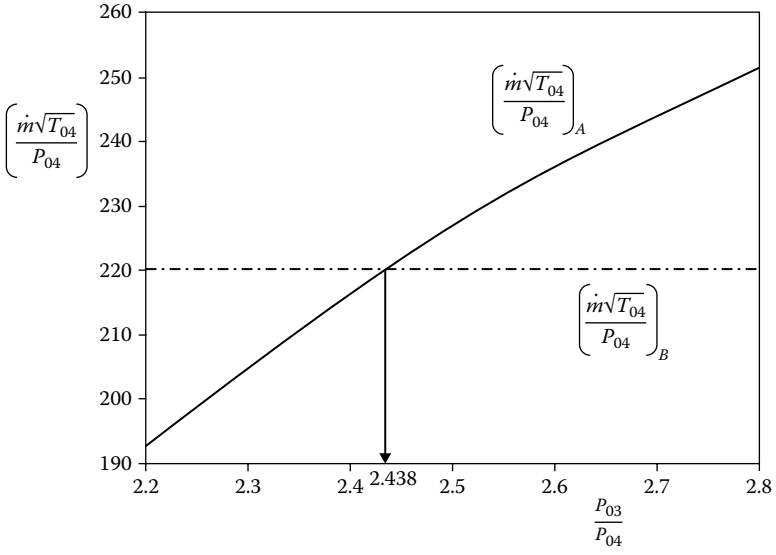


FIGURE 16.13
Matching point.

Next, matching between the compressor and gas generator turbine may proceed as follows:

Continuity equation:

$$\frac{\dot{m}\sqrt{T_{01}}}{P_{01}} = \frac{\dot{m}\sqrt{T_{03}}}{P_{03}}\sqrt{\frac{T_{01}}{T_{03}}}\frac{P_{03}}{P_{02}}\frac{P_{02}}{P_{01}} = \frac{\dot{m}\sqrt{T_{03}}}{P_{03}}\sqrt{\frac{T_{01}}{T_{03}}}\pi_b\pi_c = 98.967 \times 0.97\sqrt{\frac{T_{01}}{T_{03}}} \times \pi_c$$

$$\frac{\dot{m}\sqrt{T_{01}}}{P_{01}} = 96\sqrt{\frac{T_{01}}{T_{03}}} \times \pi_c \tag{2}$$

Power balance:

$$\dot{m}C_{P_c}T_{01} \times \frac{1}{\eta_C}\left[\pi_c^{G_c} - 1\right] = \dot{m}C_{P_t}T_{03}\eta_m\eta_t\left[1 - \left(\frac{1}{\pi_t}\right)^{G_t}\right]$$

where $G_c = \gamma_c - 1/\gamma_c$, thus

$$\frac{T_{01}}{T_{03}} = \frac{C_{P_t}}{C_{P_c}}\eta_t\eta_m\left[1 - \left(\frac{1}{\pi_t}\right)^{G_t}\right]\frac{\eta_C}{\pi_c^{G_c} - 1}$$

$$\frac{T_{01}}{T_{03}} = 0.19\frac{\eta_C}{\pi_c^{G_c} - 1} \tag{3}$$

Equations 2 and 3 are used to calculate the mass flow parameter of the compressor, which is shown in the following table against the given input values for the compressor map.

π_c	η_c	T_{01}/T_{03}	$\left(\dot{m}\sqrt{T_{01}}/P_{01}\right)_{calculated}$	$\left(\dot{m}\sqrt{T_{01}}/P_{01}\right)_{map}$
6.0	0.83	0.2356	279.60	250
5.6	0.84	0.2506	269.19	270
5.2	0.83	0.2618	255.50	290

The graphical solution of both values $\left(\left(\dot{m}\sqrt{T_{01}}/P_{01}\right)_{calculated}\right.$ and $\left.\left(\dot{m}\sqrt{T_{01}}/P_{01}\right)_{map}\right)$ gives the following results for the compressor operating point.

$$\pi_c = 5.6, \quad \eta_c = 0.84, \quad \frac{T_{01}}{T_{03}} = 0.2506, \quad \text{and} \quad \frac{\dot{m}\sqrt{T_{01}}}{P_{01}} = 269.5$$

The turbine inlet temperature is then

$$T_{03} = \frac{T_{01}}{0.2506} = \frac{288}{0.2506} = 1149.24 \text{ K}$$

16.4 Off-Design of Turbojet Engine

There is similarity between the flow characteristics of a nozzle and a turbine [2]. The static operation of the turbojet engine is similar to the operation of a free power turbine. The equilibrium running line of the compressor (see Figure 16.12) can be obtained using the

same method described in the previous section. During flight, the forward speed produces a ram pressure dependent on the flight speed (Mach number) and intake efficiency

$$\frac{P_{01}}{P_a} = \left(1 + \eta_d \frac{\gamma - 1}{2} M_a^2\right)^{\gamma/\gamma - 1} \tag{16.14}$$

The temperature ratio is

$$\frac{T_{01}}{T_a} = \left(1 + \frac{\gamma - 1}{2} M_a^2\right) \tag{16.15}$$

The ram pressure will increase the compressor delivery pressure, which in turn increases the outlet pressure of the turbine and thus increases the pressure ratio of the nozzle. Once the nozzle is choked, the non-dimensional flow will reach its maximum value and will be independent of the nozzle pressure ratio and in turn the forward speed. This then fixes the turbine operating point due to compatibility conditions between the turbine and the nozzle. The present aeroengines operate with a choked nozzle for the whole flight except during taxiing, approaching, and landing. The nozzle map is illustrated in Figure 16.14.

The mass flow parameter of the nozzle is related to the ram pressure by the relation

$$\frac{P_{04}}{P_a} = \frac{P_{04}}{P_{03}} \times \frac{P_{03}}{P_{02}} \times \frac{P_{02}}{P_{01}} \times \frac{P_{01}}{P_a} \tag{16.16}$$

where P_{01}/P_a is obtained from Equation 16.14.

Referring back to Figure 16.5, the constant temperature ratio (T_{03}/T_{01}) has a straight line pattern. When these lines are drawn when the gas generator is coupled to a nozzle, each line has a fan of equilibrium running lines, one each for a fixed flight Mach number. These lines are found at the region of low compressor pressure ratios and consequently are low mass flow rates. As the pressure ratio increases these lines merge into the single running line as before, which represents the choked nozzle operation.

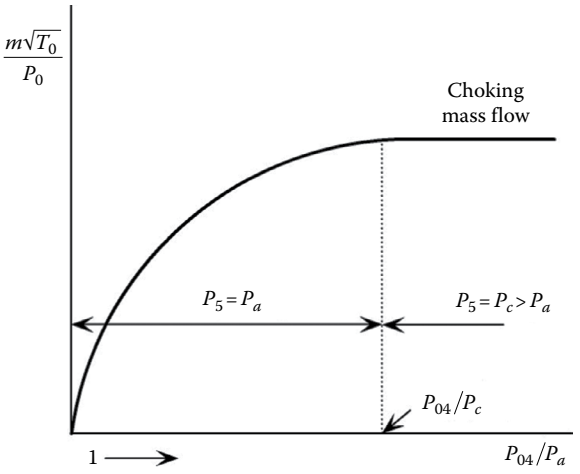


FIGURE 16.14
Nozzle map.

The engine thrust force is then calculated from the relation

$$T = \dot{m}_5\left(V_5 - V_f\right) + A_5\left(P_5 - P_a\right) \tag{16.17}$$

The flight speed is given by the relation

$$V_f = M_a\sqrt{\gamma R T_a} \tag{16.18}$$

The exhaust speed (V_5) depends on the nozzle choking.

For a choked nozzle

$$V_5 = \sqrt{\gamma R T_5} = \sqrt{\frac{2\gamma R T_{04}}{\gamma + 1}} \tag{16.19a}$$

For an unchoked nozzle

$$V_5 = \sqrt{2Cp\left(T_{04} - T_5\right)} = \sqrt{2CpT_{04}\left[1 - \left(\frac{P_a}{P_{04}}\right)^{\gamma-1/\gamma}\right]} \tag{16.19b}$$

For choked conditions

$$P_5 = P_c = P_{04}\left(1 - \frac{1}{\eta_n}\frac{\gamma - 1}{\gamma + 1}\right)^{\gamma/\gamma-1} \tag{16.20}$$

For unchoked conditions $P_5 = P_a$.

The performance of a turbojet engine looks like it is dependent on the non-dimensional engine speed, but in fact it is dependent on the actual *mechanical speed*, which is controlled by the turbine stresses and by governors [2]. The mechanical speed at takeoff represents the maximum speed that may be withstood due to stress limitations. The climbing speed will be lower, say at 98%, and the cruising speed may be less, by some 95%. Ambient conditions also have pronounced effects. An increase in ambient temperature will decrease $N/\sqrt{T_a}$ and consequently $N/\sqrt{T_{01}}$. This will move the operating point toward lower values of the pressure ratio and mass flow parameter, or be equivalent to lower mechanical speeds. This results in an appreciable decrease in the available thrust.

Example 16.3

During a ground test for a turbojet engine at ambient condition of 1 bar and 288 K, the following data were recorded as the engine accelerated from 90% to 100% of the design point.

$N/\sqrt{T_{01}}$ Percent of Design	$\dot{m}\sqrt{T_{01}}/P_{01}$	P_{02}/P_{01}	η_c
90	370	3.60	0.8580
95	421	4.07	0.8585
100	454	4.60	0.8600

The turbine inlet temperature at 90% of design speed was 1000 K. Both the turbine and nozzle were choked throughout and had constant efficiencies of 0.9 and 0.95, respectively.

For a choked turbine, the following conditions are to be satisfied.

$$\frac{P_{04}}{P_{03}} = \text{constant}, \quad \frac{T_{04}}{T_{03}} = \text{constant}, \quad \text{and} \quad N \text{ is proportional to } \sqrt{T_{03}}.$$

There is a requirement to

- Calculate the turbine inlet and outlet temperatures at 95% and 100% of the design speed
- Calculate the specific thrust of the engine $T/\dot{m}$
- Plot the parameters $T_{03}, T_{04}, T_e, V_e, T/\dot{m}$ against the non-dimensional speed parameters $N/\sqrt{T_{01}}$ % of the design

Solution

The ambient conditions are the same as the compressor inlet conditions when the engine is commencing the ground run.

$$T_{01} = 288 \text{ K}, \quad P_{01} = 1 \text{ bar}$$

At 90% of design speed:

$$\Delta T_{012} = \frac{T_{01}}{\eta_c}\left[\left(\frac{P_{02}}{P_{01}}\right)^{\gamma_c - 1/\gamma_c} - 1\right] = 148.5 \text{ K}$$

$$W_c = W_t$$

$$\Delta T_{034} = \Delta T_{012} \times \frac{Cp_a}{Cp_g} = 130 \text{ K}$$

$$\left(\frac{P_{04}}{P_{03}}\right) = \left[1 - \frac{\Delta T_{034}}{\eta_t T_{03}}\right]^{\gamma_h/\gamma_h - 1} = 0.535$$

$$\frac{P_{03}}{P_{04}} = 1.866$$

$$T_{04} = T_{03} - \Delta T_{034} = 870 \text{ K}$$

$$\frac{T_{03}}{T_{04}} = 1.149$$

During acceleration, the pressure and temperature ratio across the turbine is constant for a choked condition. Moreover, the rotational speed is proportional to the square root of the turbine inlet temperature, thus

$$\frac{P_{04}}{P_{03}} = \text{constant}, \quad \frac{T_{04}}{T_{03}} = \text{constant} \quad \text{and} \quad N \alpha \sqrt{T_{03}}$$

At 95% of design speed:

$$\sqrt{\frac{T_{03}}{1000}} = \frac{0.95}{0.9}$$

$$\therefore T_{03} = 1114 \text{ K}$$

At 100% of design speed:

$$\sqrt{\frac{T_{03}}{1000}} = \frac{1.0}{0.9}$$

$$\therefore T_{03} = 1234.6 \text{ K}$$

The specified thrust during the ground run and choked nozzle is given by the relation

$$\frac{T}{\dot{m}} = V_c + \frac{A_e}{\dot{m}}\left(P_c - P_a\right)$$

Here, the governing equations for $\dot{m}$, V_c, and P_c are given by

$$\frac{P_c}{P_{04}} = \left(1 - \frac{1}{\eta_n}\frac{\gamma - 1}{\gamma + 1}\right)^{\gamma/\gamma - 1}$$

$$P_C = \frac{P_C}{P_{04}}\frac{P_{04}}{P_{03}}\frac{P_{03}}{P_{02}}\frac{P_{02}}{P_{01}}P_{01}$$

$$T_{04} = T_{03} \times \frac{T_{04}}{T_{03}} = \frac{T_{03}}{1.149}$$

The exhaust speed is calculated from Equation 16.19a

$$\dot{m} = \left(\frac{\dot{m}\sqrt{T_{01}}}{P_{01}}\right)\left(P_{01}\right)\left(\frac{1}{\sqrt{T_{01}}}\right) = \left(\frac{\dot{m}\sqrt{T_{01}}}{P_{01}}\right) \times \frac{1}{\sqrt{288}} = \frac{\left(\dot{m}\sqrt{T_{01}}/P_0\right)}{16.97}$$

$$\frac{A_e}{\dot{m}} = \frac{0.5}{\dot{m}}$$

Calculations are arranged in the following table. Plots for the temperature at the inlet and outlet of the turbine as well as at the nozzle outlet against the rotational speed are shown in Figure 16.15. Plots for the (here critical) exhaust speed and the specific thrust against the rotational speed ratio are given in Figure 16.16.

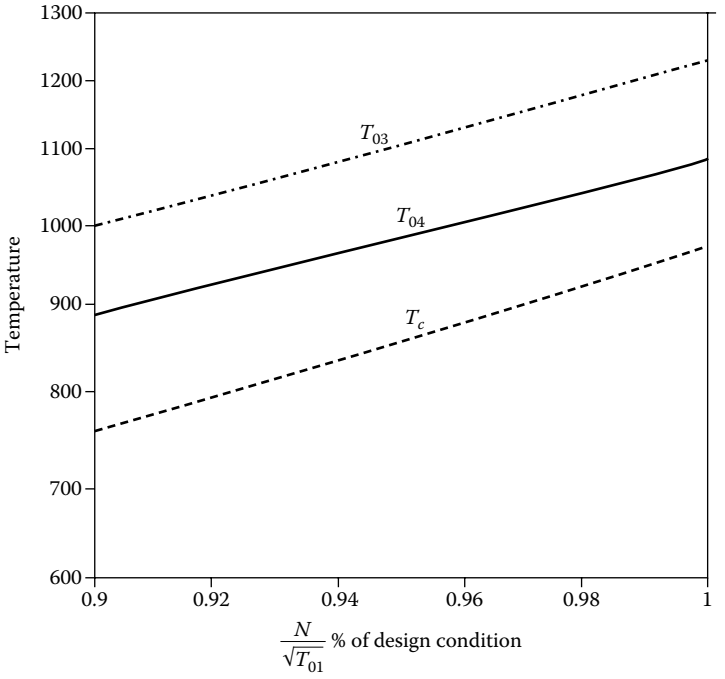


FIGURE 16.15
Turbine inlet and outlet temperature and exhaust temperature versus the engine speed percentage.

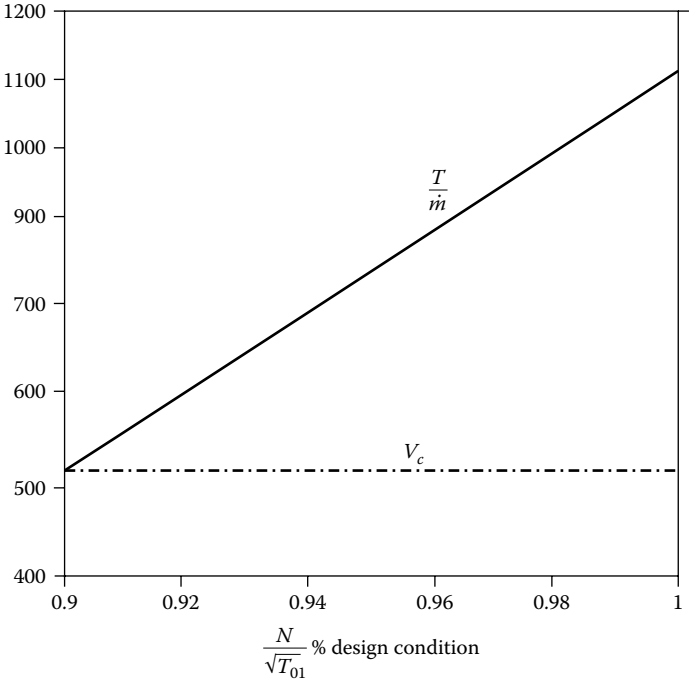


FIGURE 16.16
Specific thrust and exhaust speed versus engine speed percentage.

$N/\sqrt{T_{01}}$ Percentage of Design Value	90%	95%	100%
$P_{02}/P_{01} = P_{03}/P_{01}$	3.6	4.07	4.6
P_{04}/P_{03}	0.535	0.535	0.535
P_{04}/P_c	1.919	1.919	1.919
P_c (bar)	1.0036	1.1346	1.28243
T_{03} (K)	1000	1114	1234.6
T_{04} (K)	870	969.5	1074.4
T_c (K)	745.7	831	920.9
V_c (m/s)	534.18	563.9	593.6
$\dot{m}$ (kg/s)	21.802	24.8	26.752
$A_e/\dot{m}$ (m²·s/kg)	0.02293	0.02015	0.01869
$T/\dot{m}$ (N·s/kg)	542.4	835.119	1121.46

Example 16.4

Figure 16.17 illustrates a triple spool turbofan engine, which operates during takeoff where the ambient conditions are 288 K and 1 bar. It has a bypass ratio of 10.0. A low-pressure turbine (LPT) drives the fan. Gases enter the LPT at a temperature of 900 K and a pressure (P_{03}) of three folds that of the air exiting the fan ($P_{02} = 3P_{03}$).

Fan map data:

$\frac{P_{02}}{P_{01}}$	$\frac{\dot{m}_1\sqrt{T_{01}}}{P_{01}}$	η_f
1.2	12,000	0.88
1.5	10,000	0.90
1.8	9,000	0.91

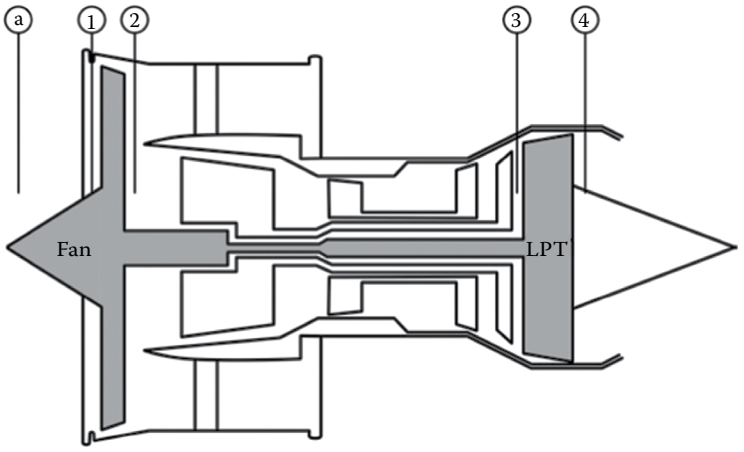


FIGURE 16.17
Three-spool turbofan engine.

Turbine map: Choked turbine, mass flow parameter 350, efficiency 0.91.
Calculate

1. The fan operating point (mass flow parameter, pressure ratio)
2. The fan air flow rate
3. The pressure ratio in the LPT

Solution

The mass flow compatibility is given by

$$\frac{\dot{m}_3\sqrt{T_{03}}}{P_{03}} = \frac{\dot{m}_1\sqrt{T_{01}}}{P_{01}}\frac{P_{01}}{P_{02}}\frac{P_{02}}{P_{03}}\frac{\dot{m}_3}{\dot{m}_1}\sqrt{\frac{T_{03}}{T_{01}}}$$

The relation between the turbine flow rate and the fan mass flow rate is given by

$$\dot{m}_3 = \frac{\dot{m}_1}{\beta+1}$$

$$\dot{m}_3 = \frac{\dot{m}_1}{10+1} = \frac{\dot{m}_1}{11}$$

The relation between fan exit pressure and turbine inlet pressure is given by

$$P_{03} = 3 * P_{02}$$

Substituting T_{03} = 900 K and T_{01} = 288 K,

$$\frac{\dot{m}_3\sqrt{T_{03}}}{P_{03}} = \frac{\dot{m}_1\sqrt{T_{01}}}{P_{01}}\frac{P_{01}}{P_{02}}\frac{P_{02}}{4 * P_{02}}\frac{1}{11}\sqrt{\frac{900}{288}}$$

$$\frac{\dot{m}_3\sqrt{T_{03}}}{P_{03}} = 0.0401765\frac{\dot{m}_1\sqrt{T_{01}}}{P_{01}}\frac{P_{01}}{P_{02}}$$

Since the turbine is choked, the mass flow parameter will always be constant and equal to 400:

$$350 = 0.0401765\frac{\dot{m}_1\sqrt{T_{01}}}{P_{01}}\frac{P_{01}}{P_{02}}$$

$$\frac{\dot{m}_1\sqrt{T_{01}}}{P_{01}} = 8711.55\frac{P_{02}}{P_{01}} \tag{5}$$

The mass flow parameter is calculated from Equation 5 for different pressure ratios and tabulated along with the values given in the data earlier in the following table:

$\frac{P_{02}}{P_{01}}$	$\frac{\dot{m}_1\sqrt{T_{01}}}{P_{01}}$ **From Data**	$\frac{\dot{m}_1\sqrt{T_{01}}}{P_{01}}$ **From Equation 5**
1.2	12,000	10,453.86
1.5	10,000	13,067.33
1.8	9,000	15,680.80

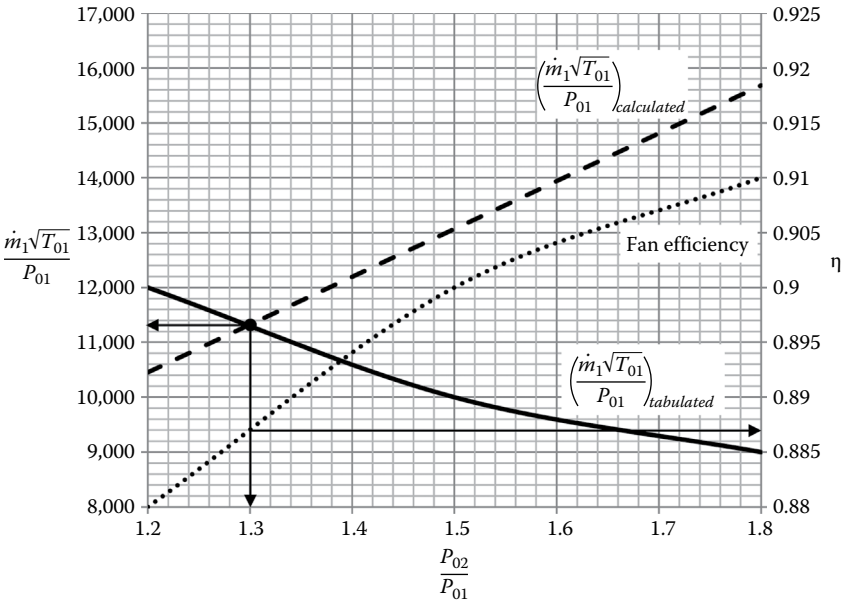


FIGURE 16.18
Matching between the fan and low-pressure modules.

The two sets of fan mass flow parameters are plotted in Figure 16.18.

$$\frac{\dot{m}_1\sqrt{T_{01}}}{P_{01}}$$

$$\left(\frac{\dot{m}_1\sqrt{T_{01}}}{P_{01}}\right)_{tabulated}$$

From the figure, the equilibrium between the turbine and the fan occurs at $\frac{P_{02}}{P_{01}} = 1.3$ and the mass flow parameter = 11,300, where the fan efficiency = 0.887.

The fan flow rate is then calculated:

$$\left(\frac{\dot{m}_1\sqrt{T_{01}}}{P_{01}}\right)_{calculated}$$

Fan efficiency

$$\dot{m}_1 = \frac{\dot{m}_1\sqrt{T_{01}}}{P_{01}}\frac{P_{01}}{\sqrt{T_{01}}}$$

$$\dot{m}_1 = 11{,}300 * \frac{1}{\sqrt{288}}$$

$$\dot{m}_1 = 665.856\,\mathrm{kg/s}$$

The corresponding turbine pressure ratio is calculated by equalizing the power required to operate the fan with the turbine power:

$$\dot{m}_3 W_t = \dot{m}_1 W_c$$

$$\dot{m}_3 = \frac{\dot{m}_1}{11} = 60.533\,\text{kg/s}$$

$$\dot{m}_3\,\eta_t C_{pt} T_{03}\left[1 - \frac{1}{\left(P_{03}/P_{04}\right)^{\gamma_t - 1/\gamma_t}}\right] = \frac{\dot{m}_1 C_{pc} T_{01}}{\eta_c}\left[\left(P_{01}/P_{02}\right)^{\gamma_c - 1/\gamma_c} - 1\right]$$

$$60.533 * 0.91 * 1148 * 900\left[1 - \frac{1}{\left(P_{03}/P_{04}\right)^{1.33-1/1.33}}\right] = \frac{665.856 * 1005 * 288}{0.887}\left[(1.3)^{1.4-1/1.4} - 1\right]$$

$$\frac{P_{03}}{P_{04}} = 4.14$$

A check on the solution is the following.

The assumed turbine mass flow parameter was 350.

The actual flow parameter can now be calculated,

$$\frac{\dot{m}_3\sqrt{T_{03}}}{P_{03}} = \frac{60.533 * \sqrt{900}}{4 * 1.3} = 349.23 \approx 350$$

Example 16.5

A turbojet engine (see Figure 16.19) is used to power a plane flying at a speed of 300 m/s at an altitude of 12,000 m, where the ambient temperature and pressure conditions are T_a = 216.7 K, P_a = 19.3 kPa. The engine has an air flow rate equal to 20 kg/s, a fuel-to-air ratio of 0.025, and a turbine inlet temperature of 1350 K.

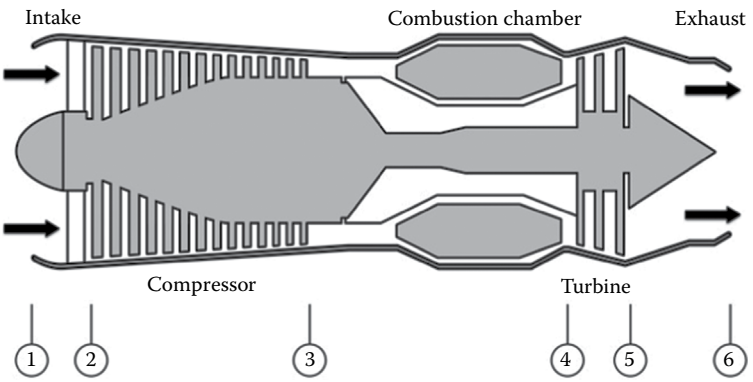


FIGURE 16.19
Turbojet engine.

The pressure drop across the combustion chamber is 5% and the fuel heating value is 43,000 kJ/kg.

The components efficiency is given in the following table:

η_{intake}	η_c	η_{cc}	η_t	η_n
0.9	0.9	0.98	0.9	0.95

Calculate

1. Compressor pressure ratio
2. Exhaust gas velocity
3. Exhaust nozzle area
4. Engine thrust
5. Thrust specific fuel consumption (TSFC)
6. η_p, η_{th}, η_0

If an afterburner (Figure 16.20) is used to reheat the turbine gases to 2100 K, recalculate these items showing the need for a variable area nozzle and a percentage increase in thrust.

Compute the compressor operating point and turbine pressure ratio at flight conditions if the compressor and turbine have the following data.

Compressor map

P_{03}/P_{02}	$\dot{m}_2\sqrt{T_{02}}/P_{02}$	η_c
9	1100	0.88
10	950	0.90
11	850	0.89

Turbine map: Choked turbine, mass flow parameter 225, efficiency 0.9.

Solution

At an altitude of 12,000 m, the ambient conditions are T_a = 216.7 K and P_a = 19.3 kPa.

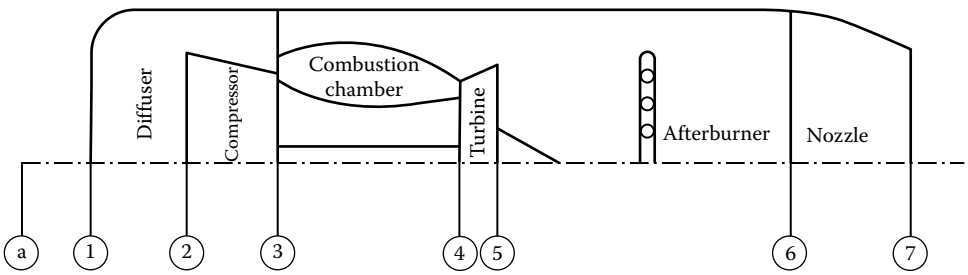


FIGURE 16.20
Turbojet engine with afterburner.

1. Turbojet engine without afterburner
   Diffuser (*state 1–2*):

$$T_{02} = T_a + \frac{V^2}{2C_{pc}}$$

$$T_{02} = 216.7 + \frac{300^2}{2*1005} = 261.5\,\text{K}$$

$$P_{02} = P_a\left[1 + \eta_i\left(\frac{T_{02} - T_a}{T_a}\right)\right]^{\gamma_c/(\gamma_c - 1)}$$

$$P_{02} = 19.3*\left[1 + 0.9*\left(\frac{261.5 - 216.7}{216.7}\right)\right]^{1.4/(1.4-1)} = 35.07\ \text{kPa}$$

Combustion chamber (*state 3–4*): Since fuel-to-air ratio is expressed as

$$f = \frac{C_{pt}T_{04} - C_{pc}T_{03}}{\eta_{cc}Q_R - C_{pt}T_{04}}$$

$$0.025 = \frac{1148*1350 - 1005*T_{03}}{0.98*43*10^6 - 1148*1350}$$

$$T_{03} = 532.4\,\text{K}$$

Compressor (*state 2–3*):

$$T_{03} = T_{02}\left[1 + \frac{\pi_c^{(\gamma_c - 1)/\gamma_c} - 1}{\eta_c}\right]$$

$$532.4 = 261.5*\left[1 + \frac{\pi_c^{(1.4-1)/1.4} - 1}{0.9}\right]$$

$$\pi_c = 10$$

$$P_{03} = P_{02} * \pi_c$$

$$P_{03} = 35.07*10 = 350.7\ \text{kPa}$$

Combustion chamber (*state 3–4*):

$$P_{04} = P_{03}\left(1 - \Delta P_{cc}\right)$$

$$P_{04} = 350.7*\left(1 - 0.05\right) = 333.165\ \text{kPa}$$

$$T_{04} = 1350\,\text{K}$$

Turbine (*state 4–5*):

$$T_{05} = T_{04} - \frac{C_{pc}\left(T_{03} - T_{02}\right)}{C_{pt}\left(1+f\right)}$$

$$T_{05} = 1350 - \frac{1005*\left(532.4 - 261.5\right)}{1148*\left(1+0.025\right)} = 1118.63\ \text{K}$$

$$P_{05} = P_{04}\left[1 - \frac{T_{04} - T_{05}}{\eta_t T_{04}}\right]^{\gamma_t/(\gamma_t - 1)}$$

$$P_{05} = 333.165*\left[1 - \frac{1350 - 1118.63}{0.9*1350}\right]^{1.33/(1.33-1)} = 142.2\ \text{kPa}$$

Tail pipe (*state 5–6*): With ideal conditions and an inoperative afterburner

$$P_{06} = P_{05}, \quad T_{06} = T_{05}.$$

Nozzle (*state 6–7*): Check whether the nozzle is choked or not.

$$\frac{P_{06}}{P_c} = \frac{1}{\left[1 - \left(\frac{1}{\eta_n}\right)\left(\frac{\gamma_n - 1}{\gamma_n + 1}\right)\right]^{\gamma_n/(\gamma_n - 1)}}$$

$$\frac{142.2}{P_c} = \frac{1}{\left[1 - \left(\frac{1}{0.95}\right)\left(\frac{1.33 - 1}{1.33 + 1}\right)\right]^{1.33/(1.33-1)}}$$

$$P_c = 74.185\ \text{kPa}$$

$P_c > P_a$ then the nozzle is choked.

$$P_7 = 74.185\ \text{kPa}$$

$$T_7 = \frac{T_{06}}{\gamma_n + 1/2}$$

$$T_7 = \frac{1118.63}{\left(\frac{1.33+1}{2}\right)} = 960.2\ \text{K}$$

$$V_7 = \sqrt{\gamma_n R T_7}$$

$$V_7 = V_{ex} = \sqrt{1.33*287*960.2} = 605.4\ \text{m/s}$$

The nozzle area is calculated from the air flow rate

$$\dot{m}_e = \rho_7 V_7 A_7$$

$$\dot{m}_e = \dot{m}_a (1 + f)$$

$$\dot{m}_e = 20 * (1 + 0.025) = 20.5 \text{ kg/s}$$

$$\rho_7 = \frac{P_7}{R T_7}$$

$$\rho_7 = \frac{74{,}185}{287 * 960.2} = 0.27 \text{ kg/m}^3$$

$$A_7 = \frac{\dot{m}_e}{\rho_7 V_7}$$

$$A_7 = \frac{20.5}{0.27 * 605.4} = 0.1258 \text{ m}^2$$

Now we calculate the engine's thrust

$$T = \dot{m}_a \left[(1 + f) V_7 - V \right] + A_7 (P_7 - P_a)$$

$$T = 20 * \left[(1 + 0.025) * 605.4 - 300 \right] + 0.1258 * (74{,}185 - 19{,}300)$$

$$T = 13{,}315 \text{ N} = 13.315 \text{ kN}$$

Then for the TSFC:

$$TSFC = \frac{\dot{m}_f}{T} = \frac{f * \dot{m}_a}{T}$$

$$TSFC = \frac{0.025 * 20}{13{,}315} = 3.755 * 10^{-5} \text{ kg/N} \cdot \text{s}$$

And for the efficiencies:

$$\eta_p = \frac{T * V}{T * V + 0.5 \dot{m}_e (V_{ex} - V)^2}$$

$$\eta_p = \frac{13{,}315 * 300}{13{,}315 * 300 + 0.5 * 20.5 * (605.4 - 300)^2} = 0.807$$

$$\eta_p = 80.7\%$$

$$\eta_{th} = \frac{T * V + 0.5 \dot{m}_e (V_{ex} - V)^2}{\dot{m}_f Q_R}$$

$$\eta_{th} = \frac{13,315 * 300 + 0.5 * 20.5 * (605.4 - 300)^2}{0.5 * 43 * 10^6} = 0.23$$

$$\eta_{th} = 23\%$$

$$\eta_o = \eta_p * \eta_{th}$$

$$\eta_o = 0.807 * 0.23 = 0.1856$$

$$\eta_o = 18.565\%$$

2. Turbojet with operative afterburner
   Tail pipe (*state 5–6*):

$$T_{06} = 2100 \text{ K}$$

$$P_{06} = P_{05}(1 - \Delta P_{ab})$$

$$P_{06} = 142.2(1 - 0.02) = 139.35 \text{ kPa}$$

The additional fuel-to-air ratio in the afterburner,

$$f_{ab} = \frac{C_{pt}T_{06} - C_{pt}T_{05}}{\eta_{ab}Q_R - C_{pt}T_{06}}$$

$$f_{ab} = \frac{1148 * 2100 - 1148 * 1118.63}{0.98 * 43 * 10^6 - 1148 * 2100} = 0.02836$$

Nozzle: Check whether it is choked or not.

$$\frac{P_{06}}{P_c} = \frac{1}{\left[1 - \left(\frac{1}{\eta_n}\right)\left(\frac{\gamma_n - 1}{\gamma_n + 1}\right)\right]^{\gamma_n/(\gamma_n - 1)}}$$

$$\frac{139.35}{P_c} = \frac{1}{\left[1 - \left(\frac{1}{0.95}\right)\left(\frac{1.33 - 1}{1.33 + 1}\right)\right]^{1.33/(1.33 - 1)}}$$

$$P_c = 72.699 \text{ kPa}$$

$P_c > P_a$ then the nozzle is choked.

$$P_7 = 72.699 \text{ kPa}$$

$$T_7 = \frac{T_{06}}{\gamma_n + 1/2}$$

$$T_7 = \frac{2100}{\left(\frac{1.33 + 1}{2}\right)} = 1802.6 \text{ K}$$

$$V_7 = \sqrt{\gamma_n R T_7}$$

$$V_7 = V_{ex} = \sqrt{1.33 * 287 * 1802.6} = 829.5 \text{ m/s}$$

The nozzle area is calculated from the air flow rate,

$$\dot{m}_e = \rho_7 V_7 A_7$$

$$\dot{m}_e = \dot{m}_a \left(1 + f + f_{ab}\right)$$

$$\dot{m}_e = 20 * \left(1 + 0.025 + 0.02836\right) = 21.0672 \text{ kg/s}$$

$$\rho_7 = \frac{P_7}{R T_7}$$

$$\rho_7 = \frac{72,699}{287 * 1,802.6} = 0.1405 \text{ kg/m}^3$$

$$A_7 = \frac{\dot{m}_e}{\rho_7 V_7}$$

$$A_7 = \frac{21.0672}{0.1405 * 829.5} = 0.18077 \text{ vm}^2$$

The change in the nozzle area confirms the need for using a variable area nozzle for turbojet engines fitted with afterburners, where the area required for operative afterburners is much larger than the case of an inoperative afterburner.

Now we calculate the new engine's thrust:

$$T = \dot{m}_a \left[\left(1 + f + f_{ab}\right) V_7 - V\right] + A_7 \left(P_7 - P_a\right)$$

$$T = 20 * \left[\left(1 + 0.025 + 0.02836\right) * 829.5 - 300\right] + 0.18077 * \left(72,699 - 19,300\right)$$

$$T = 21{,}128 \text{ N} = 21.128 \text{ kN}$$

The percentage increase in the engines thrust,

$$\Delta T\% = \left(\frac{T_{with\ ab} - T_{witout\ ab}}{T_{witout\ ab}}\right) * 100$$

$$\Delta T\% = \left(\frac{21,128 - 13,315}{13,315}\right) * 100$$

$$\Delta T\% = 58.68\%$$

Then for the TSFC,

$$TSFC = \frac{\dot{m}_f}{T} = \frac{\left(f + f_{ab}\right) * \dot{m}_a}{T}$$

$$TSFC = \frac{(0.025 + 0.02836) * 20}{21{,}128} = 5.05 * 10^{-5}\ \text{kg/N} \cdot \text{s}$$

Efficiencies:

$$\eta_p = \frac{T * V}{T * V + 0.5\dot{m}_e (V_{ex} - V)^2}$$

$$\eta_p = \frac{21{,}128 * 300}{21{,}128 * 300 + 0.5 * 21.0672 * (829.49 - 300)^2} = 0.682$$

$$\eta_p = 68.2\%$$

$$\eta_{th} = \frac{T * V + 0.5\dot{m}_e (V_{ex} - V)^2}{\dot{m}_f Q_R}$$

$$\eta_{th} = \frac{21{,}128 * 300 + 0.5 * 21.0672 * (829.49 - 300)^2}{1.0672 * 43 * 10^6} = 0.2016$$

$$\eta_{th} = 20.16\%$$

$$\eta_o = \eta_p * \eta_{th}$$

$$\eta_o = 0.682 * 0.2016 = 0.1375$$

$$\eta_o = 13.75\%$$

Summary

Case	Thrust (kN)	Fuel Mass Flow Rate (kg/s)	Exhaust Velocity (m/s)	Exhaust Area (m^2)	TSFC (kg/N·s)	η_p (%)	η_{th} (%)	η_o (%)
Inoperative afterburner	13.315	0.5	605.4	0.1258	$3.755 * 10^{-5}$	80.7	23.0	18.565
Operative afterburner	21.128	1.0672	829.5	0.18077	$5.05 * 10^{-5}$	68.2	20.16	13.75

Matching: In either cases of inoperative or operative afterburner, the flow compatibility between compressor and turbine is given by

$$\frac{\dot{m}_4 \sqrt{T_{04}}}{P_{04}} = \frac{\dot{m}_2 \sqrt{T_{02}}}{P_{02}} \frac{P_{02}}{P_{03}} \frac{P_{03}}{P_{04}} \frac{\dot{m}_4}{\dot{m}_2} \sqrt{\frac{T_{04}}{T_{02}}}$$

The relation between the turbine flow rate and compressor mass flow rate is given by

$$\dot{m}_4 = \dot{m}_2 (1 + f)$$

$$\frac{\dot{m}_4}{\dot{m}_2} = 1 + f = 1.025$$

The relation between the compressor exit pressure and the turbine inlet pressure is given by

$$P_{04} = P_{03}\left(1-\Delta P_{cc}\right)$$

$$P_{04} = P_{03}\left(1-0.02\right)$$

$$P_{04} = 0.95\,P_{02}$$

Substituting T_{04} = 1350 K and T_{02} = 261.5 K,

$$\frac{\dot{m}_4\sqrt{T_{04}}}{P_{04}} = \frac{\dot{m}_2\sqrt{T_{02}}}{P_{02}}\frac{P_{02}}{P_{03}}\frac{P_{03}}{0.95\,P_{03}}(1.025)\sqrt{\frac{1350}{261.5}}$$

$$\frac{\dot{m}_4\sqrt{T_{04}}}{P_{04}} = 2.4515\frac{\dot{m}_2\sqrt{T_{02}}}{P_{02}}\frac{P_{02}}{P_{03}}$$

Since the turbine is choked, the mass flow parameter will always be constant and equal to 225:

$$225 = 2.4515\ \frac{\dot{m}_2\sqrt{T_{02}}}{P_{02}}\frac{P_{02}}{P_{03}}$$

$$\frac{\dot{m}_2\sqrt{T_{02}}}{P_{02}} = 91.78\frac{P_{03}}{P_{02}} \qquad \text{(A)}$$

The mass flow parameter is calculated from Equation A for different pressure ratios and tabulated along with the values given in the data earlier in the following table.

P_{03}/P_{02}	$\dot{m}_2\sqrt{T_{02}}/P_{02}$ From Data	$\dot{m}_2\sqrt{T_{02}}/P_{02}$ From Equation A
9	1100	826.02
10	950	917.80
11	850	1009.60

The two sets of compressor mass flow parameters are plotted in Figure 16.21.

From the figure, the equilibrium between the turbine and the compressor occurs at P_{03}/P_{02} = 10.15 and mass flow parameter $\dot{m}_2\sqrt{T_{02}}/P_{02}$ = 916, while the compressor efficiency η_c = 0.90.

The corresponding turbine pressure ratio is calculated from the equality of the power required to operate the compressor with the generated turbine power,

$$\dot{m}_3 W_t = \dot{m}_1 W_c$$

$$\dot{m}_4\,\eta_t C_{pt} T_{04}\left[1-\frac{1}{\left(P_{04}/P_{05}\right)^{\gamma_t-1/\gamma_t}}\right] = \frac{\dot{m}_2 C_{pc} T_{02}}{\eta_c}\left[\left(P_{02}/P_{03}\right)^{\gamma_c-1/\gamma_c}-1\right]$$

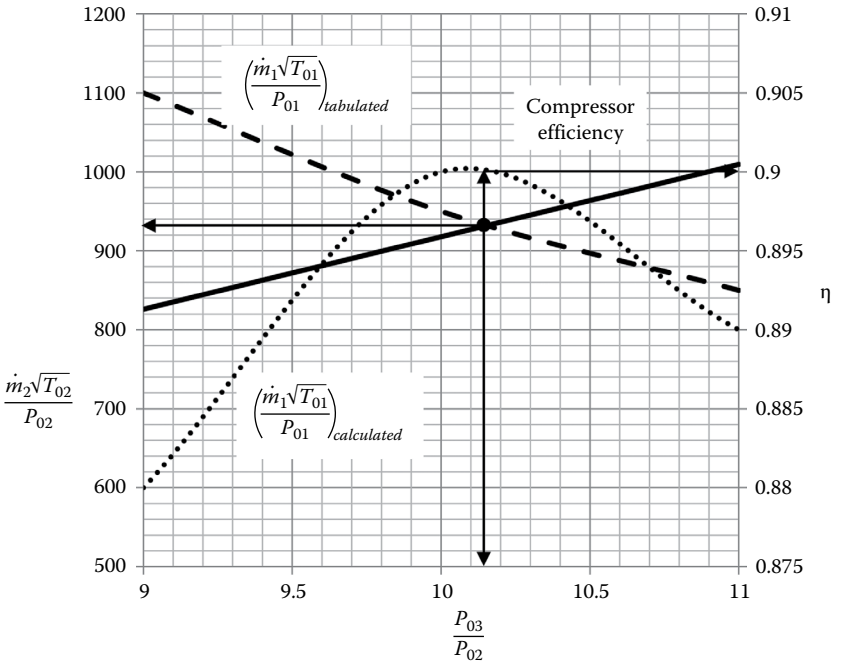


FIGURE 16.21
Matching between compressor and turbine.

$$20.5*0.9*1148*1350\left[1-\frac{1}{\left(P_{04}/P_{05}\right)^{0.25}}\right]=\frac{20*1005*261.5}{0.9}\left[\left(10.15\right)^{0.286}-1\right]$$

$$\frac{P_{04}}{P_{05}}=2.358$$

Problems

16.1 A two-spool gas turbine is fitted with a free power turbine driving a load; the other spool is a typical gas generator. If the compressor pressure ratio is 2.7, the combustion chamber pressure loss is 3% of the compressor delivery pressure; exhaust pressure loss can be ignored. The turbine characteristics are given as

Gas Generator Turbine			Power Turbine	
P_{03}/P_{04}	$\dot{m}\sqrt{T_{03}}/P_{03}$	η_t	P_{04}/P_a	$\dot{m}\sqrt{T_{04}}/P_{04}$
1.35	25	0.85	1.50	65
1.60	50	0.86	1.70	90
1.85	65	0.85	1.85	100

The non-dimensional flows quoted are based on $\dot{m}$ in kg/s and P in bar and T in K. Calculate the gas generator turbine pressure ratio at this condition.

16.2 The following data refer to the single shaft of a turboprop engine during a ground run. The gas turbine is running at its design point.

Compressor Characteristics			Turbine Characteristics		
P_{02}/P_{01}	$\dot{m}_1\sqrt{T_{01}}/P_{01}$	η_C	$\dot{m}_3\sqrt{T_{03}}/P_{03}$	P_{03}/P_{04}	η_t
3.8	320	0.77	110	4.0	0.88
4.3	300	0.80	135	4.4	0.90
4.8	290	0.83	135	4.8	0.91

The compressor inlet conditions are 1.01 bar and 288 K. The non-dimensional flows are based on $\dot{m}$ in kg/s and P in bar and T in K. The mechanical efficiency is 0.98. The pressure losses in the combustion chamber are 2%. Assume that the bled air is 3% of the compressor outlet mass flow rate. Calculate the power consumed in the propeller when the turbine inlet temperature is 1200 K.

16.3 A turbojet engine when tested at ambient conditions of 1.0 bar and 288 K gives the following results:

$N/\sqrt{T_{01}}$ (% Design)	$\dot{m}\sqrt{T_{01}}/P_{01}$	P_{02}/P_{01}	η_C
90	380	3.7	0.855
95	430	4.3	0.865
100	460	4.7	0.860

The units of the mass flow rate, temperature, and pressure are kg/s, K, and bar.

The turbine inlet temperature at 100% design speeds is 1100 K. The turbine efficiency remains constant in all cases at a value of 0.92. Calculate at 100% design speed

1. The mass flow rate
2. The thrust force

If a similar test is performed on a hot day where the ambient temperature is 303 K and the pressure is also 1.0 bar and the mechanical speed is 100% of the design condition, calculate

1. The new design speed
2. The new mass flow rate
3. The thrust force

Assume that the nozzle is choked during all these tests on cold and hot days and has an exit area of 0.4 m^2. The efficiency of the turbine on the hot day remains at 0.92.

16.4 A turbojet engine when tested at ambient conditions of 1.0 bar and 288 K gives the following results:

$N/\sqrt{T_{01}}$ Percent of Design	$\dot{m}\sqrt{T_{01}}/P_{01}$	P_{02}/P_{01}	η_c
90	380	3.7	0.855
95	430	4.3	0.865
100	460	4.7	0.860

The units of the mass flow rate, temperature, and pressure are kg/s, K, and bar. The turbine inlet temperature at 100% design speed is 1100 K. The turbine efficiency remains constant in all cases at a value of 0.92.

Calculate at 100% design speed

1. The mass flow rate
2. The thrust force

If a similar test is performed on a hot day where the ambient temperature is 303 K, the pressure is 1.0 bar, and the mechanical speed is 100% of the design condition, calculate

1. The new design speed
2. The new mass flow rate
3. The new thrust force

Assume that the nozzle is choked during all these tests on cold and hot days and has an exit area of 0.4 m^2. The efficiency of the turbine on the hot day remains at 0.92.

16.5 The following data refer to a gas turbine with a free power turbine, operating at design speed.

Compressor Characteristic			Gas Generator Turbine Characteristic		
P_{02}/P_{01}	$\dot{m}\sqrt{T_{01}}/P_{01}$	η_C	P_{03}/P_{04}	$\dot{m}\sqrt{T_{03}}/P_{03}$	η_t
6.2	250	0.83	2.9	110	0.85
5.8	270	0.84	2.5	110	0.85
5.4	290	0.83	2.1	100	0.85

Assuming that the power turbine is choked, the value of $\dot{m}\sqrt{T_{04}}/P_{04}$ being 230, determine the design values of the compressor pressure ratio and turbine inlet temperature. Assume pressure losses in the combustion chamber are 3% and assume the mechanical efficiency of the gas generator rotor to be 0.98 and take the ambient temperature to be 288 K. The non-dimensional flows quoted are based on $\dot{m}$ in kg/s and P in bar and T in K, all pressures and temperatures being stagnation values.

16.6 Figure 16.22 illustrates a geared turbofan. The fan (1) is driven by a low-pressure turbine (3), through a reduction gearbox (2). The fan rotates at a smaller speed than that of the low-pressure turbine to decrease losses. Part of the power generated

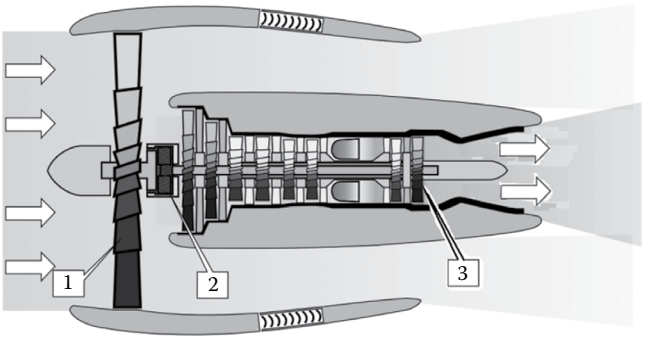


FIGURE 16.22
Geared turbofan engine.

by turbine (3) is used to drive the fan. Matching between fan (1) and low-pressure turbine (3) has the following characteristics:

1. Mass flow ratio: $\frac{\dot{m}_1}{\dot{m}_3} = \beta$
2. Speed ratio: $\frac{N_3}{N_1} = \lambda$
3. Power ratio: $\mathscr{P}3/\mathscr{P}1 = \delta$

   where all the variables (β, λ, δ) are greater than unity and the inlet and outlet states of the fan are denoted by (1, 2), while the inlet and outlet states of the turbine are (3, 4).

   a. Draw the fan and turbine maps.

   b. State the three compatibility conditions.

16.7 Figure 16.23 illustrates a C-12 Huron aircraft powered by two PT6A-42 turboprop engines (Figure 16.24). The engine has a single compressor and two turbines. The gas generator turbine is coupled to the compressor and the free (power) turbine drives the propeller.



FIGURE 16.23
C-12 Huron aircraft.

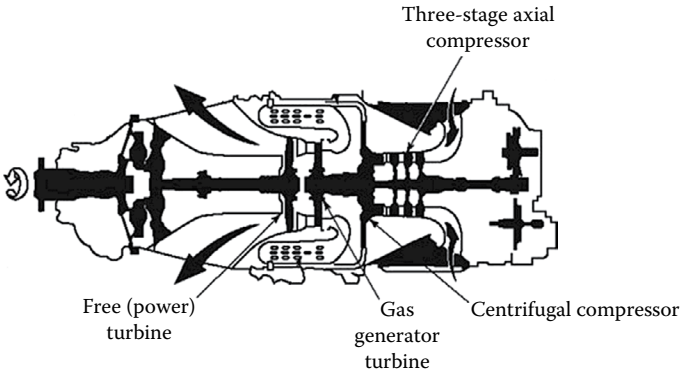


FIGURE 16.24
PT6A-42 turboprop engines.

The gas generator is running at its design speed and has the following data:

Compressor Characteristics			Gas Generator Turbine Characteristics		
P_{02}/P_{01}	$\dot{m}_1\sqrt{T_{01}}/P_{01}$	η_C	$\dot{m}_3\sqrt{T_{03}}/P_{03}$	P_{03}/P_{04}	η_t
9.0	50	0.83	18	3.0	0.85
8.0	66	0.84	18	2.6	0.85
7.0	80	0.83	15	2.2	0.84

The free (power) turbine is choked and the value of $\dot{m}\sqrt{T_{04}}/P_{04} = 40$.

The efficiency of the free (power) turbine is 0.85. Assume that the pressure loss in the combustion chamber is 3% and the mechanical efficiency of the gas generator rotor is 0.98. The ambient temperature and pressure are 288 K and 1.0 bar. The non-dimensional flows quoted are based on $\dot{m}$ in kg/s and P_0 in bar and T_0 in K.

Determine

1. The operating point for the compressor, gas generator, and free turbines
2. The mass flow rate through the compressor
3. The power generated from the free power turbine

16.8 The following data refer to the compressor and turbine of a high-pressure spool running at its design speed:

Compressor Characteristics			Turbine Characteristics		
P_{02}/P_{01}	$\dot{m}\sqrt{T_{01}}/P_{01}$	η_C	P_{03}/P_{04}	$\dot{m}\sqrt{T_{03}}/P_{03}$	η_t
6.5–6.5	330	0.80	3.2	110	0.92
6–6.0	350	0.79	2.8	110	0.92
5.6	370	0.77	2.4	110	0.92

The combustion pressure loss is 5% of the compressor delivery pressure and the inlet conditions of the compressor are 7.23 bar and 540 K. Mechanical losses can be neglected. The inlet total temperature for the turbine is 1570 K. The non-dimensional flows are based on $\dot{m}$ in kg/s and P in bar and T in K; all pressures and temperatures being stagnation values.

Calculate

1. The characteristics of the design point of the axial compressor
2. The characteristics of the design point of the turbine when the power of the compressor and turbine is equal

16.9 A gas generator is composed of a compressor, combustion chamber, and turbine. The inlet conditions are 288 K and 1.0 bar. The turbine inlet temperature is 1200 K. The fuel-to-air ratio is equal to the bleed air from the compressor at 2%. The pressure drop in the combustion chamber is 3%. Data for one of the operating points of the compressor and turbine are given here. State whether these conditions represent a *matching condition* between compressor and turbine or not.

Compressor	$\dot{m}_1\sqrt{T_{01}}/P_{01}$	π_c	η_c	$N/\sqrt{T_{01}}$
	339.4	4.0	0.85	29.46
Turbine	$\dot{m}_3\sqrt{T_{03}}/P_{03}$	π_t	η_t	$N/\sqrt{T_{03}}$
	178.6	1.776	0.9	14.43

Units for mass flow rate, temperature, pressure, and rotational speed are kg/s, K, bar, and rev/s, respectively.

References

1. W.W. Bathie, *Fundamentals of Gas Turbines*, 2nd edn., John Wiley & Sons, Inc., New York, 1996.
2. H.I.H. Saravanamuttoo, G.F.C. Rogers, and H. Cohen, *Gas Turbine Theory*, 5th edn., Prentice Hall, Harlow, U.K., 2001, 387pp.
3. P. Hill and C. Peterson, *Mechanics and Thermodynamics of Propulsion*, 2nd edn., Addison-Wesley Pub. Co., Inc., Reading, MA, 2010, 402pp.

17

Selected Topics

17.1 Introduction

One of the main challenges for the aeroengine designer is to develop new power systems that fulfill the requirements of both civil and military aircraft. The main issues now are the reduction of fuel burn, emissions, and noise while maintaining very high power/thrust levels and high propulsive and thermal efficiencies. Such engines, characterized by great power/thrust and low fuel consumption, directly affect an aircraft's payload, maneuverability, and maximum range. Perhaps the obvious way to reduce emission is to reduce the fuel burnt. Increasing the bypass ratio (BPR) of turbofan engines minimizes the kinetic energy of the exhaust gas and thus increases the propulsive efficiency. Then the value of the BPR is near its limit, and it is difficult to think of ways to continue this trend indefinitely [1]. However, the ultra-bypass ratio (UBPR) is a feasible proposal. With compressor and turbine efficiencies near plateauing, and turbine inlet temperatures paced by materials and blade cooling technologies, improvements in thrust specific fuel (SFC), specific power, and weight for conventional engines (including turboprop and turboshaft engines and larger turbofans) will likely be incremental compared with the past [2].

The most feasible action, and that meets the performance, economic, and environmental goals of future aeroengines, is to change some features of the basic cycle. Several ideas have been suggested and researched over the last decade, and others are under investigation. These include

1. Introducing more complex thermodynamic cycles involving recuperation (for turboprop and turboshaft engines) and intercooling, together with recuperation for higher-pressure ratio turbofan engines. The terms "regenerating" and "recuperating" are used alternatively in gas turbine/jet engine applications.
2. Inter-turbine burners.
3. Three-stream turbofans.

Intercoolers and recuperators are widely used in ground-based power plants and marine engines, and their benefits in reducing fuel consumption and increasing output power are well known. In regenerators (recuperators), a part of the heat available in the exhaust stream is recovered, which would otherwise be lost to preheat air from the compressor before it is introduced into the combustion chamber to save fuel. Though a negligible amount of the output power is reduced, due to the pressure loss in the heat exchanger, the thermal efficiency increases. However, the presence of the heat exchanger introduces two main problems, namely, the extra size and weight of the component, which are always prohibited on an aircraft, and the complexity of the flow pattern.

Intercooling is a practice that reduces the compression work, allowing as a consequence more power/thrust to be available at the output shaft or at the exhaust nozzle. The compression work depends, among other factors, on the air temperature at the compressor inlet. The flow pattern imposed by the presence of the intercooler is less complicated than that in regenerators, since the two flows do not need to be turned from the rear to the leading direction.

Currently, the intercooled recuperative aeroengine is being investigated in some European research programs such as Advisory Council for Aeronautical Research in Europe (ACARE) and New Aero Engine Corp Concepts (NEWAC) [3,4].

The second method for improving the engine efficiency and pollutants reduction is to employ an inter-turbine burner (ITB), which is an additional burner between the high-pressure turbine (HPT) and the low-pressure turbine (LPT). More heat can be added in the ITB station since the temperature of the gases is reduced by expansion through the HPT. The major advantages associated with the addition of an ITB are the improvement of thermal efficiency and a reduction in the NOx emission. Lower-temperature peaks in the main combustor result in a lower NOx emission, with a reduced requirement for cooling air. Continuous research work to improve performance in turbojet and turbofan engines by evaluating the placement of an auxiliary combustor between the stages of the turbine started in the late 1990s [5] and is ongoing today [6]. One possibility is to use the transition duct between the HPT and LPT stages. Another possibility is to use the turbine stator (nozzle) passages as combustors (one combustor between each set of vanes). This would imply that significant acceleration of the flow would occur while mixing and reaction are underway. The third choice is for both the transition duct and the first stators (turbine nozzles) in the LPT to serve as the combustion chamber. That is, combustion processes would begin in the transition duct but extend into the stators. Most recently, three-stream turbofan engines have been examined.

The continuous development of aircraft and aeroengines, including future speculation, over the 60 years from 1960 to 2020 is illustrated in Figures 17.1 through 17.4. The reduction of fuel consumption for different generations of turbojet/turbofan engines is illustrated in Figure 17.1. On average, the reduction in fuel consumption reached some 70%–80% in 60 years. Moreover, an additional 10%–15% reduction is expected when recuperator engines come to be employed.

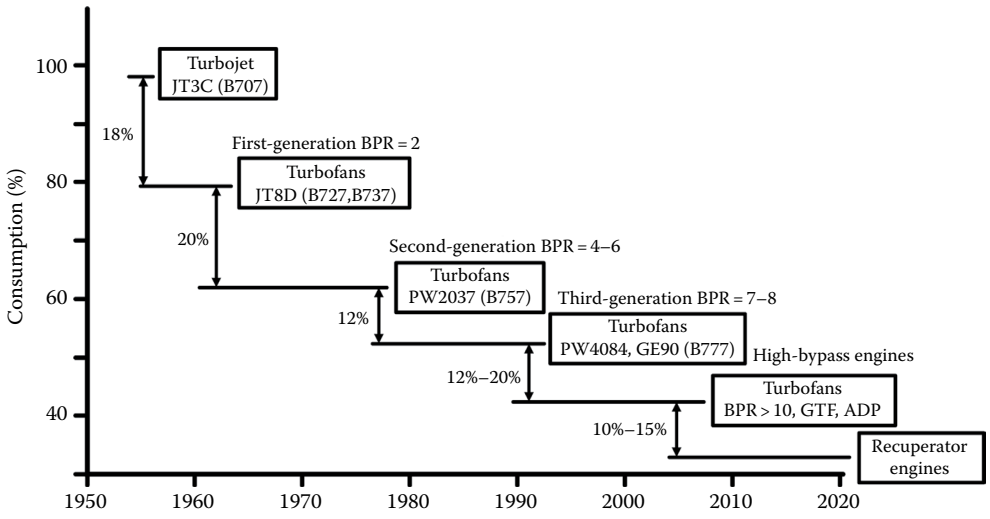


FIGURE 17.1
Reductions in fuel consumption for aeroengines over 60 years.

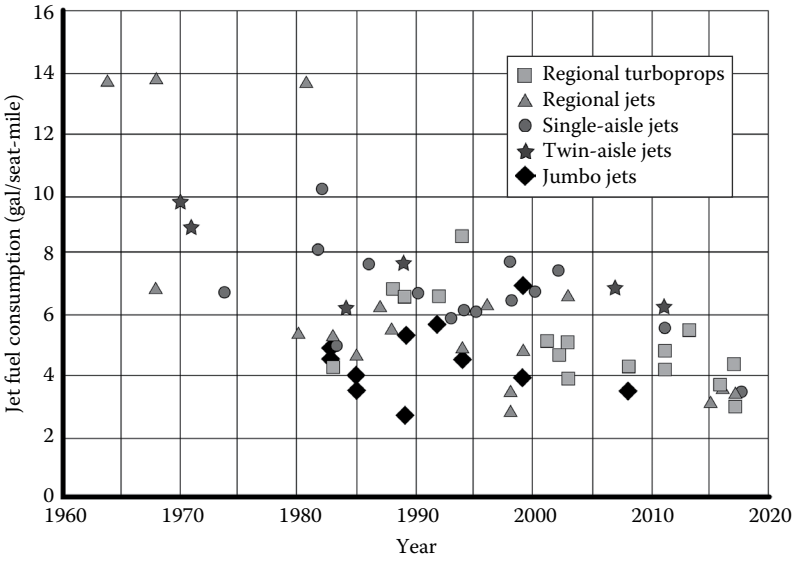


FIGURE 17.2
Reductions in fuel burn for different aircraft over 60 years. (From http://www.compositesworld.com/articles/composites-in-commercial-aircraft-engines-2014-2023.)

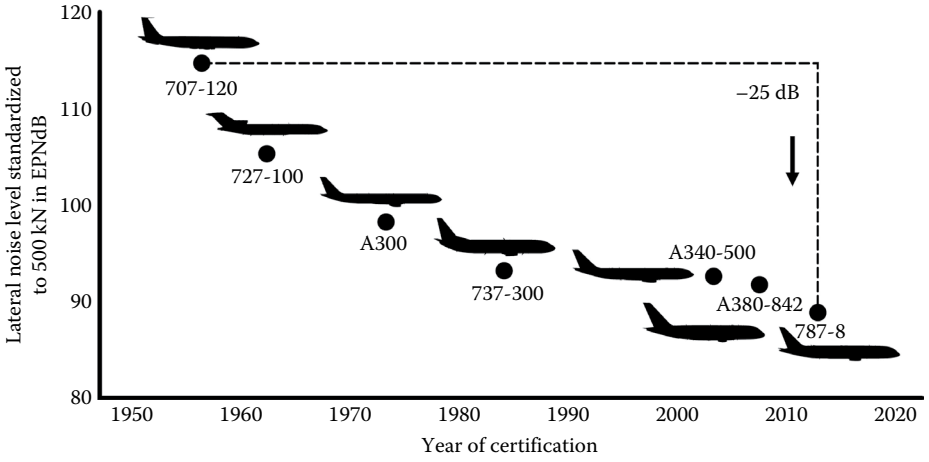


FIGURE 17.3
Reductions in noise levels for aeroengines over 60 years. (From http://www.bdl.aero/en/bdl-reports-en/aircraft-noise-report.)

Figure 17.2 shows the continuous reduction in fuel burn, if estimated in gallons/seat-mile. Since 1980, the average fuel burn per aircraft seat-mile has been reduced [7] by the following percentages:

- Regional turboprops 14%
- Regional jets 22%

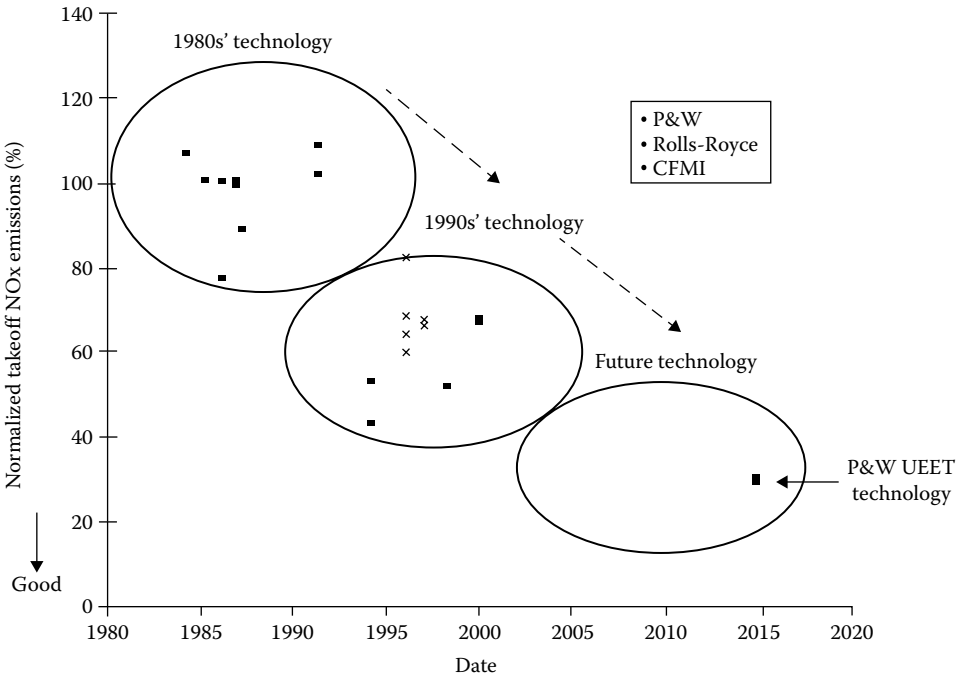


FIGURE 17.4
Reductions in emissions for aeroengines over the last 40 years.

- Single-aisle jets 22%
- Twin-aisle jets 17%
- Jumbo jets 6%

Reductions in noise have continuously been achieved over the last 50 years [8] as shown in Figure 17.3.

Reductions in emission have also been achieved over the last 40 years as shown in Figure 17.4.

Finally, special development has been devoted to aviation biofuel as a method for reducing the human impact on climate change. Sustainable biofuels are crucial in providing a cleaner source of fuel to power the world's fleet of aircraft and helping the billions of people who travel by air each year to reduce the impact of their journey on our planet.

On July 1, 2011, airlines won final approval from ASTM International to power airplanes with a blend made from traditional kerosene and biofuels derived from inedible plants and organic waste.

This decision allows airlines to fly passenger jets using derivatives of up to 50% biofuel made from feedstocks such as algae and woodchips. This will help carriers that account for 2% of global carbon dioxide emissions to reduce pollution blamed for damaging the Earth's atmosphere.

Airlines already have conducted test flights using the fuel. The Air France–KLM Group on June 29, 2011 operated the world's first commercial flight using a blend including cooking oil. KLM Airlines launched a series of around 80 biofuel flights from Oslo to Amsterdam operated

with an Embraer 190 in the period during March–April, 2016. Boeing performed a trans-Atlantic flight with fuel from the camelina plant, and on December 2, 2014 completed the world's first flight using "green diesel," a sustainable biofuel that is widely available and used in ground transportation. The company powered its ecoDemonstrator 787 flight test airplane with a blend of 15% green diesel and 85% petroleum jet fuel in the left engine. Sustainable green diesel is made from vegetable oils, waste cooking oil, and waste animal fats.

With a production capacity of 800 million gal (3 billion L) in the United States, Europe, and Asia, green diesel could rapidly supply as much as 1% of global jet fuel demand, with a wholesale cost of about $3/gal.

Airplane performance with the green diesel blend is exactly the same as conventional jet fuel.

17.2 New Trends in Aeroengines

After seven decades of continuous development in jet engines, present and future innovations are concerned with the following [2] topics:

1. Cycle parameter(s) optimization
2. Aerodynamic improvements (use of more sophisticated computational fluid dynamics (CFD) software, advanced blading, active tip clearance control, minimizing seal leakage)
3. Refined mechanical features (e.g., active blade vibration control)
4. Use of smart metals and structures
5. Focused thermal management (e.g., reduced cooling air flow, use of heat exchangers to reduce the temperature of bleed air for turbine cooling)
6. Improved combustor design
7. Use of alternate fuels
8. Use of improved environmental technologies
9. 3D printing

In this chapter, only some of these points will be discussed. These are cycle optimization via intercoolers, recuperators, and inter-turbine burners), smart materials, and biofuel such as alternative green fuel.

Intercoolers and recuperators fitted to aeroengines in military and civil aviation provide lower fuel burn, reduced emissions, and infrared (IR) signature attenuation [2,9]. Intercoolers [2] are proposed for novel turboprop engines (military transport aircraft), high bypass ratio (HBPR) turbofan engines (future airliners), and moderate bypass ratio (high-altitude unmanned air vehicles [UAVs]). Recuperators [2] are planned for turboshaft engines (military helicopters), turboprop engines (military transport and commuter aircraft), small turboprop engines (small and advanced UAVs), HBPR turbofan engines (future airliners), and moderate bypass ratio (high altitude UAVs and cruise missiles).

The drawbacks of both added modules are an increase in size/weight and complex engine architecture.

17.2.1 Intercooler

An intercooler is a heat exchanger located in the cold section of aeroengines and is similar to that used in gas turbine power plants, which was analyzed in detail in Section 8.4.4. In two-spool turbojet or turboprop engines, an intercooler is located between the low-pressure compressors (LPC) and high-pressure compressors (HPC) compressors. For a turbofan engine, an intercooler is also located between the booster (low-pressure compressor coupled to the fan in a low-pressure spool) and the high-pressure compressor; see Figure 17.5.

The convergence of lines of constant pressure on a *T*–*S* diagram indicates that compression at low temperatures reduces compression work. Intercoolers and recuperators (regenerators) are heat exchangers. Their performance depends on their effectiveness. This parameter compares the actual heat transfer rate to the maximum heat transfer rate attainable in a counter-flow heat exchanger of infinite heat transfer surface. Actual heat exchangers do not exchange all the heat that they could as a function of the two fluids temperature difference and mass flow rate. Denoting by ε the effectiveness of the heat exchanger we have the ideal intercooler (100% effectiveness) reduces the temperature of the air at the HPC back to the value at the inlet of the LPC. Intercooler effectiveness (defined in Section 8.4.4), which is normally less than unity (0.6–0.8), will yield a higher temperature at the inlet of the HPC than that at the inlet to the LPC. Air leaving the LPC and entering the intercooler is either cooled by ambient air (turboprop engines [10] as shown in Figure 17.9) or the compressed air in the fan outlet duct in turbofan engines as shown in Figure 17.5.

The effectiveness and drawbacks of intercoolers are illustrated by the following example.

Example 17.1

A two-spool turbofan engine is operating on the Brayton cycle; see Figure 17.6. The low-pressure spool is composed of a fan and a low-pressure compressor driven by an LPT. The high-pressure compressor is driven by the HPT. The cycle overall pressure ratio (π_T) is 23.6, the fan pressure ratio (π_f) is 1.57, and the pressure ratio of the low-pressure compressor (π_{LPC}) is 1.53. The fan mass flow rate ($\dot{m}_a = 280$ kg/s). The bypass ratio (β) is 5.44. The maximum and minimum cycle temperature limits are 1559 K. Consider the ground operation of the turbofan where the ambient pressure and temperature are 101 kPa and 288 K, and the Mach number is zero. The fuel lower heating value (Q_{HV}) is 45,000 kJ/kg. Consider the following efficiencies: $\eta_f = \eta_{LPC} = \eta_{HPC} = \eta_{LPT} = \eta_{HPT} = 0.9$, $\eta_b = 0.96$, $\eta_n = \eta_{fn} = 1$.

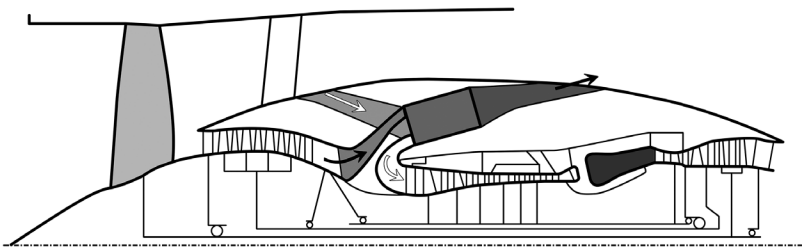
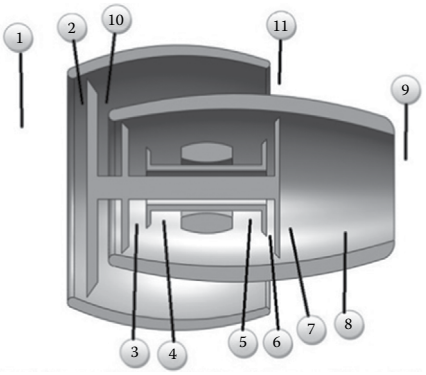


FIGURE 17.5
Turbofan engine fitted with intercooler.



Layout of two-spool turbofan engine
(fan and compressor driven by LPT)

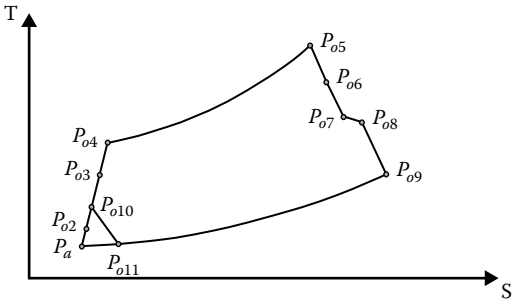
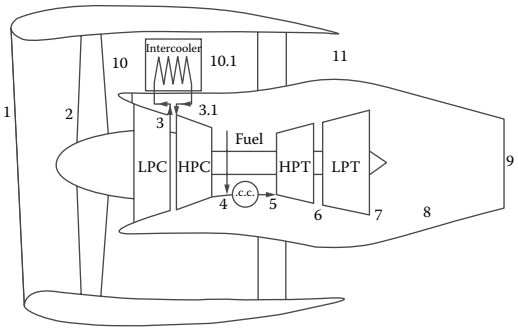


FIGURE 17.6
Two-spool turbofan engine.

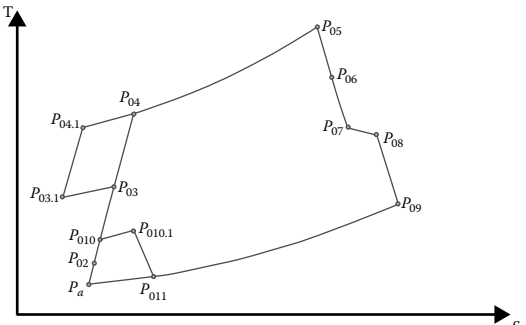
The flow properties at different modules are $\gamma_{air} = 1.4, \gamma_{gas} = 1.33, C_{pc} = 1.005$ kJ/kg, $C_{pt} = 1.05$ kJ/kg.

The following need to be calculated:

1. For the conventional Brayton cycle
   a. The fuel mass flow rate $\dot{m}_f$
   b. The combustion chamber heat addition $\dot{q}_{in}$
   c. The engine thrust
   d. The cycle thermal efficiency η_{th}
   e. The thrust specific fuel consumption (TSFC)
2. Consider an intercooler having effectiveness (=0.8) installed between the low- and high-pressure compressor where the air leaving the fan is used for cooling in the intercooler; see Figure 17.7.
   With the same cycle temperature limits
   A. Recalculate as in (1)
   B. Comment



Scheme of a turbofan engine with intercooling



T–S diagram of two-spool turbofan engine with intercooling

FIGURE 17.7
Two-spool turbofan engine with intercooler.

Solution

1. Conventional Brayton cycle: Takeoff flight phase

Intake

$$P_{o2} = P_a = 101 \text{ kPa}$$

$$T_{o2} = T_a = 288 \text{ K}$$

Fan

$$P_{o10} = \pi_f P_{o2} = 101 \times 1.57 = 158.57 \text{ kPa}$$

$$T_{o10} = T_{o2} \times \left[1 + \frac{1}{\eta_f} \left(\pi_f^{\frac{\gamma_{air}-1}{\gamma_{air}}} - 1 \right) \right] = 288 \times \left[1 + \frac{\left(1.57^{0.2857} - 1 \right)}{0.9} \right] = 332.014 \text{ K}$$

$$\dot{W}_f = \dot{m}_a C_{pt} \left(T_{o10} - T_{o2} \right) = 280 \times 1.005 \times \left(332.014 - 288 \right) = 12,385.5396 \text{ kW}$$

LPC

$$P_{o3} = \pi_{LPC} P_{o10} = 158.57 \times 1.53 = 242.6121 \text{ kPa}$$

$$T_{o3} = T_{o10} \times \left[1 + \frac{1}{\eta_f} \left(\pi_{LPC}^{\frac{\gamma_{air}-1}{\gamma_{air}}} - 1 \right) \right] = 332.014 \times \left[1 + \frac{\left(1.53^{0.2857} - 1 \right)}{0.9} \right] = 379.672 \text{ K}$$

$$\beta = \frac{\dot{m}_a}{\dot{m}_c} \quad \dot{m}_c = \frac{\dot{m}_a}{\beta} = \frac{280}{5.44} = 52.94 \text{ kg/s}$$

$$\dot{W}_{LPC} = \dot{m}_c C_{pt} \left(T_{o3} - T_{o10} \right) = 52.94 \times 1.005 \times \left(379.672 - 332.014 \right) = 2535.629 \text{ kW}$$

HPC

$$\pi_t = \pi_f \pi_{LPC} \pi_{HPC} \qquad \pi_{HPC} = \frac{23.6}{1.57 \times 1.53} = 9.82$$

$$P_{o4} = \pi_{HPC} P_{o3} = 242.6121 \times 9.82 = 2382.332 \text{ kPa}$$

$$T_{o4} = T_{o3} \times \left[1 + \frac{1}{\eta_{HPC}} \left(\pi_{HPC}^{\frac{\gamma_{air}-1}{\gamma_{air}}} - 1 \right) \right] = 379.672 \times \left[1 + \frac{\left(9.82^{0.2857} - 1 \right)}{0.9} \right] = 768.05 \text{ K}$$

$$\dot{W}_{HPC} = \dot{m}_c C_{pt} \left(T_{o4} - T_{o3} \right) = 52.94 \times 1.005 \times \left(768.05 - 379.672 \right) = 20,663.62 \text{ kW}$$

$$\dot{W}_c = \dot{W}_f + \dot{W}_{LPC} + \dot{W}_{HPC} = 12,385.5396 + 2,535.629 + 20,663.62 = 35,584.788 \text{ kW}$$

Combustion chamber: Assume no pressure loss, so

$$P_{o5} = P_{o4} = 2382.332 \text{ kPa}, \quad T_{o5} = 1559 \text{ K}$$

$$f = \frac{\frac{C_{pt}}{C_{pc}} \times \frac{T_{o5}}{T_{o4}} - 1}{\eta_b \frac{Q_R}{C_{pc} T_{o4}} - \frac{C_{pt}}{C_{pc}} \times \frac{T_{o5}}{T_{o4}}} = \frac{\frac{1.05}{1.005} \times \frac{1559}{768.05} - 1}{0.96 \times \frac{45{,}000}{1.005 \times 768.05} - \frac{1.05}{1.005} \times \frac{1{,}559}{768.05}} = 0.0208.$$

a. $\dot{m}_f = f\dot{m}_c = 0.0208 \times 52.94 = 1.1018 \text{ kg/s}$

b. $\dot{q}_{in} = \dot{m}_f \times Q_R = 1.1018 \times 45{,}000 = 49{,}581 \text{ kW}$

HPT

$$\dot{m}_c C_{pC} \left(T_{o4} - T_{o3}\right) = \dot{m}_c \left(1 + f\right) C_{pt} \left(T_{o5} - T_{o6}\right)$$

$$T_{o6} = 1559 - 364.1587 = 1194.84 \text{ K}$$

$$P_{o6} = P_{o5}\left(1 - \frac{T_{o5} - T_{o6}}{\eta_t \times T_{o5}}\right)^{\gamma_h/\gamma_h - 1} = 2382.332\left(1 - \frac{364.1587}{0.9 \times 1559}\right)^{3.5} = 832.263 \text{ kPa}$$

LPT

$$\dot{W}_f + \dot{W}_{LPC} = \dot{m}_c \left(1 + f\right) C_{pt} \left(T_{o6} - T_{o7}\right)$$

$$12{,}385.5396 + 2{,}535.629 = 52.94 \times 1.05 \times \left(1.0208\right)\left(1{,}194.84 - T_{o7}\right)$$

$$T_{o7} = 1194.84 - 262.959 = 931.88 \text{ K}$$

$$P_{o7} = P_{o6}\left(1 - \frac{T_{o6} - T_{o7}}{\eta_t \times T_{o6}}\right)^{\gamma_h/\gamma_h - 1} = 832.263\left(1 - \frac{262.959}{0.9 \times 1194.84}\right)^{3.5} = 311.89 \text{ kPa}$$

$$P_{o8} = P_{o7} = 311.89 \text{ kPa} \quad T_{o8} = T_{o7} = 931.88 \text{ K}$$

Turbine nozzle

$$\frac{P_{o8}}{P_c} = \left(\frac{\gamma_h + 1}{2}\right)^{\gamma_h/\gamma_h - 1}$$

$$P_c = \frac{311.89}{1.2^{3.5}} = 164.77 \text{ kPa}$$

$$P_c \geq P_a$$

Nozzle is *choked*

$$\frac{T_{o8}}{T_9} = \frac{\gamma_h + 1}{2}$$

$$T_9 = \frac{931.88}{1.165} = 799.896 \text{ K}$$

$$\rho_9 = \frac{P_9}{RT_9} = \frac{164.77}{0.287 \times 800} = 0.7176 \text{ kg/m}^3$$

$$V_9 = \sqrt{\gamma_h RT_9} = \sqrt{1.33 \times 287 \times 799.896} = 552.565 \text{ m/s}$$

Hot nozzle area

$$\dot{m}_9 = 52.94 + 1.1018 = 54.042 \text{ kg/s}$$

$$A_9 = \frac{\dot{m}_9}{\rho_9 V_9} = \frac{54.042}{0.7176 \times 552.565} = 0.13627 \text{ m}^2$$

Fan nozzle

$$\frac{P_{o10}}{P_c} = \left(\frac{\gamma_c + 1}{2}\right)^{\gamma_{air}/\gamma_{air}-1}$$

$$P_c = \frac{158.57}{1.2^{3.5}} = 83.769 \text{ kPa}$$

$P_c < P_a$ nozzle is unchoked

$$V_{11} = \sqrt{\frac{2\gamma_{air} RT_{o10}\,\eta_{fn}}{\gamma_C - 1}\left[1 - \left(\frac{P_a}{P_{o10}}\right)^{\gamma_{air}-1/\gamma_{air}}\right]} = 283.991 \text{ m/s}$$

c. Engine thrust, neglecting pressure term

$$\tau = \beta \dot{m}_c V_{11} + \dot{m}_c (1 + f) V_9 + A_9 (P_9 - P_a)$$

$$\tau = 5.44 \times 52.94 \times 283.991 + 52.94 \times 1.0208 \times 552.565 + 0.13627 \times (357.34 - 101) \times 10^3$$

$$\tau = 111{,}648.8396 + 34{,}932 \text{ N} = 146{,}579 \text{ N} = 146.579 \text{ kN}$$

d. Engine thermal efficiency η_{th}

$$\eta_{th} = \frac{\tau v + 0.5\dot{m}_c (1 + f) V_9^2 + 0.5\beta \dot{m}_c V_{11}^2}{\dot{q}_{in}} = 0.4$$

e. *TSFC*

$$TSFC = \frac{\dot{m}_f}{\tau} = \frac{1.1018}{146{,}579} = 0.7516 \times 10^{-5} \text{ kg/Ns}$$

2. Using an intercooler at takeoff phase
Intake

$$P_{o2} = P_a = 101 \text{ kPa}$$

$$T_{o2} = T_a = 288 \text{ K}$$

Fan

$$P_{o10} = \pi_f P_{o2} = 101 \times 1.57 = 158.57 \text{ kPa}$$

$$T_{o10} = T_{o2} \times \left[1 + \frac{1}{\eta_f}\left(\pi_f{}^{\gamma_{air}-1/\gamma_{air}} - 1\right)\right] = 288 \times \left[1 + \frac{\left(1.57^{0.2857} - 1\right)}{0.9}\right] = 332.014 \text{ K}$$

$$\dot{W}_f = \dot{m}_a C_{pt}\left(T_{o10} - T_{o2}\right) = 280 \times 1.005 \times \left(332.014 - 288\right) = 12,385.5396 \text{ kW}$$

LPC

$$P_{o3} = \pi_{LPC} P_{o10} = 158.57 \times 1.53 = 242.6121 \text{ kPa}$$

$$T_{o3} = T_{o10} \times \left[1 + \frac{1}{\eta_f}\left(\pi_{LPC}{}^{\gamma_{air}-1/\gamma_{air}} - 1\right)\right] = 332.014 \times \left[1 + \frac{\left(1.53^{0.2857} - 1\right)}{0.9}\right] = 379.672 \text{ K}$$

$$\beta = \frac{\dot{m}_a}{\dot{m}_c} \quad \dot{m}_c = \frac{\dot{m}_a}{\beta} = \frac{280}{5.44} = 52.94 \text{ kg/s}$$

$$\dot{W}_{LPC} = \dot{m}_c C_{pt}\left(T_{o3} - T_{o10}\right) = 52.94 \times 1.005 \times \left(379.672 - 332.014\right) = 2535.629 \text{ kW}$$

Intercooler analysis

For high-pressure compressor

HPC work in both cases can be calculated from

$$\dot{W}_{C.Conventional} = \dot{m}_c C_{pt} T_{o3}\left(\pi_{HPC}{}^{\gamma_{air}-1/\gamma_{air}} - 1\right)$$

$$\dot{W}_{C.Intercooler} = \dot{m}_c C_{pt} T_{o3.1}\left(\pi_{HPC}{}^{\gamma_{air}-1/\gamma_{air}} - 1\right)$$

From T–S diagram it is clear that π_{HPC} is the same in both cases but $T_{o3.1} < T_{o3}$, so the HPC power in the intercooler case is smaller than the HPC power in the conventional case

$$\dot{W}_{C,intercooler} < \dot{W}_{C,conventional}$$

where

$\dot{W}_{C,intercooler}$ is the compressor work using intercooler

$\dot{W}_{C,conventional}$ is the compressor work using intercooler

HPC

From T–S diagram $P_{o4} = P_{o4.1}$ and $P_{o3} = P_{o3.1}$

Intercooler effectiveness

$$x = \frac{T_{o3} - T_{o3.1}}{T_{o3} - T_{o10}}$$

For effectiveness $x = 0.8$

$$T_{o3} - T_{o3.1} = 0.8 \times \left(T_{o3} - T_{o10}\right)$$

So

$$T_{o3.1} = 341.546 \text{ K}$$

Energy balance in intercooler

$$\beta\left(T_{010.1} - T_{010}\right) = \left(T_{03} - T_{03.1}\right)$$

$$T_{010.1} = T_{010} + \frac{\left(T_{03} - T_{03.1}\right)}{\beta} = 339.022 \text{ K}$$

$$\pi_t = \pi_f \pi_{LPC} \pi_{HPC} \qquad \pi_{HPC} = \frac{23.6}{1.57 \times 1.53} = 9.82$$

$$P_{o4.1} = P_{o4} = \pi_{HPC} P_{o3} = 242.6121 \times 9.82 = 2382.332 \text{ kPa}$$

$$T_{o4.1} = T_{o3.1} \times \left[1 + \frac{1}{\eta_{HPC}}\left(\pi_{HPC}{}^{\gamma_{air}-1/\gamma_{air}} - 1\right)\right]$$
$$= 339.022 \times \left[1 + \frac{\left(9.82^{0.2857} - 1\right)}{0.9}\right] = 687.972 \text{ K}$$

$$\dot{W}_{HPC} = \dot{m}_c C_{pt}\left(T_{o4.1} - T_{o3.1}\right) = 52.94 \times 1.005 \times \left(687.972 - 341.546\right) = 18,431.5 \text{ kW}$$

$$\dot{W}_{C,intercooler} = \dot{W}_f + \dot{W}_{LPC} + \dot{W}_{HPC} = 12,385.5396 + 2,535.629 + 18,431.5 = 33,352.04278 \text{ kW}$$

Combustion chamber: Assume no pressure loss, so

$$P_{o5} = P_{o4.1} = 2382.332 \text{ kPa}, \quad T_{o5} = 1559 \text{ K}$$

$$f = \frac{\frac{C_{pt}}{C_{pc}} \times \frac{T_{o5}}{T_{o4.1}} - 1}{\eta_b \frac{Q_R}{C_{pc} T_{o4.1}} - \frac{C_{pt}}{C_{pc}} \times \frac{T_{o5}}{T_{o4.1}}} = \frac{\frac{1.05}{1.005} \times \frac{1559}{687.972} - 1}{0.96 \times \frac{45,000}{1.005 \times 687.972} - \frac{1.05}{1.005} \times \frac{1,559}{687.972}} = 0.022748$$

a. $\dot{m}_f = f\dot{m}_c = 0.022748 \times 52.94 = 1.2043 \text{ kg/s}$
b. $\dot{q}_{in} = \dot{m}_f \times Q_R = 1.2043 \times 45,000 = 54,194.24882 \text{ kW}$

HPT

$$\dot{m}_c C_{pC}\left(T_{o4.1} - T_{o3.1}\right) = \dot{m}_c\left(1 + f\right) C_{pt}\left(T_{o5} - T_{o6}\right)$$

$$T_{o6} = 1559 - 338.72 = 1220.279 \text{ K}$$

$$P_{o6} = P_{o5}\left(1 - \frac{T_{o5} - T_{o6}}{\eta_t \times T_{o5}}\right)^{\gamma_h/\gamma_h - 1} = 2382.332\left(1 - \frac{338.72}{0.9 \times 1559}\right)^{4.03} = 782.41 \text{ kPa}$$

LPT

$$\dot{W}_f + \dot{W}_{LPC} = \dot{m}_c\left(1 + f\right)C_{pt}\left(T_{o6} - T_{o7}\right)$$

$$12,385.5396 + 2,535.629 = 52.94 \times 1.05 \times \left(1.022748\right)\left(1,220.279 - T_{o7}\right)$$

$$T_{o7} = 1220.279 - 262.458 = 957.82 \text{ K}$$

$$P_{o7} = P_{o6}\left(1 - \frac{T_{o6} - T_{o7}}{\eta_t \times T_{o6}}\right)^{\gamma_h/\gamma_h - 1} = 782.41\left(1 - \frac{262.458}{0.9 \times 1220.279}\right)^{4.03} = 281.616 \text{ kPa}$$

$$P_{o8} = P_{o7} = 281.616 \text{ kPa} \quad T_{o8} = T_{o7} = 957.82 \text{ K}$$

Turbine nozzle: Assume $\eta_n = 1$

$$\frac{P_{o8}}{P_c} = \left(\frac{\gamma_h + 1}{2}\right)^{\gamma_h/\gamma_h - 1}$$

$$P_c = \frac{281.616}{1.8505} = 152.183 \text{ kPa}$$

$P_c \geq P_a$ nozzle is choked

$$\frac{T_{o8}}{T_9} = \frac{\gamma_h + 1}{2}$$

$$T_9 = \frac{957.82}{1.165} = 822.163 \text{ K}$$

$$\rho_9 = \frac{P_9}{RT_9} = \frac{152.183}{0.287 \times 822.16} = 0.645 \text{ kg/m}^3$$

$$V_9 = \sqrt{\gamma_h RT_9} = \sqrt{1.33 \times 287 \times 822.163} = 560.2 \text{ m/s}$$

$$\dot{m}_9 = 52.94 + 1.2043 = 54.1443 \text{ kg/s}$$

$$A_9 = \frac{\dot{m}_9}{\rho_9 V_9} = \frac{54.1443}{0.645 \times 560.2} = 0.1498 \text{ m}^2$$

Fan nozzle: Assume $\eta_n = 1$

$$\frac{P_{o10.1}}{P_c} = \left(\frac{\gamma_c + 1}{2}\right)^{\gamma_{air}/\gamma_{air} - 1}$$

$$P_c = \frac{158.57}{1.2^{3.5}} = 83.769 \text{ kPa}$$

$P_c < P_a$ nozzle is unchoked

$$V_{11} = \sqrt{\frac{2\gamma_{air} RT_{o10.1}\eta_n}{\gamma_C - 1}\left[1 - \left(\frac{P_a}{P_{o10.1}}\right)^{\gamma_{air}-1/\gamma_{air}}\right]} = 303.69036 \text{ m/s}$$

c. Engine *thrust*

$$\tau = \beta \dot{m}_c V_{11} + \dot{m}_c (1+f) V_9 + A_9 (P_9 - P_a)$$

$$\tau = 5.44 \times 52.94 \times 303.69036 + 52.94 \times 1.022748 \times 560.2 + 0.1498 \times (152.183 - 101) \times 10^3$$

$$\tau = 125{,}459.61 \text{ N} = 125.46 \text{ kN}$$

d. Engine *thermal efficiency* η_{th} using intercooler

$$\eta_{th} = \frac{\tau v + 0.5\dot{m}_c (1+f) V_9^2 + 0.5\beta \dot{m}_c V_{11}^2}{\dot{q}_{in}}$$

$$\eta_{th} = \frac{0 + 8{,}495{,}888.21 + 13{,}280{,}481.59}{54{,}194.24882 \times 1{,}000} = 0.4018$$

e. *TSFC using intercooler*

$$TSFC = \frac{\dot{m}_f}{\tau} = \frac{1.2043}{125{,}459.61} = 0.96 \times 10^{-5} \text{ kg/Ns}$$

Property	Conventional	Intercooler
η_{th}	0.4	0.4018
$\dot{m}_f$ (kg/s)	1.1018	1.2043
TSFC (kg/Ns)	0.7516×10^{-5}	0.96×10^{-5}
$\dot{q}_{in}$ (MW)	49.581	54.194
$\dot{W}_C$ (MW)	35.588	33.35
τ (kN)	127.76	125.46
$\dot{W}_{HPC}$ (MW)	20.66	18.43

Comments: All the results are for the takeoff mission for the same maximum and minimum temperature limits and compressor pressure ratio, assuming maximum intercooler effectiveness $x = 1$.

- There is little increase in thermal efficiency (0.0018).
- The fuel mass flow rate increased by 0.1025 kg/s.
- The thrust specific fuel consumption increased by 0.2084×10^{-5} kg/Ns.
- The heat addition power increased by 4613 kW.

- The high-pressure compressor power reduced by 2231.8 kW and as a result compressor power decreased by the same amount.
- The thrust force decreased by 2.3 kN.

These results match with findings in Reference 11 for turbofan engines having overall pressure ratios greater than 18. The thermal efficiency increases by adding an intercooler.

17.2.2 Intercooler and Recuperator

The intercooler is a heat exchanger located between the low-pressure compressor (LPC) in two-spool turboprop/turbofan engines or the intermediate-pressure compressor (IPC) in three-spool turbofans and the HPC. Thus, air leaving the LPC is routed to the intercooler, which cools down the flow before it enters the HPC. Again the cooler air from the intercooler is easier to compress, so less power is used to drive our HPC, which saves work energy for our shaft output. The general arrangement of a typical intercooled turbofan is an array of intercooler modules around the core of the engine and inboard of the bypass duct.

Extensive studies are being performed now in Europe and the United States for the design of efficient, compact, and lightweight intercooled compression systems with enhanced operability. These include the EU Framework 6 NEWAC program. The "Intercooled Core" subprogram SP3 is researching the key technologies needed for an intercooled turbofan to meet the specifications set in SP1. The component technologies include an effective, compact, and lightweight low-loss intercooler; low-loss inlet and outlet ducting systems for the intercooler, stiff engine, and intercase structures to support the intercooler modules and to maintain rotor tip clearances; and new systems and blading designs to maintain compressor efficiency and operability in these higher overall-pressure ratio (OPR) intercooled engine cycles [11].

A "recuperator" is a special-purpose high-temperature counter-flow heat exchanger that extracts heat from the hot engine exhaust and transfers it to the compressed engine air before combustion [12]. Depending on the specific implementation, this can sometimes double the overall thermal efficiency of the engine. The historical challenge with recuperators in aircraft applications centers around three key aspects—low-weight materials that can withstand the pressure, thermal shock, and heat-transfer efficiency. Recuperators are used in UAV [12] and cruise missile applications [13].

A combined intercooler and recuperator (regenerator) are suggested for future turbofan engines; see Figure 17.8. However, some turboprop engines incorporated both modules a

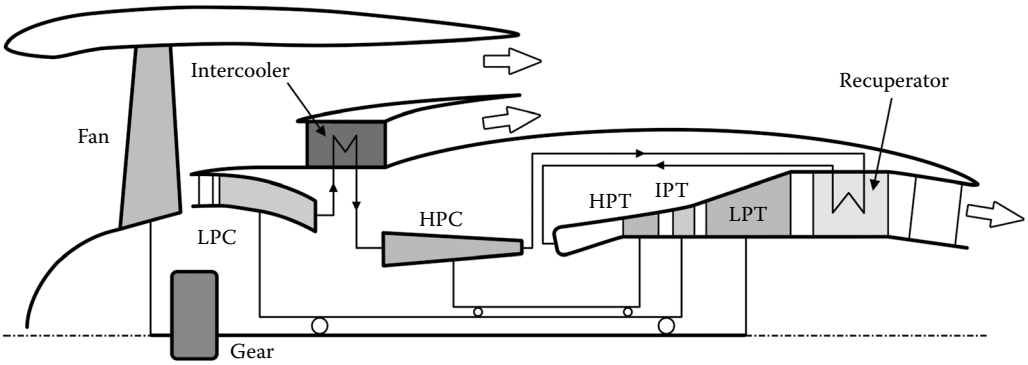


FIGURE 17.8
Turbofan with intercooler and recuperator.

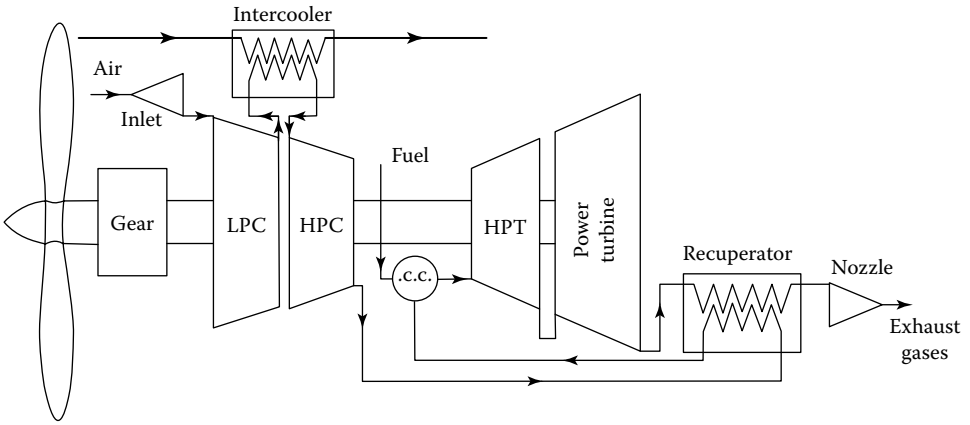


FIGURE 17.9
Scheme of a turboprop engine with intercooler and recuperator.

long time ago (see Figure 17.9), which proved the advantages of better thermal efficiency. This is due to the small mass flow through the core engine, which reduces the size and weight of the heat exchangers. Moreover, the heat regenerator downstream of the power turbine does not reduce significantly the thrust provided. Regenerators, by reducing fuel consumption, reduce pollutant emissions at the same time.

The regeneration employed in turboprop engines may be accomplished with a rotating heat-storage matrix or a fixed-surface heat exchanger.

In a rotating heat exchanger, the matrix absorbs heat from the hot turbine exhaust gases and transfers it to the cooler air leaving the compressor. Ideally, it will raise the outlet temperature of the compressor airflow to the turbine-exit gas temperature, but in order for this ideal condition to be achieved the mass and the surface area of the heat-transfer matrix would have to be very large.

Performance requirements for the recuperator in micro-turbines: As stated in References 14 and 15, the desired performance requirements are

- High exchanger effectiveness ε (≥ 90%) and low total pressure drop ($\Delta p/p < 5\%$)
- High operating temperatures and fluid pressures (about 675°C and 4 bar)
- A desired 40,000 h operation life without any maintenance for stationary power generation applications
- Compact (small hydraulic diameter surfaces) and lightweight matrix with integral manifolds and mass producible low-cost design

Example 17.2

Figure 17.10 illustrates a two-spool HBPR turbofan engine fitted with an intercooler between two compressors. A recuperator is installed within the nozzle, where hot gases leaving a low-pressure turbine are used to heat the air leaving the HPC prior to entering the combustion chamber to reduce fuel consumption.

At ground operation ($P_a = 1.0$ bar and $T_a = 288$ K), the following data apply:

$$\dot{m}_a = 540 \text{ kg/s}, \quad \beta = 8.0, \quad \pi_f = 1.3, \quad \pi_{LPC} = 1.2, \quad \pi_{HPC} = 10.0,$$

$$TIT = 1500 \text{ K}, \quad Q_R = 45 \text{ MW/kg}.$$

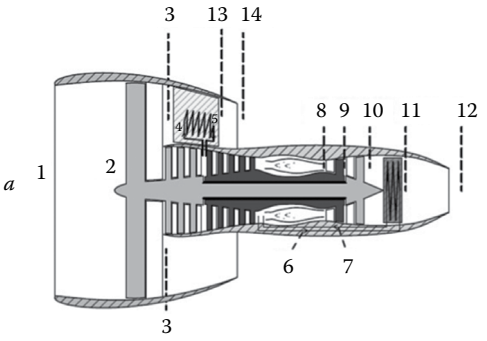


FIGURE 17.10
Schematic diagram of a turbofan with intercooler and recuperator (regenerator).

Intercooler efficiency = recuperator efficiency = 60%.
Assume no pressure drop in combustion chamber and recuperator.
Assume all processes are ideal.

Calculate

1. Fuel mass flow rate
2. Thermal efficiency
3. If the same turbofan engine was not fitted with intercooler and recuperator, recalculate the fuel mass flow rate and thermal efficiency
4. The contribution of intercooler and recuperator

Solution

Figure 17.11 illustrates the T–S diagram for the engine fitted with intercooler and recuperator.

Case 1: Turbofan with intercooler and recuperator intake (*state a-2*)
For ground operation:

$$T_{02} = T_a \times \left(1 + \frac{\gamma - 1}{2} M^2\right)$$

$$P_{02} = P_a \times \left(1 + \frac{\gamma - 1}{2} M^2\right)^{\gamma/\gamma - 1}$$

$$M = 0.0$$

$$P_a = P_{0a} = P_{02} = 1.0 \text{ bar} \quad \text{and} \quad T_a = T_{0a} = T_{02} = 288 \text{ K}$$

Fan (*state 2–3*):

$$P_{03} = P_{02} \times \pi_f = 1.3 \text{ bar}$$

For ideal fan ($\eta_f = 1.0$), then

$$T_{03} = T_{02} \times \pi_f^{\gamma - 1/\gamma} = 310 \text{ K}$$

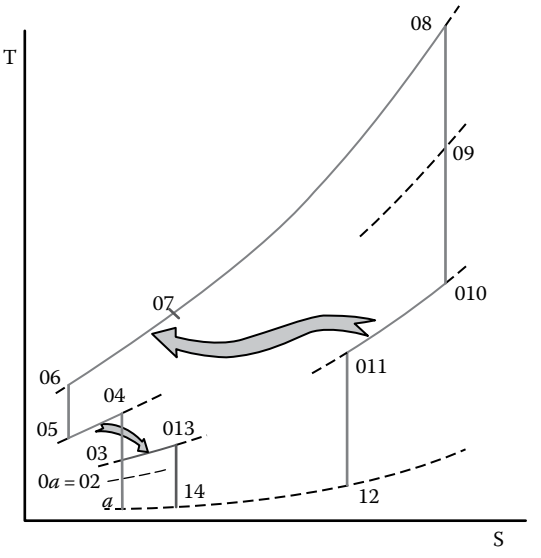


FIGURE 17.11
Thermodynamic cycle of a turbofan engine with intercooling and regeneration.

LPC (*state 3–4*):

$$P_{04} = P_{03} \times \pi_{LPC} = 1.56 \text{ bar}$$

For ideal LPC ($\eta_{LPC} = 1.0$), then

$$T_{04} = T_{03} \times \pi_{LPC}^{\gamma-1/\gamma} = 327 \text{ K}$$

Intercooler (*4–5*): Intercooler efficiency:

$$\varepsilon_{ic} = \frac{T_{04} - T_{05}}{T_{04} - T_{03}}$$

Thus,

$$T_{05} = T_{04} - \varepsilon_{ic} \times \left(T_{04} - T_{03}\right) = 327 - 0.6 \times \left(327 - 310\right) = 316.8 \text{ K}$$

$$P_{05} = P_{04} = 1.56 \text{ bar}$$

HPC (*5–6*):

$$P_{06} = P_{05} \times \pi_{HPC} = 15.6 \text{ bar}$$

For ideal HPC ($\eta_{HPC} = 1.0$), then

$$T_{06} = T_{05} \times \pi_{HPC}^{\gamma-1/\gamma} = 612 \text{ K}$$

HPT (*8–9*):

$$P_{08} = P_{07} = P_{06} = 15.6 \text{ bar}$$

$$W_{HPT} = W_{HPC}$$

For simplification assume $f \approx 0$, then

$$T_{09} = T_{08} - \frac{C_{pc}\left(T_{06} - T_{05}\right)}{C_{ph}} = 1500 - \frac{1.005 \times \left(612 - 316.8\right)}{1.148} = 1241.6 \text{ K}$$

$$P_{09} = P_{08}\left(1 - \frac{T_{08} - T_{09}}{\eta_{HPT} T_{08}}\right)^{\gamma_h/\gamma_h - 1}$$

For ideal HPT ($\eta_{HPT} = 1.0$), then

$$P_{09} = P_{08}\left(\frac{T_{09}}{T_{08}}\right)^{\gamma_h/\gamma_h - 1} = 15.6 \times \left(\frac{1241.6}{1500}\right)^4 = 7.322 \text{ bar}$$

LPT (*9–10*):

$$W_{LPT} = W_f + W_{LPC}$$

Also assuming $f \approx 0$, then

$$C_{ph}\left(T_{09} - T_{010}\right) = \left(1 + \beta\right)C_{pc}\left(T_{03} - T_{02}\right) + C_{pc}\left(T_{04} - T_{03}\right)$$

$$T_{010} = T_{09} - \frac{C_{pc}}{C_{ph}}\left[\left(1 + \beta\right)\left(T_{03} - T_{02}\right) + \left(T_{04} - T_{03}\right)\right]$$

$$T_{010} = 1241.6 - \frac{1.005}{1.148}\left[\left(9\right)\left(310 - 288\right) + \left(327 - 310\right)\right] = 1053.4 \text{ K}$$

$$P_{010} = P_{09}\left(1 - \frac{T_{09} - T_{010}}{\eta_{LPT} T_{09}}\right)^{\gamma_h - 1/\gamma_h}$$

For ideal LPT ($\eta_{LPT} = 1.0$), then

$$P_{010} = P_{09}\left(\frac{T_{010}}{T_{09}}\right)^{\gamma_h - 1/\gamma_h} = 7.322 \times \left(\frac{1053.4}{1241.6}\right)^4 = 3.793 \text{ bar}$$

Recuperator

$$\varepsilon_R = \frac{T_{07} - T_{06}}{T_{010} - T_{06}}$$

$$T_{07} = T_{06} + \varepsilon_R \times \left(T_{010} - T_{06}\right) = 612 + 0.6 \times \left(1053.4 - 612\right) = 876.84 \text{ K}$$

Since there is no pressure drop in the combustion chamber and recuperator, then

$$P_{08} = P_{07} = P_{06} = 15.6 \text{ bar}$$

Combustion chamber (*7–8*): Fuel-to-air ratio:

$$f = \frac{C_{ph}T_{08} - C_{pc}T_{07}}{Q_R - C_{ph}T_{08}} = \frac{1.148 \times 1,500 - 1.005 \times 876.84}{45,000 - 1.148 \times 1,500}$$

$$f = 0.0194$$

The fuel mass flow rate is then

$$\dot{m}_f = f \times \dot{m}_h = 0.0194 \times 60 = 1.166 \text{ kg/s}$$

Hot nozzle: The recuperator is installed inside the nozzle, where hot gases leaving the LPT are used to heat the air leaving the HPC prior to entering the combustion chamber to reduce fuel consumption.

Energy balance in the recuperator:

$$C_{ph}(1+f)(T_{010} - T_{011}) = C_{pc}(T_{07} - T_{06})$$

$$T_{011} = T_{010} - \frac{C_{pc}}{(1+f)C_{ph}}(T_{07} - T_{06}) = 1053.4 - \frac{1.005 \times (876.84 - 612)}{1.0194 \times 1.148}$$

$$T_{011} = 825.96 \text{ K}$$

$$P_{010} = P_{011} = 3.793 \text{ bar}$$

Jet speed:

$$V_{12} = \sqrt{2C_{ph}(T_{011} - T_{12})} = \sqrt{2C_{ph}T_{011}\left(1 - \left[\frac{P_{12}}{P_{011}}\right]^{\gamma-1/\gamma}\right)}$$

With $P_{12} = P_a$, then

$$V_{12} = \sqrt{2 \times 1148 \times 825.96\left(1 - \left[\frac{1}{3.793}\right]^{0.25}\right)} = 733.2 \text{ m/s}$$

Cold nozzle: Energy balance within the intercooler:

$$\beta C_{pc}(T_{013} - T_{03}) = C_{pc}(T_{04} - T_{05})$$

$$T_{013} = T_{03} + \frac{T_{04} - T_{05}}{\beta} = 310 + \frac{327 - 316.8}{8} = 311.27 \text{ K}$$

Cold air prior to leaving the cold nozzle is heated slightly (+1.27 K), while the compressed air leaving the LPC is cooled prior to entering the HPC (–10.2 K). The *jet speed* of the cold stream is

$$V_{14} = \sqrt{2C_{pc}(T_{013} - T_{14})} = \sqrt{2C_{pc}T_{013}\left(1 - \left[\frac{P_{14}}{P_{013}}\right]^{\gamma-1/\gamma}\right)}$$

With $P_{14} = P_a$, then

$$V_{14} = \sqrt{2 \times 1005 \times 311.27\left(1 - \left[\frac{1}{1.3}\right]^{0.286}\right)} = 212.7 \text{ m/s}$$

The *thrust force* is then

$$T = \dot{m}_c \times V_{14} + \dot{m}_h (1+f) \times V_{12}$$

$$T = 480 \times 212.7 + 60 \times 1.0194 \times 733.2 = 149{,}040 \text{ N} = 146.94 \text{ kN}$$

TSFC

$$TSFC = \frac{\dot{m}_f}{T} = \frac{1.166}{146.94} = 7.94 \times 10^{-3} \text{ kg/(kNs)}$$

Thermal efficiency:

$$\eta_{th} = \frac{\dot{m}_c V_{14}^2 + \dot{m}_h (1+f) V_{12}^2}{2\dot{m}_f Q_R} = \frac{480 \times (212.7)^2 + 60 \times 1.0194 \times (733.2)^2}{2 \times 1.166 \times 45 \times 10^6}$$

$$\eta_{th} = 52\%$$

Case 2: Turbofan without intercooler and recuperator

Figure 17.12 illustrates the T–S diagram for an ideal turbofan engine without heat exchangers.

HPC (*4–5*):

$$P_{05} = P_{04} \times \pi_{HPC} = 15.6 \text{ bar}$$

$$T_{05} = T_{04} \times \pi_{HPC}^{\gamma - 1/\gamma} = 631 \text{ K}$$

Combustion chamber (*5–6*):

$$f = \frac{C_{ph} T_{06} - C_{pc} T_{05}}{Q_R - C_{ph} T_{06}} = \frac{1.148 \times 1{,}500 - 1.005 \times 631}{45{,}000 - 1.148 \times 1{,}500}$$

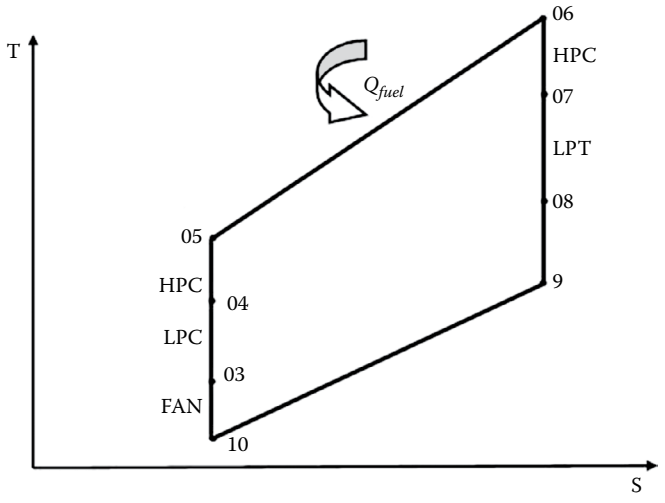


FIGURE 17.12
T–S diagram without intercooler and recuperator.

$$f = 0.0251$$

$$\dot{m}_f = f \times \dot{m}_h = 0.0251 \times 60 = 1.506 \text{ kg/s}$$

HPT (*6–7*):

$$T_{07} = T_{06} - \frac{C_{pc}\left(T_{05} - T_{04}\right)}{C_{ph}\left(1+f\right)} = 1500 - \frac{1.005 \times \left(631 - 327\right)}{1.148 \times 1.0251} = 1240 \text{ K}$$

$$P_{07} = P_{06}\left(\frac{T_{07}}{T_{06}}\right)^{\gamma_h/\gamma_h - 1} = 15.6 \times \left(\frac{1240}{1500}\right)^4 = 7.285 \text{ bar}$$

LPT (*7–8*):

$$T_{08} = T_{07} - \frac{C_{pc} \times \left[\left(1+\beta\right)\left(T_{03} - T_{02}\right) + \left(T_{04} - T_{03}\right)\right]}{C_{ph} \times \left(1+f\right)} = 1056 \text{ K}$$

$$P_{08} = P_{07}\left(\frac{T_{08}}{T_{07}}\right)^{\gamma_h/\gamma_h - 1} = 3.83 \text{ bar}$$

Hot nozzle:

$$V_9 = \sqrt{2C_{ph}\left(T_{08} - T_9\right)} = \sqrt{2C_{ph}T_{08}\left(1 - \left[\frac{P_a}{P_{08}}\right]^{\gamma - 1/\gamma}\right)}$$

With $P_9 = P_a$, then

$$V_9 = \sqrt{2 \times 1148 \times 1056\left(1 - \left[\frac{1}{3.83}\right]^{0.25}\right)} = 831.5 \text{ m/s}$$

Cold nozzle:

$$V_{10} = \sqrt{2C_{pc}\left(T_{03} - T_{10}\right)}$$

With $T_{10} = T_a$, then

$$V_{10} = \sqrt{2 \times 1005 \times 22} = 210.3 \text{ m/s}$$

Thrust force:

$$T = \dot{m}_c \times V_{10} + \dot{m}_h\left(1+f\right) \times V_9$$

$$T = 480 \times 210.3 + 60 \times 1.0251 \times 831.5 = 152{,}079 \text{ N} = 152.1 \text{ kN}$$

Thermal efficiency:

$$\eta_{th} = \frac{\dot{m}_c V_{10}^2 + \dot{m}_h (1+f) V_9^2}{2\dot{m}_f Q_R} = \frac{480 \times (210.3)^2 + 60 \times 1.0251 \times (831.5)^2}{2 \times 1.506 \times 45 \times 10^6}$$

$$\eta_{th} = 46.95\%$$

Comparison

1. Improvement in thermal efficiency due to intercooler and recuperator

$$\Delta\eta_{th} = \frac{52 - 46.95}{46.95} = +10.76\%$$

This result also matches with results presented in [11] where adding intercooler and recuperator increases the thermal efficiency for any overall pressure ratio in turbofan engines.

2. Reduction in fuel consumption due to intercooler and recuperator

$$\Delta\dot{m}_f = \frac{1.288 - 1.506}{1.506} = -14.46\%$$

17.2.3 Inter-Turbine Burner

Inter-turbine burners have been extensively studied following the pioneering work of Sirignano and Liu [5].

They demonstrated by thermodynamic analysis augmented combustion in aircraft turbojet and turbofan engines. A comparison of such inter-burners and after-burners was examined, which led to the following conclusions:

1. A reduction in after-burner length and weight
2. A reduction in specific fuel consumption compared to after-burner engines
3. An increase in specific thrust

The increase in specific thrust implies that larger thrust can be achieved with the same cross section or that the same thrust can be achieved with a smaller cross section (and therefore smaller weight). Another potential gain due to the turbine burner is to accept a reduction in the number of turbine stages without reducing thrust or increasing fuel consumption substantially. For the ground-based gas turbine, benefits have been shown by thermodynamic analysis to occur in power/weight and efficiencies [5].

One or two inter-turbine burners (1-ITB or 2-ITB) as well as continuous turbine burners (CTBs) were examined. Results showed that at Mach number 1, the 2-ITB engine produces 80% more specific thrust while incurring only about a 10% increase in the specific fuel consumption rate; the CTB engine is capable of producing 120% more thrust with about a 15% increase in the fuel rate compared to the base engine. More significantly, the 2-ITB and the CTB engines are capable of operating over the entire 0–2 flight Mach number range, while the conventional base engines cannot operate beyond Mach 1.25 [16]. The same analysis was extended to turbofan engines.

Turbine-burner engines provide significantly higher specific thrust with no or only small increases in the TSFC compared to conventional engines. Turbine-burner engines also widen the operational ranges for the flight Mach number and compressor pressure ratio. The performance gain of turbine-burner engines over conventional engines increases with compressor pressure ratio, fan bypass ratio, and flight Mach number [17].

The following two examples will clarify these findings.

Example 17.3

Consider an unmixed two-spool short-duct turbofan engine. The operating conditions are a flight speed of 250 m/s at an altitude of 20,000 m, where the ambient conditions are $T_\infty = 216.16$ K and $P_\infty = 5.476$ kPa. The modules have the following characteristics:

$$\dot{m}_a = 540 \text{ kg/s}, \quad \beta = 5.0, \quad \pi_f = 1.3, \quad \pi_{LPC} = 15,$$

$$\text{TIT} = 1500 \text{ K}, \quad Q_R = 45 \text{ MW/kg}.$$

Component efficiencies and pressure losses for the engine modules are listed in Table 17.1.

Figures 17.13 and 17.14 illustrate a turbofan with and without an inter-turbine burner. We need to plot TSFC for different values of overall pressure ratio and turbine inlet temperature (TIT).

a. *Cycle calculation for turbofan without turbine burner*: Here is a cycle analysis and the performance calculations for a two-spool turbofan engine with a short duct without turbine burner. Figure 17.15 describes the T–S diagram for this cycle.

Intake: The process of intake is treated as a polytropic compression with isentropic efficiency.

$$M_\infty = \frac{V_\infty}{\sqrt{\gamma_c R T_\infty}} = 0.8474$$

$$T_{o2} = T_{o1} = T_\infty \left(1 + \frac{\gamma_c - 1}{2} M_\infty^2\right) = 247.7 \text{ K}$$

$$P_{o2} = P_\infty \left[1 + \eta_I \frac{\gamma_c - 1}{2} M_\infty^2\right]^{\gamma_c/\gamma_c - 1} = 8.454 \text{ kPa}$$

TABLE 17.1

Modules' Efficiencies and Pressure Drop

Intake	η_I	92%
Fan	η_F	92%
Compressors	η_{LPC}	92%
Burners	η_{bcc}	99%
	ΔP_{cc}	2.5%
Turbine burner	η_{tb}	99%
	ΔP_{tb}	3%
Turbines	η_{HPT}	92%
	η_{LPT}	91%
	η_m	99%
Nozzle	η_{HN}	99%
	η_{CN}	98%

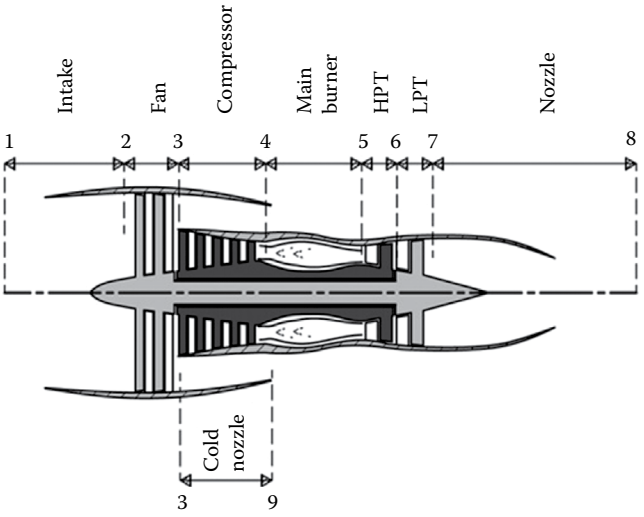


FIGURE 17.13
Turbofan without turbine burner.

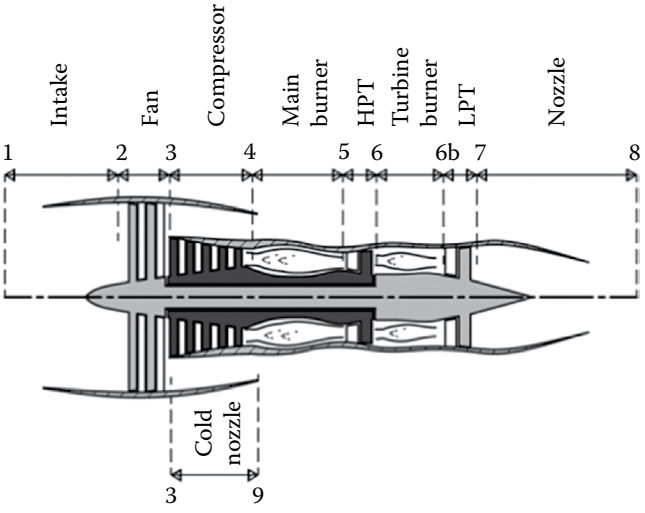


FIGURE 17.14
Turbofan with inter-turbine burner.

Fan: The fan is a compression component that raises the pressure of the bypass flow, so it can be used to develop extra thrust. The compression process in the fan is ideally isentropic and is treated as polytropic compression with isentropic efficiency to simulate real flow.

$$P_{o3} = \pi_F P_{o2} = 11 \text{ kPa}$$

$$T_{o3} = T_{o2}\left[1 + \frac{\left(\pi_F^{\gamma_c - 1/\gamma_c} - 1\right)}{\eta_F}\right] = 268.6 \text{ K}$$

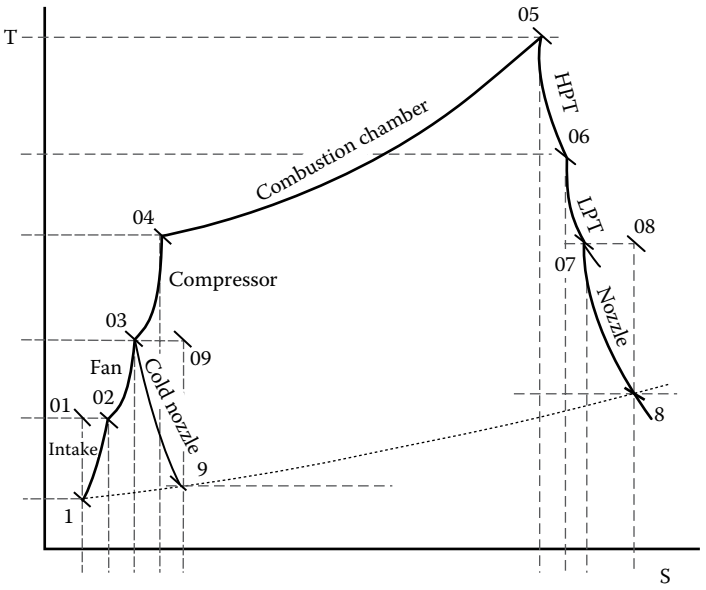


FIGURE 17.15
T–S diagram for a turbofan without turbine burner.

Compressor: The compressor is the main compression component that raises the pressure of the core flow upstream of the combustion chamber. The flow in the compressor is treated as polytropic compression with isentropic efficiency.

$$P_{o4} = \pi_C P_{o3} = 165 \text{ kPa}$$

$$T_{o4} = T_{o3}\left[1 + \frac{\left(\pi_C^{\gamma_c - 1/\gamma_c} - 1\right)}{\eta_C}\right] = 610 \text{ K}$$

Main burner "combustion chamber": The combustion process is supposed to be a constant pressure process. However, due to friction and fuel–air mixing, a drop in pressure takes place inside the burner. Fuel burning is simulated as a heat addition process to avoid the complication of chemical reaction. Burning efficiency will be taken into consideration to represent unburned hydrocarbons.

$$P_{o5} = P_{o4} - \Delta P_{occ} = 160.05 \text{ kPa}$$

$$f = \frac{\dot{m}_h}{\dot{m}_f} = \frac{C_{ph}T_{o5} - C_{pc}T_{o4}}{\eta_b Q_{HV} - C_{ph}T_{o5}} = 0.0259$$

where

$\dot{m}_h$ is the air mass flow rate passing through the core "hot flow"
$\dot{m}_f$ is the fuel mass flow rate injected in the combustion chamber

HPT: The HPT extracts power from hot gases downstream of the combustion chamber and delivers it through the shaft to the HPC. The expansion process in the turbine is treated as isentropic expansion with isentropic efficiency to simulate losses in the actual flow.

From balance of the high-pressure spool

$$C_{pc}\dot{m}_h\left(T_{o4}-T_{o3}\right)=C_{ph}\eta_m\left(\dot{m}_h+\dot{m}_f\right)\left(T_{o5}-T_{o6}\right)$$

$$T_{o6}=T_{o5}-\frac{C_{pc}\left(T_{o4}-T_{o3}\right)}{C_{ph}\eta_m\left(1+f\right)}=1205.7\ \text{K}$$

$$P_{o6}=P_{o5}\left[1-\frac{1}{\eta_{HPT}}\left(1-\frac{T_{o6}}{T_{o5}}\right)\right]^{\gamma_h/\gamma_h-1}=61.32\ \text{kPa}$$

LPT: The LPT extracts power from hot gases downstream of the HPT and delivers it through the shaft to the fan. The expansion process in the turbine is treated as isentropic expansion with isentropic efficiency to simulate losses in the actual flow.

From balance of the low-pressure spool

$$C_{pc}\dot{m}_h\left(1+\beta\right)\left(T_{o3}-T_{o2}\right)=C_{ph}\eta_m\left(\dot{m}_h+\dot{m}_f\right)\left(T_{o6}-T_{o7}\right)$$

$$T_{o7}=T_{o6}-\frac{C_{pc}\left(1+\beta\right)\left(T_{o3}-T_{o2}\right)}{C_{ph}\eta_m\left(1+f\right)}=1082.2\ \text{K}$$

$$P_{o7}=P_{o6}\left[1-\frac{1}{\eta_{LPT}}\left(1-\frac{T_{o7}}{T_{o6}}\right)\right]^{\gamma_h/\gamma_h-1}=38.03\ \text{kPa}$$

Hot nozzle: The nozzle converts the pressure and thermal energy to kinetic energy in the exiting hot gases jet, which generates the thrust. Flow in the nozzle is treated as polytropic expansion with isentropic efficiency, and the flow through it is assumed to be unchoked (complete expansion to ambient pressure).

$$T_8=T_{o7}\left[1-\eta_{hN}\left(1-\left[\frac{P_\infty}{P_{o7}}\right]^{\gamma_h-1/\gamma_h}\right)\right]=700\ \text{K}$$

$$V_8=\sqrt{2C_{ph}\left(T_{o7}-T_8\right)}=936.8\ \text{m/s}$$

Cold nozzle

$$T_9=T_{o3}\left[1-\eta_{cN}\left(1-\left[\frac{P_\infty}{P_{o3}}\right]^{\gamma_c-1/\gamma_c}\right)\right]=224.4\ \text{K}$$

$$V_9=\sqrt{2C_{pc}\left(T_{o3}-T_9\right)}=298\ \text{m/s}$$

Performance
Thrust

$$T = \dot{m}_h \beta V_9 + \dot{m}_h (1+f) V_8 - \dot{m}_h (1+\beta) V_\infty$$

$$\frac{T}{\dot{m}_h} = \beta V_9 + (1+f) V_8 - (1+\beta) V_\infty = 951.4 \text{ N} \cdot \text{s/kg}$$

$$TSFC = \frac{\dot{m}_f}{T} = \frac{f}{T/\dot{m}_h} = 0.000027223 \text{ kg}/(\text{N} \cdot \text{s}) = 0.098 \text{ kg}/(\text{N} \cdot \text{h})$$

b. *Cycle calculation for turbofan with inter-turbine burner*: Here is an analysis and the performance calculations for a two-spool turbofan engine with a short duct and inter-turbine burner. Figure 17.16 illustrates the T–S diagram for this cycle.

The same procedure and results are obtained for the modules up to the turbine burner; see Figures 17.17 and 17.18.

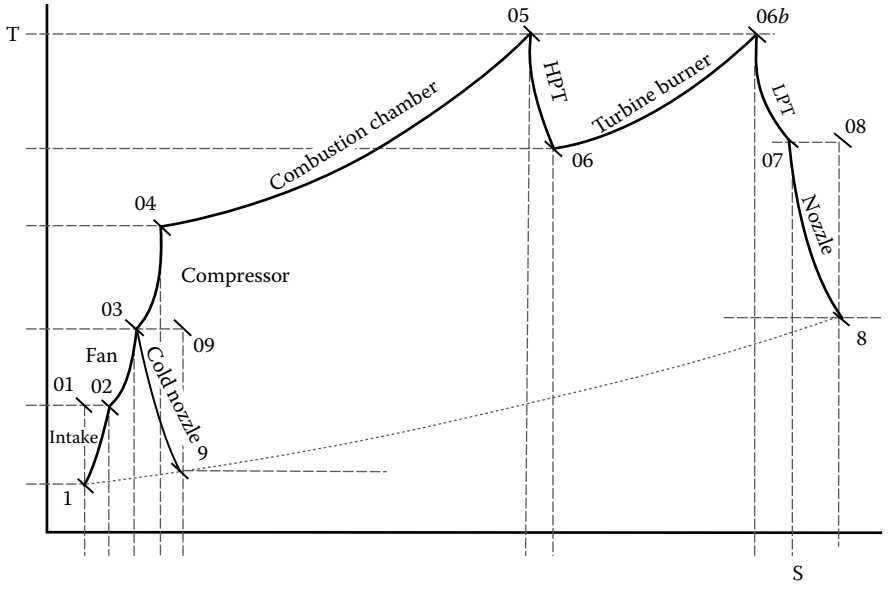


FIGURE 17.16
T–S diagram for a turbofan with turbine burner.

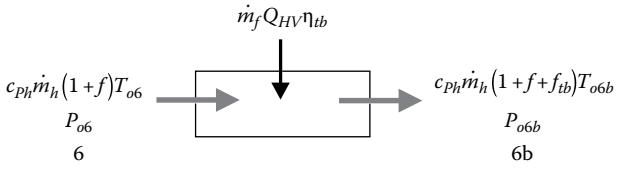


FIGURE 17.17
Main combustion chamber.

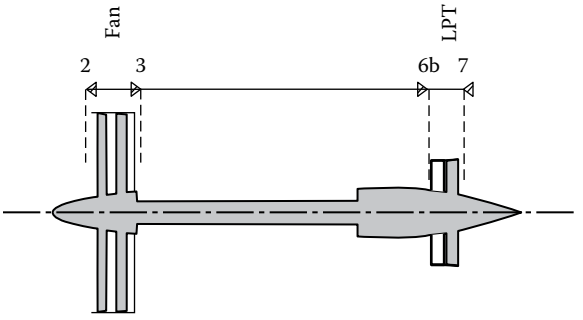


FIGURE 17.18
Low-pressure spool.

Turbine burner "reheat"

$$P_{o6b} = P_{o6} - \Delta P_{otb} = 59.48 \text{ kPa}$$

$$T_{o6b} = TIT = 1500 \text{ K}$$

$$f_{tb} = \frac{\dot{m}_{ftb}}{\dot{m}_h} = \frac{T_{o6b} - T_{o6}}{\eta_{tb} Q_{HV} - C_{ph} T_{o6b}} C_{ph}\left(1 + f\right) = 0.008$$

LPT: From balance of low-pressure spool

$$C_{pc}\dot{m}_h\left(1+\beta\right)\left(T_{o3} - T_{o2}\right) = C_{ph}\eta_m\left(\dot{m}_h + \dot{m}_f\right)\left(T_{o6b} - T_{o7}\right)$$

$$T_{o7} = T_{o6b} - \frac{C_{pc}\left(1+\beta\right)\left(T_{o3} - T_{o2}\right)}{C_{ph}\eta_m\left(1+f\right)} = 1392 \text{ K}$$

$$P_{o7} = P_{o6b}\left[1 - \frac{1}{\eta_T}\left(1 - \frac{T_{o7}}{T_{o6b}}\right)\right]^{\gamma_h/\gamma_h - 1} = 42.76 \text{ kPa}$$

Hot nozzle

$$T_8 = T_{o7}\left[1 - \eta_{hN}\left(1 - \left[\frac{P_\infty}{P_{o7}}\right]^{\gamma_h - 1/\gamma_h}\right)\right] = 883 \text{ K}$$

$$V_8 = \sqrt{2C_{ph}\left(T_{o7} - T_8\right)} = 1081 \text{ m/s}$$

Cold nozzle

$$T_9 = T_{o3}\left[1 - \eta_{cN}\left(1 - \left[\frac{P_\infty}{P_{o3}}\right]^{\gamma_c - 1/\gamma_c}\right)\right] = 224.4 \text{ K}$$

$$V_9 = \sqrt{2C_{pc}\left(T_{o3} - T_9\right)} = 298 \text{ m/s}$$

Performance: Thrust

$$T = \dot{m}_h \beta V_9 + \dot{m}_h \left(1 + f + f_{tb}\right) V_8 - \dot{m}_h \left(1 + \beta\right) V_\infty$$

$$\frac{T}{\dot{m}_h} = BV_9 + \left(1 + f + f_{tb}\right) V_8 - \left(1 + B\right) V_\infty = 1108 \text{ N} \cdot \text{s/kg}$$

$$TSFC = \frac{\dot{m}_{f-total}}{T} = \frac{f_{total}}{T/\dot{m}_h} = 0.000030595 \text{ kg}/\left(\text{N} \cdot \text{s}\right) = 0.11 \text{ kg}/\left(\text{N} \cdot \text{h}\right)$$

Comments: From these results, adding one inter-turbine burner led to

1. Increase of specific thrust by 16.5%
2. Increase of thrust specific fuel consumption by 12%

However, this increase in thrust force has a drawback in increased fuel burn.

Example 17.4

An ultra-high bypass ratio UHBPR two-spool turbofan engine has the same module efficiencies and pressure drops as in Example 17.3 as well as a fan pressure ratio of

$$\pi_f = 1.4 \text{ and a bypass ratio of } \beta = 15,$$

for a range of overall pressure ratio $\pi_o = 5 - 30$ and a range of TIT = 1250 – 1600 K.

Plot the TSFC against the specific thrust (with respect to the core flow rate) for different TITs and overall pressure ratios.

Solution

The same equations and procedure followed in Example 17.3 are used here. The final results are plotted in Figure 17.19.

17.2.4 Double-Bypass/Three-Stream Turbofan

The advanced performance of "sixth-generation" combat aircraft requires the adoption of variable-cycle, or adaptive engine, technology. The future fighter will be required to fly farther than today's aircraft and require more speed and power when engaging the enemy. Longer-range and subsonic loiter require lower fuel burn and good cruise efficiency, while higher thrust for supersonic dash demands larger cores and much higher operating temperatures, neither of which is good for fuel burn or stealth [18].

To solve this conundrum and combine both capabilities in one propulsion system, the Adaptive Engine Technology Development Program was adopted by the U.S. military. This generated the adaptive versatile engine technology (ADVENT) engine; see Figure 17.20. In this engine, the high-pressure core exhaust and the low-pressure bypass streams of a conventional turbofan are joined by a third, outer flowpath of both standard bypass duct and core that can be opened and closed in response to flight conditions. The bypass ratio ranges from 0.3 to 5.0 [19,20].

For takeoff, the third stream is closed off to reduce the bypass ratio. This sends more of the airflow through the high-pressure core to increase thrust [21]. For cruising, the third

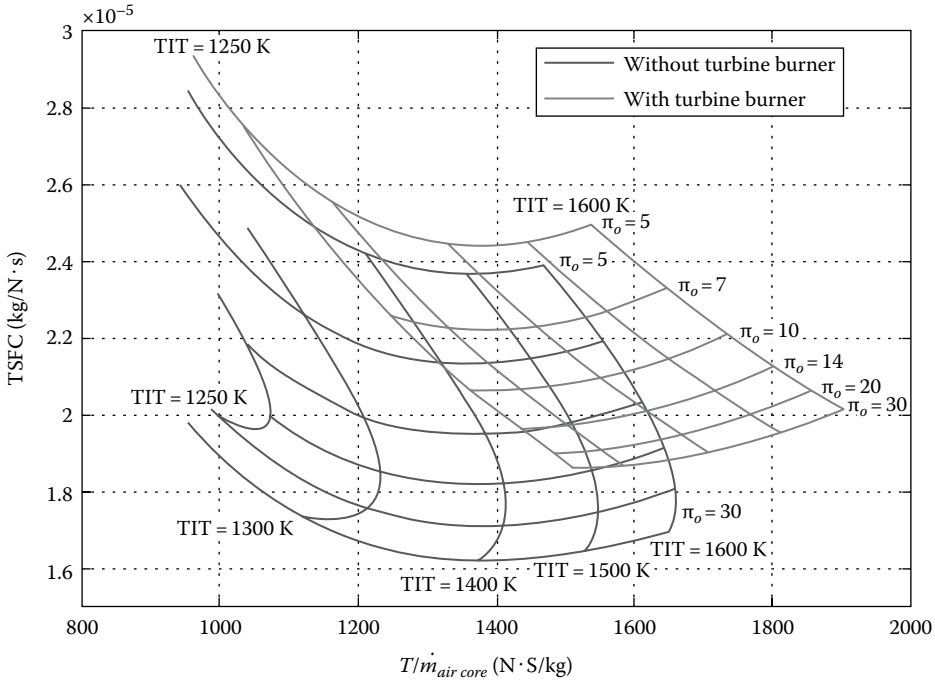


FIGURE 17.19
Performance map for a UHBPR turbofan engine with and without inter-turbine burner.

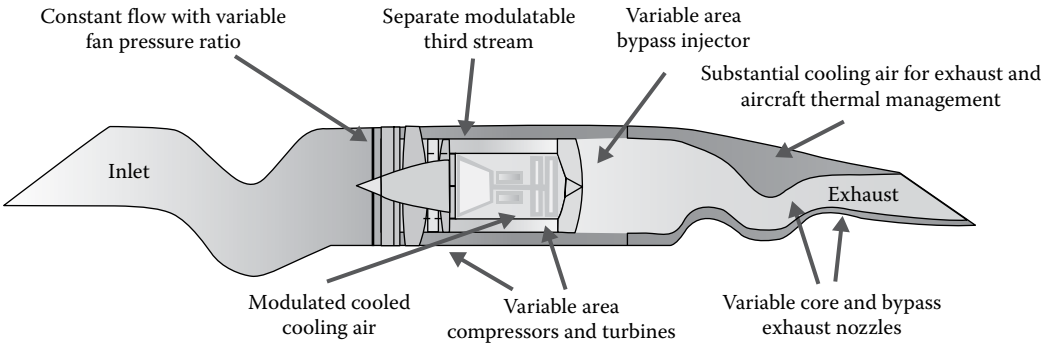


FIGURE 17.20
General Electric ADVENT three-stream turbofan engine.

bypass stream is opened to increase the bypass ratio and reduce fuel consumption and increase propulsive efficiency.

This third duct will be opened or closed as part of a variable cycle to transform the engine from a strike aircraft one to a transport type one. If the duct is open the bypass ratio will increase, reducing fuel burn and increasing the subsonic range by up to 40%, leading to 60% longer loiter times on the target [22].

If the ducts are closed, additional air is forced through the core and HPC, enabling thrust and speed to increase and providing world-class supersonic performance.

The ADVENT engine uses an array of variable geometry devices to alter dynamically the fan pressure ratio and overall bypass ratio—the two key factors influencing specific fuel consumption and thrust. The fan pressure ratio is changed by using an adaptive, multistage fan. This increases the fan pressure ratio to fighter-engine performance levels during takeoff and acceleration, and in cruise it lowers it to airliner-like levels for improved fuel efficiency.

The ADVENT Program aimed at cutting combat-engine SFC by 25% compared with early 2000 baseline fighter engines. It also developed methods for modulating cooling air that was itself cooled, and newer, simpler exhaust system designs.

ADVENT engine architecture displays a cold section composed of two fans (each has one stage) and an HPC; see Figure 17.20. The first fan is driven by an LPT and the second fan by an IPT. The second fan's discharge is sent to the engine core and the inner bypass duct. Core air is compressed by the seven axial compressors, increasing the pressure by a ratio of approximately 30:1. Compressed air is fed to the annular combustor. Combustion gases are fed to the single stage, axial, HPT, then to the IPT and LPT. The HPT drives the compressor and the accessory drive. After passing through the inner duct the inner bypass air serves to cool the engine core as it passes around it and it also reduces the temperature of the gases in the jet nozzle. The gases are accelerated and expanded through the convergent–divergent nozzle. The rest of the air that passes the first fan is sent to the outer bypass duct which it passes until it reaches the convergent nozzle, which accelerates the air providing more thrust.

GE's ADVENT designs are based on new manufacturing technologies like 3D printing of intricate cooling components and superstrong but lightweight ceramic matrix composites. These allow the manufacture of highly efficient jet engines operating at temperatures above the melting point of steel.

17.2.5 3D Printing as the Future of Manufacturing Aircraft and Aircraft Engines

3D printing is an additive manufacturing technique that lifts the constraints of traditional manufacturing processes and gives designers the ability to grow practically any shape. Thus, it enables the use of fully optimized lightweight designs that do not sacrifice performance. Consequently, the *use of additive manufacturing is the basis for optimizing an existing aircraft engine module*.

A laboratory at GE Aviation's Additive Development Center outside Cincinnati focused on developing additive manufacturing. This next-generation technique can make complex 3D structures by melting metal powder layer upon layer. In contrast to traditional machining methods that typically cut parts out of larger pieces to get to a finished shape, additive manufacturing uses lasers to fuse thin layers of metal on top of each other to build parts from the ground up. This advanced technique means less material waste and more complex parts that can be built precisely to work efficiently inside a machine.

17.3 Aviation Environmental Issues

17.3.1 Introduction

Noise and emission are the critical issues that concern mankind's development and welfare. Noise is generated by transport and industrial activities on land and in the air. It directly affects the health of exposed humans and wildlife. Consequently, environmental authorities

are concerned with noise mapping as well as developing and implementing action plans to reduce exposure in large cities and locations close to major transport infrastructure.

Aircraft engines emit various pollutants of which carbon dioxide (CO_2) is the most significant greenhouse gas influencing climate change. Other pollutants include nitrogen oxide (NOx) that can lead to the formation of other air pollutants that harm health, such as particulates and ground-level ozone. They also cause the acidification and eutrophication of waters and soils.

Particulate matter (PM) is one of the most harmful pollutants for health, as it penetrates into sensitive regions of the respiratory system and can cause or aggravate cardiovascular and lung diseases and cancers.

Emissions from combustion processes are CO_2—carbon dioxide, H_2O—water vapor, NOx—nitrogen oxide, HCs—hydrocarbons, CO—carbon, SOx—sulfur oxide, particulates (in solid or liquid that form as a result of incomplete combustion), and O_3—ozone.

Emissions from a typical two-engine jet aircraft during a 1 h flight with 150 passengers are 8500 kg carbon dioxide, 30 kg nitrogen oxides, 2.5 kg sulfur dioxide, 2.0 kg carbon monoxide, 0.4 kg hydrocarbons, and 0.1 kg of PM and soot.

In order to improve fuel efficiency, engine pressures and temperatures are increased, which can lead to higher NOx emissions. However, more stringent NOx limits have been periodically introduced in order to mitigate the potential trade-off with market-driven fuel burn improvements. Consequently, NOx emissions have been reduced by 15% within the last 4 years.

The regulatory limits for smoke, HC, and CO have not changed from their original value as they are considered to provide adequate environmental protection. These regulatory limits provide a design space for aircraft engine technology within which both NOx emissions and fuel burn can be reduced.

17.3.2 Sustainable Alternative Fuels

17.3.2.1 Introduction

While the uptake of sustainable alternative fuels in the aviation sector is still in its infancy, it is assumed that these fuels will play a large role in reducing aviation greenhouse gas emissions in the coming decades. The European Advanced Biofuels Flightpath provides a roadmap to achieve an annual production rate of two million tons of sustainably produced biofuel for civil aviation by 2020.

This sustainable biofuel is crucial for providing a cleaner source of fuel to power the world's fleet of aircraft and help the billions of people who travel by air each year to lower the impact of their journey on our planet.

Biofuel is produced from renewable biological resources [23] such as plant or animal material (rather than traditional fossil fuels like coal, oil, and natural gas). It absorbs carbon dioxide from the atmosphere as the plant matter (biomass) is grown, which is then released back into the atmosphere when the fuel is burnt.

The two most common feedstock sources for making biofuels are plants rich in sugars and bio-derived oils.

There are two types of biofuels:

1. First-generation biofuel
2. Second-generation biofuel

Crops that are rich in sugars (such as sugar cane) or starch (such as corn) can be processed to release their sugar content to make ethanol, which can be used directly as a petroleum

substitute or additive. These fuels, known as first-generation biofuels, are not suitable for use in aircraft. Bio-derived oil, from plants such as corn, soybeans, algae, jatropha, halophytes, and camelina, is processed and can either be burned directly or converted by chemical processes to make high-quality jet and diesel fuels. These are known as second-generation biofuels and can be used for aviation [24–26].

17.3.2.2 Potential Second-Generation Biofuel Feedstocks

Jatropha: This is a plant that produces seeds containing inedible lipid oil that can be used to produce fuel. Each seed produces 30%–40% of its mass in oil. Jatropha can be grown in a range of difficult soil conditions, including arid and otherwise non-arable areas, leaving prime land available for food crops. The seeds are toxic to both humans and animals and are therefore not a food source.

Camelina: This is primarily an energy crop, with high lipid oil content.

Algae: This is potentially the most promising feedstock for producing large quantities of sustainable aviation biofuel. These microscopic plants can be grown in polluted or salt water, deserts, and other inhospitable places. One of the biggest advantages of algae for oil production is the speed at which the feedstock can grow. It has been estimated that algae produces up to 15 times more oil per square kilometer than other biofuel crops. Another advantage of algae is that it can be grown on marginal lands that are not used for growing food, such as on the edges of deserts.

Halophytes: These are salt marsh grasses and other saline habitat species that can grow either in salt water or in areas affected by sea spray where plants would not normally be able to grow.

17.3.2.3 Key Advantages of Second-Generation Biofuels for Aviation

1. *Environmental benefits*: Reduction in CO_2 emissions across their life cycle.
2. *Diversified supply*: Offer a viable alternative to fossil fuels and can substitute traditional jet fuel with a more diverse geographical fuel supply through nonfood crop sources.
3. *Economic and social benefits*: Provide a solution to the price fluctuations related to fuel cost volatility that faces aviation. Biofuels can provide economic benefits to parts of the world, especially developing nations that have unviable land for food crops and that is suitable for second-generation biofuel crop growth.

17.3.2.4 Commercial and Demonstration Flights

Since 2008, a large number of test flights have been conducted, and since American Society for Testing and Materials (ASTM) approval in July 2011, several commercial flights with passengers have also occurred. Examples are given in Table 17.2.

17.3.2.5 Biofuels for Aviation Economic Viability

First, fossil fuels are forecast to become increasingly scarce and as a result will become more expensive. Second, advanced biofuels that stem from sustainable feedstocks will become less expensive as the relevant science and business models mature.

TABLE 17.2

Data for Some Flights using Biofuels

Date	Operator	Platform	Biofuel	Notes
February 2008	Virgin Atlantic	Boeing 747	Coconut and Babassu	Flight between London and Amsterdam (20% biofuels in one engine)
December 2008	Air New Zealand	Boeing 747	Jatropha	A 2 h flight (50–50 mixture of biofuel with Jet A-1)
January 2009	Continental Airlines	Boeing 737	Algae and jatropha	Houston's George Bush Intercontinental Airport completed a circuit over the Gulf of Mexico at 38,000 ft (12,000 m)
January 2009	Japan Airlines	Boeing 747	Camelina, jatropha, and algae	Japan Airlines conducted a one and a half hour flight with one engine burning a 50/50 mix of Jet-A and biofuel from the camelina plant
June 2010	EADS	Diamond D42	Algae	Occurred at an air show in Berlin in June 2010.
November 2010	TAM	Airbus 320	Jatropha	A 50/50 biofuel blend of conventional and jatropha oil
June 2011	Honeywell	Gulfstream G450	Camelina	The first transatlantic biofuels flight using a 50/50 blend of camelina-based biofuel and petroleum-based fuel
October 2011	Air China	Boeing 747-400	Jatropha	The flight used Chinese grown jatropha oil from PetroChina; 2 h in duration above Beijing and used 50% biofuel in one engine
January 2012	Etihad Airways	Boeing 777-300ER	Vegetable cooking oil	Etihad Airways conducted a biofuel flight from Abu Dhabi to Seattle using a combination of traditional jet fuel and fuel based on recycled vegetable cooking oil
March 13, 2013	KLM	Boeing 777-206ER	Used cooking oil	Weekly between John F. Kennedy Airport, United States and Amsterdam, Netherlands (biofuel supplied by SkyNRG)
May 16, 2014	KLM	Airbus A330-200	Used cooking oil	Weekly flights by Airbus A330-200 (Queen Beatrix International Airport, in Oranjestad Aruba and Amsterdam's Netherlands) using biofuel supplied by SkyNRG

It is difficult to project when biofuels might become competitive, but there are strong indications that they will become cost comparable with traditional jet fuel, Jet A-1, by around 2020.

17.4 Unmanned Aircraft Vehicles

17.4.1 Introduction

An unmanned aerial vehicle (UAV) is an aerial vehicle capable of sustained flight without need of a human operator onboard. Its flight is either controlled autonomously by computers in the vehicle or under the remote control of a pilot on the ground or in another vehicle [27].

The history of unmanned aircraft dates back to about AD 200 [28], when used by the Chinese General Zhuge Liang. The name assigned to unoccupied aircraft has changed over the years as viewed by civil and military authorities. Aerial torpedoes, radio controlled,

remotely piloted, remote control, autonomous control, pilotless vehicle, UAVs, and drones are but some of the names used to describe a flying machine absent of humans.

In the last century, UAVs had been around for many years, starting with the Kettering Bug in 1918. In the past decade or so, UAVs have truly demonstrated their military utility, particularly in Desert Storm and the conflicts in the former Yugoslavia [29]. Now, UAVs are extensively used in military applications. They are also employed in several civil applications such as firefighting, surveillance of pipelines, scientific research, public safety and commercial tasks that acquire images of disaster areas, map building, communication relays, search and rescue, traffic surveillance, and so on. UAVs are often preferred for missions that are too "dull, dirty, or dangerous" for manned aircraft.

UAVs have much in common with manned aircraft. However, there are several unique differences as well. These differences often result from operational requirements, for example, the need to take off from remote, short, unprepared airstrips or to fly for long periods at very high altitudes [30]. UAVs often have enhanced performance because they do not have to carry the weight of the equipment and structures required by an aircraft in order to accommodate an aircrew; further, they have a lower aerodynamic drag. Additionally, UAVs benefit from advantageous scale effects associated with smaller aircraft. Moreover, they are not drones, which are a radio-controlled model aircraft used for sport and which remain within sight of the operator. Usually, the operator is limited to instructing the aircraft to climb or descend and to turn left or right. A drone aircraft can fly out of sight of the operator, but has no intelligence; it merely is launched with a preprogrammed mission on a preprogrammed course and a return to base. It does not communicate, and the results of the mission usually are not obtained from it until it is recovered at base.

The following comparison can be made between manned and unmanned aircraft and the control station [30]:

- A UAV incurs 20%–40% of the manned aircraft cost.
- A UAV control station consumes 20%–40% of the manned aircraft.
- The cost of a UAV plus its control station is 40%–80% of the manned aircraft cost.

UAVs are fixed-wing, rotor-wing air vehicles (RUAVs), such as the MQ-8B Fire Scout (see Figure 17.21), or lighter-than-air vehicles that fly without a human on board.

Finally, the key benefits of a UAV are

- Low fuel consumption
- Long endurance
- Easy operation and control
- Wide operation profile
- Low maintenance, robust system
- The longer the mission, the larger the benefit for diesel piston engines in unmanned systems

17.4.2 Categorization of UAV

Various organizations have used different categories to distinguish various types of UAVs. These categories have varied between organizations and at different times even within one



FIGURE 17.21
MQ-8B Fire Scout rotor wing (RUAVs).

organization [31]. These categories are often related to the usage of UAVs (e.g., strategic or tactical) or the organizations using them (corps or platoons) rather than that affect propulsion methods.

17.4.2.1 Based on Function

UAVs typically fall into one of six categories (although multi-role airframe platforms are becoming more prevalent):

1. *Target and decoy*—Providing for ground and aerial gunnery a target that simulates an enemy aircraft or missile
2. *Reconnaissance*—Providing battlefield intelligence
3. *Combat*—Providing attack capability for high-risk missions (UCAV or unmanned or uninhabited combat air vehicle)
4. *Logistics*—UAVs specifically designed for cargo and logistics operations
5. *Research and development*—Used to develop further UAV technologies to be integrated into field deployed UAV aircraft
6. *Civil and Commercial UAVs*—UAVs specifically designed for civil and commercial applications.

17.4.2.2 Based on Range/Altitude

UAVs can be classified into the following types:

- Handheld 2000 ft (600 m) altitude, with about a 2 km range
- Close range/battle field (sometimes identified as LOCAL), 5000 ft (1500 m) altitude, up to 10 km range, and used for reconnaissance, target designation, monitoring, security, surveillance, among other applications

- NATO type 10,000 ft (3,000 m) altitude, up to 50 km range
- Tactical (medium range) 18,000 ft (5,500 m) altitude, about 160 km range
- MALE (medium altitude, long endurance, long range) up to 30,000 ft (9,000 m) and range over 200 km
- HALE (high altitude, long endurance, long range) over 30,000 ft (9,100 m) and indefinite range
- HYPERSONIC high-speed, supersonic (Mach 1–5) or hypersonic (Mach 5+) 50,000 ft (15,200 m) or suborbital altitude, range over 200 km
- ORBITAL low earth orbit (Mach 25+)
- CIS Lunar Earth–Moon transfer
- CACGS Computer Assisted Carrier Guidance System for UAV

Figure 17.22 illustrates Predator B, a MALE UAV, which has the following characteristics. Length: 11 m, wingspan: 20 m, height: 3.81 m, empty weight: 2223 kg, maximum takeoff weight: 4760 kg, fuel capacity: 1800 kg, power plant: 1 × Honeywell TPE331-10 turboprop, 900 hp (671 kW), maximum speed: 482 km/h, cruising speed: 313 km/h, range: 1852 km, endurance: 14 h fully loaded, service ceiling: 50,000 ft (15,240 m), operational altitude: 25,000 ft (7.5 km).

Figure 17.23 illustrates one of the famous HALE UAVs, namely, the Northrop Grumman RQ-4 Global Hawk. This has the following specifications. Length: 14.5 m, wingspan: 39.9 m, height: 4.7 m, empty weight: 6,781 kg, gross weight: 14,628 kg, power plant: 1 × Rolls-Royce F137-RR-100 turbofan engine, 34 kN thrust, maximum speed: 629 km/h, cruise speed: 575 km/h, range: 22,779 km, endurance: 32+ h, service ceiling: 60,000 ft (18,288 m).

As an alternative and in more recent years there has been a push to change the term of "unmanned aircraft" (UA) to "remotely piloted aircraft" (RPA) or remotely piloted vehicles (RPVs). RPAs are categorized into five groups by the U.S. Department of Defense [28] as illustrated in Table 17.3.



FIGURE 17.22
Predator B.



FIGURE 17.23
Northrop Grumman RQ-4 Global Hawk.

TABLE 17.3
Characteristics of Different Groups of UAS

UAS Category	Max Gross Takeoff Weight (lb)	Normal Operating Altitude (ft)	Airspeed (knots)
Group 1	<20	<1,200 above ground level (AGL)	<100
Group 2	21–55	<3,500 AGL	<250
Group 3	<1,320	<18,000 mean sea level (MSL)	Any airspeed
Group 4	>1,320	>18,000 MSL	
Group 5	18,000 MSL		

17.4.2.3 Based on Size

Nano Air Vehicles (*NAVs*): These are proposed to be of the size of seeds and used in swarms for such purposes as radar confusion or ultra-short-range surveillance. They normally have dimensions of less than 5 cm in any direction, an all-up mass (AUM) of less than 10 g, including a payload of 2 g. One example is the Prox Dynamics Picoflyer, which has a rotor diameter of 85 mm with a 10 min endurance and an AUM of 7.8 g.

Micro Air Vehicles (*MAVs*): MAVs are principally required for operations in urban environments, particularly within buildings. It is required to fly slowly and preferably to hover and "perch"; that is, it must be able to stop and sit on a wall or post. Generally, MAVs are launched by hand. They have very low wing loadings, which make them very vulnerable to atmospheric turbulence.

They should be of no more than a 150 mm (6 in.) span/diameter. Although small, they are required to carry a surveillance camera and a means of control and of image transmission. Their use is seen primarily for urban and indoor surveillance.

Mini-Unmanned Air Vehicles (*MUAVs also called SUAS*): These are approximately less than 25 kg. However, they are not as small as MAVs, which are capable of being

hand launched and can operate at ranges of up to about 30 km. The concept of the MUAV system was that it could be back-packed, assembled, and deployed by no more than two persons.

Example: Lockheed Martin Desert Hawk III, all-up-mass: 3.86 kg, mass empty: 2.95 kg, wingspan: 0.32 m, wing area: 0.323 m^2, cruise speed: 92 km/h, endurance: 90 min operating, range up to 15 km, payload mass/volume 0.91 kg/4720 cc, and payload Optical, LLL, or IR TV.

Other UAVs: Another classification for UAVs greatly used in Europe will be described hereafter.

17.4.2.4 European Classifications (EUROUVS)

1. Micro- and mini-UAVs
2. Tactical UAVs—close/short/medium/long range/MALE
3. Strategic UAVs—HALE
4. Special Task UAVs—lethal/decoys/stratospheric/exo-stratospheric

17.4.3 Power Plant of UAV

The power system for a UAV, as for any aircraft, includes an energy source, a means of converting that energy into mechanical energy, and a means of converting that into a lift or thrust force. Three types of engines are found, namely, electric engines, intermittent combustion (IC) engines, and gas turbine engines (turboprop, turbojet, and turbofan).

Unless a jet engine is employed (turbojet or turbofan), a propeller or rotor has to be added to generate thrust or lift force for fixed-wing or rotary-wing UAVs. The great majority of UAVs in operation are powered by internal combustion engines and most of those have piston engines. Table 17.4 lists the different possible power plants for different types of UAVs.

17.4.3.1 Electric Engine

An electric propulsion installation generally consists of an electric motor as a prime mover, wiring, a power controller device, and an energy storage and/or a generation device. Power storage is generally accomplished with a secondary battery. Energy generation is accomplished by means of solar cells or fuel cells. In brief, fuel cells are a promising alternative power source for UAVs. Two of the most promising types of fuel cells for use in aviation are proton exchange membrane fuel cells and solid oxide fuel cells [32].

TABLE 17.4

Power Plants for UAVs

UAV	Engine Type	Power Range (hp)	Power (Thrust)/ Weight
Micro	Lithium-ion batteries + electrical motor	1	Low
Mini	Piston (2 × 2)	1–10	Lowest
TAC, CR	Rotary (Wankel)	20–90	Low
MALE	Piston (4 × 4)	90–250	Low
MALE	Turboprop	250–500	High
HALE/TCUAV	Turbojet/turbofan	Above 500	High

Abbreviations: TAC, Target air controller; CR, close range; TCUAV, train cable unmanned aerial vehicle.

Electric motors convert electrical energy into mechanical energy to drive a propeller, fan, or rotor. The electrical power may be supplied by a battery, a solar-powered photovoltaic cell, or a fuel cell [37]. They have the particular advantage of being the quietest of all the engines and with the smallest thermal signature. The most famous examples for solar-powered photovoltaic cell are the NASA Helios developed from the NASA Pathfinder, NASA Pathfinder Plus, and NASA Centurion. They were built to develop the technologies that would allow long-term, high-altitude aircraft to serve as "atmospheric satellites" to perform atmospheric research tasks as well as serve as communications platforms. AeroVironment, Inc. developed the vehicles under NASA's Environmental Research Aircraft and Sensor Technology (ERAST) program, which had two goals, namely, sustained flight at altitudes near 100,000 ft (30,000 m) and endurance of at least 24 h, including at least 14 of those hours above 50,000 ft (15,000 m) [33]. Power is generated by 10 electric engines (1.5 kW each). Another solar-powered UAV is the SoLong from AC Propulsion [34], which recently flew over 48 h nonstop, and is fueled only by solar energy. The plane sports a wingspan of 4.75 m and weighs 12.6 kg.

A third famous example is the Atlantik Solar designed by ETH Zurich's Autonomous Systems Lab. Its objective is to be the first-ever crossing of the Atlantic Ocean using a solar-powered UAV. It is hand launched, has a wingspan of 5.6 m, and can fly up to 10 days continuously. Its structure is made of lightweight carbon fiber and Kevlar. It is powered by 1.4 m^2 solar panels with Li-ion batteries. Its payload is a digital HD camera, providing live-image transmission. For this power source, battery electric propeller power is constant with speed and altitude.

Micro- and mini-UAVs are powered by batteries that drive electric motors. The Desert Hawk (see Figure 17.24) is a typical example. The flight endurance and speed of such UAV



FIGURE 17.24
Desert Hawk UAV.

systems and the capability of their payload and communication systems are limited. The propulsion systems are compact, portable, low cost, need minimum support equipment, and light enough to be back packed, so they have a place in very short-range operations under relatively benign conditions. Back-up batteries must be carried and regularly charged to ensure an electrical supply.

A hybrid propulsion system might consist of a fossil-fueled engine that generates power for an electric system.

17.4.3.2 Internal Combustion (IC) Engines

IC engines are intermittent combustion engines that burn and exhaust their charge in repeating or intermittent cycles. The three major types of IC engines are as follows:

1. *Spark ignition engine*: The common automotive-type gasoline engine where a throttled homogeneous charge is ignited by a spark plug.
2. *Compression ignition engine*: The common diesel engine in which an unthrottled charge is introduced into the combustion chamber and compressed to a high pressure and temperature. Fuel auto-ignites when injected into the charge.
3. *Assisted ignition engine*: A low compression ratio engine that operates on the heavy fuels common to a diesel engine.

Since the compression ratio is not high enough for auto-ignition, a spark plug is used to assist ignition. Such a lower compression ratio permits a lighter engine structure than true diesel.

IC engines also exist in four main types:

1. Two-stroke (two-cycle) engines
2. Four-stroke engines
3. Rotary engines
4. Turbo-charging and supercharging

A piston engine is coupled to a propeller to generate thrust force for fixed-wing UAVs. Similarly piston engines may be coupled to rotors for rotorcraft types of UAVs (RUAV).

17.4.3.2.1 Two-Stroke and Four-Stroke Engines

There is probably a greater number of two-stroke engines than four-stroke units [35].

Some two-stroke units achieve lubrication by mixing oil with fuel. Others have a separate oil system, as do four-stroke units. Both types can be designed to use petroleum fuels or, with higher compression, to use diesel or other "heavy" fuels. Both types can be equipped, if necessary, with turbo-charging.

The two-stroke unit tends to run hotter than the four-stroke unit and may require more cooling facilities. The four-stroke unit tends to be heavier than the two-stroke unit.

Both types will pay for higher performance and higher fuel efficiency. Moreover, both types may be air cooled or water cooled [36]. A detailed comparison between both types has been discussed previously in Chapter 6.

17.4.3.2.2 Rotary Engines

This type of engine is little used in UAVs. There appear to be no rotary engines below a power rating of about 28 or above 60 kW available for aircraft. The reasons are its low mass/power ratio, high fuel consumption, noise, and high cost of operation.

Reciprocating props combine the engine and the propeller, thereby collocating the power plant and propulsor into a single system. As discussed in Chapter 6, the propeller and engine can be coupled directly or with a gearbox or shaft extension, but they are mechanically a single unit. The propeller can be arranged as a tractor or a pusher. Numerous installation options exist for single and multiple engines integrated as tractors or pushers. There are two advantages to a tractor configuration, namely, higher propeller efficiency due to clean airflow to the propeller, and it is quieter as there is no wake impingement upon the propeller. However, it has also two drawbacks, namely, it can obstruct the payload forward field of regard and preclude missile installation behind the propeller disk. Moreover, the forward engine exhaust and leaked fluids can contaminate payloads such as optical systems and airborne samplers.

17.4.3.3 Gas Turbine Engines

This is an engine operating by the Brayton cycle. It incorporates a gas generator, in which air is compressed in a compressor, before fuel is added and burned in a combustion chamber; finally, the products of combustion expand in a turbine that drives the compressor. The remaining energy in the hot gas is then used to provide shaft power or propulsive thrust. The three major types of aviation gas turbines are as follows:

1. *Turboprop/turboshaft*: As discussed in Chapter 6, a turboprop engine couples the gas generator turbine (or free power turbine) to a propeller that develops the thrust force necessary for propelling the aircraft. Moreover, a turboshaft couples one turbine (either the gas generator or free power) to any other propulsor (like a rotor).
2. *Recuperative turboshaft*: As discussed earlier in this chapter, in this category heat is extracted from the exhaust gases and used to add heat to the compressed air prior to combustion. Thus, the temperature of the air entering the combustion chamber is elevated and thus saves fuel.
3. *Turbojet/turbofan*: Both types develop thrust force by accelerating gases leaving the turbine(s) through a nozzle as discussed in Chapters 4 and 5. However, in turbofan engines a part of the sucked air is slightly compressed in the fan, bypasses the combustion chamber, and is exhausted through a second cold nozzle.

17.4.3.4 Engine Characteristics

The primary engine characteristics are weight, power, and specific fuel.

1. *Weight*: For a power range of less than 100 hp, mostly electric and spark ignition engines are used. Electric engines have the least weight, while spark ignition engine follow in second place. For a power range greater than 100 hp, turbine engines have the smallest weight and spark/assisted ignition engines are heavier. The heaviest is the diesel engine.
2. *Power*: Electric engines have the smallest power as well as a low power to weight ratio. Spark ignition gasoline engines are advantageous for a small power range. Moreover, two-stroke air-cooled type engines provide simplicity and lightweight in smaller sizes. However, they are less durable, require frequent overhauls, and

emit dirty exhaust. As outlined in Table 17.4, they have the lowest power to weight ratio. Diesel engines develop high power but their power to weight ratio is very poor. Turbine engines are available in greater power and have the highest power to weight ratio.

3. *Specific fuel consumption*: Generally, a lower specific consumption implies high efficiency. Concerning brake specific fuel consumption, four shaft engines can be compared [35], namely, SI gasoline, CI diesel, turboshaft, and recuperative turboshaft. For power less than 100 hp, the best engine is the CI diesel followed by the SI gasoline, recuperative turboshaft, with turboshaft being the worst.

Adding recuperators to turboshaft engines will improve its fuel consumption. However, it will increase its weight, cost and complexity.

Example 17.5

A small UAV is powered by an internal combustion engine. Thrust is generated by a propeller of diameter 1.8 m. When aircraft speed is 55 m/s it produces a thrust of 2070 N under standard sea-level conditions. Calculate the velocity of the slip stream far behind the propeller and the ideal efficiency of the propeller.

Solution

Diameter of propeller = d = 1.8 m
Free stream velocity = 55 m/s
Thrust

$$T = \dot{m}_a\left(V_j - V_f\right)$$

Air mass flow rate

$$\dot{m}_a = \rho\pi\frac{D^2}{4}\left(\frac{V_j + V_f}{2}\right)$$

$$T = \rho\pi\frac{D^2}{4}\left(\frac{V_j + V_f}{2}\right)\left(V_j - V_f\right) = \rho\pi\frac{D^2}{8}\left(V_j^2 - V_f^2\right)$$

$$V_j = \sqrt{\frac{8T}{\rho\pi D^2} + V_f^2} = \sqrt{\frac{8\times 2100}{1.225\times\pi\times 1.8^2} + 55^2} = 66.12 \text{ m/s}$$

Ideal propeller efficiency

$$\eta_p = \frac{2V_f}{V_f + V_j} = \frac{2\times 55}{55 + 66.12} = 90.82\%$$

Example 17.6

A UAV flies with a velocity of 79.2 km/h at an altitude of 300 m. It has a total drag coefficient for all parts equal to 0.02 and a wing area of 0.7 m^2.

A three-bladed propeller of diameter 30 cm is directly coupled to the piston engine that rotates at 9000 rpm. The performance of the propeller is illustrated in Figure 17.25. Determine the minimum power of the piston engine to drive the propeller.

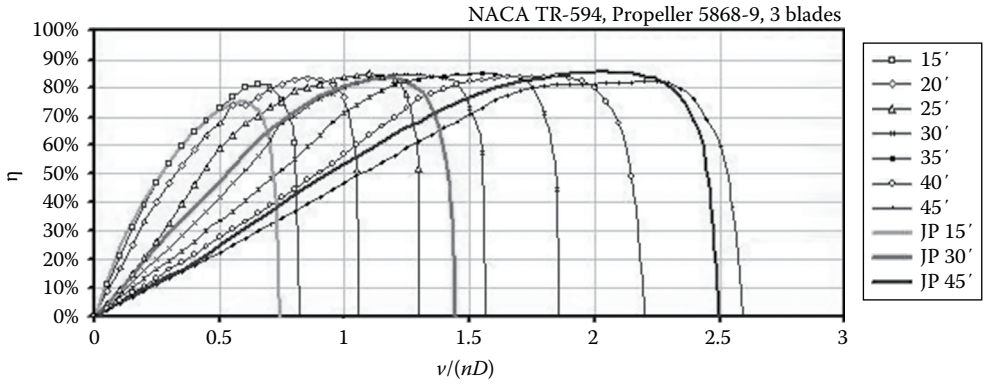


FIGURE 17.25
Characteristics of a three-bladed propeller.

Solution

From atmospheric tables at 300 m, the air density is

$$\rho = 1.1901 \text{ kg/m}^3$$

With flight speed of $V_{cruise} = 79.2$ km/h = 22.0 m/s and drag coefficient $C_D = 0.02$, the drag force on UAV is calculated as

$$D = \frac{1}{2}\rho V^2 S C_D = \frac{1}{2} \times 1.1901 \times 22^2 \times 0.7 \times 0.02 = 3.23 \text{ N}$$

Thrust required (T_r) = total drag on UAV (at cruising altitude)

$$T_r = D = 3.23 \text{ N}$$

The power required to drive the UAV is P_r and is calculated as

$$P_r = T_r \times V_{cruise} = 3.23 \times 22 = 70.96 \text{ W} = 0.1 \text{ hp}$$

To evaluate the required shaft power (P_{shaft}) for the engine, we must first choose a propeller type and determine its efficiency from Figure 17.25.

For a propeller diameter of 30 cm and a rotational speed of 3000 rpm, the advance ratio J is calculated as

$$J = \frac{V}{nD} = \frac{22}{9000 \times \left(\frac{2\pi}{60}\right) \times 0.3} = 0.08$$

Then assuming that a blade angle equals 15 degrees, the propeller efficiency $\eta_{pr} = 0.15$ (max)

$$\text{The required shaft power } \left(P_{shaft}\right) = \frac{P_r}{\eta_{pr}} = \frac{0.1}{0.15} = 0.67 \text{ hp}$$

So the selected engine must have a shaft power equal to or greater than 0.67 hp at 9000 rpm.

Problems

17.1 A two-spool turbofan engine is operating by the Brayton cycle. The low-pressure spool is composed of a fan and LPC driven by an LPT. The HPC is driven by the HPT; cycle overall pressure ratio ($\pi_{OPR} = 26$), fan pressure ratio ($\pi_f = 1.57$), while the pressure ratio of the LPC ($\pi_{LPC} = 1.53$). Fan mass flow rate ($\dot{m}_a = 180$ kg/s). Bypass ratio ($\beta = 5.44$). The maximum cycle temperature is 1500 K. Consider a cruise flight condition at an altitude of 10.0 km and flight Mach number = 0.86. Fuel lower heating value ($Q_{HV} = 45{,}000$ kJ/kg). Consider the following efficiencies: $\eta_f = \eta_{LPC} = \eta_{HPC} = \eta_{LPT} = \eta_{HPT} = 0.9$, $\eta_b = 0.96$, $\eta_n = \eta_{fn} = 1$.

Flow properties at different modules are

$$\gamma_{air} = 1.4, \quad \gamma_{gas} = 1.33, \quad C_{pc} = 1.005 \text{ kJ/kg}, \quad C_{pt} = 1.05 \text{ kJ/kg}$$

We need to calculate the following:

1. For a conventional Brayton cycle
   a. Fuel mass flow rate $\dot{m}_f$
   b. Combustion chamber heat addition $\dot{q}_{in}$
   c. Cycle thermal efficiency η_{th}
   d. Engine thrust
   e. TSFC
2. Consider an intercooler with effectiveness ($x = 0.8$) installed between the LPC and HPC where the air leaving the fan is used for cooling in the intercooler. With the same cycle temperature limits
   a. Recalculate as in (1)
   b. Comment

17.2 A two-spool HBPR turbofan engine is fitted with an intercooler between the LPC and HPC. A recuperator is installed within the nozzle, where hot gases leaving the LPT are used to heat the air leaving the HPC prior to entering the combustion chamber to reduce fuel consumption.

At ground operation ($P_a = 1.0$ bar and $T_a = 288$ K), it has the following data:

$$\dot{m}_a = 540 \text{ kg/s}, \quad \beta = 8.0, \quad \pi_f = 1.3, \quad \pi_{LPC} = 1.2, \quad \pi_{HPC} = 10.0,$$

$$TIT = 1500 \text{ K}, \quad Q_R = 45 \text{ MW/kg}$$

Intercooler efficiency = recuperator efficiency = 60%.

Assuming that the air inlet speed in the intake is 60 m/s, module efficiencies are $\eta_f = \eta_{LPC} = \eta_{HPC} = 0.9$, $\eta_b = 0.96$, $\eta_{LPT} = \eta_{HPT} = 0.92$, $\eta_n = \eta_{fn} = 0.95$, and the pressure drop in the intake and combustion chamber is 3%. Assume no pressure drop in the recuperator.

Calculate

1. Fuel mass flow rate
2. Thermal efficiency
3. If the same turbofan engine was not fitted with *intercooler* and *recuperator*, recalculate the fuel mass flow rate and thermal efficiency. What is the contribution of intercooler and recuperator?

17.3 Consider an unmixed two-spool short-duct turbofan engine operating at sea level at a Mach number of zero. The ambient conditions are $T_\infty = 288.15$ K and $P_\infty = 101.325$ kPa.

An ITB is installed between the HPT and LPT. Modules have the following characteristics:

$$\dot{m}_a = 200 \text{ kg/s}, \quad \beta = 1.0, \quad \pi_f = 2.3, \quad \pi_{LPC} = 2.4, \quad \pi_{HPC} = 8.4,$$
$$\text{TIT} = 1400 \text{ K}, \quad T_{0-ITB} = 1350 \text{ K}, \quad Q_R = 43.1 \text{ MW/kg}$$

Component efficiencies and pressure losses for the engine modules are listed in Table 17.5.

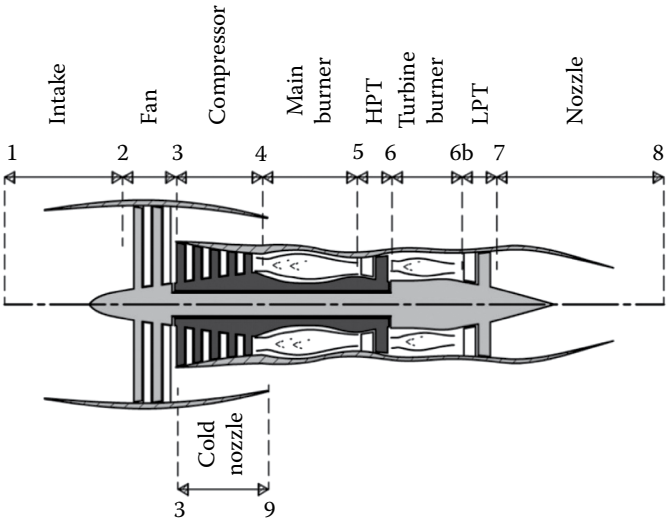


FIGURE P17.3

TABLE 17.5

Characteristics of Different Modules

Intake	$\eta_I = 0.92$, $\pi_i = 0.99$
Fan	$\eta_F = 0.91$
Compressors	$\eta_{LPC} = 0.92$, $\eta_{HPC} = 0.93$
Main burner	$\eta_{cc} = 0.99$, $\pi_{cc} = 0.98$
Inter-turbine burner	$\eta_{ITB} = 0.99$, $\pi_{ITB} = 0.97$
Turbines	$\eta_{HPT} = 0.92$, $\eta_{LPT} = 0.91$, $\eta_m = 0.99$
Nozzle	$\eta_{HN} = 0.96$, $\eta_{CN} = 0.95$

We need to plot the TSFC for different values of overall pressure ratio and TIT.

1. Operative inter-turbine burner:
   a. Calculate the thrust force.
   b. Calculate the total burnt fuel.
   c. Calculate the thermal efficiency.
2. Inter-turbine burner is shut down:
   a. Calculate the thrust force and the change in its value compared to operative inter-turbine burner.
   b. Calculate the thermal efficiency and change in its value compared to operative inter-turbine burner.

17.4 In a conventional turbofan engine, fuel is burned in the main combustor. You are required to investigate the inter-turbine burner concept in which combustion is continued inside the turbine.

The engine is a two-spool, unmixed, high bypass turbofan with the following data:
Flight conditions: T_a = 288 K, P_a = 1 bar
Bypass ratio = 8
TIT = 1500 K and maximum temprature (operative *a*/*b*) T_{06} = 1900 K
Fuel heating value Q = 45 MJ/kg

Component		**γ**
Diffuser	$r_d = 0.98$	1.4
Fan	$\eta_f = 0.88$, $\pi_f = 1.75$	1.4
LPC	$\eta_{LPC} = 0.89$, $\pi_{LPC} = 55$	1.4
HPC	$\eta_{HPC} = 0.90$, $\pi_{HPC} = 6$	1.4
Burner	$\eta_b = 0.98$, $r_b = 0.98$	1.33
HPT	$\eta_{HPT} = 0.92$	1.33
LPT	$\eta_{LPT} = 0.9$	1.33
Shaft	$\eta_m = 0.99$	
Hot gases nozzle	$\eta_{nozzle} = 0.95$	1.33
Fan nozzle	$\eta_{Fan_nozzle} = 0.97$	1.4

Calculate the specific thrust and the specific fuel consumption of the turbofan engine for the two cases (with and without inter-turbine burner) and state your conclusions.

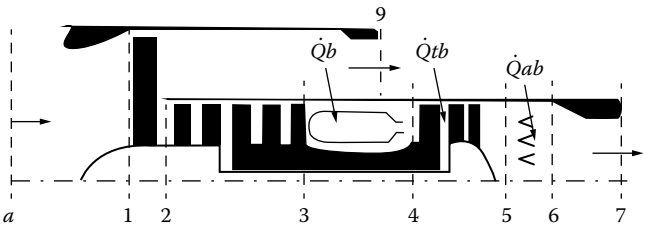


FIGURE P17.4

17.5 A UAV flies with a velocity of 90 km/h at an altitude of 600 m. It has a total drag coefficient for all parts equal to 0.05 and a wing area of 1.7 m^2.

A three-bladed propeller of diameter 30 cm is directly coupled to the piston engine that rotates at 16,000 rpm. The performance of the propeller is illustrated in Figure 17.25. Determine the minimum power of the piston engine to drive the propeller.

References

1. R. Andriani, F. Gamma, and U. Ghezzi, Main effects of intercooling and regeneration on aeronautical gas turbine engines, *46th AIAA/ASME/SAE/ASEE Joint Propulsion Conference and Exhibit*, Nashville, TN, July 28, 2010.
2. C.F. McDonald and C. Rodgers, Heat exchanged propulsion gas turbines: A candidate for future lower SFC and reduced emission; Military and Civil Aeroengines, GT2009-59156, *Proceedings of ASME Turbo Expo 2009: Power for Land, Sea and Air GT2009*, Orlando, FL, June 8–12, 2009.
3. G. Wilfert, J. Sieber, and A. Rolt, New environmental friendly aero-engine core concepts, ISABE-2007-1120, Beijing, China, 2007.
4. http://www.newac.eu/uploads/media/NEWAC_Flyer_01.pdf.
5. W.A. Sirignano and F. Liu, Performance increases for gas turbine engines through combustion inside the turbine, *Journal of Propulsion and Power*, 144, 111–118, January–February 1999.
6. W.A. Sirignano, D. Dunn-Rankin, F. Liu, B. Colcord, and S. Puranam, Turbine burners: Flame holding in accelerating flow, *AIAA 2009-5410, 45th AIAA/ASME/SAE/ASEE Joint Propulsion Conference and Exhibit*, Denver, CO, August 2–5, 2009.
7. http://www.compositesworld.com/articles/composites-in-commercial-aircraft-engines-2014-2023.
8. http://www.bdl.aero/en/bdl-reports-en/aircraft-noise-report.
9. G. Hao and W. Zhan-xue, Effects of intercooling and recuperation on turbofan engine performance, *2011 International Conference on Electronic and Mechanical Engineering and Information Technology*, August 12–14, 2011, pp. 2482–2485.
10. R. Andriani, U. Ghezzi, and F. Gamma, Parametric thermal analysis of regenerated and intercooled turboprop engine, *AIAA 2011-6099, 47th AIAA/ASME/SAE/ASEE Joint Propulsion Conference & Exhibit*, San Diego, CA, July 31–August 3, 2011.
11. A.M. Rolt and N.J. Baker, Intercooled turbofan engine design and technology research in the EU framework 6 NEWAC programme, ISABE-2009-1278.
12. V-STAR™ pocket guide VTOL-swift tactical aerial resource, http://frontlineaerospace.com/wp-content/uploads/2015/11/VSTAR_Guide_web_2_4.pdf.
13. M.R. Vanco, W.T. Wintucky, and R.W. Niedzwiecki, An overview of the small engine component technology (SECT) studies, NASA USAAVSCOM Technical Memorandum 88796, *22nd Joint Propulsion Conference*, Huntsville, AL, June 16–18, 1986.
14. C.F. McDonald, Low cost recuperator concept for microturbine applications, ASME Paper No. 2000-GT-167, ASME, New York, 2000.
15. A. Muley and B. Sunden, Advances in recuperator technology for gas turbine systems, ASME Paper No. IMECE2003-43294, ASME, New York, 2003.
16. W.A. Sirignano, D. Dunn-Rankin, F. Liu, B. Colcord, and S. Puranam, Turbine burners: Flameholding in accelerating flow, *AIAA 2009-5410, 45th AIAA/ASME/SAE/ASEE Joint Propulsion Conference and Exhibit*, Denver, CO, August 2–5, 2009.
17. F. Liu and W.A. Sirignano, Turbojet and turbofan engine performance increases through turbine burners, *Journal of Propulsion and Power*, 17, 695–705, 2001.
18. G. Norris, GE details sixth-generation adaptive fighter engine plan, Issue of aviation week and space technology, February 2–15, 2015.

19. http://www.flightglobal.com/news/articles/full-advent-engine-tests-meet-fuel-heat-goals-ge-408182/.
20. http://www.flightglobal.com/news/articles/general-electric-completes-advent-core-testing-382542/.
21. S.T. Ford, Aerothermodynamic cycle design and optimization method for aircraft engines, MSc thesis, Georgia Institute of Technology, Atlanta, GA, December 2014.
22. R.J. Simmons, Design and control of a variable geometry turbofan with an independently modulated third stream, PhD dissertation, The Ohio State University, Columbus, OH, 2009.
23. European Aviation Agency, European aviation environmental report 2016, TO-01-15-323-EN-N. http://ec.europa.eu/transport/sites/transport/files/modes/air/aviation-strategy/documents/european-aviation-environmental-report-2016-72dpi.pdf.
24. Air Transport Action Group (ATAG), *Beginner's Guide to Aviation Biofuels*, 2nd edn., Geneva, Switzerland, 2011.
25. Aviation Fuel Efficiency Technology Assessment, Prepared for *The International Council on Clean Transportation*, Washington, DC, December 26, 2015.
26. F. Cha, Desert plants and green diesel: Meet the jet fuels of the future, CNN, January 2014. http://edition.cnn.com/2014/01/23/travel/boeing-biofuel/.
27. C. Howard, Boeing, South African Airways Partner to develop, implement sustainable aviation biofuel, Intelligent Aerospace, October, 2013. http://www.intelligent-aerospace.com/articles/2013/10/boeing-biofuel.html.
28. ICAO's circular 328 AN/190: Unmanned Aircraft Systems (PDF), ICAO, Retrieved February 3, 2016.
29. R.K. Barnhart, S.B. Hottman, D.M. Marshal, and E. Shappee (Eds.), *Introduction to Unmanned Aircraft Systems*, CRC Press, Taylor & Francis Group, Boca Raton, FL, 2012.
30. B. Holder, *Unmanned Air Vehicles: An Illustrated Study of UAVs*, Schiffer Military/Aviation History, Atglen, PA, 2001.
31. D.W. Pepper, L.F. Dube, W. McElroy, and A.M. Frappier, Design and fabrication of a thin-filmed solar-powered unmanned aerial vehicle, *First Aviation Engineering Innovations Conference, AEIC-2015-01*, Luxor, Egypt, March 21–22, 2015.
32. AC propulsion technology—SoLong UAV. Retrieved August 10, 2007, from http://www.acpropulsion.com/solong/, February 2, 2006.
33. J. Gundlach, *Designing Unmanned Aircraft Systems: A Comprehensive Approach*, AIAA Educational Series, American Institute of Aeronautics and Astronautics, Reston, VA, December 2011.
34. NASA, NASA dryden fact sheet—Solar-power research. Retrieved June 02, 2008, from http://www.nasa.gov/centers/dryden/news/FactSheets/FS-054-DFRC.html, February 10, 2005.
35. R. Austin, *Unmanned Aircraft Systems UAVs Design, Development and Deployment*, John Wiley & Sons Ltd., Chichester, U.K., 2010.
36. A. Cifone and W. Parsons, The development and operational challenges of UAV and UCAV airbreathing propulsion. In: *Development and Operational Challenges of UAVs for Military and Civil Applications*, von Katrman Institute, Lecture Series, RTO-EN-9, AC/323(AVT)TP/24, April 2000.
37. K.M. Spencer, Investigation of potential fuel cell use in aircraft, IDA Document D-5043, https://www.ida.org/~/media/Corporate/Files/Publications/IDA_Documents/SED/2014/D-5043.pdf, December 2013.

Section III

Rocket Propulsion



Space Shuttle Atlantis takes flight on its STS-27 mission.
(Courtesy of NASA Image and Video Library.)


Taylor & Francis
Taylor & Francis Group
http://taylorandfrancis.com

18

Introduction to Rocketry

18.1 Introduction

In Chapter 1, propulsion systems were classified as either airbreathing or non-airbreathing (rocket) engines. All engines discussed so far belong to the category of airbreathing engines. In this chapter, non-airbreathing engines (or rockets) will be discussed.

A rocket is a propulsive device that produces a thrust force F on a vehicle by ejecting mass at a high relative velocity. Non-airbreathing engines carry an oxidizer as well as fuel on board.

Rocket propulsion engines have the following advantages over airbreathing engines [1]:

1. The thrust of rockets is essentially independent of speed, whereas the operation of airbreathing engines does depend on flight speed. Some types of airbreathing engines like ramjets, scramjets, turbojets, and turbofans can operate at supersonic speeds. Ramjets as well as afterburning turbojets and turbofan engines have a maximum Mach number of 4.0, while scramjet engines can operate at higher Mach numbers (around 5–7). Rockets, however, can operate at very high speeds in the hypersonic range.
2. Rockets have no altitude ceiling (or depth floor). They can function within and outside the atmosphere, while airbreathing engines are limited to altitudes of about 100,000 ft or less.
3. The thrust/frontal area is the largest of all known propulsion systems.
4. The thrust/weight of the engine is the largest of all known propulsion systems.

Rockets can be classified into chemical and nonchemical rockets. Chemical rockets can be further categorized into many types. The most famous of them are liquid, solid, and hybrid types. Nonchemical rockets are also classified into several types including electrical, thermal, solar, and nuclear. Some flight vehicles use a dual-mode engine, which has an airbreathing mode (either ramjet, turbojet, or turbofan engine) and a non-airbreathing or rocket mode. One of the latest applications is the SABRE engine [2].

Schematics of rocket engines are shown in Figure 18.1. Chemical rockets consist of a container or containers for a propellant, a combustion chamber (frequently identified as a thrust chamber), an exhaust nozzle, igniter, navigational equipment, payload, etc. Chemical rocket propellants are either solid or liquid. In a liquid system, the fuel and oxidizer are separately stored and are sprayed under high pressure (1900–5500 kPa) into the combustion chamber, where burning takes place that produces gases at high temperature (around 4000 K). The products of combustion expand through the nozzle at high velocities, which in turn generates very high thrust.

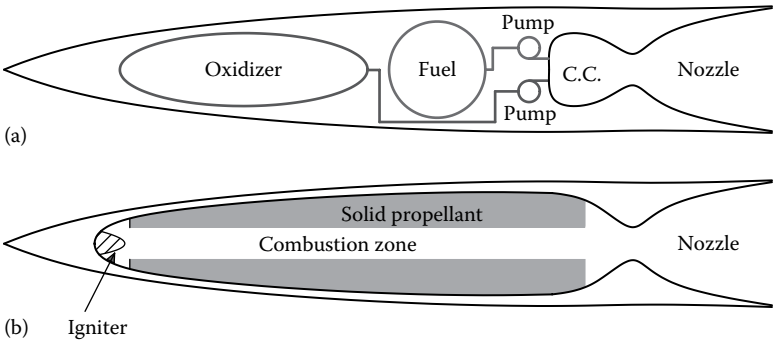


FIGURE 18.1
Basic parts of a rocket engine: (a) liquid-propellant rocket and (b) solid-propellant rocket.

When solid propellants are used, both fuel and oxidizer are contained in the same casing or combustion chamber. The propellant charge is called the "grain" and contains the entire chemical ingredients for complete burning. Once ignited, it usually burns smoothly at a nearly constant rate on the exposed surface of the charge. Because there are no feed systems or valves such as those that are in liquid units, solid-propellant rockets are relatively simple in construction.

Thus, the earliest rockets were solid-fuel rockets powered by gunpowder; they were used in warfare by the Chinese, Indians, Mongols, and Arabs, as early as the thirteenth century [2].

18.2 History

18.2.1 Important Events

Different books, publications, and websites give timelines of rocket history. These include Sutton [3], Turner [4], Yahya [5], NASA [6], and von Braun [7]. A brief history of important dates is given here:

400 BC	Archytas, a Greek, lived in Southern Italy and used the reaction principle to fly a wooden pigeon.
AD 67	Hero, another Greek, lived in Alexandria, Egypt, and invented the rocket principle. His aeolipile machine worked on the reaction principle (discovered later on by Isaac Newton) and steam power (also discovered later by James Watt).
First century AD	The Chinese used a simple form of gunpowder made from saltpeter, sulfur, and potassium nitrate (saltpeter). They put the gunpowder in bamboo tubes and tossed them in fire, mostly for fireworks in religious and other festive celebrations.
AD 970	Feng Jishen, a Chinese, is considered the real inventor of rockets.
1232	The Chinese repelled the Mongol invaders during the battle of Kai-Keng by a barrage of "arrows of flying fire." These fire arrows were a simple form of a solid-propellant rocket. A tube, capped at one end, contained gunpowder. The other end was left open and the tube was attached to a long stick. Wan Hu tried to fly in a rocket propelled chair, but died in the explosion before taking off.

(*Continued*)

1200s	Tatars and Moors used rockets in their invasion of Europe.
1275	Kublai Kahn used rockets in the Japanese invasion.
1650	A Polish artillery expert, Kazimierz Siemienowicz, published a series of drawings for a staged rocket.
1700s	Hyder Ali and his son Tipoo Sultan, of Mysori, India, used rockets against the British invasion of India.
1642–1727	Sir Isaac Newton laid the scientific foundations for modern rocketry through his three laws of motion.
1806	William Congreve's incendiary rocket used black powder, an iron case, and a 16-ft guide stick. The British used Congreve rockets in 1806 to attack Napoleon's headquarters in France.
1807	Congreve directed a rocket attack against Copenhagen; approximately 25,000 rockets were fired.
1875–1935	Konstantin Tsiolkovsky, a mathematician, developed rocket equations and wrote on multistage rockets, artificial satellites, and space travel.
1923	Herman Oberth, a Romanian, published a book on rocket travel into outer space.
1926	Robert Goddard, an American, launched the first liquid-propellant (gasoline and liquid oxygen LOX) rocket [8]. He was granted 214 patents on liquid-fueled rocket engines. He conducted practical experiments in rocketry and developed the single-stage and multistage rocket engines for both rocket and jet-assisted takeoff (JATO) aircraft in 1945.
1930	Wernher von Braun assisted Oberth in his early experiments in testing a liquid-fueled rocket with about 15 lb of thrust.
1942	The V-2 was the world's first long-range ballistic missile; see Figure 18.2. The liquid-propellant rocket was developed during the Second World War in Germany as a "vengeance weapon," designed to attack Allied cities as a form of retaliation for the ever-increasing Allied bombing effort against German cities. The V-2 rocket was also the first man-made object to enter the fringes of space.
(Oct 4, 1957)	The Soviet Union stunned the world by launching an Earth-orbiting artificial satellite called *Sputnik I*, which also made the first successful reentry.
(Nov 3, 1957)	The Soviets launched the satellite *Sputnik II* carrying a dog named Laika on board.
(Jan 31, 1958)	The Jupiter-C rocket carried the U.S. satellite *Explorer I* into space.
(Apr 12, 1961)	Yuri Alekseyevich Gagarin (Russian) was a Soviet pilot and cosmonaut. He was the first human to journey into outer space, when his Vostok spacecraft completed an orbit of the Earth.
(May 5, 1961)	Alan Shepard was the first American astronaut and traveled inside a Mercury space capsule on top of a Redstone rocket.
1965	NASA's Scout rocket (a four-stage solid rocket booster) carried the Explorer 27 scientific satellite.
(Mar 1965)	Virgil I. Grissom and John W. Young traveled into orbit inside a Gemini spacecraft mounted at the top of a Titan rocket. The spacecraft reached an orbit ranging from 161 to 225 km.
(Jul 20, 1969)	Apollo 11 was launched by a Saturn V rocket (111 m high) from the Kennedy Space Center and landed the first humans on the Moon, the Americans Neil Armstrong and Buzz Aldrin, on July 20, 1969, at 20:18 UTC. Armstrong became the first to step onto the lunar surface 6 h later on July 21 at 02:56 UTC.
(Aug 17, 1970)	Venera-7 (USSR) was launched for Venus, which landed on December 15.
(Dec 7, 1972)	Apollo 17 took a three-man crew to the Moon, who landed on December 11, 1972, had a total stay of 75 h, and traversed 26 km on the lunar surface.
(Sep 5, 1975)	A Titan III Centaur rocket carried Voyager 1, the first interplanetary spacecraft.
(Sep 21, 1984)	NASA's rocket Delta lifted the Galaxy-C communication satellite into space.
(Apr 5, 1990)	The Pegasus air-launched space booster roars toward orbit following its release from a NASA B-52 aircraft.
(Dec 2, 1992)	NASA astronauts are launched into space onboard the Space Shuttle. The Shuttle consists of a winged orbiter that climbs into space as a rocket, orbits Earth as a satellite, and lands on a runway as an airplane.
(1981–2011)	A total of 135 missions from 1981 to 2011 of the Space Shuttle; see Figure 18.3.

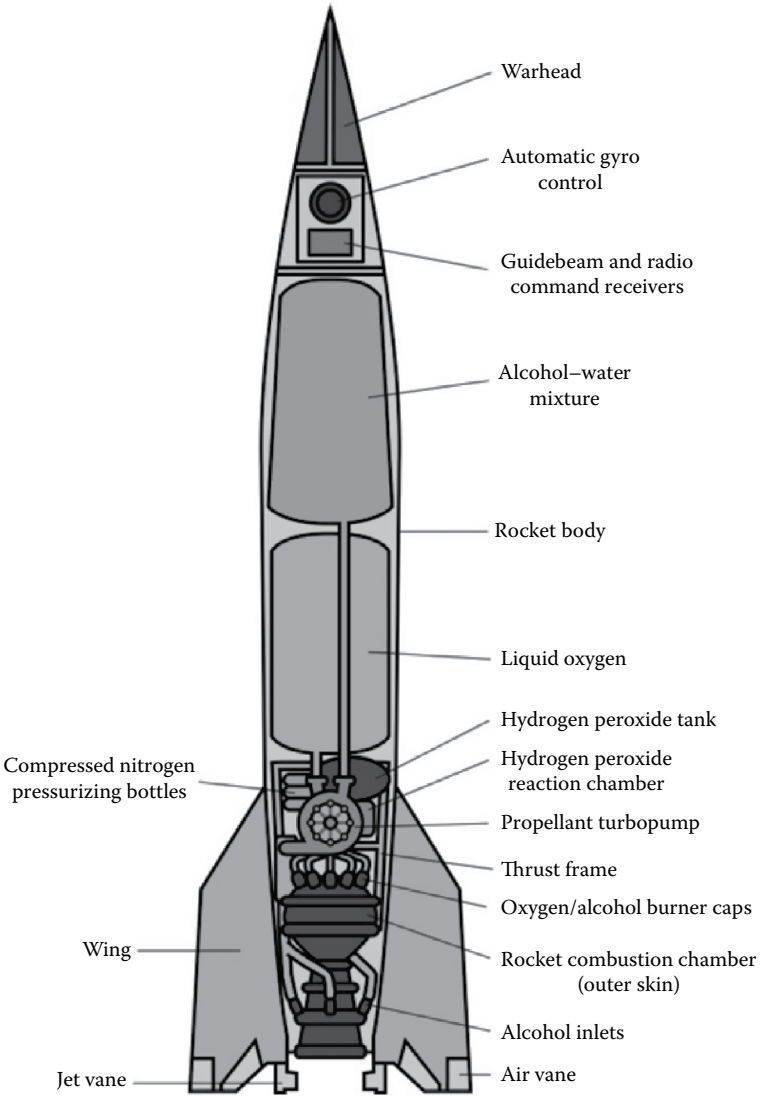


FIGURE 18.2
V2 rocket.

18.2.2 Recent and Future Plans for Rocket and Space Flights (2014 and Beyond)

- NASA's Dawn spacecraft to enter orbit around Ceres
- NASA's MAVEN spacecraft to enter orbit around Mars
- NASA to send three small landers to the surface of the Moon
- United States to launch the Next Gen NEAR mission aiming to land on an asteroid
- European Rosetta spacecraft to enter orbit around comet Churyumov-Gerasimenko



FIGURE 18.3
Space shuttle.

- India's unmanned probe to enter orbit around Mars
- The Rosetta spacecraft to drop the Philae lander on the surface of comet Churyumov-Gerasimenko
- Japan to launch Hayabusa-2 spacecraft on a mission to a carbon-rich asteroid
- Bigelow and Boeing companies to start assembling a 690 m^3 space station in Earth orbit. NASA to launch a visible-light coronagraph to search for planets outside the solar system
- Brazil to conduct its fourth attempt to orbit a satellite with a domestically built vehicle from Alcantara
- Russia to launch the Luna-Glob spacecraft toward the Moon
- China to test fly the Chang Zheng 5 (CZ-5) rocket, capable of delivering 25 tons into low Earth orbit

18.3 Missile Configuration

18.3.1 External Configuration

Missiles must have a feasible and efficient external configuration, which has three main parts (sections) with some auxiliary components, as shown in Figure 18.4. The three main parts are

1. Nose section (fore-body)
2. Mid-section
3. Tail section (after-body)

The auxiliary components are

- Canards, on the fore-body
- Wings (with or without ailerons) on the mid-section
- Fins (with or without elevators or radars) on the tail section

There are some important factors affecting missile configuration such as

- Missile requirements (range, accuracy, speed)
- Structural loads (axial loads, bending loads, shear forces, thermal loads)
- Maneuverability and response
- Development and production cost

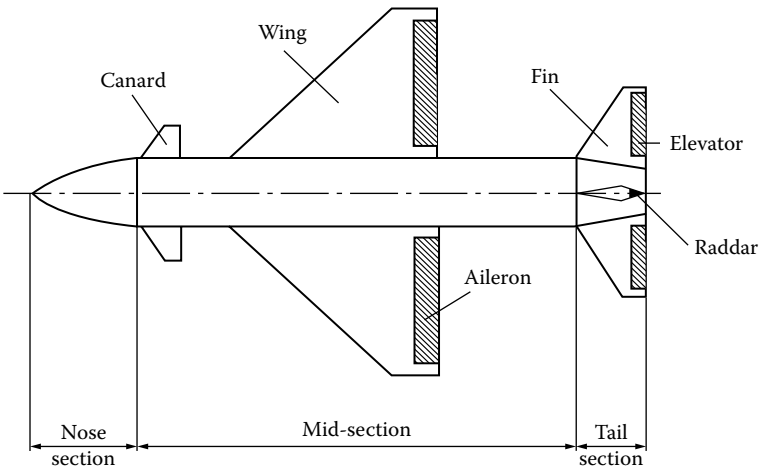


FIGURE 18.4
Missile external configuration.

18.3.2 Main Sections of a Missile Body

18.3.2.1 Nose Section (Fore-Body)

The nose is the most forward part of the missile. It may contain a warhead or a guidance system (target seeking and tracking devices, for guided missiles). There are different nose configurations, as illustrated in Figure 18.5:

Conical	Power series
Ogival	Parabolic series
Hemisphere	Von Karman series

The Conical Nose (Figure 18.5a) is represented by a linear equation as

$$\frac{r}{r_o} = \frac{x}{x_o} \tag{18.1}$$

The Ogive Nose (Figure 18.5b) has a plane-form shape as an arc of a circle; its equation is

$$R = \frac{1}{2r_o}\left(x_o^2 + r_o^2\right) \tag{18.2}$$

The Power Series Nose (Figure 18.5c) is presented by the following equation:

$$\frac{r}{r_o} = \left(\frac{x}{x_o}\right)^n \tag{18.3}$$

where the power (n) is taken to be 0.75 for Newtonian bodies.

The Parabolic Series Nose (Figure 18.5d) is defined by the following equation according to the factor k:

$$\frac{r}{r_o} = \frac{2\left(x/x_o\right) - k\left(x/x_o\right)^2}{2-k} \tag{18.4}$$

where $k = 0$ for the conical nose and $k = 1$ for the parabolic nose.

The Von Karman Series Nose (Figure 18.5e) is derived as

$$\frac{r}{r_o} = \frac{1}{\sqrt{\pi}}\sqrt{\cos^{-1}\left(1 - 2\left(\frac{x}{x_o}\right)^2\right)} \tag{18.5}$$

The Hemisphere Nose is illustrated in Figure 18.5f.

The selection of one of these nose shapes in the missile design depends on the following characteristics:

(a) Drag properties	(e) Minimum radar signature
(b) Missile length	(f) Guidance requirements
(c) Aerodynamic heating	(g) Internal volume
(d) Structural considerations	(h) Cost of production

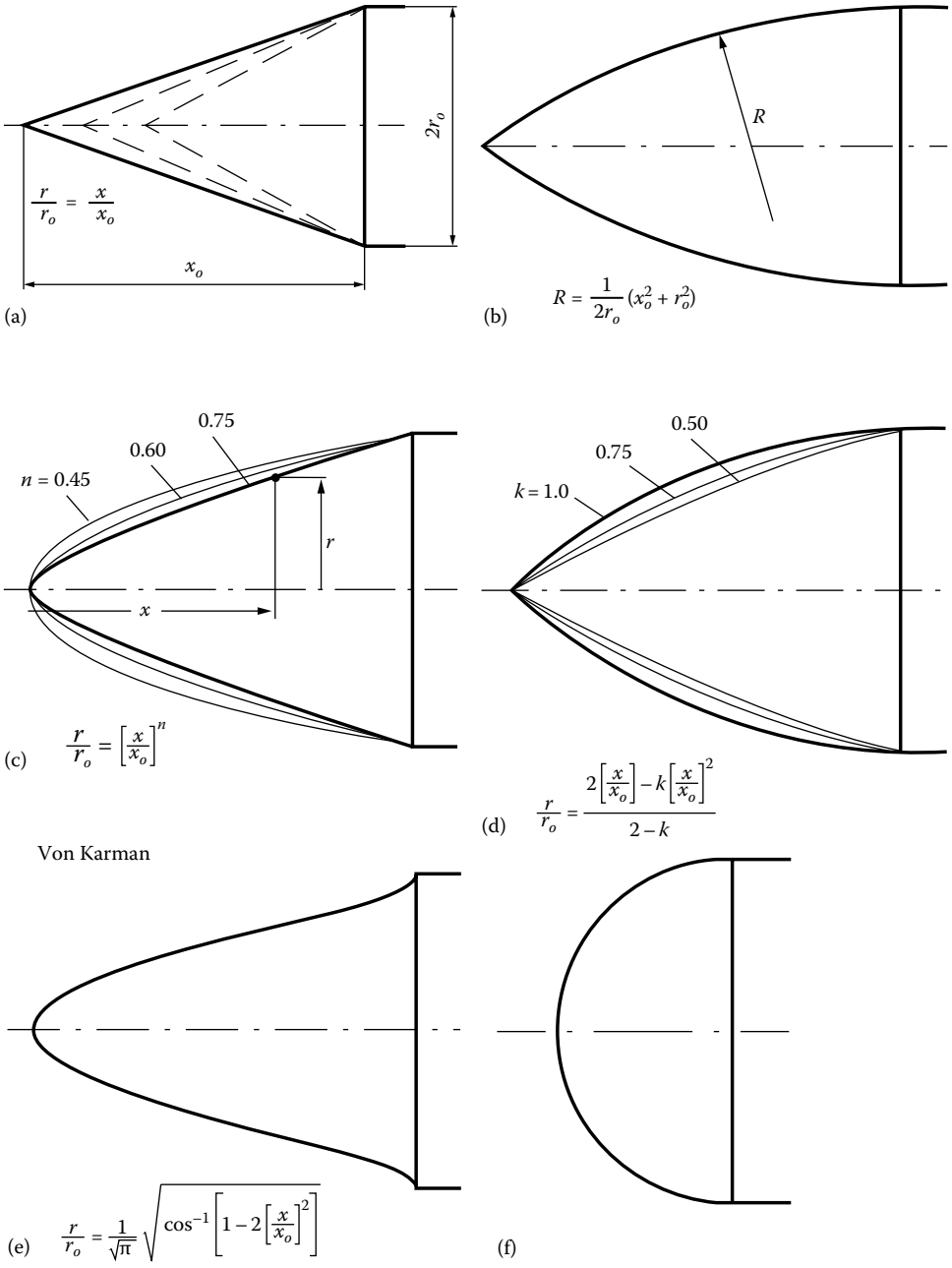


FIGURE 18.5
The most common nose shapes: (a) conical nose, (b) ogival nose, (c) power series, (d) parabolic series, (e) Von Karman, and (f) hemisphere.

Note:

- Conical and ogive shapes of nose are the most common design used in supersonic or higher-speed rockets.
- The conical nose is simple in production while the ogive nose has less drag and contains a larger internal volume.

18.3.2.2 Mid-Section

The mid-section is the principal part of the rocket body. In general, the mid-section takes a cylindrical shape with a circular cross section. It contains some of the main components in addition to the rocket motor. In the case of a winged rocket (fin-stabilized rocket), the wings are assembled on the mid-section.

18.3.2.3 Tail Section

There are different shapes of the tail section, as shown in Figure 18.6.

The selection of one of these tail sections or after-body designs depends on the rocket design requirements, which are summarized as

- Base drag
- Internal volume
- Static stability

Brief highlights of each type are described here.

Conical (*boat*) tails are characterized by

- Lower base drag
- Smaller internal volume
- Negative static stability

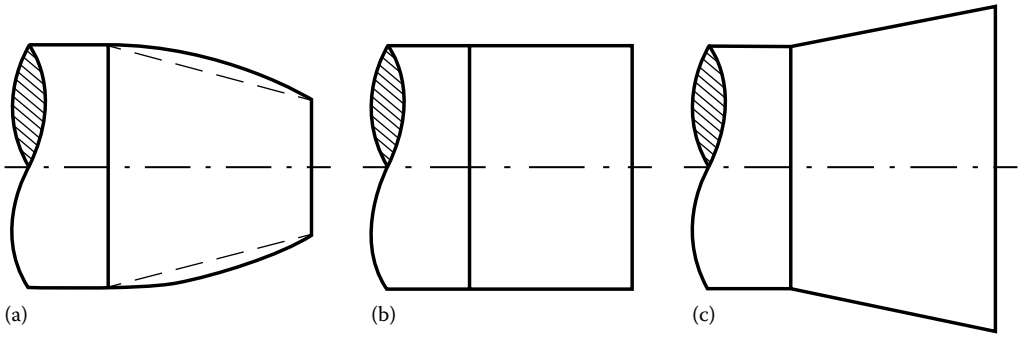


FIGURE 18.6
The most common tail shapes: (a) conical (boat), (b) cylindrical (straight), and (c) flared (skirt).

Cylindrical (*straight*) tails are characterized by

- Large internal volume
- Medium base drag
- Zero static stability

Flared (*skirt*) tails are characterized by

- Greater internal volume
- Greater base drag
- Positive static stability

18.3.3 The Auxiliary Components (Wings, Fins, and Canards)

18.3.3.1 Wings

Wings are the main lifting surfaces in a fin-stabilized rocket (winged rocket). Their task is to produce the required lift force, which depends mainly on the wings' area, thickness, and cross section. According to the wing plane form, wings can be grouped as shown in Figure 18.7.

A rocket may contain two, three, or four wings as presented in Figure 18.8. The control surfaces (movable surfaces) in a wing are called "ailerons" that are used to control the rocket rotation (left or right) and motion (up or down, when the rocket does not have fins) as shown in Figure 18.9.

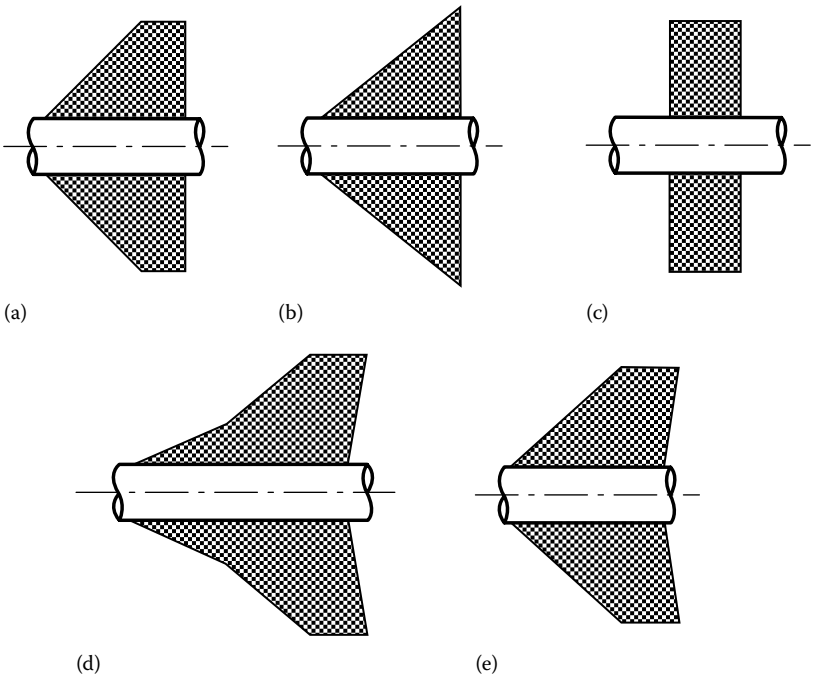


FIGURE 18.7
Common wing plane forms: (a) cropped delta, (b) delta, (c) rectangular, (d) double delta, and (e) straight delta.

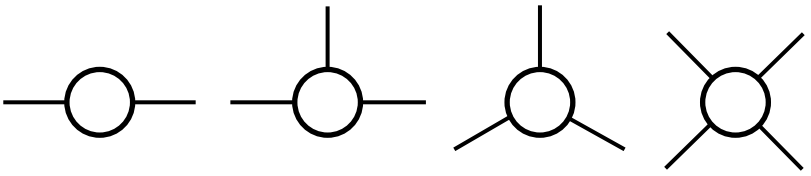


FIGURE 18.8
Rocket with two, three, or four wings.

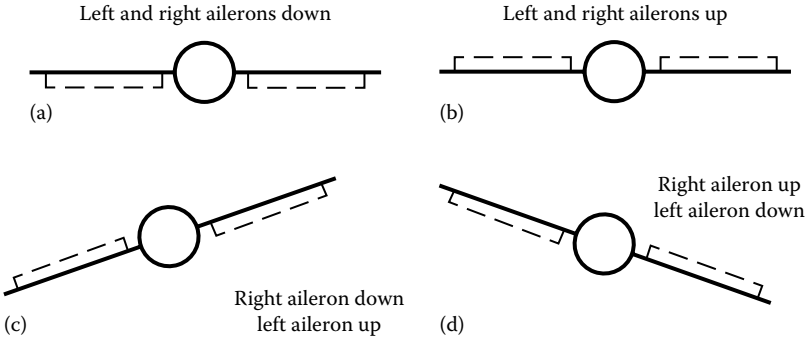


FIGURE 18.9
Aileron positions for different types of motion (two wings): (a) moving up, (b) moving down, (c) left rotation, and (d) right rotation.

The main factors affecting the wing design are

- Required maneuverability
- Structural efficiency
- Maximum possible span
- Rocket Mach number
- Minimum drag
- Stability
- Trim angle

18.3.3.2 Fins

The surfaces in the tail section are called fins. The control surfaces in the horizontal fins are called "elevators" that are used to control the missile motion up or down as illustrated in Figure 18.9. The control surfaces in the vertical fin are called "rudders" that are used to control the missile flight direction left or right, as shown in Figure 18.10a and b. In the case of four wings or fins, all control surfaces are called elevators. Figure 18.11a through d presents the positions of elevators (in four-wing rockets) for different types of direction changing.

The following example shows how to determine the position of the elevators to allow the missile to move upward. When the missile is moving upward, it needs a force on the rear

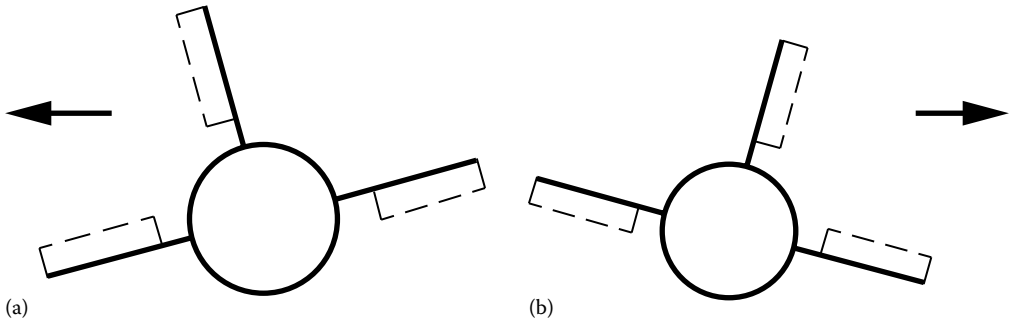


FIGURE 18.10
Rudder positions for direction changing (a) left motion and (b) right motion.

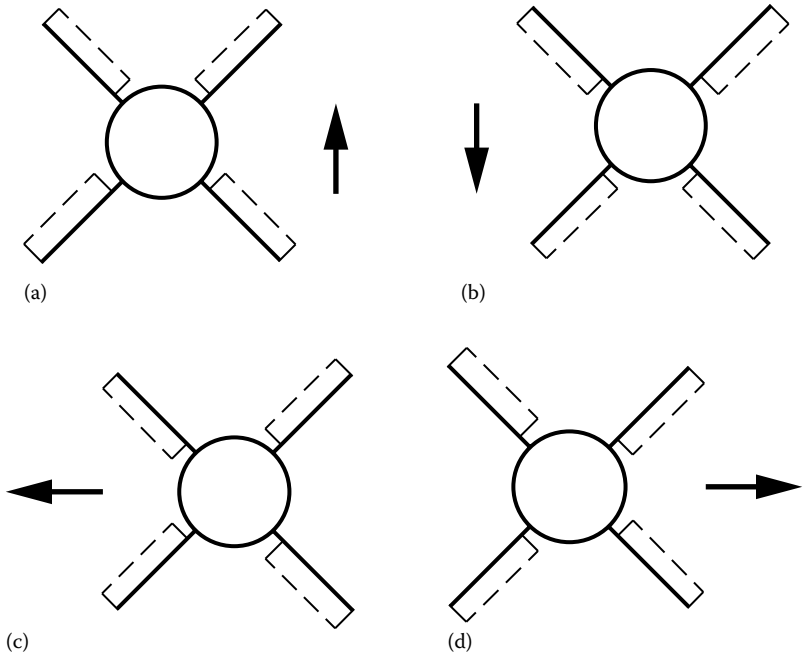


FIGURE 18.11
Control of missile motion by four elevators: (a) upward motion, (b) downward motion, (c) left motion, and (d) right motion.

part in the direction opposite to the direction of movement (down force). The elevator deviation causes a perpendicular force on the fin (or wing) opposite to the direction of deviation; see Figure 18.12.

Each elevator causes an applied force perpendicular to its surface. This applied force is analyzed into two perpendicular components (vertical and horizontal); one of them is required to cause the required motion and another is canceled out by another force (in the opposite direction) by another elevator. The summation of the required forces has to be equal to the required applied force on the rear part to cause the desired motion.

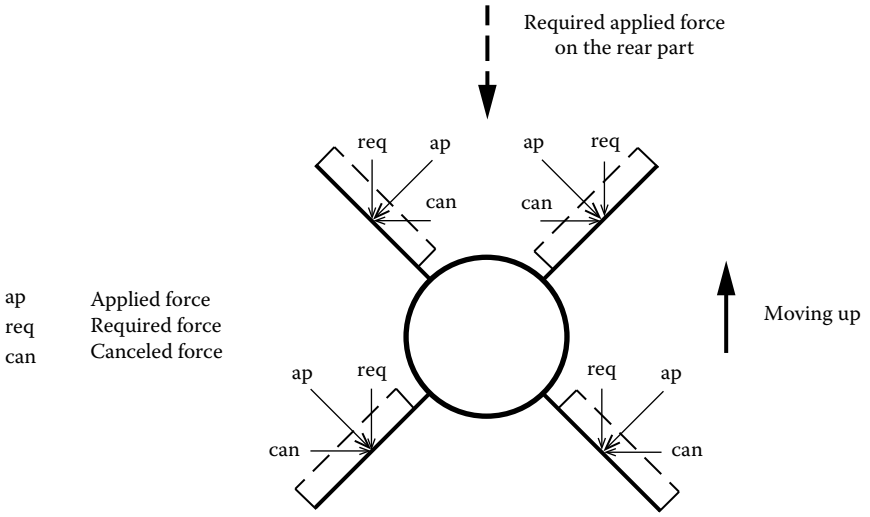


FIGURE 18.12
Analysis of the forces caused by the elevator deviation.

18.4 Classification

Rockets can be classified based on different parameters as described in this section.

18.4.1 Propulsion

Propulsion means "the act of driving forward or away."
Rockets are propelled using one of the following two ways:

1. A rocket engine (motor).
2. A combination of rocket engine and ducted jet engine (such as a ramjet, turbojet, or turbofan engine). A Tomahawk surface-to-surface missile combines a solid-propellant booster rocket for liftoff and a small turbojet for sustained flight.

18.4.2 Energy Source

Energy is generated through one of the following sources:

- Chemical (solid, liquid, and hybrid)
- Solar (solar sail rocket, solar heated rocket)
- Nuclear (nuclear fission rocket, nuclear fusion rocket, photon rocket)
- Electrical

18.4.3 Types of Missiles

- Cruise missile
- Ballistic missile

18.4.4 Launch Mode

A launch mode can be defined as how and in which way the missile will be fired. There are five types of missiles:

1. Surface-to-surface missiles
2. Surface-to-air missile
3. Air-to-surface missile
4. Air-to-air missile
5. Anti-tank missile

Surface-to-surface missiles (SSM) include sea-to-sea missiles, sea-to-surface (coast) missiles, and surface (coast)-to-sea missiles. Surface-to-air missiles include anti-ballistic missiles (ABM).

18.4.5 Range

"Range" means how long a missile will fly to hit the target. As per range, there are five types of missiles:

1. Battlefield short range (up to 150 km)
2. Short range (150–799 km)
3. Medium range (800–2399 km)
4. Intermediate range ballistic (2400–5499 km)
5. Intercontinental ballistic (over 5500 km)

18.4.6 Warheads

"Warhead" means the front part of a missile (or projectile, torpedo, rocket), which contains either the nuclear or thermo-nuclear high explosive system, chemical or biological agents, or inert materials intended to inflict damage.

There are two types of warhead:

1. Conventional
2. Strategic

18.4.7 Guidance Systems

There are eight types:

1. Wire guidance
2. Command guidance
3. Terrain comparison guidance
4. Terrestrial guidance
5. Inertial guidance
6. Beam rider guidance
7. Laser guidance
8. RF and GPS reference

18.4.8 Number of Stages

- Single-stage rockets
- Multistage rockets.

18.4.9 Application

Based on application, rockets are classified as

- Space rockets
- Military rockets (missiles)
- Weather or sounding rockets
- Aircraft propulsion, turbo-rocket engines, ramjet-rocket engines
- Booster rockets
- Sustainer rockets
- Retro rockets

18.4.10 Military Rockets

18.4.10.1 According to Purpose and Use

18.4.10.1.1 Combat Rockets

Combat rockets are used for destroying enemy troops, fortifications, and military equipment. They can be classified as

- Army rockets, including
  - Anti-tank rockets (RPG, Kobra, Shmell, Maljutika, Swingfire, Hot, Milan, Tow)
  - Artillery salvo rockets (130 mm, 132, 240, Grad B, BM21, Sakr36)
  - Tactical rockets (Lona)
  - Operational rockets (Skud-A, Skud-B)
  - Strategic rockets
- Air defense rockets (surface-to-air missiles)
  - SAM-2, -3, -4, -6, -7, Hawk, Crotale, Sparrow.
- Air force rockets
  - Air-to-surface missile (ASM)
    - 57 mm, 80 mm VAP, 68 mm, Hirda 70 mm, 100 mm
  - Air-to-air missile (AAM)
    - K5, K13, Sparrow, Sidewinder
- Naval rockets
  - Sobka, B-15, Otomate, Harpoon

18.4.10.1.2 Auxiliary Rockets

Auxiliary rockets are used as an indirect means for achieving successfully completed military activity. They can be classified into

- Sounding rockets
- Communication rockets (satellites)

- Reconnaissance rockets
- Mine cleaning rockets
- Countermeasure rockets
- Experimental and research rockets
- Training rockets
- Illuminating rockets
- Smoke rockets
- Flying targets for training air-defense units

18.4.10.2 According to the Location of the Launching Site and Target

Location of Launching	Type of Target
Ground (surface)	Tanks
Air (aircraft)	Aircraft
Sea (ships, destroyers, submarines)	Building
	Ships
	Others

18.4.10.3 According to the Main Characteristics

1. Guidance system: guided or unguided
2. Stabilization: fin-stabilized or spin-stabilized rockets

18.5 Rocket Performance Parameters

The main rocket performance parameters are

- Thrust
- Specific impulse
- Total impulse
- Effective exhaust velocity
- Thrust coefficient
- Characteristic velocity

18.5.1 Thrust Force

The thrust force for an airbreathing engine was derived in Chapter 2 and expressed as

$$T = \dot{m}_e u_e - \dot{m}_a u + \left(P_e - P_a\right) A_e$$

Figure 18.13 illustrates the control volume selected in deriving the thrust equation for both airbreathing and non-airbreathing (rocket) engines.

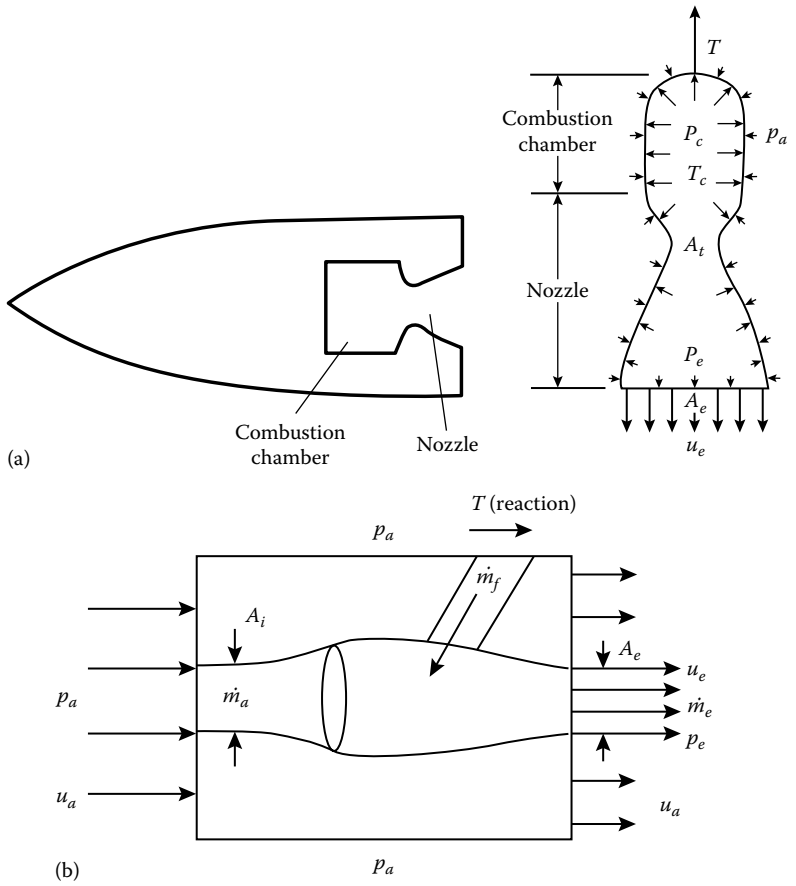


FIGURE 18.13
Control volume for a (a) rocket and (b) airbreathing engines.

The following assumptions are followed for analyzing the flow in an ideal rocket:

- Steady flow of gases within rocket engine, thus mass flow rate through the whole rocket ($\dot{m}$ = constant).
- All the species of the working fluid are gaseous. Any condensed phases (liquid or solid) in the nozzle flow have negligible volume.
- There is no heat transfer across the rocket walls; therefore, the flow is adiabatic.
- The working substance (propellant products) is homogeneous and invariant in composition throughout the rocket chamber and nozzle (thus, they have constant specific heat, specific heat ratio, and molecular weight).
- There is no friction, thus no pressure loss in the combustion chamber.
- The flow in the nozzle is isentropic, thus the total temperature and pressure in the combustion chamber and nozzle are constants.
- The flow in the nozzle is assumed to be one dimensional and exhaust gases exit in an axial direction.

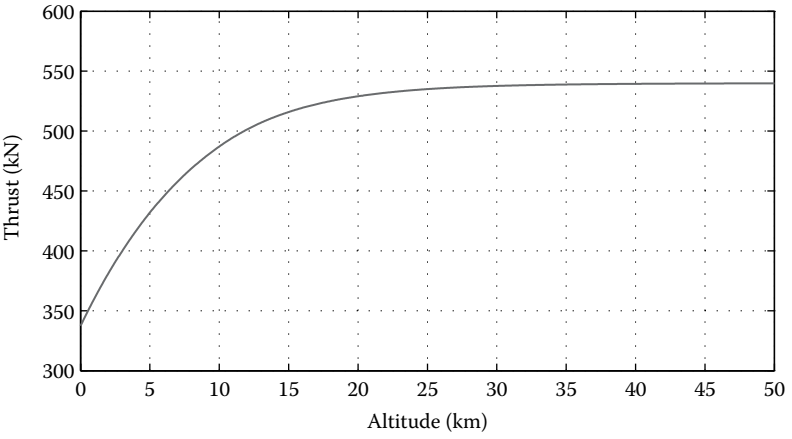


FIGURE 18.14
Variation of thrust with altitude.

For non-airbreathing engines, no inlet air is ingested; thus, the inlet momentum term vanishes ($\dot{m}_a u = 0$). The thrust equation is reduced to the relation

$$T = \dot{m}u_e + \left(P_e - P_a\right)A_e \tag{18.6A}$$

The thrust force is independent of vehicle speed and depends on the atmospheric pressure (P_a) as well as the exhaust parameters, mass flow rate ($\dot{m}$), speed (u_e), and pressure (P_e).

In the vacuum of space ($P_a = 0$) and the thrust is expressed as

$$T = \dot{m}u_e + P_e A_e \tag{18.6B}$$

For a given design of nozzle, the value of the exit pressure (P_e) is fixed. Thus, during flight through the atmosphere, the ambient pressure (P_a) decreases continuously. As a result, the thrust increases with altitude. However, beyond a certain altitude the variation is negligible and the thrust is nearly constant as illustrated in Figure 18.14.

18.5.2 Effective Exhaust Velocity (V_{eff})

The thrust force can be related to the effective velocity (as described earlier in Chapter 2) with

$$T = \dot{m}u_e + \left(P_e - P_a\right)A_e = \dot{m}V_{eff}$$

Thus,

$$V_{eff} = u_e + \frac{\left(P_e - P_a\right)A_e}{\dot{m}} \tag{18.7A}$$

The same equation was derived earlier for airbreathing engines.

The mass flow rate is expressed by

$$\dot{m} = \rho_e u_e A_e$$

$$V_{eff} = u_e \left[1 + \frac{(P_e - P_a) A_e}{u_e (\rho_e u_e A_e)} \right]$$

$$V_{eff} = u_e \left[1 + \frac{(P_e - P_a) A_e}{u_e (\rho_e u_e A_e)} \right]$$

$$V_{eff} = u_e \left[1 + \frac{P_e}{\rho_e} \frac{1}{u_e^2} \left(1 - \frac{P_a}{P_e} \right) \right]$$

$$V_{eff} = u_e \left[1 + \frac{RT_e}{\gamma RT_e} \frac{1}{M_e^2} \left(1 - \frac{P_a}{P_e} \right) \right]$$

$$V_{eff} = u_e \left[1 + \frac{1}{\gamma M_e^2} \left(1 - \frac{P_a}{P_e} \right) \right] \tag{18.7B}$$

The effective velocity ($V_{eff} = u_e$) when ($P_e = P_a$). Generally, in Equation 18.7A, if

$$\frac{(P_e - P_a) A_e}{\dot{m}} \ll u_e$$

Then

$$V_{eff} \cong u_e$$

Example 18.1

A rocket powered by a liquid-propellant rocket motor has the following characteristics:

Thrust force of 500 kN at sea level
Propellant consumption rate = 175 kg/s
Gas exit static pressure = 60.0 kPa
Exhaust area = 0.6 m^2.

Calculate the effective exhaust speeds and thrust force in the following cases:

1. Sea-level operation ($P_a = 101$ kPa)
2. At an altitude of 4.2 km, ambient pressure is ($P_a \sim 60$ kPa)
3. In-space operation ($P_a = 0.0$ kPa)

Solution

The thrust force is

$$T = \dot{m}u_e + \left(P_e - P_a\right)A_e$$

$$\therefore u_e = \frac{T - \left(P_e - P_a\right)A_e}{\dot{m}}$$

Case (*1*): Sea-level operation:

$$u_e = \frac{500{,}000 - \left(60.0 - 101\right)\times 10^3 \times 0.6}{175} = 2{,}997.7 \text{ m/s}$$

The effective exhaust speed:

$$V_{eff} = u_e + \frac{\left(P_e - P_a\right)A_e}{\dot{m}} = 2997.7 + \frac{\left(60.0 - 101\right)\times 10^3 \times 0.6}{175} = 2857.1 \text{ m/s}$$

Case (*2*): The ambient pressure is equal to the exhaust gas pressure of the nozzle ($P_e = P_a$), thus the effective exhaust speed is

$$V_{eff} = u_e + \frac{\left(P_e - P_a\right)A_e}{\dot{m}} = u_e = 2997.7 \text{ m/s}$$

The thrust force is then

$$T = \dot{m}V_{eff} = 175 \times 2{,}997.7 = 524{,}597 \text{ N} \sim 524.6 \text{ kN}$$

Case (*3*): In space where $P_a = 0$, the effective exhaust speed is

$$V_{eff} = u_e + \frac{P_e A_e}{\dot{m}} = 2997.7 + \frac{60 \times 10^3 \times 0.6}{175} = 3203.4 \text{ m/s}$$

The thrust force is

$$T = \dot{m}V_{eff} = 175 \times 3{,}203.4 = 560{,}597 \text{ N} \sim 560.6 \text{ kN}$$

These results are summarized in Table 18.1.

Comments: For sea-level operations, in case (1) the nozzle is somewhat too long for sea-level conditions, which is indicated by the fact that (P_e) is smaller than (P_a). Thus, a pressure "undershoot" and an exhaust velocity "overshoot" occurred. The "penalty" of incorrect nozzle length simply appears as the negative pressure thrust term. From Equation 18.6A and B, the difference in thrust between space and sea level resides in the term ($A_e P_a$). Since the nozzle selected was too long at sea level, this thrust increase ($A_e P_a$) during rocket ascent will be obtained in two steps. First, the *negative* thrust term $(P_e - P_a)A_e$ has to be reduced to zero; in case (2) when the rising vehicle reaches an altitude of 4.2 km

TABLE 18.1

Variation of Rocket Characteristics with Altitude

Altitude	Ambient Pressure (kPa)	Effective Velocity V_{eff} (m/s)	Thrust T (kN)
Sea level	101	2857.1	500.00
4.2 km	~60	2997.7	524.6
Space	0	3203.4	560.6

having equal exit and ambient pressures ($P_e = P_a = 60$ kPa). This represents an ideal expansion in the nozzle as described in Chapter 2. Second, as the vehicle continues to ascend farther and eventually reaches "empty space" ($P_a = 0$); in case (3), the pressure thrust will attain a positive value equal to ($P_e A_e$). The combined effect of the two phases is simply the elimination of ($P_a A_e$) provided the nozzle is filled at all times.

18.5.3 Exhaust Velocity (u_e)

The propellants enter the combustion chamber, mix, and are ignited. The gas produced is heated by the chemical energy released during combustion and expands through the nozzle. Applying the first law of thermodynamics, the change in enthalpy of exhaust gases is equal to its kinetic energy. The temperature of the gases in combustion chamber (T_c) will be equal to the total temperature of the gases exhausting the nozzle ($T_c = T_{oe}$). The change in specific enthalpy is

$$Cp\left(T_{0e} - T_e\right)$$

where Cp is the specific heat at constant pressure [9]. The gain in kinetic energy of exhaust gases per unit mass is ($1/2u_e^2$). Equating both quantities

$$u_e^2 = 2Cp\left(T_{oe} - T_e\right)$$

$$u_e = \sqrt{2Cp\left(T_{oe} - T_e\right)}$$

$$u_e = \sqrt{2CpT_{oe}\left(1 - \frac{T_e}{T_{oe}}\right)}$$

Assuming isentropic expansion, $TP^{\gamma - 1/\gamma}$ = constant. Moreover, the specific heat can be expressed as

$$Cp = \frac{\gamma}{\gamma - 1} R = \frac{\gamma}{\gamma - 1} \frac{\bar{R}}{M}$$

where

R is the gas constant
$\bar{R}$ is the universal gas constant
M is the molecular weight of the exhaust gases

$$u_e = \sqrt{2\frac{\gamma R}{\gamma - 1} T_{oe}\left[1 - \left(\frac{P_e}{P_{oe}}\right)^{\gamma - 1/\gamma}\right]} \tag{18.8A}$$

or

$$u_e = \sqrt{2\frac{\gamma}{\gamma - 1}\frac{\bar{R}}{M} T_{oe}\left[1 - \left(\frac{P_e}{P_{oe}}\right)^{\gamma - 1/\gamma}\right]} \tag{18.8B}$$

The maximum exhaust speed occurs when ($P_e = 0$), thus

$$u_{e_{\max}} = \sqrt{2\frac{\gamma R}{\gamma - 1} T_{oe}} \equiv \sqrt{2\frac{\gamma R}{\gamma - 1} T_c} \tag{18.8C}$$

From Equation 18.8A, the mass flow rate is

$$\dot{m} = \rho_e u_e A_e = \rho_e A_e \sqrt{\frac{2\gamma R}{\gamma - 1} T_{oe}\left[1 - \left(\frac{P_e}{P_{oe}}\right)^{\gamma - 1/\gamma}\right]} \tag{18.9A}$$

$$\dot{m} = \rho_e u_e A_e = \rho_e A_e \sqrt{\frac{2\gamma}{\gamma - 1}\frac{\bar{R}}{M} T_{oe}\left[1 - \left(\frac{P_e}{P_{oe}}\right)^{\gamma - 1/\gamma}\right]} \tag{18.9B}$$

18.5.4 Important Nozzle Relations

The combustion chamber is frequently identified in rocket literature as the thrust chamber. Gases leaving the chamber flow at nearly zero speed are then accelerated in a convergent divergent nozzle. They reach sonic speed at the throat and keep their accelerating motion to attain supersonic or even hypersonic speeds at their exit.

Though flow in the nozzle was previously described, a brief review of its governing equations is reviewed here. The total temperatures and pressures in the combustion chamber and nozzle are equal ($T_c = T_{oe}$ and $P_c = P_{oe}$); thus, the temperature, pressure, and area at the nozzle throat (Mach number is unity) are given by the relations

$$\frac{T^*}{T_{0e}} = \frac{2}{\gamma + 1} \tag{18.10}$$

$$\frac{P^*}{P_{0e}} = \frac{1}{\left[(\gamma + 1)/2\right]^{\gamma/\gamma - 1}} \tag{18.11}$$

$$A^* = \frac{\dot{m}\sqrt{RT^*/\gamma}}{P^*} \tag{18.12}$$

The nozzle throat diameter is given by

$$D^* = \sqrt{4A^*/\pi} \tag{18.13}$$

The mass flow rate is expressed as

$$\dot{m} = \rho^* u^* A^* = \rho_e u_e A_e \tag{18.14}$$

$$\frac{\dot{m}\sqrt{T_{0e}}}{A^* P_{0e}} = \sqrt{\frac{\gamma}{R}}\left(\frac{2}{\gamma+1}\right)^{\gamma+1/2(\gamma-1)} \tag{18.15}$$

At exit, the static pressure, temperature, Mach number, and velocity are given by the relations

$$\frac{P_e}{P_{0e}} = \left(\frac{1}{1+\frac{\gamma-1}{2}M_e^2}\right)^{\gamma/\gamma-1} \tag{18.16}$$

$$\frac{T_e}{T_{0e}} = \frac{1}{1+\frac{\gamma-1}{2}M_e^2} \tag{18.17}$$

$$M_e^2 = \left(\frac{\gamma+1}{\left(P_e/P^*\right)^{\gamma-1/\gamma}} - 2\right)\left(\frac{1}{\gamma-1}\right) \tag{18.18A}$$

$$u_e = M_e\sqrt{\gamma R T_e} = \sqrt{\frac{2\gamma}{\gamma-1}RT_{0e}\left(1-\left(\frac{P_e}{P_{0e}}\right)^{\gamma-1/\gamma}\right)} \tag{18.18B}$$

$$u_{e\max} = \sqrt{\frac{2\gamma}{\gamma-1}RT_{0e}} \tag{18.18C}$$

The density, exhaust area, and diameter at exit are then

$$\rho_e = \frac{P_e}{RT_e} \tag{18.19}$$

$$A_e = \frac{\dot{m}}{\rho_e V_e} \tag{18.20A}$$

The exhaust diameter:

$$D_e = \sqrt{4A_e/\pi} \tag{18.20B}$$

The ratio between the exit area and the throat area is given by

$$\frac{A_e}{A^*} = \frac{1}{M_e}\left(\frac{2}{\gamma+1} + \frac{\gamma-1}{\gamma+1}M_e^2\right)^{\gamma+1/2(\gamma-1)} \tag{18.21}$$

18.5.5 Characteristic Velocity (C^*)

The characteristic velocity is defined as

$$C^* = \frac{P_{0e}A^*}{\dot{m}} = \frac{\sqrt{\gamma RT_{0e}}}{\gamma\left(\frac{2}{\gamma+1}\right)^{\gamma+1/2(\gamma-1)}} \tag{18.22A}$$

18.5.6 Thrust Coefficient (C_F)

The thrust coefficient is defined as

$$C_F = \frac{T}{P_{0e}A^*} \tag{18.23A}$$

Now from Equations 18.6A, 18.8A, and 18.15,

$$C_F = \sqrt{\left(\frac{2\gamma^2}{\gamma-1}\right)\left(\frac{2}{\gamma+1}\right)^{\gamma+1/\gamma-1}\left[1-\left(\frac{P_e}{P_{oe}}\right)^{\gamma-1/\gamma}\right]} + \left(\frac{P_e-P_a}{P_{oe}}\right)\frac{A_e}{A^*} \tag{18.23B}$$

A plot for the thrust coefficient versus the area ratio (A_e/A^*) for a different pressure ratio (P_e/P_{oe}) and a constant specific heat $\gamma = 1.2$ is shown in Figure 18.15.

The first term is the contribution of the exit velocity, while the second term is the contribution of the exit pressure. For a perfect expansion of the nozzle ($P_e = P_a$), the optimum thrust coefficient is then

$$C_{F,opt} = \sqrt{\left(\frac{2\gamma^2}{\gamma-1}\right)\left(\frac{2}{\gamma+1}\right)^{\gamma+1/\gamma-1}\left[1-\left(\frac{P_e}{P_{oe}}\right)^{\gamma-1/\gamma}\right]} \tag{18.23C}$$

The ideal thermal efficiency of a Brayton cycle operating between the two pressures (P_e) and (P_{oe}) is expressed as

$$\eta_{th} = 1-\left(\frac{P_e}{P_{oe}}\right)^{\gamma-1/\gamma}$$

For a very large total pressure (P_{oe}) and low exit pressure (P_e)

$\eta_{th} \cong 1$, and

$$C_{F,opt,\text{Max}} = \sqrt{\left(\frac{2\gamma^2}{\gamma-1}\right)\left(\frac{2}{\gamma+1}\right)^{\gamma+1/\gamma-1}} \tag{18.23D}$$

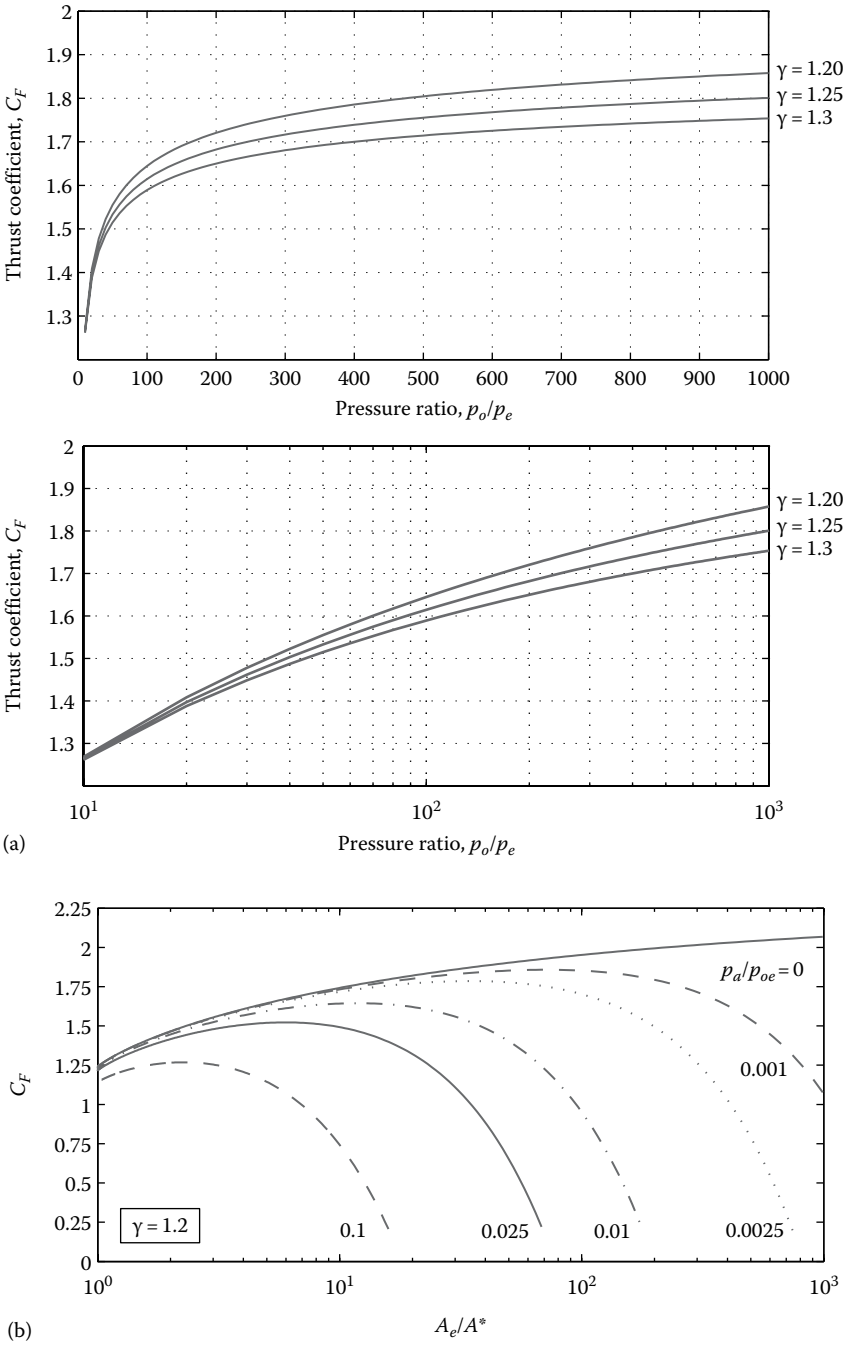


FIGURE 18.15
Variation of thrust coefficient versus (a) pressure ratio and (b) area ratio.

18.5.7 Total Impulse (I_t)

Figure 18.16 depicts typical thrust-time profiles for the three cases of propellant burning. Neutral burning generates approximately a constant thrust profile, while the two cases of increasing and decreasing thrust profile are identified as progressive and regressive profiles, respectively.

The total impulse is the thrust force integrated over the burning time (t):

$$I_t = \int_0^t T\,dt \tag{18.24}$$

For a constant thrust and negligible start and stop transients,

$$I_t = Tt \tag{18.25}$$

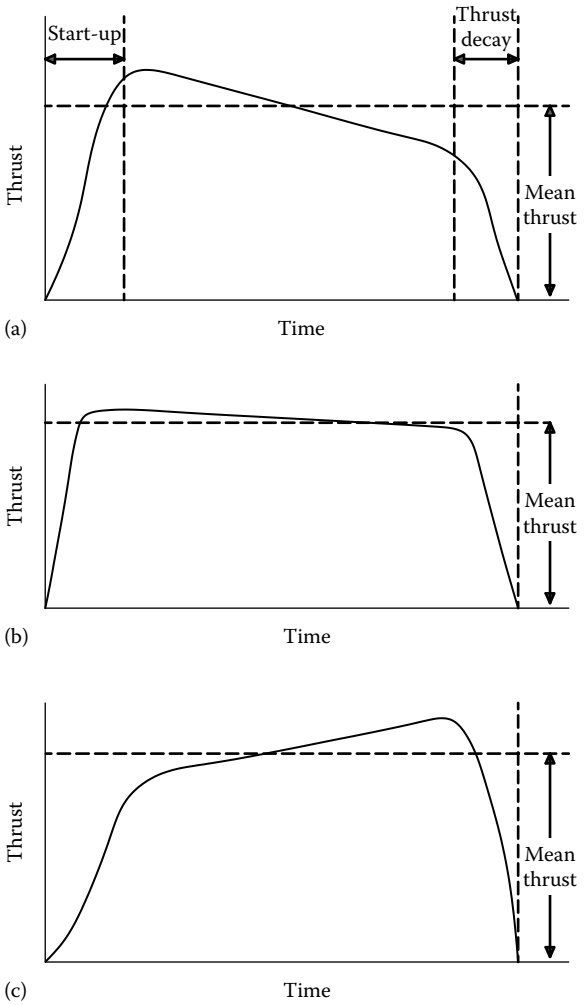


FIGURE 18.16
Typical thrust-time curves: (a) regressive burning, (b) neutral burning, and (c) progressive burning.

18.5.8 Specific Impulse (I_{sp})

$$I_{sp} = \frac{I_t}{g\int_0^t \dot{m}dt} = \frac{\int_0^t T\,dt}{g\int_0^t \dot{m}dt}$$

For a constant thrust and propellant mass flow rate,

$$I_{sp} = \frac{I_t}{m_p g} = \frac{Tt}{\dot{m}tg} = \frac{T}{\dot{m}g} \tag{18.26}$$

where m_p is the total propellant mass

$$m_p = \dot{m}t$$

with

$$T = \dot{m}V_{eff}$$

Thus,

$$I_{sp} = \frac{\dot{m}V_{eff}}{\dot{m}g} = \frac{V_{eff}}{g}\,\text{s} \tag{18.27}$$

The characteristic velocity (C^*) can be expressed as

$$C^* = \frac{I_{sp}g}{C_F} \tag{18.22B}$$

Example 18.2

Consider the data given in Table 18.2 for a rocket engine.
The total propellant mass m_p = 13.6 kg
Determine the total impulse, specific impulse, the average thrust and effective speed, and the propellant mass flow rate of the rocket motor.

Solution

The total impulse is the thrust force integrated over the burning time (t):

$$I_t = \int_0^t T\,dt$$

TABLE 18.2

Time (s)	0	0.5	1.0	2.0	2.5	3.0	3.25	3.3
Thrust (N)	7000	9400	8500	8400	8300	7900	7600	0

The total impulse is the area under the curve of thrust versus time. Since the thrust is given at discrete time intervals and not as a mathematical relation, the total impulse is approximated by a trapezoidal area.

The total impulse is the sum of the trapezoidal area.

The area of each trapezoid is calculated based on

$$\text{Area} = \text{Base} \times \left(\text{Height 1} + \text{Height 2}\right)/2$$

The total impulse is

$$I_t = 0.5 \times \left[0.5 \times (7000 + 9400) + 0.5 \times (9400 + 8500) + 1.0 \times (8500 + 8400) + 0.5 \times (8400 + 8300) + 0.5 \times (8300 + 7900) + 0.25 \times (7900 + 7600) + 0.05 \times (7600 + 0)\right]$$

$$I_t = 0.5 \times (8,650 + 8,950 + 16,900 + 8,350 + 8,100 + 3,875 + 380)$$

$$I_t = 27,602.5 \text{ N} \cdot \text{s}$$

Note that the accuracy of the calculation improves as the number of trapezoids used increases.

The specific impulse is

$$I_{sp} = \frac{I_t}{m_p g} = \frac{27,602.5}{13.6 \times 9.8065} = 206.96 \text{ s}$$

Average thrust is

$$T = \frac{I_t}{t} = \frac{27,602.5}{3.3} = 8,364 \text{ N}$$

Effective speed is

$$V_{eff} = I_{sp} \times \text{g} = 206.96 \times 9.8065 = 2029.6 \text{ m/s}$$

Propellant mass flow rate is

$$\dot{m} = \frac{m_p}{t} = \frac{13.6}{3.3} = 4.12 \text{ kg/s}$$

Example 18.3

The thrust-time profiles for the three cases of propellant burning are expressed by the following expressions:

1. Neutral profile: $T = 6000N$
2. Progressive profile: $T = 6000 + 500t$
3. Regressive profile: $T = 6000 - 600t$

For a burning time of 3 s in all cases, calculate the total impulse.

TABLE 18.3

Thrust Profile	Progressive	Neutral	Regressive
$T(0)$ N	6,000	6,000	6,000
$T(3)$ N	7,500	6,000	4,200
Total impulse second	20,250	18,000	15,300

Solution

The thrust is first calculated at the beginning and end of burning. Next, the total impulse is calculated as the area:

$$I_t = t_b \times \frac{\left[T(0)+T(3)\right]}{2}$$

Results are tabulated in Table 18.3.

The total impulse is a maximum for progressive burning and minimum for regressive burning.

Example 18.4

The thrust force of a rocket is 500 kN and the specific impulse is 300 s. Determine the gas mass flow rate.

Solution

From Equation 18.40, the mass flow rate is

$$\dot{m} = \frac{T}{I_{sp}g} = \frac{500,000}{300 \times 9.80665} = 169.95 \text{ kg/s}$$

Example 18.5

Calculate the specific thrust for the three cases discussed in Example 18.1.

Solution

The specific impulse is expressed as

$$I_{sp} = \frac{V_{eff}}{g}$$

Results are listed in Table 18.4.

TABLE 18.4

Altitude	Effective Velocity V_{eff} (m/s)	Specific Impulse I_{sp} (s)
Sea level	2857.1	291.34
3 km	2997.7	305.6
Space	3203.4	326.66

Example 18.6

A rocket motor has a combustion chamber with temperature 3300 K and pressure 22 atmospheres. The throat area is 0.2 m^2. The exit pressure is equal to atmospheric pressure at an altitude of 30 km. The specific heat ratio $\gamma = 1.23$ and the specific heat at constant pressure Cp = 2520 J/kg/K. Calculate

- Exit velocity
- Mass flow through the motor
- Thrust force
- Specific impulse

Solution

The ambient pressure at an altitude of 30 km is

$$P_e = 1.172 \text{ kPa}$$

$$P_{oe} = 22 \times 101.325 = 2229.15 \text{ kPa}$$

with

$$\frac{\gamma - 1}{\gamma} = \frac{0.23}{1.23} = 0.187,$$

then

$$R = \frac{\gamma - 1}{\gamma} Cp = 0.187 \times 2520 = 471.2 \text{ J/kg} \cdot \text{K}$$

Exhaust velocity:

$$u_e = \sqrt{2CpT_{oe}\left(1 - \left(\frac{P_e}{P_{oe}}\right)^{\gamma-1/\gamma}\right)} = \sqrt{2 \times 2520 \times 3300\left(1 - \left(\frac{1.172}{2229.15}\right)^{0.187}\right)}$$

$$u_e = 3546.7 \text{ m/s} \equiv \text{equivalent speed}$$

Mass flow rate:

$$\dot{m} = \rho_e u_e A_e$$

First evaluate the static temperature

$$T_e = T_{oe}\left(\frac{P_e}{P_{oe}}\right)^{\gamma-1/\gamma} = 3300\left(\frac{1.172}{2229.15}\right)^{0.187} = 804 \text{ K}$$

$$\rho_e = \frac{1172}{471.24 \times 804} = 0.0031 \text{ kg/m}^3$$

Exhaust Mach number is

$$M_e = \frac{u_e}{\sqrt{\gamma R T_e}} = \frac{3546.7}{\sqrt{1.23 \times 471.24 \times 804}} = 5.195$$

Area ratio between throat and exhaust sections is

$$\frac{A_e}{A^*} = \frac{1}{M_e}\sqrt{\left[\left(\frac{2}{\gamma+1}\right)\left(1+\frac{\gamma-1}{2}M_e^2\right)\right]^{\gamma+1/\gamma-1}}$$

$$A_e = \frac{0.1}{5.195}\sqrt{\left[\left(\frac{2}{2.23}\right)\left(1+0.115\times\left(5.195\right)^2\right)\right]^{2.23/0.23}} = 0.01925\times\left(3.68\right)^{4.848}$$

$$A_e = 10.66\ \text{m}^2$$

$$\dot{m} = \rho_e u_e A_e = 0.0031\times 3546.7\times 10.66 = 117.2\ \text{kg/s}$$

Thrust force is

$$T = \dot{m}u_e + \left(P_e - P_a\right)A_e$$

Since $P_e = P_a$,

$$T = \dot{m}u_e = 117.2\times 3546.7$$

$$T = 415.69\ \text{kN}$$

Specific impulse is

$$I_{sp} = \frac{T}{\dot{m}g} = \frac{\dot{m}u_e}{\dot{m}g} = \frac{u_e}{g} = \frac{3546.7}{9.80665}$$

$$I_{sp} = 361.686\ \text{s}$$

18.5.9 Specific Propellant Consumption

Specific propellant consumption is

$$SPC = \frac{1}{I_s} = \frac{\dot{m}g}{T} = \frac{\dot{w}}{T}\,\text{s}^{-1} \tag{18.28}$$

18.5.10 Mass Ratio (MR)

The mass ratio is defined as the final mass (m_f) after rocket operation (or after propellants are consumed) divided by the initial mass (m_0) before rocket operation:

$$MR = \frac{m_f}{m_0} \tag{18.29}$$

18.5.11 Propellant Mass Fraction (ζ)

The propellant mass fraction (ζ) is the ratio of propellant mass (m_p) to the initial mass (m_0)

$$\zeta = \frac{m_p}{m_0} = \frac{m_0 - m_f}{m_0} = \frac{m_p}{m_p + m_f} \tag{18.30}$$

18.5.12 Impulse-to-Weight Ratio

$$\frac{I_t}{w_o} = \frac{I_{sp}t}{\left(m_f + m_p\right)g} = \frac{I_{sp}}{\left(\frac{m_f g}{t}\right) + \dot{m}g} \tag{18.31}$$

Example 18.7

Prove that $\zeta = 1 - MR$

Solution

$$\zeta = \frac{m_p}{m_o} = \frac{m_o - m_f}{m_o} = 1 - \frac{m_f}{m_o} = 1 - MR$$

$$\zeta = 1 - MR$$

18.5.13 Efficiencies

Though efficiencies are not commonly used in rocket design as in aircraft, it is useful to understand energy conversion processes. Similar to airbreathing engines, rocket engines also have both internal and external efficiencies. Internal energy is normally identified as thermal efficiency, while external efficiency is also denoted as propulsive efficiency. The product of both is also identified as overall efficiency. For chemical rockets, energy stored in fuel is released via a specific chemical reaction process. This available energy depends on the combustion efficiency. However, a part of this energy is lost through heat dissipation from the combustor. The remaining energy is now available to the nozzle, though not all of it is convertible into kinetic energy.

The efficiency of converting this chemical energy into kinetic energy is identified as internal or thermal efficiency. This kinetic energy of the exhaust gases is employed in propelling the rocket. The efficiency of converting this kinetic energy into thrust power is identified as external or propulsive efficiency.

18.5.13.1 Thermal Efficiency

The maximum energy available per unit mass of chemical propellant is the heat of the combustion (Q_R). The power input to a chemical engine is

$$P_{chem} = \dot{m}Q_R$$

The actual power of combustion is obtained by multiplying the combustion efficiency (η_c) by the power input P_{chem}. Combustion efficiency is approximately 94%–99%.

The thermal (or internal) efficiency of a rocket propulsion system is an indication of the effectiveness of converting the chemical power input to the propulsion device into engine output power.

$$\text{Engine output power} = \text{propulsion}\left(\text{or thrust}\right)\text{power} + \text{power loss in exhaust gases}$$

Thus,

$$\text{Engine output power} = Tu + \frac{\dot{m}\left(V_{eff} - u\right)^2}{2} = \dot{m}V_{eff}u + \frac{\dot{m}\left(V_{eff} - u\right)^2}{2}$$

$$\text{Engine output power} = \dot{m} \times \left(V_{eff}^2 + u^2\right)/2$$

$$\eta_{th} \equiv \eta_{int} = \frac{\text{Engine power output}}{\text{Available chemical power developed by combustion}}$$

$$\eta_{th} \equiv \eta_{int} = \frac{Tu + \dfrac{\dot{m}\left(V_{eff} - u\right)^2}{2}}{\eta_c P_{chem}} = \frac{Tu + \dfrac{\dot{m}\left(V_{eff} - u\right)^2}{2}}{\eta_c \dot{m} Q_R} \tag{18.32A}$$

$$\eta_{th} \equiv \eta_{int} = \frac{\dot{m} \times \left(V_{eff}^2 + u^2\right)/2}{\eta_c \dot{m} Q_R}$$

Thus, the thermal efficiency is then expressed as

$$\eta_{th} \equiv \eta_{int} = \frac{\left(V_{eff+u^2}^2\right)}{2\eta_c Q_R} \tag{18.32B}$$

18.5.13.2 Propulsive Efficiency

For a rocket flying at a speed of (u) and gases' exhaust speed (u_e), the propulsive efficiency is expressed as in airbreathing engines:

$$\eta_p = \frac{\text{Propulsion (or thrust) power}}{\text{Engine output power}}$$

$$\text{Propulsion power} = Tu$$

$$\text{Engine output power} = \text{propulsion power} + \text{power lost in exhaust}$$

$$\eta_p = \frac{Tu}{Tu + \dot{m}\left(V_{eff} - u\right)^2/2} \tag{18.33A}$$

$$\eta_p = \frac{\dot{m}V_{eff}u}{\dot{m}V_{eff}u + \dot{m}\left(V_{eff} - u\right)^2/2}$$

$$\eta_p = \frac{V_{eff}u}{V_{eff}u + \left(V_{eff} - u\right)^2/2} = \frac{V_{eff}u}{V_{eff}u + \dfrac{1}{2}\left(V_{eff}^2 + u^2\right) - V_{eff}u}$$

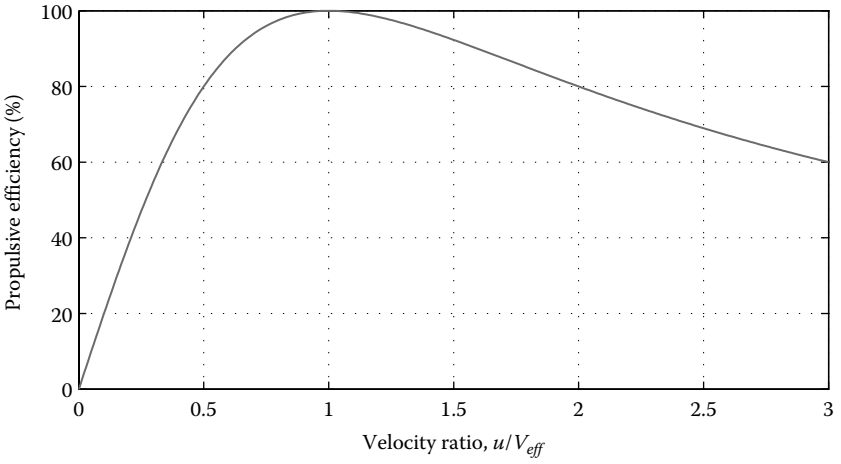


FIGURE 18.17
Propulsive efficiency versus the velocity ratio (u/V_{eff}).

$$\eta_p = \frac{2V_{eff}u}{V_{eff}^2 + u^2} = \frac{2\left(u/V_{eff}\right)}{1+\left(u/V_{eff}\right)^2}$$

$$\eta_p = \frac{2\sigma}{1+\sigma^2} \tag{18.33B}$$

where $\sigma = \dfrac{u}{V_{eff}}$, the flight to effective jet velocity ratio.

The propulsive efficiency $\eta_p = 1$(or 100%), when $u = V_{eff}$, or $\sigma = 1$. Figure 18.17 illustrates the propulsive efficiency versus the velocity ratio (u/C).

18.5.13.3 Overall Efficiency (η_0)

$$\eta_0 = \frac{\text{Thrust power}}{\text{Power developed by combustion}}$$

$$\eta_0 = \frac{Tu}{\dot{m}Q_R} = \frac{\dot{m}V_{eff}u}{\dot{m}Q_R} = \frac{V_{eff}u}{Q_R} \tag{18.34A}$$

In general, the overall efficiency is equal to the product of thermal and propulsive efficiencies; or

$$\eta_0 = \eta_{th}\eta_p \tag{18.34B}$$

It is worth mentioning here that the overall efficiency can also be obtained by multiplying Equations 18.32A and 18.33A.

Example 18.8

A certain rocket has the following data: thrust = 9000 N, propellant combustion rate = 3.9 kg/s, rocket speed $u = 420$ m/s, heat of combustion: $Q_R = 7.0$ MJ/kg, combustion efficiency: $\eta_c = 99\%$. Calculate

1. Effective exhaust velocity
2. Thermal (internal) efficiency
3. Propulsive (external) efficiency
4. Overall efficiency
5. Specific propellant consumption

Solution

The effective velocity is

$$V_{eff} = \frac{T}{\dot{m}} = \frac{9000}{3.9} = 2307.7 \text{ m/s}$$

Thermal efficiency is

$$\eta_{th} \equiv \eta_{int} = \frac{V_{eff}^2 + u^2}{2\eta_c Q_R} = \frac{(2307.7)^2 + (420)^2}{2 \times 0.99 \times 7 \times 10^6} = 39.7\%$$

Propulsive efficiency is

$$\eta_p = \frac{2\sigma}{1+\sigma^2}$$

with

$$\sigma = \frac{u}{V_{eff}} = \frac{420}{2307.7} = 0.182$$

Then

$$\eta_p = \frac{2\sigma}{1+\sigma^2} = \frac{2 \times 0.182}{1+(0.182)^2} = 35.23\%$$

Overall efficiency is

$$\eta_0 = \eta_{th}\eta_p = 39.7 \times 35.23 = 13.98\%$$

Specific propellant consumption is

$$SPC = \frac{1}{I_s} = \frac{g}{V_{eff}} = \frac{9.80665}{2307.7} = 4.2495 \times 10^{-3} = 0.00425 \text{ s}^{-1}$$

Example 18.9

A small liquid-fuel rocket engine operates from sea level ($P_a = 101$ kPa) and uses gaseous oxygen and gasoline propellants. It has the following data:

Combustion chamber pressure = 2070 kPa
Combustion chamber temperature = 3445 K

Thrust generated = 89 N
Specific heat ratio $\gamma = 1.2$
Gas constant $R = 280\ \text{J/kg}\cdot\text{K}$
Specific impulse = 260 s
Optimum O/F (oxygen/fuel) ratio is 2.5

Full expansion in nozzle to ambient pressure is assumed. We need to calculate

- Total propellant mass flow rate
- Fuel and oxygen mass flow rates
- Temperature and pressure at nozzle throat
- Area and diameter of nozzle throat
- Mach number at exit of nozzle
- Exit area and diameter

Solution

The total propellant weight flow rate is given by the relation

$$w_t \equiv \dot{m}_t g = \frac{T}{I_{sp}} = \frac{89}{260} = 0.342\ \text{N/s}$$

$$\dot{m}_t = 0.035\ \text{kg/s}$$

Since the mixture ratio (r) is 2.5, the fuel mass flow rate is

$$\dot{m}_f = \frac{\dot{m}_t}{r+1} = \frac{0.035}{3.5} = 0.01\ \text{kg/s}$$

The oxygen mass flow rate is

$$\dot{m}_{ox} = \dot{m}_t - \dot{m}_f = 0.035 - 0.01 = 0.025\ \text{kg/s}$$

As a check, we divide the oxygen flow rate by the fuel flow rate and the result is 2.5, as it should be.

Since $T_c = T_o$ is the total temperature in the combustion chamber and nozzle, the temperature of gases at the nozzle throat (Mach number is unity) is given by the relation

$$T^* = \frac{2T_0}{\gamma+1} = \frac{2\times 3445}{1.2+1} = 3132\ \text{K}$$

Moreover, with $P_c = P_o$ as the gas pressure at combustion chamber and nozzle is equal, then at the nozzle throat the pressure (P^*) is given by the relation

$$P^* = \frac{P_0}{\left[(\gamma+1)/2\right]^{\gamma/\gamma-1}} = \frac{2070}{(1.1)^6} = 1168.5\ \text{kPa}$$

The nozzle throat cross-sectional area may be computed from the relation

$$A^* = \frac{\dot{m}_t\sqrt{RT^*/\gamma}}{P^*} = \frac{0.035\times\sqrt{280\times 3{,}132/1.2}}{1{,}168{,}500} = 2.56\times 10^{-5}\ \text{m}^2$$

The nozzle throat diameter is given by

$$D^* = \sqrt{4A^*/\pi} = 6.04 \times 10^{-3} \text{ m}$$

The Mach number at exit may be calculated as follows:

$$\frac{P_e}{P^*} = \frac{P_e}{P_0}\frac{P_0}{P^*} = \left[\left(\frac{1}{1+\frac{\gamma-1}{2}M_e^2}\right)\left(\frac{\gamma+1}{2}\right)\right]^{\gamma/\gamma-1}$$

From this relation, we get

$$M_e^2 = \left(\frac{\gamma+1}{\left(P_e/P^*\right)^{\gamma-1/\gamma}} - 2\right)\left(\frac{1}{\gamma-1}\right)$$

$$M_e^2 = \left(\frac{2.2}{\left(101/1168.5\right)^{0.1667}} - 2\right)\left(\frac{1}{0.2}\right)$$

$$M_e = 2.56$$

Now, the static temperature at exit is easily determined as

$$T_e = \frac{T_0}{1+\frac{\gamma-1}{2}M_e^2} = \frac{3445}{1+0.1\times\left(2.56\right)^2} = 2081 \text{ K}$$

The exhaust density is

$$\rho_e = \frac{P_e}{RT_e} = \frac{101{,}000}{280 \times 2{,}081} = 0.173 \text{ kg/m}^3$$

The exhaust velocity is

$$V_e = M_e\sqrt{\gamma RT_e} = 2.56 \times \sqrt{1.2 \times 280 \times 2081} = 2140 \text{ m/s}$$

The exhaust area is

$$A_e = \frac{\dot{m}_t}{\rho_e V_e} = 9.451 \times 10^{-5} \text{ m}^2$$

The exhaust diameter is

$$D_e = \sqrt{4A_e/\pi} = 10.97 \times 10^{-3} \text{ m}$$

18.6 The Rocket Equation

18.6.1 Single-Stage Rocket

The equation of motion of a rocket is derived here [10]. Newton's second law of motion is used. The forces governing the motion of a rocket are thrust (T), drag (D), lift (L), and gravitational force (mg). Here, (m) is the instantaneous rocket mass. First, it is assumed that both

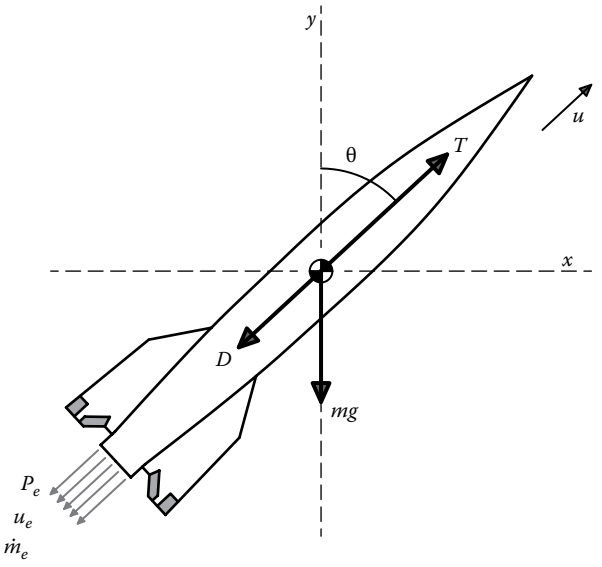


FIGURE 18.18
Forces on the rocket.

the thrust and drag are aligned in the flight direction, which is inclined at an angle (θ) to the vertical direction; see Figure 18.18.

The forces acting on the rocket may be resolved in the flight direction to give

$$m\frac{du}{dt} = T - D - mg\cos\theta \tag{18.35}$$

The thrust force in this equation can be either expressed as

$$T = \dot{m}V_{eff}$$

or

$$T = \dot{m}gI_{sp}$$

Thus from Equation 18.35,

$$m\frac{du}{dt} = \dot{m}V_{eff} - D - mg\cos\theta$$

Noting that a large fraction (typically 90%) of the mass of a rocket is propellant, it is important to consider the change in mass of the vehicle as it accelerates. Since the rate of mass flow through the nozzle is equal to the negative rate of change in rocket mass, thus

$$\dot{m} = -\frac{dm}{dt}$$

$$du = -\left(\frac{dm}{m}\right)V_{eff} - \left(\frac{D}{m}\right)dt - g\cos\theta\, dt$$

Integrating this equation over a period of time equal to the burning time (τ_b), to get the increment change in rocket velocity:

$$\frac{\Delta u}{V_{eff}} = \ell n \frac{m_0}{m_0 - m_p} - \int_o^{\tau_b} \frac{D}{mV_{eff}} dt - \int_o^{\tau_b} \frac{g \cos\theta}{V_{eff}} dt \tag{18.36A}$$

$$\frac{\Delta u}{V_{eff}} = \ell n \frac{1}{\text{MR}} - \int_o^{\tau_b} \frac{D}{mV_{eff}} dt - \int_o^{\tau_b} \frac{g \cos\theta}{V_{eff}} dt \tag{18.36B}$$

where as mentioned previously m_0 is the rocket initial mass and m_p is the propellant burnt mass.

Moreover, the first integral in the RHS is the drag loss, while the second integral is the gravity loss.

Consider the following simple cases.

18.6.1.1 Negligible Drag

$$\frac{\Delta u}{V_{eff}} = \ell n \frac{1}{\text{MR}} - \int_o^{\tau_b} \frac{g \cos\theta}{V_{eff}} dt$$

Assuming also constant gravitational acceleration and $(\theta = 0)$

$$\Delta u = V_{eff}\ \ell n \frac{m_0}{m_0 - m_p} - \int_o^{\tau_b} g \cos\theta\, dt = g I_{sp}\ \ell n \frac{m_0}{m_0 - m_p} - gt$$

$$\Delta u = g\left(I_{sp}\ \ell n \frac{m_0}{m_0 - m_p} - t \right) \tag{18.37A}$$

$$\Delta u = g\left(I_{sp}\ \ell n \frac{1}{\text{MR}} - t \right) \tag{18.37B}$$

18.6.1.2 Negligible Drag and Gravity Loss

The increment change in rocket velocity is

$$\Delta u = V_{eff}\ \ell n \frac{m_0}{m_f} = V_{eff}\ \ell n \frac{m_0}{m_0 - m_p} \tag{18.38A}$$

From Equation 18.41,

$$\Delta u = g I_{sp}\, \ell n \frac{m_0}{m_0 - m_p} \tag{18.38B}$$

From Equation 18.27,

$$\Delta u = V_{eff}\,\ell n\frac{1}{MR} \tag{18.39A}$$

or

$$\Delta u = gI_{sp}\,\ell n\frac{1}{MR} \tag{18.39B}$$

Equations 18.38A, B, 18.39A, and B are known as the "Tsiolkovsky rocket equation." A plot of Tsiolkovsky for different effective speeds is shown in Figure 18.19.

Another important parameter is the burn time. Since the final mass is related to the original mass by the relation,

$$m_f = m_0 - m_p = m_0 - \dot{m}t$$

Then, from Equation 18.38A,

$$m_0 = m_f e^{\Delta u/V_{eff}} \tag{18.40}$$

Moreover,

$$m_0 = \left(m_0 - \dot{m}t\right)e^{\Delta u/V_{eff}}$$

The burning time is then

$$t = \frac{m_0}{\dot{m}}\left(1 - \frac{1}{e^{\Delta u/V_{eff}}}\right) \tag{18.41}$$

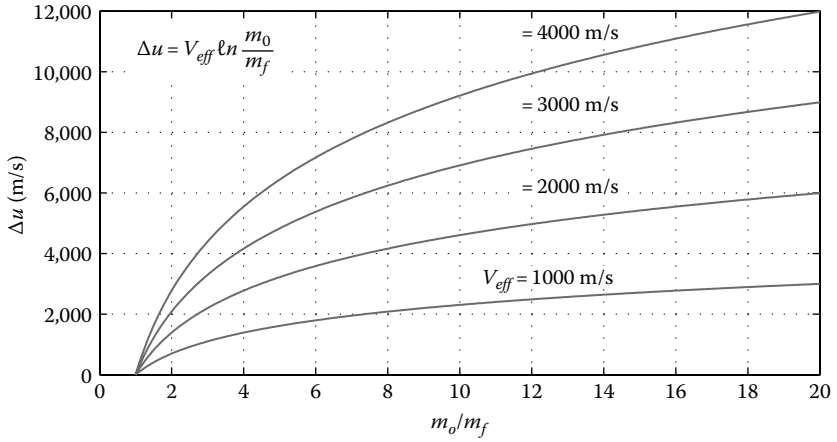


FIGURE 18.19
Tsiolkovsky rocket equation.

Introducing the payload ratio or fraction (λ) and structural (dead) weight ratio or structural fraction (δ),

$$\lambda = \frac{m_L}{m_0} \quad \text{and} \quad \delta = \frac{m_s}{m_0}$$

where

m_s is the structural mass of the rocket if a single stage or the (i_{th}) stage alone including the mass of its engine, controllers, and instrumentation as well as any residual propellant that is not expended by the end of the burn

m_L is the payload mass (which may be a satellite, space probe, or astronauts/cosmonauts)

Note that

$$m_0 = m_L + m_s + m_p$$

Dividing by (m_0), we get

$$1 = \lambda + \delta + \zeta \tag{18.42}$$

Thus,

$$\frac{m_0}{m_0 - m_p} = \frac{m_0}{m_d + m_L} = \frac{1}{\lambda + \delta} \tag{18.43}$$

Then from Equation 18.38A,

$$\Delta u = V_{eff}\, \ell n \frac{1}{\lambda + \delta} = g I_{sp}\, \ell n \frac{1}{\lambda + \delta} \tag{18.44}$$

Example 18.10

A spacecraft's dry mass is 75,000 kg and the effective exhaust gas velocity of its main engine is 3100 m/s. How much propellant must be carried if the propulsion system is to produce a total Δv of 700 m/s?

Solution

Since

$$\Delta u = V_{eff}\, \ell n \frac{m_0}{m_f}$$

$$m_0 = m_f e^{\Delta u / V_{eff}} = 75{,}000 \times e^{700/3{,}100} = 94{,}000 \text{ kg}$$

$$m_p = m_0 - m_f = 94{,}000 - 75{,}000 = 19{,}000 \text{ kg}$$

Example 18.11

A spacecraft having a mass of 5000 kg is traveling at a velocity of 8000 m/s in Earth orbit. Its propellant is burned to accelerate it to a velocity of 12,000 m/s placing it on an escape trajectory. The engine expels mass at a rate of 10 kg/s and at an effective velocity of 4000 m/s. Calculate the duration of the burn.

Solution

Given the data

$$m_0 = 5000 \text{ kg}$$

$$\dot{m} = 10 \text{ kg/s}$$

$$V_{eff} = 3000 \text{ m/s}$$

$$\Delta u = 12{,}000 - 8{,}000 \text{ m/s} = 4{,}000 \text{ m/s}$$

From Equation 18.41,

$$t = \frac{m_0}{\dot{m}}\left(1 - \frac{1}{e^{\Delta u / V_{eff}}}\right)$$

$$t = \frac{5000}{10}\left(1 - \frac{1}{e^{4000/3000}}\right) = 368.2 \text{ s}$$

18.6.2 Multistage Rockets

A multistage rocket is a rocket that uses two or more stages, each of which contains its own engines and propellant [11]. Thus, we have two or more rockets stacked on top of or attached next to each other. Multistaging is used in space launch vehicles and long-range ballistic missiles. Two-stage rockets are quite common. However, rockets with as many as five separate stages have been successfully launched. An example is the Saturn V rocket, which used three distinct stages in order to send its payload of astronauts and equipment toward the Moon.

Rocket staging comes in two types; see Figure 18.20:

1. Series
2. Parallel

For serial staging (sometimes identified as tandem or vertical staging), the first stage is at the bottom and is usually the largest, the second stage and subsequent upper stages are above it, usually decreasing in size. The first-stage engines are always electronically ignited. As this stage runs out of propellant, the upper retaining cap splits, sending hot gas into the next stage, burning it, and throwing the lower stage back to Earth. This leaves a smaller rocket, with the second stage on the bottom, which then fires. This operates at high altitude and thus under very minimal atmospheric pressure [12]. This process is repeated until the final stage's motor burns to completion. Both Saturn V and Explorer I are examples of series staging.

A popular method for producing a large first stage has been to cluster several rockets together to provide greater combined thrust without having to build a larger rocket. *Clustering* is the act of using two or more motors in a group (or cluster) and having them all ignite simultaneously; as opposed to *staging*, which ignites motors in succession (one after the other). The Saturn IC is an example of engine clusters fed from a single set of propellant tanks; see Figure 18.21.

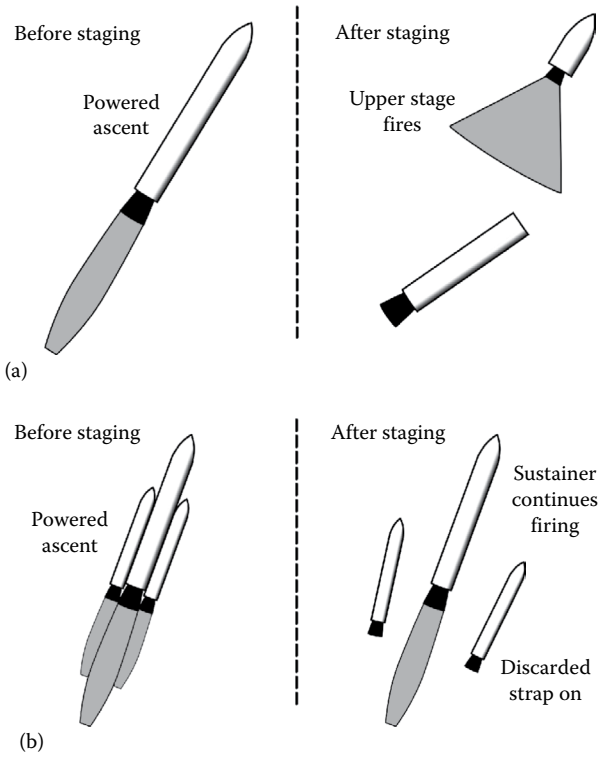


FIGURE 18.20
(a) Serial and (b) parallel staging of rockets.

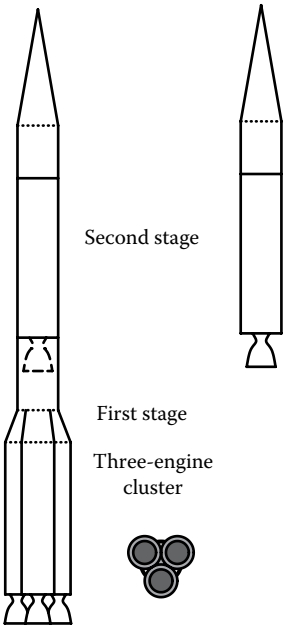


FIGURE 18.21
Clustered rocket.

In parallel staging schemes (Figure 18.20), solid or liquid rocket boosters are used to assist with liftoff. These are sometimes referred to as "stage 0." In the typical case, the first stage and booster engines fire to propel the entire rocket upward. When the boosters run out of fuel, they are detached from the rest of the rocket and fall away. The first stage then burns to completion and falls off. For example, the Atlas is parallel staged; it has two booster engines that are fired along with the central sustainer engine at launch.

18.6.3 Rocket Equation for a Multistage Series Rocket

If (i) refers to the ith of a total of N stages, then the total change in velocity is

$$\Delta u = \sum_{i=1}^{N} \Delta u_i = \sum_{i=1}^{N} \left(V_{eff}\right)_i \times \ell n \left(\frac{m_0}{m_f}\right)_i = \sum_{i=1}^{N} \left(V_{eff}\right)_i \times \ell n \left(\frac{1}{\mathrm{MR}}\right)_i \tag{18.45A}$$

$$\Delta u = \sum_{i=1}^{N} \left(V_{eff}\right)_i \times \ell n \frac{1}{\lambda_i + \delta_i} \tag{18.45B}$$

$$\Delta u = g \sum_{i=1}^{N} \left(I_{sp}\right)_i \times \ell n \left(\frac{m_0}{m_0 - m_p}\right)_i = g \sum_{i=1}^{N} \left(I_{sp}\right)_i \times \ell n \left(\frac{m_0}{m_f}\right)_i \tag{18.45C}$$

$$\Delta u = g \sum_{i=1}^{N} \left(I_{sp}\right)_i \times \ell n \frac{1}{\lambda_i + \delta_i} \tag{18.45D}$$

When the effective speed (V_{eff}) and mass ratios are the same for all the stages, this simplifies to

$$\Delta u = N \times V_{eff} \times \ell n \left(\frac{1}{\mathrm{MR}}\right) \tag{18.46}$$

Moreover, the payload of the ith stage is the sum of all the succeeding stages. Thus, the overall payload ratio (λ_0) is equal to the product of all payloads (λ_i). Thus,

$$\lambda_0 = \prod_{i=1}^{N} \lambda_i \tag{18.47}$$

18.6.4 Rocket Equation for a Parallel Multistage Rocket

For (N) stages, we have the total thrust as the sum of all engines:

$$T_t = \sum_{i=1}^{N} \dot{m}_i \left(V_{eff}\right)_i$$

Total mass flow is

$$\dot{m}_t = \sum_{i=1}^{N} \dot{m}_i$$

Thrust force is then

$$T_t = \dot{m}_t \left(V_{eff}\right)_{ave}$$

where $\left(V_{eff}\right)_{ave}$ is the average exhaust speed and is given by

$$\left(V_{eff}\right)_{ave} = \frac{T_t}{\dot{m}_t} = \frac{\sum_{i=1}^{N} \dot{m}_i \left(V_{eff}\right)_i}{\sum_{i=1}^{N} \dot{m}_i}$$

The rocket equation is then

$$\Delta u = \left(V_{eff}\right)_{ave} \times \ell n\left(\frac{m_0}{m_f}\right) \tag{18.48}$$

18.6.5 Advantages of Staging

For multistage rockets and boosters, once the fuel is exhausted, the space and structure that contained it and the motors themselves are dropped as being no longer useful. Thus, the rocket lightens itself. The thrust of the next stages is able to provide more acceleration than if the earlier stage were still attached, or a single, large rocket was used. Thus, rocket performance is improved by eliminating dead weights.

Each stage can use a different type of rocket motor that is appropriate for its particular operating conditions. Thus, the lower stage motors are designed for use at atmospheric pressure, while the upper stages can use motors suited to near-vacuum conditions. Lower stages tend to require more structure than upper ones as they need to bear their own weight plus that of the stages above them. Optimizing the structure of each stage decreases the weight of the total vehicle and provides further advantage.

Finally, staging provides the capability of a rocket to reduce thrust in mid-flight, thus avoiding severe acceleration for both astronauts and instruments.

18.6.6 Disadvantages of Staging

Staging requires the vehicle to lift motors that are not yet being used. This means that the first stages must produce higher thrusts than they would otherwise have to do.
Staging also makes the entire rocket more complex and harder to build.
In addition, each staging event is a significant potential point of failure during a launch, with the possibility of separation failure, ignition failure, and stage collision.

Example 18.12

A three-stage rocket is designed to place a small satellite into low Earth orbit, having a payload weight of 200 kg; see Figure 18.22. Data for the rocket are given in Table 18.5. Calculate the increase in its speed (Δu).

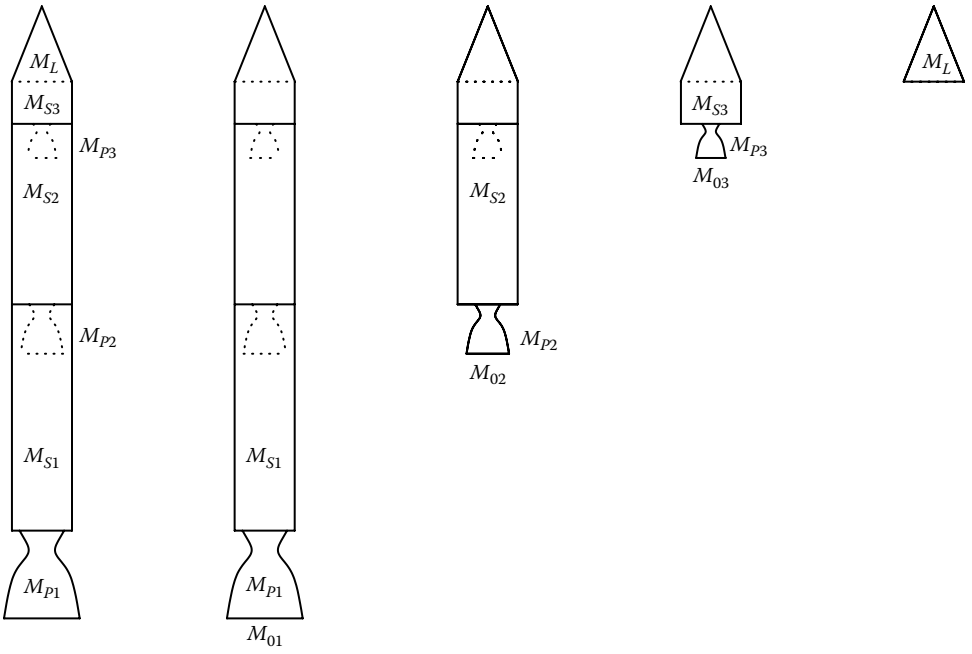


FIGURE 18.22
Three multistage rockets.

TABLE 18.5

Stage Number	Specific Impulse I_{sp} (s)	Total Mass (kg)	Propellant Mass (kg)
1	230	14,000	12,800
2	250	4,500	3,700
3	250	1,000	700

Solution

Calculations will be done using the relation

$$\Delta u = g\sum_{i=1}^{N}\left(I_{sp}\right)_i \times \ell n\left(\frac{m_0}{m_0 - m_p}\right)_i$$

As seen from Table 18.5, most of the weight of the rocket is the weight of the propellants.

First stage: Since the payload is carried atop the third stage into orbit, the total mass of the first stage is

$$m_{01} = m_{t1} + m_{t2} + m_{t3} + m_L$$

$$m_{01} = 14{,}000 + 4{,}500 + 1{,}000 + 200 = 19{,}700 \text{ kg}$$

$$m_{01} - m_{p1} = 19{,}700 - 12{,}800 = 6{,}900 \text{ kg}$$

$$\left(I_{sp}\right)_1 \times \ell n\left(\frac{m_{01}}{m_{01}-m_{p1}}\right) = 285 \times \ell n\left(\frac{19{,}700}{6{,}900}\right) = 285 \times 1.049 = 299 \text{ s}$$

Second stage: As the propellant of the first stage is burned off during powered ascent, the near-empty tank and structure of the first stage are dropped off to reduce the weight of the vehicle to achieve orbital velocity. A smaller amount of propellant is retained in the second- and third-stage tanks.

Thus,

$$m_{02} = m_{t2} + m_{t3} + m_L$$

$$m_{02} = 4500 + 1000 + 200 = 5700 \text{ kg}$$

$$m_{02} - m_{p2} = 5700 - 3700 = 2000 \text{ kg}$$

$$\left(I_{sp}\right)_2 \times \ell n\left(\frac{m_{02}}{m_{02}-m_{p2}}\right) = 265 \times \ell n\left(\frac{5700}{2000}\right) = 265 \times 1.0473 = 277.5 \text{ s}$$

Third stage: The second stage is also dropped off, thus

$$m_{03} = m_{t3} + m_L$$

$$m_{03} = 1000 + 200 = 1200 \text{ kg}$$

$$m_{03} - m_{p3} = 1200 - 700 = 500 \text{ kg}$$

$$\left(I_{sp}\right)_3 \times \ell n\left(\frac{m_{03}}{m_{03}-m_{p3}}\right) = 290 \times \ell n\left(\frac{1200}{500}\right) = 290 \times 0.875 = 253.8 \text{ s}$$

$$\Delta u = 9.81 \times \left(219 + 277.5 + 253.8\right) = 8152.8 \text{ m/s} = 8.15 \text{ km/s}$$

Example 18.13

A small three-stage rocket is designed, having a payload weight of 10 kg; see Figure 18.22. Data for the rocket are given in Table 18.6. Calculate the increase in its speed (Δu).

Solution

Calculations will be done using Equation 18.38B.

$$\Delta u = g \sum_{i=1}^{N} \left(I_{sp}\right)_i \times \ell n\left(\frac{m_0}{m_0 - m_p}\right)_i$$

TABLE 18.6

Stage Number	Specific Impulse I_{sp} (s)	Structural Mass m_{si} (kg)	Propellant Mass m_{pi} (kg)
1	285	40	50
2	265	22	15
3	290	12	9

As seen from Table 18.6, most of the weight of the rocket is the weight of the propellants.

First stage: Since the payload is carried atop the third stage into orbit, the total mass of the first stage is

$$m_{01} = m_L + \sum_{i=1}^{3} m_{si} + m_{pi}$$

$$m_{01} = 10 + 40 + 50 + 22 + 15 + 12 + 9 = 158 \text{ kg}$$

$$m_{01} - m_{p1} = 158 - 50 = 108 \text{ kg}$$

$$\left(I_{sp}\right)_1 \times \ell n\left(\frac{m_{01}}{m_{01} - m_{p1}}\right) = 230 \times \ell n\left(\frac{158}{108}\right) = 230 \times 0.380549 = 87.5 \text{ s}$$

Second stage: As the propellant of the first stage is burned off during powered ascent, the near-empty tank and structure of the first stage are dropped off to reduce the weight of the vehicle to achieve orbital velocity. A smaller amount of propellant is retained in the second- and third-stage tanks.

Thus,

$$m_{02} = 10 + 22 + 15 + 12 + 9 = 68 \text{ kg}$$

$$m_{02} - m_{p2} = 68 - 15 = 53 \text{ kg}$$

$$\left(I_{sp}\right)_2 \times \ell n\left(\frac{m_{02}}{m_{02} - m_{p2}}\right) = 250 \times \ell n\left(\frac{68}{53}\right) = 250 \times 0.2492 = 62.3 \text{ s}$$

Third stage: The second stage is also dropped off, thus

$$m_{03} = 10 + 12 + 9 = 31 \text{ kg}$$

$$m_{02} - m_{p2} = 31 - 9 = 22 \text{ kg}$$

$$\left(I_{sp}\right)_3 \times \ell n\left(\frac{m_{03}}{m_{03} - m_{p3}}\right) = 250 \times \ell n\left(\frac{31}{22}\right) = 250 \times 0.5596 = 85.74 \text{ s}$$

$$\Delta u = 9.81 \times \left(87.5 + 62.3 + 85.74\right) = 2310 \text{ m/s} = 2.31 \text{ km/s}$$

Example 18.14

Figure 18.23 illustrates the European rocket Ariane 5, used to deliver payloads into geostationary transfer orbit (GTO) or low Earth orbit (LEO). Initially at liftoff of an ARIANE 5 launch vehicle two P230 solid-propellant boosters plus the main Vulcain engine



FIGURE 18.23
European rocket Ariane 5.

are ignited. The two different components of the launch vehicle have the following characteristics:

Engine	Vulcain (Main Engine)	Booster P230
Type	Liquid propellant	Solid propellant
Thrust (kN)	1114	6470
Specific impulse (second)	430	275

Calculate

1. Effective velocity for each engine
2. Exhaust mass flow rate
3. Average effective exhaust velocity
4. Average specific impulse

Solution

As described previously, Ariane 5 has two boosters (stage 0) employing solid-propellant engines and a liquid-propellant engine. Thus, the propulsion system here resembles parallel staging.

1. Effective velocity:

$$I_{sp} = \frac{V_{eff}}{g}$$

$$V_{eff} = gI_{sp}$$

For the main engine (Vulcain):

$$\left(V_{eff}\right)_{Vulcain} = 9.81 \times 430 = 4218 \text{ m/s}$$

For the booster (P230):

$$\left(V_{eff}\right)_{\text{P230}} = 9.81 \times 275 = 2698 \text{ m/s}$$

2. Exhaust mass flow rate:

$$\dot{m} = \frac{T}{V_{eff}}$$

For the main engine (Vulcain):

$$\left(\dot{m}\right)_{Vulcain} = \frac{T}{V_{eff}} = 264 \text{ kg/s}$$

For the booster (P230):

$$\left(\dot{m}\right)_{\text{P230}} = \frac{T}{V_{eff}} = 2398 \text{ kg/s}$$

3. Average effective exhaust velocity:

$$\left(V_{eff}\right)_{ave} = \frac{T_t}{\dot{m}_t} = \frac{\left(1114 + 2 \times 6470\right) \times 1000}{264 + 2 \times 2398} = 2777 \text{ m/s}$$

4. Average specific impulse:

$$\left(I_{Sp}\right)_{ave} = \frac{\left(V_{eff}\right)_{ave}}{g} = 283 \text{ s}$$

Example 18.15

In the previous example, launching of Ariane 5 was analyzed. It is now required that we calculate the total change in rocket velocity when it is used to deliver payloads into low Earth orbit (LEO). Details of masses of its 0 stage (boosters), first stage, and second stage are given in the following table:

Stage	0 Stage (Two Boosters)	First Stage	Second Stage
Propellant mass (ton)	237	170	15
Dry mass (ton)	268	16.3	4.7
Specific impulse I_{Sp} (s)	283		446

Pay load or mass to LEO = 10.5 tons

Solution

An Ariane 5 rocket will be handled as parallel and series staging. A parallel staging procedure is followed for boosters (0 stage) and the first stage, then series with the second stage. In the previous example, we calculated the average value for the specific impulse as 283 s.

The increase in rocket speed is calculated using the relation

$$\Delta u = g\sum_{i=1}^{N}\left(I_{sp}\right)_i \times \ell n\left(\frac{m_0}{m_0 - m_p}\right)_i$$

First stage (*including boosters*): Since the payload is carried atop the second stage into orbit, the total mass of the first stage is

$$m_{01} = m_L + \sum_{i=1}^{2} m_{si} + m_{pi}$$

$$m_{01} = 10.5 + \left(268 + 16.3 + 237 + 170\right) + \left(15 + 4.7\right) = 721.5 \text{ tons}$$

$$m_{01} - m_{p1} = 721.5 - \left(237 + 170\right) = 314.5 \text{ kg}$$

$$\left(I_{sp}\right)_1 \times \ell n\left(\frac{m_{01}}{m_{01} - m_{p1}}\right) = 238 \times \ell n\left(\frac{721.5}{314.5}\right) = 238 \times 0.83 = 197.5 \text{ s}$$

Second stage:: As the propellant of the first stage is burned off during powered ascent, the near-empty tank and structure of the first stage are dropped to reduce the weight of the vehicle and achieve orbital velocity. A smaller amount of propellant is retained in the second-stage tank.

Thus,

$$m_{02} = 15 + 4.7 + 10.5 = 30.2 \text{ tons}$$

$$m_{02} - m_{p2} = 30.2 - 10.5 = 19.7 \text{ tons}$$

$$\left(I_{sp}\right)_2 \times \ell n\left(\frac{m_{02}}{m_{02} - m_{p2}}\right) = 446 \times \ell n\left(\frac{43.6}{28.6}\right) = 446 \times 0.4272 = 190.5 \text{ s}$$

$$\Delta u = g\sum_{i=1}^{2}\left(I_{sp}\right)_i \times \ell n\left(\frac{m_0}{m_0 - m_p}\right)_i = 9.81 \times \left(197.5 + 190.5\right) = 3806.3 \text{ m/s}$$

$$\Delta u = 3.8 \text{ km/s}$$

18.7 Space Flight

18.7.1 Orbital Velocity

Rockets are used to launch space stations or satellites (which will be identified here as a space vehicle) into Earth orbits. These revolve round the Earth's atmosphere in a circular orbit of radius (R)

$$R = R_0 + h$$

where
R_0 is the Earth's radius (≅6000 km)
h is the space vehicle altitude above the Earth (≥100 km)

At such an altitude, drag force is absent. A vehicle of mass (m) experiences two equal forces, namely, a gravitational force (which pulls the vehicle toward the Earth and has a radial direction) and a centrifugal force (which pushes the vehicle away from the Earth and also has a radial direction). Therefore, when these forces have equal magnitudes, the vehicle can remain in the orbit forever, without any expenditure of energy. The orbital velocity of the space vehicle (u_{orb}) is then obtained from the relation

$$m\frac{u_{orb}^2}{R} = mg$$

Thus,

$$u_{orb} = \sqrt{Rg} \tag{18.50A}$$

The variation of the gravitational force along the radius (R) is given by

$$g = \left(\frac{R_0}{R}\right)^2 g_0 = \left(\frac{R_0}{R_0 + h}\right)^2 g_0 \tag{18.51}$$

Thus,

$$u_{orb} = \sqrt{\frac{R_0^2}{R} g_0} = R_0\sqrt{\frac{g_0}{R_0 + h}} \tag{18.50B}$$

To calculate a rough estimate for such an orbital velocity and orbital Mach number, assume $h = 100$ km, $R = 6100$ km, and $g \cong 9.8$ m/s^2, then $u_{orb} \cong \sqrt{6.1\times10^6 \times 9.8} \cong 7732$ m/s.

If the sonic speed is approximately equal to 300 m/s, then the orbital Mach number ≅25.77.

From this simple analysis, it is proved that a vehicle requires a flight Mach number ≅25 to achieve a circular low Earth orbit.

If the orbital velocity of say an Earth satellite is equal to the angular velocity of the Earth, then it has a zero velocity relative to the Earth. Such a satellite is identified as a stationary

satellite and can be used for several scientific and technological programs like remote sensing as well as military missions and communications.

18.7.2 Escape Velocity

A rocket provides a means for escaping the Earth (for lunar or interplanetary travel) or the solar system. It may then be used to build a stationary or moving station in space. The following assumptions are made first:

- Vertical flight of the rocket
- Gravitational pull of other planets on the rocket is negligible
- Drag force is negligible

The velocity required to escape from the Earth can be found by equating the kinetic energy of a moving body to the work necessary to overcome gravity. Then

$$\frac{1}{2}mu_{esc}^2 = m\int_R^\infty g\,dR$$

From Equation 18.51,

$$g = \left(\frac{R_0}{R}\right)^2 g_0 = \left(\frac{R_0}{R_0 + h}\right)^2 g_0$$

$$u_{esc}^2 = 2g_0R_0^2\int_R^\infty \frac{dR}{R^2} = 2g_0R_0^2\left(\frac{1}{R}\right)_\infty^R = \frac{2g_0R_0^2}{R}$$

$$u_{esc} = R_0\sqrt{\frac{2g_0}{R_0 + h}} \tag{18.52}$$

$$u_{esc} = \sqrt{2}\,u_{orb} \tag{18.53}$$

It is worth mentioning here that

- The lowest altitude where a stable orbit can be maintained is at an altitude of 185 km.
- This requires an orbital velocity of approximately 7777 m/s.
- To reach this velocity from a space center (on Earth), a rocket requires an ideal velocity increment of 9050 m/s.
- A hydrogen–oxygen system with an effective average exhaust velocity (from sea level to vacuum) of 4000 m/s would require $M_i/M_f = 9.7$.
- A geostationary orbit maintains the same position relative to the Earth's surface. If one could see a satellite in geostationary orbit, it would appear to hover at the same point in the sky. It has an orbital velocity of 11,066 km/h = 3.07 km/s (6,876 miles/h).

Example 18.16

Calculate the escape and orbital velocities of a rocket at an altitude (h = 200 km) using the following data:

Radius of Earth R_0 = 6341 km

Acceleration due to gravity at sea level g_0 = 9.81 m²/s

Solution

From Equation 18.52, the escape velocity is

$$u_{esc} = 6,341 \times 10^3 \times \sqrt{\frac{2 \times 9.81}{(6,341 + 200) \times 10^3}} = 10,982 \text{ m/s}$$

From Equation 18.53,

$$u_{orb} = \frac{u_{esc}}{\sqrt{2}} = 7766 \text{ m/s}$$

Problems

18.1 A rocket powered by a liquid-propellant rocket motor has the following data:

1. Thrust force of 450 kN at sea level
2. Propellant consumption rate = 150 kg/s
3. Gas exit static pressure = 70.0 kPa
4. Exhaust area = 0.5 m²

Calculate the effective exhaust speeds and thrust force in the following cases:

1. Sea-level operation (P_a = 101 kPa)
2. At an altitude of 3 km, ambient pressure is (P_a ~ 70 kPa)
3. In space operation (P_a = 0.0 kPa)
4. Write an explanation

18.2 Calculate a rough estimate for such an orbital velocity and orbital Mach number flight to achieve a circular low Earth orbit for the following case:

1. Height above ground h = 250 km
2. Sonic speed 310 m/s
3. Average gravitational acceleration g = 9.8 m/s²

What is the velocity required to escape from Earth?

18.3 An ideal rocket chamber is to operate at sea level using propellants whose combustion products have a specific heat ratio of 1.30. Determine the required chamber pressure and nozzle area ratio between throat and exit if the exit nozzle Mach number is 2.40. The nozzle inlet Mach number may be considered to be zero.

18.4 Consider two rockets, one a single stage and the other a two stage. The two rockets are designed so that they have identical propellant mass, identical total mass, and

identical specific impulse. Assuming that both are launched vertically, gravity is constant, and drag is zero. Which of the following is correct:

1. The two rockets will go the same distance
2. The single-stage rocket will go farther
3. The two-stage rocket will go farther
4. Cannot be determined

18.5 The ratio of propellant mass to total vehicle mass of a rocket is

1. Greater than
2. Less than
3. About the same as the ratio of fuel mass to total vehicle mass of an airplane
4. Cannot be determined

18.6 A single-stage rocket has the following design parameters:

1. Combustion chamber temperature = 4000 K
2. Combustion chamber pressure = 5 MPa
3. Nozzle throat area = 0.0006 m^2
4. Nozzle exit area = 0.01 m^2
5. Propellant mass = 35 kg
6. Total mass at takeoff = 50 kg
7. Gas constant = 300 $J/kg \cdot K$
8. Ratio of specific heats = 1.35
   a. What is the I_{sp} and takeoff thrust for this rocket?
   b. Assuming the rocket is launched vertically, and neglecting drag, how high will it go?

18.7 A rocket with a mass of 2000 kg is placed vertically on the launching ramp. If the rate at which the propellants are consumed is equal to 4 kg/s, find the rocket exhaust velocity if the rocket just begins to rise.

18.8 A rocket's supersonic nozzle is to be designed with a combustion chamber pressure of 3.8 MPa and an ambient pressure of 101 kPa. Find the ratio between the thrust at sea level to the thrust in space (0 kPa). Assume that $R = 0.4$ $kJ/kg \cdot K$ and $\gamma = 1.3$.

18.9 Given the following data for a rocket:

Time (s)	0	0.5	1.0	2.0	2.5	3.0	3.25	3.35
Thrust (N)	5500	7000	6500	6400	5800	5400	5000	0

determine the total impulse of the motor.

18.10 A rocket has the following characteristics:

1. Initial mass = 250 kg
2. Mass after rocket operation = 140 kg
3. Mass of payload and structure = 120 kg
4. Specific impulse = 285 s
5. Rocket operation = 3.5 s

Calculate

a. Mass ratio
b. Propellant mass flow rate
c. Thrust
d. Exit velocity
e. Total impulse

18.11 A rocket flies at 7500 km/h where the ejected propellant mass flow rate is 5.0 kg/s. The propellant heating value is 7.1 MJ/kg. Draw the propulsive, thermal, and overall efficiencies for a flight to the effective jet velocity ratio $\sigma = 0 - 3$.

18.12 A rocket is fired from a flying airplane. The Mach number of the aircraft is 0.85 and the speed of the exhaust gases from the rocket relative to the fixed station on the ground is 2600 m/s. Exhaust gases from the rocket have a pressure of 85 kPa and a density 0.62 kg/m^3. The diameter of the nozzle exit is 220 cm^2. If the aircraft is flying at 6 and 12 km, calculate

1. Exhaust speed
2. Effective exhaust speed
3. Thrust force

18.13 Prove that the thrust force of a rocket motor is expressed by the relation

$$\frac{T}{P_{0t}A_t} = \sqrt{\left(\frac{2\gamma^2}{\gamma-1}\right)\left(\frac{2}{\gamma+1}\right)^{\gamma+1/\gamma-1}\left[1-\left(\frac{P_e}{P_{0t}}\right)^{\gamma-1/\gamma}\right]} + \left(\frac{P_e}{P_{0t}} - \frac{P_a}{P_{0t}}\right)\frac{A_e}{A_t}$$

where

P_{0t} is the total pressure in the combustion chamber
P_e is the nozzle exit pressure
A_t is the nozzle throat area
A_e is the nozzle exit area
γ is the ratio of specific heats

18.14 Prove that if the payload ratio (λ) and the structural ratio (ε) are defined as

$$\lambda = \frac{m_L}{m_0 - m_L} \quad \text{and} \quad \varepsilon = \frac{m_s}{m_0 - m_L}$$

then

$$\lambda = \frac{e^{-(\Delta u/V_{eff})} - \varepsilon}{1 - e^{-(\Delta u/V_{eff})}}$$

Next, plot (λ) versus ($\Delta u/V_{eff}$) for $\varepsilon = 0.06 - 0.24$ and $\Delta u/V_{eff} = 1.8 - 3.6$.

18.15 Calculate the total speed (Δu) of a three-staged rocket having the following data:

Stage	Structural Mass m_s (tons)	Propellant Mass m_p (tons)	Effective Speed V_{eff} (m/s)
1	5.5	44	2450
2	1.2	12	2650
3	0.25	1.25	3100

The payload mass that has to be put into orbit is 850 kg.

a. If a simple single stage to orbit (SSTO) rocket having the same payload, total structural mass, and total propellant mass is used, calculate the rocket speed.

b. What is the gain in rocket speed when a three-stage case is used compared to the SSTO rocket?

18.16 A two-stage rocket has the following data:

Stage	Propellant Mass m_p (tons)	Dry Mass m_s (tons)	Specific Impulse (s)
1	125	10	265
2	31	3.5	325

If the payload mass is 3000 kg, calculate the total speed (Δu) of this two-staged rocket.

18.17 A rocket engine that has an exhaust velocity of 3400 m/s is used to accelerate a vertically launched rocket vehicle to a speed of 4000 m/s. Find the approximate ratio of the propellant mass to the dry vehicle mass that is required.

References

1. J.M. Lyon, Introduction to rocket propulsion, Technical Report RD-PR-91-17, http://www.reactionengines.co.uk/index.html, US Army Missile Command, Redstone, Arsenal, AL, December 1991.
2. M. Gruntman, *Blazing the Trail: The Early History of Spacecraft and Rocketry*, AIAA, Reston, VA, Chapters 1 and 2, 2004.
3. G.P. Sutton and O. Biblarz, *Rocket Propulsion Elements*, 8th edn., Wiley, New York, 2010.
4. M.J.L. Turner, *Rocket and Spacecraft Propulsion—Principles, Practice and New Development*, 3rd edn., Springer, Berlin, Germany, 2009.
5. S.M. Yahya, *Fundamentals of Compressible Flow with Aircraft and Rocket Propulsion*, SI edn., New Age International Publisher, New Delhi, India, 1982.
6. Marshal Space Flight Center (MSFC, History Center), NASA, Huntsville, AL, http://history.msfc.nasa.gov/rocketry/.
7. W. von Braun and F. Ordway, In Y. Thomas (Ed.), *History of Rocketry and Space Travel*, 3rd edn., Crowell, New York, 1974.
8. R.H. Goddard, In E.C. Goddard and G.E. Pendray (Eds.), *A Method of Reaching Extreme Altitudes*, Three volumes, McGraw Hill Book Company, Smithsonian Miscellaneous Collections, 1970, Vol. 71(2), 1919pp.
9. M.J. Moran, H.N. Shapiro, D.D. Boettner, and M.B. Bailey, *Fundamentals of Engineering Thermodynamics*, 8th edn., John Wiley & Sons, New York, 2013.
10. J.W. Cornelisse, H.F.R. Schoyer, and K.F. Wakker, *Rocket Propulsion and Space Flight Dynamics*, Pitman Publishing, London, U.K., 1979.
11. Multi-stage rockets, Valkyrie Report No. 5105. Vashon Industries Inc.
12. J.J. Pocha, *An Introduction to Mission Design for Geostationary Satellites*, Kluwer Academic Publishers, Hingham, MA, 1972.


Taylor & Francis
Taylor & Francis Group
http://taylorandfrancis.com

19

Rocket Engines

Rocket propulsion is the means of providing power to accelerate the rocket and sustain it, if necessary, to reach the required target. The basis for the working of missile propulsion systems is Newton's three laws of motion.

As discussed previously, rockets are propelled using one of the following two ways:

1. Non-airbreathing or rocket engines. Thrust is produced by the expulsion of hot gases from a combustion chamber through an exhaust nozzle. Oxygen for burning the fuel would normally be carried in the vehicle, not collected from the atmosphere.
2. A combination of airbreathing (ramjet, turbojet, or turbofan engines) and non-air breathing (rocket) engines. A Tomahawk surface-to-surface missile combines a solid-propellant booster rocket for liftoff and a small turbojet for sustained flight.

Energy is generated through one of the following sources (see Figure 19.1):

1. Chemical (solid, liquid, and hybrid)
2. Electrical (electrostatic, electrothermal, and electromagnetic)
3. Solar (solar sail rocket, solar-heated rocket)
4. Nuclear (nuclear fission rocket, nuclear fusion rocket, photon rocket)

19.1 Chemical Rocket Engines

19.1.1 Introduction

All types of rocket propulsion engines contain a chamber, a nozzle, and an igniter. A chemical rocket is unique in being a carrier for the whole energy source necessary for its acceleration.

The chemical reaction of propellant chemicals (usually a fuel and an oxidizer) takes place in the chamber and produces gases. The energy due to this high-pressure reaction permits the heating of the product gases to a very high temperature (2000°C–3500°C). These hot gases subsequently are expanded in the convergent–divergent nozzle and accelerated to high velocities (2000–4500 m/s). The nozzle design (shape and size) is critical for the efficient function of the propulsion system.

Chemical rockets are either

- Solid propellant
- Liquid propellant
- Hybrid propellant

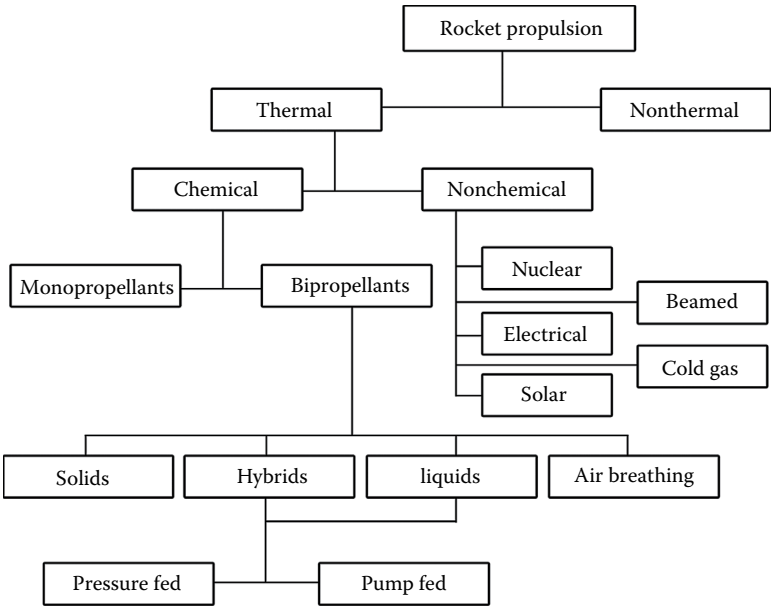


FIGURE 19.1
Classification of rocket propulsion systems.

19.1.2 Performance Characteristics

The engine's main components are composed of two elements, namely, a combustion chamber and a CD nozzle. Figure 19.2 illustrates these two modules as well as the corresponding processes on a T–S diagram. The combustion process is assumed to be a heat addition process at constant pressure or with a certain total pressure drop, ΔP_c. Flow in the

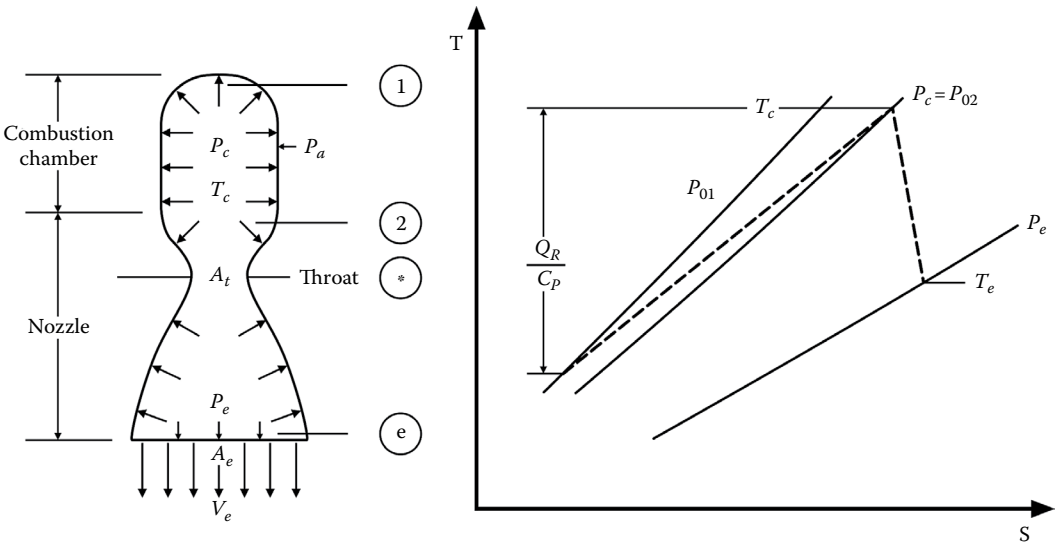


FIGURE 19.2
Rocket engine.

nozzle expansion is assumed to be an isentropic expansion or an adiabatic process with a certain isentropic efficiency. Thus, flow in both modules can be described as follows.

Combustion chamber:

$$\Delta P_c = P_{01} - P_c$$

where P_c is the combustion chamber or the chamber's total pressure. If $\Delta P_c = 0$, then $P_{01} = P_c$.

Heat added is

$$\dot{m}_p Q_R = \dot{m}_p C_p \left(T_{02} - T_{01}\right)$$

19.2 Solid Propellants

19.2.1 Introduction

Solid-propellant rockets are the oldest type of rocket and date back to ancient China. They are relatively simple in construction as shown in Figure 19.3. The term "motor" is used for solid rockets while the term "engine" is used for liquid rockets. A simple solid rocket motor consists of a casing, propellant charge, igniter, and nozzle. They contain both the solid fuel (e.g., plastic or resin material) and solid oxidizer (nitrates, perchlorates, etc.) components, which are combined into a single solid-propellant mixture within a cylindrical combustion chamber or case. The propellant charge contains all of the chemical elements required for complete burning and is formed into a solid mass called the grain. The propellant is cast into the rocket shell with a central cavity that may have different shapes including a star-shape as shown in Figure 19.3. The thrust-burning time profile depends on this cavity. A liner provided between the case and the propellant protects the case from high temperatures developing inside the propellant layers.

Under normal temperature conditions, the propellant does not burn. An electrical signal is sent to the igniter, which creates hot gases that ignite the main propellant grain. Once the flame front is established, combustion is self-sustaining. The rate of burning is proportional to the exposed surface area. As the propellant burns, hot exhaust gas is produced, which is used to propel the rocket, and a "flame front" is produced, which moves into the propellant. Once the burning starts, it will continue until all the propellant is expended. Once grain design and propellant composition is fixed for a rocket motor, the nozzle and its design become the controlling factors for its performance.

When selecting solid propellant, the rocket must have the following features:

1. High chemical energy to generate maximum thrust and specific impulse
2. High density to enable packing a large quantity of propellant in a small volume
3. Low molecular weight so that the exhaust gases achieve high acceleration
4. Easy to ignite
5. Burns steadily at a predictive rate
6. Easy to fabricate
7. Smoke free and nontoxic

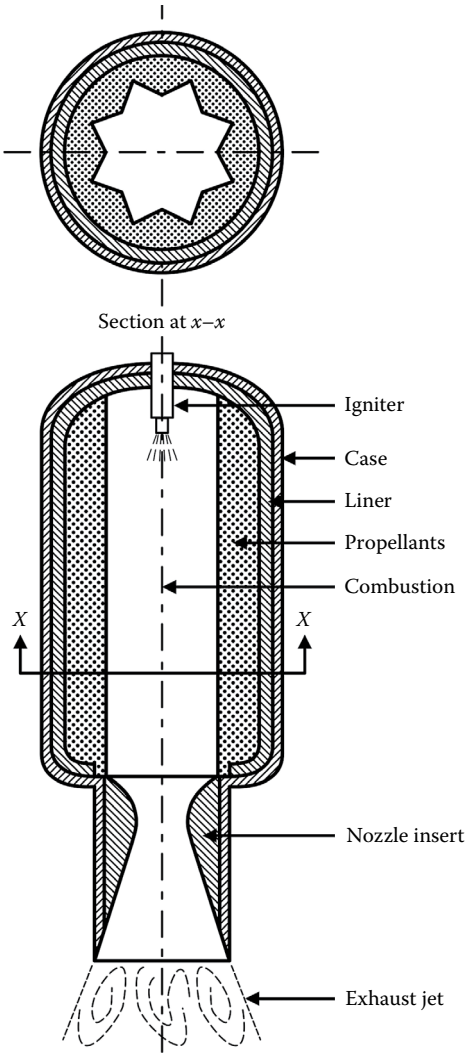


FIGURE 19.3
Typical solid-propellant rocket motor.

Space Shuttle solid rocket boosters (SRBs) are the largest solid-propellant motors ever flown and the first designed for reuse. Each measures 18.17 ft in diameter and 149.16 ft high and generates 3,300,000 lb of sea-level thrust. Its weight with the propellant is 1,300,000 lb. Its propellant is ammonium perchlorate/aluminum and has an 11-point star shape in the forward motor segments and a double truncated cone in the aft segments. The burn time is 75 s and its expansion ratio is 11.3. After burnout at approximately 150,000 ft, the spent cases separate from the vehicle, arc up to approximately 220,000 ft before parachuting to the ocean for recovery and reuse.

Solid rockets have the following advantages:

1. Compact and smaller in size with a comparable liquid rocket
2. Do not require a propellant feeding system or turbo-pumps as in liquid rockets

3. High thrust to weight ratio
4. Require little maintenance
5. Safe and reliable, thus can sit for years before firing

Disadvantages of solid rockets:

1. Once ignited they cannot be shut off since they contain all the ingredients necessary for combustion within the combustion chamber.
2. They can only be used once.

19.2.2 Composition of a Solid Propellant

There are basically three types of propellant grains:

1. *Homogeneous or colloidal propellants*: These are found in the early solid rockets. Here, fuel and oxidizer are contained in the same molecule that decomposes during combustion. Typical examples are nitroglycerine (NG) and nitrocellulose (NC). Most propellants are double-based, though a few single-based and triple-based propellants are found. Double-based propellants are combinations of nitroglycerine (NG) and nitrocellulose (NC); examples are [$C_3H_5(NO_2)_3$ and $C_6H_7O_2(NO_2)_3$], with a small quantity of additives. It has nontoxic and smokeless exhausts.
2. *Composite or heterogeneous propellants*: These are mixtures of oxidizing crystals and a powered fuel (usually aluminum) held together in a binder typically of synthetic rubber (or plastic). Sometimes, light metal powders are added to the propellant to increase the energy of the combustion process as well as fuel density. They are more stable than homogeneous propellants and are preferred in long-term stored rockets. However, the addition of light metals makes their exhaust toxic and smoky.
3. *Composite modified double-based propellants*: These are a heterogeneous combination of the double-based homogeneous (colloidal) propellants and composite propellants. Usually, they are powdered aluminum fuel held in a matrix of (NG)–(NC) and a crystalline oxidizer (ammonium perchlorate).

19.2.3 Basic Definitions

Some definitions concerning grain are given here:

1. *Cylindrical grain*: A grain in which the internal cross section is constant along the axis regardless of perforation shape.
2. *Perforation*: The central cavity port or flow passage of a propellant grain; its cross section may be cylindrical, tubular, or rod or star shaped (see Figure 19.4). All have a circular outer boundary due to the rocket casing shape.
3. *End burning* (*or cigarette burning*): This grain is the most common.
4. *Neutral burning*: Motor burn time during which thrust, pressure, and burning surface area remain approximately constant, typically within about +15%; see Figure 19.5.

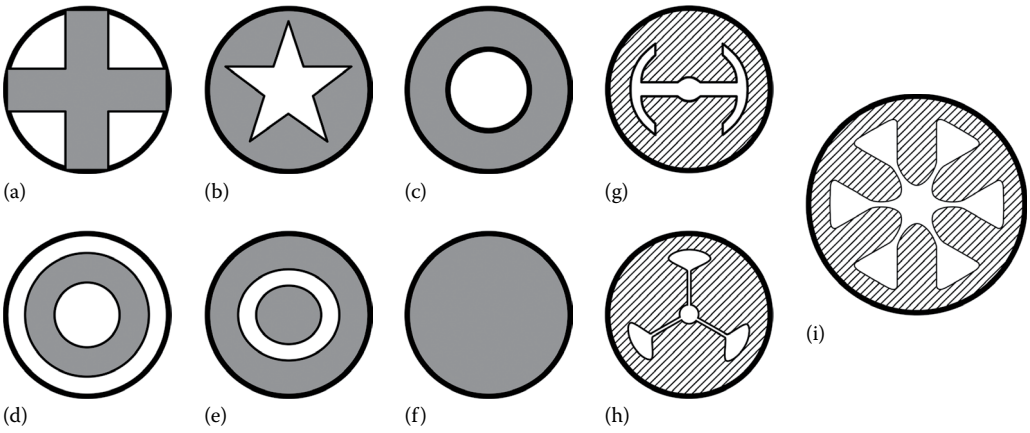


FIGURE 19.4
Grain cross sections: (a) cruciform grain, (b) start grain, (c) cylindrical grain, (d) tubular grain, (e) rod and tube grain, (f) end-burning grain, (g) anchor, (h) dogbone, and (i) wagon wheel.

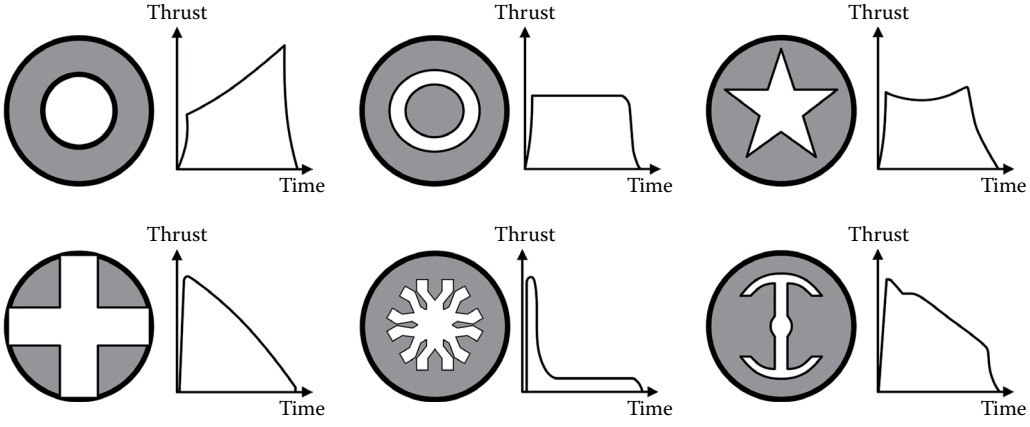


FIGURE 19.5
Thrust profile for different grain cross sections.

5. *Progressive burning*: Burn time during which thrust, pressure, and burning surface area increase (Figure 19.5).
6. *Regressive burning*: Burn time during which thrust, pressure, and burning surface area decrease (Figure 19.5).
7. *A stoichiometric mixture of fuel and oxidizer*: This is the correct proportion for complete combustion. Thus, the fuel is identified as oxygen balanced. If the propellant contains insufficient oxygen for complete burning it is called underoxidized, and if it contains too much oxygen, it is called over-oxidized.
8. *Sliver*: Unburned propellant remaining (or lost—that is, expelled through the nozzle).

19.2.4 Burning Rate

The burning rate in a full-scale motor depends on [1]

1. Combustion chamber pressure
2. Initial temperature of the solid-propellant prior to start
3. Combustion gas temperature
4. Velocity of the gas flow parallel to the burning surface
5. Motor motion (acceleration and spin-induced grain stress)

The burning rate r for a solid propellant is defined as the recession of the propellant surface in a direction perpendicular to this burning surface per unit time. The burning surface regresses by burning parallel layers in a direction perpendicular to the surface itself. The burning rate is dependent only on propellant composition and its initial temperature as well as the chamber pressure. At any given initial temperature, the empirical relationship between pressure and burning rate, known as Vielle's law, may be written as

$$\dot{r} = aP_c^n \tag{19.1A}$$

where

$\dot{r}$ is the burn rate, usually given in mm per second
P_c is the chamber pressure given in MPa
n is the burning rate pressure exponent, sometimes called the combustion index, which is independent of the initial grain temperature and describes the influence of chamber pressure on the burning rate
a is an empirical constant influenced by the initial propellant temperature prior to ignition (T_p)

It is also known as the temperature coefficient, which is dimensional quantity, and is expressed by the relation

$$a = \frac{A}{T_1 - T_p} \tag{19.2}$$

where both (A) and (T_1) are empirical constants.

Thus,

$$\dot{r} = \frac{A}{T_1 - T_p} P_c^n \tag{19.1B}$$

Here, some few remarks concerning the exponent (n) can be summarized [1]:

- The burning rate is very sensitive to the exponent (n).
- For stable operation, (n) has values greater than 0 and less than 1.0.
- A propellant having a pressure exponent of zero displays essentially zero change in burning rate over a wide pressure range.
- Most production propellants have a pressure exponent (n) ranging between 0.2 and 0.6.

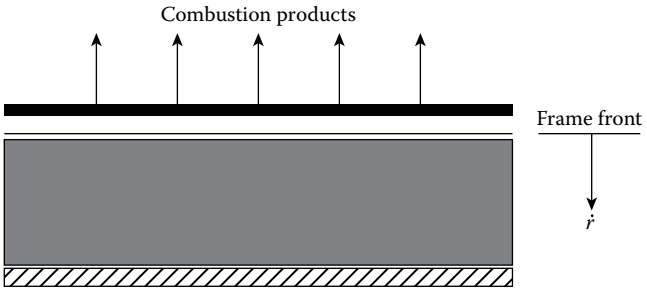


FIGURE 19.6
Surface regression and gas generation.

- As (n) approaches 1, the burning rate and chamber pressure become very sensitive to one another and disastrous rises in the chamber pressure can occur in a few milliseconds.
- When the (n) value is low and comes closer to zero, burning can become unstable and may even extinguish itself.
- Some propellants display a negative (n), which is important for "restartable" motors, the burning rate, and chamber pressure.

The mass flow rate of gas generation from the motor (see Figure 19.6) is

$$\dot{m}_g = \rho_p A_b \dot{r} \tag{19.3}$$

where
ρ_p is the solid-propellant density
A_b is the area of the burning surface
$\dot{r}$ is the burn rate or surface regression speed
$\dot{m}_g$ is the rate of gas generation at the propellant surface

The total burned mass of propellant (m_g) can be determined by integrating Equation 19.3:

$$m_g = \int \dot{m}_g dt = \rho_p \int A_b \dot{r} dt \tag{19.4}$$

From the principle of conservation of matter, the rate of propellant mass flow is equal to the rate of mass flow through the exhaust nozzle. Then from Equation 18.22A, with $P_c = P_{0e}$ and $T_c = T_{0e}$,

$$\dot{m}_g = \rho_p A_b \dot{r} = \frac{A^* P_c}{C^*} = A^* P_c \sqrt{\frac{\gamma}{RT_c}\left(\frac{2}{\gamma+1}\right)^{\gamma+1/\gamma-1}} \tag{19.5}$$

$$P_c = \rho_p C^* a P_c^n \frac{A_b}{A^*}$$

The pressure of the combustion chamber is then

$$P_c = \left[\rho_p C^* a \left(\frac{A_b}{A^*}\right)\right]^{1/1-n} \tag{19.6}$$

The ratio between the burn area and the throat area is

$$\frac{A_b}{A^*} = \frac{P_c}{\rho_p \dot{r}} \sqrt{\frac{\gamma}{RT_c}\left(\frac{2}{\gamma+1}\right)^{\gamma+1/\gamma-1}} \tag{19.7A}$$

Since $P_c \equiv P_{0e}$, then from Equation 19.1A,

$$\frac{A_b}{A^*} = \frac{P_c^{(1-n)}}{\rho_p a} \sqrt{\frac{\gamma}{RT_c}\left(\frac{2}{\gamma+1}\right)^{\gamma+1/\gamma-1}} \tag{19.7B}$$

Example 19.1

For a combined end and radial burning of a solid-propellant rocket, prove that the rate of change of combustion pressure (P_c) is expressed by both the equations:

$$\frac{dP_c}{dt} = \left(\frac{8P_c}{1-n}\right)\left(\frac{\dot{r}}{D}\right)\left(\frac{\left(\frac{L}{D}-\frac{d}{D}\right)}{4\left(\frac{d}{D}\right)\left(\frac{L}{D}\right)+1-\left(\frac{d}{D}\right)^2}\right)$$

and

$$\frac{dP_c}{dt} = \left(\frac{8P_c^{n+1}}{1-n}\right)\left(\frac{a}{D}\right)\left(\frac{\left(\frac{L}{D}-\frac{d}{D}\right)}{4\left(\frac{d}{D}\right)\left(\frac{L}{D}\right)+1-\left(\frac{d}{D}\right)^2}\right)$$

where $\dot{r} = aP_c^n$ is the burning rate.

The grain in such a solid propellant is a hollow cylinder having a length (L), inner radius (d), and outer radius (D).

Evaluate this rate in the following case:

$$\dot{r} = 10P_c^{0.7}\ \text{mm/s}, \quad P_c = 8.0\ \text{MPa}, \quad L/D = 10, \quad d/D = 0.4, \quad \text{and} \quad D = 2.0\ \text{m}.$$

Solution

$$A_b = \pi dL + \frac{\pi}{4}\left(D^2 - d^2\right)$$

$$\frac{dA_b}{dt} = \pi L\frac{d(d)}{dt} + \pi d\frac{dL}{dt} + \frac{\pi}{4}\left[-2d\frac{d(d)}{dt}\right] \tag{a}$$

Due to the regression in the radial direction,

$$\frac{d(d)}{dt} = 2\dot{r}$$

And also due to the regression in the axial direction,

$$\frac{dL}{dt} = -\dot{r}$$

$$\frac{dA_b}{dt} = \pi L(2\dot{r}) + \pi d(-\dot{r}) + \frac{\pi}{4}\left[-2d(2\dot{r})\right] = 2\pi\dot{r}(L-d)$$

$$\frac{1}{A_b}\frac{dA_b}{dt} = \frac{2\pi(L\dot{r} - d\dot{r})}{\pi dL + \frac{\pi}{4}(D^2 - d^2)} = \frac{8\pi\dot{r}(L-d)}{\pi(4dL + D^2 - d^2)}$$

$$\frac{1}{A_b}\frac{dA_b}{dt} = \frac{8\dot{r}(L-d)}{(4dL + D^2 - d^2)} = \frac{8\frac{\dot{r}}{D}\left(\frac{L}{D} - \frac{d}{D}\right)}{4\left(\frac{d}{D}\right)\left(\frac{L}{D}\right) + 1 - \left(\frac{d}{D}\right)^2} \tag{b}$$

Since the combustion pressure is expressed by

$$P_c = \left(\frac{A_b}{A^*}\frac{a\rho_p}{\sqrt{\frac{\gamma}{RT_c}\left(\frac{2}{\gamma+1}\right)^{\gamma+1/\gamma-1}}}\right)^{1/1-n}$$

Differentiating w.r.t. time,

$$\frac{dP_c}{dt} = \frac{P_c}{1-n}\frac{1}{A_b}\frac{dA_b}{dt} \tag{c}$$

From Equations b and c,

$$\frac{dP_c}{dt} = \left(\frac{8P_c}{1-n}\right)\left(\frac{\dot{r}}{D}\right)\left(\frac{\left(\frac{L}{D} - \frac{d}{D}\right)}{4\left(\frac{d}{D}\right)\left(\frac{L}{D}\right) + 1 - \left(\frac{d}{D}\right)^2}\right)$$

Substituting for ($\dot{r}$),

$$\frac{dP_c}{dt} = \left(\frac{8P_c^{n+1}}{1-n}\right)\left(\frac{a}{D}\right)\left(\frac{\left(\frac{L}{D} - \frac{d}{D}\right)}{4\left(\frac{d}{D}\right)\left(\frac{L}{D}\right) + 1 - \left(\frac{d}{D}\right)^2}\right)$$

Now from the relation $\dot{r} = 10P_c^{0.7}$ mm/s, P_c = 8.0 MPa, L/D = 10, d/D = 0.4, and D = 2.0 m

$$\frac{dP_c}{dt} = \left(\frac{8\times 8^{1.7}}{1-0.7}\right)\left(\frac{10\times 10^{-3}}{2}\right)\left(\frac{10-0.4}{4(0.4)(10)+1-(0.4)^2}\right) = 2.6068 \text{ MPa/s}$$

This time the rate for combustion chamber pressure represents a *progressive* type of burning.

Example 19.2

Deduce two relations for the following burning cases:

1. End burning only (the hollow core of the solid propellant remains uniform during burning)
2. Radial burning only (the length of the propellant remains constant during burning)
3. Recalculate the rate of change of combustion chamber having the same data in Example 19.1 in these two cases

Solution

The rate of change of the burning area is expressed by Equation a

$$\frac{dA_b}{dt} = \pi L \frac{d(d)}{dt} + \pi d \frac{dL}{dt} + \frac{\pi}{4}\left[-2d\frac{d(d)}{dt}\right]$$

Case (1): End burning only.

$$\frac{d(d)}{dt} = 0, \quad \text{thus} \quad \frac{dA_b}{dt} = \pi d \frac{dL}{dt} = -\pi d\dot{r}$$

$$\frac{1}{A_b}\frac{dA_b}{dt} = \frac{\pi d\dot{r}}{\pi dL + \frac{\pi}{4}\left(D^2 - d^2\right)} = \frac{-4\pi d\dot{r}}{\pi\left(4dL + D^2 - d^2\right)}$$

$$\frac{dP_c}{dt} = \left(\frac{P_c}{1-n}\right)\left(\frac{1}{A_b}\frac{dA_b}{dt}\right) = \left(\frac{P_c}{1-n}\right)\left(\frac{-4\pi d\dot{r}}{\pi\left(4dL + D^2 - d^2\right)}\right)$$

$$\frac{dP_c}{dt} = -\left(\frac{4P_c}{1-n}\right)\left(\frac{\dot{r}}{D}\right)\left(\frac{\frac{d}{D}}{4\left(\frac{d}{D}\right)\left(\frac{L}{D}\right) + 1 - \left(\frac{d}{D}\right)^2}\right)$$

$$\frac{dP_c}{dt} = -\left(\frac{4P_c^{n+1}}{1-n}\right)\left(\frac{a}{D}\right)\left(\frac{\frac{d}{D}}{4\left(\frac{d}{D}\right)\left(\frac{L}{D}\right) + 1 - \left(\frac{d}{D}\right)^2}\right)$$

For the same data in Example 19.1,

$$\frac{dP_c}{dt} = -\left(\frac{4 \times 8^{1.7}}{1-0.7}\right)\left(\frac{10 \times 10^{-3}}{2}\right)\left(\frac{0.4}{4(0.4)(10) + 1 - (0.4)^2}\right) = -0.054 \text{ MPa/s}$$

This resembles a *regressive* burning.

Case (2): Radial burning only.

$$\frac{dL}{dt} = 0$$

$$\frac{dA_b}{dt} = \pi L \frac{d(d)}{dt} + \frac{\pi}{4}\left[-2d\frac{d(d)}{dt}\right]$$

$$\frac{dA_b}{dt} = \pi L(2\dot{r}) + \frac{\pi}{4}\left[-2d(2\dot{r})\right] = \pi\dot{r}(2L-d)$$

$$\frac{1}{A_b}\frac{dA_b}{dt} = \frac{\pi\dot{r}(2L-d)}{\pi dL + \frac{\pi}{4}(D^2-d^2)} = \frac{4\pi\dot{r}(2L-d)}{\pi(4dL+D^2-d^2)}$$

$$\frac{dP_c}{dt} = \left(\frac{P_c}{1-n}\right)\left(\frac{1}{A_b}\frac{dA_b}{dt}\right) = \left(\frac{4P_c}{1-n}\right)\left(\frac{\dot{r}}{D}\right)\left(\frac{2\frac{L}{D}-\frac{d}{D}}{4\left(\frac{d}{D}\right)\left(\frac{L}{D}\right)+1-\left(\frac{d}{D}\right)^2}\right)$$

$$\frac{dP_c}{dt} = \left(\frac{4P_c^{n+1}}{1-n}\right)\left(\frac{a}{D}\right)\left(\frac{2\frac{L}{D}-\frac{d}{D}}{4\left(\frac{d}{D}\right)\left(\frac{L}{D}\right)+1-\left(\frac{d}{D}\right)^2}\right)$$

Now for the same data listed in Example 19.1

$$\frac{dP_c}{dt} = \left(\frac{4\times 8^{1.7}}{1-0.7}\right)\left(\frac{10\times 10^{-3}}{2}\right)\left(\frac{2\times 10-0.4}{4(0.4)(10)+1-(0.4)^2}\right) = 2.661\ \text{MPa/s}$$

This resembles a *progressive* burning.

The sum of both the pure radial and end burning cases yields the combined case, as is clear from the results in Examples 19.1 and 19.2.

Example 19.3

A solid-propellant rocket has the following data:

Combustion chamber temperature = 2600 K
Combustion chamber pressure = 20 MPa
Propellant density = 1600 kg/m^3
Throat diameter = 46 mm
Exhaust gas constant $R = 400$ J/(kg·K)
Gas specific heat ratio $\gamma = 1.2$
Vielle's law constants $\dot{r} = 0.0025\,\text{m/s}$
Burn time = 14 s
Exit pressure = 100 kPa

Calculate

1. The solid fuel grain diameter
2. Characteristic velocity
3. Optimal thrust coefficient
4. Thrust force

5. The mass flow rate and total burnt mass of the propellant
6. The specific impulse
7. The total impulse

Solution

1. From Equation 19.7A,

$$\frac{A_b}{A^*} = \frac{P_c}{\rho_p \dot{r}} \sqrt{\frac{\gamma}{RT_c}\left(\frac{2}{\gamma+1}\right)^{\gamma+1/\gamma-1}}$$

$$\frac{A_b}{A^*} = \frac{(20)\times 10^6}{1600\times 25\times 10^{-4}} \sqrt{\frac{1.2}{400\times 2600}\left(\frac{2}{2.2}\right)^{2.2/0.2}} = (3.1796)\times 10^3$$

$$\frac{d_b}{d^*} = 56.388$$

Since the throat diameter = 0.046 m, the throat area A^* = 0.00166 m^2.
The grain area is then = 5.278 m^2.

2. The characteristic velocity

$$C^* = \sqrt{\frac{RT_c}{\gamma\left(\frac{2}{\gamma+1}\right)^{\gamma+1/\gamma-1}}} = \sqrt{\frac{400\times 2600}{1.2\times\left(\frac{2}{2.2}\right)^{2.2/0.2}}} = 1572.5 \text{ m/s}$$

3. Optimal thrust coefficient.
From Equation 18.23C,

$$C_{F,opt} = \sqrt{\left(\frac{2\gamma^2}{\gamma-1}\right)\left(\frac{2}{\gamma+1}\right)^{\gamma+1/\gamma-1}\left[1-\left(\frac{P_e}{P_{oe}}\right)^{\gamma-1/\gamma}\right]}$$

$$C_{F,opt} = \sqrt{\frac{2\times 1.2^2}{0.2}\times\left(\frac{2}{2.2}\right)^{11}\times\left[1-\left(\frac{100}{20{,}000}\right)^{0.2/1.2}\right]} = 1.72$$

4. The thrust force is

$$T = C_{F,opt} P_c A^* = 1.72\times 20\times 10^6 \times 0.00166 = 57{,}104 \text{ N}$$

5. The mass flow rate of the exhaust gases is calculated from Equation 11.15 as

$$\dot{m} = \frac{A^* P_c}{\sqrt{T_c}}\sqrt{\frac{\gamma}{R}}\left(\frac{2}{\gamma+1}\right)^{\gamma+1/2(\gamma-1)} = \frac{0.00166\times 20\times 10^6}{\sqrt{2600}}\times\sqrt{\frac{1.2}{400}}\times\left(\frac{2}{2.2}\right)^{\frac{2.2}{0.4}} = 21.11 \text{ kg/s}$$

The total burnt mass of the propellant is

$$m = \dot{m}\times t_b = 295.6 \text{ kg}$$

6. The specific impulse is

$$I_{sp} = \frac{T}{\dot{m}g} = \frac{57{,}104}{21.11 \times 9.81} = 275.74 \text{ s}$$

7. The total impulse is

$$I_t = \overline{T} t_b$$

where $\overline{T}$ is the average thrust over the burning duration. Assuming $\overline{T} = 57{,}104$ N, then the total impulse will be

$$I_t = 57{,}104 \times 14 = 7.995 \times 10^5 \text{ N} \cdot \text{s}$$

Example 19.4

Consider two solid-propellant rockets (1) and (2) having the same combustion chamber temperature of 2600 K.

	Rocket 1	**Rocket 2**
Combustion pressure P_c (MPa)	18	9
Burning time (s)	12	?

What is the burning time of rocket (2)?

Solution

Since the propellant mass flow rate depends on the combustion chamber pressure,

$$\dot{m} \sim P_c$$

Moreover, the total burnt mass of the propellant is defined by

$$m = \dot{m} \times t_b$$

$$t_b \sim \frac{1}{P_c}$$

or

$$\frac{t_{b2}}{t_{b1}} = \frac{P_{c1}}{P_{c2}}$$

The burning time is then

$$t_{b2} = \frac{12 \times 18}{9} = 24 \text{s}$$

A plot for pressure variation versus burning time for the two cases of combustion chamber pressure is illustrated in Figure 19.7.

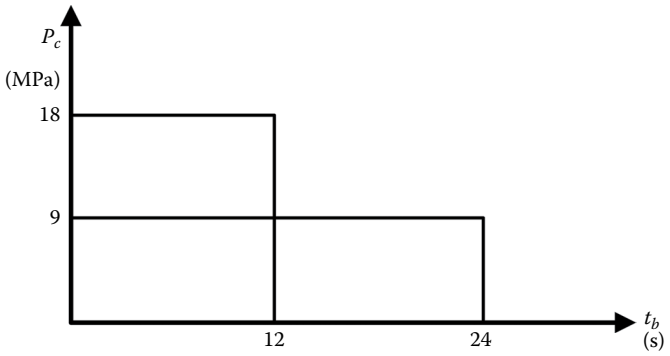


FIGURE 19.7
Variation of combustion pressure versus burning time.

Example 19.5

A solid rocket motor burns along the face of a central cylindrical channel 10 m long and 1.0 m in diameter. The propellant has a burn rate coefficient $a = 5.6$, a pressure exponent of $n = 0.4$, and a density of 1700 kg/m^3. Calculate the burn rate and the product generation rate when the chamber pressure is 7.0 MPa.

Solution

Given the data:
$a = 5.6, \quad n = 0.4, \quad P_c = 7.0$ MPa, $\quad \rho_p = 1760$ kg/m^3
The burning area is $A_b = \pi dL = \pi \times 1.0 \times 10.0 = 31.416$ m^2
The burning rate is $\dot{r} = aP_c^n = 5.6 \times 7^{0.4} = 12.196$ mm/s
The mass of propellant generated is

$$\dot{m}_p = \rho_p A_b \dot{r} = 1700 \times 31.416 \times 12.196 \times 10^{-3} = 651.4 \text{ kg/s}$$

Example 19.6

Tests of a solid-propellant grain showed the following results:

Test Number	Chamber Pressure P_c (MPa)	Burn Rate $\dot{r}$ (mm/s)
1	18	23.8
2	8	12.5

Calculate

1. The combustion pressure if the burning rate is 20 mm/s
2. The propellant consumption rate per square meter of burning surface if the combustion pressure is 15 MPa, the density of propellant ρ_p is 1700 kg/m^3, and the grain diameter is 0.2 m

Solution

1. Since the burning rate is expressed by the relation

$$\dot{r} = aP_c^n$$

$$\frac{\dot{r}_1}{\dot{r}_2} = \left(\frac{P_{c1}}{P_{c2}}\right)^n$$

$$\ln\left(\frac{\dot{r}_1}{\dot{r}_2}\right) = n\ln\left(\frac{P_{c1}}{P_{c2}}\right)$$

$$n = \frac{\ln\left(\frac{P_{c1}}{P_{c2}}\right)}{\ln\left(\frac{\dot{r}_1}{\dot{r}_2}\right)} = \frac{\ln\left(\frac{18}{8}\right)}{\ln\left(\frac{23.8}{12.5}\right)} = \frac{0.9109}{0.6439} = 1.415$$

$$n = \frac{\ln\left(\frac{\dot{r}_1}{\dot{r}_2}\right)}{\ln\left(\frac{P_{c1}}{P_{c2}}\right)} = \frac{\ln\left(\frac{23.8}{12.5}\right)}{\ln\left(\frac{18}{8}\right)} = \frac{0.2536}{0.3613} = 0.7$$

Moreover,

$$a = \frac{\dot{r}}{P_c^n} = \frac{12.5}{(8)^{0.7}} = 2.916$$

Now the pressure in the combustion chamber with a burning rate of 20 mm is

$$P_c = \left(\frac{\dot{r}}{a}\right)^{1/n} = \left(\frac{20}{2.916}\right)^{1/0.7} = 15.654 \text{ MPa}$$

2. For a grain diameter of 0.2 m, the mass flow rate of the propellant is given by Equation 19.3 as

$$\dot{m}_g = \rho_p A_b \dot{r}$$

The burning rate is to be calculated at first as

$$\dot{r} = aP_c^n = 2.916 \times (15)^{0.7} = 19.411 \text{ mm/s} = 0.0194 \text{ m/s}$$

Then, the propellant consumption rate per square meter of burning surface is

$$\frac{\dot{m}_g}{A_b} = \rho_p \dot{r} = 1700 \times 0.0194 = 33 \text{ kg/m}^2\cdot\text{s}$$

19.2.5 Characteristics of Some Solid Propellants

Data for some important characteristics of solid propellants [1] are given in Table 19.1.

19.2.6 Liquid-Propellant Rocket Engines (LRE)

19.2.6.1 Introduction

A liquid-propellant rocket engine (LRE) is a direct reaction engine using the liquid propellants (fuel and oxidizer) in liquid form stored on a flight vehicle board for thrust creation. Since propellant flow rates are extremely large for high-thrust engines

TABLE 19.1

Data for Several Solid Propellants

Propellant Type	Specific Impulse I_{sp} (s)	Chamber Temperature (K)	Metal Content (wt.%)	Pressure Exponent n	Burning Rate (mm/s)	Density (kg/m^3)
DB	220–230	2530	0	0.3	11.43	1605
DB/AP/Al	260–265	3870	20–21	0.4	19.81	1800
DB/ AP-HMX/Al	265–270	3975	20	0.49	13.97	1800
PVC/AP	230–240	2820	0	0.38	11.43	1688
PVC/AP/Al	260–265	3370	21	0.35	11.43	1772
PS/AP	230–240	2870	0	0.43	8.9	1716
PU/AP/Al	260–265	3265–3615	16–20	0.15	6.86	1772
CTPB/AP/Al	260–265	3370–3475	15–17	0.4	10.16	1772
HTBP/AP/Al	260–265	3370–3475	4–17	0.4	10.16	1855

Symbols: Al, aluminum; AP, ammonium perchlorate; CTPB, carboxy-terminated polybutadiene; DB, double base; HMX, cyclotetramethylene tetranitramine; HTPB, hydroxyl-terminated polybutadiene; PS, polysulfide; PU, polyurethane; PVC, polyvinyl chloride.

(often hundreds of gallons per second), liquids are desirable because their reasonably high density allows the volume of the propellant tanks to be relatively low. When the liquid rocket propellant (LRP) is converted from a liquid state to gaseous state, it then discharges from the engine and creates thrust as a result of the exothermal reaction associated with heat release.

A liquid-propellant rocket propulsion system is commonly called a rocket engine. It consists of

1. Tanks to store the propellants
2. One or more thrust chambers
3. A complex feed mechanism to force the propellants from the tanks into the thrust chamber(s), which includes propellant pumps, turbines, or a propellant-pressurizing device
4. A power source to furnish the energy for the feed mechanism
5. Suitable plumbing or piping to transfer the liquids and a structure to transmit the thrust force
6. Control devices to initiate and regulate the propellant flow and thus the thrust

In some applications, an engine may also include a thrust vector control system, various instrumentation, and a residual propellant (trapped in pipes, valves, or wetting tank walls).

Liquid-propellant rockets can be throttled (thrust varied) in real time and have control of the mixture ratio (ratio at which oxidizer and fuel are mixed); they can also be shut down, and, with a suitable ignition system or self-igniting propellant, restarted.

Some commonly used liquid fuels are liquid hydrogen, UDMH, hydrazine, and alcohol.

Some common oxidizers are liquid oxygen, red fuming nitric acid (RFNA), liquid fluorine, and WFNA. Most of the liquid propellants are toxic and require very high combustion temperatures, which demand special materials for the handling system and cooling of

the walls of the chamber and exhaust nozzle. For better mixing and efficient combustion, the fuel and the oxidizer are atomized into small droplets through the injectors, then mixed, evaporated, and ignited. Ignition is achieved by chemical, pyrotechnical, and electrical means. The propellant can often be hypergolic. The ignited propellants burn under high pressure, sometimes greater than the MPa.

Upon combustion, high-temperature gaseous combustion products (CPs) are formed and discharged through the nozzle. The temperature of the CPs continuously decreases while its velocity increases to sonic speed at the nozzle throat and supersonic speeds (2700–4500 m/s) at the nozzle exit.

19.2.7 Applications

The LRE is the main type of engine used for booster rockets and space modules. It is widely used in high-altitude research rockets, long-range ballistic missiles, guided anti-aircraft missiles, and combat missiles. Examples of such LREs are

- The three Space Shuttle main engines (SSMEs), which are sequentially started at launch, combust a mixture of propellants consisting of hydrogen and oxygen, which are stored and delivered in a cryogenic liquid state from the external tank (ET)
- The U.S. Saturn V booster rocket first stage (F-1) engine
- The Russian "Energy" booster rocker (RD-170) engine

19.2.7.1 Propellant Feed System of LREs

The propellant feed system of a liquid rocket engine determines how the propellants are delivered from the tanks to the thrust chamber. The functions of the propellant feed system in both types are

1. To raise the pressure of the propellants
2. To feed the propellant to the thrust chambers

LREs are generally classified based on the propellant feed system as either pressure fed or pump fed. Pressure fed is performed using gas pressurization while pump fed relies upon pumps [2]. These two systems are shown in Figure 19.8.

19.2.7.1.1 Pressure-Fed Rocket Engines

In the first system (pressure fed), a high-pressure gas like helium or nitrogen is stored in a high-pressure tank (at say 35 MPa) and used to force the propellants to the thrust chamber. Pressurized gas is warmed by a heat exchanger to avoid its cooling down.

The advantages of this system are its simplicity, reliability, and avoidance of turbomachinery. Moreover, the procedure for engine cutoff and restart is very simple.

However, its great disadvantages are as follows:

1. Large tanks having heavier and more robust tanks are needed. Thus, they are rarely applied in the first stages, but were used in the second stage of the Delta II rocket.
2. The gas pressure must be greater than the pressure in the thrust chamber (say 15%–20% more), to maintain adequate flow.

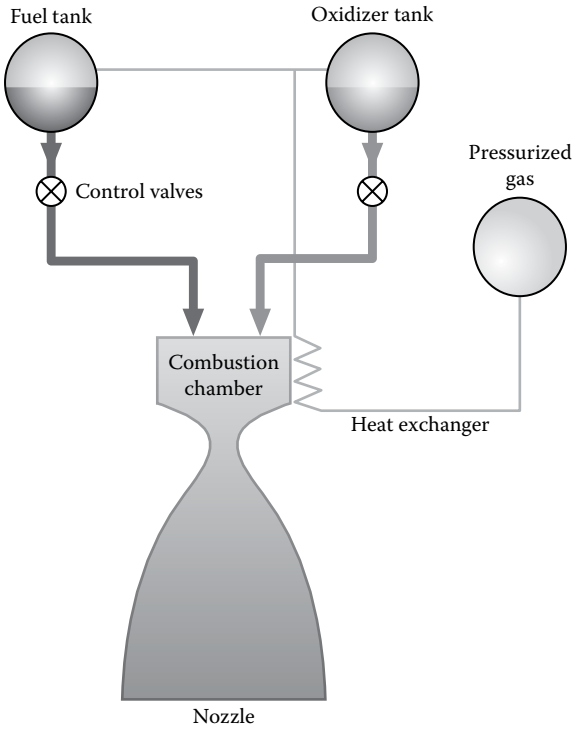


FIGURE 19.8
Propellant feed systems.

Due to these advantages, this type of system is typically used for space propulsion applications and auxiliary propulsion applications requiring low system pressures and small quantities of propellants. Maneuvering and attitude control thrusters of satellites and space probes are mostly pressure fed since they are restarted thousands of times. Other famous applications are all the engines of the Apollo CSM and Apollo LM.

19.2.7.1.2 Pump-Fed Rocket Engines

The pump-fed system is used for high-pressure, high-performance applications. A several thousand horsepower engine is needed to drive the feeding pumps. The selection of one propellant feed system over another is determined by design trade studies at both the engine and vehicle levels. The selection of a particular feed system and its components is governed primarily by the application of the rocket, duration, number or type of thrust chambers, past experience, mission, and by the general requirements of simplicity of design, ease of manufacture, low cost, and minimum inert mass.

19.2.7.1.3 Pressure-Fed Engine

The main elements of liquid rockets are

- High-pressure tanks (one or more)
- Pumps
- Turbines
- Gears

- Bearings
- Feeding lines (plumbing or piping)
- Regulators, valves, and control devices
- Thrust chamber or thruster (one or more combustion chambers)
- Nozzle

There are two categories of liquid-propellant rocket engines, namely,

1. Boosting propulsion (hours, days, and months in space)
2. Auxiliary propulsion (10 years or more in space)

19.3 Liquid Propellants

Liquid propellants are classified into two types:

1. Monopropellant
2. Bipropellant

In rare cases, tripropellant rockets using three types of propellant are used.
This classification is written as mono-, bi-, and multiphase propellants.

19.3.1 Monopropellant

A monopropellant contains an oxidizing agent and combustible matter in a single substance; see Figure 19.9a. It may be a mixture of several compounds or it may be a homogeneous material, such as hydrogen peroxide H_2O_2, ethylene oxide $(CH_2)_2O$, and hydrazine N_2H_4. Monopropellants are stable at ordinary atmospheric conditions but decompose and yield hot combustion gases when heated or catalyzed.
It has the following features:

1. Monopropellant is passed through a catalyst.
2. The catalyst causes a reaction, which generates heat.
3. The heated products of this reaction are expelled through a nozzle.
4. The exhaust speed = 2.3 km/s.
5. Usually used for altitude control of spacecraft.

Advantages:

1. Simple design
2. Robust design
3. Reliable
4. Not a lot of plumbing
5. Flight heritage
6. Can turn them off

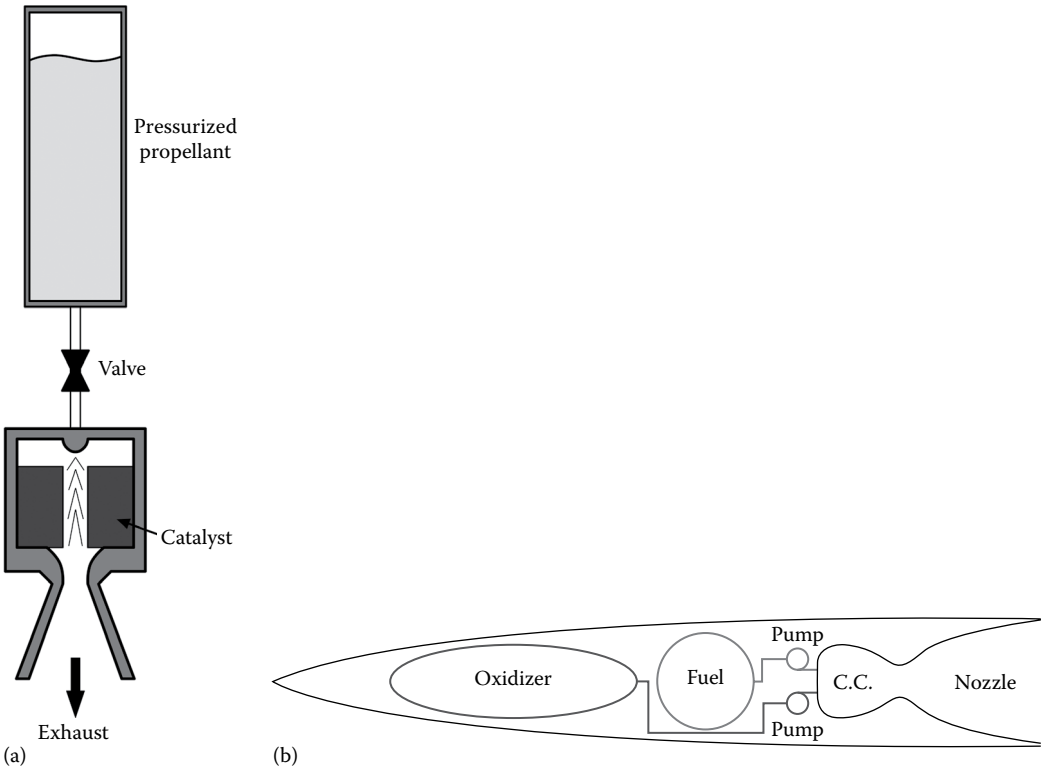


FIGURE 19.9
(a) Monopropellant engine and (b) bipropellant engine.

Disadvantages:

1. Most fuels are toxic
2. Catalyst lifetime issues
3. Low thrust
4. Low exhaust speeds
5. Low specific impulse

Some monopropellants are called "hypergolic" if the propellants ignite smoothly on contact with each other. An example is hydrazine.

19.3.2 Bipropellant

A bipropellant rocket unit has two separate liquid propellants: an oxidizer and a fuel; see Figure 19.9b. They are stored separately and are not mixed outside the combustion chamber [1]. The majority of liquid-propellant rockets have been manufactured for bipropellant applications, which have the following features:

1. Fuel and oxidizer are pumped into the combustion chamber.
2. Often use turbopumps.

3. Power tapped from main combustion.
4. Injectors mix propellant to provide stable and thorough combustion.
5. Heat is generated from combustion.
6. Heated products are expelled out of the nozzle.

Advantages:

1. Typically more efficient than solid or hybrid rockets
2. High exhaust velocity (3.6–4.4 km/s)
3. Throttled
4. Can turn them off
5. Lots of flight heritage

Disadvantages:

1. More complex than hybrids or solid rockets
2. Cryogenic systems often needed (icing issues)
3. Difficulty storing
4. System complexity

Some bipropellants are called "cryogenic" if they have to be kept at a low temperature to remain in a liquid state in propellant tanks. Examples are liquid hydrogen (LH2), liquid oxygen (LOX), liquid methane, and liquid fluorine.

Some bipropellants are also "hypergolic" like nitrogen tetroxide.

Table 19.2 illustrates some data for some bipropellant engines and their applications.

TABLE 19.2

Bipropellant Engines

Fuel	Oxidizer	Example
Liquid hydrogen H_2 (LH2)	Liquid oxygen O_2 (LOX)	Space Shuttle main engine Saturn V upper stage Delta IV first stage Centaur Ariane second stage
RPI liquid hydrocarbon (kerosene)	LOX	Atlas rockets Delta Titan rockets Voyager 1 & 2
Aerozine 50	Dinitrogen tetroxide	Apollo service module Lunar module Titan rockets Voyager 1 & 2
MMH (Monomethyl hydrazine CH_3NHNH_2)	Dinitrogen tetroxide	Space Shuttle Orbital Maneuvering System (OMS)
MMH (Monomethyl hydrazine CH_3NHNH_2)	Dinitrogen tetroxide	Space Shuttle Orbital Maneuvering System (OMS)

19.3.3 Fundamental Relations

The propellant mixture ratio for a bipropellant is the ratio at which the oxidizer and fuel are mixed and react to give hot gases. The mixture ratio (r) is defined as the ratio of the oxidizer mass flow rate rho and the fuel mass flow

$$r = \frac{\dot{m}_o}{\dot{m}_f}$$

The total propellant mass $(\dot{m})$ is

$$\dot{m} = \dot{m}_o + \dot{m}_f$$

The oxygen and fuel mass flow rates are related to the propellant mass flow rate by the equations

$$\dot{m}_o = \frac{r\dot{m}}{r+1}$$

$$\dot{m}_f = \frac{\dot{m}}{r+1}$$

As derived in Chapter 18, the thrust force is expressed by the relation

$$T = \dot{m}V_{eff}$$

For full expansion in the nozzle

$$u_e = V_{eff}$$

Since the chamber total pressure and temperature are equal to the nozzle exit conditions, then the exit velocity is expressed by Equation 18.18B, rewritten hereafter as

$$u_e = \sqrt{2CpT_c\left(1-\left(\frac{P_e}{P_c}\right)^{\gamma-1/\gamma}\right)} = \sqrt{2\frac{\gamma}{\gamma-1}RT_c\left[1-\left(\frac{P_e}{P_c}\right)^{\gamma-1/\gamma}\right]} \qquad (18.18B)$$

Example 19.7

A liquid oxygen–liquid hydrogen rocket engine has a mixture ratio of 3.51. The combustion chamber temperature and pressure are 3510 K and 22.1 atmospheres. The exit area is 3.225 m^2. The exit pressure is equal to the atmospheric pressure at an altitude of 20.2 km. The specific heat ratio $\gamma = 1.23$ and the specific heat at constant pressure $Cp = 2520$ J/kg/K. Other data are

$$P_{oe} = 2230 \text{ kPa}, \quad u_e = 3450.0 \text{ m/s}, \quad \rho_e = 0.0102 \text{ kg/m}^3,$$

$$\dot{m} = 113.5 \text{ kg/s}, \quad T = 392 \text{ kN}, \qquad I_{sp} = 352 \text{ s}$$

1. Calculate the oxygen and fuel mass flow rate.
   If the propellant mass flow rate is constant, examine the effects.
2. The nozzle efficiency (η_n), which varies from 93% to 99%.
3. The pressure drop in the combustion chamber (ΔP_c), which varies from 1% to 5% on the exhaust speed, thrust force, and specific impulse.

Solution

1. Since the mixture ratio is 3.51, the oxygen mass flow rate is calculated as

$$\dot{m}_o = \frac{r\dot{m}}{r+1} = \frac{3.51 \times 113.5}{3.51+1} = 88.334 \text{ kg/s}$$

The hydrogen fuel mass flow rate is then

$$\dot{m}_f = \frac{\dot{m}}{r+1} = \frac{113.5}{4.51} = 25.17 \text{ kg/s}$$

2. The effect of nozzle efficiency ($\eta_n = 93\% - 99\%$).
   The exit velocity is recalculated after adding the nozzle efficiency from the relation

$$u_e = \sqrt{2\eta_n CpT_{oe}\left(1 - \left(\frac{P_e}{P_{oe}}\right)^{\gamma-1/\gamma}\right)}$$

When nozzle efficiency η_n= 93%

$$u_e = \sqrt{2 \times 0.93 \times 2520 \times 3510\left(1 - \left(\frac{5.36}{2239.28}\right)^{0.187}\right)} = 3336.1 \text{ m/s}$$

The propellant mass flow rate is constant at 113.5 kg/s.
The thrust is $T = \dot{m}u_e = 113.5 \times 3,336.1 = 378,645 \text{ N} = 378.65 \text{ kN}$.
The specific impulse is

$$I_{sp} = \frac{u_e}{g} = \frac{3336.1}{9.80665}$$

$$I_{sp} = 340.19 \text{ s}$$

Other values for nozzle efficiency are calculated and tabulated in Table 19.3, where it is shown that the worst performance is associated with the smallest nozzle efficiency of 93%. In such a case, a drop in both thrust and specific impulse by 3.6% is encountered.

3. Effect of pressure drop in the combustion chamber.
   Since the exhaust velocity is expressed by

$$u_e = \sqrt{2CpT_c\left(1 - \left(\frac{P_e}{P_{0e}}\right)^{\gamma-1/\gamma}\right)}$$

TABLE 19.3

Effect of Nozzle Efficiency and Pressure Drop in Combustion Chamber on Rocket Characteristics

	Effects of Nozzle Efficiency				Effects of Pressure Drop in CC	
Nozzle efficiency (%)	93	95	97	99	100	100
Combustion pressure drop ΔP_c	0	0	0	0	0	5%
Exhaust velocity (m/s)	3336.1	3371.7	3407.1	3442.0	3459.4	3451.4
Thrust (kN)	378.65	382.70	386.70	390.66	392.64	391.74
Specific impulse (s)	340.19	343.82	347.42	351.00	352.76	351.95

Here,

$$P_{0e} = P_c\left(1 - \Delta P_c\%\right)$$

For a combustion pressure drop of 5%,

$$P_{0e} = 2239.28 \times \left(1 - 0.05\right) = 2127.3\,\text{kPa}$$

The exhaust speed is then

$$u_e = \sqrt{2 \times 2520 \times 3510\left(1 - \left(\frac{5.36}{2127.3}\right)^{0.187}\right)} = 3451.4\ \text{m/s}$$

$$T = \dot{m}u_e = 113.5 \times 3,451.4 = 391,735 = 391.74\ \text{kN}$$

The specific impulse is

$$I_{sp} = \frac{u_e}{g} = \frac{3451.4}{9.80665}$$

$$I_{sp} = 351.95\ \text{s}$$

As can be seen, even for the maximum value of pressure drop (5%), there are almost no changes in exhaust velocity and specific impulse if the nozzle efficiency is kept constant (100%); see Table 19.3.

19.4 Pump-Fed System

The main element in a pump-fed system is the turbopumps. A turbopump is a gas turbine that comprises basically two main components: a rotodynamic pump that delivers fuel or oxidizer to the thrust chamber and a driving turbine, usually both mounted on the same shaft, or sometimes geared together. The purpose of a turbopump is to produce a high-pressure fluid for feeding a combustion chamber where propellants react and produce high-temperature gases. A turbopump can comprise either a single- or multistage centrifugal pump or multistage axial flow pump.

The main challenges in the design of turbopumps are to deliver very high power in a small machine, which implies

- High pressure (up to 55 MPa)
- Large mass flow rate (some 2500 kg/s)
- Small mass turbomachinery

Pump-fed systems overcome the limitations of the pressure-fed system outlined earlier. Propellant is forced into the thrust chamber using pumps. Pumps are driven by a gas turbine to form together turbopumps. A turbopump is the high-speed and high-power turbomachinery that raise the pressure of cryogenic fluid to one higher than the combustion chamber. The gas driving the turbine may be generated in a gas generator by pre-burning some amount of the propellant, by burning separate propellant (like hydrogen peroxide in the RD-107/108 engines on the Soyuz), or gasification of some propellant in the cooling jacket of the thrust chamber and the nozzle. Pumps should rotate at tens of thousands rpm. Either single- or multistage centrifugal or multistage axial flow pumps are used. Turbopumps may also include booster pumps. In general, turbopump assembly is the most complex part of an LRE.

Advantages of turbopumps:

1. High specific impulse due to its high pressure in thrust chamber
2. Compact and lightweight compared to pressure-fed engines
3. More efficient, thus spend less propellant

Disadvantages of turbopumps:

1. Complexity
2. More expensive compared to pressure fed
3. Less reliable compared to pressure fed

Turbopumps are used in all stages of launch vehicles. The following Soviet flight vehicles used turbopumps: Lunar probes E8 (Lunokhods, soil sample missions), Lunar modules for the manned expeditions, the Salyut space stations, and the Soyuz manned spacecraft.

Important data on the RD-170/171 Turbopump are

- Propellants: LOX/kerosene
- Mass flow rate: ~2.4 tons/s
- Pressure of thrust chamber: ~250 bar
- Turbine power: ~200 MW
- Rotational speed:~14,000 rpm
- Pressure of gases driving the turbine: ~500°C

Figure 19.10 illustrates three kinds of turbopump systems used for pump-fed liquid-propellant rockets. Figure 19.10a shows a gas generator cycle. A part of the fuel and

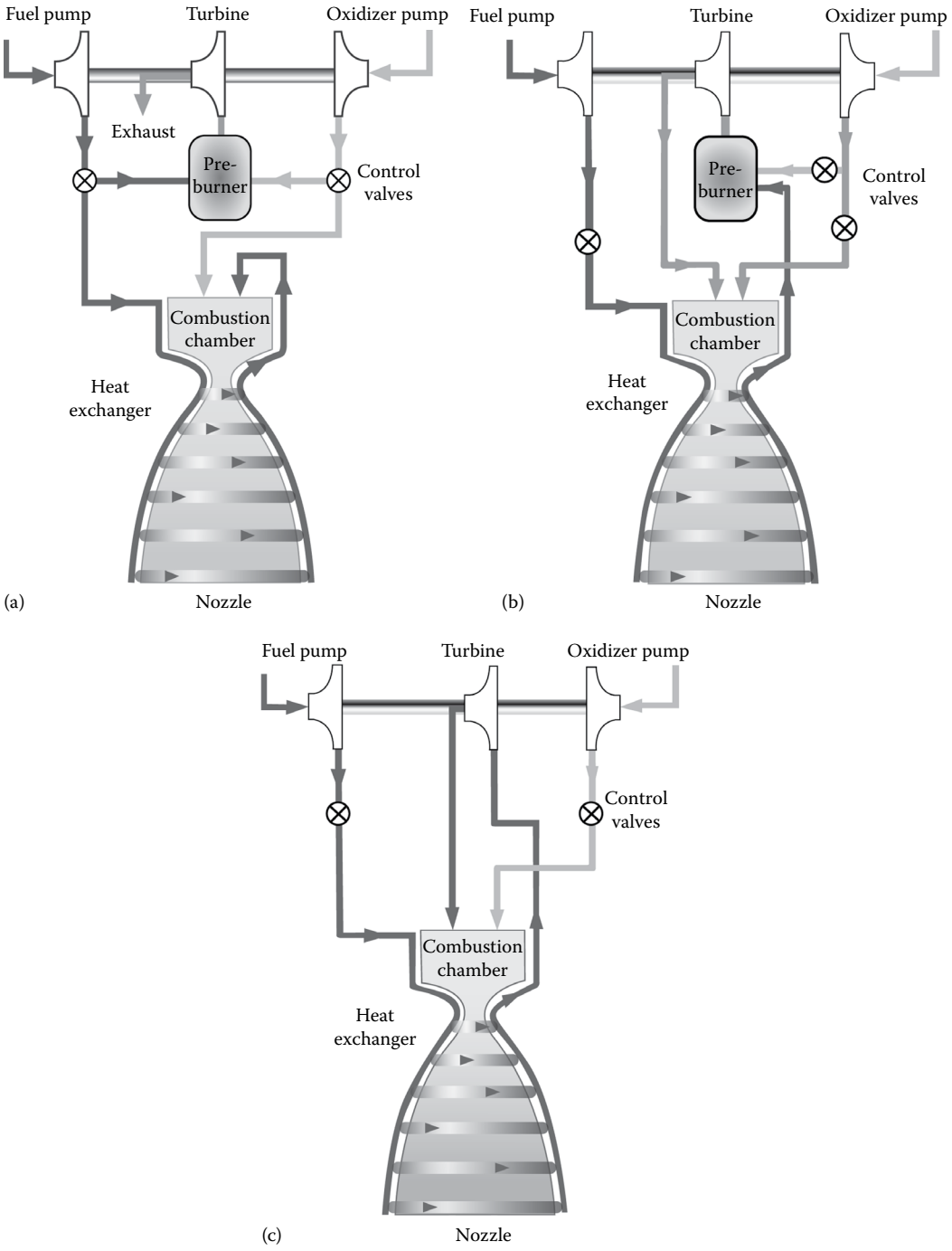


FIGURE 19.10
(a) Gas generator type of turbopump systems. (b) Staged combustion type of turbopump systems. (c) Expander cycle type of turbopump.

oxidizer is burnt in a separate combustion chamber identified as pre-burner. The products of combustion of this small chamber are used to drive the turbine before exhausted to ambient pressure. For this reason, it is identified as open cycle [3]. The gas turbine has a high-pressure ratio. To minimize weight, a small number of stages are employed; thus, a moderate turbine efficiency is attained. Combustion pressure is also moderate on the order of 5.0 MPa. Examples are the Japanese LE-5 engine, which was used in the second stage of the H-1 rocket, the Vulcain 2 engine (European first-stage rocket engines for the Ariane 5), and many U.S. engines, including the Rocketdyne J-2 and the F-1 engines.

Figure 19.10b shows a staged combustion cycle. The turbine exhaust gases are not dumped but fed into the main combustion chamber. So, all propellant and all heat pass through the thrust chamber and nothing is wasted. The fuel–oxidizer ratio in the main engine need not be the same as in the pre-burner. The turbine pressure ratio is less than that of the gas generator case. Since the turbine driving gas is not efficiently changed into a thrust, like the gas generator cycle, high engine performance is not obtained. High chamber pressure is achieved compared with the previous gas generator, here more than 40 MPa. This system first appeared in the USSR. It was then employed in the LE-5A engine, which succeeded the LE-5. Moreover, the space shuttle main engine (SSME) uses staged combustion arrangements, though a separate turbine is used for both fuel (hydrogen) and oxygen turbopumps.

The third type is the "expander" configuration shown in Figure 19.10c. Its advantages are making use of all propellant and not requiring a separate gas turbine. The gas employed in driving the turbine is produced from the fuel vaporized in the cooling jacket of the thrust chamber and nozzle. The cycle may be opened or closed. For an open cycle, a small portion of fuel is used to drive the turbine and then dumped. In a closed cycle (shown in Figure 19.10c), fuel is redirected into the thrust chamber after leaving the turbine. An example is SNECMA VINCI upper stage engine.

A comparison between these three cycles (gas generator, expander, and stage combustion) is given in [4].

1. The gas generator cycle is the easiest to control and least sensitive since it works against atmospheric or low pressure. The turbine is a low-flow high-pressure ratio machine. The discharge pressure of the pump is slightly above chamber pressure.
2. In the expander cycle, the heat source is the nozzle cooling. All the flow passes through the turbine and is injected into the chamber. Chamber pressure depends on how much pumping power can be delivered given the heat input. This makes it sensitive to the turbine efficiency. The turbine discharge pressure is higher than the chamber pressure.
3. A staged combustion cycle allows for extremely high chamber pressures. As a consequence, the discharge pressure from the pumps has to be extremely high. Thus, multiple pumps are used in some cases.

From NASA SP-8107 [5], a summary graph is given in Figure 19.11 for reasonable choices of cycle for different chamber pressures along with the resulting pump discharge pressure.

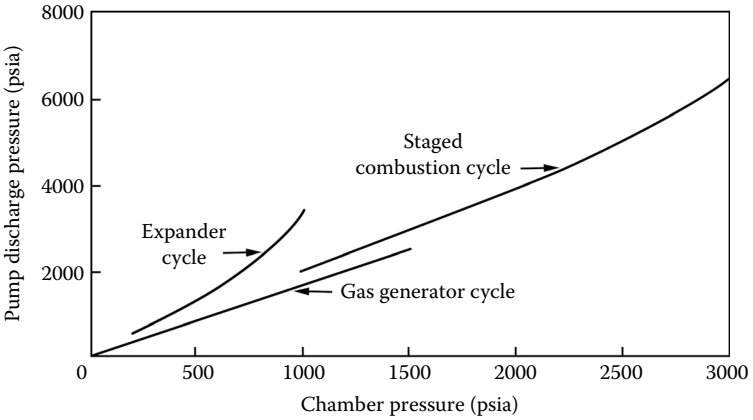


FIGURE 19.11
Pump discharge pressure versus chamber pressure. (From Mårtensson, H. et al., Rocket engines turbomachinery, in: *Advances on Propulsion Technology for High-Speed Aircraft*, Educational Notes RTO-EN-AVT-150, Paper 5, pp. 5-1–5-28.)

19.5 Rocket Pumps

19.5.1 Introduction

The principal requirements of a rocket engine propellant pump are reliability of optimum speed, lightweight, high delivery rate at maximum pressure head, smooth flow for a wide range of operating conditions, and high efficiency. The most widely used pump types are centrifugal (or radial) flow, axial flow, and mixed flow pumps. Centrifugal pumps are generally designed with a single stage, while axial pumps are primarily of multistage design. However, multistage centrifugal pumps with crossover-type volutes have also been considered. Various pump configurations are shown schematically in Figure 19.12.

The selection of a pump configuration is influenced by operational, hydrodynamic, and mechanical considerations that include inlet pressure, impeller tip speed, limiting pressure ratio per stage, engine system compatibility, and flow-range, working fluid, and weight requirements.

Pumps, like other steady flow rotating machinery, consist essentially of two basic elements: the rotor and the stator. Their working principle is similar to compressors. They develop acceleration of the fluid flow by imparting kinetic energy to it in the rotor and then decelerating or "diffusing" it in the stator. This results in an increased fluid pressure head.

19.5.2 Centrifugal Pumps

Almost all existing chemical as well as nuclear rockets have centrifugal turbopumps. This is due to their simplicity, reliability, wide operating range (without stall or surge), and their ability to handle large flows at high pressures efficiently. They are also economical in terms of weight and size. Regarding head and flow rate, centrifugal pumps can generate more than 100,000 ft and up to 30,000 gpm at 5800 rpm. Liquid hydrogen pumps for example have delivered safe operation at 46,000 rpm over the range of 800–13,000 gpm [6].

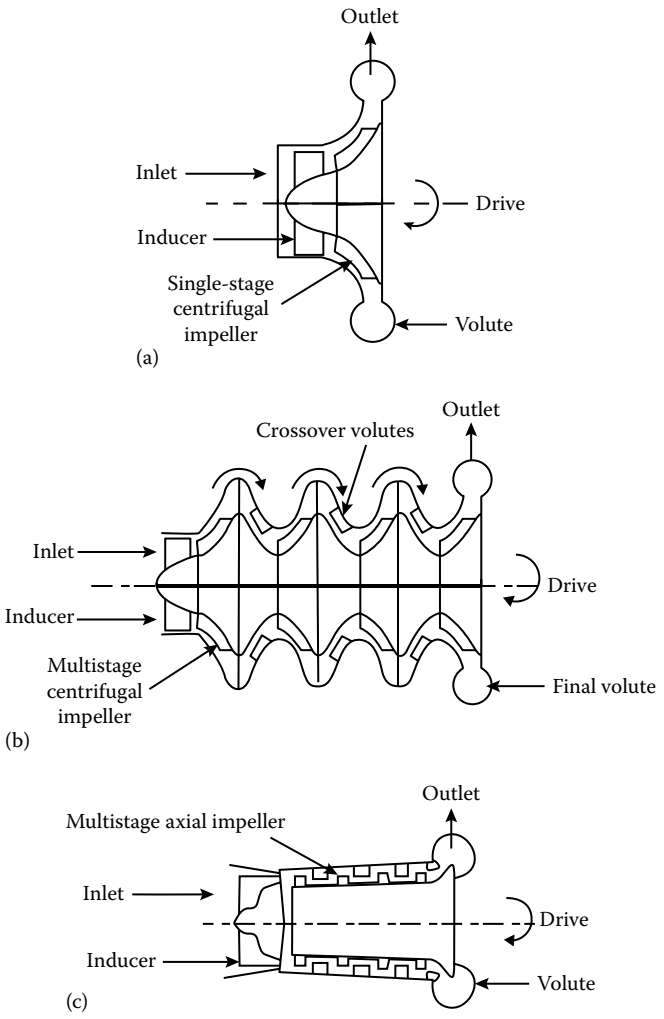


FIGURE 19.12
Various pump configurations: (a) single-stage centrifugal pump, (b) multistage centrifugal pump, and (c) multistage axial pump.

The elements of a centrifugal pump are shown in Figure 19.13. The rotor assembly usually includes an inducer, an impeller, and a shaft. The stator assembly consists of a casing with stationary diffuser vanes, a volute with discharge outlet, shaft bearings, and seals. An inducer is an axial-flow-type impeller. Its main function is to increase the static pressure of the entering fluid sufficiently to permit normal operation of the main impeller. The inducer blades are like thin, sharp-edged, flat plates formed in spirals around the hub. The inducer's leading edge is swept back toward the tip of the impeller at the inlet.

The succeeding element is the impeller, which is basically a rotating wheel. Fluid is admitted axially to the impeller, which, when rotating in an enclosure, ejects it at the periphery with increased velocity. The impeller may have either forward-leaning, radial,

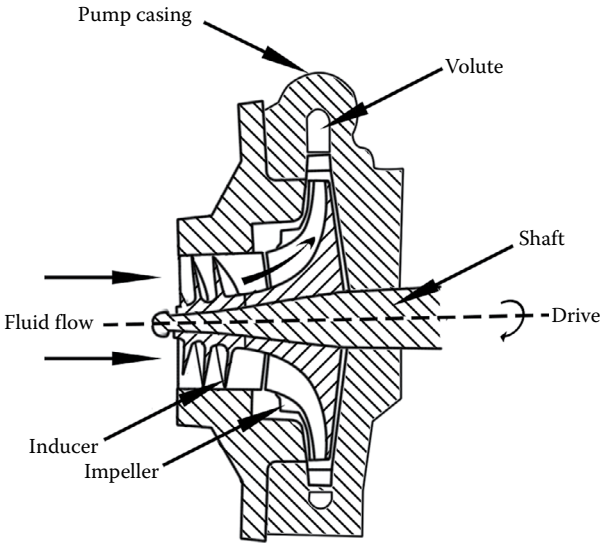


FIGURE 19.13
Elements of a centrifugal pump.

or backward-leaning geometry, the same as in a centrifugal compressor; see Figure 19.14. Flow leaving the rotor is admitted to the stator assembly, whose primary functions are diffusing (i.e., decelerating) the fluid to convert the velocity head into the pressure head, collecting and redirecting the fluid to the pump discharge outlet, and providing structural support and a pressure enclosure for the pump. Fluid leaving the stators flows into the volute.

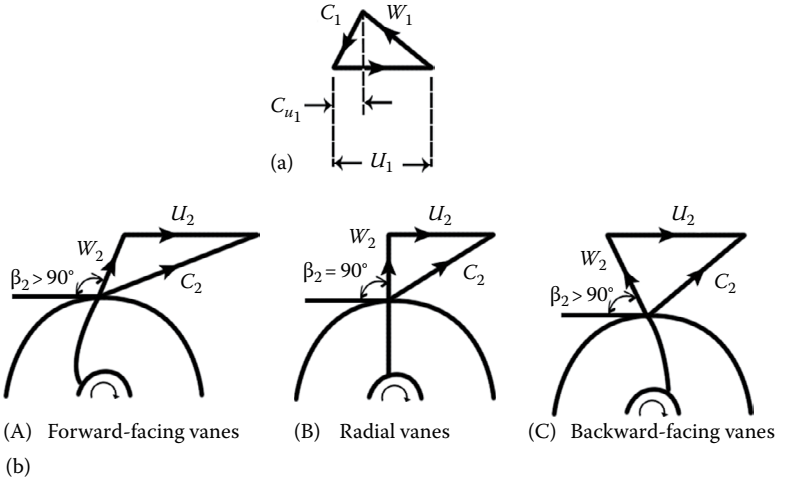


FIGURE 19.14
(a) Velocity triangles at the inlet and (b) outlet of the impeller of a centrifugal pump.

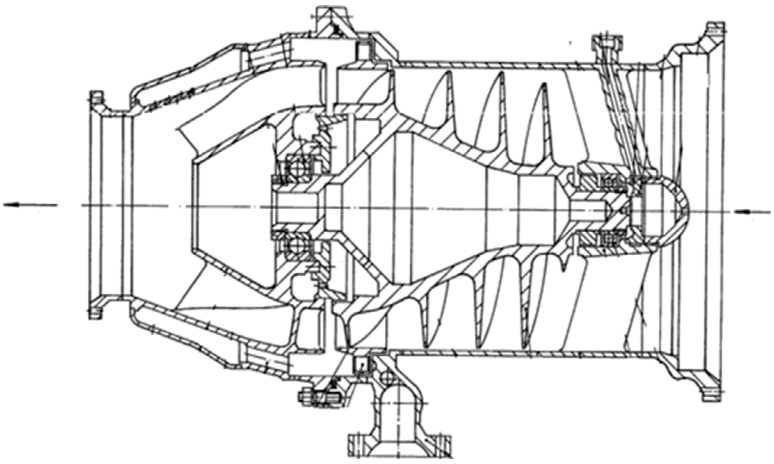


FIGURE 19.15
Axial fuel turbopump.

19.5.3 Multistage Centrifugal Pumps

For higher-pressure rises, multiple-stage centrifugal pumps can be designed if a single stage proves to be limited. The basic construction of a multistage pump is similar to that of a single-stage pump, except that proper channeling of the fluid between stages is added [7].

In the next section, performance of a centrifugal pump will be discussed and some dimensionless parameters associated with incompressible fluids will be introduced.

19.5.4 Multistage Axial Pumps

Axial types become competitive to centrifugal ones when multistaging or maximum efficiency is of paramount consideration [8]. This design is well suited to liquid hydrogen service, which entails the problems of extremely low fluid temperature and density. Low fluid density results in high-volume flow and in high-pressure head-rise requirements. For such applications, a multistage axial flow pump is generally superior with respect to construction and performance. Elements of an axial flow pump are shown in Figure 19.15. The rotor assembly consists of an inducer, a cylindrical rotor with multiple rows of rotating blades, and a rotor shaft. The stator assembly includes a cylindrical casing with rows of stationary blades spaced between the inducer and rotating blades, a volute casing, bearings, and seals. An inducer is placed at the pump inlet to supply the fluid to the main-pump section at the required pressure and velocity. The main function of the rotor blades is to accelerate the flow (or increase the kinetic energy of the fluid), while the stator blades, acting as diffusers, convert the velocity head of the fluid into a pressure head. The axial speed of flow is kept constant throughout the various stages of the pump.

19.6 Performance of Centrifugal Pumps

For a centrifugal compressor, and from Euler's equation, the enthalpy rise in the pump is

$$\Delta h = \left(U_2 C_{u2} - U_1 C_{u1}\right) \tag{19.8a}$$

The corresponding power is

$$P = \dot{m}\Delta h = \dot{m}\left(U_2 C_{u2} - U_1 C_{u1}\right) \tag{19.9a}$$

where
C_u is the tangential component of the absolute velocity
subscripts 1 and 2 refer to the inlet and outlet

Figure 19.14 shows the velocity triangle at the inlet together with the velocity triangles for the three types of centrifugal impeller (forward facing, radial, and backward facing). As in centrifugal compressors, forward-facing (or leaning) pumps are rejected as they lead to pump instability.

Neglecting slip and blockage of flow at the impeller tip, the tangential component of absolute velocity is

$$C_{u2} = U_2 - W_{r2}\tan\beta_2$$

The mass flow rate $(\dot{m})$ is then expressed by the relation

$$\dot{m} = W_{r2}\rho A_2 = W_{r2}\rho\pi D_2 b$$

Then the swirl velocity is expressed by

$$C_{u2} = U_2 - \frac{\dot{m}}{\rho\pi D_2 b}\tan\beta_2 \tag{19.10}$$

where
b is the blade width at the impeller tip
β_2 is the angle of relative velocity radial

From Equations 19.9a and 19.10, the power is

$$P = \dot{m}\left[U_2^2\left(1 - \frac{\dot{m}}{\rho\pi D_2 b U_2}\tan\beta_2\right) - U_1 C_{u1}\right] \tag{19.9b}$$

For an isentropic process and incompressible flow,

$$Tds = dh - \frac{dp}{\rho} = 0$$

The rise in enthalpy is then expressed by

$$\Delta h = \frac{\Delta p}{\rho} \tag{19.11a}$$

$$\Delta h = \left(U_2 C_{u2} - U_1 C_{u1}\right) \tag{19.8a}$$

$$C_{u2} = U_2 - \frac{\dot{m}}{\rho \pi D_2 b} \tan \beta_2 \tag{19.10}$$

The pressure rise across the pump is then derived from Equations 19.8a and 19.10 as

$$\frac{\Delta p_0}{\rho} = \left(U_2 C_{u2} - U_1 C_{u1}\right) = U_2^2 \left(1 - \frac{\dot{m}}{\rho \pi D_2 b U_2} \tan \beta_2\right) - U_1 C_{u1} \tag{19.11b}$$

"Head rise" is used commonly instead of "pressure rise" to express the performance of pumps and is defined as

$$H = \frac{\Delta h}{g} = \int_{P_1}^{P_2} \frac{dp}{\rho g} = \frac{\Delta p_0}{\rho g}$$

From Equation 19.8a, the head (H) or the term ($\Delta p/\rho g$) is then

$$H = \frac{\Delta p_0}{\rho g} = \frac{\left(U_2 C_{u2} - U_1 C_{u1}\right)}{g} \tag{19.12}$$

If there is no inlet swirl, then the flow is axial at the inlet as shown in Figure 19.15; then

$$C_{u1} = 0 \tag{19.13}$$

The input power is then

$$P = \dot{m} U_2^2 \left(1 - \frac{\dot{m}}{\rho \pi D_2 b U_2} \tan \beta_2\right)$$

The pressure rise across the pump is expressed as

$$\frac{\Delta p_0}{\rho} = U_2^2 \left(1 - \frac{\dot{m}}{\rho \pi D_2 b U_2} \tan \beta_2\right) \tag{9.11c}$$

The ideal head is

$$H = \frac{U_2^2}{g} \left(1 - \frac{\dot{m}}{\rho \pi D_2 b U_2} \tan \beta_2\right)$$

The relation between the ideal head and the volume flow rate is shown in Figure 19.16.

The same configurations stand for the pressure rise term ($\Delta P_0/\rho$) as the ordinate and the mass flow parameter ($\dot{m}/\rho \pi D_2 b U_2$) as the abscissa.

The overall pump efficiency (η_P) is a measure of the hydraulic work (or power) transmitted to the input shaft work (or power).

$$\eta_P = \frac{P_h}{P_{sh}} \tag{19.14}$$

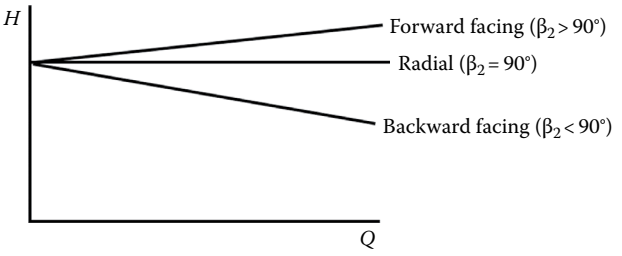


FIGURE 19.16
Head of a centrifugal pump.

The shaft power is then, from (19.9b),

$$P_{sh} = \frac{1}{\eta_P}\left[\dot{m}U_2^2\left(1 - \frac{\dot{m}}{\rho\pi D_2 b U_2}\tan\beta_2\right) - U_1 C_{u1}\right]$$

or

$$P_{sh} = \frac{1}{\eta_P}\frac{\Delta P_0}{\rho}$$

The overall efficiency in Equation 19.14 can be decomposed into three constituents as follows:

$$\eta_P = \eta_h \eta_v \eta_m \tag{19.15}$$

where η_h is the hydraulic efficiency defined as the measure of the actual head rise (H) to the ideal head rise (H_i):

$$\eta_h = \frac{H}{H_i} \tag{19.16}$$

η_v is the volumetric efficiency, which is a measure of the flow losses that occur between the impeller discharge and the volute output:

$$\eta_v = \frac{Q_{delivered}}{Q_{impeller\ discharge}} \tag{19.17}$$

η_m is the mechanical efficiency, which is the measure of the mechanical losses in the pumps:

$$\eta_m = \frac{P_a}{P_{sh}} = \frac{\text{Power available for hydrodynamic work}}{\text{Shaft power}} \tag{19.18}$$

where P_a is the shaft power minus mechanical losses.

19.7 Pump Performance Parameters

19.7.1 Pump Specific Speed (N_s)

For any given pump design, the relation between fluid flow rate (Q), developed fluid head, H (sometimes written as ΔH), required driving power (P), and rotating speed (N) can be defined by three expressions called the affinity laws of a pump. These laws state that

1. The pump volume flow rate varies directly with speed:

$$Q \sim N$$

2. The pump developed head varies directly as the square of the speed:

$$H \sim N^2$$

3. The pump driving power varies directly as a cube of the speed:

$$P \sim N^3$$

These three relationships permit us to derive a useful pump design parameter, the pump specific speed (N_s):

$$N_s = \frac{NQ^{1/2}}{(gH)^{3/4}} = \frac{\Omega Q^{1/2}}{\left(\frac{\Delta P_0}{\rho}\right)^{3/4}} \tag{19.19}$$

where
N_s is the pump specific speed (dimensionless)
N is the pump rotating speed (rpm)
Q is the pump volumetric flow rate (m^3/s)
H is the pump developed head (m)
Ω is the rotational speed of the pump (s^{-1})
ΔP_0 is the stagnation pressure rise (Pa)
ρ is the fluid density (kg/m^3)

Using these units, the specific speed for centrifugal pumps ranged from 0.05 to 1.0. Other pump parameters are defined here.

1. *Pump specific diameter* (d_s)

$$d_s = \frac{D_2(gH)^{1/4}}{Q^{1/2}} = \frac{D_2\left(\frac{\Delta P_0}{\rho}\right)^{1/4}}{Q^{1/2}} \tag{19.20}$$

where D_2 is the pump impeller tip diameter (m).

2. *Pump head coefficient* (*or dimensionless pressure*); ψ

$$\psi = \frac{gH}{\Omega^2 D^2} \quad \text{or} \quad \psi = \frac{gH}{U_2^2} \tag{19.21a}$$

Sometimes, this is expressed as

$$\psi = \frac{\Delta P_0}{\rho U_2^2} \tag{19.21b}$$

where
g is the gravitational acceleration
U_2 is the impeller discharge tip speed

3. *Pump flow coefficient* (*or dimensionless flow*); ϕ

$$\phi = \frac{W_{r2}}{U_2} \tag{19.22}$$

where W_{r2} is the radial (or meridional) component of relative velocity at the impeller tip expressed as

$$W_{r2} = \frac{\dot{m}}{\rho A_2} \tag{19.23}$$

where
$\dot{m}$ is the pump mass flow rate
ρ is the fluid density
A_2 is the discharge area normal to the meridional direction

Figure 19.17 represents a pump map expressed as constant efficiency lines on the specific diameter—specific speed coordinates. Best efficiency operation occupies a narrow zone on the $(N_s - d_s)$ plane.

4. *Net Positive Suction Head* (*NPSH*)
The steady flow operation of a pump creates a low-pressure area at the pump inlet, thus allowing the static head upstream of the pump to push fluid into the inlet at a continuous rate. If the static pressure of the fluid at the pump inlet or any regions within the pump drops below the local fluid vapor pressure level, these regions will cavitate, that is, the fluid will pass from liquid to vapor and form bubbles. The formation of vapor alters the effective flow passages of the fluid and hence seriously affects normal pump performance. Cavitation or the spontaneous formation of bubbles of vapor in the liquid may seriously decrease the pressure rise of the pump (even to zero values) as well as erode the impeller blades.
The NPSH is defined as

$$NPSH = \frac{p_{01} - p_v}{\rho g} \tag{19.24}$$

where
p_{01} is the pump inlet total pressure
p_v is the vapor pressure

Cavitation can cause significant structural damage when the vapor bubbles collapse (implode), particularly with high-density fluids.

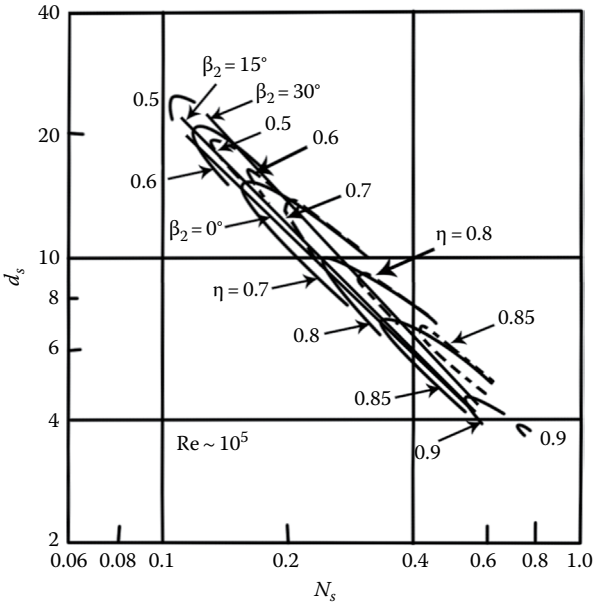


FIGURE 19.17
Comparison between calculated and measured efficiency for centrifugal pump. (From Balje, O.M., Study of turbine and turbopump design parameters, Vol. IV: Low specific speed turboprop study, S/TD No. 1735, No.20, The Sundstrand Corp., Rockford, IL, 1959.)

5. *Suction specific speed* (S_s)
Suction specific speed is defined as

$$S_s = \frac{\Omega\sqrt{Q}}{(g \times NPSH)^{3/4}} = \frac{N\sqrt{Q}}{(NPSH)^{3/4}} \tag{19.25}$$

Example 19.8

Figure 19.18 illustrates a turbopump of the gas generator type. It has the following data:
Fuel pump

$$p_{01} = 0.15 \text{ MPa}, \quad p_{02} = 3.5 \text{ MPa}, \quad \dot{m}_f = 25 \text{ kg/s}, \quad \eta_{fp} = 0.7, \quad \rho_f = 800 \text{ kg/m}^3$$

Oxygen pump

$$p_{06} = 0.2 \text{ MPa}, \quad p_{07} = 3.5 \text{ MPa}, \quad \dot{m}_{02} = 60 \text{ kg/s}, \quad \eta_{02} = 0.66, \quad \rho_{O2} = 1150 \text{ kg/m}^3$$

Turbine

$$p_{010} = 1.3 \text{ MPa}, \quad T_{010} = 800 \text{ K}, \quad \dot{m}_{10} = 1.7 \text{ kg/s}, \quad \eta_t = 0.72, \quad C_p = 1.06 \text{ kJ/kg} \cdot \text{K},$$

$$\gamma = 1.3, \quad \text{mechanical efficiency } \eta_m = 0.99$$

Combustion chamber

$$p_c = p_{05} = p_{09} = 3.0 \text{ MPa}, \quad T_c = 3000 \text{ K}$$

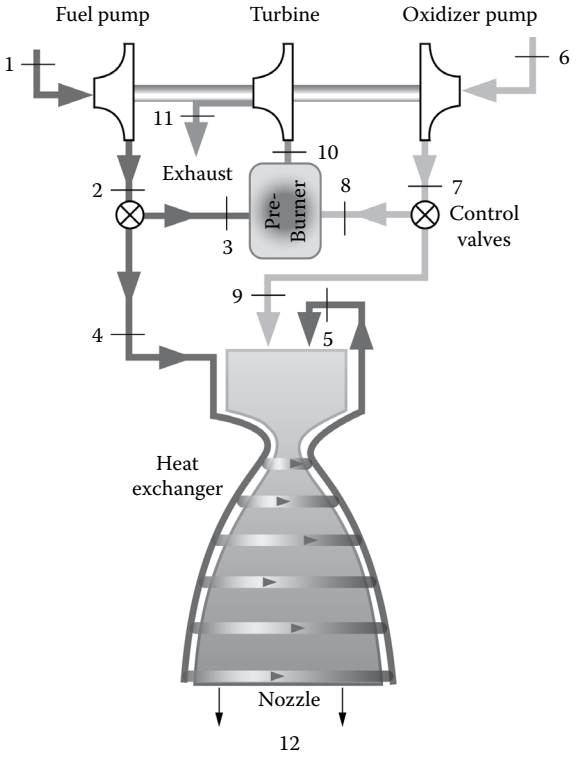


FIGURE 19.18
Layout of a turbopump of the gas generator type.

Nozzle: Full expansion to ambient pressure

$$p_{12} = p_a = 0.1\,\text{MPa}, \quad \eta_n = 0.9, \quad C_p = 1.05\,\text{kJ/kg}\cdot\text{K}, \quad \gamma = 1.28$$

Calculate

1. The turbine exhaust pressure
2. The exhaust velocity
3. Thrust force

Solution
Fuel pump

$$\Delta p_{0f} = 3.5 - 0.15 = 3.35\ \text{MPa}$$

Fuel pump power

$$P = \frac{\dot{m}_f}{\eta_{fp}}\left(\frac{\Delta p_{0f}}{\rho_f}\right) = \frac{25\times 3.35\times 10^6}{0.7\times 800} = 149.55\ \text{kW}$$

Oxygen pump

$$\Delta p_{o2} = 3.5 - 0.2 = 3.3 \text{ MPa}$$

Oxygen pump power

$$P = \frac{\dot{m}_{o2}}{\eta_{o2}}\left(\frac{\Delta p_{02}}{\rho_{o2}}\right) = \frac{60 \times 3.3 \times 10^6}{0.66 \times 1150} = 260.87 \text{ kW}$$

Total pumps power P_{total} = 149.55 + 260.87 = 410.42 kW

Turbine: Turbine power (P_t) is related to total power driving the fuel and oxygen pumps by the relation

$$P_t = \frac{P_{total}}{\eta_m} = \frac{410.42}{0.99} = 414.57 \text{ kW}$$

$$P_t = \eta_t \dot{m}_t C_p T_{oi}\left[1 - \left(\frac{p_e}{p_{010}}\right)^{\gamma-1/\gamma}\right]$$

Turbine exit pressure is then

$$p_e = p_{010}\left(1 - \frac{P_t}{\eta_t \dot{m}_t C_p T_{oi}}\right)^{\gamma/\gamma-1} = 1.3 \times \left(1 - \frac{414.57 \times 10^3}{0.72 \times 1.7 \times 1060 \times 800}\right)^{1.3/0.3} = 0.142 \text{ MPa}$$

Nozzle: Exit velocity

$$u_e = \sqrt{2\eta_n C p T_c\left(1 - \left(\frac{p_e}{p_{0e}}\right)^{\gamma-1/\gamma}\right)} = \sqrt{2 \times 0.9 \times 1050 \times 3000\left[1 - \left(\frac{0.1}{3}\right)^{0.28/1.28}\right]}$$

$$u_e = 1725 \text{ m/s}$$

Thrust force: Propellant mass flow rate:

$$\dot{m}_p = 25 + 60 - 1.7 = 83.3 \text{ kg/s}$$

$$T = \dot{m}_p u_e = 83.3 \times 1725 = 143.69 \text{ kN}$$

Example 19.9

A liquid hydrogen pump of the centrifugal type has the following data: Volume flow rate Q=1.25 m^3/s, pressure rise = 20.0 MPa, liquid hydrogen density ρ=69 kg/m^3. Rotational speed U_2=500 m/s, swirl speed at impeller outlet C_{u2}=200 m/s, and absolute angle of flow at impeller outlet α_2=45°.

Does this pump suffice to obtain the required pressure rise? If not, what is the number of pumps needed?

If the shaft rotational speed does not exceed 3000 s^{-1} and the impeller tip diameter does not exceed 0.35 m, calculate

1. Specific speed and specific diameter
2. The impeller width b_2

Solution

Assuming flow enters the pump axially, then

$$C_{u1} = 0$$

The pressure rise for a single-stage pump is

$$\left(\frac{\Delta p}{\rho}\right)_{stage} = U_2 C_{u2} = 500 \times 200 = 100{,}000 \text{ m}^2/\text{s}^2$$

Overall pump pressure ratio is

$$\left(\frac{\Delta p}{\rho}\right)_{pump} = \frac{20 \times 10^6}{69} = 289{,}985 \text{ m}^2/\text{s}^2$$

Number of stage is then

$$N = \frac{\left(\frac{\Delta p}{\rho}\right)_{pump}}{\left(\frac{\Delta p}{\rho}\right)_{stage}} = \frac{289{,}985}{100{,}000} = 2.89$$

Then $N = 3$.

Thus, the new value for pressure rise per stage is

$$\left(\frac{\Delta p}{\rho}\right)_{stage} = 96{,}618 \text{ m}^2/\text{s}^2$$

The specific speed is

$$N_s = \frac{\Omega Q^{1/2}}{\left(\frac{\Delta P_0}{\rho}\right)^{3/4}} = \frac{3{,}000 \times 1.25}{(96{,}618)^{3/4}} = 0.684$$

since $\Omega \not> 3000$ s^{-1} and $U_t = 500$ m/s,

$$D_2 = \frac{2U_t}{\Omega} = \frac{2 \times 500}{3000} = 0.333 \text{ m}$$

Specific diameter is

$$d_s = \frac{D_2\left(\frac{\Delta P_0}{\rho}\right)^{1/4}}{Q^{1/2}} = \frac{0.333 \times (96{,}618)^{1/4}}{\sqrt{1.25}} = 5.24$$

The width of impeller at tip is

$$b = \frac{Q}{\pi D_2 C_r}$$

since $\alpha_2 = 45°$, then $C_{r2} = C_{u2} = 200$ m/s.

$$b = \frac{1.25}{\pi \times 0.333 \times 200} = 5.97 \times 10^{-3}\ \text{m} \sim 6\ \text{mm}$$

19.8 Features of Modules of the Space Shuttle Main Engine (SSME)

Table 19.4 lists most features of the four turbopumps available in the SSME.

19.9 Axial Pumps

Figure 19.14 illustrates a typical axial pump and is of the multistage type. It has nearly constant blade height and a large hub-to-tip ratio. The pump head coefficient ψ has values up to 1.5–2.0 for multistage axial pumps. Normally, such a pump has typical stages with the same velocity triangles. A typical velocity triangle is shown in Figure 19.19.

TABLE 19.4

Rocketdyne SSME Turbopumps

		Low-Pressure Turbopump		High-Pressure Turbopump	
Feature		**Hydrogen**	**Oxygen**	**Hydrogen**	**Oxygen**
Pump	Type	Axial with inducer	Axial	Centrifugal pump	Centrifugal pump
	Number of stages	1	1	3	1 (double entry)
	Flow rate (kg/s)	70.3	424	67.7	407
	Inlet pressure (kPa)	207	689.5	1724	8,280
	Outlet pressure (MPa)	2.0	2.863	42.1	49.7
	Efficiency (%)	71.3	67.7	75	72
	rpm	15,400	5050	34,386	27,263
	Power (kW)			49,200	19,600
Turbine	Type	Axial gas turbine	Axial hydraulic	Axial	Axial
	Number of stages	2	6	2	2
	Turbine inlet temperature	−17°F	−272°F	997 K	3,620 K
	Turbine inlet pressure (MPa)			33.6	34.7
	Flow rate (kg/s)	13.2	84.8	74.1	27.3
	Pressure ratio	1.3	—	1.48	1.53
	Efficiency (%)	58	67.7	81.1	74.6
	rpm	15,400	5050	34,360	22,220
	Power (kW)	2,486	1203	47,039	17,062

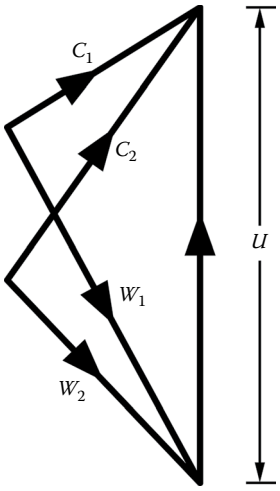


FIGURE 19.19
Velocity triangle for axial pump stage.

Example 19.10

A seven-stage axial flow pump is used for pumping liquid hydrogen. It has the following data:

$$d_m = 0.23\text{m}, \quad d_t = 0.25\ \text{m}, \quad N = 20{,}000\ \text{rpm}, \quad \eta = 0.7, \quad C_a = 70\ \text{m/s}, \quad C_{u1} = 60\ \text{m/s},$$

$$C_{u2} = 160\ \text{m/s}, \quad \rho_{H2} = 69\ \text{kg/m}^3$$

Calculate

1. Pump pressure rise
2. Power required to drive pump

Solution

1. Pump pressure rise:

$$u_m = \frac{\pi d_m N}{60} = \frac{\pi \times 0.23 \times 20{,}000}{60} = 240.9\ \text{m/s}$$

$$\Delta c_u = c_{u2} - c_{u1} = 160 - 60 = 100\ \text{m/s}$$

$$(\Delta h)_{stage} = u_m \Delta c_u = 240.9 \times 100 = 24{,}090\ \text{J/kg}$$

$$(\Delta p)_{stage} = \rho_{H2} \eta \Delta h = 69 \times 0.7 \times 24{,}090 = 1{,}163{,}331\ \text{Pa}$$

$$(\Delta p)_{stage} = 1.163\ \text{MPa}$$

For identical stages:

$$(\Delta p)_{pump} = 7 \times (\Delta p)_{stage} = 7 \times 1.163 = 8.143\ \text{MPa}$$

Mass flow rate: The blade height h is calculated from the relation

$$h = \left(d_t - d_m\right) = 0.02 \text{ m}$$

The hub diameter is then

$$d_h = d_m - h = 0.21 \text{ m}$$

$$\dot{m} = \rho c_a A = \rho c_a \frac{\pi\left(d_t^2 - d_h^2\right)}{4}$$

$$\dot{m} = 69 \times 70 \times \frac{\pi\left(0.25^2 - 0.21^2\right)}{4} = 69.8 \text{kg/m}^3$$

$$\left(\Delta h\right)_{pump} = 7 \times \left(\Delta h\right)_{stage} = 7 \times 24{,}090 = 168{,}630 \text{J/kg}$$

2. Power

$$P = \dot{m} \times \left(\Delta h\right)_{pump} = 69.8 \times 168{,}630 = 11{,}770{,}374 \text{ W} = 11.77 \text{ MW}$$

19.10 Parallel and Series Connections

Two or more pumps, either identical or nonidentical pumps, may be connected in series or in parallel to achieve a set of required flow conditions.

For series connections, the head (or pressure) is added, while in parallel connections, the mass (or volume) flow rate is added. The objective of a combination of pumps is to ensure that the operating point of the combination is close to the maximum efficiency of the combination. The effect of each pump on the combined characteristics is illustrated for a pair of identical pumps connected in series in Figure 19.20.

Example 19.11

The following table depicts the characteristics of a pump used in compressing liquid hydrogen in a typical turbopump of rockets:

Q (m³/s)	0	0.4	0.8	1.2	1.6	2.0
Δp (MPa)	11	10	8	6	4	2
η (%)	0	25	75	76	73	70

The external resistance against which the pump is working is represented by the following system data:

Q (m³/s)	0	0.4	0.8	1.2	1.6	2.0
Δp (MPa)	13.4	14	14.7	15.4	16.1	16.8

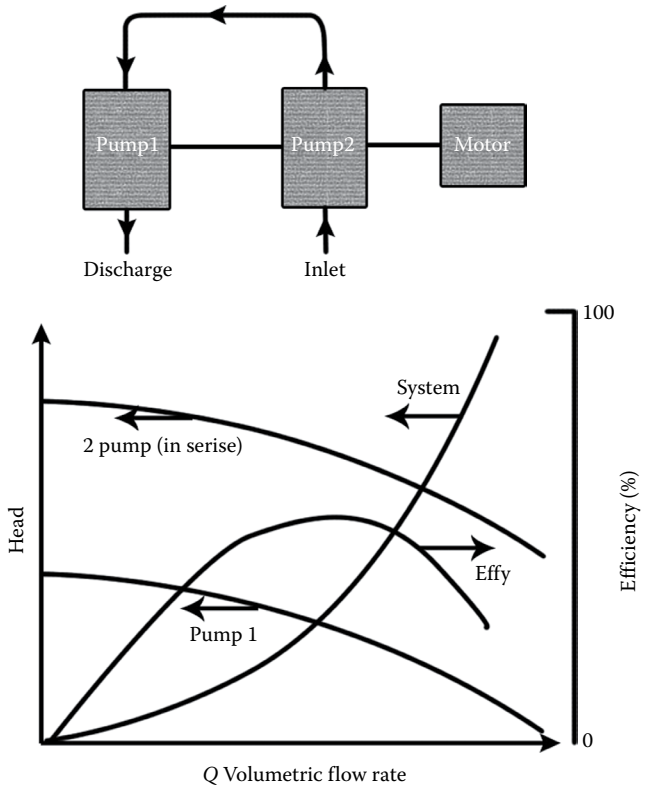


FIGURE 19.20
Performance of parallel and series pumps.

Density of liquid hydrogen: $\rho = 69\ \text{kg/m}^3$

1. Does one pump afford the system resistance?
2. If two pumps are connected, whether series or parallel, which connection is appropriate?
3. Determine the discharge and power required for the appropriate choice.

Solution

1. Single pump
   From these two tables, the minimum system resistance (represented by $\Delta p = 13.4$ MPa) is greater than the maximum pressure rise that can be developed by a single pump ($\Delta p = 11$ MPa). Thus, the system and pressure rise plots do not intersect. Consequently, a single pump will not afford the system resistance.
2. Two pumps
   a. Parallel connection
      Parallel pumps will generate the sum (here double, as both are identical pumps) of the volume flow rate, but the same pressure rise. Their performance is shown in the following table:

Q (m^3/s)	0	0.8	1.6	2.4	3.2	4.0
Δp (MPa)	11	10	8	6	4	2

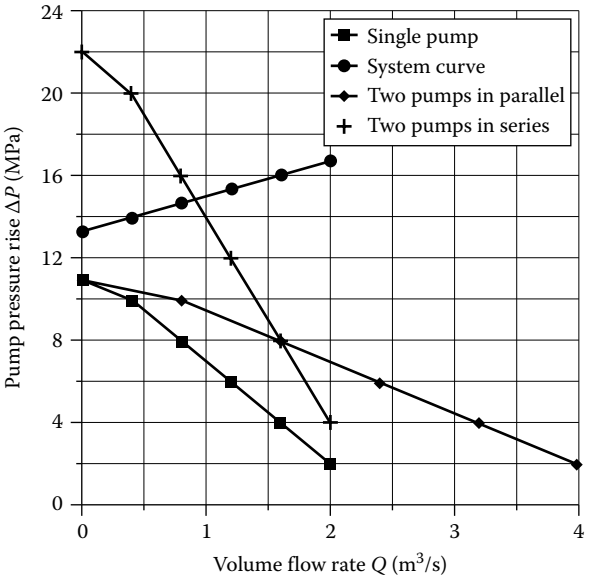


FIGURE 19.21
Two pumps in parallel and series.

Again, this arrangement will not solve the problem as the system demands are still greater than the available pressure rise. Thus, this arrangement is not suitable, and both system and pump curves will not intersect.

b. Series connection
Series pumps will generate the total (here double, as both are identical pumps) pressure rise for the same volume flow rate. Their performance is shown in the following table:

Q (m³/s)	0	0.4	0.8	1.2	1.6	2.0
Δp (MPa)	22	20	16	12	8	4

As a result, the two pumps in series connection generate a pressure rise exceeding the system demands, as shown in Figure 19.21.

Point of intersection from Figure 19.21 provides the following information.
Volume flow rate is

$$Q = 0.95 \text{ m}^3/\text{s}$$

Pressure rise is

$$\Delta p = 15 \text{ MPa}$$

The corresponding pump efficiency is

$$\eta = 0.755$$

The power needed for driving the two pumps in series is then

$$P = \frac{Q\Delta p}{\eta} = \frac{0.95 \times 15}{0.755} = 18.874 \text{ MW}$$

19.11 Pump Materials and Fabrication Processes

The first set of pumps used in turbopumps were made of aluminum, either machined forgings or castings [10]. When the pressures went up, they were made of titanium, steel alloys, and then superalloys like Inconel or Hastelloy. In the early 2000s, a few pump impellers were beginning to be made by powder metallurgy processes with new material properties (equal or slightly better than machined wrought material of a similar kind) and with smooth surfaces in the flow passages. Physical properties were equal or perhaps slightly better than a hogged out forging, but perhaps lower in cost. Design safety factors are today considerably smaller. Old pumps manufactured some 65 years ago are two to four times as heavy and considerably larger than a modern newly designed version with better materials.

19.12 Axial Turbines

The turbines that provide shaft power to the propellant pumps derive their energy from the expansion of a high-pressure, high-temperature gas to lower pressures and temperatures.

Turbines are divided into two major types: impulse and reaction turbines; see Figure 19.22. Impulse turbines can be either single or multiple stages. Reaction turbines are usually multistage.

Various turbines employed in rocket engine applications are described as follows.

19.12.1 Single-Stage Impulse Turbine

This turbine consists of a nozzle (or stator) followed by rotor blade rows. Gas is fed to the rotating blades through stationary nozzles. In the nozzles, the gas pressure is converted into kinetic energy (velocity head) while the static pressure drops. The absolute velocity is at a maximum upon entering the rotating blades, where the kinetic energy of the gas is imparted to the turbine rotor as mechanical energy of rotation. Static pressure drops in the rotor passage if the turbine is of the reaction type. For the impulse type, ideally, the static pressure of the gas remains constant (except for the effects of friction). Velocity diagrams are shown in Figure 19.23 for the impulse stage. Relative velocity remains constant in this case.

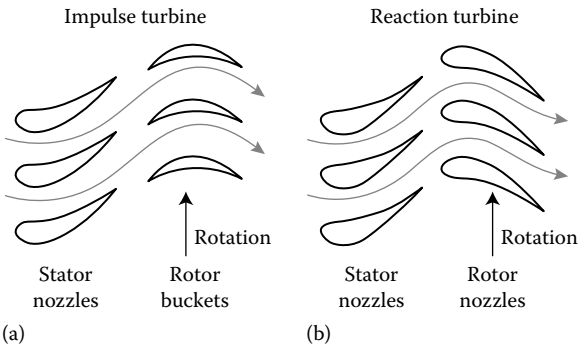


FIGURE 19.22
(a, b) Impulse and reaction single-stage axial turbine.

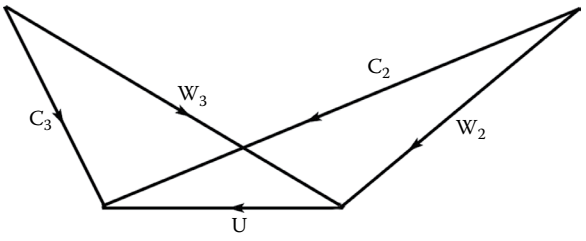


FIGURE 19.23
Velocity triangles for an impulse turbine stage.

19.12.2 Multispool Impulse Turbines

The expansion of the gas is accomplished in steps, through two or more rows or stages of stationary nozzles, each set being followed by a row of rotating blades. A design objective is that the velocity, and thus the kinetic energy, of the gas flow is the same at the entrance of each row of rotating blades. This results in equal energy being transferred to each rotating blade row, while the pressure drop in each stationary nozzle row will vary.

19.12.3 Reaction Turbines

The main difference between an impulse turbine and a reaction turbine is that in an impulse turbine no static pressure drop occurs in the rotating blades, whereas in a reaction turbine the pressure does drop. Both impulse and reaction wheels are driven by a change in momentum of the gas. In a pure reaction-type turbine, the driving force is derived entirely from the reaction due to gas expansion within the rotating blades (similar to the gas expansion in a rocket nozzle).

Denoting the inlet and outlet states of turbine as (1) and (2), then the turbine power is given by

$$P = \dot{m}_t \left(h_{01} - h_{02}\right) = \dot{m}_t C_p \left(T_{01} - T_{02}\right) \tag{19.26a}$$

where $\dot{m}_t$ is the turbine mass flow rate. If the turbine total-to-static efficiency is denoted as (η_t), then for a real expansion process of gases in the turbine from inlet total pressure p_{01} to exit static pressure p_2:

$$\eta_t = \frac{h_{01} - h_{02}}{h_{01} - h_{2s}} = \frac{1 - T_{02}/T_{01}}{1 - \left(\dfrac{p_2}{p_{01}}\right)^{\gamma - 1/\gamma}}$$

The turbine power is then

$$P = \dot{m}_t \eta_t C_p T_{01} \left[1 - \left(\frac{p_2}{p_{01}}\right)^{\gamma - 1/\gamma}\right] \tag{19.26b}$$

Denoting the turbine expansion ratio as

$$\pi_t = \frac{p_{01}}{p_2}$$

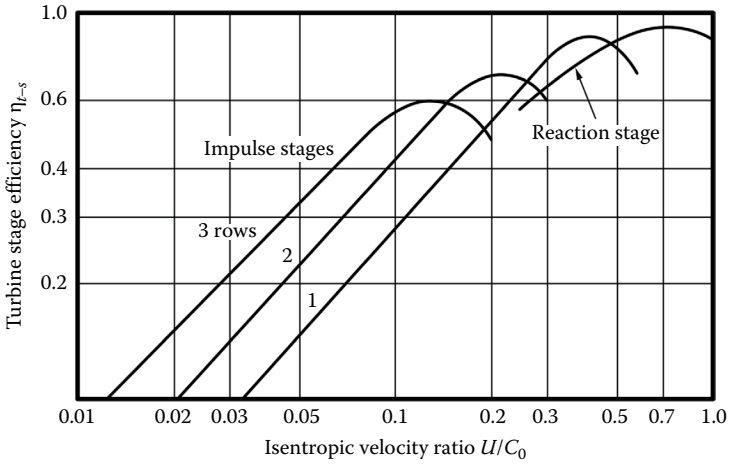


FIGURE 19.24
Turbine efficiency as a function of blade velocity and gas spouting velocity ratios. (From Stangeland, M.C., *Threshold*, 3, 34, 1988; Cannon, J.L., Liquid propulsion: Propellant feed system design, in: *Encyclopedia of Aerospace Engineering*, *Vol. 2: Propulsion & Power*, Wiley Publishers, Chichester, U.K., Chapter 2.3.11.)

The turbine power will be

$$P = \dot{m}_t \eta_t C_p T_{01} \left[1 - \left(1/\pi_t \right)^{\gamma - 1/\gamma} \right] \tag{19.26c}$$

Overall performance of the turbine depends upon three variables: the available energy content per pound of drive gas, the blade tip tangential velocity (U_t), and the number of turbine stages. The available energy for the turbine pressure ratio can be expressed as an ideal velocity, C_0. The turbine velocity ratio, (U_t/C_0), is used to characterize empirically these two variables versus the turbine efficiency. Typical efficiencies of several types of turbines are illustrated in Figure 19.24.

The design selection is made to maximize efficiency and minimize the weight compatible with the selected shaft speed. In general, when a direct drive turbopump configuration is selected, the shaft speed is less than optimum for the turbine and additional stages must be added to utilize the available energy.

Blade tip diameter is selected to optimize the (U_t/C_0) for efficiency within the blade height-to-diameter performance limits and within the tip speed structural limits. If the blade height-to-diameter ratio gets too small, the tip clearance and secondary flow losses become large, decreasing the turbine efficiency.

As described in Chapters 12 through 15, for a constant cross-sectional area of blade along its height, the maximum bending stress at the blade root is given by the relation

$$\sigma_{\max} = 2\pi \rho_b A N^2 = \frac{\rho_b U_t^2}{2}\left(1 - \zeta^2\right) = \frac{\rho_b \Omega^2 D_t^2}{8}\left(1 - \zeta^2\right) \tag{19.27}$$

From these relations, the tip speed structural limit is based on the centrifugal pull that can be carried at the base of the blade airfoil for the selected material ($\rho_b, \sigma_{\max}$) and is generally expressed as an allowable annulus area (A) multiplied by the square of rotational speed (N^2).

If the flow through the stator blade row is assumed to be ideal, and the axial velocity within the turbine blade rows is also assumed to be constant, then the spouting velocity C_0 will be calculated as

$$C_2 = C_0 = \sqrt{2C_P T_{01}\left(1 - \frac{1}{\pi_t^{\gamma-1/\gamma}}\right)}$$

and

$$C_a = C_2 \cos\alpha_2$$

The mass flow rate is expressed as

$$\dot{m} = \frac{\rho_2 C_a \pi D_t^2}{4}\left(1-\zeta^2\right) = \frac{\rho_2 C_0 \cos\alpha_2 \pi D_t^2}{4}\left(1-\zeta^2\right) \tag{19.28}$$

From Equations 19.27 and 19.28,

$$\Omega = \sqrt{\frac{2\pi\sigma_{\max}}{\dot{m}}\frac{\rho_2}{\rho_b}C_0\cos\alpha_2} \tag{19.29}$$

Example 19.12

An axial turbine is used as a power source in a rocket turbopump. The turbine is a single stage and of the impulse type. It has a mean diameter $d_m = 0.24$ m and a rotational speed $N = 14{,}000$ rpm. Hot gases flow at the rate of 90 kg/s into the turbine having a total inlet temperature and pressure of $T_{01} = 960$ K, $P_{01} = 7.5$ MPa. The turbine pressure ratio is $\pi_t = 1.5$. Flow in the stator is assumed to be ideal and the flow has an axial absolute exit velocity from the rotor blade row.

The working fluid is a molecular weight $M = 26.5$ and specific heat ratio $\gamma = 1.3$.

1. Draw the velocity diagram for the rotor blade row.
2. Calculate the blade height of the rotor at the inlet and outlet.

Solution

For the impulse turbine

$$W_2 = W_3, \quad P_2 = P_3$$

Flow leaves axially, then $\alpha_3 = 0$.

Velocity triangles are shown in Figure 19.25.

The flow in the stator is ideal, so

$$T_{01} = T_{02} \quad \text{and} \quad P_{01} = P_{02}$$

The gas constant is $R = \bar{R}/M = \dfrac{8314}{26.5} = 313.7$ J/kg·K.

Specific heat is $C_p = \gamma R/\gamma - 1 = 1359.5$ J/kg·K.

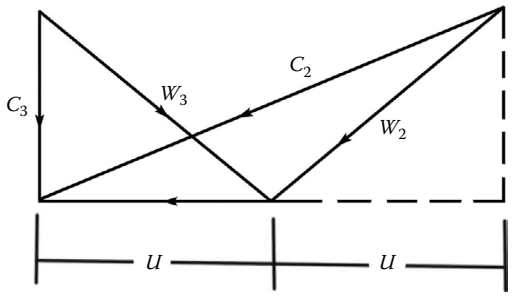


FIGURE 19.25
Velocity triangles for impulse turbine with axial exit.

The absolute outlet velocity from the stator is calculated from the relation

$$C_2 = C_0 = \sqrt{2C_P T_{01}\left(1 - \frac{1}{\pi_t^{\gamma-1/\gamma-1}}\right)}$$

$$C_2 = C_0 = \sqrt{2 \times 1359.5 \times 960\left(1 - \frac{1}{1.5^{0.3/1.3}}\right)} = 483 \text{ m/s}$$

$$U_2 = \frac{\pi d_2 N}{60} = \frac{\pi \times 0.24 \times 14{,}000}{60} = 176 \text{ m/s}$$

From the velocity triangle

$$\sin\alpha_2 = \frac{2U_2}{C_2} = \frac{2 \times 176}{483}$$

$$\alpha_2 = 46.8°$$

Then $C_3 = C_a = C_2 \cos\alpha_2 = 330.9$ m/s.

Assuming $C_1 = C_3$, $C_1 = 330.9$ m/s.

The static temperature at the stator outlet is

$$T_2 = T_{01} - \frac{C_2^2}{2C_P} = 960 - \frac{(483)^2}{2 \times 1359.5} = 874.2 \text{ K}$$

The static pressure at the stator outlet is

$$P_2 = \frac{P_{01}}{\pi_t} = \frac{7.5}{1.5} = 5.0 \text{ MPa}$$

The density at the stator outlet is

$$\rho_2 = \frac{P_2}{RT_2} = \frac{5 \times 10^6}{313.7 \times 874.2} = 18.23 \text{ kg/m}^3$$

Since $\dot{m} = \rho_2 C_a A_2$ and $A_2 = \pi d_m h_2$,

$$h_2 = \frac{\dot{m}}{\rho_2 C_a \pi d_m} = \frac{90}{18.23 \times 330.9 \times \pi \times 0.24} = 0.0198 \text{ m}$$

The tip diameter is then

$$d_{t2} = d_m + h_2 = 0.24 + 0.0198 = 0.2598 \text{ m}$$

The rotational speed at the tip is then

$$U_{2t} = U_{2m} \times \frac{d_t}{d_m} = 176 \times \frac{0.2598}{0.24} = 190.5 \text{ m/s}$$

The speed ratio is then

$$\frac{U_{2t}}{C_0} = \frac{190.5}{483} = 0.394$$

From Figure 19.24, the turbine efficiency is

$$\eta_t = 0.85$$

and is defined as

$$\eta_t = \frac{T_{01} - T_3}{T_{01} - T_2}$$

$$0.85 = \frac{960 - T_3}{960 - 874}$$

$$T_3 = 887 \text{ K}$$

With $P_2 = P_3 = 5$ kPa, the density at the rotor outlet is

$$\rho_3 = \frac{P_3}{RT_3} = \frac{5 \times 10^6}{313.7 \times 887} = 17.97 \text{ kg/m}^3$$

The blade height at the rotor outlet is then

$$h_3 = \frac{\dot{m}}{\rho_3 C_3 \pi d_m} = \frac{90}{17.97 \times 330.9 \times \pi \times 0.24} = 0.02 \text{ m}$$

19.13 Hybrid Propulsion

19.13.1 Introduction

Hybrid propellant engines represent an intermediate group between solid- and liquid-propellant engines. One of the substances used is solid, usually the fuel, while the other, usually the oxidizer, is liquid, although reverse hybrids such as liquid hydrogen burning

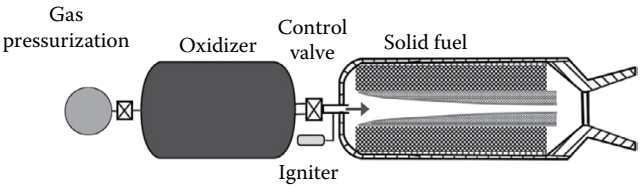


FIGURE 19.26
Hybrid rocket engine.

with solid oxygen have been studied; see Figure 19.26. Such engines have a performance similar to that of solid propellants, but the combustion can be moderated, stopped, or even restarted. It has a better specific impulse than solid rocket engines.

The liquid oxidizer is injected into the solid, whose fuel case also serves as the combustion chamber. An igniter starts the combustion process, which develops heat to vaporize the surface layer of solid fuel. The expanding hot fuel gas expands away from the solid surface and meets the spray of liquid oxidizer; the combustion process continues in a self-sustaining manner. The hot fuel gas layer and the combustion layer grow downstream in a boundary layer pattern until they merge at the centerline at nearly five diameters from the initial station. At some point, on the order of several tens of diameters in the downstream direction, the oxidizer supply has been fully used and no further combustion can be maintained. Figure 19.27 illustrates the combustion process in a hybrid motor.

Typically, the fuel is a polymeric hydrocarbon solid such as HTPB (which stands for hydroxyl-terminated polybutadiene) and the oxidizer can be any of the oxidizers used with liquid bipropellant engines (hydrogen peroxide H_2O_2). HTPB has slow burning rates, thus a number of holes, or ports, exposing more surface area of the fuel for burning are added. Unfortunately, so many holes make the solid fuel structurally weak and subject to dangerous breakup as the combustion chamber builds up pressure and gas flow. Research on new fuels has been carried out.

It is difficult to make use of this concept for very large thrusts, and so hybrid propellant engines are applied to missions requiring throttling, restart, or long-term propellant storage.

The hybrid rocket has been known for over 50 years, but was not given serious attention until the 1960s, when the European programs in France and Sweden involved small sounding rockets, whereas the American flight programs were target drones.

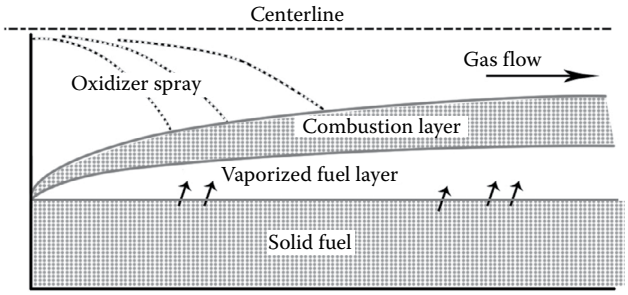


FIGURE 19.27
Combustion process in a hybrid motor.

TABLE 19.5

Fuel–Oxidizer Combinations for Hybrid Propellant Rockets

Number	Fuel	Oxidizer
1	Beryllium hydride (Be–H_2)	Fluorine (F_2)
2	Lithium hydride (Li H)	Chlorine trifluoride (CIF_3)
3	Lithium hydride (Li H)	Nitrogen tetroxide (N_2O_4)
4	Hydrocarbon $(CH_2)n$	Nitrogen tetroxide (N_2O_4)

Several hybrid propulsion programs were initiated in the late 1980s and early 1990s. The Joint Government/Industry Research and Development (JIRAD) program involved the testing of 11 and 24 in. diameter hybrid motors at the Marshall Space Flight Center. Another hybrid program initiated during the early 1990s was DARPA's Hybrid Technology Options Project (HyTOP). The Hybrid Propulsion Demonstration Program (HPDP) began in March 1995, which included the design and fabrication of a 250,000 lb thrust test bed. The most recent advance in hybrid rockets occurred in the fall of 2004 when Space Ship One carried a pilot to over 328,000 ft in a new era of space tourism. The propulsion system used for this project used a four-port motor fueled by HTPB with nitrous oxide (N_2O) as the oxidizer.

Some fuel–oxidizer combinations for hybrid propellant rockets are shown in Table 19.5.

19.13.2 Mathematical Modeling

The surface recession rate may be described by a general empirical relation

$$\dot{r} = a\left(\frac{\dot{m}}{A}\right)^n \tag{19.30}$$

where

a is a constant
$\dot{m}$ is the *combined* oxidizer and fuel mass flux
A is the cross-sectional area of the combustion chamber
the exponent n has the range $0.6 < n < 0.8$

Assuming that the fuel has a cylindrical area (A_b) with diameter (D) and length (L), the rate of fuel mass generation is

$$\dot{m}_f = \rho_f A_b \dot{r} = \rho_f \pi D L \dot{r} \tag{19.31a}$$

where ρ_f is the fuel density.

Now following the procedure of Loh [11], who assumed that the recession rate is proportional to the oxidizer only and not to the combined mass flow of the fuel and oxidizer, then, from (19.30), the fuel regression rate is

$$\dot{m}_f = \rho_f \pi D L a\left(\frac{\dot{m}_o}{A}\right)^n \tag{19.31b}$$

Substituting for the cross-sectional area A,

$$\dot{m}_f = \rho_f \pi D L a \left(\frac{4\dot{m}_o}{\pi D^2} \right)^n$$

Now, it is interesting to note that if $n = 0.5$, then the rate of fuel mass recession is

$$\dot{m}_f = 2a\rho_f L\sqrt{\pi \dot{m}_o} \tag{19.32}$$

which is independent of the fuel diameter (D) and means that the fuel mass flow is constant, even though d is increasing as the fuel is consumed.

Example 19.13

A hybrid rocket has the following data:
Propellant density = 1600 kg/m^3
Thrust force = 55 kN
Specific impulse $I_{sp} = 275$ s

$$\frac{O}{F} = 1.0$$

Constants: $a = 0.001, n = 0.6$
Burn time = 10 s
Initial propellant diameter $D(0)$ = 0.1 m
Calculate

1. The solid-propellant length
2. The final propellant diameter

Solution

The propellant flow rate is

$$\dot{m} = \frac{T}{gI_{sp}}$$

$$\dot{m} = \frac{55{,}000}{9.8 \times 275} = 20.4 \text{ kg/s}$$

Since the ratio between oxidizer and fuel flow rates

$$O/F = 1.0, \quad \text{then } \dot{m}_f = \dot{m}_o = 10.2 \text{ kg/s}$$

From Equation 19.32,

$$L = \frac{\dot{m}_f}{2a\rho_f\sqrt{\pi \dot{m}_o}} = \frac{10.2}{2 \times 0.001 \times 1600 \times \sqrt{10.2\pi}} = 0.56 \text{ m}$$

From Equation 19.30, with $n = 0.5$,

$$\dot{r} = a\left(\frac{\dot{m}_o}{A}\right)^{0.5} = 2a\sqrt{\frac{\dot{m}_o}{\pi D^2}}$$

Moreover,

$$\dot{r} = \frac{1}{2}\frac{dD}{dt}$$

Then

$$\frac{1}{2}\frac{dD}{dt} = 2a\sqrt{\frac{\dot{m}_o}{\pi D^2}}$$

$$D\frac{dD}{dt} = 4a\sqrt{\frac{\dot{m}_o}{\pi}}$$

Integrating this equation from $t = 0$ to $t = t_b$, then

$$D^2(t_b) - D^2(0) = 8at_b\sqrt{\frac{\dot{m}_o}{\pi}}$$

With $t_b = 10$ s, then

$$D^2(t_b) = 0.1^2 + 8 \times 0.001 \times 10 \times \sqrt{\frac{10.2}{\pi}} = 0.1541$$

$$D(t_b) = 0.393 \text{ m}$$

19.13.3 Advantages and Disadvantages of Hybrid Engines

The main advantages of hybrid rockets are as follows:

1. Lighter than the corresponding liquid-propellant types due to fewer propellant pumping equipment and higher fuel density.
2. The regression rate is independent of the chamber pressure, which is an important characteristic in the motor design.
3. Inherently safe due to the nonexplosive character of the fuel. Thus in the event of a structural failure, the oxidizer and fuel cannot mix intimately, leading to a catastrophic explosion that might endanger personnel or destroy a launch pad.
4. Thrust control is comparatively easier because only the flow of the liquid oxidizer need to be regulated.
5. Greater choices in the selection of grain configuration compared to solid-propellant rockets.
6. Less constituents as it uses only one liquid containment and delivery system.
7. Less complexity due to omission of a regenerative cooling system for both the chamber and nozzle.

8. A large cost saving could be realized both in manufacture and launch operation as the fuel could be fabricated at any conventional commercial site.

Additional advantages over the solid rocket are

1. Greatly reduced sensitivity to cracks and de-bonds in the propellant
2. Better specific impulse
3. The products of combustion are environmentally benign unlike conventional solids that produce acid-forming gases such as hydrogen chloride

19.14 Nuclear Rocket Propulsion

19.14.1 Introduction

Nuclear rockets have never developed or flown due to the grave risk of spreading radioactive debris if an accident occurred.

Nuclear sources include

- Radioactive isotope decay
- Fission reactor
- Fusion reactor

Nuclear rocket engines may be divided into two general classes based on the type of reactor used:

1. Solid-core systems
2. Fluid-core systems, which may be further subdivided based on its core into
   a. Liquid core
   b. Gas core
   c. Plasma

19.14.2 Solid-Core Reactors

Solid-core reactor systems have been under active investigation since 1955 [11]. These engines utilize reactors with graphite, metal, or metal-carbide cores capable of operating at temperatures ranging from 2000 to 3000 K.

Such a solid-core rocket engine is an adaptation of liquid-propellant engine, but with the combustion chamber replaced by a reactor (which resembles a heat exchanger) and the oxidizer-feeding system eliminated.

It includes a propellant tank, feeding system, reactor, and a convergent–divergent nozzle. As described in Section 19.6, the feeding system cycles may be (1) a gas generator system, (2) a staged combustion system, or (3) an expander cycle. An expander cycle is shown in Figure 19.28 where liquid propellant is pumped from its tank to the reactor through the shell jacketing the exhaust nozzle. Then it flows upward through the neutron reflector surrounding the reactor core, cooling both the reflector and the control drums contained

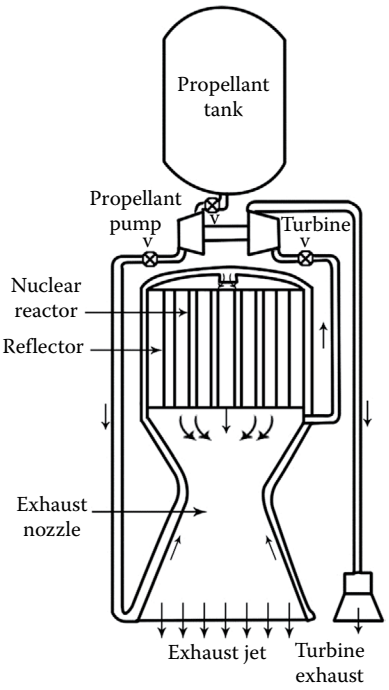


FIGURE 19.28
Simple layout of a nuclear rocket engine.

within it, before passing through a neutron and gamma ray shield placed at the upper end of the reactor assembly to limit the radiation heating of the propellant in the tank. Flowing downward, the propellant cools the reactor support structure and is heated to the design temperature, exiting into the nozzle plenum chamber prior to being discharged through the exhaust nozzle. A small portion of the heated gas (propellant) is bled off from this chamber and is cooled (by mixing the heated material with cold fluids) to an acceptable inlet temperature for the pump drive turbine. The turbine exhaust expands in a small nozzle and provides a small portion of total thrust.

Nuclear thermal propulsion (NTP) has the following main advantages:

1. High specific impulse capability, which reduces the in-orbit mass requirements for staging high ΔV missions
2. High thrust level, which increases interplanetary trip times
3. Ability to utilize any gaseous propellant, thus having the best potential for use in in situ planetary propellant resources

Both the specific impulse and thrust are proportional to the exhaust speed u_e, which in turn is proportional to the chamber temperature T_c and inversely proportional to the molecular weight M, or

$$u_e \sim \sqrt{\frac{T_c}{M}} \tag{19.33}$$

TABLE 19.6

Characteristics of Propellants for Nuclear Propulsion

Propellant	T_c (K)	Molecular Weight (M)	Max I_{sp} (s)
H_2	2800	2	1000
C_3H_8	2800	5.8	530
NH_3	2800	8.5	460

Equation 19.33 indicates the desirability of using hydrogen ($M_{H2}=2$) as a propellant. Its low molecular weight is the source of the superiority of the nuclear engine over its chemical rival. Table 19.6 shows these facts for some nuclear propellants.

Due to close similarity between the solid-core nuclear engine and liquid-propellant engine, the same analyses for feeding systems including turbopumps and nozzles will not be repeated again here. However, it is worth saying that these components differ from similar components found in liquid chemical rockets only in the modifications required to allow them to survive and function properly in the reactor radiation environment.

For this reason, only the reactor will be briefly discussed. Nuclear reactors are assemblies containing sufficient fissionable material (uranium or plutonium) to produce a self-sustaining chain-fission reaction. Figure 19.29 illustrates a generalized nuclear rocket reactor system. It is designed as a heat exchanger. The central core contains a dispersal of fissionable uranium in a high-temperature matrix material. It is supported by structural members attached to a support plate at the cold (coolant entry) end of the core. The core is surrounded by a neutron reflector material that reduces neutron losses from the core region by "reflecting" neutrons back into the core. Neutron poison (absorbing) material is incorporated into rotating drum elements to control the number of neutrons returning to the core.

Core design is a very complicated procedure that includes thermal, mechanical, and nuclear design procedures. Furthermore, control mechanisms must be provided to start up, regulate, and shut down the system on demand. Since the core material must perform at a very high temperature, selected materials must have a very high melting point like

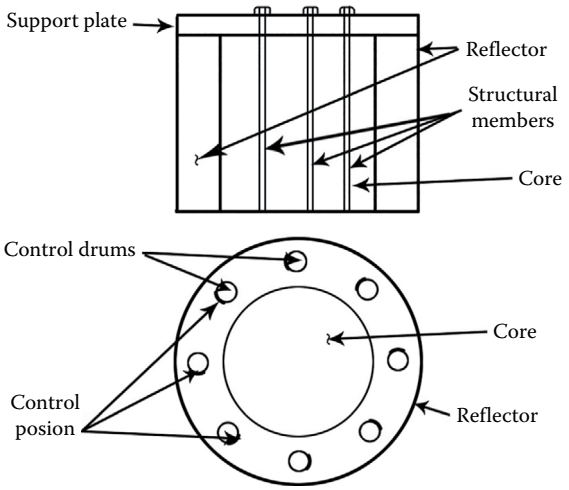


FIGURE 19.29
Rocket reactor.

graphite (7050° R), zirconium carbide (6880° R), hafnium carbide (7500° R), and tantalum carbide (7460° R).

The melting point together with data pertaining to thermal conductivity and the mechanical properties of the carbides are required to determine the maximum temperatures that might be realized in a nuclear rocket reactor.

A large cross section is a serious disadvantage, which limits the utility of hafnium, tantalum, and niobium carbides. Chemical compatibility of the reactor core with the hydrogen coolant is another criterion of material selection. Hydrogen and graphite react rapidly to form methane and other hydrocarbon gases at the temperatures of interest.

19.14.3 Gas-Core Reactor

A gas-core reactor uses the nuclear fuel in the gas phase, for example, uranium hexafluoride. Heat transfer takes place between the hot fuel and the cool propellant while both are in the gaseous state. The heated mixture of propellant and fuel is exhausted through a nozzle at much higher temperatures than that in a solid-core reactor. The gas-core rocket is an open cycle system and therefore radioactive fuel is exhausted into the ambient. Thus, gas-core application is used for interplanetary missions in the deep space environment in which such emissions are acceptable [12]. A typical gas-core nuclear rocket can operate with a gas temperature of about 8600 K at around 3.5 MPa, which when exhausted from the nozzle with an expansion ratio $\varepsilon = 40$ produces a specific impulse $I_{sp} = 2200$ s. Part of the increase in specific impulse can be attributed to the hydrogen being completely dissociated so that the effective molecular weight of the nozzle exhaust gas is approximately unity.

19.15 Electric Rocket Propulsion

19.15.1 Introduction

Electric propulsion is defined as "the acceleration of gases for spacecraft propulsion by electric heating and/or by electric and magnetic body forces" [13]. Electric thrusters typically use much less propellant than chemical rockets because they have a higher exhaust speed and higher specific impulse over long periods compared with chemical rockets. Thus, electric propulsion can work better than chemical rockets for deep space missions. However, it is not usually suitable for launches from the Earth's surface, because of its very small thrust.

Historically, the idea of electric propulsion for spacecraft was introduced by Konstantin Tsiolkovsky in 1911 [14]. The first in-space demonstration of electric propulsion was an ion engine carried on board the SERT-I (Space Electric Rocket Test-I) spacecraft, launched on July 20, 1964. Russian satellites have used electric propulsion for decades, while only recently have other countries employed it. However, presently it is extensively used. As of 2013, over 200 spacecraft operated around the world using electric propulsion for station keeping, orbit raising, or primary propulsion. In the future, the most advanced electric thrusters may be able to impart a velocity increase Δv of nearly 100 km/s, which is enough to take a spacecraft to the outer planets of the solar system. A useful overview of electric propulsion for spacecraft was presented in Reference 15.

Electric propulsion thrusters for spacecraft may be grouped into three families based on the type of force used to accelerate the ions of the plasma, namely,

- Electrostatic
- Electrothermal
- Electromagnetic

In *electrostatic* thrusters, discrete particles are charged by electron bombardment and then accelerated by electrostatic Coulomb forces. Electrostatic propulsion depends on the attraction or repulsion of electrically charged particles (by electron bombardment) and uses this effect to accelerate a stream of positively charged ions in order to produce thrust [16]. Spacecraft SERT-II (Space Electric Rocket Test-II) used electrostatic ion propulsion and operated for 10,000 h in space. Its different types are

1. Ion thrusters (IT)
2. Field emission electric propulsion (FEEP)
3. Colloidal thrusters

Electrothermal rockets are very similar in principle to chemical and nuclear rockets as the propellant is a fluid (like hydrazine) which is heated in some chamber prior to its acceleration in a nozzle to convert its thermal energy to a directed stream that delivers reactive thrust power to the vehicle. Heating may be achieved by

1. An electrical heating through the chamber wall or a heater coil (Resistojets)
2. An electrical arc through the fluid (Arcjets)
3. Inductively and radiatively heated devices, wherein some form of electrode, less discharge or high-frequency radiation, heats the flow

Electromagnetic propulsion devices depend on the creation of a magnetic force on a conducting fluid (gas or plasma) by passing it through a field with crossed electric and magnetic fields. Its different types are

1. Magneto plasma dynamic (MPD) thrusters
2. Hall thrusters (HT)
3. Pulsed plasma thrusters (PPT)
4. Pulsed inductive thrusters (PIT)

A brief comparison between the three families may be summarized as follows:

1. An electrostatic thruster generates the highest specific impulse (from 2,000 to over 10,000 s), efficiency (from 60% to >80%), and the smallest thrust (5 μN – 0.5 N). An example of the electrostatic thruster is the Deep Space-1 Ion Engine [17].
2. Resistojet electrothermal types develop the minimum specific impulse (<500 s) and moderate thrust (0.05–5 N), exhaust velocity~3.5 km/s, and efficiency ~80%. However, the electrothermal Arcjet has a specific impulse (<700 s), higher exhaust velocity ~5–6 km/s, and lower efficiency ~40%.
3. The electromagnetic (MHD) type generates the maximum thrust (25–200 N), a very high specific impulse (2000–5000 s), and efficiency (30%–50%).

19.15.2 Electrostatic Propulsion

19.15.2.1 Introduction

The appropriate propellants for electrostatic thrusters are cesium, mercury, neon, argon, and krypton, while the most commonly used is xenon. They are the most amenable sources of ions as they provide the requisite efficiency, reliability, and uniformity. The propellant introduced into the engine is electrically neutral because charged particles cannot be stored in appreciable amounts.

The engine or thruster has three basic elements, which are an ion source, an accelerator section, and a beam neutralizer (electron injector); see Figure 19.30.

A cylindrical discharge chamber containing a hollow centerline cathode emits electrons. By stripping off one or more electrons from it, the neutral propellant molecule becomes a single- or multiple-charged positive ion. Emitted electrons are forced to interact with the gaseous propellant flow in a suitable ionization chamber.

Emitted electrons will then generate neutral atoms, positive ions, and electrons in the chamber. Such electrons are attracted toward the cylindrical anode but are forced by the axial magnetic field to spiral in the chamber, causing numerous collisions with propellant atoms, which leads to ionization.

A radial electric field removes the electrons from the chamber and an axial electric field moves the ions toward the accelerator grids. These grids act as porous electrodes, which electrostatically accelerate the positive ions.

The positive ion is then accelerated by the electric field and ejected from the engine at a high speed.

Electrons are routed from the cylindrical anode through an external circuit to another hot cathode at the exhaust beam in order to neutralize the exit ion beam.

To summarize, the ion rocket accomplishes this by using an ion source to produce a stream of positively charged particles, a negatively charged grid electrode to accelerate the ions electrostatically, and an electron source to neutralize the accelerated ions.

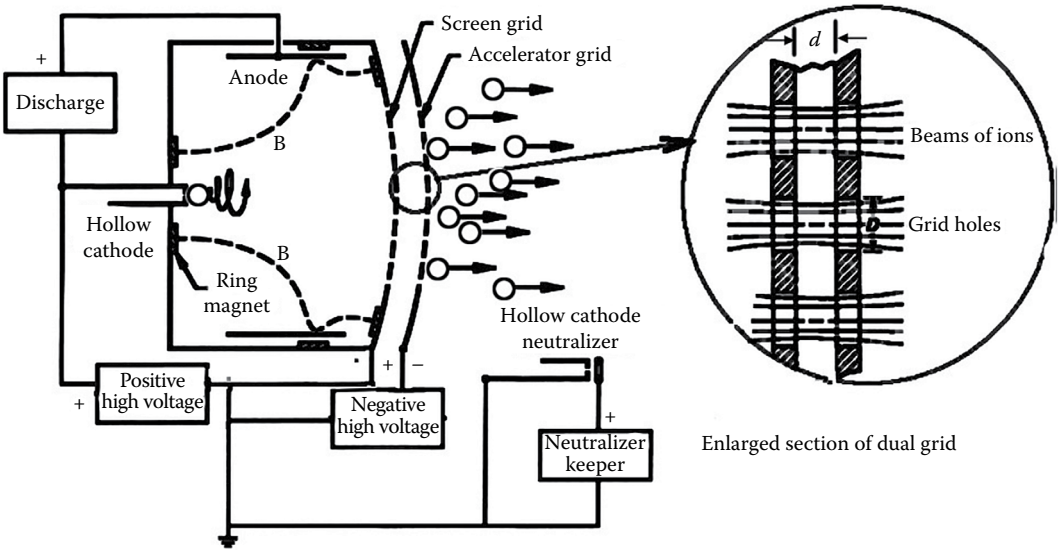


FIGURE 19.30
Elements of electrostatic thrusters.

Thus, there is no physical nozzle or pressure chamber, and the only temperature limitations are on the ion source device.

19.15.2.2 Mathematical Modeling

For mathematical modeling of electrostatic rockets, consider an ion of mass m_i (kg), an individual charge of q (Coulomb, C), and a negligible initial velocity that passes through an electric potential difference ΔV (V) and acquires an exhaust speed u_e (m/s). The acquired kinetic energy will be equal to its loss of electric potential energy, or

$$\frac{m_i u_e^2}{2} = q\Delta V$$

The ion exhaust velocity and specific thrust are given as

$$u_e = \sqrt{2\left(\frac{q}{m_i}\right)\Delta V} \tag{19.34}$$

The corresponding specific impulse is then

$$I_{sp} \equiv \frac{u_e}{g} = \frac{1}{g}\sqrt{2\left(\frac{q}{m_i}\right)\Delta V}$$

The thrust force for a singly charged particle is

$$T = \dot{m}_i u_e$$

Specific thrust is

$$\frac{T}{\dot{m}_i} = u_e = gI_{sp}$$

Denote

I_b as the ion beam current

j as the current density or flux (which is ions flux per unit area)

$$I_b = jA$$

where A is the beam cross-sectional area.

For 100% single ionization, the ion beams' current, I_b, is expressed by the relation

$$I_b = m_i \frac{q}{\dot{m}_i} \tag{19.35a}$$

The mass flow rate of ions is then

$$\dot{m}_i = \frac{I_b m_i}{q} \tag{19.35b}$$

From Equations 19.34 and 19.35b, the thrust force is then

$$T = \frac{I_b m_i}{q}\sqrt{2\left(\frac{q}{m_i}\right)\Delta V}$$

$$T = I_b\sqrt{2\left(\frac{m_i}{q}\right)\Delta V}\ \text{N} \tag{19.36a}$$

Thus,

$$\frac{T}{I_b} = \sqrt{2\left(\frac{m_i}{q}\right)}\sqrt{\Delta V} \tag{19.36b}$$

For xenon $\sqrt{2\left(\frac{m_i}{q}\right)} = 1.65\times10^{-3}$, then

$$T = 1.65\times10^{-3}\times I_b\times\sqrt{\Delta V}\ \text{mN}$$

where I_b is in amperes and ΔV is in volts.

The current density (j) is expressed by the relation

$$j = \frac{4}{9}\varepsilon_0\sqrt{2\left(\frac{q}{m_i}\right)}\frac{(\Delta V)^{3/2}}{d^2} = \frac{4}{9}\varepsilon_0\left(\frac{\Delta V}{d}\right)^2\sqrt{2\left(\frac{q}{m_i}\right)\left(\frac{1}{\Delta V}\right)}\left(\text{A/m}^2\right) \tag{19.37}$$

where

ε_0 is the electrical permittivity of free space ($\varepsilon_0 = 8.85\times10^{-12}$ farad/m $= 8.85\times10^{-12}$ C/m·V)

d is the distance between grids

Equation 19.37 is the charge-limited current and is called Child–Langmuir's law.

This limits the maximum ion current density that can be extracted from the ionization stage (ion source) for a given potential drop across a specified gap. With

$$T = \frac{I_b m_i}{q}\sqrt{2\left(\frac{q}{m_i}\right)\Delta V}$$

then

$$T = jA\sqrt{2\left(\frac{m_i}{q}\right)\Delta V}$$

and

$$\frac{T}{A} = \frac{8}{9}\varepsilon_0\left(\frac{\Delta V}{d}\right)^2$$

The maximum thrust density does not depend on the mass flow rate.

Example 19.14

Consider the case of the propellant xenon (which has $q/m_i = 0.735 \times 10^6$ C/kg). If the electric potential $\Delta V = 700$ V, $d = 0.0025$ m, $D = 0.002$ m, and the number of holes in the grid is 2000, calculate the exhaust speed, specific impulse, electric flux, and thrust force.

Solution

The exhaust speed:

$$u_e = \sqrt{2\frac{q\Delta V}{m_i}} = \sqrt{2 \times 0.735 \times 10^6 \times 700} = 3.2078 \times 10^4 \text{ m/s}$$

Specific impulse:

$$I_{sp} \equiv \frac{u_e}{g} = \frac{3.2078 \times 10^4}{9.81} = 3270 \text{ s}$$

Electrical flux:

$$j = \frac{4}{9}\varepsilon_0\sqrt{2\left(\frac{q}{m_i}\right)\left(\frac{1}{\Delta V}\right)}\left(\frac{\Delta V}{d}\right)^2 = \frac{4}{9} \times 8.85 \times 10^{-12} \times \sqrt{\frac{2 \times 0.735 \times 10^6}{700}} \times \left(\frac{700}{0.0025}\right)^2$$

$$j = 14.131 \text{ A/m}^2$$

Thrust force:

$$\frac{T}{A} = \frac{8}{9}\varepsilon_0\left(\frac{\Delta V}{d}\right)^2 = \frac{8}{9} \times 8.85 \times 10^{-12} \times \left(\frac{700}{0.0025}\right)^2 = 0.6167 \text{ N/m}^2$$

Cross-sectional area $A = \frac{\pi}{4}D^2 = 3.141 \times 10^{-6}$ m^2
Thrust force is then $T = 1.937 \times 10^{-6}$ N/hole
Total ideal thrust force $F = 2000 \times T = 2000 \times 1.937 \times 10^{-6} = 3.874$ mN

19.15.2.3 Multiply Charged Ion Species

Doubly charged ions can also be produced by a second ionization collision [18], described this simply as

$$e^{-1} + X^+ \rightarrow X^{++} + 2e^- \quad \text{or} \quad e^{-1} + X \rightarrow X^{++} + 3e^-$$

The velocity of a doubly ionized ion is $\sqrt{2}$ times the singly charged ion velocity.

Now for a beam containing both singly charged and doubly charged ions, the total beam current is

$$I_b = I^+ + I^{++}$$

where
I^+ is the singly charged ion current
I^{++} is the doubly charged ion current

The total thrust for the multiple species, T, is the sum of the thrust from each species:

$$T = I^{+}\sqrt{2\left(\frac{m_i}{q}\right)\Delta V} + I^{++}\sqrt{\left(\frac{m_i}{q}\right)\Delta V} \tag{19.38}$$

The thrust correction factor α, for doubly ionized atoms, is defined as [19]

$$\alpha = \frac{I^{+} + \frac{1}{\sqrt{2}}I^{++}}{I^{+} + I^{++}} = \frac{1 + 0.707\left(\frac{I^{++}}{I^{+}}\right)}{1 + \left(\frac{I^{++}}{I^{+}}\right)} \tag{19.39}$$

where I^{++}/I^{+} is the fraction of the double ion current in the beam.

The corrected thrust force is then

$$T = \alpha I_b\sqrt{2\left(\frac{m_i}{q}\right)\Delta V} \tag{19.40}$$

The specific impulse is also expressed as

$$I_{sp} = m^{++}\sqrt{4\left(\frac{m_i}{q}\right)\Delta V} + \left(1 - m^{++}\right)\sqrt{2\left(\frac{m_i}{q}\right)\Delta V} \tag{19.41}$$

Example 19.15

A thruster produces 2 A of xenon ions at 1500 V and a 10% doubles-to-singles ratio. If $q/m_i = 7.35 \times 10^5$, what is the developed thrust?

Solution

From Equation 19.39, the thrust correction factor is

$$\alpha = \frac{I^{+} + \frac{1}{\sqrt{2}}I^{++}}{I^{+} + I^{++}} = \frac{1 + 0.707\left(\frac{I^{++}}{I^{+}}\right)}{1 + \left(\frac{I^{++}}{I^{+}}\right)} = \frac{I^{+} + 0.707 \times 0.1}{1 + 0.1} = 0.973$$

The thrust force is then

$$T = \alpha I_b\sqrt{2\left(\frac{m_i}{q}\right)\Delta V} = 0.937 \times 2 \times \sqrt{\frac{2 \times 1500}{7.35 \times 10^5}} = 124.4 \times 10^{-3}\ \text{N}$$

or

$$T = 124.4\ \text{mN}$$

19.15.2.4 Total Efficiency

The total efficiency of an electrically powered thruster is defined as the jet power divided by the total electrical power in the thruster (η_t)

$$\eta_t = \frac{P_{jet}}{P_{in}}$$

with

$$P_{jet} = \frac{1}{2}\dot{m}_i u_e^2 \quad \text{and} \quad T = \dot{m}_i u_e,$$

then

$$P_{jet} = \frac{T^2}{2\dot{m}_i}$$

$$\eta_t = \frac{T^2}{2\dot{m}_i P_{in}} = \frac{TgI_{sp}}{2P_{in}}$$

Example 19.16

Consider a 1 kW ion thruster working with hydrogen as a gas. If the exhaust speed is 10,000 m/s and efficiency is 50%, what will be the specific impulse, mass flow rate, thrust, and jet power?

Solution

Specific impulse $I_{sp} = \frac{u_e}{g} = \frac{10,000}{9.81} = 1,019.4$ s

Mass flow rate $\dot{m}_i = \frac{2\eta_t P_{in}}{u_e^2} = \frac{2 \times 0.5 \times 1000}{(10^4)^2} = 10^{-5}$ kg/s

Thrust $T = \dot{m}_i u_e = 10^{-5} \times 10^4 = 0.1$ N

Jet power $P_{jet} = \eta_t P_{in} = 0.5 \times 1 = 0.5$ kW

19.15.2.5 Electrical Efficiency

Let us first define the electrical power consumed by the beam as the product of the current and voltage drop. Then from Equation 19.37,

$$P_E = I_b \Delta V$$

$$\frac{P_E}{A} = j\Delta V = \frac{4}{9}\varepsilon_0 \sqrt{2\left(\frac{q}{m_i}\right)} \frac{(\Delta V)^{5/2}}{d^2}$$

Since

$$\frac{T}{A} = \frac{8}{9}\varepsilon_0 \left(\frac{\Delta V}{d}\right)^2$$

then

$$\frac{P_E}{T} = \frac{1}{2}\sqrt{2\left(\frac{q}{m_i}\Delta V\right)} = \frac{u_e}{2} = \frac{gI_{sp}}{2} \tag{19.42a}$$

The electrical efficiency is defined as

$$\eta_E = \frac{\frac{1}{2}m_i u_e^2}{\frac{1}{2}m_i u_e^2 + E_{Ion}} = \frac{\frac{1}{2}m_i\left(gI_{sp}\right)^2}{\frac{1}{2}m_i\left(gI_{sp}\right)^2 + E_{Ion}} \tag{19.43}$$

where E_{Ion} is the energy loss consumed in the neutralization of gas molecules. The electric power is then replaced by $\eta_E P_E$ and the power-thrust ratio; Equation 19.42a is then modified to be

$$\frac{P_E}{T} = \frac{u_e}{2\eta_E} = \frac{gI_{sp}}{2\eta_E} \tag{19.42b}$$

Example 19.17

Compare the two propellants xenon and krypton, if the specific impulse $I_{sp} = 3000$ s and the loss in an ion thruster is expressed by

$$E_{Ion} = 100 + 0.1\Delta V \text{ eV}$$

By determining

1. The electrical efficiency
2. The power-to-thrust ratios

Propellant	Mass m (kg)	q/m (C/kg)
Xenon	2.18×10^{-25}	7.34×10^{5}
Krypton	1.39×10^{-25}	11.5×10^{5}

Solution

Electrical efficiency: Since

$$\Delta V = \frac{\left(gI_{sp}\right)^2}{2\left(\frac{q}{m_i}\right)}$$

then

$$E_{Ion} = \left[100 + 0.1\frac{\left(gI_{sp}\right)^2}{2\left(\frac{q}{m_i}\right)}\right]\times 1.6\times10^{-19}\text{J}$$

$$E_{Ion} = \left[100 + \frac{4\times10^{7}}{\left(\frac{q}{m_i}\right)}\right]\times1.6\times10^{-19}$$

From Equation 19.43,

$$\eta_E = \frac{1}{1+\dfrac{E_{Ion}}{\frac{1}{2}m_i\left(gI_{sp}\right)^2}} = \frac{1}{1+\dfrac{\left[100+0.1\dfrac{\left(gI_{sp}\right)^2}{2\left(\frac{q}{m_i}\right)}\right]\times1.6\times10^{-19}}{\frac{1}{2}m_i\left(gI_{sp}\right)^2}}$$

then

$$\eta_E = \frac{1}{1+\left[\dfrac{200}{m_i\left(gI_{sp}\right)^2}+\dfrac{0.1}{m\left(\frac{q}{m_i}\right)}\right]\times1.6\times10^{-19}}$$

or

$$\eta_E = \frac{1}{1+\dfrac{3.69\times10^{-26}}{m_i}+\dfrac{1.6\times10^{-20}}{m_i\left(\frac{q}{m_i}\right)}}$$

For xenon:

$$\eta_E = \frac{1}{1+0.1692+0.1} = 78.79\%$$

For krypton:

$$\eta_E = \frac{1}{1+0.265+0.1} = 73.23\%$$

Power-to-thrust ratio: From Equation 19.42b,

$$\frac{P_E}{T} = \frac{gI_{sp}}{2\eta_E}$$

For xenon: $\dfrac{P_E}{T} = \dfrac{9.81\times3{,}000}{2\times0.7879} = 18{,}676\,\text{W/N} = 18.7\,\text{kW/N}$

For krypton: $\dfrac{P_E}{T} = \dfrac{9.81\times3{,}000}{2\times0.7323} = 20{,}094\,\text{W/N} = 20.1\,\text{kW/N}$

As seen from the example, an ion rocket offering 3000 s of specific impulse and using xenon would require 18.7 kW of electric power to produce 1 N of thrust. Higher electric power (20.1 kW) is needed by krypton for the same requirements.

19.15.3 Electrothermal

19.15.3.1 Introduction

As described earlier, in this category the electric energy is used to heat the propellant, which is then thermodynamically expanded through a nozzle. The gross performance of any electrothermal thruster depends on the chamber temperature ($u_e \leq \sqrt{2C_pT_c}$) where T_c is the maximum tolerable temperature. Complex molecular gases like ammonia and hydrazine, which dissociate into low effective molecular weight and high specific heat ratios, are more popular these days. Its three types will be briefly discussed hereafter.

19.15.3.2 Resistojets

Components of resistojets are illustrated in Figure 19.31. Their earliest use in space dates to 1965 (the Air Force Vela satellites). However, their adoption on commercial spacecraft did not start until the 1980 launch of the first satellites in the INTELSAT-V series. A more recent application has been for orbit insertion, attitude control, and the deorbit of LEO satellites, including the 72 satellites in the Iridium constellation.

Resistojets are the simplest type of electrical thruster as they depend on typical heat transfer methods. Resistojets are similar to liquid rockets, which are composed of storable propellants, chamber, and nozzle. The propellant is heated in the chamber by flowing over an ohmically heated refractory metal surface using either an AC or DC voltage. The chamber temperature is limited by the materials of the walls and/or heater coils to some 3000 K or less, and hence the exhaust velocities cannot exceed 10,000 m/s. A nozzle with a high expansion ratio is connected to the chamber to generate a high-velocity exhaust stream, as do chemical rockets. Thrust can be steady or intermittent as programmed in the propellant flow.

Though the highest specific impulse has been achieved with hydrogen (due to its lowest molecular mass), its low density causes propellant storage to be bulky and inappropriate for space missions. A large variety of different gases have been used, such as O_2, H_2O, CO_2, NH_3, CH_4, and N_2. However, hydrazine and ammonia are more commonly employed because of their overall system advantages. Another advantage is their low operational voltage, which, unlike that in other EP systems, does not require complex power processing.

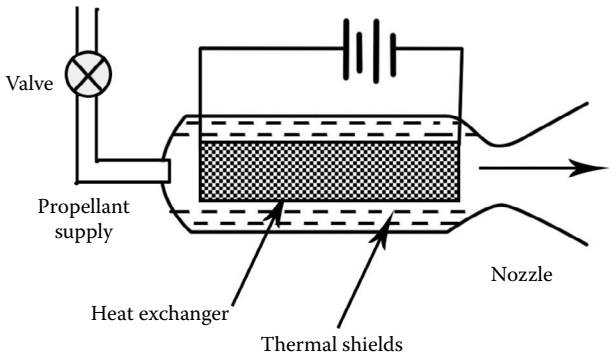


FIGURE 19.31
Schematic diagram of a resistojet.

For these reasons, and the fact that satellites in GEO often have excess electrical power, resistojets were among the first EP options to be used for the NSSK of communication satellites.

Typical characteristics of resistojets:

- Power level: 0.5–1.0 kW
- Thrust level: 0.005–0.5 N
- Exhaust velocity: 3.5 km/s (<10.0 km/s)
- Efficiency: 65%–90%
- Specific impulse: 150–700 s
- Propellant: N_2, NH_3 (ammonia), N_2H_4 (hydrazine)
- Chamber temperature: ≈3000 K

19.15.3.3 Arcjets

In the arc heating rocket engine, electrical energy is transformed into heat in an arc that is struck between two electrodes and, thus, the temperature of the working fluid is raised as it passes through the arc. The heated gas then expands thermodynamically through a nozzle and, thus, is accelerated and ejected at high velocities; see Figure 19.32. The design of the arcjet is described by Vaugh and colleagues [20].

Typical characteristics of arcjets are as follows:

- Power level: 2 kW (hydrazine), 26 kW (ammonia)
- Thrust level: 0.2–2.0 N
- Specific impulse: ≤800 s
- Exhaust velocity: 5–6 km/s
- Chamber temperature: 4000 – 5000 K
- Efficiency: 30%–40%
- Propellants: Hydrazine (N_2H_4), ammonia (NH_3), and hydrogen (H_2)

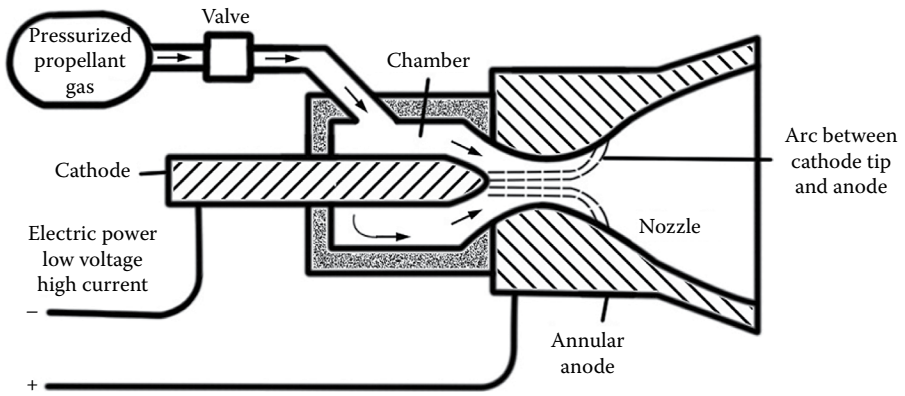


FIGURE 19.32
Schematic diagram of arcjet electrical propulsion system.

19.15.3.4 Electromagnetic Engines

One may go beyond simple electrostatic forces to accelerate charged particles and include the body force arising from crossed electric and magnetic fields. One such device is a magnetoplasmadynamic (MPD) accelerator. Usually, the electrical conductivity of the plasma must be enhanced by the addition of an easily ionized species, such as potassium chloride, a process known as "seeding." These devices have the same limitation of composition "freezing" common to all mechanically accelerated flows and, in addition, the problem of excessive wall temperatures. In these systems, the applied electric and magnetic fields are steady, although pulsed versions are also being studied.

Different thruster configurations have been studied along with various propellants. Lithium vapor gave a high performance in studies performed in Russia at power levels around 100 kW with jet velocities up to 50 km/s and propulsive jet efficiencies of up to 45%, yielding a specific impulse up to 3700 seconds. This third major type of electric propulsion device accelerates propellant gas that has been heated to a plasma state. Plasmas are mixtures of electrons, positive ions, and neutrals that readily conduct electricity at temperatures usually above 5000 K or 9000 R. According to electromagnetic theory, whenever a conductor carries a current perpendicular to a magnetic field, a body force is exerted on the conductor in a direction at right angles to both the current and the magnetic field. Unlike the ion engine, this acceleration process yields a neutral exhaust beam. Another advantage is the relatively high thrust density, or thrust per unit area, which is normally about 10–100 times that of the ion engines.

This third category relies on the interaction of an electric current pattern driven through a conducting propellant stream with a magnetic field permeating the same region to provide the accelerating body force. The propellant gas is heated to a plasma state (plasmas are mixtures of electrons, positive ions, and neutrals that readily conduct electricity at temperatures usually above 5000 K or 9000 R).

It has two main advantages:

1. Produces exhaust speeds considerably higher than those of the electrothermal devices
2. Thrust densities are much larger than those of the electrostatic thrusters

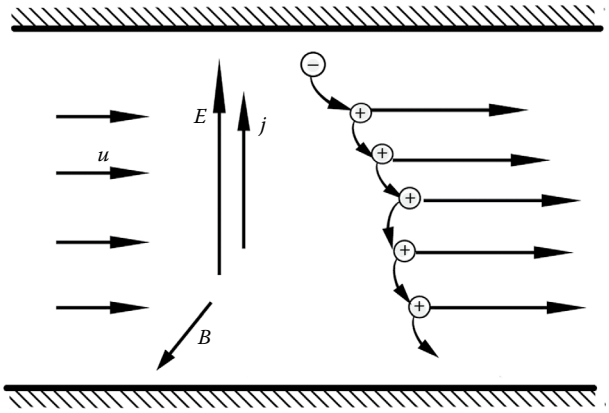


FIGURE 19.33
Crossed-field electromagnetic thruster.

However, it is more complex and analytically less tractable than either of these alternatives. The essence of an electromagnetic thruster is sketched in Figure 19.33, where some electrically conducting fluid, usually a highly ionized gas, is subjected to an electric field E and a magnetic field B, perpendicular to each other and to the fluid velocity u. The current density j driven by the electric field interacts with B to provide a streamwise body force that accelerates the fluid along the channel. It is important to note that the working fluid, although highly ionized, is macroscopically neutral, hence not constrained in its mass flow density by space-charge limitations as in the electrostatic accelerators.

Problems

19.1 For a solid-propellant rocket having the following properties:

$$\dot{r} = 15P_c^{0.7}\ \text{mm/s}, \quad P_c = 10\,\text{MPa}, \quad L/D = 12, \quad d/D = 0.4, \quad \text{and} \quad D = 1.6\,\text{m}$$

Evaluate the rate of change of combustion chamber pressure in the three cases of

1. End burning
2. Radial burning
3. Combined burning

19.2 Mission planners used a xenon ion thruster placed on a spacecraft. It has a total power of 5.5 kW, a 1200 V, 3.75 A beam with 15% double ions, and a total efficiency of 68%.

1. What is the thrust-to-power ratio (usually expressed in mN/kW)?
2. What is the I_{sp}?

19.3 A rocket engine uses liquid hydrogen and liquid oxygen propellants. It operates at a mixture ratio of 5 at a combustion chamber pressure of 7.5 MPa (T_c = 3310 K, γ = 1.21, and molecular weight = 11.8). Calculate the area of the exhaust nozzle throat if the thrust at sea level is to be 80 tons. The engine is designed for full expansion at sea level. What is the specific impulse at sea level?

19.4 A rocket engine uses liquid nitrogen tetroxide/dimethyl-hydrazine propellants. It operates at a mixture ratio of 2.1 at a combustion chamber pressure of 10 MPa (T_c = 3320 K, γ = 1.23, and molecular weight = 21.9).

Calculate the area of the exhaust nozzle throat if the thrust at sea level is to be 100 tons. The engine is designed for full expansion at sea level. What is the specific impulse at sea level?

19.5 A rocket motor has been designed with a nozzle expansion ratio of 8.5. What is the ratio of exit pressure to chamber pressure for the motor? The ratio of specific heats for the combustion gas is 1.19.

19.6 During a static test of a ballistic motor the following were measured, recorded directly, or computed:

1. Time integral of combustion chamber pressure over the equilibrium burning time of the propellant = 34 MPa·s
2. Throat area of the nozzle = 6.2 cm^2
3. Nozzle expansion ratio = 8.5

4. Atmospheric pressure = 100 kPa
5. Mass of propellant burned = 2.5 kg
6. Equilibrium burning time = 0.621 s
7. Ratio of specific heats of combustion gases = 1.20
8. Average molecular weights of exhaust = 20

Determine

a. The characteristic velocity
b. The average specific impulse delivered
c. The average thrust delivered
d. The flame temperature of the propellant

19.7 Determine the ratio of the burning area to the nozzle throat area for a solid-propellant rocket motor with the following characteristics.

1. Burning rate data: $n = 0.4$ and $a = 0.0076$
2. Chamber pressure: 6.9 MPa
3. Propellant weight density: 1600 kg/m^3
4. Specific heat ratio of combustion products: 1.19
5. Gas constant: 400 J/(kg·K)
6. Propellant flame temperature: 2750 K

19.8 An axial turbine is used as a power source in a rocket turbopump. The turbine is a single stage and of the impulse type. The maximum tip speed $U_t = 500$ m/s and a rotational speed $N = 72{,}600$ rpm. Liquid oxygen flows at the rate of 5.27 kg/s into the turbine having a total inlet temperature and pressure of $T_{01} = 1000\,\text{K}, P_{01} = 10\,\text{MPa}$. The exit static pressure $P_2 = 1.0$ MPa. Flow in the stator is assumed ideal and flow has an axial absolute exit velocity from the rotor blade row.

The working fluid has a specific heat: $C_P = 7757$ J/kg·K and specific heat ratio: $\gamma = 1.357$

1. Calculate the spouting velocity
2. Calculate the power generated
3. Calculate the rotor tip diameter

19.9 Figure P19.9a illustrates a liquid propeller rocket. Fuel and oxygen pumps are driven by a counter-rotating gas turbine; see Figure P19.9b. A counter-rotating turbine offers advantages on weight, volume, efficiency, and maneuverability relative to traditional multistage turbines. The nozzle of the second turbine is removed and the direction of rotation of the two rotors are opposite to each other.

Speed of rotation of fuel pump: $N_1 = 90{,}000$ rpm

Speed of rotation of oxygen pump: $N_2 = 18{,}000$ rpm

Other data:

$$R_1 = 0.052\,\text{m}, \quad R_2 = 0.095\,\text{m}, \quad W_{u1} + W_{u2} = 960\ \text{m/s}, \quad W_{a1} = 350\ \text{m/s}$$

$$W_{u3} = 269\,\text{m/s}, \quad \dot{m} = 5\,\text{kg/s}, \quad C_p = 1.07\,\text{kJ/kg}\cdot\text{K}, \quad \gamma = 1.3, \quad T_{01} = 1500\,\text{K}$$

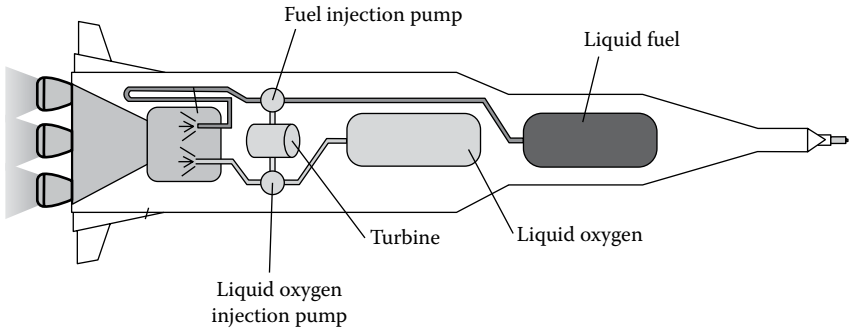


FIGURE P19.9a

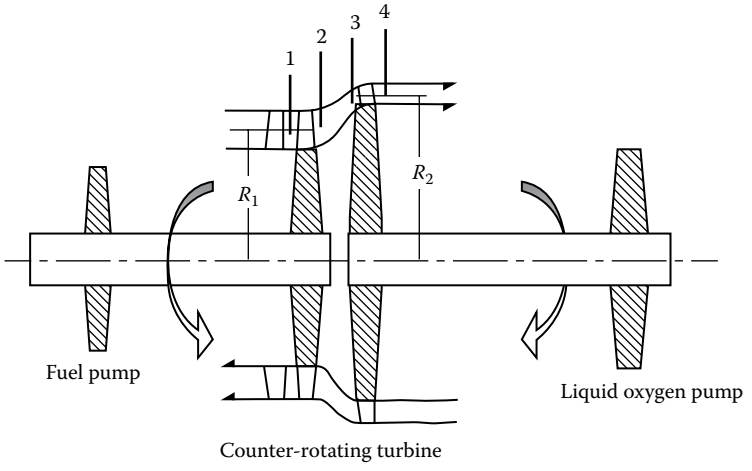


FIGURE P19.9b

Efficiencies of both turbines are equal at 0.7.

1. Draw the velocity triangles for both turbines using a common base layout.
2. Calculate
   a. Specific work generated by each turbine
   b. Temperature drop in each turbine
   c. Pressure ratio of each turbine
   d. ψ_1, ψ_2, ϕ_1

19.10 For the propellant hydrogen, for which $q/m_i = 0.91 \times 10^6$ C/kg, $d = 0.0025$ m, and $D = 0.002$ m, calculate the exhaust speed, specific impulse, electrical flux, and cross-sectional area and diameter of a round beam producing 0.001 N thrust.

19.11 A thruster has a specific impulse of 6000 s when it is singly ionized. If it is 85% singly ionized and 15% doubly ionized, what is the new specific impulse?
Calculate the exhaust speed in both cases.

19.12 A liquid oxygen–liquid hydrogen rocket engine has a mixture ratio of 3.5. The combustion chamber temperature and pressure are 3500 K and 22 atmospheres. The exit area is 3.224 m^2. The exit pressure is equal to atmospheric pressure at an altitude of 20 km while the exit total pressure is 2230 kPa. The exit speed is 3450 m/s while the exhaust density is 0.0102 kg/m^3. The generated thrust is 392 kN, specific impulse is 352 s, and the exit mass flow rate is 113.5 kg/s. Propellant characteristics are specific heat ratio $\gamma = 1.23$ and specific heat at constant pressure Cp = 2520 J/kg·K.

1. Study the effect of nozzle efficiency on the thrust and specific impulse, if the nozzle efficiency (η_n) varies from 90% to 98% and the propellant mass flow rate is constant.
2. Study the effect of pressure drop in the combustion chamber on thrust force and specific impulse, if the pressure drop in the compustion chamber (ΔP_c) varies from 1% to 5%.

References

1. G.E.P. Sutton and O. Biblarz, *Rocket Propulsion Element*, 7th edn., John Wiley & Sons, Inc., 2001.
2. P. Hill and C. Peterson, *Mechanics and Thermodynamics of Propulsion*, 2nd edn., Addison-Wesley Publishing Co., Reading, MA, 1992.
3. Y. Demyanenko, A. Dmitrenko, A. Ivanov, and V. Pershin, Turbopumps for gas generator and staged combustion cycle rocket engines, AIAA 2005-3946, *41st AIAA/ASME/SAE/ASEE Joint Propulsion Conference & Exhibit*, July 10–13, 2005, Tucson, AZ.
4. H. Mårtensson, S. Andersson, S. Trollheden, S. Brodin, and R. Engines, Rocket engines turbomachinery. In: *Advances on Propulsion Technology for High-Speed Aircraft*. Educational Notes RTO-EN-AVT-150, Paper 5, Neuilly-sur-Seine, France: RTO, pp. 5-1–5-28.
5. Turbopump systems for liquid rocket engines, NASA/SP-8107, National Technical Information Service Springfield, VA, August 1974.
6. *Liquid Rocket Engine: A Centrifugal Flow Turbopumps*, NASA SP 8109, National Technical Information Service Springfield, VA.
7. D.K. Huzel and D.H. Huang, *Design of Liquid Propellant Rocket Engines*, NASA SP-125, Washington, DC, 1967.
8. M.C. Huppert and K. Rothe, Axial pumps for propulsion systems, In *Fluid Mechanics, Acoustics and Design of Fluid Machinery*, Vol. 2, NASA SP-304, Washington, DC, 1974, pp. 623–654.
9. O.M. Balje, Study of turbine and turbopump design parameters, Vol. IV: Low specific speed turboprop study, S/TD No. 1735, No. 20, The Sundstrand Corp., Rockford, IL, 1959.
10. G.P. Sutton, Turbopumps: A historical perspective, *42nd AIAA/ASME/SAE/ASEE Joint Propulsion Conference & Exhibit*, Sacramento, CA, July 9–12, 2006.
11. W.H.T. Loh, *Jet, Rocket Nuclear Ion and Electric Propulsion, Theory and Design*, Springer-Verlag, New York, 1968.
12. R. Ragsdale, Open cycle gas core nuclear rockets, *Proceedings of the Nuclear Thermal Propulsion Workshop*, NASA Lewis Research Center, 1990, pp. 343–357.
13. R.G. Jahn, *Physics of Electric Propulsion*, McGraw-Hill, New York, 1968.
14. M. Van Pelt, *Space Tethers and Space Elevators*, Springer, U.K., 2009, p. 24.
15. M. Martinez-Sanchez and J.E. Pollard, Spacecraft electric propulsion: An overview, *Journal of Propulsion Power*, 14(5), 688–699, September–October 1998.
16. D.M. Goebel and I. Katz, *Fundamentals of Electric Propulsion: Ion and Hall Thrusters*, Wiley, 2008.

17. J.R. Brophy, NASA's deep space 1 ion engine, *Review Scientific Instruments*, 73, 1071–1078, 2002.
18. C. Charles, Topical review: Plasmas for spacecraft propulsion, *Journal of Physics D: Applied Physics*, 42, 163001, 2009.
19. D. M. Goebel and I. Katz, *Fundamentals of Electric Propulsion: Ion and Hall Thrusters*, JPL Space Science and Technology Series, 2008.
20. C.E. Vaughn, R.J. Cassady, and J.R. Fisher (1993). The design fabrication and test of a 26kw arcjet and power conditioning unit, *Proceedings of the International Electric Propulsion Conference, IEPC 93-048*, 1993, Seattle, WA, pp. 448–459.
21. M.C. Stangeland, Turbopump for liquid rocket engines, *Threshold*, 3, 34–43, 1988.
22. J.L. Cannon, Liquid propulsion: Propellant feed system design. In: *Encyclopedia of Aerospace Engineering, Volume 2 Propulsion & Power*. Wiley Publishers, Chichester, U.K., Chapter 2.3.11, October 2010.


Taylor & Francis
Taylor & Francis Group
http://taylorandfrancis.com

Appendix A: Glossary

3D design: Today, 3D methods are used to design the blading of turbomachinery components (compressors and turbines). This means that the airfoils are no longer designed section by section to obtain the necessary deflection of the gas flow, but over their entire radial height so that a rather uniform load distribution is achieved and local flow separations and excessive losses are prevented.

Absolute pressure: The total pressure measured from absolute zero (i.e. from an absolute vacuum).

Absolute temperature: The temperature of a body with reference to absolute zero, at which point the volume of an ideal gas theoretically becomes zero. (Fahrenheit scale is −459.67°F/Celsius scale is −273.15°C.)

Adiabatic efficiency: The ratio between the measured shaft power and the adiabatic compression power, referring to measured mass flow.

Afterburner: The afterburner is a second combustion chamber. Afterburning (or reheating) is a method of augmenting the basic thrust of an engine to improve the aircraft's takeoff, climb, and (for military aircraft) combat performance. Afterburning consists of the introduction and burning of fuel between the engine turbine and the jet pipe-propelling nozzle; utilizing the unburned oxygen in the exhaust gas increases the velocity of the jet leaving the propelling nozzle and therefore increases the engine thrust.

ATFI: The abbreviation ATFI stands for Advanced Technology Fan Integrator, a revolutionary propulsion concept for future aircraft that features a reduction gearbox between the low-pressure turbine and the fan.

Augmenter: Augmenters are afterburners on low-bypass turbofan engines. Core airflow and bypass (fan) airflow are mixed aft of the turbines, in the exhaust. Fuel nozzles supply atomized fuel into the airflow and an igniter ignites the fuel–air mixture. Augmenters are used on low-bypass turbofan engines to increase thrust for short periods during takeoff, climb, and combat flight.

Augmenter exhaust nozzles: Augmenter exhaust nozzles make up the aft end of augmented low-bypass turbofan engines. Augmenter has a flame holder, fuel nozzles, an igniter, and a variable exhaust nozzle. The fuel nozzles supply atomized fuel into the exhaust airflow, and the igniter makes the fuel–air mixture burn. Augmenter exhaust nozzles are used on low-bypass turbofan engines to increase thrust.

Axial-flow compressor: A compressor through which the air passes mostly in an axial direction, that is, along the engine axis; in a centrifugal-flow compressor, the airflow direction is transverse to the engine axis. Both variants are still in use today. Their application depends on the engine concept in each case.

Blade load: Blade load is the ratio between the static pressure differential upstream and downstream of the cascade and the dynamic inlet pressure or, more generally, the total of the aerodynamic loads acting on the airfoil.

Booster compressor: Machine for compressing air or gas from an initial pressure which is above atmospheric pressure, to a still higher pressure.

Brake horsepower (BHP): The maximum rate at which an engine can do work as measured by the resistance of an applied brake, expressed in horsepower.

Bypass ratio (BPR): With commercial engines, the ratio between cold and hot airflow is very high. A BPR of 6:1, for example, means that the air volume flowing through the fan and bypassing the core engine is six times the air volume flowing through the core engine.

Can-type combustion chamber: Can-type combustion chambers are particularly suitable for engines with centrifugal-flow compressors as the airflow is already divided by the compressor outlet diffusers. Each flame tube has its own secondary air duct. The separate flame tubes are all interconnected. Ignition problems may occur, particularly at high altitudes. The entire combustion section consists of 8–12 cans that are arranged around the engine. Individual cans are also used as combustion chambers for small engines or auxiliary power units.

Cascade spacing: Distance between the skeleton lines of two adjacent airfoils.

Centrifugal-flow compressor: The direction of the flow of compressed air discharges outward at 90° to the spool axis. The centrifugal compressor consists of a rating impellor, a fixed diffuser, and a manifold that collects and turns the compressed air.

Centrifugal-flow turbojet: A turbojet engine with a centrifugal compressor rather than an axial-flow compressor.

Cogeneration: (1) Any of several processes that either use waste heat produced by electricity generation to satisfy thermal needs, or process waste heat to electricity, or produce mechanical energy; or (2) the use of a single prime fuel source in a reciprocating engine or gas turbine to generate both electrical and thermal energy to optimize fuel efficiency. The dominant demand for energy may be either electrical or thermal. Usually it is thermal, with excess electrical energy, if any, being transmitted into the local power supply lines.

Combustion chamber: The purpose of the combustion chamber is to provide a stream of hot gas that releases its energy to the turbine and nozzle sections of the engine. There are three types of combustion chamber; namely, can, canannular and annular combustion chambers.

Component efficiency: Component efficiency is the efficiency of individual engine components, such as compressor, combustion chamber, or turbine. One constituent of the component efficiency is the mechanical efficiency, which takes bearing losses and friction between gas and air flows and engine components into account.

Compressor: The compressor is the first component in the engine core. The compressor squeezes the air that enters it into smaller areas, resulting in an increase in the air pressure. This results in an increase in the energy potential of the air. The normal parts of a compressor include compressor front frame, compressor casing with stator vanes, a rotor with rotor blades, and a compressor rear frame.

Core: The core engine module is aft of the fan module and forward of the turbine stator case and is made up of three components: compressor rotor and stator, combustion liner, and stage 1 HPT nozzle. The core is responsible for supplying approximately 20% of the total engine thrust and the torque for operation of all accessories.

Cowling: A removable metal covering placed over and around an airplane's engine(s).

Degree of reaction: The degree of reaction is the ratio between the specific flow in the rotor (static change over rotor) and the specific flow work between the inlet and outlet of the stage (static change over stage).

Diffuser: A stationary passage surrounding an impeller in which velocity pressure imparted to the flow medium by the impeller is converted into static pressure.

Engine 3E: Engine 3E is a German government-sponsored research program where the three Es stand for environment, efficiency, and economy. Under this program,

Motoren- und Turbinen-Union (MTU) is maturing technologies to reduce noise levels by 10%, carbon dioxide emissions by 20%, and NOx emissions by 85% by the year 2020.

Engine price: The price of a production engine for the Airbus A320 aircraft family, for example, amounts to approximately US $5.5 million, and that of a jumbo jet engine is in the region of US $10 million.

Exhaust: The exhaust section is located behind the turbine section and at the rear of the engine. It is made up of either a fixed or variable nozzle assembly, depending on the aircraft application. The exhaust section directs the exhaust gases aft and further accelerates the exhaust gases to produce forward thrust. Variable nozzles are usually found on military engines, while fixed ones are typically associated with commercial turbofans.

Fan: The fan is the first component on the engine. Most blades of the fan are made of titanium. The spinning fan sucks in large quantities of air. It then speeds this air up and splits it into two parts. One part continues through the "core" or center of the engine, where it is acted upon by the other engine components. The fan module typically supplies approximately 80% of the engine thrust. The second part "bypasses" the core of the engine. It goes through a duct that surrounds the core to the back of the engine, where it produces much of the force that propels the airplane forward. This cooler air helps quiet the engine, as well as adding thrust to the engine.

Fuel consumption: This is the fuel consumed in liters for traveling 100 km, per passenger seat. For a medium-range aircraft it is 5–6 L/seat, while for a long-range aircraft—like the Airbus A340—it is 3.7 L/seat.

Gas generator: The combination of the compressor, combustion chamber, and the turbine.

Gas turbine: The turbine converts gas energy into mechanical work to drive the compressor by a rigid shaft.

Geared fan: Normally the fan, the low-pressure compressor, and the low-pressure turbine are fitted on one shaft. In contrast, a geared fan is "uncoupled" from the low-pressure system by means of a reduction gearbox. Thus the low-pressure turbine and the low-pressure compressor can be operated at their respective optimum high speeds, whereas the fan rotates at a much lower speed (ratio approx. 3:1). Advantages of the geared fan concept include a markedly improved overall engine efficiency and signification noise reduction.

High-pressure turbine (HPT): The HPT module is aft of the compressor rear frame and forward of the LPT stator case. The HPT module is made up of the HPT rotor and HPT stator, and it removes energy from the combustion gases to turn the high-pressure compressor and accessory gearbox.

Horsepower (HP): A unit of power equal to 33,000 ft·lb of work per minute.

Hydrocarbons: Chemicals containing carbon and hydrogen.

Hypersonic: Very fast speed of flight, 3500–7000 mph (or Mach 5–10). The space shuttle travels this fast once it is in space.

Inlet guide-vane valve (IGV): A valve assembly at the air inlet of a "blower" (single-stage, low-pressure, centrifugal air compressor) usually advised to be mounted in *very close proximity* to the "blower" impeller. Provides "pre-swirl" of airflow in the same rotational direction as a "blower" impeller. Proven to improve efficiency (reduce BHP) during *throttled-down modulation* of "blowers." Effectiveness, when used with multistage centrifugal air compressors, degrades rapidly.

Impeller: The part of the rotating element of a dynamic compressor that imparts energy to the flowing medium by means of centrifugal force. It consists of a number of blades mounted so as to rotate with the shaft.

Impingement cooling: A high-velocity cold air jet is directed from a hole vertically onto the component surface to be cooled. As the cooling air jet hits the surface, it is diverted in all directions parallel to the impingement surface. The cooling effect is high but decreases continuously as the distance from the point of impingement increases.

Industrial gas turbine: The operating principle of an individual gas turbine is essentially the same as that of an aeroengine. However, a so-called power turbine is used in place of the low-pressure turbine of an aeroengine that drives the fan. This power turbine delivers the necessary power—directly or via a gearbox—to a generator or pump, and so forth. Nearly all industrial gas turbines of the lower and intermediate power classes are aero engine derivatives.

Jet engine: Any of a class of reaction engines that propel aircraft by means of the rearward discharge of a jet of fluid, usually hot exhaust gases generated by burning fuel with air drawn in from the atmosphere. The aircraft engine provides a constant source of thrust to give the airplane forward movement.

Low-pressure compressor: To achieve pressure ratios of over 30 in present-day engines, two different types of compressors are used: low-pressure compressors and high-pressure compressors. These compressors, which rotate at different speeds, are driven by their counterparts in the turbine via concentric shafts.

Low-pressure turbine (LPT): The LPT module is in the rear of the engine, aft of the HPT stator case. LPT components include the LPT rotor, LPT nozzle stator case, and turbine rear frame. The LPT removes energy from the combustion gases to drive the low-pressure compressor (N1) rotor assembly.

Mixer: A mixer is a sheet-metal cone at the rear end of some engines which, owing to its special wavy form, ensures intensive mixing of the high-velocity exhaust gases exiting the low-pressure turbine with the slowly flowing bypass air. This results in a marked reduction of noise levels.

Multistage centrifugal compressor: A machine having two or more impellers operating in series on a single shaft and in a single casing.

Multistage compressor: A machine employing two or more stages.

Normal turbine stage: The normal turbine stage consists of a stator and a rotor, with the rotor being arranged downstream of the stator.

Nozzle: The nozzle is the exhaust duct of the engine. This is the engine part that actually produces the thrust for the plane. The energy depleted airflow that passes the turbine, in addition to the colder air that bypasses the engine core, produces a force when exiting the nozzle that acts to propel the engine, and therefore the airplane, forward. The combination of the hot air and cold air is expelled and produces an exhaust, which causes a forward thrust.

Pressure ratio: The pressure ratio indicates the ratio between the pressure of the air entering the engine and the pressure of the air leaving the compressor. A pressure ratio of 30:1 (1 being the pressure of the inlet air), or just 30, means that the air pressure at the compressor exit (just upstream of the combustion chamber inlet) is 30 times the pressure value at the compressor inlet (the first compressor stage or, in most engines, the fan).

Principle of energy transfer: To allow the transfer of energy in a turbomachine, the flow of the working fluid must be deflected in bladed rotors. This means that the

generation of energy (compressor) and absorption of energy (turbine) take place in the rotors only, with the absolute flow being unsteady.

Propeller spinner: A cone-shaped piece of an airplane, mounted on a propeller, which reduces air resistance or drag.

Prop fan: The prop fan features a huge fan propeller that is driven by a turbine and allows bypass ratios of 15:1 or more to be achieved. Fuel consumption, noise, and emissions are significantly reduced.

Propulsion: (as a field of study in relation to aeronautics): This is the study of how to design an engine that will provide the thrust that is needed for a plane to take off and fly through the air.

Propulsion efficiency: The propulsion efficiency—also called external efficiency—is a measure of the quality of an engine. It depends on the outlet velocity/flight velocity ratio, so the smaller this ratio the higher the propulsion efficiency.

Pusher engine: A turboprop engine with a propeller mounted behind the engine so that the generated thrust forces push the airplane. This type of engine is identified as a pusher, while an engine with the propeller in front is called a puller because it pulls the airplane.

Radial-flow machine: The flow direction is predominantly radial. Radial-flow machines feature centrifugal stages (flow from inside to outside) and centripetal stages (flow from outside to inside). With a view to ensuring the necessary energy transfer, the centrifugal principle is used in the compressor and the centripetal principle in the turbine.

Ram: The amount of pressure build-up above ambient pressure at the engine's compressor inlet due to the forward motion of the engine through the air–air's initial momentum.

Ramjet: A jet engine with no mechanical compressor, consisting of specially shaped tubes or ducts open at both ends. The air necessary for combustion is shoved into the duct and compressed by the forward motion of the engine.

Ram ratio: The ability of an engine's air inlet duct to take advantage of ram pressure.

Regimes of flight: The ranges of speed at which airplanes fly. Subsonic: 100–350 mph; transonic: 350–750 mph; supersonic: 760–3500 mph; hypersonic: 3500–7000 mph.

Reheaters: Heat exchangers for raising the temperature of compressed air to increase its volume.

Reverse-flow annular combustion chamber: Reverse-flow annular combustion chambers are used mainly in engines whose last compressor stage is a centrifugal-flow compressor. The advantages and disadvantages of reverse-flow annular combustion chambers are the same as with annular combustion chambers. They reduce the length of the engine but do so at the expense of a larger cross-section.

Single-crystal turbine blades: Single-crystal turbine blades have been developed for use in the high-temperature environment of advanced aeroengines. With single-crystal blades the cooling process is controlled such that a single crystal is produced.

Slip: The internal leakage within a rotary compressor. It represents gas at least partially compressed but not delivered. It is experimentally determined and expressed in cubic feet per minute (CFM) to be deducted from the displacement to obtain capacity.

Solar-powered aircraft: Solar-powered aircraft such as the Pathfinder use photovoltaic cells to convert energy from the sun into electricity to power electric motors that drive the aircraft.

SPC: Specific power consumption. It is the power produced per unit mass of fuel consumed in a power plant.

Specific fuel consumption: The ratio of fuel consumption to compressor capacity.

Specific work of a stage: The mechanical work of a stage per 1 kg mass flow is the specific work of a stage.

Speed of sound: When a plane travels faster than 760 mph, a sound barrier forms in front of the plane. If a plane is going at the speed of sound, it is traveling at Mach 1.

Stage: A stage is the combination of a stator and a rotor.

Stall: A flight condition wherein the airflow separates from the airfoil surface, or the airflow around the airfoil becomes turbulent, causing the airfoil to lose lift. It is usually a result of insufficient airspeed or excessive angle of attack.

Straight cascade: Blades/vanes arranged at regular intervals along a straight line, that is, the cascade axis (two-dimensional geometry).

Surge: The reversal of flow within a dynamic compressor that takes place when the capacity being handled is reduced to a point at which insufficient pressure is being generated to maintain flow (also known as pumping).

Thermal barrier coatings: During operation, engine components are subjected to a combination of mechanical, thermal, and chemical loads. They must therefore be protected by high-temperature-resistant coatings capable of withstanding temperatures as high as 2500°C. Thermal barrier coatings are mainly used in combustion chambers and on turbine blades and vanes.

Thermal efficiency: The thermal or internal efficiency of an aeroengine is the ratio between the amount of heat converted to work and the total amount of heat supplied. The thermal efficiency is a measure of the quality of an engine.

Thrust: The forward force that pushes the engine and, therefore, the airplane forward. Sir Isaac Newton discovered that for "every action there is an equal and opposite reaction." Aircraft engines use this principle.

Thrust class: Turbojet engines are grouped into three thrust classes: engines with a thrust of up to 20,000 lb, engines with a thrust between 20,000 and ~50,000 lb, and engines with a thrust in excess of 50,000 lb.

Thrust, gross: The thrust developed by the engine, not taking into account any presence of initial air–mass momentum.

Thrust, net: The effective thrust developed by the engine during the flight, taking into consideration the initial momentum of the aircraft speed mass before entering the influence of the engine.

Thrust reverser: Thrust reversers serve as an aircraft's main brakes on landing. There are three types of thrust reversers: translating cowl, clamshell, and turboprop reverse pitch. All three literally reverse the engine's thrust by closing in when deployed by the pilot, pushing the air out the front of the engine rather than the back. This motion decreases the speed of the aircraft and is the loud noise you hear when landing.

Thrust, specific fuel consumption: The fuel that the engine must burn to generate 1 lb of thrust.

Thrust, static: Thrust developed by the engine without any initial air–mass momentum due to the engine's static state.

Thrust-to-weight ratio: The thrust-to-weight ratio is a characteristic value indicating the technical standard of an engine. The thrust-to-weight ratio of present-day military engines, for example, is 10:1.

Turbine: The high-energy gas flow coming out of the combustor goes into the turbine, causing the turbine blades to rotate. This rotation extracts some energy from the high-energy flow that is used to drive the fan and the compressor. The gases

produced in the combustion chamber move through the turbine and spin its blades. The task of a turbine is to convert gas energy into mechanical work to drive the compressor.

Turbofan engine: In turbofan engines only a small part of the thrust is generated in the core engine. The major part is produced by the bypass flow through the fan. The fan feeds large air volumes downstream that surround the engine like an envelope and thus reduce the engine noise. With increasing bypass ratio—that is, the ratio between internal and external airflow—operating costs, emissions, and noise are reduced. Bypass ratios of turbofans for modern airlines are now about 6:1, that is, the bypass flow through the fan and around the engine is six times the airflow through the core engine.

Turbojet engine: Turbojet engines—the first jet engine generation—are single-flow engines in which the total volume of air ingested flows through the compressor, the combustion chamber, and the turbine. The thrust is then produced by the exhaust gases exiting the engine at high velocities. Because of the low efficiency and the high noise levels, turbojet engines are no longer produced today.

Turboprop: A turboprop is a jet engine attached to a propeller. The turbine at the back is turned by the hot gases generated by the engine, and this turns a shaft that drives the propeller. A variety of smaller aircraft are powered by turboprops. Like the turbojet, the turboprop engine consists of a compressor, combustion chamber, and turbine, and the air and gas pressure is used to run the turbine, which then creates power to drive the compressor. Compared with a turbojet engine, the turboprop has better propulsion efficiency at flight speeds below about 500 mph. Modern turboprop engines are equipped with propellers that have a smaller diameter but a larger number of blades for efficient operation at much higher flight speeds. To accommodate the higher flight speeds, the blades are scimitar-shaped with swept-back leading edges at the blade tips. Engines featuring such propellers are called propfans.

Turboshaft engine: Turboshaft engines are mainly used to power helicopters. They may include an additional free power turbine with a gearbox to convert the thrust into driving power for the rotor.

Two-stage compressor: Machines in which air or gas is compressed from initial pressure to an intermediate pressure in one or more cylinders or casings.

Variable-pitch propeller: An engine-driven device designed to drive an airplane forward, whose efficiency can be improved by turning its blades in midflight.

Velocity triangle: The velocity triangle is the geometric representation of the kinematics condition.

Zeppelin: Named after its German inventor, this airship craft is controllable, powered, and lighter than air, with a rigid structure.


Taylor & Francis
Taylor & Francis Group
http://taylorandfrancis.com

Appendix B: Turbofan

B.1 High-Thrust Class Turbofan Engines (>200 kN)

	GE-90	CF6-50C2	CF6-80C2
Company	General Electric (USA)	General Electric (USA)	General Electric (USA)
In use since	September 1995	July 1980	October 1985
First flew on	Airbus A-340 and B-777	KC-10 (Military)	A-300/310, 747/767
Description	Two-shaft high BPR TF	Two-shaft high BPR TF	Two-shaft high BPR TF
Weight (dry) (kg)	—	3960	4144
Overall length (mm)	4775	4394	4087
Intake/fan diameter (mm)	3124	2195	2362
Pressure ratio	39.3	29.13	30.4
Bypass ratio	8.4	5.7	5.05
Thrust at takeoff (kN)	388.8	233.5	276
Thrust during cruise (kN)	70	50.3	50.4
Specific fuel consumption (S.F.C.) at sea level standard (SLS) (mg/N·s)	8.30	10.51	9.32
Air mass flow rate (kg/s)	1350	591	802
Presence of FADEC[a]	Yes	No	Yes
Other information	33% lower NO_x emission. Less noise than other TFs in its class (due to low fan tip speed)	Turbine entry temperature (TET) of low pressure turbine (LPT) is 1144 K	Lower fuel burn (S.F.C.) than other engines, long life, high reliability

	RB-211-524G/H	Trent-882	JT-9D-7R4
Company	Rolls Royce (UK)	Rolls Royce (UK)	Pratt & Whitney (USA)
In use since	February 1990	August 1994 (Cert.)	February 1969 (first)
First flew on	747-400 and 767-300	Boeing 777	Boeing 747/767, A310
Description	Three-shaft axial TF	Three-shaft TF	Twin-spool TF
Weight (dry) (kg)	4479	5447	4029
Overall length (mm)	3175	4369	3371
Intake/fan diameter (mm)	2192	2794	2463
Pressure ratio	33	33+	22
Bypass ratio	4.3	4.3+	5
Thrust at TO (kN)	269.4	366.1	202.3
Thrust during cruise (kN)	52.1	72.2	176.3

(*Continued*)

	RB-211-524G/H	Trent-882	JT-9D-7R4
S.F.C. (mg/N·s)	15.95 (cruise)	15.66 (cruise)	10.06
Air mass flow rate (kg/s)	728	728+	687
Presence of FADEC	No	Yes	No
Other information	—	Most powerful conventional a/c engine in contract in the world (until September 1995) (Trent 772)	—

Source: http://www.anirudh.net/seminar/ge90.pdf.
[a] FADEC: Full authority digital electronic control.

B.2 Low-Thrust Class Turbofan Engines (<200 kN)

	CFM56-5C2	JT-8D-17R	V 2500-A1
Company	CFM International (France) and GE (USA)	Pratt & Whitney (USA)	Intl. Aero Engines (USA)
In use since	Late 1992	February 1970	July 1988
First flew on	Airbus A-340	Boeing 727/737 and DC-9	Airbus A-320
Description	Two-shaft subsonic TF	Axial-flow twin-spool TF	Twin-spool subsonic TF
Weight (dry) (kg)	2492 (bare engine), 3856 (approx.)	1585	2242 (bare engine), 3311 (with power plant)
Overall length (mm)	2616	3137	3200
Intake/fan diameter (mm)	1836	1080	1600
Pressure ratio	37.4	17.3	29.4
Bypass ratio	6.6	1.00	5.42
Thrust at TO (kN)	138.8	72.9	111.25
Thrust during cruise (kN)	30.78	18.9	21.6
S.F.C. (mg/N·s)	16.06	23.37	16.29
Air mass flow rate (kg/s)	466	148	355
Presence of FADEC	Yes	No	Yes
Other information	—	—	—

Source: http://www.anirudh.net/seminar/ge90.pdf.

Appendix C: Samples of Gas Turbines (Representative Manufacturers)

Model	Year	Rating (kW)	Pressure Ratio	Mass Flow (lb)	Turbine Speed (rpm)	Turbine Inlet Temperature	Exhaust Temperature	Approximate Dimensions $L \times W \times H$
ABB Alstom Power								
GT35	1968	17,000	12.0	203.0	3,000/3,600	—	374°C	14.1 × 4.0 × 3.7 m
GT 11 N2	1993	113,700	15.1	842.0	3,000	—	524°C	8.5 × 5.5 × 10.0 m
GT 26	1994	265,000	30.0	1238.0	3,000	—	640°C	12.3 × 5.0 × 5.5 m
AlliedSignal								
ASE40	1978	3,284	8.8	28.1	15,400	2022°F	1116°F	4.3 × 2.5 × 3.0 ft
ASE120	2000	9,784	20.5	69.2	7,910	2321°F	970°F	8.5 × 5.9 × 4.0 ft
Bharat Heavy Electronics								
PG6561(B)	2000	42,100	12.2	311.0	5,163	—	1011°F	11.6 × 5.0 × 3.8 m
PG9351(FA)	1996	255,600	15.4	1422.0	3,000	—	1129°F	22.6 × 5.0 × 5.4 m
Dresser-Rand								
DR60G	1990	13,958	21.5	103.0	7,000	1358°F	909°F	42.0 × 11.5 × 10.5 ft
DR61GP	1998	28,429	21.5	186.3	3,600	1490°F	941°F	48.0 × 11.5 × 18.0 ft
Ebara								
PW-12E	1990	1,180	7.3	14.1	1,500/1,800	—	598°C	5.5 × 3.2 × 2.2 m
FT8 Twin	1990	51,500	20.2	371.0	3,000/3,600	—	458°C	39.0 × 12.0 × 9.0 m
GE Energy Products, Europe								
PG6101(FA)	1993	70,140	15.0	437.0	5,235	—	1107°F	120.0 × 20.0 × 34.0 ft
PG9351(FA)	1996	255,600	15.4	1375.0	3,000	—	1129°F	112.0 × 25.0 × 50.0 ft
GE Industrial Aeroderivative Gas Turbine								
LM1600-PB STIG	1991	16,900	25.1	116.0	7,000	1355°F	878°F	15.0 × 8.0 × 7.0 ft
LM6000-PC	1997	44,090	29.4	280.0	3,600	1540°F	842°F	16.3 × 7.0 × 7.0 ft
GE Power Systems								
PG9351(FA)	1996	255,600	15.4	1475.0	3,000	—	1129°F	112.0 × 25.0 × 50.0 ft
Hitachi								
PG6101(FA)	1993	70,140	15.0	433.0	5,247	—	1107°F	120.0 × 20.0 × 34.0 ft
PG9331(FA)	1995	243,000	14.8	1422.0	3,000	—	1106°F	112.0 × 25.0 × 50.0 ft
Ishikawajima-Harima Heavy Industries								
LM1600PA	1988	13,900	22.3	103.6	7,000	1406°F	914°F	4.3 × 2.6 × 2.2 m
STIG-IM5000	1986	51,160	30.6	344.0	3,600	1450°F	727°F	—
Kawasaki Heavy Industries								
M1A-11	1989	1,235	9.3	18.0	1,500/1,800	—	463°C	2.5 × 1.6 × 2.0 m
M7A-02	1997	6,958	15.9	59.8	1,500/1,800	—	525°C	3.7 × 1.5 × 1.7 m

(*Continued*)

Model	Year	Rating (kW)	Pressure Ratio	Mass Flow (lb)	Turbine Speed (rpm)	Turbine Inlet Temperature	Exhaust Temperature	Approximate Dimensions $L \times W \times H$
Mitsubishi Heavy Industries								
ASE40	1996	2,600	8.4	27.1	15,400	—	1042°F	1.3 × 0.9 × 1.1 m
M501G	1997	254,000	20.0	1250.0	3,600	—	1105°F	15.2 × 4.6 × 5.0 m
M701g	1997	334,000	21.0	1625.0	3,000	—	1089°F	18.2 × 6.2 × 6.2 m
Mitsubishi Engineering and Shipbuilding								
MSC100	1989	10,690	17.1	91.8	1,500/1,800	—	488°C	14.5 × 2.8 × 3.3 m
MTU Motoren- und Turbinen-Union Friedrichshafen GmbH								
LM6000PC	1997	20,070	29.4	280.0	3,600/1,500	1540°F	842°F	16.3 × 7.0 × 7.0 ft
Nuovo Pignone-Turbotecnica								
MS9001FA	1991	255,600	15.4	1406.5	3,000	—	1129°F	—
Pratt & Whitney Canada								
ST6L-813	1978	848	8.5	8.6	300,000	—	1051°F	4.2 × 1.4 × 1.6 ft
ST40 Water Inj.	1999	4,547	19.0	32.9	14,875	—	1010°F	5.4 × 2.2 × 3.2 ft
Rolls-Royce								
Avon	1964	14,580	8.8	173.0	5,500	—	827°F	50.0 × 13.5 × 13.5 ft
Siemens, Siemens Westinghouse								
RB211-6562DLE	1992	27,516	20.8	202.2	4,800	—	932°F	71.0 × 13.5 × 13.5 ft
Trent	1996	51,190	35.0	351.0	3,600	—	800°F	65.9 × 14.1 × 14.3 ft
V94.2	1981	157,000	11.1	1122.0	3,000	2150°F	999°F	45.9 × 41.0 × 27.6 ft
V94.3A	1995	258,000	17.0	1398.0	3,000	2400°F	1054°F	41.0 × 20.0 × 24.6 ft
Solar Turbines								
Mercury 50	1998	4,072	9.1	37.1	14,170	—	663°F	35.1 × 10.1 × 13.7 ft
Titan 130	1998	13,500	16.0	110.1	11,200	—	913°F	48.0 × 10.4 × 13.4 ft
Sulzer Turbo								
R7	1970	10,600	7.7	140.0	6,400	925°C	342°C	38.0 × 12.0 × 13.0 ft
Toshiba								
PG7231FA	1994	171,700	15.5	925.0	3,600	—	1116°F	180.0 × 75.0 × 31.0 ft
PG9351FA	1996	255,600	15.4	1375.0	3,000	—	1129°F	112.0 × 25.0 × 50.0 ft
Turbo Power								
FT8 Twin Pac	1990	51,290	20.2	376.0	3,000/3,600	—	851°F	130.0 × 40.0 × 30.0 ft
Volvo Aero								
VT4400	1999	4,400	12.4	44.5	7200	1052°C	481°C	1.5 × 1.0 × 1.0 m

Index

A

AAI RQ-7 Shadow, 430–431
A-40 Albatros aircraft, 48–49, 685
Acoustic jet engine, *see* Valveless pulsejet engine
Acoustics model theory, 826–827
Activity factor (AF), 483–484
Actuator disk theory
  assumptions and definitions, 470
  axial inflow factor, 471
  pressure and velocity distribution, 470–471
  propulsive efficiency, 474–475
  slipstream factor, 471–472
  thrust, 472–474
Adaptive Engine Technology Development Program, 1250
Adaptive versatile engine technology (ADVENT) engine, 1250–1252
Adour Mk.104 afterburning engine, 332
Advanced supersonic transport (AST), 569
Advanced Technology Fan Integrator (AFTI), 308–309
Advisory Council for Aeronautical Research in Europe (ACARE), 1222
Aeolipile, 4–5
Aerion company, 573
Aeroderivative engine, 659–661
Aeroengines; *see also* Jet engines
  aerospace engines, classifications of, 34–35
  evolution of, 62
  historical events, 60–61
  pre–jet engines, history of, 4–15
  propulsion system and flight speeds, 62
  reductions in
    emissions, 1224
    fuel burn, 1223–1224
    fuel consumption, 1222
    noise levels, 1223–1224
  sustainable biofuels, 1224–1225
Aero piston engine
  classification, 428
  compression-ignition engine, 429
  definition, 426
  piston-powered aircraft and helicopters, 426–427
  reciprocating engines
    horizontally opposed engine, 431–432
    H-type engine, 432
    in-line engine, 431–432
    radial type engine, 432–433
    V-type engines, 432
    X-type engines, 432
  rotary engine
    conventional types, 429
    Wankel engine, 429–431
  spark-ignition engine, 428
  supercharging and turbocharging, 433–436
Aerospace engines, classifications of, 34–35
Aft-engine, *see* Fuselage installation
Afterburning nozzles, 792
Afterburning turbojet engine, 204
  single-spool engine, 207
    ideal cycle, 210–211
    operative *vs.* inoperative afterburner, 234–238
    real cycle, 224, 227
  statistical analysis, 249–250
  supersonic, 257–260
  thrust augmentation
    pressure loss, 252–257
    thrust-specific fuel consumption, 252–253
  two-spool engine, 205
    examples for, 244–245
    layout of, 239
    stations and cycle for, 245–246
    thermodynamic analysis, 245–249
Afterburning two-spool turbofan engine, 332–333
Aft-fan turbofan engines, 43, 45, 335–338, 357–361
AGM-86 ALCM, 377–380
AGT1500 gas turbine, 33
AI-24, 23
Air bleed, 1013–1019
Airbreathing engines, 34–35, 55–58
Airbus A380, 53, 55
Airbus A400 M aircraft, 467
Aircraft-derivative gas turbines, 622
Aircraft fuels; *see also* Biofuels
  combustion chamber requirements, 767
  fuel system requirements, 767
  operation requirements, 766–767
  safety fuels, 767

Aircraft propellers
axial momentum/actuator disk theory
assumptions and definitions, 470
axial inflow factor, 471
pressure and velocity distribution, 470–471
propulsive efficiency, 474–475
slipstream factor, 471–472
thrust, 472–474
blade element theory
dimensionless radius, 479
geometric pitch, 479
propulsive efficiency, 480–481
three-bladed propeller, 476–477
thrust and torque, 479–480
velocity and force components, 477–478
classifications
blades, number of, 470
contra-rotating propellers, 466–467
direction of rotation, 467
fixed pitch, 465–466
material, 464–465
output shaft, 465
propulsion method, 468–469
source of power, 463–464
variable pitch, 466
cross-sections, 463–464
definitions, 462
dimensionless parameters
activity factor, 483–484
advance ratio, 482
four-bladed propeller, 484–486
Mach number, 482
power coefficient, 482–483
power loading, 483
Reynolds number, 482
speed power coefficient, 482–483
thrust coefficient, 482–483
torque coefficient, 482
history, 463
installation, 462–463
modified momentum/simple vortex model, 475–476
performance
four-bladed propeller, 491–495
NACA, 486–487
power coefficient *vs.* advance ratio, 488–490
propeller efficiency *vs.* advance ratio, 487–488
speed-power coefficient, 490–492
thrust coefficient *vs.* advance ratio, 488–490
Aircraft range, 104–108
Air defense rockets, 1287
Airframe noise, 825
Airscrew turbine engine, *see* Turboprop engines
Airship, 9, 14
Air-standard analysis, 438
Air-standard diesel cycle, 455–456
Air-to-air missile (AAM), 1287
Air to fuel ratios (AFRs), 739
Air-to-surface missile (ASM), 1287
Al-21 engine, 245
Algae, 1254
Allied Signal 331 turbofan engines, 840
Allied Signal 731 turbofan engines, 840
Allison 501-K17 engine, 664
American Society for Testing and Materials (ASTM) International, 1224, 1254
AN-24 aircraft, 23
AN-32 aircraft, 23
Anglo-French aircraft
BAe-Aerospatiale AST, 569
Concorde, 568–569
Annular combustion chambers, 743–744
Annular nozzles, 832–833
radial inflow nozzles, 834
radial out-flow nozzles, 833–834
Annulus loss, 1131
Anti-ballistic missiles (ABM), 1286
Antonov
An-70, 513, 543, 690
AN-180, 514, 542, 691
An-225, 481
An-140-100 aircraft, 468–469
Archytas, 1274
Arcjets, 1401
Ariane 5 rocket, 1320–1323
Armstrong Siddeley double Mamba, 22
Armstrong Siddeley Mamba, 22
Armstrong Siddeley Python, 22
Army rockets, 1287
Assisted ignition engines, 1262
Atlantik Solar UAV, 1261
ATREX turboramjet engine, 590, 592–593
Auxiliary power units (APUs), 741, 840
Auxiliary rockets, 1287–1288
Aviadvigatel D-30KPV turbofan engines, 48
Axial-flow compressors and fans, 927
air angle determination at mean section
first stage, 977–978
last stage, 979–980
stages from (2) to (n – 1), 978–979

air angle variation, 980–981
vs. axial turbines, 980–981, 1062–1063
blade design
airfoil type, 987
casecade measurements, 982–987
stage performance, 988–994
vs. centrifugal compressors, 930–932
complete design process, 972–973
compressibility effects, 994–1003
design parameters
centrifugal stress, 945–947
degree of reaction, 951–954
flow coefficient, 951
fluid deflection, 949–950
stage loading, 951
tip Mach number, 945, 948–949
erosion, 1023, 1028–1034
layout of, 928
mean flow (two-dimensional approach)
enthalpy velocity variations, 937–945
tangential plane, 933
velocity triangle types, 935–937
performance
compressor map, 1006–1008
multistage compressor, 1006
single stage, 1003–1006
stall and surge, 1008–1011
surge controls methods, 1011–1019
rotational speed and annulus dimensions, 973–976
seven-stage axial compressor
blades and stresses, 1021, 1028
flow details, in stage number 2, 1021–1027
layout, 1023, 1028
mean section data, 1019
variations from hub to tip, 1019–1021
stage determinations, 976–977
three-dimensional flow, 954–955
axisymmetric flow, 955–956
free vortex method, 958–963
general design procedure, 963–972
simplified radial equilibrium equation, 956–957
Axial rocket pumps, 1372–1374
Axial rocket turbines, 1377
multispool impulse turbines, 1378
reaction turbines, 1378–1382
single-stage impulse turbine, 1377–1378
Axial turbines, 1059
vs. axial-flow compressors, 1062–1063
design point, case study, 1138–1145
blade material selection, 1144
blade numbers for nozzle and rotor, 1139–1140
chord length, 1140–1144
loss coefficients, 1145
mean line flow, 1138
stresses on rotor blades, 1144
three-dimensional variations, 1138–1139, 1141–1144
turbine efficiency, 1145
preliminary design
aerodynamic design, 1109–1110
blade profile selection, 1109, 1111–1112
design steps, 1109
loss and efficiency, 1129–1132
mathematical modeling, 1123–1129
mechanical and structural designs, 1112–1120
turbine cooling, 1109, 1120–1129
three dimensional analysis
constant nozzle angle design, 1088–1091
constant specific mass flow stage, 1092–1108
free vortex design, 1088
general case, 1091–1092
simplified radial equilibrium equation, 1087
vortex blading, 1087
three-stage, 1077–1080
turbine map, 1133–1137
two-dimensional flow, aerodynamics and thermodynamics
Euler's equation, 1065–1067
loss coefficient, 1071–1072
nondimensional quantities, 1072–1080
pressure ratio, 1070
remarks, 1081–1087
stage efficiency, 1069–1070, 1072
velocity tirangles, 1062–1065

B

BAe-Aerospatiale AST, 569
B-2 aircraft, 680–681
Balanced-beam nozzle, 792
Balloon (aeronautics), 7–8
Barber, John, 7
Barber's gas turbine, 7–8
Bell nozzles, 831–832
Biofuels
aviation economic viability, 1254–1255
commercial and demonstration flights, 1254–1255

first-generation, 1253–1254
second-generation, 1254
types, 1253
Bipropellant rocket, 1351–1353
Blade element theory
dimensionless radius, 479
geometric pitch, 479
propulsive efficiency, 480–481
three-bladed propeller, 476–477
thrust and torque, 479–480
velocity and force components, 477–478
Blade material selection, 1144
Blade numbers for nozzle and rotor, 1139–1140
Blade profile selection, 1109, 1111–1112
Bleriot, Louis, 11–12
Boeing 2707-100/200, 570–571
Boeing 2707-300, 571
Boeing 737 aircraft, 993–994
Boeing CH-47 Chinook, 537–539
Boeing 787 Dreamliner, 53–55
Boeing Pelican ULTRA, 52
Boeing X-43A, 596
Bombardier CSeries, 55
Bottom dead center (BDC), 434, 436
Boundary-layer infrared suppression system (BLISS), 666
BPR, *see* Bypass ratio
Brake mean effective pressure (BMEP), 446
Brake power, 443–444
Brake-specific fuel consumption (BSFC), 104
Branca's stamping mill, 6–7
Breguet's equation, 106–107
Bristol 198, 568–569
Bristol 223, 569
Bristol Theseus, 22
British Aircraft Corporation (BAC), 569
Buckingham's theory, 897
Buried wing installation, 680–682
Burning rate, solid propellants, 1337–1346
Bypass jet engines, 25
Bypass ratio (BPR), 93, 396–397, 400–403, 1221

C

Camelina, 1254
Casing, 929
Cayley, Sir George, 8
Center-engine installation, 687
Central plug, nozzle, 790
Centrifugal bending stress, 1119
Centrifugal compressors, 930–932, 1157; *see also* Radial inflow turbines
axial-centrifugal compressor, 840
characteristic performance of, 897–899
classification of
dual-entry/double-face entry, 846–847
impeller vanes, 848
inducers types, 847
shrouded/unshrouded impeller, 847
single-entry/single-face entry, 846–847
single/multiple stages, 845–846
discharge system, 896–897
erosion
brittle mode erosion, 903
compressor–pressure ratio and efficiency, 901
constants, 904
continuum approach, 902
discrete approach, 902
ductile mode erosion, 903
engine performance, 900
particle trajectories, 902
particulate flows, 899–900
problems, 902
rate, 902
sand/dust particles, 901
target material, 904
theoretical estimation, 905–908
turbomachines, 899
two-stage mechanism, 903
volcanic ash, 901
governing equations
continuity equation, 853
energy equation/first law of thermodynamics, 854–858
impeller types, 874–883
Mach number, 851
momentum equation/Euler's equation, 853–854
prewhirl, 862–874
radial impeller, 883–885
slip factor, 858–862
thermodynamics and velocities, 851–852
T–S diagram, 849, 851
velocity triangles, 850
layout of
bell casing, 849
diffuser, 844–845
double-sided centrifugal compressor, 844
exit-guide vanes, 849
horizontally/vertically split casing, 849
IGVs, 848
impeller, 843–844, 848
inducer duct, 843
nomenclature, 842

scroll/manifold, 845
scroll/volute, 848–849
PT6 turboprop engine, 841
vaned diffuser
channel diffuser, 888–889
conical diffuser, 890–892
isentropic vaned diffuser, 893–894
performance maps, 889–890
vs. vaneless diffuser, 895–896
vaneless diffuser
compressible flow, 887–888
incompressible flow, 886–887
Centrifugal rocket pumps, 1359–1365
Centrifugal stress, 945–947, 1113
on blades, 1113–1114
on disks
inner rim, 1117
outer rim, 1115–1116
segment, 1116
CFM56-5C mixed high-BPR turbofan engine, 321–325
CF700 turbofan engine, 335
Chang Zheng 5 (CZ-5) rocket, 1277
Chemical rocket engines, 1273, 1331–1332
Child-Langmuir's law, 1394
Chimney jack, 6
Chinese fire arrows, 4–5
Clamshell door system, 811–813
Clearance volume, 434
Clustered rocket, 1314–1315
Colloidal propellants, 1335
Combat rockets, 1287
Combustion chamber
aerodynamics
conical diffusers, 750–751
diffuser, shapes of, 748
flow patterns, 749
ideal diffuser, 748, 750
straight core annular diffuser, 751–753
components, 746–748
performance
combustion efficiency, 760–761
combustion intensity, 762–763
combustion stability, 762
convection-film cooling, 764
effective cooling, 765–766
film cooling, 763–764
impingement-film cooling, 764–765
louver cooling, 763
pressure loss, 760
splash cooling, 763–764
transpiration cooling, 765
subsonic combustion chambers
annular combustion chambers, 743–744
tubo-annular combustion chambers, 742–743
tubular/multiple combustion chambers, 740–741
supersonic combustion chamber, 744
Combustion systems
afterburner, 770–773
aircraft fuels, 766–767
chemistry of, 756–758
Arrhenius equation, 753
combustion equation, 754
fuel–air ratio, 754–755
gravimetric analysis, 755
reaction rate, 753–754
stoichiometric ratio, 754
first law analysis of, 757–759
materials, 766
pollutant formation
NO_x emissions, 768–769
SO_2 emissions, 769–770
process, 744–746
requirements, 739–740
supersonic combustion system, 773–775
Commercial supersonic technology (CST), 572–573
Composite modified double-based propellants, 1335
Composite propellants, 1335
Compression-ignition (CI) engine, 428–429, 1262
Compression ratio, 436
Compressor map, 898–899
Computational fluid dynamics (CFD), 604
Computational fluid mechanics (CFD), 739
Concorde aircraft, 239, 244, 568–569, 692
Congreve, William, 1275
Conical nose, missiles, 1279–1281
Conical nozzle, 830–831
Conservation of energy, 853, 1183
Conservation of mass, 77, 211, 853, 1081, 1183
Constant nozzle angle design, 1088–1091
Constant specific mass flow stage, 1092–1108
Continuous turbine burners (CTBs), 1243
Contra-rotating aft propfan, 540
Contra-rotating forward propfan, 540
Convair BJ-58, 571–572
Convection cooling, 1126–1129, 1176–1177
Convergent-divergent (C-D) nozzle, 179–180, 784–785, 793–794
adiabatic efficiency, 786–787
behavior of, 788–789
exit Mach number, 787

exit velocity, 787
mass flow rate, 788
pressure ratio, 787
T–S diagram, 786
velocity and static pressure distribution, 788
Convergent nozzles, 87, 179–180, 785, 794–795
chocked nozzle, variations of
flow, aerodynamic and thermodynamic properties of, 798
Mach number, 799
static density, 801
static pressure, 800
static ratios, 799
static temperature, 800
static total pressure, 801
total density, 802
design steps, 796–797
efficiency, 789
pressure ratio, 790
temperature ratio, 789
Conway engine, 25
Cooling technique, 763–766
Counterrotating advanced ducted fan, 49–50
Critical point (CP), 120–121
Cruise, switch-in deflector system, 344
afterburner, 348
combustion chamber, 346
compressor, 346
fan, 345–346
HPT, 347
intake, 345
LPT, 347
mixing process, 347–348
nozzle, 348
thrust force, 348
Cs-1 engine, 21
CST, *see* Commercial supersonic technology
CTBs, *see* Continuous turbine burners
Cylindrical grain, definition, 1335

D

D-27, 28–29
da Vinci, Leonardo, 6
Dawn spacecraft, 1276
DC-10 aircraft, 687
Degree of reaction, 951–954, 1073–1075
DeHaviland Comet 4, 680
Desert Hawk UAV, 1261
Diffuser efficiency, 254, 258, 702–703, 1161
Divergent nozzle
expansion Mach number, 809
expansion waves inside nozzle, drawing procedure, 808
expansion zone, 802
graphical design, 805
Mach angles distribution, 803–805
minimum length divergent nozzle, design procedure, 807–808
nozzle contours
analytical determination of, 805–807
and expansion waves, 809
parallel flow, 802–803
sharp corner nozzle, 803
straightening section, 802–803
Double-shaft gas turbine engine
free-power turbine, 645–647, 649–650, 653–655
regenerative cycle, 652–653
thermal efficiency of gas, 650–652
two-discrete shafts (spools)
combustion chamber, 648
high-pressure spool, 648
HPT, 648
low-pressure spool, 647–648
LPT, 648–649
Double-throat ramjet (DTR) engine, 192
Down-pitch thrust vectoring, 819–820
Dual annular combustor (DAC), 769
Dual-mode ramjet (DRM), *see* Dual ram-scramjet engine
Dual ram-scramjet engine
aero-thermodynamics, 607–613
configuration and station, 606–607
isolator, 606–607
T–S diagram of, 606–608
Du Temple, Felix, 9
Dynamic compressors, 839

E

ecoDemonstrator 787 flight test airplane, 1225
Ejector nozzle, 790–791
Electrical generator, 1190
Electric engines, 1260–1262
Electromagnetic rocket engines, 1391, 1402–1403
Electron Beam (EB)-welded rotor, 627–628
Electrostatic rocket propulsion, 1392–1393
charged ions, 1395–1396
electrical efficiency, 1397–1399
mathematical model, 1393–1395
total efficiency, 1397

Electrostatic thrusters, 1391
Electrothermal rockets, 1391, 1400
  arcjets, 1401
  electromagnetic engines, 1402–1403
  resistojets, 1400–1401
Elevators, 1283–1285
Endurance factor (EF), 108–110
Enthalpy of combustion, 759
Environmental Research Aircraft and Sensor Technology (ERAST) program, 1261
Equal time point (ETP), *see* Critical point (CP)
Equivalent brake-specific fuel consumption (EBSFC), 104
Equivalent shaft horsepower (ESHP), 511–512
Equivalent shaft power (ESP), 98
Equivalent thrust power (ETP), 98
Erosion, 1023, 1028–1034
  brittle mode erosion, 903
  compressor–pressure ratio and efficiency, 901
  constants, 904
  continuum approach, 902
  discrete approach, 902
  ductile mode erosion, 903
  engine performance, 900
  particle trajectories, 902
  particulate flows, 899–900
  problems, 902
  rate, 902
  sand/dust particles, 901
  target material, 904
  theoretical estimation, 905–908
  turbomachines, 899
  two-stage mechanism, 903
  volcanic ash, 901
ETV, *see* External-thrust vectoring
Eulerian solution technique, 902
Euler's equation, 853–854, 1065–1067, 1160
European classified UAV (EUROUVS), 1260
European hypersonic transport vehicle (EHTV), 596
Exhaust system
  for afterburning engines, 781, 783
  for low BPR afterburning turbofans, 781, 783
  noise, 784, 823–829
  nozzles
    annular nozzles, 832–834
    axisymmetric nozzles, 781
    bell nozzles, 831–832
    C-D nozzle, 784–789, 793–794
    conical nozzles, 830–831
    convergent nozzle, 785, 789–790, 794–802
    divergent nozzle, 802–809
    mass flow rate, 785–786
    requirements, 785
    variable geometry nozzles, 790–792
  supersonic aircraft, 781–782
  thrust reversal, 784, 810–818
  thrust vectoring, 781, 784, 819–823
Expansion-deflection (E-D) radial outflow nozzle, 833
External-thrust vectoring (ETV), 819–820

F

Fabri, Henri, 11–12
Fan laws, 856
Fan-on-blade (Flade) engine, 59
Federal Aviation Administration (FAA), 826
Federal Aviation Regulations (FAR), 826
F-15 engine, 694
F-16 engine, 694
F-101 engine, 694
Ffowcs Williams and Hawkings (FW-H) model, 826–827
Fieseler Fi-103 Reichenberg (Fi103R), 136
Film cooling, 763–764, 1122, 1125
Fire arrows, 4–5, 1274
Fire turbine, 620
First-generation biofuels, 1253–1254
Fixed geometry ramjets, 153–154
Fixed pitch propellers, 465–466
Flameholding, 775
Flap blowing turbofan engine, 302–307
Flight fuel available (FFA), 119
F-35 Lightning II, 53
Flow coefficient, 1073, 1163
  definition, 1072
  vs. temperature loading and, 1075–1076
Fluidic-thrust vectoring, 819, 822
Flying bombs, 30, 136, 141–143
F117 Nighthawk, 53
Ford Trimotor, 13–14
Foreign object damage (FOD), 682
Forward fan mixed-flow turbofan engine
  single-spool engine, 317–318
  two-spool engine, 317–318
    CFM56-5C mixed high-BPR, 321–325
    energy balance, 319–320
    layout, 318–319
    mixed and unmixed types, 325–332
    with mixer, 319–320
    mixing process, 318–321
    temperature-entropy diagram, 318–319

Forward fan unmixed turbofan engines
single-spool configuration
BPR, 290, 295–296
combustion chamber, 292
compressor, 292
fan nozzle, 294–295
forward fan, 291
intake, 291
turbine, 292–293
turbine nozzle, 293–294
three-spool engine, 310–317
two-spool engines
fan and LPC on one shaft, 296–307
fan driven by LPT and compressor driven by HPT, 307–308
geared fan driven by LPT and compressor driven by HPT, 308–310
Four-engine fuselage installation, 686
Four-stroke engines, 8, 1262
diesel cycle
air-to-fuel ratio, 457
CI engine, 453–454
constant pressure exhaust stroke, 456
constant-pressure heat addition, 455
constant-volume heat rejection, 456
fuel injection process, 454
isentropic compression, 455, 457
isentropic expansion, 456
P–v and *T–S* diagrams, 454–455
thermal efficiency, 456, 458
Otto cycle
air/fuel and fuel/air ratios, 446–447
constant pressure exhaust stroke, 441
constant pressure suction, 439
constant-volume heat addition, 440
constant volume heat rejection, 441
isentropic compression stroke, 440
isentropic power/expansion stroke, 440–441
performance parameters, 449–453
power generation and fuel consumption, 443–446
propulsive efficiency, 449
P–v and *T–S* diagrams, 439
SFC, 447–448
thermal efficiency, 441–443, 446
vs. two-stroke engines, 453–454
volumetric efficiency, 448–449
terminology
compression ratio, 436
piston execution, 436–437
pressure–volume diagram, 436–437
TDC and BDC, 434, 436
F-22 Raptor, 53
Free power turbine
and gas generator turbine, 1195
map of, 1194
mass flow parameter, 1196–1197
matching procedure for, 1192, 1194
operating line for, 1194
parameters, 1192
pressure ratio, 1192
Free turbine engine, off-design of
free power turbine, 1192–1197
gas generator, 1190–1193
temperature–entropy diagram, 1190–1191
Free vortex design, 958–964, 969–970, 972, 1020
Friction mean effective pressure, 446
Front frame, 928–929
F.2/4 turbofan engines, 28
Fuel burn reductions, 1223–1224
Full Authority Digital Electronic Control (FADEC) system, 57
Fuselage installation, 684, 686–687
military aircraft, 693
over/under turboramjet, 581–582

G

Gas bending stress, 1117–1119
Gas-core rocket, 1390
Gas generator matching
flowchart for, 1192–1193
parameters, 1191–1192
Gasoline engine, 8
Gas turbine engines, 1059, 1263; *see also* Industrial gas turbine engines
advanced ducted fan, 49–50
Barber's gas turbine, 7–8
propfan engines, 48–50
representative manufacturers, 1419–1420
turbofan engine, 43–49
turbojet engines, 39–42
turboprop engines, 42–43
turboshaft engines, 42–43
Geared turbofan engines, 308–309
advantages, 389
Lycoming ALF502R, 309–310
PW1000G, 389–394
fuel mass flow-rate, 395
overall efficiency, 396
propulsive efficiency, 395, 397–398
specific thrust, 395, 397–398, 400–402
thermal efficiency, 396–397, 399
thrust, 394
TSFC, 396, 398, 400–403

General Electric (GE)
ADVENT engine, 1250–1252
CF6 engines, 26, 296
CT58, 24
F118-GE-110, 680
GE-90, 743
GE CF6-80C2, 902
GE CF700 turbofan engine, 335
GEnx turbofan engine, 751
I-A engine, 17–18
I-16 engine, 18
J-31 engine, 18
J-47 engine, 19, 206–207
J-73 engine, 19
J-79 engines, 20
J79-GE-17, 244
LM2500, 666–668
LM Series, 33
SNECMA CFM56 engines, 26
T-31, 22
T56, 22
T64, 22
T700/CT7, 25
T700 engine, 840
TF-39, 25
variable stator concept, 19–20
General electric unducted fan (GE UDF), 28–29
German sänger space transportation systems, 596
Gliders
human-carrier glider, 8
Lilienthal, Otto, 9
triplane glider, 8
Wright brothers, 10
Gloster E28/39 aircraft, 16–17, 203
Gnome-Monosoupape, 14–15
Goddard, Robert, 1275
Gravesand, Jacob, 6
Green diesel, 1225

H

Halophytes, 1254
Harpoon missile, 272–273
Harrier engine, 339–341
Hartzell propeller, 500–501
Hawker Siddeley Nimrod, 680
Hayabusa-2 spacecraft, 1277
Heat-recovery steam generator (HRSG), 662
Heavy-duty gas turbines, 622
Heinkel He 178 aircraft, 16–17, 203
Hemisphere nose, missiles, 1279–1280
Hero, 4, 1274
He S-3 engine, 203
Heterogeneous propellants, 1335
High altitude, long endurance, long range (HALE) UAVs, 1258
High-bypass turbofan engine, 43, 45
High-pressure compressor (HPC), 205, 241–242, 296, 298–300, 638
High-speed civil transport (HSCT), 58, 572
High-speed supersonic and hypersonic engines, 55–57
hypersonic flight
commercial transports, 596–597
history of, 594–596
military applications, 598
propulsion
hybrid-cycle engine, 574–576
multi-stage vehicle, 574
scramjet engine, 598–613
supersonic aircraft
Anglo-French activities, 568–569
Bell X-1, 567–568
Blackbird SR-71, 567–568
CST, future of, 572–573
NACA, conceptual design of, 568
Russian activities, 570
U.S. activities, 570–572
technology challenges, 573
turboramjet engine, 575–576
ATREX turboramjet engine, 590, 592–593
case study, 585–593
dual mode, 584–585
over/under turboramjet, 576, 580–583
P&W J58-1, 590
ramjet mode, 584
turbojet mode, 576, 583–584
wraparound turboramjet, 576–580
High-thrust class turbofan engines, 1417–1418
Homogeneous propellants, 1335
Horizontally opposed engine, 431–432
Hot-air balloon, 7–8
HPC, *see* High-pressure compressor
H-type engine, 432
Human-carrier glider, 8
Hybrid-cycle engine, 574–576
Hybrid propellant rockets, 1382–1383
advantages and disadvantages, 1386–1387
combustion process, 1383
empirical relation, 1384–1386
fuel–oxidizer combinations, 1384
Hybrid Propulsion Demonstration Program (HPDP), 1384
Hybrid Technology Options Project (HyTOP), 1384

HYCAT-1 aircraft, 581–582
Hydraulic/water turbines, 1059
Hydravion, 11–12
Hydrogen-filled balloon, 8
Hydroxyl-terminated polybutadiene (HTPB), 1383
Hyper-soar aircraft, 55–56
Hypersonic aurora aircraft, 55, 57
Hypersonic flight
  commercial transports, 596–597
  history of, 594–596
  military applications, 598

I

IC engines, *see* Internal combustion (IC) engines
Ideal Brayton cycle
  air inlet assembly, 627
  CBT, 626
  combustion chamber, 628
  compressor, 627–628
  single-spool gas turbine, 627
  temperature-entropy and pressure-specific volume diagrams, 627
  turbine, 628–630
Impeller
  absolute velocity, 875, 880–881
  aerodynamic performance, 874
  backward-leaning blades, 882–883
  forward-leaning blades, 876
  impeller isentropic efficiency, 878
  pressure ratio, 877–878
  radial impeller, 883–885
  shrouded/unshrouded impellers, 874
  slip factor, 877
  swirl velocity ratio, 877
  temperature rise, 879–880
Impingement cooling, 1121–1122, 1176–1177
Impingement-film cooling, 764–765
Impulse-to-weight ratio, 1304
Impulse turbine, 1077, 1084
Industrial gas turbine engines, 32–33
  advantages, 619–620
  classification of, 622–624
  combined gas turbine, 662–663
  disadvantages, 620
  double-shaft engine
    free-power turbine, 645–647, 649–650, 653–655
    regenerative cycle, 652–653
    thermal efficiency of gas, 650–652
    two-discrete shafts (spools), 647–649
  GE-7B gas turbine, 50–51
  GE-7H combined-cycle gas turbine, 50–51
  history of, 620–622
  marine gas turbines
    additional components for, 665–666
    advantages, 664
    examples, 666–668
    split-shaft gas-turbine engines, 664
  micro-gas turbines
    bearings, selection and design of, 671
    compressor and turbine, 671
    electric generation, 671–672
    manufacturing process, 670
    power generation, 669
    vs. typical-gas turbines, 670
  offshore gas turbines, 669
  single-shaft engine
    combined intercooling, regeneration, and reheat, 639–645
    ideal cycle, 626–630
    intercooling, 638–639
    real cycle, 630–633
    regeneration, 633–635
    reheat, 635–638
  three-spool gas turbine
    aeroderivative gas turbine, 659–661
    equal efficiencies, 656
    free-power turbine, intercooler, regenerator and reheater, 656–659
    overall compression work, 655
  types of, 624–626
Inlet guide vanes (IGV), 666, 848, 862
In-line engines, 14, 431
Intercoolers
  applications, 1221–1222, 1225
  design technologies, 1235
  drawbacks, 1225
  effectiveness, 1226–1235
Intermediate-pressure turbine (IPT), 659
Internal combustion (IC) engines, 1262–1263
  aerodynamics and thermodynamics
    air-standard analysis, 438
    four-stroke diesel engine, 453–458
    four-stroke engine, terminology, 434, 436–437
    four-stroke spark ignition Otto cycle, 439–453
    piston engines, 458
    superchargers/turbochargers, 458–462
  aero piston engine
    classification, 428
    compression-ignition engine, 429
    definition, 426

piston-powered aircraft and helicopters, 426–427
reciprocating engines, 431–433
rotary engine, 429–431
spark-ignition engine, 428
supercharging and turbocharging, 433–436
airship, 9
aviation statistics, 426–427
development of, 8
single-cylinder gas engine, 8
Internal thrust vectoring (ITV), 819–820
International Standard Atmosphere (ISA), 88
Inter-turbine burners (ITB)
pollutants reduction, 1222
thermodynamic analysis, 1243–1244
turbofan engine, cycle calculation for, 1244–1250
Inward-flow radial (IFR), 1157
Iris variable nozzle, 791
Isentropic compression, 628, 713
Isentropic flow, 196
Ishikawajima Ne-20, 20
ITB, *see* Inter-turbine burners

J

Jatropha, 1254
Jet Bomb 2 (JB-2), 136
Jet engines
advantages, 34–35
axial compressors, 927
performance parameters
aircraft range, 104–108
endurance factor, 108–110
mission segment weight fraction, 114–117
overall efficiency, 99–102
propeller efficiency, 98
propulsive efficiency, 91–96
range factor, 108
route planning, 117–121
specific fuel consumption, 103–104
specific impulse, 110–114
takeoff thrust, 75, 102–103
thermal efficiency, 96–98
reaction engines, 75
thrust force
air mass flow rate, 77
airspeed, 87–88
air temperature and pressure, 87–88
altitude, 88–89
control volume, 76–78
fuel-to-air ratio, 77
inlet air mass flow rate, 87
jet nozzle, 87
net thrust, 78
outlet gas mass flow rate, 87
ram effect, 89–90
thrust, lift, drag, and weight, 76
thrust power, 79–80
turbojet engine, 79–86
turboprop engines, 79
for two-stream engines, 79
Joint Government/Industry Research and Development (JIRAD) program, 1384
Joint strike fighter (JSF), 52
JT8, 695
JT9, 695
Jumo 004B turbojet engines, 17–18
Junker Jumo 004 turbojet engines, 17
Jupiter Flyer, 191–192

K

Kirchhoff (K) equation, 827
Kuznetsov NK-12, 24
Kuznetsov NK-32 triple-spool afterburning mixed turbofan engine, 372–377

L

Lagrangian approach, 902
Lift-to-drag ratio, 106–107
Lilienthal, Otto, 9
Liquid-fuel ramjet (LFRJ), 154
Liquid oxygen–liquid hydrogen rocket engine, 1353–1355
Liquid-propellant rocket engine (LRE), 1346–1347
combustion products, 1348
liquid fuels, 1347
oxidizers, 1347
propellant feed system
pressure-fed engines, 1348–1350
pump-fed system, 1349
Liquid propellants
bipropellant, 1351–1353
liquid oxygen–liquid hydrogen rocket engine, 1353–1355
monopropellant, 1350–1351
Lockheed Martin
Desert Hawk III UAV, 1260
F-35 Lightning II, 52
F-22 Raptor, 53
X-31, 53
X-35, 52

Lockheed Tristar, 687
LoFlyte, 596
Loss coefficient, 999, 1071–1072
Louver cooling technique, 763
Low emissions combustor (LEC), 769
Low-pressure compressor (LPC), 205, 241, 296–307, 639
Low-thrust class turbofan engines, 1418
LRE, *see* Liquid-propellant rocket engine
Luna-Glob spacecraft, 1277
Lycoming ALF502R, 47, 309–310
Lyulka AL-7, 19
Lyulka AL-21, 19

M

Magnetoplasmadynamic (MPD) accelerator, 1402
Marine gas turbines
  additional components for, 665–666
  advantages, 664
  examples, 666–668
  split-shaft gas-turbine engines, 664
Mass ratio (MR), 1303
MAVEN spacecraft, 1276
Mean effective pressure (MEP), 445–446
Mean flow (two-dimensional approach), 933–945
  enthalpy velocity variations, 937–945
  tangential plane, 933
  velocity triangle types, 935–937
Mechanical thrust vectoring, 819–820
Medium altitude, long endurance, long range (MALE) UAVs, 1258
Messerschmitt Me 262 jet fighter, 17
Micro air vehicles (MAVs), 1259, 1261
Micro-gas turbines
  bearings, selection and design of, 671
  compressor and turbine, 671
  electric generation, 671–672
  manufacturing process, 670
  power generation, 669
  vs. typical-gas turbines, 670
Micro turbojet engines
  C802 missile, 272
  cross-section of, 271–272
  data for, 271–272
  dimensions and weight, 271
  Harpoon missile, 272–273
  Storm shadow missile, 273–275
  US Tomahawk missile, 272
Military rockets
  auxiliary rockets, 1287–1288
  characteristics, 1288
  combat rockets, 1287
  launching site, location of, 1288
  target type, 1288
Mini-unmanned air vehicles (MUAVs), 1259–1261
Missiles
  auxiliary components
    fins, 1283–1285
    wings, 1282–1283
  external configuration, 1278
  mid-section, 1281
  nose section, 1279–1281
  range, 1286
  tail section, 1281–1282
  types of, 1285–1286
  warheads, 1286
Mission segment weight fraction, 114–117
Mixed-flow turbofan (MFTF) engine, 59
  single-spool engine, 317–318
  two-spool engine, 317–318
    CFM56-5C mixed high-BPR, 321–325
    energy balance, 319–320
    layout, 318–319
    mixed and unmixed types, 325–332
    with mixer, 319–320
    mixing process, 318–321
    temperature-entropy diagram, 318–319
Mixed turbofan with afterburner, 332–333
  Adour Mk.104, 332
  high specific thrust engines, 332–333
  ideal cycle, 333–335
  RD-133, 333
  real cycle, 335
Modified momentum model, 475–476
Module matching
  definition, 1183
  off-design operation
    of free turbine engine, 1190–1197
    of single-shaft gas turbine, 1183–1190
    of turbojet engine, 1197–1215
Momentum equation, 853–854
Monopropellants, 1350–1351
MQ-8B Fire Scout rotor wing, 1256–1257
MUAVs, *see* Mini-unmanned air vehicles
Multiple-stage centrifugal rocket pumps, 1360, 1362
Multi-spool compressor, 1011–1012
Multispool impulse rocket turbines, 1378
Multistage aircraft, 574
Multistage axial rocket pumps, 1360, 1362

N

NACA, *see* National Advisory Committee for Aeronautics
Nano air vehicles (NAVs), 1259
NASA AD-1, 571–572
NASA Helios, 1261
National Advisory Committee for Aeronautics (NACA), 486–487, 568
National Aerospace Plane (NASP), 594–595
Naval rockets, 1287
Navier–Stokes equations, 827
Nene turbojet engine, 18–19
Net positive suction head (NPSH), 1367
Neutral burning, definition, 1335–1336
New Aero Engine Corp Concepts (NEWAC), 1222
Newton, Sir Isaac, 4, 6, 1275
Newton's steam wagon, 6–7
Nimrod aircraft, 681
Nitrogen oxide (NO_x) emissions, 768–769, 1222, 1253
Noise, 1223–1224, 1252–1253
  acoustics model theory, 826–827
  aircraft, sources of, 784, 824
  corrugated perimeter noise suppressor, 828
  definition, 823
  eccentric coannular nozzle, 829
  ejector-suppressor, 828
  exhaust mixing and shock structure, 824–825
  FAA regulations, 826
  jet engine, 824
  lateral noise level, improvement in, 826–827
  lobe-tube nozzle, 828–829
  sonic boom, 825–826
  suppressor-reverser, 828
  turbofan engines, 825–827, 829
  turbojet engines, 825–826
  unit, 823
Non-airbreathing engines, 34–35, 50, 52; *see also* Rocket engines
Nonchemical rockets, 1273
Non-nuclear turbojet engine, 203–204
North American Aviation, 594
Northrop Grumman RQ-4 Global Hawk, 1258–1259
Nose installation, 467
Nose-mounted turboprop engine, 690
Nozzles
  aft-fan, 338
  annular nozzles, 832–834
  axisymmetric nozzles, 781
  bell nozzles, 831–832
  C-D nozzle, 784–789, 793–794
  conical nozzles, 830–831
  convergent nozzle, 785, 789–790, 794–795
  mass flow rate, 785–786
  requirements, 785
  rocket engine, 1294–1296
  scramjet engine, 604–606, 612
  single-spool turbojet engine
    ideal cycle, 211–213
    real cycle, 227–229
  switch-in deflector system
    cruise, 348
    takeoff/lift thrust, 351
  thrust vectoring, 781, 784, 819, 821
  two-dimensional supersonic nozzle
    convergent nozzle, 796–802
    divergent nozzle, 802–809
  two-spool turbojet engine, 243–244
  variable geometry nozzles
    for afterburning engine, 792
    central plug, 790
    ejector nozzle, 790–791
    iris nozzle, 791
Nuclear-powered jet engines, 203–204
Nuclear ramjet engine, 32, 191–192
Nuclear rocket propulsion
  gas-core reactor, 1390
  solid-core reactor, 1387–1390
  sources, 1387
Nuclear thermal propulsion (NTP), 1388
Nuclear turbojet engine, 41–42

O

Offshore gas turbines, 669
Ogival nose, missiles, 1279–1280
Otto cycle engines, 8
  air/fuel and fuel/air ratios, 446–447
  constant pressure exhaust stroke, 441
  constant pressure suction, 439
  constant-volume heat addition, 440
  constant volume heat rejection, 441
  isentropic compression stroke, 440
  isentropic power/expansion stroke, 440–441
  performance parameters, 449–453
  power generation and fuel consumption, 443–446
  propulsive efficiency, 449
  P–v and *T–S* diagrams, 439
  SFC, 447–448
  thermal efficiency, 441–443, 446
  vs. two-stroke engines, 453–454
  volumetric efficiency, 448–449

Overall efficiency
definition, 99
ramjet engines, 181, 186, 189
rocket engine, 1306
scramjet engine, 613
turbofan engines, 99–102
turbojet engine, 99
Over-oxidized, definition, 1336
Over/under turboramjet, 576, 580
dual mode, 581–583
fuselage installation, 581–582
layout of, 581
ramjet mode, 583
T–S diagram of, 581
turbojet mode, 582
wing installation, 581

P

Parabolic series nose, missiles, 1279–1280
Particulate matter (PM), 1253
Pegasus booster rocket, 595–596
Pegasus engine, 339–341
Perforation, definition, 1335
Piaggio P-180 Avanti Rennes, 468
Piston engines, 3, 34, 426, 428–429
Piston speed, 448
Pluto reactor, 191
Point of no return (PNR), 118–120
Pollutants
NO_x emissions, 768–769
SO_2 emissions, 769–770
Power Jet W.1., 16–17
Power loading (PL), 483
Powerplant installation
airframe manufacturer, 680
air intakes/inlets, 695
intake and engine, 719–721
propulsion-airframe integration, 679
subsonic aircraft
turbojet and turbofan engines, 680–688
turboprop installation, 688–691
subsonic intakes
inlet performance, 697–701
isentropic efficiency, 701
pitot intakes, 696–697
stagnation-pressure ratio, 702
turbojet/turbofan engines, 695
turboprop inlets, 695, 704–705
supersonic aircraft
civil transports, 692
military aircraft, 693–695
supersonic intakes
axisymmetric and two-dimensional intakes, 706
diffuser design, 705–706
examples, 714–716
external compression intakes, 710–713
fixed-geometry intakes, 707
internal compression inlet, 716–717
internal, external and mixed-compression, 707–708
mixed compression intakes, 717–719
normal shock waves, 708–709
oblique shock waves, 709–710
stratosphere adiabatic efficiency, 705
variable-geometry intakes, 707–708
turbo ramjet engine
eight-oblique-shocks, 723, 725–726
fighter aircraft (F-111A), 724–731
four oblique shocks, 722–724, 727
intake geometry, 721
Power plants, UAVs
electric engines, 1260–1262
engine characteristics, 1263–1265
gas turbine engines, 1263
internal combustion engines, 1262–1263
Power series nose, missiles, 1279–1280
Pratt & Whitney
FT-4, 33
J-57 engine, 19
J57-P-23, 244
JT8D-200 engine, 25
JT9D engine, 25–26
powerplant developments, 57–58
PT6 and PT6A engine, 23–24, 840
PW8000, 308–310
P&W JT 9D-7As, 902
PW4000 series, 695, 743
Predator B, 1258
Pre–jet engines
airship, 9
Barber's gas turbine, 7–8
Branca's stamping mill, 6–7
da Vinci's chimney jack, 6
Du Temple's airplane, 9
fire arrows, 4–5
Ford Trimotor, 13–14
four-stroke engines, 8
glider of Otto Lilienthal, 9
Hero's aeolipile, 4–5
hot-air balloon, 7–8
human-carrying glider, 8
hydravion, 11–12

internal combustion engines, development of, 8
marine flying, 12
Newton's steam wagon, 6–7
reciprocating engines, 14–15
reciprocating hot-air engine, 8
single-cylinder gas engine, 8
triplane glider, 8
Vickers Gunbus, 12–13
Wan Hu's chair, 4–5
Wright brothers, 10–11
XI monoplane, 11–12
Zeppelin airships, 14
Pressure-fed rocket engine, 1348–1350
Pressure loss factor (PLF), 760
Prewhirl
axial velocity, 869
bending stress, 863
curved-beam nomenclature, 863
IGV, 862
iteration procedure, 867–868
Mach number, 862
radial compressors, 864
stress, curved beams, 868–869
velocity triangle
constant inlet relative angle, 872–874
constant prewhirl angle, 871–872
inlet with slip, 866
no prewhirl, 870–871
Primary combustion zone, 746
Profile loss, 1129–1131
Progress D-27 engines, 542–543
Progressive burning, definition, 1336
Propellant feed system
pressure-fed engines, 1348–1350
pump-fed system, 1349
Propellant mass fraction, 1303
Propeller efficiency, 98
Propfan engines
counterrotating propfan, 48–50
D-27, 28–29
578-DX engine, 28
F.2/4, 28
features of, 28
GE UDF, 28–29
NASA HamStan, 28
NK-93, 28
Progress D-27 propfan, 542–543
propulsive efficiency, 93–94
single rotation, 48–49
thermal efficiency, 97
vs. turboprop engines, 541
types, 540
UDF, 543–546
578-DX, 541
GE36 UDF, 541, 543
MD-80, 541–542
UHB, 539
Propulsion-airframe integration, *see* Powerplant installation
Propulsion rocket system
electrostatic, 1392–1393
charged ions, 1395–1396
electrical efficiency, 1397–1399
mathematical model, 1393–1395
total efficiency, 1397
hybrid, 1382–1384
advantages and disadvantages, 1386–1387
empirical relation, 1384–1386
nuclear, 1387
gas-core reactor, 1390
solid-core reactor, 1387–1390
Propulsive efficiency, 449, 474–475
aircraft range, 106
definition, 91
effective jet velocity, 95–96
external efficiency, 91
ramjet engines, 91–92, 181, 185, 188
rocket engine, 1305–1306
scramjet, 91–92
single and contrarotating propfan engines, 93–94
turbofan engine, 92–93, 95–96
turbojet engines, 91–95
turboprop engines, 92–93
Prox Dynamics Picoflyer, 1259
PT6 turboshaft engine, 33
Pulse detonation engine (PDE), 135
Pulsejet engines, 28, 30
Fieseler Fi-103 Reichenberg, 136
flow parameters, pulsating nature of, 144–146
JB-2, 136
Jumo 226, 30
Ka-10, 30
operation, 36–37
PJ-31-1, 30
pulse detonation engine, 135
combined cycle, 148
example, 149–151
hybrid PDEs, 148–149
objective of, 146
pure PDEs, 147
specific impulse for, 147–148
thermodynamic cycle, 146–147

RD-13/D-10, 30
stationary modules, 135
in tethered and radiocontrol model aircraft, 136
valved engine
combustion chamber, 139
cycle, 137–138
drawback of, 136
examples, 140–143
German V-1 missile, 36, 135–136
intake/diffuser, 138–139
one-way/check valves, 135–136
valveless engine, 135–136, 143–144
Pump-fed rocket engines, 1349, 1355–1359
Pumps, rocket, 1359
axial pumps, 1372–1374
centrifugal pumps
configurations, 1359–1360
elements of, 1360–1361
head and flow rate, 1359
performance, 1362–1365
velocity triangles, 1361
materials and fabrication process, 1377
multiple-stage centrifugal pumps, 1362
multistage axial pumps, 1362
parallel and series, 1374–1376
pump-fed system, 1355–1359
specific speed, 1366–1372
SSME, 1372

R

Radial engines, 14, 432–433
Radial inflow turbines
applications, 1157
characteristics, 1157, 1169
cooling techniques, 1176–1177
dimensionless parameters
flow coefficient, 1163
rotor meridional velocity ratio, 1163
specific speed, 1164
stage loading, 1163
history, 1157
isentropic efficiency, 1161
layout of, 1157–1158
losses, breakdown of, 1168–1171
one-dimensional design procedure, 1171–1176
operating conditions, 1169
power, 1162–1163
preliminary design, 1164–1167
thermodynamics
temperature–entropy diagram, 1158–1159
total-to-total efficiency, 1161
velocity triangles in, 1159–1160
Ram effect, 89–90, 151–152
Ramjet engines, 194, 598
advantages, 152
contributors, 31
disadvantages, 152, 203
DTR engine, 192
elements, 35
fixed geometry, 153–154
ideal ramjet
fuel-to-air ratio, 157
modules, states of, 154–155
specific thrust, 161, 168–170
thermal efficiency, 166–168
thermodynamic cycle, 155–157
thrust force, 157–158
TSFC, 158, 161
isentropic flow, 196
Leduc 010, 31
liquid-fuel ramjet, 154
nuclear ramjet engine, 32, 191–192
in operational missile programs, 32
performance parameters, 180–191
pioneers, 31
ram effect, 151
Rayleigh flow, 195–196
real ramjet, 158–161, 170–173
shock waves
normal shock wave, 175–180, 195
oblique shock wave, 195
solid-fuel ramjet, 154, 193–194
speed, 30–31, 151
subsonic ramjets, 31, 35, 151–153
supersonic ramjets, 35–36, 151–153, 161–166
thermal efficiency, 97
variable geometry, 153–154, 173–175
Ramp injectors, 603
Range factor (RF), 108
Rankine-Froude theory, *see* Actuator disk theory
Rayleigh flow, 195–196
RD-133 afterburning turbofan TVC engine, 333
RD-60K booster turbojet engines, 48–49
Reaction engines, 75
Reaction rocket turbines, 1378–1382
Real Brayton cycle
combustion chamber, 630–631
compressor, 630
turbine, 631–633

Rear frame, 929
Reciprocating engines, 34
  examples, 8–9
  horizontally opposed engine, 431–432
  H-type engine, 432
  in-line engine, 431–432
  radial type engine, 432–433
  V-type engines, 432
  X-type engines, 432
Recuperative turboshaft engines, 1263
Recuperators
  applications, 1221, 1235
  drawbacks, 1225
  performance requirements, 1236
  turbofan engine, thermodynamic cycle of, 1237–1243
Regressive burning, definition, 1336
Remotely piloted aircraft (RPA), 1258–1259
Resistojets, 1391, 1400–1401
Rocket engines; *see also* Rocket pumps
  advantages, 1273
  axial turbines, 1377
    multispool impulse turbines, 1378
    reaction turbines, 1378–1382
    single-stage impulse turbine, 1377–1378
  chemical rockets, 1273, 1331–1332
  classification of, 1331–1332
    application, based on, 1287
    energy source, 1285
    guidance systems, 1286
    launch mode, 1286
    military rockets, 1287–1288
    missiles, types of, 1285
    number of stages, 1287
    propulsion, 1285
    range, 1286
    warheads, 1286
  definition, 34
  electrostatic propulsion, 1392–1393
    charged ions, 1395–1396
    electrical efficiency, 1397–1399
    mathematical model, 1393–1395
    total efficiency, 1397
  electrothermal, 1400
    arcjets, 1401
    electromagnetic engines, 1402–1403
    resistojets, 1400–1401
  history of
    important events, 1274–1277
    recent and future plans, 1276–1277
  hybrid propulsion, 1382–1383
    advantages and disadvantages, 1386–1387
    combustion process, 1383
    empirical relation, 1384–1386
    fuel–oxidizer combinations, 1384
  liquid propellants, 1273–1274
    bipropellant, 1351–1353
    liquid oxygen–liquid hydrogen rocket engine, 1353–1355
    monopropellant, 1350–1351
  missile configuration
    external configuration, 1278
    factors affecting, 1278
    fins, 1283–1285
    mid-section, 1281
    nose section, 1279–1281
    tail section, 1281–1282
    wings, 1282–1283
  nonchemical rockets, 1273
  nuclear rocket propulsion
    gas-core reactor, 1390
    solid-core reactor, 1387–1390
    sources, 1387
  performance characteristics, 1332
  performance parameters, 1307–1309
    characteristic velocity, 1296
    effective exhaust velocity, 1290–1293
    exhaust velocity, 1293–1294
    impulse-to-weight ratio, 1304
    mass ratio, 1303
    nozzle relations, 1294–1296
    overall efficiency, 1306
    propellant mass fraction, 1303
    propulsive efficiency, 1305–1306
    specific impulse, 1299–1303
    specific propellant consumption, 1303
    thermal efficiency, 1304–1305
    thrust coefficient, 1296–1297
    thrust force, 1288–1290
    total impulse, 1298
  pump-fed system, 1355–1359
  solid propellants, 1273–1274
    advantages, 1334–1335
    burning rate, 1337–1346
    characteristics, 1347
    composition, 1335
    data for, 1347
    definitions, 1335–1336
    disadvantages, 1335
    features, 1333
    liquid-propellant rocket engine, 1346–1349
    motor, 1332–1334
  space flight
    escape velocity, 1325–1326
    orbital velocity, 1324–1326

staging
advantages and disadvantages, 1317
Ariane 5 rocket, 1320–1323
multistage series rocket, 1314–1316
parallel multistage rocket, 1314–1317
single-stage rocket, 1309–1314
three-stage rocket, 1317–1320
Rocket pumps, 1359
axial pumps, 1372–1374
centrifugal pumps
configurations, 1359–1360
elements of, 1360–1361
head and flow rate, 1359
performance, 1362–1365
velocity triangles, 1361
materials and fabrication process, 1377
multiple-stage centrifugal pumps, 1362
multistage axial pumps, 1362
parallel and series, 1374–1376
specific speed, 1366–1372
SSME, 1372
Rolls-Royce, 55–57
AE1107C-Liberty, 25
Avon and Olympus engines, 33
Conway engine, 25
DART, 22, 840
Gem, 25
Industrial Trent, 33
MT30, 668
Nene engine, 18–19, 206
Pegasus, 339–341
Proteus gas turbine engines, 33
RB211, 25, 33, 311
RB50 Trent, 22
Spey engine, 25
Tay engine, 18
Trent 1000, 27
Trent series, 743
Tyne, 22
Rolls Royce/SNECMA Olympus 593 turbojets, 21, 239, 244–245, 692
Rosetta spacecraft, 1276–1277
Rotary engines, 14–15, 425, 1263
conventional types, 429
Wankel engine, 429–431
Rotational speed (RPM) and annulus dimesnsions, 973–976
Rotor blade, 927–929, 946, 1060
characteristics, 1074
hub-to-tip variations in, 1096
material selection, 1144
mechanical stresses, 1082
row layouts, 1113–1114
stresses on, 1144
vibration analysis, 1112
vibration stresses, 1082–1083
Rotor meridional velocity ratio, 1163
Rotor-wing unmanned air vehicles (RUAVs), 1256–1257
Route planning, 117–118
CP/ETP, 120–121
PNR/PSR, 118–120
track, 118
Rudders, 1283–1284

S

Safety fuels, 767
Sand-erosion tests, 908
Saturn V rocket, 1275, 1314
SCR, *see* Selective catalytic reduction
Scramjet engine, 36–37, 744
applications, 598
combustion chamber, 601–604, 611–612
disadvantages, 599–600
dual-mode, 32
dual ram-scramjet engine
aero-thermodynamics, 607–610
configuration and station, 606–607
isolator, 606–607
T–*S* diagram of, 606–608
intake of, 601–602
layout of, 600, 610
nozzle, 604–606, 612
overall efficiency, 613
vs. ramjet, 598–599
schematic representation, 598–599
thermodynamics, 600
thrust force, 612
X-43A, 32
Secondary flow loss, 1131
Second-generation biofuels, 1254
Selective catalytic reduction (SCR), 768–769
Selective noncatalytic reduction (SNCR), 768–769
SFC, *see* Specific fuel consumption
SFRJ, *see* Solid-fuel ramjet
Shaft horsepower (SHP), 511
Shaft power (SP), 98
Shenyang J-8 Chinese fighter, 20
Shock loss model, 999
Shock thrust-vector control, 822

Short takeoff and landing (STOL), *see* Vertical/short takeoff and landing (V/STOL)
Simple vortex model, 475–476
Simplified radial equilibrium equation (SRE), 956–957
Single-cylinder gas engine, 8
Single-expansion ramp nozzle (SERN), 580
Single-shaft gas turbine engine, 1183–1184
  combined intercooling, regeneration, and reheat, 639–645
  different loads, 1190
  intercooling, 638–639
  layout, 1184
  procedure, 1185–1189
  regeneration, 633–635
  reheat, 635–638
  single compressor and turbine
    ideal cycle, 626–630
    real cycle, 630–633
Single-spool turbofan engines, 403–404
  BPR, 290, 295–296
  combustion chamber, 292
  compressor, 292
  fan nozzle, 294–295
  forward fan, 291
  intake, 291
  turbine, 292–293
  turbine nozzle, 293–294
Single-spool turbojet engine
  at altitude of 8 km for inoperative afterburner
    afterburner fuel-to-air ratio, variations in, 265–266
    fuel-to-air ratio and propulsive efficiency, variations in, 265–266
    specific thrust and TSFC, variations in, 265
  at altitude of 8 km for operative afterburner
    fuel-to-air ratio and afterburner fuel-to-air ratio, variations in, 266–267
    propulsive efficiency, variations in, 266, 268
    specific thrust and TSFC, variations in, 266–267
  axial/centrifugal compressors, 205–206
  examples of, 206–207
  ideal cycle, 207
    afterburner, 210–211
    combustion chamber, 209
    compressor, 208–209
    examples, 214–223
    intake/inlet, 208
    nozzle, 211–213
    turbine, 209–210
  layout and modules of, 205
  operative *vs.* inoperative afterburner, 234–238
  real cycle
    adiabatic efficiencies, 225
    combustion chamber, 226
    compressor, 226
    examples, 229–234
    general description, 223–225
    inoperative afterburner, 224, 227
    intake, 225–226
    nozzle, 227–229
    operative afterburner, 224, 227
    turbine, 226–227
  at sea level for inoperative afterburner
    fuel-to-air ratio and propulsive efficiency, variations in, 262–263
    specific thrust and TSFC, variations in, 260–262
  at sea level with operative afterburner
    fuel-to-air ratio and propulsive efficiency, variations in, 264–265
    specific thrust and TSFC, variations in, 263–264
  statistical analysis, 249
  thermodynamic analysis, 207
Single-stage centrifugal rocket pump, 1360
Single-stage impulse rocket turbine, 1377–1378
Slip phenomenon, 858–862
SNCR, *see* Selective noncatalytic reduction
Solar-electric Helios Prototype, 53–54
Solar Impulse aircraft, 53–54
Solar-powered UAV, 1261
Solid-core rocket engine, 1387–1390
Solid-fuel ramjet (SFRJ), 154, 193–194
Solid-propellant rocket
  advantages, 1334–1335
  burning rate, 1337–1346
  characteristics, 1347
  composition, 1335
  data for, 1347
  definitions, 1335–1336
  disadvantages, 1335
  features, 1333
  liquid-propellant rocket engine, 1346–1349
  motor, 1332–1334
Solid rocket boosters (SRBs), 1334–1335
SoLong UAV, 1261

Space Electric Rocket Test-II (SERT-II) spacecraft, 1391
Space Electric Rocket Test-I (SERT-I) spacecraft, 1390
Space flight
  escape velocity, 1325–1326
  orbital velocity, 1324–1326
Space shuttle main engine (SSME), 1372
Space shuttles, 3, 1275, 1277
Spark-ignition (SI) engine, 428, 1262
  four-stroke engine
    air/fuel and fuel/air ratios, 446–447
    constant pressure exhaust stroke, 441
    constant pressure suction, 439
    constant-volume heat addition, 440
    constant volume heat rejection, 441
    isentropic compression stroke, 440
    isentropic power/expansion stroke, 440–441
    performance parameters, 449–453
    power generation and fuel consumption, 443–446
    propulsive efficiency, 449
    P–v and *T–S* diagrams, 439
    SFC, 447–448
    thermal efficiency, 441–443, 446
    volumetric efficiency, 448–449
  two-stroke engines, 453–454
Specific fuel consumption (SFC), 632
  four-stroke engine, 447–448
  ramjet, turbojet, and turbofan engines, 103–104
  turboprop engines, 104
  UAV, 1264
Specific impulse, 110–114
  vs. Mach number, 575–576
  for pulse detonation engine, 147–148
  rocket engines, 1299–1303
Specific propellant consumption (SPC), 1303
Spey engines, 25
Spike Aerospace, 573
Spike motion, 173, 175
Spike nozzles, 834
Splash cooling, 763–764
Sputnik I, 1275
Sputnik II, 1275
SR-71 aircraft, 694–695
SRBs, *see* Solid rocket boosters
SSME, *see* Space shuttle main engine (SSME)
SSTs, *see* Supersonic transports
Stage efficiency, 1069–1070, 1072
Stage loading, 1163
Stamping mill, 6–7
Stanitz formula, 859
Stanton number, 1125–1126
Starship aircraft, 689
Stator blade, 928–929, 1012–1013
Steady-state stress, 1112
Steam turbine, 620–621, 1059
Steam wagon, 6–7
Storm shadow missile, 273–275
Subsonic aircraft
  turbojet and turbofan engines
    combined fuselage and tail installation, 688
    combined wing and tail installation, 687–688
    fuselage installation, 684, 686–687
    wing installation, 680–684
  turboprop installation, 688–691
Subsonic intakes
  inlet performance, 697–701
  performance parameters
    examples, 703–704
    isentropic efficiency, 701
    stagnation-pressure ratio, 702
  pitot intakes, 696–697
  turbojet/turbofan engines, 695
  turboprop inlets, 704–705
Subsonic ramjet engine, 31, 35, 151–153
Suction specific speed, 1368
Sulfur dioxide (SO_2) emissions, 769–770
Super Caravelle, 569
Supercharging engine
  aerodynamics and thermodynamics, 458–462
  aero piston engine, 433–436
Supersonic aircraft
  Anglo-French activities
    BAe-Aerospatiale AST, 569
    Concorde, 568–569
  Bell X-1, 567–568
  Blackbird SR-71, 567–568
  civil transports, 692
  CST, future of, 572–573
  exhaust system, 781–782
  military aircraft, 693–695
  NACA, conceptual design of, 568
  Russian activities, Tupolev Tu-144, 570
  U.S. activities
    Boeing 2707-100/200, 570–571
    Boeing 2707-300, 571
    Convair BJ-58, 571–572
    HSCT, 572

Lockheed L-2000, 570–571
NASA AD-1, 571–572
Supersonic combustion ramjet, *see* Scramjet engine
Supersonic ramjet engines, 35–36, 151–153, 161–166
Supersonic Transport Aircraft Committee (STAC), 568
Supersonic transports (SSTs), 58–59, 570–571, 692
Supersonic turbojet, 257–260
Super VC-10, 686
Surface film ejection, 1177
Surface-to-air missiles, 1286
Surface-to-surface missiles (SSM), 1286
Sustainable biofuels, *see* Biofuels
Switch-in deflector system
  cruise, 344–348
  takeoff/lift thrust, 344, 349–351
  vectored thrust engine, 343–344
Swiveling nozzles, 339–343

T

Takeoff/lift thrust, 75, 102–103, 344
  afterburner, 350–351
  combustion chamber, 350
  compressor, 349–350
  fan, 349
  HPT, 350
  intake, 349
  LPT, 350
  mixing process, 350
  nozzle, 351
  thrust force, 351
Tay engine, 18
TBE, *see* Turbine bypass engine
Teledyne CAE J402 turbojet engine, 272–273
Temperature drop coefficient
  definition, 1072
  vs. flow coefficient, 1075–1076
Thermal efficiency, 629–630, 632–633, 635
  internal efficiency, 96
  ramjet engines, 97, 166–168, 180, 186, 189
  rocket engine, 1304–1305
  turbofan and propfan engine, 97
  turbojet engine, 97
  turboprop/turboshaft engine, 98
Thermal stress, 1113, 1120
Three-dimensional flow, 954–955
  axisymmetric flow, 955–956
  free vortex method, 958–963
  general design procedure, 963–972
  simplified radial equilibrium equation, 956–957
3D printing, 1252
Three-spool gas turbine engine
  aeroderivative gas turbine, 659–661
  equal efficiencies, 656
  free-power turbine, intercooler, regenerator and reheater, 656–659
  overall compression work, 655
Three-spool turbofan engine, 310–317, 1203–1204
Three-stream turbofans, 1222
Thrust coefficient, 1296–1297
Thrust force, 75
  airbreathing engine, 1288–1289
  air mass flow rate, 77
  airspeed, 87–88
  air temperature and pressure, 87–88
  altitude, 88–89
  control volume, 76–78
  convergent nozzles, 87
  fuel-to-air ratio, 77
  inlet air mass flow rate, 87
  net thrust, 78
  outlet gas mass flow rate, 87
  ram effect, 89–90
  ramjet engines, 157–158
  rocket engine, 1288–1290
  scramjet engine, 612
  specific thrust, 79
  switch-in deflector system
    cruise, 348
    takeoff/lift thrust, 351
  thrust, lift, drag, and weight, 76
  thrust power, 79–80
  turbojet engine
    constant mass flow rate, variations with, 81–82
    exhaust and flight speed, 79
    idling engine, forward thrust, 80
    single-spool axial-flow engine, 83–86
    variable mass flow rate, variations with, 81–83
  turboprop engines, 79
  for two-stream engines, 79
Thrust reversal, 784, 815–817
  aircraft engine, control volume, 814–815
  blocker doors, 811–813
  bucket-type doors, 811–812
  civilian transport, 810–811
  clamshell door system, 811–813
  conditions, 811
  exhaust jet, control volume, 813–814

ground roll distance calculation, 817–818
military aircraft, 810
turbojet engines, 811
Thrust-specific fuel consumption (TSFC), 75, 103–104, 229, 247, 252, 260
pulsejet engine, 139, 141, 150
ramjets
different fuel heating values, 181, 184
different maximum temperatures, 181–182
ideal ramjet, 158, 161
real cycle, 161
subsonic ramjets, 153
for single-spool turbojet at altitude of 8 km
inoperative afterburner, 265
operative afterburner, 266–267
for single-spool turbojet at sea level
inoperative afterburner, 260–262
operative afterburner, 263–264
vs. specific thrust, 268
turboramjet engines
dual mode, 585
hybrid engine, 587–588, 590–591
ramjet mode, 584
turbojet mode, 583
Thrust vectoring
applications, 819
definition, 819
fluidic-thrust vectoring, 819, 822
forces on aircraft, 823
mechanical thrust vectoring, 819–820
3-D thrust vectoring, 821–822
two-dimensional nozzles, 781, 784, 819, 821
Tin Goose, 13
Tip clearance loss, 1131–1132
Tip Mach number, 945, 948–949
T53 Lycoming engine, 840
Top dead center (TDC), 434, 436
Total equivalent horsepower (TEHP), 511
TPF331 turboprop engine, 23
Trailing edge ejection, 1177
Trans-Atlantic flight, 1225
Transpiration cooling, 765
Trent 1000 turbofan engines, 27
Triplane glider, 8
Triple-spool unmixed turbofan engine (Trent 700), 381–388
TSFC, *see* Thrust-specific fuel consumption
Tsiolkovsky rocket equation, 1312
Tubo-annular combustion chambers, 742–743
Tupolev Tu-144 aircraft, 570
Tupolev TU-160 aircraft, 372–377
Turbine-burner engines, 1244
Turbine bypass engine (TBE), 58–59
Turbine cooling
convection, 1121
film cooling, 1122
impingement cooling, 1121–1122
Turbine map, 1133–1137
Turbocharging engine
aerodynamics and thermodynamics, 458–462
aero piston engine, 433–436
Turbofan engines, 289, 405–406, 927, 1263, 1417–1418
advantages, 25, 289–290
aft-fan, 335–338
AI-25 TD, 28
CF6 engines, 26
CFM56 engines, 26
classification of
aft fan, 43, 45
booster turbojets, 48–49
double-spool turbofan engines, 46
forward-fan, 43–44
F-100 two-spool afterburning turbofan engine, 48
geared fans, 47
low/high bypass ratio, 43, 45–46
mixed engine, 46
nuclear and nonnuclear engines, 48
single-spool turbofan engines, 46
three-spool engines, 47
unmixed turbofan, 46
combined fuselage and tail installation, 688
combined wing and tail installation, 687–688
Conway engine, 25
D-436, 27
D-30KP, 27
D-20P, 27
D-36 series 1, 1E, 2A and 3A, 28
D-18T Series 1 and 3, 27
forward fan mixed-flow engine
single-spool engine, 317–318
two-spool engine, 317–332
forward fan unmixed
single-spool configuration, 290–296
three-spool engine, 310–317
two-spool engines, 296–310
fuselage installation, 684, 686–687
GE90, 27

geared turbofan engines, PW1000G, 389–394
advantages, 389
fuel mass flow-rate, 395
overall efficiency, 396
propulsive efficiency, 395, 397–398
specific thrust, 395, 397–398, 400–402
thermal efficiency, 396–397, 399
thrust, 394
TSFC, 396, 398, 400–403
GP7000 series, 26
high-thrust class, 1417
hybrid PDEs, 148–149
JT8D-200, 25
JT9D, 25–26
layout, 43–44
low-thrust class, 1418
mixed turbofan with afterburner, 332–333
Adour Mk.104, 332
high specific thrust engines, 332–333
ideal cycle, 333–335
RD-133, 333
real cycle, 335
noise, 825–827, 829
overall efficiency, 99–102
performance analysis
aft-fan, 357–361
AGM-86 ALCM, 377–380
forward fan, 357
GE90, 351–356
high-bypass turbofan, 351–356
Kuznetsov NK-32 triple-spool afterburning mixed turbofan engine, 372–377
new and deteriorated high-BPR engines, 362–365
propulsive efficiency and TSFC, 363, 365–367
TIT and OPR, effect of, 368–372
unmixed three-spool engine (Trent 700), 381–388
propulsive efficiency, 92–93, 95–96
RB211, 25
Spey engine, 25
TF-39, 25
TFE731, 27
thermal efficiency, 97
transonic speeds, 3
Trent 1000, 27
types, 405–406
V2500, 26
V/STOL, 338–339
switch-in deflector system, 343–351
swiveling nozzles, 339–343
wing installation
above the wing, 682–684
buried in the wing, 680–682
pod installation, 682–683
Turbojet engines, 40, 204, 276–277, 1263
centrifugal compressor for, 930
combined fuselage and tail installation, 688
combined wing and tail installation, 687–688
Comet, 19
double-spool engine, 19
afterburning, 244–249
layout and modules of, 205
non-afterburning, 239–244
statistical analysis, 249
front frame in, 928
fuselage installation, 684, 686–687
gas generator, 203
GE I-A engine, 17–18
GE I-16 engine, 18
GE J-31 engine, 18
GE J-47 engine, 19
GE J-73 engine, 19
GE J-79 engine, 20
Ishikawajima Ne-20, 20
J33 engine, 20
Jumo 004 jet engine, 17–18
Lyulka AL-7, 19
Lyulka AL-21, 19
microengines
C802 missile, 272
cross-section of, 271–272
data for, 271–272
dimensions and weight, 271
Harpoon missile, 272–273
Storm shadow missile, 273–275
US Tomahawk missile, 272
module matching off-design, 1206–1207
with afterburner, 1207–1213
between compressor and turbine, 1213–1215
exhaust speed and specific thrust *vs.* rotational speed ratio, 1201–1202
between fan and low-pressure modules, 1205
ground test, 1199–1201
nozzle map, 1198
performance, 1199
three-spool turbofan engine, 1203–1204
Nene engine, 18–19
noise, 825–826
nuclear/non-nuclear engine, 41–42, 203–204
overall efficiency, 99

performance map, 268–271
Pratt & Whitney J-57 engine, 19
propulsive efficiency, 91–95
RDT-1/VDR-2, 18
Rolls-Royce/Snecma Olympus 593
turbojet, 21
Shenyang J-8 Chinese fighter, 20
single-spool engine
axial/centrifugal compressors, 39–40, 205–206
examples of, 206–207
ideal cycle, 207–223
layout and modules of, 205
operative *vs.* inoperative afterburner, 234–238
optimization, 260–268
real cycle, 223–234
statistical analysis, 249
thermodynamic analysis, 207
supersonic, 257–260
S-18/VDR-3, 18
Tay engine, 18
thermal efficiency, 97
thrust augmentation methods, 249–250
afterburning engine, 252–257
water injection, 250–252
thrust reversal, 811
variable stator concept, 19–20
Viper, 20
von Ohain, Hans, 3, 15–17
Whittle, Frank, Sir, 3, 15–17
wing installation
above the wing, 682–684
buried in the wing, 680–682
pod installation, 682–683
Turboprop engines, 495–496, 1263
advantages, 498–499
AI-24, 23
AI-20D Series, 23
Allison T56-A-11, 22
Armstrong Siddeley Mamba and double Mamba, 22
Armstrong Siddeley Python, 22
Bristol Theseus, 22
classification
engine-aircraft configuration, 499–500
Hartzell propeller, 500–501
intakes, 501–502
propeller-engine coupling, 501
propeller type, 501
spools, 501
core engine and propeller, 21
counterrotating propellers
empennage installation, 691
nose installation, 690
disadvantages, 499
equivalent engine power
flight operation, 511–512
static condition, 511
free-power turbine, 21, 42–43
fuel consumption, 512–513
GE T-31, T56, T64, 22
650 hp Bastan, 23
400 hp Marcadau, 23
installation, 513–514
Jendrassik Cs-1, 21
Kuznetsov NK-12, 24
performance analysis
ESHP and ESFC, 522, 524
flight Mach number, 521, 523
thrust and power contribution, 521–523
propeller requirements, 688
propulsive efficiency, 92–93
PT6, 23–24
PT6A-67A pusher engines, 689
PT 6B, 497
PW120 puller engines, 689
PW200, 497–498
RB50 Trent, 22
RR Dart puller engines, 689
Russian Tu-95, 496
800–1100 shp Astazou, 23
single-spool engine, 515–520
combustion chamber, 504
compressor, 503
enthalpy-entropy diagram, 505
exhaust gas speed, 505, 507
fuel-to-air ratio and bleed ratio, 506
intake, 503
layouts, 501–502
power transmission, 504
propeller thrust, 506
shaft power, 506
temperature–entropy diagram, 501, 503
turbine, 504
specific fuel consumption, 104
speed, 21
thermal efficiency, 98
T56-IHI-14, 24
T58-IHI-110, 24
T64-P4D, 24
TP400-D6, 24
TPF331, 23
Tu116, 525–529
turbine driving compressor and propeller, 42–43

turbofan engines, 510–511, 524
vs. turbojet, 524
TV-12 engines, 23
TV3 VK-1500, 24
two-spool engine
combustion chamber, 507
compressor, 507
free power turbine, 508–510
gas generator turbine, 508
intake, 507
Tyne, 22
Turbopump system, 1356–1357
Turboramjet engine, 37–38, 152, 575–576
ATREX turboramjet engine, 590, 592–593
hybrid engine
air mass flow rate, 590, 592
fuel mass flow rate, 590, 592
HYCAT-1-A, 586
procedure, 585–586
propulsive, thermal, and overall efficiencies, 590, 593
regions, 588–590
specific thrust, 587
thrust *vs.* drag, 590–591
TSFC for, 587–588, 590–591
over/under turboramjet, 576, 580–583
performance
dual mode, 584–585
ramjet mode, 584
turbojet mode, 576, 583–584
P&W J58-1, 590
wraparound turboramjet, 576–580
Turborocket engine, 38
Turboshaft engines, 1263
AE1107C-Liberty turboshaft, 25
definition, 42, 529
double-spool turboshaft, 530–535, 537–539
D-136 Series 1, 25
D-25V, 25
free power turbine, 42–43
GE CT58, 24
Gem, 25
GE T700/CT7, 25
land and sea applications, 24
PT6, 33
100 shp 782, 23
single-spool turboshaft, 529–531, 535–537
T406, 22
TB3-117 BMA, 25
thermal efficiency, 98
Two-dimensional supersonic nozzle
convergent nozzle, 796–802
divergent nozzle, 802–809
Two-engine fuselage installation, 686
Two-spool afterburning turbojet engines, 248–249
examples for
Al-21, 245
J79-GE-17, 244
Pratt & Whitney J57-P-23, 244
Rolls-Royce/SNECMA Olympus 593 Mrk 610, 244–245
layout of, 239
stations and cycle for, 245–246
thermodynamic analysis, 245–248
Two-spool mixed afterburning engine, 333–334
Two-spool non-afterburning turbojet engine
cycle for, 240
GE J57-P-43 WB, 239–240
layout of, 205, 239–240
thermodynamic analysis
combustion chamber, 241–242
high-pressure compressor, 241
high-pressure turbine, 242
intake, 241
jet pipe, 243
low-pressure compressor, 241
low-pressure turbine, 242–243
nozzle, 243–244
Two-spool turbofan engines, 1226–1235
fan and LPC, one shaft, 299–302
combustion chamber, 298
fan, 297
flap blowing engine, 302–307
high-pressure turbine, 298
HPC, 298
intake, 296–297
LPC, 297
LTP, 298–299
LPT and compressor driven, HPT
fan driven, 307–308
geared fan driven, 308–310
Two-stroke engines, 1262
diesel cycle, 458
Otto cycle, 453–454

U

UAVs, *see* Unmanned aerial vehicles
Ultra-bypass ratio (UBPR), 1221
Ultra-high bypass (UHB) engines, 539
Underoxidized, definition, 1336
Unducted fan (UDF) engine, 543–546
578-DX, 541
GE36 UDF, 541, 543
MD-80, 541–542

United States, supersonic aircraft
Boeing 2707-100/200, 570–571
Boeing 2707-300, 571
Convair BJ-58, 571–572
HSCT, 572
Lockheed L-2000, 570–571
NASA AD-1, 571–572
Unmanned aerial vehicles (UAVs), 52
benefits, 1256
categorization
European classifications, 1260
function, 1257
range/altitude, 1257–1259
size, 1259–1260
vs. manned aircraft, 1256
military and civil applications, 1256
power plants
electric engines, 1260–1262
engine characteristics, 1263–1265
gas turbine engines, 1263
internal combustion engines, 1262–1263
solar-and fuel-cell systems, 53

V

Valved pulsejet engine
combustion chamber, 139
cycle, 137–138
drawback of, 136
examples, 140–143
German V-1 missile, 135–136
intake/diffuser, 138–139
one-way valve/check valves, 135–136
Valveless pulsejet engine, 135–136, 143–144
Vaned diffuser
channel diffuser, 888–889
conical diffuser, 890–892
isentropic vaned diffuser, 893–894
performance maps, 889–890
vs. vaneless diffuser, 895–896
Vaneless diffuser
compressible flow, 887–888
incompressible flow, 886–887
Variable-cycle engine (VCE), 58–59
Variable geometry nozzles
for afterburning engine, 792
central plug, 790
ejector nozzle, 790–791
iris nozzle, 791
Variable geometry ramjets, 153–154, 173–175
Variable pitch propellers, 466
Variable stator vanes (VSV), 666
VCE, *see* Variable-cycle engine
Vectored thrust engine, 343–344
Velocity triangles, 962, 967
for axial turbine, 1062–1067, 1079, 1097–1104, 1106, 1141
and blade shape, 960–961
for different degree of reaction, 951–954
of first stage, 943–944
for high turning supersonic impulse cascade, 996
low turning supersonic compressor cascade, 996–997
over stage, 939–940
in radial inflow turbines, 1159–1160
single stage, inlet and outlet of, 933–934
types, 935–937
Venera-7, 1275
V2500 engine, 695, 743
Vertical/short takeoff and landing (V/STOL), 338–339
switch-in deflector system
cruise, 344–348
takeoff/lift thrust, 344, 349–351
vectored thrust engine, 343–344
swiveling nozzles, 339–343
V-1 flying bomb, 135–136, 141–143
Vickers Gunbus, 12–13
Viper, turbojet engine, 20
Volumetric efficiency, 448–449
Volute
geometry, 896
shapes of, 846
Von Karman series nose, missiles, 1279–1280
von Ohain, Hans, 3, 15–17, 203
von Ohain engine, 844
V-22 Osprey aircraft, 22–23, 25, 498–499, 908
V-2 rocket, 1275–1276
V-type engines, 14, 432

W

WAC Corporal, 594
Wan Hu, 4–5, 1274
Wankel engine, 429–431
Water injection, 250–252
Westland Wyvern TF MK2 long-distance ship airplane, 690
Wet rating, 250
Whittle, Sir Frank, 3, 203
patent of, 15–16
W.1 engine and Gloster E28/39, 16–17
Whittle engine, 844
Williams F107-WR-402 turbofan engine, 377–378

Wind turbines, 1059
Winged rocket, 1282–1283
Wing installation, 467
  above the wing, 682–684
  buried in the wing, 680–682
  over/under turboramjet, 581
  pod installation, 682–683
  turboprop engine, 513–514
Wraparound turboramjet engine, 576–577
  in Convair BJ-58 and SR-71 aircraft, 576
  operation
    as ramjet engine, 579–580
    as turbojet engine, 577–579
  temperature-entropy plane, 576–577
Wright brothers
  Flyer I, 3, 10–11
  Flyer II and III, 11
  Gliders I, II, and III, 10
  Wright type A, 11
W.1 turbojet engine, 203

X

X-2, 594
X-7, 594
X-10, 594
X-15, 32, 594
X-30, 594–595
X-31, 53
X-35, 52
X-43, 595–596
X-43A scramjet, 32
XB-70 aircraft, 810
XB-42 engine, 690
XI monoplane, 11–12
X39 nuclear turbojet engine, 41–42
X-planes, 3
X-type engines, 432

Z

Zeppelin LZ-1 airship, 14
Zero-lift drag coefficient, 106


Taylor & Francis
Taylor & Francis Group
http://taylorandfrancis.com